Journal of Sensors

Recent Advances in Smart Sensor Networks and 5G

Lead Guest Editor: Gengxin Sun
Guest Editors: Chih-Cheng Chen and Fatih Özyurt

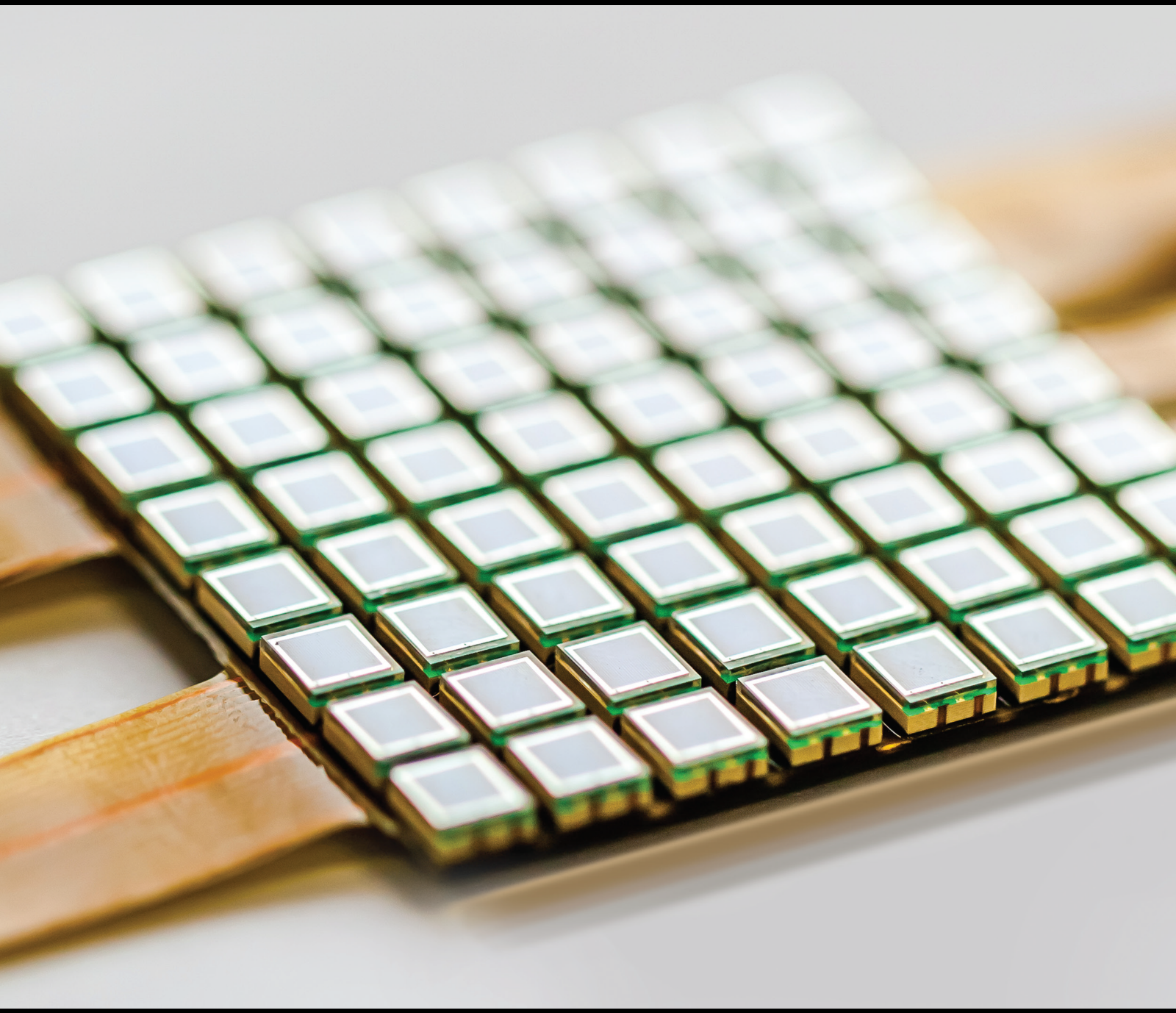

Recent Advances in Smart Sensor Networks and 5G

Journal of Sensors

Recent Advances in Smart Sensor Networks and 5G

Lead Guest Editor: Gengxin Sun
Guest Editors: Chih-Cheng Chen and Fatih Özyurt

Contents

Contents

Contents

Contents

Contents

Hindawi
Journal of Sensors
Volume 2023, Article ID 9801242, 1 page
https://doi.org/10.1155/2023/9801242

Retraction

Retracted: An Inertial Sensing-Based Approach to Swimming Pose Recognition and Data Analysis

Journal of Sensors

Received 31 October 2023; Accepted 31 October 2023; Published 1 November 2023

This article has been retracted by Hindawi following an investigation undertaken by the publisher [1]. This investigation has uncovered evidence of one or more of the following indicators of systematic manipulation of the publication process:

(1) Discrepancies in scope
(2) Discrepancies in the description of the research reported
(3) Discrepancies between the availability of data and the research described
(4) Inappropriate citations
(5) Incoherent, meaningless and/or irrelevant content included in the article
(6) Peer-review manipulation

The presence of these indicators undermines our confidence in the integrity of the article's content and we cannot, therefore, vouch for its reliability. Please note that this notice is intended solely to alert readers that the content of this article is unreliable. We have not investigated whether authors were aware of or involved in the systematic manipulation of the publication process.

Wiley and Hindawi regrets that the usual quality checks did not identify these issues before publication and have since put additional measures in place to safeguard research integrity.

We wish to credit our own Research Integrity and Research Publishing teams and anonymous and named external researchers and research integrity experts for contributing to this investigation.

The corresponding author, as the representative of all authors, has been given the opportunity to register their agreement or disagreement to this retraction. We have kept a record of any response received.

References

[1] S. Xu and S. Lee, "An Inertial Sensing-Based Approach to Swimming Pose Recognition and Data Analysis," *Journal of Sensors*, vol. 2022, Article ID 5151105, 12 pages, 2022.

Hindawi
Journal of Sensors
Volume 2023, Article ID 9864012, 1 page
https://doi.org/10.1155/2023/9864012

Retraction

Retracted: Sports Injury Risk Assessment Based on Blockchain and Internet of Things

Journal of Sensors

Received 10 October 2023; Accepted 10 October 2023; Published 11 October 2023

This article has been retracted by Hindawi following an investigation undertaken by the publisher [1]. This investigation has uncovered evidence of one or more of the following indicators of systematic manipulation of the publication process:

(1) Discrepancies in scope
(2) Discrepancies in the description of the research reported
(3) Discrepancies between the availability of data and the research described
(4) Inappropriate citations
(5) Incoherent, meaningless and/or irrelevant content included in the article
(6) Peer-review manipulation

The presence of these indicators undermines our confidence in the integrity of the article's content and we cannot, therefore, vouch for its reliability. Please note that this notice is intended solely to alert readers that the content of this article is unreliable. We have not investigated whether authors were aware of or involved in the systematic manipulation of the publication process.

In addition, our investigation has also shown that one or more of the following human-subject reporting requirements has not been met in this article: ethical approval by an Institutional Review Board (IRB) committee or equivalent, patient/participant consent to participate, and/or agreement to publish patient/participant details (where relevant).

Wiley and Hindawi regrets that the usual quality checks did not identify these issues before publication and have since put additional measures in place to safeguard research integrity.

We wish to credit our own Research Integrity and Research Publishing teams and anonymous and named external researchers and research integrity experts for contributing to this investigation.

The corresponding author, as the representative of all authors, has been given the opportunity to register their agreement or disagreement to this retraction. We have kept a record of any response received.

References

[1] J. Liu, "Sports Injury Risk Assessment Based on Blockchain and Internet of Things," *Journal of Sensors*, vol. 2021, Article ID 6820728, 13 pages, 2021.

Hindawi
Journal of Sensors
Volume 2023, Article ID 9847567, 1 page
https://doi.org/10.1155/2023/9847567

Retraction

Retracted: Piano Automatic Composition and Quantitative Perception under the Data-Driven Architecture

Journal of Sensors

Received 10 October 2023; Accepted 10 October 2023; Published 11 October 2023

This article has been retracted by Hindawi following an investigation undertaken by the publisher [1]. This investigation has uncovered evidence of one or more of the following indicators of systematic manipulation of the publication process:

(1) Discrepancies in scope
(2) Discrepancies in the description of the research reported
(3) Discrepancies between the availability of data and the research described
(4) Inappropriate citations
(5) Incoherent, meaningless and/or irrelevant content included in the article
(6) Peer-review manipulation

The presence of these indicators undermines our confidence in the integrity of the article's content and we cannot, therefore, vouch for its reliability. Please note that this notice is intended solely to alert readers that the content of this article is unreliable. We have not investigated whether authors were aware of or involved in the systematic manipulation of the publication process.

Wiley and Hindawi regrets that the usual quality checks did not identify these issues before publication and have since put additional measures in place to safeguard research integrity.

We wish to credit our own Research Integrity and Research Publishing teams and anonymous and named external researchers and research integrity experts for contributing to this investigation.

The corresponding author, as the representative of all authors, has been given the opportunity to register their agreement or disagreement to this retraction. We have kept a record of any response received.

References

[1] C. Ren, "Piano Automatic Composition and Quantitative Perception under the Data-Driven Architecture," *Journal of Sensors*, vol. 2022, Article ID 9038427, 12 pages, 2022.

Hindawi
Journal of Sensors
Volume 2023, Article ID 9784172, 1 page
https://doi.org/10.1155/2023/9784172

Retraction

Retracted: Physiological Index Monitoring of Wearable Sports Training Based on a Wireless Sensor Network

Journal of Sensors

Received 3 October 2023; Accepted 3 October 2023; Published 4 October 2023

This article has been retracted by Hindawi following an investigation undertaken by the publisher [1]. This investigation has uncovered evidence of one or more of the following indicators of systematic manipulation of the publication process:

(1) Discrepancies in scope
(2) Discrepancies in the description of the research reported
(3) Discrepancies between the availability of data and the research described
(4) Inappropriate citations
(5) Incoherent, meaningless and/or irrelevant content included in the article
(6) Peer-review manipulation

The presence of these indicators undermines our confidence in the integrity of the article's content and we cannot, therefore, vouch for its reliability. Please note that this notice is intended solely to alert readers that the content of this article is unreliable. We have not investigated whether authors were aware of or involved in the systematic manipulation of the publication process.

In addition, our investigation has also shown that one or more of the following human-subject reporting requirements has not been met in this article: ethical approval by an Institutional Review Board (IRB) committee or equivalent, patient/participant consent to participate, and/or agreement to publish patient/participant details (where relevant).

Wiley and Hindawi regrets that the usual quality checks did not identify these issues before publication and have since put additional measures in place to safeguard research integrity.

We wish to credit our own Research Integrity and Research Publishing teams and anonymous and named external researchers and research integrity experts for contributing to this investigation.

The corresponding author, as the representative of all authors, has been given the opportunity to register their agreement or disagreement to this retraction. We have kept a record of any response received.

References

[1] Z. Lu, Z. Li, and L. Zhang, "Physiological Index Monitoring of Wearable Sports Training Based on a Wireless Sensor Network," *Journal of Sensors*, vol. 2021, Article ID 7552510, 10 pages, 2021.

Hindawi
Journal of Sensors
Volume 2022, Article ID 7027086, 12 pages
https://doi.org/10.1155/2022/7027086

Research Article

Wearable Psychological Stress Monitoring Equipment and Data Analysis Based on a Wireless Sensor

Huixiang Xu,[1] **Nan Zhang**,[2,3] **and Qiuju Liu**[4]

[1]*School of Information Engineering, Zhengzhou University of Technology, Zhengzhou, Henan 450044, China*
[2]*Beijing Sport University, School of Psychology, Beijing 10084, China*
[3]*Zhengzhou University of Technology, Physical Education Institute, Zhengzhou, Henan 450000, China*
[4]*School of Information Engineering, Zhengzhou University of Technology, Zhengzhou, Henan 450000, China*

Correspondence should be addressed to Qiuju Liu; delight@njau.edu.cn

Received 26 November 2021; Revised 20 April 2022; Accepted 22 April 2022; Published 9 June 2022

Academic Editor: Gengxin Sun

With the rapid development of social economy, human psychological pressure is an important factor affecting human health. Excessive psychological pressure will lead to serious psychological diseases such as depression and anxiety. The traditional psychological stress monitoring method is mainly limited to the psychological scale. This method has a certain subjectivity, so its corresponding test data is not representative. At the hardware design level, this paper will select miniaturized, low-power, and low-cost microphysiological sensors to monitor the psychological pressure level discrimination indicators such as heart rate, body temperature, and heart rate waveform and fully optimize the layout of wireless sensors at the hardware layout level to achieve the high efficiency of the whole system. The detection of human pulse signal and heart rate signal is mainly carried out through microsensors, and the temperature signal is filtered and amplified, and analog-to-digital conversion is carried out to realize the accurate measurement of key signal waveform. At the level of hardware system and software algorithm, this paper creatively proposes a psychological stress recognition algorithm based on evidence theory. By extracting the collected key signal features, we can identify the primary stage of psychological stress and finally realize the evaluation and analysis of individual psychological stress through evidence theory. The experimental results show that the trust degree of an individual psychological stress test is improved by 0.187 compared with the traditional algorithm, and the corresponding psychological stress trust degree is up to 0.988, which has obvious advantages.

1. Introduction

As an important factor affecting human mental health in modern society, the monitoring and data analysis of its key indicators have attracted more and more attention of research institutions and researchers. The traditional psychological stress monitoring is mainly a psychological scale. The commonly used psychological stress scale mainly includes a perceived stress scale, psychological stress scale, and related stress scale. It needs human subjective intervention in identifying and analyzing the level of human psychological stress. Therefore, the corresponding discrimination results often have serious subjective performance, which cannot represent the real situation of individual psychological pressure in a certain sense [1–3]. At the level of traditional psychological stress observation factors, it mainly involves human physiological measurement and physical means measurement. At the level of corresponding physiological measurement, it mainly needs the help of some external instruments and equipment to obtain by sampling and analyzing the corresponding physiological data of the human body. Based on this, the traditional evaluation indexes of human psychological stress include ECG, heart rate, human temperature and photoelectric pulse, speech, and EEG signals [4, 5]. Based on the above relevant indicators, the traditional psychological stress assessment methods include an interview method, psychological detection method, and questionnaire method, but such assessment algorithms often require the active response and cooperation of participants to achieve a more ideal assessment state.

Therefore, the traditional psychological stress monitoring and assessment algorithms have serious subjectivity and lose some authenticity [6–8]. Therefore, how to monitor and analyze human physiological data in real time through sensors, so as to objectively and accurately analyze and study individual psychological pressure and realize the objective quantitative evaluation of individual psychological pressure, is the focus of this study.

Microphysiological sensor network technology with the continuous development of artificial intelligence and pattern recognition technology and low-power, miniaturized, and high-precision wireless physiological sensors provide the possibility for real-time monitoring of key evaluation indicators of psychological stress [9, 10]. The wearable intelligent device formed by miniaturized sensors greatly reduces the cost of real-time monitoring of human physiological characteristics, and its corresponding wearable device operation tends to be simpler and simpler [11]. Through the real-time monitoring of a heart rate sensor, temperature sensor, blood pressure sensor, and acceleration sensor integrated on wearable intelligent devices, individual physiological data can be accurately obtained [12, 13]. The emergence of a microwireless physiological sensor network further reduces the difficulty of data processing. It can realize the real-time transmission of the corresponding physiological data of the human body to the base station or data processing center in a cooperative manner, so as to realize the accurate evaluation and real-time tracking analysis of individual psychological stress. At the same time, individuals can also adjust and treat themselves through real-time data, so as to timely alleviate their own psychological pressure [14].

Based on the above psychological stress detection situation, this paper will design a wearable psychological stress monitoring and data analysis system based on low-power small physiological wireless sensors and conduct detailed research from the software and hardware levels. In terms of system hardware, this paper will select miniaturized, low-power microphysiological sensors to monitor human heart rate, temperature, heart rate waveform, and other psychological stress level discrimination indicators and comprehensively optimize the layout of wireless sensors to achieve high efficiency, high system transmission rate, and anti-interference performance; the sensor data acquisition module collects the human pulse signal and heart rate signal, filters and amplifies the temperature signal, and performs analog-to-digital conversion to achieve accurate measurement of key signals; at the system software level, this paper innovatively proposes a system based on a psychological stress recognition algorithm based on multiphysiological parameter fusion decision-making based on evidence theory. Compared with the traditional algorithm, the algorithm can perform comprehensive judgment and analysis based on more key signals, thereby improving the accuracy and reliability of the judgment and analysis. In this algorithm, multiple physiological data indicators need to be collected and quantified by extracting the key signal features collected, identifying the primary stage of psychological stress, and finally realizing the evaluation and analysis of individual psychological stress through evidence theory. The experimental results show that the trust degree of the individual psychological stress test is 0.187 higher than that of the traditional algorithm, and the corresponding psychological stress trust degree is as high as 0.988, with obvious advantages.

Based on this, the main contents of the article are arranged as follows: the second section of the article will focus on the current research status of wearable psychological stress monitoring devices based on wireless sensors. The third section will focus on the analysis and research of the psychological stress recognition algorithm based on the fusion decision of multiple physiological parameters based on evidence theory and design the software and hardware of wearable psychological stress monitoring equipment. In the fourth section of this paper, the wearable devices designed in this paper will be tested and verified, and the data analysis will be given. Finally, this paper will be summarized.

2. Correlation Analysis: Research Status of Wearable Psychological Stress Monitoring Equipment and Data Analysis Based on a Wireless Sensor

At the level of psychological stress monitoring and data analysis, a large number of scientific research institutions and researchers have analyzed from different angles and also designed a large number of individual psychological stress assessment systems. At the level of corresponding indicators for evaluating the level of psychological stress, relevant researchers in the United States have analyzed and studied individual EEG signals, which mainly study the correlation between EEG asymmetry and psychological stress and depression level. The corresponding experimental results show that EEG asymmetry can indeed be used as an important indicator of individual psychological stress; however, it is relatively difficult to monitor EEG signals [15]. Relevant scientific research institutions in Japan have focused on the correlation between individual psychological stress and individual voice expression and workload. The corresponding fundamental frequency and fundamental frequency jitter of voice signal can best reflect the current pressure faced by individuals. At the same time, with the increase in workload, the corresponding fundamental frequency jitter is more severe [16]. At the level of psychological stress assessment, the mainstream research focuses on human intervention and physiological parameter monitoring. At the level of corresponding physiological parameter monitoring, the mainstream research includes physiological parameter monitoring technology, psychological stress inducing factor setting, and individual psychological stress assessment algorithm. Relevant researchers in the United States have established physiological stress identification models based on four different stressors. At the same time, the stability and reliability of the model are verified [6, 17, 18]. Relevant European institutions assess human psychological stress based on ECG, skin surface temperature, skin surface impedance, and other parameters monitored by individuals,

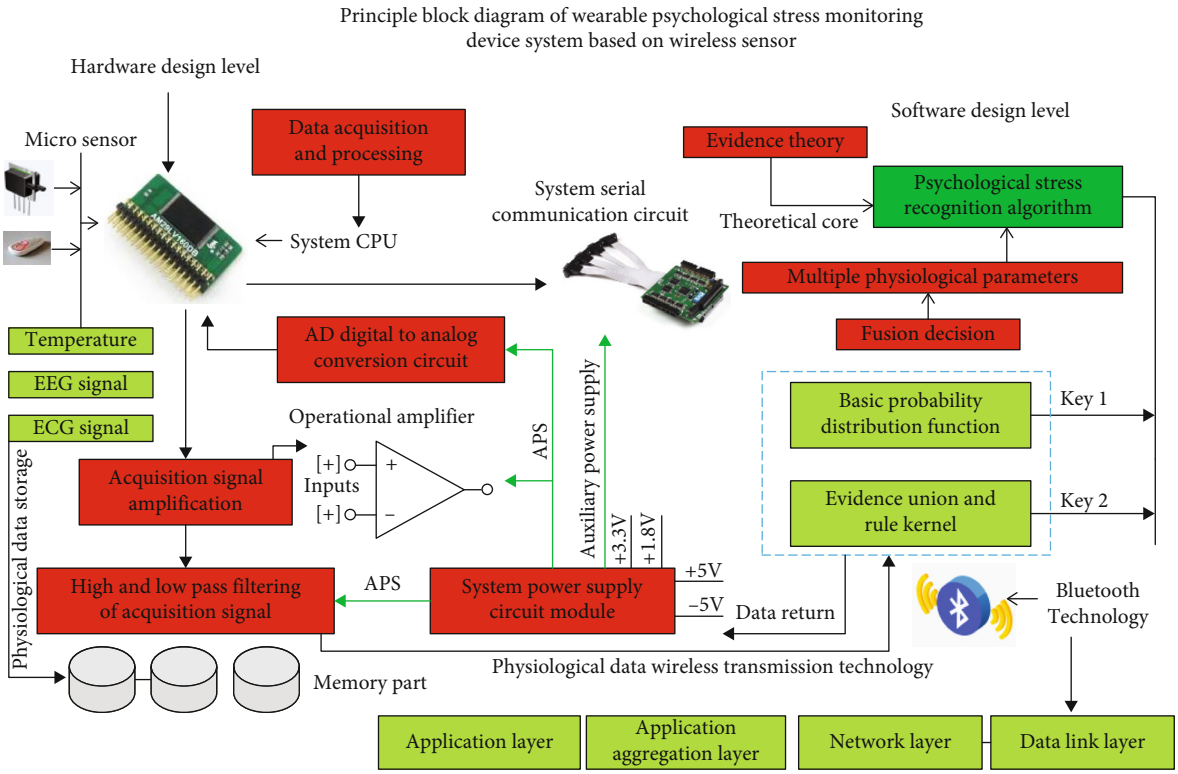

Figure 1: Principle block diagram of the wearable psychological stress monitoring device system based on a wireless sensor.

and the corresponding reliability of psychological stress assessment is about 90%, but this method relies too much on participants' subjective emotional memory ability. At the same time, the response time of EEG signal to psychological stress and the initial emotional representation time are uncertain, so the reliability of the result is low [19, 20]. Relevant American research institutions have proposed a plethysmogram technology to evaluate individual psychological stress. It mainly obtains the plethysmogram of individual heart under static and pressure conditions and then evaluates individual stress by analyzing image features [21, 22]. The advantage of this method is that it does not require individual contact with relevant sensors. However, the reliability of psychological stress corresponding to this method is low [23, 24].

3. Research on Wearable Psychological Stress Monitoring Equipment and Data Analysis Based on a Wireless Sensor

This section mainly analyzes and studies the software and hardware design of the wearable psychological stress monitoring system based on a microwireless sensor network. The corresponding system design principle block diagram is shown in Figure 1. It can be seen from the figure that at the hardware design level, this paper selects the physiological signal acquisition circuit with a single-chip microcomputer as the core, in which the corresponding core module includes a signal acquisition circuit, signal amplification circuit, signal filter circuit, digital-to-analog conversion circuit, serial communication circuit, and power supply circuit. The core algorithm at the corresponding software architecture level is mainly the psychological stress identification algorithm based on evidence theory and multiphysiological parameter fusion decision. The algorithm mainly realizes the evaluation and analysis of individual stress based on the elements collected by the sensor. The main purpose of the algorithm is to establish the psychological stress evaluation and identification model. The core elements include the basic probability distribution function kernel and the evidence association and rule kernel.

3.1. Analysis and Research on the Psychological Stress Recognition Algorithm Based on Evidence Theory and Multiphysiological Parameter Fusion Decision. In order to solve the evaluation accuracy and objectivity of an individual psychological stress evaluation algorithm, a psychological stress recognition algorithm based on evidence theory and multiphysiological parameter fusion decision-making is constructed in this paper. A variety of physiological information such as ECG, skin temperature, and EEG are collected by wireless sensors, and the three kinds of information are combined to form an information fusion body. Before the physiological information fusion, each physiological information acquisition sensor needs to preprocess and analyze the corresponding data and extract its corresponding features; then, the corresponding preprocessing results are evaluated and calculated through the multievidence theory, so as to obtain the probability value of the recognition target corresponding to each physiological parameter compared with other sensors. Finally, the final

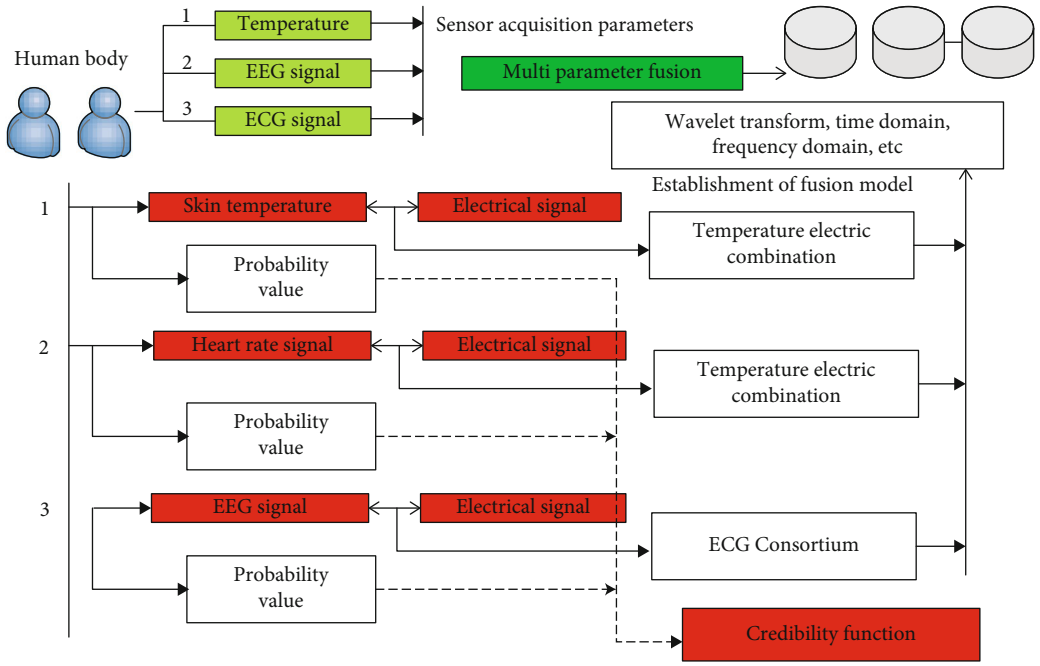

Figure 2: Operation block diagram of the psychological stress recognition algorithm based on evidence theory and multiphysiological parameter fusion decision.

evaluation result is obtained through the psychological pressure credibility function given by the fusion model. The operation block diagram of the psychological stress recognition algorithm based on evidence theory and multiphysiological parameter fusion decision-making proposed in this paper is shown in Figure 2.

It can be seen from the figure that the main core of the algorithm proposed in this paper is two parts, corresponding to the analysis of basic probability distribution function of sensor physiological characteristics, model evidence fusion, and standard definition.

The basic probability distribution function of sensor physiological characteristics is the basis of evidence theory. Combined with the psychological stress characteristics, the target of physiological characteristics to be detected is set as q, and the corresponding b is set as the judgment process of sensor local feature analysis. Therefore, it can be concluded that the representation framework of individual psychological stress recognition corresponds to [d1, d2, d3, d4], and the corresponding d1 represents individual psychological stress. The corresponding d2 represents that the individual does not have psychological stress, d3 represents that the individual does not have any state, and the corresponding d4 represents that the two states of the individual exist at the same time. In the setting of this paper, it is assumed that d3 does not exist, and the combination of d3 and d4 into an individual psychological stress state is not clear. According to the evidence theory, based on this, a specific sensor needs to be assigned probability in an identification space, and the corresponding probability function needs to meet formula (1), where the corresponding c represents the identification space and the corresponding $w : 2^{c-[0,1]}$ represents the basic probability assignment according to the specific algorithm.

$$0 < w(c) < 1 \longrightarrow w(\partial) \longrightarrow w(c1) + w(c2) + \cdots w(c_n) = 1. \tag{1}$$

Based on formula (1), the formula corresponding to the trust function of the specific physiological sensor and its corresponding basic probability assignment relationship is shown in formula (2). A in the corresponding formula (2) represents the specific monitoring physiological index in the sensor and the identification target in the evidence theory:

$$w(b1) + w(b2) + w(b3) + \cdots w(bn) = \mathrm{Bel}(b). \tag{2}$$

Based on formula (2), the calculation formula of a likelihood function of target recognized by a specific sensor is further deduced. The corresponding likelihood function is shown in

$$P(b) = 1 - \left[w\left(\overline{b1}\right) + w\left(\overline{b2}\right) + w\left(\overline{b3}\right) + \cdots w\left(\overline{bn}\right)\right]. \tag{3}$$

Based on this, the uncertainty of psychological stress assessment conveyed by the physiological characteristics monitored by specific sensors is mainly composed of formulas (1) and (2), and the corresponding uncertainty function calculation formula is shown in

$$\begin{cases} \mathrm{error}_1 = P(b_1) - \mathrm{Bel}(b_1), \\ \mathrm{error}_2 = P(b_{\ldots}) - \mathrm{Bel}(b_{\ldots}), \\ \mathrm{error}_3 = P(b_n) - \mathrm{Bel}(b_n). \end{cases} \tag{4}$$

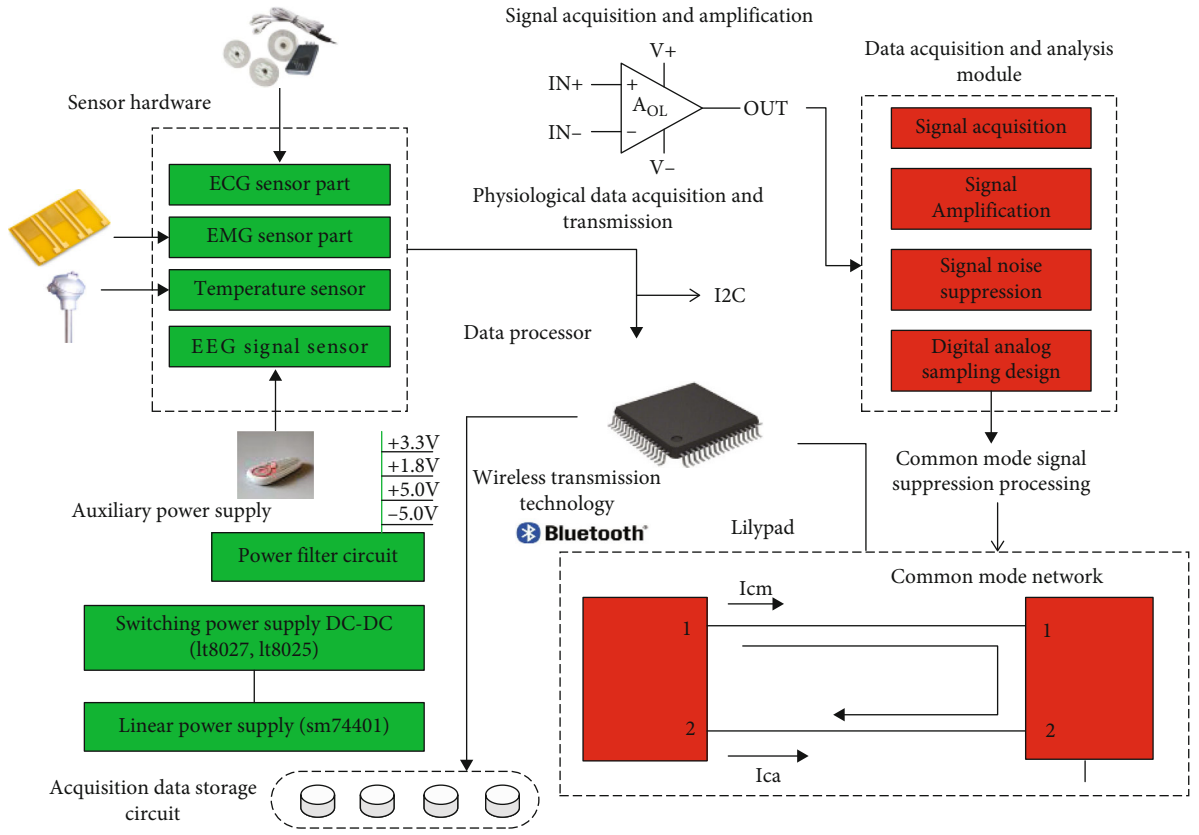

Figure 3: Hardware principle block diagram of wearable psychological stress monitoring based on a wireless sensor.

Combining formulas (1)–(4) can basically determine the basic probability distribution function of sensor physiological characteristics.

At the level of model evidence fusion and standard definition, it is mainly discussed that multiple physiological features are combined and analyzed according to certain laws, so as to realize the multiparameter fusion of psychological stress assessment. The corresponding fusion function is shown in formula (5). The corresponding k in the formula represents the degree of conflict after the judgment of physiological features among multiple sensors, and the closer the corresponding value is to 1, the more intense the conflict between the preliminary judgment results corresponding to the sensor. When the corresponding value is greater than or equal to 1, it is determined that the judgment result is completely excluded. The calculation formula of the corresponding conflict coefficient k is shown in formula (6).

$$\text{error}(b) = \frac{[(\text{error}_1(x_1) * \text{error}_2(x_1)) + \cdots + (\text{error}_i(x_i) * \text{error}_i(x_i))]}{1-k}, \tag{5}$$

$$k = 1 - [[(\text{error}_1(x_1) * \text{error}_2(y_1)) + \cdots + (\text{error}_i(x_i) * \text{error}_i(y_i))] \longrightarrow x_i \cap y_i. \tag{6}$$

For the preliminary identification results of multiple sensors, it needs to meet a certain exchange law and combination law. The corresponding satisfaction formula is shown in formula (7). The corresponding x, y, and z in the formula represent the physiological characteristics monitored by specific sensors, that is, the evidence body in evidence theory.

$$x \otimes y \otimes z \longrightarrow y \otimes x \otimes z \longrightarrow y \otimes z \otimes x. \tag{7}$$

Based on the above theory, the final evaluation principle of psychological stress is as follows, which is also the conclusion of this algorithm:

(1) The trust function value corresponding to the psychological stress of the final decision is the largest among all the sensor trust function values

(2) The value of the trust function corresponding to the final evaluation of psychological stress is greater than 1/2, and the trust function under the fusion is more than twice the value of the trust function of each specific sensor

3.2. Design and Research of a Wearable Psychological Stress Monitoring Device Based on a Wireless Sensor. At the hardware level, this paper designs a wearable psychological stress monitoring system based on the above data processing algorithm. The system mainly monitors individual heart rate, EEG signal, skin temperature, and heart rate waveform based on microphysiological sensors. The corresponding hardware system mainly includes various physiological sensors, power supply module, data acquisition module, data

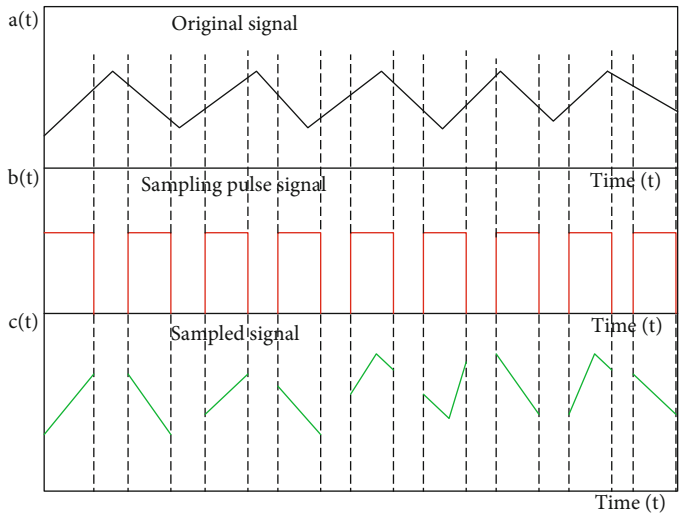

Figure 4: Waveform diagram of digital-to-analog acquisition conversion form of the wearable psychological stress monitoring system based on a wireless sensor.

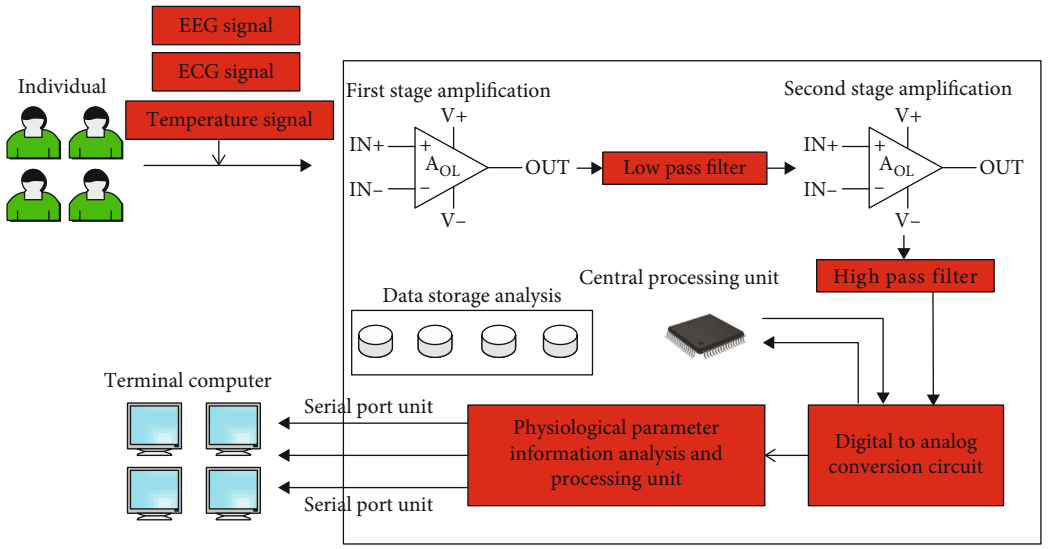

Figure 5: Hardware circuit principle block diagram of the data acquisition and analysis module.

analysis module, and wireless transmission module. The core module includes data acquisition module, data analysis module, and wireless transmission module. Figure 3 is the hardware block diagram of the system. It can be seen from the figure that the hardware system mainly focuses on the design of physiological data information acquisition circuit, and its key indicators include signal acquisition and amplification factor, signal noise and interference suppression processing, digital-to-analog sampling, and conversion rate design.

The central processor part of the system, that is, the signal data processor part, mainly selects STM32 as the core data processor, which can receive the data corresponding to the data acquisition chip using the I2C interface and transmit the data based on the I2C transmission mode. At the same time, the processor selected in this paper also has the function of connecting with the wireless sensor network. Based on this, the single-chip microcomputer model selected in this paper is LilyPad, which has obvious interface and volume advantages as a wearable intelligent device.

In the corresponding data acquisition and analysis module, we need to focus on signal acquisition and amplification, signal noise and interference suppression processing, digital-to-analog sampling, and conversion rate design. In the corresponding signal amplification part, this paper fully combines the weak characteristics of ECG and EEG signals to design the corresponding amplification factor (300 times in this paper) to meet the size of subsequent voltage window and corresponding analysis requirements. At the corresponding noise and interference suppression level, it mainly prints common mode signals mixed in ECG and EEG signals, power frequency power supply clutter signals, and

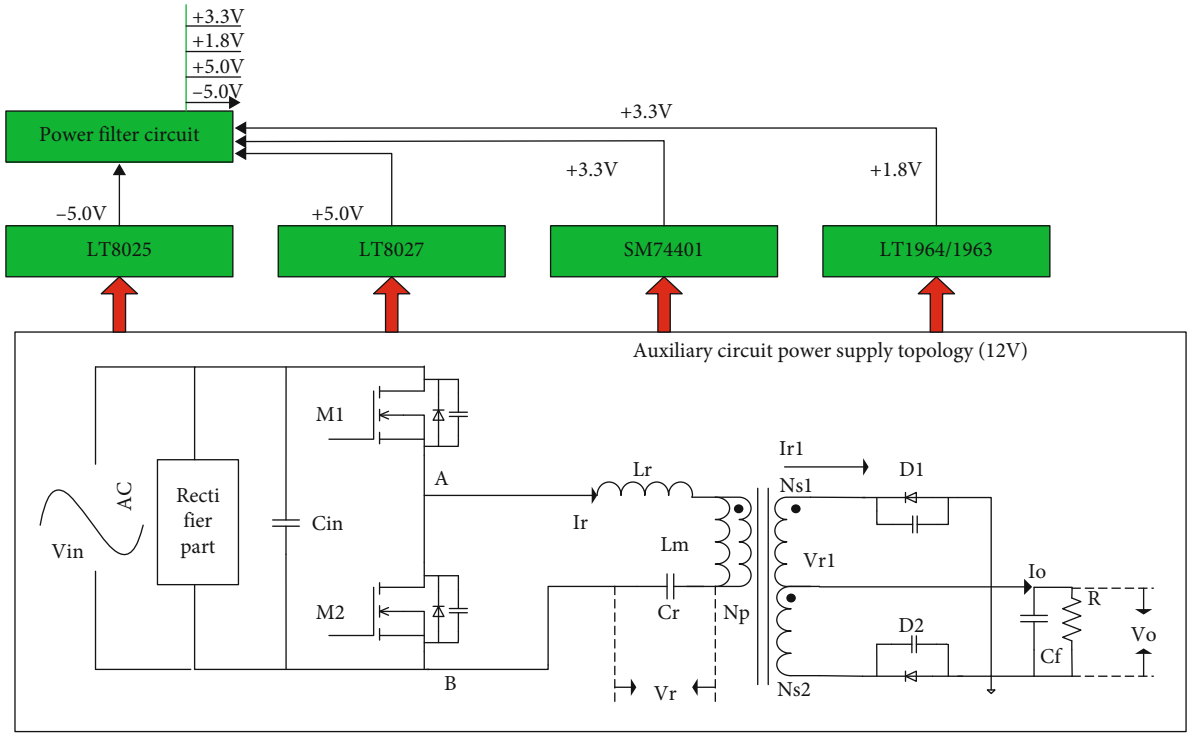

Figure 6: Schematic diagram of the auxiliary power circuit of the hardware system of the data acquisition and analysis module.

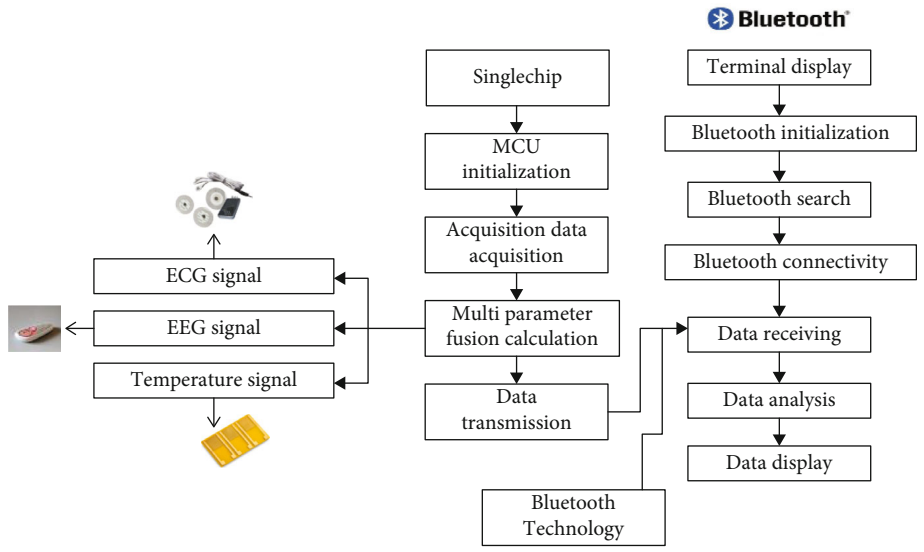

Figure 7: Schematic diagram of hardware system software algorithm flow architecture of the data acquisition and analysis module.

certain interference signals. At the level of corresponding digital-to-analog conversion and sampling rate, the sampling accuracy needs to be considered. The form of digital-to-analog conversion signal used in collecting ECG, EEG, and skin temperature in this paper is shown in Figure 4. In the corresponding figure, $a(t)$ represents the original signal, $b(t)$ represents the sampled pulse signal, and $c(t)$ represents the sampled signal. It can be seen from the formula that the sampling accuracy is mainly determined by the resolution of the sampling chip.

The hardware circuit of data acquisition and analysis module mainly includes front-end circuit module (including front-end amplification module, high-pass filter part, rear-end amplification part, and low-pass filter part), analog-to-digital conversion part, auxiliary power supply part, serial port circuit module part, etc. The corresponding hardware circuit transmission mode of each part is shown in Figure 5. It can be seen from Figure 5 that the precircuit module needs a total of 40 amplifiers. At the same time, the amplification factor of the prestage amplification circuit

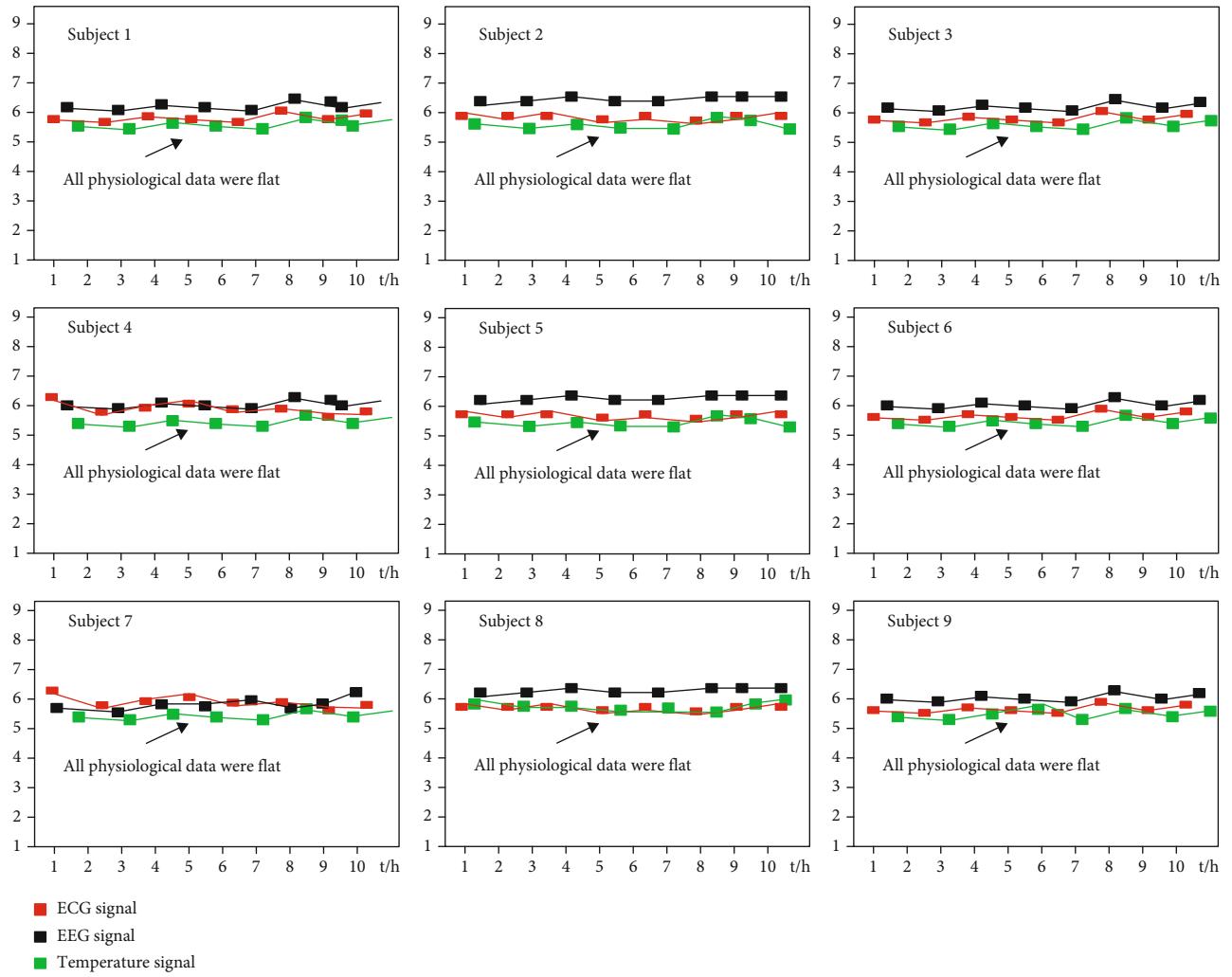

Figure 8: ECG signal, EEG signal, and skin temperature sampling waveform in a calm period.

designed in this paper is 7 times, and the voltage amplitude collected by the corresponding original circuit is 1 mv; then, the signal amplitude amplified by the amplification circuit is 7 mv. At the corresponding differential mode signal elimination level, the differential circuit is mainly used to eliminate the corresponding interference signal. Based on this, the magnification calculation formula of the primary amplification circuit can be obtained, as shown in formula (8). The corresponding resistance in the formula is the amplification factor matching resistance.

$$G = \frac{R_1 + R_0}{R_0}. \tag{8}$$

Based on the above primary amplification, filter processing is carried out, and enter the secondary amplification part at the same time. The magnification selected in the corresponding secondary amplification part is 8 times. At this time, the calculation formula of the corresponding system signal magnification is shown in formula (9), and the corresponding magnification is 56 times.

$$G_{\text{all}} = \left[G_1 : \left(\frac{1 + R_1}{R_0}\right)\right] * \left[G_2 : \left(\frac{1 + R_2}{R_0}\right)\right]. \tag{9}$$

The high-pass filter used in this paper is RC structure, which mainly uses the resonance of resistance and capacitance to filter the high-frequency signal. At the same time, the circuit design of this high-pass filter is simple and the cost is low. Based on equations (10) and (11), the filtering time constant and the corresponding minimum frequency of the high-pass filter used in this paper can be calculated.

$$\begin{cases} f_1 = \dfrac{1}{(2 * \pi * R_1 * C_1)}, \\ f_2 = \dfrac{1}{(2 * \pi * R_2 * C_2)}, \end{cases} \tag{10}$$

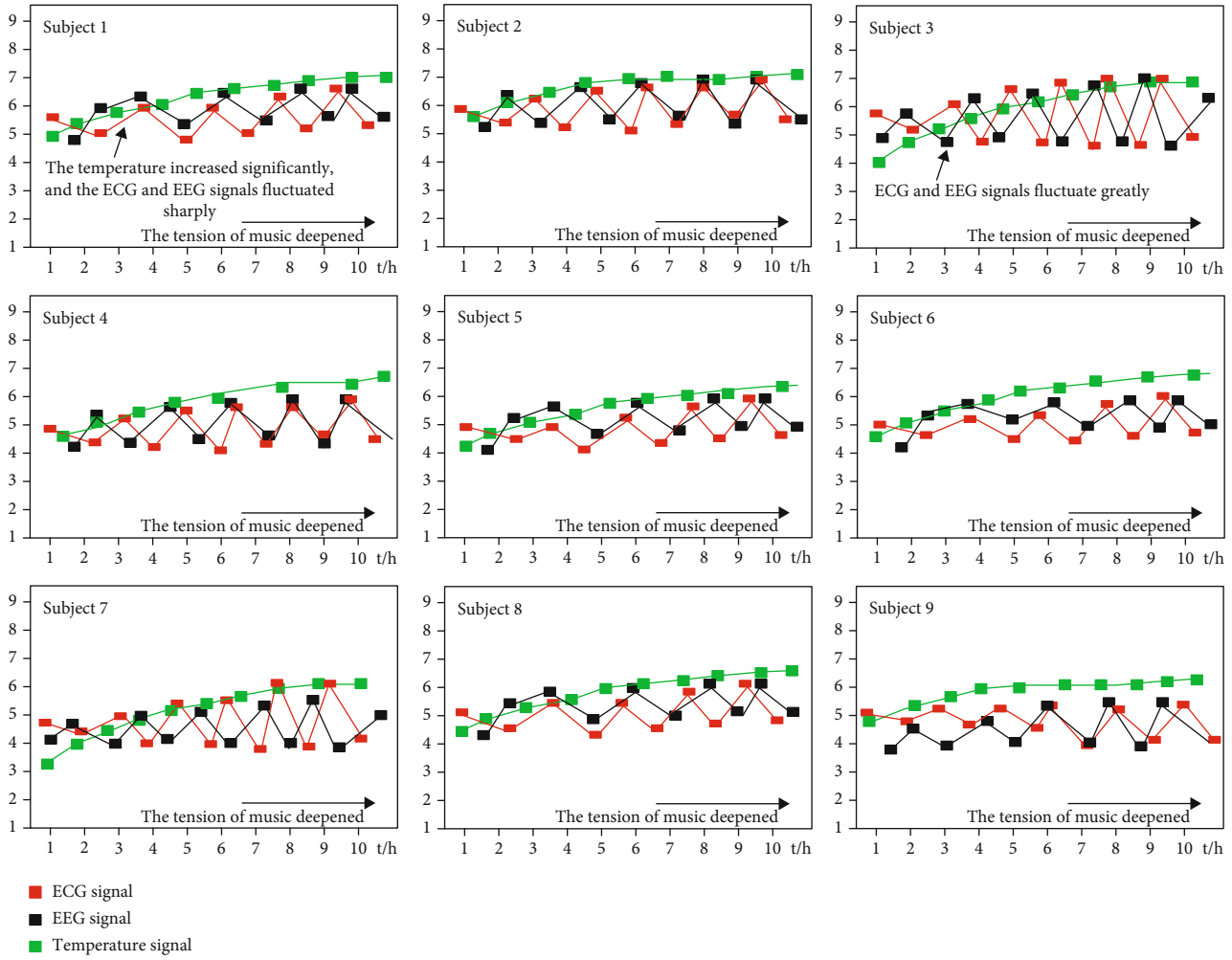

Figure 9: ECG, EEG, and skin temperature sampling waveforms of experimental participants in the psychological stress simulation period.

$$\begin{cases} t_1 = R_1 * C_1, \\ t_2 = R_2 * C_2, \\ t = t_1 + t_2. \end{cases} \tag{11}$$

In the corresponding auxiliary power supply circuit, the conventional DC-DC power chip is mainly used to set up the corresponding auxiliary circuit. The main level of the system designed in this paper includes conventional voltages such as 3.3 V, 5 V, 1.8 V, and -5 V. The chips mainly selected in this paper include power chips such as LT8025, LT8027, and SM74401. The schematic diagram of the corresponding auxiliary power supply circuit is shown in Figure 6.

At the level of corresponding wireless transmission module circuit design, this paper mainly selects Bluetooth technology to realize the circuit design of the wireless transmission module. The corresponding Bluetooth module selected in this paper is HC-09, its corresponding transmission rate can reach 1 Mbps, and the corresponding maximum transmission distance is about 100 m. When the Bluetooth module enters the data transmission working mode, its corresponding four pins are voltage pin VCC, data output pin TX, data input pin RX, and module GND. When the hardware circuit is connected, the data input pin TX of the corresponding Bluetooth module shall be connected with the data output pin RX of the single chip microcomputer, and the corresponding Bluetooth data receiving pin RX shall be connected with the data output pin TX of the single-chip microcomputer.

In the corresponding software algorithm flow architecture part, the corresponding algorithm implementation flow is shown in Figure 7. The main software algorithm flow includes the MCU initialization process, physiological data acquisition and analysis process, algorithm calculation and evaluation process, data transmission process, and data display and interaction process.

At the PCB design level of the hardware part, it mainly reduces the loss caused by reducing the corresponding parasitic parameters by simulating the corresponding parasitic parameters. At the same time, in the aspect of device selection, this paper mainly selects the chip with lower power consumption and reduces the loss of the overall hardware as much as possible in the aspect of device selection.

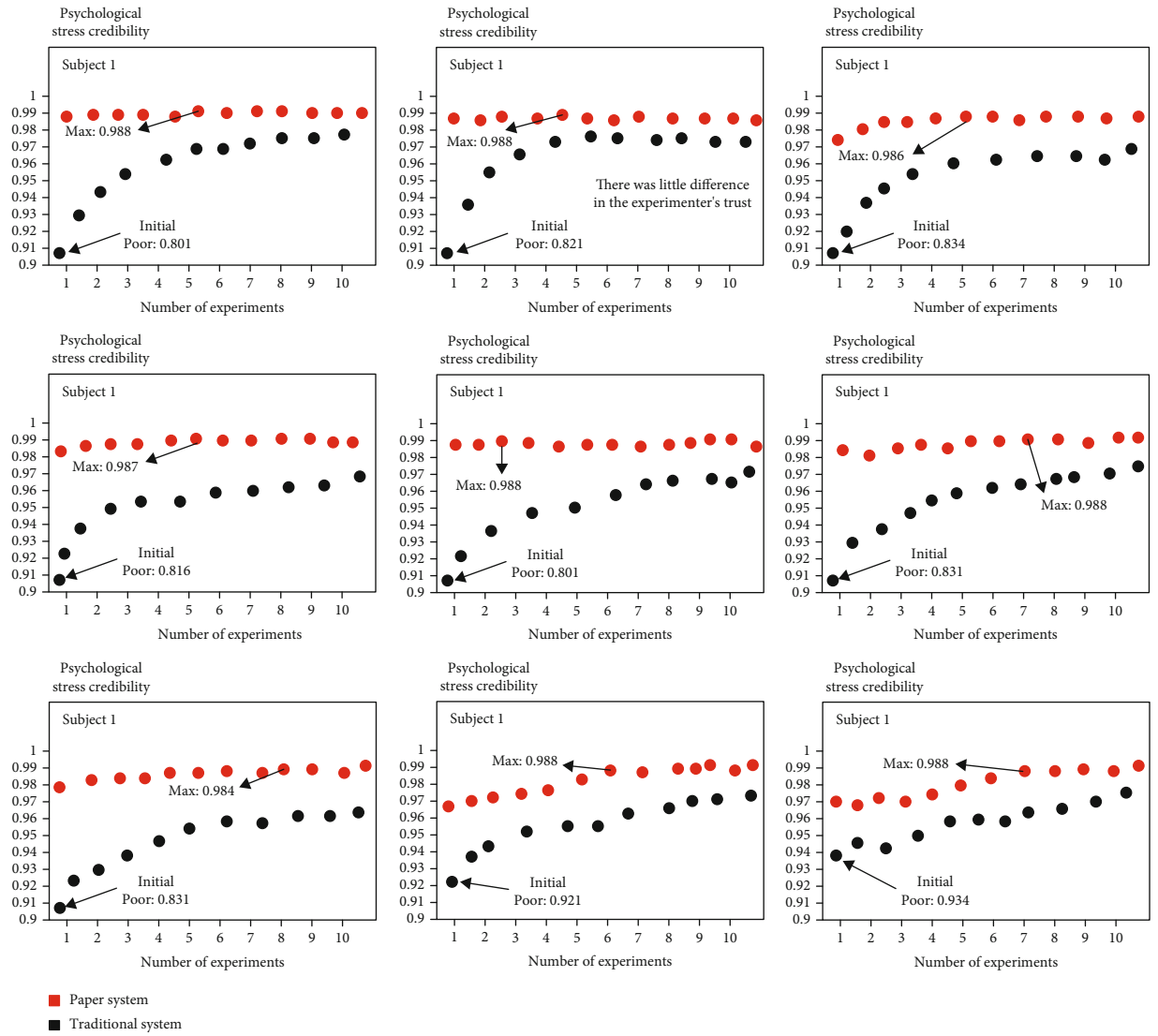

Figure 10: Psychological stress trust curve.

4. Experimental Verification and Data Analysis

The corresponding experimental environment and experimental conditions are as follows: the experimental subjects selected 9 students from related majors of a university as the experimental objects, mainly based on the system designed in this paper to collect their corresponding physiological parameters, such as ECG, EEG, and skin temperature, so as to ensure the normal mental health of the subjects before the corresponding experiment. There were no obvious emotional abnormalities. The corresponding experimental process is as follows: the wearable psychological stress monitoring system equipment based on a wireless sensor designed in this paper is worn to the participants, which calms the experimenters' mood for about 10 minutes before officially entering the experiment, records and stores the corresponding physiological parameter characteristics, and starts playing music from slow to fast after the calm transition period. The physiological parameters of the experimenters were recorded in real time, and their psychological stress level was evaluated.

The ECG, EEG, and skin temperature sampling values of the corresponding 10 college students in the quiet period are shown in Figure 8. It can be seen from the figure that the physiological parameters of the participants in the experiment are basically stable in the current state. At the same time, the psychological stress measurement under the psychological stress evaluation algorithm is a low value, which is more in line with the actual phenomenon.

After the calm period, the corresponding physiological parameters of the experimental participants in the corresponding psychological stress simulation period are shown in Figure 9. It can be seen from the figure that during this period, the corresponding physiological parameters of each participant generally accelerated, the corresponding ECG and EEG signal fluctuations increased significantly, and the skin temperature of the corresponding participants increased significantly.

Based on the above monitoring data and compared with the traditional psychological stress assessment algorithm, the corresponding psychological stress trust curve is shown in Figure 10. It can be seen from the figure that the corresponding psychological stress trust value of most experimental participants in the psychological stress simulation period is improved by 0.187 percentage points compared with the corresponding accuracy of the traditional algorithm, and part of the trust can reach 0.988. Therefore, the wearable psychological stress monitoring system based on a wireless sensor and its corresponding psychological stress evaluation algorithm proposed in this paper have obvious advantages.

Based on the experimental results and experimental data analysis, it can be concluded that the wearable psychological stress monitoring system based on a wireless sensor and the psychological stress identification algorithm based on multiphysiological parameter fusion decision-making based on evidence theory have obvious advantages over the traditional psychological stress estimation system, and its corresponding system reliability and analysis accuracy are significantly improved; therefore, the system has popularization value.

5. Conclusion

This paper mainly analyzes the current research status of individual psychological stress monitoring equipment and data analysis and expounds the problems existing in the traditional psychological stress monitoring technology. Based on the research status, based on the continuous development of microwireless sensor network technology, a wearable psychological stress monitoring device based on a wireless sensor is proposed, and an analysis algorithm is proposed based on the corresponding data analysis. At the hardware level of the system, this paper selects miniaturized and low-power microphysiological sensors to monitor the psychological pressure level discrimination indicators such as human heart rate, temperature, and heart rate waveform, fully optimize the layout of wireless sensors, realize the high efficiency, high transmission rate, and anti-interference performance of the system, and collect human pulse signals and heart rate signals through the sensor data acquisition module. The temperature signal is filtered and amplified, and analog-to-digital conversion is carried out at the same time, so as to realize the accurate measurement of key signals. At the system software level, this paper innovatively proposes a psychological stress identification algorithm based on multiphysiological parameter fusion decision-making based on evidence theory. By extracting the collected key signal features and identifying the primary stage of psychological stress, this paper finally realizes the evaluation and analysis of individual psychological stress through evidence theory. The experimental results show that the trust degree of an individual psychological stress test is improved by 0.187 compared with the traditional algorithm, and the corresponding psychological stress trust degree is up to 0.988, which has obvious advantages. In the follow-up, this paper will comprehensively analyze individual psychological stress based on more physiological data and further optimize the wearable psychological stress monitoring and data analysis system to realize the intellectualization and sustainable development of the system.

Data Availability

The data used to support the findings of this study are available from the corresponding author upon request.

Conflicts of Interest

The authors declare that they have no known competing financial interests or personal relationships that could have appeared to influence the work reported in this paper.

Acknowledgments

This work was financially supported by the Key Scientific Research Projects of Colleges in Henan Province (project name: Research on Gear Fault Feature Analysis and Detection Technology Based on Multisource Information, project number: 21A520045) and Henan Education Science Planning Project (research on the training mode of innovative electronic information talents in Colleges and Universities under the background of new engineering) (2020YB0289).

References

[1] M. Berthelot, F. P. Henry, J. Hunter et al., "Pervasive wearable device for free tissue transfer monitoring based on advanced data analysis: clinical study report," *Journal of Biomedical Optics*, vol. 24, no. 6, pp. 11–16, 2019.

[2] R. Miura, K. Yoshioka, T. Miyamoto, H. Nogami, H. Okada, and T. Itoh, "Estrous detection by monitoring ventral tail base surface temperature using a wearable wireless sensor in cattle," *Animal Reproduction Science*, vol. 180, no. 4, pp. 50–57, 2017.

[3] G. Xu, X. Yang, Q. Yang, J. Zhao, and Y. Li, "Design on magnetic coupling resonance wireless energy transmission and monitoring system for implanted devices," *IEEE Transactions on Applied Superconductivity*, vol. 26, no. 4, pp. 1–4, 2016.

[4] R. Wu, L. Ma, A. B. Patil et al., "A facile method to prepare a wearable pressure sensor based on fabric electrodes for human motion monitoring," *Textile Research Journal*, vol. 89, no. 23-24, pp. 5144–5152, 2019.

[5] M. Brodie, M. Coppens, S. R. Lord et al., "Wearable pendant device monitoring using new wavelet-based methods shows daily life and laboratory gaits are different," *Medical & Biological Engineering & Computing*, vol. 54, no. 4, pp. 663–674, 2016.

[6] M. A. Brodie, E. M. Pliner, A. Ho et al., "Big data vs accurate data in health research: large-scale physical activity monitoring, smartphones, wearable devices and risk of unconscious bias," *Medical Hypotheses*, vol. 119, no. 2, pp. 32–36, 2018.

[7] J. Feng, C. Zhou, C. He, Y. Li, X. Ye, and H. Cheng, "Development of an improved wearable device for core body temperature monitoring based on the dual heat flux principle," *Physiological Measurement*, vol. 38, no. 4, pp. 652–668, 2017.

[8] S. Buijs, F. Booth, G. Richards et al., "Behavioural and physiological responses of laying hens to automated monitoring

equipment," *Applied Animal Behaviour Science*, vol. 199, no. 5, pp. 17–23, 2018.

[9] D. Maity, K. Rajavel, and R. Kumar, "MWCNT enabled smart textiles based flexible and wearable sensor for human motion and humidity monitoring," *Cellulose*, vol. 28, no. 4, pp. 2505–2520, 2021.

[10] F. Wang, S. Liu, L. Shu, and X. M. Tao, "Low-dimensional carbon based sensors and sensing network for wearable health and environmental monitoring," *Carbon*, vol. 121, pp. 353–367, 2017.

[11] E. Pittella, S. Pisa, and M. Cavagnaro, "Breath activity monitoring with wearable UWB radars: measurement and analysis of the pulses reflected by the human body," *IEEE Transactions on Biomedical Engineering*, vol. 63, no. 7, pp. 1447–1454, 2016.

[12] S. J. Paul, I. Elizabeth, and B. Gupta, "Ultrasensitive wearable strain sensors based on a VACNT/PDMS thin film for a wide range of human motion monitoring," *ACS Applied Materials & Interfaces*, vol. 13, no. 7, pp. 8871–8879, 2021.

[13] M. C. Caccami, M. Y. S. Mulla, C. D. Natale, and G. Marrocco, "Graphene oxide-based radiofrequency identification wearable sensor for breath monitoring," *IET Microwaves Antennas & Propagation*, vol. 12, no. 4, pp. 467–471, 2018.

[14] I. C. Jeong, D. Bychkov, and P. C. Searson, "Wearable devices for precision medicine and health state monitoring," *IEEE Transactions on Biomedical Engineering*, vol. 66, no. 5, pp. 1242–1258, 2019.

[15] F. Ferreira, G. Luxardi, B. Reid, L. Ma, V. K. Raghunathan, and M. Zhao, "Real-time physiological measurements of oxygen using a non-invasive self-referencing optical fiber microsensor," *Nature Protocols*, vol. 15, no. 2, pp. 207–235, 2020.

[16] A. Asif, S. H. Park, A. M. Soomro et al., "Microphysiological system with continuous analysis of albumin for hepatotoxicity modeling and drug screening," *Journal of Industrial and Engineering Chemistry*, vol. 98, pp. 318–326, 2021.

[17] W. Schlotz, R. Kumsta, I. Layes, S. Entringer, A. Jones, and S. Wüst, "Covariance between psychological and endocrine responses to pharmacological challenge and psychosocial stress: a question of timing," *Psychosomatic Medicine*, vol. 70, no. 7, pp. 787–796, 2008.

[18] H. R. Al Ghayab, Y. Li, S. Siuly, and S. Abdulla, "Epileptic EEG signal classification using optimum allocation based power spectral density estimation," *IET Signal Processing*, vol. 12, no. 6, pp. 738–747, 2018.

[19] B. H. Yilmaz, C. M. Yilmaz, and C. Kose, "Diversity in a signal-to-image transformation approach for EEG-based motor imagery task classification," *Medical & Biological Engineering & Computing*, vol. 58, no. 2, pp. 443–459, 2020.

[20] H. Jebelli, S. Hwang, and S. H. Lee, "EEG signal-processing framework to obtain high-quality brain waves from an off-the-shelf wearable EEG device," *Journal of Computing in Civil Engineering*, vol. 32, no. 1, article 04017070, 2018.

[21] A. E. Bennett and J. M. Kearney, "Maternal sociodemographic and health behaviours associated with adiposity in infants as measured by air displacement plethysmography," *Early human development*, vol. 140, pp. 104887–104892, 2020.

[22] N. Sugita, M. Akay, Y. M. Akay, and M. Yoshizawa, "Noise reduction technique for single-color video plethysmography using singular spectrum analysis," *IEEE Journal of Biomedical and Health Informatics*, vol. 24, no. 6, pp. 1788–1795, 2020.

[23] W. J. Chang, L. B. Chen, C. Y. Sie, and C. H. Yang, "An artificial intelligence edge computing-based assistive system for visually impaired pedestrian safety at zebra crossings," *IEEE Transactions on Consumer Electronics*, vol. 67, no. 1, pp. 3–11, 2021.

[24] K. Kuru, D. Ansell, M. Jones, C. de Goede, and P. Leather, "Feasibility study of intelligent autonomous determination of the bladder voiding need to treat bedwetting using ultrasound and smartphone ML techniques," *Medical & Biological Engineering & Computing*, vol. 57, no. 5, pp. 1079–1097, 2019.

Hindawi
Journal of Sensors
Volume 2022, Article ID 1255850, 10 pages
https://doi.org/10.1155/2022/1255850

Research Article

Computing Cluster and Intelligent Sensor Network in the Analysis and Application of College Students' Physical Exercise Behavior

Lei Zhu

Wuhu Institute of Technology, Wuhu Anhui 241003, China

Correspondence should be addressed to Lei Zhu; z_l@whit.edu.cn

Received 27 October 2021; Accepted 19 November 2021; Published 5 May 2022

Academic Editor: Gengxin Sun

Based on computing cluster and intelligent sensor network technology, in view of network delay, this paper uses first-in-first-out buffers to be built at the node sending and receiving ports to convert the random delay of the physical exercise behavior network control system into a fixed delay. First, we analyze and model the controller design of the physical exercise behavior network control system. Through the analysis and synthesis of the current situation and methods of the physical exercise behavior network control system controller at home and abroad, the sensor is driven by time, and the controller and actuator are used. In the event-driven method, the sending and receiving buffers are set on the network ports of the nodes, the delay is changed from random to fixed at the same time, and the problem of data packet timing disorder is improved. Secondly, through the analysis of the internal control system node, the internal AD, DA conversion, data storage, CPU internal tasks, and task scheduling algorithm modules are implemented in the model. Experimental simulations show that, in view of the difficulty of unsatisfactory tracking effect caused by the aliasing of multiple target signals collected by sensor nodes, a combined tracking strategy is adopted; that is, multiple tracking dynamic clusters are combined into one for tracking when the sports behavior is close. In order to avoid the heavy communication and computing requirements in the centralized mode, mobile sensor networks usually adopt a distributed fusion architecture. The dynamic cluster maintenance and positioning strategy are given. In the stage of separation of multiple sports behaviors, a dynamic cluster decomposition algorithm based on boundary search is proposed, which can effectively determine the degree of separation of sports behaviors and provide a basis for establishing new dynamic clusters for follow-up tracking. The results show that the algorithm can effectively realize the merging and decomposition of dynamic clusters of multiple sports behaviors and effectively realize the dynamic tracking of multiple sports behaviors.

1. Introduction

With the development of electronic computers, network communication technology, and sensor technology, the structure of the control system is becoming more and more complex, the network topology is increasing day by day, and the complexity of the exchange and sharing of information between the various components of the system has increased sharply. The centralized control system can no longer meet the increasingly complex control performance requirements [1]. In order to effectively solve the above problems, a networked control system was created, namely, the Netwoked Control System (NCS). The emergence of the NCS effectively solved the limited limitations of the traditional centralized control system. The limitations of computing and communication resources and the spatial layout of system components reduce the structural complexity of the control system to a certain extent and save operation and maintenance costs. It is used in aerospace, vehicle systems, remote control robots, and industrial control with high risks [2–5]. The physical exercise behavior capture system is a technical device used to measure the physical exercise behavior status of physical exercise behavior objects in three-dimensional space. The physical exercise behavior capture system is

widely used in the fields of film digital special effects and animation, games and human-computer interaction, training and simulation, health monitoring and rehabilitation training, and navigation. There are many ways to capture physical exercise behavior. The current mainstream is the acquisition of human physical exercise behavior based on multicamera and the acquisition of human physical exercise behavior based on microsensor. Research on the physical exercise behavior network control system is far from enough to study the control strategy. It is also necessary to fully consider the influence of network factors. Through the research on related scheduling algorithms, the control strategy and network scheduling algorithm can be reasonably modeled and systematically. This analysis has important practical significance for the development of physical exercise behavior network control system [6–9].

Guleria and Verma [10] take some time-varying delay physical exercise behavior network control systems, and the corresponding random delay is converted into a fixed delay by setting the receiving first-in first-out buffer queue at the front end of the controller and the actuator. On this basis, Otoum et al. [11] designed a "delay compensation state observer." The main idea is to use the observer to estimate the state of the object, use the predictor to predict the system state in advance, calculate the corresponding control signal, and realize the delay compensation. The measurement data is stored in the first-in-first-out buffer queue on the controller side, and the controller's signal is stored in the queue. Zhu [12] converts the delay caused by the network in the system into a fixed delay, which can be based on the fixed delay. Aiming at the random physical exercise behavior network control system model where the random time delay is greater than one sampling period and the controller and the actuator are both event-driven, Verma et al. [13] studied single input single output and multiple input multiple. The closed-loop stability of the output is based on the known conditions of the network state variables. Bhushan et al. [14] designed the optimal controller of a long-delay network control system to make the exponential mean square of the system stable. Some researchers have proposed the MEF-TOD dynamic scheduling algorithm. In the event of a network conflict, the sensor message with the largest error is transmitted first, and the message that is not transmitted will be discarded. Research has shown that it is ensuring sufficient network transmission rate. Under the premise of this method, the performance of the system can be guaranteed by using this method. At the same time, the appropriate use of predictors or linear prediction techniques is an effective supplement to the algorithm [15–18]. Some scholars have proposed the MTS (Mixed Traffic Scheduler) scheduling algorithm for the physical exercise behavior network control system using the controller area network (CAN) and combined with the earliest time limit dynamic scheduling algorithm (Earliest Deadline, ED) and time limit monotonic static scheduling; it has higher schedulability than the DM scheduling algorithm and a smaller network load than the ED scheduling algorithm. The effectiveness of the algorithm is verified by comparison [19–25].

This paper analyzes and models the communication system of the physical exercise behavior network control system and analyzes the current status and methods of the network scheduling research of the physical exercise behavior network control system at home and abroad. The network protocol is the CAN network protocol with high real-time performance. We implement the CAN network protocol data frame format, network scheduling algorithm (CSMA/AMP), model the storage queue system, data encapsulation function, and network message scheduling function involved in the communication process. The core hardware of the physical exercise behavior capture system in this article is the sensor node and the communication base station, to realize the human physical exercise behavior monitoring system based on the human sensor network as the sports behavior, with low cost, low power consumption, high modularity, high reliability, high-precision, and easy-to-wear, and other characteristics are the design guidelines. A set of human physical exercise behavior monitoring system based on a nine-axis wireless sensor platform was developed, which initially achieved the purpose of real-time physical exercise behavior monitoring. One of these sensor nodes will serve as the central node, which is also responsible for the networking and control of the human sensor network; the base station is responsible for controlling the start and stop of the physical activity capture of the human sensor network, as well as receiving physical activity data and transfer it to the computer.

2. Construction of Analysis Model of College Students' Physical Exercise Behavior Based on Computing Cluster and Intelligent Sensor Network

2.1. Computing Cluster Hierarchical Distribution. The computing cluster hierarchical network consists of a large number of deployed sensor nodes and information gathering nodes. Through wireless communication, they form a multihop self-organizing distributed network system that can autonomously complete designated tasks based on environmental information. Figure 1 shows the hierarchical distribution of computing clusters.

In the physical exercise behavior network control system, the driving mode of the node is divided into time-driven and event-driven. The time-driven working mode refers to the node sampling the signal according to the sampling clock and then performing related data operations. The clock driving mode needs to pay attention to that the nodes must be synchronized; otherwise, it will cause the action of different nodes in the system. There is a time difference; event-driven means that the activation of a node is related to the arrival of the signal. When a certain node receives a certain signal, the node is activated immediately, and then the data is processed and sent; that is, the node executes a specific mode. The action is "driven" by the arrival of a certain "signal;" so, this working method is called event-driven. Under the premise of comprehensively considering system control performance and system real-time

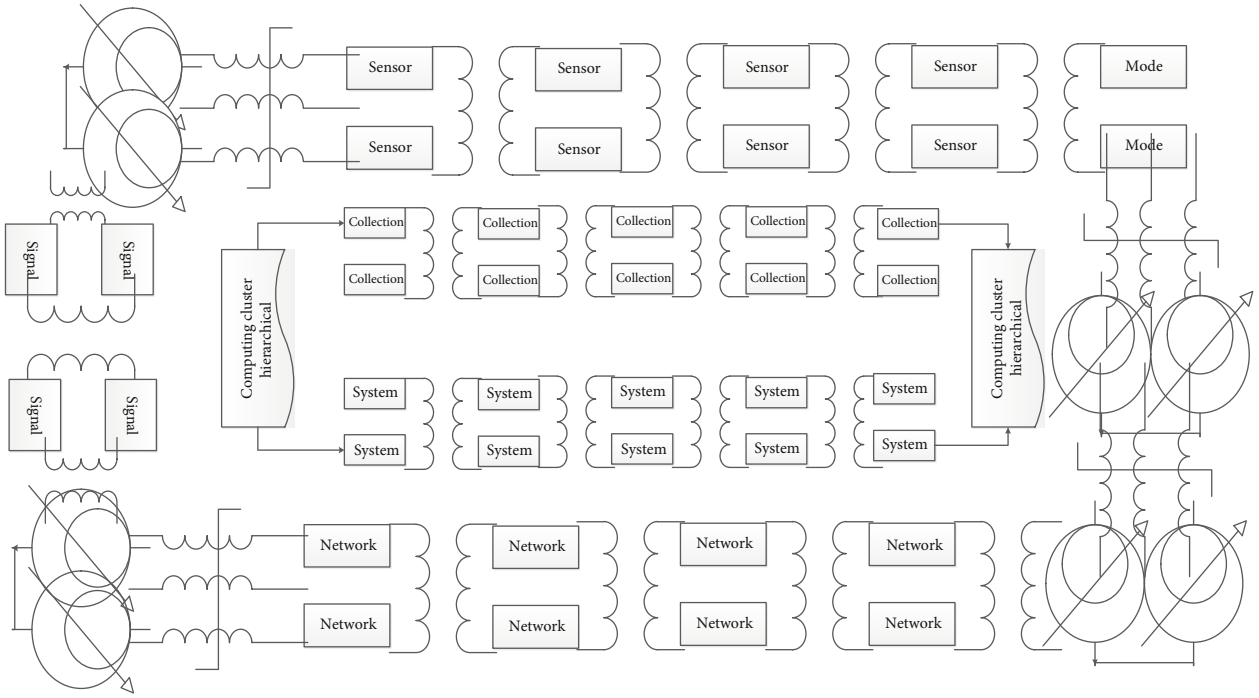

Figure 1: Computing cluster hierarchical structure distribution.

performance, the sensor in this paper is selected as time-driven, timed sampling model data, and controllers, and actuators are event-driven.

$$tf + idf - tf \times idf = 0,$$
$$tf(w_i, D_i) = N_{w_1,D_j} \times \sum_{n=1}^{K} N_{w_n,D_j} \times N. \tag{1}$$

The sensor nodes, controller nodes, and actuator nodes of this system are the final application objects of the control system model. The internal structure of the control system is different for different nodes. The sensor node adopts a time-driven mechanism to realize the function of data collection and package transmission. Its internal AD converter will periodically sample certain parameters of the physical process, and the results will be stored in the RAM inside the CPU. Each task inside the CPU can be used for this purpose. The data is read and written, but at a certain moment, only one task is allowed to read and write.

$$f(m,t) = \frac{n * f(m,t)}{\sum_{i=1}^{n} f(i,t)},$$
$$g(m,t) = \frac{n * (h(m,t)/k(i,t))}{\sum_{i=1}^{n} h(i,t)/k(i,t)}. \tag{2}$$

The controller node uses an event-driven mechanism to achieve the following functions: read data from the network, calculate the control amount, encapsulate it into a network message frame, and send it to the transmission network. Specifically, the internal network message receiving task of the controller node reads the network message frame from the network through the port connected to the network inside the controller, decapsulates it by the internal transceiver of the controller, reads the valid data therein, and stores it in the internal RAM of the CPU. This RAM is shared by all nodes inside the CPU. It is the same as the sensor node. Only one task is allowed to obtain the right to use the CPU at a time and read and write the RAM.

$$\begin{cases} V_{(i,f)} = \dfrac{J_i^f + J_i^{f-1}}{T}, \\ V_i = \left(V_{(i,\mathrm{i})}, \cdots, V_{(i,f)}\right), \end{cases}$$
$$\min \sum_{i=1}^{N} a_i + \frac{1}{2} \times \sum_{i=1}^{N} \sum_{j}^{N} a_i y_j a_j y_i k\left(x_i^2, x_j^2\right) = 0. \tag{3}$$

The data acquisition process of the physical exercise behavior capture system in this article is as follows: the system starts and keeps the node in the standby state, then the PC sends the start physical exercise behavior capture command wirelessly through the base station, and the node in the BSN starts after receiving the start capture command. The centralized tracking system is suitable for the situation where the number of sensors is small. In this state, the node transmits the data wirelessly to the base station while collecting and storing data, and the base station then transmits the data back to the computer for corresponding processing.

2.2. Smart Sensor Network Topology. The physical exercise behavior network control system has a delay between the sensor controller and the controller actuator. When calculating the control amount inside the controller, there is also a

certain delay. The cause of network data packet loss is that during the process of data packet transmission, transmission errors caused by network congestion, transmission timeout exceeding a certain error rate, connection interruption caused by node failure, etc. are caused by unknowable reasons. If the error rate is not set, the default error rate of the network is 0, and no loss will occur during data packet transmission; if the error rate of the network is set to 0.1, it will be transmitted after 10 times. During the process, there will be a transmission error. In this case, you can choose to resend or discard the data packet. This measure can simulate the network data packet loss and the corresponding processing error. Figure 2 shows the distribution of nodes in a smart sensor network.

The sensor node in this article is mainly composed of microcontroller, physical exercise behavior sensor, wireless module, power management module, and so on. Because the node needs to be small (easy to wear) and must be able to work continuously for a long time, the microcontroller must support low power consumption mode; the node integrates a nine-degree-of-freedom physical exercise sensor, and the amount of data that needs to be processed is large; so, the microcontroller memory is required; due to the real-time requirements of the system, the microcontroller needs to have a fast processing speed. According to whether the coordinate location information is obtained or not, the network nodes can be divided into beacon nodes and nodes with unknown locations. A beacon node is a node that actively obtains its own location information in some way after being deployed and sends its own information to the location node for other nodes to locate its location; nodes with unknown locations need the location information of the beacon node. Usually, triangulation, trilateral measurement, and maximum likelihood estimation method can be used to accurately calculate the position of the node.

2.3. Analysis of College Students' Physical Exercise Behavior. When the human physical exercise behavior capture system is working, the measured person wears more than a dozen sensor nodes for physical exercise behavior capture. We need to implement network interconnection between these nodes to compensate for the rather limited sensor software and hardware resources to realize the optimal use of resources. In addition, the system needs to integrate the data collected by each node at the same time at the data processing end; otherwise, it will cause incoherent and deformed movements when restoring the physical exercise behavior data. It is only designed for channel resource allocation and conflict avoidance. Therefore, the traditional synchronization mechanism cannot guarantee that the data collected at the same time can reach the data processing end at the same time. Figure 3 is the composition of the physical exercise behavior module.

The sampling frequency of the physical exercise behavior data of the sensor node mainly depends on the application, the type of physical exercise behavior, or the different parts of the joint. In general, we believe that the lowest sampling frequency that can be used to describe people's daily activities is 20 Hz, and the medium sampling frequency is about

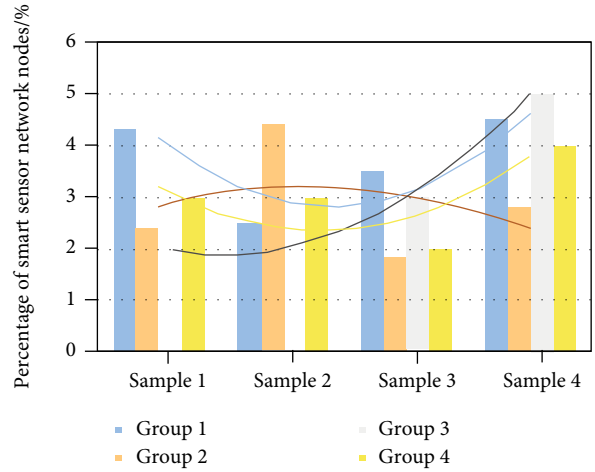

Figure 2: Distribution of smart sensor network nodes.

50~100 Hz; it can be seen that the communication data volume of the network in the data transmission state is quite large; so, the communication protocol must minimize its overhead in other states. However, the network access of nodes and network control will occasionally require communication time slots. In order to make more reasonable use of channel resources, we introduce a competition mechanism in TDMA communication based on the scheduling mechanism, referring to the multisuperframe structure of the MedMAC protocol. A single-hop star network is formed between all nodes and the central unit (CU)/central node. Each measured object has a central unit/central node responsible for data relay from node to base station and control from base station to node. This method has many advantages. First, all nodes except the central node do not need a large transmission power, which not only ensures the effective use of resources but also reduces the radiation hazard to the human body. Second, the star-shaped network is simple in networking, reducing routing overhead. Third, if we need to capture long-distance and large-scale physical exercise behaviors, we can increase the transmission power of the central node, since the signal coverage of nodes other than the central node is very small, which ensures the transmission distance and the stability of the system.

2.4. Model Iteration Factor Update. The sequence of messages transmitted in the network is out of order, indicating that the order in which the destination node receives the message is different from the order in which the sending node sends it. That is, the message sent after the sending node arrives at the destination node before the message sent by the node before. That is, if the above situation occurs, if it is a multipacket transmission, it will cause the sending node to send data disorder, disturb the corresponding controller to calculate the corresponding control amount, and have a greater impact on the control effect. In this study, using internal time, messages transmitted in the network have corresponding timestamps, namely, the generation time and the reception time. If the generation time is late and the reception time is early, it means that the data packet sequence is disordered, and the message is discarded. The sending and

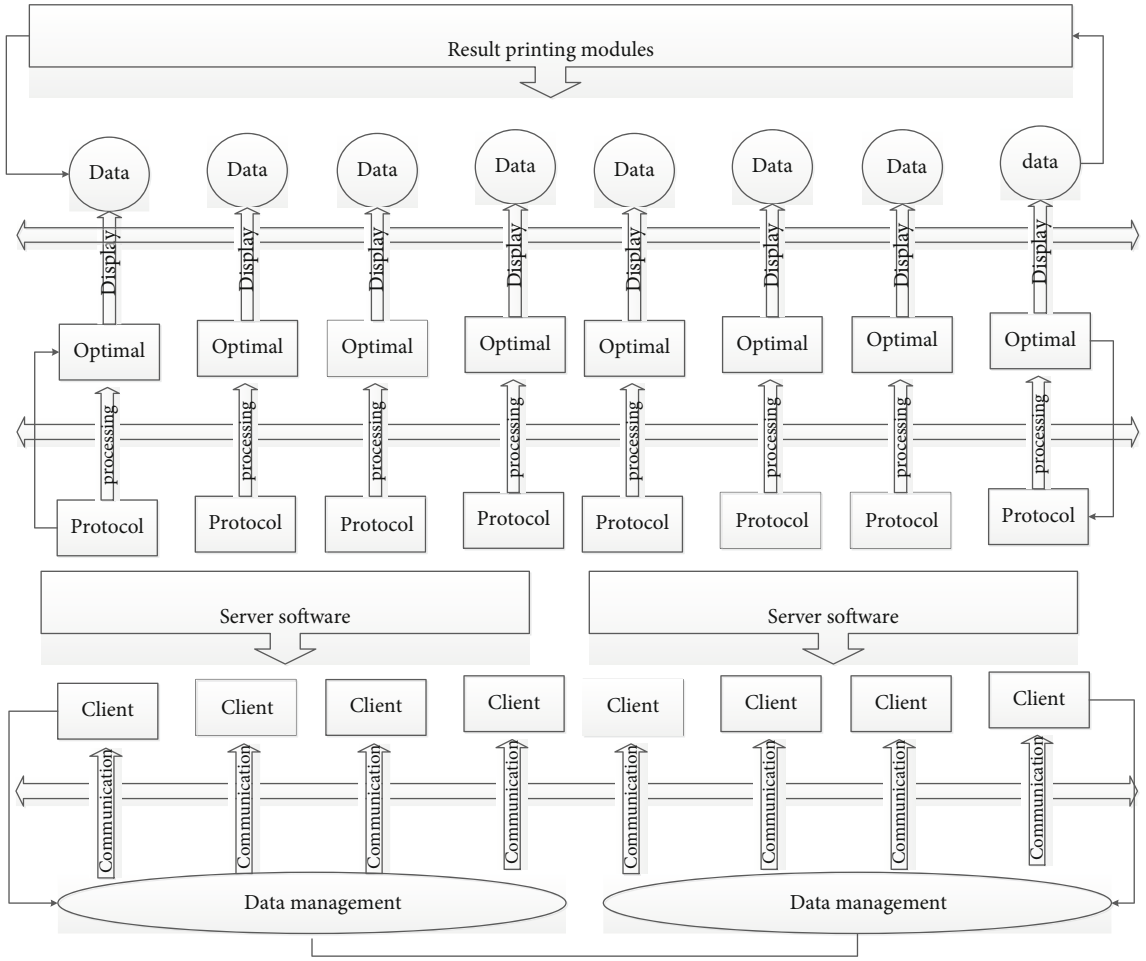

Figure 3: The composition of the physical exercise behavior module.

receiving buffer queues are, respectively, used inside the node, so that the messages sent from the node enter the network in the corresponding order, which reduces the disorder of the data packet sequence to a certain extent. Its accuracy greatly depends on the distribution density of nodes and the distribution of node positions and is easily affected by the accumulation of errors. Based on this, someone proposed to use a weighted method to weigh the impact of sports behaviors on network nodes. After using the weighted centroid algorithm, the positioning accuracy weakens the impact of uneven distribution of nodes on positioning, but the positioning effect still depends more on the distribution density of nodes. Figure 4 shows the iterative factor distribution of the calculated cluster model.

The sensor network can be regarded as a distributed database, and each node is a storage unit. Applying the database management method to the sensor network, the virtual view seen by the end user can represent the actual node information in the network. The user only needs to care about the event information of the terminal interface and does not need to care about the status information of each node in the implementation. This data management method based on database technology can significantly enhance the usability and practicability of the sensor network, making the management of network nodes more convenient and more efficient. The service life of sensor networks is limited by energy supply, and reducing the amount of transmitted data can effectively save energy. In the centralized tracking architecture, the measurement values of all sensors are sent to the central tracker or the fusion center, and the fusion center performs measurement-trajectory correlation and fusion. Therefore, data can be fused during the process of collecting and forwarding data from various sensor nodes to reduce the length of data packets and remove redundant information. At the same time, the forwarded data and the locally collected data can be analyzed and processed to improve the accuracy of the information. The microembedded system of sensor nodes has the following characteristics: one is the high degree of concurrency; that is, sometimes, there are multiple simultaneous tasks, but the execution time of a single task is very short; so, the operating system should have a mechanism to handle such concurrent tasks. The operating system is required to simplify the difficulty of operating the hardware of the application program and to release more operation permissions to the application program.

3. Results and Analysis

3.1. Data Preprocessing of Smart Sensor Network. When the polling algorithm is used in the experiment, the scheduler

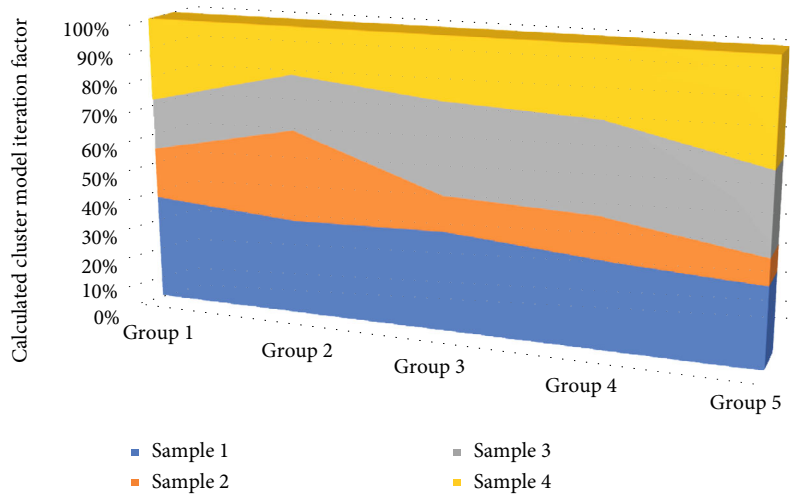

Figure 4: Calculating the distribution of the iterative factor of the cluster model.

usually uses time-sharing technology to give each process a time slice (a single allowable CPU execution time). If the process cannot complete the task at the end of the time slice, it will be replaced by other processes. When the CPU execution processing time is regained through scheduling next time, the process will be executed from the current interrupted location. If the time slice is 20 milliseconds, and process 1 needs 50 milliseconds to complete, at the end of 20 milliseconds, the system sends a signal to notify the scheduler. The scheduler stops the execution of the process according to this signal, temporarily suspends the task, and stops the execution of the CPU processing time is given to other processes. When all other processes have sequentially obtained 20 milliseconds of running time, process 1 will regain 20 milliseconds of CPU execution time and so on. This method can ensure that all processes in the run queue can obtain a time slice of CPU processing time within a given time period. Figure 5 is the data progress curve of the smart sensor network.

If the relative position of the sports behaviors in the multisports behavior dynamic cluster does not change much during the progress, and the sports behaviors are relatively evenly distributed, the weighted centroid positioning method is used to determine the geometric centroid of the sports behavior cluster as the positioning result based on all the measurement information. Regarding the sports behavior cluster as a whole, the measurement received by the nodes in the edge area of the sports behavior cluster should be smaller than the measurement of the nodes in the central area. Therefore, the geometric center of mass of the sports behavior cluster can be roughly determined according to the node coordinates of the edge area and its measurement. As the error rate increases, the overshoot increases, and the response time becomes longer. In the case of an error rate of 0.3, the inverted pendulum system can eventually remain stable; but when the error rate is 0.5, the inclination angle of the inverted pendulum cannot remain stable. The network cannot transmit the sensor collection data information and the controller node control information in time, so that the actuator node cannot obtain the control amount that acts on the inverted pendulum model at the corresponding time.

3.2. Simulation of Physical Exercise Behavior Model Based on Computing Cluster. The output of the IDG650 dual-axis gyroscope and ISZ650 single-axis gyroscope used in the simulation system are both analog voltage values, which need to be converted into corresponding measured values by the 12-bit ADC sampling module of the microcontroller. When the operating voltage of the microcontroller is 3.6 V, the accuracy of the 12-bit ADC is about 0.25 mV, which is higher than that of the gyroscope. The three-axis magnetometer uses PNI's MicroMag module, which reduces the development difficulty and shortens the development cycle. The working current of this module is only 500A at 3VDC, the magnetic field range is ±11, the resolution is 0.015, and SPI digital interface is provided. The experimental design controller contains three tasks, namely, the network message sending task, the network message receiving task, and the control quantity calculation task. Therefore, the internal scheduler of the controller must schedule these three subtasks. It can be seen that the time is 0.2 s. Inside, three concurrent tasks compete for CPU time. At a certain time, only one task can get the right to use the CPU. Using the FIFO scheduling algorithm, to apply for scheduling a new task, first find out whether the waiting task queue already contains the task. If the task does not exist in the queue, add the task to the end of the queue; otherwise, go directly to the next step and schedule it through query. If there is no task and the task queue is not empty, then take out a task at the head of the task queue and schedule its running parameter to run. Otherwise, if there is a task running, but the task is already running at the moment when it is finished, it is judged whether the task queue is empty. If the task queue is not empty, the first task of the task queue is taken out for scheduling operation; otherwise, the next scan scheduling is performed. Figure 6 shows the distribution of task scheduling in computing clusters.

For the continuous long-term physical exercise behavior of the measured object, the posture estimation mainly relies

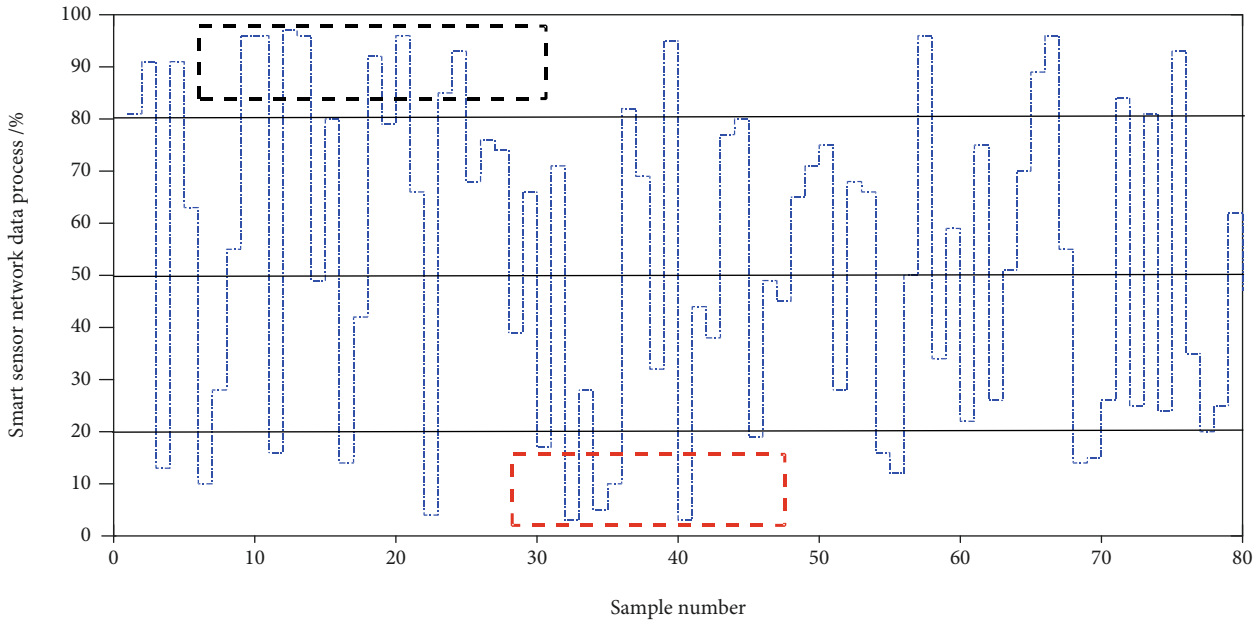

Figure 5: Data process curve of smart sensor network.

on the integration of the output value of the gyroscope. If the system cannot get the acceleration and magnetometer attitude correction over time, the deviation and drift of the gyro will make the attitude estimation accuracy. In the case of continuous motion of the object under test, we separately analyze the attitude output of the gyroscope, and the error of its Euler angle is as follows. They can not only estimate the state of multiple targets but also realize trajectory correlation. During the experiment, we used 4 miniature sensors to capture and reproduce the physical exercise behavior of the lower body of the human body. The node on the calf is fixed on the outer side above the ankle 10era, the node on the thigh is fixed on the outer side 10 cm above the knee, and two sensor nodes are placed on the torso. The sampling frequency of the node is 50 Hz. Each sensor node collects the physical exercise behavior information of the corresponding limbs, such as the thigh sensor collects the physical exercise behavior information of the thigh, and the calf sensor collects the calf physical exercise behavior information. Figure 7 is the cluster distribution of physical exercise behavior information calculation.

The multisports behavior test plan in this article is defined in the area plane with a range of $2\,\Omega = 100 \times 100$ m . 400 network nodes are randomly scattered in the area as the test environment for the content of this section. The nodes all belong to a cluster, and the network environment and the physical location information of the nodes are as written. Starting from nodes A, B, C, and D, each node starts to traverse the information of its surrounding nodes in a clockwise direction. After a round of boundary traversal, if it is a complete continuous dynamic cluster, there should be four traversal results $A \longrightarrow B$, $B \longrightarrow C$, $C \longrightarrow D$, and $D \longrightarrow A$. If not, it means that the dynamic cluster is separated, and a new dynamic cluster head management should be established. The separated dynamic cluster nodes continue to track sports behaviors.

3.3. Analysis of Experimental Results. The MSP430 series single chip microcomputer used in the experiment is a 16-bit ultra-low power mixed signal processor, which is called a mixed signal processor. It is integrated with a microprocessor on a chip to provide a "single-chip" solution. In terms of operating speed, MSP430 series single-chip microcomputers can realize 125 ns instruction cycle under the drive of 8 MHz crystal. The 16-bit data width, 125 ns instruction cycle, and the multifunctional hardware multiplier (which can realize multiplication and addition) can realize certain algorithms of digital signal processing (such as FFT). The MSP430 series single-chip microcomputers have many interrupt sources and can be nested arbitrarily, which is flexible and convenient to use. When the system is in a power-saving standby state, it only takes 6us to wake it up with an interrupt request. Due to the instability of wireless transmission, the physical exercise behavior data sent by the node to the base station may be lost; so, an external expansion storage device is required for data backup. In this way, even if the wireless communication is not smooth, the upper computer can send a repacking command to upload the missing data. The expansion storage device selects the flash chip of AT25DF641, which is fast to write and erase, the working voltage is 2.7 V-3.6 V, the capacity is 64 Mbit, the minimum erasable capacity is 4 K bytes, and the SPI digital interface is provided. Figure 8 shows the periodic data distribution of the smart sensor network.

In this system, 4 frequencies are allocated to each base station for frequency hopping, and the intervals between frequencies are equal. Frequency hopping is started when the number of data packets received by the base station in 1 s is less than the threshold, and the threshold is selected through experiments. The algorithm framework and solution for the joint search and tracking of regional multimaneuvering targets can handle situations where the number of targets is unknown and may change dynamically. If the

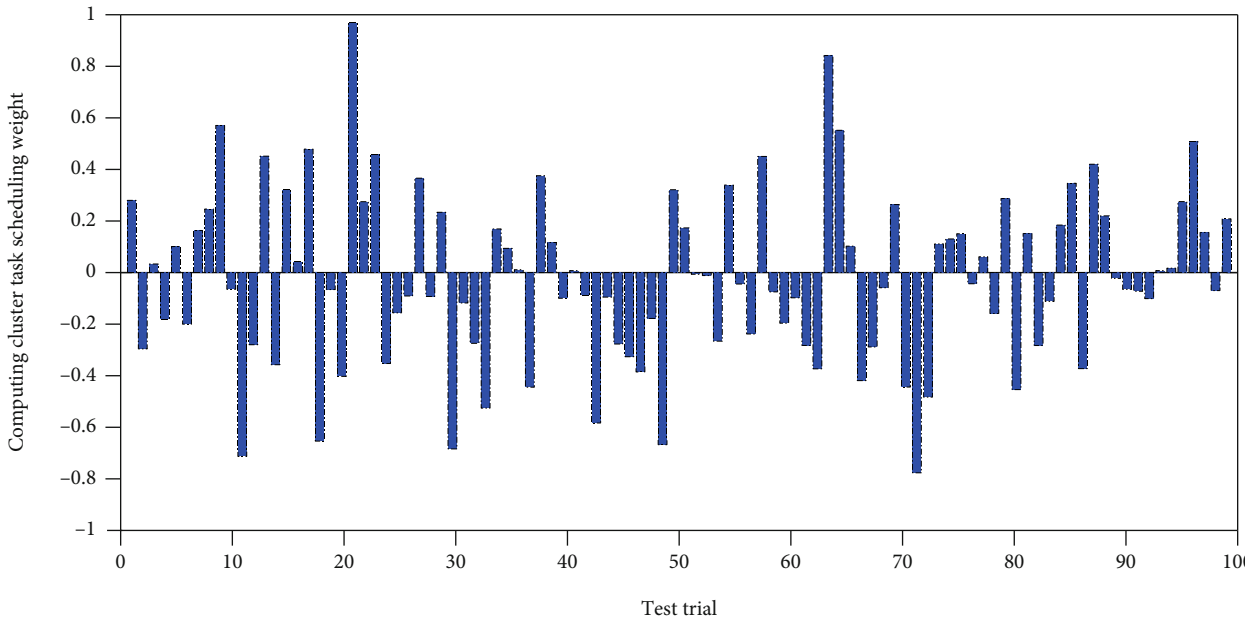

Figure 6: Computing cluster task scheduling distribution.

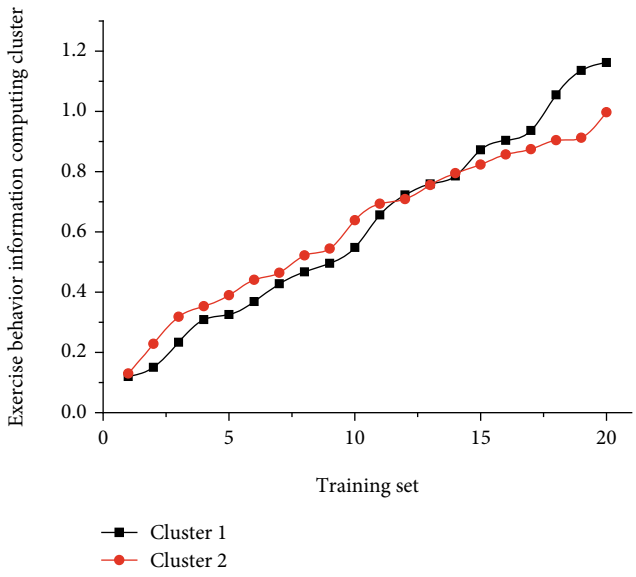

Figure 7: Physical exercise behavior information computing cluster distribution.

threshold is too large, the packet loss rate cannot be effectively controlled; if the threshold is too small, frequency hopping will occur frequently, and the chance of frequency hopping disorder will increase significantly. After the frequency hopping is disorderly, the base station and the node lose communication, the base station will hop back until it establishes communication with the node after hopping to a certain frequency. In this system, the longest time required for reestablishing the connection after frequency hopping is 4 s, the shortest time is 1 s, and 200 data packets will be lost during this time. For this reason, the frequency hopping threshold must be selected reasonably. The system has undergone repeated tests, and the selected frequency hopping threshold is 5 data packets lost within 18. Figure 9 shows the distribution of thresholds for selection of smart sensor networks.

The three-axis gyroscope and the three-axis magnetometer, respectively, measure the angular velocity component and the magnetic field component in the three-dimensional space. The gyroscope uses a combination of a single-axis gyroscope and a dual-axis gyroscope, and their sensitive axes are perpendicular to each other. Randomly, we simulate the composition of dynamic clusters from different physical exercise behaviors to different positions. Because the nodes are not evenly distributed in the two-dimensional space, the size, scope, and composition of the dynamic clusters are always changing dynamically. When the node density is sparse, because the number of nodes that can be judged is small or no, and the sports behavior positions are already very close, it is easier to cause misoperation in this case. The analog data of the gyroscope on the node bottom board is sent to the microcontroller on the node core board through the interface with the node core board. The sampled signal value of the angular velocity measured by the sensor obtained by ADC conversion needs to be converted into the corresponding measured value, and the measured value represents the obtained angular velocity component value. Strictly speaking, the resolution of the ADC should be higher than the resolution of the sensor; otherwise, the high-resolution sensor will not be effectively used.

4. Conclusion

Based on computing clusters and smart sensor network technology, this paper designs college students' physical exercise behavior experiments, using the output of posture tracker as a reference signal, taking the acceleration signal of physical exercise behavior as an example to analyze and

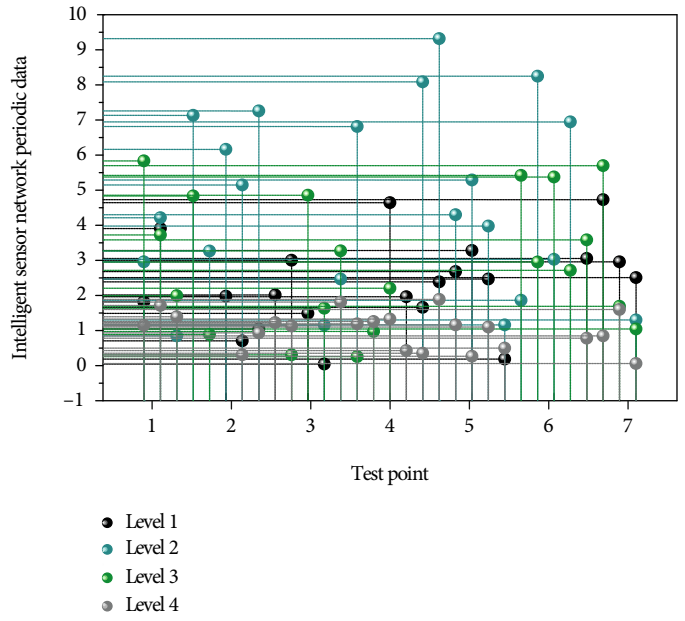

Figure 8: Periodic data distribution of smart sensor network.

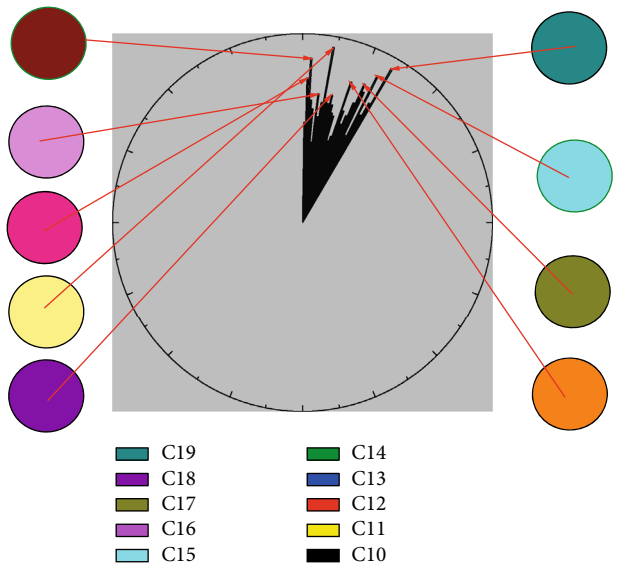

Figure 9: Distribution of thresholds for selection of smart sensor networks.

compare the commonly used data filtering methods of physical exercise behavior sensors. The experiment builds an inverted pendulum model based on CAN network protocol and a control model of continuous control system inverted pendulum and analyzes and studies the timing of the physical exercise behavior network control system model based on CAN network. The phenomenon of unexpected loss of behavior gives a recovery strategy. The simulation results show that the combination of these two methods for mobile sports behavior tracking improves the effect of sports behavior positioning and sports behavior location prediction and obtains the effects of higher tracking accuracy and lower network computing overhead. At the same time, the control communication system model of a certain type of obstacle avoidance car is built, and the delay of the communication process, data packet loss, single-packet and multipacket transmission, data packet timing disorder, and network scheduling are simulated and analyzed. It effectively proves the effectiveness of the unified modeling method of the control and communication model proposed in this paper. At the same time, two simple experiments are designed to analyze the errors of the two methods, use the real-time attitude angle calculation method to try the physical exercise behavior and physical exercise behavior of human bones and initially realize the physical behavior of real-time physical exercise behavior supervision.

Data Availability

All data, models, and code generated or used during the study appear in the submitted.

Conflicts of Interest

The author declares that he has no conflicts of interest.

Acknowledgments

This study was supported by the Provincial Massive Open Online Course (MOOC) Demonstration Project (No. 2019MOOC402).

References

[1] K. Lin, Y. Li, J. Sun, D. Zhou, and Q. Zhang, "Multi-sensor fusion for body sensor network in medical human-robot interaction scenario," *Information Fusion*, vol. 57, pp. 15–26, 2020.

[2] A. Tolba, O. Said, and Z. Al-Makhadmeh, "MDS: Multi-level decision system for patient behavior analysis based on

wearable device information," *Computer Communications*, vol. 147, pp. 180–187, 2019.

[3] B. M. Sahoo, H. M. Pandey, and T. Amgoth, "GAPSO-H: a hybrid approach towards optimizing the cluster based routing in wireless sensor network," *Swarm and Evolutionary Computation*, vol. 60, article 100772, 2021.

[4] N. Kumar and D. P. Vidyarthi, "A green routing algorithm for IoT-enabled software defined wireless sensor network," *IEEE Sensors Journal*, vol. 18, no. 22, pp. 9449–9460, 2018.

[5] A. Rajagopal, S. Somasundaram, B. Sowmya, and P. Cerna, "Performance analysis for efficient cluster head selection in wireless sensor network using RBFO and hybrid BFO-BSO," *International Journal of Wireless Communications and Mobile Computing*, vol. 6, no. 1, pp. 1–9, 2018.

[6] S. Ramakrishnan and S. Prayla Shyry, "Distributed fuzzy logic based cluster head election scheme (DFLCHES) for prolonging the lifetime of the wireless sensor network," *International Journal of Engineering & Technology*, vol. 7, no. 1.5, pp. 111–117, 2017.

[7] R. N. Yadav, R. Misra, and D. Saini, "Energy aware cluster based routing protocol over distributed cognitive radio sensor network," *Computer Communications*, vol. 129, pp. 54–66, 2018.

[8] S. Otoum, B. Kantarci, and H. T. Mouftah, "On the feasibility of deep learning in sensor network intrusion detection," *IEEE Networking Letters*, vol. 1, no. 2, pp. 68–71, 2019.

[9] S. Verma, N. Sood, and A. K. Sharma, "Genetic algorithm-based optimized cluster head selection for single and multiple data sinks in heterogeneous wireless sensor network," *Applied Soft Computing*, vol. 85, article 105788, 2019.

[10] K. Guleria and A. K. Verma, "Meta-heuristic ant colony optimization based unequal clustering for wireless sensor network," *Wireless Personal Communications*, vol. 105, no. 3, pp. 891–911, 2019.

[11] Z.H. Song and Y.X. Zhang, "Research on School Sports Health Promotion Based on Healthy China 2030," *J.Sports World(Academic Edition)*, vol. 788, no. 2, pp. 174-175, 2019.

[12] X. Zhu, "Complex event detection for commodity distribution Internet of Things model incorporating radio frequency identification and Wireless Sensor Network," *Future Generation Computer Systems*, vol. 125, pp. 100–111, 2021.

[13] Q. Liu, Y. F. Chen, S. Z. Fan, M. F. Abbod, and J. S. Shieh, "Quasi-periodicities detection using phase-rectified signal averaging in EEG signals as a depth of anesthesia monitor," *IEEE Transactions on Neural Systems and Rehabilitation Engineering*, vol. 25, no. 10, pp. 1773–1784, 2017.

[14] S. Bhushan, R. Pal, and S. G. Antoshchuk, "Energy efficient clustering protocol for heterogeneous wireless sensor network: a hybrid approach using GA and K-means," *Data Stream Mining & Processing*, pp. 381–385, 2018.

[15] S. Rani, S. H. Ahmed, and R. Rastogi, "Dynamic clustering approach based on wireless sensor networks genetic algorithm for IoT applications," *Wireless Networks*, vol. 26, no. 4, pp. 2307–2316, 2020.

[16] T. A. Alghamdi, "Energy efficient protocol in wireless sensor network: optimized cluster head selection model," *Telecommunication Systems*, vol. 74, no. 3, pp. 331–345, 2020.

[17] K. Sarangi and I. Bhattacharya, "A study on data aggregation techniques in wireless sensor network in static and dynamic scenarios," *Innovations in Systems and Software Engineering*, vol. 15, no. 1, pp. 3–16, 2019.

[18] A. Mehmood, A. Khanan, M. M. Umar, S. Abdullah, K. A. Z. Ariffin, and H. Song, "Secure knowledge and cluster-based intrusion detection mechanism for smart wireless sensor networks," *IEEE Access*, vol. 6, pp. 5688–5694, 2017.

[19] I. G. A. Poornima and B. Paramasivan, "Anomaly detection in wireless sensor network using machine learning algorithm," *Computer Communications*, vol. 151, pp. 331–337, 2020.

[20] F. Alvarez, M. Popa, V. Solachidis et al., "Behavior analysis through multimodal sensing for care of Parkinson's and Alzheimer's patients," *IEEE Multimedia*, vol. 25, no. 1, pp. 14–25, 2018.

[21] S. Arjunan and P. Sujatha, "Lifetime maximization of wireless sensor network using fuzzy based unequal clustering and ACO based routing hybrid protocol," *Applied Intelligence*, vol. 48, no. 8, pp. 2229–2246, 2018.

[22] B. Ahmad, W. Jian, Z. A. Ali, S. Tanvir, and M. S. A. Khan, "Hybrid anomaly detection by using clustering for wireless sensor network," *Wireless Personal Communications*, vol. 106, no. 4, pp. 1841–1853, 2019.

[23] B. Cao, X. Kang, J. Zhao, P. Yang, Z. Lv, and X. Liu, "Differential evolution-based 3-D directional wireless sensor network deployment optimization," *IEEE Internet of Things Journal*, vol. 5, no. 5, pp. 3594–3605, 2018.

[24] Y. Harold Robinson, E. Golden Julie, S. Balaji, and A. Ayyasamy, "Energy aware clustering scheme in wireless sensor network using neuro-fuzzy approach," *Wireless Personal Communications*, vol. 95, no. 2, pp. 703–721, 2017.

[25] M. Faheem and V. C. Gungor, "Energy efficient and QoS-aware routing protocol for wireless sensor network- based smart grid applications in the context of industry 4.0," *Applied Soft Computing*, vol. 68, pp. 910–922, 2018.

Hindawi
Journal of Sensors
Volume 2022, Article ID 3112170, 19 pages
https://doi.org/10.1155/2022/3112170

Research Article

A Hybrid Selection Strategy Based on Traffic Analysis for Improving Performance in Networks on Chip

Mohammad Trik,[1] **Ali Mohammad Norouzzadeh Gil Molk**,[2] **Fatemeh Ghasemi**,[3] **and Pourya Pouryeganeh**[4]

[1]*Department of Computer Engineering, Boukan Branch, Islamic Azad University, Boukan, Iran*
[2]*Department of Computer Engineering, University of Guilan, Rasht, Iran*
[3]*The Institute of Higher Education, Ministry of Science, Research and Technology, Computer Engineering Department Qazvin, Iran*
[4]*Electrical& Computer Faculty, Isfahan University of Technology, Iran*

Correspondence should be addressed to Mohammad Trik; trik.mohammad@gmail.com

Received 16 November 2021; Revised 21 March 2022; Accepted 31 March 2022; Published 25 April 2022

Academic Editor: Gengxin Sun

Networks on chip (NoCs) are an idea for implementing multiprocessor systems that have been able to handle the communication between processing cores, inspired by computer networks. Efficient nonstop routing is one of the most significant applications of NOC. In fact, there are different routes to reach from one node to another node in these networks; therefore, there should be a function that can help to build the best route to reach the destination. In the current study, a new hybrid algorithm scored regional congestion-aware and neighbors-on-path (ScRN) is introduced to choose better output channel and thus improve NOC performance. Having utilized the ScRN algorithm, first an analyzer is used to inspect the traffic packets, and then the *NoC traffic* locality or nonlocality is determined based on the number of the hops. Finally, *if the traffic is local*, a scoring technique will choose better output channel; however, if the traffic is nonlocal, the best output channel will be chosen based on a particular parameter introduced here as well as the system status using NoP or RCA selection functions. In the end, via Nirgam simulation, the proposed approach was assessed in traffic scenarios through various selection functions. The simulation results showed that the solution was more successful in terms of delay time, throughput, and energy consumption in comparison to other solutions. It showed a reduction of 38% in packet latency, and the throughput increased by 20%. By considering these two parameters, energy consumption decreased by 10% on average.

1. Introduction

The growing need for more effective chips has currently led to an increase in complexity of designing integrated circuits (IC) [1]. Some issues have been resolved with the use of smaller transistor manufacturing technology; however, smaller manufacturing technology has led to the problem of imbalance between the connection wire delays and the gate delays [2]. Besides, as the frequency of chips' performance increased, the power consumption rises as well. To deal with these challenges, IC designers focused on increasing efficiency rather than speed, and this change of attitude resulted in placing multiple individual processors in one chip and establishing communication between them through a single bus. The result was so satisfactory that after a short time, the systems consisted of several sections that ran on a board, relocated in a single chip. This architecture of processor construction became popular as system on chip or SoC [3–5]. However, SoC had issues emerging over time. As the number of separated sections, known as Intellectual Property (IP), increased, the SoC was not responsive [6]. The issues such as unscalability and massive power consumption in the bus encouraged new efforts among IC designers. The solution to these challenges led to a novel architecture named NoC. NoC is a connectional subsystem inside an IC (normally called "chip"), which typically provides the connection between IP cores of the system in a chip [7]. NoC technology uses network theory and in-chip

connection approaches and provides significant progress compared with bus and crossbar-based connections. NoC improves the scalability of SoCs and optimizes the energy usage in complicated SoCs in comparison to other models [8]. The factors that affect NoC design are energy consumption limit, delay, and throughput [9]. In fact, in NoC applications, due to present limits, the proposed algorithms must be designed in a way that reduces the overall energy consumption of the network and packet latency, causes an increase in performance and throughput of the network, and has a sufficient overhead-implementation. One of the important factors which affect NoC performance is the process of selecting the best output channel [10]. By designing and applying efficiently, the selection function can reduce packet latency and, due to more uniform traffic distribution on the network, increase the network throughput, and as a result, decrease the energy consumption [11]. Another challenge of NoC is the discussion of routing in these types of networks. The problem may occur in routing algorithms for instance deadlock, livelock, and starvation. Our proposed method in this study covers all cases so that the deadlock does not get excited and prevents packages from livelock. Also, the ScRN selection strategy makes that there is never any starvation. The performance requirements of today's NoC are also felt to severely affect the performance of these networks, which can be summarized as such: latency, throughput, power consumption, and fault and distraction tolerance. The key contributions of this paper are as follows: (i) Introduce a new hybrid selection function, which is able to use appropriate strategies for each mode depending on the local or nonlocal status of the packets. (ii) Introduce a new density awareness method called ScRN to select the best output channel for packet distribution. (iii) Improve the use of local and nonlocal congestion information: The output selection strategy uses a traffic analyzer to examine packets and then determine whether the packet is local or nonlocal based on the number of hops, and this can improve the network. The major goal of this paper is to develop a hybrid selection strategy with the aim of allocating the best channel that will allow packets to be routed to their destination along a path that is as free of congested nodes as possible. Networks on chip can use dedicated control lines to transport data between routers, unlike traditional computer networks, which can only communicate internode information through packets. This allows useful information about congestion-related aspects like the buffer status of individual nodes to be exchanged without adding additional traffic overhead.

1.1. Motivation. The importance of this research is in applying a hybrid solution in order to select the best output channel in routing networks on the chip. For this purpose, first, a traffic analyzer is used, and according to the number of hops of a package, it is determined whether it is local or nonlocal; then through it, a decision is made about the type of selection strategy. Accordingly, if the package is local, the optimized strategy is used for local packages, and in the nonlocal case, special strategies are used for nonlocal packages. Using this technique, packets can be routed through the best output channel, and as a result, network-level balance can be established. This can prevent hotspots, increased energy consumption, and long delays. The function of our solution is to use the information of the neighbors close to the node to which the packet has reached, to dynamically check the local and global network traffic and route the route in such a way that traffic and congestion are minimized. As a result, by creating a kind of load balance through the distribution of traffic in different routes, heat is generated, and thus energy consumption is increased. This solution is independent of the type of topology and can be used in network on chip based on neuromorphic and even wireless networks.

1.2. Paper Organization. Our paper is organized as follows. In the next section, a list of related works is stated in two groups: the previously used algorithms in NoC along with selection functions and performance techniques. In Section 3, we propose a definition of the system model in a descriptive way and network architecture. In Section 4, the proposed hybrid method is stated to propose a hybrid selection function (ScRN). In Section 5, the results of analyzing the proposed model in different scenarios are shown, and finally, we explain these scenarios in Section 6.

2. Related Works

The content of related works is divided into two parts. The first part belongs to the examination of previously utilized algorithms in NoC along with selection functions, which in the end, we explain them briefly in the form of a table. The second part evaluates some performance techniques, including energy consumption, throughput, and delay. Also, the comparison between these techniques in various previous studies is summarized in a table.

2.1. Previous Designs Related to Routing Algorithms and Selection Functions. Over recent years, numerous researchers have studied different utilized algorithms along with selection functions for different fields in NoCs, and we examine some of the performed works in these subjects in the following sections. A selection strategy named EnPSR is introduced in [12] for better performance of the network. This approach has the ability to reduce the hardware overhead through access to the data aware of the output channels. The evaluation results showed that compared to other methods, this method is significantly improved in terms of packet latency, throughput, area, and the energy consumption. A congestion-aware routing algorithm called DBAR is proposed in [13]. This approach overcomes local and global adaptive routing problems and provides an entirely adaptive, efficient routing to avoid congestion. In another study, researchers proposed an adaptive nonminimum routing algorithm called LEAR, which avoids congested routes from source to destination [14]. In reference [15], an MILP approach is proposed for unicast and multicast traffic distribution in networks on 3D mesh-based chip. This method was based on the Hamiltonian path and proposed to avoid congestion. In order to increase fault tolerance for NoCs in [16], the EDAR algorithm was introduced. This approach is based on the weighted path selection strategy, which

Table 1: Summary of utilized algorithms in NoC along with selection functions.

Work	Outlines	Features	Selection strategy name
[12]	Locally congestion-aware	Hardware overhead optimization	EnPSR
[18]	Input selection strategy	Throughput and latency improvement	DCA
[16]	Fault-tolerant improve	Higher throughput, low overhead	Weighted path
[15]	Distribute the unicast and multicast traffic	Performance improvement	—
[17]	Congestion detection	Fast evaluation	—
[13]	Congestion avoidance locally	Better performance	NoP
[14]	Congestion avoidance locally	Reducing energy consumption	—
[20]	New selection strategy	Performance improvement	NoP-OE
[21]	Congestion controlled	Traffic estimation	Fuzzy controller
[22]	Congestion avoidance locally	Load balancing	CADA

provides NoC true traffic conditions through monitoring modules. In the proposed EDAR, real-time input weights are calculated according to the channel states like idle/busy/congested/false, and least-weighted input is ranked as the near-optimal path toward the sets. In [17], the author proposed a congestion detection algorithm called CACBR that selects the best route using two methods of candidate paths and cluster's congestion information and also uses virtual channels to ensure avoidance of deadlock. In another study, the researchers attempted to decrease packet latency and increase network throughput using an output selection method named DCA. One of the advantages of this method is the capability of utilizing it on any kind of topology and network of different dimensions [18]. The researchers in [19] proposed the adaptive routing method called PT-BAR which uses temperature conditions for packet routing. In this algorithm, the high and low priority packets are routed from high- and low-heat regions, respectively. In [20], a selection function named OE-NoP is proposed which has adaptability with any routing. The purpose of introducing this function is packet routing during traffic creation toward the destination. In order to establish traffic control and balance in [21], a selection function based on the fuzzy controller is introduced. Traffic estimation for free packet routing is one of the properties of this method. Congestion control in wireless sensor networks, especially wireless network on chip, is one of the main challenges for effective performance in these networks. In [22], researchers have proposed a resource control mechanism using the Q learning method with an alternative path approach to reduce congestion. This congestion-aware data acquisition (CADA) mechanism initially identifies the congestion node (CN) where the nodes' buffer occupancy ratio is higher. Devanathan et al. [23] provides a solution for WiNoC communications that minimizes congestion by using effective wireless communication between output channels and routers. In [24], a wireless network architecture is presented on the chip to prevent congestion and load balancing. To do this, they have adopted a virtual output queue scheme to handle HOL blocking, which has significantly improved the network throughput. The list, properties, and type of selection strategy from utilized algorithms for NoC are given in Table 1.

As indicated in Table 1, some of the algorithms use selection function, while presence of a selection strategy can have a significant effect on the performance of routing algorithms and as a result the performance of the entire network.

2.2. Previous Designs Related to Performance Techniques. As was mentioned in the first section, NoCs are primary adaptive connection infrastructures for system on chips (SoCs). One of the important issues in NOC is system performance, such as delay, throughput, and energy consumption of the system, which, along with scalability in these networks, have special importance [25]. In [26], the microkernel idea was introduced to reduce energy consumption in multicore-based operating systems (OS). The proposed method is in such a way that OS is divided into microkernel and other system modules and distributes in the network to provide service for user applications. In [27], a self-adaptive mapping named SCSO is introduced based on the mapping method. The proposed method uses the k-NN method to significantly improve system performance in terms of energy consumption level, delay, and throughput. In [28], the ALO routing method is proposed to deal with energy loss routers in which routing evaluation is ran using spin, octagon, and cliché topologies. In [29], an intelligent task mapping algorithm on protocol-level is introduced to optimize energy consumption. This method evaluates the energy modeling in the protocol level so that the energy consumption level minimizes based on the protocol activity. Since links of the on-chip networks consume about 50% energy, and this issue has great importance in NoC, in [30], an energy consumption estimation method for links using virtual channels is proposed for precise estimation of energy consumption from data-dependent links. In [31], two NoC architectures are proposed, which are based on the circuit and packet switching. For both architectures, energy consumption models are proposed in which the energy consumption levels of them are estimated based on the prediction in each transferred bit. Another method for decreasing energy loss is proposed in [32]. In this research, the dissipated energy in links (links lose a large portion of energy in on-chip network although this energy loss can increase in future technologies) is reduced using some set of encrypted programs. Researchers in [33] proposed a method for reducing the

Table 2: A summary of used techniques for optimizing the system performance for NoC.

Technique(s)	Reduced latency	Reduced area	Energy efficient	Ref.
Microkernel	√	—	√	25
SCSO	√	—	√	26
ALO-bufferless	—	√	√	27
Smart protocol-level task mapping	√	—	√	28
Estim-NoC	√	—	√	29
EA-NoC	—	—	√	32
HS	—	√	√	33

energy consumption named EA-NoC that avoids unnecessary energy consumption using the most optimized path between source and destination and also optimizes the dynamic energy. Moreover, the proposed method can be efficient for parameters such as delay and throughput. In [34], the author examined the energy consumption in asynchronous NoCs. In that research, five optimizing approaches are analyzed for reducing energy consumption. Among these methods, the HS algorithm is the most efficient method which consumes the least energy by recognizing the shortest path. This research offers a multihop routing algorithm based on path tree (MHRA-PT) to minimize network energy consumption by addressing difficulties such as random cluster head selection, redundancy of working nodes, and building of cluster head transmission path. The suggested algorithm may successfully minimize network energy consumption, balance network resources, and extend network life cycle, according to simulation results [35]. In [36], on the assumption that the number of available channels is infinite, this study offers a one-shot time division multiple access (TMDA) scheduling with unlimited channels. To resolve slot conflict, the study presents scheduling with limited channels (SLC) and employs a lookahead search technique. A distributed implementation based on token change is offered for the algorithm's scalability. In Table 2, a summary of this section is presented based on different parameters for optimizing the system performance in NoC.

3. System Model

3.1. Network on Chip Architecture. NoC is a standard approach for multicore applications which consists of four main sections of routers, routing algorithms, IP cores, and network adaptor. These four sections are the major backbone of this type of network which exist in a node and are connected by wires. IP cores are processing units of the network. The network adaptor is used for connection of one core with other cores, and routers are responsible for network routing [1]. The task of routers is to navigate and transit the packets using routing algorithms in the network; more details of which are presented in the next section. NoC architecture is designed based on virtual channels and wormhole-based switching. Figure 1 presents the standard 4×4 mesh network along with details of a router [4, 37–39].

3.2. Switch and Router Structure in NoC. Routers play an essential role in the performance and efficiency of network on-chips. For instance, the design accuracy and use of routers can reduce the consumption power and delay and increase the NoC performance [3]. As can be seen in Figure 2, a router consists of different sections, including a switch, input and output buffers, routing and judgment unit, link controller, and injection and output channels. Buffers must be able to save data temporarily to prevent congestion for input and output routers during the network chaos. The switch establishes the connection between input and output buffers [18, 25, 40]. The routing unit is responsible for running the routing algorithms. The link controllers coordinate the packets flux on the channels, and output and input channels establish the connection of one processor with adjacent routers.

3.3. Selection Function. When the routing algorithm returns more than one output channel, the selection function is used to choose the output channel to which the packet is sent because the adequate selective pattern has a significant impact on the overall performance of selection routing. Namely, the adaptive routing algorithm measures a set of acceptable output channels regarding the paths that the packet can pass through to reach the destination. Afterwards, according to the network characteristics, including the congestion rate or the length of one of the routes of the output channel, the selection function will be utilized to choose the output channel from a set of permitted output channels. The overall schematic of using the routing algorithm and selection function in ScRN is presented in Figure 3 [4, 20, 25].

4. The ScRN Algorithm

In this section, an efficient selecting approach is proposed for choosing adaptive routing algorithms. In this approach, the local and global traffic condition of the network is dynamically examined by using the information obtained from neighbors near the node which the flit reached. This method routes the packet in a way that the traffic and congestion minimize, which consequently prevents heat generation in one section and unnecessary energy consumption by establishing a load balance through traffic distribution in different routes. First, Figure 4 presents the overall architecture of the approach where the routing algorithm finds output paths and the selection function with defined strategy selects the best output channel. This architecture comprised of input/output ports, input buffers, units for Traffic Analyzer

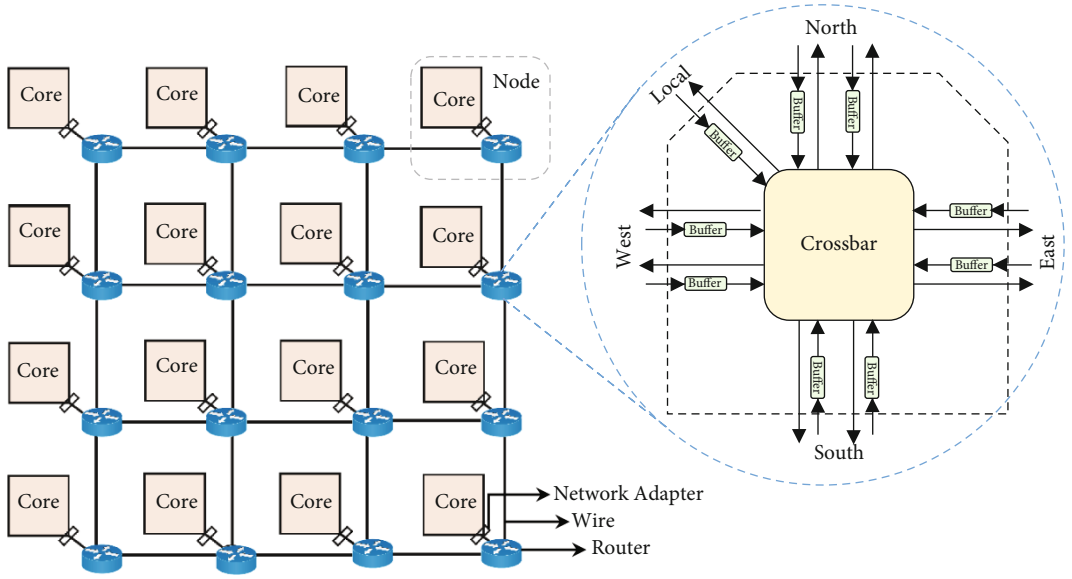

Figure 1: The standard 4 × 4 mesh network.

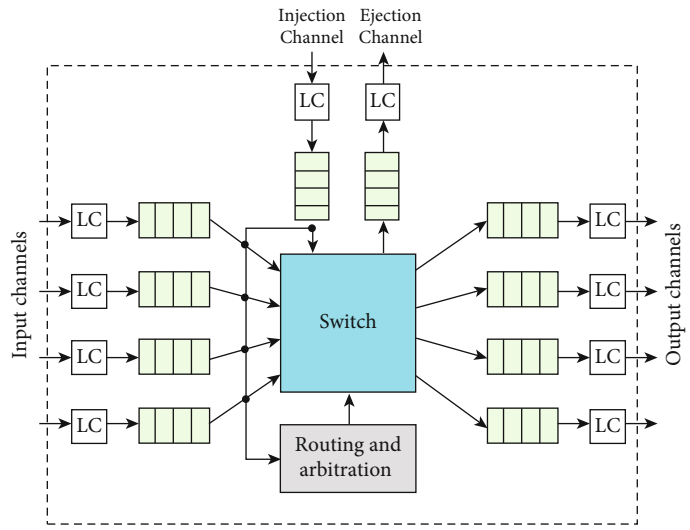

Figure 2: The internal structure of a router [8].

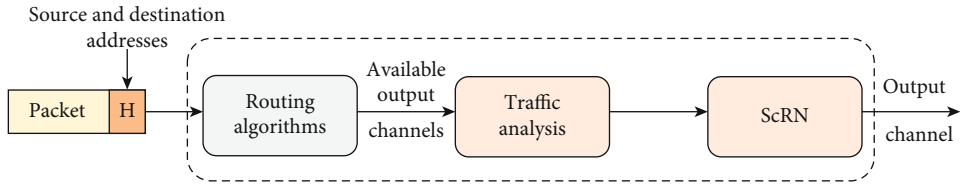

Figure 3: Routing structure and selection route blocks.

(TA), NoP,RCA and Scored selection strategy, and a crossbar switch. Then, Figure 5 shows the flow chart of the proposed approach. In the first hop, a traffic analyzer is utilized, and with the help of this analyzer, first, the traffic type is defined, and then, the best selection function corresponding to traffic type is used. In this case, the locality condition of the traffic is examined, and if the hop length corresponding to the packet is less than 2, the traffic is local, and otherwise, it is nonlocal. Also, in the nonlocality case, the hop number is examined, and if it is equal to 2, the NoP function is used, and if it is more than 2, the RCA selection function is employed to determine the best route. If the traffic is local, a scoring-based strategy (scored strategy) is applied to determine the output.

4.1. Formulation of Energy Consumption. In this study, first, the mean energy consumption of sending a data flit between two neighbor tiles, including energy consumption in both

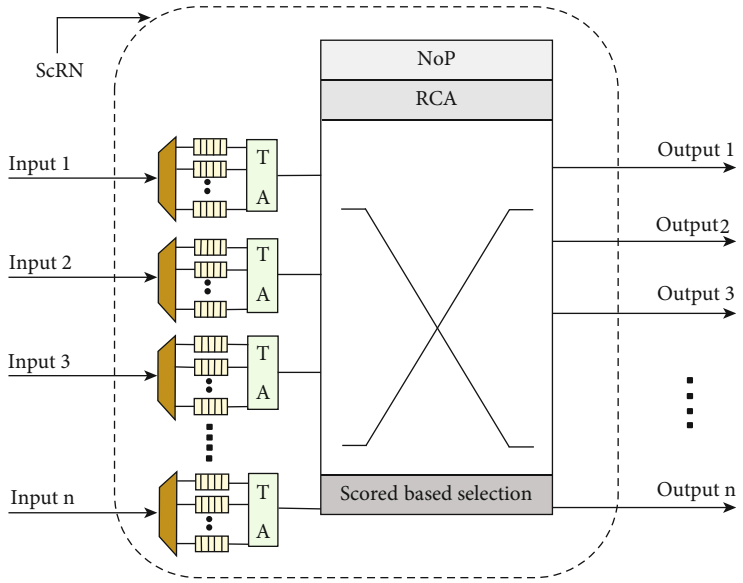

Figure 4: ScRN router and selection architecture.

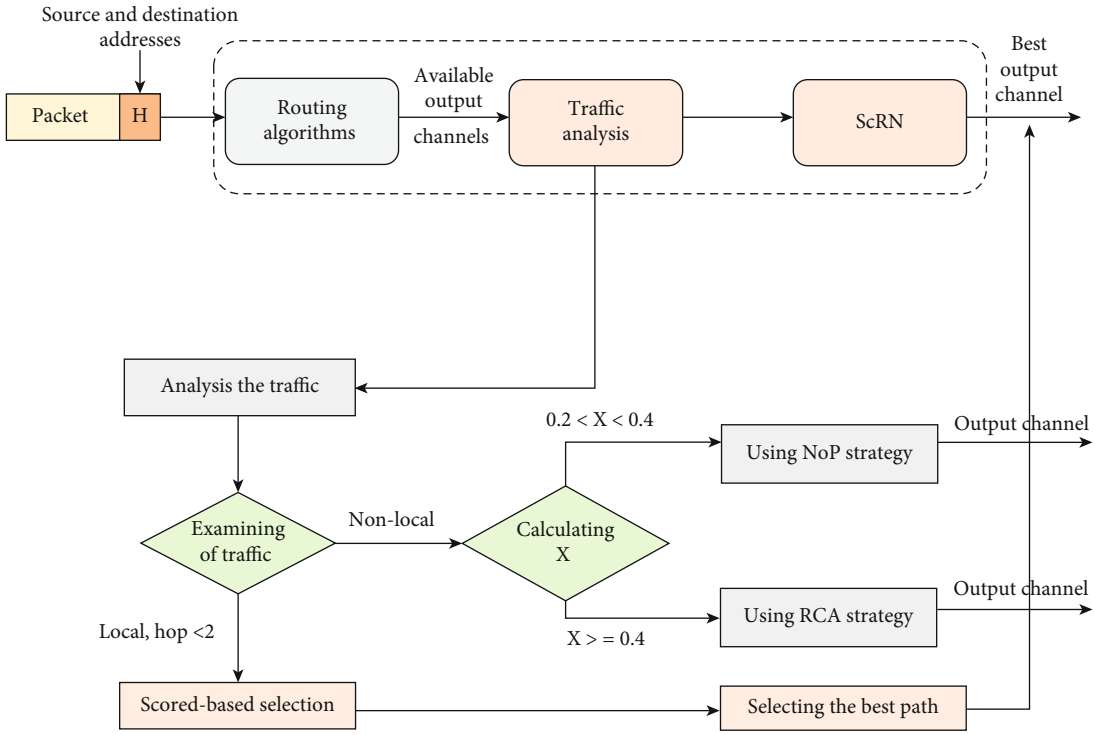

Figure 5: Flow chart of the proposed approach for ScRN algorithm.

router and connection links of them, is presented in Figure 6 to model energy consumption for each flit which is the smallest physical unit of data exchange in NoC. We have used Ref. [14] to calculate energy consumption.

$$E_{Neighboring-routers} = E_{1-hop} = E_{Intra-router} + E_{Inter-router} \quad (1)$$

In Equation (2), exchange energy between two neighboring routers is divided into two parts of the inside of the router and between routers. The inside-router energy consists of three sections of intersection switch, the buffer related to virtual channels, and wirings inside the router, according to Figure 1. Hence,

$$E_{Intra-router} = E_{Crossbar} + E_{buffer} + E_{wire}. \quad (2)$$

On the other hand, the connection between two routers depends on the defined number of bits for flits on NoCs,

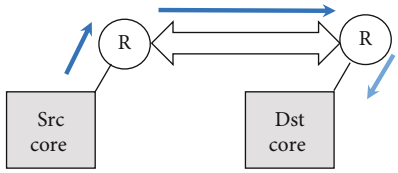

Figure 6: Route with a hop.

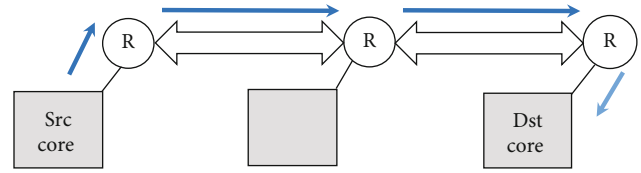

Figure 7: Route with two hops.

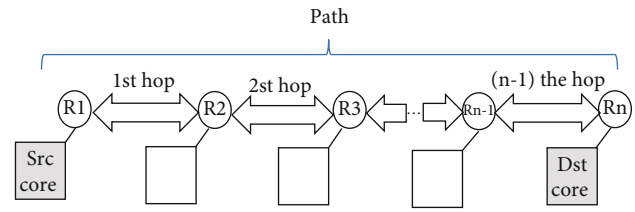

Figure 8: Route with n hops.

and showing the energy consumption in each of these wires with $E_{\text{Inter-tile-Link}}$, we have

$$E_{Inter-router} = phit\_size \times E_{Inter-tile-Link}. \quad (3)$$

Therefore, NoC energy consumption in the simple case of connection of two neighboring routers can be calculated as

$$E_{NoC-1hop} = E_{Crossbar} + E_{buffer} + E_{wire} + E_{Inter-router}. \quad (4)$$

The length of the connection wires of each pair of tiles in NoC is usually in millimeters (mm), while the length of the router wires is usually in micrometers (μm). Therefore, energy consumption in the internal buffers of the router (E_{buffer}) and internal wires of the router (E_{wire}) is insignificant compared with energy consumption between routers ($E_{\text{Inter-tile-Link}}$):

$$E_{buffer} + E_{wire} \ll E_{Inter-tile-Link}. \quad (5)$$

Thus, Equation (5) is simplified as

$$E_{NoC-1hop} = E_{Crossbar-1hop} + E_{Inter-router}. \quad (6)$$

The energy consumption $E_{\text{crossbar-1hop}}$ includes energy consumption of two intersecting sections of source and destination routers, in other words:

$$E_{Crossbar-1hop} = E_{Crossbar-Src} + E_{Crossbar-Dst}. \quad (7)$$

Thus, in homogenous architecture, the routers' structure is similar. Equation (8) is simplified as

$$E_{Crossbar} = 2 \times E_{Cross-router}. \quad (8)$$

As a result, the exchange energy consumption between two neighboring routers will be

$$E_{NoC-1hop} = 2 \times E_{Cross-router} + E_{Inter-router}. \quad (9)$$

According to Figure 7, Equation (9) for a route with a length of 3 changes as

$$E_{2-hop} = 3 \times E_{Cross-router} + 2 \times E_{Inter-router}. \quad (10)$$

Equations (9) and (10) can be generalized, and considering Figure 8, the average energy consumption of sending data flit from tile_{Src} to tile_{Dst} in general can be calculated as

$$E_{Path} = E_{n-hop} = n \times E_{Cross-router} + (n-1) \times E_{Inter-router}. \quad (11)$$

In Equation (11), variable n indicates the number of routers existing in route. Hence, this equation shows that the mean energy consumption of sending data from the source core to the destination core depends on the number of hops of the route. Hop number in the mesh between source and destination is determined by Manhattan distance between two cores. Manhattan distance is an indicator of distance between two points and is equal to the sum of the absolute values of the difference between width and length of those two points.

If a vector of length n is to be used for addressing the routers in the n-dimensional case,

$$V = (v_1, v_2, \cdots, v_n),$$
$$W = (w_1, w_2, \cdots, w_n). \quad (12)$$

The Manhattan distance of the two vectors is

$$|V - w| = \sum |v_i - w_i|. \quad (13)$$

4.2. Identification of Traffic Type. A traffic analyzer is used to identify the traffic type. This analyzer obtains the destination address of each package, which is directed through the router and examines its data in each T hour cycle. Based on this, a two 5-bit counter is used for the determination of locality or nonlocality of requests in the router. If the desired destination packet is two hops or farther from the current router, it is regarded nonlocal; otherwise, it is local. In fact, the analyzer calculates the hops associated with packet periodically and, based on that, updates the local (L) and nonlocal (N) counters. This data is sent to switch for decision-making regarding the selection strategy. The

```
1: Input: Packet hops (pkt_dst_hops),
2: Output: Local and Non-Local value (L = Local value, N = non_Local value)
3 Initializing: L = 0, N = 0
4:      if pkt_dst_hops ≧ 2 then
5:          N++;
6:      else
7:          L++;
8:      end
```

Figure 9: Pseudocode corresponding to traffic type recognition.

counter is erased after each T hour cycle. Figure 9 shows the pseudocode corresponding to the traffic analyzer.

In fact, using the analyzer, proper information about traffic rate and their convergence toward local or nonlocal traffics can be obtained, and then based on that, routing can be performed in the next hop.

4.3. Selecting the Best Output Channel. Using this approach, it will be possible to use the best selection strategy based on the traffic type. The considered condition is examined in each T hour cycle. It should be noted that if the T value is assumed large, network response to changes in traffic patterns reduces, and if this value is considered low, high switches cause a reduction in the efficiency. Overall, studies have shown that if the value of T is assumed a 32 cycle hour, the maximum efficiency is achieved. Based on this, at the end of each 32 cycle hour, the traffic pattern is determined using the output of the analyzer. According to the evaluations, this has been achieved that if traffic pattern tends toward local traffic destinations, scoring-based selection strategy is activated. Consequently, the score of one output channel is calculated through

$$Score[d] = \alpha \times Const[d] + \beta \times (B[d]/\max\ buffer + \gamma) \times (\Delta P/\max\ power), \tag{14}$$

where α, β, and γ are the weight factors for the probability of link selection, free buffer rows, and instantaneous power consumption, respectively. Since free buffer rows (B) and instantaneous power consumption (Δp) have different units, they are normalized using max-buffer and max-power factors. Also, considering that *Const* is in the range of (0,1), no normalization is needed. Afterward, the score of adaptive routing functions and all possible values of α, β, and γ are evaluated, and the adequate coefficients for each of the routers are obtained through

$$\alpha + \beta + \gamma = 1, \tag{15}$$

$$\gamma = 1 - (\alpha + \beta), \tag{16}$$

$$\beta = 0, 0.1, \cdots, (1 - \alpha), \tag{17}$$

$$\alpha = 0, 0.1, \cdots, 1. \tag{18}$$

For instance, the best values for α, β, and γ in even/odd routing under the MMS traffic scenario are 0.3, 0.4, and 0.3, respectively. Another important property of ScRN is its adaptability to any network topology and adaptive routing function. However, if traffic is nonlocal, a strategy based on RCA and NoP is activated as a proposed strategy for nonlocal traffics. In other words, under these conditions, the locality and nonlocality of the router will be determined based on the traffic pattern rate based on the traffic pattern rate. For non-edge routers in an 8×8 mesh, the local traffic penetration coefficient to nonlocal traffic is considered higher because it affects the overall network performance. Based on this, provided that a minimum rate of nonlocal traffic exists in routers, the ScRN method is activated. As a result, the local to nonlocal traffic rate (X) should be considered an effective parameter. Based on the evaluations, this parameter is considered a constant equal to $X = 0.4$, and it has been argued that it can induce maximum performance in the network. In other words, if at least 40% of the router's traffic is routed toward nonlocal destinations, the intended strategy needs to be activated. Therefore, following these principles in this study, the operations regarding the switching are expanded as

$$\begin{cases} 0.2 < X < 0.4 & \text{NoP Switching} \\ X \geq 0.4 & \text{RCA Switching} \end{cases}. \tag{19}$$

The ScRN algorithm associated with switching operation based on the traffic analyzer is shown in Figure 10. The input data to this algorithm are the type of local or nonlocal data, and the output is the best selection strategy. Also, it should be noted that since analyzer and switch receive only router data at once, consequently, no overhead in network communications is produced. In this Figure N and L represent Local and Non-Local packets and T represent clock cycels.

5. Evaluation and Simulation Environment

A Nirgam simulator is used to evaluate the proposed algorithm whose capabilities are listed in Table 3 [5]. Nirgam is a scalable, modular simulator based on the system C hardware description language, enabling various options at every stage of NoC design, including topology, switching methods, virtual channels, buffer parameters, and tested routing mechanisms. Moreover, the configuration parameters for

```
forevery T clock cycles do
    Catch L and N value from analyzer;
    Compute x = N/(L+N);
    If x = 0.2 < x < 0.4 then
        Switch to NoP;
    elseif x ≧ 0.4 then
        Switch to RCA;
    else
        Using score strategy;
    end
end
```

Figure 10: Pseudocode of switching procedure and strategy type selection in ScRN.

Table 3: Main capabilities of Nirgam simulator.

Types of production traffic	Routing algorithms type	Switching mechanism	Topology type
Constant bit rate trace and Bursty based	Odd-even, XY	Wormhole	Torus, mesh

Table 4: Simulation parameters.

Parameter	Configuration
Network size	8*8 mesh
Schemes	DICA [18], RCA [21], NoP [10], ScRN
Packet size	8 flits
Buffer size	4 flits
Traffic profile	Random, transpose, hotspot-center, hotspot-row
Simulation time	10

the analysis and simulation of the proposed method are given in Table 4. For the type and size of the utilized network in simulation, an 8×8 mesh network with a wormhole switching mechanism is considered [20, 41]. The routing function used in evaluations is odd-even algorithm, and the capacity of input buffers was 4 flits; the queue type was FIFO, and the size of each packet was defined as 8 flits. Simulation was performed for 200,000 cycles, and the first 20,000 cycles were determined as the warm-up time for stabilization of results. The entire simulation scenario was repeated ten times for more accuracy of the results whose average was calculated [18].

5.1. Traffic Scenarios Used in Algorithm Evaluation. In simulations performed to evaluate the selection functions, traffic scenarios are utilized. In a random traffic pattern, a node sends the packets with the same probability to other nodes. In transpose traffic pattern, a node in position (x, y) only sends the packets to coordinates (n-1-y,n-1-x). In this traffic pattern, n is the mesh network size (number of columns or rows). The performance of the proposed algorithm is studied for hotspot traffic as well. The hotspot traffic is like random traffic, which receives more traffic percentage than other nodes, in addition to nodes from the network. As shown in Figure 11, two types of hotspot traffic patterns are utilized in evaluations. One is named the hotspot-center traffic, and the nodes which are located in position (4,4) and (5,5) receive 10 percent more traffic than other nodes. The other hotspot traffic pattern is hotspot-row in which the points located in one row with coordinates (2,2), (3,2), (4,2), (5,2), (6,2), and (7,2) receive two percent more traffic than other nodes of the network.

5.2. Evaluated Parameters. The average packet latency, network throughput, and energy consumption in various injection rates and under different traffic patterns are evaluated to show the performance of the ScRN algorithm. The average packet latency is equal to the average delay of all packets received at the destination. In other words, the interval between injection of header flit in the network of the source node and receiving one flit sequence in the destination node is packet latency. In Equation (20), K is the total number of delivered messages in the destination node, and Li is the delay of the i^{th} message [5]:

$$L = \frac{1}{k}\sum_{i=0}^{k} L_i. \tag{20}$$

The network throughput is mainly based on the maximum number of packets delivered in a specific interval and is determined via the equation given below [20, 42] . In Equation (21), the total number of received flits, i.e., the total number of delivered flits to the destination and cycles, is the number of simulation cycles between injection of the first message into the network and reception of the last message delivered to the destination node:

$$TP = \frac{Total\ received\ flits}{Number\ \text{of}\ nodes \times Total\ cycles}. \tag{21}$$

5.3. Simulation Results. To evaluate the proposed method, parameters of throughput, average packet latency, and

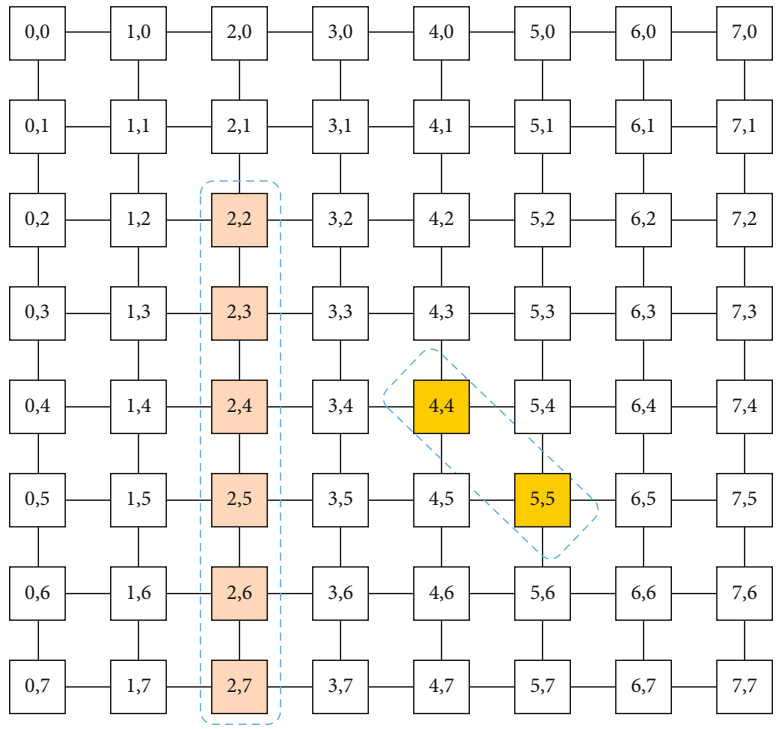

Figure 11: Performance of ScRN algorithm in 8×8 mesh.

energy consumption level were taken into account for each scenario in different modes of packet injection. Figure 12(a) shows the simulation results for average latency of the packets in the transpose traffic pattern. As shown in Figure 12(a), all algorithms are in the same level of delay in the first three points; however, in other points, the ScRN algorithm performed better than other algorithms. The improvement in average latency of the packets through the proposed ScRN algorithm is 34.64%, 11.85%, and 32.81% compared with NoP, DICA, and RCA, respectively. Figure 12(b) presents the simulation results for the average latency of the packets in the random traffic pattern. As indicated, the ScRN algorithm outperformed other algorithms at every point. The improvement in average latency of the packets using the proposed ScRN algorithm was 46.56%, 6.03%, and 22% compared with NoP, DICA, and RCA, respectively. Figure 12(c) shows the simulation results for average latency of the packet in the hotspot-center traffic pattern. As shown in the figure, the average latency of the packets using ScRN was improved by 20%, 5.92%, and 13.20% in comparison with NoP, DICA, and RCA, respectively. Figure 12(d) shows the simulation results for the average latency of the packets in the hotspot-row traffic pattern. As seen in this figure, improvement for average latency of the packets through the proposed ScRN algorithm was 15.51%, 6.87%, and 22.41% compared with NoP, DICA, and RCA, respectively.

In the performed evaluations, the ScRN output selection algorithm had a lower average latency than all other algorithms. The reason behind this is the usage of channel congestion information and the selection of packet output depending on the traffic type. According to Figures 12(a) to 12(c), in transpose, random, and hotspot-center patterns, the RCA algorithm, succeeding ScRN and DICA algorithms, and better than NoP had lower average packet latency, which is due to having more global congestion information. However, in Graph 12d, the RCA algorithm performed worse than other algorithms. This is because the selection process is made by putting separate values for traffic in all four quarters of the network. By using this, the RCA algorithm has access to additional congestion information, which is off the short route associated with node addresses of source and destination and utilized it in output selection [41] . Moreover, under hotspot-row traffic, due to the sequence of nodes with hotspot traffic in the same row, this congestion can accumulate throughout a row. Therefore, it can easily cause the output selection function to carry out an unfair selection during the time that hotspot nodes are off the short routes. This unfair selection can cause more congestion and higher packet latency. On the other hand, using congestion information on the route, ScRN can effectively prevent packets from passing through congested routes, which leads to decrease in the average packet latency and improvement in network performance [35] . Table 5 shows the level of improvement in the ScRN algorithm for random, transpose, hotspot-center, and hotspot-row traffic patterns. In this table, the ScRN delay is measured in an injection point which is not network saturated. As can be seen in the table, for all scenarios, including the hotspot-center scenario, our algorithm performed better than similar algorithms because in this scenario, there are important parts such as computing unit, memory unit, and control unit, so the percentage traffic is higher than other scenarios. Selecting the best output channel, the packets arrive at their destination with less delay. On average, the proposed ScRN

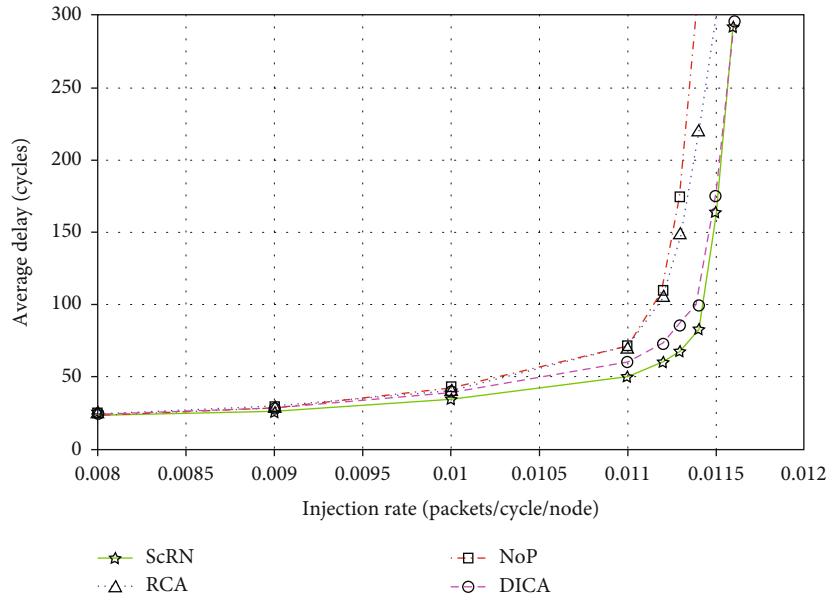

(a)

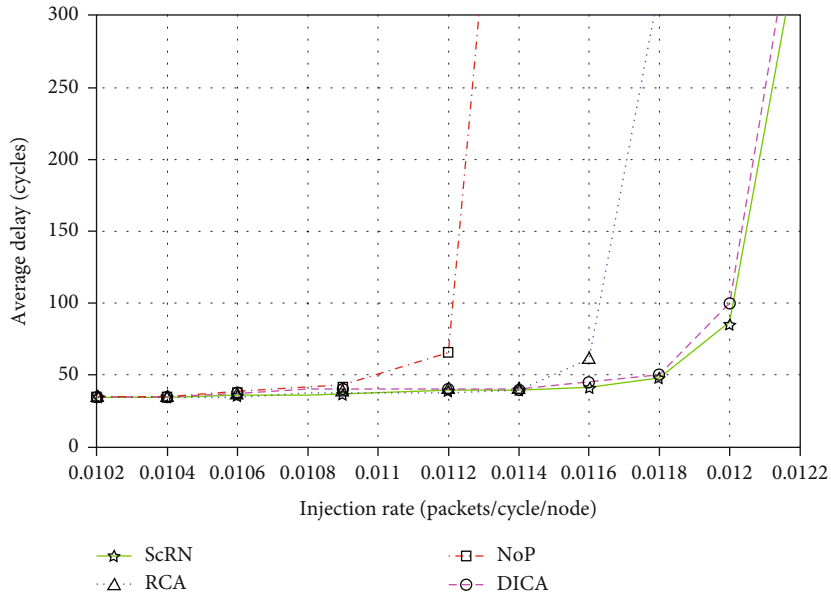

(b)

Figure 12: Continued.

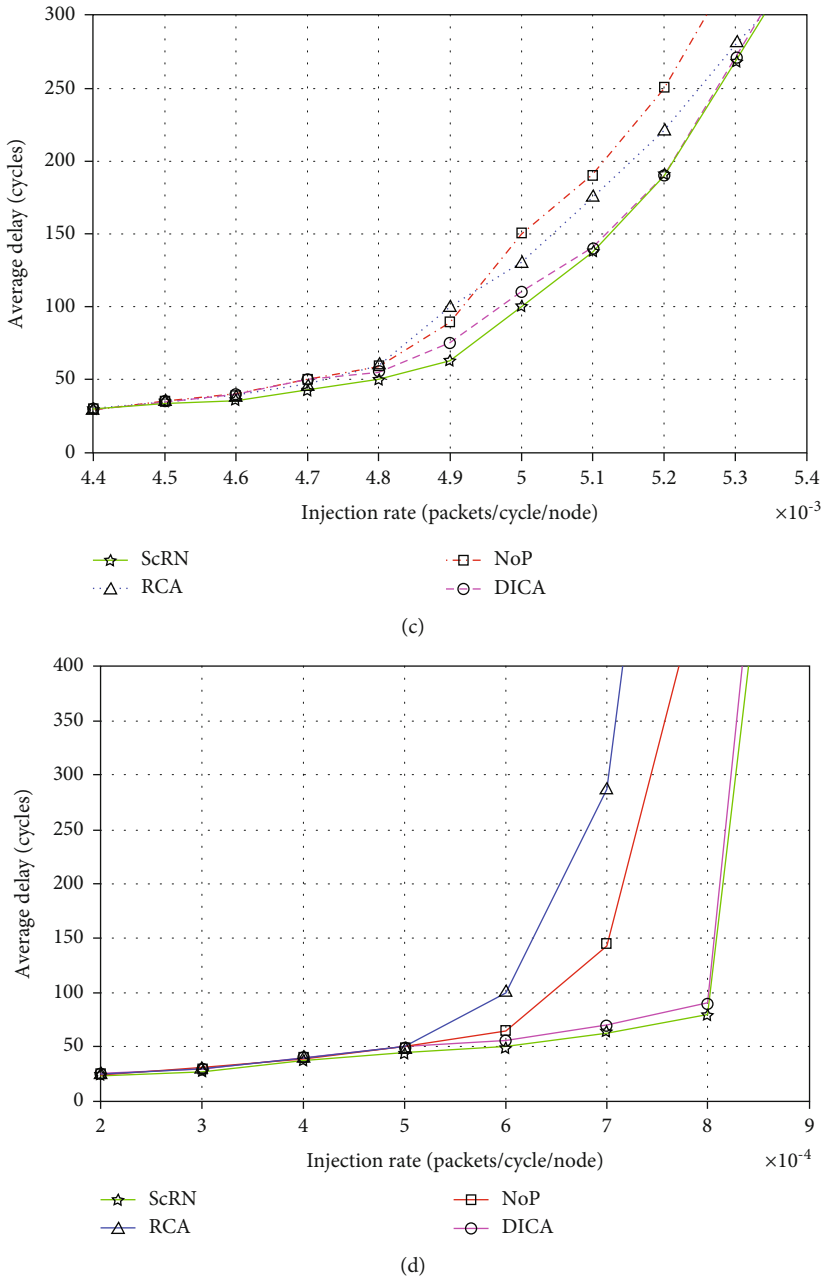

Figure 12: (a) Comparison of average packet latency in the transpose traffic pattern. (b) Comparison of average packet latency in the random traffic pattern. (c) Comparison of average packet latency in the hotspot-center traffic pattern. (d) Comparison of average packet latency in the hotspot-row traffic pattern.

Table 5: Improvement level of average latency of packets in the proposed ScRN algorithm.

Traffic patterns	Packet injection rate (packet/cycle/node)	Average latency (cycles)				Latency reduction by ScRN		
		DICA	RCA	NoP	ScRN	Versus DICA	Versus RCA	Versus NoP
Random	0.0114	36	42	866	28	22.22%	33.34%	96.76%
Transpose	0.0113	84	145	174	86	2.38%	40.68%	50.57%
Hotspot-center	0.005	109	132	147	94	13.76%	28.78%	36.5%
Hotspot-row	0.0007	70	285	146	75	7.14%	73.68%	48.63%
Average latency reduction						**11.37%**	**44.12%**	**58%**

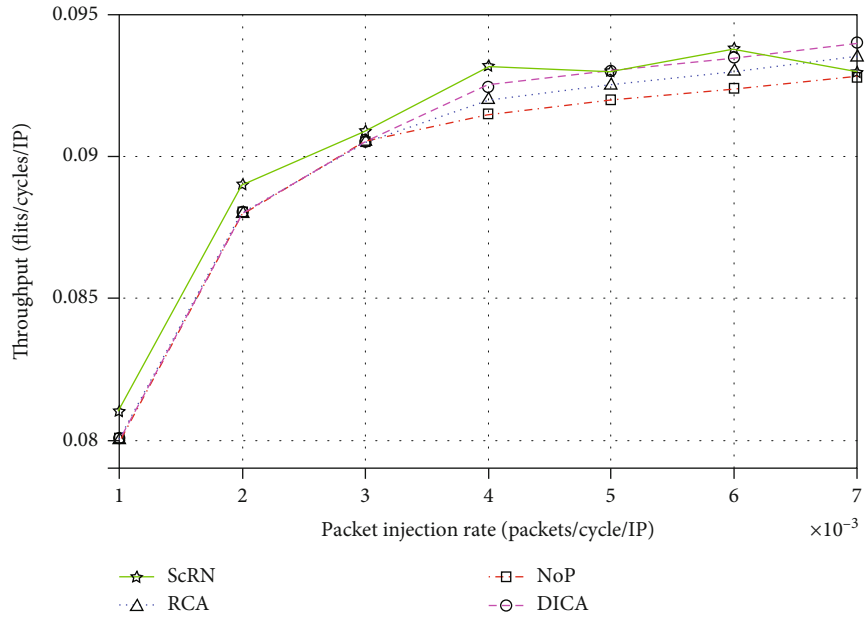

(a)

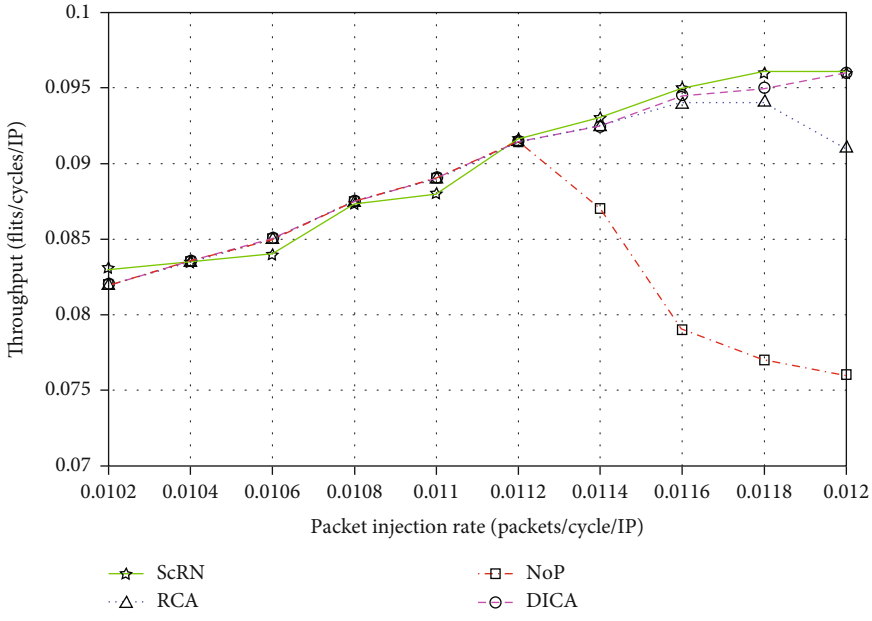

(b)

Figure 13: Continued.

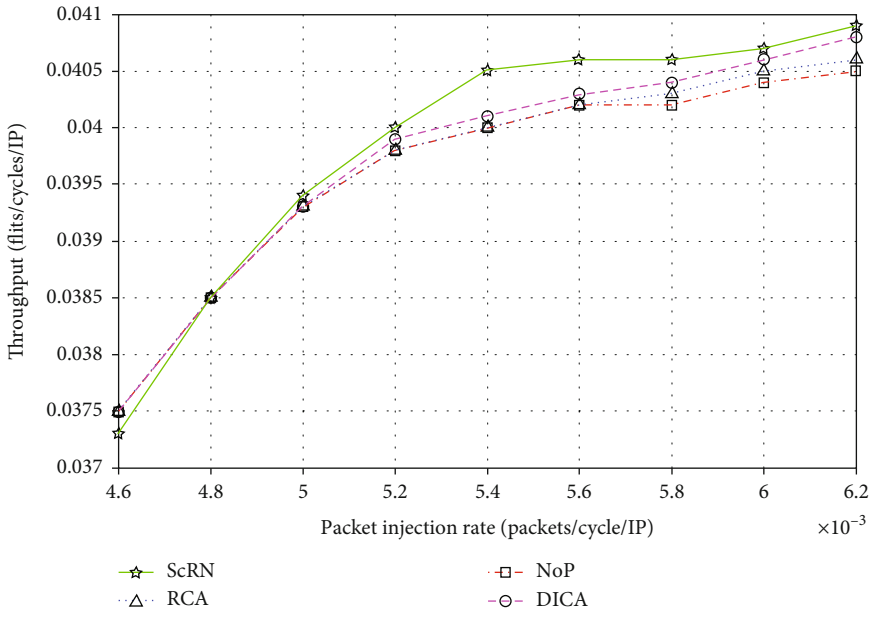

(c)

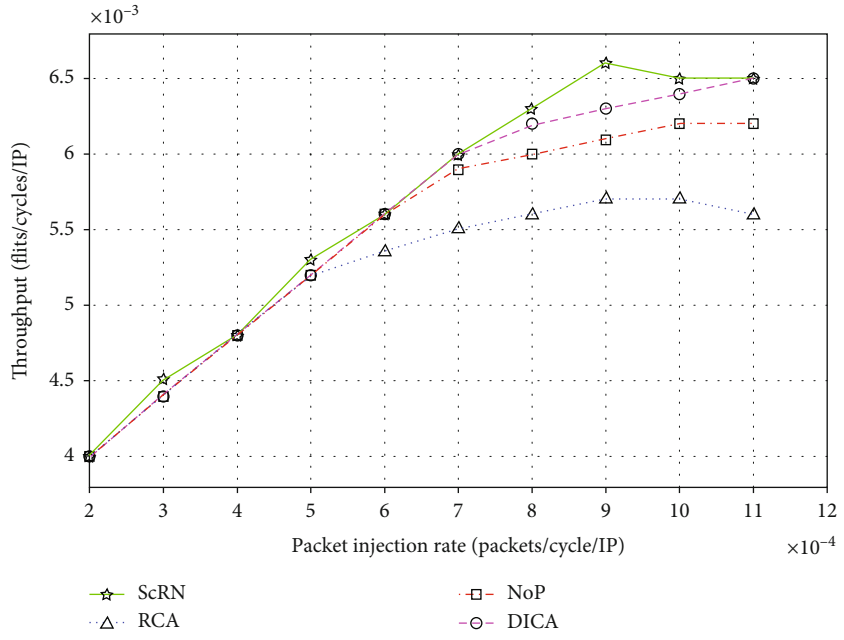

(d)

Figure 13: (a) Comparison of network throughput in the transpose traffic pattern. (b) Comparison of network throughput in the random traffic pattern. (c) Comparison of network throughput in the hotspot-center traffic pattern. (d) Comparison of network throughput in the hotspot-row traffic pattern.

Table 6: Comparison of the improvement level of throughput in saturated point for the proposed algorithm.

Traffic patterns	Saturation throughput (packet/ns/node)				ScRN improvement		
	DICA	RCA	NoP	ScRN	Versus DICA	Versus RCA	Versus NoP
Random	0.0117	0.0113	0.0106	0.0123	5.12%	8.85%	16.03%
Transpose	0.0114	0.01	0.01	0.0111	2.63%	11%	11%
Hotspot-center	0.0050	0.0049	0.0048	0.0056	12%	14.28%	16.67%
Hotspot-row	0.0008	0.0005	0.00059	0.0009	12.50%	80%	52.54%
Average improvement					**8.06%**	**26.49%**	**24.06%**

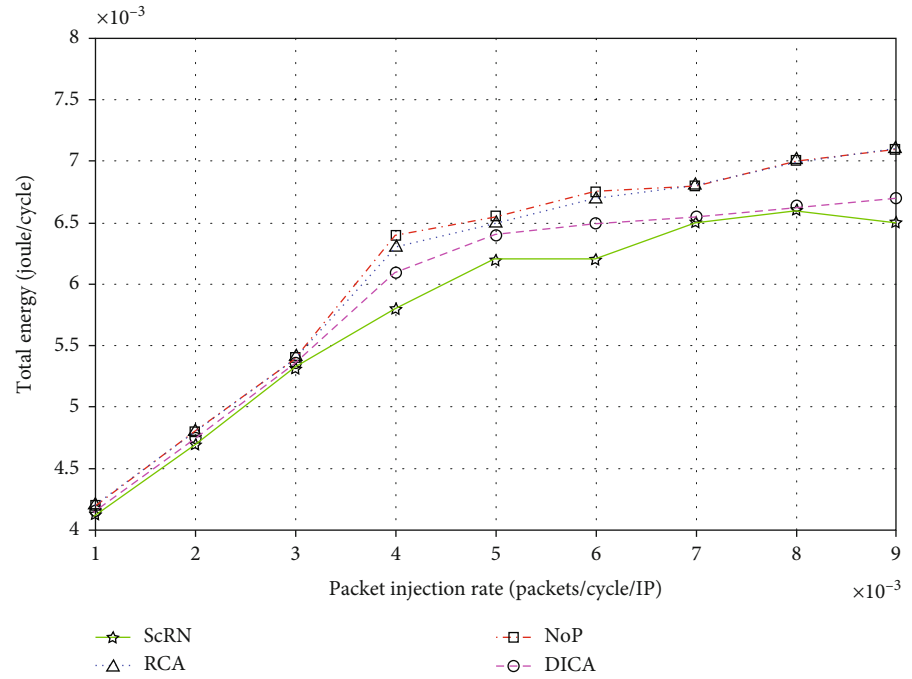

(a)

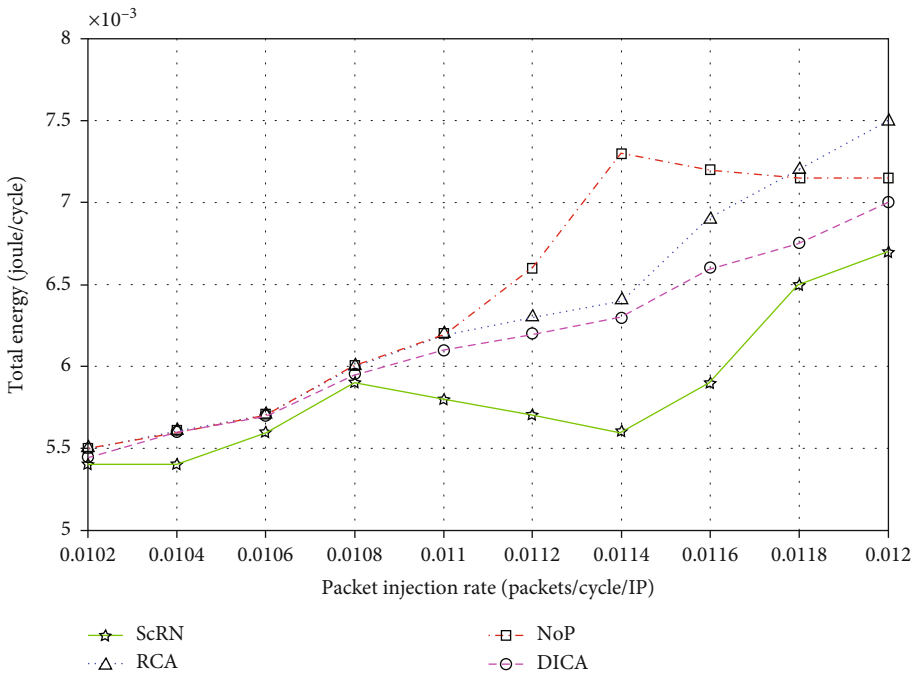

(b)

Figure 14: Continued.

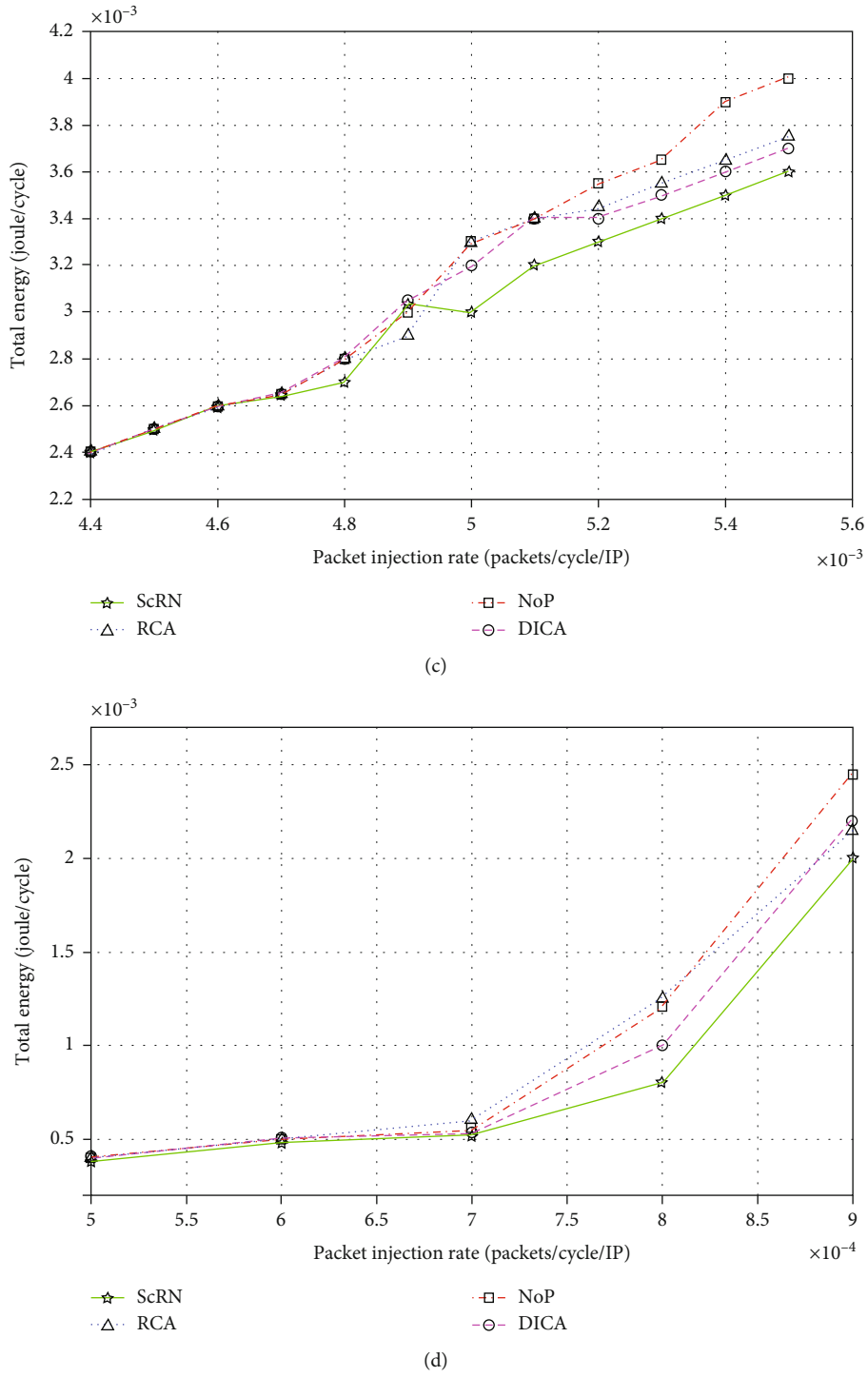

Figure 14: (a) Comparison of energy consumption in the transpose traffic pattern. (b) Comparison of energy consumption in the random traffic pattern. (c) Comparison of energy consumption in the hotspot-center traffic pattern. (d) Comparison of energy consumption in the hotspot-row traffic pattern.

algorithm was able to improve the average latency from 11.37% to 58% compared with other algorithms.

Figures 13(a) to 13(d) present the throughput results for all traffic patterns. Simulation results prove that improvement in average delay can enhance the throughput. As can be concluded from the analyses, the ScRN selection strategy caused a reduction in average packet latency and an increase in throughput for all traffic patterns. This improvement is due to a more uniform distribution of traffic compared with other algorithms and also utilization of local and nonlocal congestion information, which led to more comprehensive information associated with network conditions.

Table 7: Comparison of reduction level in energy consumption for the proposed ScRN algorithm.

Traffic patterns	Packet injection rate (packet/cycle/node)	Average energy consumption (cycles)				Energy consumption by ScRN		
		DICA	RCA	NoP	ScRN	Versus DICA	Versus RCA	Versus NoP
Random	0.0116	0.0066	0.0069	0.0072	0.0059	10.60%	18.05%	14.49%
Transpose	0.0113	0.0065	0.0067	0.00675	0.0062	4.61%	8.14%	7.46%
Hotspot-center	0.00506	0.0035	0.00355	0.00365	0.0034	2.85%	6.84%	4.22%
Hotspot-row	0.0009	0.0022	0.00215	0.00245	0.0020	9.09%	18.36%	6.97%
Average energy consumption						**6.78%**	**12.84%**	**8.28%**

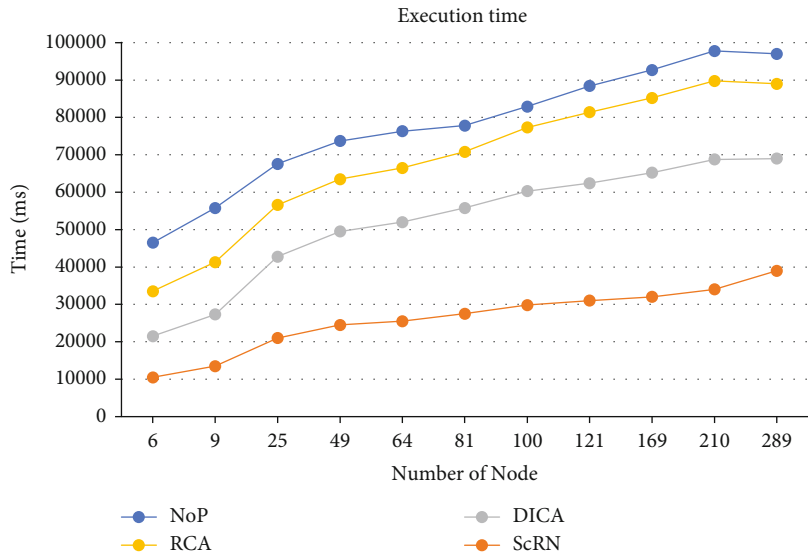

Figure 15: Execution time comparison for routing algorithms.

Table 6 presents the details of network throughput improvement for the ScRN algorithm. As can be seen in this table, the throughput for all scenarios has increased. Because the proposed algorithm first examines the amount of empty buffer of each neighboring node in question, and if the amount of buffer is less than normal or not empty, the weight of the node congestion increases, and thus the probability of selecting it decreases. This ensures that, as far as possible, congested or busy routes will have lower priority for closed selection and routing, resulting in reduced latency and increased throughput. The results of the evaluations in all scenarios show the same. Simulation results show that the proposed algorithm had one more throughput in saturated point in the range of 8.06% to 26.49% compared with other algorithms, or in other words, the network is saturated in a higher injection point.

The results show that the improvement level in network throughput can impact total energy consumption. In the present study, the Nirgam simulator is used to calculate energy consumption. As an architecture-level simulation tool, the Nirgam [5] is utilized to assess the energy consumption of the router's main operations like routing, incoming, and forwarding the flits and the output selection. SystemC which is a system description language based on C ++ is used to develop the Nirgam simulator. In Nirgam, Equation (11) has been used to estimate the average power, and each component has been applied in HDL. The ScRN strategy was implemented in VHDL, and synthesis was carried out through the Synopsys Design Compiler. Afterwards, ScRN average power in Synopsys Design Compiler was added to the Nirgam. In the Nirgam which is a signal level and cycle accuracy simulation, each wire is defined as a signal; therefore, energy consumption is computed by taking the overhead of ScRN logic and wiring. As shown in Figures 14(a) to 14(d), the mean network energy consumption using the proposed method is reduced for all traffic patterns. For example, the proposed ScRN algorithm had lower energy consumption with an average improvement of 5% compared with other algorithms in transpose traffic pattern. This decrease is the result of avoiding congested routes using the information provided by the ScRN strategy.

Table 7 presents the reduction in energy consumption of the ScRN algorithm for random, transpose, hotspot-center, and hotspot-row traffic patterns compared with other algorithms. As seen, by an increase in the injection rate, the average energy consumption rises as well. According to the results of previous evaluations, for all traffic scenarios, a reduction in energy consumption was also predictable, because in the proposed solution, the choice of crowded channels is always avoided, that is, routes with high

probability of congestion are in the lowest priority for routing. Avoiding crowded paths can create an optimal balance across the network, thus avoiding congestion of thermal bottlenecks due to congestion, and one of the important results is the reduction of energy consumption, which is shown by the results of the above diagrams. On average, the proposed ScRN algorithm was able to reduce energy consumption from 6.78% to 12.84% compared with other algorithms.

In the following, we compared the execution time of the proposed algorithm in comparison with other algorithms. Figure 15 shows the execution time and energy reductions for all routing algorithms, taking into account NoC size variation. When compared to other algorithms, ScRN achieve an average execution time reductions of over 80% while keeping energy savings to no more than 12% of the best results.

6. Conclusion

In this research, a novel output selection strategy called ScRN was proposed based on the parameters that affect the NoC performance. The basis of the proposed approach is using a traffic analyzer in which the traffic type is determined, and then, the best selection function associated with traffic type is used. Based on this, in this approach, if traffic pattern tends toward the destination of local traffics, the scoring-based selection strategy is activated, and otherwise, the strategy based on RCA and NoP is activated as proposed strategies for nonlocal traffics. In other words, in these conditions, the traffic pattern rate determines the local or nonlocal performance of the router. In the end, in the Nirgam simulation environment, and in different traffic scenarios, the proposed ScRN method was compared with and evaluated against other selection functions. Evaluations were done based on different traffic patterns. The most important features of this solution compared to previous works are as follows:

(i) Use of new hybrid selection function to increase NoC performance

(ii) Use of analyzer to evaluate local and nonlocal packet traffic

(iii) Use of scoring strategy to select the best output channel

Based on this, considering the latency and throughput parameters, it was concluded that the proposed approach was effectively able to reduce the energy consumption and delay by analyzing the traffic type and determining the most appropriate function. As a result, it enhanced the throughput in NoCs. Also, Our proposed method includes the following limitations:

(i) Calculate output channel scores can affect runtime

(ii) Only works on adaptive algorithms and mesh topology

Data Availability

Data is available on the following link: https://s21.picofile.com/file/8443990850/codes.rar.html.

Conflicts of Interest

The authors declare that they have no conflicts of interest.

References

[1] P. K. Sahu and S. Chattopadhyay, "A survey on application mapping strategies for network-on-chip design," *Journal of Systems Architecture*, vol. 59, no. 1, pp. 60–76, 2013.

[2] A. B. Achballah and S. B. Saoud, "A survey of network-on-chip tools," https://arxiv.org/abs/1312.2976.

[3] A. Abbas, M. Ali, A. Fayyaz et al., "A survey on energy-efficient methodologies and architectures of network-on-chip," *Computers & Electrical Engineering*, vol. 40, no. 8, pp. 333–347, 2014.

[4] M. Trik, S. Pour Mozaffari, and A. M. Bidgoli, "Providing an adaptive routing along with a hybrid selection strategy to increase efficiency in NoC-based neuromorphic systems," *Computational Intelligence and Neuroscience*, vol. 2021, Article ID 8338903, 2021.

[5] P. Mukherjee and S. Chattopadhyay, "Low power low latency floorplan-aware path synthesis in application-specific network-on-chip design," *Integration*, vol. 58, pp. 167–188, 2017.

[6] J. Wu, D. Dong, X. Liao, and L. Wang, "Energy-efficient NoC with multi-granularity power optimization," *The Journal of Supercomputing*, vol. 73, no. 4, pp. 1654–1671, 2017.

[7] P. Lotfi-Kamran, A.-M. Rahmani, M. Daneshtalab, A. Afzali-Kusha, and Z. Navabi, "EDXY–a low cost congestion-aware routing algorithm for network-on-chips," *Journal of Systems Architecture*, vol. 56, no. 7, pp. 256–264, 2010.

[8] X. Zhou, L. Liu, Z. Zhu, and D. Zhou, "A routing aggregation for load balancing network-on-chip," *Journal of Circuits, Systems and Computers*, vol. 24, no. 9, article 1550137, 2015.

[9] L. Zhang, E. E. Regentova, and X. Tan, "Packet switching optical network-on-chip architectures," *Computers & Electrical Engineering*, vol. 39, no. 2, pp. 697–714, 2013.

[10] G. Ascia, V. Catania, M. Palesi, and D. Patti, "Neighbors-on-path: a new selection strategy for on-chip networks," in *2006 IEEE/ACM/IFIP Workshop on Embedded Systems for Real Time Multimedia*, pp. 79–84, IEEE, 2006.

[11] A. Osmani, J. B. Mohasefi, and F. S. Gharehchopogh, "Sentiment classification using two effective optimization methods derived from the artificial bee colony optimization and imperialist competitive algorithm," *The Computer Journal*, vol. 65, no. 1, pp. 18–66, 2022.

[12] L. Liu, R. Ma, and Z. Zhu, "An encapsulated packet-selection routing for network on chip," *Microelectronics Journal*, vol. 84, pp. 96–105, 2019.

[13] S. Ma, N. E. Jerger, and Z. Wang, "DBAR: an efficient routing algorithm to support multiple concurrent applications in networks-on-chip," *Proceedings of the 38th annual international symposium on Computer architecture*, vol. 39, no. 3, pp. 413–424, 2011.

[14] P. Kullu and S. Tosun, "Energy-aware and fault-tolerant custom topology design method for network-on-chips," *Nano Communication Networks*, vol. 19, pp. 54–66, 2019.

[15] N. Chatterjee, P. Mukherjee, and S. Chattopadhyay, "Reliability-aware application mapping onto mesh based Network-on-Chip," *Integration*, vol. 62, pp. 92–113, 2018.

[16] J. Liu, J. Harkin, Y. Li, and L. Maguire, "Low cost fault-tolerant routing algorithm for networks-on-chip," *Microprocessors and Microsystems*, vol. 39, no. 6, pp. 358–372, 2015.

[17] F. Bahman, A. Reza, M. Reshadi, and S. Vazifedan, "CACBR: congestion aware cluster buffer base routing algorithm with minimal cost on NOC," *CCF Transactions on High Performance Computing*, vol. 2, no. 3, pp. 297–306, 2020.

[18] A. Mehranzadeh, A. Khademzadeh, N. Bagherzadeh, and M. Reshadi, "DICA: destination intensity and congestion-aware output selection strategy for network-on-chip systems," *IET Computers & Digital Techniques*, vol. 13, no. 4, pp. 335–347, 2019.

[19] R. Suraj and P. Chitra, "PT-BAR: prioritized thermo-buffer based adaptive routing protocol for network-on-chip," *Procedia Computer Science*, vol. 93, pp. 324–335, 2016.

[20] G. Ascia, V. Catania, M. Palesi, and D. Patti, "Implementation and analysis of a new selection strategy for adaptive routing in networks-on-chip," *IEEE Transactions on Computers*, vol. 57, no. 6, pp. 809–820, 2008.

[21] A. Arora and N. K. Shukla, "A congestion controlled and load balanced selection strategy for networks on chip," *International Journal of Distributed Systems and Technologies (IJDST)*, vol. 11, no. 1, pp. 1–14, 2020.

[22] P. K. Donta, T. Amgoth, and C. S. R. Annavarapu, "Congestion-aware data acquisition with q-learning for wireless sensor networks," in *2020 IEEE International IOT, Electronics and Mechatronics Conference (IEMTRONICS)*, pp. 1–6, IEEE, 2020.

[23] M. Devanathan, V. Ranganathan, and P. Sivakumar, "Congestion-aware wireless network-on-chip for high-speed communication," *Automatika*, vol. 61, no. 1, pp. 92–98, 2020.

[24] C. Sun, Y. Ouyang, and H. Liang, "Architecting a congestion pre-avoidance and load-balanced wireless network-on-chip," *Journal of Parallel and Distributed Computing*, vol. 161, pp. 143–154, 2022.

[25] M. Trik, S. Pour Mozafari, and A. M. Bidgoli, "An adaptive routing strategy to reduce energy consumption in network on chip," *Journal of Advances in Computer Research*, vol. 12, no. 3, pp. 1–12, 2021.

[26] W. Hu, H. Guo, K. Zhang, J. Liu, X. Liu, and Q. Shi, "An energy-efficient design of microkernel-based on-chip OS for NOC-based many core system," *The Journal of Supercomputing*, vol. 73, no. 8, pp. 3344–3365, 2017.

[27] A. Alagarsamy, L. Gopalakrishnan, S. Mahilmaran, and S.-B. Ko, "A self-adaptive mapping approach for network on chip with low power consumption," *IEEE Access*, vol. 7, pp. 84066–84081, 2019.

[28] N. L. Venkataraman, R. Kumar, and P. Mohamed Shakeel, "Ant lion optimized bufferless routing in the design of low power application specific network on chip," *Circuits, Systems, and Signal Processing*, vol. 39, no. 2, pp. 961–976, 2020.

[29] J. Wang and D. Wang, "A smart protocol-level task mapping for energy efficient traffic on network-on-chip," *Microprocessors and Microsystems*, vol. 65, pp. 69–78, 2019.

[30] J. M. Joseph, L. Bamberg, I. Hajjar, R. Schmidt, T. Pionteck, and A. Garcia-Ortiz, "Simulation environment for link energy estimation in networks-on-chip with virtual channels," *Integration*, vol. 68, pp. 147–156, 2019.

[31] O. I. Khalaf, C. A. T. Romero, S. Hassan, and M. T. Iqbal, "Mitigating hotspot issues in heterogeneous wireless sensor networks," *Journal of Sensors*, vol. 2022, Article ID 7909472, 14 pages, 2022.

[32] A. B. Gabis, P. Bomel, and M. Sevaux, "Application-aware multi-objective routing based on genetic algorithm for 2D network-on-chip," *Microprocessors and Microsystems*, vol. 61, pp. 135–153, 2018.

[33] A. V. Salazar and G. Patiño, "Reducing dynamic energy in networks on chip," in *2019 Congreso Internacional de Innovación y Tendencias en Ingenieria (CONIITI)*, pp. 1–6, IEEE, 2019.

[34] K. Ilamathi and P. Rangarajan, "Intelligent computation techniques for optimization of the shortest path in an asynchronous network-on-chip," *Cluster Computing*, vol. 22, no. S1, pp. 335–346, 2019.

[35] J. Yong, Z. Lin, W. Qian, B. Ke, W. Chen, and L. Ji-fang, "Tree-based multihop routing method for energy efficiency of wireless sensor networks," *Journal of Sensors*, vol. 2021, Article ID 6671978, 14 pages, 2021.

[36] Z. Bo, Y. Dong, J. He, and L. Dongming, "An energy-efficient one-shot scheduling algorithm for wireless sensor networks," *Journal of Sensors*, vol. 2021, Article ID 9999403, 15 pages, 2021.

[37] E. L. Prasad, M. N. Giri Prasad, and A. R. Reddy, "HSRDN: high-speed router design for various NoC topologies," *Chinese Journal of Electronics*, vol. 29, no. 2, pp. 281–290, 2020.

[38] H. Zhao, F. Zhang, L. Chen, and M. Lu, "A method of fast evaluation of an MC placement for network-on-chip," *Journal of Circuits, Systems and Computers*, vol. 30, no. 7, article 2150115, 2021.

[39] M. R. Naqvi, "Low power network on chip architectures: a survey," *Computer Science and Information Technologies*, vol. 2, no. 3, pp. 158–168, 2020.

[40] T. S. Das, P. Ghosal, and N. Chatterjee, "VCS: a method of in-order packet delivery for adaptive NoC routing," *Nano Communication Networks*, vol. 28, article 100333, 2021.

[41] M. Trik and B. Boukani, "Placement algorithms and logic on logic (LOL) 3D integration," *Journal of Mathematics and Computer Science*, vol. 8, no. 2, pp. 128–136, 2014.

[42] M. Jalalifar and G.-S. Byun, "An energy-efficient multi-level RF-interconnect for global network-on-chip communication," *Analog Integrated Circuits and Signal Processing*, vol. 102, no. 1, pp. 131–143, 2020.

Hindawi
Journal of Sensors
Volume 2023, Article ID 9847567, 1 page
https://doi.org/10.1155/2023/9847567

Retraction

Retracted: Piano Automatic Composition and Quantitative Perception under the Data-Driven Architecture

Journal of Sensors

Received 10 October 2023; Accepted 10 October 2023; Published 11 October 2023

This article has been retracted by Hindawi following an investigation undertaken by the publisher [1]. This investigation has uncovered evidence of one or more of the following indicators of systematic manipulation of the publication process:

(1) Discrepancies in scope
(2) Discrepancies in the description of the research reported
(3) Discrepancies between the availability of data and the research described
(4) Inappropriate citations
(5) Incoherent, meaningless and/or irrelevant content included in the article
(6) Peer-review manipulation

The presence of these indicators undermines our confidence in the integrity of the article's content and we cannot, therefore, vouch for its reliability. Please note that this notice is intended solely to alert readers that the content of this article is unreliable. We have not investigated whether authors were aware of or involved in the systematic manipulation of the publication process.

Wiley and Hindawi regrets that the usual quality checks did not identify these issues before publication and have since put additional measures in place to safeguard research integrity.

We wish to credit our own Research Integrity and Research Publishing teams and anonymous and named external researchers and research integrity experts for contributing to this investigation.

The corresponding author, as the representative of all authors, has been given the opportunity to register their agreement or disagreement to this retraction. We have kept a record of any response received.

References

[1] C. Ren, "Piano Automatic Composition and Quantitative Perception under the Data-Driven Architecture," *Journal of Sensors*, vol. 2022, Article ID 9038427, 12 pages, 2022.

Hindawi
Journal of Sensors
Volume 2022, Article ID 9038427, 12 pages
https://doi.org/10.1155/2022/9038427

Research Article

Piano Automatic Composition and Quantitative Perception under the Data-Driven Architecture

Chao Ren

Music and Dance Department, Zhoukou Normal University, East Wenchang Street, Chuanhui District, Zhoukou City, Henan Province 466001, China

Correspondence should be addressed to Chao Ren; 20151049@zknu.edu.cn

Received 6 December 2021; Revised 5 January 2022; Accepted 10 January 2022; Published 25 March 2022

Academic Editor: Gengxin Sun

This paper combines automatic piano composition with quantitative perception, extracts note features from the demonstration audio, and builds a neural network model to complete automatic composition. First of all, in view of the diversity and complexity of the data collected in the quantitative perception of piano automatic composition, the energy efficiency-related state data of the piano automatic composition operation is collected, carried out, and dealt with. Secondly, a perceptual data-driven energy efficient evaluation and decision-making method is proposed. This method is based on time series index data. After determining the time subjective weight through time entropy, the time dimension factor is introduced, and then the subjective time weight is adjusted by the minimum variance method. Then, we consider the impact of the perception period on the perception efficiency and accuracy, calculate and dynamically adjust the perception period based on the running data, consider the needs of the perception object in different scenarios, and update the perception object in real time during the operation. Finally, combined with the level weights determined by the data-driven architecture, the dynamic manufacturing capability index and energy efficiency index of the equipment are finally obtained. The energy efficiency evaluation of the manufacturing system of the data-driven architecture proves the feasibility and scientificity of the evaluation method and achieves the goal of it. The simulation experiment results show that it can reduce the perception overhead while ensuring the perception efficiency and accuracy.

1. Introduction

In the field of composition, human work music needs to master basic music theory, musical style, harmony, and other professional knowledge. For ordinary users, the professionalism and threshold of composition are too high [1]. Automatic composition allows more ordinary users to participate in the production of piano automatic composition, which improves the entertainment of piano automatic composition. At the same time, automatic composition is random, which can bring creative inspiration to professionals. Driven by new theories, new technologies, and social development needs, artificial intelligence has accelerated its development, showing new characteristics such as quantitative perception and cross-border integration. These problems cause these methods to be helpless when dealing with complex class structure data. However, in the process of driving the architecture, the degree of compactness within the class is also the key to measuring the success of the driving architecture. Therefore, increasing the distance between classes and increasing the compactness within classes are the goals of our drive architecture [2–5]. In order to solve this problem, we improved DSC and KNNG, taking the distance information between points into consideration, and got new measurement methods, density-aware DSC and density-aware KNNG. Using these two measurement methods, this paper designs a new linear drive architecture algorithm: PDD (perception-driven DR using density-aware DSC) uses the density DSC visual perception-driven supervisory drive architecture algorithm and PDK (perception-driven DR). The visual perception-driven supervisory-driven architecture algorithm uses density-aware KNNG [6–8].

In order to test whether our method is effective for such data, we tried our method as follows. When calculating the global dDSC and dKNNG, we no longer directly calculate the mean value of dDSC(dKNNG) of all sample points but take the class as the unit to calculate the mean of each class and then calculate the mean of all classes. The driving architecture algorithm can project data into a low-dimensional space that is easier for humans to recognize, which will make it more convenient for users to explore the distinction between different types of data and the spatial distribution of data [9–11]. However, in the currently widely used unsupervised drive architecture algorithm, such as PCA, its drive architecture goal is not to maximize the class spacing as much as possible. The supervised driving architecture algorithm, such as LDA, is only suitable for data that conforms to the Gaussian distribution and does not take human knowledge into consideration. Second, we use our method to process high-dimensional data without class labels. Third, star coordinates are well-acclaimed in the field of visual analysis. Unlike traditional drive architecture algorithms, star coordinates can be extended with many interactive methods in two-dimensional or three-dimensional space. Incorporating the user's prior knowledge into the drive architecture process is conducive to the user's exploration and learning of data. We combine the drive architecture algorithm with the star coordinates and provide users with a series of interaction methods, such as point interaction, class interaction, and axis interaction, to facilitate users' interactive data exploration [12–15].

In order to fill the gap in this regard, this paper proposes a linear drive architecture algorithm driven by automated arrangement perception. This method is aimed at maximizing the class spacing of data that conforms to the automated arrangement perception in the process of driving the architecture. Recently, the perception-based measurement method of class spacing has made a big breakthrough in the ability of simulating automatic arrangement perception. We further improve these methods, incorporate class density information, and combine them into the simulated annealing algorithm to find an approximate optimal solution. Based on the manufacturing service technology, an effective dynamic evaluation system of piano automatic composing running energy driven by perception data is designed and realized. The system mainly has four modules: equipment information management module, energy consumption data monitoring module, equipment capability evaluation module, and equipment service combination module. Each module realizes the addition, deletion, modification, and inspection of basic equipment information, monitoring and display of energy consumption data, and dynamic assessment of equipment capabilities and equipment historical service portfolio information. We provide enterprises with readily available and on-demand manufacturing resources and capabilities during the manufacturing process. We compare the algorithm with the most commonly used driving architecture algorithms on 93 data sets at the numerical level and the perceptual comparison of user scores and analyze the performance of the algorithm. At the same time, the algorithm is also extended to data with uneven class distribution and classless label data. Finally, it is combined with the star coordinate system to provide a series of interactive methods to facilitate users to further explore the data.

2. Related Work

In terms of micro resources, Machado et al. [16] define manufacturing capability as the integration of effective manufacturing resources in the realization of manufacturing tasks. It consists of processing capability and production capability. The processing capability represents the types of workpieces that can be processed under a specific machine tool, and the production capability represents the workpieces that can be produced per unit time and gives a new evaluation model and evaluation method for manufacturing capabilities. Scirea et al. [17] believe that manufacturing decision-making, resources, and manufacturing capabilities are mutually influencing. Under the common influence, manufacturing capabilities are jointly improved to achieve the goal of improving innovation performance and corporate performance. Based on this theory, manufacturing is established in the capability strategy model, but in the case proof, Größler et al. did not give out the relationship between manufacturing decision-making, resources, and manufacturing capacity but only discussed the influence of various elements of manufacturing capacity. They elaborated on the connotation of manufacturing capabilities under the cloud manufacturing model, gave the concept and classification of manufacturing capabilities under cloud manufacturing, and believed that manufacturing capabilities reflect the configuration and integration of manufacturing resources by enterprises.

Jeong et al. [18] proposed the perceptron model. Unlike the M-P model, which requires artificial setting of parameters, the perceptron can automatically determine the parameters through training. The training method is supervised learning. It is necessary to set the training samples and expected output and then adjust the error between the actual output and the expected output. After training, the computer can determine the connection weight of the neuron. Harrison and Pearce [19] proposed an error back propagation algorithm, which solved the linear inseparability problem by setting up a multilayer perceptron. Although the use of error backpropagation algorithms can be used for hierarchical training, there are some problems, such as too long training time, parameters need to be set based on experience, and there is no theoretical basis for preventing overfitting. Convolutional neural networks are widely used in the field of image recognition. Compared with traditional methods, the accuracy has been greatly improved. Raman et al. [20] proposed a method that combines pretraining and autoencoding with deep neural networks. During this period, hardware has been rapidly developed. Through high-speed GPU parallel computing, deep network training can be completed in just a few days. With the development of the Internet, the collection of training data sets has become more convenient, and researchers can obtain a large amount of training data, thereby suppressing overfitting.

Scholars analyzed the connotation of manufacturing capability in the cloud manufacturing environment, gave

the definition and basic framework of manufacturing capability service, defined the metamodel and specific description attributes of manufacturing capability service, and used object-value-attribute for manufacturing capability service. The data model is formalized and heterogeneous. Some people believe that improving the manufacturing capabilities of enterprises should mainly start from the five aspects of quality assurance capabilities, cost control capabilities, flexible response capabilities, timely delivery capabilities, and innovation capabilities, and they have carried out in-depth ways to improve the manufacturing capabilities of enterprises under different types of strategies. It also compares the direct and indirect effects of quality, cost, flexibility, delivery capabilities, and innovation capabilities and gives the best paths for cost-oriented and innovation-oriented companies' manufacturing capabilities [21]. Researchers introduced monitoring methods based on mobile agents, using forward graphs to continuously collect and update the global information of the system to support the self-repair function of distributed applications, and established MonALISA, a monitoring framework based on large-scale integrated service architecture sensing agents, to achieve a scalable dynamic perception of complex software systems, and based on this framework, the perception of complex application execution processes, workflow applications, and network resources has been successively realized. Considering that the system state can reflect whether the system is malfunctioning, we proposed a large-scale complex software system perception scheme based on an abstract state machine from a state perspective, using perception data as a calculation metric to establish a diagnosis for the system. Some researchers describe manufacturing capabilities as design and manufacturing capabilities, ascertained manufacturing capabilities, and actual manufacturing capabilities. According to manufacturing tasks, piano automation, equipment, and the relationship between roles, the model of the solution model of manufacturing capability from task expectation to demand deployment and the relationship model of piano automation composition from capability to role are established, and the piano automation composition hierarchical configuration model is proposed [22–24].

3. Data-Driven Architecture Awareness

3.1. Data-Driven Algorithm. In order to maintain different data characteristics, data scientists propose a large number of different forms of objective functions. For example, the objective function of PCA is to obtain a mapping matrix P, so that the projected result is reconstructed as much as possible with the original data. Cross-entropy is a concept in information theory that is used to measure the distance between two probability distributions. Generally speaking, the output result of the neural network output layer does not satisfy the concept distribution, so the cross-entropy loss function is generally used together with the softmax function. After regression processing through the softmax function, the final output of the neural network will become a probability distribution.

$$\pi(u,s,t) - \partial \frac{\left(\beta u - \lambda\mu_x - \lambda\mu_y\right)}{\alpha - r} / \partial r = 0. \tag{1}$$

According to whether the indicators can be directly quantified, the evaluation indicators of piano automatic composition ability are divided into qualitative indicators and quantitative indicators. According to the value of the evaluation index, the indicators are divided into extremely large and extremely small types. In the process of constructing the index system, we should fully consider the extremely small and extremely large indexes and make overall plans to make the evaluation index system more comprehensive.

$$\sqrt{(\beta u + A)^2 + \left(\sqrt{\lambda\left(\mu_x + \mu_y + 2\mu_x\mu_y\right)} \times \frac{\alpha - \beta}{b}\right)^2} = 1. \tag{2}$$

The coefficient is used to determine the degree of weight connection adjustment. If the learning rate is too large, it may be overcorrected, leading to errors that cannot converge, and the neural network training effect is not good; on the contrary, if the learning rate is too small, the convergence speed will be very slow, resulting in too long training time. Generally, the learning rate is determined based on experience. First, set a larger value, and then gradually decrease the value. TensorFlow provides an interface of exponential decay function, which can flexibly and automatically adjust the learning rate during the training process and improve the stability of the network model.

3.2. Linear Drive Architecture Framework. This new method takes into account the density of the classes, and has a continuous description of the degree of separation. When a point is very close to the center of this category, the value of dDSC at that point will be larger, and vice versa, the value of dDSC will be smaller.

$$\iint \psi(u,t)dudt - \int_0^u \exp^{\pi(u)}du = 0. \tag{3}$$

The article shows the performance of dDSC and DSC in describing the degree of data separation, and it can be found that dDSC is more sensitive to different degrees of separation. In addition, the computational complexity of dDSC is the same as that of DSC, both are $O(C_{\mathrm{n}})$, where C represents the number of classes. The high efficiency of dDSC allows dDSC to be applied to many interactive scenarios. The commonly used error direction propagation algorithm is the gradient descent algorithm, but this method cannot guarantee that the final result is the global optimal solution. If the initial value of the parameter is not set properly, the local optimal solution may be obtained instead of the global optimal solution. At the same time, the gradient descent method needs to minimize the loss function on all training data sets. Generally, in order to obtain a good network model in Figure 1, the training data set is massive, and calculating the loss function of all training data will cause the algorithm time for the complexity and space complexity.

Its overall structure is a tree topological structure, which is flexible in structure and convenient for subsequent addition of nodes. Among them, the wireless transmission

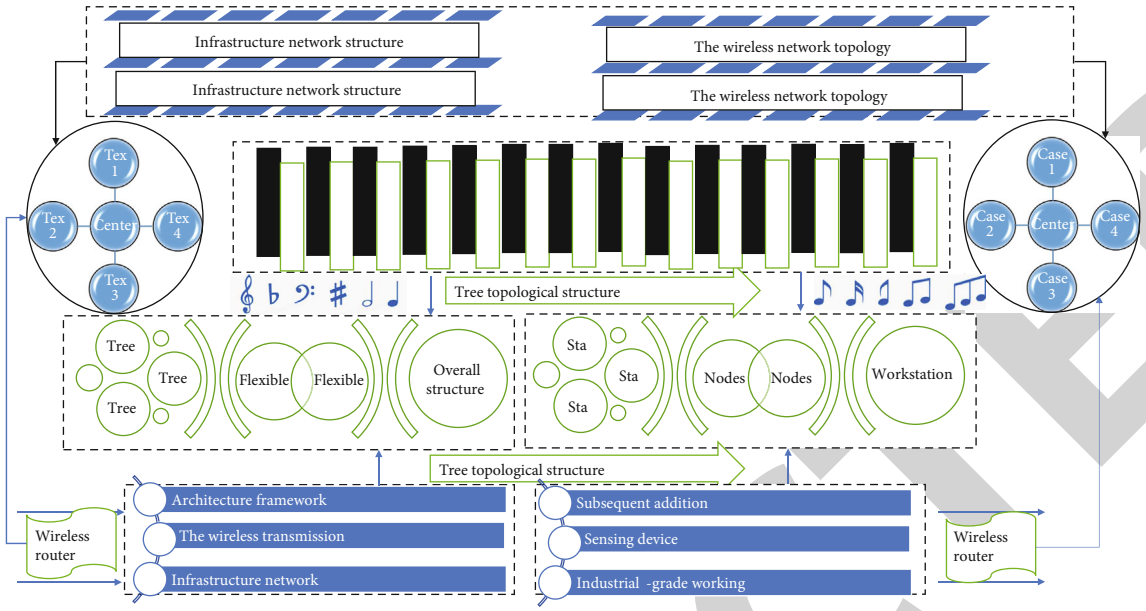

Figure 1: Linear drive architecture framework topology.

network formed between the energy consumption-sensing device and the wireless router is the infrastructure network structure in the wireless network topology, which is built together by STA (workstation) and wireless AP. The router acts as a wireless AP to form a network and is responsible for each STA site. The convergence of data and the energy consumption monitoring node is connected to the AP as a STA (workstation) node, acting as a client in the network; the energy consumption-sensing device adopts the USR-WiFi232 serial port to the WiFi module, which meets the temperature range of industrial-grade working environment.

3.3. Separable Measure of Composition. The most important thing in the entire composition evaluation process is how to obtain the capability evaluation result from the evaluation index. Only by considering the index data under the whole time sequence can the effective dynamic evaluation of the equipment operating energy be realized. The obtained energy performance index data at N moments (or stages) is formed into a set of decision-making plans for n piano automated composing objects to be evaluated, and m evaluation indexes or attribute constituent index sets are used as initial data for dynamic adjustment. Thus, the manufacturing task data of the equipment at nearly N times (or stages) is formed as the data basis, and the j-th attribute value of the equipment at the time (or stage) to be evaluated, so that the index values of each equipment at the near N times constitute a set.

$$\frac{f(p,t,x)}{p(t)} = \frac{\int_0^{\infty} \exp\left[\pi(u)\right]du}{\int_0^{\infty} \exp\left[p(t)\right]du}. \tag{4}$$

In estimating the frequency of the pitch, the pitch value will be determined according to the highest energy. But the actual situation is that the key in the low range is not the peak of the time domain. On the contrary, the maximum amplitude value appears between the second and the fifth overtones. To the mid-low range, the envelope is basically parallel to the frequency axis and then downwards.

As the pitch increases, the amplitude proportion of the fundamental tone will gradually increase, and the amplitude of other overtones will relatively gradually decrease. The keys of the piano can be divided into low range, midrange, and high range. The distribution of the number of overtones in different ranges is different. The energy in the low range is mainly concentrated in the low frequency. The number of overtones is large, and the amplitude is large. The energy distribution in the middle range is more uniform, while the number of high-order overtones in the high range is significantly reduced. And the amplitude decays quickly.

$$\psi(u) = \int_0^u \psi'(u)du = \begin{cases} \psi'(0)dt, u < t \\ 1, u > t. \end{cases} \tag{5}$$

The stochastic gradient descent algorithm does not need to optimize all the data in the training set like the gradient descent method. Instead, in each round of iteration, a piece of training data is randomly selected for optimization to minimize its loss function. In this way, the time of a single training can be shortened, and the update speed of the parameters can be improved. However, the loss function of some samples does not represent the loss function of all data and may also cause interference, so that each iteration does not update the coefficients in the direction of overall optimization, and the final solution may not be the global optimal solution.

3.4. Data Simulation Perception. When the output of the data simulation neuron is close to the upper limit of the activation function, the neuron state is called the activated state, and vice versa is the inhibited state. When the input signal is

a nonsparse signal and the measurement matrix is a real-valued matrix, most of the neurons in the hidden layer are in an active state. Then when a certain constraint or rule makes the state of most of the neurons in the neural network inhibit, the constraint is called "sparse inhibition." We mainly impose this sparsity constraint in two ways, both of which involve measuring the hidden layer activation of each training batch and adding some items to the loss function that penalize excessive activation, mainly L1 regularization and KL-scattering (relative entropy).

$$\psi'(0)\int_0^u \exp\left(\frac{\alpha-\beta}{b^2}\int_0^u \frac{1}{\pi(\theta)}d\theta\right)du - f(a,b) = 0. \quad (6)$$

For the measurement method to be evaluated, first we use this method to score 828 scatter plots. After the scoring result is obtained, the result of the measurement method and the artificial scoring result are combined to calculate the AUC value. The output range of AUC is from 0% to 100%. 50% means that the result of the method to be evaluated is equivalent to random guessing, and 100% means that the result of the method to be evaluated is in perfect agreement with the result of manual scoring. The AUC results of dDSC and DSC are 83.1% and 83.2%, and the AUC results of dKNNG and KNNG are both 92.1%. This shows that, compared with DSC and KNNG, dDSC and dKNNG have a basically equivalent effect of reflecting the perception ability of automatic arrangement.

$$\sum\psi'(u) - \sum\psi'(0) = \lim_{x\longrightarrow\infty}\left[\psi'(u) - \psi'(0)\right]. \quad (7)$$

This result does not surprise us, because in this evaluation framework, the focus is on whether the classes are clearly separated or not. What can now be determined is that for clearly divided examples, the new method has the same performance as the original measurement method. Of course, our focus should be whether we can describe the examples that are not separated in more detail and accurately. In the iterative solution process of the driving architecture in Table 1, it is particularly important to accurately describe the nuances between the two results; especially in the early stages of the iteration, the class structure is not very clear.

For energy consumption data, there are mainly errors or abnormalities, so the processing measures taken here are mainly data-cleaning processing to remove noise and abnormal data. Considering that the energy consumption data includes the working status of equipment standby, response, and processing, the data interval will change with the inconsistency of the working status, so the user-defined interval binning method is adopted here, and the relevant interval is defined according to the data law and classified energy consumption data accordingly.

Therefore, forming a dynamic constraint on the learning rate, the learning rate has a definite range, and the weight update is relatively stable. The parameter setting of the algorithm is relatively easy compared to other optimization algorithms, and usually, setting the default value has excellent performance. When constructing an automatic composition neural network model, it is necessary to combine the characteristics of the data set and the complexity of the network to select the best optimization algorithm, which can speed up the network training speed, shorten the network convergence time, and improve the quality of the network model.

Table 1: Iterative solution of drive architecture.

Number	Code name	Meaning	Type	Default value
1	Consumption	Time	INT	0
2	Learning rate	Index number	INT	0
3	Errors T	Data law	CHAR	Increment
4	C-Q	Class structure	CHAR	Increment
5	M-rate	Architecture	FLOAT	Increment
6	Energy-value	Clearly-divided	CHAR	1
7	CompreIndex	Performance	INT	1

4. Piano Automatic Composition and Quantitative Perception Model Construction under the Data-Driven Architecture

4.1. Data-Driven Architecture. The core idea of the data-driven architecture is to obtain the score of the point by comparing the distance $a(y)$ from any point Y to the midpoint of its class and the minimum distance $b(y)$ from the point to the center point of other classes $s(x)$. Here, when calculating the DSC, the calculation is performed directly in the visible space. The data used here is the data after driving the architecture to the two-dimensional visualization space through the driving architecture algorithm.

$$\prod \exp(a-b) \times \exp\left(\frac{\alpha-\beta}{b^2}\int_0^u \frac{1}{\pi(u)}du\right) = \prod \sqrt{a^2+b^2}. \quad (8)$$

DSC and KNNG incorporating density information are named dDSC and dKNNG. Correspondingly, the visual perception-driven supervisory-driven architecture algorithm using dDSC is named pDR. dDSC is PDD for short; and the visual perception-driven supervisory-driven architecture algorithm using dKNNG is named pDR. dKNNG is referred to as PDK. An important feature of wireless sensor networks is that homogeneous or heterogeneous sensor nodes can be deployed in the monitoring area at the same time.

According to the mapping relationship between the fundamental frequency and the keys, specific notes can be obtained; the length of the piano expresses the change in the length of the piano tone, which affects the choice of the time resolution in the automatic framing process of the piano composition signal. The pitch of the piano keys is determined according to the twelve equal laws, and the fundamental frequency of the keys is arranged according to the geometric progression shown in Figure 2. String vibration is a complex resonance. After the string is struck and

vibrated, it will produce not only a fundamental tone but also overtones. Overtones will have an impact on the estimation of the fundamental tone, as well as the number distribution in different zones.

After that, the amplitude discrimination method is used to determine the abnormal data, that is, the difference between the i-th power or electric energy data sampling value, and the i-th sampling value is used for judgment. If the data consumption threshold is different, it is judged that the i-th sampling value is the true value at this time; if it exceeds the specified threshold, the i-th data is considered an abnormal point; and for abnormal data, it can be considered missing value data. In the value processing, the classical regression interpolation method is used for processing, and the regression model is usually expressed as the text.

4.2. Performance Analysis of Quantitative Perception Algorithm. In the decision-making process of the quantitative perception system, it is necessary to abstract the human logical thinking process as a mathematical function and carry out quantitative analysis of qualitative analysis problems. The analytic hierarchy process (data-driven architecture) is a commonly used multicriteria decision-making method. This paper uses this method to analyze the subjective weight and finally obtains the importance of different indicators to the evaluation target. PcAE combines the advantages of model-driven and data-driven and uses data to jointly optimize the construction of sparse binary measurement matrix and noniterative reconstruction, thereby simultaneously obtaining lower coding complexity and higher signal reconstruction quality.

$$\begin{cases} A(x) = -\lambda\mu_x - \lambda\mu_y \\ A(y) = \lambda\mu_x + \lambda\mu_y. \end{cases} \tag{9}$$

Experiments on neural spikes in the application of wireless neural recording show that the PcAE algorithm has extremely low computational complexity and better reconstruction effect at the encoding end compared to several others based on compressed sensing algorithms and based on quantized sensing algorithms. For example, when the measured value is low sampling rate, the value of the signal-to-noise distortion ratio (SNDR) of the PcAE algorithm is 25, which is much higher than the SNDR value of the traditional BSBL reconstruction algorithm when the value is measured. When the deployment density of nodes is relatively high, multiple pieces of information in the same space can be collected.

$$\begin{cases} B(x-y) = \sqrt{\lambda\left(\mu_x + \mu_y + 2\mu_x\mu_y\right)} \\ B(x+y) = \sqrt{\lambda\left(\mu_x + \mu_y - 2\mu_x\mu_y\right)}. \end{cases} \tag{10}$$

At the same time, the receiving rate of the serial port can reach 460800 bps, and the uploading rate can reach 150 M. The performance is superior. Its UART pin is connected with STM32, which can easily receive the packaged information processed by STM32 and convert it into IEEE 802.11 protocol

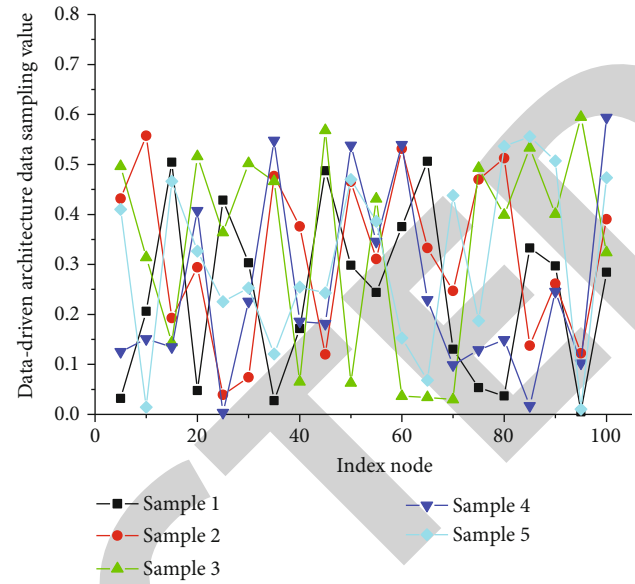

Figure 2: Data sampling value distribution of data-driven architecture.

data for transmission. As for the equipment work-related information, it is read and processed by the industrial computer connected to the equipment PLC and then transmitted to the wireless router via the network cable through the SOCKET transmission method in Table 2 to realize the aggregation of sensing data.

Since the length of the same sound in different audio files changes, the step length should also be changed synchronously, but this is difficult to control. A good method is to take the step length short enough and use equal step length to segment the audio. Then the adjacent subsegments are judged. If the pitch is the same and it is not the end of the note, it means that it is the same note, and the adjacent subsegments with the same note need to be merged. In this way, the method of merging equal steps is used to realize the change of the length of the sound.

4.3. Evaluation of Numerical Indexes of Automatic Composing. For most of the data, the algorithm is initialized by randomly generating P, and the algorithm can quickly find the ideal solution. In addition, referring to other drive architecture algorithms, we also used the results of other existing drive architecture algorithms as initialization. Therefore, the following experiments are done to select the randomly generated P and use the mapping matrix of PCA, LDA, and LPP as initialization to drive the architecture. It turns out that although the initialized P differs greatly, the results obtained are basically the same. Sometimes, the solution obtained by randomly generated P still has a slight advantage. It can be concluded that the initialization method of P has little effect on the result. Therefore, in the algorithm, we choose to randomly generate the mapping matrix P as the default option.

$$\frac{\partial\pi(u)}{\partial u} - \int \frac{1}{\alpha - r}[(\beta u + A) + (\beta u - B)]du = 0. \tag{11}$$

Table 2: Convergence algorithm of perception data.

Step number	Algorithm input	Code text
1	Since the length $B(x-y)$	For $a = [1 - 1.8237\ 0.9801]$
2	The same sound in $\partial\pi(u)$	$B = [1/100.49\ 0\ 1/100.49]$
3	The measured value is μ_x	$N = 0:30$
4	Equal step length to segment the audio	Subplot (211)
5	We choose to randomly generate x	$X1 = \mathrm{udt}(n)$
6	A good method is to take μ_y	$Y1 = \mathrm{filter}(b, a, x1);$
7	The receiving rate of $x + y$	Stem (n,$y1$,"fill," "g"), grid on
8	The method of merging equal steps	Void bigsort(int *arr,int len)
9	The industrial computer connected $1/\alpha - r$	{adjust-downmy(arr,0,len-i-1);
10	It turns out that $\mu_x\mu_y$	For(int $i = 0$; $i \le$ len; i++)
11	Referring to other drive architecture	{void merge(int *A,int low,int mid,int high)
12	The adjacent subsegments are judged	Int temp = arr[0]
13	It needs to be extracted $\mu_x + \mu_y$	Arr[0] = arr[len − i]

The demonstration audio is a piano automatic composing in the wav file format, and the features of these audio files need to be extracted as the training set of the automatic composition neural network model. For the piano automatic composition signal, there are four basic characteristic quantities of pitch and timbre. Among them, pitch and pitch are commonly used as extraction features. Modern pianos are tuned according to the twelve equal laws. The 88 keys of the piano have a certain fundamental frequency, and the fundamental frequencies of the keys are arranged in a geometric progression. For the fundamental frequency extraction process, the most widely used MFCC feature extraction method in the field of speech recognition and speech reconstruction is analyzed first.

$$\forall \lim_{x \longrightarrow \infty} \left\{ \sqrt{a^2 + b^2} \in R(c,t) \right\}, \exists \sqrt{(\beta u + A)^2 + \left(B \frac{\alpha - \beta}{b} \right)^2} = 0. \tag{12}$$

The data-driven architecture can decompose a problem, decompose a multiattribute problem into many small elements, and generate a hierarchical structure based on the affiliation between the elements, which can reflect the associated information between the elements. At the top of the structure is the target layer, which represents the objective of the evaluation; the next layer is the criterion layer, which represents the characteristic attributes of the target; and then the index layer and its subindicator layer, which can represent the criterion layer. The bottom layer is the scheme layer, which is composed of the objects to be evaluated. By calculating the relative importance of each element of each layer and its adjacent two layers, the weight between each subindicator and the total indicator can be obtained.

Based on the overall process of the system in Figure 3, we analyze the number of interactions of each computer node, run the BookStore system, count the interaction frequency and interaction time of each computer node, calculate the interaction frequency and interaction density, and quantify the importance of each computer node. Based on BookStore's initial set of perception objects, we analyze the relationship between perception objects, filter and refine perception objects, and generate a new set of perception objects. Finally, we compare the system overhead and accuracy of the new set of sensing objects and the initial sensing objects.

The specific method is as follows: adopt the method of comparing each other in sequence, corresponding to the ratio scale value in the article, and then generate a judgment matrix. If the matrix is a consistent matrix, it means that the obtained weight is the normalized eigenvector of the matrix. Specifically, the weight value of this layer and the weight value of the upper layer are multiplied and calculated in sequence until the uppermost layer stops. In this way, the sub indicators of each target layer correspond to a relative weight.

5. Application and Analysis of Piano Automatic Composition and Quantitative Perception Model under Data-Driven Architecture

5.1. Quantitative Perception Data Preprocessing. The quantitative perception data scores the scatter plot drawn from the results of 744 drive architectures. These results are obtained by applying 8 drive architecture methods to 93 data sets. In the experiment, different types of dots in the scatter diagram need to be distinguished by different colors. Due to the large number of points in some data sets, many points will overlap during the process of drawing the scatter plot, which will seriously affect the user's judgment on the indexability. In order to alleviate this problem, the order of the original points was carried out in the experiment. The shuffling operation completely disrupts the original

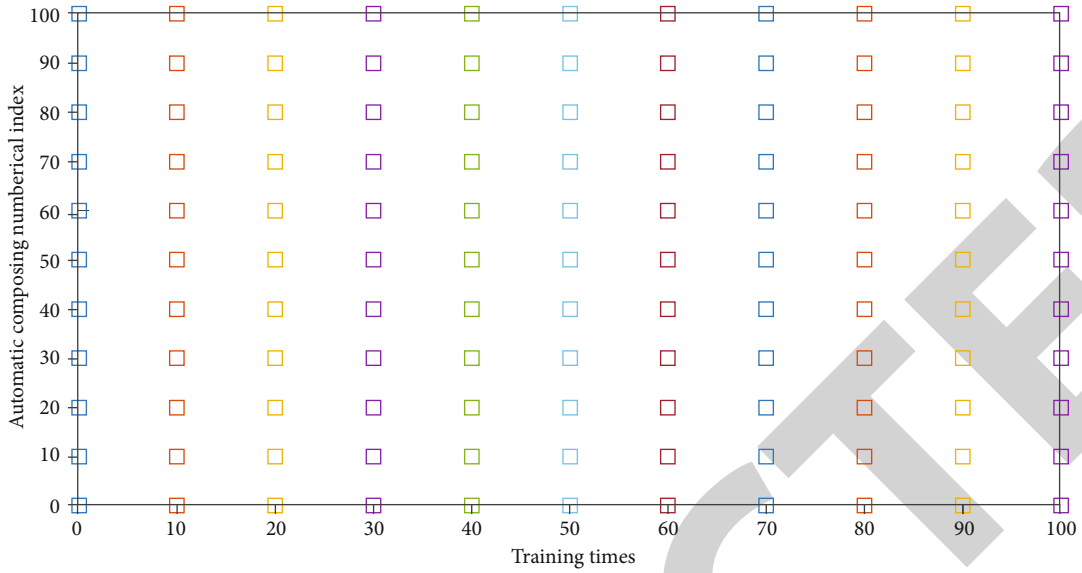

Figure 3: The distribution of the numerical index of the automated composition.

order of the points and then draws the points in the order after shuffling.

$$\prod_{A+B}(\beta u + A)\psi' + \frac{1}{2}(B)^2\psi'' = \begin{cases} \frac{1}{2}(A+B)^2, A > B \\ \frac{1}{2}(A-B)^2, A < B. \end{cases} \quad (13)$$

In addition, when the space of the monitoring environment or other factors cause a single router to fail to complete the aggregation and transmission of all information to the server, the layout of the wireless relay node can be planned according to the monitoring environment space and actual needs, wireless router signal coverage, etc. After adding routers to the nodes, we use the router's WDS wireless bridging function to set the relevant relay parameters to form a relay transmission network, realize the aggregation of the node information in the tree topology and the expansion of the transmission distance, and sense the aggregation of the information of each node in the network. It is sent to the server, and the server realizes the fusion processing and storage of the aggregated information. The data transmitted in the transmission network in Table 3 above are all encrypted by WPA2-PSK (AES), which ensures the security of the transmission channel.

The autoencoder can be regarded as a special feed-forward neural network, which is usually trained using the minibatch gradient descent method like the feed-forward neural network, so as to learn useful features of the data. AE is mainly composed of two important structures: encoder represented by and decoder represented by. Obviously, it can be concluded that the biggest feature of the encoder structure is that the input layer and output layer have the same number of neurons, and the number of neurons in the middle hidden layer is less than the number of neurons in the input layer and output layer. Experiments

Table 3: Fusion processing of aggregated information.

Processing index	Channel 1	Channel 2	Channel 3
1	0.94	0.01	0.56
2	-0.43	0.03	0.19
3	3.07	0.00	0.29
4	-0.12	0.02	0.04
5	-5.43	0.02	0.07
6	0.66	0.00	0.48
7	-0.56	0.01	0.38

have proved that the number of neurons in the hidden layer of the autoencoder can be much smaller than the number of neurons in the input layer, so a very high compression ratio can be achieved.

5.2. Data-Driven Architecture Simulation. In terms of the running time of the data-driven architecture algorithm, all linear methods have inherent advantages. For most data, the results can be solved quickly, while the nonlinear method has a slower solution speed. Since some methods are developed by the MATLAB environment, some methods are developed by C++; in addition, there are big differences between the results of many methods and the new method. Here, when comparing the running time, this article focuses on the comparison with the new method. The results of the two methods are not much different, LDA and t-SNE.

$$\begin{cases} \psi(t) = \sqrt{t^2 - 4ac}, \lim_u \psi(t) = 1 \\ \psi(0) = 0, \lim_u \psi(u) = 0. \end{cases} \quad (14)$$

For the above-mentioned perception data, this paper uses 200 as the base and records the time of data collection and data processing for every 200 pieces of perception data. The

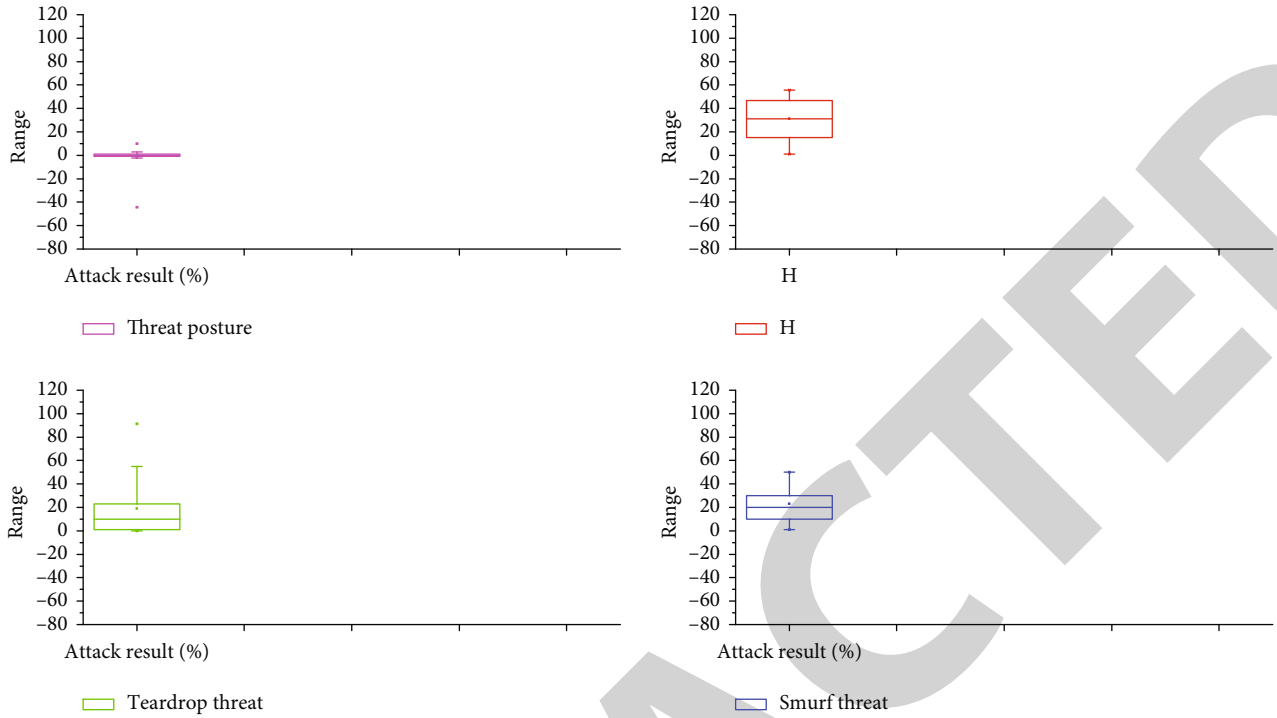

Figure 4: Data-driven architecture input note sequence distribution.

statistics of 200 pieces of perception data, 400 pieces of perception data, 600 pieces of perception data, and 800 pieces of perception data are, respectively, counted. The collection time and processing time of data, 1000 pieces of perception data and 1200 pieces of perception data, and the number of changes that occurred in them were recorded. We use these data as different sets of perception data to test the perception efficiency and accuracy of different amounts of perception data.

$$a.b.f(c,t|\nabla c\text{^}2+\nabla t\text{^}2=1),\min_{\pi}\left[(\alpha-\beta)\pi\psi'+\frac{1}{2}b^2\pi^2\psi''\right]=0. \tag{15}$$

The duration of each ECG recording is ten seconds, the sampling frequency is 1000 Hz, that is, 1000 signal points are sampled per second, and the length of a single record is 10000. According to the window size, each record intercepts the same number of windows to obtain a total of 9975 ECG signals. Randomly, they divided them into training data set and test data set, of which training data set and test data set accounted for 80% and 20% of the total data, respectively. The accuracy of data collection is improved, and the redundant information collected by nodes can also be used as fault-tolerant detection of information.

The input note sequence and the expected output note should be reasonably selected from the training set according to a certain correlation, that is to say, it needs to be formulated reasonably training rules. Finally, combined with the demonstration audio note feature data set, in order to obtain a better prediction network model in Figure 4, there will be multiple gated loop unit network layers in the network.

Table 4: Description of adaptive sensing process.

Range number	Sensing music	Data types	Process name	Score
1	Demo_10	INT	MS	29.41
2	Demo_12	CHAR	MS	3.89
3	Demo_09	CHAR	MS	7.39
4	Demo_11	INT	GRU	47.67
5	Demo_05	INT	GRU	37.59
6	Demo_02	INT	GRU	11.98
7	Demo_06	INT	PC	46.53
8	Demo_07	CHAR	PC	31.07
9	Demo_01	CHAR	GRU	26.43

There are different types of perception objects in the software system, and adaptive perception uses different perception tools to collect runtime data of different perception objects. Considering the diversity of these perception data, in order to analyze and process aspects, this article adopts extensible markup language XML to establish a formal description specification and uses this specification to formally describe different perception data, so as to realize the unification of different perception data.

$$\lim_{x\longrightarrow\infty}U(r,t)dU=\lim_{x\longrightarrow\infty}[\beta U+(\alpha-r)\pi_t+A]dt. \tag{16}$$

Online audition evaluation requires the development of an online audition effect scoring platform, which adopts

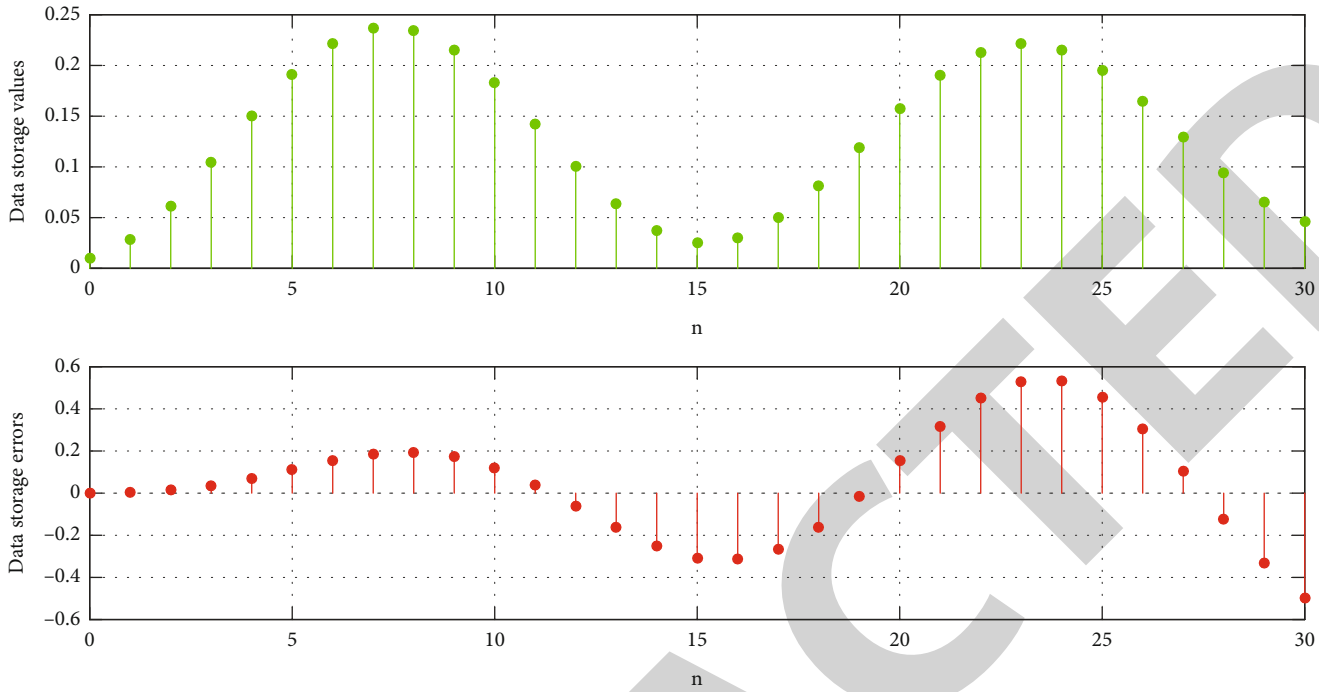

Figure 5: Distribution of adaptive sensing data storage values.

the development form of separation of front and back ends. The evaluation method of piano music effect is based on the principle of Turing test. The automatically generated piano music and the piano music created by the human work composer are randomly combined and placed on the platform. Audition users can audition the piano music on the platform, according to their own judgments of each piano piece. Through this platform, users' feedback can be collected to help optimize the model and do further research.

5.3. Case Application and Analysis. Considering that the adaptive sensing process in Table 4 will produce a large amount of sensing data that needs to be stored, and the adaptive process itself is a real-time process, the storage and reading of the sensing data are required to be fast. Therefore, this article chooses the MySQL database to store the perception data obtained by the adaptive perception process. Compared with other databases, the MySQL database is small in size and fast in running speed, which can meet the needs of fast sensory data storage. Moreover, the MySQL database is open source, which greatly reduces the cost of use. In addition, MySQL provides more data types.

In the part of automatic composition quality evaluation, this article develops an online audition effect scoring platform and invites piano music lovers to make scores based on their subjective listening feelings. The offline performance evaluation invites professionals to designate 5 indicators, use the entropy weight method to assign weight to each indicator, and then conduct a comprehensive evaluation of each song. The scoring results show that the piano music automatically created in this paper has a high score, and some works can pass the Turing test in Figure 5.

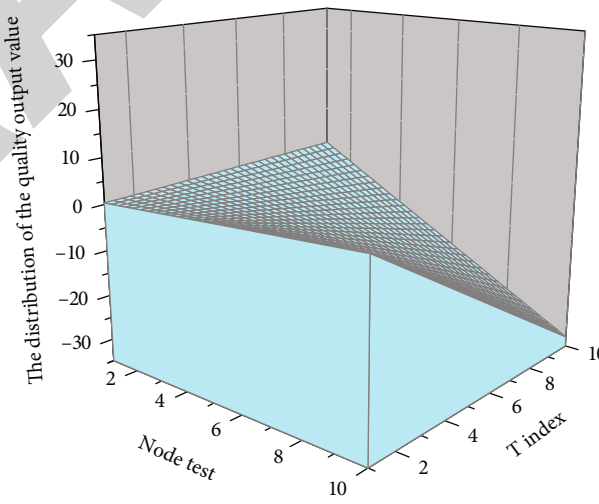

Figure 6: The distribution of the quality output value of the drive architecture algorithm.

The construction of the automatic composition neural network model first studies the cyclic neural network, which has short-term memory capabilities. This structure allows the cyclic neural network to theoretically process the sequence data of any length. However, the simple recurrent neural network can only learn short-term dependencies due to the explosion or disappearance of gradients. In the process of piano automatic composition, the dependence interval between notes is relatively large.

This type of data is usually measured by the imbalance rate (IR), which is the number of samples in the class with the most samples divided by the number of samples in the

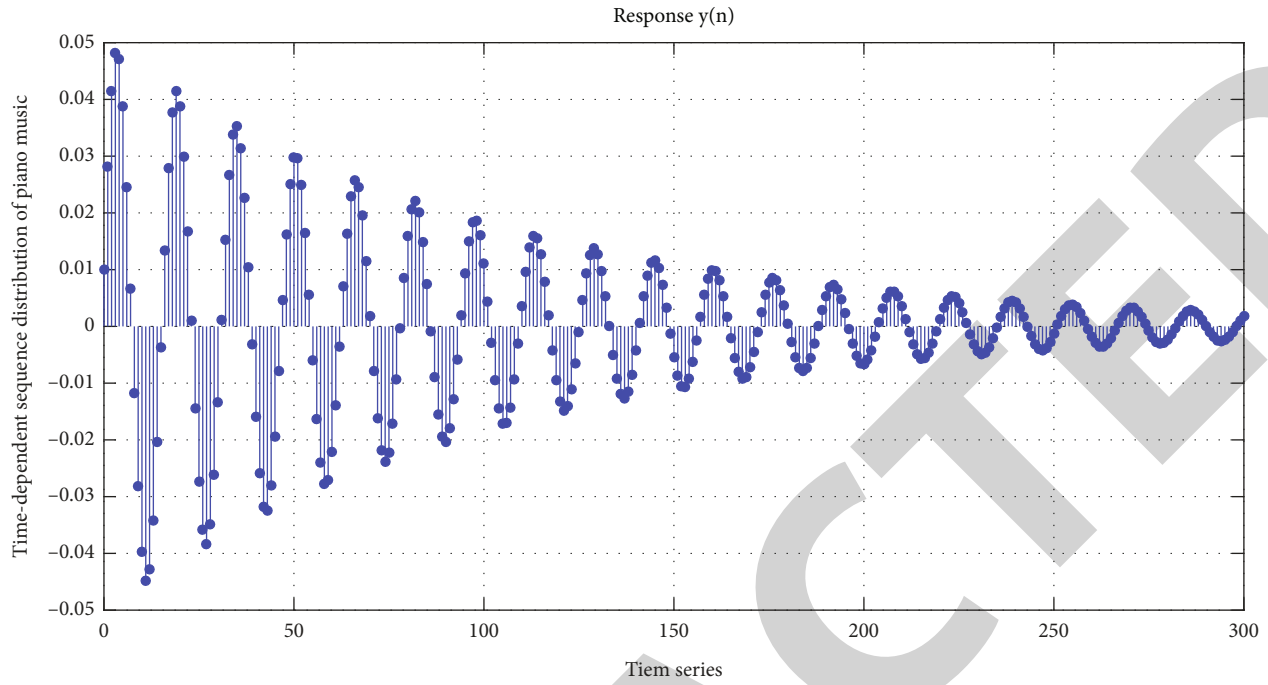

Figure 7: Time-dependent sequence distribution of piano composition.

class with the least samples. If you really use drive architecture algorithms for such data, then the final result must be largely affected by the class with more samples. In order to solve this problem, we improved the method of calculating the global $s(y)$ in PDD. After obtaining the $s(y)$ of each sample point, we first solve an average value for all sample points in each class, and then use several class averages to continue solving the global average.

$$\lim_{t\longrightarrow\infty}\frac{\nabla(a\pi_t dW_t + b\pi_t dW_t)-\nabla(AdAt + BdBt)}{\nabla F(A,B)} - \lim_{t\longrightarrow\infty}\frac{A+B}{A-B} = 0. \tag{17}$$

Users are allowed to move some points in the low-dimensional space to feed back to the drive architecture algorithm to improve the quality of the drive architecture. Specifically, the steps of the experimental program are as follows: If the distance between the unmarked data and the center point of the marked data is closer, then the unmarked point will be classified as this type. Visuals of the final classification results are shown to the users. Figure 6 uses the same classification method to test with LDA.

At the same time, the length of the same sound in different audio files also changes. This article will take the step length to be short enough and then combine the same notes in the adjacent subsegments to achieve this change in the length of the sound. After each frame that passes through the filter array, a set of output values will be obtained, and the maximum output value will be found. First, we judge with the set threshold to see if it is a silent segment, then index the filter bank corresponding to the maximum output value to the fundamental frequency of the frame, and determine whether adjacent subsegments need to be merged. There is a mapping relationship between the extracted fundamental frequency and piano notes, and the note sequence of the demonstration audio can be obtained through conversion, which can be used as the training set of the neural network.

Finally, we use alice.XPT and the corresponding alice.wav audio file to verify the design in Figure 7 based on the twelve equal laws of this article. The final experimental results show that, except for a few multifundamental moments, the extracted values of note features at other moments are completely consistent with the original file.

6. Conclusion

In this paper, by studying the collection and processing methods of massive sensing data in the manufacturing process, this paper proposes a sensing data-driven piano automatic composition operation energy efficiency evaluation model and applies these methods to the actual engineering application of the automated composing system. First of all, for the feature extraction part, using the design process of Mel frequency cepstral coefficient extraction for reference, combined with the characteristics of the piano automatic composition signal, designs based on the twelve equal temperaments are proposed. Secondly, for the network model construction part, the cyclic neural network has a memory function and is good at processing sequence data. Piano music can be regarded as a sequence composed of multiple notes according to the rules of music theory, and there is a certain dependency between the notes. Automatic composition allows the neural network model to learn these hidden rules and then predict and generate the note sequence. On

Hindawi
Journal of Sensors
Volume 2022, Article ID 8175834, 9 pages
https://doi.org/10.1155/2022/8175834

Research Article

Digital Music Feature Recognition Based on Wireless Sensing Technology

Xiaoning Wang,[1] **Wei Guo**,[2] **and Weiwei Tong**[3]

[1]*School of Music, Fujian Normal University, Fuzhou, Fujian 350108, China*
[2]*School of the Arts, Xiamen University, Xiamen, Fujian 361005, China*
[3]*School of Education, Mahasarakham University, Mahasarakham 44150, Thailand*

Correspondence should be addressed to Wei Guo; wguo@xmu.edu.cn

Received 11 November 2021; Accepted 12 January 2022; Published 18 March 2022

Academic Editor: Gengxin Sun

With the rapid development of information technology, digital music is subsequently increasing in large quantities, and how a good integration of vocal input and recognition technology can be transformed into digital music can greatly improve the efficiency of music production while ensuring the quality and effect of music. This paper focuses on the implementation and application of human voice input and recognition technology in digital music creation, enabling users to generate digital music forms by simply humming a melodic fragment of a piece of music into a microphone. The paper begins with an introduction to digital music and speech recognition technology and goes on to describe the respective characteristics of various audio formats, which are selected as data sources for digital music creation based on the advantages of the files in terms of retrieval. Following that, the method of extracting musical information from music is described, and the main melody is successfully extracted from the multitrack file to extract the corresponding musical performance information. The feature extraction of humming input melody is further described in detail. The traditional speech recognition method of using short-time energy and short-time overzero rate features for speech endpoint detection is analyzed. Combining the characteristics of humming music, the method of cutting notes by two-stage cutting mode, i.e., combining energy saliency index, overzero rate, and pitch change, is adopted to cut notes, which leads to a substantial improvement in performance. The algorithm uses the melody extraction algorithm to obtain the melody line, merges the short-time segments of the melody line to reduce the error rate of emotion recognition, uses the melody line to segment the music signal to generate segmented segments, then abstracts the features of the segmented segments through a CNN-based structural model, and inputs the output of the model to the regressor in cascade with the melody contour features of the corresponding segmented segments to finally obtain the emotion *V*/*A* value of the segmented segments.

1. Introduction

In today's digital and networked era, multimedia data has become a major part of the data transmitted on the Internet information superhighway. Multimedia technology is characterized by interactive and integrated processing of audio, text, and graphic information [1]. In multimedia systems, multimedia content such as audio, image, and video currently occupies 70% of the network, and the number is growing rapidly. Voice and music are the most familiar and accustomed ways to deliver information, and sound media is the most important media other than visual media, occupying 20% of the total information volume [2]. Large-capacity, high-speed storage systems provide the basic guarantee for massive storage of sound, and the use of sound media in various industries is becoming more and more widespread [3]. Also, the implementation and application of human voice input and recognition technology in digital music creation become increasingly important. With the improvement of computer performance and Internet bandwidth, as well as the development of multimedia information compression technology and video/audio streaming

technology, the realization and application of vocal input and recognition technology in digital music creation provide a good basis and guarantee [4]. However, in the process of digital music creation, the old traditional music production methods were followed, which could not reflect the advantages and strengths of digital music and could not improve the efficiency of music production as well as the quality and popularity of music [5]. Therefore, people are no longer satisfied with music creation through the general traditional mode, and human voice input and recognition technology provides a more efficient method for digital music creation. Music as an important media resource, music creation has a very important significance for music database and digital library construction.

The sheer volume of multimedia resources on the web has prompted digital music creation to become a mainstream mode of music production [6]. People need efficient ways to compose digital music, which in turn meets the demand for massive music resources on the web. In addition, digital music composition has broad research prospects and great application value in karaoke retrieval and assisted video retrieval [7]. Given the characteristics of music itself, digital music creation is completely different from traditional music creation. The current digital music creation is based on text, which includes the name of the music, the lyricist, the singer, and the instrument played, and this information is integrated in the computer [8]. The recognition of music based on similar singers' voices or similar styles and rhythms or even similar background music sounds has become a digital music creation method that is gaining attention. This problem is cross-cutting, involves a wide range of content, and is comprehensive, involving computer science, information science, acoustics, musicology, psychology, and so on. Speech is the most dominant form that people use to communicate [9]. Therefore, speech recognition has an extremely important position in digital music creation. Sometimes we can naturally identify the singer when we hear a piece of music because their voices are different, and in general, the technology of speech recognition includes research in many fields such as acoustics, linguistics, and information processing. The scope of application is very wide. It is widely used and has been researched for a long time and has achieved very good scientific results [10]. Nowadays, audio retrieval is a kind of application related to audio information, and music as a very special kind of audio, its retrieval has been in the retrieval for lyrics, and the process of retrieval is also through a certain music or simply humming a certain lyric to find music in the music library. Up to now, the use of audio for retrieval is still very rare [11]. Therefore, the use of related technology to achieve similar music retrieval can not only change the current manual retrieval method but also singers can use the system to retrieve songs similar to their own according to their own voice and style, which not only can save a lot of time and achieve better results but also users can automatically select their favorite songs from a large number of song music libraries to meet personalized music recommendations and services.

With the development of speech signal processing technology, the system used to process audio signals now relies more and more on the effective content of the processed signal, which first and foremost is to preprocess the audio signal, extract its effective signal part (meaningful part), remove the useless part, provide an effective preprocessing method for removing the unwanted part of the audio, and can better improve the data processing. The efficiency and performance of data processing can be improved. At the same time, due to the rapid development of multimedia technology and network technology, audio resources such as songs are becoming more and more abundant, and the access to them is becoming more and more diversified and simple. How to retrieve the songs you need accurately and conveniently in the vast library of song resources has become an urgent problem. At present, there are two major types of song retrieval methods: text-based annotation methods and content-based methods. At present, all practical song retrieval systems use text-based methods, such as Baidu Music Search, JiuKuMusic.com, and Search.com. This method requires first manually annotating songs in the song database with characteristics such as song name, singer, and song classification, and then using keyword matching methods to find them. This method has some defects that are difficult to make up in practice. First, many features of songs are difficult to be accurately described by text (e.g., singer's voice characteristics, song style, rhythm, and background music tone), so it is difficult to search for these features; second, the search accuracy of text matching depends largely on the accuracy of text annotation, while the evaluation of many features (e.g., song classification and mood) is highly subjective and the accuracy is difficult to be guaranteed. Third, the text-based approach cannot be realized for the similar song retrieval demand of "finding songs by songs."

2. Related Work

For quite a long time in the past, music composition required a high level of musical theoretical knowledge and practical skills, so it has always been the case that only those who had specialized education in music were able to do so [12]. By now, many music lovers are familiar with digital music creation. Music creation has developed mainly with the development of computers, from the initial creation of music by professionals, to the creation of music by people with their own hobby of music, which is full of personalized colors, to the music that affects all aspects of people's lives now. The history of music creation also began with the emergence of electronic instruments in the 1930s and later in the 1980s with the birth of MIDI technology, which is now more widely seen in the establishment of various music studios [13]. Nowadays, more people use digital music technology to create music, so it is convenient for more composers to get rid of the old way of creating music manually, and instead, composers can use the Internet to find more factors and ways to create music, and it is convenient and fast to create music. Sonar is just one of the powerful computing software in the computer, which has more information about music creation and also provides a broader platform for musicians to show themselves; they only need to copy, paste, and other simple operations by

clicking the mouse to create music, they do not need to imagine the music performance, tone, etc., and then modify it again and again; the new way of music creation has greatly changed the way of composers in the past. The new way of composing music has greatly changed the way composers used to compose [14].

Composers do not have to worry about the difficulty of playing their works, the complexity of the scoring process, and other technical concerns [15]. Many nonmusic majors are now using their computer skills to compose music according to their own understanding of music and hobbies. And they have achieved very good results. Thus, the use of digital technology for music composition is characterized by diversity, which is manifested in many aspects, including the genre, content, and style of music [16]. Moreover, with the rapid development of computers today, digital diversity is also reflected in the important influence that computing technology brings to the field of music composition, for example, the style of composition and aesthetic orientation. Nowadays, people use computers to digitally process the audio of music in order to get the rhythm they want. People use music creation software to create music according to their own preferences so that every music lover can easily and conveniently record, edit, and other digital processing of audio in the process of creation. The digital process requires a thorough knowledge of digital audio processing technology. Among the many software programs that use computing software to create and debug MIDI music, the most practical one is Cakewalk, which is not only a tool for music lovers to create music but also for nonmusic majors to become composers by using the software to create high-quality music [17]. It requires a systematic study of music knowledge and continuous exploration of music itself. The advantage of computer software is to satisfy the dream of ordinary people to create music [18].

The process of editing audio digitally is mainly done on traditional audio, but this is very difficult for audio programs. The whole editing process is very troublesome, and the editing and processing methods are very limited and imprecise, mainly because it needs to be done with external equipment [19]. Because there are many ways to edit and process audio in this way, there are many ways to process audio in any way one can think of. In addition, this method of processing is characterized by the speed of the audio processing and the promptness of the feedback, and the success of the creation can be played and auditioned immediately. At the same time, the quality and accuracy of the audio in the editing are very high [20]. The range of adjustment for each editing-related function of the software is large. The last feature is that in the editing and processing process, no work is required from the creator, just a simple pair of computers and music editing software can do all the work, so you can get professional-grade results at a civilian price [21].

3. Digital Music Based on Recognition Technology

3.1. Algorithm for the Implementation of Human Voice Input Recognition System. The first basis for judgment is to calculate the features at the audio frame level and at the segment level; using certain regulations, the actual calculated feature values are compared with the set thresholds to identify segments of a piece of audio into three parts: silence, pure music, and speech-music mix. In the song, the sound can be divided into three categories: silence, pure music except silence, and speech-music mixture.

It is very difficult to classify the recognition of pure music and speech-music mixed segments in the music signal (the same song) because of the high confusion susceptibility of pure music and speech-music mixture. So only using two features, short-time energy and overzero rate, cannot achieve the classification effect well. In this paper, we propose a new algorithm based on human voice input and recognition technology, as shown in Figure 1.

In music signal preprocessing and feature extraction, the commonly used feature parameters are frame average energy, overzero rate or average overzero rate, resonance peak, fundamental frequency, linear prediction coefficient, and other parameters. Short-time energy is the main energy accumulated in a signal about the sampling point within a short-time audio frame, and its short-time energy calculation formula is as follows:

$$E_n = \sum_{i=1}^{n} [a(q)w(n-q)]^2. \tag{1}$$

In the formula, n is the nth short-time frame, $a(q)$ indicates the nth short-time frame within the mth sample point signal value, N is the window length, and $w(n)$ indicates the length of the N window function. The above equation can also be rewritten as

$$E_n = \sum_{i=1}^{n} [a(q)w(n-q)]^2 = \sum_{i=1}^{n} x^2(q) * h(q). \tag{2}$$

The formula $h(n)$ is defined as follows:

$$h(q) = e^2(j) + q^2. \tag{3}$$

The short-time energy can be regarded as the output of the square of the speech signal after a linear filter with impulse response $h(n)$ by the formula. Therefore, the nature of the short-time energy is to some extent related to the choice of the window function, that is, what type of window function is used and how long the window function should be chosen; if the window length is very long, the smoothing effect of the grant window will be obvious, and the corresponding curve of the short-time energy also changes slowly with time so that the characteristics of the change about the language is not well reflected; if the window length is too short, it will appear that the short-time energy changes. If the window length is too short, there will be a dramatic change in the short-time energy with time, so it becomes very difficult to get the smoothing energy function, so, in general, the window length is chosen within 10 ms-30 ms.

Short-time overzero rate refers to the number of times the value of the sampled signal changes between positive

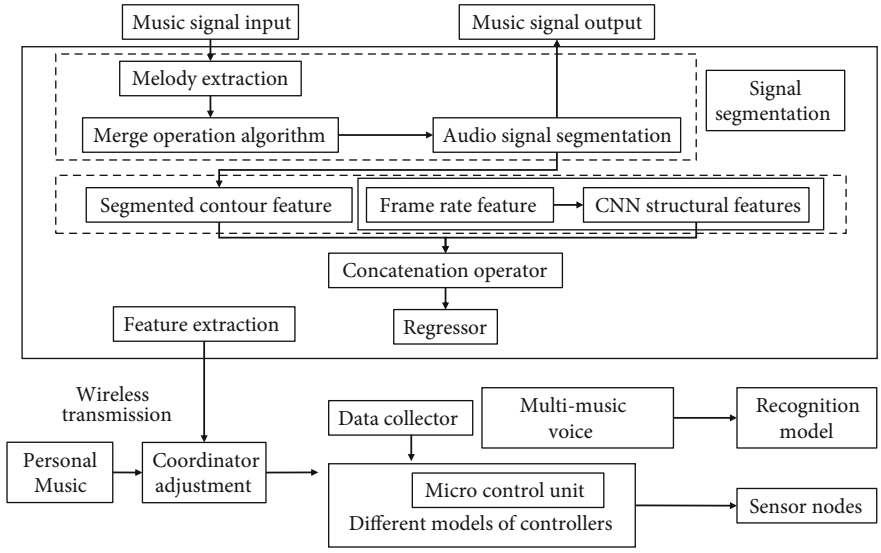

Figure 1: Principle of recognition model for pure music and speech-music hybrid clips.

and negative in a short time frame, i.e., the number of times it crosses the zero value (horizontal axis). It is the response of the average frequency of the audio signal over a short period of time and is calculated by the formula

$$Z_q = \sum_{i=1}^{n} w(q-m), \tag{4}$$

where sgn [] is the symbolic function defined as follows:

$$\text{sgn}\,[q] = \begin{cases} 1, & x(q) > 0, \\ -1, & x(q) < 0. \end{cases} \tag{5}$$

As mentioned above, the short-time overzero rate is sensitive to noise, and if the noise crosses the axes randomly and repeatedly in the computer application, many overzero artifacts can occur, which can have an important impact on the results. Therefore, in order to improve the robustness, the original signal is bandpass filtered during the operation and certain permissions can be set for the overzero rate, as shown in Figure 2. By calculating the average short-time energy and the standard deviation of the excess zero rate of the audio fragment to be recognized, we can distinguish whether the music fragment is a pure music fragment or a speech-music hybrid fragment.

3.2. Wireless Sensor-Assisted Identification. Here, the signal oscillation of the noise is guaranteed to be unaffected by the result of the overzero rate as long as it is kept within the overthreshold. Audio fragments are proposed on the basis of audio frame features. For all audio frames that make up audio, calculating the mean, variance, standard deviation, and other statistics of their audio frame features is the basic method to obtain audio fragments. In terms of audio recognition rules, the purpose of audio recognition is to roughly classify the extracted audio clips into three parts: silence, pure music, and speech-music mix. Since there is a clear distinction between these three audio categories, the recognition can be performed by the method based on the average short-time energy and the standard deviation of the overzero rate of the audio clips. Through experimental analysis, the average short time energy and overzero rate are the main two features of the standard deviation, as shown in Figure 3. The values of these two features of the pure music signal are smaller than those of speech, and by comparing the basic standard deviation of the speech waveform and the overzero rate, it can be found that there are obvious differences in their standard deviations of the overzero rate, where the music segment is located on the left side of the dotted line and the speech segment is on the right side.

The amplitude of the audio signal is small and inaudible to the human ear is the mute. The energy spectrum is characterized by low energy over a long period of time and is particularly distinctive in that the overzero rate of the mute is very different from the rest of the spectrum. Although there are also very short intervals of lower energy between each word, so it cannot be used as a silent zone. The feature of silence ratio is used here with the following rule.

(1) A silent clip is defined as when the share of silent frames in a clip exceeds the threshold value ST

(2) The definition of a silent frame is when the energy of an audio clip is well below a certain threshold. The frequency of the current sound and the loudness of the sound have a relationship to the threshold setting, the louder the sound, the higher the threshold

For this reason, the method used for extraction is the threshold ET determination method: an audio frame is considered to be silent when its temporal energy is below the threshold RT when the average ratio of the temporal energy within a 3-second window for sliding is shorter than the threshold RT. An audio clip is considered to be a pure music clip if the two characteristic values of the average short-term energy and the standard deviation of the overzero rate meet

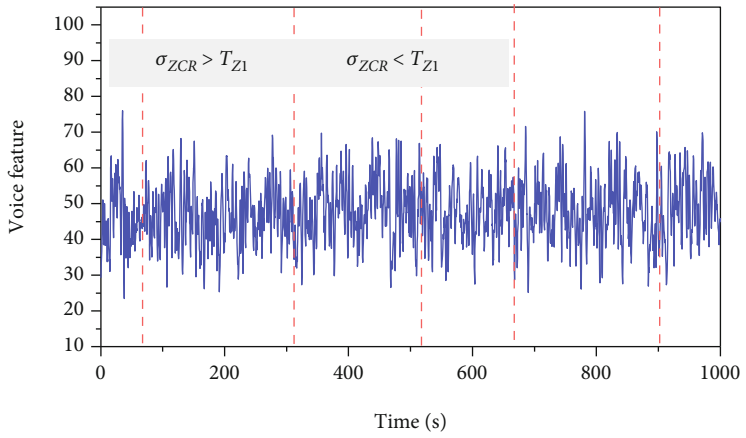

Figure 2: Threshold overzero rate diagram.

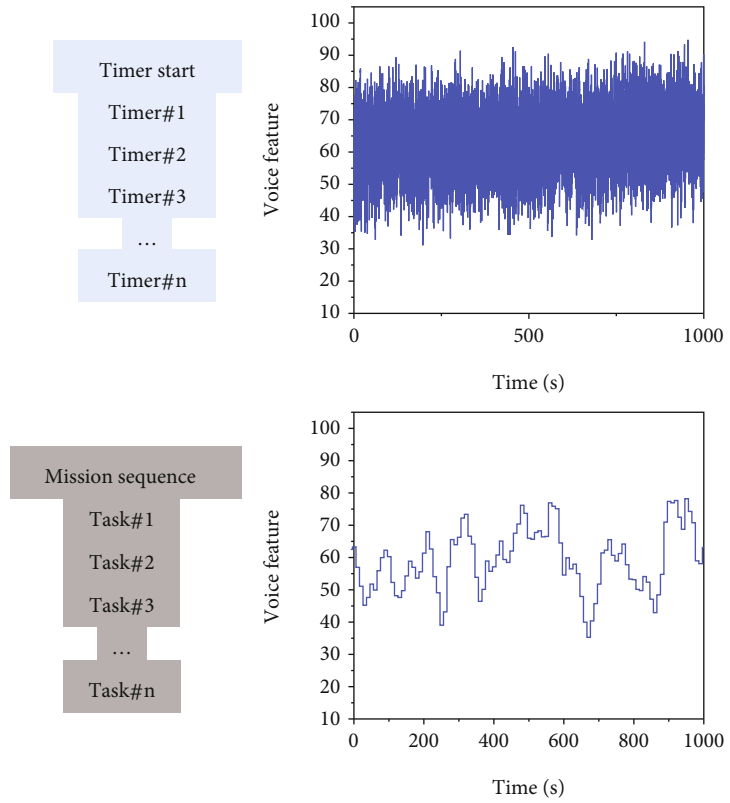

Figure 3: Feature decision table.

certain conditions; otherwise, it is a mixed speech-music clip.

3.3. Human Voice Input Recognition System. In nature, the wide variety of sounds that humans can perceive is ultimately generated by oscillations. Therefore, the first thing you come across when performing audio signal processing, and the most intuitive description of an audio signal, is the time domain waveform of the audio signal. The sound is converted into an electrical signal after passing through the transducer, and the audio signal acquisition is realized, which is the first job to be done in all audio processing systems. The electrical signal can be visually observed with an oscilloscope as the external sound changes. Since computers can only process digital signals, to draw the waveform of an audio signal in a computer, the analog audio signal must first be digitized, and then, the waveform of the audio signal is drawn based on the sampling values of each sampling point. In the waveform diagram, the changes in the energy of the audio signal can be observed very clearly, and even the time period of each note can be identified. The specific steps of digital music creation are as follows.

Sampling theorem: a time-continuous signal $m(t)$ with a frequency band limited to $(0, f)$ Hz, if $T \leq 1/2f$ seconds is the criterion for equally spaced sampling, then $m(t)$ will be completely determined by the resulting sampling value. 300 to

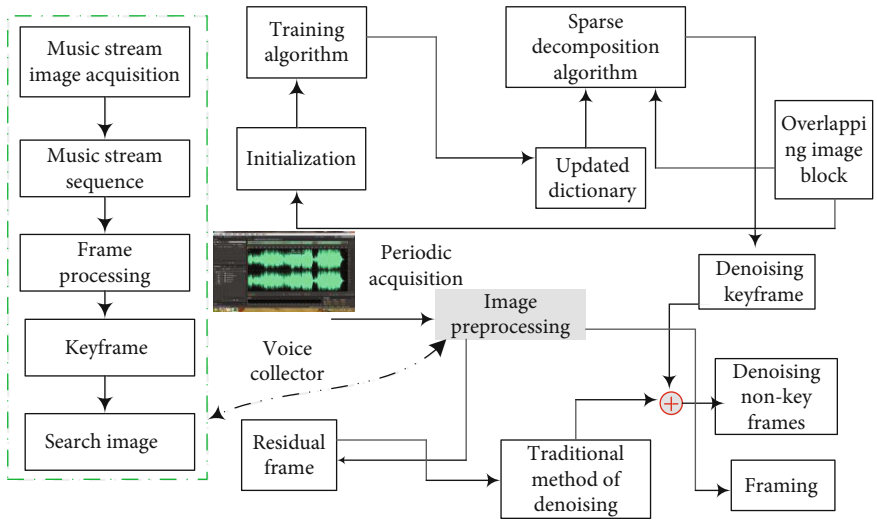

Figure 4: Architecture of the human voice input recognition system.

3400 Hz is the normal value of the human speech signal frequency band. Therefore, when the voice signal is digitally transformed, there are certain regulations for the sampling frequency, which is generally not more than 8000 Hz. 0.016~16 kHz is the most basic range according to the analysis of normal human hearing; as a young person hears more clearly, he can hear the sound of 20 kHz, so in general, equipment is often used much higher than 8000 Hz sampling frequency, so that is more enough to get a higher quality sound. The frequency range of music is related to a specific instrument. The frequency range of piano is relatively wide, from 27.5 Hz to 5000 Hz, so 10 kHz is enough to contain all the information, and the frequencies used are 22.05 kHz, 44.1 kHz, etc. What is quantization? It is mainly a process of representing the analog sampling value, which is represented by a preselected level. For the level of the analog signal according to the need for sampling, the sampling value $X(T)$ is infinite; if the size of this sample value is to be expressed in N binary digital signal, then N binary signal is expressed in M (2 of the nth power) level value. So the sampling value is divided into M discrete levels, and this process is the quantization level.

Based on what was described in the previous sections, a system was studied and developed to accept vocal humming input, retrieve it through a database, and get the user's humming name. The flow of the whole prototype system is divided into three modules. The following figure shows the functional block diagram of the system, and Figure 4 shows the block diagram of the system implementation. The higher the sampling frequency, the more accurately the discrete signal sequence will reflect the input continuous signal, which is easy to understand because the higher the sampling frequency, the less information will be lost.

After calculating the pitch saliency to obtain melodic pitch candidates, the algorithm proposes to use the continuity of pitch saliency, i.e., combining the continuity of auditory stream cues and pitch saliency to create pitch contours to reduce the problem of discontinuity of the same sound source pitch sequence due to the difficulty of distinguishing similar pitches by auditory stream cues, on top of creating pitch contours based on auditory stream cues that maintain continuity in time and pitch. Considering that the accompaniment is generally used for the modification of main notes or for the repetition of musical fragments, the repetition property of the accompaniment is proposed in the selection of melodic pitch contours. Since the repetition property is expressed in the set of pitch contours as pitch contours of equal length and pitch at different times, the dynamic time regularization (DTW) algorithm will be used to calculate the similarity between pitch contours and reduce the nonlinear deviation introduced by the difference of note length. Finally, based on the long-time relationship between adjacent pitch contours, octave errors are proposed to be detected based on the average of the pitch-weighted mean values of adjacent pitch contours in time for each frame, and melodic pitch lines are formed by smoothing melodic pitch contours using the Viterbi smoothing algorithm. Since there are strict inequalities in the pitch contours in terms of time length, the length difference range of the pitch contours satisfying the period relationship is set to. In order to remove the nonlinear deviation caused by unequal pitch contour lengths when calculating the period of pitch contours, the DTW algorithm is used to calculate the similarity between pitch contours. Considering that the difference in pitch saliency between pitch contours satisfying the period relationship is not very different, the DTW algorithm is used to calculate the difference in pitch saliency between the two pitch contours Cm and Cn, and the satisfying pitch contour is removed from the period for which the pitch contour mC is calculated, since the melodic pitch contour belonging to the dominant also has a certain long periodicity. Secondly, the system uses MFCC coefficients and short-time energy and overzero rate as feature parameters and audio retrieval technology as the recognition framework and uses GMM algorithm to train model parameters of songs, carries out the calculation of model similarity between sample songs and song feature library, realizes a song personality calculation and recommendation system, and verifies the system performance through experiments.

Programming sound in computers: the main part of programming sound in computers is the recording, playback, and operation of wa files through the sound card. In the main system of the computer, Windows, the API is used to support multimedia operations, which can be divided into two main types: low-level interfaces and high-level interfaces. The low-level interface consists of a lot of functions starting with wave, while the high-level interface is applied in two ways: they are sending messages and sending strings. When programming sound using the low-level pretext, the low-level API functions and the data structures used for sound programming and thus the handles are used.

4. Simulation Experiments and Result Analysis

Thirty humming audio clips of 10 to 15 seconds in length were used for the experiment of retrieval, and the retrieval results were output as the top three closest songs. The audio acquisition device was an external microphone. The experimental results are shown in Figure 5. From the experimental results, it can be seen that in the ideal case, the retrieval system can obtain an accuracy rate of nearly 60% for humming retrieval. The ideal situation is a situation where the user hums notes with small pauses between notes, the hummed notes are accurate, and the sampling environment is less noisy. The accuracy of system retrieval is highly dependent on the accuracy of the hummed pitch, the consistency of the hummed rhythm, and the accuracy of the MIDI information in the database. When the complexity of the MIDI file is high, such as more chord tones, and the MIDI file producer adds more subsidiary information, the retrieval rate decreases significantly. The phenomenon is related to the method of automatic extraction of MIDI file features, which is still to be improved by future research work. The hummer should have obvious pauses when humming, and the retrieval result is not satisfactory if the humming is too continuous. For the retrieval of continuous humming, more in-depth research on the note segmentation algorithm is needed.

Firstly, the system uses average short-time energy and standard deviation of overzero rate as feature parameters to accurately distinguish pure music and speech-music mixed fragments in the same song according to audio recognition rules, to achieve the function of removing pure music parts in songs. The dataset for the simulation experiments was taken from the introduced dataset DEAM15, containing a total of 489 tracks in MP3 format. Of these, 431 tracks of 45 seconds in duration were used as the development set, while the remaining 58 tracks were used as the test set. The sentiment annotation of the dataset is based on the Thayer sentiment model, with each annotation having a V/A value in the range $[-1, 1]$ and an annotation interval of 0.5 seconds. The simulations are run on Ubuntu 14.04 in the PyTorch framework, with an Intel Core i7-5930k 3.4 GHz CPU, 32 GB RAM, and TITANX 12G graphics card, and a total of 5 different random divisions of the development set are used for model training. Among them, 411 firsts were divided as the training set and 20 firsts as the validation set, and the validation set had to be randomly selected according to the genre distribution of the test dataset to ensure that the datasets matched. The evaluation index is evaluated by RMSE, which is the standard deviation of the difference between the predicted and true values of the dataset. The algorithm uses the openSMILE toolbox to extract the frame-level features of the segmented segments. The features are composed of 65 low-level acoustic descriptors, including MFCC, spectral features, and features related to the human voice. To use melodic contour features for emotion recognition, melodic contour features based on pitch, duration, vibrato, and contour type are extracted, totaling 10 features. To prevent overfitting of the model, a regularization method with random deactivation of 0.5 is used. The sequence information of short time segments is relatively small, which is prone to produce wrong emotion recognition results, so this chapter proposes the method of merging short time segments. In order to verify the effectiveness of this merging method, simulation experiments are conducted before and after the merging of short time segments, and the experimental results shown in Figure 6.

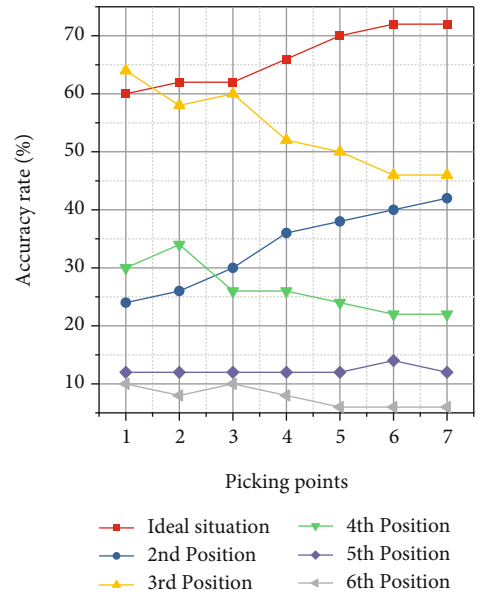

Figure 5: Audio picking experiment results.

It can be concluded from this that comparing the values of pleasantness and activation before and after merging, the merging method reduces their values, indicating that the merging method can reduce the false recognition of short-time segments. To identify the emotions of segmented segments, the features of the segmented segments need to be extracted first. To verify the effectiveness of the features extracted based on the CNN structural model and the melodic contour features, the two methods will be removed separately for testing and compared with the complete algorithm in this chapter, and the final results are shown in Figure 7. The dynamic music emotion recognition algorithm based on melody extraction and convolutional neural network is proposed for music emotions that are not uniformly distributed with time points and in order to abstract the features within adjacent emotion change points. The experimental results show that the algorithm in this chapter

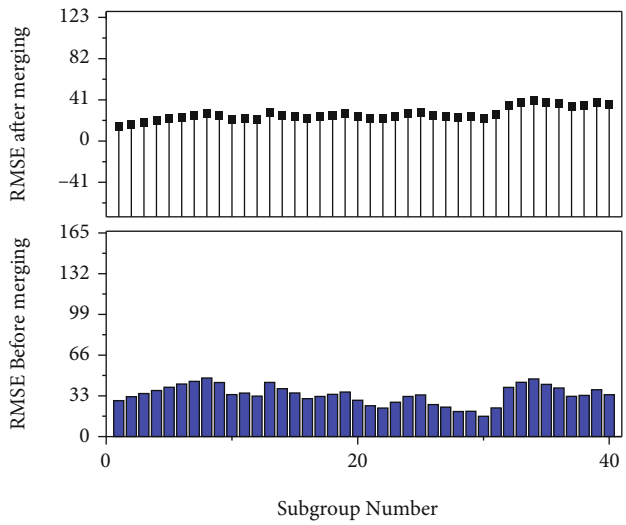

Figure 6: RMSE before and after merging short time periods.

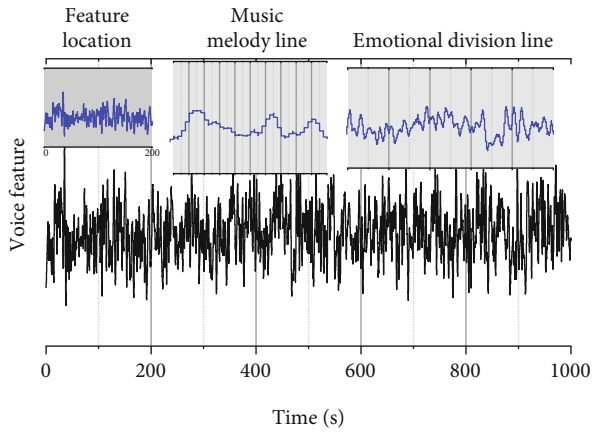

Figure 7: Music melody line and emotional division line.

achieves results close to the best recognition algorithm and greatly reduces the number of parameters of the model. The audio fragment feature used in this method is the zero-percentage standard deviation (ZCR_STD), which is defined as the standard deviation of the zero percentage of each frame in an audio fragment.

From this, it can be concluded that removing the CNN structural model significantly reduces the recognition accuracy of *V*/*A* compared to the algorithm in this chapter, which illustrates the importance of the CNN structural model for the algorithm recognition, and this result also reflects the effectiveness of the segmentation method in this chapter. For the melodic contour feature, adding this feature can further improve the recognition accuracy of the algorithm, which illustrates the effectiveness of the feature. The regressor, as the last stage of the algorithm, has many methods to choose from. To improve the recognition accuracy of the algorithm, this chapter compares regressors such as multivariate linear regression (MLR), SVR, and neutral network (NN). Among them, SVR has a 3rd polynomial kernel and NN is a single hidden layer network with 14 units.

Design and implement a prototype system that uses an audio recognition algorithm based on average short-time energy and standard deviation of overzero rate and a song personality calculation algorithm based on MFCC and GMM. The system can achieve the function of accurately removing the mute and pure music parts of a song by extracting feature parameters such as short-time energy and overzero rate of the song, extracting the speech features of the song using MFCC technique and generating the template of the song using GMM algorithm, and then performing similarity calculation of the song file using the song template library for similar song retrieval, which can accurately retrieve from the music library the songs that are similar to the sample songs that are similar (have the same characteristics or style) to the sample songs from the music library, which can achieve the requirement of personalized music recommendation. The system is developed in C++ language using VC++ compilation environment, and all functional modules are encapsulated by dynamic link libraries. The modular design of the system is realized to enhance the scalability of the system. All functions are processed by multithreaded processing technology to improve the calculation speed of the system, and at the same time, the fault tolerance and the ability to handle abnormal errors of the system are fully considered to realize the design of the reliability of the system and the ability to handle data resources.

5. Conclusion

This paper researches the implementation of human voice input and recognition technology in digital music creation, studies and analyzes the key technologies such as preprocessing technology, feature parameter extraction technology, and Gaussian mixture model algorithm of music retrieval system, and proposes the concept of "song personality" to summarize features such as song style, rhythm, and background music. We propose an audio recognition algorithm based on average short-time energy and standard deviation of overzero rate, which can distinguish pure music and mixed speech-music fragments in the same song more accurately and achieve high accuracy in processing songs of different styles, different singers, and different languages. Meanwhile, according to the need of similar song creation, a method of song personality calculation and creation based on MFCC and GMM is proposed and designed to realize the digital music creation and retrieval function to better realize the requirement of personalized digital music creation. A high accuracy recognition algorithm for pure music and speech-music hybrid audio clips based on average short time energy and standard deviation of overzero rate is proposed. The method of accurately distinguishing pure music and speech-music mixed fragments in the same song is investigated, which solves the problem of high confusion susceptibility of pure music and speech-music mixed fragment recognition and provides an effective preprocessing method for removing unwanted parts of the song. The experimental results show that by processing songs with different styles, different singers, and different languages, the average detection rate is 92.08% for pure music fragments and 96.33% for

speech-music hybrid fragments after smoothing, and the average recognition correct rate is 92.30% for pure music and 96.36% for speech-music hybrid.

By processing each note, the intensity, length, and relative pitch characteristics of the whole humming melody are extracted for the implementation of vocal input and recognition technology in digital music composition. In the melody retrieval part, a combination of exact matching algorithm and fuzzy matching algorithm is used according to the special characteristics of the humming melody to finally design the system for the implementation and application of vocal input and recognition technology in digital music composition.

Data Availability

The data used to support the findings of this study are available from the corresponding author upon request.

Conflicts of Interest

The authors declare that they have no known competing financial interests or personal relationships that could have appeared to influence the work reported in this paper.

References

[1] J. H. Barnes, G. Choby, A. J. Smith et al., "Creation of a new educational podcast: headmirror's ENT in a nutshell," *Otolaryngology head and neck surgery*, vol. 163, no. 4, pp. 623–625, 2020.

[2] S. Belikovetsky, Y. A. Solewicz, M. Yampolskiy, J. Toh, and Y. Elovici, "Digital audio signature for 3D printing integrity," *ieee transactions on information forensics and security*, vol. 14, no. 5, pp. 1127–1141, 2019.

[3] M. Bender, E. Gal-Or, and T. Geylani, "Attracting artists to music streaming platforms," *European journal of operational research*, vol. 290, no. 3, pp. 1083–1097, 2021.

[4] T. Bhangale and R. Patole, "Tampering detection in digital audio recording based on statistical reverberation features," in *Advances in Intelligent Systems and Computing*, pp. 583–591, Springer, Singapore, 2019.

[5] A. Goyal, S. K. Shukla, and R. K. Sarin, "Identification of source mobile hand sets using audio latency feature," *Forensic science international*, vol. 298, pp. 332–335, 2019.

[6] A. Goyal, S. K. Shukla, and R. K. Sarin, "A comparative study of audio latency feature of Motorola and Samsung mobile phones in forensic identification," *Indian journal of science and technology*, vol. 14, no. 4, pp. 319–324, 2021.

[7] T. Hodgson, "Quantifying music: imagined metrics in digital startup culture," *Culture theory and critique*, vol. 61, no. 4, pp. 424–439, 2020.

[8] G. Hua, H. Liao, Q. Wang, H. Zhang, and D. Ye, "Detection of electric network frequency in audio recordings-from theory to practical detectors," *ieee transactions on information forensics and security*, vol. 16, pp. 236–248, 2021.

[9] B. R. Ismanto, T. M. Kusuma, and D. Anggraini, "Indonesian Music classification on folk and dangdut genre based on rolloff spectral feature using support vector machine (SVM) algorithm," *Indonesian journal of computing and cybernetics systems*, vol. 15, no. 1, pp. 11–20, 2021.

[10] S. Li, Q. Luo, L. Qiu, and S. Bandyopadhyay, "Optimal pricing model of digital music: subscription, ownership or mixed?," *Production and Operations Management*, vol. 29, no. 3, pp. 688–704, 2020.

[11] J. Wu, B. Chen, W. Luo, and Y. Fang, "Audio steganography based on iterative adversarial attacks against convolutional neural networks," *ieee transactions on information forensics and security*, vol. 15, pp. 2282–2294, 2020.

[12] Z. Xie, W. Lu, X. Liu, Y. Xue, and Y. Yeung, "Copy-move detection of digital audio based on multi-feature decision," *in Workshop on Information Security Applications*, vol. 43, pp. 37–46, 2018.

[13] Z. Liu, Y. Huang, and J. Huang, "Patchwork-based audio watermarking robust against de-synchronization and recapturing attacks," *ieee transactions on information forensics and security*, vol. 14, no. 5, pp. 1171–1180, 2019.

[14] A. McPherson and K. Tahiroglu, "Idiomatic patterns and aesthetic influence in computer music languages," *Organised sound*, vol. 25, no. 1, pp. 53–63, 2020.

[15] L. M. Meier and V. R. Manzerolle, "Rising tides? Data capture, platform accumulation, and new monopolies in the digital music economy," *new media & society*, vol. 21, no. 3, pp. 543–561, 2019.

[16] M. Ritts and K. Bakker, "Conservation acoustics: animal sounds, audible natures, cheap nature," *Geoforum*, vol. 124, pp. 144–155, 2021.

[17] A. Rodman and S. Trivedi, "Podcasting: a roadmap to the future of medical education," *Seminars in Nephrology*, vol. 40, no. 3, pp. 279–283, 2020.

[18] G. Rodríguez-Arauz, N. Ramírez-Esparza, A. García-Sierra, E. G. Ikizer, and M. J. Fernández-Gómez, "You go before me, please: behavioral politeness and interdependent self as markers of Simpatía in Latinas," *Cultural Diversity & Ethnic Minority Psychology*, vol. 25, no. 3, pp. 379–387, 2019.

[19] A. Roper, "From print to digital: first steps in collecting digital music publications in UK legal deposit libraries," *Alexandria the journal of national and international library and information issues*, vol. 30, no. 1, pp. 32–53, 2020.

[20] J. Shen, M. Tao, Q. Qu, D. Tao, and Y. Rui, "Toward efficient indexing structure for scalable content-based music retrieval," *multimedia systems*, vol. 25, no. 6, pp. 639–653, 2019.

[21] T. Shen, J. Jia, Y. Li et al., "PEIA: personality and emotion integrated attentive model for music recommendation on social media platforms," *in National Conference on Artificial Intelligence*, vol. 34, no. 1, pp. 206–213, 2020.

Hindawi
Journal of Sensors
Volume 2022, Article ID 8445816, 11 pages
https://doi.org/10.1155/2022/8445816

Research Article

Intelligent Intersection Vehicle and Pedestrian Detection Based on Convolutional Neural Network

Senlin Yang,[1,2] **Xin Chong**,[3] **Xilong Li**,[2] **and Ruixing Li**[2]

[1]*Shaanxi Key Laboratory of Surface Engineering and Remanufacturing, Xi'an University, Xi'an, Shaanxi 710065, China*
[2]*School of Mechanic & Material Engineering, Xi'an University, Xi'an, Shaanxi 710065, China*
[3]*Vertiv Technology Ltd., Xi'an, Shaanxi 710075, China*

Correspondence should be addressed to Senlin Yang; linsenyang@xawl.edu.cn

Received 8 November 2021; Revised 4 January 2022; Accepted 26 January 2022; Published 11 March 2022

Academic Editor: Gengxin Sun

The preprocessed images are input to a pretrained neural network to obtain the corresponding feature mapping, and the corresponding region of interest is set for each point in the feature mapping to obtain multiple candidate feature regions; subsequently, these candidate feature regions are fed into a region proposal network and a deep residual network for binary classification and BB regression, and some of the candidate feature regions are filtered out, and the remaining feature regions are subjected to ROIAIign operation; finally, classification, BB regression, and mask generation are performed on these feature regions, and full convolutional nerve network operation is performed in each feature region and output. To further identify the specific model of the vehicle, this paper proposes a multifeature model recognition method that fuses the improved model with the optimized Mask R-CNN algorithm. A vehicle local feature dataset including vehicle badges, lights, air intake grille, and whole vehicle outline is established to simplify the network structure of model. Meanwhile, its detection frame generation process and the adjustment rules of overlapping frame confidence in nonmaximum suppression are improved for coarse vehicle localization. Then, the generated vehicle detection frames after localization are output to the Mask R-CNN algorithm after further optimizing the RPN structure. The localized vehicle detection frames are then output to the Mask R-CNN algorithm after further optimization of the RPN structure for local feature recognition, and good recognition results are achieved. Finally, this paper establishes a distributed server-based vehicle recognition system, which mainly includes database module, file module, feature extraction and matching module, message queue module, WEB module, and vehicle detection module. Due to the limitations of traditional region generation methods, this paper provides a brief analysis of the region generation network in the Faster R-CNN algorithm and details the loss calculation principle of the output layer.

1. Introduction

The number of motor vehicles has exceeded 350 million, cars reached 229 million, motor vehicle drivers exceeded 420 million, including 360 million car drivers, and cars have gradually replaced bicycles and other as one of the main means of transportation for travel, appearing in various scenes such as streets, highways, and communities [1]. The rapid growth of motor vehicles not only brings many conveniences to people's lives but also generates road congestion and criminal cases involving cars, bringing invisible effects to our living environment and travel speed [2]. As the number of motor vehicles grows at a rate of about 10% per year, urban building congestion leads to slow development of road construction. The urbanization of China makes more and more rural population flock to the city, which leading to road congestion, traffic accidents, environmental pollution and other problems [3]. The rapid growth of vehicles not only makes urban traffic overload but also makes the frequent occurrence of criminal cases involving vehicles, bringing new challenges to public safety, and the current management and identification of vehicles basically rely on the existing road traffic management methods and manual judgment [4]. In order to reduce manual operations, automatically detect vehicles, and identify their corresponding areas of interest, so as to make timely responses to traffic

problems occurring in highways, communities, and other environments, the research of intelligent traffic system (ITS) has emerged [5].

The rapid development of artificial intelligence has laid a good foundation for ITS, which integrates technologies such as computer processing, automation, data communication transmission technology, big data, and machine vision into the traffic management system and can replace manual operations with intelligent systems in traffic scenarios such as highways, toll stations, railway stations, and airports to reduce congestion, transportation failures, and other problems, as well as save energy and manpower and reduce economic waste [6]. The core of the vehicle detection and automatic identification system construction lies in the license plate, vehicle color, vehicle brand, and specific model recognition and the matching problem. At present the license plate positioning and recognition system is very mature, the precision and accuracy rate is very high, and it has been widely used in various traffic intersections, neighborhoods, highways, and other places; the body color recognition technology is relatively simple to achieve and also has a good recognition rate; for the specific model recognition, because the similarity of different vehicles may be larger, the vehicle detail recognition aspect has a certain degree of difficulty, the current model recognition technology cannot reach a high industrialization degree, and there is no more perfect model recognition system [7]. In order to solve the above problems, more and more experts and scholars have devoted themselves to the research of vehicle model and vehicle brand recognition in recent years, and certain progress has been made. Due to the difference of application occasions and demand objects, there is also a certain difference in the fine degree and algorithm framework for model recognition [8]. In the general highway, community and parking management system, it generally only needs to determine whether it belongs to large vehicles or small vehicles. In the public security criminal investigation for the search of the set of vehicles or illegal criminal vehicles, it requires for the vehicle detail characteristics that are extremely detailed; model recognition specific to the model and year can provide more effective clues for the public security organs [9].

The improved YOLOv3 coarse vehicle localization method is incorporated in the vehicle detection stage of fine vehicle recognition, and a distributed system is used to assign each local feature to different servers for feature extraction and recognition using the improved Mask R-CNN method, and then, the total server aggregates and outputs the recognition results, which not only improves the generalization ability and robustness of the detection method but also improves the efficiency of detection and recognition. Finally, a model recognition system is established to further verify the feasibility of the algorithm proposed in this paper. For the problem of vehicle-specific model recognition, a fine model recognition algorithm with improved YOLOv3 algorithm is considered as the detection model, while the RPN module in Mask R-CNN that is further optimized and used for recognition is proposed, and the established local feature dataset is introduced. In order to improve the detection efficiency, a method of multithreaded feature recognition using a distributed server system is proposed, and the superiority of this paper compared with other target detection methods is analyzed. Finally, the hardware system for vehicle model recognition built in this paper is introduced, mainly including database module, file module, feature extraction and comparison module, message queue module, WEB module, and vehicle detection module, and the algorithm proposed in this paper is implanted into the system to verify the practical value of the method. This paper mainly focuses on deep learning and convolutional neural network algorithms to optimize the network structure to train the detection and recognition models of large class vehicles and fine vehicles, respectively. Based on the algorithm development of R-CNN and Faster R-CNN and the design of convolutional layer, the superiority of convolutional neural network in target detection and recognition is illustrated, and the advantages and disadvantages of different methods and network frameworks in target detection are analyzed.

2. Related Work

The interframe difference method, background difference method, and optical flow method are the three most traditional methods in target detection [10]. The basic principle of the frame difference method is to determine the moving target area based on the pixel change between frames in the video, and the pixels between adjacent frames are compared by the difference and threshold operation to obtain the moving object [11]. The overall accuracy of the overall model is affected. Based on the three-frame difference method, the researchers binarized the vehicle image after extracting the contour of the moving target vehicle, then applied morphological processing to it, and finally performed line-by-line scanning to obtain the overall binarized image and reconstructed the vehicle image using the connection of contours to obtain the region of the moving vehicle, whose limitation is that it can only detect the moving vehicle, and for the stationary vehicle recognition, there is still a need for further research [12].

Background difference method is the most commonly used method in the early development of target detection. The principle is to first obtain the video or image that does not contain information such as vehicles in the background to generate a background model, and then, the image or video to be measured that inputs and subtracts the information corresponding to the background model can obtain the possible vehicle information you want to identify, finally, the information image for binarization can get more complete vehicle information [13]. Researchers in the background difference method based on the use of background model in obtaining the specific location information of the target vehicle take the labeling technology to give the video frame or image of each vehicle corresponding to the label and then do further processing; the experiment shows that the method has good detection effect in the fixed scene [14]. The optical flow method is very different from the two target detection methods mentioned above, the method is based on giving the velocity vector corresponding to all pixel points in the video frame to achieve the purpose of transforming the

original image into a variable motion field, and each coordinate in the video frame can find its corresponding coordinate on the target to be identified at any moment when training is carried out [15].

Researchers proposed to introduce Lucas-Kanade based on the parallel optical flow method to identify and track moving vehicles in video [16]. The main process is to detect moving targets using optical flow detectors and then perform binarization similar to the background difference method and use the target frame to detect the range of the target, but the limitation of this method is that it can generally only be used for target localization and tracking, not for recognition [17]. In addition to the traditional target detection methods mentioned above, feature-based target detection methods are also used in vehicle model recognition, and more commonly, vehicle detection is performed using features such as histogram of oriented gradient, scale-invariant feature transform, and Haar. The feature-based vehicle recognition methods are generally divided into two major categories: the first one is to directly extract and train features on the whole original image and the other one is to segment the original image into multiple images of appropriate size, perform feature extraction on each small image, and then use classifiers such as SVM to classify the extracted individual features before proceeding to the next step of detection [18]. This method requires a high level of dataset richness and a large number of samples with different environments, angles, and the presence of occlusions for training, which is a huge amount of engineering [19].

As one of the representative algorithms of deep learning, convolutional neural network (CNN) was first proposed in 1987, but it did not have much application at that time; with the hot development of deep learning and the wide application of GPU in recent years, CNN has been used in image processing and target detection [20]. The R-CNN network is derived from the CNN network with improvements, using automatic selection search to obtain the candidate range of the target, then feeding the target candidate range into the convolutional neural network for feature extraction and classification, and finally outputting the recognition results with rectangular boxes. Although RCNN has a great improvement in detection accuracy compared with CNN, it also has the limitation of being more time-consuming [21]. Fast R-CNN changes the convolution of the feature area for each candidate region on the basis of R-CNN, and uses shared whole image for feature extraction, which greatly reduces the detection time. Researchers improve the algorithm on the basis of Fast R-CNN and used a candidate frame extraction network to extract the target range and identify it, which further accelerated the detection speed. In addition to these networks, SPP-Net, R-FCN, GoogLeNet, etc. can be used for target detection and recognition [22].

3. Feature Extraction and Result Output for Vehicles and Pedestrians at Road Junctions

3.1. Feature Extraction. The basic process is shown in Figure 1. Firstly, the key points and key regions of the input image are located using image processing technology, then the feature descriptors in the regions are extracted, and finally the feature descriptors are input to the classifier to realize the classification and recognition of car models. According to the degree of refinement of model recognition, the model recognition technology can be divided into coarse-grained model recognition and fine-grained model recognition. Since different types of vehicles have different appearance shapes, coarse-grained model recognition can be classified mainly based on the appearance shapes of vehicles. In addition, some key parts on the car in the coarse-grained model recognition process also differ greatly (e.g., doors, front end, body, and windows), and these characteristics can also be used as the basis for discriminating coarse-grained models.

The fine-grained model recognition process often requires more detailed features to be considered because of the type and model of the vehicle to be discerned. It is understood that the fine-grained model recognition tends to pay more attention to the vicinity of the license plate as well as the vicinity of the lights and emblem, because these parts are the biggest difference in distinguishing from the same type of vehicles. First of all, the area near the license plate will be the target area, because the license plate is located in the front of the vehicle and is also the main performance part of the appearance design, so it will be the main candidate area of the model fine-grained recognition. Then, in order to carry out model recognition more effectively, the license plate image or the headlight image is usually segmented out separately for processing. Finally, in order to recognize the vehicle type effectively, the extracted features such as edge and color are classified using classifiers (softmax, SVM, etc.). With the increasing ability of feature descriptors to characterize images, such as histogram of gradients (HOG), scale-invariant feature transform (SIFT), and hybrid features, model recognition methods based on such feature extraction have very good robustness. The above vehicle recognition method based on feature extraction is inevitably limited by some external factors, such as fixed image capture view, artificially set feature extraction parameters and so on. In order to effectively solve this problem, some scholars try to apply geometric methods to car model recognition. With the help of computer-aided design (CAD) technology, the authors perform a series of preprocessing (including template matching and selecting viewpoint parameters) before feature extraction of images, so that they can better detect car license plates. The model recognition method based on geometric estimation mainly equates the vehicle area into a rectangle of certain length, width, and height, as shown in Figure 2. Firstly, the vehicle in the image is segmented to generate a rectangle of its smallest outside world, and its length, width, height, and center coordinates are output. Then, the correspondence between the key points in the reconstructed 3D space and the input 2D image is determined according to various parameters (including camera focal length and mapping relationship between coordinate systems). Finally, the inverse projection technique is used to compare the constructed 3D dimensions with the actual dimensions of the vehicle, so as to determine the type of the actual vehicle.

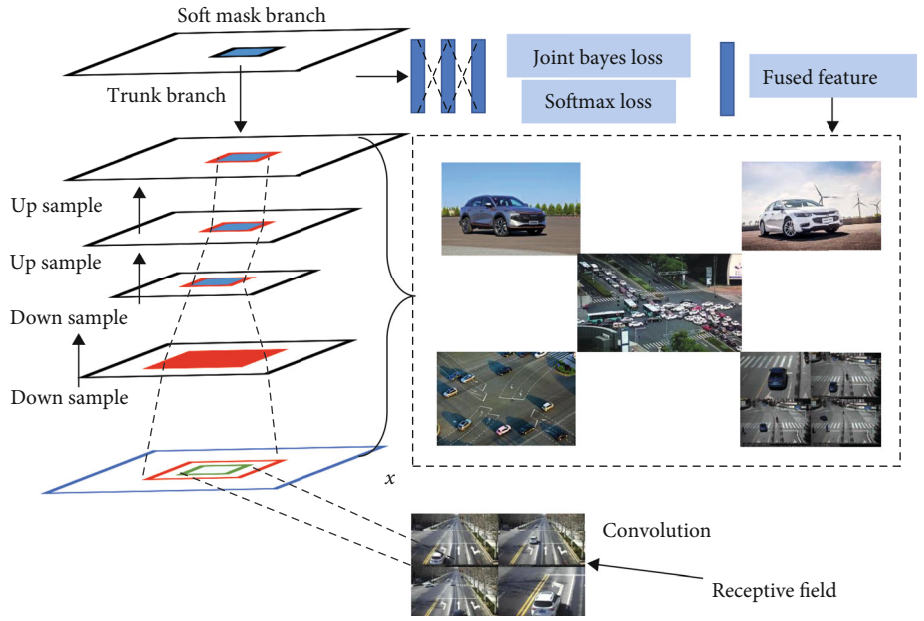

Figure 1: Feature extraction-based model recognition.

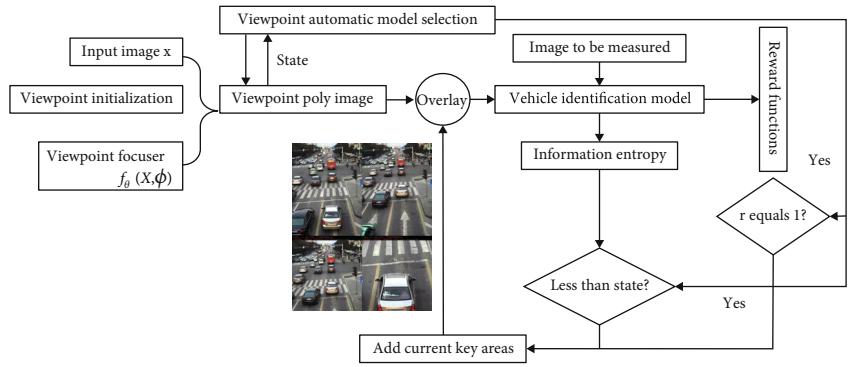

Figure 2: Geometric estimation-based model identification.

3.2. Neural Network to Enhance Recognition. In the fully connected layer, the main role is to reduce the error between the labeled samples in the dataset and the output of the generated model in order to achieve the purpose of continuously fitting the generated network to the original image in this paper.

The neural network-based model recognition method is a method that enables a neural network model to detect and recognize autonomously based on the learned capabilities by constructing it. With the outstanding contributions of neural network technology in the fields of image processing, target detection, and scene analysis, the application of neural networks in model recognition has been gradually promoted. In the research of using neural networks for car model recognition, it is usually done by extracting key frames from surveillance videos as the input of neural networks and then predicting their probabilities. This method, which involves a lot of human intervention, is called supervised training method, and semisupervised and unsupervised methods have also been studied in the literature to train neural networks for car model recognition. However, as far as the current research results are concerned, the neural network-based model recognition technique still does not effectively address the problem of low detection efficiency when dealing with multiangle and complex scenes. In the literature, the authors use images from two specific viewpoints as the infants of the neural network, which makes the neural network model possess higher detection accuracy than a single viewpoint. However, the model still cannot be used for other problems that deviate from the normal viewpoint. The literature uses CompCars, a dataset containing complex scenes and multiple perspectives, to train a neural network model with better robustness, but the model is not very efficient for vehicle detection and recognition because the constructed model is shallow. The literature proposes a car model recognition model with many complex image preprocessing means added to the network, yes the model can be converted from the input two-dimensional image to the unit space for processing, and also small datasets were constructed to verify the effectiveness of the method. However,

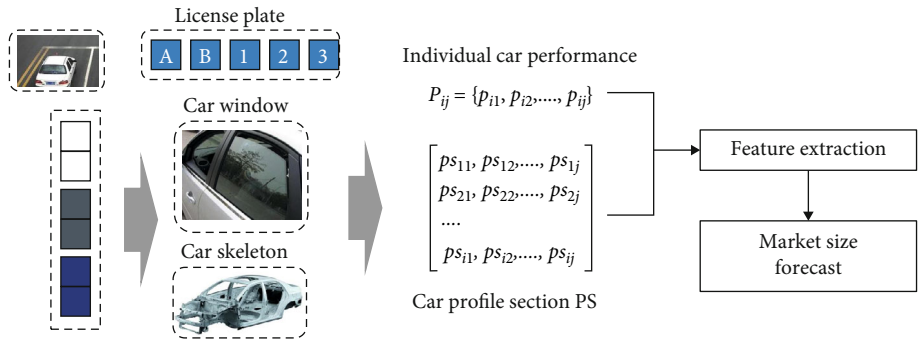

Figure 3: Global VR real estate market size forecast.

this complex preprocessing technique also requires much higher input data and therefore cannot be validated effectively on publicly available datasets, limiting its usage performance and application prospects. Therefore, it is of great interest to investigate a model for vehicle identification that can cope with complex weather, complex scenes, and high robustness.

In this paper, we propose an improved Mask R-CNN-based target detection and recognition method, whose network structure is shown in Figure 3. The original image is preprocessed and input to the pretrained convolutional layer neural network to obtain the corresponding feature map, and the region of interest is set for each point in the feature map to obtain several candidate feature regions, and then, these candidate feature regions are fed into the region suggestion network and the deep residual network (ResNet) for binary classification and BB regression. Finally, the fully convolutional network (FCN) operation is performed in each feature region to classify these feature regions by Mask and predict the target regions.

As a target detection method derived from CNN networks, the Mask R-CNN algorithm originally used feature pyramid networks (FPNs) to achieve efficient use of features at different scales, and FPNs employ top-down lateral connections to fuse (up-sample and sum) features connected at different scales and then perform 3×3 convolution to eliminate the blending phenomenon and then predict the features at different scales, repeating this process continuously until the best resolution is obtained. This feature mapping is shared for the subsequent region recommendation network layer and the fully connected layer. The advantages of FPN are its ability to localize and extract features more accurately for small targets and its shorter detection time, but it has limitations in detecting objects with low pixels or small distinctions. Deep residual network (ResNet) is a deep convolutional network with outstanding performance in target localization, target feature extraction, and target recognition proposed by four scholars from Microsoft Research in 2015, which well solves the problem of network depth and performance degradation. In this paper, we synthesize the special characteristics of vehicle targets and the applicability of other feature extractors in Mask R-CNN. The feature extraction module introduces a deep residual network with ResNet101 to extract vehicle feature information, and ResNet is based on the traditional AlexNex network, adding convolutional layers to achieve the purpose of extracting features more accurately and having stronger learning ability during model training. However, due to the large differences in the proportion of different vehicles in the video or image, background noise, and external contours, in order to better process the samples in the vehicle dataset and make the final generated model extract the vehicle features as much as possible, this paper combines the respective advantages of the deep residual network and the feature pyramid network and fuses the two for the extraction of vehicle features, and the network structure is more concise and modular. The network structure is also more concise and modular, and the convolutional network has fewer manually adjustable hyperparameters to facilitate training.

The activation functions used in this paper are the sigmoid function and the tanh function as follows:

$$\mathrm{sim}(x) = \frac{1}{1 + \exp(-x)}, \tag{1}$$

$$\tan(x) = \frac{\exp(x) - \exp(-x)}{\exp(x) + \exp(-x)}, \tag{2}$$

where 1 is the number of convolution layers, which is set to 5 in this paper; k_{lij} and b_{lj} (for) denote the convolution kernel and the offset of the feature map, respectively; the operation symbol x denotes the convolution operation; M_j is the set of input images. The convolution kernel convolves on the feature map output from the above convolution layer, and then, the new output feature map can be obtained after the sigmoid function and tanh function. The output feature map of each layer in the convolution layer of this paper through the activation function can be represented by multiple preactivation feature maps in the form of a sum, which is calculated as shown in the following equation:

$$x_i = f(q), \tag{3}$$

$$q = \sum_{i=1}^{i \in M_j} x_i * K_{ij}. \tag{4}$$

After preprocessing the original image and passing it through the convolutional layer, a common feature map can be obtained. In the more initial convolutional neural

network target detection frameworks (such as R-CNN and Fast R-CNN), the method of selective search is usually used to extract the candidate frames, which is more time-consuming and takes about 2 s to process an image on the CPU. CNN proposes the RPN method in the part of extracting candidate frames, which only takes about 10 ms to extract the candidate frames of an image, greatly speeding up the detection speed. The regional recommendation network requires less size and pixels of the input image, and its output increases the target frame of classification ratio compared with the convolutional neural network methods such as CNN, which makes the detection results easier to express. The convolutional kernel mentioned in the convolutional layer above is the key to generate the target candidate regions for RPN. The preprocessed image produces the output feature map after the operation of the convolutional layer, and sliding a small window of preset size to this feature map to obtain the corresponding large dimensional feature vector. The window of the sliding operation will generate different candidate regions after the RPN, which will then be input to the fully connected layer for localization and identification, as described below. Simply put, RPN relies on a sliding window on a shared feature map to generate nine target frames with preset aspect ratios and areas for each location, and the Mask R-CNN algorithm is inherited from this network for region prediction.

$$L_i(t, v) = \sum_{i=1}^{i\in\{x,y,w\}} s^2(t_1 - v), \tag{5}$$

$$s_i(x) = \begin{cases} 0.5x^2, & \text{if}, \quad x > 1, \\ |x| - 1, & \text{if}, \quad x \le 1. \end{cases} \tag{6}$$

The training function for training RPN is as follows:

$$L\left(\left\{p_1, p_2, \cdots, p_j\right\}\right) = \frac{p_i\{t_i, t_i^*\}}{L_{ij}}. \tag{7}$$

The network parameters can be determined by the objective function, and the network parameters in the fully connected layer are continuously updated as the objective function decreases. When the objective function reaches convergence, the signal distribution generated by our trained generative model is closest to the label distribution at the time of labeling, and the convolutional neural network for target detection can be well fitted to the original image and data to achieve accurate localization and identification. In the fitting process, the acquisition of the network parameters is essentially the problem of optimizing the nonlinear function, which is simply the problem of finding the best set of parameters $W*$ and $b*$ that can satisfy the following equation.

$$W^*, b^* = \underset{\min}{J}(W, q). \tag{8}$$

The training loss function in this paper is as follows:

$$J_{\text{fix}} = L(\{p_i\}, \{t\}). \tag{9}$$

Linear interpolation for the x-direction is calculated as follows:

$$f\left(R_1 = \frac{x_1 - x_2}{x_1 + x_2}\right) = f(Q_{11}) + f(Q_{12}), \tag{10}$$

$$f\left(R_2 = \frac{x_1 + x_2}{x_1 - x_2}\right) = f(Q_{22}) + f(Q_{12}). \tag{11}$$

Then, linear interpolation for the y-direction is calculated as follows:

$$f(P) = f(x, y), \tag{12}$$

where $f(x, y)$ is the pixel value of the point P to be solved, $f(Q_{11})$, $f(Q_{12})$, $f(Q_{21})$, and $f(Q_{22})$ are the pixel values of the four known points $Q_{11} = (x_1, y_1)$, $Q_{12} = (x_1, y_2)$, $Q_{21} = (x_2, y_1)$, and $Q_{22} = (x_2, y_2)$, respectively, and $f(R_1)$ and $f(R_2)$ are the pixel values obtained by interpolation in the x-direction.

3.3. Dataset Creation. The richness and effectiveness of the dataset is an important part of the car identification research. In this paper, we use the BIT-Vehicle dataset, the Cars dataset, and some data from the CompCars dataset as the basis and expand the dataset by traditional transformation, Gaussian noise, web crawler crawling data, and generative adversarial network (GAN) approach to expand the dataset. In order to ensure the generalization ability of the final model of this experiment, the dataset is expanded in addition to the three car datasets mentioned above, as follows.

(1) Traditional transformation. (a) Random cropping, image flipping, mirror transformation, and image color random dithering are used to change the angle, proportion, brightness, and saturation of vehicles in the original images to achieve the purpose of dataset expansion, and finally, 1800 vehicle pictures are generated

(2) Web crawlers. Web engines (such as Baidu and Google) contain a large amount of vehicle information and images, but manual search and preservation of such images are more time-consuming. Data can be crawled on a specific web page according to user-defined matching rules, parsing and analyzing the acquired page data, parsing out the hyperlinks (URLs) in the page, and downloading the text information, pictures, videos, and other information in the links. In this paper, based on the pyspider crawler framework, we use python to realize the crawler function and finally obtain 1200 vehicle images and keep 600 images of high quality after screening. Since the quality of the

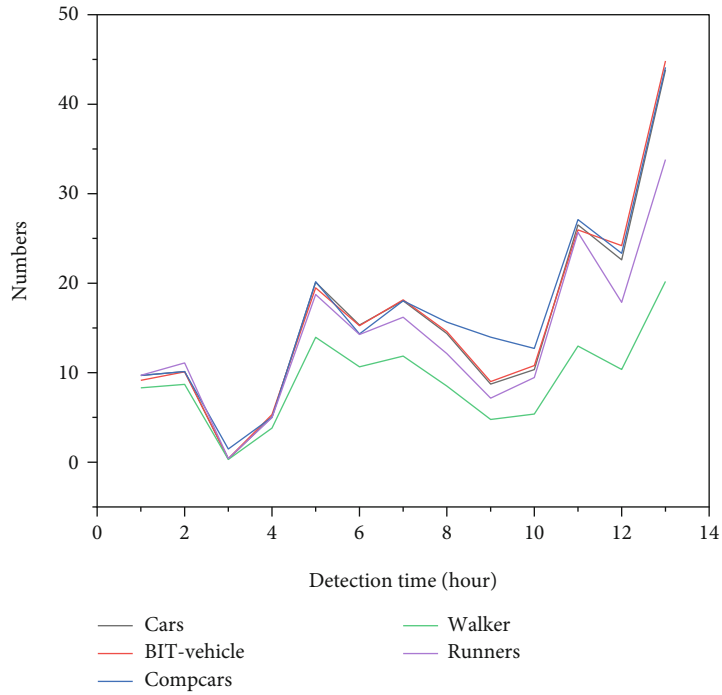

Figure 4: Classification of large categories of vehicle datasets.

images obtained using web crawlers varies, they are directly added to the dataset for use, without extending the data

(3) Generative adversarial network (GAN). In essence, the images generated by traditional transformations and the addition of Gaussian noise do not differ much from the vehicles in the original images, and the web crawler acquires the images slowly and requires manual screening, so this paper proposes to use GAN for data expansion. GAN is a method for training to generate two mutual adversarial models, where a generative model G is used to fit the sample data distribution, and a discriminative model D is used to estimate whether the input samples are from the real training data or the generative model G

(4) This paper uses convolutional neural network to construct generator G and discriminator D. Among them, discriminator D uses 4 convolutional layers with ReLU activation function and 1 fully connected layer to extract features from the input images; generator G uses 4 deconvolutional layers with ReLU activation function to generate false sample images with the same width and height as the input images by deconvolution of the noise generated using Gaussian distribution. Finally, 1500 vehicle images were generated. Based on the above dataset expansion method, this paper finally builds up a dataset including 8600 training set and 4300 test set samples, and the composition of the dataset is shown in Figure 4

4. Experiments and Analysis of Results

Network training requires setting the hyperparameters of the corresponding network, and hyperparameters are the preset values of network training, which are determined manually to achieve the parameters of the specific network training requirements; this experiment is trained from scratch for all networks, in deep learning, epoch represents the number of training steps, and the learning rate controls the learning progress of the model; the smaller the learning rate, the slower the loss gradient decreases and the convergence. The smaller the learning rate, the slower the loss gradient decreases and the longer the convergence time. After debugging, the final number of epochs is set to 50000, the learning rate is set to 0.005, the number of validations after each training step is set to 30, and the learning rate is kept constant at the beginning and decays to 0 in the last 5000 epochs. The weights are randomly initialized with Gaussian distribution, the mean value is 0, and the standard deviation is 0.02, and the specific hyperparameter values are shown in Figure 5. The network parameters can be determined by the objective function, and the network parameters in the fully connected layer are continuously updated as the objective function decreases.

At present, the evaluation indexes for the results in target recognition are precision rate, recall rate, average precision, average precision mean, etc. The average precision is the average of all accurate prediction rates of the car model under different recall rates, which is the best evaluation index of the performance of the target detection algorithm and reflects the comprehensive performance of the algorithm; meanwhile, this paper compares the pixel precision,

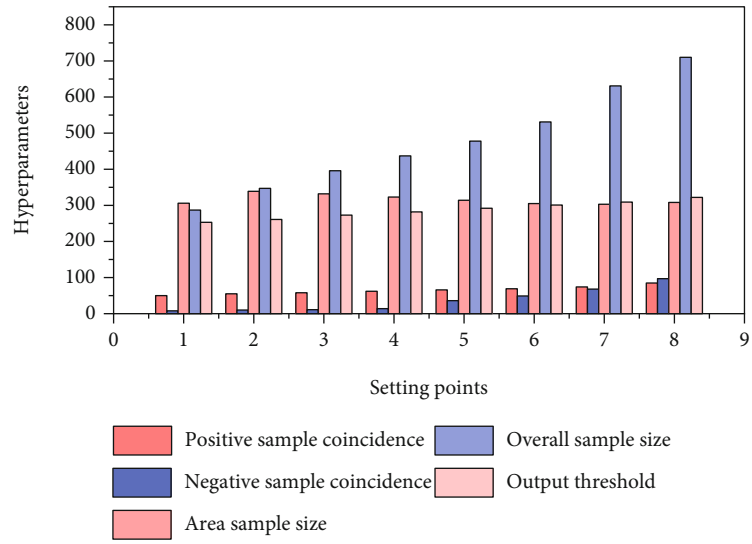

Figure 5: Hyperparameters of the large class vehicle recognition model.

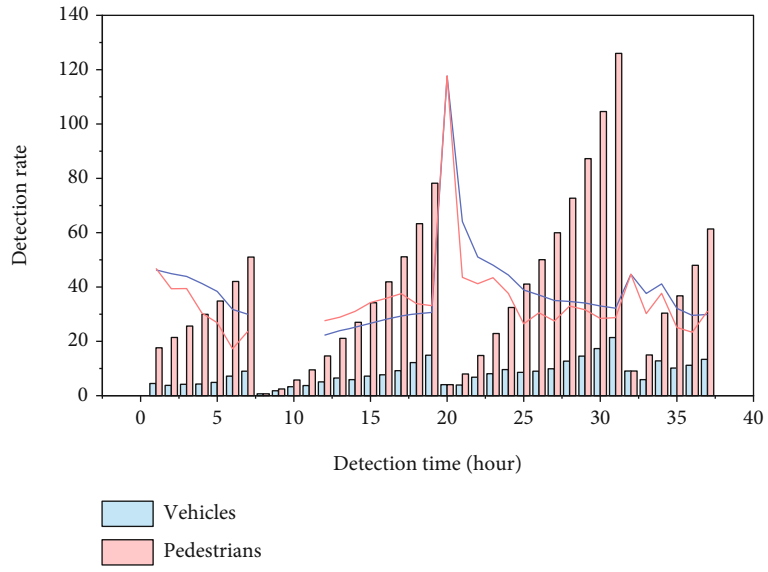

Figure 6: Detection rate of vehicles and pedestrians at smart intersections.

average interaction ratio, and detection recognition. This paper also compares the pixel accuracy, average interaction ratio, and detection recognition speed of this method with the mainstream target detection algorithms to verify the robustness and application value of this model.

In this experiment, the established 12900 datasets are divided into 8600 training sets and 4300 test sets. In common recognition systems, the workload of producing datasets is huge, requiring teamwork and time consumption. However, this system can reduce the time consumption compared with other labeling methods. Different samples can be generated randomly according to the corresponding labels during labeling and unified directly according to the labels during testing, which saves the time of unification processing after the labeling is finished. In order to test the generalization performance of the proposed model, the pictures of vehicles in different environment monitoring and different time and perspective are specially selected for recognition during the test. And the selected scenes also include the case of harsh environment, such as the bad situation of not strong light and too strong light, reflecting the difference between the model of the article and the target detection one-stage mainstream algorithm SSD, YOLO, and other method detection results. As shown in Figure 6, the experimental results show that the detection results of the model in this paper are better when the threshold is set to 0.8, and the improved algorithm has improved about 2.8% compared with the test results before the improvement in the dataset with a total of 50000 images on the KITTI public dataset. As can be seen from the figure, when there are no other occluding objects near the vehicle, the confidence of recognizing the vehicle is all above 92%, and when the

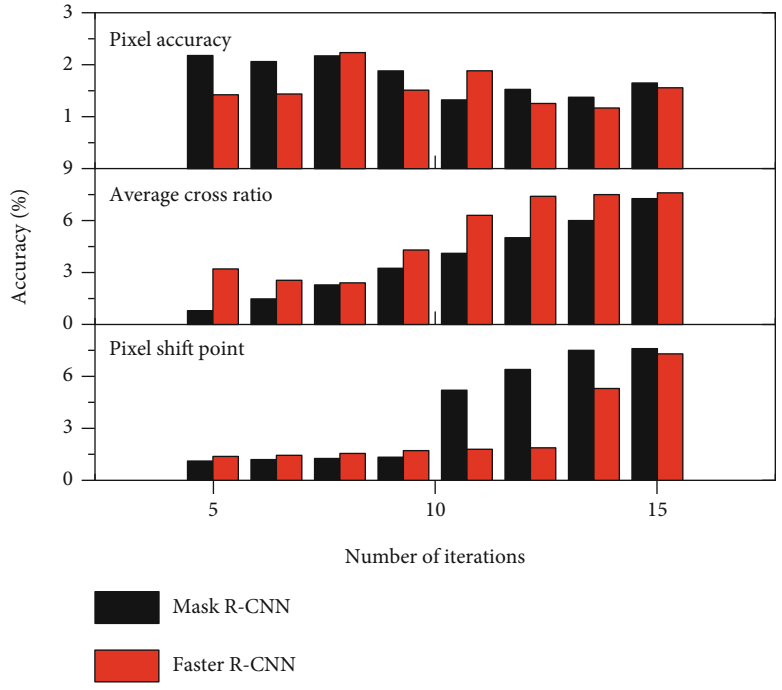

Figure 7: Scores for testing the dataset using different methods.

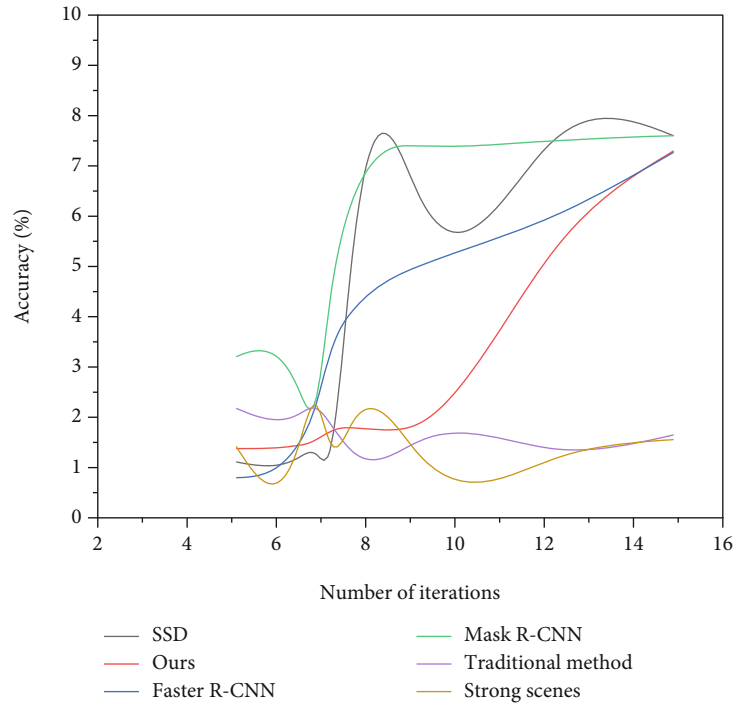

Figure 8: Trend of accuracy of different methods with the number of iterations.

vehicle is partially occluded or the vehicle has more than half of the area within the surveillance, the confidence is also above 82%, and the recognition accuracy can reach above 78%. In addition, the combination of labeled images and recognition results shows that the unlabeled vehicles and vehicles with small pixels in the training set can be recognized well, which again verifies the feasibility of the model.

In order to further verify the generalization ability of this experimental model and the recognition accuracy for different scenes, when testing the model, in addition to the above-mentioned images in the training set, this experiment also selected images in the same scene that were not in the training set and images in other scenes in different scenes for testing, and the test results are shown in Figure 7. It can be seen

that the vehicle recognition accuracy is high, and the recognition confidence for the images with low pixel in the back of the position can still reach 0.843 and the recognition result is accurate, which illustrates the strong generalization ability and high accuracy of the model. In the fully connected layer, the main role is to reduce the error between the labeled samples in the dataset and the output of the generated model in order to achieve the purpose of continuously fitting the generated network to the original image in this paper.

The experiments also selected the current open-source SSD, R-CNN, Faster RCNN, and the improved pre-Mask R-CNN algorithms for vehicle recognition detection. Figure 8 shows the scores of the test on the dataset using different methods, from which it is concluded that the recognition method used in this paper generates more reliable and more realistic results for the images and can get better results for all the scenarios described above. In addition, for the unlabeled vehicles in the training images, the method can still detect them well, which reflects the good robustness of the algorithm in this paper. Although the results of Faster R-CNN algorithm applied to this vehicle recognition also have better recognition results, but the method does not have better robustness, for most of the unlabeled vehicles are not detected, and similar to the traditional convolutional neural network-based CNN method, more postprocessing techniques are required, which increases the complexity of visualization operation, and the authenticity of the detection results is lower. When comparing with the Mask R-CNN algorithm before improvement, we found a more obvious improvement in pixel accuracy, while there is not only little difference in the average interaction ratio, but also a small improvement. Therefore, it can be seen from the above comparison tests that our algorithm has better superiority.

As can be seen from the figure, the accuracy of each method increases and stabilizes with the increase of iterations, among which the SSD method is the fastest to stabilize, and its accuracy stabilizes at about 76% after 10000 iterations, the accuracy of R-CNN is the lowest, and its accuracy stabilizes at about 74.5% after 12500 iterations; the Faster R-CNN method Mask R-CNN algorithm and the improved Mask R-CNN are more effective for car model recognition, and the recognition accuracy of Faster R-CNN method can reach about 84% for seven categories of car models; since Mask R-CNN algorithm requires higher quality of dataset and is more sensitive to pixel extraction, the accuracy of this algorithm is low when the number of iterations is small. However, after the number of iterations reaches 22500, the recognition accuracy of the algorithm for the seven categories of car models is about 86.2%, and the improved algorithm is stable at about 89% after the number of iterations reaches 25000, which is a considerable improvement compared with that before the improvement, further indicating the practical value of this algorithm.

5. Conclusion

This paper mainly focuses on deep learning and convolutional neural network algorithms to optimize the network structure to train the detection and recognition models of large class vehicles and fine vehicles, respectively. Based on the algorithm development of R-CNN and Faster R-CNN and the design of convolutional layer, the superiority of convolutional neural network in target detection and recognition is illustrated, and the advantages and disadvantages of different methods and network frameworks in target detection are analyzed, and the improved Mask R-CNN method is proposed to recognize large classes of vehicles, and the components and functions of the improved algorithm are introduced in detail. In the application of fine vehicles, we propose to use the improved YOLOv3 for detection and optimize Mask R-CNN algorithm for further recognition with good results. To further verify the practicality of the two methods proposed in this paper for engineering applications, a car model recognition system was built based on the existing equipment in the laboratory, and the algorithm was implanted in the server to achieve faster detection and recognition speed. The development of neural networks and the principle of deep learning are explained, and the algorithms related to artificial neural networks, convolutional neural networks, and target detection are introduced, and the advantages and shortcomings of each method are discussed. The speed and accuracy of convolutional neural networks in target candidate region generation, border regression, and feature extraction are discussed in detail, the improvements of new algorithms for target detection in recent years are analyzed, and the network framework of deep learning is introduced. Due to the limitations of traditional region generation methods, this paper provides a brief analysis of the region generation network in the Faster R-CNN algorithm and details the loss calculation principle of the output layer. For fine model recognition, this paper continues to expand on the basis of the CompCars dataset, establishes a vehicle dataset containing 18 common car brands such as Volkswagen, Buick, Audi, and BMW with a total of 76 common models, whose samples include vehicle badges, lights, air intake grilles, and overall contours, which can be trained with different detection models according to different needs, and finally uses labeling. Finally, we use labeling software to label all samples and build a more comprehensive model recognition dataset. In the future, the feature descriptors in the regions are extracted, and finally, the feature descriptors are input to the classifier to realize the classification and recognition of car models.

Data Availability

The data used to support the findings of this study are available from the corresponding author upon request.

Conflicts of Interest

The authors declare that they have no known competing financial interests or personal relationships that could have appeared to influence the work reported in this paper.

Acknowledgments

This work was partially supported by the Natural Science Fund of China (Grant No. 61401356), the Technological Innovation Guidance Project of Shaanxi Province (Grant 2020CGXNG-015), the Science and Technology Project of Xi'an (Grant 2020kjrc0104), the Youth Innovation Team Building Scientific Research Project of Shaanxi Province (Grant 21JP106), and the Intelligent Perception and Control Research Team of Xi'an University (Grant XAWLKYTD019).

References

[1] R. Arnay, J. Hernández-Aceituno, J. Toledo, and L. Acosta, "Laser and optical flow fusion for a non-intrusive obstacle detection system on an intelligent wheelchair," *IEEE Sensors Journal*, vol. 18, no. 9, pp. 3799–3805, 2018.

[2] L. C. Bento, R. Parafita, H. A. Rakha, and U. J. Nunes, "A study of the environmental impacts of intelligent automated vehicle control at intersections via V2V and V2I communications," *Journal of Intelligent Transportation Systems*, vol. 23, no. 1, pp. 41–59, 2019.

[3] W. Cao, J. Zhang, C. Cai et al., "CNN-based intelligent safety surveillance in green IoT applications," *China Communications*, vol. 18, no. 1, pp. 108–119, 2021.

[4] L. W. Chen and Y. F. Ho, "Centimeter-grade metropolitan positioning for lane-level intelligent transportation systems based on the Internet of vehicles," *IEEE Transactions on Industrial Informatics*, vol. 15, no. 3, pp. 1474–1485, 2018.

[5] A. Daeichian and A. Haghani, "Fuzzy Q-learning-based multiagent system for intelligent traffic control by a game theory approach," *Arabian Journal for Science and Engineering*, vol. 43, no. 6, pp. 3241–3247, 2018.

[6] T. Enokido, D. Taniar, and O. K. Hussain, "Special Issue: Intelligent edge, fog and Internet of Things (IoT)-based services," *Future Generation Computer Systems*, vol. 109, pp. 710-711, 2020.

[7] C. E. Framing, F. J. Heßeler, and D. Abel, "Learning scenario-specific vehicle motion models for intelligent infrastructure applications," *IFAC-PapersOnLine*, vol. 52, no. 8, pp. 111–117, 2019.

[8] L. Hu, J. Ou, J. Huang, Y. Chen, and D. Cao, "A review of research on traffic conflicts based on intelligent vehicles," *IEEE Access*, vol. 8, pp. 24471–24483, 2020.

[9] S. K. Kumaran, S. Mohapatra, D. P. Dogra, P. P. Roy, and B. G. Kim, "Computer vision-guided intelligent traffic signaling for isolated intersections," *Expert Systems with Applications*, vol. 134, pp. 267–278, 2019.

[10] K. Liu, "Bi-level optimisation model for greener transportation with intelligent transport system," *International Journal of Reasoning-based Intelligent Systems*, vol. 10, no. 1, pp. 26–31, 2018.

[11] S. Mohamad, F. M. Nasir, M. S. Sunar et al., "Intelligent agent simulator in massive crowd," *Indonesian Journal of Electrical Engineering and Computer Science*, vol. 11, no. 2, pp. 577–584, 2018.

[12] E. Namazi, J. Li, and C. Lu, "Intelligent intersection management systems considering autonomous vehicles: a systematic literature review," *IEEE Access*, vol. 7, pp. 91946–91965, 2019.

[13] H. Namazi and A. Taghavipour, "Traffic flow and emissions improvement via vehicle-to-vehicle and vehicle-to-infrastructure communication for an intelligent intersection," *Asian Journal of Control*, vol. 23, no. 5, pp. 2328–2342, 2021.

[14] I. O. Olayode, L. K. Tartibu, M. O. Okwu, and U. F. Uchechi, "Intelligent transportation systems, un-signalized road intersections and traffic congestion in Johannesburg: a systematic review," *Procedia CIRP*, vol. 91, pp. 844–850, 2020.

[15] Y. Sang, J. Tan, and W. Liu, "Research on many-objective flexible job shop intelligent scheduling problem based on improved NSGA-III," *IEEE Access*, vol. 8, pp. 157676–157690, 2020.

[16] M. Song, R. Li, and B. Wu, "Intelligent control method for traffic flow at urban intersection based on vehicle networking," *International Journal of Information Systems and Change Management*, vol. 12, no. 1, pp. 35–52, 2020.

[17] Q. Wu, F. He, and X. Fan, "The intelligent control system of traffic light based on fog computing," *Chinese Journal of Electronics*, vol. 27, no. 6, pp. 1265–1270, 2018.

[18] H. Xiao, M. A. Sotelo, Y. Ma et al., "An improved LSTM model for behavior recognition of intelligent vehicles," *IEEE Access*, vol. 8, pp. 101514–101527, 2020.

[19] Q. Xin, R. Fu, W. Yuan, Q. Liu, and S. Yu, "Predictive intelligent driver model for eco-driving using upcoming traffic signal information," *Physica A: Statistical Mechanics and its Applications*, vol. 508, pp. 806–823, 2018.

[20] H. Yang and K. Oguchi, "Intelligent vehicle control at signal-free intersection under mixed connected environment," *IET Intelligent Transport Systems*, vol. 14, no. 2, pp. 82–90, 2020.

[21] N. Yao and F. Zhang, "Contention-resolving model predictive control for an intelligent intersection traffic model," *Discrete Event Dynamic Systems*, vol. 31, no. 3, pp. 407–437, 2021.

[22] R. Zhang, A. Ishikawa, W. Wang, B. Striner, and O. K. Tonguz, "Using reinforcement learning with partial vehicle detection for intelligent traffic signal control," *IEEE Transactions on Intelligent Transportation Systems*, vol. 22, no. 1, pp. 404–415, 2021.

Hindawi
Journal of Sensors
Volume 2022, Article ID 7244856, 10 pages
https://doi.org/10.1155/2022/7244856

Research Article

Real-Time Collection and Analysis of Sports Index Time Series Based on Multimodal Sensor Monitoring

Yang Li, Ying Huang, and Qianqi Zhao

Department of Sports Art, Hebei Institute of Physical Education, Shijiazhuang 050041, China

Correspondence should be addressed to Yang Li; 1993009@hepec.edu.cn

Received 29 November 2021; Accepted 23 December 2021; Published 7 March 2022

Academic Editor: Gengxin Sun

With the further development of microelectronics technology and sensors, sensors can be widely embedded in mobile phone devices and portable devices. The use of acceleration sensors for human motion monitoring has broad application prospects. Monitoring the daily exercise of the human body is of great significance for formulating scientific exercise and fitness plans and improving physical health. This paper uses the measurement data of multiple types of sensors to propose an index recognition method based on the fusion of multiple types of sensor information. We take the measurement value of a single type of sensor as input and output the index value of the moving part without a strain sensor. The pattern recognition method is used to establish a pattern library, a recognition library, and a measurement library. This article considers noise interference or malfunction of sensor measurements. Aiming at uncertain factors such as the error of the finite element model, a pattern matching method considering the uncertainty is proposed. This article takes aerobics as an example to simulate and analyze the dynamic response of aerobics under wind load. In addition, by simulating the recognition results under different levels of noise interference, the robustness and anti-interference of the pattern matching method are verified.

1. Introduction

With the rapid development of wireless sensor technology and wireless communication technology, the main problem of data transmission is to choose which wireless communication technology to transmit data [1]. Information fusion refers to the process of decision-making and estimation task information processing through automatic analysis and comprehensive realization of multiple sensor observation information obtained according to time sequence in the relevant criteria by computer technology, because information fusion process has multiple sensors to obtain information connection and processing. An information fusion system is a processing system that obtains information as objects through sensors. In addition to sensors, the information fusion system also includes other links, each of which has special functions and characteristics [2]. The development cycle realizes the design of an information fusion analysis system through object-oriented thought and realizes the standardization in the process of system design. Due to the particularity of terminal nodes, how to ensure less data and energy consumption in the process of data transmission is a difficult problem in the current wireless transmission process. The current wireless communication technologies include Bluetooth, UWB, WiFi, and Zigbee. In the specific environment to choose a reasonable way, or even a combination of transmission mode, another problem is how to design high-performance transport protocols.

The so-called multisensor information fusion (MSIF) is an information processing process that uses computer technology to automatically analyze and synthesize the information and data from multiple sensors or sources under certain criteria to complete the required decisions and estimates [3]. The basic principle of multisensor information fusion technology is to make the multilevel and multispace information complementary and optimal combination processing of various sensors and finally produce consistent interpretation of the observation environment. This process should make full use of multisource data for reasonable control and utilization. The ultimate goal of information fusion is to separate observation information obtained from each sensor and extract more useful information through multilevel and

multidirectional information combination. It not only takes advantage of the cooperative operation of multiple sensors but also comprehensively processes the data of other information sources to improve the intelligence of the whole sensor system. Fusion methods include neural network, decision theory, information theory, statistical reasoning, and evidence theory. It can analyze data according to certain criteria and obtain reliable and accurate prediction results, which is the multisource information fusion technology. The core of big data technology is the remote large server cluster. In order to solve the problem of large amount of data, it is necessary to apply a data fusion algorithm to a cloud server. In this way, the stability and efficiency of the system can be improved, and problems such as poor scalability, high cost, poor data sharing, and difficult system maintenance can be solved in the monitoring platform [4, 5]. Cloud server processing technology plays a very important role in the current monitoring platform, which can classify, store, manage and share the explosive growth of data and provide a platform for subsequent data fusion.

2. Related Work

Sports is one of the important means to ensure people's health, among which, aerobics is popular among people in recent years [6]. The perception of the teaching effect of aerobics is the key factor to learn aerobics, but the current aerobics exercise method is not professional, and the teaching effect cannot be effectively evaluated in the process of fitness. Deng and Jiang identified the motion features of calisthenics decomposition by the feature extraction method, solved the optical flow between adjacent difference frames and by the Laplace method, reduced the impact of clutter, set the similarity threshold, extracted the motion features of calisthenics decomposition by similarity detection, and output the actions with high similarity as the results [7]. Wichit and Choksuriwong realized the design of a multisensor-based athlete training information fusion analysis system. Based on the acquisition and analysis of movement information, it analyzed the ground reaction information, motion image analysis, human surface mechanics, and so on in the process of athletes' movement, so as to further study the extraction of athletes' information features [8]. Bharti et al. proposed an image-based method to monitor the movement accuracy of calisthenics. The kindest depth image acquisition method was used for preanalysis of calisthenics movements, and HOG3D was used to extract the movement characteristics of calisthenics [9]. Mohsin et al. use GPRS network transmission and embedded system to collect sports information in real time and generate monitoring process diagram of sports training parameters, providing scientific basis for targeted training [10]. Physical education teaching evaluation is an important part of physical education teaching, which plays an important role in the process of physical education teaching. It provides information that controls and adjusts physical activity as a whole and ensures that it develops towards its intended goals. With the development of the popularization of physical education, people's demand for the quality of physical education is constantly improving, and the role and status of evaluation in teaching are becoming increasingly obvious, and evaluation has become an indispensable process in teaching activities.

With the progress of science and technology, human-computer interaction is more and more widely used in our daily life [11]. It has become a current development trend to study human-computer interaction system that meets current needs and to introduce human body as a reference coordinate system to directly map some actions and patterns of human body to a computer with a coordinate system. Traditional human-computer interaction technology research focusses on computer as the centre; now, human-computer interaction technology research focusses on human-computer interaction technology, all-round development, multimode, and deep coexistence, to achieve the interaction system between the user and the system. Line of sight is one of the most intuitive ways for human to receive information from the outside world. Body movements based on human eyes are characterized by directness, authenticity, and simplicity. However, visual judgment of some subtle actions shows great limitations. A human-computer interaction system based on microaction information acquisition module can effectively make up for the deficiency of visual judgment.

With the rapid development of electronic industry, especially computer, the development of the human-computer interaction system is not only reflected in the hardware but also has great progress in software. At present, research based on the human-computer interaction system not only tends to be practical and aesthetic but also the ease of operation and the degree of fitting with people will become a very important development direction [12, 13]. Human-computer interaction (HCI) refers to a technology in which the information to be tested is exchanged with a certain algorithm by certain input and output devices between human and computer and finally realizes the mutual communication between human and machine. The system consists of a computer providing some useful information to people through a display device or an output device, while people providing some instruction information to the server through some input devices. In human-computer interaction technology, interface design is very important, to realize the media and carrier of interaction between people and computers; users can receive information through the most intuitive way.

Data fusion is from multiple channels, multiple sources, and various data or information accurately, to determine the organic relation, comprehensive analysis, the overall evaluation, and the organic fusion of multiple parameters, multilevel, many elements of the process, and then get fused state, as well as the processing object, a comprehensive evaluation in the end gets information or data. Data fusion is regarded as the organic combination of data or information of different information sources, forms, media, time, and presentation, so as to accurately understand the object state [14]. The advantage of multisensor data and information fusion is that the characteristics of the object to be measured can be obtained in a very short time by a relatively simple method. The multisensor fusion information has strong

reliability, timeliness, and robustness. In the process of data fusion, it involves the processing of many uncertain factors, the decision-making mechanism and process, and the analysis of the characteristics of the information source, and it will be different with the environment of the demander.

Multisensor data fusion technology has three important characteristics: multisensor data fusion is based on the different abstraction degree of information source, multilevel processing of information; the process of multisensor data fusion includes detection, correlation, tracking, analysis, evaluation, and merger [15]. The output of multisensor data fusion can be divided into initial assessment of identity and status at low level and advanced assessment of situation and decision at high level. The target object of the multisensor data fusion system is the different information collected by various types of sensors, which has various forms of expression, such as sound, text, image, or electrical signal. The information collected by the multisensor system is called source information [16]. The purpose of multisensor data fusion is to obtain the optimal estimation of target state and properties by analyzing and processing various original information from different sensors through specific models and algorithms. Multisensor data fusion technology arises at the historic moment; it is to use computer technology to the time sequence of number of sensor observation information, and information database and knowledge base, to a certain criterion, which automatically collected, relevant, analysis and synthesis for a representation, to complete the required for estimation and decision task of information processing. Information fusion has always played an important role in the evolution of any life.

According to the data fusion structure, there are many kinds of classification. One of these methods is divided into sensor-level (distributed), central-level (centralized), and hybrid mode according to the way data is processed before finally entering data fusion. Sensor-level fusion architecture works: different sensors are used to collect information for the same target, and they are independent signals. First, each individual sensor captures and analyzes information; then, the analysis results of all sensors are transmitted to the fusion centre. Finally, the fusion results are used for state estimation. Because the structural model deals with feature vector data in the fusion centre, it does not require much computer and reduces the computing pressure. At the same time, sensor-level fusion has good stability and low system cost, so it is widely used in most projects. Central-level data fusion means that each terminal sensor transmits the preprocessing results to the fusion centre after minimal processing [17, 18]. In the fusion centre, the information obtained by each sensor is checked, correlated, fused, and decided. In most cases, this structure is the best data fusion method in the case of smooth data association and fusion in the fusion centre. The structure also requires powerful CPU processing power and high storage capacity at the convergence centre. If the sink fails, the whole system collapses. Therefore, although the structure is very good, there are some disadvantages such as poor stability. Hybrid fusion is a combination of the first two. It is the algorithm processing of adding and subtracting sensors before data reaches the convergence point and fusion [19]. In general, if the measurement of each terminal node cannot be completely independent of each other, the hybrid fusion method is the best way to classify the data. The advantage of this structure is that the sensor fusion is added in the fusion process and it has strong adaptability. However, due to the increased sensor fusion, the hybrid structure increases the complexity of data processing, reduces the transmission efficiency, and increases the cost of data processing and wireless communication.

3. Support Vector Machine Algorithm

Support vector machine (SVM) algorithm was first developed from the generalized portrait method in pattern recognition algorithm. It is a kind of generalized linear classifier that performs a binary classification of data according to supervised learning, and its decision boundary is the maximum margin hyperplane of sample data to perform a solution. If a sample data can be correctly divided into two categories, then there must be an optimal hyperplane in between which can be expressed by

$$g(x) = W^t \times x + b, \tag{1}$$

where W represents a vector of weights and b is a constant term. In general, training for sample data is to get an optimal hyperplane and classify it correctly. A standard SVM model satisfies formula (2) in order to classify samples correctly.

$$\begin{cases} W^t \times x + b \geq 0, y = 1, \\ W^t \times x + b < 0, y = -1. \end{cases} \tag{2}$$

The farther away it is, the more obvious the classification of "normal" and "abnormal" states is, and the classification results can be easily distinguished. In order to achieve the maximum classification effect, the distance between $H1$ and $H2$ is defined as

$$M = \frac{2}{\sqrt{w^2}}. \tag{3}$$

The magnitude of M is determined by the points closest to H, which are called support vectors. Let $H1$ and $H2$ from the farthest be equivalent to the value of M which is the largest, also to make the $|W|$ minimal. So, finding the optimal hyperplane is equivalent to solving the optimization constraint problem. For the above case, it is transformed into a quadratic normalization problem.

$$\min \phi(w) = \frac{1}{2} w^t w. \tag{4}$$

The constraint conditions are expressed by

$$y\left(W^t W + b\right) \geq 1. \tag{5}$$

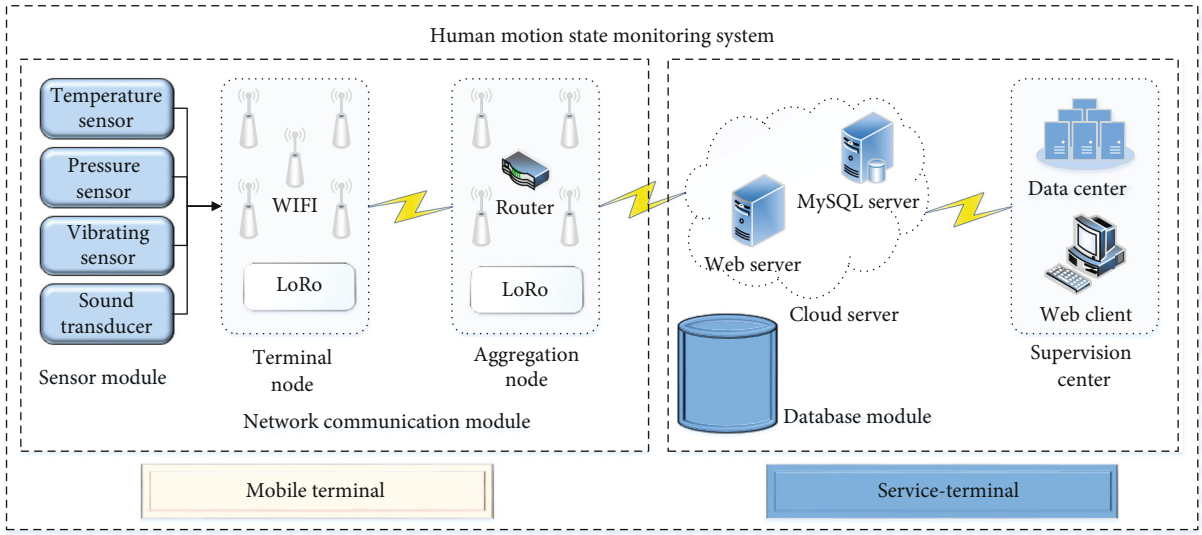

Figure 1: Monitoring system hardware design block diagram.

It is usually solved using Lagrange multipliers, so formula (4) becomes

$$L(w, b, a) = \frac{1}{2} W^t W - \sum \left[\partial y \left(W^t x + b \right) - 1 \right]. \quad (6)$$

The optimal solution is the inflection point of equation (6).

$$\begin{aligned} \frac{\partial L}{\partial W} &= w - \sum \alpha y x = 0, \\ \frac{\partial L}{\partial W} &= -\sum \alpha y x = 0. \end{aligned} \quad (7)$$

Meanwhile, the solution of the quadratic optimization problem must satisfy

$$\beta \{ y [(w \times x) + b] \} = 0. \quad (8)$$

The training sample points with medium values are called support vectors, which are usually only a small part of the total sample. For SVM, support vector is the key factor in training process. Finally, the optimization function of the classification problem is obtained as

$$f(x) = \operatorname{sgn} \left\{ \sum y \alpha + b \right\}. \quad (9)$$

4. Teaching Effect Monitoring System Based on Multisensor Information Fusion

4.1. Overall System Design Architecture. The monitoring system is designed according to several principles, including data acquisition part, data transmission, and monitoring centre part. The data acquisition part is mainly composed of terminal nodes based on a STM32 microprocessor, including LoRa wireless communication module and various sensor modules. The data transmission part is composed of a stM32-based microprocessor, which includes LoRa wireless communication module and WiFi module. The monitoring centre is mainly constructed based on the server, and the corresponding monitoring function can be realized by deploying the Web server. The monitoring system architecture mainly consists of two parts: hardware and software. The hardware unit mainly includes terminal node and sink node. Terminal nodes and sink nodes communicate through LoRa to realize wireless data transmission. After the sink node receives the data, the MQTT communication protocol is used to send the data of the sink node to the cloud server for monitoring through Web pages. The hardware design block diagram of the monitoring system is shown in Figure 1.

The system software includes the design of terminal node data acquisition terminal, aggregation node, and cloud server. In the monitoring system, the sensor terminal node is located at the bottom of the whole system, responsible for the collection of various parameters. It determines the efficiency of subsequent data collection. Cloud server processing technology plays a very important role in the current monitoring platform, which can classify, store, manage, and share the explosive growth of data and provide a platform for subsequent data fusion. The sink node is mainly composed of a processor, wireless communication module, and storage module to realize wireless data interaction with sensor node and cloud.

4.2. Aerobic Aerobics Monitoring System Based on Multisensor Information Fusion. In the process of fitness, dynamic information can be obtained through sensors, which has an important influence on fitness analysis. Dynamic parameters generally include human body displacement, plantar pressure, joint force, angle, and acceleration, which can be obtained by force sensor, displacement sensor, speed sensor, accelerometer, inertial sensor, and goniometry. The six-dimensional force testing platform can be divided into three modules: force sensor, signal processing module, and computer module. The measuring area is large, and the data of force cabinet and three-dimensional space can be obtained at the same time.

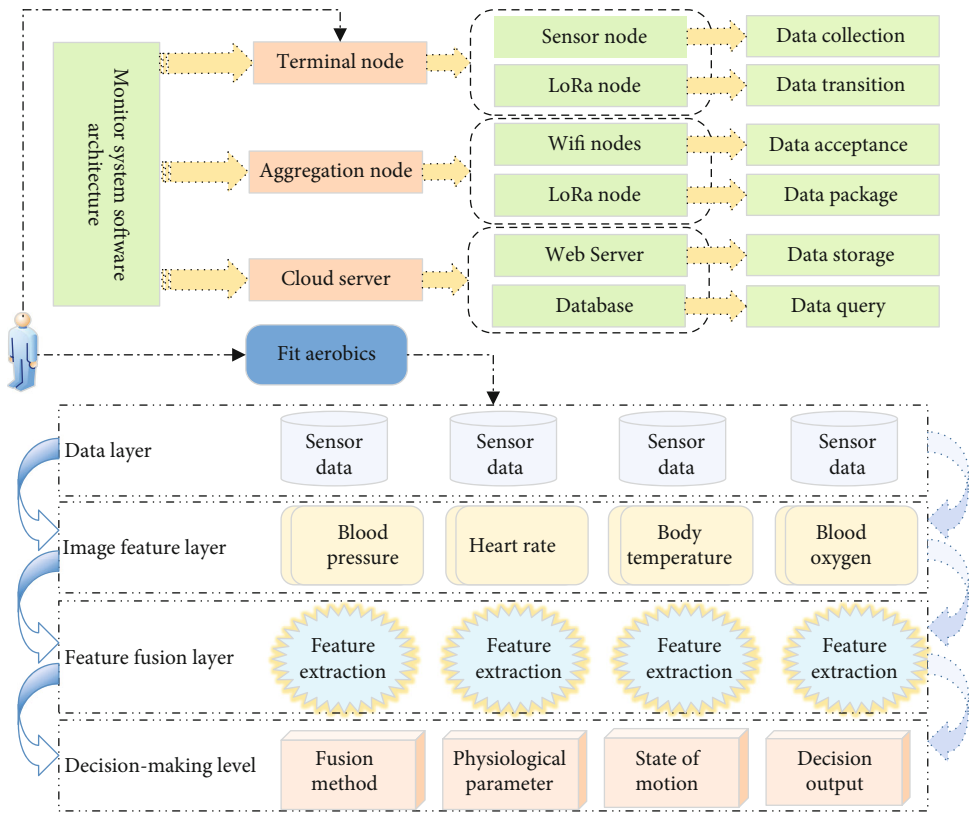

Figure 2: Architecture diagram of aerobics monitoring system.

The aerobics' monitoring platform is mainly based on a wireless sensor network, which collects and transmits the physical signs data of guardians by wearing different kinds of sensors on people [20]. The data collected by different sensors are signed and sent to the cloud through the wireless sensor network server. After receiving the corresponding algorithm for data processing, the processed data is sent back to the server for storage. Data and statement results were simultaneously sent to the mobile device of the monitored object and the hospital database of community service, so as to monitor the aerobics teaching. The overall framework of the system is shown in Figure 2.

As can be seen from the figure, the system consists of four layers: data layer, feature layer, feature fusion layer, and decision layer. The results of teaching and training are obtained by fusion analysis based on the information acquisition and processing of human movement. The multiobjective and multiparameter data in the training process of athletes can be obtained for effective fusion analysis. The system can transfer the physiological information parameters of the measured target to the server for corresponding processing and analysis, which makes the remote diagnosis more convenient, accurate, and low cost.

4.3. Terminal Node Design. In WSN, the terminal node is a full-function device, which perfectly combines the sensing technology, embedded technology, and wireless communication technology to realize the collection of human physiological parameters. Temperature, heart rate, blood pressure, respiration, and blood oxygen were collected [21]. An end node is a device that specifically performs data collection transmission and cannot transmit messages from other nodes. The terminal node adopts a modular design idea, and its main function is divided into two parts: various types of sensors for data collection; the LoRa module is responsible for sending and receiving data. Other parts also include the design of serial communication and power supply modules. The hardware structure of terminal node mainly includes a multisource sensor, STM32 processor, LoRa wireless communication module, and power module. The power module of the system uses USB power supply to provide normal working voltage for terminal node components. The terminal node as the data acquisition end, its power supply design adopts battery power. In addition to the master control chip, the peripheral circuit of the terminal node only retains the basic LoRa wireless data transceiver module, JTAG debugging module, and power reset and other basic circuits.

In the aerobic aerobics monitoring system, the terminal node of the physical sign sensor is located at the bottom of the whole system, which is responsible for collecting various parameters of the human body. It determines the efficiency of subsequent data collection. The wearable terminal nodes in the monitoring platform include motion sensors and biosensors. Motion sensors include accelerometers and gyroscopes; biosensors include blood pressure, heart rate, blood oxygen, and body temperature. The terminal node is one of the core parts of the whole system, which is now developing towards miniaturization and low power consumption.

4.4. Sink Node Design. The sink node is mainly composed of a processor, wireless communication module, and storage module. STM32F103ZET6 chip is used as the processor. The chip is a 32-bit processor product based on armCortex-M3 architecture kernel, and the maximum operating frequency can reach 72 MHz, with rich resources and low power consumption and cost. The wireless communication module consists of a LoRa module and a WiFi module. Both modules connect to the processor through a serial port for wireless data interaction with the sensor node and the cloud. The FLASH module and EEPROM module are used to store data such as WiFi hotspot name and password to prevent loss after power failure. The function of sink node mainly includes the following two aspects: LoRa module receives data of terminal node; the WiFi module packages and sends data from the terminal node to the server. The sink node is mainly used to forward the data of the terminal node. Besides the master control chip, it also contains LoRa wireless data transceiver module, WiFi module, JTAG debugging module, and power reset and other basic circuits.

As the core of the entire network, the sink node is mainly responsible for network construction, maintenance, information aggregation, and data uploading. The program design of sink node includes LoRa wireless communication program and WiFi transmission program. LoRa module mainly receives data transmitted from terminal nodes, while WiFi module sends data to the cloud server. Sink node software and networking program.

4.5. Server Design. Based on the functional requirements of a server layer, establish a data server. The data server is used to receive sensor data information to ensure that all sensor data can be stored in the cloud server in real time and accurately, providing data support for subsequent fitness effect analysis and human-computer interaction [22]. The aggregation node communicates with the cloud server using the MQTT protocol and using the JavaScript Object Notation (JSON) data format, which is a lightweight data exchange format that is easy to parse and generate by machines and can effectively improve network transmission efficiency. The TCP/IP protocol is designed for poor hardware performance and poor network conditions of the remote device; it is designed as a publish/subscribe messaging protocol. An MQTT protocol typically has two roles, publisher and subscriber. The cloud server is mainly responsible for data processing, analysis, storage, and visual display uploaded by the sink node. Based on the object-oriented language Java development, the server program uses Java Web development framework JFinal as the project framework; it uses Maven for project development and management, using MySQL as a database. The web client of the monitoring centre is designed in the form of a webpage, which is convenient for multiscreen display and remote viewing. The DataV of Aliyun is used for the front-end interface design.

The server program provides the data interface, and the monitoring centre provides real-time data display and historical data display. The server is mainly composed of a data server, human-computer interaction server, and corresponding database. A database server is built on the basis of a database system and has the characteristics of a database system. Its functions include system configuration and management and data access and update management. Similarly, a human-computer interaction server is built on the basis of a human-computer interaction system, responsible for receiving data from the data server after processing released to the client display through visual processing.

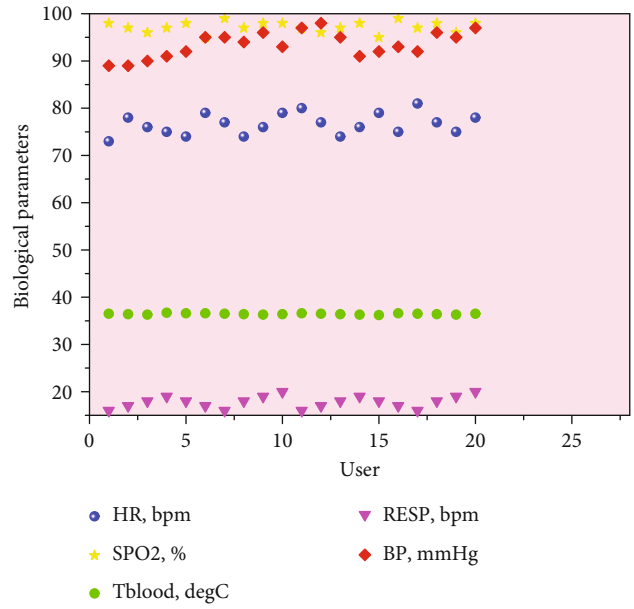

Figure 3: Infographic of physiological parameters.

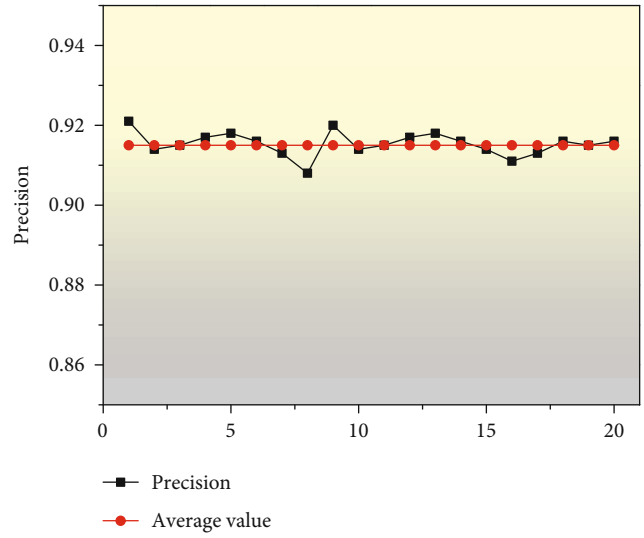

Figure 4: Collect the statistical chart of accuracy of some physiological parameters of users.

5. Monitoring System Testing and Effect Analysis

After completing the design of the overall hardware and software of the monitoring system, the function and stability of the monitoring system are tested on this basis. It is very important to test the functionality and stability of the whole

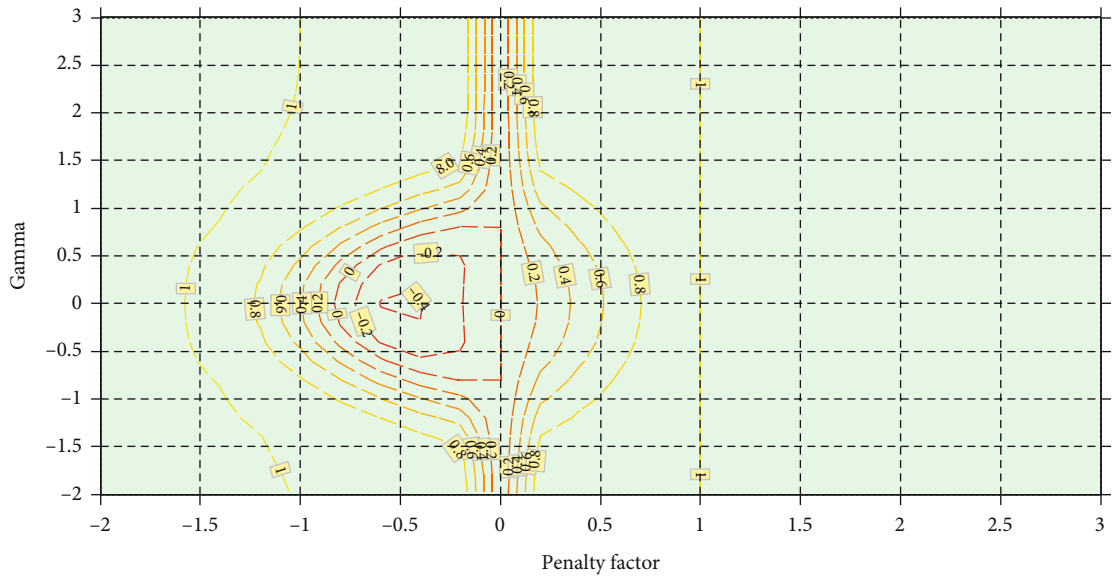

Figure 5: The relationship between the parameter gamma and the penalty factor.

system in the development process. Through the test of the system, we can find and deal with some problems that may exist in the whole system, so as to ensure that the whole system can run stably and smoothly when users use it.

5.1. Server Testing. The server test mainly tests whether the server can receive and display the uploaded hardware data. For normal operation of the overall system, testing system, adopted two terminal nodes, a gathering node, each kind of sensor mounted on sign parameter collection, will gather the node to receive data transmission via a serial port to display data from serial port assistant, by the MQTT protocol to TIO server parsed. The parsed data will be added to the message queue MQ, and then, the corresponding API of the platform stores the data in MQ into the database. Finally, APP obtains the historical data in the API through RPC for visual display. The scene of this experiment is to collect human body parameters in the room under normal conditions. You can obtain the current data information by entering the corresponding address in the browser of the PC. Basic physiological parameters of users in the current monitoring system, including temperature (degC), blood pressure (mmHg), blood oxygen (%), respiration (bpm), and heart rate (bpm), are shown in Figure 3.

As can be seen from the figure, the sensor data mounted on the terminal node is collected, and these are uploaded to the server for storage and display. After a period of operation test, the system can run stably and continuously through the test of the overall operation of the system, indicating that the system is normal. Sensors provide accurate data for the monitoring system. The sensor measurement can correctly determine the effect of aerobics teaching. The system can be collected, transmitted, stored, and displayed and can achieve the purpose of human monitoring.

5.2. Data Fusion Algorithm Testing and Result Analysis. The data fusion algorithm used to mimic the public data sets was tested, in order to state the general algorithm and the single exception of experiments, the same to 20 times the simulation model and data, using the data acquisition of the system for the user's physiological parameter acquisition and validated using data fusion algorithm, and the results are necessary analysis. Part of physiological parameters of multiple users collected by the system in a conventional environment is shown in Figure 4.

The test results show that the accuracy of the model based on real user data is basically consistent with the calculated results, and the algorithm proposed in this paper is feasible in practical application. The accuracy of the data fusion model is above 90%, and the difference is not large. Basically, it fluctuates within a very small range of average accuracy, which indicates the high stability of the algorithm in this paper. Ensure that the system can run continuously and stably, the measured physiological data is accurate and reliable, and the physiological parameters of human body are obtained. In addition, the relationship between the parameter gamma and the penalty factor is shown in Figure 5.

5.3. Trimming Fuzzy Neural Network. In order to verify that the monitoring system has a direct influence on the physical quality of aerobic aerobics students, the physical quality of students who have not carried out aerobic aerobics teaching was counted as after 30 days of aerobic aerobics teaching, the physical quality statistics were carried out. The statistical data analysis results of aerobic aerobics teaching before and after are shown in Figure 6.

As can be seen from the figure, in the aerobics movement, there are jumping movement, V-step, cross step, parallel step, jumping jacks low-impact movements, students' physical quality has also been improved to a certain extent, and aerobics project in enhancing people's strength, flexibility, and coordination plays a significant role.

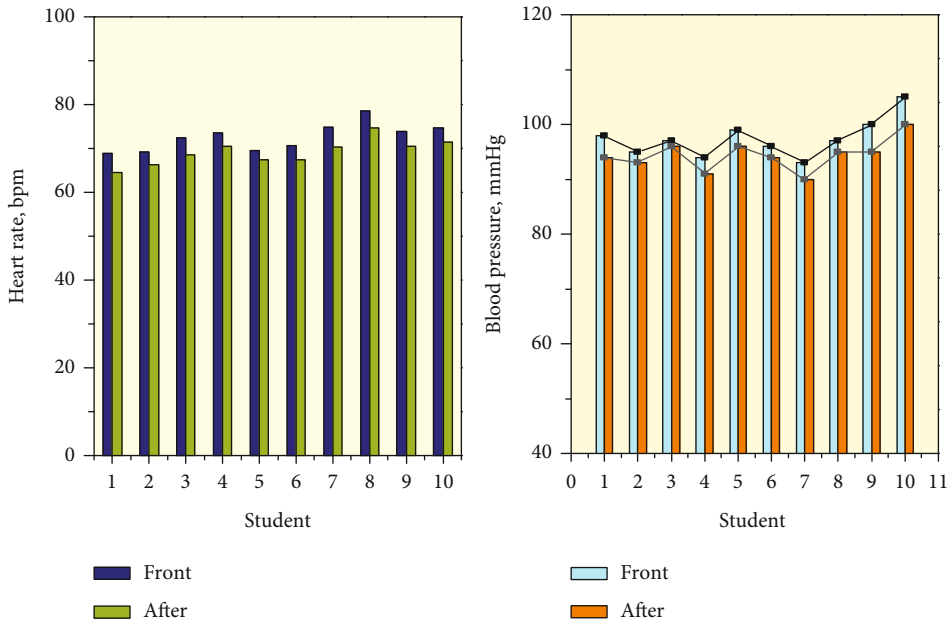

Figure 6: Figure of comparative analysis results of body parameter data.

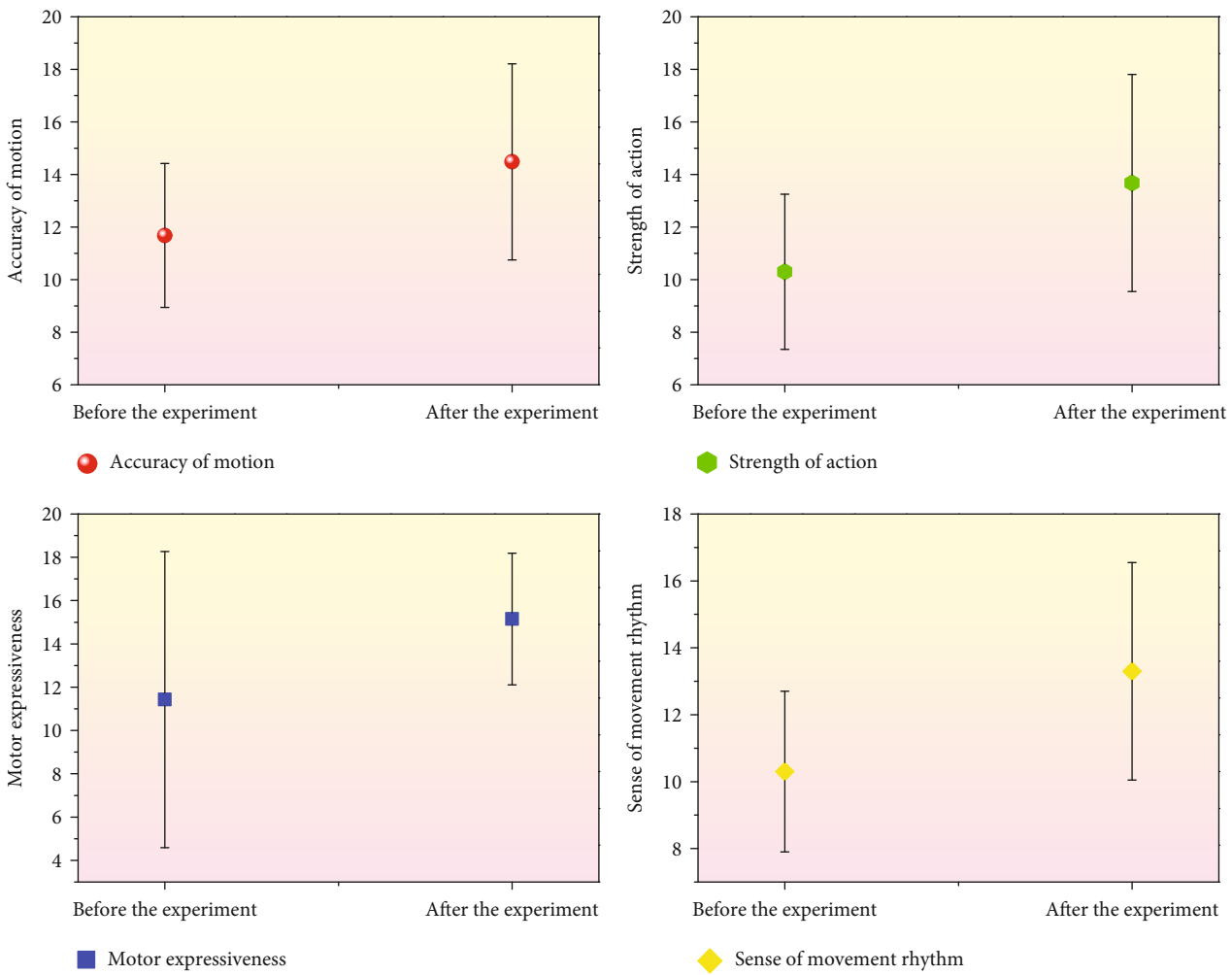

Figure 7: Teaching effect analysis and contrast chart.

5.4. Analysis on the Teaching Effect of Students' Movement Skills in Calisthenics. Before the experiment, according to the teaching objectives and requirements of the teaching task of calisthenics class, the prescribed level 1 calisthenics movement is selected as the teaching content. Before the experiment, the students' simply four eight-beat calisthenics movements are examined once. In the assessment from the following aspects of the students' technology monitoring: the accuracy of movement, the strength of the action, dexterity of movement, a sense of rhythm of movement, and the expressiveness of movement, the comparison results are shown in Figure 7.

From the figure analysis, it can be seen that after the experiment, the control group had significant changes in movement intensity, accuracy, proficiency, rhythm, and expression, indicating that the control group also had significant differences before and after the experiment. In action on the total score, which also has a very significant change, after the experiment by comparing two groups of aerobics skill test indicators, it can be seen that experimental class students of aerobics skills to the test indexes were higher than that in comparative classes of students, the experimental group and control group in action on the strength and rhythm, expressive differences are more obvious than movement accuracy and movement skill, and the effect is more prominent. For the comprehensive aerobics movement, in order to achieve significant teaching effect, in the teaching process to pay attention to the aerobics movement structure, movement characteristics and time and space effect, monitoring system to show each student's movement accuracy, enhance the students' ability to understand the movement.

6. Conclusion

The progress of science and technology brings about the improvement of people's quality of life, and people pay more attention to aerobic exercise. The perception of the teaching effect of aerobics is the key factor to learn aerobics, but the current aerobics exercise method is not professional, and the teaching effect can not be effectively evaluated in the process of fitness. This paper discusses the basic theory of human-computer interaction and multisensor information fusion, designs the multisensor information fusion system framework from software and hardware, respectively, and puts forward the monitoring system of aerobic aerobics teaching effect based on multisensor information fusion. On the basis of computer simulation, the accuracy of the data fusion model is above 90%, and the difference range is not big and basically fluctuates within a very small range of average accuracy. The results show that the designed system can achieve the acquisition and fusion of information, the use of multisensor equipment to collect the characteristics of aerobics data, movement strength, sense of rhythm, and expressiveness of the difference is more obvious than the accuracy of movement and movement proficiency, and the effect is more significant. The monitoring system designed in this paper can basically meet the monitoring needs of human physiological parameters, but the functions of some modules are not perfect, the overall hardware structure of the system is slightly complex, the overall volume is not small enough, and the system is not intelligent enough to collect and process data. The model is only simulated on a computer and tested on a simple hardware platform. How to transplant the model to a more advanced hardware platform and the miniaturization of the terminal is the direction of development. After using big data, the research direction should be structured, miniaturized, and intelligent.

Data Availability

The data used to support the findings of this study are available from the corresponding author upon request.

Conflicts of Interest

The authors declare that they have no known competing financial interests or personal relationships that could have appeared to influence the work reported in this paper.

References

[1] A. N. Patel, T. P. Jung, and T. J. Sejnowski, "A wearable multimodal bio-sensing system towards real-world applications," *IEEE Transactions on Biomedical Engineering*, vol. 66, no. 4, pp. 1137–1147, 2018.

[2] J. Zhang, Z. Yin, P. Chen, and S. Nichele, "Emotion recognition using multi-modal data and machine learning techniques: a tutorial and review," *Information Fusion*, vol. 59, pp. 103–126, 2020.

[3] F. Ali, S. el-Sappagh, S. M. R. Islam et al., "A smart healthcare monitoring system for heart disease prediction based on ensemble deep learning and feature fusion," *Information Fusion*, vol. 63, pp. 208–222, 2020.

[4] E. Kanjo, E. M. G. Younis, and C. S. Ang, "Deep learning analysis of mobile physiological, environmental and location sensor data for emotion detection," *Information Fusion*, vol. 49, pp. 46–56, 2019.

[5] J. Zhou, X. Hong, and P. Jin, "Information fusion for multisource material data: progress and challenges," *Applied Sciences*, vol. 9, no. 17, p. 3473, 2019.

[6] H. Wang and Q. Zhang, "Dynamic identification of coal-rock interface based on adaptive weight optimization and multisensor information fusion," *Information Fusion*, vol. 51, pp. 114–128, 2019.

[7] X. Deng and W. Jiang, "Fuzzy risk evaluation in failure mode and effects analysis using a D numbers based multi-sensor information fusion method," *Sensors*, vol. 17, no. 9, p. 2086, 2017.

[8] N. Wichit and A. Choksuriwong, "Multi-sensor data fusion model based Kalman filter using fuzzy logic for human activity detection," *International Journal of Information and Electronics Engineering*, vol. 5, no. 6, pp. 450–453, 2015.

[9] P. Bharti, D. de, S. Chellappan, and S. K. Das, "HuMAn: complex activity recognition with multi-modal multi-positional body sensing," *IEEE Transactions on Mobile Computing*, vol. 18, no. 4, pp. 857–870, 2019.

[10] A. H. Mohsin, A. A. Zaidan, B. B. Zaidan et al., "Real-time remote health monitoring systems using body sensor information and finger vein biometric verification: a multi-layer

systematic review," *Journal of Medical Systems*, vol. 42, no. 12, pp. 32–36, 2018.

[11] J. O. de Oliveira de Souza, M. D. Bloedow, F. C. Rubo, R. M. de Figueiredo, G. Pessin, and S. J. Rigo, "Investigation of different approaches to real-time control of prosthetic hands with electromyography signals," *IEEE Sensors Journal*, vol. 21, no. 18, pp. 20674–20684, 2021.

[12] X. Yan, H. Liu, G. Xin, H. Huang, Y. Jiang, and Z. Guo, "Research on real-time elimination of ultra-wideband radar ranging abnormal value data," *Geoscientific Instrumentation, Methods and Data Systems*, vol. 10, no. 2, pp. 153–160, 2021.

[13] M. Wang, X. Wang, L.-T. Yang, X. Deng, and L. Yi, "Multi-sensor fusion based intelligent sensor relocation for health and safety monitoring in BSNs," *Information Fusion*, vol. 54, pp. 61–71, 2020.

[14] M. Chen, Y. Zhang, M. Qiu, N. Guizani, and Y. Hao, "SPHA: smart personal health advisor based on deep analytics," *IEEE Communications Magazine*, vol. 56, no. 3, pp. 164–169, 2018.

[15] X. Wu, J. Duan, L. Zhang, and S. M. AbouRizk, "A hybrid information fusion approach to safety risk perception using sensor data under uncertainty," *Stochastic Environmental Research and Risk Assessment*, vol. 32, no. 1, pp. 105–122, 2018.

[16] G. Chen, Q. Pei, and M. M. Kamruzzaman, "Remote sensing image quality evaluation based on deep support value learning networks," *Signal Processing: Image Communication*, vol. 83, article 115783, 2020.

[17] O. AlShorman, B. Alshorman, and M. S. Masadeh, "A review of physical human activity recognition chain using sensors," *Indonesian Journal of Electrical Engineering and Informatics*, vol. 8, no. 3, pp. 560–573, 2020.

[18] A.-A. AlZubi, A. Abugabah, M. al-Maitah, and F. Ibrahim AlZobi, "DL multi-sensor information fusion service selective information scheme for improving the internet of things based user responses," *Measurement*, vol. 185, article 110008, 2021.

[19] T. Li, Z. Zhao, C. Sun, R. Yan, and X. Chen, "Hierarchical attention graph convolutional network to fuse multi-sensor signals for remaining useful life prediction," *Reliability Engineering & System Safety*, vol. 215, article 107878, 2021.

[20] R. Dinesh Jackson Samuel, E. Fenil, G. Manogaran et al., "Real time violence detection framework for football stadium comprising of big data analysis and deep learning through bidirectional LSTM," *Computer Networks*, vol. 151, pp. 191–200, 2019.

[21] M. L. Shuwandy, B. B. Zaidan, A. A. Zaidan et al., "mHealth authentication approach based 3D touchscreen and microphone sensors for real-time remote healthcare monitoring system: comprehensive review, open issues and methodological aspects," *Computer Science Review*, vol. 38, article 100300, 2020.

[22] K. I. Mohammed, A. A. Zaidan, B. Zaidan et al., "Real-time remote-health monitoring systems: a review on patients prioritisation for multiple-chronic diseases, taxonomy analysis, concerns and solution procedure," *Journal of Medical Systems*, vol. 43, no. 7, p. 223, 2019.

Hindawi
Journal of Sensors
Volume 2022, Article ID 8118605, 9 pages
https://doi.org/10.1155/2022/8118605

Research Article

A Deployment Strategy of Nodes in WSN Based on "X" Partition

Jinxue Liu and Gengxin Sun

College of Computer Science and Technology, Qingdao University, Qingdao 266071, China

Correspondence should be addressed to Gengxin Sun; sungengxin@qdu.edu.cn

Received 28 September 2021; Revised 24 January 2022; Accepted 15 February 2022; Published 7 March 2022

Academic Editor: Giuseppe Maruccio

In order to reduce the energy consumption and the cost of wireless sensor networks (WSNs) deployed in linear areas and prolong the life of the network, a deployment strategy of nodes in WSNs based on "X" partition was proposed in this paper. The monitored area was partitioned based on "X" shape, and the sensor nodes were deployed, so as to make the whole area be covered and the number of nodes deployed be reduced. At the same time, the monitoring units are divided and compressed to balance and save energy of the network and prolong life of the network. Through experiment verification, compared with traditional partition deployment strategy, the deployment cost of network can be reduced effectively by the proposed strategy. In terms of the life of the network, the proposed strategy is longer than the diamond partition strategy more than 50%.

1. Introduction

At present, wireless sensor networks are widely used in various scenes. Many sensor nodes are deployed in the area to be monitored according to the established strategy and cooperated with each other to complete the task of collecting, processing, and transmitting [1]. Sensor nodes are usually deployed in complex environments and cannot be reused. Therefore, when a node is unavailable due to its own energy depletion or other factors, the whole wireless sensor network will be seriously affected.

When wireless sensor networks are used for monitoring in tunnels, mines, rivers, or large bridges, the sensor nodes are also distributed linearly because of the linear shape of these areas. Moreover, in this kind of environment, the base station is often set at one end of the area to be monitored. When the information collected by sensor nodes is sent to the base station in the form of multihops, more data forwarding tasks and greater energy consumption need to be undertaken by sensor nodes closer to the base station, while few data forwarding tasks and low energy consumption are on sensor nodes farther away from the base station, which leads to an "energy hole" in the whole wireless sensor network [2, 3], and the life of the network is ended prematurely. In addition, the similarity of data collected by close nodes in the network is high, which makes the data redundancy of the whole network larger; the energy of sensor nodes is wasted; and the life of network is greatly shortened.

Aiming at the problem of network deployment and optimization, many efforts were made and a series of results were achieved by researchers. The node deployment density function under linear network was proposed in reference [4, 5]; the sensor nodes were arranged according to the density formula. By arranging sensor nodes in this way, the ratio of total energy and energy consumption speed in each region can be balanced, so as to effectively prolong the life of the system. However, in many practical application scenarios, its density cannot be accurately controlled. Yen et al. [6] adopted isosceles triangle partition to realize K-coverage of monitoring region, and sensor nodes were grouped to balance the overall energy consumption of the network, but the coverage rate is not high. Liu and Wu [7] proposed a hierarchical wireless sensor network routing protocol for mine roadway environment, which can cluster in large scale in areas with large data forwarding volume. However, the existence of cluster heads necessarily becomes a network bottleneck that restricts the performance of the networks. Muthusenthil and Kim [8] proposed a hierarchical wireless sensor network model for underground working environment. The topology control method based on static node controllable deployment is adopted, and

the nodes are arranged on one side of the roadway in a straight line; thus, the double coverage of the roadway was realized. Rejinaparvin and Vasanthanayaki [9] proposed the cluster node competition algorithm; the network was divided into several clusters with different sizes and combined with intercluster routing to save network energy. This protocol considers the influence of the remaining power, so it is able to balance the node power. Regular triangle partition, rectangular partition [10], and diamond partition [11] are included in common deployment strategies of wireless sensor network nodes. There are some problems in existing node deployment methods and strategies, such as high node deployment density, high network deployment cost, and large data redundancy. The data compression in wireless sensor networks [12–14] can make the transmission energy consumption be effectively reduced and the life of the network be prolonged. Aiming at the problems of uneven distribution of directed sensing nodes scattered in the designated monitoring area by random deployment in the monitoring task of directed wireless sensor networks in a two-dimensional environment, the characteristics of directed sensor nodes, probabilistic sensing model, and cooperative sensing model of multiple sensor nodes for monitoring target points are analysed. In this paper, a deployment strategy of nodes in WSN based on "X" partition is proposed; the area to be monitored can be divided by "X" partition; then, the number of sensor nodes in the network and network deployment cost can be reduced on the premise of realizing full network coverage. At the same time, the data of the monitoring unit is compressed to balance the network energy consumption and prolong the network life. The proposed method can guide the direction adjustment and perception optimization of two-dimensional oriented sensor nodes, so as to improve the perception ability of network nodes.

The main contributions of this study are summarized as follows:

(1) We propose a new a deployment strategy of nodes in WSN based on "X" partition, which can improve the coverage of the region to be monitored and the perceived quality of service and reduce the overall energy consumption of the network

(2) The proposed deployment strategy can adjust and optimize the location distribution of wireless sensor nodes according to the demand characteristics of the area to be monitored, meet the sensing needs of different areas, and improve the energy efficiency of the network and nodes

The rest of this paper is organized as follows. The energy consumption model is introduced in Section 2. Node deployment strategy is presented in Section 3. Simulation results and analysis are given in Section 4. Finally, conclusions are given in Section 5.

2. Energy Consumption Model

The requirements of node connectivity in wireless sensor networks are roughly the same as those in ad hoc networks: (1) the information must have one or enough paths to forward from the information source to the destination node; (2) the delay of information forwarding shall be as small as possible. The more information forwarding paths, the more reliable the system is. However, due to the need for multiple intermediate nodes to work at the same time, the node energy consumption increases and the system life decreases. The energy consumption of wireless transmitting devices increases exponentially with the increase of transmitting and receiving distance. Using multihop information forwarding instead of point-to-point communication can save a lot of energy. However, too many hops will increase the number of information receiving and forwarding and will also bring additional energy consumption. Therefore, the key to reduce energy consumption is to compromise the above two contradictory factors and appropriately control the number of forwarding nodes. The following definitions are given:

Definition 1. Connectivity between sensor nodes. If in the deployment area of wireless sensor network, nodes can always transmit information to each other in some way, it is said that nodes are connected in the network coverage area.

Definition 2. Connectivity of wireless sensor networks. If in the wireless sensor network deployment area, for a large subset of all nodes, the base station can always transmit relevant control information to any node in the node set by some routing method and any node in the node set is also connected, the wireless sensor network composed of this large node set in the network coverage area is connected.

The set composed of all sensor nodes is divided into $\{h_1, \ldots, h_m\}$, $s_i \in \cup_{1 \le j \le m} h_j$, and $h_i \cap h_j = \varnothing$, where h_i represents a set of sensor nodes that make up the backbone connection network and s_i is a sensor node. Each nonbackbone node in the sensing state can communicate with at least one backbone to save power. There must be one and at least one direct or indirect path between the backbone nodes to connect the two.

In wireless sensor networks, the energy of sensor nodes is mainly spent on the conversion and processing of external signals and the overhead of data communication. The wireless communication energy consumption model in the data transmission stage and the data compression algorithm in the data processing stage are adopted by the deployment strategy of nodes in wireless sensor network based on "X" partition.

When l – bit data is sent by the sensor node, its energy consumption formula is

$$E_{Tx}(l, d) = \begin{cases} l\left(E_{\text{elec}} + \xi_{fs} d^2\right), & d < d_0, \\ l\left(E_{\text{elec}} + \xi_{mp} d^4\right), & d \ge d_0, \end{cases} \quad (1)$$

where $E_{Tx}(l, d)$ is the node energy consumption, which is generated in the transmission circuit and signal amplifier.

E_{elec} is the energy consumption of transmitting unit data by transmitting circuit or receiving circuit. ξ_{fs} and ξ_{mp} are amplifier coefficients, d_0 is the distance threshold, and the corresponding channel model is selected by the node according to the relationship between data transmission distances d and d_0.

When $l-$bit data is received by the sensor node, the receiving circuit is the only source of its energy consumption, so the energy consumption E_{Rx} of the receiving node is

$$E_{Rx}(l) = lE_{\text{elec}}. \tag{2}$$

In the data processing stage, data compressing is processed by sensor nodes to filter out the repeated useless data. In the data compression algorithm, the energy consumed by each node for compressing unit data is E_{DA}.

$$E_p = lE_{DA}. \tag{3}$$

3. Node Deployment Strategy

Sensor node deployment strategies are mainly divided into two categories: random deployment strategy and fixed deployment strategy. In the random deployment strategy, the sensor nodes are randomly deployed in the area to be monitored, and then, the optimization of the network is studied. In the fixed deployment strategy, the sensor nodes are deployed in the designated position of the area to be monitored according to the established strategy, and the optimization of the network is studied. In the actual environment, roads, rivers, mines, and other shapes can be regarded as linear areas. Considering the rules of linear region morphology comparison, fixed deployment strategy is adopted in this paper.

In order to facilitate subsequent research and analysis, the following assumptions are made here:

(1) Many sensor nodes and one basic sensor are contained in the network. The initial energy, sensing radius, communication radius, transceiver power, and data processing energy consumption of sensor nodes are all the same

(2) The sensing rate of sensor nodes for data within the sensing radius is 100%, and the sensing rate for data outside the sensing radius is 0%

(3) The energy consumption of sensor nodes mainly occurs in the data processing and transmission stage, without considering the energy consumption of nodes in sensing data

The monitored area is equally divided into a plurality of "X" partitions, as shown in Figure 1. The distance of each "X" partition is the same, and sensor nodes are deployed at the vertices and intersections of "X." The full coverage of the region can be realized by this step.

3.1. "X" Partition Coverage Strategy. The linear area which is monitored is partitioned based on the "X" shape, sensor nodes are deployed at boundary vertices, and intersections of "X" make the node position as the center of the circle and the sensing distance as the radius; the coverage area is the sensing area of each sensor node. The sensor nodes of four vertices at the boundary of the region and the center crossing position are included in each partition. As shown in Figure 2, A, B, D, and E are common sensor nodes, which are responsible for sensing surrounding data. In addition to sensing data, the sensor node at position C is also responsible for processing and transmitting data, which is called the master node.

The area sensed by the master node in the "X" partition and its ordinary node far away from the base station is divided into a monitoring unit; as shown in Figure 2, the area covered by circles A, B, and C is a monitoring unit, which ensures that the nodes transmit data towards the base station and redundant energy consumption can be avoided. The perceived information is transmitted to the master node by ordinary nodes in the monitoring unit, and then, the information is received by the master node, which obtains the data of the whole monitoring unit.

The length and width of the linear region are a, and the sensing radius of sensor nodes is r; the region is divided into "X" shape according to the value L, which can realize the full coverage of the network and minimize the number of nodes.

$$L = 2\left(r + \sqrt{r^2 - \left(\frac{b}{2}\right)^2}\right). \tag{4}$$

As shown in Figure 3, it is an "X" partition according to the distance L, with A, B, C, D, and E as five sensor nodes; A, B, D, and E are all located on the boundary of the region; and C is located on the center of "X." At this time, the intersection point H of circle A and circle C is located on one boundary of region, and the intersection point N of circle B and circle C is located on another boundary of region, and the circles A, B, and C just intersect at point M. Circle D and circle E are the same as circle A and circle B. Any point in the whole "X" partition can be sensed by sensor nodes. If $L > 2(r + \sqrt{r^2 - (b/2)^2})$, the intersection points of H and N are located within the boundary of the region, which leads to some regions not being sensed by any sensor nodes; that is, the full coverage of the network cannot be realized. If $L < 2(r + \sqrt{r^2 - (b/2)^2})$, although the network can achieve complete coverage, the deployment number of sensor nodes cannot reach the optimal value. Therefore, $L = 2(r + \sqrt{r^2 - (b/2)^2})$ is the best partition distance.

According to the previous definition of monitoring units, monitoring units are corresponded to "X" partition one by one, so when the network is fully covered, the number of monitoring units in the network is equal to the number of "X" partitions. The number of monitoring units in the network is $N_d = N_X = (a/L) = (a/(2(r + \sqrt{r^2 - (b/2)^2}))2(r$

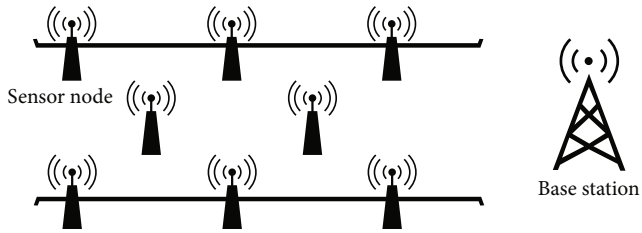

Figure 1: Node deployment model of linear area.

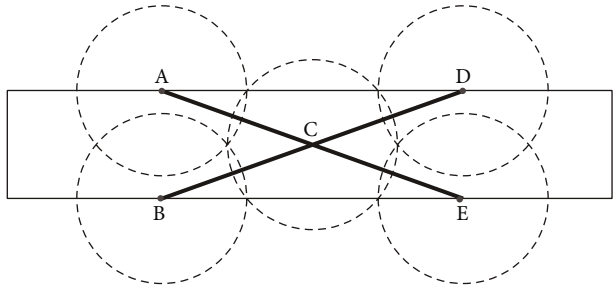

Figure 2: The deployment strategy of nodes based on "X" partition.

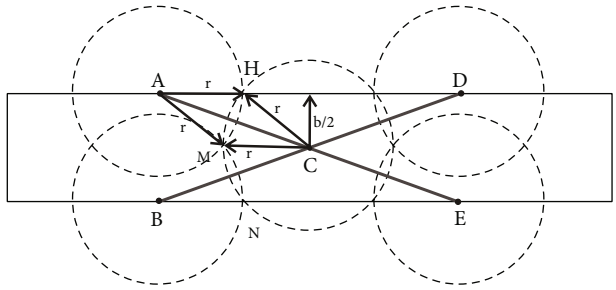

Figure 3: Node coverage effect diagram.

$+\sqrt{r^2-(b/2)^2}))$, the number of basic nodes needed to achieve full coverage of the network is $3a/L = (3a/(2(r+\sqrt{r^2-(b/2)^2}))2(r+\sqrt{r^2-(b/2)^2}))(a/L)$, the number of master nodes is a/L, and the master nodes are numbered $i = 1, 2, 3, \cdots, a/L$.

The dimensions of the wireless sensor network can be reduced by division of monitoring units from a two-dimensional plane area to a one-dimensional straight line. Based on the "X" partition, the size of all monitoring units is the same and all monitoring units are arranged in sequence. The data of the whole monitoring unit is stored in the master nodes, and the relative positions and distances of the master nodes in monitoring units are the same; that is, they are evenly distributed on a straight line. According to the distance from the base station, the monitoring units and master nodes are numbered. Data is transmitted to the base station through other master nodes in a multihop manner, and the problem of data return caused by the traditional clustering method is solved.

3.2. Data Compression. Sensing, processing, and transmitting are the functions of sensor nodes. And the energy consumption of data processing is much smaller than that of data transmission. Therefore, the energy consumption of the network can be balanced and the life of the network can be prolonged by processing the data before transmitting the data. Data compression is the main work of data processing; that is, sensor nodes compare and analyze the data they sense and receive, filter redundant data, and integrate main data. However, data compression is at the expense of the accuracy of data transmission to reduce the energy consumption of data transmission. Moreover, the more the data compression times, the greater the network delay. In the deployment strategy of nodes in WSN based on the "X" partition, each monitoring unit has a master node, and the number of sensor nodes is small. Data compression can be performed only inside the monitoring unit: after the data sent by the sensor nodes in the unit is received by the master node, it is integrated and compressed with the data sensed by the master node and then transmitted by multihop. Because the monitoring range of each monitoring unit is small and the sensing areas of each sensor node overlap, the principal component analysis method [15] is adopted in this paper to reduce data redundancy and compress data. The main process is as follows: in the monitoring unit, the data sensed by the nodes are sent to the master node and then received by the master node to generate corresponding data matrices. After analyzing and comparing these matrices, the principal components in the matrices are extracted and transmitted.

According to the energy consumption formula of the data compression, the compression energy consumption of each master node in the network is

$$E_p = 3lE_{DA}. \tag{5}$$

3.3. Network Energy Consumption Optimization. After the size of the monitoring unit and the number of the main node were determined, the network energy consumption is further optimized. In wireless sensor networks, the biggest energy consumption of nodes is in the data transmission stage. In a linear area, data is transmitted in multihops; there is a great relationship between energy consumption of nodes and the transmission step. By comparing the energy consumption under different transmission distances, the optimal value is selected to optimize the network energy consumption.

The distance d between two adjacent master nodes is taken as the basic step length for data transmission, and the step length is written as $D = nd(n = 1, 2, 3)$. Since the data has been compressed by each master node in the monitoring unit before data transmission, the energy consumption of each master node when transmitting data to the base station is the same under each step length, so it is only necessary to calculate the energy consumption E_i of the master node i acting as a relay node and the energy consumption $E_k{}^n$ of the whole network when l – bit data is transmitted to the base station by the No. 1 master node under different

Table 1: Sensor node parameter settings.

Parameter name	Numerical
Sense radius r	20 m
Initial energy E_0	0.5 J
Energy consumption per unit data transmission E_{elec}	50 nJ
Amount of data l	1200 bits
ξ_{fs}	$10\,\text{pJ}\cdot\text{bit}^{-4}\cdot\text{m}^{-2}$
ξ_{mp}	$0.0013\,\text{pJ}\cdot\text{bit}^{-4}\cdot\text{m}^{-2}$
E_{DA}	50 pJ

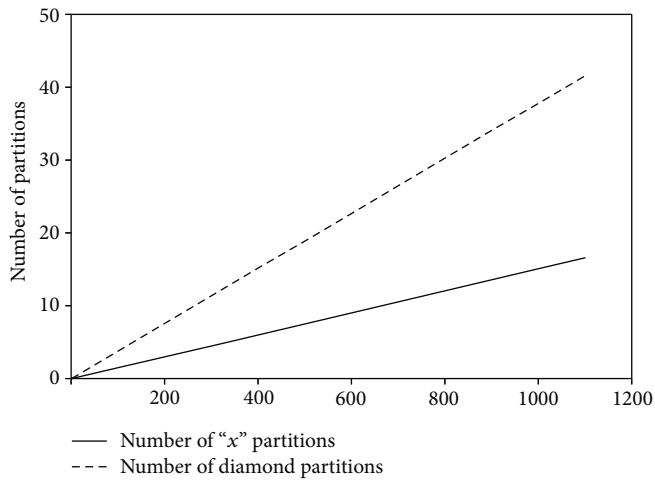

Figure 4: Relationship between the number of nodes and the length of regions.

step values n, and then, the optimal step value can be selected.

$$\begin{aligned}
&n=1, E_i=E_{RX}(l)+E_{TX}(l,d), E_k{}^1=(m-1)\left(2lE_{\text{elec}}+l\xi D^{t\cdot}\right),\\
&n=2, E_i=E_{RX}(l)+E_{TX}(l,2d), E_k{}^2=\left\lfloor\frac{(m-1)}{2}\right\rfloor\left[2lE_{\text{elec}}+l\xi D^t\right],\\
&n=3, E_i=E_{RX}(l)+E_{TX}(l,3d), E_k{}^3=\left\lfloor\frac{(m-1)}{3}\right\rfloor\left[2lE_{\text{elec}}+l\xi D^t\right].
\end{aligned} \tag{6}$$

Derive the formula for selecting the available step length:

$$n=\{n\mid \min \mathrm{E}_k{}^n\},$$
$$E_k{}^n=\left\lfloor\frac{\left(\left(a/2\left(r+\sqrt{r^2-(b/2)^2}\right)\right)-1\right)}{n}\right\rfloor\left[2lE_{\text{elec}}+l\xi(nd)^t\right], \tag{7}$$

where the value t depends on ξ and ξ is related to the value n .

After the transmission step is determined, when the data of the i-th master node is transmitted to the base station for each round of data transmission, the energy consumption of the network is

$$E_k{}^n(i)=\left\lfloor\frac{\left(\left(a/\left(2\left(r+\sqrt{r^2-(b/2)^2}\right)\right)\right)2\left(r+\sqrt{r^2-(b/2)^2}\right)\right)-i\right)}{n}\right\rfloor \cdot\left[2lE_{\text{elec}}+l\xi(nd)^t\right]. \tag{8}$$

The sum of transmission energy consumption of each master node in the network is the total energy consumption $E_{\text{total}}{}'$ of transmission in the network; then,

$$E_{\text{total}}{}'=\sum_{i=1}^{a/\left(2\left(r+\sqrt{r^2-(b/2)^2}\right)\right)}E_k{}^n(i). \tag{9}$$

For comprehensive data compression and data transmission, the total energy consumption E_{total} of the network is

$$E_{\text{total}}=E_{\text{total}}{}'+\frac{a}{2\left(r+\sqrt{r^2-(b/2)^2}\right)}E_p. \tag{10}$$

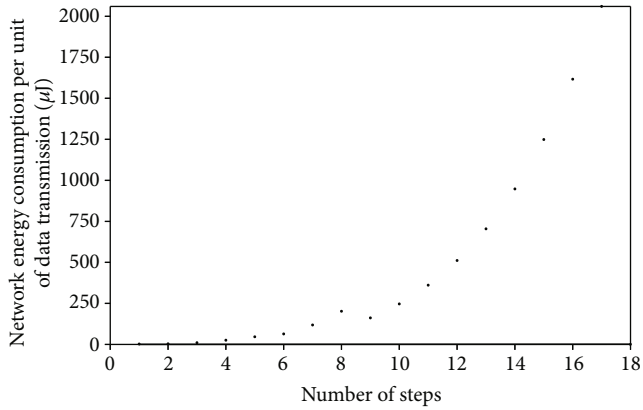

Figure 5: Relationship between energy consumption per unit data transmission and step length.

Table 2: Partition effect based on "X" partition deployment strategy and diamond partition deployment strategy.

Deployment strategy	Number/number of network partitions (clusters)	Number of network nodes	Partition distance d (m)
X-shaped partition	18	54	66
Diamond partition	20	60	60

3.4. Deployment of Spare Nodes. In order to ensure the life and performance of the network, spare nodes are properly deployed for each master node according to its energy consumption. Because the energy consumption of the master node in the network is related to the hop count j, $j = i/n$, the later the hop count, the greater its energy consumption. Under a certain step length, the life of the whole network is equal to that of the master node in the last hop [9]. The energy consumption E_i of each master node in the network is

$$E_i = E_{RX}(l) + E_{TX}(l, d) = (i-1)lE_{\text{elec}} + ilE_{\text{elec}} + il\xi d^t. \quad (11)$$

Therefore, the closer the energy consumption of the master node that initially transmits information is to that of the master node in the last hop, the more balanced the network energy consumption is. That is, the smaller the value of $|E_1 - E_{a/L}|$, the more balance the network energy consumption and the longer its life. The formula for calculating the number of spare nodes of each master node is [9]

$$\text{Num}_i = \frac{E_i}{E_1}. \quad (12)$$

3.5. Steps of Node Deployment. Assuming that the base station is on the right side of the linear area, the specific steps of the deployment strategy of nodes in WSN based on the "X" partition are as follows:

Table 3: The number of spare nodes of each master node.

Node number	Number of spare nodes	Node number	Number of spare nodes
1	0	10	5
2	1	11	6
3	1	12	6
4	2	13	7
5	2	14	8
6	3	15	8
7	4	16	9
8	4	17	9
9	5	18	10

(1) The linear area to be monitored is initialized, and its length is a, width is b, and node perception radius is r

(2) The linear area is divided into "X" partitions by length $L = 2(r + \sqrt{r^2 - (b/2)^2})$, so as to realize the full coverage of the network

(3) The divided "X" partitions are divided into monitoring units, and the master nodes in each monitoring unit are numbered $1, 2, 3, 4 \cdots \cdots, i$ from left to right

(4) The optimal step size n of data transmission and network energy consumption E_{total} are calculated

(5) The position j of each master node in the transmission path is calculated

(6) Sensor nodes and spare nodes are deployed in the linear area to be monitored based on the "X" partition strategy

(7) Run the network; when the energy of the master node is unavailable, replace it with a spare node

4. Experiment and Analysis

4.1. Experiment Environment and Parameter Setting. In order to verify the rationality of this method, *Python 3.7* is used for simulation experiment, ignoring packet loss and other problems in the process of data forwarding, comparing with diamond partition strategy. All experimental environments assume that the signal transmission range of sensor nodes is a regular circle. In order to ensure the accuracy of the experiment, all data adopt the average value of 20 rounds of experimental data. The nodes are initially randomly distributed in the monitoring area, and the number of nodes is 70. The parameters of the sensors used in the experiment are shown in Table 1. Transmission threshold $d_0 = 87$.

4.2. Analysis of Network Cost. In practice, the number of network partitions is directly affected by the length of the area to be monitored. The width of the area to be monitored and the sensing radius of the sensor nodes are set as fixed values. According to formula (4), the number of partitions

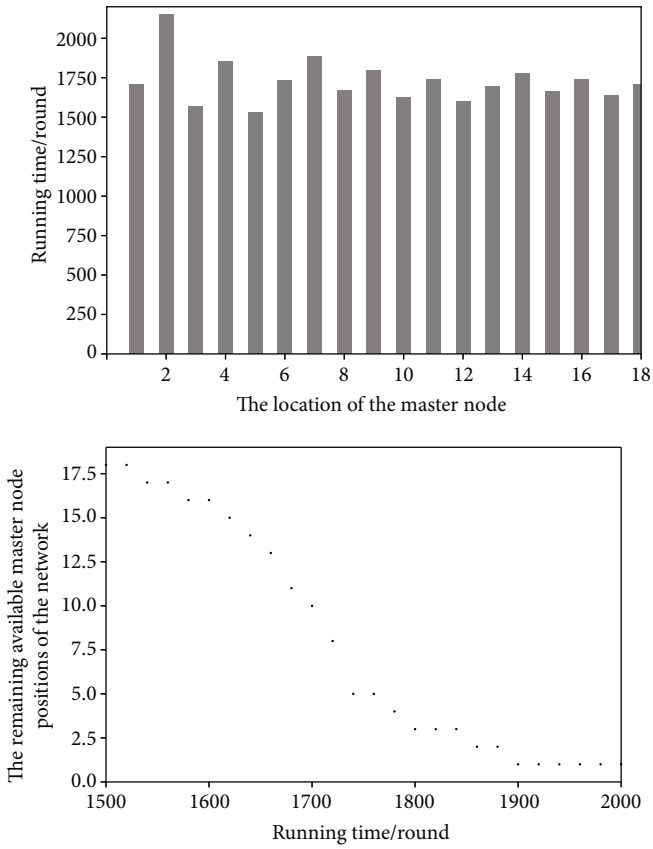

Figure 6: The life of master nodes in network.

obtained by the "X" partition deployment strategy and the diamond partition strategy is compared under different region lengths. As shown in Figure 4, the number of partitions based on the "X" partition deployment strategy is significantly less than the diamond partition, and the difference between the two strategies is more significant with the increase of the length of the area to be monitored. When the length of the area to be monitored is long, it is more suitable to choose the "X" partition deployment strategy for network deployment. At this time, the number of basic sensor nodes needed to achieve complete network coverage is less than that of the diamond partition deployment strategy; that is, the cost of network deployment is lower.

In the traditional diamond partition deployment strategy, after partitioning the area to be monitored, it is necessary to calculate the optimal cluster spacing and the location of cluster nodes, so that sensor nodes are often deployed according to the approximate value of the optimal solution instead of the optimal solution. However, in the "X" partition deployment strategy, the nodes can be only deployed according to the partition location and then filter out the master nodes.

4.3. Analysis of Network Energy Consumption. In the experiments, the length and width of the area to be monitored are set as 1200 m and 30 m, respectively, and the number of basic sensor nodes needed under the "X" partition deployment strategy and diamond partition strategy is shown in Table 2.

Based on the "X" partition deployment strategy, 18 monitoring units are divided in the area to be monitored, and the master nodes are numbered as $i = 1, 2, 3, \cdots, 18$. Then, the optimal step length of data transmission is calculated according to the selected function of transmission step length. The network energy consumed of the No. 1 master node in transmitting data under different step lengths is shown in Figure 5, so the optimal transmission distance is 66 m, that is, $n = 1$.

According to the experiment in reference [2], the data transmission effect is best when the area to be monitored is divided into 20 clusters in the experimental environment set in this paper; that is, the optimal distance of data transmission in the network is 60 m.

The energy consumption of the network can be directly reflected by the energy consumed by each round of data transmission in the network. According to the selected optimal data transmission distance, the energy consumed by the network for one round of data transmission under different deployment strategies is calculated. In the "X" partition deployment strategy, the data in the monitoring unit is firstly compressed by the master node. According to the energy consumption formula of data compression, 324 nJ energy will be consumed by the master node for each round of network operation. According to the energy consumption

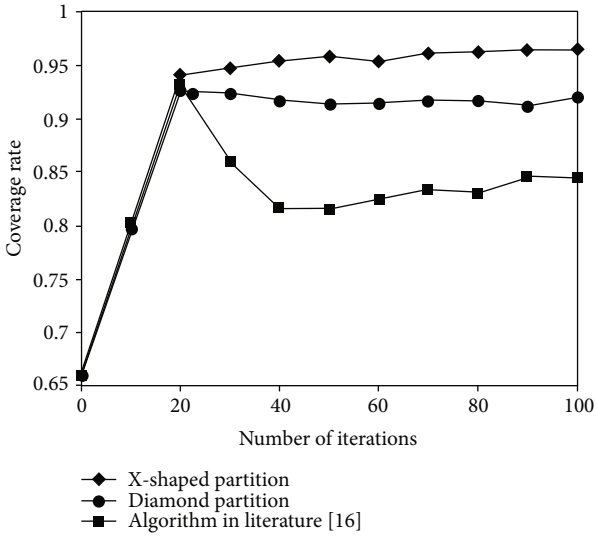

Figure 7: The coverage rate comparison results of different algorithms.

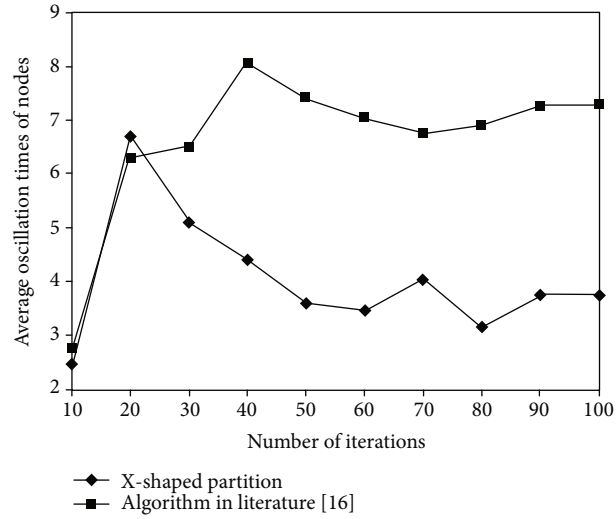

Figure 8: Average oscillation times of nodes.

formula of data transmission, the energy consumed by the network for data transmission is 26357616 nJ. In the "X" partition deployment strategy, the total energy consumption of the network is 26360856 nJ. In the diamond partition deployment strategy, the energy consumption of each round of network processing is 8252400000 nJ, which is much higher than the "X" partition deployment strategy.

4.4. Life of Network. The life of network is another important basis for measuring network performance. The number of spare nodes required by the network is calculated according to Equation (12). At first, the energy consumption of the No. 1 master node in the basic network is calculated to be 1710.74 nJ per round, and then, the number of spare nodes to be deployed near each master node is obtained, as shown in Table 3.

Based on the "X" partition deployment strategy, nodes are deployed in the area to be monitored to form a network. And the life of nodes is calculated in the network, as shown in Figure 6. When more than one-third of the nodes in the network run out of energy, the network performance will decrease sharply; that is, the life of the network is exhausted. It can be seen from Figure 6 that under this deployment strategy, the life of each master node in the network can reach 1500 rounds. On the premise of ensuring the network performance, the network can run more than 1650 rounds at most; that is, the life of the network exceeds 1650 rounds. Under the same experimental environment, the network composed of diamond partition deployment strategy can run for 1000 rounds. Therefore, the network life of the strategy proposed in this paper is superior to the diamond partition strategy.

4.5. Connectivity Rate and Coverage Rate. Wireless sensor network coverage must consider multiple performance indicators in order to make network coverage more reliable and effective, including coverage rate, connectivity rate, energy consumption, signal strength, fault tolerance, scalability, and reliability.

Table 4: Partition effect based on the "X" partition deployment strategy and diamond partition deployment strategy.

	$t = 20$	$t = 40$	$t = 60$	$t = 80$	$t = 100$
X-shaped partition	1.37%	3.76%	9.54%	4.66%	4.51%
Diamond partition	7.72%	13.38%	13.68%	13.18%	11.77%

During the experiment, Monte Carlo method is used to calculate the area coverage to measure the coverage ability of three algorithms (X-shaped partition, diamond partition, and the algorithm in literature [16]). The comparison results are shown in Figure 7.

When the number of iterations is $t < 20$, it can be seen from Figure 7 that the coverage rate of the X-shaped partition in this paper is similar to that in the diamond partition and literature [16]. When the number of iterations is $20 \leq t \leq 40$, many nodes of the algorithm in literature [16] oscillate back and forth. The number of node oscillations is shown in Figure 8.

The algorithm in literature [16] did not analyze and deal with the problem of continuous oscillation of nodes in detail, resulting in slow and unstable convergence speed of the algorithm, and the regional coverage decreased.

Table 4 shows the change of coverage growth rate of the X-shaped partition in this paper compared with the diamond partition with the number of iterations.

When the number of iterations of the algorithm is $20 \leq t \leq 60$, most nodes are in the optimization state. The growth rate of the coverage of the X-shaped partition in this paper is larger than that of the diamond partition. When the number of iterations $t > 60$, the coverage algorithm basically tends to be stable. Therefore, the growth coverage rate of the X-shaped partition is slower than that of the Diamond partition.

The focus of this paper is how to balance the network load and improve the network lifetime through the

deployment strategy of nodes. However, this paper does not use the previous method of calculating the distance according to the received signal strength but only determines the angle of nodes in different center coordinate systems according to the signal strength, which will lead to low positioning accuracy and complex mobile path and positioning methods.

5. Conclusions

In this paper, a deployment strategy of nodes in WSN based on the "X" partition is proposed, the linear area is equally divided into some "X" partitions, and the sensor nodes are deployed at fixed positions to achieve full coverage of the area to be monitored. According to the position of the node and base station, the monitoring unit is divided, the master node is determined, and the data is compressed by the master nodes in the monitoring unit; then, the data is transmitted, so as to balance the network load and improve the utilization of the network. According to the difference of node energy consumption, spare nodes are deployed to prolong the life of the network. Through theoretical analysis and experimental verification, the deployment cost of the network can be effectively reduced in the "X" partition deployment strategy and the life of the network can be prolonged. The aim of subsequent research is reducing the network delay and transmission accuracy caused by data compression in this deployment strategy.

Data Availability

The basic data used in this paper can be downloaded from https://gitee.com/hwang_zc/asdasd/blob/master/dataset.csv.

Conflicts of Interest

The authors declare that there are no conflicts of interest regarding the publication of this paper.

Acknowledgments

This work was supported by a grant from Humanities and Social Science Project of Ministry of Education of China (No. 21YJA860001).

References

[1] S. Bin and G. Sun, "Optimal energy resources allocation method of wireless sensor networks for intelligent railway systems," *Sensors*, vol. 20, no. 2, p. 482, 2020.

[2] P. S. Mann and S. Singh, "Improved metaheuristic-based energy-efficient clustering protocol with optimal base station location in wireless sensor networks," *Soft Computing*, vol. 23, no. 3, pp. 1021–1037, 2019.

[3] G. Nishi, P. M. Pawar, and S. Jain, "Improve performance of wireless sensor network clustering using mobile relay," *Wireless Personal Communications*, vol. 110, no. 2, pp. 983–998, 2020.

[4] K. Xu, H. Hassanein, and G. Takahara, "Relay node deployment strategies in heterogeneous wireless sensor networks," *IEEE Transactions on Mobile Computing*, vol. 9, no. 2, pp. 145–159, 2010.

[5] R. C. Luo and O. Chen, "Mobile sensor node deployment and asynchronous power management for wireless sensor networks," *IEEE Transactions on Industrial Electronics*, vol. 59, no. 5, pp. 2377–2385, 2012.

[6] L. H. Yen, W. Y. Chang, and Y. M. Cheng, "Expected _k_ -coverage in wireless sensor networks," *Ad Hoc Networks*, vol. 4, no. 5, pp. 636–650, 2006.

[7] Y. Liu, Q. Wu, T. Zhao, Y. Tie, F. Bai, and M. Jin, "An improved energy-efficient routing protocol for wireless sensor networks," *Sensors*, vol. 19, no. 20, p. 4579, 2019.

[8] B. Muthusenthil and H. Kim, "SHRP - secure hybrid routing protocol over hierarchical wireless sensor networks," *International Journal of Computers Communications & Control*, vol. 12, no. 6, pp. 854–870, 2017.

[9] J. Rejinaparvin and C. Vasanthanayaki, "Particle swarm optimization-based clustering by preventing residual nodes in wireless sensor networks," *IEEE Sensors Journal*, vol. 15, no. 8, pp. 4264–4274, 2015.

[10] G. Sun and C. C. Chen, "Influence maximization algorithm based on reverse reachable set," *Mathematical Problems in Engineering*, vol. 2021, Article ID 5535843, 12 pages, 2021.

[11] G. Sun and S. Bin, "Router-level internet topology evolution model based on multi-subnet composited complex network model," *Journal of Internet Technology*, vol. 18, no. 6, pp. 1275–1283, 2017.

[12] M. A. Alsheikh, S. Lin, and D. Niyato, "Rate-distortion balanced data compression for wireless sensor networks," *IEEE Sensors Journal*, vol. 16, no. 12, pp. 5072–5083, 2016.

[13] G. Sun, C. C. Chen, and S. Bin, "Study of cascading failure in multisubnet composite complex networks," *Symmetry*, vol. 13, no. 3, p. 523, 2021.

[14] S. Bin, G. Sun, N. Cao et al., "Collaborative filtering recommendation algorithm based on multi-relationship social network," *CMC-Computers, Materials & Continua*, vol. 60, no. 2, pp. 659–674, 2019.

[15] G. L. Tian, S. Zhou, G. X. Sun, and C. C. Chen, "A novel intelligent recommendation algorithm based on mass diffusion," *Discrete Dynamics in Nature and Society*, vol. 2020, Article ID 4568171, 9 pages, 2020.

[16] D. Sah, K. Cengiz, P. K. Donta, V. N. Inukollu, and T. Amgoth, "EDGF: empirical dataset generation framework for wireless sensor networks," *Computer Communications*, vol. 180, pp. 48–56, 2021.

Hindawi
Journal of Sensors
Volume 2022, Article ID 3383685, 11 pages
https://doi.org/10.1155/2022/3383685

Research Article

Multimodal Intelligent Acoustic Sensor-Assisted English Pronunciation Signal Acquisition and Phonetic Calibration

Nan Hu[1,2] **and Yongyi Bi**[3]

[1]*Public Teaching Department Nanyang Medical College, Nanyang Henan 473000, China*
[2]*School of Public Health Wuhan University, Wuhan Hubei 430000, China*
[3]*Wuhan University Medical School, Wuhan Hubei 430000, China*

Correspondence should be addressed to Yongyi Bi; yongyib@whu.edu.cn

Received 22 November 2021; Revised 16 December 2021; Accepted 6 January 2022; Published 2 March 2022

Academic Editor: Gengxin Sun

In this paper, a multimodal intelligent acoustic sensor is used for an in-depth study and analysis of English pronunciation signal acquisition and calibration analysis of English phonetic symbols based on the acquired sound signals. This paper proposes a bimodal fusion algorithm around the direction of feature extension and fusion of acoustic recognition features. After each unimodal classification error cost is minimized, the current fusion process is determined by adaptive weights to fix its one decision layer on the fusion. The adaptive weight approach in this algorithm improves the drawback of always identifying one mode as the optimal mode in fixed-weight fusion and further improves applicability and performance compared to unimodal recognition. The random network generation algorithm is used to generate a random network for sound source data acquisition; then, the algorithm is investigated using the decomposition containing fusion center algorithm to each node, and data preprocessing is implemented at each node; finally, the distributed consistency algorithm based on average weights is used for consistent averaging iterations to achieve a consistent speech enhancement effect at each node. The experimental results show that this distributed algorithm can effectively suppress the interference of noncoherent noise, and each node can obtain an enhanced signal close to the source signal-to-noise ratio. In this study, factors that may affect the readability of spoken texts are summarized, analyzed, defined, and extracted, and the difficulty of spoken items obtained from the divisional scoring model is used as the dependent variable, and the extracted influencing factors are used as independent variables for feature screening, model construction, and tuning, and the generated results are interpreted and analyzed. From this, it was found that phonological features have a strong influence on the readability of spoken texts, mainly in features such as phonemes, syllables, and stress. This study is summarized, and the shortcomings of location-based contextual mobile learning of spoken English in terms of student management, device deployment, and empirical evidence are pointed out, to provide references and lessons for the research on IT-supported language learning.

1. Introduction

In acoustic emission detection systems, resonant piezoelectric transducers are often used as acoustic receivers, which convert the measured changes into resonant changes. Resonant piezoelectric transducers use resonance technology to analyze parameters such as amplitude, vibration frequency, and phase for resonant oscillators to achieve measurements of parameters such as acoustic pressure and displacement, an algorithm that has the advantage of enabling high accuracy and resolution [1]. Despite the significant advantages of such sensors, they cannot be used in extreme environments, such as high voltage environments and environments subject to electromagnetic interference, and are difficult to embed inside materials. Compared with resonant piezoelectric sensors, fiber optic sensors have many unique properties. Fiber optic sensors have a series of unique advantages: good electrical insulation performance, strong resistance to electromagnetic interference, noninvasive, high sensitivity, easy to achieve long-distance monitoring of the measured

signal, corrosion resistance, explosion-proof, the optical path can be flexed, and easy to connect with the computer. They have high sensitivity, strong immunity to electromagnetic interference, extreme corrosion resistance, etc. At the same time, they are simple, compact, and lightweight, can be transmitted over long distances, and can be used as an important part of online telemetry systems. Since the 20th century, fiber optic sensors have received special attention from scholars in various countries; fiber optic sensors have been applied to measure temperature, stress, current, and hundreds of physical quantities, but also in high temperature, corrosion, and other special environments, and with the practical significance of traditional electronic sensors, they cannot be replaced. For solid-state sensors due to the manufacturing process and cost and other factors, the induction area is also smaller [2]. And with the development of embedded and a variety of mobile wearable devices, fingerprint capture devices are also towards the trend of smaller and smaller. For example, Apple's Touch ID fingerprint capture device is only 6.35 mm × 6.35 mm, and the universal smartphone at the same time, with the development of the trend, is bound to make the size of the fingerprint image capture also becomes smaller, and thus, the information contained in the fingerprint image is also greatly reduced. Multimodal biometrics refers to the integration or fusion of two or more biometric technologies, utilizing the unique advantages of its multiple biometric technologies and combining with data fusion technology to make the authentication and recognition process more accurate and secure. Multimodal biometrics can realize the combination of multiple biometrics such as face, fingerprint, finger vein, iris, and voice print, so as to carry out more accurate identity authentication.

It has been shown that when the sensing area of the acquisition device becomes small, the performance of the traditional fingerprint feature point matching recognition method will be greatly affected due to the low number of captured detail points. Therefore, the problems of missing features and recognition accuracy of small-area fingerprints have become the focus of scholars' research, and feature extension or fusion is the trend to compensate for the missing features [3]. Multimodal biometrics is a new biometric technology that overcomes some drawbacks of unimodal biometrics by fusing no less than two unimodal biometric features (or behavioral features) as data objects, which can get rid of the limitations of usage scenarios with higher stability and security, making the authentication process more accurate and secure. Multimodal fusion also overcomes, for example, the situation where kind of biometric features is lost, such as fingerprints due to cuts, wear, and tear, dryness, or inconspicuous innate features. Multimodal biometrics makes up for the deficiency [4]. One of the more typical methods is the beamforming method, which can obtain different performances depending on different beam constraints, such as minimum variance and minimum mean square error criteria [5]. The speech enhancement performance is proportional to the number of microphones, which means that more microphones will usually result in better speech enhancement performance. Speech recognition technology has a very wide range of application areas and market prospects, such as for voice-activated voice dialing system, voice-activated smart toys, and smart home appliances. It can also be applied to information network inquiries, medical services, banking services, etc. In beamforming algorithms, the microphone array is generally located relatively close to the sound source, which makes both the signal-to-noise ratio and the direct reverberation ratio of the received signal sufficiently large to obtain a better enhancement performance. The pronunciation calibration engine A/D circuit is designed to improve the data sampling efficiency by using analog to digital signal conversion for English pronunciation information acquisition.

With the continuous development of speech recognition technology, various derivative technologies based on speech recognition, such as keyword recognition, language recognition, speaker recognition, and ambient sound recognition, have also been devoted increased attention and have made promising progress. At the same time, speech recognition is also penetrating increasingly into our common life. The biggest advantage of speech recognition is that it makes human-computer interaction more natural and convenient. Nowadays, speech recognition technology has been widely used in voice communication systems, data inquiry, ticket booking systems, medical systems, banking services, computer control, industrial control, and many other fields, providing us with a more convenient way of life and playing a significant role in human progress. Social development plays a pivotal role. In summary, speech recognition technology has great research value and application prospects, especially phonetic recognition technology with phonetic symbols as the basic recognition unit, which is outstanding in practical applications under large vocabulary. This has led many researchers to actively participate in the research of phonetic recognition technology.

In the second part of the paper, we organize and summarize the existing research, and in the third part, we provide a detailed description of the specific implementation. In the fourth section, we provide a detailed analysis of the results of the implementation and illustrate the advantages of our results.

2. Related Work

Speech enhancement research based on distributed microphone arrays is a hot topic in speech signal processing that has emerged in recent years. Scholars initially studied this problem based on the topology of distributed microphone placement and proposed some distributed noise cancellation algorithms, when microphones are distributed throughout the observation area to form an array, still transmitting the received signal from each microphone to the fusion center for unified processing [6]. The spoken language evaluation algorithm models the randomness of natural language pronunciation and the instability of speech processing systems through fuzzy measures and plausibility and then integrates them into the Sugeno integral framework to evaluate the language score rather than specific scores. A delay-free subband adaptive filter is used to implement multichannel speech

enhancement in MRI devices. This speech enhancement algorithm is based on a minimum variance estimation criterion to remove noise using a minimum mean square error adaptive filter, where one microphone is used as the reference microphone to receive the noise-containing signal and the other microphones receive only the noise, using the noise as the target signal for the adaptive filter to estimate the source signal [7]. Based on the minimum mean square error criterion to estimate the speech source spectral amplitude and phase, this algorithm assumes that the signal conforms to the Rayleigh distribution and the noise conforms to the Gaussian distribution, which in turn estimates the speech source short-time amplitude spectrum, logarithmic amplitude spectrum, and phase spectrum using the statistical model and the minimum mean square error criterion [8].

Two steps are typically followed in the training of speaking assessment algorithms, namely, score generation and score calibration. Score calibration involves adjusting machine scores and combining scores from multiple divisions, to develop scores that match expert judgments as closely as possible [9]. To achieve this goal, it was necessary to collect data including ratings of pronunciation by human expert evaluators to test the validity of this type of assessment algorithm or system. For reliability assessment, it usually means that the scores obtained by the same test-taker after taking the same test under different test conditions are consistent or highly correlated [10]. Device sensing technology can be divided into five basic categories: vector pressure sensing technology touch screen, resistive technology touch screen, capacitive technology touch screen, infrared technology touch screen, and surface acoustic wave technology touch screen. Traditional speaking tests have experts as scorers, where more factors can lead to unfair scoring, such as scorer evaluation concerns, experience, and ability, age, gender, and psychology. Machine-based speaking assessments, on the other hand, exclude a range of subjective factors that can cause problems, thus ensuring that the speaking assessment algorithm or system has high reliability [11]. Most of these systems are based on ubiquitous learning theory and generally push location-related content information to learners based on their different location information [12].

The focus of research has shifted to the construction of ubiquitous learning environments with a rich variety of implementation technologies [13]. The gradual integration of mobile phones, radios, and sensor technologies into learning activities has facilitated the formation of new learning environments that are highly location-portable and context-aware. From foreign studies, it is found that technologies such as mobile phones, wireless networks, and multimedia are popular in language teaching and learning research. Many researchers had placed RFID tags on top of many objects, and sensors can sense these objects when learners are near, allowing the learners' mobile devices to receive information about these objects [14]. Most of the platforms targeting language learning or context awareness lack and should have empirical studies and rarely do long-term tracking of the systems, but there is no shortage of new technologies introduced and applied. The corresponding system platforms pay attention to theoretical guidance, as well as the analytical design and implementation techniques of the whole system [15]. In addition, although domestic language learning systems make use of the characteristics of mobile devices, they seldom point to specific should-Chan scenarios or contextual information as well as lack specific feedback mechanisms and are rarely integrated with specific speaking instruction.

3. Analysis of English Pronunciation Signal Acquisition and Phonetic Calibration with Multimodal Intelligent Acoustic Sensors

3.1. Multimodal Intelligent Acoustic Sensor Sound Acquisition Design. Acoustic emission is a type of elastic wave, and in the real environment, it can be divided into transverse waves, longitudinal waves, and surface waves, depending on how the sound waves propagate in the medium and the direction of vibration. When propagating in solids, it causes local deformation of the medium, and two types of waves appear simultaneously: longitudinal (compressional) and shear (transverse) waves, which have different speeds and are automatically separated after leaving the source [16]. When the acoustic signal propagates to the junction of air and solid media, the acoustic wave is reflected and refracted, which causes it to undergo a waveform transition, followed by the simultaneous appearance of two waveforms. On free surfaces, acoustic emission waves also form surface waves, and plate waves are generated when the thickness of the solid medium is like the wavelength. After reflection and other transformations of the acoustic signal, the various forms of sound waves will be transmitted to the sensor according to their wave speed, time sequence, and wave range, so that the pulsed signals generated by the acoustic emission sources can be superimposed on each other to produce long and complex waveforms. The online learning environment provides course resources for learning management. Students carry out independent learning, teachers assist through inspiration and demonstration, and students learn cooperatively, communicate with each other, and share wisdom.

When the device receives an acoustic signal, the alternating forces during the resonance of the sound on the piezoelectric film will cause deformation of the PVDF-TrFE piezoelectric film, which causes a piezoelectric effect and generates an electrical charge. To accurately measure the voltage signal generated on the PVDF-TrFE piezoelectric film due to the piezoelectric effect of the acoustic device in operation, we use function generators, ultrasonic transducers, loudspeakers, high sampling rate voltage data acquisition cards, electronic computers, and software data analysis to build a test platform for acoustic device performance characterization, and as shown in Figure 1, the working principle of the experimental platform is as follows: use function generator to generate alternating voltage and frequency-controlled electrical signal, through the ultrasonic transducer electroacoustic conversion, the electrical signal into the required acoustic signal, or use the electronic

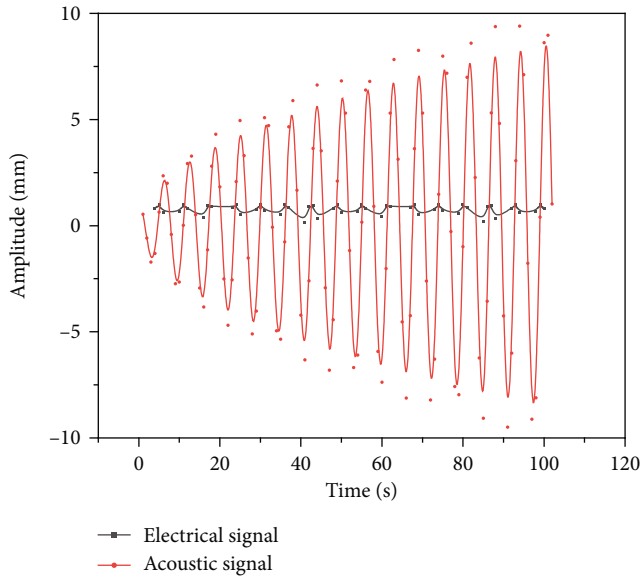

Figure 1: Simplified waveform diagram of the acoustic emission signal.

computer connected to the speaker to play the required sound samples, the acoustic signal reached the PVDF-TrFE thin-film acoustic device, through the high sampling rate voltage data acquisition card for the device response voltage signal acquisition. The voltage signal is recorded, analyzed, and processed by an electronic computer and software.

An acoustic emission signal is a process in which the emission signal reaches its highest amplitude and then gradually decays. The ringing count reflects the number and frequency of acoustic emission events, and the amplitude is the maximum amplitude of the signal waveform, which is used to distinguish the type of wave source as well as to measure the strength of the wave. The duration is the time from when the acoustic signal first rises above the threshold limit to when it falls to the threshold. The rise time is the time when the acoustic emission signal first exceeds the threshold to reach its maximum amplitude. The mathematical expression can be expressed as a decaying sine function as shown in Equation (1).

$$x(t) = A_0 \exp(\alpha t) \cos(\pi f_0 t). \quad (1)$$

A is the amplitude of the acoustic signal P_a; α is the attenuation factor of the signal; f_0 is the resonant frequency of the acoustic emission sensor (Hz). When there is acoustic emission generation, the acoustic emission sensor located on the surface of the component or inside the component converts the acoustic signal into an electrical signal, amplifies it through a signal amplifier, and then after acquisition and data processing, analyzes the relevant characteristic parameters and calculates the specific location of the measured acoustic emission source by combining mathematical geometric formulae with data analysis.

The MZI-based wavelength demodulation technique is based on the sensing principle of fiber optic interferometer, by converting the DFB fiber laser sensor wavelength drift into phase change after entering the nonequilibrium fiber interferometer, and using the high-resolution phase demodulation technique can finally get the sensor weak wavelength change [17]. It transmits the narrow-band laser to the MZI by exciting the 980 nm pump light source and 980/1550 nm fiber wavelength division multiplexer (WDM) guide and DFB fiber laser sensor output, and then convert its optical signal into an electrical signal output by photodetector; by the demodulation system for the analysis of data processing, the output electrical signal is proportional to the magnitude of the acoustic signal.

In the actual environment, the speech signal observed by each microphone in the array will be disturbed by some environmental signals such as noise and reverberation, and there are two common microphone array signal models, the ideal model and the actual reverberation model. The ideal model considers an array of N microphones, and the array structure is chosen to be either one of the structures, and let the source signal be $s(t)$; then, the signal observed by the ith microphone $y_i(t)$ can be expressed as follows:

$$y_i(t) = \alpha_i s(t + \tau_i) - n_i(t), \quad (2)$$

where α_i is the attenuation coefficient of the source signal due to distance, τ_i is the time delay of the source signal to the ith microphone, $n_i(t)$ represents the background noise at the ith microphone, and t is the time factor. Since the actual environment contains other disturbances such as reverberation and multipath effects, for an array of N microphones, let the source signal be $s(t)$ and the acoustic transfer function from the source to the ith microphone be h_i; then, the signal observed by the ith microphone $y_i(t)$ can be expressed as follows:

$$y_i(t) = h_i s(t) * s(t) - n_i(t). \quad (3)$$

For the ideal model, the acoustic transfer function can be equated as follows:

$$h_i s(t) = \alpha_i s(t + \tau_i), \quad (4)$$

where $z(t)$ is the output beamforming result and α_i is the weighting factor, generally taken as $1/N$. This can be described by the following expression.

$$z(t) = \sum_{i=1}^{N} \alpha_i y_i(t + \tau_i). \quad (5)$$

Wireless sensor networks (WSNs) consist of multiple inexpensive miniature sensor nodes, and each node contains one or more sensors, which constitute a distributed network with less power consumption and lower cost through wireless collaborative information sharing, which are used in a wide range of applications such as environmental science, medical health, space exploration, remote environmental monitoring, and target tracking. Especially in recent years, the development of smaller, cheaper, and smart sensors has greatly enhanced the scope of wireless sensor network

applications [18]. Sound wave is a mechanical wave, generated by the vibration of an object (sound source); the space in which the sound wave propagates is called the sound field. It is a longitudinal wave when propagating in gas and liquid media but may be mixed with transverse waves when propagating in solid media. These wireless sensors are equipped with wireless interfaces for communicating with each other to form a network. These sensors are smaller and are capable of only limited computation and processing of information or data at a low cost compared to conventional sensors. These sensor nodes can collect information by sensing and measuring in the environment and can transmit the sensed data to the user based on some local discriminant criterion. In this paper, we focus on speech processing; at this point, the sensors become microphone sensors, so this network is also called wireless acoustic sensor networks (WASNs).

Acoustic sensors are mainly used for sensing and measuring environmental information; processors and memories perform limited processing and storage of data; power supplies are generally composed of batteries, which are the main energy for this sensor network and are limited in energy; wireless transmitter-receiver devices are used for information transmission between nodes, and actuators are mainly for local discrimination (see Figure 2 for the specific structure).

For unstructured WASNs, network maintenance management and detection of faults are more difficult due to many nodes. In contrast, for structured WASNs, some or all the sensor nodes are arranged in a way that is required for certain purposes. The advantage of structured networks is the ability to deploy fewer nodes to obtain smaller network maintenance and management costs. But fewer nodes mean that providing network coverage is significantly reduced.

Unlike traditional networks, wireless acoustic sensor networks are subject to design and resource constraints. Resource constraints include limited energy per node, short communication range, low bandwidth, and limited computational and storage capacity. Design constraints are application-dependent and based on the environment being monitored. The environment plays a key role in the size of the network, the deployment scheme, and the network topology. The size of the network varies with the environment being monitored. For an indoor environment, a network can be formed with fewer nodes, while an outdoor environment may require more nodes to cover a larger area. Obstacles in the environment can also limit communication between nodes, which in turn can interfere with the connectivity of the network. Acoustic measurement software is a measurement software that runs on a smartphone or tablet PC. It is paired with an instrument to achieve accurate measurements and supports acquisition of measurement data from WIFI and analysis of calculations.

3.2. Experimental Design for English Pronunciation Phonetic Calibration. Due to the coarticulation phenomenon, phonetic pronunciations do not exist completely independently in time, and neighboring phonetic pronunciations partially overlap and influence each other [19]. These indicate the need to apply features that can capture long-time information in speech recognition. To address the above problem, we try to extend the spectral features in the time domain by combining the Mel subband energy of the current frame and the subband energies of multiple frames before and after it to obtain the time-domain extended features, which are called temporal pattern (TRAP) features. The extraction process of TRAP features is shown in Figure 3.

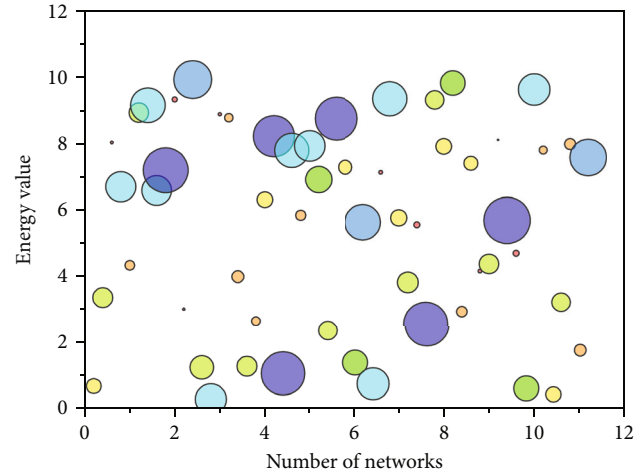

Figure 2: Wireless acoustic sensor network with 20 nodes.

First, the speech signal is windowed in frames, and the energy value of the output of each frame through the Mayer filter bank is calculated. And with the current frame as the center point, the same number of frames is taken before and after, and these several frames' features are concatenated to get a long-time feature. Then, the DCT method is used for dimensionality reduction, and the features are normalized on the mean and variance to finally obtain the TRAP features. TRAP reflects the long-time feature variation and effectively exploits the correlation between speech signals. Compared to short-time features such as MFCC, TRAP features effectively exploit the correlation between speech signal contexts, which not only improves the noise robustness of acoustic features, but it helps to solve the copronunciation phenomenon among phonetic features, which can improve the performance of speech recognition.

Phoneme posterior probability features are commonly used feature representations in speech recognition with high discriminative and robust features. Define the phoneme model space to consist of M classes (for an English corpus with 39 phonemes); then, $M = 39$. Then, the phoneme posterior probability feature vector for a frame of speech at moment t is as follows:

$$P_t = \{p(s_1|o_t), p(s_2|o_t), \cdots, (s_i|o_t), \cdots, (s_M|o_t)\}, \quad (6)$$

where o_t denotes the corresponding speech frame at that moment and s_i denotes the corresponding ith phoneme; then, $p(s_1|o_t)$ denotes the posterior probability that the

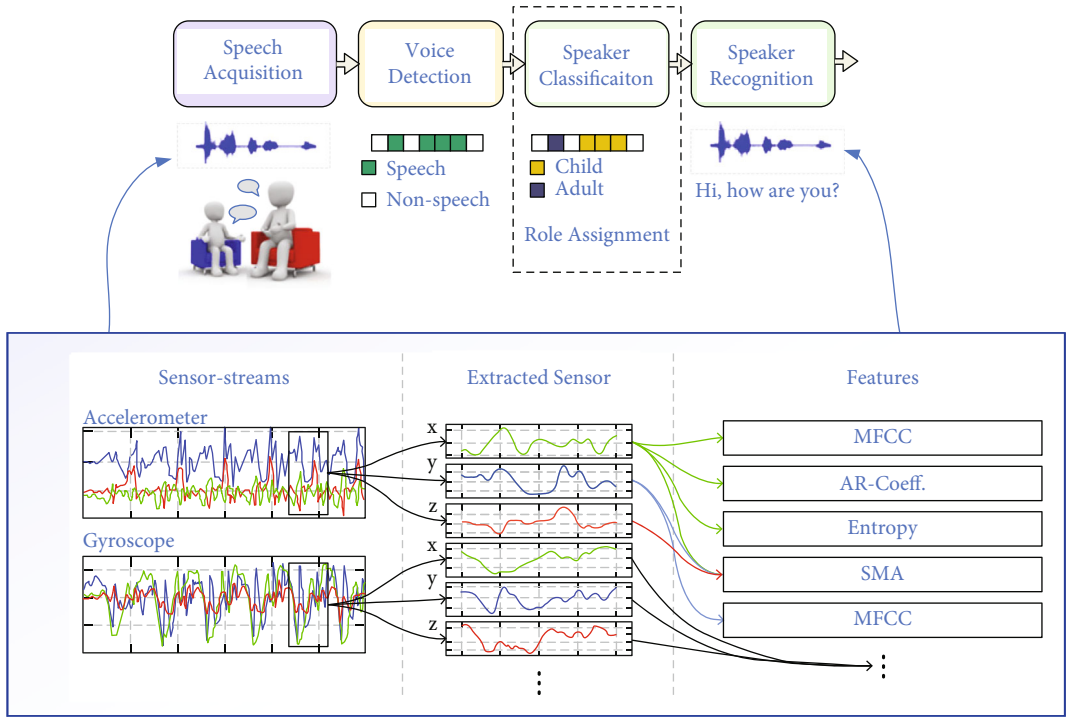

Figure 3: TRAP feature extraction process.

corresponding phoneme is s_i for a known speech frame o_t.

$$\sum_{i=1}^{M} p(s_1|o_t) = 2. \tag{7}$$

Rhythmic features are a typical feature of natural human language, with many common features across languages. When people communicate with each other using language, it is not only the phonetic sounds of the words but also the suprasegmental information of the language, i.e., the rhythmic features, which play a very important role in the naturalness and intelligibility of the language. Rhythmic features respond to variations in pitch, length, and intensity in addition to phonetic features: variations in pitch form the tone of speech, variations in length from the length of speech, and variations in intensity from the stress. Speech rhythm features are widely used in the fields of speech recognition, speaker recognition, and language recognition because of the rich dynamic information they carry. No state can be transferred to any of the previous states:

$$a_{ij} = 0, j \geq i. \tag{8}$$

A GMM model is a multidimensional probability density function model that utilizes a weighted sum of multiple Gaussian probability density functions to represent arbitrary probability distributions. For example, Equation (9) is a GMM model with M Gaussian components:

$$p\left(\vec{x}|\lambda\right) = \sum_{i=1}^{M} w_i p\left(\vec{x_i}|\mu_i\right), \tag{9}$$

$$\sum_{i=1}^{M} w_i = 2. \tag{10}$$

The ball in Equations (9) and (10) is a D-dimensional eigenvector, $p(\vec{x_i}|\mu_i)$ is the probability density function of one of the Gaussian components, μ_i denotes the mean vector of the Gaussian components, and $\vec{x}$ is the covariance matrix and is calculated in Equation (11).

$$p\left(\vec{x_i}|\mu_i\right) = \frac{1}{2\pi\sum_i i^2} \exp\left[\frac{1}{2}\left(\vec{x} - \mu_i\right)^T \sum_i i^2 \left(\vec{x} - \mu_i\right)\right]. \tag{11}$$

The observed probability distribution is what is characterized using the GMM model, and the superiority of the GMM as an observed probability model is that the continuous distribution model provides a more accurate description of the probability distribution compared to the discrete or semicontinuous model. This is because the characteristics of the inputs in the continuous distribution model do not need to be quantified. In addition, GMM models can fit arbitrary distributions infinitely accurately by increasing or decreasing the number of mixing components. Thus, the CMU-SPHINX phoneme recognition mechanism sees distribution of a single Gaussian distribution when the state is not bound at the beginning of parameter training. The state binding complicates the model parameters by Gaussian splitting, which in turn leads to more accurate parameter estimates, as shown in Table 1.

According to the dynamic programming principle, the optimal path has the property that if the optimal path passes through node r_i at time t_i, then the partial path of this path

Table 1: Steps of Viterbi algorithm.

(1) Initialization	$\delta_1 = \pi_i b_i(o_1), i \in N$ $\psi_i(i) = 1, i \in N$
(2) Recursion	For $t = 2, 3, \cdots, T$ $\psi_{it}(i) = \arg\min \pi_i b_i(o_1), i \in N$ $\delta_t(i) = \min \pi_i b_i(o_1), i \in N$
(3) Termination	$P^* = \max \psi_{it}(i)$ $S^* = \arg\max \psi_{it}(i)$
(4) Optimal path backtracking	For $t = T-1, T-2, \cdots, 0$ $s_t = \psi_{t+1}(s_i)$
(5) Find the optimal path S^*	$S^* = (s_1, s_2, \cdots, s_N)$

from node r_i to endpoint p_i must be optimal for all possible partial paths from t_i to r_i. For if this is not the case, then another better partial path exists from t_i to r_i. If it is connected to the partial path from t_i to p_i, it will form a path that is better than the original path, which is contradictory. According to this principle, we only need to compute recursively the maximum probability of each partial path with state i at moment $t = 1$ until we get the maximum probability of each path with state i at moment $t = T$. The maximum probability at moment $t = T$ is the probability of the optimal path, and the endpoint p_i of the optimal path is obtained at the same time. After that, to find the individual nodes of the optimal path, starting from the endpoint r_i, the nodes are gradually solved from back to front $i_{T-1}, i_{T-2}, \cdots, i_T$, and the optimal path is obtained $I = (i_{T-1}, i_{T-2}, \cdots, i_T)$.

The preparation of data has always been a prerequisite and key to system experiments. Especially in systems using fully connected neural networks as the underlying model, when the number of input and hidden layer neurons is relatively large and the number of model parameters is huge, the need for a large amount of training data is more urgent. Only by collecting enough training data can the acoustic model be trained more adequately and accurately. In addition, the quality of the data preparation is also essential for the training of good acoustic models. When the quality of the prepared data is poor, it will lead to the existence of outliers, which will affect the accuracy of the model training. Resource limitation is the speed of program execution limited by computer hardware resources or software resources during concurrent programming. In concurrent programming, the principle of making code execution faster is to turn the serial part into concurrent execution. A tree network can contain branches, and each branch can contain multiple nodes. The tree topology is an expanded form of the bus topology, and the transmission medium is an unclosed branch cable. The tree topology is the same as the bus topology, where one station sends data and all other stations can receive it.

The meaning of tree topology network is the network left by removing the edges that form a circle (ring) in the network, like the spanning tree algorithm [20]. This network has a minimum connection structure and most efficient information transfer rate and is suitable for information transfer between nodes. This topological network uses the knowledge of tree to divide the adjacent nodes into parent and child nodes so that information transfer can be divided into two processes: convergence and dispersion. Convergence starts from the leaf nodes, and the child nodes converge their information to the parent nodes to the root node; dispersion is exactly the opposite, starting from the root node and the parent node disperse their information to the child nodes, all the way to the leaf nodes, to achieve all nodes can get consistent fusion results, and due to the use of spanning-tree structure, in each node, just convergence or dispersion process can greatly reduce the duplication of information transmission, improve the efficiency of information transmission, and reduce the energy overhead of the sensor network, as shown in Algorithm 1.

Students can easily use the online communication function provided by mobile terminals for discussion and interaction when learning English speaking around the location context. According to the participating objects, this communication includes teacher-student and student-student communication; according to the timeliness of communication, the communication can be divided into synchronous and asynchronous communication; according to the form of communication, it can be divided into text communication, voice communication, and video communication. Learners can ask questions online about the problems they encounter in learning spoken English, and they can also answer other people's questions, making communication more convenient. In addition, learners can also expand the field of interaction through the social sharing function provided by the system. Through discussion and interaction, learners can enhance their internalization of speaking knowledge.

The first layer is the response layer, which considers the system's response and satisfaction to the learners; while the second layer is the learning layer assessment, which measures the users' understanding and proficiency in English-speaking learning such as English knowledge, speaking skills, and attitudes. Given the minimum period of two years required for the assessment of the behavioral and outcome layers of the Koch model, the period is too long, and the students who participated in this experiment have already graduated. Therefore, this study assessed the effects of the positional context in terms of the first two layers of learner response and cognitive transfer. It is important to note that this implementation is not a true, rigorous experiment in the true sense of the word, but rather a design-based research approach to explore the effects of positional contexts to be closer to natural contexts and closer to reality.

4. Analysis of Results

4.1. Performance Results of Multimodal Smart Acoustic Sensors. From Figure 4, the 20 nodes of the simulated wireless acoustic sensor network are relatively evenly distributed, and there is no node overlap, and cover the whole 10 m * 10 m plane area. The whole network edge connection is more reasonable, satisfying the experimental hypothesis, and closer to the real environment. It can also be found that no matter for noise-containing sources or clean noise-free sources, it is clearer to distinguish the speech-free segments

1: Input: The matching scores of the two classifiers are respectively denoted as X=(X, X), X=Px, |R), X,=Py, R), i=1,2.... N, j =1,..,k; N represents a total of N categories, and k represents a total of k samples. α is the weight of the fingerprint identification system; α is the weight of the voiceprint system: o is the quality threshold. In addition, set o to be the average score value obtained by the current user paired with N templates.
2: output: which category the feature belongs to
3: loop
4: if $\delta_t(i) = \min \pi_i b_i(o_1), i \in N$
5: if $h_i s(t) = \alpha_i s(t + \tau_i)$
6: return $\sum_{i=1}^{M} p(s_1|o_t) = 2$
7: else $p(\vec{x}|\lambda) = \sum_{i=1}^{M} w_i p(\vec{x_i}|\mu_i)$
8: return z(t) = $\sum_{i=1}^{N} \alpha_i y_i(t + \tau_i)$

Algorithm 1: Algorithm pseudocode.

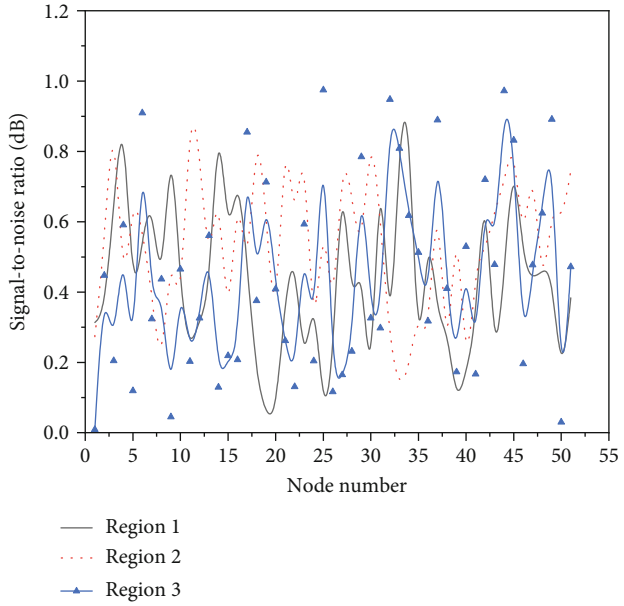

Figure 4: Nodal signal-to-noise ratio.

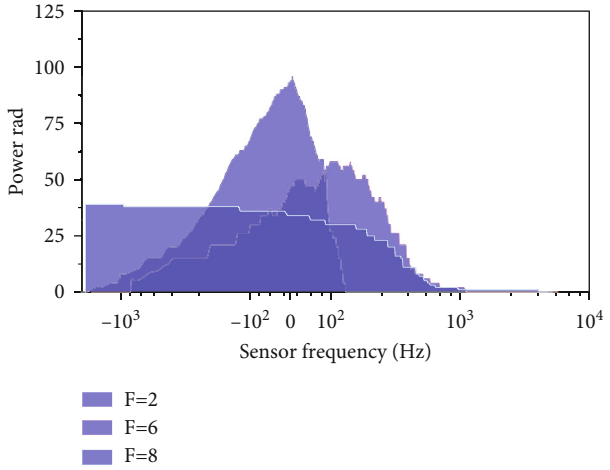

Figure 5: Bandwidth test results of fiber laser sensor demodulation system.

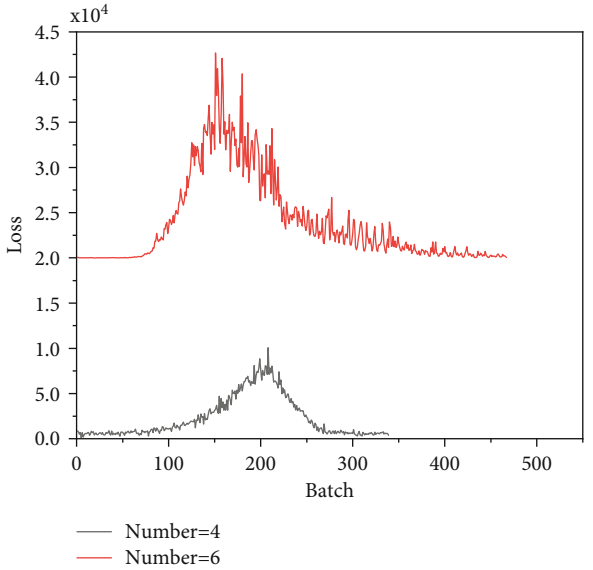

Figure 6: Variation of loss function.

from speech-containing segments, which is more conducive to estimating the noise power spectrum by VAD method and paving the way for the subsequent speech enhancement by using beamforming algorithm.

After transmission noise addition, the signal received by each node contains significant noise and has a large difference in signal-to-noise ratio, some are still higher, such as 12.5 dB for node 5, and some are lower, such as -1.18 dB for node 18. At this point, speech enhancement must be performed to obtain a better output for the whole node. So, after that, these two special cases are selected for experimental observation to confirm the effectiveness of the algorithm in this paper. Neural networks have a wide and attractive prospect in the fields of system identification, pattern recognition, and intelligent control. Especially in intelligent control, people are particularly interested in the self-learning function of neural networks and regard this important feature of neural networks as one of the keys to solve the difficult problem of controller adaptability in automatic control.

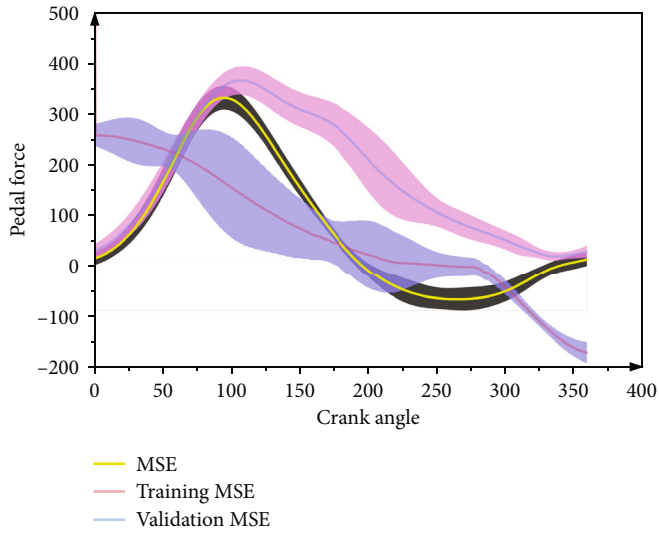

Figure 7: Phonetic calibration change curve.

Due to the unique directivity characteristics of the DFB fiber laser sensor, the acoustic emission sensor was pressed onto the pigtail of the DFB fiber laser sensor, allowing for a complete acoustic emission signal with maximum responsiveness in the axial direction, and a 100 mW pump laser output was loaded on the DFB fiber laser sensor, allowing the DFB fiber laser sensor to reflect a sufficiently large light intensity. The bandwidth of the demodulation system was tested using a 2 MHz wide band acoustic emission sensor transmitting acoustic wave signals from 20 kHz to 2 MHz as shown in Figure 5. The results of the bandwidth test of the fiber demodulation system are shown in Figure 5. The signals of the acoustic emission transducer operating at 20 kHz, 40 kHz, 100 kHz, 1000 kHz, 1500 kHz, and 2000 kHz were tested separately. It was able to obtain that the DFB demodulation system can stably demodulate acoustic waves from 20 kHz to 2 MHz frequency, and the small resonance does not have a large impact on the main frequency. Also, when the sampling rate is F and the number of sampling points is set to N, the frequency resolution can be derived from the fast Fourier change equation.

The delay caused by the system is unavoidable and will have a large impact on the accuracy during the positioning process, so the system delay needs to be calibrated. A self-transmitting signal generator was used to transmit a signal with a center frequency of 100 kHz from the acoustic emission sensor for the experiment. The fiber laser sensor is placed on a 2 cm thick Plexiglas plate, impedance matching is performed using an ultrasonic coupling agent, and the acoustic emission sensor is placed on the back of the Plexiglas plate to emit a 1 kHz pulse signal.

Sixteen acoustic emission signal points at fixed locations were acquired and demodulated and localized by the hyperbolic localization method, with 10 measurements per point and averaged as the result. The minimum error of the 16 acoustic emission sources of the hyperbolic localization algorithm is 0.35 cm, and the maximum error is 0.98 cm, in which the average error of the horizontal axis is 0.39 cm and the average error of the vertical axis is 0.45 cm, and the summation of the errors of these 16 sources is averaged to obtain the overall localization error of 0.67 cm. The model constructs the initial load of a node from the global and local perspectives by combining the node mesonumber, node degree, node weight, and neighbor node weight and establishes the proportional relationship between the node capacity and the initial load. When a node fails, the load redistribution rules are formulated by combining the capacity of the neighbors of the failed node, and then, the evolutionary process of the load parameters is deduced through the analysis of the network cascade failure, resulting in the parameters in the model.

4.2. English Pronunciation Phonetic Calibration Results. It can be seen from Figure 6 above that the loss function of the training process of the neural net will occur a steep drop in the initial stage of training, after which it will gradually smooth out. However, the change of the loss function in this experiment is still drastic near the end of the training, indicating that the learning rate is set too large in the end stage, causing the loss function to oscillate too much and make it difficult to converge. Since the learning rate of the neural network is updated in epochs, Figure 6 shows the change of the loss function at the end of each epoch. It is seen through Figure 6 that the number of iterations in this experiment is low, and there is still a large reduction in the loss function at the end of training. Therefore, an attempt was made to change the training end condition to make the model more fully trained and to increase the initial learning rate to prevent a local optimum.

It is seen that the number of iterations becomes more in this experiment, and the value of the final loss function is smaller than that of the last experiment, indicating that the training is more adequate this time. It can also be seen that the recognition rate of the system has been improved after the network parameters have been adjusted.

To test whether the model has high variance or high bias and whether collecting more data would help solve this problem, we use learning curve in sci-kit-learn, which is used to return test scores for different size datasets, and use matplotlib's plot with the "fill_between" function to add the standard deviation of the MSE to the plot to obtain the learning curve of the model as shown in Figure 7. The scores obtained by using 10-fold cross-validation are calculated. For the mean and standard deviation of MSE, the fold line represents the corresponding mean MSE at the size of this dataset, and the band around the fold line indicates the fluctuation range of MSE, where blue represents the training set and the green represents the test set. It can be found that the MSE of the model is stable around 0.0026, compared to the slightly larger standard deviation of MSE in the test set, but the fluctuation range is between 0.0022 and 0.0031 with less variation in the values.

It can be found that the learning effect in the elastic network has been greatly improved. The linear regression results are more unstable, and the reasons for this result are that there is still covariance in the parameters of the model or the model is overfitted, which makes the model ineffective, but these problems are well circumvented in the elastic network. In the learning layer, students' attitude towards learning spoken English through M-Oral was more positive and they imitated the pronunciation of authentic spoken English more during the interaction. The observation shows that compared to the control group, the experimental group is more motivated to learn spoken English due to the simulation of contextual perception.

5. Conclusion

Around the feature extension perspective, vocal recognition technology is introduced and a Bayesian decision-based dynamic weight bimodal fusion algorithm is proposed to alleviate the unimodal biometric feature acquisition; recognition generic drawbacks in addition to making the recognition rate of the small area improved and improving the performance of the algorithm. The algorithm determines the classification weights of the two recognition modalities in that environment by adaptive weights and finally fuses them at the decision level based on the weights. The theory of the algorithm is based on Bayesian decision-making which minimizes the cost of classification errors and improves the inflexibility problem caused by traditional fixed-weight fusion. Distributed consistency-based and distributed speech enhancement algorithm: this algorithm decomposes the traditional array algorithm to each wireless acoustic sensor network node, transforms distributed speech enhancement into a distributed consistency problem, and then achieves consistency averaging based on a distributed consistency iterative algorithm. In the process of consistency averaging, an average Metropolis right is proposed in this paper, and the experimental results show that the efficiency of iteration based on this right can be second only to the consistency iteration algorithm based on the optimal constant right and outperforms the consistency iteration algorithm based on the maximum degree right and Metropolis right. The speech enhancement effect of this algorithm can achieve the effect of the algorithm containing the fusion center, and the signal-to-noise ratio of the enhanced speech of each node can approximate the source, which can offset the signal energy attenuation caused by the distance. For English speech sound data, the changes of the loss function during the training of the neural network of the LC-RC system are tracked, and the learning rate and iterations of the benchmark system are optimized as necessary according to their changes, and certain results are achieved.

Data Availability

The data used to support the findings of this study are available from the corresponding author upon request.

Conflicts of Interest

The authors declare that they have no known competing financial interests or personal relationships that could have appeared to influence the work reported in this paper.

Acknowledgments

This work was supported by the Henan Province Curriculum Ideological and Political demonstration course project, Higher Vocational English course, Jiaozhicheng (2021), No. 138 document No. 65.

References

[1] K. Saito, "Individual differences in second language speech learning in classroom settings: roles of awareness in the longitudinal development of Japanese learners' English/ɹ/pronunciation," *Second Language Research*, vol. 35, no. 2, pp. 149–172, 2019.

[2] K. Saito, "The role of aptitude in second language segmental learning: the case of Japanese learners' English/ɹ/pronunciation attainment in classroom settings," *Applied PsychoLinguistics*, vol. 40, no. 1, pp. 183–204, 2019.

[3] K. Saito, Y. Suzukida, and H. Sun, "Aptitude, experience, and second language pronunciation proficiency development in classroom settings: a longitudinal study," *Studies in Second Language Acquisition*, vol. 41, no. 1, pp. 201–225, 2019.

[4] I. G. Jayantini, I. B. Yadnya, I. N. Suparwa, and I. A. Puspani, "Translating English medical terms into Indonesian: a study of phonological translation and spelling adjustment," *International Journal of English Language & Translation Studies*, vol. 5, no. 3, pp. 86–95, 2017.

[5] C. Nance, "Bilingual language exposure and the peer group: acquiring phonetics and phonology in Gaelic Medium Education," *International Journal of Bilingualism*, vol. 24, no. 2, pp. 360–375, 2020.

[6] A. M. Al-Rubaat and H. A. Alshammari, "Analysis of phonetic and phonological constraints of Saudi EFL learners," *English Language Teaching*, vol. 13, no. 1, pp. 63–72, 2019.

[7] P. Fabre-Merchan, G. Torres-Jara, F. Andrade-Dominguez, M. J. Ortiz-Zurita, and P. Alvarez-Munoz, "A phenomenological study: the impacts of developing phonetic awareness through technological resources on English language

learners'(ELL) communicative competences," *English Language Teaching*, vol. 10, no. 12, pp. 83–87, 2017.

[8] W. L. Law, O. Dmitrieva, and A. L. Francis, "Language attitudes modulate phonetic interactions between languages in bilingual speakers in diglossic settings," *Linguistic Approaches to Bilingualism*, vol. 11, no. 3, pp. 289–322, 2021.

[9] J. Suntornsawet, "Problematic phonological features of foreign accented English pronunciation as threats to international intelligibility: Thai EIL pronunciation core," *Journal of English as an International Language*, vol. 14, no. 2, pp. 72–93, 2019.

[10] T. Zarifian and M. Fotuhi, "Phonological development in Persian-speaking children: a cross-sectional study," *International Journal of Speech-Language Pathology*, vol. 22, no. 6, pp. 614–625, 2020.

[11] J. Fouz-González, "Podcast-based pronunciation training: enhancing FL learners' perception and production of fossilised segmental features," *ReCALL*, vol. 31, no. 2, pp. 150–169, 2019.

[12] T. A. Barriuso and R. Hayes-Harb, "High variability phonetic training as a bridge from research to practice," *CATESOL Journal*, vol. 30, no. 1, pp. 177–194, 2018.

[13] T. Cadierno, M. Hansen, J. T. Lauridsen et al., "Does younger mean better? Age of onset, learning rate and shortterm L2 proficiency in young Danish learners of English," *Vigo International Journal of Applied Linguistics*, vol. 17, no. 17, pp. 57–86, 2020.

[14] E. L. Zen, "Role of regional language background and speech styles on the production of Voice Onset Time (VOT) in English among Indonesian multilinguals," *Indonesian Journal of Applied Linguistics*, vol. 10, no. 2, pp. 359–368, 2020.

[15] R. Mayr, L. Roberts, and J. Morris, "Can you tell by their English if they can speak Welsh? Accent perception in a language contact situation," *International Journal of Bilingualism*, vol. 24, no. 4, pp. 740–766, 2020.

[16] S. Kirkham and K. M. McCarthy, "Acquiring allophonic structure and phonetic detail in a bilingual community: the production of laterals by Sylheti-English bilingual children," *International Journal of Bilingualism*, vol. 25, no. 3, pp. 531–547, 2021.

[17] J. Fouz-González and J. A. Mompean, "Phonetic symbols vs keywords in perceptual training: the learners' views," *ELT Journal*, vol. 75, no. 4, pp. 460–470, 2021.

[18] K. Saito, J. M. Dewaele, M. Abe, and Y. In'nami, "Motivation, emotion, learning experience, and second language comprehensibility development in classroom settings: a cross-sectional and longitudinal study," *Language Learning*, vol. 68, no. 3, pp. 709–743, 2018.

[19] P. Eckert and W. Labov, "Phonetics, phonology and social meaning," *Journal of SocioLinguistics*, vol. 21, no. 4, pp. 467–496, 2017.

[20] R. Kopečková, C. Dimroth, and U. Gut, "Children's and adults' initial phonological acquisition of a foreign language," *Journal of Second Language Pronunciation*, vol. 5, no. 3, pp. 374–401, 2019.

Hindawi
Journal of Sensors
Volume 2022, Article ID 1308615, 12 pages
https://doi.org/10.1155/2022/1308615

Research Article

Design of Centralized Heating Monitoring System Based on Wireless Sensor Networks

Xiangting Jiang,[1] **Yaojun Lv**,[1] **and Haoran Yan**[2]

[1]*School of Energy and Power Engineering, Changchun Institute of Technology, Changchun, Jilin 130012, China*
[2]*School of Management, Changchun Institute of Technology, Changchun, Jilin 130012, China*

Correspondence should be addressed to Yaojun Lv; 1817300035@e.gzhu.edu.cn

Received 9 November 2021; Revised 9 December 2021; Accepted 16 December 2021; Published 2 March 2022

Academic Editor: Gengxin Sun

Current centralized heating monitoring system has realized the collection and control of working condition data in heating power stations, but there are still some shortcomings, such as the inability to collect data on the working conditions of user sides, and the inability to meet the further demand of heating enterprises for the refinement of heating network monitoring data. A wireless sensor network is a fully distributed sensor system with no central node, which can intensively deploy many sensor nodes to monitoring area through random placement, and integrates sensors, data processing and communication modules to form a self-organized network system. Therefore, in order to realize the intelligence of heating system and improve the flexibility of node data collection, the monitoring system can use wireless sensor network technology to realize wireless collection of node data, and display the collected data on a man-machine interface in real time. On the basis of research results from previous scholars, this paper expounds the research status and significance of centralized heating monitoring system design, elaborates the development background, current status and future challenges of wireless sensor network technology, introduces the methods and principles of wireless network communication protocol and heating and heat balance flow analysis, proposes a structural model of a centralized heating monitoring system based on wireless sensor networks, carries out the design of perception and convergence nodes, analyzes the layout of wireless sensor networks, explores the design scheme of centralized heating monitoring system based on wireless sensor networks, conducts the hardware and software design of the monitoring system, implements the software testing and hardware debugging of the centralized heating monitoring system, and finally discusses the relationship between data transfer related tasks and task scheduling. The study results show that the application of the centralized heating monitoring system based on the wireless sensor networks can not only more conveniently monitor, control and manage the entire heating networks, but also make full use of the centralized monitoring and quantitative management functions of the wireless sensor networks. This achieves dynamic tracking and monitoring of heating operation, real-time diagnosis of hidden dangers in heating operation, and safe, normal and energy-saving operation of the centralized heating system. The study results of this paper provide a reference for further researches on the design of centralized heating monitoring system based on wireless sensor networks.

1. Introduction

Centralized heating has become a main method for house heating in many areas. Centralized heating technology is currently relatively mature, has high safety, can effectively reduce environmental pollution, and is easy to achieve scientific management of heating. However, traditional centralized heating has problems such as uneven heating, local overheating, and outdated monitoring systems [1]. Therefore, centralized heating monitoring systems developed based on information technology have been widely promoted and applied. The current centralized heating monitoring system realizes the data collection and control of the heating power station, but there are still some shortcomings [2]. The wireless sensor network technology collects processes and displays the operating data of the thermal station, automatically adjusts, detects faults, diagnoses and alarms, calculates cumulative heat consumption, and prints reports.

For example, it cannot realize the user-side data collection and cannot meet the further requirements of the heating enterprise for the refinement of the heating network monitoring data. Therefore, it is important to use more advanced information technology to design a centralized heating monitoring system with more comprehensive functions, more accurate data, and more sensitive operations [3]. In order to realize the intelligence of heating and improve the flexibility of node data collection, the monitoring system can use wireless sensor network technology to realize wireless collection of node data, and display the collected data on the man-machine interface in real time [4].

The wireless sensor network is a self-organized system structure composing a large number of micro sensor nodes deployed in monitoring areas through radio communication. Its purpose is to cooperatively perceive, collect and process the information from the monitored objects and feedback them to observers [5]. These sensor nodes integrate sensors, data processing and communication modules, which are connected through wireless channels and form a self-organized network system [6]. The protocol stack is designed after the investigation of the remote monitoring environment of the urban heat pipe network and the in-depth research on the commonly used communication technologies of wireless sensor networks, and is used for data collection at the user end of the heat network. Some or all of the nodes in the sensor network can be moved and the topology of the sensor network will also dynamically change with the movement of nodes [7]. Wireless sensor network integrates sensor technology, embedded technology, distributed information processing technology and network communication technology. It can monitor, perceive and collect information of various environmental objects in real time collaboratively, and transmit the information to the system user host for analysis and processing [8].

On the basis of research results from previous scholars, this paper expounds the research status and significance of centralized heating monitoring system design, elaborates the development background, current status and future challenges of wireless sensor network technology, introduces the methods and principles of wireless network communication protocol and heating and heat balance flow analysis, proposes a structural model of a centralized heating monitoring system based on wireless sensor networks, carries out the design of perception and convergence nodes, analyzes the layout of wireless sensor networks, explores the design scheme of centralized heating monitoring system based on wireless sensor networks, conducts the hardware and software design of the monitoring system, implements the software testing and hardware debugging of the centralized heating monitoring system, and finally discusses the relationship between data transfer related tasks and task scheduling. Specifically, Section 2 introduces the methods and principles of wireless network communication protocol and heating and heat balance flow analysis; Section 3 proposes a structural model of a centralized heating monitoring system based on wireless sensor networks; Section 4 explores the design scheme of centralized heating monitoring system based on wireless sensor networks; Section 5 discusses the relationship between data transfer related tasks and task scheduling; Section 6 is conclusion.

2. Methods and principles

2.1. Wireless network communication protocol. As the network scale becomes larger, the delay caused by the long back-off time will increase exponentially; and choosing a suitable back-off time strategy can increase opportunistic routing transmission and reduce the end-to-end transmission delay. Suppose the back-off time interval of node i is a_i, the delivery rate between sending node i and node j is a_j, and the forwarding probability of node i continuing to forward to the destination node k after receiving the packet is a_k, then the back-off time A_i is:

$$A_i = \frac{1}{b}\sum_{i=1}^{n}\frac{a_k\left(\|a_i\|^2\right)}{a_j[c(a_i)-c(a_k)]} \tag{1}$$

Where $c(a_i)$ and $c(a_k)$ are the processing time of data packets at nodes i and k, which are determined by the sending node in the data packet; b is a random number that changes with time to prevent node back-off time and the selected node conflicts with other backups.

Assuming that the setting of sensor nodes is basically a relatively uniform random distribution, for any non-empty sub-area b_i in the monitoring area B, $N(b_i)$ represents the number of objects falling in the monitoring area B, then the probability of $N(b_i) = m$ is:

$$P\{N(b_i)=m\} = \frac{1}{l}\frac{(c_i\|b_i\|)^m(b_i-d_i)}{\left[h_i-e^{-m\|g_i\|}\right]f_i[(o_i-p_i)]} \tag{2}$$

Where c_i is the intensity of the random process; d_i is the area of area B; f_i is the input vector, which is the influencing factor; g_i is the output vector, which is the temperature value corresponding to each influencing factor in the time series; l is the correlation coefficient between the influencing factor and the indoor temperature; o_i and p_i are the average values of input parameters and output parameters.

In a wireless heat metering network system, suppose that the heat meter source node needs to transmit q-bit data to the concentrator after multiple hops, and the wireless transmission power can be adjusted. Data transmission needs to be forwarded by q-1 intermediate heat meter nodes, so the total energy consumption $C(q_i)$ of the node transmitting q_i bit data to the concentrator is:

$$C(q_i) = \frac{(q_i-r_i)\cdot(q_i-s_1)}{\sqrt{(q_i-s_2)^2+(q_i-s_3)^2}} \tag{3}$$

Where r_i is the correlation coefficient between the i-1-th hop intermediate node and the i-th hop intermediate node; s_1, s_2, and s_3 are constant factors related to energy consumption, respectively.

The monitoring system uses the existing public facilities in the city to construct a monitoring network. According to

the characteristics of convenient cable wiring inside the heating station, a field bus is used to lay out the local area network. The wireless low-speed network of the wireless sensor network is used at the user end of the centralized heating and the wireless sensor network includes a monitoring center. The sensor nodes are installed on the roof of the building on the user side of the centralized heating that needs to collect data, and the convergent nodes are installed in the heating station. Each sensor local area network is composed of a sink node and multiple sensor nodes. After the nodes are turned on, they automatically form a tree-like hierarchical network with the sink node as the root node. The user-side working condition data of the centralized heating collected by the sensor node is aggregated to the data relay aggregation node by means of wireless jump transmission. The thermal station sensor collects the field working condition data in the thermal station and converge it to the data relay convergent node by the field bus. The protocol stack is designed after the investigation of the remote monitoring environment of the urban heat pipe network and the in-depth research on the commonly used communication technologies of wireless sensor networks, and is used for data collection at the user end of the heat network.

2.2. Flow analysis of heating balance. Considering that the heating network pipes will dissipate heat to the surrounding space uninterruptedly, resulting in significant high-temperature hot spots on the pipe shell or certain components, which constitutes a suitable environmental heat source. The terminal generates an available temperature difference to drive its output power. When the impedance of the load and the thermoelectric module match, the maximum output power D_i can be expressed as:

$$D_i = \left[\frac{z(t_i)}{x(t_i) - y(t_i)}\right] \frac{t_i(u) - v_i(u+1)}{t_i(u) - w_i(u+1)} t_i \in [t_i(u), t_i(u+1)] \tag{4}$$

Where t_i is the material insulation coefficient; u is the pulse interval; v_i is the pulse time interval; w_i is the temperature difference between the hot and cold ends; x is the cross-sectional area of the thermoelectric arm; y is the length of the thermoelectric arm; z is the number of thermocouple pairs inside the thermoelectric device.

When a heat meter is installed in the heating user and the hot water flows through the heating user, the heat meter can calculate and display the heat absorbed by the heating user E_i:

$$E_i = \int_{i=1}^{n} \frac{B_i|C(i)|^2 + D(i)|F(i)|^2}{G(i)|H(i)|^2} \tag{5}$$

Where B_i is the heat absorbed by the heating user; $C(i)$ is the mass flow of water flowing through the heat meter; $D(i)$ is the volume flow of water flowing through the heat meter; $F(i)$ is the heat flowing through the density of the water in the table; $G(i)$ is the difference in enthalpy between the inlet and outlet temperatures of the heating user; $H(i)$ is the time.

During the operation of the centralized heating system, there is unavoidable parameter perturbation due to friction and changes in resistance and capacitance; the system parameters at this time behave as the nominal parameters with an additional amount of change. If the system sensitivity function J is the ratio of the system output change to the controlled object change, then the compensation sensitivity function $J(i)$ is:

$$J(i) = \sum_{i=0}^{t}[K(i)L(i)] = \sum_{i=0}^{t} \frac{M(i)N(i)}{O(i)P(i)} \tag{6}$$

Where $K(i)$ is the nominal transfer function of the controlled system; $L(i)$ is the multiplicative perturbation; $M(i)$ is the perturbation bound function; $N(i)$ is the amplifier coefficient; $O(i)$ is the input voltage control signal; $P(i)$ is the voltage signal returned by the position feedback.

The server collects and stores data from each client site in real time, and monitors the operation of each site in real time. The control layer is located in the substations of each thermal power company. After the software is started, it is initialized first. The node is in a sleep state by default, waiting to receive data. When the node receives data through the radio frequency module or its own sensor senses the data, it is awakened, processed data and sent to the next node when the sending cycle arrives or the cluster head node. The automatic processing is the ability to automatically perform self-adjustment control or alarm by means of text messages, phone calls, sound and light, email, etc., and notify the computer room management personnel in time. In this protocol, the sensing node has four states: sensing, forwarding, sensing and forwarding, and inactive. The protocol also divides the time frame into a data transmission phase, a refresh phase, a recombination phase caused by a refresh, and an event-triggered recombination phase. The sink node exchanges data with the cluster head node through the radio frequency module, and communicates with the host computer through the serial port. Therefore, the sink node can be awakened by radio frequency data, and it can also be awakened by serial port data. The processed data is placed in the sending buffer. When the data sending cycle comes, the data in the buffer is sent out through the radio frequency module, or the data is sent to the upper computer.

3. Structure model of the centralized heating monitoring system based on wireless sensor network

3.1. Sensing and convergence node design. The wireless ad hoc network in the centralized heating monitoring system is a wireless communication network composed of wireless communication nodes such as monitoring terminal nodes, building byte points, community nodes, and relay nodes distributed in different locations in the centralized heating area. The temperature data reported by the wireless temperature sensor is first stored on the relay module, and then the temperature data is reported to the database server through the gateway according to the patrol instruction of the central

monitoring system. It is widely used in technical fields such as communication, electronics, measurement and control with its strong self-organizing network capability and unique multi-hop routing and transmission advantages [9]. The wireless temperature sensor has two working states, heating period and non-heating period, and set up unmanned house management. As a host, it can complete the wireless sending and receiving of instructions and data information according to the terminal's realization function; as a route, it can refer to parameters such as wireless link quality and route hops to select an optimal path for data transmission. Therefore, in the entire wireless sensor network, without base station support, any communication node can interact with neighboring nodes for data (Figure 1). Therefore, the wireless sensor network is a true self-maintenance and self-management multi-hop network.

The software control makes the sensor node sleep for most of the time, wake up every once in a while and the system uses hardware address allocation method to allocate node addresses. Daily management tasks include report generation and printing, centralized heating metering management, controller working parameter setting, remote data collection, summary and comprehensive analysis of operating data. Some circuits will be turned off, and only the timer and interrupt will be retained, and the timer will be started in the dormant state. The process scheduling module completes the control flow of the operating system, and it is related to the initialization of the entire wireless sensor and the system operating state. The energy consumption management unit supports the energy consumption status control of processors, radio frequency transceivers, sensors and other components. Some data collection nodes can also act as routing nodes and act as relay bridges. Its function is to connect data collection nodes beyond the influence range of the central data collection node. Therefore, the functions of each node are distinguished by different physical address information. When the main collection node performs a query operation, it needs to determine the physical address of the destination node in the first place.

The central monitoring station needs to receive the data packets sent by centralized station and display the data for monitoring personnel and heating users to access and view. The former sends the data collected by the interface to its own application layer for frame structure organization, which realizes the data collection function; the latter sends the application layer data application serial communication program to the serial port of the module sends data to the network through its data transfer function. The module is more convenient to use, can automatically complete all information exchange with the network, and can be directly connected to various configuration software without special drivers [10]. The sensor part is in a dormant state when there is no data collection. Once the collected heating information needs to be transferred, the sensor starts to work, transfers the heating packages to the wireless sensor network and then resumes the dormant state. Once the node data comes in, it will immediately pass the information to the monitoring center through the module to process the incoming data. The pressure sensor is small in size, lights enough in weight, and adopts a stainless steel sealed structure, which can work in harsh environments with a high degree of corrosion.

3.2. Layout of wireless sensor network. The centralized heating monitoring system can monitor heating information and record operating parameters of centralized heating in real time, and carry out over-limit alarms for parameters such as temperature, pressure and flow. Daily management tasks include report generation and printing, centralized heating metering management, controller working parameter setting, remote data collection, summary and comprehensive analysis of operating data, and historical data backup. Through the automatic control of the centralized heating, the monitoring system will make the entire system heat evenly, meet the comfort requirements, reduce heat consumption, and achieve the purpose of energy saving. The management layer is located in the main station of the thermal power company and consists of a network with industrial control machines as the core (Figure 2). The industrial control machines operate around the clock. The industrial control machine is not only the server of the dispatch center, but also the client relative to the collection and control stations. The server collects and stores data from each client site in real time, and monitors the operation of each site in real time. The control layer is located in the substations of each thermal power company. It collects, stores, monitors and processes signals from smart sensors in real time, completes the network transmission of collected data, and can set parameters such as over-limit alarms at any time.

Adding a data analysis thread to the main process can play a role in the first-level monitoring of the physical quantity of the pipe network. The processor receives the physical quantity collected by the terminal device and compares it with the threshold first. Control commands and transfer the heating information to the server to display error information on the control center web page. Since four threads are running in the main process and frequent data interaction and transmission are required between the threads, a global variable structure is defined in the main process, and the variable values required by each thread are obtained from the global area. In order to prevent conflicts in multi-threaded operation of the global area, each thread uses semaphores to mutually exclusive access to global variables. The central monitoring station needs to receive the data packets sent by centralized station and display the data for monitoring personnel and heating users to access and view. The content of the beacon frame includes information such as the network number of the network and the communication channel occupied by the network. The control center obtains the corresponding network number and channel information according to the received beacon frames of different networks, and selects the appropriate network number and communication channel to establish a new wireless sensor network [11].

Automatic monitoring is real-time online monitoring in the unattended situation, and can automatically deal with abnormal situations. The automatic processing is the ability to automatically perform self-adjustment control or alarm by means of text messages, phone calls, sound and light,

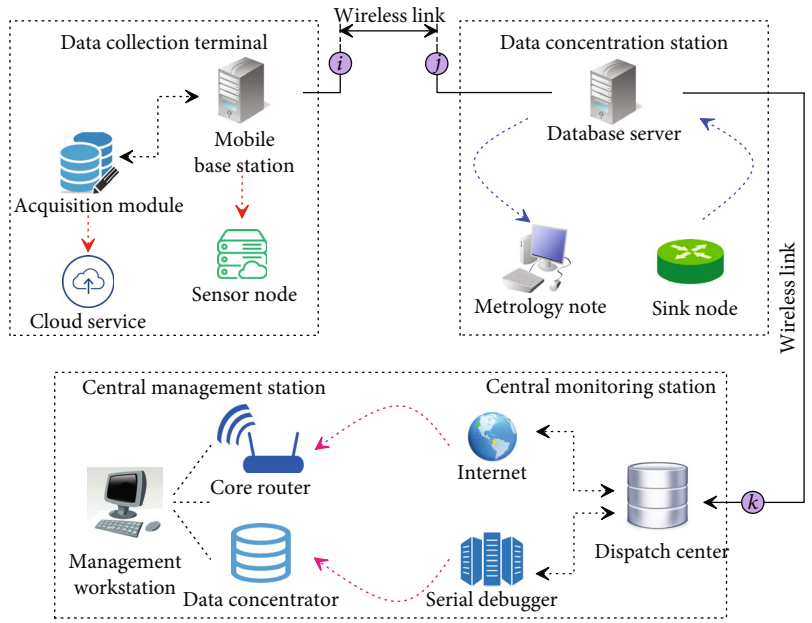

Figure 1: Structure model of the centralized heating monitoring system based on wireless sensor network.

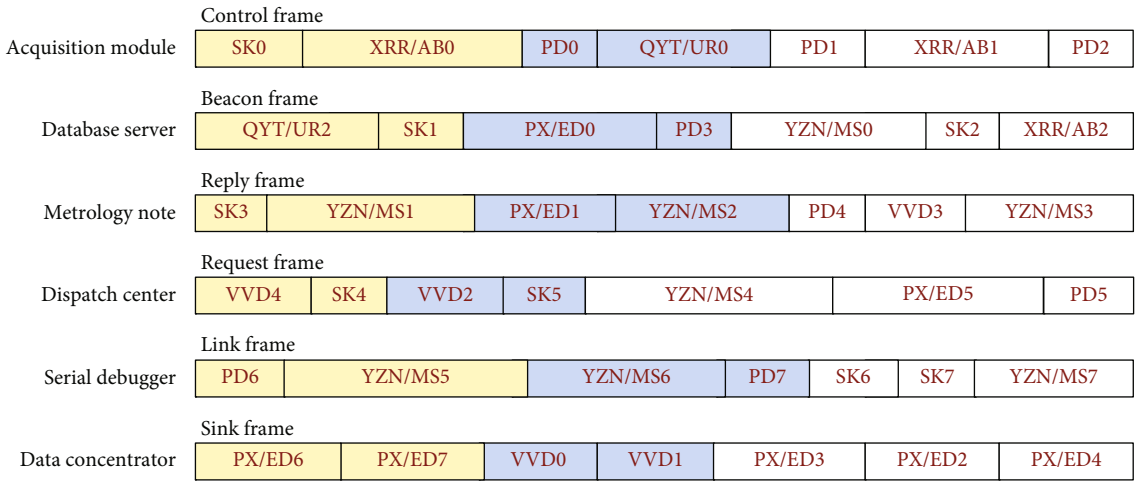

Figure 2: Sensing and convergence node design for the layout of wireless sensor network.

email, etc., and notify the computer room management personnel in time. The real-time performance and stability are mutually restricted. Too high real-time performance will inevitably reduce stability; therefore, the system can flexibly configure real-time performance. In the case of limited system resources, as the collection parameters increase, the load on the data collection terminal and the data collection management center will also increase, which affects the real-time performance and even stability of the system, and therefore requires scalability of the system [12]. The data processing part is the core of the entire network. The main tasks it completes are information processing, storage, data transmission and reception, and control of the components of the data collection part. This system requires the setting of thresholds and ranges for important parameters of the computer room environment.

4. Design scheme of centralized heating monitoring system based on wireless sensor network

4.1. Hardware design of centralized heating monitoring system. In the centralized heating monitoring system, the wireless sensor node data collection part includes temperature sensors, humidity sensors, light intensity sensors, smoke sensors, water immersion sensors, etc., which collect temperature, humidity, light, fire alarm, and water immersion parameters in the computer room. The research and development of a single sensor node self-organizing dynamic multi-directional wireless data transmission sensor network cannot work alone, because its wireless communication distance is limited, and it is impossible to directly send the

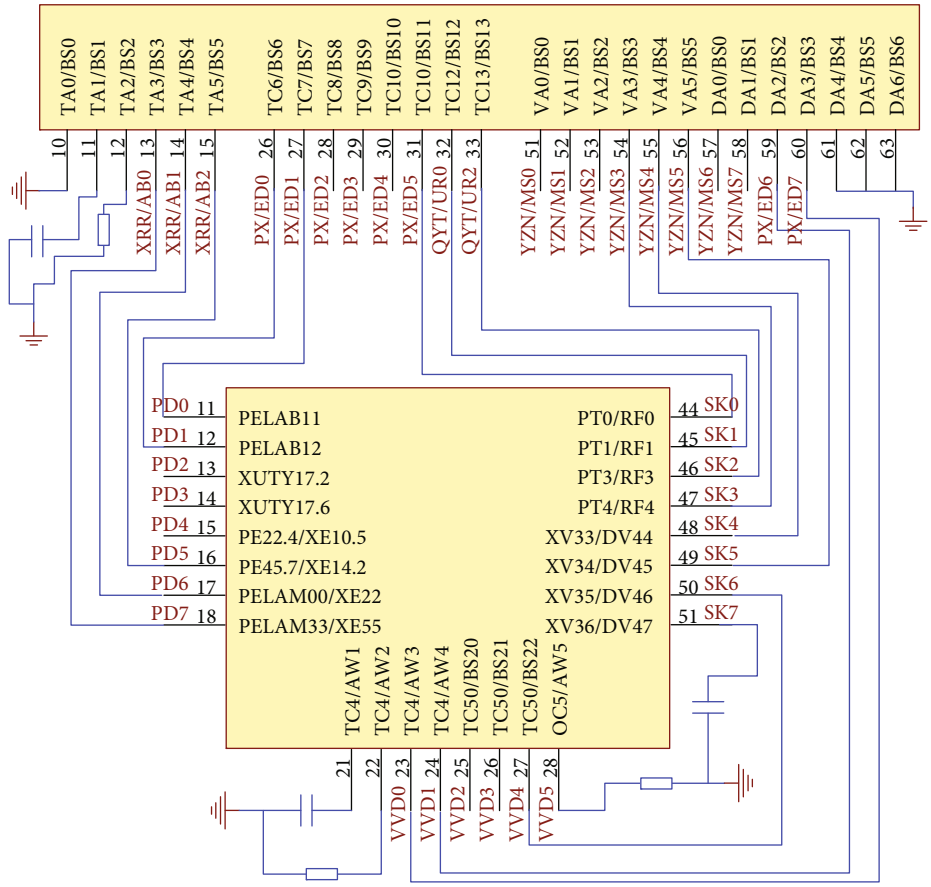

Figure 3: Design result of core monitoring circuit in the centralized heating monitoring system based on wireless sensor network.

collected monitoring data to the computer network system. This requires a certain protocol and technology to interconnect multiple sensor nodes to form a wireless data transmission sensor network to realize data forwarding through neighboring nodes and change short-distance to long-distance transmission [13]. The upper-level computer management software is deployed on the monitoring host. It is designed to transfer the temperature information by the wireless sensor network, forming an intuitive monitoring view, and real-time alarming according to the preset alarm strategy (Figure 3). The wireless sensor network subsystem and the upper computer system rely on the gateway to interconnect. A gateway node is a wireless sensor node with relatively complex functions. It can naturally communicate with other heating information in the sensor network and it can also design a hierarchical data transfer mode for multi-level gateway nodes.

The wireless household on-off solenoid valve adopts a normally-open on-off solenoid valve to control the on-off of the heating water to realize the regulation of the heating temperature, and keep it normally open when it is not controlled or when the power is cut off, and does not control the heating water flow. When the heating water is closed, the wireless household on-off solenoid valve activates the automatic protection function, and automatically opens the heating water according to the temperature to ensure the normal heating of the user. The temperature data reported by the wireless temperature sensor is first stored on the relay module, and then the temperature data is reported to the database server through the gateway according to the patrol instruction of the central monitoring system [14]. The wireless household on-off solenoid valve control is used in conjunction with the wireless temperature sensor, and the point-to-point binding is realized by setting on the central control system. When the wireless temperature sensor receives the switch command sent by the central monitoring system through the wireless repeater, or controls the switch of the wireless household on-off solenoid valve according to the temperature data and time period, realizes the on-off control of the heating household water inlet solenoid valve to achieve the regulation of heating temperature (Figure 4). The wireless temperature sensor has two working states, heating period and non-heating period, and set up unmanned house management. The wireless gateway is connected to the server in a wired manner, and the wireless gateway can be set with different Ethernet addresses, as long as it is on the same network segment as the database server.

In order to save energy, terminal monitoring nodes are dormant most of the time. When the monitoring heating information is not been packed and not been transferred, they turn off the node communication module and data acquisition module to save energy. After the coordinator receives the data packet, it will return the original route and send the confirmation message to the terminal

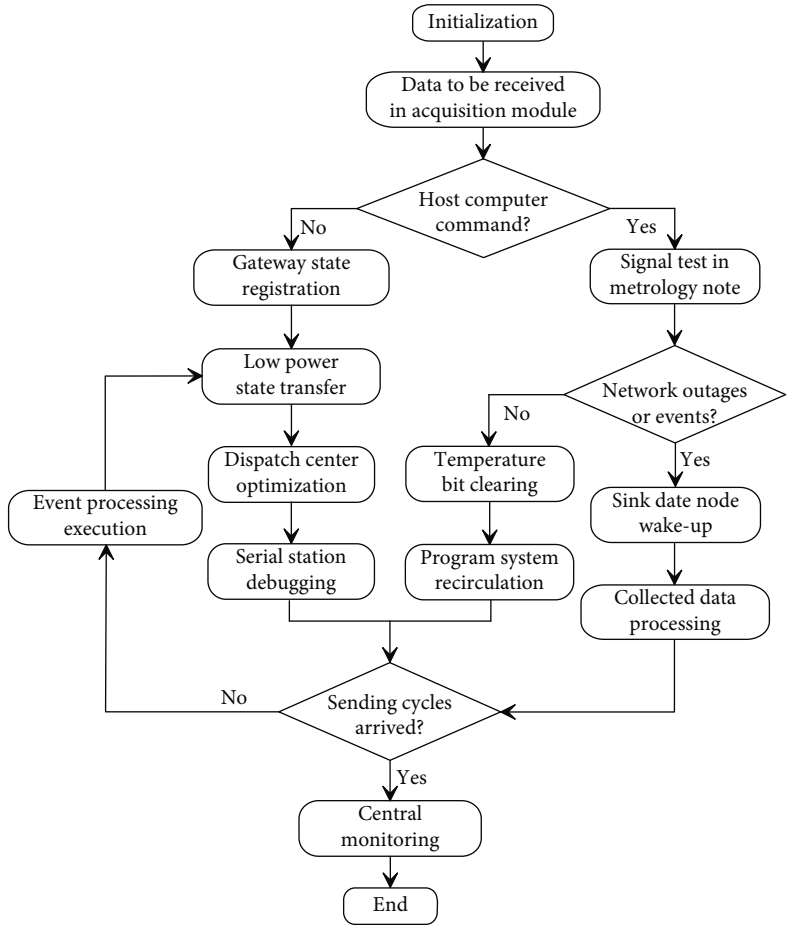

Figure 4: Design scheme flowchart of centralized heating monitoring system based on wireless sensor network.

monitoring node to realize handshake communication with the monitoring node. If the heating information does not transfer confirmation, the coordinator continues to send data until it receives the confirmation message. The main job of the coordinator is to transfer heating information, upload them to monitoring hosts, and forward commands from the monitoring center. In addition, considering that in the same centralized system, different heating pipes have different energy requirements and consumption. In order to balance the electricity consumption of each heating pipe, the centralized heating monitoring system uses a clustering network to perform mean clustering on the sensor network. The system then combines the remaining heating information and uses the global optimization capability of the genetic algorithm to select the appropriate cluster heating pipe. As a result, the sink node is a sensor node with rich memory resources, strong computing power, and sufficient energy supply.

4.2. Software design of centralized heating monitoring system. Since wireless sensor networks are usually highly related to applications, each protocol has its own uniqueness and shortcomings. Through the analysis and comparison of the protocol and the actual situation of the system itself, a set of routing protocols for multi-hop adaptive routing path selection are designed. In the parent node selection of the same level, the only parent node will be selected according to the estimated value of the received signal power level in the current street. The maximum number of relay router hops for transmitting messages is inversely proportional to the maximum number of nodes connected to a router node. Therefore, each node can only have one parent node, but it can have multiple child nodes (Figure 5). The heating information is related to the establishment and maintenance of routing and the basic functions to be realized by routing protocol are routing. After simple processing operations, the microcontroller unit uses the channel access mechanism specified by the network protocol to transfer heating information to the system via the radio frequency transceiver unit. It sends the target pipe address and transmission path instruction to the subnet heating pipe in centralized system and the heating pipe that receives the instruction corresponds to its own address to determine whether to execute it. The client's data reading process corresponds to the server's data writing process, and the client's data writing process corresponds to the server's data reading process.

The star structure is relatively easy to implement, but its functions are limited. If the central node fails, the entire network will be paralyzed. The tree structure can form a network with a relatively wide coverage, but if one route fails,

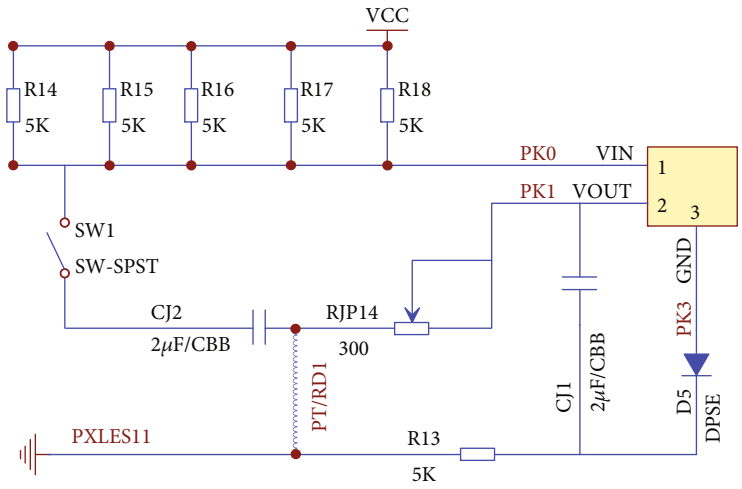

Figure 5: Design result of core interface circuit in the centralized heating monitoring system based on wireless sensor network.

there is no route that can be replaced. This kind of function is usually used as the communication interface between heating information and centralized system. It is the interface that transfers the control right to the application program when the protocol stack is running, if the application program needs to perform corresponding processing. In the mesh network topology, nodes have dynamic networking and automatic routing functions. All sensor node devices in the network not only complete the task of data collection, but also forward the data of other nodes and transfer heating information to the centralized system. The greater the number of router node hops, the greater the vertical coverage area of the network, and the greater the data delay at the terminal data collection node; the greater the maximum number of nodes that the router can connect to, the greater the horizontal coverage of the network. In the actual development process, the developer adds the user's application logic to the required interface, defines the user's data processing process, and calls it at the appropriate time through the corresponding interface function to realize the application code [15].

According to the location of the centralized heating equipment, an appropriate number of terminal temperature collection control nodes and router nodes are arranged in different areas. After doing the corresponding judgment processing, it forwards the collected device temperature to the centralized system, and finally uploads the temperature data to upper computer monitoring software. The heating information is related to the establishment and maintenance of routing and the basic functions to be realized by routing protocol are routing [16]. The maximum number of relay router hops for transmitting messages is inversely proportional to the maximum number of nodes connected to a router node. Therefore, the larger the maximum router hop number is set, the fewer detectors and routing nodes that each router node can connect to them. The greater the number of router node hops, the greater the vertical coverage area of the network, and the greater the data delay at the terminal data collection node; the greater the maximum number of nodes that the router can connect to, the greater the horizontal coverage of the network. However, the probability of data transmission conflicts between router nodes has also increased, and the delay of data transmission has also increased. Therefore, the system needs to set appropriate network parameters according to the scale and structure of the communication centralized heating to optimize the performance of the entire monitoring network.

5. Discussions

5.1. Relationship between data transfer related tasks and task scheduling. The application of the centralized heating monitoring system can not only more conveniently monitor, control and manage the entire heating network, and coordinate scheduling, but also can give full play to the computer's centralized monitoring and scientific quantitative management functions. The heating information is related to the monitoring system in the centralized heating program, and the eating program need to optimize the censor layout styles for the operation of the centralized heating pipes. The main task of the coordinator is to transfer heating information, upload them to monitoring hosts, and forward commands from the monitoring center. The wireless household on-off solenoid valve control is used in conjunction with the wireless temperature sensor, and the point-to-point binding is realized by setting on the central control system. After simple processing operations, the microcontroller unit uses the channel access mechanism specified by the network protocol to transfer heating information to the system via the radio frequency transceiver unit. The sink node uses the routing algorithm to forward data to the management node through multiple hops to realize the exchange of information [17]. Therefore, the design of sensor networks must take improving the heating pipes of the centralized system as primary goal (Figure 6).

The data collection function will display the operating status of all circulating pumps, make-up pumps, electric regulating valves and other operating equipment on site in real time, and parameters of the heat exchange unit. The frequent alarm function will display the abnormal conditions

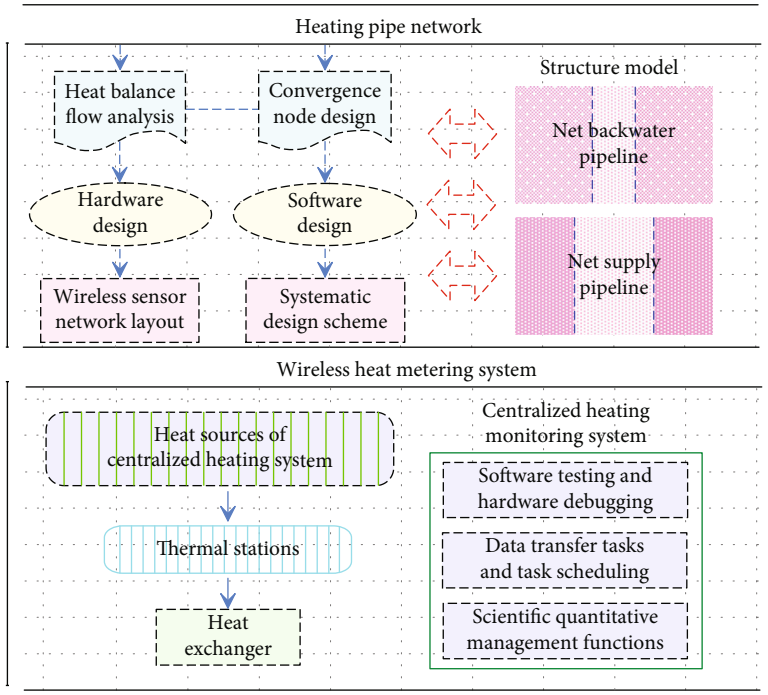

Figure 6: Relationship between data transfer and task scheduling of the centralized heating monitoring system.

or alarms of the on-site heat exchange unit from time to time and promptly notify the station patrol personnel to solve the problem on the spot, and the operator can confirm and manage the alarm information that appears from time to time. The remote setting function will send equipment operation instructions remotely and remotely set the parameters of the field equipment, which provides a very convenient means for equipment maintenance. When the data collection equipment changes, the software can update the instrument and wireless sensor network node information in real time, and has the adaptive capability of equipment update. The application of the centralized heating monitoring system can not only more conveniently monitor, control and manage the entire heating network, and coordinate scheduling, but also can give full play to the computer's centralized monitoring and scientific quantitative management functions. This realizes dynamic tracking and monitoring of heating operation, real-time diagnosis of hidden dangers in heating operation, and enables the heating system to operate safely, normally and energy-saving.

The coordinator first needs to select idle channels for the entire network, and then generate beacon frames and send them regularly, and at the same time process other device association or disassociation requests, data transmission, etc. The association operation refers to the process of registering with the coordinator and identity authentication when a device joins a specific network. The time allocation of super-frames is defined by the network coordinator, which mainly includes active periods and inactive periods. All communications in the network must be carried out during heating process; and during the optimizing stage, the device can revoke the heating information [18]. The physical layer is designed to realize the transparent transmission of various heating information between data link entities on a physical transmission medium. The transmission mechanism of each data transmission also depends on whether the network supports beacon transmission. When there is no low-latency device in the network, the system can choose not to use beacon transmission in data transmission. In this case, although data transmission a beacon is not used, but when the network is connected, a beacon is still needed to complete the network connection.

5.2. Software testing and hardware debugging of the centralized heating monitoring system. The management layer uses a carrier sense algorithm to avoid shared channel conflicts caused by multiple nodes sending data at the same time. In addition, the management layer searches for the next hop address based on the address information provided by the network layer to cooperate with the physical layer to complete the single-hop data transmission. Sensor nodes are divided into router nodes and leaf nodes. Among them, heating pipes and heating devices are designed to address allocation, and the leaf nodes are at the end of this local area network and do not have the function of address allocation [19]. The network layer implements routing management in the protocol, and its functions also include address allocation and routing table management for new nodes in the process of wireless sensor network ad hoc networking. From the function, it uses the network to complete the two data aggregation of the sensor local area network and the internal field bus of the heating station, and the aggregation node automatically completes the registration and login to the network after a period of time (Figure 7). The structure

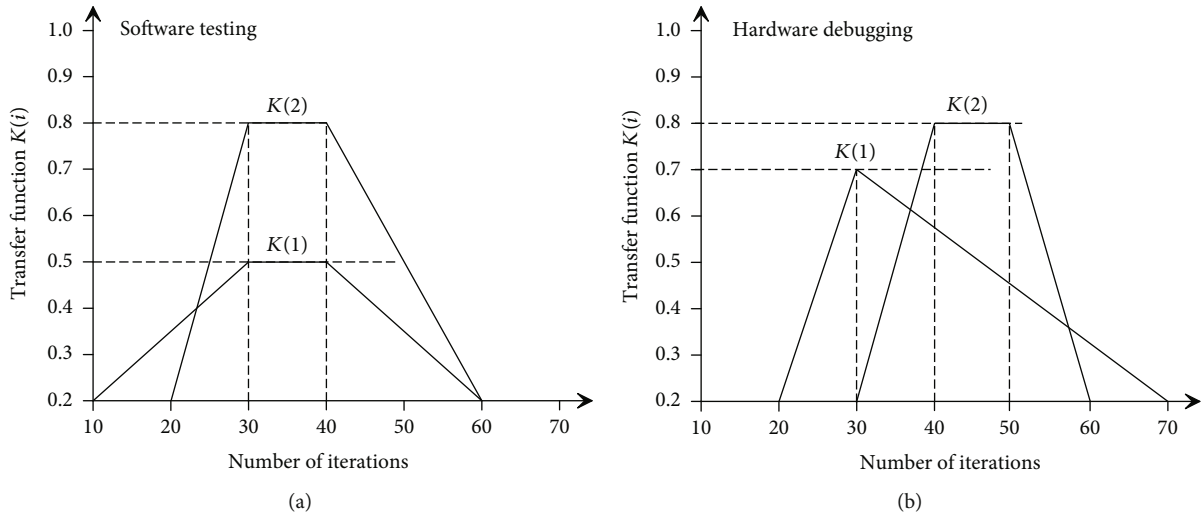

Figure 7: Transfer functions of numbers of iterations in software testing (a) and hardware debugging (b) of the centralized heating monitoring system.

defines the menu description string members, and the menu description string is sent through the serial port to display the menu items. The protocol stack of the heating pipe and the centralized system is different according to the heating devices. The sensor node is divided into a router node and a leaf node according to the address that can be allocated and the address that cannot be allocated.

The heating operation management software collects the temperature, pressure, flow, heat, valve opening, outdoor temperature and other data of the thermal station site, weighs and calculates the operation of the entire network, and issues control instructions to the on-site control equipment. The on-site controller is equipped with a communication interface, which is used to realize the data transmission with the dispatch center and the signal transmission of the on-site heat meter, soft water and other equipment. The on-site controller not only accepts the instructions issued by the central control machine and adjusts the control, but also can work independently within the specified range [20]. It collects processes and displays the operating data of the thermal station, automatically adjusts, detects faults, diagnoses and alarms, calculates cumulative heat consumption, and prints reports. The monitoring system converts the collected analog signals such as temperature, pressure, and flow into digital signals to optimized the basic function of the heating surrounding environment, circulation pump and primary network valve, and maintain the stability of the system. After the data collection front-end computer obtains the data of the user's heat meter, the data must be analyzed first to remove the abnormal data, and the processed information will be archived in the data server.

The wireless sensor network protocol uses the routing algorithm to initiate the message node, and establishes an appropriate routing path by querying neighboring nodes. This query propagates in the network like a wave until the destination node is found and a response is obtained. This response reaches the message originating node in the reverse direction and save important routing data all the way. After a period of time, this new routing message will become old and expired, and new routing information will be needed to ensure that the routing result is based on the new information [21]. The interruption or failure of any node will cause some nodes to leave the network. Since the transmission path between nodes is processed in a preprogrammed manner, no matter whether there are other nodes within the communication range, the information will be transmitted according to a predetermined procedure. Therefore, the potential for communication time is very high. Finally, the tree network must provide configurable range attributes to indicate how many resources the wireless network device has to support the tree topology. This range attribute includes the maximum number of layers of the tree structure and the maximum number of allowed child nodes.

6. Conclusions

This paper introduces the methods and principles of wireless network communication protocol and heating and heat balance flow analysis, proposes a structural model of a centralized heating monitoring system based on wireless sensor networks, carries out the design of perception and convergence nodes, analyzes the layout of wireless sensor networks, explores the design scheme of centralized heating monitoring system based on wireless sensor networks, conducts the hardware and software design of the monitoring system, implements the software testing and hardware debugging of the centralized heating monitoring system, and finally discusses the relationship between data transfer related tasks and task scheduling. The centralized heating monitoring system based on the wireless sensor network can monitor measure and record the operating parameters of the centralized heating in real time, and carry out over-limit alarms for parameters such as temperature, pressure and flow. The heating operation management software collects the temperature, pressure, flow, heat, valve opening, outdoor temperature and other data of the thermal station site, weighs and

calculates the operation of the entire network, and issues control instructions to the on-site control equipment. The sink node exchanges data with the cluster head node through the radio frequency module, and communicates with the host computer through the serial port. Therefore, the sink node can be awakened by radio frequency data, and it can also be awakened by serial port data. The processed data is placed in the sending buffer. After simple processing operations, the microcontroller unit uses the channel access mechanism specified by the network protocol to transfer heating information to the centralized monitoring system via the radio frequency transceiver unit. The study results show that the application of the centralized heating monitoring system can not only more conveniently monitor, control and manage the entire heating networks, but also make full use of the centralized monitoring and scientific quantitative management functions of the wireless sensor networks. This achieves dynamic tracking and monitoring of heating operation, real-time diagnosis of hidden dangers in heating operation, and safe, normal and energy-saving operation of the centralized heating system.

Data Availability

The data used to support the findings of this study are available from the corresponding author upon request.

Conflicts of Interest

The authors declare that they have no known competing financial interests or personal relationships that could have appeared to influence the work reported in this paper.

Funding

The study was supported by School of Energy and Power Engineering, Changchun Institute of Technology.

References

[1] A. P. Svintsov, E. L. Shchesnyak, V. V. Galishnikova, and R. S. Fediuk, "Monitoring of heating systems as a factor of energy safety of buildings," *Journal of Building Engineering*, vol. 31, article 101384, 2020.

[2] M. Borowski, P. Mazur, S. Kleszcz, and K. Zwolińska, "Energy monitoring in a heating and cooling system in a building based on the example of the Turówka hotel," *Energies*, vol. 13, no. 8, p. 1968, 2020.

[3] O. van Pruissen, A. van der Togt, and E. Werkman, "Energy efficiency comparison of a centralized and a multi-agent market based heating system in a field test," *Energy Procedia*, vol. 62, pp. 170–179, 2014.

[4] M. Ravina, D. Panepinto, M. C. Zanetti, and G. Genon, "Environmental analysis of a potential district heating network powered by a large-scale cogeneration plant," *Environmental Science and Pollution Research*, vol. 24, no. 15, pp. 13424–13436, 2017.

[5] M. F. Othman and K. Shazali, "Wireless sensor network applications: A study in environment monitoring system," *Procedia Engineering*, vol. 41, pp. 1204–1210, 2012.

[6] P. Zhou, G. Huang, L. Zhang, and K. F. Tsang, "Wireless sensor network based monitoring system for a large-scale indoor space: data process and supply air allocation optimization," *Energy and Buildings*, vol. 103, pp. 365–374, 2015.

[7] A. Salleh, M. K. Ismail, N. R. Mohamad, M. A. Abd Aziz, M. A. Othman, and M. H. Misran, "Development of greenhouse monitoring using wireless sensor network through ZigBee technology," *International Journal of Engineering Science Invention*, vol. 2, no. 7, pp. 6–12, 2013.

[8] B. Risteska Stojkoska, A. Popovska Avramova, and P. Chatzimisios, "Application of wireless sensor networks for indoor temperature regulation," *International Journal of Distributed Sensor Networks*, vol. 10, no. 5, Article ID 502419, 2014.

[9] V. M. Krishna and T. Anuradha, "A QoS improvement in P2P based Wireless Mesh Network using Hybrid Swarm Intelligence," *Indian Journal of Science and Technology*, vol. 9, no. 1, pp. 1–6, 2016.

[10] O. Friman, P. Follo, J. Ahlberg, and S. Sjökvist, "Methods for large-scale monitoring of district heating systems using airborne thermography," *IEEE Transactions on Geoscience and Remote Sensing*, vol. 52, no. 8, pp. 5175–5182, 2014.

[11] L. Liu, D. Wang, L. Gao, and R. Duan, "Distributed heating/centralized monitoring mode of biomass briquette fuel in Chinese northern rural areas," *Renewable Energy*, vol. 147, pp. 1221–1230, 2020.

[12] C. Yang, B. Gunay, Z. Shi, and W. Shen, "Machine Learning-Based Prognostics for Central Heating and Cooling Plant Equipment Health Monitoring," *IEEE Transactions on Automation Science and Engineering*, vol. 18, no. 1, pp. 346–355, 2021.

[13] J. Moreno, O. Morales, R. Tejeida, J. Posadas, H. Quintana, and G. Sidorov, "Distributed learning fractal algorithm for optimizing a centralized control topology of wireless sensor network based on the hilbert curve l-system," *Sensors*, vol. 19, no. 6, p. 1442, 2019.

[14] C. Liu, T. Zhao, J. Zhang et al., "Operational electricity consumption analyze of vrf air conditioning sys-tem and centralized air conditioning system based on building energy monitoring and management system," *Procedia Engineering*, vol. 121, pp. 1856–1863, 2015.

[15] H. R. Kolvir, A. Madadi, V. Safarianzengir, and B. Sobhani, "Monitoring and analysis of the effects of atmospheric temperature and heat extreme of the environment on human health in Central Iran, located in southwest Asia," *Air Quality, Atmosphere and Health*, vol. 13, no. 10, pp. 1179–1191, 2020.

[16] M. Ravina, D. Panepinto, and M. Zanetti, "District heating system: evaluation of environmental and economic aspects," *International Journal of Environmental Impacts*, vol. 1, no. 4, pp. 420–432, 2018.

[17] R. Priyadarshini, S. Reddy, and R. Mehra, "Design, development and deployment of multi-sensor node based wireless sensor network for campus monitoring," *International Journal of Applied Engineering Research*, vol. 10, no. 3, pp. 5599–5615, 2015.

[18] N. Aste, M. Buzzetti, P. Caputo, and M. Manfren, "Local energy efficiency programs: A monitoring methodology for heating systems," *Sustainable Cities and Society*, vol. 13, pp. 69–77, 2014.

[19] C. Bo, C. Xin, Z. Chengwen, L. Ying, and C. Junliang, "Wireless machine to machine based mobile substation monitoring

for district heating system," *International Journal of Distributed Sensor Networks*, vol. 10, no. 6, Article ID 242907, 2014.

[20] A. M. Pawar, S. N. Patil, A. S. Powar, and B. P. Ladgaonkar, "Wireless sensor network to monitor spatio-temporal thermal comfort of polyhouse environment," *International Journal of Innovative Research in Science, Engineering and Technology*, vol. 2, no. 10, pp. 4866–4875, 2013.

[21] W. S. Jang, W. M. Healy, and M. J. Skibniewski, "Wireless sensor networks as part of a web-based building environmental monitoring system," *Automation in Construction*, vol. 17, no. 6, pp. 729–736, 2008.

Hindawi
Journal of Sensors
Volume 2022, Article ID 9047737, 9 pages
https://doi.org/10.1155/2022/9047737

Research Article

Optimization of Mobile Edge Computing Offloading Model for Distributed Wireless Sensor Devices

Songyue Han,[1,2] **Dawei Ma**,[1] **Chao Kang**,[3] **Wei Huang**,[1] **Chaoying Lin**,[1] **and Chunyuan Tian**[1]

[1]*Communications Non-Commissioned Officer School, Army Engineering University of PLA, Chongqing 400035, China*
[2]*32705 Unit of PLA, Xi'an, Shaanxi 710086, China*
[3]*Xi'an University of Posts & Telecommunications, Xi'an, Shaanxi 710061, China*

Correspondence should be addressed to Songyue Han; colincooper@sina.com and Chao Kang; kangchao@stu.xupt.edu.cn

Received 2 December 2021; Revised 17 January 2022; Accepted 26 January 2022; Published 28 February 2022

Academic Editor: Gengxin Sun

The development and popularization of mobile Internet and wireless communication technology have spawned a large number of computation-intensive and delay-intensive applications. Limited computing resources and existing technologies cannot meet the performance requirements of new applications. Mobile edge computing technology can use wireless communication technology to offload data to be stored and computing tasks to the nearby assistant or edge server with idle resources. Based on the data offloading of distributed wireless sensor device to device communication, the architecture is designed and the basic framework of distributed mobile edge computing is constructed. To solve the problem of high mobile cloud computing technology, the offloading model of optimized mobile edge computing was proposed, and the stability and convergence of the proposed algorithm were proved. Finally, the system performance of the proposed algorithm is verified by simulation. The results show that the proposed algorithm can converge within a finite number of steps. Compared with other benchmark schemes, the proposed algorithm has better performance in reducing system energy consumption, reducing moving edge response delay and system total delay.

1. Introduction

With the growth of mobile web services and the growth of social networking applications, mobile data traffic is experiencing explosive growth. The increasing mobile traffic is mainly caused by emerging mobile device applications that require higher network throughput and more stringent network latency, something that current 4G wireless networks cannot achieve. 5G wireless networks will be standardized, increasing network capacity by a factor of 1,000 compared to 4G networks, and latency will be less than one millisecond. It now runs efficient and powerful applications with more computing power, storage, bandwidth, and power. Applications typically include computer vision image processing, optical character recognition, and augmented reality [1]. Mobile cloud computing is a collection of servers located in remote data centers that provide sufficient computing, storage, and network resources for mobile devices [2]. MCC delays are caused by backhaul links, so long delays between users and the cloud become a challenge. In order to meet the network latency requirements of 5G wireless networks on MCC, a new network architecture is needed. Therefore, moving edge computing came into being [3]. Edge distributed devices use low-level signaling to share information. MEC discovers the location of devices by receiving information, provides network information and real-time network data service applications, and implements MEC through the model to benefit business and events [4]. The application estimates radio and network bandwidth congestion based on RAN real-time information, helping to make informed decisions to better serve customers. How to enhance the space of MEC cloud server and storage capacity has become the focus of research.

As wireless sensor networks begin to attract great interest of researchers, the footprint of wireless sensor networks can be seen in various fields [5]. The application provides

real-time information to estimate congestion in radio and network bandwidth, enabling informed decisions and better service for customers. Wireless sensor network is a technology generated through the miniaturization of radio components and sensor devices [6]. It is a wireless communication network composed of sensor nodes composed by some small devices with certain communication and sensing capabilities. Wireless sensor network (WSN) technology, as a more intelligent information technology after the Internet, has been concerned by many fields. Wireless sensor network technology is attracting more and more attention. MEC allows direct mobile communication between the core network and end users, while connecting users directly to the nearest cloud-enabled edge network [7]. Deploying MECs on base stations enhances computing power and avoids bottlenecks and system failures. How to optimize the offloading model of mobile edge computing by distributed wireless sensor devices has become a hot issue.

2. Related Work

Thanks to the continuous progress of information and communication technology, a large number of emerging intelligent Internet of Things applications have emerged, which require a large number of wireless devices to quickly perform low-latency and high-complexity computing tasks. Generally, wireless devices are small in size and have limited battery power supply, so the key challenge to be solved is how to increase the computing power of these devices and reduce computing latency [8]. At present, cloud computing can provide rich computing resources and powerful computing power, but the physical distance between cloud server and wireless terminal device is long, and the multihop routing and addressing transmission from the access network to the core network is required, which make cloud computing generally unable to meet the low latency requirements of some emerging applications run by wireless devices. For this reason, mobile edge computing technology came into being. In mobile edge computing, by configuring servers on the edge of wireless networks, computing resources are deployed on the side of wireless access networks to reduce the transmission time between wireless devices and computing servers and effectively meet the requirements of low-latency computing. It can be seen that mobile edge computing effectively integrates wireless communication network and mobile computing technology. Wang et al. realized PROFINET fieldbus communication based on edge devices and integrated the information collected by a large number of island devices together. Edge computing refers to the network edge perform calculations of a new type of calculation model, object at the edge of the computing operations including downstream data from cloud services, and uplink data from all Internet services [9]. Liu et al. carried out a scheme of computing offloading of multiple mobile devices and joint management of wireless network resources, but the main optimization objective of the literature was to minimize energy consumption without paying too much attention to system delay [10]. Chen et al. proposed a mobile device offloading algorithm, which can effectively reduce system delay of the algorithm by taking advantage of linear characteristics limited by inequality in the optimization problem. A strong assumption is made in the algorithm, assuming that wireless network resources are sufficient. Moreover, the network resources allocated to each mobile device are in a fixed proportion to the computing tasks offloaded by the mobile device. However, in the actual mobile edge system environment, wireless network resources are limited, so the actual feasibility of this algorithm needs to be considered [11].

Wireless communication technology has also been rapidly developed, data acquisition system relying on wireless communication technology, and began to develop to wireless sensor network. The main working mode of wireless sensor network is to collect information through nodes and carry out communication and data transmission among nodes through wireless communication [12]. With the continuous research on wireless sensor network, its application is no longer limited to the military field and gradually extends from military weapons to antiterrorism and disaster relief, large-scale structural health monitoring, environmental monitoring, medical care and transportation support, and other fields. Moreover, the integrated circuit technology is becoming more and more mature, the reliability of hardware electronic components of various functional modules is becoming more and more high, and the reliability of wireless sensor network is becoming more and more stable. It can provide accurate information at different times, places, and environments, making wireless sensor networks gradually get more and more applications in people's lives [13]. Since MEC servers are not deployed on a large scale to cellular networks, most of the literature is theoretical. Due to the communication between mobile devices and MEC servers, computational offloading will incur extra costs in terms of delay and energy consumption [14]. Siavoshi and others proved the existence of game equilibrium, and put forward an effective balance algorithm, each mobile devices according to their own situation decision computing tasks uninstall strategy. The goal is to minimize their own application execution time delay. Total system delay is not taken into account [15]. Zeng et al. such as the main research Gui multiple mobile devices at the edge of the service node case computing tasks offload and resource allocation optimization problem put forward a kind of low time complexity of the algorithm for calculation of mobile equipment offloading and mobile edge server selection, and main optimization goal is to improve computing offloading efficiency and save mobile offloading at the edge of the cloud resources [16]. Li et al. proposed a mobile edge computing system architecture based on the central cloud, which further expanded the resources of mobile devices by utilizing the sufficient computing resources of the central cloud. This architecture is mainly applied to the mobile network, and the offloading strategy is designed according to the real-time situation of the central cloud to improve the practicability of the network. However, the limitation of wireless network resources and the allocation of network resources are not taken into account [17]. The allocation of wireless resources and computing resources is particularly important for MEC systems.

This paper uses wireless communication technology to unload the data to be stored and the tasks to be calculated to the edge server, designs the architecture of mobile edge computing, and constructs the basic framework of distributed mobile edge computing. Solve the problem of high delay caused by existing high mobile cloud computing technology.

3. Distributed Mobile Edge Computing Offloading Model

Mobile devices can use mobile edge computing technology to offload their computing tasks to THE MEC server, which performs computation-intensive or time-delay sensitive tasks instead of MD by collecting a large number of idle resources and storage space distributed at the edge of the network, thus, saving energy for the device.

3.1. MEC Architecture. To meet the ever-increasing device requirements, cloud services are being moved to the vicinity of mobile devices, the emerging edge computing paradigm considered in mobile networks. By moving computing tasks to edge servers rather than remote clouds, service response times can be significantly reduced, thereby improving the user experience. The traffic through the return link can also be alleviated [18]. The structure of the MEC is shown in Figure 1. Business processing time on the server is to compensate for long wireless transmission delays.

The architecture of mobile edge computing usually consists of user layer, edge computing layer, and cloud layer. The user layer is composed of mobile devices, and the edge computing layer is composed of mobile edge cloud servers located at the edge of the network. The cloud layer is mainly composed of cloud servers. Mobile devices at the user layer can make full use of computing, communication, and storage resources of mobile edge cloud through wireless access network. Mobile devices transmit their basic information to mobile edge cloud servers through wireless access networks. Edge of a mobile service node may be equipped with one or more edges in the cloud, compared with the computing and storage resources of mobile devices, mobile communications at the edge of the cloud server have richer, computing, and storage resources, can support mobile devices running time delay sensitive, large amount of calculation, or cache, etc, and also can carry out data real-time interaction [19]. The mobile edge cloud server in the edge computing layer receives real-time information and computing tasks unloaded by mobile devices. Mobile edge cloud servers are deployed on the edge of the network, and the distance between mobile devices is relatively short. At the same time, affected by physical scene factors, it has certain limitations compared with public cloud computing resources. Mobile edge cloud server can transfer part of computing tasks to the clouds, which can be executed by public cloud computing, which can realize clouds centralized management. Cloud refers to public cloud servers deployed in remote clouds. The mobile edge cloud server can send information to the cloud. The cloud can not only store long-term useful information but also carry out task processing and get

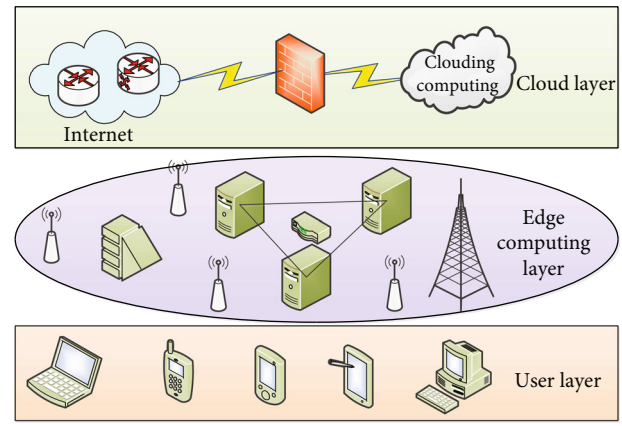

Figure 1: MEC architecture diagram.

the overall complete view of the covered area. However, offloading tasks from the mobile edge cloud server to the cloud also requires a certain transmission delay, so only nondelay-sensitive computing tasks can be offloaded. By providing global management and centralized control, the cloud's public cloud server provides a great help for the mobile edge cloud server to decide the optimal resource allocation strategy and the optimal computing offload strategy.

3.2. Distributed Mobile Edge Computing Framework. In distributed sensor network, each sensor can process its own information independently, provide a large amount of data, further obtain the classification characteristics of the target, and avoid the serious performance degradation of the single sensor system caused by electronic countermeasures. In the distributed fusion structure, each sensor can process its own information independently and then send each decision result to the data fusion centre for fusion. The basic architecture of edge computing is shown in Figure 2. Cloud servers are typically located in the core network, different from cloud computing, edge computing combines edge computing nodes into the network [20]. Edge computing can be run as a single computing platform or a collaboration platform with other components (including cloud).

To support real-time and interactive applications, mobile edge computing can store data on mobile devices on the edge, and the storage is distributed. The storage capacity of edge servers is still very limited compared to the resource-rich cloud. The storage types of data required by devices are extremely diverse. Therefore, edge servers need to have multiple types of storage policies to meet users' requirements. Different from the simple calculation provided by traditional caching and access technology, the calculation of edge server is more independent and tends to be intelligent [21]. Edge computing is closer to the terminal device, reducing the time delay and energy consumption of uploading computing tasks to the cloud, thus improving the quality of user experience. Mobile edge computing processes large amounts of raw data collected near different applications and performs real-time data analysis to generate valuable information. The ability to analyse data at the edge reduces the latency required to send data to the cloud and

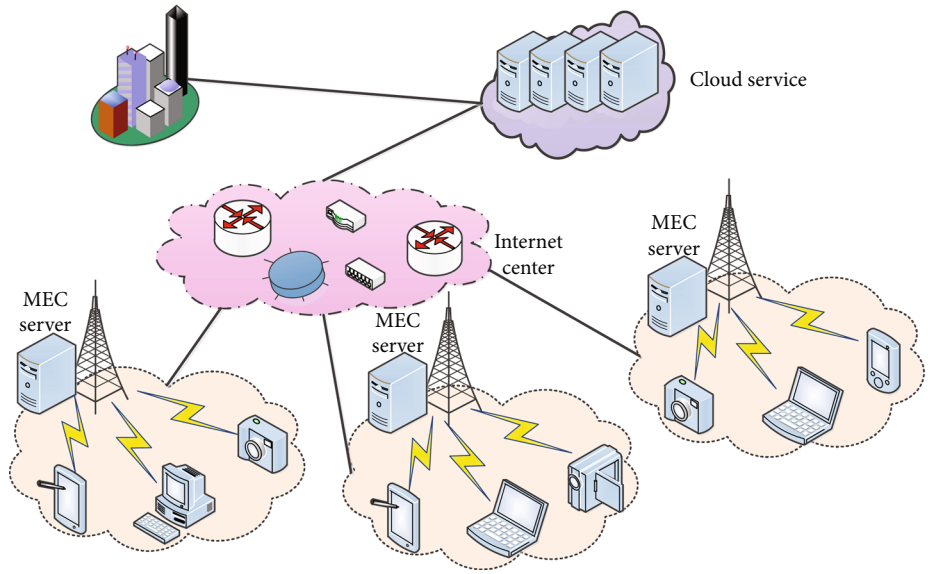

Figure 2: Distributed mobile edge computing framework diagram.

wait for responses from the cloud. The results of local data analysis are then used to make decisions. The results of local data analysis are then used to make decisions. Mobile edge computing helps entities make real-time decisions and actions based on well-processed data in an automated manner. Its decision-making ability improves system availability by reducing the exchange of components and data. Mobile edge computing enables remote control and monitoring, especially of critical equipment in insecure environments, including remote or more comfortable or secure locations. Mobile edge computing acts as an additional layer between the cloud and mobile devices to improve network security. Edge Cloud can be used as a secure distributed platform, providing security credential management, malware detection, software patch distribution, and trusted communications to detect, verify, and counter attacks. Because of the close proximity of mobile edge computing, it can quickly detect and isolate malicious entities and can initiate real-time responses to reduce the impact of attacks. This will help minimize service disruptions.

3.3. Offloading Model of Moving Edge Computing System. Assume that each user has a queue buffer that stores incoming but unprocessed computing tasks. In each time slot, the arrival process of user computing task is independent and identically distributed, and the average arrival rate is $\lambda I = E[Ai(t)]$. Meanwhile, each computing task can be processed locally or uninstalled to the MEC server [22]. Therefore, when the time gap t is fixed, the length vector of the household queue is

$$Q(t) = [Q_1(t), Q_2(t), \cdots Q_n(t)]. \tag{1}$$

The update process of $Q_i(t)$ is as follows:

$$Q_i(t) = \max\left\{\frac{Q_i(t)+Y_i(t)}{D_{\sum,i}(t)}\right\}, \tag{2}$$

where the total amount of computing tasks processed by user I at time t is expressed as

$$D_{\sum,i}(t) = \frac{\tau f_i(t)}{L_i} + \frac{\sum_{j\in S} R_{ij}(t)}{L_i}. \tag{3}$$

The first part on the right of equation (3) is the amount of computing tasks processed locally by the user. $F_i(t)$ is the computing resources allocated by user i to process the computing tasks, that is, the CPU cycle frequency. L_i is the CPU cycle required to execute each bit of the computing task. The second part is the amount of computing tasks processed by offloading to MEC server. $R_{ij}(t)$ is the transmission rate when user i offloads computing tasks to MEC server J at time t, and its expression is

$$R_{ij}(t) = \zeta_{ij}(t)\mathrm{W}\tau lb + \frac{p_{ij}(t)h_{ij}(t)}{\zeta_{ij}(t)NW}, \tag{4}$$

where W is the bandwidth of MEC server, $\xi_{ij}(t)$ represents the proportion of bandwidth allocated by MEC server j to user i, $p_{ij}(t)$ and $h_{ij}(t)$, respectively, represent the transmission power and channel gain from user i to MEC server j, and N is the power spectral density of Gaussian white noise. In addition, since each base station is connected to a MEC server, j also refers to a MEC server in this article. Task request is dynamic, and the length of the task queue may exceed the user cache space, resulting in packet loss. Therefore, the task requirements of low delay and high reliability, a probability constraint, are added to the user queue length [20], namely,

$$\lim_{t\longrightarrow\infty} p(Q_i(t) \geq Q_i^{\max}) \leq \varepsilon_i, \tag{5}$$

where $Q_i^{\max}$ stands for the queue threshold of user i, and ε_i stands for the overspill tolerance threshold of the task queue of user i, whose value is much less than 1. There are multiple queue buffers in each MEC server that can simultaneously store computing tasks offloaded by multiple users but not yet processed by the MEC server. Define the task queue of user i in MEC server j as $X_{ji}(t)$, and its update process is as follows:

$$X_{ji}(t+1) = \max\left\{\frac{X_{ji}(t) - Y_{ji}(t)}{L_j} - \frac{\tau f_{ji}(t)}{L_i}, 0\right\}, \quad (6)$$

$$Y_{ji}(t) = \min\left\{Q_i(t) + Y_i(t) + \frac{\tau f_{ji}(t)}{L_i}, R_{ij}(t)\right\}, \quad (7)$$

where formula (7) represents the calculation that user i offloads to server j at time t, and $f_{ji}(t)$ represents the calculation that server j assigns to user i. Because MEC servers are deployed to provide users with more computing power, this article assigns the CPU cores of each server to at most one user to perform computing tasks. This paper also adds a probability constraint to the MEC server task queue length, namely,

$$\lim_{t\longrightarrow\infty} p\left(X_{ji}(t) \geq X_{j_i}^{\max}\right) \leq \varepsilon_i, \quad (8)$$

where $X_{ji}^{\max}$ represents the task queue threshold of user i in MEC server j, and ε_{ji} represents the task queue overflow tolerance threshold of user i in MEC server j, whose value is much less than 1.

3.4. Offloading Model Optimization of Moving Edge Computing System. According to the multitask distributed offloading method oriented to moving edge computing, its characteristics lie in that the uplink and downlink transmission rates in the steps are calculated by the following formula:

$$R_m^{y_1} = \log_2\left(1 + P_{y_2}\eta\right), m = 1, 2, \cdots M. \quad (9)$$

Among them, the superscript $y_1 \in \{\mathrm{UL}, \mathrm{DL}\}$, respectively, ascending and descending link subscript m calculation the serial number of access points, the subscript $y_2 \in \{T, R\}$, respectively, transmitting and receiving mode, according to different mode of transmission rate of different transmission link, P_{y2} said transmitting and receiving power, and m said system service count the number of access points of the current mobile station.

According to the moving edge computing-oriented multitask distributed offloading method described by rights, its characteristics lie in the mathematical optimization problems in the steps described are as follows:

$$T(x) = \max_{m\in i}\sum_{n\in j} x_{nm}\left\{\frac{R_m^{UL}}{\alpha_n} + \frac{R_m^{DL}}{\beta_n} + \frac{r_m}{\gamma_n}\right\}, \sum_{n\in j} x_{nm} = 1, \quad (10)$$

where $i = \{1, 2\cdots, A\}$ and $j = \{1, 2\cdots, B\}$, respectively, represent the set of tasks generated by mobile station and computing access points serving the mobile station, where elements A and B, respectively, represent the total number of tasks generated by mobile station and computing access points serving the mobile station; $X = [X_{nm}]B \times (A+1)$ is the task offloading access matrix; element X_{nm} represents the element in the NTH row and the m column of matrix X, which represents the access parameter of the access point A when the access parameter task B is offloaded. $\psi(x) = \lambda t\, T(x) + \lambda e E(x)$, the elements λt and λe, respectively, represent the effects of delay and energy loss in the objective function in the current scenario, and the elements $T(x)$ and $E(x)$ represent delay and energy loss in the current scenario.

$$E(x) = p\sum_{n\in j} x_n \frac{\gamma_n}{r} + p\sum_{n\in j} x_{nm}\frac{\alpha_n}{R_m^{UL}} + p\sum_{n\in j} x_{nm}\frac{\beta_n}{R_m^{DL}}. \quad (11)$$

Elements α_n, β_n, and γ_n, respectively, represent the initial data size, the size of the task to be calculated, and the size of the output task after calculation. Element R_m represents the working rate of the computing access point M, and element P represents the power loss of the mobile station's local computing task, transmission task, and receiving task.

According to the said multitask distributed offloading method oriented to moving edge calculation, its characteristics lie in that the said method includes the following processes: reconstructing the matrix X, vectorizing the matrix X as x, where

$$x = [x_0, x_1, \cdots x_{\mathrm{A}}] = [x_l]_{l\times(\mathrm{BA}+B)}, \quad (12)$$

$$x_m = [x_{1m}, x_{2m}, \cdots x_{Bm}]. \quad (13)$$

Element $L = \mathrm{AB} + B$ is the dimension of vector x, that is, the total number of elements of matrix x. The auxiliary variable $u = [x_1]_{1\times(\mathrm{AB}+B)}$ is introduced, where ul represents the probability of $x_l = 1$. It is transformed into a problem of finding the optimal probability u, constrained by $X_{Bm} \in \{0, 1\}$, and the probability density function of decision set x is defined as Bernoulli distribution:

$$p(x, u) = \prod_{i=1}^{L} u_l^{x_l}(1 + u_l)^{(1-x_l)}. \quad (14)$$

Transform the original equation into the minimum cross-entropy:

$$\min_{\pi} H = \max_{\pi}\frac{1}{S}\sum \ln p(x, u). \quad (15)$$

4. Simulation Results and Analysis

The effectiveness of the proposed offloading optimization algorithm for moving edge computing is verified by statistics and comparative analysis of simulation results. The edge computing system optimizes the computational unloading model of mobile devices and verifies whether the proposed

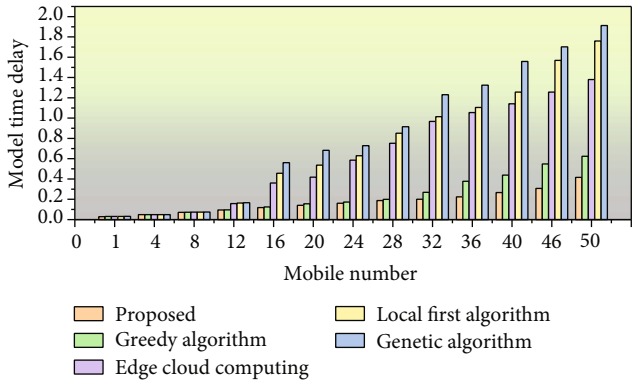

Figure 3: The influence of different mobile devices and different algorithms on total delay of the system.

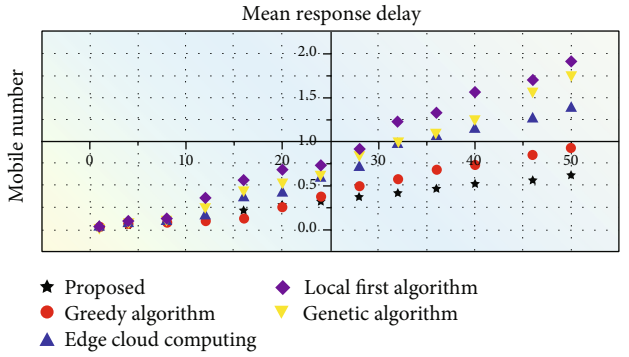

Figure 4: Effect of different mobile devices on average moving edge response delay.

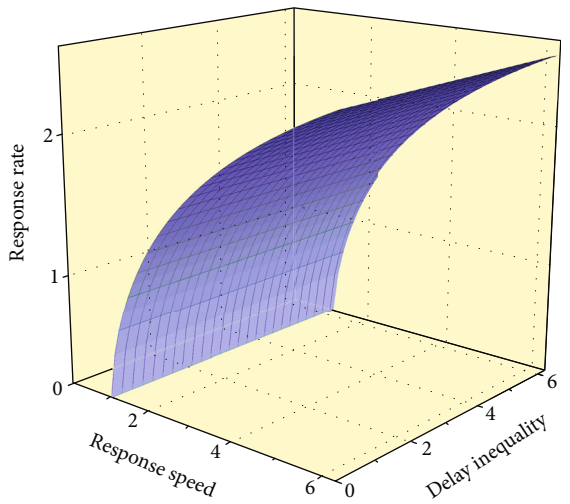

Figure 5: Effect of different mobile devices on average moving edge response delay.

optimization algorithm can reduce the total delay of system execution applications.

4.1. Model Validity Analysis. The analysis of the effectiveness of the offloading optimization algorithm for moving edge computing is mainly carried out through the following steps: in the case of different numbers of mobile devices, the influence of different algorithms on the average moving edge response delay. The influence of different algorithms on the total delay of the system is analyzed by line graph under different arrival rates of computational tasks. When the mobile device's own computing resources are different, the influence of different algorithms on the total delay of the system is analyzed by line chart.

The influence of different algorithms on the total system delay under different numbers of mobile devices is shown in Figure 3. In this simulation experiment, the range of numbers is [5,50], and the step size of the changing device is 4.

The experimental results show that the total system delay increases with the increase of the number of mobile devices. This is because the total amount of computing resources provided by wireless network resources and mobile edge cloud is fixed, and the competition for system resources increases when the number of mobile devices is large, so the total system delay also increases. The greedy algorithm only focuses on the shortest task execution delay of the device itself, and the total system delay is large. The competition for mobile edge cloud resources increases, and the total system delay required to perform all computing tasks increases. The total delay increases the fastest. In this algorithm, because all computing tasks are executed locally on mobile devices, computing resources of mobile edge cloud are not used, and mobile devices have limited resources. When a large number of computing tasks are executed, a large application execution delay will occur. For example, when the number of mobile devices is 50. In the mobile edge cloud first computing algorithm, all computing tasks generated by mobile devices are offloaded to the mobile edge cloud for execution. The execution delay of computing tasks is divided into two parts: wireless transmission delay and mobile edge cloud execution delay. Mobile edge cloud can expand computing resources for mobile devices, but the offloading of too many computing tasks will cause serious network congestion for wireless network transmission, thus bringing large transmission delay. In addition, the computing resources of mobile devices themselves are also idle in the mobile edge cloud priority computing algorithm, resulting in a waste of resources. The optimization algorithm makes full use of the wireless sensor and mobile edge cloud computing in the system to make a decision on the offloading of mobile devices. Therefore, the total system delay required for application execution is less than the other three benchmark algorithms.

The influence of different numbers of mobile devices on average moving edge response time is shown in Figure 4. In this simulation experiment, the range of the number is set from [5,50], and the change step is 4.

The experimental results can be roughly observed in the moving edge computing system, the more mobile devices, the longer the average moving edge response time of the system. In the local first computing algorithm, all computing tasks of mobile devices are executed locally, so the moving edge response delay in the local first computing algorithm is always zero. Compared with greedy computing algorithm and mobile edge cloud first computing algorithm, the

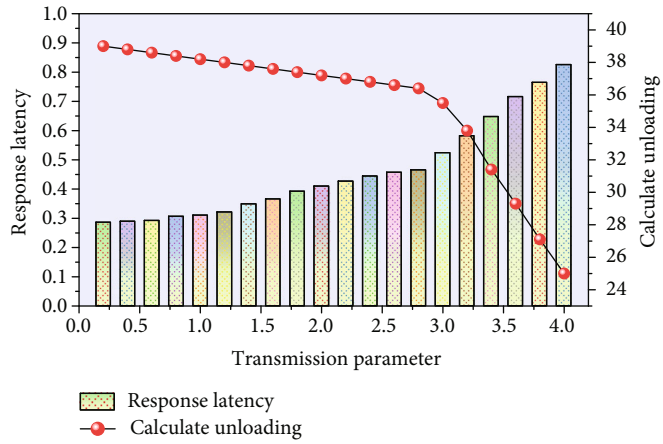

Figure 6: Effect of transfer parameters on mobile computing offloading.

optimal computing offloading optimization algorithm proposed in this paper avoids the idle and waste of system computing resources, so the effect is better.

The impact of the average rate of task arrival on the total system delay is shown in Figure 5. The abscissa in the figure of experimental results is the average arrival rate of computing tasks for mobile devices. The range of average rate of computing tasks is controlled at [0, 6], and the step size of change is 1.

It can be seen from the experimental figure that in the dynamic edge computing system, with the increase of computing requirements, the total system delay required to perform computing tasks also increases accordingly. The analysis results show that when the arrival rate of computing tasks increases, the total delay of the system does not increase significantly, and the average delay required for the execution of computing tasks decreases significantly. The optimization algorithm combining the optimal computing offloading and resource allocation can make full use of the wireless transmission and computing resources in the system, avoid the waste of resources, and reduce the total delay of the system.

4.2. Model Performance Analysis. The mobile edge computing system has a large number of mobile devices arriving every time, and the mobile devices are loaded with delay-sensitive applications, which will generate a large number of intensive computing tasks according to the use requirements of mobile devices. The transmission resources in the mobile edge computing system are not fixed, so the optimal computing unloading optimization algorithm needs to maintain good stability to ensure that the decision results of the algorithm have less impact on the whole system when the resources in the system change. This paper mainly focuses on the influence of the change of transmission parameter C on mobile device computing task offloading and system delay. The influence of the change of transmission parameter C on mobile device computing offloading is shown in Figure 6. The abscissa in the figure of experimental results is the transmission parameters of wireless network transmission resources, that is, the amount of data actually needed to transmit a single computing task, and the ordinate in the figure is the sum of all computing tasks offloaded by mobile devices.

The number of mobile devices in this simulation experiment is set to 50. As can be seen from the experimental results, with the forcing-port of transmission parameter C, the offloading amount of total computing tasks of mobile devices shows a downward trend. This is because the transmission parameter C represents the transmission cost. The larger c is, the larger the actual data amount required by the calculation task of the transmission unit is. In this case, the congestion of the network will be aggravated and the transmission delay of the system will be longer. The experimental results show that when the transmission parameter C is less than 3.0, there is no significant impact on the computing offloading strategy of mobile devices. When the transmission parameter C is greater than 3.0, mobile devices in the system are more inclined to perform computing tasks locally, because offloading computing tasks at this time will bring large transmission delay.

Analysis results can be found that the transmission parameter c smaller, less than 2, had no significant effect on the system time delay, prove that the change of the transmission parameter c in the edge of mobile computing system calculation uninstall not significantly affect the decision-making organ, and wireless network at this time the actual transmission data volume is low, so the transmission lower than the proportion of the total delay system. With the increase of transmission parameter C, especially when parameter C is greater than 3.0, the actual transmitted data volume of wireless network increases significantly. At this time, mobile devices will have a large transmission delay in offloading computing tasks. Therefore, the optimal computing offloading optimization algorithm is more inclined to leave computing tasks in the local execution of mobile devices.

4.3. Influence of Model Iteration Times on Total Energy Consumption. The performance of this algorithm is verified in offloading model optimization, and different strategies of offloading optimization algorithm based on moving edge

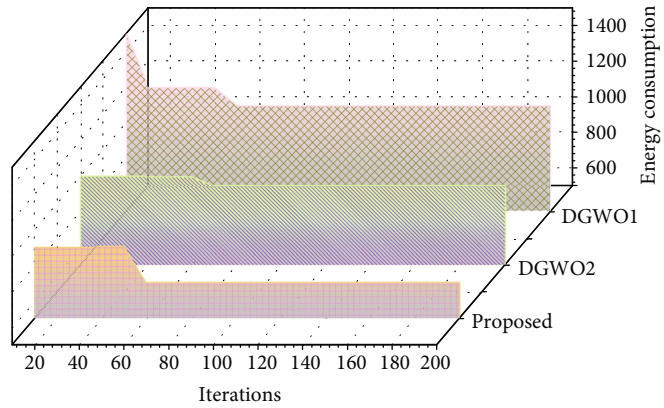

Figure 7: The influence of iteration times on total energy consumption of the system.

computing are compared. Simulation experiments were carried out in Matlab software, and simulation scenes were built based on the described multiuser system model. Figure 7 shows the influence of the number of iterations of simulation experiment on the total energy consumption of the system.

The convergence performance of different algorithms is compared in the figure. DGWO1 algorithm and DGWO2 algorithm converge gradually to the local optimal solution after the 50th and 60th iterations, respectively, and the convergence trend is slow. This is because the operation of crossover function may lead to the loss of the optimal individual in the next generation population, and the phenomenon of losing the optimal individual may occur repeatedly in the whole position update process. The algorithm in this paper increases the amount of information contained in each individual by expanding dimensions, so the accuracy is higher. Moreover, the algorithm in this paper combines cosine convergence factor, which can make the algorithm better jump out of local optimum.

5. Conclusion

In mobile edge computing technology, the time delay required to perform computing tasks is very important. When mobile devices uninstall computing tasks, it may occur those multiple mobile devices uninstall computing tasks through the same wireless access point, and the offloaded computing tasks are executed in the same mobile edge cloud service section. By optimizing the offloading model of mobile edge computing, the wireless transmission parameters in the system are well supported, and the impact on the whole system is small. The performance meets the system requirements of mobile edge computing. The optimal computing offloading optimization algorithm can make full use of mobile device's own computing resources, wireless network transmission resources, and mobile edge cloud computing resources in the mobile edge computing system to avoid waste and idle resources. At the same time, compared with the local computing first algorithm and the mobile edge cloud computing first algorithm, the joint optimization algorithm of optimal computing offload and resource allocation can better reduce the mobile edge response delay and the total delay of the system. Computing, storage, network, and communication resources are deployed at the edge of the mobile network, reducing network operations and service delivery delays, and improving user experience. In addition, MEC reduces the transmission bandwidth requirements for the core network by deploying servers at the edge of the network, reducing operating costs. In the next step, the combination of deep reinforcement learning and computational unloading is considered to design a more intelligent unloading algorithm to adapt to the complex and changeable edge unloading environment.

Data Availability

The data used to support the findings of this study are available from the corresponding author upon request.

Conflicts of Interest

The authors declare that they have no known competing financial interests or personal relationships that could have appeared to influence the work reported in this paper.

Acknowledgments

This work was supported by Army Engineering University of PLA.

References

[1] X. Cao, G. Zhu, J. Xu, and K. Huang, "Optimized power control for over-the-air computation in fading channels," *IEEE Transactions on Wireless Communications*, vol. 19, no. 11, pp. 7498–7513, 2020.

[2] W. Z. Khan, E. Ahmed, S. Hakak, I. Yaqoob, and A. Ahmed, "Edge computing: A survey," *Future Generation Computer Systems*, vol. 97, pp. 219–235, 2019.

[3] Z. Ziming, L. Fang, and C. Zhiping, "Edge computing: platforms, applications and challenges," *Journal of Computer Research And Development*, vol. 55, no. 2, p. 327, 2018.

[4] Y. He and Z. Tang, "Strategy for task offloading of multi-user and multi-server based on cost optimization in mobile edge

computing environment," *Journal of Information Processing Systems*, vol. 17, no. 3, pp. 615–629, 2021.

[5] G. Li, Q. Lin, J. Wu, Y. Zhang, and J. Yan, "Dynamic computation offloading based on graph partitioning in mobile edge computing," *IEEE Access*, vol. 7, pp. 185131–185139, 2019.

[6] Z. Lv, D. Chen, and Q. Wang, "Diversified technologies in internet of vehicles under intelligent edge computing," *IEEE Transactions on Intelligent Transportation Systems*, vol. 22, no. 4, pp. 2048–2059, 2020.

[7] D.-R. Chen, L.-C. Chen, M.-Y. Chen, and M. Y. Hsu, "A coverage-aware and energy-efficient protocol for the distributed wireless sensor networks," *Computer Communications*, vol. 137, pp. 15–31, 2019.

[8] Q. Liu, Z. Chen, J. Wu, Deng, Liu, and Wang, "An efficient task scheduling strategy utilizing mobile edge computing in autonomous driving environment," *Electronics*, vol. 8, no. 11, p. 1221, 2019.

[9] R. Wang, M. Li, L. Peng, Y. Hu, M. M. Hassan, and A. Alelaiwi, "Cognitive multi-agent empowering mobile edge computing for resource caching and collaboration," *Future Generation Computer Systems*, vol. 102, pp. 66–74, 2020.

[10] M. Liu, K. Yang, and N. Zhao, "Intelligent signal classification in industrial distributed wireless sensor networks based industrial internet of things," *IEEE Transactions on Industrial Informatics*, vol. 17, no. 7, pp. 4946–4956, 2021.

[11] C. Chen, L. Chen, L. Liu et al., "Delay-optimized v2v-based computation offloading in urban vehicular edge computing and networks," *IEEE Access*, vol. 8, pp. 18863–18873, 2020.

[12] Y. Sun, C. Song, S. Yu, Y. Liu, H. Pan, and P. Zeng, "Energy-efficient task offloading based on differential evolution in edge computing system with energy harvesting," *IEEE Access*, vol. 9, pp. 16383–16391, 2021.

[13] H. Sun, M. Liu, Z. Qing, X. Li, and Li, "Energy consumption optimisation based on mobile edge computing in power grid internet of things nodes," *International Journal of Web and Grid Services*, vol. 16, no. 3, pp. 238–253, 2020.

[14] A. H. Sodhro, S. Pirbhulal, and V. H. C. De Albuquerque, "Artificial intelligence-driven mechanism for edge computing-based industrial applications," *IEEE Transactions on Industrial Informatics*, vol. 15, no. 7, pp. 4235–4243, 2019.

[15] S. Siavoshi, Y.-S. Kavian, M. Tarhani, and H. F. Rashvand, "Geographical multi-layered energy-efficient clustering scheme for ad hoc distributed wireless sensor networks," *IET Wireless Sensor Systems*, vol. 6, no. 1, pp. 1–9, 2016.

[16] F. Zeng, Y. Chen, L. Yao, and J. Wu, "A novel reputation incentive mechanism and game theory analysis for service caching in software-defined vehicle edge computing," *Peer-to-Peer Networking and Applications*, vol. 14, no. 2, pp. 467–481, 2021.

[17] H. Li, K. Ota, and M. Dong, "Learning IoT in edge: deep learning for the Internet of Things with edge computing," *IEEE Network*, vol. 32, no. 1, pp. 96–101, 2018.

[18] C. Wang, Y. Lv, Q. Wang, D. Yang, and G. Zhou, "Service-oriented real-time smart job shop symmetric CPS based on edge computing," *Symmetry*, vol. 13, no. 10, p. 1839, 2021.

[19] L. Lombardo, S. Corbellini, and M. Parvis, "Wireless sensor network for distributed environmental monitoring," *IEEE Transactions on Instrumentation and Measurement*, vol. 67, no. 5, pp. 1214–1222, 2018.

[20] M. Chen, Y. Miao, and H. Gharavi, "Intelligent traffic adaptive resource allocation for edge computing-based 5G networks," *IEEE Transactions on Cognitive Communications and Networking*, vol. 6, no. 2, pp. 499–508, 2020.

[21] A. Chatterjee, P. Venkateswaran, and D. Mukherjee, "A unified approach of simultaneous state estimation and anomalous node detection in distributed wireless sensor networks," *International Journal of Communication Systems*, vol. 30, no. 9, p. e3191, 2017.

[22] Z. Lv, D. Chen, R. Lou, and Q. Wang, "Intelligent edge computing based on machine learning for smart city," *Future Generation Computer Systems*, vol. 115, pp. 90–99, 2021.

Hindawi
Journal of Sensors
Volume 2022, Article ID 2482638, 13 pages
https://doi.org/10.1155/2022/2482638

Research Article

Model Analysis of Sandstone Tunnel Cracking Based on Fracture Mechanics Theory and Sensor Testing Technology Research

Hu Jin, Bo Gao, and Yusheng Shen

Key Laboratory of Transportation Tunnel Engineering, MOE, Southwest Jiaotong University, Sichuan Chengdu 610031, China

Correspondence should be addressed to Hu Jin; jinhu@home.swjtu.edu.cn

Received 22 November 2021; Revised 14 January 2022; Accepted 21 January 2022; Published 14 February 2022

Academic Editor: Gengxin Sun

In this paper, we survey sandstone tunnels using sensor testing technology and conduct an in-depth analysis and research on the model of sandstone tunnel cracking based on the theory of fracture mechanics. This paper systematically investigates the static mechanical properties, energy evolution and distribution law, acoustic emission monitoring, and digital image correlation methods of intact and jointed rock chamber enclosures (including parallel jointed rock chamber enclosures and cross jointed rock chamber enclosures) under static loads, based on physical simulation test methods and combined with other technical means such as acoustic emission monitoring and digital image correlation methods. In this paper, the effects of parallel and cross-joint angles on the static mechanical properties, energy evolution and distribution, acoustic emission variability, progressive destabilization, and their mechanisms are compared and analyzed. This paper takes fiber Bragg grating (FBG) sensing theory and technology research as a breakthrough, relies on major underground engineering geohazard model tests, and proposes a grating spectral reconstruction theory based on the wavelength position constraint of the spectral center and its improvement based on an in-depth analysis of the influence of fiber grating intrinsic parameters and strain distribution on the reflection spectral properties. Based on an in-depth analysis of the influence of spectral center wavelength location and strain distribution on the reflectance spectral properties, we propose the grating spectral reconstruction theory based on the spectral center wavelength location constraint and its improved genetic algorithm optimization method; realize the fast and accurate identification and rejection of the melancholy effect of fiber grating; propose the sensor numerical simulation optimization design method; develop the high sensitivity seepage pressure sensor, new strain sensor, target flow sensor, microdisplacement sensor, and multipoint displacement sensor; and build a large capacity, multi-parameter fiber grating real-time monitoring network.

1. Introduction

After entering the 21st century, with the implementation of the modernization strategy and continuous deepening, the national investment in some important fields related to the national economy and people's livelihood has increased greatly, and the fields of transportation and civil engineering, water conservancy, and hydropower, mineral resources, electric power and energy, aerospace, machinery, and chemical industry have ushered in an unprecedented leap forward, which has brought great opportunities for the development and progress of science and technology in various fields [1]. However, at the same time, engineering disasters and geological disasters, as well as major production safety accidents, have become the main challenges for the construction and development of various fields, which are very likely to cause serious casualties, huge economic losses, and bad social impacts. Especially in the field of underground engineering, the frequent occurrence of geological disasters has become a bottleneck restricting the construction of underground engineering [2]. After entering the 21st century, with the implementation and continuous deepening of the modernization strategy, the state's investment in some important areas related to the national economy and people's livelihood has increased significantly. The fields of transportation and civil engineering, water conservancy and hydropower, mineral resources, electric energy, aerospace, machinery, and chemical industries are all welcome. An unprecedented leap-forward development

has brought huge opportunities for the development and progress of science and technology in various fields. In mines, sudden water accidents have become a major disaster that endangers mine safety, with more than 250 pairs of mines flooded in the past 20 years and direct economic losses amounting to hundreds of millions of yuan, and 285 of the country's key coal mines are threatened by water hazards, accounting for 47.5% of the total. To deal with water hazards in coal mines, discharges 5.6 billion m^3 of mine water every year, causing serious water depletion and environmental damage. In the field of transportation and hydropower, as the construction of water conservancy and hydropower projects and railway and highway projects have shifted their focus to the western mountainous areas under complex terrain and geological conditions, many tunnel caves with significant characteristics such as "large depth of burial, long cave lines, strong karst, high water pressure, high risk of disasters and construction difficulties" have emerged, and the complex hydrogeological conditions and sudden water, landslides, and other major geological hazards are a major concern. The complex hydrogeological conditions and major geological hazards such as sudden water and landslides are considered world-class engineering problems [3]. At the same time, engineering catastrophes, geological disasters, and major production safety accidents have become the main challenges for the construction and development of various fields in our country, which can easily cause serious casualties, huge economic losses, and bad social impacts.

The twenty-first century is the century of underground space. The development and utilization of underground space are an inevitable choice for human social development, economic construction, and the strategic needs of national security. In recent years, the construction of mining, traffic tunnels, water conservancy, hydropower, oil caverns, nuclear waste disposal, carbon dioxide geological storage, and national defence is developing at an unprecedented speed, and the underground chambers (such as tunnels, tunnels, mine tunnels, and shafts) are "long, large, deep and group." The number of "long," "large," "deep," and "massed" underground chambers (e.g., tunnels, tunnels, mine tunnels, and shafts) has increased to an unprecedented scale. With the introduction of the "deep earth" science strategy, it is predicted that the construction of large-scale, high-depth rockwork will become the norm, and underground engineering will become increasingly complex [4]. At the same time, the problems of strong disturbances and high ground stresses in rockwork chambers are becoming more serious, posing a significant challenge to the analysis and maintenance of the stability of the refuge envelope. The design and safe operation of underground chambers in rock engineering is directly dependent on an in-depth study of the deformation and damage characteristics and destabilization mechanisms of the project rock mass. The excavation of an underground chamber disrupts the original equilibrium stress state of the rock mass, causing a series of complex mechanical response behaviours associated with stress redistribution in the surrounding rock mass. In the fields of transportation and hydropower, as the focus of construction of water conservancy and hydropower projects and railway and highway projects has shifted to the western mountainous areas under complex terrain and geological conditions, a number of large buried depths, long tunnel lines, strong karst, high water pressure, tunnels with distinctive features such as high disaster risk and high construction difficulty, complex hydrogeological conditions, and major geological disasters such as water inrush and landslides can be regarded as world-class engineering problems. The deformation of the refuge rock is characterized by the emergence and expansion of cracks and the interpenetration of multiple cracks, which in turn leads to varying degrees of damage at the excavation face, ranging from flaking and spalling to major inward extrusion [5]. The present stage of the construction of infrastructure projects has avoided the contact between the engineering body and the geological body, of which the geological body is mainly rocking, soil, and the engineering body is the most common concrete. The application of concrete has been an essential part of engineering construction at this stage. Traditional support theory, design method, and construction technology are more based on normal temperature conditions, or not recommended for construction in low temperature, but cold zone engineering construction inevitably to accept the cold zone low-temperature impact, the traditional design method has been unable to meet the cold zone engineering construction needs [6]. As the frontier technology of modern science and technology, sensing technology, computer technology, and communication technology are considered as the three technical pillars of modern information technology and become the high point of human competition for high-tech technology in the 21st century.

2. Related Works

For the freeze-thaw damage of porous rocks and concrete, the theory of volume expansion was proposed in 1909. This theory suggests that water undergoes about 9% volume expansion during freezing. In confined pore spaces, damage can occur due to ice pressure that breaks the skeleton of the rock particles. However, the volume expansion theory has been questioned by other scholars as rocks under natural conditions are more likely to have connected pores [7]. The hydrostatic pressure theory was proposed in the study of concrete freeze-thaw damage due to the connectivity of pores within the rock. In addition, in the 1930s, it was found that unfrozen water in the soil migrates towards the ice surface, which in turn continuously forms subcondensed ice at the ice surface. It has also been found that water condensation ice can also form in frost-prone rocks with small mineral grains. The phenomenon of pore water freezing in different types of rocks was studied, and it was found that some of the pore water did not produce freezing at low temperatures [8]. It was found that the unfrozen water phenomenon is mainly due to the formation of an unfrozen water film between the ice and the rock skeleton, and the unfrozen water keeps migrating to the unfrozen water film during the freezing process [9]. With the proposal of the "deep ground" scientific strategy, it can be predicted that in the future, large-scale, high-burial rock mass engineering construction

will become normal, and underground engineering will become increasingly complicated. At the same time, the problems of strong disturbance and high ground stress faced by chambers in rock mass engineering have become more serious, which brings great challenges to the stability analysis and maintenance of chamber surrounding rocks. The existence of adsorption of unfrozen water in rocks to ice crystals was subsequently confirmed. Many studies have been done by related scholars on water migration under the freeze-thaw action of rocks. From the previous studies, it is known that the migration of water inside the rock or concrete under the action of freeze-thaw cycles can cause its local damage fracture phenomenon. For the rock-concrete binary, the interface is usually a naturally weak surface with low tensile strength and is therefore susceptible to moisture migration, which can lead to unpredicted freeze-thaw damage. Furthermore, due to the peculiarities of the interface presence, the mode of moisture migration behavior is not well established [10]. Thus, the study of moisture migration and damage debonding at the rock-concrete binary interface under freeze-thaw action is a good academic prospect in terms of binary interface bonding in cold regions.

There are two main branches of fiber optic sensing technology, which are fully distributed fiber optic sensing technology based on Raman scattering or Brillouin scattering and quasi-distributed fiber optic sensing technology based on fiber grating. The fully distributed fiber optic sensing technology uses an optical fiber as an extended sensitive element, and any unit on the fiber is both a sensitive unit and an information transmission channel for other sensitive units, which fundamentally breaks the traditional single point measurement mode limitation, but its disadvantage is that due to the extremely fast propagation speed of light, the technology requires a very high signal acquisition speed, and the signal processing usually takes a section of the optical fiber multiple acquisitions signals [11]. The average value of the signals collected on a section of the fiber is usually taken, which makes the spatial resolution low and therefore not suitable for the detection of abrupt fields; at the same time, the Raman and Brillouin scattering signals are extremely weak, so the signal processing is very tedious, which also makes the price of the sensing system high, which seriously limits the further application of the technology. The most widely used is based on fiber grating quasidistributed fiber optic sensing technology, because the fiber grating is a reflective optical device, able to produce several different center wavelength grating in an optical fiber, and time division multiplexing and wavelength division multiplexing technology combined to form a sensor array, suitable for buried in the material and structure or mounted on its surface, to achieve quasidistributed temperature, pressure, strain, and displacement parameters [12]. They are suitable for quasidistributed measurements of parameters such as temperature, pressure, strain, and displacement, either buried inside or mounted on the surface of materials and structures. The deformation and failure of the surrounding rock of the chamber are mainly manifested by the initiation and propagation of cracks and the interpenetration of multiple cracks, which leads to different degrees of damage to the rock mass of the excavation surface,such as extrusion and large deformation. At this stage, basic engineering construction cannot avoid the contact between engineering bodies and geological bodies. The geological bodies are mainly rock and soil bodies, and concrete is the most common form of engineering bodies.

In the field of current measurement, current sensors based on the tunnel magnetoresistance (TMR) effect have also received extensive attention. The designed current sensor with Wheatstone bridge structure is based on a magneto resistive element with magnetic tunnel junction structure, the current sensor has a DC measurement range of ±30 A, the sensitivity of 9.8 mV/A, and -3 dB bandwidth of 200 kHz for AC sensor, and the temperature coefficient of sensitivity is 0.031%/°C under different temperature tests, which is lower than the giant magnetoresistance current sensor based on spin valve structure [13]. Related scholars have applied TMR current sensors to current detection in integrated circuits to achieve current measurements from μA to mA levels, but there are strict requirements on the geometric design of the sensor chip, fabrication process, and testing methods. The TMR current sensor has been explored for high-frequency current testing, achieving a maximum current of 2.1 kA at operating frequency with a sensitivity of 35 μV/A and a nonlinearity of 1.5%. The application of TMR current sensor in the leakage current detection of high-voltage bushings is explored; the jointly developed TMR sensing chip shows good performance in the leakage current detection test of ZnO valve piece in surge protector, which provides a new idea and method for the noncontact measurement of leakage current of high-voltage devices [14].

2.1. Analysis of Sandstone Tunnel Cracking Model Based on Fracture Mechanics Theory. According to the different stress states of the geotechnical body, the stress path can be divided into two mechanical states, loading, and unloading. According to the subdivision of loading rate and unloading rate, it can be further divided into various combinations of loading and unloading. The mechanical properties of the rock body vary with different combinations of mechanical states. For rock loading or unloading, the difference in the process of stress change leads to the same transformation of total energy [15]. The loading damage process is equivalent to the external energy input to the rock mass, while for the rock mass with a certain ground stress field, during which there is residual strain energy, the excavation, and unloading of the rock mass is a process of energy release, resulting in changes in the mechanical properties of the rock mass and its integrity. In the study of practical problems, the actual stress conditions of the rock project should be distinguished, and different rock stress-strain paths should be selected for analysis according to the specific stress conditions. The biggest difference between rock loading and unloading is shown by the different stress paths. Fully distributed optical fiber sensing technology uses an optical fiber as an extended sensitive element. Any unit on the optical fiber is both a sensitive unit and an information transmission channel for other sensitive units. It fundamentally breaks through the limitation of the traditional single-point measurement mode. The

disadvantage is that due to the extremely fast propagation speed of light, this technology requires extremely high signal acquisition speed, and in signal processing, the average value of multiple acquisition signals on a piece of optical fiber is usually taken to make its spatial resolution low, so it is not suitable for use. For the detection of mutation field, if $\sigma 3$ remains unchanged and keeps increasing the maximum principal stress $\sigma 1$, i.e., when changing from B $\longrightarrow$ B1 $\longrightarrow$ B2 $\longrightarrow$ B3, the Mohr stress circle also keeps increasing, i.e., the partial stress is a gradually increasing process, so with the increase of load, the partial stress keeps increasing until the rock body is damaged. If the rock is unloaded, if $\sigma 1$ remains unchanged, as $\sigma 3$ decreases from A $\longrightarrow$ A1 $\longrightarrow$ A 2 $\longrightarrow$ A3, the Mohr stress circle becomes larger in the reverse direction, and even $\sigma 3 < 0$ may occur, i.e., it changes from the compressed state to the tensile state, which eventually leads to the destruction of the rock mass. If both $\sigma 1$ and $\sigma 3$ are changed during loading or unloading, more complex stress-strain states will be evolved. As shown in Figure 1, the Mohr stress circle is displayed.

According to the classification of the structural form of rock engineering, open-pit mine slope engineering belongs to the ground engineering in rock engineering, which is different from another ground engineering because of its special mechanical nature and conditions. When the open pit slope is excavated and exposed, the original ground stress equilibrium is broken, and the rock slope has the tendency to move to the stable state, at this time, its mechanical state is mainly manifested as unloading, and at this time, if the construction of external discharge field is carried out along the help, the vertical compressive stress is produced on the slope, that is, the rock slope is adjusted from the original ground stress equilibrium state to the stress state of tension and compression. Therefore, the analysis of hand-excavated slopes should not ignore the damage and deformation caused by unloading [16]. At present, the most widely used is the quasidistributed optical fiber sensing technology based on fiber gratings. Because fiber gratings are reflective optical devices, multiple gratings with different central wavelengths can be continuously produced in a single fiber. The multiplexing technology is combined to form a sensor array, which is suitable for being embedded in materials and structures or mounted on the surface, and realizing quasidistributed measurement of parameters such as temperature, pressure, strain, and displacement.

Conventional structural mechanics theory usually treats structural materials as isotropic homogeneous materials, but materials can have cracks or crack-like defects due to their own or external reasons, and crack-containing structures may be damaged when the stress of the member is far from reaching the yield stress, and such damage shows that it is difficult to accurately evaluate the performance and service state of a structure by using conventional mechanical theory analysis alone, no matter how accurately it is done. Therefore, scholars have proposed fracture mechanics on this basis. Fracture mechanics is an important theoretical basis for analyzing the strength and life prediction of engineering materials and components, and it is a new discipline to study the equilibrium, expansion, and destabilization laws of cracks and their strength of components containing cracks under the action of external forces. In online elastic fracture mechanics, concrete is no longer considered as a damage-free structure, but as a crack, model to study the conditions of crack extension and the process of crack extension, and its main mechanical parameter characterizing crack extension is the strength factor K, which represents the stress field at the crack tip and can describe cracking more accurately. Fracture mechanics is widely used in the study of crack extension in concrete.

Crack fracture criteria can be divided into two categories depending on whether the crack extends along the crack direction or not: single type crack fracture criteria and compound type crack fracture criteria. The essential difference between composite crack and single type crack is that the cracking direction no longer expands along the original crack surface, but has a certain angle with it. So composite cracks need to determine the angle of crack expansion based on a single crack. There are three commonly accepted ones: (1) the maximum energy release rate criterion, (2) the minimum strain energy density criterion, and (3) the maximum circumferential stress criterion. The three fracture criteria are based on energy-based parameters, strain-parameter, and stress-parameter types in turn.

(1) Guidelines for maximum energy release rate

The maximum energy release rate criterion considers that the idea of crack expansion can be considered from the point of view of energy release, and this criterion has two basic assumptions: the crack begins to expand when the maximum energy release rate reaches a critical value, and the crack expands in the direction of the maximum energy release rate generated by the crack tip. This fracture criterion is related to the fact that, by derivation, the maximum energy release rate is obtained as follows.

$$G_{\min} = \frac{1+\nu^2}{E} k^2. \tag{1}$$

(2) Minimum strain energy density criterion

Similarly, the basic assumption of this fracture criterion is that crack expansion along the direction of minimum strain energy density is associated with it reaching a critical. The minimum strain energy can also be obtained by analogous reasoning.

$$s(\theta) = c \cdot S_{\min}, \tag{2}$$

$$S_{\min} = \frac{1+2\nu}{2\pi s} k. \tag{3}$$

This chapter aims to architect a fully automated statistical analysis system for structural surface parameters based on digital image processing techniques. The choice of "fully automated" as the research objective makes the elimination of manual intervention an important consideration in the

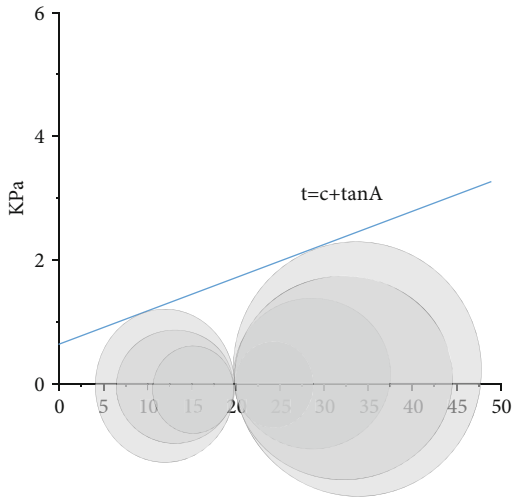

Figure 1: Mohr stress circle.

development process. The loading failure process is equivalent to the external energy input to the rock mass, and for the rock mass with a certain in situ stress field, there is residual strain energy during it. The excavation and unloading of the rock mass are a process of energy release, which leads to changesin the mechanical properties completeness of the rock mass..

A digital camera is first used to image the unsupported roof face, followed by image preprocessing with local histogram equalization, adaptive gamma correction, and median filtering, then, the structural face contour is extracted by area growth segmentation and Hough transform, and the structural face skeleton is obtained by contour refinement and interrupted point connection, and finally, the structural face characteristic parameters are calculated and the GSI rating is calculated. The flow of the digital image analysis system is shown in Figure 2.

A Go-Pro digital camera (model: CHDHX-601-RW) was used for image acquisition. This digital camera has excellent waterproof, dustproof, and impact resistance properties, which is conducive to image acquisition in underground coal mines and meets the needs of posttesting. The camera lens is placed in the vertical direction of the rock face during the shooting process, which can avoid the image distortion caused by the angle error during the inclined shooting process. When the open-pit mine slope is excavated and exposed, the original ground stress balance is broken, and the rock slope tends to move to a stable state. At this time, its mechanical state is mainly shown as unloading. The construction of the external dump site produced vertical compressive stress on the slope, that is, the rock slope was adjusted from the original in situ stress balance state to the tension and compression stress state. The lack of effective lighting equipment at the roadway excavation working face and a suitable light source is an extremely important part of the imaging system. The current light source for the camera can be divided into three categories: direct light source, diffuse light source, and reflective light source, the difference is whether the light in the process of propagation from the light source to the object changes direction, a simple schematic diagram is shown in Figure 3. Direct light from the light source directly to the object surface, direct light is very easy to cause uneven distribution of image brightness, in the imaging of uneven rock surface, and direct light will cause many high-contrast shadow areas, hindering the subsequent image processing work. Diffuse light travels through a translucent diffuse plate during propagation, causing light to be emitted irregularly in different directions. Diffuse light softens shadow areas in the image, and at high luminance, it is even possible to achieve shadow elimination. The reflected light reaches the object after it has been reflected by an opaque surface. Both reflective and diffuse light can soften the light, but additional reflective surface controls need to be added during implementation, adding to the complexity of the system. In addition, reflection attenuates light intensity, which is not conducive to imaging work in dark environments.

2.2. Sensor Testing Technology Research. A wireless sensor network is a network system consisting of many intelligent sensor nodes deployed in a monitoring area, whose purpose is to collaboratively sense, collect, and process information about the sensed objects in the network coverage area. Compared with traditional monitoring methods, wireless sensor networks have the following advantages: (1) wireless communication. Therefore, scholars put forward fracture mechanics on this basis. Fracture mechanics is an important theoretical basis for analyzing the strength and life prediction of engineering materials and components. It is to study the balance, growth, and instability of cracks in components with cracks under the action of external forces,which is a new discipline of law and intensity. Smart sensor nodes are wirelessly connected and self-organized communication networks, which brings great convenience to instrument installation and greatly reduces installation cost and installation workload; (2) large-scale network. Small size, flexible arrangement, and many sensor nodes can be deployed in the monitoring area to form a large-scale network, through different spatial perspectives to obtain information with greater signal-to-noise ratio, reducing the accuracy requirements of individual sensor nodes, making the system has a strong fault-tolerant performance; (3) scalability and robustness (relative stability). Wireless sensor networks have the advantages of self-organization and self-healing, and sensor nodes can be randomly arranged and nodes are automatically configured and managed to form a multihop wireless network. Therefore, new expansion nodes can be added to the network at will, with good scalability, when a node failure, other nodes automatically find a new transmission path, does not affect the normal work of the entire network, to ensure the overall network robustness; (4) have local computing and processing capabilities. Sensor nodes integrated microprocessor and memory can achieve self-calibration, self-diagnosis, and other functions, the original data processing, extraction of useful information, greatly reducing the amount of data to be transmitted wirelessly; (5) damage recognition and localization capabilities. Wireless sensor network that enables node localization. Combined with the structural state information measured by sensors, the

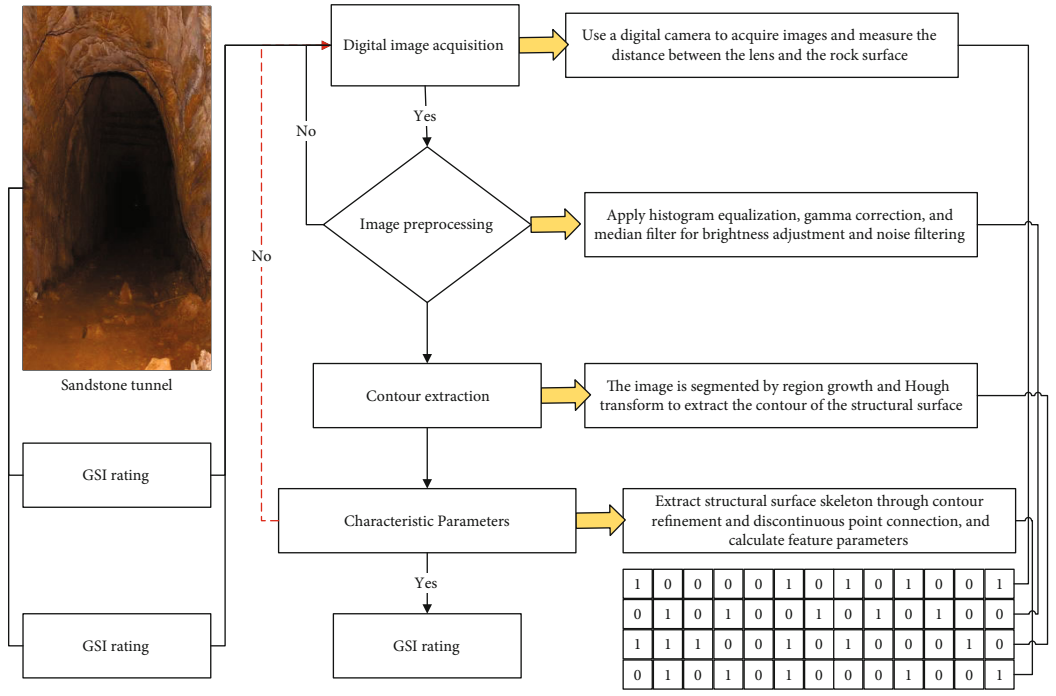

Figure 2: Flow chart of the digital image analysis system.

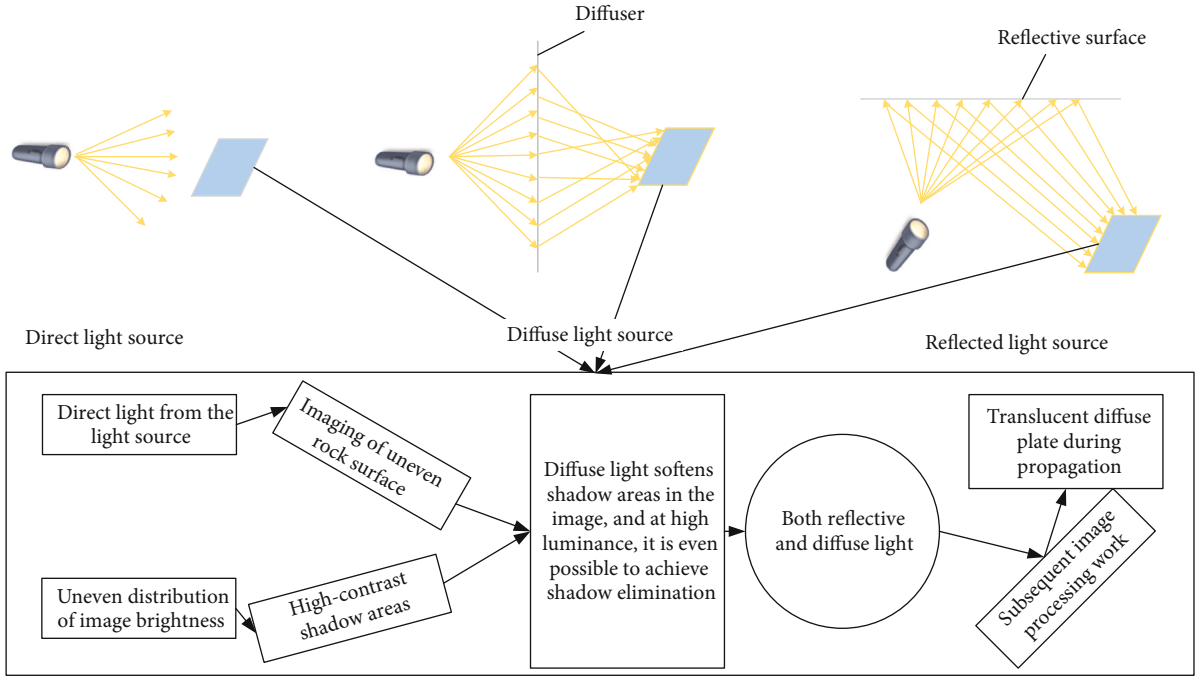

Figure 3: Schematic diagram of a direct light source, diffuse light source, and reflected light source.

damage recognition theory can be applied to automatically detect damage and accurately locate the damage location, which greatly promotes the intelligence of structural monitoring and maintenance.

At this stage, there are two types of inclination sensors, synchronous acquisition, and asynchronous acquisition, which in turn is important for deformation measurement. The method of achieving synchronization can be achieved by hardware and software methods, and the software method can be achieved by interpolation. The hardware synchronous acquisition technique is a bit-synchronous communication technique, and to achieve synchronization in hardware, the sender and receiver need to have clock signals of the same frequency and phase [17]. When no data

acquisition is required, the connection line is in MARK state. At the start of a measurement, the sender first sends one or two of the synchronization characters. Once both parties have achieved synchronization, large blocks of data can be sent in single character succession, thus, eliminating the need for start and stop bits. During transmission, both parties take a clock for coordination, which is used to determine the position of each bit in the serial transmission. The essential difference between compound cracks and single type cracks is that the cracking direction no longer extends along the original crack surface, but has a certain angle with it. Therefore, compound cracks need to determine the crack propagation angle based on a single crack. To start the measurement, both sides use the sync character to keep the clock internally synchronized with the sender, then the data following the sync character is shifted in bit by bit while converting to a parallel format for the CPU to read, and the data is not available until the end character is received. Synchronous acquisition uses a common clock, and synchronous acquisition has a high transmission frequency, to achieve high-speed, high-capacity data transmission. When data transmission is performed, both sides must maintain complete synchronization, requiring the receiving and sending devices to have the same clock and maintain strict synchronization. In summary, the system consists of a complete system topology consisting of a data processing platform on the server-side, a database station, and an inclination sensor, as shown in Figure 4.

To further analyze the characteristics of the open-loop and closed-loop structures, a mathematical model is developed to analyze both separately. First, the transfer function block diagram of the open-loop structure is established, where the voltage V is the out output of the system and the primary current Ip is the input of the system. b denotes the magnetic induction intensity generated by the primary current I in the paleomagnetic loop, and the coefficient K is used to define the relationship between Ip and Bp: $K =$ Bp/Ip. According to the ampere-loop theorem, K can also be expressed as

$$K = \frac{3u_0}{2d}. \tag{4}$$

The static gain SI (0) represents the sensitivity of the entire system, which is also the turn ratio of the primary coil to the feedback coil. Since the number of turns of the primary coil is generally 1, the turn ratio is determined by the number of turns of the feedback coil only. Therefore, when the number of turns of the feedback coil is certain, the feedback current is always proportional to the primary current even though the nonlinear error or temperature drift of the TMR sensor affects the open-circuit sensitivity coefficient Ka of the TMR sensor, which improves the measurement accuracy of the TMR current sensor, eliminates the offset and drift associated with the chip temperature, and greatly reduces the error caused by the hysteresis phenomenon. Based on the transfer function of the closed-loop TMR current sensor, the cutoff frequency of the system can be obtained as

$$f(0) = \frac{K_a + K_s + K_b}{2\pi R_{t0}}. \tag{5}$$

The cutoff frequency $f0$ indicates the bandwidth of the TMR current sensor, which is determined by the operational amplifier parameters τA, Ka, the feedback magnetic field coefficient Kb, the open-loop sensitivity coefficient Ks, and the feedback resistance Rm. In practical design, due to the high sensitivity of the TMR chip, the bandwidth of the closed-loop TMR current sensor can be as high as MHz when a suitable feedback magnetic field coefficient K and feedback resistance Rm are selected some time, it should be ensured that the feedback resistance Rm is large enough to obtain a good output voltage resolution. Increasing the value of K allows a wider bandwidth of the closed-loop TMR current sensor, but at the same time, the size of the number of turns N of the feedback 2coil should be limited to ensure a good current sensitivity of the system. Compared with traditional monitoring methods, wireless sensor networks have the following advantages: (1) wireless communication. The use of wireless connection between intelligent sensor nodes and self-organizing communication network brings great convenience to the installation of the instrument, greatly reducing installation cost and installation workload; (2) large-scale network. Small size, flexible layout, and many sensor nodes can be deployed in the monitoring area to form a large-scale network, obtain information with greater signal-to-noise ratio through different spatial perspectives, reduce the accuracy requirements for a single sensor node, and make the system highly fault-tolerant performance; (3) scalability and robustness (relative stability). Wireless sensor networks have the advantages of self-organization and self-healing. Sensor nodes can be randomly arranged, and nodes can be automatically configured and managed to form a multihop wireless network. Therefore, new expansion nodes can be added arbitrarily in the network, which has good scalability. When a node fails, other nodes automatically find a new transmission path, which does not affect the normal operation of the entire network and ensures the robustness of the overall network nature; (4) have local computing and processing capabilities. The integrated microprocessor and memory of the sensor node can realize self-calibration, self-diagnosis, and other functions, process raw data, extract useful information, and greatly reduce the amount of data that needs to be wirelessly transmitted; (5) damage identification and location capabilities. Wireless sensor network can realize node positioning. Combining the structural status information measured by the sensors and applying the damage recognition theory can automatically detect damage and accurately locate the damage location, which greatly improves the detection accuracy.

The sensitivity of the TMR current sensor is low when using the single wire measurement model, and it is difficult to ensure that the relative positions of the wire and the TMR chip are fixed, so the effect of a change in the relative

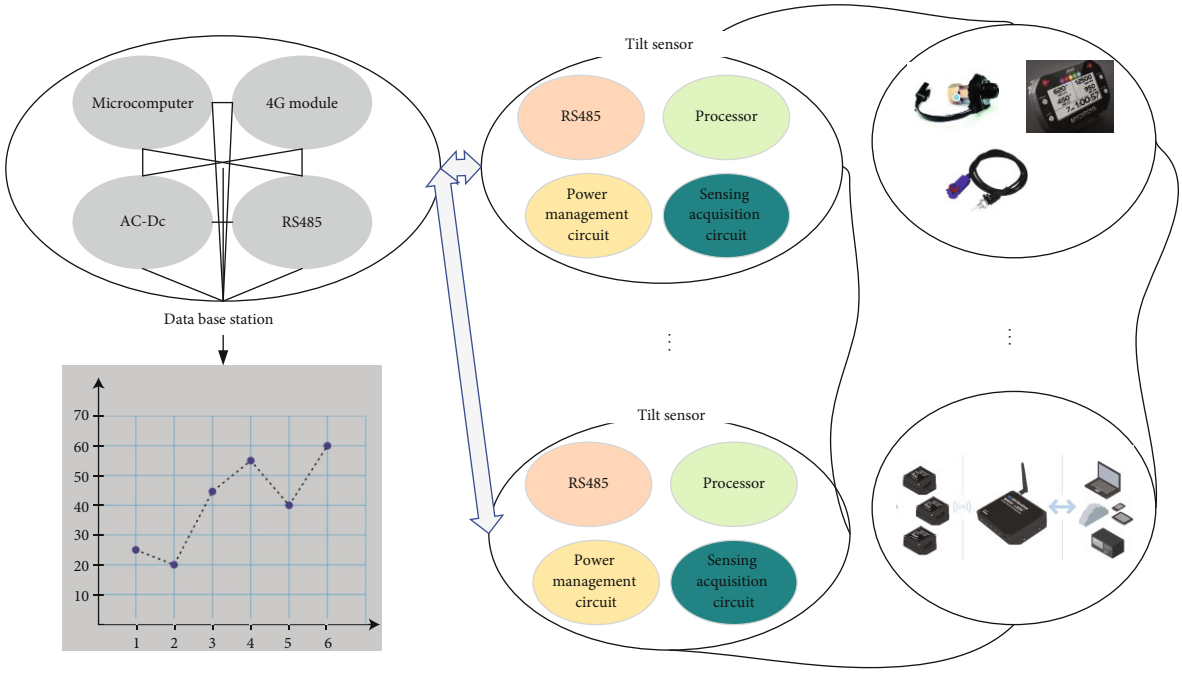

Figure 4: Sensor acquisition system topology diagram.

positions of the two on the measurement accuracy is further analyzed. The position of the wire is taken as the center of the circle, the TMR is the point on the circle, and the effect of the wire deviating from the center of the circle on the measurement is analyzed [18]. The simulation model is built in COMSOL simulation software, the radius of the wire is 5 mm, the length is 0.5 m, the size of the TMR chip is 0.8 mm × 5 mm × 3.5 mm, the distance between the TMR chip and the wire is $r0$ is 30 mm, and the magnetic field distribution at the TMR chip is analyzed at different positions of the wire. Since the magnetic sensitivity axis of the TMR chip is in the $+X$ direction, the magnetic flux on the surface of the TMR chip is used as a comprehensive measure of the magnetic field distribution at the TMR chip. The magnetic field distribution at the TMR chip is considered for the two cases of the wire moving along the $+X$ direction and the wire moving along the $+Y$ direction, respectively. Analyze the case of the wire moving along the $+X$ direction. As shown in Figure 5, the X-coordinate of the wire is changed so that the wire moves along the $+X$ direction. The X-coordinate of the wire is scanned parametrically with the X-coordinate ranging from -18 mm to 18 mm, and the wire is made to move 1 mm along the $+X$ direction each time to find the magnetic flux at the surface of the TMR chip.

3. Results and Analysis

3.1. Performance Testing of Sandstone Tunnel Cracking Model with Fracture Mechanics Theory. The rock is a highly typical nonhomogeneous rock mass, and the expansion and changes of its internal microjoint fractures are closely related to time. The deterioration process of the sloping rock in open-pit mines is a nonlinear cumulative process closely related to time, and the slope stability is typically time-dependent. During the whole cycle from open pit excavation, slope exposure to final backfill and burial, changes in the external environment, such as blasting vibration, mining disturbance, weathering, groundwater infiltration, frost, and cold shrinkage, may cause the destruction and accumulation of the internal microstructure of the rock, and with time, the mechanical strength of the rock body continues to decay and gradually converge to a low limit value of stable convergence, resulting in the overall stability of the slope. Therefore, it can be considered that the stability of slopes in open-pit mines is dynamic [19]. The external factors affecting the exposure time of slopes can be summarized in the following two major aspects: (1) synthetic mining disturbance factors. It is mainly reflected in the whole mining process system of the open-pit mine, including the perforation of coal rock near the slope, loose blasting vibration, and excavation and transportation of ore and soil discharge along with the gang. When there is no need to collect data, the connection line is in the MARK state. At the beginning of the measurement, the sender first sends one or two synchronization characters. When the two parties reach synchronization, they can continuously send large blocks of data with a single character, so that the start bit and stop bit are no longer needed. These operational processes will produce certain damage to the geotechnical body, and the degree of damage accumulation is closely related to the slope exposure time. (2) Natural environmental factors. Mainly reflected in the geotechnical body is located in the natural environment changes, the impact on the physical and mechanical properties, and strength of the slope geotechnical body, including groundwater level, temperature changes, rainfall erosion, and physical and chemical weathering. Take temperature change as an example, for the slope of the open-pit mine located in the seasonal freezing area, due to the

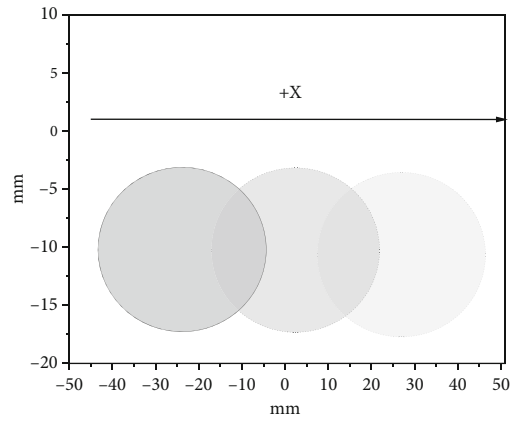

Figure 5: Simulation model of guidewire movement along +*X* direction (top view).

seasonal and temperature changes, the water in the slope constantly freezes and melts, changing the structure and distribution of the original joint fissures and weakening the stability of the slope.

$$t = \frac{(\cot \alpha - \cot \beta) - D}{v_p}. \tag{6}$$

The fracture behavior of a chambered and jointed rock mass can be considered as a complex flawed rock mass, which depends mainly on the emergence, extension, and agglomeration of cracks during loading. The fracture behavior of a rock mass containing a jointed chamber is closely related to the stress distribution around the chamber under the corresponding loading conditions. To gain insight into the damage pattern and crack evolution of the specimens from chambers containing parallel joints, it is necessary to first conduct a brief analysis of the stress distribution around the chamber. To facilitate the theoretical derivation, the chamber is usually simplified to a planar stress problem, the stress distribution around the chamber is calculated based on two-dimensional elastic theory for biaxial stress conditions, and the theoretical analysis model is shown in Figure 6.

To study the deformation evolution and crack extension process of composite defective rock specimens from a fine viewpoint, the image evolution characteristics of the specimens during deformation and damage were recorded by a digital image correlation system, and after postprocessing, the change characteristics of deformation fields (displacement field and strain field) during deformation and damage of the specimens were obtained, and then the crack extension evolution law of the specimens at different stress stages under static load was analyzed and compared [20]. Changes in the external environment, such as blasting vibration, mining disturbance, weathering, groundwater infiltration, frost heave, and cold shrinkage, may cause the damage and accumulation of the fine structure of the rock. As time goes by, the mechanical strength of the rock mass continues attenuation and gradually approaching a stable and convergent low limit value, resulting in a gradual decrease in the overall stability of the slope. Therefore, it can be considered that the slope stability of the open-pit mine changes dynamically. Due to the high strength of the composite defective rock material used in this paper, the deformation field on the surface of the specimen does not change significantly in the preloading stage, and the obvious crack extension phenomenon generally occurs only in the stable crack extension stage and the unstable crack extension stage. Therefore, according to the development characteristics of the stress-strain curve of the specimen and combined with the evolution characteristics of AE events, some key stress points of the specimen in the crack stable extension stage and the crack unstable extension stage are selected to analyze the evolution characteristics of the deformation field.

The results of the NMR analysis show that the sandstone, the concrete side, and the interface have significantly different pore distribution evolution patterns under the freeze-thaw action. The sandstone and the interface show variation characteristics that are distinct from those of single materials. In contrast, sandstone near the interface is more susceptible to the effects of interfacial action. This chapter focuses on the effect of the presence of interface on the sandstone side and refers to it as Interface Influence Zone (IIZ). The extent of the interface influence zone is further identified and related to different freeze-thaw environments, and the evolutionary mechanism of the interface influence zone is explored from a fine-scale perspective. Based on the NMR signal intensity, the pore volume of the sandstone part is much larger than that of the concrete part. For the initial state, i.e., 0 freeze-thaw cycles, the sandstone-concrete binary exhibits a significant difference along the longitudinal direction. This phenomenon can be attributed to the original individual variability within the test. The NMR signal intensities at different numbers of freeze-thaw cycles are considered in conjunction with the NMR signal intensities at 0 freeze-thaw cycles. At the 14–17-layer position, i.e., within 13.6 mm of the interface in the sandstone, the freeze-thaw effect on the NMR signal is evident. In this range, the NMR signal intensity increases by about 50,000 a.u. with an increasing number of freeze-thaw cycles. However, at other locations in the sandstone-concrete diatom, the NMR signal intensity changes less. This analysis shows that under the effect of freeze-thaw cycles from -10°C to 10°C, the sandstone portion near the interface (layers 14-17) shows significant pore volume changes, exhibiting significant water aggregation and water migration to the interface. To deeply understand the failure mode and crack evolution of the chamber sample of rock mass with parallel joints, it is necessary to briefly analyze the characteristics of the stress distribution around the chamber. To facilitate theoretical derivation, the chamber is usually simplified as a plane stress problem, and the stress distribution around the chamber under biaxial stress conditions is calculated based on the two-dimensional elastic theory.

Analyzed at the interface, the interface is the cemented surface of the sandstone and concrete, and an interfacial transition zone is formed at the interface. The hydration of the cement in the part of the interface transition zone is

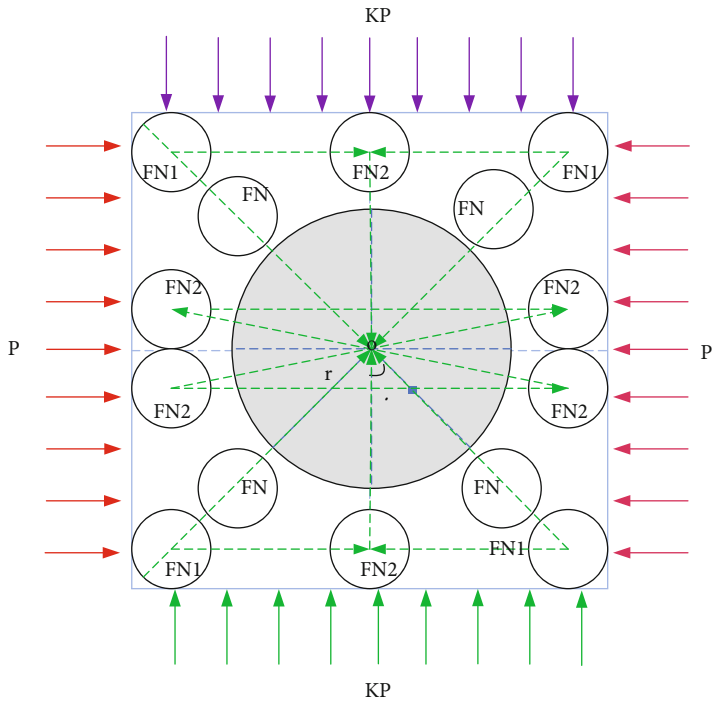

Figure 6: Simplified diagram of the stress distribution in the plane of the chamber under stress conditions.

different from the interior of the concrete. The interfacial transition zone is distributed with more calcium alumina crystals, and the interfacial fracture toughness is low. It should be noted that the interface transition zone has less distribution of both pores due to the intrusion of cement at the interface. However, at the same time, based on the pore distribution, a small number of large pores occur at the interface. Therefore, the analysis suggests that at the beginning of the freeze-thaw cycle, the hydraulic fracturing phenomenon mainly arises within the interface-influenced zone. The freeze-swelling force is not yet sufficient to cause fracture extension at the interface, or there are few newborn fractures at the interface part relative to the sandstone end. The water pressure inside the pore space is sufficient to crack the interface under repeated freeze-thawing action. And after the interface cracking, the later freeze-thawing has more influence on the interface cracking because the large pores of the interface have penetration, and the internal water pressure is more easily released along with the interface.

The extent of the interfacial zone of influence varies at different temperature intervals. At relatively high temperatures, the range of the interface influence zone is larger; at lower temperatures, the range of the interface influence zone is smaller. This phenomenon can be attributed to the combined effect of interface and freezing temperature. As shown in Figure 7, for low freezing temperature, the freeze swell force curve shows an increase and then a decrease, and there is a peak freeze swell force; for low freezing temperature, the same is true for the freeze swell force. However, for the low freezing temperature state, it produces a larger freeze swell force. In the sandstone near the interface, the low freezing temperature causes damage and cracking of the sandstone more easily and quickly. However, based on the test results, the low freezing temperature does not produce an increased area of influence at the interface under multiple freeze-thaw cycles.

3.2. Results of Sensor Testing Techniques. The static characteristics of the TMR current sensor mainly include sensitivity, range, linearity, accuracy, and other parameters, which must be calibrated before using the TMR current sensor. The TMR current sensor was sent to the Municipal Institute of Metrology and Quality Inspection for testing and calibration, and the testing equipment was a special clamp meter calibration device and a digital multimeter of type 8846A. The input and output curves of the TMR current sensor can be obtained by changing the current of the clamp meter calibration device and recording the corresponding output voltage of the TMR current sensor at different currents. The sensitivity of the sensor is defined as the ratio of the increment of the output quantity to the corresponding increment of the input quantity that causes the increment, so the sensitivity of the TMR current sensor is the ratio of the change of the output voltage to the change of the measured current. The current test range was first set to -60 A to 60 A, and the data from the test was imported into the origin plotting software for a linear fit, and the input and output curves were drawn as shown in Figure 8. The black curve is the input and output curve of the open-loop TMR current sensor, and the red curve is the input and output curve of the closed-loop TMR current sensor.

The maximum deflection error between the inclination sensor and the measured deformation curve of the total

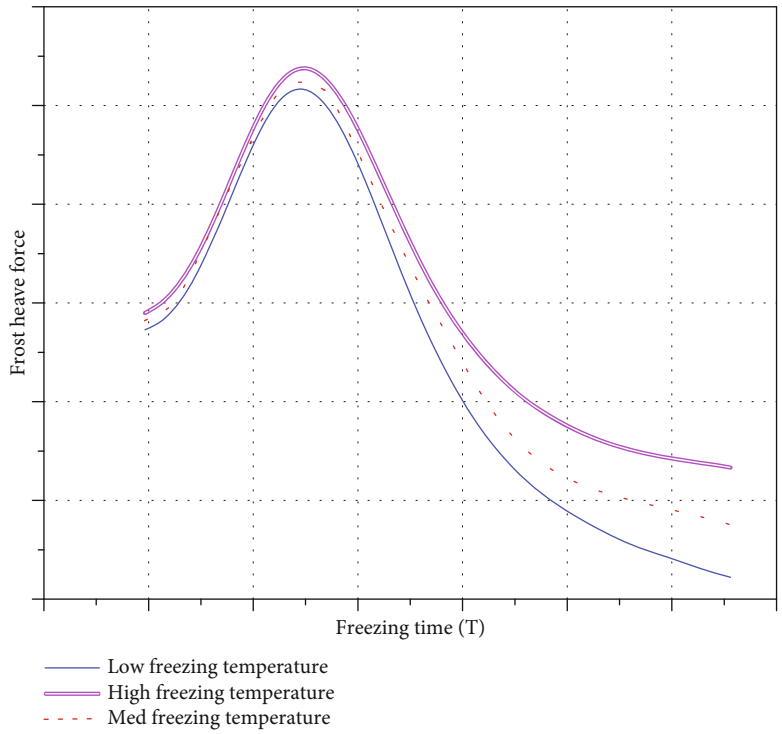

Figure 7: Schematic diagram of the development of internal freezing and swelling forces in sandstone at different freezing temperatures.

station is 0.7 mm, and the difference in the deformation curve is not significant. The inclination sensor for measuring tunnel deflection has the following advantages.

(1) The tilt sensor is small and easy to carry. Its size is 120 mm∗150 mm∗40 mm, which can be carried in large quantities band

(2) The inclination sensor is easy to install, the measuring point is not easy to damage, the aluminium housing can guarantee its long-term use, and not subject to measurement conditions, it can be used in unlit conditions

(3) Inclination sensors are less costly instruments compared to total stations and can be recycled

(4) The inclination sensor has high testing accuracy, and the measured inclination can be up to 9 decimal places, while the total station measures the deflection values can only be measured to an accuracy of two decimal places

(5) Inclination sensors can be realized in the office under the premise of unattended, real-time monitoring can be achieved. Using the user platform, through the computer control, you can achieve real-time monitoring, greatly reducing the workload, as well as the test time on site. And the tilt sensor acquisition can be achieved high frequency, that is, 1 s acquisition of 20, 50, and 100 numbers, real-time monitoring. This chapter introduces the application of the inclination sensor in the subway deformation monitoring

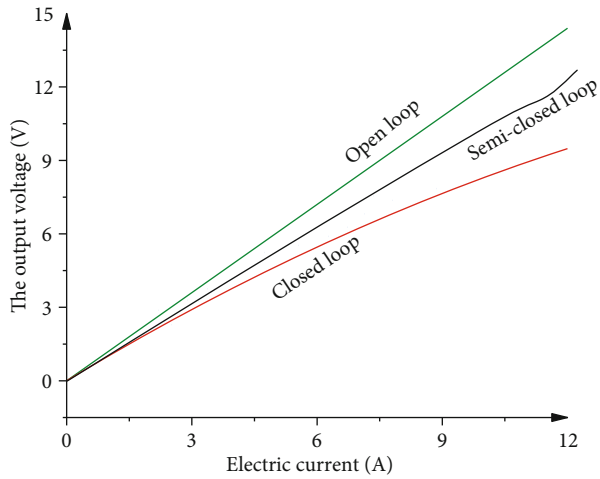

Figure 8: Input and output curves for open-loop and closed-loop structures.

example, through the inclination sensor and the total station measured data with the theoretical curve for comparison and analysis, know the inclination sensor and the total station measured data deformation curve difference is not large, the inclination sensor applied to the tunnel deformation measurement is feasible. The data in this chapter show that the maximum deflection value measured by the inclination sensor is 1.86 mm, which is less than the theoretically calculated value of 8.23 mm and less than the warning value of 10 mm, and the existing tunnel will be affected by the tunnel excavation, but overall, it is

safe. Compared with the traditional total station monitoring method, the inclination sensor has several advantages such as small size, easy installation, high testing accuracy, and realizing real-time monitoring

4. Conclusion

The development and utilization of underground space are an inevitable choice for human social development, economic construction, and strategic security needs. As a nonlinear, noncontinuous, nonhomogeneous, and anisotropic natural geological body, the rock body is randomly distributed with discontinuous structural surfaces such as joints, fractures, weak interlayers, and faults of different scales inside after a long period of geological action. The mechanism of rock instability damage and its stability and control problems is some of the key scientific problems that are currently focused on and urgently need to be solved in the field of rock mechanics. Compared with traditional wired monitoring methods, wireless sensor networks can overcome many drawbacks of traditional wired monitoring methods and have obvious advantages in many aspects such as instrument installation, data measurement, condition assessment, and cost control, which provide convenience for health monitoring work and are the future development direction of structural health monitoring. This paper discusses the model of sandstone tunnel cracking based on fracture mechanics theory with the help of sensor testing technology, and some results have been achieved. However, due to the complexity of sandstone tunnels themselves and the environment, there are very few studies dedicated to the application of wireless sensor networks in the intelligent monitoring of sandstone tunnels. The actual geography of sandstone tunnels is more complex, and further research work is still needed for a comprehensive analysis of their interface debonding characteristics. Therefore, a more in-depth study on the application of wireless sensor networks in tunnelling is of great significance for both human society and economic development.

Data Availability

The data used to support the findings of this study are available from the corresponding author upon request.

Conflicts of Interest

The authors declare that they have no known competing financial interests or personal relationships that could have appeared to influence the work reported in this paper.

Acknowledgments

The study was supported by Southwest Jiaotong University.

References

[1] F. Zhao, Z. Shi, and Q. Sun, "Fracture mechanics behavior of jointed granite exposed to high temperatures," *Rock Mechanics and Rock Engineering*, vol. 54, no. 5, pp. 2183–2196, 2021.

[2] W. Guo, F. Yu, Y. Tan, and T. B. Zhao, "Experimental study on the failure mechanism of layer-crack structure," *Energy Science & Engineering*, vol. 7, no. 6, pp. 2351–2372, 2019.

[3] L. Zhang, D. Yang, Z. Chen, and A. Liu, "Deformation and failure characteristics of sandstone under uniaxial compression using distributed fiber optic strain sensing," *Journal of Rock Mechanics and Geotechnical Engineering*, vol. 12, no. 5, pp. 1046–1055, 2020.

[4] X. Fu, Y. X. Ban, Q. Xie, R. A. Abdullah, and J. Duan, "Time delay mechanism of the Kaiser effect in sandstone under uniaxial compressive stress conditions," *Rock Mechanics and Rock Engineering*, vol. 54, no. 3, pp. 1091–1108, 2021.

[5] J. Chen, J. Zhao, S. Zhang, Y. Zhang, F. Yang, and M. Li, "An experimental and analytical research on the evolution of mining cracks in deep floor rock mass," *Pure and Applied Geophysics*, vol. 177, no. 11, pp. 5325–5348, 2020.

[6] D. Liu, K. Ling, D. Li et al., "Evolution of anisotropy during sandstone rockburst process under double-faces unloading," *Journal of Central South University*, vol. 28, no. 8, pp. 2472–2484, 2021.

[7] Y. H. Huang, S. Q. Yang, and J. P. Dong, "Experimental study on fracture behaviour of three-flawed sandstone specimens after high-temperature treatments," *Fatigue & Fracture of Engineering Materials & Structures*, vol. 43, no. 10, pp. 2214–2231, 2020.

[8] P. Zhou, J. Li, Y. Jiang et al., "Damage mechanism of tunnels in the high-content salt rock stratum," *Bulletin of Engineering Geology and the Environment*, vol. 80, no. 10, pp. 7633–7652, 2021.

[9] C. Niu, Z. Zhu, F. Wang, P. Ying, and S. Deng, "Effect of water content on dynamic fracture characteristic of rock under impacts," *KSCE Journal of Civil Engineering*, vol. 25, no. 1, pp. 37–50, 2021.

[10] Q. Xie, S. Li, X. Liu, F. Q. Gong, and X. B. Li, "Effect of loading rate on fracture behaviors of shale under mode I loading," *Journal of Central South University*, vol. 27, no. 10, pp. 3118–3132, 2020.

[11] W. Yu, G. Wu, B. Pan, Q. Wu, and Z. Liao, "Experimental investigation of the mechanical properties of sandstone–coal–bolt specimens with different angles under conventional triaxial compression," *International Journal of Geomechanics*, vol. 21, no. 6, 2021.

[12] Y. Zhang, X. Yao, P. Liang et al., "Fracture evolution and localization effect of damage in rock based on wave velocity imaging technology," *Journal of Central South University*, vol. 28, no. 9, pp. 2752–2769, 2021.

[13] H. Wu, B. Dai, L. Cheng, R. Lu, G. Zhao, and W. Liang, "Experimental study of dynamic mechanical response and energy dissipation of rock having a circular opening under impact loading," *Mining, Metallurgy & Exploration*, vol. 38, no. 2, pp. 1111–1124, 2021.

[14] A. Sedmak, "Computational fracture mechanics: an overview from early efforts to recent achievements," *Fatigue & Fracture of Engineering Materials & Structures*, vol. 41, no. 12, pp. 2438–2474, 2018.

[15] X. Li, F. Gong, M. Tao et al., "Failure mechanism and coupled static-dynamic loading theory in deep hard rock mining: a

review," *Journal of Rock Mechanics and Geotechnical Engineering*, vol. 9, no. 4, pp. 767–782, 2017.

[16] X. Zhang, Z. Li, E. Wang, B. Li, J. Song, and Y. Niu, "Experimental investigation of pressure stimulated currents and acoustic emissions from sandstone and gabbro samples subjected to multi-stage uniaxial loading," *Bulletin of Engineering Geology and the Environment*, vol. 80, no. 10, pp. 7683–7700, 2021.

[17] Z. Jinhao, C. Hongkai, W. He, and Z. Zheng, "Experimental study on damage evolution characteristics of rock-like material," *Arabian Journal for Science and Engineering*, vol. 44, no. 10, pp. 8503–8513, 2019.

[18] K. Zhang, X. Liu, Y. Chen, and H. Cheng, "Quantitative description of infrared radiation characteristics of preflawed sandstone during fracturing process," *Journal of Rock Mechanics and Geotechnical Engineering*, vol. 13, no. 1, pp. 131–142, 2021.

[19] S. Fereshtenejad, J. Kim, and J. J. Song, "The effect of joint roughness on shear behavior of 3D-printed samples containing a non-persistent joint," *Petrophysics-The SPWLA Journal of Formation Evaluation and Reservoir Description*, vol. 62, no. 5, pp. 553–563, 2021.

[20] L. Li, Y. Liu, W. Liu et al., "Crack evolution and failure modes of shale containing a pre-existing fissure under compression," *ACS Omega*, vol. 6, no. 39, pp. 25461–25475, 2021.

Hindawi
Journal of Sensors
Volume 2022, Article ID 2124462, 10 pages
https://doi.org/10.1155/2022/2124462

Research Article

Effect Evaluation of Biomedical Experiment Teaching Based on Intelligent Sensor

Zhicong Ma

Department of Medical College, Xuchang University, Henan Xuchang 461000, China

Correspondence should be addressed to Zhicong Ma; 12014131@xcu.edu.cn

Received 11 November 2021; Revised 5 January 2022; Accepted 22 January 2022; Published 14 February 2022

Academic Editor: Gengxin Sun

With the continuous development and progress of nanotechnology, its biosensors have been widely used in biomedical experimental teaching, and good experimental results have been achieved. Graphene, as a new nanomaterial with large surface area, good thermal conductivity, and unique electrical conductivity, has unique advantages in the field of biosensor preparation. Based on this, this paper will prepare the electrochemical sensor applied to biomedical experimental teaching based on graphene, optimize the detection sensitivity and detection range of graphene electrochemical sensor based on the corresponding experimental conditions, and improve its corresponding stability and reusability. At the level of electrochemical activity of biosensors, this paper innovatively uses the electric AC impedance method to detect the electrochemical activity, so as to accurately evaluate the key characteristics of biosensors. Based on the preparation of biosensors and the results of biological experiments, this paper will design a network-based biomedical experiment teaching effect evaluation system, and realize the basic functions of teacher-student interaction, teaching effect evaluation, sensor performance evaluation and so on. Based on the above, the electrochemical sensor based on graphene and a conductive polymer solution is actually prepared in this paper. At the same time, the electrocatalysis experiment is carried out based on the sensor, and the experimental teaching effect is systematically evaluated. The experimental results show that the sensitivity of the biosensor proposed in this paper is increased by about 10% compared with the traditional biosensor, the corresponding preparation complexity is reduced by nearly 1/3, and the corresponding reusability is increased by 30%. Therefore, the biomedical experiment teaching effect evaluation system proposed in this paper has good evaluation effect. It can provide accurate reference for the evaluation of biological experiment teaching effect, so it has important value and significance.

1. Introduction

As an important means of modern biomedical experiments, the biosensor is essentially a high-precision biosensor formed by combining the sensitive parts of organisms and their derivatives through physical and chemical energies. It linearizes the intensity of the detected biological signal with the physicochemical characteristics of the detected related organisms and converts it into a digital signal for processing [1, 2]. The cell biosensor is mainly composed of two parts: a molecular factor recognition processor and an energy converter, in which the corresponding energy converter is the main core module, which essentially converts biological signals into electrical signals, optical signals, thermal signals, and acoustic signals. In addition, molecular factors commonly used in biomedical experimental teaching include the detected organisms, tissues, nucleic acids, and organelles and corresponding biological derived materials [3–5]. The preparation technology of biosensors includes the cross-integration of biology, physics, chemistry, and other disciplines. Therefore, the corresponding biosensors in conventional biomedical experiments mainly include sound sensors, optical sensors, electrical sensors, semiconductor sensors, and electrochemical sensors [6–8]. As the most commonly used biosensor in biomedical experimental teaching, electrochemical sensors are mainly divided into cell tissue sensors, cell sensors, RNA sensors, microbial sensors, and enzyme sensors [9, 10]. Electrochemical sensors

often have the advantages of high sensitivity, fast response, convenient operation, and miniaturization and integration in biological teaching experiments. Therefore, it is of obvious value to study the sensor and its effect in biomedical experimental teaching [11, 12].

As an important biological material for biosensors, nanomaterials have unique biological detection advantages due to their quantum size effect, surface effect, small size effect, and macroquantum tunnel effect [13–15]. Graphene, as a new material for preparing biosensors in nanomaterials, has high charge carrier mobility [16]. Due to its large surface area, high electrochemical activity, and high electron mobility, it has obvious structural advantages as an electrochemical biosensor. A conventional graphene electrochemical biosensor can detect the dose of hydrogen peroxide with high sensitivity, so as to fix the electrochemical behavior of egg white matter [17]. The detection of biological glucose can be realized by using the electron migration of graphene derivatives between the electrode substrate and the redox active center of glucose. The detection of dopamine similar to a nerve substance can be realized based on microwave plasma enhancement technology, and the biosensor technology based on graphene can accurately detect the low concentration of dopamine in the biological system. High concentrations of interfering substances are eliminated in a wide range. Therefore, compared with traditional sensors, graphene-based biosensor technology can achieve high-precision detection of dopamine and other nerve substances and achieve good biomedical teaching experimental results [18, 19]. In the corresponding biomedical experiment teaching of deoxyribonucleotide, the detection of deoxyribonucleotide is very important and meaningful. The corresponding biomedical experiment teaching effect also directly affects the learning effect of students and reflects the teaching quality of teachers. Based on this, the excellent electrochemical characteristics of the graphene biosensor can detect with high precision deoxyribonucleotides and double-stranded deoxyribonucleotides. Graphene biosensors can provide ultrahigh-density active edge sites [20].

In view of the above corresponding research status and existing problems, this paper focuses on the preparation technology and application of the biosensor based on graphene and systematically gives the design and implementation of the biomedical experiment effect evaluation system and experimental verification. The specific research details are as follows: the electrochemical sensor applied to biomedical experiment teaching based on graphene is prepared and verified to optimize the detection sensitivity and detection range of the graphene electrochemical sensor under the corresponding experimental conditions and improve its corresponding stability and reusability. At the level of the electrochemical activity of the biosensor, this paper innovatively uses the electric AC impedance method to detect the electrochemical activity, so as to accurately evaluate the key characteristics of the biosensor, based on the preparation and production of the biosensor. The advantages of the corresponding electrochemical analysis method are as follows: high sensitivity. The lowest detection limit is 10-12 mol/L. *High accuracy*: for example, coulometric analysis and electrolytic analysis have high accuracy. The former is especially suitable for the determination of trace components, and the latter is suitable for the determination of high content components. *Wide measuring range*: potentiometric analysis and microcoulometric analysis can be used for the determination of trace components. Electrolytic analysis, capacitance analysis, and Coulomb analysis can be used for the analysis of medium content components and pure substances. The instrument and equipment are simple, the price is low, the debugging and operation of the instrument are simple, and it is easy to realize automation. *Poor selectivity*: the selectivity of electrochemical analysis is generally poor, but the selectivity of the ion selective electrode method, polarography, and controlled cathodic potential electrolysis method is high. According to the different electrical quantities measured, electrochemical analysis methods can be divided into conductivity analysis, potential analysis, voltammetry and polarography, and electrolysis and coulometry. Based on the above, an electrochemical sensor based on graphene and the conductive polymer solution is actually prepared and tested based on the sensor electrocatalysis experiment, and the experimental teaching effect is systematically evaluated. The experimental results show that the biosensor proposed in this paper has the advantages of high sensitivity, simple preparation, and high availability. At the same time, it also further verifies that the biomedical experimental teaching effect evaluation system proposed in this paper has good evaluation effect and can provide accurate information for the evaluation of biological experimental teaching effect reference resources.

The structure of this paper is arranged as follows: the second section of the article will analyze and study the preparation technology of the biosensor and the research status of biomedical teaching experimental effect evaluation system; the third section of this paper will focus on the preparation technology and optimization process of the graphene biosensor and give the design process of the biomedical teaching experimental effect evaluation system;the fourth section is mainly the validation experiment and analysis; finally, this paper will be summarized.

2. Correlation Analysis: Analysis of the Research Status of Sensor-Based Biomedical Experimental Teaching

At present, the research on biomedical experiment teaching based on sensors mainly focuses on the preparation technology of the biosensor and the evaluation of the teaching effect. At the level of biosensor preparation, a large number of researchers and research institutions have studied and analyzed it. Relevant researchers in Asia have prepared a graphene-based bioelectrochemical sensor based on host guest supramolecular interaction and achieved certain experimental results, At the same time, at the level of graphene biosensor preparation, relevant Japanese scientists have realized high-precision detection of hydrogen peroxide based on the graphene biosensor modified by gold nanoparticles. This detection technology has simplified the detection

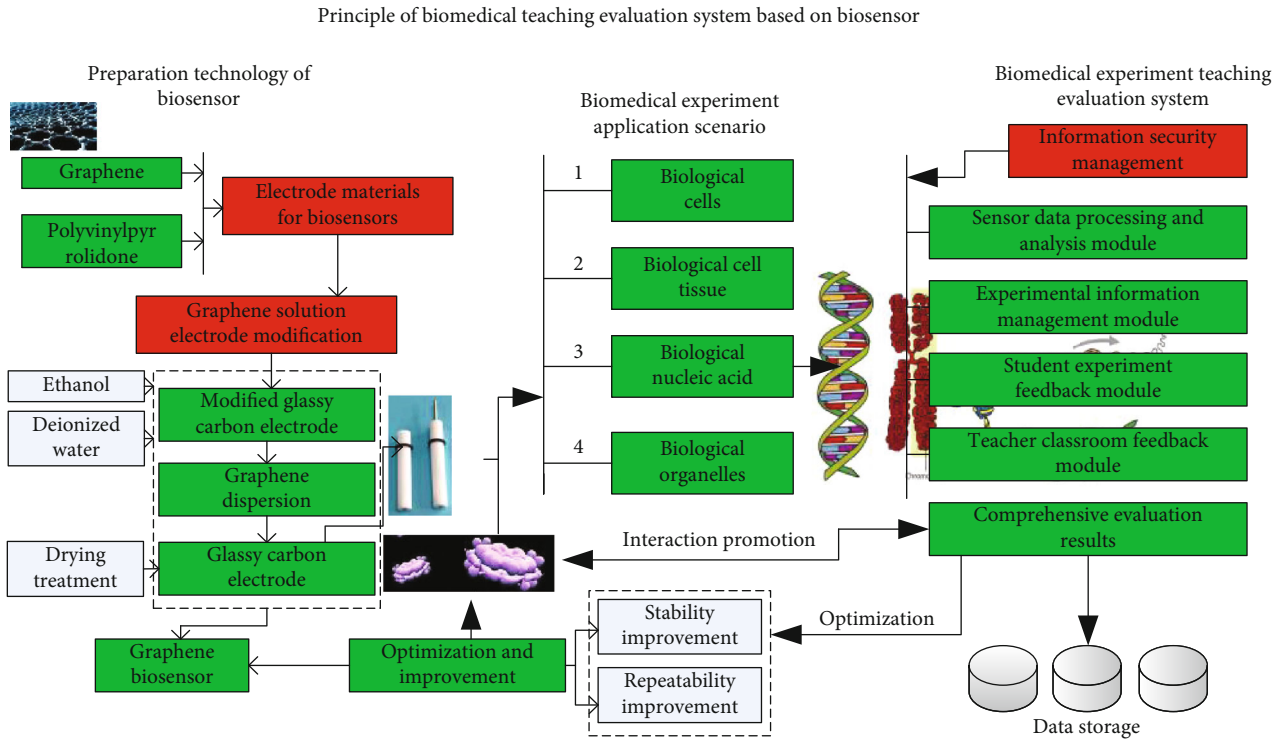

Figure 1: Principle block diagram of biomedical teaching evaluation system based on biosensor.

and has certain popularization value [21, 22]. Relevant European scientists have modified the glassy carbon electrode by the interaction of gold nanoparticles and graphene, so as to realize the high-precision detection of hydrogen peroxide. At the same time, the biosensor has a highly flexible detection response and experimental repeatability [23]. Based on the combination of gold nanoparticles and graphene, relevant scientific institutions in the United States have improved it. It uses gold nanoparticle clusters to modify the corresponding electrode, so as to realize the preparation of a semiamino acid biosensor. This biosensor successfully improves the electron migration rate on the electrode surface, greatly improves the sensitivity of the sensor, and further improves the detection range [24]. Relevant Chinese scientists have also conducted a lot of research on the preparation of biosensors. Relevant research mainly uses the self-assembly technology of gold nanoparticles and plasma polymer deposition technology to prepare immunosensors. The biosensor constructed based on this technology can improve the biological activity of fixed antibodies. At the same time, its corresponding sensor interface can be quickly activated, and its corresponding repeatability can be improved [25]. Relevant scientists in the United States have prepared a biosensor at the level of deoxyribonucleotide biological detection, which mainly uses the irregular edge characteristics of the deoxyribonucleotide to provide high-density active edge sites, so as to expand the detection range [26]. At the research level of the biomedical teaching experiment effect evaluation system, the main system technology includes the computer network and its distributed database management system. At the design level of the biomedical teaching effect evaluation system, a large number of scientists and research institutions have studied and analyzed it, and its main experimental effect is also based on biosensor preparation technology [27].

3. Preparation of Biosensor and Design of Biomedical Experiment Teaching Evaluation System

This section mainly analyzes and studies the preparation technology and optimization technology of the graphene biosensor. At the same time, this section will also give the design idea of the corresponding biomedical experiment teaching evaluation system. The corresponding principle block diagram is shown in Figure 1. As can be seen from Figure 1, at the level of biosensor preparation, this paper mainly prepares the electrochemical sensor applied to biomedical experimental teaching based on graphene, optimizes the detection sensitivity and detection range of the graphene electrochemical sensor based on the corresponding experimental conditions, and improves its corresponding stability and reusability. In the aspect of electrochemical activity of biosensors, this paper innovatively uses the electrochemical impedance method to detect the electrochemical activity, so as to accurately evaluate the key characteristics of biosensors. At the design level of the corresponding biomedical experiment teaching evaluation system, the biomedical experiment teaching effect evaluation system is mainly constructed based on the information network.

3.1. Analysis and Study on Preparation Technology of Graphene Biosensor. In this section, the corresponding biosensor in the biomedical experimental teaching system is

Table 1: Experimental reagents and equipment for graphene biosensor preparation.

Serial number of experimental equipment	Name of experimental equipment	Serial number of test reagent	Name of experimental reagent
1	Ultrasonic cleaning machine	1	Mechanical stripping graphene
2	Electron microscope	2	Polyvinylpyrrolidone
3	Centrifuge	3	Secondary distilled water
4	Balance	4	Sodium hydroxide
5	Precision pH meter	5	H_3PO_4
6	Laser spectrometer	6	
7	Electrochemical workbench		

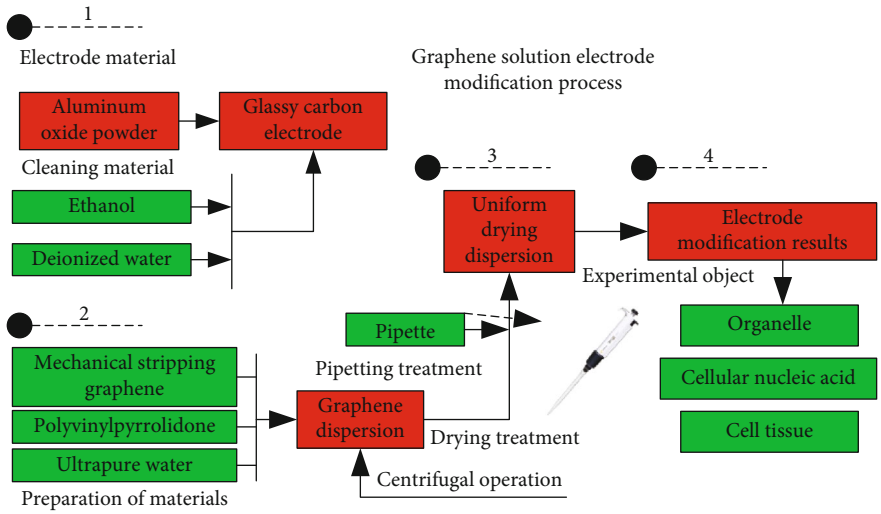

Figure 2: Principle block diagram of graphene solution electrode modification process.

designed based on graphene. Graphene and polyvinylpyrrolidone are used as the electrode materials of the biosensor in the preparation process, and the electrochemical sensitivity of the sensor prepared in this paper is optimized based on the characteristics of this material. The water used in the actual preparation process in this paper is distilled water. The corresponding experimental reagents and equipment used are shown in Table 1.

The above conditions are necessary for the preparation of the graphene biosensor. Based on the above experimental reagents and experimental instruments, the key part of the preparation of the graphene biosensor is the graphene solution electrode modification process. The corresponding process principle block diagram is shown in Figure 2. It can be seen from Figure 2 that the graphene preparation process is mainly divided into four key steps. Each corresponding step has its corresponding key technology. The first step is mainly cleaning, the corresponding second step is mainly centrifugation, the corresponding third step is mainly drying treatment technology, and the corresponding fourth step is mainly modification. From Figure 2, it can be seen that the corresponding preparation technical steps are as follows.

Step 1: continuously modify the glassy carbon electrode with aluminum oxide powder, and continuously clean the glassy carbon electrode with ethanol and deionized water. After cleaning, blow dry with nitrogen.

Step 2: graphene dispersion is prepared based on mechanical stripping of graphene, polyvinylpyrrolidone, and corresponding ultrapure water, and uniform dispersion is obtained by centrifugation based on this dispersion.

Step 3: based on the pipette, place the corresponding dispersion on the surface of the glassy carbon electrode for drying treatment.

Step 4: the electrode modification results of the graphene solution were obtained.

In order to further optimize the electrochemical performance of the graphene biosensor, cyclic voltammetry is used to verify and optimize the selection of the graphene surface area. The core significance of the optimization algorithm is to characterize the corresponding electron mobility on the electrode surface through the oxidation current on the glassy carbon electrode. The electrochemical sensitivity of the graphene biosensor is positively represented based on electron mobility. In this paper, when cyclic voltammetry is used, the linear voltage characteristic is used to continuously scan from high voltage to low voltage and then repeatedly scan back. The corresponding scanning function curve is shown in Figure 3. It can be seen from the figure that the corresponding detection curve includes two parts: first, when the potential sweeps to the cathode, the detected substance will get electrons, so that the reduction peak can be detected; second, when the corresponding potential sweeps to the

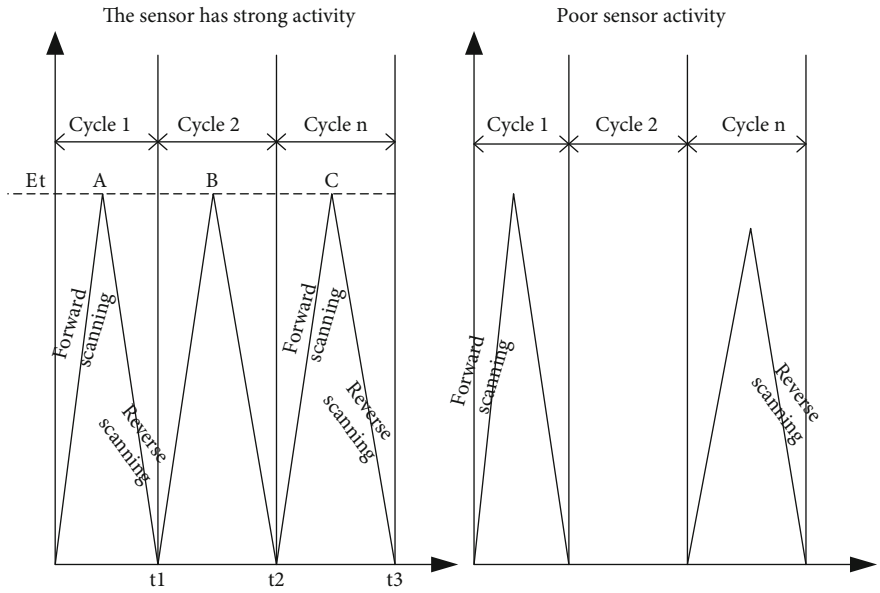

Figure 3: Scanning function curve of cyclic voltammetry.

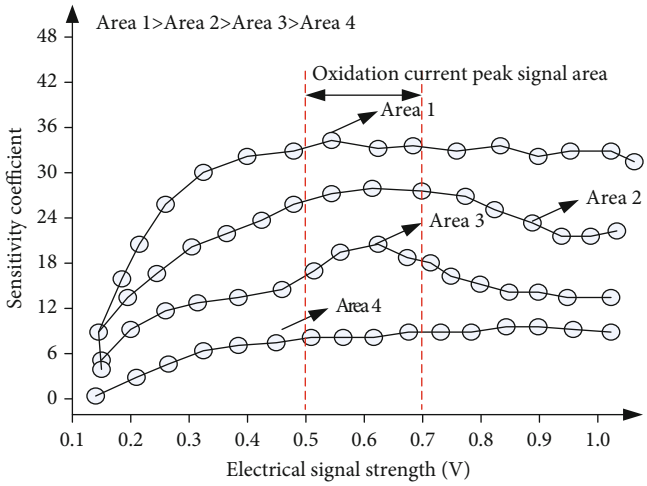

Figure 4: Electrochemical sensitivity curves of graphene biosensors with different surface areas.

anode, an oxidation peak will appear. Based on this repeated scanning, the process of continuous gain and loss of electrons is realized. At this time, when the activity of the corresponding detected substance is high, the corresponding two peaks are symmetrical and the corresponding amplitude difference is small. When the activity of the corresponding substance is poor, only one corresponding oxidation or reduction reaction will occur; thus, there is only one corresponding oxidation peak and reduction peak. Therefore, based on the above principle, the performance of the selected biosensor can be sensitively reflected.

In order to further optimize the electrochemical performance of the graphene biosensor, cyclic voltammetry is used to verify and optimize the selection of the graphene surface area. The core significance of the optimization algorithm is to characterize the corresponding electron mobility on the electrode surface through the oxidation current on the glassy carbon electrode; the electrochemical sensitivity of graphene biosensor is positively represented based on electron mobility. The corresponding electrochemical sensitivity curves of graphene biosensors with different surface areas are shown in Figure 4. It can be seen from Figure 4 that selecting a larger graphene surface area is conducive to improving the electrochemical sensitivity of the biosensor and can give full play to the good crystal structure and catalytic performance of graphene to the greatest extent.

3.2. Design and Analysis of Biomedical Experiment Teaching Evaluation System. The biomedical teaching evaluation system designed in this paper is mainly to better evaluate biological experimental teaching and reflect the practical role of biosensors in biomedical experimental teaching. The system designed in this paper includes five modules: sensor data processing and analysis module, experimental information management module, student experimental feedback module, teacher classroom feedback module, and overall evaluation module. The principle framework of the corresponding biomedical experimental teaching evaluation system is shown in Figure 5.

In the corresponding sensor data processing module, the graphene biosensor prepared above is mainly used as the medium for students to perceive biological characteristics such as microbiological organelles, so as to help students better understand the conceptual elements in biomedical experiments and corresponding biomedical phenomena. By transforming the biological information sensed by the biosensor into physical signals such as electrical signals and sending them to the computer for processing and analysis, students can more comprehensively and intuitively understand the relevant experimental steps and implementation phenomena, so as to deeply quantify the experimental results, so as to further improve the effect of biomedical experimental teaching.

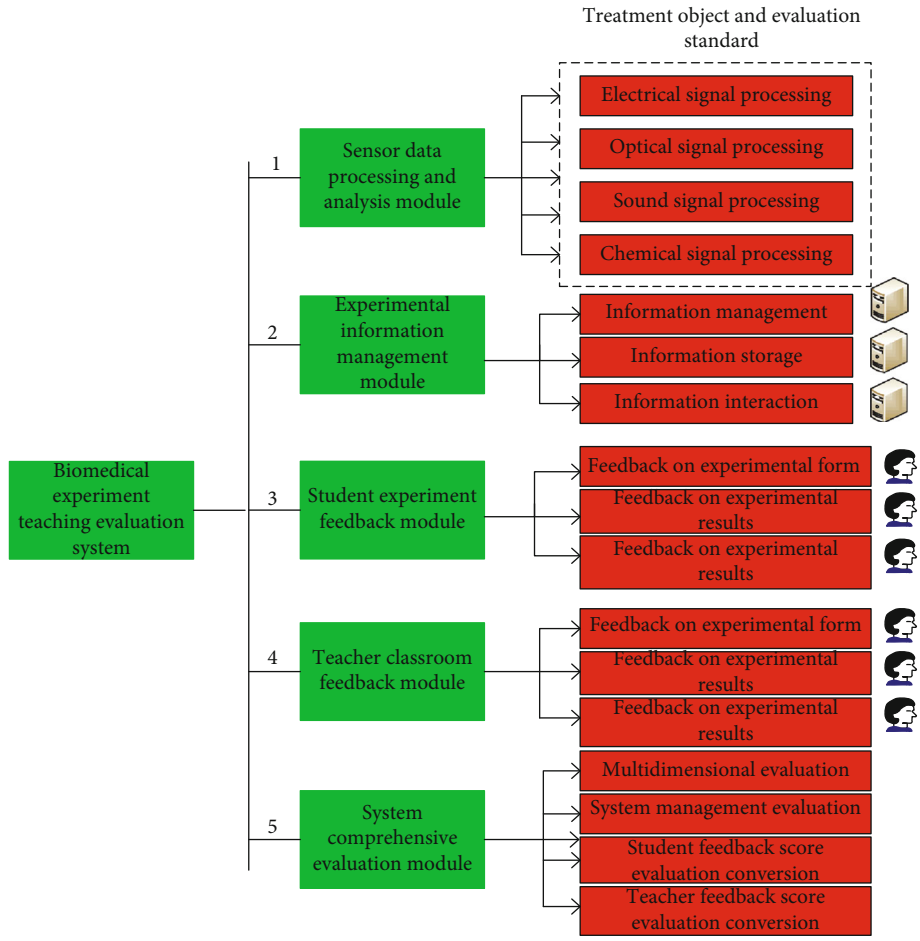

Figure 5: Principle frame diagram of biomedical experiment teaching evaluation system.

The corresponding information system management level mainly adopts the C/S architecture, the corresponding physical architecture adopts the LAN form, the corresponding database level adopts the dynamic database technology, and the network communication protocol mainly adopts the TCP/IP protocol. The information system management module is mainly used to comprehensively manage the biological data collected by biosensors, as well as various biomedical experiments and the information of students and teachers. At the same time, the information system management module also needs to comprehensively deal with the evaluation of students and teachers on biomedical experiments and form final opinions.

The student experiment feedback module is mainly used to provide an interface for students to timely feed back the current biomedical experiment teaching effect. It is mainly used to store and analyze students' opinions and evaluation on the experiment and also test the current experimental situation of students, Thus, students' evaluation results of biomedical experimental teaching are given at the subjective and objective levels and finally outputted to the evaluation module for integration with teachers' evaluation opinions.

The teacher classroom feedback module mainly provides a subjective teaching effect evaluation interface for teachers. It records, stores, and analyzes the teachers' subjective evaluation of this biomedical teaching experiment and finally converts it into a score calculated according to a certain proportion as the evaluation index of the current biomedical teaching experiment at the teacher level.

The overall evaluation module mainly integrates the contents of the student experimental feedback module and the teacher classroom feedback module for comprehensive processing and analysis. At the same time, the results of the comprehensive processing and analysis are displayed in the form of final scores as the evaluation results of the current biomedical experimental teaching.

In the security level of the whole biomedical teaching evaluation system, this paper mainly controls the operation of the system based on user authentication and key and realizes the safe operation of the system by designing hierarchical permissions for the application system.

4. Experimental Verification and Analysis

In order to verify the advantages of the graphene biosensor prepared in this paper compared with the traditional biosensor in biomedical experiments, and to verify the practicability of the biomedical evaluation system proposed in this paper, this section will analyze and discuss the detection experiment and experimental effect evaluation based on tryptophan.

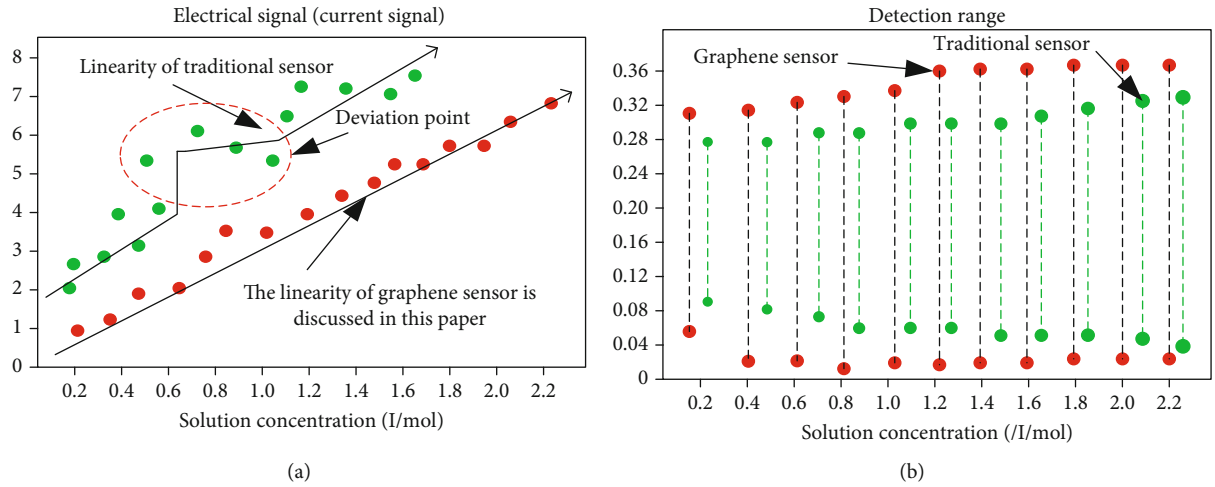

Figure 6: (a) Detection linearity curve; (b) monitoring range curve.

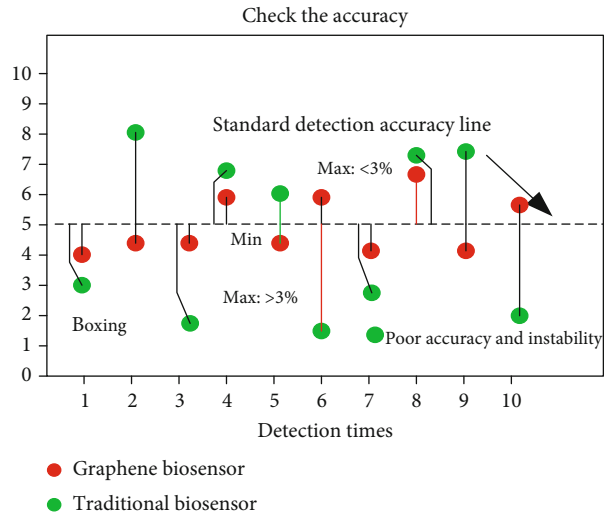

Figure 7: Detection curve of reproducibility characteristics of biosensor.

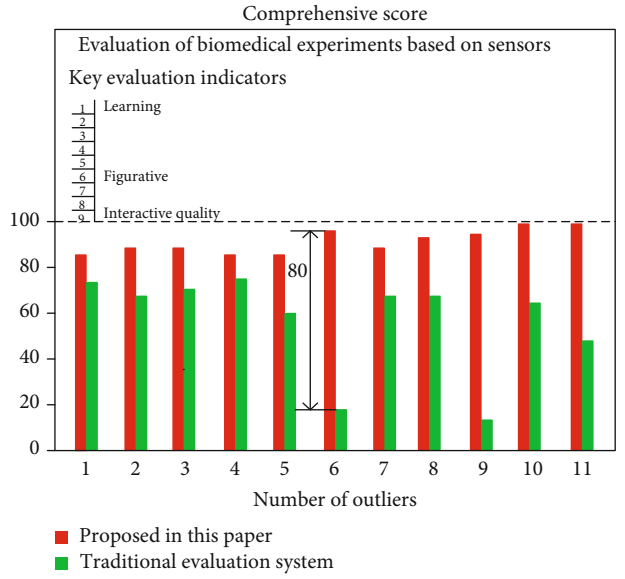

Figure 8: Effect curve of biomedical experiment evaluation.

The superiority of the sensor is mainly verified by analyzing its corresponding linear detection range and corresponding detection limit. Based on this, experiments are carried out on tryptophan detection solutions with different concentrations. The corresponding experimental results are shown in Figures 6(a) and 6(b). It can be seen from the figure that the graphene biosensor used in this paper has better detection linearity than the traditional biosensor, and its corresponding detection range is also relatively wide.

In order to further verify the reproducibility advantages of the graphene biosensor proposed in this paper, the same modified electrode is used to measure the solution of the same concentration for 10 times, and the corresponding biosensor current signal deviation is recorded. The corresponding experimental result curve is shown in Figure 7. It can be seen from the figure that the graphene biosensor proposed in this paper has better repeatability than the traditional biosensor, and the corresponding deviation is less than 3%.

In order to reflect the advantages of this biomedical teaching evaluation system, the teaching experiment evaluation is carried out based on the tryptophan experiment, and the corresponding evaluation index is mainly the comprehensive evaluation score. The evaluation effect of biomedical experiments based on the two biosensors is shown in Figure 8. It can be seen from the figure that the evaluation effect of biomedical experiments based on graphene biosensors is due to the similar experiments carried out by traditional biosensors.

According to the above experimental results, the sensor-based biomedical experiment is analyzed. The main analysis contents include the following: description of the modification characteristics of biosensor electrode, analysis of the advantages of the electrochemical characteristics of graphene biosensor, the impact of pH on the biomedical experiment, and the impact of the performance of biosensor on the effect of biomedical teaching experiment. For the

Table 2: Optimization and improvement of graphene biosensor and biomedical teaching experiment.

Optimization part	Optimization level details
Optimization direction of graphene biosensor	Optimization of electrode modification parameters
	Optimization of material deposition
	pH optimization
	Polarization voltage optimization
	Selection and optimization of biosensor
Optimization of biomedical teaching experiment	Optimization of teacher-student interaction
	Optimization of biomedical experiment teaching evaluation system

electrode modification characteristics of biosensors, compared with ordinary biosensors, the large-area graphene biosensor proposed in this paper can better adsorb and fix biological macromolecules in biomedical experiments, so as to promote the sensitivity of biomedical experimental detection and enable students to obtain more real detection results; at the same time, it also provides a guarantee for the follow-up experimental conclusions. In terms of the advantages of the electrochemical characteristics of the graphene biosensor, the above experiments further prove that the electrochemical performance detection based on cyclic voltammetry has higher accuracy; at the same time, the experimental results under cyclic voltammetry further prove that the mechanical stripping graphene corresponding to the graphene biosensor proposed in this paper has more advantages than the corresponding crystal structure of the traditional biosensor (detection of tryptophan and such biological experiments), and its corresponding catalytic performance is better. In terms of the impact of pH on biomedical experiments, this paper does not give the experimental results in the experimental part, but it is important to analyze the pH from the experimental process, but this paper controls the pH of the same experiment. In terms of the performance of biosensors on the effect of biomedical teaching experiments, good biosensors play an important role in improving the quality of biomedical teaching. Through the introduction of biosensors with high precision, high reproducibility, and fast response speed, students' interest in learning can be significantly improved, and the reliability of experiments and the accuracy of experimental conclusions can be increased; at the same time, it can also provide good teaching support for experimental teachers and improve classroom quality.

Based on the above analysis, the graphene biosensor is optimized, and the biomedical teaching experiment based on the biosensor is improved, so as to further improve the experimental teaching effect. The corresponding optimization direction is shown in Table 2. The optimization of electrode parameters in the corresponding table mainly considers the optimization of electrode modification parameters to obtain high sensitivity. The optimal solution of this parameter depends on the experimental results and analysis. The material deposition parameters will seriously affect the corresponding polymerization state, polymerization morphology, and corresponding polymerization density on the surface of glassy carbon electrode, which has an important restriction on the sensitivity of the sensor. Therefore, at the level of material deposition parameter optimization, based on cyclic voltammetry, it is found that when the corresponding electrode scanning is about 20 cycles, the corresponding biosensor has the highest sensitivity. At the corresponding pH optimization level, when the corresponding pH is neutral or near neutral, the corresponding biosensor sensitivity is the highest. The corresponding experimental results also show that when the corresponding electrolyte is too acidic or alkaline, the corresponding biosensor sensitivity will be greatly reduced. At the corresponding polarization voltage level, the corresponding polarization voltage will seriously affect the detection sensitivity of the biosensor. The polarization voltage corresponding to different electrolytes needs to be obtained through experiments. In the experiment, it is found that the corresponding biosensor has the highest sensitivity when the polarization voltage is maintained at about 0.1 V. When the corresponding polarization voltage is higher than 0.1 V, the corresponding sensor sensitivity will be greatly reduced, but the polarization voltage should not be too small, which will affect the adequacy of the reduction reaction of the experiment. In the aspect of biomedical experimental teaching optimization, it is necessary to emphasize the selection and optimization of biosensors in the experiment, enhance the interaction between teachers and students in the experimental process, and optimize the biomedical experimental teaching evaluation system.

5. Conclusion

This paper mainly analyzes the research status of the biosensor and its biomedical experimental teaching evaluation system and summarizes its corresponding existing problems. In view of the current characteristics of low precision, poor repeatability, and unsystematic evaluation system of biomedical experimental teaching, this paper mainly prepares the electrochemical sensor for biomedical experimental teaching based on graphene and optimizes the detection sensitivity and detection range of graphene electrochemical sensor based on the corresponding experimental conditions; at the same time, its corresponding stability and reusability are improved. At the level of electrochemical activity of biosensors, this paper innovatively uses the electric AC impedance method to detect the electrochemical activity, so as to accurately evaluate the key characteristics of biosensors. Based on the preparation of biosensors and the results of biological experiments, this paper will design a biomedical experiment teaching effect evaluation system based on the network and realize the basic functions of teacher-student interaction,teaching effect evaluation, sensor performance evaluation and so on. Based on the above, the electrochemical sensor based on graphene and conductive polymer solution is actually prepared in this paper. At the same time, the electrocatalysis experiment is carried out based on the

sensor, and the experimental teaching effect is systematically evaluated. The experimental results show that the biosensor proposed in this paper has the advantages of high sensitivity, simple preparation, and high availability; at the same time, it also further verifies that the biomedical experimental teaching effect evaluation system proposed in this paper has good evaluation effect and can provide accurate reference for the evaluation of biological experimental teaching effect. In the follow-up research, this paper will focus on the accuracy of the graphene sensor in biological detection and its corresponding biomedical teaching effect in other harsh environments. At the same time, this paper will continue to study the application of other nanomaterials in the preparation of biosensors and continuously improve its accuracy and repeatability.

Data Availability

The data used to support the findings of this study are available from the corresponding author upon request.

Conflicts of Interest

The author declares that they have no conflicts of interest.

Funding

This work was supported by the 2021 Education and Teaching Reform Research and Practice Project of Xuchang University (general project) "Project Name: Application of TBL Teaching Method and Experiential Teaching Method in Physiology Teaching in Colleges and Universities" (No.: XCU2021-YB-060).

References

[1] H. Zhao, X. Ji, B. Wang et al., "An ultra-sensitive acetylcholinesterase biosensor based on reduced graphene oxide-Au nanoparticles-β-cyclodextrin/Prussian blue-chitosan nanocomposites for organophosphorus pesticides detection," *Biosensors & Bioelectronics*, vol. 65, no. 4, pp. 23–30, 2015.

[2] E. Mehmeti, D. M. Stankovi, and S. Chaiyo, "Wiring of glucose oxidase with graphene nanoribbons: an electrochemical third generation glucose biosensor," *Microchimica Acta*, vol. 184, no. 4, pp. 1127–1134, 2017.

[3] S. Han, T. Du, J. Hui, and X. Wang, "Synergistic effect of pyrroloquinoline quinone and graphene nano-interface for facile fabrication of sensitive NADH biosensor," *Biosensors & Bioelectronics*, vol. 89, no. 1, pp. 422–429, 2017.

[4] S. Beyranvand, M. F. Gholami, A. D. Tehrani, J. P. Rabe, and M. Adeli, "Construction and evaluation of a self-calibrating multiresponse and multifunctional graphene biosensor," *Langmuir*, vol. 35, no. 32, pp. 10461–10474, 2019.

[5] C. Wang, Y. Li, Y. Zhu et al., "High-kappa solid-gate transistor configured graphene biosensor with fully integrated structure and enhanced sensitivity," *Advanced Functional Materials*, vol. 26, no. 47, pp. 8575–8575, 2016.

[6] L. Klukova, J. Filip, and T. Belick, "Graphene oxide-based electrochemical label-free detection of glycoproteins down to aM level using a lectin biosensor," *Analyst*, vol. 141, no. 14, pp. 4278–4282, 2018.

[7] T. Hu, L. Zhang, W. Wen, X. Zhang, and S. Wang, "Enzyme catalytic amplification of miRNA-155 detection with graphene quantum dot-based electrochemical biosensor," *Biosensors & Bioelectronics*, vol. 77, no. 4, pp. 451–456, 2016.

[8] J. B. Maurya, Y. K. Prajapati, V. Singh, J. P. Saini, R. Tripathi, and V. Singh, "Improved performance of the surface plasmon resonance biosensor based on graphene or MoS_2 using silicon," *Optics Communications*, vol. 359, no. 4, pp. 426–434, 2016.

[9] M. S. Khan, S. K. Misra, Z. Wang et al., "Paper-based analytical biosensor chip designed from graphene-nanoplatelet-amphiphilic-diblock-co-polymer composite for cortisol detection in human saliva," *Analytical Chemistry*, vol. 89, no. 3, pp. 2107–2115, 2017.

[10] H. Zhang, Y. Wang, D. Zhao et al., "Universal fluorescence biosensor platform based on graphene quantum dots and pyrene-functionalized molecular beacons for detection of microRNAs," *ACS Applied Materials & Interfaces*, vol. 7, no. 30, pp. 16152–16156, 2015.

[11] T. C. Lin, Y. S. Li, W. H. Chiang, Z. Pei, and W. H. Chiang, "A high sensitivity field effect transistor biosensor for methylene blue detection utilize graphene oxide nanoribbon," *Biosensors & Bioelectronics*, vol. 89, no. 1, pp. 511–517, 2017.

[12] S. Eissa, M. Zourob, and M. Zourob, "In vitro selection of DNA aptamers targeting β-lactoglobulin and their integration in graphene-based biosensor for the detection of milk allergen," *Biosensors & Bioelectronics*, vol. 91, no. 4, pp. 169–174, 2017.

[13] Q. Wu, Y. Sun, P. Ma et al., "Gold nanostar-enhanced surface plasmon resonance biosensor based on carboxyl-functionalized graphene oxide," *Analytica Chimica Acta*, vol. 913, no. 4, pp. 137–144, 2016.

[14] M. S. Rahman, M. R. Hasan, K. A. Rikta, M. S. Anower, and K. A. Rikta, "A novel graphene coated surface plasmon resonance biosensor with tungsten disulfide (WS_2) for sensing DNA hybridization," *Optical Materials*, vol. 75, no. 6, pp. 567–573, 2018.

[15] M. S. Rahman, M. S. Anower, M. R. Hasan, M. B. Hossain, M. I. Haque, and M. R. Hasan, "Design and numerical analysis of highly sensitive Au-MoS_2-graphene based hybrid surface plasmon resonance biosensor," *Optics Communications*, vol. 396, no. 5, pp. 36–43, 2017.

[16] J. Sethi, M. V. Bulck, A. Suhail, M. Safarzadeh, A. Perez-Castillo, and G. Pan, "Correction to: a label-free biosensor based on graphene and reduced graphene oxide dual-layer for electrochemical determination of beta-amyloid biomarkers," *Microchimica Acta*, vol. 187, no. 6, pp. 12–16, 2020.

[17] A. A. Ensafi, M. Sohrabi, M. Jafari-Asl, B. Rezaei, and M. Jafari-Asl, "Selective and sensitive furazolidone biosensor based on DNA-modified TiO_2-reduced graphene oxide," *Applied Surface Science*, vol. 356, no. 11, pp. 301–307, 2015.

[18] K. Nakama, M. Sedki, A. Mulchandani, and A. Mulchandani, "Label-free chemiresistor biosensor based on reduced graphene oxide and M13 bacteriophage for detection of coliforms," *Analytica Chimica Acta*, vol. 1150, no. 15, article 338232, 2021.

[19] Y. H. Nien, T. Y. Su, C. S. Ho et al., "The analysis of potentiometric flexible arrayed urea biosensor modified by graphene oxide and γ-Fe_2O_3 nanoparticles," *IEEE Transactions on Electron Devices*, vol. 67, no. 11, pp. 5104–5110, 2020.

[20] D. Chauhan, Pooja, V. Nirbhaya et al., "Nanostructured transition metal chalcogenide embedded on reduced graphene

oxide based highly efficient biosensor for cardiovascular disease detection," *Microchemical Journal*, vol. 155, no. 3, article 104697, 2020.

[21] J. Dong, M. Sang, S. Wang et al., "Ultrasensitive label-free biosensor based on the graphene-oxide-coated-U-bent long-period fiber grating inscribed in a two-mode fiber," *Journal of Lightwave Technology*, vol. 39, no. 12, pp. 4013–4019, 2021.

[22] M. Devaraj, S. Rajendran, J. N. Jebaranjitham et al., "Horseradish peroxidase-immobilized graphene oxide-chitosan gold nanocomposites as highly sensitive electrochemical biosensor for detection of hydrogen peroxide," *Journal of the Electrochemical Society*, vol. 167, no. 14, article 147517, 2020.

[23] F. N. Ajeel, A. M. Khudhair, M. H. Mohammed, K. M. Mahdi, and M. H. Mohammed, "DFT investigation of graphene nanoribbon as a potential nanobiosensor for tyrosine amino acid," *Russian Journal of Physical Chemistry A*, vol. 93, no. 4, pp. 778–785, 2019.

[24] M. Zhao, L. Bai, W. Cheng, X. Duan, H. Wu, and S. Ding, "Monolayer rubrene functionalized graphene-based eletrochemiluminescence biosensor for serum cystatin C detection with immunorecognition-induced 3D DNA machine," *Biosensors and Bioelectronics*, vol. 127, no. 55, pp. 126–134, 2019.

[25] H. Borah, S. Gogoi, S. Kalita, P. Puzari, and S. Kalita, "A broad spectrum amperometric pesticide biosensor based on glutathione S-transferase immobilized on graphene oxide-gelatin matrix," *Journal of Electroanalytical Chemistry*, vol. 828, no. 4, pp. 116–123, 2018.

[26] S. Proa-Coronado, J. R. Vargas-García, A. Manzo-Robledo et al., "Platinum nanoparticles homogenously decorating multilayered reduced graphene oxide for electrical nanobiosensor applications," *Thin Solid Films*, vol. 658, no. 7, pp. 54–60, 2018.

[27] J. White, K. Costilow, J. Dotson et al., "Guided-inquiry experiment for teaching the calibration method of standard addition in the analysis of lead with graphite furnace atomic absorption spectroscopy," *Journal of Chemical Education*, vol. 98, no. 2, pp. 620–625, 2021.

Hindawi
Journal of Sensors
Volume 2022, Article ID 1048914, 12 pages
https://doi.org/10.1155/2022/1048914

Research Article

Analysis of Dynamic System of Exercise Load Condition Monitoring Based on Characteristic Parameters

Yunlan Ren[1] **and Shang Wu**[2]

[1]*School of Applied Engineering Henan University of Science and Technology, Zhengzhou Henan 472000, China*
[2]*School of Police Sport Henan Police College, Zhengzhou Henan 450046, China*

Correspondence should be addressed to Shang Wu; 20170472@hnp.edu.cn

Received 10 November 2021; Revised 10 January 2022; Accepted 17 January 2022; Published 14 February 2022

Academic Editor: Gengxin Sun

According to the algorithm of time difference and threshold value, this paper selects the more valuable data for motion state recognition and selects the characteristics, respectively selects the data of the combined acceleration and the combined angular velocity, and uses the data of the pitch angle and the roll angle more novelly. In the aspect of data preprocessing, the sliding segmentation window method is used for feature processing, and the time domain and frequency domain features of the data are extracted. A total of 108 dimensional features are extracted. In order to improve the calculation performance, PCA technology is used for data dimensionality reduction. In this paper, we collected data on changes in physiological parameters of 24 experimenters before and after exercise, collected 14 self-evaluated severely fatigued volunteers and self-evaluated severely stressed volunteers' resting heart rate and blood pressure data as unhealthy data samples, and collected physiological data of 14 healthy experimenters as unhealthy data samples. For healthy samples, three sets of experiments were set up to analyze the changes of exercise heart rate, exercise blood pressure and exercise body temperature, and the effectiveness of fusion of physiological data to improve the performance of exercise recognition and the analysis of the health status of physiological parameters that introduce exercise interference. The experimental results show that during exercise, monitoring changes in systolic blood pressure is more meaningful than monitoring changes in diastolic blood pressure; it verifies the effectiveness of improving the performance of exercise recognition by fusion of physiological parameters. The addition of physiological data can effectively improve the recognition rate of exercise. The recognition rate has been increased from 93.7% to 96.3%; the effectiveness and applicability of the algorithm in this paper are analyzed through design experiments, and the results show that the recognition accuracy of the algorithm in this paper is above 87%. This result has a good classification recognition rate for a small sample.

1. Introduction

With the continuous improvement of living standards, people's living habits and eating habits are also changing. Excessive diet, intake of high-calorie food, and lack of exercise due to staying indoors for a long time are increasing, causing the human body to consume too much energy every day, leading to diseases such as obesity, high blood pressure, and hyperlipidemia [1]. Developing a healthy diet and taking an active part in outdoor activities can not only enhance the body's immunity but also consume excess energy, so that the body's energy supply and demand can reach a balance [2]. Monitoring the daily exercise status of the human body can guide people to formulate a healthy and reasonable diet plan, rationally arrange daily exercise, and improve people's healthy living standards [3]. There are many types of daily activities of the human body, including running, walking, going up and down the stairs, sitting down, standing, and many other exercise methods. The energy consumption relationship corresponding to these different daily exercises is also different. Therefore, it is very important to monitor and identify these daily exercises, and it is also the main research topic of many researchers at present [4].

The acceleration phenomenon has always existed in human body movement; for example, daily human body movements such as washing face, brushing teeth, walking, running, and riding a bicycle will produce corresponding acceleration. The use of acceleration to monitor human motion status has received extensive attention from domestic and foreign researchers [5]. The acceleration signal is the corresponding action signal generated by the body movement in the daily life of the human body. By effectively processing this signal, it can be judged what kind of action the human body has made [6]. With the continuous improvement of microelectronic system technology, acceleration sensors are becoming smaller and cheaper, and they have been widely embedded in mobile phone devices, notebooks, electronic game consoles, etc., and are based on acceleration sensors [7]. Various studies provide a broader platform. The human action recognition mechanism and fall detection algorithm proposed in this paper are based on a single acceleration sensor [8]. Most of the current popular smartphones and other devices have a single acceleration sensor embedded, so the research in this paper has a certain practical value [9].

Wearable health monitoring devices are often greatly affected by the state of human movement. Through the identification and analysis of different exercise states, the real health conditions contained in the health data can be better mined. Recognition of human motion status has development prospects in many fields such as health field, medical monitoring, fall monitoring, competitive sports, and indoor positioning. In daily life, different motion states will produce different accelerations. Accurate identification of individual motion states can be achieved by acquiring acceleration signals in different motion states and performing corresponding preprocessing and feature identification. The rapid development of artificial intelligence technology provides a strong support for solving feature recognition and improving the ability to identify behaviors autonomously. Various intelligent mobile terminal devices that are widely used contain a wealth of sensors, which provide the possibility for convenient monitoring of physiological parameters, but the monitoring data is often greatly affected by the state of human movement. Through the identification and analysis of different motion states, the real physiological information contained in the monitoring data can be better mined.

This paper uses the random forest classification algorithm to classify the movement state. Using variable-scale sliding window segmentation technology, 27 time-domain and frequency-domain features of total acceleration, total angular velocity, pitch angle, and roll angle are extracted, respectively. A total of 108 features are extracted for each action, and the PCA algorithm is used to do feature extraction. This paper collects data from 24 experimenters and analyzes the changes in exercise heart rate, blood pressure, and body temperature. The results show that human body sweat evaporation and other factors lead to insignificant changes in human body temperature monitoring values. Exercise blood pressure changes according to a certain rule. The above reflects the health of the human body. In predicting the health status based on the physiological data of the monitored human body's real-time exercise status, the physiological parameter health status analysis that introduces exercise interference can be used to distinguish the changes in the physiological parameters caused by the individual exercise and the changes caused by the abnormal physical health of the individual. After counting the changes in blood pressure and heart rate of 24 experimenters, it can be concluded that after 5 minutes of vigorous exercise, most of the experimenters' systolic blood pressure will increase to a certain extent, but the diastolic blood pressure basically remains unchanged or has a small extent decrease; the heart rate rises sharply. Therefore, during exercise, it is more meaningful to monitor changes in systolic blood pressure than to monitor changes in diastolic blood pressure. Exercise can lower the body's diastolic blood pressure. In terms of diastolic blood pressure monitoring, the overall stability of diastolic blood pressure of female experimenters is higher than that of men. Changes in blood pressure during exercise can reflect the health of the human body to a certain extent, and the changes are also related to the height and weight of the experimenter.

2. Related Work

The multisensor strategy is to place acceleration sensors, gyroscopes, height sensors, air pressure sensors, skin conductivity sensors, heart rate sensors, etc., on the head, wrist, waist, ankle, sole, or skeletal muscle joints of the human body. It collects data collaboratively and uploads data to the analysis platform in real time through data transmission equipment such as Bluetooth. The advantage of the multipoint arrangement is that detailed and comprehensive data can be obtained, and the corresponding algorithm can be used to accurately identify the complex action process. It is often used in the fields of game modeling, athlete's posture analysis, and training correction. Judging from commercialization results, there are many successful cases [10]. Taking wearable devices as an example, wristbands with pedometer functions are all the rage. The main implementation mode of this type of product does not only analyze the data of the motion sensor alone but also analyzes the mileage and step frequency through the GPS function of the mobile phone to compensate for the step error [11]. Accelerometers, gyroscopes, and magnetometers are generally integrated into mobile phones. In response to the upsurge of motion recognition research, many companies have introduced special equipment for data sampling, such as Microsoft's band2 [12].

Relevant scholars observe the impact of a six-week virtual reality exercise experiment on cognitive ability [13]. In the experiment, six weeks of virtual reality exercises such as stretching exercises, archery exercises, and balance exercises was used. The 32-lead Brain Vision Analyzer produced by BP in Germany was used for ERP P300 evaluation. The results showed that six weeks of virtual reality exercises was used during exercise. Undergraduates' cognitive ability has a certain selective influence, and it is believed that these selective changes should be adaptive changes to the exercise style [14]. Related scholars have observed the effect of high-

intensity interval training on the ability of adolescents to exercise control [15]. Using six weeks of high-intensity interval training or choosing aerobic continuous training can significantly shorten the stroop reaction time of young children, but the effect of the high-intensity interval training group is significantly better than that of continuous aerobic training.

The single-sensor strategy undergoes data processing and algorithm recognition and outputs the judgment result of the motion state. The data processing capacity of a single sensor is relatively small, and although it cannot recognize complex human movements, the recognition of walking, running, falling, and other movements can reach a high degree of accuracy. It is mainly used in the fields of elderly fall detection, medical rehabilitation, exercise assistance, and other fields.

In the research of motion recognition, the preprocessing of accelerometer data mainly includes data transformation, filtering, and sample collection [16]. The main purpose of data transformation is to decompose or merge the original data that is not convenient for analysis to obtain target values that are beneficial for analysis or feature extraction. At present, the main analysis object of domestic and foreign researchers is the resultant acceleration derived from the three-axis acceleration, and a small number of studies use the raw data of the three-axis acceleration for comprehensive analysis [17]. For data filtering, some researchers have analyzed the influence of median filtering, moving average filtering, and Kalman filtering on the signal [18]. At present, the windowing method is commonly used at home and abroad to process acceleration sampling data. Researchers mainly conduct testing and research on the time length and overlap ratio of windows to find the best window setting form [19]. Other data set extraction methods include the key event cut-off method, which is mainly a supplement to the continuous recognition of the window method. This method selects certain feature points as the settlement signal for the feature value extraction of the window data, such as points with a higher rate of change.

The motion recognition algorithm is the core of motion recognition research [20]. The algorithms used by domestic and foreign researchers mainly include naive Bayes algorithm, K-nearest neighbor algorithm, threshold algorithm, decision tree algorithm, random forest algorithm, SVM support vector machine algorithm, and BP neural network [21]. Among them, the decision tree algorithm is actually a tree topology representation of the threshold algorithm, and the entropy gain calculation of the split node is more reliable than a single threshold. The random forest algorithm has absorbed the naive Bayesian algorithm's thoughts on the probability processing of classified events and the advantages of a simple and efficient decision tree algorithm [22]. The naive Bayes algorithm is highly efficient and concise, and the time complexity and space complexity of the program are extremely low. However, the calculation of its prior probability requires a lot of statistical work. At present, with the increasing popularity of machine learning and artificial intelligence, more researchers use the BP neural network. The BP neural network has many advantages. Related scholars use context-aware technology to identify feedback and optimize control of robot motion processes [23]. However, its algorithm has high complexity, high requirements for system hardware resources, and slow speed, and the training results are affected by many factors. At present, the relevant literature is only seen in laboratory simulations, and no mature products have been launched [24].

3. Method

3.1. The Overall Architecture of the Monitoring Dynamic System. According to functional requirements, the system needs the implementation of the data acquisition module, low power consumption module, positioning module, system alarm module, remote communication module, and other software. The working mode of the dynamic system of exercise load status monitoring is shown in Figure 1.

After the system switch is turned on and powered on, in the main function, initialize the clock, USART, timer 2, timer 7, IIC, MPU9250, MAX30102, SD card, and open the MTK serial port to communicate with the remote server. After the connection is successful, the system obtains the initial data. If the system detects that the user is not exercising, the heart rate is normal, and there is no abnormality after 3000 times (30 s) of information monitoring, it will enter the low power consumption mode, and no exercise status recognition will be performed at this time; if the user is detected in motion state, the MPU9250 interrupt pin will wake up the STM32F4. At this time, the system enters the high-speed motion mode. According to the acceleration, angular velocity, attitude angle, and time difference data, it recognizes the user's walking, running, sitting, standing, falling danger, and falling. When the result is recognized, a flag bit specified by the system will be returned, then send it to MTK through the serial port, and MTK will broadcast the corresponding action voice. At the same time, MTK will package the corresponding signs of the corresponding action information, positioning information, power, and other information into the form of BSN data packets and upload them to the server. The BSN data packet format is a data transmission protocol defined by humans. If the user has a fall or an abnormal heart rate, the system will give an alarm and send its location information to the guardian in order to get timely help. If the user is rescued in time and the alarm state is released (press the release alarm button), then the system will continue to enter the motion monitoring mode and continue to work. The data package in the upload server mode is shown in Table 1.

3.2. Feature Extraction and Selection. There are many features that can be extracted by motion state recognition, which are mainly divided into time domain and frequency domain features. Time domain features (TDF) mainly refer to the time-related features that the signal has during the change of the signal with time; frequency domain features (FDF) are mainly used to find some periodic signals in the signal, and the frequency domain is mainly calculated by Fast Fourier Transform (FFT). Taking the resultant

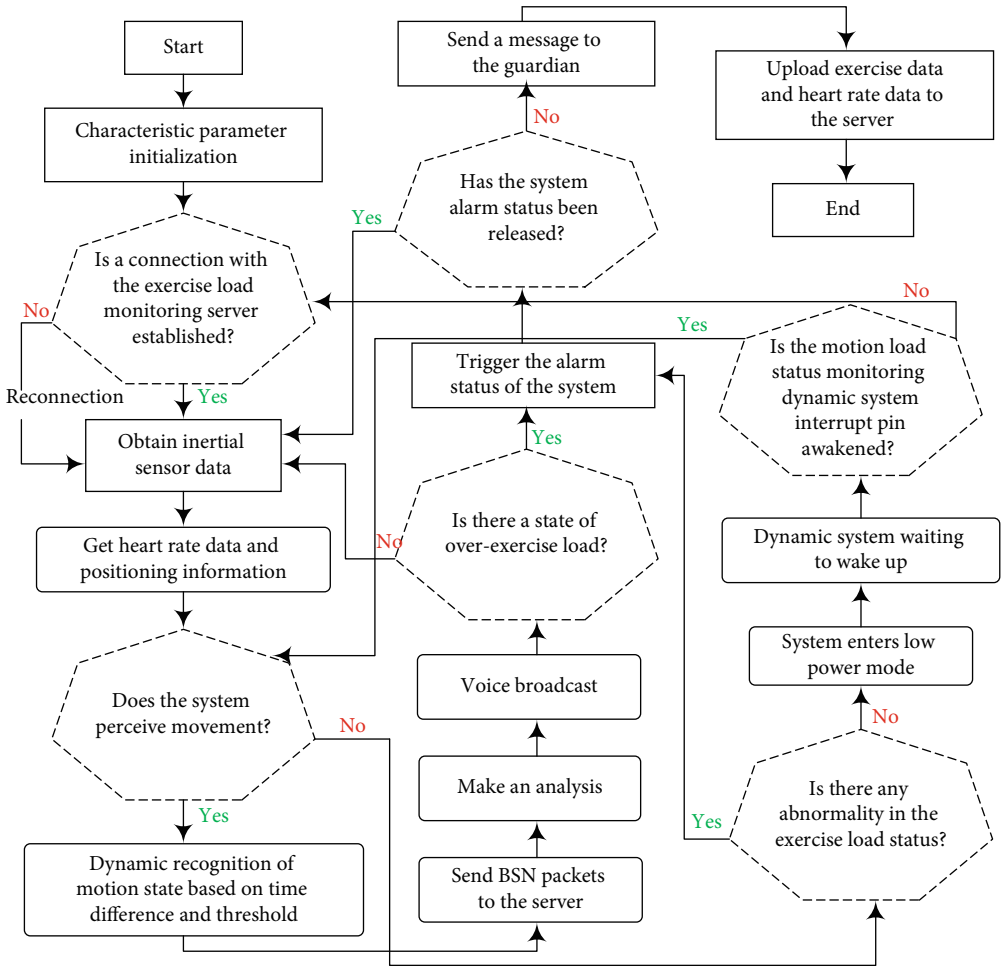

Figure 1: Work flow chart of the dynamic system for monitoring the exercise load state.

acceleration data as an example, the features that can be extracted are shown in Figure 2.

The mean value is often used to identify sitting and standing states, while the root mean square is used to distinguish walking patterns, and the signal amplitude area is used to distinguish motion to determine when the subject is engaged in activity and when in static state. Energy and entropy are used to distinguish different types of daily life states. The signal amplitude vector is used to indicate the degree of exercise intensity, and it is an important indicator of fall detection. Standard deviation has also been widely used for activity classification.

For a given set of signals: $Y = \{y1, \cdots, yn\}$, we perform FFT transformation, where Fi is the ith component of the Fourier transform of Y. The calculation method of each feature is as follows.

The standard deviation is

$$\text{std} = \left[\frac{1}{n}\sum_{i=1}^{n}(y_i - \text{mean})^2\right]^{1/2}. \quad (1)$$

Table 1: Upload data package in server mode.

Frame header	BSN
System ID	SIM card number
1	Battery voltage level
2	Exercise status
3	GPS positioning information
4	Base station location information
5	WIFI location information
6	Battery voltage
End of frame	@

The energy is

$$\text{Energy}(Y) = \frac{1}{n}\prod_{i=1}^{n}F_i^2. \quad (2)$$

The calculation methods of mean uamp, standard deviation σamp, skewness γamp, and kurtosis ηamp of amplitude

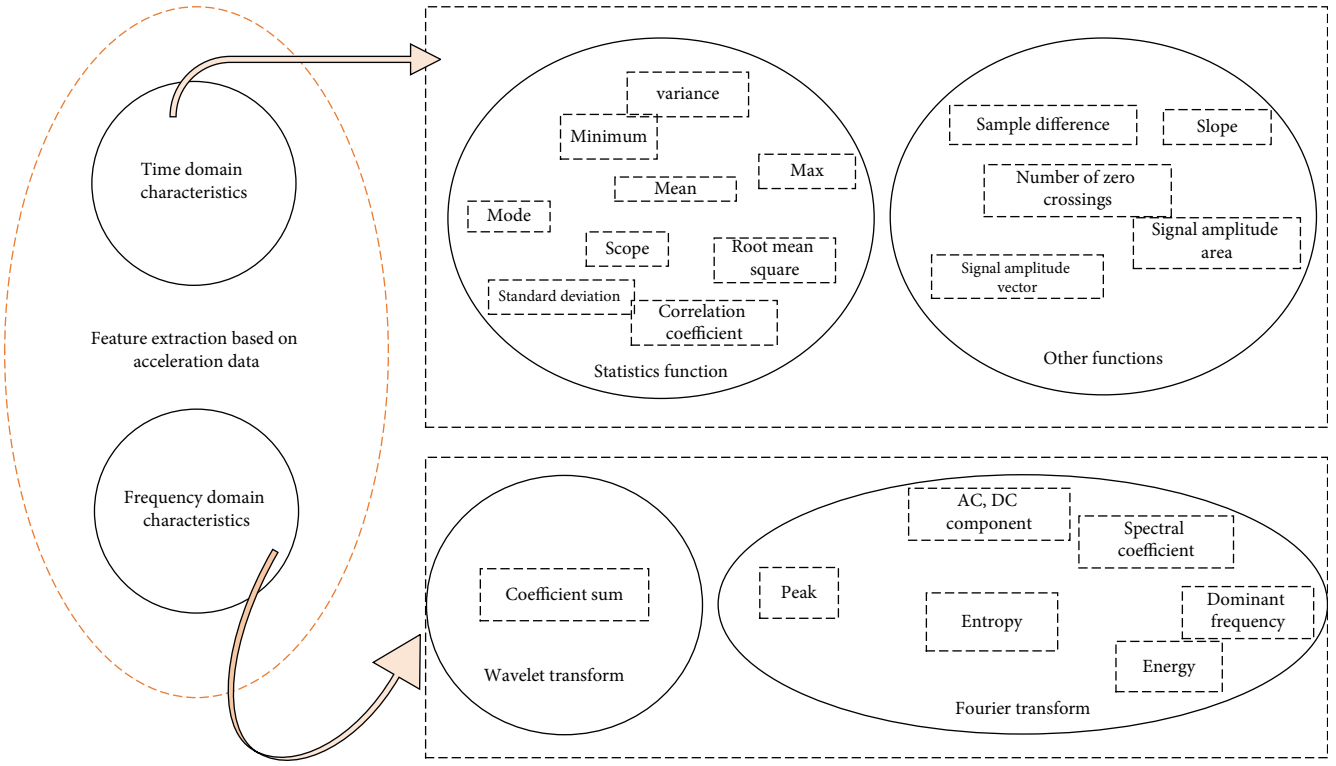

Figure 2: Schematic diagram of feature extraction of acceleration data.

statistical characteristics are as follows:

$$\text{uamp} = \frac{1}{M-1}\prod_{i=0}^{M-1}[D(i)\cdot D(i+1)], \tag{3}$$

$$\sigma\text{amp} = \left\{\frac{1}{M-1}\prod_{i=0}^{M-1}[D(i)\cdot D(i+1) - \text{uamp}]^2\right\}^{1/2}, \tag{4}$$

$$\gamma\text{amp} = \frac{1}{M-1}\prod_{i=0}^{M-1}\left[D(i)\cdot D(i+1) - \frac{\text{uamp}}{\sigma\text{amp}}\right]^3, \tag{5}$$

$$\eta\text{amp} = \frac{1}{M-1}\prod_{i=0}^{M-1}\left[\frac{D(i)\cdot D(i+1)}{\sigma\text{amp} - \text{uamp}} - 1\right]^2. \tag{6}$$

This paper extracts the time-domain and frequency-domain features of the combined acceleration, combined angular velocity, pitch angle, and roll angle. 27 features are extracted from each type of data. A total of 108 features are extracted for each action, and these features are combined into feature vectors. Each row represents a sample, and each column represents a feature, which constitutes a data set for motion state recognition.

3.3. Use PCA for Data Feature Extraction. After the data is preprocessed and feature extracted, it is necessary to reduce the dimensions of the data features, retain the most important features, and input the machine learning algorithm for training, which can reduce the computational overhead of the algorithm and make the data set easier to use. Dimensionality reduction is a way to retain some of the most important features of high-dimensional data and remove unimportant features and noise, so as to achieve the purpose of improving the data processing speed.

Principal component analysis is a type of unsupervised dimensionality reduction method. Its goal is to reduce a set of N-dimensional vectors to K-dimensional and to ensure that the variance of any two vectors is as large as possible. In order to ensure that the two vectors represent as much of the original information as possible, there should be no linear correlation between the vectors. This requires the selection of K orthogonal features, the principal components. It is a k-dimensional feature reconstructed on the basis of the original n-dimensional feature. This is to find a set of mutually orthogonal principal components in turn from the original space.

The first principal component selects the direction with the largest variance in the original data, and the second principal component selects the direction with the second largest variance in the data. For the third principal component, we choose the plane with the largest variance on the planes orthogonal to the directions of the first and second principal components. By analogy, K principal components are selected.

The variance is mainly contained in the K principal components, and the variance of the remaining principal components is almost zero. Therefore, we use K principal components to transform the original data into a new space, realizing dimensionality reduction of data features.

Through PCA dimensionality reduction, the percentage of the total variance of each principal component in the

feature matrix can be calculated, that is, the contribution rate. The percentage of the total variance of the first few principal components is called the cumulative contribution rate. In general, the first few principal components whose cumulative contribution rate reaches 90% are selected to ensure that all important feature information is included. In addition, the included noise and irrelevant information are removed to make the data clearer.

3.4. Recognition of Exercise Load State Based on Random Forest. This paper chooses the random forest (RF) classifier as the algorithm of motion state recognition. Random forest is an ensemble learning algorithm, it belongs to the bagging type, and the bagging structure is shown in Figure 3. It mainly combines multiple weak classifiers, and each classifier votes to get the final result. A random forest is actually a classifier with multiple decision trees, and each decision tree is not related. When the data to be tested enters the random forest, each tree in it will be classified, and the output category is determined by the mode of the output results of some trees; the final classification result in all decision trees is the final classification. Because "random" can make it have the ability to resist overfitting and "forest" makes it more accurate, it can achieve a good classification effect.

Suppose that the set S contains n different samples $\{x1, x2, \cdots, xn\}$. If one sample is randomly selected from the set S each time and it is sampling with replacement, a total of n times are drawn, and the new set $S*$ is formed. Then, the probability that a certain sample $xi\,(i = 1, 2, \cdots, n)$ is not included in the set $S*$ is

$$p = \left(\frac{1-1}{n}\right)^{n}. \tag{7}$$

When n tends to infinity,

$$\lim_{n\Rightarrow+\infty} p = \lim_{n\Rightarrow+\infty}\left(\frac{1-1}{n}\right)^{n+1} = e^{-1} \longrightarrow 0.368. \tag{8}$$

Therefore, although the total number of samples in the new set is equal to that in the original set, the new set is obtained by randomly sampling S samples with replacement n times, so it may have duplicate samples. If the duplicate samples are removed, the new set contains 0.63 samples in the original set.

The random forest algorithm is based on the bootstrap method of resampling to generate multiple training sets, and when constructing the decision tree, a method of randomly selecting a split attribute set is used. When inputting the feature matrix into the classifier, each sample in the training set and the test set needs to be labeled with a corresponding label for subsequent recognition.

4. System Test and Result Analysis

4.1. Data Preprocessing. The data includes three-axis acceleration, three-axis angular velocity, three-axis magnetometer, and attitude angle. The motion data used in this article mainly includes the combined acceleration, combined angular velocity, pitch angle, and roll angle, which can better reflect the human body's movements. However, the data collected is a period of time, and the amount of information is relatively large, which is not conducive to subsequent feature extraction. Therefore, window segmentation is required; that is, given a time series and a limited sample set characterized by time points, the sample set is divided into segments (windows) of continuous samples between two time points a and b. These two time points are internally homogeneous for the program.

How to determine the segmentation window is a key issue when performing window segmentation. For example, activities with a relatively short duration, such as sitting down, cannot be effectively recognized if the window is too long or too short. In fact, many classification errors in motion state recognition are caused by improper selection of the size of the segmentation window. If the window is too short, it may not cover the span of an action. If the window is too long, it may overlap two unrelated activities. This article uses sliding window segmentation technology and takes different sliding windows F according to different actions. Each sliding step $F/2$ means that each window segmentation will have a 50% overlap rate for the previous time window. This ensures that each action has better integrity. In this article, according to the different actions and the collected data analysis, the window chooses 100 and 200, such as falling, sitting, and standing. It takes about 2 s for the completeness of the data, so the segmentation window is selected as 200. It takes about 1 s to go upstairs, go downstairs, and stand still, so the split window is selected as 100, as shown in Figure 4. It can be seen that when the sliding window is selected as 100, the integrity of the action will not be destroyed.

4.2. Exercise Heart Rate and Exercise Blood Pressure Monitoring Test. Before the measurement, the experimenter should avoid strenuous exercise, keep calm, and conduct the experiment in a quiet environment. The experimenter needs to fill in basic personal information, including gender, age, height, and weight, and needs to clearly inform whether he has cardiovascular-related diseases and whether he has any medication records in the near future. After completing the basic information collection, it needs to wear the collection equipment correctly. We collect ECG signals, PPG signals, and blood pressure signals. After wearing the equipment correctly, first, we ask each experimenter to stay calm and maintain a resting state for 1 minute. After 1 minute, we record the physiological data within one minute, in which blood pressure is measured three times repeatedly, and use an electronic thermometer to measure the experimenter's resting state before exercise.

After the initial data collection is completed, take off the measurement equipment worn and exercise vigorously for 5 minutes in a running state. After finishing the exercise, the experimenter wears the measuring equipment again and immediately starts data collection in the same way as the initial data collection. We record the changes of data every 2 minutes until the measured values are basically stable.

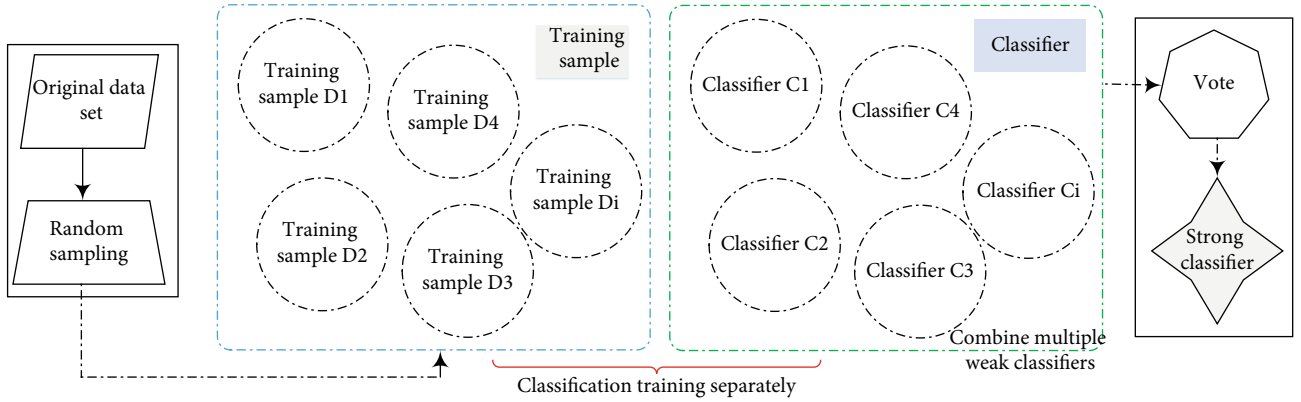

Figure 3: Bagging structure.

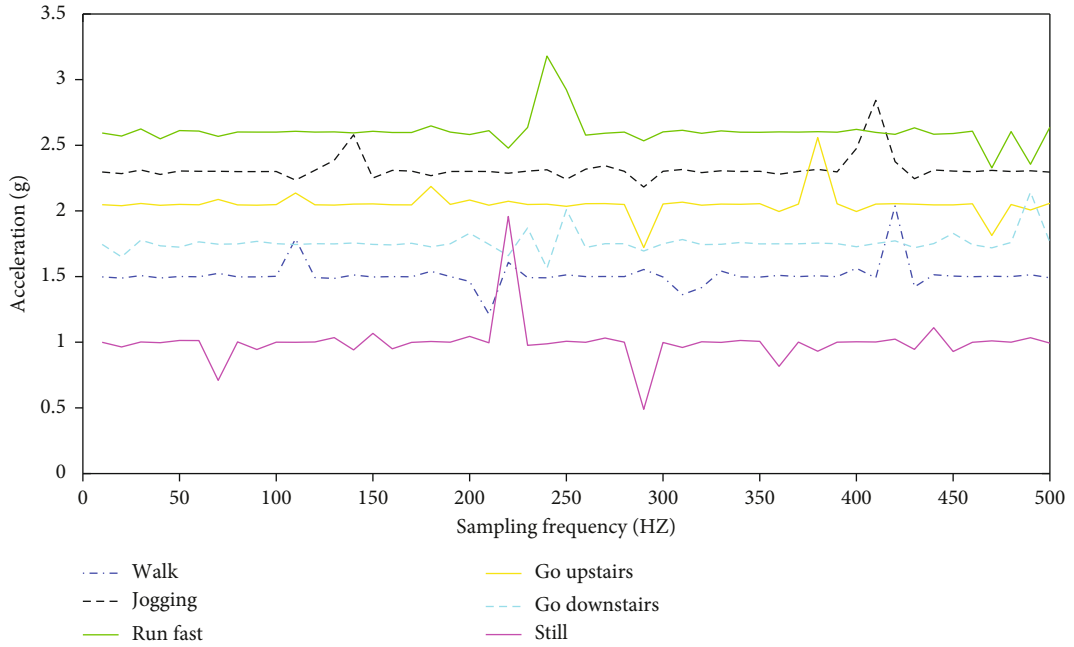

Figure 4: The acceleration of the sliding window segmentation when the overlay rate is 50% and the window is 100.

Table 2: Measurement data of the first experimenter.

Motion state	HR (bpm)	T (°C)	SBP (mm Hg)	DBP (mm Hg)
Resting state before exercise	90.2	36.1	113.1	69.1
	93.3	35.9	111.4	68.1
	91.0	36.2	115.1	68.3
After exercise	119.1	36.3	129.3	67.1
	117.4	36.1	128.1	65.3
	118.1	36.4	129.3	68.1
Resting after exercise	109.1	36.4	116.1	71.2
	105.0	36.3	114.1	69.3
	108.1	36.5	118.3	70.1

This section focuses on the analysis of the changes in the blood pressure of the experimenter before and after exercise. A total of 24 experimenter sample data were collected, and the measurement data of one experimenter was randomly selected as an example for analysis and explanation. Table 2 shows the systolic blood pressure, diastolic blood pressure, and heart rate of the first experimenter before and after exercise and after recovery. It can be seen from Table 1 that after 5 minutes of strenuous exercise, both blood pressure and heart rate values will change significantly, and after 10 minutes of rest recovery, the measured data basically return to a stable state.

After statistical analysis, it is found that using a forehead thermometer to measure human body temperature before and after exercise, the value of the change is small. The main reason is that the selected experimental environment is relatively open, the body surface temperature is greatly affected by the environment, and the human body sweat evaporation and other factors lead to the human body temperature. The

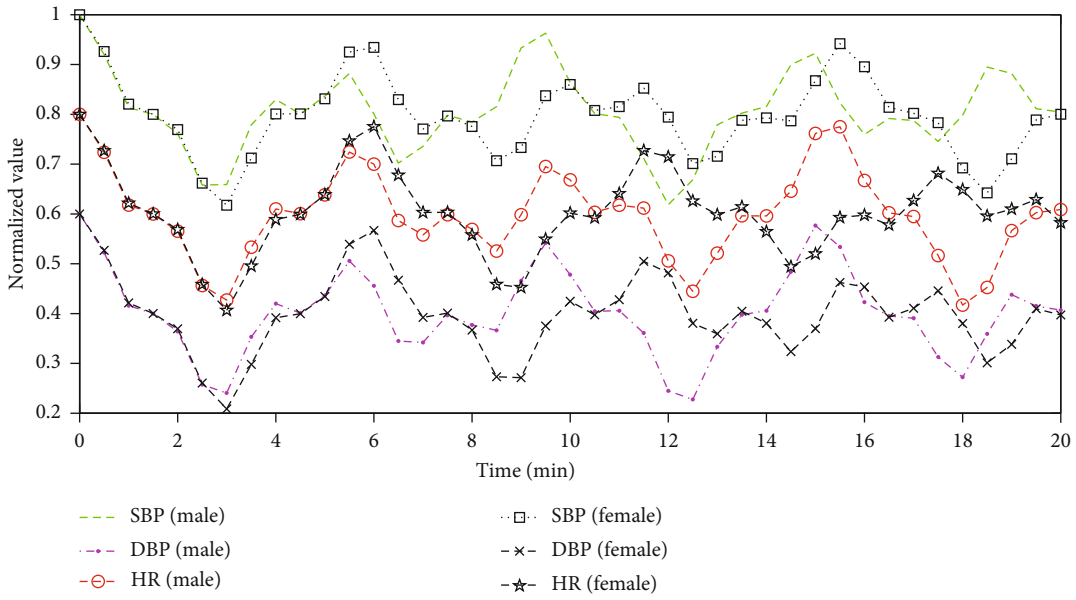

Figure 5: Normalized SBP, DBP, and HR changes of male and female experimenters before and after exercise.

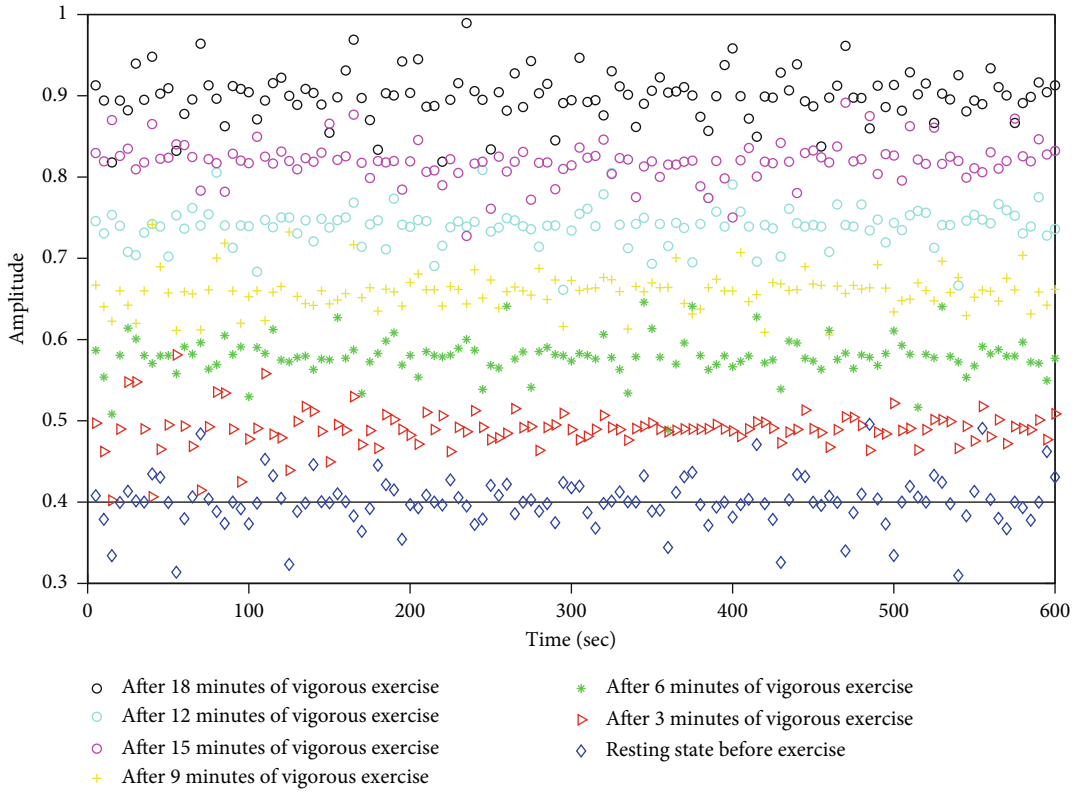

Figure 6: Changes of characteristic points of pulse wave waveform before and after exercise.

monitoring value has not changed significantly. After statistical analysis, it is found that the blood pressure changes of the 24 experimenters can be divided into three categories: (1) after exercise, the systolic blood pressure increased while the diastolic blood pressure decreased; (2) the systolic blood pressure decreased after exercise, while the diastolic blood pressure increased; (3) the diastolic blood pressure increased after exercise, while the diastolic blood pressure did not change significantly.

The two situations (1) and (2) mostly occurred in young male experimenters, and situation (3) occurred more frequently in young female experimenters. Among them, the

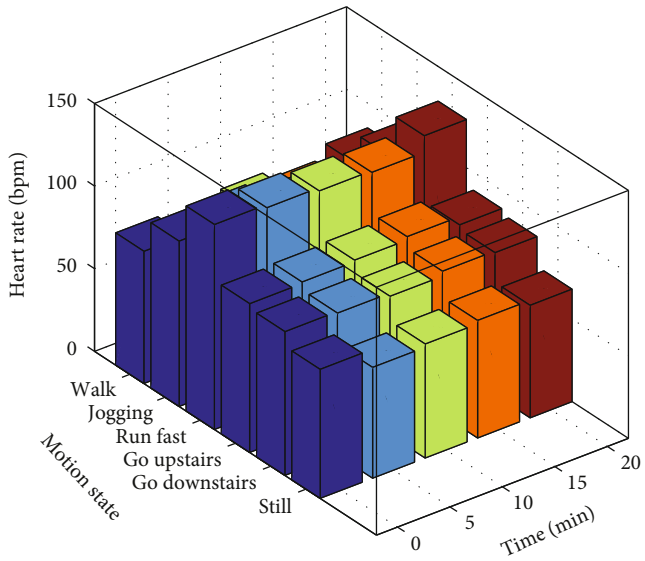

Figure 7: Changes in center rate data during different exercises.

normalized diastolic blood pressure, systolic blood pressure, and heart rate changes of male and female healthy experimenters before and after exercise are shown in Figure 5.

Through analyzing the data, it is found that after 5 minutes of vigorous exercise, the experimenter's diastolic blood pressure dropped from 75 mmHg to 65 mmHg, systolic blood pressure rose from 120 mmHg to 136 mmHg, and heart rate rose from 89 bpm at rest to 130 bpm. After 5 minutes of rest, the experimenter's heart rate began to recover, and the diastolic blood pressure increased, and the systolic blood pressure also began to show a downward trend; after 10 minutes of rest, the diastolic and systolic blood pressure basically returned to their preexercise state. The waveform characteristics of the pulse wave before and after the exercise of this experimenter were collected synchronously as shown in Figure 6. Figure 6 shows the pulse wave waveform feature points in the resting state before exercise and the distribution of waveform feature points after strenuous exercise.

It can be seen from the pulse wave waveform that the wave crest becomes narrower, the pulse rate increases, and the myocardial contractility is strengthened, resulting in an increase in the heart rate. Therefore, it can be seen that exercise leads to faster heart rate, increased myocardial contractility, increased cardiac output, and a certain increase in systolic blood pressure. After exercise, the vascular muscles relax, the peripheral blood vessels dilate, the diameter of the blood vessels increases, and the resistance decreases, which leads to a decrease in diastolic blood pressure. However, in the test, it was also found that after strenuous exercise of the same intensity, the blood pressure of some experimenters was opposite to the above phenomenon. Compared with the resting state before exercise, the systolic blood pressure decreased to a certain extent, and the diastolic blood pressure increased.

4.3. Motion Recognition and Monitoring Incorporating Multiple Physiological Characteristic Parameters. In this section, the physiological data and acceleration data of 12 people standing, squatting, jumping, walking, running, going upstairs, and going downstairs were collected. All 12 people were healthy and free of cardiovascular disease. There was no disease and no disease in the week before the test. We take medication records, and they sleep well and did not stay up late three days before the test. We collect acceleration data worn on the waist of a person wearing physiological signal measurement equipment during exercise. The data includes ECG signals, blood pressure data, and body temperature data.

Before the measurement of each set of exercise data, the experimenter should avoid strenuous exercise and maintain a resting state for 5 minutes. It is necessary to correctly wear a belt-type ECG and acceleration sensor, which can collect ECG signals and acceleration data synchronously, and correctly wear a finger clip blood pressure measuring instrument, which can realize the measurement of blood pressure data during exercise. We perform zero calibration on the acceleration sensor node fixed in the middle of the waist. After being worn correctly, we collected the physiological data and acceleration data of the experimenter in a standing state and recorded it. Each exercise lasts for three minutes, and there are at least 10 rests between the two exercises.

In this section, we will focus on the effectiveness of using physiological data to recognize exercise status. This section introduces blood pressure and heart rate data, mainly discussing the effectiveness of physiological data to improve the performance of exercise recognition. To this end, this section conducts a comparative experiment: only uses acceleration data to recognize sports and uses acceleration data, blood pressure data, and heart rate data to recognize sports. We select 7 experimenters with representative data changes among 12 experimenters for analysis and record the changes of systolic blood pressure, diastolic blood pressure, and heart rate obtained by 7 experimenters after 7 exercises, ECG signal, and acceleration during exercise. In this paper, the RF classification algorithm is used to identify the movement. Figure 7 records the heart rate changes of one of the experimenters during the six exercises. From the data waveform in the figure, it can be seen that the amplitude of the change of the different action data waveforms is obviously different, which verifies the effectiveness of the physiological data to improve the performance of motion state recognition from the data layer.

In this group of experiments, the acceleration data adopts the same set of data samples. The data in the first 20 seconds of the heart rate is eliminated, and the data within 50~230 seconds is selected for analysis. The data collection frequency of the ECG equipment is 360 Hz, and the data collection frequency of the acceleration sensor is 60 Hz. The sample data is intercepted for 5 seconds. There are 4000 sampling points for ECG data and 220 sampling points for acceleration data. A total of 3000 sets of sample data are obtained. 80% of the data is selected for training and 20% for testing. The results of random forest exercise load status monitoring and recognition are shown in Figure 8. It can be seen from the figure that when

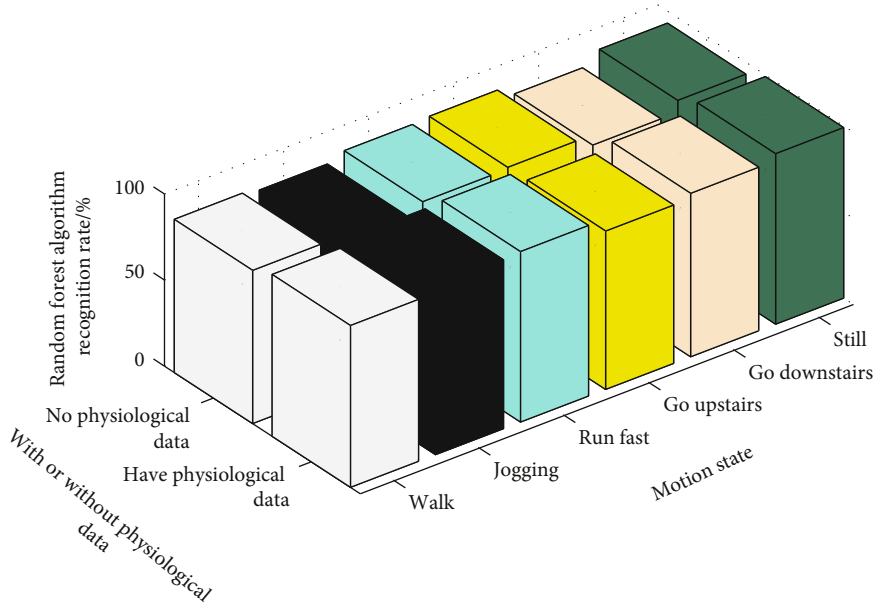

Figure 8: Experimental comparison of the validity of physiological data.

Table 3: Effectiveness classification results.

		Recognition rate (%)	
		Healthy sample	Unhealthy sample
Actual sample	Healthy sample	90.2	6.7
	Unhealthy sample	9.8	93.3

Table 4: Applicability classification results.

		Recognition rate (%)	
		Healthy sample	Unhealthy sample
Actual sample	Healthy sample	91.6	7.9
	Unhealthy sample	8.4	92.1

recognizing motion based on acceleration data, adding physiological data can effectively improve the recognition rate of the motion state.

4.4. Introducing Physiological Parameter Health Monitoring of Exercise Interference

4.4.1. Analysis of the Effectiveness of the Algorithm. We randomly selected a severe fatigue experimenter and collected resting heart rate and blood pressure data in the experimenter's fatigue state. Data was collected every 10 minutes for three minutes each, and a total of 6 sets of data were collected. Resting heart rate and blood pressure data were measured in 6 groups of subjects with unhealthy physiological parameters. In addition, the acceleration data in the stationary state was measured. After the experimenter returned to the awake state, the acceleration data and physiological parameter data in the six exercise states were collected as the data of the healthy group.

We select 216 groups of unhealthy samples (1 person × 6 times × 180 seconds/5 seconds) and select the same number of healthy samples. The classification results are shown in Table 3.

It can be seen from Table 2 that the recognition accuracy of the positive class of the designed classifier is above 89%. For a small sample, the classification recognition rate is ideal. It can be used for doctors or professionals to predict the health status; it can be used to distinguish whether the change of individual physiological parameters is caused by exercise or due to abnormal health of the individual. For example, it can be extended to actual application scenarios to analyze based on a large amount of accurate data.

4.4.2. Analysis of the Applicability of the Algorithm. In this section, the resting heart rate and blood pressure data of 10 severe fatigue experimenters and 4 self-evaluated severe stress experimenters were collected. The data of 14 unhealthy samples were measured to collect the resting heart rate and blood pressure data of the experimenter, as well as the acceleration data in the resting state. The data of the healthy group was collected from the awake state and relaxed state of 14 experimenters as healthy samples. We select 1176 groups of healthy samples (14 people × 7 actions × 60 seconds/5 seconds) and also select 1176 groups of unhealthy samples. The classification results are shown in Table 4.

It can be seen from Table 3 that the recognition accuracy rate of the positive class is above 87%. At the same time, comparing the effectiveness of the algorithm, it can be seen

that the recognition accuracy rate of this group of experiments is slightly lower, but it is also above 87%. Considering the experimenter differences in height, weight, gender, etc., the correct rate is within a controllable range. It shows that the algorithm in this paper is applicable to different experimenters.

5. Conclusion

In this paper, a random forest classification algorithm is selected to classify the motion state. The 27 time-domain and frequency-domain features of the human body's combined acceleration, combined angular velocity, pitch angle, and roll angle are, respectively, extracted to form a 108-dimensional feature vector; when extracting features, a sliding window segmentation method is used for feature extraction. Different actions use appropriate sliding windows to ensure the integrity of each action; the PCA dimensionality reduction method is used to optimize the feature matrix to make the data set cleaner and more concise and improve the calculation performance. This article sets up three sets of experiments to collect data from 24 people to study the changes in exercise heart rate, blood pressure, and body temperature, collect data from 12 people to analyze the effectiveness of fusion of physiological parameters to improve the recognition rate of exercise, and collect data from 14 people to discuss the physiological parameters that introduce exercise interference. The experimental results show that motion recognition with physiological features can effectively improve the recognition rate of motion, and the average recognition rate is increased from 94.8% to 95.7%; the recognition accuracy of the SVM-based blood pressure and heart rate abnormality judgment algorithm is more than 87%. This paper uses a depth camera to obtain depth images to build a human knee joint motion data set and uses neural networks to realize the training of the motion model and the positioning of the main human joints, but there is still a deviation from the motion data obtained by the wearable device. There are two main reasons for this situation: one is that the existing data set is not complete; the other is that the performance of the neural network structure is not strong enough. In order to avoid the shortcomings of the above basic work, the number of samples for the data set can continue to be expanded, including the number of people collected and the number of images, and the network structure can be further optimized. By adjusting the structure and parameter settings, a fast and accurate motion model can be trained. At present, the collection of acceleration sensor data and multiphysiological parameter data cannot be synchronized online and can only be synchronized offline. Next, we will build an integrated motion data and physiological data collection system.

Data Availability

The data used to support the findings of this study are available from the corresponding author upon request.

Conflicts of Interest

The authors declare that they have no known competing financial interests or personal relationships that could have appeared to influence the work reported in this paper.

Acknowledgments

The study was supported by the School of Applied Engineering Henan University of Science and Technology.

References

[1] T. Yang, X. Jiang, Y. Zhong et al., "A wearable and highly sensitive graphene strain sensor for precise home-based pulse wave monitoring," *ACS sensors*, vol. 2, no. 7, pp. 967–974, 2017.

[2] C. Carling, M. Lacome, A. McCall et al., "Monitoring of post-match fatigue in professional soccer: welcome to the real world," *Sports Medicine*, vol. 48, no. 12, pp. 2695–2702, 2018.

[3] L. Djaoui, M. Haddad, K. Chamari, and A. Dellal, "Monitoring training load and fatigue in soccer players with physiological markers," *Physiology & Behavior*, vol. 181, pp. 86–94, 2017.

[4] N. Dey, A. S. Ashour, F. Shi, S. J. Fong, and R. S. Sherratt, "Developing residential wireless sensor networks for ECG healthcare monitoring," *IEEE Transactions on Consumer Electronics*, vol. 63, no. 4, pp. 442–449, 2017.

[5] W. Jeong, J. Song, J. Bae, K. R. Nandanapalli, and S. Lee, "Breathable nanomesh humidity sensor for real-time skin humidity monitoring," *ACS Applied Materials & Interfaces*, vol. 11, no. 47, pp. 44758–44763, 2019.

[6] A. Fornasiero, A. Savoldelli, D. Fruet, G. Boccia, B. Pellegrini, and F. Schena, "Physiological intensity profile, exercise load and performance predictors of a 65-km mountain ultra-marathon," *Journal of Sports Sciences*, vol. 36, no. 11, pp. 1287–1295, 2018.

[7] A. A. Flatt, M. R. Esco, J. R. Allen et al., "Heart rate variability and training load among national collegiate athletic association division 1 college football players throughout spring camp," *The Journal of Strength & Conditioning Research*, vol. 32, no. 11, pp. 3127–3134, 2018.

[8] O. Selmi, H. Marzouki, I. Ouergui, W. BenKhalifa, and A. Bouassida, "Influence of intense training cycle and psychometric status on technical and physiological aspects performed during the small-sided games in soccer players," *Research in Sports Medicine*, vol. 26, no. 4, pp. 401–412, 2018.

[9] H. Kim, J. Lee, and J. Kim, "Electromyography-signal-based muscle fatigue assessment for knee rehabilitation monitoring systems," *Biomedical Engineering Letters*, vol. 8, no. 4, pp. 345–353, 2018.

[10] J. L. Viana, P. Martins, K. Parker et al., "Sustained exercise programs for hemodialysis patients: the characteristics of successful approaches in Portugal, Canada, Mexico, and Germany," *Seminars in Dialysis*, vol. 32, no. 4, pp. 320–330, 2019.

[11] Y. Huo, G. Prasad, L. Atanackovic, L. Lampe, and V. C. M. Leung, "Cable diagnostics with power line modems for smart grid monitoring," *IEEE Access*, vol. 7, pp. 60206–60220, 2019.

[12] P. Sansone, H. Tschan, C. Foster, and A. Tessitore, "Monitoring training load and perceived recovery in female basketball: implications for training design," *The Journal of Strength & Conditioning Research*, vol. 34, no. 10, pp. 2929–2936, 2020.

[13] Y. T. Jao, P. K. Yang, C. M. Chiu et al., "A textile-based triboelectric nanogenerator with humidity-resistant output characteristic and its applications in self-powered healthcare sensors," *Nano Energy*, vol. 50, pp. 513–520, 2018.

[14] O. Postolache, D. J. Hemanth, R. Alexandre, D. Gupta, O. Geman, and A. Khanna, "Remote monitoring of physical rehabilitation of stroke patients using IoT and virtual reality," *IEEE Journal on Selected Areas in Communications*, vol. 39, no. 2, pp. 562–573, 2021.

[15] N. Xing, L. Ji, J. Song et al., "Cadmium stress assessment based on the electrocardiogram characteristics of zebra fish (*Danio rerio*): QRS complex could play an important role," *Aquatic Toxicology*, vol. 191, pp. 236–244, 2017.

[16] A. A. Flatt and D. Howells, "Effects of varying training load on heart rate variability and running performance among an Olympic rugby sevens team," *Journal of Science and Medicine in Sport*, vol. 22, no. 2, pp. 222–226, 2019.

[17] H. Peltonen, S. Walker, A. Lähitie, K. Häkkinen, and J. Avela, "Isometric parameters in the monitoring of maximal strength, power, and hypertrophic resistance-training," *Applied Physiology, Nutrition, and Metabolism*, vol. 43, no. 2, pp. 145–153, 2018.

[18] R. Zacca, R. Azevedo, P. Chainok et al., "Monitoring age-group swimmers over a training macrocycle: energetics, technique, and anthropometrics," *The Journal of Strength & Conditioning Research*, vol. 34, no. 3, pp. 818–827, 2020.

[19] A. S. Martorelli, F. D. de Lima, A. Vieira et al., "The interplay between internal and external load parameters during different strength training sessions in resistance-trained men," *European Journal of Sport Science*, vol. 21, no. 1, pp. 16–25, 2021.

[20] D. Conte, N. Kolb, A. T. Scanlan, and F. Santolamazza, "Monitoring training load and well-being during the in-season phase in national collegiate athletic association division I men's basketball," *International Journal of Sports Physiology and Performance*, vol. 13, no. 8, pp. 1067–1074, 2018.

[21] L. T. Starling and M. I. Lambert, "Monitoring rugby players for fitness and fatigue: what do coaches want?," *International Journal of Sports Physiology and Performance*, vol. 13, no. 6, pp. 777–782, 2018.

[22] M. J. Buller, A. P. Welles, and K. E. Friedl, "Wearable physiological monitoring for human thermal-work strain optimization," *Journal of Applied Physiology*, vol. 124, no. 2, pp. 432–441, 2018.

[23] M. M. Kolokoltsev, S. S. Iermakov, and K. Prusik, "Motor skills and functional characteristics of students of different somatotypes," *Physical Education of Students*, vol. 22, no. 1, pp. 31–37, 2018.

[24] M. Zhu, Q. Shi, T. He et al., "Self-powered and self-functional cotton sock using piezoelectric and triboelectric hybrid mechanism for healthcare and sports monitoring," *ACS Nano*, vol. 13, no. 2, pp. 1940–1952, 2019.

Hindawi
Journal of Sensors
Volume 2022, Article ID 9741906, 10 pages
https://doi.org/10.1155/2022/9741906

Research Article

Research on Intelligent Control System of Indoor Greening Based on Wireless Sensor Network

Chen Su and Zhen Wang

Hubei University of Technology, Hubei Wuhan 430068, China

Correspondence should be addressed to Zhen Wang; 101910943@hbut.edu.cn

Received 19 November 2021; Revised 31 December 2021; Accepted 7 January 2022; Published 11 February 2022

Academic Editor: Gengxin Sun

With the acceleration of urbanization, people living in cities have a fast pace of life, great work pressure, and difficult to form a regular work and rest. As an emerging industry, indoor greening began to develop rapidly, which is of great significance to increase the area of urban green space and improve the living environment in a specific range. Aiming at the contradiction between urban resources and demand, the existing indoor greening automatic management system is studied, and an indoor greening intelligent management system based on wireless sensor network is designed. After careful study of indoor greening and wireless sensor technology, the design scheme is obtained by comprehensively considering the factors of intelligent management and resource saving. The hardware and software are designed from four parts: acquisition end, control end, gateway, and host computer. The plant growth environment parameters such as light intensity are obtained in real time. Using analytic hierarchy process and fuzzy comprehensive evaluation method to evaluate and analyze the plant growth environment, it can collect the relevant data of light, temperature, humidity, gas, and soil in real time and transmit the collected data to the host computer through wireless sensor network. The quantitative environmental suitability index is put forward, and the intelligent management of indoor greening plants is realized through the feedback control system. This topic combines wireless sensor technology with indoor greening, which can provide a new application field for the existing indoor greening. Once mature products are launched into the market, it can save time and energy for people to raise plants and better beautify and optimize the living environment.

1. Introduction

Indoor greening refers to the use of foliage plants and other ornamental materials to break the monotony of the indoor environment, adjust the indoor temperature and humidity, purify the air, and create a vibrant, beautiful, and comfortable indoor environment. Indoor greening mainly adopts three types of plants, namely, foliage plants, bonsai, and potted flowers [1]. The leaf of foliage plants is the main ornamental part, or the leaf shape is strange, or the leaf color is beautiful and has low requirements for sunlight and simple management, which is very popular all over the world [2]. Bonsai is a traditional Chinese art with high ornamental value, but it needs careful maintenance and high cost. It is mostly used for rent. Potted flowers have good decorative effect. Because they have high requirements for light and need more care, they are mostly used in festivals to set off the festival atmosphere. Indoor greening can absorb poison gas, relieve mood, and beautify the room, and the indoor space has the function of reconstruction [3]. Indoor plants can absorb harmful toxic gases emitted by household appliances and plastic products, such as carbon monoxide and nitrogen peroxide. Indoor plants can make people feel relaxed, regulate people's optic nerve and heart rhythm, and alleviate neurological fatigue. Indoor greening can beautify the room, make the room present the beauty of artistic conception and art, and make the indoor atmosphere more flexible [4]. It is an indispensable part of indoor decoration. The size and height of indoor plants can adjust the sense of proportion of space, and the flower walls, flower pools, and potted plants placed indoors can separate the room into small spaces that are both

transparent and slightly hidden, so as to achieve the effect of mutual integration [5]. Naturally, people living in downtown areas yearn for a comfortable, quiet, natural, and harmonious living environment, so they begin to greening the environment to varying degrees [6]. As an emerging industry, indoor greening began to develop rapidly, which is of great significance to increase the area of urban green space and improve the living environment in a specific range. In recent years, some cities have frequently held family greening and decoration design competitions, family gardening seminars, exchange meetings, and other activities, which have greatly inspired people's enthusiasm for family gardening activities [7].

Since the 21st century, wireless sensor network (WSN) has developed rapidly under the leadership of wireless communication technology. WSN network researchers have also successfully developed micro sensor nodes with low power consumption, low cost, and wireless communication capability. Therefore, it is possible to build a low-cost WSN network. At the same time, with the development and progress of society, WSN network has a significant application demand in the fields of ecological protection, energy conservation and emission reduction, and modern services [8]. People's application needs for the network show diversity and continue to move closer to the direction of personalization and intelligence. The current network structure has the coexistence of a variety of heterogeneous network coverage and complex and diverse access technologies. The limitations of this network organization structure are constantly expanding, making heterogeneous network interconnection, that is, heterogeneous network integration, become the main direction of the development of the next generation network. The interconnection and interworking of heterogeneous networks and the cooperative work of network nodes are also an important topic that must be solved in the research process of next generation networks [9]. At present, the problems of small coverage and limited network capacity are gradually emerging in wireless networks. The emergence of heterogeneous wireless network integration technology not only solves the limitations of existing networks but also becomes an effective means for network terminal nodes to provide network access services anytime and anywhere and mobile computing power. Moreover, this technology has attracted the continuous attention of people from all walks of life [10]. It has great development potential in various application fields in the future. As a new generation of wireless network technology, wireless sensor network integrates computer technology, wireless communication technology, intelligent embedded technology, and sensor technology. In the monitoring area, the staff scatter the sensor nodes freely [11]. These sensor nodes are automatically built into a WSN network through self-organization. The network can complete the collection, transmission, processing, and transmission of the physical parameters of the perceived objects in the monitoring area [12]. The WSN wireless sensor network finally transmits the perceived physical information to the host computer monitoring software and provides decision support for users. Because the sensor nodes scattered in the monitoring area can form communication links through self-organization, WSN network does not have high requirements for infrastructure construction. Even without infrastructure construction, nodes work together to complete the information acquisition process of sensing objects [13]. A large number of sensors deployed in the monitoring area are single nodes. In addition to the functions of sensing object information acquisition and data processing, it can also process the information transmitted from adjacent nodes for simple dump and processing [14]. However, due to the limitations of low microprocessor processing rate, limited storage space, and limited energy supply, the communication ability of sensor nodes is relatively weak [15]. Therefore, we cannot rely on a single sensor node to complete the task of collecting, processing, and transmitting the information of the monitoring area, so we need to cooperate with adjacent nodes to process the information of the sensing object and finally transfer the sensing object information to users to provide decision support [16]. Intelligent control is a control mode with intelligent information processing, intelligent information feedback, and intelligent control decision-making. It is an advanced stage of the development of control theory. It is mainly used to solve the control problems of complex systems that are difficult to be solved by traditional methods. The main characteristics of intelligent control research object are uncertain mathematical model, high nonlinearity, and complex task requirements.

Through research and practice, this paper applies wireless sensor technology to indoor greening and develops indoor greening application module in command and control system. In addition, this paper also uses wireless sensor technology to develop a convenient, intelligent and cost-effective maintenance management control system suitable for family greening, so as to realize the intelligent management and control of humidity, light, temperature and landscape lights.

The rest of this article is organized as follows. Section 2 discusses related work. Section 3 introduces the experimental method. Section 4 analyzes the results. Section 5 gives the conclusion.

2. Related Work

Indoor greening and decoration refer to the use of ornamental materials based on indoor foliage plants in accordance with the characteristics of the indoor environment, combined with people's daily needs, to beautify the utensils and places used. This kind of beautification decoration is based on the needs of people's material and spiritual life. The entire indoor environment is designed, decorated, and arranged to integrate indoor and outdoor, reflecting the combination of dynamic and static and achieving the integration of people, indoor environment, and nature. Harmony and unity, it is an important breakthrough in traditional architectural decoration. Indoor greening and decoration refer to the use of ornamental materials based on indoor foliage plants in accordance with the characteristics of the indoor environment, combined with people's daily needs, to beautify the utensils and places used. This kind of beautification decoration is based on the needs of

people's material and spiritual life and is designed, decorated, and arranged in line with the entire indoor environment, so that indoor and outdoor are integrated, reflecting the combination of dynamic and static and reaching people, indoor environment, and nature. It is an important breakthrough in traditional architectural decoration. In the field of agriculture, wireless sensor networks can be used to monitor the environment and soil moisture in orchards, vegetable gardens, greenhouses, greenhouses, and other places in real time, so as to realize the functions of automatic collection, wireless transmission, real-time monitoring, network release, and remote monitoring of soil moisture information in farmland, orchards, and nurseries and formulate management plans for producers [17, 18]. Wireless sensor network can quickly and effectively obtain soil moisture information and transmit information with low cost and high reliability, which is helpful to scientific planting and improve yield [19]. Air humidity, temperature, ambient light intensity, CO2 concentration, water content in soil, pH value, etc. are important parameters for monitoring [20]. At present, researchers have developed and designed a variety of wireless sensor network monitoring systems using different technologies and methods to monitor the field, orchard, vegetable greenhouse, and greenhouse environment in real time [21]. Si and Yang [22] developed the remote monitoring system of citrus orchard soil and realized the remote and real-time monitoring of citrus orchard by using XBee PRO module with ZigBee wireless data transceiver. Shao et al. [23] developed and designed a low-power greenhouse monitoring system based on ZigBee, which can accurately collect environmental information such as illumination, air temperature and humidity, soil moisture, and carbon dioxide concentration in the greenhouse and well avoid the problems of complex construction, many lines, and difficult maintenance in the traditional greenhouse wired monitoring system [24]. Alsamhi et al. [25] use wireless sensor network to collect soil moisture content in each irrigation area of farmland, analyze and process the collected data, and formulate water use plan by using correct prediction and decision-making methods. Agricultural irrigation accounts for 70% of China's total water consumption. Wireless sensor network realizes automatic water saving and energy saving through environmental monitoring and can build an efficient, low energy consumption, low investment, and multifunctional agricultural water-saving irrigation platform. Jing et al. [26] studied farmland information collection and automatic drip irrigation based on ZigBee technology and implemented zoned precision irrigation on farmland by collecting information such as plant soil humidity, ambient temperature, and light intensity. Odiyur et al. [27] used ZigBee wireless communication technology to design the garden automatic water-saving irrigation system, which can collect the soil temperature and humidity in the garden and control the sprinkler and drip irrigation valves according to the temperature and humidity. Bai et al. [28] used GSM network to send short message instructions through mobile phone to realize micro irrigation remote control of garden ornamental plants. Mobile phone keys or short message instructions can start and stop irrigation. Han et al. [29] used ZigBee wireless sensor network and GPRS network to design and develop a water-saving irrigation control system based on CC2530 and MSP430 to automatically carry out farmland water-saving irrigation according to the collected soil moisture content information.

3. Experimental Method

3.1. Principles of Indoor Greening and Construction of Wireless Sensor Network. The automatic maintenance system of indoor greening is different from the widely used farmland intelligent irrigation system and the artificial climate room used in the laboratory. Although they all control the three factors of light, humidity, and temperature, they also pay attention to the requirements of multiple systems due to different application fields and purposes. Farmland conservation focuses on income, and laboratory scientific research conservation focuses on accuracy. However, indoor greening is based on the premise of facilitating home and improving the living environment. The maintenance system needs to be integrated with the home environment to meet people's needs in beauty and convenience. In order to make rational use of resources, the accuracy control can be relaxed appropriately. Many horticultural lovers like plants, but they do not easily try to raise plants. Many people move plants from flower shops to their homes and soon dry up. Some people can feed for a few months, while others can only feed for a week or two. Raising plants is a difficult problem for many people. First, people lack plant knowledge.

In addition, plant conservation needs long-term careful care. Plants are different from pets. Pets can be called and spoiled. Plants are different. They only grow quietly and are easy to be ignored. The pace of modern life is too fast, people's energy is very scattered, and it is easier to forget to maintain the flowers and plants at home. Although many people clearly know the benefits of plants to mankind, they still flinch. Therefore, the first problem to be solved by the maintenance system is to realize automatic maintenance, share worries for growers, and make indoor greening simple.

The indoor greening maintenance system is applied to home life without professional maintenance, which requires the system to have high stability and long-lasting durability. Due to the wide geographical distribution of family horticulture and different climates in different regions, for example, families in tropical areas do not need to consider the problem of cold protection, and there is no need to take lighting supplement measures for maintenance under full light.

The planting sites are free to play by the head of household, and the climatic environment is different. Different families carry out horticultural activities on different scales, and their living areas are large and small, and some species are few. Only plants are planted on the balcony, with small area and concentration. Some are arranged with greening on the villa roof, courtyard, and indoor. The area to be managed is large and scattered. This requires that the system has different configurations, and the acquisition end and control end can be expanded and reduced according to the needs to adapt to different home gardening scenarios. Therefore, the

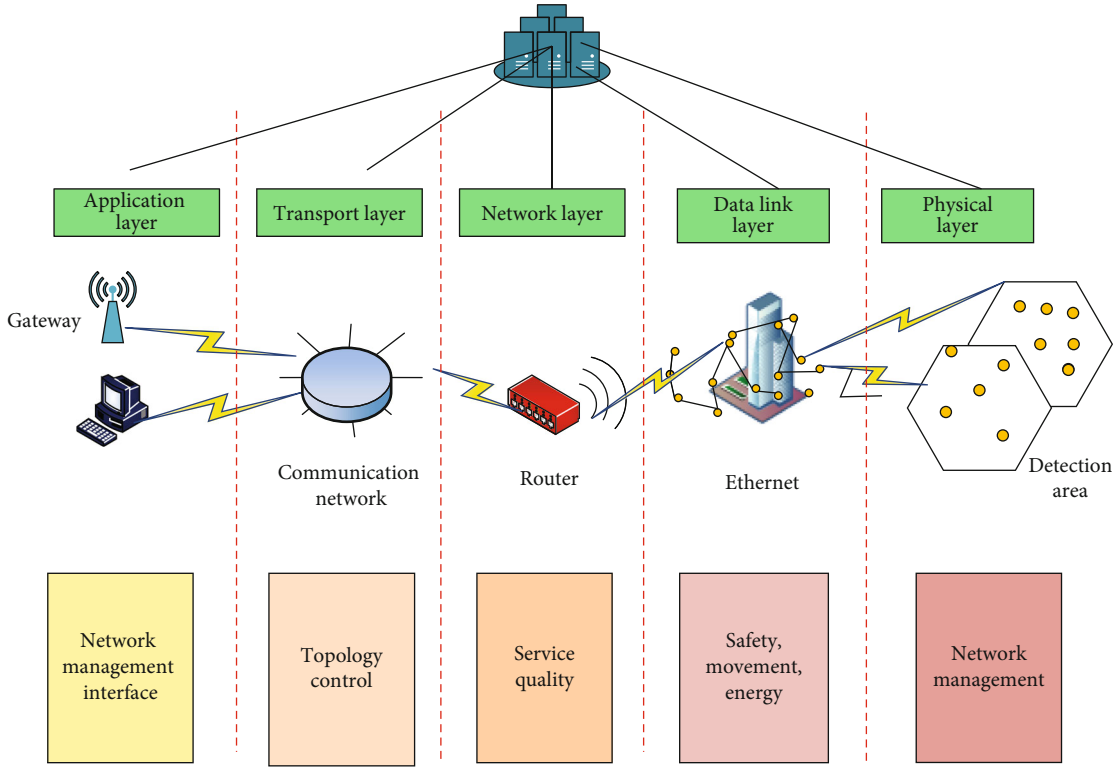

Figure 1: Network structure diagram of wireless sensor.

system is required to have good scalability and reassembly, so as to be applied to different home environments.

Wireless sensor network applications are characterized by low cost, low power consumption, and wide range. It is a special ad hoc network composed of sink node, task management node, and sensor node. In the monitoring area, these nodes are deployed effectively, and the physical quantities to be measured are collected, recorded, and analyzed in real time and continuously, so as to complete real-time control. Sensor node is usually a micro embedded system with relatively weak storage, communication, and data processing capabilities. Its main task is to collect data. Wireless sensor network system adopts hierarchical structure, which is composed of network management platform, network communication protocol, and application support platform. A typical wireless sensor network structure is shown in Figure 1.

3.2. Architecture Design of Indoor Greening Intelligent Control System. The indoor greening automatic control system is divided into five parts: acquisition terminal, control terminal, gateway, host computer, and wireless communication network. In the system, the acquisition terminal is equivalent to nerve endings, which is responsible for feeling "stimulation" and transmitting perceptual information to the host computer. Wireless communication network is equivalent to neural network, which provides a channel for the transmission of information. Gateway is the hub, which can receive and convert information and connect the host computer and other ports. The upper computer is the brain of the whole system, which is responsible for receiving signals, making final accounts and issuing commands. The control end is equivalent to muscle tissue, which is used to realize the command of the system and make practical operation. The system architecture is shown in Figure 2.

The acquisition terminal of the system includes the acquisition of three parameters: humidity, temperature, and light. The wireless sensor network adopts nRF24L01. The gateway adopts a simple gateway, which only performs data conversion without data processing. Its main function is to connect the nRF24L01 network with the host computer. The upper computer uses LabVIEW to design the virtual instrument, which is responsible for data calculation and judgment. It is a bridge between the acquisition end and the control end. The control end mainly includes watering control, cooling control, lighting control, and landscape lamp control. It also communicates with the host computer through the gateway.

3.3. Design of Acquisition Terminal of Intelligent Control System. The sensor senses physical information and generates measurable electrical signals. It is a necessary device for parameter detection in the control system. The information of various parameters in the system can be obtained through the sensor. The accuracy of the information is directly related to the measurement accuracy and control accuracy of the whole system, so as to further reasonably control the plant growth parameters according to the growth requirements of various plants, so that the plants can grow smoothly. Selecting appropriate sensors is the premise and foundation of automatic control. The information

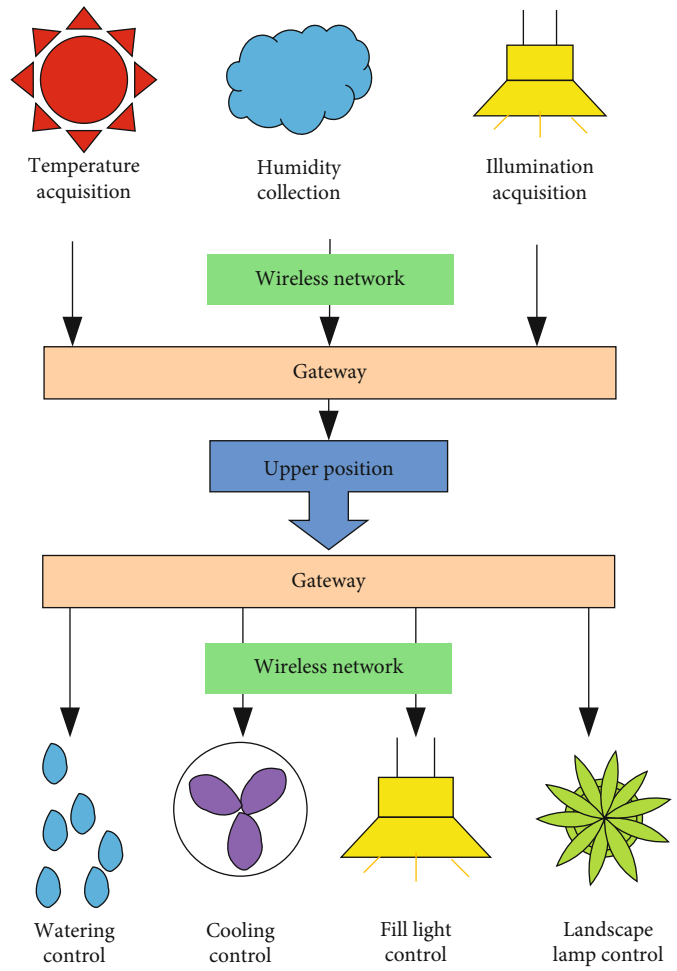

Figure 2: Indoor greening intelligent maintenance system structure diagram.

collected by the home gardening maintenance system mainly includes light intensity, soil humidity, and temperature. The information is collected through photosensitive sensing resistance, temperature sensor, and soil humidity sensor. The selection of the sensor at the acquisition end determines the implementation mode of the acquisition module, affects the complexity of the circuit and program, and also affects the overall performance of the system in operation.

The software design of the acquisition end is relatively simple compared with the control end. Mainly, the information can be uploaded after receiving the acquisition command of the upper computer, which can be realized through C51 programming of the single chip microcomputer. In addition, it can also realize the recognition of three types of sensing data and the processing of corresponding sensing data, including AD conversion and hexadecimal conversion. The outputs of soil moisture sensor and photosensitive sensor are analog signals. Before data processing, the analog signals must be transformed into digital signals for transmission and calculation. AD conversion is divided into parallel comparison type and feedback comparison type. There is no accurate digital soil moisture sensor module in the market. This design uses an ordinary

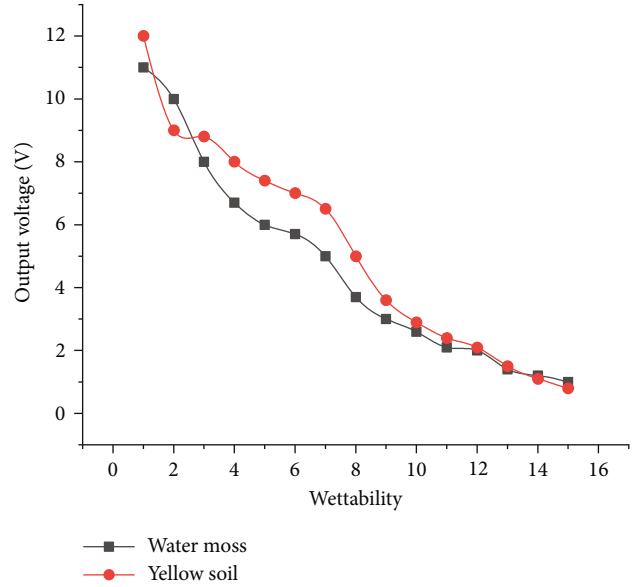

Figure 3: Corresponding relationship between soil humidity sensing output voltage and humidity.

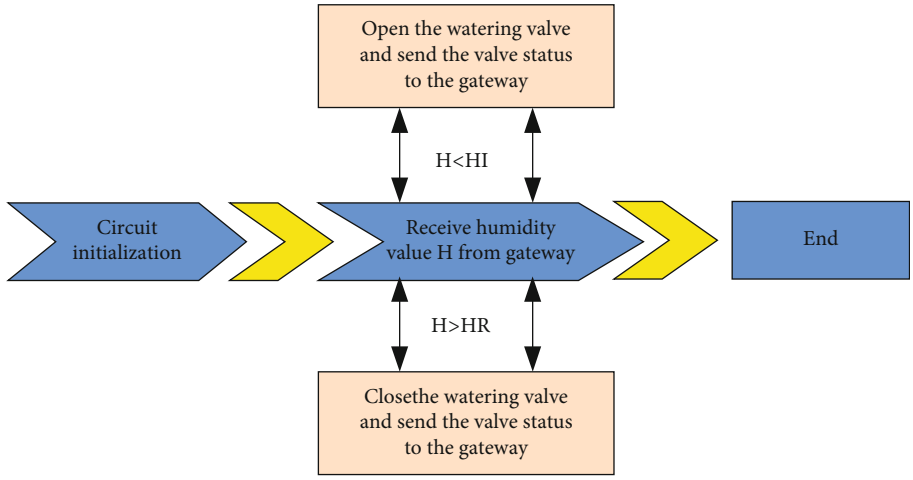

Figure 4: Flow chart of soil moisture automatic control.

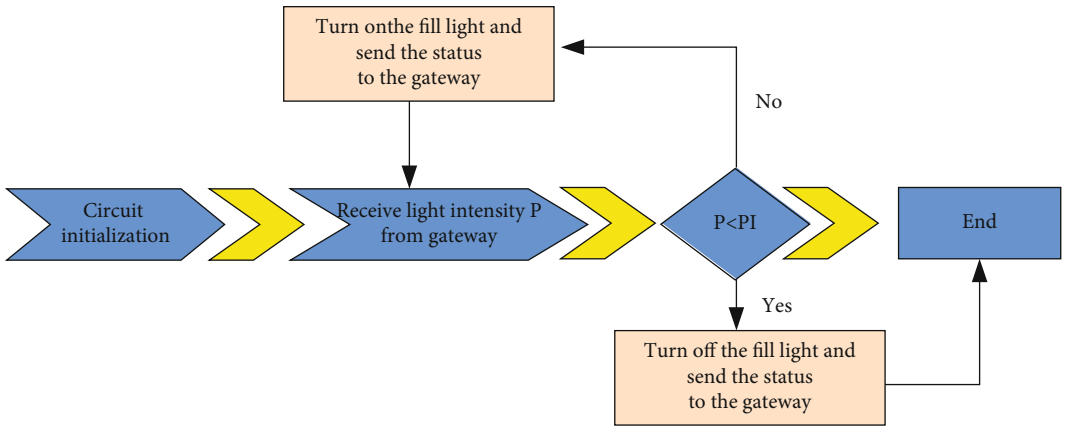

Figure 5: Flow chart of fill light control.

analog output soil moisture sensor, model yl-69. Two types of substrates, water moss and yellow soil, are used for verification. The test method is to water the dried substrate one by one, measure the sensor output every time, and observe the appearance change of the substrate until the water content of the substrate reaches saturation, and the sensor output will not change.

By detecting the moisture of two substrates of water moss and yellow soil, it is concluded that the output of yl-69 soil moisture sensor is roughly the same as that of yellow soil. With the increase of humidity, the output voltage of the sensor decreases. When dry yellow soil and yellow soil are used for detection, the output voltage is 11.0 V, which is the same as the output of detection air. When wet yellow soil and yellow soil are detected, the output voltage is less than 1.5 V, which is the same as the output of detection pure water. As shown in Figure 3. Similarly, with the increase of the humidity of the yellow soil, the output voltage of the sensor decreases. It is observed that when the yellow soil is relatively wet, the output voltage is about 5 V. When the output voltage drops to about 2.0 V, the yellow soil is obviously wet, and there is water exposed at the lower part of the flower pot below 1.5 V. Due to the different water retention between yellow soil and water moss, there are slight differences in the calibration process. For example, the water demand of yellow soil is larger, and the change of output voltage is slower.

3.4. Design of Intelligent System Control Terminal. The software design determines whether the automatic control of various functions can be realized. In the wireless transceiver protocol, watering, spraying, lighting, and landscape lighting controllers all have their own command formats. Various controllers send or receive commands in their own format to achieve control effectiveness. And each controller has a switch to set the address; that is, there can be multiple control areas. For example, if a family has a balcony and indoor green space, two watering controllers with different addresses can be used to control watering, and the upper computer can distinguish the area where the controller is located. Under specific needs, users can flexibly choose to control one or more locations. However, the maximum capacity of nodes in a system is 256, which is sufficient for indoor greening.

Watering is the most important maintenance content of family horticulture. The biggest difference between the

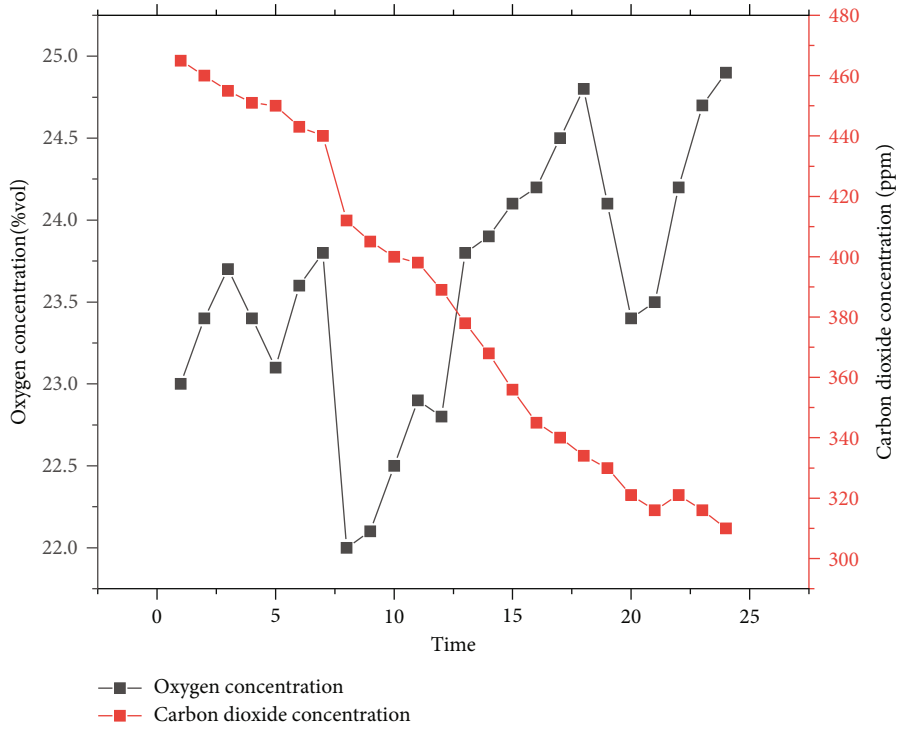

Figure 6: 24-hour change curve of air quality.

indoor environment and the outdoor environment is rainfall. The water in the soil of family horticulture is supplied by growers. Domestic plants are often dried or drowned under human factors. Watering is the most important maintenance content of family horticulture. The biggest difference between the indoor environment and the outdoor environment is rainfall. The water in the soil of family horticulture is supplied by growers. Domestic plants are often dried or drowned under human factors. Considering the characteristics of small home space and high requirements for environmental sanitation, the system adopts drip irrigation, which can not only save water but also prevent excess water from overflowing and soiling the room. The switch of drip irrigation is controlled by the solenoid valve, which is connected with the wireless module and the control module. The control of soil humidity is to send the humidity value collected by the sensor to the gateway through the wireless module. The gateway transmits the data to the upper computer. The upper computer compares the collected humidity value with the minimum humidity threshold. If it is lower than the minimum threshold, open the valve for irrigation until the soil humidity is higher than the maximum threshold, close the valve. Thus, the soil humidity is controlled within the more suitable range between the maximum humidity threshold and the minimum humidity threshold, as shown in Figure 4.

Light is a major limiting factor for indoor greening, and the layout and maintenance of indoor plants should be determined according to the light intensity. For example, the light in the porch and walkway is too dark, and it is difficult for general plants to survive. Greening and decoration can be carried out only under the condition of light supplement. The light supplement control is similar to the watering air control and cooling control in front. It also uses wireless communication technology to transmit information and commands between the acquisition end, the upper computer, and the control end, as shown in Figure 5. The upper computer compares the light intensity from the acquisition end with the minimum light intensity threshold. If it is higher than the threshold, there is no need to turn on the light; if it is lower than the threshold, it is necessary to turn on the fill light and then send the control command of the fill light to the wireless light on.

4. Result Analysis

4.1. Evaluation Algorithm of Indoor Greening Evaluation Factor Collection and Monitoring System. We choose an algorithm combining fuzzy comprehensive evaluation method and analytic hierarchy process. The improved comprehensive evaluation algorithm model in fuzzy comprehensive evaluation method and the index weight determined by analytic hierarchy process are used for comprehensive evaluation, which can not only avoid the loss of effective information but also realize the comprehensive measurement of operation. Through the combination of the two algorithms, we can give full play to the advantages of the two algorithms, which can not only relatively divide "good" and "bad" at the appropriate threshold and make the fuzzy phenomenon clear but also accurately measure the relative importance of the evaluation index. In this way, the combination of qualitative and quantitative can not only comprehensively consider various factors affecting

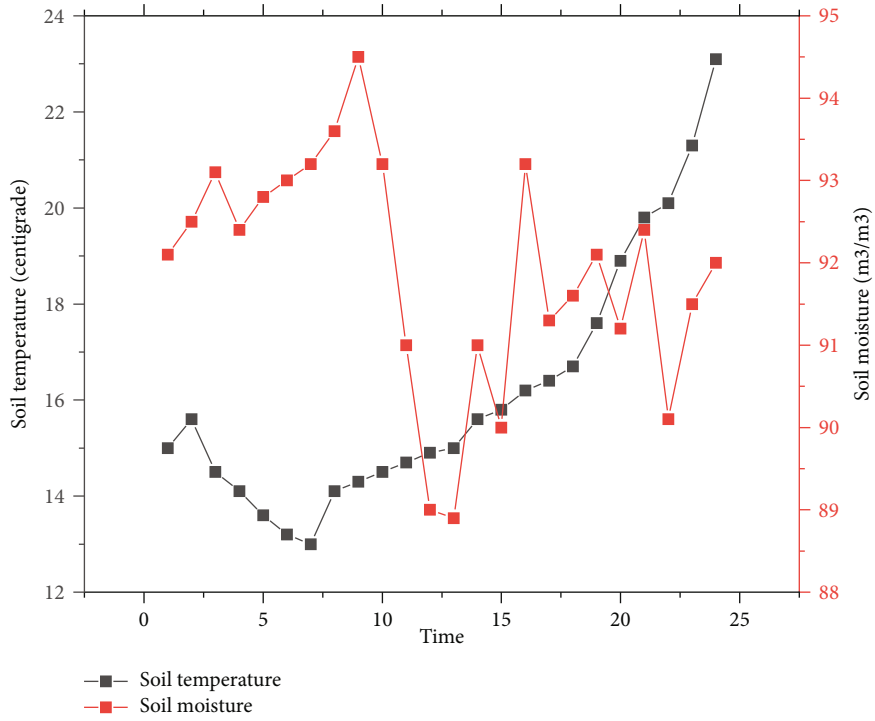

Figure 7: 24-hour variation curve of soil quality.

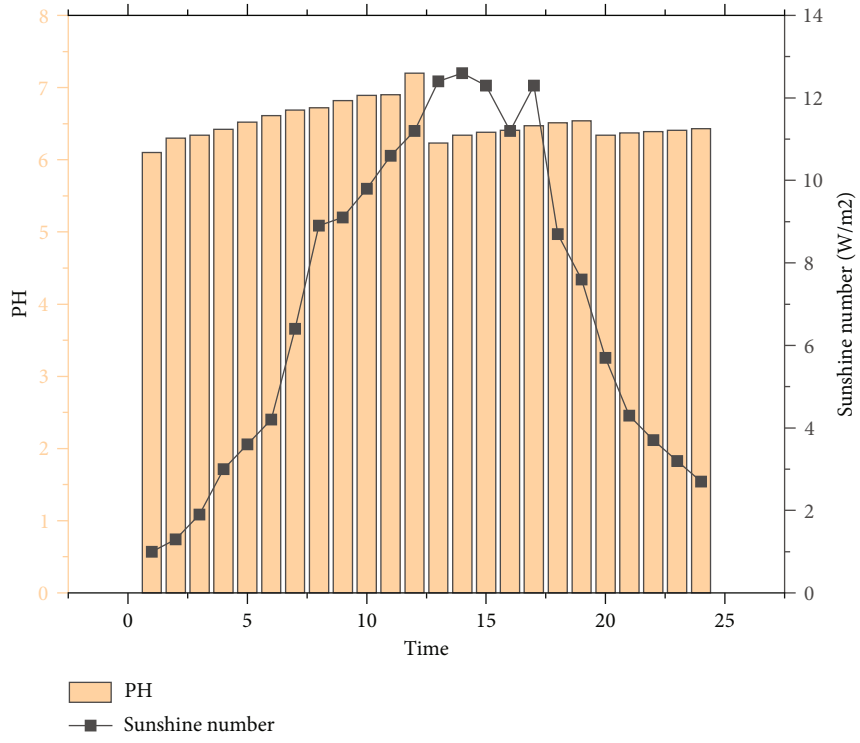

Figure 8: 24-hour curve of water pH and sunshine.

the ecological environment assessment of urban green space but also fully reflect the fuzziness of evaluation factors and evaluation process. Minimize the impact caused by personal experience or preferences, and be able to give evaluation results objectively.

4.2. Evaluation Results of Indoor Greening. The following figure shows some data obtained from the actual monitoring of the monitoring system in summer by using the indoor greening ecological evaluation factors, which provides data support for the practical application of the algorithm.

Figure 6 shows the change curve of 24-hour air quality, in which the concentration of CO2 decreases continuously with the passage of time, and the concentration of oxygen fluctuates and increases. Figure 7 shows the change curve of soil quality within 24 hours. With the passage of time, the soil temperature generally increases, but from 2 o'clock to 6 o'clock, the soil temperature decreases. The soil moisture is in a relatively high state at the beginning, but with the passage of time, it is in a process of fluctuation and decline.

The improved single level comprehensive evaluation algorithm model in fuzzy comprehensive evaluation method and the index weight determined by analytic hierarchy process are used for comprehensive evaluation. It is the weight vector of four elements calculated by analytic hierarchy process, and R is the fuzzy set calculated by fuzzy comprehensive evaluation method. The grade of comprehensive evaluation of urban green space eco-environmental quality will be determined by the membership degree of each level after matrix calculation and finally depends on the grade with the largest membership value in the environmental evaluation set. Using the data collected by the system and through the calculation of the algorithm, we can conclude that the evaluation result of the selected area is excellent; that is, the air quality is good, the soil quality is good, the water quality is good, and the sunshine is moderate (Figure 8).

5. Conclusion

Wireless sensor networks are like the human body's sensing system, and each node is the nerve endings of the sensing system. Through the data they return, we can accurately understand the changes in the monitored area. This course applies wireless sensor network technology to indoor greening to realize intelligent remote management of indoor greening. By consulting the literature and investigating the indoor greening products and wireless sensor network technology in the market, the author has completed the design and debugging of the home gardening automatic maintenance system based on nRF24L01 wireless communication module. The main work includes hardware design and software design of acquisition end and control end, host computer program design, PCB proofing and welding, and system debugging. The hardware of home gardening intelligent maintenance system includes four parts: acquisition end, control end, gateway, and host computer. The acquisition end includes wireless transceiver module, three sensors (soil humidity sensor, temperature sensor, and photosensitive sensor), and data processing module. The system consists of four independent control points, which control watering, spraying, lighting, and landscape lights, respectively. Each control terminal has the same circuit structure but different programming. The hardware of control terminal includes wireless transceiver module, voltage conversion module, and data processing module. The gateway communicates with the host computer through RS232 serial port. The gateway circuit mainly includes wireless transceiver module and USB to serial port module. The system composed of wireless network has the characteristics of strong flexibility, safety, reliability, and low power consumption. It does not need manual operation, eliminates the tedious and hidden dangers of wired access, and can work stably for a long time. It is a supplement to wired control mode. This topic combines wireless sensor technology with indoor greening, which can provide a new application field for the existing indoor greening. Once mature products are launched into the market, it can save time and energy for people to raise plants and better beautify and optimize the living environment. Introducing the latest information technology into indoor greening can create convenience for indoor greening management and speed up the intellectualization of home gardening. Home gardening management technology still follows the traditional way. Management by experience and feeling requires a lot of investment in time and energy. Some irrigation timers are not common in automation. People are looking forward to a control system that can automatically manage home gardening. Although automatic management and remote control have been applied in the greenhouse with a high degree of intelligence, the system is expensive, bulky, and complex, so it is not suitable for family use. The research on the intelligent maintenance system of indoor greening based on wireless sensor network is based on the maintenance of family horticulture. It has strong applicability and is a customized maintenance system for indoor greening.

The research of indoor greening intelligent maintenance system can provide new ideas and new application fields for horticultural maintenance of smart home domain. In recent years, the Internet of Things has been widely used in home life, and smart home has emerged as an emerging industry, which can realize intelligent security system, home theater and intelligent remote control of home appliances, making life more comfortable and convenient. However, smart home does not involve gardening and maintenance. Indoor greening maintenance system can attract the interest of many smart home system developers, and it is a promising development field.

Data Availability

The data used to support the findings of this study are available from the corresponding author upon request.

Conflicts of Interest

The authors declare that they have no known competing financial interests or personal relationships that could have appeared to influence the work reported in this paper.

Acknowledgments

The study was supported by the Hubei University of Technology.

References

[1] W. Wei, H. Song, and W. Li, "Gradient-driven parking navigation using a continuous information potential field based on wireless sensor network," *Information Sciences*, vol. 408, pp. 100–114, 2017.

[2] U. Gogate and J. Bakal, "Healthcare monitoring system based on wireless sensor network for cardiac patients," *Biomedical & Pharmacology Journal*, vol. 11, no. 3, p. 1681, 2018.

[3] H. Li, G. Xu, and G. Xu, "Mechanical vibration monitoring system based on wireless sensor network. International Journal of Online," *International Journal of Online Engineering*, vol. 14, no. 6, p. 126, 2018.

[4] J. H. Seo, "Temperature data visualization for condition monitoring based on wireless sensor network," *The Journal of the Korea Institute of Electronic Communication Sciences*, vol. 15, no. 2, pp. 245–252, 2020.

[5] P. Song, C. Hao, and J. Wu, "Acoustic source localization using 10-microphone array based on wireless sensor network," *Sensors and Actuators A: Physical*, vol. 267, pp. 376–384, 2017.

[6] B. Shi, V. Sreeram, D. Zhao et al., "A wireless sensor network-based monitoring system for freshwater fishpond aquaculture," *Biosystems Engineering*, vol. 172, pp. 57–66, 2018.

[7] Y. Kuo, C. L. Li, and J. H. Jhang, "Design of a wireless sensor network-based IoT platform for wide area and heterogeneous applications," *IEEE Sensors Journal*, vol. 18, no. 12, pp. 5187–5197, 2018.

[8] D. Zhang, T. Zhang, J. Zhang, Y. Dong, and X. D. Zhang, "A kind of effective data aggregating method based on compressive sensing for wireless sensor network," *EURASIP Journal on Wireless Communications and Networking*, vol. 2018, no. 1, 15 pages, 2018.

[9] J. Qi and G. P. Liu, "A robust high-accuracy ultrasound indoor positioning system based on a wireless sensor network," *Sensors*, vol. 17, no. 11, p. 2554, 2017.

[10] S. A. Kumar and P. Ilango, "The impact of wireless sensor network in the field of precision agriculture: a review," *Wireless Personal Communications*, vol. 98, no. 1, pp. 685–698, 2018.

[11] M. Faheem and V. C. Gungor, "Energy efficient and QoS-aware routing protocol for wireless sensor network-based smart grid applications in the context of Industry 4.0," *Applied Soft Computing*, vol. 68, pp. 910–922, 2018.

[12] A. D. Salman, O. I. Khalaf, and G. M. Abdulsahib, "An adaptive intelligent alarm system for wireless sensor network," *Indonesian Journal of Electrical Engineering and Computer Science*, vol. 15, no. 1, pp. 142–147, 2019.

[13] S. Rani, S. H. Ahmed, and R. Rastogi, "Dynamic clustering approach based on wireless sensor networks genetic algorithm for IoT applications," *Wireless Networks*, vol. 26, no. 4, pp. 2307–2316, 2020.

[14] S. C. Chu, T. K. Dao, and J. S. Pan, "Identifying correctness data scheme for aggregating data in cluster heads of wireless sensor network based on naive Bayes classification," *EURASIP Journal on Wireless Communications and Networking*, vol. 2020, no. 1, 15 pages, 2020.

[15] J. Chu and W. Han, "Internet communication system protocol based on wireless sensor," *Radioelectronics and Communications Systems*, vol. 62, no. 8, pp. 422–429, 2019.

[16] H. Li and A. V. Savkin, "Wireless sensor networ kbased navigation of micro flying robots in the industrial Internet of Things," *IEEE Transactions on Industrial Informatics*, vol. 14, no. 8, pp. 3524–3533, 2018.

[17] S. Bhushan, M. Kumar, P. Kumar, T. Stephan, A. Shankar, and P. Liu, "FAJIT: a fuzzy-based data aggregation technique for energy efficiency in wireless sensor network," *Complex & Intelligent Systems*, vol. 7, no. 2, pp. 997–1007, 2021.

[18] S. P. Singh and S. C. Sharma, "A PSO based improved localization algorithm for wireless sensor network," *Wireless Personal Communications*, vol. 98, no. 1, pp. 487–503, 2018.

[19] B. Wang, X. Gu, L. Ma, and S. Yan, "Temperature error correction based on BP neural network in meteorological wireless sensor network," *International Journal of Sensor Networks*, vol. 23, no. 4, pp. 265–278, 2017.

[20] T. Y. Ling and Y. C. Chiang, "Well-being, health and urban coherence-advancing vertical greening approach toward resilience: a design practice consideration," *Journal of Cleaner Production*, vol. 182, pp. 187–197, 2018.

[21] H. Li, Y. Liu, C. Wu, and L. Jia, "Design method of green ecological building considering light environmental pollution," *Ekoloji*, vol. 28, no. 108, pp. 1301–1306, 2019.

[22] H. F. Si and Z. Yang, "Research of the application of virtual reality in green construction," *Advanced Materials Research*, vol. 462, pp. 592–597, 2012.

[23] S. Shao, A. Khreishah, and I. Khalil, "Joint link scheduling and brightness control for greening VLC-based indoor access networks," *Journal of Optical Communications and Networking*, vol. 8, no. 3, pp. 148–161, 2016.

[24] O. Franek and Č. Jarský, "On implementation of plants in the indoor environment in intelligent buildings," *Environmental Research, Engineering and Management*, vol. 77, no. 3, pp. 66–73, 2021.

[25] S. H. Alsamhi, O. Ma, M. S. Ansari, and Q. Meng, "Greening Internet of Things for greener and smarter cities: a survey and future prospects," *Telecommunication Systems*, vol. 72, no. 4, pp. 609–632, 2019.

[26] X. Jing, S. Li, J. Cheng, and J. Guo, "Multidimensional situational information fusion method for energy saving on campus," *Journal of Intelligent & Fuzzy Systems*, vol. 38, no. 4, pp. 4793–4807, 2020.

[27] G. S. Odiyur Vathanam, K. Kalyanasundaram, R. M. Elavarasan et al., "A review on effective use of daylight harvesting using intelligent lighting control systems for sustainable office buildings in India," *Sustainability*, vol. 13, no. 9, p. 4973, 2021.

[28] Y. Bai, W. Zhang, X. Yang, S. Wei, and Y. Yu, "The framework of technical evaluation indicators for constructing low-carbon communities in China," *Buildings*, vol. 11, no. 10, p. 479, 2021.

[29] G. Han, Y. Wen, J. Leng, and L. Sun, "Improving comfort and health: green retrofit designs for sunken courtyards during the summer period in a subtropical climate," *Buildings*, vol. 11, no. 9, p. 413, 2021.

Hindawi
Journal of Sensors
Volume 2022, Article ID 3683723, 11 pages
https://doi.org/10.1155/2022/3683723

Research Article

A Data-Driven Approach for Electric Energy Equipment Using Wireless Sensing Technology in the Context of Carbon Neutrality

Zichen Hu and Lixing Zhou

Changsha University of Technology, Hunan Changsha 410114, China

Correspondence should be addressed to Zichen Hu; wuwb@csust.edu.cn

Received 13 November 2021; Revised 8 January 2022; Accepted 17 January 2022; Published 10 February 2022

Academic Editor: Gengxin Sun

In this paper, we use wireless sensing technology to conduct an in-depth study and analysis of data-driven power energy equipment in the context of carbon neutrality. For the high-order uncertainty of renewable energy power generation and the nonlinearity of the tidal equation, a set of orthogonal bases under arbitrary probability space can be constructed by itself using the high-order information of renewable energy power generation statistics, and then, polynomials fit the state variables such as voltage in the tidal equation using the orthogonal bases and calculate the fitting parameters using the stochastic Gallatin integration method. Based on the analysis of the online monitoring project of the main power equipment in the substation, a substation power equipment condition monitoring system is designed to realize the real-time monitoring of the temperature status of power equipment, substation smoke and temperature, and humidity environment, and the feasibility and advanced of the system are verified by elaborating the analysis. Using wireless transmission to send real-time temperature information to the monitoring background, the infrared thermal imaging online monitoring system is designed around the front-end data acquisition system, transmission network, background data processing, and display module. Saving-investment equilibrium means that total investment equals total savings; government budget balance can be achieved through government savings or deficits. When both supply chain approaches enter into the same environmental competition, the added value that consumers value the product because of the carbon-neutral approach becomes smaller in the coefficient constraint of green effort investment cost due to the competition between the two supply chains, which in turn increases the green investment cost of the supply chain with the green effort carbon-neutral approach, indicating that in the case of competition, consumers, when faced with two products produced by two supply chains, are interested in the product with the carbon-neutral approach has less value-added, and some of the demand is shifted to the product not produced with the carbon-neutral approach.

1. Introduction

In the new round of global scientific and technological revolution and industrial upgrading, energy Internet has become the focus of competing development in the world, and accelerating the construction of energy Internet based on the smart grid is the necessary way to promote the common construction, cofinancing, and sharing of electric energy and the intelligent upgrading of the electric power industry, which is of great significance to enhance the competitiveness of equipment manufacturing industry [1]. The construction of intelligent substations has attracted wide attention from researchers. However, with the rapid growth of the scale of distribution automatic control, precise load control, and power consumption information collection of power grids; the gradual expansion of power grid control to the end; the increasing number of new businesses and applications such as distributed power supplies, clean energy, electric vehicles, and smart households, prompting a significant increase in the information collection points and collection volume of power communication systems; and the explosive growth of information collection demand for the security, reliability, real-time, ubiquity, and broadband have put forward higher requirements [2]. However, manual inspection requires a lot of workforce and time due to the large workload, and the quality of inspection is affected by subjective factors such

as the work experience of operation and maintenance personnel, making the monitoring results unreliable. It caused a huge threat to the personal safety of operation and maintenance personnel. And substation intelligent inspection robot instead of manual inspection to make up for the above defects and shortcomings greatly guarantees the objectivity and reliability of inspection, but inspection robot also has some shortcomings, such as expensive, monitoring accuracy and precision by the environment, and some equipment inspection by site restrictions. Based on the above factors, in the large-scale intelligent substation construction and transformation, real-time online monitoring of substation power equipment status comes into being, using practical sensing elements to continuously monitor power equipment in operation in real-time and obtain relevant data, and combined with certain expert system software to judge the operating status of the equipment and predict the remaining life of the equipment, to timely find the failure of power equipment precursors and provide data support for equipment maintenance [3]. The total operating time is about 2498.5 days or about 6.8 years. If the collection period is extended to 30 min/time, and the report is reported every 6 hours, the collection terminal can work continuously for more than 10 years. Condition monitoring of power equipment can greatly reduce equipment failure during the maintenance period; provide the technical basis for equipment maintenance, timely discovery of equipment defects, and abnormal symptoms; ensure safe operation of equipment; and improve power supply reliability.

In the process of achieving the 2050 carbon neutrality target, global carbon emissions will gradually rise to the highest value and then gradually achieve carbon-neutral growth and eventually achieve carbon neutrality completely [4]. From the perspective of the fashion supply chain, for a secondary supply chain consisting of a manufacturer and a retailer, the game theory approach is applied in the model to establish a noncooperative influence on the supply chain to construct different models of manufacturer-retailer profit demand inputs, and after a preliminary exploration of the supply chain performance after the application of carbon neutrality, the impact of the carbon neutrality approach on market demand, retailer pricing, manufacturer pricing, retailer, and manufacturer profits. We also consider the competition between two supply chain strategies without and with the carbon-neutral approach to explore the impact of the carbon-neutral approach on market demand when consumers have a choice of two products [5]. Finally, we examine the cost of green inputs and offsetting carbon neutrality concerning the intensity of environmental gains and losses, the environmental gains and losses due to carbon emissions under both approaches, and the change in the intensity of environmental gains and losses as a percentage of manufacturer revenue.

The achievement of energy conservation, emission reduction, and energy and environmental constraint targets cannot simply be rigidly achieved at the cost of slowing down economic growth but requires attention to internal adjustments. Energy consumption intensity, expressed by the amount of energy consumed per unit of output, reflects the degree of dependence of economic development on energy, as well as the efficiency of energy utilization. Reducing energy consumption intensity has long been one of the important ways to achieve energy conservation and emission reduction, and China's energy consumption intensity is still at a high level, with great reduction potential. Against the above background, this paper takes energy consumption intensity as the research object and studies the characteristics of changes in China's energy consumption intensity in terms of historical trends, volatility shocks, and industry elasticity, respectively. Secondly, the influencing factors of energy consumption intensity changes and their regional differences are further studied. Finally, the reduction rate of energy consumption intensity in the industry in the future is predicted, and the carbon emissions and carbon intensity reduction potential are predicted based on this. The study of the above issues can provide a basis for the formulation of energy conservation and emission reduction and energy efficiency improvement policies. The analysis of energy fee intensity at the regional level helps to understand spatial differences and to develop targeted policies for different regional development to gain competitive advantages. Overall, by studying the characteristics and connotations of energy consumption intensity and carbon emissions in China, this study can provide policymakers with feasible methods to solve practical problems from a scientific perspective and has significant practical significance and reference value for formulating energy economic policies, promoting low-carbon development, and implementing sustainable development strategies. It also helps to achieve the energy-saving and emission reduction targets set by the Chinese Government in an efficient and high-quality manner.

2. Related Works

Carbon neutrality, also known as offsetting carbon emissions, is a system that aims at carbon neutrality by planning and sorting out the processes that may generate carbon emissions, understanding the carbon emission levels of different parts of the system from multiple aspects, and then making the overall net carbon emissions of the system zero or keeping them within the scope of the system's target through carbon collection/capture [6]. The data-driven polynomial chaotic expansion method can be applied to the situation with limited statistical data. It is necessary to point out that the main difference between the generalized polynomial chaotic expansion method and the data-driven polynomial chaotic expansion method is that the calculation methods of the polynomial basis of the two are different. The former is selected from the Wiener-Askey mechanism, and the latter directly uses several moments of statistical data. Construct a polynomial basis. Only if these factors can have a reasonable range of values under the premise of the existence of optimal solutions can the goal of a green supply chain be achieved [7]. Therefore, the current problem of green supply chain channel selection and pricing is less related to the luxury industry but more a comprehensive study of channel selection plus energy efficiency, supply chain coordination, and uncertain environment [8].

The basic idea of wireless sensor networks first originated in the United States military to meet its own operational needs, the traditional sensors using point-to-point signal transmission, connected to sensing controllers, constituted the prototype of sensor networks in human history [9], that is, the distributed sensor network with comprehensive information processing ability, which uses modern micro sensor nodes to monitor the activities of the enemy. Subsequently, several studies on wireless sensor networks have been carried out, and corresponding results have been achieved [10]. Condition monitoring technology for substation power equipment is developing very rapidly, and most of the power equipment has developed various condition monitoring schemes to varying degrees [11]. Compared with preventive testing, condition monitoring systems use more sensitive sensors to collect insulation deterioration information in power equipment operation and rely on computer networks and rich software support to process and identify the information [12]. The online condition monitoring system uses some online preventive test programs to reflect the operating status of power equipment more accurately, to achieve a comprehensive diagnosis of the operating status of power equipment, and to promote the transition from periodic maintenance to condition maintenance of power equipment [13].

The stability of the renewable energy power generation system itself is not as stable as that of the traditional synchronous machine, and the system stability margin also fluctuates greatly when the system operating state changes randomly in a wide range, which makes it difficult to apply the system stability analysis results based on the determined operating state with small disturbances in practice. Considering that uncertainty is an inherent characteristic of renewable energy power generation systems and the common probability distribution model is difficult to accurately describe the uncertainties in the actual system, it is necessary to research the uncertainty analysis method of high proportional renewable energy power systems for higher-order uncertainties. The significance and necessity of condition monitoring of power equipment, the principle of infrared temperature measurement of power equipment, the development and application of wireless communication technology, and the progress of domestic and international research on wireless sensing network and substation power equipment condition monitoring technology are described, and the research on existing online condition monitoring technology of power equipment is elaborated.

3. Wireless Sensing Technology for Carbon-Neutral Data-Driven Analysis of Electric Energy Equipment

3.1. Design of Data-Driven Wireless Sensing Technology Based on. Various equipment in power systems often has abnormal temperature states due to the occurrence of equipment faults, and temperature monitoring using infrared thermography can diagnose the fault conditions of the equipment to a certain extent. However, in terms of the current development level, the application of infrared thermal imaging camera in power equipment condition monitoring has its one-sidedness, mainly for the power equipment internal diagnosis of certain faults; there are still some difficulties that need to cooperate with other conventional methods to make a comprehensive diagnosis of the fault [14], such as reading, writing, adding, and deleting. Permission means permission to perform these operations in a protected system and data source, such as publishing and subscribing. The distribution relationship between permissions and executive roles is a many-to-many relationship. LoRa technology is based on chirp pulse coded modulation, which has the low power consumption characteristic of FSK modulation used in traditional wireless communication technology and at the same time greatly improves the communication distance, minimizes power consumption, and saves transmission cost; LoRa adopts frequency hopping spread spectrum technology, and the link budget is as high as 157 dB, which makes its communication distance greatly increased.

The basic principle of the frequency hopping spread spectrum scheme is that part of each LoRa packet is sent through a hopping channel selected in a frequency lookup table managed by the microcontroller, and at the end of the scheduled hopping cycle, the transmitter and receiver switch to the next channel in the hopping predefined list to continue sending and receiving the next part of the packet. The frequency hopping transmitting and receiving process starts at channel 0 [15]. The preamble and header are first transmitted in channel 0. After the transmission is completed, the first interrupt signal is generated, and the microcontroller responds to the interrupt by jumping to channel 1 according to the preagreed frequency, and the first hop is completed. While jumping, the channel counter reading located in the register increases and generates an interrupt signal, and the microcontroller responds to the interrupt by jumping to channel 2 and repeating the above frequency hopping process. The frequency hopping reception process starts from channel 0. After the detection of the valid preamble code is completed, the receiver starts the above frequency hopping process as well.

$$w \approx \sum_{k} C_k^2 P_2^k(X), \tag{1}$$

where C_k^2 is a constant corresponding to the polynomial basis P_2^k.

Explicit header mode is the default mode of LoRa operation, in which the header contains payload information such as payload length in bytes and forward error correction code rate and whether optional 16-bit cyclic redundancy check is turned on. The header sends the payload information according to the maximum error correction code, including the payload length in bytes, the forward error correction code rate, and whether to turn on the optional 16-bit cyclic redundancy check. The header is sent following the maximum error correction code and additionally contains its cyclic redundancy check to cause the receiver to discard invalid header packets. In specific cases where the payload

length, coding rate, and cyclic redundancy checks are fixed or known, the implicit header mode is typically invoked to shorten the transmission time by manually setting the payload length, coding rate, and cyclic redundancy checks at both ends of the wireless link, as shown in Figure 1. In the profit of retailers, because the best results of carbon neutralization methods that do not use green inputs are numerical and lack the impact of the corresponding cost coefficient, only when the cost coefficient of green inputs is less than the added value of consumers to carbon neutral products the mathematical result of the coefficient.

The wireless sensing system mainly monitors the status of power equipment in real-time, and the sensor device and LoRa wireless communication module cooperate to realize the real-time collection of power equipment status data, and each sensor node in the system has a wireless communication function. The system is mainly composed of terminal nodes, gateway nodes, and a back-end equipment monitoring centre [16]. The overall structure of the LoRa wireless communication technology-based power equipment status monitoring system is shown in Figure 1. The LoRa gateway node is equivalent to a router, which can collect and process the information and transmit the processed information to the backend equipment monitoring centre to realize the management of each LoRa node; in the backend equipment monitoring centre, the operation and maintenance personnel can base on the real-time collected equipment status information and decide on the status of the power equipment. In the background equipment monitoring centre, operation and maintenance personnel can make timely judgments on the operation status of power equipment based on the real-time collected equipment status information to effectively avoid power equipment accidents and bigger disasters.

Since in traditional methods such as the generalized polynomial chaos expansion method, only orthogonal bases are considered for the probability space of independent univariate variables (e.g., Gaussian distribution); the original correlated multidimensional probability space needs to be removed from correlation by the Nataf transform before the generalized polynomial chaos expansion method can be used. In the framework of the generalized polynomial chaos expansion method, the orthogonal basis in the multidimensional probability space is the tensor product of the orthogonal bases of the independent univariate probability space.

$$P_2^k(X) = \prod_{i=1}^{n} K_i^2 P^{(k_1,k_2,\cdots,k_n)}(X), \tag{2}$$

where $P_2^k(X)$ represents the kth order polynomial basis associated with a one-dimensional random variable x; the main components of the terminal node are the sensor acquisition module, wireless communication module, microprocessor module, and power supply module [17]. The functions of the sensor acquisition module are mainly to use the ultrasonic signal sensor to receive the ultrasonic signal generated by radiation in the process of partial discharge to realize the online monitoring of partial discharge, to use the smoke sensor to monitor the smoke situation of the substation in real-time, and to use the temperature and humidity sensor to monitor the temperature and humidity situation of the substation in real-time; the wireless communication module refers to the use of LoRa wireless communication module to transfer the sensor module collected. The LoRa wireless communication module is used to transmit the data information collected by the sensor module to the LoRa gateway node; the power module provides energy supply to the whole terminal node module.

This part is the data guarantee of the big data platform. The data integration part is the foundation of the entire big data platform. It analyses the sources, characteristics, storage, and usage requirements of various types of big data in power and designs and adopts corresponding collection strategies, methods, tools, and interfaces according to its data characteristics. Since the Schmidt orthogonalization method constructs a set of orthogonal bases in a given inner product space from a set of bases in an arbitrary inner product space, a set of bases needs to be chosen as initial conditions. Without loss of generality, the initial polynomial basis is first chosen to be composed of linearly independent monomials concerning a d-dimensional random variable X and represented by a set, the elements of which are defined as follows.

$$e_j(X) = \prod_{i=1}^{n} X_i^2, j_i \in N, \tag{3}$$

where e is the maximum order of the polynomial basis; the goal of the energy Internet is to personnel social welfare services process, with the assistance of big data, can be based on the needs of consumers, the formation of their internal processes for in-depth reanalysis and redesign of interactive real-time feedback. Therefore, the process reengineering brought by the energy Internet is not ordinary resource allocation, but a deep management change, from the original one-way transmission of energy services, consumers passively accept to a two-way interactive intelligent network, including not only the consumer orientation of the energy provider but also the adaptation of consumers to the emerging energy network, until reaching a dynamic balance between the two sides of the common demand, as shown in Figure 2.

Power station big data sources are mainly defined as data from various business systems or offline measurements in the current power production process, and professional data from cross fields and qua industries such as meteorological data, demographic data, and urban planning data may be accessed in the future. Grid control is gradually expanding to the end. The increasing number of new services and applications such as distributed power, clean energy, electric vehicles, and smart homes has greatly increased the information collection points and collection volume of the power communication system, and the demand for information collection has exploded. The security, reliability, real-time, ubiquity, and broadbandization of smart grids put forward

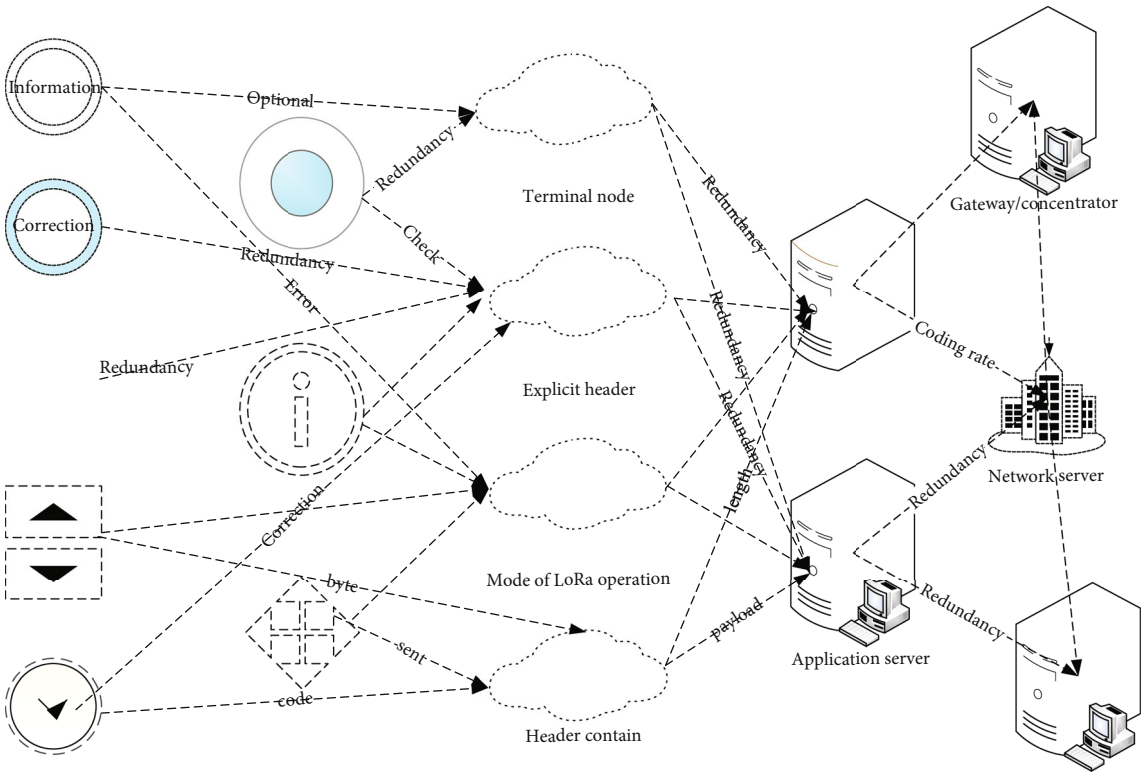

Figure 1: LoRa WAN network architecture.

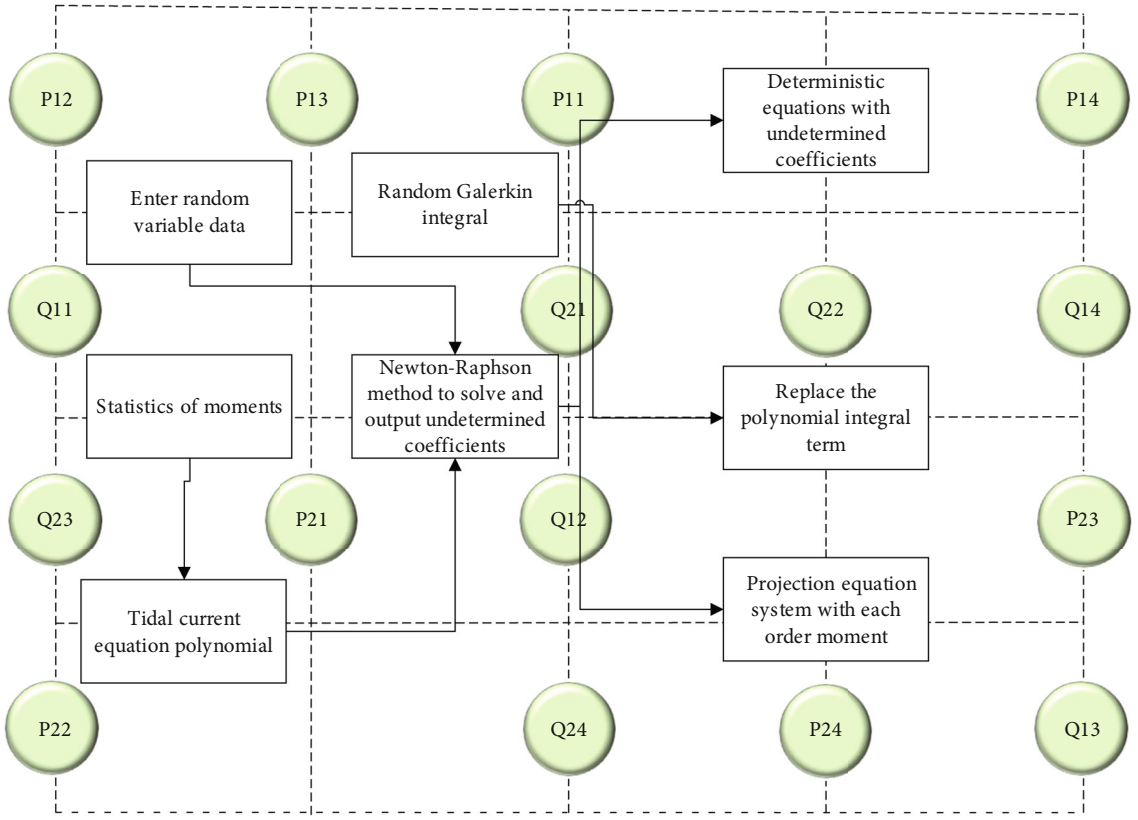

Figure 2: Data-driven design.

higher requirements. These data types not only contain a large amount of structured data but also more unstructured data such as documents and images, which is the data guarantee of the big data platform. The data integration part is the foundation of the whole big data platform, which deeply analyses the sources, characteristics, storage, and usage requirements of various types of power big data and designs and adopts corresponding collection strategies, methods, tools, and interfaces according to their data characteristics, to ensure the integrity and efficiency of the big data collection process. Data integration technology mainly uses message queues, data import tools, data extraction tools, data replication tools, and other methods to realize structured/unstructured, massive historical/real-time/quasi-real-time, and internal/external data access.

Considering that there is a weak local discharge signal when partial discharge monitoring is carried out, at this time, to improve the reliability of partial discharge monitoring, it is necessary to use a high-gain amplifier to amplify the original output ultrasonic signal; this design uses a multistage amplification circuit to amplify the useful information in the sensor acquisition signal and suppress noise interference, improve the signal-to-noise ratio of the system, and ensure the whole analogy channel bandwidth, at the same time by the influence of the substation monitoring environment interference, the need to apply band-pass filtering of the acquisition signal in the environmental noise and other filtering processing, and the effective filtering of the monitoring site interference signal.

3.2. Carbon Neutral Electric Energy Equipment Data-Driven Analysis. The status information data of the power equipment collected by each monitoring node is received by the wireless transceiver module of the gateway node and sent to the microprocessor module through its serial port, and the microprocessor module receives this data information for corresponding processing, and the processed data transmits the data information to the upper computer through the USB to the serial port [18]. The data acquisition module is completed by two modules: the sensor module and the microprocessor. The sensor mainly collects analogy current signals and needs to be able to collect multiple data at the same time; the main controller module is mainly responsible for controlling the status of the sensor and processing the collected data. The interconnection between the energy Internet has a more complex energy transfer relationship. The energy supply of the energy internet can be produced either within the region or from other regions. Similarly, on the energy consumption side, the energy produced in the region can be consumed as well as energy supplied by other regions. When the energy supply within the region is greater than the energy demand, energy can be exported through the energy transmission pipeline to supply energy to other regions to achieve interregional energy interconnection optimization and coordinated operation. Therefore, the energy Internet has the characteristics of the bilateral flow of energy between electrical and other forms of energy and the coordinated and optimal allocation of energy across regions. Practical sensor elements are used to continuously monitor the power equipment under operating conditions in real time and obtain relevant data, combined with certain expert system software to judge the operating status of the equipment and predict the remaining life of the equipment.

$$Y_t = \alpha - \sum_{i=1}^{p} \beta_i^2 Y_{t-1} + \varepsilon_t^2, \tag{4}$$

where Y is the k-dimensional endogenous variable and is the k-dimensional error vector and $\beta_i^2 Y_{t-1}$ is the matrix of coefficients to be estimated. In practical applications, the VAR model is more theoretical than empirical. At the same time, the VAR model can estimate the lagged terms of all endogenous variables, describing the dynamic correlation between them. Using this model, it is possible to analyse the impact of a shock on the system dynamics when the model encounters shock. The impulse response function can test for this "contagious" diffusion effect [19]. The impulse response function reflects the behaviour of the variables themselves, as well as other variables in the system, when the errors in the system subjected to a shock, and the impact on their future performance, etc. Using variance decomposition, the degree of influence of each structure on the endogenous variables can be analysed to further evaluate the importance of different structural shocks. This approach can verify the evolution of the dynamic behaviour of the variables over time. However, the VAR model also has drawbacks, as the model construction is not based on actual economic theory and lacks structural constraints imposed on the variables of interest, resulting in variable estimation and correlation tests that are often not accurate enough. Also, when major shocks occur, the VAR model is not stable, resulting in an impulse response function that is not unique, as shown in Figure 3.

Fuel transfer personnel should pay attention to the dynamic information of the production and transportation links in the mine in real-time, do a good job of docking with the information of receiving and unloading and storage in the plant, and communicate and coordinate well to ensure the normal and smooth operation of all links of shipping, transportation, and coal unloading. With the goal of not incurring demurrage as much as possible, we should grasp the berth and leaning dynamics of loading port in real-time, reasonably transfer vessels, and the efficiency of unloading port should be improved year by year. Employees with strong execution should be selected as shunting staff, which should be adequately equipped and zoned to ensure that the plan is executed. Game theory is used in the model to establish supply chain structure under noncooperative influence. Different manufacturers and retailers profit demand input models, after preliminary exploration of the supply chain performance after carbon neutrality and application.

$$\beta \geq \frac{(1-\theta)(1+\varepsilon)}{6\theta}. \tag{5}$$

Using the optimal results for the supply chain without the green effort carbon-neutral approach in a noncompetitive environment, we can see that only a quarter of the

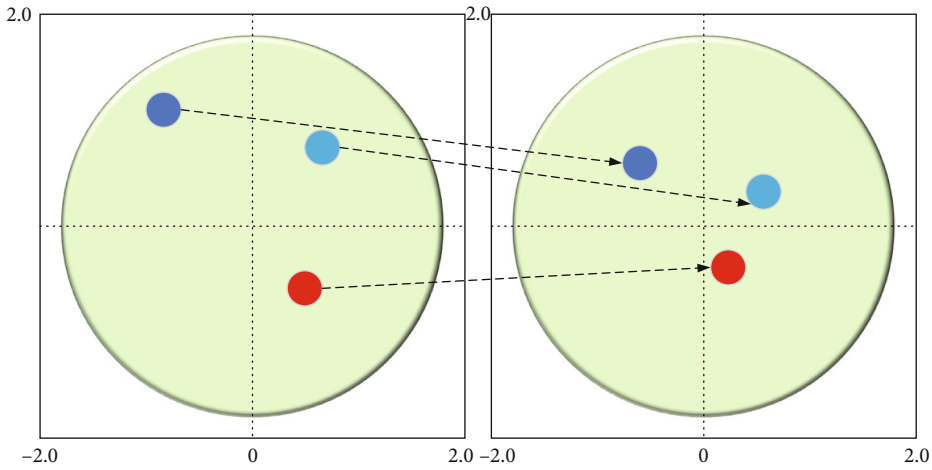

Figure 3: AR root test plot.

market demand is met, the green effort is zero relative to the supply chain with the carbon-neutral approach, carbon emissions are not reduced by any measures at the production stage, the cost of offsetting carbon emissions depends on consumer demand, and the intensity of environmental gains and losses is the greatest, suggesting that manufacturers' profit maximization and sustainability are opposites. In the comparison of individual items, except for the retail price and wholesale price where we can visually compare the size, in market demand, manufacturer's profit, and retailer's profit, because the optimal results of the carbon-neutral approach without green inputs are numerical and lack the influence of the corresponding cost coefficients, the cost coefficients of green inputs can only be reduced if they are smaller than the mathematical results containing the added value coefficients of consumers to carbon-neutral goods. The cost coefficients of carbon emissions are in the constraint of the cost coefficients of green inputs, so that the performance of one of the outcomes of market demand, manufacturer, and retailer can be optimized. But in a comparison of two supply chains collectively, only the smallest needs to be chosen as the benchmark for comparison to obtain consistent results for market demand, manufacturer, and retailer sizes.

Roles represent a set of access rights, and the node-to-role assignment relationship is a many-to-one relationship [20]. A node can be granted only one execution role; however, a role can be assigned to multiple nodes. A node that is a publisher will be granted an execution role based on the topic, and if it is a subscriber, it will be granted its corresponding execution role based on the agent. Publishers of different topics will need different permissions to handle data and resources. Operations mean different commands to be executed on the data source, such as read, write, add, and delete. Permissions denote permission to perform these operations in a protected system and data source, such as publish and subscribe. The relationship between permissions and the assignment of executive roles is a many-to-many relationship. Thus, the system can assign multiple access rights to a role. The publisher role is granted publish-related permissions, and the subscriber is granted subscription-related permissions.

$$S_k^a(u,v) = \frac{1}{n}\sum_{i=1}^{m} P_2^k(u,v). \tag{6}$$

In different cases, we can adjust the structure and attribute similarity weights. If the attribute information is more helpful than the structure information for interest prediction, S_k^aset to greater than 0.5 nodes in the same community are more likely to have similar interests. The more common communities, the higher the likelihood that nodes have similar interests, i.e., the higher the similarity, as shown in Figure 4.

The method of carbon neutral will have an impact on market demand. Finally, it studies the green investment and the cost of offsetting carbon neutrality according to the intensity of environmental gains and losses and discusses the environmental gains and losses caused by carbon emissions under the two methods and the changes in the proportion of environmental gains and losses in the manufacturer's income. It is necessary to point out that the main difference between the generalized polynomial chaos expansion method and the data-driven polynomial chaos expansion method is that the polynomial bases of the two are computed differently that the former is chosen from the Wiener-Askey mechanism and the latter constructs the polynomial bases directly using the information of several order moments of the statistical data.

Although the generalized short-circuit ratio of a power electronic multifeeder system can analyse the system's small disturbance stability margin analytically, however, the system is subject to random fluctuations of renewable energy power and uncertainty in the stability margin during operation. The generalized short-circuit ratio determined under deterministic operating conditions cannot quantify the small disturbance stability margin under stochastic conditions. Therefore, calculating the small disturbance probabilistic

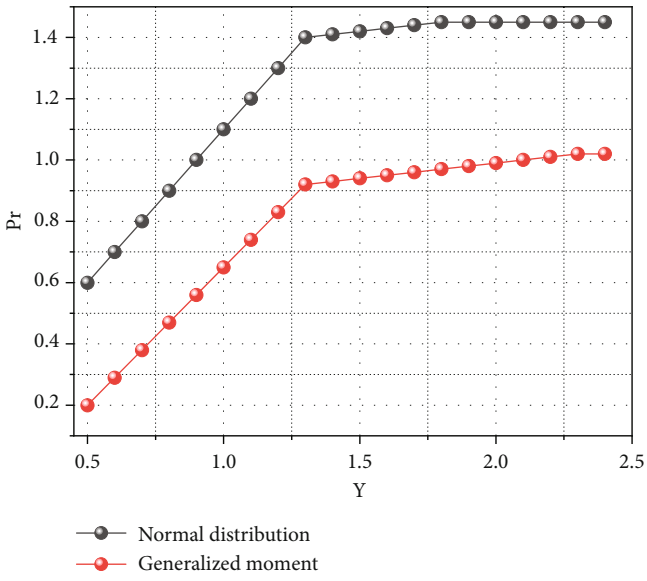

Figure 4: Comparison of generalized moments and normal distribution results.

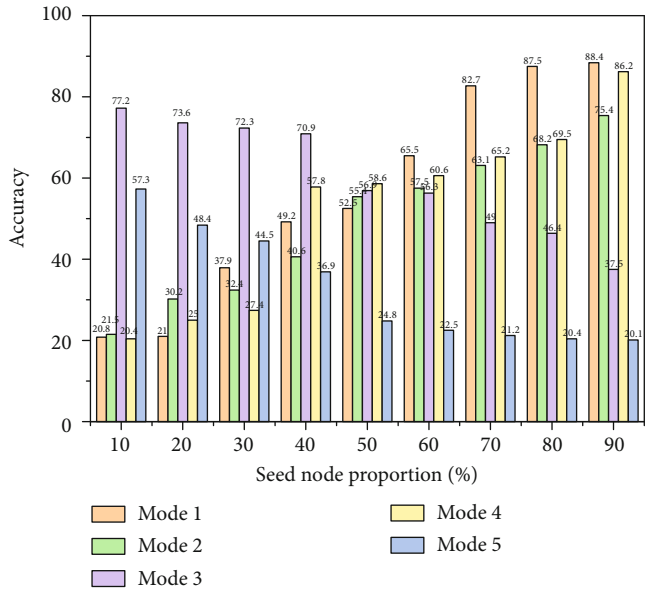

Figure 5: Effect of seed node ratio on accuracy.

stability margin for multifeeder systems is important for the dynamic stability assessment of multifeeder systems.

4. Results and Analysis

4.1. Data-Driven Wireless Sensing Performance Results. Figure 5 demonstrates the effect of the proportion of seed nodes on prediction accuracy. The initial probability distribution of interest is predicted based on the interest of the seed nodes within the community, and after updating the algorithm iteratively, a significant improvement in prediction accuracy is achieved. Due to the randomness of seed node selection, the initial accuracy showed a decrease in the 40% to 50% interval. However, the final performance was improved after the update iterations, proving the robustness of the model. As the percentage of seed nodes increases, the prediction accuracy also becomes higher.

The results of comparing this paper's work with other models shown to verify the importance of overlapping communities on prediction accuracy. The most significant difference between the models is the calculation of similarity in the overlapping communities. In this paper, the combined similarity of nodes under overlapping communities is higher than the similarity computed in individual communities. Through the analysis of the intensity of energy charges at the regional level, it is helpful to understand spatial differences, formulate targeted policies for the development of different regions, and gain competitive advantages. In Models 1 and 2, the combined similarity is the maximum and minimum similarity under common communities, respectively. Model 3 does not consider community division, and all nodes are in one large community. The testing of the communication function of the terminal shows that the communication module works properly. Then, the power consumption of the terminal system needs to be tested in combination with hardware and software. From the power consumption analysis, it is known that the test includes the current in the sleep state of the acquisition terminal, the current in the acquisition state, and the current during data upload, and the current consumption in these states directly determines the power consumption performance of the remote acquisition terminal. The terminal needs a certain discharge time to enter the sleep state from the working state, and it takes about 2 minutes for the terminal to be completely discharged after the discharge voltage test by the voltmeter; therefore, after entering the sleep state, the terminal needs to ensure at least 2 minutes of sleep time, and the power consumption test is shown in Table 1.

The acquisition terminal designed in this paper accesses the hibernation state immediately after processing data and is in the sleep state when there is no work, and the set terminal has no standby power consumption, and the standby power consumption of the terminal is negligible. Therefore, the power consumption of the remote acquisition terminal is composed of three parts: the sleep state, the data acquisition state, and the data upload state. In actual application, assuming that the acquisition cycle of the remote acquisition terminal is 15 minutes/time and the upload cycle is 6 hours/time, the remote data acquisition terminal consumes about 13717.772 mA∗s of electric energy in the acquisition state, 372.211 mA∗s of electric energy in the sleep state, and 591.907 mA∗s of electric energy in the transmission state every day, so the total daily electric energy consumption of the acquisition terminal is about 14678.772 mA∗s. Therefore, the total daily power consumption of the collection terminal is about 14678.89 mA∗s. Minimize power consumption and save transmission costs; LoRa adopts frequency hopping spread spectrum technology, and the link budget is as high as 157 dB, which greatly increases its communication distance.

The collection terminal adopts the lithium battery of the EAST'FIR brand, the specification of which is 3.7 V∗

Table 1: Measurement data sheet.

Group	Sleep state (μA)	Sleep state (μA)	Sending status (mA)
1	34.5	78	86.9
2	53.1	42.5	39.4
3	86.2	60.5	71
4	83.9	31.7	41.4
5	74.6	34.5	59.7
6	57.8	58.6	55.5
7	56.8	42.7	64.6
8	54.6	46.9	80.5
9	25	81.7	89.1
10	45.2	21.3	69.6

9800 mAh. Taking this power supply as an example, it can be calculated that the total time that the low-power collection terminal can operate is about 2498.5 days, i.e., about 6.8 years. If the acquisition cycle extended to 30 min/time and reported every 6 hours, the acquisition terminal can work continuously for more than 10 years. The calculation results show that the designed NB-IoT-based low-power remote acquisition terminal can meet the operating index requirement of more than 5 years of operation. For the low-power acquisition terminal device, the device is in the dormant state for a long time, so the power consumption level of the sleep state is of vital significance and is an important indicator of the low-power performance of the remote acquisition terminal.

5. Carbon Neutral Electric Energy Equipment Data-Driven Results

The development of the energy Internet is not an easy task in terms of the specific technologies needed for its discovery and must require a high level of technical support. Without the perfection of these technologies, the maturation and large-scale application of the energy Internet is unlikely to be successful. Therefore, to achieve significant development of the energy Internet, it is necessary to carry out large-scale technological innovation and breakthrough the core technical limitations of these applications, to successfully carry out large-scale commercial applications and promotion. The development of the energy Internet requires a high degree of technical difficulty and spans a wide range of industries that cannot be accomplished by a few companies. Therefore, technological innovation in the energy Internet industry is a huge and complex system project, which requires cross-border cooperation among different industries and enterprises, as well as the formation of closer technological innovation alliances among enterprises and industries, to jointly carry out technological innovation activities around the core technology of the energy Internet, promote the innovation and change of energy science and technology, and drive the great development of energy Internet-related industries.

To clarify whether carbon trading has a significant impact on corporate renewable energy development, it is necessary to compare the difference in the degree of corporate renewable energy development before and after the implementation of the carbon trading market. However, many factors can have some impact on corporate renewable energy development, such as firm size, the number of patents, the share of technicians, environmental regulations, and market share. The development of corporate renewable energy may be based on government subsidies to companies, which reduce investment costs and thus promote their development, or companies may sell their excess carbon allowances in the carbon trading market to gain additional revenue, thus reducing costs and promoting their development. The header sends the relevant information of the payload according to the maximum error correction code, which mainly includes the payload length expressed in bytes and the forward error correction code rate and whether the optional 16-bit cyclic redundancy check is turned on. Therefore, it is necessary to use the double-difference method to test whether it is because the establishment of the carbon trading market has had an impact on the development of renewable energy by firms, as shown in Figure 6.

This module mainly covers product market equilibrium, saving-investment equilibrium, government budget balance, and balance of payment equilibrium and follows neoclassical macro closure conditions. According to neoclassical theory, investment and all prices are endogenously determined by the model, and labour and capital fully utilized, which is also referred to as factor market equilibrium. Specifically, product market equilibrium requires that aggregate supply and demand for goods are balanced; factor market equilibrium includes equilibrium in labour and capital markets; saving-investment equilibrium means that aggregate investment equals aggregate savings, and government budget equilibrium can be achieved by government savings or deficits. In addition, the balance of payments is defined as imports equalling exports plus net inflows of foreign capital.

The humidity of the substation environment can effectively reduce the floating sink existing in the air of the substation and reduce the harm to the operation of the equipment, while the substation power equipment needs to be in a suitable temperature environment to achieve normal and stable work, so a suitable temperature and a humidity environment are important to ensure the long-term stable work of the entire substation power equipment, and it is necessary to monitor the temperature and humidity environment of the substation. The results of satisfaction assessment based on confidence uncertainty are shown in Figure 7 and the trends of the predicted happy probability distribution, uncertainty, and unhappy probability distribution in satisfaction. The experimental results show that the uncertainty decreases with the increase of trip records.

Given the high-order uncertainty of the renewable energy power and the nonlinearity of the tidal equation, a set of orthogonal bases in any probability space can be constructed by using the high-order moment information of the renewable energy power statistics, and then, the orthogonal bases can be used to polynomials fit the voltage and other state variables in the tidal equation, and the fitted parameters are calculated by the stochastic integration method.

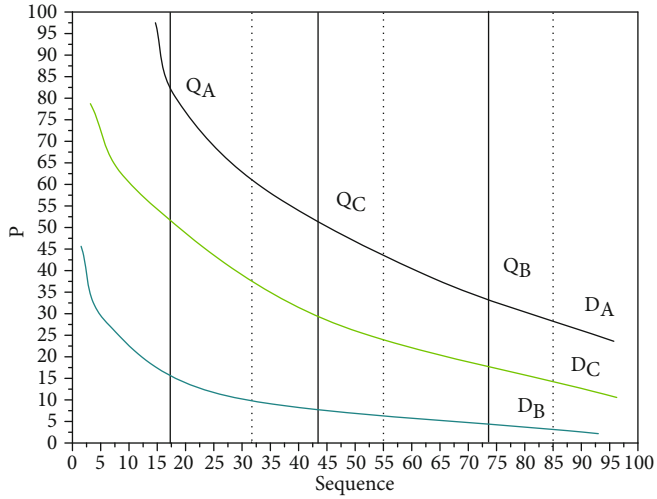

Figure 6: Carbon emission results.

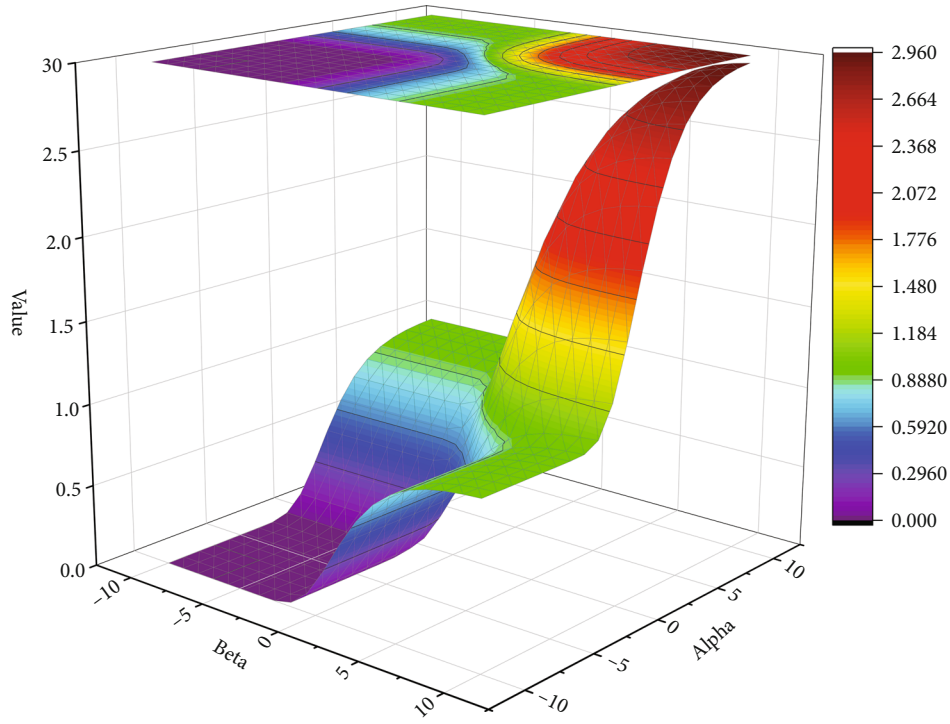

Figure 7: Data-driven results for electric energy equipment.

The analysis of the algorithm shows that the proposed method can effectively handle the stochastic tidal analysis with correlation and is more accurate than the traditional transformation method.

6. Conclusion

A time series-based structural vector autoregressive model, combined with impulse effect function and variance decomposition methods, is used to study the fluctuation characteristics of energy consumption intensity and the dynamic impact of energy structure on energy consumption intensity changes and the degree of shocks. Realize the online monitoring of partial discharge, use the smoke sensor to monitor the smoke condition of the substation in real time, and use the temperature and humidity sensor to monitor the temperature and humidity condition of the substation in real time; the wireless communication module refers to the use of the LoRa wireless communication module to transmit the data information collected by the sensor module to LoRa gateway node. The information advantage and trading platform of the energy Internet, the sharing economy derived from it, also optimize the allocation of resources. As the energy Internet perfectly bridges the gap between energy demanders and energy producers, it allows

some energy consumers to share part of their temporarily inexhaustible energy with energy demanders through the energy Internet. On the one hand, incentive policies are used to increase the motivation of enterprises to take the initiative in technological innovation, energy-saving, and emission reduction and to guide them to invest more money and energy in low-carbon production through the establishment of preferential policies. On the other hand, it regulates industry behaviour through binding policies, promotes the establishment of environmental management standards for enterprises, and strengthens the access threshold for key industries such as high energy consumption and high pollution.

Data Availability

The data used to support the findings of this study are available from the corresponding author upon request.

Conflicts of Interest

The authors declare that they have no known competing financial interests or personal relationships that could have appeared to influence the work reported in this paper.

Acknowledgments

This work was supported by the Changsha University of Technology.

References

[1] T. Kannan, C. Lork, W. Tushar et al., "Energy management strategy for zone cooling load demand reduction in commercial buildings: a data-driven approach," *IEEE Transactions on Industry Applications*, vol. 55, no. 6, pp. 7281–7299, 2019.

[2] B. Yan, F. Hao, and X. Meng, "When artificial intelligence meets building energy efficiency, a review focusing on zero energy building," *Artificial Intelligence Review*, vol. 54, no. 3, pp. 2193–2220, 2021.

[3] M. A. Sadeeq and S. Zeebaree, "Energy management for Internet of Things via distributed systems," *Journal of Applied Science and Technology Trends*, vol. 2, no. 2, pp. 59–71, 2021.

[4] X. Zhang, J. Wang, J. Vance, Y. Wang, J. Wu, and D. Hartley, "Data analytics for enhancement of forest and biomass supply chain management," *Current Forestry Reports*, vol. 6, no. 2, pp. 129–142, 2020.

[5] C. S. Lai, Y. Jia, Z. Dong et al., "A review of technical standards for smart cities," *Clean Technologies*, vol. 2, no. 3, pp. 290–310, 2020.

[6] W. Tushar, N. Wijerathne, W. T. Li et al., "Internet of Things for green building management: disruptive innovations through low-cost sensor technology and artificial intelligence," *IEEE Signal Processing Magazine*, vol. 35, no. 5, pp. 100–110, 2018.

[7] Z. Y. Dong, Y. Zhang, C. Yip, S. Swift, and K. Beswick, "Smart campus: definition, framework, technologies, and services," *IET Smart Cities*, vol. 2, no. 1, pp. 43–54, 2020.

[8] O. Inderwildi, C. Zhang, X. Wang, and M. Kraft, "The impact of intelligent cyber-physical systems on the decarbonization of energy," *Energy & Environmental Science*, vol. 13, no. 3, pp. 744–771, 2020.

[9] G. Deconinck and K. Thoelen, "Lessons from 10 years of demand response research: smart energy for customers?," *IEEE Systems, Man, and Cybernetics Magazine*, vol. 5, no. 3, pp. 21–30, 2019.

[10] M. S. Stein, M. Neumayer, and K. Barbé, "Data-driven quality assessment of noisy nonlinear sensor and measurement systems," *IEEE Transactions on Instrumentation and Measurement*, vol. 67, no. 7, pp. 1668–1678, 2018.

[11] C. L. Gargalo, I. Udugama, K. Pontius et al., "Towards smart biomanufacturing: a perspective on recent developments in industrial measurement and monitoring technologies for bio-based production processes," *Journal of Industrial Microbiology & Biotechnology: Official Journal of the Society for Industrial Microbiology and Biotechnology*, vol. 47, no. 11, pp. 947–964, 2020.

[12] J. A. Sanguesa, V. Torres-Sanz, P. Garrido, F. J. Martinez, and J. M. Marquez-Barja, "A review on electric vehicles: technologies and challenges," *Smart Cities*, vol. 4, no. 1, pp. 372–404, 2021.

[13] W. Zhang, N. B. Tooker, and A. V. Mueller, "Enabling wastewater treatment process automation: leveraging innovations in real-time sensing, data analysis, and online controls," *Environmental Science: Water Research & Technology*, vol. 6, no. 11, pp. 2973–2992, 2020.

[14] S. Mustapha, Y. Lu, C. T. Ng, and P. Malinowski, "Sensor networks for structures health monitoring: placement, implementations, and challenges—a review," *Vibration*, vol. 4, no. 3, pp. 551–584, 2021.

[15] T. Alam, "Cloud-based IoT applications and their roles in smart cities," *Smart Cities*, vol. 4, no. 3, pp. 1196–1219, 2021.

[16] A. I. Torre-Bastida, J. Del Ser, I. Laña, M. Ilardia, M. N. Bilbao, and S. Campos-Cordobés, "Big data for transportation and mobility: recent advances, trends and challenges," *IET Intelligent Transport Systems*, vol. 12, no. 8, pp. 742–755, 2018.

[17] J. P. Giraldo, H. Wu, G. M. Newkirk, and S. Kruss, "Nanobiotechnology approaches for engineering smart plant sensors," *Nature Nanotechnology*, vol. 14, no. 6, pp. 541–553, 2019.

[18] S. Aslam, M. P. Michaelides, and H. Herodotou, "Internet of ships: a survey on architectures, emerging applications, and challenges," *IEEE Internet of Things Journal*, vol. 7, no. 10, pp. 9714–9727, 2020.

[19] A. S. Syed, D. Sierra-Sosa, A. Kumar, and A. Elmaghraby, "IoT in smart cities: a survey of technologies, practices and challenges," *Practices and Challenges. Smart Cities*, vol. 4, no. 2, pp. 429–475, 2021.

[20] B. Anthony Jnr, "Smart city data architecture for energy prosumption in municipalities: concepts, requirements, and future directions," *International Journal of Green Energy*, vol. 17, no. 13, pp. 827–845, 2020.

Hindawi
Journal of Sensors
Volume 2022, Article ID 1841066, 12 pages
https://doi.org/10.1155/2022/1841066

Research Article

Optimization and Simulation of a Dynamic Management System for Building Construction Based on Low-Power Wireless Sensor Networks

Ning Qi

School of Architecture and Design, Changchun Institute of Technology, Jilin Changchun 130021, China

Correspondence should be addressed to Ning Qi; jz_qn@ccit.edu.cn

Received 10 November 2021; Revised 18 January 2022; Accepted 22 January 2022; Published 9 February 2022

Academic Editor: Gengxin Sun

In this paper, we use a low-power wireless sensor network to conduct in-depth research and analysis on the optimization simulation of the dynamic management system of building construction and study the specific application of BIM technology in the information management of building construction sites. By analysing the classical delustering routing and combining the advantages in the delustering routing protocols, we propose a two-level Mesh wireless sensor network delustering routing protocol in terms of cluster head uniformity, energy consumption and balance, working mode, and handling of isolated nodes. The most important feature of this protocol compared to other delustering protocols is that it retains the design of flat network topology and designs three routing methods with the corresponding functions of wireless sensor networks to achieve better network performance. The supported personnel location technology and construction measures and environmental monitoring technology are introduced, the applicability of the technology in the building construction process is compared and analysed, the topology of construction measures and environmental monitoring technology is designed, and finally, the targeted development of the collection scheme for personnel, scaffolding, formwork, pits, cranes, construction hoists, and physical environment is completed. Firstly, it analyses the development status of BIM-based building construction site information management technology and application and discusses the basis of BIM technology implementation and the advantages of BIM technology application in information management. Then, this paper constructs the framework of a BIM-based building construction site information management system from three dimensions: functional, logical, and physical. To ensure the realizability and operability of the system, this paper discusses the operation mechanism of the BIM-based building construction site information management system, studies the key technology of system operation, designs the basic operation process of each application system of the system, and elaborates the organizational structure of the building construction site and the functional division of the relevant personnel.

1. Introduction

The construction industry is a labour-intensive industry; its operating environment is complex; there are more unsafe factors; the volume of the production of construction products is large; the operating time is long; there are many types of safety accidents at construction sites; and falls from height, object strikes, mechanical injuries, collapses, and electric shock are the five major injury accidents in the construction industry. Falls from height are the most frequent type of accident, accounting for 53% of accidents, followed by object strikes. The probability of safety accidents becomes greater because safety managers alone cannot detect safety hazards and solve them in time by relying on on-site inspections, while the probability of safety accidents becomes greater due to the rapid renewal of personnel in the construction industry and low safety awareness of personnel and formal safety education of workers by managers [1]. Competition will inevitably occur, resulting in the failure of some of the data to be sent, and the data must be sent through multiple retransmissions. Construction safety accidents not only bring huge loss of life and property to society, enterprises, individuals, and their families but also bring serious negative impacts to the image

of enterprises and social stability. The economic losses caused by safety accidents include not only the compensation costs for the families of the accident victims, the rescue and medical costs, and the costs of accident penalties but also the losses caused by the stoppage of work due to the accident and the losses caused by the replacement of workers [2]. The low level of attention to technological innovation in construction technology and management and the low investment in technological research has left the development of construction technology in a stagnant state [3]. Most of the construction machinery and safety protection used in construction currently have no essential improvements, and the way of safety management is almost indistinguishable from before, leading to a lack of safety control on site. The use of emerging technologies in the construction industry can shift the focus of safety management to the prior, to achieve preventive management, based on emerging technologies of safety warning management can not only monitor in real-time human behaviour and the state of things the identification of unsafe factors in construction and early warning but also serve as a platform for safety management, to support other safety management-related work content, such as safety education, safety training, and safety records.

Safety is not just an issue for the construction industry but also an issue that needs to be a key concern for the whole society. Modern information technology is developing at a high speed, bringing immeasurable impact to the construction industry, so construction safety management needs the information technology industry to assist and to develop a clear strategic plan when the country builds a construction safety system. This paper delves into the application of construction safety management based on BIM technology, exploring how the use of building information modelling can make the construction safety management level improve, prevent and reasonably control the safety accidents that occur with the construction site in advance, and promote the construction industry to the road of sustainable development [4]. The construction industry is in a state of rapid development, and the characteristics of modern buildings are reflected in the large volume, large span, complex structure, and deep foundation, resulting in a higher accident rate in the construction stage. BIM technology applied in the construction stage can effectively find out the safety hazards and danger sources in construction management and technology and deal with the construction safety hazards through simulation [5].This paper deeply analyses BIM technology application management and engineering safety management, which makes it possible to further improve the relevant safety management procedures; improve and adjust safety programs and safety plans several times which can make the rate of safety accidents before and during construction decrease; meet the national construction development policy; promote construction informatization; strengthen the information communication between building designers, owners, and construction, etc.;and reduce the cost of resources invested. Information technology should be used throughout the whole period of construction and maintenance.

Due to the complex and variable operating environment faced by the passive sensing nodes, the magnitude of the input signal faced by the power amplifier is not stable and constant. In this case, the overall efficiency of the amplifier over the entire input signal power range becomes more important than the optimal efficiency. To improve the overall amplifier efficiency, this paper proposes a method for input RF power monitoring and intelligent control of the bias voltage. Based on ensuring that the amplifier itself has a high peak efficiency, its efficiency in the case of a small signal input is improved by intelligent bias control techniques. WSNs are typically task-based networks with the data collected by all nodes in the network as the core, and WSNs are generally said to be data-centric networks. WSN can also serve as a good backbone network in the monitoring area under the condition of restricted communication methods, and if it can be converged with other networks, it can carry more functions and enhance the flexibility of WSN. The construction personnel and management personnel on the construction site need a lot of construction information to support the construction activities. The use of a protocol conversion interconnection scheme is more convenient; you need to complete the protocol conversion between the interconnection nodes while providing the appropriate support in the backbone network protocol. Therefore, you can let the WSN in the sensing nodes as interconnection nodes to complete the protocol conversion, while designing the corresponding WSN routing protocol. In terms of protocol design, the focus should be on adding network convergence support and extending the network lifetime of WSNs. With the network fusion of WSN as the research objective and the optimization direction of improving the energy usage efficiency, the WSN routing protocols applicable in different applications are proposed. Through protocol design and optimization, simulation testing, and physical testing, the convergence of WSNs with individual domain networks is achieved. This paper tentatively explores the field of WSN network convergence and further verifies the feasibility of WSN network convergence through hardware platforms in addition to simulation and explores the potential applications of WSN as a backbone network for monitoring areas.

2. Related Works

Among the many technical difficulties of wireless sensor networks, the most important one is the characteristic of their limited energy supply. In recent years, wireless sensor networks have been facing many challenging problems in the process of rapid development, among which, energy consumption is the core issue, which is one of the main differences between wireless sensor networks and traditional wireless networks [6]. Traditional wireless networks are mainly focused on meeting the increasing requirements of users for network service quality, and the energy of its network equipment terminals can be replenished, and the energy consumption is not the main issue that restricts the development of network technology. In contrast, due to the

limited energy supply of the nodes, the energy of the nodes becomes the biggest factor limiting their continued development [7]. Once the node energy is exhausted, the node will stop working immediately. To be able to extend the life of the node, it is necessary to improve the efficiency of the entire node for energy utilization. The battery is the core of providing energy to the node; however, the technology level of the battery is relatively slow to develop, and in the past long time, the energy density of the battery has improved to a very limited level [8]. Therefore, in addition to using environmental energy such as solar energy, mechanical energy, wind energy, electromagnetic energy, vibration energy, and temperature difference energy to supplement the node battery energy, so that the node will achieve a certain degree of self-power, the main way is to reduce the energy consumption of wireless sensing nodes or wireless sensing nodes for low-power design [9]. Therefore, research on low-power technologies for nodes in wireless sensing networks is important to promote the level of performance of wireless sensing networks revealing that the chain reaction of factors with cause-and-effect relationships is the basic process that causes accidents and has a great impact on safety management [10].

Scholars are more advanced in their research on safety management and have developed visual 4D technology models to link personnel in various departments thereby increasing team safety awareness. Traditional construction safety management systems and practices are analysed, and a cloud-based safety information and communication system is designed and developed using a free online web server with features including preinitiation safety meeting minutes, access requests and approvals, job safety analysis, and safety incident reporting, and prospects for cloud computing in construction safety management are indicated [11]. At the same time, the transmission is fast and the information fidelity is high. However, due to the need for cables to be laid in the monitoring area, it is difficult to arrange the monitoring sites with complex environments. At the same time, maintenance during the later period is also difficult. The idea of establishing a set of construction safety management systems based on China's national conditions is proposed, and how to do a good job of construction safety management in China is analysed from the legal level, political level, economic level, and cultural level. Some scholars believe that the development of China's construction safety production management is not stable enough, the safety management responsibilities are not clear, and there is a lack of scientific basis and favourable theoretical guidance in construction safety production management; the main defects of the construction safety production regulation system are that the legal normative documents do not play a full role, the laws and regulations supporting the formulation of slow laws and regulations are too principled and not strong in science, and the entire regulation system is still lacking in content [12].

The government should improve safety legislation and strengthen safety law enforcement, based on the focus on highlighting the service guidance function, and complemented by the role of market mechanisms to guide construction enterprises to consciously pay attention to safety production. The process of improving the efficiency of safety management should pay attention to the importance of construction safety management personnel training mechanism and also needs to improve the supporting mechanism for the development of safety management personnel in construction enterprises; some scholars from universities, enterprises, and government form three levels of in-depth analysis of countermeasures and measures to train safety management personnel and to provide analysis and reference for the establishment of domestic construction safety management personnel training mechanism. Wireless sensing in the disaster site monitoring data collection applications is also very extensive at present; it can achieve not only early warning of landslide geological disasters but also wireless sensing network monitoring system, deployed in areas prone to secondary disasters, to assist in the implementation of search and rescue tasks, to improve the safety and reliability of rescue.

3. Simulation Analysis for Optimization of Dynamic Management System for Low-Power Wireless Sensor Network Building Construction

3.1. Design of a Dynamic Management System for Low-Power Wireless Sensor Network Building Construction. Construction safety early warning data information collection is the key problem that needs to be solved for the whole early warning system, and only if the data has authenticity and timeliness can the practicality of the whole early warning be guaranteed [13]. Data information collection in the traditional way is obtained through human inspection or measuring instruments, which not only consumes a lot of workforce and material resources but also has limitations and errors in the data obtained, which cannot meet the needs of managers for first-hand data. With the progress of science and technology, information technology is developing rapidly, and wireless sensor network technology has brought a breakthrough to data collection, which can not only meet the various needs of data acquisition but also preprocess and analyse the data.

$$RQ = k_1 \cdot \mathrm{Hop} - k_2 \cdot (\alpha_1 \cdot RSSI_{\max} - \alpha_2 \cdot LQI_{\max} + \alpha_3 \cdot UI_{\max}),$$
$$\mathrm{Hop} = \left(1 + \frac{\mathrm{Hopnum} + 1}{\mathrm{Hopnum}_{\min}}\right) \times 256. \tag{1}$$

Wireless sensor network (WSN) technology refers to a distributed sensing network composed of various types of sensor nodes with physical information collection functions, data processing functions, and wireless communication functions. The various types of small sensing devices at the end of the sensing network are small but fully equipped with sensing devices, embedded microprocessors, and radio transceivers, so they can not only sense any relevant physical information but also have sensing capabilities, data

processing, and communication capabilities for automatic transmission to wireless base stations [14]. This can speed up the progress of construction. Therefore, the level of construction technology is also a key factor in determining the construction progress. Thanks to developments in the field of microelectronics and wireless communication technologies, miniature, inexpensive, and intelligent sensors are deployed in physically monitored areas through wireless connections, offering great convenience over the previous wired connections. Wireless sensor network technology is now widely used in various fields, and it is bound to become a bridge between the physical world and the computer world and will revolutionize the way we live, work, and interact with the physical world.

$$AMPR = \frac{\sum_{i=1}^{M} \max P w r_i^2}{N},$$
$$CH_{\text{prob}} = \min\left(C_{\text{prob}} \cdot \frac{E_{\text{residual}}^2}{E_{\max}}, P_{\min}\right). \tag{2}$$

The design of wireless sensing networks is mainly applied in harsher environments, and the number of nodes required is generally much more than that of traditional communication systems, which are high-density wireless sensing networks. The sensing nodes in wireless sensing networks not only take the responsibility of collecting data but also take the responsibility of receiving data transmitted by other nodes. The networking method of wireless sensing networks is self-organization and multihop etc., which is more flexible. Self-organization is equivalent to plug-and-play, while the topology will be affected by the joining or withdrawal of sensing nodes, which belong to the dynamic topology. If the sensing nodes move, the topology is also updated according to the relative position of the sensor nodes. This also ensures the stability of the system; when one or more of the sensing nodes in the sensing network fails, it does not lead to stagnation of the entire sensing network system [15]. The sensing network is divided into wired sensing networks and wireless sensing networks. A wired sensing network establishes a channel for information transmission through a line connection, which is highly resistant to interference, and the information transmission process is less affected by the outside world. Wireless sensing networks can carry out information transfer between nodes through a wireless network and aggregate to the gateway for conversion to achieve the self-organized connection between the wireless network and wired network, as shown in Figure 1.

The sensor node layer is composed of a data acquisition hardware unit, a processing control hardware unit, a communication hardware unit, and an energy hardware unit that implements the data acquisition, preprocessing storage, and transmission functions of the sensor nodes. The sensor node layer is implemented by arranging many sensors in the monitoring area, thus requiring the sensors to provide as much power as possible with minimum expense, minimum size, minimum weight, and maximum lifetime.

$$CI = w_1^2 \frac{E}{E_{\max}^w} - w_2 \frac{C}{C_{\min}}. \tag{3}$$

The topology discovery request sent by the aggregation node and the broadcast sent by the cluster head election completion use the cluster head broadcast; the cluster head broadcast contains the hop count and the information used to calculate the route quality; the hop count is used to limit the range of the broadcast; and other sensing nodes in the cluster can calculate the route quality and establish the route to the cluster head based on the data in the message. There is no safety problem; otherwise, it is necessary to warn the safety management personnel to check the relevant mechanical equipment and arrange maintenance personnel to repair. The cluster head sends a reelection broadcast message when it is reelected; the node receives it, calculates the cluster head index using the route control message, and notifies the cluster head node with a node election information reply message. The cluster head node elects a new cluster head based on the cluster head index of the nodes in the cluster and notifies the node with a cluster head election confirmation message; upon receipt of the notification, the node sends a cluster head broadcast message; if the previous cluster head receives the message, then the election is successful; if not, then it is sent several times. If the previous cluster head does not receive the cluster head broadcast message several times, then this election fails and the cluster head election is conducted again. Additional information about the transport method, the list of transport methods, and the status of the route are added to the four base messages in the previous chapter. The transmission method indicates whether the route is a long-range route or a close-range route. The aggregation node can be regarded as an intermediate gateway node connecting the sensing network and the extranet, realizing the conversion and interoperability between different protocols, and the data information from the sensing node is delivered to the aggregation node using a single-hop or multihop approaches [16].

The convergence node layer is in the middle layer between the sensing node layer and the management node layer and plays a role in the organizational structure to carry on the task to the sensing node layer according to the requirements of the management node, whose physical structure is essentially equivalent to the enhanced function of the sensing node. At the same time, the aggregation node is also responsible for the establishment of the network and the joining or withdrawing of sensors in the sensing network. The management node layer is in the uppermost layer of the whole wireless sensing network and its authority level is the highest; the user can use the management node to achieve information resource access to the wireless sensing network system; if the user needs to change the settings in the wireless sensing network, it also operated through this layer, as shown in Figure 2. It accounted for 53%, followed by object strikes. Simply relying on safety management personnel to patrol the site cannot find and solve potential safety hazards in a timely manner.

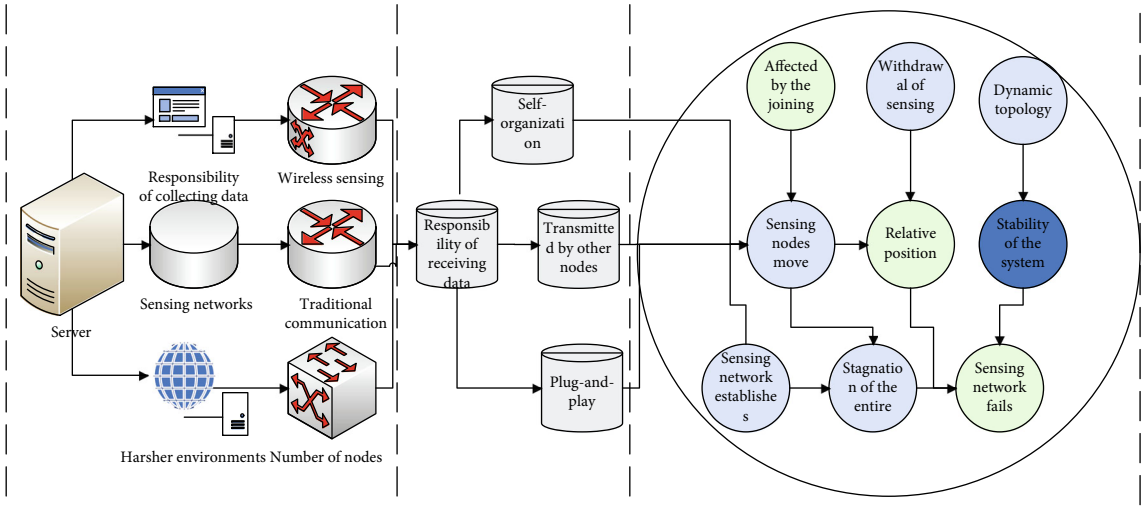

Figure 1: WSN three-level network structure.

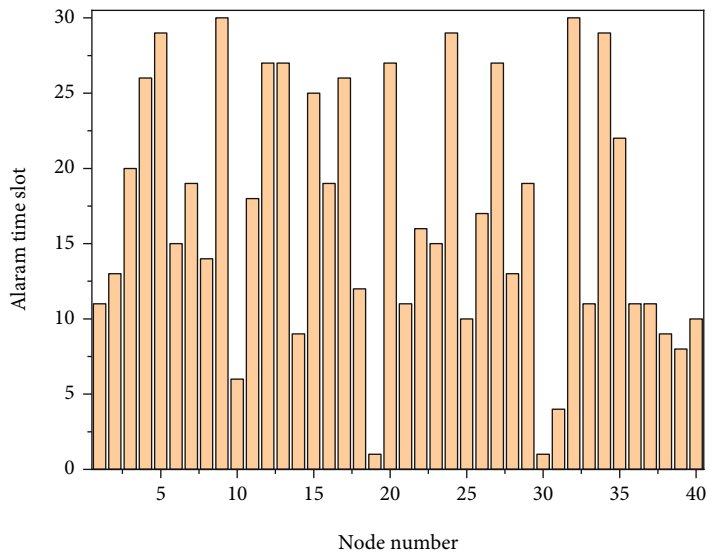

Figure 2: Node alarm time slot.

When multiple nodes are ready to send data at the same time, contention will inevitably occur as they go to occupy the transmit channel at the same time, failing to send some of the data and having to finish sending the data by multiple retransmissions [17]. The collision of data not only causes a delay in the working of the whole system but also increases the extra power consumption and increases the energy consumption of the whole system due to multiple retransmissions. Wireless channels have broadcast characteristics; when a node sends a message, the nodes within the entire network can receive the information it sends. For nondestination nodes, receiving these messages that are not valid for themselves not only consumes extra energy but also may disrupt their own. During wireless communication, nodes have four states, which are sleep, listening, receiving, and sending.

$$w_1 - w_2 = 1. \tag{4}$$

Among them, the sleep state has the least power consumption, and the power consumption for sending data and receiving data is relatively high. When in the listening state, the node constantly listens to the wireless channel to determine whether the channel is idle or not. Since wireless sensor networks are relatively small data networks, it is not necessary for the nodes to always listen to the channel, and they can completely go into a dormant state when there is no task. The design concept of WSN is data-centric. Data from all nodes are transmitted to the aggregation node. Compensation expenses, rescue and medical expenses, accident penalty expenses, etc., also include the loss of shutdown and rectification caused by the accident and the loss caused by the replacement of workers. The user is

mainly concerned with monitoring the data collected by the sensing nodes in the area, and the protocol design needs to consider the management and processing of the data. With limited energy, how to minimize energy consumption and increase the network life cycle while discovering routes and transmitting data is the focus of the routing protocol design.

The communication between sensing nodes is improved on the original communication flow. The communication flow finds the proximity route first when discovering the route and then further discovers the distance route if there is no proximity route for the destination node. The advantage of this is that when the nodes are close to each other, only a small amount of network and energy resources are consumed to establish a route to communicate with each other. For distant nodes, the additional consumption in finding proximity routes is only a very small part of the complete route-finding process and has less impact on network lifetime and network performance.

3.2. Simulation Analysis of Construction Dynamic Management System Optimization. Information refers to news, intelligence, knowledge, etc. transmitted (conveyed, transmitted) by oral, electronic voice, mail, or other relevant written means, usually manifested as sound, text, figures, and images, etc. In the field of engineering project management science, a large amount of engineering information is formed with the flow of workflow, coordination, capital flow, etc. in the process of project implementation, which are processed and formed into specific forms of data to provide the basis for decision-makers to control the project implementation process [18]. At the same time, the information flow also forms an interrelated whole of the project's capital flow, coordination, project organization, and various management functions, as well as the external project environment, which influences and controls the workflow, coordination, and capital flow. Only when the information flow is smooth can the project be implemented smoothly. The building construction site is the convergence place where various construction operations and construction activities are carried out and completed at the same time, and it is also the centralized place where building construction information is generated, transmitted, and applied. Construction personnel and managers at building construction sites need a large amount of construction information to support construction activities. To explore a new system of construction site information management, it is necessary to identify and categorize construction site information. The building construction site is the gathering place where the design results of different professions such as architecture, structure, HVAC, water supply, and drainage are transformed into the physical building, and it is also deeply influenced by the decisions of project planning, design, and construction. So, the construction site of the building construction information sources is wide, and the content is complex and changeable, and lack of on-site security controls. The use of emerging technologies in the construction industry can shift the focus of safety management to advance management and realize preventive management. Safety early warning management based on emerging technologies can not only monitor the behaviour of people and the state of things in real-time. Construction project construction lasts for a long time, with many uncertainty factors and a high frequency of information changes [19]. Construction site engineering information is also updated in real-time with the progress of the project, and the updated engineering information can be used as the next stage of information. Therefore, the engineering information is interdependent and transforms and influences relationships, which often involves the whole and is highly correlated, as shown in Figure 3.

In general, on-site information can be divided into structured and unstructured information. Structured information refers to information data that is stored and described by open data standards, and such information data can form multiple components with clear hierarchical structure and interconnection. In the application of BIM technology in building construction sites, structured information can be searched quickly by determining its characteristic nodes, which has the advantages of improving information utilization rate, completing information search efficiently, and reducing missing information; unstructured information refers to information data with relatively unclear form, poor correlation, and blindness when querying information, and at present, it mainly relies on manual means to modify and update and organize, such as electronic document reports, e-mails, web pages, video files, and BIM model information of nonpublic data standards. Wireless monitoring technology for construction measures and environment can be classified into two categories according to the transmission method; one is the wired transmission method.

Because the data information is transmitted by way of cable, it is less interfered with by the outside world, while the transmission is faster and the information fidelity is high, but because the cable needs to be laid in the monitoring area, the arrangement is more difficult for the monitoring place with a complex environment, while a certain degree of difficulty also exists with the later maintenance in the process of use.

Especially on the construction site, many cables lying about will affect the normal construction of the operator, while the operator might easily to destroy the cable during the construction process. Prevent and reasonably control the safety accidents on the construction site in advance, and promote the sustainable development of the construction industry. The construction industry is in a state of rapid development, and modern buildings are characterized by large volumes, large spans, complex modeling structures, and deep foundations. The other type is the wireless transmission method; the wireless transmission method is transmitted by wireless signal; the signal carries monitoring information, relying on the current rapid development of wireless transmission information technology, and can be applied to the monitoring of harsh environments; therefore, the wireless transmission method has been favoured by the field of structural monitoring and

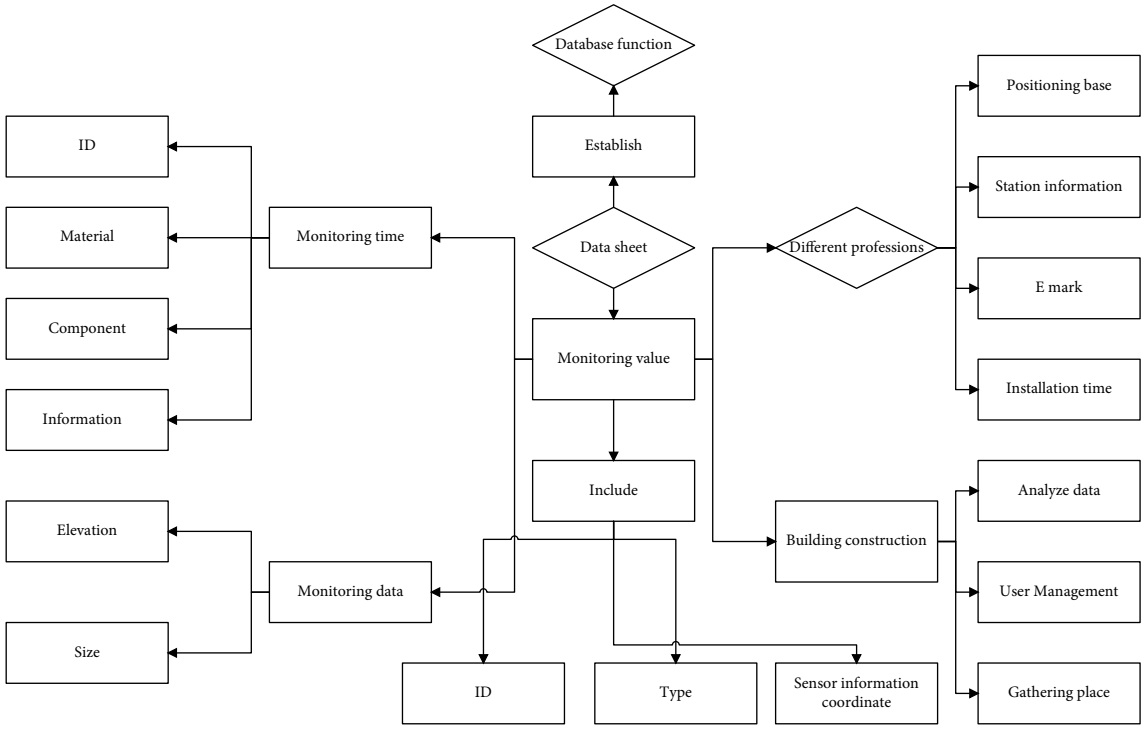

Figure 3: Monitoring information database ER diagram.

is slowly replacing the wired transmission method. The research on the construction methods of digital terrain and 3D hydraulic building models is an important part of the research on dynamic 3D total view management methods for construction, and this section will carry out the research on digital terrain construction methods, 3D model construction methods, and ground coupling methods based on BIM ideas and combined with the characteristics of hydraulic construction modelling.

There are many components in the construction of the sea trial terminal, the construction process is complex, the volume of work is large, and the duration is long. In the actual construction process, it is easy to have factors affecting the construction schedule, such as problems in the supply of construction materials during the construction process, unexpected weather, typhoons, and rainstorms encountered during the construction process; an insufficient number of construction personnel will lead to delays in the construction schedule. Construction schedule management generally refers to the analysis of relevant influencing factors and making reasonable adjustments, using certain measures to achieve the project schedule adjustment optimization, as shown in Figure 4.

The influencing factors of construction schedule and construction schedule optimization methods are closely related, and the constraints of the construction optimization model can be determined by investigating and analysing the influencing factors of the construction schedule. Resources such as workforce, material supply, and quantity of machinery and equipment have a great influence on the construction progress; if the resources are insufficient, the construction progress will be delayed because of the inability to increase the construction input; on the contrary, if the construction resources are in excess and greater than the construction capacity, it will cause the waste of resources, thus increasing the construction cost and management difficulty. Sufficient funds are the guarantee that the project can be carried out smoothly, and in the case of sufficient funds, the project can be reasonably accelerated. Construction costs are composed of direct costs and indirect costs, and direct costs include labour, materials, and machinery, while indirect costs include management and site expenses. Therefore, it can not only sense any relevant physical information but also have sensing capabilities, data processing and communication capabilities and can automatically transmit to wireless base stations. Due to the development in the field of microelectronics and wireless communication technology, tiny, inexpensive, and intelligent sensors are deployed in the physical monitoring area through wireless connection. Therefore, the level of construction technology is also a key factor in determining the construction schedule.

In this regard, the system will define the structure of data and composes an Extensible Markup Language (XML) schema to achieve structured information storage; similarly, a special unstructured data architecture will be established to centralize the storage and management of unstructured data. In the whole process of building construction site information management, the system will establish different BIM database tables to record information metadata according to information categories and formats, thus forming a complete BIM-based data storage [20]. The IFC standard is the de facto data description standard of BIM technology, and most of the BIM professional application

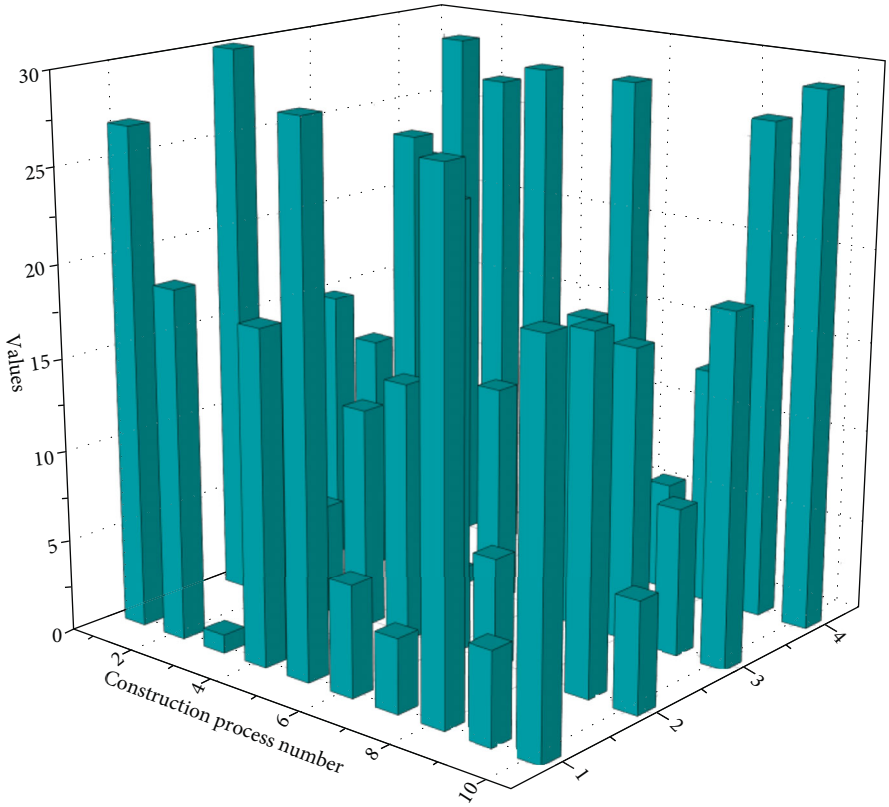

Figure 4: Construction schedule and costs.

software can support the input and output of the IFC building information model.

Through this module, the information manager issues instructions related to material and equipment management; the relevant personnel view the instruction information and generate the instruction feedback information; when the difference with the BIM data exceeds a certain area, the difference part is highlighted in the BIM model and the alarm information is quickly submitted to the front-end system and the information manager, while the module can be configured by the user to respond to the alarm linkage option according to the actual demand. In the process of BIM-based construction site information management, the information manager can implement comprehensive BIM-based information management of the quality, quantity, and use plan of materials and equipment at the construction site through the system, while nonconstruction site information managers such as material and equipment suppliers, equipment leases, and supervisors can only view and feedback the instruction information or make inquiries about contracts, inventory and other information.

4. Results and Analysis

4.1. Performance of Dynamic Management System for Low-Power Wireless Sensor Network Building Construction. According to the data in Table 1, it can be learned that when the transmission distance is farther, the received power is lower. When the transmission distance from the receiving antenna to the transmitting antenna is 10 m, the received wireless energy is -18 dBm; when the transmission distance is more than 20 m, the wireless energy received by the antenna is less than -20 dBm. When the received infinite energy is lower than -20 dBm, the converted DC energy is less efficient and difficult to collect. Therefore, in the simulated system, due to the limitation of the RF source transmitting power, the effective wireless transmission distance is limited to 20 m, while in the actual shed application environment, the effective system receiving distance can be extended by increasing the RF source transmitting power.

From a theoretical point of view, the relationship between the effective transmission distance of a directional wireless transmission system and the transmitting power of the RF source is analysed. In this section, however, the focus will be on flexible receiving antennas that can be closely integrated with the greenhouse agricultural environment. Flexible antennas, usually nonplanar antennas that conform to the shape of a specific object, have been used as part of the surface of moving objects such as aircraft. Due to its conformal characteristics, it can be well applied under some nonregular objects or special application scenarios, satisfying the characteristics of concealment and not easy to destroy, and in recent years, conformal antennas have gradually become a hot spot for research. It is a dynamic topology. If the sensor nodes move, the topology is also updated based on the relative positions of the sensor nodes. As a high gain circularly polarized array world is used as the RF transmitting antenna in this paper, to avoid the polarization mismatch problem, the receiving antenna should also

Table 1: Analysis of the wireless energy transmission link.

Input signal power	Output signal power	PAE
8	22.3	10.7
9	39.2	41.2
10	16	30
11	15.8	46.6

conform to the characteristics of circular polarization. A circularly polarized rectifier antenna is proposed, which is made of flexible material and can be applied on cylindrical surfaces such as pipes to achieve a conformal effect and provide power to wireless sensing nodes. This section will mainly discuss the structure and simulation results of the rectified antenna.

The design of this paper includes three sensing nodes for data collection, while the relay nodes are in broadcast mode to continuously poll the data to send data requests to the slave nodes, and when the sensing nodes get the corresponding data requests, they send the data to the relay nodes. The conventional data communication is based on relay nodes, which are polled continuously through a single channel according to the sensor node number, and the polled sensor nodes send data to the relay nodes, while the unpolled sensor nodes are in the sleep state, waiting for the polling signal. And when the sensing node collects monitoring data to reach the alert point, a second channel is opened for alarm data transmission in order not to crowd the channel with normal communication, as shown in Figure 5.

An envelope tracking power amplifier is a kind of dynamic bias amplifier, which synchronizes the bias voltage of the amplifier after detecting the amplitude and phase information of the input signal so that the amplifier can always work in the region of higher efficiency. The envelope tracking technique has high requirements for envelope tracking power supply, and according to the actual requirements of this system, it was decided to use the control role of the microcontroller to achieve the function of dynamic biasing based on the idea of envelope tracking. Since the bias voltage needs to change according to the input signal power, the input signal needs to be detected first, and since the detection process is not expected to have too much impact on the final output signal, a small portion of the signal needs to be separated by a power divider or coupling module for detection. The detector unit directly uses a circuit module composed of detector chips, and the MCU at the back end converts and processes the analogy signal generated by the detector circuit after the detector is completed to obtain the input signal power and then controls the DC voltage generation module at the back end to generate a suitable bias voltage to power the power amplifier according to the power magnitude value.

5. System Optimization Simulation Results

To read and judge the electronic tag information on the mechanical equipment using the fixed or portable method, the permission information of the mechanical equipment includes the annual inspection information, maintenance information, whether there are maintenance problems, etc. The implementation of this function is also using the C# language nested If statement; for the annual inspection information, maintenance information, etc. which belong to the date and time information, it is impossible to directly calculate the date difference; it needs to be converted to seconds It needs to be converted into seconds and then calculated. As shown in Figure 6, it is the same way as the judgment of personnel authority identification, when all the return values are True after the execution of the nested. It proves that the machinery and equipment can be used normally, and there is no safety problem; otherwise, it is necessary to notify the safety management personnel to check the relevant problem machinery and equipment and arrange the maintenance personnel to carry out maintenance. After the inspection is completed, the label information in the label of the machinery and equipment needs to be updated, and the return value is True for the nested If statement execution structure identified by the authority, and the warning reminder ends, as shown in Figure 6.

The principle of this construction safety early warning system for the structural warning is to collect construction data from the site and compare it with the design safety values, to warn when the collected data exceeds the design range, and to consider the site in a safe construction state if it is within the design safety values. Therefore, the use of the early warning system requires the project department of the construction unit to establish good communication with the design unit and the design department of the construction unit, to carry out the design and safety technical briefing based on the construction safety early warning system, to accurately account for the initial value (safety design value) of this early warning system, and to improve the practicality of the safety early warning system.

This construction safety early warning system has four modules; considering the actual situation on-site and cost factors, the required module functions can be used selectively, and the monitoring of site personnel, machinery, structure, and physical environment can also be selectively installed and monitored according to the actual situation of the project; for example, the construction project undertaken by the construction unit has low floors, the external scaffolding is relatively simple to erect and the danger is minimal; considering the cost reasons, the structural monitoring of external scaffolding is not required, as shown in Figure 7.

The construction progress management module consists of two parts: two-dimensional construction progress management and three-dimensional construction progress management. The two-dimensional construction progress management function module is designed based on dynamic chart technology and database mining technology, which outputs the construction progress data optimized by the system as visual charts. The system's two-dimensional construction progress management generates the plan dynamically into a Gantt chart, which shows the total

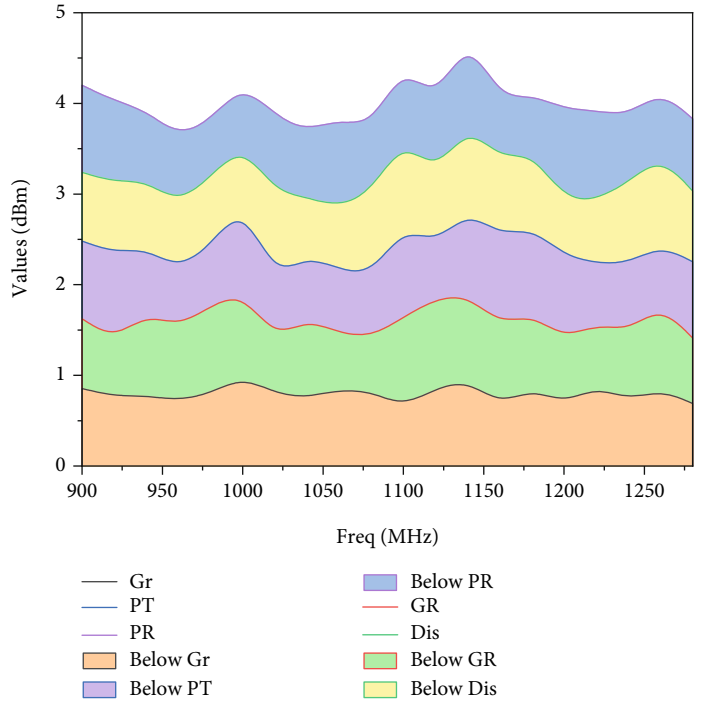

Figure 5: Output signal power-in, gain, and PAE test data plot.

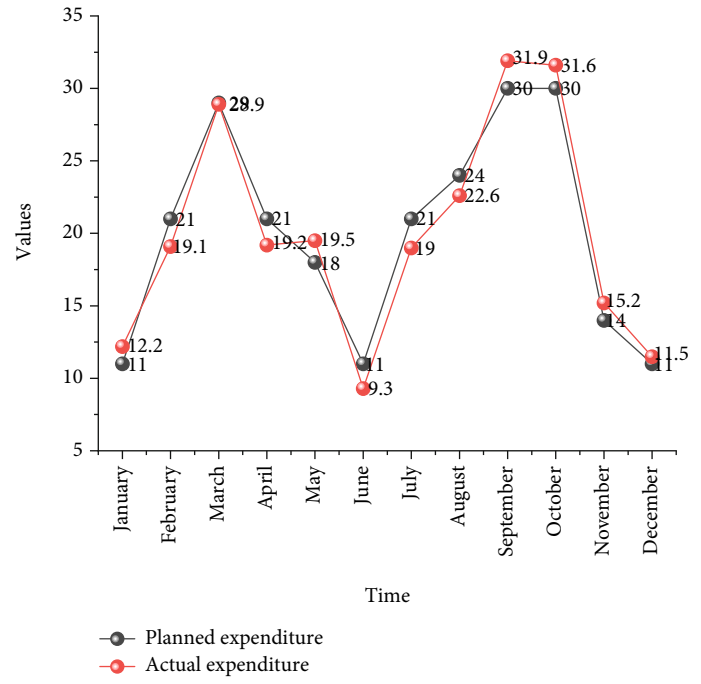

Figure 6: Use of funds and resources.

construction progress at the top and the unit project progress and schedule at the bottom, where the green part indicates that the section has completed construction and the red part indicates that the section is not yet under construction. After the node receives the notification, it will immediately send the cluster head broadcast message. If the previous cluster head receives the message, the election is successful, and if it does not receive the message, it will be sent multiple times. The left side of the construction progress Gantt chart shows the unit project progress plan attributes and the project progress display time zone; the unit project construction progress plan attributes include project progress, project start time, project duration, project end time, and the project name of the project; click on a unit project in the right side of the Gantt chart; the left-side attribute information column will display the corresponding

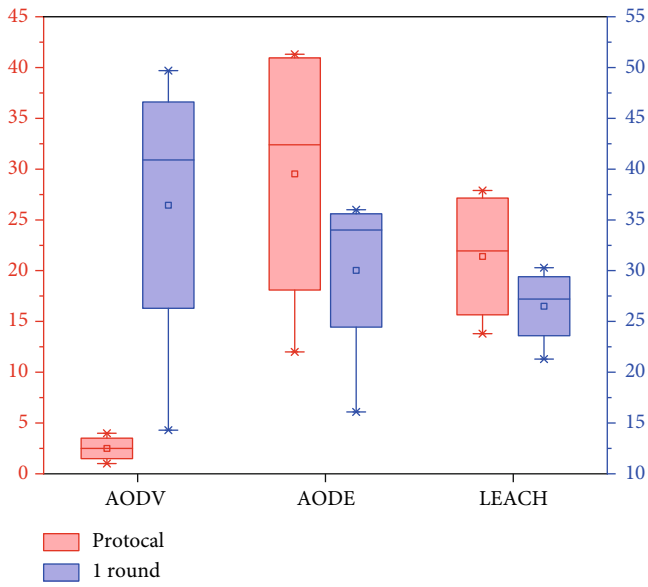

Figure 7: Protocol simulation results.

attribute information and the project progress display time zone. You can adjust the start and end time of the chart displayed on the right, and you can adjust the time unit of the construction progress Gantt chart display. Based on the above functions, the design of the two-dimensional construction progress management of the sea trial pier is completed. The spring-rectangular piezoelectric cantilever beam has a wide resonance range at the resonance point, and the bridge is in low-frequency vibration most of the time, so more energy can be collected by designing a piezoelectric energy harvesting device to integrate the triangle and spring-rectangular piezoelectric cantilever beam.

6. Conclusion

The collection of construction site data information is realized through WSN technology, including the information collection of people supported by WSN technology for personnel positioning technology; the information collected is mainly location information and attribute information; For the information collection of things supported by WSN technology for construction measures and environmental monitoring technology, the information collected mainly measures structure information, location information and environmental information. At the same time, comparative analysis and algorithm research on location technologies are conducted, topological network structure design for construction measures and environmental monitoring technologies is completed, and information collection schemes targeting people and objects at construction sites are developed. The design of the construction safety early warning system includes the determination of design principles, system framework design, initial value design, functional module design, process design, and use authority design. The construction safety early warning system mainly takes the site personnel of the construction unit as the monitoring object of the occurrence of safety accidents, and the use of this early warning system can realize the behaviour or state of reminding and informing people and objects of possible safety accidents and realize the functions of safety education, daily attendance management, and safety reward and punishment management. The physical framework of the system is then designed from the actual situation of the building construction site, and the physical equipment architecture and construction site network of the BIM-based building construction site information management system are designed. The construction of this system provides a solution for applying BIM technology to the whole construction site and accelerates the information management process of the whole process of the construction industry.

Data Availability

The data used to support the findings of this study are available from the corresponding author upon request.

Conflicts of Interest

The author declares that they have no known competing financial interests or personal relationships that could have appeared to influence the work reported in this paper.

References

[1] V. Freschi and E. Lattanzi, "A study on the impact of packet length on communication in low power wireless sensor networks under interference," *IEEE Internet of Things Journal*, vol. 6, no. 2, pp. 3820–3830, 2019.

[2] R. Chéour, S. Khriji, D. El Houssaini, M. Baklouti, M. Abid, and O. Kanoun, "Recent trends of FPGA used for low-power wireless sensor network," *IEEE Aerospace and Electronic Systems Magazine*, vol. 34, no. 10, pp. 28–38, 2019.

[3] S. Bin and G. Sun, "Optimal energy resources allocation method of wireless sensor networks for intelligent railway systems," *Sensors*, vol. 20, no. 2, p. 482, 2020.

[4] K. Guleria and A. K. Verma, "Comprehensive review for energy efficient hierarchical routing protocols on wireless sensor networks," *Wireless Networks*, vol. 25, no. 3, pp. 1159–1183, 2019.

[5] H. H. Mahmoud, H. M. ElAttar, A. Saafan, and H. ElBadawy, "Optimal operational parameters for 5G energy harvesting cognitive wireless sensor networks," *IETE Technical Review*, vol. 34, no. sup1, pp. 62–72, 2017.

[6] H. Keshmiri and H. Bakhshi, "A new 2-phase optimization-based guaranteed connected target coverage for wireless sensor networks," *IEEE Sensors Journal*, vol. 20, no. 13, pp. 7472–7486, 2020.

[7] I. Mandourarakis and E. Koutroulis, "Unified system-and circuit-level optimization of res-based power-supply systems for the nodes of wireless sensor networks," *IEEE Transactions on Industrial Informatics*, vol. 14, no. 2, pp. 598–607, 2018.

[8] S. Rani, S. H. Ahmed, and R. Rastogi, "Dynamic clustering approach based on wireless sensor networks genetic algorithm for IoT applications," *Wireless Networks*, vol. 26, no. 4, pp. 2307–2316, 2020.

[9] X. Song, Y. Gong, D. Jin, and Q. Li, "Nodes deployment optimization algorithm based on improved evidence theory of underwater wireless sensor networks," *Photonic Network Communications*, vol. 37, no. 2, pp. 224–232, 2019.

[10] G. Shabbir, A. Akram, M. M. Iqbal, S. Jabbar, M. Alfawair, and J. Chaudhry, "Network performance enhancement of multi-sink enabled low power lossy networks in SDN based Internet of Things," *International Journal of Parallel Programming*, vol. 48, no. 2, pp. 367–398, 2020.

[11] K. Vijayalakshmi and P. Anandan, "A multi objective Tabu particle swarm optimization for effective cluster head selection in WSN," *Cluster Computing*, vol. 22, no. S5, pp. 12275–12282, 2019.

[12] X. Cao, S. Madria, and T. Hara, "Multi-model Z-compression for high speed data streaming and low-power wireless sensor networks," *Distributed and Parallel Databases*, vol. 38, no. 1, pp. 153–191, 2020.

[13] F. Gara, L. B. Saad, R. B. Ayed, and B. Tourancheau, "A new scheme for RPL to handle mobility in wireless sensor networks," *International Journal of Ad Hoc and Ubiquitous Computing*, vol. 30, no. 3, pp. 173–186, 2019.

[14] A. Karaagac, E. De Poorter, and J. Hoebeke, "In-band network telemetry in industrial wireless sensor networks," *IEEE Transactions on Network and Service Management*, vol. 17, no. 1, pp. 517–531, 2020.

[15] S. Bin and G. Sun, "Matrix factorization recommendation algorithm based on multiple social relationships," *Mathematical Problems in Engineering*, vol. 2021, 8 pages, 2021.

[16] J. Joy Winston and M. Nivas, "Optimal energy efficient connected coverage wireless sensor networks," *Annals of the Romanian Society for Cell Biology*, vol. 25, no. 6, pp. 20812–20817, 2021.

[17] H. Wang, K. Li, and W. Pedrycz, "An elite hybrid metaheuristic optimization algorithm for maximizing wireless sensor networks lifetime with a sink node," *IEEE Sensors Journal*, vol. 20, no. 10, pp. 5634–5649, 2020.

[18] G. Sun, C. C. Chen, and S. Bin, "Study of cascading failure in multisubnet composite complex networks," *Symmetry*, vol. 13, no. 3, p. 523, 2021.

[19] X. Liu, Z. Sheng, C. Yin, F. Ali, and D. Roggen, "Performance analysis of routing protocol for low power and lossy networks (RPL) in large scale networks," *IEEE Internet of Things Journal*, vol. 4, no. 6, pp. 2172–2185, 2017.

[20] A. Pegatoquet, T. N. Le, and M. Magno, "A wake-up radio-based MAC protocol for autonomous wireless sensor networks," *IEEE/ACM Transactions on Networking*, vol. 27, no. 1, pp. 56–70, 2019.

Hindawi
Journal of Sensors
Volume 2022, Article ID 1551118, 9 pages
https://doi.org/10.1155/2022/1551118

Research Article

Virtual Reality (VR) Advertising Communication Design Based on 3D Wireless Active Visual Sensing

Yunshan Geng [1,2]

[1]*School of Art, Xi'an University of Architecture and Technology Huaqing College, Xi'an, Shaanxi 710055, China*
[2]*Silliman University, Philippines 999005*

Correspondence should be addressed to Yunshan Geng; gengyunshan@su.edu.ph

Received 10 November 2021; Revised 13 January 2022; Accepted 17 January 2022; Published 7 February 2022

Academic Editor: Gengxin Sun

With the vigorous development of the advertising industry, advertising in the era of intelligent media fills all aspects of our lives, and more and more intelligent media are applied to the advertising industry. The current three-dimensional advertising and interactive advertising are too fragmented in form, with three-dimensional advertising having a strong sense of three-dimensionality but lacking interactivity and interactive advertising having strong interactivity but lacking visual attraction. How to integrate 3D advertising and interactive advertising in order to make advertising in the future has greater development potential and market, whether in the visual or interactive experience can attract the target consumers becomes very necessary. It is found that VR technology has a wide range of application prospects, and intelligent media advertising mediated by VR technology follows the trend of advertising industry development. This thesis uses VR (virtual reality) technology as a medium to study the integration of 3D advertising and interactive advertising in the smart media era. In the second phase, the development direction of VR as an advertising medium in the era of intelligent media is identified. The research on the integration of 3D animated ads and interactive ads under VR technology is launched, and the research on 3D stereoscopic and interactive design of advertisements in the era of smart media is a reflection and exploration of the future language of advertising design. And through the comparison with traditional advertising, it is concluded that the aesthetic subject of VR advertising is "polycentric," the aesthetic object. Then, we analyze the theoretical roots of the formation of the aesthetic characteristics of VR advertising from three levels: media technology, communication theory, and audience psychology. Finally, we return to the general environment of visual culture and explore the deconstruction of visual culture by the aesthetic characteristics of VR advertising in three levels: "symbol collapse," "audience reshaping," and "immersive communication."

1. Introduction

The continuous development of advertising media, in the practical sense, can make the form of advertising more three-dimensional and interactive; with the continuous change of advertising media, VR (virtual reality) technology has become the media of the intelligent media era; virtual reality (VR) technology is a new image technology that integrates three-dimensional sense of picture and interactive forms, is an important direction for the future development of advertising, and is also one of the current hot topics of image research [1]. Since the emergence of advertising media, there have been different media in different times, from print media to radio media, from TV media to computer media, in the era of intelligent media with interactive functions of cell phone media, and finally developed to three-dimensional advertising and interactive advertising integration of VR media [2]. At present, VR advertising has a unique advantage; at the end of 2016, the famous international virtual advertising company, Airpush, released the world's first research report on the effectiveness of VR advertising. Based on objective data, the researchers quantified the effectiveness of VR advertising versus traditional advertising [3]. The report describes: "If VR is used as the technical support for the advertising effect, advertising will increase by 1.5 to 1.8 times, especially in terms of product memory, VR-based advertising as a new type of advertising message will increase the message memory effect by 5 times and advertising message sharing will increase by 2 times. As the cycle of media replacement becomes

shorter and shorter, the advertising industry itself should adapt to the general trend and make changes to itself [4]."

It is of great relevance to provide rich information for advertisers to create VR advertisements, to analyze the existing technical bottlenecks and future development expectations for technology platforms, and to guide the correct perception of VR advertisements for advertising audiences [5]. Visual culture is an interdisciplinary and emerging term that involves many disciplines such as literature, art, and philosophy. The study of visual culture as a systematic theory began in the West in the 1980s, while visual culture as a research branch was really grafted into the field of communication after the 1990s [6]. After human beings left the traditional tribal society of "face-to-face communication" and "oral transmission," and after the birth of writing, the communication of information began to be done through media. The printing press realized the visualization of spoken expression, and the radio, television, and Internet after the printing press all made the enhancement of the "visualization" of information the ultimate goal of technological change [7]. The popularity of visual culture is in line with the pace of media technology, and because visual communication is inseparable from the role of media, visual culture research has become an important area of media research. At present, the number of consumers using traditional media is decreasing, and there is a lack of supply and demand between functional distribution and consumer demand [8]. According to the statistical analysis of relevant data, mobile terminals account for 38%, computer terminals account for 35%, TV media accounts for 16%, and paper media only accounts for 11% of the forms in which consumers get advertisements, and people over 50 years old are bit traditional media consumers. In addition, the traditional media also lacks technical support and is not strong enough for development. The media is single, information is scarce, information is closed, and advertising requires technical processing [9]. However, in the era of growing intelligent media, on the one hand, advertising presents the characteristics of audience communication, dispersal communication, and infinite communication, and on the other hand, consumer needs are becoming more and more personalized, participation and interaction are becoming stronger, and the concept of experience is becoming more and more diversified [10]. Under the radical change of the external situation of advertising, many traditional advertisements still follow a single boring communication mode, and the development situation, theme setting, language mode, means of communication, skill innovation, situation layout, and other aspects do not follow the trend to keep up with the frontier of technological development, which leads to the advantages of traditional media decreasing compared with intelligent media [11]. One of the main reasons why traditional advertising is difficult to develop is that there is no key technology support and a lack of wisdom media technology-oriented advertising such as three-dimensional, interactive experience, ergonomics, and personalized services, which is out of touch with the times in terms of technological innovation [12].

Three-dimensional production technology is not the only way of film and television advertising production; in film and television advertising, we have to correctly play the computer's three-dimensional technology in order to effectively highlight its highlights, so that the production level of film and television advertising and the creation of the magnitude of greater improvement. In the computer three-dimensional technology performance level, will focus on the consideration of film and television advertising production supply and demand, for some live-action risk factor is large, it is difficult to take the content of the field, can consider using three-dimensional technology to produce. In short, in the production process of film and television advertising to rational use of three-dimensional technology.Only by making appropriate use of the benefits of three-dimensional technologycan we give full play to the appeal of three-dimensional technology and make the explosive power of film and television advertisingenter a new stage. This paper takes advertising aesthetics as a research clue, analyzes the subject of advertising aesthetics, the object of advertising aesthetics, and the standard of advertising aesthetics, and seizes the core of advertising marketing from the audience's point of view, and the conclusions and proposed development strategies provide reference materials and case examples for advertisers to understand VR advertising and get involved in VR communication. In addition, the paper is also relevant in educating the advertising audience about the emerging VR advertising, and it provides a reference for the advertising audience to improve their media literacy. Therefore, the relevance of this paper exists at three levels: advertisers, technology platforms, and advertising audiences, and the conclusions of the study provide development strategies for the three main actors of advertising campaigns to understand VR advertising.

2. Related Work

VR advertising is the most emerging form of advertising nowadays, but few books have been written on this topic, and most of the relevant discussions are focused on journals and online platforms with high timeliness. VR online marketing advertising is a form of advertising in which audiences wear VR headsets to experience products or services online using cell phones or computers and other Internet terminal devices. Because of its convenience, large audience, and ease of data statistics, it has attracted the attention of many brands, and various kinds of online experiential advertising have also let audiences have a "VR addiction" [13]. A typical example of VR online marketing advertising is the new Mercedes-Benz "long wheelbase E-Class" VR ad launched by Sohu and Mercedes-Benz, which has also become an innovative move in the new media industry and automotive advertising. The format of the ad is to jump into the "VR Panorama Ad" page through the Sohu page ad, a new E-Class sedan parked in front of a glass office building; the user can swipe the phone 360 degrees to "walk" around the car to observe; when the user clicked on the LED headlights, the car lights will automatically light up and pop up. When the user clicks on the LED headlights, the lights will automatically light up and a detail page introducing its performance will pop up [14]. In addition, users can also remotely experience the "autoparking" function and can also click "scene switch" to experience the steering wheel details and stereo sound effects inside the car.

In order to ensure the advertising effect and user experience, the ad has impeccable details, and any component in the car can be felt by the users by clicking and popping up the details page. This VR live-action experience ad breaks away from the conventional film and TV commercial format and dares to break through the experiment, making the ad itself with a strong sense of immersion and technology [15]. At the same time, the contemporary and intelligent form of the ad coincides with the slogan of the Mercedes-Benz E-Class long wheelbase car, "The wise, the great," making the ad a technology news at the same time and spreading the effect with half the effort. The ads are usually in the form of paid experiences [16]. The audience wears VR glasses with a gamepad, and the VR glasses are interconnected with the computer terminals. The content of the ads is mainly in the form of VR live-action games and live-action homes, aiming to sell VR equipment and promote VR technology. The audience can experience the latest technology through the many projects in this offline "VR experience"; the most common forms of VR games are VR surgery, VR brush, VR CS, etc., in addition to VR smart home, VR bike, VR live roller coaster, etc. Unlike gamers sitting in front of computers and TVs, VR games are set in an exceptionally realistic scenario, where the audience is stimulated by a combination of auditory, visual, tactile, and other senses, seeing objects and scenes beyond reality, so the audience will hide, run, and attack as in real games; they can also walk around freely in the kitchen of VR smart homes, open cabinets, and unscrew faucets [17].

The VR offline experiential advertising also defines this new technology as a "toy," penetrates into the audience with a game, and takes "live experience" as the biggest attraction for "attention economy" marketing [18]. The biggest highlight is the "attention economy" marketing. The advertisers have opened the door to a new world for their audiences and at the same time have profited from the new technology as a marketing tool and have made a significant contribution to the promotion and popularization of "VR for all." Although TV and online ads can easily restore or recreate scenes, VR goes beyond TV and the Internet in that it is no longer limited to visual perception but rather to deeper sensory stimulation, such as smell, touch, taste, and other stimuli [19]. Therefore, the "scene" and "experience" have become the pursuit of VR advertising, changing the traditional advertising pursuit of images, words, and symbols corresponding to the framework of the constraints, which lighten the unnecessary auxiliary factors, the "scene" and "experience" in the first place. At the same time, traditional advertising needs to abstract the core value elements of products or services for symbolic packaging, in order to achieve the correspondence between products and symbols, so as to create the symbolic qualities as the unique selling point of the brand [20]. Therefore, traditional advertisements need to use words, music, colors, and other elements to make comprehensive packaging, but VR advertising no longer needs such meaningless blind packaging, nor does it need brands to shape the spiritual value or symbolic connotation of products [21]. Instead, through the sensory stimulation brought by the "immersive and interactive" all-round scenes, audiences can experience the brand culture and stimulate the desire to buy.

3. 3D Visual Communication of VR Advertising

3.1. MediaSmart Media Advertising Fusion. VR is immersive, and it allows consumers to be fully engaged in the real world virtualized by VR and can attract consumers in a short period of time, giving them a strong sense of immersion and enabling them to have an extremely realistic and authentic experience in contact with the virtual environment. It can be said that VR (virtual reality) technology combines the advantages of three-dimensional advertising and interactive advertising to demonstrate the functions and characteristics of the products. People can not only view the performance and appearance of the product through VR (virtual reality) devices but also experience the fun of the product firsthand. The VR medium is three-dimensional, and the three-dimensional images of the images can bring a great visual experience to the consumers. In the traditional media era, we capture content through the eyes. When people read advertisements, they will start to associate the things that newspapers, books, and other media make to describe, and consumers can form imagination in their minds after receiving the content of the advertisement. The textual description of the original appearance of things can be endless imagination, in this age of seeing is believing, and cannot let consumers really understand the appearance of goods and the use of VR three-dimensional technology. In order to allow consumers more intuitively see the appearance and even internal structure of goods, the intelligent media era of virtual reality advertising was born, as shown in Figure 1. The VR media has characteristics, advanced VR technology based on modern platforms public media products based on modern platforms, flexible media portfolio becomes a reality, and messages can be put into carefully prepared advertising content in each VR device at any time. So the result of the integration of 3D advertising and interactive advertising is not to simplify advertising but to give it more personalization and appeal. The VR media change consumer information contact behavior; in the age of smart media, the change of consumer information contact behavior is accompanied by changes in the media.

If the existing 3D advertising and interactive advertising can be integrated and gradually form a unified model, then it can provide consumers with "personalized" information and bring a fashion culture to the young consumer group, such as 3D images to attract consumers' attention and interactive advertising to follow up the satisfaction of today's trends. The interactive ads follow the satisfaction of today's trends.

In the era of intelligent media how to integrate three-dimensional advertising and interactive advertising, the author found after research, first of all, from sensory integration to experience integration. Most of the current advertisements are in the visual aspect, which are brought by simple advertising design and special effects operation, and consumers can only stay in the sensory visual experience of advertising. With the continuous development and application of VR technology, the future immersion experience will be more realistic. Second, from one-way communication to interactive communication integration, despite the advantages of traditional media advertising in creativity and special effects, but cannot change the status quo of one-way communication of advertising, it is

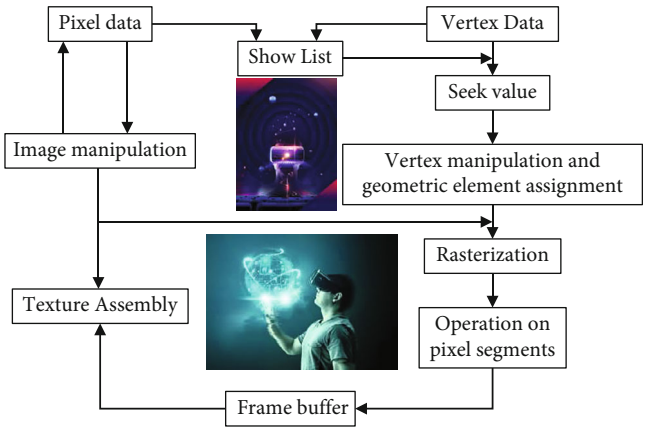

Figure 1: 3D VR technology and the evolution of 3D advertising.

difficult for consumers to interact with advertising. However, at this stage, too many experience technologies can only stay on some websites or touch screen and other devices.If you want to have an interactive experience in advertising films, you must use the interactive characteristics of VR media to integrate 3D advertising and interactive advertising. Advertising not only has a three-dimensional display technology, but also can interact with consumers, so that consumers are actively choose the need for advertising, enjoy the fun brought by advertising. In the process of using VR media technology to integrate three-dimensional advertising and interactive advertising, advertisers will slowly reduce the use of traditional media. As VR technology becomes more and more mature, consumers are no longer just passive recipients.In other words, advertising is truly people-oriented. After the above analysis, I believe that when designing VR advertising, we need to focus on consumer immersion experience and interactive experience, using the characteristics of VR to design a real interactive environment to give consumers a better experience.

3.2. Stimulate Consumption and Reduce Costs Based on VR Technology. VR media change the behavior of consumer motivation.In the traditional media advertising era, most consumers will think that the media broadcast on the product has no problem.Often the advertising goods and brands equivalent to advertising companies, so when the consumers need to buy advertising goods, they will get information from the ads. But with the advent of the era of smart media, countless commodity ads broadcast on a variety of media has entered the era of ubiquitous advertising, especially the price reduction of electronic display products, the cost of advertising media is getting lower and lower, and the consumers began to change the past existing advertising viewing habits, from the beginning of passive acceptance of advertising to take the initiative to understand advertising and thus better able to search for the goods they need through the use of smart media VR. The use of intelligent media VR equipment forms of a sense of immersion in the real world. For advertisers, paying close attention to and even predicting the development trend of advertising and media make them willing to invest more time, money, and attention to advertising media. Because VR as a medium of advertising is a full-sensory immersive experience, with the advantages of both three-dimensional advertising and interactive advertising, allowing people to enter a fully immersive virtual reality realm, in this real "world," consumers can experience advertising more deeply and realistically, thus attracting a large number of consumers. Among the media used by young people, due to the rapid improvement of the performance and functions of electronic products, young people have more interest and dependence on the use of smart media, as shown in Figure 2. Nowadays, young advertising consumers are more attracted to 3D display media and media with interactive features, and advertisers are constantly trying to integrate the two technologies. As VR technology matures, VR-based media is becoming more available and, of course, more affordable. The use of VR technology not only allows consumers to view immersive 3D images but also allows consumers to independently select the ads they want, experience the interactivity of the product at home, and share their experiences and feelings in a timely manner, using consumer interactive reviews to advocate for the ad, making it better for promotion and distribution.

From the current technology, traditional media advertising has now formed a certain scale and experience, technology is also more mature, there is a fixed consumer base, and the popularity of VR devices is not high, so the study of VR technology is not very deep. The market use is not mature enough, because the development of three-dimensional advertising and interactive advertising has been more common.However, as for how to really put three-dimensional advertising and interactive advertising together, I think designers need to constantly upgrade their technical experience, think about how to improve the high level of consumer interaction and experience, and expand the influence of VR advertising on the market gravity, so that advertisers can create and design ads based on the characteristics of VR (virtual reality).By attracting consumers to promote VR devices and VR advertising, the integration will be faster and faster. Virtual reality advertising is popular in China and other countries as a new marketing model. In recent years, the 3D technology of VR has been widely used, using various techniques of virtual reality technology. For example, in the case of fierce competition in the real estate industry, the original form of real estate display has been difficult to meet the actual needs of consumers. Therefore, the real estate industry must grasp the trend of market development, making full use of the latest technology at present, breaking the original monolithic three-dimensional display on customers through the virtual reality sensors, and giving customers a strong three-dimensional sense of scene, which allows customers to walk in different house types and rooms and at the same time choose different decoration styles and furniture according to their preferences through the interactive function and to really feel the scene after decoration, which not only saves a lot of investment in model rooms and different decoration for the real estate industry but also greatly stimulates customers' desire to buy, which makes the sales of origin products grow rapidly (as shown in Figure 3).

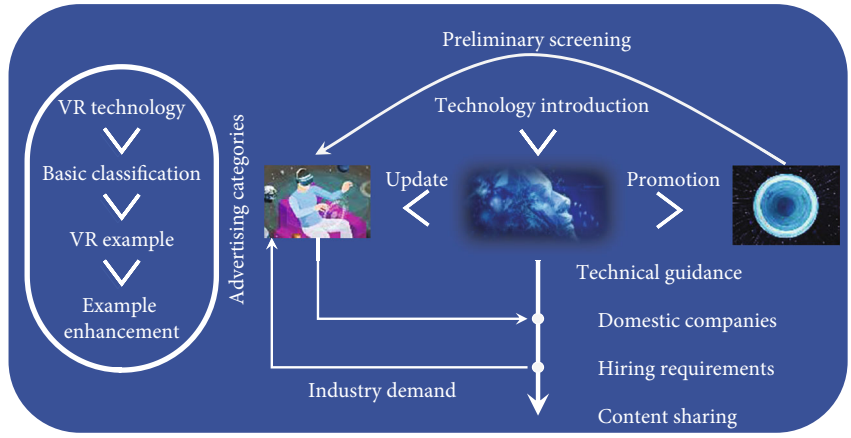

Figure 2: 3D VR media evolution process.

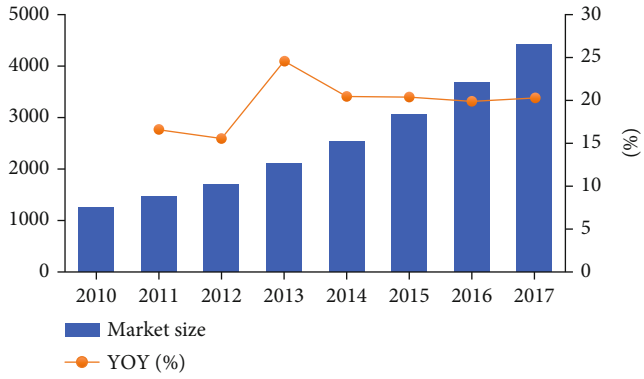

Figure 3: Global VR real estate market size forecast.

3.3. VR Display Advertising Design Practice. This advertisement is designed based on VR (virtual reality) technology as the medium. Through the analysis and research of the previous article, the author uses the design methods and design ideas summarized in the previous article as a practical guide; adopts the form of 3D immersive design interface, which can intuitively represent the real campus landscape and facilities; and adopts interactive design, which can interactively experience each landscape and facility and flexibly display each part of the campus to achieve the advertising. Because of its excellent immersion and immersion, the audience experiences the sensory stimulation even beyond the real, so the VR offline experience game is called "black technology" by users. The interactive design allows for interactive experience of each landscape and facility and flexible display of each part of the campus and achieves the advertising effect. This time, I did not choose ads with commercial nature but chose noncommercial ads with humanistic nature, hoping to promote the school with the help of VR media, so that more people can understand the charm of Ningjunyuan and integrate the culture of Ningjunyuan. In this advertisement, users can browse and watch the advertisement through computer or VR display device, and the typical buildings can be operated interactively. In order to reflect the authenticity of the display ads, the campus is filmed with an aerial camera for a bird's-eye view, and 3D max software is used to model the internal scenes of important buildings, especially the university's Union Building, and Pano2VR software is used to create hotspot interactions, so that users can use the virtual elevator to reach each floor and start consulting and answering questions with relevant university departments, or they can reach each branch of the university and become familiar with its specialties and advantages. That is to say, when a technology is applied to real life, its subsequent effects and consequences will not belong to the scope of human control; at the same time, people are addicted to the technological pleasure brought by technology on the one hand and are manipulated by this technological "pleasure" on the other hand.

The audience's sensory perception of information is roughly divided into the following five stages (Figure 4). The first stage is the initial stimulation stage of external physical information, and there is no great difference in the audience's perception of information at this stage; the second stage is the physiological filtering layer of the audience, i.e., the sensory stage. The third stage is the audience's psychological filtering layer; that is, the audience's own personalization and personality characteristics will be the second screening of information, and the role of emotion is the most important part of the link; the fourth stage is the audience's awareness of the product or brand. The fifth stage is the establishment of the cognitive profile, which has a certain chance; the audience's cognitive profile is not in the inevitable state that it will be established, but the confirmation is after the audience's perceived positioning of the brand or commodity awareness. It is a confirmation stage. In addition, the establishment of this stage will also provide feedback to the previous stages, and the desire for information generated by the establishment of the cognitive profile will have a rebound effect on the audience's mental and physical filters and continue to influence the audience's subsequent perception process.

In the eyes of "technological determinists," "technology is an independent force that develops according to its own logic, and although it arises from human needs, once it becomes a climate, it can easily become a wild horse out of human control." For example, before the technology of television was invented, there were no "TV people" and "container people."

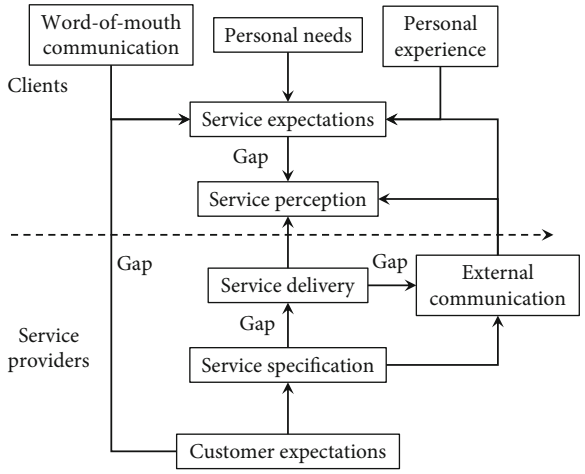

Figure 4: Consumer perception process model.

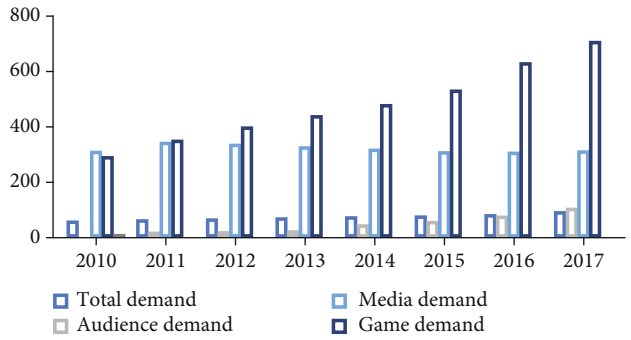

Figure 5: Demand generation in the dissemination process.

Before the technology of computer was popularized, there were no such terms as "mouse hand" and "Internet-addicted teenager." Once people reach this stage of "being controlled by technology," they become "puppets," that is, according to the logic of technology itself to change the human living environment and lifestyle and even to change the human value system. Therefore, VR advertising, as a hot new medium and technology, will also have a large or small impact on people's real life, and audiences should clearly understand that the "good" nature of technology and its "evil" nature exist together. The "change" of "technology changes life" is also neutral. VR advertising has opened a new chapter in people's understanding of the virtual world, but at the same time, it is also changing people's value identity, and the new trend in the aesthetic characteristics of advertising is the best reflection.

4. The Development of Three-Dimensional Visual Psychology in Practice

The "use and satisfaction" theory "views audience members as individuals with specific needs, and their media exposure activities as a process of using media based on specific needs and motivations, so that these needs can be satisfied." (1) From the concept, we can know that the theory involves three key words: demand, use, and satisfaction, and both "demand" and "satisfaction" are the psychological feelings

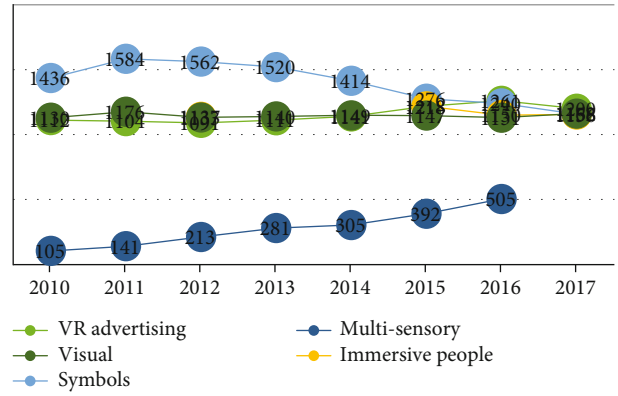

Figure 6: Sensory stimulation changes.

of the audience with autonomous and emotional characteristics, but "use" however is a dynamic process compared with the two and is a practical part of the construction of the audience's aesthetic psychological mechanism. After the construction of audience aesthetic mechanism based on audience sensory perception is completed, the subsequent behavior and psychology of the audience will also have a greater impact on the communication effect. The "use and satisfaction" communication process model shows the two main factors of demand generation (Figure 5), namely, social conditions and personal characteristics; after demand generation, the audience will choose the type of media based on media impressions and media contact possibilities and then engage in media contact. The whole process is bifurcated at the media contact stage, where the media that satisfies the audience's needs will in turn act on the media impression, and the audience will continue to seek other means of satisfaction if the media does not satisfy their needs.For advertising planners, VR creative will further unleash the imagination. Currently, there is only one way to combine VR and mobile marketing, so VR advertisers should work to innovate and inspire a richer and more diverse form of VR advertising.

From the above analysis, we can see that media impressions and media exposure possibilities are the key aspects of audience needs to be satisfied. In today's society, the richness of media forms gives audiences enough mobility and variety in their choices, so they pay more attention to their own physical and psychological pleasure of communication. This "selective exposure" gives audiences a great sense of pleasure and power, and they are more likely to follow their own media logic for media selection. This sensory perception also influences the image of VR media, and the positive image of the media attracts more and more attention from the audience. The development of VR advertising has received a great deal of attention in the past year, and it is very important for the audience to have a sense of satisfaction. The development of VR advertising has received a lot of attention in the past year, and people are full of curiosity and expectation for the new technology which is extremely human and interesting.

The derivation of new media and technologies represents a major advancement in human technology, and human beings have made remarkable achievements in the process of

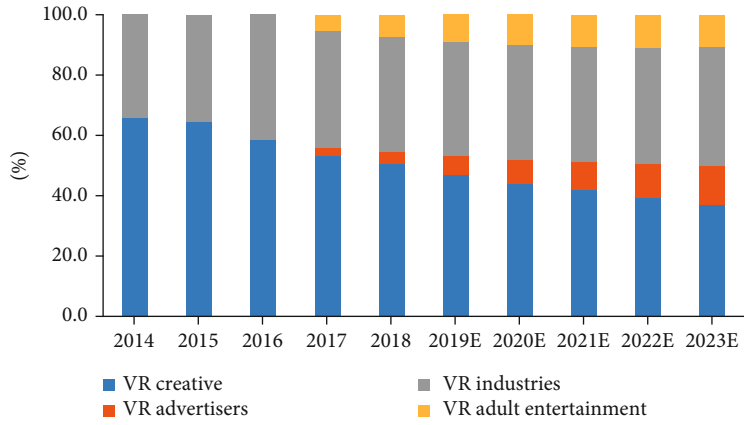

Figure 7: VR users' votes on "adult entertainment."

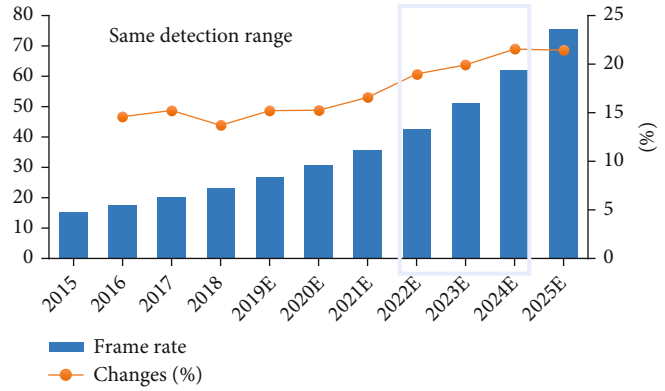

Figure 8: Frame rate variation of VR ads.

transforming the world. What we need to do is to take a high theoretical and global view of the transformation of real life by the new medium of VR advertising and to compare the properties of the new medium with those of the old medium, trying to understand the development of the new medium at its inception, as shown in Figure 6. The emergence of "immersive people" has reshaped the aesthetic psychology of advertising audiences; we are moving away from the "visual is king" approach. We are changing from a "visual" cognitive approach to a "multisensory-stimulating experience"-based exploration channel. All these changes prove that the change of media technology eventually leads to the renewal of the aesthetic characteristics of advertising.

First, VR advertisers should reject the temptation to strengthen their own ethical awareness. The Chinese VR user research report launches storm magic mirror in conjunction with the national advertising research institute on March 18, 2016.Now, Meng Consulting Agency has released the "Chinese VR user behavior research report," which report on China's VR users to conduct in-depth research; and in a comprehensive analysis of the current VR user behavior for the first time.The survey involved 15 provinces and cities across the country, and a total of 5,626 analysis samples were taken. The survey involved 5,626 samples taken from 15 provinces and cities for analysis. One of the survey data for the "top 10 VR industries of interest to users" showed that heavy users and light users voted 54.2% and 44.8%, respectively, for "VR adult entertainment" (Figure 7). At present, more and more technology companies are investing in VR adult entertainment. Facing such audience and market situation, VR advertisers must strengthen their own ethical awareness, pay attention to their own moral shape, and not disrupt the whole VR market communication order because of immediate self-interest. Second, VR advertisers should strengthen their own strengths and improve their ability to innovate. In the face of the burgeoning VR market, advertisers should break the limits of the format and be willing to try more and fresher ways of communication. Fu Chuanzhi, general manager of Airwave mobile marketing at Omnicom Media Group, said, "For brand owners, VR devices will become the main link to consumers."

By focusing on the aesthetic characteristics of VR advertising as an object of study, the new aesthetic trends that emerge will have implications for both VR advertising research and the development of the advertising industry itself. The new characteristics of the aesthetic characteristics of advertising are inevitably disruptive to the existing visual culture: the role of "symbols" is gradually weakened. VR advertising has extremely demanding technical requirements, and any substandard

equipment will have a direct impact on the effectiveness of VR advertising, so VR advertisers should improve their business capabilities, learn from the early start of VR technology and the development of mature foreign technology companies, and develop a series of technical development strategies combined with their own. First, technology platforms should improve their strengths and overcome technical barriers. Although VR advertising represents the most technological advertising available, there are still inevitable embarrassments in the technical equipment level. For example, the high price of VR devices, compared to smartphones, poses a barrier to audience reception, as shown in Figure 8; in addition, VR devices are prone to vertigo and discomfort due to their ultra-realistic panoramic views. How to break the price barrier and pave the way for the popularity of VR are the problems that VR technology platform needs to face.How to overcome the technical problemsand make the audience's experience reach an extremelyforgetful level is the proposition that the technology platform should be developed first.

First of all, VR advertising audience should strengthen their own media literacy. First, they should learn and master the ability to use new media means or equipment, which is the most basic ability that VR advertising audience should have; second, they should have the ability to read media information, that is, the reading and understanding of information; third, they should develop their own critical and questioning ability of media information, so that they will not be blinded by the complex information; fourth, they should strengthen the ability to collect, process, produce, and publish information. This is also the core ability that "immersion people" should have when they evolve to the stage of integration with the media. The shaping of the audience's "media literacy" is also an extremely important part of bridging the "digital divide." The audience should be aware of their "self-media" identity and strengthen their sense of responsibility and existence, so that they can sharpen their eyes in the face of temptation. Secondly, "opinion leaders" should also play their own role in guiding and cultivating the aesthetic ability of the audience. VR is currently the hottest medium of communication, and the trend has just emerged so that many companies and individuals cannot help but follow a trend, so the current communication market VR ads are numerous and mixed, not without some collective and individual exploit. The law has been broken, and some groups and individuals are taking advantage of it to disseminate information that is contrary to social mores. Mainstream media and opinion leaders should be aware of their own orientation and promote risk awareness to their advertising audiences. They should also be aware of their social responsibility to not promote VR ads that contain bad information in order to attract attention.

5. Conclusion

VR (virtual reality) has created a unique advertising logic, and its extension and experience in the field of advertising integration fully combine the immersion, three-dimensionality, and special services of VR (virtual reality) into the field of advertising, demonstrating its distinctive consumer attributes, which are released as a consumer attribute of communication. But the continued maturity and development of technology will give rise to more advanced communication media, and each new media replacing the old media is a huge test for human beings. The change of media has its own "constant": we have to follow the old media, use the existing communication theory to verify the new media, and find the fit between communication theory research and social development in order to move forward in the turbulent stream of media change. "Whereas in the past interaction was the darling of a particular scenario, now consumption defines the properties of a certain product, a certain kind of release or liberation, and these dogmas are readily available whenever and wherever they are." In terms of broader content, it can be said that VR (virtual reality) or its equivalent is the perfect interplay of media people and crowds' tastes. The research on the integration of 3D animated ads and interactive ads under VR technology is launched, and the research on 3D stereoscopic and interactive design of advertisements in the era of smart media is a reflection and exploration of the future language of advertising design. In the era of smart media, the ads realized through the fusion of VR technology will become a new trend in the future development of advertising. The integration of 3D advertising and interactive advertising makes VR as a new medium in the age of intelligent media that has a new way out in the advertising industry, which can more easily and quickly replace the traditional media-based advertising methods, allowing consumers to have a more realistic and personalized advertising experience. In the future, mainstream media and opinion leaders should be aware of their own orientation and promote risk awareness to their advertising audiences.

Data Availability

The data used to support the findings of this study are available from the corresponding author upon request.

Conflicts of Interest

The authors declare that they have no known competing financial interests or personal relationships that could have appeared to influence the work reported in this paper.

Acknowledgments

This work was supported by the Shaanxi new liberal arts research and reform practice project:innovative research and practice of mixed teaching methods for art majors from the perspective of intelligent education.

References

[1] V. Bogicevic, S. Seo, J. A. Kandampully, S. Q. Liu, and N. A. Rudd, "Virtual reality presence as a preamble of tourism experience: the role of mental imagery," *Tourism Management*, vol. 74, pp. 55–64, 2019.

[2] K. Cowan, N. Spielmann, E. Horn, and C. Griffart, "Perception is reality... How digital retail environments influence brand perceptions through presence," *Journal of Business Research*, vol. 123, pp. 86–96, 2021.

[3] S. Crawford-Holland, "Virtual healing: militarizing the psyche in virtual reality exposure therapy," *Television & New Media*, vol. 20, no. 1, pp. 56–71, 2019.

[4] L.-E. Dubois and C. Gibbs, "Video game-induced tourism: a new frontier for destination marketers," *Tourism Review*, vol. 73, no. 2, pp. 186–198, 2018.

[5] M. F. Farah, Z. B. Ramadan, and D. H. Harb, "The examination of virtual reality at the intersection of consumer experience, shopping journey and physical retailing," *Journal of Retailing and Consumer Services*, vol. 48, pp. 136–143, 2019.

[6] L. de Gauquier, M. Brengman, K. Willems, and H. van Kerrebroeck, "Leveraging advertising to a higher dimension: experimental research on the impact of virtual reality on brand personality impressions," *Virtual Reality*, vol. 23, no. 3, pp. 235–253, 2019.

[7] S. H. Jeong, S. Kim, J. Y. Yum, and Y. Hwang, "Effects of virtual reality news on knowledge gain and news attitudes," *International Journal of Mobile Communications*, vol. 18, no. 3, pp. 300–313, 2020.

[8] J. Jung, J. Yu, Y. Seo, and E. Ko, "Consumer experiences of virtual reality: Insights from VR luxury brand fashion shows," *Journal of Business Research*, vol. 130, pp. 517–524, 2021.

[9] K. Kilic, M. G. Saygi, and S. O. Sezer, "Exact and heuristic methods for personalized display advertising in virtual reality platforms," *Journal of Industrial & Management Optimization*, vol. 15, no. 2, pp. 833–854, 2019.

[10] K. W. Lau and P. Y. Lee, "Shopping in virtual reality: a study on consumers' shopping experience in a stereoscopic virtual reality," *Virtual Reality*, vol. 23, no. 3, pp. 255–268, 2019.

[11] Y.-J. Lee, W. Zhao, and H. Chen, "Consumer response to virtual CSR experiences," *Journal of Current Issues and Research in Advertising*, vol. 42, no. 1, pp. 102–122, 2021.

[12] W. H. Lo and K. L. B. Cheng, "Does virtual reality attract visitors? The mediating effect of presence on consumer response in virtual reality tourism advertising," *Information Technology & Tourism*, vol. 22, no. 4, pp. 537–562, 2020.

[13] A. Marasco, P. Buonincontri, M. van Niekerk, M. Orlowski, and F. Okumus, "Exploring the role of next-generation virtual technologies in destination marketing," *Journal of Destination Marketing and Management*, vol. 9, pp. 138–148, 2018.

[14] S. Okolo, "Can virtual reality improve the health of older sports fans," *IEEE Potentials*, vol. 38, no. 3, pp. 17–19, 2019.

[15] J. Park, J. Choi, and C. Rhee, "Futuristic VR image presentation technique for better mobile commerce effectiveness," *Virtual Reality*, vol. 25, no. 2, pp. 341–356, 2021.

[16] G. Pizzi, V. Vannucci, and G. Aiello, "Branding in the time of virtual reality: are virtual store brand perceptions real?," *Journal of Business Research*, vol. 119, pp. 502–510, 2020.

[17] N. Spielmann and U. R. Orth, "Can advertisers overcome consumer qualms with virtual reality?," *Journal of Advertising Research*, vol. 61, no. 2, pp. 147–163, 2021.

[18] C.-Y. Ung, M. Menozzi, C. Hartmann, and M. Siegrist, "Innovations in consumer research: the virtual food buffet," *Food Quality and Preference*, vol. 63, pp. 12–17, 2018.

[19] P. Vishwakarma, S. Mukherjee, and B. K. Datta, "Antecedents of adoption of virtual reality in experiencing destination: a study on the indian consumers," *Tourism Recreation Research*, vol. 45, no. 1, pp. 42–56, 2020.

[20] R. Yung, C. Khoo-Lattimore, and L. E. Potter, "Virtual reality and tourism marketing: conceptualizing a framework on presence, emotion, and intention," *Current Issues in Tourism*, vol. 24, no. 11, pp. 1505–1525, 2021.

[21] R. Yung, C. Khoo-Lattimore, G. Prayag, and E. Surovaya, "Around the world in less than a day: virtual reality, destination image and perceived destination choice risk in family tourism," *Tourism Recreation Research*, vol. 46, no. 1, pp. 3–18, 2021.

Hindawi
Journal of Sensors
Volume 2022, Article ID 3436530, 11 pages
https://doi.org/10.1155/2022/3436530

Research Article

Optimization of the Intelligent Asset Management System Based on WSN and RFID Technology

Yunyue Chen[1] **and Guanggui Chen**[2]

[1]*Stern School of Business, New York, 10001 NY, USA*
[2]*Yangzhou University Yangzhou College of Science and Technology, Jiangsu Yangzhou 225001, China*

Correspondence should be addressed to Guanggui Chen; 101293@yzpc.edu.cn

Received 15 November 2021; Revised 8 January 2022; Accepted 17 January 2022; Published 4 February 2022

Academic Editor: Chih-Cheng Chen

With the development of Internet of Things (IoT) technology, especially the promotion of perception layer radio frequency identification (RFID) technology and wireless sensor network (WSN), a new way of thinking is provided for asset management. Applying both to the management technology of assets is an effective way to achieve intelligent asset management. This paper proposes an intelligent network applied to an asset management system based on WSN and RFID technologies. The whole intelligent asset management is divided into four layers according to the functional structure. From the top layer downward, the layers are the management and dispatch center, communication network, intelligent gateway, and data collection layer in order. Meanwhile, the functions and hardware composition of each layer are described. The data acquisition butcher is the sensing terminal of the whole intelligent asset management network. Smart nodes are its key devices to collect RFID data and sensing data to realize the intelligent sensing capability of the assets. The paper uses the MSP430 control chip, MFRC522 RF read/write chip, CC2425 wireless communication chip, temperature sensor, data memory, and voltage regulator chip to design the smart nodes in the system and details the working principle of the smart nodes and the networking process of the system. The newly designed intelligent asset management network can be deployed independently in asset management or can be integrated into the technical design of existing asset management systems. The management scheduling also collects and manages the RFID and sensing information of the area through the data collection layer, which improves the intelligent construction of the assets.

1. Introduction

The corresponding work involved in asset management is tedious, and the process is relatively fixed. It has to involve all kinds of work-related to equipment storage, equipment inquiry, equipment monitoring, equipment maintenance, and equipment change and asset loss analysis [1]. In traditional asset management, a lot of daily management work is done in the traditional manual way, such as regular inventory check of fixed assets, registering the relevant asset and equipment data collected with paper materials, and then entering these data into the computer memory file after manual collation. Fixed assets used in enterprises are characterized by a wide range of types, high values, and a large number of people handling them, a long life cycle, and a wide distribution of locations [2]. The traditional way of management often leads to problems such as incomplete registration information, data not being updated in time, inconvenient information inquiry, and difficulties in integrating information in isolation. By deploying and controlling the various base stations and locators in the area, it is possible to know the asset location and distribution of a certain indoor and outdoor attached asset card in time and record its historical location information [3]. The administrator can query the real-time location of the specified asset in real-time and mark it on the electronic map of the system. The distribution of assets in each depository can be inquired in real-time, and the detailed asset

information of a certain distribution can be viewed [4]. It can query and replay the historical movement tracks of assets and historical data reports.

This paper carries out research work such as understanding and analyzing the fixed asset and equipment management technology existing in enterprises, using advanced object-oriented technical means to analyze and model the needs of asset management, applying RFID technology to track and locate important equipment, and using smartphones as tools to manage asset information in a timely and convenient manner. Radiofrequency identification technology (RFID) has gradually become a hot research area of concern for current information technology, and a variety of various applications based on this technology are emerging [5]. Radiofrequency identification technology (RFID) works in a very different way from the traditional way, and it uses a noncontact way to automatically acquire and identify the required data. Since RFID technology is not limited by physical location and can communicate with multiple objects at the same time, it has been widely promoted in various applications related to location. Asset management using various technologies is well organized to achieve information and standardized management of assets [6]. The asset management system mainly has functions such as asset registration, data inquiry, change management, asset review, asset inventory, asset statistics, and report printing. The key issues in the development of this system are the setting of network security access rights, diversity of data query, performance optimization of the system, QR code generation and report printing, etc. This paper adopts the scheme of enterprise fixed asset management system with WSN and RFID, taking into full consideration to reduce manual work intensity and improve the management level and efficiency [7]. The choice of WSN and RFID technology program, using its technical advantages of real-time positioning monitoring of valuable fixed assets, can effectively prevent the loss of valuable assets and damage to the enterprise and improve the security of assets and equipment and efficiency of use.

The separation of system operation and maintenance personnel from basic operation and maintenance personnel reduces the cultural and operational requirements of basic operation and maintenance personnel and reduces the personnel requirements for daily operation and maintenance of the system, thereby saving the cost of high-end operation and maintenance manpower. This paper proposes to apply the wireless sensor network and RFID fusion technology to the intelligent asset management system and design the fusion wireless sensor network node and RFID electronic label status monitoring, the main contents of this paper and the related chapters are arranged as follows [8]. The first chapter analyzes the background of this paper and the practical significance of the research in detail and introduces the research work of the paper. The second chapter analyzes the research status of various intelligent asset management systems and condition monitoring devices at home and abroad, explains the advantages of integrating RFID technology with WSN technology, summarizes the advantages and disadvantages of existing research results, and puts forward the research direction and objectives of this paper. Chapter 3 analyzes the intelligent asset management system based on WSN and RFID technology. This paper proposes a new intelligent asset management network, which mainly consists of a condition monitoring IED fusing WSN nodes and RFID tags and a master IED fusing aggregation nodes and readers, and focuses on analyzing the data communication mode between the condition monitoring IED and the master IED. An RFID technology prioritization strategy and RFID and ZigBee communication technology switching algorithm are designed for the intelligent asset management network. Chapter 4 analyzes the research of this paper, tests the intelligent asset management network model and system constructed in this paper, and summarizes the test results. Chapter 5 concludes and outlooks this paper, summarizes the work and research results done in this paper, analyzes the shortcomings that still exist in the system design and implementation, and proposes further research improvement solutions for these shortcomings.

2. Related Work

Asset management is an indispensable part of business management, and all companies are paying more attention to equipment assets. A variety of advanced technologies are used to continuously improve the management of assets and the efficiency of use, domestic, and foreign enterprises to reduce the rate of idleness of assets, especially the use of valuable assets, to avoid various losses [9]. Kinnunen et al. used WSN nodes and reader fusion for security monitoring of fixed assets. WSN nodes are responsible for collecting environmental parameters such as temperature, humidity, and pressure of the warehouse where fixed assets are stored and establishing a transmission network to transfer this sensory information to the host computer system simultaneously with the fixed asset information read by RFID technology, thus achieving a real-time mastery of fixed asset warehouse information. In the WSN node and reader fusion network, the reader can join the WSN network; however, RFID tags are still only able to communicate with the reader through RFID technology, which limits the communication range [10]. Andreacchio et al. proposed WSN node and RFID electronic tag fusion for monitoring fixed assets, the information stored in the electronic tag is also regarded as a kind of sensing data, and Zigbee star topology network is used to transmit the sensing data of WSN node and RFID tag information. It is proved through experiments that only 2.44 W-2.5 W more power consumption is consumed by embedding RFID tags into fixed assets. In the network of WSN nodes fused with electronic tags, the data transmission mainly relies on the WSN network, but the power consumption of the WSN network to transmit data is higher [11]. Çeken et al. used RFID tag and sensor fusion so that the RFID electronic tag can sense environmental information; however, the fused RFID tag sensor is only able to communicate with the reader single-hop through RFID technology and cannot join the WSN network, and the communication distance is short [12].

Barcode-based asset management systems are generally used to manage assets in physical form, characterizing an

asset with a barcode tag to achieve asset management. However, barcodes are not as efficient as RFID technology because they are prone to breakage and can only be read one by one [13]. Chen et al. proposed the structure of WSN and RFID convergence, which includes distribution streamlined sensor-reader structure, hybrid network structure, and intelligent active tag network structure, and analyzed the problems of technology faced by these three systems structures [14]. Chen et al. extended the architecture design of the fusion network and improved the network of intelligent nodes effectively to achieve intelligent management of the location management system of the warehouse and adopted an adaptive system structure used to improve the efficiency and reliability of the inventory goods, and this system has the characteristics of flexibility and stability [15]. Lee et al. fused sensor nodes and RFID tags and divided them into two types of tags, active, and passive and solved the synergistic working mechanism of the two as a key problem [16]. The effective fusion of WSN and RFID technologies can fully solve the existing deficiencies of the existing research, and the wireless RFID devices can work in harsh environments, have a small size, are resistant to interference, have strong penetration, can quickly identify moving objects, and can identify multiple tags simultaneously [17].

The above research shows that RFID and WSN technologies have been widely used in various fields, but the application of these two technologies in the coal industry has just begun, and the application prospects are broad [18]. The RFID system integrated with WSN has the advantage of wireless communication. Compared with wired communication, it is convenient to transmit and process key data and save valuable time. Portable RFID readers can further speed up data collection. From the relevant literature at home and abroad, all the above applications are relatively single, and only two technologies are used separately. The research work of RFID and WSN fusion technology has not fully considered the interference of RFID to ZigBee wireless sensor networks, RFID anticollision algorithms, optimized RFID positioning and tracking technology for intelligent asset management environment. This project will further study the key theories of RFID and WSN fusion technology, establish the positioning model, and play an important role in complementing the positioning algorithm for intelligent asset management. Due to the need for long-distance reading, asset management usually uses UHF RFID technology [19]. This thesis analyzes and studies the architecture composition and function module of RFID technology and studies the interface call and functional interaction between the reader and the two terminals of client and handheld. At the same time, since assets are scattered inside and outside the enterprise, the enterprise does not want the data in the RFID tags attached or installed on the assets not to be known by unauthorized users [20].

2.1. Multipath Routing Method for Video Streams in Wireless Multimedia Sensor Networks Based on Optimized Ant Colony Algorithm

2.1.1. General Analysis of the Intelligent Asset Management System. Through the functional and business logic analysis of the asset management system, a deep requirement analysis of the system designed and implemented in this thesis is conducted. The four main functional modules of this system are summarized to include system management function, asset management function, asset query function, and report management function. The user rights are divided into the following types: system administrator, departmental asset manager, and general user. The system administrator has all the system privileges and can perform the following four functional operations: system management, asset management, asset inquiry, and report management. The departmental asset manager has three functional rights: asset management, asset inquiry, and report management. Ordinary users have only two basic functional privileges: asset inquiry and report management.

We set the QR code to consist of a UUID (universal unique identification code) and an information part, whose functions correspond as shown in Table 1.

Smart tag is a fusion of RFID tag and wireless sensor node together. Its main structure is divided into a tag module, a processor module, sensor module, wireless communication module, storage circuit, power supply, voltage regulator circuit, etc. The tag is not only able to communicate with RFID readers through tag antenna but also able to communicate with each other through node antenna and other nodes. Smart tags and radio frequency read-write devices by RFID standards for data transmission between the smart tags are by the WSN protocol networking communication. The data forwarded between smart tags include unique electronic code information and monitored environmental dynamic information.

The monitoring and scheduling center is the top department of the whole monitoring network, where the monitoring and display platform can query and monitor all RFID and sensing data in the current network; the linkage response mechanism can quickly execute the order to eliminate faults. The communication network in terms of hardware facilities is mainly for signal towers and related communication devices in the network, and its direct purpose is to transmit the data gathered by the intelligent gateway to the monitoring and scheduling center safely and reliably, while the monitoring and scheduling center is often deployed in the asset management Midwest or comprehensive monitoring system management platform according to the actual situation of rail transit. In the data collection layer, each node will monitor a large amount of raw data, which is a no small task for both the node processor and the data transmission between each intelligent node due to the large scale and poor accuracy. And for some occasions, often only the results of monitoring events are concerned, not the data itself. Therefore, in this part, data fusion techniques need to be designed. Data fusion techniques can be combined in the data acquisition layer, which reduces the amount of data transmission and saves energy overhead, or in the gateway and application layers.

In the communication mode, when the CC2425 sends data, it first writes the data into the sending buffer and starts data transmission when the wireless channel is free. When receiving data, the same data is first stored in the receive buffer, and the status of the received data is output through

Table 1: Composition of QR code encoding.

Serial number	Constitute	Function	Occupied digits
1	UUID	Describe the unique identifier of the QR code	Top 16
2	Information to be encrypted	Store QR code transmission information	Available digits (total capacity-16)

the FEFO and FEFOP ports. The flow chart of initialization, sending, and receiving data of the communication module is shown in Figure 1. MF RC522 supports all layers of ISO14443A, and the transmission speed is up to 424 kbps. The internal transmitter part can directly drive the short-distance antenna without adding an active circuit. The receiving part provides solid and effective demodulation and decoding circuit for receive ISO14443A compatible response signal.

2.2. Intelligent Model Construction Based on WSN and RFID Technology. In this paper, the three-dimensionally arranged beacon nodes are projected on a horizontal plane, and an improved localization algorithm is proposed by using the traditional RSSI trilateral measurement algorithm and combining the fusion technology of WSN and RFID. The positioning of blind areas and incomplete coverage of RF signals ineffectively compensated, and the positioning accuracy of RF coverage and motion trajectory is improved.

The format of the localization vector in the localization algorithm is designed as (tag, node ID, X_{first}, X_{last}), where tag denotes the electronic tag carried by the miner and has a unique EPC code, node ID denotes the ID number of the beacon node, tatar denotes the time when the asset is first monitored within the range of the beacon node, and tend denotes the time when the asset is last monitored by the beacon. The time when the asset was last monitored by the beacon node, and the positioning vector after group ordering is shown in Table 2.

Assuming that the current position of the unknown node is not within the range of any beacon node signal, let the unknown node pass through beacon nodes x_1, x_2, and x_3 in turn with signal radii $d(x_1)$, $d(x_2)$, and $d(x_3)$, and the unknown node is $d(k, x_1)$ at the signal range boundary to x_1, $d(k, x_2)$ at the signal range boundary to x_2, and $d(k, x_3)$ at the signal range boundary to x_3. The moment to be located is known to be T_x and the unknown node. The last monitored moment Tend at x_1 is $T(x_1)$, as in Equation (1). The distance from the unknown node to the beacon node N1 can be obtained from Equation (1).

$$d(k, x_1) = f(v, d) * (T(x_n) - T(x_1). \tag{1}$$

The last monitored moment Tend of the unknown node at x_2 is $T(x_2)$, as in Equation (2). From Equation (2), the distance from the unknown node to the beacon node is x_2.

$$d(k, x_2) = f(v, d) * (T(x_n) - T(x_2). \tag{2}$$

The moment X_{first} when entering x_3 is monitored for the first time that is $T(x_3)$, as in Equation (3). From Equation (3), the distance from the unknown node to x_3 is obtained.

$$d(k, x_3) = f(v, d) * (T(x_n) - T(x_3). \tag{3}$$

Based on the above three assumptions, then the traditional trilateral measurement algorithm is improved to Equation (4).

$$\begin{cases} (d(i) + d(k, i))^2 = \left(f(x) - f(x_i)\right)^2 + \left(f(y) - f(y_i)\right)^2 \\ G(m) = \sum_{j=1}^{N} \left(T(x_j) - T(m)\right)^2 \end{cases}, i = 1, 2, 3, \tag{4}$$

where the unknown node is within the range of a smart node x_i, and then $d(k, i) = 0$. The joint cubic equation system can calculate the coordinates (x, y) of the unknown node, as shown in Equation (5).

$$\begin{cases} x_1^3 - x_2^3 + y_1^3 - y_2^3 = (d(x_1) + d(k, x_1))^3 - (d(x_2) + d(k, x_2))^3, \\ x_1^3 - x_3^3 + y_1^3 - y_3^3 = (d(x_1) + d(k, x_1))^3 - (d(x_3) + d(k, x_3))^3, \\ x_2^3 - x_3^3 + y_2^3 - y_3^3 = (d(x_2) + d(k, x_2))^3 - (d(x_3) + d(k, x_3))^3. \end{cases} \tag{5}$$

The service life of the sensing tag can be calculated by Equation (6), where D is the battery capacity, M is the duty cycle, and the MCU indicates the state "0" when it is working and "1" when it is sleeping, and the probability of "0" and "1" is the same as 0.5. The duty cycle is $M = 0.5$.

$$P(h) = \frac{D}{(L_{\text{active}} * M) + L_{\text{sleep}} * (1 - M)}. \tag{6}$$

The carrier frequency is set to grow from 810 MHz to 950 MHz in 5 MHZ steps. The reader antenna is placed at a distance of $d = 1$ m from the sensing tag antenna (H (reader) = 6.5 dBi), and the reader transmits at a power of P (on). The sensitivity of the sensing tag can be obtained by Equation (7), where P (on) denotes the minimum power that can activate the RFID tag. H (ide) takes the maximum antenna gain of the sensing tag as 1.8 dBi, H (ide) = 1.8 dBi, α is the wavelength, and β is the polarization loss factor of the reader antenna and the sensing tag antenna.

$$\begin{cases} L(\text{ide}) = \beta * Q(\text{on}) * H(\text{ide}) * \left(\dfrac{\lambda * \alpha}{3\pi d(k, i)}\right)^2, \\ Q(\text{on}) = P(\text{reader}) * H(\text{reader}). \end{cases} \tag{7}$$

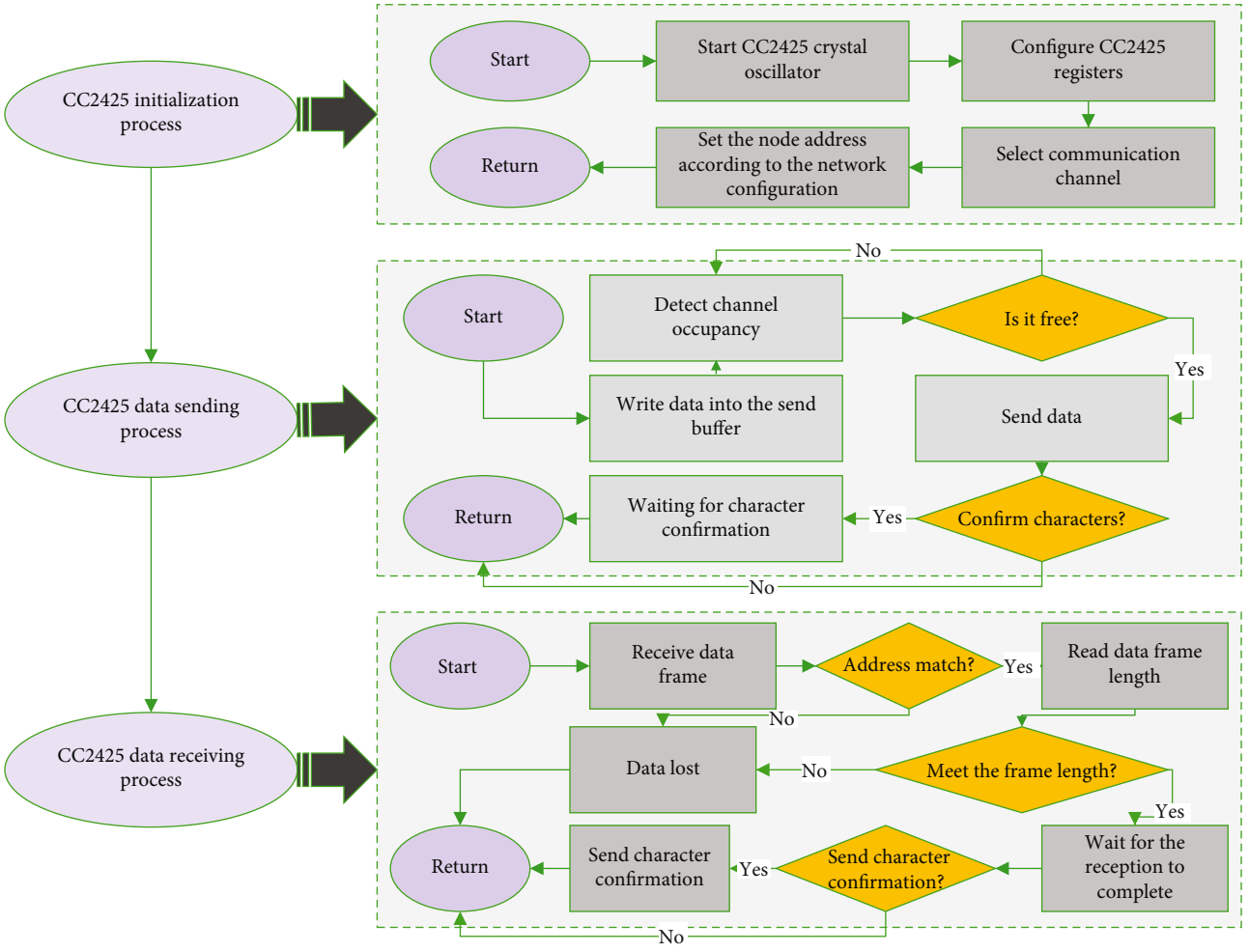

Figure 1: CC2425 program flow chart.

Table 2: Table of positioning vectors.

Serial number	Tag	Node ID	X_{first}	X_{last}
1	Tag 1	Node 1	First 1	Last 1
2	Tag 2	Node 2	First 2	Last 2
…	…	…	…	…
4	Tag N	Node N	First N	Last N

The read/write distance of UHF RFID tags is an important index for testing the performance of the tags. The maximum read/write distance of the sensing tag is calculated by Equation (8). Evaluate the position of the mobile terminal equipment entering the positioning area and determine the range of the area in which the pending node can exist, and when the RFID reader recognizes the RFID tag of the entered RF area, the reader's data will be related to itself.

$$\max(d) = \alpha * \frac{\lambda}{3\pi d}\sqrt{\frac{\max(Q(\text{on})) * H(\text{ide}) * \beta}{U(\text{ide})}}. \quad (8)$$

The main basis for switching between RFID and ZigBee technologies is the advantages and disadvantages of the communication conditions of the two technologies, and a communication condition detection loop is proposed. The communication condition detection loop consists of two detection tasks for detecting the real-time communication conditions between RFID and ZigBee, and the two detection tasks are defined as RFID_test_loop() and ZigBee_test_loop(). Firstly, RFID_test_loop() is used to detect the RFID communication conditions, if the RFID communication environment is good, the status monitoring IED and the main IED use RFID technology to communicate, if RFID test task RFID_test_loop0 detects that RFID technology cannot meet the communication requirements, then ZigBee technology is used. If the status monitoring IED and the main IED cannot communicate even if they try to use ZigBee technology, then the communication between them fails and the next test task loop will be carried out.

2.3. Intelligent Asset Management System Design and Implementation. The asset management system realizes the

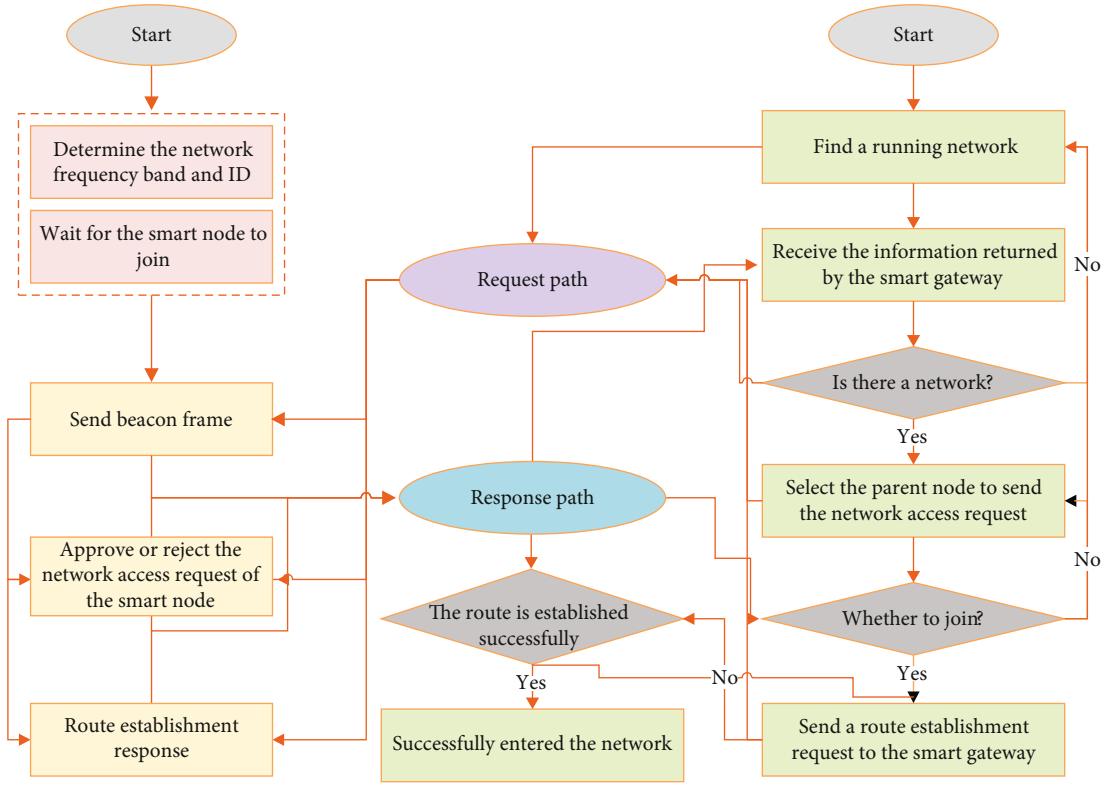

Figure 2: Flow chart of network formation.

modules of business management, information inquiry and analysis, system setting, and cell phone application. Before running the system, an initial setup is performed, and some necessary basic information is entered, after which the system can run normally [21, 22]. To use the system, the identity of the user has to be determined by logging in, and the functional interaction interface is given according to the user's authority. After logging in, you enter the operation interface of the asset management system, which includes the system setting module, business processing module, and system message management module.

The ZigBee coordinator of the smart gateway is responsible for the information collection of the whole data collection layer. Therefore, it needs to be responsible for the networking of smart nodes with the gateway. After successful networking, each node is then responsible for its task under the management of the operating system. The ZigBee protocol has a clear process for the networking process of the system. First, the coordinator module scans and selects all available 2.4 GHz bands in the protocol stack configuration. Then, the band with less noise is selected to build the network, or this step is skipped if there is a present. The coordinator assigns a network address packet of limited capacity to each smart node that is to join the network. The flow chart of the network formation procedure of the smart gateway and the network entry procedure of the smart nodes are shown in Figure 2.

The uppermost layer in the traceability system is the application layer, which is responsible for the management, storage, and display of data. The database is responsible for data collection and storage, and the webserver is responsible for business logic processing and data presentation. The system is designed in B/S mode with MySQL database, Nginx web server, Python+Django framework as the development language, and Bootstrap+Jquery as the front-end development, and the design of the application layer mainly include coding design, database design, and website logic design.

The data transmission module is mainly responsible for collecting, organizing, and uploading data. This module is mainly composed of sensing nodes that upload the collected data to the database through the data transmission module. For systems with a large number of data collection nodes, it is appropriate to use a wireless sensor network as the medium for data transmission and collection. Wireless sensor networks are highly integrated and involve a variety of cutting-edge science and technology. The network itself consists of multiple stationery or mobile sensing nodes that collaborate to collect and process data information. Since they transmit simple data, they require low bandwidth, but low latency and power consumption. Very low power consumption can greatly extend the working time of nodes. And ZigBee has the advantages of low complexity, low power consumption, low rate, and low cost; so, this paper uses ZigBee wireless sensor network as a medium for data transmission. ZigBee wireless sensor network has three main logical device types: coordinator (coordinator) router (router), and end-device. Usually, a ZigBee network consists of a coordinator as well as multiple routers and end devices. The functions of each part in the ZigBee network composition are shown in Table 3.

Table 3: Functions of each node in the ZigBee network.

Serial number	Equipment name	Hardware name	Function
1	Coordinator	CC2425 core board	Network configuration
		CC2425 base plate	Start-up and maintenance
2	Router	CC2425 core board	Node verification
		CC2425 base plate	Data forwarding
3	Terminal node	CC2425 core board	Data upload
		CC2425 base plate	Data forwarding
		Multiple sensors	Data collection

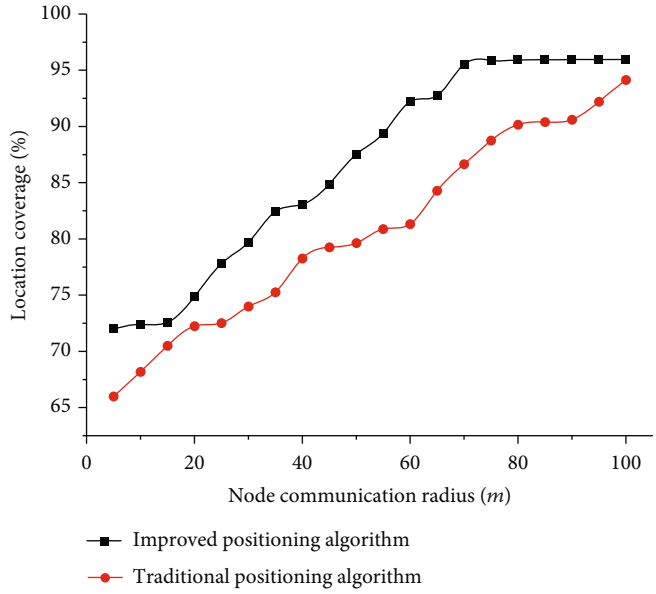

Figure 3: Positioning coverage map.

3. Analysis of Results

3.1. Intelligent Model Analysis. Comparing the improved localization algorithm in this paper with the traditional localization algorithm, the coverage of the improved localization algorithm approximates 95% when the localization radius of the beacon nodes is gradually increased. In the traditional localization algorithm, the coverage of localization is only about 70% when the radius of beacon node communication is short because the beacon node arrangement has a great influence on the localization accuracy, but as the radius of beacon node communication increases, the coverage of the traditional algorithm and the improved algorithm will converge. From Figure 3, it can be shown that the coverage rate of the improved algorithm can be significantly higher than that of the traditional algorithm.

In the experiment, the communication radius is set to 10 M in this paper, and the Markov chain is effectively used for localization trajectory prediction, using the localization coordinates of a known moment to predict the localization coordinates of the next unknown moment, in turn. The experiment will be run using 50 times of the same data and take its average. The localization error of one of the experiments is shown in Figure 4(a). Using the same method, the average error of the predicted 50, 70, and 100 motion trajectories is compared, as shown in Figure 4(b). From Figure 4, it can be obtained that the X-axis and Y-axis coordinates of the localization coordinates are stable in the range of 100 meters, and the error values are more stable. However, in the subsequent time slot prediction, the error value gradually increases. It is found that it is due to the accumulation error of the Markov chain itself. In practical applications, the combination of the positioning algorithm and the prediction algorithm in this paper can effectively reduce the prediction error.

According to Figure 5, it can be seen that the improved algorithm in this paper significantly reduces the localization error when there are fewer nodes compared with the traditional algorithm. This is because when the reference nodes are relatively few, the influence coefficient of environmental errors on system localization is larger, and the RSSI filtering model, as well as the location filtering in this paper, just reduces the influence of environmental factors on localization. As the number of reference nodes increases, both the

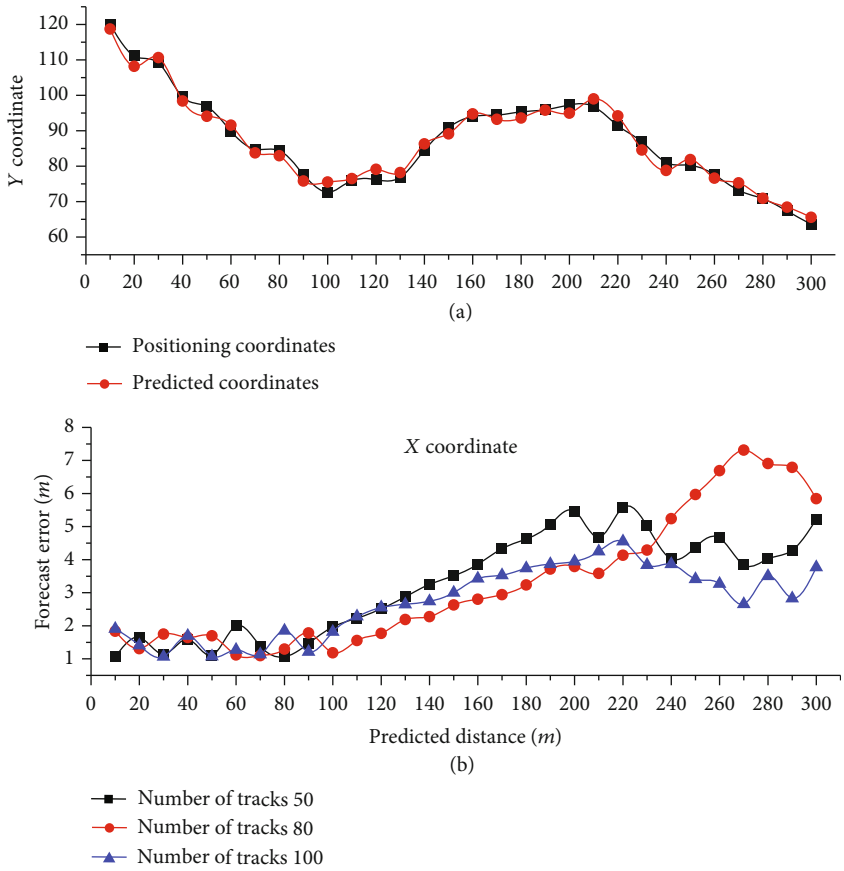

Figure 4: Comparison of predicted position with localized position and overall predicted localization error analysis.

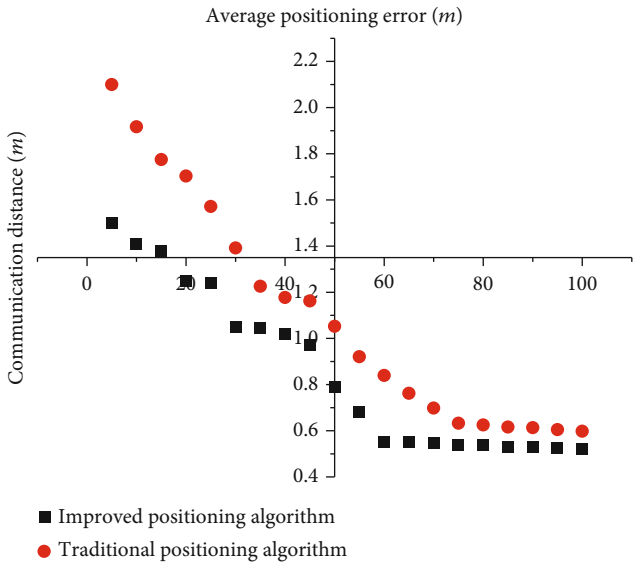

Figure 5: Average positioning error.

improved algorithm and the traditional algorithm improve inaccuracy. The reason for this phenomenon is that the algorithm takes the geometric mean at the end so that the environmental error has less influence on the final localization results.

3.2. Analysis of the Intelligent Asset Management System. Simulation experiments of wireless sensor networks use 5-hop binary tree static topology. In practical applications, the topology of wireless sensor networks is often irregular and changing. In this paper, a typical 5-hop binary tree static topology is used to study the energy consumption of the RFID RF wake-up mechanism, IEEE802.16.4 MAC protocol, and C-MAC protocol. The energy consumption of the RFID RF wake-up mechanism, IEEE802.16.4 MAC protocol, and C-MAC protocol when S is set to 50 s is shown in Figure 6. From Figure 6, the energy consumption of the RFID RF wake-up mechanism is the lowest, and the energy consumption of the three protocols is independent of the number of hops. The minimum power consumption of the RFID radio frequency wake-up mechanism reaches 0.53, and the maximum power consumption of the IEEE802.15.4 MAC protocol reaches 2.71.

Figure 7 shows the simulation and test results of the system antenna return loss; as shown in Figure 7, the test results are very close to the simulation results. The test result shows that the antenna center frequency is 600 MHz, and S11 minimum is about -14.91 dB. The simulation result shows that the antenna center frequency is 900 MHz, and S11 minimum is about -14.54 dB. The rationality of RFID tag antenna design depends on, whether the antenna impedance and chip impedance to achieve a perfect match, the antenna impedance, and chip impedance to achieve matching can

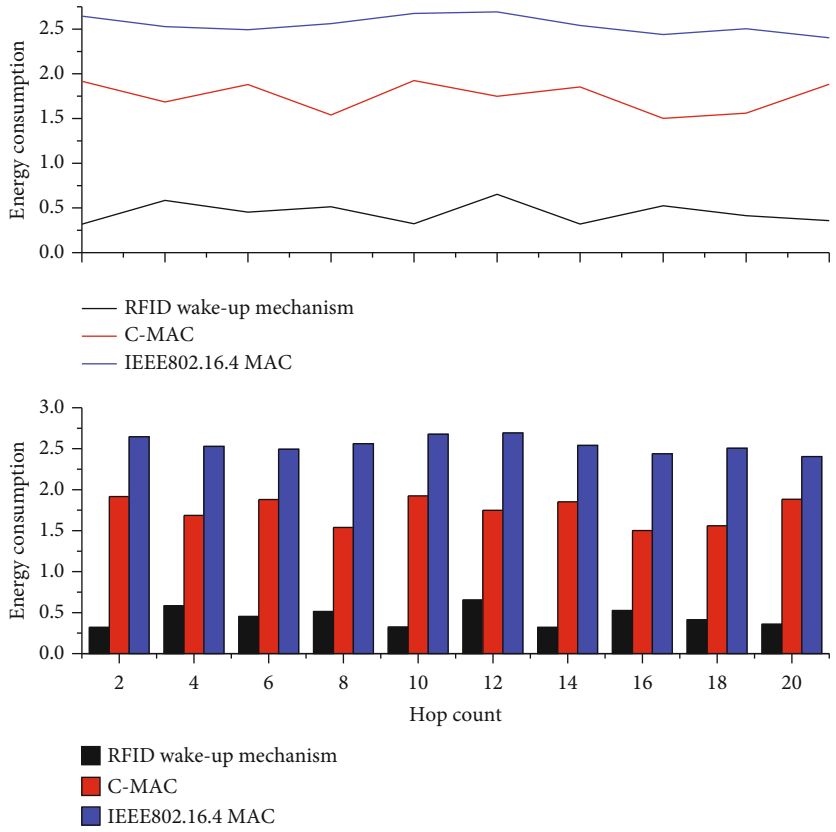

Figure 6: Comparison of energy consumption of the 3 protocols.

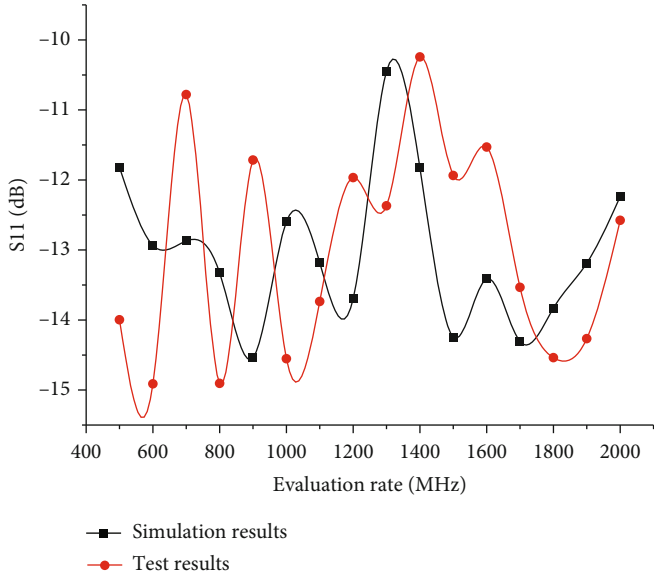

Figure 7: System antenna return loss.

improve the power supply efficiency and read-write distance of the tag antenna. The input impedance of the antenna should be designed as the common impedance of the tag chip, to achieve the maximum energy transfer.

In the performance testing of the fixed asset equipment system, since the system may be used by multiple users at the same time, multiple users are simulated to conduct random access operations to each server of the system at the same time, the corresponding processing time of each server operation is recorded, and the performance of the test results is evaluated and compared. The designed test scenario is as follows: the database is initially entered with

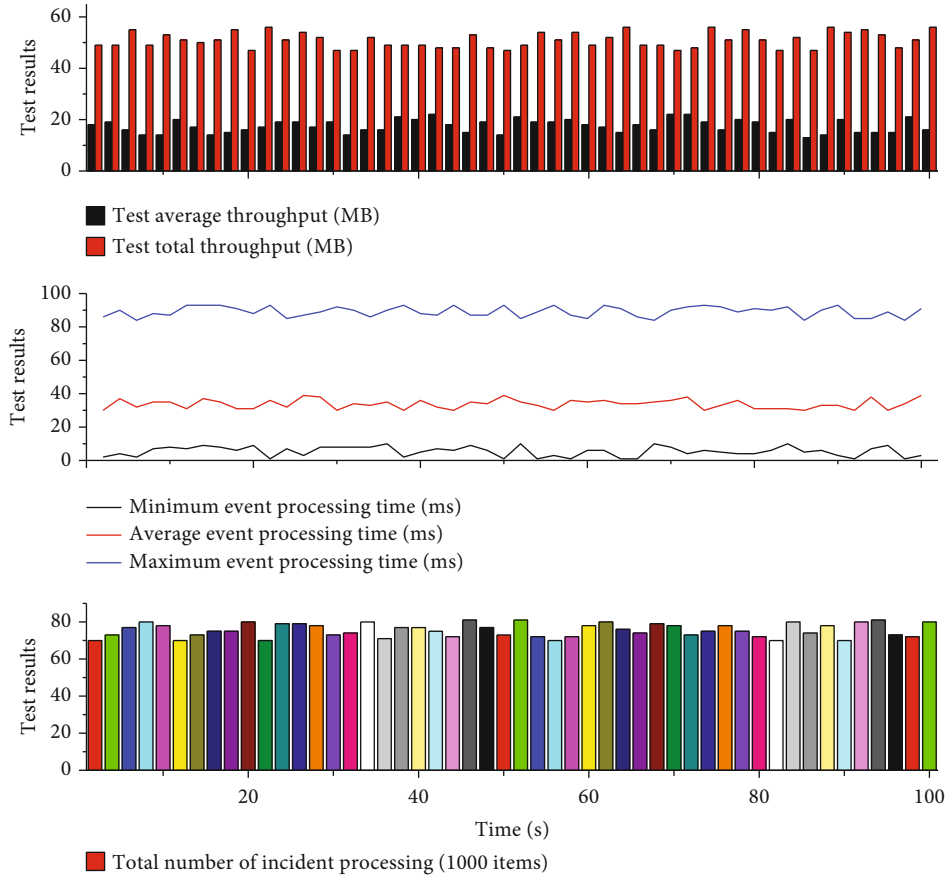

Figure 8: Asset system performance test chart.

more than 10000 basic data, and more than 200 users with different roles are simulated to access the fixed asset equipment management system concurrently and randomly, and the test access time is tested by random access to these users (Figure 8).

4. Conclusion

Based on the discussion of RFID technology and WSN technology, this paper finds that RFID technology and WSN technology are two functional complementary technologies and therefore consider the fusion of RFID technology and WSN technology. An intelligent asset management system architecture based on RFID and WSN fusion technology is proposed, which is divided into information sensing layer, data communication layer, information fusion layer, and integrated application layer, and the functions realized by each layer are introduced in detail. The system in this paper has been analyzed and designed to complete the development work, and in this design implementation process, the development status and background of the asset system are introduced. The corresponding software development techniques are applied. It also follows the software program design concepts, such as the system can run permanently, the system security performance is reliable, the user is easy to operate, the system has strong scalability, and other program development design theories. The main functional modules are implemented by analyzing the requirements of the asset system. For example, the system management, asset management, asset query, and report management modules finally realize the whole system from front-end UI to back-end logic code writing. After the system development was completed, the functional and performance tests of the fixed asset management system were conducted according to the common testing methods and theoretical principles of the system. The results fully demonstrate that the developed asset system is safe and reliable and can ensure the efficient management of assets. For the intelligent asset management network proposed in this paper, a comprehensive and detailed analysis is not carried out, and the hardware design involved is only the introduction of the design method, which is not relevant. In the design of an intelligent asset management system, a reasonable hardware scheme should be adopted according to the demand. Especially sensor module, RF read/write module, the choice of different locations has great variability.

Data Availability

The data used to support the findings of this study are available from the corresponding author upon request.

Conflicts of Interest

The authors declare that they have no known competing financial interests or personal relationships that could have appeared to influence the work reported in this paper.

Acknowledgments

This study was supported by the National Social Science Foundation of China: research on the coordination of monetary policy and macro prudential policy from the perspective of operational tools (13BJY165).

References

[1] F. Wan and M. Li, "RFID based intelligent traffic information acquisition system," *International Journal of RF Technologies*, vol. 11, no. 1, pp. 45–58, 2020.

[2] X. Gaofeng, "Low financial cost with ant colony optimisation in intelligent agriculture," *International Journal of Wireless and Mobile Computing*, vol. 18, no. 2, pp. 111–115, 2020.

[3] A. Dawson, "Robotic wireless sensor networks, big data-driven decision-making processes, and cyber-physical system-based real-time monitoring in sustainable product lifecycle management," *Economics, Management, and Financial Markets*, vol. 16, no. 2, pp. 95–105, 2021.

[4] R. Granillo-Macías, I. Simón-Marmolejo, I. J. González-Hernández, and J. Zuno-Silva, "Traceability in Industry 4.0: A Case Study in the Metalmechanical Sector," *Acta Logística*, vol. 7, no. 2, pp. 95–101, 2020.

[5] F. Molaei, E. Rahimi, H. Siavoshi, S. G. Afrouz, and V. A. Tenorio, "A comprehensive review on internet of things (IoT) and its implications in the mining industry," *American Journal of Engineering and Applied Sciences*, vol. 13, no. 3, pp. 499–515, 2020.

[6] K. Leng, L. Jin, W. Shi, and I. van Nieuwenhuyse, "Research on agricultural products supply chain inspection system based on internet of things," *Cluster Computing*, vol. 22, Supplement 4, pp. 8919–8927, 2019.

[7] P. Gibson and J. Macek, "Sustainable industrial big data, automated production processes, and smart networked factories in cyber-physical system-based manufacturing," *Economics*, vol. 9, no. 3, pp. 22–34, 2021.

[8] M. A. M. Sadeeq and S. Zeebaree, "Energy management for internet of things via distributed systems," *Journal of Applied Science and Technology Trends*, vol. 2, no. 2, pp. 59–71, 2021.

[9] E. Cunningham, "Artificial intelligence-based decision-making algorithms, sustainable organizational performance, and automated production systems in big data-driven smart urban economy," *Economics*, vol. 6, no. 1, pp. 31–41, 2021.

[10] S. K. Kinnunen, A. Ylä-Kujala, S. Marttonen-Arola, T. Kärri, and D. Baglee, "Internet of things in asset management," *Management, Engineering, and Technology (IJSSMET)*, vol. 9, no. 2, pp. 104–119, 2018.

[11] M. Andreacchio, A. Bekrar, R. Benmansour, and D. Trentesaux, "Assessing cyber-physical systems to balance maintenance replacement policies and optimise long-run average costs for aircraft assets," *IET Cyber-Physical Systems: Theory & Applications*, vol. 4, no. 2, pp. 148–155, 2019.

[12] C. Çeken and D. Abdurahman, "Simulation modeling of an iot based cold chain logistics management system," *Sakarya University Journal of Computer and Information Sciences*, vol. 2, no. 2, pp. 89–100, 2019.

[13] L. Qin, S. Feng, and H. Zhu, "Research on the technological architectural design of geological hazard monitoring and rescue-after-disaster system based on cloud computing and internet of things," *International Journal of System Assurance Engineering and Management*, vol. 9, no. 3, pp. 684–695, 2018.

[14] J. I. Z. Chen and K. L. Lai, "Machine learning based energy management at Internet of Things network nodes," *Journal: Journal of Trends in Computer Science and Smart Technology September*, vol. 2020, no. 3, pp. 127–133, 2020.

[15] J. Chen, "Composition rule perception algorithm of national art plane system based on wireless sensor network communication technology," *International Journal of Wireless Information Networks*, vol. 28, no. 3, pp. 243–251, 2021.

[16] C. K. Lee, Y. Lv, K. K. Ng, W. Ho, and K. L. Choy, "Design and application of internet of things-based warehouse management system for smart logistics," *International Journal of Production Research*, vol. 56, no. 8, pp. 2753–2768, 2018.

[17] W. Zhang, M. Kumar, and J. Liu, "Multi-parameter online measurement IoT system based on BP neural network algorithm," *Neural Computing and Applications*, vol. 31, no. 12, pp. 8147–8155, 2019.

[18] M. Ben-Daya, E. Hassini, and Z. Bahroun, "Internet of things and supply chain management: a literature review," *International Journal of Production Research*, vol. 57, no. 15-16, pp. 4719–4742, 2019.

[19] A. I. Vlasov, P. V. Grigoriev, A. I. Krivoshein, V. A. Shakhnov, S. S. Filin, and V. S. Migalin, "Smart management of technologies: predictive maintenance of industrial equipment using wireless sensor networks," *Entrepreneurship and Sustainability Issues*, vol. 6, no. 2, pp. 489–502, 2018.

[20] B. S. Awoyemi, A. S. Alfa, and B. T. J. Maharaj, "Resource optimisation in 5G and internet-of-things networking," *Wireless Personal Communications*, vol. 111, no. 4, pp. 2671–2702, 2020.

[21] B. Bhushan, C. Sahoo, P. Sinha, and A. Khamparia, "Unification of Blockchain and Internet of Things (BIoT): requirements, working model, challenges and future directions," *Wireless Networks*, vol. 27, no. 1, pp. 55–90, 2021.

[22] Y. Ding, M. Jin, S. Li, and D. Feng, "Smart logistics based on the internet of things technology: an overview," *International Journal of Logistics Research and Applications*, vol. 24, no. 4, pp. 323–345, 2021.

Hindawi
Journal of Sensors
Volume 2022, Article ID 8367387, 12 pages
https://doi.org/10.1155/2022/8367387

Research Article

Virtual Reconstruction of Visually Conveyed Images under Multimedia Intelligent Sensor Network Node Layout

Qi Yang[1,2] **and Jong Hoon Yang**[2]

[1]*School of Journalism and Media, Chongqing Normal University, Chongqing 401331, China*
[2]*Department of Digital Image, Sangmyung University, Seoul 03016, Republic of Korea*

Correspondence should be addressed to Qi Yang; 20131736@cqnu.edu.cn

Received 13 November 2021; Revised 5 January 2022; Accepted 15 January 2022; Published 2 February 2022

Academic Editor: Gengxin Sun

In this paper, multimedia intelligent sensing technology is applied to the virtual reconstruction of images to construct or restore images to the communication media for visual communication. This paper proposes image virtual reconstruction theory based on visual communication research, treats image virtual reconstruction content as open data links and customized domain ontology, establishes an interdisciplinary interactive research framework through the technical means of visual communication, solves the problem of data heterogeneity brought by image virtual reconstruction, and finally establishes a three-dimensional visualization research method and principle of visual communication. The research firstly visual communication cuts into the existing conservation principles and proposes the necessity of image virtual reconstruction from the perspective of visual communication; secondly, the thinking mode of digital technology is different from human thinking mode, and the process of calculation ignores the emotional and spiritual values, but the realization of value rationality must be premised on instrumental rationality. This requires a content judgment and self-examination of the technical dimensional model of image virtual reconstruction on top of comprehensive literature and empirical evidence. In response to the research difficulties such as the constructivity of visual communication, the solution of image virtual reconstruction of visual communication is proposed based on the data collection method and literature characteristics. The process of introducing the tools of computer science into humanity research needs to be placed in a continuous critical theory system due to the uncontrollable and subjective nature of visual content, and finally, based on the construction of information models for image virtual reconstruction, the ontology and semantics of information modeling are thoroughly investigated, and the problems related to them, such as interpretation, wholeness, and interactivity, are analyzed and solved one by one. The transparency of image virtual reconstruction is enhanced through the introduction of interactive metadata, and this theoretical system of virtual restoration is put into practice in the Dunhuang digital display design project.

1. Introduction

With the rapid progress of society and the continuous development of technology, the world has now fully entered the information age. The information age, also known as the digital age, is a period in which the generation and transmission of digital information is the main mode of operation of society [1]. Under the impetus of such a development trend, electronic data has gradually replaced some previously indispensable material elements, the form of production has been transformed from manual labor to computer manipulation, the cultural form has been transformed from materialization to informatization, and the world economic system has been transformed from physical exchange to digital exchange [2]. It can be said that the widespread use of information technology has fundamentally changed the functioning of all aspects of society and has been integrated into different fields, significantly changing the way of production and life of human beings. With the application of virtual image reconstruction, the continuous emergence of new exhibit forms such as digital exhibits and digital media art has enriched today's display methods, and the mode of display

activities has gradually begun to shift to two-way information interaction modes such as interactive experience. Each change of the times provides a more efficient way to disseminate information and drives the evolution and renewal of media forms. From oral transmission in ancient times to written communication in ancient times to radio and television in the electric age, each communication era has its unique form of media. From the technical point of view of digital media technology, digital media technology is applied in a wide range of fields, so this article combines its research scope to collate and summarize the relevant research results of digital media technology used in the display field. In the information age, people access information and express and exchange ideas through different digital technology devices. The widespread popularity of digital technology has greatly enhanced the mobility and integration of information, and with the maturity of computer technology and network technology, image virtual reconstruction technology has emerged [3].

In the era of more open technology development, product competition no longer depends solely on the quality and price competition but begins to gradually expand to the brand and corporate image; marketing methods have gradually become an aspect of competition [4]. With the continuous development and innovation of computer technology, information network, and intelligent devices, the conventional display methods alone cannot satisfy the contemporary people who are full of various design concepts, so we need to always walk in the front of technology and seek more innovative and creative ways to attract people's attention [5]. With the application of image virtual reconstruction, digital exhibits, digital media art, and other new exhibit forms have emerged to enrich today's display methods, and the mode of display activities has gradually begun to shift to interactive experience and other two-way information interaction modes. Window adjustment of two-dimensional images is a necessary operation for medical image processing. The main reason is the limitation of human eye recognition. Human eyes can only recognize 16 gray levels, but CT can recognize 2000 gray levels. Degree, there is a huge gap between the two. The display activities under the intervention of image virtual reconstruction realize the transmission of information through the two-way interaction between exhibits and audiences with a multidimensional expression. The development of image virtual reconstruction technology has entered various fields and achieved very significant results [6].

The ever-changing digital media technology takes new technologies such as multimedia technology, virtual reality technology, and interactive technology to realize the transformation of information dissemination from text to image, from delayed time to instant, from the one-way transmission to two-way transmission, which has completely changed the way of information dissemination, communication efficiency, and communication effect. Every change of the times will provide a more efficient way of dissemination of information and promote the evolution and update of the media form. From word of mouth in ancient times to written dissemination in ancient times, to the electric power dissemination form of radio and television in the electric age, each dissemination age has its unique media form. In the information age, people obtain information through different digital technology devices to express and exchange ideas. With each innovation in media form, we gradually realize that media technology is not only a tool to carry information but also a language to express information. In general, the development of the field of the virtual reconstruction of images has made great progress, and it is believed that soon there will be a great breakthrough in this field.

2. Related Works

With the rapid development of computer information technology, augmented reality has gradually come into people's lives. By establishing a relationship between real scenes and computer-generated virtual environments, augmented reality technology has played a great role in the medical field, industry, military field, education field, and monument protection field. Augmented reality (AR) is a brand-new technology further developed based on virtual reality technology, first proposed in 1992, which extends the human visual perception of the real environment by accurately superimposing computer-generated virtual objects or other auxiliary information into the real scene (three-dimensional registration) and allowing users to interact with this virtual information fused to the real world in real-time [7]. By establishing a relationship between the real scene and the virtual environment generated by the computer, augmented reality technology has fully played a huge role in the medical field, industrial field, military field, education field, and historical site protection field. It allows users to interact with this virtual information fused to the real world in real-time, extending the human visual perception of the real environment, thus completing the "augmentation" of the real world. At the same time, thanks to the rapid improvement in the performance of smartphones, tablets, and other wearable mobile devices, as well as the increasing maturity of computer vision and mobile cloud computing technologies on mobile devices, combined with a variety of advanced sensors and ubiquitous and stable network connections, augmented reality technology continues to move towards the more convenient mobile augmented reality (MAR) direction [8].

The scientific (deterministic and integrity level) process of 3D visualization documentation has facilitated the creation of interactive and immersive information models, enabled by more than a decade of technological development, that allow users to visually isolate themselves from the real world through external devices, thus manipulating the digital virtual environment and creating a sense of belonging [9]. These immersive information models transform the digital environment "perception" into a metric of the real environment. Web-based solutions and applications enable efficient 3D digitization methods, as well as postprocessing tools for rich semantic modeling. This is a complex "reverse engineering" where data must be processed without losing important information such as metadata and interaction metadata [10]. When using interactive solutions for

mobile devices such as AR glasses, the main considerations are the limitations of mobile device performance, the visual interference caused by too many tissue models during surgery, and the single issue of auxiliary information interaction. In medicine, a handheld augmented reality neuronavigation (AR-IGNS) with three navigation modes was proposed and built in 2013, which first precisely segments the tumor target area in the original 2D image of the patient and then combines the segmented tumor information with the actual surgery scene to generate the corresponding navigation image and display it on the iPad to assist the surgeon in the surgery. Professor Xiaorong Xu's team proposed to apply mobile augmented reality technology to the treatment of breast cancer surgery and developed a Google Project Glass-based dual-modality ultrasound and fluorescence image navigation system and a HoloLens-based breast reconstruction navigation system to assist doctors in locating and removing anterior lymph nodes, and the latter to guide physicians in mammoplasty reconstruction [11]. On June 26, 2017, a complex hip fracture surgery guided by augmented reality technology was completed, and a mobile augmented reality surgical planning and navigation system based on the visor ST60 headset was researched and developed, and a series of calibration algorithms were proposed to improve the problems of insufficient positioning accuracy, poor intuition, and poor real-time interactivity in the clinical application of augmented reality surgical navigation systems.

From the technical perspective of digital media technology, which is applied in a wide range of fields, this paper thus collates and summarizes the relevant research results on digital media technology corresponding to its use in the field of display, considering the scope of its research [12]. Distinguishing immersion in the age of digital media from earlier forms of illusionary art, drawing on actual works by contemporary artists and groups in the analysis, it summarizes how the use of technological tools such as 3D, IMAX, and virtual reality can create immersive illusions and outlines the impact of virtual reality on the conception of contemporary art, outlines and discusses information about augmented reality and its functions, and introduces people to augmented reality from various perspectives [13]. Functional design is the core part of the entire mobile augmented reality application development, and a good interaction design helps to improve the overall application display effect. The three-dimensional virtual model and multimedia resources are integrated into the application, and the effect of virtual and real fusion is realized through buttons and human-computer interaction, and the user experience is improved. In 2013, we introduced the types of haptic sensors and described how to build holistic and localized haptic display systems, brought together the research of advanced practitioners in the VR field, and outlined the main hardware and software technologies that currently make up. The main hardware and software technologies that make up virtual reality systems are described, and the main developments and issues in the field are elaborated, exploring how digital media technology tools can be used to incorporate olfactory, tactile, and thermal sensations into media objects, thereby enriching traditional multimedia content and enhancing immersion [14].

3. Multimedia Intelligent Sensor Image Virtual Reconstruction Model Design

3.1. Smart Sensor Model Construction. By analyzing the whole experimental system, the key modules related to it are introduced in the following, which contain six types of image acquisition module, recognition tracking module, 3D registration module, virtual-real fusion module, terminal display module, and human-computer interaction module, and also, this chapter gives detailed explanations of the key modules.

(1) Image acquisition module: the image acquisition module is the first step in the whole system; it is like the "eyes" of the system, using the camera to acquire the image in the scene and using the optical components inside the camera to obtain the real-world position and finally store it in pixel representation and display it through the terminal display device

(2) Recognition and tracking module: the recognition and tracking module is necessary in augmented reality systems to perceive the real world through cameras, track real scenes in real-time, use features in the environment for recognition, and clarify the location and direction of objects, thus enhancing information about the real world

(3) Virtual and real registration module: the virtual and real registration module is the core module of the whole system, its purpose is to draw the virtual model in the real environment, and tracking registration is an important step to achieve this process, usually based on two-dimensional identifiers or certain features in the field, through the calculation of the corresponding matrix to achieve the purpose of real-time registration

(4) Virtual-real fusion module: the virtual-real fusion module is to seamlessly integrate the computer-generated virtual objects with the real world, which includes the optimization of the generated virtual model and lighting processing, and the accurate addition of the location of the virtual objects. The relationship between the key modules of the system is shown in Figure 1

In the current environment of the scarcity of medical resources, sometimes, medical staff may need to diagnose diseases at all times and in all places, and medical staff needs to use a variety of devices, such as in the office to read films on PC, and on business trips, off-site consultations or special emergencies need to use mobile devices such as mobile phones and pads for office work and also take into account the existence of different operating platforms for PC and mobile devices such as Windows, iOS, and Android. So,

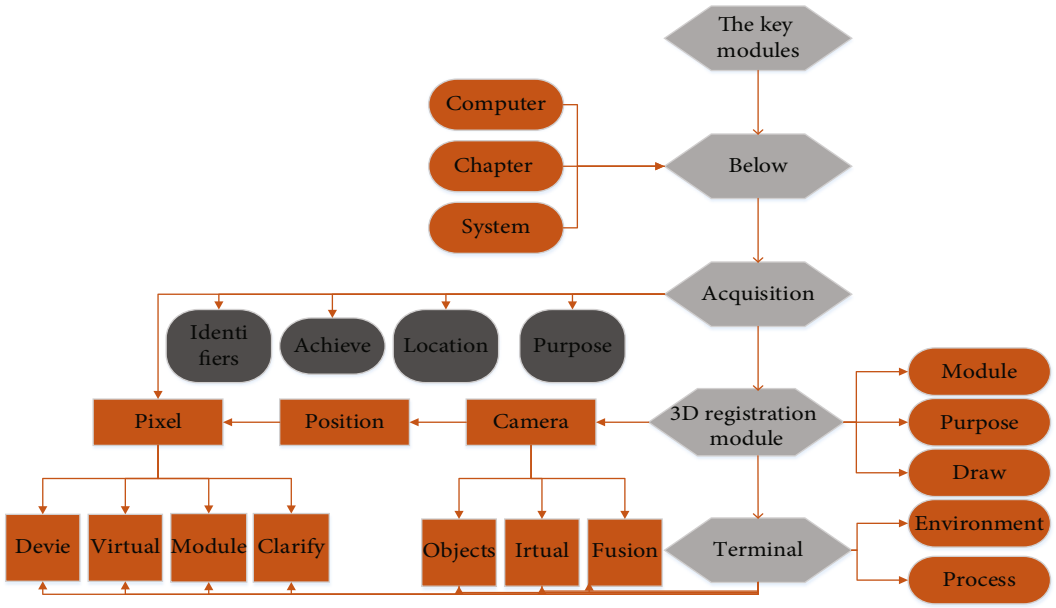

Figure 1: Relationship diagram of key modules of the system.

the image viewing solution designed in this paper must be cross-platform and multidevice support, this paper through the Web-based approach to achieve cross-platform; the solution is designed as a pure Web solution, without any installation [15]. However, in contemporary exhibition activities, due to the intervention of digital media technology, some of the information display methods formed by it also show the characteristics of large scale in addition to the characteristics of publicity. The exhibition space to accommodate this kind of exhibition activity is relatively large. If the vertical free space is not fully utilized, it will form a waste of space and limit people to a single level for viewing. Part of the information available in front of you can be obtained in a way, and it is impossible to fully understand the content of the display. The browser-side also does not need to install plug-ins and can independently complete the 2D and 3D image viewing and interactive operations. When using mobile devices such as AR goggles, the main considerations are the performance limitations of mobile devices, the visual interference caused by too many tissue models during surgery, and the single interaction of auxiliary information. This is because in intraoperative scenarios, when choosing to apply mobile device solutions such as AR goggles, the processing power of mobile devices is somewhat different from that of PC terminals, resulting in a certain delay in the model rendering speed, which affects the real-time tracking display in surgical navigation; a large number of tissue models are not differentiated, and if all of them are displayed, they will have an obscuring effect on the parts that have already passed, causing visual interference to the medical staff. If only the dangerous tissue models around the surgical path are retained, but not selectively rendered, the problem of model occlusion will arise; only obtaining the distance information between surgical instruments and the target tumor, the offset value of surgical instruments and the surgical path, the minimum distance of dangerous tissues and other auxiliary information without reasonable interactive display will not provide effective help.

$$U(D) = \begin{cases} 0 \\ \dfrac{u}{W}\left(D - \dfrac{W}{2}\right) \\ u_m \end{cases}. \tag{1}$$

In the system in which the camera is located, the key problem to be solved is to place the virtual objects drawn by the computer in the correct position, through the alignment and then achieve the purpose of accurate fusion, so to clarify the conversion relationship between the various coordinate systems is the key to achieve this problem. The meaning of space technology is not simply to mechanize the assembly of installations and space but to inform and media space at a deeper level. The purpose is to use the advantages of technology to create an intelligent space environment, which is fundamentally realized. Communication between people and space. The whole augmented reality system mainly involves four kinds of coordinate systems, respectively, the image plane coordinate system (image coordinate system), the camera coordinate system (video camera coordinate system), the physical coordinate system (world coordinate system), and the virtual object in the coordinate system (virtual object coordinate system). This includes the conversion between real-world and camera coordinate systems, the conversion between camera coordinate system and image plane coordinate system, and the transformation between virtual coordinate system and real coordinate system. The conversion relationship between the four coordinate systems is shown in Figure 2.

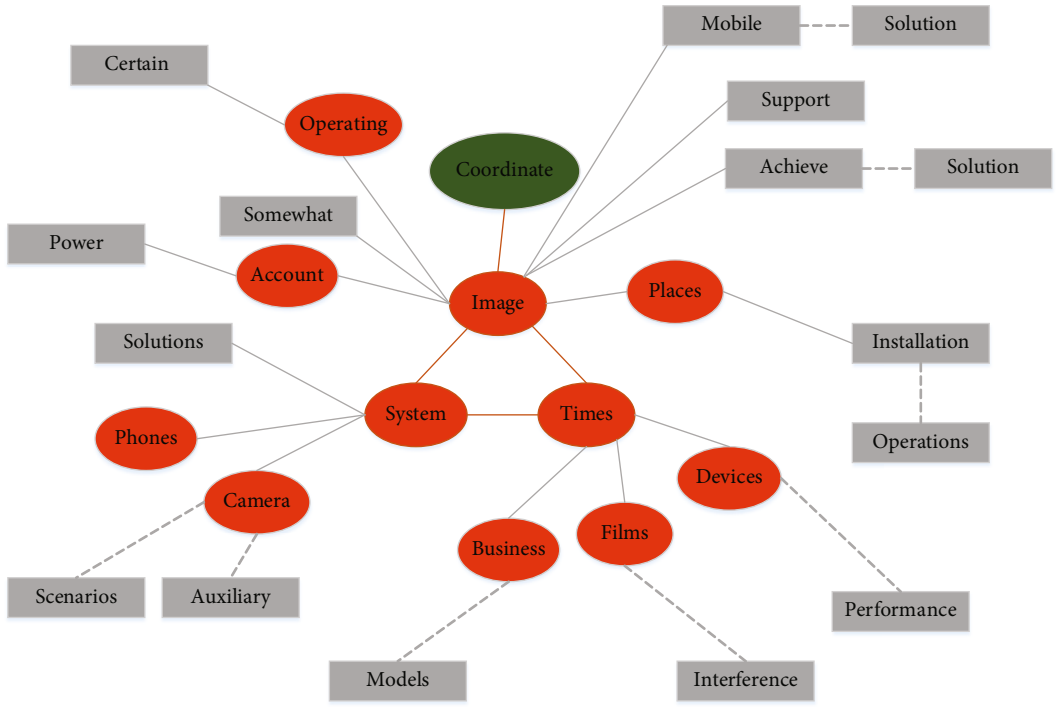

Figure 2: Schematic diagram of coordinate system conversion relationship.

Windowing of 2D images is a necessary operation for medical image processing, mainly because of the limitations of human eye recognition. The human eye can only recognize 16 gray levels, but CT can recognize 2000 gray levels, and there is a huge gap between the two. This means that the CT value recognized by the human eye is 125 Hu, which is calculated by 2000/16. When a doctor looks at a CT slice, he or she can only distinguish different tissues in the image if they differ by more than 125 Hu and cannot accurately distinguish those below 125 Hu. However, the CT values of human tissues and organs are often between 20 and 50 Hu, whether 20 or 50 Hu is far less than the 125 Hu standard, so the result will be unrecognizable to the doctor. Windowing is an image display technique that facilitates the physician's ability to view different densities of tissue structures when diagnostically reviewing medical imaging slides and is designed to fully utilize the rendering space from 0 to 255, within which important voxel values are mapped. The basic principle is to obtain the window widths and window positions that need to be displayed utilizing preset window widths and window positions and to convert the values within the brightest and darkest ranges of the display, setting them to the brightest for parts above the grayscale range of the window, and vice versa. In mathematical terms, windowing is the conversion of an image grayscale value to a screen display value.

$$K_{pi} = pi \times sl + os. \tag{2}$$

The current tension between doctors and patients is mainly due to poor communication. First, there is a huge difference in the amount of medical knowledge and medical information held by doctors and patients, which makes it sometimes difficult for patients and their families to understand the specific conditions of patients. Secondly, in traditional doctor-patient communication, patients play a passive role and lack effective interaction with doctors. The advent of mobile augmented reality technology provides excellent solutions to both problems. Using the patient's computed tomography, magnetic resonance imaging, and other image data, the patient's lesion model is segmented and reconstructed in three dimensions by medical image processing software, and then, the patient-specific personalized medical 3D model is presented directly to the patient or the patient's family using the MAR system based on the mobile device side (mobile phone and tablet) [16]. Through the visual demonstration and operation of the model (pan, rotate, and zoom) and the doctor's explanation, the patient will have a deeper understanding of the condition, and this new way of medical interaction will make the traditional doctor-patient communication more simple, clear, and direct. Most of the existing medical augmented reality systems based on mobile devices are based on the 3D registration technology of manual signs and applied to intraoperative navigation, while the 3D registration technology based on manual signs can only be applied to scenes with signs, resulting in a limited tracking area, which not only affects the scope of use of medical mobile augmented reality systems but also makes the system not convenient and stable enough. Therefore, in this paper, we choose to use the ARKit framework of SLAM technology to complete the development of a mobile augmented reality convenient display system, which can be used by medical personnel to display the lesion model for patients and their families anytime and anywhere without the limitation of markers. In addition, the system can also be applied to medical education, so that the complex structure of two-dimensional medical images on paper is more conducive to the understanding and memory of learners.

3.2. Image Virtual Reconstruction Model Design. The design of multimedia resources contains three parts: audio, video, and 3D model. Audio is an important component, and this topic selects the intelligent voice generated by reading aloud female in the processing of voice and plays the voice by scanning the text to enhance the user's memory of the text; integrates video elements and plays the promotional video of the property by scanning the graphics of the property, which has more visual impact relative to the image; and produces a realistic virtual 3D model, so that the user can view house models and indoor roaming without leaving home [17]. Through these multimedia resources, the user can interact with the computer in real-time, which is a new model of human-computer interaction. The mobile augmented reality application consists of three major interfaces, the main interface, AR scanning interface, and indoor roaming interface; the key to interface design is icon design and interaction design; icon design should have the role of content orientation and impact while paying attention to the color and style of unity; interaction design should follow the logical relationship between the interface and the buttons. The logical relationship between interfaces is shown in Figure 3.

Functional design is the core part of the whole mobile augmented reality application development, and good interaction design helps to improve the overall application presentation. The 3D virtual model and multimedia resources are integrated with the application, and the effect of virtual-reality integration is achieved through buttons and human-computer interaction to enhance the user experience. The functional design of this subject mobile-augmented reality application contains basic display functions and extended functions: (1) basic display not function basic display function contains graphic recognition, voice explanation, model interaction. Graphic recognition function scans the brochure on [18]. The two-dimensional house pictures display the corresponding three-dimensional housing model; you can watch the house model in 360 degrees; voice explanation function scans the text content on the brochure, automatically plays intelligent voice, and enhances the user's memory of the text content; model interaction function, by zooming, rotating, and moving the model, to achieve real-time interaction with the model, at the same time, the off-card function makes the user do not need to point the camera at the scanned object, which enhances the user's experience effect; (2) extended functions include video demonstration, 3D scanning, house roaming, and furniture replacement. The video demonstration function integrates video elements into the application, and the promotional video can be played by scanning the corresponding video introduction image; the house roaming function enables jumping from the bird's eye view in AR to indoor roaming through interactive buttons; the furniture replacement function replaces different materials for the floor through interactive buttons.

$$a_i = \sqrt{a_X{}^2 + a_y^2} + g. \tag{3}$$

Image segmentation technology refers to the process of segmenting an image into some disjoint regions (segmentation of selected features showing consistency in the same region) based on features such as grayscale, color, spatial texture, and geometry and extracting the region of interest, which is the basis for fields such as image processing and computer vision. In the medical field, due to the differences in the imaging principles of medical imaging devices, the complexity of human anatomy, and the diversity of human tissue and organ shapes, the formation of images is often affected by, for example, noise, tissue motion, field offset effects, and local body effects, and thus has characteristics such as blurring and inhomogeneity, which brings great difficulties to the segmentation of medical images. To date, there is still no universal medical image segmentation technique for clinical applications, but scholars at home and abroad have reached a consensus on the general rules of image segmentation, and a considerable number of research results and methods have been produced as a result. At present, various medical image segmentation methods widely used around the world can be mainly classified into edge-based, region-based, and combined with specific theoretical image segmentation according to their segmentation characteristics. The typical ones are threshold segmentation, region growth, wavelet transform, statistics-based, and Artificial Neural Network- (ANN-) based methods. Image segmentation technology refers to the segmentation of an image into several disjoint regions based on features such as grayscale, color, spatial texture, and geometric shapes (the selected features of the segmentation show consistency in the same region), and the region of interest is extracted The process is the foundation of image processing and computer vision. Based on the theory of the above methods, two types of image segmentation have also arisen, namely, automatic segmentation and manual segmentation. Automatic intelligent segmentation is mainly done with the help of high-performance computers' understanding of medical images and many operations to complete fully automatic image segmentation; manual segmentation requires human participation in the division and calibration in advance, and then computer operations to complete the medical image segmentation.

4. Analysis of Results

4.1. Smart Sensor Model Performance Analysis. In the past, when the museum exhibition halls were laid out, due to the size of the physical exhibits and the spatial organization of the museum in pursuit of economic efficiency and other factors, thus, the display space was mainly unfolded in the form of a single-level space so that visitors and exhibits were always in the same horizontal level, and visitors appreciated the exhibits from a height perspective in the space. However, in contemporary display activities, due to the intervention of digital media technology, certain information display methods formed by it have the characteristics of publicness in addition to the characteristics of large scale. The traditional display space relies on the introduction of sound

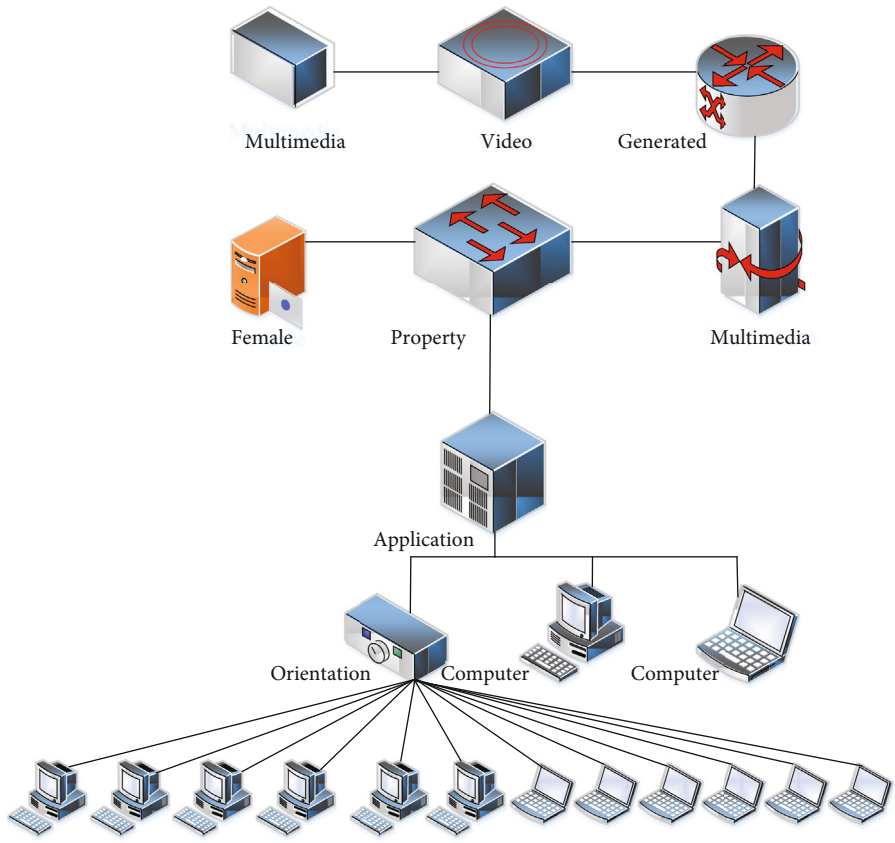

Figure 3: Interface logic relationship diagram.

and light elements in the natural environment to create an environmental atmosphere, while the contemporary display space can be simulated by technical means, which can be created in real-time according to the information content displayed in the space. The corresponding light environment and sound environment form an on-site atmosphere that fits the theme. If the vertical space is not fully utilized, it will form a waste of space, and people are limited to a single level of viewing; they can only get some of the information in front of them and cannot fully understand the content of the display. In addition, the number of viewers in the same horizontal space at the same time is limited, and digital media displays hope to attract more people to participate in them, forming people's sharing and communication.

$$T = [Ta, Tb, Tc]^2. \quad (4)$$

The principle of integration into the technical means, on the other hand, is reflected in the creation of sound and light atmosphere. The traditional display space is dependent on the introduction of sound and light elements in the natural environment to create the environment atmosphere, while the contemporary display space can be achieved through technical means to achieve its simulation, according to the information content displayed in the space in real-time to create a light environment and sound environment that echoes it, forming a suitable theme of the scene atmosphere [19]. The use of intelligent sound and photoelectric technology simulates a more realistic scene environment, infecting visitors from an audio-visual perspective and bringing them an all-around multilevel experience. At the same time, in the soundscape atmosphere, in addition to the use of equipment technology, it is also necessary to take certain architectural acoustic technology means in equipment arrangement, reverberation, noise, and other aspects to support the perfect restoration of technical effects. The principle of integration mainly promotes the display of space design from two aspects of materiality integration and sound and light atmosphere creation, enriching the expression of space and forming a new design vocabulary. The shaping of space differentiation is the main way for landscape installations to shape the landscape space and stimulate the public to participate in the experience. Use a variety of alienation methods to break the inherent thinking and present a personalized visual effect. While expressing the design concept, the landscape installation becomes unique and full of personality, making the entire landscape space more attractive. The significance of space technologization is not simply the mechanized assembly of devices and space, but deeper informatization and mediatization of space, the purpose of which is to use the advantages of technology to create an intelligent space environment and fundamentally realize the communication between people and space. The three-dimensional display space is not simply to increase the height of space but to enrich the vertical level of space, vertical organization

of visitors' activity space so that they can participate in the experience of digital media display with different height perspectives in a multidimensional way, to enrich people's visual experience.

$$\phi = \arcsin\left(\frac{g(x)}{g}\right). \tag{5}$$

One way to create a vertical three-dimensional display space model is to use the placement of mezzanine space or the hollowing out of each layer of space and other techniques to form a display space with multiple layers of "viewing platforms" in the vertical direction. The multilayered space increases the space area that can accommodate the audience and divides several clear vertical levels in the display space, which is convenient for the audience to stay. At the same time, each level is relative. Independent and visually connected, it allows the people gathered on each platform to view the exhibition from different perspectives while forming an interactive exchange between the layers, exchanging the information acquired under their respective perspectives and thus guiding the flow of visitors between the layers. For example, in the design of the Kerkrade Museum in Limburg, the architects created a half-underground, half-above-ground spherical space for the display of digital images and used the hemispherical part of the ground floor to form an inverted spherical gallery. To make full use of the space to accommodate more visitors, a circular glass platform was inserted to form a mezzanine space to accommodate the audience, and a staircase was used to form a link between the levels inside the exhibition hall, so that people can look down on the dome at different heights in the space, creating a visual experience as if they were looking back at the Earth from space, as shown in Figure 4.

The shaping of spatial differentiation is the main way for landscape installations to shape the landscape space and stimulate public participation in the experience. The use of a variety of alienation methods to break the inherent thinking presents a personalized visual effect, while expressing the design concept, so that the landscape installation becomes unique and individual, making the whole landscape space more attractive. The intervention of virtual image technology provides more means for the shaping of spatial differentiation. In landscape space, strong color contrast will produce certain visual signals to the public, and in the subjective world of human beings, color also has certain symbolic meaning, cultural meaning, warning meaning, etc., according to the designer's concept of expression and the needs of the landscape space atmosphere for image color saturation, contrast, and the brightness of different collocation, to cause different color feelings and connotations to the public. In the 2013 Sydney Christmas light show, St. Mary's Cathedral became the protagonist of the light show; the designer used wall projection technology in the church facade projection show, by changing the color of the church, so that the audience's visual experience of the church and the inner feelings have changed; green projection makes the church warm and romantic, and when the dark red projection in the church appears, in the audience's heart is a majestic green projection that makes the church warm and romantic, while when the dark red projection appears in the church, it creates a majestic visual and inner feeling in the audience. The meaning of color is complex and has different meanings in different regions, as shown in Figure 5.

The common coordinate systems used in visual-inertial navigation are the world coordinate system, the camera coordinate system, and the IMU coordinate system. The world coordinate system is a fixed reference coordinate system, the camera coordinate system is a coordinate system bound to the camera with the shooting viewpoint as the coordinate origin, and the IMU coordinate system is bound to the IMU device and is a moving coordinate system. Since the reconstruction method used in this paper is single-view reconstruction, the camera coordinate system is used as the reference coordinate system, and the world coordinate system is not considered, and only the camera coordinate system and the IMU coordinate system are fused to solve the motion trajectory and pose of the camera in the indoor scene. In pure visual SLAM, the camera coordinate system of the first frame is generally used as the world coordinate system. In this paper, the camera coordinate system of the first panoramic image is used as the reference coordinate system, and the 3D model reconstructed from subsequent panoramic images is converted to the reference coordinate system to realize the stitching of the model. The layout models reconstructed by single panoramic images are all in their respective camera coordinate systems as the reference coordinate systems, i.e., the coordinate systems of the models reconstructed by different panoramic images are relatively independent. To realize the stitching of multiple 3D models, it is necessary to obtain the position relationship between each model, i.e., the relative position relationship of each panoramic image shooting viewpoint. When the IMU device is fixed to the camera device, the relative position relationship between the two viewpoints, i.e., the relationship between the two camera coordinate systems, can be calculated from the IMU data when switching the shooting viewpoints. The relationship between the two coordinate systems can be represented by a rotation matrix and a translation matrix, and the camera model between the two coordinate systems can be converted to the same coordinate system after obtaining the camera model between the two coordinate systems to achieve model stitching. This is shown in Figure 6.

In the real scene, the objects in the ground area will obscure the contour lines of the ground area, resulting in the incomplete acquisition of the contour line segment of the ground area. In the ceiling area, there are relatively few objects and the contour lines are clearer, so it is easier to obtain the contour lines of the ceiling area. In most indoor scenes, the top region has the same shape as the ground region, so the ground region line segments can be mapped by the ceiling region line segments. The indoor scene model proposed in this chapter is top and bottom symmetric, i.e., the floor region has the same shape as the ceiling region, but due to the camera height, the mapping of the top and bottom regions of the indoor scene cannot be done directly by changing the sign of the vertical coordinates, because the distance from the camera to the floor is different from

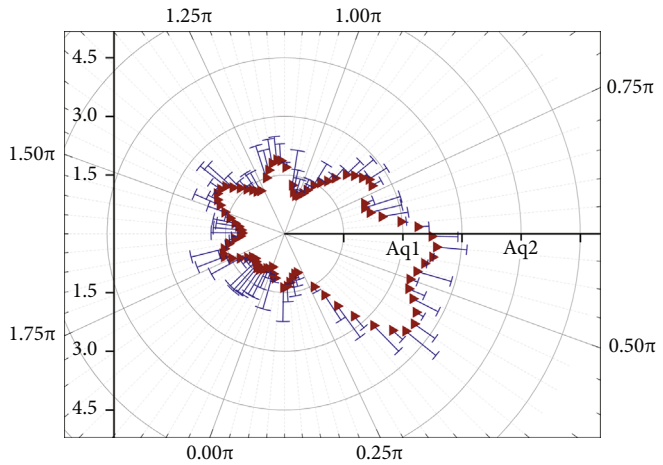

Figure 4: Schematic diagram of the reference coordinate system.

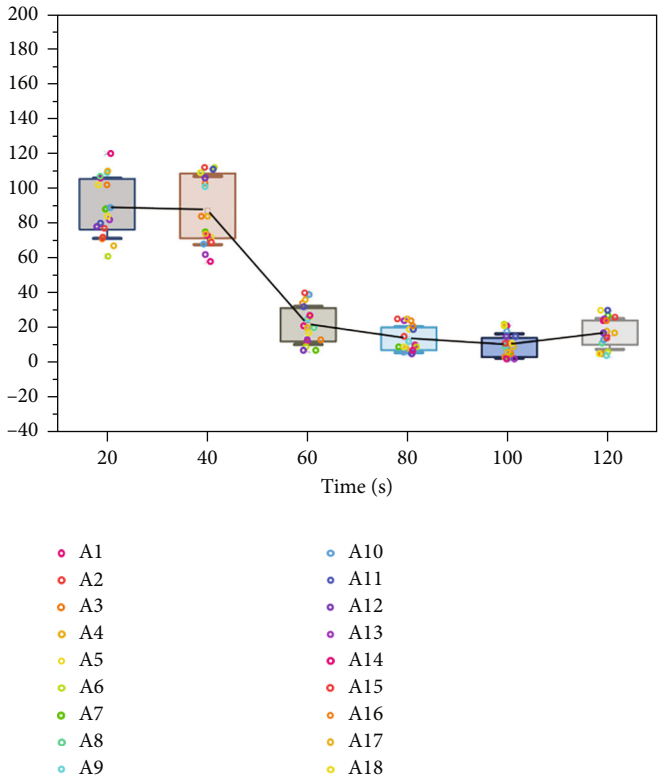

Figure 5: Sensor performance data graph.

the distance to the ceiling causes the two regions to be projected on the image in different proportions. The layout models reconstructed by a single panoramic image all use the respective camera coordinate system as the reference coordinate system, that is, the coordinate systems of the models reconstructed from different panoramic images are relatively independent. To realize the stitching of multiple three-dimensional models, it is necessary to obtain the positional relationship between each model, that is, the relative positional relationship of the viewpoint of each panoramic image. If the camera height and the room height are known, the projection ratio of the floor area to the ceiling area in the panoramic image can be obtained, and the projection ratio can then be used to calculate the contour line segment of the floor area in the indoor scene.

$$C_2 = R_c C_1 - T. \tag{6}$$

4.2. Image Virtual Reconstruction Implementation. The ARKit-based mobile-augmented reality system for medical imaging mainly interacts with virtual medical models through user gestures and contains three main interaction methods: panning, rotating, and zooming. In the actual interaction

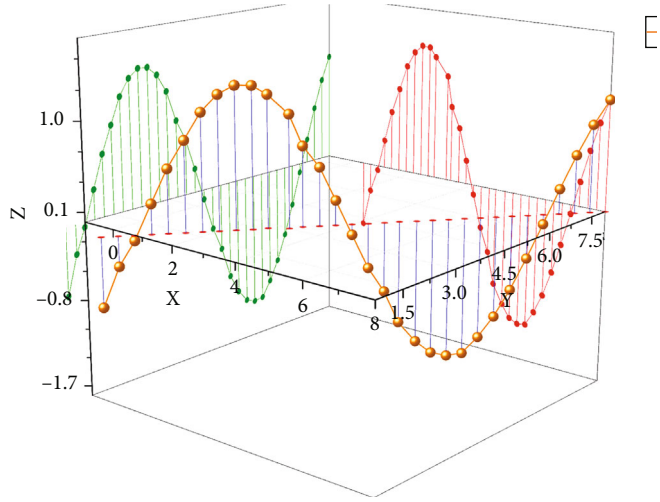

Figure 6: Mobile terminal posture data.

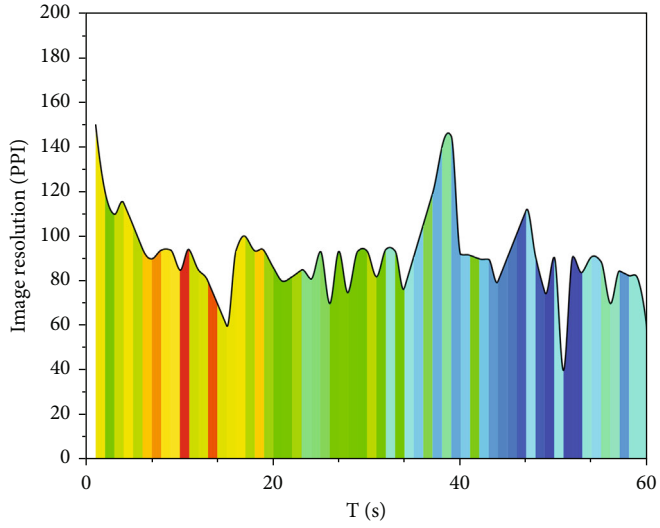

Figure 7: Virtual reconstruction detection results.

process, the user interaction gestures are essentially two-dimensional (i.e., the movement of the user's finger on the display screen of the mobile device), but the MAR experience involves three dimensions in the real world [20]. Therefore, the choice in this system was made to simplify the interaction between the user and the virtual object by limiting the rotation of the virtual medical model to a single axis and the translation range to the plane in which the virtual object was initially placed. The chi-square coordinate representation is one of the most important tools in computer graphics that can be used not only to clearly distinguish between points and vectors but also to perform affine (linear) geometric transformations. In ARKit, the representation of flush coordinates is used to implement linear spatial transformations of virtual objects through a 4×4 transformation matrix with translation matrix T, rotation matrix Y_r (around the Y-axis), and scaling matrix S. The principle of the gesture interaction algorithm is to convert the change of user-specific gestures on the screen of the handheld device into the required transformation coefficients in the affine transformation matrix and then complete the interactive display of the virtual object.

$$R_y = \begin{bmatrix} \cos\theta & 0 & \sin\theta & 1 \\ 0 & 0 & 1 & 1 \\ \sin\theta & 1 & -\cos\theta & 0 \\ 0 & 0 & 0 & 1 \end{bmatrix}. \tag{7}$$

The projection ratio of the ceiling area to the wall area on the panoramic graphic, C_h is the camera height, R^h is the room height, and an $_f$, a_g denotes the vertical offset angle when the corresponding points of the ceiling area and the floor area are projected onto the sphere, respectively. The camera height and the height of the room scene affect the relationship between the projection of the ceiling area and the wall area

on the image. The camera calibration ensures that the horizontal vanishing line in the scene is the x-axis of the image coordinate system and that the x-coordinate of the image coordinates of the two points corresponding to the floor and wall points in a real scene is the same when projected onto the panoramic image, and the relationship between the y -coordinates is determined by the projection scale. It mainly includes three interactive methods: translation, rotation, and zoom. In the actual interaction process, user interaction gestures are essentially two-dimensional (that is, the movement of the user's finger on the display screen of the mobile device), but the MAR experience involves three dimensions in the real world. Therefore, this system chooses to limit the rotation of the virtual medical model to a single axis, and the translation range is limited to the plane where the virtual object was originally placed, to simplify the interaction between the user and the virtual object. This property is used to calculate the ground contour lines corresponding to the contour line segment of the ceiling area in the image. After determining the contour line segments of the ceiling and the floor, it is possible to find the ceiling area and the floor area in the image by the contour line segments. The closed-loop area enclosed by the contour line segments is the ceiling area, and in a panoramic image, the ceiling area contour line segments often span the entire image. When projected onto the sphere, it appears as a spherical region made up of several spherical triangles, each of which is enclosed by a line segment connecting the contour line segment to the upper vertex P of the sphere. When converted to the image coordinate system, the spherical triangles are represented as image regions above the contour line segments, combining this property. The ability to find the ceiling area in an image is shown in Figure 7.

This chapter focuses on a comprehensive verification of the entire experimental system, using a real-life scenario built on an experimental platform. The corresponding error analysis is given for some of the experiments covered in this paper. In the section on camera calibration, the internal parameters of the camera are calculated using two calibration plates. In the image correction section, the symmetry axis errors obtained for the six images are within 0.3 pixels. In addition, the two measurements of the long and short axes of the images before and after correction were compared with a difference of 0.0934 pixels and 0.1229 pixels, respectively, and the ratio of the two was compared with the ratio of the length and width of the real artifacts, and the maximum error value obtained was 0.0018, and the average error value was 0.0012, which has high accuracy and can be used for 3D plotting using the bus data obtained by the algorithm of this paper. Finally, the plotted model is imported into the real scene to realize the virtual reality alignment. The object of the experimental study is a rotating ceramic vase with a maximum circumference of 43 cm and a height of 23 cm, and the diameter of the belly diameter is 13.6873 cm. The ratio of the maximum diameter length to the height is calculated to be approximately equal to 0.5954, and the maximum error value is 0.0018, and the average error value is 0.0012 when compared with the data in the above table.

5. Conclusion

The progress of digital technology has brought about an information revolution, the medium of information dissemination has achieved digital transformation, and people can access the information resources they need through various means at any time and anywhere. In the context of the intelligent era, development and innovation must be the integration and innovation of technology and art, technology leads the transformation of art and design concepts, and technology realizes art and design goals. The diversified functions and experience need of the public in the intelligent era are the internal driving force that drives continuous innovation and development. Based on the policy guidance of public digital culture construction, virtual image technology has been widely used. Virtual image technology effectively solves the technical constraints, form constraints, application constraints, and site constraints of visual communication and has the characteristics of digital technology in the intelligent era, forming a dynamic display, game entertainment, and auxiliary daily diversified functions, bringing a multisensory immersive experience of vision, hearing, and touch, thus enhancing the cultural value and commercial value, making the visual product better serve the interactive cultural experience zone. The visual products can better serve the construction of interactive cultural experience zones, enhance the interactivity and fun of public cultural services, meet the diversified functional and experiential needs of the public, and realize the multisensory immersive experience innovation, emotional experience innovation, service experience innovation, and commercial value innovation of visual products.

Data Availability

The data used to support the findings of this study are available from the corresponding author upon request.

Conflicts of Interest

The authors declare that they have no known competing financial interests or personal relationships that could have appeared to influence the work reported in this paper.

Acknowledgments

The study was supported by School of Journalism and Media, Chongqing Normal University.

References

[1] Y. Lou, L. Y. Duan, Y. Luo et al., "Towards efficient front-end visual sensing for digital retina: a model-centric paradigm," *IEEE Transactions on Multimedia*, vol. 22, no. 11, pp. 3002–3013, 2020.

[2] G. Chen, H. Cao, J. Conradt, H. Tang, F. Rohrbein, and A. Knoll, "Event-based neuromorphic vision for autonomous driving: a paradigm shift for bio-inspired visual sensing and perception," *IEEE Signal Processing Magazine*, vol. 37, no. 4, pp. 34–49, 2020.

[3] M. Liu, L. Nie, X. Wang, Q. Tian, and B. Chen, "Online data organizer: micro-video categorization by structure-guided multimodal dictionary learning," *IEEE Transactions on Image Processing*, vol. 28, no. 3, pp. 1235–1247, 2018.

[4] H. H. Hadi, B. F. Neamah, and M. K. Farhan, "Energy efficient routing protocall by one way multi-hope sensor nodes," *Turkish Journal of Computer and Mathematics Education (TURCOMAT)*, vol. 12, no. 7, pp. 3401–3410, 2021.

[5] X. Xie, X. Cai, J. Zhou, N. Cao, and Y. Wu, "A semantic-based method for visualizing large image collections," *IEEE Transactions on Visualization and Computer Graphics*, vol. 25, no. 7, pp. 2362–2377, 2018.

[6] K. Bai, X. Liao, Q. Zhang, X. Jia, and S. Liu, "Survey of learning based single image super-resolution reconstruction technology," *Pattern Recognition and Image Analysis*, vol. 30, no. 4, pp. 567–577, 2020.

[7] T. Akilan and Q. M. J. Wu, "Sendec: an improved image to image cnn for foreground localization," *IEEE Transactions on Intelligent Transportation Systems*, vol. 21, no. 10, pp. 4435–4443, 2019.

[8] H. Xiong, W. Ma, X. Zheng, J. Gong, and D. Abdelalim, "Indoor scene texturing based on single mobile phone images and 3D model fusion," *International Journal of Digital Earth*, vol. 12, no. 5, pp. 525–543, 2019.

[9] F. Li, J. Hao, J. Wang et al., "VisioMap: lightweight 3-D scene reconstruction toward natural indoor localization," *IEEE Internet of Things Journal*, vol. 6, no. 5, pp. 8870–8882, 2019.

[10] C. Sur, "Survey of deep learning and architectures for visual captioning—transitioning between media and natural languages," *Multimedia Tools and Applications*, vol. 78, no. 22, pp. 32187–32237, 2019.

[11] M. R. Khosravi and S. Samadi, "Reliable data aggregation in internet of ViSAR vehicles using chained dual-phase adaptive interpolation and data embedding [J]," *IEEE Internet of Things Journal*, vol. 7, no. 4, pp. 2603–2610, 2019.

[12] M. Liu, D. Li, C. Xu, J. Zhou, and W. Huang, "Discovery of multimodal sensor data through webpage exploration," *IEEE Internet of Things Journal*, vol. 6, no. 3, pp. 5232–5245, 2019.

[13] L. Turchet, G. Fazekas, M. Lagrange, H. S. Ghadikolaei, and C. Fischione, "The internet of audio things: state of the art, vision, and challenges," *IEEE Internet of Things Journal*, vol. 7, no. 10, pp. 10233–10249, 2020.

[14] T. Wang, "Intelligent employment rate prediction model based on a neural computing framework and human–computer interaction platform," *Neural Computing and Applications*, vol. 32, no. 21, pp. 16413–16426, 2020.

[15] M. Kaur and L. Singh, "A survey on mobile sensing technology and its platform," *International Journal of Advanced Networking and Applications*, vol. 9, no. 4, pp. 3523–3536, 2018.

[16] J. Li, X. Feng, and H. Fan, "Saliency-based image correction for colorblind patients," *Computational Visual Media*, vol. 6, no. 2, pp. 169–189, 2020.

[17] E. A. Naeem, A. E. A. Abdelaal, A. A. Eyssa et al., "Efficient signal and protocol level security for network communication," *International Journal of Speech Technology*, vol. 23, no. 2, pp. 399–424, 2020.

[18] H. Zhang, S. Wang, X. Xu, T. W. S. Chow, and Q. M. J. Wu, "Tree2Vector: learning a vectorial representation for tree-structured data," *IEEE transactions on neural networks and learning systems*, vol. 29, no. 11, pp. 5304–5318, 2018.

[19] M. Grard, E. Dellandréa, and L. Chen, "Deep multicameral decoding for localizing unoccluded object instances from a single rgb image," *International Journal of Computer Vision*, vol. 128, no. 5, pp. 1331–1359, 2020.

[20] J. Guo, B. Song, Y. He, F. R. Yu, and M. Sookhak, "A survey on compressed sensing in vehicular infotainment systems," *IEEE Communications Surveys & Tutorials*, vol. 19, no. 4, pp. 2662–2680, 2017.

Hindawi
Journal of Sensors
Volume 2022, Article ID 9002533, 11 pages
https://doi.org/10.1155/2022/9002533

Research Article

Wireless Music Playing Buzzer Sensor-Assisted Music Tone Adaptive Control

Suipeng Li[1] **and Dan Shen**[2]

[1]*Zhengzhou Technology and Business University, Henan Zhengzhou, 451400, China*
[2]*Harbin University, Heilongjiang Harbin, 150086, China*

Correspondence should be addressed to Dan Shen; shendan@hrbu.edu.cn

Received 16 November 2021; Revised 8 January 2022; Accepted 15 January 2022; Published 2 February 2022

Academic Editor: Gengxin Sun

Aiming at the problem of adaptive change of auxiliary music tones, this paper proposes a MAC protocol with a common music tone listening/sleeping type based on a wireless music buzzer sensor. First of all, the new MAC protocol adopts network-wide synchronization, and all sensor nodes in the entire network use the same scheduling table, so that the entire network nodes enter the music tone listening period and the sleep period at the same time. Secondly, the node adaptively adjusts the duty cycle of the node according to the number of data packets in the sending queue, increases the node's music tone listening time, reduces the end-to-end delay of data packets, and improves the throughput of the network. Then, the experiment adopts a new backoff strategy to adjust the contention window according to the backoff times and collision times of data packets sent by nodes in the last five working cycles, increase the backoff time of sending data packets under high network load, and reduce the appearance of data packets. We build four simulation experiments on the NS2 simulation platform: unassisted music tone adaptive network, single auxiliary music tone adaptive network, auxiliary music tone adaptive convergence network, and random deployment network, which will be based on the auxiliary music tone adaptive MAC protocol, and IEEE802.11 protocol and SMAC protocol are run in four simulation experiments, respectively, and the performance of the three protocols is analyzed according to the tracking files in the simulation experiment. The analysis results show that the simulation wireless sounding buzzer sensor network is adaptive to different auxiliary music tones and different topologies.

1. Introduction

Since the wireless music buzzer sensor network is an extremely limited energy network, reducing the energy consumption of the sensor network is the research focus of the wireless music buzzer sensor network protocol [1]. Among the various layer protocols of the wireless music buzzer sensor network, the design of the media access control (MAC) layer and the network layer routing protocol plays a decisive role in the energy efficiency of the sensor network. The wireless music buzzer sensor network is composed of a large number of energy-limited sensor nodes through self-organization, and the nodes cooperate to improve its detection rate, and finally combine the two to get the final feature subset [2–5]. However, due to the limitation of node size and cost, sensor nodes are usually greatly affected in terms of computing power, communication ability, and energy. The energy consumption of nodes comes from batteries with limited capacity. How to minimize the energy consumption of the wireless music buzzer sensor network and maximize the network lifetime is the optimization goal of the wireless music buzzer sensor network. Existing research work extends the survival time of wireless music buzzer sensor networks from different directions. This article starts from the MAC protocol in the link layer and studies the method of optimizing the MAC protocol in wireless music buzzer sensor networks to extend the network.

With the continuous development of science and technology, the form of network existence is also constantly changing, from the initial local area network to the wide area network, to today's Internet, and the Internet of Things that is gradually taking shape. As the name suggests, the Internet

of Things is the "Internet of Things Connected". That is to say, the core and foundation of the Internet of Things is still the existing Internet, and a network extended and expanded on the basis of the Internet: its user end extends to any object and object to exchange and communicate some information. As an extension technology of the Internet of Things in the Internet, the wireless sensor network (WSN) has become a research hotspot in the academia and industry. The wireless music buzzer sensor network integrates sensor technology, embedded computing technology, network technology, distributed information processing technology, and wireless communication technology [6–8].

The paper proposes a wireless music buzzer sensor network MAC protocol based on low-power music tone listening (LPL) to reduce preamble crosstalk energy consumption and increase data transmission throughput. This protocol is aimed at the wireless music buzzer sensor network MAC protocol in low-power music tone listening (LPL) using too long preamble to wake up the node, resulting in unnecessary "crosstalk" energy consumption for the sensor network. The target node information in the received data packet start message received in the preamble sequence is compared with the node information (DS-MAC), and it is determined whether to continue to receive subsequent messages and data according to the comparison result. At the same time, in LPL, in each transmission cycle, the node receives a fixed data packet, consumes the energy required to send a too long preamble. Extending the time sequence of a single receiving data cycle increases the amount of data received by the receiving node in each cycle. The simulation results show that the protocol not only improves the energy consumption of the sensor network but also increases the network throughput.

2. Related Works

The throughput rate, delay, packet delivery rate, and energy consumption are usually the main performance indicators of the WSN MAC protocol. Since the nodes in WSN are usually powered by batteries, energy consumption has become the primary principle of the MAC protocol design. At the same time, when WSN is used in industrial control, military reconnaissance, medical diagnosis, and other fields, the reliability of its data transmission has also become a key indicator that the MAC protocol has to consider. For the WSN that uses IEEE 802.15.4 CSM ~ CA default parameters for channel access, the increase in the number of network nodes and the data load will make it unable to withstand the fierce channel competition, resulting in serious data transmission reliability and energy consumption decline. For the deterioration problem, relevant researchers work to solve this problem as the research goal, aimed at designing an adaptive optimization strategy, so that each sensor node can adjust channel access parameters according to network load changes, so as to meet the application layer's requirements for packet delivery rate and low power consumption [9–11].

Regarding the MAC protocol using the fixed multiplexing access mode, Aguilera et al. [12] proposed a MAC protocol based on the TDMA mechanism for WSN with a clustered structure. The protocol divides the nodes in the network into multiple clusters. Each cluster has a cluster head. The cluster head allocates sending time slots for the ordinary nodes managed by itself and collects the data sent by the ordinary nodes and merges the data and then sent to the sink node. Although the MAC protocol based on the clustered network reduces the energy consumed by the common node competing channels, the energy consumption of the cluster head is too large, so further research is needed. Distributed energy-aware node activity protocol is also one of the classic protocols that uses time division multiplexing access. The timeframe is divided into a scheduled access phase and a random access phase according to the cycle. The scheduling access phase is divided into multiple time slots. A certain time slot is allocated to a specific node to send data, while the random access phase is only used for the transmission of control frames. However, the DEANA protocol does not consider how to allocate time slots reasonably according to the needs of nodes to send data.

In terms of MAC protocols that use random contention access methods, the sensor MAC protocol based on the IEEE 802. 11 MAC protocol of wireless local area networks is known as one of the most classic WSN MAC protocols. The protocol uses a fixed periodic music tone listening/sleep scheduling mechanism to reduce energy consumption and uses the CSMA/CA access mechanism to compete for channels during the active period. Under the premise of ensuring low power consumption, Shi et al. [13] minimized delay and increase throughput. Aiming at the problem that the relatively fixed scheduling period cannot adapt to the adaptive changes of network-assisted music tones, a MAC protocol that adaptively adjusts the duty cycle is proposed: T-MAC (timeout MAC) protocol, which dynamically adjusts the scheduling. The length of the active time in the cycle changes the duty cycle. However, the T-MAC protocol may have the problem of the destination node going to bed early, so further improvement is needed. Gupta et al. [14] proposed the wiseMAC protocol, which was originally designed for the WiseNET low-power WSN platform. The protocol introduced preamble sampling technology on the CSMA mechanism and improved the protocol to the network communication control node in idle music by minimizing the preamble mechanism. Compared with MAC and T_MAC, it has higher energy efficiency. Nozawa et al. [15] proposed the SiR MAC protocol. The basic idea of the protocol is to use a fixed-size contention window and select an appropriate transmission probability distribution for nodes at different time slots, so that different nodes that detect the same event can be within the contention window to send messages without conflict in each time slot. Cannard et al. [16] found the problem of excessive energy consumption by the boundary nodes of MAC virtual clusters is brought forward by algorithm, which effectively improves the network life of boundary nodes. Researchers are concerned with synchronous periodic music tone listening/sleeping mechanism. If the underreporting rate is high, it will lead to deviations between the evaluation results and the actual ones. The MAC protocol and the x-MAC protocol adopting the asynchronous periodic music tone listening sleep mechanism establishes

a Markov queuing model. Through this model, the network throughput, delay, and energy consumption in the synchronous and asynchronous conditions are analyzed, and the theory is provided for the optimization of the WSN protocol [17–20].

3. Wireless Playing Buzzer Sensor-Assisted Music Tone Adaptive Control Model Construction

3.1. The Level of Wireless Music Network Space. When a wireless music buzzer sensor network faces different applications, the hardware components selected by the sensor nodes are also slightly different. The difference lies in the size, cost, and energy consumption of the nodes. The functions of the main four unit modules of a node are as follows: (1) The sensor module is used to sense and obtain the information of the monitoring area and the related physical quantities of some objective objects and pass the analog signal through the analog to digital converter (analog-to-digital (A/D) converter) signal. (2) The processor module is used to process the information data collected by the sensor and the data sent by other sensor nodes and is responsible for coordinating the work of various parts of the node. (3) The wireless communication module converts the digital signal output by the processor into an analog signal through a digital-to-analog converter (D/A) and sends it to the equivalent node through the wireless medium. Usually, the transceiver adopts low-power consumption and short-distance communication. The wireless communication module has four states: sending, receiving, idle, and sleeping. Figure 1 shows the hierarchy of wireless music network space.

The MAC layer is the first layer above the physical layer, so the performance of the MAC protocol is strongly affected by the physical layer. In wireless sensor networks, the MAC protocol determines the use of wireless channels and allocates limited wireless communication resources between sensor nodes to build the underlying infrastructure of the sensor network system. In fact, the medium in a wireless environment is usually a wireless channel, and the essence of wireless channel transmission is broadcasting. In other words, within the communication range, any ongoing transmission may be interfered by other transmissions. Interference means the loss of data packets. In this case, the MAC protocol needs to provide a suitable retransmission mechanism.

$$C(r,t)-\sum\left(C(r,t)/C(s,t)+\frac{C(r,t)-C(s,t)}{C(r,t)\times C(s,t)}\right)\times 100\%=0. \tag{1}$$

The use of scheduling-based MAC protocols will also cause some problems. In a network without infrastructure, huge energy needs to be spent to maintain global clock synchronization, and a highly complex distribution algorithm calculates conflict-free time slots. The conflict-free schedule needs to understand the topology of the two hops around the node and place the topology within the two hops in the node with limited memory, which will consume additional energy to maintain the topology.

$$F(x,t)=\lim_{x\longrightarrow\infty}\sum_{i=1}^{N}a_i-\frac{1}{\prod a_i y_j a_j y_i}\sum_{i=1}^{N}\sum_{j}^{N}a_i y_j a_j y_i k\left(x_i^2,x_j^2\right). \tag{2}$$

It can be seen that most of the energy consumption of sensor nodes is in the wireless communication module. The wireless communication module consumes the most energy in the sending state, followed by idle and receiving states. The wireless communication module always monitors the usage of the channel in the idle state, checks whether there is data sent to it, and turns off the radio transceiver in the sleep state, reducing unnecessary forwarding and receiving, and entering the sleep state as much as possible when there is no communication requirement can make the communication of sensor nodes more efficient.

3.2. Tone Adaptive Analysis of Auxiliary Music Data. Before the auxiliary music data node receives the start symbol (start symb01), the sender's information is received at least twice. The first time is the semaphore information, and the second time is the reception start information. From the perspective of energy consumption, the semaphore information is received earlier than the reception start signal, which is more conducive to preventing nodes from responding to signals from nondestination nodes.

In the MAC protocol mechanism, multiple nodes will compete for the same destination node, that is, the destination node will receive multiple semaphore information. At this time, the amount of information will be interfered, and the semaphore will be adjusted through related methods (used in an analog environment). If it is judged whether it is the destination node in the received semaphore information, at this time, multiple nodes are competing for the same channel time sequence, so when the received semaphore information is selected to determine the sender may affect the channel competition, and when the reception start information is received, at this time, the competition ends and the radiofrequency signal has stabilized, which is conducive to the stability of the sensor network information transmission, so the reception start information is used as the basis for selecting the destination node. Figure 2 shows the distribution of auxiliary music data.

In the process of designing energy-efficient network protocols, it is often not related to a certain layer of the protocol stack, but to achieve the best energy efficiency through the integration of multiple layers of functions and data, which is the crosslayer design mentioned above layer design, because it is difficult to apply multiple energy efficiency strategies together at a certain layer. In a whole receiving cycle, different timing intervals or time slots apply different methods to control energy consumption, so there may be conflicts in the same layer. For example, the method of applying asynchronous purpose LPL in the synchronization protocol TMAC protocol cannot be implemented at the same time at the MAC layer. All data units in the data packet

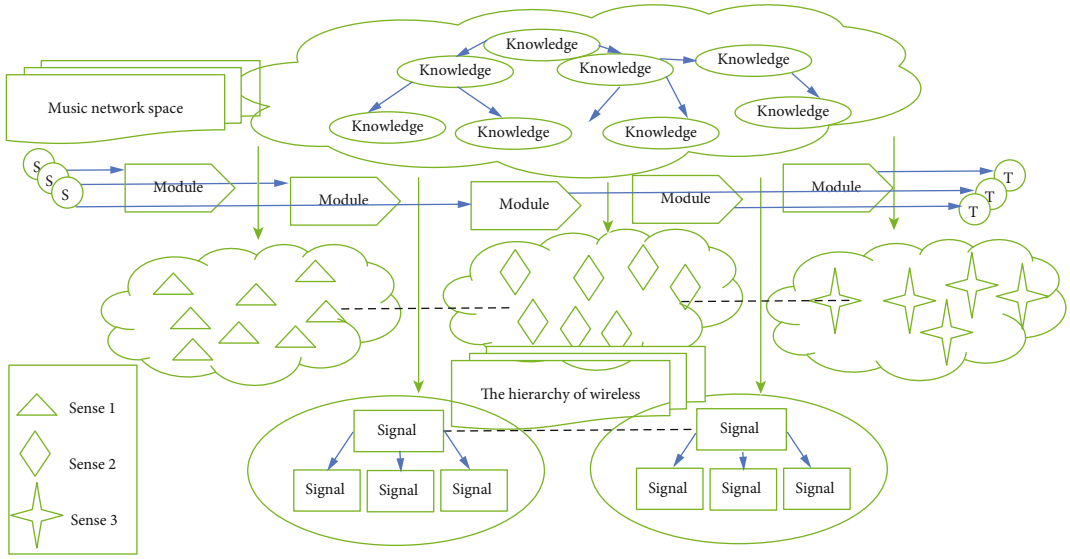

Figure 1: The hierarchy of wireless music network space.

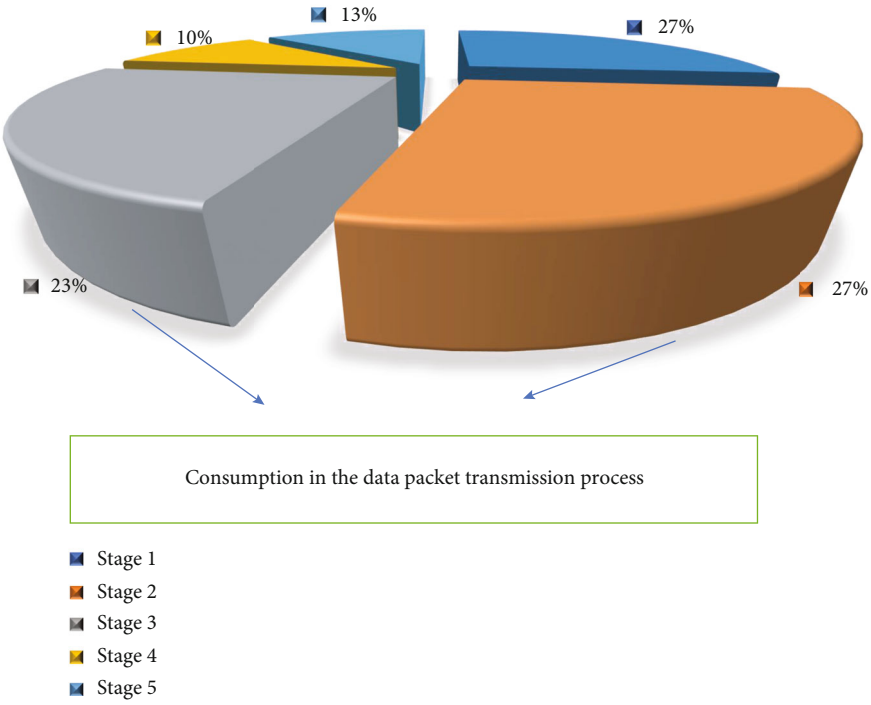

Figure 2: Distribution of auxiliary music data.

transmission process can only be analyzed at the physical layer, so that the proposed new protocol can transmit data.

The mechanism in which sending nodes compete to send wake-up signals in SCP mode is much less expensive than the mechanism of continuous preamble transmission in LPL. However, if the length of the data packet to be sent is too short, the ratio of the energy cost of the wake-up signal to the energy consumption of data transmission is still relatively small. In order to further reduce overhead and improve protocol performance, the improved SCP working mode of MA-MAC adds a short data burst function, that is, when multiple data to the same destination node plus an ACK frame (if ACK needs to be sent), the total transmission time is less.

Security elements are the input part of the network security assessment system, and its classification accuracy affects the results of the assessment. When the protocol supports the maximum length of data packet transmission time, multiple short data packets can be continuously transmitted in bursts. If there are multiple short data packets to be sent

continuously, the node sets the BURST_XMIT_BIT flag in the packet header when sending the previous data packet, and the receiving node does not enter sleep after receiving the data packet with this flag set but continues to wait.

3.3. Buzzer Sensor Network Parameter Setting. The protocol stack of a buzzer sensor node usually includes five layers: application layer, transport layer, network layer, data link layer, physical layer, and three management planes, namely, energy management plane, mobility management plane, and task management plane. The result can be obtained according to

$$\begin{cases} V_{(i,f)} - \dfrac{\sum J_i^f + J_i^{f-1}}{\sin\left[\omega(x,t)\right]} = 0, \\ V_i = \left(V_{(i,i)}, \cdots, V_{(i,f)}\right). \end{cases} \tag{3}$$

The role of the sensor's network protocol stack is roughly the same as that of the Internet protocol stack, coordinating the transmission of data packets in the network. The main role of the three management planes is to enable sensor nodes to work together in an energy-efficient manner, coordinate the forwarding of data packets between mobile nodes in the network, and support multitasking and resource sharing. The functions of the protocols and management planes of each layer are as follows: (1) The main function of the physical layer is to determine the modulation mode and transceiver architecture so that it has simple, low-cost characteristics and can provide the required sufficiently robust services. (2) The main function of the data link layer is to ensure the correctness of transmission, adjust the data transmission rate, and media access control of the MAC layer (the MAC layer is usually considered a part of the data link layer, but in the MAC layer and the rest is a clear boundary between the data link layer). (3) The network layer is responsible for forwarding data packets from the source node to the destination node through the network. The main function is to find the optimal path and forward it correctly along the optimal path. Table 1 shows the applicability of auxiliary music data.

At the end of the backoff time, the wireless channel is always in an idle state, and then, the node will send the RTS packet. The RTS control packet includes the time NAV required for this data transmission. After the transmission is completed, the channel will listen to the music tone and wait for the destination node of the data packet. As the sent CTS control packet, when the clock of the CTS waits for a timeout, the node performs timeout processing and enters the dormant state.

The LEACH protocol clusters the network by first selecting the cluster head and then dividing the cluster area. When receiving the CTS packet sent by the destination node, the sending node immediately sends the data packet to the destination node and waits for the ACK control packet. When the sending node waits for the ACK to time out, the node will also perform timeout processing and retransmit. When the number of retransmissions exceeds 3 times, the node

Table 1: Description of the applicability of auxiliary music data.

Index number	First level indicator	Second level weight	Third level weight
1	Auxiliary function rate	0.12	0.34
		0.24	0.25
		0.09	0.26
2	Optimal network layer	0.13	0.25
		0.05	0.41
		0.14	0.52
3	Network auxiliary capabilities	0.22	0.17
		0.31	0.09

enters the dormant state. When the sending node receives the ACK control packet from the destination node, the sending node checks to see if there is still data to be sent. If not, it enters the dormant state. If there is still data to be sent in the buffer queue, the node needs to reapply for the channel and enter again in idle music tone listening state, after successful channel competition, repeat the above steps to send data packets.

3.4. Tone Adaptive Clustering Control. Since the tone adaptive communication module consumes most of the energy of the node, and the MAC protocol determines the state of the radio, the quality of the MAC protocol will affect the lifetime of the entire network. In addition, different nodes sometimes use different power supply modes, such as the use of non-rechargeable batteries, the use of regularly charged equipment (sunlight, etc.), and the use of irregular charging equipment (the ion in the soil, etc.).

In short, under the limited energy and hardware of the node, the MAC protocol design of the wireless music buzzer sensor network should try to ensure the life of the node. Secondly, the MAC protocol is concerned with the quality of service. The service attributes of the wireless music buzzer sensor network are basically determined by the specific application. Therefore, the MAC protocol in the wireless music buzzer sensor network focuses on the lifetime, reliability, fairness, scalability, and delay of the network, and throughput is rarely regarded as the main factor in the design of the MAC protocol. Figure 3 shows the distribution of pitch adaptive clustering data.

To support the mobility of network nodes, the node information management module should include a mobile information management submodule and a neighbor table management submodule, while providing corresponding management and data access interfaces to each layer of the protocol stack. The main function of the mobile information management submodule is to manage the status information of the node itself and nearby mobile nodes. The mobile information is stored in the mobile information database, and the mobile information management routine is responsible for changing and querying it. The function that the mobile information management routine should have is to estimate the node's mobile state based on the information provided by the MAC layer and the application layer. In

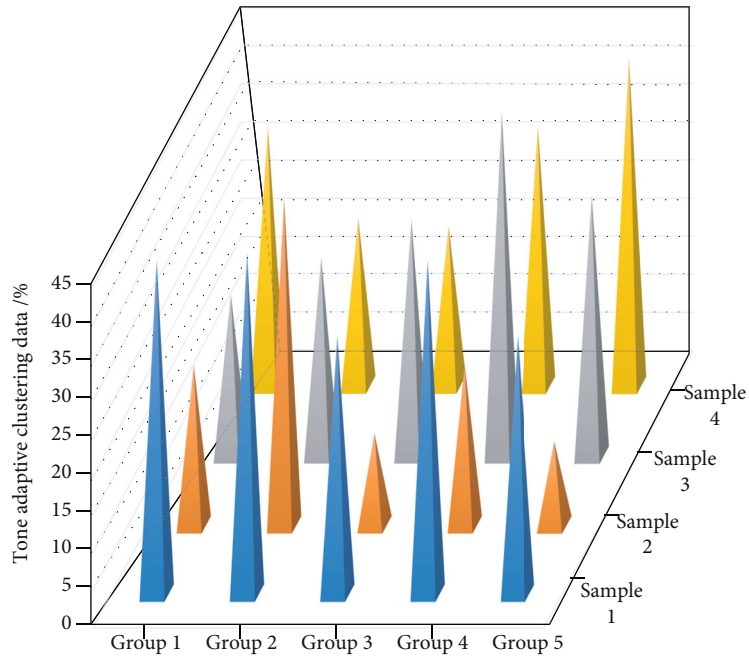

Figure 3: Data distribution of pitch adaptive clustering.

addition, the crosslayer status information of some nodes should also be managed uniformly by the node information management module and provide access and control interfaces for each layer of the protocol stack.

4. Application and Analysis of Wireless Music Playing Buzzer Sensor-Assisted Music Tone Adaptive Control Model

4.1. Buzzer Sensor Network Data Preprocessing. Since in this protocol, all network link constructions and data transmissions are initiated and controlled by the receiving node sending a beacon frame after waking up, the information about the destination address, beacon type, and predicting the next wake-up should be set in the beacon frame. The average load on sensor nodes within 2 hops from the sink node is much higher than the average load on nodes outside 2 hops. Among them, the load of the node within 1 hop from the sink node is the largest, which is about 5 times that of the 3-hop node. For a network with a clustered structure, the network load is mainly concentrated on the cluster head, and the communication bottleneck effect on the cluster head near the sink node is more serious than in a flat structure network. The result can be obtained according to

$$\oint F(x,t) \times L_{(\mathrm{emg},k)} dxdt - \int \left(f_{(\mathrm{emg},n)} + C_{(\mathrm{emg},k)} \right) dkdt = 0. \quad (4)$$

From this beacon structure, it can be seen that compared with other asynchronous MAC protocols; this protocol only adds a rand bit to the beacon structure adjustment, which is used to complete the calculation of the next wake-up time and control the beacon's behavior by setting different values of the DST bit type values, and complete the broadcast update operation; this protocol beacon has the feature of low overhead.

Regardless of whether there are new nodes or dead nodes in the later stage of the network, n is used as a normal value for calculation, but the value of n must be greater than or equal to the initial total number of nodes. After the nodes in the network start to work, they need to determine their approximate scheduling cycle through the initial broadcast beacon frame, and the cycle only starts to run after a node successfully broadcasts the beacon frame. In order to avoid the collision of the node's broadcast frame in the initial stage of the network, in the first original period TPrim, the node randomly selects a moment TRand as the time for sending the broadcast beacon frame. Figure 4 shows the data distribution of the buzzer sensor network.

The average energy consumption of each node in the entire network changes with the increase of the CBR interval. The calculation method is the same as that of the single auxiliary music tone adaptive simulation experiment. Due to the change of the topology, the auxiliary music tone adaptive convergence experiment is different. There is a big difference in the energy consumption of a single auxiliary music pitch adaptation experiment. It can be seen from the simulation performance curve that similar to the simulation result of the single auxiliary music tone adaptation experiment, when the CBR interval is different, the average energy consumption of the nodes in the SMAC protocol and the new MAC protocol changes slowly.

The selection of the cluster head is based on the relationship between the self-generated random number and the threshold. All nodes selected as the cluster head broadcast the cluster head message. At the same time, the sending node sends an RTS data transmission request to the target

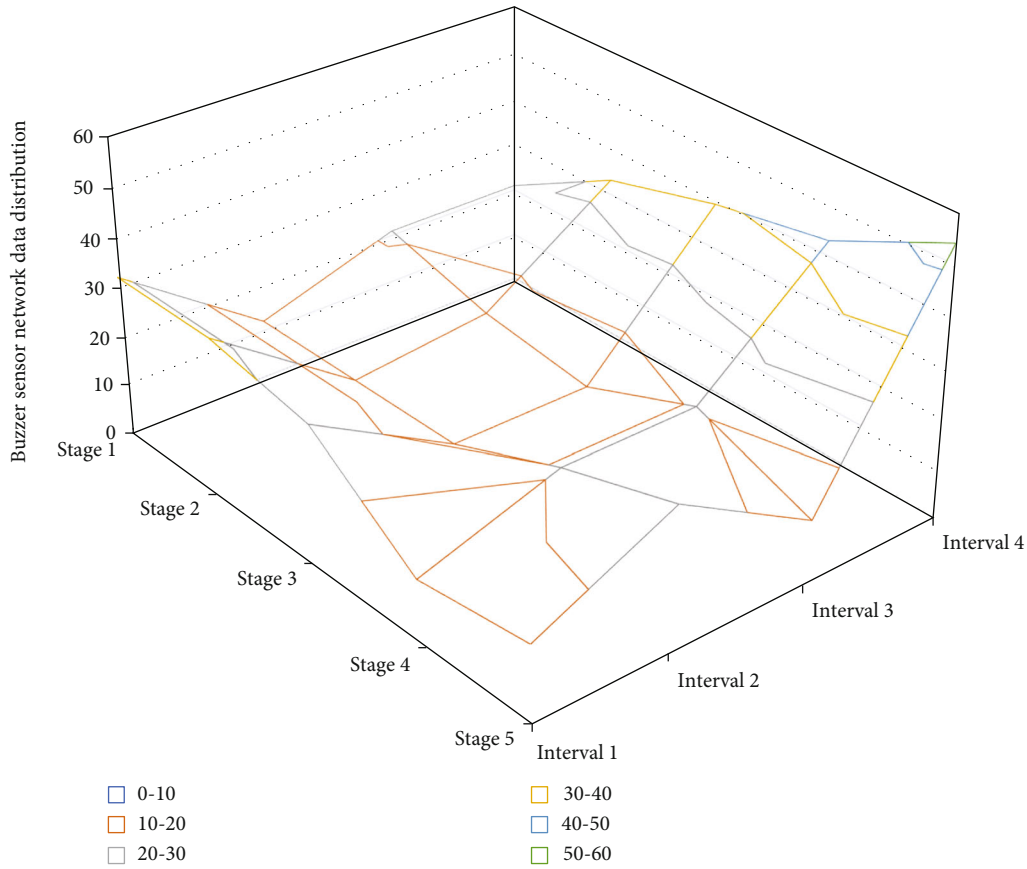

Figure 4: Data distribution of buzzer sensor network.

node and establishes a reliable communication link and completes data transmission through the RTS/CTS/DATA/ACK mechanism. After receiving the data and sending the confirmation frame ACK, the target node still keeps the music tone listening channel for one TKeep time. If there is a data sending request, it will continue to receive data. If there is no request, it will enter the sleep state. However, it can be clearly seen from the simulation results that the new MAC protocol and the SMAC protocol are not converging. The reason for this is that the fixed duty cycle in the SMAC protocol cannot properly handle the funneling phenomenon.

4.2. Auxiliary Music Pitch Adaptive Model Simulation. This paper carries out simulation experiments on the MAC protocol on the NS2 (Network Simulator Version 2) simulation platform. NS2 is a free software that can run on Windows X. All source codes are open and easy to expand. These features are useful for wireless. The research and expansion of the music buzzer sensor network are very convenient, and the research results obtained by this method are also generally recognized by the academia, so this article uses NS2 as a simulation tool. This method first uses the maximum correlation minimum redundancy method to initially filter irrelevant features to reduce the data dimension. The main purpose of the simulation experiment is to verify the feasibility and performance of the protocol on the establishment of a simulation platform and to compare and analyze with the existing mature MAC protocol. The main aspects of the comparison are energy, delay, throughput, etc. Figure 5 is the architecture of the auxiliary music tone adaptive model.

Unbalanced network load distribution results in unbalanced energy consumption of nodes. Nodes near the sink node consume energy faster than peripheral nodes, and routing holes are easily formed near the sink node, which greatly shortens the lifetime of the entire network. The bottleneck effect caused by the sensor data generated by peripheral nodes cannot be correctly and timely reported to the aggregation node. The use of hierarchical fusion and data compression can reduce the total amount of network data and alleviate the communication bottleneck problem to a certain extent, but this method is only suitable.

In addition, since a small number of cluster heads are responsible for most of the network's auxiliary music tone adaptation, the above two problems are more obvious in clustered networks. There are three transmission links in the simulation scenario and all need to be forwarded by high-rate node 0 to complete the data transmission, and node 4 is the destination node of the three links. Therefore, the simulation of this network scenario can achieve the purpose of verifying the optimization effect of the contention

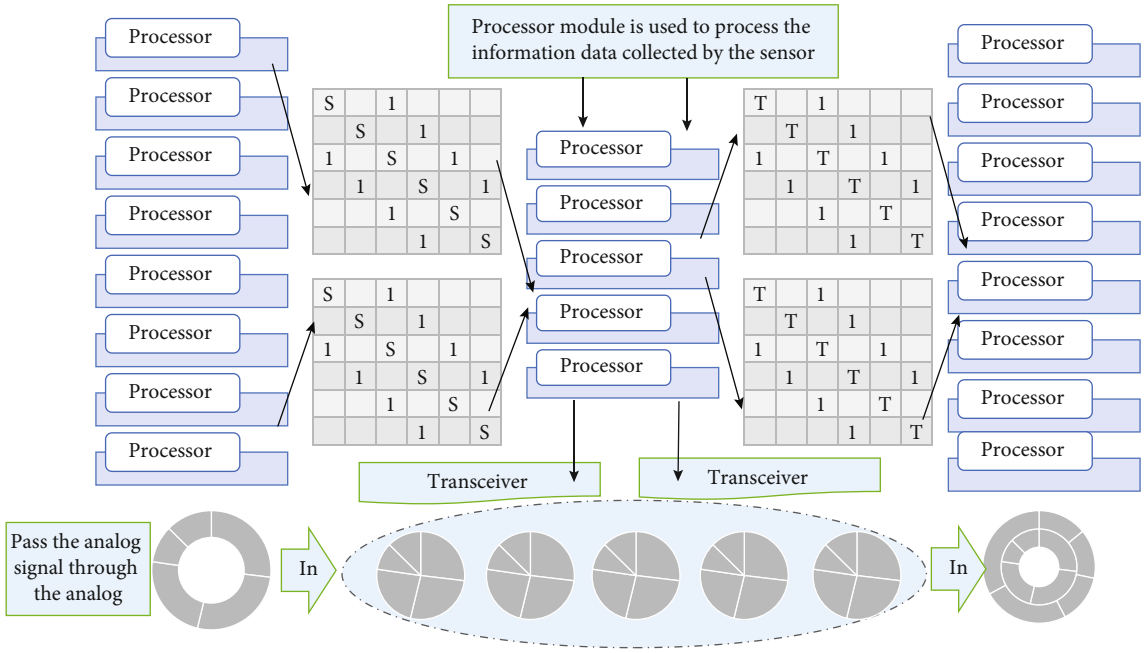

Figure 5: Auxiliary music tone adaptive model architecture.

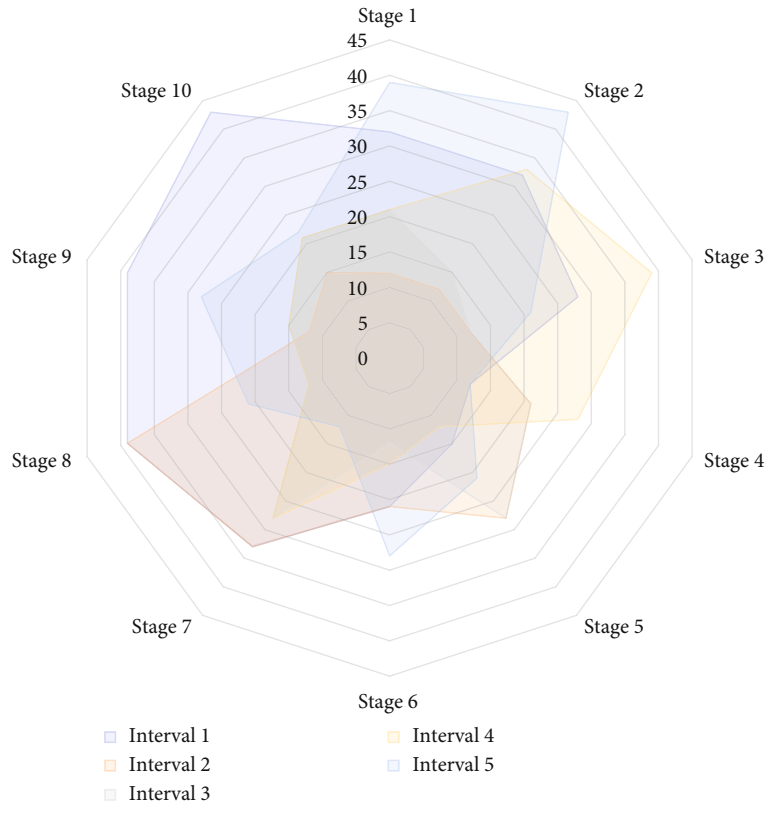

Figure 6: Energy consumption distribution of wireless sensor network nodes.

window white adaptation mechanism of the multirate MAC protocol based on congestion control in this paper. Figure 6 shows the distribution of energy consumption of wireless sensor network nodes.

It can be seen that the performance of this protocol is exactly the same as that of the competition window adaptive protocol. This is because in the hidden terminal scenario, there are only two nodes on the data link, one receiving

and one transmitting, and there is no congestion in the network. The protocol in this paper has been using the competition avoidance mode of the competition window adaptive mechanism, so the mechanism is the same.

A common node usually receives information from multiple cluster heads. In the original S-MAC protocol, when the packet sending interval is less than 5 s, the throughput per child is maintained at around 180 bps, and it does not get better until the packet sending interval is 5 s. This shows that under high load conditions, due to the low duty cycle and the overly simple backoff mechanism, the throughput performance of S-MAC cannot be improved when it reaches a limit value. Under high load, the throughput performance of the optimized protocol in this paper is significantly higher than that of the original S-MAC protocol. The result can be obtained according to

$$\cup_{x-t=1} f(x,t) - \operatorname{sign}\left(\sum_{i=1}^{N} a_i \times y_i \times k\left(x_i, x_j\right) - b\right) = 0. \quad (5)$$

As the auxiliary music tone adaptation decreases, the performance curves of the two protocols tend to be consistent. When the packet transmission interval is less than 0.006 s, the three performance: packet arrival rate, throughput and delay of the protocol in this paper are better than those of the RBAR protocol. The advantage is weakened, and the performance of the three protocols is not much different. In terms of more important throughput performance indicators, when the packet sending interval is less than 0.006 s, the throughput of the RBAR protocol is basically maintained at 1100 Kbps, while the protocol and contention window adaptation mechanism in this paper are higher than RBAR. The simulation results show that the multirate MAC protocol based on congestion control in this paper solves the problem of abnormal performance of multi-rate networks.

4.3. Example Application and Analysis. Most mobile sensing application scenarios require that a small range of sensor nodes near the mobile node can report sensor data at a high rate and high success rate in a short period of time. Maintaining a high transmission success rate under local heavy load is the goal pursued by a mobile sensor network protocol design. Simulation results show that the combination of the AOCMSN optimization strategy and MA-DC-MAC design can achieve better transmission performance than DC-MAC.

At this time, it determines its own attribution based on the received signal strength. Sending one data in 2 seconds to sending one data every 5 seconds, that is, the average data occurrence rate gradually decreases from 5 packets/s to 0.2 packets/s. In the first ten experiments, each sending interval increased by 0.2 seconds compared to the previous one, and l s was increased each time after the sending interval reached 2 s. A total of 13 experiments were carried out. The 5 rounds of experimental data are averaged to get the final result. Figure 7 is the distribution of the communication rate of the buzzer sensor network.

Because the data in DC-MAC is concentrated in a time period for transmission, the collision is very serious when the data transmission rate is high. Because it adopts the data response ACK mechanism, the data packet must be retransmitted continuously after the transmission fails, resulting in a decrease in throughput and an average delay increases. A-DC-MAC only uses the RTS/cTS mechanism near the sink node (data response is not enabled by default). After the node wins the TONE or RTS/CTS competition, it will send multiple data packets continuously in a burst mode to increase the channel utilization. Then, we use the information gain to calculate the feature that has the greatest correlation with the classification result. When the packet transmission interval is less than 0.06 s, the protocol in this paper solves the deficiencies of the competition window adaptive protocol in a network with a relatively complex topology and gives full play to the advantages of the high-rate nodes in the multirate protocol and achieves the highest throughput performance at the same time.

When the packet sending interval is greater than 0.06 s, due to the decrease in network load, the performance of the three protocols is not much different, and the throughput and the packet arrival rate are basically the same. The simulation results prove that the multirate MAC protocol based on control in this paper has realized the optimization of the adaptive mechanism of the contention window. Figure 8 is the load capacity distribution of the buzzer sensor network.

It can be seen that the optimized protocol in this paper consumes less energy than the original S-MAC protocol when the packet sending interval is less than 5 s. Because under high load conditions, the fixed duty cycle and contention window mechanism of the original S-MAC protocol cannot meet the demand for a large amount of data to be sent in the network. The collision and retransmission phenomenon is serious, and a lot of energy is wasted. The optimization of this article improve the network efficiency of the protocol under high load, thereby saving energy. The result can be obtained according to

$$\begin{bmatrix} g(x) * [0,x,1] & 1 & 1 \\ 1 & g(x) * [0,x,1] & 1 \\ 1 & 1 & g(x) * [] \end{bmatrix} [0,x,1] \times \begin{bmatrix} f(x) \times [x,1,0] & -1 \\ -1 & f(x) \times [x,1,0] \end{bmatrix} = 1. \quad (6)$$

When a gateway node receives a data packet in the virtual grid, it first determines whether any adjacent node in the same virtual grid has received the data packet. This can be done by comparing the node directory and the adjacent node list in the data packet. To finish, if it is not received, the gateway node appends the IDs of these nodes to the node directory in the data packet and forwards the data packet to the neighboring node that has not received the information.

In the first ten experiments, each sending interval increased by 0.2 seconds compared to the previous one, and l s was increased each time after the sending interval reached 2 s. A total of 13 experiments were carried out. When a gateway node receives a data packet from other

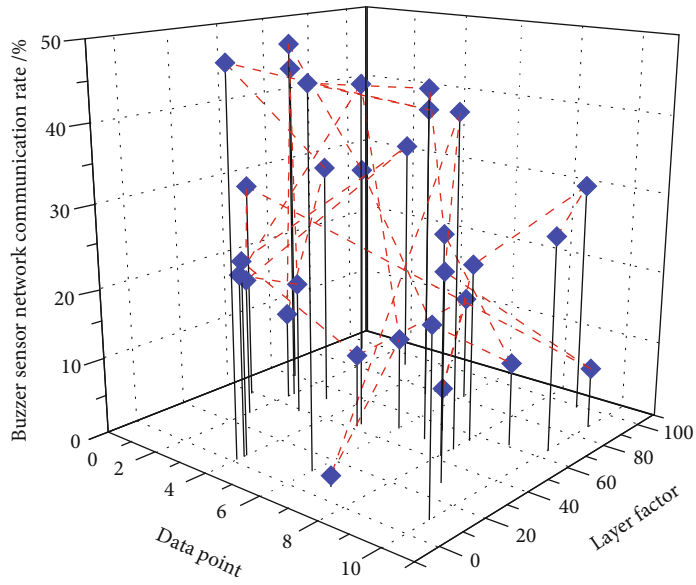

Figure 7: Communication rate distribution of buzzer sensor network.

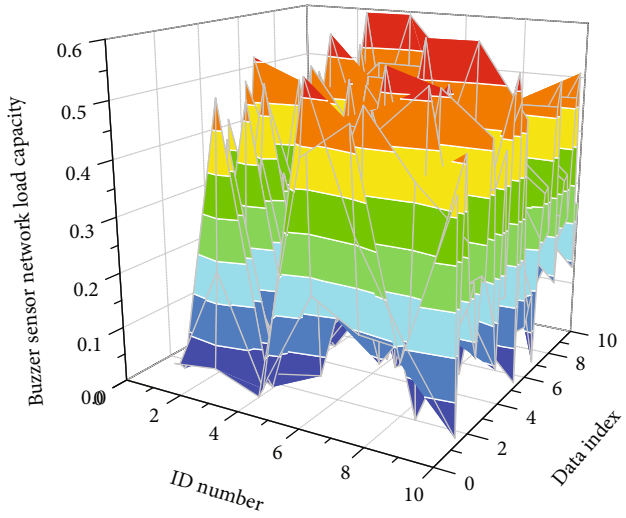

Figure 8: Load capacity distribution of buzzer sensor network.

gateway nodes, it first separates the node directory of the data packet, then adds its own ID and the directories of all its adjacent nodes, and forwards the data packet to all adjacent nodes. In this way, when a data packet is transmitted between virtual grids, its information length will become shorter, but when a data packet is transmitted between the same virtual grid, the information length will increase, so the basic idea of location-assisted flooding is fine.

5. Conclusion

This paper proposes a new wireless music buzzer sensor network positioning-assisted flooding algorithm, which uses positioning information to reduce unnecessary data transmission and divides the sensor network into multiple virtual grids. The internal nodes only send data in the virtual grid, and the gateway node is responsible for data forwarding between grids. Aiming at the problem of multidimensional service load balancing in wireless music and buzzing sensor networks, the experiment established a mathematical model of network load balancing based on a swarm particle optimization algorithm and proposed the application of swarm particle optimization algorithm (PSO algorithm) to sensor network load balancing algorithm. In the optimization protocol of this article, the duty cycle mechanism of auxiliary music tone adaptation, with the cooperation of the competition window adjustment algorithm, will effectively improve the performance of the S-MAC protocol under high load. The increase in duty cycle is conducive to meeting the needs of large amounts of data transmission, while the improved backoff mechanism can reduce collisions caused by fierce competition between nodes, and improve network efficiency. Through the proof of the integrity of the data distribution process, the analysis of the energy consumption of different types of networks, and the results of the actual deployment test on the ZigBee platform, it is proved that the auxiliary location flooding routing algorithm has good energy efficiency. At this time, the duty cycle of the optimized protocol is the same as that of the original S-MAC protocol, and the improved backoff mechanism is not effective. The PSOB algorithm balances the network traffic load by adaptively adjusting the service load bundle on the network node according to the network load.

Data Availability

The data used to support the findings of this study are available from the corresponding author upon request.

Conflicts of Interest

The authors declare that they have no known competing financial interests or personal relationships that could have appeared to influence the work reported in this paper.

Acknowledgments

This work was supported by the Harbin University.

References

[1] S. Ren, D. Yan, X. Yang, Y. Liao, W. Yang, and Z. Liu, "Design of intelligent meridian magnetotherapy instrument and monitoring system based on TCM," *Intelligent Computing and Signal Processing*, pp. 945–951, 2021.

[2] C. Cai, M. Hu, and X. Ma, "Accurate ranging on acoustic-enabled IoT devices," *IEEE Internet of Things Journal*, vol. 6, no. 2, pp. 3164–3174, 2019.

[3] A. Krestanova, M. Cerny, and M. Augustynek, "Review: Development and technical design of tangible user interfaces in wide-field areas of application," *Sensors*, vol. 21, no. 13, p. 4258, 2021.

[4] J. Esparza, P. Gudimetla, S. De Silva, and C. A. Unsworth, "An early warning system for diabetic automobile drivers with peripheral neuropathy," *Disability and Rehabilitation: Assistive Technology*, vol. 16, no. 6, pp. 624–631, 2021.

[5] S. Márquez-Sánchez, I. Campero-Jurado, J. Herrera-Santos, S. Rodríguez, and J. M. Corchado, "Intelligent platform based on smart PPE for safety in workplaces," *Sensors*, vol. 21, no. 14, p. 4652, 2021.

[6] T. Sumida, S. Hirai, and D. Ito, "RapTapBath: user interface system by tapping on a bathtub edge utilizing embedded acoustic sensors," *Interactive Surfaces and Spaces.*, pp. 181–190, 2017.

[7] I. Lashkov and A. Kashevnik, "Smartphone-based intelligent driver assistant: context model and dangerous state recognition scheme," *Intelligent Systems Conference*, pp. 152–165, 2019.

[8] X. Li, L. Teng, H. Tang et al., "ViPSN: a vibration-powered IoT platform," *IEEE Internet of Things Journal*, vol. 8, no. 3, pp. 1728–1739, 2021.

[9] Y. Ye, Q. Wang, and J. Wang, "Green city air monitoring and architectural digital art design based on IoT embedded system," *Environmental Technology & Innovation*, vol. 23, article 101717, 2021.

[10] L. E. Hartman, *DIY in Early Live Electroacoustic Music*, J. Cage, G. Mumma, and D. Tudor, Eds., the Migration of Live Electronics from the Studio to Performance, 2019.

[11] M. Hudec and Z. Smutny, "RUDO: a home ambient intelligence system for blind people," *Sensors*, vol. 17, no. 8, p. 1926, 2017.

[12] T. Aguilera, F. Seco, and F. J. Álvarez, "Broadband acoustic local positioning system for mobile devices with multiple access interference cancellation," *Measurement*, vol. 116, pp. 483–494, 2018.

[13] H. Shi, L. Chen, and Z. Xu, "Personalized location recommendation using mobile phone usage information," *Applied Intelligence*, vol. 49, no. 10, pp. 3694–3707, 2019.

[14] S. Gupta, G. Singal, and D. Garg, "Deep reinforcement learning techniques in diversified domains: a survey," *Archives of Computational Methods in Engineering*, vol. 28, no. 7, pp. 4715–4754, 2021.

[15] T. Nozawa, K. Sakaki, S. Ikeda et al., "Prior physical synchrony enhances rapport and inter-brain synchronization during subsequent educational communication," *Scientific Reports*, vol. 9, no. 1, pp. 12-13, 2019.

[16] C. Cannard, T. Brandmeyer, H. Wahbeh, and A. Delorme, "Self-health monitoring and wearable neurotechnologies," *Handbook of Clinical Neurology*, vol. 168, pp. 207–232, 2020.

[17] S. M. R. Guérin, M. A. Vincent, C. I. Karageorghis, and Y. N. Delevoye-Turrell, "Effects of motor tempo on frontal brain activity: an _f_ NIRS study," *NeuroImage*, vol. 230, article 117597, 2021.

[18] G. K. J. Antara, "Peripherals using in working area," *International Research Journal of Management, IT and Social Sciences*, vol. 2, no. 5, 2015.

[19] J. Brereton, H. Daffern, and M. Green, "Enhancing student employability through innovative program design," *Audio Education: Theory, Culture, and Practice*, vol. 275, 2020.

[20] D. Damianidou, J. Foggett, M. L. Wehmeyer, and M. Arthur-Kelly, "Features of employment-related technology for people with intellectual and developmental disabilities: a thematic analysis," *Journal of Applied Research in Intellectual Disabilities*, vol. 32, no. 5, pp. 1149–1162, 2019.

Hindawi
Journal of Sensors
Volume 2022, Article ID 2348573, 9 pages
https://doi.org/10.1155/2022/2348573

Research Article

Research on Smart City Environment Design and Planning Based on Internet of Things

Zijia Wang

Changchun Humanities and Sciences College, The College of Art, Changchun 130117, China

Correspondence should be addressed to Zijia Wang; wangzijia@ccrw.edu.cn

Received 30 September 2021; Accepted 6 December 2021; Published 1 February 2022

Academic Editor: Gengxin Sun

With the economic construction of human cities entering the era of Internet of Things, people can better build cities, make better use of information resources, and put forward high requirements for smart city environmental design. However, there are serious problems in the construction of smart cities due to the problems of talents, technology, energy, and capital in urban construction. Therefore, in the era of Internet of Things, urban construction needs to take the Internet of Things as the foundation of intelligent construction and constantly form an optimized processing model of urban construction through intelligent excellent methods and the association of all things. In this paper, the smart city of Internet of Things is taken as the research point, and the urban population density and public infrastructure are taken as the optimization objects. The population of four districts in the city is taken as the research object. The population density under 18 years old accounts for 25% of the whole city, the population density between 18 and 65 years old accounts for 41%, the population density over 65 years old accounts for 34%, and the population density over 18 years old accounts for about 80% of the population density in the East District and South District. The research results show that under the premise of population and infrastructure, adding medical and recreational resources can rationally allocate and optimize resources, thus improving the utilization rate of public resources.

1. Introduction

In the information age, national science and technology are becoming more and more developed, and our life may become more and more convenient. The key to facilitation is the development of smart cities, and the planning of public facilities is particularly important in the environmental design and development of smart cities. However, the design and planning of smart city environment under the Internet of Things environment also face many difficulties, such as technology, talents, funds, and laws and regulations. In order to solve the following problems, we must accumulate experience and update methods and technologies in the development of smart cities.

The combination of big data and 5G [1] can improve the competitiveness and efficiency of small- and medium-sized enterprises, enhance the security of the Internet of Things, and solve the technical problems of the Internet of Things. The development of Internet of Things [2] cannot be separated from telecommunications, computing, and social sciences. The essence of the Internet of Things includes wired and wireless sensors and tracking technology. The technology used in the Internet of Things is still the main content of research. Internet of Things [3] connects digital and physical objects. The Internet of Things envisions a future in which digital and physical entities can be linked to form a brand-new intelligent facility, so we will conduct research and investigation on this issue. The Internet of Things provides practical urban management services for citizens and supports the development of smart cities [4]. This paper will discuss the technologies adopted by Padua Smart City. However, the structure of the Internet of Things is very cumbersome and varied. The prospect of the Internet of Things is to provide value-added for citizens. With the rapid development of society [5], communication technology and high-performance technology are associated with smart cities to support various market services. This paper also discusses the relationship between the Internet of Things and other emerging technologies and finally explains in detail how to provide the required TOT services in different protocols.

In order to bring faster services to citizens [6], the development of cities relies more and more on smart facilities, but smart cities have a wide range and are a new architecture. Therefore, this paper discusses the development planning of smart cities and proposes a new architecture from the perspective of data provided by smart cities. At the same time, smart cities are using scientific [7] and technological means to meet the challenges of urban governance and governance. This paper outlines the future of smart cities through examples based on geospatial information science and technology. Smart cities solve urban governance for us through technical services [8] and provide more effective services for aging cities. Literature [9] takes the integration of 5G networks in smart cities and the research of self-driving trucks as examples. Self-driving trucks in smart cities are studied. Literature [10] studies the influence of supply chain management on the development of smart cities. In the final analysis, the development of smart cities [11] is an inevitable requirement, and smart cities should be included in urban management planning. Literature [12] from the experience of smart cities in Japan, smart cities can be combined with renewable energy to realize new energy power generation. Literature [13] looks at the top ten smart cities in the world; we can see that smart cities still face many difficulties and challenges. In order to improve the quality of life in cities [14], we need to change our way of thinking from "city" to "smart city." It greatly facilitates people's lives [15]. From Lecce's experiments, we can know that residents play a vital role in smart cities. Residents are one of the keys to a smart city.

2. Specific Content of Smart City Development

2.1. Smart City and Industry 4.0. Compared with traditional information systems and physical hardware systems, the new generation of information technologies, such as Internet of Things, electronic tags, RMID, and embedded sensors, has more compatibility and no need for manual input. It makes the boundary between information and physics smaller and smaller and can be integrated almost directly, which improves factory efficiency, shortens construction period, reduces cost and energy, and at the same time, it can be customized and improves flexibility.

Industry 4.0 is not limited to the industrial field but also related to smart cities. We hope to realize smart factories, smart grids, smart buildings, and smart homes. In addition, in the field of architecture, the integration of software informationization and hardware automation leads to intelligent building, and the integration of surgical robot and medical automation leads to intelligent medical treatment, which fully shows that Industry 4.0 can be applied in a wide range of fields. In the future, the extension of Industry 4.0 will be in agriculture and so on, and we should form a complete smart city. The schematic diagram of human Internet is shown in Figure 1.

2.2. Essence of Internet of Things. Internet of Things is (NSID+NB + OID)∗N=IOT. In common terms, objects can be connected to each other if they contain NSID/NB/OI. Objects with three characteristics at the same time can be called interconnected bodies. When everything becomes an interconnected system, it can realize the interconnection of all things, which is called the network of information interaction—the Internet of Things. The core of smart city is shown in Figure 2.

Figures 1 and 2 have some similarities in description, but the application scenarios are different. Figure 1 is based on the application of Industry 4.0 and smart city in different scenarios, while Figure 2 is based on the application of the Internet of Things in different scenarios, from eight different scenarios to the smart city application scenarios under the Internet of Things. In Figure 1, there is a wide range of application scenarios, with industrial technology in smart cities as the application. The important technology and means of smart city implementation are realized through industrial 4.0 and Internet of Things technology. Therefore, the given urban application scenarios under different technical frameworks have certain scientific significance.

2.3. Planning and Research Steps. According to the investigation and summary of the city and the set development plan, we can make a blueprint for the development of smart cities.

The blueprint of a smart city is shown in Figure 3.

In Figure 3, the implementation classification of smart city describes the application blueprint of smart city from the aspects of Government affairs, Economy, Traffic, Capital construction, Life, and Resources. This classification is applied to different fields of smart cities to realize the core applications and important scenarios of smart cities. To realize the blueprint of smart city, we need to realize it from the above application scenarios in order to plan and construct smart city.

The specific implementation steps are shown in the following Figure 4.

2.4. Convenience Brought by Smart Cities

2.4.1. Convenience of People's Livelihood. The building of a smart city makes it easier and faster for ordinary people to do things, which is close to the needs of ordinary people. Through a series of computing connected by the Internet of Things, such as cloud computing, people, and the core of cities, such as communities, enterprises, enterprises, and public facilities, are uniting to share information, facilitate people's lifestyles, and better understand the development of smart cities.

2.4.2. Transportation. An intelligent monitoring system is built through sensors, which can monitor whether there are vehicle violations and calculate the current traffic volume in conjunction with big data. When the traffic volume reaches a certain standard, it is designated as a congested road section to remind drivers to travel around. You can also find spare parking spaces in conjunction with big data to facilitate travel.

2.4.3. Security Aspects. Relying on the intelligent monitoring system, intelligent alarm devices are installed at the corresponding positions in the streets, and when personal safety is threatened, they can go to the nearest alarm point to give an alarm. Safeguard the safety and interests of the people.

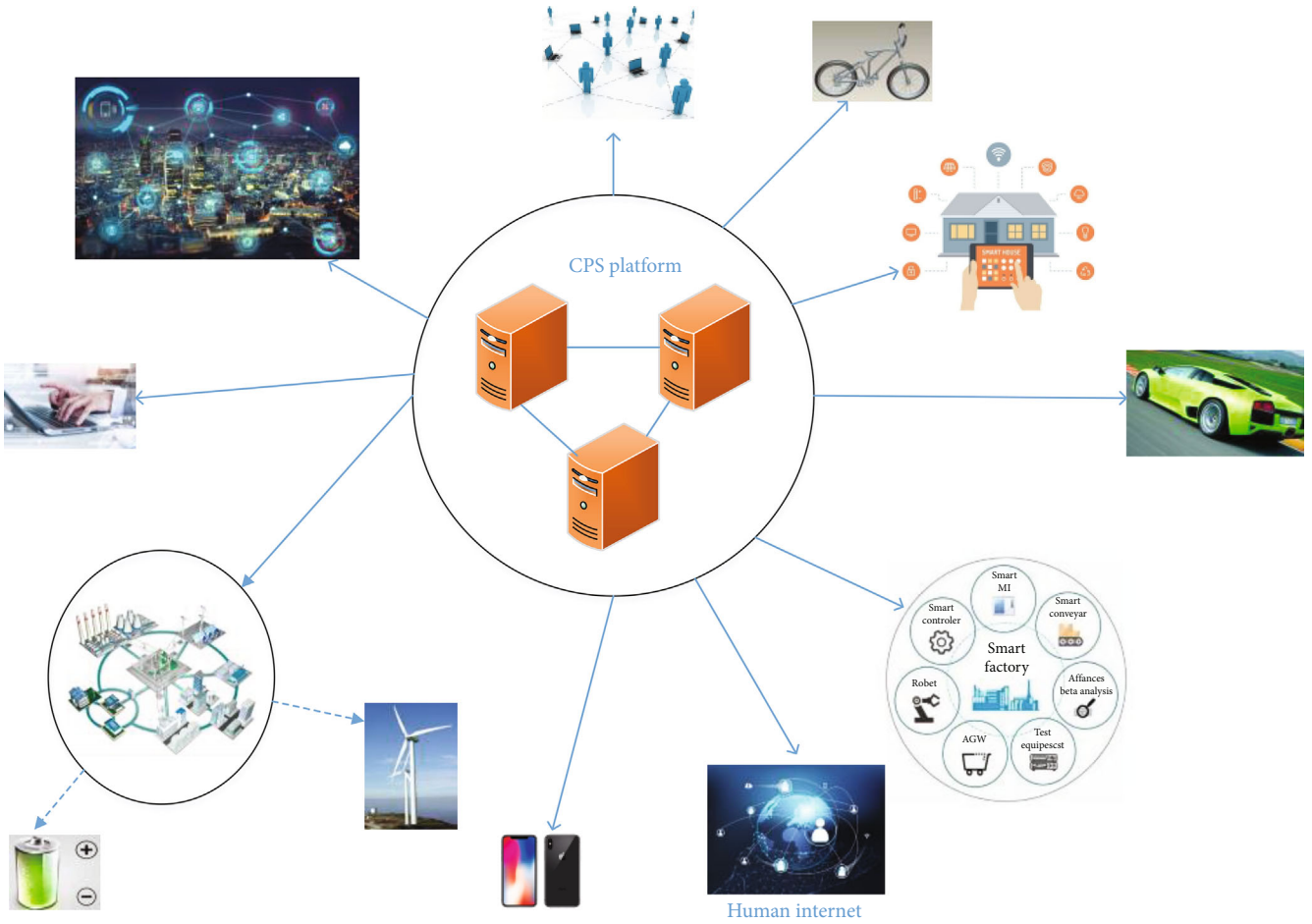

Figure 1: Schematic diagram of Internet of Things and smart city.

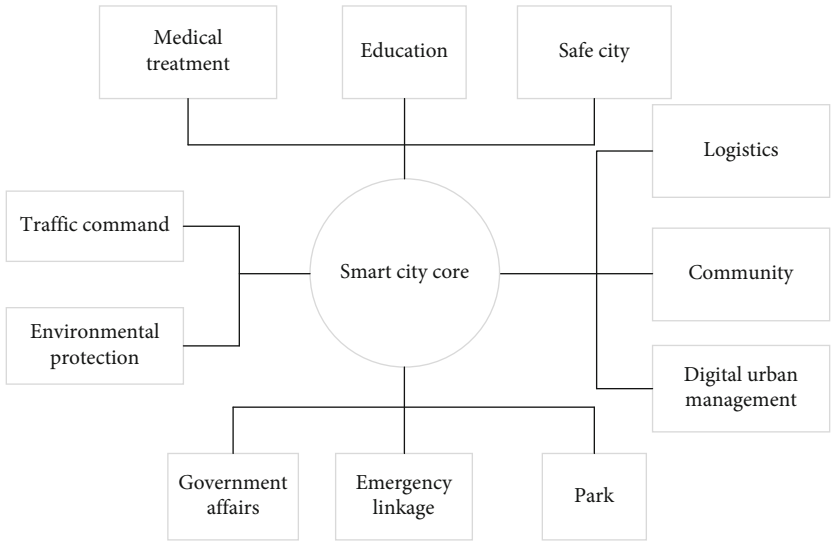

Figure 2: The core of a smart city.

2.4.4. Architectural Aspects. With the building of smart cities, smart buildings have gradually entered everyone's field of vision, mainly including face recognition, voiceprint recognition, motion recognition, and the wide application of service robots. Artificial intelligence technology of intelligent building has sensing function. The comfort of the building

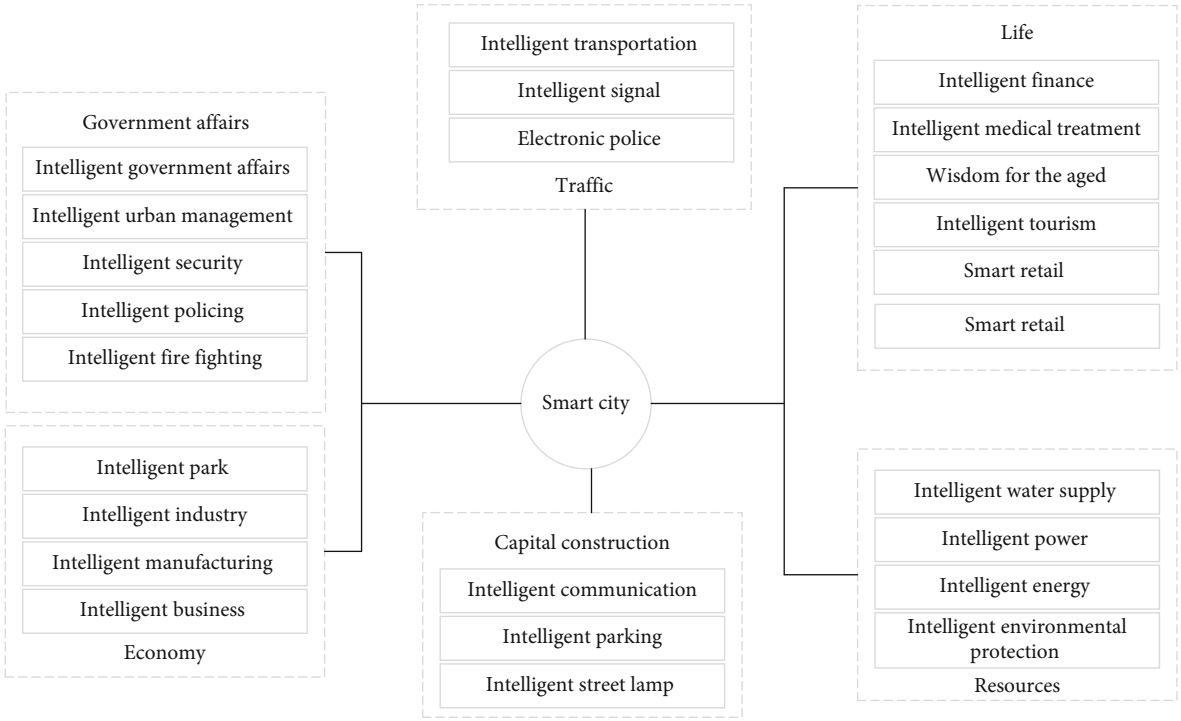

Figure 3: The blueprint of a smart city.

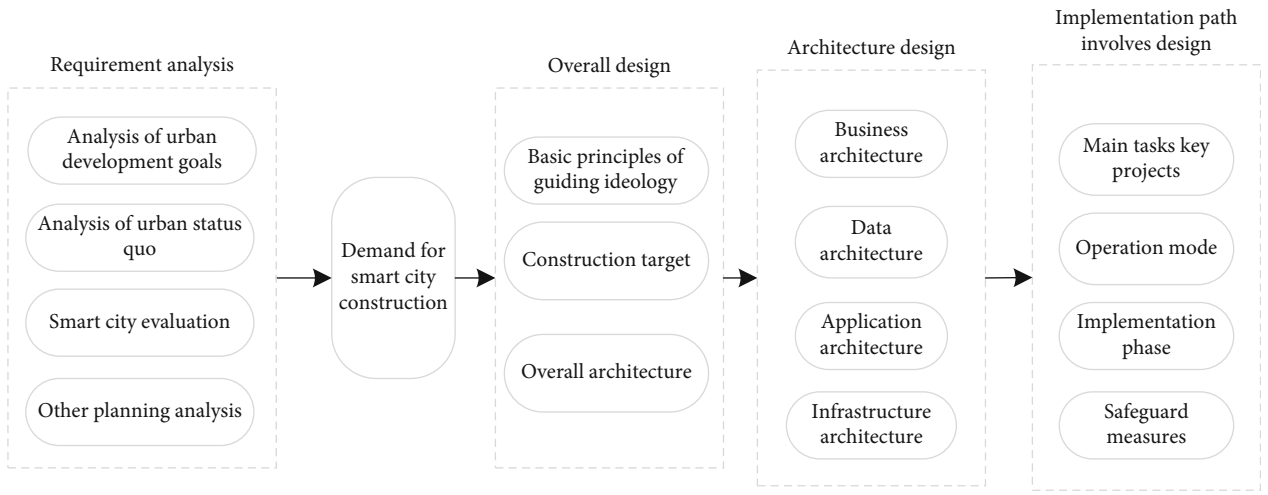

Figure 4: Implementation steps.

is improved. Combining architecture with intelligent technologies such as 5G and 3D modeling to form an intelligent building, the building configuration can be designed and viewed by using the network method, reflecting the perfect sense of intelligent building.

2.4.5. Network Security. In the information age opened by cloud computing, users enjoy convenience but also pose a serious threat to personal privacy. A homomorphic encryption algorithm requires a pair of encryption and decryption algorithms E and D to satisfy plaintext P. In addition, if the decryption algorithm D is regarded as a mapping D: $C \longrightarrow P$, the relation can be satisfied for any ciphertext

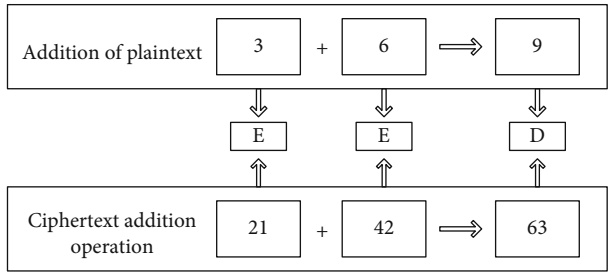

Figure 5: Plaintext ciphertext addition operation.

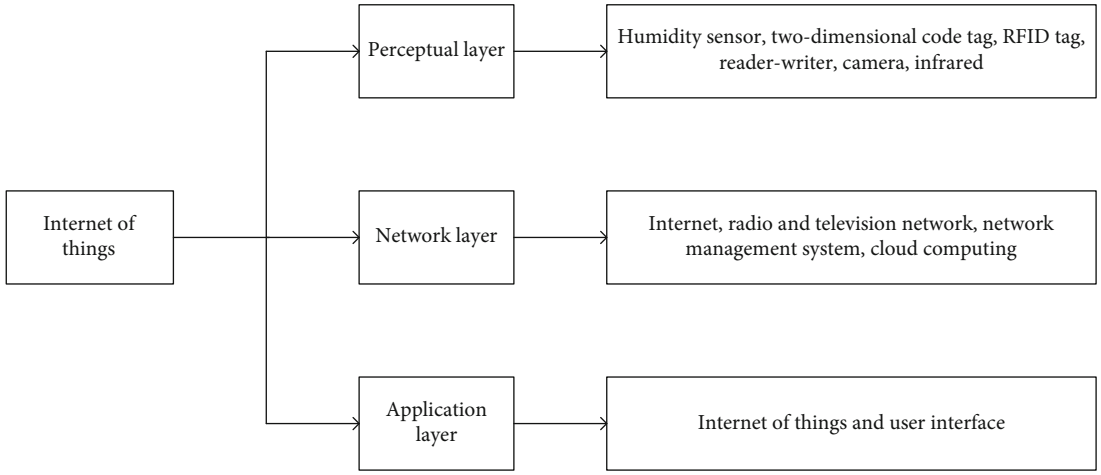

Figure 6: IoT applications.

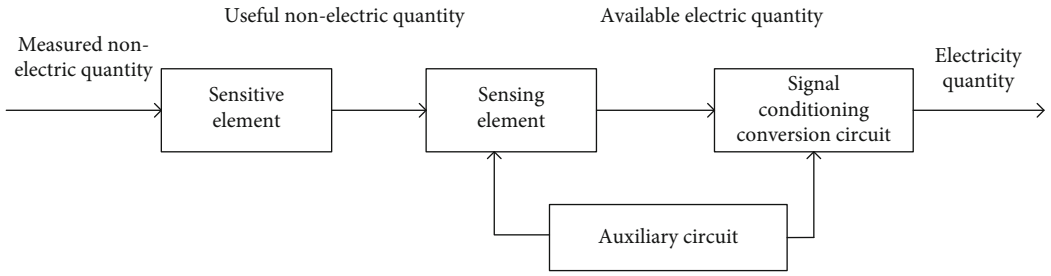

Figure 7: Sensor principle.

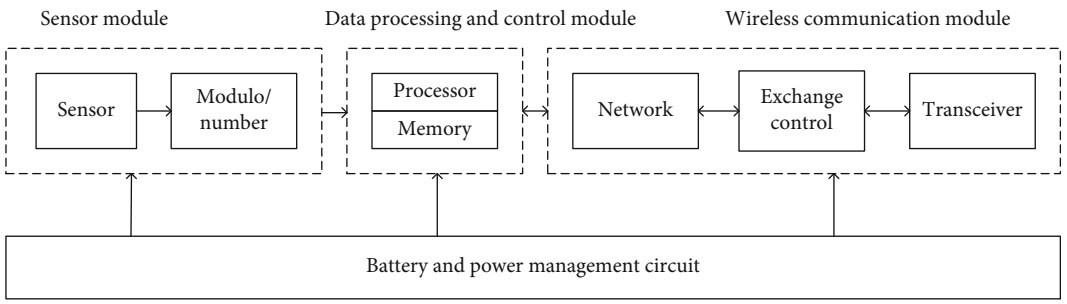

Figure 8: Sensor node structure.

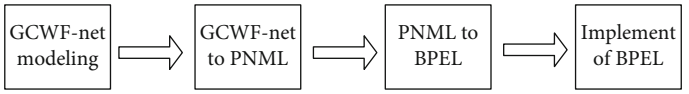

Figure 9: Modeling process.

sequence c, $c1$, and cn belonging to the ciphertext space C:

$$D\left(f'(c, c1, \cdots cn)\right) = f(D(c), D(c1), \cdots D(cn)). \quad (1)$$

f stands for plaintext, f' stands for ciphertext, and f is of the same nature as f'.

For example, set an encryption algorithm, Set Key, if $E(p) = \text{key} \cdot p$, $D(c) = c/\text{key}$.

Then, when key = 7, for plaintexts 3 and 6, their plaintext and ciphertext addition operations are shown in Figure 5.

2.4.6. Care for the Elderly. Physiologically, with the increase of age, the elderly will have problems such as slow response and inconvenient movement; visceral decline, sensory weakness, and other symptoms. Psychologically, the elderly are prone to feel loneliness and other negative emotions. In behavior, they prefer outdoor sports. At present, there are

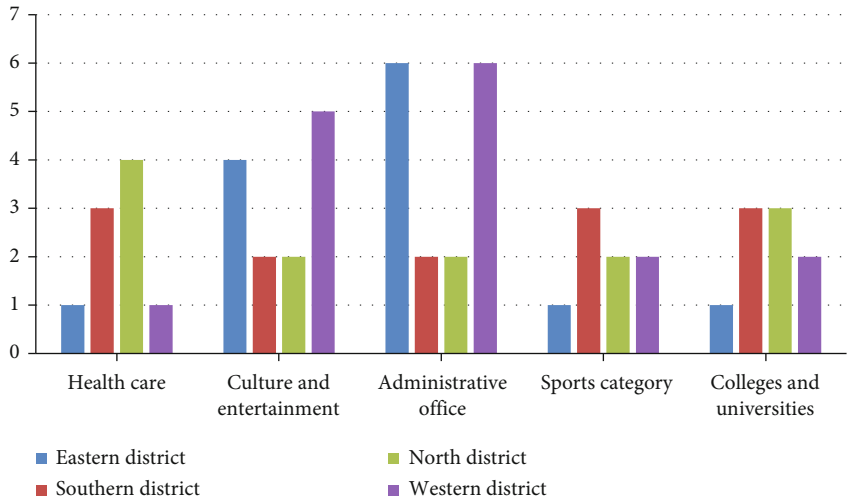

Figure 10: Number of public places in cities.

Table 1: Statistics of people by age group.

Label	Community name	Total population in 2020	Under 18 years old	18~65 years old	Over 65 years old
1	Eastern District	113240	26780	43520	42940
2	Southern District	83970	13259	34507	36141
3	North District	97035	26712	49520	20803
4	Western	109875	33567	39602	36706
Total	C City	404120	100318	167230	136590

many defects in outdoor facilities. In order to create a better outdoor experience for the elderly, intelligence is applied to outdoor facilities to improve the safety and comfort of facilities.

2.5. Problems in Smart City Design and Research Planning

2.5.1. Idea Problem. In the promotion of smart cities in China, more attention is paid to the technical problems related to the construction of smart cities, while the concept of smart cities is ignored. Residents have deviations and confusions about the concept of smart cities. It is necessary to strengthen the main concept of smart cities to facilitate the people.

Smart city construction needs a lot of start-up capital. Investment can be made through communities, enterprises, and residents. However, for some cities, the investment situation is not clear, and the development of smart cities still needs a long time of exploration and research, which is full of many unknown problems.

2.5.2. Technical Issues. The development of smart cities is the simultaneous action of various technologies. However, there are still immature technologies, and some technologies have not been popularized nationwide. The direct deviation of technologies cannot provide stability and accuracy for the planning of smart cities under the Internet of Things environment. Because smart cities under the Internet of Things environment are still in the early stage of development, there are still many unknown problems to be explored, and there are too many uncertain factors, so it is unrealistic to promote smart cities nationwide at this stage in Figure 6.

2.5.3. Talent Problem. The rapid development of intelligent technology leads to the shortage of talents. Most technicians engaged in management, automation, IT, and other fields have changed careers to solve some talent vacancies. However, these technicians have not systematically studied the professional knowledge of Internet of Things and the related knowledge of smart city construction and lack comprehensive talents such as technology and strategy. Therefore, the construction of smart cities still needs a large number of professionals.

2.5.4. Laws and Regulations. Government information and national information often involve private information. Once leaked, it is very important to the development and security of the country. And to build a smart city, there are still technologies provided to foreign enterprises. In order to ensure the security of information and data and prevent information from being artificially monitored and leaked, the privacy of information should be strictly controlled.

2.5.5. Energy Problem. Energy plays a key role in the development of smart cities. However, renewable energy is often accompanied by instability, such as being affected by extreme weather. Therefore, the supply of energy is unstable.

Without standards, Fiona Fang cannot be achieved. The construction of smart cities should plan corresponding standards and improve them according to them.

2.5.6. Postoperation and Maintenance Management. The stable use of the Internet of Things depends on the support of big data, and the acquisition of big data depends on the combination of various technologies, which requires later

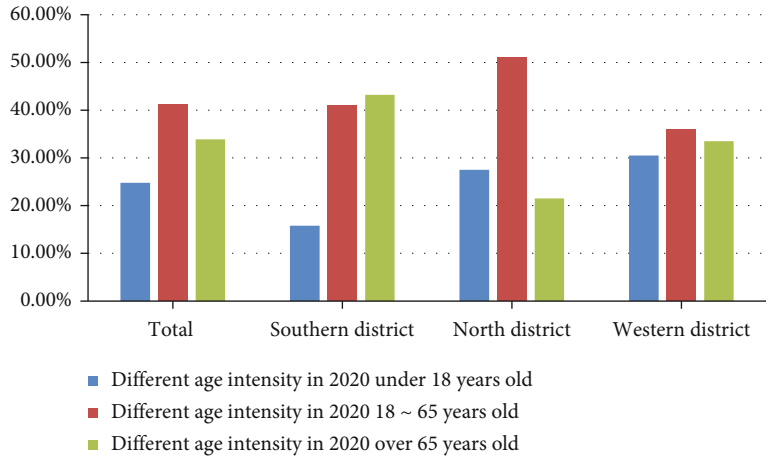

Figure 11: Age density statistics.

operation and maintenance management to manage system development, data collection, data analysis, collation, etc. However, urban affairs are complicated and scattered, which need to be managed by multiple departments. The instability of urban information services will lead to biased data and paralysis of various technical facilities, which will have an impact on urban affairs and residents' lives. The development of smart cities in the later period of operation and maintenance should not be underestimated.

In order to improve people's life satisfaction, the concept of smart city should be widely known by people in the form of community lectures and leaflets. Establish the system, structure, and direction of building a smart city.

The second part of the article focuses on the different applications and classification of the city to give the corresponding technical support. This paper studies the development and planning of the city, puts forward the corresponding structure method, and puts forward the solution from the whole. It has important research significance and application value. The construction process of smart city is to take social and economic prosperity as the goal, social harmony and stability as the premise, and people's livelihood happiness as the assessment criteria and fully apply new information technology to all walks of life in the city, so that human beings can manage production and life in a more sophisticated and dynamic way to achieve the state of "wisdom."

3. Propose a Solution to the Problem

3.1. Concept Promotion. In order to make citizens understand the concept of smart city, we should promote the concept of smart city to citizens by explaining in the community or distributing brochures, facilitating people's lives, displaying the blueprint of smart city, and improving residents' happiness index and satisfaction.

We can attract investment by making investment manuals and advertisements, promoting them through the Internet, and constructing the development plan of smart cities, so as to attract more enterprises to settle in cities and invest in smart cities.

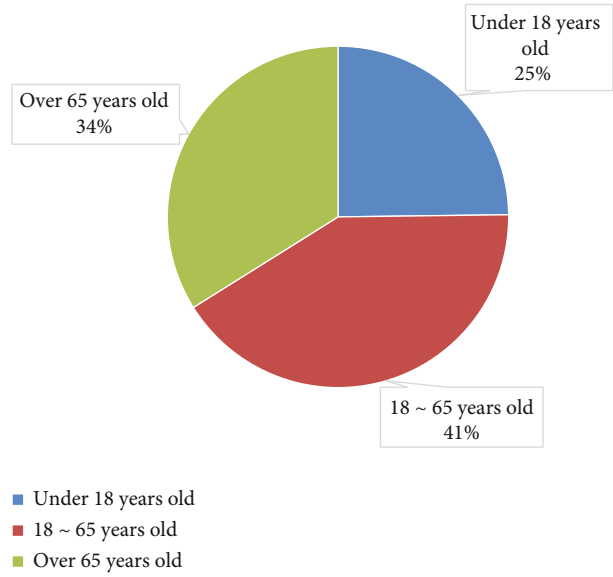

Figure 12: Population density by age group.

The principle of the sensor is shown in Figure 7.

The sensor node structure is shown in Figure 8.

In order to obtain stable technical support and make the information more accurate, more technical enterprises can be settled in the city through investment promotion.

Talent is the key to the implementation of smart cities, and researchers promote the sustainable development and smooth development of smart cities. Therefore, we should set up related majors to train a large number of technical personnel. At the same time, it is necessary to protect the related welfare of technical personnel and retain talents. At the same time, senior technical personnel are regularly hired to popularize the latest science and technology for the vast number of personnel, so as to enhance their own abilities. We should advocate the rotation system and the combination of work and rest, so as to ensure the health of technicians and increase the guarantee for building a smart city.

There are still many uncertain factors in the development of smart cities. And there are different differences in

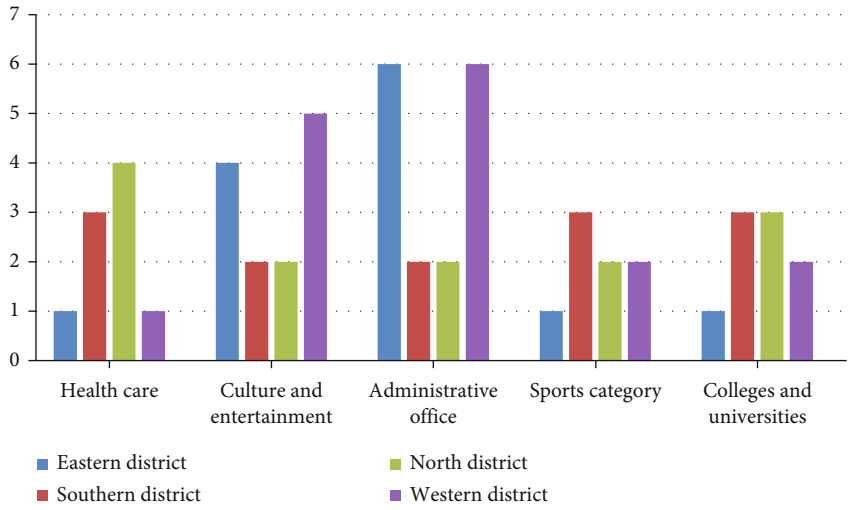

Figure 13: Public facilities around the city.

different cities, so we can take the lead in implementing smart city transformation in one city through pilot projects and then plan other smart city transformation according to successful cases.

3.2. Analysis on the Present Situation of Intelligent City

3.2.1. Problems in the Layout of Public Facilities. GIS database explores spatial and attribute data in spatial domain. Among them, buffer analysis is an important technology in GIS. Set the radius according to points, lines, and planes. Analyze within a specific range. The formula is as follows:

$$D = \{x \mid d(x, s) \leq R\}, \tag{2}$$

where s is the analysis object, d is the Euclidean distance, and R is the radius.

3.2.2. GCWF-net Modeling. Spatial constraint GCNet = (E, T, R, W_r, G, B). If the following conditions are met, it is a spatial information constraint network.

$$\begin{gathered} E \cup T \neq \varnothing \wedge E \cup T = \varnothing, \\ R \subseteq E \times T \wedge W_r \subseteq T \times E, \\ \text{dom}\,(R) U cod(W_r) = E \wedge \text{dom}\,(R) \cup cod(W_r) = T, \end{gathered} \tag{3}$$

where $|T| = 1$ and $\forall t \in T : G(t) \in \{\text{true}, \text{false}\}$, E represents the place, R and W_r are read arc and write arc, respectively, T is the basic unit constrained by spatial information, G is Boolean expression, and B is function body.

The process is shown in Figure 9.

The number of public facilities in different fields is shown in Figure 10.

According to the research, induction, and summary, the table is obtained. Among them, the health and medical facilities in the Southern and Northern Districts are higher than those in the Eastern and Western Districts, which are more suitable for the elderly, while the cultural, recreational, and administrative office facilities in the Eastern and Western Districts are more suitable for young people. As there are more scientific research facilities in the south, north, and west of colleges and universities, there will be a large number of young students living in groups, so cultural, entertainment, and administrative office facilities in the north, south, and west can be increased.

Combine the present situation of public facilities in each district with GIS model. Through the GIS database, the relative population density of teenagers, adults, and the elderly in each street of each community is analyzed, and the urban public facilities are rationally planned according to the population density.

Different age groups use community public facilities differently, so we should make reasonable planning for public facilities with reference to the population density of different age groups to improve the use of public facilities.

In this paper, the number of people of each age group is counted in the community in Table 1.

It can be seen from the chart that the population density aged 18-65 in Eastern District is the highest, the population density aged over 65 in Southern District is the highest, the population density aged 18-65 in Northern District is the highest, and the population density aged 18-65 in Western District is the highest. Population density represents the density of population. Public facilities can be planned in corresponding communities according to age density. Health care will be added in places with high population density of the elderly, recreational facilities and administrative offices will be added in dense areas aged 18-65, and leisure and entertainment facilities will be added under the age of 18. Maximize the utilization of facilities.

4. Comparison of Improved Effects

4.1. Analysis of Improved Public Facility Layout. A survey of the age density, number of facilities, and planning of each community can be found in Figures 11 and 12.

As shown in Figures 11 and 12, in the proportion of population density in the city, the population aged 18-65 and over 65 accounts for a large proportion, so the focus of improving public facilities is to facilitate the population aged 18-65 and over 65 and maximize the use of facilities.

The planned urban public facilities enable the elderly to be treated nearby when they are sick, adults to work nearby, and students to study nearby without having to work across regions. Make the geographical location of public facilities just right in Figure 13.

4.2. Analysis of Improved Intelligent City Planning. Nowadays, the planning of public facilities should also face many difficulties due to the complexity of the environment, so we should combine relevant technologies to explore from various aspects to maximize the use of public facilities.

Handle the relationship between facilities and people, enterprises, and communities, use government resources to improve the quality and geographical location of public facilities, select excellent managers, better manage public facilities, use laws and other relevant regulations to safeguard the interests of public facilities, use science and technology to accelerate the development of public facilities, and promote the masses and social forces to upgrade public facilities.

The basic need of the people is the convenience of life, and the planning of public facilities in smart cities is to meet this need and make people know more intelligent facilities in smart cities.

5. Conclusion

Through GIS model, this paper calculates the population density of each age level to calculate the population of the age level with relatively large living density in each district and then designs and plans the construction of public facilities to maximize the use of facilities.

Data Availability

The experimental data used to support the findings of this study are available from the corresponding author upon request.

Conflicts of Interest

The author declared that there are no conflicts of interest regarding this work.

References

[1] N. L. Fantana, T. Riedel, J. Schlick et al., *Internet of Things: Converging Technologies for Smart Environments and Integrated Ecosystem*, River Publisher, Denmark, 2013.

[2] L. Atzori, A. Iera, and G. Morabito, "The Internet of Things: a survey," *Computer Networks*, vol. 54, no. 15, pp. 2787–2805, 2010.

[3] D. Miorandi, S. Sicari, F. de Pellegrini, and I. Chlamtac, "Internet of Things: vision, applications and research challenges," *Ad Hoc Networks*, vol. 10, no. 7, pp. 1497–1516, 2012.

[4] A. Zanella, N. Bui, A. Castellani, L. Vangelista, and M. Zorzi, "Internet of Things for smart cities," *IEEE Internet of Things Journal*, vol. 1, no. 1, pp. 22–32, 2014.

[5] A. al-Fuqaha, M. Guizani, M. Mohammadi, M. Aledhari, and M. Ayyash, "Internet of Things: a survey on enabling technologies, protocols, and applications," *IEEE Communications Surveys & Tutorials*, vol. 17, no. 4, pp. 2347–2376, 2015.

[6] R. Wenge, X. Zhang, C. Dave, L. Chao, and S. Hao, "Smart city architecture: a technology guide for implementation and design challenges," *China Communications*, vol. 11, no. 3, pp. 56–69, 2014.

[7] H. Min and L. Chang, "Design smart city based on 3S, Internet of Things, *grid computing and cloud computing technology*," vol. 8, no. 4, pp. 25–27, 2012.

[8] H. Zhang, M. Babar, M. U. Tariq, M. A. Jan, V. G. Menon, and X. Li, "SafeCity: toward safe and secured data management design for IoT-enabled smart city planning," *IEEE Access*, vol. 8, pp. 145256-1–14145267, 2020.

[9] F. Sartipi, "Influence of 5G and IoT in construction and demolition waste recycling - conceptual smart city design," *Journal of Construction Materials*, vol. 1, no. 4, pp. 2031–2163, 2020.

[10] K. Gazzeh, E. Hammad, and H. H. Eldien, "Sustainable supply chain management in smart city design: a case study of Al Khobar City Centre," *Journal of Supply Chain Management*, vol. 9, no. 4, pp. 2031–2163, 2020.

[11] F. Zhen, X. I. Guangliang, and X. Qin, "Smart city planning and construction based on geographic perspectives: some theoretical thinking," *Progress in Geography*, vol. 34, no. 4, pp. 402–409, 2015.

[12] T. Kobayashi and S. Ikaruga, "Development of a smart city planning support tool using the cooperative method," *Frontiers of Architectural Research*, vol. 4, no. 4, pp. 277–284, 2015.

[13] L. Liu, H. L. Liu, Q. Wang, and Y. Long, "Smart city planning in the era of big data: international experience," *Urban Planning International*, vol. 29, no. 6, pp. 38–43+65, 2014.

[14] O. Gervasi, D. Taniar, B. Murgante, A. Laganà, and Y. Mun, "Computational science and its applications-ICCSA 2009," *Computational Science and Its Applications--ICCSA 2009: International Conference, Seoul, Korea, June 29–July 2, 2009, Proceedings, Part I (Vol. 5592)*, Lecture Notes in Computer Science, Springer Science & Business Media, 2009.

[15] V. Chetta, L. Marasso, E. Giangreco, D. Storelli, and S. Francesco, "Idea management system for smart city planning," *Interdisciplinary Studies Journal*, vol. 21, no. 4, pp. 312–389, 2014.

Hindawi
Journal of Sensors
Volume 2022, Article ID 4606128, 9 pages
https://doi.org/10.1155/2022/4606128

Research Article

Digital Planning and Design of Landscape Based on Intelligent Sensor Network

Wei Wu[1] **and Jiaxi Zou**[2]

[1]*School of Civil Engineering, Architecture and Environment, Hubei University of Technology, Yingshan, Hubei 438700, China*
[2]*School of Arts & Design, Hubei University of Technology, Xianning, Hubei 437000, China*

Correspondence should be addressed to Wei Wu; 19961047@hbut.edu.cn

Received 23 November 2021; Revised 11 January 2022; Accepted 15 January 2022; Published 1 February 2022

Academic Editor: Gengxin Sun

According to the development of landscape digitization and the actual market demand, a digital landscape system based on intelligent sensor network is designed and implemented. The system consists of two parts: sensor node and display terminal, forming a star intelligent sensor network. Sensor node measurement is sent to display control terminal through intelligent sensor network. The display control terminal serves as the aggregation node. Based on geometry transformation, free form, and bionics, the method of constructing complex surface and the method strategy of optimizing complex surface are put forward from geometry and bionics theory. Then, the material types and construction methods of landscape composite surface are discussed and studied. According to the process and project of site cognition and landscape planning and design, six special models are established: ecological sensitivity evaluation model, construction suitability evaluation model, project site selection model, road line selection model, quasinatural waterscape construction model, and vertical design model. According to the characteristics of each landscape planning and design project, the logic generation and parameter composition of the model are discussed, and the application of the model is empirically studied and discussed based on actual cases.

1. Introduction

With the advent of the digital era, the form and connotation of design have undergone significant changes, and the concept of design is also constantly changing. Modern design is the organic combination of science and art and technology and human nature; there is no correlation between one and the other, so it is not one-sided. The progress of science and technology and the development of scientific theories provide a scientific platform and means for design and promote the design industry to be rational from another aspect [1]. The emphasis on rationality shows that practitioners in the field of design take a more mature view of design and explore the essential laws and methods of design. To grasp things with a rational attitude is a dynamic way of development, which is also in line with the complexity and systematic needs of living environment subjects. Landscape design has the dual attributes of art and science, always walking between sensibility and rationality. Facing the changing trend of contemporary design from sensibility to "rationality and sensibility interwoven," it is inevitable to seek theories and methods in the new era for the development of landscape planning and design.

Sensor network is composed of many on the space distribution of automatic device of a computer network, collaboration [2] by sensors, microchip processors, wireless sensor network node interface, and the power of four modules. Compared with general sensors, intelligent sensors have the following three advantages: through software technology it can achieve high-precision information collection and low cost, with a certain degree of programming automation ability [3], function diversification. Intelligent sensor network is a computer network composed of many spatially distributed intelligent sensors, which can realize high-precision information acquisition and share the huge amount of data processing in the network with intelligent sensors. A number of intelligent sensors can be composed of high-precision, powerful red energy measurement and control network

and low cost, easy installation, configuration, upgrade, and maintenance.

Corresponding to the planning and design mechanism of digital landscape architecture, the model is the prototype of specific methods and paths. Aiming at the process of digital landscape planning and design based on coupling principle, this paper discusses the digital evaluation of landscape planning and design and the construction of planning and design model. The digital evaluation model includes ecological sensitivity evaluation model and construction suitability evaluation model. The digital planning and design model consists of four parts: project positioning model, road route selection model, waterscape construction model, and vertical design model. From ecological sensitivity model to vertical design model, it is consistent with the process of design promotion, interlocking and with feedback upon each other. The model reflects the logic of the algorithm. The research of this paper focuses on the construction of the above six digital models, and ArcGIS and Civi13D are selected as the platform of model operation. Combined with engineering examples, the practical application of digital model in planning and design is explained in detail.

2. Related Work

Chaos theory, system theory, emergence theory, and fractal theory have exerted great influence on modern architectural theories and methods. Under the background of the great development of computer and information technology, architecture has entered the digital era together. A group of architects have actively explored digital design and construction. Academic circles have shown unprecedented enthusiastic response to the advent of the digital era. Many famous universities have carried out research, application, and practice of digital technology in architecture and planning and achieved fruitful results [4]. Landscape architecture is a compound discipline that coordinates the relationship between man and nature. It is both artistic and scientific. It requires scientific analysis and establishment of all objective elements related to it, and art is also required to describe and carry specific semantic meanings of places [5]. The complexity of objects and targets has more or less resulted in the slow adoption of digital technology in the landscape architecture industry compared to architecture and urban planning.

This paper discusses the application and trend of digital technology in landscape design and successively discusses 3D model and visual technology in landscape design [6, 7], communication and collaboration in landscape planning and design [8], digital methods developed in geographical design [9], landscape planning and design of systematic thinking [10], and other digital landscape themes. In the conference held, we discussed on Representing, Evaluating, and Designing Landscapes: Digital Approaches [11]. In recent years, they gradually shift their focus to using digital technology to solve the practical problems of landscape architecture. Under the framework of digital technology, a heated discussion on landscape information modeling (LIM) and GeoDesign (GeoDesign) has emerged [12]. The proposed concept of building information modeling (BIM), design and construction innovation, Building Information Modeling-Transforming Design and Construction to Achieve Greater Industry Productivity pointed out: BIM is a process of designing, constructing, and operating a project using digital information model [13]. BIM has become a hot topic in the field of architecture, and how BIM can be applied in the planning and design of landscape architecture has been discussed in the field of landscape architecture. Some scholars believe that BIM cannot support the study of large-scale environment and is not good at site design [14], so they put forward the concept of LIM. LIM is similar to BIM in terms of concept and connotation. For landscape architecture projects, LIM focuses on a relatively large scale. LIM is a practical technique and tool for collaborative design and life cycle management through the creation of digital information models; as a systematic solution, part of the digitalization ideas and technologies is included [15]. Geographical design adopts multidisciplinary comprehensive research and provides a unified platform for communication in these fields through information technology, which is used to solve outstanding problems through optimization of geographical location and orientation at regional and global scales. Taking site design into account is the basis of geographical design research and development [16]. As a response to the "geographic design framework," the biggest highlight is that it can realize the rapid iteration of the "geographic design process change model." A number of scholars around the world have carried out research on geographical design, and several thematic conferences have been held at home and abroad [17]. In literature [18], related concepts of digital strategy of landscape architecture are elaborated, major digital design methods and application software platforms are analyzed, and flowcharts of digital planning and design of landscape architecture are summarized. He pointed out that the digital process of landscape architecture planning and design can be subdivided into four basic steps: environmental cognition, design construction, design evaluation, and design media, including environment space simulation of landscape architecture, analysis technology: simulation and prediction of plant landscape; numerical analysis and evaluation of landscape architecture ecology; landscape planning, design, and management information system; theory and technology of digital generation and digitization in landscape architecture planning and design; landscape planning and design visualization and digital simulation technology, virtual reality technology; digital construction technology of landscape architecture; BIM application in landscape architecture; numerical evaluation method of landscape architecture; numerical control construction system; innovative digital technology, interdisciplinary research in digital technology, experimental design, and construction; and landscape architecture theory in digital age. Literature [19] discusses the auxiliary role of computer technology in landscape planning and design from three aspects: geographic information system, eco-aided design technology, and model construction. From the perspective of the current research situation, the research on geographical design is still in its infancy, mostly focusing on the definition of its concept, the framework and the

discussion of possible content, and the prediction of the future development trend. There are few concrete empirical studies and few practical applications.

At present, domestic ZigBee technology and intelligent sensor network technology combined with the application of intelligent landscape research are more and more common. For example: (1) combining the characteristics and advantages of ZigBee technology and GPRS technology, a wireless ZigBee sensor network capable of remote monitoring of the water environment in the field was realized [20]. And the solar power supply system is applied to the network; the ZigBee network in the system is a tree network, using the air temperature and humidity sensor, soil moisture sensor, rainfall sensor to detect environmental information, using Delphi 7.0 programming environment to develop upper computer monitoring software. (2) Design an intelligent sensor network based on CC2430 to automatically control the landscape system [21], which can monitor abundant environmental information, such as soil moisture, environmental temperature, and illumination, and transmit the information sent by the sensor to the processor in combination with the sensor fusion technology to make accurate judgment of irrigation behavior. (3) Build a ZigBee intelligent sensor network-based landscape control system, focusing on the AD (Altium Designer) hoc network process of intelligent sensor network [22, 23]. The node uses the competition mechanism in the channel for communication channel, each node periodically in a state of sleep and to monitor channel switching, when nodes be wakened from sleep began scanning around each node, until the monitoring signal to other nodes, first of all nodes to establish a list of adjacent nodes, then there will be a signal of node address added to the list. Ad hoc networking is reflected in that nodes update the routing list and reselect routes at an interval, thus forming the topology of the entire network [24]. Intelligent sensor network is a distributed network system composed of a large number of sensor nodes that integrates monitoring, control, and wireless communication functions [25]. The basic purpose of network design is to collaboratively perceive, collect, process, and transmit the monitoring information of perceived objects in the geographical area covered by the network and report it to users [26]. Intelligent sensor network has many nodes and limited energy and requires long-term work. It has the characteristics of large network scale, self-organization, self-maintenance, low rate, low power consumption, low cost, and short distance. Intelligent sensor network, supported by microelectromechanical technology, embedded technology, and communication technology, has become one of the fastest developing wireless network technologies and plays an important role in the era of Internet of Things.

3. Research on Landscape Planning Model Based on Intelligent Sensor Network Analysis

3.1. Intelligent Sensor Network Architecture. A typical smart sensor network is shown in Figure 1. A large number of sensor nodes are densely deployed inside or on the edge of the monitoring area to perceive the information of the monitored area, conduct preliminary processing, and transmit it to the sink node. According to different network topologies, sensor nodes may communicate directly with sink nodes or transmit data to sink nodes in the way of multihop relay. The sink node sends data to the management node through the mobile Internet or the Internet. Users can manage and configure the sensor network, view the collected monitoring data, and publish monitoring tasks through the management node.

Smart sensor node is the basic functional unit of wireless sensor network, and its processing ability, storage ability, and communication ability are relatively weak. In multihop networks, each sensor node has the dual functions of terminal and router in traditional networks. In terms of hardware composition, sensor module can be divided into sensor module, processor module, communication module, and electric-only module, as shown in Figure 2.

The power module provides power for the sensor node and other modules. Sensor nodes are generally powered by miniature batteries. For energy-saving and cost considerations, embedded processors with low power consumption and low cost are usually selected. Based on actual monitoring task requirements, determine whether to transplant an embedded operating system for task allocation and scheduling, a dedicated network management device with more adequate energy supply, memory, and computing resources or a wireless communication interface without detection function. According to different requirements, the topology of wireless sensor network is different, and the realization form of sink node is different. In general, the sink node selects the CPU with strong performance, rich hardware resources, and stronger processing capacity, storage capacity, and communication capacity than the sensor node. For simple tasks, the sink node uses a single program (no operating system) for software design. For some special applications, such as extremely complex functions or high concurrency of control logic, you can transplant an appropriate operating system to allocate hardware and software resources and schedule tasks of the entire device to ensure system reliability and stability.

3.2. Optimization of Complex Surface in Landscape Design. Before the optimization of complex surface, it is necessary to analyze the characteristics of the surface to be optimized, including the analysis of the curvature of the surface, the analysis of the continuity of the surface, and the analysis of the structure of the surface. Curvature and continuity can be visualized in the form of maps. The analysis of complex surface is a necessary stage, which is the process of checking surface quality. Through this process, we can find the defects or defects of surface structure and optimize the surface according to these defects or defects so that the surface can meet the construction requirements.

The concept of surface continuity is proposed for spliced surfaces. The quality of interfacing between surfaces affects the smoothness of surfaces. In general, the geometric continuity of surface can be roughly divided into five degrees, respectively, G0, G1, G2, G3, and G4. From G0 to G4, the

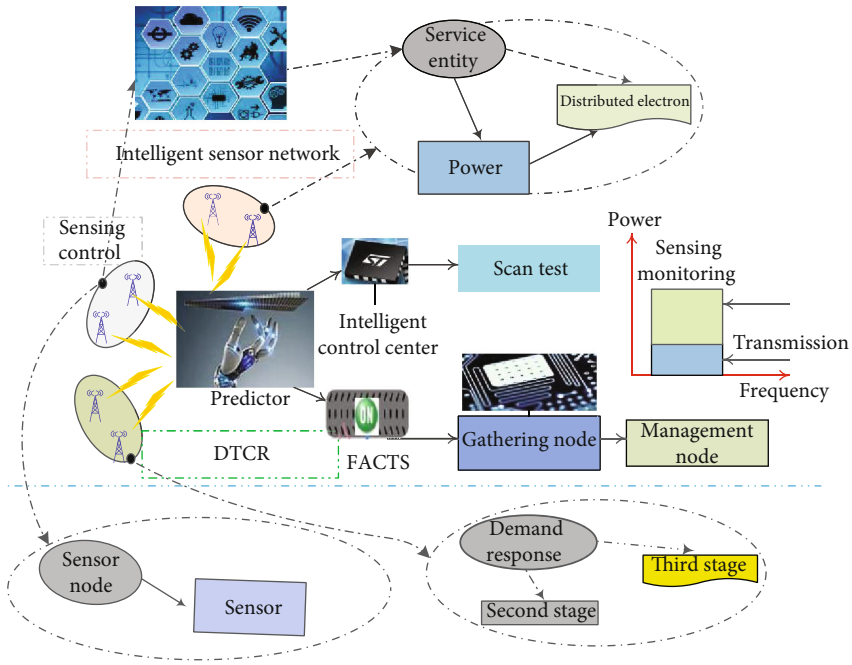

Figure 1: Architecture of intelligent sensor network.

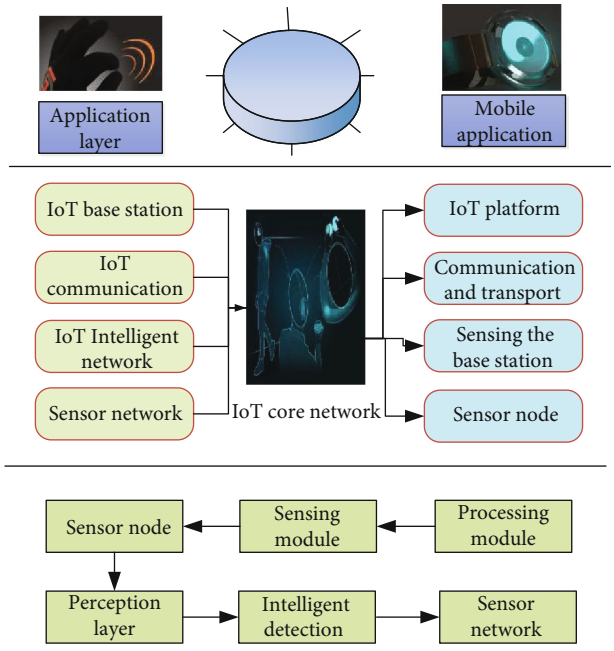

Figure 2: Sensor node composition.

smoothness of surface connection becomes higher and higher, and the precision of surface modeling is also higher and higher. G0 refers to the continuity of dots on the curve or surface, no breakpoint in the middle of the curve, and the surface is connected but has obvious joints. G1 means that the dots on a curve or surface are continuous and all connected curves or faces are tangent. G2 means that the dots on the curve or curve are continuous, and the curvature at the contact points of the curve or surface is the same: G3 and G4 are more complex, involving higher-order curves, and their curvature change rates are continuous. Some industrial products are required to achieve the accuracy of G3 and G4. Compared with industrial design, landscape design has a larger scale. From the perspective of construction and crowd use and visual experience, the continuity of music I (I) is not required to be very high, and generally, the accuracy of G3 and G4 is not required (Table 1).

The paradigm and model together form the basis of understanding the planning and design mechanism of digital landscape architecture and explain the planning and design of digital landscape architecture from the theoretical and technical aspects, respectively. See Figure 3.

The traditional design process mainly relies on the designer's experience and feelings: first of all in your mind for design of general conception and strategy and then manually sketch map, using the 3D design software modeling of the preliminary program, in the process repeatedly, adjust and modify the plan, and in the solution after the final drawings. This design process is divided into several stages. Only after the completion of the previous stage can we enter the next stage of work. There are relatively clear boundaries between the processes. At the same time, due to the fact that the design completely depends on the experience of the designer which will inevitably reflect a strong personal will, it is difficult to fully reflect the situation of the site, the design process is ambiguous, and the design results are subjective. The introduction of digital models has changed that. Relying on the digital model, the designer determines the factors affecting the design as parameters, connects the elements of the design system through the construction of the model, describes the design process, and finally controls the generation of the final design result by adjusting the parameters with the computer platform. This design approach is based on process logic thinking and is more rational and accurate,

Table 1: Comparison between the degrees of continuity of surfaces.

Surface continuity	G0	G1	G2	G3	G4
Characteristics	Position to contact	Tangent continuous	Continuous unsmoothness	Curvature	Curvature
Curvature	Discordance of direction	Curvature lines break in the same direction	Curvature line position continuous	Curvature line position continuous	Curvature line position continuous
Explain		Continuity of derivative	Second-derivative continuity	The third derivative is continuous	
A zebra crossing	Staggered discontinuity	Continuous corner	Continuous and smooth	Continuous and smooth	Continuous and smooth

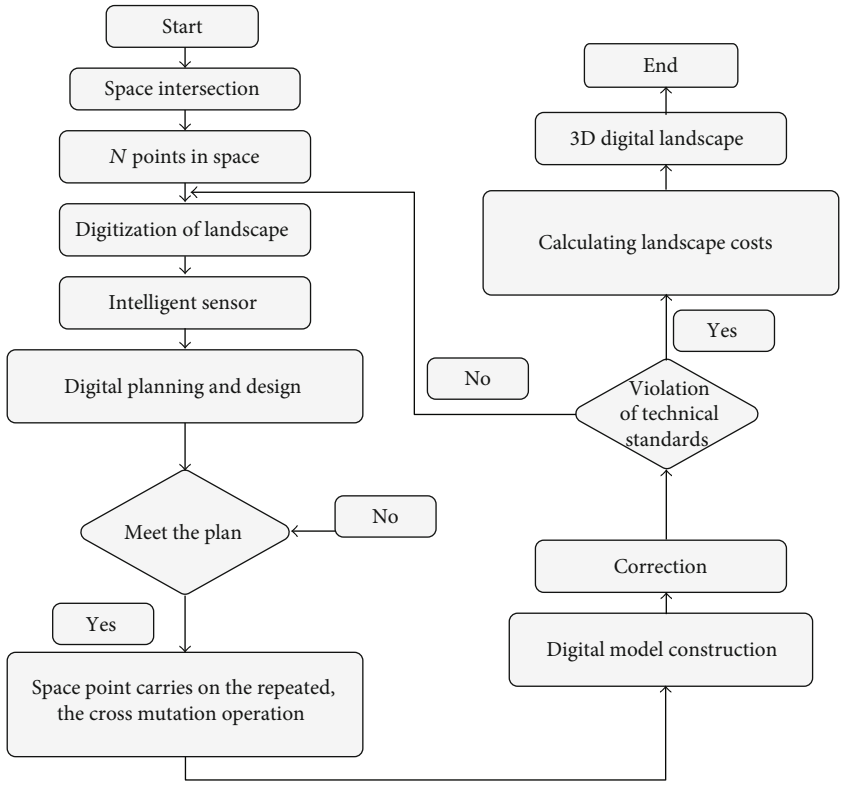

Figure 3: Digital landscape planning and design mechanism diagram.

considering the actual situation of the site and the role played by various elements of the system in the design.

Modeling research is closely linked to the needs of qualitative and quantitative research in landscape architecture. There are two kinds of relations between qualitative and quantitative research in the research method of combining qualitative and quantitative research. The first is the time relation, which refers to the sequence of occurrence of both in the research. The second is the primary and secondary relationship, that is, the primary and secondary methods used in the research. Therefore, there are three types of mixed research methods: one is sequential; qualitative research and quantitative research are in the same position, including qualitative to quantitative, quantitative to qualitative, and both simultaneous use; the second is the primary and secondary type, including qualitative, quantitative, and vice versa; the third is the comprehensive model, namely, the above two kinds of mixed, multilevel use. The model of digital landscape planning and design embodies the comprehensive relationship between qualitative and quantitative methods. Qualitative and quantitative methods appear alternately and complement each other in the operation of the model.

4. Construction of Digital Landscape Planning and Design System Based on Intelligent Sensor

The design of landscape architecture not only refers to the surrounding of a certain structure, a certain space, a certain

plant community, and some independent pieces but also for things in a certain regional scope; not only planners and landscape architects are needed but also ecological experts, soil experts, geographers, etc., to gather information from different fields. It not only applies landscape architecture, ecology, and planning but also integrates various disciplines for guidance. The integrated theory of landscape architecture design is the life cycle process in the planning and design process. Landscape architects should grasp the whole process of design projects from preliminary design, preliminary design to design construction and management, and integrate them into management. Even if the designer is only involved in one part of the design, when the whole project design is integrated, the information transmission should reduce a lot of unnecessary mistakes and waste.

(1) Digitally express the physical and functional characteristics of a facility

(2) A shared knowledge resource

(3) The process of sharing information related to the facility and providing a reliable basis for all countermeasures throughout the life cycle of the facility

(4) In the different stages of the construction project, the participants support and reflect the coordination of various responsibilities by embedding, extracting, updating, and modifying information in the information model

In order to achieve the design effect of "digital landscape" presenting perfect landscape image, designers should collect, measure, and record relevant environmental, natural, and human activity data, including terrain, landform, elevation, rivers, lakes, hills, types, and quantity and quantity of ground buildings and plants. Natural data include air quality, soil properties, snow and rain, wind, light, and other data; human activities include crowd, behavior, business, assembly, production, and other data. "Digital landscape" must digitize these data, and this process is digital landscape information collection. It is the image, video, sound, text, and related landscape information for digital processing or through digital equipment (such as digital camera, video camera, and scanner) the image, sound, text, and related landscape information digitization and in accordance with certain rules, classification of the establishment of information database, recorded in memory, for future analysis, evaluation, production, design, planning, and management services.

In addition to the characteristics of iteration, systematicness and nonlinearity are also important characteristics of modern landscape planning and design process. System analysis is to regard all elements in the landscape site as interrelated whole and pay attention to the analysis of the correlation between elements on the basis of independent analysis of elements. Comprehensive judgment is based on the results of system analysis, after integrated analysis, weighing each element to make a design judgment. System analysis and comprehensive judgment are dialectical unity; system analysis is the premise of comprehensive judgment; only through analysis can we provide the basis for the design to solve problems and deepen the understanding of the design. Comprehensive judgment is the summary, induction, perfection, and improvement of analysis. The interaction between the two activities is described above. The discussion about linearity and nonlinearity originated in nature, and for a long time, the study of nature was limited to linear methods. However, the achievements of natural science show that human beings are faced with a complex nonlinear world, not only linear can be covered. The discussion of nonlinearity quickly extends to all fields, and the design world is no exception. Landscape architecture planning and design are faced with a complex nonlinear world, so it is necessary to treat design problems with nonlinear thinking. Nonlinear thinking brings complexity of design process and nonlinearity and uncertainty of design result. The open and uncertain design results bring about multiple solutions, but the final implementation of the scheme is really unique. It is difficult for designers to judge the quality of the scheme simply through subjective evaluation, so the selection and evaluation mechanism in the regular design process is inevitable and necessary. Figure 4 shows the design process of digital landscape planning of intelligent sensor network.

From Figure 4, the six special models correspond to the main special design content of landscape planning and design, which belong to the process of digital landscape planning and design and have close logical connection. A special study is aimed at more clearly analyzing and interpreting the digital design process, guided by various special models for building intelligent sensor networks, realizing each special "coupling" and manifesting the connection between special designs and site, but also reflected in the tracking and coordination between different special process, unified in digital landscape planning and design system.

5. Example Verification

At present, the road route selection methods based on ArcGIS software platform are mostly used in the study of highway route selection problems of transportation majors. Most of them are based on digital elevation model (DEM), using cost distance algorithm tools to calculate, combined with genetic algorithm and other methods to carry out auxiliary optimization of route selection. Whether the cost distance algorithm can be applied to road route selection in landscape environment is worth further discussion and research.

The first step of constructing digital landscape planning and design road route selection model based on intelligent sensor network is to determine the primary and secondary factors influencing road route selection in the site, determine the cost of secondary factors, and determine the weight of impact factors through Delphi method, analytic hierarchy process, and other evaluation methods. The second step is to make each factor dimensionless and assign values through the reclassification function of ArcGIS software. The third step is to make use of the superposition analysis function to superimpose the cost graph of second-level and first-level factors in turn to obtain the comprehensive cost graph. The last step is to use the shortest path analysis tool of ArcGIS software to calculate the optimal path. Because road

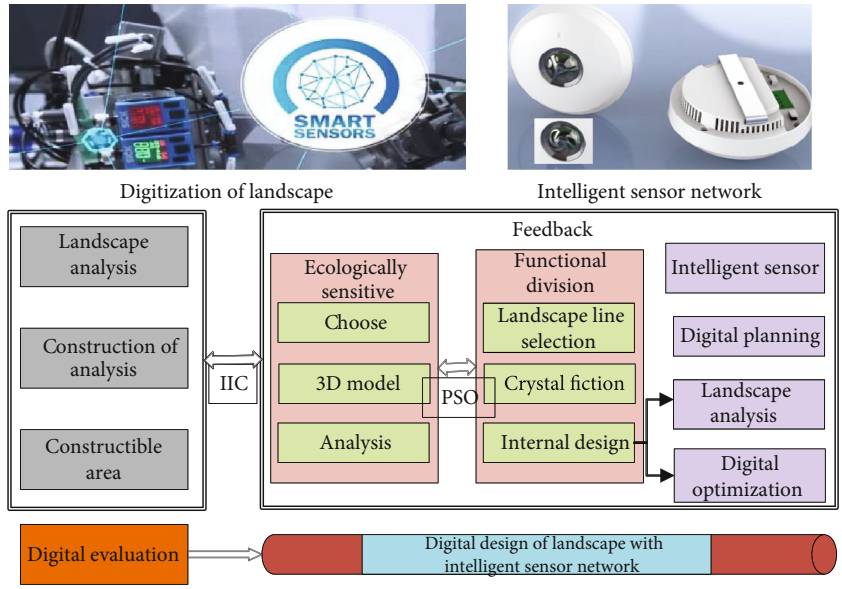

Figure 4: Landscape architecture digital planning and design process based on intelligent sensor network.

alignment is a complex system problem, it is not possible to obtain the optimal road alignment scheme completely by a computer. After determining the initial route selection scheme, it is necessary to optimize the road alignment scheme in the way of human-computer interaction, which is also one of the important steps in the process of road selection. According to the above process, the variables involved in this model include influence factor, grading, and grading assignment. The following is to study and discuss the line selection results generated by different parameter inputs of the above three variables. The hierarchical comparison of the comprehensive cost map in this paper is reflected in the comparison of grade 3, grade 6, grade 9, and grade 12 of slope single factor cost, as shown in Figure 5.

In order to analyze the difference of spatial heterogeneity of each landscape type with scale change, the slide-frame algorithm was used to calculate the voidness index of each landscape type in 1987 and 2003, and the double natural logarithmic curve was made, as shown in Figure 6. As can be seen from the void index curves of 1987 and 2003, the void index values and curve shapes of different landscape types in 2003 changed greatly compared with 1987, that is, the void index of 2003 decreased to different degrees compared with 1987, and the size order and curve shapes of different landscape types were different. It indicates that the spatial heterogeneity of landscape pattern has changed greatly in the past 16 years.

Through the intelligent landscape network distribution mode, design a variety of viewing guide routes (guide theme), dynamically analyze the mutual information difference between each viewing path and landscape network resource layout, and increase the experience of visitors. Four tourist routes were selected in the experiment, and the distribution of emotional factors of landscape routes is shown in Table 2.

Emotional variation factors (emotional edge and emotional node changes) were obtained randomly, and the emotional regulation items were gradually expanded from 50 to 600. The applicability detection curve of landscape network resource items was calculated as shown in Figure 7, which was used to judge the effectiveness of landscape elements after they were put into ornamental activities.

(1) In dynamic path landscape planning and design, the initial emotional magnitude of electric "novelty" landscape route is not the largest, but with the regulation of emotional variation factors, it can improve the landscape viewing efficiency

(2) In the design of landscape sightseeing routes, the rationality of sentiment difference and landscape route design can be obtained through emotional observation, and the most satisfactory sightseeing routes can be designed for customers by combining the characteristics of emotional changes

6. Conclusion

This article is based on the guidance of intelligent sensor network to the digital landscape architecture planning and design process as the main body, building the system of digital landscape architecture planning and design, including the six interrelated special model; the digital landscape architecture planning and design process was described in detail: starting from the place of cognitive, in the workplace, on the basis of full research and information collection, quantifiable elements obtained from analysis are transformed by software calculation and analysis algorithm to form variables and parameters, which accurately describe various environmental factors and reflect the place faithfully. According to the characteristics of each design, such as type and target, appropriate special design model is selected to build the association between design elements and site conditions. The generated parameters are input into algorithm

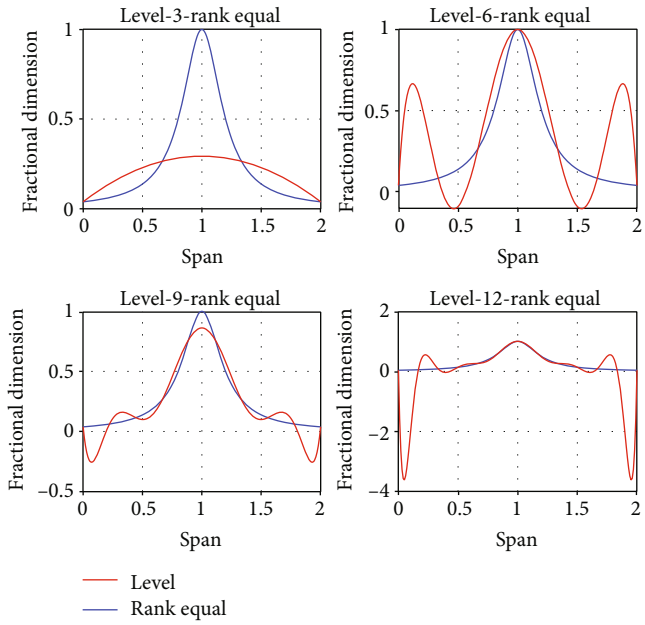

Figure 5: Line chart of assignment growth corresponding to different numbers of grades.

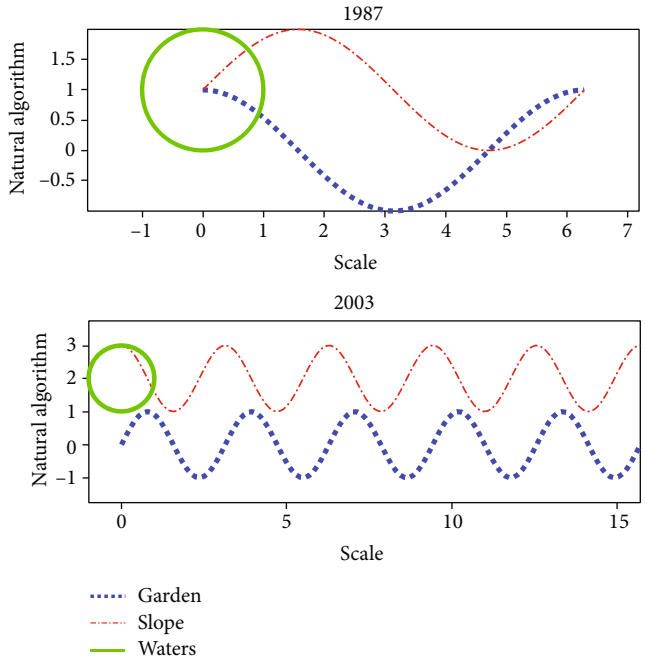

Figure 6: Voidage curves of different landscape types.

Table 2: Composition of mood factors of landscape routes.

Landscape line	$Z1$ such emotions	$Z2$ such emotions	$Z3$ such emotions	$Z4$ such emotions
1	60	20	25	15
2	15	50	35	25
3	15	15	20	30
4	10	15	20	30

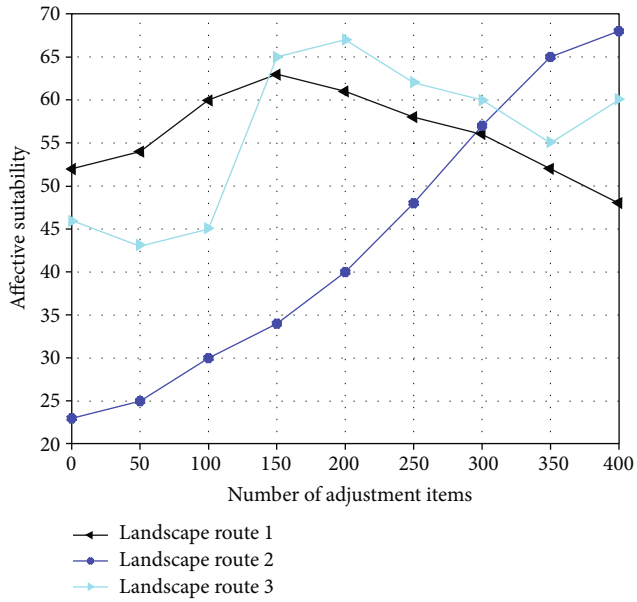

Figure 7: Suitability test curve of tour routes.

software and auxiliary design software, and the design result is finally formed, which is presented in the form of full data model. In the design evaluation stage, the data model can be analyzed and evaluated by means of digital analysis, and the results of analysis can be fed back to the design for further adjustment and optimization. The parametric vertical model of landscape architecture embodies all elements of vertical design in the same digital terrain model and constructs the dynamic relationship between elements. Starting from the three main components of the vertical design of road, water system, and site and taking earthwork balance as the vertical optimization target, the construction of parameter vertical optimization model will be the next research focus.

Data Availability

The data used to support the findings of this study are available from the corresponding author upon request.

Conflicts of Interest

The authors declare that they have no known competing financial interests or personal relationships that could have appeared to influence the work reported in this paper.

Acknowledgments

This work was supported by the project of Hubei University of Technology.

References

[1] X. Liu, "Three-dimensional visualized urban landscape planning and design based on virtual reality technology," *IEEE Access*, vol. 8, no. 9, pp. 149510–149521, 2020.

[2] X. Song and Y. Guo, "Featured town planning based on FPGA and sensors," *Microprocessors and Microsystems*, vol. 81, no. 2, pp. 103670–103687, 2021.

[3] L. Jia and L. Li, "Research on core strength training of aerobics based on artificial intelligence and sensor network," *EURASIP Journal on Wireless Communications and Networking*, vol. 2020, no. 1, 26 pages, 2020.

[4] B. Bechtel, P. Alexander, J. Böhner et al., "Mapping local climate zones for a worldwide database of the form and function of cities," *International Journal of Geo-Information*, vol. 4, no. 1, pp. 199–219, 2015.

[5] A. Agarwal, K. Jain, and A. Dev, "Modeling and analysis of data prediction technique based on linear regression model (DP-LRM) for cluster-based sensor networks," *International Journal of Ambient Computing and Intelligence*, vol. 12, no. 4, pp. 98–117, 2021.

[6] R. Jia, "Design of a simulation platform for intelligent marine search and rescue based on wireless sensors," *Microprocessors and Microsystems*, vol. 80, pp. 103572–103586, 2021.

[7] D. Nallaperuma, R. Nawaratne, and T. Bandaragoda, "Online incremental machine learning platform for big data-driven smart traffic management," *IEEE Transactions on Intelligent Transportation Systems*, vol. 20, no. 12, pp. 4679–4690, 2019.

[8] J. Song, Z. H. Wang, S. W. Myint, and C. Wang, "The hysteresis effect on surface-air temperature relationship and its implications to urban planning: an examination in Phoenix, Arizona, USA," *Landscape & Urban Planning*, vol. 167, pp. 198–211, 2017.

[9] B. Mayton, G. Dublon, S. Russell et al., "The networked sensory landscape: capturing and experiencing ecological change across scales," *Presence: Teleoperators and Virtual Environments*, vol. 26, no. 2, pp. 182–209, 2017.

[10] F. Susanto, S. Budi, P. de Souza, U. Engelke, and J. He, "Design of environmental sensor networks using evolutionary algorithms," *IEEE Geoscience and Remote Sensing Letters*, vol. 13, no. 4, pp. 575–579, 2016.

[11] D. Mourtzis, K. Angelopoulos, and V. Zogopoulos, "Mapping vulnerabilities in the industrial Internet of things landscape," *Procedia CIRP*, vol. 84, pp. 265–270, 2019.

[12] A. Vangala, S. Pandey, P. Parwekar, and I. A. Ukaegbu, "Intelligent authentication model in a hierarchical wireless sensor network with multiple sinks," *International Journal of Natural Computing Research*, vol. 9, no. 3, pp. 30–53, 2020.

[13] F. Tan, "The algorithms of distributed learning and distributed estimation about intelligent wireless sensor network," *Sensors*, vol. 20, no. 5, pp. 1302–1324, 2020.

[14] X. Yan, J. Gong, and Q. Wu, "Pollution source intelligent location algorithm in water quality sensor networks," *Neural Computing and Applications*, vol. 33, no. 1, pp. 209–222, 2021.

[15] Y. Chen, X. Xu, and Y. Wang, "Wireless sensor network energy efficient coverage method based on intelligent optimization algorithm," *Discrete & Continuous Dynamical Systems*, vol. 12, no. 4-5, pp. 887–900, 2019.

[16] C. Choi, G. D'Angelo, and F. Palmieri, "Special issue on intelligent systems in sensor networks and Internet of things," *Sensors*, vol. 20, no. 11, pp. 3182–3196, 2020.

[17] S. D. Achanta and T. Karthikeyan, "A wireless IOT system towards gait detection technique using FSR sensor and wearable IOT devices," *International Journal of Intelligent Unmanned Systems*, vol. 8, no. 1, pp. 43–54, 2020.

[18] H. Wang, L. Song, J. Liu, and T. Xiang, "An efficient intelligent data fusion algorithm for wireless sensor network," *Procedia Computer Science*, vol. 183, no. 3, pp. 418–424, 2021.

[19] X. Liu, R. Zhu, A. Anjum, J. Wang, H. Zhang, and M. Ma, "Intelligent data fusion algorithm based on hybrid delay-aware adaptive clustering in wireless sensor networks," *Future Generation Computer Systems*, vol. 104, pp. 1–14, 2020.

[20] S. Preeth, R. Dhanalakshmi, and P. M. Shakeel, "An intelligent approach for energy efficient trajectory design for mobile sink based IoT supported wireless sensor networks," *Peer-to-Peer Networking and Applications*, vol. 13, no. 6, pp. 2011–2022, 2020.

[21] P. S. Banerjee, S. N. Mandal, D. de, and B. Maiti, "iSleep: thermal entropy aware intelligent sleep scheduling algorithm for wireless sensor network," *Microsystem Technologies*, vol. 26, no. 7, pp. 2305–2323, 2020.

[22] N. Gao, Q. Ni, D. Feng, X. Jing, and Y. Cao, "Physical layer authentication under intelligent spoofing in wireless sensor networks," *Signal Processing*, vol. 166, pp. 107272–107286, 2020.

[23] J. Cho and M. Lee, "Building a compact convolutional neural network for embedded intelligent sensor systems using group sparsity and knowledge distillation," *Sensors*, vol. 19, no. 19, pp. 4307–4325, 2019.

[24] C. Jia, H. Ding, and C. Zhang, "Design of a dynamic key management plan for intelligent building energy management system based on wireless sensor network and blockchain technology," *AEJ - Alexandria Engineering Journal*, vol. 60, no. 1, pp. 2073–2085, 2020.

[25] D. K. Bangotra, Y. Singh, A. Selwal, N. Kumar, P. K. Singh, and W. C. Hong, "An intelligent opportunistic routing algorithm for wireless sensor networks and its application towards e-healthcare," *Sensors*, vol. 20, no. 14, pp. 3887–3896, 2020.

[26] C. Jamroen, P. Komkum, C. Fongkerd, and W. Krongpha, "An intelligent irrigation scheduling system using low-cost wireless sensor network toward sustainable and precision agriculture," *IEEE Access*, vol. 8, pp. 172756–172769, 2020.

Hindawi
Journal of Sensors
Volume 2022, Article ID 5969130, 10 pages
https://doi.org/10.1155/2022/5969130

Research Article

Semantic Interaction Strategy of Multiagent System in Large-Scale Intelligent Sensor Network Environment

Xi Chen,[1] **Zhaoyang Yin**,[2] **and Miaomiao Zhu**[3]

[1]*School of Art and Media, Hubei University of Business and Commerce, Hubei Wuhan, 430073, China*
[2]*School of Art, Hubei University, Hubei Wuhan, 430062, China*
[3]*School of Fine Arts and Design, Huainan Normal University, Anhui Huainan, 232038 Anhui, China*

Correspondence should be addressed to Miaomiao Zhu; zmm@hnnu.edu.cn

Received 20 November 2021; Revised 21 December 2021; Accepted 10 January 2022; Published 30 January 2022

Academic Editor: Gengxin Sun

In a multiagent system, the semantic interaction between agents is an important aspect affecting multi-intelligence. The purpose of interaction is to reasonably arrange task objectives and behaviors through information sharing and communication interaction, so as to maximize the overall performance of multiagent system. This paper analyzes the communication and interaction process between agents from the perspective of semantic layer and introduces the BDI (belief, desire, intention) model of agent's thinking state into the communication and interaction process. Furthermore, we propose a multiagent semantic interaction strategy model based on a large-scale intelligent sensor network, which supports various types of negotiation and interaction on the basis of basic interaction behavior to solve the problem of information operational conflicts. In addition, this paper limits the scale of historical information through the definition of equivalence and the merging theorem of history, and it uses reinforcement learning algorithm to detect possible conflicts and delay communication and makes rational use of limited resources to improve system revenue and coordination efficiency. The experimental results show that compared with the previous methods such as debate and negotiation, the strategy model can realize the flexible interaction based on scene and is more practical. At the same time, the existence of reinforcement learning improves the efficiency analysis and the convergence performance of semantic interaction strategy.

1. Introduction

With the development of artificial intelligence (AI), a multiagent system (MAS) has become a research hotspot. A multiagent system is composed of a group of independent and interactive autonomous agents [1, 2]. As an interactive autonomous learning paradigm, reinforcement learning provides an effective method to solve the distributed collaboration of multiagent systems [3]. Multiagent Reinforcement Learning (marl) has attracted extensive attention [4]. Drawing on the technologies and concepts of artificial intelligence, game theory, psychology, and sociology, marl provides a promising method to learn satisfactory agent behavior in complex environment, which is widely used in distributed control, multirobot system, resource allocation management, and automatic transaction [5].

In the past, the research on agent interaction in multiagent system (MAS) can be divided into two main parts: communication mechanism and negotiation method, but they lack connection and universality [6]. In the design of MAS system, in order to enable agents to obtain semantic information from exchange data, it is necessary to have a new understanding of the content and mode of communication interaction [7]. Firstly, communication should not be a passive behavior determined by the protocol, but the behavior that one agent wants another agent to accept some kind of belief or intention in the scene of communication [8]. The specific answer to each communication should be determined by the interactive target [9]. This interaction model can be applied to flexible interaction scenarios and provide means for communication based on target requirements [10]. Secondly, interaction is to share the information of

both sides, understand the intention of both sides, and adjust their plans in a certain order [11]. As long as the transmission and inquiry of information, intention and planning adjustment are expressed; a considerable number of interactive processes can be expressed [12]. And its scope of application is only limited to the planning ability of agent to take interactive action to achieve its purpose [13].

Due to environmental uncertainty, incomplete information, distributed learning, concurrent learning, and other problems, multirobot system (MRS) is widely used in UAV, spacecraft, autonomous underwater vehicle, ground mobile robot, and other practical problems [14]. As an interaction-oriented autonomous learning paradigm, Multiagent Reinforcement Learning (RL) allows robots to learn the mapping from state to action through the reward obtained by interaction with the environment, so as to cooperate with robot behavior and complete specific tasks, which is widely used in multirobot systems [15–17]. In reinforcement learning, each agent learns the optimal strategy by interacting with its dynamic environment [18]. When single agent reinforcement learning is applied to a multiagent system, reinforcement learning faces some challenges. The centralized learning method regards the multiagent system as a whole [19]. Through the observation of the global environmental information, the single agent reinforcement learning method is applied to learn the joint optimal behavior of the multiagent system [20]. Because it depends on the scale of real problems, centralized learning methods usually face scalability problems. Therefore, the centralized learning method can not be applied to multirobot systems. In a multirobot system, each robot needs to have complete control over the individual robot, that is, the distributed control of multirobot system. As a model-free reinforcement learning method, Q-learning has been widely used in multirobot systems such as soccer robot, chasing robot [21], chasing robot prey, and moving target observation robot [22]. The literature [23] applied the independent Q-learning algorithm to the soccer robot to realize the cooperation of robot behavior. The documenters [24] improved the learning efficiency through robot cooperative learning. This research work accelerated the learning process by sharing perceptual information and learning experience [24]. The distributed independent learning method models each agent, and each agent only observes its local environment. The distributed independent learning method does not rely on the observation of global environment information. It has the characteristics of high robustness and good scalability. At the same time, it can solve the dimensional disaster problem faced by centralized learning [25]. The contributions of this paper are summarized as follows: (1) this paper analyzes the communication and interaction process between agents from the perspective of semantic layer and introduces the BDI model of agent thinking state into the communication and interaction process; on the basis of basic interaction behavior, it supports various types of negotiation and interaction to solve the problem of information operation conflict. (2) This paper limits the scale of historical information through the definition of equivalence and historical merging theorem, uses reinforcement learning algorithm to detect possible conflicts and delayed communication, and makes rational use of limited resources to improve system revenue and coordination efficiency. (3) This paper constructs a large-scale intelligent sensor network system to verify the superiority and reliability of the algorithm.

In this paper, for the behavior coordination problem in multiple environments, an improved reinforcement learning mechanism based on planning fusion is proposed. The history and belief information are expressed as a function of the state. On the premise of ensuring that there is no loss of effective information, the historical information is combined by the methods of possible conflict detection and delayed communication, and the limited resources are reasonably used to obtain more system benefits. The mechanism takes the belief pool as the basic way of inter coordination and uses the strategy merging theorem to losslessly merge the historical information, so as to improve the efficiency of solving the problem with large-scale historical information. At the same time, the mechanism of conflict detection and delayed communication is adopted to effectively use the limited communication resources to strengthen the resolution of behavior conflicts and the exchange of important information.

2. Architecture Design of Multiagent System

2.1. Multiagent System Architecture. A multiagent system is an important field in the application of multiagent technology. The multiagent system is a group organization with multiple independent abilities. Each has a certain thinking state, such as belief, knowledge, and intention, and they will perform some actions according to their thinking state. The necessity of coordination lies in the existence of other intentions. The purpose of coordination is to change individual intentions and enable all individuals in the system to work together in a consistent and harmonious way. The goal of multiagent system is to make several systems with simple intelligence but easy to manage and control realize complex intelligence through mutual cooperation, so as to reduce the complexity of system modeling and improve the robustness, reliability, and flexibility of the system. The main characteristics of multiagent system are as follows:

(1) Autonomy: in the multiagent system, each agent can manage its own behavior and achieve independent cooperation or competition.

(2) Fault tolerance: agents can jointly form a cooperative system to achieve independent or common goals. If some agents fail, other agents will independently adapt to the new environment and continue to work, and the whole system will not fall into a failure state.

(3) Flexibility and scalability: MAS system itself adopts distributed design, and the agent has the characteristics of high cohesion and low coupling, which makes the system show strong scalability.

(4) Ability to collaborate: the multiagent system is a distributed system. Agents can cooperate with each

other to achieve the global goal through appropriate strategies.

Deliberative type is also called knowledge type or cognitive type. Its biggest feature is to use symbols to realize the representation and reasoning of entities in the real world and make decisions according to the reasoning at a certain stage. There are only some simple actions in reactivity-perceptual behavior pattern. The above two are extreme representations of two ways of thinking. The cautious type requires strict theoretical background such as knowledge representation, behavior planning, and decision-making strategies. The real implementation process is too complex. Although the reactive type is simple, it only makes reasoning and decision-making according to local perceived information, and empirical knowledge can not be effectively used, so it is difficult to effectively solve practical problems. Therefore, there is a hybrid type. It integrates the characteristics of the above two types and can make up for each other to a certain extent. It is the most ideal structural model. The architecture diagram is shown in Figure 1.

As shown in Figure 1, the multiagent architecture mainly includes environment awareness module, information processing module, communication module, decision and control module, and execution module. In addition, when an agent predicts environmental changes, it should consider that the activities of other agents are generally not controlled by themselves and difficult to predict. In order to better predict environmental changes, enhance their own action ability, and realize their own needs, agents must communicate. The capability of a single agent is limited, but multiple agents can be organized through an appropriate architecture to make up for the shortcomings of each agent and make the capability of the whole system exceed that of any single agent. A multiagent system means that a problem needs multiple solving entities. This system has the advantages of traditional distributed and concurrent problem solving and has complex interaction mode. Communication ability is not a necessary characteristic of rational agents; it is the embodiment of agent sociality. Communication action is also a specific planning action, which is scheduled in the process of completing agent requirements. From the semantic level, communication interaction is the transmission of thinking state between agents.

2.2. Structure of Multiagent System Based on Large-Scale Sensors. A distributed cooperative control method based on multiagent system is shown in Figure 2, which is characterized by the following steps: (1) build a multiagent three-level control architecture, that is, a control architecture of "local droop control-secondary power optimization control-centralized optimization and regional autonomy." Each network using droop control installs agents to realize the semantic interaction of multiagents. (2) The dispatching decision-making function module is designed to coordinate the adjustable resources with different control response rates, which respond to the internal and external energy demand of the LAN and quickly stabilize the power fluctuation of the tie line in the process of power failure, parallel, and off network switching in the energy LAN. (3) A distributed sparse communication network based on the multiagent system is constructed. Furthermore, the generation and completion of communication must have certain objective conditions, such as the existence of communication carrier and other factors. At the same time, there must be explicit intention for information exchange in communication. No matter whether the communication medium is language or action, the sender knows that its intention will be received by the other agents; the receiver of communication must also have the need to receive information. Communication is also a group behavior between two agents, which cannot be fully represented by only one agent sending information. The occurrence and implementation of communication depend on the existence of agents similar to themselves in the world information of other agents following the same communication processing mode and thinking mode. In addition, a large-scale intelligent sensor network is an information collection platform. It is a multihop self-organizing network system formed by a large number of cheap sensor nodes. Sensor nodes can collect the information of the monitoring area in real time, transmit the collected information to multiagent through multihop routing, and realize the semantic interaction between multiagent. Therefore, the large-scale intelligent sensor network is cooperation an important part of multiagent cooperation.

Intention transfer has a direct impact on agent behavior and can be used for behavior coordination among agents. Intention is expressed as the expected world state in the thinking state of agent, which has the same expression as observation information and knowledge, and can be transmitted as information and knowledge. After the intention is transferred to an agent a, a should decide whether to take it as his intention and start planning and action Starting from the self-interest principle of autonomous agent, agent adopting the intention of other agents should help to improve its effectiveness. There are many choices in which criteria the agent chooses the acceptable intention. Therefore, the construction of large-scale wireless sensor networks is the basis of multiagent intention transmission.

3. Research on Semantic Interaction Strategy of Multiagent System Based on Planning Fusion

When an agent predicts environmental changes, it should consider that the activities of other agents are generally not controlled by themselves and difficult to predict. In order to better predict environmental changes, enhance their own action ability, and realize their own needs, agents must communicate. Communication ability is not a necessary characteristic of rational agents. It is the embodiment of agent sociality. Communication action is also a specific planning action, which is scheduled in the process of completing agent requirements. From the semantic level, communication interaction is the transmission of thinking state between agents. Reinforcement learning is based on the premise that the interaction between agent and environment is regarded as a Markov decision-making process; that is, the next system state is determined only by each current state and

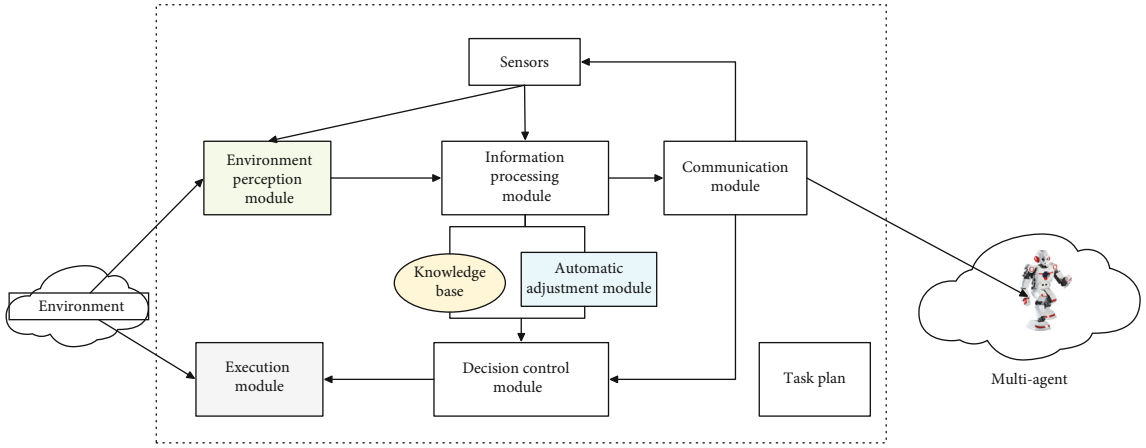

Figure 1: Multiagent architecture diagram.

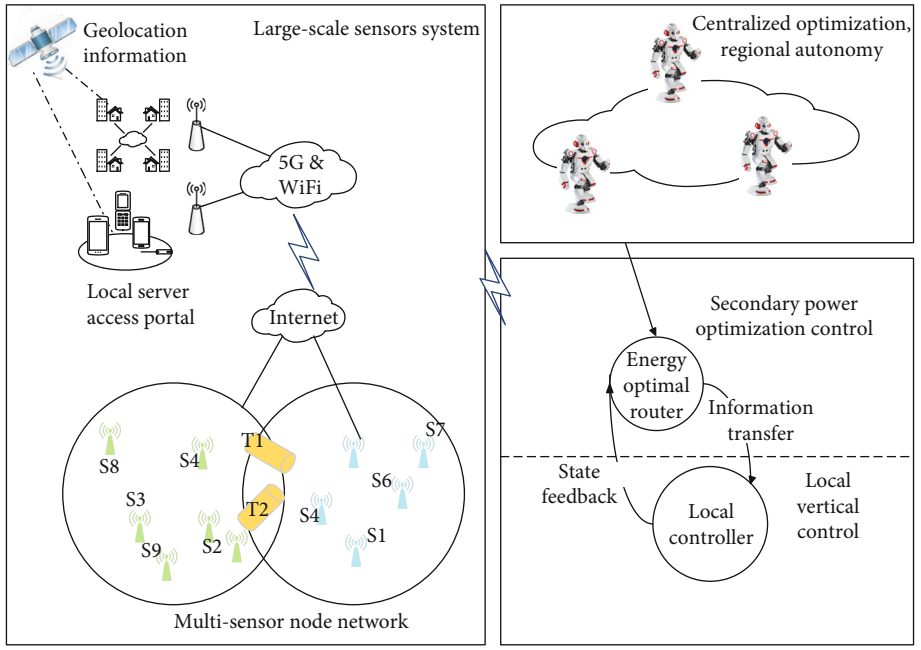

Figure 2: A distributed cooperative control framework based on multiagent system.

selected action, and a fixed state transition probability distribution is determined, which is independent of the previous historical state. The goal of learning is to find a strategy to maximize future reward by sampling the environment. Experience is an important basis for future behavior selection. Learning accumulated experience is an effective way to solve the problem of semantic interaction. The overall framework of the algorithm is shown in Figure 3.

As shown in Figure 3, the algorithm framework mainly includes reinforcement learning units, BP agent decision, and candidate model. The whole multisystem has gone through a stage of reinforcement learning process. The system stores the corresponding knowledge system and has the ability to adapt to the changes of the external environment. When it is determined that the system enters the emergency state, the management compares the historical data stored in the database with the real-time data sent by the guidance office, finds out the similarities, and assists in the decision-making according to the optimal decision made when the historical data occurs. If there is no similar historical data, the management will combine other reinforcement learning processes, make tentative action attempts, obtain the feedback of the environment, and then modify the decision judgment and cycle to obtain the optimal solution. Since it is set in this section that the system has been running for a long time and has corresponding knowledge base for data and decision support, it is assumed that the management can directly make the optimal decision for this accident.

3.1. Improved Reinforcement Learning Mechanism Based on Planning Fusion. The perceptron can sense the changes of the external environment and other actions and states. When encountering a learned situation, take action directly

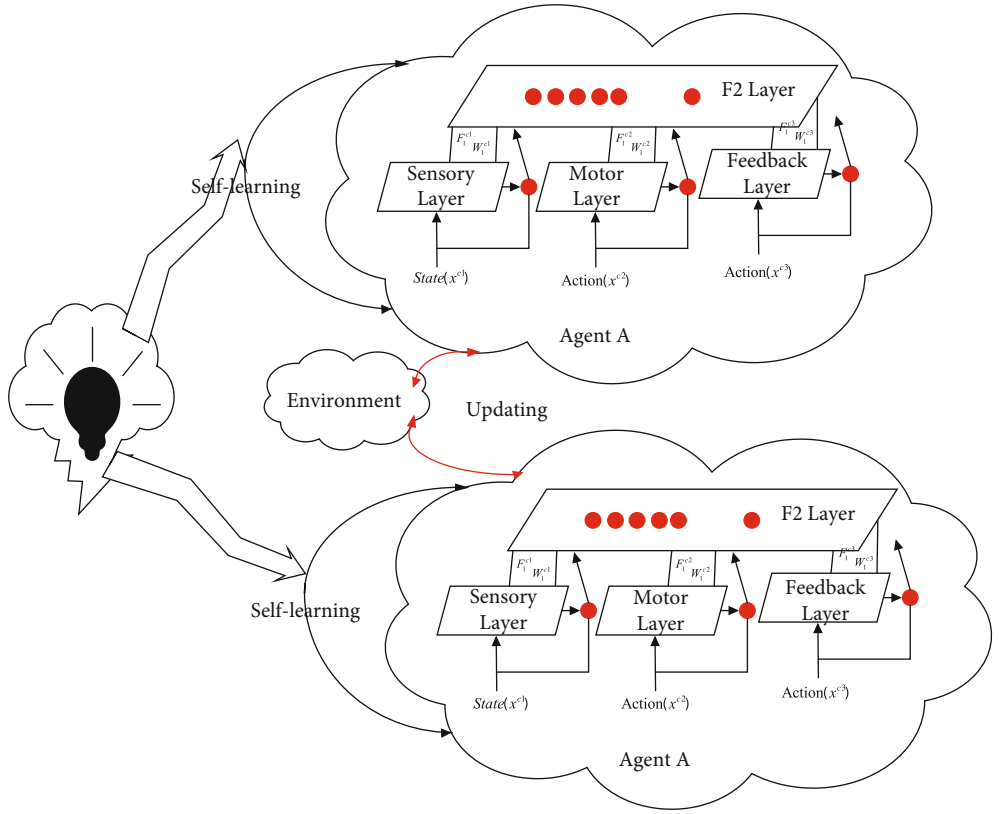

Figure 3: Improved reinforcement learning structure based on planning fusion.

through reflection. When encountering a new, learned, and more complex situation, combined with other behaviors and states, make behavioral decisions and take optimal actions through cooperative reinforcement learning strategy.

In some cases, the behavior selection of multiagent depends partly on the past behavior history, and h is defined as the action sequence executed and its observation sequence. At the time when the time step is t, the history of agent i can be expressed as

$$h_i^t = \left(a_i^0, o_i^1, a_i^0, \cdots, o_i^{t-1}, a_i^{t-1}, o_i^t\right), \tag{1}$$

where $h' = [h_1, h_2, \cdots, h_n]$ is the joint matrix of multiagent semantic interaction.

The joint belief b of multiagent is a function of joint history h', that is, $b(h) \in \Delta(S)$. Its essence is a probability distribution of environmental state, which is composed of initial belief state and sufficient statistics of joint history. If the joint history h^{t-1} before time t is known, the method of calculating the joint belief b^t at the current time can be obtained by using Bayesian rules:

$$\forall s' \in S, b^t\left(s' \mid h'\right) = \frac{O\left(o^t, s', a^{t-1}\right)\sum_{s\in S} P\left(s' \mid s, a^{t-1}\right) b^{-1}\left(s \mid h^{-1}\right)}{\sum_{s\in S} O\left(o^t, s'', a^{t-1}\right)\sum_{s\in S} P\left(s'' \mid s, a^{t-1}\right) b^{-1}\left(s \mid h^{-1}\right)}. \tag{2}$$

3.1.1. Local Joint Strategy δ. It is set that δ_i is a mapping from the history set h to the action set A. This mapping is determined and becomes the local determination strategy of agent i. It is easy to understand that $\delta(h) = \langle \delta_1(h_1), \delta_2(h_2), \cdots, \delta_n(h_n)\rangle$ means multiple joint determination strategies at a certain time and $\delta(h) = \vec{a}$. The local random strategy $\pi_i(a_i|h_i)$ represents the mapping from the historical set to the action probability distribution. It is different from the local determination strategy, because the uniqueness of the selected action cannot be determined according to the historical information but can only make the action selection process obey a certain probability distribution $\pi(h) = \langle \pi_1(h_1), \pi_2(h_2), \cdots, \pi_n(h_n)\rangle$ representing the local joint random strategy of multiagent.

3.1.2. Belief Pool. The belief pool at time t is represented as a binary array $\langle \{H_i^t(i \in I)\}, B^t\rangle$, where H_i^t is represented as the history of agent I at time t, and B^t is represented as the joint belief of multiagent at time t. The purpose of setting belief pool is to provide a medium for information sharing and coordination among multiagents.

In a MAS environment, due to the multifunction and heterogeneous structure, it is impossible to determine the behavior rules of other agents in many cases, so agents must interact and coordinate to jointly complete the overall goal. Therefore, agents need to be able to understand the strategies and knowledge of other agents through online learning, so as to determine the optimal behavior strategy and adapt to the changes of system environment. In this case, the state

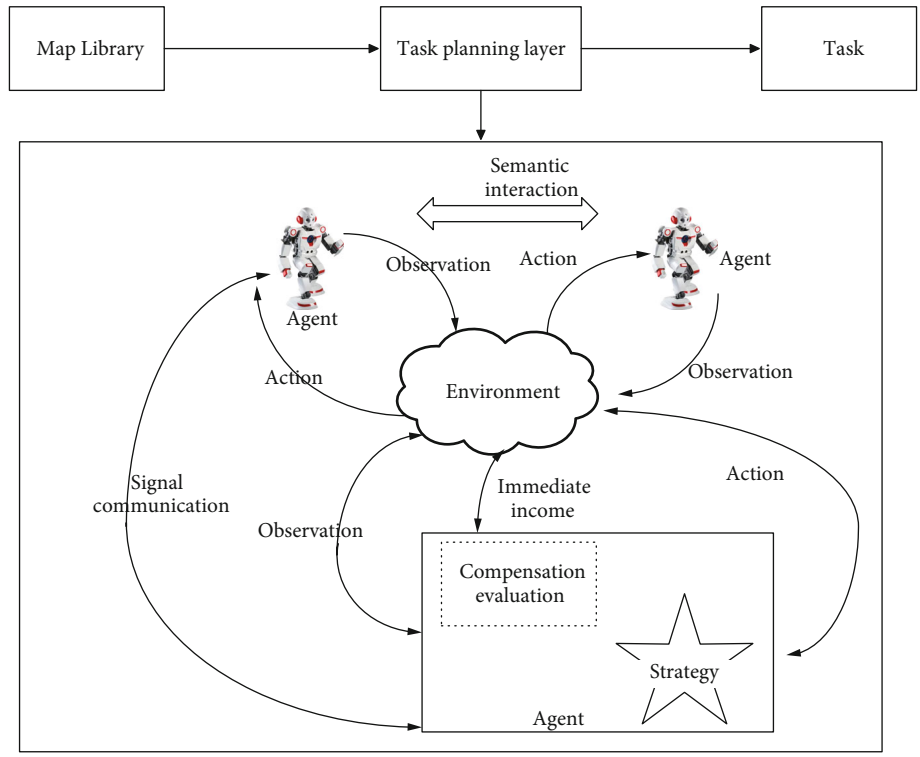

Figure 4: Improved Q-reinforcement learning model of multiagent.

change of a single agent is affected by the joint action of agents, so the traditional Q-learning formula needs to be extended. The q-reinforcement learning model under MAS is shown in Figure 4.

The immediate reward function under the defined environment is $R(s, \vec{a})$, where $\vec{a}$ is the joint action of system. The state transition function is $P(s_i, \vec{a}, s_j)$. The corresponding modification of the value function by the action of state i is as follows:

$$Q^{\pi}(s,a) = R\left(s, \vec{a}\right) + \gamma \sum_{s \in S} P\left(s' \mid s, \vec{a}\right) \max\left(s', \vec{a}'\right). \quad (3)$$

Equation (3) represents the discount income obtained by executing the joint action in the state and iteratively executing it according to the principle of optimal reward value. Therefore, Q function update formula is

$$Q_{t+1}\left(s, \vec{a}\right) = (1-\alpha_i) Q_t\left(s, \vec{a}\right) + \alpha_i \left[r_i + \gamma \max Q_t\left(s', \vec{a}'\right)\right], \quad (4)$$

where α_i is the dynamic learning rate or discount factor and t represents the number of iterations.

3.2. Research on Communication of Semantic Interaction. In the planning fusion framework, agents learn each other's knowledge by sharing belief pool, so as to maintain the coordination between agents. However, there is such a problem that we need to focus on considering that the belief pool contains all the historical information, but in some cases, there may be conflicts between these historical information and the local observation of the agent. At this time, communication can be used to deal with these conflicts more effectively and improve the efficiency of coordination.

If the agent understands the current system state, the detection will become easy, but in the planning fusion environment discussed above, these states cannot be known. Each agent can understand in the execution stage which is its local observation of the environment, and the local observation can only provide part of the information about the current system state. However, we can determine whether there is conflict by detecting the relationship between these local observations and belief pool. Equation (5) formally defines the conflict between the two agents.

When the belief pool B^t satisfies the following formula, we call the conflict degree ε between B^t and local observation o_i^t.

$$\max\left\{\sum_{s' \in S} O\left(\vec{o} \mid s', \vec{a}\right) \sum_{s \in S} P\left(s' \mid s, \vec{a}\right) b(s)\right\} \le \varepsilon. \quad (5)$$

In essence, it is to test the conflict between the local history of agent i and its observation. The value of ε is determined by the observation function. If the observation uncertainty is very small, the value of ε is correspondingly small. Nevertheless, the above method cannot detect all conflicts in the belief pool, but only conflicts based on current observations. The number of communication times is determined by two factors: the observed structure and the heuristic

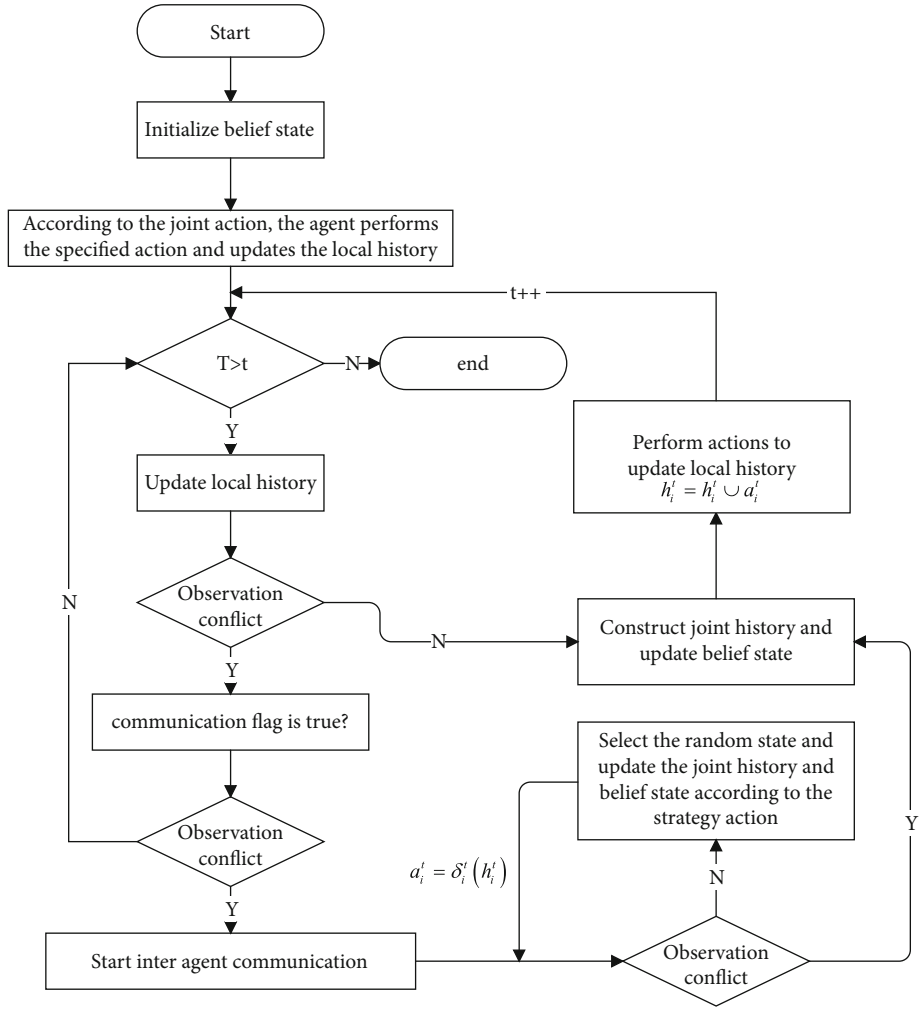

Figure 5: Implementation flow chart of algorithm.

function. The advantage of adopting this communication coordination method is that when the communication conditions are not available, it is allowed to delay until it meets the communication conditions. In many previous communication coordination methods, when the number of failures exceeds a certain limit, they tend to adopt extreme methods for coordination processing or ignore local observation information and completely rely on history, alternatively relying entirely on the current local observation to derive adverse results. To sum up, the implementation flow chart of the algorithm is shown in Figure 5.

As is shown in Figure 5, the main work is carried out in the first two stages. In the behavior planning stage, the local history of each agent in the belief pool is used to calculate the joint strategy δ'. In the execution stage, each agent updates the local historical information and first updates the historical information of the previous step according to its latest observation o. Then, according to the joint strategy δ' calculated in the planning stage and the current local history h pair, the corresponding actions are performed through $h_i^t = h_i^t \cup a_i^t$ calculation, and $a_i^t = \delta_i^t(h_i^t)$ is used at the same time. Update the current local history for the last update stage, and update the old local history of each in the belief pool with the foot of the execution stage.

4. Experiment and Result Analysis

4.1. Experimental Setup and Experimental Environment

4.1.1. Environment State. Each agent may be in any grid other than the obstacle grid. The state of the machining center can be either idle or working, so the environment state space of a single agent is $13 * 2$ and the joint state space of two agents is $13 * 13 * 2$.

4.1.2. Action Space. Each action has a kind of move up, move down, turn left, turn right, and maintain the original position. Therefore, the size of action space is $5 * 5$.

4.1.3. Observation Set. Bit binary characters are used to represent each observation. The first bit indicates whether there are obstacles in the upper, left, lower, and right directions. The obstacles here include obstacles and surrounding walls. The second bit indicates whether it is currently in the top grid. For two agent systems, the observed set size is $2^{5\times2}$.

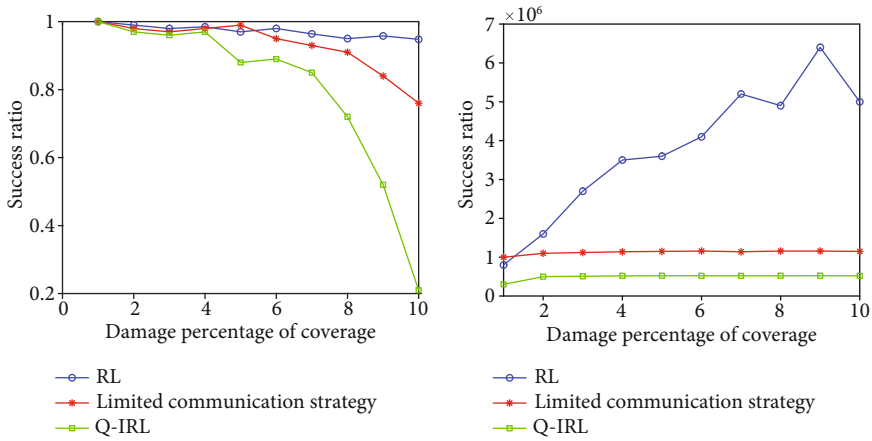

(a) Fault tolerance success ratio (b) Communication loss

Figure 6: Efficiency comparison of three semantic interaction strategies.

4.1.4. Historical Information. In MAS, the joint observation of agents in some observable environments can not accurately reflect the current state information of the group, and it is also necessary to express the trust of each observation through belief. The popular understanding of belief is a subjective view of what actions should be performed in a certain state according to the laws of experience or historical statistics.

4.1.5. Revenue Function. The immediate return value of each step is $r = -1$ when hitting an obstacle. Cooperation to achieve the goal is$r = 10$. Other return values are $r = 0$.

Assuming that the processing time of the product is small enough, it can be ignored that each agent does not know the return value of its other agents at the beginning of learning, obtains the return through learning, and guides the next step. At the end of a round of experiment, agent 1 sends the goods from the processing center to the processing center, and agent 2 takes the goods back from the processing center to u.

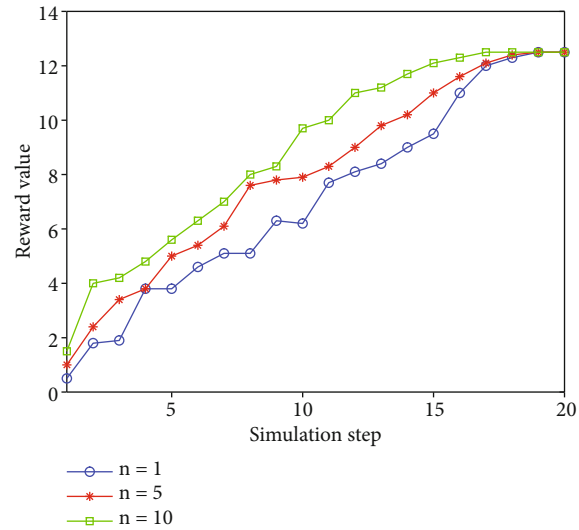

Figure 7: Relationship between discount reward and simulation step size.

4.1.6. Simulation Environment and Parameters. The simulation process is realized by MATLAB. With the help of POMDP solver open source software package, the time step of the problem is set to $t = 200$, and the discount return is calculated every 10 steps. The simulation parameters are as follows: $\alpha = 0.8$; $\varepsilon = 0.74$; and $l = 8$. The simulation parameter n is a parameter that can only be determined by experiment.

4.2. Efficiency Analysis of Semantic Interaction Strategy. In this section, Java language is still used to design multiagent sensor system simulation platform in Eclipse: within the rectangular range of $800 * 600$, 50-38, the fourth plane is randomly distributed to activate 300 sensor agents in the cluster fault-tolerant method. The number of agents in different experiments is different and increases with the step value of 50. Agents have unique identification IDS, but their performance is the same. The sensing and communication range is set to a circle with a radius of 100. At the beginning of the experiment, the system is initialized, and each agent generates NT table information and saves it separately. The abscissa in Figure 6 shows that the number of agents gradually increases from 50 to 300, and the density of node distribution in the experiment is briefly explained. Figure 6(a) describes the difference in fault tolerance success rate between the three methods. Figure 6(b) describes the different communication losses of the three methods and takes all the communication times during the experiment as the reference standard of communication loss.

It is obvious from Figure 6(a) that there is no obvious difference in the fault tolerance of the three methods at the beginning. However, as the error model is closer and closer to large-scale centralized errors, this paper proposes that the error tolerance success rate of the semantic interaction strategy of multiagent system in the environment of large-scale intelligent sensor network is getting lower and lower, and there is no obvious advantage in communication loss. Because the conventional reinforcement learning and the activation cluster under the semantic interaction mechanism

Table 1: Convergence performance.

Case number	Strategy	Minimum iterations	Maximum iterations	Average iterations	Success rate
Case 1	Our	11	46	22.6	20/20
	Traditional	26	103	62.8	20/20
Case 2	Our	22	51	29.5	20/20
	Traditional	51	286	104.4	17/20
Case 3	Our	8	28	18.7	20/20
	Traditional	12	200	56.8	19/20

do not care about the size of errors and the number of failed nodes. In addition, the range of errors in the experiment is fixed, the range of activation cluster is relatively fixed and the change of communication loss is not obvious. Under the semantic interaction strategy mechanism of multiagent system in a large-scale intelligent sensor network environment, the activated clusters are divided into each other by the ID of failed nodes. Although it can prevent the overflow of information between different clusters, such activated clusters cannot fully reflect the scale of errors. Therefore, the communication loss is greatly increased, but the success rate of fault tolerance is greatly reduced. According to Figures 6(a) and 6(b), it can also be found that although the conventional algorithm is designed for large-scale centralized errors, it can also deal with a single centralized error well and better take into account the fault-tolerant success rate and communication loss.

The word reinforcement learning comes from behavioral science. It imitates the natural learning process of human and animals and establishes the mapping from environmental state to behavior through repeated exploration of the environment Therefore, simulation step size is one of the most important parameters of reinforcement learning algorithm. In order to verify the effect of the strategy in this paper, this paper verifies the variation law between the reward values harvested. The relationship between the discount reward and the simulation step n is shown in Figure 7.

It can be seen from Figure 7 that when the number of experiments is divided into 1, 5, and 10, the change trend of the reward value was obtained through reinforcement learning. Since the last belief state is calculated as the next initial belief state value, the learning effect will gradually become ideal after multiple rounds of experiments. In this paper, the simultaneous interpreting strategy is adopted in the improved learning mechanism of planning and integration. Compared with the traditional distributed communication strategy, the most important feature of the scheme is to make timely and appropriate use of communication resources with limited resources and large unit communication costs. The coordination between them is mostly carried out by means of information sharing. In addition, in reality, we often encounter a series of optimization problems under different parameters In the case of a specific structure, the optimization problem under all parameters is solved by training a model for different parameters. Different from the traditional method, we do not train our model by multiple independent sampling of different parameters but use reinforcement learning to accelerate the training process. In a reinforcement learning algorithm, the strategy network is used to obtain the optimization results and the value network is used to evaluate the strategy. The two networks are trained iteratively to optimize the strategy.

4.3. Comparison of Convergence Performance of Strategies. In order to verify the performance indexes of the improved algorithm, reinforcement learning algorithm and improved Q-reinforcement learning algorithm are selected as reference in the experiment. If the algorithm reaches the set accuracy within the specified number of iterations, the convergence of the algorithm is recognized. If the number of iterations exceeds and the set accuracy is not reached, the algorithm terminates, and it is considered that the algorithm does not converge. The test results of 20 times are shown in Table 1.

As can be seen from Table 1, the improved Q-reinforcement learning algorithm achieves better experimental results than the basic reinforcement learning algorithm. Under the same precision, for the three test functions, although the two algorithms can successfully complete the optimization task, the difference in optimization speed is obvious. The proposed algorithm has more advantages in the number of iterations required for algorithm convergence.

5. Conclusion

In the multiagent system, the coordination degree between agents has an important impact on the overall intelligence of multiagent system. The purpose of coordination is to reasonably arrange task objectives and behaviors through information sharing and communication interaction, so as to maximize the overall performance of multiagent system. The communication of agent is to change the information carrier and send the carrier to the observable environment receiving Ag NT. This communication view can expand the form of communication, not limited to language communication. The transmission of intention has a direct impact on the behavior of agents and can be used for behavior coordination among agents. Intention is expressed as the expected world state in the thinking state of agents. After the intention is transmitted to agent a, a should decide whether to take it as his intention and start planning and action. An improved learning mechanism based on planning fusion is proposed to express the history and information as a function of the state. On the premise of ensuring no loss of effective information, the method of possible conflict detection and delayed communication is adopted for historical information merging, and the limited resources are reasonably

used to obtain more system benefits. Through experiments, the effectiveness of above strategies is analyzed and compared. In addition, how to use reinforcement learning and the reinforcement learning process before cooperation to deal with a virtual event to illustrate how the agent system determines the accident, makes decisions, and solves the accident after the accident and how the agents cooperate with each other is the focus of the next research.

Data Availability

Data are available on request.

Conflicts of Interest

The authors declare that they have no conflicts of interest.

Acknowledgments

This work was supported by Hubei University of Business and Commerce.

References

[1] S. Listopad, "Architecture of the hybrid intelligent multi-agent system of heterogeneous thinking for planning of distribution grid restoration," *Baltic Journal of Modern Computing*, vol. 7, no. 4, pp. 487–499, 2019.

[2] F. Yang, Y. Qiao, S. Wang, X. Wang, and X. Wang, "Blockchain and multi-agent system for meme discovery and prediction in social network," *Knowledge-Based Systems*, vol. 229, 2021.

[3] Q. Wu, J. Wu, J. Shen, B. Yong, and Q. Zhou, "An edge based multi-agent auto communication method for traffic light control," *Sensors*, vol. 20, no. 15, 2020.

[4] A. Benayache, A. Bilami, K. Benaggoune, and H. Mouss, "Industrial IoT middleware using a multi-agent system for consistency-based diagnostic in cement factory," *International Journal of Autonomous and Adaptive Communications Systems*, vol. 14, no. 3, pp. 291–310, 2021.

[5] D. Wu, Q. Liu, H. Wang, D. Wu, and R. Wang, "Socially aware energy-efficient mobile edge collaboration for video distribution," *IEEE Transactions on Multimedia*, vol. 19, no. 10, pp. 2197–2209, 2017.

[6] E. Ahmed and H. Gharavi, "Cooperative vehicular networking: a survey," *IEEE Transactions on Intelligent Transportation Systems*, vol. 19, no. 3, pp. 996–1014, 2018.

[7] A. Belhadi, Y. Djenouri, G. Srivastava, and J. C. W. Lin, "Reinforcement learning multi-agent system for faults diagnosis of mircoservices in industrial settings," *Computer Communications*, vol. 177, pp. 213–219, 2021.

[8] Z. Bouattou, H. Belbachir, and R. Laurini, "Multi-agent system approach for improved real-time visual summaries of geographical data streams," *International Journal of Intelligent Systems Technologies and Applications*, vol. 17, no. 3, pp. 255–271, 2018.

[9] Z. Yahouni, A. Ladj, F. Belkadi, O. Meski, and M. Ritou, "A smart reporting framework as an application of multi-agent system in machining industry," *International Journal of Computer Integrated Manufacturing*, vol. 34, no. 5, pp. 470–486, 2021.

[10] Z. Ma, M. J. Schultz, K. Christensen, M. Værbak, Y. Demazeau, and B. N. Jørgensen, "The application of ontologies in multi-agent systems in the energy sector: a scoping review," *Energies*, vol. 12, no. 16, 2019.

[11] K. Tazi, F. M. Abbou, and F. Abdi, "Multi-agent system for microgrids: design, optimization and performance," *Artificial Intelligence Review*, vol. 53, no. 2, pp. 1233–1292, 2020.

[12] B. Teixeira, T. Pinto, F. Silva, G. Santos, I. Praça, and Z. Vale, "Multi-agent decision support tool to enable interoperability among heterogeneous energy systems," *Applied Sciences*, vol. 8, no. 3, 2018.

[13] E. Serrano and J. Bajo, "Discovering hidden mental states in open multi-agent systems by leveraging multi-protocol regularities with machine learning," *Sensors*, vol. 20, no. 18, p. 5198, 2020.

[14] S. Howell, Y. Rezgui, J. L. Hippolyte, B. Jayan, and H. Li, "Towards the next generation of smart grids: semantic and holonic multi-agent management of distributed energy resources," *Renewable and Sustainable Energy Reviews*, vol. 77, pp. 193–214, 2017.

[15] R. Kamdar, P. Paliwal, and Y. Kumar, "A state of art review on various aspects of multi-agent system," *Journal of Circuits, Systems and Computers*, vol. 27, no. 11, 2018.

[16] B. Okreša Đurić, J. Rincon, C. Carrascosa, M. Schatten, and V. Julian, "MAMbO5: a new ontology approach for modelling and managing intelligent virtual environments based on multi-agent systems," *Journal of Ambient Intelligence and Humanized Computing*, vol. 10, no. 9, pp. 3629–3641, 2019.

[17] V. Mascardi, D. Weyns, A. Ricci et al., "Engineering multi-agent systems," *ACM SIGSOFT Software Engineering Notes*, vol. 44, no. 1, pp. 18–28, 2019.

[18] L. S. Melo, R. F. Sampaio, R. P. S. Leão, G. C. Barroso, and J. R. Bezerra, "Python-based multi-agent platform for application on power grids," *International Transactions on Electrical Energy Systems*, vol. 29, no. 6, 2019.

[19] W. Du and S. Ding, "A survey on multi-agent deep reinforcement learning: from the perspective of challenges and applications," *Artificial Intelligence Review*, vol. 54, no. 5, pp. 3215–3238, 2021.

[20] B. S. Sami, "Intelligent energy management for off-grid renewable hybrid system using multi-agent approach," *IEEE Access*, vol. 8, pp. 8681–8696, 2020.

[21] S. H. Choi, M. Kim, and J. Y. Lee, "Situation-dependent remote AR collaborations: image-based collaboration using a 3D perspective map and live video-based collaboration with a synchronized VR mode," *Computers in Industry*, vol. 101, pp. 51–66, 2018.

[22] S. Mariani, A. Omicini, R. Calegari, and E. Denti, "Logic programming as a service in multi-agent systems for the Internet of Things," *International Journal of Grid and Utility Computing*, vol. 10, no. 4, pp. 344–360, 2019.

[23] X. Zhang, S. Tang, X. Liu, R. Malekian, and Z. Li, "A novel multi-agent-based collaborative virtual manufacturing environment integrated with edge computing technique," *Energies*, vol. 12, no. 14, 2019.

[24] S. Munawar, S. Khalil Toor, M. Aslam, and E. Aimeur, "Pacaits: a multi-agent system for intelligent virtual laboratory courses," *Applied Sciences*, vol. 9, no. 23, p. 5084, 2019.

[25] E. Amador-Domínguez, E. Serrano, and D. Manrique, "A hierarchical multi-agent architecture based on virtual identities to explain black-box personalization policies," *Expert Systems with Applications*, vol. 186, 2021.

Hindawi
Journal of Sensors
Volume 2022, Article ID 4909942, 11 pages
https://doi.org/10.1155/2022/4909942

Research Article

Dynamic Analysis of Alternative Elements in an Automated Packaging System Based on 5G Internet of Things

Jian Long

School of Art & Design, Guilin University of Electronic Technology, Guilin 541000, China

Correspondence should be addressed to Jian Long; lomjian@guet.edu.cn

Received 6 December 2021; Revised 28 December 2021; Accepted 3 January 2022; Published 28 January 2022

Academic Editor: Gengxin Sun

The arrival of 5G will usher in an era of "Internet of Everything." Massive Internet of Things data contains great value in the dynamic analysis of alternative elements of automated packaging systems. From the perspective of the realization of personalized customization functions, this article solves the problem of dynamic analysis of alternative elements in the automated packaging system. We analyze the connection mechanism and interaction method between the cloud service system layer and the mobile terminal service layer, and carry out the corresponding software design. From the perspective of the realization of the intelligent production of the system in this paper, this topic mainly studies the information interaction mechanism and production control mechanism of the cloud service system and the manufacturing system. Based on the hardware of the manufacturing system layer, a flexible production implementation mechanism is formulated to make it the basis for the implementation of intelligent production of the system. Based on the massive data processing capabilities of the cloud service system, the information processing mechanism and the production planning decision-making mechanism are formulated for it, so as to realize the intelligent adjustment of the manufacturing system layer in the production process. For the connection scenario of IoT group paging, based on the application of NB-IoT technology in the next-generation mobile communication network, the focus of network optimization is to ensure the random access performance of IoT devices as much as possible. To this end, this paper proposes a random access optimization strategy for IoT group paging based on time slot scattering. We establish a mathematical model based on queuing theory for the connection scenario of the Io T group paging, then use the mathematical formula to derive the number of IoT devices scattered to each time slot in the initial state, thereby deriving the specific time slot scattering algorithm. This paper establishes a list of credit nodes, changes the participation mode of consensus nodes from static to dynamic, and supports voting to select trusted nodes. We designed a credit evaluation mechanism as a basis for consensus node elections to improve system's fault tolerance rate. The algorithm process was simplified, and the PBFT algorithm process was simplified from a 3-phase protocol to a 2-phase protocol to further reduce communication bandwidth overhead and algorithm time. Simulation analysis shows that, compared with the PBFT algorithm, the proposed algorithm improves node flexibility and fault tolerance while reducing communication bandwidth overhead by about 45%, packaging throughput by about 4%, and latency by about 3%.

1. Introduction

The Internet of Things is known as the third revolutionary wave of innovation in the information industry after computers and the Internet [1]. Driven by such a wave, any object in the world is connected to the Internet according to a preagreed agreement, and communications and information exchange services are provided [2]. The research on the architecture of the information and communication technology Internet of Things information service system represented by the Internet of Things is developing rapidly at an unprecedented speed, greatly affecting world's technological landscape [3]. Under the service of 5G network, the amount of data information that the Internet of Things information service system needs to serve in the future will increase exponentially. According to HIS statistics, by 2025, there will be 150 billion wireless terminal devices connected to the network worldwide, among which the wireless terminal devices connected to the Internet of Things will reach about 85 billion [4]. By then, more than 90% of

world's wireless terminal devices need to seek services in the Internet of Things information service network. In the future, the number of mobile terminals and Internet of Things terminal devices will far exceed the total population of the world. The Internet of Things information service network will carry a large amount of data traffic growth [5]. Faced with such a huge demand for data services, wireless terminal equipment directly connected to the network has large interference, high power consumption, low spectrum utilization of system communication links, inability to achieve compatibility between mobile terminals and IoT terminals, and inability to integrate into the Internet application ecosystem. The problem is becoming more and more obvious.

The development of the packaging industry requires continuous research and development of more advanced packaging technologies to meet the ever-increasing demand of market competition, and the innovation of packaging technology is more reflected in the degree of intelligence of packaging equipment [6]. Therefore, the design and development of a more economical and smarter new packaging system is of great significance to the development of the packaging industry [7]. This topic fully considers the actual needs of manufacturers and the packaging market and ensures that the packaging process is simple; the equipment is stable and easy to operate while ensuring that the system is fully functional. From the perspective of the enterprise, the design of the packaging system solves the problems of high packaging cost, low efficiency, and poor precision from the root and effectively improves the market competitiveness of the enterprise [8]. From an industry perspective, the design of the packaging system provides a good reference platform for the research and development of automatic packaging technology for small rubber products, fills the current technical gap in automatic packaging for small products, and promotes the rapid development of the packaging industry [9]. At present, the labor cost of manufacturing transformation and upgrading is increasing year by year, and the degree of automation and informationization in the packaging field is low [10]. This article combines mainstream packaging methods and selects objects to be packaged for research. This article can improve the competitiveness of enterprises, liberate people from simple and repetitive labor, and can reduce production costs and improve the controllability of product quality. Therefore, studying the dynamic analysis of alternative elements in the automated packaging system has important theoretical and practical significance.

This article summarizes the overall functional requirements and implementation basis of the automated packaging system for personalized customization of this topic, carries out a structured and layered design, and at the same time, gives the basic architecture and platform of each level of system's subsystems. Through the introduction of these platforms and technologies, the platform foundation of "intelligence," "flexibility," and "personalized service" to be realized in the case design of this article is completed. This paper analyzes the limitations of NB-IoT cellular sites when processing group paging IoT device connection requests, and then, in the IoT group paging model based on queuing theory, studies the random access optimization of the scattering of the arrival rate of the IoT devices in the scattered group paging plan. In order to obtain the interval value of the time slot scattering, the upper limit of the arrival rate in each RA-slots in the random access process is studied, and starting from the expected IoT arrival rate, according to the current number of IoT devices, iteratively, we calculate each RA-slot initial IoT arrival rate and then get the IoT slot scattering algorithm. At the same time, according to the maximum processing capacity of the current NB-IoT cell site, the critical value for starting the IoT time slot scattering algorithm is given. This paper establishes a list of credit nodes and improves the participation mode of consensus nodes from static to dynamic, and nodes can enter or exit dynamically. A node credit evaluation mechanism is designed to follow the consensus node election and improve system's fault tolerance rate. Based on the credit evaluation mechanism, the three-phase protocol of the PBFT algorithm is simplified into two phases, which further reduces communication overhead and algorithm delay.

2. Related Work

Compared with the previous generations of mobile communication technologies, the biggest difference of the 5G system is that it does not reform and upgrade the key technologies used in the previous communication systems, but integrates many technologies to make them complement each other and play their respective strengths. The rapid growth of network service traffic and the number of devices connected to the network will make the spectrum resources in the future communication network more tense. Although some new spectrum resources will be unearthed, the real key is to allocate the existing spectrum resources reasonably to maximize the value of the limited resources.

The packaging industry is a service-oriented manufacturing industry. It is the last process in enterprise production [11]. It is a necessary link for all manufacturing engineering to make finished products. It is an inaccessible part of the manufacturing process. Therefore, automated packaging is very important for enterprises. With the development of robotics, vision technology, modern control technology, computer technology, artificial intelligence technology, and material technology, automated packaging has emerged [12]. Automated packaging not only improves labor production efficiency, reduces product costs, and enhances the competitiveness of enterprises. Moreover, the packaging quality can be more controllable, and at the same time, a lot of work injuries can be reduced [13]. As more functions are integrated in the automated packaging system, automated packaging is more favored by enterprises, such as anticounterfeiting technology, intelligent sorting systems, and intelligent detection systems [14].

At present, automated packaging is used in beverages, food, medicine, nonfood industrial products and industrial products [15]. Automated packaging is developing in terms of multiple functions, aesthetics and personalization, light and smart equipment, and material saving. As the automated packaging industry in foreign countries started earlier

than the domestic development, packaging in Western countries has been fully automated. In the packaging field, there are famous companies such as ABB, EPSON, KUKA, Omron, and FANUC [16].

Packaging equipment control technology refers to an advanced technology in which packaging equipment can complete packaging work in accordance with a preplanned work flow without human intervention. At present, most of the truss packaging equipment at home and abroad adopts a distributed control method with programmable logic control technology as the main and embedded control technology as the supplement [17]. On the one hand, it can retain the advantages of programmable logic control technology in an industrial environment with more stable performance, better safety, and better compatibility with electrical equipment; on the other hand, it can ensure that the system has better economic efficiency and applicability.

Relevant scholars apply Pro/E behavioral modeling technology to the optimization of packaging machinery parts, by modeling the drive mechanism of the plug-in plate and establishing measurement features, inserting motion analysis features and relationship analysis features, and performing sensitivity analysis to obtain the optimal parameters, and then improve the design efficiency of packaging machinery [18]. Relevant scholars have conducted algorithmic research on the packing problem of irregular objects and put forward some constructive algorithms that can solve various two-dimensional packing problems [19]. He proposed several integer programming models to determine the degree of association between irregular parts and packaging boxes and then established a mixed integer programming model to solve the problem of packing irregular parts into packaging boxes.

Swiss ABB's robotic automated packaging is mainly used in three aspects: picking, packaging, and palletizing [20–22]. In terms of picking technology, ABB's picking solutions are used in many types of products, applications, and packaging lines. It includes various industries such as frozen food, bread candy, ice cream, meat and fish products, cheese, pet food, medical supplies, shampoo bottles, and perfume bottles [23, 24]. In the picking solution, there are subdivisions for different scenarios. Aiming at high-precision picking and unloading operations, ABB currently launches the IRB360 FlexPicker TM second-generation triangular robot solution [25]. For applications that need to achieve six-axis flexibility, require slightly lower cycle time, and have a payload of no more than 5 kg, ABB has launched the IRB 140 robot solution; in the packaging industry, ABB has launched the IRB260 robot solution. The packaging system is equipped with ABB's unique visual assisted conveyor tracking system to maintain continuous product passing and rapid packaging [26, 27]. ABB also provides a series of high-speed bag stacking, box stacking, and palletizing robots [28].

3. Methods

3.1. 5G Private Network Networking Technology. According to the evolution of the network architecture, 3GPP has defined two networking modes for 5G services: nonindependent networking NSA and independent networking SA. NSA uses 4G base stations as control plane anchor points to access 4G core network or 5G core network, that is, use existing 4G infrastructure for 5G network deployment. NSA is a transitional solution that can only support Ultra Mobile Broadband (e MBB) services, and most 5G features cannot be realized. At this stage, 5G services for public users will run in NSA mode; SA is a standard 5G networking mode. 5G base stations are used as control plane anchor points to access the 5G core network. 5G's new core technologies, such as end-to-end slicing, can support various innovative business operations in the SA mode and meet the guaranteed service-level agreements (SLA) for different businesses.

The 5G network architecture mainly includes two parts, the 5G core network 5GC and the radio access network NG-RAN. Currently, the NSA networking mode is adopted, and it is evolving to the SA networking mode. The 5G core network mainly has three functional logical network elements or virtual network elements to undertake, namely, UPF, SMF, and AMF. The 5G radio access network includes two types of network elements: gNB and ng-eNB, where gNB provides NR user plane and control plane functions and protocols, and ng-eNB provides E-UTRA user plane and control plane functions and protocols. Among the two main interfaces, NG belongs to the interface between the wireless access network and the core network, and Xn belongs to the interface between wireless network nodes.

3.2. 5G Mobile Edge Computing. The deployment locations of mobile edge computing nodes are mainly divided into three types: edge level, location level, and regional level. The three have different characteristics, respectively. Among them, the transmission delay is edge level < location level < regional level; the overall transmission bandwidth is regional level > location level > edge level. To determine the specific location of the mobile edge computing node deployment, it needs to be determined according to the specific service type, the specific characteristics, and requirements of the service scenario.

Mobile edge computing (MEC) refers to the deployment of IT service environments and computing capabilities on the edge of the network closer to users or data sources and provides users with a call interface for underlying communication services. In the 4G era, operators and equipment manufacturers have initiated MEC technical research, product development, and live network deployment. 5G is a new generation of mobile communication technology proposed in response to the rapid increase in data traffic, massive device connections, and deep industry integration brought about by the development of the mobile Internet and the Internet of Things. It becomes a native capability in 5G and plays an important role in the three major application scenarios of 5G (e MBB, mMTC, and URLLC). At present, on a global scale, MEC has become a focus of attention and research in the industry. In various links such as technical standardization, operator 5G planning, and manufacturer 5G equipment product development, mobile edge

computing is regarded as an important and indivisible component of 5G networks. Mobile edge computing, together with core functions such as network slicing, serve as an important foundation for global operators to provide services to users in the 5G era.

5G edge computing is a multilevel edge computing technology system deployed in scenarios. The system is oriented to the diverse needs of intelligence, deploying edge computing nodes on the base station side, base station convergence side, or core network edge side to provide a variety of intelligent network access and high-bandwidth, low-latency network bearer. It relies on open and reliable connection, computing, and storage resources to support the flexible carrying of multiecological services on the access edge side. Facing the application needs of medical scenarios, smart medical multilevel edge computing provides basic capabilities such as massive terminal management, high-reliability and low-latency networking, hierarchical quality assurance, real-time data computing and cache acceleration, application container services, and network capability opening. Based on the smart medical multilevel edge computing system, operators can provide real-time, reliable, intelligent, and ubiquitous end-to-end services for smart medical.

3.3. Overall Functional Architecture of the Automated Packaging System. The functional architecture of the personalized customization-oriented automated packaging system is shown in Figure 1. The system architecture is divided into three levels of subsystems according to executive functions. The definitions of these three levels of subsystems from top to bottom are as follows: (1) mobile terminal service layer is the service part of the application of information interaction between people and the system, responsible for the execution of information interaction functions between customers or administrators using mobile terminal equipment and the system; (2) cloud service system layer is responsible for the reception and transmission of business information and the execution of related information processing functions for production scheduling; (3) manufacturing system layer is the production execution part of the entire system; it is responsible for product processing and manufacturing within the business scope of the enterprise.

(1) Mobile terminal service layer

The mobile terminal service layer is the user-end application access layer of the automated packaging system, which provides methods and tools for receiving user service information. With the rapid development of communication technology, various services of mobile terminal products have begun to occupy people's daily lives. With the advent of the 4G/5G network era, the network transmission rate is no longer the bottleneck of mobile communication network information transmission. With the expansion of cloud computing applications, mobile cloud services (MBaaS) have become a way to connect mobile applications to cloud services.

We connect mobile applications to the back-end cloud storage by using a unified application programming interface (API). At present, people can use mobile terminals to complete various activities such as information inquiry, shopping, entertainment, learning, and sports. Therefore, this article combines mobile terminal services in the design of intelligent manufacturing systems to complete the mobile information interaction between humans and automated packaging systems.

Relying on mobile communication technology to achieve flexible information interaction between humans and automated packaging systems is a good choice. That is, smart phones are connected to the cloud through the mobile Internet, and the corresponding APP provided by the enterprise is used to realize the remote operation of the internal resources of the factory. Intelligent matching provides users with convenient and friendly interaction methods, so as to achieve the most direct and personalized information interaction anytime, anywhere, and then, realize the mobile terminal service layer of the automated packaging system for personalized application and management needs.

(2) Cloud service system layer

The cloud service system layer, as the information hub center of the automated packaging system, must possess the key features of computing, communication, and control integrated by the Cyber-Physical System (CPS). The cloud service system layer provides data interaction, storage, and analysis methods and interfaces for heterogeneous resource management existing in the industrial environment through cloud computing technology, web service technology, etc. and provides corresponding data computing functions. The terminal service layer and the manufacturing system layer are interrelated to form a unified and coordinated whole, so as to realize the information integration and resource sharing of the entire system.

The cloud service system layer realizes that the cloud receives personalized order information and query instructions from customer's mobile terminal through the data channel interface provided by the web service and performs order classification and integration processing on the back-end server. According to the characteristics of the query instruction, the corresponding product information is mined, and then, the information processing result is pushed to the corresponding client terminal to complete the information interaction task between the client and the smart factory.

The cloud service system layer provides a data channel interface to receive equipment status information from the manufacturing system layer. According to the result of customer order integration, the decision-making information of the corresponding production plan is formulated and then issued to the control module center of the workshop production equipment. In order to facilitate the production management of the workshop manager, the cloud service system layer needs to organize the historical data information of all orders and the status information of the workshop production unit, so as to provide functions such as workshop status monitoring, equipment startup and shutdown, and raw material inventory forecasting.

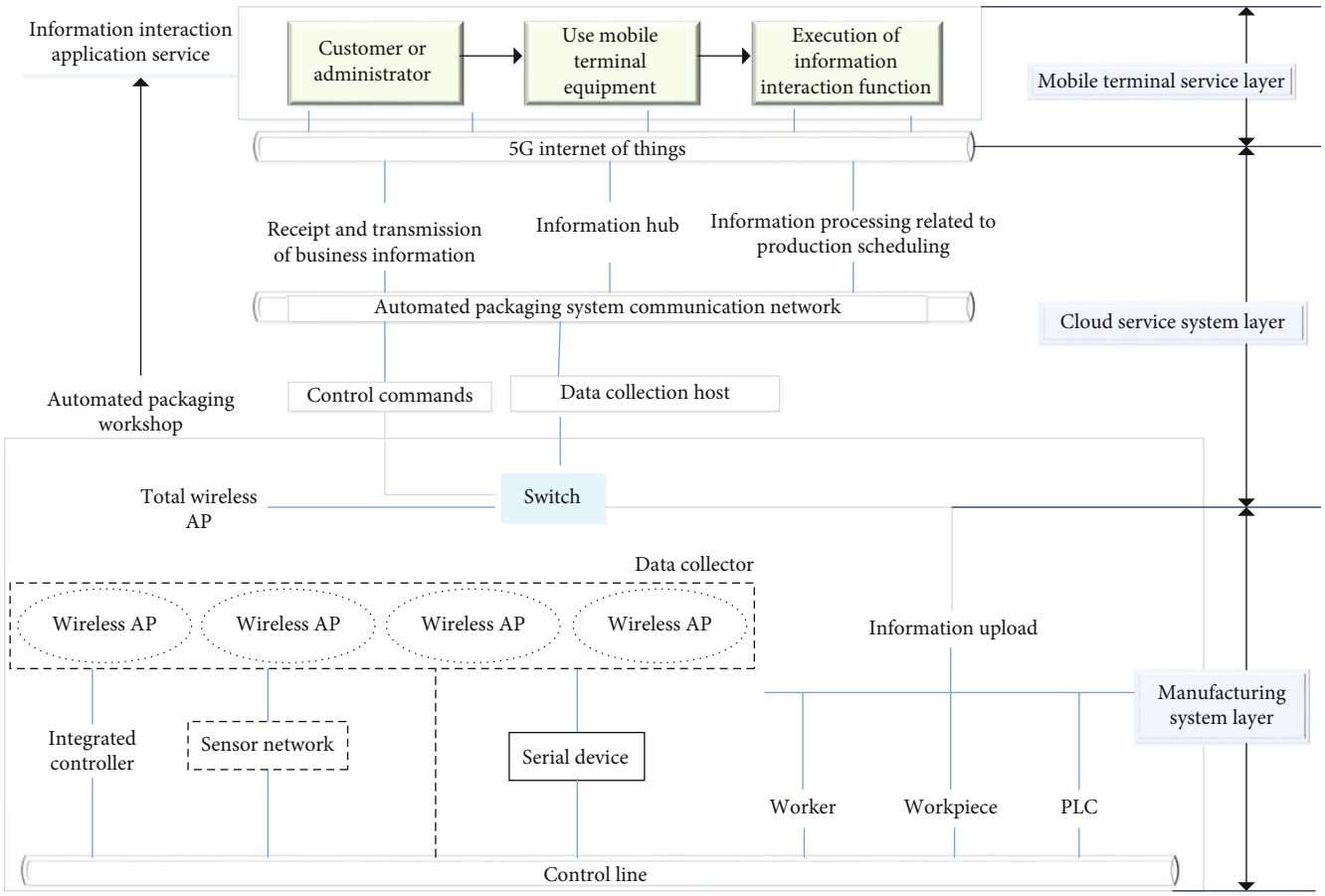

Figure 1: System architecture diagram.

(3) Manufacturing system layer

As the production execution part of the automated packaging system, the manufacturing system layer needs to have execution functions that can be automated and intelligent. Therefore, the manufacturing system layer needs to associate various manufacturing-related processing equipment and sensors and other components for flexible design to realize the coordinated adjustment of workshop production units. Collaborative production between workshop production units needs to be considered from two design perspectives at the manufacturing system level, namely, IoT design and reconfigurable design.

In terms of IoT design, it mainly relies on sensor networks, radio frequency, and other related industrial IoT technologies to connect discrete processing equipment, sensor components, and product parts in the factory workshop. We use sensor technology to detect the operating status of the equipment to realize the calibration and tracking of the workstation information of the processing object; rely on communication methods such as WiFi, ZigBee, and Ethernet to connect the items, processing units, cloud platforms, so as to solve the interoperability problem caused by the heterogeneity of resources in the production process.

In the reconfigurable design, the equipment and components that can complement each other's functions and can complete a set of production operations in the workshop are modularized and packaged to form a relatively independent production and processing unit. Each such independent unit is connected with other independent units by means of corresponding communication, so that they can cooperate with each other to complete industrial production tasks. The cloud service system is used as the instruction decision center for all independent production and processing units in the workshop, so as to realize the production planning and ordering of the workshop. This realizes that all equipment of the manufacturing system can adjust the working mode by itself and then quickly respond to the small batch and diversified production needs of the product.

3.4. Optimization of Random Access for IoT Group Paging Based on Queuing Theory. Under the NB-IoT cell site group paging mechanism, the service requests of IoT devices with the same GID are consistent, and the delay requirements are not high. Suppose that after the NB-IoT cell site initiates a group paging, it only processes access requests for IoT services with a certain GID in one RA-slots, and IoT devices with the same GID will initiate the same in the first RA-slots access request. Therefore, the number of access requests initiated by IoT devices in I RA-slots is different, but it will decrease with the increase of time. Considering the processing capacity of NB-IoT cellular sites, it is

necessary to scatter a large number of IoT devices on different RA-slots in order to control the number of IoT devices that initiate access requests in each RA-slots. The number of IoT devices requested for access is the same.

We define the connection rate for the first access in a RA-slots $\theta_{\mathrm{RA}}(\lambda)$ as the arrival rate in the current RA-slots multiplied by the probability of the first access success, then:

$$\theta_{\mathrm{RA}}(\lambda) = (1-\lambda)e^{-\lambda/2R}. \tag{1}$$

Obviously, the value of θ_{RA} changes with the change of the parameter λ, and the maximum value of θ_{RA} can be obtained by seeking its extreme value:

$$\theta_{\max} = (1+R)\bullet e^{-\lambda}. \tag{2}$$

Through analysis, it can be known that the NB-IoT cellular site system can achieve the largest first-time successful connection rate when the value of λ is R. In order to keep the NB-IoT cellular site at a relatively high connection performance in I RA-slots, the arrival rate of access requests in I_{RA}-slots must be scattered control processing, and the scattered interval value is equal to R.

Define λ_{TH} as the maximum capacity of the current NB-IoT cellular site to handle massive IoT traffic services, then:

$$\lambda_{\mathrm{TH}} = 1-\lambda = e^{-u}. \tag{3}$$

Regardless of the processing capacity of the current NB-IoT cellular site, as long as there are more than one IoT devices initiating access requests in each RA-slots, theoretically, the IoT conflicts in Msg1 always exist. For each RA-slots, the number of IoT devices that fail to access in the traditional LTE random access model will randomly select a RA-slots within the random back-off window to initiate an access request again, in the random access strategy for IoT group paging based on time slot scattering proposed in this chapter. Since the number of IoT devices allocated for the first time in each RA-slots is the same, the IoT devices that fail to access will randomly back off to the total access time. A certain RA-slots in the slot initiates an access request again.

Assuming that the initial arrival rate set of each RA-slot in the total access slot I is represented by EN, when the random access request of an IoT device n in the ith RA-slot fails, the IoT device n should be in $[i+1, I_{\mathrm{TH}}]$ randomly selecting an access slot k as the RA-slot for reinitiating random access request. Therefore, the initial arrival rate and actual arrival rate set of each RA-slot have the following inequality relationship:

$$\begin{cases} \lambda_1 = \lambda_{\mathrm{TH}} = \varepsilon_1, & i = 1, \\ \lambda_i = \lambda_{\mathrm{TH}} > \varepsilon_i, & i = 2, 3, \cdots, I-1, I. \end{cases} \tag{4}$$

Obviously, with the exception of the first RA-slot, each RA-slot in the total access slot I will be equally probabilistically selected by the IoT device that failed to access in the previous RA-slots as its new initiator. Therefore, the relationship expression between the initial arrival rate and the actual arrival rate set can be further obtained:

$$\begin{cases} \lambda_1 = \lambda_{\mathrm{TH}} = \varepsilon_1, & i = 1, \\ \lambda_i = 1 - \varepsilon_i + \prod_{k=1}^{i-1} k\lambda_k\left(1 - e^{R\lambda_k}\right), & i = 2, 3, \cdots, I-1, I. \end{cases} \tag{5}$$

The expression of the total access times Ω under the total access time slot I is as follows:

$$\Omega = (N-1)(I-1)\lambda_{\mathrm{TH}} e^{-R\lambda_{\mathrm{TH}}}. \tag{6}$$

When the value of σ_I appears, the E^N set greater than the access time slot σ_I is set to 0, that is:

$$E^N = \begin{pmatrix} \varepsilon_1 & \varepsilon_2 & \varepsilon_3 \cdots \varepsilon_{\sigma_I} & 0 \end{pmatrix}. \tag{7}$$

I_{TH} is the time slot scattering threshold, and its mathematical expression is as follows:

$$I_{\mathrm{TH}} = (N-1)R\lambda_{\mathrm{TH}}. \tag{8}$$

When $I_{\mathrm{TH}} < 1$, the number of IoT devices does not exceed the maximum processing capacity of the NB-IoT cellular site. At this time, there is no need to perform actual scattering processing on the IoT devices, just initiate an access request according to the traditional LTE random access process. The system flow chart of the random access optimization strategy for IoT group paging based on time slot scattering is shown in Figure 2.

4. Simulation Analysis

4.1. Throughput and Delay Analysis. In order to evaluate the throughput and latency of the IOT group paging random access optimization algorithm, this article is configured with an Intel Core i7-6700M @3.40 GH processor and 16 G memory, installed on a PC with a 64-bit Windows7 system, through the Eclipse2020 platform. The PBFT and IOT group paging random access optimization algorithm was implemented by programming in Java language, and the delay and throughput test were carried out. Among them, the implementation and testing of the PBFT algorithm uses part of the code shared by the PbftSimulator project on the Github platform. Each group of experiments was run 25 times independently and averaged as the test result. The main parameter settings are shown in Table 1. In particular, in order to ensure higher consensus efficiency, the number of consensus nodes of the PBFT algorithm is selected less, usually less than 30.

As the number of packages increases, the overall throughput of the two algorithms is increasing; when the number of packages is less than 100, the throughput of the IOT group paging random access optimization algorithm is slightly higher than that of the PBFT algorithm; when the number of packages is greater than 1000, the throughput

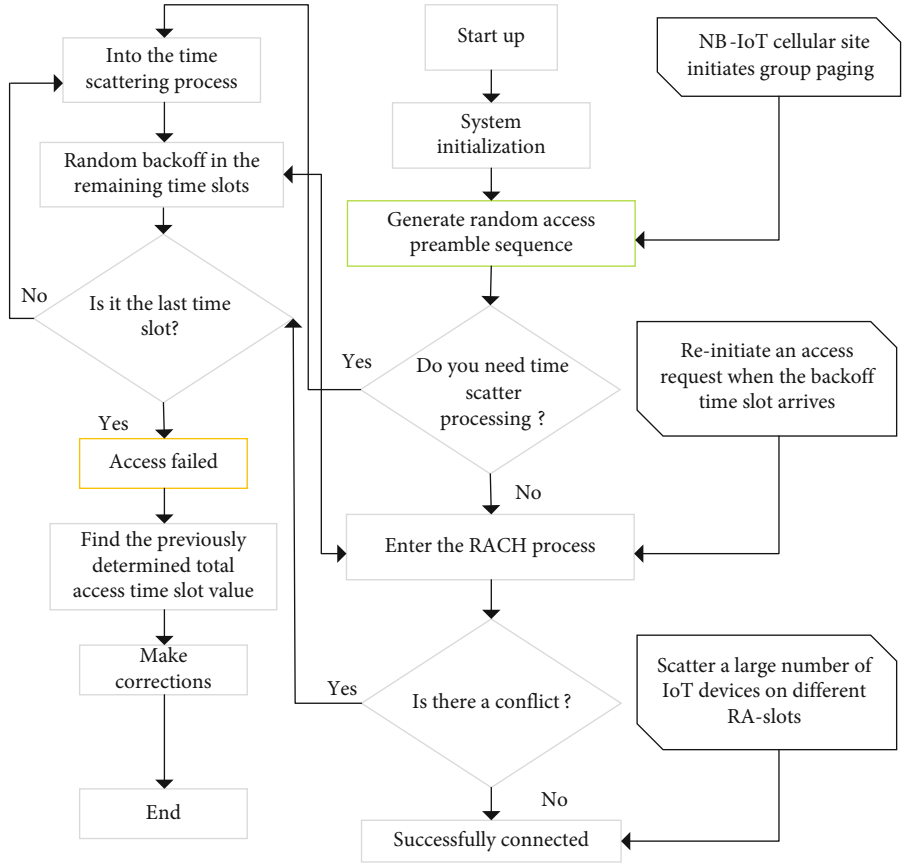

Figure 2: Flow chart of random access system for IoT group paging based on time slot scattering.

Table 1: Simulation parameter table for evaluating algorithm throughput and delay.

Simulation parameters	Values
Maximum number of simultaneous requests	6500
Total number of request messages	3000~8000
Malicious consensus node	1
Number of consensus nodes	7
Number of failed nodes	1
The size of the request message	300 bytes
Rated bandwidth of the network between nodes	7500 bytes
Basic network delay between nodes	3 ms
Network delay disturbance range between nodes	0.5 ms

of the IOT group paging random access optimization algorithm is significantly greater than that of the PBFT algorithm, and as the number of packages increases, the throughput difference gradually increases. Figure 3 shows the relationship between throughput and packaging quantity.

Without considering the delay, it is not rigorous and meaningless to discuss the throughput, and the delay is also an indicator to measure the responsiveness of the algorithm, so this article also tests the relationship between the delay and the number of packages. As the number of packages increases, the delays of both algorithms increase. It can be seen from Figure 4 that the time delay of the IOT group paging random access optimization algorithm is less than that of the PBFT algorithm.

As the number of packages increases, both throughput and delay increase linearly. However, in actual alliance chain applications, the delay is generally required to be less than 3 seconds. Therefore, based on practical application considerations, the discussion of the throughput and delay comparison between the algorithm in this paper and the PBFT algorithm should be limited to the range of delay less than 3 seconds. Under the simulation conditions of this article, when the number of packages is 4000, the delay of the IOT group paging random access optimization algorithm is 2812 milliseconds, and the delay of the PBFT algorithm is 2900 milliseconds; and the throughput of the PBFT algorithm is 1379 transactions/sec. At this time, compared with the PBFT algorithm, the throughput of the IOT group paging random access optimization algorithm is increased by about 3.12%, and the delay is reduced by about 3.03%.

4.2. Analysis of Communication Bandwidth Overhead. In order to evaluate the communication bandwidth overhead of the IOT group paging random access optimization algorithm, on a PC configured with Intel Core i7-6700M @3.40 GH processor and 16 G memory, installed with a 64-bit Windows7 system, the algorithms are used for mathematical calculation simulation, and the parameter settings are shown in Table 2.

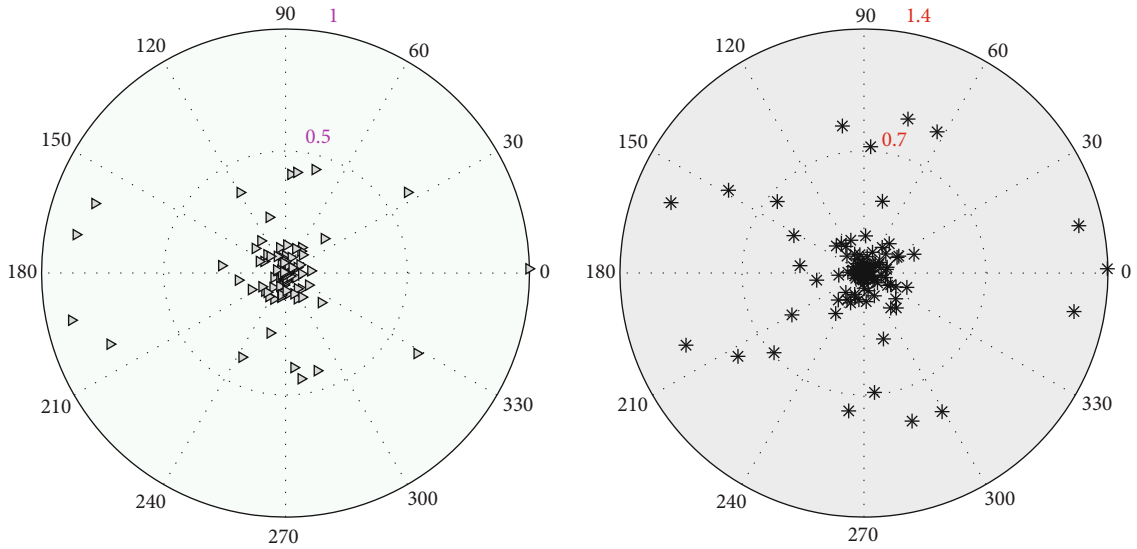

Figure 3: The relationship between throughput and packaging quantity. (1) PBFT algorithm. (2) IOT group paging random access optimization algorithm.

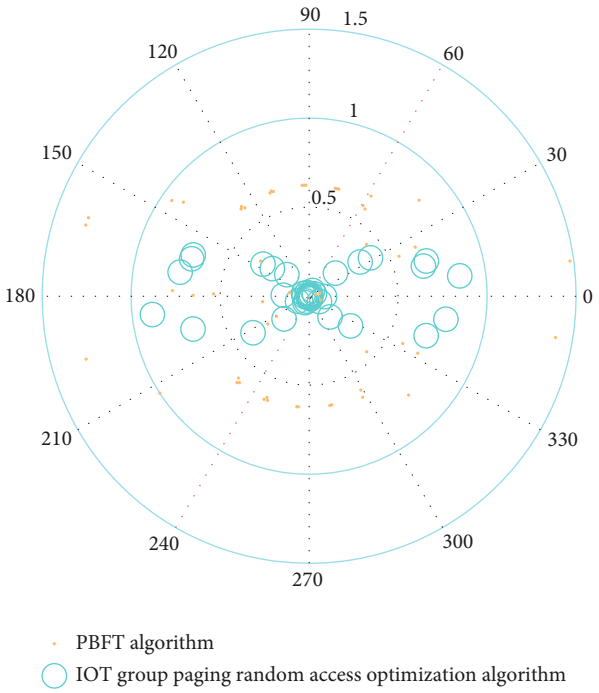

Figure 4: The relationship between delay and packaging quantity.

Table 2: Simulation parameter table of algorithm bandwidth overhead.

Simulation parameters	Values
Vote	0.1 KB
N	<60
Message	0.3 KB
k	<20
Size block	512 KB

The first set of simulations is to compare the bandwidth overhead of different algorithms. In this experiment, the number of fixed voting nodes $N_V = 1000$, and the number of consensus executions in a round of voting cycle is $k = 5$. With the increase of the number of consensus nodes N, the bandwidth cost of the three algorithms increases exponentially, and the growth rate of the algorithm in this paper is small, and the growth rate of the PBFT algorithm is larger; when the number of consensus nodes $N < 15$, the size relationship is that the algorithm in this paper> PBFT. This is because the algorithm in this paper increases the bandwidth overhead of the election process compared with the PBFT algorithm. Under the experimental conditions of this paper, when the number of consensus nodes is 7, this algorithm reduces the bandwidth cost of the PBFT algorithm by about 45%. It can be analyzed that in the case of a large number of consensus nodes, the IOT group paging random access optimization algorithm has lower bandwidth overhead. The relationship between communication bandwidth overhead and the number of consensus nodes is shown in Figure 5.

The second set of tests is to compare the bandwidth overhead of different algorithms when applied to automated packaging systems. When applied to an automated packaging system, consensus is based on a block containing multiple packages as the smallest unit. This is different from the consensus process in the first set of experiments where one package is the smallest unit, and the test results are also different. Figures 5 and 6 have different trends. Under the simulation conditions of this article, when the number of nodes is 7, the bandwidth overhead between the IOT group paging random access optimization algorithm and the PBFT algorithm is relatively large.

4.3. Complexity Analysis. In order to measure the growth relationship between algorithm execution efficiency and resource overhead and data scale, time complexity and space complexity are used as indicators to analyze the complexity

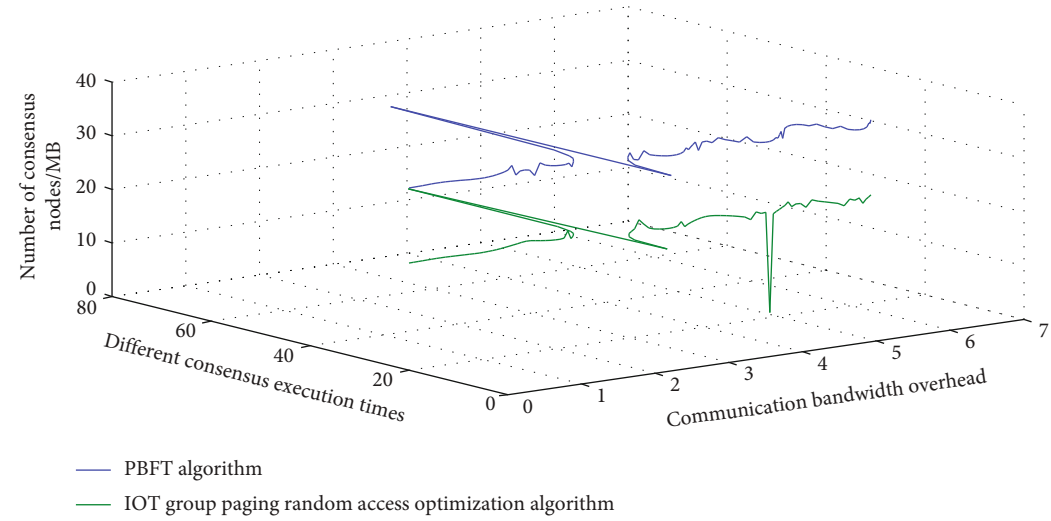

Figure 5: The relationship between communication bandwidth overhead and the number of consensus nodes.

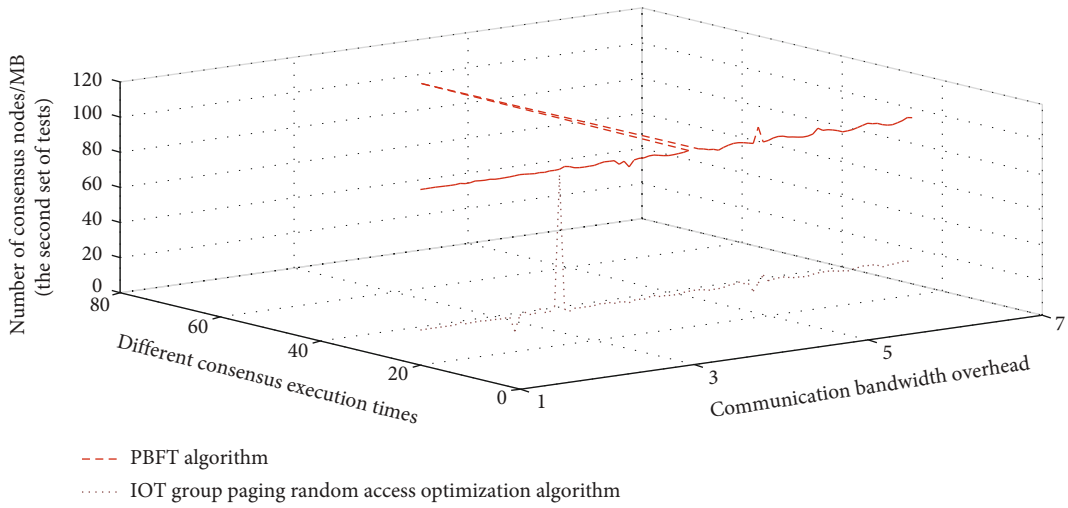

Figure 6: The relationship between communication bandwidth overhead and the number of consensus nodes (the second set of tests).

of the IOT group paging random access optimization algorithm.

Time complexity represents the growth relationship between the execution time of an algorithm and the size of the data and is a measure of the amount of time the algorithm occupies during its operation. For the time complexity analysis of the IOT group paging random access optimization algorithm, this section is measured by the number of basic operations performed by the algorithm under a given input scale. The IOT group paging random access optimization algorithm implements two processes of election and consensus, and one election process supports multiple rounds of consensus. The election process includes 4 stages of voting request, preparation, response, and broadcast results. The consensus process includes 4 stages of request, prepreparation, submission, and response.

Given the input size n, assuming that an election process supports m $(m < n)$ rounds of consensus, then the basic operation number of the algorithm in the voting request phase is 1, the basic operation number of the algorithm in the preparation phase is $n-1$, and the operand is n, the basic operand of the algorithm in the broadcast phase is n, the basic operand of the algorithm in the request phase is m, the basic operand of the algorithm in the pre-preparation phase is $m*(n-1)$, and the basic operand of the algorithm in the submit phase is $m*n*(n-1)$; the basic operand of the algorithm in the response phase is $m*n$.

Space complexity represents the growth relationship between the storage space of the algorithm and the data size and is a measure of the storage space temporarily occupied by the algorithm during operation. For the space complexity analysis of the IOT group paging random access optimization algorithm, this section is measured by the size of the storage space occupied by the algorithm under a given input scale. Similar to the analysis of algorithm's time complexity,

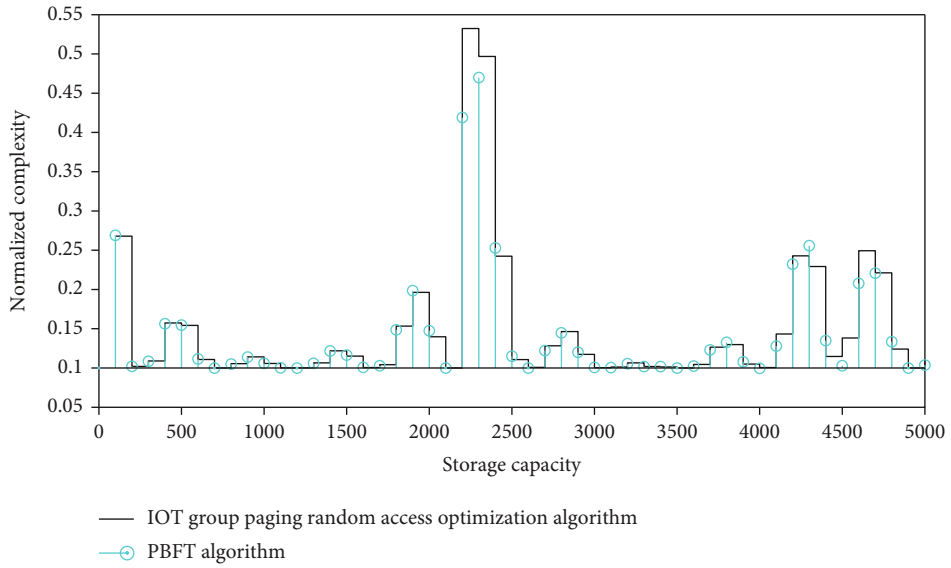

Figure 7: Simulation results of normalized complexity.

given the input size n, assuming that an election process supports $m\,(m < n)$ rounds of consensus, then the storage size of the voting request phase is 1, and the storage size of the preparation phase is $n - 1$; the storage size of the response phase is n, the storage size of the broadcast phase is n, the storage size of the request phase is m, the storage size of the pre-preparation phase is $m * (n - 1)$, and the storage size of the commit phase is $m * n * (n - 1)$; the storage size of the response stage is $m * n$. The stages are carried out in sequence. The simulation result of complexity normalization is shown in Figure 7. It can be seen from Figure 7 that the complexity of the IOT group paging random access optimization algorithm and the PBFT algorithm are not much different.

5. Conclusion

This paper studies the information interaction mechanism between the cloud service system and the mobile terminal and uses web service technology to implement the application channel for users to obtain system services and the interface design for terminal device data interaction. The information interaction mechanism between the cloud service system and the manufacturing system is studied, the Hadoop system is used to classify and mine the order information of the cloud service system, the design of the information interaction between the cloud platform and the manufacturing layer equipment is completed, and the manufacturing system layer flexibility is planned and designed. For the implementation process of automated production, the design of the cloud-assisted decision-making mechanism of the cloud service system for the production activities of the manufacturing system is designed, so as to realize the intelligent production function of the automated packaging system. In the 5G network architecture using NB-IoT technology, this paper proposes a random access optimization strategy based on time slot scattering for the access scenario of IoT group paging. First, a mathematical model based on queuing theory is established for the access scenario of IoT group paging, and on the basis of this model, the scattering threshold and scattering time slot of IoT devices are derived through mathematical formulas. According to the actual application scenario, the time slot scattering algorithm is modified to make it closer to the ideal value. This article builds a list of credit nodes. The credit node list has two functions. One is to improve the participation mode of consensus nodes from static to dynamic, and nodes can enter or exit dynamically; the other is to support the selection of trusted nodes by voting. During the voting period, all nodes can vote, and the top nodes with the most votes form a list of trusted nodes, which will be the candidate list of consensus nodes. This paper designs a credit evaluation mechanism. This mechanism is the follow-up of consensus node election, including credit value calculation model and node election strategy. Through this mechanism, a trusted consensus node (master node and replica node) can be elected from the list of credit nodes. Trusted consensus nodes will improve system fault tolerance and reduce communication overhead. Based on the credit evaluation mechanism, the credibility of the consensus node is ensured, thereby simplifying the three-phase protocol of the PBFT algorithm into two phases to further reduce communication overhead and algorithm delay.

Data Availability

The data used to support the findings of this study are available from the corresponding author upon request.

Conflicts of Interest

The authors declare that they have no known competing financial interests or personal relationships that could have appeared to influence the work reported in this paper.

Acknowledgments

This research supported by "Research on interactive intelligent packaging design under the background of 5G era" (project no. 2021ky0178), which is the project to improve the basic scientific research ability of young and middle-aged teachers in colleges and universities in Guangxi in 2021.

References

[1] T. Taleb, K. Samdanis, B. Mada, H. Flinck, S. Dutta, and D. Sabella, "On multi-access edge computing: a survey of the emerging 5g network edge cloud architecture & orchestration," *IEEE Communications Surveys & Tutorials*, vol. 19, no. 3, pp. 1657–1681, 2017.

[2] D. Soldani and A. Manzalini, "Horizon 2020 and beyond: on the 5G operating system for a true digital society," *IEEE Vehicular Technology Magazine*, vol. 10, no. 1, pp. 32–42, 2015.

[3] A. Al-Fuqaha, M. Guizani, M. Mohammadi, M. Aledhari, and M. Ayyash, "Internet of things: a survey on enabling technologies, protocols, and applications," *IEEE Communications Surveys & Tutorials*, vol. 17, no. 4, pp. 2347–2376, 2015.

[4] S. Zhang and T. N. Wong, "Integrated process planning and scheduling: an enhanced ant colony optimization heuristic with parameter tuning," *Journal of Intelligent Manufacturing*, vol. 29, no. 3, pp. 585–601, 2018.

[5] J. A. Warren, M. E. Riddle, D. J. Graziano et al., "Energy impacts of wide band gap semiconductors in U.S. light-duty electric vehicle fleet," *Environmental science & technology*, vol. 49, no. 17, pp. 10294–10302, 2015.

[6] J. Moura and D. Hutchison, "Game theory for multi-access edge computing: survey, use cases, and future trends," *IEEE Communications Surveys & Tutorials*, vol. 21, no. 1, pp. 260–288, 2019.

[7] S. A. A. Shah, E. Ahmed, M. Imran, and S. Zeadally, "5G for vehicular communications," *IEEE Communications Magazine*, vol. 56, no. 1, pp. 111–117, 2018.

[8] K. S. E. Phala, A. Kumar, and G. P. Hancke, "Air quality monitoring system based on ISO/IEC/IEEE 21451 standards," *IEEE Sensors Journal*, vol. 16, no. 12, pp. 5037–5045, 2016.

[9] S.-Y. Wang and L. Wang, "An estimation of distribution algorithm-based memetic algorithm for the distributed assembly permutation flow-shop scheduling problem," *IEEE Transactions on Systems, Man, and Cybernetics: Systems*, vol. 46, no. 1, pp. 139–149, 2016.

[10] X. She, A. Q. Huang, O. Lucia, and B. Ozpineci, "Review of silicon carbide power devices and their applications," *IEEE Transactions on Industrial Electronics*, vol. 64, no. 10, pp. 8193–8205, 2017.

[11] M. Mehrabi, D. You, V. Latzko, H. Salah, M. Reisslein, and F. H. P. Fitzek, "Device-enhanced mec: multi-access edge computing (mec) aided by end device computation and caching: a survey," *IEEE Access*, vol. 7, pp. 166079–166108, 2019.

[12] R. Zhang, Z. Zhong, J. Zhao, B. Li, and K. Wang, "Channel measurement and packet-level modeling for V2I spatial multiplexing uplinks using massive MIMO," *IEEE Transactions on Vehicular Technology*, vol. 65, no. 10, pp. 7831–7843, 2016.

[13] A. Ali, G. A. Shah, M. O. Farooq, and U. Ghani, "Technologies and challenges in developing machine-to-machine applications: a survey," *Journal of Network and Computer Applications*, vol. 83, no. 4, pp. 124–139, 2017.

[14] X.-L. Zheng and L. Wang, "A collaborative multiobjective fruit fly optimization algorithm for the resource constrained unrelated parallel machine green scheduling problem," *IEEE Transactions on Systems, Man, and Cybernetics: Systems*, vol. 48, no. 5, pp. 790–800, 2018.

[15] C. Chen, F. Luo, and Y. Kang, "A review of sic power module packaging: layout, material system and integration," *CPSS Transactions on Power Electronics and Applications*, vol. 2, no. 3, pp. 170–186, 2017.

[16] K. Zhang, S. Leng, Y. He, S. Maharjan, and Y. Zhang, "Mobile edge computing and networking for green and low-latency internet of things," *IEEE Communications Magazine*, vol. 56, no. 5, pp. 39–45, 2018.

[17] K. Liu, J. K. Y. Ng, V. C. S. Lee, S. H. Son, and I. Stojmenovic, "Cooperative data scheduling in hybrid vehicular ad hoc networks: VANET as a software defined network," *IEEE/ACM transactions on networking*, vol. 24, no. 3, pp. 1759–1773, 2016.

[18] M. Centenaro, L. Vangelista, A. Zanella, and M. Zorzi, "Long-range communications in unlicensed bands: the rising stars in the IoT and smart city scenarios," *IEEE Wireless Communications*, vol. 23, no. 5, pp. 60–67, 2016.

[19] G. Mejia, J. P. Caballero-Villalobos, and C. Montoya, "Petri nets and deadlock-free scheduling of open shop manufacturing systems," *IEEE Transactions on Systems, Man, and Cybernetics: Systems*, vol. 48, no. 6, pp. 1017–1028, 2018.

[20] S. Ji, Z. Zhang, and F. Wang, "Overview of high voltage sic power semiconductor devices: development and application," *CES Transactions on Electrical Machines and Systems*, vol. 1, no. 3, pp. 254–264, 2017.

[21] P. Kourouthanassis, C. Boletsis, C. Bardaki, and D. Chasanidou, "Tourists responses to mobile augmented reality travel guides: the role of emotions on adoption behavior," *Pervasive and Mobile Computing*, vol. 18, pp. 71–87, 2015.

[22] T. Qiu, X. Wang, C. Chen, M. Atiquzzaman, and L. Liu, "TMED: a spider web-like transmission mechanism for emergency data in vehicular ad hoc networks," *IEEE Transactions on Vehicular Technology*, vol. 67, no. 9, pp. 8682–8694, 2018.

[23] M. Ndiaye, G. P. Hancke, and A. M. Abu-Mahfouz, "Software defined networking for improved wireless sensor network management: a survey," *Sensors*, vol. 17, no. 5, pp. 1031-1032, 2017.

[24] M. Gen, W. Zhang, L. Lin, and Y. Yun, "Recent advances in hybrid evolutionary algorithms for multiobjective manufacturing scheduling," *Computers and Industrial Engineering*, vol. 112, pp. 616–633, 2017.

[25] C. Durand, M. Klingler, D. Coutellier, and H. Naceur, "Power cycling reliability of power module: a survey," *IEEE Transactions on Device and Materials Reliability*, vol. 16, no. 1, pp. 80–97, 2016.

[26] J. Pan and J. McElhannon, "Future edge cloud and edge computing for internet of things applications," *IEEE Internet of Things Journal*, vol. 5, no. 1, pp. 439–449, 2018.

[27] T. Qiu, R. Qiao, and D. O. Wu, "EABS: an event-aware backpressure scheduling scheme for emergency internet of things," *IEEE Transactions on Mobile Computing*, vol. 17, no. 1, pp. 72–84, 2018.

[28] C. Chen, Y. Chen, Y. Li, Z. Huang, T. Liu, and Y. Kang, "An sicbased half-bridge module with an improved hybrid packaging method for high power density applications," *IEEE Transactions on Industrial Electronics*, vol. 64, no. 11, pp. 8980–8991, 2017.

Hindawi
Journal of Sensors
Volume 2022, Article ID 5013905, 10 pages
https://doi.org/10.1155/2022/5013905

Research Article

A Data-Driven WSN Security Threat Analysis Model Based on Cognitive Computing

Xinyan Huang

School of Computer Science and Technology, Shandong University of Finance and Economics, Shandong Jinan 250014, China

Correspondence should be addressed to Xinyan Huang; 20063462@sdufe.edu.cn

Received 24 November 2021; Revised 21 December 2021; Accepted 22 December 2021; Published 27 January 2022

Academic Editor: Gengxin Sun

In this paper, we use cognitive computing to build a WSN security threat analysis model using a data-driven approach and conduct an in-depth and systematic study. In this paper, we develop a simulation platform (OMNeT++-based WSN Security Protocol Simulation Platform (WSPSim)) based on OMNeT++ to make up for the shortcomings of current WSN simulation platforms, improve the simulation capability of WSN security protocols, and provide a new technical means for designing and verifying security protocols. The WSPSim simulation platform is used to simulate and analyze typical WSN protocols and verify the effectiveness of the platform. In this paper, we mainly analyze the node malicious behavior by listening and judging the communication behavior of the nodes, and the current trust assessment is given by the security management nodes. When the security management node is rotated, its stored trust value is used as historical trust assessment and current trust assessment together to participate in the integrated trust value calculation, which improves the reliability of node trust assessment; to increase the security and reliability of the management node, a trust value factor and residual energy factor are introduced in the security management node election in the paper. According to the time of management node election, the weights of both are changed to optimize the election. Using the WSPSim simulation platform, a typical WSN protocol is simulated and analyzed to verify the effectiveness of the platform. In this paper, the simulation results of the LEACH protocol with an MD5 hash algorithm and trust evaluation mechanism and typical LEACH protocol as simulation samples are compared; i.e., the correctness of the simulation platform is verified, and it is shown that improving the security of the protocol and enhancing the security and energy efficiency of wireless sensor networks provide an effective solution.

1. Introduction

A wireless sensor network (WSN) is a key technology for IoT and has been widely used in many fields. WSN is characterized by many sensor nodes and a large network size, which is usually deployed in an exposed external environment and therefore vulnerable to various forms of attacks [1]. Authentication is the basis for securing the network, and traditional authentication mostly uses centralized authentication, but such an authentication mechanism has many drawbacks: the security of the network depends entirely on the authentication center, and once the authentication center is maliciously attacked, the whole authentication system will fall into collapse; when the scale of the network is expanded, the performance of the network will be affected due to the limited computing power and storage capacity of the authentication center. With the development of WSN, the topology of the network is ever-changing, and centralized authentication is not flexible enough. Therefore, the security of centralized authentication is not high and scalability is poor. This security problem can be effectively solved by establishing a distributed trust model in WSN [2].

With the rapid development of information technology, the Internet of Things has come into being. IoT is an application expansion based on the Internet, which extends its application end from the object to object, enabling information exchange and communication between people and things. The wireless sensor network is the key technology of IoT, which is oriented to the perception layer in the three-layer structure of IoT [3, 4]. The wireless sensor network is a new multihop self-organizing network composed of numerous sensor nodes with the characteristics of overall

sensing, reliable transmission, and intelligent processing. The data acquisition unit is responsible for collecting information in the monitoring area and converting it; the data transmission unit mainly sends and receives that collected data information in the form of wireless communication [5]. To establish a wireless sensor network environment, many sensors, a data transmission center, and a base station are required. Sensors are devices with detection, computing, and communication capabilities. Wireless sensor networks integrate the acquisition, processing, and execution of information with sensing, processing, communication, and storage functions and can measure indicators [6]. Wireless sensor networks have a wide range of applications in many fields such as military battlefield and smart home with their self-organization and fast deployment. Due to the limited computing resources and long-term operation of the IoT sensor device nodes converged and accessed by the edge computing terminal, the traditional "patch" security reinforcement mechanism cannot be applied to the IoT sensor device node and the IoT sensor device in an uncontrolled environment. The risk of malicious use of nodes is extremely high, making edge computing terminals extremely easy to become attack targets or springboards for IoT sensor device nodes.

In the era of big data, improving the cognitive ability of large-scale data is an urgent need for technological development. Cognitive computing is a set of theoretical studies that includes the whole process from the sample input, processing, and output. Cognitive computing is based on mathematical methods, computer technology, and biological neurology, and it can analyze data by simulating the mechanism of the human brain [7]. The application of cognitive computing for data value mining will help people to discover potential laws and improve the way they work. In the era of big data, it is of great practical importance to study the cognitive ability of knowledge acquisition and experiential learning for massive data [8].

2. Related Works

The research on wireless sensor networks first started in the 1970s and 1980s, and with the rapid development of the Internet, wireless sensor networks have also been developed. Centralized authentication is generally used in traditional networks for authentication, thus ensuring network security. The communication parties identify each other with the help of an authoritative authentication center to establish a trust relationship. The structure of centralized authentication is relatively simple, so there are many problems: the security of the entire network depends on this authentication center, and the authentication center is easily identified by malicious nodes and attacked; there is a great security risk; in the case of large network size and limited performance of the authentication center, the network may collapse at any time [9]. There are many sensor nodes in the WSN, the node topology is very variable, and the centralized authentication is not flexible enough to meet this variable topology. WSN has become one of the key technologies for information access in the information age, attracting close attention from academia and industry, and has become a research hotspot in the fields of automation, computing, and communication. WSN is listed as one of the top ten technologies that will change the world in the 21st century and is also listed as one of the four new technologies in the future. At present, with the widespread promotion of the Internet of Things and "Internet Plus," the application research of WSN has entered a new climax [10].

The trust management approach, first proposed in 1996, is based on a simple language that specifies trust operations and trust relationships and solves the problem of trusting one node over another by developing a security policy and delegating it to third-party nodes; it also follows the principles of uniformity, flexibility, locality control, and separation of mechanisms and policies to develop a general framework that can be applied to any service that requires encryption [11]. The approach considers the dynamic variability of nodes in the network and meets the open needs of the network. Based on this, scholars have proposed trust models such as EigenTrust, Peer Trust, and Power Trust, all of which have improved the calculation related to trust values to some extent. Although these trust models are more accurate in the calculation of trust values, the structure of many of them does not apply to wireless sensor networks [12].

With the continuous changes of attack methods, the concealment of malicious attacks has become stronger and stronger. On the one hand, terminal identity execution authentication and identification technology has been easily forged or bypassed; on the other side, legitimate terminals that have passed identity authentication are used as a springboard; it is difficult to detect and identify infiltration attacks. As the network security situation becomes increasingly complex, the technical means to launch attacks on the network are becoming more sophisticated, although at this stage, there are different intrusion prevention technology models to deal with. However, for unknown attacks, the existing intrusion prevention solutions cannot completely solve these unknown network attacks, and there is no "one size fits all" intrusion prevention model to solve all kinds of unknown network attacks [13]. In this context, active defense technology is gradually gaining great attention. It does not depend on the characteristics of the attack code and attack behavior but rather on the technical means of providing the operating environment, changing the static and deterministic nature of the system, to minimize the successful utilization of vulnerabilities, disrupt the implementation ability of network vulnerability exploitation, and block or interfere with the accessibility of the attack, thus significantly increasing the difficulty and cost of the attack [14]. Although the idea of active defense has been around for a long time, as an attack defense concept, there is still no standardized definition to date. A summary based on relevant literature is broadly divided into security defense models and active defense techniques [15].

3. Data-Driven WSN Security Threat Analysis Model Construction Based on Cognitive Computing

3.1. Cognitive Computing Model Design. Due to the limited computing resources and long-term operation of the IoT sensing device nodes aggregated and accessed by the edge

computing terminals, the traditional "patch" security hardening mechanism cannot be applied to the IoT sensing device nodes, and the risk of malicious exploitation of the IoT sensing device nodes in uncontrolled environments is extremely high, which makes the edge computing terminals extremely easy to become the target or springboard of the IoT sensing device nodes. Therefore, how to effectively conduct the active defense of edge computing endpoints and detect and defend remote penetration attacks from IoT sensing device nodes in advance is often the first step in edge computing network security protection [16]. To address this, several terminal defense techniques have been proposed in related research, and the main implementation idea of these techniques is to use digital certificate authentication technology and trusted access technology to evaluate and authenticate the identity legitimacy, software and hardware integrity, and security of terminal entities, and only terminals that satisfy the access control policy specified by the system are allowed to access the network. However, with the continuous changes in the means of attack, malicious attacks are becoming increasingly covert; on the one hand, the terminal identity execution authentication and identification technology has been easily forged or bypassed; on the other hand, the legitimate terminal after welcoming the identity authentication is used as a springboard, so that the implementation of penetration attacks is difficult to be detected and identified.

Based on the idea of mimetic defense, a mimetic defense model for edge computing terminals is established based on the dynamic heterogeneous redundancy characteristics of the network attack chain and the mimetic defense system, and the possibility of successful attacks on each key component in the mimetic defense model can be solved based on this model, so that different parameters can be used to analyze the security defense effectiveness of the mimetic defense model for edge computing terminals, facilitating a better insight into how to use mimetic defense techniques designed to improve the security of edge computing endpoints. Figure 1 illustrates the relevant components studied in this chapter. As the network security situation becomes more complex, the technical means to launch attacks on the network are increasingly emerging, although at this stage, there are different intrusion prevention technology models to deal with. However, for unknown attacks, the existing intrusion prevention solutions cannot completely solve these unknown network attacks. At present, there is no "one size fits all" intrusion prevention model to solve all kinds of unknown network attacks. In this context, active defense technology has gradually gained people's attention.

The active defense model constructed based on the idea of mimetic defense is an IPO model; when the submitted request input enters the system, it is copied into n copies by the input agent unit and forwarded to the set of executors, which contains n similar redundant executors (k_1, k_2, k_3, …, k_m). By taking advantage of the dependency of cyberattacks on the environment, one attack against a specific vulnerability cannot be effectively played in heterogeneous executors (k_1, k_2, k_3, …, k_m) at the same time, thus achieving the defense effect against vulnerability attacks. The multiredundancy voter mainly compares the execution results of redundant executors in terms of discrepancy, to vote whether the mimetic defense system suffers from network intrusion and achieves the purpose of intrusion detection [17]. At present, the mimetic defense technology has formed a variety of systems with mimetic defense structure routers.

A cluster analysis algorithm is a statistical analysis method that can be used to deal with sample classification problems. It is based on similarity and does not require sample labeling. The cluster analysis algorithm tries to discover the implied relationships between different data in the sample space and classify the data into different groups by calculating the similarity between the data, which are more similar within the groups and less similar between the groups. The clustering algorithm is a very important and commonly used data mining algorithm in machine learning, which does not require prior knowledge of the characteristics of the sample categories which can be very good at discovering "unknown" relationships from "known" data. The clustering algorithm puts similar samples together in one category by calculating the similarity. The clustering analysis algorithm has the characteristics of clear computational logic and good sample classification.

The calculation of vector distances in competitive neural network algorithms usually uses the Euclidean distance method or the cosine method. The Euclidean distance method calculates the distances between vectors with the following formula:

$$\|X + X_i\| = \sqrt{(X_i - X)} - \sqrt{(X - X_i)}^T. \quad (1)$$

The algorithm to implement the "winner takes all" competition mechanism in competitive neural networks is as follows.

(1) Vector normalization

Vectors with different angles and lengths or too much difference will increase the computational complexity of the algorithm. Therefore, the vector is normalized to a unit vector with direction and length of 1.

(2) Finding the winning neuron

After the competing layer neurons acquire the sample objects in the input layer, the weights of all competing layer neurons are calculated for similarity with the input objects, and the competing layer neuron with the greatest similarity receives the highest weight to become the winning neuron.

(3) Adjustment of weights

Weights are adjusted for the winning neuron and wait for the next input. Competitive neural networks can arrive at the final winning neuron through the competition rule, but if the initial value of a neuron deviates from all samples to a large extent, then these neurons will still not be able to obtain a higher weight in the process of weight adjustment for as long as they are trained, and as a result, these neurons

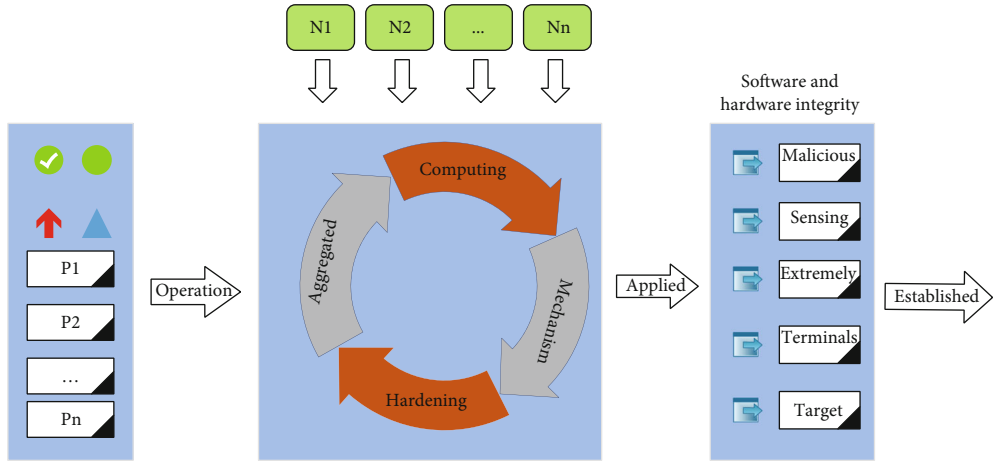

Figure 1: Framework of remote access anti-infiltration technology for computing endpoints.

will never win and will naturally not be activated. Such inactivated neurons are called "dead neurons." The problem of dead neurons is solved by adding a threshold learning rule to the weight adjustment rule of the competing layer neurons of the competitive neural network [18]. The threshold learning rule sets a higher threshold for neurons with a low probability of winning to improve the competitive ability of the neuron and a smaller threshold for neurons that win frequently to make each neuron likely to win. Finally, the average degree of neuron weight adjustment is calculated to output the final winning neuron.

$$P_1 = \frac{3}{\beta_2}\left(P' + \beta_1 p_2\right). \tag{2}$$

After taking the direct trust value, the weight of the direct trust value is then calculated. The weight of the direct trust value is used to indicate the reliability of the direct trust value, and its value is related to the dispersion of the historical interaction trust value and the adequacy of the historical interaction. The relationship between the number of interactions and the sufficiency is shown in Figure 2. When the number of interactions N is 30, the interaction sufficiency reaches 95%, and when the number of interactions reaches 50, the sufficiency is almost close to 100%. Clustering analysis algorithms are very important and commonly used data mining algorithms in machine learning. They do not need to know the characteristics of sample categories in advance and can find "unknown" relationships from "known" data. The clustering algorithm puts similar samples together into one category through the calculation of similarity. The cluster analysis algorithm has the characteristics of clear calculation logic and good sample classification effect.

The weight formula can be expressed as shown in equation (3). This setting enables the weight of the direct trust value to be inversely proportional to std and positively proportional to freq, where $\omega_{ji}^{\mathrm{DT}}$ denotes the direct trust weight of the node numbered j to the node numbered i. Multiplying by 1/2 is to normalize the weights between 0 and 1. Up to this point, the direct trust value and direct trust weight are

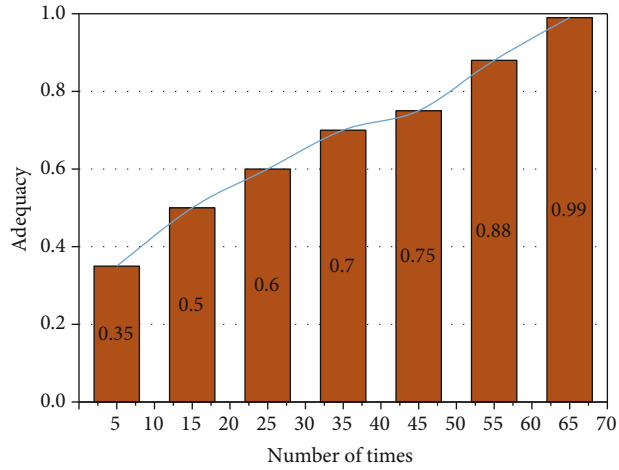

Figure 2: Relationship between the number of interactions and adequacy.

calculated and the whole direct trust module has been designed.

$$\omega_{ij}^{\mathrm{TD}} = 2(\mathrm{freq} + \mathrm{std} - 1). \tag{3}$$

3.2. WSN Security Threat Analysis Model Construction. The Internet of Things (IoT) is a fusion of automation systems and IoT systems, which features comprehensive sensing, interconnected transmission, intelligent processing, intelligent handling, and self-organization and maintenance, and its applications span many fields such as intelligent transportation, smart factories, smart grids, and intelligent environmental detection [19]. The IoT can be viewed as a subset of the IoT and can be structurally divided into three layers: data collection layer, data transmission layer, and data processing layer. The security of the entire network relies on this certification center, and the certification center is easily identified by malicious nodes and is attacked, which poses great security risks; when the network is large and the performance of the certification center is limited, the

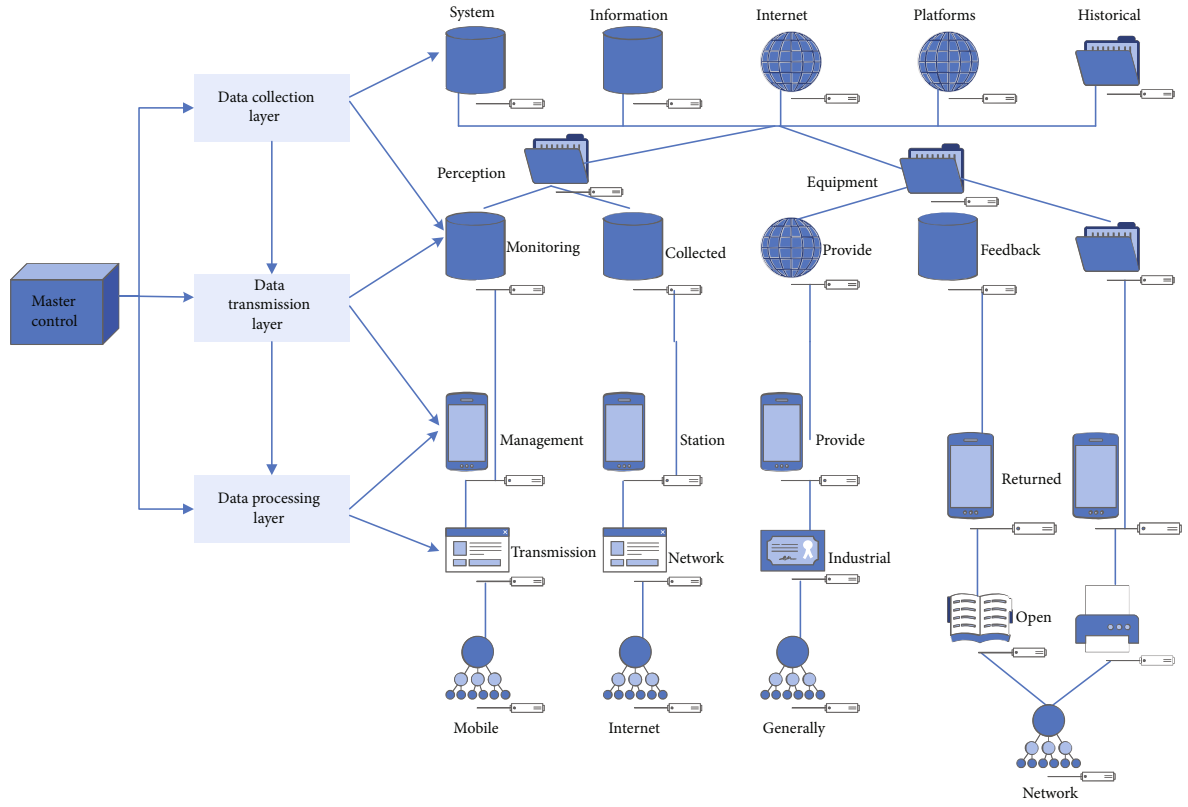

Figure 3: IoT system architecture.

network may collapse at any time. A typical system architecture for a wireless network is shown in Figure 3.

The blockchain infrastructure has six main layers, each layer completes a part of the core tasks, and the layers collaborate to achieve a decentralized trust model; from bottom to top, there are mainly data layers, network layers, consensus layers, incentive layers, contract layer, and service layer. The data layer represents the physical form of the blockchain technology and is the basic technical structure for designing the blockchain ledger, describing which parts the blockchain consists of. Each block contains many technologies, such as timestamp technology and hash cryptography function, which is used to ensure that the blocks are connected in sequential order and that the data saved in the blockchain is not tampered with; the main function of the network layer is to enable communication between the nodes in the blockchain network and to achieve a distributed record of information [19]. The purpose of the blockchain network is to create a P2P (peer-to-peer network) to solve the problem of single-point congestion and failure in traditional networks, where each node is both a sender and a receiver of messages; the knowledge layer is responsible for efficiently reaching a consensus on a certain aspect in a decentralized system through information exchange between highly decentralized and distrustful nodes, which is the core idea of blockchain. Commonly used consensus algorithms are the proof-of-workload algorithm, proof-of-share authorization algorithm, practical Byzantine fault tolerance algorithm, etc. Cognitive computing is based on mathematical methods, based on computer technology, and guided by the results of bioneurology to realize the analysis of data by simulating the mechanism of the human brain. The application of cognitive computing to mine the value of data will help people discover potential patterns and improve working methods.

$$y^2 + bx - ay^2 \leq x^2 + cy^3 - dx + e. \tag{4}$$

Hashing is a method of applying a hash function to data that maps an input of any size (file, text, or image) into a fixed-length binary value. The hashed hash value is very different if the original information is slightly modified, so hash functions are commonly used in blockchains to verify the integrity and accuracy of data.

Hash functions have several important security properties as follows:

(1) They are reverse resistant. This means that they are one-way irreversible, and computing the correct input value given some output value does not work here with hash functions. For example, given digest, finding hash (x) = digest is infeasible

(2) They have a second inverse. This means that it is impossible to design a hash function to find a second input that produces the same output by giving a particular input

The latter block in the blockchain holds the hash value of the previous block to form a chain structure, and once the data in the previous block changes, the hash pointer in the block header of the latter block will follow, so it is difficult to tamper with the data in the blockchain. The Internet of Things is the integration of automation systems and Internet of Things systems. It has the characteristics of comprehensive perception, interconnected transmission, intelligent processing, intelligent processing, and self-organization and maintenance. Its applications are widespread in intelligent transportation, smart factories, smart grids, smart environment detection, etc. In the field, the Internet of Things can be regarded as a subset of the Internet of Things.

As symmetric encryption is difficult to solve the key management and digital signature problems, asymmetric encryption was born. In the process of asymmetric encryption, X represents the plaintext, which indicates the input of the algorithm; the public key used for encryption and the private key used for decryption are different; Y is the ciphertext, which indicates the data obtained after encryption. The steps of the public key cryptosystem are shown below [20].

The encryption algorithm gets the encrypted ciphertext based on the input plaintext and the public key, which is delivered to the destination through the network, and the receiver decrypts the received ciphertext with the private key to get the same plaintext as the one sent by the sender. This completes the entire process of asymmetric encryption. The most widely used asymmetric encryption regimes are the RSA algorithm, ElGamal algorithm, etc. The advantages of the asymmetric encryption system are as follows: unlike symmetric encryption, the sender and the receiver need to share the same password and each has its key, eliminating the link of transmitting the key and reducing the security risks in the network; even if the public key is intercepted by the attacker in the process of transmission, the ciphertext cannot be decrypted even if the public key is obtained because there is no private key matching the public key, ensuring that the n users only need n pairs of keys, which is easy to manage as the key distribution is simple, and only need to distribute the encryption key to each other and keep the decryption key by themselves. But the disadvantage is that the encryption algorithm is complex and the encryption and decryption speed is slow.

$$3a^4 + 15b^2 \leq 0. \tag{5}$$

Wireless sensor networks have many sensor nodes and large network sizes and are usually deployed in exposed external environments, making them vulnerable to various forms of attacks. Distributed authentication by establishing a trust model can effectively reduce attacks. The node trust mechanism is the basis of the trust model. Wireless sensor networks are mainly used to transmit data information through mutual aid forwarding between nodes, and establishing trust mechanisms between nodes can effectively resist malicious attacks. In the network, nodes choose whether to interact with the target node by judging its trustworthiness.

There are many and dense nodes in WSNs with large network sizes; due to the low cost of sensors, the computational capacity, storage capacity, and power supply are limited; it is difficult to perform authentication and cannot guarantee network security. Establishing an authentication model can effectively solve this security problem. The authentication model is divided into centralized authentication and distributed authentication, and the centralized authentication mechanism has many drawbacks: the network structure is simple and not strong against attacks, the network scalability is poor, the performance of the authentication center is limited, and the network will collapse at any time when the network scale is expanded; therefore, the security of centralized authentication is not high. Therefore, this section also focuses on the principle and current research status of distributed authentication models and compares the existing models with the RRCTM model proposed in this paper.

4. Analysis of Results

4.1. Cognitive Computing Model Results. For some samples that can be identified by the "naked eye" based on experience and criteria, the number of classifications can be identified. The K-DB algorithm is chosen to not only determine the radius and density thresholds more accurately but also to identify core, boundary, and outlier points in the sample. The analysis based on the analysis of sample points of different nature can make the study of the sample more comprehensive and targeted. The core points with the smallest average distance in the density clustering results can be used to characterize the nearest similar objects of all samples of the cluster, which to some extent reflects the overall characteristics of the cluster [21]. The boundary points in the clustering results are used to characterize the farthest similar objects of all samples in the cluster and are suitable for judging the extreme attributes and characteristics of the cluster; outliers can be used to determine the reason for the occurrence of the sample and analyze the problems in the data information; in practical applications, outliers can be dealt with, or they can be selectively discarded. The boundary points in the clustering results are used to characterize the farthest similar objects of all samples of the cluster, which are applicable to determine the extreme properties and characteristics of the cluster; outlier points can be used to determine the reasons for the appearance of the sample and analyze the problems in the data information, and the outlier points can be processed or selectively discarded in practical applications.

Cluster quality assessment methods use the Cluster Validity Index (CVI) to assess the effectiveness of clustering. Cluster quality assessment is commonly performed by internal, external, and expert evaluation. The internal evaluation assesses the effectiveness of clustering by obtaining assessment quality scores according to calculation rules. When a node is subject to intermittent attacks or random errors, the reputation value of the node will decrease. This type of node is an abnormal node, but due to the low frequency of attacks or errors, it does not affect the normal

communication of the node. The reputation value of the node is also maintained above 0.8. External assessment is a controlled assessment using public standards, and expert assessment is a manual assessment method that indirectly assesses the effect of clustering through expert knowledge. This experiment uses internal evaluation to verify the effectiveness of the K-DB algorithm. The circle blob dataset contains 6000 data items, which can be roughly divided into 3 clusters according to the sample distribution, and the DBSCAN algorithm adjusts the density threshold Mats to 40 after the 4th iteration to obtain better clustering results. The clustering results of the density clustering algorithm with a density radius of 0.13 and a density threshold of 60 are calculated according to the K-DB algorithm in Figure 4.

To further verify the superiority of the K-DB algorithm, this paper selects real datasets from the UCI database for experimental validation of algorithm accuracy and efficiency. The experiments are compared with K-means, DBSCAN, and K-DB algorithms on the real datasets Iris, Wine, and Glass, and this experiment uses the Davidson-Fortin Index (DBI) and accuracy (ACC) to compare and validate the performance of the K-DB algorithm. The experimental results are shown in Table 1.

From the table, the K-DB algorithm outperforms K-means and DBSCAN algorithms in terms of clustering accuracy on all three real datasets, and the K-DB algorithm effectively improves the accuracy of density radius and threshold setting. The K-DB algorithm combines the advantages of the two algorithms to achieve complementary advantages and has higher accuracy and a smaller DBI than the single K-means and DBSCAN algorithm. Experimental results show that the K-DB algorithm has superiority in improving algorithm efficiency and clustering accuracy and can identify core points, boundary points, and outliers in sample clusters. The K-DB algorithm combines the advantages of both algorithms to achieve complementary strengths and has higher accuracy and smaller DBI than single K-means and DBSCAN algorithms. The experimental results show that the K-DB algorithm is more accurate than the single K-means and DBSCAN algorithms. The experimental results show that the K-DB algorithm is superior in improving the efficiency and clustering accuracy of the algorithm and can identify core points, boundary points, and outliers in the sample clusters.

$$a_{ij} = p\left(q_{j-i} = \mathrm{IS}_i\right), \sum_{i=1}^{m} a_{ij} = 1. \tag{6}$$

To predict the security reliability of all the reachable paths in the network topology mimetic association graph, this paper classifies the network security reliability hidden state level into 5 values. The reliability of each reachable path will be transferred with probability among these 5 states. The observation sequence $O = \{o_1, o_2, L, o_3\}$ is obtained after t moments of observation. For example, for the network throatiness metric, the observation sequence is the network anomaly measure obtained after t moments. From the HMM definition, it is known that

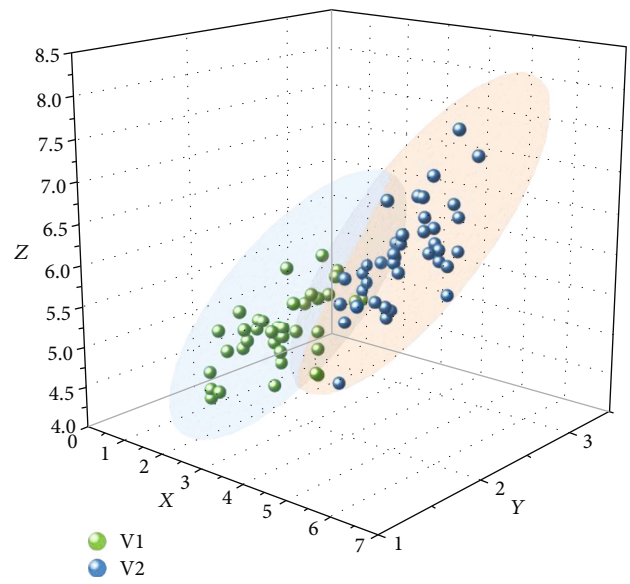

Figure 4: K-DB clustering data distribution for the circle blob dataset.

Table 1: Accuracy of clustering results for real datasets.

	K-D		K-E		K-F		K-G	
	ab	ce	ab	ce	ab	ce	ab	ce
UCI	0.92	3.53	0.821	3.62	0.786	3.89	0.694	2.94
DBSCAN	0.83	3.15	0.795	3.54	0.754	3.75	0.678	2.84
K-DB	0.76	2.71	0.734	3.41	0.722	3.61	0.662	2.74
ACC	0.71	3.21	0.756	3.45	0.696	3.47	0.646	2.64
GLASS	0.65	2.92	0.712	3.67	0.658	3.33	0.635	2.54

a total of 2 posture prediction models for 2 observable metrics need to be constructed and integrated into four steps to determine the network security reliability transfer probability at the next moment.

4.2. WSM Security Threat Analysis Model Simulation Experiment. To facilitate the modeling, the following assumptions are made in this paper related to the network model properties of wireless sensor networks.

(a) All nodes deployed in the monitoring area are statically deployed, and the node locations can be moved at will

(b) Each node has a unique network-wide identification ID, and its residual energy and geographic coordinates are sensed

(c) All nonbase station nodes have the same energy at the initial moment, and the energy cannot be replenished

(d) Each node has the same storage, computing, and communication capabilities except for the base station

(e) The sensor nodes can dynamically adjust the node transmit power to accommodate different communication distance requirements

WSN is characterized by many sensor nodes and large network scale. It is usually deployed in an exposed external environment, so it is vulnerable to various forms of attacks. Authentication is the basis for ensuring network security. Traditional authentication mostly uses centralized authentication. Since the research proposal in this paper focuses on the hierarchical security model, a simple energy consumption model involving only communication is used here and does not consider the energy consumption of the nodes in the process of computing and storing data. The energy consumption of the node sending data is divided into two parts: RF transmitting consumption and signal amplifier consumption; the energy consumption of the node receiving data is only the consumption of the receiving circuit. Security is an important metric to evaluate the merits of a defense method, and this section analyzes the resistance to attacks of the proposed edge computing network attack active defense technique based on network topology mimetic correlation.

The attack method is a SYN flood for guided DoS attacks, and the average service response time of the network topology mimetic correlation system is tested under different SYN flood attack rates to reflect the service availability performance. Figure 5 shows the results showing that the network topology mimetic association strategy proposed in this paper can better resist DoS attacks because the network topology mimetic association technique dynamically measures network anomalies for the strength of network attacks and performs automatic adjustment of the network topology mimetic association graph and communication paths, which increases the path hitting difficulty of DDoS attacks. This is because when the network topology mimetic association graph space is squeezed to almost zero, the DDoS attack enters an unguided blind attack state; i.e., the attacker detects all nodes in the reachable paths and attacks them on average.

A comparison of the change in reputation value of different types of nodes in the network under the condition that no management node rotation is performed showed that the reputation value of normal nodes that are not under attack does not change significantly throughout the cycle and the node reputation value remains normal. When a node is subjected to intermittent attacks or random errors, the reputation value of the node decreases and this type of node is an abnormal node, but due to the low frequency of attacks or errors, it does not affect the normal communication of the node, and the reputation value of the node is maintained above 0.8. The security of the network completely relies on the certification center. Once the certification center is maliciously attacked, the entire certification system will collapse; when the network scale is expanded, the computing power and storage capacity of the certification center will be limited, which will affect the performance of the network; with the development of WSN, the topology of the network is ever-changing, and the flexibility of centralized authentication is not enough. When the node is

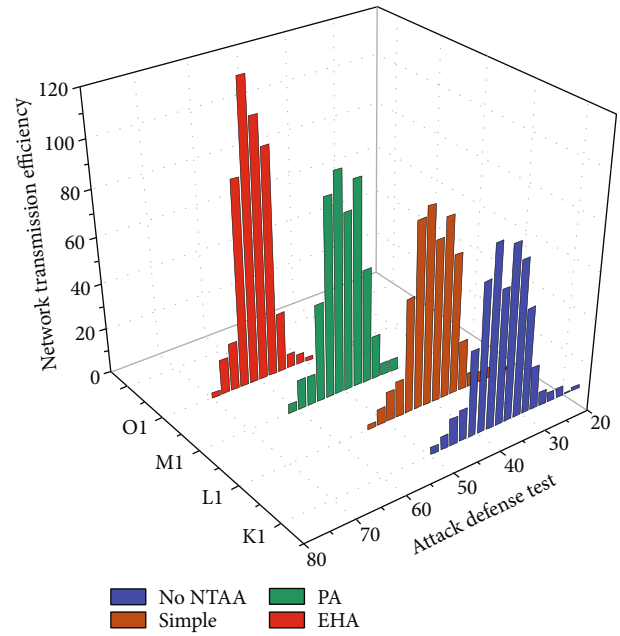

Figure 5: DOS attack defense test results.

under continuous uninterrupted attacks, after about 50 s, the node reputation value starts to drop exponentially and rapidly to below the threshold value of 0.2 and the node is cut out of the network.

In this section, with the help of TOSSM, a simulation tool for WSNs, the physical and link layer protocols of IEEE 802.15.4 are used and ACK/NACK is disabled to experimentally evaluate and compare the transmission performance of GCCT with existing typical protocols such as CTPII and SHMT0. The wireless channel uses a random erasure channel; i.e., the MAC layer discards the received packets with a certain probability, thereby generating Bernoulli-distributed packet loss. Simulation results (averaged over 100 simulations) are given below for end-to-end single data stream communication and many-to-one aggregated data stream communication, respectively.

For single-stream communication, the protocol performance is evaluated here in terms of 3 aspects: packet loss rate, node density, and transmission hops, where node density refers to the average number of neighboring nodes of the nodes in the network. Three metrics are used to evaluate the algorithm performance: (a) packet delivery success rate, i.e., the percentage of packets successfully received by the sink node from the source node; (b) transmission delay, i.e., the time used for packets to be received from the source node to the sink time; and (c) communication overhead, i.e., the total number of packets sent by the network nodes during transmission. In terms of energy balance, the first two schemes have some advantages and the number of nodes that die in the early stage is less; although Figure 6 shows that at 500 s the SCM scheme still has close to 100 nodes surviving, the experimental results show that due to the high energy consumption of the nodes in the early stage, most of the nodes are on the verge of death and at 530 s the nodes all die. In terms of node

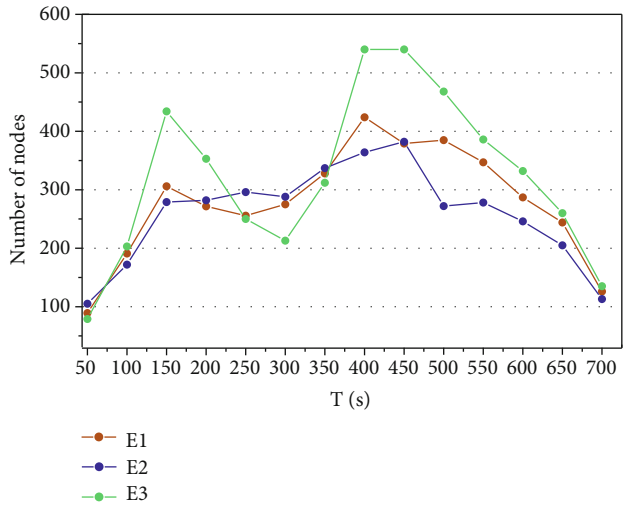

Figure 6: Comparison of the number of nodes surviving at different points in time.

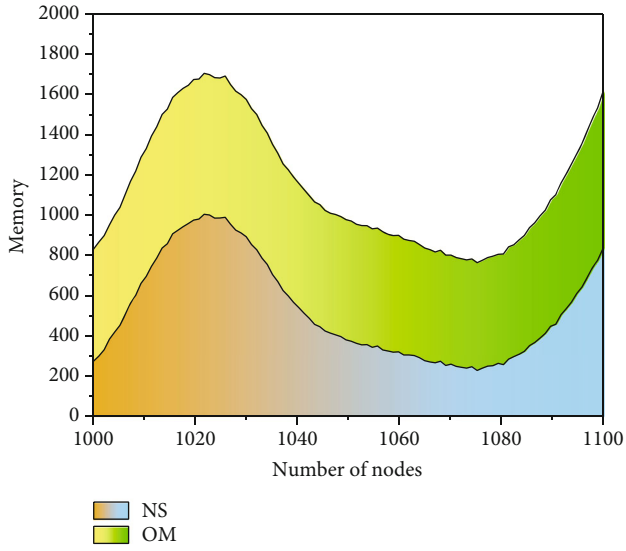

Figure 7: Simulation performance comparison.

survival time, the survival of nodes in this model is better than the first two scenarios in the later stage.

The comparison of the total energy consumed by the network with a capacity of 400 nodes over time shows that the initial energy of a single node in the network is set to 2 J and the total energy of the nodes in the network is 800 J. The comparison of this method with the SCM scheme and the improved LEACH protocol shows that the total energy consumed by the nodes in this model is significantly lower in 500 s of survival time. In terms of the remaining energy, the node energy in the SCM and LEACH schemes is depleted, while the total energy of the network in this model is about 25% remaining, mainly since the cluster head election is performed inside the subnet in this model, which reduces the energy consumption of communication with nodes at longer distances. The energy-saving effect will be more significant for wireless sensor networks deployed over large areas. The data collection unit is responsible for collecting and converting the information in the monitoring area; the data transmission unit mainly sends and receives the collected data information in the form of wireless communication. To establish a wireless sensor network environment, many sensors, a data transmission center, and a base station are required.

Under the same conditions, the performance of the two simulation platforms is compared mainly by their memory consumption through experiments with the improved LEACH protocol on NS-3 and WSPSim based on OMNeT++, and the performance comparison is shown in Figure 7. Therefore, this system is more advantageous for large-scale WSN.

This section improves the classical LEACH protocol by adding an MD5 hash encryption mechanism and trust evaluation mechanism, which is modeled and simulated by the functional modules already developed in this simulation platform. The simulation results are compared to verify the correctness of the module and the security of the improved protocol and verify that through simulation experiments, this platform can correctly simulate WSN-related protocols and algorithms and has good adaptiveness and ease of use compared to other simulation platforms.

5. Conclusion

The security of wireless sensor networks as an important carrier in the future era of the Internet of everything is becoming more prominent, and maintaining the security of wireless sensor networks is as important as human beings protecting their nervous system. By dividing the modules through a clustering analysis algorithm, the intelligent mechanism of "functional separation" of the cerebral cortex is introduced into the practice of a single neural network to solve the problems of oversized structure, high computational complexity, and weak interpretation in neural network problem processing engineering. A modular neural network-based feature combination recommendation model is designed to achieve the extraction of important features from sample data and help people make fast and accurate decisions. The experimental results show that the computational overhead of the RRCTM model is significantly reduced, and the RRCTM model is more accurate for the evaluation of trust values and has strong dynamic adaptivity and high sensitivity, which can effectively resist various malicious node attacks and ensure the security of wireless sensor networks. Some progress has been made in this research work, but there are still some security issues that need further research. The current studies have focused on the security of over-the-air data distribution based on network-coded data distribution protocols, neglecting the security management of the code image after it is received by the sensor nodes. If the new code image is an update about a military application code, its content is sensitive and special treatment of the code image is required to secure it. Thus, security mechanisms for the storage, use, and destruction of code images on sensor nodes will be investigated in the future.

Data Availability

The data used to support the findings of this study are available from the corresponding author upon request.

Conflicts of Interest

The author declares that he has no known competing financial interests or personal relationships that could have appeared to influence the work reported in this paper.

Acknowledgments

This work was supported by Shandong University of Finance and Economics.

References

[1] D. Sivaganesan, "A data driven trust mechanism based on blockchain in IoT sensor networks for detection and mitigation of attacks," *Journal of Trends in Computer Science and Smart Technology*, vol. 3, no. 1, pp. 59–69, 2021.

[2] A. Williams, P. Suler, and J. Vrbka, "Business process optimization, cognitive decision-making algorithms, and artificial intelligence data-driven internet of things systems in sustainable smart manufacturing," *Journal of Self-Governance and Management Economics*, vol. 8, no. 4, pp. 39–48, 2020.

[3] M. S. Munir, S. F. Abedin, N. H. Tran, and C. S. Hong, "When edge computing meets microgrid: a deep reinforcement learning approach," *IEEE Internet of Things Journal*, vol. 6, no. 5, pp. 7360–7374, 2019.

[4] A. Clark, "Big data-driven transportation planning and engineering: smart urbanism, autonomous vehicle algorithms, and network connectivity systems," *Contemporary Readings in Law and Social Justice*, vol. 12, no. 2, pp. 70–78, 2020.

[5] M. Mahmud, M. S. Kaiser, M. M. Rahman et al., "A brain-inspired trust management model to assure security in a cloud based IoT framework for neuroscience applications," *Cognitive Computation*, vol. 10, no. 5, pp. 864–873, 2018.

[6] S. Tripathi and S. De, "Data-driven optimizations in IoT: a new frontier of challenges and opportunities," *CSI Transactions on ICT*, vol. 7, no. 1, pp. 35–43, 2019.

[7] D. Watkins, "Real-time big data analytics, smart industrial value creation, and robotic wireless sensor networks in Internet of things-based decision support systems," *Economics, Management, and Financial Markets*, vol. 16, no. 1, pp. 31–41, 2021.

[8] W. Xu, Y. Xu, C. H. Lee, Z. Feng, P. Zhang, and J. Lin, "Data-cognition-empowered intelligent wireless networks: data, utilities, cognition brain, and architecture," *IEEE Wireless Communications*, vol. 25, no. 1, pp. 56–63, 2018.

[9] C. Morgan, "Can smart cities be environmentally sustainable? Urban big data analytics and the citizen-driven Internet of things," *Geopolitics, History, and International Relations*, vol. 12, no. 1, pp. 80–86, 2020.

[10] F. Shi, H. Ning, W. Huangfu et al., "Recent progress on the convergence of the Internet of things and artificial intelligence," *IEEE Network*, vol. 34, no. 5, pp. 8–15, 2020.

[11] I. Yaqoob, K. Salah, M. Uddin, R. Jayaraman, M. Omar, and M. Imran, "Blockchain for digital twins: recent advances and future research challenges," *IEEE Network*, vol. 34, no. 5, pp. 290–298, 2020.

[12] B. Hyman, Z. Alisha, and S. Gordon, "Secure controls for smart cities; applications in intelligent transportation systems and smart buildings," *International Journal of Science and Engineering Applications*, vol. 8, no. 6, pp. 167–171, 2019.

[13] Y. J. Qu, X. G. Ming, Z. W. Liu, X. Y. Zhang, and Z. T. Hou, "Smart manufacturing systems: state of the art and future trends," *The International Journal of Advanced Manufacturing Technology*, vol. 103, no. 9-12, pp. 3751–3768, 2019.

[14] A. Toma, A. Krayani, M. Farrukh et al., "AI-based abnormality detection at the PHY-layer of cognitive radio by learning generative models," *IEEE Transactions on Cognitive Communications and Networking*, vol. 6, no. 1, pp. 21–34, 2020.

[15] L. Yang, W. Li, M. Ghandehari, and G. Fortino, "People-centric cognitive Internet of things for the quantitative analysis of environmental exposure," *IEEE Internet of Things Journal*, vol. 5, no. 4, pp. 2353–2366, 2018.

[16] M. M. Hussain, M. S. Alam, and M. M. S. Beg, "Fog computing model for evolving smart transportation applications," *Fog and Edge Computing: Principles and Paradigms*, vol. 22, no. 4, pp. 347–372, 2019.

[17] F. Kong and Y. Wang, "Multimodal interface interaction design model based on dynamic augmented reality," *Multimedia Tools and Applications*, vol. 78, no. 4, pp. 4623–4653, 2019.

[18] Y. Liu, X. Ma, L. Shu, G. P. Hancke, and A. M. Abu-Mahfouz, "From Industry 4.0 to Agriculture 4.0: current status, enabling technologies, and research challenges," *IEEE Transactions on Industrial Informatics*, vol. 17, no. 6, pp. 4322–4334, 2021.

[19] W. Shi, W. N. Chen, Y. Lin, T. Gu, S. Kwong, and J. Zhang, "An adaptive estimation of distribution algorithm for multipolicy insurance investment planning," *IEEE Transactions on Evolutionary Computation*, vol. 23, no. 1, pp. 1–14, 2019.

[20] J. Keane, "Can self-driving cars lead to sustainability? Autonomous smart sensors, perception and planning algorithms, and data processing efficiency," *Contemporary Readings in Law and Social Justice*, vol. 12, no. 1, pp. 9–15, 2020.

[21] C. Zhou, B. Hu, Y. Shi, Y. C. Tian, X. Li, and Y. Zhao, "A unified architectural approach for cyberattack-resilient industrial control systems," *Proceedings of the IEEE*, vol. 109, no. 4, pp. 517–541, 2021.

Hindawi
Journal of Sensors
Volume 2022, Article ID 6232267, 12 pages
https://doi.org/10.1155/2022/6232267

Research Article

Optimization of a Wireless Sensor-Based Tennis Motion Pattern Recognition System

Haoxuan Ruan[1] **and Xinchen Zhang**[2]

[1]*Institute of Sports and Health, Tianjin University of Sport, Tianjin 301617, China*
[2]*Department of Sociology, Yeungnam University, Gyeongsan, Gyeongsangbuk 38541, Republic of Korea*

Correspondence should be addressed to Haoxuan Ruan; ruanhaoxuan@tjus.edu.cn

Received 11 November 2021; Revised 17 December 2021; Accepted 6 January 2022; Published 27 January 2022

Academic Editor: Gengxin Sun

With the rapid development of information technology in today's era, the application of the Internet, big data, and smart bracelet information technology in the field of sports has enhanced the intelligence of sports and plays an important role in promoting sports performance. This paper focuses on the application of wireless sensors in the field of tennis, using research methods such as literature research, video analysis, comparative research, and mathematical statistics, to explore and analyze the application of wireless sensors in the field of tennis big data, tennis robotics, and the implementation of tennis teaching and training, to provide a theoretical basis for promoting the application of wireless sensors in the field of tennis and also for the broader application of wireless sensors in sports to provide a theoretical reference. For the problem of multiple scales of motion targets in action videos, two video action recognition methods based on high- and low-level feature fusion are proposed, which are the video action recognition methods based on top-down feature fusion and the video action recognition methods based on bottom-up feature fusion. The multipowered mobile anchor nodes are allowed to move along a prescribed route and broadcast multiple power signals, and then, the location of the unknown node is estimated using a four-ball intersection weight center-of-mass algorithm. Simulations show experimentally that the algorithm reduces the average localization error and requires fewer anchor nodes.

1. Introduction

The wireless sensor network is one of the hot spots of rapid development in recent years; it combines the sensor field, wireless communication field, computer field, and a large number of other different fields of advanced technology and constantly developed into a new field of integrated technology. Many tiny low-power nodes constitute the wireless sensor network; tiny nodes can monitor complex external information in real time and transmit the monitoring results to the embedded system and after the system processing, by sending to the user terminal, so that these nodes can intelligently sense the outside world. However, these nodes can locate themselves in addition to sensing information such as temperature, humidity, and light intensity. Using this property, wireless sensor network technology quickly entered the wireless communication industry, giving rise to many new technologies and applications that have attracted widespread attention worldwide [1]. The heavy use of sensors requires lower cost, better scalability, and more power savings than traditional technologies. Motion analysis allows one to learn the motion patterns of target objects and use them for analytical modeling. For example, in the field of medical rehabilitation, remote monitoring networks can be established for patients to enhance the monitoring of their behavior and thus provide timely feedback on medical data, while in the field of ergonomics it can also provide sufficiently accurate human posture data for research; in the field of sports, motion analytics can be used to simulate training, record athletes' movement data, and compare it with quasi-templates to generate corrective information for reference; in the entertainment industry, motion analysis technology is used in 3D graphics production to restore the movement of the target object, which can lead to lifelike character

modeling. In addition, distributed sensor architectures for motion capture can be installed on different mechanical devices, thus offering the possibility of achieving intelligent interaction [2].

Wireless sensor networks, as one of the important technologies for the new Internet of Things (IoT), have become the communication hub of society with their efficient, fast, and comprehensive features. The popularity of IoT has led to the rapid development of the wireless communication industry and the ubiquity of sensor networks. Compared to traditional technologies, the massive use of sensors demands low cost, good scalability, and more energy-efficient power consumption. WSN is usually a unified joint system consisting of communication, microelectronics, semiconductor, and embedded computer technologies. The ability of WSNs to reconfigure intelligently and dynamically allows them to collect and process the information sent by the nodes in large quantities and transmit it to the control center, which is the user terminal [3]. In this paper, around the theme of wireless sensors in the field of tennis, we use literature research, video analysis, comparative research, and mathematical statistics to explore and analyze the implementation of wireless sensors in tennis big data, tennis robotics, and tennis teaching and training approaches, to provide a theoretical basis for promoting the application of wireless sensors in the field of tennis and also to provide broader applications to provide theoretical references [4].

2. Related Work

The development of video action recognition methods relies on the progress of fundamental research on video representation learning. Video representation can be divided into two aspects, manual feature representation and deep feature representation. The dense trajectory method (DT) was proposed in the literature [5] and applied to the video action recognition task. The basic idea of the dense trajectory method is to first use the optical flow field to obtain the trajectory in the video sequence, then extract motion descriptors HOF, HOG, MBH, and trajectory features along the trajectory, then encode the features using the Fisher Vector method, and finally train the SVM classifier based on the encoding results to give recognition results. An improved version of the dense trajectory method (IDT) is proposed in the literature [6]. IDT uses the SURF matching algorithm to match the key points of the optical flow between two frames before and after the video to attenuate the effect of camera motion on the video content and becomes the most effective method among traditional video motion recognition methods. Manual features mainly characterize low-level visual information, underrepresent high-level semantic information, and have the disadvantage of difficulty in handling large amounts of data and unsatisfactory recognition accuracy. To solve this problem, the literature [7] proposes the concept of intermediate-level features, which represent behavioral features through a set of action attributes learned from the training dataset, which is referred to as an intermediate concept in the paper. The literature [8] uses motion phrases and motion atoms to represent the features of actions in videos. For high-level feature representation, the literature [9] uses an ordering function to model the evolution of motion over time. To better capture spatiotemporal information, literature [10] uses hidden Markov models to capture temporal information in videos and uses fixed dimensional vectors as descriptors of motion videos. The literature [11] uses a structural trajectory learning approach to extract relevant motion features.

The four methods based on ranging localization are angular arrival, timely arrival, time difference arrival, and received signal strength indication; AOA uses the angular relationship between two anchor nodes concerning the unknown node for localization, TOA and TDOA use the product of signal propagation time and propagation speed to calculate the distance, and trilateral localization or great likelihood estimation becomes the method to estimate the coordinates in the latter step. RSSI uses the received signal strength to measure the distance and then the base positioning method to achieve positioning. The main ones that are not based on ranging are the DV-HOP localization algorithm, APIT, center-of-mass localization, MDS-MAP, and amorphous localization: amorphous uses network connectivity as a basis for calculation. In indoor localization by WSN, the literature [12] can detect a single intruder through Wi-Fi devices with a high detection rate and small false-positive results; mobile anchor nodes can plan the path to achieve high coverage and are more flexible than static anchor nodes and do not depend on the topology of the network. The literature [13] proposes adaptive framework structures thus detecting variable speed objects in indoor environments. The authors conducted a series of experiments to learn empirically the effect of different speeds on localization accuracy and thus improve the accuracy of localization at different speeds. A novel indoor passive localization system in a wireless environment is proposed in the literature [14]. It provides low overhead and accurate and robust motion detection and gives tracking capability, using coordinates of different unknown nodes with the same anchor node to construct a new coordinate system to calculate the distance and then using trilateral localization for localization of nodes, which cleverly simplifies a large number of calculations using the coordinate method. In the literature [15], large-scale indoor passive localization and tracking are proposed. Although it has relatively high localization accuracy under multipath effect, the literature [2] better describes the localization classification model for passive localization, improves the quality of the dataset, and reduces the error caused by the multipath effect; mostly, the distance between the anchor node and unknown node is estimated by network connectivity, information passed between nodes, etc.; the accuracy is not very high, but it does not need to carry extra equipment so the cost is low and the power consumption is relatively low. The literature [16] proposes three passive indoor localization methods and discusses the effect of multiple targets on the results. Once the packet enters that grid, it is forwarded to the grid head node which also becomes the phantom source. If no node exists in the grid where the random location is located, the head node of the grid where the node that last cached the packet is located will become the phantom source.

3. Optimization of a Wireless Sensor-Based Tennis Motion Pattern Recognition System

3.1. Node Localization Algorithm for Wireless Sensor Networks. Wireless sensor network node localization algorithms can usually be divided into two categories: range-based localization algorithms and range-free localization algorithms. Range-based algorithms use geometric relationships to derive node unknowns by measuring the wireless signal angle or propagation time between the unknown node and the signal transmitting node. The measured information includes received signal strength, signal arrival time, signal arrival time difference, and signal arrival angle. These algorithms usually require the deployment of special components to obtain these variables and improve the localization accuracy by taking multiple measurements, resulting in incurring higher deployment costs. In contrast, range-free localization algorithms require only information about the anchor node and network connectivity and thus are cheaper to deploy and require no additional hardware support but have limited localization accuracy. The fingerprint localization algorithm belongs to the range-free localization algorithm, which requires several anchor nodes and reference nodes with fixed locations to be predeployed in the localization area. The anchor nodes continuously transmit wireless signals with rated power, and the signal RSS (Really Simple Syndication) of each anchor node is measured at each reference node location. The individual reference node locations and their measured RSS form a location fingerprint or fingerprint for short. The unknown node also measures the RSS of each anchor node and pattern matches it with the existing fingerprint to determine the node location. Fingerprint location algorithms not only are cheap to deploy but also have more accurate localization performance in complex and variable propagation environments, such as multipath and NLOS environments, and thus have been widely studied and applied in recent years.

Such algorithms use network-wide connectivity information to make location decisions. One of the best-known algorithms is DV-hop. This algorithm has distance vector routing at its core, where each anchor node broadcasts a beacon message containing its location coordinates. The initial value of the number of hops in the beacon is 1, and 1 is added for each node passed. When beacons from multiple anchor nodes are transmitted in the network, each node on the transmission path records the minimum number of hops for each anchor node. Due to the diversity of action modes covered in the set, the energy base of each action varies, and even the magnitude difference between different performers under the same type of action is huge, so it is unrealistic to use a constant value as a threshold to complete the interception of all actions. Therefore, it is necessary to propose a threshold determination scheme with self-adaptive capability. In an isotropic sensing network, the single-hop physical distance of the signal is approximately the same in all directions. Unknown nodes estimate the distance to each anchor node based on the number of hops. However, in complex networks, the presence of interference and other factors lead to large differences in the single-hop distances in each direction, making it difficult to achieve precise positioning, as in Figure 1 bit wireless sensor network node localization process.

Fingerprint localization is a localization algorithm that has gained more attention among the range-free localization algorithms. A certain number of anchor nodes are deployed in the localization area with a fixed location and known coordinates with the signal transmitting function. The sensor nodes measure the wireless signal strength RSS of each anchor node. The measured HSS value and the position coordinates of that node are called the signal fingerprint of that position. The fingerprint localization approach does not derive the node location based on RSS and distance equations but rather fuses RSS with the anchor node approximation algorithm to derive the sensor node location. The fingerprint localization algorithm requires a fingerprint database in the localization space, i.e., the location coordinates of each point in the space are linked to the RSS information of different anchor nodes at that location. The fingerprint localization process is to convert the RSS information received by the unknown node into location information based on the fingerprint and location relationship information in the fingerprint database. The process of converting RSS into a target location is known as fingerprint matching and fingerprint localization. Fingerprint localization can also be described as a multiple hypothesis testing problem, where the best hypothesis (location of the target) is deduced based on the preobtained observations (i.e., fingerprints). The fingerprint localization process can also be considered a decision process, where the decision target is the unknown node location based on the information available (fingerprint database) and the RSS measured by the unknown node. The fingerprint localization algorithm requires two phases: an offline measurement phase and an online localization phase:

$$P(\theta \mid k) = \frac{\int \alpha \cdot (\theta - \mu)/\sigma d\theta}{kr}. \tag{1}$$

Figure 2 shows the basic process of fingerprint localization. In the offline measurement phase, firstly, a certain number of reference nodes are laid out in the current localization environment and the location coordinates of all reference points are recorded. Usually, the reference nodes are laid out in a grid-like manner, and the reference nodes can be either physical or virtual nodes. Then, the RSS values of each anchor node are measured and collected in some way at all reference nodes, called raw observation data, or samples. Due to the inevitable signal interference in the localization area, the RSS measurements are subject to errors and certain methods are needed to preprocess the samples. The preprocessed RSS data and the coordinates of the reference node establish a correspondence to form a fingerprint database. In the online localization phase, the target node measures the RSS value of each anchor node at its location and sends it to the backend localization service. The localization algorithm matches this RSS value with all samples of the fingerprint database according to the set algorithm and finds one or more reference nodes with the highest matching

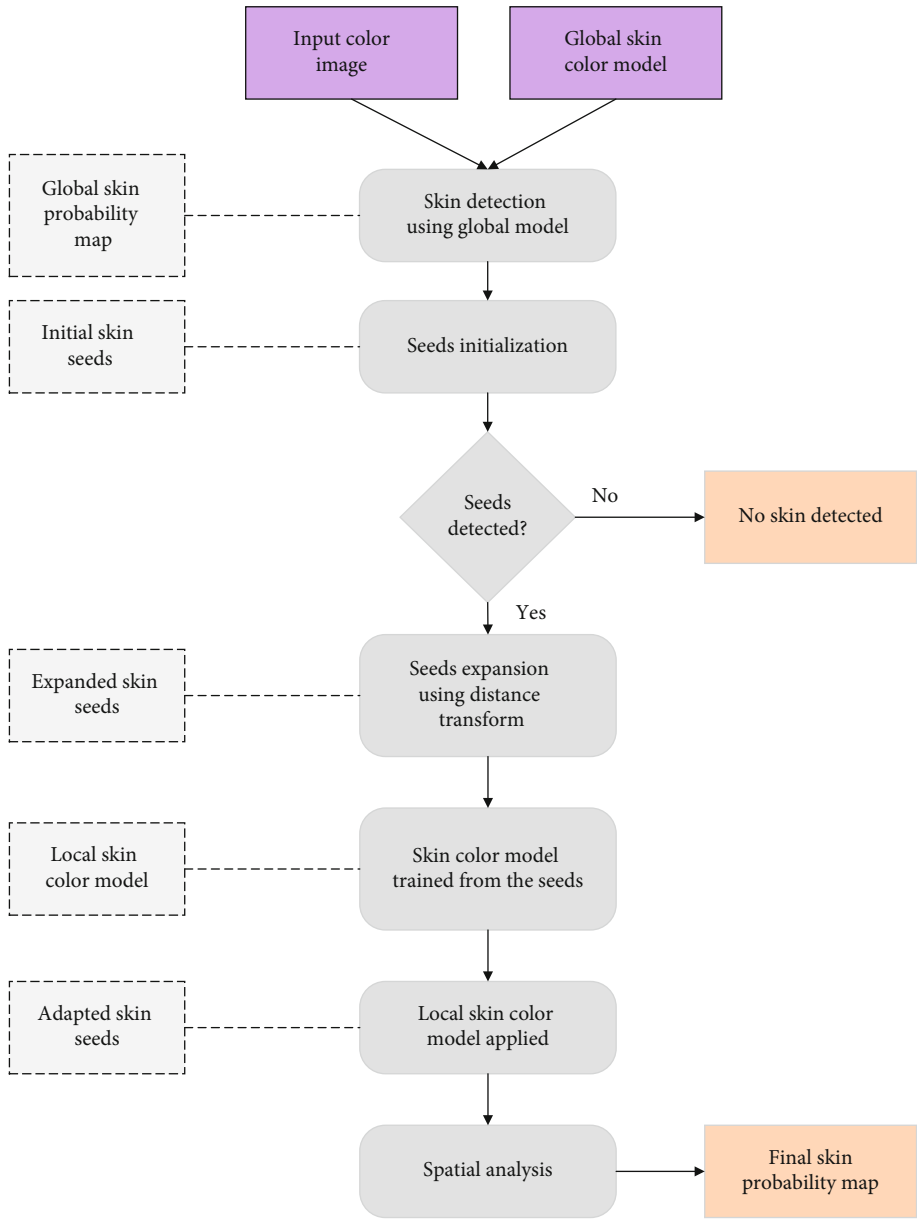

Figure 1: Flowchart of wireless sensor network node localization.

degree. Finally, these reference point location coordinates are converted to the location corresponding to the target node according to the characteristic algorithm, i.e., the location estimate of the target node.

In a fixed localization environment, RSS samples usually obey some probability distribution. This is usually described using a joint probability distribution and assuming that the RSS of each anchor node measured by the reference node is independent of each other and does not interact with each other, using the product of the edge distributions of the RSS as the joint distribution. A common data form is the basis for sharing research results. This paper gives a common inertial device standard, motion recording scheme, and data storage form and establishes a simple error calibration scheme for MEMS devices in motion capture application scenarios and a data cleaning method for the low automation of the data acquisition process. The RSS vector measured by the unknown node is set, the probability of getting this vector at each reference node is obtained, and the reference node with the highest probability is selected as the estimated location. Probabilistic algorithms are mainly based on Bayesian theory, or Bayesian combined with clustering algorithms, to calculate the location estimate of the unknown node on the posterior probability of the unknown node. Plain Bayes, hidden Bayes, Bayesian networks, and maximum likelihood estimation are also widely used methods. The process of node localization based on RSS fingerprinting is usually divided into two phases: an offline measurement phase and an online localization phase. In offline measurement, the RSS data of the anchor node is measured at multiple reference nodes to build a fingerprint database.

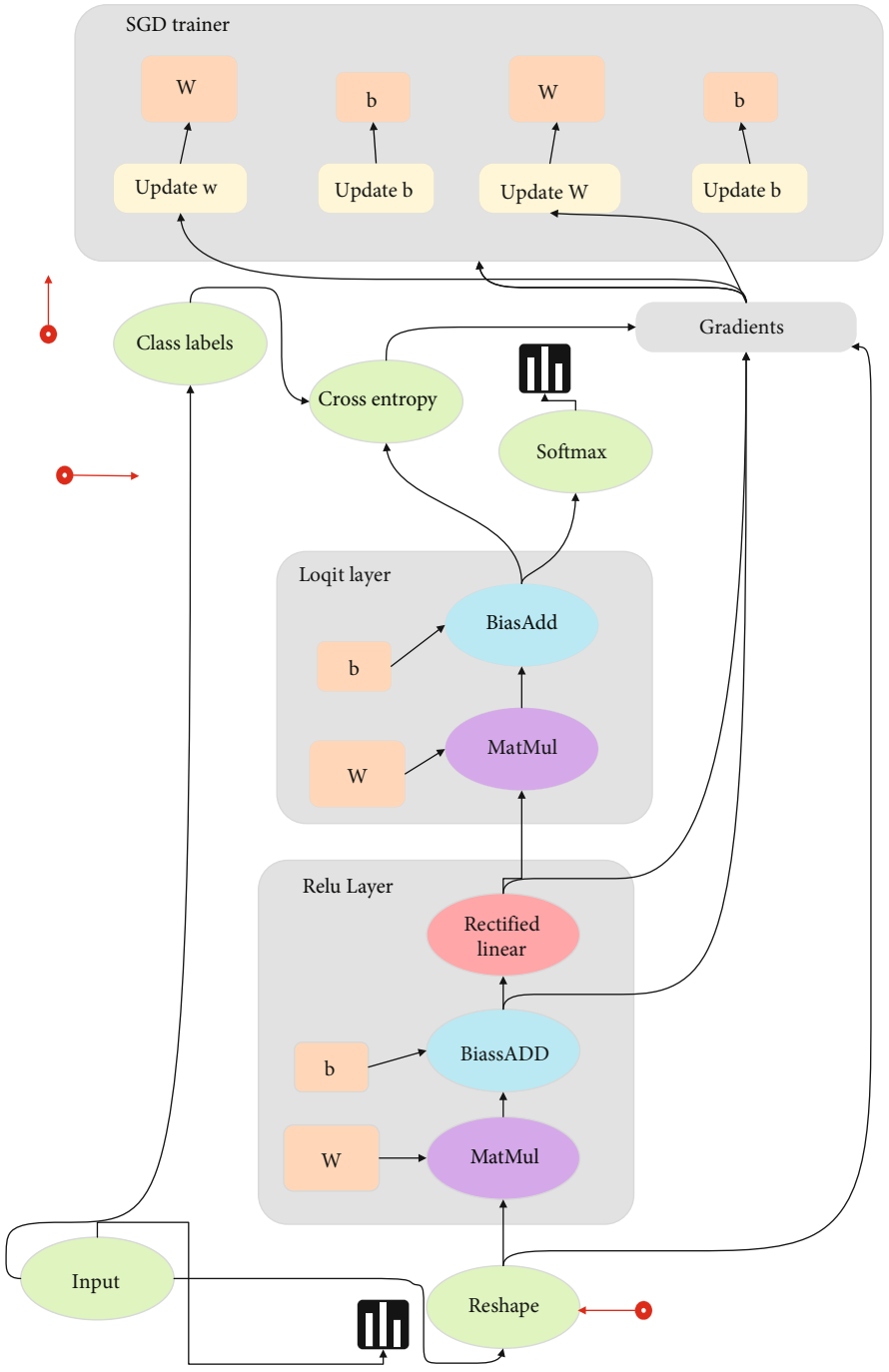

Figure 2: Fingerprint location process.

Since environmental noise and obstacles interfere with the wireless signal propagation, it is also necessary to remove the noise in the fingerprint database using statistics, filtering, and fitting; in the online measurement phase, the location of the unknown node is estimated by matching the RSS data collected from the unknown node with the fingerprint database. Therefore, the research of fingerprint localization algorithms mainly includes two aspects: enhancing fingerprint data accuracy and improving localization accuracy.

3.2. Wireless Sensor-Based Algorithm for Tennis Motion Pattern Recognition. The fundamental research in the field of tennis motion analysis can be divided into two directions: namely, motion analysis based on the pose layer and analysis based on the action primitive layer, the essential difference being whether the extraction of data meaning is more focused on positional or velocity information. We can know that tennis sports actions from two perspectives. One way of thinking is to consider it as a continuous-time sequence, i.e., the body joints complete a spatial displacement, then the

velocity information of the point movement can be a complete response to the movement. The other idea is to consider the serving action as a segment of motion with wrist force and posture change, then we can achieve the recognition of a segment of motion by keeping continuous detection of body posture. The two ideas focus on different motion information; the first idea is more concerned about the absolute motion of space differential information; if you use the video capture scheme, you need to extract the spatiotemporal motion trajectory of the moving target and then only through the position information interest inverse calculation of the speed information, resulting in the calculation accuracy being seriously limited by the number of frames shot and a large amount of calculation. The inertial motion sensor can be worn to directly capture the velocity information of the moving object, and the video capture does not have the advantage in this scheme. The second idea is more concerned about the location of the target point information; using the video program is roughly the data processing process: first from a single frame image to extract the relative position of the target feature points and then compared with the standard template to determine the former human pose, and for the inertial sensor program, the need to use inertial navigation integration algorithm from the device output to measure the location of the target point and posture information, so the integration of inertial data. The accuracy of the operation determines the feasibility of the scheme, which is also the core focus of almost all inertial guidance research.

The wireless sensor network is a combination of four components which are sensor nodes, aggregation nodes, mobile communication network, and task management desk. The sensor nodes are mainly placed in the monitoring area and are responsible for the collection of the required information, such as temperature and humidity. There are a small number of anchor nodes carrying self-locating hardware and a large number of unknown nodes whose locations are not known in advance. The main role of the aggregation nodes is to gather the information propagated from the nodes in the monitoring area and then deliver it to the higher level, similar to the role of a gateway. The mobile communication network is mainly responsible for carrying the transmission of information. Usually, the reference nodes are laid out in a grid-like pattern, and the reference nodes can be physical nodes or virtual nodes. Then, the RSS value of each anchor node is measured and collected in some way at all reference nodes, which is called raw observation data or called sample. The task management desk is mainly responsible for processing the collected information for use in higher-level applications.

From a mathematical point of view, an important issue that must be considered in algorithm selection is the trade-off between bias and variance. Classification models with high bias have a high error rate in prediction, while models with high variance will perform erratically across different datasets. Bias and variance are defined in statistics as follows: bias describes the difference between the predicted value and the true value as shown in

$$I^{\alpha}f(\eta) = m(z)(i\omega)^{\alpha}f(\omega) = |\omega|^{\alpha}e^{i2\pi\alpha}f(\omega). \tag{2}$$

Variance describes the instability of the model predictions themselves as shown in

$$Rf(x) = \int\int g(t)dt = \left(\frac{1+\gamma}{n}\right)\cdot\sum(x-1)f(t). \tag{3}$$

Ideally, with an infinitely large sample size of training data and a model algorithm that tends to be perfect, we could obtain models with small bias and variance, but in real engineering problems, this ideal situation does not often exist. Learning algorithms with low bias values tend to be more "flexible" and respond to the higher complexity of the model, thus being able to fit the data very accurately. The feature space is divided into two, with positive and negative classes on each side of the plane, and the specific classification decision function is as follows:

$$R^{m}f(x) = \int\int g(t)dt = \left(\frac{m+\gamma}{n}\right)\cdot\sum\left(x^{m}-t^{m-1}\right)f(t). \tag{4}$$

For linearly differentiable problems, the sample points in T that are closest to (w, b) are called support vectors, and they are mathematically characterized in such a way that equation (5) holds

$$L^{n}_{R-D}f(x) = \frac{1}{\eta(\alpha)}\int\int(x-\eta)^{\alpha}g(\eta)d\eta. \tag{5}$$

Since the coverage of node M_i contains the intersection A, we have

$$Mi = \begin{vmatrix} A\cdot\sin u\cos x & I_n\cdot\cos\gamma \\ I_m\cdot\sin\gamma & -\sin y \end{vmatrix}. \tag{6}$$

In the process of covering the void repair, the void is not split if the NNICI generated by all nodes in the set of the mobile nodes and the void boundary nodes that make up the covering void is not more than 2, based on the guarantee that the void inferior arc of the driving node is completely covered, with

$$\overline{v_i} = \frac{\delta x}{\delta t}\left(\frac{n!}{r!(n-r)!}x^{\gamma}+\mu\right). \tag{7}$$

The input signal is computed in the network in a forward direction: the very front of the network is the input, where each input sample corresponds to a definite known ideal output, while at the output at the very end of the network, the error information is formed between the predicted value and the ideal value, while the gradient information of the error signal can be passed backward from back to front according to the chain rule. At the end of a round of iterations, the new prediction results in an error value whose gradient information is fed back to the layers of the network

through the reverse conduction law, and the parameter values of each neuron will be corrected based on the error gradient according to the established update strategy. This cycle is repeated until the network reaches the accuracy index.

Since the professional basic action division in the tennis field has less ambiguity arising, it can be presumed that the similarity between feature vectors of similar actions is high and the clustering effect of action features is more obvious, i.e., the linear differentiability of the dataset is high. Definitely, the training data sample size is infinitely large, the model algorithm tends to be perfect, and we can obtain models with small bias and variance; however, in real engineering problems, this ideal situation often does not exist. Learning algorithms with low bias values tends to be more "flexible," responding to the higher complexity of the model and thus being able to fit the data very accurately. However, overly flexible learning algorithms will fit different training sets in completely different ways, resulting in higher variance values as well. This phenomenon is often also referred to as overfitting: that is, models that use too many parameters can bring the loss function values down to very low during training but instead have a higher error rate when predicting new samples.

Figure 3 shows the comparison diagram of action recognition process under traditional machine learning algorithm and deep learning algorithm, from which it can be found that compared with the traditional machine learning algorithm which requires a lot of manual feature extraction work, the deep learning algorithm often takes the original data as input directly, extracts the abstract features of the data layer by layer through the hierarchical structure of the network, and finally realizes the mapping to the target output. From the input of raw data to the acquisition of the task target, deep learning automatically completes the integrated work of feature representation, feature selection, and model learning.

The first step in a sports analysis study is to break down the underlying movements for the specific sport in the context of the project. This part often requires a combination of expertise in the field of sport. The most famous application of this aspect is the Laban dance score, which laid the foundation of human kinetics and was one of the first cases of using computer notation to record human movement and analyze it logically. The greater the continuity of movement and the greater the degree of freedom of the limbs, the more difficult it is to disassemble. Ideally, with an infinitely large sample size of training data and a near-perfect modeling algorithm, we could obtain a model with very small bias and variance, but in real engineering problems, this ideal situation does not often exist. Learning algorithms with low bias values tend to be more "flexible," responding to the complexity of the model and thus being able to fit the data very accurately. The vast majority of sports in the matter are far less difficult to disassemble than dance, so there is a well-established system of disassembling basic movements in the field of their teaching long ago. Under the premise of focusing only on the geometric nature of the movement, the human body can be reduced to a skeleton model, while completely ignoring muscle movement, trunk movements can mostly be described more accurately with a combined rigid body model, and only movements that are suitable for rigid-body modeling expression and more concerned with the movement process are suitable for the inertial analysis scheme. Under the rigid body kinematic model, inertial data is the most natural and suitable data for quantitative analysis of human movement form.

3.3. Experimental Verification and Conclusion. The application of human action data collected by inertial sensors to action recognition, whether online or offline, is a pattern recognition process; we can summarize the overall process specification as follows: first for the modeling of the motion background, to complete the basic action classification system, followed by the design of the acquisition and tagging scheme, in addition to recording the inertial data of each action sample, which must also record the matching action tags, in addition to using inertial motion capture devices to capture human body information, it is necessary to ensure that the devices have a certain accuracy and sampling rate to reflect the real action situation as realistically as possible. The specific capture device is called an inertial measurement unit, which captures the linear acceleration signal of the movement through an accelerometer, the rotation rate of the movement through a gyroscope, and in some cases a magnetometer for heading reference. A typical configuration has a single-axis accelerometer, gyroscope, and magnetometer on each of the three airframe axes (pitch, roll, and yaw). The three-axis IMU allows for the complete recording of point motion information at fixed parts of the body. In this way, the inertial sensor converts the rich and complex motion information into a finite-dimensional digital signal. Figure 4 illustrates the inertial data for two types of action examples in the tennis action dataset collected in this experiment, and observation of the above figure reveals that very little information can be obtained from the action curves. From a cognitive point of view, there is no intuitive connection between the curves and the specific "forehand lunge" and "forehand serve high" movements, although the raw signals collected by the inertial sensors are a faithful record of the real movements, which are complete and comprehensive enough. Some studies in motion modeling have shown that motion reduction can be achieved with inertial data. But the sensor data does not directly reflect the properties of the tennis action. A clear correspondence between it and the actual motion cannot be easily established at the human cognitive level; in other words, the correspondence between the raw data and the actual problem is difficult to understand, especially for algorithmic models that are less intelligent than humans.

The determination of the threshold parameters is at the heart of the interception algorithm. Due to the diversity of action modes covered in the collection, the energy base of each action varies, and even the magnitude difference between different performers under the same class of actions is huge, so it is not practical to use a constant value as the threshold to complete the interception of all actions. The equipment mounting solution of fixing the measurement

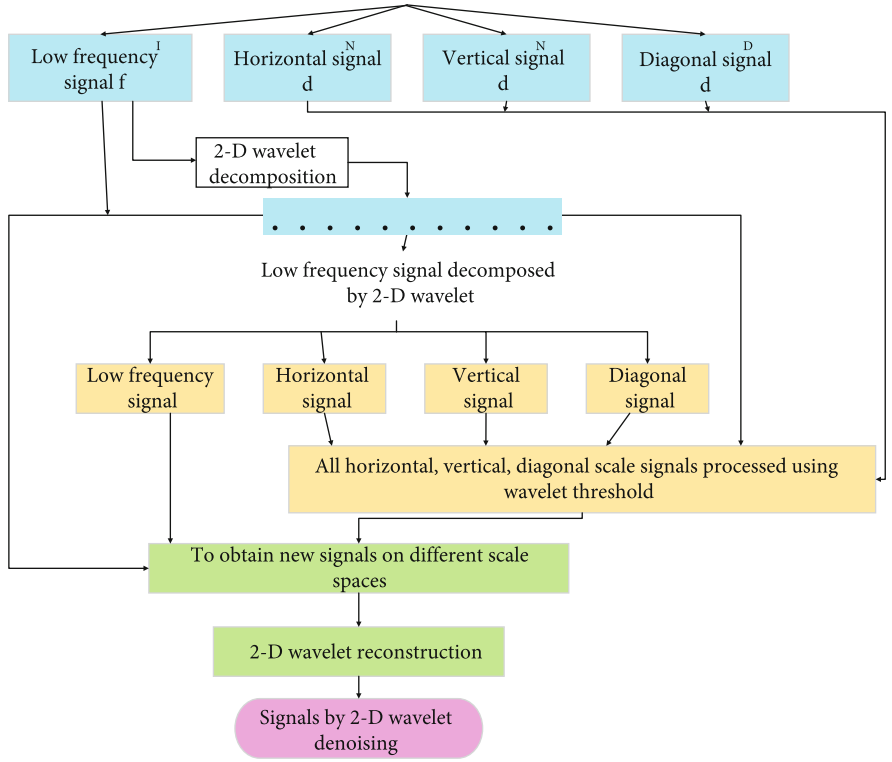

Figure 3: Comparison of action recognition process under traditional supervised learning and deep learning.

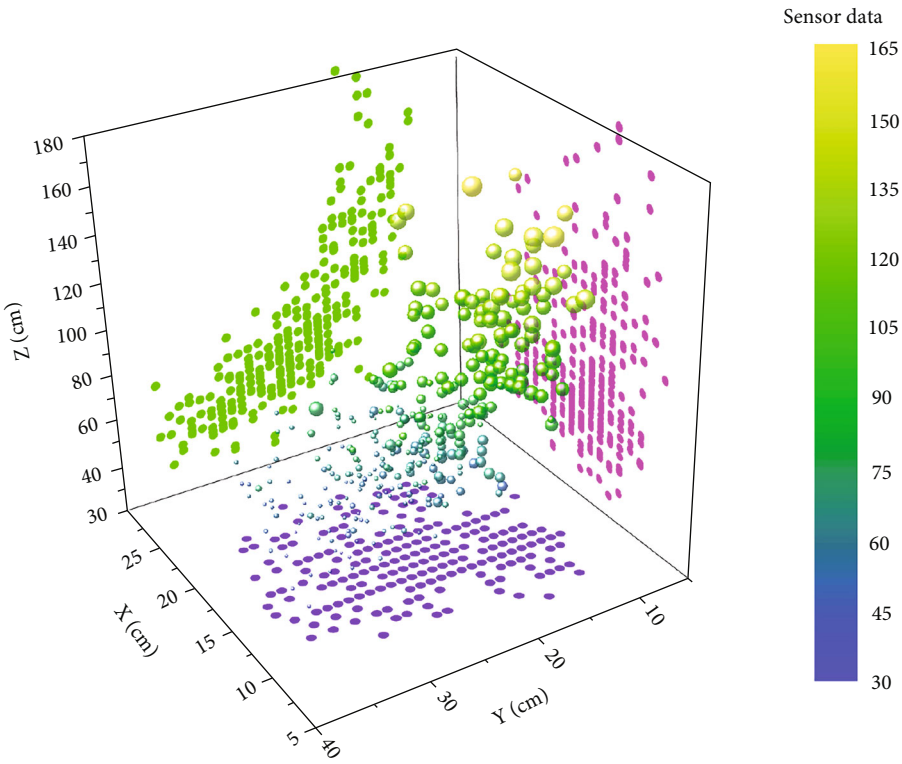

Figure 4: Raw inertial sensor data plot.

device to the sports equipment, while minimizing the obstruction to the collector's movement, can also lead to the resulting tennis action dataset not being sensitive enough to the distinction between grip styles, and based on this situation, mounting the motion acquisition equipment set on different sides of the racket is a viable solution. So, a

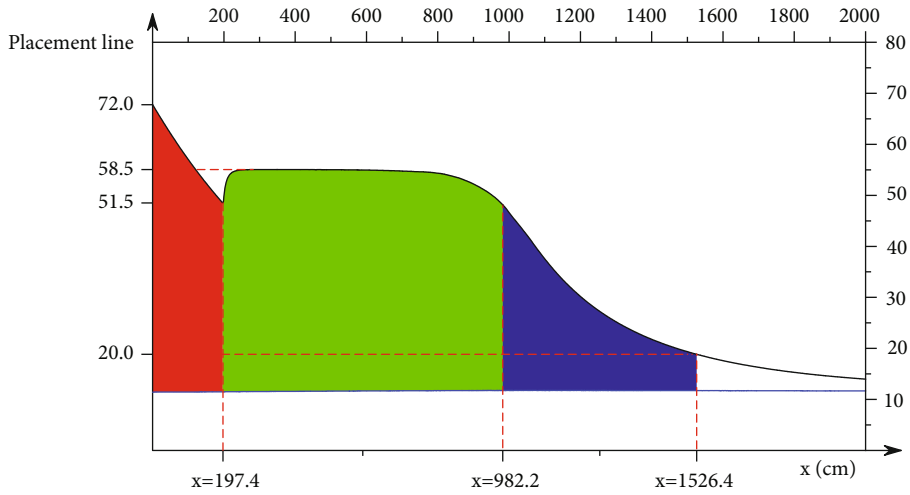

Figure 5: Gyroscope data energy curve.

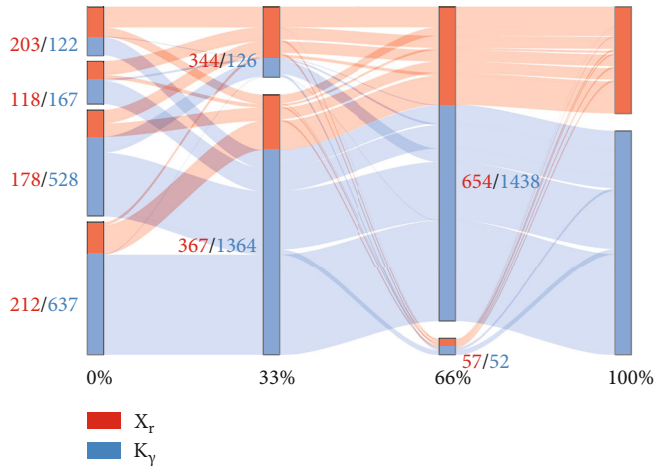

Figure 6: Schematic diagram of the variation pattern of quantile values.

threshold determination scheme with adaptive capability needs to be proposed. First, observe the gyroscope data energy profile for a sample action as shown in Figure 5. A series of quantile arrays are calculated for the energy sequence (before smoothing), and the quantile lines at different percentiles are plotted, from which it can be found that the distribution of energy values for a segment of the action is mainly concentrated in the smooth segment of the action, the reason being that the action signal in this segment is mainly caused by random body jitter of the wearer and the degree of fluctuation of the data points is high.

The experimental hypothesis for the variation pattern of the quantile values is that the quantile values increase dramatically at the beginning of the action segment. To confirm this hypothesis, the variation curves of the quantile values and their difference curves were plotted for uniform increases of X_r values from 1% to 100% as shown in Figure 6. By the experiment, it can be observed that there is a steep increase in the quantile values near 50%. Substituting the quantile values at this point into the inertial data plot to do the verification basically matches with the starting and ending thresholds of the data, and the pattern is verified on the data of other kinds of actions. The particular quantile point obtained throughout the hypothetical process experiment was then referred to as the maximized group clustering quantile value, in the sense that it maximizes the concentration effect of the low-amplitude motion segment and continues to increase the quantile increasing the spacing between quantile values significantly. The mathematical determination method of maximizing the cluster clustering quantile value not only requires first plotting the quantile value change curve but also requires the minimization of the squared difference as the objective function for the line fitting and taking its inflection point, and such a calculation process is undoubtedly very complicated in practical application.

The number of anchor nodes is the number of attributes in the localization decision. The anchor node ratio is the ratio of the number of anchor nodes to the total number of nodes in the localization area. Adjusting the anchor node ratio will affect the localization performance. Increasing the ratio of anchor nodes will increase the deployment cost. Therefore, the performance of the proposed algorithm with different anchor node ratios is simulated to find the best value that meets the localization accuracy requirements and saves energy. In performing the simulation, three neural

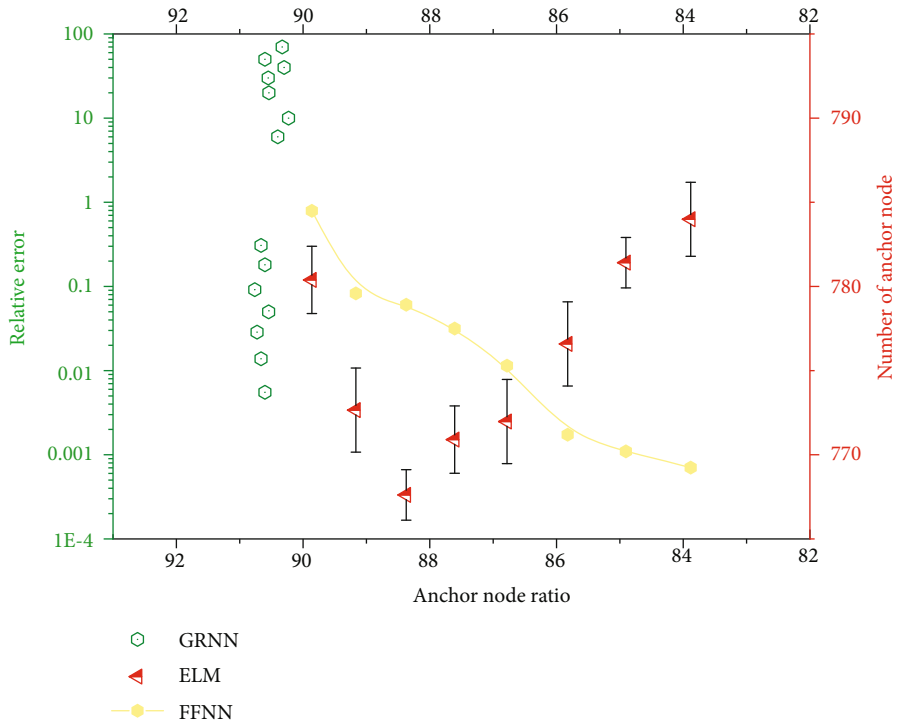

Figure 7: RLE of different algorithms with different anchor node ratios.

network-based localization algorithms, GRNN, FFNN, and ELM, are selected as the comparison algorithms. As can be seen in Figure 7, the RLE of all four localization algorithms in different localization areas decreases as the proportion of anchor nodes increases. With the transition from underground parking lots and indoor office areas to relatively less crowded areas such as campus roads and open activity areas, the reduction in crowd density reduces electromagnetic interference and small-scale fading in the surrounding environment, leading to a decrease in the RLE of all algorithms. From the figure, it can be seen that the relative localization error of the algorithm in this paper is the smallest, which is better than the three comparison algorithms and shows a stable decreasing trend in different regions. It indicates that the algorithm in this paper has the best localization performance; GRNN is slightly inferior, while ELM and FFNN have the worst performance.

In a multiarea localization scenario, the population density and geographic location of buildings affect the ambient noise level in the localization space, while the localization performance of the algorithm varies with the noise standard deviation. A larger noise standard deviation indicates a more disturbing environment and a harsher wireless environment in which it is located. To verify the adaptability of the localization algorithm to different regions in the localization space and the robustness to environmental interference, the variation of RLE with noise standard deviation in different regions is simulated. The simulation results are shown in Figure 8. In the four localization regions, the RLE of all four algorithms increases more significantly with the increase of the noise standard deviation. From the figure, it can be seen that the relative error of the FFNN algorithm fluctuates the most in the four regions, and the rising trend is more obvious. The localization error of the ELM algorithm also increases rapidly with the increase of noise standard deviations, especially in the underground sports field and the open region where the stability is poor. In contrast, the relative localization error (RLE) of the GRNN algorithm and the algorithm in this paper grows steadily. The RLE of the

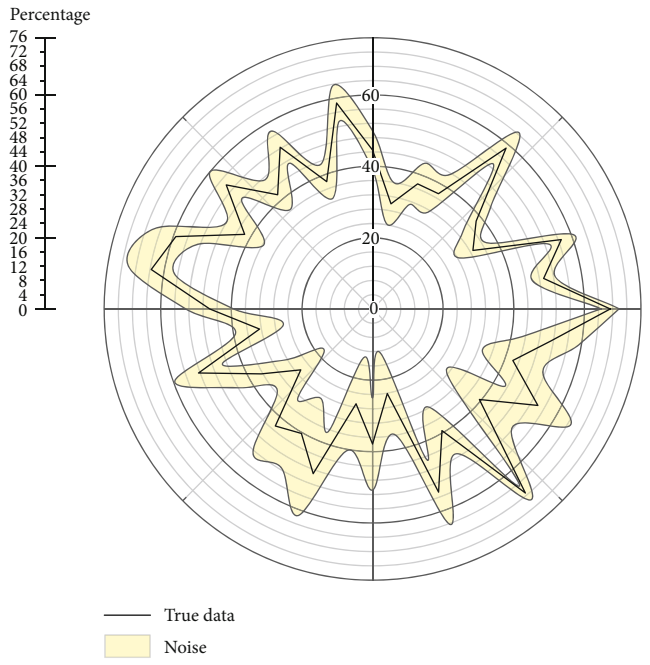

Figure 8: The effect of noise on the algorithm RLE.

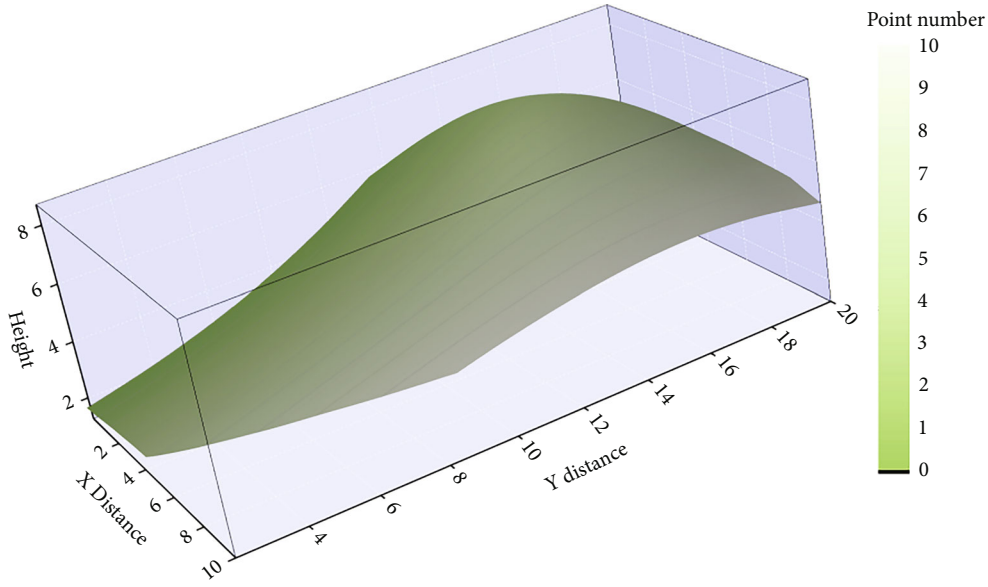

Figure 9: Accelerometer output graph.

algorithm proposed in this paper is significantly better than the comparison algorithm in four regions, and the difference value between regions is the smallest. The fluctuation range of RLE of the algorithm in this paper is smaller in the indoor sports area, underground sports field, campus sports field, and open area. It indicates that the algorithm in this paper has better robustness in different regions, can adapt to the changes of environmental noise, and has better stability of positioning accuracy.

The sequence length of tennis action data is unified to 128 samples by the resampling algorithm, i.e., each segment of action data is saved in the form of a 12×128 matrix, and the data matrix is expanded and spliced into a one-dimensional vector to be fed into the network learning. In addition, due to the translation property of sliding window segmentation, a segment of tennis action may be segmented into multiple data windows. A common data form is the basis for sharing research results. This paper gives a common inertial device standard, motion recording scheme, and data storage form and establishes a simple error calibration scheme for MEMS devices in motion capture application scenarios and a data cleaning method for the low automation of the data acquisition process. Observing the grayscale plot of the confusion matrix, it can be found that both recognition schemes are relatively easy to cause misjudgment for two types of tennis actions: forehand lunge and backhand lunge. From a practical perspective, this is because the two types of tennis actions are relatively close to each other, the trajectory of the racket is a lunge action, and the difference only lies in whether the player's grip is forehand or backhand. Figure 9 shows an example of the accelerometer output curve for the two motions.

Such experimental results reflect the fact that the device mounting solution of fixing the measurement device to the sports apparatus, while minimizing the hindrance to the collector's movement, can also lead to the resulting tennis action dataset being less sensitive to the differentiation of grip patterns, and based on this situation, mounting the motion acquisition device set on different lateralities of the racket is a viable solution.

4. Conclusion

This paper focuses on the study of motion recognition algorithms based on inertial motion capture schemes through wireless sensors. Since most of the current motion analysis is a shallow use of general algorithmic models, often not combined with expertise in the field of inertial guidance to target the characteristics of inertial data, and the research results are limited to small-scale motion datasets, this paper establishes a standardized motion recognition research process that best fits inertial motion capture schemes. This paper establishes a standardized motion recognition research process that best fits the inertial motion capture scheme, including a summary of data processing experience and a generalization of ideas for decomposing the emotion recognition task.

The main research work is divided into the following parts: (1) Acquisition and preprocessing of inertial datasets: a common data form is the basis for sharing research results; this paper gives a common inertial device standard, motion recording scheme, and data storage form and establishes a simple error calibration scheme for MEMS devices in motion capture application scenarios and a data cleaning method for the low automation of data acquisition process. (2) Motion interception algorithm research: from the offline recognition and online recognition of two research modes, focus on the needs of this paper and the implementation of the motion interception algorithm under the event window and motion window, respectively. To accurately detect the starting and ending points of motion, a stable motion amplitude indicator function is established using the Teager

operator combined with Gaussian smoothing filtering, a parametric modeling method for motion thresholds is derived, and an adaptive threshold determination scheme based on energy peaks is determined, which can accurately intercept the effective signal segments of various motions. Based on the professional research foundation in the field of statistics and signal processing, we designed a set of feature calculation schemes that can cover the motion characteristics to the maximum extent, including a total of 19 types of features under statistical features, signal time-frequency features, and system modeling features, and proposed a set of scientific feature contribution evaluation indexes based on the principle of information gain, and optimized and adjusted the applied feature combination scheme by combining the tennis action dataset, and the feature dimension was reduced by 20.78% under the streamlined combination. The feature dimensionality was reduced by 20.78%, while the classification accuracy only decreased from 97.99% to 97.60%.

Data Availability

The data used to support the findings of this study are available from the corresponding author upon request.

Conflicts of Interest

The authors declare that they have no known competing financial interests or personal relationships that could have appeared to influence the work reported in this paper.

References

[1] M. A. K. Quaid and A. Jalal, "Wearable sensors based human behavioral pattern recognition using statistical features and reweighted genetic algorithm," *Multimedia Tools and Applications*, vol. 79, no. 9-10, pp. 6061–6083, 2020.

[2] S. S. Tabrizi, S. Pashazadeh, and V. Javani, "Comparative study of table tennis forehand strokes classification using deep learning and SVM," *IEEE Sensors Journal*, vol. 20, no. 22, pp. 13552–13561, 2020.

[3] E. E. Cust, A. J. Sweeting, K. Ball, and S. Robertson, "Machine and deep learning for sport-specific movement recognition: a systematic review of model development and performance," *Journal of Sports Sciences*, vol. 37, no. 5, pp. 568–600, 2019.

[4] M. Batool, A. Jalal, and K. Kim, "Telemonitoring of daily activity using accelerometer and gyroscope in smart home environments," *Journal of Electrical Engineering and Technology*, vol. 15, no. 6, pp. 2801–2809, 2020.

[5] A. Jalal, S. Kamal, and C. A. Azurdia-Meza, "Depth maps-based human segmentation and action recognition using full-body plus body color cues via recognizer engine," *Journal of Electrical Engineering and Technology*, vol. 14, no. 1, pp. 455–461, 2019.

[6] J. Sena, J. Barreto, C. Caetano, G. Cramer, and W. R. Schwartz, "Human activity recognition based on smartphone and wearable sensors using multiscale DCNN ensemble," *Neurocomputing*, vol. 444, pp. 226–243, 2021.

[7] M. Rana and V. Mittal, "Wearable sensors for real-time kinematics analysis in sports: a review," *IEEE Sensors Journal*, vol. 21, no. 2, pp. 1187–1207, 2021.

[8] G. Lan, W. Xu, D. Ma, S. Khalifa, M. Hassan, and W. Hu, "Entrans: leveraging kinetic energy harvesting signal for transportation mode detection," *IEEE Transactions on Intelligent Transportation Systems*, vol. 21, no. 7, pp. 2816–2827, 2020.

[9] A. Switonski, H. Josinski, and K. Wojciechowski, "Dynamic time warping in classification and selection of motion capture data," *Multidimensional Systems and Signal Processing*, vol. 30, no. 3, pp. 1437–1468, 2019.

[10] M. R. Keyvanpour, S. Vahidian, and M. Ramezani, "HMR-vid: a comparative analytical survey on human motion recognition in video data," *Multimedia Tools and Applications*, vol. 79, no. 43-44, pp. 31819–31863, 2020.

[11] P. Wang, G. Li, J. Liu, Z. Hou, C. Meng, and S. Guo, "Flexible, freestanding, ultrasensitive, and iontronic tactile sensing textile," *ACS Applied Electronic Materials*, vol. 3, no. 5, pp. 2195–2202, 2021.

[12] X. Li, Y. J. Fan, H. Y. Li et al., "Ultracomfortable hierarchical nanonetwork for highly sensitive pressure sensor," *ACS Nano*, vol. 14, no. 8, pp. 9605–9612, 2020.

[13] X. Chen, L. Gong, L. Wei et al., "A wearable hand rehabilitation system with soft gloves," *IEEE Transactions on Industrial Informatics*, vol. 17, no. 2, pp. 943–952, 2021.

[14] X. He, W. P. Tay, L. Huang, M. Sun, and Y. Gong, "Privacy-aware sensor network via multilayer nonlinear processing," *IEEE Internet of Things Journal*, vol. 6, no. 6, pp. 10834–10845, 2019.

[15] B. Ning and L. Na, "Deep spatial/temporal-level feature engineering for tennis-based action recognition," *Future Generation Computer Systems*, vol. 125, pp. 188–193, 2021.

[16] M. Oshita, T. Inao, S. Ineno, T. Mukai, and S. Kuriyama, "Development and evaluation of a self-training system for tennis shots with motion feature assessment and visualization," *The Visual Computer*, vol. 35, no. 11, pp. 1517–1529, 2019.

Hindawi
Journal of Sensors
Volume 2023, Article ID 9801242, 1 page
https://doi.org/10.1155/2023/9801242

Retraction

Retracted: An Inertial Sensing-Based Approach to Swimming Pose Recognition and Data Analysis

Journal of Sensors

Received 31 October 2023; Accepted 31 October 2023; Published 1 November 2023

This article has been retracted by Hindawi following an investigation undertaken by the publisher [1]. This investigation has uncovered evidence of one or more of the following indicators of systematic manipulation of the publication process:

(1) Discrepancies in scope
(2) Discrepancies in the description of the research reported
(3) Discrepancies between the availability of data and the research described
(4) Inappropriate citations
(5) Incoherent, meaningless and/or irrelevant content included in the article
(6) Peer-review manipulation

The presence of these indicators undermines our confidence in the integrity of the article's content and we cannot, therefore, vouch for its reliability. Please note that this notice is intended solely to alert readers that the content of this article is unreliable. We have not investigated whether authors were aware of or involved in the systematic manipulation of the publication process.

Wiley and Hindawi regrets that the usual quality checks did not identify these issues before publication and have since put additional measures in place to safeguard research integrity.

We wish to credit our own Research Integrity and Research Publishing teams and anonymous and named external researchers and research integrity experts for contributing to this investigation.

The corresponding author, as the representative of all authors, has been given the opportunity to register their agreement or disagreement to this retraction. We have kept a record of any response received.

References

[1] S. Xu and S. Lee, "An Inertial Sensing-Based Approach to Swimming Pose Recognition and Data Analysis," *Journal of Sensors*, vol. 2022, Article ID 5151105, 12 pages, 2022.

Hindawi
Journal of Sensors
Volume 2022, Article ID 5151105, 12 pages
https://doi.org/10.1155/2022/5151105

Research Article

An Inertial Sensing-Based Approach to Swimming Pose Recognition and Data Analysis

Shaofeng Xu and Somi Lee

Physical Education Sangmyung University, Seoul 03016, Republic of Korea

Correspondence should be addressed to Somi Lee; 161842032@masu.edu.cn

Received 17 November 2021; Revised 6 January 2022; Accepted 8 January 2022; Published 27 January 2022

Academic Editor: Gengxin Sun

In this paper, inertial sensing is used to identify a swimming stance and analyze its swimming stance data. A wireless monitoring device based on a nine-axis microinertial sensor is designed for the characteristics of swimming motion, and measurement experiments are conducted for different intensities and stances of swimming motion. By comparing and analyzing the motion characteristics of various swimming stances, the basis for performing stroke identification is proposed, and the monitoring data characteristics of the experimental results match with it. The stance reconstruction technology is studied, PC-based OpenGL multithreaded data synchronization and stance following reconstruction are designed to reconstruct the joint association data of multiple nodes in a constrained set, and the reconstruction results are displayed through graphic image rendering. For the whole system, each key technology is organically integrated to design a wearable wireless sensing network-based pose resolution analysis and reconstruction recognition system. Inertial sensors inevitably suffer from drift after a long period of position trajectory tracking. The proposed fusion algorithm corrects the drift of position estimation using the measurement of the visual sensor, and the measurement of the inertial sensor complements the missing measurement of the visual sensor for the case of occlusion of the visual sensor and fast movement of the upper limb. An experimental platform for upper-limb position estimation based on the fusion of inertial and visual sensors is built to verify the effectiveness of the proposed method. Finally, the full paper is summarized, and an outlook for further research is provided.

1. Introduction

Human motion capture technology uses sensor devices to track, measure, and record the motion information of key limbs of the human body in 3D space and then uses this information to reconstruct, edit, and analyze the human motion process. Human motion capture technology has a broad market space and application prospects and has been widely used in film and television animation production, human-computer interaction, virtual reality, sports training, medical rehabilitation, and other cross-disciplinary fields. As an emerging multimedia data, the technical research of editing, analysis, and recognition of human motion data has attracted extensive attention from many scholars and researchers [1]. Nowadays, the main methods of movement analysis are visual movement observation and video movement observation, both of which require managers to subjectively observe, analyze, and evaluate the operator's operation process and then develop improvement plans. Human posture recognition has a wide range of applications, including human-computer interaction, film and television production, motion analysis, games, and entertainment. The visual action observation method is a direct analysis method in which the observed operation is recorded directly on a special form for analysis, provided that the operator's original operating condition is not affected. This method is intuitive but has the disadvantage of being difficult to measure subtle movements and requires more energy. The video motion observation method is recorded and retained, which is susceptible to a variety of factors when recording human motion images due to the fixed location of the video equipment, and it is difficult to directly measure some motion parameters, such as acceleration and angular velocity [2]. Compared with the above methods, the human motion

monitoring recognition method based on an inertial sensor module can monitor human motion at any time and place, the motion recognition results are highly accurate, the motion parameters can be directly calculated by the collected inertial data and physiological data, and it has the advantages of simple operation and portable wearing. Motion analysis is another element of the method study, which focuses on analyzing the body movements of people while performing various operations in order to eliminate redundant movements, reduce labor intensity, make operations easier and more effective, and thus develop the best action procedures.

The study of an LPMS-B2-based swimming data acquisition and monitoring system is very significant for detailed recording and analysis of swimming movements [3]. The swimming monitoring studied in this paper specifically refers to the recognition of swimming strokes, arm strokes, and turns and generates detailed swimming data. In competitive sports, detailed data analysis can help athletes to track and analyze their movements. For the average person, recording their daily swimming log and monitoring their swimming data in detail can help them to plan their workouts and improve their swimming performance [4]. As the third most popular sport in the world, swimming also needs a mature product that can help users to complete their daily monitoring work. Water therapy has become a recognized form of physical therapy because of the buoyancy of water movement to offset some of the effects of gravity, the human joints, the spine, and other very good protection. Swimming is an important exercise in rehabilitation because it can reflect sports injuries and many spinal disorders through the coordination and symmetry of movements [5]. However, it has been difficult to effectively extract information on physical conditions from human swimming data. Initially, the assessment of swimming movements relied mainly on the visual observation and experience of professional instructors in the field, which was inefficient. Subsequently, a class of video image-based swimming movement recording systems has emerged, where the professional instructor no longer needs to be physically present but still needs to make judgments based on the video, and the cost of this method is generally very high. The image action observation method is a method of recording the execution of the operation through video and photography, using film and audio tapes, and then observing and analyzing the operation action through the method of video and image playback.

Swimming is a sport that involves many parts, and early studies would obtain complete motion information by fixing multiple sensors to multiple parts of the body and obtaining the acceleration rate of each part. This method has improved the recognition rate, but too many devices are very uncomfortable for the wearer and can interfere with the movement, and the experimental cost is high, so this paper acquires acceleration data through a single sensor [6]. The purpose of this paper is to use a single inertial measurement unit to comprehensively monitor swimming movements and to explore a method to assess the physical condition of swimmers, which can provide some reference basis for the application of physical rehabilitation therapy in water, training injury assessment, etc. A single inertial sensor-based wireless swimming motion monitoring experimental device was built and worn on the lower back of swimmers in the form of a belt. Human motion detection is to input video images and then detect the location, scale size, and pose of the moving human body. A series of processing methods such as low-pass filter denoising, background differencing, morphological image processing, and regional connectivity analysis can be used to extract the moving object from the video image, and then, the features of human body height and width and its ratio are used for human body recognition. The motion characteristics of various swimming stances are analyzed, and the basis for stroke recognition is proposed and verified by comparing them with the experimental monitoring data. The link between the monitoring data and the information of human body condition (fatigue and injury level) was established for the strong movement symmetry characteristic of the freestyle and backstroke sports.

2. Related Works

Inertial sensors inevitably encounter certain difficulties because of their sensor characteristics. For example, gyroscope integration introduces attitude drift, accelerometers are susceptible to external linear acceleration, and magnetometers are susceptible to external magnetic field interference. The Kalman filter-based multisensor fusion algorithm enables the fusion of multisensor information with complementary information to improve the estimation accuracy [7]. The decomposition of acceleration measurements and magnetometer measurements reduces the effect of magnetic field interference on the gravitational direction attitude angle. The threshold-based approach uses the gyroscope measurements as the process equation and the quaternions obtained from attitude decomposition as the observation equation to achieve the fusion of information. The inverse operation imposes a large computational burden on the system [8]. It is more difficult for embedded devices to perform such operations while ensuring real-time performance. This algorithm replaces the inverse operation with an operation of one complexity [9]. In attitude estimation applications, due to the nature of magnetic-inertial sensors, the measurement noise covariance matrix is often assumed to be a diagonal array, and the terms on the diagonal are large to ensure convergence. This results in the new interest covariance matrix being naturally a diagonally dominant matrix, thus ensuring convergence of the Taylor series expansion [10]. Even without the interference of linear acceleration, the accelerometer can only measure two rotational degrees of freedom and cannot be used for measurements of the multi-rotational degree of freedom joints.

There are several universities dedicated to the establishment of an inertial motion capture laboratory, to a certain extent, to promote the development of domestic inertial motion capture technology. Due to the late start of domestic research in this field, in both the system architecture and core algorithms and similar foreign products, there is a significant gap; there are obvious distortions and jams in motion capture [11]. At present, most of the inertial motion

capture systems appearing on the market are still at the stage of experimental prototypes, with low capture accuracy, poor reliability, immature supporting software, and other problems, and there is still a long way to go from marketization [12]. Not only the continuous development of the human posture recognition algorithm but also human posture recognition technology is applied in various fields. Inertial motion capture is a new type of human motion capture technology, in which human posture recognition is the core of motion capture technology, divided into three parts: data acquisition equipment, data transmission equipment, and data processing unit [13]. The data acquisition equipment is to collect the pose information of the body parts using inertial sensors such as accelerometer, gyroscope, and magnetometer, the data transmission equipment is to transmit the data collected by the inertial sensors to the data processing end, and the data processing unit is to process the collected data and recover the human motion model using the human kinematics principle to present in the computer software [14].

Firstly, the basics of inertial sensors are described, and the current data fusion algorithms are briefly introduced. Then, according to the nine-axis sensor chip used in this paper and the usage scenario, the extended Kalman filtering algorithm is selected to correct the angle with the data collected from the gyroscope as the main data and the measured data from the accelerometer and magnetometer as the supplement to reduce the error of the attitude module. Swimming exercise promotes physical health, healthy mental development, and social adaptability in adolescents in a way that other sports cannot replace the benefits. Long-term swimming can lead to healthy chest development and improved lung capacity, and swimming can also shape a healthy form and improve physical fitness. Swimming can provide a physical foundation for adolescent health and promote good psychological development. For swimming drives, rotation means applying asymmetric driving forces to both sides of the drive. The traditional method is to focus the beam on a noncenter part of the actuator, generating an unbalanced driving force to achieve rotation. However, for microscale actuators, it is difficult to maintain a specific point on which the light is also focused during the motion. The collected attitude data are processed and analyzed, and the features of each attitude data are extracted by the commonly used time-domain analysis method and frequency domain analysis method, and then, the measured attitude data are classified and recognized, which proves that the attitude recognition device designed in this paper can meet the basic requirements of recognition. The algorithmic problem of using inertial sensors for attitude resolution and reconstruction under high dynamic motion conditions with low cost and limited sensor accuracy is mainly studied, and experiments are designed to verify the correctness of the relevant algorithms. The theory related to this system is introduced as the basis for the subsequent chapters; secondly, the algorithmic part of this paper is investigated, mainly including the study of the calibration algorithm of the nine-axis sensor, the gradient descent-based attitude solving algorithm, and the attitude angle-based attitude recognition algorithm.

3. Analysis of Swimming Attitude Data Recognition with Inertial Sensing

3.1. Swimming Inertial Sensor System Design. The accelerometer and gyroscope in the ICM-20948 chip can be activated by triggering the self-test register, and the chip will automatically simulate the external force applied to the accelerometer and gyroscope. After the self-test, the output value will be changed compared to the value without the self-test [15]. When the self-test function is activated, the sensor generates an output signal to observe the self-test condition. The self-test response value is equal to the difference between the sensor output value with the self-test and the output value without the self-test. When the self-test reply value is within a reasonable range, the self-test passes; when the self-test reply value is outside the specified range, it indicates a self-test failure. The action of a particular job is a succession of changes in several job postures over a continuous period. This series of successive changes is produced by instructions from the brain acting on the muscles of the body. For a specific operational posture, it is important to maintain its momentary stability. If this stability is disrupted during the action, the correct posture will be lost and this will lead to an operational accident. The continuous collection of such stability in the operating posture is the stability of the operating action, and the stability of the action can be well enhanced by repetitive training.

Motion analysis, also known as motion study, is the process of studying and analyzing each action to ensure the effectiveness and reasonableness of the operator's actions during the work process and to achieve the highest return on the work at the lowest cost. An action analysis is generally based on the actions performed by the operator, recording the contents of each limb action cantered on the operator's hands and eyes according to specific marks, charting the actual action, and using this as a basis for analysis and improvement [16]. Because the motion sensor is very sensitive to movements, even for the same swimming stroke, each person's subtle hand movements are very different, resulting in a limited coverage of the population and a very complex algorithm model. On the other hand, because the motion sensor can only sense the movement, it is difficult to distinguish accurately between the stroke movement in swimming and similar movement in a nonswimming state, and the data is easily disturbed to reduce the accuracy rate. At present, most accidents in production operations are caused by improper movements of the operator. Therefore, the analysis and improvement of movements, the orderly combination of operational movements, the improvement of inadequate movements, and the elimination of dangerous movements are powerful means of preventing accidents.

Based on the above requirements, this experimental device adopts a system structure consisting of a measurement device, wireless network, and data processing software, as shown in Figure 1. The measurement device includes a three-axis acceleration sensor, a three-axis gyroscope sensor, and an embedded WIFI module, which is mainly responsible for real-time acquisition of human swimming motion data and real-time uploading of measurement data using the

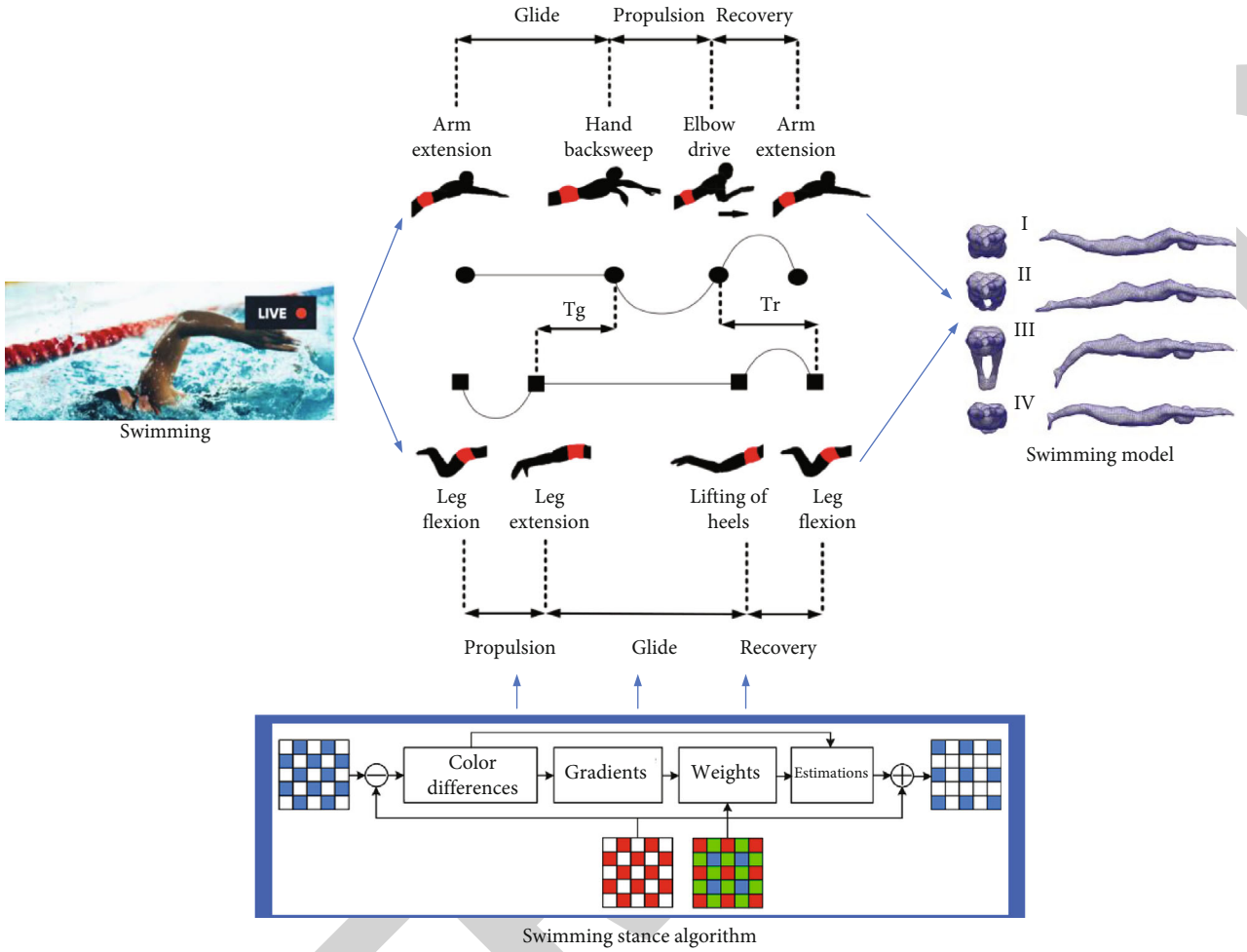

Figure 1: Structure of the IoT-based swimming attitude measurement system.

embedded WIFI module. The wireless network can be used to cover the wireless network, which is responsible for forwarding the data uploaded by the embedded WIFI module to the terminal data processing software. Due to the manufacturing process, data measured by inertial sensors are usually subject to some errors. Offset error is also known as gyroscope and accelerometer will have nonzero data output even when they are not rotating or accelerating. To get the displacement data, we need to integrate the output of the accelerometer twice. After two integrations, even small offset errors will be amplified, and as time progresses, displacement errors will accumulate, eventually causing us to no longer be able to track the position of the object. In statistics and probability theory, each element of the covariance matrix is the covariance between the individual vector elements, a natural generalization from scalar random variables to higher dimensional random vectors. The terminal data processing software includes three modules: network communication, data monitoring, data processing, and display, as shown in Figure 1, which is mainly responsible for establishing data communication and data monitoring with the measurement device, as well as simple processing and display of the measurement data.

Complementary filters are analyzed in the frequency domain to fuse the signal to obtain a better estimate of a particular quantity. Assuming that the signal is driven by noise at two different frequencies, two filters with appropriate bandwidths can be constructed to cover the useful frequencies with these two filters. For this system, the complementary filters perform high-pass filtering on the direction estimated by the gyroscope data affected by low-frequency noise and low-pass filtering on the accelerometer data and magnetometer data affected by high-frequency noise. The fusion between the two filter estimates will ideally result in an all-pass and noise-free pose estimate.

$$R(s) = G_L(S)R_0(s) - G_H(S)R_0(s),$$
$$C(s) = k_p - \frac{k_i}{s^2}, \tag{1}$$

where $R(s)$ determines the cut-off frequency of the complementary filter and G_L determines the time taken to suppress the static error; in general, k_p is 10-100 times larger than k_i. The complementary filter performs high-pass filtering on the direction line estimated from gyroscope data affected by low-frequency noise and low-pass filtering on

accelerometer data and magnetometer data affected by high-frequency noise. Fusion between the two filtered estimates will ideally result in an all-pass and noise-free pose estimate. Consider the unconstrained optimization problem min $f(x)$, where $f(x)$ is a continuously differentiable function. If one can construct a sequence $x_1, x_2, x_3, \cdots, x_t$ satisfying

$$f(x_{t+1}) \geq f(x_t), \quad t = 0, 1, \cdots, t, \tag{2}$$

thus, to satisfy $f(x - \Delta x) \geq f(x)$, one may choose

$$\Delta x = \gamma \nabla f(x), \tag{3}$$

where the step size γ is a constant. However, if γ is obtained too small, the convergence process of gradient descent will take a long time and will show poor following results in this system, while if γ is obtained too large, the gradient descent will overshoot and may sometimes converge quickly, but most cases will have repeated oscillations. In a gradient descent algorithm, a loss function is generally given first and a starting point is chosen; next, the gradient of the loss curve at the starting point is calculated, a step is taken in the direction of the negative gradient, a fraction of the gradient size is added to the starting point, and the process is iterated over and over, gradually approaching the lowest point of the loss curve.

The problem of calibration of inertial and vision sensors without connection is studied [17]. The calibration method introduces the ground coordinate system and the calibration plate coordinate system to establish the relationship between the ground coordinate system and the vision sensor coordinate system. The rotation relationship between the ground coordinate system and the visual sensor is solved by the camera calibration method and the pose estimation method. Finally, a set of wrist part motion tracking experiments are designed to verify the effectiveness of the proposed method.

For the inevitable cumulative error and position drift problems of the inertial sensor-based positional estimation system, a multisensor information fusion method based on an event-triggered mechanism is designed to use the position information obtained from vision sensors to constrain the cumulative error of inertial sensors and use the high-frequency measurement information of inertial sensors to supplement the visual data in the interval between two frames of vision sensors and in the case of occlusion loss, as shown in Figure 2. The cost of the entire set of optical motion capture equipment is extremely expensive, cumbersome to set up, and vulnerable to blocking or light interference, bringing a lot of trouble to the postprocessing work. For some serious obstruction of the action, optical motion capture cannot accurately restore the action of, for example, squatting, hugging, and twisting in real time. The emergence of motion capture technology based on an inertial sensor system has greatly improved the status quo.

These three methods of pose solving have their characteristics and can be chosen according to different situations and can be converted to each other. The Eulerian angle is easy to understand and convenient to represent, but the phenomenon of gimbal deadlock will occur, and it cannot display the pose information of the object in all directions; quaternion can avoid gimbal deadlock compared with the Eulerian angle, but it has one more dimension, which is relatively difficult to understand and cannot be displayed intuitively; the rotation matrix can be easily represented by arbitrary vectors, but the operation is relatively large and consumes time and memory. Computer vision-based recognition mainly uses various feature information to recognize human posture movements, such as video image sequences, human contours, and multiple viewpoints. Computer vision-based recognition can easily obtain the trajectory and contour information of human motion, but there is no specific way to express the details of human motion, and it is easy to have problems such as recognition errors due to occlusion.

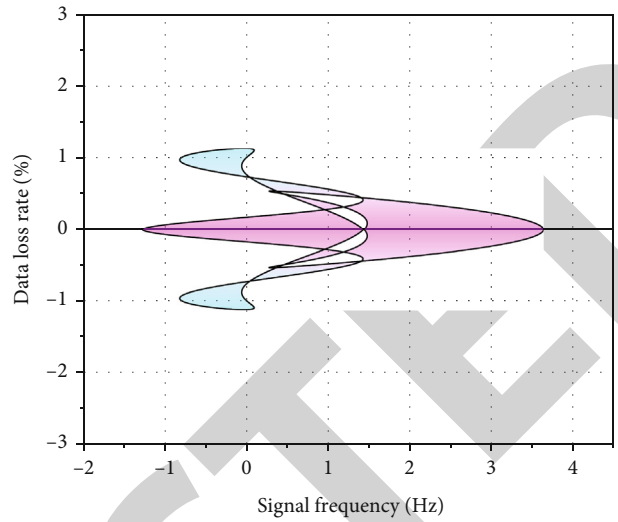

Figure 2: Ellipse around the axis of rotation and data.

Since the size of the filter window used by the conventional median filter is fixed, causing the above contradiction cannot be solved. This problem can be solved by using the filtering method of an adaptive median filter. First, a threshold is set in advance for the adaptive median filter, and when the data point in the center of the window is judged to be noisy, the current median window value is replaced by the output of the filter; otherwise, its value is up to retention. The adaptive median filter can produce a good suppression of the impulse noise that often occurs in acceleration data, and the details are well preserved.

$$Z_{\text{med}} = \begin{cases} a_k^2, n \in (1, 3, 5, \cdots 2n+1), \\ \dfrac{a_k^2 - a_{k+1}^2}{2}, n \in (2, 4, \cdots 2n), \end{cases} \tag{4}$$

where n is the size of the sliding window, a_k^2 denotes the number in the middle of the current sliding window after arranging the data in numerical order one by one, and a_k^2 is the input window acceleration data. Define $Z_{\max}$ as the minimum value of the acceleration data a_k^2, $Z_{\min}$ as the maximum value of the acceleration data a_{k+1}^2, Z_{med} as the median

signal, and Z_{max} as the maximum window size allowed. In this way, the adaptive median filter has two processes that can be summarized: determining whether the median obtained within the current window is noise and determining whether the acceleration a_k^2 is noise. If the relation $Z_{min} < Z_{med} < Z_{max}$ is satisfied, the median Z_{med} is not determined to be noise and the acceleration data at the center of the current window is continued to be checked. Compensation for hard and soft iron distortion depends on the materials in the sensor and its surroundings. While we can compensate for the presence of materials around the sensor that may distort the magnetic field relative to the sensor at rest or moving with the sensor, this compensation becomes much more difficult when the distorted materials in the external environment are changing, especially when the object is in motion and compensation for this external environment is almost impossible.

3.2. Design of Swimming Stance Data Identification and Analysis. The LPMS-B2 nine-axis sensor chosen for this paper is powerful, with a three-axis accelerometer, three-axis gyroscope, three-axis magnetometer, and barometric and humidity sensors, small enough to be easily worn by the user, and easy to connect using an app via Bluetooth communication [18]. Swimming is a sport that involves many parts, and early studies would obtain complete motion information by attaching multiple sensors to multiple parts of the body and obtaining the acceleration velocity of each part. This method does improve the recognition rate, but too many devices are very uncomfortable for the wearer and can interfere with the movement, and the cost of the experiment is also high.

The different parts of the individual sensors can also have a great influence on the results. For swimming, the motion characteristics of the hands and feet are more obvious for different strokes, and from the perspective of daily use, wearing the sensor on the hand is more in line with people's habits, so in this paper, the sensor is worn on the wrist to acquire data. For the most popular backstroke and freestyle in rehabilitation, the body rotates around the longitudinal axis of the body with the left and right arm strokes and has strong left and right symmetry, so the body rotation angle during swimming can be used to represent the left and right arm movements. y-axis gyroscope data represents the angular velocity of the left and right body rotation during swimming, which is a simple periodic signal with strong regularity, and can be calculated by using equation (5). Its integration to calculate the body rotation angle during swimming is also a simple periodic signal.

$$\varphi_Y = \int w_Y^2 dt, \tag{5}$$

where φ_Y is the body rotation angle in the left and right directions and w_Y^2 is the angular velocity in the left and right directions. By analyzing the basic characteristics of the rotation angle signal in swimming, the amplitude and time to complete the corresponding swimming stroke can be determined, in which the maximum and minimum values of the human body rotation angle can reflect the amplitude of the left and right arm strokes, respectively; the stroke period of the left and right arm strokes can be extracted according to the time when the rotation angle crosses the zero point. During the swimming exercise, the maximum rotation angle and the stroke period of the left and right arms of the swimmer will remain relatively stable. If the swimmer has some spinal disease, injury, or limb injury, it will produce some asymmetry in the left and right arm movements, and the higher the degree of injury, the greater the corresponding asymmetry, so we can calculate the difference between the maximum left and right rotation angles and the difference between the left and right movement cycles during the whole swimming process to comprehensively evaluate the degree of human injury, as shown in

$$\eta = \frac{\sum(\varphi_{Y-max})_i + (\varphi_{Y-min})_i}{\sum(\varphi_{Y-max})_i - (\varphi_{Y-min})_i/2}, \tag{6}$$

where η denotes the combined asymmetry of the left and right swimming movements, i.e., the degree of human injury; D denotes the combined variance of the left and right swimming movements, i.e., the degree of human fatigue. $(\varphi_{Y-max})_i$, (φ_{Y-min}), $(TL)_i$, and $(TR)_i$ denote the maximum and minimum values of the rotation angle and the left-handed and right-handed action cycles in the i-th action cycle, respectively; n denotes the number of action cycles in a certain time.

This compensation for magnetic field distortions ensures that magnetic field disturbances are limited to affect only the direction to be estimated. This approach eliminates the need to predetermine the reference direction of the Earth's magnetic field, overcoming the potential drawbacks of other direction estimation algorithms, as shown in Figure 3.

Attitude estimation requires fusing information from the gyroscope, accelerometer, and magnetometer inside the magnetic-inertial sensor to determine the attitude of the target under test [19]. The second part is the estimation of the motion position of the upper limb joints. The results of the pose estimation in the first part can be obtained by transferring the accelerometry measurement to the ground coordinate system and excluding the gravitational acceleration to obtain the motion acceleration of the object under test. Once a uniformly accelerated motion model is established, the motion acceleration can be fused with the position information provided by the vision sensor, and a more robust and more accurate wrist motion trajectory can be obtained. Diagnostic research focuses on the study of the action itself. It may be a pilot study that explores how an action is applied and may be received in practice, or it may describe the action process itself. Diagnostic research is primarily for the benefit of the leaders of the organization being diagnosed, and the research report is for their reference only. Therefore, it is mostly conducted before or after the action has been implemented.

The accuracy of posture estimation is very dependent on the accuracy of sensor measurements; however, sensor measurements are subject to linear acceleration and external

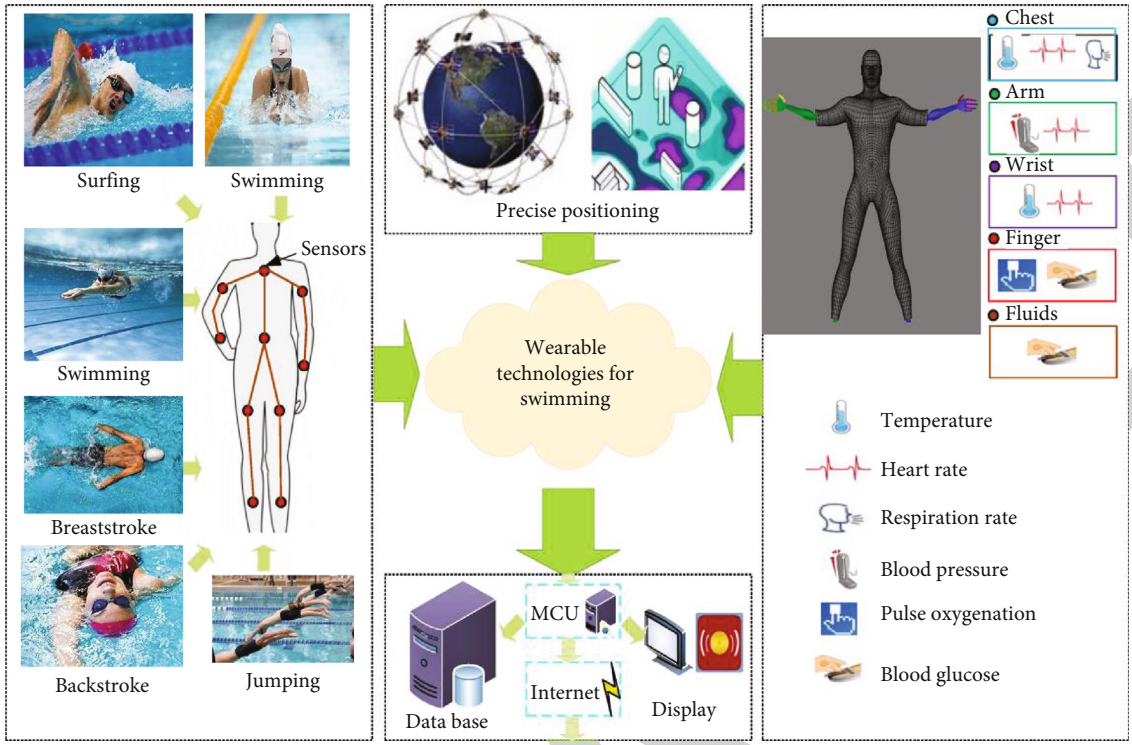

Figure 3: Overall structure of the recognition algorithm.

magnetic field interference. For example, when the human arm is moving rapidly, the acceleration measurements will contain large linear acceleration disturbances and the measurements cannot be trusted. And in the case of rapidly changing magnetic fields, the assumption of a uniform magnetic field does not hold, and then, the attitude angle calculated from the magnetometry measurement will be inaccurate. Also, numerical integration of the angular velocity measured by the gyroscope can give attitude information, but this method is only valid for short periods and gradually deviates as the integration time becomes longer and longer or even becomes an incorrect attitude estimate.

Based on the above characteristics of inertial sensors, threshold-based methods are a mainstream approach to reduce the effects of external disturbances. The core idea of this type of approach is that during a measurement, for accelerometers, if there is a measurement that deviates significantly from the acceleration of gravity, which indicates that the sensor's measurement cannot be trusted, it is rejected, and the gyroscope measurement is then used to predict the direction of gravity at that moment. Similarly, in magnetometer measurements, if the measurement deviates too much from the geomagnetic intensity or if the measured measurement deviates significantly from the declination of gravity and the initial moment, it is rejected and replaced with the predicted value of the previous moment's measurement again.

From the division of the gait cycle in the Figure 3, the user takes two steps in a gait cycle and the situation where the difference between the posture angles at the two thighs is the largest once in each step, so the situation where the absolute value of the difference between the posture angles is the largest can be used as the discrimination criterion for each step, thus achieving the recognition of the number of steps in the walking posture. This approach overcomes the drawbacks of a single sensor and takes full advantage of the multisensor network of this system. The raw data and difference curves of the collected left and right leg posture angles in the actual measurement experiment are shown in Figure 4.

In the attitude reconstruction thread, the source IP is first obtained; then, the quaternions used for attitude transformation are initialized and blocked to determine if data is received from the inertial acquisition node, and if so, the node number, raw nine-axis data, Euler angles, and other information in the resulting data frame are parsed. The next step after getting the data is to start the work of attitude reconstruction [20]. First, determine if the pose has been initialized; if it has been initialized, then find the pose transformation matrix of the node before and after two times relative to the reference point of the node, find the pose transformation matrix, and then send a drawing message to the view to drive the corresponding node motion and update the pose data to the aggregated pose structure for the next call. Median filtering is a nonlinear digital filtering technique often used to remove noise from images or other signals. The design idea is to examine a sample in the input signal and determine if it represents the signal, using a viewing window consisting of an odd number of samples to achieve this function. The values in the viewport are sorted, and the median value in the middle of the viewport is used as the output. Then, the earliest value is discarded, a new sample is obtained, and the above calculation process is repeated.

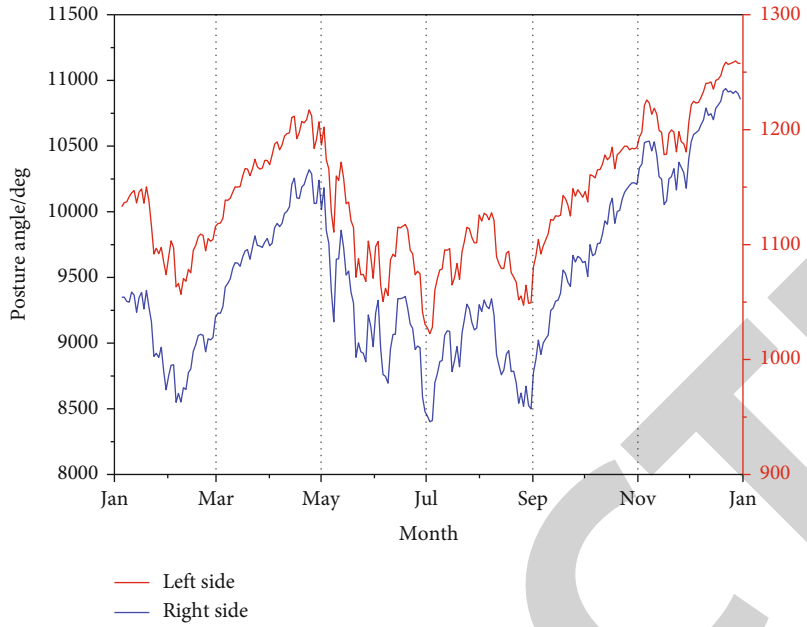

Figure 4: Raw data and difference curves of left and right leg posture angles.

4. Results and Analysis

4.1. Test Results of the Swimming Inertial Sensor System. The experimental design of stillness and motion recognition in posture recognition is as follows: the user will wear the hardware used in this system and power it up and the user performs the following operations, respectively: stand still for 5 seconds, do casual motion for 10 seconds, sit still for 5 seconds, do casual motion for 10 seconds, lie still for 5 seconds, do casual motion for 10 seconds, lie down for 5 seconds, do casual motion for 5 seconds, lie down for 5 seconds, do casual motion for 10 seconds, and so on for 5 times; that is, the number of times of stillness and motion is 10 times, respectively, and each posture at rest occurs 5 times, and the statistical recognition results are shown in Figure 5.

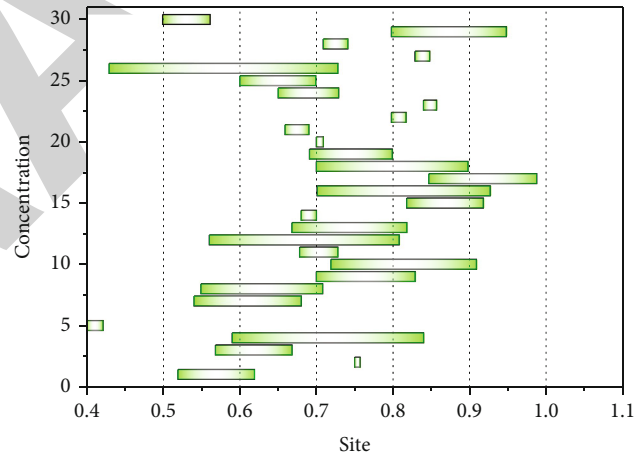

Figure 5: Experimental statistics of stationary and motion pose recognition.

From the above experimental results, only one "sitting at rest" action was not recognized, but the recognition rate of rest and motion reached 100%, which is because the trend of the change of the posture angle in the process of rest and motion in this experiment based on the posture angle recognition method is very different. The reason the sitting posture is not recognized in the experiment is that the user does not reach the set threshold value during the experiment after inspection and analysis. In this paper, a multisensor information fusion method based on an event-triggered mechanism is used. The measurement of inertial and visual sensors is used as a trigger condition to perform sensor information fusion, specifically expressed as: once the position filter receives the data from inertial and visual sensors, it is fused with the predicted values of the past moments to estimate the position information at this moment.

Once the sensor measurements reach the position filter, then the position filter performs information fusion to estimate the 3D spatial position of the wrist part at that moment. This allows all data to be used efficiently, improving the dynamic performance of the wrist position estimation system and enhancing the stability of the system in the absence of Kinect data. The inertial sensor can maintain good estimation accuracy even at high motion speeds. However, after 5 seconds, the velocity deviates to some extent and cannot be compensated. As time increases, the deviation gets larger showing the disadvantages of using the inertial sensor alone for position tracking. After the inertial sensor does two integrations, the accumulated error gets larger and larger and soon deviates from the true value. Inertial sensors can only provide acceleration information and cannot compensate for the drift on their own. Therefore, it is necessary to fuse inertial sensors and vision sensors for human position estimation (Figure 6).

And after position filtering, the interrupted position data can be effectively compensated by the data from inertial

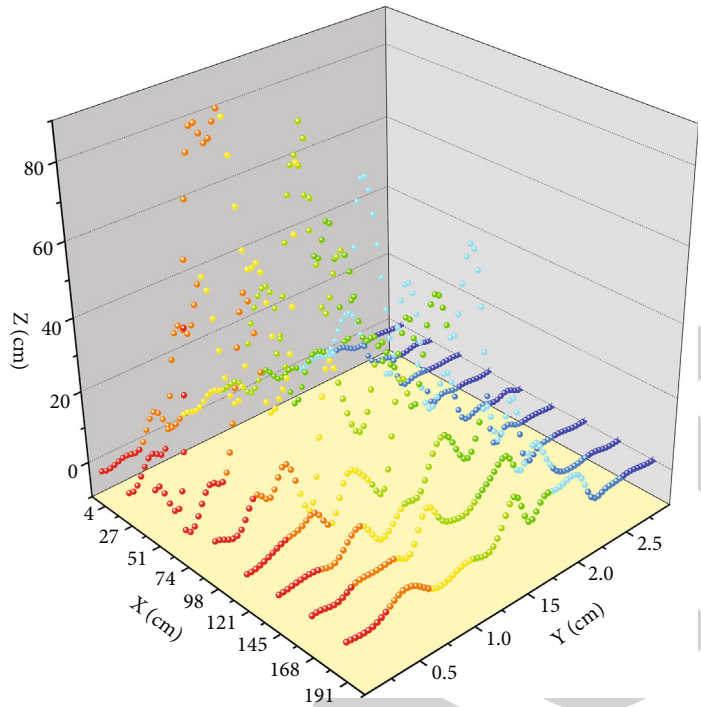

Figure 6: System location estimation.

sensors, avoiding rapid and drastic changes in the tracking trajectory. This algorithm enhances the robust performance of the tracking system, which helps to ensure safety performance in human-machine collaboration or teleoperation scenarios. However, the single use of inertial sensors does not guarantee that the tracking effect is effective for a long time. This is because inertial sensors can only rely on double integration to obtain position information in space, a process that inevitably introduces the problem of drift, causing the position to eventually deviate from the true value. In general, do not use the inertial sensor integration alone for some time greater than 1 second. At the same time, a wrist joint position filter can achieve good results in other periods and can effectively improve the estimation accuracy of the wrist joint position.

After differencing, the Kinect sensor obtains a large noise in the velocity valuation, while the position filtering is almost unaffected by it and can track the upper motion velocity better, avoiding the impact of the visual sensor measurements on the system. Under the control application of teleoperation, the velocity affects the torque of the robot, and once the velocity changes drastically, it may affect the estimation accuracy of teleoperation and damage the robot's motor to some extent. Therefore, the velocity estimation experiments demonstrate that the present algorithm has better dynamic performance than the single vision sensor human pose estimation algorithm.

4.2. Results of Identification and Analysis of Swimming Stance Data. Vision sensors have a low sampling frequency and are somewhat lacking in detail for motion. The high sampling frequency of the inertial sensor can complement the sampling interval of the visual sensor well. This experiment is aimed at verifying the position tracking of the performance of the proposed fusion algorithm in the case of fast motion. The experiment requires the test subject to slide his arm in front of his body as fast as possible to provide a fast-motion experimental scenario.

Figure 7 shows the 2D wrist position estimation for the front of the tester, which is the view of the human arm motion from the camera perspective. The blue dots are the sampled wrist joint points obtained by the Kinect vision sensor, the red plus signs are the wrist joint motion trajectory points obtained by the position filter, and the green line is the wrist joint motion position obtained by the OptiTrack system. All the above estimates are transformed in some way and are in the Kinect sensor coordinate system. The inertial and visual sensor fusion algorithm provides more motion trajectory points, i.e., richer human motion data. In addition, the fusion results are closer to the true values of wrist motion provided by the OptiTrack system than the position estimates from the vision sensor only. Therefore, the experimental results show that the upper limb position estimation algorithm based on the fusion of inertial and visual sensors can obtain better tracking results in the case of fast movements.

Figure 8 shows the average deviation distance and average time distortion for the DBA and ADBA algorithms, respectively, when different initial averaging sequences are chosen. The ADBA algorithm always obtains a smaller average deviation distance and average time distortion than the DBA algorithm when the same initial averaging sequence is chosen. Regardless of how the initial averaging sequence is chosen, the average deviation distance and average time distortion obtained by the ADBA algorithm are very stable and fluctuate very little, while the average deviation distance

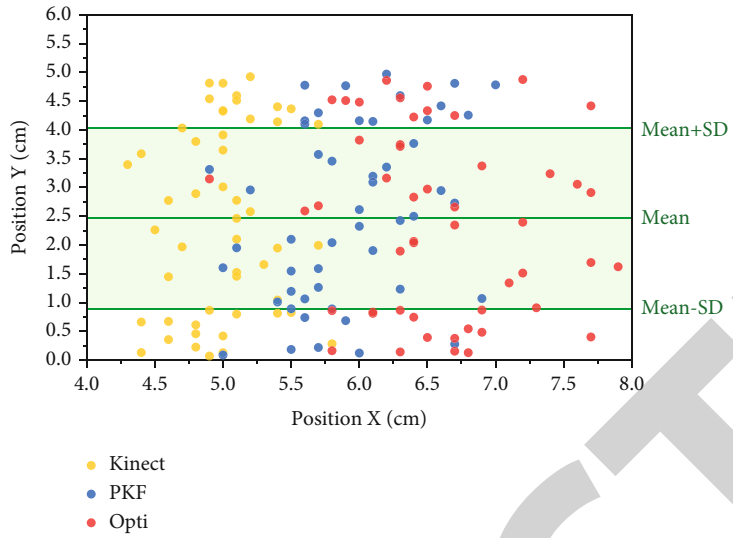

Figure 7: Wrist motion position tracking.

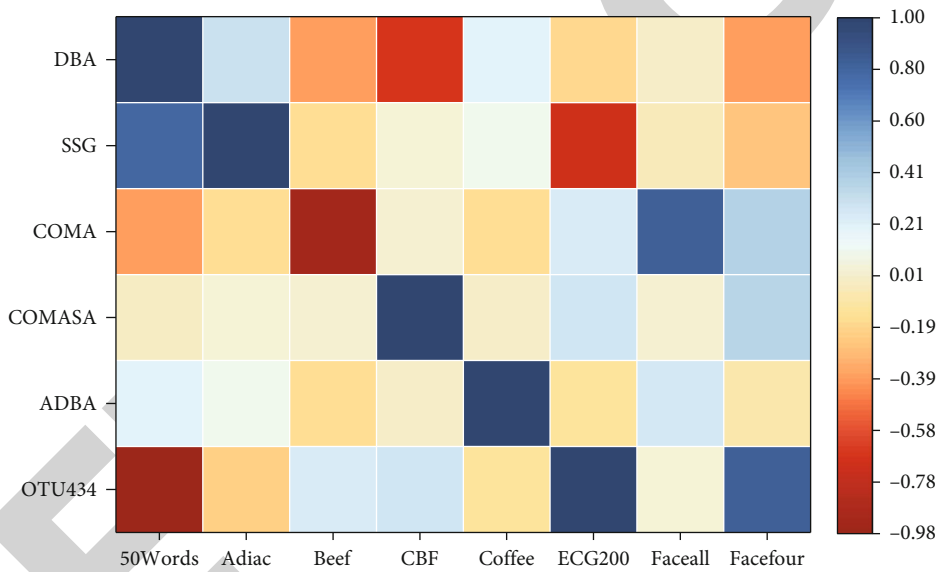

Figure 8: Comparison of mean deviation distances for ten experiments.

and average time distortion obtained by the DBA algorithm vary more significantly and fluctuate more.

To further evaluate the impact of the initial averaging sequences on the ADBA and DBA algorithms, 30 different sequences are selected as the initial averaging sequences, respectively. Due to the large amount of computation required for this experiment, only eight of these sequence sets are selected for testing in this paper. The mean and variance of the mean deviation distance and meantime distortion of the ADBA algorithm and DBA algorithm are shown for 30 different initial conditions, respectively. The mean and variance of the mean deviation distance and meantime distortion can be used to measure the sensitivity of both algorithms to the initial mean sequence selection. For all sets of test sequences, the ADBA algorithm always results in smaller mean deviation distances and meantime distortions relative to the DBA algorithm, regardless of the choice of initial averaging sequence. Even the computational results of the DBA algorithm at the best time are not as good as those of the ADBA algorithm at the worst time. The above experimental results show that the ADBA algorithm is more robust than the DBA algorithm under different initialization conditions.

The human rotation angle is obtained by integrating the y-axis angular velocity data for the medium-intensity backstroke and freestyle of Figure 8 using equation (6), which reveals the period and rhythm characteristics of the swimming action. The maximum and minimum curves can be obtained by the envelope extraction of the rotation angle signal, which corresponds to the left and right action rotation angles in swimming, respectively. Then, according to the zero-point detection method in signal processing, the time

corresponding to when the rotation angle signal passes the zero point is determined, which in turn leads to the period of the left and right-hand movements, i.e., the duration of the left- and right-hand movements. Using the same processing method, the motion data of backstroke and freestyle of three intensities were processed in turn to obtain the rotation angle signals corresponding to them, and the maximum and minimum rotation angles and action periods were extracted.

5. Conclusion

In this paper, a wireless swimming posture measurement experimental device is implemented, which can upload the measurement data in real time with low cost and without affecting the exercise process. The characteristics of swimming motion data are also analyzed, the identification method of swimming posture and intensity is proposed, and the period and amplitude of swimming motion are used as the basis for extracting human body condition. The XYZ acceleration data corresponding to different strokes of equal intensity are significantly different, which can be used as the basis for the identification of human swimming posture. For freestyle and backstroke, the left and right rotation angles of the human body are a simple periodic signal from which the period and amplitude of the human body movements on both sides can be extracted, and the difference and variance between the left and right sides can be used to evaluate the degree of impairment and fatigue of the human body, respectively. In this paper, we designed a swimming data recording and analysis system based on a single LPMS-B2 nine-axis sensor. The user wears the LPMS-B2 sensor on his wrist, collects data such as acceleration during swimming, uploads it to a mobile app and then uploads it to a server to calculate data such as stroke, stroke arm, time, and distance, and displays it on the mobile. The final experimental results prove that the recognition accuracy of the system can meet the actual demand, and the system has a lower development cycle and development cost, which has some application value.

Data Availability

The data used to support the findings of this study are available from the corresponding author upon request.

Conflicts of Interest

The authors declare that they have no known competing financial interests or personal relationships that could have appeared to influence the work reported in this paper.

Acknowledgments

The study was supported by Physical Education Sangmyung University.

References

[1] G. McNarry, J. Allen-Collinson, and A. B. Evans, "Reflexivity and bracketing in sociological phenomenological research: researching the competitive swimming lifeworld," *Qualitative Research in Sport, Exercise and Health*, vol. 11, no. 1, pp. 138–151, 2019.

[2] J. F. Kooij, F. Flohr, E. A. Pool, and D. M. Gavrila, "Context-based path prediction for targets with switching dynamics," *International Journal of Computer Vision*, vol. 127, no. 3, pp. 239–262, 2019.

[3] A. Nassauer and N. M. Legewie, "Video data analysis: a methodological frame for a novel research trend," *Sociological Methods & Research*, vol. 50, no. 1, pp. 135–174, 2021.

[4] M. L. Gavrilova, Y. Wang, F. Ahmed, and P. P. Paul, "Kinect sensor gesture and activity recognition: new applications for consumer cognitive systems," *IEEE Consumer Electronics Magazine*, vol. 7, no. 1, pp. 88–94, 2018.

[5] E. E. Cust, A. J. Sweeting, K. Ball, and S. Robertson, "Machine and deep learning for sport-specific movement recognition: a systematic review of model development and performance," *Journal of Sports Sciences*, vol. 37, no. 5, pp. 568–600, 2019.

[6] W. Chen, B. Liu, H. Huang, S. Guo, and Z. Zheng, "When UAV swarm meets edge-cloud computing: the QoS perspective," *IEEE Network*, vol. 33, no. 2, pp. 36–43, 2019.

[7] C. Xu, K. Wang, P. Li, R. Xia, S. Guo, and M. Guo, "Renewable energy-aware big data analytics in geo-distributed data centers with reinforcement learning," *IEEE Transactions on Network Science and Engineering*, vol. 7, no. 1, pp. 205–215, 2020.

[8] R. E. Johnson, S. Linderman, T. Panier et al., "Probabilistic models of larval zebrafish behavior reveal structure on many scales," *Current Biology*, vol. 30, no. 1, pp. 70–82.e4, 2020.

[9] J. Ren, Y. Guo, D. Zhang, Q. Liu, and Y. Zhang, "Distributed and efficient object detection in edge computing: challenges and solutions," *IEEE Network*, vol. 32, no. 6, pp. 137–143, 2018.

[10] F. Ni, J. Zhang, and M. N. Noori, "Deep learning for data anomaly detection and data compression of a long-span suspension bridge," *Computer-Aided Civil and Infrastructure Engineering*, vol. 35, no. 7, pp. 685–700, 2020.

[11] P. J. Phillips, A. N. Yates, Y. Hu et al., "Face recognition accuracy of forensic examiners, superrecognizers, and face recognition algorithms," *Proceedings of the National Academy of Sciences*, vol. 115, no. 24, pp. 6171–6176, 2018.

[12] R. Ranjan, S. Sankaranarayanan, A. Bansal et al., "Deep learning for understanding faces: machines may be just as good, or better, than humans," *IEEE Signal Processing Magazine*, vol. 35, no. 1, pp. 66–83, 2018.

[13] C. M. Ackerman, C. Myhrvold, S. G. Thakku et al., "Massively multiplexed nucleic acid detection with Cas13," *Nature*, vol. 582, no. 7811, pp. 277–282, 2020.

[14] G. T. Reddy, M. P. K. Reddy, K. Lakshmanna, D. S. Rajput, R. Kaluri, and G. Srivastava, "Hybrid genetic algorithm and a fuzzy logic classifier for heart disease diagnosis," *Evolutionary Intelligence*, vol. 13, no. 2, pp. 185–196, 2020.

[15] M. A. K. Quaid and A. Jalal, "Wearable sensors based human behavioral pattern recognition using statistical features and reweighted genetic algorithm," *Multimedia Tools and Applications*, vol. 79, no. 9-10, pp. 6061–6083, 2020.

[16] Z. Tian, C. Luo, J. Qiu, X. Du, and M. Guizani, "A distributed deep learning system for web attack detection on edge

Hindawi
Journal of Sensors
Volume 2022, Article ID 4378718, 11 pages
https://doi.org/10.1155/2022/4378718

Research Article

Construction of an Intelligent Evaluation Model of Mental Health Based on Big Data

Zhang Wei and Liang Yan

Yantai Vocational College, Yantai Shandong 264670, China

Correspondence should be addressed to Zhang Wei; 0613@ldu.edu.cn

Received 6 December 2021; Revised 5 January 2022; Accepted 8 January 2022; Published 27 January 2022

Academic Editor: Gengxin Sun

In this paper, mental health data were used to evaluate the educational effects, in which the high and low scorers of three emotions, autism, positivity, and anxiety, are compared separately to explore the subtle differences in the long-term trends of the sensing traits of people with opposite characteristics. Based on the fusion of multiple kinds of sensing traits, the differences in physical and mental health assessment of positive and negative emotions by different fusion trait approaches are explored, and speech and behavioural traits are fused to build a physical and mental health assessment system for positive and negative emotions. Energy gravity uses physical distance to estimate the residual energy of nodes and considers the energy distribution of downstream nodes. The main work is to combine the data of mental health of higher education students using data mining techniques, to analyze the feasibility study of mental health education of college students. Relevant definitions, classifications, tasks, processes, and application areas of data mining techniques are introduced, and the basic principles of data mining are analyzed in detail. Taking the mental health assessment data of new students as the research object, the decision tree algorithm is used to construct a decision tree model for students with depressive symptoms, and an association rule algorithm is used to data mine the relationship between factors of psychological dimensions. Finally, it can find out the hidden laws and knowledge behind the data information and analyze the relationship that exists between psychological problems and students.

1. Introduction

However, at present, the psychological crisis early warning means in most universities are still relatively traditional and the effect of early warning is limited. On the one hand, the widely used psychological crisis prevention measures include SCL psychological scale screening at the early stage of new students, holding general psychological knowledge lectures and courses, and opening psychological counseling rooms with low penetration rates. However, to a certain extent, these practices do not enable student managers to grasp students' psychological conditions in a timely and effective manner, to make timely interventions for possible crises [1]. The evaluation process and methods should also be simple and practical. Through the research on the construction model of college students' psychological quality and the analytic hierarchy process, the basic process of psychological evaluation of college students based on the analytic hierarchy process can be obtained. On the other hand, with the rapid development of Internet technology, "Internet Education" has made great achievements in the process of modernizing education, and major universities have basically realized the informatization of student management, but the current informatization mostly stays in simple collection, storage, and management of student information by using basic information technology means, combined with literature. It is found that there are relatively few research applications in the screening and early warning of psychological crisis using the precise, real, timely, and effective data brought by informatization to deeply dig the hidden correlation relationship behind. Some of the student data samples most encountered by student managers in their daily work are collected, a psychological crisis early warning model is constructed through data mining related methods, and a related application system is designed and developed with the early warning model as the centre [2]. The

application of this system to student management at the grassroots level can not only make up for some of the missing links in the current electronic office, but more importantly, student managers can use the system to combine several scattered and fragmented student attribute behaviour data to achieve dynamic screening of the list of students who may have psychological crisis from the objective data of daily management informatization and to carry out targeted psychological crisis intervention in combination with the warning rules based on psychological crisis intervention, providing certain decision support and reference for grassroots student management.

Mental health problems are not as easy to detect as physical illnesses, and some people are not subjectively aware of mental illnesses, especially in younger children; some adults are too shy to seek psychological treatment for their abnormal mental conditions, which can seriously affect their quality of life. Secondly, it has been found in studies that people with long-term negative emotions have lower immunity [3]. Further improve the generalization ability of the decision tree model. The system management module is used for administrators to manage the roles, users, and classes in the system; the information collection module is used to collect and manage the basic personal attribute data of students; the performance management module is divided into two parts: course performance and extracurricular activity quantitative score. For some people suffering from chronic diseases, such as hypertension and hyperlipidaemia, long-term negative emotions can accelerate the development of these chronic diseases and lead to more complications. These negative effects due to mental illness may make people more negative and form a negative cycle. That is why physical and mental health conditions need to be identified and treated promptly. Not only have wearable devices been developed, but the high speed of the Internet has made transmission faster. In recent years, based on the Internet, the Internet of Things (IoT) has been birthed, expanding the original network functions as well as developing more functions to be used in more scenarios, bringing interoperability between people and things one step closer. The IoT refers to the interconnection of various sensing devices with sensors and communication with the Internet and telecommunication networks to build a unified network system for the interconnection of everything [4]. Currently, most wearable devices transmit data through Bluetooth, which collects a single type of data and a small amount of data. If wearable devices can be made to combine with IoT technology with longer transmission distance and faster connection to build an online physical and mental health assessment system, it can solve the problem of insufficient real-time questionnaire-based psychological assessment methods.

At present, mental health education has been taken as an indispensable part of higher vocational quality education. As a base for cultivating skilled talents, schools take the comprehensive promotion of quality education as an important work goal, and mental health education is not only the foundation and premise of quality education but also the result of quality education [5]. The interaction of the main functions of each module is analyzed in the form of sequence diagram. The main function points of the score management module include the administrator downloading the course score template and the single quantitative score template and uploading the course score sheet and the single quantitative score sheet, and the head teacher downloads the course score sheet and automatically generates the quantitative total score sheet. Cultivating the health level of higher vocational students is an important guarantee for them to adapt to the market economy and face the future. Institutions have incorporated mental health education into the moral education curriculum system, established special mental health counseling centres, and opened mental health education courses, as well as counseling and psychological census activities for school students. Most schools conduct mental health assessments for students every year, collect psychological questionnaires online through the Internet, store the results in the database, and use school mental health assessment software to conduct a simple situation analysis and result statistics on college students' psychological problems. However, these traditional data analysis methods can only obtain superficial psychological information, not scientific and important knowledge, resulting in low accuracy of prediction. In this paper, we attempt to apply data mining techniques to the study and analysis of student mental health data. Through the application of data mining technology, valuable knowledge hidden in students' psychological problems is unearthed, and this important knowledge is used to predict the mental health status of college students, providing a scientific basis for the prevention and solution of mental health problems, making mental health education work more targeted and effective, and improving the level of mental health education workability.

2. Related Works

After more than a century of development, school mental health education has formed a more complete theoretical system and operational system, and it plays an active and important role in the education system. As a discipline with vitality and practical value, school mental health education has received wide attention and developed rapidly in developed countries. With this attention, mental health education has a good environment for development and has formed a complete system structure in theory and practice. Mental health education is a compulsory subject for students, as an important part of their learning, and its purpose is to adapt to the diversity, differences, and comprehensive development of students through mental health education [6]. The evaluation-related data is derived from the higher vocational student mental health evaluation system. The processing operation depends on the amount of data. If the data to be processed is relatively small, you can fill in the empty value according to the law; if the data to be processed is relatively large, you can find a value to fill in the empty value. Mental health educators play six main roles: counsellors of academic life, health care providers of mental health, guides of moral thinking, discoverers of psychological potential, facilitators of psychological development, and guides of career selection and employment. Mental health counseling

institutions in universities are equipped with special funds to ensure the effective implementation of activities, and a strong team of psychological educators has been formed, with the cooperation of medical staff and student administrators, which has a great influence and high status in Japanese university education [7]. Mental health education has become an important part of moral education in schools, and the psychological study of students has become an important task for educators [8].

Most of the institutions have started to conduct psychological screening activities for students at the early stage of their enrolment and have established mental health records for students, established mental health counseling centres to provide psychological counseling services for students at school, and offered mental health education courses to cultivate and improve the psychological quality of students [9]. The students must make the transition from high school to college, from adolescence to adulthood, to build up an independent and mature personality structure, and step by step to break away from financial and psychological dependence on their parents [10]. In the process of such transition, they face various difficulties and frustrations and opportunities and face competitive pressure. A considerable number of higher vocational students are unable to handle the difficulties they encounter correctly, making them feel lost and confused, and some of them even develop psychological disorders. To make students develop comprehensively, they must first have a good and healthy mind to form a stable and healthy personality [11]. With a healthy mind, we can face difficulties and setbacks in life, learning, and emotions; actively cope with challenges and competition and other pressures; face success and failure optimistically; and face gains and losses frankly. The reality shows that due to objective factors such as parental pampering and spoiling, a large proportion of higher vocational students are not capable of solving problems independently. If they cannot solve their confusion and perplexity in time, they will develop psychological disorders overall [12].

Then, realize the function of collaborative sensing, with key technologies such as context-aware technology, massive information processing technology, task-driven large-scale autonomous networking technology, and multiple communication network fusion technologies, with distributed, cross-level, and self-learning collaborative processing capabilities to provide intelligent, accurate, and diversified information services. It has some support for the selected data set. The function of the algorithm is to extract a set of items with a high degree of support and to extract a rule higher than the minimum confidence level from the generated rule. The algorithm's strategy is to repeatedly reduce the minimum support until a specified number of rules are found within the minimum confidence range. Finally, the purpose of ubiquitous aggregation is to realize the aggregation of massive information with information aggregation theory, fuzzy control technology, ubiquitous heterogeneous network, artificial intelligence, bionic sensors, nanomaterials, biochips, and other technologies to produce new information with application value; to realize the interconnection of anyone, any object, any time, and any place; and to trigger innovation of application and service modes. Thus, the purpose of ubiquitous aggregation is ultimately achieved.

3. Mental Health Data Collection and Analysis

3.1. Design of Mental Health Data Collection. A wireless sensor network (WSN) is a distributed sensor network that senses the state of an object and forms a data-based information collection using smart sensors connected to it and uses wireless communication to form a dynamic and secure full-volume transmission of information data. Its connection includes both wired and wireless and is a network that is flexibly organized according to needs and site conditions. The organization form has the ability of intelligent multipath hopping transmission and has good self-organization in functional characteristics [13]. The intelligent wireless sensor network is the product of the integration of computers, information processing, embedded computing, communication, and sensor technology, which is a new method of information acquisition and processing. Smart wireless sensor networks have many advantages such as high flexibility, low maintenance cost, high detection accuracy, high fault tolerance, and a large amount of processed information, which are widely used in national defense and security, infrastructure operation and maintenance, ecological and environmental monitoring, health management, etc. Decision support system generally consists of interactive language system, problem system, database, model library, method library, and knowledge base management system. Through the storage and processing of a large amount of information and data in the database, it can assist decision-makers to achieve a higher-level and more scientific decision-making capabilities. Increase the relevant model base and the corresponding model base management system to effectively organize and store the models, can realize the database and model base. It is different from Msl data processing. Therefore, the development and application of this system have played a very good early warning role in promoting the mental health of vocational students and provided effective technical support for the informatization of mental health management. Through the analysis and mining of the evaluation information, we have obtained many objective factors that affect the mental health of college students.

The first stage is the preparation for the long-term physical and mental health experiment, which is guided by researchers specializing in mental health, who select participants from their usual contacts and determine their suitability for the experiment through an initial questionnaire and other tests. We also sign an ethical agreement with the participant before the start of the experiment to ensure that the data is used only for this study. A common heart rate sensor is the pulse sensor, which converts the detected pressure change in the pulsating artery into a more visually observable electrical signal. There is also a noncontact heart rate sensor—an optical heart rate sensor. Light waves are first shone inside the skin through a light emitter consisting of two light-emitting diodes; then, the light frequencies refracted by the wearer are captured, and finally, these analogy signals are converted into digital signals for calculating heart rate data, as shown in Figure 1.

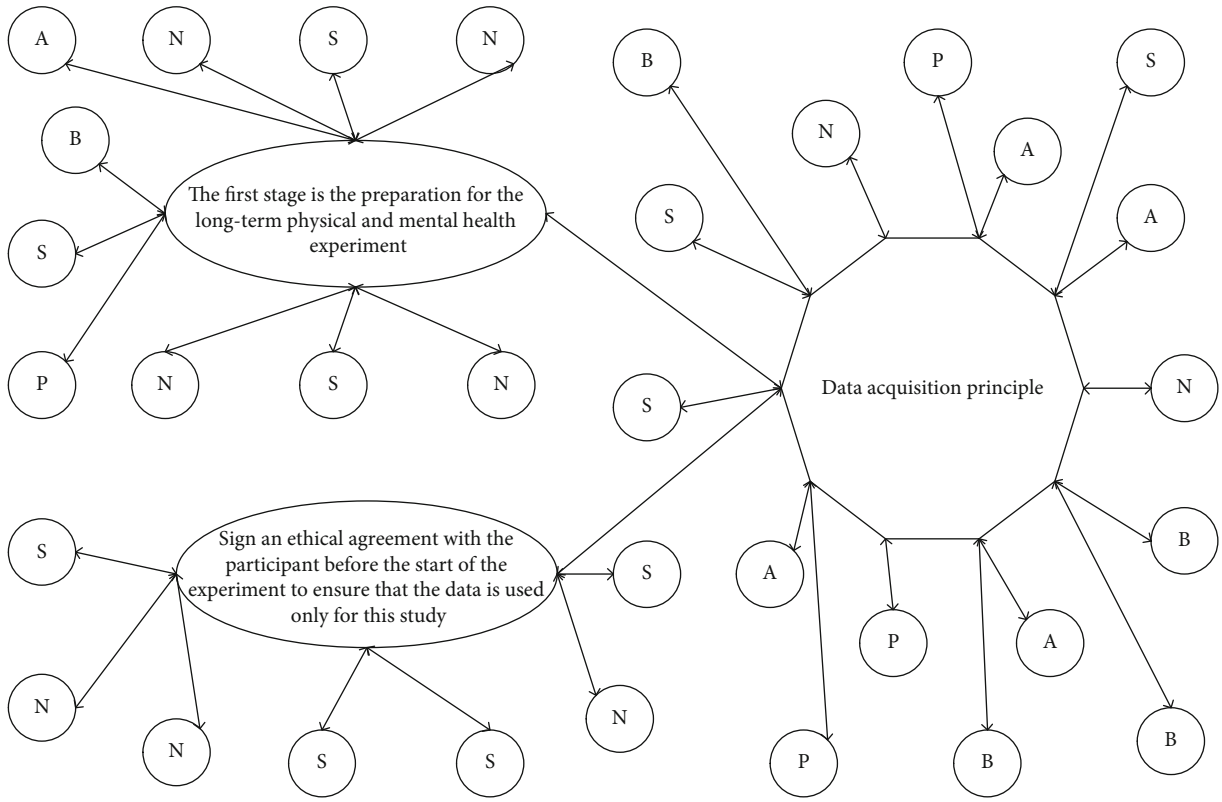

Figure 1: Data acquisition principle of 5G wireless sensor network.

In the long production process, the physical state of workers will change with the duration of work, such as relaxation or tension, energy fatigue, or fullness. These changes of workers will have a direct impact on construction safety and efficiency, so scientific means of collecting and analyzing physiological and psychological data are necessary [14]. A timely grasp of workers' status not only can better understand their work habits, reasonable adjustment of work arrangements, to achieve personalized production management. Combined with correlation analysis, people with autistic tendencies will not only close themselves psychologically but also manifest themselves in daily life activities and are often unwilling to participate in activities. It can also adjust the workers' state in time to help enterprises to do a good job in the management of workers' psychological and physical training and timely regulation of workers' emotions. To maximize the output efficiency of the production line at the lowest cost, key workstations should be managed first, because the efficiency of key workstations is directly related to the overall efficiency of the production system. In the case of sufficient funds, it can be gradually applied to the whole production line to prevent serious problems in some common workstations and bottlenecks in production, which will affect the work of subsequent lines. Based on this, neural industrial management is based on traditional industrial engineering, combined with workers' psychological and physiological data collection equipment and physical state analysis algorithms to control the overall situation and effectively achieve a more humane production and intelligent manufacturing.

The database used in this case is MySQL, which has good performance even in the case of millions of data and has a good fault-tolerant recovery mechanism with multiple levels of isolation mode. All the sensing data collected by this wearable device is uploaded to the cloud server side, and the server stores the data in the database [15]. This time, SD card is also used to persist the data considering data redundancy backup. Since each person has about 3 million sensed data per day, the data is handled in a split table, with a new data table for each person per day, and the data table naming is implemented using a combination of user number and date, as shown in Table 1.

Caching design is an important part of the server side. Data is usually stored in relational databases, and the overhead associated with each request to the database is very high because the data is persisted in the disk and frequent requests inevitably bring performance degradation. Most people request the same data for a short period, and these data are called hot data. For hot data, it can be kept in the place where the requests are faster, that is, the importance of caching; this time, Redis is used as a cache. Redis is an open-source in-memory data structure store that supports data structures like strings, hashes, lists, collections, and sorted collections with range queries. The main data structures used for this data are strings, which are used to cache user account information, and lists, which are used to cache user data for the last few days, which are bidirectional and can add or remove data left or right. For hot data in the cache, when the data in the database is updated, the cache needs to be updated at the same time, and the consistency of the data in the cache and database needs to be ensured.

Table 1: Table of users in the database.

Field	Type	Field description
id	Int	User id student number
Time_date	Int	Data generation time
Panas	Int	PANAS scale score
neo_ffi	Int	NEO_ FFI scale score
bdi	Int	BDI scale score
stai	Int	STAI scale score

That is, the attributes are closely related to each other, and a change in one or more of them leads to a change in the others. The purpose of the analysis is to find hidden relationships in large data sets and to uncover unfamiliar knowledge [16]. The analysis of association rules is to find the pattern of events that occur and lead to the occurrence of other events in time or sequence. It is mainly used to discover unknown object classes in large amounts of data. It requires the process of directly confronting the source data and classifying it into different classes so that there is a similarity between similar objects and a difference between different classes of objects. Cluster analysis is the process of dividing the data into categories based on some similarity and analyzing these constituent classes. By looking in the data set to find data that has incongruities with other classes, these small patterns of anomalous results are generally the result of problems with the information itself or execution errors. Usually, the isolated points found are generally discarded as noise or anomalous data. However, in fraud monitoring of unusual responses to unusual credit cards or disease treatments, isolated point data analysis is very important. The design of the collection device is done in terms of two parts: the energy collection antenna and the energy conditioning circuit. The specific composition and structure of the antenna model and the conditioning circuit are determined.

3.2. Evaluation of Mental Health Effectiveness. The algorithm optimal test attribute is based on the choice of information first. The selection of the test attribute is determined by the attribute with the highest value of information gain. The sample-set partitioning is determined by the values determined by the test attributes, and different values are taken to divide the sample set into multiple subsample sets [17]. Also, the nodes corresponding to the sample set on the decision tree generate new child nodes. According to the principle of decision tree algorithm, for the instability of the sample set after partitioning to distinguish the quality, if the information gain value is low, the measurement uncertainty will be large; on the contrary, the information gain value is high, the measurement uncertainty will become small. So, the decision tree algorithm generally determines the test attribute by selecting the attribute with the maximum information gain at any nonleaf node; in such an environment, we can obtain a smaller decision tree by partitioning technique operation. Major colleges and universities have basically realized student management informatization, but most of the current informatization only stays in the simple collection, storage, and management of student information using basic information technology. Combined with literature surveys, it has been found that in the screening and early warning of psychological crisis, there are relatively few research on using the accurate, true, timely and effective data brought by informatization to deeply mine the implicit relationship.

$$I\left(s_1^2, s_2^2, \cdots, s_n^2\right) = \sum_{i=1}^{n} P_i \ln\left(P_i^2\right),$$
$$E(A) = \sum_{i=1}^{n} \frac{s_1 + s_2 +, \cdots, +s_n^2}{S} I\left(s_1, s_2, \cdots, s_n^2\right). \quad (1)$$

The above process is recursively invoked for all but the selected attributes, producing other attributes as subnodes and branches when used as nodes, which in turn produces a complete decision tree model. As a more typical learning algorithm in decision trees, the focus of the algorithm is to use the information gain of the nodes to determine the measurement attributes, allowing the classification gain of the largest category to be obtained when computing all nonleaf nodes, which in turn makes the data set full after classification to be the smallest. The general depth of the tree is reduced by this solution, allowing for a reasonable increase in classification efficiency [18]. The use of hierarchical analysis as a method of psychological assessment of college students is to stratify college students' psychology from the perspective of hierarchical analysis; firstly, in order to ensure the validity of the model establishment, it is required that the logic between college students' psychological hierarchical criteria and the principle of consistency test of hierarchical analysis should be the same; secondly, the establishment of psychological quality assessment model should be based on the practical application of college student's education and training. The purpose of the psychological assessment model of college students is to provide strong data support for the psychological health assessment of trainees and ultimately serve the education and training of military colleges and universities, so the collected psychological quality data of trainees should be real and effective, and the assessment process and method should be simple and practical. Through the study of college students' psychological quality construction model and hierarchical analysis method, the basic process of college students' psychological assessment based on the hierarchical analysis method can be obtained, as shown in Figure 2. More importantly, student administrators can use the system to combine several scattered and fragmented student attribute behaviour data to dynamically screen out the list of students who may be in psychological crisis from the objective data of daily management informatization and combine it with the basis; the early warning rules carry out targeted psychological crisis intervention to provide certain decision-making support and reference for the management of grassroots students. Seventeen relevant attributes were selected as research data to further explore the mental health status of students as reflected by these attributes

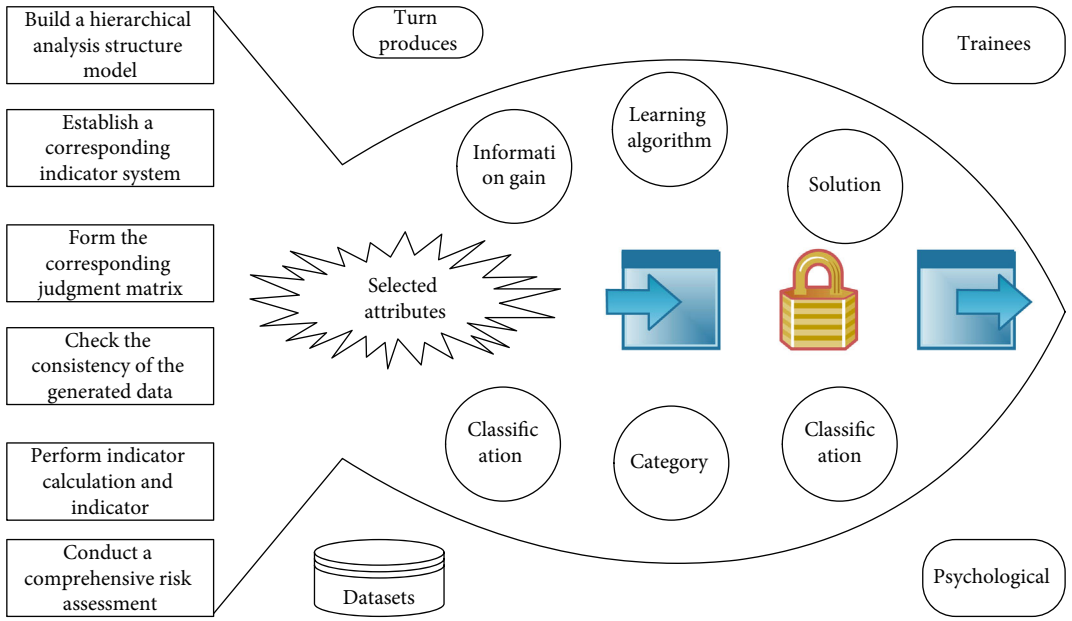

Figure 2: Basic process of psychological assessment of military cadets based on hierarchical analysis.

under different combinations of values. To ensure the accuracy of the research results, this paper simulates the data acquisition in actual student work, and 863 undergraduate students were collected as the research sample to obtain new, respondent-approved research data [19].

The data collection was conducted utilizing an online questionnaire, and the self-administered scale was used to understand students' personal information, such as gender, grade level, academic status, participation in extracurricular activities, and family situation; the results of the Family Closeness Scale were used to obtain information about the student's family of origin, which led to data related to the type of family relationships; and the scores of the Psychological Crisis Signs Checklist were used to assess whether students had a psychological crisis. Since there were some errors and missing data in the collected sample data after the data were sorted, cleaned, and integrated, a total of 847 complete records were finally obtained for the study.

$$\begin{aligned} \text{ACC} &= \frac{\text{TP} - \text{TN}}{\text{TP} + \text{TN} + \text{FN} + \text{TN}}, \\ \text{Precision} &= \frac{\text{TP}}{\text{TP} + \text{TN} + \text{TN}}, \end{aligned} \tag{2}$$

which indicates the ratio of the number of correctly classified positive samples to the total number of samples whose true class is positive.

$$\begin{aligned} \text{Recall} &= \frac{\text{TP}}{\text{TP} + \text{TN}}, \\ I(s_1, s_2, \cdots, s_n) &= -\sum_{i=1}^{n} P_i \ln\left(P_i^2\right) \end{aligned} \tag{3}$$

When applied to more scenarios, the intercommunication between people and things is one step closer. The Internet of Things means that various sensing devices with sensors are connected to each other and communicate with the Internet and telecommunication networks to construct a unified network system that connects everything. The crisis warning module is the core function of the system, which extracts the data information required for the psychological crisis warning model from the data collected and stored by the above-mentioned functional modules to carry out dynamic warning of students' psychological crisis; the article publishing module is mainly used by the administrator to issue targeted notices and articles of mental health education for student users according to the status of crisis warning, as shown in Figure 3.

After logging into the system as a super administrator, you enter the psychological crisis early warning module. To increase the extensibility of the system, considering that the training set data may be expanded to optimize the model in later work, the model update interface is set to leave a good implementation channel for future updates of the psychological crisis warning model. If the model does not need to be updated, the current model can be applied to filter the warning list of existing student users in the system through the one-click warning function, and the list will be displayed on the interface; the specific information displayed in the list includes class, student number, name, contact number, and warning rule; and the administrator can pay attention to the real state of these students who may have a psychological crisis in a timely and targeted manner according to the content of the warning rule prompt. The main functional modules of the application system centred on the early warning model include the system management module, information collection module, grade management module, leave approval module, psychological crisis early warning module, and article publishing module. It also includes psychological counseling and psychological survey activities for school students. Most schools conduct mental health assessments

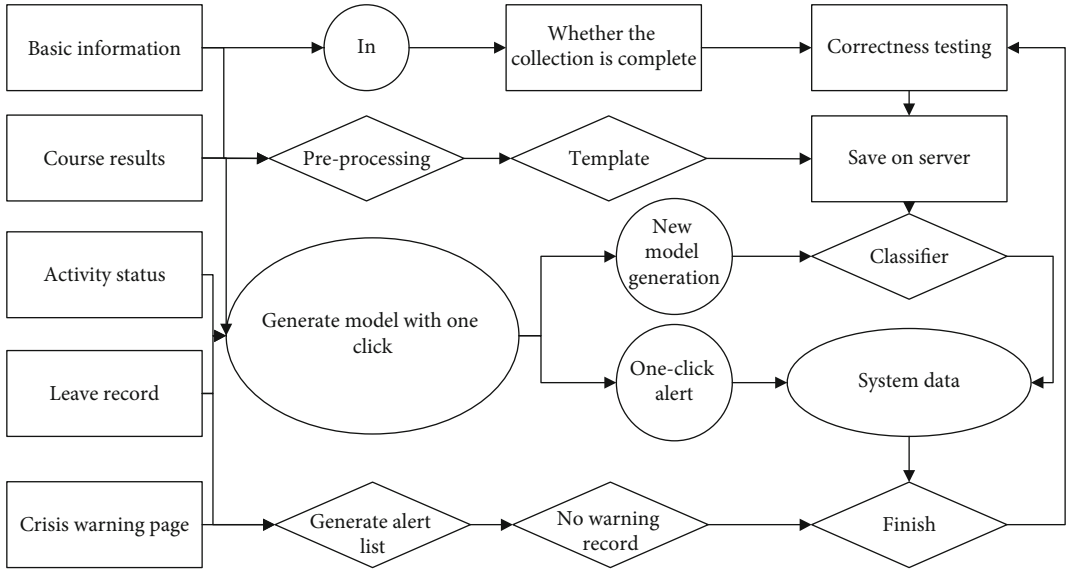

Figure 3: Flow chart of the psychological crisis warning module.

of students every year, collect psychological survey questionnaires online through the Internet, and store the results in a database. Through the school mental health assessment software, simple status analysis and result statistics of college students' psychological problems can be carried out. This subsection analyzes the process interaction of the main function points of each module in the form of a time sequence diagram. The main function points of the grade management module include downloading course grade templates and single quantitative score templates by administrators, uploading course grade sheets and single quantitative score sheets, downloading course grade sheets by classroom teachers, and automatically generating total quantitative score sheets. The main functions of the leave approval module include students initiating leave requests, class teachers, and super administrators reviewing whether the leave requests within their authority are reasonable according to the actual situation and then choosing to approve or reject the leave approval after making judgments.

The preprocessing mainly includes frame splitting and windowing operations. To ensure the effectiveness of the acquisition and the power consumption, the frequency of the voice acquisition is set to 8 KHz; i.e., there are 8000 acquisition points per second, and the original voice data is not stored in the terminal. For the voice signal, it is not suitable to process 8000 data at one time, so the data needs to be divided into 512 points for one frame, that is, 64 milliseconds, and the voice is continuous, so there will be a 25% overlap between each frame, which improves the continuity and smoothness after data processing. The change in heart rate also reflects the psychological change of people, and the calculation of heart rate is especially critical. The common methods of heart rate calculation are ECG, PPG, bioimpedance, etc. This time, the heart rate is calculated using the photoelectric volume pulse wave tracing method PPG optical signal; this method uses a small size of hardware that is easy to wear on a bracelet. Using PPG to calculate the heart rate, the signal is converted by converting the optical signal into an electrical signal and the electrical signal into a digital signal. The specific principle is that when light hits the skin tissue, the reflected light will be attenuated. The degree of attenuation varies depending on the site of irradiation; e.g., the absorption of light by skeletal veins and connecting tissues remains almost constant, corresponding to equal light irradiation, returning similar light values. Through the storage and processing of a large amount of information and data in the database, it can achieve a higher level and more scientific decision-making ability to assist decision-makers, increase the relevant model library and the corresponding model library management system, effectively organize and store the model, and make the database realize organic integration with model library. This is not the case with arterial irradiation, where there is blood flow and changes in blood flow can affect the absorption of light.

4. Results and Analysis

4.1. Results of Mental Health Data Collection in Multimodal. Data selection is a common data processing method for data analysis and mining, and it is the first step of data preprocessing operation. Due to the large size of the original data set, mining and analyzing all the data sets will take a lot of computing resources and computing cycles, so the data selection operation of the data set is needed to reduce the impact on the results. Based on the objective of the mining project, the information records in the data set can be assembled and found out, which can make the data content be streamlined, and the internal connection between the attributes and the law hidden behind the data can be discovered. If the data to be processed are relatively small, the null values can be filled according to the rules; if the data to be processed are relatively large, a value can be found to fill the null values. In this case, 48 students who did not participate in the assessment were removed, and the psychometric

information of the students who participated in the assessment met the research specification. Students' basic information data came from the school academic affairs management system because some students did not improve their personal information in time after enrolment, resulting in the absence of some family status, whether single parents and other information, of which 86 students with more missing items were no longer used as research subjects. There is also a non-contact heart rate sensor, that is optical heart rate sensor. First, the light wave is irradiated into the skin through a light emitter composed of two light emitting diodes, and then, the light frequency refracted by the wearer is captured, and finally, these analogy signals are converted into digital signals for calculating heart rate data. After the cleaning process of the data, a total of 1820 records can be used for data mining operations.

The filtering rules are filtered based on the support, which is the number of instances found that meet the rules. Confidence is the ratio of instances determined by the conclusion, and support is the number of instances that satisfy the rule. Rules with high support/confidence are found, but usually, the confidence is not set to 100% to find all rules; even if there are hundreds of rules, many of them have very low support. Typically, the minimum confidence is set to a minimum to find the maximum support at the minimum confidence level. An item set is a combination of attribute-value pairs, which has some support for the selected data set. The function of the algorithm is to extract the high support item set from the generated rules and extract the rules above the minimum confidence level. The strategy of the algorithm is to iteratively reduce the minimum support until a specified number of rules are found within the minimum confidence range. Association rules and classification rules require different skills when used, the former being significantly larger than the latter. So, support and confidence are two important metrics for association rules, as shown in Figure 4. With sufficient funds, it will be gradually applied to the entire production line to prevent serious problems in some ordinary stations and production bottlenecks, which will affect the subsequent work of the assembly line.

The algorithm energy balance is poor as it does not consider energy balance and uses the shortest path which makes the network energy consumption concentrated in important nodes, resulting in overburdening the energy consumption of important nodes too fast. The node mortality rate of the GCAR algorithm in this section ranges from 0.4% to 4.4%, and the average increase rate after 100 rounds of simulation is only 26%, which is lower than that of the MOPC algorithm and CCOR algorithm. The energy gravity introduced by the GCAR algorithm integrates the node residual energy, node forward energy density, and the sending energy consumption directly related to the distance, which can ensure the energy consumption is at a low level and make the energy consumption more evenly distributed among the nodes. When it senses that the energy consumption rate of important nodes is too large, the algorithm adaptively adopts alternative routes to temporarily protect important nodes and make full use of other nodes to slow down the death of the first node of the network and extend the network survival time, as shown in Figure 5.

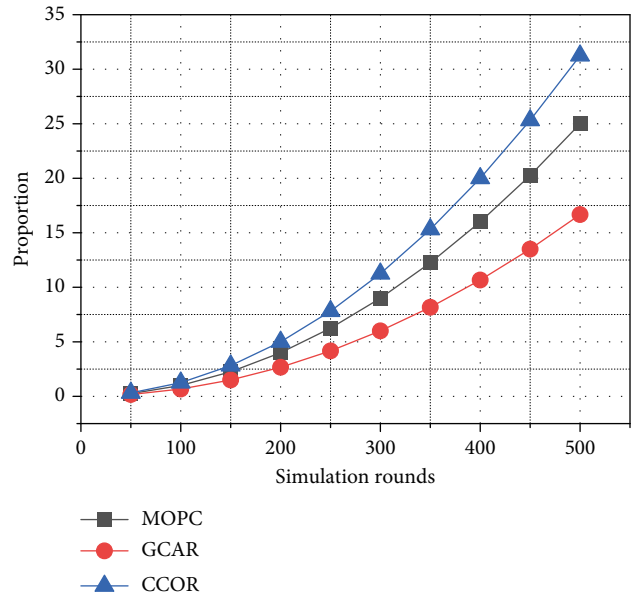

Figure 4: Comparison of the percentage of node deaths.

Figure 5 gives the variation of the average packet energy consumption with simulation time. From the beginning of the simulation to 200 seconds, the average energy consumption of all three algorithms increases, but GRCS has the fastest growth rate, up to 8.56%; the maximum growth rate of GRCS is 6.67%, and the maximum growth rate of TADR algorithm in this paper is the lowest, only 5.33%. And there are differences between objects of different types. Cluster analysis divides and categorizes data based on a certain similarity and analyzes the process of forming these categories. After 200 seconds, the average packet energy consumption of the GRCS algorithm increases slowly with time, while TADR and VFTR remain essentially the same. The reason for this is that the TADR and VFTR algorithms consider traffic balancing in routing decisions, which results in energy balancing of the nodes. Since the node queue length can effectively measure the load of nodes, the network load is balanced to a certain extent by constructing a virtual potential energy field in the TADR algorithm, which makes the average energy consumption of packets relatively low. And the contour external force is established in the VFTR algorithm based on the load difference between the current node and neighboring nodes and dynamically adjusts its occupied weight, which more effectively avoids congestion and finally makes the packet average energy consumption index benefit from the improvement of transmission success rate.

5. Results of the Evaluation of Mental Health Effectiveness

Data mining techniques were applied to the mental health data of senior students by using basic student information and SCL90 psychometric scale data as the training set. The results obtained from the analysis of mental health problems of higher vocational students were compared with the data mining results in the mental health assessment system, and

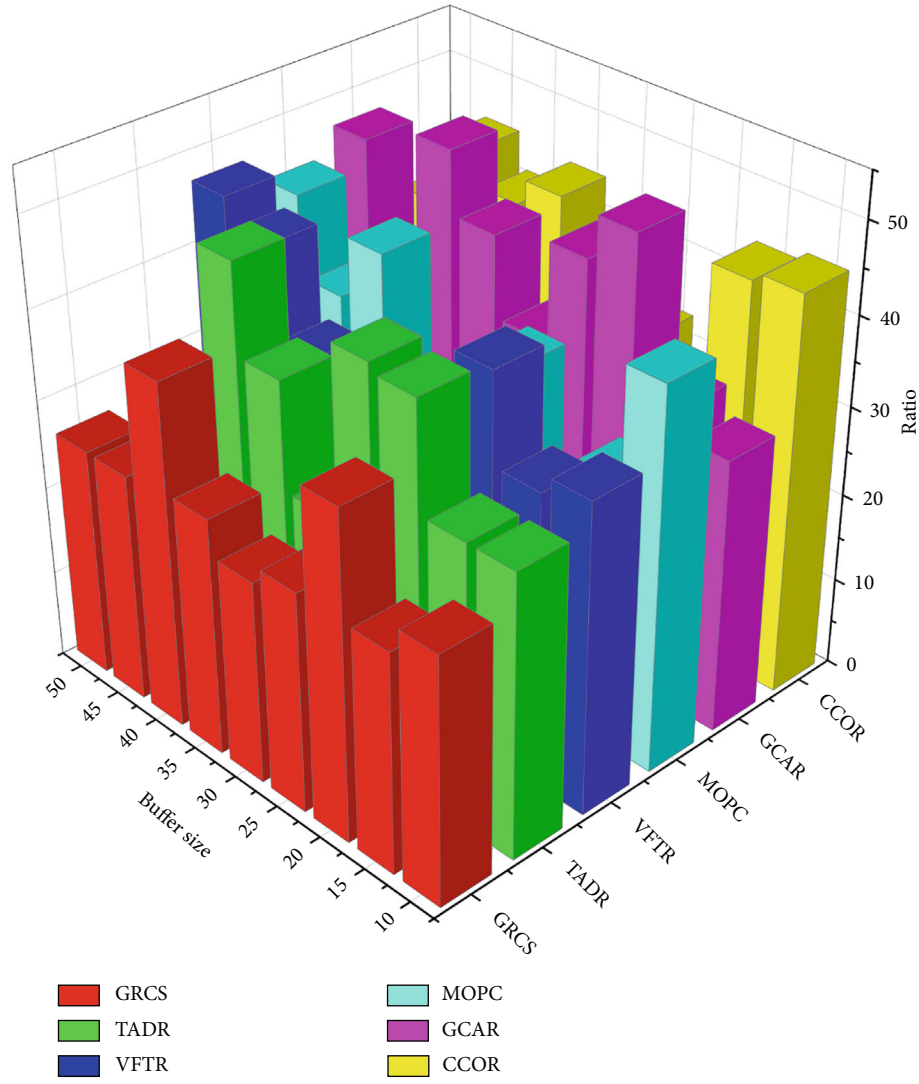

Figure 5: Network throughput rate versus node cache queue.

the analysis rules obtained from the system mining were consistent with the experience and psychological perceptions in psychological counseling, which confirmed that the data mining techniques applied to the research and analysis of mental health data of higher vocational students are implementable. Therefore, the development and application of this system play a good early warning role in promoting the mental health of higher vocational students and provide effective technical support for the informatization of mental health management. Through the analysis and excavation of the assessment information, we obtain that many objective factors are affecting the mental health of college students. Therefore, in the future mental health consultation work of college students, we target to improve the awareness of college students' mental health through many ways and help them solve the problems in psychological aspects, as shown in Figure 6.

Both TADR and VFTR are characterized by finding idle or less congested you-back paths based on node queue length, which reduces the occurrence of congestion to some

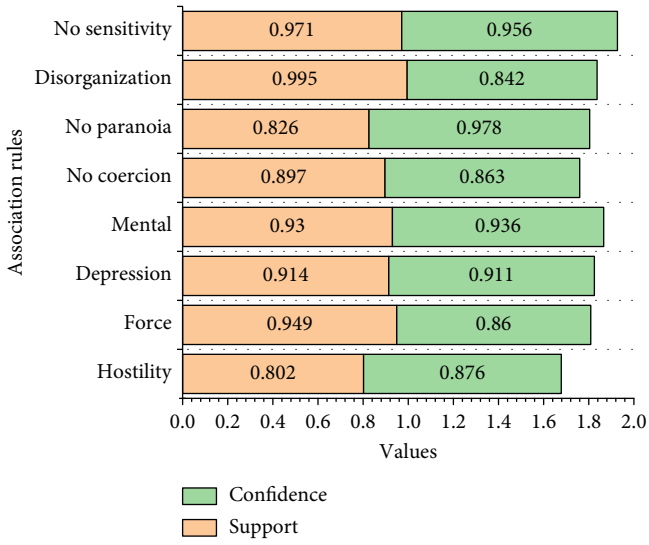

Figure 6: Generating association rules.

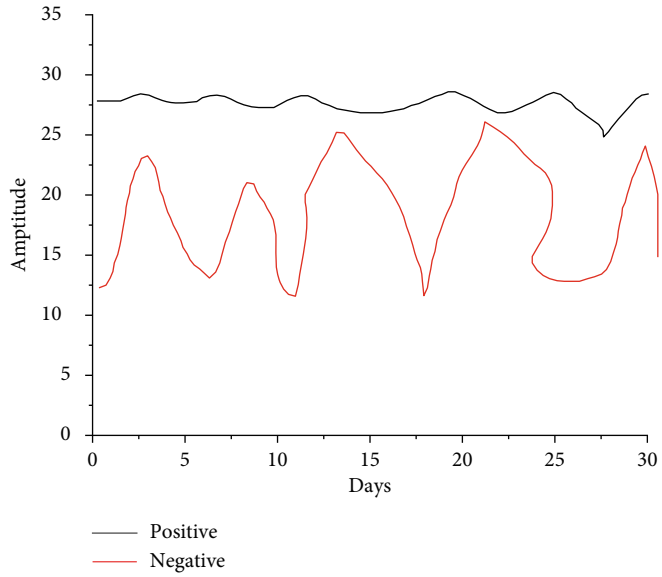

Figure 7: Comparison of the characteristics of positive and negative emotional.

extent but causes an increase in the number of packet transmission hops, so both have relatively the highest average delay. Moreover, since the potential field of TADR based on node hops only ensures that the route satisfies the minimum number of hops and avoids route backhaul, while in VFTR routing, decisions need to be made based on the geographical location of the nodes and route backhaul is avoided by defining forward transmission nodes; the average delay of VFTR is 181 ms, which is slightly lower than that of TADR at 192 ms. The experimental participants will be subjected to testing; the purpose of conducting preexperimental testing is to test whether the participants' are honest, useful for long-term drug use, and have bad habits, which will ensure that the selected participants will be able to complete the whole experiment properly. In addition, all participants are selected after an initial assessment by a psychological professional. All selected volunteers will sign an experimental informed agreement before conducting the experiment, which describes the detailed experimental steps, the use of the equipment and instructions for the use of the IoT platform. In addition, ethics are included in the experimental informed agreement to ensure that this collected experiment is not disclosed and all data used are for this study, as shown in Figure 7.

Figure 7 shows the curves of the average sum of the acceleration characteristic frequency domain amplitudes and the maximum value of the acceleration shape characteristic variance for the two experimenters with high and low scores, respectively. As can be seen in the left panel, except for the high scorer who has a large rise and fall (probably due to interference from high frequencies), the amplitude of up to several days is below that of the low scorer, and the high scorer has a much flatter rise and fall of data variation. In the right panel, the high scorers are slightly below or equal to the low scorers for some time but contain a few days where the high scorers have low values. Combined with the correlation analysis, people with autistic tendencies not only close themselves off psychologically but also show it in their daily life activities, often being reluctant to participate in them.

In most cases, the luminance minima for the positive emotion participants were greater than those for the negative emotion participants. The classification gain of the largest category can be obtained, so that the data set is the smallest after classification. The general depth of the tree is reduced by this solution, so that the classification efficiency is reasonably increased. In the left panel, which shows the speech feature energy maxima, the data for the positive emotion participants are also largely larger than the negative emotion participants in the graph, and the fluctuations are more pronounced for the negative emotion participants. This is also consistent with the usual life perception that optimistic people speak loudly and are more communicative in their daily speech. The negative mood group, on the other hand, was more passive and would appear rushed when communicating and speaking, and their voices appeared low.

6. Conclusion

The wearable bracelet with integrated multisensors is designed, and based on IoT technology, the system number of physical and mental health characteristics with high correlation with sensor features was as high as 20, which further provides a basis for using multiple features to assess multiple physical and mental health conditions. The application system was designed and implemented with the psychological crisis early warning model in mind. The detailed requirement analysis, general design, and detailed design of the system were carried out in conjunction with the actual work of the users. It was determined that the system users are divided into three roles: students, class teachers, and super administrators, and contain six functional modules, namely, system management module, information collection module, grade management module, leave approval module, psychological crisis warning module, and article publishing

module. The system is developed with Spring MVC as the back-end framework, JSP as the front-end language, and MySQL as the database, which realizes all the functions required by users. The system provides a good platform for the effective application of the psychological crisis early warning model. In addition to providing data support for the early warning model, the basic module also optimizes the module functions after the actual user demand research, which enhances the practicality of the system and provides some assistance for the electronic office of student managers and the dynamic monitoring of student psychology.

Data Availability

The data used to support the findings of this study are available from the corresponding author upon request.

Conflicts of Interest

The authors declare that they have no known competing financial interests or personal relationships that could have appeared to influence the work reported in this paper.

References

[1] V. Badiger, S. Bhalerao, A. Mankar, and A. J. Nimbalkar, "Wireless sensor network-assisted forest fire detection and control firefighting robot. SAMRIDDHI: A Journal of Physical Sciences," *Engineering and Technology*, vol. 12, Supplement 2, pp. 50–57, 2020.

[2] L. Yan, Y. He, and Z. Huangfu, "A fish swarm inspired holes recovery algorithm for wireless sensor networks," *International Journal of Wireless Information Networks*, vol. 27, no. 1, pp. 89–101, 2020.

[3] Y. Zhang, X. Ma, J. Zhang, M. S. Hossain, G. Muhammad, and S. U. Amin, "Edge intelligence in the cognitive Internet of Things: improving sensitivity and interactivity," *IEEE Network*, vol. 33, no. 3, pp. 58–64, 2019.

[4] J. Liu, J. Wan, B. Zeng, Q. Wang, H. Song, and M. Qiu, "A scalable and quick-response software defined vehicular network assisted by mobile edge computing," *IEEE Communications Magazine*, vol. 55, no. 7, pp. 94–100, 2017.

[5] K. M. Kumaran and M. Chinnadurai, "Cloud-based robotic system for crowd control in smart cities using hybrid intelligent generic algorithm," *Journal of Ambient Intelligence and Humanized Computing*, vol. 11, no. 12, pp. 6293–6306, 2020.

[6] M. Wu, X. Huang, B. Tan, and R. Yu, "Hybrid sensor network with edge computing for AI applications of connected vehicles," *Journal of Internet Technology*, vol. 21, no. 5, pp. 1503–1516, 2020.

[7] J. Wang, F. Wang, Y. Wang, D. Zhang, L. Wang, and Z. Qiu, "Social-network-assisted worker recruitment in mobile crowd sensing," *IEEE Transactions on Mobile Computing*, vol. 18, no. 7, pp. 1661–1673, 2019.

[8] H. Cheng, L. Wu, R. Li, F. Huang, C. Tu, and Z. Yu, "Data recovery in wireless sensor networks based on attribute correlation and extremely randomized trees," *Journal of Ambient Intelligence and Humanized Computing*, vol. 12, no. 1, pp. 245–259, 2021.

[9] H. Yao, P. Gao, J. Wang, P. Zhang, C. Jiang, and Z. Han, "Capsule network assisted IoT traffic classification mechanism for smart cities," *IEEE Internet of Things Journal*, vol. 6, no. 5, pp. 7515–7525, 2019.

[10] B. Bhushan and G. Sahoo, "E^2SR^2E 2 S R 2 : an acknowledgement-based mobile sink routing protocol with rechargeable sensors for wireless sensor networks," *Wireless Networks*, vol. 25, no. 5, pp. 2697–2721, 2019.

[11] A. Mehto, S. Tapaswi, and K. K. Pattanaik, "A review on rendezvous based data acquisition methods in wireless sensor networks with mobile sink," *Wireless Networks*, vol. 26, no. 4, pp. 2639–2663, 2020.

[12] A. Carie, M. Li, B. Marapelli, P. Reddy, H. Dino, and M. Gohar, "Cognitive radio assisted WSN with interference aware AODV routing protocol," *Journal of Ambient Intelligence and Humanized Computing*, vol. 10, no. 10, pp. 4033–4042, 2019.

[13] S. Liu, Z. Gao, J. Zhang, M. Di Renzo, and M. S. Alouini, "Deep denoising neural network assisted compressive channel estimation for mmWave intelligent reflecting surfaces," *IEEE Transactions on Vehicular Technology*, vol. 69, no. 8, pp. 9223–9228, 2020.

[14] V. Sneha and M. Nagarajan, "Localization in wireless sensor networks: a review," *Cybernetics and Information Technologies*, vol. 20, no. 4, pp. 3–26, 2020.

[15] A. Mukherjee, N. Dey, R. Kumar, B. K. Panigrahi, A. E. Hassanien, and J. M. R. Tavares, "Delay tolerant network assisted flying ad-hoc network scenario: modeling and analytical perspective," *Wireless Networks*, vol. 25, no. 5, pp. 2675–2695, 2019.

[16] Y. Jin, Z. Qian, S. Gong, and W. Yang, "Learning transferable driven and drone assisted sustainable and robust regional disease surveillance for smart healthcare," *IEEE/ACM Transactions on Computational Biology and Bioinformatics*, vol. 18, no. 1, pp. 1–125, 2020.

[17] D. D. Nguyen, H. X. Nguyen, and L. B. White, "Reinforcement learning with network-assisted feedback for heterogeneous RAT selection," *IEEE Transactions on Wireless Communications*, vol. 16, no. 9, pp. 6062–6076, 2017.

[18] Y. Yao and Y. Mizuno, "Neural network-assisted signal processing in Brillouin optical correlation-domain sensing for potential high-speed implementation," *Optics Express*, vol. 29, no. 22, pp. 35474–35489, 2021.

[19] M. Erdelj, E. Natalizio, K. R. Chowdhury, and I. F. Akyildiz, "Help from the sky: leveraging UAVs for disaster management," *IEEE Pervasive Computing*, vol. 16, no. 1, pp. 24–32, 2017.

Hindawi
Journal of Sensors
Volume 2022, Article ID 6599720, 10 pages
https://doi.org/10.1155/2022/6599720

Research Article

Example Analysis of Digital Wireless Mapping Applied to Construction Engineering Measurement

Pengfei Wang, Yanli Wang, and Maohui Wang

Shandong Labor Vocational and Technical College, Jinan 250022, China

Correspondence should be addressed to Pengfei Wang; wangpengfei@sdlvtc.cn

Received 1 November 2021; Accepted 13 December 2021; Published 27 January 2022

Academic Editor: Gengxin Sun

This paper provides an in-depth study and analysis of the measurement of construction projects using digital wireless mapping and illustrates it using examples. Static measurements determine the relative positions between ground points with high accuracy using a baseline vector network composed of simultaneous observations by multiple receivers, using the correlation of errors in space and time. Technology-based on this error correlation, then the distance observation error or coordinate observation error measured by the base station is sent to the mobile station through the data chain to correct the station star distance observation or coordinate value of the mobile station, improving the operational accuracy and efficiency of the mobile station. The measurement avoids the tedious measurement organization work and long-time data collection and postcomputation work of static measurement, and the coordinates of the mobile station can be obtained in real-time. To verify whether the accuracy of the 3D model built by the 3D reconstruction method integrating UAV and camera (air ground) images can meet the accuracy requirements for the installation deviation detection of the assembled building components, the 3D reconstruction of the physical objects was completed by this method. The accuracy of the 3D model built by this method was evaluated by comparing the measurement coordinates of 25 prearranged checkpoints in the 3D model with those of the total station. The test results show that the maximum point accuracy of the 3D model is 2.305 mm, and the average medium error is 2.147 mm, which can meet the accuracy requirements of the installation deviation detection of the assembled building components. The detection of installation deviation of wooden columns was completed by measuring the 3D model, and it was verified that the method is intuitive, fast, accurate, and batch completion of the deviation detection of axis position, elevation, small labour, batch detection of components, and contactless mapping compared with the traditional detection methods.

1. Introduction

New instruments and technologies are needed to improve the traditional surveying and mapping technology to obtain spatial three-dimensional information. Unlike the traditional surveying and mapping measurement technology such as total station and GPS through a single point measurement way to collect data, three-dimensional laser scanning technology can obtain many point cloud data information, to obtain a more fine, complete information data of the object under test [1]. 3D laser scanning technology does not need to contact the measured object when measuring the target object, which can reach the number of hundred thousand points per second, and this efficiency of point collection is incomparable to traditional measurement technology [2]. Point cloud data can express the measured target object in more detail and accurately because of its huge amount of data and strong point density, but this also brings greater difficulties for data computing, processing, use, and storage [3]. A large amount of point cloud data requires high computer configuration, and it often leads to computational crashes and crashes when processing, which affects the efficiency of point cloud data processing and use, and then affects the efficiency of 3D model reconstruction of point cloud data, so point cloud data streamlining is especially important. It is of great significance for the application and development of 3D laser scanning technology and points cloud data to compress the data volume of point cloud data to the maximum extent while ensuring that the target object model features and reconstruction are not

affected [4]. In turn, it affects the efficiency of point cloud data 3D model reconstruction, so point cloud data streamlining is particularly important. In this paper, we take the point cloud data of Nanjing subway station as experimental data, propose an improved method for the deficiency of not being able to retain the target area for point cloud data streamlining, and carry out the streamlining and compression of discrete point cloud data under the condition of avoiding the establishment of a topological relationship between points and points, which preserves the original format of point cloud data from being destroyed and provides a good data basis for the later processing and reconstruction of point cloud data.

The existing data exchange and storage management mode have obvious drawbacks, poor integration and management, and poor visualization. The monitoring of high-speed railway in operation period has the characteristics of long-term, complexity, and wide area, and there is less research on the monitoring data management of high-speed railway in operation period [5]. At the same time, the engineering department, measurement unit, evaluation unit, and the evaluation unit, as the hub to link all units, is an important link for data communication, data quality control, and progress control, while the evaluation system has not been systematically studied. Urban control measurement in urban surveying and mapping projects, and other work and control measurement, are mainly divided into two aspects of plane control measurement and elevation control measurement. Urban control survey is mainly divided into three stages of design, construction. The first is the establishment of the engineering control network and the mapping of the engineering topographic map [6]. These two kinds of measurements are mostly used in the preconstruction survey and design stage of urban construction. The second is the positioning of construction release. The last is the as-built measurement and deformation measurement, which are used for project quality inspection and later evaluation after the construction is finished.

The software system supporting them has been continuously improved, which makes the UAV tilt photogrammetry system have technical support and quality guarantee in various engineering applications. UAVs are widely used in many industries for their advantages such as good stability. Especially in the field of surveying and mapping, UAVs can acquire ground images with high efficiency and are used in many aspects such as drawing high precision medium and large-scale mapping and generating DEM (Digital Elevation Model) models. The various building components obscure each other, and it is difficult to use a single UAV to complete a full range of image data collection of the components, resulting in the lack of data on the obscured parts, holes, and other phenomena in the corresponding parts of the three-dimensional model established based on image data, affecting the measurement accuracy. The camera, with its advantages of free shooting angle and flexible operation, can provide an effective complement to the UAV image. Combining the characteristics and advantages of the UAV and camera, it can complete all-around and high-efficiency image data acquisition of the completed installation.

2. Status of Research

3D reconstruction is an important method to obtain 3D information of an object. In recent years, the technical theory of 3D reconstruction and related software has been increasingly improved, and 3D reconstruction models of physical objects are widely used in mapping engineering, digital earth, urban planning, and other fields. The acquired point cloud data is subjected to a series of operations such as denoising, alignment, thinning, and encapsulation to realize the construction of a 3D point cloud model of the target object [7]; the 3D reconstruction method based on image data is to collect the image data of the object using unmanned aerial vehicles, cameras, and other equipment, based on the photogrammetry principle combined with relevant 3D reconstruction software to realize the automatic reconstruction work of the 3D model of the photographed object [8]. When using 3D laser scanners for all-around measurement of buildings, due to the restricted scanning angle of the instrument, it is often necessary to arrange multiple scanning sites, and the on-site data collection is time-consuming; later, the point cloud data from different sites need to be spliced, and the amount of manual intervention is large; moreover, the amount of point cloud data is huge, and the processing and preservation costs of the data are high [9]. The image-based 3D reconstruction method is becoming more popular with the continued development of drones, cameras, and other equipment, the sensor accuracy continues to improve, and the corresponding technical theory and supporting software continues to improve, with its high-cost performance, high stability, good accuracy, and other advantages in the construction, mapping, and other engineering fields of application [10].

Point cloud data segmentation based on edges is investigated, and an algorithm for point cloud data segmentation using different judgments of point cloud data contours using information gradients and unit normal vector directions is proposed [11]. The original format of the point cloud data is not destroyed, providing a good data foundation for later point cloud data processing and reconstruction. An edge-based point cloud data segmentation method is proposed to use a three-dimensional moving boundary model for data segmentation to reduce the influence of noise in the judgment of point cloud data contours, but the computational efficiency is relatively slow. A region-based point cloud data segmentation study is conducted, proposing point cloud data segmentation based on the normal vector of points and their redundancy as a basis for region growth [12]. The second segmentation uses edge-based segmentation for point cloud data after the first segmentation, which improves the accuracy of the point cloud data segmentation algorithm [13]. The study of multiple point cloud data segmentation is carried out, based on edge and then face-based segmentation of point cloud data, first, the geodesic lines between different points in the point cloud data model are calculated, the contours formed by the segmentation lines are used as separation boundaries, and the point cloud data segmentation is carried out using region growing method [14].

The full building lifecycle is dynamic and includes the full cycle of design, production, construction, and operation and maintenance, up to demolition and recycling. In different stages of this process, the required spatial information of prefabricated components will be different according to specific project tasks, such as the outline dimensions of components in the component production stage, the timely access to transportation routes, vehicle locations, and yard unit locations in the transportation stage, the component positioning control points and lines in the construction and installation, and the floor and room numbers to which the components belong in the operation and maintenance stage, etc. In addition, many scholars consider component coding as an important element of component location information, which is the main basis for quickly identifying, locating, and managing target components from many similar prefabricated components in each project phase.

3. Analysis of Digital Wireless Mapping Applied to Construction Engineering Measurement

3.1. Digital Wireless Mapping Design for Construction Projects. The determination of the appropriate number of elevation and planimetric control points as the basis for topographic mapping is known as control surveying. In the case of plate meter mapping, there are two types of control surveys, namely, root and first-level control surveys. The latter is based on geodetic control points, combined with wire or triangulation methods, in the determination area of relatively uniform distribution, with a high degree of accuracy of the control points to determine; while the former is based on the first level of control, combined with small triangulation of fixed points to measure the way, the mapping needs of control points to encrypt to meet [15]. In addition, it can also be combined with the way of triangulation and elevation measurement to determine the elevation of the control point of the root of the map. Fragmentation measurement is a way of giving the topography as well as the mapping of the features. The terrain or feature points obtained during the mapping process are called fragmentation points. The location of the fractional point planes can be determined in conjunction with the polar method, and the elevation can also be determined by the rules of apparent distance measurement. As a hub for contacting various units, the evaluation unit is an important link in data communication, data quality control, and progress control, and the evaluation system has not yet been systematically studied. The mapping methods can be classified according to the type of instrument used, such as the latitude and longitude instrument and the plate meter mapping method. All the above methods have similar operational processes. Before the mapping work is carried out, mylar or drawing paper is fixed on the mapping board, the coordinate grid is drawn, the control points and contour points are spread, and the mapping operation is carried out after confirming that they are correct. In this process, the plotted or temporarily determined points are used as stations, the levelling plate is placed at the station and oriented, then the telescope is used to align the fragmented points, and the elevation and horizontal distance from the station to the fragmented points are determined in combination with the straight edge, and the edge length is intercepted along the straight edge in combination with the mapping scale, which is the plane position of the fragmented points on the map, and the elevation is marked. Thus, the topographic map is mapped by carrying out mapping activities at each station.

$$\begin{cases} S = T\left(r^2\right), 0 \le r \le 1, \\ P_s(s) = P_r(\mathrm{r})\dfrac{dr}{ds}, r > 1, \end{cases} \tag{1}$$

$$T(r) = \int_0^T \frac{P_r(\mathrm{r})}{dr}. \tag{2}$$

The need to carry out the corresponding measurement work in the preconstruction preparation. This is to get the spatial location of each line to facilitate the construction of the project, especially in the construction process, it is necessary to restore the centreline of each pipeline in the design drawings to the reality of construction accurately. Let us take the construction of a railway as an example. When railway construction is carried out, several measurements are first taken, and the initial measurement data is obtained and then corrected to obtain accurate mapping data. In the preliminary surveying and mapping, the main task point is for the geographical condition along the way, and the mileage data and the corresponding pile numbers are obtained by calculation [16]. Two kinds of cross-sections are drawn out according to the illustrated elevation, and the corresponding engineering data are calculated to obtain a relatively feasible plan, which is then applied in the later construction. The so-called actual measurement is to implement the designed scheme in practice.

$$\frac{dT(r)}{dr} = \frac{d}{dr}\left[\int_0^T \frac{P_r(\mathrm{r})}{dr}\right], \tag{3}$$

$$\left[\int_0^T \frac{P_r(\mathrm{r})}{dr}\right] = \frac{P_r(\mathrm{r})}{dr}\frac{3}{P_r(\mathrm{r}^2)}. \tag{4}$$

But the calculation process cannot be adjusted; parameters are not easy to control. In contrast, histogram matching can select the image with excellent effect as the matching object and correct the histogram of the original image to make it into a prescribed shape. Histogram correction and matching are particularly effective for low brightness image processing. When the sun altitude angle and light conditions in the same period and the same area are the same, the difference between the histogram distribution of the two images near is small. Conversely, there are large differences in the histograms of feature images taken by the camera when the time and external environment are different. In this paper, the target image to be corrected is radiometrically corrected according to the histogram of the reference image (the image with the most suitable image brightness and contrast are selected), so that the gray level interval of the target

image and the reference image is the same, and the purpose of histogram correction is accomplished. Image matching is the process of finding homonymous points between two or more images, and image matching problems are generally solved using image correlation techniques in early research. In UAV photogrammetry, image matching technology is the key to automatically finding homonymous image points and generating orthophoto by null-three calculation, and the matching work can be carried out only through feature information, which mainly points feature, line feature, and area feature, among which, point feature extraction is the mainstream method for feature extraction due to its simple algorithm and low implementation difficulty, as shown in Figure 1. Due to its good stability and low cost, drones can complete large-scale and high-efficiency image data collection of ground objects, and the advantages of data timeliness and scientific have been widely used in many industries, especially in surveying and mapping. In the field, drones can obtain ground images efficiently.

Model light-weighting refers to the compression and extraction [17]. The methods for BIM data model lightweight can be broadly divided into two categories: internal lightweight and external lightweight of the model. Internal lightweight is mainly to delete the redundant information in the model, which usually includes information that is used infrequently, too detailed information, duplicated information, etc., to achieve the purpose of reducing the database [91]. A series of studies have been conducted in this area. They investigated lightweight methods based on component merging and discretization. Among them, in internal lightweight, by parsing the basic attribute information of the components, the corresponding attribute sets are extracted and the same attribute data are deleted; at the same time, the duplicate geometric representations in the model are deleted and a unified representation is established through the spatial location relationship to identify the components with the same geometric shape in the BIM model. In terms of internal lightweight, the main purpose is to identify the information in the O&M phase and delete other unnecessary information (unnecessary information generated in the design and construction phases), which can be done by obtaining the set of data to be deleted through the provided filters and deleting them. It is difficult for a single UAV to collect all-round image data of the components, resulting in missing data in the occluded parts, and resulting in distortions and holes in the corresponding parts of the three-dimensional model established based on the image data, which affects the measurement accuracy.

$$V = AX + Bt + L, \tag{5}$$

$$t = A^T A + A^T B. \tag{6}$$

It signals that the interpolated midpoint has shifted to its neighbouring loci, so the position of the currently significant point needs to be shifted. Also, interpolate multiple times on the new loci until convergence; perhaps exceeding the set frequency of iterations or exceeding the extent of the picture edges, when such points should be eliminated. In scale-space polar detection, because of the variable quality of polar points, there will inevitably be points among these polar points that do not satisfy the conditions. A poorly defined Gaussian difference algorithm has limits with great principal curvature at locations that span the boundary and little principal curvature in the direction of the vertical boundary, requiring the removal of fluctuating boundary response points, as shown in Figure 2.

The accuracy of digital results plays a decisive role in the feasibility of applying low-altitude photogrammetry to earth change monitoring. The accuracy analysis of digital results generally contains two aspects: theoretical accuracy and the real difference value of checkpoints. The calculation principle of theoretical accuracy is to regard the coordinate correction values of encrypted points as random errors, calculate the variance-covariance matrix of the correction numbers of coordinate points, and thus find out the levelling accuracy. The theoretical accuracy analysis reflects the error distribution law. The theoretical accuracy can be viewed in the levelling log under the project file. When the residuals are higher than 3 times the medium error, the point is treated as a rough point [18]. The true difference of checkpoint is compared by comparing the coordinate value of checkpoint with the field measurement value to find out the medium error of all checkpoints and control points. In general, this true difference value can reflect the real error more directly, and this method is also used in production for product quality analysis.

The amount of earth change is calculated from repeated measurements in a specific measurement area [19]. Therefore, its feasibility needs to consider not only the accuracy (precision) of measurement data but also the stability of each measurement data, both of which are indispensable, and the accuracy and stability of monitoring data depend on the absolute precision of single measurement and the relative precision of multiple measurements, respectively. The absolute accuracy of a single measurement can be obtained by checking the true difference of point coordinates, while the relative accuracy of multiple measurements is analysed by comparing data of multiple periods.

3.2. Design Analysis of Construction Engineering Measurement Examples. The 3D laser scanner acquires a huge amount of point cloud data of the target object, although a large amount of data provides very complete and detailed information of the target object, at the same time, it also brings great difficulties to the processing and application of the data, which is of great help to the application, processing, operation, and storage of point cloud data. Point cloud data streamlining and compression according to the data format are mainly divided into grid data and discrete data, based on the triangular grid streamlining is the first point of cloud data to establish the topological grid relationship to form triangular grid data, and then the triangular grid for data compression and deletion. The streamlining based on discrete point cloud data is to directly calculate the information of point cloud data and directly compress and delete the point cloud data according to the information. The streamlining based on point cloud data directly is more efficient, better, and more widely used, as

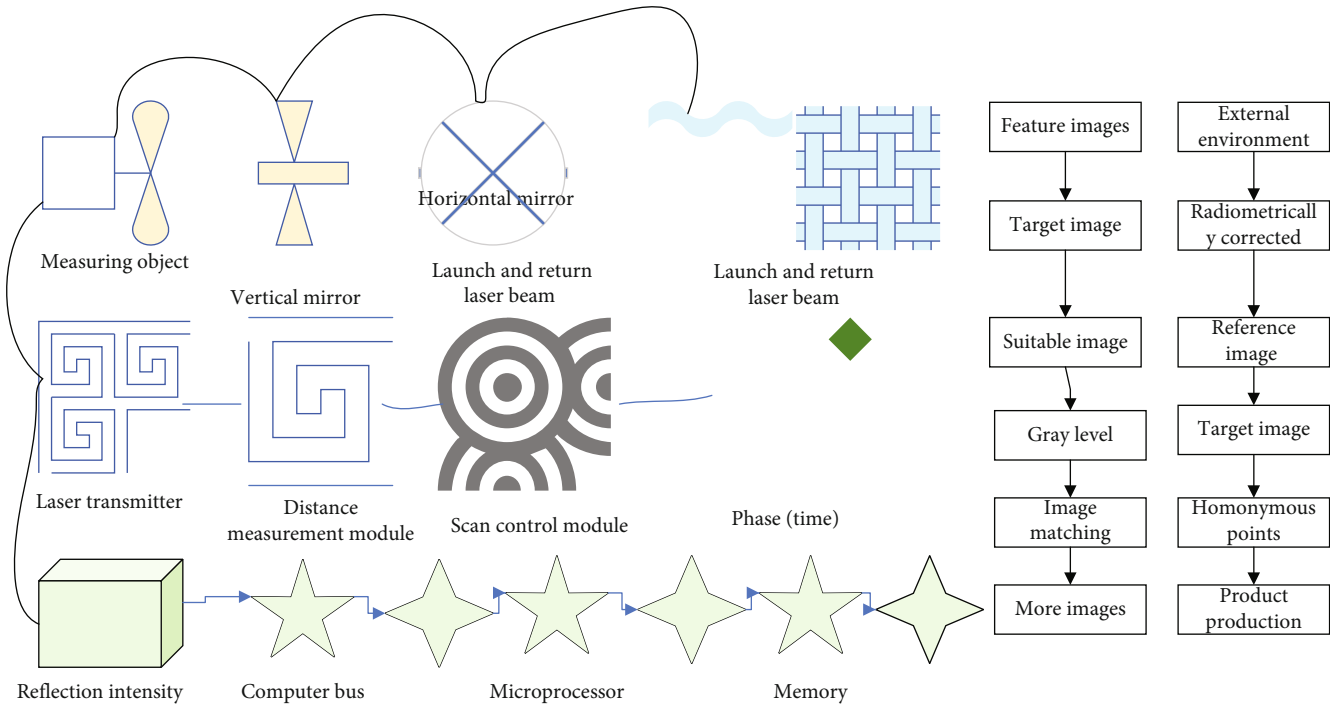

Figure 1: Working principle of 3D wireless mapping of buildings.

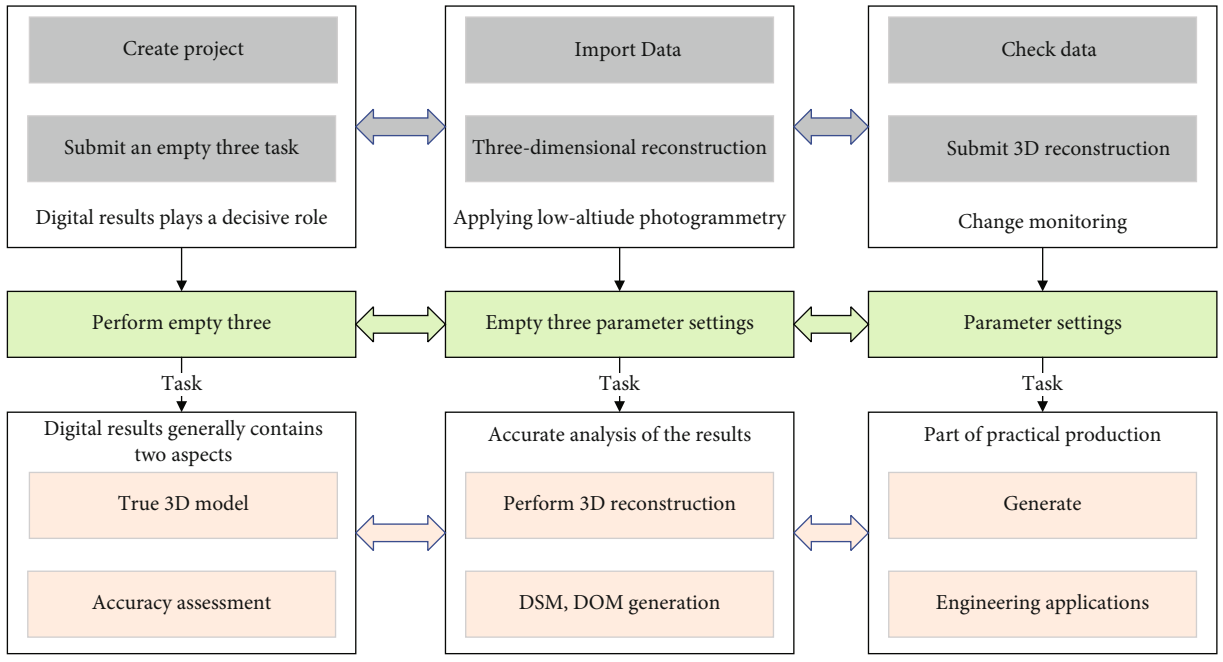

Figure 2: Data production process.

shown in Figure 3. Provide accurate data for the preliminary design. In the predesign, generally according to the position corresponding to the turning point, use the curve to connect the two adjacent straight lines to each other, according to the radius value given by the design and the steering angle obtained by the measurement, the element value of the curve is obtained through calculation.

The structural members of the assembled building should be positioned and installed following the modal grid, and the location of the datum (line) can be determined by the centreline positioning method, the interface positioning method, or the method of mixing the centreline and interface positioning methods. These three positioning methods have their characteristics and are suitable for different

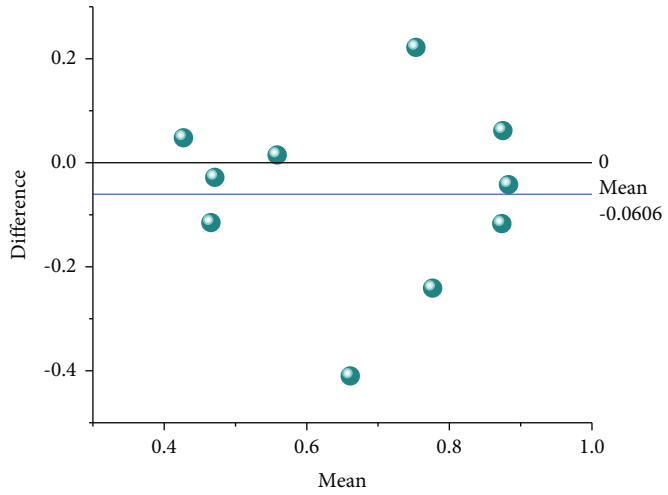

Figure 3: Building modulus coordination criteria.

component positioning and modulus grid space requirements. The centre positioning method is to coincide the positioning datum (line) with the physical centre of the member. This method is beneficial to the prefabrication, positioning, and installation of the member, so when the structural members are not connected adjacent to other members, the centre positioning method can generally be used, beams, and load-bearing walls. However, when the centre positioning method is used for the main structural members, it may cause the nonmodularity of the interior decoration space, which is not convenient for the setting of the decoration space grid and the positioning and installation of the decoration members, and the modal decoration space needs to be formed by adjusting the thickness of the walls. The use of the interface positioning method can make the interface of the members overlap with the positioning datum (line) to avoid the unevenness of the space interface or the formation of nonmodular space due to the different sizes of structural members and space dividing members. When the structural members are installed continuously, the interface of the previous member is the installation datum of the next member, the members along a certain interface need to be installed completely flat, and the interface positioning method should be used, such as the positioning of floor slabs and roofs. Make the gray level interval of the target image and the reference image the same, and achieve the purpose of completing the histogram correction. Image matching is a process of finding points with the same name between two or more images. In early research, image-related technologies are generally used to solve image matching problems. In practical application, only one positioning method often cannot meet the requirements of construction, such as the main structural member positioning and installation requirements at the same time to meet the datum surface positioning, or the main structure wall installation thickness needs to meet the modulus size, often use the method of centre positioning axis, interface positioning line superimposed on the same modulus grid.

The deepening design of the assembled building refers to the construction drawings with implement ability based on the original design scheme and condition drawings, should complete the design of a flat and vertical section of the building, the design of cross-section and reinforcement of structural members, the designers should refine the parameters of the components and determine reasonable production and installation tolerances according to the comprehensive requirements of various professions and project links, such as architecture, structure, and equipment, and the content and depth should meet the requirements of component processing, as shown in Figure 4.

When only orthophoto is used in the modelling, the elevation accuracy is gradually improved with the encryption of image control points, but the improvement effect is gradually weakened, and the medium error in the elevation of image control points is the same in scheme e and scheme f, both of which is 0.014 m, and the medium error in the elevation of checkpoints is 0.029 m and 0.023 m, respectively, which is not much different. This indicates that increasing the density of the image control points can improve the accuracy of the null-three solution, but it is not the case that the greater the density of control points is better, and a reasonable layout plan and number of image control points should be chosen according to the project requirements [20]. Theoretically, the weakest point of the model should be around the survey area, and the error control around the survey area should be mainly considered when setting up the image control points, so the mid-error of the elevation is 0.067 m when using scheme c, i.e., the image control points are evenly set up around the area, which is a significant improvement in accuracy compared with schemes a and b. However, in the actual modelling, if the survey area is not evenly set up, the accuracy of the model can be improved. Calculate the variance-covariance matrix of the correction number of the coordinate point to find the accuracy of the adjustment. Theoretical accuracy analysis reflects the law of error distribution, and the theoretical accuracy can be viewed in the adjustment log under the engineering file. However, in the actual modelling, if the elevation error in some areas inside the survey area is still high, adding internal control points can effectively control the internal

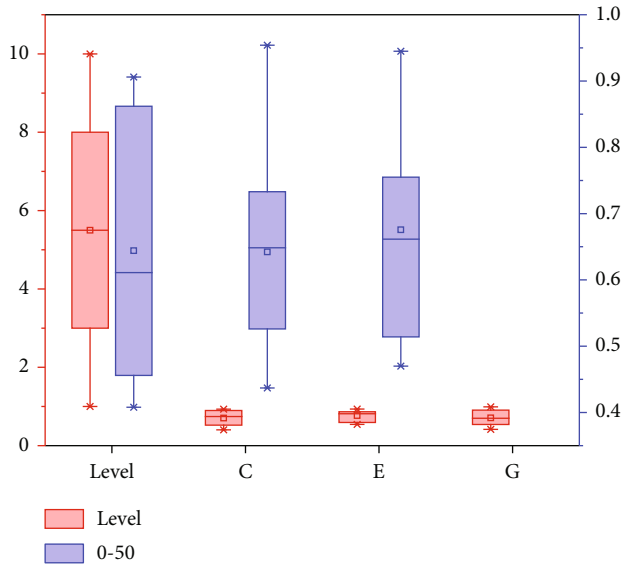

Figure 4: Elevation errors for different scenarios.

accuracy. When the tilted image is included in the modelling and option a is used, i.e., the single point layout at the four corners, the mid-elevation error of the control point is 0.018 m and the mid-elevation error of the checkpoint is 0.026 m, which is slightly worse than the mid-elevation errors of 0.014 m and 0.023 m when only the orthophoto and option f is used in the modelling, and the maximum residual value of both options is 3 cm. This indicates that the inclusion of tilted images in the modelling has an obvious binding effect on the model elevation error.

As we all know, before collecting image data for the first time, we need to use GNSS-RTK to measure the coordinates of image control points for internal processing, and the coordinates of the first measured image control points are also used in the later processing of multiphase data, but in actual engineering, the previously laid out image control points are often destroyed, and if the image control points are relaid, it will affect the operation efficiency and the accuracy of data processing. In the calculation of multiperiod DSM data overlay, the sampling points with elevation differences less than 1 cm can be selected as relatively stable image control points for subsequent internal modelling, which can effectively reduce the inconvenience caused by image control points remeasurement and improve the relative elevation accuracy of DSM overlay.

4. Results and Analysis

4.1. Digital Wireless Mapping Performance of Construction Projects. The image data captured by the UAV gimbal camera is first stored on a memory card carried by the camera, while the wireless image transfer module is used to transfer the captured image data back to the staging database of the automated airport system. The camera's memory card has limited memory, and the memory card is cleared after the mission to make sure that the data has been completely returned to the staging database. The staging database has much more memory than the memory card carried by the camera, but also has limited storage space and will also be cleared after multiple phases of data collection to ensure that the data has been fully uploaded to the backend cloud database. It plays a great role in the measurement of historical sites, cultural relics and historical sites restoration, archaeological site reproduction simulation, cultural relics and historical sites data storage, and large-scale historical site surveying and mapping. The image data collected by the UAV gimbal camera and other process data of the system will eventually be uploaded to the cloud database for professional staff to download and process. The cloud database should have a large storage space, and through the continuous accumulation of data, it will eventually form engineering monitoring big data and provide the possibility for big data analysis. The automatic skylight realizes the function of automatic opening and closing of the UAV before and after take-off and before and after landing, using a stepper motor and a limit switch to control the movement of the skylight. The stepper motor drives the skylight movement through gears and chains, and the limit switch controls the closing motor according to the position of the skylight movement to complete the task of opening or closing the skylight, as shown in Figure 5.

Each point has 2 groups of data acquisition, each group with a different instrument height, more than 15 data acquisition, each data acquisition time of 3 seconds, two groups of data count 30 data through the levelling calculation, you can get the point after the levelling correction of the coordinate value. After the collection, you can use the instrument to do the preliminary calculation in the field and check whether the data is acceptable. If not, collect one or two more sets until you can pass the calculation. Ideally, the data collection time for each point is about 2 minutes. Adding the time of erecting stations, walking between points, and waiting for the fixed solution of the instrument between groups, it takes about 20 minutes at most, and 480 minutes for 8 hours of work a day, which can collect more than 24 points a day it took 3 days to complete the field control measurement data collection of 65 points.

In the actual measurement, the orientation is carried out with disk-left and disk-right observations, resulting in observation data, which are checked by the software site to see if the observation data exceeds the limits and if there are errors in the control point spacing. If the orientation is correct, then the data collection of pipeline points is carried out. When the pipeline point data is measured, the attribute data of each pipeline point can be input directly on the EPS software, and the connection relationship of the pipeline point can be outlined in the field so that the graph can be directly compared with the current situation, and errors such as connection and flow direction can be found and solved in the field. It is necessary to form a modular decoration space by adjusting the thickness of the wall. Using the interface positioning method can make the interface of the component coincide with the positioning reference plane (line) and avoid the unevenness of the space interface or the formation of a non-modular space due to the different sizes of structural components and space division components. The

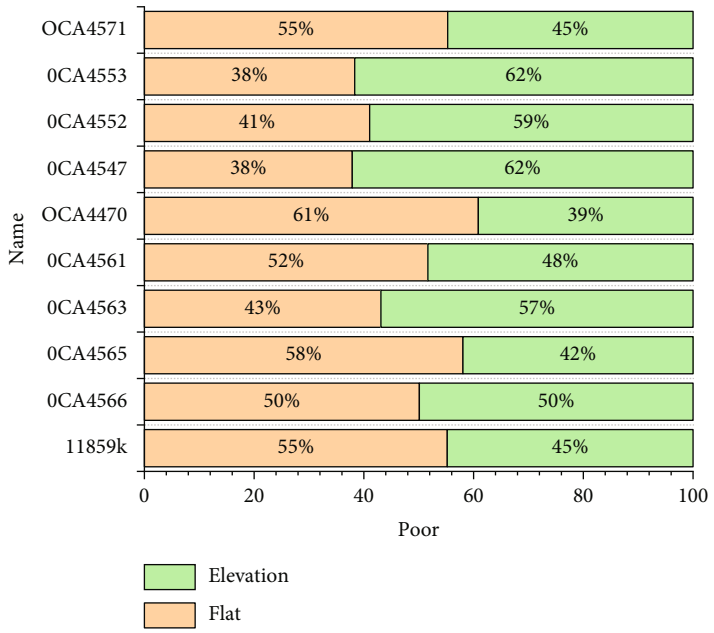

Figure 5: Accuracy of the observed data.

pipeline diagrams, which have been measured and initially edited externally, are imported into the EPS software on the PC for further editing and finishing. Add markups and solve problems such as landing on the drawing surface. After self-checking and checking and modifying by the quality inspector, the final topographic pipeline result map was formed as shown in Figure 6.

The landing deviation is mainly concentrated around 10 cm at wind level 1, within 20 cm, at wind level 3, and within 30 cm at wind level 4. In wind level 4, the landing deviation was around 30 cm, and in wind level 5, only a small portion of the landing deviation was greater than 40 cm. This indicates that the M100 drone achieves good landing accuracy in this simulation environment, and the landing error has certain randomness as the wind speed increases. The landing deviation of the drone is related to its ability to land safely and accurately on the designed automatic landing pad, which is a prerequisite for the monitoring system to realize the functions of collection and autocontinuation. Therefore, the simulation experiments initially verify the technical feasibility of the monitoring system in the absence of the M100 real aircraft.

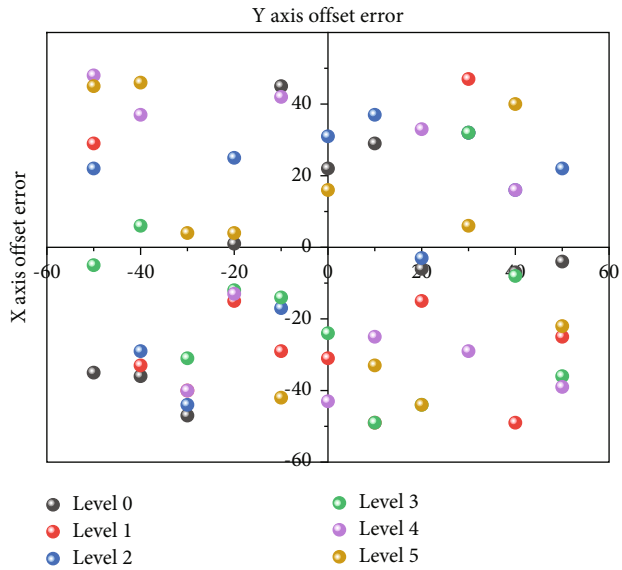

Figure 6: Offset error.

5. Design Results of Construction Engineering Measurement Examples

UAV automatic landing pad, communication, and data management and processing are designed; the functional layers of the system and their interlogical relationships are elaborated; the automatic landing pad of the system, including the general structure of the box-type dock and the automatic range function settings. Meanwhile, considering the limitation of weather conditions on the unattended UAV operation mode, the composition and functional design of the environmental sensing system were discussed, and the detailed operation process of the UAV and the automatic landing pad was determined. Finally, the technical feasibility of the unattended UAV monitoring system was initially verified by simulating the landing process and landing accuracy of the UAV and comparing it with the actual landing deviation of DJI Genie.

The first type is the splicing target, which is mainly used to increase the accuracy of automatic splicing because of the automatic splicing operation by the professional point cloud processing software, and the additional targets are mainly needed in the case of difficult viewing conditions and little information transmission between two adjacent stations, which is deployed according to the coordinate alignment

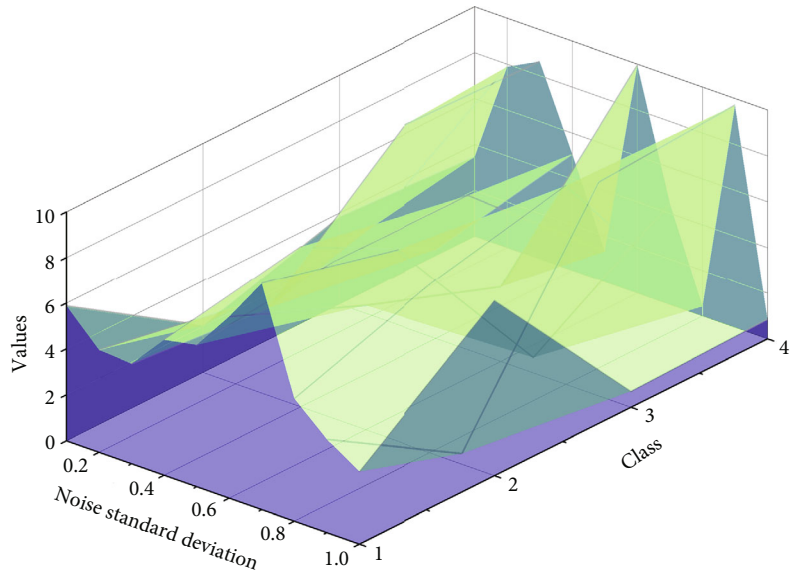

Figure 7: Rotational transformation parameter error.

requirements, which is deployed according to the coordinate alignment requirements, usually at the entrance and exit of the subway station or at the ground or underground level. After setting up the instrument, insert the battery, open the protective cover of the storage disk, insert the storage disk, the scanner starts to scan and rotate with itself, after one week of rotating and scanning, the scanner stops and stands still, indicating the completion of the current station, turn off the instrument and move to the next station to collect and scan, as shown in Figure 7.

Under the same noise standard deviation condition, the quaternion method outperforms the singular value decomposition method for the solution of the rotation transformation parameters. As the noise standard deviation keeps increasing, the error of the rotation parameters solved by both algorithms increases, and the error of the rotation parameters solved by the indicated quaternion is consistently lower than the error of the rotation parameters solved by the indicated singular value decomposition method. It shows that the accuracy of the solution of the quaternion method is higher than that of the singular value decomposition method in the solution of the rotation transformation parameters under the same noise conditions. Point cloud data alignment, also known as point cloud data stitching. The target object structure is complex, the target object exists between the occlusion and the limited view angle of the instrument itself, so in a single station set up, 3D laser scanner cannot collect the complete target object point cloud data and need to carry out multistation point cloud data scanning. Since the point cloud data of multiple stations are collected under separate coordinate systems, the point cloud data of multiple stations need to be stitched into one coordinate system, which requires point cloud data alignment processing, as shown in Table 1.

The average error of the x-axis is 0.0121 m, y-axis is 0.0105 m, and z-axis is 0.0159 m. The overall error in each coordinate direction is no more than 0.02 m, and the maximum error in the z-axis direction is 0.0159 m, because the subway station is divided into a negative one and negative two layers, and in the point cloud data. This is because the subway station is divided into two layers: negative one and negative two, and the error is increased due to the splicing between different layers when the point cloud data is spliced.

Table 1: Comparison of coordinates of target points.

Point name	X	Y	Z	Error
$Z1$	2.5	4.8	4.7	3.4
$Z2$	4.2	2.2	2.1	4.1
$Z3$	3.1	4.9	3.2	4.8
$Z4$	2.7	2.4	3.4	3.9
$Z5$	4.6	2.4	4.8	3.1
$Z6$	4.2	4	4.6	3.9

Point cloud data unification is a way to optimize the overall point cloud data, to unify the overall point cloud of multiple stations after stitching into the overall point cloud data of a single station, and after the point, cloud unification process is completed, the operation of point cloud data selection and browsing becomes smoother on the original basis. In the process of point cloud data unification, point cloud data thinning parameters can be set according to the needs of modelling and point cloud data application to adjust the density and size of point cloud data.

6. Conclusion

The requirements of urban surveying on measurement technology are increasing, the operation environment of urban surveying is complex and changeable, due to the influence of visibility and operation conditions, the traditional measurement operation mode can no longer well meet the needs of urban surveying, TREK technology can be widely used in

many fields of urban surveying because of its flexible and convenient work and fewer operation conditions, but its reliability is worse than the conventional static relative measurement. Some, so in using CORES technology measurement especially in control measurement operations, it is necessary to conduct repeat measurements appropriately and consider using different observation instruments and distributing repeat measurements at different observation times to improve the reliability of CORES measurements. There is no obvious systematic error, but the plane error leads to a large relative error in elevation in areas with abrupt elevation changes such as the edges of buildings and the edges of pits. By comparing the distribution and number of point clouds with elevation differences in different intervals, it was found that the number of high-precision sampling points with elevation differences less than 0.01 m in three groups accounted for 21.99%, 21.5%, and 23.3% of the total, respectively. This can improve the relative accuracy of multiphase image modelling and reduce the negative impact caused by the destruction of the resurvey of image control points.

Data Availability

The data used to support the findings of this study are available from the corresponding author upon request.

Conflicts of Interest

The authors declare that they have no known competing financial interests or personal relationships that could have appeared to influence the work reported in this paper.

References

[1] M. Mahmood, D. Mzurikwao, Y. S. Kim et al., "Fully portable and wireless universal brain-machine interfaces enabled by flexible scalp electronics and deep learning algorithm," *Nature Machine Intelligence*, vol. 1, no. 9, pp. 412–422, 2019.

[2] S. Bi, J. Lyu, Z. Ding, and R. Zhang, "Engineering radio maps for wireless resource management," *IEEE Wireless Communications*, vol. 26, no. 2, pp. 133–141, 2019.

[3] R. Ponuma and R. Amutha, "Compressive sensing based image compression-encryption using novel 1D-chaotic map," *Multimedia Tools and Applications*, vol. 77, no. 15, pp. 19209–19234, 2018.

[4] A. Rashidi, M. Maghiar, and M. H. Sigari, "Capturing geometry for labeling and mapping built infrastructure: an overview of technologies," *Iranian Journal of Science and Technology, Transactions of Civil Engineering*, vol. 41, no. 4, pp. 415–428, 2017.

[5] T. R. Ray, J. Choi, A. J. Bandodkar et al., "Bio-integrated wearable systems: a comprehensive review," *Chemical Reviews*, vol. 119, no. 8, pp. 5461–5533, 2019.

[6] Z. Ma, J. Xie, H. Li et al., "The role of data analysis in the development of intelligent energy networks," *IEEE Network*, vol. 31, no. 5, pp. 88–95, 2017.

[7] K. Lee, X. Ni, J. Y. Lee et al., "Mechano-acoustic sensing of physiological processes and body motions via a soft wireless device placed at the suprasternal notch," *Nature Biomedical Engineering*, vol. 4, no. 2, pp. 148–158, 2020.

[8] S. M. Sepasgozar, H. Li, S. Shirowzhan, and V. W. Tam, "Methods for monitoring construction off-road vehicle emissions: a critical review for identifying deficiencies and directions," *Environmental Science and Pollution Research*, vol. 26, no. 16, pp. 15779–15794, 2019.

[9] M. Shafiei Dizaji, M. Alipour, and D. K. Harris, "Leveraging full-field measurement from 3D digital image correlation for structural identification," *Experimental Mechanics*, vol. 58, no. 7, pp. 1049–1066, 2018.

[10] C. Z. Dong and F. N. Catbas, "A review of computer vision–based structural health monitoring at local and global levels," *Structural Health Monitoring*, vol. 20, no. 2, pp. 692–743, 2021.

[11] S. M. Won, H. Wang, B. H. Kim et al., "Multimodal sensing with a three-dimensional piezoresistive structure," *ACS Nano*, vol. 13, no. 10, pp. 10972–10979, 2019.

[12] A. Buffi, A. Michel, P. Nepa, and B. Tellini, "RSSI measurements for RFID tag classification in smart storage systems," *IEEE Transactions on Instrumentation and Measurement*, vol. 67, no. 4, pp. 894–904, 2018.

[13] E. van der Kruk and M. M. Reijne, "Accuracy of human motion capture systems for sport applications; state-of-the-art review," *European Journal of Sport Science*, vol. 18, no. 6, pp. 806–819, 2018.

[14] M. Carminati, O. Kanoun, S. L. Ullo, and S. Marcuccio, "Prospects of distributed wireless sensor networks for urban environmental monitoring," *IEEE Aerospace and Electronic Systems Magazine*, vol. 34, no. 6, pp. 44–52, 2019.

[15] J. Koo, M. R. MacEwan, S. K. Kang et al., "Wireless bioresorbable electronic system enables sustained nonpharmacological neuroregenerative therapy," *Nature Medicine*, vol. 24, no. 12, pp. 1830–1836, 2018.

[16] A. K. Srivastava, A. Dev, and S. Karmakar, "Nanosensors and nanobiosensors in food and agriculture," *Environmental Chemistry Letters*, vol. 16, no. 1, pp. 161–182, 2018.

[17] T. Kokulnathan, T. Sakthi Priya, and T. J. Wang, "Surface engineering three-dimensional flowerlike cerium vanadate nanostructures used as electrocatalysts: real time monitoring of clioquinol in biological samples," *ACS Sustainable Chemistry & Engineering*, vol. 7, no. 19, pp. 16121–16130, 2019.

[18] E. Bakhtavar, M. Valipour, S. Yousefi, R. Sadiq, and K. Hewage, "Fuzzy cognitive maps in systems risk analysis: a comprehensive review," *Complex & Intelligent Systems*, vol. 7, no. 2, pp. 621–637, 2021.

[19] J. Y. Dai, W. Tang, L. X. Yang et al., "Realization of multi-modulation schemes for wireless communication by time-domain digital coding metasurface," *IEEE Transactions on Antennas and Propagation*, vol. 68, no. 3, pp. 1618–1627, 2020.

[20] S. Wolny, A. Mazak, C. Carpella, V. Geist, and M. Wimmer, "Thirteen years of SysML: a systematic mapping study," *Software and Systems Modeling*, vol. 19, no. 1, pp. 111–169, 2020.

Hindawi
Journal of Sensors
Volume 2022, Article ID 6492566, 13 pages
https://doi.org/10.1155/2022/6492566

Research Article

Text Data Processing and Classification Algorithm Based on Data Fusion and Granular Computing

Duo Ji[1] **and Peng Zhang**[2]

[1]*College of Public Security Information Technology and Intelligence, Criminal Investigation Police University of China, Shenyang, 110854 Liaoning, China*
[2]*Institute of Information Engineering, Chinese Academy of Sciences, Beijing 100093, China*

Correspondence should be addressed to Duo Ji; jiduo@cipuc.edu.cn

Received 19 November 2021; Revised 29 December 2021; Accepted 3 January 2022; Published 24 January 2022

Academic Editor: Gengxin Sun

With the rapid expansion of network information and the emergence of a large number of electronic texts, how to organize and manage this massive information has become a major challenge. Automatic text categorization technology is to study how to let the machine classify unknown text through self-learning, thus solving the difficulties encountered in manual classification. Because granular computing can reduce the knowledge in solving complex problems, it is more convenient to summarize and acquire knowledge. It has become a hotspot in recent years, and it also provides new ideas for text classification research. The rough set model of granular computing can acquire knowledge by mining decision rules. The decision process is more transparent and easy to understand. It has been paid attention to and applied in text classification research. Based on the research of existing achievements, this paper makes a further study on the application of granular computing in text categorization. After analyzing the existing feature selection methods, the feature distribution is proposed based on the relationship between feature words and categories. By calculating the distribution distance between any two feature words, the feature words with similar distribution distances are aggregated, which effectively reduces the dimension of the feature space and also avoids the individual samples caused by the existing feature selection algorithm. A phenomenon that is discarded due to features. The experimental results show that the clustering method can obtain higher classification accuracy than other feature selection methods when using SVM as the classifier. SVM performs best, and the final text classification accuracy rate can reach 85.46%. According to the correlation principle of the rough set, feature selection is made for each information granularity, the selected feature is used as the condition attribute and the coordination matrix is constructed, and the most similar sample is heuristically searched to obtain the attribute reduction set.

1. Introduction

The rapid development of information technology, especially the development of the Internet, has brought people into the era of information exchange. The Internet provides a platform for people to exchange and share information and has become an indispensable part of modern life tools and work tools. In February 2019, the China Internet Network Center (CNNIC) released the "43th Statistical Report on Internet Development in China," showing that as of December 2018, the number of Internet users in China was 829 million, and the number of new Internet users was 56.53 million. The penetration rate reached 59.6%, an increase of 3.8% from the end of 2017. The number of mobile Internet users in China reached 871 million, and the number of mobile Internet users increased by 64.33 million. The proportion of Internet users using mobile phones increased from 97.5% at the end of 2017 to 98.6% at the end of 2018. Mobile Internet access has become one of the most commonly used Internet channels. With the continuous increase in the number of Internet users and the continuous growth of online information, people have encountered the problem of massive information such as retrieval and management brought about by information expansion.

How to effectively organize and manage this information has become an area facing the information science. With the continuous development of technology, text classification has gradually changed from a knowledge-based method to a method based on statistics and machine learning.

Most of the information on the Internet appears in the form of text or can be converted into text. Therefore, as a key technology for processing and organizing large amounts of text data, text categorization has become information filtering, information security, mail classification, information retrieval, and search. Basic technologies in the fields of engines, web forums, digital libraries, etc. and many research teams at home and abroad have conducted in-depth research on text classification algorithms. Tian [1] proposed that in text categorization, the performance of the classifier decreases as the feature dimension increases. The main purpose of feature selection is to remove irrelevant and redundant features in the function and to reduce the functional dimensions. Based on the word vector generated by Word2-Vec, the Word2Vec-SM algorithm is proposed to reduce the dimension of the feature. Bei [2] proposed an improved tf-idf-miow algorithm based on the traditional tf-idf algorithm and mutual information algorithm to meet the requirements of marine big data text classification. The results of automatic text classification experiments show that the tf-idf-miow recall rate in the oceanography field is 10.33% higher than the traditional tf-idf algorithm, and the f1 score is increased by 6.92%. Ni et al. [3] studied in detail the influence of parameters on classification accuracy when using support vector machine (SVM) and K-nearest neighbor (KNN) text automatic classification algorithm. The advantages and disadvantages of the two text classification algorithms are presented in the field of petrochemical processes. Chen [4] proposed a new classification model LDA- (Latent Dirichlet Allocation-) KNN (K-nearest neighbor). LDA is used to solve the problem of semantic similarity measurement in traditional text categorization. The sample space is modeled and selected by this model. Lianhong et al. [5] proposed a short text semantic extended representation method based on concept map. Firstly, the degree of association between the text feature words and the concepts in the concept map is calculated, and the concept with high degree of relevance is selected to form a conceptual dictionary of the current text. Then, the concept dictionary is added to the feature word set to obtain a semantic extended representation of the short text. Weiyin and Li [6] proposed a text classification model CNN-XGB based on convolutional neural network and XGBoost. Firstly, Word2Vec is used to represent the preprocessed data, followed by multi-scale convolution kernel convolutional neural network for data feature extraction. Finally, XGBoost is used to classify the features of deep extraction. Man et al. [7] fully validated the model by using multiple indicators to evaluate the model in the test data set. Compared with other models, the proposed model has better classification performance in the two-class and multiclassification tasks. Wang et al. [8] proposed a new feature word extraction algorithm based on chi-square statistics by extracting the feature words of text method and evaluated the text classification model through the improved new method. The experimental results show that the new method is significantly better than the traditional feature extraction methods in the evaluation results such as precision, recall, F1, and ROC_AUC. Yao et al. systematically study the web/text classification problem by combining sparse representation with random measurement. First, a very sparse data measurement matrix is used to map the original high-dimensional text feature space to a low-dimensional space without losing key information. Then, a general sparse representation method is proposed, which obtains the sparse solution by decoding the semantic correlation between the query text and the entire training sample. The authors conducted a large number of experiments using real-world data sets to check the proposed method, and the results showed the effectiveness of the proposed method [9]. Wang et al. [10] to improve the text classification effect and introduce the deep neural network isomorphic with BP neural network to initialize the initial weight of BP neural network. Experiment on multiple data sets it shows that this text method obviously improves the accuracy of text classification. Chaolei and Junhua [11] conducted experiments on the same data set. The results show that simulated annealing has stable global search performance and is an effective way to optimize SVM parameters. Chao and Junhua [12] show through experiments that compared with the traditional KNN algorithm, the improved algorithm has improved accuracy, recall rate, and F value. Compared with other classification algorithms, it has certain advantages. Junhong et al.'s [13] simulation experiments show that the proposed method can effectively solve the problem that the incompletely labeled text classifier can not effectively identify the boundary between the incompletely labeled text category and other categories under the current classification system, resulting in low data classification performance. Kai [14] introduced the process of text categorization and an overview of the three classifiers. Finally, the three classifiers were tested separately, and the experimental results were analyzed to find out the classification effect of the support vector machine classifier in the experimental environment, better than the other two classifiers. J. Ma and Y. Ma [15] showed that the method is superior to the commonly used long- and short-term memory models, multicategory logistic regression, and support vector machines in terms of accuracy and recall rate.

Although many research teams at home and abroad have their own research plans for text categorization methods, they all have some shortcomings: single method, low efficiency, and complicated calculation process. The granularity calculation method just has the advantages that these methods do not have. The calculation process is simple and clear, the operation is simple, the feature recognition efficiency is high, and subtle changes can be detected. Many research teams have seized the opportunity and made extensive calculations on the granularity.

The method of granular computing can reduce the dimension of knowledge when solving complex problems, which makes it easier to generalize and acquire knowledge. It has become a hotspot in recent years, and it also provides new ideas for the study of text classification. Xingguo et al.

[16] applied the granularity calculation to the vehicle identification. Aiming at the problem that the classification of fine-grained vehicle identification images has low recognition rate due to redundant features, a fine-grained vehicle identification algorithm based on singular value decomposition and central metric is proposed. The research shows that the method uses the Residual Network (ResNet) framework to test on the Cars-196 fine-grained model data set, and the accuracy rate can reach 93.02%, which is better than the current bilinear and attention model. Extended experiments prove that this method is equally applicable to other network frameworks. Haoru et al. [17] used the granular algorithm to screen out images with great influence on the recognition results to prevent overfitting; input the filtered images into the RPN network improved by soft-nms (Soft Nonmaximum Suppression) to obtain object-level image annotation. Dangwei et al. [18] applied the granularity algorithm to search for isolated regions. Aiming at the shortcomings of traditional particle swarm optimization algorithm for searching isolated regions and low search accuracy, a subgroup hierarchical coarse-grained particle swarm optimization algorithm was proposed. On the basis of the coarse-grained model, the subgroup is divided into several common subgroups, adaptive subgroups, and elite subgroups. Different subgroups adopt different evolution strategies in the evolution process. Jingrui and Dongyang [19] completed the multigranularity search of the initial layer data source through statistical expectation calculation, imported the initial layer probability calculation result into the multigranularity variable distribution calculation, and completed the multigranularity search of the middle layer data source. In order to ensure the effectiveness of the proposed method, the proposed method is compared with two traditional methods, and the efficiency is obviously improved and has high efficiency. The experimental results of Jinshuo et al. [20] and others show that the multithreading strategy based on CPU can achieve a 4x speedup ratio, and the parallel algorithm based on the unified computing device architecture (CUDA) can achieve a maximum speed up of 34 times and the proposed strategy. Based on the CUDA parallel strategy, it achieves a 30% performance improvement and can be used to quickly schedule computing resources in other areas of big data processing. Suzhi et al. [21] introduced the granularity idea to divide the initial data set into multiple subsets. Secondly, the improved similarity matrix was calculated for each subset combined with intraclass and interclass distance. Finally, the improved parallel AP aggregation was implemented based on MapReduce model. Experiments on real data sets show that the IOCAP algorithm has better adaptability on large data sets and can effectively improve the accuracy of the algorithm while maintaining the AP clustering effect. Ronghu and Yunjie [22] in order to improve coarse-grained parallel inheritance algorithm performance, shortening the solution time for the stereo warehouse path optimization problem, applying a single program multiple data stream (SPMD) parallel structure to the coarse-grained parallel genetic algorithm, and improving the algorithm. Yingjian et al. [23] use the granular algorithm to divide the circuit into multiple regions and use the logical fingerprint feature as the identifier of the region. By comparing the multivariant logical fingerprints of the partition in two dimensions of time and space, the hardware Trojan detection without gold chip is realized and diagnosed. Jin and Jianhua [24] designed a fine-grained remote attribute proof algorithm to solve the problem of large-scale remote identification of traditional attributes. For different remote proof requirements, the attribute was remotely proved and the terminal platform was more detailed. Yilin et al. [25] proposed the theory of the degree of weighted granularity superiority relationship pessimistic multigranularity rough set and weighted granularity dominant degree optimistic multigranular rough set. On this basis, a dynamic parallel updating algorithm based on the degree-weighted rough set approximation set of weighted granularity and dominant relationship is presented.

In order to solve the problem of complex data, difficult operation, cumbersome recognition process, and incomplete feature extraction in a text categorization method, this paper studies the text classification method based on granular algorithm. Based on the existing results, the application of granular computing in text categorization is further studied. The existing feature selection methods are analyzed. According to the relationship between feature words and categories, the feature distribution distance is proposed. The distribution distance is similar. Feature words are aggregated, which effectively reduces the dimension of the feature space and avoids the phenomenon that individual samples caused by the existing feature selection algorithm are discarded because they do not contain the selected features; the clustering method can be obtained when using SVM as the classifier has higher classification accuracy than other feature selection methods.

2. Method

2.1. Data Fusion

2.1.1. Introduction to Data Fusion. Data fusion in text data processing is to carry out multilevel comprehensive optimization and intelligent analysis through certain rules and finally complete the needs of users, that is, a process of obtaining more accurate description of perceptual object fusion information. In text data processing, the perceptual information obtained by data fusion technology is usually more persuasive than the data collected and analyzed by a node. The data fusion center fuses information from multiple sensors; it can also fuse information from multiple sensors and the observation facts of the human-machine interface (this fusion is usually a decision-level fusion). Extract the symptom information, under the action of the inference engine. Match the symptoms with the knowledge in the knowledge base, make fault diagnosis decisions, and provide them to users. Data fusion can ensure the accuracy of perceived data, reduce the network data traffic in processing, reduce the redundant data in the network, and play an important role in making reasonable decisions for applications.

2.1.2. Hierarchy of Data Fusion. According to the level of data abstraction in the fusion system, the fusion can be divided into three levels: data level fusion, decision level fusion, and feature level fusion.

(1) Data Level Fusion. The information processing of data level fusion is shown in Figure 1. Data level fusion is the fusion directly on the original data layer. The data is synthesized and analyzed before various sensors are preprocessed. Because the sensor detects the same feature data in the same environment, different types of feature data cannot be fused. The advantage of data level fusion is that it can maintain the complete amount of information of data without data preprocessing. However, it also has the disadvantages of large traffic, long analysis time, poor anti-interference ability, and poor real-time performance. In order to solve this problem, efforts should be made to develop a fusion algorithm model that has both robustness and accuracy. Focus on research on related processing, fusion processing, and system simulation algorithms and models, and conduct research on evaluation techniques and metrics for data fusion systems.

(2) Feature Level Fusion. Feature level fusion belongs to the middle level fusion. It first extracts the features of the original information from each sensor (the features can be the edge, direction and speed of the target) and then classifies, collects, and synthesizes the multisensor data according to the feature information. The information processing process is similar to the feature level fusion process. Because the extracted feature information is generally directly related to decision analysis, the fusion result can assist decision analysis to the greatest extent. Feature level fusion has low requirements for communication bandwidth; as long as the broadband reaches above 2 MHz, normal operation can be guaranteed. It realizes considerable information compression and is conducive to real-time processing, but its accuracy is reduced due to data loss. At present, many methods have been applied to feature level fusion. Common methods include image fusion, data compounding, information compounding, data compounding, and image compounding.

(3) Decision Level Fusion. Decision level fusion is the highest level of data fusion. Firstly, after each sensor preprocesses the original data and makes a decision, it fuses their decision results to make the final decision results consistent as a whole. The information processing process of decision level fusion is shown in Figure 2. The advantage of decision level fusion is that it has good real-time and fault tolerance, less dependence on sensors, and less traffic. It can still work even when one or several sensors fail. However, because decision level fusion needs to preprocess the original data obtained by sensors to make their own decision results, the preprocessing cost is high.

Because different levels of fusion algorithms have different advantages, disadvantages, and scope of application. For choosing the fusion algorithm at which fusion level, it is necessary to comprehensively consider the sensor performance, computing power, communication bandwidth, detection parameters, and capital budget of each system. There is no universal structure that can be applied to all application backgrounds. In practical applications, different levels of fusion algorithms often appear in one system at the same time. The characteristics of three different levels of fusion methods are compared as follows.

2.1.3. Data Fusion Classification. In the existing data fusion applications, data fusion technology can be divided into different categories according to different standards. Data fusion technology is divided into data layer fusion, feature layer fusion, and decision layer fusion. See Figure 3 for details.

2.1.4. Common Data Fusion Methods. With the rapid development of information theory, artificial intelligence, target recognition and other fields, more and more data fusion algorithms also appear. At present, data fusion algorithms can be divided into three categories: methods based on physical model, methods based on parameter classification, and methods based on cognitive recognition model. There are many common data fusion methods in text data processing. The typical ones are neural network, fuzzy theory, D-S evidential reasoning, and principal component analysis. This paper chooses the method of parameter classification to solve the problem of massive information retrieval and management caused by information expansion.

We choose the data fusion algorithm of principal component analysis. Principal component analysis (PCA) is a simple and effective data compression algorithm, which is very consistent with the characteristics of text data processing. Principal component analysis is to project the perceptual data onto a new coordinate axis and calculate its eigenvector, so that the eigenvector corresponding to the largest eigenvalue becomes the first coordinate vector (called the first principal component); the eigenvector corresponding to the second largest eigenvalue becomes the second coordinate vector (called the second principal component), and so on. In this way, its main components are retained, which not only ensures the main characteristics of the data but also reduces the amount of data transmission. The data fusion algorithm based on principal component analysis divides the text data into multiple clusters. The cluster head will collect the information of its cluster members and then put the data into the observation matrix, which can be projected into a new space. The nodes of the cluster are evenly distributed in the sensing area. After clustering, the observation matrix in the cluster meets $a_{\text{value}} = 25$, $a_{\text{value}} = 50$, $a_{\text{value}} = 75$, respectively. The relationship with the standard reconstruction error and data fusion rate is shown in Table 1.

The table shows the following characteristics: (1) the standard reconstruction error rate decreases with the increase of data fusion rate. (2) When the data fusion rate in the control cluster is certain, the smaller the value of a_{value}, the smaller the standard reconstruction error rate of data, which also shows that the data similarity affects the reconstruction error rate of data.

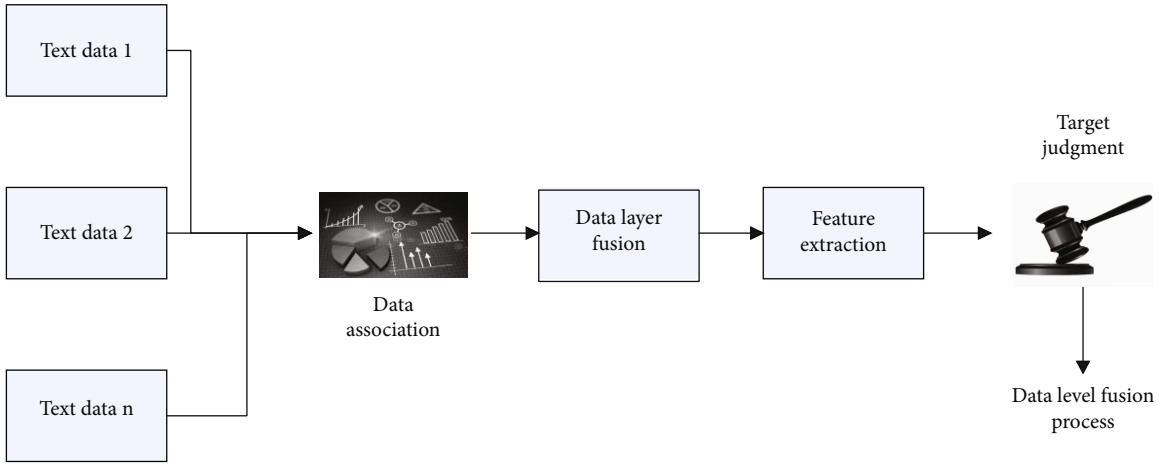

Figure 1: Data level fusion process.

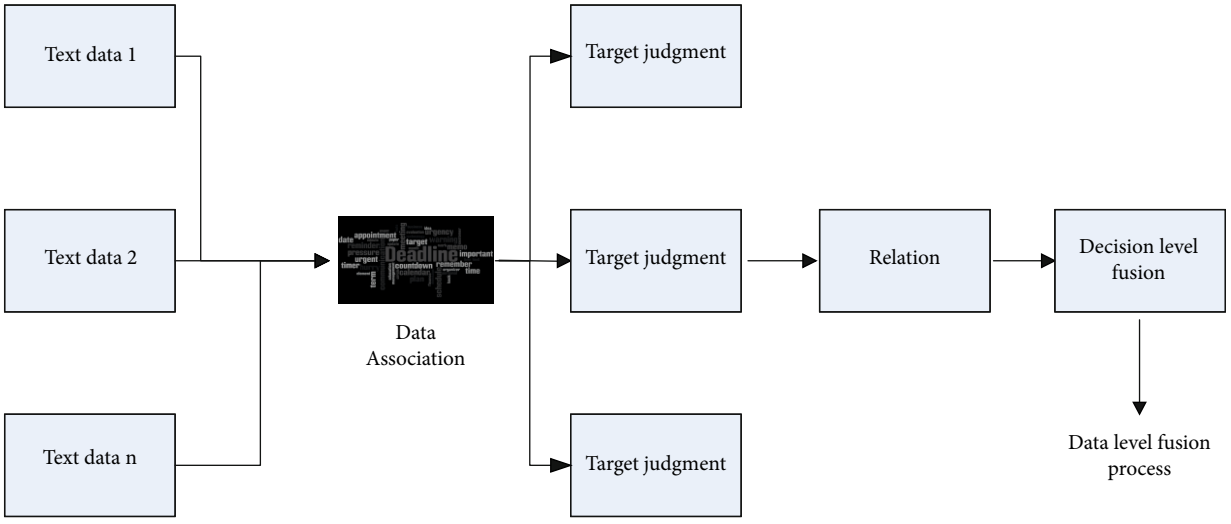

Figure 2: Decision level fusion process.

2.2. Feature Selection and Feature Extraction

2.2.1. Document Frequency (DF). The document frequency is determined according to the number of documents containing feature items, and the feature whose document frequency is higher than a certain threshold is selected as the feature item. The calculation formula is as follows:

$$\mathrm{DF}(f_k, c_i) = p(f_k \mid c_i). \tag{1}$$

2.2.2. Information Gain. The information gain indicates the average amount of information of the document class when the document contains a certain feature value. The calculation formula is as follows:

$$\begin{aligned}\mathrm{IG}(f_k) = \sum_{i=1}^{d}\left(p(f_k \mid c_i)\log\left(\frac{p(f_k \mid c_i)}{p(c_i)p(f_k)}\right)\right) \\ + p(\bar{f}_k \mid c_i)\log\left(\frac{p(\bar{f}_k \mid c_i)}{p(c_i)p(\bar{f}_k)}\right).\end{aligned} \tag{2}$$

2.2.3. Expected Cross Entropy (ECE). It is expected that the cross entropy is similar to the information gain, but it only

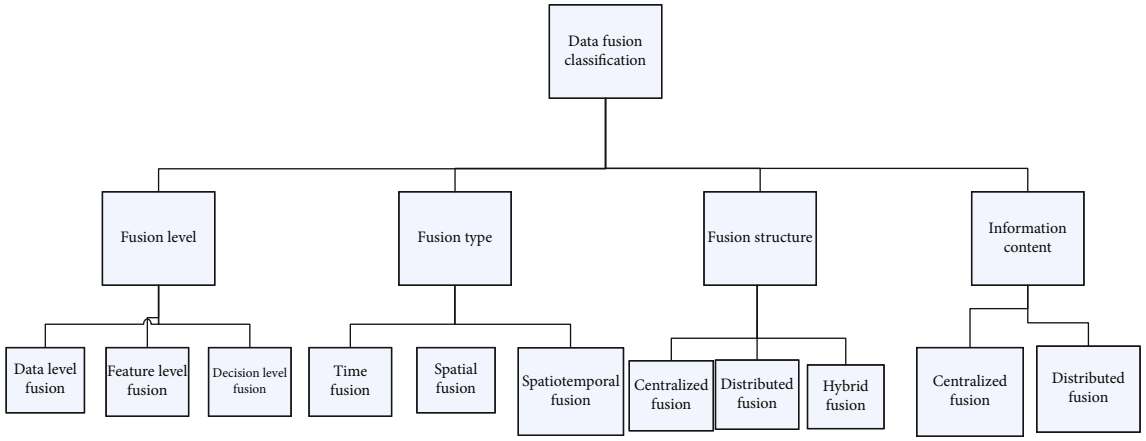

Figure 3: Classification of data fusion.

Table 1: Characteristics of principal component analysis.

Data fusion rate	0	15	30	45	60	75	90
$a_{\text{value}} = 25$	0.1	0.075	0.05	0.03	0.02	0	0
$a_{\text{value}} = 50$	0.16	0.13	0.08	0.05	0.035	0.02	0
$a_{\text{value}} = 75$	0.18	0.16	0.12	0.055	0.04	0.025	0

considers the occurrence of features in the text, and the formula is as follows:

$$\text{ECE}(f_k) = \sum_{i=1}^{|d|} p(c_i \mid f_k) \log \frac{p(c_i \mid f_k)}{p(c_i)}. \tag{3}$$

2.2.4. Mutual Information. Mutual information represents the correlation between text features and text classes. The formula is as follows:

$$\text{MI}(f_k, c_i) = \log\left(\frac{p(f_k \mid c_i)}{p(c_i)p(f_k)}\right). \tag{4}$$

2.2.5. CHI Statistic. The CHI statistic, also known as x2 statistic, assumes that the x2 distribution with the first degree of freedom between the feature and the category, the x2 statistic, is calculated as follows:

$$\text{CHI}(f_k, c_i) = \frac{N \times \left[p(f_k \mid c_i) \times p(\bar{f}_k \mid \bar{c}_i) - p(f_k \mid \bar{c}_i) \times p(\bar{f}_k \mid c_i)\right]^2}{p(f_k) \times p(\bar{f}_k) \times p(c_i) \times p(\bar{c}_i)}, \tag{5}$$

where A represents the number of texts containing the feature f_k and belongs to the category c_i, B represents the number of texts containing the feature f_k but not belonging to the category c_i, C represents the number of texts that do not contain the feature f_k but belongs to the category c_i, and D represents the number of texts containing feature f_k and does not belong to the category c_i.

2.3. Support Vector Machine (SVM). The most important point in SVM is the choice of kernel functions. The performance of different kernel functions is different. In the era of big data, a lot of data is linear and inseparable. In order to make performance better at this time, we must choose the most suitable kernel function. The main role is to map the linearly inseparable numbers in the input space into a high-dimensional space so that the feature data is separable. But to construct a kernel function V, you must know the mapping of input space to feature space. To know this kind of mapping, you should understand the distribution of the data set, but in many cases, you do not know the specific distribution of the processed data set, so it is difficult to choose a kernel function that conforms to the input space. You can choose the following common kernel function to replace your own kernel function:

2.3.1. Linear Kernel Function.

$$\kappa(x, x_i) = x \cdot x_i. \tag{6}$$

The linear kernel function is used to solve the problem of linear separability. From the above formula, we can know that the dimension of the feature space to the input space is the same. The parameters are small and fast. It is suitable for linearly separable numbers. When you first choose a linear kernel function, if the effect is not ideal, then switch to another kernel function.

2.3.2. Polynomial Kernel Function.

$$\kappa(x, x_i) = \left((x \cdot x_i) + 1\right)^d. \tag{7}$$

The polynomial kernel function can realize the mapping of low-dimensional feature data to high-dimensional data, but there is an obvious disadvantage that there are many parameters. When the order of the polynomial is high, the element value of the kernel matrix approaches infinity or infinity, and the calculation is performed. The complexity is too big to calculate.

2.3.3. Gaussian (RBF) Kernel Function.

$$\kappa(x, x_i) = \exp\left(-\frac{\|x - x_i\|^2}{\delta^2}\right). \quad (8)$$

The Gaussian kernel function is a highly localized function that maps a sample of data into a high-dimensional space. The advantage of this kernel function is that its performance is better regardless of the number of samples, large or small, relative to the polynomial kernel. There are fewer function parameters. Therefore, in most cases, when you do not know which kernel function to use, you can choose the Gaussian kernel function first.

2.3.4. Sigmoid Kernel Function.

$$\kappa(x, x_i) = \tanh(\eta < x, x_i > + \theta). \quad (9)$$

If sigmoid is a kernel function, the support vector machine is equivalent to a multilayer neural network. In the actual machine learning modeling, if you have a certain prior knowledge of the data in advance, you should choose a kernel function suitable for the data distribution. If you cannot know, you should use the cross-validation method to try different kernel functions. The smaller the effect, the better the kernel function with the smallest error. Of course, when using SVM modeling, multiple kernel functions can also be combined to form a mixed kernel function. Of course, according to the experience of predecessors, the number of selected features and the size of the sample must follow certain rules. Figure 4 is the classification principle of the sample linear separable support vector machine in two dimensions.

The machine finds a decision boundary and separates the positive and negative categories. Then, the machine will find the distance from all sample points to this decision boundary and find the closest points to this decision boundary. Among them, the larger the distance, the better the decision boundary.

2.4. Rough Set. The rough set was proposed by Z. Pawlak, a professor at the Warsaw University of Technology in Poland. As a mathematical theory for dealing with uncertain, incomplete data and inaccurate problems, rough sets have been widely used in artificial intelligence, pattern recognition, data mining, and machine learning and knowledge discovery. It examines knowledge from a new perspective and uses knowledge as a classification ability. The size of classification ability is determined by the granularity of knowledge. The uncertainty of knowledge is caused by the large granularity of the composition domain knowledge, and this granularity of knowledge will represent the classification by the division of equivalence classes of equivalence relations. The following are the advantages of rough sets: the mathematical foundation is mature; no prior knowledge is required; the operation is simple; and the theories for dealing with other uncertain problems are strongly complementary. The following is the disadvantage of rough set: rough set can only solve discrete data.

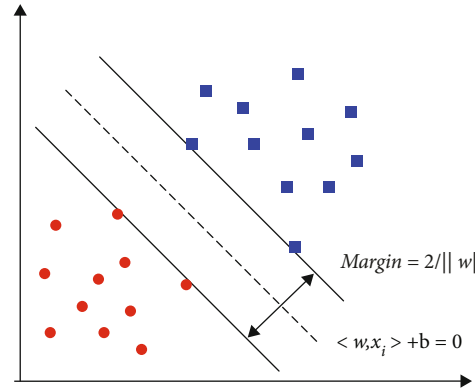

Figure 4: Optimal classification surface in the case of two-dimensional linear separability.

A rough set uses an information system as a description object. An information system is a collection of objects described by a set of multivalued attributes. Each object and its attributes have a value as its descriptive symbol. The information system can be represented by an information table, the rows of the information table corresponding to the research object, the columns corresponding to the attributes of the object, each row containing the descriptors representing the attributes of the corresponding object feature items, and the category information of the corresponding objects. Rough sets can also represent classification rules in decision information tables and attribute reduction based on the importance and dependencies of attributes to generate decision rules for each class. The test data set is used to calculate the confidence and gain of the candidate rule to verify the extracted candidate rule as the final classification rule. Before establishing candidate rules, the decision table is divided into two groups in a random manner: a% of the data is regarded as the training data group; 1-a% of the data is regarded as the test data group. Figure 5 is a rough set flow chart.

Firstly, the demand data is processed. Based on the similarity definition in the algorithm definition, the equivalent item is calculated for each demand item; based on the rough set, the similarity threshold is calculated, and the initial equivalence class is modified; and the validity index of the cluster is calculated. Judge the quality of the clustering results, and obtain the clustering results that meet the needs of customers through repeated calculations.

2.5. Definition of Text Classification Method Based on Granularity Calculation. The particle size calculation mainly includes three parts: particles, grain layer, and grain structure. Among them, the particle is the most basic element that constitutes the particle size calculation model and is the primitive of the particle size calculation model. The grain layer is the overall composition of all the particles obtained according to the granulation criterion of a practical demand and is an abstract description of the problem space. The grain structure is the relationship structure formed by the interconnections between the grain layers. The complexity of the grain structure determines the complexity of the

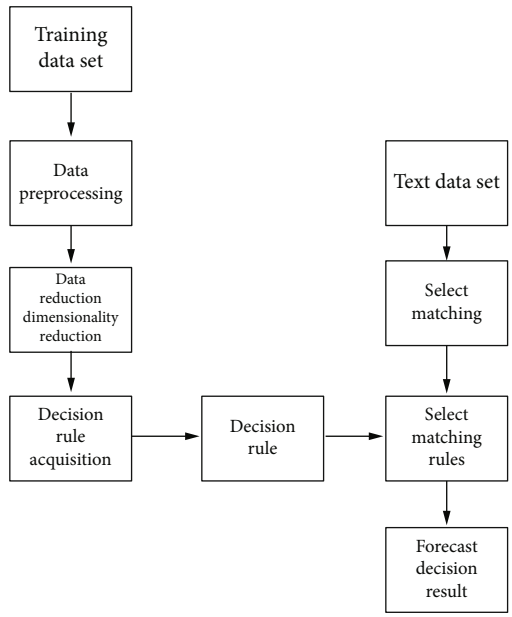

Figure 5: Rough set flow chart.

problem solving. Granularity calculations can be solved in two ways, namely, granulation and particle calculation.

Definition 1. Set a corpus D, where D contains m texts d; that is, after each word of D is segmented, multiple feature words w are obtained, and then each feature word w is trained by Gensim library. The corresponding feature word vector w is obtained, and the dimension is k-dimensional. Set the word vector set obtained by the entire corpus $W = \{w_1, w_2, \cdots, w_n\}$. Based on the perspective of granular computing, this set of word vectors is called the word vector space.

Definition 2. For a word vector space, the feature word similarity $W = \{w_1, w_2, \cdots, w_n\}$ based on the space is defined as

$$R_W^{\lambda} = \left\{ \left(\mathbf{w}_i, \mathbf{w}_j \right) \in W \times W \mid S\left(w_i, \mathbf{w}_j \right) \geq \lambda \right\}, \quad (10)$$

where $S(w_i, w_j)$ represents the similarity between the word vector w_i and w_j; this paper uses the Euclidean distance to measure the similarity; λ is a threshold, which satisfies $0 < \lambda \leq 1$. It can be seen that the definition of the similarity of the characteristic words is a special binary relationship. Responsiveness and symmetry are satisfied, but the transfer characterization is not necessarily satisfied, so it can induce an overlay on the word vector space W.

It can be seen that the feature word similarity segmentation divides the whole word vector space into one feature word class, which is equivalent to granulating the entire word space. Each granulated word class maintains a high similarity inside, and the similarity the definition is embodied by the threshold λ, so the lambda value has a significant influence on the final granulation result.

3. Experiment

3.1. Data Source. The experiment uses the TanCropusV1.0 Chinese corpus, firstly classifying the corpus into 12 text granularity sets by class. Then, the stop words and 1-gram words of 12 text granularity sets (5504 total) were removed, and the characteristics of 12 text granularity sets were evaluated by DF, GSS, ECE, and CHI. In a descending order, select the top 20 features as the condition attributes for each granularity set and calculate the purity of each granular set.

Select five from any of the 12 text granularity sets (e.g., G1, G4, G7, G8, and G11) to experiment; first, divide the five text granularity sets into test sets and training sets in a ratio close to 3 : 2, and select the characteristics of the training set separately, select the top 20 features of each CHI evaluation in the granularity set, and then "compress" the text set; that is, remove the text with the same result after feature selection, and count the number of texts and missing text after feature selection.

3.2. Experimental Platform

3.2.1. Skip-Gram Model Experimental Environment Configuration. There are many practical and convenient libraries. This article uses the Word2Vec in the Gensim library to complete the training process of word embedding. From the data preprocessing of the text to the completion of the word embedding training, the environment of the whole experimental process is shown in Table 2.

In this experiment, in addition to the user's comment data, I also added Wikipedia data as a library to train the word embedding of each word. The reason for this is that the corpus has a certain scale, and the effect of training is more. Well, it can fully reflect the correct position of these words in the vector space, so that a higher degree of word embedding can be obtained.

3.2.2. Skip-Gram Model Parameter Configuration. When using the Skip-Gram model to train the word embedding of each word, it mainly involves setting two parameters: first is the size c of the training window, and second is the length of the word vector, that is, the k of the word embedding. In theory, the larger the window c, the better the completeness of the model, but if c is too large, it will lead to many irrelevant words being trained. Therefore, in the course of the experiment, the random selection window is selected, and the window size is generally less than or equal to 10. For example, after determining the size of c, for a word, the distance $R = \text{rand}(1, c)$ is selected as the result of selecting the R words before and after the word as the final generated prediction result. Because of the corpus involved in this article, each text contains only a few to dozens of words, and the text is relatively short, so the size c of the window is set to 8.

3.3. Classification Algorithm Calculation

3.3.1. Information Granularity Rule Acquisition. Input: information system $S = (U, A, V, f)$

Output: rule set RUL

Table 2: Data preprocessing and extraction feature experimental environment.

Lab environment	Environmental configuration
Operating system	Centos6.5
CPU	Intel Core I5-650 3.20 GHz
RAM	8GB
Programming language	Python3.6
Word segmentation tool	ICTCLAS2016
Training tool	Word2Vec

(Step 1) The first step is to divide the domain according to the decision attribute value into different information granularities $G = \{G_{d_1}, G_{d_2}, \cdots, G_{d_s}\}$.

(Step 2) Determine if impurities are included between the particle sizes.

(Step 3) The third step is to perform attribute reduction on each information granularity in G, set the rule preamble length including the impurity attribute, and obtain the intragranular rule RUL.

(Step 4) Combine the rules between the granularities $\mathrm{RUL} = \bigcup_{G_F \in G} \mathrm{RUL}_{G_G}$.

(Step 5) Output RUL

3.3.2. Information Granularity Attribute Reduction. Input: information granularity G_i

Output: reduction attribute set REUDi

(Step 1) Calculate the coordination matrix H_i of G_i.

(Step 2) The second step is to find the most similar samples x_i, x_j in H_i, determine the elements $H_{i,j}$, delete other elements in sub H_i containing subscript i (or j), and initialize the reduction attribute subset R_i and the sample division subset X_i.

$$\begin{aligned} R_i &\longleftarrow H_{i,j}, \\ X_i &\longleftarrow x_i, x_j. \end{aligned} \tag{11}$$

(Step 3) The third step is to search for the sample x_k which is the most similar to H_{ij} and simultaneously update the reduction attribute subset R_i and the sample division subset X_i and delete the other elements in the H_i subscript containing k.

$$\begin{aligned} R_i &\longleftarrow H_{ij} \cap x_k, \\ X_i &\longleftarrow X_i \cup x_k. \end{aligned} \tag{12}$$

Table 3: The purity of the granularity of the text information corresponding to the four feature extraction methods.

Granular set number	DF	GSS	ECE	CHI
G1	35%	65%	35%	100%
G2	80%	95%	80%	100%
G3	60%	90%	60%	95%
G4	30%	70%	30%	95%
G5	40%	50%	40%	85%
G6	70%	80%	60%	100%
G7	55%	75%	55%	100%
G8	60%	95%	60%	100%
G9	60%	85%	60%	90%
G10	30%	80%	30%	95%
G11	20%	30%	20%	70%
G12	45%	65%	45%	100%
Mean	48.75%	73.33%	47.92%	94.17%

Table 4: Word2Vec.

Tunable parameter	Value
Number of iterations	20
Model selection	Skip-Gram
Method selection	HS
Context window	8
Sample value	Le-4
Lowest frequency	5

(Step 4) Repeat step 3 until the length of R_i is less than or equal to the specified threshold and add R_i to REUDi, and if $G_i = X_i$, terminate the search.

(Step 5) Output the reduced attribute set REUDi.

4. Results

4.1. Feature Extraction Purity Analysis. The experiment uses the TanCropusV1.0 Chinese corpus, firstly classifying the corpus into 12 text granularity sets by class. Then, the stop words and 1-gram words of 12 text granularity sets (5504 total) were removed, and the characteristics of 12 text granularity sets were evaluated by DF, GSS, ECE, and CHI. In a descending order, select the top 20 features as the conditional attributes of each granularity set, and calculate the purity of each granularity set. The results are shown in Table 3.

As can be seen from Table 2, the text granularity set obtained by DF and ECE for feature selection has a lower average value of 48.75% and 47.92%, respectively, and when ECE is used, the purity of a single text size set is up to 80%. The minimum is 20%. The text granularity set obtained by CHI feature selection has the highest average value, reaching 94.17%, wherein the single text granularity set has the highest purity of 100%, the lowest is 85%, and the six text granularity sets have a purity of 100%. It can be seen that among

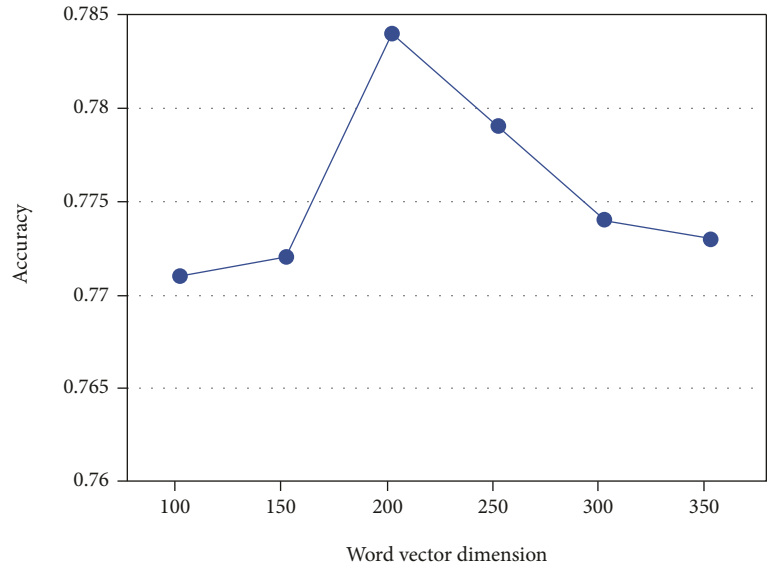

Figure 6: Accuracy rate results.

the four feature selection methods, the 12 feature granularity sets have the same feature words in the top 20 feature words obtained by DF and ECE, and the same top 20 feature words obtained by CHI are the same. There are fewer feature words, so CHI is more suitable as a feature selection method for text granularity sets.

4.2. Influence of Vector Dimensions and Thresholds on Experimental Results. This experiment mainly considers the influence of the word vector dimension on the experimental results. In this experiment, Wikipedia is used as the training set, and the Word2Vec tool is used to train the word vector. The setting of each parameter is shown in Table 4. The word vector dimension is a multiple of 5 from 100 to 350. Experiments are performed using Word2Vec+SVM to determine the influence of the word vector dimension on the experiment. The experimental results are shown in Figure 6. Table 5 is a comparison table of experimental results.

From the above comparative experimental results, table analysis is as follows:

(1) In the traditional machine learning model experiment, linear SVM performs best, and the final text classification accuracy can reach 85.46%. The reason is analyzed: the objective function of the support vector machine model is to minimize the structural risk, which greatly reduces the model's requirements for data volume and data distribution, so the performance is the best when the number of samples is small. Compared with the traditional machine learning algorithm, this method is more excellent in performance, even higher than the best performing SVM, which is nearly 8% higher in classification accuracy

(2) In the three traditional convolutional neural network model experiments, the best performance is the CNN-non-static model. Moreover, the model is nearly 3% higher in final classification accuracy than the CNN-rand model. The reason is as follows: on the one hand, the artificial random initialization feature representation can not be very abstract data input distribution; on the other hand, the Word2Vec trained word vector is used as the CNN input feature in advance, and in iterative training, the input feature is keep up to date

Table 5: Comparison of experimental results.

Model	Accuracy (%)
Word embedding+linear SVM	85.46
Word embedding+LR	85.20
Word embedding+random forest	82.61
CNN-rand	88.52
CNN-static	90.36
CNN-non-static	91.79
Text method	93.25

4.3. Classification Accuracy Analysis. After text classification for all 1918 test texts using the improved rough set text classification technique, the classification results of Tables 3 and 4 were obtained according to the evaluation methods given. The comparison shows the following:

(1) For small-scale test sets, the correct number of recalls and precision of texts have increased significantly

(2) There are significant reductions in the number of false recalls and nonrecalls in all test sets, such as environmental, educational, and economic; the wrong recall rate for computers and transportation is even reduced to zero

Table 6: Test results analysis table.

	G1	G4	G7	G8	G11
Number of test texts	207	50	263	193	178
Correct match number	174	50	231	182	168
Error match number	32	0	32	11	9
Number of lost text	1	0	0	0	1
Recall rate	84.45%	100%	87.83%	94.30%	94.92%
Precision rate	86.14%	84.75%	89.53%	100%	89.36%

(3) The recall and F1 values of all test sets are increased. The improved text classification technology reduces the false recall rate of computer and traffic to zero. Therefore, the recall rate of these two types reaches 100%

(4) The overall recall rate and precision rate of the overall ten text categories are improved to varying degrees

According to Bayesian theory, this is equivalent to the introduction of prior knowledge, which guides the model to converge to the optimal solution along a better direction during the training process. The CNN model is characterized in that it does not require manual feature selection in advance, which greatly reduces manpower consumption, and the input features are continuously updated during the training process, which indicates that the CNN text classification process is a combination of feature selection and training.

4.4. Text Test Results. During the test, the test set is divided into five groups according to the category, and then the five groups are matched with the rules in the rule base, and the classification results are statistically analyzed. The results are shown in Table 6.

It can be seen from Table 6 that the total number of texts participating in the test is 891, of which 807 are correctly classified and 84 are classified incorrectly. Since the test text set does not contain the feature words in the rule base, 2 articles are lost (unable to be judged). The macro average accuracy of the five categories is 89.96%, the macroaverage recall rate is Macro.r. 92.30%, and the macro average F1 is 91.11%. The microaverage accuracy Micro_p of the five categories is equal to the microaverage recall rate of Micro_r of 90.55% and the microaverage F1 of 90.55%.

5. Discussions

According to the degree of similarity of the conditional attributes between the particle sizes, the concept of particle size purity is proposed. It is proved by experiments that the top 20 features obtained by CHI are evaluated as the conditional attributes of each information granularity. Different from the traditional method of attribute reduction by constructing discernible matrix, this chapter constructs the attribute matrix by deconstructing the decision matrix. According to the search method proposed in this chapter, the five categories are trained to obtain attribute reduction sets, and 34 rules with rule precedence greater than or equal to 2 are obtained. Experimental results show that these classification rules have a high classification ability.

There are significant reductions in the number of false recalls and nonrecalls in all test sets, such as environmental, educational, and economic; the wrong recall rate for computers and transportation was even reduced to zero; for the overall ten text categories, the recall rate and precision rate have been improved to different extents; for small-scale test sets, the correct number of recalls and precision of texts have increased significantly.

Linear SVM performs best, with a final text classification accuracy of 85.46%. Compared with the traditional machine learning algorithm, this method is more excellent in performance, even higher than the best performing SVM, which is nearly 8% higher in classification accuracy. In the three traditional convolutional neural network model experiments, the best performance is the CNN-non-static model. Moreover, the model is nearly 3% higher in final classification accuracy than the CNN-rand model.

Through three sets of comparative experiments, it can be known that compared with the traditional machine learning classification algorithm, the proposed method achieves better results in classification effect; using word embedding to initialize text features, compared with artificial randomization, text feature initialization is more excellent in classification effect; the method of this paper also achieves better classification accuracy than the traditional best convolutional network model. Finally, this chapter gives a detailed conclusion analysis for the experimental parameter settings and experimental results.

6. Conclusion

(1) In terms of feature dimension reduction, unlike the existing methods of selecting features by evaluation function, this paper proposes a new feature clustering method, which aggregates different feature words by calculating the distribution distance between features. To reduce the feature dimension, this can prevent part of the sample caused by the feature evaluation function from being discarded because it does not contain the selected feature. The experiment also proves that the clustering method can obtain higher classification accuracy through SVM test

(2) Using the Skip-Gram neural network language model to train the word embedding of each word, that is, the word vector of the feature word, construct the word vector space based on the word vector of all feature words, and then construct the relevant granulation relationship to the word vector space. As a result of granulation and granulation, each feature word in the word vector space has a feature word class, also called feature word granule, and the feature words inside each feature word class maintain a high degree of similarity, so the feature words in the feature word class are selected to expand, and the purpose of text expansion is achieved

(3) In terms of classification algorithm, this paper combines the relevant theory of granular computing with text classification. Firstly, the test text set is granulated, which reduces the complexity of attribute reduction in rough set. Second, for a single information granularity, by constructing a synergistic matrix and heuristic search attribute reduction set. The experiment extracted 34 rules from 1811 training samples. These rules were used to test 891 unknown samples. The average macroaccuracy was 89.96%, and the microaverage accuracy was 90.55%

(4) The experimental results show that the clustering method can obtain higher classification accuracy than other feature selection methods when using SVM as the classifier. According to the correlation principle of the rough set, feature selection is made for each information granularity, the selected feature is used as the condition attribute and the coordination matrix is constructed, and the most similar sample is heuristically searched to obtain the attribute reduction set

The experimental results show that in the three traditional convolutional neural network model experiments, the best performance is the CNN-non-static model. Moreover, the final classification accuracy of this model is nearly 3% higher than that of the CNN rand model.

Data Availability

This article does not cover data research. No data were used to support this study.

Conflicts of Interest

The authors declare that they have no conflicts of interest.

Acknowledgments

This work was supported by Liaoning Collaboration Innovation Center for CSLE, National Natural Science Foundation of China (Grant No. 61832004), and Projects of International Cooperation and Exchanges NSFC (Grant No. 62061136006).

References

[1] W. Tian, "A method of feature selection based on Word2Vec in text categorization," in *2018 37th Chinese Control Conference (CCC)*, pp. 9452–9455, Wuhan, China, 2018.

[2] L. I. U. Bei, "Oceanographic big data text categorization algorithm based on improved mutual information," in *Proceedings of 2017 2nd International Conference on Artificial Intelligence: Techniques and Applications (AITA 2017)*, p. 5, Shenzhen, Guangdong, China, 2017.

[3] J. Ni, G. Gao, and P. Chen, "Chinese text auto-categorization on petro-chemical industrial processes," *Cybernetics and Information Technologies*, vol. 16, no. 6, pp. 69–82, 2016.

[4] W. Chen, "Research on text categorization model based on LDA-KNN," in *Proceedings of 2017 IEEE 2nd advanced information technology, electronic and automation control conference (IAEAC 2017). IEEE Beijing Section, global union academy of science and technology, Chongqing global union academy of science and technology, Chongqing geeks education technology co., ltd: IEEE BEIJING SECTION (multinational Institute of Electrical and Electronics Engineers Beijing Branch)*, p. 8, Chongqing, China, 2017.

[5] D. Lianhong, S. Bin, and Z. Hongwei, "A short text classification method based on knowledge graph extension," *Information Engineering*, vol. 4, no. 5, pp. 38–46, 2018.

[6] G. Weiyin and W. Li, "Text classification based on convolutional neural network and XGBoost," *Communication Technology*, vol. 51, no. 10, pp. 2337–2342, 2018.

[7] Z. Man, X. Zhanguo, L. Bing, and Z. Yong, "A character-level text classification method for full convolutional neural networks," *Computer Engineering and Applications*, vol. 56, no. 5, p. 7, 2020.

[8] L. Wang, Z. Tao, C. Cai, A. Zhu, and Q. Luo, "Study on text classification of TF-IDF based on chi-square statistics improvement," *Electronic World*, vol. 6, pp. 24-25+28, 2019.

[9] L. Yao, Q. Z. Sheng, X. Wang, S. Wang, X. Li, and S. Wang, "Collaborative text categorization via exploiting sparse coefficients," *World Wide Web*, vol. 21, no. 2, pp. 373–394, 2018.

[10] T. Wang, Z. Long, L. Huaiquan, L. Li, and C. Siqi, "Text classification method based on key word learning," *Journal of Shandong Normal University(Natural Science)*, vol. 34, no. 1, pp. 54–60, 2019.

[11] G. Chaolei and C. Junhua, "Study on Chinese text classification based on SA-SVM[J].," *Computer applications and Software*, vol. 36, no. 3, pp. 277–281, 2019.

[12] H. Chao and C. Junhua, "Chinese text classification based on improved K nearest neighbor algorithm," *Journal of Shanghai Normal University(Natural Science)*, vol. 48, no. 1, pp. 96–101, 2019.

[13] D. Junhong, L. Xiaoyu, and M. Dejun, "A text classification training method based on incomplete labeling," *Microprocessor*, vol. 40, no. 1, pp. 20–24, 2019.

[14] L. Kai, "Study on Chinese text classification method," *Computer Knowledge and Technology*, vol. 15, no. 4, pp. 242–244, 2019.

[15] J. Ma and Y. Ma, "Semantic-driven classification of judicial document learning methods," *Computer Applications*, pp. 1–6, 2019.

[16] J. Xingguo, J. Wan, C. Xiaodong, L. Haiou, and C. Yi, "A fine-grained vehicle identification algorithm based on singular

value decomposition and central metric," *Journal of Xidian University*, pp. 1–6, 2019.

[17] Z. Haoru, Z. Yong, and L. Guozhu, "Study on fine-grained image classification algorithm based on RPN and B-CNN," *Computer Applications and Software*, vol. 36, no. 3, pp. 210–213+264, 2019.

[18] L. Dangwei, Z. Yongzhe, L. Kewen, and C. Zhenwen, "The coarse-grained particle swarm optimization algorithm for subgroup stratification," *Computer Engineering and Design*, vol. 40, no. 2, pp. 389–393, 2019.

[19] L. Jingrui and P. Dongyang, "Research on data source multigranularity search algorithm based on probability and statistics," *Computer Products &Circulation*, vol. 2, pp. 89–152, 2019.

[20] L. Jinshuo, L. Yangmei, J. Zhuangyi, J. Deng, Q. Haigang, and J. Pan, "A large-scale data fine-grained parallel optimization method based on PMVS algorithm," *Journal of Wuhan University(Information Science Edition)*, vol. 44, no. 4, pp. 608–616, 2019.

[21] Z. Suzhi, Y. Wei, C. Xiaoni, and L. Penghui, "A coarse-grained parallel AP clustering algorithm based on intra-class and inter-class distance," *Journal of Central China Normal University(Natural Science)*, vol. 52, no. 6, pp. 781–787+797, 2018.

[22] C. Ronghu and H. Yunjie, "Application of SPMD-based coarse-grained parallel genetic algorithm in path optimization of solid warehouse," *Software Guide*, vol. 17, no. 12, pp. 108–112, 2018.

[23] Y. Yingjian, L. Min, and Q. Yiyang, "Design and implementation of a hardware Trojan detection algorithm for coarse-grain reconfigurable arrays," *Journal of Electronics & Information Technology*, pp. 1–8, 2019.

[24] Q. Jin and L. Jianhua, "A fine-grained attribute analysis algorithm for terminal trusted remote proof," *Computer and Digital Engineering*, vol. 46, no. 10, pp. 1970–1973, 2018.

[25] Z. H. A. O. Yilin, J. I. A. N. G. Lin, M. I. Yunlong, and L. I. Jinhai, "A dynamic parallel updating algorithm for degree-grained rough set approximation sets based on weighted granularity and dominance relation," *Computer Science*, vol. 45, no. 10, pp. 11–20, 2018.

Hindawi
Journal of Sensors
Volume 2022, Article ID 4327414, 9 pages
https://doi.org/10.1155/2022/4327414

Research Article

Optimization of Heterogeneous Clustering Routing Protocol for Internet of Things in Wireless Sensor Networks

Shun Yang, Xian'ai Long, Hao Peng, and Haibo Gao

Hunan International Economics University, Changsha Hunan 410205, China

Correspondence should be addressed to Shun Yang; bobyang520@163.com

Received 26 October 2021; Accepted 16 December 2021; Published 19 January 2022

Academic Editor: Gengxin Sun

Wireless sensor network technology is widely used in various modern scenarios, and various industries have higher and higher requirements for the performance indicators of wireless sensor networks. A reasonable and effective layout of wireless sensor networks is conducive to the monitoring of environmental quality, various transactions, and status and transmits a large number of sensing data to the data aggregation center for processing and analysis. However, the operation and development of traditional wireless sensor networks are extremely dependent on the energy supply of the network. When the corresponding supply energy is limited, the operation life of the corresponding wireless sensor network will be greatly reduced. Based on the above situation, this paper proposes a nonuniform clustering routing protocol optimization algorithm from the energy loss of cluster head and clustering form algorithm in wireless sensor networks. At the level of cluster head calculation in wireless sensor networks, firstly, based on the adaptive estimation clustering algorithm, the core density is used as the estimation element to calculate the cluster head radius of wireless sensor networks. At the same time, this paper creatively proposes a fuzzy logic algorithm to further solve the uncertainty of cluster head selection, integrate the residual energy of cluster head nodes, and finally complete the reasonable distribution of cluster heads and realize the balance of node energy consumption. In order to further reduce the algorithm overhead of transmission between cluster heads and realize energy optimization, an intercluster routing optimization algorithm based on the ant colony algorithm is proposed. The pheromone is updated and disturbed by introducing chaotic mapping to ensure the optimal solution of the algorithm, and the optimal path is selected from the perspective of energy dispersion coefficient and distance coefficient, so as to optimize the energy consumption between cluster heads. The experimental results show that compared with the traditional algorithm, the proposed nonuniform clustering routing protocol optimization algorithm prolongs the corresponding life cycle by 75% and reduces the total network energy consumption by about 20%. Therefore, the algorithm achieves the purpose of optimizing network energy consumption and prolonging network life to a certain extent and has certain practical value.

1. Introduction

A wireless sensor network is formed by a large number of wireless sensors through reasonable layout. It is widely used in national defense, military, industrial production, and other activities. The traditional wireless sensor network communication protocol mainly includes an application layer, transmission layer, network layer, data link layer, physical layer, energy management layer, mobile management layer, and task management layer. In the corresponding energy management layer, the wireless sensor network realizes the management of system energy and prolongs the service life of the system as much as possible. A wireless sensor is a small unit constituting wireless sensor network, which is mainly used for specific data acquisition, data processing, data storage, and transmission of the monitored environment. Its corresponding structure is usually small, so its corresponding power supply part often uses small battery for power supply [1–3]. When the corresponding wireless sensor network is arranged in a harsh environment, the timeliness of the corresponding battery replacement is weak, resulting in the downtime of the wireless sensor network once the battery energy in the environment is exhausted, so the wireless sensor will not be able to collect, compress,

and transmit data in a specific area; therefore, it will seriously affect the whole wireless sensor network [4, 5]. Therefore, based on the above analysis, the energy balance of wireless sensor networks, the optimization of energy nodes, and the maximization of network life cycle are important problems that need to be solved urgently in wireless sensor networks for the Internet of things [6]. How to optimize the energy consumption of each node from the whole wireless sensor network, so as to optimize the energy consumption of the whole network, realize the balance of energy consumption of wireless sensor network, and avoid the problem of excessive energy consumption of individual nodes, so as to prolong the service life of the network, is very important and meaningful.

From the routing protocol algorithm level of wireless sensor networks, its main research contents focus on two levels: hierarchical routing protocol and planar routing protocol [7]. The corresponding plane routing protocol mainly takes the data as the center and continuously sends the corresponding data to the corresponding adjacent data nodes in the form of broadcasting. Generally speaking, the plane routing protocol is relatively simple, and its corresponding application scenarios are mostly concentrated in the case of a small number of nodes. It has no advantages in network scalability, network delay, and energy consumption balance [8, 9]. The corresponding hierarchical routing protocol is mainly based on the idea of clustering. It divides the nodes into cluster head nodes and conventional nodes. The corresponding conventional nodes are mainly used to collect sensing data and send it to the corresponding cluster head nodes. The cluster head nodes are responsible for transmitting the corresponding merged data to the base station for processing [10]. Based on this conventional hierarchical routing protocol, the corresponding data transmission modes are divided into two modes: intracluster transmission and intercluster transmission. On the problem of corresponding cluster formation, the current main strategies include clustering algorithm, uniform clustering algorithm, and nonuniform clustering algorithm. The main purpose of the corresponding clustering algorithm and uniform clustering algorithm is to effectively balance the corresponding load among clusters, so as to balance the energy consumption of each cluster head. The corresponding nonuniform clustering algorithm is mainly used to deal with the uneven location distribution and energy distribution of network nodes. Its classical nonuniform clustering algorithm includes distributed competitive nonuniform clustering algorithm and fuzzy logic nonuniform algorithm [11, 12]. However, the above traditional wireless sensor network routing protocol algorithms have more or less the randomness of cluster head selection, the subjectivity of cluster head size selection, and the corresponding routes between cluster heads fall into the dilemma of local optimization rather than global optimization. Therefore, the routing protocol algorithm of wireless sensor networks with excellent performance is very meaningful.

Based on the above analysis, the current wireless sensor networks still have unreasonable energy consumption allocation at the level of energy management. At the same time, the traditional nonuniform clustering routing protocol algorithm can not solve the current problem of reasonable energy consumption allocation. Based on this, this paper will start with the cluster head energy consumption and clustering algorithm of wireless sensor networks and propose a nonuniform clustering routing protocol optimization algorithm. Firstly, based on the adaptive estimation clustering algorithm, the core density is used as the estimation element to calculate the cluster head radius of wireless sensor networks. At the same time, a fuzzy logic algorithm is innovatively proposed to further solve the uncertain problem of cluster head selection and integrate the residual energy of cluster head nodes, The comprehensive factors such as node density and corresponding node energy consumption finally complete the reasonable allocation of cluster heads and realize the balance of node energy consumption. In order to further reduce the algorithm overhead of transmission between cluster heads and realize energy optimization, this paper proposes an intercluster routing optimization algorithm based on the ant colony algorithm, which updates and perturbs the pheromone by introducing chaotic mapping, so as to ensure the optimal solution of the algorithm, and selects the optimal path from the perspective of energy dispersion coefficient and distance coefficient, so as to optimize the energy consumption between cluster heads. The experimental results show that the proposed nonuniform clustering routing protocol optimization algorithm for wireless sensor networks extends its corresponding life cycle by 75% compared with the traditional algorithm, and its corresponding total network energy consumption speed is improved. Therefore, the algorithm achieves the purpose of optimizing network energy consumption and prolonging network life to a certain extent and has certain practical value.

The chapters of this paper are arranged as follows: Section 2 mainly analyzes the current research status of clustering routing protocol algorithm for wireless sensor networks for the Internet of things and points out the existing problems. In Section 3, the cluster head allocation problem will be analyzed and studied based on adaptive estimation clustering algorithm and fuzzy logic algorithm. At the same time, the intercluster head routing optimization algorithm will be optimized based on the ant colony algorithm, so as to optimize the energy consumption between cluster heads, and finally realize the optimization of nonuniform clustering routing protocol algorithm in wireless sensor networks. Section 4 will verify the algorithm and analyze the experimental results. Finally, a summary of this paper is made.

2. Related Research Work: Analysis of the Research Status of Clustering Routing Protocol Algorithm for Wireless Sensor Networks for the Internet of Things

In order to solve the energy consumption problem of traditional wireless sensor networks, the current mainstream energy management algorithms include random clustering

routing protocol algorithm, uniform clustering routing protocol algorithm, and nonuniform clustering routing protocol algorithm [13–15]. Based on the above three algorithms, a large number of research institutions and researchers have studied and analyzed them. This paper only discusses uniform clustering algorithm and nonuniform clustering algorithm. For the uniform clustering algorithm, relevant Japanese scientists first proposed a hybrid energy-efficient clustering protocol, which fully considers not only the residual energy but also the average value of the minimum achievable energy consumption. The cluster heads with large energy will compete to select clusters. The cluster heads corresponding to the algorithm are evenly distributed and support scalable data fusion, thus effectively prolonging the data life cycle [16]. Relevant European researchers have proposed a hybrid energy efficient clustering protocol with fuzzy energy consumption characteristics based on the hybrid energy-efficient clustering protocol. The corresponding fuzzy energy consumption depends on the node density and node centripetality. The cluster head can be determined by comparing the corresponding fuzzy energy consumption. The corresponding clustering speed of the algorithm is fast, and the corresponding clustering is relatively uniform, Therefore, the corresponding energy consumption is also relatively uniform [17]. However, the uniform clustering routing protocol algorithm has the phenomenon of large energy consumption of nodes near the base station and premature downtime of nodes. Therefore, relevant researchers proposed a nonuniform clustering routing protocol algorithm to prolong the life cycle of wireless sensor networks in the form of nonuniform clustering [18]. Relevant Asian researchers have proposed an improved nonuniform clustering routing protocol algorithm based on the traditional nonuniform clustering routing protocol algorithm. The algorithm randomly selects candidate shots, competes for the final cluster head within its own cluster radius by comparing the residual energy, and carries out adaptive calculation based on the calculation formula of nonuniform clustering radius; the algorithm avoids the energy waste caused by long-distance data transmission and further improves the hot spot problem caused by excessive forwarding energy consumption of cluster heads [19]. Based on the above analysis, the above algorithms have more or less problems, such as unreasonable selection of cluster heads and excessive energy consumption during transmission between cluster heads.

3. Analysis of Nonuniform Clustering Routing Protocol Optimization Algorithm in Wireless Sensor Networks

This section mainly starts with the cluster head energy consumption and clustering algorithm of wireless sensor networks and proposes a nonuniform clustering routing protocol optimization algorithm. At the level of clustering algorithm, it is mainly based on the adaptive estimation clustering algorithm and takes the kernel density as the estimation element to calculate the cluster head radius of wireless sensor networks. At the same time, it further solves the uncertain problem of cluster head selection based on fuzzy logic algorithm and integrates the residual energy of cluster head nodes; the comprehensive factors such as node density and corresponding node energy consumption finally complete the reasonable allocation of cluster heads and realize the balance of node energy consumption. In order to further reduce the algorithm overhead of transmission between cluster heads and realize energy optimization, this section proposes an intercluster routing optimization algorithm based on ant colony algorithm, which updates and perturbs the pheromone by introducing chaotic mapping, so as to ensure the optimal solution of the algorithm, and selects the optimal path from the perspective of energy dispersion coefficient and distance coefficient, so as to optimize the energy consumption between cluster heads. The principle block diagram corresponding to the nonuniform clustering routing protocol optimization algorithm of wireless sensor networks analyzed in this section is shown in Figure 1:

3.1. Cluster Head Selection Optimization Algorithm Analysis. Before the algorithm runs, three models of the algorithm are established, which correspond to the network model, data aggregation model, and node energy consumption model. The corresponding network model is mainly the assumption of wireless sensor network algorithm. The corresponding data model is mainly to reduce the corresponding node data redundancy. The corresponding model is an *Ia* model mechanism. The length of the data packet after the aggregation of the corresponding model is shown in Formula (1), where the corresponding D represents the length of the data packet after the data aggregation and the corresponding L_r represents the packet length received by the corresponding node.

$$L_{\mathrm{DATA}} = (L_{r1} + L_{r2} + \cdots + L_{r3} + L_{ri}) * \varepsilon + L_D. \tag{1}$$

At the level of corresponding energy consumption model, the model used by this algorithm is the first-order wireless communication model, and the corresponding model principle block diagram is shown in Figure 2. From the principle block diagram, it can be seen that the corresponding node energy consumption includes transmission energy consumption and reception energy consumption, the corresponding transmission energy consumption includes a transmission circuit and transmission amplifier, and the corresponding reception energy consumption includes a signal receiving circuit. The corresponding mathematical calculation output energy consumption and receiving energy consumption is shown

$$\begin{aligned} \mathrm{Power}(L, d) &= L * \mathrm{Power}_{\mathrm{elec}} + L * d * d, d < d_0, \\ \mathrm{Power}(L, d) &= L * \mathrm{Power}_{\mathrm{elec}} + L * d^4, d \geq d_0, \end{aligned} \tag{2}$$

$$L * \mathrm{Power}_{\mathrm{elec}} = P_R(L, D) \tag{3}$$

Based on this calculation formula, the energy consumption distribution formula corresponding to the cluster head

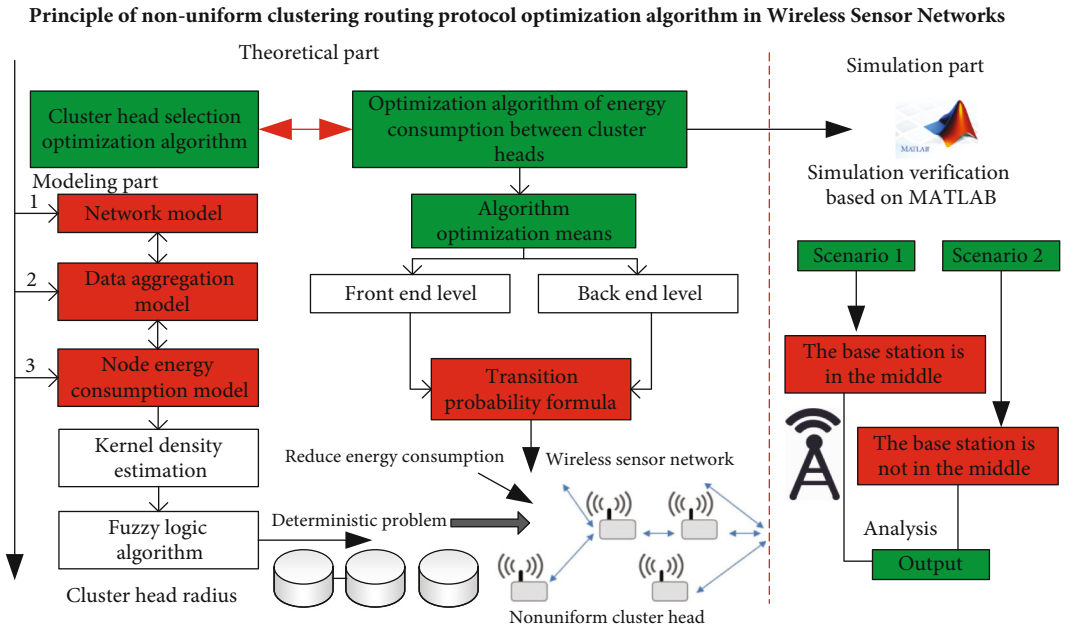

Figure 1: Schematic diagram of nonuniform clustering routing protocol optimization algorithm for wireless sensor networks.

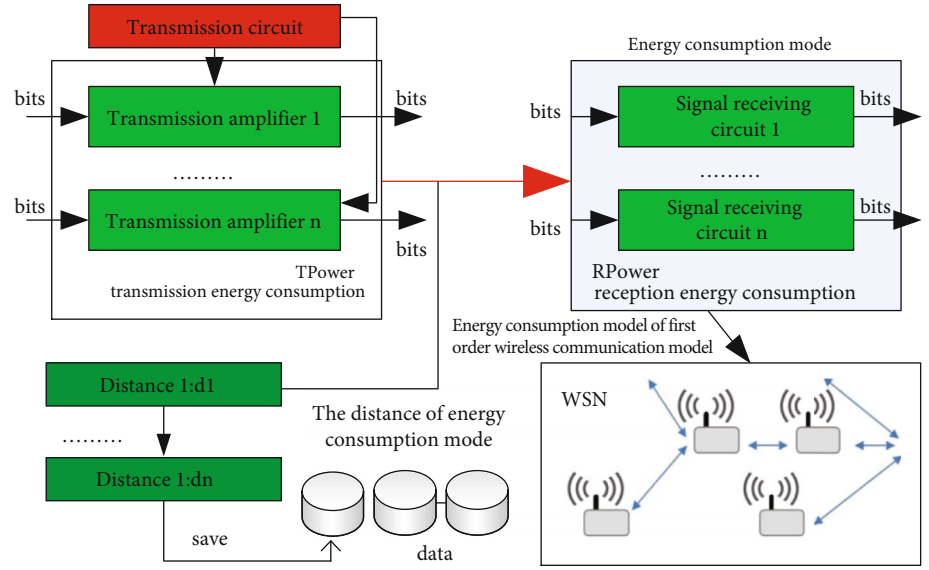

Figure 2: Principle block diagram of the energy consumption model of the first-order wireless communication model.

node can be further obtained. The calculation formula is shown in

$$Power_{all} = Power_R + Power_T + Power_{route} + Power_{DATA}. \quad (4)$$

When calculating the cluster head radius of the system network, it is mainly estimated based on the kernel density. The corresponding cluster head size mainly depends on the density of node distribution, the dispersion of node distribution, and the relative residual energy of nodes. At the node distribution density level, when the corresponding nodes are densely distributed, the corresponding load of the cluster head can be reduced by reducing the cluster head radius, so as to avoid the rapid failure of the system cluster head. On the contrary, for the local area with sparse node distribution, the corresponding cluster head radius can be appropriately increased; the dispersion of the corresponding cluster head node will affect the radius of the cluster head node. When the corresponding wireless sensor network system transmits data to the cluster head node, the corresponding energy loss is positively correlated with the distance to the cluster head node. When the distribution of the corresponding cluster head nodes is relatively discrete, the wireless sensor network needs to consume a lot of energy to transmit to the cluster

head node, at this time, the cluster head radius can be appropriately reduced to realize the energy consumption of data transmission in the cluster head. The amount of residual energy of the corresponding cluster head node is related to the cluster head radius. The larger the corresponding residual energy is, the larger the corresponding cluster head radius is. However, with the continuous consumption of energy of wireless sensor network nodes, the corresponding cluster head radius is decreasing. Therefore, based on the analysis of the above influencing factors, the corresponding node adaptive cluster head radius algorithm steps are as follows:

Step1: the kernel density estimation is calculated based on the above influencing factors. The corresponding estimation function is shown in formula (5), where the corresponding L_i represents I data nodes in the wireless sensor network and the corresponding k represents the normal kernel function, which reflects the dispersion of the distribution of data nodes.

$$\begin{aligned}\text{Dispersion}(L/\text{Power}, D) &= \left(\frac{1}{M}\right) * \left[\left[\frac{ND(1)}{((DS(1) * \text{Power}(1))}\right] * k(L - L_1)\right], \\ &\cdots\cdots \\ \text{Dispersion}(L/\text{Power}, D) &= \left(\frac{1}{M}\right) * \left[\left[\frac{ND(1)}{((DS(N) * \text{Power}(N))}\right] * k(L - L_N)\right].\end{aligned} \tag{5}$$

Step 2: estimate the local bandwidth of the wireless sensor network. The local bandwidth is still estimated by using the relevant factors analyzed above. Adaptive bandwidth estimation is performed after local bandwidth estimation. The corresponding calculation formula of adaptive bandwidth estimation is shown in formula (6), where the corresponding y represents the sensitive factor factor. The larger the corresponding sensitive factor, the more sensitive the function estimated based on kernel density is.

$$H_i = \left(\text{Dispersion}\left(\frac{L}{\text{Power}}, D\right)\right)^{-y} * p^y. \tag{6}$$

Step3: fit and estimate the cluster head radius based on the adaptive bandwidth. At this time, the calculation formula of the corresponding cluster head radius is shown in formula (7). Control the corresponding cluster head radius between the minimum cluster head radius and the maximum cluster head radius. It can be seen from the function that the cluster head radius is inversely correlated with the kernel density estimation function.

$$\begin{aligned}Radius(1) &= H_1 * bandwidth, \\ &\cdots \\ Radius(i) &= H_i * bandwidth.\end{aligned} \tag{7}$$

Based on the above determination of cluster head radius, this paper reconfirms the uncertain cluster head based on fuzzy algorithm. The core algorithm is as follows: firstly, we calculate the distance between each node of the sensor network and the base station. The closer the corresponding node is to the base station, the greater the probability that it will become an important cluster head node. At the same time, it is proved that the competitiveness of this cluster head is strong. Therefore, based on this characteristic, fuzzy rules are used to further deal with the uncertainty of competition between cluster heads. The fuzzy inputs used in this paper correspond to the residual energy of cluster heads and the distance from nodes to base stations, and the corresponding fuzzy output variables are only limited to the ability of competing cluster heads. The logic block diagram of the corresponding cluster head deterministic algorithm based on fuzzy logic is shown in Figure 3. It can be seen from the figure that the main two core mechanisms of the fuzzy logic algorithm are fuzzification processor and defuzzification processor, respectively, and the corresponding core analysis module is fuzzy reasoning module.

Based on the above, we can further determine the cluster head of wireless sensor network and optimize the selection of cluster head.

3.2. Analysis of Energy Consumption Optimization Algorithm among Cluster Heads. In order to further optimize the energy optimization between cluster heads of wireless sensor networks, this section optimizes the routing algorithm between cluster heads of wireless sensor networks based on ant colony algorithm, so as to reduce the output transmission energy consumption between cluster heads. This paper mainly optimizes the transition probability formula in the traditional ant colony algorithm. In the traditional algorithm, only a single distance index is used as the heuristic factor, which will essentially lead to the excessive consumption of node energy between cluster heads. Therefore, this section considers the transfer probability formula of the ant colony algorithm from the front-end and back-end levels. At the corresponding front-end level, the pheromone heuristic factor and distance factor between cluster heads are mainly considered. At the back-end, the balance degree of cluster heads between nodes and the tolerance of the balance degree are mainly considered. Combined with the factors of the front-end and back-end, the corresponding transfer probability formula of the improved ant colony algorithm is shown in formula (8), in which the corresponding B represents the concentration heuristic factor of information elements, the corresponding C represents the path heuristic factor of cluster head transmission, and the corresponding W represents the importance of the above two heuristic factors.

$$TP(B, C, W) = \frac{w * \left(c * b_j(1)\right)}{c * b_i(1)^{\left(1+d_{jb}/\sum d\right)}} + \cdots + \frac{w * \left(c * b_j(t)\right)}{c * b_i(t)^{\left(1+d_{jb}/\sum d\right)}}. \tag{8}$$

Based on this, the principle and steps of the intercluster energy consumption optimization algorithm based on the improved ant colony algorithm are shown in Figure 4 below. It can be seen from the figure that the details of the corresponding algorithm are as follows:

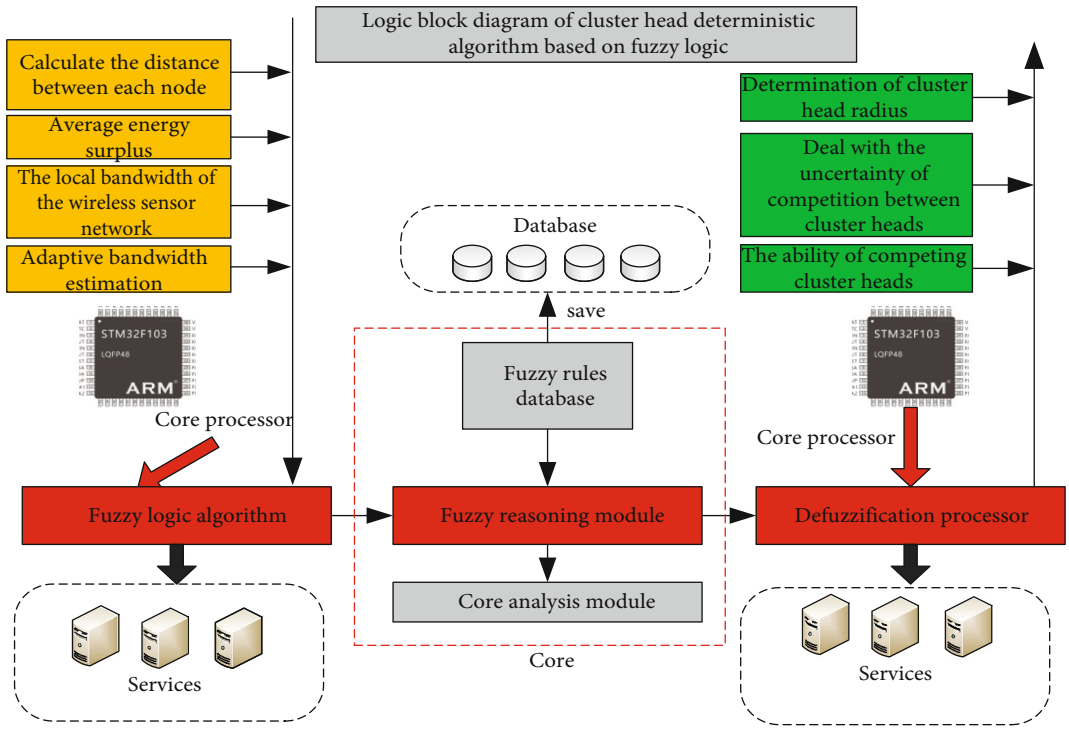

Figure 3: Logic block diagram of cluster head deterministic algorithm based on fuzzy logic.

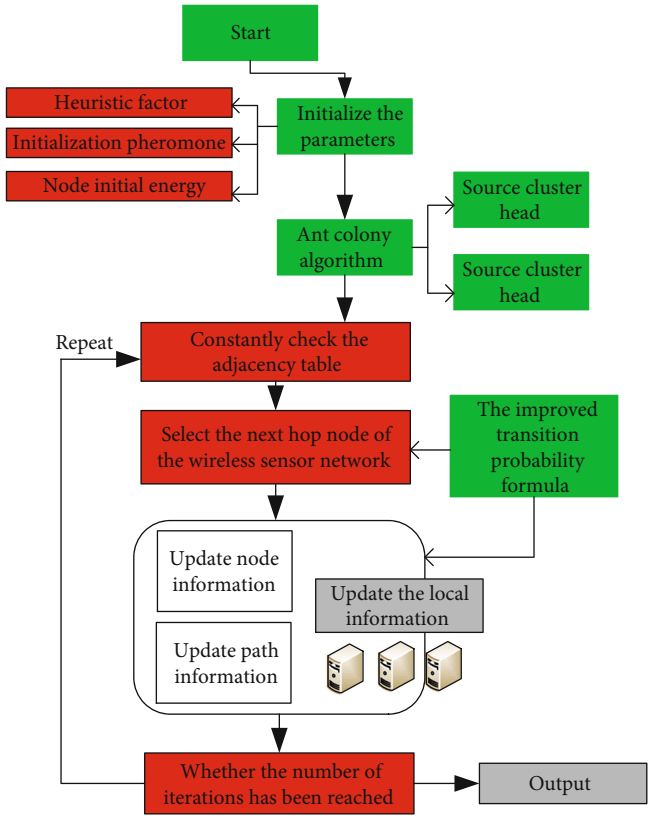

Figure 4: Principle block diagram of energy consumption optimization algorithm between cluster heads based on improved ant colony algorithm.

Step 1: initialize the parameters of the wireless sensor system. The corresponding initialization information includes initialization pheromone, node initial energy, heuristic factor, and other parameters.

Step 2: perform iterative processing based on ant colony algorithm on the corresponding source cluster head and update it in time.

Step 3: constantly check whether there is a next hop node to be selected in the adjacency table. If it does not exist at this time, continuously expand the search radius and update the adjacency status in time until it is found.

Step4: select the next hop node of the wireless sensor network based on the improved transition probability formula, record the corresponding update node and path information, and update the local information.

Step 5: judge whether the number of iterations has been reached. If not, repeat steps 2-4 until the algorithm is terminated.

4. Experiment and Data Analysis

In order to verify the algorithm proposed in this paper, it is simulated and verified based on MATLAB. The corresponding verification experiments mainly include two cases: the base station of wireless sensor network is located in the middle of the network and the base station of wireless sensor network is not located in the middle of the network. In order to further control the variables, the corresponding simulation sensor is set to 200, and the traditional cluster head selection mechanism is introduced into the cluster head selection mechanism for comparative experiments. In the algorithm evaluation index, this paper selects the wireless

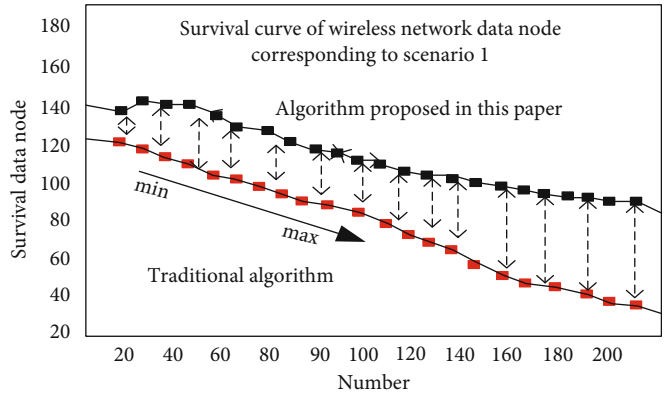

Figure 5: Survival curve of wireless network data node corresponding to scenario 1.

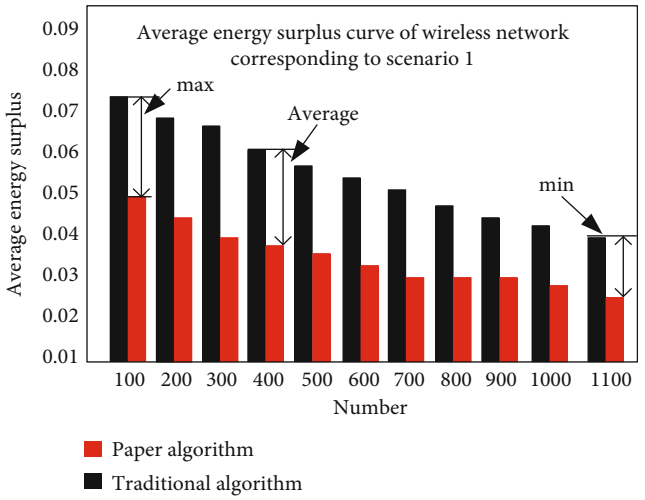

Figure 6: Average energy surplus curve of wireless network corresponding to scenario 1.

sensor network life and energy consumption efficiency as the evaluation index.

Experiment 1. The base station of wireless sensor network is located in the middle of the network.

Based on the comparative experiment between the algorithm proposed in this paper and the traditional algorithm, the corresponding node survival number experimental results are shown in Figure 5. It can be seen from the figure that the corresponding node failure rate of the algorithm proposed in this paper is low, and the corresponding node failure rate continues to slow down with the passage of time, while the traditional algorithm is still relatively steep, so the overall network life becomes longer.

The corresponding Figure 6 shows the corresponding network average energy residual curve under the two algorithms. From the figure, it can be seen that the algorithm proposed in this paper has more residual energy than the traditional algorithm. At the same time, the gap between the residual energy is further widened with the passage of time, which further highlights the advantages of this algorithm at the level of node energy consumption balance.

Experiment 2. The base station of wireless sensor network is not located in the middle of the network.

Based on the comparison experiment between the proposed algorithm and the traditional algorithm, the corresponding node survival number experimental results are shown in Figure 7. It can be seen from the figure that in this case, the corresponding node failure rate of the proposed algorithm and the traditional algorithm is not different, but on the whole, the failure rate of the proposed algorithm is still slightly lower, At the same time, its corresponding node failure rate decreases with the passage of time, so the overall network lifetime still has advantages over traditional algorithms.

The corresponding Figure 8 shows the corresponding network average energy residual curve under the two algorithms. It can be seen from the figure that the algorithm proposed in this paper still has advantages over the traditional algorithm in terms of the corresponding node residual energy. At the same time, the gap between the residual energy and the traditional algorithm is further widened with the passage of time. Therefore, it further highlights the advantages of this algorithm in node energy consumption balance.

In the verification of the corresponding intercluster head routing algorithm, this paper makes an experimental analysis on the energy efficiency between cluster heads based on scenario 2. The experimental results also verify that the clustering routing optimization algorithm under this algorithm consumes less energy than the traditional algorithm in data transmission between cluster heads, so the corresponding wireless sensor network has better stability at this time. According to the above experimental results, it can be further analyzed that the corresponding uniform algorithm and the traditional nonuniform algorithm have the problem of excessive energy consumption. At the same time, it also further proves the disadvantages of the uniform algorithm in the nonuniform scene and the uncertainty problem of the traditional nonuniform algorithm.

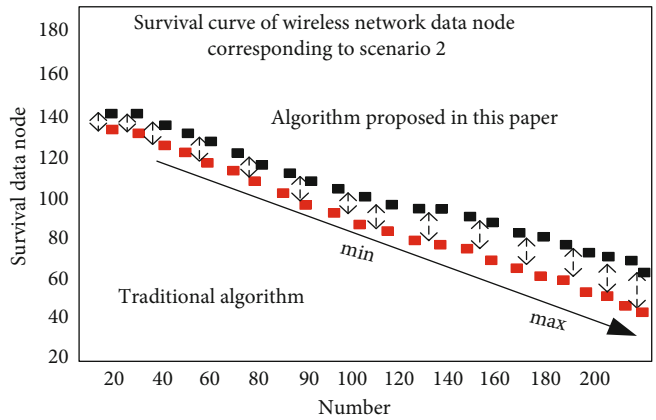

Figure 7: Survival curve of wireless network data node corresponding to scenario 2.

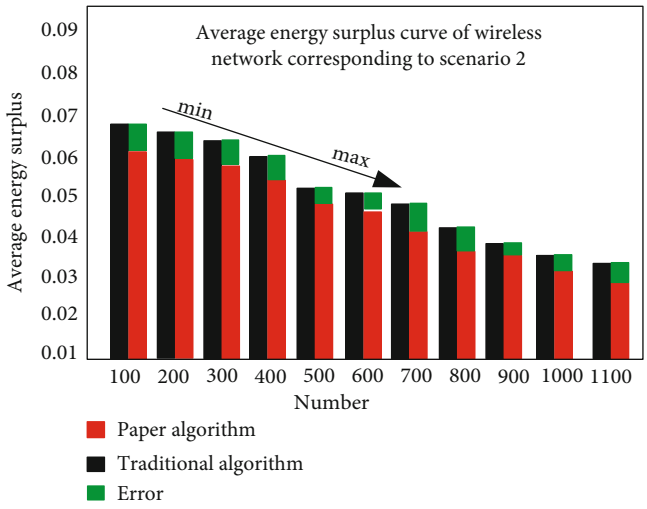

Figure 8: Average energy surplus curve of the wireless network corresponding to scenario 2.

Based on the above experimental results, it can be seen that the proposed algorithm has obvious advantages over the traditional algorithm.

5. Conclusion

This paper mainly analyzes and studies the current research status of clustering routing protocol algorithms for wireless sensor networks for the Internet of things, focuses on the problems existing in nonuniform cluster routing protocol algorithms, and optimizes and improves the traditional algorithms for the corresponding energy management problems. This paper uses the adaptive estimation clustering algorithm and takes the kernel density as the estimation element to realize the optimal selection of cluster heads and the establishment of cluster head mechanism in wireless sensor networks. At the same time, a fuzzy logic algorithm is innovatively proposed to further solve the uncertain problem of cluster head selection and integrate the residual energy of cluster head nodes, and the comprehensive factors such as node density and corresponding node energy consumption finally complete the reasonable allocation of cluster heads and realize the balance of node energy consumption. In order to further reduce the algorithm overhead of transmission between cluster heads and realize energy optimization, a routing optimization algorithm between cluster heads is proposed based on the ant colony algorithm. The pheromone is updated and disturbed by introducing chaotic mapping, so as to ensure the optimal solution of the algorithm, and the optimal path is selected from the perspective of energy dispersion coefficient and distance coefficient; thus, the energy consumption between cluster heads is minimized. The experimental results show that compared with the traditional algorithm, the corresponding life cycle of the proposed nonuniform clustering routing protocol optimization algorithm for wireless sensor networks is prolonged by 75%, and the total energy consumption speed of the corresponding network is improved. In the follow-up research, this paper will focus on more factors affecting the selection of cluster heads, control and deal with their factors, and study the corresponding processing algorithms to realize the global optimization of system network parameters, so as to further reduce the energy consumption of wireless sensor networks and prolong the life cycle of the system.

Data Availability

The data used to support the findings of this study are available from the corresponding author upon request.

Conflicts of Interest

The authors declare that they have no known competing financial interests or personal relationships that could have appeared to influence the work reported in this paper.

Acknowledgments

The work was supported by the Hunan Provincial Research Foundation of Education Bureau of China (Grant Nos. 18B529 and 18A481).

References

[1] M. Elhoseny, X. Yuan, Z. Yu, C. Mao, H. K. el-Minir, and A. M. Riad, "Balancing energy consumption in heterogeneous wireless sensor networks using genetic algorithm," *IEEE Communications Letters*, vol. 19, no. 12, pp. 2194–2197, 2015.

[2] A. E. Assaf, S. Zaidi, S. Affes, and N. Kandil, "Low-cost localization for multi-hop heterogeneous wireless sensor networks," *IEEE Transactions on Wireless Communications*, vol. 15, no. 1, pp. 472–484, 2016.

[3] K. Okano, Y. Aoki, and T. Ohta, "An inter-domain routing protocol based on autonomous clustering for heterogeneous mobile ad hoc networks," *IEICE Transactions on Communications*, vol. 98, no. 9, pp. 1768–1776, 2015.

[4] S. Karimi-Bidhendi, J. Guo, and H. Jafarkhani, "Energy-efficient deployment in static and mobile heterogeneous multi-hop wireless sensor networks," *IEEE Transactions on Wireless Communications*, vol. 13, no. 9, pp. 1–12, 2021.

[5] A. S. Rostami, M. Badkoobe, F. Mohanna, H. keshavarz, A. A. R. Hosseinabadi, and A. K. Sangaiah, "Survey on clustering in heterogeneous and homogeneous wireless sensor networks," *Journal of Supercomputing*, vol. 74, no. 1, pp. 277–323, 2018.

[6] N. Nelson and D. K. Schwartz, "Unbiased clustering of molecular dynamics for spatially resolved analysis of chemically heterogeneous surfaces," *Langmuir*, vol. 31, no. 22, pp. 6099–6106, 2015.

[7] S. Kim, C. Kim, H. Cho, Y. Yim, and S. H. Kim, "A hole self-organization real-time routing protocol for irregular wireless sensor networks," *Journal of the Acoustical Society of America*, vol. 39B, no. 5, pp. 281–290, 2014.

[8] I. Nevat, G. W. Peters, F. Septier, and T. Matsui, "Estimation of spatially correlated random fields in heterogeneous wireless sensor networks," *IEEE Transactions on Signal Processing*, vol. 63, no. 10, pp. 2597–2609, 2015.

[9] S. Deepak and A. P. Bhondekar, "Traffic and energy aware routing for heterogeneous wireless sensor networks," *IEEE Communications Letters*, vol. 22, no. 4, pp. 1608–1611, 2018.

[10] H. Qabouche, A. Sahel, and A. Badri, "Hybrid energy efficient static routing protocol for homogeneous and heterogeneous large scale WSN," *Wireless Networks*, vol. 27, no. 1, pp. 575–587, 2021.

[11] N. Shahid, I. H. Naqvi, and S. B. Qaisar, "Characteristics and classification of outlier detection techniques for wireless sensor networks in harsh environments: a survey," *Artificial Intelligence Review*, vol. 43, no. 2, pp. 193–228, 2015.

[12] M. T. Nuruzzaman and H. W. Ferng, "Design and evaluation of an LQI-based beaconless routing protocol for a heterogeneous MSN," *Wireless Networks*, vol. 26, no. 1, pp. 699–721, 2020.

[13] I. Santos-González, A. Rivero-García, M. Burmester, J. Munilla, and P. Caballero-Gil, "Secure lightweight password authenticated key exchange for heterogeneous wireless sensor networks," *Information Systems*, vol. 88, no. 2, article 101423, 2020.

[14] J. Joung and J. Choi, "Operation strategy for wireless-powered heterogeneous sensor networks," *Electronics Letters*, vol. 53, no. 21, pp. 1437–1439, 2017.

[15] M. Rovcanin, E. de Poorter, D. van den Akker, I. Moerman, P. Demeester, and C. Blondia, "Experimental validation of a reinforcement learning based approach for a service-wise optimisation of heterogeneous wireless sensor networks," *Wireless Networks*, vol. 21, no. 3, pp. 931–948, 2015.

[16] T. Kour and P. Sharma, "Maximizing lifetime of heterogeneous wireless sensor network using heed protocol," *Thin Solid Films*, vol. 97, no. 2, pp. 12–15, 2014.

[17] X. Liang, J. Liang, and W. Zhang, "Construction of quality virtual backbones with link fault tolerance in wireless sensor networks," *IEEE Transactions on Mobile Computing*, vol. 2021, no. 34, pp. 1–20, 2021.

[18] F. Deniz, H. Bagci, I. Korpeoglu, and A. Yazıcı, "Energy-efficient and fault-tolerant drone-BS placement in heterogeneous wireless sensor networks," *Wireless Networks*, vol. 27, no. 1, pp. 825–838, 2021.

[19] N. Madhavi and M. Madheswaran, "Enhanced lifetime of heterogeneous wireless sensor network using stable election protocol with region-based energy-conscious sink movement," *The Journal of Supercomputing*, vol. 76, no. 8, pp. 5715–5731, 2020.

Hindawi
Journal of Sensors
Volume 2022, Article ID 5491876, 11 pages
https://doi.org/10.1155/2022/5491876

Research Article

Construction of Wireless Sensor Model for Carbon Neutralization and Environmental Protection from the Perspective of Energy Internet of Things Transformation

Huawen Tian,[1] **Liwen Jiang**,[2] **and Jie Zhang**[3]

[1]*School of Grammar and Law Shandong University of Science and Technology, Qingdao 266590, China*
[2]*School of Economics and Management, Shandong University of Science and Technology, Qingdao 266590, China*
[3]*School of Management, Shandong University of Technology, Zibo 253770, China*

Correspondence should be addressed to Huawen Tian; skd992912@sdust.edu.cn

Received 10 November 2021; Revised 6 December 2021; Accepted 9 December 2021; Published 17 January 2022

Academic Editor: Gengxin Sun

Carbon neutral environmental protection is an important way to effectively control the rapid rise of global temperature, promote the green transformation of energy utilization, and promote green, low-carbon, and other technological progress. It is a new driving force for world economic development and growth. This paper explores the construction of wireless sensor model for carbon neutralization and environmental protection from the perspective of the transformation of energy Internet of things. This paper analyzes the development background and research status of energy Internet of things technology at home and abroad and determines the overall design scheme of environmental monitoring Internet of things system. Then, we design the overall scheme of wireless sensor model under the environment monitoring Internet of things system. An experimental test platform was built to test the performance of the environmental monitoring Internet of things system. The test results show that the wireless sensor can monitor and respond to physical impact, and the generated energy can realize wireless data transmission of about 20 m; the regional coverage and fixed-point Internet of things system can realize the real-time monitoring of environmental parameters such as light, temperature, humidity, and dust, interact with the data and instructions of the cloud platform normally, and work stably. The basic functions of the whole Internet of things system have been realized, including the alarm function of passive wireless impact sensing, the cloud real-time monitoring function of environmental data and the real-time sending function of cloud instructions, and the real-time monitoring of indoor and outdoor environment under two working modes. The task objectives set in the early stage of the whole system are realized.

1. Introduction

Climate change has a profound impact on the earth's environment, which is a great challenge facing mankind [1]. In order to cope with global climate change and realize the progress of human civilization and the sustainable development of the earth's ecosystem, the 21st United Nations Climate Change Conference adopted the Paris climate agreement, which proposed to achieve the goal of "net zero emission" of CO_2 around 2050, that is, carbon neutralization [2]. Broadly speaking, carbon neutralization refers to the dynamic balance between carbon source systems such as human fossil energy utilization, land use, and natural volcanic eruption carbon emission and carbon sink systems such as earth's carbon cycle system, marine carbon dissolution, and biosphere carbon absorption. In a narrow sense, carbon neutralization refers to the CO2 emission of an organization, group, or individual in a period of time, which is offset by forest carbon sink, artificial transformation, geological storage, and other technologies to achieve "net zero emission" [3]. Carbon neutralization is an important way to effectively control the rapid rise of global temperature, promote the green transformation of energy utilization, and promote green, low-carbon, and other technological progress [4]. It is a new driving force for world economic development and growth [5]. Realizing carbon neutralization will improve

the earth's ecological environment on which human beings depend and reduce environmental problems caused by human activities [6]. In 2019, the World Health Organization announced that air pollution and climate change ranked first among the top ten health threats in the world [7]. It is estimated that from 2030 to 2050, climate change will cause about 250000 new deaths from malnutrition, malaria, diarrhea, and excessive temperature in the world every year, and 7 million people will die prematurely from diseases such as cancer, stroke, heart disease, and lung disease every year [8]. Carbon neutralization will promote the transformation of human energy system to green, low-carbon, and carbon-free, realize the substitution of carbon-free new energy for high-carbon fossil energy, and drive the growth of jobs and GDP in the field of new energy industry [9]. It is estimated that by 2050, the average annual investment in the field of global energy low-carbon transformation will exceed US $3.2 trillion, the cumulative investment will exceed US $95 trillion, and more than 100 million jobs will be provided [10]. Carbon neutralization is the common goal and pursuit of all mankind. The global cooperation mechanism with consultation as the main body is the premise and guarantees to achieve carbon neutralization [11]. In the process of actively promoting carbon neutralization all over the world, it is necessary to carry out carbon neutralization research guided by scientific issues [12].

The automatic identification center established by MIT proposed a radio frequency identification system-item loading sensing equipment [13]. Through the application of RF technology, it is connected with other objects to realize the interconnection of objects and form an intelligent control system [14]. Internet of things is another widely concerned network in the network field after the Internet. It is based on standards and has the ability of self-configuration and management [15]. The Internet of things supports the direct information interaction between people and things, and wireless sensor networks only support the information exchange between things, in order to provide users with the environmental information they need [16]. Therefore, wireless sensor network is the technical basis of the Internet of things and a branch network of the Internet of things. From the historical background of the emergence of wireless sensor network technology, wireless sensor network has experienced wireless data network, wireless ad hoc network, and wireless sensor network [17]. The traditional environmental detection method is to manually obtain various material samples in the environment, such as air, water, and soil, and test the collected samples on the instruments in the laboratory [18]. Such a sample acquisition method can only collect limited data, and the data is not reliable. In order to meet people's demand for various resource monitoring in the future and maintain the sustainable development of economy and environment, we need to obtain a large amount of environmental information timely and accurately [19]. Because of its own characteristics, wireless sensor networks are different from traditional fixed networks. They have the characteristics of limited resources, self-organization, dynamic network, wide scale, and high density [20]. The characteristics of wireless sensor network, such as single deployment, low cost, network self-configuration, and no manual maintenance, make it suitable for the field of environmental monitoring. Multiple nodes carrying various sensors are distributed in the required monitoring environment, and the nodes cooperate to complete the remote monitoring task [21]. Although the research time of wireless sensor network is very short, a large number of sensor network research and application make its technology develop rapidly. With the continuous exploration of wireless sensor networks all over the world, the application of wireless sensor networks has widely existed in all fields of production and life [22]. It is the research focus and application technical basis of wireless networks in the future. Wireless sensor networks (WSNs), which combine sensor technology, microelectronics technology, and wireless technology, are a powerful network. It has been widely used in road traffic, military safety, environmental monitoring, intelligent life, and other aspects. Today's society is affected by the technology and application of WSN [23]. Wireless sensor networks play an important role in monitoring, such as the concentration of carbon dioxide in the air, air humidity, and light intensity. The monitoring of these indicators can well reflect the results of carbon neutralization and provide an important basis for the early realization of carbon neutralization. This paper analyzes the development background and research status of energy Internet of things technology at home and abroad and determines the overall design scheme of environmental monitoring Internet of things system. Then, the wireless sensor network model is applied to the detection of air quality in the environment to detect the content of CO2 in the air more accurately, which is of great significance to achieve the goal of carbon neutralization as soon as possible.

2. Related Work

The Internet of things takes data networking as the essential core, while the energy Internet of things has a large number of users and devices, and the data collected by its measurement and perception is very valuable. On the one hand, the use of massive data enables the energy industry to fully understand its own characteristics and provide new technical support means for low-carbon green development, energy efficiency improvement, energy conservation and consumption reduction, economic operation, and system planning of the energy industry; on the other hand, data analysis and processing based on deep learning, artificial intelligence and other technologies can improve the production efficiency of the energy system, provide better consumer services for users, and provide more efficient decision support for system operators. The Internet of things and wireless sensor networks have been widely favored all over the world. In 1991, the concept of "pervasive computing" proposed by the United States involved perceptual technology, and then, MIT first proposed the "Internet of things" [24]. IBM announced the "smart earth" plan to the outside world in November 2008. Immediately, the plan received strong support from the government and jointly developed smart grid and smart medicine [25]. Carbon neutralization

means that enterprises, groups, or individuals calculate the total amount of greenhouse gas emissions directly or indirectly generated within a certain period of time to offset their own carbon dioxide emissions through afforestation, energy conservation, and emission reduction, so as to achieve "zero emission" of carbon dioxide. As a new form of environmental protection, carbon neutralization has been adopted by more and more large-scale events and conferences. Some other developed countries have also set development goals and taken a number of feasible measures to promote their rapid development. In the field of agricultural environmental monitoring, data transmission technology and environmental data acquisition technology have been developed [26]. In terms of data transmission, there are two measures to ensure the correctness of data transmission: the optimal network protocol and the appropriate network deployment [27]. The correctness of agricultural environmental data transmission first needs the optimal network protocol. The agricultural environment monitoring based on wireless sensor network needs to deploy the network according to the characteristics of the monitoring area. When wireless sensor networks need a single network in a small-scale agricultural monitoring environment, the physical layer and data link layer of the network protocol are the same [28]. However, when wireless sensor networks need composite networks in complex environments, different network layer and application layer specifications are formulated due to specific network protocols. It can be seen from the literature that the fusion between networks requires standards to agree on the communication between different networks [29]. According to different monitoring environments, the research focus of routing algorithm is also different. It can be seen from the literature that the protocols related to wireless sensor networks are appropriately tailored to meet the characteristics of agricultural monitoring environment. Second, select the appropriate topology to deploy the network nodes to make the network reach the optimal state, so as to transmit data reliably [30]. Wireless sensor networks deployed in various regions as the experimental field of project research have promoted the rapid development of Internet of things related technologies. Gong and Jiang [31] proposed a smart city Internet of things system for monitoring indoor temperature, humidity, and CO_2. It uses PIC24F16KA102 chip as the main control and NRF24L01 RF module with 2.4 GHz bandwidth as the transmitting and receiving node to collect temperature, humidity, CO_2, and other sensing data, transmit it to PC through USB, and transmit the data to mobile phone app through the Internet, so as to obtain, save, and process environmental data. Liu et al. [32] proposed a low-power Internet of things system for long-term monitoring of outdoor environment. It is composed of sensor node, gateway node, application server, and back-end alarm equipment. The sensor node collects temperature data through the main control and sends the sensor data to the gateway equipment through CC1150 RF module; the gateway device collects RF data through the 433 module and drives the GPRS module to transmit the data to the application server through the main control module; the application server stores and provides data support for the back-end alarm device; the back-end alarm device runs data query and alarm functions. Vijayalakshmi et al. proposed a real-time environment monitoring Internet of things system using solar energy self-power supply [33]. It is composed of solar panel, power management module, main control module, XBee RF module, and sensor module. Solar panels generate electric energy during the day, provide electric energy for system operation, and charge 50 f capacitors; The main control module collects the information of temperature, humidity, CO, CO_2, and LDO sensors and transmits the data through XBee module. The power consumption of the whole system is about 4.907 mW. At the same time, the 50 F capacitor can be charged to 4.6 V by the solar module during the day; when the operating voltage of the system is between 3.6 V and 4.6 V, the 50 F capacitor can provide the power of the whole system for 12 hours at night [34]. Muthukumaran et al. [35] put forward a cloud service monitoring system for diabetes patients. In the system, the sensor node layer is composed of two parts. One part collects indoor environmental information, such as temperature, humidity, time, location, and air quality, and the other part collects patient information, such as heart rate and body temperature; the gateway is responsible for local data storage, data packaging, data push, and other functions; the cloud service layer is responsible for cloud data storage, data query, and other functions; the equipment terminal can view the information of patients and rooms in real time. The sensor node layer communicates through a 2.4 GHz radio frequency module; the sensor node and gateway transmit data through WiFi module.

3. Research Methods and Key Technologies

3.1. Transformation of Energy Internet of Things. This paper will explore the path description and research methods of energy Internet of things transformation and discuss how to use power system, Internet of things, and social factors to strongly support energy transformation. In 2015, the proportion of nonfossil energy power generation was 30%. The schematic diagram of energy transfer path is shown in Figure 1, showing the change curve of the proportion of renewable energy in primary energy. Under the goal that the proportion of nonfossil energy power generation will reach 80% in 2050, there can be different paths to achieve this goal, and different paths will have different effects on the national economy. How to plan the energy transfer path can take into account the constraints of coordinated economic development and carbon emission, which is worthy of in-depth research.

In many paths, the transformation task can be allocated to each year by linear method; we can also increase the amount of renewable energy as soon as possible, so as to obtain carbon emission benefits as soon as possible and save resources. However, due to immature technology and other reasons, the investment will increase. Or use the opposite method to accumulate experience at the beginning and accelerate the pace of transformation when the technology is mature. Therefore, among many paths, how to find a feasible method to compare different paths and select the

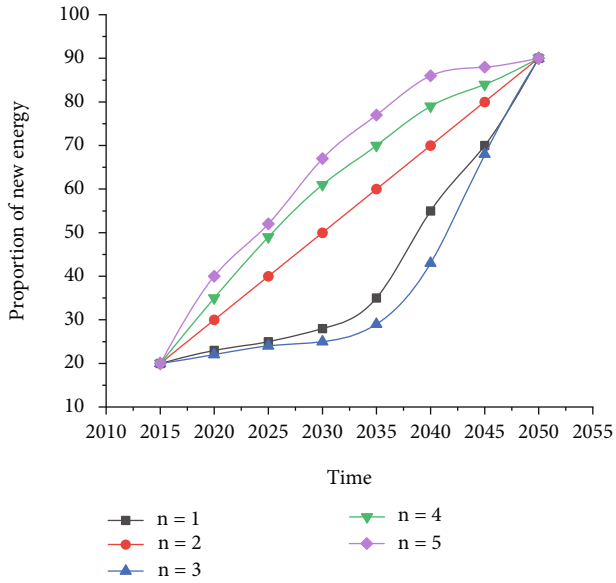

Figure 1: Schematic diagram of energy transfer path.

optimal path has become an urgent problem to be solved. The proportion of nonfossil energy power generation is used as the characteristic quantity of energy transformation, as shown in Figure 1. The time series trajectories of different transformation curves are marked with typical power functions. The power of the transformation curve is represented by n, the linear transformation curve is a special case where the power is equal to 1, and n represents the power of the transformation curve. $R0$ represents the initial proportion of new energy, Rf represents the target proportion, $t0$ and tf represent the starting year and target year, respectively. In year t, the proportion of new energy can be expressed as

$$C(t) = C0 + \left(\frac{A1 + A0}{A1A0}\right)\sqrt{\frac{(t1 - t0)^2}{2}}, \quad (1)$$

$$C0 = \int_{t=0}^{n} A0(1 + 2.3a\%)^n t, \quad (2)$$

$$a = \frac{C(t) - C0}{C(t)}. \quad (3)$$

3.2. Key Technologies of Energy Internet of Things. The network nodes in the energy Internet of things can ensure the comprehensive monitoring of the external environment and improve the overall quality of data transmission. In environmental monitoring, we need to improve the security and stability of data transmission. Combined with the actual characteristics of the Internet of things, we can optimize the design of link layer data transmission and enhance the security of data. We can also establish the reliability analysis method of data transmission of the Internet of things system and take corresponding management measures to ensure the overall effect of data transmission of the Internet of things. The Internet of things system mainly includes three parts: application layer, perception layer, and network layer. The sensing layer is composed of various sensor devices, including reader, terminal camera, and GPS. It can sense the external environment and collect a variety of signals and physical information. The network layer refers to the IOT network communication system, including information processing center and intelligent control center, which can process information quickly and timely.

A large number of microsensor nodes are arranged in the monitoring area to realize the self-organizing network system by means of wireless communication. Various microsensors can be integrated to realize the real-time reception and transmission of information. Wireless communication transmits various data information, and the information obtained by the sensor can also realize the development of integration, miniaturization, and networking, as shown in Figure 2. Wireless sensor network integrates embedded computing, sensor technology, wireless communication technology, and modern network technology, which can enhance the perception ability of the whole device. It is an important prospect in the field of Internet of things.

3.3. Construction of Wireless Sensing Model under Energy Internet of Things Technology. Under the condition of Internet of things technology, it is necessary to analyze the application characteristics of ecological environment, meet the overall needs of system architecture, and improve the overall quality of service monitoring. Wireless sensor nodes with self-organizing function are connected in the form of wireless transmission, which can conduct three-dimensional and comprehensive monitoring of the ground, underground, and air environment, forming a 3D Internet of things environment monitoring system, as shown in Figure 3. The detection system uses Ethernet to monitor different indicators in the environment, such as temperature and humidity. Then, it is transmitted to the remote client through the network.

The core node design of the Internet of things needs to be composed of control and information processing unit, storage unit, and communication unit, and the distributed power supply is used to provide support. Build a monitoring system suitable for the ecological environment of different villages and towns, analyze it combined with the Internet of things node technology and ecological environment sensing data, and develop a sensor module to meet the monitoring of multi environmental parameters such as gas, water, and soil. In order to improve the security and reliability of data and information transmission in the Internet of things, it is necessary to effectively control the nodes of the whole data transmission, design specific methods such as error recovery, congestion control, and flow control, establish sensor models, comprehensively optimize the deployment and coverage of regional sensor nodes, and take corresponding management measures to ensure the quality of information transmission.

The whole IOT monitoring system can realize two working modes to adapt to different application environments.

The situation in the working mode of the area coverage monitoring system is as follows. As shown in

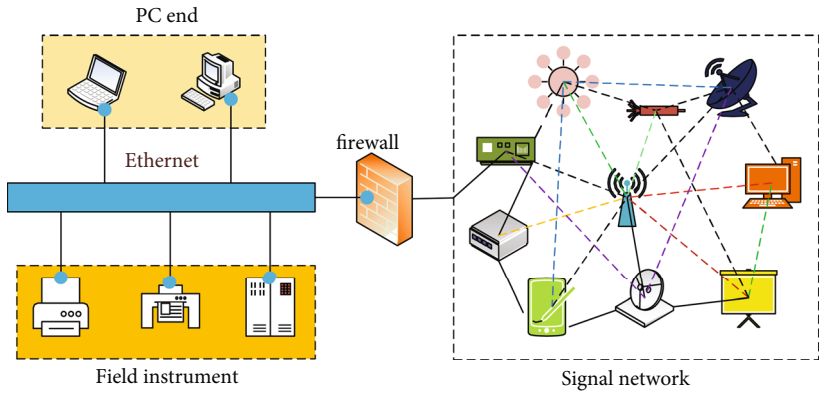

Figure 2: Wireless network sensor.

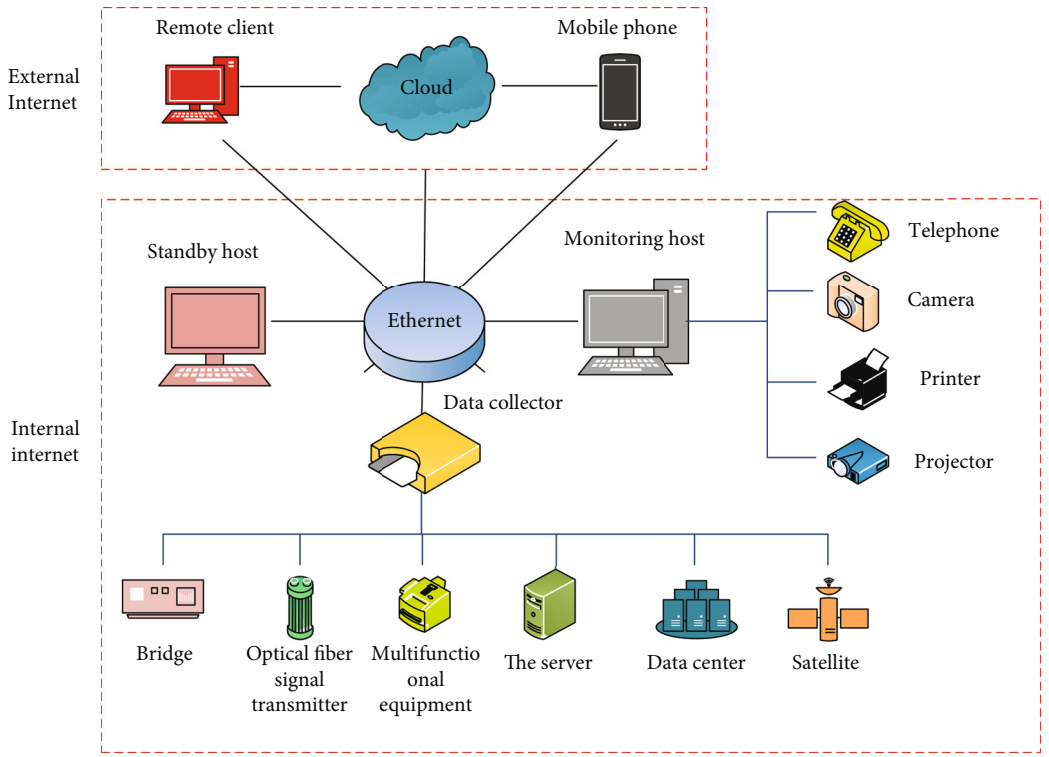

Figure 3: Environmental monitoring system.

Figure 4, the regional monitoring system includes LAN nodes, main control module, and data cloud platform. It can carry out real-time environmental monitoring for large areas, upload data to the data platform in real time, and synchronously monitor the information of each node (impact, temperature, humidity, light and general ad data, etc.).

The working mode of the fixed-point direct connection monitoring system is as follows. Based on the regional coverage monitoring system, the fixed-point direct connection monitoring system removes the monitoring ability of multi-node environment and retains the passive wireless impact sensor node network. Its environmental data collection mainly comes from the data collection of the main control module (impact, temperature, humidity, light, dust, general AD data, etc.). At this time, the monitoring range of fixed-point direct monitoring becomes smaller, but the data acquisition frequency increases, which is mainly applicable to scenes with high data requirements. Its design architecture is shown in Figure 5.

4. System Test and Analysis

This chapter mainly tests the environment monitoring Internet of things system, including passive wireless impact sensing module, area coverage monitoring system, and fixed-point direct connection monitoring system, tests and detects the overall function of the system, and verifies the function of the whole system.

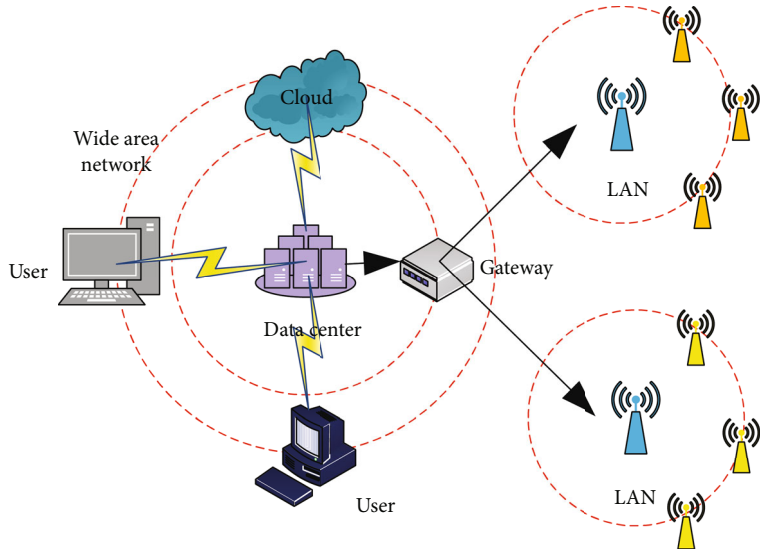

Figure 4: Schematic design architecture of regional coverage monitoring system.

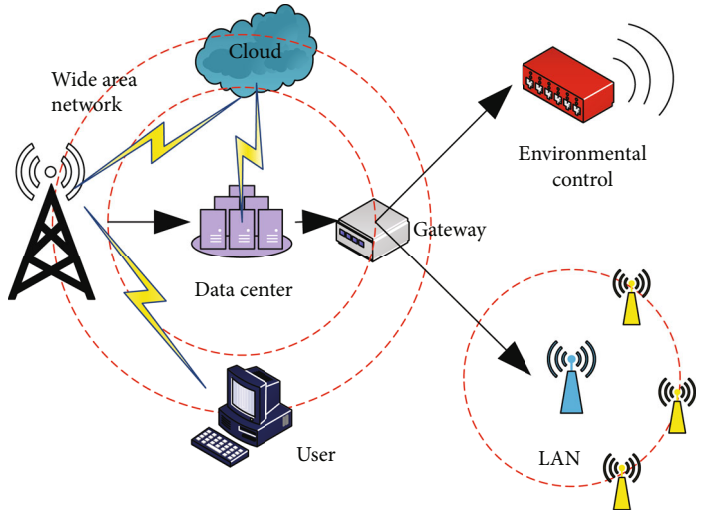

Figure 5: Overall scheme design architecture of fixed-point monitoring system.

4.1. Node Circuit Test. For the node circuit, it is necessary to test the energy storage capacitance and the operation of the control circuit. The energy storage capacitor is a 10 uF tantalum capacitor. After receiving the DC voltage converted by the impulse signal, its voltage test is shown in Figure 6. As can be seen from the figure, the maximum output voltage can reach about 7.2 V, and the voltage shows an exponential attenuation trend with time, which can realize the storage of electric energy and meet the power supply of ultralow power RF module. Since the back-end control circuit will turn on when it is above 3.2 V, the output voltage is the energy storage capacitor voltage, and the voltage of 7.2 V will burn the ultralow power RF module chip, a voltage stabilizing diode must be added at the output voltage to protect the RF chip.

Add the control circuit after the energy storage capacitor and test its output voltage, as shown in Figure 7. When the energy storage voltage of the energy storage capacitor increases from 0 V to 3.2 V, the voltage of the control circuit is 0 V; when the voltage of the energy storage capacitor is greater than 3.2 V, the voltage of the control circuit changes with the voltage of the energy storage capacitor; after that, the voltage of the control circuit will always follow the voltage of the energy storage capacitor to drop to about 1.6 V, and then turn off the output. The control time of the whole control circuit is about 40 ms, that is, the normal working time of ultralow power RF circuit; the voltage output is 1.6 V to 3.2 V, closely following the voltage change of the energy storage capacitor. The design function of the control circuit is verified.

4.2. Overall Function Test. In the overall function test, the fixed-point direct monitoring Internet of things system will be tested in the field. Through the real-time monitoring of the surrounding environment, the data of dust, temperature, humidity, and illumination of the surrounding environment

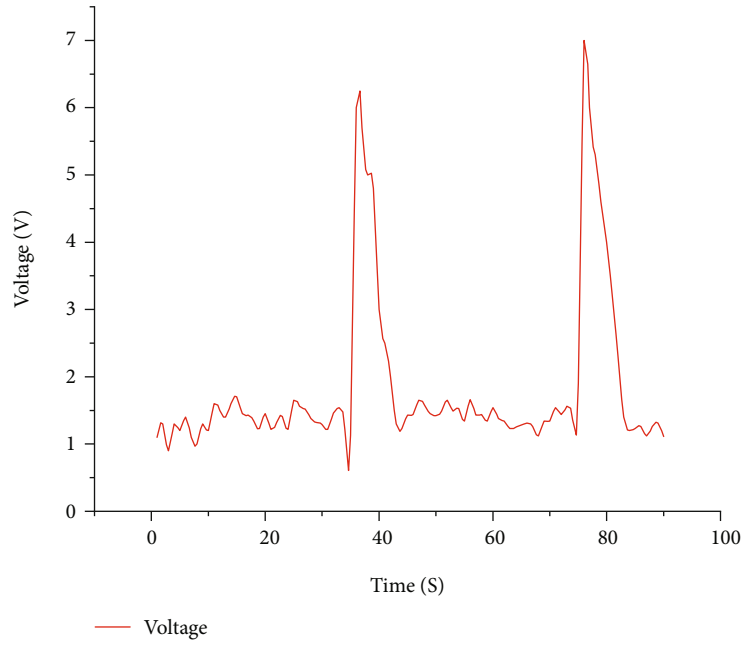

Figure 6: Voltage signal of energy storage capacitor.

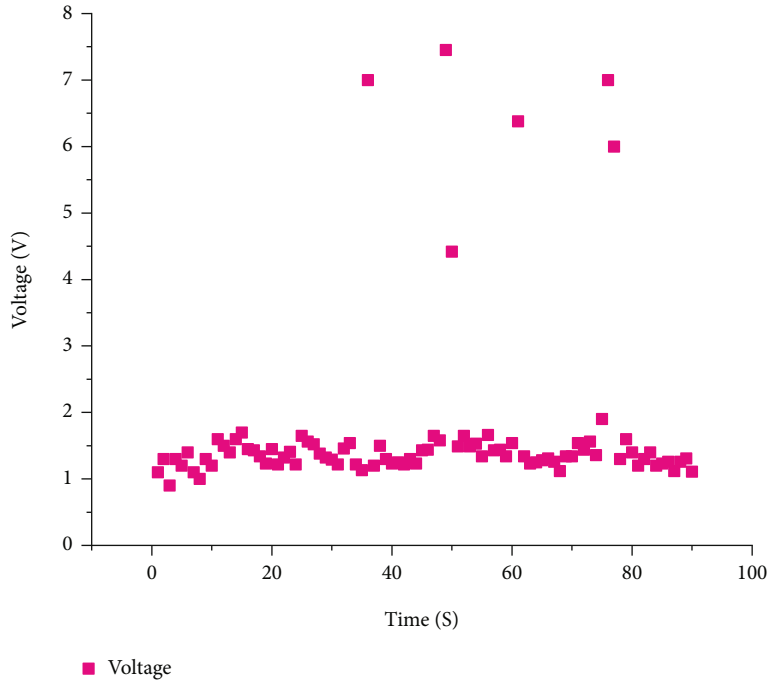

Figure 7: Voltage signal diagram of control circuit.

will be collected in real time to verify the working condition and stability of the whole system. The monitoring time is one hour, and the change curve of each environmental information is obtained, as shown in Figure 8. The system works stably, and all sensing data curves are displayed and saved in real time. At the same time, it can be seen from the data that the system can stably monitor all kinds of data information in the outfield environment.

According to the above tests, the basic functions of the whole Internet of things system have been realized, including the alarm function of passive wireless impact sensing, the cloud real-time monitoring function of environmental data, and the real-time sending function of cloud instructions. The real-time monitoring of indoor and outdoor environment has been realized under two working modes, and the task objectives set in the early stage of the whole system

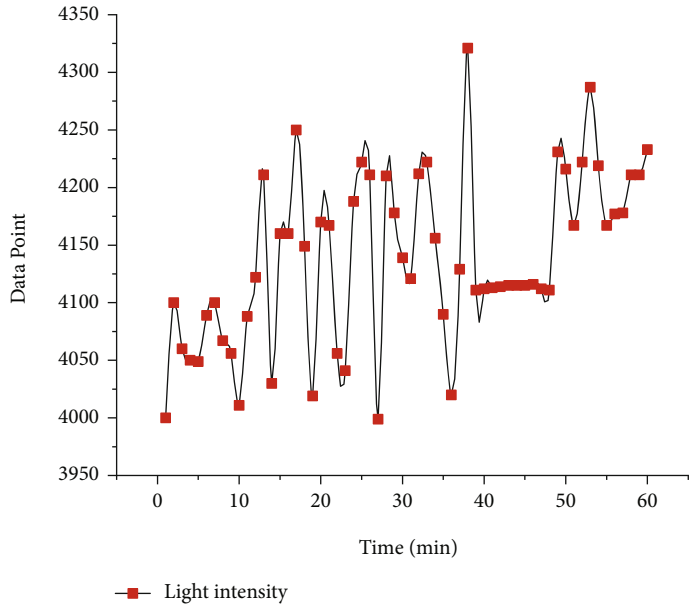

(a)

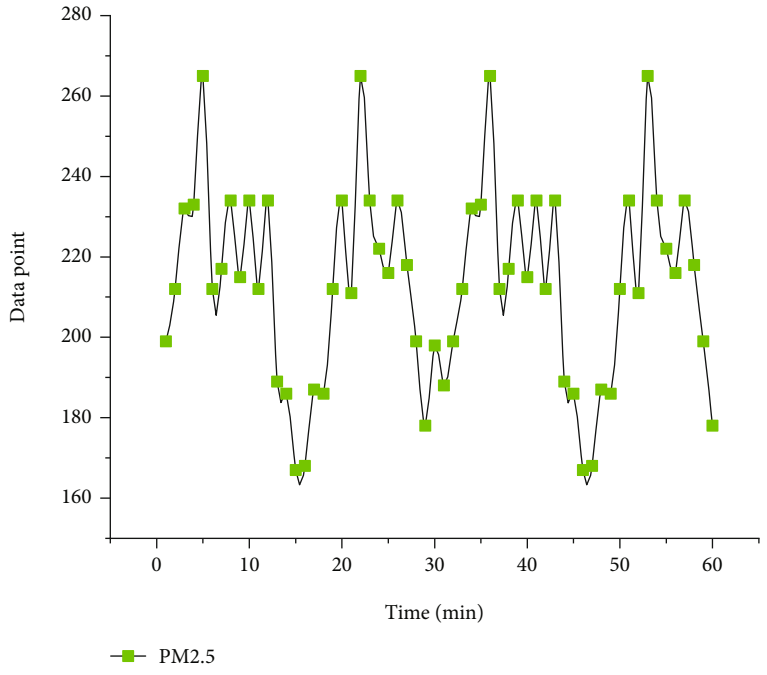

(b)

Figure 8: Continued.

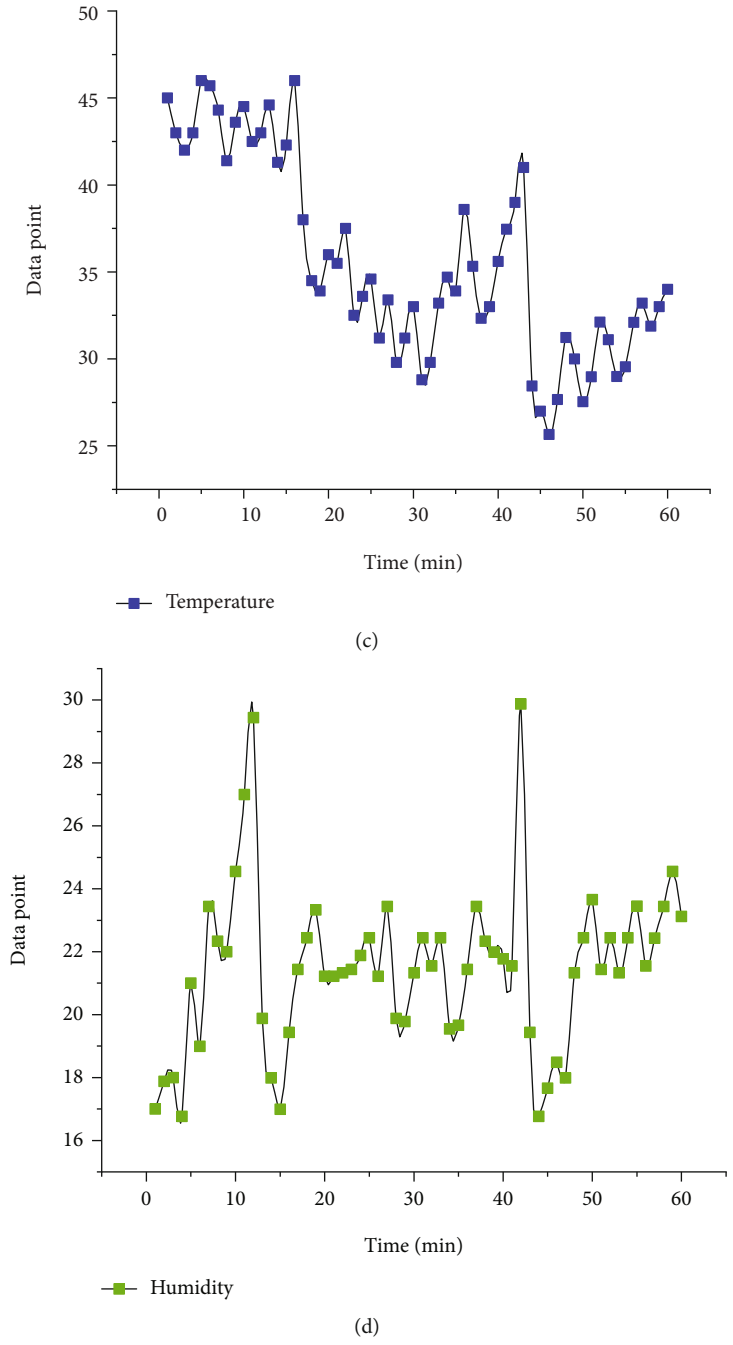

Figure 8: Environmental monitoring data curve 4.3 analysis of test results.

have been realized. The test results show that the environmental monitoring Internet of things system can realize the real-time acquisition and data transmission of passive wireless impact sensing signals, use 10 uF tantalum capacitor to store energy and complete about 20 m RF data transmission with about 42 uJ energy supply; the completed area coverage monitoring system uses five ZigBee sensor nodes and master control nodes to collect a variety of sensor data (temperature, humidity, and light) and interact with the data instructions of ONENET cloud platform, with stable operation and reliable performance; the completed fixed-point direct connection monitoring system can collect a variety of sensing data and interact with the data instructions of Alibaba cloud platform, with strong reliability and stable operation. The system achieves the expected design and functional objectives.

5. Conclusion

Internet of things technology can automatically analyze the concentration, emission, and emission speed of toxic and harmful substances in the natural environment. It can also transmit data information to the environmental monitoring and management department in real time, formulate

scientific and reasonable pollution management strategies, and ensure the rapid and timely treatment of pollution problems. Wireless sensor networks are widely used in environmental monitoring. Atmospheric monitoring is mainly online monitoring or mobile monitoring. Online monitoring can realize synchronous monitoring and monitoring prediction. Comprehensively analyze the future atmospheric environment conditions, and install fixed monitoring equipment at the discharge of pollution sources to form a distributed network to comprehensively control specific pollutants. Various wireless sensor network devices can be used to collect the data of sulfur dioxide and inhalable particles of nitrogen oxides in the atmospheric environment in an all-round way and use the network to transmit the real-time data to the monitoring center to automatically analyze the environmental quality and clarify the overall effect of environmental data processing. Aiming at the environment under the background of carbon neutralization, this paper carries out the research on the technology of environmental monitoring Internet of things system, focuses on the key technologies such as multisensor terminal, local area network communication, wide area network communication, and data cloud platform, and develops a complete set of Internet of things system, which realizes the monitoring of dust, light, temperature, and real-time monitoring of humidity and other environmental parameters, and on this basis, support the scalability of the system to meet the needs of different environmental conditions. We have added relevant contents as follows: today's world is experiencing great changes that have not been seen in a century. The ecological environment is related to human survival and sustainable development, which requires the unity and cooperation of all countries to jointly meet the challenges. Carbon neutralization is a consensus reached by mankind in response to global climate change. Countries all over the world actively commit to achieving the goal of carbon neutralization. Carbon substitution, carbon emission reduction, carbon sequestration, and carbon cycle are the four main ways to realize carbon neutralization, and carbon substitution is the backbone of carbon neutralization.

Data Availability

The data used to support the findings of this study are available from the corresponding author upon request.

Conflicts of Interest

The authors declare that they have no known competing financial interests or personal relationships that could have appeared to influence the work reported in this paper.

Acknowledgments

This work was supported by 2019 Shandong Social Science Popularization and Application Research Project "Life Community and Green Life" (2019-SKZZ-13), Shandong Natural Science Foundation Project "O2O Supply Chain Channel Coordination Strategy and Consumer Behavior in the context of mobile Internet" (ZR2019PG001), and 2021 Qingdao Social Science Planning and Research Project "Research on the Collaborative Development Path of Intelligent Connected Automobile Industry in Qingdao under 5G Empowerment" (QDSKL2101119).

References

[1] G. Bedi, G. K. Venayagamoorthy, R. Singh, R. R. Brooks, and K. C. Wang, "Review of internet of things (IoT) in electric power and energy systems," *IEEE Internet of Things Journal*, vol. 5, no. 2, pp. 847–870, 2018.

[2] C. Zou, H. Xue, B. Xiong et al., "Connotation, innovation and vision of "carbon neutrality"," *Natural Gas Industry B*, vol. 8, no. 5, pp. 523–537, 2021.

[3] E. Viciana, A. Alcayde, F. G. Montoya, R. Baños, F. Arrabal-Campos, and F. Manzano-Agugliaro, "An open hardware design for internet of things power quality and energy saving solutions," *Sensors*, vol. 19, no. 3, p. 627, 2019.

[4] A. T. Chatfield and C. G. Reddick, "A framework for internet of things-enabled smart government: a case of IoT cybersecurity policies and use cases in U.S. federal government," *Government Information Quarterly*, vol. 36, no. 2, pp. 346–357, 2019.

[5] H. Hamidi and M. Jahanshahifard, "The role of the internet of things in the improvement and expansion of business," *Journal of Organizational and End User Computing*, vol. 30, no. 3, pp. 24–44, 2018.

[6] G. Beier, S. Niehoff, and B. Xue, "More sustainability in industry through industrial internet of things?," *Applied Sciences*, vol. 8, no. 2, p. 219, 2018.

[7] M. Babar, A. Rahman, F. Arif, and G. Jeon, "Energy-harvesting based on internet of things and big data analytics for smart health monitoring," *Sustainable Computing: Informatics and Systems*, vol. 20, pp. 155–164, 2018.

[8] S. S. Reka and T. Dragicevic, "Future effectual role of energy delivery: a comprehensive review of internet of things and smart grid," *Renewable and Sustainable Energy Reviews*, vol. 91, pp. 90–108, 2018.

[9] P. Spachos, I. Papapanagiotou, and K. N. Plataniotis, "Microlocation for smart buildings in the era of the internet of things: a survey of technologies, techniques, and approaches," *IEEE Signal Processing Magazine*, vol. 35, no. 5, pp. 140–152, 2018.

[10] U. Paukstadt and J. Becker, "Uncovering the business value of the internet of things in the energy domain–a review of smart energy business models," *Electronic Markets*, vol. 31, no. 1, pp. 51–66, 2021.

[11] S. Navulur and M. N. G. Prasad, "Agricultural management through wireless sensors and internet of things," *International Journal of Electrical and Computer Engineering*, vol. 7, no. 6, p. 3492, 2017.

[12] E. Manavalan and K. Jayakrishna, "A review of internet of things (IoT) embedded sustainable supply chain for industry 4.0 requirements," *Computers & Industrial Engineering*, vol. 127, pp. 925–953, 2019.

[13] D. H. Bui, D. Puschini, S. Bacles-Min, E. Beigne, and X. T. Tran, "AES datapath optimization strategies for low-power low-energy multisecurity-level internet-of-things applications," *IEEE Transactions on Very Large Scale Integration (VLSI) Systems*, vol. 25, no. 12, pp. 3281–3290, 2017.

[14] D. Wu, H. Shi, H. Wang, R. Wang, and H. Fang, "A feature-based learning system for internet of things applications," *IEEE Internet of Things Journal*, vol. 6, no. 2, pp. 1928–1937, 2019.

[15] W. F. Cheung, T. H. Lin, and Y. C. Lin, "A real-time construction safety monitoring system for hazardous gas integrating wireless sensor network and building information modeling technologies," *Sensors*, vol. 18, no. 2, p. 436, 2018.

[16] S. Bin and G. Sun, "Optimal energy resources allocation method of wireless sensor networks for intelligent railway systems," *Sensors*, vol. 20, no. 2, p. 482, 2020.

[17] X. Hao, L. Wang, N. Yao, D. Geng, and B. Chen, "Topology control game algorithm based on Markov lifetime prediction model for wireless sensor network," *Ad Hoc Networks*, vol. 78, pp. 13–23, 2018.

[18] E. Oda, K. Kawauchi, and T. Hamasaki, "Wireless sensor networks construction support application–estimation of RSSI prediction model formula," *IEICE Technical Committee Submission System*, vol. 120, no. 261, pp. 13–16, 2020.

[19] C. Luo, J. Yu, D. Li, H. Chen, Y. Hong, and L. Ni, "A novel distributed algorithm for constructing virtual backbones in wireless sensor networks," *Computer Networks*, vol. 146, pp. 104–114, 2018.

[20] W. Wen, S. Zhao, C. Shang, and C. Y. Chang, "EAPC: energy-aware path construction for data collection using mobile sink in wireless sensor networks," *IEEE Sensors Journal*, vol. 18, no. 2, pp. 890–901, 2018.

[21] Z. Gao, W. Li, Y. Zhu et al., "Wireless channel propagation characteristics and modeling research in rice field sensor networks," *Sensors*, vol. 18, no. 9, 2018.

[22] T. Bin and C. Jiang, "A cost-sensitive method for wireless sensor network min beacon node set construction," *Cluster Computing*, vol. 22, no. S5, pp. 11551–11559, 2019.

[23] T. Yang, X. Xiangyang, L. Peng, L. Tonghui, and P. Leina, "A secure routing of wireless sensor networks based on trust evaluation model," *Procedia Computer Science*, vol. 131, pp. 1156–1163, 2018.

[24] R. Yarinezhad and S. N. Hashemi, "An efficient data dissemination model for wireless sensor networks," *Wireless Networks*, vol. 25, no. 6, pp. 3419–3439, 2019.

[25] L. Kong and B. Ma, "Intelligent manufacturing model of construction industry based on internet of things technology," *The International Journal of Advanced Manufacturing Technology*, vol. 107, no. 3-4, pp. 1025–1037, 2020.

[26] X. Wang, S. Garg, H. Lin, M. Jalilpiran, J. Hu, and M. S. Hossain, "Enabling secure authentication in industrial IoT with transfer learning empowered blockchain," *IEEE Transactions on Industrial Informatics*, vol. 17, no. 11, pp. 7725–7733, 2021.

[27] X. Zhu, "Complex event detection for commodity distribution internet of things model incorporating radio frequency identification and wireless sensor network," *Future Generation Computer Systems*, vol. 125, pp. 100–111, 2021.

[28] Z. Hong, R. Wang, X. Li, and N. Wang, "A tree-based topology construction algorithm with probability distribution and competition in the same layer for wireless sensor network," *Peer-to-Peer Networking and Applications*, vol. 10, no. 3, pp. 658–669, 2017.

[29] J. Gui and J. Deng, "A topology control approach reducing construction cost for lossy wireless sensor networks," *Wireless Personal Communications*, vol. 95, no. 3, pp. 2173–2202, 2017.

[30] L. Kong, J. S. Pan, V. Snášel, P. W. Tsai, and T. W. Sung, "An energy-aware routing protocol for wireless sensor network based on genetic algorithm," *Telecommunication Systems*, vol. 67, no. 3, pp. 451–463, 2018.

[31] F. Gong and X. Jiang, "RETRACTED ARTICLE: Wireless sensor-based soil composition detection and high-efficiency water-saving irrigation in agricultural water conservancy applications," *Arabian Journal of Geosciences*, vol. 14, no. 16, pp. 1–12, 2021.

[32] J. Liu, F. Chen, and D. Wang, "Data compression based on stacked RBM-AE model for wireless sensor networks," *Sensors*, vol. 18, no. 12, p. 4273, 2018.

[33] P. Vijayalakshmi, K. Selvi, K. Gowsic, and K. Muthumanickam, "A misdirected route avoidance using random waypoint mobility model in wireless sensor network," *Wireless Networks*, vol. 27, no. 6, pp. 3845–3856, 2021.

[34] J. S. Pan, L. Kong, T. W. Sung, P. W. Tsai, and V. Snášel, "α-Fraction first strategy for hierarchical model in wireless sensor networks," *Journal of Internet Technology*, vol. 19, no. 6, pp. 1717–1726, 2018.

[35] M. K, C. K, and S. C, "An energy efficient clustering scheme using multilevel routing for wireless sensor network," *Computers & Electrical Engineering*, vol. 69, pp. 642–652, 2018.

Hindawi
Journal of Sensors
Volume 2022, Article ID 5348222, 11 pages
https://doi.org/10.1155/2022/5348222

Research Article

Visual Communication Design Based on Collaborative Wireless Communication Video Transmission

Cong Ma and Wonjun Chung

Department of Design, Tongmyong University, Pusan 612022, Republic of Korea

Correspondence should be addressed to Cong Ma; mamacong@tu.ac.kr

Received 11 November 2021; Revised 14 December 2021; Accepted 21 December 2021; Published 15 January 2022

Academic Editor: Gengxin Sun

With the development of wireless communication technology, video and multimedia have become an integral part of visual communication design. Designers want higher interactivity, diversity, humanization, and plurality of attributes in the process of visual communication. This makes the process of visual communication have high requirements for the quality and real-time data transmission. To address the problem of transmitting HD video in a heterogeneous wireless network with multiple concurrent streams to improve the transmission rate and thus enhance the user experience, with the optimization goal of minimizing the system transmission delay and the delay difference between paths, the video sender and receiver are jointly considered, and the video transmission rate and the cache size at the receiver are adaptively adjusted to improve the user experience, and a cooperative wireless communication video transmission based on the control model for video transmission based on cooperative wireless communication is established, and video streams with self-similarity and long correlation are studied based on Pareto distribution and *P*/*P*/*l* queuing theory, based on which an adaptive streaming decision method for video streams in heterogeneous wireless networks is proposed. Simulation results show that the proposed multistream concurrent adaptive transmission control method for heterogeneous networks is superior in terms of delay and packet loss rate compared with the general load balancing streaming decision method, in terms of transmission efficiency and accuracy.

1. Introduction

Visual communication design is a planned, effect-oriented design image generation and communication activity that people carry out to achieve certain purposes (such as information transmission, promotion, expression, and influence). The design of design images and transmission methods are a marginal discipline that integrates art, science, and technology [1, 2]. It can be seen that visual communication design, as the study of visual information transmission as the main destination, plays a vital role in people's lives. The term "visual communication design" was popularized in the 1960s, and at the World Design Conference in Tokyo, Japan, the participants recognized that print art design could no longer cover new information dissemination media such as images, so visual communication design was born, and it was the expansion of media forms that gave design a new connotation [3, 4]. With 50 years of design life, he has witnessed the transformation of designer's identity from "commercial artist," "graphic designer," to "visual communicator" [5]. The scope of design is expanding, the content and means of design are enriching, and design activities are not limited to a single fixed field, but a cross-cutting, multifaceted, and comprehensive design practice and research are expanding.

The main function of visual communication design is to convey information, which is conveyed by visual symbols, unlike the abstract concept conveyed by language [6, 7]. The process of visual communication is designer's process of transforming ideas and concepts into the form of visual symbols, while for the receiver, it is an opposite process. Visual communication design is precisely the design that uses visual symbols to communicate, the designer is the sender of the information, and the receiver of the information [8]. It can be seen that visual communication design is a design that uses visual media as a carrier to convey information to the public. Visual communication contains two

levels of meaning: visual symbols and communication. Visual symbols are the formal language composed of graphics, words, colors, and other design elements, which is the medium to carry information [9, 10]. Therefore, visual communication design not only includes the meaning of design level but also includes the process of information dissemination [11].

Real-time multimedia transmission usually has high network bandwidth requirements, especially real-time HD video services require strict end-to-end delay and delay jitter requirements, while a single wireless access technology cannot provide users with a better user experience due to limited communication capabilities and different working methods [12–14]. Wireless heterogeneous network environment is an important feature of next-generation wireless networks, and there are many different heterogeneous wireless networks, such as 5G, LTE, and WLAN. Multipath parallel transmission systems, by aggregating the transmission performance of multiple links, can effectively improve network resource utilization, service transmission rate, and load balancing capability [15].

Reference [16] proposed an adaptive traffic distribution strategy under the collaboration of wireless WAN and wireless LAN, which minimizes the system transmission delay through internetwork load balancing and extends the communication function of single-mode terminals to support high-rate data streams. 1 queue, while a large number of studies on network traffic presented in reference [17] show that data packet arrivals do not obey exponential distribution and are not Poisson, but have self-similarity and long correlation. Reference [18] also suggested that data packet arrival and packet length obey exponential distributions are not suitable for modeling different kinds of network traffic and pointed out that heavy-tailed distributions are more suitable for data packet arrival and data packet length. In network performance analysis, data flows obeying the heavy-tailed distribution have distinctly different characteristics from those obeying the Poisson distribution. Reference [19] points out that understanding the nature of traffic is essential for the design of wireless networks and wireless services and that the traditional model of network traffic (Poisson traffic) leads to underestimation or overestimation of wireless network performance, and simulation results show that the latency of real-time polling services and best-effort services increases for self-similar traffic, and the request collision probability increases for best-effort services compared to Poisson traffic. The different types of network traffic proposed in Reference [20] exhibit self-similarity characteristics, and their performance characteristics are significantly different from those of traffic that obeys typical Poisson or exponential distributions. Reference [21] proposes a path traffic allocation algorithm that satisfies the delay-constrained jitter optimization, which allocates each path traffic proportionally according to the maximum allowable inflow rate of the path, while minimizing the delay jitter between paths. Reference [22] proposed a traffic adaptive allocation strategy in heterogeneous networks, decomposing data flows into multiple flows and aggregating them at terminals, parallel data transmission using $M/M/1$ queuing theory modeling, and solving the optimization problem by Lagrange multiplier method. However, recent research on the measurement of network communication flows has overturned the traditional communication model based on Berzon theory, and many papers have reported that modern data communication flows have self-similarity properties. Reference [23] established an equivalent queueing theory model for the end-to-end delay of concurrent transmission in heterogeneous multiaccess networks and obtained the theoretical delay bound for concurrent transmission systems from this model. However, the packet arrival is regarded as exponential distribution and the service process as Poisson distribution. References [24, 25] investigated the impact of self-similar traffic in various wireless LAN scenarios using the $P/P/1$ queuing model for the self-similar characteristics of network traffic. Network services with self-similarity pose new challenges to network design. Instead of smoothing the network service, the multiplexing overlay of self-similar services increases its burstiness, and the burstiness of time-aggregated fractal services diminishes much more slowly than Poisson services, so more resources need to be allocated in network design to ensure the quality of service. For solving the problem of transmitting HD video in heterogeneous wireless networks with multiple concurrent streams, improve the transmission rate, enhance the user experience, and minimize the system transmission delay and the delay difference between paths; the main contributions are summarized as follows: (1) based on Pareto distribution and $P/P/L$ queuing theory, video streams with self-similarity and long correlation are studied. On this basis, an adaptive stream decision method for video streams in heterogeneous wireless networks is proposed. (2) GSO algorithm is used to adaptively solve the number of visual transmission to reduce the system delay and system burden; (3) experiments verify the effectiveness and reliability of the visual communication strategy based on cooperative wireless communication video transmission.

In this paper, we address the above issues by first expressing the meaning of visual communication and the need of visual communication itself for interactivity, communication, and diversity of interface display. Then, the link between visual communication and wireless video transmission is developed, and the process of interaction and presentation of visual communication with users is introduced. Then, it focuses on minimizing the system link delay and as well as the delay difference between paths as the optimization objective; firstly, the system model is proposed, and a mathematical model of concurrent video multistream transmission control for heterogeneous wireless networks is established to form an optimization problem of adaptive video traffic distribution in heterogeneous wireless networks, so as to obtain a more reasonable traffic distribution strategy to ensure the quality of service. It also integrates the conditions at the sender and receiver sides and adjusts the rate at the sender side as feedback to improve the user experience. To solve this optimization problem, an artificial firefly swarm optimization algorithm is used to solve the optimization problem. Finally, we compare the effect of the proposed algorithm with that of the visual communication and show

that the visual communication has better performance with the application of cooperative wireless communication technology.

2. Visual Communication Design Architecture Based on Wireless Communication Video Transmission

2.1. Structure of Visual Communication Based on Cooperative Wireless Communication. Visual communication design requires designers to put themselves in user's shoes as much as possible, reflecting the concept of human-oriented design. At the level of humanized design, designers need to consider the psychological feelings brought by the form of content writing and presentation. At the level of humanized design, designers mainly consider the feelings brought by external factors such as platform function, influence, and value. At the interpersonal design level, designers mainly consider the relationship between the microplatform, users, and the social environment. These requirements also put higher demands on the video itself. From the old noise-filled black and white images, to the current high definition video and lossless sound quality. The visual communication itself also requires a higher quality and real-time video transmission.

As shown in Figure 1, visual users usually view video in two ways: wired and wireless. Wired is usually in a fixed place and location, connected to the video playback terminal through optical fiber or network cable, which usually has a larger bandwidth, faster transmission speed, and relatively better video quality. The wireless way is usually the video transmission in the process of moving, compared to the wired transmission method; the video quality will be relatively low. Video playback site by collecting the window of the user to watch the video, with geographic location and other information for fusion. The fused information is handed over to the data server for collation and decision-making to match the best visual communication patterns for the user. The server hands these patterns and decisions to the data organization server, which finds the information to be displayed from the servers it manages for video, audio, images, text, etc., and organizes and transmits it. And after users receive it at different terminals, they all need to decode it correspondingly to achieve the optimal display effect on the corresponding terminal.

2.2. Principle of Wireless Cooperative Communication. Joint source channel coding (JSCC) is considered as an effective solution for the above-mentioned problem of reliable transmission of video streams in wireless network environments [26]. However, the main problem of existing JSCC approaches is that the network between the server and the client is considered as a single transmission link, which is more complicated in the multipath case [27]. Therefore, a simpler but equally reliable data transmission method is needed for video transmission. Therefore, in this paper, with the optimization objective of minimizing the system link delay and the delay difference between paths, we first propose a system model to establish a mathematical model for concurrent video multistream transmission control in heterogeneous wireless networks and form an optimization problem for adaptive video traffic distribution in heterogeneous wireless networks. In this paper, collaborative infinite communication video transmission method is designed in Figure 2. As is shown, the self-similarity characteristics of video streams are applied to the multistream concurrent distribution strategy of heterogeneous networks. And the data packet arrival interval and data packet size are modeled using a more realistic self-similarity distribution to obtain a more reasonable distribution strategy to ensure the quality of service by better matching the actual time delay of video streams. And considering the condition of the sender and receiver side, the buffer length of the receiver side is used as feedback to adjust the rate of the sender side to improve the user experience. To solve this optimization problem, an artificial firefly swarm optimization algorithm is used to solve the optimization problem.

3. Collaborative Wireless Communication Video Transmission Algorithm and Implementation Framework

3.1. HD Video Transmission Model Based on Cooperative Wireless Communication. The heterogeneous wireless network video multistream concurrent transmission control system model is shown in Figure 3. The HD video streams are split at the video source side, and through adaptive splitting decision, the video streams are transmitted through different links and multiple heterogeneous wireless terminals; multiple wireless networks work together and finally played after the buffer is integrated at the video playback side. The video source side uses H.264 to compress and encode the video, and the 5G network is used for transmission [28]. Multiple users can use the available terminals in the vicinity to complete the video service with concurrent transmission of multiple streams. Heterogeneous single-mode terminals from different users form virtual multimode terminals, which use different standard networks, such as cdma2000, WCDMA [29]. These cooperative terminals are aggregated into an organic whole with enhanced capabilities, more interfaces, and external collaboration through Wi-Fi networking controlled by terminal controllers, forming a user-centered super terminal, i.e., virtual terminal, to achieve service diversification and enhancement. The virtual terminal can be used to realize service diversification and enhance user experience [30].

Suppose there are K links between the transmitter and the receiver, and the performance of each transmission path varies, such as the packet loss rate and transmission delay of different paths may be different. Assuming that the smallest unit of service transmission is data packet, the transmission rate of service on each path is adjusted by reasonably arranging the rate at which data packets leave the transmission. R is the total data traffic; R_1, R_2, and R_3 are the data traffic divided into individual links; and D_1, D_2, and D_3 are the time delay of each link.

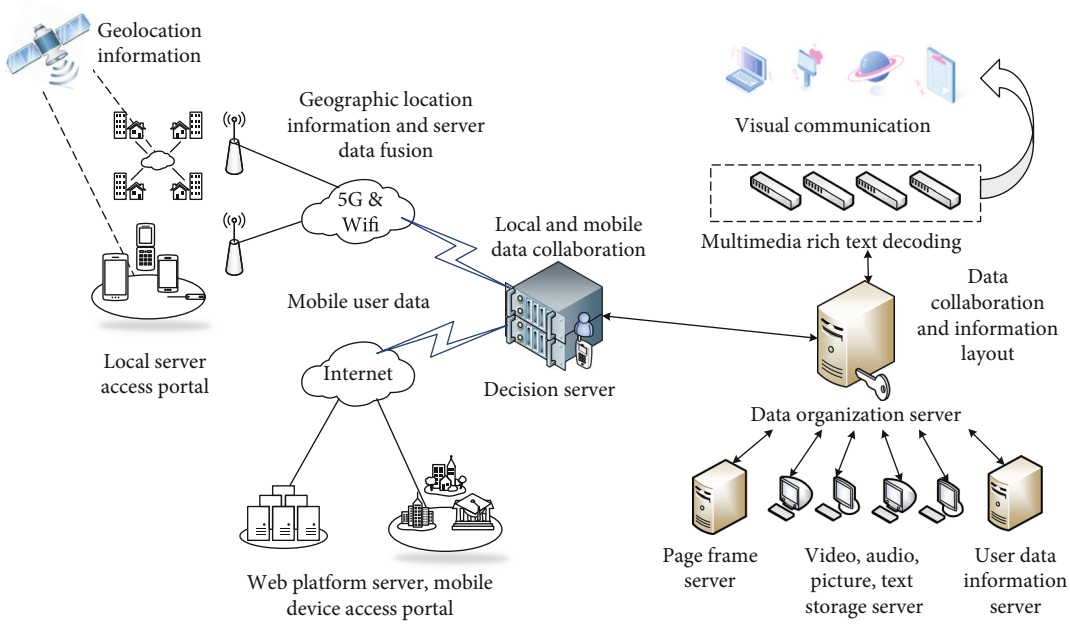

Figure 1: Visual communication framework for collaborative infinite communication video transmission.

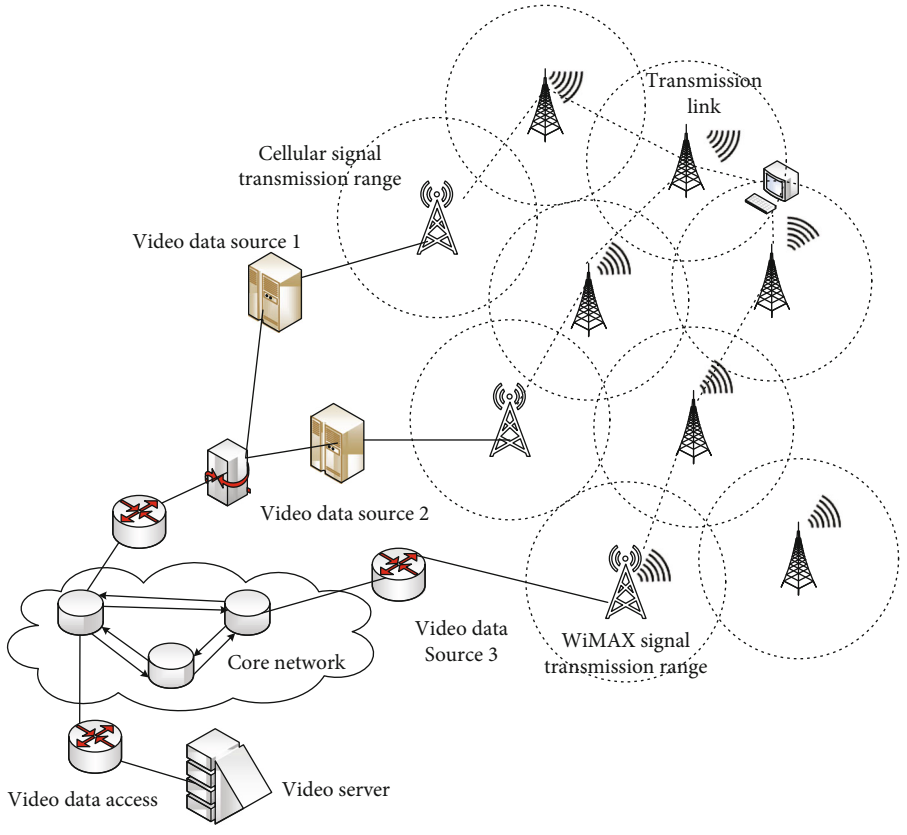

Figure 2: Collaborative infinite communication video transmission method.

A buffer with dynamically adjustable length is set at the video playback end. The video received at the video playback end is temporarily stored in the playback buffer, where short-time rate and bandwidth mismatches can be absorbed to mitigate video interruptions, and video data grouping can be reordered in this playback buffer to absorb the delay jitter between paths. The buffer forms a cache feedback loop between the video playback end and the video source end, and the video source can adjust the sending rate R according to the buffer length at the video playback end, thus keeping

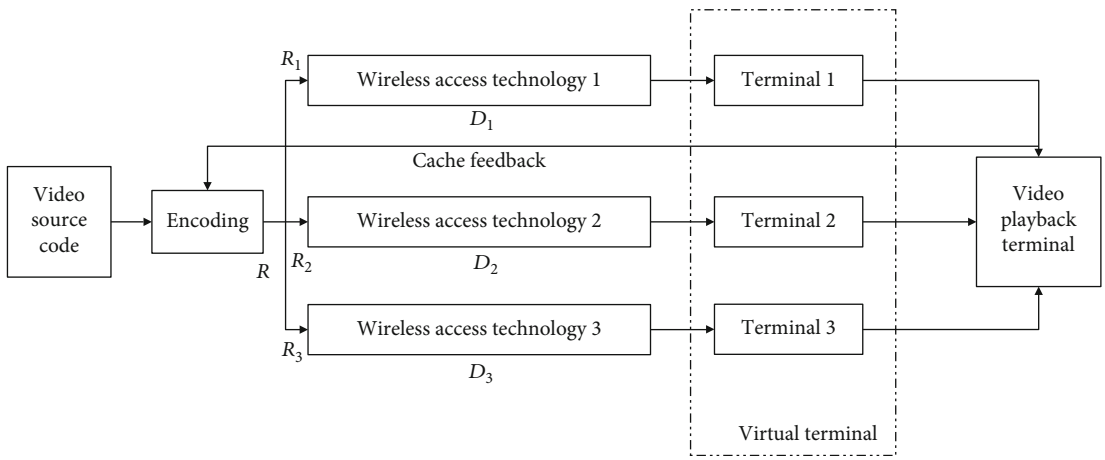

Figure 3: Concurrent video multistream transmission control model in heterogeneous wireless networks.

the buffer length in a normal state and improving the user experience.

Video traffic is self-similar and long-correlated, and long-correlated traffic has a negative impact on network performance, the most important result being that the queue length distribution decays more slowly with self-similar traffic than with short-correlated service sources (e.g., Poisson model). It has also been shown that the self-similarity of traffic leads to high buffer overflow rates, time lengthening, and persistent periodic congestion, which directly affects the design, control, analysis, and management of next-generation networks, while the use of Poisson or Markov business models does not accurately reflect the long correlation of actual traffic and can lead to underestimation of the average packet delay or maximum queue length in the analysis.

3.2. Truncated Pareto Distribution. The self-similarity of traffic has a direct impact on the design, control, analysis, and management of next-generation networks, and the self-similarity of data flows is receiving increasing attention in network performance analysis. Although the cause of the service self-similarity process is not conclusively established, the heavy-tailed distribution is a major cause of the self-similarity process. The commonly used heavy-tailed distributions are Pareto, Weibull, and Log-normal. As shown in reference [31], the video data group size obeys the truncated Pareto distribution, and the arrival interval also obeys the truncated Pareto distribution. By applying a more realistic self-similar distribution to the data group arrival interval and the data group size, we can obtain a delay that is more consistent with the actual video stream.

The tail function of the Pareto distribution is:

$$P(X > x) = \left(\frac{k}{t}\right)^{a}. \tag{1}$$

It is a hyperbolic function, which decays much more slowly than the exponential function. In this paper, the Pareto distribution is used to represent the video stream to fully consider the self-similarity of the video stream. And because x is infinite, the truncated Pareto distribution is used instead of the Pareto distribution, and the actual truncated Pareto distribution is used.

$$F(x) = P[X \le x] = \frac{\left[1 - (k/x)^{a}\right]}{\left[1 - (k/L)^{a}\right]}, \quad k \le x \le L, \tag{2}$$

where $k > 0$ is the position parameter and a is the shape parameter.

Each concurrent link in a heterogeneous wireless network video multistream concurrent system can be modeled as a $P/P/1$ queuing model, and the whole system is a parallel $P/P/1$ queuing model. The delay of a single link in a heterogeneous wireless network is the sum of the average waiting time and the average service time.

$$\begin{aligned} D &= t_w + t_s, \\ t_w &= t_s \frac{\rho}{(1-\rho)} \cdot \frac{{C_a}^2}{{C_s}^2}, \\ t_s &= \frac{8M_s}{B}, \end{aligned} \tag{3}$$

where t_w is the average waiting time, t_s is the average service time, and ${C_a}^2$ and ${C_s}^2$ are the squared variance coefficients of the video stream data packet arrival interval and data packet service time, respectively. ρ, M_s, and B represent the transmission proportion, transmission volume, and total transmission volume, respectively.

3.3. Adaptive Streaming Decision Based on GSO Method. The adaptive streaming decision for video streams in heterogeneous wireless networks proposed in this paper is to design the optimal streaming strategy to minimize the delay of the system while minimizing the delay jitter in the difference of each link. In concurrent transmission, the delay jitter of data packets mainly comes from the difference in transmission capability between different wireless access technologies.

The transmission delay of data packets on different paths D_i is not only related to the transmission capability of the

paths but also related to the traffic allocation strategy between the paths. When the transmission capacity of the path is poor, allocating more traffic to it will lead to a sharp increase in D_i. When the transmission capability of the path is good, increasing its transmission traffic appropriately does not have a great impact on the transmission delay D_i. By reasonably allocating the traffic among the paths, the difference in delay between the paths can be reduced, thus achieving the purpose of reducing jitter.

Suppose there are K links between the sender and the receiver, and the performance of each transmission path varies, such as the packet loss rate and transmission delay of different paths may be different. Assuming that the smallest unit of video service transmission is the data packet, the transmission rate of video service on each path is adjusted by reasonably arranging the rate at which the data packet leaves the transmission.

The artificial firefly swarm optimization algorithm originates from the study of the behavior of fireflies in nature such as luminous courtship and communication. It is a swarm intelligence optimization algorithm, which is widely used in resource scheduling. Its bionic principle is that it uses individual fireflies in nature to simulate the points in the search space, and the process of mutual attraction and movement of individual fireflies is simulated as the process of target seeking, and the superiority of the position of individual fireflies is used to measure the objective function of solving the problem, the iterative process of the feasible solution of the function in the process of optimization.

The GSO algorithm is mainly used to simulate the optimal value of the solution function by operating on fireflies through the equation of fluorescein value update in Equation (4) and the equation of probability distribution in Equation (5).

$$l_i(t) = \max\{(0, (1-\rho)\cdot l_i(t-1) + \gamma \cdot J(x_i(t)))\}, \quad (4)$$

$$P_j(t) = \frac{l_i(t)}{\sum_{k\in N_i(t)} l_k(t)}, \quad (5)$$

where $l_i(t)$ means fluorescein value in ith time. $P_j(t)$ means probability distribution. The implementation process of the GSO algorithm is as follows. Relative attraction between fireflies is defined:

$$\beta(r) = \beta_0 e^{-\gamma r^2}. \quad (6)$$

β_0 is its initial attraction, that is, the attraction when the distance between two fireflies is 0, and r is the distance between two fireflies. A firefly will move towards all fireflies with higher brightness than itself, and its moving distance is calculated by the following formula (7):

$$X_i' = X_i + \beta_0 e^{-\gamma r^2}\left(X_i - X_j\right) + \alpha \text{ rand }(), \quad (7)$$

where represents the position of a firefly with higher brightness than the ith individual, and R represents the distance between the ith firefly and the jth firefly. Rand () is a random disturbance and is the step factor of the disturbance. Generally, the value of rand () is the uniform distribution within the range of [-0.5, 0.5], or the value of standard normal distribution a of U (0, 1) is between [0, 1].

The GSO-based wireless video transmission path optimization algorithm is shown in Figure 4. From the principle of GSO algorithm, the running time of the adaptive triage decision process is mainly consumed by the firefly position update, and its time complexity is mainly determined by the maximum number of iterations M and the number of fireflies n. In one iteration, the frequency of firefly position update operation is $f = 1 + 2 + 3 + \cdots + n = n \times (n+1)/2$, and its time complexity is $O(n^2)$, so after M iterations, the total time complexity of adaptive diversion decision is $O(M \times n^2)$, where M is the maximum number of iterations and n is the number of fireflies.

4. Transmission Experimental Results

4.1. Experiment of HD Video Transmission Based on Cooperative Wireless Communication. In this paper, the performance of the proposed adaptive streaming strategy is evaluated by extensive MATLAB simulation experiments. Assuming three parallel transmission data with transmission capacities of 4 Mbit/s, 2 Mbit/s, and 3 Mbit/s, respectively, the initial population size of the artificial firefly swarm optimization algorithm is 20, and the maximum number of iterations is 300. In this simulation, the video sender rate changes from 2 Mbit/s to 6 Mbit/s. The adaptive shunting decision proposed in this paper is compared with the general load balancing shunting decision The proposed adaptive streaming decision is compared with the general load balancing streaming decision. The general load-balanced streaming decision is shown in Equation (6):

$$R_i = R\frac{R_{a,i}}{\sum_{j=1}^{3} R_{a,j}}(i = 1, 2, 3). \quad (8)$$

Figure 5 shows the variation of the packet loss rate of the system with the transmission rate. It can be seen that the delay and delay jitter-based splitting strategy proposed in this paper has lower packet loss rate than the general load balancing splitting strategy, but the difference between them gradually decreases as the network load increases, and the packet loss rate is close when the sender rate increases to 5.5 Mbit/s and 6 Mbit/s. This is because the optimization effect decreases with higher network load. At the sender rate of 3 Mbit/s, the packet loss rate of the proposed splitting strategy is 10.6% lower than that of the general load balancing splitting strategy.

Figure 6 shows that the delay of the proposed splitting strategy is reduced by 4.67%, 5.89%, and 10.12% mode compared to the general load balancing splitting strategy, real-time multimode transmission mode, and classic video transmission. When the sender rate gradually increases, the delay in both streaming strategies increases significantly because the traffic load is close to the available resources, which will lead to unstable system performance, especially when the

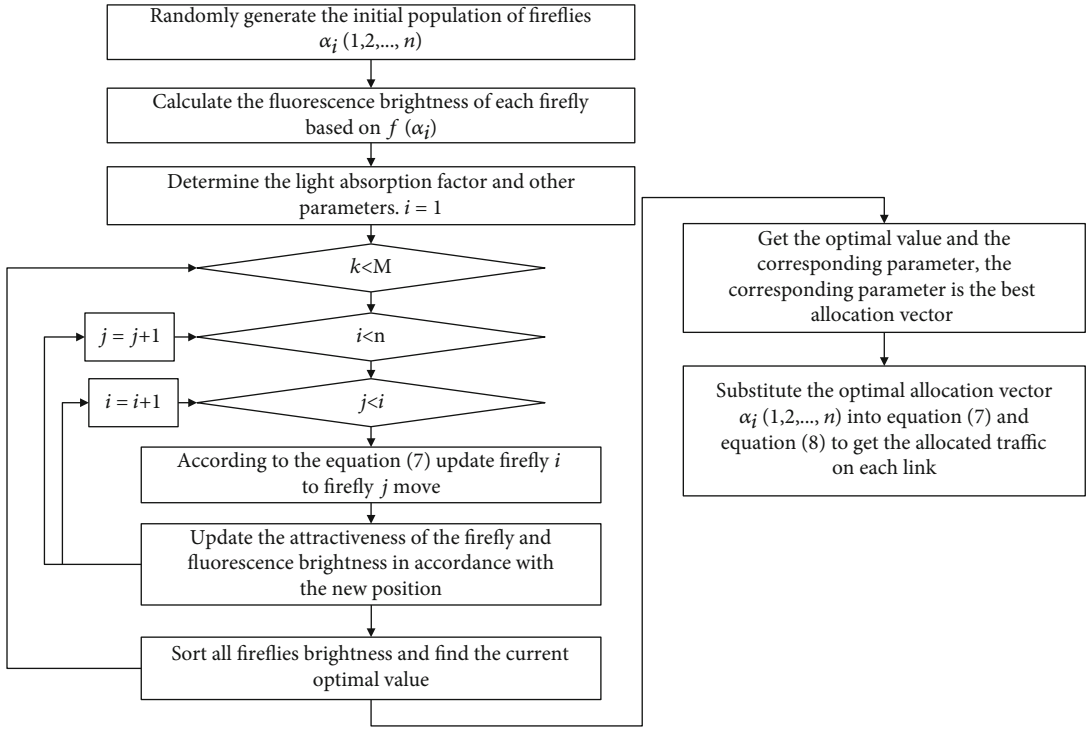

Figure 4: GSO-based wireless video transmission path optimization algorithm.

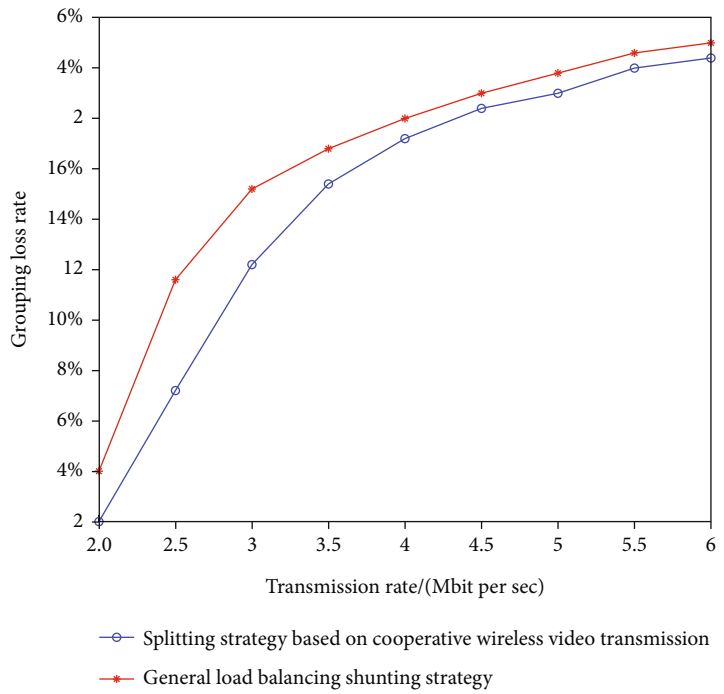

Figure 5: Comparison of packet loss rates for different splitting strategies.

sender rate exceeds 4 Mbit/s, a single wireless access technology cannot meet the requirements because of the limited communication capacity, so single-mode heterogeneous terminals from different users are expanded into user-centric superterminals through LAN networking centered superterminals with enhanced capabilities, i.e., virtual terminals, which can aggregate link resources and improve user experience.

Figure 7 shows that the delay with $P/P/1$ queuing theory is larger than the former compared with that with $M/M/1$

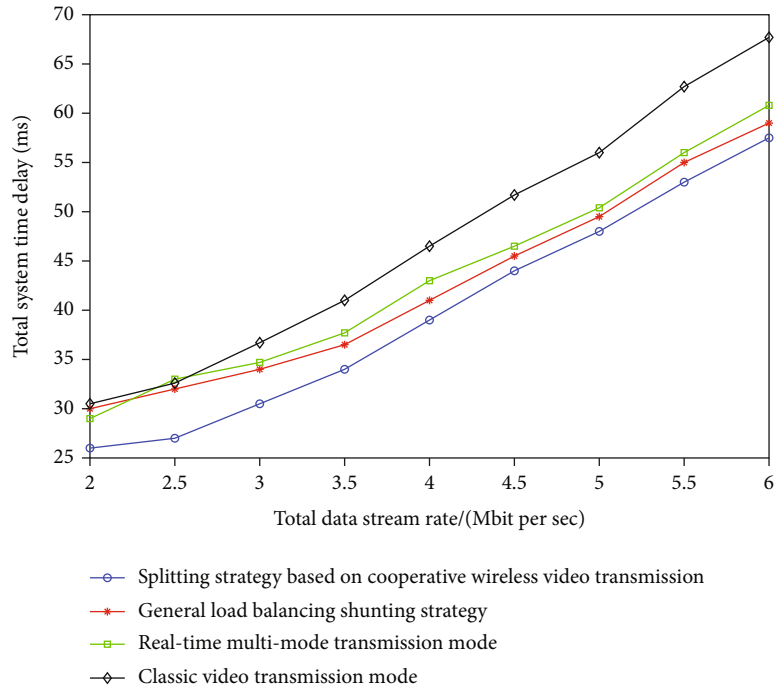

Figure 6: Delay of different splitting strategies.

queuing theory, and the difference increases with the increase of sending rate. This is because the self-similarity of video streams affects the delay, and more resources need to be allocated to ensure the quality of service, so using the $P/P/1$ queuing theory, which is more consistent with the self-similarity of video streams, for the streaming decision can provide a better experience to users.

4.2. Experiment of Visual Communication Design Based on Collaborative Wireless Communication Video Transmission. Common indicators of visual communication design are as follows: (1) video-based: video-based design is an inevitable trend for the future development of visual communication design. Through the new digital media technology and communication medium, it makes the design content richer, the information more communicative and innovative, and makes the visual communication design a new visual form. (2) Humanization: in the era of digitalization, visual communication design bids farewell to the traditional flat paper printing and wants to bring a new experience to customers visually, starting from meeting their visual needs, which is the embodiment of the concept of humanization of visual communication design [32]. (3) Diversity: nowadays, electronic technology and digital media are developing rapidly, and the design field is expanding [33]. In the field of civilian design, visual language presents people with different expressions, graphic that is flat, image that is dynamic three-dimensional, and what they pursue is a broad international vision to make the design with superb quality, so as to express the inner language logic. (4) Multisensory interface user trust: nowadays, the widespread use of mobile APP makes many designers and developers start to pay attention to the trust relationship between users and the product, the so-called user trust, which is what we usually known as "user viscosity". (5) Integrated: visual communication design itself is a discipline containing a variety of fields, modern visual communication discipline is no longer simply graphic design graphics, it is through the visual design performance and other media to convey to the audience, and the distinctive characteristics of the times and the connotation of the times are reflected in its performance.

In this study, two hundred subjects, all divided into two groups, were selected to watch 10 different videos and to rate the visual communication effect of the videos after watching them, using a ten-point scoring method. This study used the self-compiled "Questionnaire on the Performance Effect of Visual Communication Design." The questionnaire includes five dimensions: video, humanization, diversity, multisensory interface user trust, and synthesis. The internal consistency coefficient of this questionnaire was 0.969, and the split-half reliability was 0.820, and the reliability of the total scale was good. The data were collected from the participants of the test and then entered and analyzed. Correlation analysis was used to explore the correlation between the training conditions, research quality, and psychological development of master's students in Jiangsu Province. As shown in the radar (Figure 8), the subjects, without knowing what technology was used for the video, generally perceived that the video using collaborative wireless communication transmission was more visually communicative than the regular transmission video. Specifically, of the five main aspects of video communication, the three aspects of visualization, multisensory interface user trust, and synthesis were significantly better than traditional video transmission methods. The user-friendliness and diversity aspects have also been improved to a certain extent. By further analyzing the

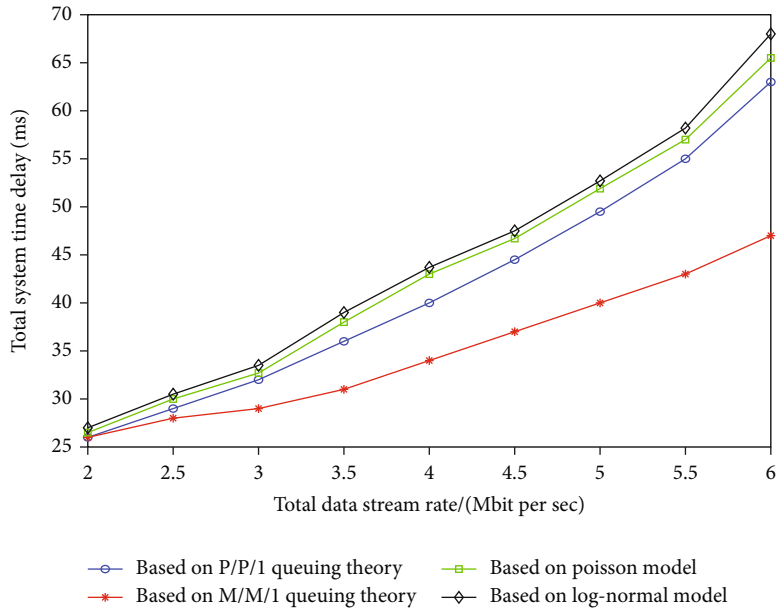

Figure 7: $P/P/1$ and $M/M/1$ transmission delay.

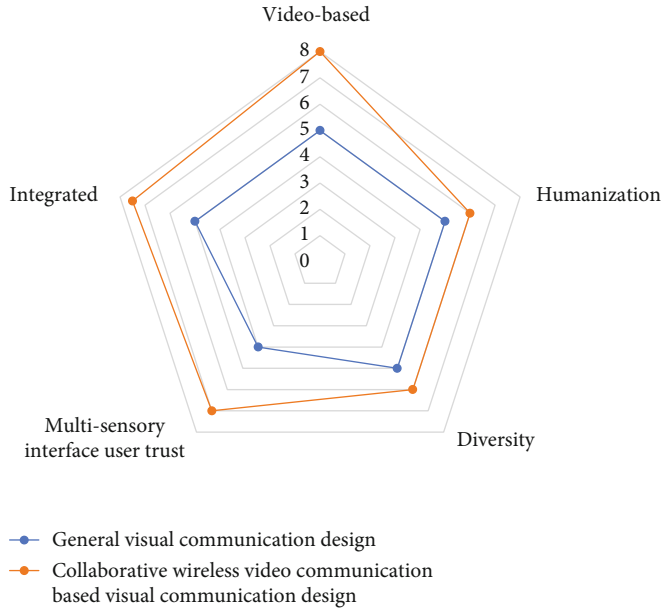

Figure 8: Experimental results of evaluation of visual communication.

user-feeling part of the questionnaire, we can learn that users generally believe that the video quality and fidelity of video transmission based on cooperative wireless communication have been significantly improved, which makes users' viewing experience more comfortable and thus feel more humane and more able to discover the diverse contents of the video.

5. Conclusion

This paper improves the expressiveness of visual communication design based on wireless communication video transmission technology. In order to improve the aspects of diversity, interactivity, and trustworthiness in the visual communication process, the proposed heterogeneous network HD video multistream concurrent transmission control consists of two stages: adaptive streaming decision and receiving buffer length feedback adaptively adjusting the rate at the sender side. The adaptive streaming decision obtains a streaming decision method by minimizing the system delay while minimizing the delay jitter. The buffer length feedback adaptive adjustment of the sender rate is a joint video source side and video playback side, and the sender rate is adaptively adjusted by the buffer length of the playback side.

The simulation results show that the proposed video adaptive streaming decision reduces the delay by 4.67% compared with the general load balancing streaming decision method, and the delay increases based on $P/P/1$ queuing theory compared with $M/M/1$ queuing theory, and the difference increases with the increase of the sender side rate, indicating that the self-similarity of video streams affects the delay, and more resources need to be allocated to ensure the quality of service, so using the $P/P/1$ queuing theory, which is more consistent with the self-similarity of video streams, for the streaming decision can provide a better experience to users. Compared with the general load-balanced streaming decision method, the proposed streaming decision method in this paper has certain superiority in terms of delay and packet loss rate. Finally, experiments on the visual communication effect are conducted based on this algorithm. The experimental results show that the visual communication based on collaborative wireless communication video transmission has a certain improvement over the usual visual communication effect, especially in the two aspects of multisensory interface user trust and synthesis.

Data Availability

The data used to support the findings of this study are available from the corresponding author upon request.

Conflicts of Interest

We declare that there is no conflict of interest.

Acknowledgments

The study was supported by the Department of Design, Tongmyong University.

References

[1] X. Liu, D. Zhai, J. Zhou, X. Zhang, D. Zhao, and W. Gao, "Compressive sampling-based image coding for resource-deficient visual communication," *IEEE Transactions on Image Processing*, vol. 25, no. 6, pp. 2844–2855, 2016.

[2] G. S. Park and H. Song, "Cooperative base station caching and X2 link traffic offloading system for video streaming over SDN-enabled 5G networks," *IEEE Transactions on Mobile Computing*, vol. 18, no. 9, pp. 2005–2019, 2018.

[3] B. Al-Hayani and H. Ilhan, "Efficient cooperative image transmission in one-way multi-hop sensor network," *The International Journal of Electrical Engineering & Education*, vol. 57, no. 4, pp. 321–339, 2020.

[4] A. Mehrabi, M. Siekkinen, and A. Ylä-Jaaski, "QoE-traffic optimization through collaborative edge caching in adaptive mobile video streaming," *IEEE Access*, vol. 6, pp. 52261–52276, 2018.

[5] D. Wu, Q. Liu, H. Wang, D. Wu, and R. Wang, "Socially aware energy-efficient mobile edge collaboration for video distribution," *IEEE Transactions on Multimedia*, vol. 19, no. 10, pp. 2197–2209, 2017.

[6] E. Ahmed and H. Gharavi, "Cooperative vehicular networking: a survey," *IEEE Transactions on Intelligent Transportation Systems*, vol. 19, no. 3, pp. 996–1014, 2018.

[7] E. Yanmaz, S. Yahyanejad, B. Rinner, H. Hellwagner, and C. Bettstetter, "Drone networks: communications, coordination, and sensing," *Ad Hoc Networks*, vol. 68, pp. 1–15, 2018.

[8] G. Zhang, J. Wang, C. Yan, and S. Wang, "Application research of image compression and wireless network traffic video streaming," *Journal of Visual Communication and Image Representation*, vol. 59, pp. 168–175, 2019.

[9] H. Sun, Y. Yu, K. Sha, and B. Lou, "mVideo: edge computing based mobile video processing systems," *IEEE Access*, vol. 8, pp. 11615–11623, 2020.

[10] D. Anton, G. Kurillo, and R. Bajcsy, "User experience and interaction performance in 2D/3D telecollaboration," *Future Generation Computer Systems*, vol. 82, pp. 77–88, 2018.

[11] A. Chriki, H. Touati, H. Snoussi, and F. Kamoun, "FANET: communication, mobility models and security issues," *Computer Networks*, vol. 163, article 106877, 2019.

[12] X. Zhu, C. Jiang, L. Yin, L. Kuang, N. Ge, and J. Lu, "Cooperative multigroup multicast transmission in integrated terrestrial-satellite networks," *IEEE Journal on Selected Areas in Communications*, vol. 36, no. 5, pp. 981–992, 2018.

[13] S. Li, J. G. Kim, D. H. Han, and K. S. Lee, "A survey of energy-efficient communication protocols with QoS guarantees in wireless multimedia sensor networks," *Sensors*, vol. 19, no. 1, p. 199, 2019.

[14] S. Kim, M. Billinghurst, and G. Lee, "The effect of collaboration styles and view independence on video-mediated remote collaboration," *Computer Supported Cooperative Work (CSCW)*, vol. 27, no. 3, pp. 569–607, 2018.

[15] W. Huang, L. Alem, F. Tecchia, and H. B. L. Duh, "Augmented 3D hands: a gesture-based mixed reality system for distributed collaboration," *Journal on Multimodal User Interfaces*, vol. 12, no. 2, pp. 77–89, 2018.

[16] K. Chen, W. Chen, C. T. Li, and J. C. Cheng, "A BIM-based location aware AR collaborative framework for facility maintenance management," *The Journal of Information Technology in Construction*, vol. 24, pp. 360–380, 2019.

[17] X. Wang, L. Kong, F. Kong et al., "Millimeter wave communication: a comprehensive survey," *IEEE Communications Surveys & Tutorials*, vol. 20, no. 3, pp. 1616–1653, 2018.

[18] S. U. Rehman, S. Ullah, P. H. J. Chong, S. Yongchareon, and D. Komosny, "Visible light communication: a system perspective—overview and challenges," *Sensors*, vol. 19, no. 5, p. 1153, 2019.

[19] N. S. Vo, T. Q. Duong, H. D. Tuan, and A. Kortun, "Optimal video streaming in dense 5G networks with D2D communications," *IEEE Access*, vol. 6, pp. 209–223, 2018.

[20] S. H. Choi, M. Kim, and J. Y. Lee, "Situation-dependent remote AR collaborations: image-based collaboration using a 3D perspective map and live video-based collaboration with a synchronized VR mode," *Computers in Industry*, vol. 101, pp. 51–66, 2018.

[21] L. Lyu, C. Chen, Z. Shanying, and X. Guan, "5G enabled co-design of energy-efficient transmission and estimation for industrial IoT systems," *IEEE Transactions on Industrial Informatics*, vol. 14, no. 6, pp. 2690–2704, 2018.

[22] H. Hamdoun, S. Nazir, J. A. Alzubi, P. Laskot, and O. A. Alzubi, "Performance benefits of network coding for HEVC video communications in satellite networks," *Iranian Journal*

of Electrical and Electronic Engineering, vol. 17, no. 3, pp. 1956–1956, 2021.

[23] A. Ali, K. S. Kwak, N. H. Tran et al., "RaptorQ-based efficient multimedia transmission over cooperative cellular cognitive radio networks," *IEEE Transactions on Vehicular Technology*, vol. 67, no. 8, pp. 7275–7289, 2018.

[24] F. Lyu, N. Cheng, H. Zhu et al., "Intelligent context-aware communication paradigm design for IoVs based on data analytics," *IEEE Network*, vol. 32, no. 6, pp. 74–82, 2018.

[25] X. Ge, L. Pan, Q. Li, G. Mao, and S. Tu, "Multipath cooperative communications networks for augmented and virtual reality transmission," *IEEE Transactions on Multimedia*, vol. 19, no. 10, pp. 2345–2358, 2017.

[26] M. F. Tuysuz and M. E. Aydin, "QoE-based mobility-aware collaborative video streaming on the edge of 5G," *IEEE Transactions on Industrial Informatics*, vol. 16, no. 11, pp. 7115–7125, 2020.

[27] M. Yao, M. Sohul, V. Marojevic, and J. H. Reed, "Artificial intelligence defined 5G radio access networks," *IEEE Communications Magazine*, vol. 57, no. 3, pp. 14–20, 2019.

[28] M. A. Khan, I. M. Qureshi, and F. Khanzada, "A hybrid communication scheme for efficient and low-cost deployment of future flying ad-hoc network (FANET)," *Drones*, vol. 3, no. 1, p. 16, 2019.

[29] H. Chen, C. Lin, L. Fu, and R. Zhang, "Collaborative optimal operation of transmission system with integrated active distribution system and district heating system based on semidefinite programming relaxation method," *Energy*, vol. 227, no. 4, article 120465, 2021.

[30] Y. Xu, J. Cheng, G. Wang, and V. C. M. Leung, "Coordinated direct and relay transmission for multiuser networks: NOMA or hybrid multiple access?," *IEEE Wireless Communication Letters*, vol. 10, no. 5, pp. 976–980, 2021.

[31] A. Ahmad and L. Atzori, "MNO-OTT collaborative video streaming in 5G: the zero-rated QoE approach for quality and resource management," *IEEE Transactions on Network and Service Management*, vol. 17, no. 1, pp. 361–374, 2019.

[32] D. Wu, F. Zhang, H. Wang, and R. Wang, "Fundamental relationship between node dynamic and content cooperative transmission in mobile multimedia communications," *Computer Communications*, vol. 120, pp. 71–79, 2018.

[33] S. Li, W. Qu, C. Liu, T. Qiu, and Z. Zhao, "Survey on high reliability wireless communication for underwater sensor networks," *Journal of Network and Computer Applications*, vol. 148, article 102446, 2019.

Hindawi
Journal of Sensors
Volume 2022, Article ID 2192186, 10 pages
https://doi.org/10.1155/2022/2192186

Research Article

Application of Data Mining Technology in Financial Intervention Based on Data Fusion Information Entropy

Cong Gu

College of Science, Zhongyuan University of Technology, Zhengzhou, 450007 Henan, China

Correspondence should be addressed to Cong Gu; gucong@zut.edu.cn

Received 19 November 2021; Revised 7 December 2021; Accepted 13 December 2021; Published 13 January 2022

Academic Editor: Gengxin Sun

Finance, as the core of the modern economy, supports sustained economic growth through financing and distribution. With the continuous development of the market economy, finance plays an increasingly important role in economic development. A new economic and financial phenomenon, known as financial intervention, has emerged in recent years, which has created a series of new problems, promoting the rapid increase both in credit and investment and causing many problems on normal operation of financial bodies. In the long run, it will inevitably affect the stability and soundness of the entire economic and financial system. In order to maximize the effect of financial intervention, in response to the above problems, this article uses a series of US practices in financial intervention as the survey content, combined with the loan data provided by the US government financial intervention department, and mines the data of the general C4.5 algorithm of the decision tree algorithm. Generate a decision tree and convert it into classification rules. Next, we will discover the laws hidden behind the loan data, further discover information that may violate relevant financial policies, provide a reliable basis for financial intervention, and improve the efficiency of financial intervention. Experiments show that the method used in this article can effectively solve the above problems and has certain practicability in fiscal intervention. With stratified sampling, the risky accuracy rate increased by 10%, probably because stratified sampling increased the number of high-risk samples.

1. Introduction

The United States is considered to be the world's most free market [1], but no country in the world has a free market economy that is completely laissez-faire and free from government regulation, and the United States is no exception [2]. In fact, American government intervention in the economy is to ensure that the market can operate more healthily and that market players can compete more fairly and freely [3]. The financial system of the United States is a financial system dominated by the capital market. Because of the normative system, well-developed financial institutions and financial instruments have formed a developed capital market by virtue of the world's leading international monetary status of the United States dollar [4]. The market should be determined by the laws of the market, not determined and controlled by administrative orders [5]. The free competition of market entities under equal conditions is very important. Antimonopoly is because monopoly harms free market competition [6]. Unified financial legislation is because fraud and misleading harm the free market competition. The way the United States handles the economic crisis shows that [7], administrative intervention is an effective way for the country to emerge from the crisis, and practice has proved this. Government intervention in the economy is inevitable for the development of market economy [8]. It is also a good remedy for "market failure" and "market self-defeat" in the process of the development of market economy [9–10]. Market mechanism and government intervention have their own time and space [11–12], which cannot be ignored and replaced [13]. A government should perform its coercive intervention management function in the economy during dramatic market changes and economic crises [14] with the purpose of curbing the damage to society caused by harmful behaviors resulting from dramatic market changes and economic crises [15].

The most basic characteristics of data mining include a large amount of data [16], which is to discover unknown

and hidden information, extract valuable information, and use this kind of information to make important decisions [17–20]. Data mining is the process of extracting useful information from data and using it to make more appropriate decisions. The key to data mining can be divided into three parts: data, information, and decision-making [21]. Data is the basis of all mining [22], but it is only when we mobilize them or convert them into useful information that they are most valuable [23–25]. It is not enough to simply obtain information [26], and it is not what data mining requires [27]. The information obtained in the decision-making application is the ultimate goal of obtaining information. Therefore, the ultimate goal of data mining is to extract useful information from data to improve the efficiency of decision-making and make more appropriate decisions. In the past few years, data mining has been used in many industries to help senior managers make important and appropriate decisions. For example, different data mining methods can be used in the banking industry to solve and help the difficulties encountered in the business process of bank cards, credit, etc. Use these advanced computer technologies to enhance or improve their decision-making security and efficiency.

The financial market is producing huge amounts of data. Analyzing these data, explaining valuable information and helping to make financial decisions are great opportunities and challenges for data mining. The essence of many financial theories is to study how to construct a prediction model which is in line with the reality and minimize the prediction error. However, traditional financial analysis and theory, the prediction models used are often established on some harsh assumptions, and the form is a model of some simple mathematical expressions. Although this model is simple, it has good interpretability and comprehensibility, but it damages the accuracy of prediction to some extent. Data mining technology has broken this limitation in some respects. Through the analysis of the characteristics of financial data, we can see its advantages more clearly. Data mining technology is produced under the background that the database cannot predict the development trend of data, and its concept was first proposed at the 1989 International Joint Conference on Artificial Intelligence (IJCAI). Its significance is the process of extracting hidden and potentially useful information and knowledge from a large amount of incomplete and noisy, ambiguous, and random practical application data. Data mining is a new information processing technology. Its main function is to extract, transform, analyze, and model a large amount of data in the database. The process of data mining is also called the process of knowledge discovery. This is a broad academic subject.

In this paper, when studying the problem of financial intervention strategies, the existence of various irregular noises in the data can cause serious interference to the experiment. In order to avoid this situation and realize the hidden laws of data, this paper adopts an effective two-way cohesive information entropy data analysis method to establish a relevant model, which can discover the hidden information and patterns in financial data and help government financial departments to make correct intervention decisions. Under the support of information entropy theory, a simulation model based on two-way clustering is proposed for simulation. After extensive analysis and theoretical demonstration, the results show that the multichannel clustering algorithm has obvious effect on improving the accuracy of data analysis, which provides a strong scientific basis for the formulation of the financial intervention policy of the modern American government. In view of the fact that traditional clustering algorithms can only deal with single attribute data and cannot deal with the clustering problem of mixed attribute data well, and that most of the current clustering algorithms of mixed attribute data are sensitive to initialization and cannot deal with arbitrary shape data, a spectral clustering algorithm of mixed attribute data based on information entropy is proposed to deal with mixed type data. Firstly, a new similarity measurement method is proposed. The traditional similarity matrix is replaced by the combination of the Gaussian kernel function matrix composed of numerical data in spectral clustering algorithm and the influence factor matrix composed of new information entropy-based classification data. The new similarity matrix avoids the conversion and parameter adjustment between numerical attribute and classification attribute data. Then, the new similarity matrix is applied to spectral clustering algorithm to process arbitrary shape data, and finally, the clustering results are obtained.

2. Proposed Method

2.1. Basic Technology of Data Mining. Following years of development, it has been gradually matured the data mining technology. There are commonly used data mining techniques and algorithms such as decision trees, neural networks, rough sets, association rules, cluster analysis, regression analysis, genetic algorithms, and rough set algorithms. Here, the focus will be on clustering analysis, association rules, and regression analysis algorithms in line with the application area of this paper. Figure 1 is a display of several common data mining methods.

2.1.1. Cluster Analysis. Among them, cluster analysis plays a role in data mining in the following aspects: First, preprocessing steps for other algorithms, and then, these algorithms are generated into new clusters and processed; second, to analyze each cluster, mainly to analyze specific clusters; and third, explore and process some relatively independent data. However, it is often ignored when mining some relatively independent data.

(1) Split Method. If a database containing n data objects or tuples is provided, the analytical method can construct c data partitions, and each partition has its own representative cluster "$c < n$". As a general rule, divisive criteria (such as distance) are used to make objects in the same cluster "similar" and to make objects in different clusters "different." It is mainly used to find spherical clusters. These are mostly used for small- and medium-sized databases. For the purpose of better management and processing of data in clusters, some new partitioning methods are urgently needed.

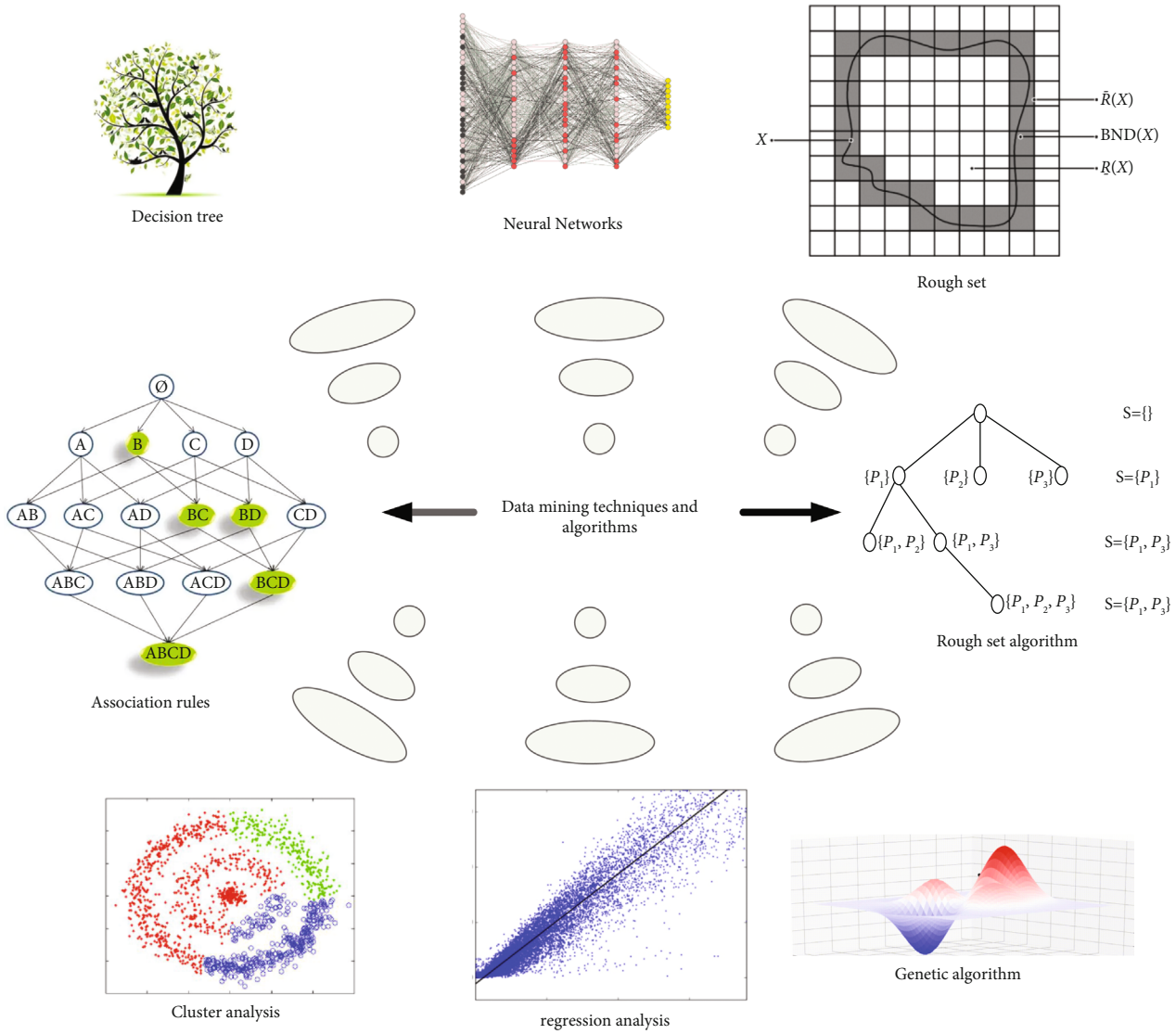

Figure 1: Several common data mining techniques.

(2) Stratification. The hierarchical method decomposes the collection of specific data objects hierarchically. According to whether the hierarchical decomposition is bottom-up or bottom-up, the hierarchical clustering technique can be divided into agglutination and segmentation. The disadvantage of hierarchical clustering is that it cannot be restored after the steps are completed, so the errors are corrected.

2.1.2. Association Rules. Association can be divided into simple association and time association. The most commonly used association rule algorithm is the Apriori algorithm proposed by R. Agrawal. Even using candidate itemsets to search for frequent itemsets, mining itemset with frequent Boolean correlation rules is the most influential algorithm.

(1) Find all frequency sets that are at least the same as the predefined minimum supported frequency

(2) Use the frequency set found in the first step to generate the target rule, and generate all the rules that only include the setting items. There is only one correct part of each rule. The definition of the intermediate rule is used here

Apriori algorithm will generate more candidate sets and may need to scan the database repeatedly. This is where the Apriori algorithm is insufficient.

2.1.3. Regression Analysis

(1) Simple Linear Regression Analysis. It is possible to determine the linear equation with a high correlation between the dependent vector a and the independent variable B if they are found to be highly correlated, with a view to making all data points as close in approximation to a straight line as possible. The model can be expressed as follows.

$$A = x + yB. \tag{1}$$

(2) Multivariate Linear Regression Analysis. What we usually see more often is that a single dependent variable corresponds to multiple independent variables. This corresponding mode is called regression. Its performance is as follows:

$$Y = a + b_1X_1 + b_2X_2 + b_3X_3 + \cdots + b_kX_k. \quad (2)$$

a represents the intercept, and $b_1, b_2, b_3, \cdots, b_k$ represents the correlation coefficient.

(3) Analysis of Nonlinear Regression Data. For linear regression problems, the sample points fall on or near a straight line in space, so a linear function can be used to represent the corresponding relationship between independent variables and dependent variables. However, in some applications, the relationship between variables is in the form of curve, so it is impossible to express the corresponding relationship between independent variables and dependent variables by linear functions, but it needs to be expressed by nonlinear functions.

2.2. Decision Tree Algorithms. It is closer to the objective function. Both leaf node classification and instance classification are performed mainly at the basis of the arrangement of nodes. On each node corresponding to one possible case, a root of a tree node is started; its attributes are measured; then, the node is changed according to its corresponding value.

2.2.1. ID3 Algorithm. On the basis of the ID3 algorithm that the attribute selection metric is the information gains when selecting on the best attribute as each node. And the measure is based on the pioneering work of C.E. in the study of information value or information theory by scientists of C.E. the Shannon:

We first compared the growth of each type of information. To choose the attribute from which the highest information is gaining (for example, maximum extraction compression) one of the tree points.

The second step is to branch according to the different values of the root node and then establish the lower nodes and branches for each branch.

The third step is to repeat the first and second steps and stop branching when the data contained in the subset are of the same category.

In this way, a decision tree can be obtained and used to classify test samples.

For the calculation description of information gain value, let D be a set of training data and define m different $C_i ni = 1n2n \cdots, mn$. The expected information for a given training data classification is given by the following formula:

$$\inf\ o(D) = -\sum_{i=1}^{m} P_i \log_2(P_i). \quad (3)$$

Note that the logarithmic function bottoms 2 because of information binary encoding.

Now, suppose you want to divide the tuples in D by attribute A, where attribute A has $V\{a_1, a_2, a_3, \cdots, a_V\}$ values according to the observation of training data. Therefore, attribute A divides D into v subsets $\{D_1, D_2, D_3, \cdots, D_V\}$, where the tuples in D_j have the same value a_j on attribute A. However, these partitions may contain tuples not from the same class but from different classes, that is, impure. After this partition, how much information is needed for the accurate classification of the generated tuples, which can be measured by the following formula:

$$\mathrm{Info}(A) = \sum_{j=1}^{V} \frac{|D_j|}{|D|} \mathrm{Info}(D_j). \quad (4)$$

Among them, item $|D_j|/|D|$ denotes the weight of the j th partition, and $\mathrm{Info}(A)$ denotes the expected information needed to classify the components of D by attribute A. The information gain obtained by branch on attribute A can be described as:

$$\mathrm{Gain}(A) = \mathrm{Info}(D) - \mathrm{info}(A). \quad (5)$$

The advantages of ID3 algorithm are as follows:

(1) The basic principle of the algorithm is clear

(2) The classification speed is faster

(3) Practical example learning algorithm

Its shortcomings are as follows:

(1) There is a bias problem. The number of feature attributes affects the amount of information

(2) A problem with training data will make the results different and more sensitive to noise

(3) The probability of error is proportional to the increase of category

2.2.2. C4.5 Algorithm. An early machine learning algorithm and a common algorithm for constructing decision tree classifiers became the basis of many decision tree algorithms later.

(1) The information gain rate is used as attribute selection measure to solve the problem of bias

(2) It can discretize attributes with continuous values and deal with incomplete data

(3) Pruning at the same time in the process of tree construction

With the extension of information gain, benefit ratio can solve the drawback of ID3. In the assumption that a variable is selected as a partitioning attribute, with a higher information gain of the variable than the information gain of its other variables is needed. The definition formula of

segmentation information is as follows:

$$\text{SplitInfo}(A) = -\sum_{j=1}^{V} \frac{|D_j|}{|D|} \times \log_2\left(\frac{|D_j|}{|D|}\right). \quad (6)$$

The ratio of the increase in information is mainly compared with the total amount of information in some segments. The formula is as follows:

$$\text{GainRatio}(A) = \frac{\text{Gain}(A)}{\text{SplitInfo}(A)}. \quad (7)$$

2.2.3. CART Algorithm. Classification and Regression Tree (CART) is a technique for generating binary decision trees. In fact, its principle is dichotomy recursive segmentation technology. In order to produce subnodes, it divides two sample subsets; that is, only two subnodes are generated, so finally, a simple binary decision tree is obtained. Unlike ID3 and C4.5, which are based on information entropy splitting technology, CART chooses the best grouping variables and splitting points based on gini coefficient and variance and chooses the attributes with the minimum gini coefficient as the current test attributes. If the gini coefficient value is smaller, the more reasonable the segmentation is, and the higher the purity of the sample set is.

If the training tuple set D contains records of m categories, then the gini index is determined as follows:

$$\text{Gini}(D) = 1 - \sum_{i=1}^{m} P_i^2. \quad (8)$$

Calculate the sum of m classes, where P_i is the probability that any record in D belongs to C_i class and is expressed by $|Ci, D|/|D|$. If D is divided into D1 and D2, the gini coefficient of this division is

$$\text{Gini}(D) = \frac{|D_1|}{|D|}\text{Gini}(D_1) + \frac{|D_2|}{|D|}\text{Gini}(D_2), \quad (9)$$

where $|D|$ is the number of samples in D and $|D_1||D_2|$ is the number of samples in D1 and D2, respectively.

The CART algorithm terminates splitting and stops constructing decision tree if the following conditions exist.

(1) The data records contained in leaf nodes belong to the same category

(2) The number of samples covered by a branch is less than a threshold set by the user in advance

3. Experiments

3.1. Selection of Experimental Platform. Through this paper, SPSSC lementine 12.0 is elected as the data mining platform in conjunction for the actual research work. For the mining platform, the selection of the platform is mainly based on the following six aspects:

(1) Clementine has the functions of classification and prediction, association analysis, time series analysis, and clustering. It provides a variety of methods, such as neural network, decision tree and regression tree, linear regression, logistic regression, self-organizing network, and fast clustering

(2) Clementine has an interactive and visual user interface, which combines intuitive user graphics interface with a variety of analysis techniques. It is a very easy software for users to build models by connecting nodes, and data mining model can be built without programming. So that users can put more energy into the application of data mining to solve specific business problems, rather than the use of software

(3) Clementine has an open database interface that provides rich data access capabilities for access to files and relational databases. It also provides the ability to input data processing and output data settings

(4) Clementine provides two ways to build models. In the simple mode, the user does not need to make any settings; the system will build the model according to the default settings; in the expert mode, the user can adjust the parameters in the model according to his own needs, so that the model achieves the best results

(5) Provide powerful publishing capabilities to export data mining models or entire data mining processes to embedded systems

(6) Provide complete data flow management and project management functions. The former can effectively manage the data flow, data mining model, and mining results in the work area. The latter can effectively manage the entire project; users can manage related project files according to different stages of data mining and can effectively manage data mining projects according to data flow, nodes, data mining models, results, and other methods

3.2. Data Acquisition. With this paper, the data are obtained from the financial data of 1500 relevant firm clients of a commercial bank, averaged over the years 2015 to 2018. The attributions in the financial information data tables provided by the bank are in the transaction database based attributes, so conversion of attributes is performed to form 18 attributes that reflect the financial indicators for a firm, as shown in Table 1. Firstly, according to the relevant indicators of enterprises and the actual situation of enterprises in 2018, the experts of financial institutions define the risks of enterprises as high, higher, medium, and low. Among them, the enterprises with high risk are those that will fail from 2017 to 2018; the enterprises with high risk are those that will produce credit default; the

Table 1: Randomly selected with 12 attributes from 18 alternatives.

Number	Attribute	Calculation formula
1	Asset-liability ratio	Total liabilities/total assets
2	Net profit margin of operating income	Major business profit/major business income
3	Return on assets	Net profit/(total shareholders' equity + total shareholders' equity in the previous period)*2
4	Fixed asset ratio	Total fixed assets/total assets
5	Liquidity ratio	Total current assets/total current liabilities
6	Quick ratio	(Total current assets - net inventory)/total current liabilities
7	Interest guarantee multiple	(Net profit + income tax + financial expenses)/financial expenses
8	Total asset turnover rate	Main business income/(total assets + total previous assets)*2
9	Inventory turnover	Main cost/(net inventory + net previous inventory)*2
10	Receivable turnover rate	Main business cost/(accounts receivable + last accounts receivable)*2
11	Receivable turnover rate	Main business income/(accounts receivable + last period accounts receivable)*2
12	Cash ratio of main business income	Cash flow/main business income from operational activities
13	Inventory current liability ratio	Net inventory/total liquidity liabilities

Table 2: Comparison table of classification accuracy of multiple random decision trees.

Verification times	High risk%	Higher risk%	Medium risk%	Low risk%
1	53.21	71.66	78.23	88.79
2	54.43	72.12	77.98	89.01
3	48.67	74.98	81.61	89.37
4	58.65	75.45	78.92	86.02
5	51.36	73.37	78.76	88.09
Average	53.34	73.46	78.94	88.57

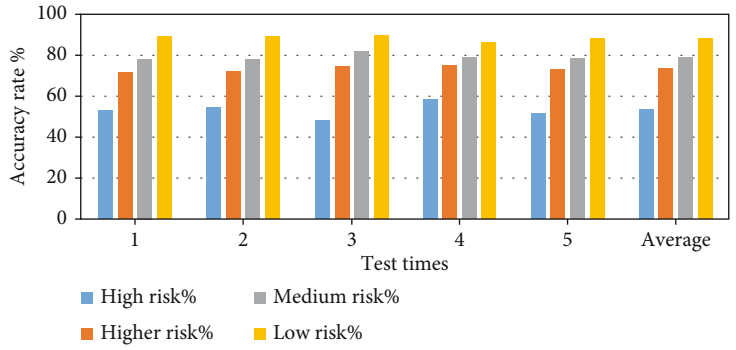

Figure 2: Comparison of classification accuracy of multiple random decision trees.

enterprises with medium risk are those that have no default but have deteriorating financial situation, and the enterprises with low risk have good financial situation and no credit default. At each tree construction, a randomized method was used. For verification of the stability of a decision tree classification, a total of 5 experiments were conducted. At each training dataset, 1200 data were randomly selected with the tree from the original dataset as training data, which was randomly selected with 12 attributes from 18 alternatives.

Table 3: Comparing table of accuracy of C4.5 algorithms.

Verification times	High risk%	Higher risk%	Medium risk%	Low risk%
1	35.24	60.62	65.29	72.75
2	37.43	62.12	66.98	73.01
3	34.67	64.98	71.61	76.37
4	38.65	65.45	70.92	76.02
5	31.36	63.37	68.76	78.09
Average	35.34	63.46	68.94	74.57

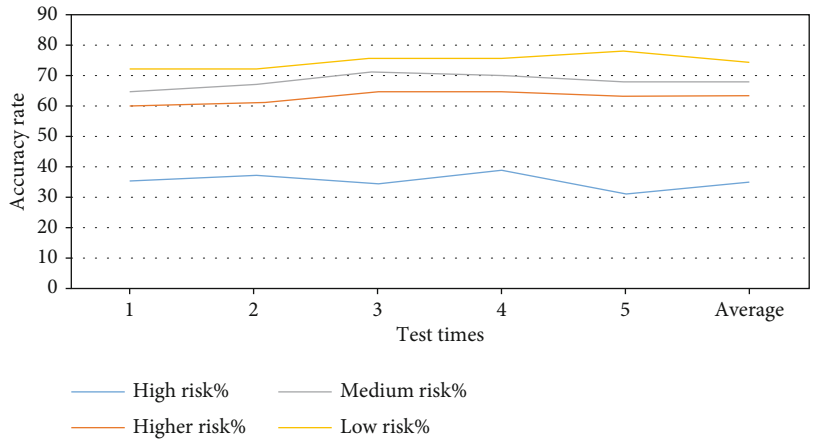

Figure 3: Comparisons of accuracy of C4.5 algorithms.

Table 4: Accuracy comparison between random decision tree algorithm and C4.5 algorithm.

	High risk%	Higher risk%	Medium risk%	Low risk%
Stochastic decision tree algorithm	52.63%	70.15%	78.89%	82.51%
C4.5 algorithm	37.26%	60.94%	65.75%	68.21%

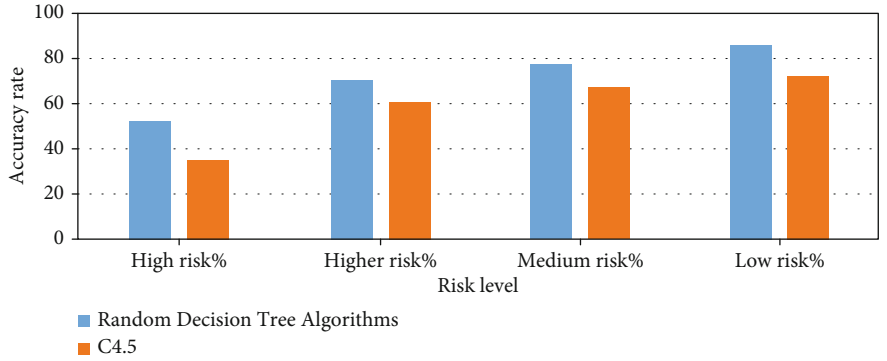

Figure 4: Comparing the accuracy of stochastic decision tree algorithm with that of C4.5 algorithm.

Table 5: Comparison table of stratified sampling accuracy of multiple random decision trees.

Verification times	High risk%	Higher risk%	Medium risk%	Low risk%
1	71.41	77.32	83.29	89.78
2	72.43	76.12	84.98	90.01
3	71.67	78.98	87.61	90.37
4	70.65	79.45	78.92	89.02
5	72.36	79.37	85.76	88.09
Average	71.34	78.46	85.94	89.57

Table 6: Accuracy comparison table of stratified sampling and random sampling.

	High risk%	Higher risk%	Medium risk%	Low risk%
Stratified sampling	71.25%	78.59%	85.12%	88.91%
Random sampling	51.69%	71.20%	79.21%	86.57%

4. Discussion

4.1. Accuracy Comparison

(1) In order to compare the data, we counted the progress of a large number of random decisions, making the data comparison between them obvious, and the comparison results are shown in Table 2 and Figure 2.

We can see that the classification accuracy is informative for bank risk prediction by the confirmation of bank personnel and based on the data presented through the graph. However, the algorithm has relatively low classification accuracy for high risks. The main reason is that the number

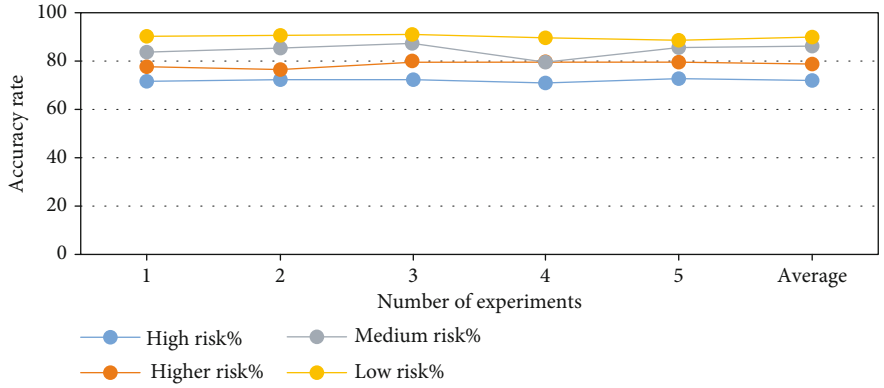

Figure 5: Comparisons of stratified sampling accuracy for multiple random decision trees.

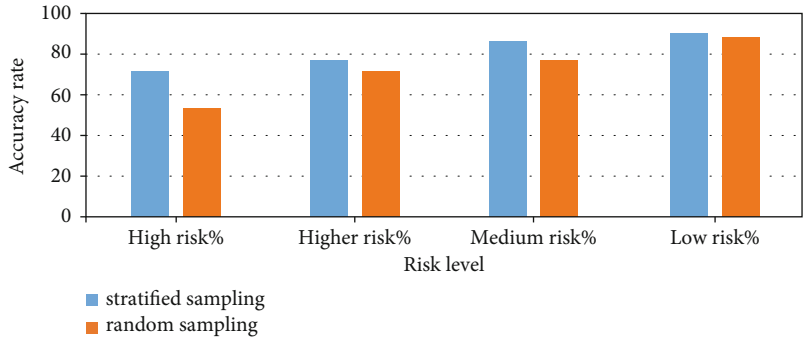

Figure 6: Comparison of stratified sampling and random sampling accuracy.

of data with high risk in the training data set is small, resulting in insufficient training of this kind of branch.

(2) Accuracy analysis of C4.5 algorithm, as shown in Table 3 and Figure 3.

The classification accuracy of the algorithm for high risk is relatively low. The main reason is that the number of data with high risk in the training data set is small, which results in insufficient training of this kind of branch. Table 4 is the accuracy comparison table between the random decision tree algorithm and the C4.5 algorithm.

According to Table 4, the accuracy comparison chart between the random decision tree algorithm and the C4.5 algorithm is obtained, as shown in Figure 4.

From Figure 4, we can see that the accuracy of random decision tree method is about 10% higher than that of C4.5. In order to improve the accuracy of high risk, 300 high risk data were added to the training data set. The original random sampling is replaced by stratified sampling. The original data are stratified according to the high, higher, medium, and low risk. Random sampling is used for each level to ensure the number of training data with high risk. The following Tables 5 and 6 and Figures 5 and 6, respectively, show the stratified sampling accuracy comparison table of multiple random decision trees, the comparison table of stratified sampling and random sampling accuracy, the comparison of stratified sampling accuracy of multiple random decision trees, and the stratified sampling.

We can see that the accuracy of high-risk increases to 10% after stratified sampling, which is mainly because stratified sampling increases the number of high-risk samples. Then, the accuracy of decision tree classification is related to the number of training data samples. By having a larger sample size, the more accurate the decision tree of classification.

5. Conclusions

With the continuous progress of computer theory and technology, more and more computer data processing and analysis methods are combined with financial intervention work efficiently and organically, which has brought revolutionary innovation to the theory, mode, and method of financial intervention work. Especially the introduction of data mining technology, it brings new ideas for financial analysts, improves the efficiency and quality of financial intervention, and plays an increasingly important role.

(1) On the basis of introducing the background of topic selection, process steps, and application fields of data mining and focuses on the commonly used algorithms of data mining

(2) Based on the theory of information entropy and through theoretical proof, this paper proposes an objective and fair method to evaluate the clustering effect and applies this method to solve practical

problems and achieves better practical results. Due to incomplete data and partial distortion in raw data acquisition, the accuracy of the model is affected to a certain extent. Further work is to increase the number of experimental samples, fully tap the potential useful information; add some derivative variables to make the results of analysis more objective and convincing; the results of analysis are more comprehensive and have greater practical value

(3) This paper analyses and studies the classification technology of decision tree in data mining, especially the application of C4.5 algorithm to loan data of a credit cooperative, establishes decision tree and classification rules, builds audit analysis model, and facilitates financial analysts to find problems and find clues to financial problems

Data Availability

This article does not cover data research. No data were used to support this study.

Conflicts of Interest

The author declares that there are no conflicts of interest.

Acknowledgments

This work was supported by the Humanities and Social Sciences Project of Henan Provincial Education Department (No. 2022-ZZJH-098), the Independent Innovation Application Research Project of Zhongyuan University of Technology (No. K2018YY023), and the Graduate Quality Engineering Project of Zhongyuan University of Technology (No. QY202102).

References

[1] C. R. Tryon, *Cluster Analysis: Correlation Profile and Orthometric (Factor) Analysis for the Isolation of Unities*, Edwards Brothers, Ann Arbor, 1939.

[2] R. B. Cattell, "The description of personality: basic traits resolved into clusters," *Journal of Abnormal and Social Psychology*, vol. 38, no. 4, pp. 476–506, 1943.

[3] D. Swingley, "Statistical clustering and the contents of the infant vocabulary," *Cognitive Psychology*, vol. 50, no. 1, pp. 86–132, 2005.

[4] U. Maulik, "Medical image segmentation using genetic algorithms," *IEEE Transactions on Information Technology in Biomedicine*, vol. 13, no. 2, pp. 166–173, 2009.

[5] A. Capozzoli, F. Lauro, and I. Khan, "Fault detection analysis using data mining techniques for a cluster of smart office buildings," *Expert Systems with Applications*, vol. 42, no. 9, pp. 4324–4338, 2015.

[6] D. Liu, M. H. Jiang, X. F. Yang, and H. Li, "Analyzing documents with quantum clustering: a novel pattern recognition algorithm based on quantum mechanics," *Pattern Recognition Letters*, vol. 77, pp. 8–13, 2016.

[7] L. A. Lopes, V. P. Machado, R. A. L. Rabêlo, R. A. S. Fernandes, and B. V. A. Lima, "Automatic labelling of clusters of discrete and continuous data with supervised machine learning," *Knowledge-Based Systems*, vol. 106, pp. 231–241, 2016.

[8] R. J. Kuo, C. H. Mei, F. E. Zulvia, and C. Y. Tsai, "An application of a metaheuristic algorithm-based clustering ensemble method to APP customer segmentation," *Neurocomputing*, vol. 205, pp. 116–129, 2016.

[9] Hung-Leng Chen, Kun-Ta Chuang, and Ming-Syan Chen, "On data labeling for clustering categorical data," *IEEE Transactions on Knowledge and Data Engineer*, vol. 20, no. 11, pp. 1458–1472, 2008.

[10] J. B. Macqueen, "Some methods for classification and analysis of multivariate observations," *Proceedings of 5th Berkeley Symposium on Mathematical Satistics and Probability*, vol. 1, no. 14, 1967.

[11] I. V. Zhihan and H. Song, "Trust mechanism of feedback trust weight in multimedia network," *ACM Transactions on Multimedia Computing, Communications, and Applications*, vol. 17, no. 4, pp. 1–26, 2021.

[12] X. Li, H. Liu, W. Wang, Y. Zheng, H. Lv, and Z. Lv, "Big data analysis of the internet of things in the digital twins of smart city based on deep learning," *Future Generation Computer Systems*, vol. 128, pp. 167–177, 2021.

[13] R. W. Hamming, "Error detecting and error correcting codes," *Bell System Technical Journal*, vol. 29, no. 2, pp. 147–160, 1950.

[14] Z. X. Huang, "Clustering large data sets with mixed numeric and categorical values," in *Proceedings of the 1st Pacific-Asia Conference on Knowledge Discovery and Data Mining*, Singapore, 1997.

[15] Z. Huang and M. K. Ng, "A fuzzy k-modes algorithm for clustering categorical data," *IEEE Transaction on Fuzzy Systems*, vol. 7, no. 4, pp. 446–452, 1999.

[16] J. Y. Yeh and C. H. Chen, "A machine learning approach to predict the success of crowdfunding fintech project," *Journal of Enterprise Information Management, Accepted Manuscript*, 2020.

[17] S. Guha, R. Rastogi, and K. Shim, "Rock: a robust clustering algorithm for categorical attributes," *Information Systems*, vol. 25, no. 5, pp. 345–366, 2000.

[18] V. Ganti, J. Gehrke, and R. Ramakrishnan, "CACTUS-clustering categorical data using summaries," *Knowledge Discovery and Data Mining*, pp. 73–81, 2000.

[19] D. Barbará, Y. Li, and J. Couto, "COOLCAT," in *Proceedings of the eleventh international conference on Information and knowledge management - CIKM '02*, New York, 2002.

[20] J. F. Brendan and D. Delbert, "Clustering by passing messages between data points," *Science*, vol. 315, no. 5814, pp. 972–976, 2007.

[21] M. K. Ng, M. J. Li, J. Z. Huang, and Z. He, "On the impact of dissimilarity measure in k-modes clustering algorithm," *IEEE Transactions on Pattern Analysis and Machin*, vol. 29, no. 3, pp. 503–507, 2007.

[22] F. Cao, J. Liang, D. Li, L. Bai, and C. Dang, "A dissimilarity measure for the k-modes clustering algorithm," *Knowledge-Based Systems*, vol. 26, pp. 120–127, 2012.

[23] G. Chen, Y. Lu, B. Li, K. Tan, and T. Moscibroda, "MP-RDMA: enabling RDMA with multi-path transport in datacenters," *IEEE/ACM Transactions on Networking*, vol. 27, no. 6, pp. 2308–2323, 2019.

[24] G. Chen, Y. Lu, Y. Meng et al., "FUSO: fast multi-path loss recovery for data center networks," *IEEE/ACM Transactions on Networking*, vol. 26, no. 3, pp. 1376–1389, 2018.

[25] Y. Zeng, G. Chen, K. Li, Y. Zhou, X. Zhou, and K. Li, "M-skyline: taking sunk cost and alternative recommendation in consideration for skyline query on uncertain data," *Knowledge Based Systems*, vol. 163, pp. 204–213, 2019.

[26] Z. Y. He, X. F. Xu, and S. C. Deng, "Squeezer: an efficient algorithm for clustering categorical data," *Journal of Computer Science and Technology*, vol. 17, no. 5, pp. 611–624, 2002.

[27] D. W. Kim, K. H. Lee, and D. Lee, "Fuzzy clustering of categorical data using fuzzy centroids," *Pattern Recognition Letters*, vol. 25, no. 11, pp. 1263–1271, 2004.

Hindawi
Journal of Sensors
Volume 2022, Article ID 3943153, 11 pages
https://doi.org/10.1155/2022/3943153

Research Article

Research on Efficacy Evaluation of Large-Scale Networked Intelligent Perception System

Suqiong Ge[1,2] and Xiaopeng Huang[2]

[1]*Business School, Hohai University, Nanjing 211100, China*
[2]*No.724 Research Institute of China Shipbuilding Industry Corporation, Nanjing 211153, China*

Correspondence should be addressed to Xiaopeng Huang; huangxp@724pride.com

Received 10 November 2021; Revised 8 December 2021; Accepted 11 December 2021; Published 13 January 2022

Academic Editor: Gengxin Sun

Under the smart engineering system (SES), there is a huge demand for evaluating the efficacy of a large-scale networked intelligent perception system (IPS). Considering the large-scale, distributed, and networked system characteristics and perception task demands, this paper proposes a conceptual system for IPS efficacy evaluation and, on this basis, designs the architecture of the efficacy evaluation system. A networked IPS model is constructed based on domain ontology, an index system is quickly established for efficacy evaluation, the evaluation methods are assembled automatically, and adaptive real-time organization strategies are generated for networked perception based on efficacy estimate. After exploring these key technologies, a prototype system is created for the service-oriented integrated efficacy evaluation platform and used to verify and integrate research results. The research provides support for the efficacy evaluation theories and methods of large-scale networked IPS.

1. Introduction

In recent years, many advanced information technologies have emerged and evolved quickly, including the Internet of things (IoT), artificial intelligence (AI), cloud computing, and big data. In the meantime, many complex issues have surfaced in urban public governance, public safety, industrial manufacturing, agricultural production, and ocean, such as energy, environmental protection, traffic and tourism, emergency management, production-service process, disaster prevention, and mitigation [1–6]. To mitigate or solve various problems, advanced information technologies are combined with physical entities and other resource elements through overall planning and optimal allocation. The optimization of advanced information technology is a very cutting-edge research problem. Many researchers have done research in this field, such as the related theories, methods, and technologies of three-way decision-making, and have made a lot of achievements in this problem. The synergy between them gives birth to smart engineering systems (SESs) of different modes, which improve the level of smart services. Typical SESs include smart cities, intelligent transportation, smart factories, intelligent agriculture, and wisdom oceans [7–13]. A three-way decision has also played a great role in some fields [14–16].

The current research on SES construction mostly focuses on the top-level design and decision application of the system, as well as the key technologies like information processing, storage, transmission, and perception [17–19]. However, there are not many in-depth studies on the efficacy of the intelligent perception system (IPS), which is based on performance and function. Few scholars have considered if the perception ability of IPS could satisfy the demand of perception tasks. There are still many indescribable difficulties in the mathematical description of intelligent sensing systems. We cannot use a very accurate formula to describe the problem, which leads to the accuracy of the intelligent sensing system.

During SES construction, the large-scale complex networked IPS with various sensors and multiple functions faces severe challenges, such as diverse perception tasks and objects, high requirement on perception ability, and

complicated perception environment. The IPS must measure, differentiate between, and track many objects accurately in a wide range. The huge amount of data perceived by the system carries obvious features of the big data, namely, complex data relationships, various types, fast storage/reading, and low application value density. IPS is characterized by a large amount of data and too complex information. It must be processed twice before it can be used as computable data to participate in efficiency evaluation.

How to evaluate the efficacy of the large-scale networked IPS under the SES becomes an unavoidable problem with theoretical, methodological, and technical challenges, because this is hard to format the question, and the theoretical, methodological, and technical challenges also have some need for research. The evaluation of perception efficacy is the guide for the construction of the large-scale networked IPS and the theoretical basis of system capacity measurement, because it exists throughout the lifecycle of such systems from planning and demonstration, design, research, and development (R&D) to testing and use, associates closely with specific conditions and tasks, and takes root on system functions and performance [20, 21].

Therefore, it is a fundamental and practical issue to explore the theories and techniques for the large-scale networked IPS efficacy evaluation under the SES. To construct high-quality large-scale networked IPS, this paper systematically investigates every aspect of efficacy evaluation environment, ranging from architecture, conceptual system, model base, index system, and method base to integrated platform construction.

2. Research Roadmap

Our research is based on relevant theories, technologies, and methods of system science and complex systems engineering, computer science, information science, IoT, cloud computing, mobile Internet, big data, service-oriented technology, and evaluation theories and methods. Driven by the demand for efficacy evaluation of the large-scale networked IPS, this paper designs the architecture of efficacy evaluation environment based on the conceptual system of efficacy evaluation and makes breakthroughs on such key techniques as the modeling, index system, and evaluation method of the IPS, as well as adaptive generation of perception strategy based on efficacy estimate. In this way, an integrated prototype system is established for efficacy evaluation to verify and integrate the research results. The technical roadmap of the research is shown in Figure 1.

3. Methodology

3.1. Conceptual System of the Large-Scale Networked IPS Efficacy Evaluation

3.1.1. Conceptual System of Efficacy Evaluation. There is not yet a unified definition for the connotation or denotation of efficacy. But it is generally agreed that the core of efficacy lies in three elements, namely, condition, time, and task, as well as their associations. The term efficacy was originally proposed for evaluating the demand for weapon systems. Later, the concept gradually extends from military application to the social economy system.

From the perspective of methodology, efficacy evaluation was initially implemented through probability statistics and military operation research and went through such stages as the coupling between qualitative and quantitative evaluations and simulation-based system evaluation. Currently, efficacy evaluation is service-oriented and big data-based, involving human-machine integration, which lays the theoretical and methodical bases for the large-scale networked IPS efficacy evaluation under the SES.

Considering the IPS performance, functions, and use efficacy of the large-scale networked IPS, the efficacy of the system is conceptualized as the comprehensive measurement of the ability to complete a specific task under given conditions, time, and environment, contraposing the task demand of the large-scale networked IPS and according to the capability bases like technical performance, functions, and application scenarios. The system efficacy can be calculated by

$$\mathrm{SE} = P * A * U, \tag{1}$$

where P is the measure of system performance, i.e., the capacity of the system under 100% utilization of system availability and ability; A is the measure of system availability, i.e., the degree of the system completing its expected functions during the application; and U is the measure of system applicability, i.e., the demonstration of system capability in executing the perception task. P, A, and U are independent of each other. These measures can be characterized by mathematical methods such as the index method and probability method. The index method and the probability method can be easy to describe the problem and get results as soon as possible, but the index method is not good at complex problems in the cost.

Based on different phases of the lifecycle of the networked IPS including the demonstration, design, R&D, testing, and use, the efficacy evaluation essentially needs to adopt unified, standard, and universal measures to evaluate each subefficacy and combine the series of subefficacy evaluations into a composite efficacy by a certain logical rule or from the bottom up.

For a given perceptual task, the composite efficacy can be calculated from several interconnected and mutually constrained efficacy elements, for example, analytic hierarchy process (AHP), fuzzy comprehensive evaluation method, gray whitening weight function method, and TOPSIS method, including the networked perception model, characterization index, and assessment and environment methods. Figure 2 shows the relationship between the efficacy elements, and the task is very complex, and each element can take charge of different tasks. Hence, that can be explained according to different questions.

The connotation representation system for the networked IPS efficacy is tailorable. It can be dynamically adjusted according to the specific phase and objective. Efficacy indices are generally used in the actual application

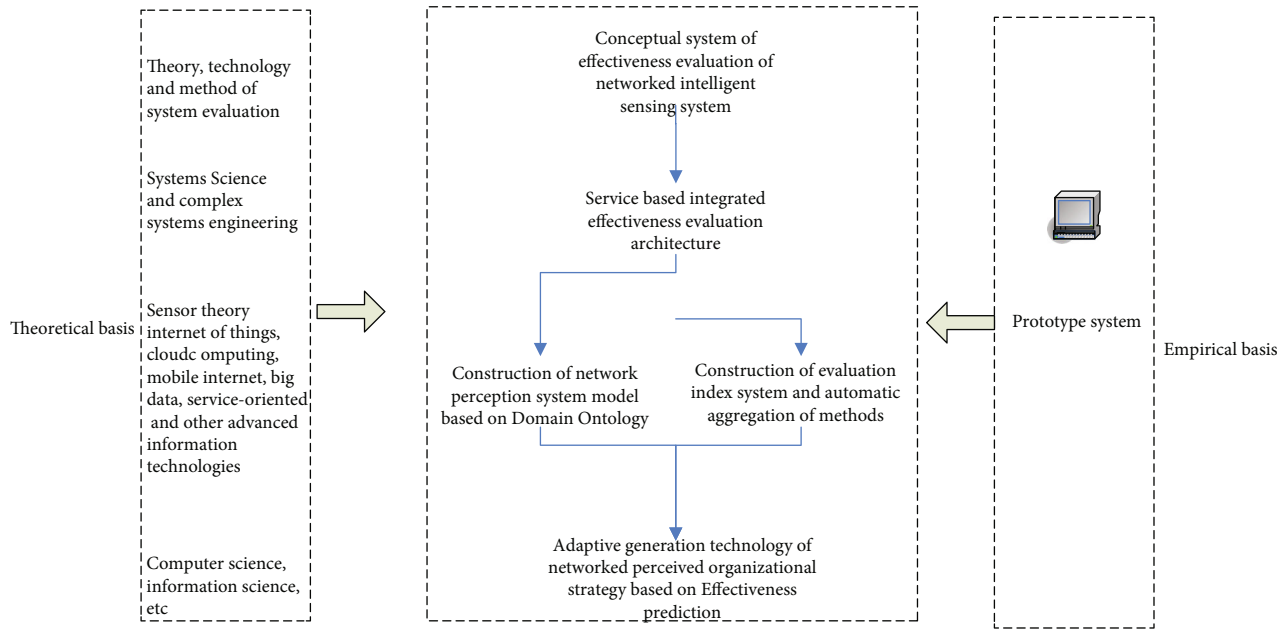

Figure 1: Technical roadmap.

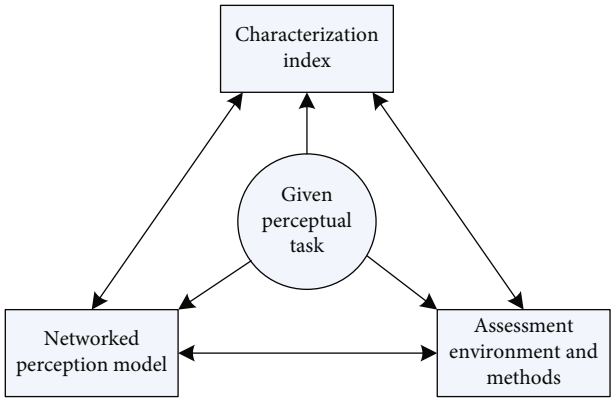

Figure 2: Relationship between efficacy elements.

phase of the networked IPS. The actual efficacy of the system needs to be tested and evaluated under complex scenarios [22]. Considering the principles and strategies for hierarchical decomposition of complex systems, i.e., wholeness, hierarchy, and completeness, the networked IPS efficacy is decomposed into a perception resource layer, a technical performance layer, an application function layer, a capability layer, a task layer, and a perception task requirement layer (Figure 3).

The understanding and demand of system efficacy evaluation vary with the task boundaries, environmental conditions, and the focuses and perspectives of subjects. Therefore, the criteria, method, and index system must be developed properly for system efficacy evaluation.

3.1.2. Composite Efficacy Index Model for Networked IPS. Drawing on the theory of index method, the composite efficacy of the networked IPS can be modeled by

$$\begin{aligned} \mathrm{SE} = P * A * U &= \left\{ \left(P_i'\right)^{w_i} * \left(A_i'\right)^{w_j} * \left(U_i'\right)^{w_k} \right\} * K_i \\ &= \left\{ \left(\frac{P_i}{P_0}\right)^{w_i} * \left(\frac{A_i}{A_0}\right)^{w_j} * \left(\frac{U_i}{U_0}\right)^{w_k} \right\} * K_i, \end{aligned} \tag{2}$$

where SE_i is the composite efficacy index, which is a dimensionless relative value; P_i', A_i', and U_i' are subefficacy indices of system performance, availability, and applicability, respectively; w_i, w_j, and w_k are the weights of subefficacy indices $(w_i + w_j + w_k = 1)$, which depend on the specific purpose and change with task conditions; K_i $(i = 1, 2, 3, 4,$ and $5)$ is the task conditions of the whole lifecycle, i.e., planning and demonstration, design, R&D, testing, and use; P_i, A_i, and U_i are the actual system performance, availability, and applicability, respectively; and P_0, A_0, and U_0 are the ideal system performance, availability, and applicability, respectively.

3.2. Service-Oriented Architecture and Flow of Networked IPS Efficacy Evaluation. System efficacy evaluation involves multiple interconnected elements: effectiveness evaluation scenario, model system, index system, methodology system data system, and display control. Among them, the sensor model and the networked IPS model should be constructed based on domain ontology. The effectiveness evaluation scenarios cover task, objectives, and environment. In addition, the networked IPS model supports the system data service; the method base provides on-demand restriction of evaluation methods. Figure 4 shows the set of elements in the networked IPS efficacy evaluation. Obviously, the efficacy evaluation environment is compatible with the hardware-in-the-loop state of sensors, i.e., in support of semiphysical simulation or full physical simulation.

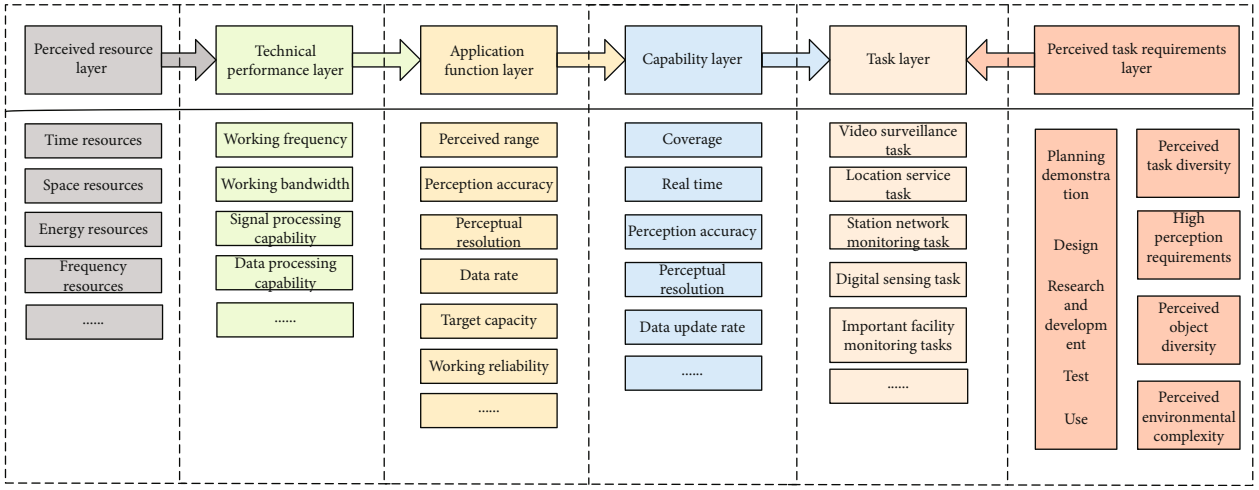

Figure 3: Hierarchical structure of networked IPS efficacy.

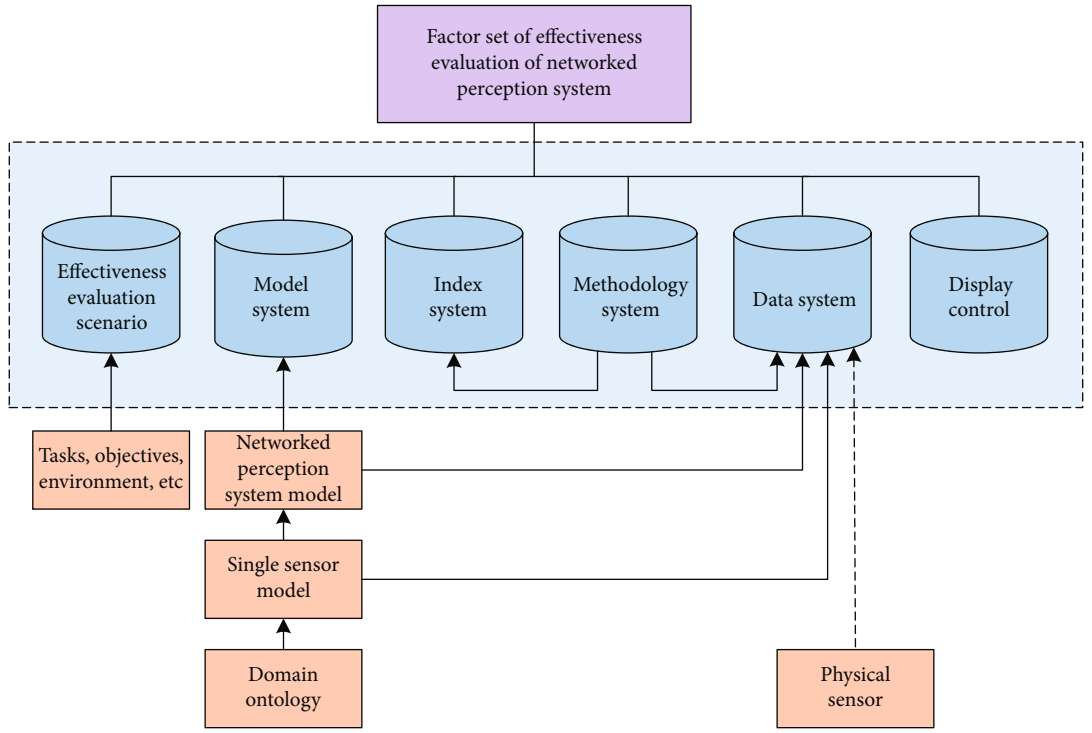

Figure 4: Element set of networked IPS efficacy evaluation.

Based on the theories and methods of complex systems, efficacy evaluation theories and techniques, web service technical framework, and ontologies and semantic network theories and methods, this paper designs a service-oriented integrated efficacy evaluation system, which consists of four layers: a resource layer, a service layer, an application support layer, and an application layer (Figure 5).

The resource layer provides the platform with basic supports like data, models, methods, and instances. This layer mainly drives all the resources in the system and visualizes them for object management. On the resource layer, the various bases could be distributed or concentrated. But all of them are centered on services, providing support for the implementation of web services.

The service layer, which is built on the resource layer, integrates the basic technical means of efficacy evaluation, offers the management tools and interface components for resources (e.g., data, models, algorithms, and knowledge), and encapsulates and calls businesses.

The application support layer encompasses the basic functional components and modules required for constructing the efficacy evaluation system and provides the application layer with consistent interfaces, thereby simplifying service development. The component technology of this

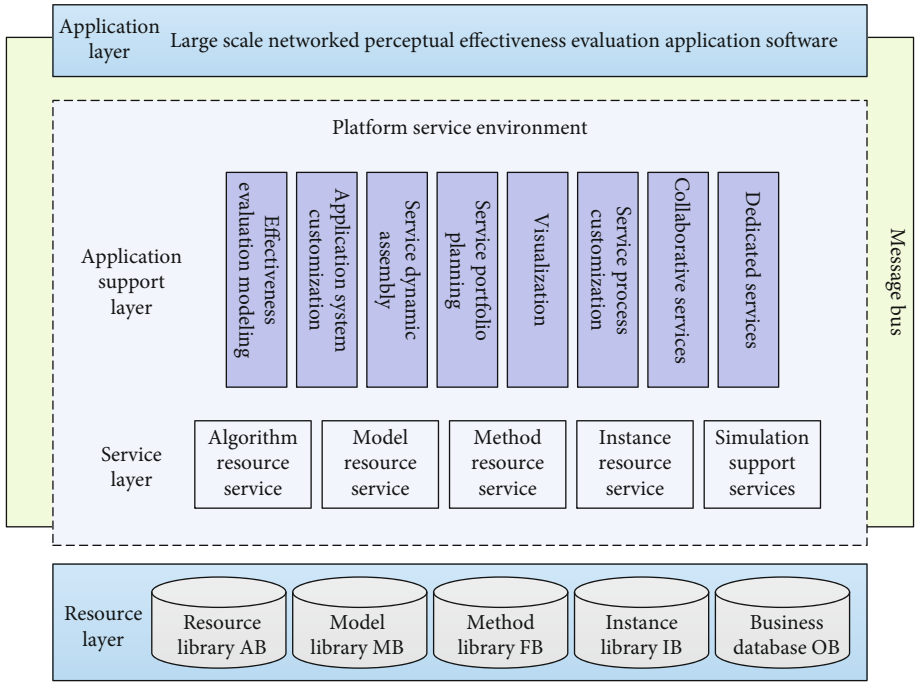

Figure 5: Four-layer architecture of effectiveness evaluation.

layer helps to manage the various business components on the superior layer and dynamically reconfigure any business components.

According to the requirements of the evaluation task, the application layer utilizes application support tools and adopts the task-based management strategy. This layer is mainly responsible for decomposing a task into the functional combination of several business components and calls the dedicated resources and services of the system to generate actual efficacy evaluation modules.

The evaluation task is executed in the following process: First, the system provides the user with a service interface, calls different services or service portfolios as per user demand for evaluation, and optimizes the called service portfolio to generate the job to be executed. Once generated, the job is decomposed, organized, scheduled, and controlled by our architecture, and the final result is fed back to the user. Under the architecture, the job scheduling module receives all the generated jobs and decomposes each job into multiple parallel subjobs via the parallel job controller. Then, the intelligent scheduling module assigns one or more virtual resources on the platform to each subjob and controls the execution of each subjob. The entire flow is illustrated in Figure 6.

3.3. Sensor and Networked IPS Modeling Based on Domain Ontology. Domain ontology, an important type of ontology, can provide unique concepts and their relations, the basic principles, and the activities in specific fields. The technical realization of ontologies relies on advanced ontology languages [23]. Currently, several ontology languages are available, such as XML-based ontology exchange language (XOL) and the web ontology language (OWL) derived from OIL and DAML+OIL (XML: extensible markup language; DAML: DARPA agent markup language; DARPA: US Defense Advanced Research Projects Agency; OIL: ontology inference layer).

The field ontology of a single sensor should be built based on clear domain concepts and their relationships. One of the key technical paths for building a macro language library is to establish a standard description of the sensor model by domain ontology.

The single sensor model can be formally depicted as

$$S_i = \{\text{Id, Name, Category, Function, Inputs, Outputs, Task, and Qos}\}, \quad (3)$$

where Id, Name, Category, Function, Inputs, Outputs, Task, and Qos are identifier, name, sensor type, functional description, inputs, outputs, task, and quality of service, respectively, and i is the system scale. Multiple S_i can be combined by the actual logic of time and space and formed into a stereo regional ocean perception system.

Figure 7 shows the domain ontology of the networked IPS, which describes the concepts and their logical relationships covered by the system. The domain ontology of the networked IPS lays the basis for sharing the knowledge of accurate model depiction and facilitates the unified control of the relevant data.

With the networked IPS modeling as the goal, the knowledge in relevant fields is acquired, described, and represented by the features of domain ontology of sensors: conceptualized, clear, formalized, and shared. The modeling involves multiple construction techniques for the model chain, namely, standard description of sensor model, model verification, model combination, model query, model matching, model management, and model generation.

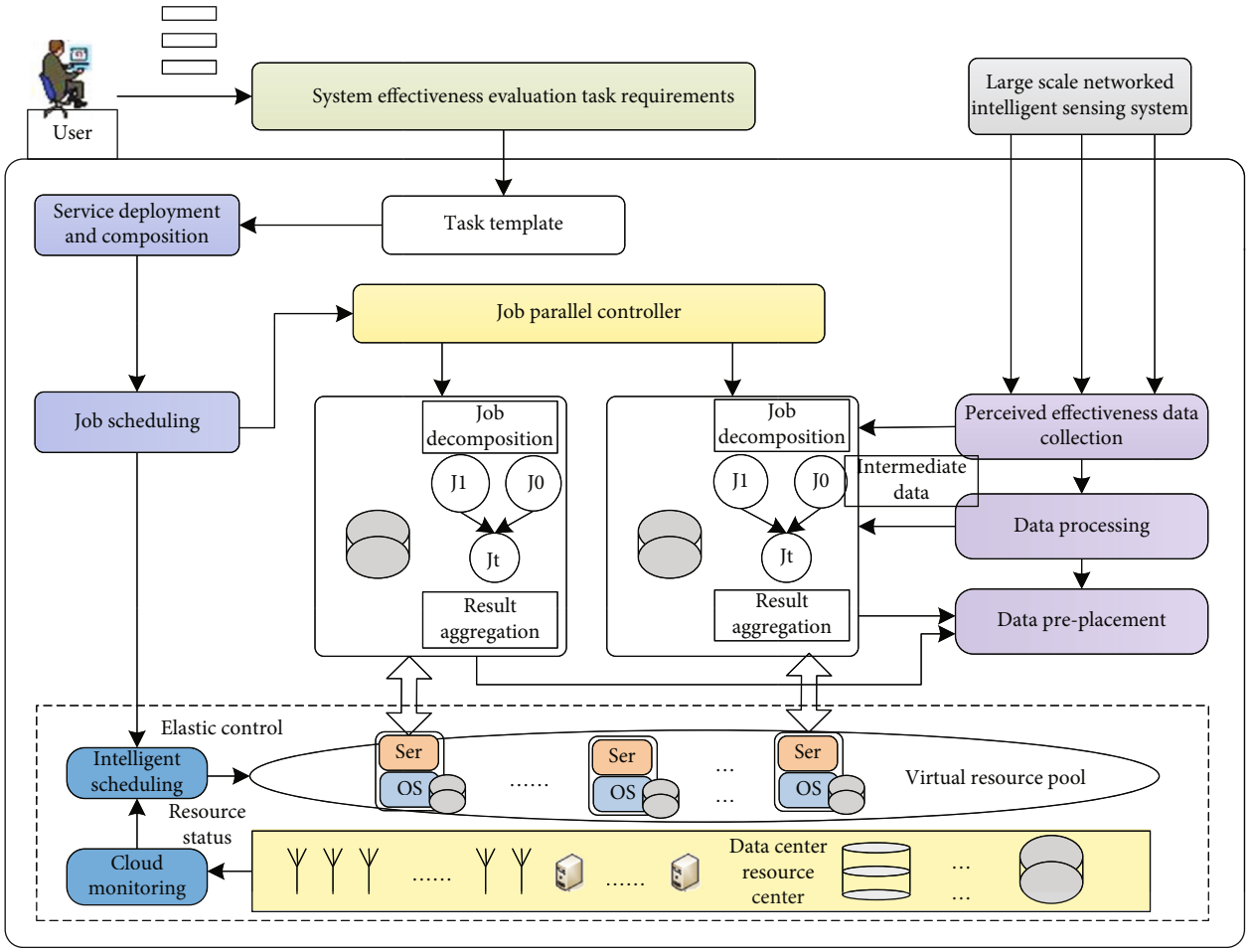

Figure 6: Execution flow of efficacy evaluation task.

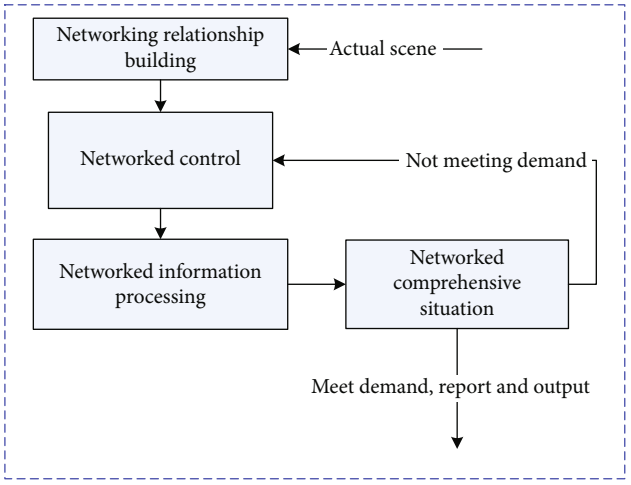

Figure 7: Domain ontology of networked IPS.

The networked IPS model can be formally depicted as

$$NS_i = \{\text{Id, Name, Number, Function, Coverage, Accuracy, Task, and Qos}\}, \quad (4)$$

where Id, Name, Number, Function, Coverage, Accuracy, Task, and Qos are identifier, name, number of sensors, functional description, coverage, data accuracy, task, and quality of service, respectively.

Networked control, as the key and focus of the networked IPS modeling, is established based on the following technologies such as sensor networking, information distribution, information fusion, state/situation awareness, resource scheduling, and network control. The elements of networked control include networking objects, structure, objectives, means, and strategies. The state/situation awareness modeling of the networked IPS mainly requires the description framework and formal modeling method of state/situation awareness knowledge and the knowledge characterization and reasoning technologies for state/situation awareness elements.

The various problems in networked perception, namely, information processing mechanism and flow, data recording and analysis, and system index evaluation, can be solved by accessing multisensor signals and data, functional reorganization, time-space integration, networked control, and networked data processing. As shown in Figure 8, networked control modeling is aimed at establishing the following models: functional reorganization model, multisensor control strategy model, perceptual task model, control model,

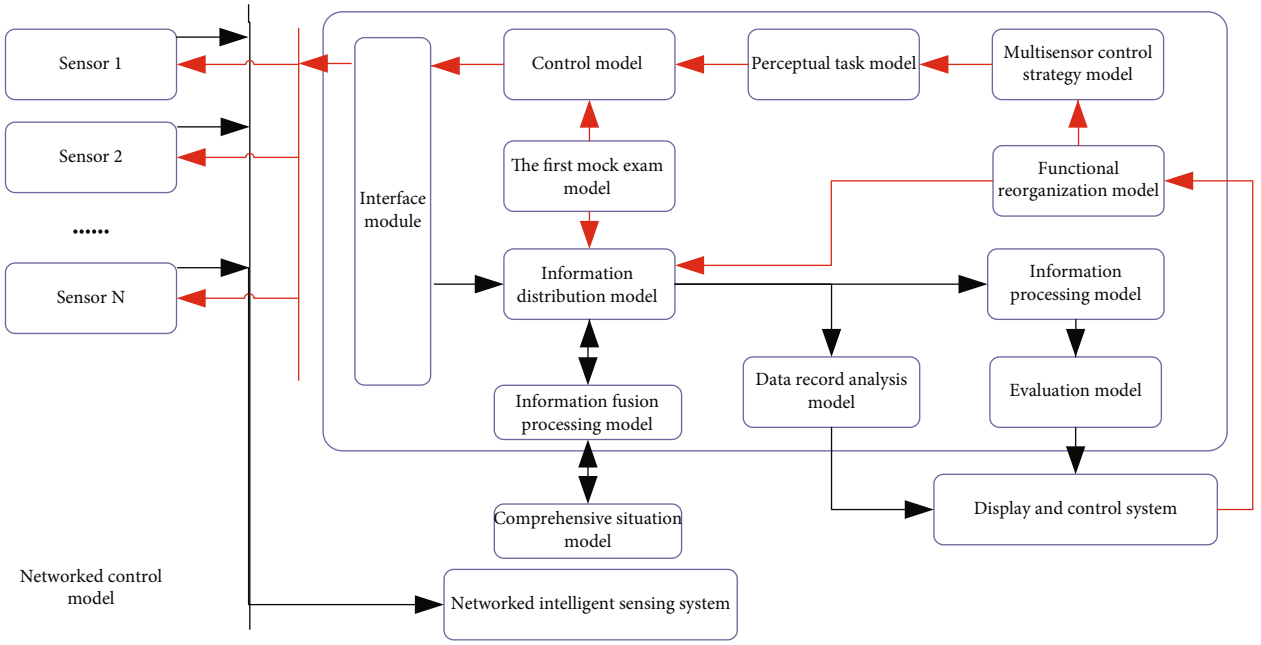

Figure 8: Architecture of networked control model.

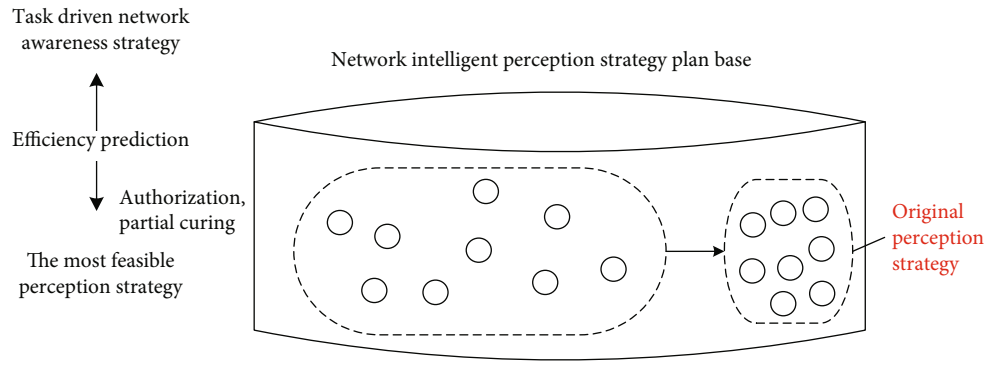

Figure 9: Real-time generation of networked IPS organization strategy based on efficacy estimate.

interface module, the first mock exam model, information fusion processing model, comprehensive situation model, data recording and analysis model, evaluation model, etc.

The model query mainly uses semantic technologies, such as model content analysis/interpretation, knowledge extraction/expression/learning, and reasoning mechanism, to match the information in model resources with the user's demand for model information, with the aim of better satisfying the query demand.

During the modeling of sensors and the networked IPS based on domain ontology, multiple roles are generally involved including perception business modeling personnel, model development personnel, model management personnel, flow planning personnel, and users.

3.4. Rapid Construction of Indices, Automatic Assembly of Methods, and Parameter Acquisition. The EIS for networked IPS efficacy is the basis for depicting and characterizing the attributes of networked perception. Following the principles of building a scientific, complete, and measurable EIS, the efficacy evaluation is divided into performance evaluation, function evaluation, and efficacy evaluation (associated with specific tasks), in view of the different roles of efficacy evaluation in different stages of the networked IPS construction. The EIS of networked IPS efficacy covers index value measurement, index weighting, sensitivity analysis, index evaluation, parameter acquisition, etc.

Currently, efficacy is generally evaluated qualitatively, quantitatively, or through both qualitative and quantitative approaches. The mainstream qualitative evaluation method is expert consultation, while the popular quantitative evaluation methods are system effectiveness analysis (SEA) [24], test statistics, and information entropy method. The combination of qualitative and quantitative approaches has been adopted more frequently than qualitative evaluation or quantitative evaluation. The combined approaches include the analytic hierarchy process (AHP), fuzzy analysis, multiattribute decision-making, gray evaluation, and cloud centroid method.

Each evaluation method applies to a specific range of issues. Since a single method has limited applicability, it is important to automatically assemble methods to improve

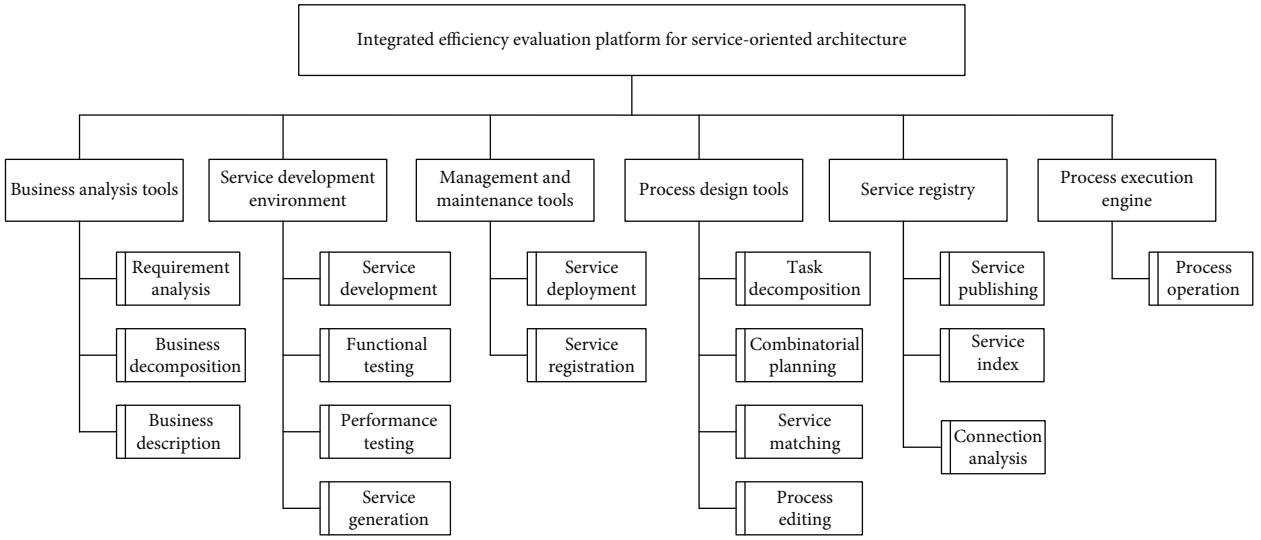

Figure 10: Components of service-oriented prototype platform for integrated system efficacy evaluation.

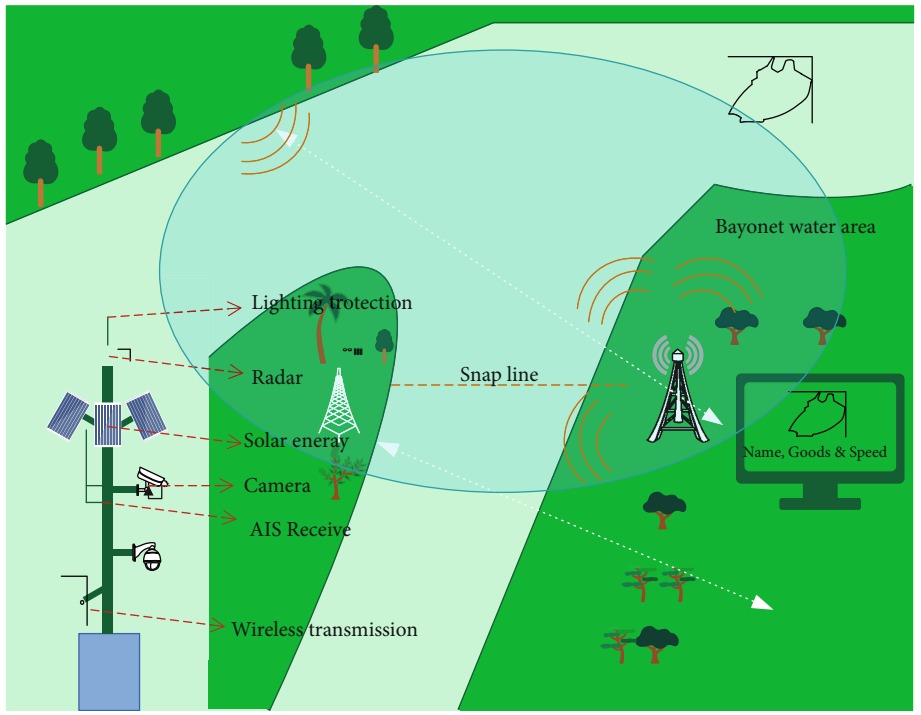

Figure 11: Intelligent sensing system of regional marine fishery environment.

evaluation efficiency and quality. Which method to choose depends on the evaluation task, given conditions, and distribution of efficacy parameters. This is the only way to obtain evaluation results that are satisfactory, scientific, and practical.

For the established EIS of networked IPS efficacy, the data could be collected in real time or not in real time during semiphysical simulation or full physical simulation. The data storage system would save multisource system data into the database and offer data storage, sorting, calling, query, and screening. The preprocessing of evaluation data is designed around the EIS. By removing abnormalities, redundancies, and noises and filling the missing terms, the quality of the collected system data reaches the requirement of the evaluation system. During data processing, the original data are fused, and the precise values of the data are obtained through time-space unification, correlation analysis, and cluster analysis. The processed data are ready to be called by the solving module of the evaluation model.

3.5. Real-Time Generation of Networked IPS Organization Strategy Based on Efficacy Estimate. According to the efficacy estimates of the network IPS obtained from different

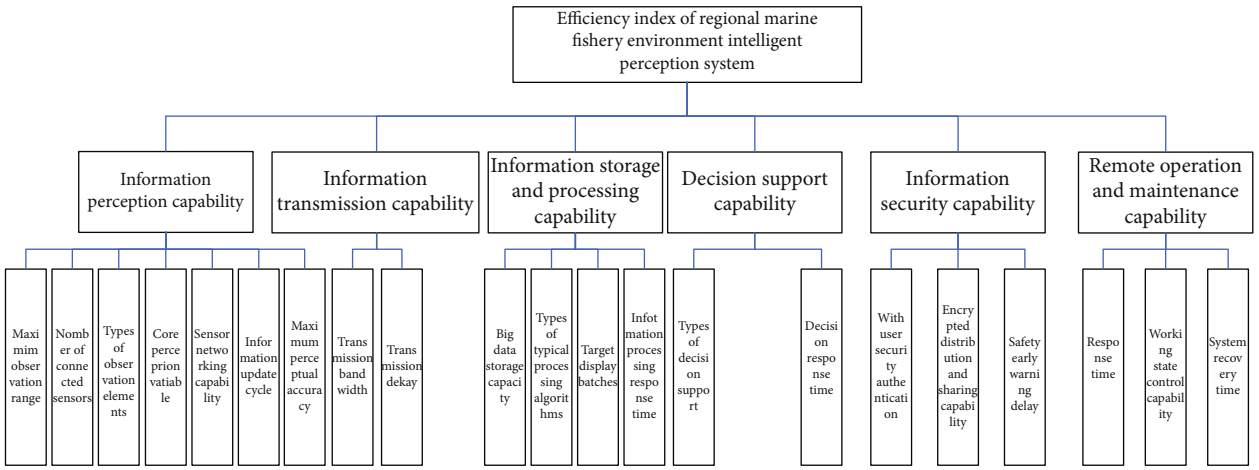

Figure 12: EIS design of regional marine fishery environment IPS.

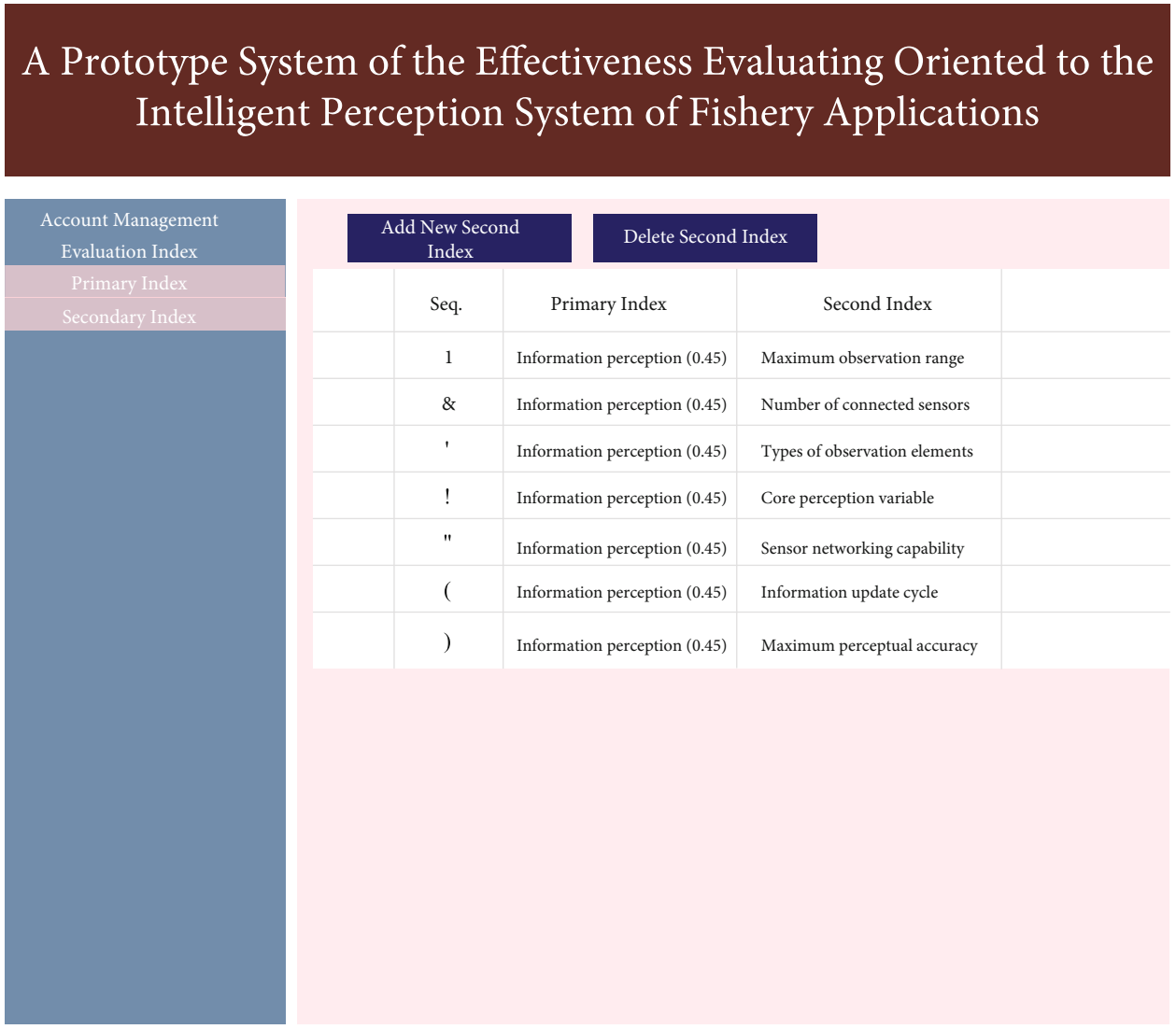

Figure 13: Prototype system of effectiveness evaluation of intelligent perception system in the regional marine fishery environment.

perception tasks,] perception efficacy and organization strategy are optimized iteratively, such that the most feasible networked perception strategy is introduced to the network intelligent perception strategy plan base.

During networked perception, the application effects of networked perception strategy are recorded in real time, perception efficacy and organization strategy are optimized iteratively, and the autonomous learning and automatic adaptation technologies are supplemented continuously. In this way, the networked perception strategy is improved, and more perception knowledge and empirical schemes are saved in the strategy plan base, providing an abundance of strategies for the networked IPS in different scenarios. Then, it is possible to generate perception strategies for different perception tasks (Figure 9).

4. Design Service-Oriented Efficacy Evaluation Platform

The system design is guided by perception demand, top-level design, comprehensive integration, domain knowledge, and real-world situation. According to the proposed novel architecture for efficacy evaluation, the findings of the networked IPS model base, index system, and method base are combined to build a service-oriented prototype platform for integrated system efficacy evaluation. The prototype platform is adopted for the technical realization, verification, and optimization of the findings above to solve the technical problems in real R&D, thereby enhancing the perception ability of the large-scale networked IPS in different scenarios.

Referring to the overall structure of mature platforms, the components of the service-oriented prototype platform for integrated system efficacy evaluation are designed from the perspective of system engineering. The functional modules of the platform include business analysis tools, service development environment, management and maintenance tools, process design tools, service registry, and process execution engine (Figure 10).

Figure 11 shows the regional marine fishery environment IPS under wisdom ocean. The system is aimed at collecting observations of marine objects and environment by using multiple instruments such as radar, photoelectric sensor, and automatic identification system (AIS). The main technical indices of the system include the multigranular stereo perception ability of marine environment, objects, and activities within 40 km, which adopt information from different sensors, and different information is transformed into stranded format data, which can be used to calculate the ability to receive and process the information from multisource sensors: 5 radars, 6 photoelectric sensors, and 5 AISs.

Based on our results on index design, method assembly, and efficacy prediction, this paper chooses information perception capacity, information transmission capacity, information storage and processing capacity, decision-making support capacity, information security capacity, and remote operation and maintenance capacity as primary evaluation indices and breaks them down into secondary indices (Figure 12). On this basis, a prototype platform of service-oriented integrated efficacy evaluation is developed to verify our research findings (Figure 13).

The research results can apply to the overall demonstration, design, joint debugging, and efficacy evaluation of the large-scale networked IPSs under the SES, such as smart city IPS and wisdom ocean IPS.

5. Conclusions

This paper mainly explores the efficacy evaluation of the large-scale networked IPS under the SES. The efficacy evaluation research starts from and is supported by the conceptual system, which mainly consists of the connotation or denotation, meaning, flow, criteria, and environment of efficacy evaluation. The evaluation architecture is studied to guide the top-level design of efficacy evaluation, so as to satisfy the demand for efficacy evaluation of the large-scale networked IPS under the SES. The model base, as the foundation and core of efficacy evaluation environment, depicts and illustrates the attributes, features, and laws of sensors and the networked IPS. Our model base mainly includes the single-sensor model and the networked IPS model, both of which are developed based on domain ontology, as well as model organization and management technology. In addition, the keys of efficacy evaluation environment, i.e., EIS and evaluation methods of efficacy, are investigated in detail. On this basis, the various elements of the efficiency evaluation system are synthesized into a service-oriented integrated physical efficacy evaluation platform, which encompasses such components as task scenes, model base, index base, method base, and display control. The physical platform provides an important tool to verify and realize our efficacy evaluation strategy, enhance the capacity of the networked IPS, and support the construction of such a system. The future research will further verify our system through semi- and full physical simulations and provide a computing environment in support of the efficacy evaluation of the large-scale networked IPS under the SES.

Data Availability

The data used to support the findings of this study are available from the corresponding author upon request.

Conflicts of Interest

The authors declare that they have no conflicts of interest.

References

[1] S. L. Yang, "Intelligent manufacturing of high-end equipment in industrial internet era," *Wisdom China*, vol. 2019, no. Z1, pp. 72–74, 2019.

[2] B. Tarchoun, A. B. Khalifa, S. Dhifallah, I. Jegham, and M. A. Mahjoub, "Hand-crafted features vs deep learning for pedestrian detection in moving camera," *Traitement du Signal*, vol. 37, no. 2, pp. 209–216, 2020.

[3] L. Chao, H. Lei, and S. Yunkui, "Deployment framework for distributed applications in cloud computing," *Computer Technology and Development*, vol. 28, no. 6, pp. 12–16, 2018.

[4] X. L. Zhang, J. H. Yang, X. Q. Sun, and J. P. Wu, "Survey of geo-distributed cloud research progress," *Ruan Jian Xue Bao/ Journal of Software*, vol. 29, no. 7, pp. 2116–2132, 2018.

[5] X. Li, C. Lin, and X. P. Xu, "A target tracking model for enterprise production monitoring system based on spatial information and appearance model," *Traitement du Signal*, vol. 36, no. 4, pp. 369–375, 2019.

[6] D. S. Miao, "'Shili', 'shili' system engineering and science of 'shili'," *Journal of Systems Science*, vol. 27, no. 1, pp. 32–40, 2019.

[7] Y. Hou, Z. J. Cao, and S. L. Yang, "Cloud intelligent logistics service selection based on combinatorial optimization algorithm," *Journal Europeen des Systemes Automatises*, vol. 52, no. 1, pp. 73–78, 2019.

[8] Z. B. Xu, Z. Y. Fen, X. H. Guo, D. J. Zeng, and G. Q. Chen, "Frontier topics of management and decision-making driven by big data," *Management World*, vol. 11, pp. 158–163, 2014.

[9] G. M. Suleiman, M. K. Younes, M. Ergun, and K. A. Omari, "Effect of transportation parameters on traffic accident in urban areas comparison study of ANFIS with statistical analysis," *International Journal of Safety and Security Engineering*, vol. 11, no. 2, pp. 129–134, 2021.

[10] J. Hua, L. Deng, and C. Z. Zhang, "Evolutionary mechanism of public participation in the social stability risk assessment of large construction project decision based on self-organization theory," *Journal of Systems Science*, vol. 25, no. 2, pp. 46–50, 2017.

[11] D. R. Li, Y. Yao, and Z. F. Shao, "Big data in smart city," *Geomatics and Information Science of Wuhan University*, vol. 6, pp. 631–640, 2014.

[12] Y. Wang, "Moving vehicle detection and tracking based on video sequences," *Traitement du Signal*, vol. 37, no. 2, pp. 325–331, 2020.

[13] A. G. Zhang, W. Q. Fan, and Y. Y. Zhang, "Cloud computing model for intelligent transportation systems: a case study of Shenzhen," *Urban Transport of China*, vol. 17, no. 3, pp. 48–52, 2019.

[14] J. Liu, H. Li, and B. Huang, "Convex combination-based consensus analysis for intuitionistic fuzzy three-way group decision," *Information Sciences*, vol. 574, no. 1, pp. 542–566, 2021.

[15] F. Tao, Y. Zuo, and L. Xu, "IoT-based intelligent perception and access of manufacturing resource toward cloud manufacturing," *IEEE Transactions on Industrial Informatics*, vol. 10, no. 2, pp. 1547–1557, 2014.

[16] J. Liu, H. Li, and X. Zhou, "An optimization-based formulation for three-way decisions," *Information Sciences*, vol. 495, pp. 185–214, 2019.

[17] W. J. Yu, Y. Li, Y. G. Xu, and J. Wang, "Design of cyber—physical system architecture for smart factory," *Modern Electronics Technique*, vol. 40, no. 5, pp. 151–154, 2017.

[18] S. J. Li, "Research on a two - way drive mechanism for intelligent agricultural development," *Science and Technology Management Research*, vol. 39, no. 10, pp. 85–90, 2019.

[19] X. Y. Jiang and D. L. Pan, "Suggestions on the development of the Smart Ocean in China," *Marine Information*, vol. 1, pp. 1–6, 2018.

[20] G. S. He and J. Li, "Top-level design framework for national marine informatization," *Marine Information*, vol. 1, pp. 11–16, 2018.

[21] J. Cheng and C. Z. Du, "An investigation of wisdom city system engineering," *Journal of CAEIT*, vol. 3, pp. 234–238, 2014.

[22] Z. J. Lu, X. Liu, Y. G. Qin, Y. Pan, J. G. Guo, and S. Huang, "An adaptive multi-sensor management method for cooperative perception," *Journal of CAEIT*, vol. 12, no. 4, pp. 353–358, 2017.

[23] Z. P. Tong and X. Liu, *Integrated Electronic Information System—Mainstay of Information Warfare (Second Edition)*, National Defense Industry Press, Beijing, 2008.

[24] N. Ma, X. Wang, and E. Hu, "Evaluation of input-output efficiency of medical postdoctoral research (work)station based on DEA model," *Forum on Science and Technology in China*, vol. 3, p. 9, 2021.

Hindawi
Journal of Sensors
Volume 2022, Article ID 8223590, 13 pages
https://doi.org/10.1155/2022/8223590

Research Article

Intelligent Measurement and Monitoring of Carbon Emissions for 5G Shared Smart Logistics

Ailing Zhang,[1] **Sha Li**,[1] **Lin Tan**,[1] **Yingchao Sun**,[2] **and Fuxiao Yao**[1]

[1]*Shandong Vocational and Technical University of International Studies, Rizhao Shandong 276800, China*
[2]*Qingdao Administrative Service and Public Resources Trading Center, Qingdao, Shandong 266071, China*

Correspondence should be addressed to Ailing Zhang; ailing.zhang@cumt.edu.cn

Received 23 November 2021; Revised 17 December 2021; Accepted 21 December 2021; Published 12 January 2022

Academic Editor: Gengxin Sun

With the upgrading of logistics demand and the innovation of modern information technology, the smart logistics platform integrates advanced concepts, technologies, and management methods, maximizes the integration of logistics resources and circulation channels, and effectively improves the efficiency of logistics transactions, but its energy consumption problem is particularly prominent. The study of intelligent measurement and monitoring of carbon emissions in smart logistics is of great value to reduce energy consumption, reduce carbon emissions in buildings, and improve the environment. In this paper, by comparing and analyzing the accounting standards of carbon emissions and their calculation methods, the carbon emission factor method is selected as the method to study the carbon emissions of the smart logistics process in this paper. The working principle of each key storage technology in the smart logistics process is analyzed to find out the equipment factors affecting the carbon emission of each storage technology in the smart logistics process, and the carbon emission calculation model of each key storage technology is established separately by using the carbon emission factor method. Meanwhile, according to the development history of energy consumption assessment, the assessment process of different stages from logistics storage energy consumption assessment to smart logistics energy consumption assessment is analyzed, and based on this, a carbon emission energy consumption assessment framework based on 5G shared smart logistics is constructed. This paper applies the supply chain idea to define the smart logistics supply chain, constructs a conceptual model of the smart logistics supply chain considering carbon emissions, and at the same time combines the characteristics of the smart logistics supply chain to analyze the correlation between the carbon emissions of the smart logistics supply chain and the related social, environmental, and economic systems.

1. Introduction

Smart logistics marked by modern information technology has become an important grasp of the supply-side structural reform of the logistics industry, which can effectively integrate social resources, reduce labor costs, meet the personalized needs of consumers, and realize the wisdom of the logistics industry upgrade; energy is the engine and power of human economic development but also an important support for modern social civilization. Historically, with the development of human society and lifestyle changes, all the energy required by humans is increasing [1]. The integration of intelligent carbon emission measurement and monitoring in the process of 5G shared smart logistics ensures the highest utilization of resources, the least impact on the surrounding environment, and the greatest overall benefits in the entire life cycle of smart logistics, including product design, product logistics, component assembly, product use, end of life, recycling, and relogistics.

In this paper, the narrow definition of shared intelligent logistics energy consumption assessment refers to the assessment of the degree of energy consumption by integrating the whole life cycle of shared intelligent logistics of products into the service industry, with the whole life cycle of services as the mainline; its broad definition refers to the assessment of the energy consumption of shared intelligent logistics in each stage of the whole life cycle of services and the waste emissions, time spent, and energy flow involved in the

dynamic tracking, and the assessment is aimed at high-quality and low-consumption logistics process, energy-saving and emission reduction process, and optimal remaining service life to improve the production efficiency and material utilization [2]. The assessment process of energy consumption such as this lacks research on the comprehensive assessment of energy consumption of logistics services throughout the life cycle with the assistance of IoT, big data, digital twin, and other high technologies, and its assessment methods are typically characterized by singularity assessment, process assessment, and fragmentation assessment. Among them, singularity refers to the singularity of the energy consumption assessment method, and the core of the assessment method is mainly the establishment of mathematical models and simulation and calculation based on energy consumption data, etc.; process refers to the fact that the assessment process has a certain time interval and cannot reflect the instantaneous energy consumption of this logistics service comprehensively; fragmentation refers to the fact that the current energy consumption assessment mainly considers the output energy consumption of machinery in the physical space alone or in the information. The modeling, simulation, and prediction of each phase of logistics are cut off in the information space, and there is a lack of efficient collaboration between the whole life cycle of logistics services and energy consumption assessment in the information space and a lack of interaction and integration of physical space and information space [3]. By increasing the investment in ecological compensation, the whole supply chain is changed. Due to the compensation policy and capital investment, the carbon emission of the production link is reduced through green raw materials, order-based production, and energy-saving manufacturing, the carbon emission of the storage link is reduced through green packaging and energy-saving storage and direct sales by manufacturers, and the carbon emission of the recycling wisdom is reduced through the optimization of transportation methods and transportation paths. The total carbon emission of the smart logistics supply chain will be reduced by optimizing the transportation method, optimizing the transportation path, and reducing the recycling of smart materials. By comparing and analyzing the accounting standards of carbon emissions and their calculation methods, the carbon emission factor method is selected as the method to study the carbon emissions of the smart logistics process in this paper. The working principle of each key storage technology in the smart logistics process is analyzed to find out the equipment factors affecting the carbon emission of each storage technology in the smart logistics process, and the carbon emission calculation model of each key storage technology is established separately by using the carbon emission factor method. This paper also analyzes the influencing factors of carbon emissions in the logistics process through the study of carbon emissions of storage technologies in the process of shared smart logistics and provides some basis for the development of energy-saving and emission reduction measures in shared smart logistics.

2. Related Work

The smart logistics platform emerges under the two-way drive of the changing demand for logistics services and the update of modern information technology such as the Internet, big data, and cloud computing, which provides intelligent modern logistics services to users by integrating groups related to logistics services such as cargo owners, vehicle owners, and storage enterprises. Kuru and Ansell constructed a basic framework of a big data cloud computing-based smart logistics platform consisting of a supply subsystem, demand subsystem, and supervision subsystem [4]. Piovesan et al. proposed to integrate and fuse modern information technology such as cloud computing with traditional logistics information systems and build a "smart cloud logistics" platform system with intelligent decision-making and automatic distribution to solve the logistics problems of e-commerce [5]. The literature [6] outlines the functional planning, target planning, and system framework design of the intelligent logistics platform and gives specific implementation methods. The literature [7] analyzed the construction needs of logistics platforms under cloud computing and constructed a logistics platform framework and functional components of logistics platforms consisting of a cloud platform layer, cloud application layer, and cloud management layer. Logistics platforms were classified according to national, provincial, municipal, and regional levels, and the operation modes and functions of different types of platforms were analyzed. The literature [8] analyzed the operation mechanism of the smart logistics platform based on the bilateral market theory, detailing the platform's incentive mechanism, pricing mechanism, and other operational mechanisms. Lu et al. [9] proposed a functional structure model of a regional logistics information platform and analyzed the role played by the platform in liaising with the government and enterprises. [10] proposed a conceptual model of a smart logistics distribution platform. Matthew [10] proposed a conceptual model of a smart logistics and distribution platform, analyzed the value creation process of the platform stakeholders, and pointed out that the logistics and distribution platform will become a new solution to the logistics and distribution problem. The literature [11] evaluated the business model of traditional logistics information platforms based on the unconfirmed measure of information entropy and other methods, and the results showed that the traditional logistics information platform business model has a single profit model, insufficient standardization of logistics information, and other problems.

The assessment of energy consumption is a key aspect of green logistics, which requires the integration and fusion of energy consumption data in the virtual and physical space to be considered based on the whole life cycle energy consumption data to provide services and applications for energy consumption assessment. As the traditional method of energy consumption assessment ignores the external environment, equipment performance, processing and transportation, and internal environment of materials in use process at different stages of logistics services, it cuts the virtual space and physical space of the assessment process, making it difficult to interact and connect data and information in real time, resulting in the current energy consumption assessment mainly considering the output energy consumption of machinery in the physical space alone or cutting the

information space. The modeling, simulation, and prediction of each stage of logistics services are not available, and there is a lack of efficient collaboration between the whole life cycle of logistics services and energy consumption assessment in the information space, as well as a lack of real-time interaction and integration between the physical space and the information space, while the carbon emission measurement and assessment based on shared intelligent logistics have greater advantages. Evans and Horak introduce a new global optimization algorithm and propose a green logistics-themed service portfolio as well as multiple data integration and sharing techniques, which provide the conditions for data integration to form a green BOM [12]. The literature [13] researched and developed a new energy estimation framework for calculating energy consumption in the product life cycle and various production processes, which can be extended to different logistics domains and customized for users. Literature [14] developed a new energy estimation framework for calculating energy consumption in the product life cycle and various logistics processes and proposed a requirement for a computational framework for evaluating energy consumption for full product life cycle integration with CAD/CAM systems. Aamir et al. illustrate how simplified design, modeling, and simulation can support the study of life cycle assessment frameworks by reviewing case studies that provide preliminary estimates for material consumption data [15]. The literature [16], on the other hand, presents a methodology for measuring energy efficiency and ecological footprint metrics for product design, modeling, and estimating the total energy consumption of a product based on its various logistical characteristics. Using a probabilistic approach, the literature [17] proposed an energy consumption method on a sequence of relogistics processes. Anser et al. developed a modular simulation model describing a multivariate production system under heterogeneous energy inputs after considering the interdependencies in the production process [18].

3. 5G Research Hypothesis for Value Creation in Shared Smart Logistics

3.1. Building 5G Shared Smart Logistics Based on the Ecological Value. The intelligent logistics enterprise is the main body of logistics value creation, which provides logistics services for customers through basic activities to achieve profitability and thus create economic value. The realization of economic value is often accompanied by the destruction of the ecological environment, leading to the reduction of ecological value, which is one of the drawbacks of traditional logistics development. Then, while creating economic value, it is necessary to maintain the ability of the enterprise to create ecological value, make the two develop in coordination, and consider the economic value of forest land resources.

Taking the conflict between value and ecological value as an example, the path to internalizing external economy into the coordinated development of both forest land owners' benefits is elaborated from the perspective of the public easement, and the path to the coordinated development of logistics economic value and ecological value is to build a smart logistics system. From the perspective of packaging, smart logistics recommends the packaging size suitable for goods through intelligent packaging technology, uses environmentally friendly materials and electronic face sheets, and implements the promotion of shared express boxes to reduce the waste of logistics packaging, improve the efficiency of packaging utilization, and realize green packaging to improve the ecological value creation ability of enterprises in the packaging link. From the perspective of transportation and distribution, the route is optimized through advanced logistics technologies such as big data and cloud computing to improve the efficiency of transportation and distribution such as vehicle scheduling and cargo monitoring, increase the actual loading rate of vehicles, reduce cargo and energy consumption, and increase the ecological value of the company's transportation and distribution links , so as to realize green transportation and distribution. From the perspective of warehousing, the intelligent warehousing system optimizes warehousing space and inventory and handles special items appropriately to avoid out-of-home situations. From the perspective of warehousing, a series of automated and mechanized equipment is used to load, unload, and sort goods, improve logistics efficiency, reduce labor costs, enhance the ecological value of the enterprise in the process of loading and unloading, and realize green loading and unloading. From the perspective of distribution processing and information service, we improve the efficiency of distribution processing through process optimization and intelligent management and collect, filter, analyze, and utilize logistics information to improve the overall operational efficiency of logistics and realize green distribution processing and information service to improve the ecological value creation ability of enterprises in distribution processing and information service [19]. The process of ecological value creation of intelligent logistics enterprises is shown in Figure 1.

The increase in economic value is the basic goal pursued by every enterprise, and the only way for logistics enterprises to achieve the increase in economic value is to improve their service quality, to improve customer satisfaction; in addition, the ability to save resources, on the one hand, can reduce the operating costs of enterprises and, on the other hand, can reflect the social responsibility of logistics enterprises and establish a good corporate image. The establishment of the corporate image can lay the foundation for long-term development in the future and can continue to bring economic value added to the enterprise. The formation of cost control advantages for the entire logistics industry has epoch-making significance, and intelligent logistics enterprises through the wisdom of technology achieve the optimization of the logistics business process, reduce the work pressure of managers at the same time, and reduce the management costs. Strengthen the effective docking between government departments and between government and enterprises to improve the efficiency of policy implementation and implementation; the level of specialized organization scale in the hub city has a low significance on the impact of comprehensive logistics service capacity in the hub city. However, with the expansion of the logistics demand market, the cost of energy consumption of logistics

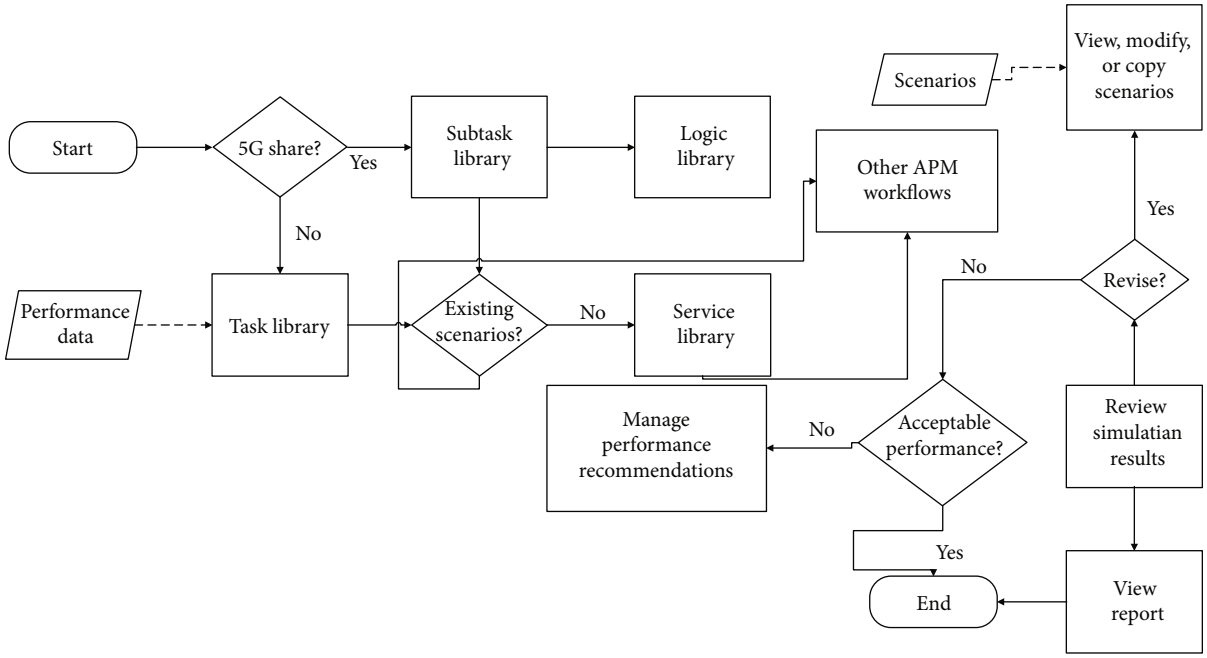

Figure 1: 5G shared intelligent logistics ecovalue creation.

enterprises is also rising year by year. The cost control advantages pursued by the intelligent logistics enterprises do not only stop at the reduction of management costs but also stop at the consumption of source costs. In addition, the reduction of the cost of intelligent logistics enterprises to save more liquidity for the development of the enterprise itself, which is conducive to intelligent logistics enterprises to invest more funds in the research and development and application of technology, and the development and successful application of new technologies will further reduce the cost of enterprises and promote the formation of cost control advantages, thus constituting a virtuous circle.

Smart logistics enterprises occupy a place in the market competition under cost control advantages and innovative technology research and development to achieve more value creation; the reduction of enterprise costs brings more intuitive feelings to customers—the reduction of perceived costs and the increase in perceived value, which in turn improves customer satisfaction with smart logistics enterprises [20]. Both the enterprise itself and the customer, through the construction of the cost control advantage, thus realize the value creation of both sides. The cost control advantage can promote the enterprise value creation ability through the indirect role, while the information platform advantage can pull the enterprise value creation through the direct role; secondly, the low-value creation ability is closely related to the business ability; the stronger the business ability, the stronger the enterprise value creation ability, so the business ability advantage is the key to support the enterprise value creation; finally, the operating environment advantage not only promotes the formation of other advantages but also provides a guarantee for the improvement of the overall value creation ability of the enterprise. Through the cultivation of cost control advantage, information platform advantage, business capability advantage, and operation environment advantage, the value addition of enterprise ecological value, brand value, customer value, and economic value will be gradually realized. The construction of an information platform is the key to building the competitive advantage of intelligent logistics enterprises, since both the enterprise and other stakeholders in the supply chain rely on the convenience brought to them by the platform [21]. First of all, the information platform crosses the spatial obstacle; the original idle logistics resources are integrated and used to improve the overall supply chain and service efficiency, which includes logistics facilities and equipment, logistics network and the community, schools, convenience stores, and other social resources together. Secondly, information sharing becomes the most important function of the information platform. Through the information platform, all participants in the supply chain cooperate and transfer information among enterprises, which alleviates the original "information island" phenomenon among enterprises and helps to improve the overall efficiency of the supply chain and the efficiency of enterprise services, thus realizing value addition. In addition, customers can also experience better logistics services with the help of the information platform, such as real-time understanding of the status of cargo transportation, real-time updating of transportation information, and door-to-door pickup of goods, to meet the diversified needs of customers and ultimately achieve the goal of customer satisfaction, improve the competitiveness of enterprises in the market, and promote value addition.

3.2. Regression Model Construction for Shared Smart Logistics. The fuzzy Borda method adopted in this paper is a method of evaluating single evaluation methods after combining the final scores and rankings derived from each evaluation method based on multiple single evaluation models.

In this paper, entropy and gray correlation methods are mainly selected to evaluate and calculate six smart logistics enterprises, respectively, and finally, the fuzzy Borda method is used to combine the entropy and gray correlation methods to combine the two evaluation results and finally combine them into a new evaluation model. Virtual space energy consumption-related data specifically includes logistics unit energy consumption simulation data, product logistics energy consumption prediction data, enterprise energy consumption prediction data, logistics energy consumption prediction data, product life cycle energy consumption data, etc.

The concept of entropy is derived from thermodynamics, and it is a measure of the degree of disorder in a system [22]. It can be used to determine the degree of dispersion of an indicator by calculating the magnitude of the entropy value. The smaller the entropy value is, the greater its dispersion degree is and the greater the weight of the indicator in the comprehensive evaluation. The specific steps are as follows.

(1) Construction of the data matrix

Define the matrix as

$$\begin{pmatrix} a_{11} & \cdots & a_{1n} \\ \vdots & \ddots & \vdots \\ a_{m1} & \cdots & a_{mn} \end{pmatrix}. \tag{1}$$

X_{ij} is the value of the jth indicator of the ith evaluation object, where $i \in (1,\cdots,n)$, $j \in (1,\cdots,m)$

(2) Calculate the weight of each evaluation object in indicator j

$$K_{ij} = \frac{\partial^2 \Omega / \partial \mathrm{x} \partial y}{\sum_{i=1}^{n} \sum_{j=1}^{m} x_i y_j} + C, \tag{2}$$

where K_{ij} is the weight of the jth indicator, C is the correction term, and Ω is the rate of change of the total indicator.

(3) Calculation of entropy values for each indicator

$$\eta = -\mu \sum_{i=1}^{n} K_{ij} \Omega_{ij} - \kappa \left| M_{ij} \right|, \tag{3}$$

where η is the entropy value and M_{ij} is the coefficient matrix.

(4) Calculation of indicator weights

$$\varphi_j = \frac{L_j \cdot \sum_{i=1}^{n} x_{ij}}{\sum_{j=1}^{m} L_j}, \tag{4}$$

where φ_j is the indicator weight and L_j is the information redundancy.

(5) Calculate the composite evaluation score for each evaluation subject

$$g^n(x) = \lim_{a \longrightarrow 0} \frac{1}{a^n} \sum \varphi_j \left(L_j - a K_{ij} \right) \binom{n}{k} (-1)^k + C, \tag{5}$$

where $M(x)$ is the electrical resistance of the fiber itself, $p(x)$ is the electrical conductivity, φ is the longitudinal length of the fiber, and A is the cross-sectional area of the fiber. The cross-sectional area A of the prepared rGO fibers varies very little during the tensile deformation process and has relatively little effect on the resistance value. The electrical conductivity $p(x)$ will vary somewhat depending on the rGO coating effect, and the preparation process will be influenced by the ratio of GO solution and the number of times the fibers are impregnated in the GO solution. rGO fibers will remain stable in electrical conductivity after forming and can be considered constant. Thus, the magnitude of the resistance of the ego fiber itself is mainly influenced by the longitudinal length φ, and within a certain range, the resistance value will increase regularly with the production when the fiber is stretched. The above equation only roughly describes some of the factors that cause changes in the resistance of rGO fibers; when the stretching range is too large, the change in resistance does not necessarily show a perfectly linear pattern.

The capacitance is given by the following expression, where C_γ is the capacitance in the ion equivalent circuit, C_μ is the capacitance per unit area, and A is the area directly opposite to the ends of the capacitor.

$$C_\gamma = C_\mu \cdot \int A \cdot M(x) dx. \tag{6}$$

Here, the capacitance of the semiconductor layer at z position in the direction and width dz is defined, and the expression is

$$C_\gamma(z) = C_\mu \cdot \int A \cdot M(x) M(z) dx dz + C_{x0}. \tag{7}$$

After applying a positive gate voltage to an organic electrochemical transistor, a dedoping mechanism is used to describe the carrier concentration in the semiconductor layer: cations from the electrolyte are injected into the semiconductor film (here the cations are the charges on this side of the organic semiconductor layer for the equivalent capacitance in the ionic circuit), and each cation injected into the semiconductor layer fills a hole, which is the hole density K_ρ. According to this mechanism, the expression for the hole density K_ρ in the organic semiconductor layer is given by

$$K_\rho(x,y) = \varphi \sum_{y \in \gamma} \sum_{x \in \chi} \left[p(x,y) \cdot \ln p(x,y) + Ax + Cy \right] + \lambda. \tag{8}$$

Therefore, the doping state is different at each part of the semiconductor layer in the direction x, so here the hole

density at each part of the $K_{\rho\text{all}}$ semiconductor layer is defined as a function of x:

$$K_{\rho\text{all}} = \frac{K_\rho(x,y)}{M(x)} = \frac{\varphi\sum_{y\in\gamma}\sum_{x\in\chi}[p(x,y)\cdot\ln p(x,y) + Ax + Cy] + \lambda}{\varphi\sum_{x\in\chi}[p^2(x)\cdot\ln p(x)] + Ax}. \tag{9}$$

The distribution capacity of the hub city has no significant impact on the scale level of the city's specialized organization, the current logistics network is highly scattered ("fishing net" distribution), various modes of transport coordination are not enough, logistics hubs in promoting industrial division of labor and supply chain synergy integration are not enough, and it is difficult to play the logistics hub agglomeration advantage. Logistics policy has no significant impact on the scale of the city's specialized organization; on the one hand, the number of relevant policies is insufficient, for the scale of the organization, agglomeration development, logistics service capacity, and other policies cannot meet the current requirements of the development of the hub city; on the other hand, the policy is not strong enough; strengthen the effective interface between government departments and government and enterprises, and improve the policy implementation and efficiency. On the one hand, the scale level of logistics organizations in hub cities is not highly specialized; on the other hand, the scale level of logistics organizations in hub cities has not formed an efficient docking channel with logistics service capacity, resulting in a low degree of positive influence.

As shown in Figure 2, the cluster supply chain is a product of the combination of industrial cluster theory and supply chain management, characterized by locality and output, and is a supply chain operation mechanism that expands horizontally based on a single type of supply chain. New business models and service modes in the logistics industry gradually emerge, as well as financing difficulties, excessive transport loads, backward infrastructure construction, and other issues. Cluster supply chain collaboration focuses not only on business cooperation between upstream and downstream enterprises in a single supply chain but also on information resource collaboration between different enterprises in different types of supply chains, so it has the characteristics of both horizontal and vertical integration of supply chains.

The core enterprises are the basis for the formation of individual supply chains, while the synergy between a huge amount of individual supply chains constitutes a more complex supply chain synergy network. Under its leading position in the industry, the core enterprise attracts upstream and downstream enterprises with certain capabilities in adjacent geographic areas to form a vertical supply chain structure. Its strong appeal may come from its strong capital reserve, strong business strength, outstanding resource integration ability, etc. This results in a certain degree of competition among core enterprises in different types of supply chains in a certain region, which negatively affects the effective synergy of clustered supply chains.

4. Intelligent Carbon Emission Measurement and Monitoring for 5G Shared Smart Logistics

The carbon emission assessment framework for 5G shared smart logistics is shown in Figure 3, including the physical entity layer and perception layer in physical space and database layer, assessment layer, and optimization layer in virtual space. Among them, the physical entity layer is the level of feedback and corresponds to the virtual model; the perception layer is used to collect and perceive the service process and energy consumption data of logistics services; the database layer is a collection of databases used to hold multisource heterogeneous data; the evaluation layer includes the process of classification, cleaning, processing, and storage of perceived data, as well as the transformation of ECBOM and the evaluation of energy consumption. The optimization layer effectively realizes the optimization of the carbon emission assessment process and results and gives feedback to the physical devices in physical space in real time.

Traditional extraction of elements of physical space entities focuses on high fidelity with virtual models in a static state in an ideal environment, i.e., under conditions of ambient temperature, humidity, air circulation, rapid human reflection, constant rotational speed at rated power, and normal machine operation. However, real physical space entities are subject to large external influences, making it difficult to ensure the accuracy of prediction results and actual output. With the application of 5G smart sharing technology to the product life cycle, the physical space entity attributes and energy consumption will be mapped into the virtual space with high fidelity and complexity and in real time, thus greatly improving the accuracy of carbon emission assessment.

The sensing layer of carbon emission assessment for 5G shared smart logistics is the collection and acquisition of multisource heterogeneous service process data and energy consumption data based on sensing devices, communication networks, IoT, and manual inputs. Different types of data are acquired in different ways, which can be divided into the perception of fixed data, perception of dynamic data, and complex perception. Among them, the perception of fixed data refers to the acquisition of data such as horizontal and vertical location information in physical space, national standard data, etc., which are fixed for a long time during logistics services, often through scene recognition, SLAM (simultaneous localization and mapping) perception and localization, intelligent collection, manual input, etc. Sensing of dynamic data refers to the flowing data that changes over time throughout the life cycle of logistics services and active monitoring and tracking of data through collaborative control of multiple devices based on the Internet of things, for example, energy consumption data, waste emission data of machinery and equipment, wear and tear of tools, and changes in temperature; in addition to this complex sensing aimed at providing more intelligent, swift, and high-quality logistics services, most of them use expert system energy consumption assessment data fused with traditional mathematical model

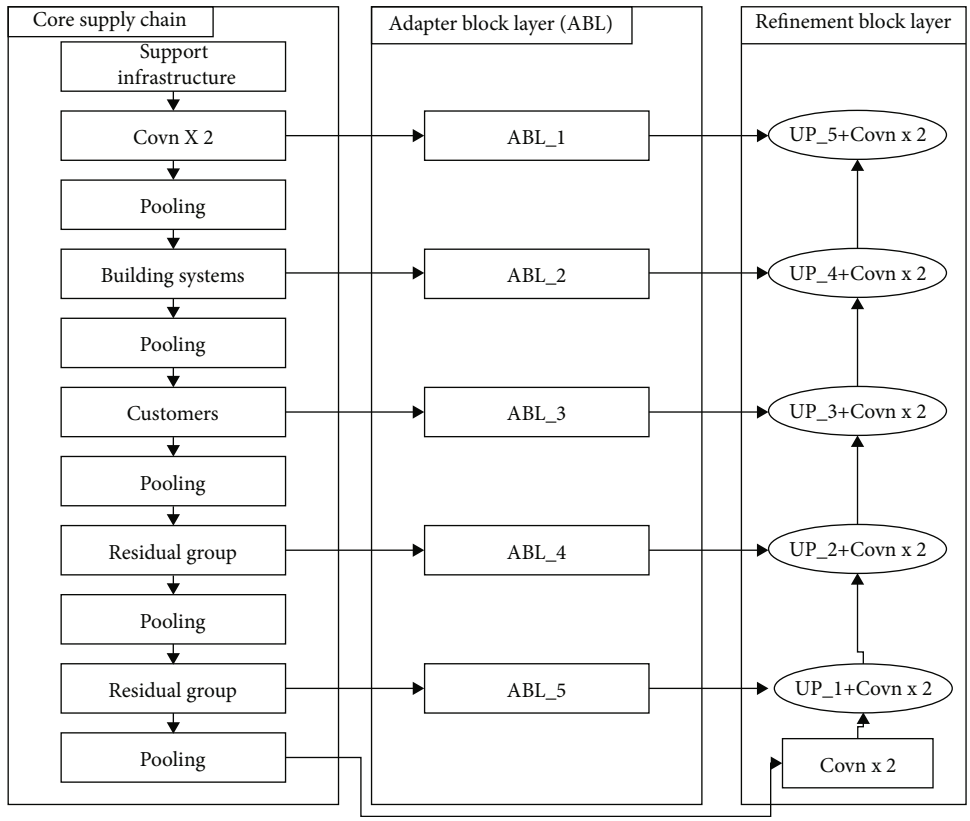

Figure 2: Clustered supply chain collaboration.

data to obtain more accurate and reasonable data. The effective sensing and integration of massive heterogeneous, multidimensional, and multisource data provide data source access methods for the application of digital twin technology, real-time mapping, and carbon emission assessment.

The database layer is the database support for carbon emission assessment for 5G shared smart logistics, which is the process of storing energy consumption-related data involved in the life cycle of logistics services on the cloud platform and is also a collection of all-sided, multiheterogeneous, and complex databases. This database layer is roughly divided into five parts: the collection of physical space data, the collection of virtual space data, the collection of service system data, the collection of fusion data, and the collection of other data. The collection of physical space data is derived from the collection and storage of real-time data in physical space, ephemeral data calls, subjective fuzzy data, etc.; the collection of virtual space data is a collection of models with high-fidelity mapping to physical entities based on the behavior, geometry, rules, etc. of physical space elements; the collection of service system data is a collection of data for energy consumption analysis, energy consumption assessment, and data management within the service system; the collection of fusion data is a collection of data for energy consumption analysis, energy consumption assessment, and data management within the service system. The traditional methods of energy consumption assessment ignore the external environment, equipment performance, processing and transportation, and internal environment of materials in the use process at different stages of logistics services, which cut the virtual space and physical space of the assessment process, making it difficult to interact and connect data and information in real time, resulting in the current energy consumption assessment mainly considering the output energy consumption of machinery in the physical space alone or cutting off in the information space. Modeling, simulation, and prediction of each phase of logistics services lack efficient coordination of the whole life cycle of logistics services and energy consumption assessment in the information space. The collection of fusion data is a collection of intelligent, multifaceted, and real-time evaluation processes based on objective energy consumption, which requires certain learning and self-decision capability to complete high-quality and low-consumption product logistics processes under certain energy consumption standards. This kind of fusion data is also stored in a distributed manner as part of the twin data; the collection of other data is the intellectualized expression of connection rules, interface types, feedback mechanisms, network protocols, optimization algorithms, etc. between different levels. Physical space energy consumption-related data specifically includes logistics unit energy consumption data, logistics service energy consumption data, interenterprise logistics data, product life cycle energy consumption real-time data, material attribute data, water, electricity, and gas and other real-time consumption data, physical space data, human resource data, storage space data, and time-scale data; virtual space energy consumption-related data specifically includes logistics unit

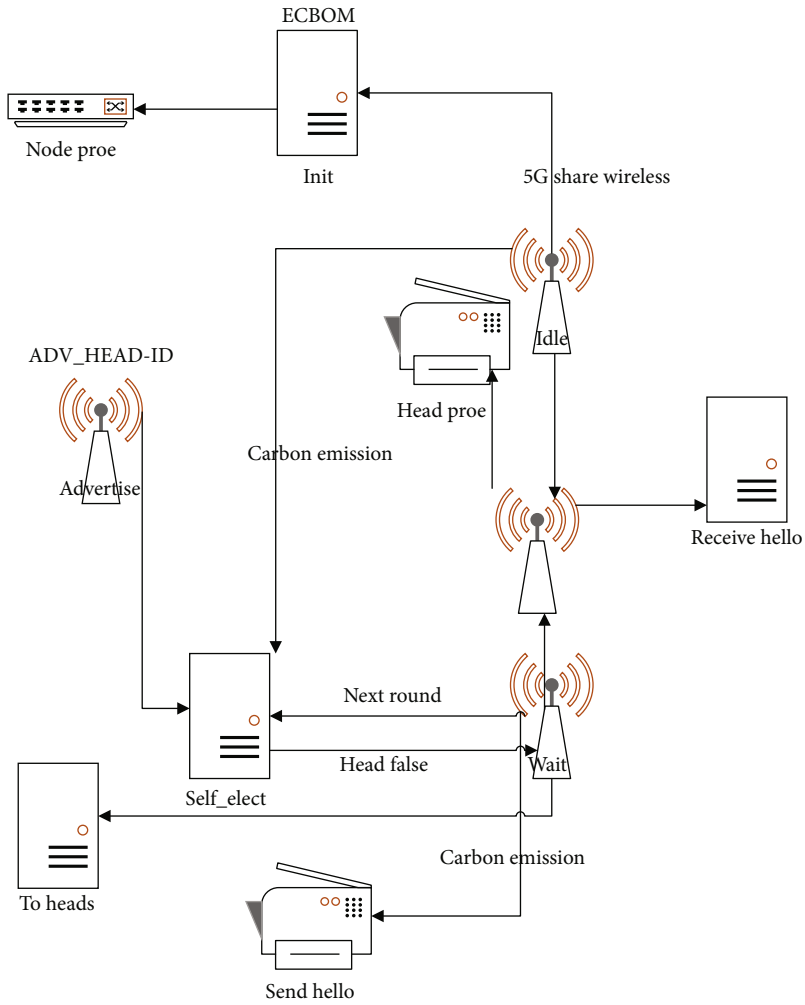

Figure 3: Carbon emission assessment framework for 5G shared smart logistics.

energy consumption simulation data, product logistics energy consumption prediction data, enterprise energy consumption prediction data, logistics energy consumption prediction data, product life cycle energy consumption data, etc.; service system-related data includes real-time energy consumption monitoring service data, energy consumption management service data, product life cycle green design service data, etc.; fusion data includes historical energy consumption optimization data, energy consumption model association fusion data, etc.; other data includes energy consumption source model data, intelligent optimization algorithm data, energy consumption evaluation rule data, etc.

5. Experimental Verification and Conclusion

The system dynamic simulation model of the carbon emission system of the smart logistics supply chain can simulate and predict the operation of the system under different policies and contexts and provide a decision basis and data reference for the low-carbon development of the smart logistics supply chain. By comparing the simulation results of carbon emissions and analyzing the extent of the resulting system changes, the best strategy to reduce carbon emissions of the smart logistics supply chain system can be explored. The relevant experimental analysis in this section will define the current state of carbon emissions of the smart logistics supply chain before the change of influencing factors as the basic model, which will be used as the reference value for comparing the simulation results. Combined with the actual situation of the smart logistics supply chain and the related research status, the simulation analysis of the change of the carbon emission factors of the smart logistics supply chain will be carried out in four aspects: increasing the ecological compensation and treatment investment, reducing the unit energy consumption, reducing the carbon emission of the packaging link, and transforming the transportation structure.

The system dynamic simulation model of the carbon emission system of the smart logistics supply chain can simulate different policies and situations to provide a basis for decision-making to reduce carbon emissions in the smart logistics supply chain. The analysis of the changes of system dynamic elements can not only give the development trend under different situations but also clearly understand the specific amount of changes, which is one of the important advantages of system dynamics for simulation. From Figure 4, it can be seen that the production link, the storage

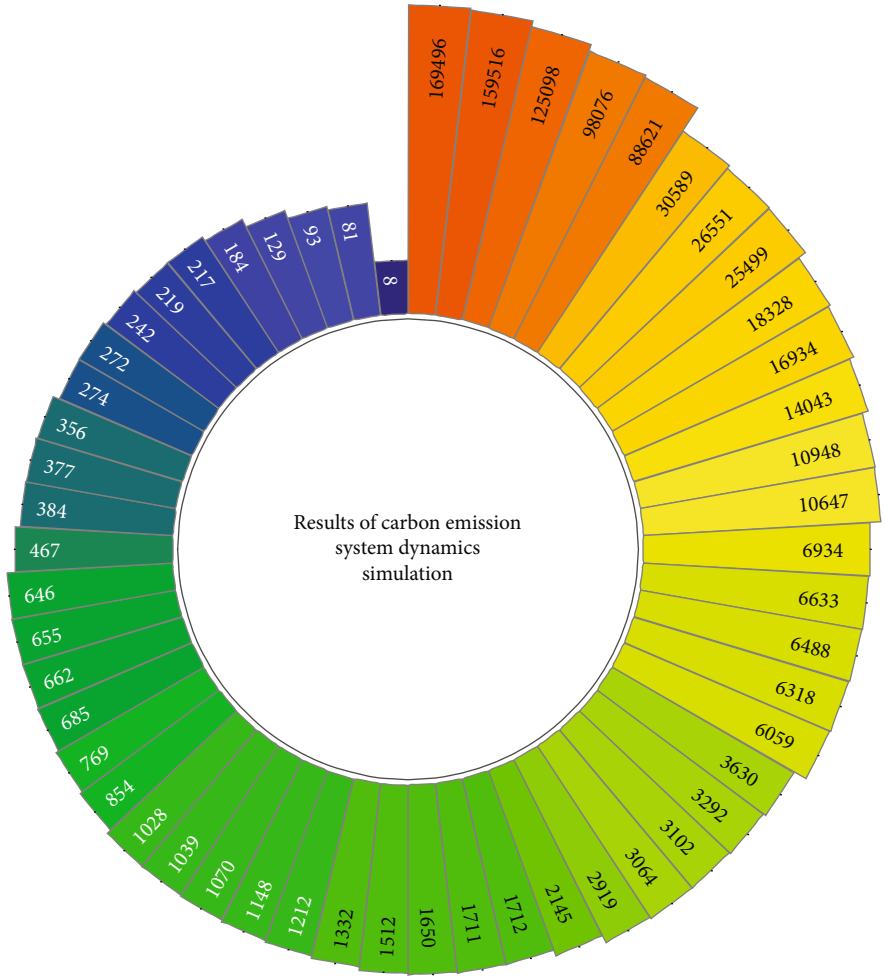

Figure 4: Results of carbon emission system dynamic simulation.

link, and the transportation link are the key links that generate more carbon emissions, so the change analysis of the main adjustable factors that generate carbon emissions will be carried out from these three links to simulate the change analysis of carbon emissions. Based on the actual results of the research and the main problems of this supply chain, the detailed question will analyze the change of factors in four aspects, such as the change of energy in the production chain, the change of storage, the change of transforming transportation structure, and the change of increasing ecological compensation investment. As shown in Figure 4, the changes of each influential element of the logistics chain, such as the use of energy-saving logistics equipment and electrical appliances, while increasing the use rate of clean energy, the use of environmentally friendly raw materials, and the use of environmentally friendly simple design to achieve the effect of improving the utilization rate of marginal materials, improve the production capacity to ultimately reduce the overall carbon emissions or to reduce the carbon emissions per unit of intelligent logistics product.

To achieve the overall goal of energy saving and emission reduction, we can start from the perspective of increasing investment in volatile gas and carbon dioxide control and ecological compensation, through increasing investment in ecological compensation, so those producers can consciously reduce their internal carbon emissions, balance the increased costs within the industry due to the increased use of green equipment and green materials, or give some material or policy compensation to those who participate in energy saving and emission reduction in the smart logistics supply chain. By investing ecological compensation funds, the government will promote institutional and energy reforms, such as the adoption of green raw materials and energy-efficient equipment; order-based production, saving production materials and reducing production waste and inventory redundancy, thus increasing the turnover rate of storage capacity; and transportation, through the vehicle management system to optimize transport routes and distribution vehicles to run more efficiently, reducing the carbon emissions of this link. In the long run, sales of products with low-carbon emissions will increase, and government subsidies will allow companies to produce low-carbon and green smart logistics without cost concerns, which will encourage people to start consuming more and more low-carbon products. Increase ecological compensation investment which is from the side or fundamental to change the carbon emissions of the smart logistics supply chain; from Figure 5, it can be seen that, through the government's ecological

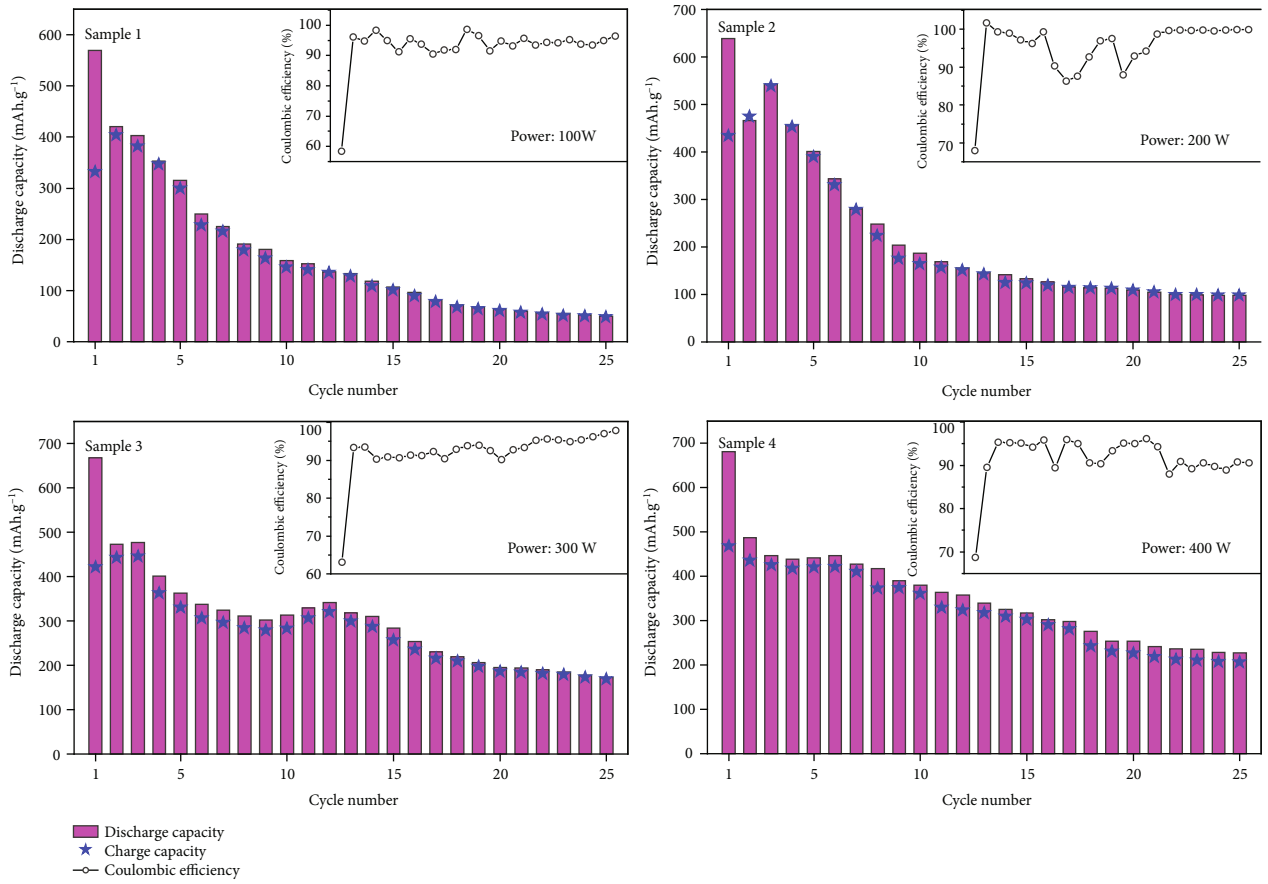

Figure 5: Analysis of the impact of changes in ecological offset investments on carbon emissions.

compensation investment, enterprises will have more part of the capital investment, which is invested in production or procurement or transport links or storage links, which can bring a great effect of emission reduction. By increasing ecological compensation investment, the whole supply chain is changed, due to the compensation policy and capital investment, the carbon emission of the production link is reduced through green raw materials, order-based production, and energy-saving manufacturing, the carbon emission of the storage link is reduced through green packaging and energy-saving storage and direct sales by manufacturers, and the carbon emission of the transportation link is reduced by optimizing transportation methods, optimizing transportation routes, and reducing the recycling of the smart materials to reduce the carbon emission of the transportation link; the total carbon emission of the smart logistics supply chain will be reduced.

The transport sector is a key sector, so it is important to control carbon emissions from transport. Figure 6 shows the analysis of carbon emissions from transport, in which the difference in carbon emissions between different modes of transport can be analyzed, and the least carbon-emitting mode of transport can be used and the price of energy can be increased through a carbon tax to reduce carbon emissions from transport. One of the main focuses of the transport chain should be on optimizing the transport structure. There are many irrational transportation processes caused by the irrational process of the smart logistics supply chain, which increases the carbon emission of the smart logistics supply chain. Reduce the intermediate links and ineffective transportation, and adjust the unreasonable process, to realize the low carbonization of the transportation link of the smart logistics supply chain; promoting the use of clean energy is an important strategy to realize the low carbonization of the transportation link. Clustered supply chain collaboration focuses not only on business cooperation between upstream and downstream enterprises in a single supply chain but also on information resource collaboration between different enterprises in different types of supply chains, so it has the characteristics of both horizontal and vertical integration of supply chains. The smart logistics supply chain involves many large and small transportation processes, and the focus of the transportation link should also be on improving transportation services and optimizing distribution routes. Incomplete transportation services and low quality are a major problem in the development of the intelligent logistics industry. The application of intelligent logistics transportation outsourcing should be promoted, regardless of the distance, it will be handed over to professional logistics companies for transportation, and vehicle scheduling will be carried out by professional logistics companies and professional vehicle information management systems. This can be scientific and reasonable, reduce waste in the transportation process, and achieve carbon reduction. The effect of reducing emissions to promote the use of

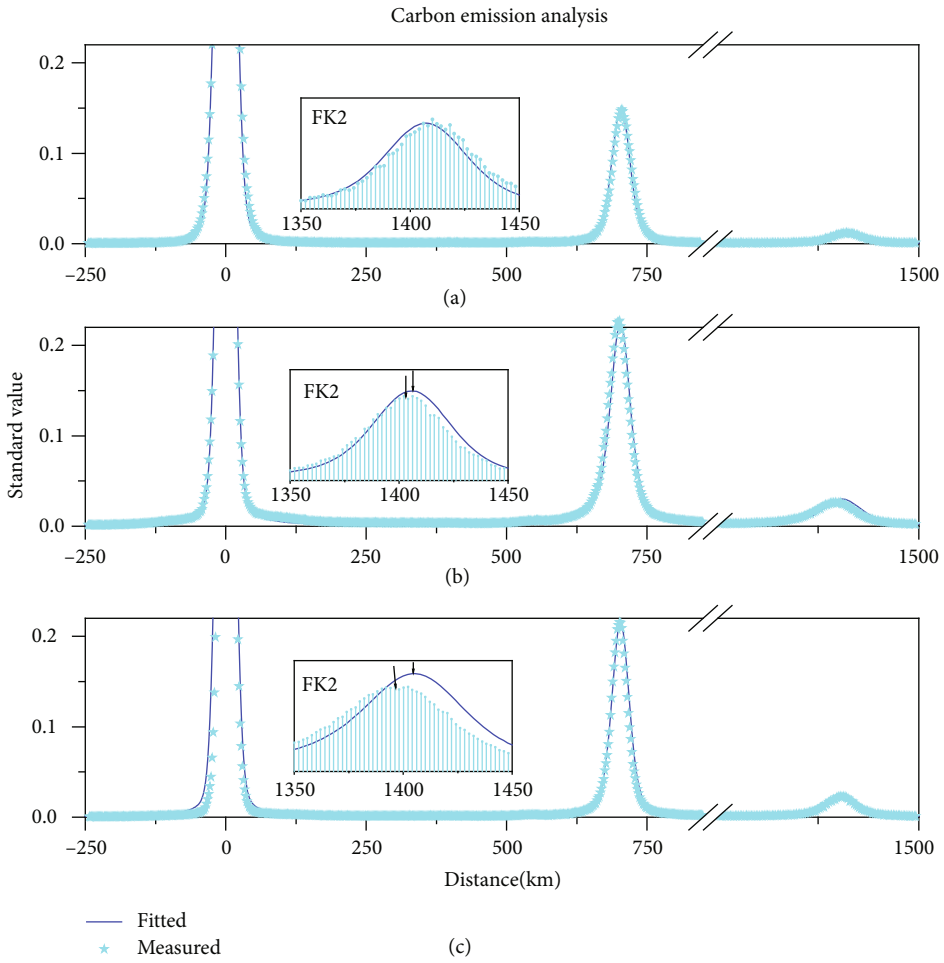

Figure 6: Carbon emission analysis of the transport chain.

clean energy is also an important choice for the low carbonization of the intelligent logistics supply chain.

Transportation, storage, and production link energy and other factors together change, these three links are more carbon emission links, and transportation link adjustment elements are the mode of transport and products with the transport put to improve the full rate, which is the way of change in transport using the same way as the previous section, for storage factors set to the impact of multiple elements: the number of cycles of packaging materials, storage space, lighting equipment, and the results of changes in a variety of elements. Similar to the results of changes in increasing ecological compensation investment, because they are the process of optimizing the overall various key links, with the cost of inputs being different, there will still be some differences in the results; the comprehensive change impact analysis is shown in Figure 7. The influence factors of the three high carbon emission rings, namely, production, warehousing and packaging, and transportation, are integrated, and the change is made comprehensive, and the impact of the change is greatly increased, which can reduce the carbon emission of the three links at the same time and optimize the whole smart logistics supply chain and indeed achieve the effect of reducing the overall carbon emission. The carbon emissions of the production and transportation of the smart logistics supply chain account for 48% and 34% of the carbon emissions of the whole supply chain, respectively, indicating that measuring and controlling the production and transportation of the smart logistics supply chain are the focus of the whole smart logistics supply chain carbon emission measurement, and optimizing the production process is also the key to controlling carbon emissions. Therefore, enterprises should improve energy efficiency, use clean production technology while promoting technological innovation, adopt low energy-consuming production equipment, and implement low-carbon production to create low-carbon smart logistics.

The control of carbon emission of the smart logistics supply chain should pay attention to the development strategy. First of all, we should achieve precise control in the measurement link, choose suitable carbon emission measurement tools, and determine the scope of reducing different greenhouse gas emissions under different environmental performances; adjust the resource structure, transform the development model of the smart logistics industry, and realize green and low-carbon management of the smart logistics supply chain; accelerate product upgrading, comprehensively promote the variety of smart logistics, and comprehensively

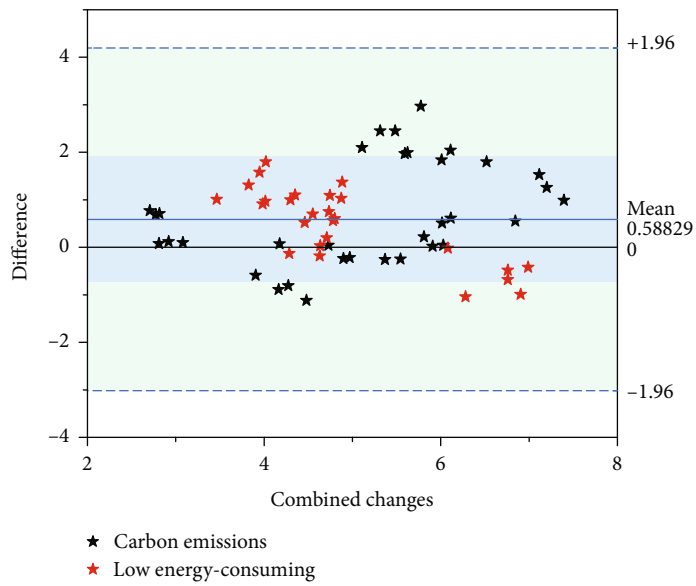

Figure 7: Analysis of the impact of combined changes on carbon emissions.

promote quality and standard improvement; choose low-carbon emission mechanization equipment to optimize the layout of facilities; and implement government subsidies to regulate the contradiction between the consumer and the supplier through the government subsidy mechanism, to achieve a common fight against carbon emission problems among all parties in the supply chain.

6. Conclusion

The logistics industry has entered the track of green development, but it is still in the primary stage. With high pollution and high carbon emission, clean production and low-carbon development are the only ways for the logistics industry, and the study of the carbon emission of the smart logistics supply chain has important theoretical and practical significance for green development and low-carbon economy. To reduce the high-energy consumption and high-carbon emission of the smart logistics industry, the smart logistics supply chain insists on the road of green manufacturing and green production and faces and solves the carbon emission problem of each link together for intelligent development which is the inevitable trend of logistics development. Because intelligence is a typical feature of intelligent logistics, it will continue to improve with the development of artificial intelligence technology, automation technology, and information technology and the degree of intelligence. This is not only limited to the current level. So with the development of the times, intelligent logistics will continue to be given new content.

In this paper, the carbon emission measurement model of the more intelligent logistics supply chain is reasonable and effective through construction. Using the supply chain idea to define the wisdom logistics supply chain, construct a conceptual model of the wisdom logistics supply chain considering carbon emissions, and at the same time combine the characteristics of the wisdom logistics supply chain, analyze the association between the carbon emissions of the wisdom logistics supply chain and the related social, environmental, and economic systems, and conclude that the influencing factors of the wisdom logistics supply chain are mainly energy consumption, production process, process technology, and industrial-scale aspects from the procurement. The model of carbon emission measurement of a smart logistics supply chain is built from five aspects: procurement, production, packaging, storage, and transportation, which enriches the theory of the smart logistics supply chain and provides a reference for carbon emission measurement of smart logistics enterprises. The carbon emission control strategies for each link of the smart logistics supply chain are of practical guidance value. Through the analysis of factor changes, it is proposed that using clean materials and energy-saving equipment instead of the original materials and equipment is an important way to reduce carbon emissions; optimizing the transportation link and using various information systems are important methods to improve the unreasonable reduction of purchasing times and single purchase volume, thus improving the unreasonable transportation situation. Optimization of packaging process and storage function, packaging process design, use of skilled labor, and good storage management are important means to reduce carbon emissions in packaging and storage.

Data Availability

The data used to support the findings of this study are available from the corresponding author upon request.

Conflicts of Interest

The authors declare that they have no known competing financial interests or personal relationships that could have appeared to influence the work reported in this paper.

References

[1] Y. Ding, M. Jin, S. Li, and D. Feng, "Smart logistics based on the Internet of things technology: an overview," *International Journal of Logistics Research and Applications*, vol. 24, no. 4, pp. 323–345, 2021.

[2] S. H. Alsamhi, O. Ma, M. S. Ansari, and Q. Meng, "Greening Internet of things for greener and smarter cities: a survey and future prospects," *Telecommunication Systems*, vol. 72, no. 4, pp. 609–632, 2019.

[3] M. S. Răboacă, N. Bizon, and P. Thounthong, "Intelligent charging station in 5G environments: challenges and perspectives," *International Journal of Energy Research*, vol. 45, no. 11, pp. 16418–16435, 2021.

[4] K. Kuru and D. Ansell, "TCitySmartF: a comprehensive systematic framework for transforming cities into smart cities," *IEEE Access*, vol. 8, pp. 18615–18644, 2020.

[5] N. Piovesan, D. A. Temesgene, M. Miozzo, and P. Dini, "Joint load control and energy sharing for autonomous operation of 5G mobile networks in micro-grids," *IEEE Access*, vol. 7, pp. 31140–31150, 2019.

[6] K. Muhammad, J. Lloret, and S. W. Baik, "Intelligent and energy-efficient data prioritization in green smart cities: current challenges and future directions," *IEEE Communications Magazine*, vol. 57, no. 2, pp. 60–65, 2019.

[7] M. A. Habibi, M. Nasimi, B. Han, and H. D. Schotten, "A comprehensive survey of RAN architectures toward 5G mobile communication system," *IEEE Access*, vol. 7, pp. 70371–70421, 2019.

[8] X. Chen, "The development trend and practical innovation of smart cities under the integration of new technologies," *Frontiers of Engineering Management*, vol. 6, no. 4, pp. 485–502, 2019.

[9] H. P. Lu, C. S. Chen, and H. Yu, "Technology roadmap for building a smart city: an exploring study on methodology," *Future Generation Computer Systems*, vol. 97, pp. 727–742, 2019.

[10] E. Mathew, "Swarm intelligence for intelligent transport systems: opportunities and challenges," *Swarm Intelligence for Resource Management in Internet of Things*, pp. 131–145, 2020.

[11] L. Belli, A. Cilfone, L. Davoli et al., "IoT-enabled smart sustainable cities: challenges and approaches," *Smart Cities*, vol. 3, no. 3, pp. 1039–1071, 2020.

[12] V. Evans and J. Horak, "Sustainable urban governance networks, data-driven Internet of things systems, and wireless sensor-based applications in smart city logistics," *Geopolitics, History, and International Relations*, vol. 13, no. 2, pp. 65–78, 2021.

[13] M. Autili, L. Chen, C. Englund, C. Pompilio, and M. Tivoli, "Cooperative intelligent transport systems: choreography-based urban traffic coordination," *IEEE Transactions on Intelligent Transportation Systems*, vol. 22, no. 4, pp. 2088–2099, 2021.

[14] Y. Noh and J. Y. Ro, "A study on the service provision direction of the National Library for Children and Young Adults in the 5G era," *International Journal of Knowledge Content Development & Technology*, vol. 11, no. 2, pp. 77–105, 2021.

[15] M. Aamir, S. Masroor, Z. A. Ali, and B. T. Ting, "Sustainable framework for smart transportation system: a case study of Karachi," *Wireless Personal Communications*, vol. 106, no. 1, pp. 27–40, 2019.

[16] H. Lu, L. Guo, M. Azimi, and K. Huang, "Oil and gas 4.0 era: a systematic review and outlook," *Computers in Industry*, vol. 111, pp. 68–90, 2019.

[17] R. Philipp, G. Prause, E. O. Olaniyi, and F. Lemke, "Towards green and smart seaports: renewable energy and automation technologies for bulk cargo loading operations," *Environmental and Climate Technologies*, vol. 25, no. 1, pp. 650–665, 2021.

[18] M. K. Anser, M. Ahmad, M. A. Khan et al., "The role of information and communication technologies in mitigating carbon emissions: evidence from panel quantile regression," *Environmental Science and Pollution Research*, vol. 28, no. 17, pp. 21065–21084, 2021.

[19] H. Treiblmaier, A. Rejeb, and A. Strebinger, "Blockchain as a driver for smart city development: application fields and a comprehensive research agenda," *Smart Cities*, vol. 3, no. 3, pp. 853–872, 2020.

[20] M. A. Adedoyin and O. E. Falowo, "Combination of ultra-dense networks and other 5G enabling technologies: a survey," *IEEE Access*, vol. 8, pp. 22893–22932, 2020.

[21] T. Yigitcanlar, N. Kankanamge, and K. Vella, "How are smart city concepts and technologies perceived and utilized? A systematic geo-Twitter analysis of smart cities in Australia," *Journal of Urban Technology*, vol. 28, no. 1-2, pp. 135–154, 2021.

[22] Z. Tong, F. Ye, M. Yan, H. Liu, and S. Basodi, "A survey on algorithms for intelligent computing and smart city applications," *Big Data Mining and Analytics*, vol. 4, no. 3, pp. 155–172, 2021.

Hindawi
Journal of Sensors
Volume 2022, Article ID 3216727, 11 pages
https://doi.org/10.1155/2022/3216727

Research Article

Clustered Wireless Sensor Network Assisted the Design of Intelligent Art System

Yue Zhao

Institute of Art and Design, Shandong Women's University, Jinan, Shandong 250300, China

Correspondence should be addressed to Yue Zhao; 29021@sdwu.edu.cn

Received 8 November 2021; Accepted 17 December 2021; Published 10 January 2022

Academic Editor: Gengxin Sun

Based on the principle of cluster wireless sensor network, this article introduces typical routing protocols in wireless sensors, and wireless sensor network protocol in detail analyzes their advantages and disadvantages and addresses their shortcomings. First, in the clustering network, a uniform clustering protocol with multiple hops in the circular network is proposed. The circular network is divided into rings of equal width, and clusters of equal size are set on different rings. Secondly, the ordinary nodes on each layer of the ring send the collected data to the auxiliary intelligent nodes in the cluster in a single-hop manner, and the auxiliary intelligent nodes located on the outer ring transfer the data to the auxiliary intelligent nodes located on the adjacent inner ring. Finally, on the basis of studying the clustering network protocol, this paper proposes a new clustering routing algorithm, a multihop adaptive clustering routing algorithm. The simulation results show that the algorithm can effectively extend the life of the network, save network energy consumption, and achieve network load balance. At the same time, the initial energy of the auxiliary intelligent node is set according to the energy consumption of the ordinary node and the relative distance between the auxiliary intelligent node and the base station on each layer of the ring. The theoretical and simulation results prove that, compared with the clustered network and auxiliary intelligent nodes, the clustered network can extend the life of the network.

1. Introduction

Wireless sensor networks (WSNs) are composed of a large number of sensor nodes, which are deployed in the target area to be monitored. These nodes cooperatively perceive and process the information in the monitoring area; that is, they can be used to obtain the information of the objective physical world [1]. Therefore, it has been widely used in military, environmental, and habitat monitoring and forecasting, smart home, fire detection, machinery monitoring, industrial and agricultural control, remote control of dangerous areas, and urban transportation in many fields in recent years. Therefore, WSNs have become a current research hotspot in the computer field [2–5]. A routing protocol is one of the current research hotspots of WSNs. Because the routing protocols applicable to traditional wired and wireless networks cannot be applied to the topology of WSNs, it is necessary to design appropriate new routing protocols for WSNs. A wireless sensor network is composed of a large number of sensor nodes, a multihop self-organizing network system formed by wireless communication, and its purpose is to cooperatively perceive, collect, and process information in the network area and send it to observers [6]. A wireless sensor network has many advantages such as fast and flexible networking, has high research value and very broad application prospects, and has attracted great attention from academic and industrial circles [7–9].

Abujubbeh et al. [10] pointed out that the robustness of the system can be improved through the multipath routing algorithm. Data packets are forwarded in the multipath path through the routing algorithm and reconstructed at the receiving end through the forward error correction technology. Kou [11] presents a mesh multipath routing protocol, in which selective forward transmission of data packets and end-to-end forward error correction decoding technology are applied in the protocol, and the mesh multipath search mechanism suitable for sensor networks can be used. Compared to the

data packet replication or limited flooding method, this method consumes less system resources (such as channel bandwidth and power). Singh and Saini [12] assume that the task of the sensor network is to provide security protection for senior politicians. In terms of specific technical implementation, Nkomo et al. [13] assume that sink always works normally and is always safe. To meet the necessary calculation speed and memory capacity, the sink power meets the requirements of encryption and routing; the communication mode is point-to-point, and the security of data transmission is guaranteed through end-to-end encryption; the radiofrequency layer always works normally. In order to reduce or eliminate the noise in the analog measurement value, the sensor data with higher accuracy can be obtained. Chéour et al. [14] deployed in the actual environment need to consider packaging issues. Different packaging forms are used according to different monitoring tasks. The sensor nodes used to collect light information need to be transparent and sealed, while the nodes that collect temperature and humidity information need to have gap for the temperature and humidity sensor to collect data. Sun et al. [15] proposed a DEEC protocol suitable for heterogeneous wireless sensor networks where nodes have initial energy differences based on clustered networks. This protocol takes the remaining energy of each node as much as the average energy of the current node when calculating the node threshold. Taking the ratio into account, as a factor that affects the election of auxiliary intelligent nodes, the greater the remaining, the higher the probability of being elected [16–19]. At the same time, nodes are divided into multiple levels. Each level of node has its own threshold calculation formula $T(i)$. The network life is longer. In the research, the researchers found that after multihop routing transmission, the nodes closer to the sink bear a greater data fusion load and consume more energy, so the nodes near the sink will die prematurely and produce the so-called around the sink [20–22]. Some scholars use the remaining energy, expected energy consumption, the distance from the auxiliary intelligent node to the base station, and the number of nearby nodes as weights and find the optimal dynamic network structure by balancing the weights of these factors and propose a self-organizing network based on genetic algorithm The clustering algorithm GASONeC, when the sink node is far from the sensor, it is preferable to form more clusters to save energy. Compared with other methods, GASONeC greatly prolongs the network survival time and shortens the average response time of the algorithm [23–25].

Aiming at the problem of WSN's stable period and half of the node death period being too short, this paper uses the distance between the node and the sink and the distance between the node and the auxiliary intelligent node as parameters to modify the node threshold. When electing the remaining auxiliary intelligent nodes, the threshold correction factor is used to appropriately increase the election probability of nodes that are far away from the existing auxiliary intelligent nodes to balance the energy consumption of auxiliary intelligent nodes and extend the stable period of WSN and half of the node death period. By optimizing the auxiliary intelligent node election process, it is ensured that the optimal number of auxiliary intelligent nodes can be elected in each round of auxiliary intelligent node elections, and the zero cluster situation can be avoided in the later stage of network operation, and the stability of the election can be improved. Compared with the genetic algorithm, the CMACP algorithm nearly doubles the fitness value through local search, effectively extending 55.66% of 100% coverage time and 28.87% of network life. Whether it is a uniform and uniform distribution of sensor nodes and MTP or a random distribution, the CMACP algorithm can extend the WSN survival time, stabilize period of network operation, and ensure good coverage.

2. Design of Auxiliary Intelligent Art System Based on Clustered Wireless Sensor Network

2.1. Hierarchical Distribution of Wireless Sensors. Wireless sensors are powered by batteries with limited energy. The goal of extending the lifetime of the entire WSN as much as possible is an important topic that requires continuous exploration and research. The energy consumption of the sensor mainly occurs in the communication phase, especially the energy consumption of the auxiliary intelligent node (cluster head, CH for short) in the clustered network is very large. A good routing protocol can effectively schedule node communication and reduce communication failure rate and communication interference, thereby improving energy utilization and extending network life. Figure 1 shows the hierarchical distribution of wireless sensors.

In the actual environment, the sensor will die due to exhaustion of energy or other unpredictable external factors, or other members will join the WSN, which will cause the number of sensors and topology in the WSN to dynamically change. So, WSN should adapt to SN to enter and leave dynamically. In addition, the reliability of WSN also depends on dynamics.

$$f_{11} = \left(\frac{1}{n} \times \sum_{i=1}^{n} x_i^2, \frac{1}{n} \times \sum_{i=1}^{n} y_i^2, \right), \quad f_1 = \|p_i + g\|_2. \tag{1}$$

A large number of sensor nodes are randomly deployed in or near the monitoring area (sensor field), which can form a network through self-organization. The data monitored by a sensor node is transmitted hop by hop along other sensor nodes. During the transmission, the detected data may be processed by multiple nodes, routed to the sink node after multiple hops, and finally reach the management node through the Internet or satellite. The user configures and manages the sensor network through the management node, releases monitoring tasks, and collects monitoring data.

$$L(y, g) = \sum_{i=1}^{n} y_i \left(g_i + \ln \sum_{j=1}^{n} \exp g_i \right), \quad f(x_i, x_2, x_3) = G(F(x_1); W) G(F(x_2); W) G(F(x_3); W). \tag{2}$$

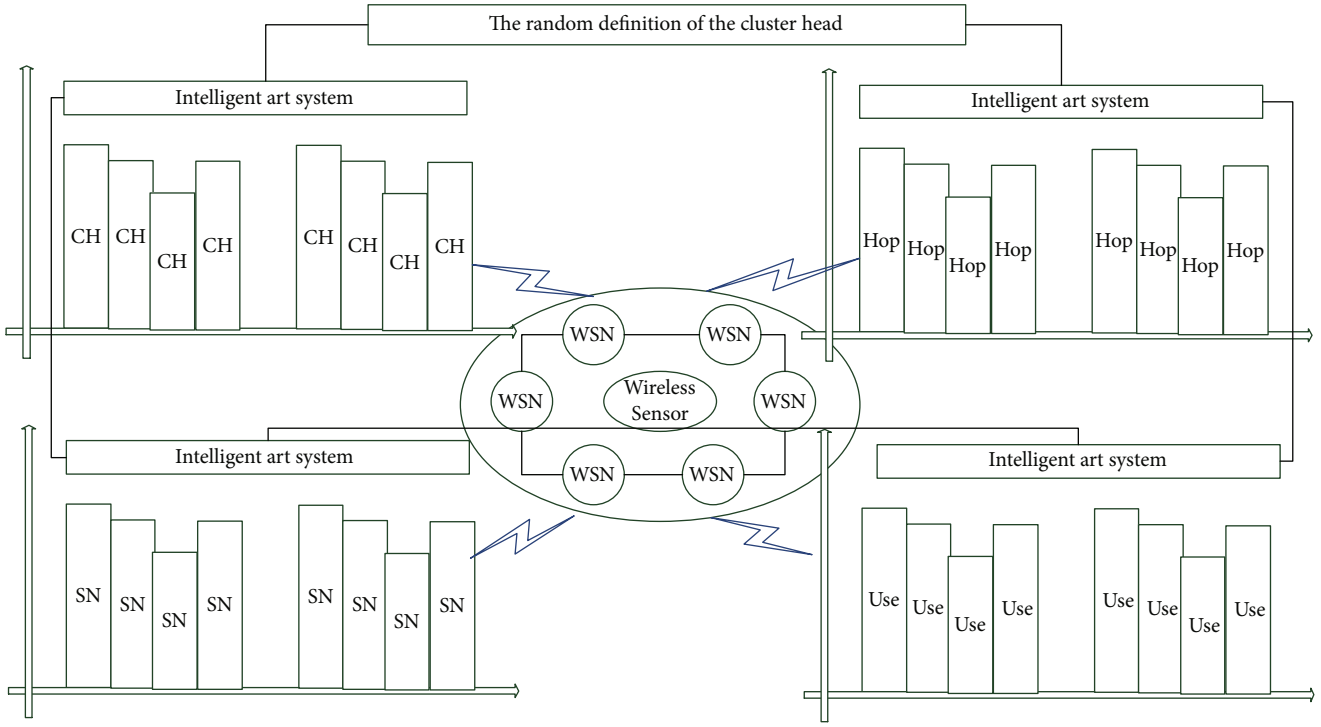

Figure 1: Hierarchical distribution of wireless sensors.

The processing capacity, storage capacity, and communication capacity of the aggregation node are relatively strong. It connects the sensor network and external networks such as the Internet to realize the communication protocol conversion of the two protocols. At the same time, it releases the monitoring tasks of the management node and forwards the collected data to the outside. The sink node can either be a sensor node with enhanced functions, sufficient energy supply, and more memory and computing resources, or it can be a special gateway device with no monitoring function but a wireless communication interface.

$$\left(\frac{x-y}{a_1}\right)^2 - \left(\frac{x+y}{a_2}\right)^2 = 1, \tag{3}$$
$$t' = [r\bullet\cos\theta, r\bullet\sin\theta, r\bullet\tan\theta_1 - t].$$

The protocol stack also includes an energy management platform, a mobile management platform, and a task management platform. These management platforms enable sensor nodes to work together in an energy-efficient manner, forward data in the sensor network where the nodes move, and support multitasking and resource sharing.

2.2. Clustering Network Routing Algorithm. In the clustering network routing protocol, each node broadcasts the data it received from the previous neighbor route to all its neighbor nodes (except the node that sent the data) until the data reaches the final destination node or does not reach the final destination node. However, the maximum number of route hops restricted during datagram transmission has been reached.

In order to overcome the implosion, overlap, and blind use of resources of traditional routing protocols, the SPIN protocol introduces two key technologies: innovative negotiation and resource adaptation. Based on the SPIN protocol, the data distribution protocol SPMS is proposed for node and link failure. The implementation process is divided into three stages: interest diffusion, initial gradient establishment, and data transmission. There are many data-centric algorithms that are improved based on this algorithm. Table 1 shows the routing description of the clustered network.

The basic idea of the algorithm is the clustering process is carried out periodically, and the auxiliary intelligent node is randomly selected with equal probability, and the node bootstraps as the auxiliary intelligent node according to its own probability value. Because the auxiliary smart nodes are burdened heavily, after one round of execution, the protocol restarts the cluster establishment process, so that each sensor node can load average energy consumption in the network, thereby reducing network energy consumption and improving the overall network survival time.

The clustering network needs to periodically perform the cluster reconstruction process during its operation. Each round is divided into two phases: cluster establishment and data transmission phase. Because the cluster reconstruction process consumes a lot of energy, in order to reduce the extra cost of cluster reconstruction, in general, the duration of the data transmission phase should be much longer than the cluster establishment phase. Figure 2 shows the topology of the clustered network routing algorithm.

Each node may receive multiple data packets from different auxiliary intelligent node nodes. According to the signal strength of the received data packets, the auxiliary intelligent

Table 1: Clustering network routing description.

Index number	First-level indicator	Second-level indicator	Third-level indicator
1	Clustering capability	0.07	Current ratio
		0.27	Clustering complaint rate
		0.33	Clustering network rate
2	Clustering service ability	0.15	The freshness of agricultural products
		0.24	The time rate of network
		0.21	Information transmission accuracy
3	Information technology capabilities	0.09	Technical network rate
		0.11	The utilization rate of refrigerated trucks

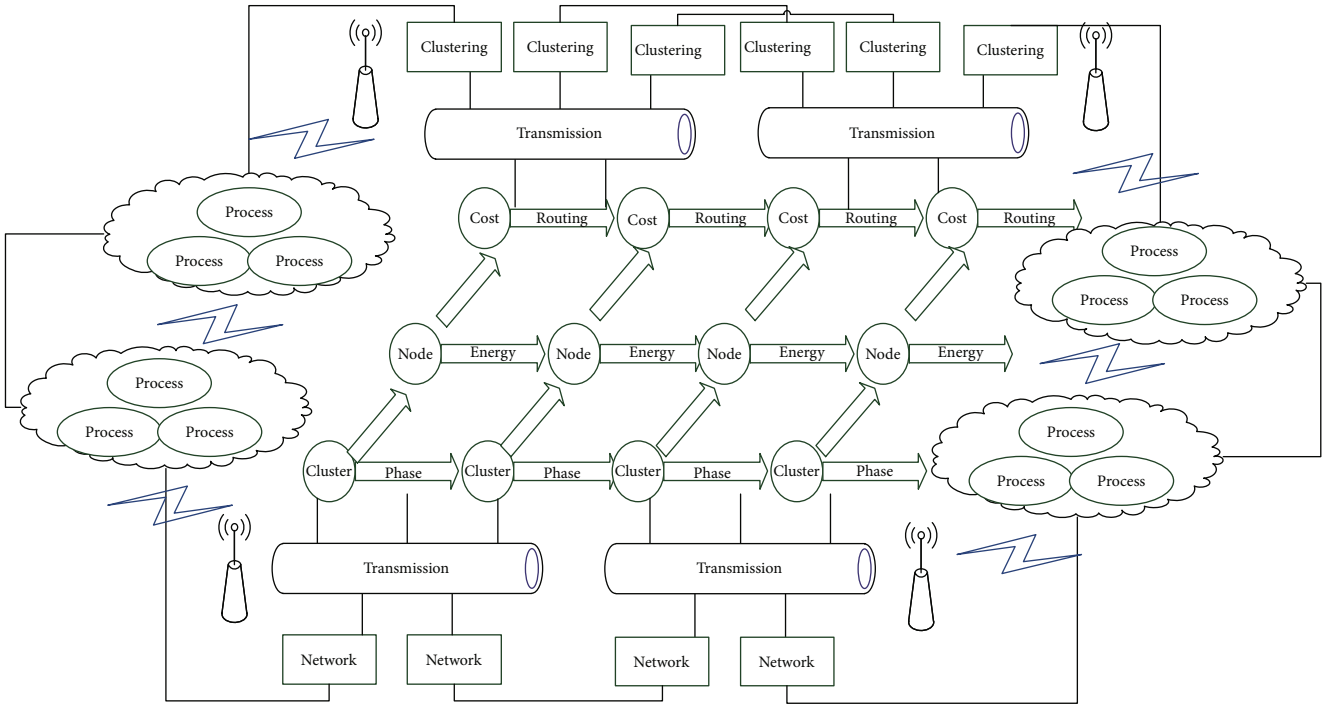

Figure 2: Clustering network routing algorithm topology.

node with the strongest broadcast signal as its auxiliary intelligent node was selected and sent to join information. The reason is that the greater the strength of the signal received by the node, the shorter the distance between the node and the auxiliary intelligent node, and the least energy consumed during communication. When all nodes in the network have selected their own auxiliary intelligent node, they will join the corresponding cluster and become a member node of this cluster. Then, the member node will notify the auxiliary intelligent that it has become a member of this cluster.

The data of a certain time interval is related to the data of the adjacent time interval. During this process, the receiving end of the cluster head will remain active and used to receive join messages from member nodes. In wireless sensor networks, the energy of nodes is limited and there is generally no energy supplement. Therefore, routing protocols need to use energy efficiently. At the same time, the number of sensor network nodes is often very large, and the nodes can only obtain local topology information. Routing protocols in different applications may be very different, and there is no universal routing protocol.

2.3. Auxiliary Intelligent Cluster Analysis. When the auxiliary intelligent cluster structure in the network is formed, the auxiliary intelligent node has calculated the TDMA time slot table and has broadcast to the member nodes and then enters the stable stage of data transmission, and the node starts to send according to the allocated TDMA scheduling time slot data. That is, only send the collected data to its own auxiliary intelligent node in its own time slot.

It is also related to the historical data at the same time of the previous day or the previous week. After a round of data transmission is completed, the cluster head node will merge the redundant data sent by the received member nodes and

then send it to the base station. In this process, the long-distance communication between the auxiliary intelligent node and the base station will consume a lot of energy. The nodes send metadata (that is, the data describing the attributes of the data collected by the sensor node, meta-data) instead of the collected data for negotiation. Since the size of metadata is smaller than the collected data, it consumes relatively little energy to transmit metadata. Before transmitting or receiving data, each node must check its own available energy status. If it is at a low energy level, some operations must be interrupted, such as acting as a data transfer station (router) and stopping data forwarding operations.

Data fusion technology can be combined with multiple protocol levels of sensor networks. Figure 3 is a pie chart of auxiliary intelligent clustering. In the application layer design, distributed database technology can be used to gradually filter the collected data to achieve the effect of fusion; in the network layer, many routing protocols incorporate data fusion mechanisms to reduce the amount of data transmission.

It saves energy by reducing the transmission conflict and header overhead of the MAC layer without losing time performance and information integrity. Data fusion technology has been widely used in the fields of target tracking and automatic target recognition. The first is the cost of delay. In the process of data transmission, finding routes that facilitate data fusion, performing data fusion operations, and waiting for the arrival of other data for fusion may increase the average delay of the network. The second is the cost of robustness. Compared with traditional networks, sensor networks have higher node failure rates and data loss rates. Data fusion can greatly reduce data redundancy. But, losing the same amount of data may lose more information, so relatively speaking, it also reduces the robustness of the network.

2.4. Art System Compilation Design. During the compilation process of the art system, due to the energy limitation of sensor nodes and the large network coverage area, the network is suitable for adopting the routing mechanism of art compilation and transmission. The wireless communication bandwidth of the sensor node is limited, usually only a communication rate of several hundred at most. Due to changes in node energy, high mountains, buildings, obstacles, and other topography and natural environments such as wind, rain, and thunder, wireless communication performance may change frequently and communication interruptions frequently occur. In such a communication environment and the limited compilation capability of nodes, special consideration should be given to meeting the communication requirements of wireless sensor networks when designing a network compilation mechanism. It can be seen that the energy consumption of the wireless compiling module in the sending state is the largest, and the energy consumption in the idle state and the receiving state is close, slightly less than the energy consumption in the sending state. Figure 4 shows the distribution of compilation nodes in the art system.

In each art system compilation subgroup, the auxiliary intelligent node is responsible for managing the common member nodes of the cluster and shares part of the management tasks of the WSN bottom layer. This layered structure is conducive to the large-scale deployment of sensor nodes and has a good network dynamic adaptability and scalability. Most of the energy of the sensor node is consumed on the wireless communication module. Sensor nodes consume more energy when transmitting information than when performing calculations.

The wireless compiler module always monitors the existence of the wireless channel in the idle state, checks whether there is any data sent to itself, and shuts down the communication module in the sleep state. The member nodes in the cluster use TDMA technology to cut nonoverlapping time slots and can be shut down or hibernated to save energy during idle periods (such as assisting the intelligent node in the data processing and sending phase). The AD analog-to-digital conversion module realizes the conversion of analog to digital, which is convenient for the postprocessing unit to perform operations; the processing unit is mainly composed of a micro, low-power embedded microprocessor and memory and is responsible for the data storage and operation of the entire node and forwarding. The data from other nodes is the function control center and data computing center of the node. In addition, because the environmental data collected between adjacent nodes has greater repetition and redundancy, the use of data fusion technology in the processing unit is conducive to reducing network traffic; the radiofrequency module is responsible for conversations and data transmission with other nodes or base stations, according to electromagnetic waves. The disposable microbattery provides energy for the stable operation of the node.

3. Results and Analysis

3.1. Data Screening of Clustered Wireless Sensor Network. The test scenario is as follows: 200 nodes are evenly distributed in a circular area with a radius of 50 m. The circular area is divided into rings of equal width, and a certain number of higher energy is deployed in an appropriate position in each divided ring. When the number of auxiliary intelligent nodes on the second layer ring is gradually increased, the life cycle of the network also gradually increases, and the slope of the curve of 4 ~ 6, 6 ~ 8, and 8 ~ 10 is greater than that of the later stages.

It is difficult to accurately predict the flow of traffic in an area. Because as the number of auxiliary intelligent nodes on the second-level ring increases, $R1$ will decrease accordingly, that is, the farthest distance between ordinary nodes and auxiliary intelligent nodes will decrease, thus reducing the number of ordinary nodes sending to the cluster head. The clustering network algorithm simulation environment uses MATLAB 8.1 platform, and $N = 100$ sensor nodes are randomly deployed in a site of $100 \times 100\,m^2$. Through simulation comparison, it is found that the value of mouth is 2, and the value of p is 4; the result is the most ideal. Figure 5 shows the energy consumption distribution of clustered wireless sensor networks.

When the clustering network protocol is running, most of the nodes in the network die quickly. The reason is that the clustering network protocol does not consider the heterogeneity of nodes. The node will still have a lot of energy remaining and can no longer be fully utilized, thus causing

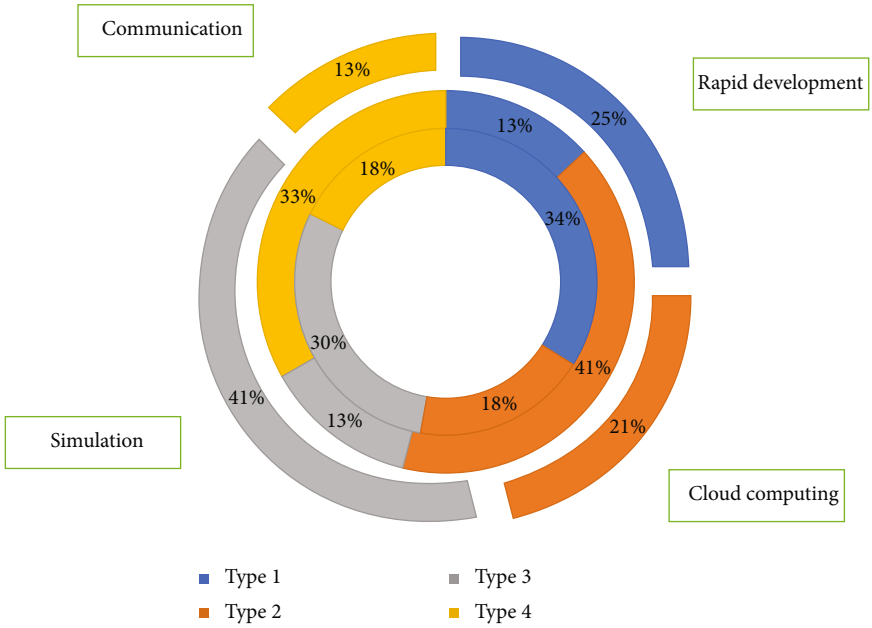

Figure 3: Auxiliary intelligent clustering fan chart.

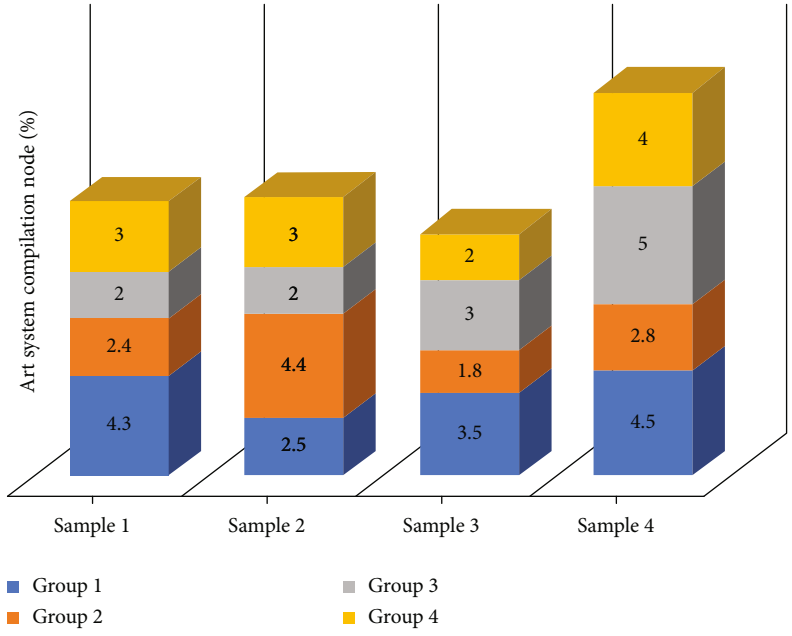

Figure 4: Distribution of compilation nodes of the art system.

a waste of energy. The centralized algorithm clustering network can obtain a more balanced distribution of auxiliary intelligent nodes than ordinary networks, and the energy consumption of nodes in the network can be balanced to a certain extent, but the clustering network also does not consider the heterogeneity of node energy. The clustering network sets the auxiliary intelligent node to a higher energy, which can make full use of the high energy of the auxiliary intelligent node. When the transmission distance is farther, the energy consumed by wireless communication is greater, and it shows an exponential growth trend as the distance d increases.

At this time, the node closer to the sink node should be selected as the auxiliary intelligent node as much as possible, so that the energy consumption of wireless transmission can be saved by shortening the distance, and the communication distance is controlled at d. The clustering network algorithm modifies the threshold of the node according to the distance between the sensor node and the sink node and the distance between the node and the auxiliary intelligent node, so that

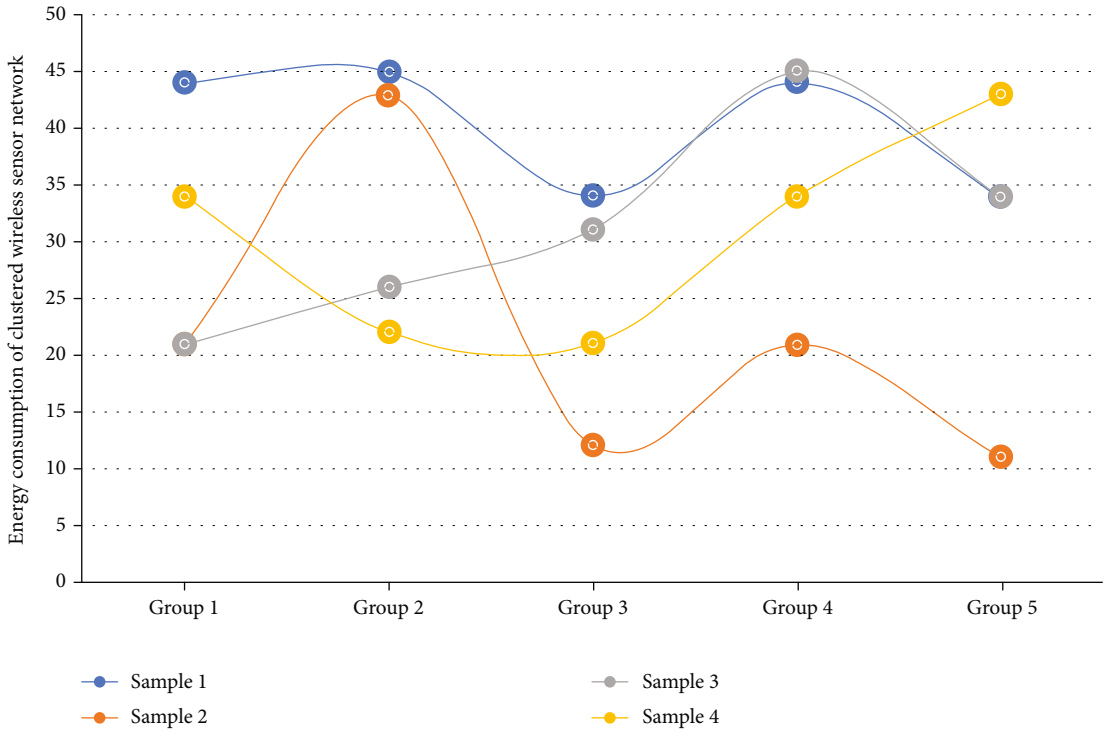

Figure 5: Energy consumption distribution of a clustered wireless sensor network.

the node closer to the sink node has a greater probability of becoming the auxiliary intelligent node to shorten the communication distance. The node that is closer to the auxiliary intelligent node has a smaller probability of being elected as the auxiliary intelligent node, avoiding too small clustering intervals and causing too many multihop transmissions of data, thereby saving the energy consumption of radio transmission.

3.2. Auxiliary Intelligent Art System Simulation. This experimental platform is built on Acer laptops with Core i5-3230M Core CPU, 4 GB DDR3 memory, and Windows 8 operating system. MATLAB is used as the simulation platform. In terms of simulation parameter setting, 200 wireless sensor nodes are distributed in 200∗200 second. The auxiliary system is an object-oriented network simulation simulator that uses C++ to write specific protocols, but in order to increase flexibility, its front end uses an OTcl interpreter.

Because the data is affected by many factors, such as spatial correlation, time dependence, and external environmental factors, the kernel of the auxiliary system simulator defines a variety of classes, which are hierarchical, which is called the compiled class structure, and the corresponding similar class structure in the OTcl interpreter is called the interpreted class structure. Before network simulation, we must first analyze the levels involved in the simulation. At the first level, the existing network elements of the auxiliary system can be used to realize simulation without modifying the auxiliary system itself. However, if there are no network elements required for simulation in the auxiliary system, you need to add the required network elements to expand the NS.

Figure 6 shows the distribution of clustered wireless sensor network elements. It can be seen that the number of rounds appearing in the clustering network are 415, 645, 796, and 917, respectively. It can be seen that the number of rounds appearing in the clustering network are 695, 783, 832, and 1026, respectively. In addition, the period from the beginning of the simulation to the appearance of the clustered network is called the network stability period. The stable period is an important indicator to measure the stability coefficient of the network. The number of surviving nodes of the improved algorithm in the same round is more than that of the other three algorithms. This is because the algorithm in this paper adopts a mixed working mode of multiple auxiliary intelligent nodes, and the selected auxiliary intelligent nodes are optimized for high energy and perform their own duties, effectively alleviating the information transmission load between clusters and reducing the communication energy consumption and burden of auxiliary intelligent nodes. The energy consumption of the nodes in the network is balanced, so that the working time of the nodes becomes longer. The other three algorithms have different degrees of defects in the election of auxiliary intelligent nodes, the distribution of auxiliary intelligent nodes, and the balance of energy consumption. As a result, the survival time of nodes cannot be effectively extended.

3.3. Analysis of Experimental Results. In the clustering network and wireless sensor network algorithm, the resource consumption is imbalanced due to the random definition of the cluster head. When the number of failed nodes gradually

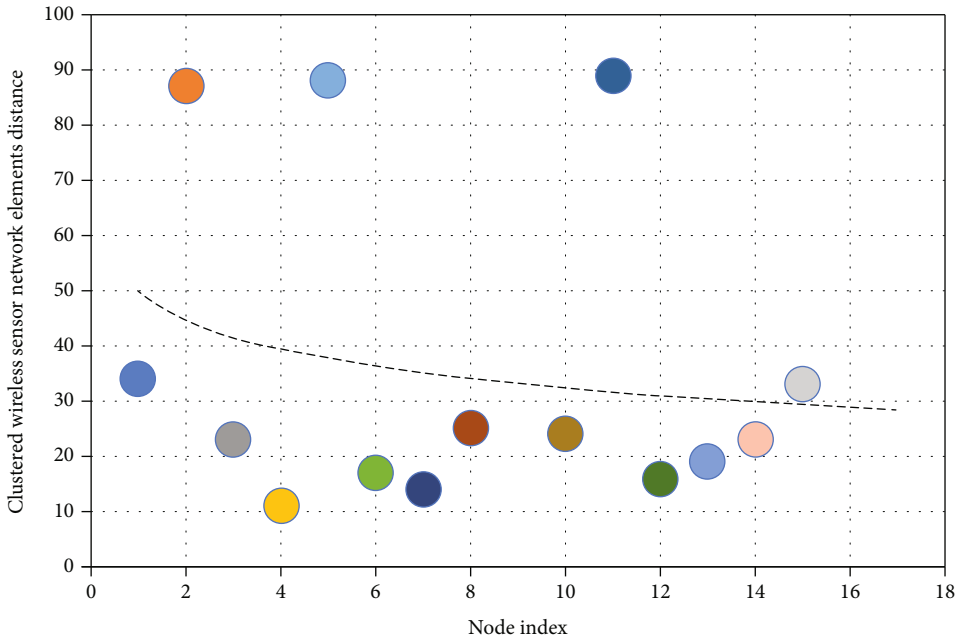

Figure 6: Distribution of clustered wireless sensor network elements.

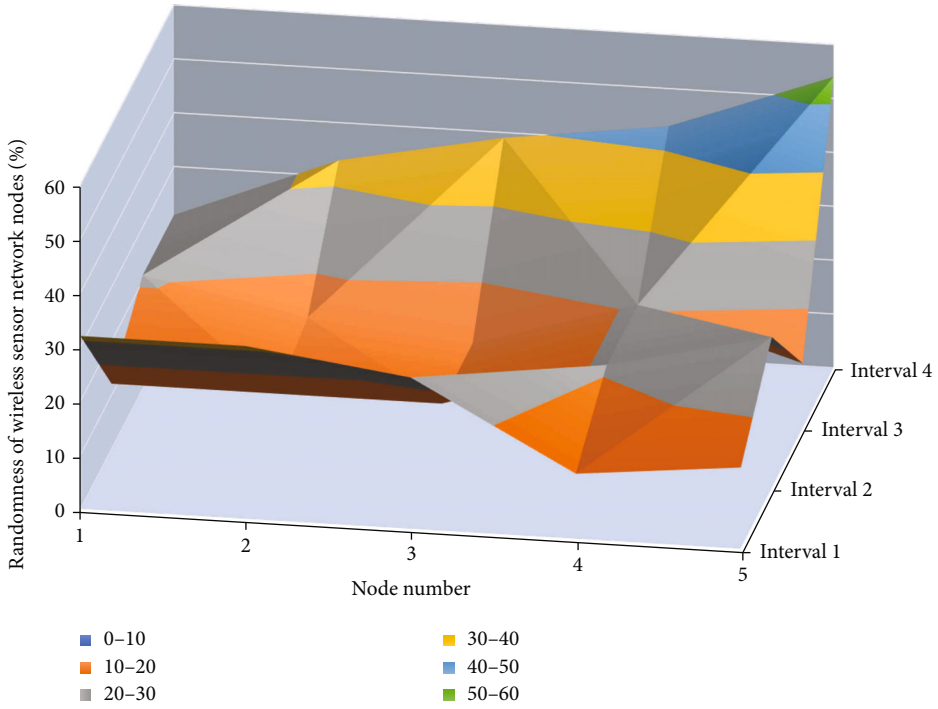

Figure 7: Randomness of node distribution in wireless sensor network.

increases, the failure rate of the nodes is higher. The clustering network and the wireless sensor network algorithm proposed in this paper both apply K-means to the formation process of the WSN logical structure and obtain clustering with relatively balanced load between clusters, and the wireless sensor network algorithm solves the problem of the number of clusters. It can be seen that the failure time of the first node in the wireless sensor network algorithm is the latest.

It can be seen that in the first round, the distribution of nodes on the clustered network and the wireless sensor network is roughly the same, because the network has just started to operate, and the factors affecting the election of auxiliary intelligent nodes are not very different at this time. At the same time, due to the randomness of the clustering network's auxiliary intelligent node election, the first round of clustering network is roughly equivalent to the effect of

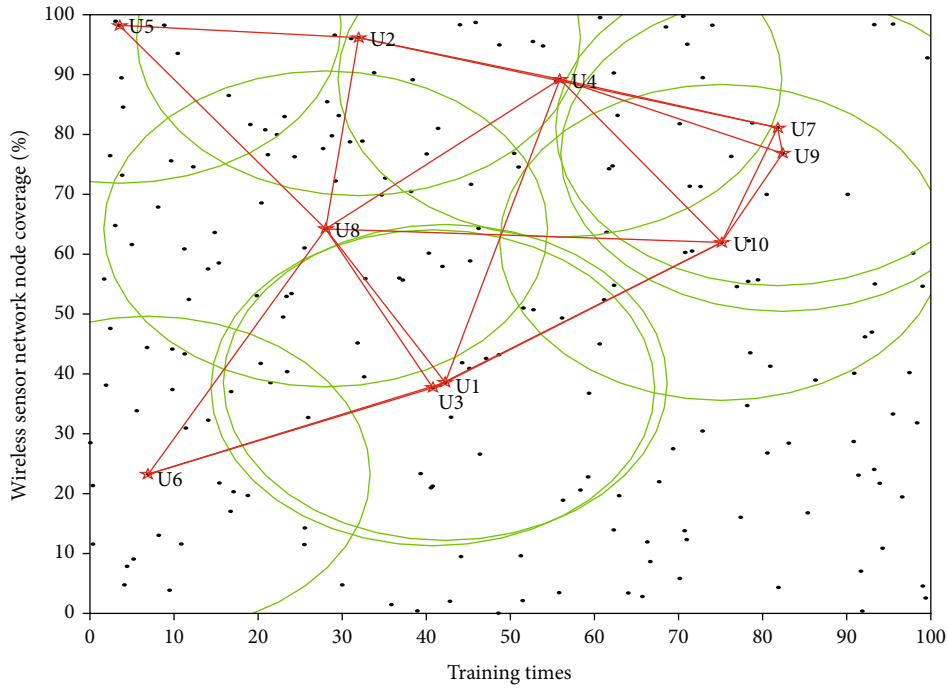

Figure 8: Node coverage distribution of wireless sensor network.

the wireless sensor network, but the performance of the clustering network will not be as stable as the network runs. Figure 7 shows the random distribution of wireless sensor network nodes.

In the stable period, half of the surviving node period, and the entire network life cycle, the improved clustering network algorithm in this paper is significantly higher than other algorithms in the stability of assisting intelligent node election. Especially when there is no node death during the stable period, the clustered network can elect 5 optimal numbers of auxiliary intelligent nodes in each round of network operation, and its average value is 5 and the variance is zero during the stable period.

Spatial correlation means that the inflow of each area varies with the outflow data of neighboring areas. The performance is the same as the ideal situation. It can be seen that the stability of the clustered network is significantly higher than that of the other three. Before the algorithm runs iteratively, the initial fitness values of the two are almost the same. After 40 population iterations, regardless of the average fitness or the maximum fitness, the algorithm with a local search algorithm has a better fitness value than the genetic algorithm.

Figure 8 shows the distribution of node coverage in the wireless sensor network. It can be seen that the clustering network node starts to die in 58 rounds, and the slope of the curve in rounds 60-120 is higher than the curve slope of the clustering network-NS, indicating that its nodes die faster than the clustering network-NS. Until the end of the simulation 200 rounds, there are still a small number of nodes in the clustered network. The clustered network extends the network survival time by more than 40%. It can be seen that in the first 60 rounds of network operation, the number of data packets received by the two algorithms assisted by the intelligent node is roughly the same.

The outflow of this area also affects the inflow of adjacent areas. This is because the data packets received by the assisted intelligent node are mainly from cluster members. Afterwards, it is obvious that the amount of data packets received by the clustered network is higher than that of the clustered network, and the gap is gradually widened. It can be seen that the number of data packets received during the entire operation time of the network using the clustering network is nearly 13% higher than that of the clustering network. It can be seen from the above that the clustering network increases the data transmission volume of the network, and it also reflects from one aspect that the clustering network reduces the energy consumption of the network.

4. Conclusion

In this paper, an energy-efficient clustering protocol is proposed in the wireless sensor network. The selection of the auxiliary intelligent node and the sending node is based on the average remaining energy of the nodes in the network and the average energy and relative distance of the member nodes in each cluster. Since the energy load of the auxiliary intelligent node is greatly reduced, there is no need to perform a global cluster reconstruction, which avoids a large amount of additional energy overhead. Therefore, the algorithm can not only balance the energy consumption of auxiliary intelligent nodes and ordinary nodes, but also avoid the huge extra cost caused by global cluster reconstruction. Aiming at the problem of WSN lifetime and coverage optimization, this paper proposes a composite cultural gene clustering protocol based on cultural gene algorithm and node wake-up strategy. The algorithm first runs the cultural genetic algorithm to initialize the nodes that need to be activated and plan adjacent redundant nodes. The genetic algorithm and the local search algorithm obtain the

optimal initial node distribution through multiple iterations. With the operation of the network, when a node loses its coverage target due to exhaustion of energy, the wake-up scheduling strategy compensates for the coverage loophole by calculating and activating the optimal adjacent redundant node. The analysis results show that the improved algorithm effectively reduces the energy consumption of the network and prolongs the survival of the network cycle. Simulation experiments show that, compared with genetic algorithm, CMACP has higher adaptability. It can better extend the 100% coverage period and network lifetime and improve the WSN's ability to control the coverage of the sensing area.

Data Availability

The data used to support the findings of this study are available from the corresponding author upon request.

Conflicts of Interest

The authors declare that they have no known competing financial interests or personal relationships that could have appeared to influence the work reported in this paper.

Acknowledgments

The study was supported by "Shandong Province Social Science Planning Research Project, China; project: Moral Education of Female Visual Symbols in Chinese Folk Art, (Grant No. 18CWYJ20)".

References

[1] T. Mahmood, J. Li, Y. Pei et al., "An intelligent fault detection approach based on reinforcement learning system in wireless sensor network," *The Journal of Supercomputing*, pp. 21–30, 2021.

[2] A. Arshad, Z. Mohd Hanapi, S. Subramaniam, and R. Latip, "A survey of Sybil attack countermeasures in IoT-based wireless sensor networks," *PeerJ Computer Science*, vol. 7, article e673, 2021.

[3] S. Roy, N. Mazumdar, and R. Pamula, "An energy optimized and QoS concerned data gathering protocol for wireless sensor network using variable dimensional PSO," *Ad Hoc Networks*, vol. 123, article 102669, 2021.

[4] O. Kanoun, S. Bradai, S. Khriji et al., "Energy-aware system design for autonomous wireless sensor nodes: a comprehensive review," *Sensors*, vol. 21, no. 2, p. 548, 2021.

[5] G. Ahmed, X. Zhao, M. M. S. Fareed, M. R. Asif, and S. A. Raza, "Data redundancy-control energy-efficient multi-hop framework for wireless sensor networks," *Wireless Personal Communications*, vol. 108, no. 4, pp. 2559–2583, 2019.

[6] R. Sivaranjani and A. V. S. Kumar, "Energy-efficient routing based distributed cluster for wireless sensor network," in *Innovative Data Communication Technologies and Application*, pp. 489–497, Springer, Cham, 2020.

[7] S. Roy, N. Mazumdar, and R. Pamula, "An optimal mobile sink sojourn location discovery approach for the energy-constrained and delay-sensitive wireless sensor network," *Computing*, vol. 12, no. 12, pp. 10837–10864, 2021.

[8] L. Liu, "Tennis assistant referee system based on intelligent sensor network and data understanding," in *2021 5th International Conference on Computing Methodologies and Communication (ICCMC)*, pp. 67–70, Erode, India, 2021.

[9] D. Ramotsoela, A. Abu-Mahfouz, and G. Hancke, "A survey of anomaly detection in industrial wireless sensor networks with critical water system infrastructure as a case study," *Sensors*, vol. 18, no. 8, p. 2491, 2018.

[10] M. Abujubbeh, F. Al-Turjman, and M. Fahrioglu, "Software-defined wireless sensor networks in smart grids: an overview," *Sustainable Cities and Society*, vol. 51, article 101754, 2019.

[11] J. Kou, "Intelligent sensing system of human physiological detection based on biosensor and WSN–A review," in *2020 International Conference on Inventive Computation Technologies (ICICT)*, pp. 647–650, Coimbatore, India, 2020.

[12] S. Singh and H. S. Saini, "Intelligent ad-hoc-on demand multipath distance vector for wormhole attack in clustered WSN," *Wireless Personal Communications*, vol. 122, pp. 1305–1327, 2022.

[13] M. Nkomo, G. P. Hancke, A. M. Abu-Mahfouz, S. Sinha, and A. J. Onumanyi, "Overlay virtualized wireless sensor networks for application in industrial internet of things: a review," *Sensors*, vol. 18, no. 10, p. 3215, 2018.

[14] R. Cheour, S. Khriji, D. El Houssaini, M. Baklouti, M. Abid, and O. Kanoun, "Recent trends of FPGA used for low-power wireless sensor network," *IEEE Aerospace and Electronic Systems Magazine*, vol. 34, no. 10, pp. 28–38, 2019.

[15] W. Sun, M. Tang, L. Zhang, Z. Huo, and L. Shu, "A survey of using swarm intelligence algorithms in IoT," *Sensors*, vol. 20, no. 5, p. 1420, 2020.

[16] P. Bezerra, P. Y. Chen, J. A. McCann, and W. Yu, "Adaptive monitor placement for near real-time node failure localisation in wireless sensor networks," *ACM Transactions on Sensor Networks (TOSN)*, vol. 18, no. 1, pp. 32–41, 2022.

[17] M. Ndiaye, G. P. Hancke, and A. M. Abu-Mahfouz, "Software defined networking for improved wireless sensor network management: a survey," *Sensors*, vol. 17, no. 5, p. 1031, 2017.

[18] S. Ahmed, M. A. Khan, A. Ishtiaq, Z. A. Khan, and M. T. Ali, "Energy harvesting techniques for routing issues in wireless sensor networks," *International Journal of Grid and Utility Computing*, vol. 10, no. 1, pp. 10–21, 2019.

[19] X. Liu, J. Yu, F. Li, W. Lv, Y. Wang, and X. Cheng, "Data aggregation in wireless sensor networks: from the perspective of security," *IEEE Internet of Things Journal*, vol. 7, no. 7, pp. 6495–6513, 2019.

[20] S. Pundir, M. Wazid, D. P. Singh, A. K. Das, J. J. Rodrigues, and Y. Park, "Intrusion detection protocols in wireless sensor networks integrated to internet of things deployment: survey and future challenges," *IEEE Access*, vol. 8, pp. 3343–3363, 2019.

[21] N. Sharma, I. Kaushik, V. K. Agarwal, B. Bhushan, and A. Khamparia, "Attacks and security measures in wireless sensor network," in *Intelligent Data Analytics for Terror Threat Prediction: Architectures, Methodologies, Techniques and Applications*, pp. 237–268, Wiley Online Library, 2021.

[22] H. S. HK, P. Kumar, D. Anil, and N. Smitha, "An efficient and robust reliable data aggregation in wireless sensor networks," in *2021 Second International Conference on Electronics and Sustainable Communication Systems (ICESC)*, pp. 1052–1057, Coimbatore, India, 2021.

[23] M. Zamini and S. M. H. Hasheminejad, "A comprehensive survey of anomaly detection in banking, wireless sensor networks, social networks, and healthcare," *Intelligent Decision Technologies*, vol. 13, no. 2, pp. 229–270, 2019.

[24] N. Javaid, Z. Ahmad, A. Sher, Z. Wadud, Z. A. Khan, and S. H. Ahmed, "Fair energy management with void hole avoidance in intelligent heterogeneous underwater WSNs," *Journal of Ambient Intelligence and Humanized Computing*, vol. 10, no. 11, pp. 4225–4241, 2019.

[25] M. O. Osifeko, G. P. Hancke, and A. M. Abu-Mahfouz, "Artificial intelligence techniques for cognitive sensing in future IoT: state-of-the-art, potentials, and challenges," *Journal of Sensor and Actuator Networks*, vol. 9, no. 2, p. 21, 2020.

Hindawi
Journal of Sensors
Volume 2022, Article ID 4199985, 12 pages
https://doi.org/10.1155/2022/4199985

Research Article

Monitoring and Analysis of Physical Exercise Effects Based on Multisensor Information Fusion

Xinliang Zhou[1] **and Shantian Wen**[2]

[1]*School of Physical Education, Xihua University, Chengdu, Sichuan 610039, China*
[2]*School of Physical Education, Huzhou University, Huzhou, Zhejiang 313000, China*

Correspondence should be addressed to Shantian Wen; wst@zjhu.edu.cn

Received 2 November 2021; Revised 10 December 2021; Accepted 15 December 2021; Published 10 January 2022

Academic Editor: Gengxin Sun

In this paper, multiple sensors are used to track human physiological parameters during physical exercise, and data information fusion technology is used to extract useful information for monitoring and analyzing the effects of physical exercise. This paper explores the interaction and developmental dynamics of multisensor information fusion technology and physical exercise data monitoring based on the interrelationship and interpenetration between the two. The design ideas and principles that should be followed for the software designed in this study are discussed from the perspective of the portable design of measurement instruments and the perspective of multisensor information fusion, and then, the overall architecture and each functional module are studied to propose a scientific and reasonable design model. The general methodological model to be followed for the development of this resource is designed, and the basic development process of the model is explained and discussed, especially the requirement analysis and structural design, and how to build the development environment are explained in detail; secondly, based on the course unit development process in this model, we clarify the limitations of the system through meticulous analysis of the measurement results, which provides a solid foundation for the next step of system optimization. Finally, with a focus on future development, we elaborate on the potential possible role and development trend of multisensor information fusion in the future period. In this paper, we propose to apply the multisensor data fusion algorithm to the monitoring, analysis, and evaluation of the effect of physical exercise, by collecting multiple human physiological parameters during physical exercise through multiple sensors and performing data fusion processing on the collected physiological parameters to finally evaluate the effect of physical exercise.

1. Introduction

The method of tracking single sensor measurement data can no longer meet the growing requirements, and people have begun to explore the use of multiple sensor measurement data combined to maximize the extraction of useful information contained in the measurement data to achieve the tracking of moving targets [1]. When using measurement data from multiple sensors for target tracking, the measurement data provided by each sensor may have different characteristics, such as the sampling time, sampling location, data expression form, sampling frequency, and confidence level of each sensor to obtain the data, and the position of each sensor in the data fusion process is also different [2]. How to effectively fuse the measurement data from multiple sensors to obtain tracking performance that cannot be achieved by a single sensor has become the focus of research and attention in multisensor data fusion technology in the field of target tracking. Due to the rich information provided by many sensor data in the system that needs to be extracted and utilized, to better process the sensor data, combining intelligent theory with information fusion technology is an inevitable trend in the development of sensor information fusion technology. The development of multisensor information fusion technology has a wide range of applications in areas such as intelligent transportation, robotics, space navigation, and even military aspects. Nowadays, information fusion is increasingly used in life, and scholars around

the world pay high attention to the development of multisensor information fusion technology. In data monitoring, it has also changed from a traditional single sensor to a multisensor composite [3].

Multisource information fusion technology, through the collection of multiple information sensors for multiple confirmations of different sensor systems, can be more conducive to improving the reliability of the sensor system and the ability to detect; conducive to improving the quality and credibility of the system's detection data and information; and conducive to improving the system's ability to perceive idiosyncratic data and data logical reasoning, accelerating the accuracy and response speed of the system, and improving the system's detection reliability; according to the data information provided by sensors of different information sources, through data fusion, it can improve the system's information decision-making and analysis capabilities, shorten the system's information response delay time, reduce the information ambiguity, and help to improve the system's information detection and processing performance [4]. Commonly used multisensor data fusion methods are the weighted average method, Kalman filter method, Bayesian estimation method, evidence inference method, fuzzy logic inference method, and artificial neural network method. Neural networks have strong nonlinear processing capability and meet the needs and technical requirements of multisensor data fusion. In the process of processing multisensor data fusion, the neural network model is used, and the learning algorithm inside learns the training samples, and eventually, through continuous learning, the neural network model is obtained, and then, the network model is used to obtain the signal processing capability, test the test samples, test the performance of the fusion model, and realize the fusion processing of multisensor data [5]. Among the many methods of data fusion, artificial neural networks have unique advantages in terms of the operating environment, information category, and applicability and a wide range of data fusion. Therefore, the research of applying neural networks for multisensor data fusion has received attention from various aspects of the world.

At this stage, in most Chinese young people, fast-paced daily life, work, and increased psychological pressure result in most Chinese young people's bodies in a state of subhealth and the emergence of some common chronic diseases; if this continues, without strengthening physical exercise and effective prevention, the physical condition of young people will become worse and worse, not conducive to the development of society. According to statistics, the number of deaths due to chronic diseases is increasing year by year, and they come rapidly, which for most of the Chinese aged people will cause huge socioeconomic and psychological pressure to their families in the light and even endanger their own lives in the heavy cases. Therefore, for the younger generation, it becomes especially important to exercise scientifically and effectively in fast-paced daily life [6].

A sports monitoring system based on multisensor information fusion is constructed in this project, which combines with IoT technology to achieve the monitoring of body temperature, blood pressure, EMG, and pulse during human exercise. The adaptive dynamic programming (ADP) data theoretical algorithm is applied in this human physical exercise monitoring system to fuse the physiological parameters obtained from the multisensors in the sensing layer of the system to realize the monitoring and judgment of the user's physical exercise condition.

2. Current Status of Research

With the rapid development of science and technology, there have been great advances in electronic technology, wireless communication technology, and biosensor monitoring. Health monitoring devices are developing towards integration, intelligence, multifunctionality, and portability [7]. The new health monitoring equipment has more comprehensive functions and monitors a wider range of human physiological parameters, and the structure and size of the whole equipment are more miniaturized. The core idea of the Bayesian filtering algorithm is to calculate the corresponding probability value according to the input data of the known sensor. According to the uncertainty of sensor measurement, it is expressed as conditional probability. Each sensor is estimated by Bayesian filtering, and finally, the calculated probability is calculated. The distribution combines a joint posterior probability distribution function. At this stage, the existing portable intelligent monitoring devices are mainly intelligent bracelets and intelligent clothing. A smart clothing company in Shenzhen, China, has developed a new type of smart clothing. This kind of clothing uses a self-developed flexible sensor, which has many different functions and soft models and can have certain deformation and other advantages [8]. It also has bioelectricity, pressure, and other sensor functions and can transmit bioelectric signals, pressure values, and respiratory frequency signals generated by human activities and obtain resting ECG/heart rate data, body posture parameters, and respiratory rate parameters. It can view the data via a mobile app and what measures should be taken for the current situation.

A smart company has developed a range of smart exercise clothing, with different kinds of clothing having different functions. Some garments can keep the body at a constant temperature, while others can make working out safer and reasonably efficient [9]. It also connects to your phone via Bluetooth and gives a more reasonable fitness plan based on data analysis. At present, smart monitoring equipment still has some shortcomings that need to be resolved, such as relatively high cost, short battery life, poor adaptability, and relatively simple functions and appearance structures [10]. Both can be made into the human body daily clothes to wear, can also be made into jewelry, and can also be made into smart helmets, smart glasses, and many other types. At present, manufacturers domestically and internationally have been using a variety of advanced technology to develop more advanced wearable clothing to meet the requirements of people's use.

The process of information processing is a core part of multisensor physical exercise monitoring through actual data reception, data processing with comparative analysis with existing knowledge and experience, and rational output results based on all acquired information [11]. Currently,

there are algorithms for information fusion such as fuzzy algorithms, neural networks, mutual correlation algorithms, and specific relational equations. The neural network algorithm is considered one of these information fusion algorithms with better accuracy in multisensor fire detection and is widely used by people in various fields. Compared with the traditional single sensor, these processing methods have obvious essential differences in the processing methods of the detection signal. It is now more common to classify according to the processing level and level of fusion, which is divided into three levels: information layer fusion, feature layer fusion, and decision-making layer fusion. Neural networks are a class of physiologically based intelligent bionic models that simulate the working principles of the human brain to deal with problems, consisting of a large number of processing units in a nonlinear adaptive dynamic system with good self-adaptability, self-organization, and strong learning, associative fault tolerance, and anti-interference capabilities [12]. The advantages of this technology are reflected in the fields of pattern classification recognition and nonlinear curve fitting. The neural network is a research hotspot in the field of artificial intelligence development. When the neural network is applied to multisensor data fusion, the first step is to select a suitable neural network model, and the selection criteria are the requirements of the fusion system and the characteristics of the sensors, including the topology of the network, neuron characteristics, and learning rules [13]. It is also necessary to establish connections between the input and sensor information and between the output and the system decision and then determine the assignment of weights based on the acquired sensor information and the corresponding system decision information to complete the training of the network [14]. When the sensor is accurate, we can correctly determine the health of the human body. If the accuracy of the sensor is insufficient, it will greatly affect the recognition of the human health and may even cause undesirable consequences. Therefore, special attention should be paid to the accuracy and stability of the sensor. After training the neural network which can then participate in the actual fusion process, the data obtained from the sensors are first processed appropriately by the process and then used as the input to the neural network, which is processed by the neural network and finally sent to the processing to interpret it as the system-specific decision behavior; the BP neural network is currently the most widely used network. Many researchers are currently working on neural networks in the field of multisensor data monitoring with satisfactory results.

3. Design of a Physical Exercise Monitoring System with Multisensor Information Fusion

3.1. Design of a Multisensor Physical Exercise Monitoring System. In the multisensor information system, the multisensor information has a variety of manifestations, huge information capacity, complex correlations between various types of multisensor information, and high requirements for the timeliness of information acquisition and processing, which requires an effective method to collect and process multisensor information acquired by multilevel sensors in the multisensor system, and through the coordination and performance complementarity among multisensors, to quickly and effectively to derive a comprehensive and correct understanding of the surveillance (detection target) object [15]. The research design of this paper is a monitoring system of human physiological parameters for physical exercise, which is mainly used for real-time monitoring of physical exercise in the daily life of families and individuals and real-time feedback of the physiological parameters of human movement. After an in-depth understanding and study of the functions to be achieved and the technical theoretical knowledge required, the overall structure and functions of the system are systematically designed and studied. The system is divided into three parts: information acquisition, information judgment, and information display as shown in Figure 1.

The system establishes a hardware architecture based on a Wi-Fi network, uses an embedded Wi-Fi microcontroller as the processing core of the system, and uses Java programming language to design and develop a software application platform for the remote health monitoring systems. The system detects four basic physiological parameters of the human body: pulse, heart rate, blood pressure, and body temperature from multiple information sources, and combines the concept of data fusion to give a judgment of whether the human body is in a healthy state. At the same time, the system also designs the functions of remote real-time monitoring of body indicators, intelligent heart rate monitoring and first aid, and automatic storage of health data according to actual needs [16]. Excessive sweating and insufficient rehydration can also lead to dehydration and affect health. In the case of heavy sweating, conditions such as thirst, oliguria, fatigue, muscle cramps, and heat cramps may occur. In severe cases, symptoms of heat stroke may occur and may even be life-threatening. Data on basic human physiological parameters of the user (pulse, EMG, blood pressure, and body temperature) are collected through wearable devices that are in contact with the body. After obtaining the data, they are sent to the processor and simply classified. The various physiological indicators of the user collected by the human body indicator sensor collection terminal are processed by the Wi-Fi module and then uploaded to the server in real time through the Wi-Fi wireless network; i.e., in this system, the Wi-Fi module acts as both the communication module and the only processor in the system. To address the binding and identification of data information, a unique ID is assigned to each registered user on the server side, and users can view their information related to this vital sign signal through the smart mobile terminal-based app. If the physiological indicators are out of the preset range, the system will display the corresponding alarm information and the alarm will be automatically alerted. At this time, the user can choose to store the abnormal physiological indicator information in the database for future analysis.

$$\frac{x_m - \sqrt{x^2 + m^2}}{x_m} \leq e. \tag{1}$$

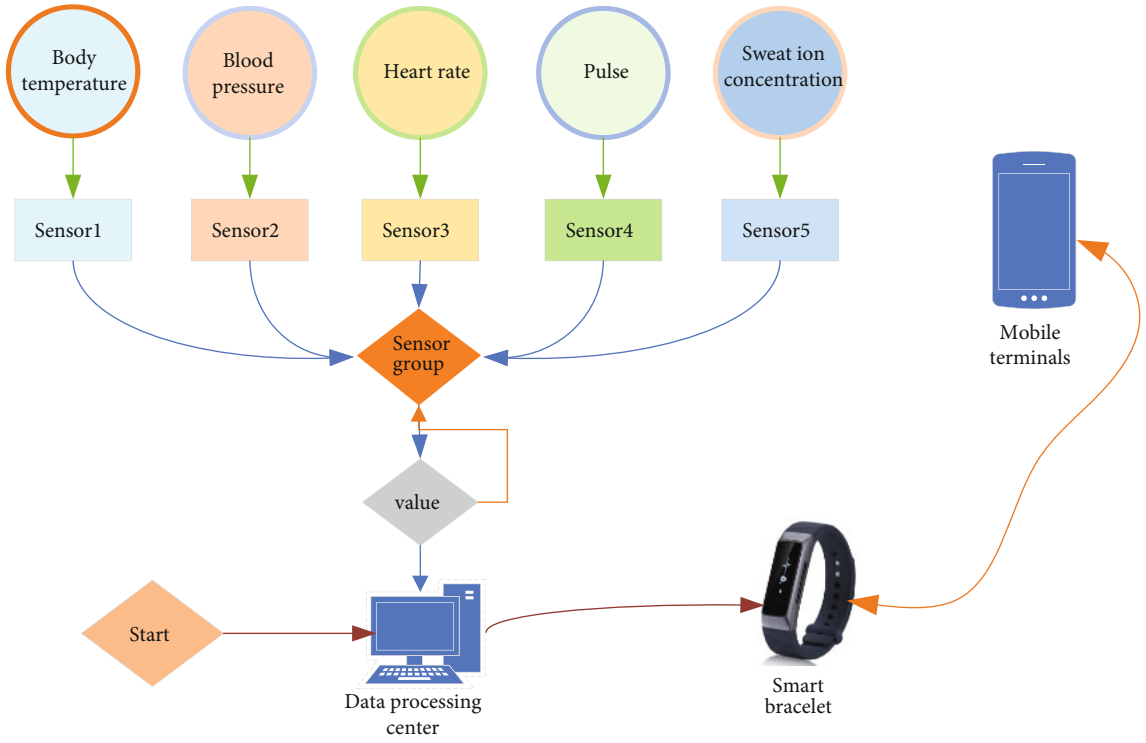

Figure 1: Structure flow of the physical exercise monitoring system.

This paper discusses a multilevel multisensor information acquisition system, which mainly completes the collection and acquisition of detection data from radar sensors, photoelectric sensors, and ground sensors, and performs the necessary data preprocessing. The multisensor information acquisition system is the basis for application-specific surveillance information systems for fusion processing, information monitoring, and information dissemination, providing them with raw surveillance data information. The information quality provided by multilevel multisensor directly affects the quality and performance of multisensor information fusion output. Multisensor systems in surveillance information systems are often covered according to partitions, which form multisensor information acquisition systems. Multilevel multisensor system partitioning is shown in Figure 2.

A fiber optic radiation temperature sensor can be used to measure the body temperature signal and output the AD value of the measured body temperature. A fiber optic absorption probe has the obvious advantages of small size, high accuracy, small interaction with the electromagnetic field, and high sensitivity, but the measurement range is relatively narrow. Because the measurement of a specific part of the human body can be obtained from this part of the human body temperature, the measurement range has small impact on the accurate measurement of body temperature, so you can choose the fiber optic radiation temperature sensor to measure body temperature. Since the fiber optic diameter is small and malleable, multiple probes can be used to measure body temperature in different parts of the body, constituting a multisource temperature measurement system. The body temperature acquisition module is selected from Huaqiang Electronics manufacturer's V1.1 body temperature acquisition sensor [17]. After comparing with other sensors in terms of accuracy, stability, size, sensitivity, and other aspects, this temperature acquisition module has certain advantages. The operating characteristic of this temperature acquisition module is that the voltage decreases as the temperature increases. The typical feature of this acquisition module is that it is sensitive to temperature and can be accurate to two decimal places, which is especially suitable for small changes in the human body temperature range under the influence of various conditions, and the temperature range is exactly in line with the human body temperature range. This section conducts an overall test of the physical exercise system and compares the stability, reliability of the system, and the accuracy of the physiological data collected by the system. Using the nonlinear fitting ability of neural network, through the nature of the data correlation between sensors in the multisensor system, the accurate prediction value is used to diagnose whether the sensor is faulty and the fault location and to repair the data of the faulty sensor. The linear range of voltage change is 30-4 degrees/voltage 2.127-1.193 V, and the temperature characteristic curve is shown in Figure 3.

Pulse check is an auxiliary test used to check the normal functional status of the circulatory system. The human circulatory system is responsible for transporting various nutrients and waste products in the body, and the blood acts as a carrier in a never-ending work. During the cardiac cycle, periodic pulses of dilation and vascular return occur because of alternating ventricular systole and diastole. The

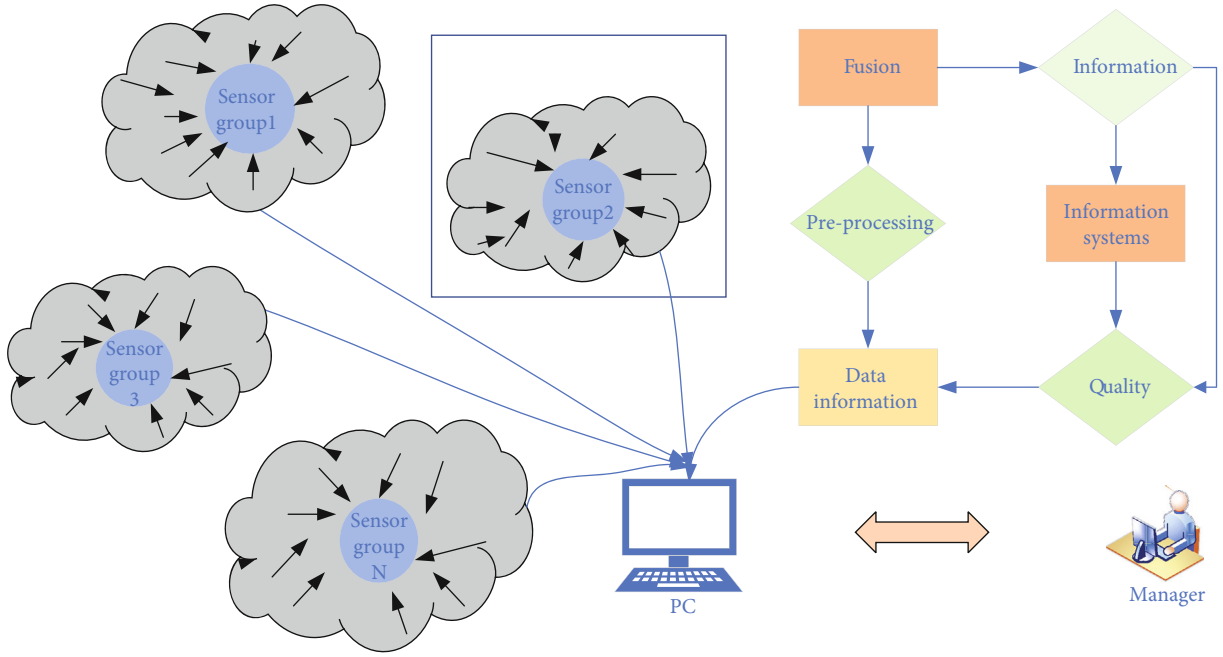

Figure 2: Schematic diagram of the partitioned coverage of a multisensor system.

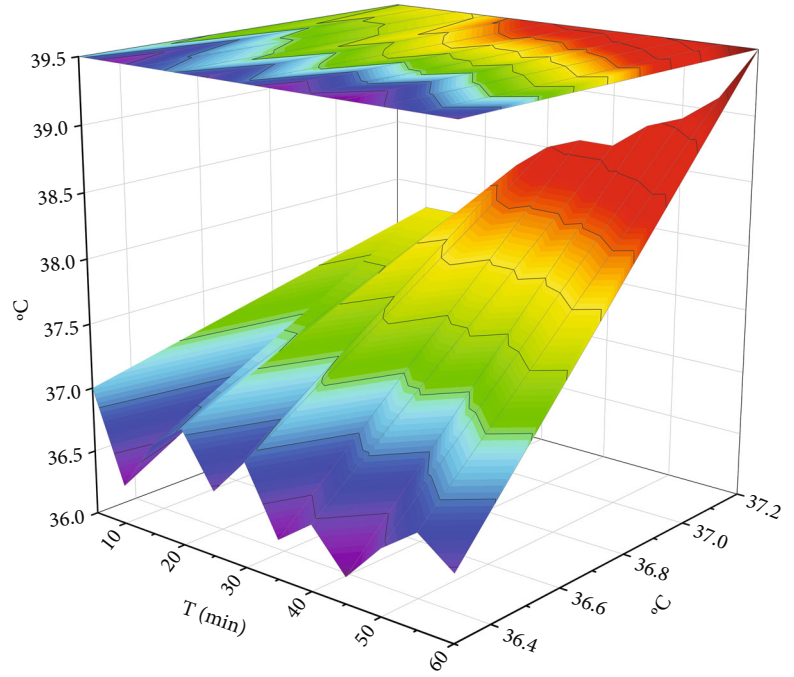

Figure 3: Temperature characteristic curve of physical exercise.

pulse rate changes significantly when the body is in poor condition, especially when critically ill. Changes in the pulse rate are also used by doctors as an important indicator in the diagnosis of a condition. A pulse check includes the examination of the rate, rhythm, strength, and waveform of the pulse. In this article, the pulse test uses a pulse sensor to detect the pulse and output a digital signal value. The probe of the sensor is applied to the skin surface where the arterial beat is strong and a certain pressure is applied. The micropressure material in the probe picks up the pressure signal of the pulse beat, and an electrical signal change is generated, which is first amplified and then processed by the adjustment circuit to obtain the complete waveform of the pulse beat, which further gives a set of pulse signals synchronized to the pulse beat. Piezoelectric and piezoresistive pulse sensors are mainly used in clinical applications for the pathological analysis of cardiovascular diseases such as atherosclerosis.

$$x = \frac{X - \max(X)}{\max\left(X^2\right) + \min(X)}. \quad (2)$$

3.2. Multisensor Data Fusion Processing. Data preprocessing is an important prerequisite for multisensor data fusion. Due to the relatively large variation in the range of variation of various physiological parameters during exercise, unprocessed raw data from sensors often have missing data, misleading data, data not in line with common sense, and other problems, resulting in data analysis being not easy. To analyze the data reasonably, we usually must perform preprocessing operations on the raw data to normalize the raw sensor data. The specific applications of multisensor information fusion technology in the military field mainly include marine surveillance and air-to-air and surface-to-air defense systems. The marine monitoring system mainly detects, tracks, and identifies military targets. Air-to-air and surface-to-air defense systems mainly detect, track, and identify enemy aircraft, missiles, and air defense weapons. After normalization of the original data, the data will be stored in plain text form after preprocessing, which is convenient for subsequent programming. The multisensor information is collected through the multisensor data collection interface, and the collected multisensor information is distributed to the upper-level monitoring center using the multisensor information distribution service, thus completing a system with two or more levels of multisensor information collection. The types of multisensor information in the system mainly include radar information, optoelectronic information, ground sensor information, and navigation and positioning information, and the multisensor information acquisition system acquires various types of multisensor information in real time by adapting different types of sensor acquisition interfaces, as shown in Figure 4.

For the "surveillance information system + RS + GPS + GIS," the core problem of research and solution is that it should make full use of the complementary or redundant multisensor in the time and space domain to carry out the relevant coordination, data processing, and synthesis of multisource information. There is no clear boundary between various sensor information sources, multisensor systems, integrated situational systems, information fusion, and auxiliary decision support systems in the whole surveillance information system, and there is information coupling and feedback between various systems [18]. Therefore, the multilevel multisensor information acquisition system can obtain two or more levels of multidimensional surveillance target information. At present, in this field, multisensor information fusion technology is mainly used to fuse the information collected by each sensor in the smart car, to determine the road position, the roadblock ahead, the speed limit, and other information of the smart car, and then, according to the information in the system, the corresponding rules can realize autonomous driving of smart cars.

$$y\left(x^i\right) = v_0' - \sum_{i=1}^{n} \kappa_i\left(x^i\right)^2. \quad (3)$$

In the target environment, a single sensor can only capture a certain type of information of the target environment and cannot form a complete description of the target environment. And the information fusion mode of a single sensor is also relatively low level, simply imitating the process of processing primary information in the human brain, and cannot extract the effective information needed for the target environment. With heterogeneous multiple sensors, the type of information collected for the target environment is different due to the different sensor types. Therefore, this rich source of information and information collection is followed by a multisensor information fusion technique that can more fully extract the valid information in the target environment, resulting in a more comprehensive and accurate description of the target environment. Each multisensor information fusion mode has its advantages and disadvantages. The multisensor data fusion algorithm is applied to the monitoring and analysis of the effect of physical exercise, a variety of human exercise physiological parameters are collected through the multisensor data network, and the collected human physiological parameters are subjected to data fusion calculation, and finally, the physical exercise effect is obtained. For example, the data-level fusion mode has the advantage of a more comprehensive amount of original information, which is what feature-level fusion lacks, and the less computational information processed by feature-level fusion is also an advantage that data-level fusion does not have. Therefore, in the process of fusing specific target environment information in specific application areas, the advantages and disadvantages of each mode can be combined and different multisensor information fusion algorithms can be used flexibly at different levels, thus improving the ability to accurately describe the target environment.

Tracking of moving objects requires filtering out noise in noise-containing data and minimizing or even eliminating the effect of noise on the tracking system to obtain an optimal estimate of the target's motion state. The Kalman filtering algorithm is the most classical and commonly used target tracking filtering algorithm, if the tracking system satisfies the linear and Gaussian white noise condition, using the minimum variance criterion to estimate the tracking object motion state recursive processing method. The Kalman filter algorithm not only calculates the optimal estimate of the tracking object's motion state at a given moment but also calculates the error covariance matrix. A theoretical framework for optimal tracker design is provided for tracking problems with known target system equations and observation equations. The method of tracking the measurement data of a single sensor can no longer meet the increasing requirements. People have begun to explore the comprehensive utilization of the measurement data of multiple sensors to maximize the extraction of useful information contained in the measurement data to achieve tracking of moving targets. However, practical target tracking systems are often nonlinear, and the traditional Kalman filtering algorithm cannot handle nonlinear tracking problems well. The nonlinear filtering of target tracking, i.e., the estimation of the posterior probability distribution of the

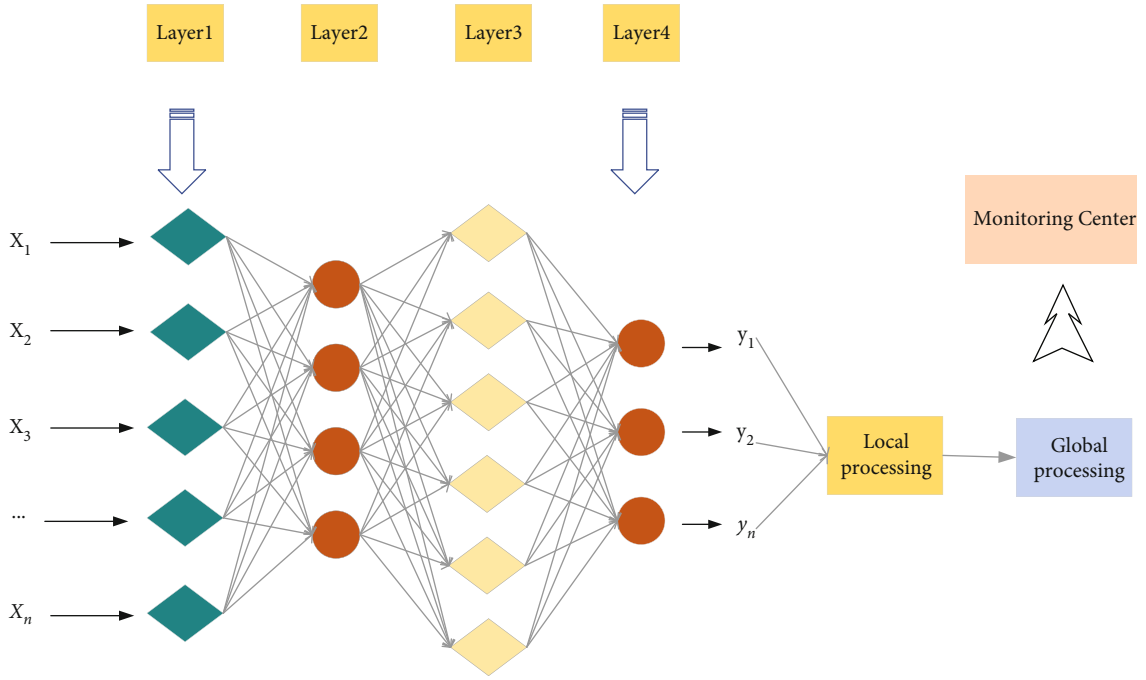

Figure 4: Network structure model of multilevel multisensor information acquisition system.

moment state under the observation sequence condition, is expressed by the formula, where the optimal method to deal with the nonlinear tracking filtering problem is to obtain the posterior probability distribution of the target motion state; however, obtaining the exact posterior probability distribution requires a large amount of data, which cannot be realized in the practical application system, and some suboptimal approximation methods which have been proposed for these commonly used nonlinear target tracking filtering algorithms are discussed below.

$$c_k = \int p(z_{k+1}|x_k)p(x_{1:k+2}|z_k)d, \quad k = 1, 2, \cdots. \tag{4}$$

Many classical filtering and fusion ideas originate from Bayesian filtering methods, such as particle filtering, Kalman filtering, and other algorithms which are specific implementations of Bayesian filtering algorithms. Multisource information fusion technology, by collecting multiple information sensors to confirm different sensor systems multiple times, can be more conducive to improving the reliability and detection capabilities of the sensor system; it is conducive to improving the quality and credibility of the system detection data and information degree and is conducive to improving the system's ability to perceive specific data and data logical reasoning, speed up the accuracy and response speed of the system, and improve the detection reliability of the system. The core idea of the Bayesian filtering algorithm is to calculate the corresponding probability values based on known sensor input data, represent the uncertainty of sensor measurements in terms of conditional probabilities, make Bayesian filtering estimates for each sensor, and finally synthesize the calculated probability distributions into a joint posterior probability distribution function. The environmental features detected by the prior model are characterized by computing the sensor fusion weights derived from the distribution function. Bayesian filtering is characterized by the fact that all estimates are based on probability distributions rather than specific values, and the goal of the Bayesian filtering algorithm is to combine the state probability distributions of the previous moment to estimate the current moment state quantities based on the control and observation model. Also, Bayesian filtering is a general term for a large class of methods, an abstract expression, and a concrete implementation of the Kalman filter fusion algorithm. The Kalman filter algorithm is based on the prerequisite that an accurate mathematical model is known. At this stage, the fast-paced daily life, work, and increased psychological pressures of most Chinese young people have caused most Chinese young people's bodies to be in a subhealthy state and have some common chronic diseases. If this goes on, they will not strengthen physical education. With exercise and effective prevention, the physical condition of young people will get worse and worse, which is not conducive to the development of society. However, building accurate mathematical models for nonlinear target tracking systems is difficult. In practical target tracking systems, it happens that the target state model and observation model do not match the actual system, which is a case of partial prior knowledge uncertainty of the target model from the estimation theory point of view. To solve the problem of mismatch between the mathematical model established in the target tracking system and the actual system, the adaptive Kalman filtering algorithm is generated. Adaptive Kalman filtering uses the information carried by the newly acquired measurement data to change the Kalman gain matrix and the system noise of the target tracking problem online to seek an approximation of the optimal filtering

and to solve the mismatch between the system modeling and the actual motion of the target.

$$\phi(k) = \begin{bmatrix} T & 0 & \frac{T}{2} \\ 1 & 0 & 0 \\ 1 & T^2 & 1 \end{bmatrix}, \quad f(x) = \operatorname{sgn}\left(\sum_{i=1}^{l} \alpha_i^x \Phi(x_i) - y_i b^*\right). \tag{5}$$

Multisensor is the basis of information fusion, multisensor information is the object of processing of information fusion, and integrated processing is the core of information fusion; multisensor information fusion is performed by combining the advantages of multiple single sensors, reasonably mining the use of the detected fire characteristic information and fusing the spatially and temporally complementary or redundant information according to certain criteria to obtain a unified conclusion about the observed object. Information fusion can be classified by its fusion structure, algorithms, techniques, etc. [19]. The neural network is a research hotspot in the field of artificial intelligence development. When the neural network is applied to multisensor data fusion, the appropriate neural network model must first be selected. The selection criteria are the requirements of the fusion system and the characteristics of the sensor, including the network, the topological structure, neuron characteristics, and learning rules etc. At the same time, it is also necessary to establish a connection between input and sensor information and between output and system decision-making and then determine the distribution of weights according to the acquired sensor information and corresponding system decision-making information to complete the training of the network. There are clear and fundamental differences in the way these processing methods treat the detection signal compared to traditional single sensors. Nowadays, it is more common to classify them by the level and hierarchy of processing of fusion, which is divided into three levels: information-level fusion, feature-level fusion, and decision-level fusion. The information fusion level system focuses on how to analyze and process the multisensor detection information at different processing stages. The higher the fusion level, the less detail is required for the original information, but the corresponding level of abstraction is also higher.

$$K(X_{1,}X_2) = \left[\left(X_1^{T^2}, X_2\right)\right]^{\ell}. \tag{6}$$

Time synchronization of different sensors in the multisensor fusion process is very important, but the basis of time synchronization is to ensure that each sensor uses the same clock source and the information to be collected in the same moment of data. Because the sensor clocks used generally have drift errors and each clock source has a different drift, initial moment timestamp alignment is required in the multisensor fusion process, but with a period of operation, the aligned timestamps will still be misaligned by drift. The timestamp synchronization method used in this thesis is to design a hardware pulse generator to unify the trigger pulses of all sensors, and each pulse trigger can correct and eliminate the clock source drift, as shown in Figure 5.

4. Performance Results of a Multisensor Physical Exercise System

The importance of body temperature to the human body is self-evident, and special attention should be paid to the monitoring of human body temperature when monitoring the health condition of the human body. When the system is running, check that the whole system is in normal connection, open the upper computer software interface, and supply power to the whole system. In the port setting interface of the upper computer LabVIEW, select the COM port and baud rate values to ensure that the Arduino is successfully connected to LabVIEW. The user enters information such as name, gender, age, mobile phone, landline, and notes in the information input interface, places the sensor on the appropriate acquisition site, and clicks start, and the system collects and reads the data and displays the acquired data and waveform graph in the data display interface. The data analysis interface will show the specific situation of human health. When detecting the body temperature signal, a fiber optic radiation temperature sensor can be used to measure the body temperature signal and output the AD value of the measured body temperature. The optical fiber absorption probe has obvious advantages such as small size, high accuracy, small interaction with electromagnetic fields, and high sensitivity, but the measurement range is relatively narrow.

By testing the overall operation of the system, the test obtained that the system can operate stably and continuously, indicating that the system is normal. After that, the stability and accuracy of the sensors are tested. The accuracy and stability of the sensor are extremely important for the whole health monitoring system. When the sensor measurement is accurate, we can correctly determine the health of the human body; if the accuracy of the sensor is not enough, it will greatly affect the identification of human health conditions and may even cause adverse consequences. Therefore, special attention should be paid to the accuracy and stability of the sensor. Body temperature usually refers to the internal temperature of the human body. In daily life, mercury thermometers are commonly used to measure the axillary body temperature, which is normally in the range of 36-37 degrees Celsius. Body temperature is susceptible to various internal and external factors, so body temperature can vary slightly within the normal range, usually by no more than 1 degree Celsius, and this change is not harmful to human health. Due to the relatively large variation range of various physiological parameters during exercise, the unprocessed raw data of the sensor often appears: data missing, disordered data, and data inconsistent with common sense, which makes data analysis difficult. To analyze the data reasonably, we usually need to preprocess the raw data to standardize the raw data of the sensor. For example, in a physiological state, the body temperature is at a low value in the morning and

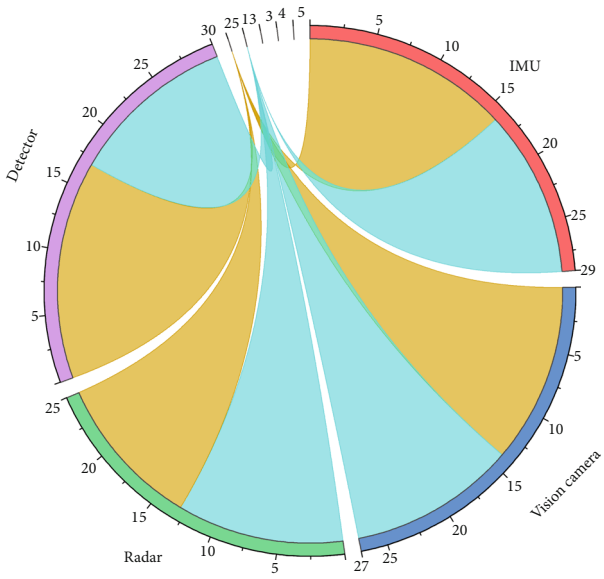

Figure 5: Multisensor time synchronization comparison schematic.

will rise slightly in the afternoon. Suddenly entering a hot environment or emotional stress can also cause a slight increase in body temperature. There are also slight differences in body temperature by age; for example, children have a slightly higher body temperature compared to adults, while older people have a slightly lower body temperature. The relative constancy of body temperature is one of the important basic conditions for maintaining normal life activities in the human body.

The information revealed by the human heart rate reflects the health of the human heart. The heart rate is the number of times the heart beats in a minute, and there are two different states. Quiet heart rate is the size of the human heart rate when in a quiet state, and the normal adult heart rate value range is generally 60-100 beats. The maximum heart rate of a person refers to the maximum number of times the heart beats in a minute. The heart rate of adults is generally between 60 and 100 times/min, most people are in the 60-80 times/min, and women generally have faster heart beat than men; for children, the heart rate may be higher generally in the 100 times/min or more; for the elderly due to the aging of the body organs, the heart rate will have a certain degree of reduction. It can be seen in heavy physical work for long periods and athletes. Athletes have a slower heart rate than the average adult, typically around 50 beats per minute. In the quiet state, there are some differences in the heart rates of adults and athletes, as shown in Table 1.

Most of the sweat is water, and this also contains minerals such as sodium, potassium, chloride, magnesium, calcium, and phosphorus. The Kalman filter algorithm can not only calculate the optimal estimation of the motion state of the tracking object at a certain moment but also calculate the error covariance matrix. It provides a theoretical framework for optimal tracker design for the tracking of known target system equations and observation equations. The most ions in sweat are sodium and chloride, with some

Table 1: Heart rate in different exercise states.

Status	Kids	Females	Male	The elderly
Normal	99	77	100	90
Slow walking	102	73	92	55
Rush walking	110	85	70	74
Jogging	96	94	81	57
Running	96	75	66	73
Vigorous exercise	100	66	80	50

amount of potassium and calcium ions also present. People sweat a lot during some strenuous physical activity, and it is mainly sodium ions that are lost with sweat. The body relies on sodium and chloride ions to regulate fluids and body temperature, and these two ions are important to the body. Although sweating is a physiological regulation, heavy sweating and insufficient rehydration will also lead to dehydration and affect your health. A relatively large amount of sweating may produce conditions such as thirst, low urination, fatigue, muscle cramps, and heat cramps. In severe cases, symptoms of heatstroke may occur and may even be life-threatening [20]. When the body exercises vigorously, it also loses large amounts of mineral ions after losing large amounts of sweat. The pH balance in the body is then affected to some extent, the pH level changes and the body's sweat ratio is lower than normal. The importance of sweat for the human body cannot be overstated, and it also reflects the health of the body to some extent. The measurement of human health can also be done by collecting and monitoring the sweating of the body and the ion concentration of sweat. The ion concentration in human sweat also reflects some of the health information of the human body, as shown in Figure 6.

This section provides an overall test of the physical exercise system, comparing the stability and reliability of the system as well as the accuracy of the physiological data collected by the system. The nonlinear fitting capability of the neural network is used to diagnose whether a sensor is faulty and the fault location by the nature of data correlation between sensors in a multisensor system using accurate predictive values and repairing the data from the faulty sensor. The role of the BP neural network in the sensor fault diagnosis structure proposed in this chapter is to fuse the correlation data between individual sensors, and the fault diagnosis relies on the prediction value errors of these fusion models to determine the fault of the system and to recover the faulty sensor data. For the three typical forms of sensor faults detected by the simulation experiments, the data fusion sensor fault diagnosis model proposed in this paper can accurately detect the faults and remedy them effectively, which proves that such a sensor diagnosis model is effective. It ensures that the system can operate continuously and stably in actual use, the measured physiological data are accurate and reliable, and the human exercise physiological parameters obtained after multiconditional judgment are correct.

The average value of the athlete's reaction to action is 46.82 ms. The IAAF's starting reaction limit is 100 ms. The

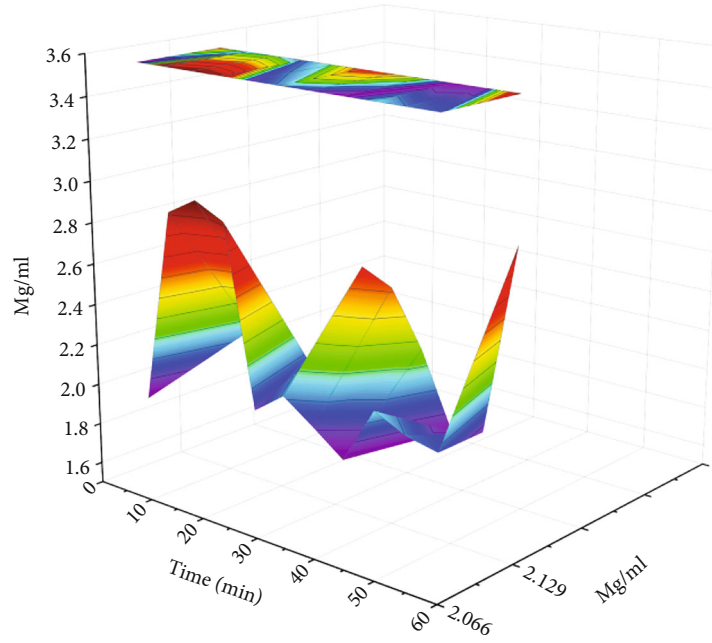

Figure 6: Sweat ion concentration in different exercise states.

average value of the athlete's reaction to action accounts for 46.82% of the starting reaction limit. The starting reaction limit includes the reaction to action, so the error of judging whether an athlete fouls a foul is also 46.82%. Athlete's reaction to action has an important influence on whether the athlete's starting reaction exceeds the limit and fouls. When reacting to the action, the fastest is the 8th track in the men's 100 m final with a time of 15 ms, and the slowest is the 4th track in the first group of the men's 200 M preliminaries with a time of 143 ms; the difference between the two is 128 ms. This shows that under the current electronic starting monitoring system, if the actual reaction time of two athletes is the same, then the first reaction time is 128 ms faster than the latter's starting reaction time. Therefore, under the same conditions, the former has a starting reaction time compared to the latter. The possibility of overlimit fouls has increased significantly.

5. Results of Multisensor Information Fusion Applications

Multisensor information fusion has a wide range of applications, and its specific applications in the military and civilian domains are briefly described below. In the military field, certain geographic locations or military activity areas are restricted by various factors, making it impossible for military personnel to make accurate judgments about the target environment. The emergence of multisensor information fusion technology is a good solution to this dilemma. Applying multisensor information fusion technology to this field can achieve accurate detection, precise positioning, tracking, and identification of the target environment, thus providing military commanders with more reliable battlefield information for effective judgment of the next military operation. The specific applications of multisensor information fusion technology in the military field are mainly marine surveillance, air-to-air and ground-to-air defense systems, etc. The ocean surveillance system mainly detects, tracks, and identifies military targets. The air-to-air and ground-to-air defense system mainly detects, tracks, and identifies enemy aircraft, missiles, and air defense weapons. At present, the main applications of sensors include marine defense, anti-submarine warfare, detection of stealth aircraft, artillery, electric warning, tracking enemy military actions, and preventing biochemical attacks as shown in Figure 7.

Multisensor information fusion technology is mainly used to fuse and reason with the information collected from video sensors, sound sensors, etc. in the robot and then combine it with the robot's own implanted operating program to perform the target task to complete the prespecified work in the field of intelligent transportation. At present, in this field, multisensor information fusion technology is mainly used to fuse the information collected from each sensor in the smart car, to determine the road location, roadblocks ahead, speed limits, and other information of the smart card, and then realize the autonomous driving of the smart card according to the corresponding rules in the system [21]. Multisensor information fusion technology is mainly through the information collected by infrared sensors, microwave sensors, etc., to detect the location of the hidden weapons or drug situation fusion analysis and finally get the fusion results to determine the site conditions. At the same time in this field, multisensor information fusion technology can also be an effective fusion of the information collected from the face, fingerprints, voice, etc., to improve the identification and authentication of the suspect, greatly improving the efficiency of crime-solving.

In the past medical diagnosis, surgeons often used visual inspection, thermometers, or stethoscopes to aid in diagnosis. More advanced and effective medical sensing

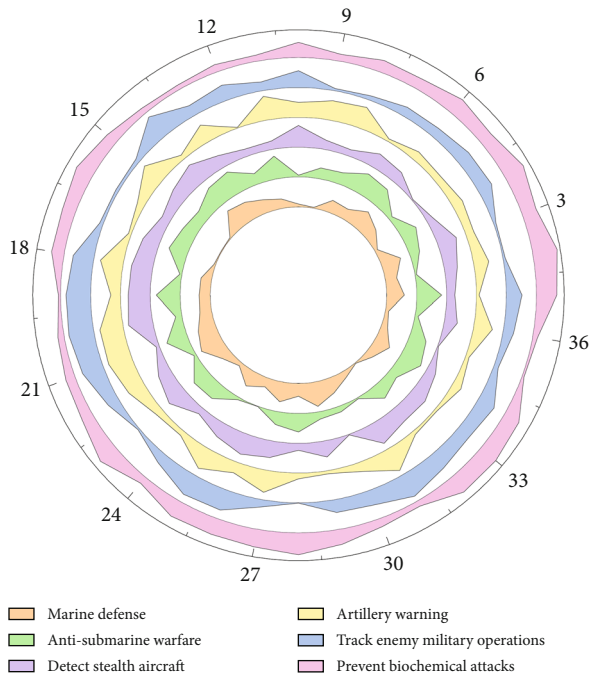

Figure 7: Application result.

technologies have now emerged, such as ultrasound imaging, localization, and identification of tumors. The use of information collected by these sensors and the effective fusion of this information has made modern medical diagnosis much more accurate and efficient.

6. Conclusion

Internet of Things (IoT) technology is rapidly booming and has become a newly developed norm in the process of modern people achieving information management in their daily lives. The integration of Internet data applied in wireless medical and health services is also increasing. Due to the high intensity of life and work pressure in modern society, people have less and less time to participate in physical exercise, and increased people are in a subhealthy or even unhealthy state. Therefore, how to carry out physical exercise scientifically and effectively is gaining increased attention. In this paper, we propose to apply the multisensor data fusion algorithm to monitor and analyze the effect of physical exercise and collect multiple human exercise physiological parameters through a multisensor data network and calculate the collected human physiological parameters by data fusion to finally derive the effect of physical exercise. Data fusion technology is a hotspot of research and attention in the field of multisensor target tracking, and multisensor target tracking data fusion technology has a broad development prospect. In general, it seems that there are still many problems that need to be studied. In this paper, for the proposed multilevel multisensor information acquisition solution, a three-level information acquisition system from the front-end multisensor to the monitoring station, the surveillance subcenter, and the surveillance center is realized by successively simulating access and accessing multisensor information. Finally, a demonstration and verification environment was built according to the system testing requirements, and the system testing was completed to demonstrate the software operation effect. The experimental results show that the system design is reasonable and feasible, and the software and algorithm research results are effectively usable, which solves the problems of multisensor information acquisition interface diversity and is not easy to expand in multilevel surveillance and achieves the purpose of the research. The research in this paper is only an initial phase of work, and many aspects deserve deeper research and improvement. At the same time, the research work in this paper is only a part of multisensor target tracking data fusion, which needs to be further improved in future research work.

Data Availability

The data used to support the findings of this study are available from the corresponding author upon request.

Conflicts of Interest

The authors declare that they have no known competing financial interests or personal relationships that could have appeared to influence the work reported in this paper.

References

[1] A. Dameshghi and M. H. Refan, "Wind turbine gearbox condition monitoring and fault diagnosis based on multi-sensor information fusion of SCADA and DSER-PSO-WRVM method," *International Journal of Modelling and Simulation*, vol. 39, no. 1, pp. 48–72, 2019.

[2] N. Xiong and P. Svensson, "Multi-sensor management for information fusion: issues and approaches," *Information fusion*, vol. 3, no. 2, pp. 163–186, 2002.

[3] Y. Lu, H. Wang, F. Hu, B. Zhou, and H. Xi, "Effective recognition of human lower limb jump locomotion phases based on multi-sensor information fusion and machine learning," *Medical & Biological Engineering & Computing*, vol. 59, no. 4, pp. 883–899, 2021.

[4] S. Sarkar, S. Sarkar, K. Mukherjee, A. Ray, and A. Srivastav, "Multi-sensor information fusion for fault detection in aircraft gas turbine engines," *Proceedings of the Institution of Mechanical Engineers, Part G: Journal of Aerospace Engineering*, vol. 227, no. 12, pp. 1988–2001, 2013.

[5] K. Jiang, D. Su, and Y. Zheng, "Intelligent acquisition model of traffic congestion information in the vehicle networking environment based on multi-sensor fusion," *International Journal of Vehicle Information and Communication Systems*, vol. 4, no. 2, pp. 155–169, 2019.

[6] I. V. Maslov and I. Gertner, "Multi-sensor fusion: an evolutionary algorithm approach," *Information Fusion*, vol. 7, no. 3, pp. 304–330, 2006.

[7] S. McLaughlin, B. Holbert, A. Fawaz, R. Berthier, and S. Zonouz, "A multi-sensor energy theft detection framework for advanced metering infrastructures," *IEEE Journal on Selected Areas in Communications*, vol. 31, no. 7, pp. 1319–1330, 2013.

[8] Y. Zhang, H. Zhang, N. M. Nasrabadi, and T. S. Huang, "Multi-metric learning for multi-sensor fusion based classification," *Information Fusion*, vol. 14, no. 4, pp. 431–440, 2013.

[9] T. D. Dixon, S. G. Nikolov, J. J. Lewis et al., "Task-based scanpath assessment of multi-sensor video fusion in complex scenarios," *Information Fusion*, vol. 11, no. 1, pp. 51–65, 2010.

[10] L. R. M. Johansson and N. Xiong, "Perception management: an emerging concept for information fusion," *Information Fusion*, vol. 4, no. 3, pp. 231–234, 2003.

[11] M. Wei, M. Chen, and D. Zhou, "Multi-sensor information based remaining useful life prediction with anticipated performance," *IEEE Transactions on Reliability*, vol. 62, no. 1, pp. 183–198, 2013.

[12] E. Nazari, R. Biviji, A. H. Farzin, P. Asgari, and H. Tabesh, "Advantages and challenges of information fusion technique for big data analysis: proposed framework," *Journal of Biostatistics and Epidemiology*, vol. 7, no. 2, pp. 189–216, 2021.

[13] J. A. Rodger, "Toward reducing failure risk in an integrated vehicle health maintenance system: a fuzzy multi-sensor data fusion Kalman filter approach for IVHMS," *Expert Systems with Applications*, vol. 39, no. 10, pp. 9821–9836, 2012.

[14] L. Gao, A. K. Bourke, and J. Nelson, "Evaluation of accelerometer based multi-sensor versus single-sensor activity recognition systems," *Medical Engineering & Physics*, vol. 36, no. 6, pp. 779–785, 2014.

[15] J. J. Guiry, P. Van de Ven, and J. Nelson, "Multi-sensor fusion for enhanced contextual awareness of everyday activities with ubiquitous devices," *Sensors*, vol. 14, no. 3, pp. 5687–5701, 2014.

[16] S. Roy, D. Sarkar, and D. De, "Entropy-aware ambient IoT analytics on humanized music information fusion," *Journal of Ambient Intelligence and Humanized Computing*, vol. 11, no. 1, pp. 151–171, 2020.

[17] O. Banos, M. Damas, A. Guillen et al., "Multi-sensor fusion based on asymmetric decision weighting for robust activity recognition," *Neural Processing Letters*, vol. 42, no. 1, pp. 5–26, 2015.

[18] J. Triloka, S. M. N. A. Senanayake, and D. Lai, "Neural computing for walking gait pattern identification based on multisensor data fusion of lower limb muscles," *Neural Computing and Applications*, vol. 28, no. S1, pp. 65–77, 2017.

[19] G. Fasano, D. Accardo, A. Moccia et al., "Multi-sensor-based fully autonomous non-cooperative collision avoidance system for unmanned air vehicles," *Journal of Aerospace Computing, Information, and Communication*, vol. 5, no. 10, pp. 338–360, 2008.

[20] F. Miao, Z. D. Liu, J. K. Liu, B. Wen, Q. Y. He, and Y. Li, "Multi-sensor fusion approach for cuff-less blood pressure measurement," *IEEE Journal of Biomedical and Health Informatics*, vol. 24, no. 1, pp. 79–91, 2020.

[21] A. Belmonte-Hernandez, G. Hernandez-Penaloza, F. Alvarez, and G. Conti, "Adaptive fingerprinting in multi-sensor fusion for accurate indoor tracking," *IEEE Sensors Journal*, vol. 17, no. 15, pp. 4983–4998, 2017.

Hindawi
Journal of Sensors
Volume 2022, Article ID 3817226, 11 pages
https://doi.org/10.1155/2022/3817226

Research Article

Research on the Construction of Human-Computer Interaction System Based on a Machine Learning Algorithm

Yu Wang

Department of Information Engineering, Chengyi College of Jimei University, Xiamen 361000, China

Correspondence should be addressed to Yu Wang; ruoque1001@jmu.edu.cn

Received 17 November 2021; Revised 10 December 2021; Accepted 16 December 2021; Published 10 January 2022

Academic Editor: Gengxin Sun

In this paper, we use machine learning algorithms to conduct in-depth research and analysis on the construction of human-computer interaction systems and propose a simple and effective method for extracting salient features based on contextual information. The method can retain the dynamic and static information of gestures intact, which results in a richer and more robust feature representation. Secondly, this paper proposes a dynamic planning algorithm based on feature matching, which uses the consistency and accuracy of feature matching to measure the similarity of two frames and then uses a dynamic planning algorithm to find the optimal matching distance between two gesture sequences. The algorithm ensures the continuity and accuracy of the gesture description and makes full use of the spatiotemporal location information of the features. The features and limitations of common motion target detection methods in motion gesture detection and common machine learning tracking methods in gesture tracking are first analyzed, and then, the kernel correlation filter method is improved by designing a confidence model and introducing a scale filter, and finally, comparison experiments are conducted on a self-built gesture dataset to verify the effectiveness of the improved method. During the training and validation of the model by the corpus, the complementary feature extraction methods are ablated and learned, and the corresponding results obtained are compared with the three baseline methods. But due to this feature, GMMs are not suitable when users want to model the time structure. It has been widely used in classification tasks. By using the kernel function, the support vector machine can transform the original input set into a high-dimensional feature space. After experiments, the speech emotion recognition method proposed in this paper outperforms the baseline methods, proving the effectiveness of complementary feature extraction and the superiority of the deep learning model. The speech is used as the input of the system, and the emotion recognition is performed on the input speech, and the corresponding emotion obtained is successfully applied to the human-computer dialogue system in combination with the online speech recognition method, which proves that the speech emotion recognition applied to the human-computer dialogue system has application research value.

1. Introduction

In recent years, with the storm of artificial intelligence sweeping through, intelligent technologies have emerged in various fields, and the innovation of human-computer interaction has also received the attention of many scholars, many of whom have begun to research and design more natural ways of human-computer interaction. And human interaction methods used to transmit information have been many elementalized, but the most basic ways are dialogue, eyes, body movements, etc. They are the most natural interaction methods formed by humans in social development, and they are also the most consistent with human behavioral habits. Thus, speech and gesture are widely recognized by scholars as important means of natural human-computer interaction. And as an older interaction method than speech, the human gesture is relatively simple and can be better understood by computers compared to the complexity of speech. The use of manual gestures in human-computer interaction has been researched and developed over a long period [1]. Human-computer interaction systems and dialogue systems are service-oriented systems that directly use voice for interaction. With the gradual maturity of HCI systems and the gradual application of speech emotion

recognition in people's lives, there is a more urgent need to make machines intelligent to understand human emotions [2]. The intensities of the peaks and valleys of the spectrum are estimated by the average values of the small neighborhoods near the maximum and minimum values, rather than the exact maximum and minimum values.

The application of speech emotion recognition to the human-computer dialogue system, on the one hand, can make the dialogue system through the human voice as input and understand the emotion it contains and communicate with humans rich in emotion, giving human-computer dialogue system humanized and intelligent interaction characteristics [3]. On the other hand, medical service systems, call centers, car systems, and other applications based on speech emotion recognition systems can help people to improve the efficiency of work and efficiently solve the practical problems encountered by people. Therefore, speech emotion recognition has an important theoretical research value and its application research value in human-robot interaction. Humans and robots use force control to achieve like curtain wall installation work. Besides, human-robot collaboration technology is also applicable to the field of medical rehabilitation, such as limb rehabilitation training for some patients with cerebral thrombosis or some other limbs that need to be recovered [4]. Due to the increasing emergence of aging countries, robots that assist in the lives of the elderly have emerged to facilitate the care of these elderly people. Various entertainment robots are beginning to use new human interaction methods to appeal to the customer base [5]. Robotics-related technologies have gradually started to enter the world of common people and into the lives of most people close to them. Because of this, our requirements for robots are becoming increasingly stringent. Due to the close contact between humans and machines, the contact method must be stable and safe, and it is better to have certain self-help recognition ability so that it can respond in time to emergencies and ensure reasonable, effective, and safe interaction between humans and machines.

Hand gesture recognition is based on human hand movements; the human hand is very flexible; according to the change of gestures to simulate the image or syllables to form a certain meaning or words, it is a body language between people and communication and exchange of ideas and is "an important auxiliary tool of audible language," for the hearing impaired and other specific. For people with hearing impairment, it is the main communication tool and has a wide range of applications and prospects [6]. In industrial production, robot teaching is a tedious and complex task, and controlling robot movement through gestures can simplify the process of teaching and operating industrial robots, which is of great value. This can make the classification process simple and can get good classification performance. It is relatively simple to extract frames through a fixed extraction frequency or interval, and it is a commonly used method in video retrieval. With the emergence of Kinect body-sensing devices, its sensitive body-sensing technology can obtain the depth image of the human body, through gesture recognition, to understand the ideas of the operator, to effectively operate some industrial equipment to carry out and learn through gesture signaling to teach the robot how to move. In this way, it can ensure the safety of carrying out some dangerous work, reduce the risk factor, simplify the number of operations, and improve productivity.

In Section 2 of this paper, the relevant research and research background of this paper are introduced. Section 3 describes the machine learning algorithm used in this paper. Section 3 constructs the human-computer interaction system, Section 4 analyzes the results of this paper, and Section 5 concludes the paper.

2. Related Work

There have also been many achievements in the application and control of robotic human-robot interaction; for example, Active Media Robotics' Centibots, related to robot organization, task assignment, and other technologies, have grown to teams of more than 100 robots choreographed to work together in the military field of reconnaissance, tracking and mapping through real-time control [7]. Many systems based on the various functions of this body-sensing device have been developed by developers. For example, body language recognition is done based on some basic image processing techniques to discriminate the movements of the human body detected by the camera [8]. In traditional gesture recognition systems, many technical difficulties for segmenting and locating hand positions have not been solved, and the systems have poor real-time performance and low robustness and basically cannot capture gestures and output correct results in real time, so until the emergence of body-sensing systems, traditional gesture systems still can only do rough recognition [9]. As an early human interaction method, gestures are still widely used as a communication tool. In the long social practice, hand gestures constantly update their specific meanings and can express human thoughts more vividly due to the good flexibility of the hand. Therefore, with the continuous development of artificial intelligence, gesture recognition has gradually been combined with machine devices and becomes one of the effective ways for computers to understand human language [10].

From the current robot interaction methods, most of the research only focuses on a single perception mode, which firstly limits the diversity of robot interaction means and contents and secondly makes the interaction process single and tedious and the interaction experience poor [11]. Therefore, how to fuse multimodal perceptual information to provide faster, more efficient, and more diverse interaction experiences is one of the current research hotspots [12]. The sixth generation of robots integrates three new sensory categories of the cosensory model of dialogue engine, full-duplex speech, and real-time vision. In the test site, Xiaobing can conduct real-time parallel interaction through vision and speech, and visual information and speech information are associated and shared in real-time during the interaction process [13]. Multiple interaction methods complement and integrate to form a complete interaction system. The gesture interaction technology is through the camera to capture the

gesture interaction process and, then through computer vision and other technologies to analyze the image, to achieve gesture recognition [14]. This gesture recognition is more natural and convenient to use, with simple equipment and a good user experience. Earlier vision-based gesture interaction is mainly based on the marker approach, i.e., by pasting or painting different colors or shapes on the hand like markers and recognizing the markers by visual means thus realizing gesture recognition.

The second is to design a set of static gesture commands to control handwriting operations, including basic commands such as start, stop, erase, and save. Liang et al. used the optical flow-based motion detection method to segment the hand region, but the optical flow method is only able to detect moving targets, so the method is only effective when the hand is in motion [15]. And when the camera is also moving, the optical flow detection will be unable to segment the situation. Parvathy et al. used color histogram information to model the background information and then used the background difference method to detect the hand region, which is computationally simple and can only be applied to scenes with stable illumination and fixed cameras [16]. In general, a gesture recognition model is a machine learning-based classifier, which can classify gestures into corresponding classes by using sample data for learning [17]. According to the motion characteristics of hand gestures, gesture recognition can be divided into static gesture recognition and dynamic gesture recognition, where dynamic gesture recognition mainly contains the trajectory motion of hands and arms, so it can also be called trajectory gesture recognition.

3. Machine Learning Algorithm Design

3.1. Gesture Recognition Algorithm. Skin color is a distinctive feature of the human body; with the development of computer vision technology, skin color segmentation is widely used in face recognition, gesture recognition, etc. Skin color-based gesture segmentation algorithms are simple and better in real-time and are not affected by changes in the shape of the gesture target, and the technology is more maturely developed. It mainly includes a histogram model as well as a classifier based on pattern recognition. The histogram model transforms the color space into a set of histogram bins, which correspond to the color orientation, and is usually divided into two types: the external lookup table method and the Bayesian method; the pattern recognition-based classifier can generalize the data and adopt the method of approximating the complex nonlinear input-output relationship [18]. The advantage of the threshold model is that the algorithm is simple and suitable for systems with high requirements for real-time, but its accuracy of detecting skin tones is low; the parametric model usually does not contain luminance information, reducing the error caused by illumination interference, but its accuracy depends on the choice of color space and the shape of skin tone distribution.

The background image B is created from the image acquired by the camera, and the differential image D is obtained by using the current frame image f to do the differential operation with the background image B, as in equation (1). The differential image D is binarized, where T denotes the appropriate threshold value for segmenting the background and foreground during target detection.

$$D(x, y) = |f(x, y) + B(x, y)|. \tag{1}$$

The time-averaging model is averaged based on the connected frame images, where the low-frequency components in the image sequence are selected as the background images. Let $B_t(x, y)$ and $f_t(x, y)$ be the background image and the image frames at time t. Update the $B_t(x, y)$ following

$$B_t(x, y) = \alpha B_{t-1}(x, y) - (1 - \alpha) f_t(x, y). \tag{2}$$

Firstly, the first frame and second frame images are treated as background image $B(x, y)$ and target image $T(x, y)$, respectively, and secondly, the possible gesture regions are obtained by an edge segmentation method for edge extraction of target image $T(x, y)$. Through the static gesture detection method designed in this article, determine the gesture category, and then execute the corresponding control command. Next, the target image is used to generate the mask map $\text{Mask}(x, y)$ and then to detect the previously obtained possible gesture regions. If more than 2/3 of the pixel points in the region are distributed within the skin tone range, we set the value of the pixel points in the range to 1 and the rest to 0. Finally, the background map is updated according to the following equation (3), and the pixel points with the value of 1 are kept and the pixel points with the value of 0 are replaced with the corresponding point pairs of the target image.

$$B_t(x, y) = \begin{cases} B_{t-1}(x, y), & \text{if } \text{Mask}(x, y) = 0, \\ T_{t-1}(x, y), & \text{if } \text{Mask}(x, y) = 1. \end{cases} \tag{3}$$

The values of the background pixel points can be described by a Gaussian model, as shown in equation (3). This method is suitable for more stable environments.

$$p(x) = \frac{1}{\sqrt{2\pi}\sigma} \exp\left[\frac{(x - \mu)^2}{2\sigma^2}\right], \tag{4}$$

where μ represents the mean and σ represents the standard deviation. Whenever a new image frame is acquired, the pixel point is firstly judged. If the pixel point satisfies equation (4), it can be determined that the pixel point is a background point; otherwise, it is a foreground point. In practical applications, the background may be changing, so the background model, which is the parameter, is updated.

$$\begin{aligned} \mu_{i+1} &= (\alpha + 1)\mu_i - a x_{i+1}, \\ \sum_{i+1} &= (\alpha + 1)_i \sum_i + \alpha(x_i - \mu_i)(x_{i+1} - \mu_{i+1})^T, \end{aligned} \tag{5}$$

where the mean value of Gaussian distribution before μ_i the update is x_{i+1}, μ_{i+1} the mean value of Gaussian distribution after the update is μ_{i+1}, the covariance matrix before the

update is denoted by $\sum_i$, and the covariance matrix after the update is $\sum_{i+1}$ denoted by, x_{i+1} is the pixel point value at $i+1$, α is the learning rate, and the value of α is between 0 and 1, which directly affects the background update speed. α is too small to cause the background update speed to be too slow, and the static objects in the background will be mistaken as gesture targets; α is too large to cause the too large causes the background update speed to be too fast, moving object targets will be considered as background, and the noise effect increases. In the grayscale image $\sum_{i+1}$ is σ^2, in the color image, the color components of each pixel point are independent, so the $\sum_{i+1}$ reduction is diag $[\sigma_R^2, \sigma_G^2, \sigma_B^2]$.

3.2. Speech Recognition Algorithm. Speech energy, resonant peak frequency, fundamental frequency, and mel-frequency cepstrum are used by some researchers because of their effectiveness in distinguishing certain emotional states. To elicit different emotions, rhythmic features such as speaking intensity, vocal gate parameters, fundamental frequency, pitch, and volume can be used. According to the results of previous studies, spectrum and rhythm are the two types of features that carry the most emotional information [19]. The rhyme continuum has features such as energy and pitch and contains most of the emotional information of the discourse. In addition, the combination of spectral and rhyme features is also believed to improve the performance of emotion recognition systems because they both contain emotion information.

The most used spectral features for various sentiment recognition systems are linear predictive coefficients (LPCs), mel-frequency cepstral coefficients (MFCCs), and linear predictive cepstral coefficients (LPCCs). For example, Linear Predictive Coding (LPC) is a digital method for encoding analog signals. LPC works by predicting the next value of a signal based on the information it has received in the past, forming a linear pattern. The main goal of LPC is to obtain a set of prediction coefficients that minimize the mean square error E_m.

$$E_m = \sum_i e_m^2 \left[n^2\right]. \tag{6}$$

$e_m^2[n^2]$ is a frame of the speech signal and the order of the LPC analysis. LPC coding typically provides satisfactory high-quality speech at a low bit rate and provides an accurate approximation of speech parameters. While LPCC can be considered a more traditional feature of speech, LPC contributes to the overall recognition of emotion, as shown in Table 1.

Ensure that the system meets user needs. The focus of the test is whether the driver's gestures can accurately complete the instructions to the in-vehicle system. The main test contents are the opening of the system application, the realization of functions in the specific application, and the correct rate of gesture recognition. Rhythmic features, also known as acoustic features, are extracted over a longer region than the typical frame and are therefore also known as "hypersegmented" features. Commonly extracted rhythmic features include pitch, energy, articulation rate, pause, spectral tilt characteristics, and duration. The contours of rhythmic features (indicating smooth, rising, or falling slopes), obtained in SER studies, generally include minimum, maximum, median, and interquartile ranges. Pitch can be measured as a change in frequency. The time between two consecutive vocal fold vibrations is called the pitch period, and the number of vibrations in a unit time is called the fundamental frequency or pitch frequency.

$$A(i) = \lim_{M \longrightarrow \infty} \frac{1}{2M} \sum_{n=-M}^{M} x\left(n^2\right) x\left(n^2 + i\right). \tag{7}$$

Gaussian mixture models are alternatively generated probabilistic models, which mean that for a particular word, a multivariate Gaussian density model representing all frames can be formed with a strong fit. Like HMM, GMM as a statistical model, GMM can also be expressed in mathematical terms. Let $P_{\mathrm{GMM}}(x_t)$ be the nth frame of the word x, the probability of generating a $G_k(x_t)$ frame using GMM can be calculated as in

$$P_{\mathrm{GMM}}(x_t) = \sum_{k=1}^{S} C_k^2 G_k(x_t). \tag{8}$$

S is the mixing number, C_k is the probability of the kth mixing, and G_k is a multivariate Gaussian density function with a mean vector and covariance matrix. Compared to HMMs, GMMs are more efficient in the overall modeling of multimodal distributions and thus have advantages in training and testing. Using GMMs in SER, the global property is the main concern [20]. However, due to this property, GMMs are not suitable when the user wants to model the temporal structure. It has been widely used in classification tasks. Although the salient local features based on the reference frame have only 256 dimensions, the result is better. The reasons for this gap can be summarized as the following two points.

In practice, the Fourier transform is calculated by dividing a longer time signal into shorter segments of equal length and then calculating the Fourier transform separately on each shorter segment, which reveals the Fourier spectrum for each small segment. One then usually plots the changing spectrum as a function of time, called a spectrogram or waterfall plot. In the discrete-time case, the data to be transformed can be decomposed into blocks or frames (they usually overlap each other to reduce special handling at the boundaries). Each block is Fourier transformed, and the complex results are added to a matrix that records the magnitude and phase at each point in time and frequency.

$$\mathrm{STFT}\{x[n]\}(m, w) \equiv \sum_{-\infty}^{\infty} x[n] w[n+m] e^{jwn}. \tag{9}$$

In this case, m is discrete and ω is continuous; however, in most typical applications performed on a computer using the Fast Fourier Transform STFT, the two variables are discrete and quantized. As m increases, the window function w

Table 1: Spectral characterization.

Extract characteristics	Advantage	Shortcoming
MFCC	Popular features.	Poor noise resistance.
LPCC	Helps to capture the voice perception of the human ear.	For different emotions (especially anger and sadness), the coefficient values usually overlap.
ZCR	Delta and double-delta values can improve recognition accuracy.	The ZCR value tends to vary greatly, depending on the amount of noise present.
Shimmer	Indicates common features of voice content.	Emotions such as anger and disgust often exhibit similar jitters and flickers.
LFPC	The observed LFPC value is not relevant, so the diagonal covariance of its value can be used as the feature input of the classifier.	Most studies only compare LFPC with MFCC and LPCC. The nonlinear changes of the speech signal are not considered.
DSCC	Simple calculation.	Anger and disgust often exhibit similar jitters and flickers.

slides to the right. For the result of the obtained frame $x[n]$ $w[n+m]$, the computational Fourier transform is performed. The resulting STFTX is a function of time m and frequency w. The raw spectral contrast feature estimates the intensities of the spectral peaks and troughs and their differences in each subband, and to ensure the stability of the feature, the intensities of the peaks and troughs of the spectrum are estimated from the average of the small neighborhoods around the maximum and minimum values, respectively, rather than the exact maximum and minimum values.

$$\begin{aligned} \text{Peak}_k &= \ln\left\{\frac{2}{\alpha N}\sum_{i=1}^{\alpha N} x'_{k,i}\right\}, \\ \text{Valley}_k &= \ln\left\{\frac{2}{\alpha N}\sum_{i=1}^{\alpha N} x'_{k,i+1}\right\}. \end{aligned} \tag{10}$$

N is the total number in the kth subband, $k \in [1, 6]$. The value of α can be different, in the interval 0.02 to 0.2 which will not have a great effect on the classification result. The most basic ways are dialogue, eye expressions, body movements, etc. They are the most natural way of interaction formed by human beings in the development of society, and they are also the way of interaction that most conforms to human behavior habits. After the K-L transformation, the feature vectors are mapped into the orthogonal space and the covariance matrix if mapped in the new feature space using a diagonal approach, which makes the classification process simple and gives good classification performance. Frame extraction by fixed extraction frequency or interval is a simpler method and is a common approach in video retrieval. However, this random extraction is baseless and there is no guarantee whether the extracted keyframes contain key information of motion. Combined with the environment in which this paper is used, the dynamic gesture operation process needs to be fast and concise, and the integrity of the information cannot be guaranteed by using the sampling method.

4. Human-Computer Interaction System Construction

4.1. Gesture Recognition System Design. Because the robot is widely used, most scenarios have their specific production environment and assembly process, and the production environment of different industrial plants is more complex and different for all kinds of gestures and movements [21]. The basic task of the system software is gesture recognition and human-robot interaction. Gesture recognition needs to complete data acquisition, data processing, data recognition, and other points of the function. Human-computer interaction needs to design interactive gestures and complete the control of upper-layer applications. Thus, according to its basic task, the system software has the following functional requirements. By calling the underlying camera device, the user's gesture data is collected and saved in a video format. With the gradual maturity of human-computer interaction systems and the gradual application of voice emotion recognition in people's lives, there is an even more urgent need for machines to intelligently understand human emotions. The gesture data needs to be processed in two ways, firstly, to extract the ROI of the region of interest of the gesture, crop the picture of the region of interest, and save the ROI parameters of the region of interest. The second is to annotate the 2D node coordinates of the gesture according to the gesture node model and save the annotated 2D node coordinate data.

The aerial handwriting module is a simple gesture interaction application, which mainly consists of the following two basic functions: first, to identify fingertip points and use fingertip point trajectories to achieve aerial font writing; second, to design a set of static gesture commands for controlling handwriting operations, including basic commands such as start, stop, erase, and save. Static gestures are judged multiple times to prevent miscalculation, and a single static gesture is kept constant for 10 consecutive frames before the current operation is executed. After entering the handwriting mode, first, start the improved KCF tracker designed in this paper to track the gesture, use the tracking result region as the gesture region, extract the gesture mask image using the hybrid GMM skin tone extraction Bye's correction

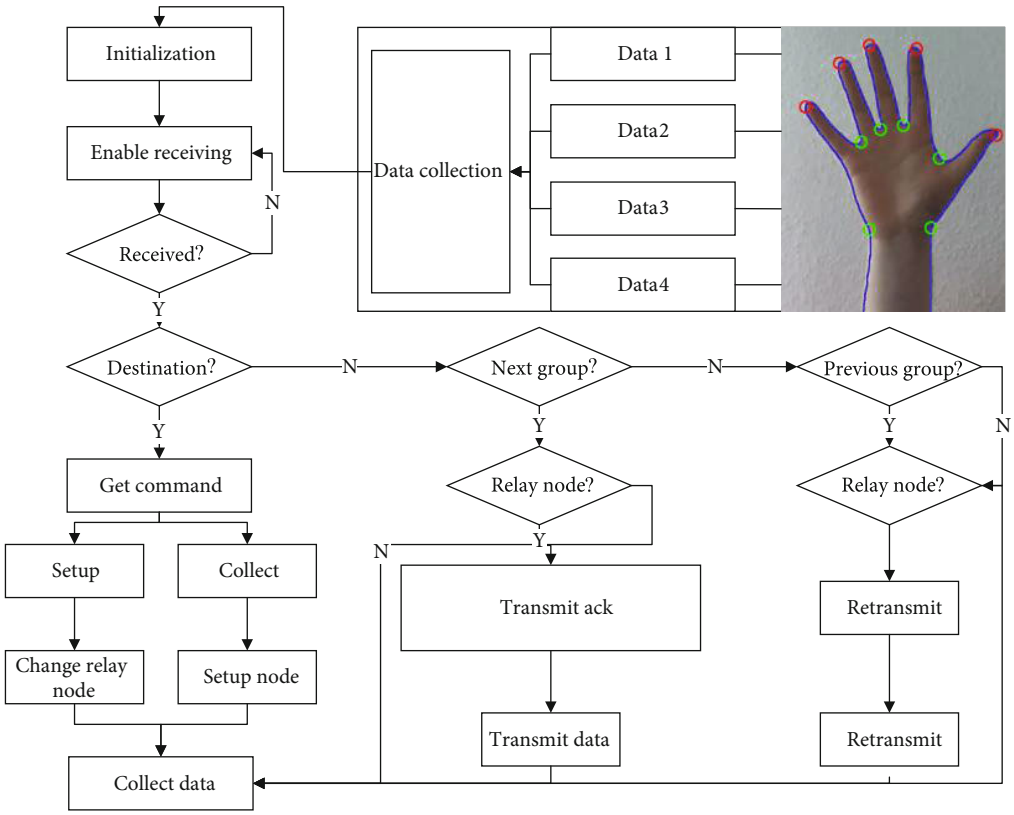

Figure 1: Flow chart of data acquisition.

proposed in this paper, and then use the convex packet detection to obtain the fingertip point of the gesture, and this paper uses a single fingertip point to achieve over-the-air handwriting. If the position of the fingertip point does not change in 20 consecutive frames or no fingertip point is detected inside 10 consecutive frames, then reenter the static gesture detection state, determine the gesture category by the static gesture detection method designed in this paper, and then execute the corresponding control command.

Based on the simple experimental system established for the human-robot collaboration model, the data acquisition flow chart shown in Figure 1 was constructed in this paper to show the acquisition of the data clearly and explicitly. First, the six-dimensional force sensor used in the system and the AC servo motor representing the robot are initialized, and to achieve consistent information about the end position of the collected robot, it is necessary to make the handle at the end have the operation of zeroing the opportunity home. Just as expressed above, the process of data acquisition is carried out using the impedance control method for the robot in the one-degree-of-freedom human-robot collaboration system.

In this simple human-robot collaboration system, because there is only one direction of motion space, so just collect the data in this direction, one of the six-dimensional pressure sensors used in this paper for the acquisition of interactive force information, and the information of the robot is mainly the three-position, velocity, and acceleration. In this paper, we mainly analyze the robot velocity information, which is calculated from the encoder acquisition. These data are built on the variable damping impedance control method to collect the data. Humans and robots use force control to achieve installation work like curtain walls. In addition, human-machine collaboration technology is also applicable to the field of medical rehabilitation, such as physical rehabilitation training for some patients with cerebral thrombosis or other patients whose limbs need to be recovered. In this paper, the mass matrix and damping matrix of the robot are set as $m = 0.02, b = 15$, $f_h = 2N$. According to the data acquisition flowchart in Figure 1, the data acquisition is repeated several times, and finally, 900 sets of data are obtained for the training of the one-degree-of-freedom human-robot collaboration system, and 100 sets of data are randomly collected as the data test data in each of the three data acquisition sessions.

4.2. Speech Recognition System Construction. A 1D CNN can be very effective when valid features are obtained from a shorter (fixed-length) segment of the overall dataset and the position of the feature in that segment is not relevant. 1D CNNs are suitable for analyzing any kind of signal data (e.g., audio signals) over a fixed-length period. Another application is natural language processing. The key difference between the 1D and 2D CNN approaches is the dimensionality of the input data and how the feature detector (or filter) slides over the data.

In Algorithm 1, an example application of a 1D CNN is presented; the set consists of 8 parts, each represented by a

Input: depth map sequence $I = [I_1^2, I_2^2, \cdots, I_N^2]$
Step 1. the initial feature point extraction
Use SURF algorithm to detect key points.
Step 2. Forward search
Initialize the reference frame of frame 1, $A_1^F = 1$
For $I_i = I_1^2 : I_N^2$ do.
If $A_1^F \neq 1$ then $R_i^F = I$
end
Step 3. Backward search
Consistent with the forward search step, get the backward reference frame
Two-way search area fusion to obtain the final saliency area
$Valley_k = \ln \{1/\alpha \sum_{i=1}^{\alpha N} x'_{k,i+1}\}$
Step 4. Feature selection and descriptor extraction
Use S to filter out invalid points, and extract HOG and HOF feature descriptions in a square area centered on key points $S_i^* = S_i^F \cap S_i^B$.
Output: extracted feature points and location information and feature description

Algorithm 1: Significance feature extraction algorithm based on bidirectional reference frame search.

vector. The feature detector always covers the complete 2 vectors, where the height of the detector determines the number of all vectors to be considered in the training process. Assuming a height of 2, the feature detector will traverse the data 7 times. Using a 1D CNN can extract features from an entire dataset of a fixed-length segment very efficiently [22]. If the user's intent is simply to say hello, thank you, goodbye, etc., there is no need to extract slot value information. Using Rasa Core for session management and behavior decision of the dialogue system, different behaviors are returned to reply for different user intents, e.g., if the user intends to greet, then reply to self-introduction/feature introduction; if the user intends to chat and communicate, then call the Turing bot interface to communicate with the user; if the user intends to move an object, but no location of the object to be moved or target location, the text is returned asking the user for information about the slot value that needs to be filled.

When using an existing preliminary dialogue model, users can train online with the bot, and new dialogue scenarios generated during the dialogue are added to this file, continuously enriching the model data and enhancing the robustness of the dialogue system.

System testing is used to check whether gestures can achieve specific functions, analyze problems, and provide feedback to system developers to ensure that the system is meeting user needs. The focus of the test is on whether the driver's gestures can accurately complete the instructions to the in-vehicle system. The main test contents are the opening of the system application, the implementation of the functions in the specific application, and the correct rate of gesture recognition. Due to funding issues, the system tested in a simulated environment with an Android operating system and a laptop camera for image acquisition and transmission to the central operating platform.

The Android system uses Java language to develop programs and has complete hardware device support, providing developers with an open and highly free development platform. In addition, Android provides developers with rich interface controls, which facilitate the development of user interfaces, while using the same design language to ensure the consistency of application interfaces. Due to the rapid development of telematics technology in recent years, Android-based in-vehicle devices and related applications have a great market share. The Android platform is highly developable and has low development cost; therefore, major automobile manufacturers are developing in-vehicle devices on the Android platform.

5. Analysis of Results

5.1. HCI Performance Results. After the gesture sample library is established, 1000 samples of 10 dynamic gestures are trained and recognized; the process is as follows: 100 samples of each dynamic gesture are divided into a training set and test set: the training set is to train the set model and adjust the model parameters, and the test set is to test the accuracy of the trained model and determine whether the trained model has been trained. The contact method must be stable and safe, and it is best to have a certain degree of self-recognition ability, so that emergencies can be dealt with in a timely manner, and a reasonable, effective, and safe interaction between man and machine is ensured. In this paper, 50 samples are selected as the training set of the HMM-NBC model, and the remaining samples are used as the test set of this model. Firstly, the motion trajectory HMM model and the gesture HMM model are trained, and the parameters in the HMM need to be set. In this paper, the number of hidden states S is set to 9, and the observed state value M is set to 10 in the gesture HMM model; for the motion trajectory HMM model, the S value is set to 9 and the M value is set to 12. When the HMM model is initialized, the training of the HMM model can be started, and when the 10 dynamic gestures are trained, the dynamic gestures are input to the test set to complete the recognition of dynamic gestures, and the experimental results are shown in Figure 2.

The recognized text information is sent to the Rasa dialogue system in the form of a service; the dialogue system understands the text information and extracts the user's

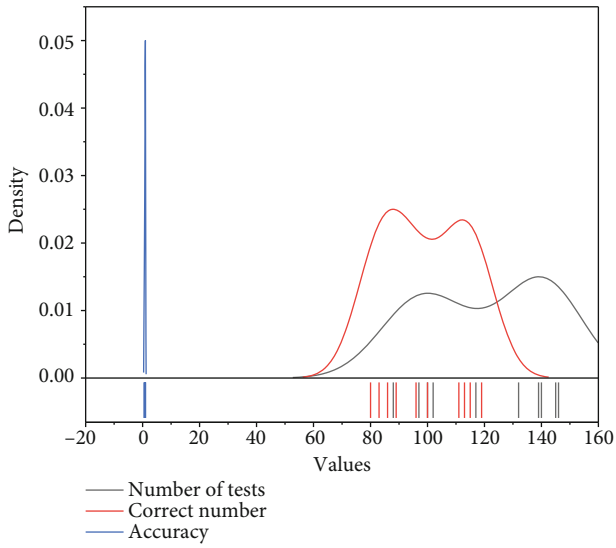

Figure 2: Dynamic gesture recognition results.

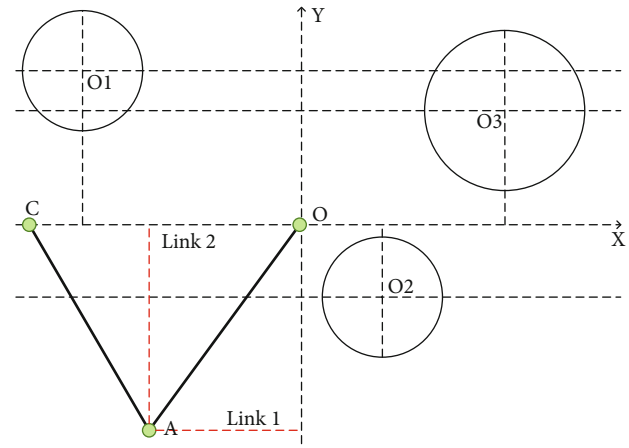

Figure 3: Three circular object detection.

intention, extracts the entity slot information needed to reply to the intention, and acts accordingly to return the reply text; the speech synthesis API is called to realize text-to-speech and plays the reply to the user through the headset.

The multimodal expression sequences are extracted, and fusion is performed to extract multiple feature descriptions, while the spatiotemporal probability distribution of the features is modeled using the 3D hidden shape model afterward; the main steps include the establishment of the target description table and the implicit shape model, where the target description table is an index entry for all features, while the implicit shape model implicitly describes the spatiotemporal distribution information of the features. In the recognition phase, after extracting all features, the spatiotemporal locations of all frames are voted in combination with the 3D implicit shape model to compose the alignment cost matrix, and finally, the dynamic programming algorithm is used to find the optimal path. It is the body language used to communicate and exchange ideas between people. It is an "important auxiliary tool for audio language." For certain people such as hearing impaired, it is the main communication tool and has a wide range of applications and prospects.

The two-way search-based saliency features focus on static information and analyze the saliency region of the current frame through contextual information and use it as a benchmark to filter out invalid feature points. The main idea is to use contextual information to extract the saliency region of the current frame and limit the feature extraction to the key region of the gesture, which improves the effectiveness of the features while increasing the feature density and then improves the characterization ability of the features, as shown in Figure 3.

After switching to the over-the-air handwriting module, the system software starts the timer and begins to monitor the gesture changes, and Figure 3 identifies the start-up gesture through the gesture detection method in this paper. After that, the system enters the over-the-air handwriting phase, and Figure 3 identifies the fingertip movement trajectory through the gesture tracking method and fingertip point recognition method in this paper. The software system flips the picture left and right after entering the handwriting so that the writing trajectory is displayed normally. The parameter model usually does not contain brightness information, which reduces the error caused by light interference, but its accuracy depends on the choice of color space and the shape of the skin color distribution. After detecting the condition of handwriting termination, the system software reenters the detection session, and Figure 3 identifies the erase gesture and stop gesture by the gesture detection method in this paper. By iteratively adjusting the feedforward forces and reference points in the reference model, as well as information on the steady-state achieved when the robotic arm interacts with the external object, the elasticity coefficients and geometric boundary locations of the external object are estimated using weighted least squares. In addition, we propose a novel learning law for updating the learning of weights in ELM that ensures fast convergence of the matching error between the closed-loop system and the reference model.

5.2. Interaction Results. The most important and basic step in building the application of speech emotion recognition to human-computer dialogue is speech emotion recognition; the speech emotion recognition model recognizes the input speech and obtains the corresponding emotion labels. The human-computer dialogue model is constructed and trained, and the speech is used as the input of the human-computer dialogue model, combined with the speech recognition, and added emotion labels as the real input of the human-computer dialogue, and the ECM human-computer dialogue gets the corresponding emotional response. The front-end acquires speech recognition text and sentiment labels and inputs them into the human-computer dialogue model and uses the acquired text and sentiment as the driver to obtain sentiment-rich responses.

Due to the excessive size of the training set, the number of features obtained is too large to use all the training sample

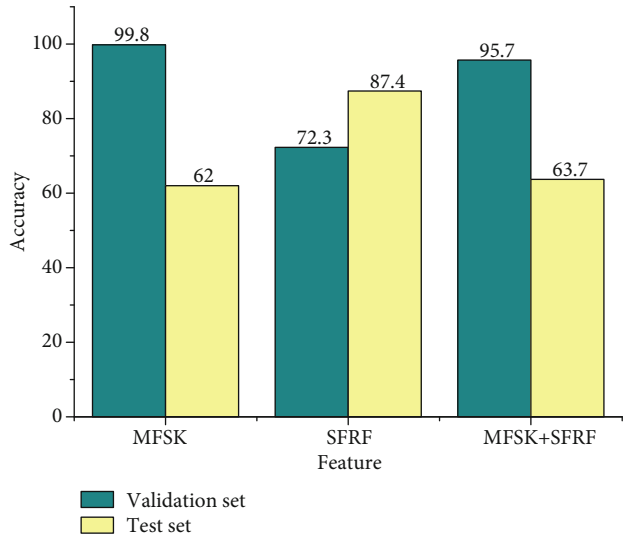

Figure 4: Comparison results of experiments in which different features were used.

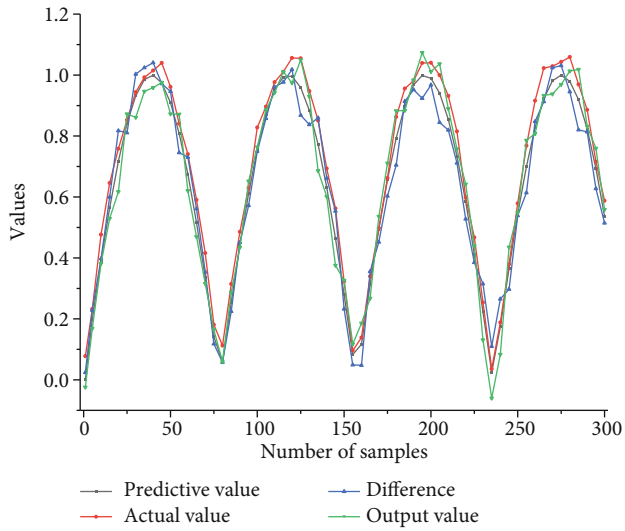

Figure 5: Results of interaction force changes.

features to train the random forest model. Therefore, in this chapter, partial training samples are used; i.e., features are extracted using some of the samples to obtain the lexicon, and later, all sample features are used to vote to obtain the spatiotemporal probability distribution of individual words. To ensure uniformity in category sampling, the number of samples for each category in the lexicon clustering process is the same. To ensure that the spatial location is not disturbed by human movement, the proposed algorithm extracts the face center as the reference center and corrects the human movement bias. In practical applications, the background may be changing, so the background model, that is, the parameters, is updated.

The DTW algorithm based on consistent voting can fuse a variety of features, such as the MFSK features used in this chapter and the significant local features based on reference frames. The results are shown in Figure 4. From the table, the MFSK features are expressive but their results are poor, while the significant local features based on reference frames have only 256 dimensions but their results are better. The reasons for this gap can be summarized as the following two points. The MFSK features adopt a uniform feature extraction and selection strategy for background and foreground, which invariably introduces many invalid features and causes a greater impact on the frame matching process. The MFSK only focuses on the motion part and static actions, especially those in the hold phase, which causes a poor impact in the context of dynamic time planning algorithms. From the data in Figure 4, the combination of the two features can effectively complement the features, and from the results, the validation set is improved by 8.87%, and the test set is improved by 7.91%, which is a more obvious improvement and shows the effectiveness of the fusion multiple modal.

To test the predictive effectiveness of the BP-based neural network model established above for identifying and predicting collaborators' intentions, the test samples collected in the impedance control in three sections were used. With 300 sets of test data, the predicted and true value data of cooperator intention based on the BP neural network were obtained as shown in Figure 5. The trained BP neural network model can predict the desired velocity well. To clarify the advantages of the BP network, the prediction results of the radial basis network are compared with it in this paper, and the same sample data and test data are also used to obtain the prediction results of the radial basis neural network in this paper.

According to previous research results, frequency spectrum and prosody are the two types of features that carry the most emotional information. The prosodic continuum has the characteristics of energy and pitch and contains most of the emotional information of the discourse. In addition, the combination of spectral features and prosodic features is also considered to improve the performance of emotion recognition systems, because they all contain emotional information. For the process of human-robot collaboration, the actual robot's tracking speed lags significantly behind the operator's desired speed, which is because the system uses impedance control, and the robot only responds to the operator's information when it receives it during the control process thus having a delay, but this delay characteristic limits the human-robot synchronization requirement we expect in the human-robot collaboration process, making the robot in the human-robot collaboration system in a passive. The robot in a human-robot collaboration system is in a passive following state.

6. Conclusion

A collaborator intention recognition method based on a fuzzy clustering BP neural network model is proposed based on the shortcomings of the experiment. Drawing on the characteristics of human-human cooperation, it is necessary to endow the robot with a certain cooperation experience before recognizing the human intention. Because of the

random and variable characteristics of collaborator intention, this paper takes the collaborator-robot dynamic collaboration information as the basis for intention estimation, uses impedance control for sample data collection, constructs a suitable network model, and achieves the prediction of human motion information by first undergoing offline training and then online for predicting the collaborator's intention. The contour of the prosody feature (representing a steady, rising or falling slope), generally obtained in the SER research, includes the minimum, maximum, median, and interquartile range. The pitch can be measured by the change in frequency. The data such as end velocity and interaction force of the robot in the human-robot collaboration system were analyzed experimentally, and the results showed that the control method based on fuzzy clustering and BP neural network prediction can accurately learn to predict the intention information of the collaborator and improve the synchronization of human and robot motion in contact human-robot collaboration. The spatiotemporal structure information of each modal feature is modeled using a three-dimensional hidden shape model, while the features are later mapped to a uniform probability space by consistency voting to form a probabilistic estimate of the spatiotemporal distribution of each frame of action, which is used to construct an alignment cost matrix. In addition, a probability-based upper bound finding method is proposed to reduce the unnecessary matching process and accelerate the computational process, which makes DTW applicable to large-sample multicategory gesture classification tasks.

Data Availability

The data used to support the findings of this study are available from the corresponding author upon request.

Conflicts of Interest

The author declares that they have no known competing financial interests or personal relationships that could have appeared to influence the work reported in this paper.

Acknowledgments

This work was supported by Young Teachers Education and Research Projects of Fujian Province (Grant No. JAT191160).

References

[1] A. Fritz, W. Brandt, H. Gimpel, and S. Bayer, "Moral agency without responsibility? Analysis of three ethical models of human-computer interaction in times of artificial intelligence (AI)," *De Ethica*, vol. 6, no. 1, pp. 3–22, 2020.

[2] M. Jarosz, P. Nawrocki, B. Śnieżyński, and B. Indurkhya, "Multi-platform intelligent system for multimodal human-computer interaction," *Computing and Informatics*, vol. 40, no. 1, pp. 83–103, 2021.

[3] F. Ren and Y. Bao, "A review on human-computer interaction and intelligent robots," *International Journal of Information Technology & Decision Making*, vol. 19, no. 1, pp. 5–47, 2020.

[4] W. Xu, "Toward human-centered AI," *Interactions*, vol. 26, no. 4, pp. 42–46, 2019.

[5] G. Ma, Z. Hao, X. Wu, and X. Wang, "An optimal electrical impedance tomography drive pattern for human-computer interaction applications," *IEEE Transactions on Biomedical Circuits and Systems*, vol. 14, no. 3, pp. 402–411, 2020.

[6] G. Ramos, C. Meek, P. Simard, J. Suh, and S. Ghorashi, "Interactive machine teaching: a human-centered approach to building machine-learned models," *Human–Computer Interaction*, vol. 35, no. 5-6, pp. 413–451, 2020.

[7] M. Klumpp, M. Hesenius, O. Meyer, C. Ruiner, and V. Gruhn, "Production logistics and human-computer interaction—state-of-the-art, challenges and requirements for the future," *The International Journal of Advanced Manufacturing Technology*, vol. 105, no. 9, pp. 3691–3709, 2019.

[8] B. K. Chakraborty, D. Sarma, M. K. Bhuyan, and K. F. MacDorman, "Review of constraints on vision-based gesture recognition for human–computer interaction," *IET Computer Vision*, vol. 12, no. 1, pp. 3–15, 2018.

[9] Q. Zhu, "Research on road traffic situation awareness system based on image big data," *IEEE Intelligent Systems*, vol. 35, no. 1, pp. 18–26, 2020.

[10] A. Memo and P. Zanuttigh, "Head-mounted gesture controlled interface for human-computer interaction," *Multimedia Tools and Applications*, vol. 77, no. 1, pp. 27–53, 2018.

[11] M. Klumpp and H. Zijm, "Logistics innovation and social sustainability: how to prevent an artificial divide in human–computer interaction," *Journal of Business Logistics*, vol. 40, no. 3, pp. 265–278, 2019.

[12] "Call for papers—special issue of information systems research—humans, algorithms, and augmented intelligence: the future of work, organizations, and society," *Information Systems Research*, vol. 29, no. 1, pp. 250-251, 2018.

[13] B. Shneiderman, "Human-centered artificial intelligence: three fresh ideas," *AIS Transactions on Human-Computer Interaction*, vol. 12, no. 3, pp. 109–124, 2020.

[14] A. A. Karpov and R. M. Yusupov, "Multimodal interfaces of human–computer interaction," *Herald of the Russian Academy of Sciences*, vol. 88, no. 1, pp. 67–74, 2018.

[15] W. Liang, "Scene art design based on human-computer interaction and multimedia information system: an interactive perspective," *Multimedia Tools and Applications*, vol. 78, no. 4, pp. 4767–4785, 2019.

[16] P. Parvathy, K. Subramaniam, G. K. D. Prasanna Venkatesan, P. Karthikaikumar, J. Varghese, and T. Jayasankar, "Development of hand gesture recognition system using machine learning," *Journal of Ambient Intelligence and Humanized Computing*, vol. 12, no. 6, pp. 6793–6800, 2021.

[17] B. Shneiderman, "Human-centered artificial intelligence: reliable, safe & trustworthy," *International Journal of Human–Computer Interaction*, vol. 36, no. 6, pp. 495–504, 2020.

[18] Y. Ye, C. He, B. Liao, and G. Qian, "Capacitive proximity sensor array with a simple high sensitivity capacitance measuring circuit for human–computer interaction," *IEEE Sensors Journal*, vol. 18, no. 14, pp. 5906–5914, 2018.

[19] A. W. Johnson, M. W. Blackburn, M. P. Su, and C. J. Finelli, "How a flexible classroom affords active learning in electrical

engineering," *IEEE Trans. Educ.*, vol. 62, no. 2, pp. 91–98, 2019.

[20] Z. Chen, Y. Wang, and H. Liu, "Unobtrusive sensor-based occupancy facing direction detection and tracking using advanced machine learning algorithms," *IEEE Sensors Journal*, vol. 18, no. 15, pp. 6360–6368, 2018.

[21] Y. F. Liao, Y. H. S. Chang, Y. C. Lin, W. H. Hsu, M. Pleva, and J. Juhar, "Formosa speech in the wild corpus for improving taiwanese mandarin speech-enabled human-computer interaction," *Journal of Signal Processing Systems*, vol. 92, no. 8, pp. 853–873, 2020.

[22] F. Sperrle, M. el-Assady, G. Guo et al., "A survey of human-centered evaluations in human-centered machine learning," *Computer Graphics Forum*, vol. 40, no. 3, pp. 543–568, 2021.

Hindawi
Journal of Sensors
Volume 2022, Article ID 6256884, 10 pages
https://doi.org/10.1155/2022/6256884

Research Article

Reliability Analysis of Social Network Data Transmission in Wireless Sensor Network Topology

Zhixue Wang

School of Mathematics and Computer Science, Ningxia Normal University, Guyuan Ningxia 756000, China

Correspondence should be addressed to Zhixue Wang; nxwzx@nxnu.edu.cn

Received 5 November 2021; Revised 6 December 2021; Accepted 10 December 2021; Published 6 January 2022

Academic Editor: Gengxin Sun

In this paper, the reliability of data transmission in social networks is thoroughly studied and analyzed using wireless sensor network topology technology. This paper, based on the introduction of sensor network reliability analysis-related technology, combined with the characteristics, and needs of the sensor network itself, focuses on the study of the reliability analysis of the sensor network under the state of perturbation scheme. Based on the idea of making full use of data changes to respond to the sensor state, this paper takes the actual monitoring data of the wireless sensor network as the research object, selects the temporal correlation and spatial correlation of the measured environmental data as the reliability index by extracting the features of the wireless sensor network data, and proposes the Evidential reasoning rule- (ER-) based wireless sensor network data reliability assessment model based on Evidential reasoning rule (ER) is proposed. The data are mined, analyzed, and quantified from the perspective of content popularity, and the interest indicators of nodes on data under content popularity are analyzed to derive stable interest quantification values. Combined with the network properties, i.e., node autoassembly community, we analyze the data dissemination characteristics of social networks in wireless sensor network topology environment and derive the upper and lower bounds of data transmission capacity under node interest-driven and its variation on network performance. Social relationships among nodes affected by social attributes are considered; in turn, the data forwarding behavior of nodes is modeled using data transmission probability and data reception probability; finally, the data forwarding process is analyzed and a closed expression for the average end-to-end transmission capacity is derived in turn.

1. Introduction

With the development of technology, social networking applications such as Weibo, YouTube, and Twitter provide people with convenient ways to communicate. Traditional social media content is mainly in the form of pictures, articles, and so on. In recent years, with the development of cloud computing, the Internet of Things, and other technologies, various new social network applications represented by new media methods such as interactive live streaming and real-time meetings have started to appear in the users' view [1]. In such applications, users are more sensitive to the access delays of various new media. At the same time, the popularity of smart mobile devices has brought hundreds of millions of users to join social networking applications for real-time communication, and the amount of data generated by them has exploded, making it increasingly important to maintain a reasonable load balance of storage systems to ensure good system performance. Although traditional social networking applications use cloud computing platforms to place user data in a way that can provide better storage services for massive amounts of user data, cloud data centers are generally far away from users, which makes it difficult to ensure users' high real-time requirements for various new social media [2]. With the development of wireless technology, the availability, coverage, and performance of wireless communication are rapidly improving, and it has become a necessity of modern life, which can effectively complete the various demands made by network users and is suitable for various long-range and short-range wireless transmissions. In addition, the shared and open nature of wireless propagation channels, which cannot simultaneously satisfy the service requests of many users, leads to lower communication quality and increases the complexity of

wireless transmission, while secure data transmission becomes a challenging issue in wireless communication.

Wireless sensor networks benefit from the technical support brought by the rise of sensor technology, embedded computing technology, distributed information processing technology, and wireless communication technology, combining features such as high sensing, computing and communication capabilities, low cost, low power consumption, multifunctionality, small size, and short-range wireless communication, making it of interest to various industries [3]. Although traditional social network applications using cloud computing platforms to place user data can provide better storage services for massive amounts of user data, cloud data centers are generally far away from users, and it is difficult to ensure that users are more comfortable with all types of new social media in real-time requirements. The flexibility, fault tolerance, and rapid deployment of sensor networks make it widely used in environmental, food, and industrial fields, and it is considered one of the most important technologies of the twenty-first century. The ten emerging technologies with the most far-reaching impact in the future and wireless sensor networks are in the first place. The pervasiveness of wireless sensor networks determines its broad application prospects, and it can be evaluated as the most important technology in the twenty-first century, which is enough to represent its huge potential. A wireless sensor network by many inexpensive sensors randomly installed in the area to be observed, in the form of a multihop self-organizing network system, with only a small cost to the complex monitoring area for real-time monitoring, mastering the regional environment of each attribute data. Wireless sensor networks become a medium for indirect connection between users and the objective world, extending the way people and nature interact.

Wireless sensor network (WSN) reliability is the premise to ensure the normal operation of the network and is the basis for improving the performance of the network. WSN reliability not only is a key indicator of the network design but also ensures the normal operation of the network and management and maintenance of an important basis [4]. In the WSN, the sensor individual computing power, storage resources, and battery capacity are limited; sensor communication line bandwidth is limited, the transmission rate is low, there is mutual interference between signals, and transmission signal with the communication distance is constantly reduced; sensors are vulnerable to adverse weather, electromagnetic radiation, and other environmental factors; WSN is vulnerable to passive eavesdropping, active intrusion, denial of service, and other network attacks from the Internet [5]. For WSN reliability, research focuses on the difficulty of research in today's academic community and still has not formed a completer and more mature theoretical framework. Therefore, this study has important theoretical and practical value.

2. Related Works

Many types of research have been done to address the wireless sensor network reliability issues, such as proposing a method based on automatic fault tree generation from the perspective of analyzing sensor failures to evaluate the reliability and availability of wireless sensor networks when failures occur on network devices. A reliability assessment method based on a hierarchical confidence rule base is proposed to analyze WSN reliability assessment from both internal faults and external attacks [6]. A detection method based on time series data of sensor networks is proposed to determine the source of faults using calculating the degree of difference between the test data and the normal interval. Object-oriented colored Petri nets are used as a modeling tool for heterogeneous wireless sensor networks, and a new quantitative method for the reliability assessment of heterogeneous wireless sensor networks is proposed. The above method has good analysis results for sensor failures, i.e., when the data changes drastically; however, satisfactory results cannot be achieved for insignificant data fluctuations.

According to research on WSN-based communication networks, the reliability of WSNs is mainly studied in terms of routing problems, reliable transmission problems, and network connectivity problems. A reliable method for evaluating WSNs in a malware environment is considered to guarantee the effectiveness of WSN data transmission. After comparing the reliability and performance of different routing algorithms for WSNs, a dynamic routing algorithm is proposed to achieve end-to-end reliable transmission. The problem of data reliability in event-driven WSNs is investigated [7]. Considering network connectivity, an uncertainty random spectrum is established to evaluate the survivability of mobile WSN. To meet the user's needs for WSN transmission reliability assessment, a task-oriented transmission path-based WSN transmission reliability assessment model is proposed. To address the inefficiency of transmitting multimedia data over WSNs, the WSN packet congestion control protocol is modified and a lightweight reliability mechanism is proposed. A reliability-improving cooperative communication data collection scheme is designed to achieve improved network communication reliability without degrading the network survival cycle.

One of the major characteristics of nodes in wireless sensor networks is that they have limited energy, and in the process of practical applications, the nodes are centrally powered by batteries. From the existing research, the early research on wireless sensor networks mainly focused on energy saving, that is, to ensure the normal and stable operation of wireless sensor networks by extending the life cycle of the network as much as possible by practical means [8]. The sharing and openness of wireless communication channels cannot meet the service requests of many users at the same time, resulting in lower communication quality and increasing the complexity of wireless transmission. At the same time, secure data transmission in wireless communication has become a challenging issue. However, the operational characteristics of the wireless sensor network itself can easily reduce the reliability of its transmission, so it is necessary to ensure the reliability of its transmission under the premise of energy saving. When applied to the monitoring of hazardous sources, because the node energy is limited and the node deployment location is not easy to replace the

battery, so it is necessary to ensure the balance of net energy during the monitoring process. In addition, it is necessary to avoid excessive use of a node prematurely exhausting energy and affecting data transmission. [9]. The birth of emerging technologies is usually associated with the context of a particular era, and the same is true for wireless sensor network technology. Today, many fields are in dire need of new technologies to help them evolve rapidly and achieve higher efficiency with as few human and material resources as possible. And many frontier fields of technology are usually closely related to IoT, and many research topics related to IoT have emerged, such as smart bracelets, smart homes, smart hotels, smart transportation, and smart manufacturing [10]. Not only that, wireless sensor network technology plays an extremely important role in diverse fields such as environmental monitoring, emergency rescue, natural disaster warning, and industrial and agricultural automation.

3. Wireless Sensor Social Network Data Transmission Reliability Model Design

3.1. Reliability Transmission Techniques. For the data forwarding process, not only the forwarding efficiency but also the stability needs to be considered. To ensure that data is received by the destination node stably and reliably, the trust degree among nodes needs to be considered when selecting relay nodes. Generally, the more frequent nodes with similar interests interact with each other, indicating a high trust degree and a more intimate relationship between them; therefore, the trust degree is crucial to the reliability of data forwarding [11]. To accurately quantify trustworthiness, this paper uses similarity and interaction degrees, which reflect the similar interests and frequency of interactions between nodes, respectively. To accurately measure the similarity between nodes, common neighbor nodes are used as the same or similar interest of two nodes; the main reason is that the more common neighbor nodes of two nodes, the closer they are in the network, which can ensure the reliability of data forwarding. The similarity sim is used to denote the proportion of the number of common neighbor nodes of two nodes i and j, in which, to ensure transmission efficiency, then the selected node should have better forwarding ability than the carrying node, which means the influence degree of node j should be greater than that of node i. Secondly, to ensure the stability and reliability of data forwarding, then the selected node has a strong enough relationship with the carrying node, which means the trust degree of node j and node i should be greater than the average trust degree of node i and its neighbors; in addition, node$j$of the destination node relationship is better than that of the carrying node, which means that the trust between node j and destination node D is greater than the trust between node i and destination node D, as shown in the following equation:

$$\mathrm{sim}_{ij} = \frac{1}{\sqrt{d_i + d_j}}. \tag{1}$$

Task reliability is defined as "the ability of a product to perform a specified function within a specified task profile." The definition of task reliability shows that task reliability is determined by the prescribed task profile; i.e., task reliability is related to the rules for determining task success or failure, the task time, and the stress conditions experienced by the product in chronological order during the task period and the environmental conditions, and task reliability reflects the success of the product in completing the task [12]. Therefore, when assessing mission reliability, it is only necessary to count the failures that occur during the mission period that jeopardize mission success. When judged from a "maintenance" perspective, any event or condition that causes a product to be repaired is considered a failure. This is the criterion for identifying faults that correspond to basic reliability. Such a failure may or may not affect the completion of the product's task. If considered from the point of view of "mission accomplishment," only the state or event that affects mission accomplishment is considered a fault or a fatal fault. This is the criterion for fault discrimination that corresponds to task reliability. The scope of failure in the former is greater than and includes the latter. Task profile means "A chronological description of the events and environment experienced by a product during the time it takes to complete a defined task." One or more task profiles should be developed for each product that accomplishes one or more tasks. The task profiles include the elements shown in Figure 1.

This chapter considers a large-scale high-conflict WSN environment, which consists of hundreds of sensor nodes that are divided into different levels of clusters from high to low by a hierarchical clustering algorithm, where the nodes within each cluster send the sensed data information to a cluster head node generated through an election, and finally, the cluster head node forwards the collected data information of all the nodes within the cluster to the aggregation node through a multihop nodes. Different clusters can cause conflicts in the process of data transmission, resulting in the loss of data information, and the failure of the node responsible for forwarding can also cause the loss of data information. To facilitate the study, it is agreed that the WSN network model has the following properties.

(1) High-density characteristics, with no isolated nodes under initial conditions

(2) The base station is unique and has no energy limitations

(3) The initial energy of the sensor nodes is all, and the energy cannot be increased

(4) Sensor nodes have some data fusion capability and are uniquely identified

(5) Sensor nodes have localization capability

The structural model diagram of the network is shown below, the sensor node sends the sensed data information to the cluster head node of that cluster, the cluster head divides the packet into several subpackets based on the local routing table information and transmits the subpackets to

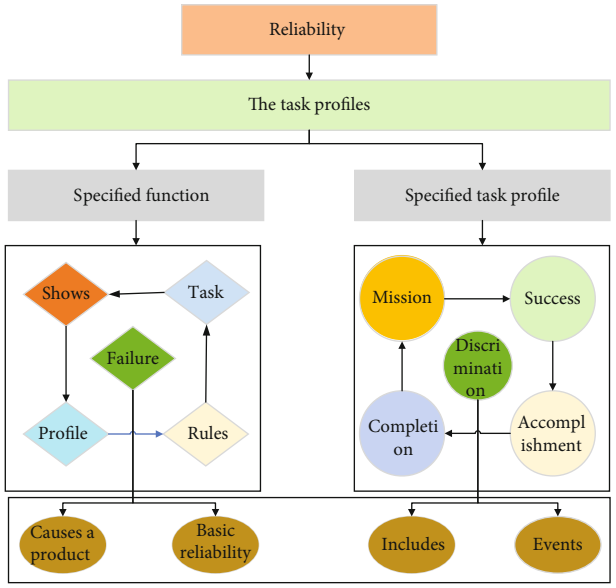

Figure 1: Contents of the mission profile.

the aggregation node through the intermediate node in a concurrent multipath manner, the aggregation node receives the subpackets from the same cluster and performs a simple data fusion, and if it forms the complete original packet, then all the subpackets of that cluster on the transmission line are automatically dropped, as shown in Figure 2.

The fault diagnosis of WSN contains two parts of work, fault detection and fault type judgment, for the workflow of the fault diagnosis model [13]. In fault detection, the sensor data is analyzed to find the abnormal data present; in fault type judgment, the prerequisite attributes of sensor data are extracted and the fault type of sensor data is found through a hierarchical BRB model. In WSN when a sensor node fails, it generates a large amount of abnormal data that deviates from the normal value, and the comparison of normal and abnormal data can achieve fault detection in WSN. The flexibility, fault tolerance, and rapid deployment of sensor networks make it widely used in the environment, food, industry, and other fields. It is considered one of the most important technologies in the 21st century. Among the ten emerging technologies with the most far-reaching impact in the future, wireless sensor networks rank first. The universality of wireless sensor networks determines its broad application prospects, and it can be evaluated as the most important technology in the 21st century, which is enough to represent its huge potential. To achieve reasonable fault detection requires clustering analysis of sensor nodes, similarity comparison of data between sensor nodes within a cluster, and when the cumulative deviation of sensor data exceeds the reservation threshold within a certain time, the current sensor node is possibly faulty. Through fault detection, WSN abnormal data is found and it is difficult to discover the fault type directly from the sensor data when the fault type is determined, so the data is characterized. The prerequisite attributes of the data can be extracted by data correlation features, including temporal correlation, spatial correlation, and attribute correlation. A hierarchical BRB model structure is proposed on how to reasonably utilize these prerequisite attributes to construct a BRB model while solving the rule explosion problem of the BRB model due to too many prerequisite attributes and improving the detection accuracy of the BRB model. The basic structure of the layered BRB system uses the output results of the current layer of BRB as the input of the next layer of BRB models, thus realizing the conversion of a complex BRB model into multiple simple BRB models.

$$\frac{A_I^{i-1} - a_i^{(t)}}{A_i^i - A_I^{i-1}} = l. \tag{2}$$

Wireless sensor networks can provide versatile applications and great benefits for smart cities and intelligent transportation systems. There are various types of services and applications in wireless sensor networks, such as real-time traffic monitoring, security information exchange, and seismic activity monitoring. Open wireless networks, social networks, and smart grids allow other users to easily join the system. This sharing model makes these wireless networks vulnerable to various attacks, converting them to internal attackers in case the attacker captures them internally and affects the normal operation of the network. Our approach develops availability weights based on statistical representations of internal malicious nodes and incorporates them into optimization problems that can be widely used in many practical scenarios [14].

During the work of wireless sensor networks, affected by various factors, the data collected by the sensor nodes may be different from the real environmental information and inevitably interspersed with noise. For this phenomenon, it is assumed that the reliability changes of sensor nodes due to different factors are expressed through the uncertainty of monitoring data, such network blockage will cause some node data loss, and node energy deficiency will cause data distortion. Therefore, this paper analyzes the node data reliability from the perspective of monitoring data changes. Combined with the data reliability assessment model of wireless sensor networks based on evidence-based inference rules, the possible problems in practical engineering are summarized as follows: Problem 1—WSN data reliability assessment index construction problem. In this paper, the reliability of wireless sensor networks is mainly assessed by analyzing the monitoring data of wireless sensor networks, and it is especially important to construct reasonable and credible assessment indicators. The following indicator system model is established.

$$S = (x_1, x_2, \cdots, x_n), \tag{3}$$

where S denotes the indicator system, x_i denotes the ith indicator, and I denotes the number of indicators.

3.2. Data Transmission Reliability Model Design for Wireless Sensor Social Networks. The basic structure of the data reliability assessment model for wireless sensor networks considering perturbation is based on evidence-based inference

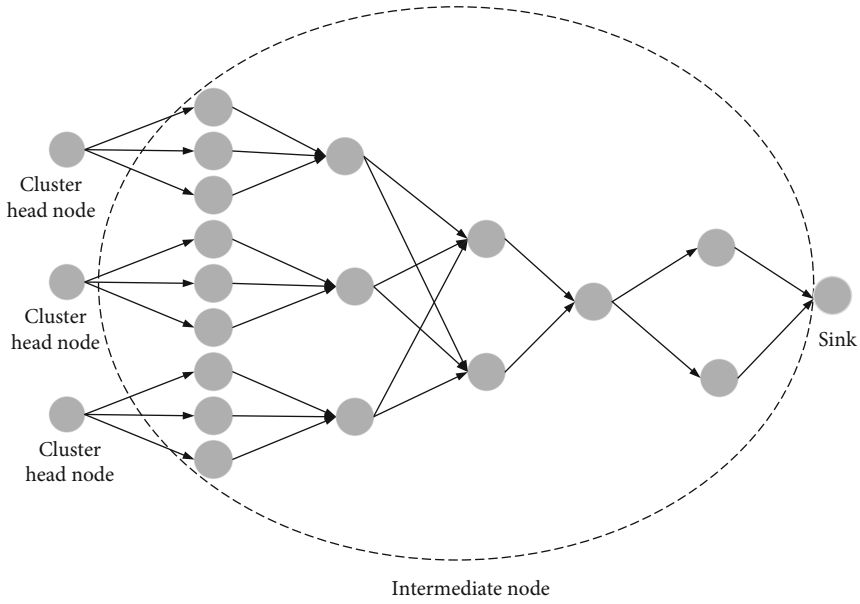

Figure 2: Model diagram of a packet structure.

rules with the model mentioned in Section 3.1. Firstly, the assessment index system is constructed, and the index data are unified by a rule-based approach to identify the framework; after that, the weights and reliability of the index data are calculated, and the data reliability is assessed by evidence-based inference rules, compared with the aforementioned model, the assessment considering perturbation. The model also requires a random variation of the data to simulate the impact of the perturbed environment on the sensor data, and the impact of the perturbation on the original data is analyzed by calculating the perturbation factor and setting the maximum perturbation error to indicate the adaptability of the sensor to that perturbed environment. The data reliability assessment method of sensor node based on evidence inference rule in the perturbed environment uses ER rule to fuse the information of indicator data and parameters based on the standardization of indicator data as well as its weight and reliability and calculates the data reliability of sensor node at a certain moment, and the following will analyze the implementation process of ER rule in detail for the calculation formula of ER rule. Suppose a node collects a total of T data, each information contains I indicators, and the evidence after data normalization can be expressed as the following confidence distribution form.

$$e_i = \left\{ \left(H_n, P_j\right), n = 1, j = -1 \right\}. \tag{4}$$

After analyzing the sensor node data reliability by ER rules, the real-time state of sensor node reliability can be observed, but the perturbation of the sensor node by external factors is not considered; however, the analysis of the sensor operating mode reveals that it is inevitably disturbed by various factors. In this subsection, based on the above-proposed sensor node data reliability assessment model considering perturbations, the nodes are evaluated for reliability to simulate the operating state of the nodes affected by different factors by adding perturbation variables to the nominal trajectory and setting perturbations of different strengths, with the perturbation variables representing the actual data of the sensor nodes relative to the perceived information in the unperturbed environment. Two laws are met: the generation of perturbations is random and irregular, and the generation of perturbation variables conforms to the characteristics of normal distribution. Analyzing the perturbation factors affecting the index data, the accuracy of temperature data is easily affected by network fluctuations and environmental confrontation. In this paper, we simulate four types of perturbed environments (weak network fluctuations and weak environmental confrontation, weak network fluctuations and strong environmental confrontation, strong network fluctuations and weak environmental confrontation, strong network fluctuations, and strong environmental confrontation), and the corresponding perturbation strengths are 0.015, 0.030, 0.045, and 0.060, respectively. After adding the perturbation, the data of each indicator changes, as shown in Figure 3.

However, data transmission is not guaranteed immediately after the nodes meet, because the resource-limited channel may be busy and the nodes can use the channel to complete data forwarding only when the channel becomes idle. Therefore, the idle waiting time of the channel after two nodes meet until they start transmitting data needs to be analyzed. Different from the general waiting rule, this paper uses the channel in the order of the priority of the nodes' influence, which is because the nodes with higher influence have a higher probability of carrying high-value data, which can make the channel resources more efficient. During data transmission, the channel will show two states: first, the channel is idle, when node i sends data directly to node j; second, the channel is busy, when node i needs to wait for the channel to become idle before competing with

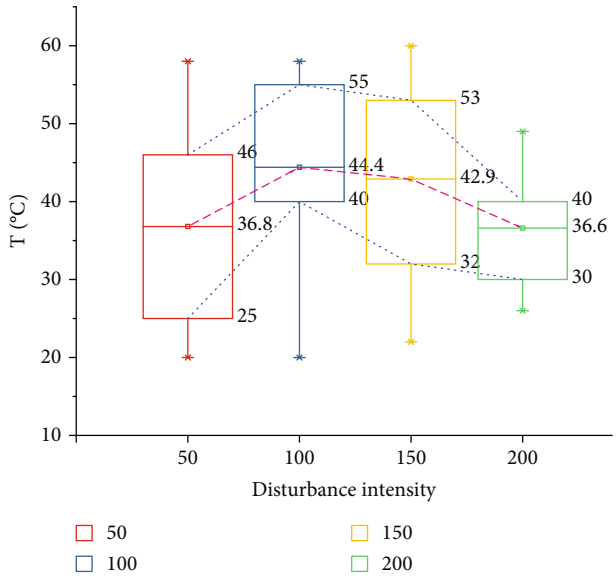

Figure 3: Temperature data corresponding to the intensity of the disturbance.

other nodes for the channel. Therefore, there are two issues to consider: whether the channel is busy or not and the waiting time when the channel is busy [15]. In general, whether the channel is busy or not is related to two factors, namely, the channel bandwidth and the number of nodes competing for the channel, which are exponentially related to the probability of the channel being busy, because channel competition decreases significantly with each doubling of the bandwidth at low bandwidths, while the number of nodes competing for the channel is the opposite.

$$R(\mathrm{t}) = \sum_{u=t}^{N_y} L(I_t : I_u) + 1. \tag{5}$$

When a cluster head node fails, if there is no other redundant node for continued transmission, then, the data of that node may be lost and will reduce the reliability of the network. If a normal node reselects another cluster head node for data delivery, it is not only a complex process for the nodes in the failed cluster, but it is also a nontrivial task for the clusters that wish to join to deal with the newly joined nodes. For example, cluster head nodes (routers) and sink nodes (coordinators) take the backup redundancy of cluster head nodes so that the overall reliability of the cluster head nodes is the best, thus improving the reliability of the whole monitoring system. At this point, when a cluster head fails, it is no longer considered a single failed body, but as a group of 1 cluster head node. When an individual node in the node group fails, a redundancy mechanism is used, and another link can be selected for the transmission of information, ensuring the connectivity of the communication link. When a cluster head node fails, another backup cluster head node takes over the work, which not only reduces the overhead of route finding but also reduces the complexity of controlling other cluster head nodes [16]. Assuming that the number of redundancies of cluster head nodes is $k = 1, 2, 3, \cdots, 10$, the relationship between cluster head node reliability and the number of redundancies is proportional, the more the number of redundancies, the higher the reliability of cluster head nodes will be, when the number of redundancies is 2, and the reliability of cluster head nodes is significantly improved, when the number of redundancies reaches 3. However, it is not better to have more redundancy because the actual deployment needs to consider the budget, and the cluster head nodes are more expensive. When the number of redundancies reaches 3 or more, the reliability of the cluster head is almost the same and does not improve significantly, as shown in Figure 4.

We assume that the source node has no prior knowledge of the abnormal behavior of the node that is working. We do not assume the policies, targets of failure behavior, or movement patterns of malicious nodes. We assume that the type of misbehavior, such as internal component failure or external failure, is not known in the network. To characterize the impact of node misbehavior on multiple types of transmissions, each source must collect information about the impact of misbehavior in the urban network. When sensor node I provides multiple types of services to the receiving node through multihop communication, there exist some candidate forwarding nodes based on node i's knowledge of the available neighbors. Each sensor node tries to maximize its revenue by sending feedback signals, and the "resource price" determines the cost of consuming these limited resources for the competing services. Therefore, each node charges a resource price and then allocates a certain number of resources to be made available to users. For various types of services or applications, each source is associated with a utility function that reflects how much of a quality of service (QoS) benefit the source receives as measured by the allocated transmission rate. Here, the network model in a distributed framework for candidate node selection and rate allocation of sources is shown in Figure 5.

4. Wireless Sensor Network Topology Reliability Assessment

4.1. Reliability Assessment. The network may be affected by various factors such as component failure, traffic changes, and routing methods; during the operation, the complexity and randomness of the network present a great challenge to network reliability analysis, and it is difficult to establish an analytical model for network reliability assessment; therefore, many researchers use simulation or statistical approach to analyze the network reliability [17]. The simulation method is the main way of current and even future network reliability assessment, by constructing a network reliability model, setting up a model of random parameters in the network such as tasks, failures, and maintenance, simulating the state changes in the network, and then statistically analyzing the corresponding reliability parameters. At present, there exist two main types of simulation methods: Monte Carlo and state machine. The Monte Carlo method is a probabilistic statistical method to obtain results by random sampling. Based on the results of the analysis of the actual problem,

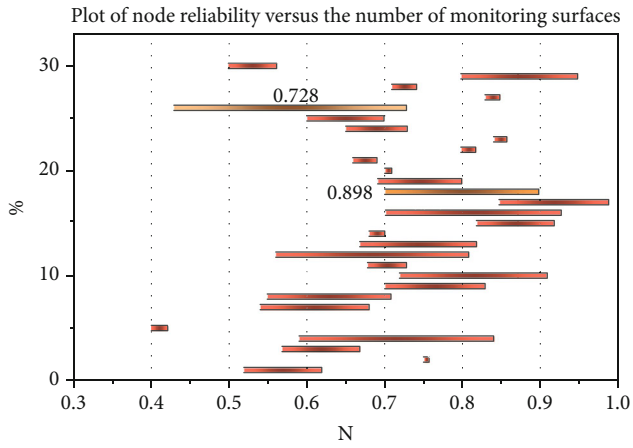

Figure 4: Plot of node reliability versus the number of monitoring surfaces.

random events are constructed to describe the probabilistic process, and the solution of the problem is obtained by sampling and calculating the random events. The process of constructing a reliability evaluation model of a network based on network topology, network protocols, and business processes by simulating the current common network performance simulation tools such as OPNET, NS2, and OMNESE is a Monte Carlo method.

$$N_e = \begin{cases} \dfrac{w}{r} > \dfrac{\sqrt{5}r}{2}, \\ \dfrac{w}{2r} \le \dfrac{\sqrt{5}r}{2}. \end{cases} \tag{6}$$

Input random parameters such as network traffic and fault distribution are sampled and calculated to obtain the relevant reliability parameters. For complex discrete events in networks, state machines are used to describe network changes and analyze the transfer process of network states to assess network reliability. Among the state machine-based modeling approaches, Petri nets, which simulate discrete-event dynamic systems, are commonly used modeling tools. Petri nets can depict multiple logical relationships and events in the system such as resource sharing, competition, and conflict in synchronous as well as asynchronous. However, when modeling large-scale complex network systems, general Petri nets are prone to the "state combination explosion" phenomenon. To address this problem, researchers have proposed various advanced models of Petri nets such as Coloring Petri Nets (CPN), Stochastic Petri Nets (SPN), and Object-Oriented Petr Nets for modeling. Aiming at the problem of low efficiency in transmitting multimedia data on WSN, the WSN data packet congestion control protocol was modified, and a lightweight reliability mechanism was proposed. A scheme of collaborative communication data collection with improved reliability is designed, which can improve the reliability of network communication without reducing the network life cycle. Redundancy is usually used in wireless sensor networks to improve reliability; however, energy saving and high reliability are two conflicting goals, so it becomes a challenge to integrate high reliability and low energy consumption for transmission task assignment in wireless sensor networks [18]. The goal of this chapter is to minimize the energy consumption of transmission task assignment in wireless sensor networks with the deadline of the task and the reliability of the task as a constraint.

To achieve this goal, a centralized reliable and efficient transmission task assignment strategy for wireless sensor networks is proposed, in which the task is taken as the malefactor object and the transmission task assignment process is executed by the sink node after the required network information is collected; based on the global network state information, the wireless sensor network transmission task assignment problem is transformed into a nonlinear mixed-integer programming problem. Many researchers have researched the transmission task allocation problem of wireless sensor networks. Since WSN nodes are resource-constrained, one of the main objectives of task assignment in this environment is to minimize energy consumption and thus maximize the system operational lifetime. Therefore, the objective of traditional wireless sensor network transmission task allocation is mainly focused on energy saving. Among the methods for solving the task assignment problem, the exact solution methods such as integer programming, branch-and-bound method, and enumeration method cannot meet the real-time requirements; while the dynamic planning-based heuristics are more efficient to solve, but they all use a local search strategy based on greedy strategy, so the obtained task assignment scheme may not be the optimal one, as shown in Figure 6.

In this paper, the message retransmission technique is used in the backbone transmission part to ensure reliable data transmission. A scheme is proposed for message delivery using hop-by-hop broadcasting and copying multiple copies of the same message with improved reliability, using wireless broadcasting to increase the packet delivery rate per-hop and to obtain the required reliability at minimum cost, and finally deriving the optimal policy used to distribute the required reliability at each hop point to obtain the required end-to-end reliability for any given. This approach can reduce the probability of packet loss, but because replicating multiple copies and sending them entails significant energy consumption, especially in large networks. To avoid duplication of messages, a new decentralized technique called Geographic Forwarding Rules (GFRs) is proposed to reduce the number of broadcast messages in mobile self-organizing networks by dividing the network into virtual regions using the location information of the nodes and avoiding duplication of messages between regions.

4.2. Simulation Verification and Analysis of Results. To be able to clearly illustrate the factors influencing the transmission capacity and to verify the accuracy of the proposed analysis process, an empirical dataset was used, which was completed by 100 volunteers during the INFOCOM06 conference, each of whom carried a mobile terminal with a Bluetooth interface and the trajectories of these volunteers and

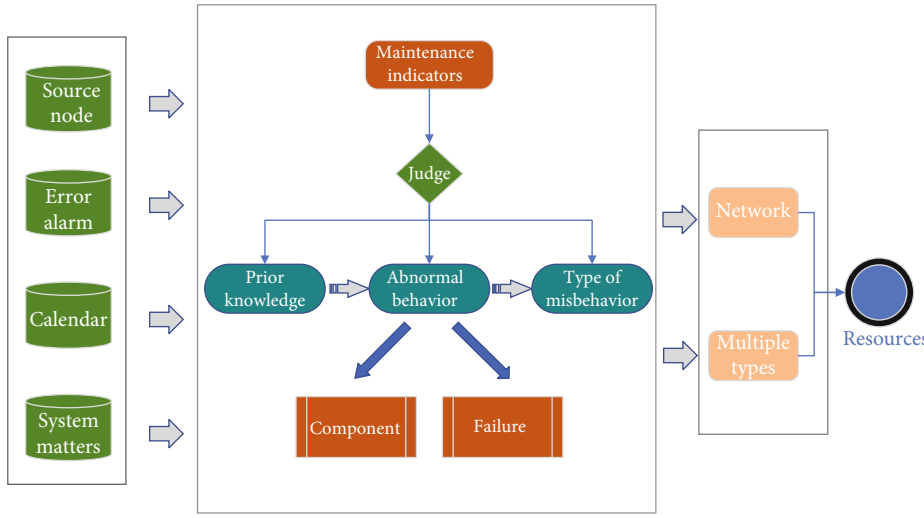

Figure 5: Multiservice transfer framework for fault activity information.

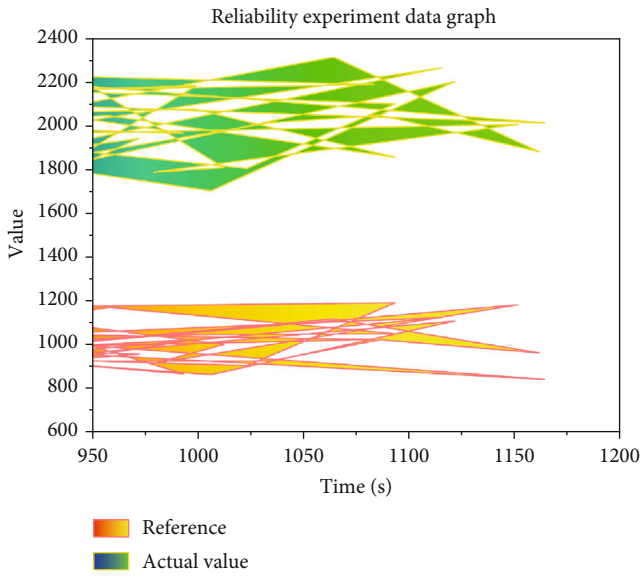

Figure 6: Reliability experiment data graph.

the contact records, which can reflect the mobile characteristics of the nodes and their social relationships. The dataset is used by several laboratories at home and abroad and has high authority [19]. In this paper, we use the MATLAB simulation platform to compare and analyze the difference between the theoretical numerical results and simulation numerical results, and the THR and SML appearing in the later figures indicate the theoretical results and simulation results, respectively. The operating characteristics of the wireless sensor network itself can easily reduce the reliability of its own transmission, so on the premise of ensuring energy saving, it is also necessary to ensure the reliability of its transmission. When applied to the monitoring of hazardous sources, because the energy of the node is limited and the location of the node is not easy to replace the battery, it is necessary to ensure that the network energy is balanced during the monitoring process, affecting the transmission of data. In this section, we analyze the relationship between the transmission capacity S and the number of network nodes N, the number of hops H, the packet loss rate P, and the delay T, respectively, and also analyze the relationship between the packet loss rate and the delay to better understand the trend between these variables. The simulation parameters are set as shown in Table 1.

According to the small world theory, any two nodes in the network can communicate with the help of a limited number of nodes, and the number of these collaborating nodes is generally 2-6, so this section first analyzes the effect of the number of network nodes N on the transmission capacity S at different hop counts ($H = 2, H = 4, H = 6$). From the results, it can be found that the transmission capacity increases with the increase in the number of network nodes at different hop counts, but the overall transmission capacity under 4 hops is higher than under 2 and 6 hops; this is because the data has the best transmission performance only when the number of hops is within a certain range; too high or too low is not good for data forwarding. In addition, as the number of nodes increases, the transmission capacity grows faster under 4 hops. Two-hop transmission capacity increases slowly and decreases to a certain extent when $N \geq 120$. This is because the network nodes increase to a certain level and fewer relay nodes make the total time required to transmit data grow, resulting in a decrease in transmission capacity. Finally, the numerical results of the simulation and theoretical analysis match with an average error of 12%.

$$\lambda_{u_{ij}=W_{u_{ij}/d_{u_1}}}. \tag{7}$$

Keeping the communication distance constant and increasing the number of nodes within the network, we can see that the traditional chance routing algorithm starts to have node failures about 1 minute into the simulation, relying solely on the geographic location information of

Table 1: Simulation parameter settings.

Simulation parameters	Reference	Actual value
Number of nodes	80-150	120
Communication module	Bluetooth	ZigBee
Network area	1000,1000	1000,1000
Subchannel rate	100	103
Node cache space	20-50	30

neighboring nodes and sink nodes to determine intermediate forwarding nodes [20]. In this case, it is considered that the closer the sink node within the transmission range, the better the path. This will result in the frequent use of a node as an intermediate node for data forwarding during the initial process of the network until the node fails with energy exhaustion, while many nodes will have energy redundancy and the energy will not be utilized after the overall failure of the network. With the improved chance routing algorithm, the network energy consumption can be evenly distributed to neighboring nodes, which increases the network survival time until the surrounding nodes are depleted of energy before they fail centrally at 14 minutes, basically reaching the maximum network survival time, as shown in Figure 7.

Due to the backbone role of the cluster head node in the network, in this paper, the cluster head node is evaluated as a separate component and both upstream and downstream transmission processes are divided into two phases using the cluster head node as the boundary and modeled in a stepwise manner to facilitate the application and extension of the reliability assessment model. Wireless sensor networks have complementary and redundant relationships in space and time between the information sent out by multiple sources when monitoring the same event or parameter. Many source nodes in a cluster topology send sensing information to the cluster head node, which determines whether the sensing task is completed based on comparison with a threshold value. In the uplink transmission phase of mesh-type (mesh) topology, multiple source nodes transmit the sensed information to the sink node, so this phase is a multisource single-homed network. For the same task in a multisource environment, it is not required that every packet sensed by each source node be successfully received by the sink node. Unlike the cluster topology where the sensed packets are prone to data fusion at the cluster head, the mesh topology is less efficient in performing data fusion at the intermediate nodes of the network. For modeling, it is assumed that the data sensed by the source nodes in the mesh-type topology is not subjected to data fusion. To accurately measure the similarity between nodes, the common neighbor node is regarded as the same or similar interest of two nodes. The main reason is that the more common the neighbor nodes of two nodes, the closer their relationship in the network can ensure data forwarding. The similarity sim_{ij} is used to represent the proportion of the number of common neighbor nodes of two nodes i and j.

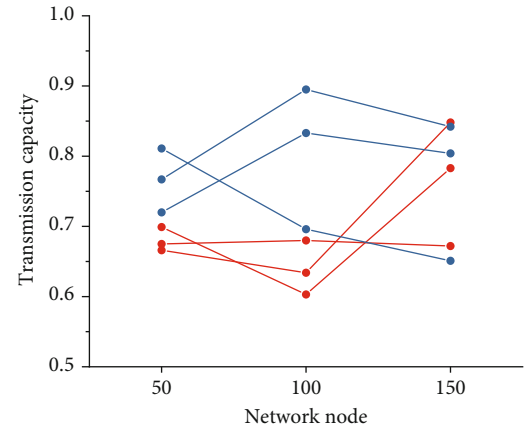

Figure 7: Transmission capacity versus network nodes.

5. Conclusion

The reliability of wireless sensor networks (WSNs) is one of the important indicators of network quality of service and requires system planning and a series of designs and verification to achieve reliability goals. Existing studies have mainly investigated the basic reliability of the network in terms of the connectivity of the network, the capacity of the network, and individual performance parameters such as delay and packet loss. However, these parameters are difficult to assess the comprehensive capability of the network when running services, which requires an overall evaluation and design of the mission reliability of the network. Task reliability is closely related to the task profile, functional requirements, state mode, and system configuration of the network; as the WSN continues to expand, the association relationships between nodes within the network become more complex and the system operation states increase, leading to increased difficulty in the analysis and design process of WSN task reliability. Task reliability is a comprehensive reflection of various characteristics of the network; therefore, the analysis and design of task reliability of WSNs are a difficult point that needs to be broken. In this paper, the hierarchical clustering protocol is designed from the perspective of saving energy consumption of WSN, and the reliable data transmission protocol is designed to ensure reliable data transmission, but the idea is not perfect, and there are still many topics to be improved or to be studied in the field of WSN.

Data Availability

The data used to support the findings of this study are available from the corresponding author upon request.

Conflicts of Interest

The author declares that they have no known competing financial interests or personal relationships that could have appeared to influence the work reported in this paper.

Acknowledgments

The study was supported by the Construction of First-Class Disciplines in Ningxia Colleges and Universities (Pedagogy) (Grant No. NXYLXK2017B11).

References

[1] Y. Liu, D. Liu, Y. Zhao, and L. Wang, "The reliability analysis of wireless sensor networks based on the energy restrictions," *International Journal of Wireless and Mobile Computing*, vol. 10, no. 4, pp. 399–406, 2016.

[2] L. Xing, "Reliability modeling of wireless sensor networks: a review," *Recent Patents on Engineering*, vol. 15, no. 1, pp. 3–11, 2021.

[3] Z. Zou and Y. Qian, "Wireless sensor network routing method based on improved ant colony algorithm," *Journal of Ambient Intelligence and Humanized Computing*, vol. 10, no. 3, pp. 991–998, 2019.

[4] M. Abdulkarem, K. Samsudin, F. Z. Rokhani, and M. F. A Rasid, "Wireless sensor network for structural health monitoring: a contemporary review of technologies, challenges, and future direction," *Structural Health Monitoring*, vol. 19, no. 3, pp. 693–735, 2020.

[5] W. Zhang, S. Zhu, J. Tang, and N. Xiong, "A novel trust management scheme based on Dempster–Shafer evidence theory for malicious nodes detection in wireless sensor networks," *The Journal of Supercomputing*, vol. 74, no. 4, pp. 1779–1801, 2018.

[6] Q. Huamei, J. Tao, J. Su, Z. Zhiwen, and X. Wangping, "QoS adaptive and energy aware cross-layer opportunistic routing protocol in wireless sensor networks," *IET Communications*, vol. 13, no. 8, pp. 1034–1042, 2019.

[7] V. Gaur, O. P. Yadav, G. Soni, and A. P. S. Rathore, "A literature review on network reliability analysis and its engineering applications," *Proceedings of the Institution of Mechanical Engineers, Part O: Journal of Risk and Reliability*, vol. 235, no. 2, pp. 167–181, 2021.

[8] S. Tamilselvi and S. Rizwana, "Optimized cluster head selection with traffic-aware reliability enhanced routing protocol for heterogeneous wireless sensor network (HWSN)," *International Journal of Computer Networks and Applications*, vol. 8, no. 2, pp. 108–118, 2021.

[9] L. Chan, K. Gomez Chavez, H. Rudolph, and A. Hourani, "Hierarchical routing protocols for wireless sensor network: a compressive survey," *Wireless Networks*, vol. 26, no. 5, pp. 3291–3314, 2020.

[10] T. A. Alghamdi, "Energy efficient protocol in wireless sensor network: optimized cluster head selection model," *Telecommunication Systems*, vol. 74, no. 3, pp. 331–345, 2020.

[11] G. Khanna, S. K. Chaturvedi, and S. Soh, "Two-terminal reliability analysis for time-evolving and predictable delay-tolerant networks," *Recent Advances in Electrical & Electronic Engineering (Formerly Recent Patents on Electrical & Electronic Engineering)*, vol. 13, no. 2, pp. 236–250, 2020.

[12] S. Din, A. Paul, A. Ahmad, and J. H. Kim, "Energy efficient topology management scheme based on clustering technique for software defined wireless sensor network," *Peer-to-Peer Networking and Applications*, vol. 12, no. 2, pp. 348–356, 2019.

[13] Nizirwan Anwar, Dewanto Rosian Adhy, Budi Tjahjono, Rudi Hermawan, Nur Widiyasono, and Muhammad Abdullah Hadi, "Reliability analysis of communication network service quality for internet of vehicles (IoV)," *International Journal of Science, Technology & Management*, vol. 2, no. 5, pp. 1588–1599, 2021.

[14] R. P. Ojha, P. K. Srivastava, G. Sanyal, and N. Gupta, "Improved model for the stability analysis of wireless sensor network against malware attacks," *Wireless Personal Communications*, vol. 116, no. 3, pp. 2525–2548, 2021.

[15] M. Mathapati, T. S. Kumaran, A. Muruganandham, and M. Mathivanan, "Secure routing scheme with multi-dimensional trust evaluation for wireless sensor network," *Journal of Ambient Intelligence and Humanized Computing*, vol. 12, no. 6, pp. 6047–6055, 2021.

[16] D. J. I. Zong Chen and K. L. Lai, "Machine learning based energy management at Internet of Things network nodes," *Journal: Journal of Trends in Computer Science and Smart Technology September*, vol. 2, no. 3, pp. 127–133, 2020.

[17] D. Hosahalli and K. G. Srinivas, "Enhanced reinforcement learning assisted dynamic power management model for Internet-of-things centric wireless sensor network," *IET Communications*, vol. 14, no. 21, pp. 3748–3760, 2020.

[18] M. Abdelhafidh, M. Fourati, L. C. Fourati, and A. Chouaya, "Wireless sensor network monitoring system: architecture, applications and future directions," *International Journal of Communication Networks and Distributed Systems*, vol. 23, no. 4, pp. 413–451, 2019.

[19] P. Joshi and A. S. Raghuvanshi, "Hybrid approaches to address various challenges in wireless sensor network for IoT applications: opportunities and open problems," *International Journal of Computer Networks and Applications*, vol. 8, no. 3, pp. 151–187, 2021.

[20] G. F. Albery, L. Kirkpatrick, J. A. Firth, and S. Bansal, "Unifying spatial and social network analysis in disease ecology," *Journal of Animal Ecology*, vol. 90, no. 1, pp. 45–61, 2021.

Hindawi
Journal of Sensors
Volume 2022, Article ID 3842722, 12 pages
https://doi.org/10.1155/2022/3842722

Research Article

Data Transmission Reliability Analysis of Wireless Sensor Networks for Social Network Optimization

Xia Xu,[1] **Jin Tang**,[1] **and Hua Xiang**[2]

[1]*School of Information Science, Changjiang Polytechnic, Wuhan, Hubei 430074, China*
[2]*School of Computer Science, Changjiang University, Jingzhou, Hubei 434023, China*

Correspondence should be addressed to Hua Xiang; xianghua@yangtzeu.edu.cn

Received 2 November 2021; Revised 6 December 2021; Accepted 7 December 2021; Published 6 January 2022

Academic Editor: Gengxin Sun

With the rapid development of the Internet in recent years, people are using the Internet less and less frequently. People publish and obtain information through various channels on the Internet, and online social networks have become one of the most important channels. Many nodes in social networks and frequent interactions between nodes create great difficulties for privacy protection, and some of the existing studies also have problems such as cumbersome computational steps and low efficiency. In this paper, we take the complex environment of social networks as the research background and focus on the key issues of mobile wireless sensor network reliability from the mobile wireless sensor networks that apply to large-scale, simpler information, and delay tolerance. By introducing intelligent learning methods and swarm intelligence bionic optimization algorithms, we address reliability issues such as mobile wireless sensor network fault prediction methods and topology reliability assessment methods in industrial application environments, the impact of mobile path optimization of mobile wireless sensor networks on data collection efficiency and network reliability, reliable data transmission based on data fusion methods, and intelligent fault tolerance strategies for multipath routing to ensure mobile wireless sensor networks operate energy-efficiently and reliably in complex industrial application environments.

1. Introduction

With the deep development of Internet technology and computer technology, the emergence of social networks has changed the traditional way of human socialization, and social networks have gradually become the main place for people's daily activities (entertainment and communication, online shopping, community Q&A, online education, etc.), and there are more and more participants in social networks, and information is spread in social networks at an unprecedented speed [1]. Through social networks, we can communicate in-depth with our friends in the form of sending messages, sharing content, etc. Due to its convenience and easy-to-use characteristics, social networks have become more and more common in people's lives and work under the environment of increasingly mature network technology. At the same time, with the rapid development of the network, the privacy issues therein are gradually attracting widespread attention. The wireless sensor network is an intelligent network that transmits data in the form of proximity multihop self-organization and collaboration and cooperation between nodes by deploying various types of sensor nodes to the monitoring area [2]. The network integrates information sensing, wireless communication, embedded computing, distributed information processing, and other technologies, the nodes preprocess the collected data and send it to the aggregation nodes in the form of multihop self-organization, and the aggregation nodes then transmit the collected information to the monitoring centre, which performs appropriate processing and finally feeds the processed data back to the decision-makers and transmits it to the required users. The physical links and capacities are mapped to traffic paths during the evaluation process, which can concisely reflect the performance degradation of the network. When evaluating the network performance reliability, the probability that the information from the source node reaches the destination node within the specified time is used as the timely reliability of this network,

the probability that the routing buffer overflows is used as the criterion to evaluate the network congestion, and the ratio of the packet received at the receiver side to the transmission at the sender side can also be used as the complete reliability of this network.

Privacy data in social networks mainly includes user's identity information, login information, friend information, the content published on the social network platform, and the dissemination of information. The root cause of privacy security risks in social networks is that the private data of data owners are distributed on social networking platforms without the direct physical control of data owners, which may cause data leakage and allow users who do not have access rights to view the content published by data owners or even users who maliciously steal information to view it. Studying how to combine data publishing methods with privacy-preserving techniques and prevent leakage of sensitive user information has become a serious challenge for current social networking services [3].

The reliability of WSNs (wireless sensor networks) is an important indicator for assessing network performance and can be classified into different categories based on different criteria. From the perspective of application requirements, dependability assessment can be divided into coverage-based and connectivity-based reliability; according to the different methods used for reliability analysis and calculation, reliability assessment can be divided into conditional probability, Markov chain, block diagram method, Monte Carlo simulation method, binary decision diagram, fault tree analysis, etc.; in addition, from the definition of division, it can be divided into task-based reliability and lifetime distribution-based reliability [4]. In this paper, we propose to carry out research on mobile wireless sensor network reliability problems and conduct an in-depth and systematic study in mobile wireless sensor network reliability assessment and optimization by introducing intelligent optimization algorithms and swarm intelligent bionic optimization methods, to address mobile wireless sensor network node hardware and network failure prediction methods, network reliability assessment methods for mesh, tree, and ribbon topologies, mobile path optimization on data collection efficiency and network reliability, reliable data transmission based on data fusion methods, and intelligent fault tolerance of multipath routing and other reliability issues, to provide an effective way to build a reliable mobile wireless sensor network suitable for the complex environment of social networks.

2. Related Work

The privacy and security of users in social networks is a pressing issue that is directly related to their safety in real life. Currently, researchers have carried out some research work on privacy metrics in social networks, but the research is still relatively lagging compared to industrial networks. The reliability of WSNs is mainly studied in terms of the failure problem of nodes and energy problem.

The problem of random failure of nodes is considered in the distributed WSN in the literature [5] for the analysis of the WSN feasibility. In the literature [6], a wireless sensor network consisting of a Sink node and n sensor nodes is considered and the reliability of the network is evaluated using probabilistic analysis. The concept of common cause failure is introduced in the literature [7], and a Monte Carlo simulation-based approach is proposed to calculate the reliability of the wireless sensor network. The Markov model is introduced in the literature [8] to evaluate the reliability of sensor nodes. A binary decision graph algorithm is proposed in the literature [9] to address the reliability of WSNs in a common cause failure environment. Common cause failure is defined as the phenomenon of simultaneous failure of multiple components in the network; for example, multiple sensor nodes in the network will fail simultaneously during an avalanche; previous WSN reliability analyses assume that sensor nodes are independent of each other and do not consider the effective correlation of sensor nodes; this analysis is not comprehensive; the literature [10] transforms the binary decision diagram into an ordered bifurcated decision diagram (OBDD) to consider the common cause events, which has been of great help to later scholars in their research. The literature [11] proposed the use of a survey questionnaire to count multiple metrics, through which users who may differ significantly in their privacy-preserving behaviours are selected to count their scores and then validate the validity of these metrics. In their study, they analyze the correlation between the scores of the survey metrics and two established privacy-preserving behaviours. Ultimately, they conclude that these metrics are a reliable and valid web management tool that can be used in research on online privacy metrics. In the literature [12], a dual objective function was constructed with the goal of shortest transport distance and highest security, and an adaptive random selection algorithm and a time adjustment algorithm were added to the ALNS heuristic to solve the transport path and improve the security of the transport path. The literature [13] combines the road class and road traffic influence factors in the actual dynamic road network and uses an improved ant colony algorithm to explore the optimal path that meets the requirements of travellers. The literature [14] proposes an algorithm to improve the reliability of paths between customers and target users in social networks, which uses a reverse ant colony algorithm with an improved pheromone update strategy in it, thus ensuring load balancing and shorter user waiting time. In the literature [15], path reachability, optimal path selection, and TOP-K path query are studied with graph data, and the objective and subjective weights of each attribute of the path are derived using information entropy technique and subjective assignment method for the case of mixing different types and characteristics of attributes such as deterministic and uncertainty in complex multiattributes, and then, the two weights are analyzed comprehensively to calculate each path's combined score and reduce the search space when optimizing the path query by graph decomposition and hierarchical shrinkage techniques. In terms of network routing, literature [16] proposed a general method to solve multiconstrained path queries by minimizing the nonlinear cost function to determine whether the found path is feasible and by minimizing

the main cost function to explore whether there are still better paths, thus ensuring QoS quality. The literature [17] proposes a difference-oriented path multiplex selection algorithm (CMT-DPS), where when the difference between paths is relatively large, paths of poorer quality are not selected to participate in data transmission, which improves the overall throughput and reduces the transmission delay to some extent. The software-defined network (SDN) path selection algorithm with dual impact factors based on the actual quality of experience (QoE) is proposed in the literature [18], which ensures link quality and load balancing by real-time state acquisition and dynamic adjustment of weights, while also applying the ant colony algorithm to improve the transmission rate.

3. Data Reliability Study of Wireless Sensor Networks for Social Network Optimization

3.1. Data Reliability Study of Wireless Sensor Networks. The basic reliability and mission reliability of a wireless network are the "one and two sides" of the product reliability work, "one" means that the main body of basic reliability and mission reliability implementation is the product design itself, "two sides 'one'" means that the main body of basic reliability and task reliability is the product design itself, and "two sides" means that basic reliability and task reliability are two objectives that should be taken into account in product design, and one is indispensable. From the definition of basic reliability and task reliability, we know that the difference between them is as follows: (1) The time definition is different. The scope of "specified time" in the definition of mission reliability is defined by the mission profile cycle. The "specified time" in the definition of basic reliability is defined by the full life cycle profile, which generally includes multiple task profiles. (2) The scope of failure statistics is different. When evaluating task reliability, only those failures that affect the "completion of the task" in the definition of task reliability are considered, and those failures that do not affect the completion of the task are not considered. However, when evaluating basic reliability, it is necessary to consider all the failures that need to be repaired during the whole system life cycle, and the scope of failures in basic reliability statistics is larger than that of mission reliability. (3) The final impact on product use is different. Basic reliability is related to maintenance coverage, and basic reliability ultimately affects the availability of equipment and the cost of maintenance coverage [19]. The continuous type of Weibull distribution and other distributions is closely related, and the range of values of shape parameters of Weibull distribution reflects the product failure characteristics, so the Weibull distribution is also quite widely used, while mission reliability affects the performance of the system's mission-related applications and is a key factor in determining whether the product can perform its mission successfully. (4) For different calculation models, mission reliability firstly establishes mission profiles based on mission descriptions, and for different missions, a system may have multiple mission profiles, based on which multiple mission reliability models are generated. In contrast, when calculating the basic reliability of a system, a system corresponds to only one reliability calculation model.

The theoretical bases of traditional research on network reliability assessment can be divided into three types: mathematical analysis methods based on graph theory and probability theory, simulation methods that simulate random events, and field experiment methods based on real scenarios. Figure 1 shows the theoretical bases and research methods of traditional network reliability assessment methods.

Connectivity reliability is the first proposed network reliability metric and is classified into active and passive networks based on the presence or absence of specified source points in the network. The classical analytical algorithms for computing network connectivity reliability include state enumeration, exclusion principle, disjoint sum, factorization, graph transformation, and delimitation methods. These algorithms usually assume that the links have only two states, fault and normal, and that the probabilities of link failures in the network are independent of each other. Network reliability design needs to consider redundancy design, fault management and prevention, data management, node and link trustworthiness, environment, destruction resistance, security, and other factors. The capacity of a link is limited at the time of transmission, and the capacity reliability refers to the probability of success in transmitting the required capacity between the two ends of the link after setting the maximum capacity for each link, as shown in the following equation:

$$P(\theta \mid k) = \frac{\int \alpha \cdot (\theta - \mu)/\sigma d\theta}{kr}. \tag{1}$$

This type of algorithm adds capacity constraints to the consideration of topological connectivity, and this network model has evolved into the "random flow network model":

$$\text{limit}C = \frac{1}{n}(3.36 + \varsigma)^3 + C_0. \tag{2}$$

Based on this model, researchers have proposed a series of computational methods. The capacity reliability assessment model is based on known conditions, such as node and link reliability information (e.g., reliability), node and link capacity information, network topology, and transmission capacity requirements, to solve for the probability of the existence of a connectivity path that satisfies certain capacity requirements for some set of nodes [20]. The connectivity reliability assessment classification is shown in Figure 2.

Performance reliability focuses on the traffic on the network path, and the physical links and capacity are mapped to the traffic path during the evaluation process, which can concisely reflect the performance degradation of the network. When evaluating the network performance reliability, the probability that the information from the source node reaches the destination node within the specified time is taken as the timely reliability of this network, the probability that the routing buffer overflows is used as a criterion to evaluate the network congestion, and the ratio of packet

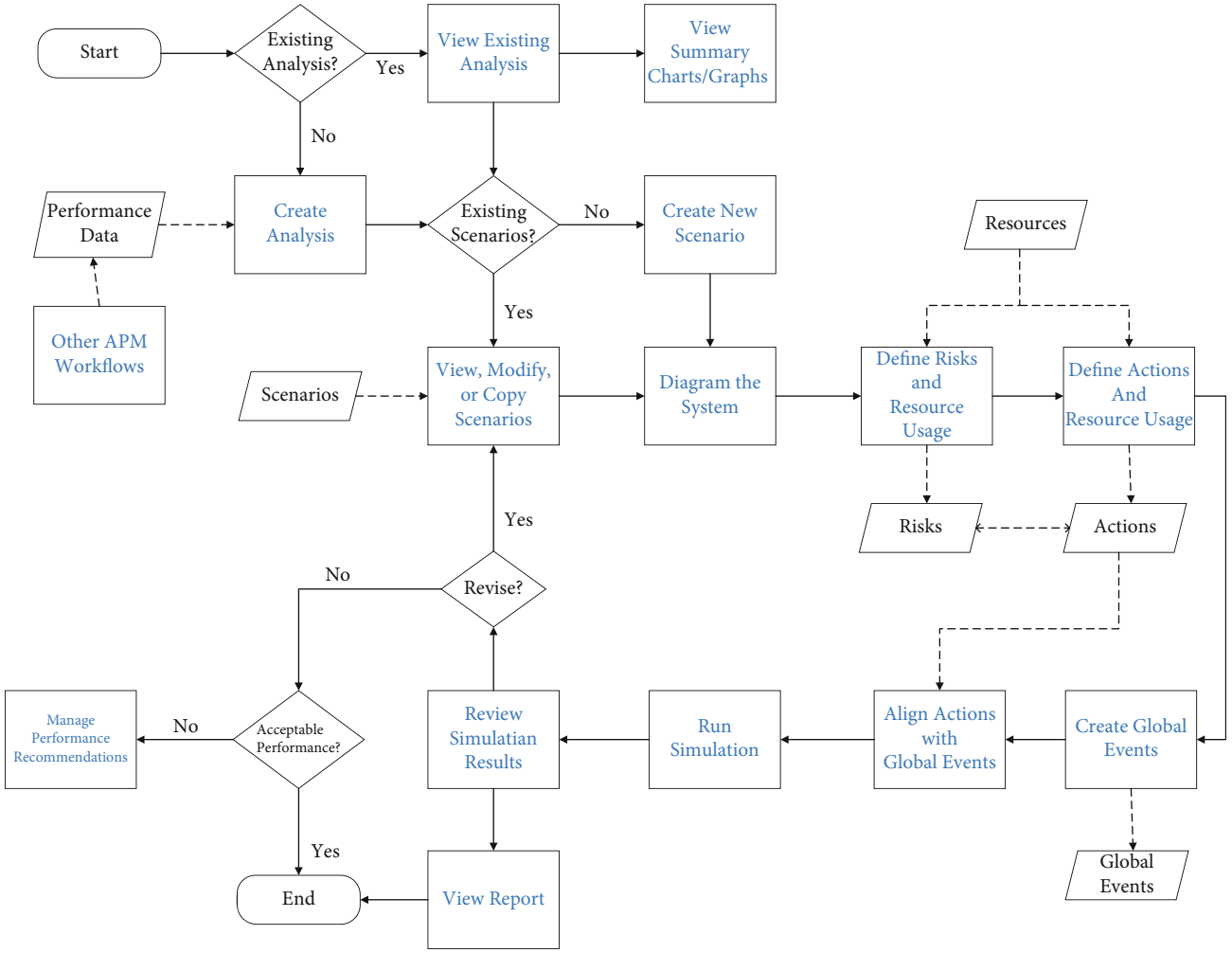

Figure 1: Classification of network reliability assessment methods.

reception at the receiving end to the amount sent at the sending end can also be used as the complete reliability of this network. Although the above three types of network reliability assessment of connectivity reliability, capacity reliability, and performance reliability can reflect the different functional requirements, metric range, and network performance of the network, it is difficult to give the comprehensive capability of the network when it is running a task. The problem of a comprehensive assessment of task-centric network reliability can be formulated as follows:

$$Y = \bigcap_{i=1}^{n} X_i + \bigcap_{i=1}^{r} U_i + c. \tag{3}$$

Many different types of lifetime distributions are used in reliability engineering, classified as discrete and continuous. Discrete distributions include mainly binomial, geometric, and Poisson distributions, and discrete distributions include mainly exponential, Weibull, normal, and log-normal distributions. The exponential distribution of continuous type is the most important type of distribution in reliability statistics and is almost exclusively used to describe the reliability of electronic equipment. The failure rate in the exponential distribution is constant and independent of time. Since the beginning of reliability studies, the exponential distribution has been the most widely used, and it has a large number of advantages such as simplicity of calculation, ease of estimation of parameters, and additivity of the failure rate, and when the failures of the components in a system satisfy the exponential distribution, its system also satisfies the exponential distribution. The continuous type of Weibull distribution and other distributions are all more closely related, and the range of values of the shape parameter of the Weibull distribution reflects the failure characteristics of the product, so the Weibull distribution is also used quite widely [21]. In this paper, the two typical continuous-type distributions that are most widely used for sensor life distribution are chosen as exponential distribution and Weibull distribution. The exponential distribution is shown in equation (4), and the Weibull distribution is shown in equation (5):

$$F(x) = \begin{cases} \lambda e^{-\lambda x}, & x > 0, \\ 0, & x \le 0, \end{cases} \tag{4}$$

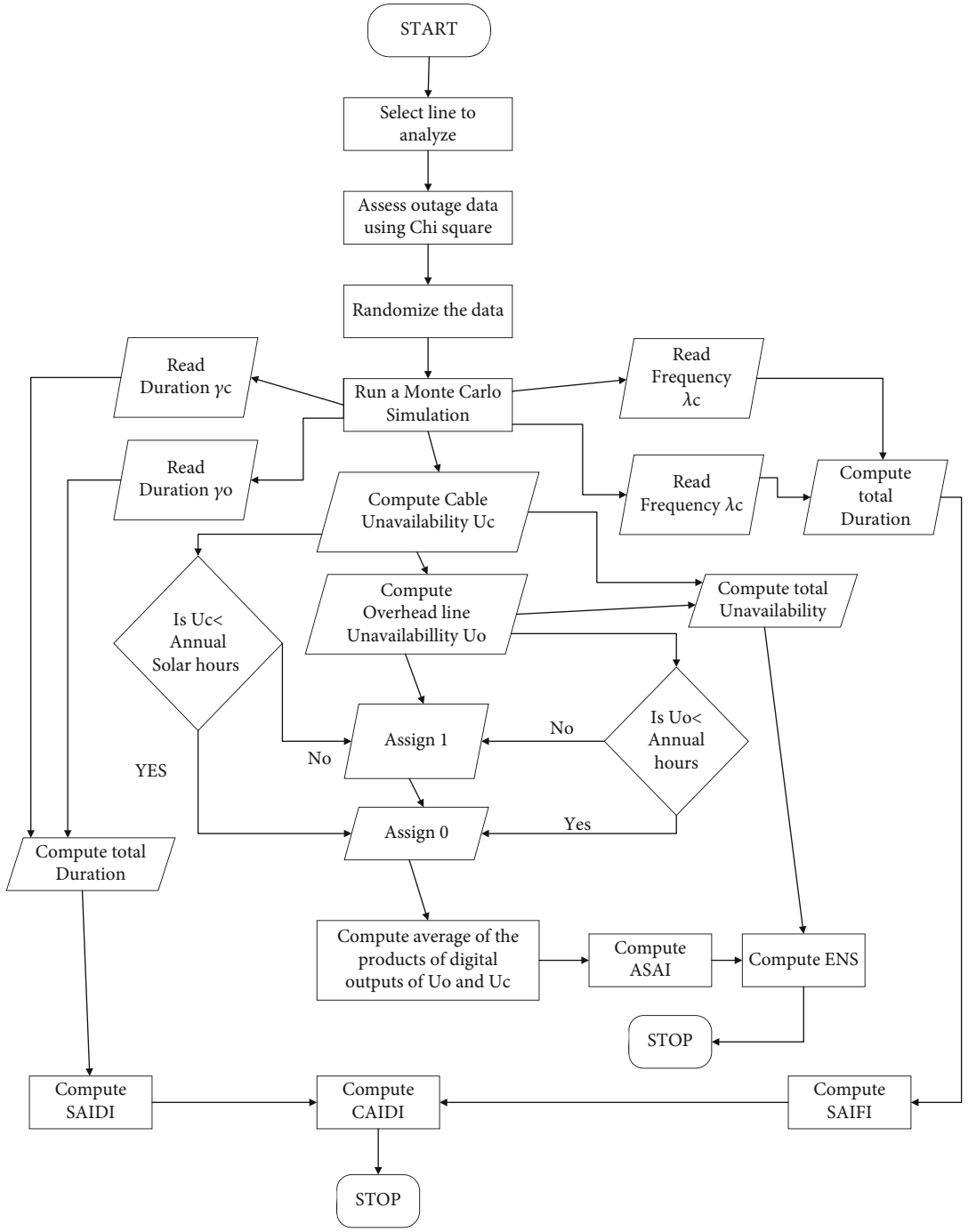

Figure 2: Classification of connectivity reliability assessment.

$$F(x) = \begin{cases} re^{-x} + \mu x, & x > 0, \\ 0, & x \le 0. \end{cases} \quad (5)$$

For WSN reliability studies, the star network topology is simple, with two-way communication between the sensor nodes and the Sink (or base station), but no communication path is established between the nodes. In addition, the data information from the sensor nodes can be sent directly to the base station, so the failure of the nodes can directly affect the normal operation of the WSN. All these advantages are good for assessing the reliability of WSNs, and the study of WSN reliability fruits of star network topology also has great reference value for later study of other network topologies. Therefore, in the WSN reliability study in this paper, the wireless sensor network topology is a star network.

The network reliability design needs to consider redundancy design, fault management and prevention, data management, node and link trustworthiness, environment,

resilience to destruction, security, and other factors. The following aspects should be considered in focus: (1) Redundancy design. Focus on considering the redundancy of key equipment and links. Decentralized deployment of multiple key devices in the same area to achieve load sharing and decentralized multiple means and multiple routing protocols are implemented on the transmission path. (2) Network protection mechanisms. For example, reliable routing protocols, hot backup protocols, route binding protocols, and automatic protection switching protocols are commonly used network protection mechanisms. (3) Fault-tolerant design. That is, the network is robustly designed so that it can still work properly or partially work in case of some errors or failures. The transmission path is selected by considering the remaining energy of neighboring nodes, data transmission distance, and network load balancing to reduce the chance of individual path overheating, reduce the probability of too many shared nodes, balance the network energy consumption, and improve the data transmission success rate and network lifetime. The main methods are fault limiting, fault detection, fault shielding, retry techniques, fault diagnosis, reorganization, recovery, reconfiguration, etc. (4) Congestion control. Through analysis or reliability simulation test to find out the "bottleneck" of network traffic, taking effective congestion control strategy can increase network resources and reduce user demand from two aspects to consider to solve the congestion problem. (5) Online maintenance guarantee design, that is, without interrupting the network operation, the maintenance, and protection of the network. Commonly used methods include hot-plug replacement of hardware and online upgrade of software. (6) Simulation-assisted design, through the network reliability simulation test method, the network completeness, resistance to destruction, availability, recovery, reliability of the auxiliary analysis, and design.

3.2. Data Transmission Reliability Analysis of Wireless Sensor Networks for Social Network Optimization. In the PPSSN model, there is a data owner (DO), a DO server, an attribute management server (AMS), an access user, and a social network platform (SNP). The DO server encrypts and stores the DO's buddy list, queries the encrypted list when the user requests access to the data, and returns the buddy relationship data, which shares the DO's overhead but does not affect the security of the data. After receiving a user's access request, the attribute management server (AMS) requests a buddy relationship from the DO, determines the buddy relationship from the data returned by the DO, and distributes the private key to the access requestor. The social network service platform SNP is the data distribution platform for users. Visitor V is a user of the social network platform and needs to obtain the appropriate access rights to access the data on the SNP when viewing the data published by the DO. When a visitor requests access to the data, he/she first needs to send a request to DO and can access the SNP data only after passing the authentication of AMS and DO and receiving the private key. Users who are not DO friends can only access the data that was last published on the SNP, and illegal users who are identified by AMS as social networks cannot access any DO publication data.

According to the extended complex network model of social networks, the concept of multiconstraint path pattern matching is proposed, i.e., finding matches in the data graph that match the pattern graph. Based on the multiconstraint optimized path selection algorithm, the multiconstraint edge matching algorithm is executed for each edge in the pattern graph, and the query results obtained are connected in the order in the pattern graph to form answers that match the user's query conditions. To improve the execution efficiency and connection efficiency, a probability-based sampling estimation algorithm is introduced to accelerate the execution of the path matching algorithm and also to provide guidance for the mapping query result connection algorithm [22]. The algorithm can be applied to pattern matching in areas such as location-based social networks, spatial crowdsourcing, and recommender systems.

Since the wireless communication link quality sequence characterized by the signal-to-noise ratio is characterized by the superposition of smooth and noisy sequences, the time series prediction model lacks accuracy for the prediction of sequence values. Therefore, in this paper, according to the complex environment of the energy grid, and combined with the characteristics of wireless communication link quality S/N sequence, a prediction algorithm based on LSTM for the confidence interval of communication link reliability is proposed, and the structure diagram is shown in Figure 3.

In this paper, we measure the attribute similarity between two users by determining whether the attribute content is the same. When matching whether the attribute contents are the same, the birthday attribute is matched only to the year, and the address and hometown are matched only to the city, and then, the result of whether these nine attributes match is defined as a nine-dimensional vector. In this vector, if the attribute contents are the same, the corresponding element has a value of 1; otherwise, the value is 0. The reason for considering names and avatars is that if the avatars and names of two accounts are very similar or identical, there is a high probability that they represent a particularly close relationship, usually a couple or the same user with multiple accounts. In determining whether avatars are similar, this paper chooses to use the perceptual hashing algorithm because avatar files are usually small. In existing studies on attribute inference, user identity linking, and link inference, the most basic approach is based on the principle of homogeneity, i.e., the information between users and their surrounding friends is similar, and the closer the friends, the higher the degree of similarity, so that the target user's undisclosed information can be inferred from the information disclosed by surrounding friends. Connectivity reliability is the first proposed network reliability index, which is divided into active and passive networks according to the presence or absence of specified source points in the network. The classical analytical algorithms for computing network connectivity reliability include state enumeration, exclusion principle, disjoint product sum, factorization, graph transformation, and delimitation method. These

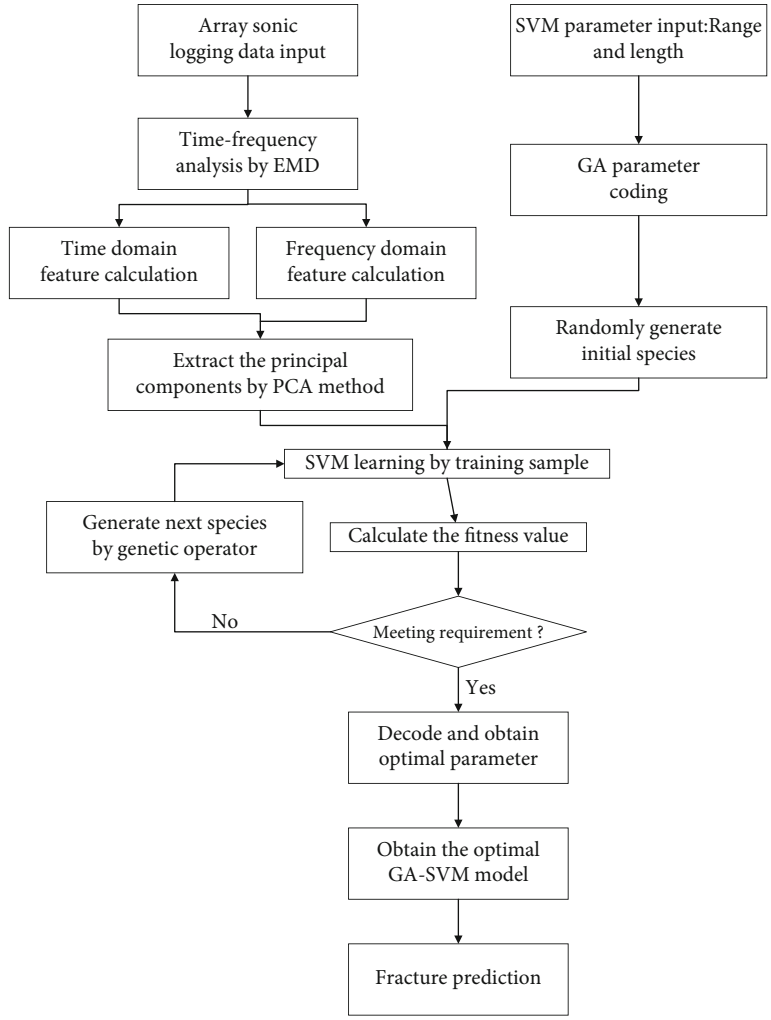

Figure 3: Confidence interval prediction algorithm for communication link reliability.

algorithms usually assume that the links have only two states, fault and normal, and the probabilities of link failures in the network are independent of each other. The most direct and effective way of this is to compare the attribute information filled in the profile of the user. Based on the above principles, this paper argues that the same attribute information between the target user and his friends is very likely to reveal the user's private information, and even if the target user himself does not disclose this information, a malicious attacker can still infer the target user's information based on the attribute content of the largest number of the same friends around. The closeness between any two participants also has similar properties as trustworthiness: self-reflexivity, asymmetry, dynamism, complexity, and transferability (not to be elaborated here). There is no subjectivity and it possesses objectivity, as the closeness is based on the interaction behaviour of the participants and can be analyzed by data mining techniques. In addition to this, it is also decaying, showing a tendency to decay as the path length increases.

When considering the spatial relationships and social identities of the participants, the following search process needs to be executed: the first step: all the nodes in the network need to be traversed to find the nodes that satisfy the location information and text information; the second step: among these nodes, find the paths in the network that meet the multiple constraints according to the multiple constraints specified by the user using one of the nodes as the source node and the other node as the target node. But with the increase in the number of nodes, the first step becomes very difficult, so the algorithm proposed above is no longer good enough to solve the optimal path selection problem for multiple constraints based on geographic location, and the search space is reduced based on location information and text information for solving the optimal path selection problem for multiple constraints regarding spatial constraints and social constraints. To speed up the filtering of geolocation information and text information, spatial text indexes need to be created for participants in social networks. Spatial text indexing can be classified as spatial indexing, text indexing, and hybrid indexing. Depending on the priority of spatial and text indexes, they can be classified as text-first and spatial-first. Text-first usually uses the inverted file as the top-level index and then arranges

each posting list in the inverted list by a spatial structure, which can be an R-Tree, a grid, or a space-filling curve. And spatial-first usually uses the spatial structure as the top-level index, with leaf nodes (or grid cells) containing inverted files or bitmaps of the object's textual information. There is also a tight combination of both indexes so that both types of information can be trimmed from the search space during the search.

4. Experimental Verification and Conclusion

The dataset used in this paper contains 2626 objects, each record contains the participant's sequence number, nickname, key text information extracted from the tweet, and the participant's spatial geographic location information (latitude and longitude). The constraint values of trust, closeness, and reputation of the participants are randomly generated through the WS small-world model. The specific generation process is as follows: (1) the network contains N (N randomly taken as 150, 300, 450, 600, 750, and 1050) nodes, and each node connects m edges (m randomly taken as 1~8) with its nearest m nodes; (2) an edge is added between a randomly selected pair of nodes with probability pr (pr randomly taken as 0.1~0.8), and any two different nodes have at most one edge between them, and each node cannot be connected to itself. The above procedure was repeatedly performed, and 24 subdatasets were synthesized. In the simulation experiments, the trust, closeness, and reputation values between participants were randomly generated, and to better model the decay of closeness in social networks, the decay factor was set to $\delta = 1.5$, and the source participants specified the bound values of trust, closeness, and reputation as $\{0.05, 0.001, 0.3\}$. The privacy data in social networks mainly includes users' identity information, login information, friend information, and the content published on social network platforms and information dissemination. The purpose of setting the parameters in this way is to allow more paths to satisfy the constraints. The weights of trust, intimacy, and reputation in the path quality function are $\{0.25, 0.25, 0.5\}$, highlighting the importance of reputation in trust assessment.

The IR-Tree-MBS algorithm is compared with the H_MCOP algorithm and the MBS algorithm, respectively. The three algorithms perform the same path query condition three times on each of the 24 randomly generated subdatasets, and each query needs to be repeated three times for averaging. Comparing the path quality and path query efficiency found by the algorithms, Figure 4 shows the comparison results of path quality.

The R-Tree-MBS algorithm and the MBS algorithm have similar path lookup quality because both algorithms use the same lookup strategy and objective function. The path quality of both algorithms is no worse than that of the H_MCOP algorithm, which is because the IR-Tree-MBS algorithm, MBS algorithm, and H_MCOP algorithm all treat the path found as optimal when it has the maximum path quality and is a feasible solution, which leads to similar pathfinding quality when finding certain paths (e.g., on datasets 9 and 15 in Figure 4). When there is a maximum path quality and it is

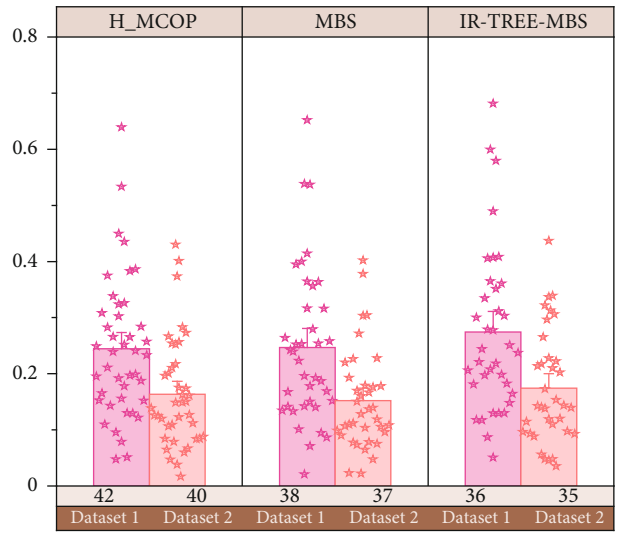

Figure 4: Comparison of path quality finding results of different algorithms on different datasets.

not a feasible solution, the H_MCOP algorithm stops searching according to the minimum cost and starts searching according to the minimum objective function $g\lambda(p) < 1$. This leads to the phenomenon that the H_MCOP algorithm cannot find the near-optimal solution or even actually has a feasible solution but H_MCOP returns no feasible solution, while the MBS and IR-Tree-MBS algorithms can find approximately optimal solutions.

From Figure 5, we can see that the H_MCOP algorithm and the MBS algorithm have higher execution efficiency when the network size is not large and the network structure is relatively simple, while the IR-Tree-MBS algorithm is relatively poor. This is because the IR-Tree-MBS algorithm needs to create IR-Tree indexes of the nodes in the network first when it is executed, which consumes about 1-5 seconds. The discrete distribution mainly includes binomial distribution, geometric distribution, and Poisson distribution. The discrete distribution mainly includes exponential distribution, Weibull distribution, normal distribution, and log-normal distribution. When the network size is small, the algorithms MBS and H_MCOP algorithms for the direct query have higher efficiency. However, as the network size increases and the complexity of the network structure increases, the efficiency of the H_MCOP algorithm and MBS algorithm gradually decreases, while the IR-Tree-MBS algorithm has good stability. The reasons include two aspects: (1) the IR-Tree-MBS algorithm utilizes the characteristics of the IR-Tree structure and does not query the path directly but performs distance pruning and keyword pruning first, narrowing the search scope to a certain extent, which is not considered by the H_MCOP algorithm and the MBS algorithm; (2) the IR-Tree-MBS algorithm does not need to be like the H_MCOP algorithm to compute $g\lambda(p) > 1$ during the forward search, especially when λ tends to ∞, resulting in a larger time overhead.

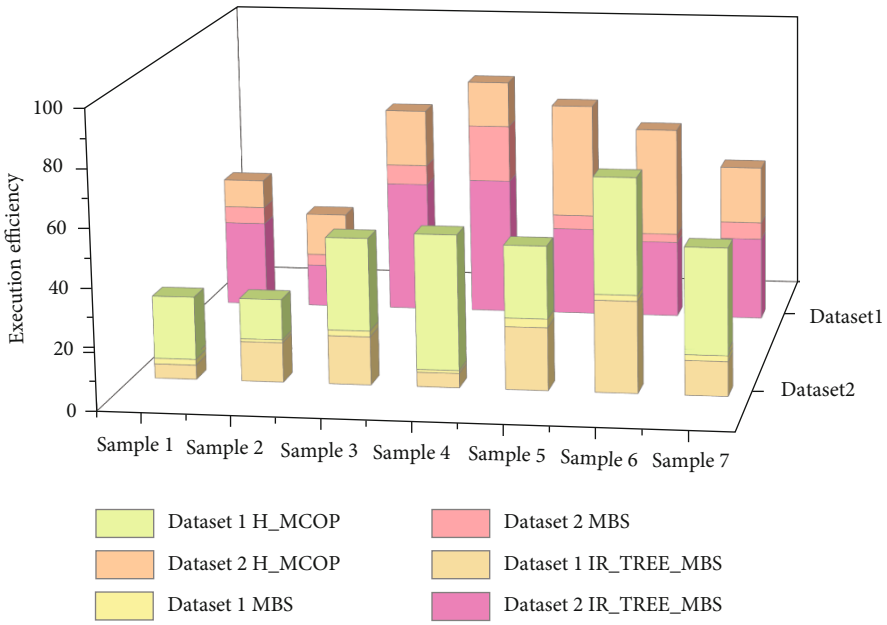

Figure 5: Execution efficiency of different algorithms on different datasets.

From Figure 6, we know that as the number of network polling increases, the total energy consumption of the network increases regardless of whether it is 100 nodes or 200 nodes, and the increase in energy consumption is greater for the AODV-SMS route recovery protocol, followed by AODV-SMS (PSO), and AODV-SMS (ABC-PSO) has the least energy consumption. And it is also seen that as the number of sensing nodes in the network increases, along with it, the density of the whole network increases, the AODV-SMS route recovery method has a single transmission path and the sensing nodes that die faster during the source node transmission are generally in the common node, the transmission path where the common node is located, and the location near the destination node Sink. At the same time, as the density of sensing nodes increases, the probability of using the same transmission path increases greatly, and the energy consumption of the common node on the same transmission path is very large, which is prone to premature "death" phenomenon, resulting in data loss and data transmission link interruption. The AODV-SMS (ABC-PSO) multipath routing recovery mechanism proposed in this paper considers the remaining energy of neighboring nodes, data transmission distance, and network load balancing in the process of the data transmission path which reduces the chance of individual path overheating, decreases the probability of too many shared nodes, balances the network nodes, balances network energy consumption, and improves data transmission success rate and network lifetime.

As can be seen from Figure 7, the energy utilization of the algorithm proposed in this paper is much higher than that of the AODV-SMS routing protocol, mainly because the adopted AODV-SMS (ABC-PSO) route recovery strategy interrupts the original data transmission path as the Sink moves; it searches for the nearest transmission path near the original path and considers the network energy consumption equalization, which makes the energy consumption of our proposed route recovery strategy lower than that of other methods. When considering the spatial relationships and social identities of participants, the following search process needs to be performed: Step 1: all nodes in the network need to be traversed to find nodes that satisfy the location information and text information; Step 2: among these nodes, one of them is used as the source node and the other as the target node to find paths in the network that meet the multiple constraints according to the multiple constraints specified by the user. Although the swarm intelligent optimization algorithm AODV-SMS (ABC-PSO) consumes a portion of energy to optimize the data transmission path, considering the remaining energy of neighboring nodes, data transmission distance, and network load balancing, the proposed multipath transmission route recovery strategy can make full use of the information provided by the original path to quickly recover an efficient and reliable transmission path, providing faster global convergence for network optimization.

As can be seen from Figure 8, the end-to-end transmission delay of the AODV-SMS protocol at a low number of nodes (100 nodes) is higher than the original. AODV-SMS (PSO) and AODV-SMS (ABC-PSO) multipath routing recovery path mechanisms are slightly larger. Mainly because the data transmission congestion is not serious in the case of the low number of nodes, the difference in transmission delay between AODV-SMS (PSO) and AODV-SMS (ABC-PSO) multipath transmission route recovery mechanisms is not significant, and the end-to-end delay of the proposed algorithm is smaller than that of the AODV-SMS method. It is also observed that as the number of sensing nodes increases, the multipath route recovery mechanism of AODV-SMS (PSO) and AODV-SMS (ABC-PSO)

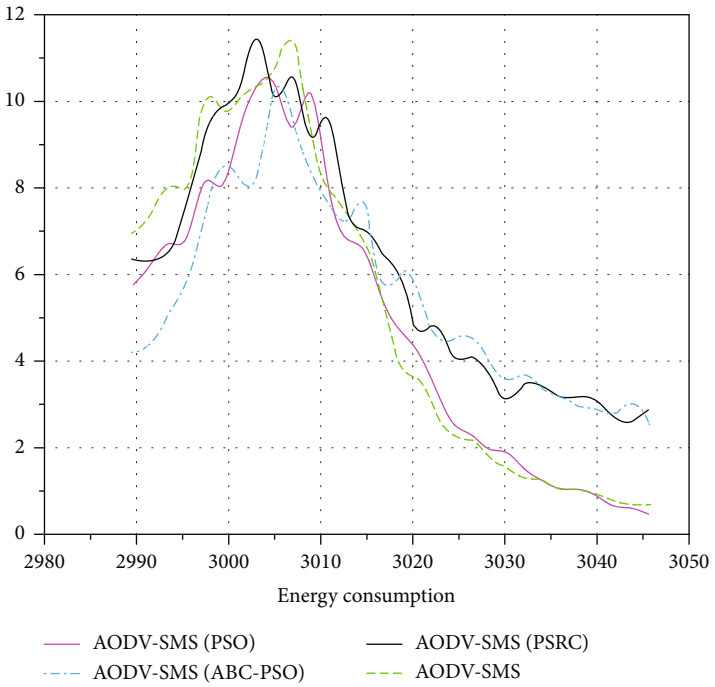

Figure 6: Network energy consumption comparison.

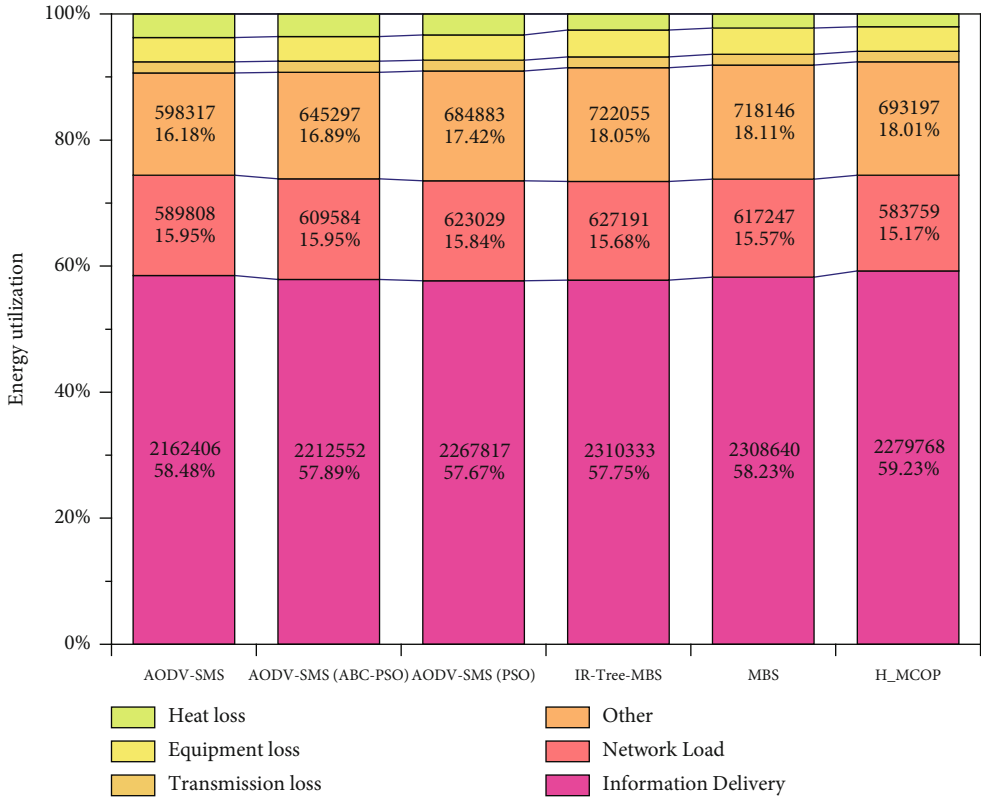

Figure 7: Algorithm energy utilization.

algorithms increases the number of transmission paths to the destination node, while the new transmission paths are constructed with comprehensive consideration of transmission AODV-SMS (ABC-PSO) routing recovery protocol showing a better packet transmission delay time than other routing recovery strategies. Packet transmission delay takes less time, and there is an increasing difference between them. This is enough to show that the larger the network size, the

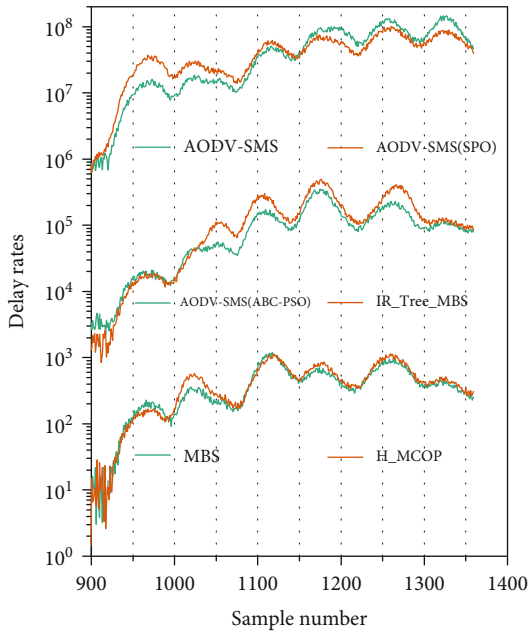

Figure 8: Comparison of network propagation delay rates.

greater the delay and transmission path length spent by the source node to transmit to the destination node, which better reflects the advantage that the multipath route recovery strategy proposed in this paper can consider the remaining energy of the neighboring nodes of the transmission link and the communication distance and the network load balance, select more suitable communication nodes to form a better alternative path, and make the network energy consumption have more balanced distribution and the longest lifetime.

5. Conclusion

With the convenience of people communicating with each other in the information age, social networks have been created and gradually become popular. Due to their convenience and easy operation, social networks have become deeply involved in people's lives and work in the context of increasingly mature network technology. At the same time, the issue of privacy in social networks has also gradually aroused people's concern. The root cause of the private security problem in social networks is that the private data of the data owner is spread on the social network platform without the direct physical control of the data owner, so it may cause the leakage of the data, which makes the users who originally do not have the access permission or even the users who maliciously steal the information to view the content published by the data owner.

In this paper, by studying the network reliability problem differently from the general study of reliability content (network failure rate, fault diagnosis, fault repair, etc.), we conduct a comprehensive study of network performance (network energy consumption, load balancing, transmission delay, network connectivity, reliability, etc.). By introducing intelligent optimization methods and artificial intelligence algorithms, we address reliability issues such as basic research on mobile wireless sensor network fault prediction and network reliability assessment methods, the impact of mobile path optimization on data collection efficiency and network reliability, reliable data transmission based on data fusion methods, and intelligent fault tolerance algorithms for multipath routing to reduce fault interference and network energy consumption, improve network efficiency, and increase network connectivity, availability, and reliability and extend the network survival cycle as the objectives to ensure energy-efficient, efficient, and reliable operation of mobile wireless sensor networks in complex application environments. The discrete distribution mainly includes binomial distribution, geometric distribution, and Poisson distribution. The discrete distribution mainly includes exponential distribution, Weibull distribution, normal distribution, and log-normal distribution. In the key issuance process of attribute encryption, the management of user rights is jointly implemented by the data owner and the attribute management server, which not only reduces the overhead of the data owner but also avoids collusion attacks between the attribute management server and illegally accessed users. To weigh the usability of data distribution and the security of information privacy protection, users are classified and designed to achieve access control for different users with different privileges. In addition to this, the caching mechanism of the buddy data is designed to improve and optimize the original scheme and reduce the decryption overhead. The model improves query efficiency, reduces the system overhead, and enhances privacy security.

Data Availability

The data used to support the findings of this study are available from the corresponding author upon request.

Conflicts of Interest

The authors declare that they have no known competing financial interests or personal relationships that could have appeared to influence the work reported in this paper.

References

[1] J. Lu, L. Feng, J. Yang, M. M. Hassan, A. Alelaiwi, and I. Humar, "Artificial agent: the fusion of artificial intelligence and a mobile agent for energy-efficient traffic control in wireless sensor networks," *Future Generation Computer Systems*, vol. 95, pp. 45–51, 2019.

[2] F. Zhang, "Research on reliability analysis of computer network based on intelligent cloud computing method," *International Journal of Computers and Applications*, vol. 41, no. 4, pp. 283–288, 2019.

[3] A. Alarifi and A. Tolba, "Optimizing the network energy of cloud assisted internet of things by using the adaptive neural learning approach in wireless sensor networks," *Computers in Industry*, vol. 106, pp. 133–141, 2019.

[4] R. P. M. Sundhari and K. Jaikumar, "IoT assisted hierarchical computation strategic making (HCSM) and dynamic stochastic optimization technique (DSOT) for energy optimization in

wireless sensor networks for smart city monitoring," *Computer Communications*, vol. 150, pp. 226–234, 2020.

[5] T. A. Alghamdi, "Energy efficient protocol in wireless sensor network: optimized cluster head selection model," *Telecommunication Systems*, vol. 74, no. 3, pp. 331–345, 2020.

[6] J. Tan, W. Liu, T. Wang et al., "An adaptive collection scheme-based matrix completion for data gathering in energy-harvesting wireless sensor networks," *IEEE Access*, vol. 7, pp. 6703–6723, 2019.

[7] S. Randhawa and S. Jain, "MLBC: multi-objective load balancing clustering technique in wireless sensor networks," *Applied Soft Computing*, vol. 74, pp. 66–89, 2019.

[8] M. Faheem, R. A. Butt, B. Raza et al., "FFRP: dynamic firefly mating optimization inspired energy efficient routing protocol for internet of underwater wireless sensor networks," *IEEE Access*, vol. 8, pp. 39587–39604, 2020.

[9] B. Pitchaimanickam and G. Murugaboopathi, "A hybrid firefly algorithm with particle swarm optimization for energy efficient optimal cluster head selection in wireless sensor networks," *Neural Computing and Applications*, vol. 32, no. 12, pp. 7709–7723, 2020.

[10] S. E. Mood and M. M. Javidi, "Rank-based gravitational search algorithm: a novel nature-inspired optimization algorithm for wireless sensor networks clustering," *Cognitive Computation*, vol. 11, no. 5, pp. 719–734, 2019.

[11] V. Gaur, O. P. Yadav, G. Soni, and A. P. S. Rathore, "A literature review on network reliability analysis and its engineering applications," *Proceedings of the Institution of Mechanical Engineers, Part O: Journal of Risk and Reliability*, vol. 235, no. 2, pp. 167–181, 2021.

[12] R. Elhabyan, W. Shi, and M. St-Hilaire, "Coverage protocols for wireless sensor networks: review and future directions," *Journal of Communications and Networks*, vol. 21, no. 1, pp. 45–60, 2019.

[13] Z. Zou and Y. Qian, "Wireless sensor network routing method based on improved ant colony algorithm," *Journal of Ambient Intelligence and Humanized Computing*, vol. 10, no. 3, pp. 991–998, 2019.

[14] M. E. Ekpenyong, D. E. Asuquo, and I. J. Umoren, "Evolutionary optimisation of energy-efficient communication in wireless sensor networks," *International Journal of Wireless Information Networks*, vol. 26, no. 4, pp. 344–366, 2019.

[15] M. Abdulkarem, K. Samsudin, F. Z. Rokhani, and M. F. A. Rasid, "Wireless sensor network for structural health monitoring: a contemporary review of technologies, challenges, and future direction," *Structural Health Monitoring*, vol. 19, no. 3, pp. 693–735, 2020.

[16] O. Deepa and J. Suguna, "An optimized QoS-based clustering with multipath routing protocol for wireless sensor networks," *Journal of King Saud University-Computer and Information Sciences*, vol. 32, no. 7, pp. 763–774, 2020.

[17] S. Sivakumar and P. Vivekanandan, "Efficient fault-tolerant routing in IoT wireless sensor networks based on path graph flow modeling with Marchenko–Pastur distribution (EFT-PMD)," *Wireless Networks*, vol. 26, no. 6, pp. 4543–4555, 2020.

[18] X. Liu, T. Qiu, and T. Wang, "Load-balanced data dissemination for wireless sensor networks: a nature-inspired approach," *IEEE Internet of Things Journal*, vol. 6, no. 6, pp. 9256–9265, 2019.

[19] G.-D. Zhou, M.-X. Xie, T.-H. Yi, and H.-N. Li, "Optimal wireless sensor network configuration for structural monitoring using automatic-learning firefly algorithm," *Advances in Structural Engineering*, vol. 22, no. 4, pp. 907–918, 2019.

[20] J. Jiang, X. Zhu, G. Han, M. Guizani, and L. Shu, "A dynamic trust evaluation and update mechanism based on C4. 5 decision tree in underwater wireless sensor networks," *IEEE Transactions on Vehicular Technology*, vol. 69, no. 8, pp. 9031–9040, 2020.

[21] A. Seyfollahi and A. Ghaffari, "Reliable data dissemination for the Internet of Things using Harris hawks optimization," *Peer-to-Peer Networking and Applications*, vol. 13, no. 6, pp. 1886–1902, 2020.

[22] S. Tabatabaei, A. Rajaei, and A. M. Rigi, "A novel energy-aware clustering method via lion pride optimizer algorithm (LPO) and fuzzy logic in wireless sensor networks (WSNs)," *Wireless Personal Communications*, vol. 108, no. 3, pp. 1803–1825, 2019.

Hindawi
Journal of Sensors
Volume 2022, Article ID 6823502, 11 pages
https://doi.org/10.1155/2022/6823502

Research Article

Optimization and Simulation of an English-Assisted Reading System Based on Wireless Sensor Networks

Shumei Huang

Department of Foreign Languages and Tourism, Guilin Normal College, Guilin Guangxi 541199, China

Correspondence should be addressed to Shumei Huang; hsm@mail.glnc.edu.cn

Received 2 November 2021; Revised 7 December 2021; Accepted 13 December 2021; Published 6 January 2022

Academic Editor: Gengxin Sun

In this paper, wireless sensor network technology is applied to an English-assisted reading system to highly simulate and restore the context and improve the performance of all aspects of the English-assisted reading system to optimize the English-assisted reading system. The product designed in this paper is based on wireless sensor network technology with Linux as the core operating system and supports POSIX (Portable Operating System Interface Standard) standard application development interface; QT is used as the component and framework of the system to support many applications. Based on player open-source multimedia audio and video technology, optimized and tailored for the hardware platform, it well supports multimedia learning and entertainment functions; this paper also adopts open-source database technology based on SQL (Structured Quevy Language) and Berkeley DB, using them as a platform for data storage and access, supporting a million-level thesaurus and high-speed, example sentence search. In this paper, we describe the user's personalized needs by creating interest models for the user, recommending the text content, and reading order that can help with understanding through the interest models and reading articles and expanding the recommended text range by making expansions to the reading content through references and related articles to further help the user understand the text. Based on the above work, this paper implements an assisted reading system; finally, a multihop self-organizing network system is formed through a wireless sensor network to make the rigid and boring English reading easy and interesting.

1. Introduction

In recent years, with the continuous development of communication technology, wireless communication methods have gained more attention with their advantages of convenience and efficiency. Multimedia technology-assisted English reading teaching is a common teaching tool, which has a certain positive effect on improving the effectiveness of language learning and teaching quality. Reading, as the main and most important means of language input, plays an important role in language learning and has always been the focus of English teaching. How well students perform in reading determines to a large extent how well they learn English [1]. In high school English teaching, reading is undoubtedly one of the most important learning contents and skills, and it takes up a considerable amount of weight in the English Advanced Placement exam papers. In English learning, students' reading ability also directly affects their learning and training of other English skills, so the basic position of reading should not be underestimated. Therefore, improving student's English reading ability is one of the priorities of high school English teaching. However, in the actual English reading teaching, grammar and vocabulary teaching is still the main content of high school English reading class, and teachers pay much more attention to language knowledge than to language skills [2]. This way of teaching also makes high school students in the process of English learning do not pay attention to the learning and training of reading skills, resulting in the wrong concept of good English learning which is to remember more words and grammar errorless, which is not difficult to explain the phenomenon that students achieve high scores in English but can not read an English article.

Psychological research shows that certain stimuli in the environment can cause people's orientation response, thus arousing people's attention and making them interested.

Multimedia technology combines text, graphics, color, sound, video images, and other information together, graphic and sound, which can activate students' perceptual organs and attention and fully mobilize students' learning interest. The goal of language learning is to cultivate the communicative ability, and the cultivation of communicative ability first requires a large amount of input of real language materials and, then through repeated practice and practical application, gradually transformed into the learners' inner language ability [3]. The specific steps for establishing an interest model are as follows: (1) users provide relevant information, including majors, courses, hobbies, and published or downloaded articles; (2) perform word segmentation, keyword extraction, deduplication, weighting, and other operations on the information to obtain a keyword set; (3) get the insertion position, get the nearest common ancestor node of the keyword and the node in the interest model in WordNet, and add it to the interest model; and (4) repeat step 3. Multimedia equipment playing audio and video materials can create a real language environment, which is conducive to the development of communicative activities in the classroom and the cultivation of students' sense of language. In English learning, the role of reading is irreplaceable and the level of English is inseparable from the amount of reading. Reading is also the most basic way of learning for students; learners can constantly improve their sense of language, increase their vocabulary, and improve their English reading comprehension and oral communication skills in reading materials; we all know the important role of vocabulary in English reading level, and reading is one of the effective means to memorize words, without relevant English language environment; it is ineffective to memorize words by rote. In the reading classroom, if we continue to use the unchanging traditional teaching method, it is far from enough for students to improve their sense of language and vocabulary; therefore, the necessity of using multimedia technology reasonably in English reading teaching is especially important.

The age of artificial intelligence demands a distinct personality and a very creative mind for each person. The difference in creativity reflects the difference between people, and for this reason, using all the advantages of artificial intelligence, we can pay attention to the personalized development of students and the differential teaching of students, so that each student does not fall behind [4]. Artificial intelligence facilitates teachers to understand the dynamics of information from individual students and provides more scientific and accurate personalized tutoring. The development of microlearning, flipped classrooms, big data analytics tools, and many other forms have given rise to a variety of intelligent interactive teaching systems that are gradually making digital teaching a reality. This real-time feedback and assessments provide intelligent suggestions for teachers to implement precise teaching strategies, effectively improving classroom teaching effectiveness and student learning efficiency.

2. Related Works

The research on the ability of multimedia technology to assist in foreign language teaching began in the United States. Because of the rapid development of information technology in the United States, the research related to multimedia technology in teaching and learning started in the United States in 1963 and was applied in a practical work. From the 1990s to the present, information technology in education has been developed rapidly worldwide, so the auxiliary function of multimedia technology in teaching has been widely recognized and fully used in the teaching of various subjects [5]. The use and development of multimedia technology in the field of education have had a development history of several decades, and the research on multimedia in language teaching has been conducted for quite some time. The earliest systematic research on multimedia-assisted teaching can be traced back to the American audiovisual educational psychologist Dale, who studied the use of audiovisual media in actual teaching and the teaching effects brought about by them [6]. The most famous of these is the "Tower of Experience" theory. He divided the sources of human learning experiences into ten levels according to different levels of abstraction and grouped these ten levels into three major categories. Among these ten levels, there are multimedia elements such as text, sound, and images. However, scholars have researched multimedia-assisted foreign language teaching, which has reflected its certain superiority in some educational practices and educational ideas and provided a good basis for our later research and development, but there is still little research on the aspects of problems arising from multimedia technology in English teaching [7].

The research on multimedia teaching and the emergence of research results are slightly behind those of advanced countries and regions, and only in the 1980s did they begin to explore the relevant aspects of multimedia-assisted teaching. However, the slow development of information technology during this period made it difficult to create good hardware conditions for practical activities, and research on related aspects of software had not yet begun. This article sets up a default value for the weight of a hobby. After each reading, you only need to determine whether there is hobby-related content in the reading content. If there is, update the weight of the hobby, so that it can be prioritized. In the first decade, theoretical research was mainly conducted in multimedia-assisted teaching, as well as translation and study of advanced theories and experiences. The two journals "Chinese Electro-Chemical Education" and "Research on Electro-Chemical Education," which were found in the nascent period of multimedia education, have provided a lot of theoretical knowledge for educators since they were first published in 1980 [8]. Through these two journals, educators were able to learn about the advanced experience and the process of technological development at the early stage of technology development, and therefore, they are known as the base of theoretical research on e-education. The first teaching aids incorporated in foreign language teaching were electronic media as well as speech labs, and it was only in the 1990s that real multimedia aids were introduced [9].

From 1981 to 1994, the annual research literature was within three digits, and from 1995 to 2000, the annual research literature did not exceed four digits, but after

entering the 21st century, from 2001 to 2014, the annual research literature in related fields has been increasing [10]. The research trend shows that multimedia-assisted English teaching has been valued since the new century and has been a hot research topic for scholars in related fields. From the content of the research, multimedia-assisted English teaching is mostly carried out from two aspects: theory and practical application. First is the theoretical research aspect. At the early introduction, whether multimedia could enter teaching had also been questioned. Dr. Yang analyzed the possibility of multimedia entering language teaching from the technical point of view, pedagogy, and the possibility of language teaching and suggested that multimedia could help language teaching and classroom to be organically integrated [11].

3. Design of English-Assisted Reading System for Wireless Sensor Networks

3.1. System Analysis and Architecture. WordNet is a cognitive linguistics-based English dictionary designed by a consortium of psychologists, linguists, and computer engineers at Princeton University. WordNet is superficially like a thesaurus in that it groups words based on their meanings. However, there are some important differences. First, WordNet is not just about word forms and strings of letters, but also about the specific meanings of words. Words that are very close to each other in the network are disambiguated semantically. Second, WordNet marks semantic relationships between words, whereas the grouping of words in a synonymy thesaurus does not follow any explicit pattern other than the similarity of meaning. WordNet is a large database of English words. Nouns, verbs, adjectives, and adverbs are grouped into cognitive synonym sets, each expressing a different concept. The synonyms are related to each other by conceptual semantics and lexical relationships. The structure of WordNet makes it a useful tool for computational linguistics and natural language processing [12]. The main relationships between words in WordNet are synonyms, such as the relationship between shut and close or car and automobile. Synonyms represent words that share the same concept and are interchangeable in many contexts, grouping text into unordered sets (synonym sets). Each of WordNet's 17,000 synonyms is linked to other synonym sets by a small number of "concept relations." In addition, a synset contains a short definition and, in most cases, one or more short sentences describing the use of a synset member. Forms of words with several different meanings are represented in as many different synsets as possible. Thus, each form-meaning pair in WordNet is unique.

$$M_i = \frac{\ln\left[1 + \left(N_{10}^{i}/2N_i^0\right)\right]}{\ln\left(1 - \left(1/f(x)\right)\right)}. \quad (1)$$

The system defaults to the basic common dictionary, in the download dictionary, can copy the dictionary to the specified directory; using a list display, the user selects any thesaurus as the current query dictionary. The system uses Unicode encoding to build a powerful word bank to support multinational languages. The picture, sound, phonetic, and example dictionaries are all built-in by default, and all dictionaries share these data. The picture library, sound library, example sentence library, and basic lexicon can be updated in a data upgrade. The lexicon is stored using SQLite, and word lookup uses the database's query function. The routing module can also act as a relay router in the entire network, so that some routing modules far away from the aggregation module can relay communications through the closer routing modules, which can reflect the large-scale deployment of the entire network and multihop routing features. The use case for analyzing the lookup dictionary is relatively simple; the user enters the word or looks it up by taking the word from the screen. The user downloads the different dictionary libraries to the machine [13]. The dictionary server receives all the word lookup requests sent to it, queries the database, or replaces the current dictionary and then sends the results back to the requesting client. The dictionary lookup function is needed in many parts of the system. If the dictionary is loaded as a dynamic library, each application that needs to look up words will link to the dynamic library and open the dictionary in its process to look up its data, which may encounter a series of synchronization problems such as resource usage. So, the dictionary needs to unify the word search interface, and this topic will be designed as a client-server model, as shown in Figure 1.

The process of interest model building includes acquiring information, processing the information, determining the insertion position, and adding to the interest model step by step. The specific steps for building the interest model are as follows: (1) the user provides relevant information, including majors, courses, interests, and published or downloaded articles; (2) the information is divided into words, keyword extraction, deweighting, weighting, and other operations to obtain the keyword set; (3) obtain the insertion position, obtain the nearest common ancestor nodes of the keywords and nodes in the interest model in WordNet, and add them to the interest model; and (4) repeat step 3, get the preliminary interest model for the professional model, and then build the interest model according to the content of the course syllabus, which generally includes the subjects that need to be studied before taking this course, the key chapters of the course, the key definition concepts, etc., and the division of class time, etc., according to the chapter where the key definition concepts are located in the course syllabus to determine the insertion position. Thus, ensure hierarchy and for linkage, examine whether this concept or definition is linked to other nodes in the model of interest, and if so, establish a connection. In the case of previously taken courses, it is determined if there is a link to other subjects based on the information taken in the course syllabus. For the hobby model, it is simple to determine the superordinate term of the hobby, i.e., the category to which the hobby belongs, and if the category of the hobby exists in the model, it is placed directly under the category, if not, the category is put into the model together with the hobby, and the weight of the hobby, based only on the hobby provided by the user, cannot determine the priority

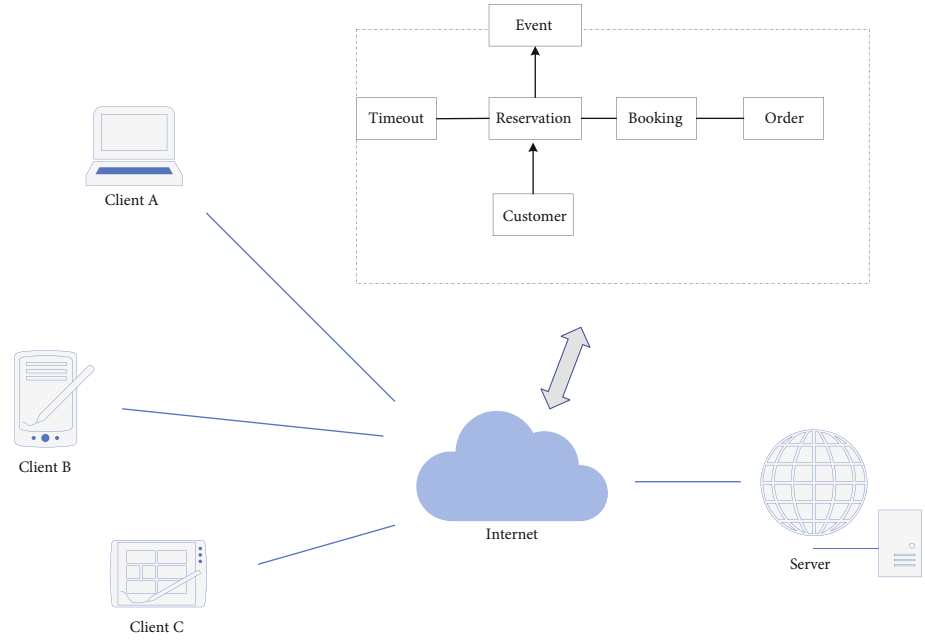

Figure 1: Domain modeling diagram for the client-server model.

of the hobby; so this paper establishes a default value for the weight of the hobby, and after each reading, in this paper, the default value of hobby is set; so after each reading, we only need to determine whether there is any hobby-related content in the reading content; if there is, then, the weight of the hobby will be updated so that the priority can be classified.

$$\omega = \frac{1}{W_1 + W_2 + \cdots + W_n}. \tag{2}$$

To reflect the characteristics of wireless self-assembling sensor networks such as large-scale deployment, self-organization, reliability as well as low-power consumption, and multihop routing, this chapter designs a LoRa-based multihop wireless sensor network. The LoRa-based wireless self-assembling sensor network mainly consists of a common module, routing module, and aggregation module. The common module is the lowest layer of the whole network and the most numerous modules in the network, so it can be externally connected to sensors and act as a data collection role, and the common nodes cannot communicate with each other. The routing module belongs to the upper layer of the common module and is responsible for the management of the surrounding common modules to form multihop communication data links. The aggregation module is the core of the whole network, managing all the routing modules in the network, which can be connected to the PC control center to complete the data collection of the whole network, and the operating instructions of the whole network are also issued by the administrator through the control center to the aggregation module and then distributed to the submodules at the lower level. The routing module can also act as a relay route in the whole network so that some routing modules that are far away from the aggregation module can relay the communication through the closer routing module so that the large-scale deployment and multihop routing characteristics of the whole network can be reflected. The aggregation module broadcasts synchronization frames periodically after powering up, and the non-logged-in routing modules will send login ACKs to the aggregation module after receiving the synchronization frames, and the aggregation module assigns an incremental route ID to each routing module and records it in the routing table according to the order of receiving the login ACKs from the routing modules. Once a routing module is dropped in the sensor network at a later stage, the corresponding ID position in the routing table will be vacated, and the vacant ID will be assigned in priority when waiting for the next new routing module to log in, reflecting the self-organization of the whole network. At the same time, in the whole network, except for the aggregation module which is not powered by an external lithium battery, the aggregation module and the common module are powered by a lithium battery. To reduce the power consumption of the modules and improve the survival cycle of the network, all the common modules and routing modules use the hibernate-wake-up-hibernation cyclic working mode, as shown in Figure 2.

3.2. Wireless Sensor Network Data Fusion. Since multisensor data fusion technology has a wide range of research components and applications, so far it does not have a standard definition that can be universally accepted. Although there are multiple definitions of data fusion, they are consistent. As a focused military area, multisensor data fusion mainly includes target detection, data correlation, target estimation, and identification and situational assessment and threat estimation to achieve multilevel integrated processing of multisensor data. Nowadays, multisensor data fusion technology

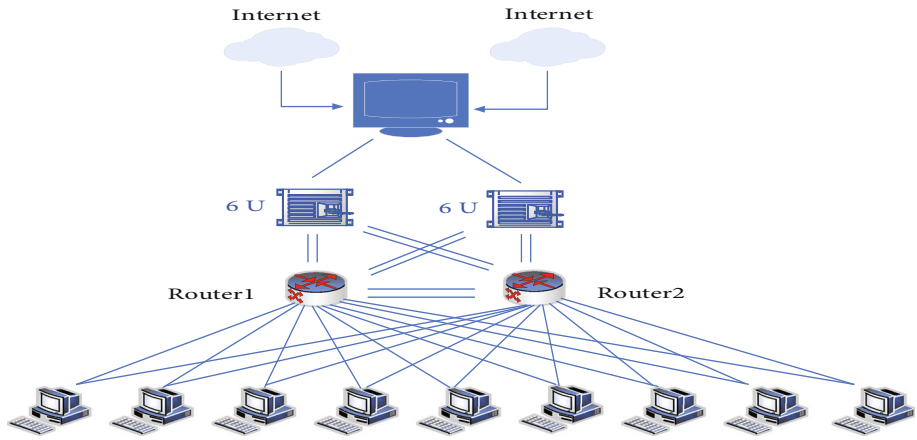

Figure 2: Network topology diagram.

has become an independent discipline, and the definitions proposed based on a particular application area are not representative. However, based on the substance of these definitions, taken together, multisensor data fusion can be simply defined as the use of computers to optimally synthesize multisensor observations to obtain more accurate and reliable target information. Multisensor data fusion techniques combine multiple sources of information according to some criterion that takes full advantage of the complementary and redundant nature of multiple sensors to obtain maximum reliable information about the target. Multisensor data fusion is divided into five levels of fusion based on the form of information abstraction, including detection-level fusion, position-level fusion, attribute-level fusion, situational assessment, and threat estimation.

$$p(k) = \left[\sum_{j=1}^{n} p_y^{-1} \times k^2\right]^{-1}. \quad (3)$$

Target tracking (TT), through the comprehensive application of modern scientific theories such as statistical estimation, stochastic decision-making, and intelligent computing, first discriminates the data detected by the sensors and forms the corresponding observation set to give the total number of targets being tracked and then uses the target observation information to reliably estimate (filter) and predict the target state. The observations are generally derived from sensor measurements, i.e., target state observations obtained in the presence of noise pollution, and the target state generally includes kinematic components (position, velocity, acceleration, etc.), other components (radiated signal strength, spectral characteristics, and "property" information, etc.), and constants or other retardation parameters (coupling coefficients, propagation velocity, etc.). Multiple target tracking (MTT) refers to the simultaneous processing of observations from multiple targets and the maintenance of state estimates for multiple targets. However, the implementation process is the same for both single target tracking and multiple target tracking, and the schematic diagram is shown in Figure 3.

In a multisensor target tracking system, target motion state estimation mainly refers to the position estimation and velocity estimation of the moving target. Target position estimation includes the estimation of distance, altitude, bearing, and elevation angle; velocity estimation contains both velocity estimation and acceleration estimation. At the same time, in the entire network, except that the aggregation module is not powered by an external lithium battery, both the aggregation module and the ordinary module are powered by lithium batteries. To reduce the power consumption of the module and increase the life cycle of the network, all common modules and routing modules adopt the sleep-wake-sleep cycle working mode. In 2002, Mitchell and House Kamer et al. processed sounding, satellite, and aircraft data using the EnKF filtering algorithm and explored the problem of the influence of the number of ensemble members, model errors on the filtering results in complex situations [14]. In 2003, Snyder et al. completed an experimental approach to assimilate radar data with ensemble Kalman filtering. In 2004, Dowel applied EnKF to assimilate actual radar measurements. Since the frequency information acquired by the sensors contains information about the relative motion velocity between the target and the observation platform, the introduction of frequency information can determine the velocity of a moving target, an important measurement in target tracking techniques. This chapter uses a multisensor target passive tracking model that jointly utilizes the angle of arrival and Doppler frequency, as shown in Figure 4.

The Monte Carlo method is a numerical method to solve the problem by mathematical simulation and statistical analysis of random variables. The Monte Carlo method first establishes a corresponding stochastic model according to the characteristics of the problem to be solved and generates random variables with known probability distribution by the stochastic model; then sample random data according to the distribution characteristics of each random variable to conduct statistical experiments to obtain a large amount of experimental data is obtained; finally, statistical analysis is performed on these experimental data to obtain the final solution of the problem being solved. As a key military field, multisensor data fusion mainly includes target detection,

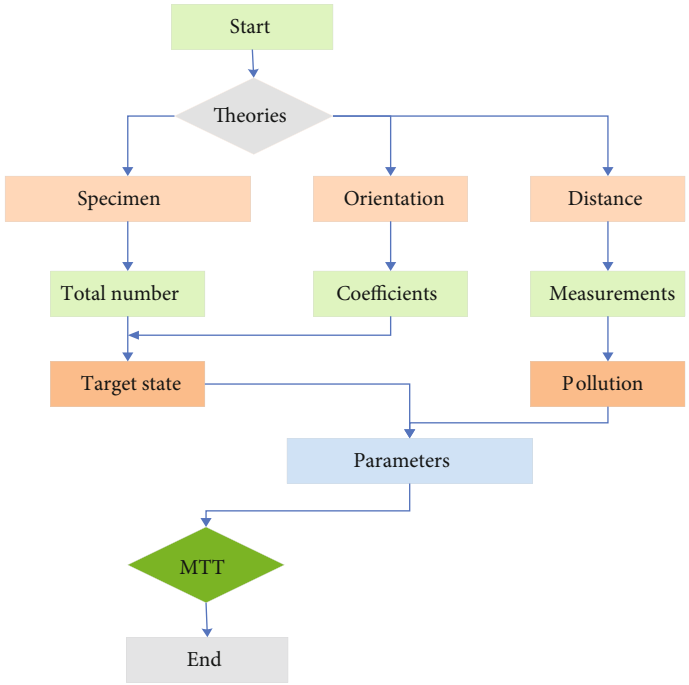

Figure 3: Basic schematic of target tracking.

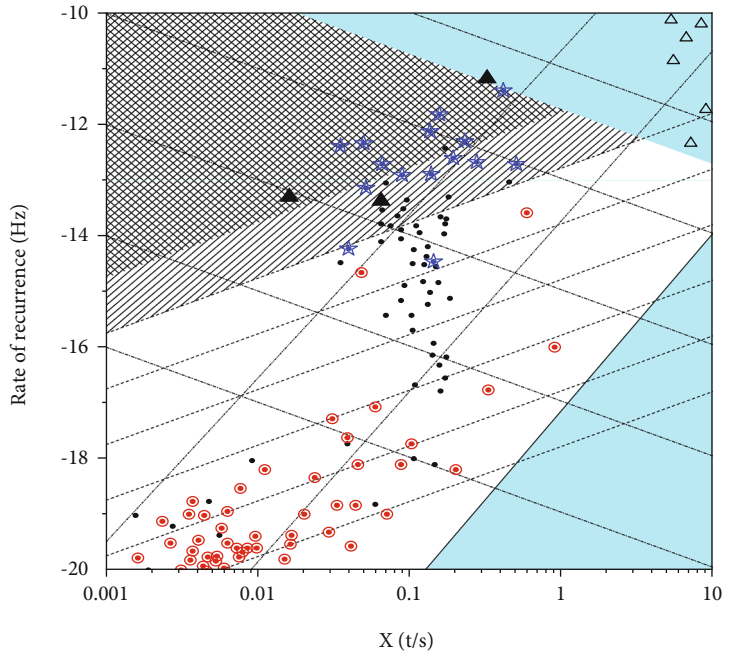

Figure 4: Model of target tracking system.

data association, target estimation and recognition, situation assessment, and threat estimation, to achieve multilevel comprehensive processing of multisensor data. The Monte Carlo stochastic simulation theory is used in the target tracking system. One place is to use Monte Carlo theory to generate the initial set $X_0 = [X_0^1, X_0^2, \cdots, X_0^N]$ of the EnKF algorithm set with membership number N. The other place is for generating the observation set by perturbing the observations using the Monte Carlo method. If the same observations and the same returns are used to update each ensemble member, the analysis error covariance will be underestimated, causing degradation of the analysis function and even leading to filter divergence. If the number of ensemble members is large, the problem of underestimation of the analytical error can be mitigated by adding the correct random perturbation to the observations to generate the ensemble of observations using the Monte Carlo method. A perturbation with a mean of 0 and a variance of the noise

scale factor multiplied by the Gaussian white noise of the observations is often applied to the observations.

$$\xi(k) = \cos\left(\frac{1}{x(k)^2 + y^2(k)}\right). \quad (4)$$

After the global observation fusion results are obtained, a smoothing estimation can be performed using a filtering algorithm to obtain the global system state fusion estimate and the corresponding error covariance. The key aspect of the weighted fusion algorithm is the determination of the weighting factors for the input information. Currently, it is common to assign weights by the method of great likelihood, least squares, etc. These methods use the measurement variance of each sensor to determine the weighting factors. However, the random interference existing in the sensors themselves and the external environment makes the observed information uncertain and correlated, which in turn leads to uncertainty in the corresponding measurement variance, making the weighted fusion effect not optimal or the effectiveness of the fusion performance reduce. In addition, when the measurement accuracy of a sensor is low, the direct use of sensor observation information for weighted fusion will cause further degradation of the track fusion performance. Based on this, by studying the weighted fusion algorithm proposed in the literature, this chapter proposes a weighted fusion algorithm based on local state estimation and uses the idea of weighted fusion algorithm to achieve an improvement on the stepwise filtered fusion algorithm proposed in the literature and reduce the impact on the performance of the fusion algorithm when directly using the observation information. The algorithm is made less effective when directly using the observed information because of some factors. The main influencing factors are as follows: first, the sensor itself performance and the external environment random interference see information uncertain and correlated, which leads to lower observation accuracy; second when the accuracy of multiple measurement devices differs greatly, the correlation leads to a large mutual influence between the observation information in the fusion process. To this end, this section proposes a weighted track fusion algorithm based on local state estimation and verifies its effectiveness through simulation comparison.

$$Z(k) = \chi_1(k) + \chi_2(k) + \cdots + \chi_n(k). \quad (5)$$

The weighted fusion algorithm based on local state estimation mainly uses the local state estimation of each sensor to complete the weighted combination of multisensor filtering to achieve the target fusion track. The specific process of the algorithm is as follows: first, the preprocessed observation information of the multisensors is used to estimate the target local state of each sensor using the filtering algorithm; then, a suitable support function is selected according to the local state estimation information of the multisensors, and the support matrix between the multisensors is established; then, the support matrix is used to calculate the weighting factor of each sensor and the weighted combination of the local state estimation information. Finally, the position fusion estimation information is filtered and estimated to compensate for the neglect of the correlation between the front and back of the data in time by the support degree matrix, and finally the fusion estimation value based on the global system is obtained. In the multisensor target tracking system, target motion state estimation mainly refers to the position estimation and velocity estimation of the moving target. Target position estimation includes estimation of distance, height, azimuth, and elevation; velocity estimation includes velocity estimation and acceleration estimation.

Table 1: Simulation parameter settings.

Area	8 m∗ 8 m	Name	Number
Number of labels	30	Positioning area	20
Reference tags	20	Reference tags	16
The position of the tags	16	Nearest reference tag	14
k	4	n	2.2

4. System Performance Testing

4.1. Analysis of Simulation Results. In the simulation of the LANDMARK positioning system, MATLAB r2014a is used for simulation, according to the previous simulation analysis, the k value; the number of reference tags and the position of the tags to be positioned in the system will affect the positioning accuracy. The final positioning area is an $8 * 8$ space, and within the positioning area, a total of 16 reference tags and 20 tags to be positioned are set, and the layout of the reference tags is all laid out according to a square. The nearest reference tag k value is selected according to the previous analysis and is chosen as 4. The channel transmission model is a log-path statistical model, where the environment factor is taken as 2.2. The simulation settings are shown in Table 1.

Root Mean Square Error (RMSE) and Cumulative Distribution Function (CDF) are mainly used in the simulation analysis of localization error in this section. To determine the localization performance of the DISTANCE-LIMIT-LANDMARK algorithm, a comparison experiment is conducted with the LANDMARK localization algorithm, VIRE-LANDMARK localization algorithm, and ADAPTIVE-SELF-LANDMARK localization algorithm to compare the localization error of each tag to be localized under the same experimental environment. The DISTANCE-LIMIT-LANDMARK localization algorithm proposed in this paper has better localization accuracy than the other three localization algorithms for most of the tags to be located; the average localization error of all tags is about 0.3596 m. However, it is obvious that the tags to be located with numbers 14 and 20 are poorly localized, and the average localization error is very high (high, which is also consistent with the conclusion that the location of the to-be-located tags at the edges). This is also consistent with the conclusion of the previous analysis that the positioning

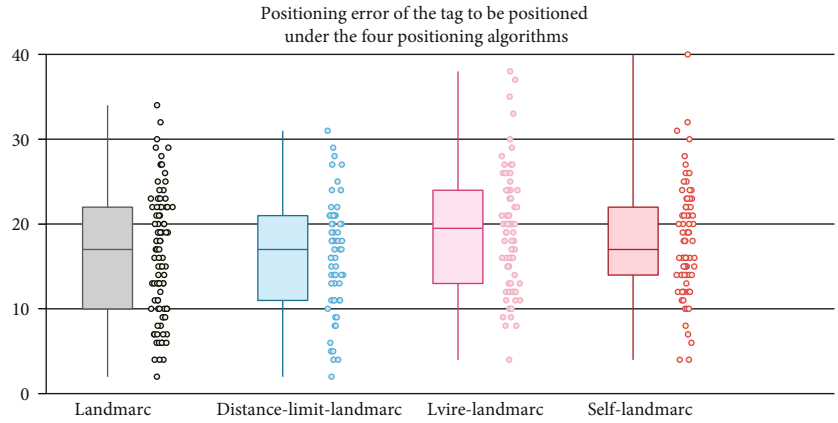

Figure 5: Positioning error of the tag to be positioned under the four positioning algorithms.

accuracy is greatly reduced when the tags are located at the edge of the positioning area, as shown in Figure 5.

In this section, this paper examines the estimation accuracy of the anomalous nodes in the key classes returned by the FDP (Fast Detection Protocol (FDP)) protocol [15]. The estimation accuracy contains two levels, firstly whether the probability of the class nodes with the highest number of anomalous nodes appearing in the set ruler is satisfied and secondly whether the number of anomalous nodes in these K classes is estimated accurately. If the most anomalous nodes appear in the top 10 classes of nodes, respectively, the experimental results show that the frequency of node class 18 appearing in the TOP~k set is 95%, which satisfies the default query accuracy of this paper, while the frequency of nodes in classes 9 and 10, appearing in the TOP~k set, seems to be lower than the expected value. Could the FDP protocol not satisfy the predefined precision? It can not. This paper can find that the probability frequency of nodes in categories 9 and 10 appearing in TOP-10 is still much higher than those of the other node categories that follow. Because the first 10 categories of nodes appear in the TOP~k set with the greatest frequency, this paper counts whether their estimated number of anomalous nodes is accurate when they appear in the TOP~k set, as shown in Figure 6.

In this paper, we aim to identify the class K nodes quickly and accurately with the highest number of anomalous nodes and accurately estimate the number of anomalous nodes in a large-scale wireless rechargeable sensor network system. To solve this problem, this paper proposes an EPC C1G2 compliant FDP protocol that can use the difference between the virtual time slot frame vector and the actual time slot frame vector to estimate the number of anomalous nodes in the corresponding class and can dynamically eliminate those node classes with a particularly small number of missing nodes, so that only the limited communication resources need to be reserved for those node classes that are more likely to belong to the TOP~K set. The specific process of the algorithm is as follows: first, use the filtering algorithm to estimate the target local state of each sensor using the preprocessed observation information of the multisensor; then, select the appropriate support function according to the local state estimation information of the multisensor, and establish the multisensor. Then, the support matrix is used to calculate the weighting factor of each sensor and the weighted combination of the local state estimation information, realizes the weighted fusion of the local state estimation, and obtains the corresponding target position fusion estimation information and, finally, the position. The fusion estimation information is filtered and estimated to compensate for the ignorance of the support matrix to the temporal relevance of the data before and after, and finally, the fusion estimation value based on the global system is obtained. This paper presents extensive theoretical analysis to ensure the accuracy of the query and optimizes the parameters involved in the FDP protocol to minimize its time cost. Extensive simulation results show that when the number of node categories is large, the FDP protocol can improve up to 80% in terms of time efficiency over existing protocols. The FDP protocol proposed in this paper is essentially a probabilistic solution, and although it can provide query results with guaranteed accuracy, it still cannot give 100% accurate query results, especially for those node classes that are at the boundary of the FDP.

$$P_{ij} = \begin{bmatrix} 0.7 & 0.02 & 0.02 \\ 0.02 & 0.88 & 0.02 \\ 0.02 & 0.02 & 0.9 \end{bmatrix}. \quad (6)$$

4.2. System Functionality Test Results. Most of the users have used handheld PDA devices, the cumbersome operation interface makes those non-professionals a headache for a while, so the interface production effect is very important for these people; these nontechnical aspects of the test are very necessary; interface friendliness is also one of the important indicators to evaluate the system [16]. To make the system interface beautiful and generous, you need the help of workers to complete and determine the background tone, with relevant pictures and text color to form the overall style and then insert a variety of functions based on this interface, the title within the page to generate static connections, relevant URLs, and database connections. At this point, the system interface has been basic.

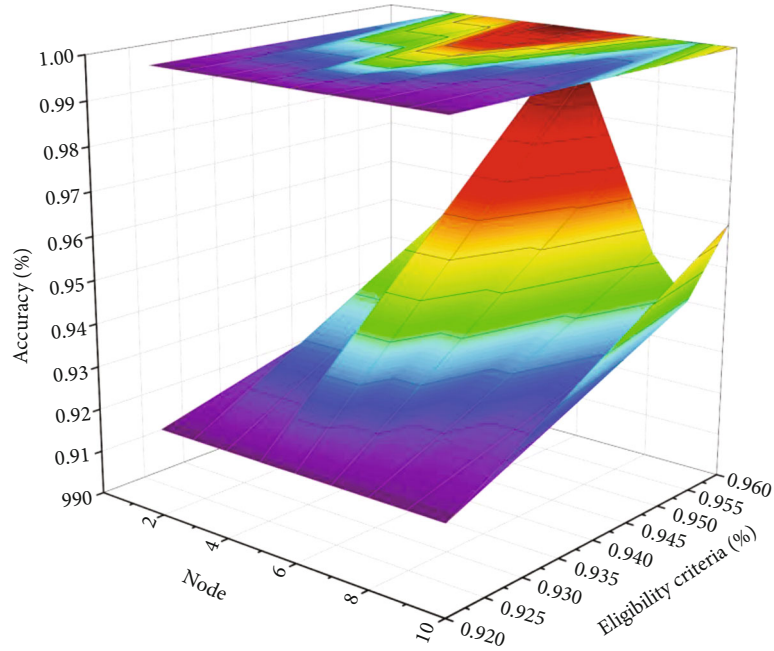

Figure 6: Frequency of the top 10 types of anomalous nodes being correctly estimated.

Table 2: Interface test protocol and results.

Test methods	Conclusion	Test methods	Conclusion
Whether the window is updated in time	Yes	Is the text accurate	Yes
Is the information standardized	Efficient	Is the password format wrong	Yes
Whether the link valid is well	Adaptation	Is the positioning accurate	Yes

Meet the public requirements; at this point, you need to get people at all levels to look at the page to correct the expenses. Finally, it is given to the client for review. For the above requirements of interface testing and performance testing, evaluate its testing index. During the testing process, many problems were found and simple solutions were concluded in the process of correction [17]. These included a variety of errors such as design flaws, coding errors, and improper hardware pairings. The corrections improved the reliability of the system and increased the corresponding speed of the system. The results from each test are listed, as shown in Table 2.

The UBLQ transmission mechanism proposed in this paper can converge quickly, and the goal of maximizing the network effect is achieved. The pairwise experiments are based on the problem of maximizing the network utility to obtain the link transmission cost parameter through the pairwise problem, which is used to find the transmission rate of the data stream. In the experiments, the algorithm chooses the same utility function as in this paper. Since the algorithm needs to know the size of the link transmission capacity, the transmission capacity of each link is set to 35 pkts/s in this paper. The UBLQ protocol in this paper converges faster compared to the distributed algorithm and can ensure that the utility of the network maintains fluctuating in the optimal value range [18]. It shows that this protocol can maximize the network utility by increasing the exploration algorithm to adjust the transmission rate of one-hop nodes and distributing the rate to multihop nodes according to the link quality in a joint algorithm. Also, by setting different transmission capacities, all the algorithms in this paper can find out the current maximized network utility faster, different link transmission capacities constrain the transmission rates of nodes in the network, and by assigning the node transmission rates so that they forward the data collected by sensor nodes to the aggregation nodes at the maximum transmission rate, the efficiency of collecting data is greatly improved. Finally, the difference between the transmission rates assigned to each node of the UBLQ transmission mechanism in this paper and the results obtained by the distributed algorithm are analyzed. The difference between the transmission rate of the nodes assigned by this algorithm and the distributed algorithm in the case of link transmission capacity is within 1 pkts/s, which increases the throughput of the network while ensuring maximum network utility, as shown in Figure 7.

In this chapter, firstly, some problems encountered during the project are analyzed and studied, and the solutions are elaborated. The method can complete the modulation identification in the multipath channel environment using only the higher-order accumulation characteristics of the received signal, which requires less a priori knowledge and

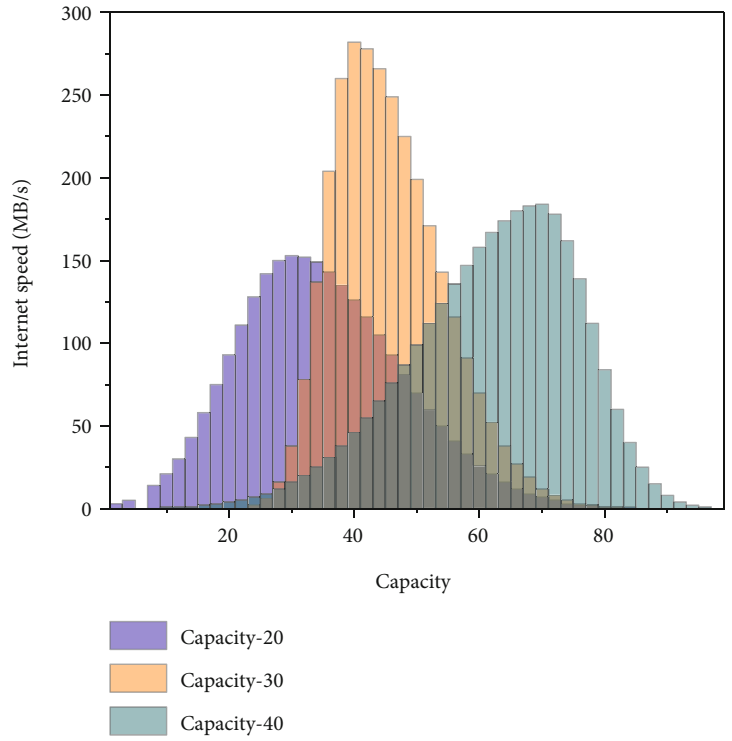

Figure 7: Maximum network utility achieved for different transmission capacity conditions.

high identification performance. Finally, the simulations are performed and the results of the simulations prove the effectiveness of the algorithm proposed in this paper, and the whole project development process is made more complete by the work in this chapter.

During the experiment, the teachers did not find the experiment to be a burden on their teaching. During the experiment, teachers could use the digital learning resources in the "Speak Easy" intelligent speech system to recommend to students to use, and students could complete the recommended practice tasks on time, and the software also provided feedback on students' completion, which was positive and effective. At the same time, students also reflect that when they use the system, they like the practice module in the system, and they can choose their favorite video clips according to their interests [19]. To solve this problem, this paper proposes an FDP protocol that conforms to the EPC C1G2 standard. It can use the difference between the virtual time slot frame vector and the actual time slot frame vector to estimate the number of abnormal nodes in the corresponding category and dynamically eliminate those with a particularly small number of missing node category, so only the limited communication resources need to be reserved for those node categories that are more likely to belong to the TOP~K set. These clips include classic movies, cartoons, speeches, and dramas, which can greatly enrich students' choice preferences, and by practicing some classic dialogue bridges, they can well stimulate their learning interests and thus improve their English listening and speaking abilities. The five aspects of clarifying the importance of students' listening ability, providing rich contexts, cultivating students' independent listening ability, attaching importance to students' listening feelings and interest in listening, and conducting diversified evaluation prove that the experimental hypothesis of this study is correct, and the applied strategies are effectively verified, and the English listening ability cultivation strategy based on intelligent speech system for junior high school students can improve students' English listening ability; i.e., the English listening ability based on intelligent speech system-based English listening and speaking ability development strategy is effective.

5. Conclusion

In this paper, we design and implement an English-assisted reading system based on a wireless sensor network. The system uses user information to construct a user interest model, maps interest communities to reading content, reconstructs the reading order of interest articles and expands reading content based on references, and updates user interest in real-time according to user reading content [20]. The study proved that applying wireless sensor network technology to an English-assisted reading system is beneficial to help students improve their reading attitudes, train their reading skills, and improve their reading performance. In conclusion, this study, through educational observations, surveys, interviews, and experiments, has demonstrated to some extent the positive impact of multimedia teaching on English reading instruction, which is worth implementing in educational practice. Although the research in this paper has obtained certain results, admittedly, this study is inevitably deficient due to the influence of objective and subjective factors. In the subsequent research, it can be summarized from the aspects that teachers themselves need to improve in the

actual teaching activities as well as the time and laws of multimedia technology used in English reading teaching, to drive students' initiative in learning English and improve students' learning ability as well as their learning autonomy in a comprehensive way, which hopefully can provide a reference for the relevant research afterward.

Data Availability

The data used to support the findings of this study are available from the corresponding author upon request.

Conflicts of Interest

We declare that there is no conflict of interest.

Acknowledgments

The study was supported by Study on Intercultural Communication in Tourism English Translation, Guijiao Research (2018) (No. 2 (2018KY0913)).

References

[1] R. Al-Zaidi, J. C. Woods, M. Al-Khalidi et al., "Building novel VHF-based wireless sensor networks for the Internet of marine things," *IEEE Sensors Journal*, vol. 18, no. 5, pp. 2131–2144, 2018.

[2] R. Klis and E. N. Chatzi, "Vibration monitoring via spectro-temporal compressive sensing for wireless sensor networks," *Structure and Infrastructure Engineering*, vol. 13, no. 1, pp. 195–209, 2017.

[3] S. Poudel, S. Moh, and J. Shen, "Residual energy-based clustering in UAV-aided wireless sensor networks for surveillance and monitoring applications," *Journal of Surveillance, Security and Safety*, vol. 2, no. 3, pp. 103–116, 2021.

[4] I. Boudali and M. B. Ouada, "Smart parking reservation system based on distributed multicriteria approach," *Applied Artificial Intelligence*, vol. 31, no. 5-6, pp. 518–537, 2017.

[5] H. Zhang, C. Jiang, R. Q. Hu et al., "Self-organization in disaster-resilient heterogeneous small cell networks," *IEEE Network*, vol. 30, no. 2, pp. 116–121, 2016.

[6] S. Chen, Z. Wang, H. Zhang, G. Yang, and K. Wang, "Fog-based optimized kronecker-supported compression design for industrial IoT," *IEEE Transactions on Sustainable Computing*, vol. 5, no. 1, pp. 95–106, 2020.

[7] E. Zimos, D. Toumpakaris, A. Munteanu, and N. Deligiannis, "Multiterminal source coding with copula regression for wireless sensor networks gathering diverse data," *IEEE Sensors Journal*, vol. 17, no. 1, pp. 139–150, 2017.

[8] B. C. Csaji, Z. Kemeny, G. Pedone, A. Kuti, and J. Vancza, "Wireless multi-sensor networks for smart cities: a prototype system with statistical data analysis," *IEEE Sensors Journal*, vol. 17, no. 23, pp. 7667–7676, 2017.

[9] F. H. Bijarbooneh, W. Du, E. C. Ngai, X. Fu, and J. Liu, "Cloud-assisted data fusion and sensor selection for internet of things," *IEEE Internet of Things Journal*, vol. 3, no. 3, pp. 257–268, 2016.

[10] C. M. Chen, J. Y. Wang, and C. M. Yu, "Assessing the attention levels of students by using a novel attention aware system based on brainwave signals," *British Journal of Educational Technology*, vol. 48, no. 2, pp. 348–369, 2017.

[11] Z. Xu, F. R. Sheykhahmad, N. Ghadimi, and N. Razmjooy, "Computer-aided diagnosis of skin cancer based on soft computing techniques," *Open Medicine*, vol. 15, no. 1, pp. 860–871, 2020.

[12] J. W. Li, S. N. Li, Y. Zhang et al., "An analytical model for coding-based reprogramming protocols in lossy wireless sensor networks," *IEEE Transactions on Computers*, vol. 66, no. 1, pp. 24–37, 2017.

[13] L. D. Xu and L. Duan, "Big data for cyber physical systems in industry 4.0: a survey," *Enterprise Information Systems*, vol. 13, no. 2, pp. 148–169, 2019.

[14] V. Agrawal, R. Rastogi, and D. C. Tiwari, "Spider monkey optimization: a survey," *International Journal of System Assurance Engineering and Management*, vol. 9, no. 4, pp. 929–941, 2018.

[15] N. Razmjooy, F. R. Sheykhahmad, and N. Ghadimi, "A hybrid neural network–world cup optimization algorithm for melanoma detection," *Open Medicine*, vol. 13, no. 1, pp. 9–16, 2018.

[16] J. Sambharia and H. S. Mali, "Recent developments in abrasive flow finishing process: a review of current research and future prospects," *Proceedings of the Institution of Mechanical Engineers, Part B: Journal of Engineering Manufacture*, vol. 233, no. 2, pp. 388–399, 2019.

[17] Q. Liu, Z. Wang, X. He, G. Ghinea, and F. E. Alsaadi, "A resilient approach to distributed filter design for time-varying systems under stochastic nonlinearities and sensor degradation," *IEEE Transactions on Signal Processing*, vol. 65, no. 5, pp. 1300–1309, 2017.

[18] F. Goudarzi, H. Asgari, and H. S. Al-Raweshidy, "Traffic-aware VANET routing for city environments—a protocol based on ant colony optimization," *IEEE Systems Journal*, vol. 13, no. 1, pp. 571–581, 2018.

[19] W. Zhou, J. Hou, L. Liu, T. Sun, and J. Liu, "Design and simulation of the integrated navigation system based on extended Kalman filter," *Open Physics*, vol. 15, no. 1, pp. 182–187, 2017.

[20] A. Moeuf, R. Pellerin, S. Lamouri, S. Tamayo-Giraldo, and R. Barbaray, "The industrial management of SMEs in the era of Industry 4.0," *International Journal of Production Research*, vol. 56, no. 3, pp. 1118–1136, 2018.

Hindawi
Journal of Sensors
Volume 2022, Article ID 6430191, 11 pages
https://doi.org/10.1155/2022/6430191

Research Article

Digitalization and Information Management Mechanism of Sports Events Based on Multisensor Node Cooperative Perception Model

Yi Liu,[1] Yaodong Wang,[1] Yuntong Tan,[2] Jie Ma,[1] Yan Zhuang,[1] and Xiangqian Zhao[1]

[1]*Department of Physical Education Teaching, China University of Mining and Technology (Beijing), Beijing 100083, China*
[2]*Department of Physical Education Teaching, Guang Dong University of Technology, Guang Zhou 510006, China*

Correspondence should be addressed to Yaodong Wang; wyd@cumtb.edu.cn

Received 29 October 2021; Revised 24 November 2021; Accepted 30 November 2021; Published 6 January 2022

Academic Editor: Gengxin Sun

In the process of developing major sports events, how to guide providers and users to provide and utilize the archives information resources of major sports events and realize the interaction between them is an important problem to be solved urgently in the development of major sports events and the archive service of major sports events. By analyzing the present situation of archive service of major sports events, especially the analysis of the opposite dependent subjects of service providers and users, we can see that the continuous development of archive services for major sports events will inevitably lead to constant changes in user groups and user needs, guided by the theory of information retrieval, knowledge management, and media effect. According to the service model of archive service of major sports events, the archive service model of specific sports events is constructed. In this paper, four kinds of event recommendation models are applied to the collected marathon event data for experiments. Through experimental comparison, the effectiveness of content-based recommendation algorithm technology in the event network data set is verified, and an algorithm model suitable for marathon event recommendation is obtained. Experiments show that the comprehensive event recommendation model based on term frequency–inverse document frequency (TF-IDF) text weight and Race2vec entry sequence has the best recommendation performance on marathon event data set. According to the recommendation target of the event and the characteristics of the event data type, we can choose a single or comprehensive recommendation algorithm to build a model to realize the event recommendation.

1. Introduction

Under the background of big data and artificial intelligence, sports and big data are in urgent need of integration and development, and the increment of sports-related information, especially sports information resources on the Internet platform, has risen sharply. In the new era, our people's demand for sports is characterized by pursuing more personalized, multilevel sports events, and sports services to meet their own needs with the improvement of living standards [1]. At the same time, facing a large number of demands, the number of sports events and services also shows a rapid growth trend. Taking marathon events as an example, in 2018, a total of 1,102 events were held nationwide, with nearly 50 million participants. Among them, there are 350 certified events of the Chinese Association of Athletics, and various interesting and characteristic theme events are also booming [2]. Therefore, a large number of race supplies provide rich choices for many marathon entry-level runners or ordinary participants, but complex race classification standards and uneven race promotion information also increase the difficulty for runners to choose races and the promotion cost of race service organizations. Beginner runners need to spend a lot of time screening race information and evaluating content, and inspecting and selecting suitable race services [3]. Today, with the rapid development of big data, the above-mentioned problem of noncirculation of sports event information resources, taking marathon event information as an example, is no longer a case, and the problem of event information resources should

be regarded as an information overload problem in essence [4].

In the digital age, the change of media urges people to get the needed sports information more quickly through the network and computer technology. However, sports information, especially sports information resources on a large number of Internet platforms, such as event data display information and text evaluation information, have not been collected and applied reasonably [5]. Fragmented network sports information, especially the text state information, makes the irrationality of traditional sports information classification and storage begin to appear, which easily leads to the dislocation of information resources intercommunication when users search for sports information, and excessive dislocation information accumulation easily leads to information overload. Facing the problem of information overload, search engine, e-commerce, and other fields have carried out in-depth research and discussion, among which the most important solution is entity recommendation technology [6]. In 1990s, some American scholars put forward the concept of recommendation system, and realized the content recommendation to forum users through recommendation technology. At present, the application of recommendation technology in sports field is not very extensive, and it is still only recommended for specific entities such as sports goods or sports news [7]. At the same time, under the current industry development background of artificial intelligence and "Internet plus," the mining and processing of sports event information resources need the introduction of new technologies. Therefore, if the fragmented sports information resources can be fully mined and applied by effectively constructing the event recommendation model and introducing a variety of algorithms to process the event network information data, it will help to improve the use efficiency of users' Internet fragmented event information taking marathon event network data as an example [8]. This fundamentally meets the needs of runners for suitable event information supply and enhances the interactive experience of users in using sports information resources [9]. At the same time, the introduction of event recommendation algorithm can promote the utilization rate and relevance of sports information resources, which will not only provide more personalized and professional information service technical support for sports enthusiasts but also help to improve the overall information intelligence level of sports and promote the development of sports industry [10].

At present, as one of the most important information exchange channels, there is still a lot of fragmented sports-related information. Under the background of the rapid increase of sports events and service information, studying the recommendation technology of competition information and the comparative application of various algorithms will help to make statistical analysis of competition network information more efficiently, realize the demand of people for competition information recommendation, and provide basic theoretical and technical support for the research of network sports information resources mining and application in a more intuitive and effective way. Internet data of sports events is a part of sports information resources, which is fragmented information data. This paper analyzes the characteristics of the current network event information to select the appropriate data recommendation algorithm, through the combination of algorithm and data to build a practical event recommendation model, in order to provide the basis and reference for the application research of fragmented sports information resources represented by competition Internet data and the use of related methods. Second, it gives the possibility of integration and development of sports event information and related information technology from the perspective of technology, which provides a broader idea for sports informationization research and enriches the technical means of sports research. For this reason, archive service providers must constantly develop service infrastructure, change service concepts, and innovate service methods: build an objective foundation of archive service that adapts to the development of the times and can continuously integrate new technologies, new equipment, and new concepts.

2. Related Work

At present, the definition of Internet data of sports events is rarely mentioned in academic circles, and the Internet data of sports events is essentially an expression form of information resources based on Internet platform in sports information resources [11]. Therefore, in the research status analysis, choose to belong to the upper level of network sports information resources for current research and analysis, searching in the full-text database of academic journals of China Knowledge Network (CNKI) with the retrieval format of "Subject = Network Sports Information Resources." Among them, there are 179 literatures in journals and master's and doctoral dissertations, among which 13 are cited more than 20, but only 3 are highly related to the research of online sports information resources, all of which are before 2005, and their reference value is not great under the current Internet development background [12]. Through all the relevant literature available for inquiry, the main research directions are divided into two categories: the construction and application of network sports information resources in colleges and universities, and the integration and development of network sports information resources [13]. Among them, the dominant research content is the integration of network sports information resources and how to use them efficiently [14].

Among them, the researchers made a clear exposition on the mining and acquisition of network sports information resources at that time, covering the use of search engines, sports authoritative websites, network databases, sports websites, or sports channels of comprehensive websites. In the research direction of improving the retrieval efficiency of network sports information resources, based on the previous information resource acquisition skills, researchers put forward a method of using professional database retrieval skills and file type retrieval on the network platform [15]. According to the problems existing in the development of network sports information resources, the researchers put forward some suggestions on building a sharing platform of network

sports information resources and analyzed the corresponding operation mechanism and feasibility [16]. However, from all the available literature, most of the research on network sports information resources is to summarize the current situation and analyze the possibility of its integration, there is a certain technical lag, and there is little in-depth research on its internal data structure and application.

To sum up, at present, there is little research on the application of Internet data of sports events in China. This study builds a reasonable event recommendation system by analyzing the characteristics of public event information of professional sports vertical websites in the Internet, which is an effective and innovative research on network sports information resources based on this [17]. At present, with the government departments at all levels vigorously promoting the development of sports and cultural undertakings, more and more major sports events are held in major cities in China. Academic circles and other people from all walks of life, government departments, and other workers on major sports events have gradually been put on the agenda and become a hot spot of current research [18]. Among them, many scholars, staff, and government departments have noticed the various influences of archives on the inheritance, holding, development, and dissemination of major sports events and have written books, expressed their views, and clarified their positions, showing a scene of a hundred flowers blooming.

In this paper, before studying the major sports event archive service, the relevant literature was consulted, and some existing journals, papers, and government documents related to the major sports event archive service were collected and combed to obtain the necessary literature support [19]. By searching the full-text database of electronic resources of China Periodical Network, Wanfang Database, domestic and foreign government, and research websites, we find the literature related to the archives of major sports events and study some related works. From the current point of view, domestic scholars are committed to study the archives of major sports events from different angles [20]. After sorting out and analyzing this paper, some conclusions are drawn. From the existing achievements, the research on the archives of major sports events by relevant workers and scholars mainly includes three aspects: the research on the concept and management of sports archives, the need for archive service support for the development of sports cultural undertakings, and the development and utilization of sports archives information resources [21]. This paper will summarize the current research status from these three aspects.

At present, the research on the application of sports information resources and sports information mainly focuses on sports information and sports literature, while the application of a large number of fragmented sports event information based on the Internet is rarely mentioned.

3. Multisensor Node Perception of Internet Data of Sports Events

3.1. Basic Characteristics of Internet Data of Sports Events. In order to effectively meet the urgent needs of the masses to participate in sports events, it is necessary to display and recommend many event information to the masses reasonably and accurately. Under the current background of "Internet plus," the event data in the Internet is multiplying day by day, and the characteristics of event information hidden behind a large amount of data and the rules of user browsing are effective information when constructing the event recommendation model. Therefore, this chapter will take the Internet data of sports events as the research object, deeply discuss the network data characteristics and reasonable data collection framework of marathon events, and collect corresponding data sets according to the framework, so as to provide basic data reference for the construction of sports event recommendation model, as shown in Figure 1.

The Internet information data storage of sports events is large, and the Internet content corresponding to a single event includes official websites, portals, professional forums, new media, and other information dissemination platforms. For example, by the end of 2019, searching for "Marathon Events" on Baidu search engine can obtain more than 30 million related web pages, covering information such as publicity, communication, and popular science of marathon events. At the same time, the content between sites is relatively independent. To obtain the corresponding event information completely, visitors need to obtain information through multiple related keywords and multiple platforms. This fragmentation feature is becoming more and more obvious in the Internet data of events with a sharp increase in data volume. Because of relying on the Internet platform for information display, the Internet data of sports events shows diversified characteristics in data type distribution, including video data, numerical data, computer language data, and other forms besides traditional text data and picture data. Taking the retrieval of "NBA Games" in Baidu as an example, the data types displayed include the text data of the victory and defeat reports of the Games, the numerical data of the players' participation information, and the video data of the wonderful performance of the Games. At the same time, the angle of each site to spread events and the scope of data collection are different, the types of sports event data transmission are different, and there is a lack of label definition for content types.

3.2. Internet Data Acquisition Based on Multisensor. The collection framework of Internet data set of sports events refers to the standardized data collection structure and rules that can be constructed according to the characteristics of network data of sports events. Among them, the common Internet data collection framework is generally realized by constructing database catalogue and metadata format. At the same time, the collection of event network data set is different from the current sports event state data collection and physiological state data collection, which is non-real-time and delayed. Common event data collection focuses on athletes' physiological state and real-time state data information during the event, while the Internet data set of sports events is generally public information set related to the event, which is published and non-real-time data information. In order to effectively collect the event network data and build

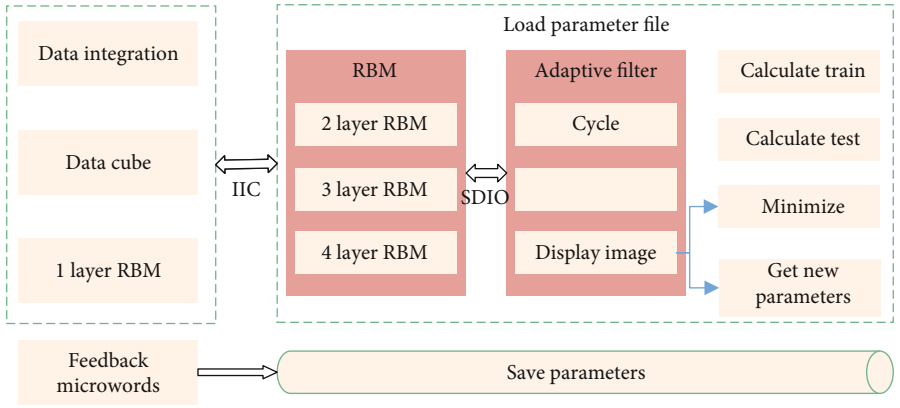

Figure 1: Recommended model for sports events.

an effective data storage warehouse, the attributes and categories of the event data in the current network should be clearly defined, so as to establish the corresponding data collection and storage table. According to the current scholars' research on the elements of sports events, events are generally composed of various elements such as event attributes, human resources, competition, and evaluation. From the perspective of sports information resources, the composition of competition network information includes many types of elements, such as competition news information, database resources, competition video resources, organizational social resources, and so on.

This paper studies the event recommendation model to meet such needs. The construction of event recommendation model first needs to clarify the current application scenarios of event recommendation and the data types required for recommendation, so as to select the appropriate recommendation model algorithm according to reasonable recommendation objectives and effective event data.

According to the research direction of this paper, the construction of event recommendation model needs to consider three elements: sports events, users, and algorithms. From the perspective of users participating in events or browsing event information, users browse event details or attribute information and upload event participation details when browsing event information. Therefore, from the perspective of the association between network users and events, the event network data can be divided into three categories: event attribute data set, user attribute data set, and user participation in events data set. As shown in Figure 2, this paper divides the event Internet data into three parts, thus constructing the corresponding data table. In each data set, there are field names to be collected under the data set. According to the standard of constructing the third normal form according to the data table, each field name is independent and does not repeat, which represents a data feature under the data set. At the same time, in the process of data storage, the network data of the three types of events contains the data corresponding to all the field information in the data table, which is regarded as the metadata of a data table, also known as tuples. In order to effectively collect the characteristic data in the network data of events and make the data set conform to the information details of sports events, this study clarifies the inherent field names under the three data sets, so that the collection framework can be matched to the network data collection process of various events.

Among them, the event attribute network data set should include five field names: event number, event name, event venue, event date, and event introduction. The event number is the primary key of the data set, that is, the necessary field name. The user attribute network data set includes four field names: user number, user name, user gender, and user location, wherein the user number is the necessary field name of the data set. The network data set of user participation in the competition is associated with the other two tables and has the competition number, user number, and necessary user participation number. As shown in Figure 3, when the collection framework is applied to the network data collection of various events, the corresponding data sets and field names should be determined according to the event-related public contents to be collected. In the data table composed of three data sets, the event number, user number, and user entry number are the primary keys of each data table, that is, this field is the key field to determine the uniqueness of data in the data set. According to the different network data of various sports events, you can choose to add other fields to form a corresponding reasonable data table.

3.3. Digital Management of Event Information. In the era of big data, data analysis cannot be separated from reasonable search and collection of data. At present, the collection of large quantities of Internet data has entered the period of automatic collection, which is also called network data collection or network crawler. Web crawler technology has played a great role in scientific research, public opinion collection, and information security. Through Web crawler technology, regular data information can be obtained in large quantities according to the set program content. At present, the crawler technology based on python language is the most widely used, and the personalized website data collection framework can be written through python language. At the same time, a large number of data are collected with the help of plug-ins, among which the commonly used plug-in modules include web page request module, scrawny crawler framework, and selenium automated web page test

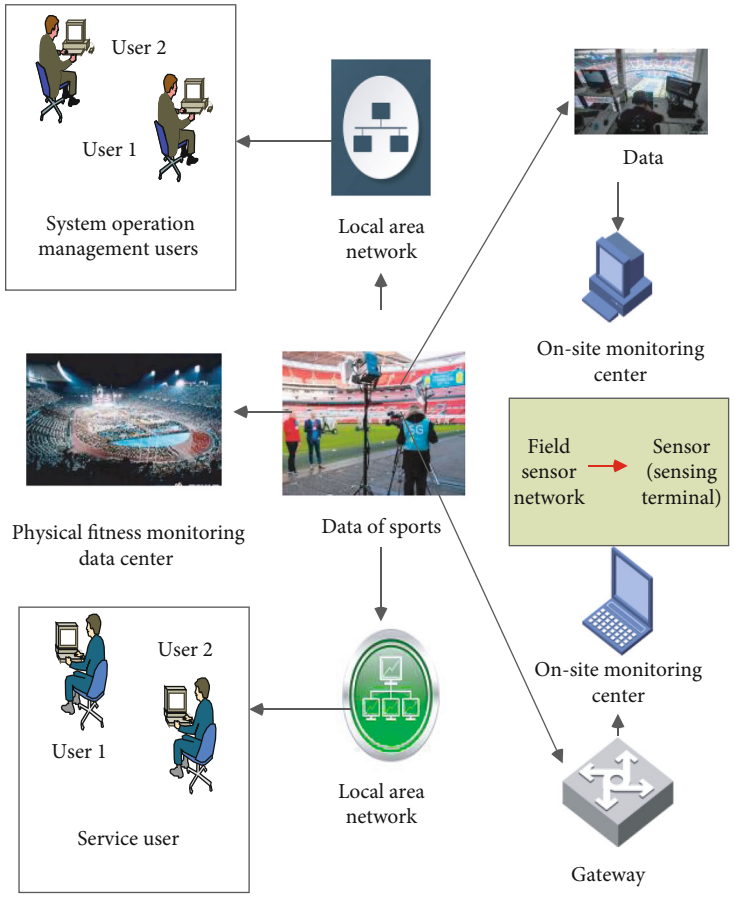

Figure 2: Event network data collection framework.

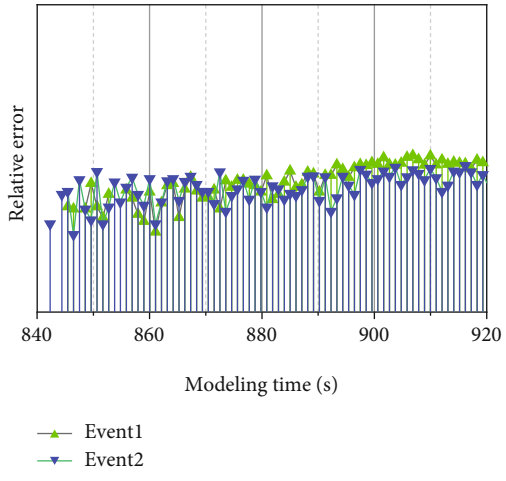

Figure 3: Collection of event attribute data sets.

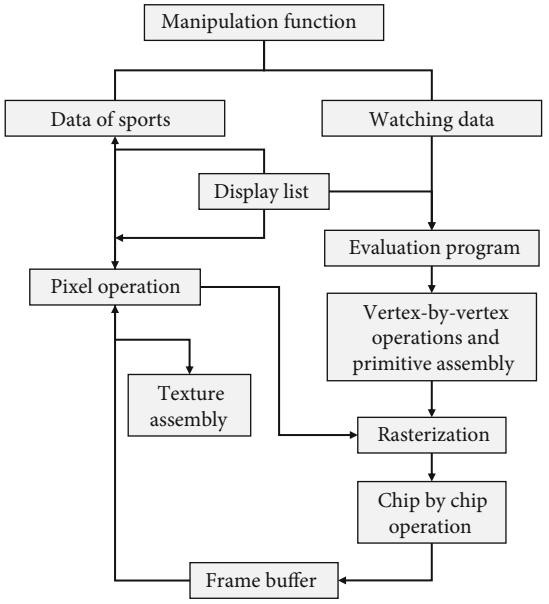

Figure 4: Implementation of web crawler.

framework. The implementation flow of web crawler is shown in Figure 4.

The collection of Internet data of sports events can also be expanded according to web crawler technology. First of all, it is necessary to determine the target website and the target content that need to collect data, through Python language or other computer language to write the corresponding website content request module code, content analysis module code, and content collection module code. Then, batch event data collection is realized according to the order of requesting or taking event data website content, analyzing event data content, and collecting corresponding field data. At the same time,

it is necessary to make it clear that the collection of corresponding data should conform to the robots protocol of the Internet and only be used for academic research, so as to ensure the reasonable and legal collection behavior.

Based on the corresponding user needs when constructing the event recommendation model, the main function of the model after construction is to realize the recommendation between the same type of sports events and have a certain accuracy to meet the basic needs of users. From the use scenarios of the event recommendation model, there are uncertain differences in the event characteristics and data characteristics of different categories of events. According to different competition requirements, it is necessary to fine-tune the algorithm under a unified framework in the construction of the competition model, so as to meet the effective recommendation under different input data conditions, different competition project recommendation requirements, and different use scenarios. Therefore, the constructed event recommendation model needs to have a statistical basic framework, and at the same time, according to the project objectives, it needs to meet the recommendation needs of different sports characteristics. In terms of actual functional requirements, the functions that the event recommendation model should realize include feature extraction of events, similarity calculation of events, and recommendation list supply of events.

4. Experiences and Results Analysis

4.1. Data Requirements Analysis. The construction of the recommended model needs to meet its usage scenarios and performance requirements, which makes the construction of the model follow the target direction and data feature dimension of the entity project. The event recommendation model constructed in this paper is based on the analysis of network data characteristics of events, which makes it clear that the current network data of events has the characteristics of large amount of text data and uneven and diversified data distribution. Under such characteristics, the construction of recommendation model needs to be as close to the characteristics of most public network data as possible. In the selection of input data, we should select characteristic data with clear classification attributes and considerable quantity. Traditional recommendation models often need a large number of data sets with standardized structure to support them. In the past studies, the information research on sports events tends to be carried out on the theoretical framework and data structure, while the research on the characteristics of event data in the current Internet is rarely mentioned. The reason lies in the lack of effective analysis means and data support. The characteristics analysis and collection of network data of current marathon events as an example can provide more suitable basic data for the research of event recommendation model. With the corresponding basic data set, the construction of the event recommendation model will be more accurate. From the technical feasibility point of view, the rapid development of artificial intelligence and big data provides more feasible directions for the selection and comparison of model algorithms, as shown in Figure 5. The rapid evolution of natural language

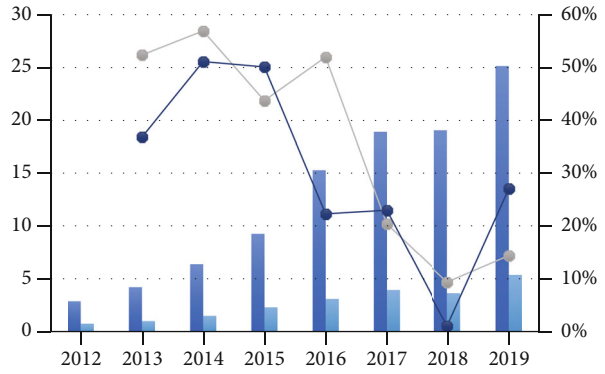

Figure 5: Model feasibility requirements.

processing technology and machine learning technology promotes the practice of various recommendation algorithms in more industrial production fields. According to the data characteristics and the needs of runners, the recommendation technology algorithm selected in this paper has been effectively proved in other fields such as commodity recommendation, text recommendation, and news recommendation, so as to ensure that the algorithm selected in the construction of event recommendation model in this study will be followed.

4.2. Recommendation System. In order to evaluate the performance of various recommendation algorithms or systems conveniently, academia and industry have a series of evaluation indexes which can be used to evaluate the reliability of recommendation algorithms or systems. Different evaluation indicators have different emphases in measuring recommendation performance and correspond to different evaluation approaches. This section summarizes some commonly used evaluation indicators in academic circles, including recommendation accuracy, recommendation coverage, and user satisfaction. Users' satisfaction with the recommended items is one of the important indicators to evaluate the recommendation model. However, user satisfaction cannot be obtained by offline calculation, which requires user survey and real-time collection. At the same time, in the online system, user satisfaction needs to be obtained by collecting some user behaviors and making statistical analysis.

Prediction accuracy is the most important index to measure the offline evaluation of recommendation system. Among them, it is mainly divided into scoring prediction accuracy and using prediction accuracy. According to different research directions, the commonly used prediction accuracy indicators are as follows: mean absolute error (MAE), precision, and recall. MAE uses absolute value to calculate the recommendation error and observes the gap between the predicted score of items given by the recommendation algorithm and the actual score of users to measure the performance of the recommendation system. Accuracy and recall rate are widely used in Top-N recommendation. Top-N recommendation gives users a recommendation list of corresponding items with the number of N, which is the

mainstream recommendation scheme of recommendation system at present. Coverage is to evaluate the mining ability of a recommendation system or recommendation algorithm for long-tail items. The most common definition is the proportion of items recommended by the recommendation system to the total collection of items. Coverage rate is often used to evaluate the recommendation performance of books, movies and other items with complex classification. Combined with the above-mentioned Internet data set characteristics of sports events taking marathon events as an example, in this study, the actual test of the event recommendation model will use the evaluation method of prediction accuracy to test the results of the event recommendation model based on the content recommendation algorithm.

According to the above research on the category of recommendation model, this paper chooses content-based recommendation model technology to build the corresponding event recommendation model according to the sports event data set on the Internet. The content-based recommendation model algorithm mainly uses the descriptive content features of the entity to be recommended and calculates the number of tags or the similarity of tags content through the tagging vector of content features. It can be seen that the content-based recommendation algorithm replaces entities with tags of feature content, and each tag has different corresponding values, thus transforming the feature distribution problem of entities into the vector value problem of entity tagging and realizing the calculation of vector value distance instead of similarity. In the Internet data of sports events, the descriptive information of sports events is mostly unstructured feature data, which is manifested as event name, event introduction, event location, and entry requirements. This kind of descriptive information is mostly distributed in text content, and the text length is different. By browsing this kind of text information, users or visitors can quickly form a preliminary understanding of the competition situation, as shown in Figure 6.

Therefore, for this kind of unstructured feature text, it is generally necessary to use the corresponding text processing algorithm to transform the feature content into space vectors. At the same time, by observing the event data set and data characteristics, we can find that there are a large number of user entry record sequence data in the Internet data of sports events. This kind of data belongs to unstructured data type, but the text in its sequence is mainly the name of the event, and the content features are hidden in the entry records. Therefore, for the application of this kind of data set, it is necessary to extract the hidden features from the sequence records by algorithms and attach them to the event entities or user entities. This transforms the feature similarity problem of events into the hidden feature distribution problem in the event sequence. In the current research, the text content feature extraction algorithms commonly used in content-based recommendation model include the LDA topic model algorithm, TF-IDF text weight model, and Word2vec model. These three algorithms have achieved the extraction of text features in sentence segments through different concepts and have achieved success in a large number of experiments and practical applications. At the same time, the algorithm idea of Word2vec model is also widely used in the data set of sequence data or behavior records, which can obtain the vector space values of each entity in the sequence. In the following, these three content text feature extraction algorithms are described and analyzed.

Vectorization of events introduces the concept of vector space model (VSM), which is defined as transforming traditional text content into dimension vectors in vector space, thus giving corresponding values for calculation, so that similar documents or paragraphs have similar vector spaces. Vector transformation makes entity content from text information to numerical information, which makes it easier to carry out statistics of entity content attributes. For example, in marathon events, "Shanghai International Marathon," "Beijing International Marathon," and "Beijing International Cross-country Running Challenge" are all top marathon events at present, but it is difficult to judge the similar intensity of the two events from the classification attributes of the events. For example, "Shanghai International Marathon" and "Beijing International Marathon" are both regular paved marathon events, but their venues belong to different cities. The "Beijing International Marathon" and "Beijing International Cross-country Running Challenge" are both held in Beijing, which are geographically similar events, but their classification is different, and the suitable participants are also different. However, as shown in the vectorization of event names in Figure 7, the vector space model transformation based on word frequency (the greater the word frequency, the weaker the feature performance and the smaller the value) can extract the values of similar texts from the text attributes and give effective space vector values to these three events. The corresponding event vector model can be constructed under a large amount of training data.

Event similarity calculation is a necessary step to achieve event recommendation, which transforms the similarity problem between events into the distance problem of spatial values, in which it is convenient to use mathematical and physical calculation forms to realize the similarity judgment of event entities. And the recommended list can be output conveniently according to the ranking of similarity between events. At present, there are many methods to calculate the similarity of VSM vector space models. Common vector space similarity algorithms include Euclidean distance, cosine similarity, and Pearson's correlation coefficient. At the same time, when using different algorithms to build vector models, the calculation of entity similarity also needs a specific adaptive similarity calculation method. For example, when using the LDA theme model to build "event-theme distribution matrix" in this study, it is necessary to use the corresponding theme proportion similarity calculation method to realize the similarity calculation of theme proportion. Therefore, in the following research, this paper will compare and analyze the commonly used vector similarity calculation methods and study their applicability, so as to choose the appropriate similarity calculation method and apply it to the modeling of each event recommendation model. As the mainstream topic generation and topic vectorization model in text content analysis, LDA model holds that a document corresponds to multiple topics, and each topic corresponds to a different vocabulary in the document.

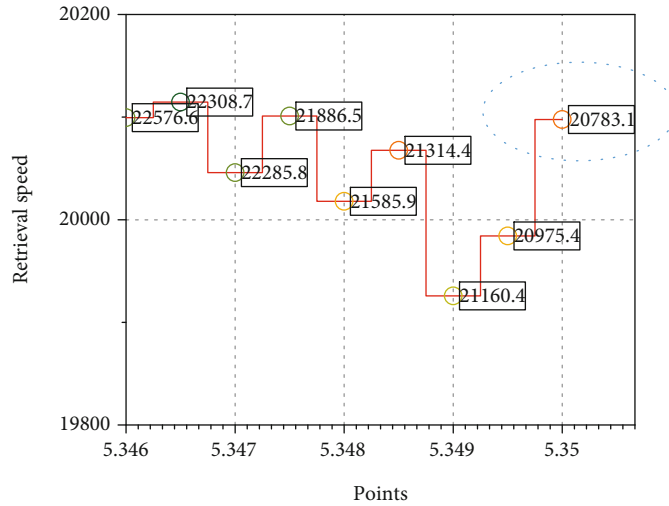

Figure 6: Text class information retrieval speed.

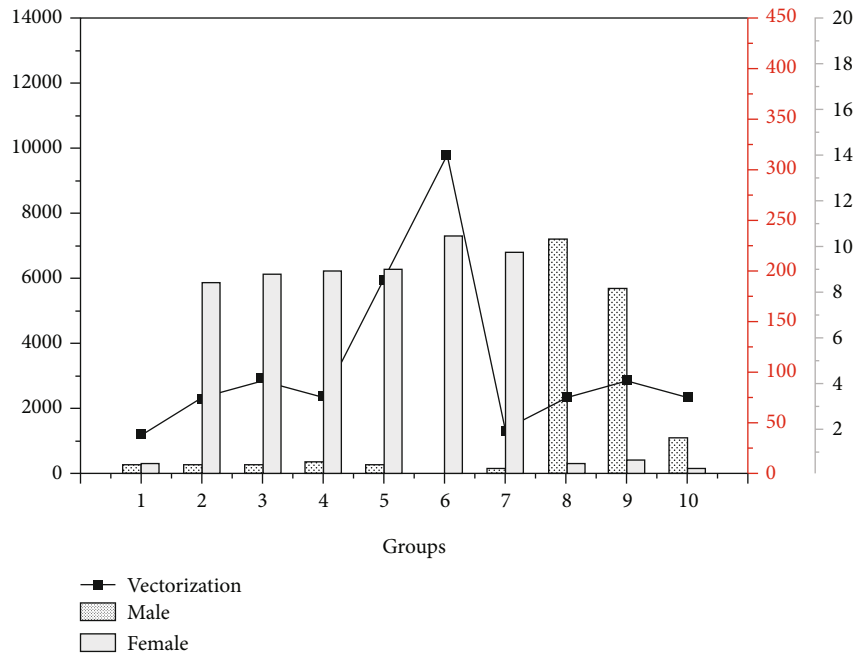

Figure 7: Vectorization of event names.

According to the lexical distribution probability within the topic, the corresponding content range of the topic can be summarized. According to the proportion of documents on different topics, the topics that account for a larger proportion can be regarded as the main topics of the document. Three-dimensional "document-topic-vocabulary" constitutes a necessary condition for the proportion of document generation vectors. When inputting the original text, the LDA topic model adopts the basic word bag representation and transforms each input document content into a corresponding word frequency vector. In LDA modeling Internet event data, it is necessary to model the text content of all events after word segmentation. In order to effectively express the characteristics of events, the characteristic text content of events generally includes the name of events, the venue of events, and the brief introduction of events. These data indicators reflect the content of events in theme characteristics, regional tendentiousness, and overall characteristics. After text preprocessing such as word segmentation, the input original event content text is changed into a content feature entry matrix for modeling. As shown in the event-theme combination content based on LDA theme model in Figure 8, when modeling the event-theme through LDA model, the characteristic contents of m events, R is input, and the number of possible themes T of a given event is k. After training the model code, the event-theme matrix and theme-content vocabulary matrix can be finally obtained.

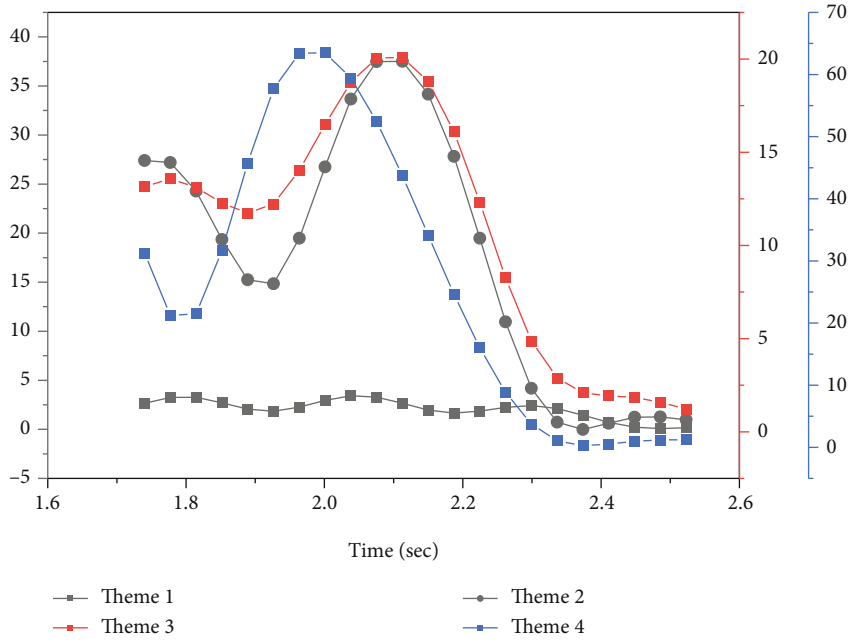

Figure 8: Theme combination of theme model.

The basic assumption of TF-IDF model is that a corpus contains multiple documents. If a word in a document appears many times in the document and is marked with the TF value at the same time, but the word appears less in the whole corpus and is marked with IDF value, then the larger TF × IDF mark value of this word may be the keyword or subject word of the document to which it belongs. According to the rules of the TF-IDF algorithm, the corresponding TF-IDF value of words in each event name can be calculated. By observing the TF-IDF vector values of words in the event corpus, we can find that "Shanghai" is the key theme of "Shanghai International Marathon Events." "Cross-country Running" and "Challenge" are the key themes of "Beijing International Cross-country Running Challenge." It also shows that TF-IDF algorithm can effectively separate the feature themes of each event in the event text corpus and endow the event with a certain vector dimension. In practice, the improved model is no different from the basic Word2vec model in algorithm principle, but the selected input data set is changed from the event feature text data in the Internet to the sequence data of users participating in the event. Then the output content changes from the vector value of constructing characteristic vocabulary to the vector value of each event in the input event sequence set. This transformation is more suitable for constructing corresponding spatial vectors for event entities and calculating the similarity of event vectors. At the same time, in the use of data, it can avoid using a single event feature text data, which cannot effectively verify the recommendation accuracy of the recommendation model and turn to using the user competition sequence data in the Internet. Finally, it can compare and analyze the performance of the recommendation models when using different data sets.

After the above description, it can be seen that the Internet data sets of sports events have the characteristics of large number and many types, and a single content-based recommendation algorithm modeling method is easy to achieve better recommendation results on specific Internet event data input samples. However, from the perspective of user selection of entities, it lacks universal applicability. For example, the LDA topic model requires a high number of feature texts in the input data set, and the selection of the number of subjects will affect the numerical size of the final topic vector space of each entity. The event recommendation model based on TF-IDF can construct the spatial vector of each event according to the feature text of the event. However, if the feature text description of sample events is too little or different language description methods are adopted, the phenomenon of vector deviation in feature space will easily occur, which will make the events with similar types or properties have a long spatial distance in vector space and affect the final recommendation efficiency. Similarly, in the event recommendation modeling based on Word2vec sequence model, the insufficient sample size of users' entry records or uncertain entry types in the network will easily affect the generation of event space vectors. If a single user only participates in the same race for many years or professional runners participate in the race with too wide type or region and large span, it is easy to have the phenomenon that two marathon events with low correlation are close in vector space. Therefore, in order to reduce the influence of single algorithm and input samples on marathon event recommendation, the author considers combining the TF-IDF model with the Word2vec sequence model, so that they can fuse and calculate the event similarity matrix after the vectorization of events and propose a comprehensive event recommendation model and compare the performance difference between the comprehensive recommendation model and other single algorithm models under the test sample data, so as to improve the performance and accuracy of

event recommendation. At the same time, when the comprehensive model carries out the event vectorization step, it can directly call the event vector matrix generated by a single TF-IDF model and Word2vec sequence model, so as to save computing resources and improve the fault-tolerant space of the comprehensive model.

5. Conclusion

Taking the marathon event data in combustion network as an example, this paper discusses the algorithm selection and model construction of event recommendation model and determines the content-based recommendation technology and three key algorithms commonly used to achieve the goal of event recommendation model construction. On the basis of the above, this paper further studies the construction framework of event recommendation model under three key algorithms, focusing on the steps of event vectorization and event similarity calculation, and makes experimental comparison on the collected marathon event data set. From the results, the constructed event recommendation model has a good performance in the marathon event recommendation, which verifies the feasibility of content-based recommendation technology in the event information recommendation. This can effectively meet the needs of the existing people for marathon event recommendation and also provide technical support and theoretical basis for the research of building an effective Internet data processing mechanism and event recommendation model of sports events. This paper studies the Internet data of current sports events, which has the characteristics of huge quantity, various types, fragmentation, and low correlation, and builds a general event data collection framework and collection method. Taking the popular marathon event among the masses as an example, this paper discusses and analyzes the similar and unique characteristics of its network information. Through the collection and statistics of marathon data, the characteristics of data diversity are verified, which provides basic data support for the construction of event recommendation model.

In the future, it gives the possibility of integration and development of sports event information and related information technology from the perspective of technology, which provides a broader idea for sports informationization research and enriches the technical means of sports research.

Data Availability

The data used to support the findings of this study are available from the corresponding author upon request.

Conflicts of Interest

The authors declare that they have no known competing financial interests or personal relationships that could have appeared to influence the work reported in this paper.

References

[1] P. Haje, A. Arystanbaeva, Z. Oralbaeva, and Z. Kupenova, "The role and importance of accounting information system in the context of digitalization," *Asian Journal of Social Sciences and Humanities*, vol. 5, no. 1, pp. 64–73, 2019.

[2] M. McKee, M. C. I. van Schalkwyk, and D. Stuckler, "The second information revolution: digitalization brings opportunities and concerns for public health," *European Journal of Public Health*, vol. 29, Supplement 3, pp. 3–6, 2019.

[3] Y. Shrayberg and K. Y. Volkova, "Features of copyright transformation in the information environment in the age of digitalization," *Scientific and Technical Information Processing*, vol. 48, no. 1, pp. 30–37, 2021.

[4] T. Pistunova, V. Slabko, K. Averina, I. Romanchenko, O. Babakina, and O. Vidomenko, "Providing the minds of the out-of-the-box digitalization as the basic component of the information culture of the teacher," *Laplage Em Revista*, vol. 7, no. 2, pp. 691–696, 2021.

[5] T. Rudakova and M. Semikolenova, "Evolution of accounting information model under conditions of changing economic formations and digitalization of the economy," *Electronic Markets*, vol. 12, no. 1, pp. 108–115, 2018.

[6] A. Rafisovich Gapsalamov, E. Munirovich Akhmetshin, R. Rashatovich Sharipov, V. Lvovich Vasilev, and T. Nikolaevna Bochkareva, "Approaches to information security in educational processes in the context of digitalization," *TEM Journal*, vol. 9, pp. 708–715, 2020.

[7] J. Tuzii, "Healthcare information technology in Italy, critiques and suggestions for European digitalization," *Pharmaceuticals, Policy and Law*, vol. 19, no. 3-4, pp. 161–176, 2018.

[8] E. Hofmann, H. Sternberg, H. Chen, A. Pflaum, and G. Prockl, "Supply Chain Management and Industry 4.0: conducting research in the digital age," *International Journal of Physical Distribution & Logistics Management*, vol. 49, no. 10, pp. 945–955, 2019.

[9] I. G. Utomo and G. S. Darma, "Measuring optimization of digital military programs: an innovation of information and communication systems in Industrial Digitalization 4.0," *International Research Journal of Engineering, IT and Scientific Research*, vol. 6, no. 2, pp. 39–46, 2020.

[10] S. D. Karakozov and N. I. Ryzhova, "Information and education systems in the context of digitalization of education," *Journal of Siberian Federal University*, vol. 12, no. 9, pp. 1635–1647, 2019.

[11] S. A. Dyatlov, O. S. Lobanov, and W. B. Zhou, "The management of regional information space in the conditions of digital economy," *Economy of Region*, vol. 14, no. 4, pp. 1194–1206, 2018.

[12] S. Treber and G. Lanza, "Transparency in global production networks: improving disruption management by increased information exchange," *Procedia CIRP*, vol. 72, pp. 898–903, 2018.

[13] Z. Wei and L. Sun, "How to leverage manufacturing digitalization for green process innovation: an information processing perspective," *Industrial Management and Data Systems*, vol. 121, no. 5, pp. 1026–1044, 2021.

[14] A. V. Nesterov, "Digitalization of society and the economy: systematization of personal data in information systems," *Scientific and Technical Information Processing*, vol. 47, no. 2, pp. 133–138, 2020.

[15] J. Y. Baek, A. Jo, S. S. Yu, T. B. Kim, and H. J. Oh, "Development and application of evaluation factors for the digitalization of intangible cultural heritage record information resources," *Journal of Korean Society of Archives and Records Management*, vol. 19, no. 3, pp. 123–153, 2019.

[16] T. M. Lappi, K. Aaltonen, and J. Kujala, "Project governance and portfolio management in government digitalization," *Transforming Government: People, Process and Policy*, vol. 13, no. 2, pp. 159–196, 2019.

[17] S. N. Bobylev, O. Y. Chereshnya, M. Kulmala et al., "Indicators for digitalization of sustainable development goals in PEEX program," *Geography, Environment, Sustainability*, vol. 11, no. 1, pp. 145–156, 2018.

[18] M. L. Martín-Peña, J.-M. Sánchez-López, and E. Díaz-Garrido, "Servitization and digitalization in manufacturing: the influence on firm performance," *Journal of Business & Industrial Marketing*, vol. 35, no. 3, pp. 564–574, 2019.

[19] M. U. Hulla, M. Hammer, H. Karre, and C. Ramsauer, "A case study based digitalization training for learning factories," *Procedia Manufacturing*, vol. 31, pp. 169–174, 2019.

[20] J. Björkdahl, "Strategies for digitalization in manufacturing firms," *California Management Review*, vol. 62, no. 4, pp. 17–36, 2020.

[21] M. Stoyanova, "Good practices and recommendations for success in construction digitalization," *TEM Journal*, vol. 9, no. 1, pp. 42–47, 2020.

Hindawi
Journal of Sensors
Volume 2022, Article ID 9675342, 10 pages
https://doi.org/10.1155/2022/9675342

Research Article

Research on Online Education Curriculum Resources Sharing Based on 5G and Internet of Things

Yang Luo[1,2] **and Kyung Yee Kim**[2]

[1]*Zhejiang Ocean University, Zhoushan, Zhejiang 316022, China*
[2]*Department of Education, General Graduate School, The Catholic University of Korea, Bucheon-si, Gyeonggi-do, 14662, Republic of Korea*

Correspondence should be addressed to Yang Luo; z19095137014@zjou.edu.cn

Received 18 September 2021; Accepted 8 December 2021; Published 5 January 2022

Academic Editor: Gengxin Sun

Information technology has brought great changes to China's education. 5G technology provides a better guarantee for the sharing of curriculum resources, facing the extreme shortage of educational resources in China. The contradiction between limited educational resources and unlimited development needs of higher education has become increasingly prominent. How to effectively realize resource sharing among universities has become a problem that must be considered in the talent development of universities. In order to solve this problem, universities must improve the utilization rate of resources, maximize resource sharing, and establish a more perfect resource sharing mechanism under the background of 5G and Internet of Things. This paper analyzes the current situation of research at home and abroad, the current situation of resources development, and the application of online courses under the background of Internet of Things, thus constructing an overall framework of curriculum resource sharing mode. According to effective experiments, the offline curriculum education resource sharing and traditional resource sharing schemes in the background of 5G and Internet are compared, and the necessity and importance of applying 5G Internet of Things are verified.

1. Introduction

With the increasing scale of higher education, whether there is a complete resource sharing mechanism is an important factor to ensure that students can receive high-quality education. Faced with limited teaching resources and unlimited development needs, universities must reasonably improve the utilization rate of resources, make use of the convenience of 5G and Internet of Things technology, maximize resource sharing, and propose solutions to the problems existing in resource sharing. The literature [1] shows that there is an extreme shortage of educational resources in China at present. According to effective investigation, most students cannot get high-quality teaching resources. On the university campus, with the convenience of 5G and the Internet, they have gradually formed a mode of sharing curriculum education resources, which can share teaching resources, teachers' resources, and curriculum resources and advanced teaching facilities. According to the investigation of college students' access to resources in the literature [2], it is concluded that the simplest way for college students to obtain high-quality learning resources is through libraries and online search tools. According to a report, college students tend to share resources among classmates and friends. Instead of directly obtaining resources, on average, students share learning resources twice or more times a week. They will share their handwritten notes and textbooks, purchased extracurricular books, and use some social software that cannot be directly shared, such as sharing learning resources on the Internet. The literature [3] studies the main ways of sharing high-quality resources inside and outside universities. The conclusions are as follows: the first one is through learning textbooks, extracurricular books, online courses, and learning websites. The other is network resources. The characteristics and differences between them are obvious. The literature [4] investigated more than 600 teachers in order to investigate

the influence of shared resources on teaching and practice. Knowing how they use shared resources and how to choose shared resources, the survey results show that shared education can not only reduce costs but also bring greater flexibility to education. The literature [5] is to verify the timeliness of the application of blog and wiki resource sharing mode. Taking "Principles and Methods of Instructional Design," one of the universities awarded by the Ministry of Education of China, as the research object, based on the research and analysis of curriculum resources sharing at home and abroad, this paper establishes a general framework of curriculum resources sharing mode. The literature [6] studies the sharing of massive open online course resources and puts forward a solution to the fragmentation of network resources. The implementation process and application framework of linked data are introduced. The literature [7] puts forward a brand-new way of education, which is called Fujian-Taiwan cooperation in construction and education. How to make full use of their respective educational resources, limited integration and sharing between the two campuses is the key to improve the education quality of talent training programs. Organizational coordination institutions and teaching quality monitoring mechanisms have been established to ensure the substantive sharing of educational resources. With the prevalence of the Internet of Things and the explosive growth of various data flows, the Internet of Things may face the problem of resource shortage. Reference [8] puts forward a scheme to solve the shortage of resources sharing. Considering the different communication requirements of various sensors, a new function is designed to drive the learning process. The results show that this algorithm can achieve good network performance. The literature [9] studies the platform of "Construction and Sharing of Moral Education Curriculum Resources in Shanghai Universities." It is found that they are realized through "1+2" operation mode, cloud storage structure, user classification management, and resource sharing scoring mechanism, which has the characteristics of intelligent resource retrieval and real-time resource evaluation and has become one of the important research achievements of "the construction and sharing of moral education curriculum resources in colleges and universities." The literature [10] describes a knowledge based on a learning development system. Used in e-learning courseware design and e-learning resource management, the distributed e-learning system development environment is developed by building a system model. The literature [11] introduces intelligent algorithms in a distributed manner to coordinate the overall goals of cellular systems with the individual goals of Internet (LOT) devices. The utility function of Internet of Things users is designed, a new incentive mechanism is constructed, and a priority queue is set for continuous actions. The literature [12] proposes a distribution protocol using blockchain technology. In the Online education resources, there are unfair distribution of teaching resources and difficulties in retrieving resources. Facing the emergence of 5G and Internet of Things technology, teaching resources can be shared and utilized in a variety of ways. With the support of 5G technology and Internet of Things technology, this paper realizes the research framework of sharing teaching resources and puts forward the theoretical model of sharing resources. This paper compares the offline curriculum educational resource sharing and traditional resource sharing schemes under the background of 5G and Internet and greatly improves the performance of teaching resources.

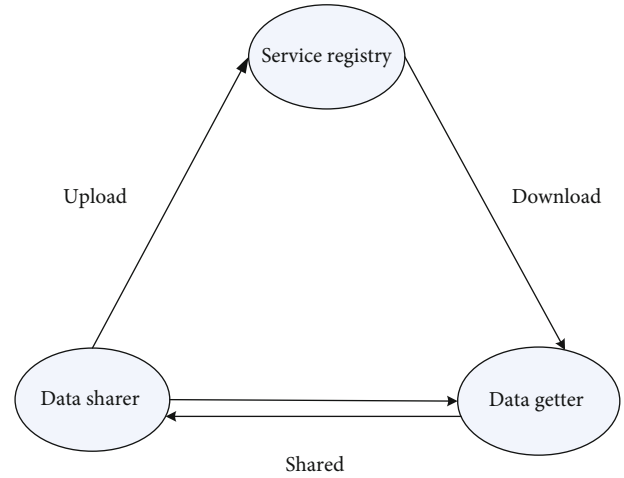

Figure 1: System model.

1.1. Research Background. With the development of science and technology and the prevalence of Internet technology, compared with traditional networks, 5G networks have the advantages of light coverage, low energy consumption, hot spots, and high capacity. It can spread data well. According to the current extremely scarce state of educational resources, some places do not have advanced teaching resources, so it is necessary to make use of the convenience of the Internet to share networks.

1.2. Significance of Research. The rise of the Internet of Things has also promoted the development of the education industry and launched a brand-new education model. The sharing of network resources has broken the traditional teaching concept, so that students are no longer limited by time and place. The sharing of network resources can not only save manpower and material resources but also quickly let more people receive high-quality educational resources.

1.3. Research Status at Home and Abroad. Effective storage and management of data is a problem that information resource sharing parties need to solve. A large number of scholars have done a lot of research on data encryption, storage, and management. Safe and efficient storage of shared data is the basis of safe sharing of resources, which can maximize the use of effective resources, maximize the value of data resources, and promote the development of society and production.

The prevalence of Internet of Things technology leads to the frequent sharing and exchange of data, and more and more people begin to pay attention to security and privacy issues. Access control is an important technology to ensure the data security of the Internet of Things. It is the control

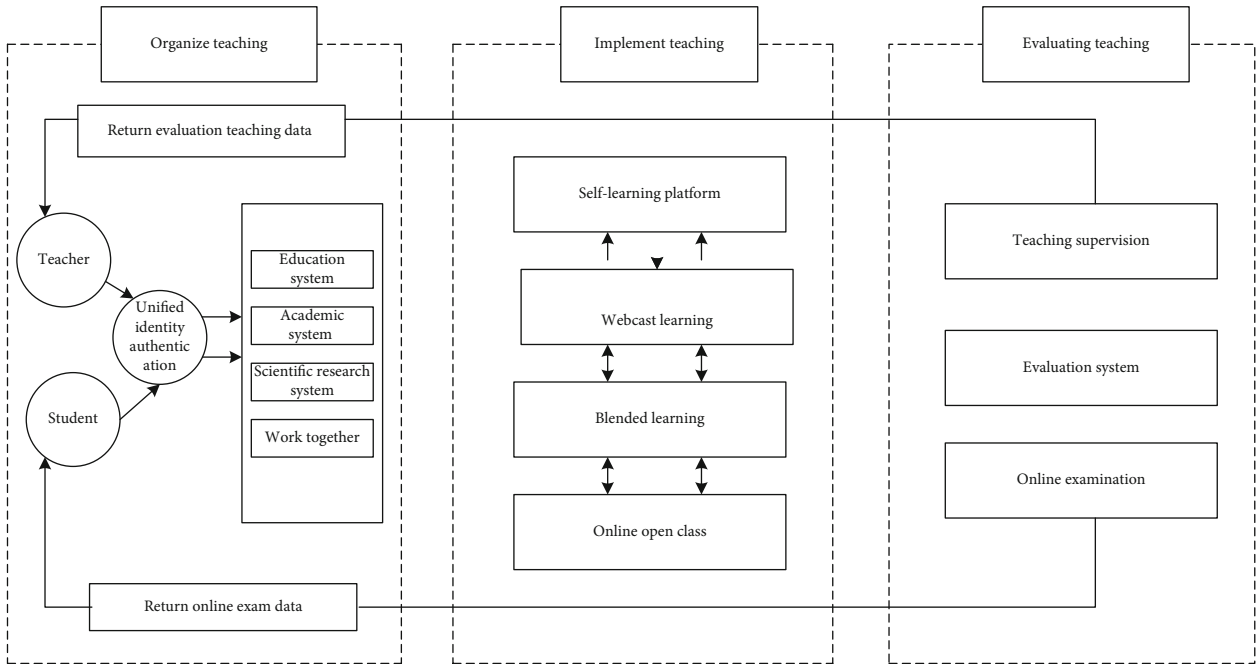

Figure 2: The educational information platform and realize resource.

of terminal access members to access shared data resources, which makes the access more secure, effective, and flexible.

1.4. Problems in Resource Sharing. In the process of resource sharing, there are also many security problems. The data processing ability of data exchange mode is poor, and the sharing security problem cannot be guaranteed. The following are the problems:

(1) Resource interconnection and interoperability in multidomain IoT scenarios. It is difficult to share data across domains. The Internet of Things is independent, and services are massively diversified and decentralized, resulting in difficult data sharing, poor service interaction, and system coordination and linkage

(2) The confidentiality and privacy of data have received a great threat. Therefore, how to ensure that information resources are not leaked and the security of shared resources has become a major challenge for Internet of Things resource sharing

1.5. Implementation Process of Curriculum Resources. We should make full use of the convenience brought by the Internet of Things to our lives. Although network teaching has been popularized, the traditional teaching methods are still deeply rooted, and some teachers do not use information technology very well. Therefore, teachers should fully feel the charm of the integration of information technology and classroom and lead teachers to recognize and utilize information teaching resources and take their essence. For some poor areas, school curriculum resources are extremely scarce. As a result, many students cannot enjoy high-quality educational resources, and then, the sharing of network resources is particularly important for them. Sharing resources is not only conducive to the reform of traditional teaching methods in some poor areas but also conducive to stimulating teachers' "want to teach" and students' "want to learn," which greatly stimulates students' interest in learning and makes the teaching quality reach a higher level.

1.6. Application of Network Sharing Courses under the Background of "Internet of Things"

1.6.1. Network Design and Development. When designing the curriculum content, we should first analyze the learning needs of different scholars and create multitype curriculum files. Before the course is officially used, it is necessary to try it out and modify and improve it according to the feedback and opinions of different auditioners.

1.6.2. Requirements of Online Courses for Teachers. In the multimedia teaching environment, teachers should not only have the basic knowledge and application skills of online courses but also use some advanced equipment. On the traditional basis, some easy-to-understand pictures and videos have been added to the network sharing course, but students cannot master knowledge without a teacher's explanation, so teachers should also have clear language expression ability.

2. Secure Resource Sharing Protocol for Ciphertext Attribute Authentication

2.1. System Model. The service registry is a data sharing platform. The shared data information is encrypted and stored in the server, and the data collector can download the data

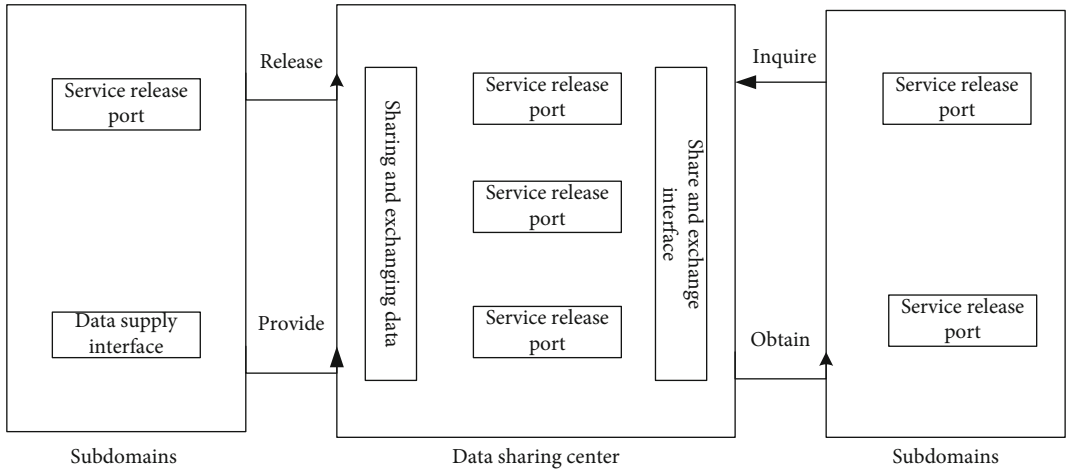

Figure 3: Data exchange framework.

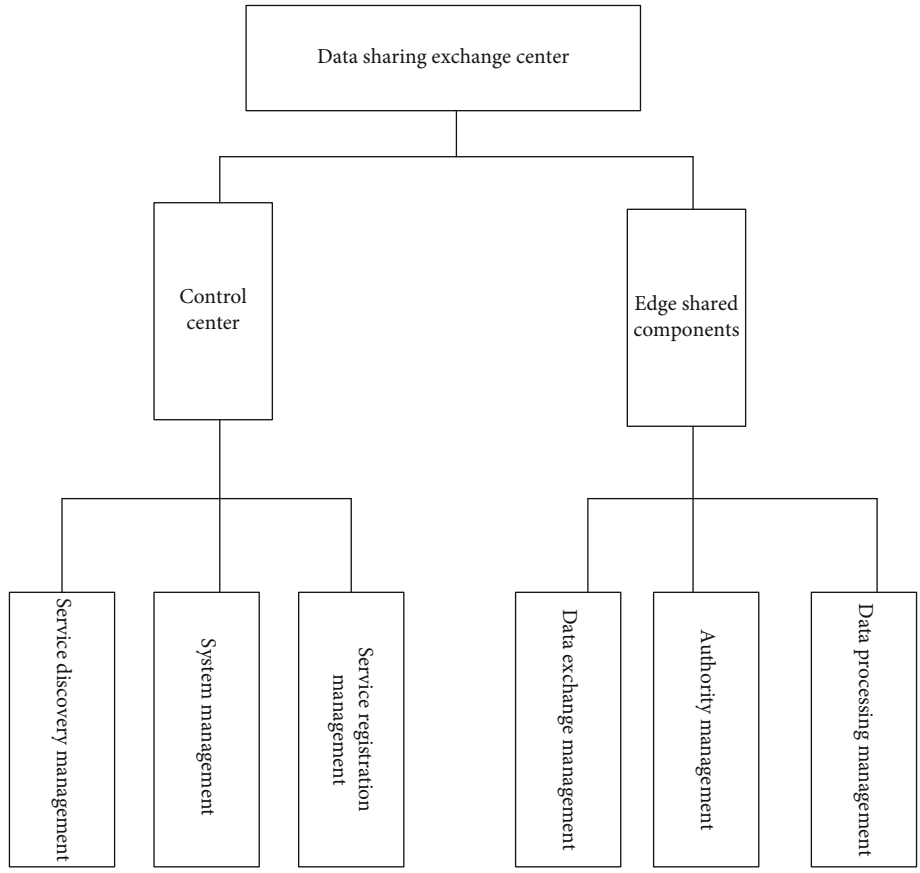

Figure 4: Data exchange center function module.

from the server. Data sharers can exchange identities with data recipients. Data sharers can share data with data collectors on the server, encrypt the provided data, and upload it to the server.

Data acquirers are members who are interested in the data on the server. They can download the corresponding data from the server. If they have data access rights, they can decrypt the ciphertext with the group key. The relationship between the three is shown in Figure 1.

In Figure 1, the data sharer uploads course resources to the Service Registry side, and the data getter downloads resources from the Service Registry side, thus realizing the sharing of teaching resources between the data sharer and the data getter.

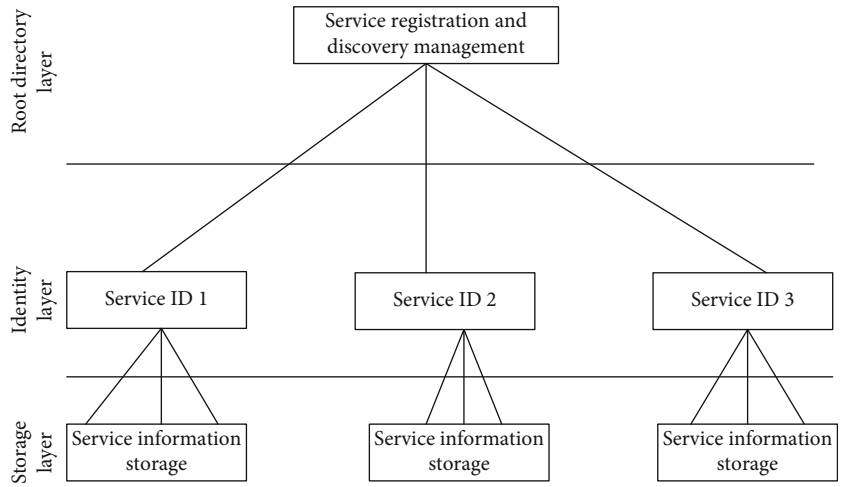

Figure 5: Service information architecture.

2.1.1. Chinese Remainder Theorem

Definition 1. In Chinese remainder theorem, suppose there are k pairwise positive integers $p_1, p_2, \cdots, p_k$ $(K \geq 2)$. Let $P = p_1 p_2, \cdots, p_k = p_1 P_1 = p_2 P_2 = \cdots = p_k P_k$; P_i is shown in

$$P_i = \frac{p}{p_i}(1 \leq i \leq k), \quad p_i > y. \tag{1}$$

The following equations are satisfied:

$$\begin{cases} x \equiv y_1 (\bmod p_1), \\ x \equiv y_2 (\bmod p_2), \\ \cdots, \\ x \equiv y_k (\bmod p_k). \end{cases} \tag{2}$$

There is a unique solution:

$$x \equiv y_1 p_1 p_1^i + y_2 p_2 p_2^i + \cdots + y_k p_k p_k^i (\bmod p) = \left(\sum_{i=1}^{K} y_t \cdot p_t^i \cdot p_t \right) \bmod p, \tag{3}$$

where $p_t^i p_t (\bmod p_t) = 1, \quad i = 1, 2. \cdots, n.$

2.1.2. Key Calculation for Shared Resources. According to the Chinese remainder theorem, the following equations are calculated:

$$\begin{cases} x_i \equiv c_{t,1} (\bmod p_2), \\ x_i \equiv T_{t,2} (\bmod p_2), \\ \cdots, \\ x_i \equiv T_{t,2} (\bmod p_2). \end{cases} \tag{4}$$

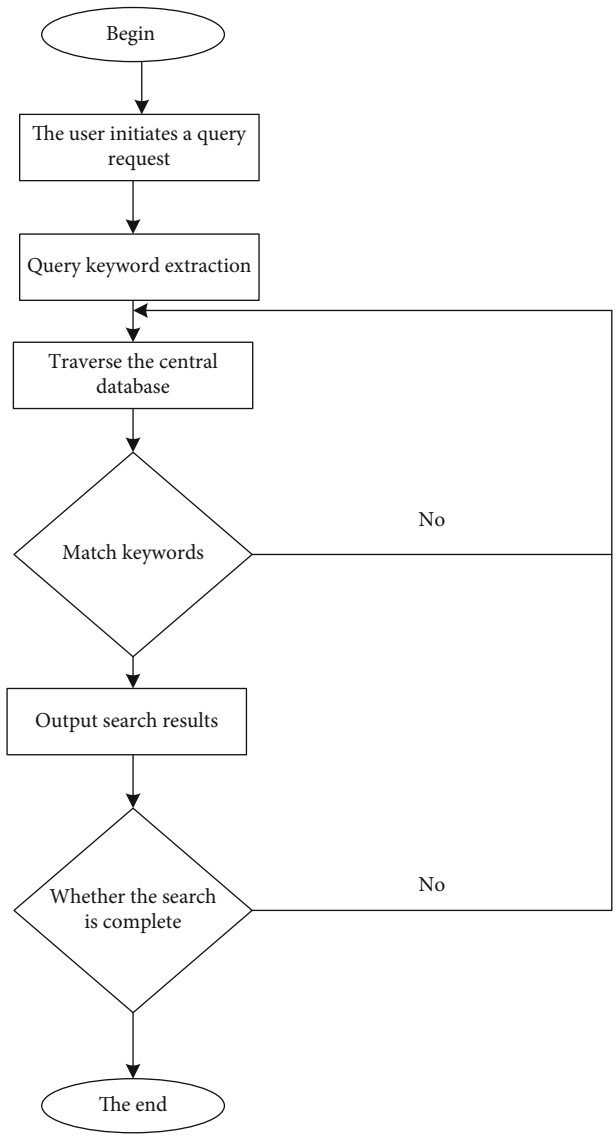

Figure 6: Resource query flow chart.

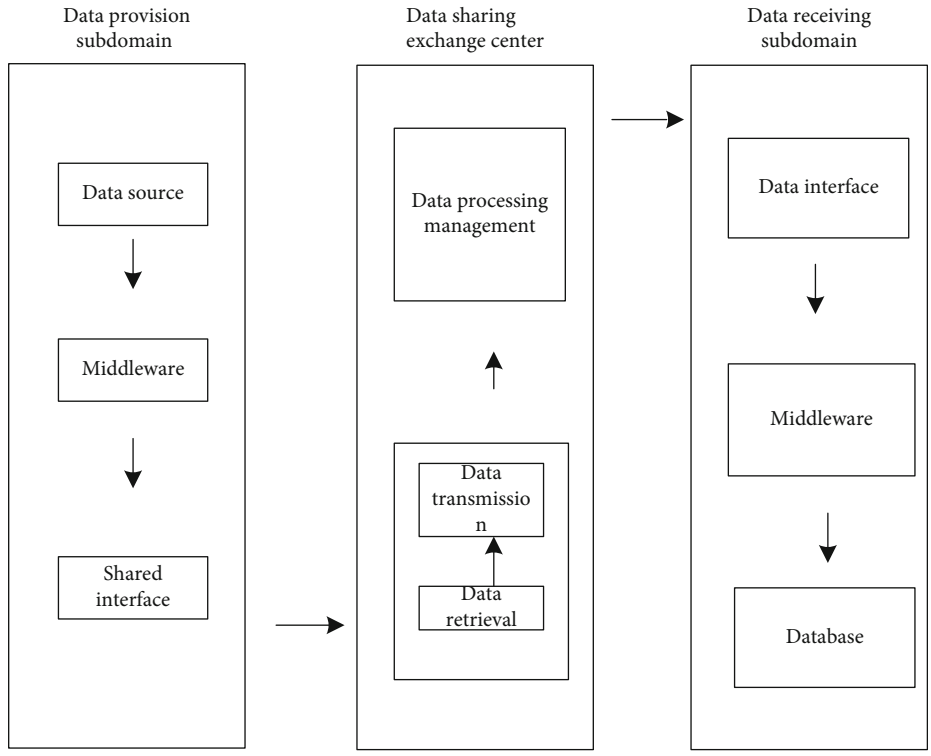

Figure 7: Data security architecture.

And get a unique solution: $x_i = (\sum_{v-1}^{t} \delta_{t,v} \bullet y_v \bullet (p/p_v)) \bmod P$ (in order to facilitate the solution, $T_{t,v} = \delta_{t,v}$, $v = 2, 3, \cdots, t$).

Among them,

$$\mathbf{P} = P_1 \times P_2 \times \cdots \times P_t = \prod_{v-1}^{t} p_v, \quad y_v \bullet \frac{p}{p_v} \bmod P_v = 1. \tag{5}$$

Results obtained

$$\text{Group}_{\text{key}} = x_i = \left(\sum_{v-1}^{t} \delta_{t,v} \bullet y_v \bullet \frac{p}{p_v} \right) \bmod P. \tag{6}$$

It can be used to encrypt the information exchange between shared resources and terminal devices to ensure the security of information exchange.

2.1.3. Encryption and Storage of Shared Resources. After the terminal members in the shared resources complete the successful registration steps, they can selectively encrypt and store the uploaded resources.

2.1.4. Download and Access to Shared Resources. Each user who logs into the system searches for corresponding resources on the platform through keyword search and related description content. If the user needs to access the shared resources, he needs to send information to the platform, download the corresponding ciphertext resources according to the ciphertext link, and then select the corresponding authority to calculate the decryption key:

$$x_i = \left(\sum_{v-1}^{t} \delta_{t,v} \bullet y_v \bullet \frac{p}{p_v} \right) \bmod P = x_i = \text{group}_{\text{key}}.. \tag{7}$$

According $\text{tom} = c_{t,2m} \oplus H_2(x_3) \quad c_{t,2m} \oplus H_2(x_3)$, get the resources of civilization.

2.2. Types of Learning Platform for Curriculum Resources. With the advent of the information age, in order to better organize platform resources, colleges and universities have successively built educational administration management systems, online learning course centers, and so on. The main categories are as follows:

(1) Students' autonomous learning: students can freely answer the discussion questions raised by teachers on the platform, and teachers can also upload exercises. It makes up for the defect that offline teachers have less communication with students and can also test students' autonomous learning ability [13, 14].

(2) Live webcast learning: on the basis of traditional classroom, live webcast learning has more intelligent functions, such as sign-in, answering first, and class inspection. During the epidemic period, live webcasts were held at home. After the outbreak, colleges and universities also maintained a live learning

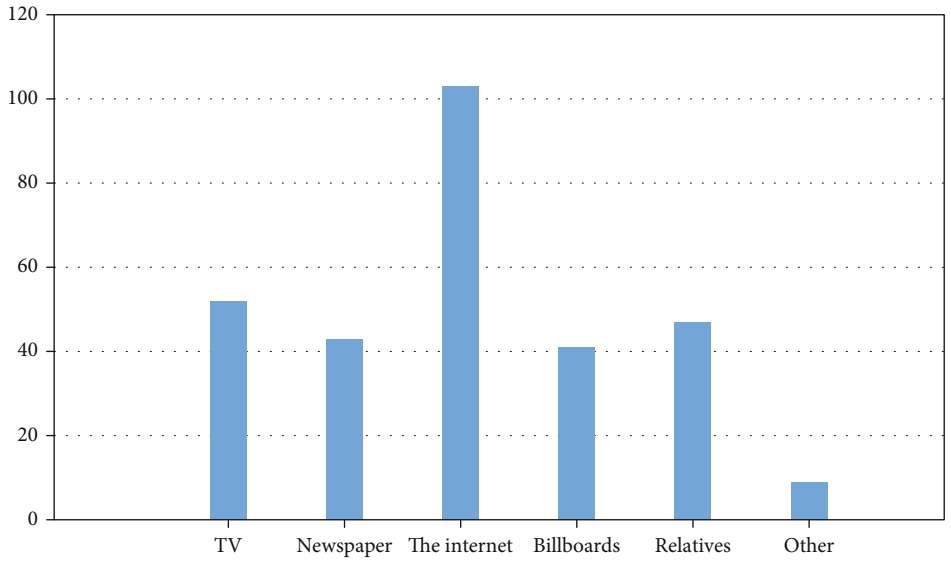

Figure 8: Understanding ways of information resource sharing construction.

platform. This is of great help to students' final review. Students can watch live playback and consolidate their knowledge.

(3) Blended learning: in blended learning platform, representative platforms are "recording and broadcasting classroom" and "smart classroom," which have the functions of recording, playback, interaction, and group discussion. Give the teaching environment intelligent, integrated teaching management and diversified teaching scenes and even introduce the Internet of Things and big data technology to open up all intelligent teaching platforms.

(4) Online open class: students can choose courses according to their own hobbies, which are not limited by time and place. As long as there is a network, they can learn. In some places, the resources of famous teachers are scarce. We can learn the courses of famous teachers through the Internet, so that more people can come into contact with the classrooms of famous teachers and share resources to the maximum extent.

(5) Calculator-assisted instruction: because the platform type has a wide audience and the needs of various universities are similar, it has become the mainstream trend to open up the educational information platform and realize resource sharing. The flowchart is shown in Figure 2.

2.3. Resource Accumulation. Traditional teaching resources basically come from teaching materials, extracurricular books, etc. With the rise of multimedia teaching, more resources come from multimedia courseware. In the information age, network resources have gradually occupied the mainstream trend. According to the learning platform, the

Table 1: Comparison table of results of different schemes.

Statistics	5G and Internet of Things	Traditional method	Other methods
Mean	269 s	304 s	325 s
Median	25.24 s	37.69 s	42.58 s
Mode	23.87 s	39.65 s	43.65 s
Standard deviation	12.65 s	18.73 s	19.65 s
Maximum	13.95 s	17.67 s	19.97 s
Minimum	59.57 s	92.67 s	97.19 s

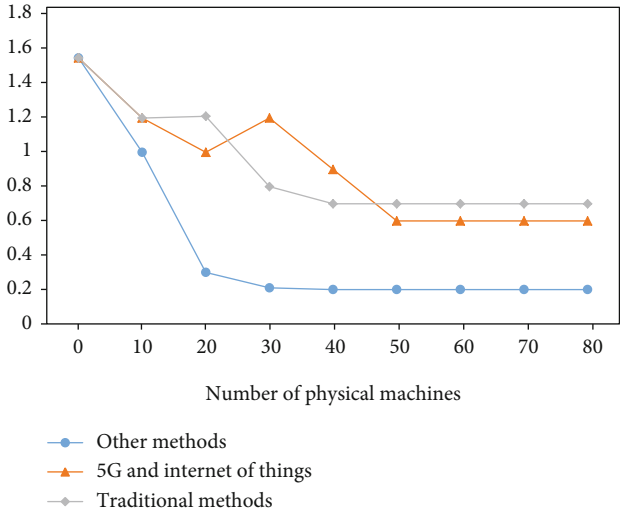

Figure 9: Evolutionary process.

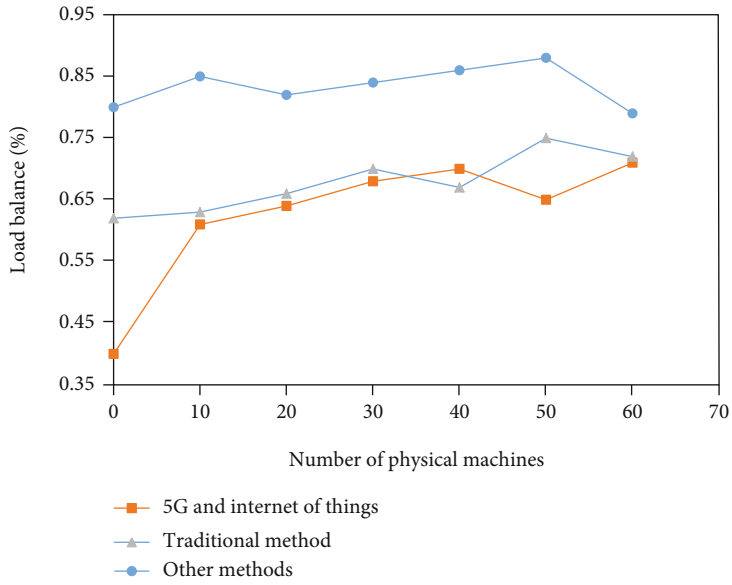

Figure 10: Resource sharing degree of different methods.

accumulated resources mainly include PPT, excellent massive open online course, question bank, and experimental material training.

(1) PPT: it is mainly written around the curriculum and helps students understand by means of some pictures and micro videos, which is beneficial to stimulate students' learning enthusiasm.

(2) Training of experimental teaching materials: it mainly focuses on the construction of experimental centers in schools and obtains medical experimental operation resources based on visual intelligent laboratories.

In the face of numerous platform resources, we should do a good job of sorting out and complete a certain amount of resource reserves according to the advantages of the Internet.

2.4. Architecture Design of Internet of Things Data Exchange System. The data exchange framework is show in Figure 3.

As can be seen from Figure 3, data sharing center is more important among several modules. Subdomains are divided into data providing and data releasing ports. Subdomains can provide teaching resources to the data sharing center and can also obtain resources to exchange data and interface with the data sharing center. Data sharing center is mainly used to provide data service and service interface, and the three modules are used to realize data exchange and sharing.

The core is the data exchange center, which plays the role of service query, service release, and data conversion. It consists of administrative center and edge shared components, as shown in Figure 4.

2.4.1. Management Center. Manage the security management of registering, publishing, and maintaining data exchange services, as shown in Figure 5.

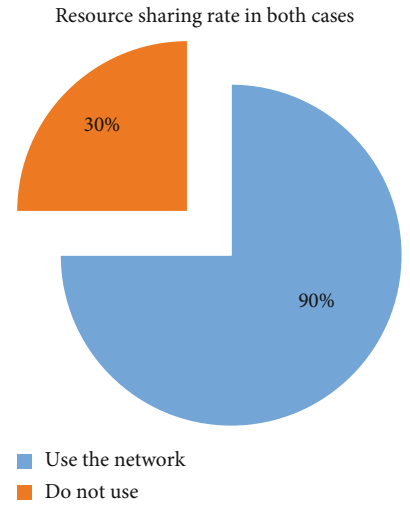

Figure 11: Statistical table of resource sharing rate.

When a user initiates a query request, keywords are usually used to search, and the operation mechanism adopts recursive mode. The flow chart is shown in Figure 6.

2.4.2. Edge Shared Components. Edge sharing component consists of three parts: data exchange management, authority management, and data processing management. Data exchange management has the functions of data retrieval and data transmission, and the data processing management module has the functions of extracting and transforming the data obtained by the management module, so as to realize the sharing and exchange of diversified data. Privilege management module is the core to ensure data security. The architecture diagram is shown in Figure 7.

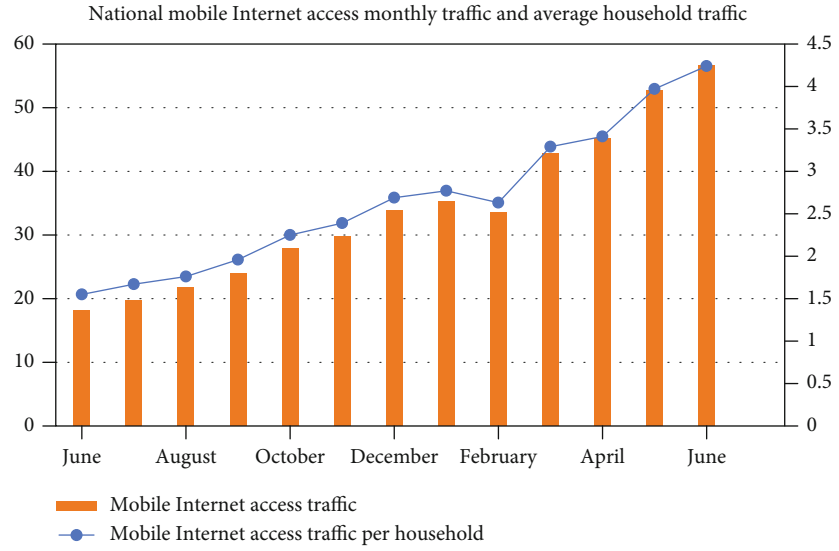

Figure 12: Traffic statistics.

3. Experimental Simulation

3.1. Data Budgeting. In order to understand the use of the Internet of Things, we conducted a questionnaire survey on the members of Hunan Literature Information Resources Co-construction and Sharing Collaboration Network. Experimental results show that compared with traditional methods, most people know new resource information through the Internet of Things. A small number of people learn about it through newspapers, relatives and friends, publicity columns, or other means. The statistics are shown in the following table. Statistics are shown in Figure 8.

3.1.1. Experimental Results and Analysis. We conducted a simulation experiment to compare the speed and universality of resource sharing in the context of 5G and the Internet of Things. The specific comparison results are shown in Table 1.

Compared with other methods, the results are shown in Figures 9 and 10.

3.2. Necessary Experimental Results. Comparing the implementation effect after adopting 5G and Internet of Things with other schemes, we designed an experiment to compare the degree of resource sharing without the background of Internet of Things with the prevalence of resources under the background of 5G and Internet of Things and obtained the following data, as shown in Figures 11 and 12.

3.3. Evaluation Results. According to the survey results, under the background of 5G and Internet of Things, information dissemination is wider, faster, and more accurate. The Internet of Things has become a mainstream trend. Of course, the requirements for 5G network are higher, so we should constantly optimize the network carrier and make sufficient preparations for the service bearing of 5G and Internet of Things.

4. Conclusion

We rationally apply the Internet of Things, which has brought great changes to the information season and maximized the sharing rate of information resources. Finally, on the basis of absorbing the theoretical research results and practical experience of foreign resource sharing, according to China's specific national conditions, proceeding from reality, this paper puts forward some new ideas on the construction of literature resources sharing network in China and especially puts forward some constructive views and suggestions on how to choose the breakthrough point of the construction of resources sharing network in China and how to establish a self-developing network operation mechanism, the guiding ideology of the construction of resources sharing network in China, and the construction of network system.

Data Availability

The experimental data used to support the findings of this study are available from the corresponding author upon request.

Conflicts of Interest

The authors declared that they have no conflicts of interest regarding this work.

References

[1] F. Wang, "College Park development and sharing of educational resources exploration mode," *Electronic Test*, vol. 14, pp. 146-147, 2013.

[2] T. Judd and K. Elliott, "Methods and frequency of sharing of learning resources by medical students," *British Journal of Educational Technology*, vol. 48, no. 6, pp. 1345–1356, 2017.

[3] Z. Li and L. Qin, "Comparison and analysis on sharing ways of high-quality curriculum resources based on modern

educational technology," *Experimental Technology and Management*, vol. 32, no. 3, pp. 25–29, 2015.

[4] B. de los Arcos, R. Farrow, R. Pitt, M. Weller, and P. McAndrew, "Adapting the curriculum: how K-12 teachers perceive the role of open educational resources," *Journal of Online Learning Research*, vol. 2, pp. 1–9, 2016.

[5] Y. Xie, J. Bai, G. Li, and R. Yin, "Research and application on Web2.0-based sharing modes of curriculum resources," in *International Conference on Hybrid Learning and Continuing Education*, pp. 30–39, 2014.

[6] X. U. Yan-Dan and Q. J. Zhang, "Research on the linked data in the sharing of MOOC educational resources based on Drupal," *Journal of Xichang College*, vol. 29, no. 4, pp. 46–49, 2015.

[7] J. H. Zheng and L. Huang, "Integration and sharing of high quality educational resources in the colleges running by Fujian and Taiwan," *Higher Education Forum*, vol. 7, pp. 34–36, 2013.

[8] Z. Shi, X. Xie, M. Kadoch, and M. Cheriet, "A spectrum resource sharing algorithm for IoT networks based on reinforcement learning," in *2020 International Wireless Communications and Mobile Computing (IWCMC)*, pp. 1019–1024, Limassol, Cyprus, 2020.

[9] S. Johnson, J. Gao, M. Bian, D. Hsu, J. Yuan, and Y. Zhou, "Informatization construction of moral education curriculum resources in schools and universities," in *2014 IEEE Workshop on Electronics, Computer and Applications*, pp. 594–601, Ottawa, ON, 2014.

[10] T. Tanigawa and T. Fuji, "The methodology for reuse of E-learning resources," *Proceedings of E-learn 2002–world conference on E-learning in corporate, government, healthcare, and higher education. Montreal, Canada: Association for the Advancement of computing in education (AACE)*, 2002, pp. 305–310, San Diego, CA, 2002.

[11] Y. Li, Z. Li, J. Liu, and R. Zhou, "Resources sharing in 5G networks: learning-enabled incentives and coalitional games," *IEEE Systems Journal*, vol. 15, no. 1, pp. 226–237, 2021.

[12] B. Hamdaoui, M. Alkalbani, A. Rayes, and N. Zorba, "IoT-Share: a blockchain-enabled IoT resource sharing on-demand protocol for Smart City situation-awareness applications," *IEEE Internet of Things Journal*, vol. 7, no. 10, pp. 10548–10561, 2020.

[13] S. Bin and G. Sun, "Matrix factorization recommendation algorithm based on multiple social relationships," *Mathematical Problems in Engineering*, vol. 2021, 8 pages, 2021.

[14] G. Sun and S. Bin, "Research on public opinion propagation model in social network based on blockchain," *CMC-Computers, Materials & Continua*, vol. 60, no. 3, pp. 1015–1027, 2019.

Hindawi
Journal of Sensors
Volume 2021, Article ID 5946228, 12 pages
https://doi.org/10.1155/2021/5946228

Research Article

Design of an Automatic English Pronunciation Error Correction System Based on Radio Magnetic Pronunciation Recording Devices

Zhang Shufang

Anyang Vocational and Technical College, Anyang Henan 455000, China

Correspondence should be addressed to Zhang Shufang; 2011020103@st.btbu.edu.cn

Received 8 November 2021; Accepted 3 December 2021; Published 27 December 2021

Academic Editor: Gengxin Sun

In this paper, a system for automatic detection and correction of mispronunciation of native Chinese learners of English by speech recognition technology is designed with the help of radiomagnetic pronunciation recording devices and computer-aided software. This paper extends the standard pronunciation dictionary by predicting the phoneme confusion rules in the language learner's pronunciation that may lead to mispronunciation and generates an extended pronunciation dictionary containing the standard pronunciation of each word and the possible mispronunciation variations, and automatic speech recognition uses the extended pronunciation dictionary to detect and diagnose the learner's mispronunciation of phonemes and provides real-time feedback. It is generated by systematic crosslinguistic phonological comparative analysis of the differences in phoneme pronunciation with each other, and a data-driven approach is used to do automatic phoneme recognition of learner speech and analyze the mapping relationship between the resulting mispronunciation and the corresponding standard pronunciation to automatically generate additional phoneme confusion rules. In this paper, we investigate various aspects of several issues related to the automatic correction of English pronunciation errors based on radiomagnetic pronunciation recording devices; design the general block diagram of the system, etc.; and discuss some key techniques and issues, including endpoint detection, feature extraction, and the system's study of pronunciation standard algorithms, analyzing their respective characteristics. Finally, we design and implement a model of an automatic English pronunciation error correction system based on a radiomagnetic pronunciation recording device. Based on the characteristics of English pronunciation, the correction algorithm implemented in this system uses the similarity and pronunciation duration ratings based on the log posterior probability, which combines the scores of both, and standardizes this system scoring through linear mapping. This system can achieve the purpose of automatic recognition of English mispronunciation correction and, at the same time, improve the user's spoken English pronunciation to a certain extent.

1. Introduction

Language is the most natural tool for human communication, and the automatic processing of speech-language information is an important research area in information science. Among them, the more important research directions include large-scale continuous speech recognition natural language understanding, speech synthesis, and machine translation [1]. Human-machine speech interaction is a human-machine dialogue technology based on speech recognition, natural language understanding, and speech synthesis. Speech synthesis is one of the cores of human-computer interaction. It is involved in many disciplines, such as acoustics and natural language processing, artificial intelligence, and signal processing. In recent years, speech information processing has developed more rapidly, and spoken pronunciation detection is one of the important research directions. Speech interaction is the most direct, natural, and effective way people use to convey information, and with the rapid development of mobile phones and other intelligent terminal products in recent years, new human-computer interaction has become a hot spot in scientific research of computers, linguistics, and communications [2]. Human-computer speech interaction is a human-

computer dialogue technology based on speech recognition, natural language understanding, and speech synthesis. Speech synthesis is one of the cores of human-computer interaction, which is involved in several disciplines, such as acoustics, natural language processing, artificial intelligence, and signal processing. A lot of English learning is carried out in the "vacuum" of the "nonlinguistic environment." Once it enters the communicative state, it is more susceptible to the inevitable pronunciation defects or poor pronunciation in the real context. Its purpose is to enable computers or other hardware devices to make natural sounds like people. In this environment, to make mobile phones, computers, and other intelligent terminal devices be completely like people that can "speak" and "listen," can understand the natural language of humans, and can get some feedback or according to the instructions to complete the corresponding operation is one of the goals of the current scientific artificial intelligence field [3]. However, for the current TTS (Text-To-Speech) system, it is the main research direction of many enterprises and universities to make it produce clear, understandable, fluent, and natural voices in different scenes to better meet the personalized needs of users.

Language learning generally includes four areas: listening, speaking, reading, and writing, each of which has its method of learning. For example, listening comprehension skills can be improved by listening to various foreign language multimedia resources, including news, movies, and audiobooks. We can also regularly read foreign language newspapers, professional papers, world famous books, and other textual resources to practice reading skills and to obtain information in other languages [4]. Many people tend to be fluent in reading and writing, but their oral English is poor, which further affects the improvement of listening. English writing can be practiced through journaling, translating English resources, etc. There is no good way to improve the ability to "speak"; although it can be practiced in "English corner" or similar places, it is very limited. In addition, a lot of English learning is done in the "vacuum" of a "nonlinguistic environment," and once you enter the real communication situation, you are more likely to be affected by the inevitable pronunciation defects or inappropriate pronunciation factors in the real context. Because "speaking" is an interactive process, it cannot be trained alone but must be interacted with. For these reasons, "speaking" often becomes a bottleneck for language learners.

Computers have brought great convenience to humans due to their powerful information processing, computing, and storage capabilities. Speech recognition technology has been developed over the years and is now starting to gradually come into different applications. Research on language learning and spoken pronunciation detection has received increased attention in recent years, and the application of speech recognition in computer-assisted language learning has become an important research direction. Especially, audio as an information medium plays an important role in the process of human-computer interaction [5]. Therefore, the study of English pronunciation monitoring and automatic correction is not only of theoretical significance but also of great help to the language learning of nonnative learners; through the detection of learners' pronunciation in language learning, it can help learners understand their pronunciation accuracy and improve their speaking level [6].

2. Related Works

The purpose of oral pronunciation testing is to provide a mechanism for learning foreign languages such as English to automatically correct country pronunciation. Many people tend to read and write fluently but speak poorly, which affects listening even more [7]. The key to improving listening and speaking skills is to practice speaking and to receive guidance and correction from English-speaking teachers, but the lack and high cost of English-speaking teachers in China leave many learners without opportunities to practice and improve, and often, after eleven years of study, they are still unable to communicate with foreigners, neither speaking nor understanding. Make use of the error rules in the learner's pronunciation and integrate these rules into the speech recognition to detect and diagnose the possible error categories in the learner's phoneme pronunciation. Given the importance of oral practice, the main means of practice for learners is to play tapes and other recording media repeatedly, and the advent of the repeater has introduced electronic English learning products to the market. The development of teaching aids using electronic and computer technology has become a key step in the transition from basic research to products, and many learning machines have received strong support and input from national education and science and technology departments [8].

The main development of pronunciation error detection as part of the CAPT system came after the 1990s. In 1996, a pronunciation scoring algorithm for speech-interactive language learning systems was proposed that combined Hidden Markov Similarity, sentence length, segment length, and segment classification to calculate scores. The important difference between this algorithm and earlier algorithms is that the content of the sentence or phrase to be read aloud by the person to be tested does not have to be specified, making it more flexible to use. The recognition system implemented the algorithm and evaluated French pronunciation in native English speakers, and experimental results showed that the duration score for the same segment was an important indicator of pronunciation fluency and was robust to background noise. In 1997, the pronunciation evaluation algorithm was improved by scoring multiple sentences from a given pronouncer and then averaging them to obtain a higher-level score, while combining different machine scores to obtain a higher correlation coefficient [9]. Experiments show that the improved algorithm requires less speech to be tested on sentence-level scores, increasing the human-machine score correlation coefficient from 0.5 to 0.88, and by combining different machine scores, increasing the human-machine score correlation coefficient by 7%. In 2000, by calculating the confidence (CM) measures derived from the Hidden Markov Model- (HMM-) based ASR system for phoneme measures (CM) for phoneme-level articulation error detection. In 2003, the articulation error

detection method was improved based on the GOP algorithm. The improved method shows that the phoneme detection recognizer can determine the correct pronunciation rate, and the lower the CM, the higher the probability of incorrect pronunciation of the speech [10]. The advantage of these CMs is that they are readily available through the ASR system; however, when analyzing individual voices, the correlation between CMs and human judgments is low over a relatively long range of speech sounds. At the phoneme level, it was found that the lack of features of CM resulted in a low correlation between assessment levels and human judgments and that these features were computed algorithmically using similar feature sets of speech sounds and were not suitable for performing pronunciation error detection. In 2004, when studying pronunciation errors in Dutch as a second language, it was found that learners of Dutch had pronunciation problems in terms of vowel length, a problem that suggests that pronunciation errors resulting from pronouncing phonemes different from the expected phonemes can cause deviations in word comprehension [11].

Since the study of automatic pronunciation detection is closely related to the study of linguistics, phonology, etc., the problems faced by different languages when learning another language such as English are different and the solutions must be targeted. In general, one of the mechanisms of oral pronunciation testing is the assessment of phonological accuracy, which has always been an important aspect of research. In early pronunciation tests, an acoustic model was created based on the standard phonetic pronunciation of native speakers, and then, the pronunciation of learners from nonnative speakers was tested [12]. Some studies have added expert speech from nonnative countries to the training data as well to improve judgments of the difficulty of pronunciation of phonemes. Many studies have only evaluated the pronunciation of limited words with limited phonemes, and less research has been conducted on the detection of continuous natural speech with larger vocabularies. We believe that it is difficult to obtain standard phoneme pronunciation scores by merely applying forcing regularization. Since the native Chinese learners of English are too far from the standard English, pronunciation recognition may fail to obtain valid phoneme pronunciation accuracy. Some studies use the output of speech recognition and regularized acoustic model scores as phoneme pronunciation scores, which are useful to reasonably assess the accuracy of phoneme pronunciation [13].

3. Design of an Automatic English Pronunciation Error Correction System Based on Radiomagnetic Pronunciation Recording Devices

3.1. Automatic Calibration System Model Design. In this paper, we propose a kind of automatic system for detecting incorrect phoneme pronunciation for continuously spoken pronunciation for English learners. The core idea of the method is to use the error patterns existing in learners' pronunciation to detect and diagnose the possible error categories in learners' phoneme pronunciation by incorporating these patterns into speech recognition. Three main problems are faced in the methodology. From the phoneme pronunciation, we summarize the typical pronunciation error rules through cross-language phonological comparison and analysis. This law is the form of confusion rules from phoneme to phoneme to predict the learner's possible wrong phoneme pronunciation.

(a) How to summarize the error pattern. It is very difficult and unnecessary to make a summary analysis of each situation one by one. The method of this paper is to summarize the cases of errors that are common in learners' pronunciation and are regular and extended. The confusion rules are represented in the form of confusion rules

(b) How to design a speech recognition system where error laws are effectively combined with speech recognition as a priori knowledge to detect and diagnose mispronunciation. Mispronunciation detection is mainly oriented to users who are nonnative speakers, and recognition requires accuracy down to the phoneme, which places high demands on the system design. The accuracy of speech recognition will be improved if error laws are integrated into speech recognition to reduce the burden on the recognizer and do recognition in a recognition range with a priori knowledge

(c) How to provide corrective feedback information. This is a basic human-computer interaction problem intelligent problem of the wrong pronunciation detection system and an important part of the system. More reasonable and intuitive feedback can make learners understand more quickly and correct pronunciation errors and achieve the purpose of computer-aided pronunciation training

For the different functional structures and approaches of the three problems, this chapter divides the system into three modules extended pronunciation dictionary generation module, speech recognition module, pronunciation detection, and feedback module; the overall system structure design is shown in Figure 1.

The main pronunciation problems faced by language learners are the inaccurate pronunciation of phonemes, inappropriate stress and intonation, and nonfluent and continuous pronunciation. The causes are mainly categorized into the following three types: (1) differences in linguistic, phonological, and phonetic pronunciation structures between learners' native language and the target language and differences in the functioning force of the articulatory organs; (2) the learner's misunderstanding of linguistics, phonology, and phonemes, not knowing the continuum, or misunderstanding the rules of letter pronunciation. For the first two reasons, based on the theory of language transfer, this paper systematically analyzes the characteristics of English mispronunciation of native Chinese speakers from linguistics, phonology, and phonemic and finds that the errors are mainly concentrated in those phoneme pronunciations that are present but not in Chinese, and learners habitually substitute the pronunciation

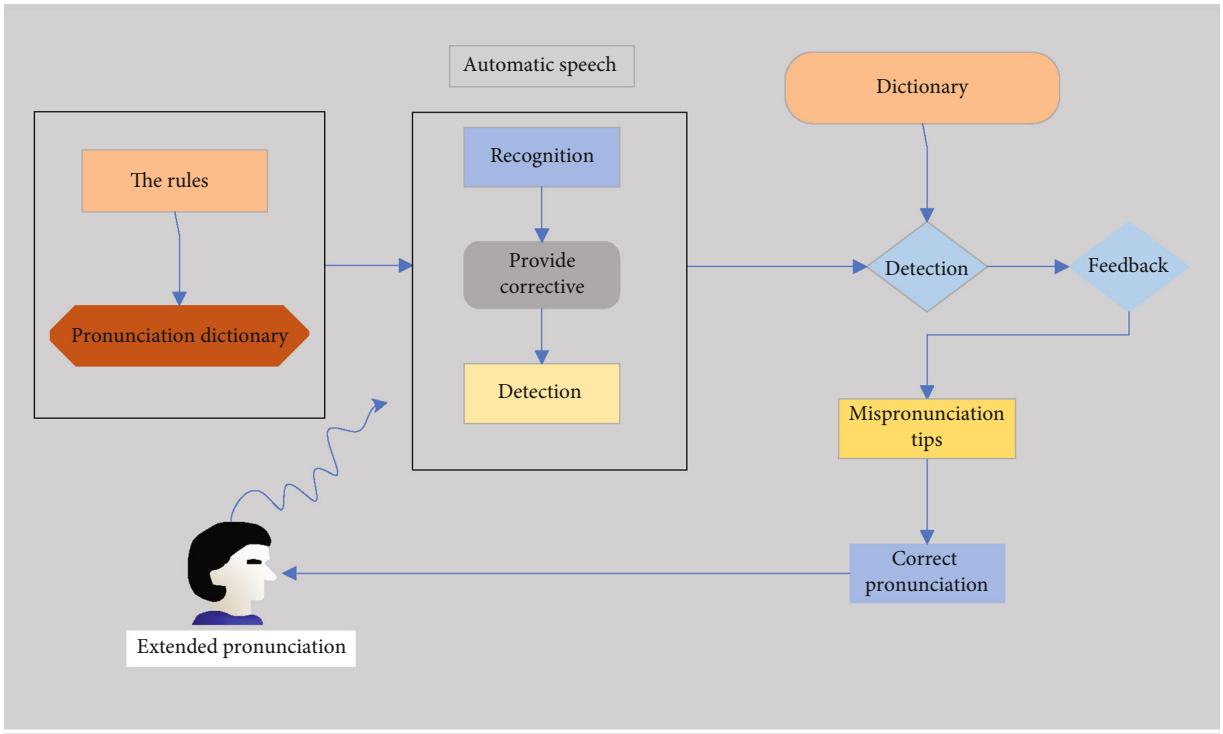

Figure 1: Overall system structure design diagram.

with the phoneme pronunciation of the native phoneme that is similar to this phoneme in linguistics and phonology, which leads to mispronunciation [14]. After the human voice is emitted from the lips, the high-frequency part will be attenuated, so that the energy of the low-frequency part is always higher than the energy of the high-frequency part, which results in a smaller spectral value of the high-frequency part, which is not convenient for analysis and processing. Preemphasis is to let the voice pass through a high-pass filter to enhance the high-frequency part so that the high- and low-frequency ranges are equal. Therefore, we generalize the typical pronunciation error patterns from phoneme pronunciation through crosslinguistic phonological comparative analysis of the differences, and this pattern is a form of phoneme-to-phoneme confusion rule to predict the possible wrong phoneme pronunciation of learners. While the third reason contains too many personal factors of the learner, Chimin's difficult mountain knowledge to predict, therefore, this paper adopts a data-driven approach that does not rely on a priori knowledge, using the identification of the learner's actual pronunciation errors to predict the possible wrong pronunciation by performing phoneme-based automatic speech-to-phoneme recognition on the learner's speech and analyzing the recognition results between the resulting wrong pronunciation phonemes and the standard pronunciation phonemes. The mapping relationships between the mispronounced phonemes and the standard pronunciation phonemes are analyzed.

$$S_n = \cos \frac{3\pi(n+1)}{N+1}. \quad (1)$$

Speech signal preprocessing is the preparation work before speech feature extraction, mainly for the frequency domain processing of speech signal features. After the analog speech signal is sampled and quantized into a digital signal, it needs to be preemphasized so that the high- and low-frequency amplitudes are equal and then, it is framed and windowed to get the speech frame. If the voice data is read directly from an audio file such as a file there is no need for sample quantization processing. Because the human voice is from the lips, the high-frequency part will be attenuated, so that the energy of the low-frequency part is always higher than the energy of the high-frequency part, which leads to a smaller spectral value of the high-frequency part, which is not easy to analyze and process. Preemphasis is to allow the speech to pass through a high-pass filter that enhances the high-frequency part, making the high- and low-frequency amplitudes comparable. Speech signals are slow time-varying signals with short-time smoothness. For a segment of the speech signal, if we take a short enough time (about 6~30 ms), we find that the characteristics of the segment remain the same, but from a long time (0.6 s or more), the speech signal characteristics keep changing, and from that, the content of what the speaker is supposed to express [15]. Because of this characteristic of speech, we need to divide the speech into several short-time segments for analysis, and this process is "framing." There is a certain overlap between two adjacent frames so that the continuity of speech features is maintained by smoothing the comparison between frames. Usually, the overlap is half or one-third of the frame length, and the size of the frame length is between 20 and 30 ms because the characteristics of the speech signal are more stable in this period. Assuming a signal sampling

frequency of 16 KHz, a frame length of 25 ms, and a frame rate of 100 frames/second, there is one sample per frame, and the framed speech signal has 40,000 samples per second.

$$S_n = S_{n+1} - aS_{n-1}. \quad (2)$$

The key aspects of text analysis in a TTS are text-to-symbol conversion, including pauses, placement of stress, and hierarchical relationships, as well as standardization of the text, division of words, and determination of the correct pronunciation of the word or phrase in that position. Although the main task in this section is not text analysis, the key to constructing a complete TTS is the transformation of text to symbols, including pauses, placement of stress, and hierarchical relationships, as well as the standardization of the text, the division of words, and the determination of the correct pronunciation of the words and phrases in that position. Although the main task of this section is not text analysis, it is also crucial to sort out the working process of text analysis to construct a complete TTS system. The main function of text analysis is to enable the subsequent synthesis stage to correctly recognize the digital expression converted from text, similar to a code, and perform a shallow analysis of the text to a certain extent according to the corresponding relationship of the text in the sentence and understanding. The main function of text analysis is to enable the subsequent synthesis stage to correctly identify the digital expressions transformed from text, like an electrical code, and to perform a somewhat shallow analysis and understanding of the text based on its correspondence in that sentence, resulting in the determination of how words and conjunctions in the text should sound, what rhyme is needed based on sentence characteristics, the interval based on semantics, and so on. These parameters will be passed on to the back end of the parametric processing process and play a large role in the effectiveness of the synthesis. The study of the whole text analysis can be divided into the following stages:

(1) Standardize the input text, find gaps and typos, and remove illegitimate characters appearing in the corpus and wrong word composition; conversion of letters or Arabic numerals for which Chinese pronunciation exists to their Chinese counterparts

(2) A participle, which can split the text according to verbs, nouns, conjunctions, and other forms

(3) Level the pauses in the utterance, and mark them based on information such as participles and punctuation

The block diagram of the text analysis system is shown in Figure 2.

In phonetic error recognition detection, each mispronounced phoneme may be due to the insertion, substitution, and deletion of new phonemes. And most of the mispronunciation problems of nonnative learners also arise due to phoneme confusion. The phonetic features of the phonemes corresponding to the associated phoneme strings, phoneme onset and end times, and ratings were obtained after recognition and forced alignment by the Sphinx system. With this resultant data, phonemes are detected for errors. Witt classifies articulation errors into two types, namely, phoneme errors and rhyme errors, and further classifies phoneme errors into three categories: mispronunciation, omission, and addition of phonemes. Generally, the recognizer only performs one recognition detection process for phoneme sequences, and after phoneme alignment, the recognizer performs one recognition process for phonemes from left to right and outputs the recognition results, but the problem of missed and false detection often occurs. To improve the correctness and accuracy of phoneme recognition detection, this paper proposes a phoneme cyclic recognition detection strategy, which converts the speech to be tested into a feature vector after feature extraction and then expands the phoneme bias pronunciation network into each phoneme recognition state, and the Sphinx recognizer performs the cyclic detection task twice for the phoneme feature vector and phoneme bias network to obtain the recognition results. The phoneme sequence SIL, K, AE, T, and SIL is obtained after phoneme alignment for the single word "cat," and the duration d and acoustic score a feature vectors of the phoneme are generated. Then, for each, three T and two D phoneme groups are identified several times, respectively, and the aligned sequences are subjected to phoneme substitution, insertion, and deletion. And to further determine the error type of the phoneme, the duration feature of the phoneme is also identified. The examination process of the cyclic recognition strategy is shown in Figure 3.

3.2. Research on English Pronunciation Detection Methods. The accuracy of pronunciation detection as the basis of speech intelligibility evaluation in this paper is directly related to the effectiveness of the speech intelligibility evaluation system. Detecting pronunciation errors and providing feedback on the error information can help learners to improve the intelligibility level of speech. In the current pronunciation recognition detection, due to the diversity of learners' pronunciation errors, similar phonemes are easily confused, which is likely to cause the situation of missing and false detection in recognition [16]. The detection methods based on mispronunciation networks are being intensively researched and applied, and this chapter proposes a phoneme recognition detection strategy based on the construction of phoneme biased pronunciation networks, which uses recognizers randomly in a cycle and performs pronunciation error differentiation detection by SVM. This chapter focuses on improving the phoneme recognition detection method for nonnative learners to improve the recognition rate and accuracy of phoneme phonetic features and to provide sufficient and accurate phoneme recognition features for subsequent speech intelligibility evaluation. To improve the correct rate and accuracy of phoneme recognition and detection, this paper proposes a phoneme cycle recognition and detection strategy. After feature extraction, the voice to be tested is converted into feature vectors, and then, the phoneme error pronunciation network is expanded into each phoneme. In the recognition state, the Sphinx recognizer performs two rounds of detection tasks on the voice feature vector to be tested and the phoneme error network to obtain the recognition result. Pronunciation error

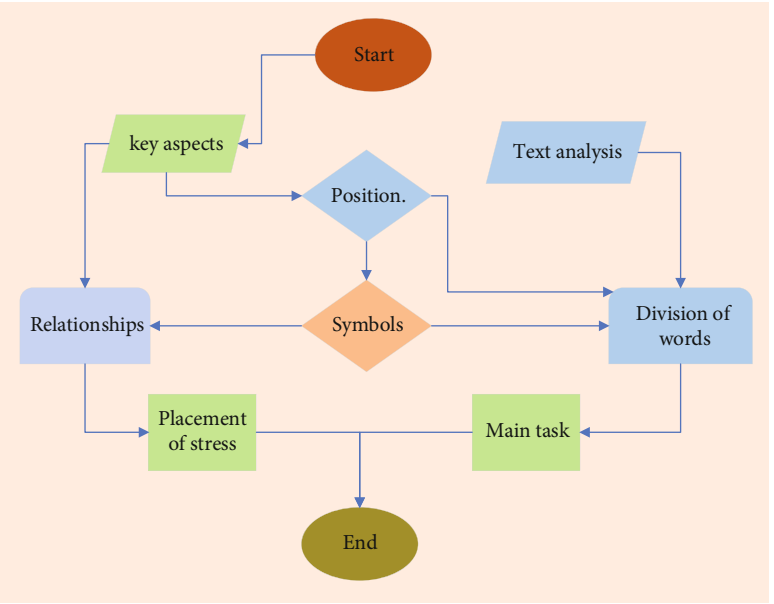

Figure 2: Flowchart of text analysis.

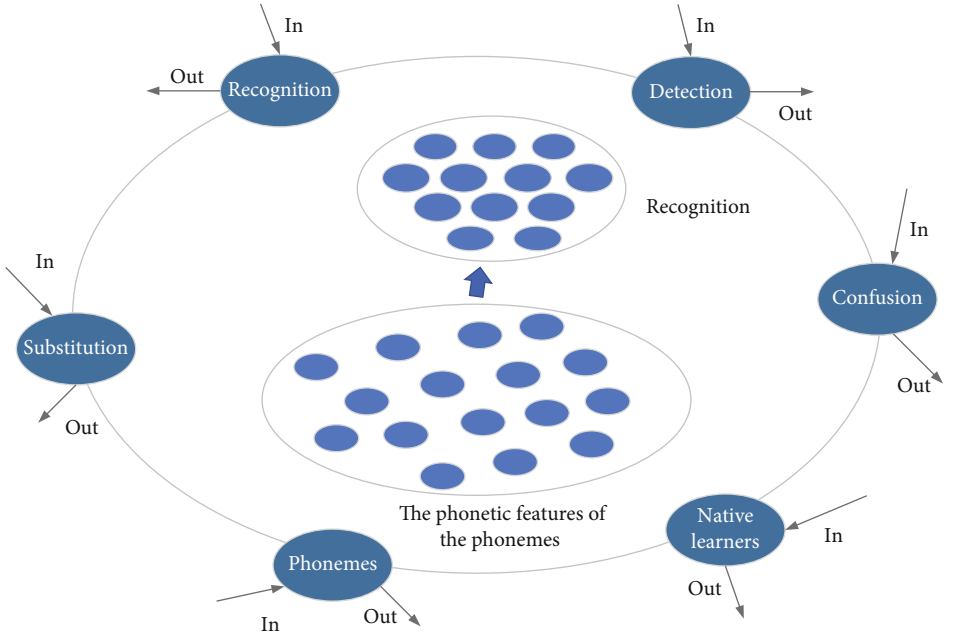

Figure 3: Schematic diagram of the process of phoneme identification test strategy.

detection requires a higher level of detail than pronunciation grading and is typically based on more phonological features such as temporal features, speech rate, articulation rate, and segmental duration that can be computed relatively more easily, and such detection of phonological temporal features is more reliable when measured for longer speech segments and has a greater correlation with human judgments of pronunciation quality. Pronunciation detection grading is often used to calculate the level of pronunciation scores at the speaker or discourse level and can also be a weighted average of native phoneme scores. And the simplest method of pronunciation error detection is to use posterior probability algorithms or GOP algorithms to define error detection by setting bounds.

$$\text{Thresh} = u_p + a\varepsilon_p + \beta. \tag{3}$$

The purpose of speech signal endpoint detection is to detect speech signal segments and noise segments from the

digital signal obtained by continuous sampling. Accurate speech endpoint detection not only reduces the computational effort but also improves the recognition rate of the system. Therefore, endpoints, as important features of speech segmentation, largely affect the performance of speech recognition systems, and thus, how to design a robust endpoint detection algorithm in a noisy environment is still a very tricky problem. Traditional endpoint detection algorithms rely on only one feature, such as signal energy, overzero rate, duration, and linear prediction energy error. These methods have good performance at high signal-to-noise ratios, but poor performance at low signal-to-noise ratios. Speech processing systems usually operate in different noise environments, and the endpoint detection methods used in the system should apply to various adverse situations to enable the system to achieve good performance [17]. First, a higher threshold amp1 is chosen based on the speech short-time energy, which is above this threshold in most cases. This allows for a coarse judgment: the speech start and endpoints lie outside the time interval corresponding to the intersection of this threshold and the short-time energy envelope. Then, a lower threshold amp2 is determined based on the average energy of the background noise, and the two points C and D where the short-time energy envelope intersects the threshold amp2 for the first time are searched forward from point A and backward from point B, respectively, so that the CD segment is the speech segment determined by the double threshold method based on the short-time energy, completing the first level of judgment. The second level of judgment is then performed, this time employing a threshold determined by the short-time excess zero rate. From points C and D, we search forward and backward, respectively, to find the two points E and F where the short-time average zero rate is below the threshold for the first time, which are the starting and ending points of the judged speech segment. This is shown in Figure 4.

The standard pronunciation models and grading models of computer-aided spoken English learning systems are obtained by corpus training. The system usually needs two types of speech databases, the standard pronunciation corpus and the nonstandard pronunciation corpus. The former of them is mainly used to train the standard pronunciation model, and the training corpus should be made to ensure the main training of the pronunciation content of spoken English learning as much as possible, and the content of the corpus is mainly obtained from several famous international corpora. The nonstandard pronunciation corpus is used to train the grading scoring model by experts manually and to test the system performance and should be widely representative. The proposed speech intelligibility evaluation method is compared with expert scores for a correlation experiment. After that, the evaluation method in this article is compared with other existing speech intelligibility evaluation methods, and finally, the intelligibility of this article is analyzed. The scoring performance of the degree evaluation method is analyzed. The content of its corpus is given by the experts, and the targets for grading scoring judgments differ according to the learning priorities of the users at different learning stages. In the study of speech recognition-based English-speaking learning systems, some focus on the common pronunciation errors of beginning pronouncers, such as various similar pronunciations and nasal sounds; some focus on pronunciation skills or difficulties specific to English speakers, such as intonation, alliteration, and stress. There is also one that focuses on a whole system of learning spoken English, following the phonetic teaching method combined with computers to make the system user-friendly and optimize its performance. Of the above, it makes sense to conduct an in-depth study of a particular problem in learning spoken English, for example, synchronic pronunciation, intonation, and intonation. Simply solving one of these problems applied to a spoken language learning system can make the system function optimally. Speech recognition is the key to performing pronunciation learning, but it is not fully suitable for English spoken pronunciation learning and many improvements are needed.

4. Analysis of Results

4.1. Automatic Calibration System Implementation. While the three raters were scoring manually, the author proposed to score the same speech documents by using speech evaluation technology. Based on the analysis of speech evaluation technology principles and speech evaluation cases, I found that Xunfei is the most advanced in the field of Chinese speech evaluation and provides free technical support for speech evaluation to the researcher, so I finally decided to use the speech evaluation function of Xunfei Open Platform to achieve the scoring of all test speech samples (hereinafter referred to as "technical scoring"). The Xunfei Open Platform provides speech evaluation technology [18]. The Xunfei Open Platform provides the speech evaluation technology SDK and explains the format of test questions, evaluation results, and frequently asked questions in the developer documentation, which provides great convenience for setting up the technical scoring environment. In the process of testing the technical scoring environment, it was found that the assessment results were on a five-point scale, which did not match the scoring requirements of HSKK Repeat After Listening (2 points for beginners and 3 points for intermediates). Therefore, the technology scoring results were processed as follows: beginner test technology scoring results = speech scoring results $*$ 0.4; beginner test technology scoring results = speech scoring results $*$ 0.6. The final descriptive analysis of the beginner and intermediate technology scoring results was conducted, and the results are shown in Table 1.

As can be seen from the above table, the technical scoring results of the primary test were controlled between 0 and 2, with the average score in the high range and the standard deviation within 0.5; the intermediate technical scoring results were all distributed between 1 and 3, with the average score around 2.3 and the standard deviation within 0.5. All the data showed that the technical scoring results met the requirements of the topic scoring and the scores showed a concentrated and stable state in general. When compared with the manual scoring results, the results of the descriptive analysis of the technical scoring results were found to show a high degree of agreement with the manual scoring, a finding

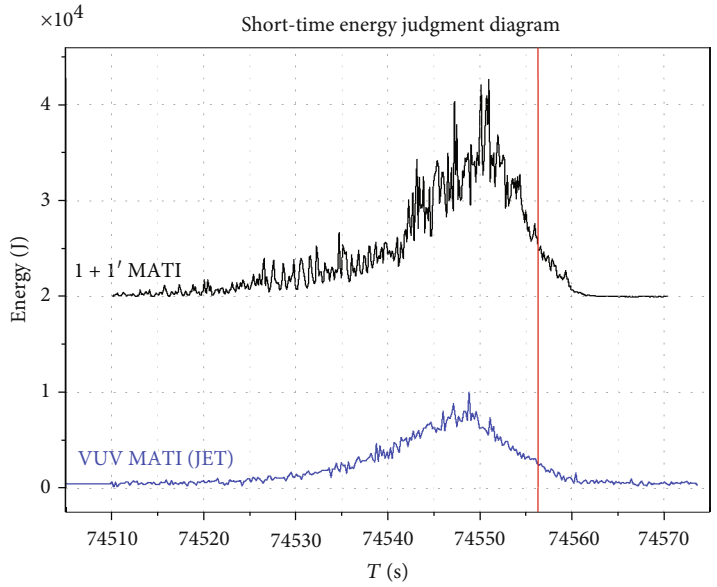

Figure 4: Short-time energy judgment diagram.

Table 1: Descriptive analysis of the results of scoring speech assessment techniques.

Level	Numerical	Minimal values	Maximum value	Average	Variance
Primary	200	0.01	1.50	0.075	0.243
Intermediate	210	0.05	1.00	0.050	0.233
Advanced	230	1.00	2.00	1.500	0.253

that well supports the conjecture of this study. However, this hypothesis needs further proof, so in Section 5, various aspects of the manual and technical scoring results are analyzed and compared to prove the research hypothesis one by one that speech assessment technology can complete the scoring of HSKK postlistening repetition questions.

$$D_j = \frac{L_j^{\mathrm{PL}} + L_j^{\mathrm{FA}}}{d_j}. \tag{4}$$

In the process of conducting experimental tests on speech intelligibility evaluation methods, an experimental database is used in this paper. Firstly, the speech intelligibility evaluation method proposed in this paper is compared with expert ratings for correlation experiments; after that, the evaluation method in this paper is compared with some other existing speech intelligibility evaluation methods, and finally, the scoring performance of the intelligibility evaluation method in this paper is analyzed. Meanwhile, this paper combines the phoneme bias pronunciation network to detect phoneme mispronunciation, and the phoneme error rate of each intelligibility level is counted to verify the effectiveness of the system's error correction feedback. The correlation between the proposed method in assessing intelligibility scores and each expert English teacher in the nonnative test set and TIMIT set is analyzed. Accurately detecting the endpoint of the voice signal can also reduce the amount of calculation for subsequent processing, and improving the utilization of communication equipment will help improve the recognition performance of the system. The experimental results show that the intelligibility evaluation method based on the combination of features proposed in this paper has a high correlation with the actual scores of human experts. The experimental results show that the combination feature-based evaluation method proposed in this paper outperforms the GOP scoring method and the AI index-based intelligibility evaluation method. This is mainly because the method proposed in this paper combines the information of both phoneme duration and phoneme acoustic score features and makes the most effective evaluation method calculation by optimizing the linear regression model. As shown in Figure 5.

For regression analysis in speech characteristics, in probability statistics, regression is the process of studying to estimate the relationship between different variables. Regression analysis studies the process by which the independent variable changes with the dependent variable and describes the trend of the dependent variable change by the characteristics of the probability distribution. And in speech signal analysis, regression analysis of feature vectors is used to explore the relationship between independent variables and dependent variables, which is generally applied to the attributes or parameters of speech for evaluation and prediction. By the

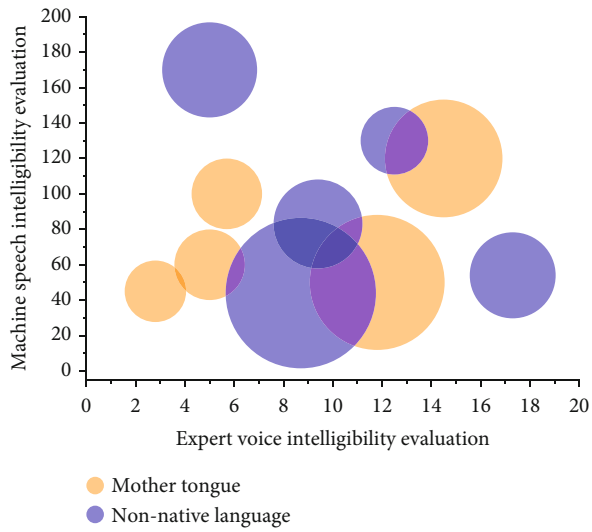

Figure 5: Machine speech intelligibility evaluation concerning expert evaluation.

relationship of different speech features, the correlation between their linear combination of features and phonology is sought, and this statistical perspective is useful for studies with sufficient correlation data. To estimate intelligibility scores, this paper uses a linear regression model, which is derived from the relationship between acoustic/phonological measures and expert scores. In this paper, independent variables (x_i) and variables Y are defined for each expert score, and the linear regression model is defined as shown in the following equation:

$$Y = \sum_{x=1}^{i} (\alpha_x + y_x) + \omega. \tag{5}$$

4.2. Analysis of Simulation Test Results. The endpoint detection is performed before feature extraction and recognition of the input speech. Experiments show that the accuracy of endpoint detection has a very important impact on the recognition rate of the speech signal; in addition, the accurate detection of the endpoints of the speech signal can also reduce the amount of computation for subsequent processing and improve the utilization of communication equipment to help improve the recognition performance of the system [19]. Endpoint detection is used to delineate the articulation and silence zones. The popular endpoint detection methods at this stage are based on short-time energy, based on short-time average overzero rate and pattern recognition, based on inverse spectral distance, based on wavelet transform, and based on other methods. In the prototype English-speaking learning system implemented in this paper, a double threshold endpoint detection method is used, which firstly sets two closed values each by short-time energy and overzero rate and obtains the endpoint detection method of speech signal content by a certain operation with the closed values. Exceeding the high threshold can basically determine the beginning of the voice, and the low threshold is used to determine the true endpoint of the voice. Exceeding the low threshold may not be the beginning of speech, and it may also be a short-term noise. Since the interval between the start of recording and the start of vocalization is generally considered to be the first 100 ms of the speech signal as a silent segment, the average energy and the average overzero rate of this segment of the speech signal can be extracted as the characteristic parameters when making a rough judgment. For the calculation of the threshold, a lower energy threshold is used, which is taken as two times the average energy of the background noise, and a higher energy threshold is taken as the average energy of multiple frames of speech data [20]. Exceeding the higher threshold identifies the beginning of the speech, and the lower threshold is used to determine the true endpoint of the speech. The low threshold being exceeded may not necessarily be the beginning of the speech but may also be short-lived noise. When the high threshold has determined the beginning of the speech, go back, and use the low threshold to determine the true beginning of the speech, and the end of speech is discriminated similarly. Sometimes, the noise is also quite energetic and may exceed the high threshold, but the noise which is generally of short duration can be used to determine whether it is noise or speech, as shown in Figure 6.

Determining the most effective error correction feedback decisions to help improve learners' phonetic intelligibility levels is the final issue to be addressed in this paper's evaluation system. In general, the overall level of pronunciation of nonnative learners when learning English pronunciation falls short of the standard pronunciation. However, for CAPT, if all the feedback is given to the learners without considering the impact value of the phonetic intelligibility of the wrong phoneme pronunciation, all the learners' key pronunciations will be judged as mispronunciations, which will weaken the learners' confidence in learning. The learner pronounces the phoneme sequence through the given lexical text, and after matching and forcing alignment with the phoneme biased pronunciation network, the possible biased pronunciation recognition sequence of the learner is obtained, where {} denotes the possible mispronunciation of phonemes. To determine which mispronounced phonemes should be improved, we define the priority $\pi(j, i)$ of the mispronounced phoneme j on intelligibility level i as the difference between the learner's error rate and the average error rate of the learners at level i as follows:

$$W(\mathrm{j}) = \sum_{j}^{2} \pi(i, j) \cdot l(i, 1). \tag{6}$$

Based on the results of phoneme detection, all potentially misleading phoneme reading detection rates are ranked, and by adjusting the priority of each phoneme to determine which phonemes are most in need of improvement, the best adjustment is made to obtain the intelligibility rating level for the entire word pronunciation. The problematic phoneme of the target word that has the greatest impact on phonological intelligibility is also given as positional feedback to the learner, informing the learner that improving the

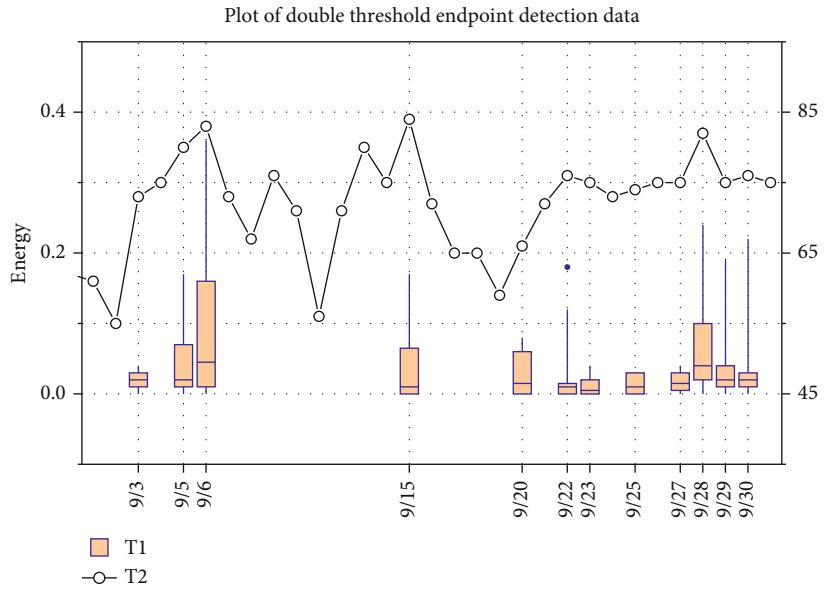

Figure 6: Plot of double threshold endpoint detection data.

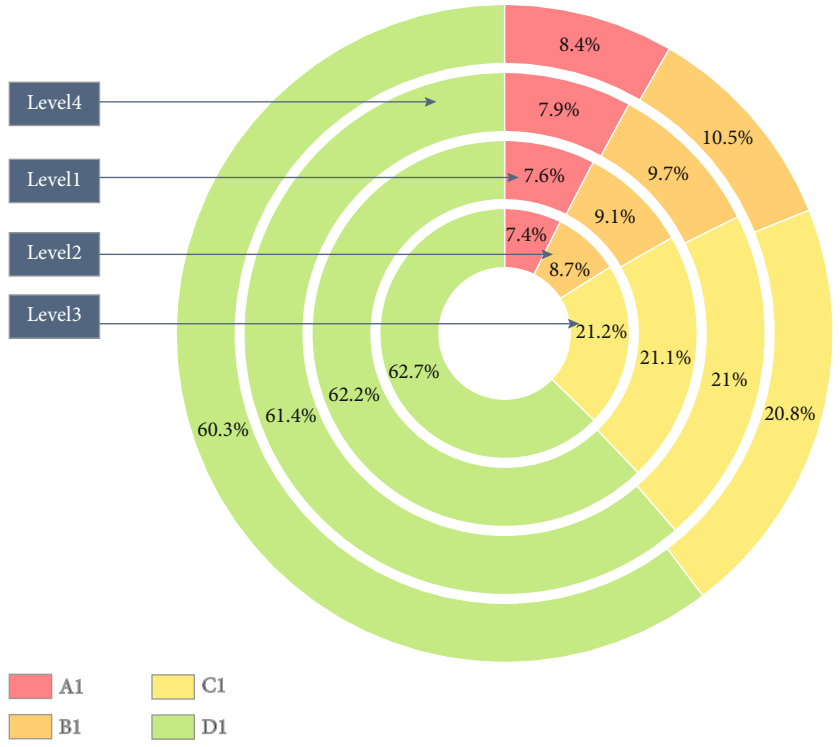

Figure 7: Phoneme recognition error rate.

offending phoneme will most effectively improve the intelligibility score of the word pronunciation.

To examine the phonological error rates of nonnative data at different intelligibility levels, this paper conducts recognition detection experiments on pronunciation. The average pronunciation error rate is used as a reference for the average error rate of subjects at each intelligibility level. The error rate of phonemes in the highest intelligibility level is only 0.22, while the error rate of phonemes in intelligibility level 1 reaches 0.53. Because of the difference between the error rate of each intelligibility level and the overall average phoneme error rate, this paper further analyzes the average error rate of phonemes in each intelligibility level and finds that, for the pronunciation of each phoneme in the lexicon,

the higher the intelligibility level is, the lower the average. This is in line with the human perception of phonological intelligibility. Also, based on the results of phoneme error detection, we calculated the influence between the trend of phoneme error rate and intelligibility and verified that the design of the online assessment system in this paper needs to consider the feedback to learners those correction suggestions that can most effectively help them improve their speech intelligibility level. This is shown in Figure 7.

5. Conclusion

Automatic assessment of pronunciation is a complex subject involving knowledge from many disciplines such as linguistics, acoustics, signal processing, and pattern recognition. The language pronunciation rules are also very complex, and it is very difficult to perform an automatic assessment of pronunciation. In this paper, we propose a system that uses automatic speech recognition technology to effectively detect incorrect phoneme pronunciations in continuous Japanese pronunciation by English learners. The research focuses on how to effectively generate an extended pronunciation lexicon to predict possible mispronunciations in learners' pronunciation, combine speech recognition to detect erroneous phoneme categories in pronunciation, and provide corrective feedback to learners to help them improve their pronunciation. This paper introduces error elimination calculation for speech recognition and proofreading, which can effectively improve the recognition ability of spoken English, avoid the data progression error in traditional recognition and proofreading methods, and optimize the feedback control system to improve the system's ability to recognize speech and fundamentally solve the speech recognition confusion problem. The system in the paper improves the pronunciation model for the influence of the native language on the pronunciation of the second language, and although it achieves better results, there are still some shortcomings, and future research can be further explored in terms of using multiple speech feature parameters for comprehensive evaluation and networking in the implementation method.

Data Availability

The data used to support the findings of this study are available from the corresponding author upon request.

Conflicts of Interest

The author declares that there are no known competing financial interests or personal relationships that could have appeared to influence the work reported in this paper.

References

[1] C. Xu, "From sonic models to sonic hooligans: magnetic tape and the unraveling of the Mao-era sound regime, 1958–1983," *East Asian Science, Technology and Society: an International Journal*, vol. 13, no. 3, pp. 391–412, 2019.

[2] X. Li and M. Mills, "Vocal features: from voice identification to speech recognition by machine," *Technology and Culture*, vol. 60, no. 2S, pp. S129–S160, 2019.

[3] M. Caprolu, S. Sciancalepore, and R. Di Pietro, "Short-range audio channels security: survey of mechanisms, applications, and research challenges," *IEEE Communications Surveys & Tutorials*, vol. 23, no. 1, pp. 311–340, 2021.

[4] Y. Li, H. Cheng, Z. Alhalili, G. Xu, and G. Gao, "The progress of magnetic sensor applied in biomedicine: a review of non-invasive techniques and sensors," *Journal of the Chinese Chemical Society*, vol. 68, no. 2, pp. 216–227, 2021.

[5] "Reviews of acoustical patents," *The Journal of the Acoustical Society of America*, vol. 144, no. 4, pp. 2022–2029, 2018.

[6] M. Romera, P. Talatchian, S. Tsunegi et al., "Vowel recognition with four coupled spin-torque nano-oscillators," *Nature*, vol. 563, no. 7730, pp. 230–234, 2018.

[7] O. S. A. Chronicle, "66th open seminar on acoustics Boszkowo, Poland, September 18–20, 2019," *Archives of Acoustics*, vol. 44, no. 3, pp. 603–622, 2019.

[8] D. Liu, S. Guo, Y. Yang, Y. Shi, and M. Chen, "Geomagnetism-based indoor navigation by offloading strategy in NB-IoT," *IEEE Internet of Things Journal*, vol. 6, no. 3, pp. 4074–4084, 2019.

[9] O. Marshall, "The maniac-making machine: a media history of delayed auditory feedback," *Technology and Culture*, vol. 62, no. 3, pp. 839–860, 2021.

[10] H. Dehra, "Acoustic signal processing and noise characterization theory via energy conversion in a PV solar wall device with ventilation through a room," *Advances in Science, Technology and Engineering Systems Journal*, vol. 3, no. 4, pp. 130–172, 2018.

[11] J. E. Huggins, C. Guger, E. Aarnoutse et al., "Workshops of the seventh international brain-computer interface meeting: not getting lost in translation," *Brain-Computer Interfaces*, vol. 6, no. 3, pp. 71–101, 2019.

[12] H. Rayes, G. Al-Malky, and D. Vickers, "The development of a paediatric phoneme discrimination test for Arabic phonemic contrasts," *Audiology Research*, vol. 11, no. 2, pp. 150–166, 2021.

[13] H. Charaf, G. Harsányi, A. Poppe et al., "BME VIK annual research report on electrical engineering and computer science 2016," *Periodica Polytechnica Electrical Engineering and Computer Science*, vol. 61, no. 2, pp. 83–115, 2017.

[14] C. DeLaurenti, "Imperfect sound forever: a letter to a young phonographer," *Resonance: The Journal of Sound and Culture*, vol. 2, no. 2, pp. 125–167, 2021.

[15] J. Pinkl, E. K. Cash, T. C. Evans et al., "Short-term pediatric acclimatization to adaptive hearing aid technology," *American Journal of Audiology*, vol. 30, no. 1, pp. 76–92, 2021.

[16] Y. Huang, X. Guan, H. Chen, Y. Liang, S. Yuan, and T. Ohtsuki, "Risk assessment of private information inference for motion sensor embedded iot devices," *IEEE Transactions on Emerging Topics in Computational Intelligence*, vol. 4, no. 3, pp. 265–275, 2020.

[17] A. F. T. Borges, A. L. Giraud, H. D. Mansvelder, and K. Linkenkaer-Hansen, "Scale-free amplitude modulation of neuronal oscillations tracks comprehension of accelerated speech," *Journal of Neuroscience*, vol. 38, no. 3, pp. 710–722, 2018.

[18] S. A. Fulop and L. Rice, "Reviews of acoustical patents," *The Journal of the Acoustical Society of America*, vol. 142, no. 1, pp. 124–133, 2017.

[19] V. G. Sardegna, J. Lee, and C. Kusey, "Self-efficacy, attitudes, and choice of strategies for English pronunciation learning," *Language Learning*, vol. 68, no. 1, pp. 83–114, 2018.

[20] H. Vančová, "Current issues in pronunciation teaching to non-native learners of English," *Journal of Language and Cultural Education*, vol. 7, no. 2, pp. 140–155, 2019.

Hindawi
Journal of Sensors
Volume 2021, Article ID 1345759, 12 pages
https://doi.org/10.1155/2021/1345759

Research Article

Construction of Enterprise Management Business Model Based on Internet of Things RFID Technology

Fang Chen

Shandong Management University, Jinan City, Shandong Province 250357, China

Correspondence should be addressed to Fang Chen; 14438120180082@sdmu.edu.cn

Received 1 November 2021; Revised 20 November 2021; Accepted 7 December 2021; Published 27 December 2021

Academic Editor: Gengxin Sun

This paper proposes a new tag anticollision algorithm. On the basis of the common query tree algorithm, this algorithm increases the number of query bits, so that the algorithm has a faster tag identification amount in the state of full time slots. Collision bit and total response bit are used to estimate the number of tags, and combined with the highest collision bit to determine whether it is continuous, the number of query crosses is adaptively adjusted, and a variable bit dynamic query tree tag anticollision algorithm is designed. In conjunction with the settlement environment, improvements have also been made in the status of the identified tags. The new algorithm has improved progress in reducing idle time slots and reducing search depth. Under the premise of ensuring stability, the recognition efficiency of the algorithm is improved. From the perspective of different dimensions of corporate network and marketing dynamic capabilities, based on the strength of network relationships and product development processes, it can promote value creation model innovation in business model innovation. That is, when the network partners communicate very frequently, they can provide new ideas and resources for enterprise product development and creation and then can better integrate innovation through product innovation, quality improvement, product development cycle shortening, and development advance management. Typed products and resources are put into the operation process of the industrial chain of product output to better create new products for customers and lay the foundation for realizing the innovation of corporate value creation models. Based on the network density and customer relationship process, it can promote the value proposition model innovation in the business model innovation. Enterprise business model innovation should not only pay attention to the collaborative innovation between different elements within the enterprise but also pay attention to the overall coordination mechanism of the company's external interest network, pay attention to the different value propositions of stakeholders through the enterprise network, and cultivate the enterprise's rapid response to market changes. Network centrality has the greatest positive impact on the supply chain process. The company develops new products, manages customer relationships across departments, and implements supply chain management across departments.

1. Introduction

Business model innovation is an exploration process of initiative, trial and error, and reshape. It is not only an important tool for companies to commercialize technology and expand into new markets but also a key driving force for companies to create competitive advantages [1]. Effective means to adapt to environmental changes. In recent years, Tencent, Alibaba Group, and other companies have achieved catch-up with leading companies through business model innovation [2]. IBM has used business model innovation to successfully transform from a global hardware giant to a world leader in information technology and business solutions. And the competitive business model has achieved leapfrog development. However, it is still unclear how companies carry out business model innovation and how to grasp the key elements of business model innovation. It is urgent to establish a logical framework for effective interpretation of business model innovation [3]. The issue of business model innovation has aroused widespread concern and discussion from scholars at home and abroad, and many results have been achieved [4]. In the existing research, scholars have defined the concept and connotation of business model innovation based on different perspectives and

summarized the business model innovation path through case analysis or existing theoretical integration research, which provides a useful reference for enterprises to carry out innovative practices [5]. However, in-depth analysis of the formation logic of business model innovation and literature on business model innovation from a methodological level are relatively rare. Therefore, it is of great significance to summarize the experience and skills in existing research, analyze the formation mechanism of business model innovation, and build a set of methods that can inspire or guide enterprises to carry out business model innovation.

No matter in the aspect of item information identification or in the aspect of cargo information tracking, radio frequency identification technology has great advantages [6]. This technology is also called RFID technology. It can not only realize fast reading of item information but also realize the modification of item-related information, so that electronic tags can be reused. Moreover, the electronic tag also has the advantages of large storage capacity and nonvisual identification, which can realize remote cargo information reading, which is convenient for the staff to manage the cargo [7]. In addition, the goods with electronic tags can realize real-time tracking and positioning of goods information when they are out of storage or transfer. And the use of this technology can realize the intelligentization of warehouse management, reduce manual operation management, improve the information accuracy of warehoused goods, and to a certain extent avoid the favoritism of some people, thus bringing the greatest benefits to the enterprise [8]. However, RFID technology still has many problems in the actual application environment, among which the collision between tag data is a key issue that needs to be studied. In the RFID system, the mutual transmission of information between the tag and the reader is the same channel. When multiple tags to be identified respond at the same time, it may cause the phenomenon of information transmission conflicts, so that the information of some tags will not be transmitted for a period of time [9]. The occurrence of such label conflicts will seriously affect the integrity of the collected physical information, cause data loss, and reduce system efficiency. Therefore, how to effectively solve the collision problem in the RFID system is an important content that needs to be solved in the further development of RFID technology.

This article has made a detailed design of the tag anticollision algorithm in the settlement environment and proposed a new tag anticollision algorithm. Based on the common query tree algorithm, adaptive query bits are added to make the algorithm in the full time slot state. It has a faster tag recognition capacity and uses collision bits and total response bits to estimate the number of tags. According to the continuous situation of the highest collision position, the number of query forks is automatically adjusted, which reduces the generation of idle time slots and collision time slots and improves the efficiency of the anticollision algorithm. This research is aimed at exploring a specific path to drive and enhance business model innovation based on the dynamic capabilities of corporate networks and marketing and is closely focused on this research purpose and theoretical mechanism. We constructed and proposed a theoretical research model of corporate network-marketing dynamic capabilities-business model innovation and used service industry companies as the research object to obtain large samples of primary data. The hypothesis of the relationship between variables is tested by empirical test and structural equation model analysis. When the network members are more densely connected with each other, it will provide a lot of convenience for managing the relationship between stakeholders including customers, then deeply explore the potential value needs of users to achieve customer segmentation and target market, and then clarify the direction for realizing the innovation of enterprise value proposition model. Based on the network scale and product development process, it can promote the value creation model innovation in the business model innovation. Through different cross-departmental business processes, market resources are transformed into enterprise's enterprising advantages, and network resources are reset and allocated again. On the basis of effectively meeting customer needs, the company's own organizational competitiveness is improved.

2. Related Work

A general RFID system contains an RFID reader and multiple RFID tags. Each electronic tag has its own unique ID. When the reader transmits a signal, the tag within the signal range will feed back its ID sequence to the reader for identification and complete tag identification. Due to the shared channel used by the reader to read the tag ID, when multiple tags feed back the ID at the same time, data transmission may be blocked, causing tag collisions, and the tag information to be identified cannot be correctly identified by the reader. The time division multiple access method has the advantages of simplicity, easy implementation, and low cost. It is widely used in most RFID systems. In the time division multiple access method, the anticollision algorithm is divided into two categories: deterministic and probabilistic.

Related scholars have proposed a binary split tracking algorithm, which effectively improves the identification efficiency of large-scale RFID systems [10]. The researchers proposed an M query tree algorithm to optimize the RFID system in terms of energy consumption and recognition speed [11]. By optimizing the binary query tree algorithm, scholars have effectively reduced the problem of data redundancy in the information transmission between the tag and the reader [12]. Researchers propose a Bayes-based query tree algorithm, which improves time efficiency by 78.5% compared to traditional query tree algorithms [13].

Related scholars pointed out that business model innovation is, in a sense, a high degree of integration of social capital, and social capital will enhance the innovation capabilities of enterprises [14]. Through case study analysis, it is believed that companies in different competitive positions choose different paths of business model innovation. Generally, companies that are in a dominant position in competition are more inclined to adopt radical methods to carry out business model innovation, and companies that lack the right to speak in competition tend to be more inclined to business model innovation for defensive purposes. Relevant

scholars collected and sorted out the operating data of 334 companies and found through model empirical research that relational and structural embedding played a key role in promoting the innovation of modern enterprise business models [15]. Researchers have concluded through empirical analysis that integrated companies can achieve long-term resource cooperation with external companies to complement resources, which will help companies to carry out process reengineering and business model innovation [16].

Relevant scholars have used the structural equation model of the influencing factors of the "Internet+" business model innovation and found that the changes in the connection, the upgrade of consumer demand, the application of network technology, and the social dividend have a significant impact on the "Internet+" business model innovation [17]. Among them, the upgrade of consumer demand, network technology application scenarios, social dividends, technology drive, and the company's willingness to innovate in the future are the main influencing factors.

Relevant scholars pointed out that the business model mainly includes elements of transaction content, transaction structure, and transaction governance to create more value for focus companies and other participants and proposed four business model design themes of efficiency, novelty, lock-in, and complementarity, and past empirical analysis found that efficiency and novel business models have a significant impact on corporate performance, while lock-in and complementary business models have no significant impact on performance [18, 19]. Researchers believe that a business model is the process of value creation, value transfer, and value acquisition by an enterprise [20]. Relevant scholars define the business model based on the perspective of value creation as the complementary combination, transaction structure, profit model, and revenue and expenditure methods formed by producers, consumers, and partners in R&D, production, marketing transactions, and service experience based on resource capabilities. Relevant scholars believe that the business model is based on the profitability of the enterprise, which gathers relevant elements to form a business "ecosystem" and a logical system that accompanies the development of the enterprise [21].

Relevant scholars have compiled a large number of academic documents and compared various viewpoints fully and pointed out that business model innovation is a comprehensive innovation and breakthrough that integrates value creation, value concept proposition, and value resource acquisition [22]. Therefore, in the process of business model innovation, it is necessary to comprehensively consider all aspects such as suppliers, purchasers, customers, and stakeholders. We must not only consider the various components but also pay attention to the management and reintegration of internal and external resources. At the same time, we must also take into account the direct or indirect impact of the micro- and macroenvironments on it. Business model innovation is a kind of business value derived from the idea of meeting consumer needs. The importance and significance of business model innovation lies not only in creating new technologies or new products but in creating new value for customers.

3. Method

3.1. IoT Platform Architecture. This design uses the Internet of Things model as the overall design framework and connects traditional devices with various sensors to the Internet to achieve information sharing and interaction between things. The Internet of Things architecture is composed of a perception layer, a network layer, and an application layer. Based on the Internet of Things architecture, the system is divided into three parts: the device side, the server side, and the monitoring side. Being equipped with RFID as the sensing layer constitutes the device side. The server is placed in the cloud, and the data is transmitted to the cloud server using 5G or Wi-Fi transmission. The web management platform is realized through the background monitoring system.

(1) *Device-side architecture design*. The device side is mainly used to realize the functions of data collection and logic control of the perception layer of the Internet of Things. The collected data and various communication protocols or business logic operations and other data will eventually be collected into the IoT gateway. In addition to the device-side and server-side data interaction, the IoT gateway can also process some raw data to complete the operation.

(2) *Server architecture design*. In this design, the server is arranged in the Alibaba Cloud server. The cloud server is usually composed of three parts: web front-end, web back-end, and middleware. The web front-end mainly implements the following functions: dynamically display the actual device data status on the site through the page, generate various data reports, and save; the main functions are user management, role management, role matching, and project template management.

(3) *Architecture design of the monitoring terminal*. As a traditional and commonly used monitoring device, a PC can be used as a network front end to monitor and control the system status. However, because of its large size and inflexibility, this design chose to place the server in the Alibaba Cloud, so that not only PCs can be used as monitoring devices but also smartphones, tablets, etc. can be used regardless of location through a web browser. It is convenient to complete the monitoring of the on-site equipment status.

3.2. The Overall Design of the System. The RFID-based intelligent tool management system is composed of an intelligent tool cart and a system back-end. Among them, the intelligent tool cart completes the life cycle tracking link of tool information collection, positioning tool from storage to scrapping, and the circulation link of daily borrowing and returning of tools. The system backstage realizes intelligent management of tools by summarizing various data of tools. Figure 1 shows the overall design of the system. The system is composed of equipment, servers, and system back-ends.

In view of the fact that some workshops did not construct the local area network, the wireless router did not

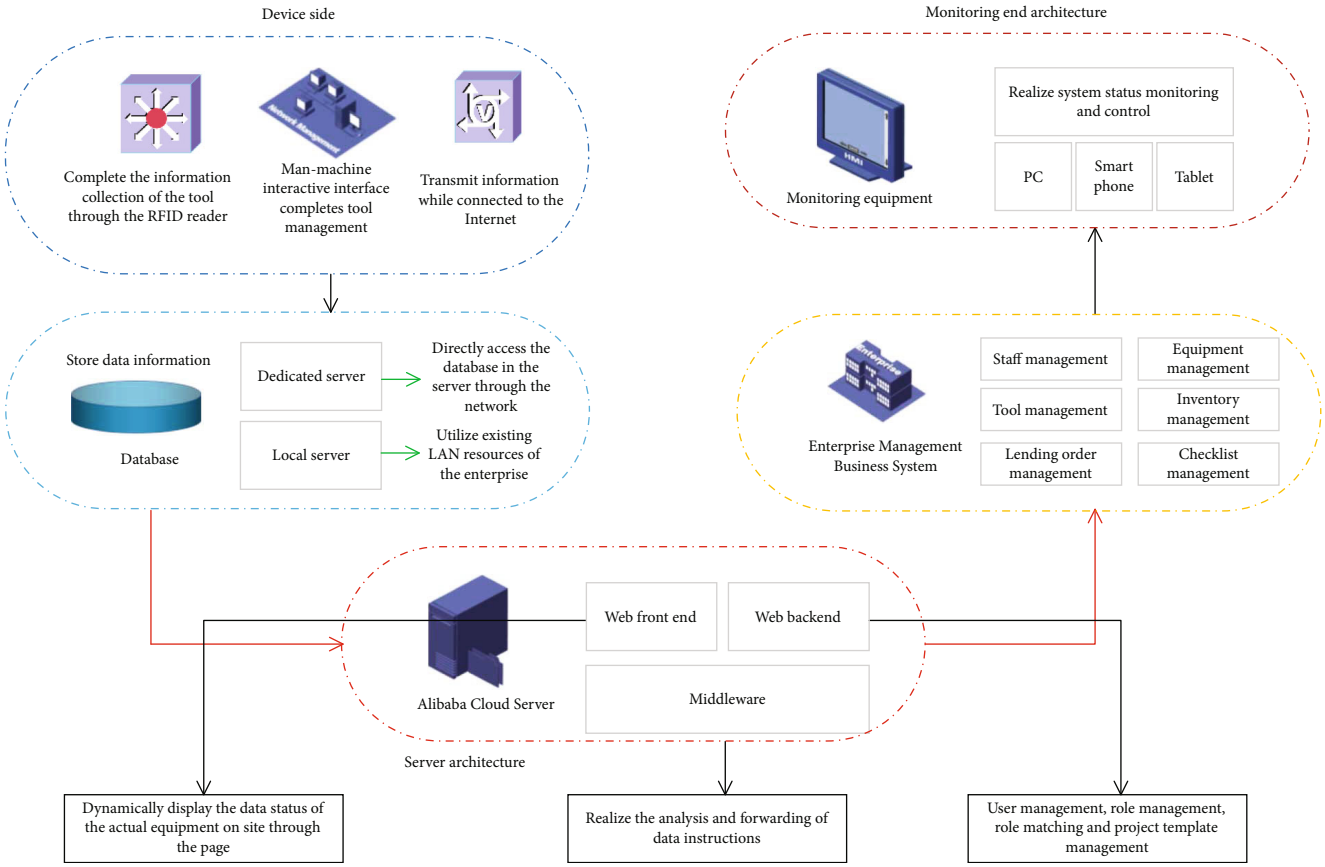

Figure 1: Overall system design scheme.

achieve full coverage, and if the local area network was rebuilt in order to implement tool management, a large amount of capital would be required, and the cost would be too high. Therefore, this prototype design chose to place the server on the cloud and adopt 5G for transmission. Considering factors such as security and convenience, the Alibaba Cloud server was finally selected.

The system background can generally be divided into mobile devices and PCs, etc. This design combines the actual situation inside the workshop, and the administrator or background operators can achieve control through the PC-side management web page. The system background is mainly used to display and operate the basic information of the operating system, complete the input of the initial data of the tools and equipment, realize the remote management and view of the intelligent tool cart, process the system logic business, and statistically summarize the various management data of the system. The system client has set up six sections of content, including employee management, equipment management, tool management, inventory management, loan order management, and inspection order management.

In order to reduce the storage pressure of the tool cart and the system back-end, this design sets the database in a dedicated server, and the tool cart and the system back-end directly access the database in the server through the network to complete information interaction. For workshops with full coverage of the enterprise's basic unit network, local servers are used, Wi-Fi is used for information transmission, and internal addresses are selected to be physically isolated from the external Internet. In this case, no changes will be made to the internal network structure of the enterprise, no new network equipment will be purchased, and all existing LAN resources of the enterprise will be used.

The application of the server is divided into two aspects: on the one hand, it provides a server port for the human-computer interaction interface system of the smart tool cart for data interaction; on the other hand, it provides a server port for the remote back-end management system to implement interface management. The embedded terminal realizes the tool borrowing, query, inventory, and human-computer interaction interface of the tool cart; the cloud server realizes the storage and interaction of information; the system background realizes real-time monitoring and background operation.

3.3. Search Depth Analysis. The search depth is the number of steps the reader sends a command during the execution of the deterministic anticollision algorithm, and it is also the number of differential levels of the multitree, which is reflected in the previous section. The search depth also indicates the complexity of the algorithm and the total number of time slots used to calculate the algorithm. Under the same

conditions, the deeper the search depth, the more complex the algorithm, and the lower the recognition speed and recognition efficiency achieved. Figure 2 shows a flow chart of the search depth of tag identification using single-bit algorithm and double-bit algorithm.

3.4. Label Estimation Algorithm. In the tag anticollision algorithm, the estimation of the number of tags to be identified is a very important link. Only when the dynamic estimation of the tags to be identified is accurate can the next step of the algorithm be accurately judged which is more efficient. The main principle of the new algorithm is to dynamically adjust the number of forks of the query tree, so that it can perform tag-by-tag identification with maximum efficiency in an environment where the number of tags is constantly decreasing. The dynamic adjustment of the number of crosses needs to design an adjustment threshold according to the real-time multifaceted situation of the system, and the dynamic estimation of the number of tags to be identified is also more important.

Because the tag recognition process obeys the Poisson distribution, Schoute gives the time slot collision probability C_{rate} as

$$C_{\text{rate}} = \frac{\theta}{1 - \Phi}. \tag{1}$$

In the formula, θ is the number of collision tags and Φ is the number of successfully identified tags. The number of collision tags in a single time slot can be expressed by the following formula:

$$C_{\text{tag}} = \frac{1 - \Phi}{\theta}. \tag{2}$$

3.5. Collision Factor. In addition to judging whether the high collision bit is a continuous collision bit to adaptively adjust the bit number of the algorithm, in the case of a large number of tags, it is also necessary to set a threshold according to the number of tags for adaptive adjustment. By judging the collision bits and tag response bits in the collision time slot by the reader, indirect tag estimation can be realized without adding a new estimation time slot, thereby determining the threshold for adaptive adjustment.

The collision factor γ is the ratio of the collision bit position α to the tag response bit position β in the collision time slot, and the collision factor can be similarly regarded as the tag estimate.

$$\gamma = \frac{1 - \alpha}{\beta}. \tag{3}$$

Assuming that there are m tags to be identified in the system that meet the query conditions, the length of the tag response is β bits, and the probability that any bit does not collide is 2^{m-1}, so

$$\gamma = \frac{\beta\left(1 - 2^{m-1}\right)}{1 - m}. \tag{4}$$

It can be seen that the larger the number of tags, the higher the collision factor. It shows that the collision factor can be similarly regarded as the estimated information of the tag to be identified. Assuming that the number of forks allocated by the system is l, when the search depth is 1, the identification probability of the tag is

$$p(1) = \left(\frac{1}{l+1} - 1\right)^{1-m}. \tag{5}$$

When the search depth is k, the recognition probability is

$$p(k) = [1 + mp(1)]^{1-k}. \tag{6}$$

The mean value of the required search depth is

$$E(k) = \prod_{k=0}^{\infty}\left\{mp(1)[k - p(1)]^{1+k}\right\}. \tag{7}$$

The algorithm flow chart is shown in Figure 3.

4. Results and Discussion

4.1. Data Collection. This research is based on service industry companies as the research object and conducts investigations on them to study the role and influence of service industry companies' network and marketing dynamic capabilities on business model innovation. From a macroperspective, Premier Li Keqiang pointed out many times in the working conferences on the development planning of service industry enterprises that adjusting the economic strategic structure to promote business model innovation is an important way to accelerate and promote China's economic development, while the development of the service industry is an adjustment. The economic structure promotes the key breakthrough point for the innovation and development of business models. Therefore, vigorously developing the service industry and actively studying the business model innovation of service industry enterprises are of self-evident importance for the adjustment of China's economic strategic structure and promoting the development of the national economy. From a microperspective, the service industry, as the tertiary industry, can create higher economic efficiency than the primary and secondary industries and can promote the accelerated development of the economy. That is, the more developed the service industry, the higher the economic labor productivity that can be created. At the same time, the higher the economic labor productivity, the faster the economic development. And with the economic globalization and the rapid development of China's economy, the service industry economy has gradually evolved into an important development symbol of the modern economy. The service industry accounts for almost half of the proportion of the three major industries, and it has become the mainstay of modern industries. It is closely related to people's living standards and has become the greatest potential for consumer demand and industrial development. It has great advantages in stimulating economic growth,

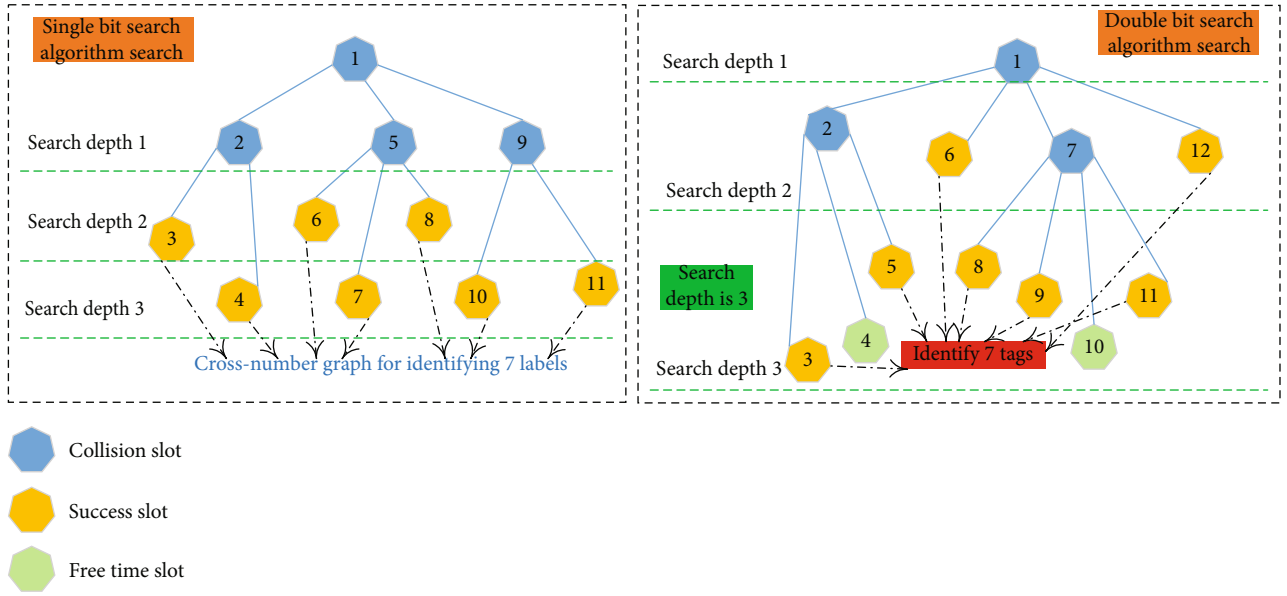

Figure 2: Comparison of search depth of single-bit search algorithm and dual-bit search algorithm.

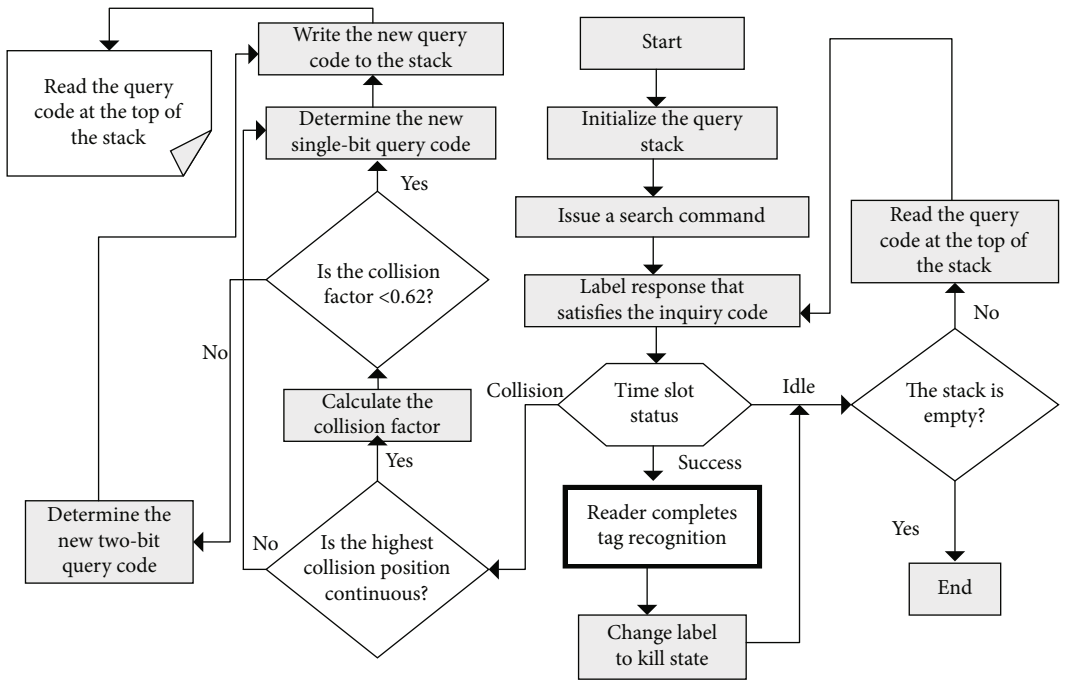

Figure 3: Algorithm flow chart.

maintaining a balance of supply and demand, stabilizing market prices, and promoting social employment. It has become the current promotion of efficient economic growth. An important driving force for improving social development has played a particularly important role in promoting China's national construction and economic strengthening, as well as improving people's living standards and quality. Therefore, this study takes service industry companies as the research object and studies the impact of business model innovation on the basis of corporate network and marketing dynamic capabilities in the specific development process of the service industry. The sampling scope of the questionnaire survey is mainly concentrated in Beijing, Xi'an, Tianjin, Hangzhou, Shanghai, Jinan, and other places, and the questionnaire is distributed based on the online platform.

4.2. Descriptive Statistical Analysis. It mainly includes the nature, age, and scale of the company, as well as the core role of the company's network, as well as the position and working years of the person filling in the questionnaire. The research objects of this study are mainly service industry

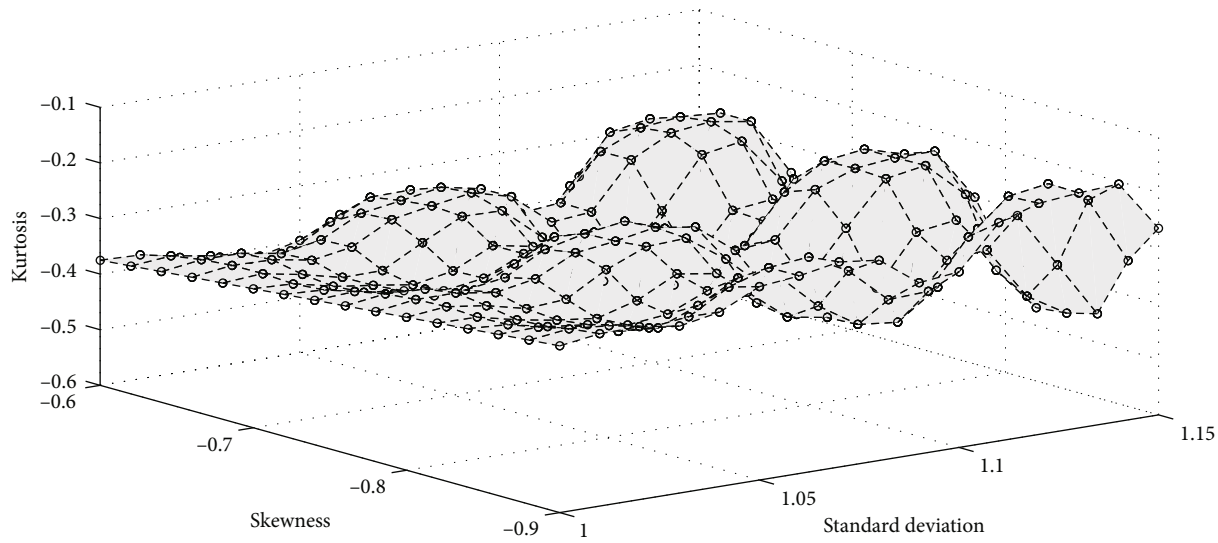

Figure 4: Descriptive statistical analysis.

enterprises, and 500 copies of questionnaire data were distributed and 487 copies of valid sample data were received. The following is a descriptive statistical analysis of the valid samples in this study. Figure 4 shows the standard deviation, skewness, and kurtosis.

4.3. Reliability Analysis. This study refers to the practice of previous scholars. The reliability test still uses the Cronbach's Alpha value to measure the reliability of the questionnaire to determine the reliability of the scale. Generally speaking, when the Cronbach's Alpha value is relatively high, the internal stability is better. After reliability analysis, the reliability coefficient values of all dimensions of the corporate network are greater than 0.8. In addition, the reliability coefficient values of all dimensions of marketing dynamic capabilities are greater than 0.8. Moreover, the reliability coefficient values of all dimensions of the business model innovation are greater than 0.8, as shown in Figure 5.

4.4. Validity Analysis. In this study, referring to previous scholars' practices, KMO and Bartlett's sphericity were analyzed and tested before the validity analysis. When the value of KMO exceeds 0.7, it is suitable for further confirmatory factor analysis. According to the SPSS 22.0 analysis result, in the enterprise network, the KMO values of the four dimensions are 0.71, 0.85, 0.72, and 0.83. In marketing dynamic capabilities, the KMO values of the three dimensions are 0.905, 0.909, and 0.906 in turn. In business model innovation, the KMO values of the four dimensions are 0.855, 0.865, 0.815, and 0.702 in order. It can be seen from the results that the KMO values of all variables in different dimensions exceed 0.7, and the results of Bartlett's test are significantly lower than 0.001, so it is suitable for the next step of confirmatory factor analysis. The results of the validity analysis are shown in Figure 6.

In the previous part of this study, a theoretical model has been constructed for each variable and related relationship assumptions have been proposed. At this time, confirmatory factor analysis is needed to test whether the collected samples and the constructed model are good enough to ensure that the structural equation model can be used. Generally speaking, the fitting indicators of the model include reference indicators such as chi-square statistics, RMSEA value, CFI, GFI, and IFI, and each indicator has a corresponding reference value. If the index reaches the standard of the reference value, it is considered that the fit is good.

The network relationship strength reliability value is 0.849, the network density reliability value is 0.912, the network size reliability value is 0.872, and the network centrality reliability value is 0.867, which all indicate that the dimensional consistency of the various variables in the enterprise network is better. In addition, the average variance extraction value also exceeded 0.5, of which the highest network density reached 0.741, and although the lowest network centrality was 0.612, it also reached the standard above 0.5, which all indicate that the convergence validity of each question item measurement is good. Figure 7 shows the test results of the convergence validity of the enterprise network.

4.5. Correlation Analysis between Variables and Structural Equation Test. From the perspective of the number of survey samples, the effective sample of this study is 487, with a capacity greater than 100, and it is suitable to use the maximum likelihood estimation method. In addition, using the maximum likelihood method to estimate the structural equation model requires that the sample must obey a normal distribution. Generally speaking, when the skewness and kurtosis values are close to 0, it indicates that the data obeys the normal distribution. At the same time, it is considered that skewness less than 2 and kurtosis less than 5 also obey normal distribution. The previous analysis of data skewness and kurtosis shows that the sample data of each item in this study meets the basic requirements of normal distribution. Therefore, comprehensively, this research is suitable for

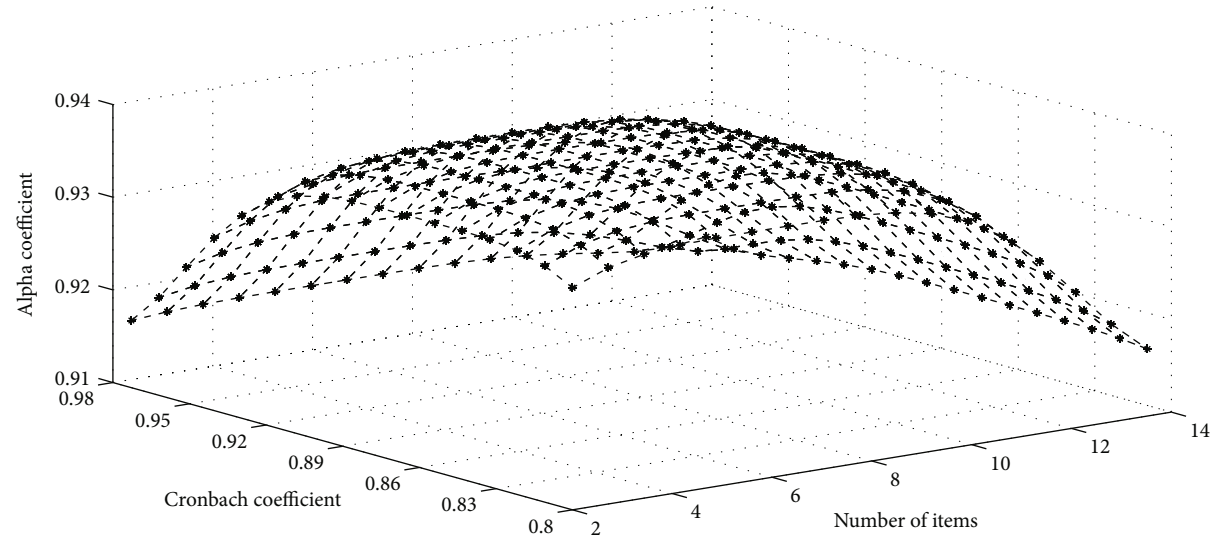

Figure 5: Reliability test of business model innovation.

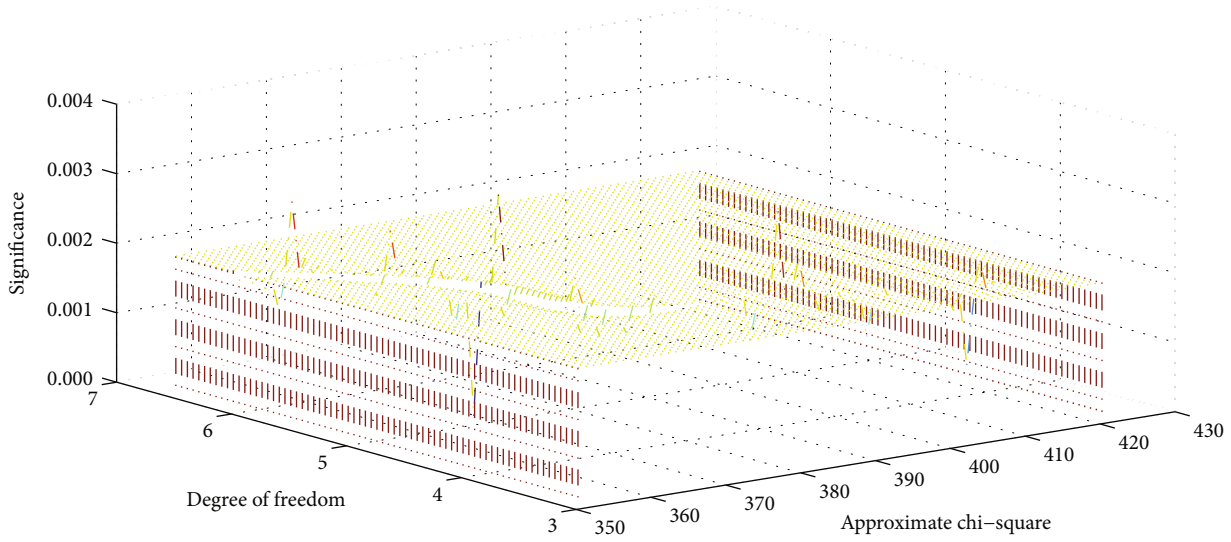

Figure 6: Bartlett's sphericity test.

structural equation modeling and analysis. The contribution ratio among variables is shown in Figure 8.

This research mainly explores the theoretical relationship between corporate network, marketing dynamic capabilities, and business model innovation and constructs a structural equation model. Structural equation model is a multivariate statistical method that deals with the relationship between multiple causes and multiple results. It can analyze the relationship between individual indicators and the overall indicators through the establishment of causal models, model parameter evaluation and later model evaluation. It can also test the causal path relationship of complex interactions between latent variables. Therefore, it can replace many methods such as multiple regression analysis and factor molecules, and is often used in the fields of social sciences, economics, and management. This research mainly explores the impact of the combination of different subdimensions of corporate network and marketing dynamic capabilities on business model innovation. It analyzes the relationship between individual indicators and their overall impact.

4.6. Path Analysis and Hypothesis Testing. It can be seen from Table 1 that the positive impact of corporate network on marketing dynamic capabilities has been initially confirmed. Looking specifically at it, the standard path coefficient of the network relationship strength on the product development process is 0.166, and it is significant at a P value less than 0.001, indicating that the network relationship strength has a positive effect on the product development process; that is, it has a positive effect. The standard path coefficient of the network relationship strength to the

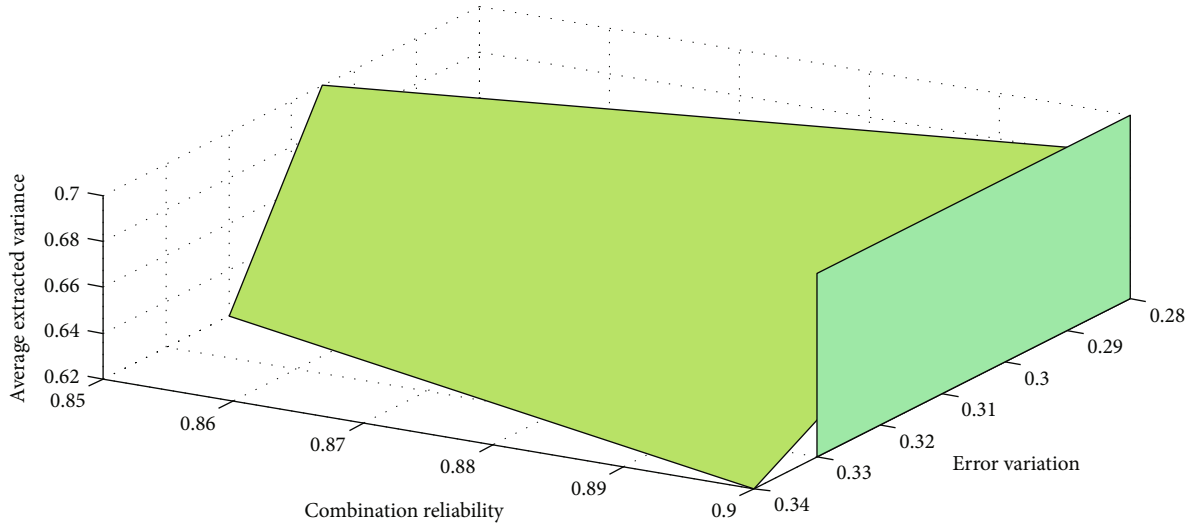

Figure 7: Convergence validity test of enterprise network.

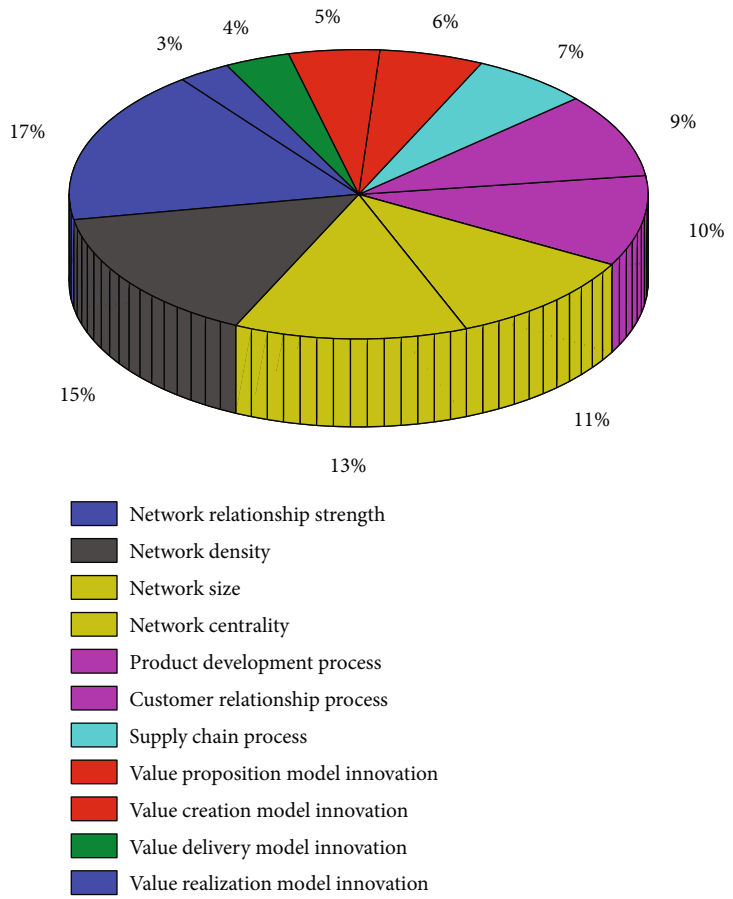

Figure 8: Contribution ratio among variables.

customer relationship process is 0.152, and it is significant at the level of P value less than 0.001, indicating that the network relationship strength has a positive effect on the customer relationship process. The standard path coefficient of the network relationship strength on the supply chain process is 0.151, and it is also significant at the level of P value less than 0.001, indicating that the network relationship strength has a positive effect on the supply chain process. But on the whole, it has the greatest positive impact on the product development process. Similarly, the standard path coefficients of network density on the three dimensions of marketing dynamic capabilities are 0.226, 0.255, and

Table 1: Hypothesis test results of the relationship between corporate network and marketing dynamic capabilities.

Relation	CR value	Standard path coefficient	Conclusion
Network relationship strength ⟶ customer relationship process	8.7	0.14	Positive impact
Network density ⟶ product development process	12	0.21	Positive impact
Network relationship strength ⟶ supply chain process	8.71	0.15	Positive impact
Network density ⟶ customer relationship process	12.1	0.25	Positive impact
Network centrality ⟶ supply chain process	11	0.21	Positive impact
Network centrality ⟶ customer relationship development process	11.2	0.19	Positive impact
Network scale ⟶ supply chain process	9.5	0.18	Positive impact
Network centrality ⟶ product development process	9.4	0.17	Positive impact
Network density ⟶ supply chain process	11.1	0.23	Positive impact
Network scale ⟶ customer relationship process	10.9	0.18	Positive impact

0.246, respectively, and they are all significant at a P value less than 0.001 and have the greatest positive impact on the customer relationship process. The standard path coefficients of the network size for the three core processes are all significant at a P value less than 0.001 and have the greatest positive impact on the product development process. The standard path coefficients of network centrality for the three dimensions are all significant at the level of P values less than 0.001 and have the greatest positive impact on the supply chain process. In summary, the four dimensions of the corporate network have positive effects on marketing dynamics.

4.7. Discussion. From the perspective of the influence of the corporate network on marketing dynamic capabilities, the four dimensions basically have a positive impact on marketing dynamic capabilities, but the degree of influence is different. Among them, the strength of the network relationship has the greatest positive impact on the product development process. The reason may be that the more frequent network partners make contact, the more they can create and provide new resources and ideas for enterprise product research and development and in turn can innovate products, enhance brands, and reduce R&D cycle and adjustment of design costs to enhance customer value, meeting effective customer needs to achieve cross-departmental business processes that drive new products. Network density has the greatest positive impact on the customer relationship process. When a company's network connection is denser, that is, the number of network partners contacted, the better it is to understand the needs of customers, stakeholders, etc., so as to actively realize the cross-departmental business process of its supply and meet the differentiated needs of customers. The scale of the network has the greatest positive impact on the product development process. The reason may be that the larger the scale of the company's network and the more network partners it cooperates with, the more conducive to the rapid expansion of the scale of development of the company. Network centrality has had the greatest positive impact on the supply chain process. The reason may be that the more important the company is in the network partners, the stronger the leadership role it exerts, and the more beneficial it is for the company to coordinate the interests of all parties. In turn, it promotes the development of new products, cross-departmental management of customer relationships, and cross-departmental supply chain management.

5. Conclusion

The product development process has a significant positive impact on business model innovation, of which the positive impact on value creation model innovation is the greatest. The reason is that product research and development and innovation are conducive to the realization of enterprises to create better value for customers and themselves. The customer relationship process has a significant impact on the four major innovation models, of which the most significant impact is on the value proposition model innovation. The reason is that cross-departmental customer relationship management is more conducive to further mining customers' potential demand points and value pursuits, which is more conducive to enterprises to clarify their value propositions and better provide customers with high-quality products and services. Supply chain process management has a positive impact on business model innovation, of which the most significant impact is on value delivery model innovation and value realization model innovation. The main reason is that the cross-departmental high-efficiency supply chain management is indeed conducive to coordinating the value proposition and interest relationship of the upstream and downstream partners of the enterprise.

Based on the common query tree algorithm, this paper adds query bits (i.e., the number of query forks), so that the algorithm has a faster tag identification under the full time slot state, and uses collision bits and total response bits to estimate the number of tags. According to the continuous situation of the highest collision bit, the number of query crosses (bit number) is automatically adjusted, and a variable bit dynamic query tree tag anticollision algorithm is designed. Combined with the settlement environment, the status of the identified tags is also improved. The new algorithm has improved progress in reducing idle time slots and reducing search depth. Under the premise of ensuring stability, the recognition efficiency of the algorithm is improved. The larger the scale of the enterprise network, the more network partners it cooperates with and the more it helps to provide various types of resources and different types of

innovative ideas for the enterprises in the network to promote the improvement of enterprise product development and quality. Based on network centrality and supply chain process, it can promote the innovation of value transmission mode and the innovation of value realization mode in business model innovation. That is to say, the positive impact of network centrality on the supply chain process is the most significant. When an enterprise is in a core and important position among network partners, the stronger the leadership role it exerts, the more beneficial it is for the enterprise to coordinate the interests of all parties and promote enterprises to develop new products and conduct cross-departmental management of customer relations and cross-departmental supply chain management. In the process of business model innovation and development, the supply of resources is undoubtedly a key prerequisite for business model innovation, especially network resources, which play an increasingly important role in business model innovation. Because in the competition of the business ecosystem, the mutual confrontation between enterprises has evolved and upgraded to the competition between enterprise networks including a series of stakeholders. However, favorable network resources, namely, strong network relationship strength, dense network density, huge network scale, and good network centrality, reflect the resource advantages that need to be recognized by enterprises in a complex and turbulent market environment. The competitive advantages are used by enterprises themselves to promote the innovative development of enterprise business models. The relationship dimension (network relationship strength) and structural dimension (network density, network scale, network centrality) of the corporate network basically have a positive impact on marketing dynamic capabilities, but the significant impact on each variable is different. Among them, network relationship strength and network scale are conducive to building the product development process in marketing dynamic capabilities, network density is conducive to building customer relationship processes in marketing dynamic capabilities, and network centrality is conducive to building supply chain processes in marketing dynamic capabilities.

Data Availability

The data used to support the findings of this study are available from the corresponding author upon request.

Conflicts of Interest

The author declares that Fang Chen have no known competing financial interests or personal relationships that could have appeared to influence the work reported in this paper.

Acknowledgments

This study was supported by the Scientific Research Launch Program of Shandong Management University: Research on the Application of Blockchain Technology in Reinsurance Transactions (Grant No. QH2021R05).

References

[1] R. Rodríguez, F. J. Molina-Castillo, and G. Svensson, "The mediating role of organizational complexity between enterprise resource planning and business model innovation," *Industrial Marketing Management*, vol. 84, pp. 328–341, 2020.

[2] I. Krawczyk-Sokolowska, A. Pierscieniak, and W. Caputa, "The innovation potential of the enterprise in the context of the economy and the business model," *Review of Managerial Science*, vol. 15, no. 1, pp. 103–124, 2021.

[3] M. Abdel-Basset, G. Manogaran, and M. Mohamed, "Retracted: Internet of Things (IoT) and its impact on supply chain: a framework for building smart, secure and efficient systems," *Future Generation Computer Systems*, vol. 86, pp. 614–628, 2018.

[4] S. Yan, B. Hu, G. Liu, X. Ru, and Q. Wu, "Top management team boundary-spanning behaviour, bricolage, and business model innovation," *Technology Analysis & Strategic Management*, vol. 32, no. 5, pp. 561–573, 2020.

[5] K. Buntak, M. Kovačić, and M. Mutavdžija, "Internet of things and smart warehouses as the future of logistics," *Tehnički glasnik*, vol. 13, no. 3, pp. 248–253, 2019.

[6] H. Gil-Gomez, V. Guerola-Navarro, R. Oltra-Badenes, and J. A. Lozano-Quilis, "Customer relationship management: digital transformation and sustainable business model innovation," *Economic research-Ekonomska istraživanja*, vol. 33, no. 1, pp. 2733–2750, 2020.

[7] X. Zhu, "Complex event detection for commodity distribution Internet of Things model incorporating radio frequency identification and wireless sensor network," *Future Generation Computer Systems*, vol. 125, pp. 100–111, 2021.

[8] A. Purusottama and Y. B. Kadarusman, "The essential benefits of an enterprise blockchain in business model innovation," *Jurnal Ekonomi Dan Bisnis*, vol. 24, no. 2, pp. 189–210, 2021.

[9] C. Z. Li, F. Xue, X. Li, J. Hong, and G. Q. Shen, "An Internet of Things-enabled BIM platform for on-site assembly services in prefabricated construction," *Automation in Construction*, vol. 89, pp. 146–161, 2018.

[10] F. A. Goni, A. Gholamzadeh Chofreh, Z. Estaki Orakani, J. J. Klemeš, M. Davoudi, and A. Mardani, "Sustainable business model: a review and framework development," *Clean Technologies and Environmental Policy*, vol. 23, no. 3, pp. 889–897, 2021.

[11] W. Liang, S. Xie, J. Long, K. C. Li, D. Zhang, and K. Li, "A double PUF-based RFID identity authentication protocol in service-centric internet of things environments," *Information Sciences*, vol. 503, pp. 129–147, 2019.

[12] M. Loon, L. Otaye-Ebede, and J. Stewart, "Thriving in the new normal: the HR microfoundations of capabilities for business model innovation. An integrated literature review," *Journal of Management Studies*, vol. 57, no. 3, pp. 698–726, 2020.

[13] B. Yan, Z. Jin, L. Liu, and S. Liu, "Factors influencing the adoption of the internet of things in supply chains," *Journal of Evolutionary Economics*, vol. 28, no. 3, pp. 523–545, 2018.

[14] M. Hock-Doepgen, T. Clauss, S. Kraus, and C. F. Cheng, "Knowledge management capabilities and organizational risk-taking for business model innovation in SMEs," *Journal of Business Research*, vol. 130, pp. 683–697, 2021.

[15] X. Li, C. Pak, and K. Bi, "Analysis of the development trends and innovation characteristics of Internet of Things technology – based on patentometrics and bibliometrics," *Technology*

Analysis & Strategic Management, vol. 32, no. 1, pp. 104–118, 2020.

[16] E. Parga Dans and P. Alonso González, "The unethical enterprise of the past: lessons from the collapse of archaeological heritage management in Spain," *Journal of Business Ethics*, vol. 172, no. 3, pp. 447–461, 2021.

[17] Y. Liu, K. D. Tong, F. Mao, and J. Yang, "Research on digital production technology for traditional manufacturing enterprises based on industrial Internet of Things in 5G era," *The International Journal of Advanced Manufacturing Technology*, vol. 107, no. 3-4, pp. 1101–1114, 2020.

[18] P. W. Moroz and E. N. Gamble, "Business model innovation as a window into adaptive tensions: five paths on the B Corp journey," *Journal of Business Research*, vol. 125, pp. 672–683, 2021.

[19] A. S. Brillinger, C. Els, B. Schäfer, and B. Bender, "Business model risk and uncertainty factors: toward building and maintaining profitable and sustainable business models," *Business Horizons*, vol. 63, no. 1, pp. 121–130, 2020.

[20] T. Haaker, P. T. M. Ly, N. Nguyen-Thanh, and H. T. H. Nguyen, "Business model innovation through the application of the Internet-of-Things: a comparative analysis," *Journal of Business Research*, vol. 126, pp. 126–136, 2021.

[21] F. Alamdar Youli, A. Mohammadi, M. Alimohammadlou, and A. Abbasi, "Designing a sustainable business model by using soft systems methodology and value triangle business model canvas (case study: Farassan Manufacturing and Industrial Company)," *Modern Research in Decision Making*, vol. 5, no. 1, pp. 95–117, 2020.

[22] C. Y. Yao and W. C. Hsia, "An indoor positioning system based on the dual-channel passive RFID technology," *IEEE Sensors Journal*, vol. 18, no. 11, pp. 4654–4663, 2018.

Hindawi
Journal of Sensors
Volume 2021, Article ID 5723567, 11 pages
https://doi.org/10.1155/2021/5723567

Research Article

Application of Heart Rate Acceleration Motion Wireless Sensor Fusion in Individual Special Competitive Sports

Bu Chang

Sports Department, China Jiliang University, Hangzhou, China

Correspondence should be addressed to Bu Chang; 10b1502038@cjlu.edu.cn

Received 28 October 2021; Accepted 2 December 2021; Published 25 December 2021

Academic Editor: Gengxin Sun

Heart rate monitoring is becoming more and more important in the development of modern health industry. At present, wireless sensor network equipment is mainly used to realize the real-time or periodic monitoring of human heart rate, so as to realize the health management of specific people. At the same time, the monitoring and analysis technology of heart rate is also widely used in special competitive sports. Through the real-time monitoring and analysis of athletes' heart rate, we can feedback and analyze their corresponding competitive state in real time, so as to monitor the sudden state of athletes, and also provide a basis for the improvement of athletes' later sports level. Based on this, this paper will use a single-chip microcomputer as the central data processing unit of the monitoring system at the hardware level, and inertial sensor and heart rate sensor at the sensor level. The system will design data acquisition module, motion positioning module, low-power module, athlete heart rate acquisition module, and motion state recognition module. Aiming at the low accuracy of traditional heart rate acceleration motion wireless sensor in competitive sports athletes' heart rate recognition and motion state recognition, this paper innovatively proposes an athlete heart rate recognition algorithm based on acceleration signal, which extracts the frequency-domain characteristics of motion signal. The time-domain and time-frequency characteristics of athletes' acceleration signal are used to realize the recognition of athletes' sports state, and the power spectrum cancellation technology is used to realize the accurate detection of athletes' heart rate. In order to verify the advantages of the hardware system and algorithm in this paper, three sports with quiet, dynamic, and random dynamic characteristics are selected for experimental verification. The experimental results show that the software algorithm proposed in this paper has obvious accuracy advantages in quiet and dynamic competitive sports compared with the traditional algorithm.

1. Introduction

The recognition, monitoring, and analysis technology of human heart rate and exercise state is widely used in health monitoring and exercise monitoring scenarios. At the same time, it is also an important index to evaluate exercise intensity and exercise quality. In professional competitive sports, real-time monitoring of human heart rate and corresponding sports status can not only fully obtain the energy consumed by athletes in the process of sports but also analyze their corresponding sports quality level. Systematic comprehensive analysis of the above two data can further improve athletes' sports level, improve defects in the process of sports, and improve sports quality [1–3]. The traditional heart rate detection of athletes is mainly based on hardware equipment such as heart rate belt, but the traditional hardware heart rate belt is inconvenient to wear, and its heart rate monitoring of athletes during exercise is not accurate [4]. The traditional athlete's movement state recognition technology is mainly embodied in three ways, which correspond to wearable sensor devices, external sensor devices, and wearable and hybrid integrated sensor devices, but these devices are more professional, and the corresponding equipment price and power consumption are relatively large, so they do not use athletes flexibly in competitive sports. It is convenient to wear, and the high price is not conducive to large-scale promotion [5–8]. Most of the detection algorithms of human heart rate and motion state also focus on the acceleration sensor algorithm, and a large number of heart rate and motion state recognition sensors are also

developed based on this kind of algorithm. However, various algorithms lack relatively unified standards, so they are subject to various factors, and their corresponding heart rate monitoring accuracy and motion state recognition accuracy are not high. Therefore, based on the above discussion, it is of great significance and practical value to analyze and develop a heart rate acceleration detection device with low power consumption and high precision [9].

As an important technology in various application scenarios, wireless sensor technology is the product of the cross development of information technology and Internet of Things technology. Wireless sensor technology can realize the real-time monitoring of a specific scene environment or the corresponding state of a specific individual [10]. In traditional wireless sensor networks, a large number of wireless sensors are arranged at specific nodes to realize the collection, monitoring, and transmission analysis of specific data. Based on this, the main characteristics of traditional wireless sensor networks are as follows. One of their characteristics is distributed and self-organized. In this process, the corresponding nodes can be connected with each other through corresponding algorithms and through mutual monitoring and analysis, the corresponding data nodes have the ability of self-organization, and the corresponding network nodes will automatically configure and manage without affecting the operation of the sensor network. The second characteristic of wireless sensor network is that the corresponding sensor network data has large scale and high density, and the redundant information between corresponding nodes can realize cooperative work [11–13]. The third characteristic of wireless sensor networks is that the corresponding node energy of wireless sensor networks is relatively limited. The main energy consumption of conventional wireless sensor networks is mainly based on communication, which increases with the communication distance. Therefore, the main data transmission mode in many wireless sensor networks is multihop mode. This paper mainly uses wireless sensors. Inertial sensor and heart rate sensor are reasonably arranged based on these two sensors, and the corresponding collected information is timely summarized into the single-chip microcomputer for data analysis, and corresponding conclusions are given [13, 14]. At the level of corresponding heart rate sensor, the main heart rate monitoring algorithms mainly include four calculation algorithms: blood oxygen heart rate monitoring, optical capacitance pulse wave heart rate monitoring algorithm, ECG algorithm, and arterial blood pressure method. These four traditional heart rate detection algorithms have various detection accuracy problems such as inaccurate detection in athletes' special competitive sports at the level of state recognition; the current inertial sensors mainly use acceleration sensors for motion state recognition. At present, such sensors have serious power consumption problems, so they do not meet the requirements of green low power consumption. At the same time, the relatively expensive price is not conducive to the wide promotion and use [15–18]. At the hardware system layout level, relevant scholars use the principle of hardware nearby layout to realize high-precision monitoring of key data, but this layout method will increase the volume of the system and the corresponding system energy consumption will increase.

In view of the above corresponding research status and existing problems, this paper will analyze and verify the hardware system and software algorithm based on wireless heart rate acceleration sensor. Based on the above situation, this paper will use a single-chip microcomputer as the core processing unit of the system and design the data acquisition system with inertial sensor and heart rate sensor as sensing equipment module, motion positioning module and low-power module, athlete heart rate acquisition module, and motion state recognition module. In view of the low accuracy of traditional heart rate acceleration wireless sensor in athletes' heart rate recognition and movement state recognition in competitive sports, this paper proposes an athlete's heart rate recognition algorithm based on acceleration signal to fully extract athletes' acceleration signal. At the same time, in the hardware design level, this paper optimizes the position of the sensor, so as to further optimize the hardware layout of the system and improve the detection accuracy of the sensor. In order to verify the advantages of hardware system and algorithm, three sports with quiet, dynamic, and random dynamic characteristics are selected for experimental verification. The experimental results show that compared with the traditional hardware and software, the hardware system and software algorithm have obvious accuracy advantages in quiet and dynamic competitive sports, but they have no obvious advantages in random competitive sports, which is also the focus of follow-up research in this paper.

The structure of this paper is arranged as follows: the second section of this paper will analyze and study the current research status of heart rate acceleration wireless sensor in competitive sports; the third section of this paper will carry out rational analysis and architecture design from the two aspects of hardware system and software algorithm of heart rate acceleration wireless sensor; the fourth section of this paper is mainly verification experiment and analysis; finally, this paper will give its summary.

2. Correlation Analysis: Current Research Status of Heart Rate Acceleration Wireless Sensor in Competitive Sports

At present, the application research of heart rate acceleration wireless sensor mainly focuses on health monitoring and sports condition detection of professional athletes. The main research contents include the design of hardware system and the research of software algorithm based on hardware system. Based on this, a large number of scientific research institutions and researchers have developed a variety of hardware systems and detection algorithms. At the hardware level, Japan and relevant European and American research institutions have developed a repeated athlete sports activity hardware system based on external sensors. It is mainly based on image sensors such as cameras and uses image sensors to recognize and detect the athlete's sports state. However, such hardware systems need a large number of

storage devices to store the recognized image data. Therefore, the corresponding equipment cost is high [19]. Relevant universities in the USA have developed a five-axis human motion recognition and heart rate monitoring hardware system based on accelerometers. Based on this hardware sensing system, the corresponding heart rate monitoring accuracy and motion recognition accuracy are gradually improved, but the human body recognition accuracy in the moving state is low, and there are many sensors corresponding to the hardware system, so the cost of the hardware system is increased [20]. In order to improve the disadvantages of the five-axis sensor network, relevant European researchers have optimized and improved the five-axis sensor. The improved sensor is set as a three-axis sensor, and its corresponding three-axis accelerometer is mainly worn at the chest position of athletes. It realizes the static, transitional, and dynamic monitoring of the human body through the human chest characteristic signal and neural network monitor and analyzes the heart rate and movement [21]. Relevant Japanese scientists have fully combined the advantages of external sensors and wearable sensors to develop hybrid motion state and heart rate monitoring equipment. It mainly uses sensors and cameras to propose a general recognition algorithm, which mainly processes various characteristic information such as image, sound, heart rate, and posture of the monitored athletes and the corresponding detection of such equipment. The accuracy is higher than the other two, but the corresponding equipment cost is higher. At the same time, the corresponding algorithm is complex and the resource consumption is large [22, 23]. At the level of corresponding heart rate monitoring and motion state recognition algorithms, the mainstream algorithms include vector machine algorithm, naive Bayesian algorithm, decision tree algorithm, k-value proximity algorithm, and other algorithms; at the level of heart rate monitoring and analysis, relevant European scholars put forward heart rate monitoring algorithm based on pulse wave, which adds accelerometer sensors to athletes during exercise; the athletes' motion information is obtained separately, and the corresponding heart rate noise is removed by using the motion signal auxiliary algorithm. Finally, the transmission of heart rate signal is realized through Bluetooth and other wireless sensing technologies [24, 25]. Based on the principle of photoelectric measurement, the corresponding researchers use multiple light-emitting diodes and photoelectric sensitive sensors to form the hardware part of heart rate monitoring. The photoelectric sensor detects the heart rate of athletes in competitive sports by sensing the change of light field intensity, but the accuracy of heart rate detected by this method still has errors [26–28].

3. Application Analysis of Heart Rate Acceleration Motion Wireless Sensor Fusion in Individual Special Competitive Sports

This section mainly analyzes the problems of heart rate monitoring and sports state recognition of athletes in competitive sports from the two aspects of hardware system and software system of heart rate acceleration motion wireless sensor. At the hardware system design level, the design is mainly based on a STM32 single-chip microcomputer. The design content includes the design of hardware module circuits such as data acquisition module, motion positioning module, low-power module, athlete heart rate acquisition module, and motion state recognition module. At the corresponding algorithm level, it mainly includes heart rate detection algorithm and motion recognition algorithm. This section mainly analyzes the principle and implementation process of the corresponding algorithm. The application principle block diagram of the corresponding heart rate acceleration motion wireless sensor in competitive sports is shown in Figure 1. From the figure, we can see the hardware and software logic block diagram of the system.

3.1. Hardware System Design of Heart Rate Acceleration Motion Wireless Sensor. At the hardware design level, the main application sensors of heart rate acceleration motion wireless sensor are inertial sensor and heart rate monitoring sensor. The corresponding core hardware includes CPU and its auxiliary circuit, data acquisition circuit, sensor circuit, wireless transmission circuit, positioning system module and its circuit, data storage part, and corresponding power management part circuit. The corresponding system hardware block diagram is shown in Figure 2. In some high-speed signal acquisition, this paper mainly depends on the related high-speed signal processing ad of ADI Company. At the same time, this paper optimizes the signal acquisition circuit on the PCB layout and fully considers the problem of signal integrity.

In the part of CPU and its auxiliary circuit design, the corresponding processor selection must have the characteristics of low price and low power consumption. Based on this, the processor selected in this paper is STM32. The processor has m4 core, which has rich resources, high cost performance, flexibility and stability, and relatively low power consumption. Based on this, the principle block diagram of the processor and its corresponding auxiliary circuit are shown in Figure 3. The corresponding data acquisition mainly collects the corresponding analog information through the ad module and transmits it to the central processing unit.

In the sensor hardware design part, it mainly includes inertial sensor and heart rate monitoring sensor. The inertial sensor mainly adopts a nine-axis inertial sensor, which integrates three-axis accelerometer, three-axis angular velocity, and three-axis magnetometer. At the same time, the sensor also has digital motion processor, so it has online programming processing function to a certain extent. Based on the sensor, the cost can be reduced, which mainly avoids the selection of complex peripherals and complex chips. The heart rate sensor used in this paper is mainly a biosensor based on pulse blood oxygen and heart rate function. Its specific composition includes LED lamp, infrared light, photoelectric detector, and subcircuit with environmental noise suppression ability. At the same time, the sensor hardware also integrates logic power supply and corresponding

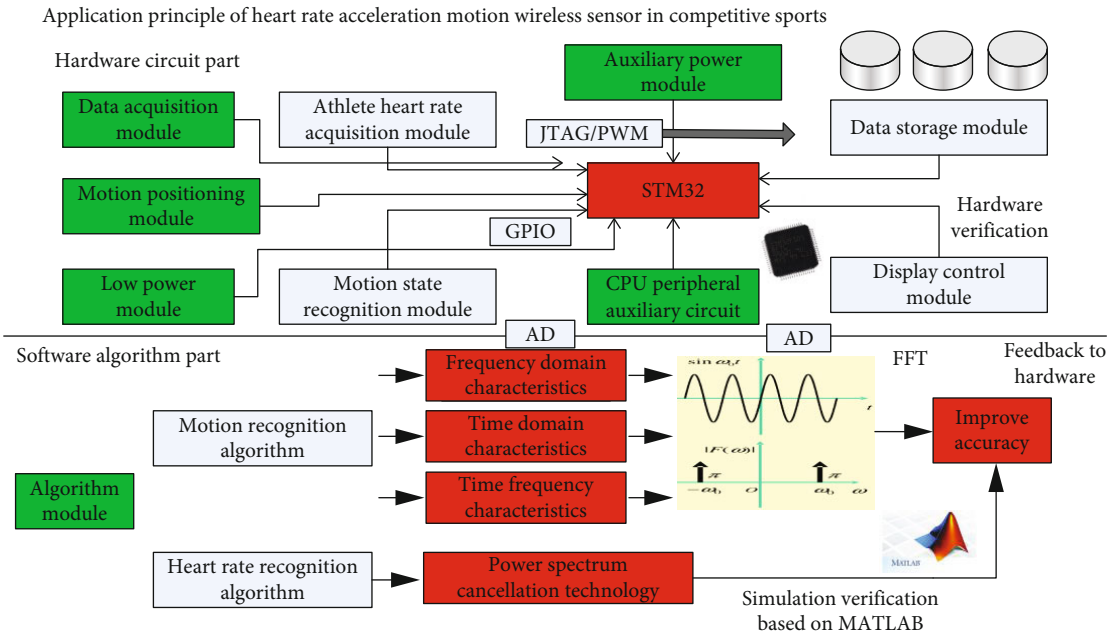

Figure 1: Application principle block diagram of heart rate acceleration motion wireless sensor in competitive sports.

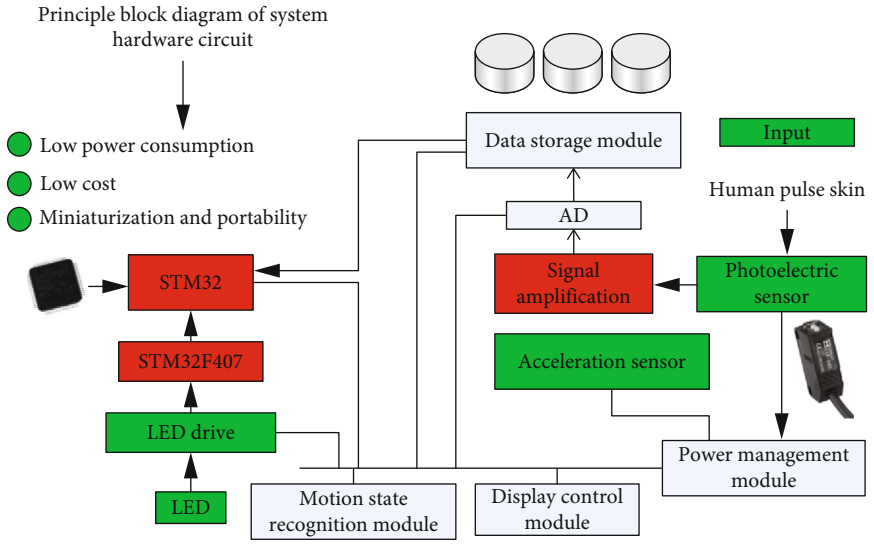

Figure 2: System hardware block diagram of heart rate acceleration motion wireless sensor in competitive sports.

subpower supply circuit. The heart rate sensor can transmit the collected data to the single-chip microcomputer through I2C interface, so as to detect and analyze the athlete's real-time heart rate through a certain data analysis algorithm. The physical sample corresponding to the sensor circuit module and the corresponding circuit principle block diagram are shown in Figure 4. From the figure, it can be seen that both the heart rate sensor and the inertial sensor have the characteristics of miniaturization and low power consumption.

In the corresponding wireless transmission and positioning part, the detection and positioning of athletes' sports state is mainly realized through GPS module, and the data transmission is realized through wireless transmission technologies such as Bluetooth or WiFi. The corresponding data storage circuit mainly realizes the basic reading and writing operation of data through SD card, which is also fully suitable for the application of a single-chip microcomputer system. C language is mainly used to read and write data storage. As an important power supply circuit of the system, the power management chip mainly selected in this paper includes mp1584 power conversion module and Texas Instruments related LDO chip. The corresponding wireless transmission module, CPU, and its auxiliary circuit are powered by LDO. The principle block diagram of the corresponding auxiliary power supply circuit and the

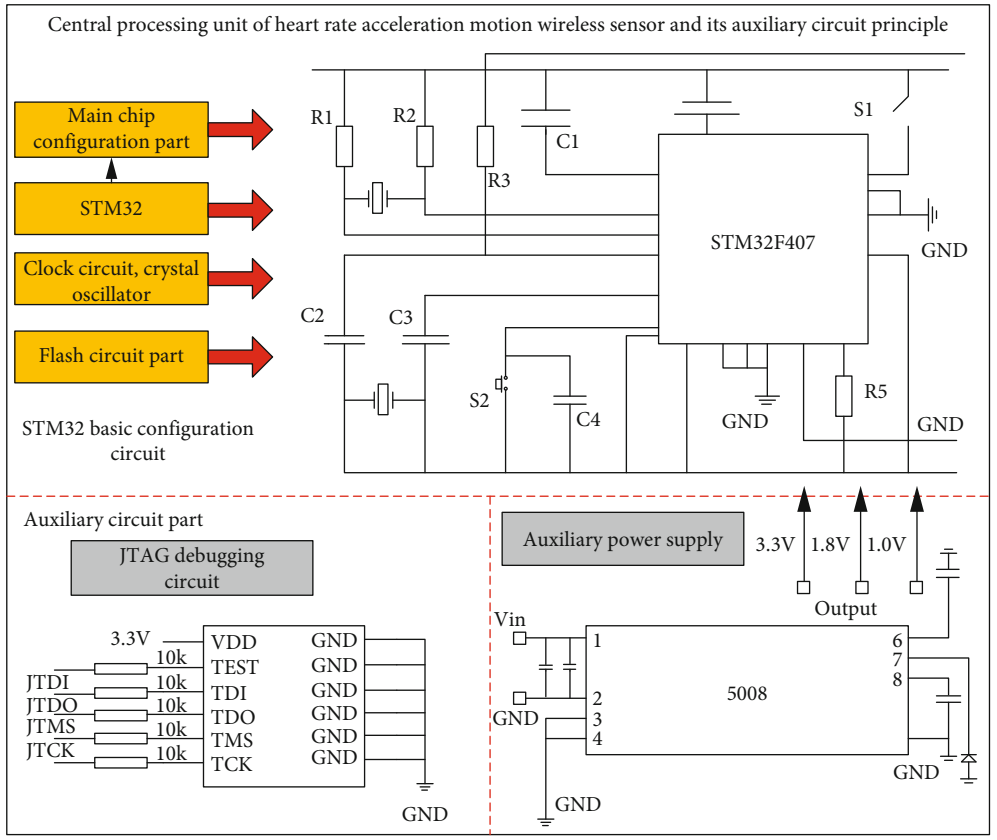

Figure 3: Heart rate acceleration motion wireless sensor CPU and its auxiliary circuit schematic diagram.

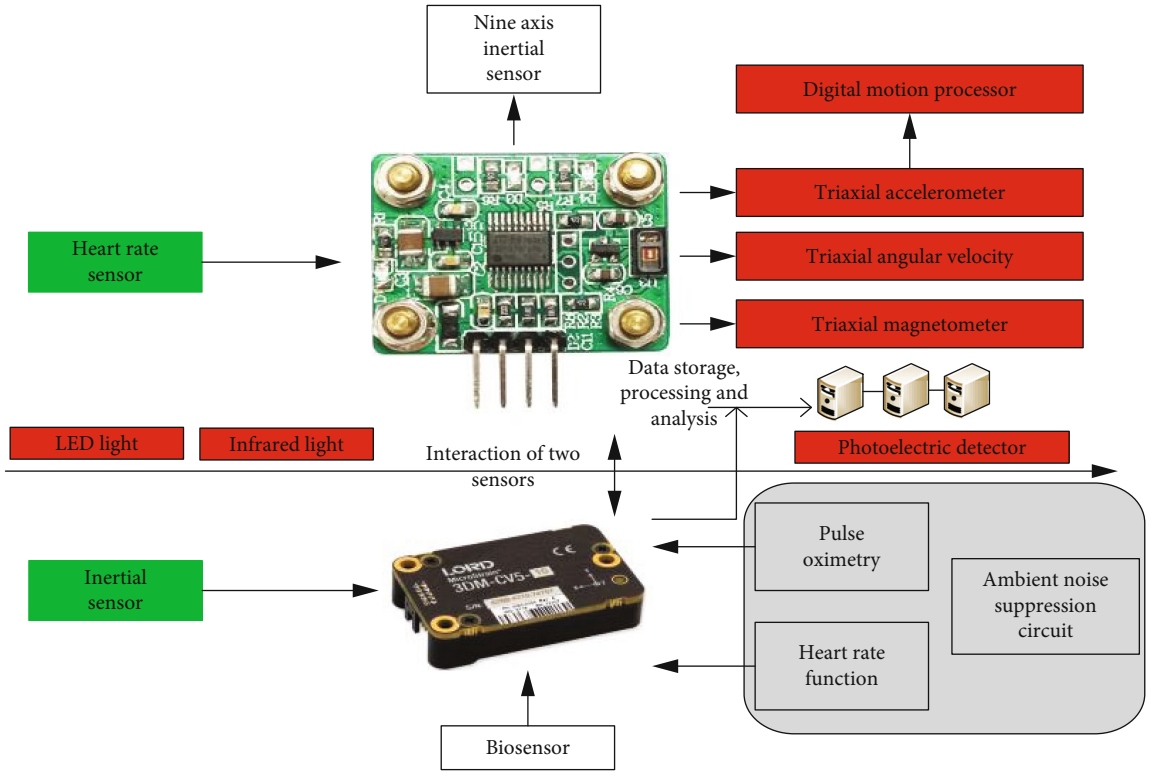

Figure 4: Circuit schematic diagram of sensor module in heart rate acceleration motion wireless sensor.

corresponding physical diagram of the module are shown in Figure 5. From the figure, we can see the power supply demand and power supply relationship of each module in the system.

In the system low-power design level, this paper selects the low-power chip selected by each subsystem circuit module for the design and verification of the peripheral circuit. At the same time, this paper also takes into account the low cost of the chip when selecting the chip, so as to achieve the low-power and low-cost characteristics of the whole hardware system.

3.2. Analysis of Heart Rate Acceleration Motion Detection Algorithm Based on Wireless Sensor. In view of the low accuracy of traditional heart rate acceleration motion wireless sensor in athlete heart rate recognition and motion state recognition in competitive sports, this paper proposes an athlete heart rate recognition algorithm based on acceleration signal, which fully extracts the frequency-domain, time-domain, and time-frequency features of athlete acceleration signal to realize the recognition of motion state; the accurate detection of athletes' heart rate is realized by power spectrum cancellation technology.

Before optimizing the algorithm, this paper first studies and analyzes the interference factors of heart rate and analyzes the static, running, random exercise, and various stimulating exercises. The results show that the human heart rate is mainly subject to the interference and drift of human motion, which will produce a lot of burrs, drift, and unclear dominant frequency caused by irregular motion. Based on the above phenomena, this paper first preprocesses and analyzes the collected signals and filters them to a certain extent before entering the optimized heart rate monitoring algorithm. Carry out accurate heart rate analysis on the processed data. The principle block diagram of the corresponding optimized heart rate monitoring algorithm is shown in Figure 6. It can be seen from the figure that the interference of the external environment on the collected information can be further reduced by power spectrum weighting.

It can be further seen from Figure 6 that the principle of the corresponding optimized heart rate detection algorithm is as follows:

Step 1. Intercept a certain length of information fragment from the collected pulse information, perform fast Fourier transform on the information fragment, and perform mathematical operation as shown in Equation (1) on the Fourier transform corresponding to the pulse wave, so as to obtain a unified and standardized Fourier spectrum.

$$X(i) = \frac{(X(1))^2}{\sum_{i=0,1,\cdots,n}^{i} (X(i))^2}, \quad X(i) = \frac{(X(i))^2}{\sum_{i=0,1,\cdots,n}^{i} (X(i))^2}. \tag{1}$$

Step 2. Considering the accuracy of the detected athlete's heart rate information, when selecting the data segment in Step 1 above, generally select a data segment of about 30 s-60 s and perform normalized Fourier transform for the data segment in this time period.

Step 3. Compare and analyze the Fourier transform of the processed pulse information with the motion Fourier spectrum and perform weighting operation. The corresponding weighting operation formula is shown in Equation (2). After the weighting operation, the corresponding motion components in the Fourier spectrum have been offset, and the spectrum information corresponding to the heart rate is highlighted.

$$Y(i) = \frac{(Y(1))^2}{\sum_{i=0,1,\cdots,n}^{i} (Y(i))^2}, \quad Y(i) = \frac{(Y(i))^2}{\sum_{i=0,1,\cdots,n}^{i} (Y(i))^2}. \tag{2}$$

Step 4. Smooth the Fourier transform of motion signal, and the corresponding processing formula is shown in the following equations:

$$F(1) = \left[\frac{1}{2 * n}\right] * [F(1+m)], \quad F(i) = \left[\frac{1}{2 * n}\right] * \left[\sum_{m=-n}^{m=n-1} (F(i+m))\right], \tag{3}$$

$$\hat{F}(1) = X(1) * Y(1), \quad \hat{F}(i) = X(i) * Y(i). \tag{4}$$

Step 5. Use the heart rate data collected before and after the time period to weigh the secondary power spectrum and use the Gaussian function to construct the weighting function. The corresponding weighted pulse spectrum curve function is shown in the following equation:

$$\hat{P}(1) = X(1) * Y(1) * W(1), \quad \hat{P}(i) = X(i) * Y(i) * W(i). \tag{5}$$

Step 6. Select the peak point in the curve as the final athlete's heart rate value, record the heart rate value in each period of time, and construct the heart rate curve.

Based on the above steps, the accurate detection of athletes' heart rate in competitive sports can be realized, and the analysis of athletes' heart rate transformation process can be realized at the same time.

At the level of motion state recognition algorithm, this paper mainly realizes the recognition of motion state based on the frequency-domain characteristics, time-domain characteristics, and time-frequency characteristics of athletes' acceleration signal. In the corresponding frequency-domain feature extraction process, the main frequency parameters of

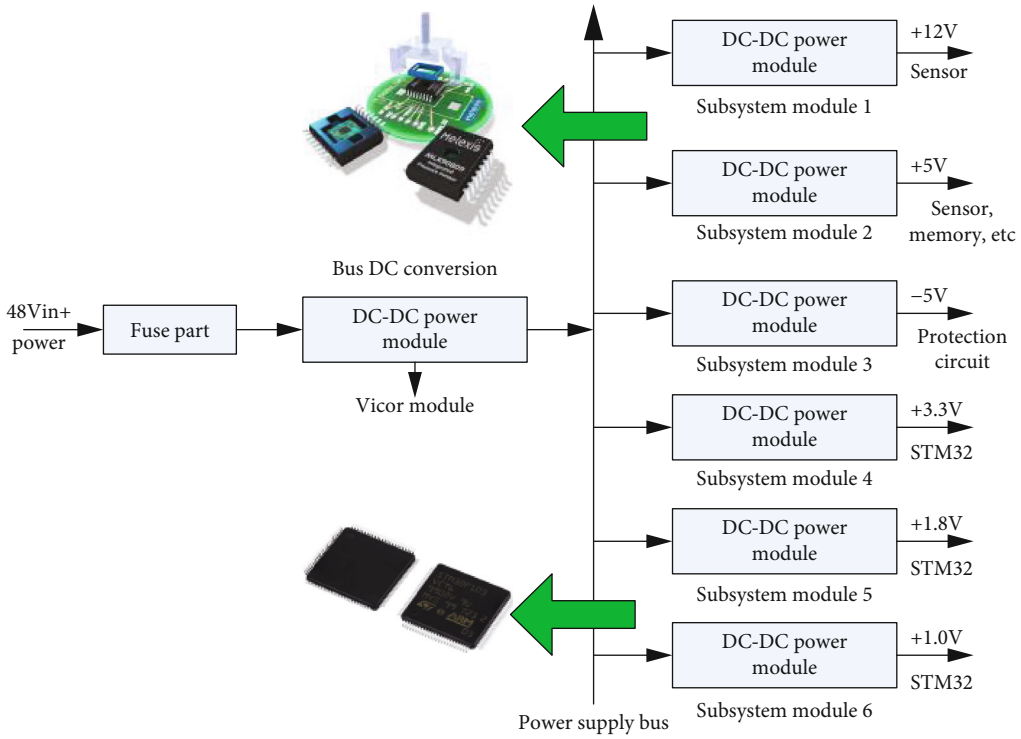

Figure 5: Circuit schematic diagram of power supply part in heart rate acceleration motion wireless sensor.

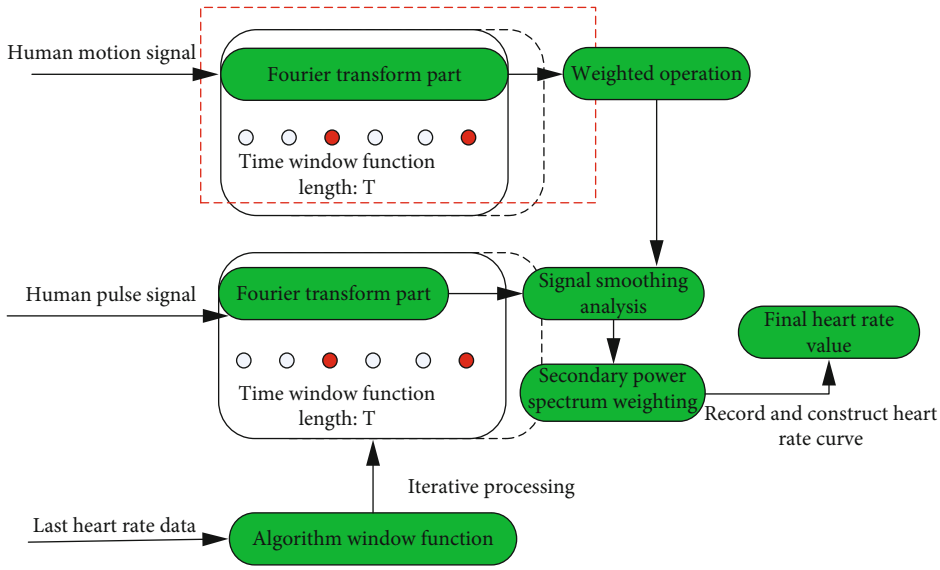

Figure 6: Principle block diagram of optimized heart rate monitoring algorithm.

motion information are extracted and taken as the main analysis object. The corresponding time-domain feature extraction mainly extracts the mainstream parameters such as the standard deviation of motion information and sample entropy. The extraction of corresponding time-frequency information is mainly based on the extraction and analysis of mixed parameters in time-domain and frequency-domain.

Based on the above two optimization algorithms and combined with the hardware design of the system, it can basically realize the accurate identification of athletes' sports state and heart rate information in competitive sports. At the same time, it has the characteristics of low power consumption, low cost, and high stability.

4. Experimental Verification and Analysis

In the experimental verification part, this paper mainly analyzes the athletes' movement state recognition and heart rate

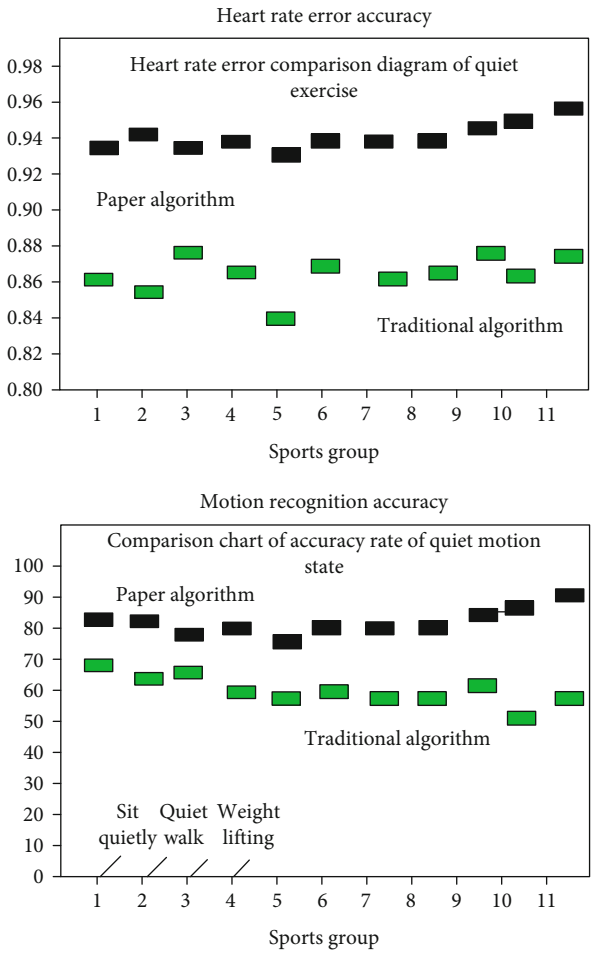

Figure 7: Comparison of heart rate error rate and exercise state accuracy under quiet exercise.

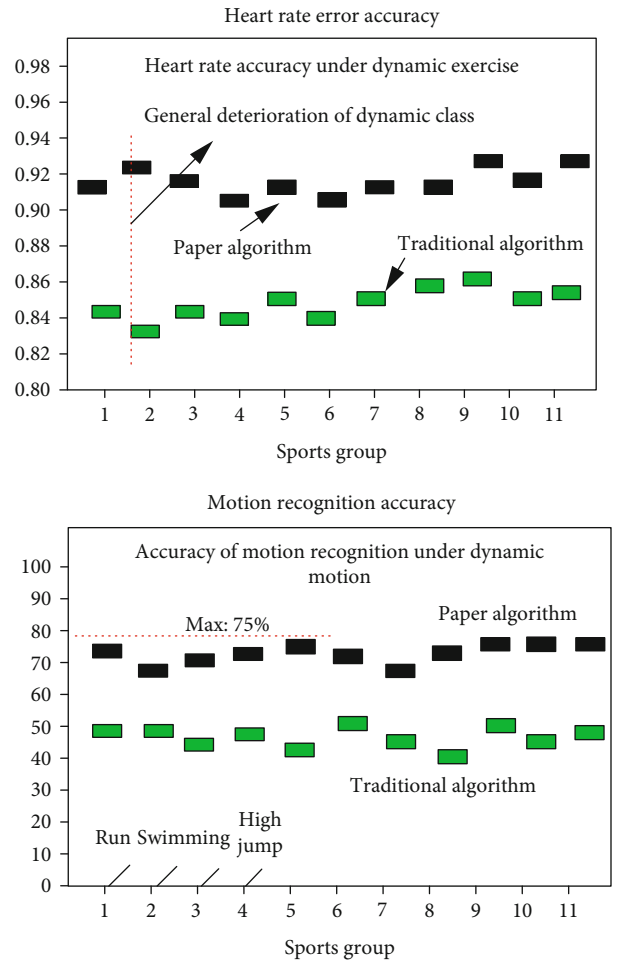

Figure 8: Comparison of heart rate error rate and exercise state accuracy under dynamic exercise.

monitoring based on the above designed hardware system. The corresponding experimental conditions are as follows: 9 athletes were selected to perform static sports, random sports, and dynamic regular sports, and three athletes were assigned to each group. Based on the above three groups of athletes and the corresponding sports, the experiment is carried out and the experimental results are analyzed. The evaluation criteria of the experiment are mainly heart rate error rate index and motion recognition accuracy index. The above three experiments have different requirements for data acquisition, but their corresponding data acquisition circuits are basically similar, but the corresponding dynamic acquisition needs antishake processing. The corresponding description is shown in the highlighted part of the article.

Firstly, three athletes in quiet sports wear the hardware system designed in this paper, and based on this, collect the athletes' corresponding heart rate information and sports information. In the case of control variables, compare it with the traditional algorithm. The corresponding experimental results are shown in Figure 7; as can be seen from Figure 7, in quiet motion, the heart rate error of the algorithm proposed in this paper is obviously low, and the recognition accuracy of the corresponding motion information is high.

For the corresponding athlete's heart rate information, heart rate error rate of sports information, and broken line diagram of sports state in the case of dynamic sports, as shown in Figure 8, it can be seen from Figure 8 that the heart rate error of the algorithm proposed in this paper is obviously low in dynamic sports, and the recognition accuracy of corresponding sports information is high. At this time, the corresponding heart rate error rate is relatively high compared with static motion, which also shows that the corresponding performance of this algorithm needs to be further improved when dealing with dynamic motion.

Heart rate information detection and motion state information monitoring experiments are carried out for random sports. The corresponding random sports in this paper mainly refer to basketball, because the dynamic and static properties of such sports are uncontrollable. The corresponding experimental results are shown in Figure 9. It can be seen from the figure that the algorithm proposed in this paper has detection accuracy and no longer has obvious advantages compared with the traditional algorithm. Therefore, it further points out the improvement of this algorithm in random motion.

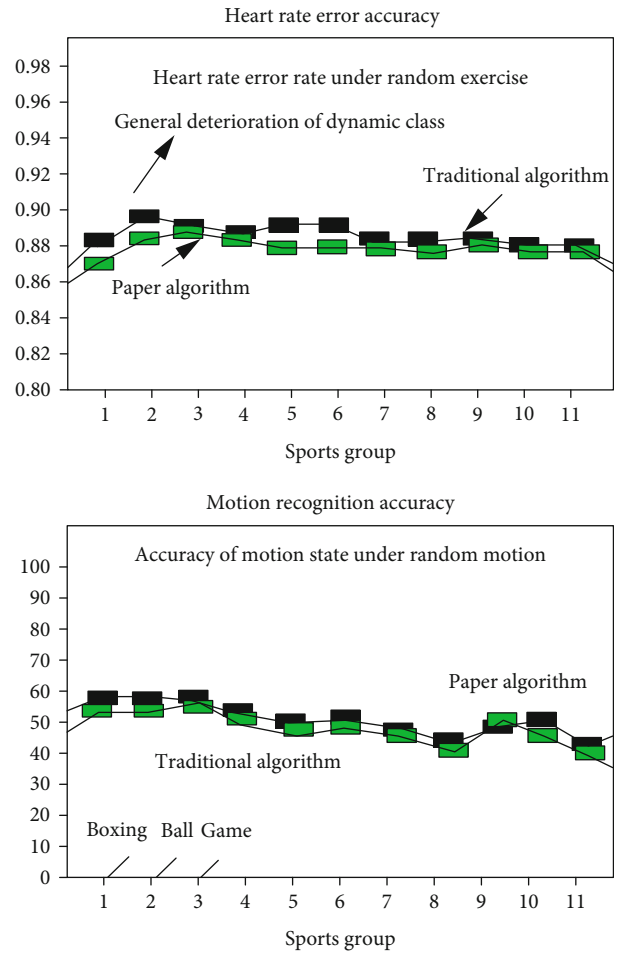

Figure 9: Comparison of heart rate error rate and exercise state accuracy under random exercise.

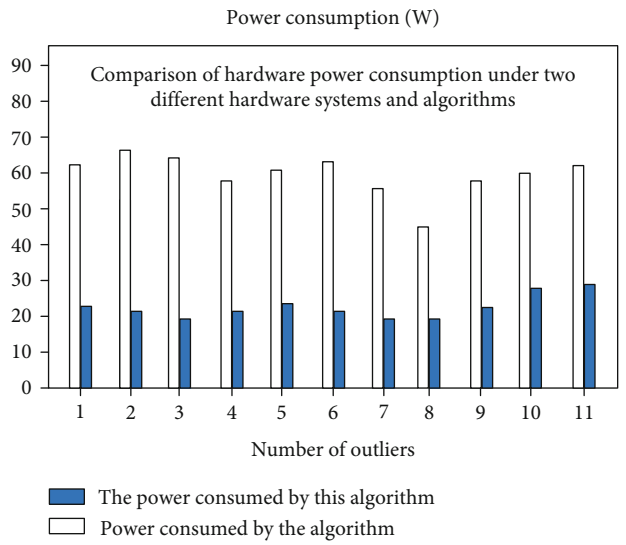

Figure 10: Comparison of hardware power consumption under two different hardware systems and algorithms.

In order to further verify the power consumption of the hardware designed in this paper, the power consumption comparison experiment is carried out with the traditional hardware system. When the control variables are guaranteed, the corresponding power consumption comparison line diagram of the corresponding two hardware systems under their respective algorithm consumption is shown in Figure 10. As can be seen from Figure 10, the hardware system and corresponding detection algorithm designed in this paper have lower power consumption under the same conditions, and their power consumption only accounts for about 70% of the traditional hardware system and its algorithm.

Based on the above experimental results and the corresponding experimental analysis, we can draw the following conclusions: compared with the traditional algorithms, the proposed algorithm has obvious detection accuracy advantages in quiet and dynamic motion, but its advantages are relatively small for random motion.

5. Conclusion

This paper mainly analyzes the research status of heart rate acceleration sensor fusion in individual special competitive sports and its disadvantages in hardware system components and detection algorithms. Aiming at the problem of low power consumption in the hardware system and the problem of low detection accuracy in the detection algorithm, this paper makes improvement and experimental verification. In the hardware part, this paper uses a single-chip microcomputer as the core processing unit of the system and uses inertial sensor and heart rate sensor as the sensing equipment. The system designs data acquisition module, motion positioning module, low-power module, athlete heart rate acquisition module, and motion state recognition module. In view of the low accuracy of traditional heart rate acceleration motion wireless sensor in athlete heart rate recognition and motion state recognition in competitive sports, this paper proposes an athlete heart rate recognition algorithm based on acceleration signal, which fully extracts the frequency-domain, time-domain, and time-frequency features of athlete acceleration signal to realize the recognition of motion state; the accurate detection of athletes' heart rate is realized by power spectrum cancellation technology. In order to verify the advantages of the hardware system and algorithm in this paper, three sports events with quiet, dynamic, and random dynamic characteristics are selected for experimental verification. The experimental results show that the hardware system and software algorithm proposed in this paper have obvious accuracy advantages in competitive sports with quiet and dynamic characteristics compared with traditional hardware and software, but they do not have obvious advantages in competitive sports with random sports characteristics, which is also the focus of follow-up research in this paper. This paper will focus on the accuracy of athletes' data acquisition in the case of irregular movement. At the same time, this paper will

continue to study the hardware optimization layout and signal integrity to make the system reach the best state.

Data Availability

The data used to support the findings of this study are available from the corresponding author upon request.

Conflicts of Interest

The author declares that there are no known competing financial interests or personal relationships that could have appeared to influence the work reported in this paper.

References

[1] N. Zhao, F. M. Li, and X. D. Liu, "Blind estimation of number of motion multi-human targets in wireless pyroelectric infrared sensor networks," *Infrared Physics & Technology*, vol. 61, no. 1, pp. 208–215, 2013.

[2] S. Z. Yu, G. Zhu, and S. Niu, "Nanometer resolution self-powered static and dynamic motion sensor based on micrograted triboelectrification," *Advanced Materials*, vol. 26, no. 11, pp. 1719–1724, 2018.

[3] H. Liu, Y. Wang, and K. Wang, "Turning a pyroelectric infrared motion sensor into a high-accuracy presence detector by using a narrow semi-transparent chopper," *Applied Physics Letters*, vol. 111, no. 24, article 243901, 2015.

[4] J. M. O'Kane and W. Xu, "Energy-efficient information routing in sensor networks for robotic target tracking," *Wireless Networks*, vol. 18, no. 6, pp. 713–733, 2012.

[5] B. H. Dobkin, "Wearable motion sensors to continuously measure real-world physical activities," *Current Opinion in Neurology*, vol. 26, no. 6, pp. 602–608, 2013.

[6] K. Martinez, J. K. Hart, P. J. Basford, G. M. Bragg, T. Ward, and D. S. Young, "A geophone wireless sensor network for investigating glacier stick-slip motion," *Computers & Geosciences*, vol. 105, no. 3, pp. 103–112, 2017.

[7] R. Tu and L. Wang, "Real-time coseismic wave retrieving by integrated Kalman filter with observations of GPS, Glonass and strong-motion sensor," *Advances in Space Research*, vol. 53, no. 1, pp. 130–137, 2014.

[8] X. Zhong, M. K. Law, and C. Y. Tsui, "A fully dynamic multimode CMOS vision sensor with mixed-signal cooperative motion sensing and object segmentation for adaptive edge computing," *IEEE Journal of Solid-State Circuits*, vol. 121, no. 99, pp. 1–14, 2020.

[9] C. H. Wu and Y. C. Tseng, "Exploiting multi-spatial correlations of motion data in a body sensor network," *IEEE Communications Letters*, vol. 16, no. 5, pp. 662–665, 2012.

[10] B. Zhang, J. Chen, L. Jin et al., "Rotating-disk-based hybridized electromagnetic-triboelectric nanogenerator for sustainably powering wireless traffic volume sensors," *ACS Nano*, vol. 10, no. 6, pp. 6241–6247, 2016.

[11] Y. Sang, X. Huang, H. Liu, and P. Jin, "A vibration-based hybrid energy harvester for wireless sensor systems," *IEEE Transactions on Magnetics*, vol. 48, no. 11, pp. 4495–4498, 2012.

[12] B. Y. Li and P. J. Chuang, "Geographic energy-aware non-interfering multipath routing for multimedia transmission in wireless sensor networks," *Information Sciences*, vol. 249, no. 8, pp. 24–37, 2013.

[13] M. Hamed, I. Paul, and M. H. Craver, "An implantable wireless inductive sensor system designed to monitor prosthesis motion in total joint replacement surgery," *IEEE Transactions on Biomedical Engineering*, vol. 4, no. 9, pp. 11–21, 2019.

[14] T. H. Kim, S. H. Kang, D. S. Kim et al., "Feasibility study of patient motion monitoring by using tactile array sensors," *Journal of the Korean Physical Society*, vol. 67, no. 1, pp. 199–203, 2015.

[15] G. Dai, T. K. Aman, and F. Dimaio, "The HCN channel voltage sensor undergoes a large downward motion during hyperpolarization," *Nature Structural & Molecular Biology*, vol. 26, no. 8, pp. 686–694, 2019.

[16] S. J. Paul, I. Elizabeth, and B. K. Gupta, "Ultrasensitive wearable strain sensors based on a VACNT/PDMS thin film for a wide range of human motion monitoring," *ACS Applied Materials & Interfaces*, vol. 13, no. 7, pp. 8871–8879, 2021.

[17] C. Mzab, D. Zy, and D. By, "Making use of nanoenergy from human-nanogenerator and self-powered sensor enabled sustainable wireless IoT sensory systems," *Nano Today*, vol. 36, no. 4, article 101016, 2021.

[18] A. M. Silva, D. A. Santos, C. N. Matias et al., "Accuracy of a combined heart rate and motion sensor for assessing energy expenditure in free-living adults during a double-blind crossover caffeine trial using doubly labeled water as the reference method," *European Journal of Clinical Nutrition*, vol. 69, no. 1, pp. 20–27, 2015.

[19] J. S. Kim, Y. H. Jeong, and J. H. Park, "A geometric approach for forward kinematics analysis of a 3-SPS/S redundant motion manipulator with an extra sensor using conformal geometric algebra," *Meccanica*, vol. 51, no. 10, pp. 2289–2304, 2016.

[20] S. Alamandala, R. L. N. Sai Prasad, R. K. Pancharathi, V. D. R. Pavan, and P. Kishore, "Study on bridge weigh in motion (BWIM) system for measuring the vehicle parameters based on strain measurement using FBG sensors," *Optical Fiber Technology*, vol. 61, no. 3, article 102440, 2021.

[21] G. Peng, X. Liu, and S. Tang, "Enabling coverage-preserving scheduling in wireless sensor networks for structural health monitoring," *IEEE Transactions on Computers*, vol. 65, no. 8, pp. 2456–2469, 2016.

[22] N. Winer, W. D. Mason, C. H. Carter et al., "Effects of atenolol on blood pressure, heart rate, renin, and norepinephrine during exercise," *Clinical Pharmacology & Therapeutics*, vol. 26, no. 3, pp. 315–325, 2016.

[23] D. Jarchi and A. J. Casson, "Towards photoplethysmography-based estimation of instantaneous heart rate during physical activity," *IEEE Transactions on Biomedical Engineering*, vol. 64, no. 9, pp. 2042–2053, 2017.

[24] C. R. Bellenger, J. T. Fuller, R. L. Thomson, K. Davison, E. Y. Robertson, and J. D. Buckley, "Monitoring athletic training status through autonomic heart rate regulation: a systematic review and meta-analysis," *Sports Medicine*, vol. 46, no. 10, pp. 1461–1486, 2016.

[25] G. Toni, M. Belvederi Murri, F. M. Piepoli et al., "Physical exercise for late-life depression: effects on heart rate variability," *The American Journal of Geriatric Psychiatry*, vol. 24, no. 11, pp. 989–997, 2016.

[26] D. Zammit-Mangion and M. Eshelby, "Evaluation of takeoff performance monitoring algorithm in large jet transport

operations," *Journal of Aircraft*, vol. 43, no. 1, pp. 201–206, 2015.

[27] L. Cadmus-Bertram, R. Gangnon, E. J. Wirkus, K. M. Thraen-Borowski, and J. Gorzelitz-Liebhauser, "The accuracy of heart rate monitoring by some wrist-worn activity trackers," *Annals of Internal Medicine*, vol. 166, no. 8, pp. 610–612, 2017.

[28] A. Yamamoto, H. Nakamoto, Y. Bessho et al., "Monitoring respiratory rates with a wearable system using a stretchable strain sensor during moderate exercise," *Medical & Biological Engineering & Computing*, vol. 57, no. 12, pp. 2741–2756, 2019.

Hindawi
Journal of Sensors
Volume 2021, Article ID 5618538, 9 pages
https://doi.org/10.1155/2021/5618538

Research Article

Design of Remote Environmental Monitoring Network Based on Intelligent Sensor Network Address Allocation and Addressing

Jinyong Liu

Guangdong University of Science and Technology, Dongguan, Guangdong 523083, China

Correspondence should be addressed to Jinyong Liu; liujinyong@gdust.edu.cn

Received 8 November 2021; Revised 26 November 2021; Accepted 2 December 2021; Published 24 December 2021

Academic Editor: Gengxin Sun

Based on the wireless sensor network, this paper combines node monitoring data with intelligent network address management. Users can view real-time environmental data through a computer or mobile phone and can manually remotely manage the environmental adjustment equipment of the network address through the mobile phone. This article first discusses the research background of the subject, introduces the current domestic and foreign research status of WSN in environmental detection, and analyzes the reasons for choosing ZigBee network as the wireless transmission environment of the intelligent monitoring system. Secondly, the structure, layered model, and key technologies of wireless sensor networks are introduced, and it is pointed out that ZigBee technology, which has the characteristics of low power consumption, reliable communication, self-organization of the network, strong self-healing ability, and low cost, is very suitable for application in the environment. Then, it analyzes TI's protocol stack Z-Stack based on the ZigBee2006 standard and analyzes the network address assignment and addressing in Z-Stack, the process and steps of node binding, the routing mechanism and routing maintenance, and channel configuration. The realization of other functions was discussed in depth. During the simulation experiment, in the hardware design of the intelligent monitoring system, the network node was divided into two parts: the core board and the backplane. The crystal oscillator, power supply, antenna, and I/O port circuits of the core board were designed, and the data acquisition, relay, and power supply of the backplane were designed. Finally, this paper studies the data security issues in the environmental monitoring network and proposes two solutions to control network access and data encryption. Experimental results show that in terms of low-power design, the energy of the entire system is calculated to determine the factors that affect the power consumption of the system and methods such as increasing the node sleep time to ensure that the system can work for a long time.

1. Introduction

Environmental monitoring has the characteristics of large number of monitoring points in the area, long monitoring time, and complicated monitoring conditions. Aiming at the shortcomings of traditional environmental monitoring methods such as difficult network layout and low node intelligence, a wireless sensor environmental monitoring network system based on the ZigBee protocol is designed [1]. The system has the advantages of large number of nodes, high reliability, convenient network layout, and remote control. However, the monitoring device using a wired network is easily affected by factors such as geographical environment and cumbersome wiring, and the cost and difficulty of installation, maintenance, and update are relatively large, which brings certain inconvenience to the majority of users, so it is of little promotion. Therefore, there is an urgent need for a wireless intelligent monitoring system that can detect environmental information and take corresponding measures according to the results during the planting process of the network address [2–5].

Considering that wireless sensor network technology is more and more used in the field, and WPAN based on IEEE 802.15.4 standard has the advantages of low speed, low cost, and low power consumption, this paper proposes based on the existing research at home and abroad. The design scheme of the visual monitoring system of the network address environment based on the wireless sensor network

is of great significance to the current network control system [6–8]. The web client can display historical data and real-time data. The Android client has the update function of real-time data, the display function of the map, and the alarm mechanism of abnormal data. The design of the client provides users with visualization intuitive data. The design of the system mainly includes the design of the lower computer for collecting network environment parameters and the design of the upper computer for intelligent monitoring of the network environment. The lower computer adopts the ZigBee wireless sensor network. In order to realize the data collection and transmission function of the wireless sensor network, the hardware node is designed in a modular way. Hardware nodes mainly include sensor modules that collect environmental parameters in the network, control modules for adjusting network environment equipment, wireless communication modules, processor modules of the CC2530 chip, serial communication modules, and power modules for hardware energy control [9–11].

In the software design of the intelligent monitoring system, IAR is used to complete the compilation of the Zigbee networking protocol stack, so that the nodes can form a network and perform data transmission in a wireless and autonomous manner; the PC monitoring platform uses Visual C++ as the development environment and uses the industrial control iocomp to realize the functions of network address environment data display, fuzzy temperature control, server construction, and alarm; Android client uses the Eclipse development platform, designed for the menu, user interface, server connection, and other modules and realizes the use of mobile phones to obtain environmental data and control network addresses. The routing protocol of wireless sensor networks is studied, RPL (Routing Protocol for Lossy and Low.power Networks) routing is implemented, and the performance of RPL routing is analyzed. The comparison with CTP (CollectionTree Protoc01) routing shows the good performance of RPL routing. Based on the RPL routing, a wireless sensor network-based environmental data collection function is designed; the function of the server and the MySQL database for storing environmental data are designed, and the network communication between the server and the client is realized.

2. Related Work

At present, researchers have many scientific research results in the fields of industrial control, intelligent transportation, smart home, environmental monitoring, etc. In the current research results, different researchers use different technologies in different directions to achieve research goals. For example, based on the research of ZigBee protocol, based on Tinyos operating system, and based on the research of embedded Linux system, some researchers used GPRS, TCP/IP, etc. to study the combination of wireless sensor network and the Internet [12–14].

Trevathan and Johnstone [15] proposed a biochemical sensor that detects hazardous substances and hazardous material information to reduce damage to human safety and designed a digital detection device for ambient temperature and light intensity to achieve real-time temperature and light in various environments and detect and display the obtained data in real time to realize human-computer interaction. Iqbal et al. [16] studied the WSN gateway and designed the interconnection between the wireless sensor network and the external network, designed the network measurement and control system, and realized the collection of network environment parameters on the hardware and the acquisition and processing of the data on the software. Yadav et al. [17] studied agricultural monitoring based on wireless sensor network technology and implemented it on hardware and designed the communication protocol. The wireless sensor node sends environmental data to the master node every 15 minutes through the GPRS gateway, and the master node uses TCP. The IP protocol forwards the data to the remote server. Mukherjee et al. [18] designed an environmental monitoring system based on wireless sensor network precision agriculture. It can automatically collect temperature, humidity, pressure, and other data and transmit the data to a remote server through GPRS. This system also includes web services, google map, and SMS (Short Messaging Service) alarm and other services. Adeel et al. [19] proposed a remote agricultural network monitoring system based on WSN and SMS. It can accurately capture the environmental information in the greenhouse and send short messages to farmers when the environmental data changes abnormally. The location environment is difficult to detect. They designed an ARM-based multilocation wireless detection system, which uses an ARM controller to control the SMS TC35i module and send and receive SMS messages.

Because the scale of sensor network deployment is very large, how to connect the nodes in the sensor network to the Internet is a difficult point. We know that IPv4 addresses are almost exhausted at present, and it is no longer necessary to allocate IPv4 addresses to sensor network nodes. Because of the huge number of IPv6 addresses, the application of IPv6 technology in wireless sensor networks will enable each node to be assigned an IP address. Therefore, IETE established the 6LoWPAN (IPv6 over Low Power WPAN) working group, committed to the standardization of the IPv6 protocol on the IEEE802.15.4 standard. The randomness of environmental monitoring is reflected in two aspects. One is that the data collected at one point is very random. Therefore, in order to obtain accurate results, it is generally necessary to collect large-scale and large data points through statistical methods. In addition, on the whole, the type, quantity, size, and temporal and spatial distribution of information are all randomly affected by people's social behavior, natural factors, and specific environmental conditions, with obvious randomness [20].

3. Design of a Network Model for Remote Environmental Monitoring Based on Address Allocation and Addressing of Smart Sensor Networks

3.1. Smart Sensor Network Topology. Intelligent wireless sensor network refers to the detection of environmental conditions in the area by sensor nodes distributed in the sensing field, and the data is fused and transmitted. Finally, the

gateway node is responsible for processing the data and passing it to the upper computer for further processing. It includes cutting-edge technology such as sensor technology, microprocessors, and wireless communication networks. Figure 1 is the smart sensor network topology.

The architecture of the WSN network is mainly composed of the following points: the terminal node is an important component of the sensor network, which contains an embedded system, which is mainly responsible for detecting and sending the data information of the detection target in the sensing field. It is generally battery-powered and located in the WSN. The routing node is more capable of data processing and forwarding than the terminal node. It can be regarded as an enhanced terminal node, which is essentially a terminal node that does not contain a detection module.

$$U\{[x(tn) > x(tn)] \mid x(tm-1) = v(tm-1), x(tm-2) = v(tm-2)\},$$
$$U_{st}^{m+n} = \begin{bmatrix} U_{11}^{m+n} & U_{12}^{m+n} & U_{1s}^{m+n} \\ U_{21}^{m+n} & U_{22}^{m+n} & U_{2s}^{m+n} \\ U_{s1}^{m+n} & U_{s2}^{m+n} & U_{ss}^{m+n} \end{bmatrix}. \tag{1}$$

The coordinator is mainly responsible for the formation, maintenance, and joining of the entire sensor network. It is generally connected to the local computer and acts as a gateway; the local computer visually displays and stores the information collected by the terminal nodes. On-site detection information is sent to a remote computer through the Internet network, so that users can remotely read information and send control information.

$$U(x, y, s, t) = \int (I(x, y) - c(1) + (s-1) \times I(x, y, s, t)) \times dA,$$
$$\begin{cases} g(s, t) = w(s, t) \times x + w(s, t) \times x(i-1), \\ w(s, t) = f(i, x). \end{cases} \tag{2}$$

The network architecture mainly refers to the layered structure of network protocols. The network protocol architecture of WSN is designed based on the Internet architecture. Due to the differences in bandwidth, node capabilities, operating environment, network scale, communication range, and specific application requirements, its network protocol architecture is somewhat different from the Internet network structure.

$$\begin{cases} U_{st}(m, n) \geq 0, \quad s, t \in R, \\ \sum_{i=1}^{k} U_{st}(m, n) < 0, \quad s, t \in R. \end{cases} \tag{3}$$

Considering the cost of equipment hardware, the carrier sense multiple-access method usually used in practical applications is Carrier Sense Multiple Access-Conflict Avoidance (CSMA-CA). In the absence of direct conflict control, the data link layer generally adopts error control methods to ensure the success rate of node transmission. The used error detection technology such as cyclic redundancy check with response signal is usually a very effective error control technology in WSN.

$$\begin{cases} \varepsilon(x, x) - \dfrac{\partial f(x, y, z)}{\partial x} = 0, \\ \varepsilon(y, y) - \dfrac{\partial f(x, y, z)}{\partial y} = 0, \\ \varepsilon(z, z) - \dfrac{\partial f(x, y, z)}{\partial z} = 0. \end{cases} \tag{4}$$

During signal transmission, the ZigBee network accesses the MAC layer. MAC selects the CSMA/CA control algorithm, which can effectively bypass the mutual interference and accumulation of signals in the transmission process. At the same time, the control layer can be compatible with the confirmed signal communication method and more efficiently confirm the safe communication of the signal.

3.2. Network Address Allocation Design. The address allocation module of the Zigbee network consists of a variety of nodes, including terminal nodes, routing nodes, and coordinator nodes (gateway nodes). The terminal nodes are divided into data collection nodes and environmental control nodes. The data collection nodes contain multiple environmental sensors. The main function is to detect various environmental factors and convert them into electrical signals. In order to detect the environmental information of the network address more comprehensively, the user data collection nodes can be placed in different locations of multiple network addresses; the environmental control node is controlled by the intelligent monitoring system and controls the environment adjustment equipment in the network through a relay to ensure that the network address always keeps the crop in the optimal growth environment.

The routing node is more capable of data processing and forwarding than the terminal node. It can be regarded as an enhanced terminal node, which is essentially a terminal node that does not contain sensors. The coordinator node is mainly responsible for the formation and maintenance of the entire sensor network and controls the joining of terminal nodes. It is generally connected to the local computer and acts as a gateway. Figure 2 shows the WSN network node address allocation.

Route selection is a process in which devices in the network cooperate to find and establish routes, usually initiated by a router. It searches all possible routes between the source address and the destination and tries to find the best route. The basis of route selection is the least link cost, that is, the route with the least consumption is selected. Each node must constantly track the link consumption of all its neighbor nodes, which is a function of the signal strength it receives. The cost of a route is to add up the cost of all the links from the source address to the destination and choose the route with the least cost. The mesh network provides route maintenance and self-repair functions. The middle

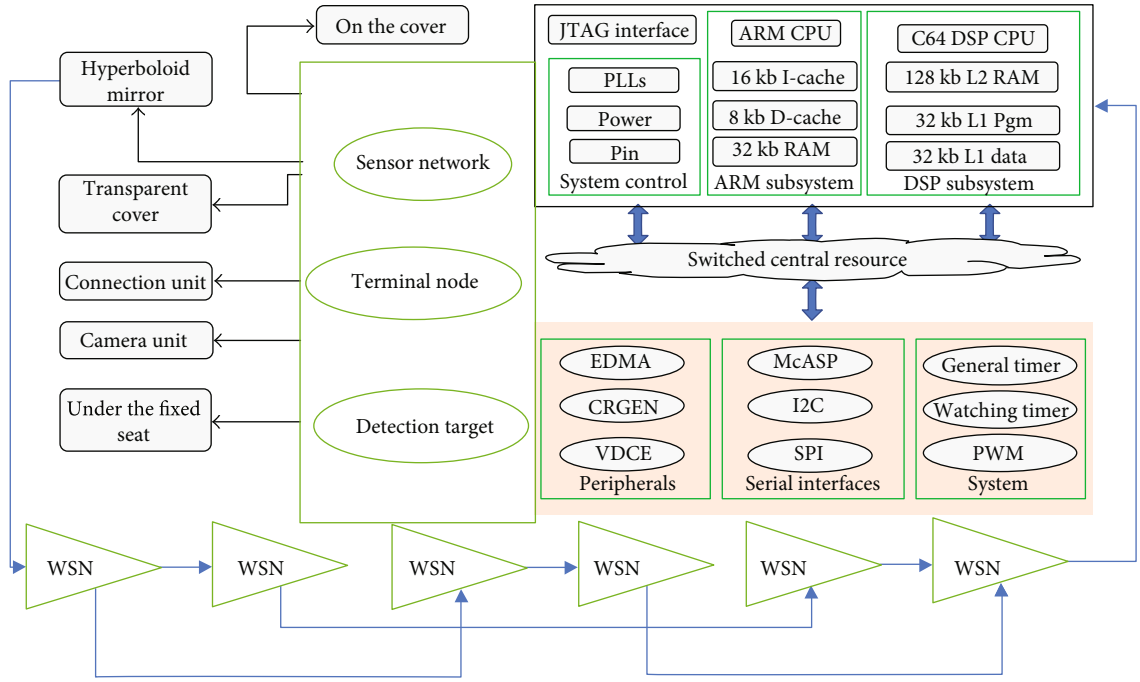

Figure 1: Smart sensor network topology.

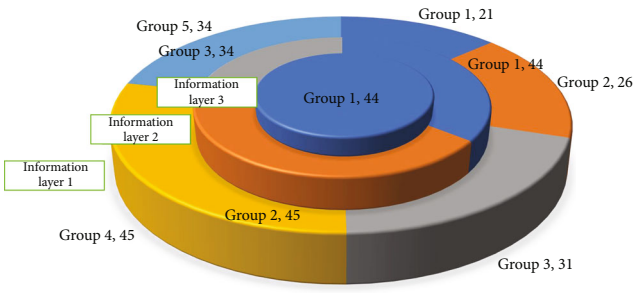

Figure 2: WSN network node address allocation.

node will record the transmission failure on the link. If a link is considered to be down, all nodes on this link will start link repair. It usually starts a rediscovery process the next time after a data packet arrives on this link. If the process of rediscovering the route cannot be started, or fails for some reason, it will send a RERR to the sending node of the data packet, and then, it will reinitiate a route discovery process. Either way, the establishment of the route will be completed automatically.

3.3. Environment Remote Monitoring Architecture. The environmental remote monitoring data link layer is responsible for the media access control (MAC) and error control of the wireless sensor network. Carrier Sense Multiple Access (CSMA) is the most commonly used data access technology in WSN, and its working principle is the network node monitors whether the communication channel is free before sending data. If the channel is occupied, the node will detect again within a certain period of time and close the circuit during the waiting period to save energy; the network layer is responsible for network connection, routing management, and congestion in the wireless sensor network cControl, etc., compared with the general network; WSN has the characteristics of high node distribution density and large number, so the network has greater limitations in computing power, storage capacity, and energy consumption.

The transmission layer is mainly responsible for the control of data stream transmission in WSN to ensure the safety and reliability of data transmission. In actual use, since WSN is relatively small compared with traditional Internet data transmission, the necessity of the transmission layer of wireless sensor network has not yet been obtained. Figure 3 is the process of environmental remote monitoring architecture.

In the network, if you want to send data or commands to other nodes, use the AF_DataRequest() function. This function requires that the sending destination address and Endpoint must be known. Endpoint is a data addressing method defined in the ZigBee communication protocol. Each device supports up to 240 Endpoints. For example, a button, a sensor, or a light can be an Endpoint. The destination address mode has the following values: AddrNotPresent (unknown address mode), Addr16Bit (short address mode), AddrGroup (group address mode), and AddrBroadcast (broadcast mode).

The concept of kernel has two purposes: one is as the calculation basis of attribute reduction, and the other is that it can be interpreted as the most important conditional attribute in attribute reduction. These address modes are all necessary, because in ZigBee, data packets can be unicast, multicast, or broadcast. The function ZDO_ProcessMgmtLeaveReq can be used to disconnect the node itself or its child nodes from this network, and it does so based on the IEEE address provided. If a node leaves itself from the network, it usually waits for 5 seconds and then restarts. After restarting, the node enters a quiescent state. It will not try

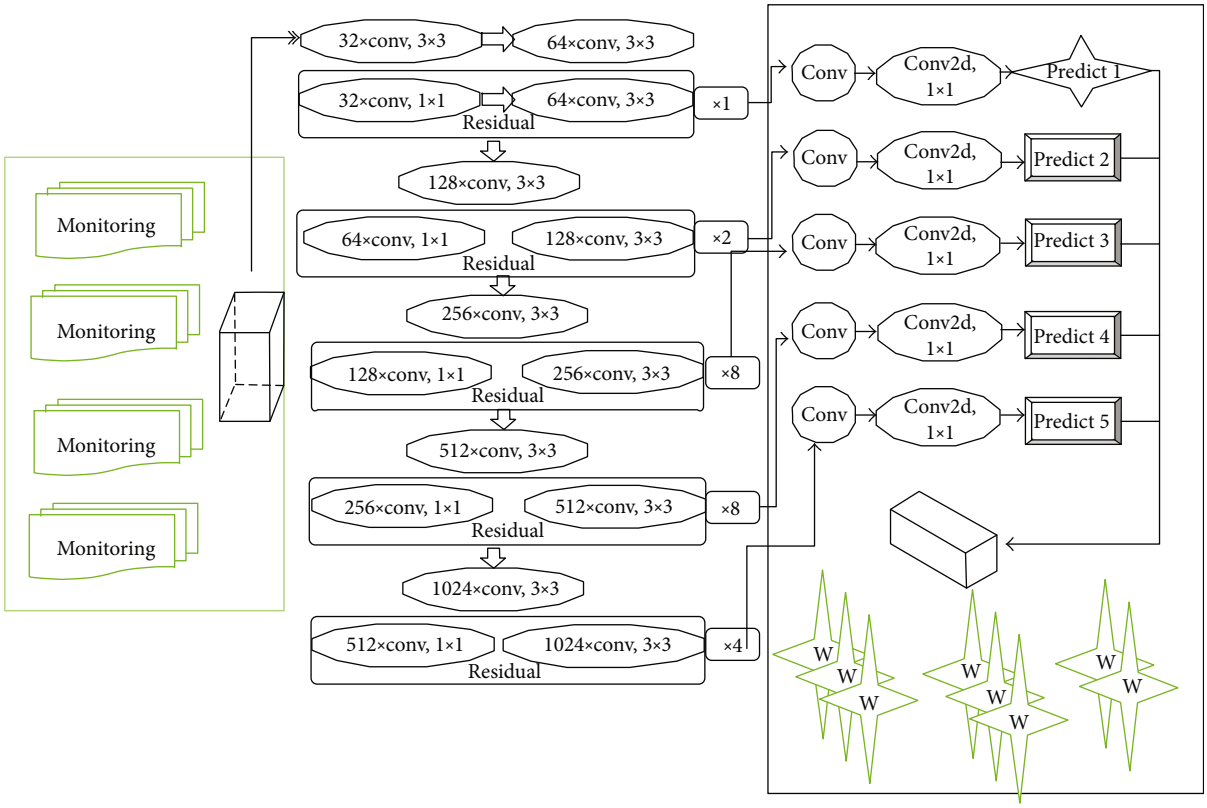

Figure 3: Process of environmental remote monitoring architecture.

to rejoin the network again. If a child node of a node leaves the network, it will delete the device from the contact list. If this address belongs to a terminal device, this address will be reassigned to other terminal devices. If it is a router, this address will no longer be used. If the parent node of a node leaves the network, it will remain in the network.

3.4. Monitoring Network Design Factor Changes. The PC monitoring network control terminal adopts Visual C++ as the development environment, and the industrial control iocomp is used to realize real-time processing and display of the data information transmitted by the gateway. After collecting the environmental information data of the terminal node and calculating the fuzzy algorithm, the PC monitoring terminal will display the result. It is converted into corresponding control information and sent to the relevant terminal control node. And when the environmental information exceeds the warning value or the human thermal infrared sensor (which can be turned on at night for anti-theft) is triggered, the PC monitoring terminal will send out an alarm message.

The Android mobile phone monitoring terminal of the intelligent monitoring system will be installed with a monitoring program compiled by Eclipse, which can connect to the Internet through a 3G/4G network to obtain real-time network address environmental information and realize direct manual control of network address environment-related adjustment equipment on the client. After confirming the coordinator, the FFD node starts the channel scan. There are two processes for channel scanning: active scanning and energy scanning. The first is to perform energy scanning. In this process, in order to reduce unnecessary interference as much as possible, the FFD node will start energy scanning on the designated channel. The function of energy scan is to select channels within the allowable range of energy levels. Figure 4 shows the WSN remote monitoring data distribution.

When sending data but do not know the destination address, the address mode needs to be set to AddrNotPresent, and the address cannot be specified. The destination address can only be searched from the binding table. After it is found, the data can be sent in a point-to-point sending mode or group sending mode. In ZigBee2004, all binding tables are stored in the coordinator. At this time, the sending node will send the data to the coordinator, and then, the coordinator will forward the data to the destination address found in the binding table. The binding mechanism usually uses key presses or other similar actions on the device to be bound to complete a binding within the specified timeout period. The default timeout period (APS_DEFAULT_MAXBINDING_TIME) is 16 seconds. The ZDApp_SendEndDeviceBindReq() function calls ZDP_EndDeviceBindReq() to send the binding information to its parent node. After the parent node receives it, it will parse the function ZDO_ProcessEndDeviceBindReq() and call ZDApp_EndDeviceBindReqCB() and ZDO_MatchEndDeviceBind() to process the request. When the corresponding Cinda is not found, the network layer will return through the corresponding

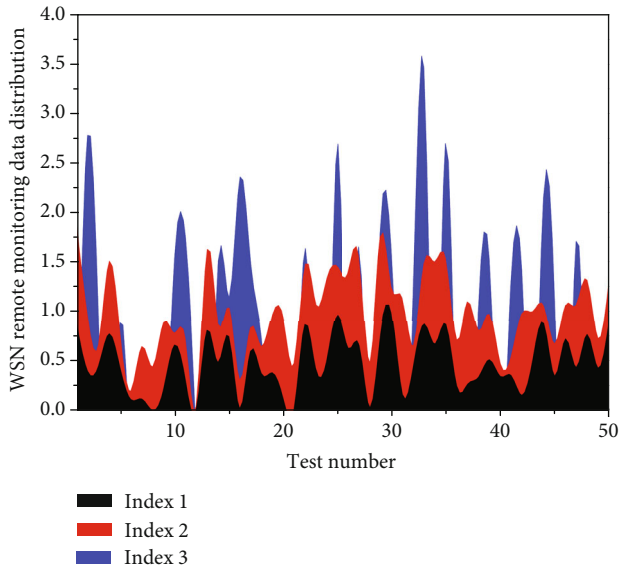

Figure 4: WSN remote monitoring data distribution.

parameters and notify the upper layer of the network initialization failure. Active scanning is to scan the network information within the communication range. Based on this information, the FFD node can determine a channel that is used by little or no equipment.

4. Application and Analysis of Environment Remote Monitoring Network Model Based on Intelligent Sensor Network Address Allocation and Addressing

4.1. Smart Sensor Network Address Data Extraction. In the design of the environmental monitoring system, TI's protocol stack Z-Stack is used. The protocol stack complies with the ZigBee2006 specification and has very rich functions, such as the ability to wirelessly download node update programs through the ZigBee network, and has positioning awareness functions, etc. For the sake of simplicity, the function of Z-Stack used in the environmental monitoring system is introduced next. JTAG (Joint Test Action Group) comes from the official inspection method of module function inspection, which belongs to the internal control method of the module. The CC2530 module part can provide JTAG module communication function test and edit the working program of the entire network in the serial communication test and software flow design of the module.

The concept of kernel has two purposes: one is as the calculation basis of attribute reduction, and the other is that it can be interpreted as the most important conditional attribute in attribute reduction. Compilation, verification, and other functions of the similar system in each module are all applied in the JTAG test window. However, the JTAG debugging module intercepted by ARM generally covers three modules: the overall structure of the test, the communication transmission interface, and the test result display module. The module can complete the signal transmission between the measuring device and the monitoring center and complete the mutual signal transmission of several parts through the acquisition and transmission circuit, the signal sensing circuit, and the power circuit. Figure 5 is the extraction of the address data space of the smart sensor network.

The microprocessor module is responsible for controlling the data processing operation, routing protocol, power consumption management, task management, etc. of the entire node. The most important thing is to implement a safe and reliable network communication protocol; the wireless communication module is responsible for wireless communication with other nodes and exchange control messaging and sending and receiving data. The configuration of network parameters is to set the ID number of the network. When the channel is determined, the FFD node will determine a PAN ID. PAN ID can set an ID that will not cause network conflicts through the monitoring function. PAN ID can also be set in a way that thinks it is. The ID of PAN ID cannot be set to 0xFFFF, which is a reserved address. The power supply module management unit has different power supply modes for different node types. On the terminal device node, the power supply consists of two 1.5 V alkaline batteries, and the power supply of the coordinator is USB power supply or AC power supply. There is an LCD on the coordinator, which can be used to display the commands sent and received and the status of the nodes. Buttons can be used to control binding and send commands. There is also an RS-232 serial port on the coordinator to communicate with the monitoring host.

4.2. Network Address Allocation and Addressing Model Simulation. In the CC2530 module, P2 terminals 1 and 2 are independently supplied to provide JTAG modules. The JTAG module design of the signal receiving end is shown in the text for details. In the process of making the module part, be careful to connect port 7 of the JTAG module to the initialization port of the CC2530 module, so as to complete the initialization of the entire system verification and simulation work.

The sensor node is used to collect various environmental parameters in the network and the data of its subnodes, including the temperature and humidity sensor SHT11 and the photoelectric sensor BPW34S. Convergence nodes are used to build networks and give instructions, converge the signals sent by the sensing nodes, and pass them to the monitoring platform at the same time. In addition, the ZigBee wireless communication part is composed of the radio frequency chip CC2530, and the monitoring center uses DSP technology. The design of the software part includes the node process and the monitoring platform program. The node process includes the sensor node workflow and the convergence node workflow. The protocol stack uses TI's ZStack-CC2530-2.3.1-1.4.0 version, implemented in C language in the Visual Studio 2010 development environment, and the monitoring center is convenient and quickly provides users with real-time online understanding of the network environment, data storage, and quantitative management of the network, etc. Figure 6 is the network address allocation and addressing information test.

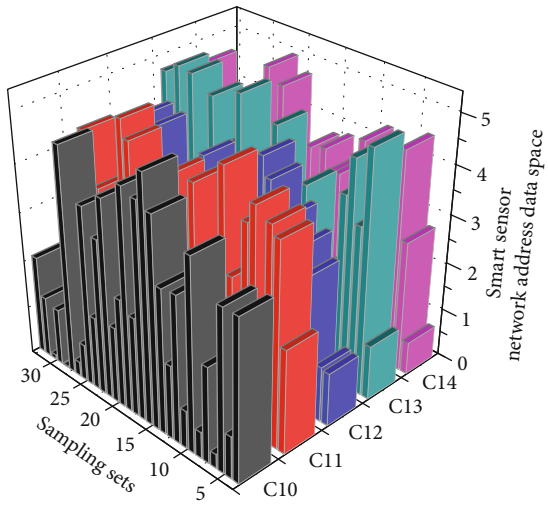

Figure 5: Extraction of address data space of smart sensor network.

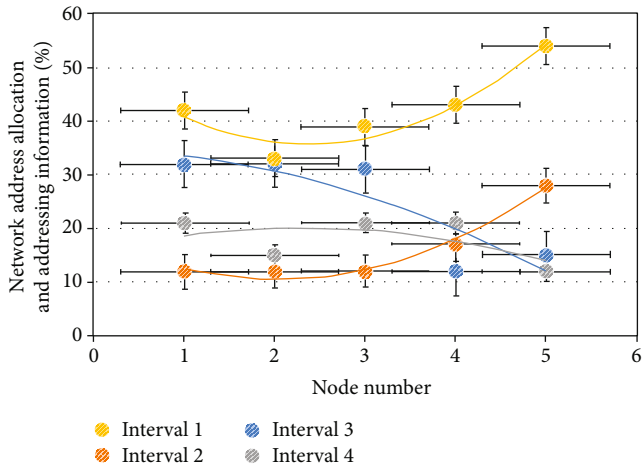

Figure 6: Network address allocation and addressing information test.

Database development realizes data storage and, at the same time, satisfies the functions of adding, deleting, modifying, and searching data. The database version used in this article is Microsoft SQL Server 2008. This article mainly uses DBHelper. The cs file realizes the corresponding function. The database stores and associates data to realize platform display, query, and control functions. The realization of data collection is under the TinyOS 2.1.2 platform, the program based on RPL routing written by NesC language that can accurately collect the temperature, humidity, light, and other information in the environment is burned to the TelosB node, and through the network address deploy TelosB nodes to form a wireless sensor network.

Because it can effectively analyze and process various incomplete information such as inaccuracy and incompleteness, the TelosB node in the network will pass the collected data in the environment to the Sink node through the RPL route. The realization of the whole network is based on BLIP 2.0 protocol stack and TinyRPL. In the nesdoc icon, a single rectangle represents a module, such as IPProtocolP, and a double-layer rectangle represents an accessory, such as MainC. Figure 7 is the distribution of network address allocation database nodes.

The B-LUX-V30B sensor provides I2C data output format, which consists of a 4-digit exponent and an 8-digit mantissa. When the device is working in the highest sensitivity mode, one count value represents 0.045 lumens. The maximum value of the mantissa is 255, and the maximum value of the exponent is 14. Therefore, the maximum range is: $255 * 2^{14} = 4177920$. The maximum lumens reading value at 0.045 lumens/LSB is 188,000. Any reading greater than this value (for example, index = 15) will be regarded as overload. The lumens value under overload conditions cannot be calculated by the conversion formula in the ambient light sensor. The basic design idea of the real-time data display module is when the real-time data display module is turned on on the website, the API interface that calls the monitoring data is transmitted to the server, and at the same time, the passed monitoring data is injected into echarts in the form of a string for visual display.

We will introduce the two important concepts of "relative reduction" and "relative core" of knowledge. At the same time, we set jS frame skipping (due to network delay and other irresistible reasons, the time interval of frame skipping is slower than) to continuously call the API interface for monitoring data to perform dynamic monitoring and visual display of data. The dashed border indicates that this component is universal and needs to be instantiated in actual use, such as TimerMilliC. The line with an arrow indicates the binding of the interface, from the user of the interface to the provider of the interface, and the text on the connection represents the bound interface, such as the Leds interface of the LedsC accessory used in the TestRPLC module, or as in the IPStackC accessory. The IP interface used is implemented by the IPProtocolsP module.

4.3. Example Application and Analysis. The microprocessor required for the experiment uses Texas Instruments (TI) CC2430, which is a system-on-chip solution for 2.4 GHz IEEE 802.15.4/ZigBee. CC2430 integrates IEEE 802. 15. 4 standard 2.4 GHz RF radio transceiver, memory, and microcontroller. It uses an 8-bit MCU (8051), which has 128 KB of programmable flash memory and 8 KB of RAM.

The SHT11 measuring terminal includes sensing equipment constructed with special equipment and special equipment constructed with fluid polyester blocks to obtain parameters. It is located in the corresponding module and completes the communication without loopholes with the 9-bit A/D switching device and the communication terminal module. At the same time, determine the analog communication module ports (SCK clock circuit and DATA transmission circuit) at both ends, and use the I 2 C circuit serial module and peripheral expansion device to connect. The SHT11 measuring device occupies a small area, consumes less space, has a particularly timely answer, and has many features such as strong resistance to external noise. This also makes it regarded as the preliminary identification of multiparameter monitoring in greenhouses. Figure 8 is the parameter distribution of the serial module of the WSN circuit.

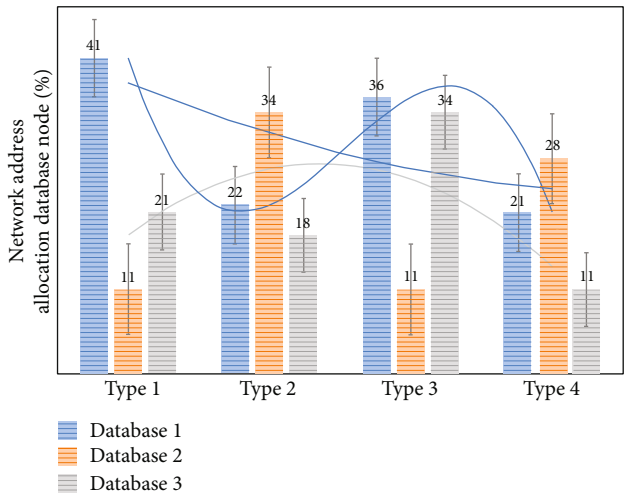

Figure 7: Network address allocation database node distribution.

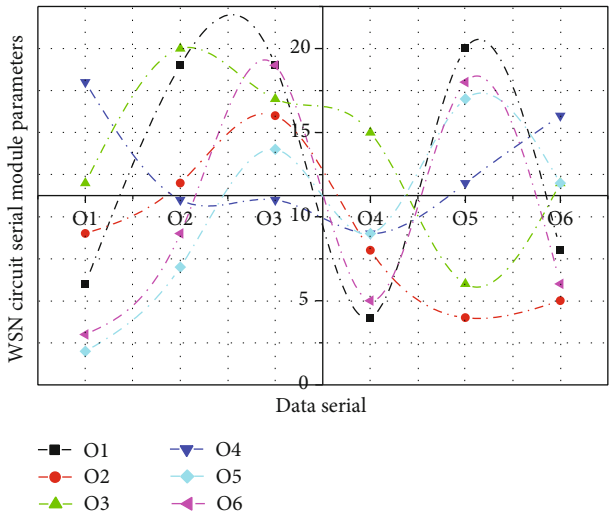

Figure 8: Parameter distribution of WSN circuit serial module.

In the design, the data acquisition module uses the ADC inside the CC2430. Its structure is shown in the text. It supports up to 12 bit analog-to-digital conversion. There is an analog multiplexer inside, which can support up to 8 configurable channels. Each sampling result is written into the memory through DMA without any intervention by the kernel. This method ensures that the ADC can capture a continuous stream of samples. It receives data from the serial port, can set the serial port and set the alarm value, has an alarm prompt, and can display the temperature curve. Serial port configuration: baud rate 38400, data bits 8 bits, no parity bit, 1 stop bit. After opening the monitoring software, you can see the data sent to the coordinator in the network. These data include the short address of the sending node and its real-time environmental data. Here is an example of temperature: according to the preset alarm temperature, for example, it is set to 18.085 degrees, and the actual temperature is 18.59 degrees, which exceeds the preset alarm line. Figure 9 shows the WSN real-time environmental data response distribution.

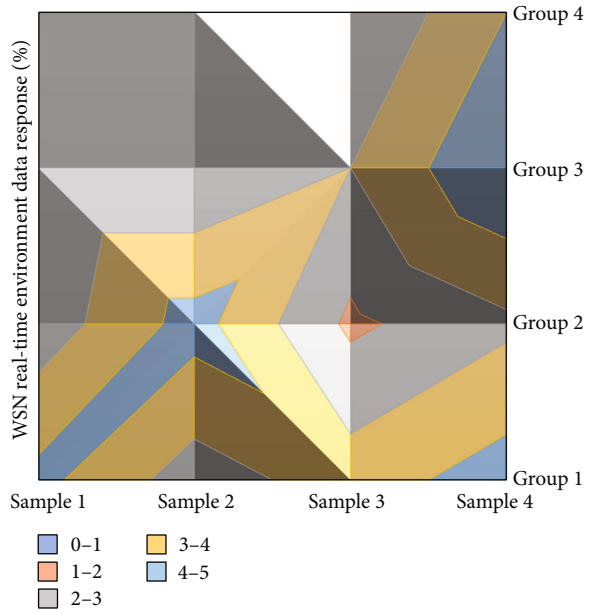

Figure 9: WSN real-time environmental data response distribution.

When receiving requests from other nodes to join the network, the coordinator will assign a network address to this node. The coordinator node is mainly used to receive the data of all nodes in this design, display it on its own LCD, and upload all the received data to the monitoring host for data analysis and storage. During this period, you can also send commands downward. If multiple device nodes send requests to the coordinator node at the same time, the coordinator node will lose some requests if it is too late to respond, and the device node that finds that its request has not been responded will send the request again after a few seconds, until it gets a response from the coordinator node until.

After the coordinator has established the network, the role of the coordinator in the network is the same as that of the router. If the coordinator is disconnected, the network can be maintained, that is, data transmission can be continued, but no new nodes can join. Since all data is sent to the coordinator in the design, if the coordinator fails, it will cause all data to be retransmitted continuously, which will affect the network operation.

5. Conclusion

The design of the environmental monitoring network in this paper includes two aspects: hardware design and software design. The hardware design mainly introduces the selection and design methods of the microprocessor module, data acquisition module, antenna module, and other peripheral circuit chips. In terms of software design, the software design of monitoring center software and ZigBee environmental monitoring network node based on Z-Stack protocol stack is introduced, including node joining, network address allocation, data collection, communication, routing management, and data encryption. During the functional test of the intelligent monitoring system, a test platform was built in the Venlo network to test the Zigbee network node networking and data transmission

capabilities, the PC monitoring terminal software data collection, intelligent environment adjustment, and alarm functions, and the Android client to remotely obtain environmental information and control the environment, and adjust the function of the equipment. Then, we define the positive domain of one category relative to the other. The final test result shows that the functions of the intelligent monitoring system in the previous design have been successfully realized. Finally, the communication, stability, and function of the system are tested. After verifying that the system is feasible, the system is installed in the entity and compared with traditional manual testing. Experimental tests show that the introduction of ZigBee-based WSN technology into the intelligent network monitoring system is achievable to control the multiparameters that affect the entire process of network address search and matching, which can shorten the plant growth cycle, increase the yield, and meet the system expectations. The system has strong stability, reliable performance, easy deployment, maintenance, and expansion and provides a new type of control method for the automation of network address environment monitoring.

Data Availability

The data used to support the findings of this study are available from the corresponding author upon request.

Conflicts of Interest

The authors declare that they have no known competing financial interests or personal relationships that could have appeared to influence the work reported in this paper.

Acknowledgments

The study was supported by the Guangdong University of Science and Technology.

References

[1] J. Aponte-Luis, J. A. Gómez-Galán, F. Gómez-Bravo, M. Sánchez-Raya, J. Alcina-Espigado, and P. Teixido-Rovira, "An efficient wireless sensor network for industrial monitoring and control," *Sensors*, vol. 18, no. 2, p. 182, 2018.

[2] E. U. Ogbodo, D. Dorrell, and A. M. Abu-Mahfouz, "Cognitive radio based sensor network in smart grid: architectures, applications and communication technologies," *IEEE Access*, vol. 5, pp. 19084–19098, 2017.

[3] X. Zhu, "Complex event detection for commodity distribution Internet of Things model incorporating radio frequency identification and wireless sensor network," *Future Generation Computer Systems*, vol. 125, pp. 100–111, 2021.

[4] S. Ramesh, C. Yaashuwanth, K. Prathibanandhi, A. R. Basha, and T. Jayasankar, "An optimized deep neural network based DoS attack detection in wireless video sensor network," *Journal of Ambient Intelligence and Humanized Computing*, pp. 12–14, 2021.

[5] D. Thakur, Y. Kumar, A. Kumar, and P. K. Singh, "Applicability of wireless sensor networks in precision agriculture: a review," *Wireless Personal Communications*, vol. 107, no. 1, pp. 471–512, 2019.

[6] L. Muduli, D. P. Mishra, and P. K. Jana, "Application of wireless sensor network for environmental monitoring in underground coal mines: a systematic review," *Journal of Network and Computer Applications*, vol. 106, pp. 48–67, 2018.

[7] N. Morozs, P. D. Mitchell, Y. Zakharov et al., "Robust TDA-MAC for practical underwater sensor network deployment: lessons from USMART sea trials," in *Proceedings of the Thirteenth ACM International Conference on Underwater Networks & Systems*, pp. 6–8, Auckland, New Zealand, 2018.

[8] C. Wu, Y. Wang, and Z. Yin, "Energy-efficiency opportunistic spectrum allocation in cognitive wireless sensor network," *EURASIP Journal on Wireless Communications and Networking*, vol. 2018, no. 1, p. 14, 2018.

[9] J. M. Williams, R. Khanna, J. P. Ruiz-Rosero et al., "Weaving the wireless web: toward a low-power, dense wireless sensor network for the industrial IoT," *IEEE Microwave Magazine*, vol. 18, no. 7, pp. 40–63, 2017.

[10] E. B. Priyanka, S. Thangavel, and X. Z. Gao, "Review analysis on cloud computing based smart grid technology in the oil pipeline sensor network system," *Petroleum Research*, vol. 6, no. 1, pp. 77–90, 2021.

[11] M. Abdulkarem, K. Samsudin, F. Z. Rokhani, and M. F. A Rasid, "Wireless sensor network for structural health monitoring: a contemporary review of technologies, challenges, and future direction," *Structural Health Monitoring*, vol. 19, no. 3, pp. 693–735, 2020.

[12] M. E. Bayrakdar, "Priority based health data monitoring with IEEE 802.11af technology in wireless medical sensor networks," *Medical & Biological Engineering & Computing*, vol. 57, no. 12, pp. 2757–2769, 2019.

[13] K. I. Mohammed, A. A. Zaidan, B. B. Zaidan et al., "Real-time remote-health monitoring systems: a review on patients prioritisation for multiple-chronic diseases, taxonomy analysis, concerns and solution procedure," *Journal of Medical Systems*, vol. 43, no. 7, pp. 16–21, 2019.

[14] R. E. Mohamed, A. I. Saleh, M. Abdelrazzak, and A. S. Samra, "Survey on wireless sensor network applications and energy efficient routing protocols," *Wireless Personal Communications*, vol. 101, no. 2, pp. 1019–1055, 2018.

[15] J. Trevathan and R. Johnstone, "Smart environmental monitoring and assessment technologies (SEMAT)—a new paradigm for low-cost, remote aquatic environmental monitoring," *Sensors*, vol. 18, no. 7, p. 2248, 2018.

[16] J. Iqbal, M. Khan, M. Talha et al., "A generic internet of things architecture for controlling electrical energy consumption in smart homes," *Sustainable Cities and Society*, vol. 43, pp. 443–450, 2018.

[17] R. N. Yadav, R. Misra, and D. Saini, "Energy aware cluster based routing protocol over distributed cognitive radio sensor network," *Computer Communications*, vol. 129, pp. 54–66, 2018.

[18] A. Mukherjee, S. Misra, A. Sukrutha, and N. S. Raghuwanshi, "Distributed aerial processing for IoT-based edge UAV swarms in smart farming," *Computer Networks*, vol. 167, 2020.

[19] A. Adeel, M. Gogate, S. Farooq et al., "A survey on the role of wireless sensor networks and IoT in disaster management," *Geological Disaster Monitoring Based on Sensor Networks*, pp. 57–66, 2019.

[20] W. Chen, "Intelligent manufacturing production line data monitoring system for industrial internet of things," *Computer Communications*, vol. 151, pp. 31–41, 2020.

Hindawi
Journal of Sensors
Volume 2021, Article ID 5753947, 12 pages
https://doi.org/10.1155/2021/5753947

Research Article

Double-Fed Wind Power System Adaptive Sensing Control and Condition Monitoring

Jing Peng,[1] **Peng Yang**,[2] **and Zhiqi Liu**[2]

[1]*Mechanical & Electrical Engineering Department of Wuhan Electrical Technology College, Wuhan 430079, China*
[2]*Hubei Branch of CGN New Energy Investment Co., Ltd., Wuhan 430223, China*

Correspondence should be addressed to Jing Peng; pengjing0210msx@st.btbu.edu.cn

Received 24 October 2021; Accepted 12 November 2021; Published 23 December 2021

Academic Editor: Gengxin Sun

This paper presents an in-depth study and analysis of improving the performance of doubly fed wind power systems using adaptive sensing control technology. The maximum wind energy tracking principle is analyzed in this paper with the wind turbine operation characteristics. Considering that the operation state and control strategy of a doubly fed wind power generation system is different before and after grid connection, the no-load simulation model and power generation simulation model are established based on the idea of separate modeling and time-sharing work. Combined with the respective control strategies and enabling modules, the overall simulation system is constituted for the continuous process from no-load operation to power generation operation. To analyze the chaotic mechanism of ferromagnetic resonance of wind farm power system and suppress the problem, based on the ferromagnetic resonance model of wind farm power system, analyze the basic conditions of the system into the chaotic state, consider the resonance phenomenon when external excitation acts, adopt the multiscale method to calculate the approximate solution at the resonance of main parameters and determine the steady-state solution and stability conditions, and explore the influence of external excitation on the dynamic characteristics of ferromagnetic resonance. In this paper, the inverse system approach, applied to the linearized decoupling of doubly fed wind power, a nonlinear, strongly coupled multivariable system, is derived for the no-load inverse system model and the inverse system model for the power control scheme and the speed control scheme to achieve maximum wind energy tracking for grid-connected power generation, respectively. The model further extended to fractional order to study the complex dynamical behavior of the system of different orders and flux chain subsquares. To suppress the system chaotic oscillation phenomenon, a fractional-order finite-time terminal sliding mode controller is proposed based on the frequency distribution model with time-frequency domain conversion, which achieves the suppression of chaotic phenomena in resonant overvoltage infinite time and is compared with the conventional sliding mode to confirm the effectiveness and superiority of the proposed controller. This paper explores and discusses the impact of adaptive sensing control technology on the practice of doubly fed wind power systems, to provide theoretical possibilities for the adaptive sensing control technology to be more effective for the practice of doubly fed wind power systems.

1. Introduction

Energy is the material basis for human survival and the driving force for social development and progress, and since the industrial revolution, global energy consumption has grown rapidly, rapidly promoting the process of world industrialization and improving the level of social development and the quality of human life. However, the reserves of nonrenewable resources such as oil, coal, and natural gas, which are the main pillars of world energy, are very limited. The rapid growth of the global economy has led to increasing demand for energy, making the energy crisis an obstacle to further human development [1]. The main advantage is that the speed can be adjusted in a wide range to keep the wind energy utilization coefficient at the best value; it can absorb and store the gust energy, reduce the fatigue damage, mechanical stress, and torque pulsation caused by the gust impact on the wind turbine, extend the life of the unit, and reduce low noise; it can also control active power and reactive power to improve power quality. With the traditional

energy shortage and environmental pollution problems aggravated, vigorously developing wind energy, solar energy, tidal energy, and other renewable energy has become an inevitable choice. In many renewable energy sources, wind energy is the most promising. In the past decades, the total installed capacity of wind power generation worldwide has grown tremendously, from only 3.5 GW in 1994 to 539.6 GW in 2017, an increase of more than one hundred times. It can be said that, by far, wind power is one of the largest developed, fastest-growing, and most technologically mature forms of renewable energy generation [2]. Wind energy is a renewable and clean energy source, and a wind power generation is an important form of wind energy utilization, by using wind turbines to obtain energy from the wind, converting wind energy into mechanical energy, and then using generators to convert mechanical energy into electrical energy suitable for long-distance transmission. All the pulses received during the sampling period are taken; whether the number of received pulses is greater than the set threshold number was determined; if the number of pulses is greater than the set threshold number, the sum of the number of pulses and the time interval between the received pulses is corrected. According to the number of corrected pulses and the sum of the time intervals between the received pulses, the motor speed is determined. Due to the randomness, variability, and uncontrollability of wind speed, to obtain the maximum wind energy, the rotational speed of the wind turbine often varies with the wind speed. The use of variable speed and constant frequency doubly fed wind power generation technology allows for a constant output frequency with varying generator speeds.

In today's wind power generation field, variable speed constant frequency technology with AC excitation has been commonly adopted. Compared with the traditional constant speed and constant frequency technology, the variable speed and constant frequency wind turbine have the advantages of wide operating range, high wind energy conversion efficiency, smooth output power, and low mechanical stress [3]. The addition of vector control, in turn, allows the stator output active and reactive power of the doubly fed motor to be decoupled and controlled, improving the flexibility and stability of the whole system. In the vector control-based doubly fed motor control system, the rotor speed and position information are the key to the decoupling and stable operation of the whole control system [4]. At present, most of the doubly fed units at home and abroad perform speed detection directly by installing speed sensors such as photoelectric encoders. But the speed encoder also brings the disadvantages of increasing system cost and reducing system reliability at the same time. Therefore, a lot of research has been conducted on the control technology of adaptive sensors, and the control technology of adaptive sensors will be a development direction for future wind turbines.

Focusing on the dynamic characteristics and control methods of wind power systems and grid-connected power systems in the form of mechanical, electrical, and magnetic oscillations, revealing their influence mechanisms and change laws, and designing fast and effective suppression methods will help to improve the stability of wind power systems and grid-connected power networks [5]. Due to the nonlocal and weak singularity of fractional-order calculus operators, the control theory of fractional-order power systems is more complex than the control theory of integer-order power systems, and how to control the system to quickly stabilize and obtain good control performance when the system is uncertain and external disturbances is a difficult research point in control theory and engineering applications. Therefore, for the dynamical models in integer-order and fractional-order wind power systems, how to quickly and effectively control complex oscillation phenomena, new control methods need to be explored to improve the robustness and dynamic response performance of the system, determine the parameter control range and elimination path, provide the more and more informative theoretical basis for wind power system nonlinear control design schemes, and also provide stability analysis of wind power systems and grid-connected power systems, theoretical basis, and technical reserve.

2. Current Status of Research

A wind power system is a typical nonlinear time-varying dynamic system, and the two common horizontal axis permanent magnet synchronous wind power systems mainly include a wind turbine, drive shaft system (direct drive and semidirect drive), permanent magnet synchronous generator, converter, and grid-connected power system [6]. Semidirect-drive wind turbines add a single-stage gearbox to the drive shaft system, which has the characteristics of the small size of permanent magnet synchronous generator, large converter capacity, and good economy, etc. It has attracted much attention. Ltd. has independently developed China's largest (7.6 MW) offshore semidirect-drive permanent magnet synchronous wind turbine, and the technology level is in the international leading position. According to the national "new energy industry revitalization plan" draft, the cumulative installed capacity of China's wind power will reach to in the year and will be proposed in six provinces and regions to build nearly ten 10,000 MW wind power base planning, respectively, Xinjiang Hami, Gansu Jaquan, coastal and northern Hebei, western Jilin, coastal Jiangsu, Mending, and Mengzi. According to the plan, the year will be completed, accounting for about the total installed capacity of the country [7]. The doubly fed induction generator is an important part of a wind power generator. To design a high-quality wind power system, it is necessary to determine the best control method. This paper takes the vector control technology as the core and takes the wind turbine unit combining the doubly fed induction generator and the AC-DC-AC dual PWM excitation converter as the research object and conducts the theoretical analysis and simulation analysis of the system. By the end of the year, the country's cumulative grid-connected capacity wind power grid-connected capacity accounted for about the total installed capacity of the national power supply, an increase of about over the year. China's wind power market is beginning to enter a period of steady development after years of rapid growth

and continues to maintain its position as the world's largest wind power market.

Doubly fed generators have become the mainstream models of variable speed and constant frequency wind power generation systems because of their superior operational performance and outstanding advantages. Compared with the permanent magnet synchronous generator wind power generation, the structure of the doubly fed wind power generation system is more complex, and the decoupling control strategy of the doubly fed power generation system through rotor AC excitation has been the focus of research by scholars at home and abroad. At present, the control of doubly fed wind power generation systems mainly include vector control, direct torque control, and nonlinear control. The industrial doubly fed induction generators usually use the traditional vector control method [8]. The basic idea of vector control, which is currently the dominant control strategy for doubly fed wind power systems, is to control the rotor current in a synchronous rotating coordinate system and to ensure that the chosen vector coincides with the horizontal axis of the coordinate system. In asynchronous motor vector control, the rotor magnetic chain orientation is usually used, and synchronous motor vector control takes the air-gap synthetic magnetic chain orientation. According to the principle of vector control, the system designed with the concept of master-slave control and cross-coupling basically solves the problem of power imbalance, but its power balance accuracy and dynamic performance are not good. To improve the power balance accuracy and improve the dynamic performance, the "differential moment feedback" link is added. In the DFIG vector control technique, the stator voltage vector and the stator magnetic chain vector are usually chosen as the orientation vectors. To achieve the goal of controlling the motor speed and reactive power, a power winding magnetic chain-directed vector control strategy without cross compensation is proposed in the literature. The literature proposes a vector control-based negative sequence compensation strategy for the excitation current with only one current loop, which can effectively suppress the pulsations of torque, power, and DC bus voltage without setting a specified target and can even minimize the current imbalance. The literature incorporates the design of a sliding mode variable structure controller based on the power winding magnetic chain directional vector control, which integrates the effect of rotor magnetic chain on electromagnetic torque and improves the accuracy of motor speed control [9].

Because of the abovementioned drawbacks and shortcomings of vector control, it is necessary to realize the fully decoupled control of active and reactive power from the nonlinear nature of a doubly fed wind power generation system to improve its static and dynamic performances. In recent years, many scholars have introduced new control strategies for the integrated control of doubly fed power generation systems. The internal mode control is a new control strategy based on the mathematical model of the controlled object, which is proved to have the advantages of simple structure, direct and clear parameter adjustment, and high robustness. In the literature, internal mode control is used to replace the general control, and a mathematical model of the doubly fed motor is established using the function, and the internal model control method is used to design the current inner loop and speed outer loop. The internal mode control reduces the requirement for system model accuracy, and the simulation results show that the control system has good steady-state performance and dynamic response speed [10].

3. Performance Testing of a Doubly Fed Wind Power System with Adaptive Sensing Control Technology

3.1. Adaptive Sensing Control System Design. Industrially, doubly fed induction generators usually use a conventional vector control method. This method is based on the principle of vector orientation and decouples the three-phase model of the doubly fed motor into two decoupled subsystems corresponding to reactive power/magnetic flux and active power/torque through a coordinate transformation from a three-phase stationary coordinate system to a two-phase rotating coordinate system and decouples the inter-system coupling relationship through a compensation term, so that the reactive power/magnetic flux and active power/torque of the doubly fed motor are, respectively, subject to only the decoupled DC voltage flux control, making its performance equivalent to that of a DC generator. Two frequently used vector control methods are stator chain-oriented vector control based on the stator and grid voltage-oriented vector control based on the grid voltage [11]. Whether stator magnet chain oriented or stator voltage oriented is used, vector control uses a double-loop control structure. Dual-loop control generally refers to power outer-loop control and current innerloop control. The doubly fed asynchronous generator we usually talk about is essentially a wound rotor motor. Since its stator and rotor can feed power to the grid, it is called doubly fed motor for short. Although the doubly fed motor belongs to the category of asynchronous motor, it can apply excitation and adjust the power factor like a synchronous motor because it has an independent excitation winding. Among them, the current innerloop control link includes PI controller and compensation term, which is responsible for decoupling between active and reactive control; the power outerloop control link is PI controller, which is responsible for generating the reference value of rotor innerloop current. For the control of the rotor-side converter, two control schemes are generally used: vector control based on stator magnetic chain oriented SFO or vector control based on stator voltage oriented SVO. The two vector control schemes have almost the same effect on the control of active and reactive power. The following will be an example of the vector control method under stator chain orientation. In this case, it is possible to control the active power part/rotor speed/electromagnetic torque of a doubly fed induction generator by controlling only the q-axis component of the rotor current and the reactive power part by controlling only the d-axis component of the rotor current.

$$P_2 + P_m = p_1 - (p_{u1} + p_{u2}). \quad (1)$$

The analysis above in this chapter, for an invertible system, can be derived to form a pseudolinear composite system with its order inverse system and the original system. However, the presence of nonlinear modeling errors and the parameter drift of the system in operation make the pseudolinear composite system not an ideal linear system, so it is necessary to design the pseudolinear system using an additional controller. The internal model control, a control strategy based on the mathematical model of the object, has the characteristics of simple design and the ability to consider the closed-loop performance and robustness compared with the traditional feedback control. If the pseudolinear composite system is formed by the inverse system of order and the original system is taken as the control object, the theoretical linearized transfer function describing the input-output relationship of the composite system corresponds to the internal model in the internal model control, and based on this idea, the internal mode control is adopted in this chapter to control the design of the above pseudolinear system [12], as shown in Figure 1.

As an important part of the wind power system, the wind turbine extracts energy from the wind and then converts it into mechanical energy to drive the wind turbine. The relationship curve between the active power of a wind turbine and its rotational speed at different wind speeds when the pitch angle β is zero. For each wind speed, the maximum power point corresponds to only one value of the wind turbine speed. The doubly fed wind turbine, as a variable speed and constant frequency wind turbine, can be operated by adjusting the rotor speed when the wind speed changes, which in turn allows the wind turbine to operate at the peak of the corresponding power curve [13]. The theoretical curve for the maximum power that a wind turbine can extract from the wind is a power-of-three function concerning the wind turbine speed, Pop = Koptω3t. The expression for the maximum electromagnetic torque is like this equation, except that it is a square function concerning the wind turbine speed. If the wind speed is below the rated value, the wind turbine operates in the variable speed mode where its rotational speed is adjusted by the doubly fed generator speed control or active power control so that Cp is maintained at the Coma point. In this mode of operation, the wind turbine pitch angle control is deactivated, when the pitch angle β is fixed. However, if the wind speed when exceeds the rated value, the pitch angle control is activated to increase the pitch angle of the wind turbine, thus reducing the mechanical energy extracted from the wind. This is shown in Figure 2.

The parameters of the proportional-integral controller used in vector control are designed based on a linearized model of the system at some stable operating point, which makes it heavily dependent on an accurate model of the system. The physical mechanical failure of IPM is largely related to the design quality defects of the device itself, from the reliability design of the device itself, the body structural design, and the internal structure layout design, comprehensive rectification, starting from the quality improvement of the device itself, to improve the quality of the device comprehensively and systematically. However, because the exact model of the system is often impossible to obtain in practice, vector control generally does not allow the system to be controlled optimally when the system is shifted from the equilibrium point [14]. The so-called equilibrium point is the state in which the turbine can operate stably, which generally refers to the rated operating state. In the system operation, due to the fluctuation of output caused by the change of wind speed and the change of grid operation status caused by the change of load, the operation points of doubly fed wind power system is constantly changing, so the vector controller designed based on a certain operation point cannot play its optimal control effect at other operation points. In recent decades, some nonlinear control methods have also been applied to the control of many power system devices, and the most representative control method is the feedback linearization method. The feedback linearization method can achieve the optimal control under the working point offset because it is a global linearization of the system model. However, its disadvantage is that it also relies on an exact model of the system and therefore lacks robustness to changes in parameters. In individual applications, the controller requires the use of many state variables that are difficult to obtain accurately in real systems, let us say in mechanical systems.

$$\frac{\left(T_s + xL_m^3/L_s^2\right)}{(3\mathrm{H}_m)}. \quad (2)$$

The parameters of the proportional-integral controller used in vector control are designed based on a linearized model of the system at some stable operating point, which makes it heavily dependent on an accurate model of the system. However, because the exact model of the system is often impossible to obtain in practice, vector control generally does not allow the system to be controlled optimally when the system is shifted from the equilibrium point. The so-called equilibrium point is the state in which the turbine can operate stably, which generally refers to the rated operating state. In the operation of the system, the operating point of the doubly fed wind power system is constantly changing due to the fluctuation of the output power caused by the change of wind speed and the change of the grid operating state caused by the change of load, so the vector controller designed based on a certain operating point cannot exert its optimal control effect at other operating points. In this section, a control strategy combining proportional-integral feedback control and feedback linearization methods is proposed, i.e., a feedback linearization method based on differential geometry theory is used to design the current inner-loop controller, while a proportional-integral feedback control method is used to design the power outerloop controller. The proportional-integral controller is used in the power outerloop control because it helps in switching control of the outerloop reference current under multiple operating conditions and helps in simplifying the overall controller

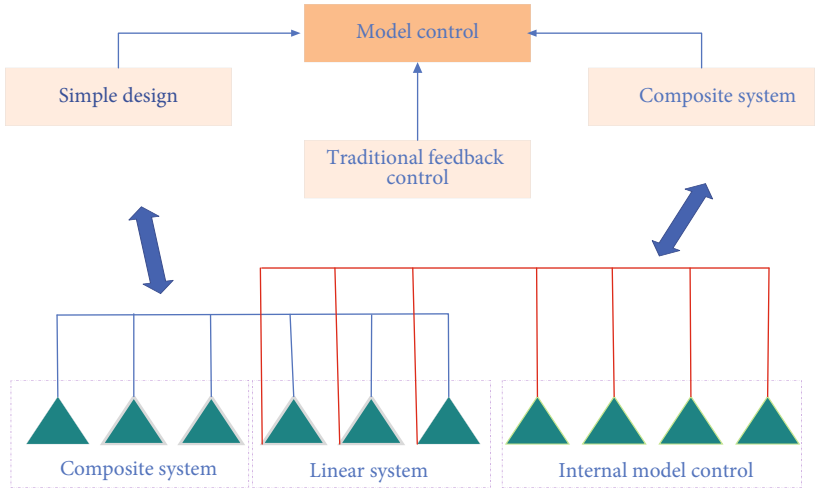

Figure 1: Control structure of internal mode of two-port structure.

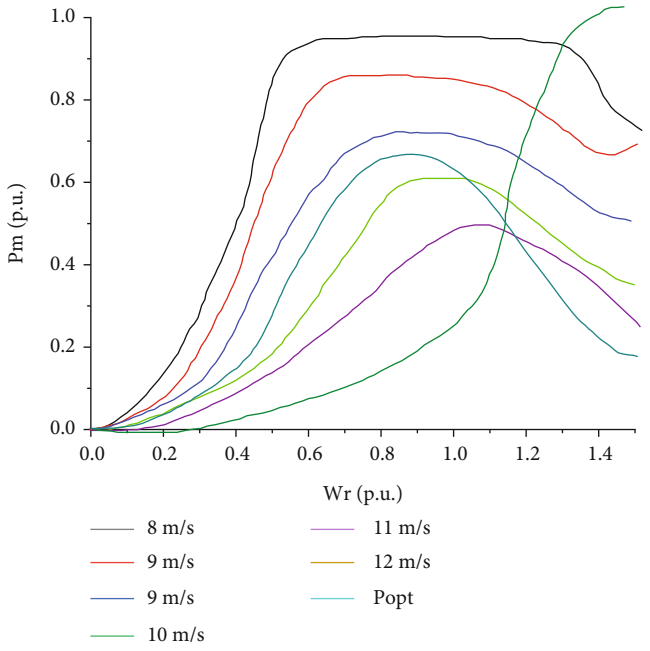

Figure 2: The relationship curve between the active power of wind turbine and its speed at different wind speeds.

design, whereas the feedback linearization method based on differential geometry is used in the current inner loop control, which ensures the responsiveness of the current inner loop controller.

3.2. Performance Testing of Doubly Fed Wind Power Systems. The name "doubly fed" is derived from the fact that both the stator and rotor of the generator can feed electricity to the grid separately. The DFIG has a rotor excitation winding and, due to its constructional advantages, offers the advantages of both synchronous and asynchronous generators. Synchronous generators are often used, but the excitation system of synchronous generators uses a DC power supply, and the excitation system can only control the amplitude of the excitation current. The DFIG excitation system uses an AC excitation power supply, which can control the frequency, amplitude, and phase of its current. The total positive electrode of the lithium battery pack is connected in series with the contactor, and the inverter and the shunt are connected to the total negative electrode of the lithium battery pack. The invention has a novel structure and a clever design; the overcurrent signal latch and reset circuit are used to memorize the overcurrent protection signal; avoiding frequent switching of the contactor can extend the life of the contactor and reduce the impact on other power devices. When the DFIG rotational speed changes, the frequency of the AC excitation power supply can be adjusted to achieve variable speed and constant frequency power generation; when the DFIG power angle needs to be changed, the phase of the AC excitation power supply output current can be controlled to produce a certain amount of displacement of the generator rotor magnetic field to ensure that the phase angle between the DFIG output voltage and the grid voltage is corrected; changing the amplitude of the AC excitation current can adjust. The magnitude of the DFIG output active power can be adjusted by changing the amplitude of the AC excitation current. By using vector control technology, the amplitude and phase of the AC excitation current in the DFIG can be controlled simultaneously, and the active and reactive power can be controlled independently, which makes the control strategy more flexible and diverse [15]. The doubly fed induction motor is an AC-excited motor, where the stator is connected to the industrial frequency grid and the rotor is excited by adjustable AC. By adjusting the frequency, amplitude, and phase of the rotor excitation current through AC excitation, the doubly fed motor can achieve variable speed and constant frequency operation, and at the same time, the active and reactive power of the stator can be adjusted. Centralized management of the servers running various e-government business systems, real-time grasp of the operation status, receiving and processing of alarm information, and timely judgment such as whether the flow of key services is normal, whether the application operation exceeds the specified threshold,

and ensuring the stability of the core e-government business. For efficient and safe operation, if the stator winding and rotor winding of the doubly fed induction motor are both symmetrically wound, and the number of motor pole pairs is, when a three-phase AC voltage is applied to the stator side, an asynchronous rotating magnetic field will be generated in the air gap of the motor due to the three-phase symmetrical current in the stator winding, and the rotating magnetic field rotates at a synchronous speed, and the speed is related to the grid frequency, and the number of motor pole pairs as follows.

$$n_1 \geq \frac{60f(x)}{2p}. \tag{3}$$

The main operational objectives of the variable speed and constant frequency doubly fed wind power system is first, to achieve maximum wind energy tracking, the core of which is the control of DFIG speed or active power, and secondly, the control of DFIG stator output reactive power. Thus, the DFIG is the object of control, and the rotor side PWM converter is the executor of the control command. To achieve effective control of the control object, the rotor side PWM converter should be designed based on the mathematical model of the DFIGURE. The mathematical model of DFIG is a high-order, multivariable, nonlinear, strongly coupled system in the same three-phase stationary coordinate system as the common three-phase AC motor, which is difficult to analyze and design the control system. To realize the effective control of the active and reactive power of DFIG, both must be decoupled. Therefore, the vector control technology in AC speed control can be applied to the active and reactive power decoupling control of DFIG, i.e., the active and reactive components of rotor current can be decoupled through coordinate transformation to realize the effective and decoupling control of active and reactive power of DFIGURE. The two objectives of the variable speed and constant frequency doubly fed wind power generation system is achieved.

$$\xi = \begin{bmatrix} ak & 1 & 0 \\ 0 & k & 0 \\ 0 & \frac{1}{t} & 0 \end{bmatrix}. \tag{4}$$

To further improve the safety and reliability of the IPM, a "multisource, multimeasure" hierarchical IPM protection scheme is designed based on the IPM's protection. As can be seen in the figure, in addition to the IPM's protection, an independent IPM AC side overcurrent protection circuit and a DC side overvoltage protection circuit have been set up in the hardware. The gain of the observer designed by the pole configuration method can be adjusted online according to the previously estimated moment of inertia and viscous friction coefficient, so that the observer can still accurately observe the sudden external load disturbance when its own mechanical parameters change drastically. Compensation has greatly improved the accuracy of the servo system. In addition to the hardware protection measures, software protection is also provided in the DSP program by judging the sampling signals. Three hardware protection sources and one software protection source are logically "combined" to form the IPM protection signal. The protection signals generate several actions now of latching: blocking the PWM signal from the DSP output to the driver circuit, setting the DSP PDPINT pin low so that it sets the PWM output pin to a high resistance state through the hardware circuit, triggering a DSP protection interrupt, and blocking the input of the optical scourge in the IPM driver circuit. This redundant protection measure improves the reliability of the IPM protection work and provides safety assurance for iterative exploratory experimental studies using the prototype system, as shown in Figure 3.

The wind turbine simulation subsystem consists of a DC motor, a thyristor governor, and a PCI bus-based data acquisition card. Under the control of the host data, the acquisition card collects the voltage and current of the DC motor and the speed signal of the unit to output the control signal of the thyristor governor to control the DC motor to realize the simulation of the wind turbine characteristics. The DFIG control subsystem and the wind turbine simulation subsystem complete the DFIG control and wind turbine simulation, respectively, is the electromechanical energy conversion (power generation) unit and the power (prime mover) unit of the experimental system. Different from the real wind power system, DC machine simulation of the wind turbine and DFIG operation has a more complex interoperability relationship to ensure the normal operation of the entire experimental prototype system must be harmonized to the two subsystems so set up a monitoring and management of the two subsystems of the host computer whose hardware configuration includes PC, data acquisition card software configuration using self-developed host monitoring, and management program. The main task of the mainframe is two: one is to monitor and control the two DSPs as slaves to realize the master-slave two-level control of DFIG; the second is to control the data acquisition card to realize the wind turbine simulation to coordinate the DFIG and the DC machine simulation of the engine (wind turbine) with each other to achieve the purpose of maximum wind energy tracking. In addition, the host computer communicates with the two DSPs in real-time to obtain real-time information on the changes of each signal so that the operation of the whole experimental prototype can be monitored.

$$U = U(1 + d)e^{itv_1}, t \leq 0^+. \tag{5}$$

To study the impact of grid-connected operation characteristics of large-scale wind turbines on the power system, a wind farm grid-connected model consisting of 20 wind turbines. This model consists of five feeders to connect the single 2.5 MW wind turbine to the wind farm substation via 690 V/35 kV transformer 1 T and then from 35 kV/110 kV transformer 2 T to the high-voltage transmission line and the grid-side substation fed into the grid. For modeling

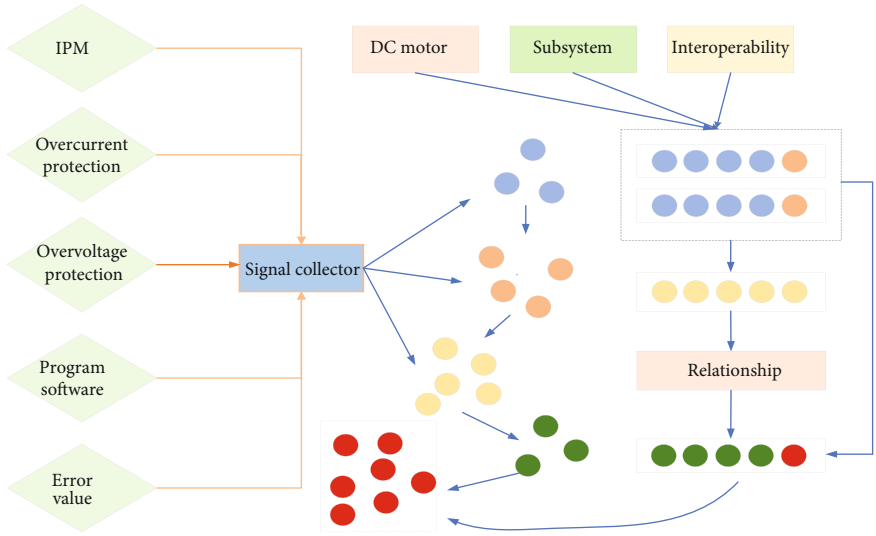

Figure 3: Schematic diagram of IPM protection scheme.

purposes, all wind turbines of the wind farm are equivalently considered as equivalent wind turbines, and the simple single interconnected power system consists of equivalent wind turbines, load model, and infinity bus. The equivalent grid-connected structure uses an IEEE3 node system, where node 1 is the equivalent wind turbine tie-in node, node 2 is the dynamic load node, and node 3 is the infinity balance node [16], where the dynamic load is usually connected in parallel with a constant P Q load. $0_E, 0_S$ are the equivalent electric potential and capacity of the infinity grid, respectively, as shown in Figure 4.

The observer is responsible for the estimation of state variables and disturbance terms, while the controller performs optimal feedback control. In addition, a compensation term is used to achieve complete decoupling between the loops. Using pole configuration techniques to select the appropriate observer gain, the perturbation observer can actively estimate and compensate for the perturbations. The rotor side controls the doubly fed generator to achieve maximum wind energy power tracking. The grid-side converter is controlled by output and grid-connected to achieve DC bus voltage stability and independent decoupling control of output power. It is worth noting that since an increase in observer gain amplifies the measurement noise, there is a trade-off between the speed of convergence and sensitivity to the measurement noise in the choice of observer gain. The stability, dynamic performance, and interference immunity of the system should be considered when selecting the observer bandwidth $\lambda\alpha$. To obtain accurate observations and satisfactory dynamic performance should be chosen as large as possible in the initial design phase. In this chapter, a nonlinear adaptive control POMAC method based on disturbance observer is proposed for the overall control of a doubly fed wind power system, and its performance is verified by simulation. Since the POMAC method compensates for the disturbances better and responds faster, it can provide more reactive power, which helps to improve the voltage outlets at the machine end.

The state and disturbance terms of the system are estimated using an extended state and disturbance high gain disturbance observer and the estimated values are used instead of the true values to achieve optimal output feedback control. The design of POMAC does not depend on an exact system model and its excellent control performance remains largely consistent under various operating conditions, which indicates its robustness to system nonlinearities and uncertainties. These advantages can be attributed to perturbation estimation and optimal output feedback control, which eliminate the effects on the system due to nonlinearities, uncertainties, and external perturbations.

4. Analysis of Results

4.1. Adaptive Sensing Control System Results. The software parts of the net-side converter and rotor-side converter control systems of the dual PWM converter are also independent of each other. Both have different control objects and processed data, but their structure is the same, both are modular designs, the whole software system is composed of the main program and various interrupt service programs, and the main program and interrupt service programs are composed of subroutines. The software system uses five priority levels, with the highest priority being protection interrupts, followed by timer interrupts, serial communication interrupts, keyboard interrupts, and the lowest level is the main program. The timer interrupt implements DFIG real-time control and is the core of the software system. The serial communication interrupt and the keyboard interrupt handle the communication and interaction between the DSP and the host and the DSP and the operator, respectively, where the serial communication interrupt has a higher priority for the machine-to-machine communication task than the keyboard interrupt has for the human-to-machine interaction task. This is shown in Figure 5.

The control unit and the DSPZ control unit are relatively independent in function and structure but have many

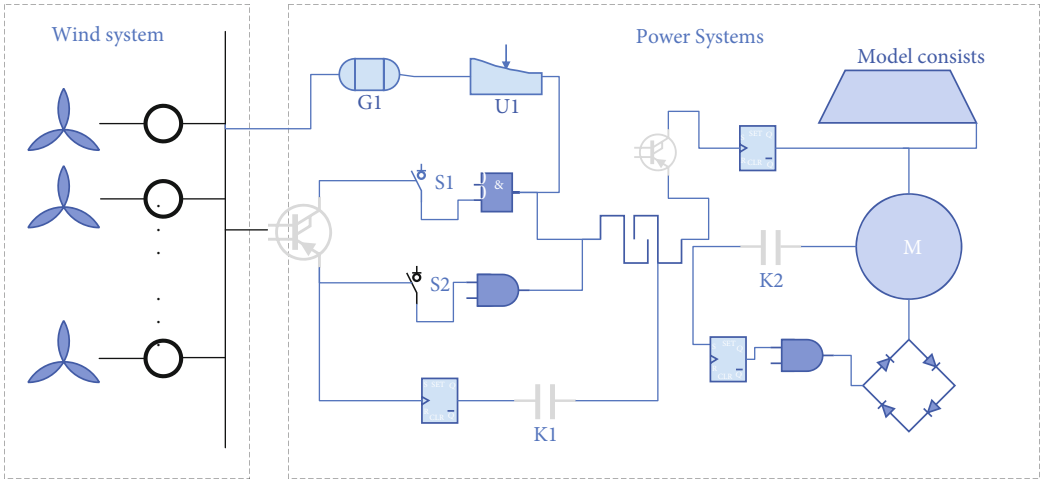

Figure 4: Simplified model of the power system of a wind farm.

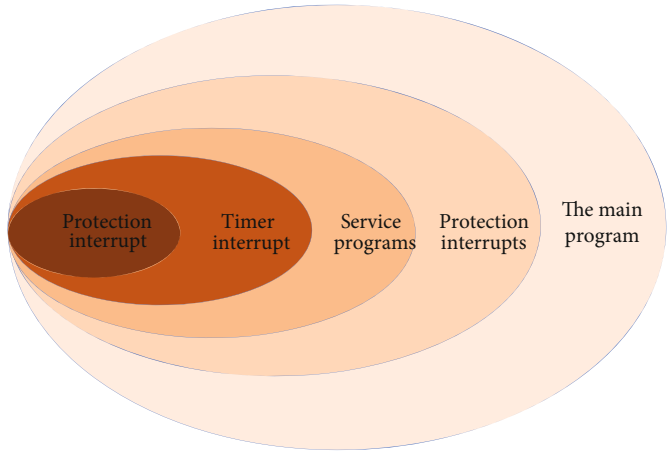

Figure 5: Module execution priority in the adaptive sensing control system.

similarities in hardware composition. The basic circuits of the two control units are the same including the DSP minimum system and extended input and output circuits, signal acquisition circuits, signal preprocessing circuits, guard M drive circuits, nd control power circuits. The DSP minimum system includes the CPU, system clock, data and program memory, and decoding circuits; extended input and output circuits are to provide interfaces for numerous peripheral circuits and extended circuits are to connect the DSP minimum The signal acquisition circuit uses voltage transformers and current transformers to convert strong power signals into weak control signals; the signal preprocessing circuit amplifies and filters the weak signals output from the signal acquisition circuit for AD conversion by the DSP. The hybrid damping suppression scheme is derived and combined with the grid impedance measurement technology to form an adaptive control strategy for grid-connected inverters based on hybrid damping, so that the grid-connected inverter can maintain relatively good performance under various grid impedance conditions. In system characteristics, the IPM driver circuit isolates and shapes the drive pulses from the DSP for driving the IPM; the control power circuit provides the 15 V and SV power supplies required by the control circuit and the four +15 V power supplies required by each IPM. The two DSP control units differ in that the DSPI control unit serves as the direct control core for the DFIG and has more functions than the DSPZ control unit and the circuitry to implement those functions. The additional circuitry for the DSPI control unit includes a keypad display circuit, a protection drives operation circuit, parallel communication, and serial communication circuits, and a DFIG speed position detection circuit. The keypad display circuit provides a 4×4 matrix keypad and a 6-digit digital tube display; parallel communication and serial communication are channels for information exchange between the slave and the host Parallel communication takes a simplex approach (data can only be passed from the slave to the host in one direction) Serial communication is a full-duplex approach (data can be passed between the slave and the host in both directions).

$$G_{\text{hfp}} = \frac{T_h s - 1}{T_h s + 2}. \quad (6)$$

By combining the power generation subsystem with the grid-connected subsystem, an overall simulation system based on the rotational speed control scheme for maximum wind energy tracking is formed. The speed control scheme is straightforward compared to the power control scheme, i.e., the optimal motor speed is calculated from the monitored wind speed, and then, the optimal motor speed is tracked and controlled. The speed control scheme is simulated by setting the doubly fed generator to run at speed for seconds at no load and then connected to the grid. The wind speed is given: the wind speed is from second to second, and the optimal speed is the one that maximizes the blade tip speed ratio at that wind speed, and the speed difference is from second to second, and the optimal speed is $\overline{\top}$, and the speed difference is from second to second, and the speed difference is from second to second. The reactive power is given: the reactive power is given from second to second and the reactive power is given from second to second and the reactive power is given from second to second [17]. It shows the waveforms of rotor three-phase current versus motor speed during the speed control scheme to achieve maximum wind energy tracking. It can be seen that as the motor speed increases, the rotor current amplitude increases accordingly; the rotor current frequency decreases as the speed gradually increases and the turndown rate gradually decreases in the first seconds; after seconds, as the speed increases and the turndown rate becomes larger, the rotor current frequency starts to gradually increase. The figure shows the waveform of the rotor three-phase voltage as the control quantity in this process, and it can be found that the rotor voltage amplitude is proportional to the rotation rate, as shown in Figure 6.

4.2. Performance Results of the Doubly Fed Wind Power System. The control software part of the variable speed and constant frequency doubly fed wind power system consists of the main program and the interrupt service program. Here, we mainly analyze the main program and the interrupt service program of the network-side converter and the machine-side converter in the AC excitation power supply. The main program mainly completes the initialization of the system, the interrupt service of the network-side converter is mainly used to stabilize the DC-side voltage, and the interrupt service program of the machine side converter mainly implements the DFIG variable speed and constant frequency power generation operation and the fault ride-through function of the doubly fed wind power generation system. According to the active power and the virtual synchronous speed, the drag torque is generated to realize the governor function; according to the wind speed and rotor speed, the torque command of the doubly fed wind turbine at the maximum wind power output is obtained, and then, the doubly fed motor is in a steady state. According to the reactive power and stator voltage, the voltage-reactive droop controller is used to generate the excitation current command to realize the excitation regulator function. The functions of the main program include initializing the DSP registers, setting the interrupt system, initializing the analog-to-digital converter ADC module, timer, event manager, CAP unit, QEP unit, comparison unit, I/O pins, etc., and displaying the program operation status. A three-level priority design is used in the software system, where the main program has the lowest priority level, followed by the timer interrupts, and the protection interrupts have the highest priority [18]. The control programs for the net-side converter and the machine-side converter are not done in the main program, but in the corresponding timer interrupt service programs, as shown in Figure 7.

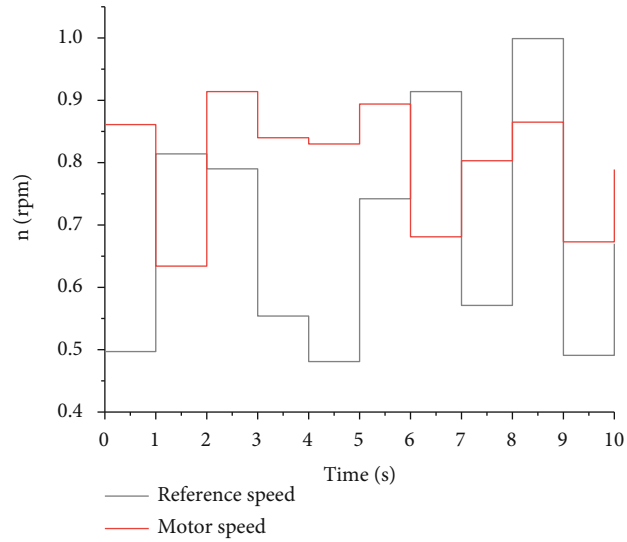

Figure 6: Motor speed tracking waveform graph.

Combined with the analysis earlier in this chapter, it is known that under weak grid conditions, although the stability and passivity of the system can be improved by further adjusting and rationalizing the PI controller parameters and phase-locked loop controller parameters of the grid-side converter system and rotor-side converter system, etc., due to the grid environment in practical applications and the requirements of a weaker grid with a lower short-circuit ratio, the practical results that can be achieved by adjusting the PI controller parameters only. However, due to the actual grid environment and the requirements of weaker grids with lower short-circuit ratios, the practical results that can be achieved by adjusting the PI controller parameters alone are very limited, so there is a need to improve and enhance the stability of the system by adding additional control structures to reshape the output conductance of the doubly fed wind power system so that it can improve the passive nature of the system. The three-step prediction method and hysteresis switch are used to detect the occurrence of grid faults, control the cut-in and cut-out of the deexcitation current, and dynamically adjust the size of the deexcitation current according to the degree of the grid fault, and effectively reduce the system shock time when the grid voltage dips. While keeping the DFIG system from leaving the network, it can also well protect the purpose of the DFIG system. From the point of view of the passive

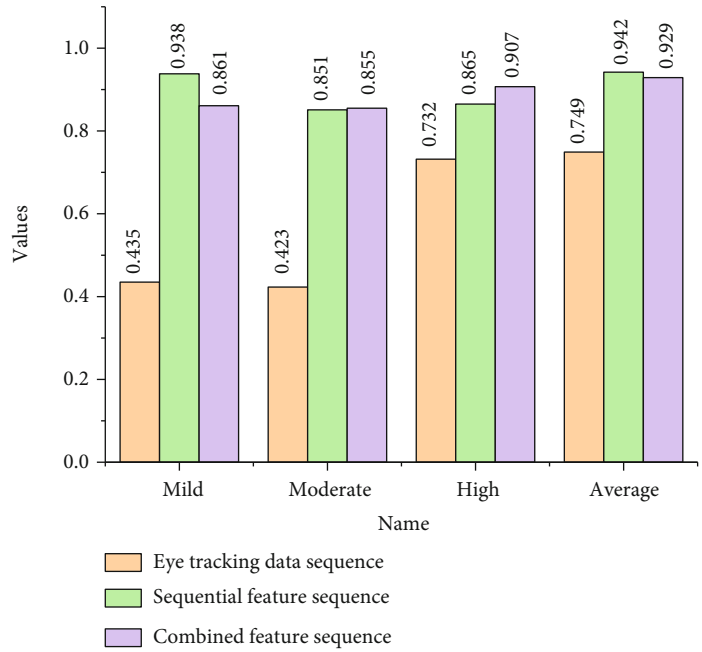

Figure 7: Flow chart of the doubly fed wind power simulation experimental system.

nature, the reason for the instability of the doubly fed wind power system when grid-connected is because its equivalent conductance has too many nonpassive regions in its dd component and Q component, active damping can be considered to suppress the nonpassive regions and reduce the conductance amplitude, the main step is to improve the damping of the system by extracting the current disturbance components after filtering and gain processing, etc., and feeding them back into the current control loop capacity, i.e., expanding the passive region of the system. To further investigate the effectiveness of the proposed control method of introducing variable dampers with the crowbar protection circuit to suppress the DFIG rotor overcurrent, the double fed wind power system can use the vector control method with the crowbar protection circuit to realize the fault ride-through when the voltage and voltage have deep symmetrical dip fault, or the control method of introducing variable dampers with the Crowbar protection circuit proposed in this paper can be used. Control method with Crowbar protection circuit is shown in Figure 8.

A disturbance observer-based OFCC method for magnetic chain compensation control is proposed for the LVRT problem of doubly fed wind power systems. Firstly, the transient characteristics of the doubly fed wind power system during voltage dips are studied, and it is concluded from the analysis that accurate compensation of the dynamics of the stator magnetic chain is the key to achieving LVRT. Based on the multiloop adaptive control proposed in Section 3, an observer-based magnetic chain compensation control method is designed considering a system model in which the stator-rotor magnetic chain interacts with each other. The disturbances caused by stator magnetic chain variations are accurately observed by using an observer, and the observed values are controlled instead of the real values. The results of the simulation lead to the following conclusions. The proposed OFCC can achieve the same control effect of low voltage ride-through as FFTCC, which is much better than the low ride-through effect of vector control [19].

To verify the feasibility of the control algorithm of doubly fed wind power system and the control algorithm of the doubly fed motor without speed sensor which will be studied later, the thesis establishes a doubly fed wind power simulation system in the environment. The doubly fed wind power system is a complex nonlinear multivariate high-order system with various symmetric relationships internally, so vector control technique is used to control the instantaneous values of voltage and current to achieve power or torque dissymmetric control.

Unlike the FFTCC method, the design of the proposed method does not rely on an accurate system model; it can well estimate the disturbances due to the magnetic chain dynamics and compensate for the control. Based on the magnetic chain compensation, the controller can output a suitable rotor voltage to offset the induced electric potential and achieve a suppression effect on the rotor overcurrent. The proposed magnetic chain compensation control method does not require accurate observation of the magnetic chain, and there is no problem with switching the control strategy during a fault.

$$h_1 = \frac{\omega_{ds}\mu_s}{L_g}. \tag{7}$$

In this paper, in the studied doubly fed wind power system without position sensor control system, firstly, the simulation study of the system is required, so the simulation models of the components that make up the doubly fed power system must be constructed. Many functional modules are provided,

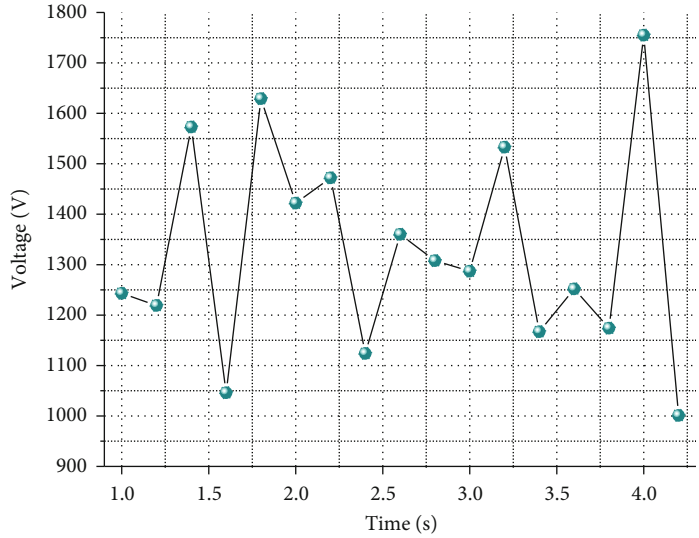

Figure 8: DC-side voltage for Crowbar+variable damper method.

and together with simple programming using the language, it is relatively easy to implement the above model and control block diagram so that the feasibility of the control strategy of the doubly fed wind power system can be verified through simulation, and the dynamic and static performances of the whole system model can be simulated and analyzed for the study. The simulation of various load cases is used to guide the design of the hardware circuit and to give viable thinking and steps for the software writing to provide adequate preparation instructions for the prototype experiments.

5. Conclusion

In this paper, the doubly fed wind power variable current system is taken as the research object, with the objective of effectively improving the grid stability of the doubly fed wind power variable current system; starting from the basic structure of the doubly fed wind power system, it is analyzed that the system can be divided into two subsystems, namely, the net-side converter system and the rotor-side converter system, and the impedance model is established for the subsystems, respectively, along these lines; in the control structure of the doubly fed wind power system, the control parameters of the net-side converter subsystem and the rotor-side converter subsystem are parametrically designed, respectively, and then, the theory of grid-connected impedance stability analysis and the theory of passivity are introduced in detail, and the port impedance characteristics of the system and the grid-connected stability under different grid strengths are analyzed by combining the resulting impedance model and the design parameters [20]. The adaptive control of the doubly fed wind power system is studied and applied to the control strategy of low voltage ride-through, mainly focusing on the poor control effect of traditional vector control at the operating point offset and the lack of robustness to the system modeling errors and external disturbances.

The adaptive sensing control method for doubly fed wind power systems mentioned in this paper considers the system under the condition of three symmetric faults. The probability of asymmetric faults in the grid is much larger than that of symmetric faults. Therefore, it is of great practical importance how to apply the proposed adaptive sensing control method to asymmetric fault conditions. Finally, how to apply the proposed adaptive control method to other power system devices and achieve coordinated control among multiple devices can be our future research direction, thus making the grid stability and robustness of the whole doubly fed wind power system optimized and improved.

Data Availability

The data used to support the findings of this study are available from the corresponding author upon request.

Conflicts of Interest

The authors declare that they have no known competing financial interests or personal relationships that could have appeared to influence the work reported in this paper.

Acknowledgments

This work was supported by the Educational Science Planning Project of Hubei Province Study on the Role of National Undergraduate Mechanical Innovation Competition in the Career Development of Higher Vocational College Students (No. 2017GB198).

References

[1] H. Zhao and L. Cheng, "Open-switch fault-diagnostic method for back-to-back converters of a doubly fed wind power generation system," *IEEE Transactions on Power Electronics*, vol. 33, no. 4, pp. 3452–3461, 2017.

[2] P. Tchakoua, R. Wamkeue, M. Ouhrouche, F. Slaoui-Hasnaoui, T. Tameghe, and G. Ekemb, "Wind turbine condition monitoring: state-of-the-art review, new trends, and future challenges," *Energies*, vol. 7, no. 4, pp. 2595–2630, 2014.

[3] S. Huang, X. Wu, X. Liu, J. Gao, and Y. He, "Overview of condition monitoring and operation control of electric power conversion systems in direct-drive wind turbines under faults," *Frontiers of Mechanical Engineering*, vol. 12, no. 3, pp. 281–302, 2017.

[4] Z. Hameed, S. H. Ahn, and Y. M. Cho, "Practical aspects of a condition monitoring system for a wind turbine with emphasis on its design, system architecture, testing and installation," *Renewable Energy*, vol. 35, no. 5, pp. 879–894, 2010.

[5] Y. Sun, J. Wu, and G. J. Li, "Influence research of wind power generation on power systems," *Power System Technology*, vol. 31, no. 20, pp. 55–62, 2007.

[6] A. Purarjomandlangrudi, G. Nourbakhsh, M. Esmalifalak, and A. Tan, "Fault detection in wind turbine: a systematic literature review," *Wind Engineering*, vol. 37, no. 5, pp. 535–547, 2013.

[7] J. Li and S. Xu, "Control strategy of low-voltage ride-through for direct-drive wind power generation system," *Electric Power Automation Equipment*, vol. 32, no. 1, pp. 29–33, 2012.

[8] W. Hu, Y. Wang, M. Li, M. Li, and Z. A. Wang, "Research on sensorless control strategy of direct drive multi-phase PMSG wind power generation system based on MRAS," *Power System Protection and Control*, vol. 42, no. 23, pp. 118–124, 2014.

[9] W. S. Hu and Y. J. Ding, "Research on new pitch control algorithm of wind power generators," *Power Electronics*, vol. 47, no. 2, pp. 53-54, 2013.

[10] G. Mu, J. Wang, G. Yan, Y. Cui, Y. Huang, and J. An, "Cascading trip-off of doubly-fed induction generators from grid at near full-load condition in a wind farm," *Dianli Xitong Zidonghua (Automation of Electric Power Systems)*, vol. 35, no. 22, pp. 35–40, 2011.

[11] J. Son, D. Kang, D. Boo, and K. Ko, "An experimental study on the fault diagnosis of wind turbines through a condition monitoring system," *Journal of Mechanical Science and Technology*, vol. 32, no. 12, pp. 5573–5582, 2018.

[12] W. Teng, W. Wang, H. Ma, Y. Liu, Z. Ma, and H. Mu, "Adaptive fault detection of the bearing in wind turbine generators using parameterless empirical wavelet transform and margin factor," *Journal of Vibration and Control*, vol. 25, no. 6, pp. 1263–1278, 2019.

[13] X. I. Wang and S. X. Zhang, "Research of a novel active power smoothing control strategy for double-fed wind turbine generator," *Gongkuang Zidonghua-Industry and Mine Automation*, vol. 37, no. 1, pp. 38–43, 2011.

[14] D. Xu, W. Wang, and N. Chen, "Dynamic characteristic analysis of doubly-fed induction generator low voltage ride-through based on crowbar protection," *Proceedings of the CSEE*, vol. 30, no. 22, pp. 29–36, 2010.

[15] F. El Hammouchi, L. El Menzhi, A. Saad, Y. Ihedrane, and B. Bossoufi, "Wind turbine doubly-fed asynchronous machine diagnosis defects using stator and rotor currents lissajous curves," *IJPEDS International Journal of Power Electronics and Drive System*, vol. 10, no. 2, pp. 961–970, 2019.

[16] K. D. Kerrouche, A. Mezouar, L. Boumediene, and A. Van den Bossche, "Speed sensor-less and robust power control of grid-connected wind turbine driven doubly fed induction generators based on flux orientation," *The Mediterranean Journal of Measurement and Control*, vol. 12, no. 3, pp. 606–618, 2016.

[17] Z. Li, P. Guo, R. Han, and H. Sun, "Current status and development trend of wind power generation-based hydrogen production technology," *Energy Exploration & Exploitation*, vol. 37, no. 1, pp. 5–25, 2019.

[18] W. Teng, H. Cheng, X. Ding, Y. Liu, Z. Ma, and H. Mu, "DNN-based approach for fault detection in a direct drive wind turbine," *IET Renewable Power Generation*, vol. 12, no. 10, pp. 1164–1171, 2018.

[19] A. Boufertella, H. Chafouk, M. Boudour, and A. Chibah, "Edge detection in wind turbine power system based DFIG using fault detection and isolation FDI," *IFAC-PapersOnLine*, vol. 51, no. 24, pp. 674–679, 2018.

[20] Y. Chang, Z. Xu, and Y. Zheng, "A comparison of the integration types of large wind farm," *Automation of Electric Power Systems*, vol. 14, no. 31, pp. 70-71, 2007.

Hindawi
Journal of Sensors
Volume 2021, Article ID 3170056, 11 pages
https://doi.org/10.1155/2021/3170056

Research Article

Wireless Pressure Sensor Assisted Orthopedic Nursing Effectiveness Evaluation

Qiufang Wang and Yumei Shen

The Fourth Hospital of Baotou, Baotou 014030, China

Correspondence should be addressed to Yumei Shen; 102009178@btmc.edu.cn

Received 2 November 2021; Revised 24 November 2021; Accepted 25 November 2021; Published 22 December 2021

Academic Editor: Gengxin Sun

This paper combines flexible pressure sensing technology, wireless sensor network, and cloud platform technology to design and manufacture a medical miniature pressure sensor and its supporting system. The problem of noninvasive monitoring of the syndrome encountered in the clinic is used for real-time monitoring and auxiliary diagnosis of the disease. Different from the current clinical use of "puncture" to measure intrafascial pressure, this system focuses on the noninvasive monitoring of compartment syndrome, using medical tape to paste a flexible microsensing unit on the injured area. The flexible sensor unit can measure the pressure here in real time and then can know the pressure in the fascia chamber. The flexible pressure sensor unit combines with the subsequent flexible circuit to send the measured data to the data in real time through wireless communication. The data aggregation node transmits the collected data to the upper computer through serial communication, and the upper computer software processes and stores the data and uploads it to the cloud server. In this experiment, it was observed that the concentrations of Ca and P showed the same fluctuating trend. With the gradual progress of the stretch, the concentrations of Ca and P increased with the increase in time, reaching approximately at the end of the extension. The peak value indicates that the osteoclast activity is enhanced at this time, the bone matrix is largely destroyed, and the Ca and P in the matrix are released into the serum in a large amount, thereby increasing the serum concentration. After the distraction ceases, it enters the healing period of the callus. At this time, the concentrations of Ca and P decrease with the increase in time and gradually reach a stable level, indicating that the osteoblast activity is enhanced at this time, the bone matrix begins to rebuild, and the Ca and P gradually increase. The deposited bone matrix gradually forms new bone and finally reaches a balance. Since the speed of extension in each experimental group is inconsistent, the time required to reach the same extension length is also inconsistent, so that the peak time is also inconsistent. After plotting the stress difference ($\triangle F$) before and after stretching against time and speed, it is found that the relationship is linear. However, these two variables affect $\triangle F$ at the same time, so they cannot be isolated. Based on this, this subject uses multiple regression equations to fit the three relationships of stress difference ($\triangle F$), time, and speed. In the process of distraction osteogenesis, with each distraction, the bone stress presents a trend from high to low. And as the stretch progresses, the measured stress value increases linearly at the same time point every day.

1. Introduction

In orthopedics trauma, trauma caused by various sudden accidents, such as car accidents, slips, falls, and industrial accidents, may cause tissue damage or loss [1]. These injuries or defects often result in the loss of body functions and ultimately lead to disability or even death. Therefore, the care of wounds has attracted much attention from medical staff. Common traumas in orthopedics include open fractures, avulsions, extensive skin abrasions, and crush injuries. Currently, researchers and medical staff have developed many methods for treating wounds and repairing skin [2]. Among them, wound dressings are widely used for wound healing because they can provide suitable healing conditions and at the same time coordinate and balance body activities such as blood vessels, connective tissues, and epithelial cells. In addition, with the rapid development of China, the contradiction between the increasing aging population and the increasingly serious

chronic diseases and China's relatively scarce medical resources has gradually become prominent [3]. At present, new concepts such as "smart medical" and "smart medical" are proposed to change the existing medical service model and improve the utilization of medical resources. Smart medical devices and wearable devices are an important part of these concepts. The research on sensors suitable for this type of equipment is of great significance to the promotion of "smart medical" and "smart medical." At the same time, this type of sensor device with the ability to perceive different external environmental parameters is also expected to be used in existing medical equipment such as artificial limbs to effectively improve the quality of life of patients [4].

When the external force is within the range of normal physiological load, in order to maintain its normal structure and function, the articular cartilage will obtain nutrients through the exchange of joint lubricating fluid and the fluid in the matrix. Therefore, normal joints usually do not cause cartilage damage when carrying loads within the bearing range, but any load that exceeds the joint bearing capacity has the risk of cartilage degeneration and osteoarthritis. For some athletes, soldiers or dancers, they often do some rapid acceleration, instant deceleration, continuous training and jumping and landing one-leg support. Therefore, due to their special activities, they may be greatly exacerbated by regular exercises in this way. The damage to the cartilage of the knee joint or the risk of worsening of the knee joint cartilage in people in China will have a serious impact on their careers. At present, for some different exercise methods, the human knee joint cartilage is subjected to different forms of loading conditions, and the mechanism of its mechanical properties has not been clearly expressed [5]. This requires us to strengthen the study of the changes in the mechanical behavior of the knee joint in different ways of movement and explore the inducing mechanism of the occurrence and exacerbation of knee cartilage damage under different loading conditions, as well as the changes in contact stress and mechanical behavior [6].

This paper designs the hardware of the flexible pressure sensor, which mainly includes the selection of the main components according to the system requirements, the design of the pressure signal conversion and reading circuit, the selection of the antenna, and the corresponding optimization processing. In the actual design, this article has been tightly focused on the requirements of flexibility, portability, and wearable. While satisfying the most basic functions of the system such as data reading and wireless communication, it can be achieved to the maximum extent. This subject observes that under the stretch strategy of extending twice a day, the stress value increases significantly after each stretch. As time goes by, this stress value gradually decreases until the next stretch (after 12 hours), approximately reaching the level before the last stretch. At this point, the second stretch is performed, and the stress value immediately increases and then gradually decreases with the passage of time. Until the first stretch on the next day, the stress value dropped to a slightly higher level than before the previous stretch. In this way, there are two stress peaks every day, and each peak appears at the moment after stretching and then gradually decreases with an exponential decay function. For each phase of distraction osteogenesis (the same number of days of extension), the experimental groups with different extension speeds showed different stress changes. The stress decreased by 8.83 N before and after the first stretch on the first day, and the stress increased by 12.52 N before and after the second stretch and then dropped by 11.21 N.

2. Related Work

Combining the patient's clinical manifestations, imaging examinations, serological indicators, infrared spectroscopy, and direct manometry are the main methods for diagnosing acute compartment syndrome. Pain, paleness, paresthesia, pulselessness, and paralysis are the five main clinical manifestations. Serological indicators are mainly accelerated erythrocyte sedimentation rate, increased white blood cell count, and increased creatine kinase. The first two are mainly caused by the body under stress conditions, and the increase in the two can appear under many stress conditions, lacking specificity. Creatine kinase is of relatively great value in the diagnosis of compartment syndrome. Normally, there is a small amount of this enzyme in serum, 25-170 U/L for women and 25-200 U/L for men. It is an important enzyme that regulates cell energy metabolism. When the body is severely traumatized or compartment syndrome occurs, resulting in muscle ischemia and necrosis, the enzyme in the cell will be released into the blood, which will significantly increase the content of serum creatine kinase. It began to rise sharply 2 hours after injury and reached a peak at 24 hours after injury, which was 42 times the normal value.

Studies by related scholars have reported that when muscle tissue develops edema and degeneration, the average creatine kinase value reaches 2400 U/L or more; the osteofascial compartment should be cut and decompressed at this time [7]. At this time, the nerve, blood vessel, and muscle ischemia time is not yet very long, without avascular necrosis, causing irreversible damage. MRI examination can mainly see manifestations such as increased volume of the osteofascial compartment, muscle edema, and loss of muscle texture. Doppler ultrasound is more valuable in the diagnosis of compartment syndrome than other auxiliary examinations. It can not only observe tissue edema and vessel diameter, but also dynamically observe arterial pulsation and fascial tissue elasticity changes. Related scholars have studied the pulsed phase-locked loop ultrasound instrument to observe the fascia displacement waveform of the arterial blood pressure pulse to estimate the pressure of the osteofascial compartment [8]. The correlation between the degree of fascia displacement in the osteofascial compartment and the perfusion pressure was confirmed by the researchers through noninvasive ultrasound. Relevant scholars have established a model of the anterior tibial compartment of the calf to study the increased pressure of the fascial compartment (infusion of 0.9% sodium chloride solution increases the pressure of the compartment) [9]. The reduced feasibility of noninvasive evaluation has made Doppler ultrasound more and more widely used in the diagnosis of compartment syndrome.

Related scholars have studied the creep behavior of articular cartilage and the mechanical behavior of depth and velocity correlation [10]. It is found that under different creep times of articular cartilage, the creep strain and creep compliance decrease along the depth of the cartilage from the surface to the depth. The depth-dependent creep compliance increases with the creep time, and the increase in creep compliance decreases along the cartilage depth. As the creep progresses, the creep compliance first increases rapidly, then increases and slows down, and decreases as the compressive stress increases. In addition, Young's modulus will gradually increase from the surface layer to the deep layer, and Young's modulus of different layers will increase with the increase in the stress rate [11]. Under the set compressive strain, the Poisson's ratio will increase with the increase in depth and the Poisson's ratio of different layers will increase with the increase in compressive strain.

Related scholars have studied the dynamic contact mechanics of the human knee tibial platform during gait and stair climbing, analyzed the magnitude and position of the maximum contact stress at different relative positions during the movement [12]. The maximum contact stress occurs in the cartilage-cartilage contact area. During climbing stairs, the maximum stress occurs on the back of the platform under the meniscus; in the early stages of gait and ladder climbing, the maximum stress on the lateral platform appears under the meniscus. At the later stage of the ladder climbing process, the maximum contact stress appears in the cartilage-cartilage contact area. Related scholars have studied the stress contact mode on the tibial plateau during the simulated gait movement [13]. The first mode occurs on the posterior side of the tibial plateau and a single peak stress occurs in the early stage; the second mode occurs in the middle and posterior part of the lateral plateau, with two peaks in the early and late stages; the third mode occurs on the medial plateau cartilage.

Relevant scholars have studied the changes of some knee joint motion parameters during walking before and after a period of kneeling position and found that the continuous static load on the knee joint will significantly affect the subsequent knee joint motion load pattern [14–16]. The motion and work style of static load applied to the joint will obviously affect the force of the knee joint movement, which will cause or aggravate the risk of arthritis [17, 18]. The researchers found through finite element simulation that even when the damage occurs only through strain-related damage mechanisms, the location and size of cartilage damage are obviously dependent on the strain rate [19–21]. In addition, experimental studies have found that for a given compression amplitude of up to 1.2 mm, the reaction force changes 6 times in the compression rate [22–24]. Although the static response is basically linear, the nonlinear behavior increases with the increase in the compression rate [25, 26].

3. Method

3.1. Flexible Pressure Sensor Terminal Architecture. The hardware part of the flexible pressure sensor mainly includes a flexible pressure sensing unit module, a pressure data reading and conversion module, a wireless communication module, and a power supply module. The overall hardware architecture is shown in Figure 1. The flexible pressure sensing unit converts the pressure signal into the resistance (conductance) signal, pressure data reading and conversion module reads and converts the resistance signal into a digital signal and sends it to the wireless communication module. The wireless communication module sends the data to the data aggregation node through the ZigBee wireless communication protocol, the data is transmitted to the upper computer by the transmission method, the upper computer software further processes the data and stores and uploads the data, and finally the power module is responsible for supplying power to the entire flexible pressure sensor.

3.2. Flexible Pressure Sensing Unit. The flexible pressure sensing unit is a flexible pressure sensing device, which has many advantages such as good flexibility, free bending and even folding, and being light and thin, portable, and wearable. It is very suitable for pressure data measurement on wearable devices. This article analyzes the advantages and disadvantages of the three mainstream flexible pressure sensing units: piezoelectric flexible pressure sensing unit, capacitive flexible pressure sensing unit, and piezoresistive flexible pressure sensing unit. Aimed at the scenario of comprehensive monitoring of the osteofascial compartment, this paper intends to use a piezoresistive flexible pressure sensing unit as the pressure acquisition device of the system.

The flexible pressure sensing unit used in this article is Flexiforce from Tekscan, USA. The thickness of the flexible pressure sensing unit is only 0.15 mm, and the diameter of the sensitive area is 0.95 cm. The range of different types of flexible pressure sensing units can range from a few Newtons to hundreds of Newtons, which can be used by different users [27, 28]. Flexiforce is very flexible, can be bent at will like paper, and is very thin, which fits the application scenarios of compartment syndrome pressure measurement in this article.

The Flexiforce flexible pressure sensing unit adopts a two-layer structure, each layer of film is made of polyester fiber material, and then silver wires are printed on this layer of film, and finally a layer of pressure sensitive material is added, and the two films are glued together. The mixture is pasted together to form the Flexiforce flexible pressure sensing unit. When no pressure is applied to the sensitive area, the Flexiforce flexible pressure sensing unit presents a high resistance state; that is, the resistance of the Flexiforce flexible pressure sensing unit is infinite, usually on the order of tens of megaohms. When a force is applied to the sensitive area, the resistance of the Flexiforce flexible pressure sensor unit will drop to the order of tens of kiloohms; that is, the resistance of the Flexiforce flexible pressure sensor will decrease as the pressure increases, and the conductance increases with the pressure.

The conductance of the Flexiforce flexible pressure sensing unit is related to the pressure; that is, there is a one-to-one correspondence between the pressure and the conductance. However, since each sample of the Flexiforce flexible pressure sensing unit is not exactly the same [29, 30]. Therefore, it is necessary to calibrate the pressure conductance

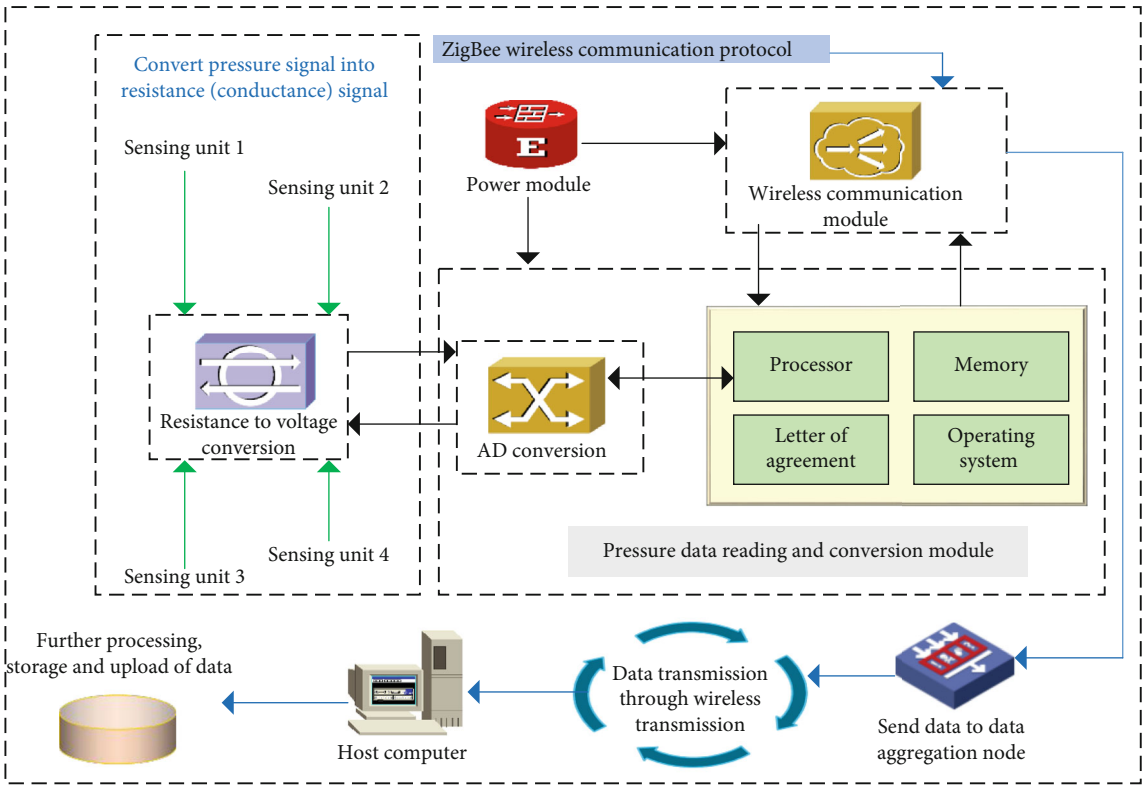

Figure 1: The overall architecture of flexible pressure sensor terminal hardware.

curve of each Flexiforce flexible pressure sensing unit sample and do the corresponding recording and storage work to process the data later.

Place the Flexiforce flexible pressure sensing unit on the rotating screw lifting platform to ensure that the sensitive unit is located directly under the push-pull force gauge. The two electrodes of the pressure sensing unit are, respectively, connected to the red and black test leads of the multimeter to measure the resistance value, and the pressure conductivity data is recorded within the pressure range of the Flexiforce flexible pressure sensing unit. Figure 2 is the pressure conductance curve of the Flexiforce flexible pressure sensing unit with a range of 5 N. It can be seen that the flexible pressure sensing unit has good repeatability within its range.

3.3. ZigBee Wireless Communication. This article intends to use ZigBee as the wireless communication protocol of the auxiliary monitoring system for compartment syndrome. There are currently four mainstream ZigBee wireless communication chips on the market: Texas Instrument (TI) CC2530, SILABS EM35x, FREESCALE MC13224, and JENNIC's JN516x. The parameters of the four chips are shown in Table 1.

According to the parameters in Table 1, combined with our application scenario of compartment syndrome, this paper intends to use the CC2530 with a smaller chip size and a lower price as the wireless communication chip of this system. CC2530 is the second-generation ZigBee wireless communication chip launched by TI. The wireless communication chip works in the 2.4 GHz frequency band and integrates modules such as a microcontroller, wireless communication, and analog-to-digital converters. CC2530 adopts the QFN40 package, the physical size is only 6 mm ∗ 6 mm, the input voltage is between 2 V and 3.6 V, and the sending and receiving data currents are relatively small, 24 mA and 29 mA, respectively.

The following mainly introduces the modules contained in the chip:

(1) Microcontrol unit: the wireless communication chip contains an enhanced 8051 microcontrol unit with three different memory access bus modes: special function registers, DATA, and CODE/XDATA. In addition, it also includes a debug interface and an input expansion interrupt unit

(2) Flash memory: the flash memory of the CC2530 is mainly used to retain program codes and constants. There are 4 different versions of the chip, which are mainly distinguished according to the memory size. The memory size is divided into 32 KB, 64 KB, 128 KB, and 256 KB

(3) Random access memory: this module can retain data when the digital part is powered down, reducing the power consumption of the entire system

(4) Analog-to-digital converter: ADC is 12 bits, supports 8 channels of analog signal input, and can choose single-ended or differential input

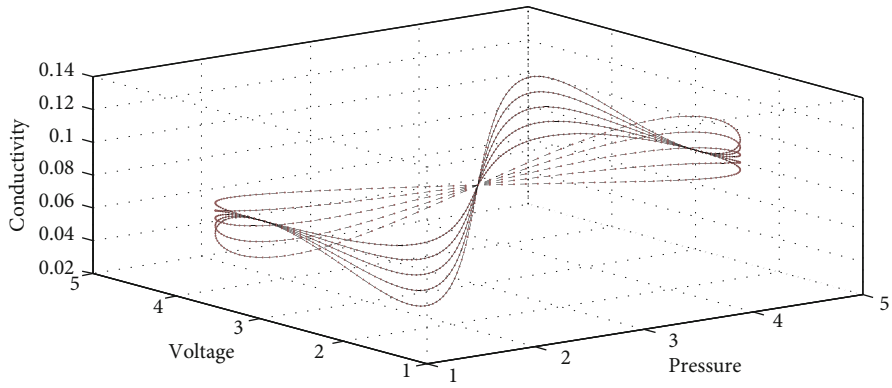

Figure 2: Flexiforce pressure conductance.

Table 1: ZigBee chip parameter table.

Chip model	MC13224	JN516x	CC2530	EM35x
Size	9.5 cm ∗ 9.5 cm	5 cm ∗ 5 cm	7 cm ∗ 7 cm	8.2 cm ∗ 8.2 cm
Maximum transmit power	4.2 dBm	2.4 dBm	5.4 dBm	9.4 dBm
Received power	-91 dBm	-95 dBm	-98 dBm	-95 dBm
Tx current	16 mA	14 mA	27 mA	19 mA
Rx current	18 mA	16 mA	22 mA	29 mA
Lowest power consumption current	0.33 μA	0.11 μA	0.51 μA	0.43 μA

(5) Watchdog: the watchdog plays the role of protecting the microcontroller, resetting the device, and waking up the device from sleep state when the software fails

(6) Sleep mode timer: this timer is an ultralow power timer with a 32 kHz frequency crystal oscillator, which can be used as a sleep wake-up timer

(7) Wireless transceiver module: this module includes an IEEE 802.15.4 radio frequency transceiver, data packet filtering, and address recognition module

3.4. Wireless Pressure Sensor Assistance. The main function of the flexible pressure sensor is to collect pressure information at the wound of compartment syndrome. The pressure is not an electrical quantity. We are not good at measuring and processing it directly. Therefore, the pressure change needs to be converted through the flexible pressure sensing unit. It is the resistance change, and then the resistance change is converted into a voltage change. In this way, we can measure and process it and finally send the data to the data aggregation node in the data center through wireless communication. The data aggregation node then transmits the pressure data to the upper computer through serial communication, and the software of the upper computer displays, graphs, stores, and uploads the data to the cloud, so as to achieve the purpose of real-time monitoring of pressure information at the wound of compartment syndrome.

The resistance of the sensitive area of the Flexiforce flexible pressure sensing unit is inversely proportional to the pressure. The greater the pressure, the lower the resistance of the Flexiforce flexible pressure sensing unit. For the measurement of resistance change, this article uses the same phase amplifier circuit to achieve. According to the knowledge in analog electronic circuits, it can be known from the "virtual short" and "virtual disconnection" that the input voltage and output voltage of the same phase amplifier circuit have the following relationship:

$$V_{\text{out}} = \left(\frac{1 - R_x}{R_{\text{ref}}}\right) \bullet (R_{\text{ref}} \bullet V_{\text{in}}), \tag{1}$$

where V_{in} is the input voltage, V_{out} is the output voltage, R_{ref} is the reference resistance, and R_x is the resistance of the piezoresistive flexible pressure sensing unit. When V_{in} and R_{ref} are constant, the output voltage V_{out} of the circuit is inversely proportional to the resistance R_x of the piezoresistive flexible pressure sensor, that is, proportional to its conductance. According to the previous content, the conductance of the piezoresistive flexible pressure sensor is proportional. Pressure is positively correlated and can be fitted with a linear function, so the output voltage of this circuit has a linear function relationship with pressure.

$$V_{\text{out}} = \frac{C_1 S_x}{R_x} + C_2 R_x - C_3(1 - F) + C_4. \tag{2}$$

In the formula, S_x is the conductance of the Flexiforce flexible pressure sensing unit, F is the pressure on the sensitive area of the Flexiforce flexible pressure sensing unit, and C_1, C_2, C_3, and C_4 are constants.

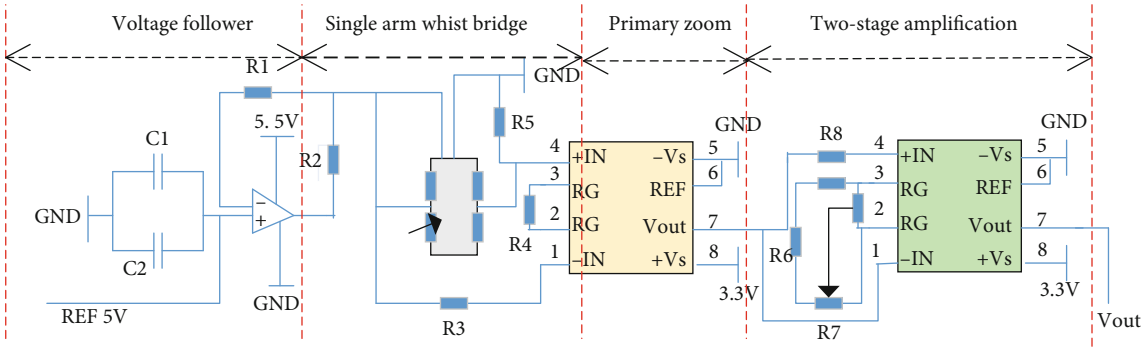

Figure 3: Two-stage amplifying circuit composed of AD8236.

The power module is one of the key modules of the flexible pressure sensor. The CC2530 chip, the operational amplifier chip (MCP6004), and the JTAG (Joint Test Action Group) interface in the flexible pressure sensor all require a stable 3.3 V power supply. Although there are many 3.3 V batteries to choose from, most of these batteries on the market have a wide range of variations and are not very stable 3.3 V voltages. For example, some 3.3 V lithium batteries have a voltage of 4.2 V when fully charged. The latter voltage becomes about 2 V, so the power supply voltage by a battery is usually unstable. And we need a stable 3.3 V power supply. If the power supply voltage is unstable, it is likely to affect the conversion accuracy of the internal analog-to-digital conversion module of the CC2530 chip and even affect the normal operation of the device, so the basic design idea of the module is 3.7 V. The output is followed by a low dropout voltage regulator chip (low dropout voltage (LDO)). Through such processing, a stable 3.3 V voltage is provided to the CC2530 chip and the operational amplifier chip. In order to reduce the size of the flexible pressure sensor power supply module as much as possible, this design uses a 3.7 V rechargeable battery with a capacity of 60 mAh. The size of the battery is 15 mm ∗ 12 mm ∗ 4 mm in length.

The signal amplification link uses the instrumentation amplifier AD8236 as the core chip. This amplifier is an instrumentation amplifier with low price, low power consumption, and output swing that can reach the power supply voltage (usually called power limit output). It has been widely used in microcurrent detection, portable equipment, and medical equipment. The input range of the sensing signal is 0~3.3 mV, and the voltage input range of the analog-digital converter (ADC) that needs to be connected to the microcontroller is 0~3.3 V; then, the required gain is $\beta = 1000$. This article uses two-stage amplification to meet the amplification requirements, and the corresponding circuit is shown in Figure 3. The power supply voltage of the system is provided by a 5 V DC-DC DC power supply circuit. A voltage follower is added to the input of the amplifier to improve the ability of the reference voltage to carry a load and to isolate interference from other modules. In order to calibrate that the input of the amplifying circuit is zero when the sensor is not working, an adjustable resistor and a zero-adjusting circuit are added before the two-stage input of the amplifying circuit.

3.5. Analysis of Error Sources. The contact pressure signal will be affected by environmental factors (such as temperature) during the process from acquisition to amplification, causing measurement errors. It is necessary to analyze the sources of system errors. In the Wheatstone bridge link, the main factor that affects the change in the output voltage of the bridge is temperature. The change of temperature will cause the sensitivity coefficient K of the strain gauge to change. According to the calculation formula of the bridge output voltage, when the temperature changes by ΔT, the output voltage of the bridge is

$$U_{\mathrm{To}} = K\frac{(1-\varepsilon_L)(1-\alpha_k\Delta T)}{(K+1)\varepsilon_L U_i(1+2\alpha_k\Delta T)}. \tag{3}$$

In the formula, α_k is the sensitivity temperature coefficient of the strain gauge.

In the signal amplification link, the amplifier is a low-speed and high-precision application in the environment described in this article. It is necessary to focus on low-frequency DC errors, such as low-frequency noise, bias current, and offset voltage. The error sources of the gain β of the amplifier used in the amplifying link include the temperature of the environment (or the measured object), the environmental noise, the voltage and current noise of the amplifying chip, and the offset voltage. Among them, the external environmental noise is extremely small in ordinary environments, usually below 0.1%, and the internal noise of the amplifier itself is in the μVp-p level, so the influence of these two items on the amplified output voltage is negligible.

The absolute error part of the amplifier mainly includes gain error S_β, common mode error S_{CMR}, and output offset voltage error S_{ao}. The temperature drift error is divided into gain drift and input offset voltage drift (ignoring input offset current drift). Combining the errors of these two parts, the expression of the sum of errors S_a of the amplification link can be obtained as follows:

$$S_a = (1-\alpha_{at})\Delta T - \alpha_{ao}S_\beta + S_{ao}S_{\mathrm{CMR}}. \tag{4}$$

In the formula, the units of S_β, S_{CMR}, and S_{ao} are ppm, and α_{at} and α_{ao} are the temperature coefficients of gain and offset

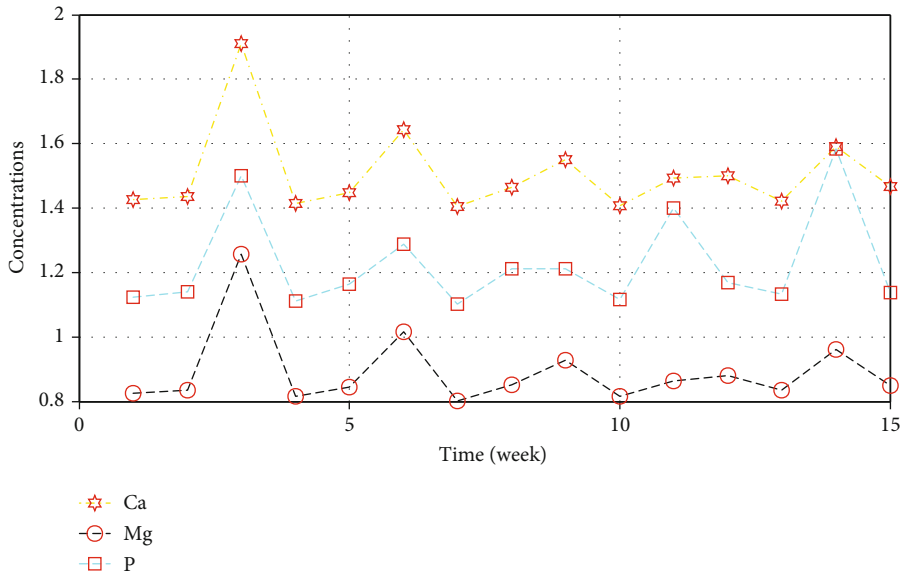

Figure 4: The change trend of serum Ca, Mg, and P concentrations with the progress of bone elongation.

voltage (in ppm/°C), respectively. For the DC amplifier circuit, the main source of error is the static error part (such as offset error), which can be eliminated by calibration.

When considering the temperature change, it is necessary to compensate for the error caused by the temperature drift. There are many methods of temperature compensation, which can be divided into two types: self-compensation and bridge compensation. Among them, the self-compensation method is to make the additional strain of the strain gauge zero by selecting the appropriate sensitive grid material and structural parameters when the linear expansion coefficient of the material to be tested is known, so that the resistance change caused by the temperature change is also zero, in order to achieve the purpose of temperature compensation. Although this compensation method can realize zero resistance change caused by temperature from the perspective of resistance deformation, it needs to know the temperature coefficient of the tested piece and other parameters, so there will be certain errors in actual use. The compensation effect of the occasion is not ideal.

The bridge compensation method uses other arms in the full bridge as reference strain gauges, which are exactly the same as the working strain gauge model parameters and are all attached to the test piece in the same temperature environment, but do not bear the effect of strain. Then, the bridge is still in equilibrium when the temperature changes, and the change in output voltage is only related to the pressure on the working strain gauge. The effect of bridge compensation is better than self-compensation, so it is also a more commonly used compensation method in engineering applications.

In a single-arm bridge, the bridge compensation method can be used for temperature compensation. R_1 is the working strain gauge, then R_2 should be selected as the reference strain gauge, and the other arms are matched resistances. The resistance change of R_1 under the action of temperature and pressure is dR_P and dR_T, respectively. R_2 is only affected by temperature, and its resistance change is dR_T. Then, the output voltage of the bridge is

$$U_o = \left[\frac{R_1 + d(R_p - R_T)}{R_1 - R_2 + (1-d)(R_p - R_T)} - \frac{R_2}{R_p - R_3}\right] U_i. \quad (5)$$

Choosing the initial resistance $R_1 = R_2 = R_3 = R_4 = R$, we can get

$$\frac{U_o}{U_i} = \frac{dR_T(R_p + dR)}{3(R_p - dR) - dR_T}. \quad (6)$$

For the resistance change caused by pressure in the same temperature environment, we can get

$$\frac{U_o}{U_i} = \frac{(1-K)\varepsilon_L}{3\varepsilon_L - KR_T}. \quad (7)$$

It can be seen from the above formula that the change in the resistance of the strain gauge caused by the temperature is offset in the bridge, and the output of the bridge is only related to the input voltage and strain. It should be noted that the premise of using this temperature compensation method is that the parameters of the working strain gauge and the reference strain gauge are exactly the same, the installation conditions are the same, and the resistance values of the other two arms always remain unchanged during temperature changes.

4. Result Analysis

4.1. Determination of Biochemical Indicators of Bone Metabolism. In this subject, various bone metabolism-related indicators in the serum of experimental samples in different experimental processes were determined. The main biochemical indicators measured include Ca, Mg, and P. In the

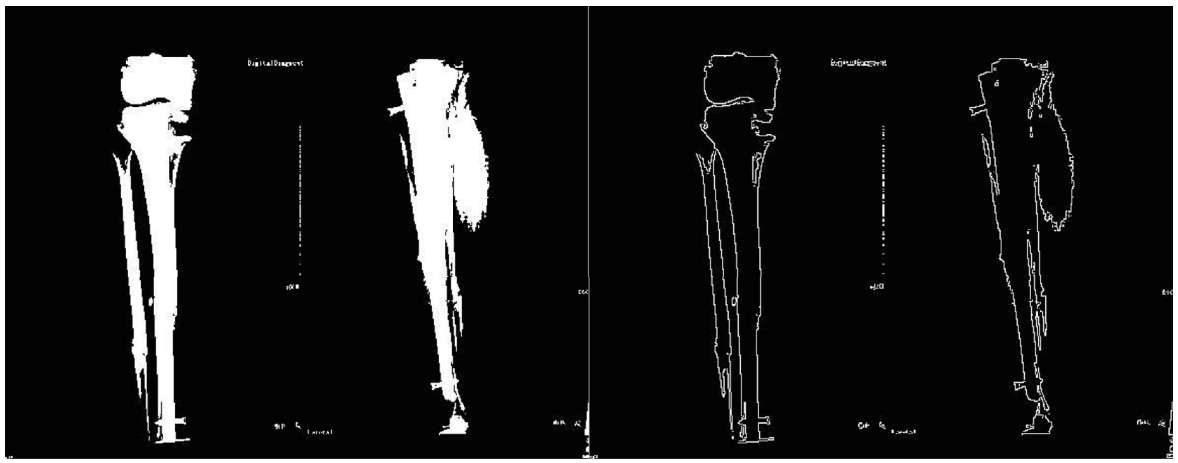

Figure 5: The edge extraction of the anterior and lateral positions of the film after the operation.

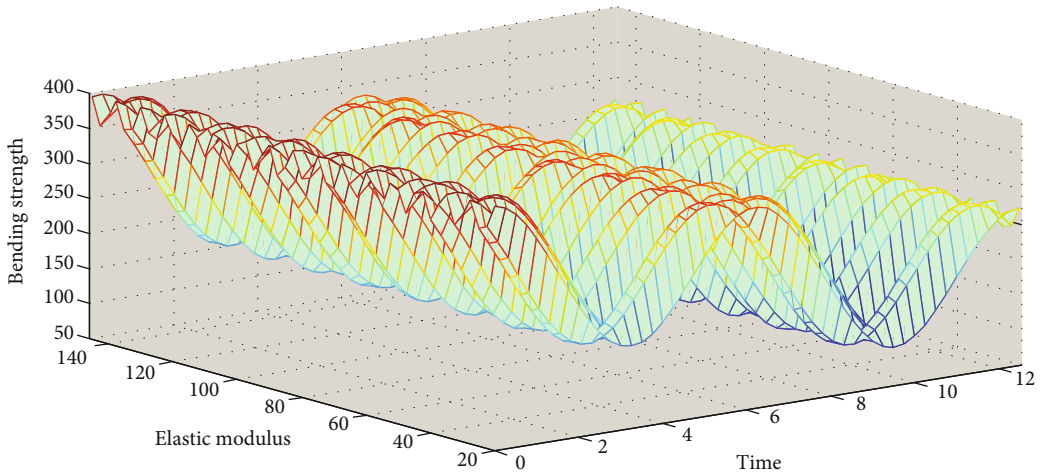

Figure 6: Mechanical properties of bone bending after elongation stops.

abscissa, "1-15" are the samples collected on the first day of the 1-15 weeks after surgery. According to the stretch strategy, extension is only performed one week after surgery.

It can be seen from Figure 4 that the concentrations of Ca, Mg, and P show similar fluctuation trends. Stretching was performed one week after the operation. With the gradual progress of the stretch, the concentrations of Ca, Mg, and P increased with time, reaching a peak at about the third week, after which the stretch stopped and the callus healing period entered. At this time, the concentration of Ca, Mg, and P fluctuates with the increase in time and gradually stabilizes. Since the speed of extension in each experimental group is inconsistent, the time required to reach the same extension length is also inconsistent, making the time of peak appearing in the graph also inconsistent.

4.2. X-Ray Judgment of Bone Healing. After the osteotomy was completed, X-ray monitoring of the surgical site was performed. The result is shown in Figure 5. It can be seen from Figure 5 that the fractured ends of the bone can be clearly seen on the X-ray film and the fracture line is clear; there is a zona pellucida of about 0.5 mm between the fractured ends (pointed by the red arrow), which is the stable fixation of the external fixation device. Regardless of whether it is in the frontal or lateral position, the alignment and alignment of the bone ends are good.

4.3. Mechanical Property Test at the Later Stage of Bone Healing. When analyzing the mechanical properties of the bone after the extension is stopped, if the material is defined as a pipe, the bending strength can be increased to 400 MPa. At the same time, the elastic modulus has also increased from 20 MPa to 140 MPa. Such a large difference in elastic modulus shows that in the same sample test, the setting of material properties in the experiment has a great influence on the results. Therefore, in this experiment, the material is set as the pipe material, and the experimental group and the control group use the same pipe diameter setting. Healed bone has strong plasticity and weaker brittleness, so it can be inferred that the bone tissue is still in the mid-healing stage at this time and cannot bear a large load. The mechanical

Table 2: Test results of bone mechanical properties 2 weeks after stopping lengthening.

Sample	Material	Elastic modulus	Bending strength	Breaking strength	Sample area	Maximum load
Test	Bar	13	23	21	165	145
	Pipe	176	433	335	95	112
Control	Bar	15	178	147	161	1178
	Pipe	1165	4556	3789	98	1177
Ratio	Bar	82	14	13	0.98	12
	Pipe	15	8	8.7	0.99	9

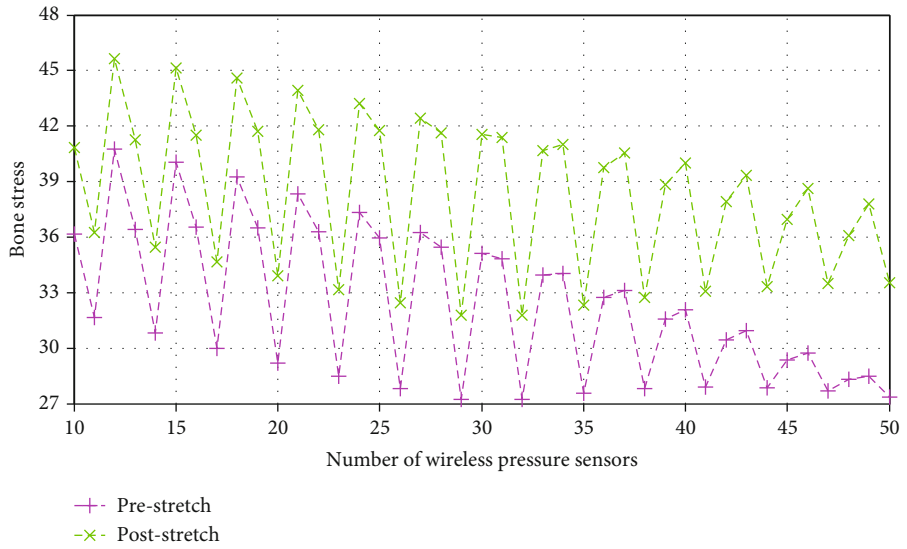

Figure 7: The change trend of bone stress value with the number of wireless pressure sensors.

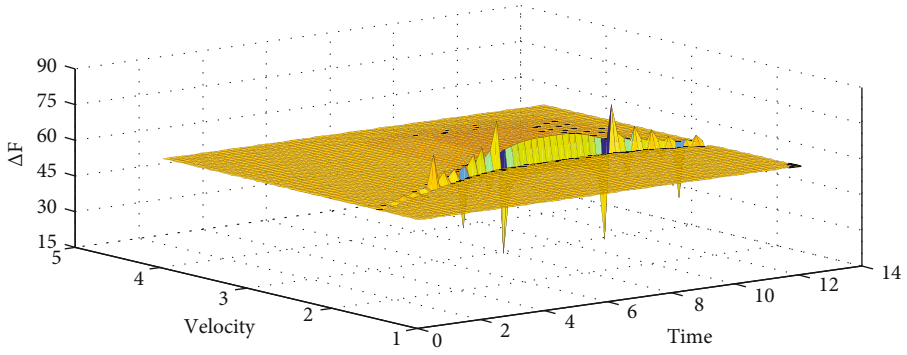

Figure 8: The 3D trend graph of $\triangle F$ changes with time and stretch speed.

properties of bone bending after the extension stops are shown in Figure 6.

It can be seen from Table 2 that in the analysis of the comparative bone mechanical properties, if the material is defined as a tube, the bending strength of the healing bone is only 184.85 MPa, and if the material is defined as a tube, the bending strength can be increased to 4,594.56 MPa. The modulus of elasticity is 1170.84 MPa. The healed bone is more rigid and less brittle. Compared with the healing bone in the experimental group, the elastic modulus of the control group is significantly higher than that of the experimental group, so the rigidity of the former is much greater than that of the latter.

4.4. Determination of Bone Stress Level. With the passage of time, this stress value gradually decreases and reaches the level before the last stretch before the next stretch. At this point, the second stretch is performed, and the stress value immediately increases and then gradually decreases with the passage of time. Until the first stretch on the next day, the stress value dropped to slightly higher than the level before the previous stretch. In this way, there are two stress peaks every day, and each peak appears at the moment after stretching and then gradually decreases with an exponential decay function. The stress value at the initial stage of decline decreases rapidly, and this speed gradually slows down. This

process just coincides with the exponential decay function model. The change trend of bone stress value with the number of wireless pressure sensors is shown in Figure 7.

The 3D trend graph of $\triangle F$ changing with time and stretching speed is shown in Figure 8. Since $\triangle F$ also changes with the change of the stretching speed, the stress-time curve alone is not enough to explain the change trend of the stress difference ($\triangle F$). The previous experiment proved that at the same time point, the stress difference ($\triangle F$) is also linear with different stretching speeds, so we used multiple linear regression fitting to simultaneously investigate the influence of two variables on $\triangle F$.

5. Conclusion

The results of this experiment show that after stopping distraction for 2 weeks, the torsion resistance and bending resistance of the healed bone are lower than those of the healthy side control group. In particular, the bending strength and breaking strength of the healed bone are only 10% of the control group. The elastic modulus is about 15% of the control group. The torsion strength, yield strength, yield shear stress, maximum shear stress and other indicators of the healing bone were only about 50% of the control group. This shows that the healing bone is in the early stage of secondary healing at this time, and the plasticity of the healing bone is strong but the rigidity is weak. If the external fixator is removed at this time, it is very prone to secondary fractures. After stopping the distraction for 10 weeks, the plasticity of the healing bone increased significantly compared with that at 2 weeks, especially the fracture strength was close to the normal bone tissue (95.4%), and there was no significant difference between the healing bone and the healthy side bone ($p > 0.01$). However, the elastic modulus is still quite different from the normal control (27.2%). Therefore, it can be inferred that the bone is already at the end of the healing period and can bear a larger load. The later recovery is mainly the recovery of the elastic modulus. As far as torsion strength is concerned, there is no significant difference between the experimental group and the control group ($p > 0.01$). The difference in shear modulus is 14%. The maximum shear stress of the healing bone is slightly higher than that of the control, and the yield shear stress is slightly lower than that of the control, indicating that the healing degree of the healing bone can bear the corresponding shear stress, but it will yield early. This suggests that its plasticity is slightly higher than its own control. It will take some time for the bone tissue to heal completely. Comprehensive analysis shows that the healing bone is currently at the end of the second stage of healing, and its callus strength has been able to withstand its own gravity and has a certain degree of resistance to torsion and bending. At this time, it is completely feasible to remove the external fixator. This subject has greatly controlled the weight difference when grouping, but later found that there are differences in the thickness of bones of the same weight, and whether these differences will also have a greater impact on the change in stress value ($\triangle F$). The next step in this topic will be to explore other factors that affect bone stress changes in order to establish an equation based on multiple parameters to prepare for preclinical experiments. In the research at this stage, the system construction and performance testing and optimization of the bone stress monitoring device have been completed, and the bone stress change curve ($\triangle F$) based on the binary regression equation has been initially established for the in-depth study of bone stress and bone healing. The relationship has laid a solid experimental foundation.

Data Availability

The data used to support the findings of this study are available from the corresponding author upon request.

Conflicts of Interest

The authors declare that they have no known competing financial interests or personal relationships that could have appeared to influence the work reported in this paper.

References

[1] P. Avaltroni, S. Nappi, and G. Marrocco, "Antennifying orthopedic bone-plate fixtures for the wireless monitoring of local deep infections," *IEEE Sensors Journal*, vol. 21, no. 18, pp. 21012–21021, 2021.

[2] P. M. S. Shimabukuro, M. L. Duarte, A. M. Imoto et al., "Environmental cleaning to prevent COVID-19 infection. A rapid systematic review," *Sao Paulo Medical Journal*, vol. 138, no. 6, pp. 505–514, 2020.

[3] S. I. Jeong, E. J. Lee, G. R. Hong et al., "Three-dimensional multistack-printed, self-powered flexible pressure sensor arrays: piezoelectric composites with chemically anchored heterogeneous interfaces," *ACS Omega*, vol. 5, no. 4, pp. 1956–1965, 2020.

[4] Y. Xiao, Y. Duan, N. Li et al., "Multilayer double-sided microstructured flexible iontronic pressure sensor with a record-wide linear working range," *ACS Sensors*, vol. 6, no. 5, pp. 1785–1795, 2021.

[5] A. Palmroth, T. Salpavaara, P. Vuoristo et al., "Materials and orthopedic applications for bioresorbable inductively coupled resonance sensors," *ACS Applied Materials & Interfaces*, vol. 12, no. 28, pp. 31148–31161, 2020.

[6] S. Li, F. Hu, Z. Xu, Z. Mao, Z. Ling, and H. Liu, "Joint power allocation in classified WBANs with wireless information and power transfer," *IEEE Internet of Things Journal*, vol. 8, no. 2, pp. 989–1000, 2020.

[7] R. Saidi, H. Heidari, M. Sedehi, and B. Safdarian, "Evaluating the effect of Matricaria chamomilla and Melissa officinalis on pain intensity and satisfaction with pain management in patients after orthopedic surgery," *Journal of Herbmed Pharmacology*, vol. 9, no. 4, pp. 339–345, 2020.

[8] X. Liu, L. Li, L. Wang, K. Herr, and Q. Chen, "Implementation and evaluation of a pain management core competency education program for surgical nurses," *International Journal of Nursing Sciences*, vol. 8, no. 1, pp. 51–57, 2021.

[9] Y. Li, W. Chen, and L. Lu, "Wearable and biodegradable sensors for human health monitoring," *ACS Applied Bio Materials*, vol. 4, no. 1, pp. 122–139, 2020.

[10] M. Beccatelli, M. Villani, F. Gentile et al., "All-polymeric pressure sensors based on PEDOT: PSS-modified polyurethane

foam," *ACS Applied Polymer Materials*, vol. 3, no. 3, pp. 1563–1572, 2021.

[11] P. W. K. Putra, I. K. A. Widiantara, and A. A. N. Kusuma, "Effectiveness of the use of acupressure wristband at Neiguan point (P 6) towards postoperative nausea vomiting (PONV) in orthopedic surgical patients," *Journal of Holistic Nursing Science*, vol. 8, no. 1, pp. 31–38, 2021.

[12] G. Xia, Y. Huang, F. Li et al., "A thermally flexible and multisite tactile sensor for remote 3D dynamic sensing imaging," *Frontiers of Chemical Science and Engineering*, vol. 14, no. 6, pp. 1039–1051, 2020.

[13] J. Y. Chen, B. S. Lin, Y. W. Luo, C. Y. Lin, and B. S. Lin, "Recovery evaluation system of bowel functions following orthopedic surgery and gastrointestinal endoscopy," *IEEE Access*, vol. 9, pp. 67829–67837, 2021.

[14] F. Y. Chang, P. T. Teng, and L. C. Chen, "Non-invasive monitoring method for lower-leg compartment syndrome using a wireless sensor system and finite element analysis," *Proceedings of the Institution of Mechanical Engineers, Part H: Journal of Engineering in Medicine*, vol. 235, no. 3, pp. 346–356, 2021.

[15] P. M. S. Shimabukuro, M. L. Duarte, A. M. Imoto et al., "Surgical Instruments Kits Orthopedic Electric Plaster Cutter Saw Price," *Sao Paulo Medical Journal*, vol. 138, no. 6, pp. 505–514, 2020.

[16] F. Gaetani, R. de Fazio, G. A. Zappatore, and P. Visconti, "A prosthetic limb managed by sensors-based electronic system: experimental results on amputees," *Bulletin of Electrical Engineering and Informatics*, vol. 9, no. 2, pp. 514–524, 2020.

[17] H. Amson, P. Lasselin, B. Naegels, G. P. Bracho, F. Aubrun, and M. Dziadzko, "Usability evaluation of sufentanil sublingual tablet analgesia in patients following enhanced recovery after surgery," *Journal of Comparative Effectiveness Research*, vol. 10, no. 9, pp. 743–750, 2021.

[18] T. A. Baldo, L. F. de Lima, L. F. Mendes, W. R. de Araujo, T. R. L. C. Paixão, and W. K. T. Coltro, "Wearable and biodegradable sensors for clinical and environmental applications," *ACS Applied Electronic Materials*, vol. 3, no. 1, pp. 68–100, 2020.

[19] H. Toda, M. Tada, T. Maruyama, and Y. Kurita, "Optimal swing support during walking using wireless pneumatic artificial muscle driver," *Journal of Robotics and Mechatronics*, vol. 33, no. 2, pp. 379–385, 2021.

[20] J. Meng, P. Pan, Z. Yang et al., "Degradable and highly sensitive CB-based pressure sensor with applications for speech recognition and human motion monitoring," *Journal of Materials Science*, vol. 55, no. 23, pp. 10084–10094, 2020.

[21] C. Weber, K. Fierz, M. Katapodi, and W. Hasemann, "An advanced practice nurse-led delirium consultation service reduces delirium severity and length of stay in orthopedic patients: a nonrandomized posttest only evaluation study," *Perspectives in Psychiatric Care*, vol. 56, no. 4, pp. 804–810, 2020.

[22] R. B. Green, M. Hays, M. Mangino, and E. Topsakal, "An anatomical model for the simulation and development of subcutaneous implantable wireless devices," *IEEE Transactions on Antennas and Propagation*, vol. 68, no. 10, pp. 7170–7178, 2020.

[23] M. Safaei, R. M. Meneghini, and S. R. Anton, "Compartmental force and contact location sensing in instrumented total knee replacements," *Medical Engineering & Physics*, vol. 83, pp. 64–72, 2020.

[24] L. Witthauer, J. P. Cascales, E. Roussakis et al., "Portable oxygen-sensing device for the improved assessment of compartment syndrome and other hypoxia-related conditions," *ACS Sensors*, vol. 6, no. 1, pp. 43–53, 2020.

[25] L. Jiang and R. E. Mendame Ehya, "Effectiveness of a collaborative nursing care model for the treatment of patients with diabetic foot disease by transverse tibial bone transport technique: a pilot study," *Journal of Peri Anesthesia Nursing*, vol. 35, no. 1, pp. 60–66, 2020.

[26] E. H. Othman, F. Shatnawi, O. Alrajabi, and J. A. Alshraideh, "Reporting nursing interventions classification and nursing outcomes classification in nursing research: a systematic review," *International Journal of Nursing Knowledge*, vol. 31, no. 1, pp. 19–36, 2020.

[27] K. Thompson, W. Griffiths-Jones, L. Frendin et al., "Interobserver agreement of sensor-derived compartmental pressure measurements in computer-assisted total knee arthroplasty," *The Knee*, vol. 27, no. 3, pp. 717–722, 2020.

[28] M. Pike, L. Campagna-Wilson, K. Sears, R. Warren, D. Legay, and D. Trudel, "Pilot study: the effectiveness of physiotherapy-led screening for patients requiring an orthopedic intervention," *Journal of Military, Veteran and Family Health*, vol. 7, no. 2, pp. 3–15, 2021.

[29] H. Tilala, P. M. Suneesh, and K. J. J. Doss, "A study to assess the effectiveness of cryotherapy on level of pain among patient with arthralgia in selected orthopedic hospital at Rajkot," *International Journal of Advances in Nursing Management*, vol. 8, no. 1, pp. 69–71, 2020.

[30] S. Chae, H. Oh, and S. Moorhead, "Effectiveness of nursing interventions using standardized nursing terminologies: an integrative review," *Western Journal of Nursing Research*, vol. 42, no. 11, pp. 963–973, 2020.

Hindawi
Journal of Sensors
Volume 2021, Article ID 5856140, 11 pages
https://doi.org/10.1155/2021/5856140

Research Article

5G Multimedia Precision Marketing Based on the Improved Multisensor Node Collaborative Filtering Recommendation Algorithm

Kai Si,[1,2] **Min Zhou**,[1] **and Yingfang Qiao**[2]

[1]*China University of Mining and Technology, Xuzhou 221116, China*
[2]*Xuzhou University of Technology, Xuzhou 221116, China*

Correspondence should be addressed to Min Zhou; xzkdzm@163.com

Received 25 October 2021; Accepted 11 November 2021; Published 21 December 2021

Academic Editor: Gengxin Sun

The rapid development of web technology has brought new problems and challenges to the recommendation system: on the one hand, the traditional collaborative filtering recommendation algorithm has been difficult to meet the personalized recommendation needs of users; on the other hand, the massive data brought by web technology provides more useful information for recommendation algorithms. How to extract features from this information, alleviate sparsity and dynamic timeliness, and effectively improve recommendation quality is a hot issue in the research of recommendation system algorithms. In view of the lack of an effective multisource information fusion mechanism in the existing research, an improved 5G multimedia precision marketing based on an improved multisensor node collaborative filtering recommendation algorithm is proposed. By expanding the input vector field, the features of users' social relations and comment information are extracted and fused, and the problem of collaborative modelling of these two kinds of important auxiliary information is solved. The objective function is improved, the social regularization term and the internal regularization term in the vector domain are analysed and added from the perspective of practical significance and vector structure, which alleviates the overfitting problem. Experiments on a large number of real datasets show that the proposed method has higher recommendation quality than the classical and mainstream baseline algorithm.

1. Introduction

With the advent and popularization of the Internet and the rapid development of information technology, the total number of users and business types of operators has also increased [1]. By the end of 2018, the total number of Internet users in China had reached 829 million. In 2018, 56.53 million new Internet users were added, and the Internet penetration rate was 59.6%, an increase of 3.8% over the end of 2017 [2, 3]. With the continuous vigorous development of the communication industry and the gradual maturity of the customer life cycle, relevant Internet enterprises and Internet technologies have sprung up, and operators are facing increasing market competition pressure. However, the marketing mode and marketing business of operators have not changed breakthrough, and the market position and traditional business model are greatly challenged. The external and internal of the enterprise are under great development pressure [4].

The stock maintenance work is not carried out in place, and the understanding of stock users is not deep enough. Furthermore, the online data of stock users are not well used for analysis, resulting in poor matching between sales products and users, no in-depth mining of user needs for marketing, and single marketing mode; recommending sales products to users often does not meet user needs, and the maintenance effect of stock users is general [5]. In addition, there is no unified control over the service quality of stock users. At ordinary times, the maintenance of users is extensive marketing [6]. Policies are issued uniformly, and

marketing activities are formulated and carried out by multiple teams at the same time [7]. In this way, it could have met the personalized policy needs of different marketing units, but there is no unified communication to record the marketing track of users [8]. Each marketing team did not coordinate and communicate during marketing, and it results in repeated pushing the same marketing activity for users, promoting different marketing promotions to the same user at the same time [9]. Different users under the same user or customers of the same unit received marketing messages with different contents, which made users become confused about 5G precision marketing, reduce their trust, and become more reluctant to accept and maintain promotion [10].

Common recommendation system algorithms mainly include content-based recommendation algorithm, association rule-based recommendation algorithm, knowledge-based recommendation algorithm, collaborative filtering recommendation algorithm, and hybrid recommendation algorithm [11]. Collaborative filtering recommendation algorithms can be divided into two categories: memory-based collaborative filtering algorithms and model-based collaborative filtering algorithms [12]. Memory-based collaborative filtering uses the nearest neighbor search, which can be divided into user-based collaborative filtering (user-based CF) and item-based collaborative filtering (item-based CF) [13]. Memory-based collaborative filtering mainly uses similarity calculation, including Pearson similarity and cosine similarity [14]. The model-based collaborative filtering algorithm establishes a prediction model according to the historical data and then uses the method of machine learning to train the parameters of the model to make the model have the ability to predict. Widely used model-based methods include singular value decomposition (SVD), Bayesian network, implicit factor model (IFM), restricted Boltzmann machine (RBM), factor decomposition machine, Bayesian personalized recommendation, and so on [15, 16]. The advantages of the memory-based collaborative filtering algorithm are that the algorithm is easy to implement and has certain prediction accuracy and the recommended results have good interpretability [17, 18]. However, this method also has significant disadvantages: it needs to maintain a similarity matrix, resulting in high computational overhead, difficult to deal with cold start and sparsity problems and poor scalability of the algorithm [19]. The model-based collaborative filtering method can alleviate the sparsity problem [20]. The model has certain scalability and good predictability, but the disadvantages of this method are as follows: the construction of the model is complex, the time complexity of the algorithm is high, and the recommended results are not reasonably interpretable [21].

The collaborative filtering recommendation algorithm is the mainstream recommendation algorithm. Most of the current research used the model-based collaborative filtering recommendation algorithm. The great success of a hidden factor model in Netflix recommendation system competition makes it one of the important models in the collaborative filtering recommendation algorithm. The basic hidden factor model is the low-rank matrix decomposition model BASEMF [22], which maps the features of users and items into low-dimensional space in the form of vectors. Based on the basic matrix decomposition algorithm, nonnegative matrix factorization (NMF) [23], maximum margin matrix factorization (MMMF) [24], and so on are also derived. Although the basic matrix decomposition model adds an L-2 penalty term to the objective function to prevent overfitting in the process of training, the fitting effect is still not ideal when the training samples are highly sparse. Therefore, researchers propose a probabilistic matrix factorization (PMF) [25] model to model the problem from the perspective of probability, in order to predict the overall sample from the observed sample, so as to alleviate the overfitting problem. Reference [26] further proposed Bayesian PMF (BPMF) on the basis of PMF. The main improvement of BPMF is the introduction of a priori user implicit factor matrix and item implicit factor matrix. Literature [27] proposed a distributed algorithm for large-scale datasets. References [28, 29] proposed two matrix decomposition frameworks based on general distribution. Good scalability makes PMF and its related models become an important model in the collaborative filtering recommendation algorithm and has achieved good application results.

With the rapid development of Internet technology, the problem of information overload is becoming more and more serious, and the 5G precision marketing recommendation system came into being [30]. The 5G precision marketing recommendation system is mainly composed of a user modelling module, recommendation object modelling module, and recommendation algorithm module, in which the recommendation algorithm is the core of the recommendation system. At present, the most widely used recommendation algorithm is the collaborative filtering recommendation algorithm. However, the collaborative filtering recommendation algorithm has unavoidable problems such as data sparsity and cold start. Aimed at the sparsity of the collaborative filtering recommendation algorithm, considering the few common scoring items and the lack of user demand information, this paper studies the film recommendation algorithm based on the collaborative filtering recommendation algorithm. Aimed at the lack of user demand information, an improved method of similarity calculation is proposed. In the similarity calculation of the UBCF recommendation algorithm, demographic information is used to integrate the demographic similarity into the traditional similarity calculation to find the nearest neighbour users more similar to the target users, so as to improve the recommendation quality. The main contributions are summarized as follows: (1) in order to alleviate sparsity and improve dynamic timeliness and recommendation quality, 5G multimedia precision marketing based on the improved multisensor node collaborative filtering recommendation algorithm is proposed in this paper. (2) In the similarity calculation of the UBCF recommendation algorithm, demographic information is used to integrate the demographic similarity into the traditional similarity calculation to find the nearest neighbour users. In this way, the data sparsity is solved. (3) The effectiveness of the above-recommended methods is verified by experimental methods.

2. The Design of the 5G Multimedia Precision Marketing System Based on Multisensor Nodes

2.1. The Structure Design of the 5G Multimedia Precision Marketing System. The structure design of the 5G multimedia precision marketing system is shown in Figure 1. The multimedia precision marketing system mainly includes a sensor layer, network layer, and application layer.

(1) The sensing layer uses multisensor node network technology to collect basic information. The main function is to identify objects and collect information through sensing equipment

(2) The network layer is mainly used to serve the network equipment and platform for aggregation, transmission, and preliminary processing of data collected from the sensor layer. Through the existing three networks (Internet, radio and television network, and communication network), seamless remote transmission of a large amount of data information is perceived by sensors. It is responsible for transmitting the information collected by the sensor safely, analysing and processing the collected information, and then providing the results to the application layer. At the same time, the application of network layer "cloud computing" technology ensures the establishment of practical, applicable, reliable, and efficient information system and intelligent information sharing platform to realize the sharing and optimal management of various information resources

(3) The application layer mainly solves the problems of information processing and man-machine interface, that is, input and output control terminals, such as controllers of mobile phones and smart appliances, mainly providing the information services people need through data processing and solutions. The relevant applications and services of the application layer are directly oriented to users and mainly provide users with personalized service requirements. Users can customize their own personalized services according to the relevant applications of the application layer, such as querying relevant information, monitoring relevant information, and controlling relevant information

2.2. Design of the General Recommendation System Model. The recommendation system is a system used by e-commerce websites to provide users with commodity information and purchase suggestions. It can simulate the salesperson and recommend what products the customer should buy according to the customer's needs. Generally, the recommendation system can be divided into three modules: user modelling, recommendation object modelling, and recommendation algorithm. The core module of the recommendation system is the recommendation algorithm. The general recommendation system model is designed in Figure 2.

(1) User modelling module: establish a user model according to user information. Analyse the user's attribute information, user input information, and user behaviour information (such as historical browsing behaviour and mouse click behaviour), and mine a computable and formal user model from these information and continuously track and update the user model in time. (2) Recommendation object modelling: the description method of recommendation objects will affect the recommendation results. Different recommendation objects have different feature expressions, so the description methods and recommendation results are different. For example, text, which is mainly text symbols, is easier to extract features than 5G multimedia marketing, so the model is closer to the user interest model. Nowadays, the mainstream recommended object description methods are a content-based method and a classification-based method. Take the text as an example to briefly summarize these two recommended object modelling methods. When using the content-based method to model the text, first use the feature extraction method to find the keyword of the text, usually use the information increment method to determine the keyword vector, then use the TF-IDF method to select the weight of the keyword, and use Bayesian to recommend. (3) The recommendation algorithm is the core of the recommendation system. The quality of the recommendation algorithm directly determines the recommendation quality of the recommendation system. This paper also focuses on the research of the recommendation algorithm and puts forward effective improvement methods for the problems existing in the current recommendation algorithm

3. The Design of the Improved Multisensor Node Collaborative Filtering Recommendation Algorithm

3.1. Collaborative Filtering Matrix and Potential Similarity. With the development of cloud computing, data storage and computing, data sharing, and data application technology, today's era has entered the era of big data. Based on the development of the above technologies, big data technology and big data application have developed rapidly. At present, data information has become a powerful competitiveness of enterprises in market competition and an advantageous asset of enterprises. Therefore, collaborative filtering of effective information from a large amount of data and the use of effective information are the key to precision marketing.

In order to solve the above problems, this section proposes a new prediction mechanism to predict the scores of items that the target users may be interested in through the organic integration of extreme scoring behaviour, nearest neighbour relationship, and recommendation method based on matrix decomposition. Specifically, by introducing extreme rating branches, in order to alleviate the failure of similarity measurement and the instability of the nearest neighbour recommendation in the context of sparse data, the robustness of recommendation performance is further

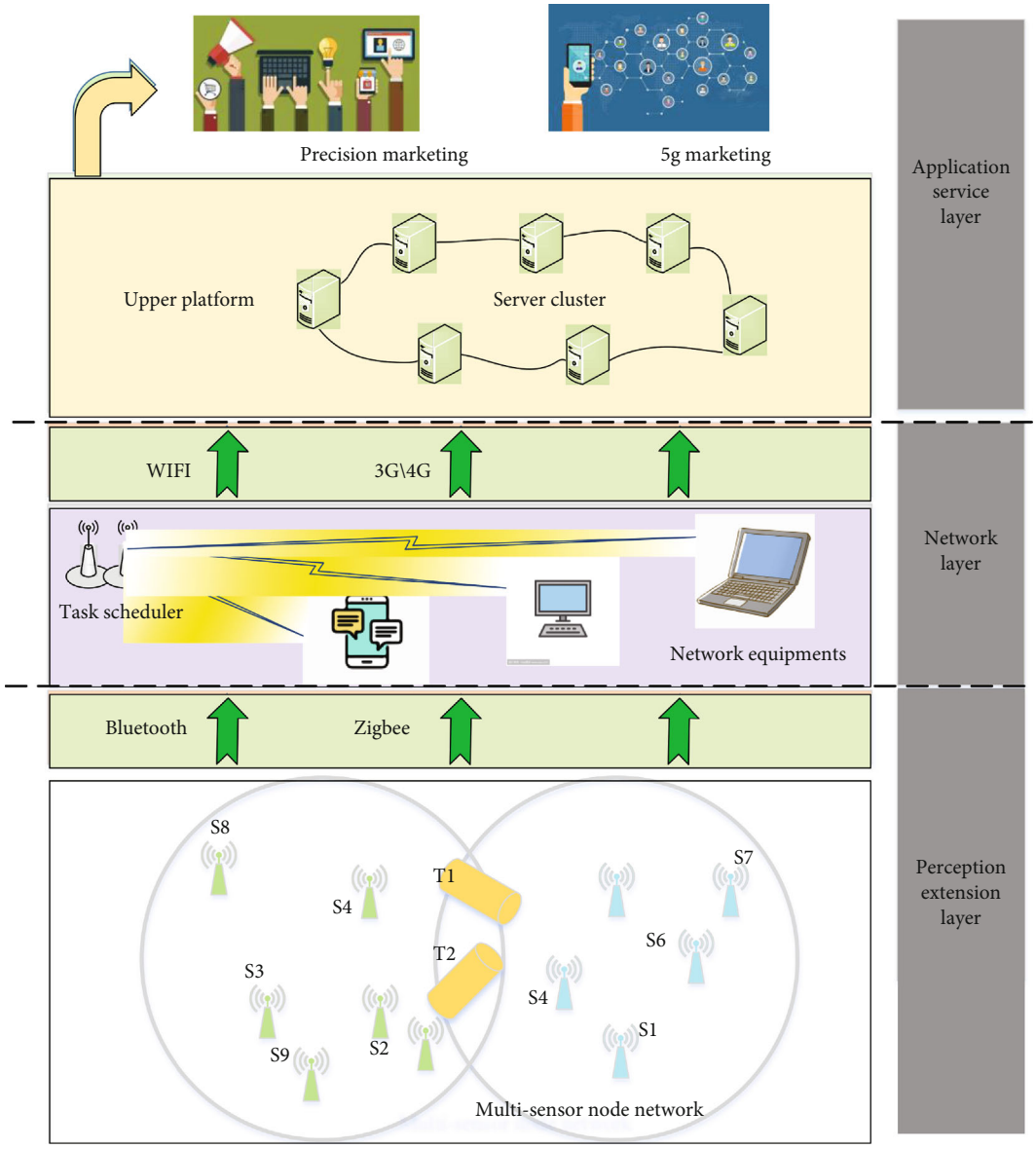

Figure 1: The structure of the 5G multimedia precision marketing system based on multisensor nodes.

improved through the introduction of the matrix decomposition method. It should be noted that probabilistic matrix decomposition is a kind of matrix decomposition method, which is consistent with the optimization objective function of regularized SVD (i.e., singular value decomposition model in the matrix decomposition method). However, considering that the probabilistic matrix decomposition model can more clearly show its prediction mechanism, the matrix decomposition method in this section selects the probability matrix decomposition model. Based on the above considerations, this paper proposes a recommendation method framework considering both extreme scoring behaviour similarity and scoring matrix information fusion. This framework integrates the user's local nearest neighbour relationship into the global scoring optimization process of matrix decomposition. It improves the prediction accuracy and robustness in sparse data situation. The knowledge matrix of collaborative filtering is shown in Figure 3. As shown in Figure 3, first of all, through implicit acquisition, the system "secretly" tracks the user's behavior and records the information that can reflect the user's interest, such as browsing records, query records, mouse clicks, and page dwell time, to record the user's preferences. Secondly, build the knowledge structure between users and preferences. Finally, build the user's scoring system and its matrix to the user's precision marketing in the next step.

The CF algorithm originated from If technology and is the most successful method to realize the recommendation system at this stage. The core idea of CF is to recommend from the perspective of people related to users. Use the scoring matrix and relevant calculation methods to predict the user's score on an item and complete the recommendation. The CF algorithm filters items through the quantitative scoring matrix of user experience and selects items that are difficult to describe (such as movies, music, and pictures) and concepts that are difficult to express (such as tastes and

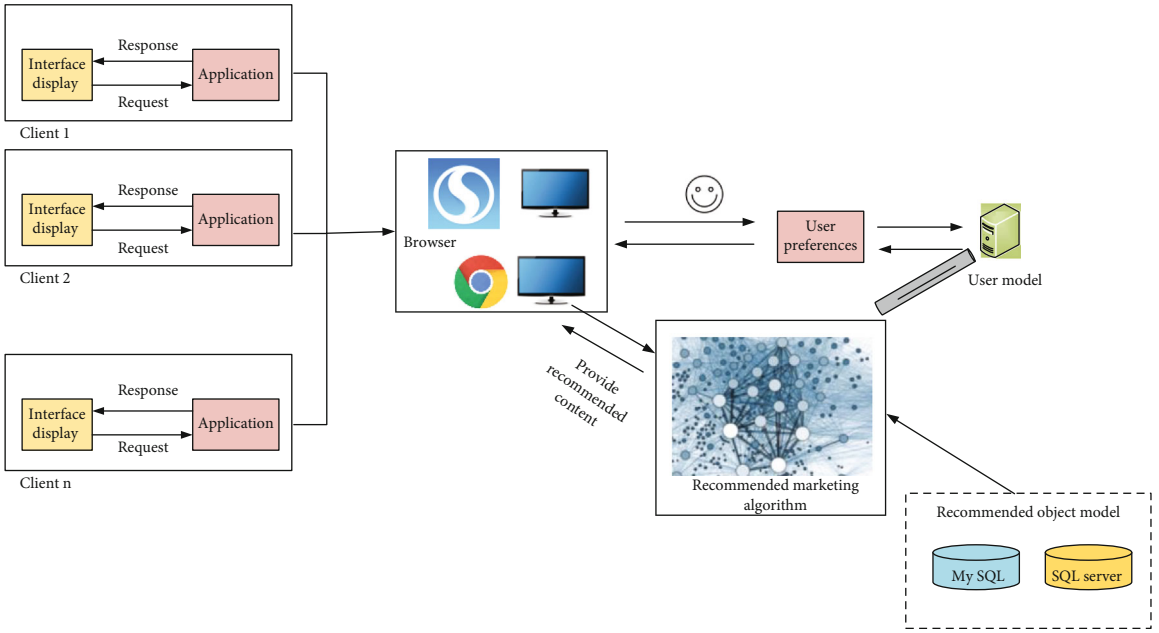

Figure 2: Recommended system structure.

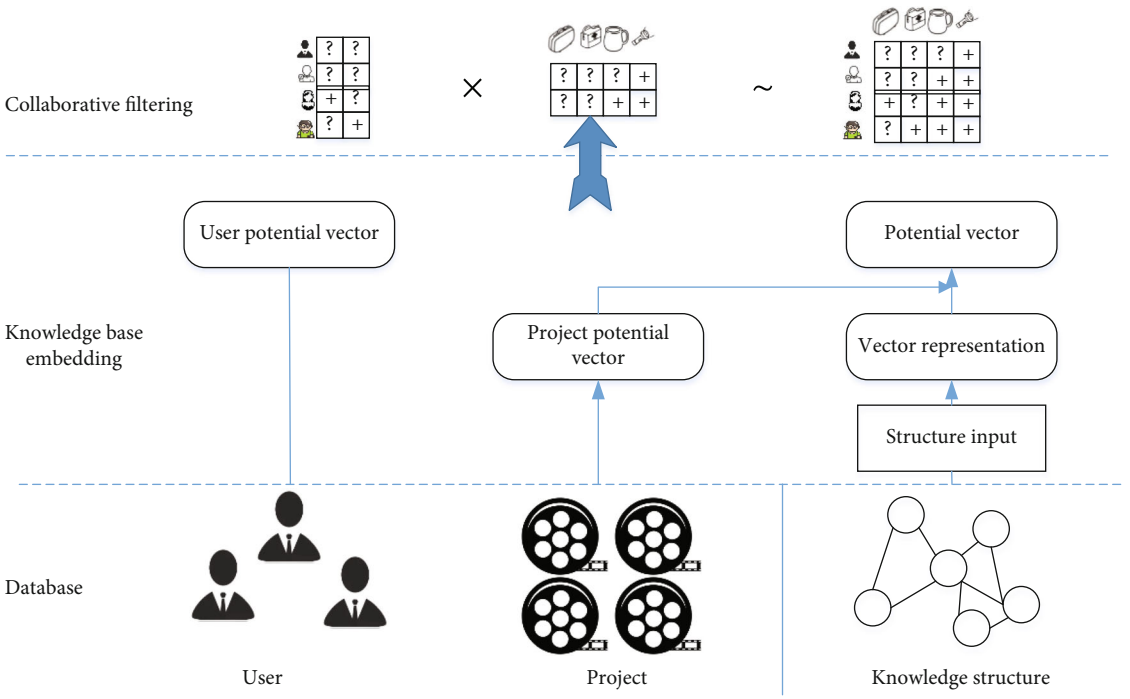

Figure 3: Knowledge architecture of the collaborative filtering algorithm.

hobbies). Compared with traditional filtering methods, it can screen out innovative items and truly achieve the purpose of personalized service. For a collaborative filtering recommendation system with n users and m movies, $R_{m\times n}$ indicates its score matrix. Spa(R) is the score matrix; therefore,

$$\mathrm{Spa}(R) = \frac{\left|r_{\mathrm{in}} \mid r_{\mathrm{iN}} \in R, r_{iw} = 0, 1 \le i \le n\right|}{n \times m} \times 100\%, \quad (1)$$

where the numerator represents the number of "0" in the scoring matrix and the denominator represents the number of elements in the scoring matrix.

It is the process of predicting the unknown user score value according to the known user score value. However, in practice, the score matrix $R_{m\times n}$ is an extremely sparse matrix, and there is still a big gap between the predicted value and the user's real preferences. Finding the nearest neighbour is actually the process of establishing the

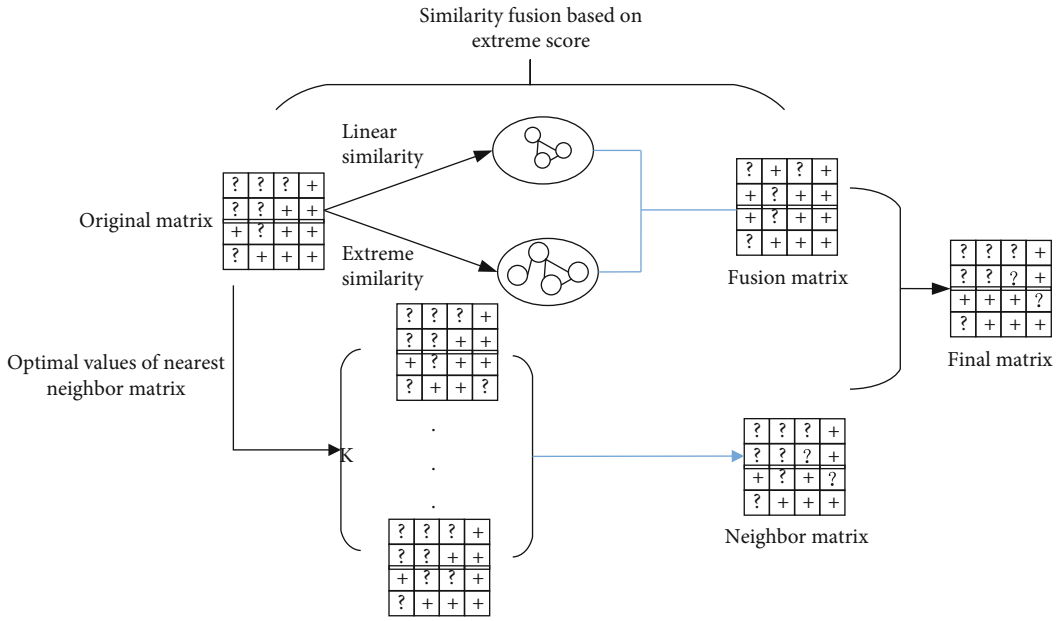

Figure 4: Structure of the improved collaborative filtering model.

algorithm model of UBCF, that is, the process of finding users similar to the target user according to the user's scoring behaviour.

Using Euclidean distance to measure the absolute distance between multidimensional vectors is the most common distance measurement method. Distance similarity believes that the smaller the distance between users, the more similar the users are. The distance similarity $\mathrm{sim}(i, \mathrm{j})$ between user i and user j is

$$\mathrm{sim}(i,j) = d\left(\vec{i}, \vec{j}\right) = \sqrt{\sum_{k=1}^{m} \left(r_{ik} - r_{jk}\right)^2}, \tag{2}$$

where $\vec{i}, \vec{j}$ represents the historical score vector of user i and user j, m is the dimension of the matrix, and r_{ik} and r_{jk} are the score matrix.

The CF algorithm based on the association rule is based on the association rule mining algorithm, which takes the items liked or purchased by the target user as the rule header (LHS) and the rule body (RHS) as the pending recommendation object. The support or confidence of association rules can be used as the similarity between items to find the nearest neighbour, and then, the final recommendation set can be obtained.

If itemset B also appears more in the scene where itemset A appears, it is considered to express an association rule $A \Rightarrow B$. Itemset A is LHS and itemset B is RHS. For all itemsets $I = \{i_1, i_2, \cdots, i_N\}$ assuming that the set of database transactions is dataset D and the set of items is t_m, there is $t_m \in I$ for $\forall m$. Let A be a set of items with $A \in t_m$. An association rule $A \Rightarrow B$, where $A \subseteq I$, $B \subseteq I$, and $A \cup B = \varnothing$.

Define the proportion of the union set of itemset A and itemset B contained in the transaction with the support degree of D in dataset D; there is

Table 1: The features of datasets.

Datasets	User number	Project number	Score number	Density (%)
Ml-100k	943	1680	100000	6.3
ML-latest-small	1508	2071	35497	1.1
Filmtrust	671	9058	100004	1.6
CiaoDVD	17615	16121	72665	0.03

$$\sup\left(A \Rightarrow B\right) = P(A \cup B) = \frac{\mathrm{count}(A \cup B)}{|D|}. \tag{3}$$

Similarly, the confidence of the defining rule $A \Rightarrow B$ in dataset D is the proportion of transactions that contain itemset A and itemset B in D; there is

$$\mathrm{con}(A \Rightarrow B) = P(B \mid A) = \frac{\sup\left(A \cup B\right)}{\sup\left(A\right)} = \frac{\mathrm{count}(A \cup B)}{\mathrm{count}(A)}. \tag{4}$$

After the confidence is obtained, the confidence is defined as the similarity between items:

$$\mathrm{sim}(A, B) = \mathrm{con}(A \Rightarrow B). \tag{5}$$

3.2. The Improved Collaborative Filtering Recommendation Algorithm. The improved collaborative filtering model (ICF model) includes three parts: (1) extreme scoring similarity is introduced to overcome the shortcomings of traditional similarity measurement. (2) By combining the proposed extreme scoring behaviour similarity with linear similarity, the similarity based on extreme scoring behaviour is established, and then, the user relevance is described more comprehensively. (3) The nearest neighbour matrix is generated by similarity based on extreme scoring behaviour,

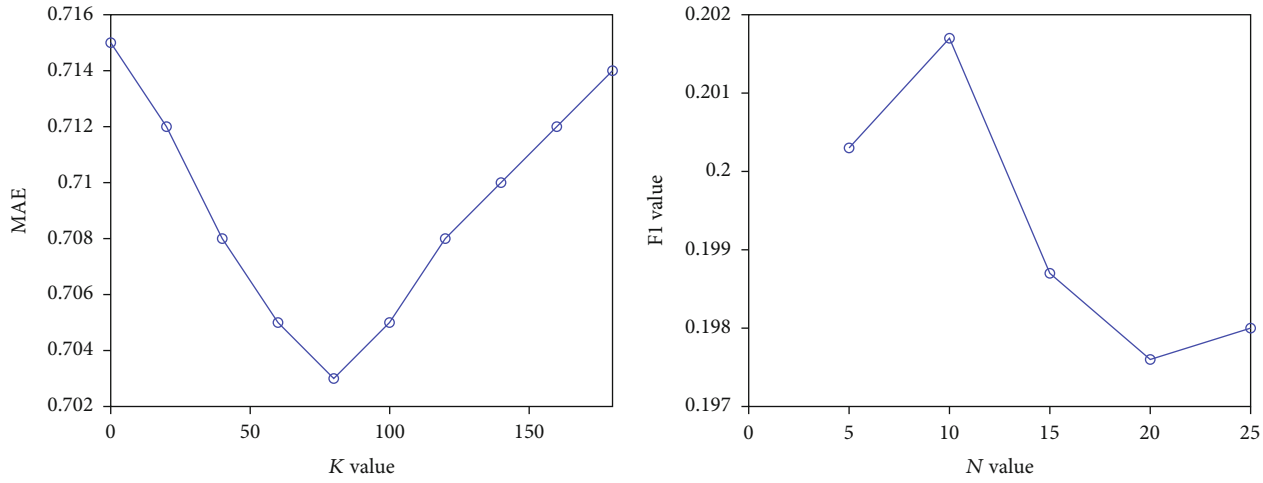

(a) MAE (b) RMSE

Figure 5: The structure of the improved sequential pattern mining algorithm.

which is fused into the original scoring matrix to improve the recommendation performance. Figure 4 is the flowchart of the ICF model. The flowchart of the algorithm is as follows: the mixed matrix of the score matrix is obtained by using the similarity theory and the limit theory. By selecting the adjacent K score matrices to solve the average, the similarity matrix is obtained. The final scoring matrix can be obtained by fusing the mixing matrix with the similarity matrix.

The probability matrix decomposition model uses the Bayesian inference method to convert the posterior probability into the product of a priori and likelihood function. Its calculation scale is linear with the number of observations. More importantly, it performs well on large-scale, sparse, and unbalanced datasets. The probability matrix decomposition model assumes that the conditional probability distribution (likelihood function) obeyed by the known score R is

$$P\left(R \mid A, B, \sigma^2\right) = \prod_{i=1}^{m} \prod_{j=1}^{n} \left[N\left(r_{ij} \mid A_i^T B_j, \sigma^2\right)\right]^{I_{ij}}. \quad (6)$$

By assuming that the potential eigenvectors of users and projects obey the mean value of zero, the variance is σ_A^2 and σ_B^2 Gaussian priori:

$$\begin{cases} p\left(A \mid \sigma_A^2\right) = \prod_{i=1}^{n} \left(N\left(A_i \mid 0, \sigma_A^2 I\right)\right), \\ p\left(B \mid \sigma_A^2\right) = \prod_{i=1}^{n} \left(N\left(B_i \mid 0, \sigma_B^2 I\right)\right). \end{cases} \quad (7)$$

The maximum log a posteriori probability is equivalent to the minimum sum of squares of error function with regularization:

$$E = \frac{1}{2} \sum_{i=1}^{m} \sum_{j=1}^{n} I_{ij} \left(r_{ij} - A_i^T B_j\right) + \frac{\lambda_A}{2} \sum_{i=1}^{m} \|A_i\|^2 + \frac{\lambda_B}{2} \sum_{j=1}^{n} \|B_i\|^2, \quad (8)$$

where λ_A and λ_B are the parameters of the regularization weight.

4. Simulation Results and Performance Analysis

4.1. Data Sources and Simulation Setting. With the in-depth study of the recommendation system, major research teams have released a series of recommendation system research and test datasets, for example, the movie lens dataset of the movie recommendation system, the Netflix dataset of the movie rental website Netflix, the jester joke dataset of the joke system, and the user browsing data Usenet newsgroups of the newsgroup. In order to evaluate the performance of the proposed method, we selected four commonly used datasets: Ml-100k, ML-latest-small, Filmtrust, and CiaoDVD. Among them, Ml-100k and ML-latest-small are two representative datasets in the movie lens dataset, which were collected by the GroupLens research group of the University of Minnesota; the scoring range is from 1 to 5. Filmtrust is a dataset captured from the Filmtrust website. Its scoring range is from 0.5 to 4 with an interval of 0.5. CiaoDVD is a DVD category dataset. The statistical data of scoring ranging from 1 to 5.4 datasets are shown in Table 1, where the density represents the available scoring proportion in the scoring matrix. We usually think that the first three datasets are sparse. The fourth dataset is very sparse.

Since the main purpose of the model is to alleviate the sparsity problem and improve the robustness of the model recommendation performance. In order to verify the effectiveness of the methods, this section randomly deletes 20%, 40%, 60%, and 80% of the scores on the dataset (Ml-100k, ML-latest-small, Filmtrust, and CiaoDVD) and constructs a series of experiments on the sparse dataset.

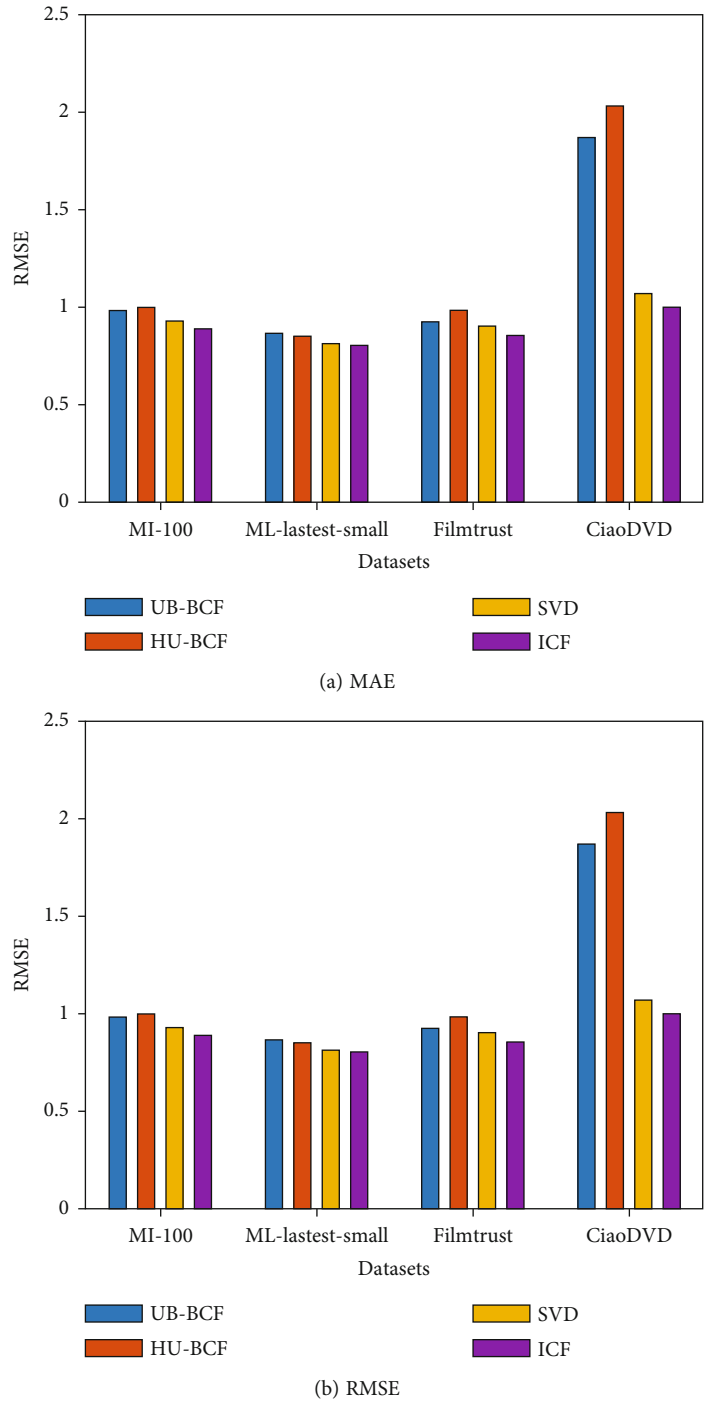

Figure 6: The structure of the improved sequential pattern mining algorithm.

In order to verify the performance of the proposed method, three groups of experiments are designed: (1) the proposed fusion model is compared with six common collaborative filtering methods. (2) For different sparse datasets, the method in this paper is compared with four common matrix decomposition methods. (3) The fusion model (ICF) in this paper is compared with some other representative similarity measurement fusion models. We use VS2010 to implement the CF and ICF algorithm on a machine with 1024 M memory, 733 MHz CPU, and Windows 10 operating system. The ICF algorithm is compared with the CF algorithm.

4.2. Optimal Parameter Selection. In order to verify the influence of the number of the nearest neighbours, the number of recommended movies N in the fixed recommendation list is 10 and the user has the least number of jointly rated movies φ. The number of the nearest neighbours K value is increased from 5 to 160 in a multiple growth mode, and

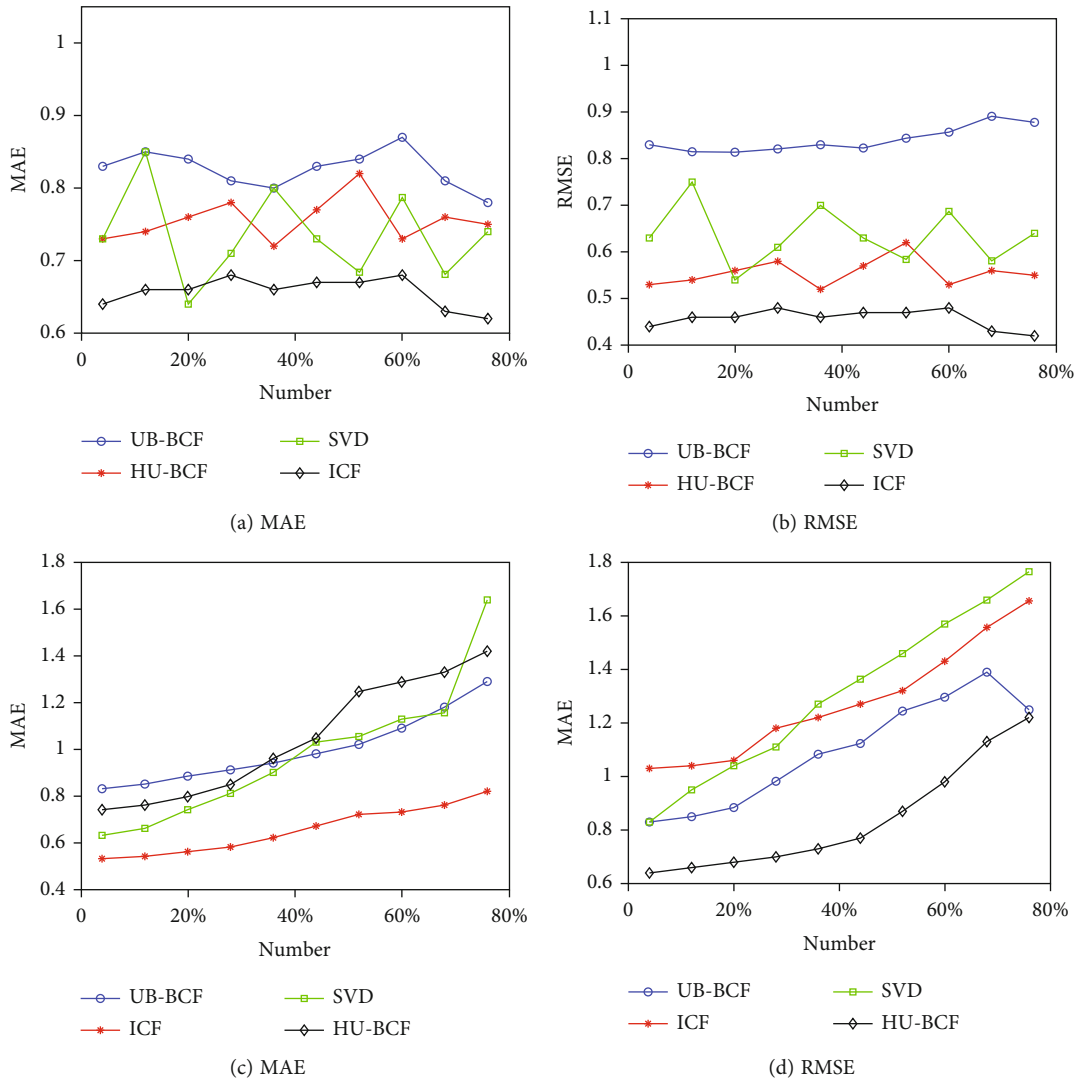

Figure 7: The simulation results of the proposed method.

the MAE-K curve is drawn to reflect the recommendation effect of the ICF algorithm under different K values. Changing the nearest neighbour number k actually changes the prediction score of the target user. The experimental results show that when the number of the nearest neighbour K increases from 5 to 80, the MAE value of the ICF algorithm gradually decreases and the recommendation accuracy gradually increases; when the number of the nearest neighbours K increases from 80 to 160, the MAE value of the ICF algorithm increases and the recommendation accuracy decreases. It can be seen from Figure 5(a) that when the nearest neighbour K is 80, the MAE value of the ICF algorithm is the smallest and the recommendation effect is the best. Therefore, the optimal K value of this dataset is 80.

Furthermore, in order to verify the relationship between the number of recommended movies in the recommendation list and the recommendation accuracy of the ICF algorithm, fix the number of the nearest neighbours K as 80, increase the number of recommended movies n in the recommendation list from 5 to 25 in steps of 5, and draw the F1-N curve accordingly. Observe the experimental results of the change of the number of recommended movies n in the recommendation list. When the number of recommended movies n increases from 1 to 10, the change trend of F1 increases, indicating that the recommendation accuracy of the ICF algorithm is improved; when the number of recommended movies n increases from 10 to 25, the change trend of F1 decreases, indicating that the recommendation accuracy of the ICF algorithm decreases gradually. It can be seen from Figure 5(b) that when the number of recommended movies n is 10, the F1 value of the ICF algorithm is the largest and the recommendation effect is the best. Therefore, the optimal n value of this dataset is 10.

4.3. Comparative Simulation of Common Collaborative Filtering Methods. The purpose of this experiment is to verify the performance of the proposed model in terms of prediction accuracy. Therefore, this section compares and analyses the proposed ICF recommendation algorithm with three commonly used collaborative filtering recommendation algorithms, such as UB_BCF [30], HU-BCF [31], and SVD [32]. As shown in Figure 6, the proposed ICF model

is obviously superior to other methods, especially in the sparse CiaoDVD dataset.

On the three datasets of Ml-100k, ML-latest-small, and Filmtrust, the MAE obtained by the ICF model is optimal and is reduced by 0.52%, 0.6%, and 0.69%, respectively, compared with the suboptimal method. In Figure 6(b), the RMSE of the ICF model is reduced by 0.11%, 0.83%, and 1.54%, respectively, compared with that of the suboptimal method. From the perspective of robustness, the ICF algorithm proposed in this paper shows relatively stable recommendation performance. Other collaborative filtering methods show unstable prediction accuracy. On the CiaoDVD dataset, the recommendation method based on the matrix decomposition model has a better recommendation effect than the user-based nearest neighbour method. The reason is that when the dataset is very sparse, the similarity is very difficult to measure. Overall, the experimental results in this section show that the organic integration of the extreme rating branch, nearest neighbour relationship, and SVD can effectively alleviate the problem of sparsity and improve the robustness of the recommended method in prediction accuracy.

4.4. Comparative Simulation of Different Sparse Levels. The purpose of this experiment is to verify that the ICF model based on the fusion of the local nearest neighbour information and global score information has robustness 5zadvantages in recommendation prediction accuracy under different sparsity situations. Figure 7 shows the MAE and RMSE results at different sparsity levels, in which different sparsity levels are obtained by randomly deleting scores. The results show that, on the datasets, MAE and RMSE increase with the increase in sparsity, which is consistent with our expectation; that is, with the increase in sparsity, the recommendation error will increase. However, the results also show that the MAE and RMSE values of the fusion model proposed in this paper are better than those of other comparison methods at different sparsity levels.

For the Ml-100k dataset, after removing the scores of 20%, 40%, 60%, and 80%, the MAE of the method in this paper is reduced by 0.68%, 1.12%, 2.85%, and 1.19%, respectively, compared with that of the suboptimal method. RMSE shows the same change trend. Figure 7 shows that for the datasets Filmtrust and ML-latest-small, the ICF model has slight advantages over other methods in MAE and RMSE when randomly deleting 20%, 40%, and 60% of the scores. However, when 80% of the scores are deleted, the advantages of the method proposed in this paper further increase on these two datasets. Overall, the ICF model proposed in this chapter has better prediction performance than other methods in different sparse situations. Further, the comparative experiments in this section verify the robustness of the ICF model.

5. Conclusion

With the development of Internet, communication, and Internet of things technologies, Internet companies are developing rapidly. The rich content applications and customer-based personalized marketing of Internet companies have brought great challenges to telecom operators. At the same time, the promotion of number carrying network transfer business and the commercialization of 5G technology have further weakened the advantages of traditional business operation of operators. The lack of exploration of customers' personalized needs, no targeted marketing activities, and the traditional extensive operation do not effectively combine operators' products with users' needs, and the marketing success rate is low, which leads to the crisis that operators may become "pipelines," so the implementation of precision marketing to meet users' personalized needs is imminent. Collaborative filtering is one of the most commonly used methods in recommendation systems. However, accurate prediction of unknown scores is still a challenging problem in the context of sparse data. Based on the user-based nearest neighbour recommendation method and probability matrix decomposition method, combined with similarity measurement based on extreme scoring behaviour, a new collaborative filtering recommendation method is constructed. This method comprehensively considers the local nearest neighbour relationship and global scoring information and establishes a probability matrix decomposition model integrating the nearest neighbour information, which effectively improves the prediction accuracy and robustness.

Data Availability

The data used to support the findings of this study are available from the corresponding author upon request.

Conflicts of Interest

The authors declare that they have no known competing financial interests or personal relationships that could have appeared to influence the work reported in this paper.

References

[1] C. Yin, L. Shi, R. Sun, and J. Wang, "Improved collaborative filtering recommendation algorithm based on differential privacy protection," *The Journal of Supercomputing*, vol. 76, no. 7, pp. 5161–5174, 2020.

[2] S. Li, X. Song, H. Lu, L. Zeng, M. Shi, and F. Liu, "Friend recommendation for cross marketing in online brand community based on intelligent attention allocation link prediction algorithm," *Expert Systems with Applications*, vol. 139, article 112839, 2020.

[3] L. Xiaojun, "An improved clustering-based collaborative filtering recommendation algorithm," *Cluster Computing*, vol. 20, no. 2, pp. 1281–1288, 2017.

[4] M. Jiang, Z. Zhang, J. Jiang, Q. Wang, and Z. Pei, "A collaborative filtering recommendation algorithm based on information theory and bi-clustering," *Neural Computing and Applications*, vol. 31, no. 12, pp. 8279–8287, 2019.

[5] P. Zhang, Z. Zhang, T. Tian, and Y. Wang, "Collaborative filtering recommendation algorithm integrating time windows and rating predictions," *Applied Intelligence*, vol. 49, no. 8, pp. 3146–3157, 2019.

[6] Y. Wang, Z. Song, and C. Xiao, "Collaborative filtering recommendation algorithm based on improved clustering and matrix factorization," *Journal of Computer Applications*, vol. 38, no. 4, pp. 1001–1006, 2018.

[7] C. Li and K. He, "CBMR: an optimized MapReduce for item-based collaborative filtering recommendation algorithm with empirical analysis," *Concurrency and Computation: Practice and Experience*, vol. 29, no. 10, article e4092, 2017.

[8] J. Deng, J. Guo, and Y. Wang, "A novel K-medoids clustering recommendation algorithm based on probability distribution for collaborative filtering," *Knowledge-Based Systems*, vol. 175, pp. 96–106, 2019.

[9] M. Ghazanfari, H. Mohammadi, M. S. Pishvaee, and E. Teimoury, "Fresh-product trade management under government-backed incentives: a case study of fresh flower market," *IEEE Transactions on Engineering Management*, vol. 66, no. 4, pp. 774–787, 2019.

[10] B. S. Neysiani, N. Soltani, R. Mofidi, and M. H. Nadimi-Shahraki, "Improve performance of association rule-based collaborative filtering recommendation systems using genetic algorithm," *International Journal of Information Technology and Computer Science*, vol. 11, no. 2, pp. 48–55, 2019.

[11] J. Xu, A. Liu, N. Xiong, T. Wang, and Z. Zuo, "Integrated collaborative filtering recommendation in social cyber-physical systems," *International Journal of Distributed Sensor Networks*, vol. 13, no. 12, Article ID 1550147717749745, 2017.

[12] M. F. Aljunid and M. Doddaghatta Huchaiah, "Multi-model deep learning approach for collaborative filtering recommendation system," *CAAI Transactions on Intelligence Technology*, vol. 5, no. 4, pp. 268–275, 2020.

[13] Y. Yun, D. Hooshyar, J. Jo, and H. Lim, "Developing a hybrid collaborative filtering recommendation system with opinion mining on purchase review," *Journal of Information Science*, vol. 44, no. 3, pp. 331–344, 2018.

[14] C. Zhang, M. Yang, J. Lv, and W. Yang, "An improved hybrid collaborative filtering algorithm based on tags and time factor," *Big Data Mining and Analytics*, vol. 1, no. 2, pp. 128–136, 2018.

[15] M. Jalili, S. Ahmadian, M. Izadi, P. Moradi, and M. Salehi, "Evaluating collaborative filtering recommender algorithms: a survey," *IEEE access*, vol. 6, pp. 74003–74024, 2018.

[16] Z. Cui, X. Xu, F. Xue et al., "Personalized recommendation system based on collaborative filtering for IoT scenarios," *IEEE Transactions on Services Computing*, vol. 13, no. 4, pp. 685–695, 2020.

[17] Y. Liu, "Data mining of university library management based on improved collaborative filtering association rules algorithm," *Wireless Personal Communications*, vol. 102, no. 4, pp. 3781–3790, 2018.

[18] M. He, M. Chang, and X. Wu, "A collaborative filtering recommendation method based on differential privacy," *Journal of Computer Research and Development*, vol. 54, no. 7, p. 1439, 2017.

[19] P. Kumar, V. Kumar, and R. S. Thakur, "A new approach for rating prediction system using collaborative filtering," *Iran Journal of Computer Science*, vol. 2, no. 2, pp. 81–87, 2019.

[20] M. Nilashi, O. Ibrahim, and K. Bagherifard, "A recommender system based on collaborative filtering using ontology and dimensionality reduction techniques," *Expert Systems with Applications*, vol. 92, pp. 507–520, 2018.

[21] R. Chen, Q. Hua, Y. S. Chang, B. Wang, L. Zhang, and X. Kong, "A survey of collaborative filtering-based recommender systems: from traditional methods to hybrid methods based on social networks," *IEEE Access*, vol. 6, pp. 64301–64320, 2018.

[22] N. Nassar, A. Jafar, and Y. Rahhal, "A novel deep multi-criteria collaborative filtering model for recommendation system," *Knowledge-Based Systems*, vol. 187, article 104811, 2020.

[23] H. Li, X. Diao, J. Cao, and Q. Zheng, "Collaborative filtering recommendation based on all-weighted matrix factorization and fast optimization," *Ieee Access*, vol. 6, pp. 25248–25260, 2018.

[24] M. K. Najafabadi, A. Mohamed, and C. W. Onn, "An impact of time and item influencer in collaborative filtering recommendations using graph-based model," *Information Processing & Management*, vol. 56, no. 3, pp. 526–540, 2019.

[25] T. Cunha, C. Soares, and A. C. de Carvalho, "Metalearning and recommender systems: a literature review and empirical study on the algorithm selection problem for collaborative filtering," *Information Sciences*, vol. 423, pp. 128–144, 2018.

[26] R. Logesh, V. Subramaniyaswamy, D. Malathi, N. Sivaramakrishnan, and V. Vijayakumar, "Enhancing recommendation stability of collaborative filtering recommender system through bio-inspired clustering ensemble method," *Neural Computing and Applications*, vol. 32, no. 7, pp. 2141–2164, 2020.

[27] X. Yu, F. Jiang, J. du, and D. Gong, "A cross-domain collaborative filtering algorithm with expanding user and item features via the latent factor space of auxiliary domains," *Pattern Recognition*, vol. 94, pp. 96–109, 2019.

[28] S. Mandal and A. Maiti, "Deep collaborative filtering with social promoter score-based user-item interaction: a new perspective in recommendation," *Applied Intelligence*, vol. 51, no. 11, pp. 7855–7880, 2021.

[29] Z. Chen, Y. Wang, S. Zhang, H. Zhong, and L. Chen, "Differentially private user-based collaborative filtering recommendation based on K-means clustering," *Expert Systems with Applications*, vol. 168, article 114366, 2021.

[30] D. Murnane, M. White, and A. G. Williams, "Exploring fine-tuning of the next-to-minimal composite Higgs model," *Journal of High Energy Physics*, vol. 2019, no. 4, pp. 1–27, 2019.

[31] F. Zhang, V. E. Lee, R. Jin et al., "Privacy-aware smart city: a case study in collaborative filtering recommender systems," *Journal of Parallel and Distributed Computing*, vol. 127, pp. 145–159, 2019.

[32] S. Yang, M. Korayem, K. AlJadda, T. Grainger, and S. Natarajan, "Combining content-based and collaborative filtering for job recommendation system: a cost-sensitive statistical relational learning approach," *Knowledge-Based Systems*, vol. 136, pp. 37–45, 2017.

Hindawi
Journal of Sensors
Volume 2021, Article ID 6800470, 11 pages
https://doi.org/10.1155/2021/6800470

Research Article

Digital Media Art Communication Based on Wireless Cooperative Routing with Minimum Energy Consumption

Shuli Song

Institute of Art and Design, Shandong Women's University, Jinan, Shandong 250300, China

Correspondence should be addressed to Shuli Song; 29040@sdwu.edu.cn

Received 2 November 2021; Accepted 26 November 2021; Published 21 December 2021

Academic Editor: Gengxin Sun

Wireless cooperative routing algorithm transmits the data collected in the target area to users, so that users can obtain monitoring information timely and accurately. In the traditional low-power adaptive clustering hierarchical routing protocol, the process of building clusters is random, the resources of nodes are not fully utilized, the node death speed is fast, the network life cycle is short, and the performance is not stable enough. In addition, the route maintenance process is cumbersome and will occupy a lot of bandwidth. In order to solve the problems of real-time transmission of digital media art communication data and network lifetime optimization, a wireless cooperative routing algorithm based on minimum energy consumption is proposed. The facts of transmission strength consumption, node residual strength, and minimal information transmission extension are analyzed, a new weight feature is proposed, and a multipath statistics routing scheme is developed by using the usage of the minimal strength consumption. All digital media art propagation sensor nodes transmit data to sink nodes along multiple transmission paths. Simulation results show that the algorithm can prolong the network lifetime, reduce and balance the node energy consumption, reduce the data transmission delay, reduce the energy consumption of wireless cooperative routing based on the minimum energy consumption by 64.5%, and increase the number of compressed images by 182%.

1. Introduction

In recent years, with the improvement of people's requirements for the diversity and accuracy of information acquisition, the simple data obtained by the original traditional wireless sensor networks cannot meet the requirements of network application, and there is an urgent need to introduce digital media services such as image, audio, and video into wireless cooperative routing [1]. Therefore, wireless cooperative routing has attracted more and more attention from academia and media. With the introduction of digital media services, wireless sensor nodes will consume more energy to ensure the quality of service of transmitted digital media services, such as greater traffic and lower communication delay. For sensor nodes with limited resources and energy, energy consumption has become one of the main bottlenecks restricting the application and popularization of wireless cooperative routing [2]. Digital media art communication based on wireless cooperative routing is a new sensing method to collect and process digital media data such as image, video, and audio. The digital media sensor node of wireless cooperative routing is equipped with cameras, microphones, and other sensors, with computing, storage, and communication capabilities. It can self-organize to form a wireless sensor network, cooperate to collect and process the digital media data in the surrounding environment, and finally transmit the data to the monitoring centre through multihop routing [3]. The monitoring centre records, analyzes, and displays various data obtained, so as to realize comprehensive and effective digital media data monitoring.

Wireless cooperative routing provides a new means for the traditional digital media monitoring system. It can effectively overcome the shortcomings of traditional monitoring system, such as high deployment cost, inflexible networking, and troublesome maintenance [4]. Wireless cooperative routing also inherits the advantages of wireless sensor network, can sense the diversified data in the network coverage area, and has flexible and rich functional scalability. Therefore, wireless cooperative routing has a very broad

application prospect in many application fields, such as battlefield monitoring, traffic monitoring, security sensitive area monitoring, smart home, target tracking, and public security monitoring [5]. However, there are still some difficulties in the industrialization of WMSN, including high bandwidth demand, high node energy consumption, and real-time requirements of digital media data transmission. Due to the complex environmental conditions of wireless cooperative routing applications, the energy consumption of digital media sensor nodes has not decreased significantly; how to develop wireless cooperative routing algorithms with low energy consumption and high network lifetime puts forward new requirements for digital media art communication [6].

In order to reduce the energy consumption of digital media art communication nodes and prolong the life cycle of the network, a wireless cooperative routing algorithm based on minimum energy consumption is proposed to solve the problems of real-time transmission of digital media art communication data and network lifetime optimization. The information transmission power consumption, node residual power, and minimal information transmission length are analyzed, a new weight feature is proposed, and a multipath fact routing scheme is built by means of the usage of the minimal strength consumption. All digital media art propagation sensor nodes transmit data to sink nodes along multiple transmission paths. Simulation results show that the algorithm can prolong the network lifetime, reduce and balance node energy consumption, reduce data transmission delay, and realize the digital media art dissemination of wireless cooperative routing based on minimum energy consumption.

The specific contents of this paper are arranged as follows: Section 1 introduces the relevant background and significance of wireless cooperative routing and analyzes the existing problems of digital media art communication. Related work is discussed in Section 2. Section 3 analyzes the algorithm and energy consumption of wireless cooperative routing based on minimum energy consumption. In Section 4, simulation experiments are carried out. Section 5 summarizes the full text.

2. Related Work

With the development of new wireless communication technology and the increasing popularity of low-cost communication equipment, wireless cooperative routing plays an important role in digital media communication because of its strong scalability and distributed self-organization. As the most critical subject in wireless networks, wireless cooperative routing technology has important research significance. According to the fading characteristics of wireless links and the limited energy of low-cost communication equipment, how to design an end-to-end routing mechanism for various potential application scenarios of wireless cooperative routing, so that data packets can be transmitted to the destination node in time reliably and efficiently, is the current research focus and difficulty. In recent years, there have been many advances in the algorithm and application research of wireless cooperative routing, some of which are as follows:

Relevant scholars study the wireless cooperative routing algorithm from the aspect of optimization, consider the data processing power, propose the constraints such as error distortion inequality constraints, traffic constraints, and energy constraints, and establish the network optimization model [7]. The subgradient algorithm is used to solve the model and obtain the optimal solution. The delay constraint and traffic constraint are analyzed, and an optimization model is established to balance lifetime, utility, and delay. The optimization model is analyzed, and the delay minimization problem, lifetime maximization problem, and utility and power allocation balance problem are derived, which are solved by the optimization method [8]. An image transmission scheme based on a two-hop cluster structure is studied to maximize the lifetime of wireless digital media sensors. In this scheme, multiple relay nodes are used to compress and forward images, so as to reduce the energy consumption of camera nodes and cluster head nodes. The network lifetime optimization model is established, and the adaptive method of camera node sending radius and the image compression task allocation method based on the residual energy of ordinary sensor nodes are proposed to balance the node energy consumption [9]. However, the implementation of these algorithms is complex, the convergence speed is slow, and the calculation workload of the optimal scheme is large, which needs to consume a certain amount of node energy.

Many scholars have made some achievements in traditional wireless routing algorithms. For example, a proportional weight routing algorithm is proposed. The algorithm considers the link energy consumption and node residual energy, constructs the link weight function, finds the minimum weight path from each node to sink node according to the algorithm, and constructs the shortest path tree [10]. Finally, all nodes transmit data along the shortest path tree. For wireless sensor networks with nodes, a clustering routing algorithm with maximum lifetime is proposed. In this algorithm, the nodes that can replace cluster heads and charge are introduced to calculate the optimal location of nodes [11]. According to the cluster head energy consumption and node to cluster head energy consumption, multiple cluster head selection and clustering methods that can maximize the network lifetime are proposed. All sensor nodes gather the data to the cluster head node, and the cluster head node relays the data to the sink node through the node [12]. The node has limited transmission rate and a large number of digital media data. Only transmitting data along one path will cause high data transmission delay, cause high energy consumption and premature failure of hub nodes, and shorten the network lifetime.

Therefore, aiming at the above problems, based on the summary of relevant references, a wireless cooperative routing algorithm based on minimum energy consumption is proposed. In this algorithm, multiple paths that weigh the network lifetime and data transmission delay are found to reduce the node energy consumption and data transmission delay and improve the network lifetime.

3. Wireless Cooperative Routing Algorithm Based on Minimum Energy Consumption

3.1. Energy Consumption Model of Wireless Cooperative Routing. Nodes can be divided into scalar sensor nodes, digital media sensor nodes, and sink nodes. The scalar sensor node is responsible for performing simple tasks, such as forwarding data from other nodes and collecting scalar data. The data processing requirements are not high. Therefore, the energy consumption of the scalar sensor node i to send and receive g_{ij} bit data through distance d_{ij} is defined as E, respectively.

$$E = \frac{g_{ij}E_{\text{elec}} + g_{ij}\varepsilon d_{ij}}{g_{ij} + d_{ij}}, \tag{1}$$

where E_{elec} represents the circuit energy consumption per bit, d_{ij} represents the distance between the wireless transmitting node i and the receiving node j, and εd_{ij} represents the amplifier energy consumption per bit depending on the amplifier model. Considering the error conditions such as timeout retransmission and packet loss in the data transmission process, the total energy consumption of the scalar sensor node is as follows:

$$E_i = \sum_{j \in N(i)} g_{ij}E_{\text{elec}} + g_{ij}\varepsilon d_{ij}^{\gamma}, \tag{2}$$

where $N(i)$ represents the set of all possible receiving nodes within the single-hop maximum communication range of the transmitting node i.

In addition to considering the energy consumption of wireless communication, digital media sensor nodes still need to collect and process digital media data such as image, video, and audio with a large amount of data, so the energy consumption of data processing needs to be considered. According to the power, speed, and distortion model, the energy consumption of data processing is as follows:

$$E_{pe}(S) = \frac{-\ln\left(D_i/\sigma^2\right)/\phi S_i}{1 - P_e}, \tag{3}$$

where D_i represents the processing distortion of digital media data, S_i represents the perceived rate of digital media data, σ represents the average input variance of digital media data, and ϕ represents the data processing efficiency coefficient. The total energy consumption of digital media sensor node is as follows:

$$E_i = \sum_{j \in N(i)} \left(g_{ij}E_{\text{elec}} + g_{ij}\varepsilon d_{ij}^{\gamma}\right) + \sum_{j \in N(i)} g_{ij}E_{\text{elec}}. \tag{4}$$

3.2. Wireless Cooperative Routing Algorithm Based on Minimum Energy Consumption. Network flow theory is a common theory in graph theory. It mainly aims at many systems including flow, such as wireless sensor network system with data flow, highway system with vehicle flow, control system with information flow, water supply system with water flow, and financial system with cash flow [13].

Each digital media sensor node collects a large number of digital media data. In order to send the digital media data to sink node in the shortest possible time, it is necessary to calculate the data routing scheme according to the network maximum flow method [14]. However, the network maximum flow method only considers the traffic maximization of data transmission, its transmission scheme is not unique, and does not consider the energy consumption and data transmission delay of nodes [15]. Therefore, in order to reduce node energy consumption and data transmission delay, in addition to considering the transmission capacity of the link, the cost is introduced on each link. On the premise of ensuring the maximum flow, find a minimum cost and maximum flow that can reduce node energy consumption and data transmission delay. Architecture and propagation of wireless cooperative routing based on minimum energy consumption are shown in Figure 1.

The algorithm can find all possible paths from the digital media sensor node to the sink node, but some paths consume a lot of energy. Choosing this route will enlarge the power consumption of the node. If there are a couple of digital media sensor nodes in the network, there may additionally be more than one replica paths between the statistics transmission paths of every digital media sensor node; that is, some links in the duplicate path appear in the transmission paths of multiple digital media sensor nodes at the same time [16]. Due to the limited data transmission rate of scalar sensor nodes, the hub node in the repeated path cannot relay the data of all digital media sensor nodes. Therefore, count the number of repetitions of each repeated path, allocate the bandwidth resources of the repeated path to multiple digital media sensor nodes, and modify the traffic of all links of each digital media sensor node on the repeated path; finally, the data routing scheme of wireless digital media sensor network is obtained [17].

3.3. Implementation of Wireless Cooperative Routing Algorithm Based on Minimum Energy Consumption. Cycle through the following steps until the first sensor node runs out of energy:

(1) Sink node obtains the position coordinates, self-address, residual energy, and other information of all sensor nodes by flooding

(2) Calculate the weight of all links. $M = 0$, $k = 0$. Initialize the feasible stream of all digital media sensing nodes. Start to calculate the minimum cost and maximum flow of digital media sensing node M

(3) If the minimum cost flow calculated in iteration $k - 1$ is $f_m(k-1)$, the structure changes with the network $W(f_m(k-1))$

(4) Find the shortest path from the digital media sensing node m to the sink node in $W(f_m(k-1))$. If there is no shortest path, skip to step (6). If there is a shortest path, skip to step (5)

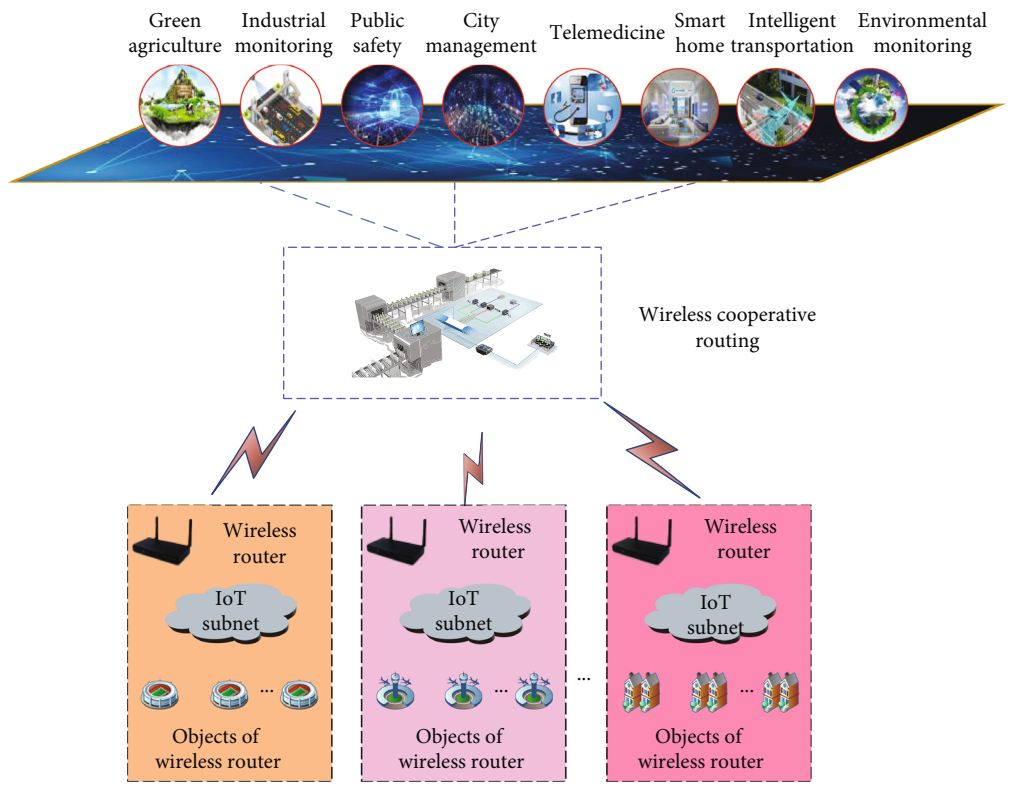

Figure 1: Architecture and propagation of wireless cooperative routing based on minimum energy consumption.

(5) Obtain the corresponding minimum cost widening path P and calculate the improvement amount

(6) $f_m(k-1)$ is the minimum cost stream of digital media sensor node M. When the minimum cost and maximum flow calculation of all digital media sensing nodes is completed, skip to step (7). Otherwise, $M = m + 1$, skip to step (3) and start a new node calculation [18]

(7) Judge whether there is a duplicate path in the data transmission path of each digital media sensing node. If it exists, depend the wide variety of repetitions of every repeated path, divide the site visitors of all hyperlinks of every digital media sensing node on the repeated direction through the wide variety of repetitions, and gain the statistics routing scheme of the wireless digital media sensing node [19]. The sink node notifies other nodes of the data routing scheme. All nodes transmit data according to the data routing scheme

(8) After the sink node collects data for a period of time, skip to step (1) again. The time complexity is mainly composed of the time complexity of minimum cost and maximum flow calculation of M digital media sensing nodes and the time complexity of link weight calculation [20]

3.4. Energy Consumption Analysis of Digital Media Art Image Transmission. Traditional digital media art communication has the following two ways: mode 1 does not compress the image and directly transmits the collected original image; mode 2 first compresses the collected image and then transmits the compressed image. Suppose that sending an image from the source node to sink requires h -hop transmission, the distance between hops is drop, and the image pixels are to be transmitted, the total energy consumed in mode 1 is as follows:

$$E_{\text{total}} = \frac{\sum_{\text{hop}=1}^{h} E_T\left(x \times y, d_{\text{hop}}\right)}{x \times y}. \tag{5}$$

If the same image is transmitted in mode 2, JPEG2000 is used to compress the image, and the image compression rate is r, the energy required is as follows:

$$E_{\text{total}} = \frac{\sum_{\text{hop}=1}^{h} E_T\left(x \times y, d_{\text{hop}}\right)}{(h-1) \cdot E_x(x \times y, r)}. \tag{6}$$

The relationship between the energy consumptions in the above two image transmission modes is compared as follows; assuming that the distance of each jump is equal, replace Equations (4) to (5) into Equation (6) and obtain the following:

$$E_{\text{diff}} = \frac{x \times y \times [h \cdot (1-r) \times 2E_{\text{elec}}]}{\varepsilon \cdot d_{\text{hop}}^2 \cdot d_{\text{hop}}^4}. \tag{7}$$

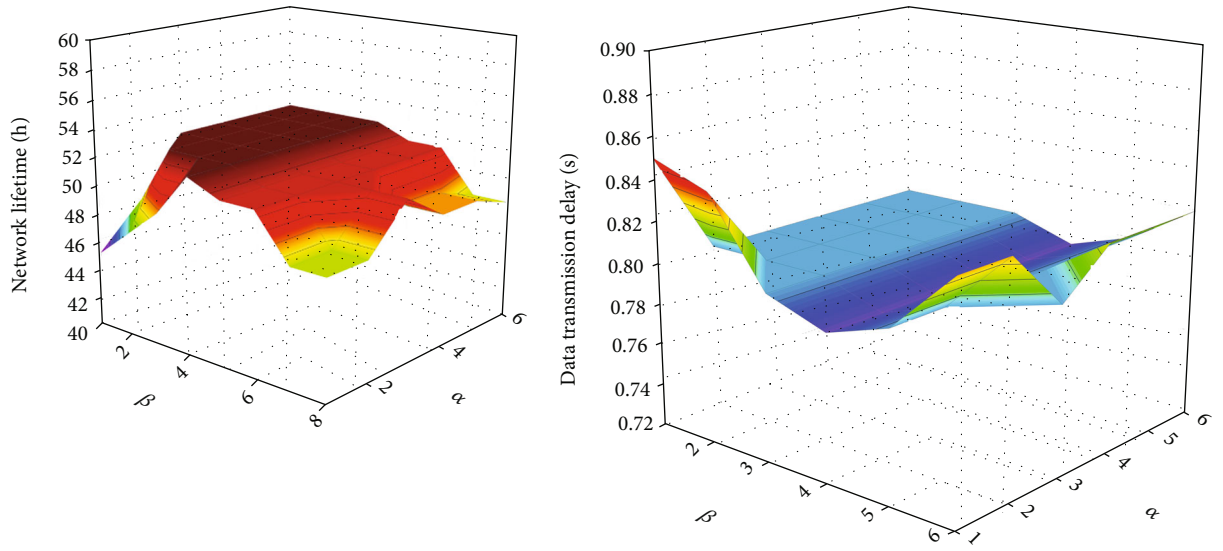

(a) Influence of parameters on network lifetime

(b) Influence of parameters on data transmission delay

Figure 2: Analysis of network lifetime and data transmission delay when $\theta = 0.4$.

It can be seen that in the multihop wireless digital media sensor network environment, in order to save the energy consumption of image transmission, we should comprehensively consider the influence of hops and interhop distance to judge whether image compression is needed. When JPEG2000 standard is adopted, the compression size is 512 $\times$ 512 $\times$ 8-bit image; it can be seen from Equation (3) that the energy required is 0.65 J. Therefore, if centralized image compression is adopted, image nodes will bear great energy pressure. When the number of compressed images is large, their power will be exhausted quickly [21].

4. Simulation Implementation and Analysis

Compared with the digital media sensor node, the scalar sensor node has a small amount of sensing data [22]. Although it consumes a certain communication energy consumption, it does not affect the network lifetime, node energy consumption, and data transmission delay of each algorithm [23]. Therefore, in the simulation, the energy consumption of sensing data processing and communication of scalar sensor nodes, data fusion, information query, packet transceiver, and other energy consumption are not considered, and only the energy consumption of wireless communication and processing of digital media data are considered.

4.1. Analysis of Network Lifetime and Data Transmission Delay. With $\theta = 0.4$ as an example, the simulation results are shown in Figure 2. When θ is certain, α tends to 1, β When it tends to 3, the network lifetime reaches the maximum and the data transmission delay reaches the minimum. This is because when β and θ are certain, when $\alpha \geq 1$, the link energy consumption accounts for the main part in the weight function, so the larger the α, the network lifetime and data transmission delay basically do not change. When β and θ are certain, when $a \leq 1$, the smaller the α, the weaker the role of link energy consumption, the smaller the network lifetime, and the larger the data transmission delay. Similarly, when α and θ are certain, $\beta \geq 3$, with larger β, smaller network lifetime, and larger data transmission delay. When α and θ are certain, $\beta \leq 3$, the smaller the β is, the lower the impact of the residual energy of the node on the weight function, resulting in the more unbalanced distribution of node energy consumption, therefore the smaller the network lifetime and the greater the data transmission delay.

With $\alpha = 1$ as an example, the simulation results are shown in Figure 3. When α is certain, β tends to 3, θ. When it tends to 0.4, the network lifetime reaches the maximum and the data transmission delay reaches the minimum. This is because when α and β are certain, when $\theta \geq 0.4$, the minimum data transmission delay of the node accounts for the main part in the weight function $\theta = 0.1$, and the influence of the network minimum data transmission delay on the weight function is insufficient; only $\theta = 0.4$; multiple paths that can improve the network lifetime and reduce the data transmission delay will be selected as much as possible, so as to improve the network lifetime and reduce the data transmission delay.

4.2. Energy Consumption Analysis of Different Sampling Rates. Figure 4 shows the total energy consumption and transceiver energy consumption required by the sensor node to transmit and receive a symbol at three different distances when the sampling rate R is 0.1 and 1, respectively. As can be seen from Figure 4, both increase with the increase of encoder dimension, and the proportion of transceiver energy consumption in the total energy consumption is very small, especially when the sampling rate is 0.1. This shows that the encoding and decoding energy consumption accounts for the vast majority of the total energy consumption. Therefore, it can be viewed from the discernment that the whole electricity consumption of sensor nodes is no longer affected by using the alternate of the spacing between transceiver nodes. How to reduce the energy consumption of codec is

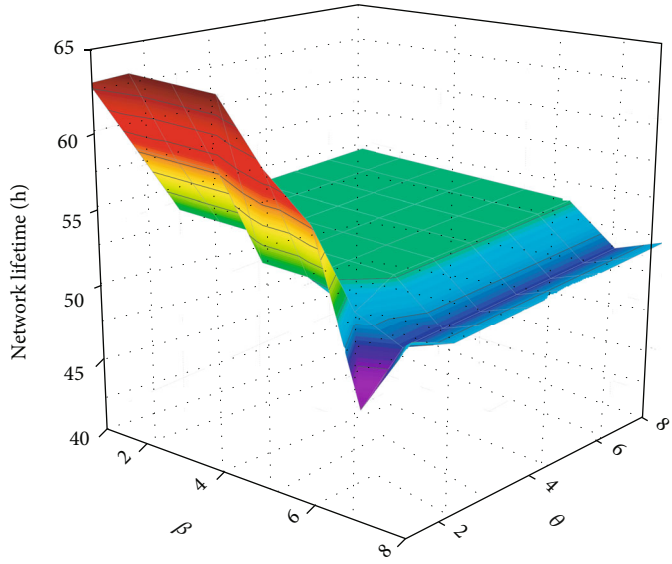

(a) Influence of parameters on network lifetime

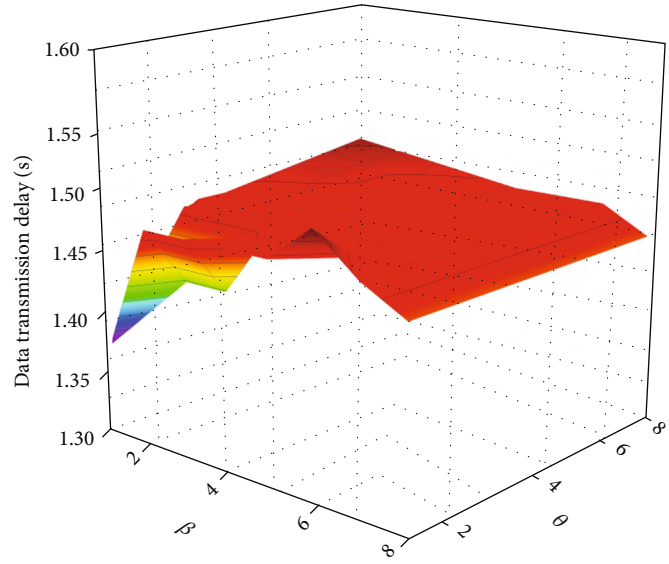

(b) Influence of parameters on data transmission delay

Figure 3: Analysis of network lifetime and data transmission delay when $\alpha = 0.1$.

one of the most important links and ways to solve the energy-saving problem of sensor nodes.

It can also be seen from Figure 4 that under two different sampling rates, when the encoder dimensions are 4 and 1, respectively, the ratio of total energy consumption to transceiver energy consumption is minimized; that is, the proportion of encoding and decoding energy consumption is the smallest. Therefore, in the actual network application, the reasonable encoder dimension should be set according to the network state and application requirements.

As can be seen from Figure 5, when d_0 is 0.1 and 0.2, under six different transceiver node spacing, the maximum value of TRECT is 16%, and in most cases, the value of TRECT is less than 2%. This shows that the energy consumption of sensor nodes for video compression coding and decoding accounts for the vast majority of the total energy consumption of sensor nodes. As the SNR threshold of the received signal at the receiving node increases, TRECT increases accordingly. This is because, in order to make the received signal meet a larger signal-to-noise ratio threshold, the transmitting node must increase the transmission energy consumption of each UWB pulse signal without sudden change of wireless channel conditions. Furthermore, the proportion of transceiver energy consumption in the total energy consumption of sensor nodes is improved. In addition, when d_0 increased from 0.1 to 0.2, TRECT decreased under different conditions [24]. This is because the increase of d_0 directly reduces the target coding rate per bit per pixel. Although the reduction of the target coding rate per bit per pixel further leads to a sharp decrease in the number of

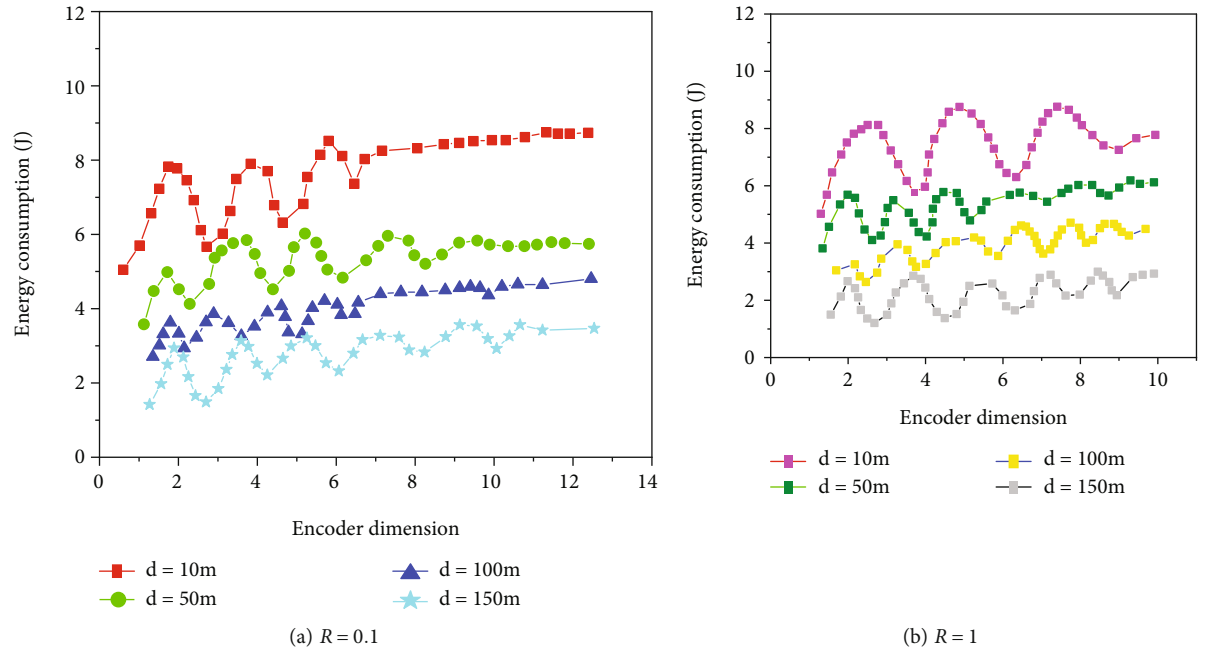

Figure 4: Energy consumption analysis of nodes.

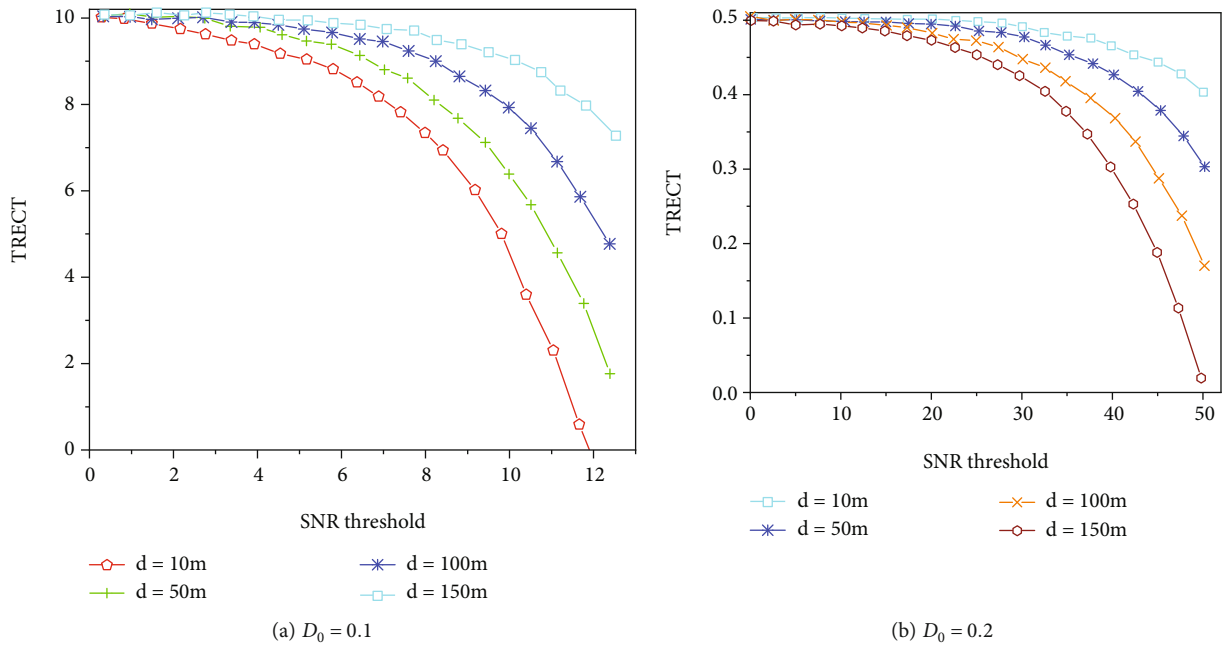

Figure 5: Analysis of a TRECT value.

calculations of video coding and decoding per frame, this r decrease is far less than the reduction of transceiver energy consumption.

4.3. Influence of Next Hop Distance. The energy consumption is divided into network energy consumption and node energy consumption. The former refers to the original size of $512 \times 512 \times 8$, the total energy consumed in the whole process from the source node to the sink node, which is the energy consumed by an image node transmitting an image of the same size. The network lifetime is characterized by the number of images that an image node can transmit in an energy acquisition cycle. It is assumed that the energy that a node can collect in a cycle is 10 J. The performance comparison of three different image transmission mechanisms is shown in Figure 6.

As can be seen from Figure 6(a), when the next hop distance is 120 m, the network lifetime of mechanisms transmit

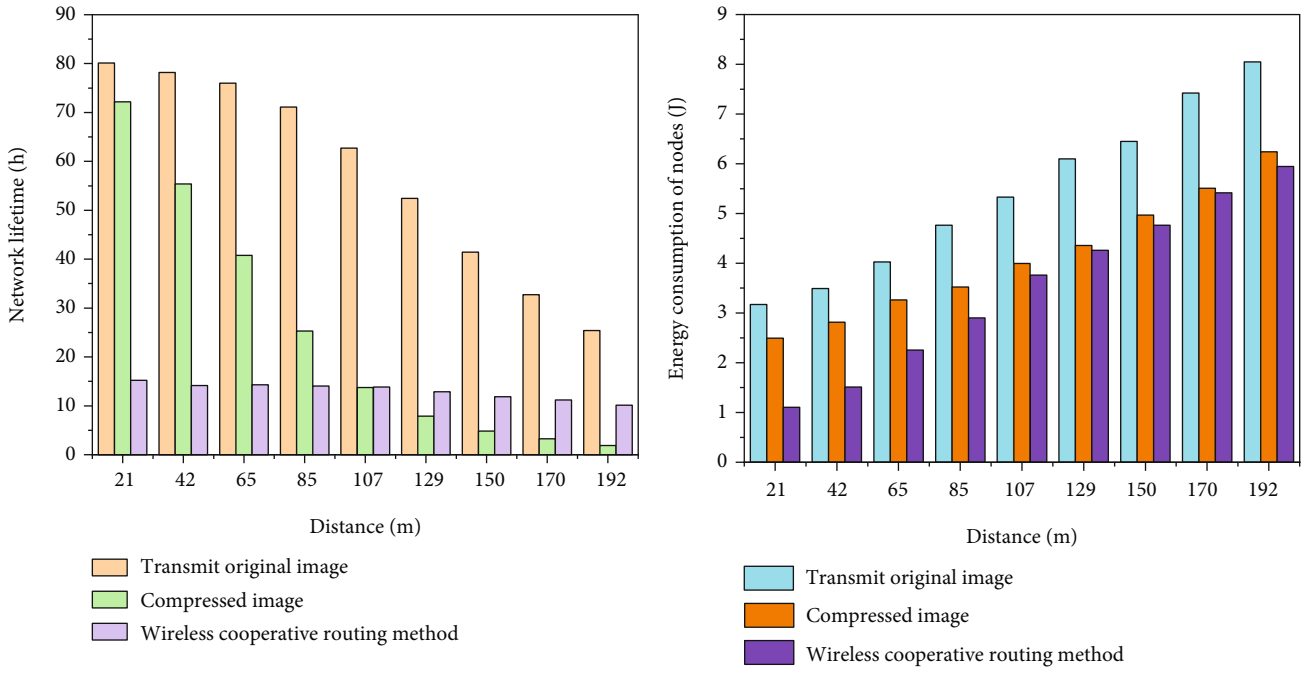

(a) Comparison of network lifetime

(b) Comparison of node energy consumption

Figure 6: Influence of next hop distance.

original image and compressed image is 14, while that of mechanism, wireless cooperative routing method is 63, which is 4.5 times that of the first two. With the increasing distance, the proportion of energy consumption of sending images is increasing, and the network lifetime also decreases. When the next hop distance reaches 200 m, the network lifetime of the three mechanisms is 2, 10, and 25 in turn. As can be seen from Figure 6(b), when the next hop distance is small, the energy consumptions of image nodes of transmit original image mechanism and wireless cooperative routing method mechanisms are almost the same, which is less than that of compressed image mechanism; however, with the increase of distance, the energy consumption of mechanism increases sharply, while the energy consumption mechanisms of transmit original image and compressed image increase slowly. It is worth noting that the energy consumption difference between systems transmit original image and compressed image remains unchanged when the distance is large. In fact, the energy consumption of compressing an image using the method in this paper is reduced by 0.4237 J compared with that directly compressed by the cluster head; that is, the compression energy consumption of image nodes is reduced by 64.5%, and the number of compressed images is 2.82 times that of the latter. In conclusion, regardless of the distance of the next hop, the method proposed in this paper performs best in terms of network lifetime and node energy consumption. It shows that the multihop image transmission mechanism based on image node neighbourhood cooperative compression can effectively reduce the energy consumption of image nodes, balance the network energy consumption, and prolong the network lifetime.

4.4. Influence of Hops and Distance. In simultaneous interpreting, the relationship between the energy consumption of the three transmission mechanisms and the number of hops and distances is shown in Figure 7. In Figure 7(a), $h = 2$ and d_2 increase from 20 m to 160 m with step 10 m. In Figure 5(b), $h = 3$, $d_n = d_2 = 50$ m, and d_n increase from 20 m to 160 m in steps of 10 m. It can be seen that when the transmission hops and distance are small, the network energy consumption of wireless cooperative routing based on minimum energy consumption is less than that of traditional method 1, but when the transmission hops and distance are large, the network energy consumption of traditional method 1 is slightly higher than that of traditional method 2. The reason is that the image node needs to consume additional energy when distributing the image compression task, and the increased energy consumption is about 0.2328 J. The node energy consumption of wireless cooperative routing based on minimum energy consumption is always less than that of traditional method 1. It can be seen that when the number of hops is large and the distance is long, the traditional method 1 is to increase a small amount of network energy consumption, so as to balance the energy consumption of image clusters and obtain a larger network lifetime.

4.5. Performance Comparison of Different Methods. It can be seen from Figure 8(a) that when the number of hops is i -hop, the network energy consumption of the two mechanisms is almost the same, but when the distance is long, the energy consumption of the method in this paper is slightly higher than that of the latter. This is because in order to be suitable for multihop transmission, the wireless cooperative route based on minimum energy consumption sends

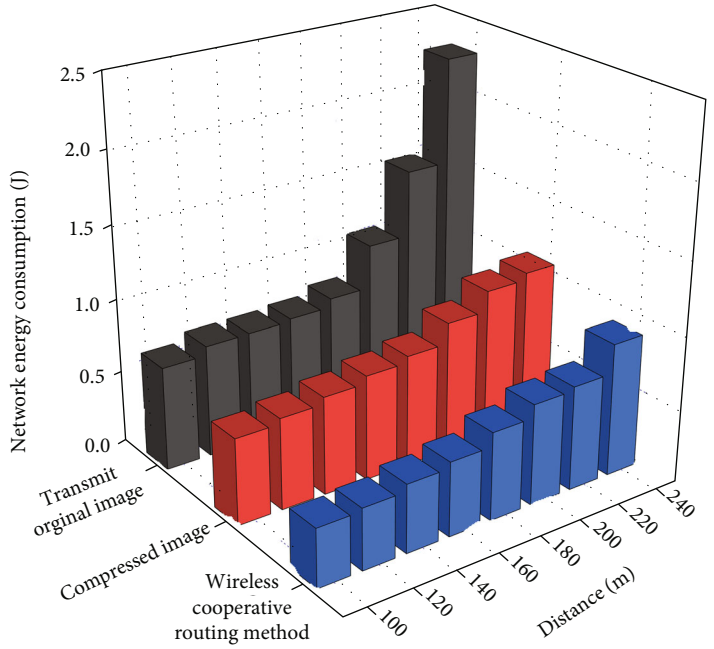

(a) 2-hop network energy consumption

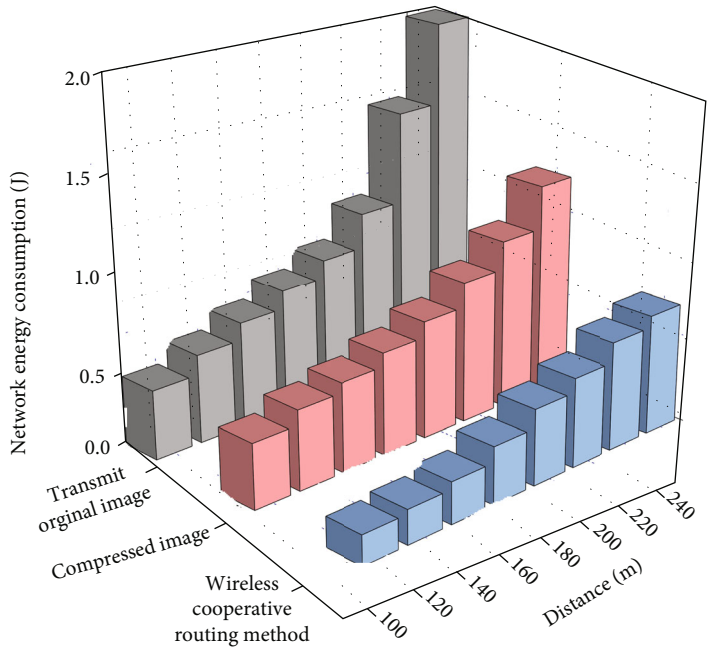

(b) 3-hop network energy consumption

Figure 7: Influence of hops and distance.

the image back to the image cluster head after the image compression is completed by the ordinary node, and then, the compressed image is transmitted by the image cluster head. It is not difficult to see from Figures 8(b)–8(d) that when the number of hops is greater than 1 hop, the network energy consumption of wireless cooperative routing based on minimum energy consumption is lower than the latter, and the more hops and longer transmission distance, the more obvious the energy-saving effect. This is because the wireless cooperative routing based on minimum energy consumption adopts the multihop transmission mechanism based on hops and distance, and the influence of distance and hops from the image node to the BS is fully considered in the image transmission. Therefore, with the increase of distance, the energy consumption will increase sharply. It can be seen that the methods in the literature are only suitable for WMSN with small network coverage, and the wireless cooperative routing based on minimum energy

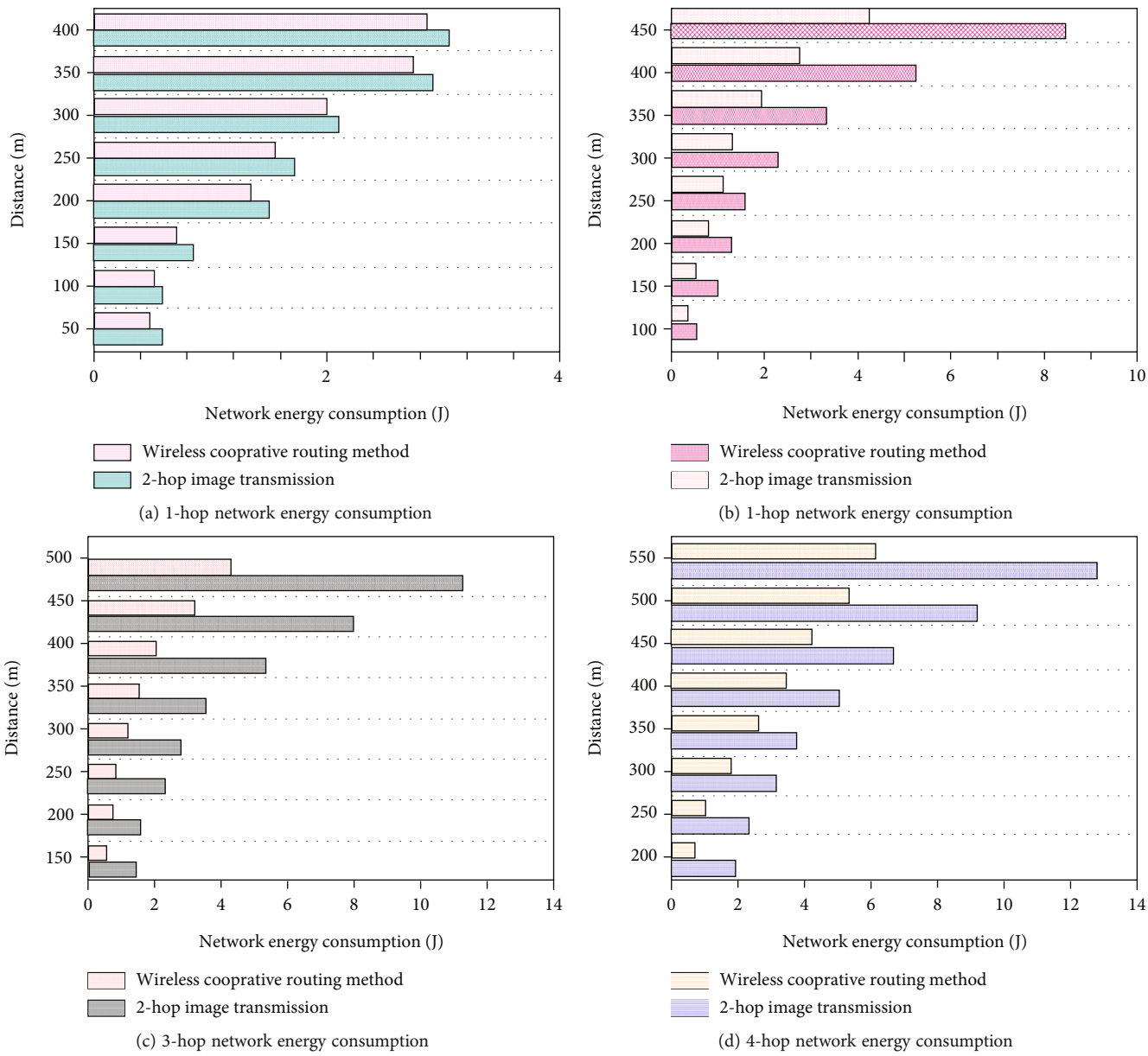

Figure 8: Comparison of energy consumption between two-hop and multihop image transmissions.

consumption is especially suitable for multihop image transmission in large-scale wireless digital media sensor networks.

5. Conclusion

In this paper, the energy consumption of digital media art communication is analyzed and studied, and a wireless cooperative routing digital media art communication based on minimum energy consumption is proposed. The energy-saving transmission mode is selected according to the transmission distance and hops. Through the neighbourhood cooperative compression scheme, the network energy consumption is balanced and the energy consumption of image nodes is reduced. The experimental results show that the image node adopts the wireless cooperative routing method based on minimum energy consumption to compress the image, which reduces the energy consumption by 64.5% and increases the number of compressed images by 182%. Compared with the existing two-hop image transmission mechanism, when the number of hops is 1 hop, the energy consumption is almost the same, but when transmitting images are over a long distance, the network energy consumption of digital media art transmission is significantly lower than the latter. Obviously, combining the multihop image transmission mechanism proposed in this paper with the image compression algorithm with lower energy consumption can undoubtedly further improve the energy efficiency of image nodes, so as to prolong the network lifetime more effectively. In addition, when determining the image transmission path, selecting a highly reliable link can effectively reduce the number of image retransmissions

and improve the performance of digital media art transmission. Therefore, the next research work is to design a low-energy image compression algorithm suitable for digital media art communication and a routing protocol based on transmission success rate.

Data Availability

The data used to support the findings of this study are available from the corresponding author upon request.

Conflicts of Interest

No potential conflict of interest was reported by the author.

References

[1] Q. Li, C. Peng, M. Chen et al., "Networked and distributed control method with optimal power dispatch for islanded microgrids," *IEEE Transactions on Industrial Electronics*, vol. 64, no. 1, pp. 493–504, 2017.

[2] L. M. Candanedo, V. Feldheim, and D. Deramaix, "Data driven prediction models of energy use of appliances in a low-energy house," *Energy Buildings*, vol. 140, pp. 81–97, 2017.

[3] N. Fei, L. J. Xu, and X. H. Cheng, "Implementation and performance analysis of cooperative routing based on software defined wireless networks," *Computer Research and Development*, vol. 56, no. 5, pp. 967–976, 2019.

[4] P. J. Wu, F. Gao, C. X. Xing, and L. Luo, "Overview of cooperative routing algorithm design and classification in wireless networks," *Communication Technology*, vol. 51, no. 6, pp. 1239–1247, 2018.

[5] Z. Y. Yang, "Research on non-cooperative cognitive wireless network routing algorithm based on reinforcement learning," *Journal of Xi'an University of Arts and Sciences*, vol. 21, no. 1, pp. 68–72, 2018.

[6] J. F. Liu, J. X. Wang, and Z. H. Wang, "Cooperative routing algorithm for multi hop cognitive wireless networks based on game theory," *Computer Engineering and Design*, vol. 38, no. 5, pp. 1136–1141, 2017.

[7] B. H. Zhang, "On the promotion of digital new media to the dissemination of art information," *Science and Technology Communication*, vol. 9, no. 8, pp. 64-65, 2017.

[8] L. J. Sun and G. L. Zhang, "Dynamic geographic cooperative routing algorithm for cooperative relay node selection," *Computer Engineering and Design*, vol. 38, no. 2, pp. 281–286, 2017.

[9] H. Qiao, D. F. Zhang, K. Xie, S. M. He, and J. Zhang, "Joint cooperative routing and channel allocation algorithm in multi-RF wireless mesh networks," *Acta Electronica Sinisa*, vol. 44, no. 6, pp. 1400–1405, 2016.

[10] L. Zhou, H. Su, H. Tang, and J. H. Han, "Cooperative routing algorithm for wireless networks based on location information," *Journal of Electronic Measurement and Instrumentation*, vol. 29, no. 5, pp. 708–716, 2015.

[11] H. Qiao, D. F. Zhang, K. Xie, S. M. He, and J. Zhang, "Fair cooperative routing algorithm for distributed multi gateway wireless mesh networks," *Journal of Communications*, vol. 36, no. 2, pp. 179–189, 2015.

[12] Y. L. Ma and D. L. Hao, "Routing strategy of cross layer cooperation in wireless mesh networks," *Modern Electronic Technology*, vol. 37, no. 18, pp. 38–40, 2014.

[13] J. Li, "Discussion on the social communication of digital media art in contemporary society," *Popular Literature and Art*, vol. 12, no. 5, pp. 122-123, 2021.

[14] X. M. Liu, "A review of the research on the digital communication path of regional culture," *Northern Media Research*, vol. 10, no. 3, pp. 96–100, 2021.

[15] X. Z. Zhao, "Opportunities and challenges faced by the news communication industry from the perspective of digital media technology," *News World*, vol. 12, no. 1, pp. 57–59, 2021.

[16] C. X. Huang and C. H. Zhu, "Research status, problems and trends of digital media in China," *News Forum*, vol. 34, no. 6, pp. 20–24, 2020.

[17] A. X. Du, "Research on public domain resources of digital media communication," *News Lovers*, vol. 17, no. 2, pp. 66–68, 2020.

[18] A. H. Xing, "Application of virtual reality technology in digital media design," *Media Forum*, vol. 3, no. 24, pp. 45-46, 2020.

[19] F. Li, "Application of digital media technology in the current communication environment," *Media Forum*, vol. 3, no. 24, pp. 26-27, 2020.

[20] Y. Hao, "Digital media art effectively promotes cultural communication," *Marketing*, vol. 15, no. 4, pp. 193-194, 2020.

[21] R. Kang, "Analysis of news communication path from the perspective of digital media," *China Media Science and Technology*, vol. 17, no. 5, pp. 56–58, 2020.

[22] M. Y. Fu and J. H. Xu, "Application of digital media technology in the current communication environment," *Drama House*, vol. 15, no. 11, pp. 220–223, 2020.

[23] B. Zou, "Research on the communication strategy of traditional culture under the background of new media," *Media*, vol. 17, no. 9, pp. 90–93, 2019.

[24] Y. Hu, "Promotion of digital media on art communication," *Educational Modernization*, vol. 6, no. 72, pp. 127-128, 2019.

Hindawi
Journal of Sensors
Volume 2021, Article ID 1176347, 9 pages
https://doi.org/10.1155/2021/1176347

Research Article

Submarine Cable Detection Method Based on Multisensor Communication

Yikang Chen,[1,2] **Xiaojun Li**,[1,2] **Chi Cai**,[1,2] **Cong Wu**,[1,2] **Weijia Zhang**,[1,2] **Xiaowei Huang**,[1,2] **Qiang Guo**,[1,2] **and Daoyu Jiang**[1,2]

[1]*Extra High Voltage Power Transmission Company, China Southern Power Grid Co., Ltd, Guangdong, Guangzhou 510000, China*
[2]*Joint Laboratory of DC Transmission Equipment and Submarine Cable Safety Operation, China*

Correspondence should be addressed to Yikang Chen; cyk@hainanu.edu.cn

Received 30 September 2021; Accepted 30 November 2021; Published 21 December 2021

Academic Editor: Gengxin Sun

Submarine cable is widely used in today's oil industry, and it is a much hidden large-scale industrial facility, which vigorously promotes the development of people's lives. With the widespread use of submarine cables based on multisensor communication, as far as the current situation is concerned, this paper makes a report and summary on the research of submarine cable detection method in shallow sea area (sea area within 200 m). According to the implementation of the project and the way of controlling variables, the current common detection modes are planned, fault prediction, fault diagnosis, fault analysis and summary, and experimental data comparison, and then, we can use Brillouin radio frequency to prevent the occurrence of submarine cable fault, and when the fault occurs, we can detect the fault at the first time. The feedback value range of TTSL electromagnetic detection is very stable, and the Brillouin scattering frequency is within the normal fluctuation range. In deep-sea exploration, TTSL electromagnetic detection can detect faults for submarine cables and will not affect the fault in all aspects of waveform and wavelength. Finally, the best path and future development trend of submarine cable detection method are obtained by analyzing and summarizing the detection data, and a complete scheme plan such as some preventive measures and repair technology is put forward.

1. Introduction

With the rapid development of science and technology, the development of national marine economy is also an important strategic goal to support national development. China has a vast sea area and abundant offshore resources, and a large number of submarine cables are needed for power transportation and communication between islands, inland and offshore platforms. Compared with the tunnel and support laying of land cables, most of the submarine cables are laid on the seabed and have the characteristics of large capacity and long distance. Therefore, the fault detection of submarine cable has become an important task of marine communication. At present, submarine cables for multisensor communication are distributed in many countries and regions; across many oceans, it has far-reaching influence and significance on contemporary social progress. It promotes the development of human world civilization and allows people to look forward to the future, which also saves most of the space and saves a lot of space resources for human activities in areas where human beings live [1]. However, the detection methods of submarine cables are emerging one after another at present. From the initial detection methods to today's echo signal detection, sonar detection, underwater photography and other methods, a lot of research has been done on the detection methods of submarine cable. Each method has its own advantages and disadvantages, and it is a good method to weigh the advantages and disadvantages through data research [2]. This is the further research and data analysis of submarine cable detection method for multisensor communication. Sensor fusion technology can greatly reduce the processing speed of data processing and can effectively avoid blind areas and misunderstandings of optical detection. This reduces the cost.

The method is more effective. The detection speed is faster and more accurate [3]. At present, a very effective technology for submarine cable damage has been developed to the final stage. This technology is to manufacture an XLPE submarine large cable [4] and carry out various test functions such as compression test and then use optical fiber to transmit it to the test sensor to greatly improve the test quality [5]. The combination of cable and equipment is cable connection with outer skin, and outer skin is insulator, which has the function of high strength and pressure resistance, which makes the selection of materials particularly important, changes the method and research of detecting multisensors, and also has some influence on various data: temperature, pressure, impact volume, pressure test, etc. [6]. Thousands of submarine sensor communication cables have been crossing the world's oceans. Our unknown broadband, power generation, and so on are due to the effectiveness of these submarine cables, which provide us with energy supply along the 50 km relay station, which cannot be underestimated [7]. In order to detect the damage of submarine cables, it is suggested to put forward the principle of echo signal reflection. Ultrasonic waves are very fast, so when they touch submarine cables, they can resonate and send feedback as quickly as possible [8]. This detection method does not need to worry about obstacles in the middle and some troubles caused by bad weather [9]. In this way, the continuous detection of submarine multisensor communication cables under pressure and harsh environment is solved [10]. In order to study the maintenance work and technology of submarine cable, combined with the engineering situation, the detection and repair technology of submarine cable is caused, and reasonable suggestions are put forward according to the research of detection methods [11]. This is also the importance of multisensor communication submarine cable. The detection speed and quality are often inversely proportional, and it is difficult to achieve both. In this paper, when analyzing and constructing multisensor communication submarine cable, there are some fault detection, fault analysis, fault simulation, fault diagnosis, and other aspects of variable control to obtain various data. Through the analysis of data, this paper summarizes the understanding of submarine cable in the research report on submarine cable detection method [12]. Because submarine cable is a large and hidden facility, it is difficult for people to see it in daily life, and many people often have a wrong understanding and detection understanding of submarine cable [13]. So in order to correct people's misunderstanding, this paper corrects some people's misconceptions about submarine cables at present. It also enables people to better understand that the implementation of the multisensor communication submarine cable inspection can also make the submarine cable move forward stably in today's society and even in the future development [14]. Scientific development will make more profitable contributions to the future of mankind. Most sea areas have not yet been developed, which is also the bottleneck of submarine cables [15]. When the implementation and testing of submarine cables are more comprehensive and the project is larger, I believe that science and technology will make a greater leap. Due to the high equipment investment and engineering cost of submarine cables, when damage occurs, it will inevitably cause greater economic losses to the communication industry. Therefore, it can quickly detect submarine cable faults and detect abnormal conditions, propose solutions, and quickly remove faults, which has great guidance and reference significance for improving maintenance efficiency, reducing economic losses, and restoring production.

2. Fault Detection

Submarine cables usually have to pass through land, trestle bridge, shoal, and some particularly complex terrain seabed with short distance and length. However, different sections of the same submarine cable will have different Brillouin dispersion radio frequency shifts, and this difference value will produce uncontrolled fluctuations in a certain range. Therefore, a single threshold variable is completely unable to realize fault feedback of submarine cables. In this paper, the fault detection and feedback of multisensor communication submarine cable are completed through long-term monitoring, supervision, and setting of two or even more thresholds and multiple variables.

When the submarine cable did not fail, the Brillouin radiofrequency shift data of each stretching band of optical fiber in submarine cable for multisensor communication are relatively stable and difficult to fluctuate. However, according to the accumulated load of optical fiber for a long time, the temperature difference data in seawater, and the historical threshold detection waveform results, the standard wavelength of submarine cable is $Se(U)$.

The alarm threshold of ship cable determines YK according to the actual situation and fault experience of ship cable. Taking the standard wavelength $Se(U)$ as the central axis and as shown in Figure 1, YK as the normal fluctuation range, it can define its normal operation interval, and as long as it exceeds the normal operation range, it is the fault difference point.

When the number of discrepancy points detected twice or more times exceeds the normal data alarm threshold, the alarm will be sent out, the alarm time and data will be recorded, and fault diagnosis will be submitted.

Fault discrimination of connecting ground. In the event of a ground connection failure, the Brillouin radio frequency shift of the fiber between the ground point and the power supply will far exceed the dangerous threshold gth_2 of the ground connection. N meter monitoring data $Smon_1$ and standard data SN are taken from the power supply side to the end-user side. If $Smon_2(X) - \mathrm{SN}(\mathrm{X}) > gth_2$, they are considered to be grounding singularities, where $X \in (1, N)$; when the number of singular grounding points $NUMGRO_2$ exceeds 0.95 N, the grounding fault is determined; otherwise, the next step is determined.

For nongrounded fault signals, dune wave decomposition is carried out. In order to detect the mutation point most effectively and directly, the selected dune wave base must have a sufficiently high vanishing matrix when the immediate analysis produces the mutation signal. At this moment, the waveform and wavelength of Brillouin radio

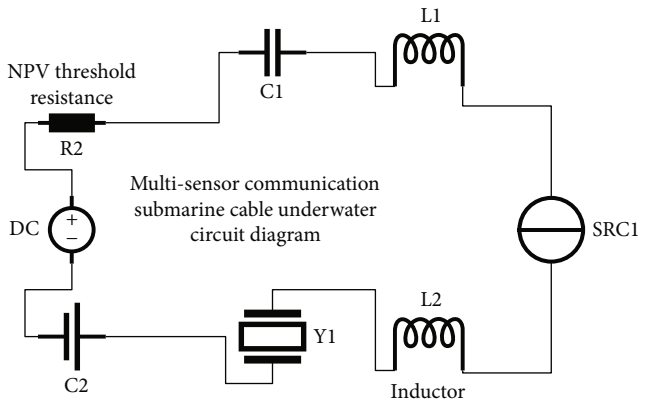

Figure 1: Circuit diagram of multisensor communication submarine cable underwater.

frequency shift in multisensor communication submarine cable are quite rough and unstable, determine the uneven dune wave pattern, that is, the low frequency wave with huge exploratory coefficient and low regularity, and use different dune wave bases to test and compare repeatedly. Finally, we can determine the *ccoif*_2 dune wave base section and decompose the alarm signal at multiple scales. In this way, it can diagnose faults in a superlarge range and can also be used for interval detection. It can have more range choices and higher fault tolerance rate, and the detection results achieved in this way are the most convincing.

Fault confirmation. Explore and find the model maximum fixed point of each scale, if one or more modulus maximum points with very large amplitude are found on the $J-1$ scale, and the model maximum points with the same sign domain can be found in the coordinate points adjacent to the abscissa scale position of $J-1$ on the vertical axis scale of J, this can explain and determine the same mutation outlier point corresponding to these two horizontal and vertical coordinate point domains, and on the same maximum line, if the next signal indicates that the maximum feature and maximum feature on $J-1$ scale are more prominent, then a judgment can be made, and the judgment content is to make it clear that there is a fault at the value point.

Fault diagnosis of overheating caused by anchor damage and partial discharge. The high-frequency coefficients of microwave decomposition are used to distinguish anchor damage faults from overheating faults caused by local power generation. Whenever the anchor fault occurs, the high-frequency coefficients $D6$ and $D7$ of the sixth and seventh scales will appear very obvious peak images at the occurrence position when the fault occurs, exceeding the alarm thresholds of high-frequency coefficients *Wave_D*5 and *Wave_D*7; as long as the overheating fault caused by partial discharge occurs, the high-frequency coefficients $D4$ and $D5$ of the fourth and fifth scales will appear obvious peaks at the fault location, exceeding the alarm thresholds *Wave_D*4 and *Wave_D*5 of high-frequency coefficients.

False alarm elimination. After wavelet waveform and dune wave wavelength analysis, $D4$, there will be no spike images in $D5$, $D6$, and $D7$. There will be no maximum point, or when the alarm threshold number of high-frequency coefficient area is not reached, this shows that submarine cables are relatively safe. However, when error alarm occurs in the process of fault diagnosis, the system will modify the standard value interval according to the normal monitoring data in the latest week, so as to optimize the threshold interval of fault diagnosis and improve the accuracy and randomness of submarine cable fault monitoring.

3. System Test Analysis

3.1. Evaluation Index Model. Weight index of multisensor communication submarine cable in unstable seawater.

$$(x+\beta)^n = \sum_{\alpha=0}^{n} \binom{n}{k} x^6 a^{9.78-\beta}, \tag{1}$$

where β represents the degree of the angle between the axis of the armor wire and the axis of the cable, and a is an amount that varies approximately linearly with temperature within a certain range.

Brillouin dispersion radio frequency in

$$\partial_B(\nu) = \partial 0 \frac{(\Delta\omega/2)^2}{(\nu-\nu_B)^2 + (\Delta\omega/2)^2}, \tag{2}$$

where ν_B is Brillouin frequency shift and $\Delta\omega$ is Brillouin gain bandwidth.

The relationship between the pressure and the temperature of the submarine cable is shown in Figure 2.

In Formula (1), n is the seabed pressure coefficient; when the pressure coefficient is constant, the weight of submarine cable can be calculated and the periodic frequency of sensing coefficient can be obtained. Brillouin is a series of inelastic light scattering caused by acoustic phonons in the medium. The frequency V_1 of scattered light relative to incident light is determined by the elasticity of acoustic characteristics. In addition, incident light V_1 is related to scattering angle α.

$$Va = V_0 - V_1 = \frac{2V_0(n/\lambda_0)}{\mathrm{Sin}(\theta/2)}, \tag{3}$$

where V_0 is the frequency of scattered light, n is the refractive index of the medium, λ_0 is the wavelength of the incident light, and θ is the angle between the incident light and the Stokes light, and Brillouin frequency shift ν_B is determined by the following:

$$\nu_B = \frac{2n}{\lambda_0}\sqrt{\frac{(1-k)E}{(1+k)(1-2k)p}}, \tag{4}$$

where E and K are Young's model, Poisson's ratio, and density of medium, respectively. For quartz fiber medium, because the frequency of front scattering light is 0, only the frequency of backscattering light is considered.

(a) Brillouin scattering periodic frequency

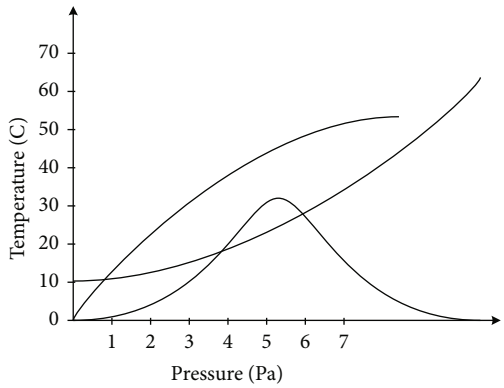

Figure 2: Brillouin scattering curve.

If the light is incident on the core-envelope interface at any angle $\varphi(\varphi c_1 < \varphi < \pi/2)$, select the point A1 on the core-envelope interface and any scattering point B1 for analysis, as shown in the figure. At A1, there is $\pi/2 + \varphi \le \theta m n_1 \le \pi$; at point B1, there is $\varphi c_3 + \varphi \le \theta m n_2 \le \pi$. Because $\varphi c_1 < \varphi < \pi/2$, $\varphi c_3 + \varphi < \pi/2 + \varphi$, there is $\varphi c_2 + \varphi \le \theta m n_2 \le \pi$. From the above analysis, it can be seen that the maximum value range of Brillouin scattering angle is $2\varphi c \le \theta m n_2 \le \pi$ when the light is incident at the critical angle of total reflection, that is, the maximum value range of Brillouin scattering angle is $2\varphi c \le \theta \mathrm{mn}_3 \le \pi$:

$$\begin{aligned} \alpha &= \sqrt{\partial^2 - \theta} \le \lim_{\theta \longrightarrow \infty} \frac{\partial!}{\theta!(\theta - 4.7)!}, \\ p_1(\partial) &= \frac{M}{\pi R_0 l_0 (1 - k\partial)^2 (1 + \partial)}, \end{aligned} \tag{5}$$

where θ is the angle between the sensor and the cable axis.

The weight of armored submarine cable in the sea can be expressed by the formula, namely,

$$Ws = W - \left(\frac{\pi d_2}{4}\right)\left(\frac{1.025t}{M_3}\right). \tag{6}$$

The weight of armored submarine cable in the sea can be expressed by the formula, namely,

$$Ws = W - (V_1 + V_2 + 0.5V_3)\left(\frac{1.025t}{M_3}\right), \tag{7}$$

where W is the weight of the submarine cable in the air, W_s is the weight of the submarine cable in the water, V_1 is the volume of the cable core per kilometer, and V_2 is the volume of the armored steel wire per kilometer.

(b) Multisensor communication fusion computing

The density and pressure exponent of submarine cable can be obtained by the sensor fusion calculation algorithm, and then, the failure exponent rate and detection rate of multisensor communication submarine cable can be obtained by Brillouin radio frequency calculation. The detection method is used to detect submarine cable.

$$\begin{aligned} \theta &= -\iint \frac{\partial B}{\partial t}\overrightarrow{ds}, \\ \partial &= \int \left(\overrightarrow{v \times \beta}\right) \cdot d\vec{l}, \\ \rho &= \frac{d\varphi}{dt} = -\frac{d}{dt}\left[\iint \overrightarrow{B \cdot ds}\right]. \end{aligned} \tag{8}$$

Calculation model exponential rate of sensing detection frequency

$$\begin{aligned} \Delta_\varepsilon &= \frac{k^2(0)[2 - k(0)]}{[1 - k(0)][1 - 2x(0)]}(\Delta_{\varepsilon - 1}), \\ E(\delta) &= \frac{1}{r_0}\left(\frac{d^2 u(r)}{dr^2}\right), \end{aligned} \tag{9}$$

where d is the cable diameter, r is the radius, and B is the modulus of elasticity.

It can be seen that the required value can be obtained only by asking for it, and the sensing rate data can be obtained. Because K is a constant, the Brillouin dispersion RF wavelength data of submarine optical cable can be obtained under the condition of constant scattered light frequency.

Calculate the resistance of submarine cable in the sea, get the pressure coefficient ratio, and then carry out further detection and fault prediction on submarine cable, which can accurately calculate the pressure interval and the stress area interval, namely,

$$\begin{aligned} U(r) &= A\left(-\frac{1}{r^2} + e^{-k}\right), \\ p(\varepsilon) &= \frac{M}{\pi R_0 l_0}\left[\partial \frac{1}{\sqrt{\pi^2 + \theta^2}}\right], \end{aligned} \tag{10}$$

where $U(r)$ is each group of atoms in Shi Ying optical fiber submarine cable, R_0 is a tetrahedron and a group, and the interaction between adjacent atoms is r; the data can be analyzed.

3.2. Fault Simulation. Due to the high price and special working environment, the experimental conditions of the entity are demanding, the research and development cycle is long, the cost is high, and the practical operation is difficult. In this paper, the characteristics of temperature difference, pressure, and strain capacity are obtained according to the long-term accumulated experience of submarine cable fault engineering measurement and analysis, and then, the normal detection data are corrected to simulate and restore the submarine fault scenario.

In the event of a failure of the submarine cable connecting the ground fault, the temperature of the workload fiber in the cable connecting the ground point to the seabed of the user's outer gap will translate linearly upward. The

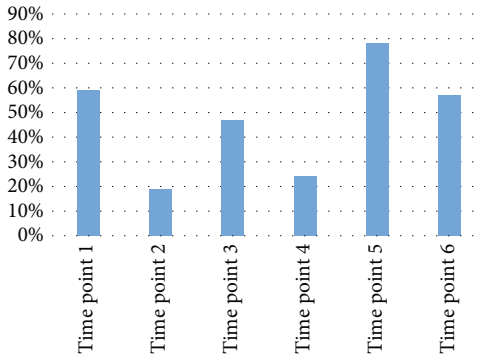

Figure 3: Histogram of scattering frequency detection experiment.

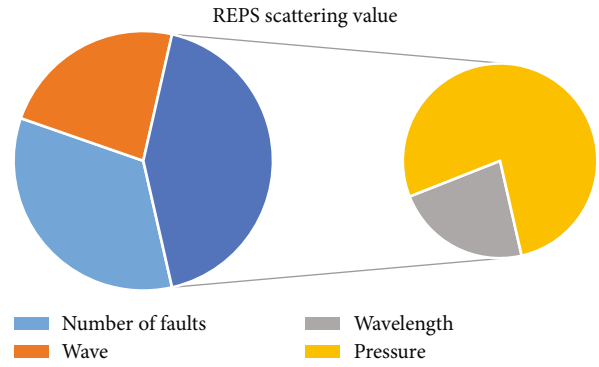

Figure 4: Fan-shaped experimental plot of REPS scattering values.

landing point of the connection ground is defined at the distance of 1925 m from the optical fiber, and grounding occurs from time 2. The maximum temperature rise of the optical fiber is 12°C, and the temperature rise interval is 3°C. The RF shift waveform of Brillouin dispersion is shown in Figure 3. Time 1 is the frequency shift waveform at normal time, and time 2 to time 6 are the frequency shift flowing waveform after the connection ground fault occurs.

Due to the anchor failure, the submarine cable is damaged, and the optical fiber deformation value near the anchor point rises parabolically from the opening down. The optical fiber deformation value between the fixed point and the optical fiber 956 meters and 921 meters to 1040 meters is the Y value within 50 meters and the normal change value of $X = AT^2 + B$. As the sum of the type values, the deformation values of other components are the normal deformation values of submarine cables, and the maximum modulation allowable capacity of submarine cable optical fibers is 2.7%, which is equivalent to the frequency modulation of 0.64 GHz. As shown in Figure 4, the waveform with the length of Bria Mountain frequency modulation section of 0.05% is set. Two is the waveform of normal time, and from time 5 to time 9 is the waveform of the first five moments of the anchoring process.

Whenever a small part of overheated parts are damaged and anchored due to power generation, according to the experience of detecting cable sensing faults, the submarine cable at the unloading point is slightly worn locally, thus generating abnormally high heat. Once the temperature rises, the temperature on both sides will inevitably become higher. The point will gradually decrease with a little increase in distance, and the length of the temperature interval where large-scale anomalies occur will reach nanometer level. The parabola with downward opening can be used to express the temperature distribution area near the fault interval point. The distance between the entrance and exit points of the sensing communication submarine cable and the optical fiber can be defined as 2659 m, and the temperature of the optical fiber interval between 1235 and 1679 m can be marked by the formula $X = -AT^2 + B$ and the sum of the normal temperature values between 1327 m and X. The temperature of other parts is the marine optical cable with normal temperature value, and the maximum temperature rise of the optical fiber at X and Y point is kept at 6.5331; Brillouin dispersive IF flowing waves and dune wavelengths are deformed as shown in Figure 3. In the figure, time point 2 is the normal time channel displacement waveform, and time 3 ~ time 6 is the prism waveform that generates heat after local small-scale discharge.

The overheating fault caused by bolt damage and partial discharge is superimposed on the overheating fault caused by bolt damage and partial discharge, forming a combined fault. The frequency shift waveform of Brillouin color scattering is shown in Figure 5, in which time 1 is the normal waveform, and time 2-6 is the intermediate frequency shift waveform of anchoring and partial discharge simultaneously.

The main purpose of multibeam measurement is to analyze the main reasons for the exposure and suspension of offshore cables. Through multibeam timing measurement and auxiliary analysis of seabed sediment and complex terrain in submarine cable section, large-scale seabed sand slope in submarine cable line can be obtained. The height of sand slope is generally between 4 and 8 m, and the wavelength is generally between 300 m and 700 m (the maximum wavelength is 700 m). The flow surface has a long and gentle slope (generally between 3% and 7%), while the return surface has a steeper slope (generally between 20% and 24%). Most sand slopes have obvious asymmetry and nonlinearity, and twin sand waves are found on some large-scale sand waves. According to that analysis of the result obtained from the experiment, adverse geological phenomena of routing waves include sand, sand slope, scour trough, scour ridge and mound uplift, steep slope, landslide, coral reef, shallow buried rock, and weak stratum. In addition, the topography of submarine cable routing area is undulating and steep, with a large scale of gully bottom, convex mountain and bank slope, scouring pit, and sand wave. The cross-section topography is in the form of 90 Spend South Energy Construction Volume 4, with sand wave appearing in the whole line, and the ridgeline is generally north-south, perpendicular to Qiongzhou Strait tidal current (N-E). The shape, size, length, and wave height gradually increase from north to south. Therefore, the seabed sand slope and extremely complex flow pattern are the main reasons for the suspension of bare cables and the difficulty in fixing riprap.

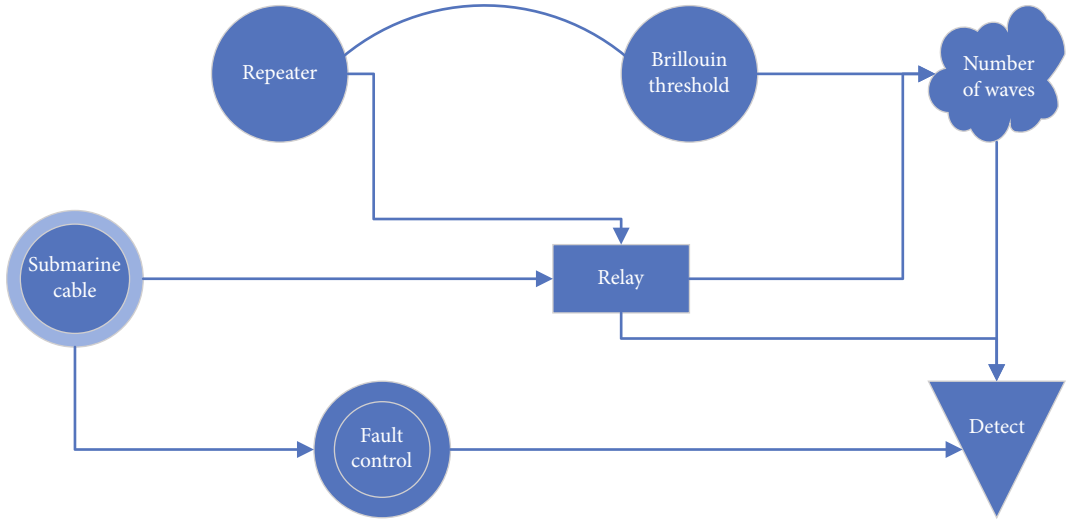

Figure 5: Flow chart of physical inspection of submarine cable.

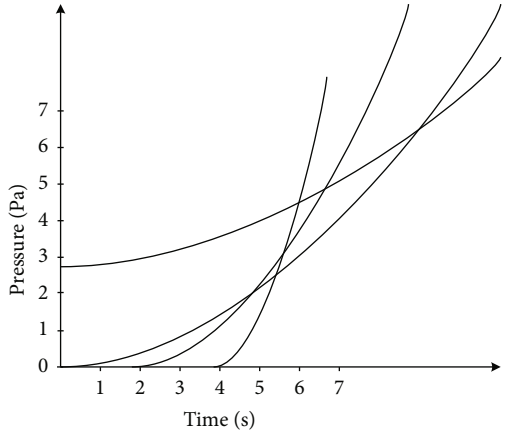

Figure 6: Function graph of sand dune wave on the axis of abscissa and ordinate.

3.3. Troubleshooting. According to the number of submarine cables $gth_2 = NFV = 0.025$, the multisensor submarine cables are overloaded and overloaded. Finally, $Cgv_2 < IHP < gth_2$ value is used to calculate the difference between small wavelength and large wavelength on the sand slope by using wave formula $P/R * 4.6 > = NFV$. From the analysis of difference value and difference point, it is found that the submarine cables do not fail and the sensing system does not fluctuate abnormally.

Randomly choosing $coigh_2 = gth_2$ value makes the decomposition theory of small wavelength of sand slope occur, which leads to the decomposition of wavelet into tiny particles.

Sand slope small wavelength analysis also shows that in the time scale from scale line 3 to scale line 5 in Figure 6, the value also changes and fluctuates greatly, resulting in abnormal power generation of the submarine cable and fluctuation caused by the decrease of the sensing degree of multisensor communication, indicating that the submarine cable fails in this time period, resulting in fault feedback.

The threshold wavelength of the alarm point for setting the high-frequency coefficient is $D4 = 0.004$ GHz, waveform $D5 = 0.006$ GHz, waveform $D6 = 0.003$ GHz, waveform $D7 = 0.005$ GHz, and *wave* $D7 = 0.005$ GHz. The high-frequency coefficients of the 4th and 5th order are $D3 > D4$ *wave* and $D4 > D5$ wave near 1789 m. In the vicinity of 1789 m, the high-frequency coefficients of the 7th and 9th segments are $D6 > D7$ and $D4 > D5$ *wave* $D5 = 0.003$ GHz. Multisensor communication submarine cable can be completely discriminated as the anchor damage and overheating effect caused by local unified power generation. From Figure 6, it can be seen that the peak value of anchored dune fault on the superlarge spatial scale is the most prominent in the microwave fine decomposition ratios 5 and 8. In wavelet decomposition ratios 6 and 7, there is a specific small part of discharge overheating, which leads to the dune fault having a particularly obvious peak value in a small space. Bolt breakage and local unloading are all completed according to the above steps. The results show that this method can effectively detect and diagnose the faults of multisensor communication submarine cables.

4. Experimental Comparison

4.1. Comparison of Mechanical Experiments. The pressure performance and environmental performance are tested, and the results are shown in Table 1.

The related test results are shown in Figures 7 and 8.

The pressure test is relatively stable and normal; control invariants and control variables will not cause wavelength waveform amplitude.

When the multisensor communication submarine cable is made of frequency conversion optical fiber, the detection methods are sonar detection, TTSL electromagnetic detection, side electromagnetic detection, ultrasonic detection, and deep-sea photography detection. The comparison of experimental results is shown in Figure 9.

The pressure of multisensor communication submarine cable in the detection method of submarine photography,

Table 1: Pressure performance and environmental performance test.

Object	Pressure performance	Environmental performance
GJB 5589-122	Overload working tension is normal; transient load index is normal; impact is normal; repeated bending under compression is normal.	The water seepage property is normal; the temperature cycle is slow; the pressure index is normal.
GB/T 18480	Overload working is normal; the transient load index is normal; the impact is normal; flattening and repeated bending are normal.	The watertight properties are normal; the temperature cycle is fast; the pressure index is overloaded.

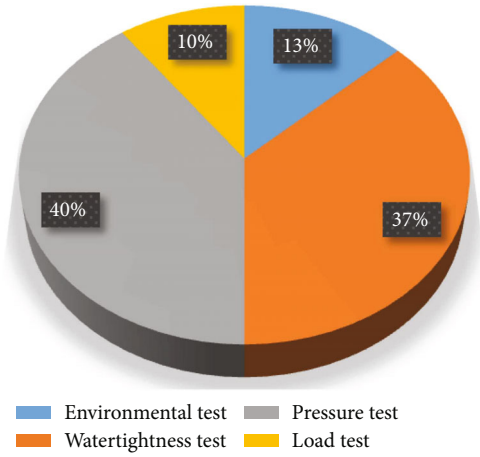

Figure 7: GJB mechanical experiment comparison data graph.

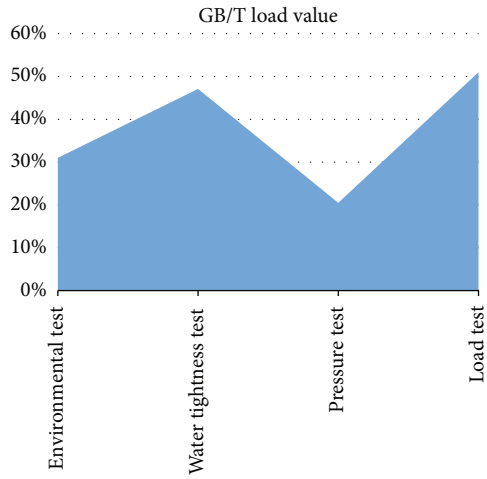

Figure 8: GB/T mechanical experiment comparison chart.

with the detection time, and fault feedback, the fault detection rate tends to be relatively stable, and waveform wavelengths tend to normal interval thresholds relatively, but the efficiency is very low. Compared with sonar detection technology and electromagnetic detection technology, it takes the longest time from the beginning to the end of detection, which leads to a limited number of detections. Moreover, when encountering complex seabed terrain and sand dunes and slopes, the seabed camera detection method is slightly weak, which greatly increases the detection difficulty and increases the detection risk in direct proportion. Fault damage is also obvious. When the number of faults is huge, the detection method of submarine camera cannot

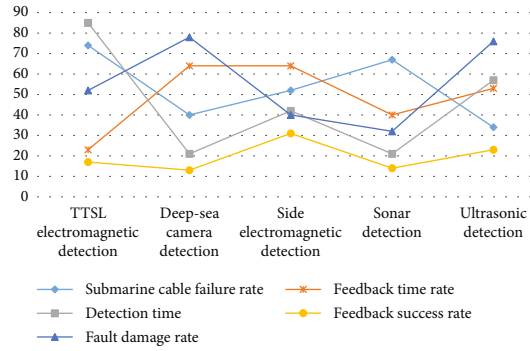

Figure 9: Comparative performance test of the five detection methods.

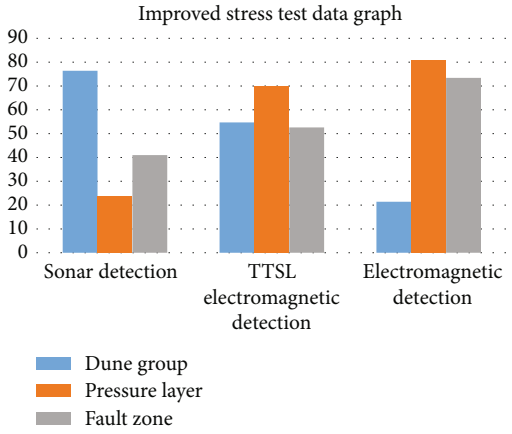

Figure 10: Improved stress test chart.

be used. Because the submarine pressure is too high in shallow sea, the submarine camera technology has no obvious abnormality, and the submarine camera sometimes cannot operate normally in the deep-sea test. The detection activity is temporarily terminated, which will make the experimental results produce errors, and the error range increases significantly in the range of $P\alpha * Z\beta$, so only the numerical interval error can be taken in Figure 10.

4.2. Pressure Contrast Test. For the pressure detection experiment of multisensor communication submarine cable on the seabed, in order to study whether the submarine cable has excessive pressure or pressure load exceeding normal value on the seabed, by studying the surface, submarine cables are in shallow sea areas. There is no difference in pressure values. All indexes of pressure are normal values. Waveform wavelength is also relatively normal. When

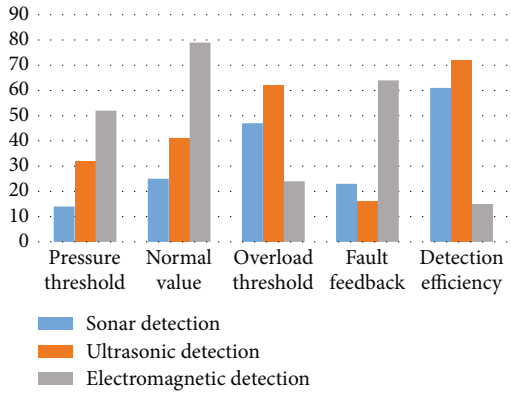

Figure 11: Three types of test data charts for submarine cables.

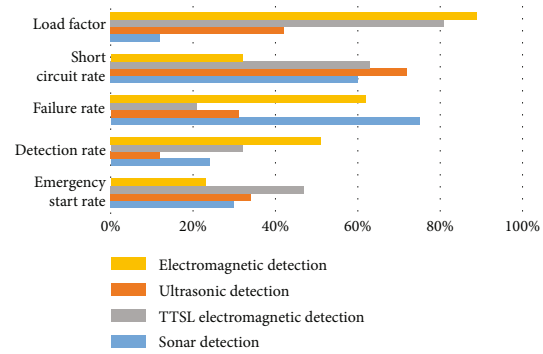

Figure 12: Short-term load detection diagram of multisensor submarine cable.

encountering complex seabed topography, there will be different choices and changes in the laying routes of submarine cables. The pressure threshold of submarine cable is normal at sand dunes, in a relatively stable state, as for that situation that there is no fluctuation in various data and the overload value increases, in order to evaluate the appropriate detection method, control relative variable method. Through the known sensing fusion formula, the scattering distribution map of Brillouin dispersion radio frequency is obtained. It can be seen from Figure 11 that the detection method can measure the pressure distribution of multisensor communication submarine cable on the seabed, which is convenient to measure and summarize the advantages and disadvantages of the detection method. The wavelet distribution, wavelength shape, and wavelength measurement are studied from the normal initial value, and the relevant conclusions are given for analysis and research. In order to further reduce the error, sonar detection technology, electromagnetic detection technology, and ultrasonic detection technology are used for experimental comparison, and the final comparison results are marked by the bottom line chart.

From the research data, it can be seen that for submarine cables with multisensor communication, sonar detection technology is not suitable for known submarine cables; for the damage of submarine cables, there is a positive advance. In view of this phenomenon, ultrasonic detection has performed abnormally well. For all aspects, wavelength fluctuation is relatively stable, and wavelet decomposition is relatively suitable and normal interval value in the region, which makes ultrasonic detection technology more comprehensive and rigorous.

4.3. Failure Rate of Short Load Detection. What is very common when working under short load in submarine cables, when large-scale demands such as large-scale power generation are needed, submarine cables will make short load working hours. At this time, when submarine cables are most prone to external interference and failure, usually, the radio frequency of Brillouin dispersion greatly exceeds the dangerous value. The submarine cable triggers emergency response measures. When the emergency response measures cannot relieve the power supply pressure, the submarine cable will generate large load power data, resulting in serious changes in wavelength waveform, which will pollute the submarine ecological environment, destroy the submarine ecological chain, and seriously cause irreversible anchor damage and large-scale short circuit. Therefore, short-term load detection of submarine cable failure rate becomes an important index, This is one of the major detection indexes of submarine cables, so for ultrasonic detection, sonar detection, electromagnetic detection, and TTSL electromagnetic detection are compared experimentally. The experimental process flow is the same as above. The control variable and invariant are short-term load rate, which increases the sensing rate of submarine cable and the working index and workload of submarine cable to achieve the effect of one-hour short-term load and starts detection. The statistical comparison detection results are shown in Figure 12.

It is concluded that when the load rate is constant, the detection rate is roughly the same. However, sonar detection technology shows drawbacks, a sharp decline. There are also many shortcomings in the display of waveform wavelength. It is not suitable for testing under short load. Other detection methods, such as the battery detection method, TTSL electromagnetic detection method, and ultrasonic detection method, will be relatively balanced, and the Brillouin dispersion wavelength rate will not change obviously. Therefore, these three detection methods can be used to detect multisensor communication submarine cables in shallow sea areas. In the submarine cable testing experiment, the data can be obtained by using the above evaluation model formula, and the data can be converted into percentages to make the experimental results more significantly reflect the advantages and disadvantages of each testing method.

4.4. Evaluation Results. To sum up, in the multisensor communication submarine cable detection method, Brillouin value judgment is used to grade the feedback rate of detection; the three elements of feedback value and feedback period are attributed to TTSL electromagnetic detection technology commonly used at present. Electromagnetic detection, sonar detection, ultrasonic detection, and submarine camera detection adopt rigorous detection methods such as controlling the number of faults, controlling the depth of shallow sea and controlling variables. Finally, the evaluation results of each detection method are obtained,

because the depth of shallow sea is similar. For seawater, density requirements tend to normal level. Sonar detection and submarine camera detection technology have good feedback values for submarine cable detection of multisensor communication in shallow sea field. Brillouin dispersion frequency fluctuation also tends to normal range, so it can be concluded that sonar detection and submarine camera are a good choice in shallow sea detection. For deep-sea detection, the feedback value range of TTSL electromagnetic detection is very stable, and Brillouin dispersion radio frequency is within normal fluctuation range. Therefore, TTSL electromagnetic detection can detect faults for submarine cables in deep-sea exploration, and the waveform and wavelength in all aspects will not affect the faults.

5. Conclusion

Because there are many ways to detect submarine cables in multisensor communication, but to sum up, this paper only uses several common methods to carry out fault feedback of submarine blue line detection. The final expected conclusion is obtained by data feedback, and the problems and defect directions of submarine cables are roughly predicted by fault prediction, so that the experiment can draw conclusions in a multivariable way, and a single variable cannot be used. The conclusions and results obtained by various variables are more convincing, scientific, and rigorous. This is also the charm of science. In this society with rapid development of science, a world with highly progressive humanities, I believe that the submarine cable for multisensor communication will be upgraded in higher technology in the future. Materials will be adopted more advanced, which also indicates that there will be more and more research on submarine cable detection in the future, and the detection types, detection methods, detection approaches, data flow analysis, and other methods will be more forward-looking and convincing, which is also the gospel of mankind and can make civilized by going up one flight of stairs. In this mysterious underwater world, I believe that there are not only the development prospects of sensing communication cables but also more opportunities and challenges, which is a necessary way for mankind to explore the world and science in the future. In the commercial market, submarine cable also has a place, and it exists in this market at a high price. Here, I also hope that the later detection methods will be studied with more and more rigorous scientific attitude.

Data Availability

The experimental data used to support the findings of this study are available from the corresponding author upon request.

Conflicts of Interest

The author declared that they have no conflicts of interest regarding this work.

Acknowledgments

This research was supported by the Science and Technology Project of China Southern Power Grid Co., Ltd. (CGYKJXM20180373).

References

[1] B. Smith, M. Hall, A. Franklin, E. S. Johansen, and O. Haldun Unalmis, "Field-wide installation of optical sensing technology yields multi-sensing benefits [J]," *World Oil Magazine*, vol. 229, no. 5, pp. 39–45, 2008.

[2] D. C. Shotton, "The radiography of polythene in submarine cable systems [J]," *Proceedings of the IEE-Part A: Power Engineering*, vol. 109, no. 3, pp. 199–202, 2010.

[3] Y. Li, L. Zhao, Z. Yang, A. Lv, and F. Wu, "Design and realization of the submarine cable three-dimensional monitoring system based on BOTDR [J]," *Yi Qi Yi Biao Xue Bao/Chinese Journal of Scientific Instrument*, vol. 35, no. 5, pp. 1029–1036, 2014.

[4] E. Ekici, Y. Gu, and D. Bozdag, "Mobility-based communication in wireless sensor networks," *IEEE Communications Magazine*, vol. 44, no. 7, pp. 56–62, 2006.

[5] C. Pandana and K. J. R. Liu, "Near-optimal reinforcement learning framework for energy-aware sensor communications," *IEEE Journal on Selected Areas in Communications*, vol. 23, no. 4, pp. 788–797, 2005.

[6] A. Sahari, T. T. Ruckh, R. Hutchings, and H. A. Clark, "Development of an optical nanosensor incorporating a pH-sensitive quencher dye for potassium imaging," *Analytical Chemistry*, vol. 87, no. 21, pp. 10684–10687, 2015.

[7] M. Weyn, G. Ergeerts, L. Wante, C. Vercauteren, and P. Hellinckx, "Survey of the DASH7 Alliance Protocol for 433 MHz wireless sensor communication," *International Journal of Distributed Sensor Networks*, vol. 9, no. 12, 2013.

[8] G. Tadesse, "Distributed particle filter for target tracking: with reduced sensor communications," *Sensors (Basel)*, vol. 16, no. 9, p. 1454, 2016.

[9] J. M. Chen, R. Z. Lin, and Y. X. Sun, "On communication architecture for wireless sensor networks [J]," *Chinese Journal of Sensors and Actuators*, vol. 17, no. 3, pp. 197–208, 2006.

[10] R. Rahman, M. Alanyali, and V. Saligrama, "Distributed tracking in multihop sensor networks with communication delays," *IEEE Transactions on Signal Processing*, vol. 55, no. 9, pp. 4656–4668, 2007.

[11] T. Kasetkasem and P. K. Varshney, "Communication structure planning for multisensor detection systems," *IEE Proc, Radar Sonar Navig*, vol. 148, no. 1, pp. 2–8, 2001.

[12] W. L. Kruer, "Nonlinear estimates of Brillouin scatter in plasma," *Physics of Fluids*, vol. 23, no. 6, pp. 1273–1275, 1980.

[13] D. W. Phillion, W. L. Kruer, and V. C. Rupert, "Brillouin scatter in laser-produced plasmas," *Physical Review Letters*, vol. 39, no. 24, pp. 1529–1533, 1977.

[14] I. V. Bogachkov, "Research properties of the Mandelstam–Brillouin scatter in the polarization maintaining single-mode fibers [J]," *Journal of Physics: Conference Series*, vol. 1210, no. 1, article 012024, p. 7, 2019.

[15] N. T. Otterstrom, S. Gertler, Y. Zhou et al., "Backscatter-immune injection-locked Brillouin laser in silicon," *Physical Review Applied*, vol. 14, no. 4, 2020.

Hindawi
Journal of Sensors
Volume 2021, Article ID 2166075, 12 pages
https://doi.org/10.1155/2021/2166075

Research Article

Digital Twin-Assisted Simulation of Complex Assembly Models in Descending Process and Implementation of Key Link Characterization

Zhuqiao Ma,[1,2] **Yifei Tong**,[1] **Linyan Liu**,[1] **Lei Huang**,[1] **and Juntang Yuan**[1]

[1]*Department of Mechanical Engineering, Nanjing University of Science and Technology, Nanjing 210094, China*
[2]*School of Intelligent Manufacturing, Nanjing University of Science and Technology Zijin College, Nanjing 210046, China*

Correspondence should be addressed to Juntang Yuan; mc106@njust.edu.cn

Received 29 October 2021; Revised 23 November 2021; Accepted 26 November 2021; Published 20 December 2021

Academic Editor: Gengxin Sun

In this paper, the simulation and key link characterization of the complex assembly model step-down process are studied and analysed in depth using the digital twin approach, and the method is used in the practical process. The physical model step-down method MORA algorithm and its physical interpretation in various simplified cases are given, and the MORA method is improved on this basis. The concept of local activeness based on knot structure is introduced, and the process of model transformation and downscaling and decomposition based on local activeness is explained in detail. The high-fidelity mapping of solid equipment is completed in virtual space, which can accurately reproduce and predict the health state of engineering equipment throughout its life cycle, effectively avoiding the huge property losses and safety risks caused by early failure of vulnerable structures and providing a safe and stable working environment for offshore oil and gas production. With the prototype monitoring data as reference, the response surface method is used to identify the parameters of the finite element model of the hinge node, which improves the fidelity of the virtual model of the hinge node. Considering the friction coefficient changes and load characteristics during the degradation of the hinge node, the dynamics simulation conditions are set, and the operating states of the hinge node at different stages of its whole life cycle are simulated by using the high-fidelity virtual model of the hinge node, and the prediction model of the hot spot stress of the hinge node is established to monitor its in-position state in real time, and the operation and maintenance overhaul method based on the health state of the hinge node is proposed. The system is divided into four modules: multilevel inverse modelling of the assembly twin, statistical shape characterization and analysis of batch parts, optimization of fixture positioning and flexible assembly of thin-walled parts, and optimization of low-stress assembly of bolted joint structure, which verifies the feasibility of the method and provides guidance for the actual product forming process.

1. Introduction

With the continuous development of the economy, people's demand for personalized products is increasing, requiring product production lines to have multispecies, small-lot, multifreedom, and high-reliability production capacity, and production lines should independently adapt to various changes brought about by-product personalization, which include changes from within and changes from outside [1]. The traditional rigid automated production line produces a single product, which can no longer meet the demand of diversified production, and industrial production line flexibility and intelligence have become the mainstream development trend. Industrial robotic arms are widely used in all aspects of flexible production lines, and robotic arms replace humans to complete the tasks of handling and assembly in the production process. In these operational tasks, the requirements for robotic arm cooperation and functionality are increasing, and the traditional single robotic arm based on the demonstration mode is already difficult to meet all the needs, while the multirobot collaborative operating system can well solve these problems [2]. For example, the cost

of designing a robotic arm that can handle large, heavy loads is very expensive. However, with a multirobotic arm system, where each arm only must carry a relatively small load, a handling system containing two or more small-cost arms can transfer heavy loads. In addition, a multirobotic arm synergistic system can perform different subtasks in parallel, thus facilitating the handling of decomposable tasks such as automated assembly in smart production. In short, a multirobotic arm system has higher load capacity and flexibility to perform coupled tasks.

The performance of complex products is closely related to the quality of assembly; the assembly error is one of the evaluation indicators of the quality of assembly, which is mainly determined by two steps of part feature modelling and assembly accuracy analysis and is affected by various factors such as part manufacturing errors, material properties, positioning forms, and coupling processes, which is difficult to be predicted by classical methods. Assembly error prediction requires the construction of a prototype including all parts and process information, and the traditional physical prototype construction method is prone to scrap parts that do not meet the performance requirements, resulting in a great waste of resources and rising product costs. However, digital prototype models often ignore many elements in the real environment, resulting in discrepancies with the actual part assembly, making it difficult to meet the performance requirements of products with high accuracy [3]. Flexible and intelligent industrial production lines have become the current mainstream development trend. Industrial robotic arms are widely used in all aspects of flexible production lines, and robotic arms replace humans in completing tasks such as handling and assembly in the production process. Therefore, the use of digital technology to truly reproduce the complex product forming process, to guide the actual production and assembly of parts, is a major research hotspot in the current manufacturing products. At present, the flat width processing method has been widely used in woven fabric dyeing and finishing processing and gradually become the development direction of knitted fabric printing and dyeing processing. Knitted fabric is a material with good air permeability and softness made of yarns trapped each other, the force deformation of knitted fabric presents a high degree of nonlinearity and complexity, due to the relatively large width of the product in the knitted fabric flat width processing, and tension pulling in the processing process is easy to produce from the edge to the centre of the contraction, as well as due to unfavourable winding control resulting in the uneven layer, wrinkles, uneven density, and other defects. In addition, the knitted fabric structure will be affected by the tension of the larger deformation which cannot restore the original weaving structure; knitted fabric flat width processing tension size needs to fully consider the size of the knitted fabric deformation [4]. Therefore, low tension and stable tension control are the key influencing factors of knitted fabric flat processing quality, and how to determine the tension setting model and stable, small fluctuation of low-tension control technology is the difficult point of knitted fabric flat printing and dyeing.

Digital twin technology is a technology proposed in recent years for the fusion of virtual simulation and physical reality, which is a technology that integrates physical reality data, integrates multidomain and multiscale mapping simulation models, and covers the whole process and product life cycle. The study of knitted fabric flat width dyeing and finishing process involves several disciplines, including product pretreatment, roll dyeing control, and product finishing, and other processing aspects. This paper applies digital twin technology to the study of key issues in textile processing, aiming to explore and provide a reference for the study of complex textile processing problems. Product digital assembly modelling and simulation is an advanced technology that uses computer theory to construct a digital model of a product in a virtual environment, to simulate the behaviour of a physical prototype in the whole life process, such as assembly and maintenance. It is important to analyse the assembly process and error transmission of the product digital model through simulation methods to verify whether the part assembly sequence, assembly path, force deformation, etc. meet the engineering requirements, which is important to guide the actual part manufacturing and assembly operations, improve the efficiency of product development, and reduce costs.

2. Status of Research

A multidomain-coupled digital twin model of CNC machine tool is established, which contains hydraulic, electrical, mechanical equipment, and its control system. The article debugs the system operation response in the established machine tool coupling system, focuses on the response characteristics of the coupling system, and studies the impact of machining tool trajectory on the product machining profile, which is the multidomain coupling modelling technology under the research idea from the equipment electromechanical control response to the product machining level, and the virtual machining and virtual control of the workpiece is realized in the article through the virtual debugging of the CNC machine tool motion trajectory, the construction of software platform [5]. If a multimanipulator system is used, each manipulator only needs to bear a relatively small load, and a handling system containing two or more low-cost manipulators can transfer heavy objects. A digital twin model architecture for machining tools on CNC machine tools is proposed, and the model is applied to tool detection, life prediction, and tool selection decision, and the tool wear amount is quantitatively analysed by using a convolutional neural network algorithm to achieve accurate prediction of tool wear amount and remaining life [6]. The research differs from the electromechanical modelling approach from a data-driven perspective, based on deep learning from multiple sample data, to optimize the detection model of tool wear, while using tool wear data to construct a mathematical model of wear degradation and life decay under actual machining conditions [7]. The product model validation method mentioned in the article is to use the existing data of tool machining milling time and remaining machining times for the unused prediction of tool life, for machining

processes with big data conditions, provides a way to predict the usage performance of products and equipment [8]. The spatial expression for the cantilever travel path of the road header is firstly calculated, and secondly, the collision conditions between the coal seam and the road header are mathematically modelled [9]. The control buttons for controlling the cantilever of the road header are designed in the virtual model to realize the simulation of the coal mining site within the virtual environment, which provides a good solution for early warning prevention of special operations and virtual equipment monitoring in special environments.

The design of complex multidisciplinary systems requires the knowledge of a collaborative group of experts, where designers with different disciplinary backgrounds work with analytical engineers, manufacturing engineers, marketing experts, and managers [10]. To support collaborative issues in simulation and design, it is important to document models, capture their semantics, and place them in a well-organized knowledge base suitable for use on the Internet [11]. A variety of unified modelling approaches and simulation languages exist, and they can be classified according to the following criteria: graphical and language-based approaches, procedural and descriptive modelling, multidomain and single-domain modelling, continuous and discrete system modelling, and function-based and object-oriented approaches [12]. Like other modelling methods, in the bonding diagram approach, complex systems are first decomposed into subsystems, and then, the subsystems are further hierarchically decomposed top-down into components with known dynamic behaviour or elements expressing physical processes, and the decomposition is based on power exchange between subsystems, components, and elements [13].

Power is distributed, transferred, stored, or converted to other forms while flowing within a system, so the bonding diagram method is best suited for modelling continuous processes and systems, but with some augmentation of the bonding diagram, discrete-time systems and continuous-discrete hybrid systems can also be modelled. A unified description of the energy distribution, storage, transfer, and consumption of the underlying physical processes makes bonding diagrams suitable for various types of physical systems and for multidomain systems that contain different forms of energy and their interactions. And, since most of the power exchange between components or subsystems in a system occurs in physical systems with couplings such as shafts, hydraulic lines, or wires, there is a clear correspondence between bonding diagram model structures and physical system mechanisms.

3. Digital Twin-Assisted Simulation Analysis of Complex Assembly Models for Step-Down Processes

3.1. Simulation Design of Digital Twin Assembly Model. A digital twin is a simulation process based on physical models, making full use of sensor-aware data, inheriting multidisciplinary, multiphysical, multiscale, and multiprobability, completing the high-fidelity mapping of physical equipment in virtual space, adding, or extending new capabilities to physical entities, and realizing health management and maintenance of physical equipment throughout its life cycle [14]. The unique virtual model of the digital twin, as an important carrier expressing all information of the physical system, can synchronize the in situ state of physical equipment and realize adaptive update according to the change of health characteristics of a physical system and realize the performance degradation detection, damage, and life prediction of a physical system by combining with the intelligent diagnosis and prediction rule model built based on big data. A study on the application framework of digital twin technology in the health management of hinge nodes of soft rigid arm mooring systems is carried out.

The five-dimensional digital twin model, as the basic conceptual model for the application of digital twin technology on the ground, can most directly reflect the specific content of digital twin technology in the application process, organically integrating the real physical system, the sensor monitoring data in the operation process, the high-fidelity twin in the virtual space, and the integrated service system into a new health management paradigm of digitization, intelligence, and visualization. In this paper, the five-dimensional digital twin model is represented by the following equation.

$$M_{\mathrm{DT}} = \left(\mathrm{PE}, \mathrm{VE}, \mathrm{Ss}, \mathrm{CN}^2\right). \tag{1}$$

The mechanical system is mainly composed of motor-driven active rollers and friction-driven idler rollers. According to the requirements of knitted fabric processing, the fabric is expanded and unfolded by the spreading rollers on the threaded surface after the fabric is finished, and the fabric is adjusted by the gravity floating rollers. After the roller rolls the dyeing liquid, it is sent to the measuring device before the roll, in which the roller and the roll spacing of the roll before the device are small, to reduce the knitted fabric curling and wrinkling, etc., the winding axis and the A-frame are connected with the frame through the slide rail, and the slide rail is equipped with a hydraulic cylinder drive at the bottom, and the variable tension winding is realized by adjusting the distance between the winding device and the roll before the device. Due to many parts and connections of the mechanical model, it is necessary to do the Boolean merging process [15]. After the model processing is completed, the kinematic subconstraints are added between each roll shaft. Rotational subconstraints are added between the shafts and the bearing base, i.e., only one direction of rotational freedom is retained, and the base of the frame is fixed to the earth by applying fixed subconstraints to keep it fixed to the ground. The winding section consists of a movable platform and winding roller, so the movable platform and the ground slide are set as a planar moving sub. In addition, the connection end of the winding drum and the motor shaft adopts the cross shaft type universal joint connection in consideration of the vertical distance difference, so for this shaft end connection, a Hooker sub for universal joint

connection rotation will be applied, allowing the up and down movement of the universal joint while rotating, which makes the winding drum have better mobility and better meet the field implementation requirements; the mechanical model and typical motion sub are shown in Figure 1.

The data of the digital twin is characterized by multitime scale, multidimensional, multisource, and heterogeneous. This has caused a great waste of resources and increased product costs; the adoption of digital technology has reduced the probability of assembly failure and improved product economic benefits. However, digital prototype models often ignore many elements in the real environment, causing them to be inconsistent with the actual assembly of parts. Meet the performance requirements of products with higher precision. The data are mainly derived from real physical systems, virtual twin models, service systems, and algorithmic fusion data. The data obtained from the real physical system includes static data and dynamic data; static data is mainly extracted from the existing database, such as material mechanics parameters, processing process, and assembly sequence of equipment, while dynamic data is the data of the operation state of the real physical system monitored by sensors in real time; the virtual model can generate auxiliary data through simulation, and these data reflect the operation of the real physical system in different connections which represent the association rules between systems, including the connection between physical system and database, the connection between the physical system and virtual model, the connection between the physical system and service system, connections between virtual models and databases, connections between virtual models and service systems, and connections between service systems and databases [16]. The virtual model relies on operational state data from the real physical system, and the virtual model is made more representative of the real physical system by tuning and optimizing the model (e.g., parameters, boundary conditions, and dynamic characteristics), driving the virtual model for state updates in real time, and establishing a real-time interactive mapping between the real physical system and the virtual model.

Data is the foundation and direct driver of the entire twinning process, and the mirror replication of the virtual system to the physical system relies on the real-time acquisition and rapid transmission of high-precision sensor data. The soft rigid arm mooring system has a complex structure and diverse features and relies on sensors with stable and durable working performance to obtain information on structural response, load change, operation, and service environment during its service. At the same time, it is also necessary to consider the information transmission efficiency between sensors and build a fast and efficient sensing network to ensure low delay and less missing data signal transmission, which is also a key factor to realizing the synchronous mapping of the virtual system to the physical system. The sensing data acquired in real time can be used not only to monitor the current state of the system but also to predict the future state of the system with the help of big data and dynamic data-driven analysis and decision-making technologies.

$$\max F = (x - x_i)^2 - (y - y_i)^2 - (z - z_i)^2, \tag{2}$$

$$\|f(x) + Q\|_2 = \sqrt{\sum_{i=1}^{n} [f(x_i) - z_i]^2}. \tag{3}$$

Starting from the physical system of the soft rigid arm mooring system, the integrated sensor data acquisition system acquires the operational state data of the physical system and establishes a multisystem-level virtual model in the virtual space with the same geometric, physical, behavioural, and rule attributes as the real physical system, then uses the historical and real-time data collected by the sensors to update the virtual model and guarantee the fidelity and reliability of the model; through the real-time data, AI intelligent algorithms are driven to diagnose the current state of the equipment and predict the degradation trend of the equipment; finally, an integrated service system is used to assist in operation and maintenance to achieve monitoring, simulation, diagnosis, prediction, and control of the equipment. The tension of open-width processing of knitted fabrics needs to fully consider the deformation of knitted fabrics. Therefore, low tension and stable tension control are the key factors influencing the quality of knitted fabric open-width processing.

$$p_k = [I\,0]\prod_{i=1}^{k}{}^{i} A_i(\theta_j)[0 \quad 0 \quad 1 \quad 1]^T. \tag{4}$$

Complex products are composed of a series of parts connected, and the assembly process not only has information on the types and quantities of parts, but also has many other types of assembly information, such as the structure, function, fit constraints, degrees of freedom, surface accuracy, dimensional tolerances, hierarchical relationships, and other basic information of parts, assembly sequence information containing the division of assembly tasks and hierarchical decomposition, and assembly scene information containing assembly tools, fixtures, and other assembly resources and the assembly environment, assembly resources such as jigs and fixtures and assembly scenario information of the assembly environment [17]. The diversity of assembly information leads to various ways of description, such as part shape information described in vector form, assembly task information described in the semantic form, and assembly process information described in diagram form. The part assembly path planning is closely associated with this assembly multisource information, and the assembly path not only depends on the starting and ending points of the assembly, but to some extent, it is also related to the coupling of the assembly multisource information, as shown in Figure 2, and how to describe the multisource information reasonably is of great significance for the reuse planning of the assembly path.

Complex products are characterized by many parts and components, so if the assembly path planning is carried out according to "assembly-parts," it will increase the complexity of the assembly path planning and the difficulty of solving the calculation. To complete the assembly

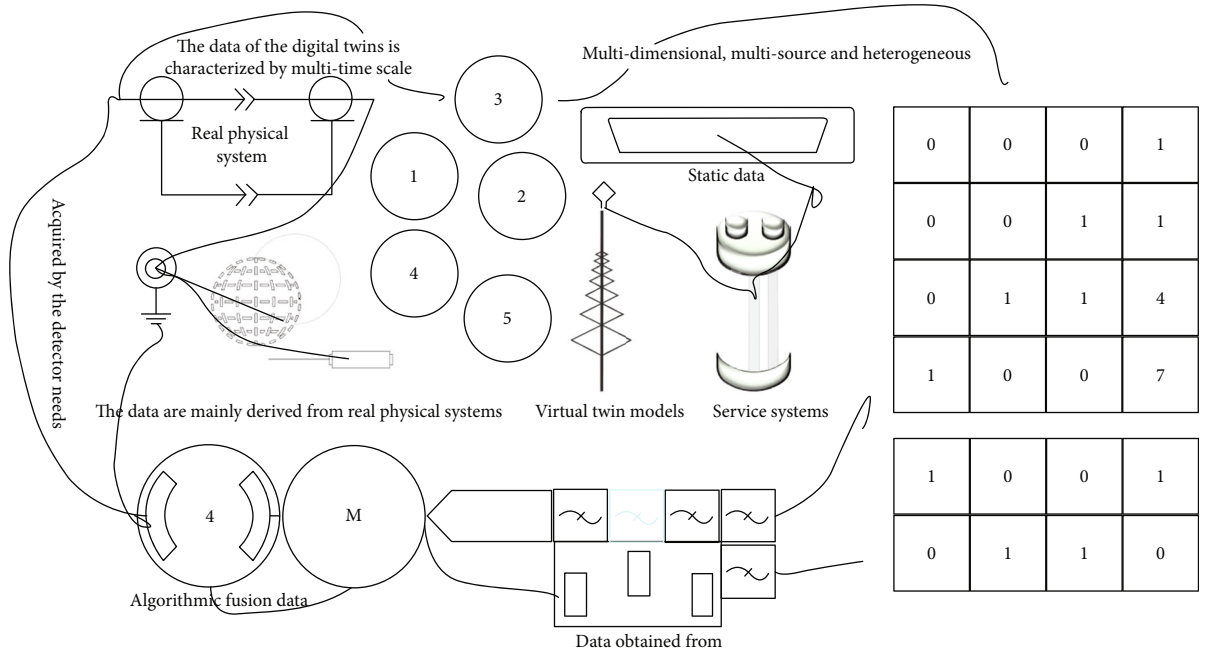

Figure 1: Simulation framework of digital twin assembly model.

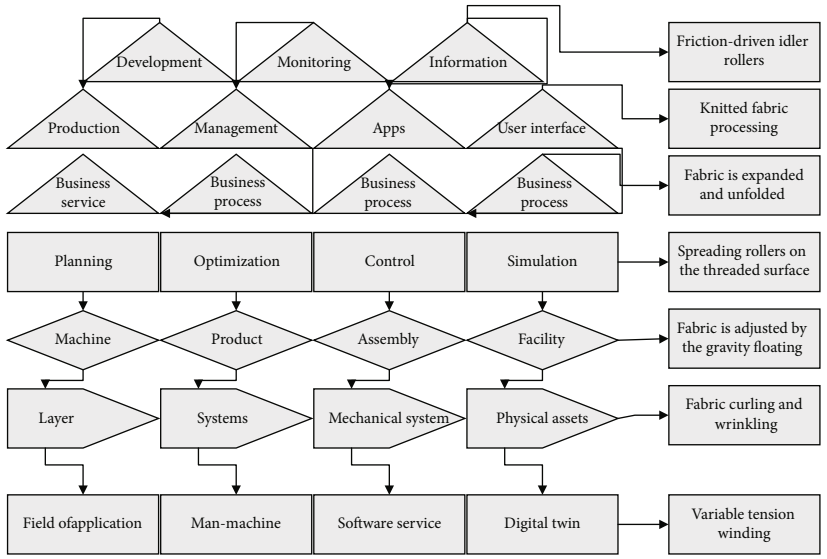

Figure 2: Schematic diagram of assembling multiple sources of information.

path planning of complex products better and more efficiently, the assembly is usually assembled according to the hierarchy of "complex assembly - subassembly - component - assembly - part."

$$\mu = \frac{1}{3n}\sum_{i=1}^{n}\left(p^i - q^i + r^i\right), \tag{5}$$

$$\mathrm{Cov}_{j,k} = \frac{1}{3n}\sum_{i=1}^{n}\left(p^i q^i - q^i r^i + r^i\right) j. \tag{6}$$

The attitude information of a component can be represented by giving a reference attitude and performing a certain attitude transformation on the reference attitude. The attitude transformation process in 3D coordinates can be represented in the form of a 3D attitude transformation matrix, which can be characterized by multiplication operations of the attitude matrix and the rotation matrix.

The fit feature information is an important parameter used to describe and constrain the fit relationship of parts in an assembly. For complex products, the fit relationship between parts is an important part of the assembly path planning for building assemblies, and the assembly paths of parts with similar fit feature constraints are reusable to a

certain extent, so the part fit features need to be analysed and reasonably represented.

$$\begin{bmatrix} a \\ b \\ c \end{bmatrix} = \begin{bmatrix} r_{11} & r_{12} & r_{13} \\ r_{21} & r_{22} & r_{23} \\ r_{31} & r_{32} & r_{33} \end{bmatrix} \cdot \begin{bmatrix} a' \\ b' \\ c' \end{bmatrix}. \quad (7)$$

Parts generally have multiple geometric features; however, generally, only individual features will interact with other parts to form the fit relationship between features; this feature fit relationship is determined by feature matching elements, so how to accurately extract these feature matching elements and match is the premise of the construction of part fit feature information. The tension of open-width processing of knitted fabrics needs to fully consider the deformation of knitted fabrics. Therefore, low tension and stable tension control are the key factors influencing the quality of knitted fabric open-width processing. Part features are divided into matching features and other features according to whether they have matching relationships with other parts, and the matching features are mainly plane features, surface features, shaft features, hole features, slot features, table features, cavity features, etc., and these features can be decomposed into three types of feature elements: point, line, and surface. By combining feature elements and contact matching, motion constraints that limit degrees of freedom are generated between mating parts.

3.2. Simulation and Characterization of the Descending Process with Key Links. When the bonding diagram causality is labelled according to the principle of preferential integral causality, sometimes, some of the energy storage elements of the system bonding diagram have differential causality. In this case, the number of state variables of the system is equal to the number of energy storage elements with integral causality. The energy variables corresponding to the energy storage elements with differential causality depend on the state variables of the system and are nonindependent variables. When writing the state equations of the system from this type of bonding diagram, one will also encounter algebraic loop problems, sometimes quite complex, especially in the nonlinear case. Since bond graph modelling emerged before object-oriented modelling, the concepts of knowledge encapsulation and inheritance are not common in bond graph modelling; however, according to the above account, these modern modelling principles are also well known in bond graph-based modelling of physical systems [18]. Early in the modelling process, bond graph models are qualitative descriptions of physical processes, and only the relevant physical mechanisms are captured, implying that models at the physical process abstraction level can have different implementations at the mathematical model abstraction level as the modelling process progresses. Organically integrate real physical systems, sensor monitoring data during operation, high-fidelity twins in virtual spaces, and integrated service systems to become a digital, intelligent, and visualized new health management paradigm. In the subsequent modelling stages, the form of the intrinsic equations remains noncausal. In contrast to the object-oriented approach to submodel connectivity, the bonding diagram submodels can be assembled into a full cause-free model that corresponds exactly to the physical structure, and the causal relationships are automatically determined in the final full bonding diagram.

The three layers are the technical component layer, the physical process layer, and the mathematical description layer. The modelling of the system starts with the identification of the technical components and the connections between them, which are usually expressed in a graphical or nonstandard notation independent of the specific implementation; in the physical process layer, the relevant physical processes occurring in the components and the interactions between them are defined, which can be expressed qualitatively by graphical methods such as key sum diagrams, generalized networks, and line diagrams; finally, in the mathematical description layer, the mathematical model is built. It is usually generated automatically from the graphical description, and the mathematical model is expressed using an object-oriented noncausal modelling language or a block diagram, etc., as shown in Figure 3.

The physical model contains information on the material parameters and constraint boundaries of the structure, and the system-level physical model is modelled using ADAMS, which has a certain current research base. The physical model of the hinge node is created using the DM module in ANSYS Workbench, and the geometric model is imported into the transient dynamic's analysis module associated with it, which can realize the simulation of the dynamical behaviour and response extraction of the related structure. The behavioural model can not only map the motion behaviour of the real structure but also stimulate its degradation behaviour. The multibody dynamics equations of the soft rigid arm mooring system can be used to build the behavioural model at the subsystem level, and this part already has a certain research foundation, and the finite element models based on the fatigue damage process can all realize the behavioural model mapping at the member level.

The first task in implementing hinge node health management for soft rigid arm mooring systems is to create high-fidelity virtual models [19]. The virtual model of the hinge node is highly consistent with the physical system in terms of the structural shape, dimensions, and relative motion relationships, but there are model simplifications in detail. Meanwhile, the environmental loads on the hinge nodes are characterized by a high degree of nonlinearity and a wide range of action, and there is a problem of simplification of the boundary conditions in the finite element virtual model simulation, which leads to deviations between the simulation results and the monitored structural response. In addition, the structure will show performance degradation, damage, and other behaviours during long-term service, and the virtual model with constant parameters cannot accurately restore the process. For this reason, a set of well-adapted and fault-tolerant virtual model parameter identification schemes is needed to address the problem of parameter changes during the service of hinged structures and to track the parameter state of the physical system in

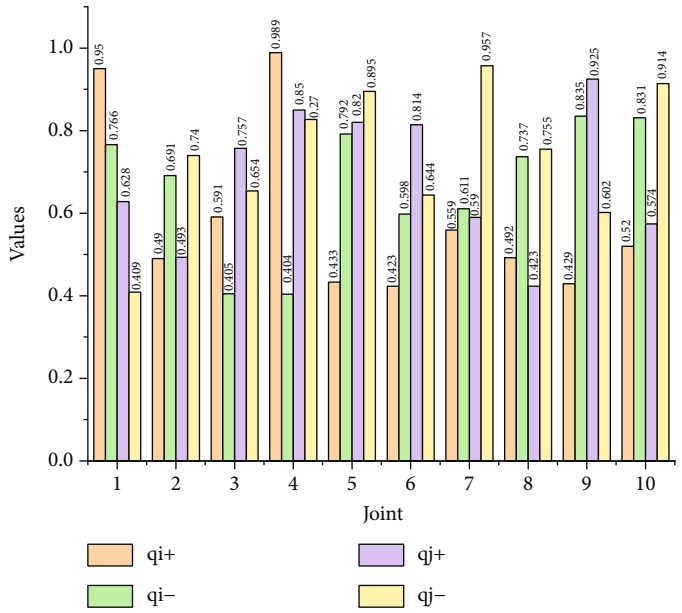

Figure 3: Physical limitations of the joints of the robotic arm.

real-time, to improve the fidelity of the virtual model. Parameter identification is to optimize the model according to the structural response and find the optimal combination of parameters that can characterize the model state within a reasonable range, involving parameters such as structural dimensions, material properties, constraints, cell types, and meshes.

After removing or transforming the relatively low active bonds, the transformed bonding diagram is obtained and some dynamic interactions of the original bonding diagram are changed or removed. The transformed bond graph can then be simulated with the same inputs, and the results obtained are compared with the original bond graph simulation results, and the small error indicates that the deleted and transformed low active bonds as well as components contribute little to the system dynamics and can indeed be deleted and transformed.

After obtaining a transformed bonding diagram with similar dynamic properties to the original bonding diagram, the driving and passive subdiagrams can be divided on the transformed bonding diagram, and if subdiagrams can be found, the dynamic properties of the obtained driving and passive submodels have been proved to be approximate to the original model by the comparison of the simulation results mentioned above and are therefore appropriate. The similarity of the simulation results is a sufficient condition for the decomposed model to approximate the original bonding graph model. The presence of subgraphs allows for further simplification of the model, rather than just removing the energy components. If the dynamic output of our interest lies in the driven subgraph, the entire passive subgraph can be removed: if the dynamic output of interest lies in the passive subgraph, the driven subgraph must be retained. In the second case, if the parameters of the passive subsystem are kept constant, or if only small changes are made in the design so that the boundaries of the subgraph remain inactive, the simulation can be done in the following two ways, including the connection between the physical system and the database, the connection between the physical system and the virtual model, the connection between the physical system and the service system, the connection between the virtual model and the database, the connection between the virtual model and the service system, and the connection between the service system and the database. First, the driven subgraph is simulated to get the input of the passive subgraph and generate a data file, and then, this data file is used to replace the driven subgraph and simulate the passive subgraph, i.e., a sequential simulation is used, and the driven and passive subgraphs are simulated in parallel (as shown in Figure 4).

A reusable conformal space construction method based on the reuse degree of the assembly path is proposed. The features of the conformal space for assembly path reuse are analyzed, the expression of the conformal space considering a priori path information is given, and the concept of a priori degree of a priori path positional point is proposed in combination with ant colony pheromone, which is introduced into the expression of a priori path information and the construction of a priori space [20]. For the problem of low reusability of conformation space of batch parts of complex products, the construction of reusable conformation space of batch parts is realized by path reusability calculation and reusability multigranularity cohesive hierarchical clustering with fused assembly multisource information. Finally, the feasibility and practicality of the method are verified by using a CNC milling machine as an example. The traditional path planning algorithm is a complete planning process for a given starting and target poses, and each planning is a complete exploration in the conformal space, ignoring the a priori path reusability existing in the conformal space, and the repeated search generates redundant consumption. The assembly path planning of batch parts of complex products,

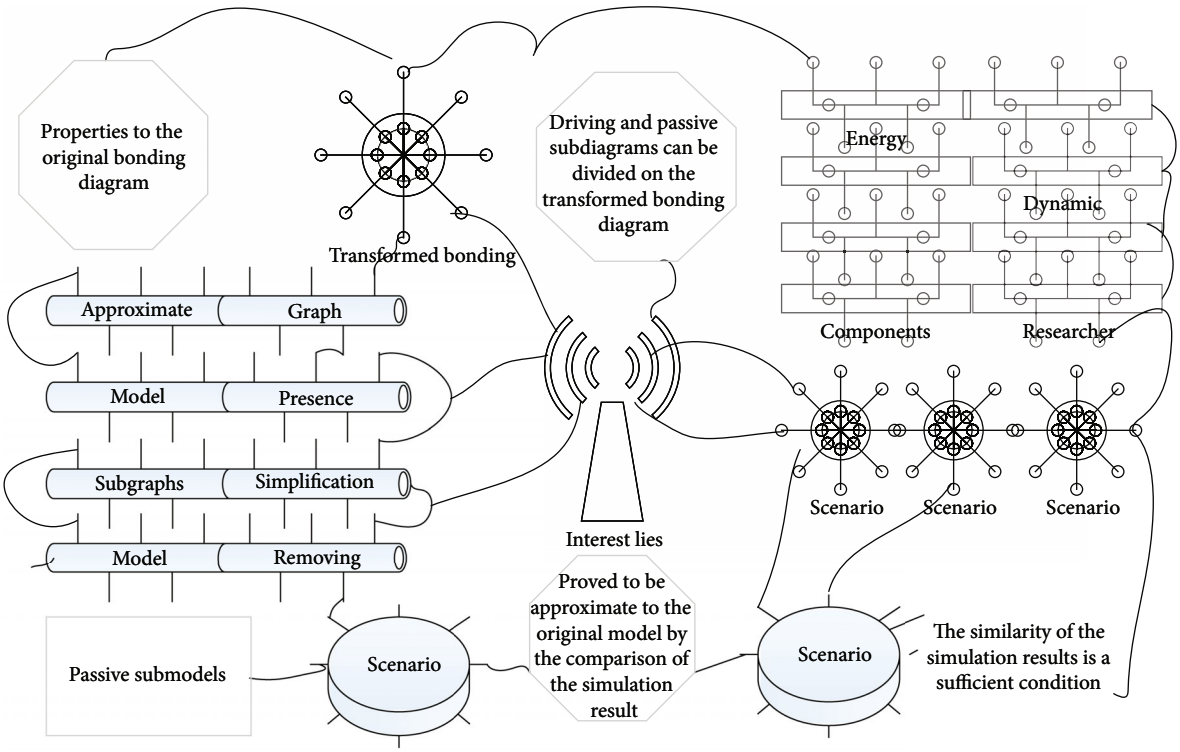

Figure 4: Flow of updating the physical parameters of the virtual model of the hinge node.

if replanned for each part, leads to a long product assembly cycle and low planning efficiency, so the constructed reusable conformal space based on the need for a method can achieve fast assembly path planning by reusing a priori paths for the characteristics of the reusable conformal space; this chapter proposes based on algorithms for path reuse in homogeneous and heterogeneous spaces. Two improved strategies are proposed to achieve reuse planning of assembly paths.

4. Results and Analysis

4.1. Simulation Results of Digital Twin Assembly Model. The cold roll pile dyeing machine control system studied in this paper has five active motors that are jointly controlled to achieve stable operation of the knitted fabric flat width process. These include the upper fabric roll drive motor, the spreading roll drive motor, the roll motor, the winding motor for winding up the dyed fabric, and the preroll motor for preroll tension control. The knitted fabric flat width processing process mainly relies on the contact between the fabric and the roll body, which is driven forward by friction. As the knitted material itself tension sensitive and easy to deformation characteristics, which requires the active motor can achieve accurate control of the front and rear tension, multimotor joint control of the difficulty is the multistage speed chain in the speed response synchronization; the current practical application of multimotor joint control strategy mainly masters order control, master-slave control, and other common ways. The tension value is less than 20 N, and the speed is within the range of 30~60 m/min, and the tension has a certain anti-interference ability before and after the flat width operation. The cold roll pile dyeing machine equipment studied in this paper uses variable frequency speed control of five motors; all motor types are three-phase asynchronous motors, using the motor reducer integrated model, using the stator current of the motor as shown in Figure 5.

The results show that the motor speed climbs rapidly with high torque and current at the instant of starting, and the output torque and current tend to stabilize when the speed is stabilized. When the target speed is adjusted from 30 r/min to 50 r/min, the output torque increases rapidly to accelerate the motor speed response, and the motor speed tends to stabilize around 0.1 s, indicating that the vector control speed regulation model has good robustness, and the frequency conversion speed regulation method under asynchronous motor vector control can meet the requirements of stable tension control for knitted fabric flat width processing operation. The target speed of all motors in the master order reference control strategy is the same, which has certain defects, that is, the target speed of each motor is from the same fixed value; when the speed of one motor in the multimotor fluctuates, the speed of the remaining motors is difficult to make timely dynamic speed adjustment according to the fluctuating motor, which cannot meet the requirements of this paper that the front and rear motors of the cold roll stack dyeing machine have associated control.

Therefore, the speed output feedback of adjacent motors is used to realize the multimotor joint control strategy. The idea of this strategy is to use the speed output value of the previous motor as the target speed input value of the next

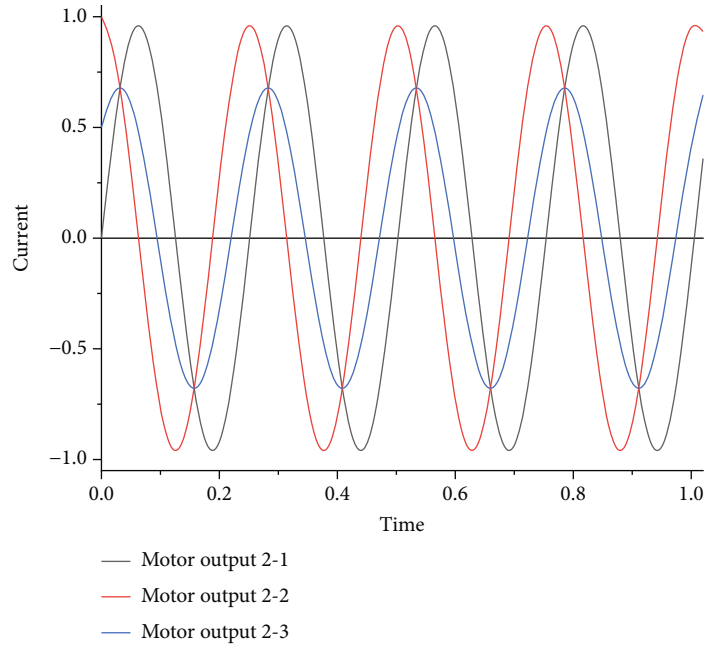

Figure 5: Stator current.

motor after the input is adjusted by PID parameters to realize the tension adjustment and complete the speed control requirement of the next motor. This strategy realizes the joint control of tension by using the input and output of multimotor speed as the correlation factor.

Subarray is the basic component unit of phased array antenna; each subarray includes base, truss, wall plate, support frame, reflecting surface and transmitting end, and other basic parts, and its assembly structure is shown in Figure 6, which is assembled from a mixture of rigid and flexible body parts. In this section, a comprehensive analysis will be carried out for the rigid error of the support parts and the flexible error of the reflecting surface of the splicing layer in the antenna subarray, and the error statistics on the target features after the subarray assembly is completed will be calculated, and the installation error of the array element layer and the positioning error during the assembly process will not be considered in this process.

For batch part assembly, it is difficult to construct a digital twin of each part to predict the overall assembly error, and it is necessary to construct a statistical feature representation of this batch of parts for error analysis. This chapter constructs an assembly twin for batch parts by hierarchically extracting part real-data statistics based on the previous work, calculating the discrete point probability distribution of batch part features based on contour similarity and proposing a hybrid vector ring method to analyse the error statistics of rigid-flexible assembly products.

4.2. Simulation and Characterization Results of the Step-Down Process with Key Links. This chapter proposes a method for predicting the positioning-assembly accuracy of complex products based on twin data, simulating the whole assembly process of real thin-walled parts from fixture positioning to welding completion, and improving on the existing method to predict the product twin assembly accuracy. Firstly, the basic process of thin-walled part assembly is described, and reasonable assumptions are made to introduce the application scenario and construction process of product twin in the positioning-assembly process. The advantages of the flexible tooling system for positioning thin-walled parts with free-form surfaces are introduced, and the adjustment method of the fixture positioning ball head based on isometric offset surfaces is proposed to analyse the influence of geometric errors and physical characteristics of the thin-walled twin on its force deformation. To minimize the mean value of deformation of the discrete point set on the thin-walled part, a hybrid particle swarm-based multiclamp positioning optimization method is proposed to ensure a strong deformation resistance of the thin-walled part at the positioning stage. The discrete error of the positioned thin-walled part is taken as the input condition, and the real assembly error of the thin-walled twin is calculated by improving on the traditional influence coefficient method and considering the flexible assembly under the action of various attributes such as feature alignment and physical interference. Finally, the feasibility of the method is verified in the flexible assembly process of the phased array antenna array (as shown in Figure 7).

The synchronization of multistage tension control can be improved by increasing the gain coefficient, and a reasonable gain coefficient can effectively enhance the followability of tension control; as shown in the figure, when the gain coefficient is 2, the change of tension of 2~4 levels with tension 1 is better. However, by adjusting the gain coefficient method will increase the peak of the follower tension; comprehensive result considered for knitted fabric low tension control applications in the gain coefficient in the range of 1~2 control effect is best. The traditional bolt joint analysis has not considered the interaction between the bolt and the

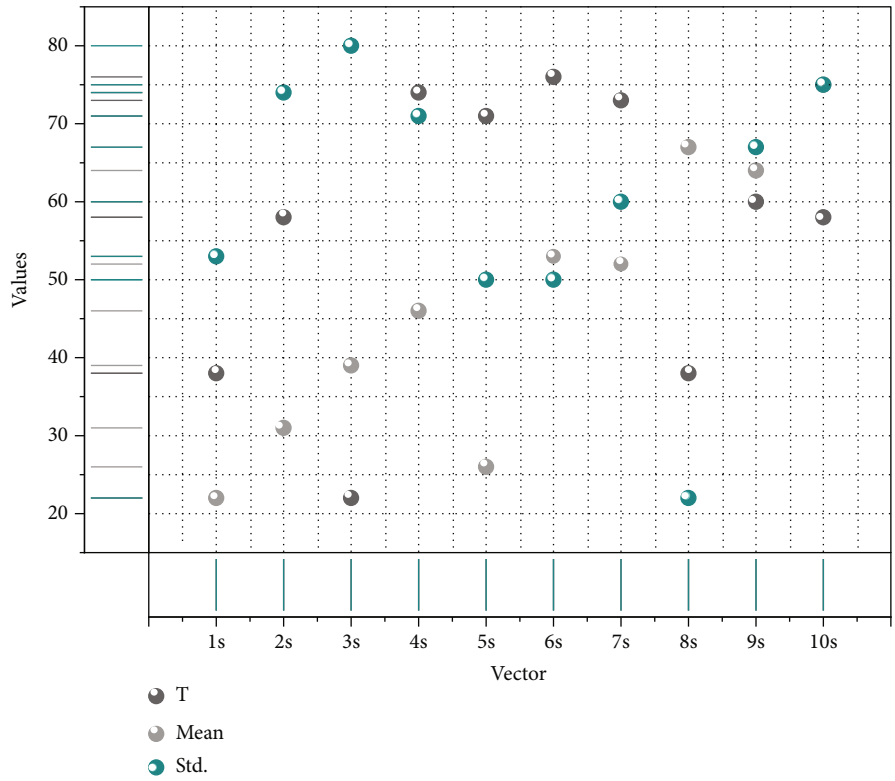

Figure 6: Discrete point statistics of the reflective surface and the lateral line of the wall plate assembly edge.

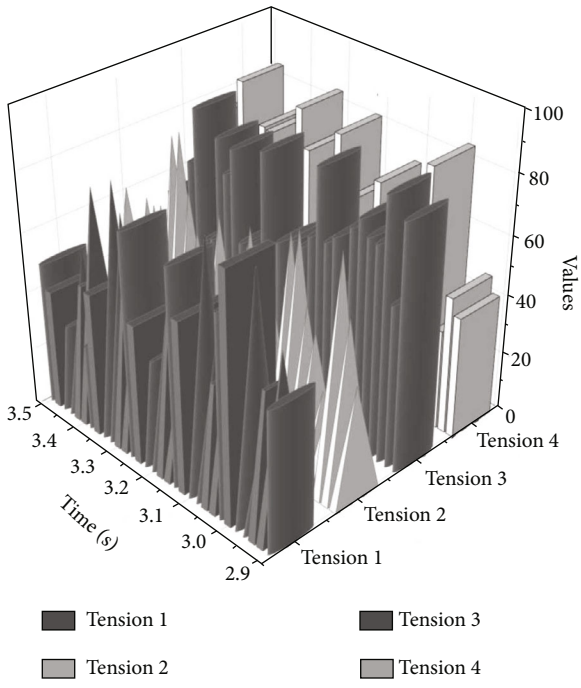

Figure 7: Gain coefficient.

transmission error in the assembly process, which makes it difficult to accurately simulate the bolt assembly stress. To a certain extent, it is also related to the coupling of assembly multisource information. In this chapter, we study the bolt assembly of the connecting plate twin based on the spring-stiffness model and construct a bolt stress model driven by multiple parameters such as part geometry and physical properties, assembly process, and service environment and achieve low-stress assembly effect by optimizing the bolting process, to guarantee the accuracy and performance stability of the product in service.

Figure 8 shows the motion response of the bracket, chassis, and cab, respectively. Based on the simulation results, the crane-related parameters in the design can be adjusted and restimulated to achieve the desired product performance. This shortens the cycle time for both product design, experimentation, change redesign, and reexperimentation and solves possible problems in the design phase, significantly reducing the design cost. This shows that it is very correct to consider systems, especially multidomain coupled systems, using bonding diagrams. Such a bonding diagram model is also very useful for detecting instabilities in vehicles and can be used for dynamic characterization of similar mechanical products, such as excavators and cranes.

CNC machine tools as typical complex customized products, widely used in ships, high-speed rail, aviation, aerospace, vehicles, and other manufacturing fields, is a basic product of China's manufacturing development. In recent years, with the rapid development of batch customization technology for complex products, the reusable design method based on product configuration design and variant design can meet the functional parameter requirements of customized products by reconfiguring some modules, leading to the serialization and modularization of CNC machine

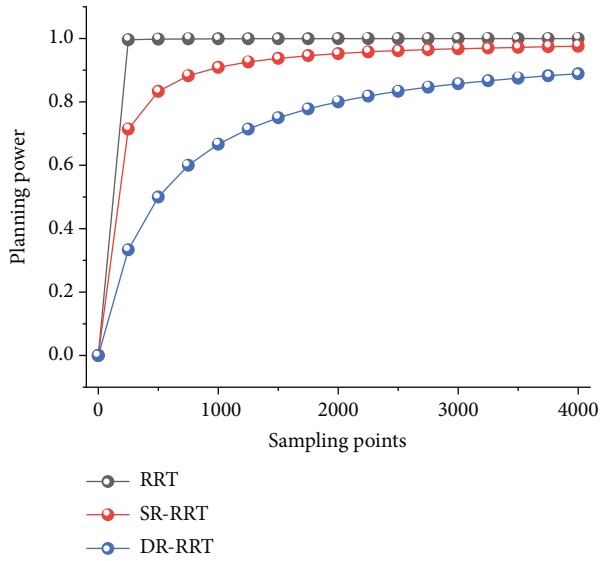

Figure 8: Path planning success rate of each algorithm with different maximum sampling points.

tools. Assembly path planning as a key link in the product life cycle of CNC machine tools, the efficiency of the assembly path planning has a great impact on the product assembly cycle, domestic machine tool enterprises due to the lack of effective support for a series of complex products digital assembly software system, and in the new model of the product assembly planning often need to replan the assembly of all the component modules, resulting in low planning efficiency. Therefore, how to improve the quality and efficiency of assembly path planning by digital means is an urgent problem for machine tool manufacturers.

5. Conclusion

Firstly, the reuse-oriented conformation space expression is analysed, and it is pointed out that the reuse-oriented conformation space should contain a priori path information, and the concept of a priori degree is defined in combination with ant colony pheromone concentration, and it is introduced into the information expression of a priori path positional points and the construction of a priori path space. The method of calculating the point distance of assembly multisource information nonlinear mapping space is proposed, and the calculation of assembly path reuse degree is realized by the many-to-many matching algorithm that fuses the assembly multisource information, and on this basis, the multigrained clustering of parts path reuse degree is realized by cohesive hierarchical clustering based on the multigrained judging criteria of assembly task coupling degree and dimensional information aggregation degree, and the uniform enclosing box dimensional information between clusters is obtained according to the clustering results. The assembly conformation space that can be reused by parts in the same cluster is constructed. Since the bond graph model describes the power flow within the system, it is suitable for power- and energy-based approach to downscaling the system, preserving the components or subsystems that make the main contribution to the dynamic behaviour of the system and the physical meaning of the parameters; comparison of the local activity of the junction structure can reveal the strength of the power or energy coupling within the system and thus can be used for decomposition and decoupling of the system, and this decomposition and decoupling have obvious physical significance. The special role of the multiport modulation converter MTF in bond diagram modelling is explored, and the bond diagram model of the mechanism is built through the motion transition relationship represented by the multiport converter MTF, while its dynamical structural characteristics are directly represented by it, which not only makes it easier to establish the equation of state of the system but also very helpful to make an intuitive force and velocity relationship between the interacting parts in the system, physical interpretation of the force and velocity relationships between the interacting components of the system. A typical mechanical-hydraulic coupled system loader is modelled in its entirety and reduced in order using a component-based bonding diagram modelling approach.

Data Availability

The data used to support the findings of this study are available from the corresponding author upon request.

Conflicts of Interest

The authors declare that they have no known competing financial interests or personal relationships that could have appeared to influence the work reported in this paper.

Acknowledgments

This work is supported by the National Key Research and Development Program of China (grant no. 2020YFB1710300).

References

[1] P. Bauer, B. Stevens, and W. Hazeleger, "A digital twin of earth for the green transition," *Nature Climate Change*, vol. 11, no. 2, pp. 80–83, 2021.

[2] J. Corral-Acero, F. Margara, M. Marciniak et al., "The 'digital twin' to enable the vision of precision cardiology," *European Heart Journal*, vol. 41, no. 48, pp. 4556–4564, 2020.

[3] K. Y. H. Lim, P. Zheng, and C. H. Chen, "A state-of-the-art survey of digital twin: techniques, engineering product lifecycle management and business innovation perspectives," *Journal of Intelligent Manufacturing*, vol. 31, no. 6, pp. 1313–1337, 2020.

[4] R. Minerva, G. M. Lee, and N. Crespi, "Digital twin in the IoT context: a survey on technical features, scenarios, and architectural models," *Proceedings of the IEEE*, vol. 108, no. 10, pp. 1785–1824, 2020.

[5] A. J. H. Redelinghuys, A. H. Basson, and K. Kruger, "A six-layer architecture for the digital twin: a manufacturing case study implementation," *Journal of Intelligent Manufacturing*, vol. 31, no. 6, pp. 1383–1402, 2020.

[6] L. Zhao, G. Han, Z. Li, and L. Shu, "Intelligent digital twin-based software-defined vehicular networks," *IEEE Network*, vol. 34, no. 5, pp. 178–184, 2020.

[7] K. T. Park, J. Lee, H. J. Kim, and S. Do Noh, "Digital twin-based cyber physical production system architectural framework for personalized production," *The International Journal of Advanced Manufacturing Technology*, vol. 106, no. 5-6, pp. 1787–1810, 2020.

[8] Y. Lu, X. Huang, K. Zhang, S. Maharjan, and Y. Zhang, "Communication-efficient federated learning for digital twin edge networks in industrial IoT," *IEEE Transactions on Industrial Informatics*, vol. 17, no. 8, pp. 5709–5718, 2021.

[9] W. Polini and A. Corrado, "Digital twin of composite assembly manufacturing process," *International Journal of Production Research*, vol. 58, no. 17, pp. 5238–5252, 2020.

[10] J. Ma, H. Chen, Y. Zhang et al., "A digital twin-driven production management system for production workshop," *The International Journal of Advanced Manufacturing Technology*, vol. 110, no. 5-6, pp. 1385–1397, 2020.

[11] K. Alexopoulos, N. Nikolakis, and G. Chryssolouris, "Digital twin-driven supervised machine learning for the development of artificial intelligence applications in manufacturing," *International Journal of Computer Integrated Manufacturing*, vol. 33, no. 5, pp. 429–439, 2020.

[12] K. T. Park, Y. H. Son, and S. D. Noh, "The architectural framework of a cyber physical logistics system for digital-twin-based supply chain control," *International Journal of Production Research*, vol. 59, no. 19, pp. 5721–5742, 2021.

[13] J. Lee, M. Azamfar, J. Singh, and S. Siahpour, "Integration of digital twin and deep learning in cyber-physical systems: towards smart manufacturing," *IET Collaborative Intelligent Manufacturing*, vol. 2, no. 1, pp. 34–36, 2020.

[14] Y. Lu, X. Huang, K. Zhang, S. Maharjan, and Y. Zhang, "Communication-efficient federated learning and permissioned blockchain for digital twin edge networks," *IEEE Internet of Things Journal*, vol. 8, no. 4, pp. 2276–2288, 2021.

[15] K. T. Park, D. Lee, and S. Do Noh, "Operation procedures of a work-center-level digital twin for sustainable and smart manufacturing," *International Journal of Precision Engineering and Manufacturing-Green Technology*, vol. 7, no. 3, pp. 791–814, 2020.

[16] R. B. Roy, D. Mishra, S. K. Pal et al., "Digital twin: current scenario and a case study on a manufacturing process," *The International Journal of Advanced Manufacturing Technology*, vol. 107, no. 9-10, pp. 3691–3714, 2020.

[17] W. Sun, H. Zhang, R. Wang, and Y. Zhang, "Reducing offloading latency for digital twin edge networks in 6G," *IEEE Transactions on Vehicular Technology*, vol. 69, no. 10, pp. 12240–12251, 2020.

[18] X. Tong, Q. Liu, S. Pi, and Y. Xiao, "Real-time machining data application and service based on IMT digital twin," *Journal of Intelligent Manufacturing*, vol. 31, no. 5, pp. 1113–1132, 2020.

[19] H. Zhang, Q. Yan, and Z. Wen, "Information modeling for cyber-physical production system based on digital twin and AutomationML," *The International Journal of Advanced Manufacturing Technology*, vol. 107, no. 3-4, pp. 1927–1945, 2020.

[20] Y. Peng, S. Zhao, and H. Wang, "A digital twin based estimation method for health indicators of DC–DC converters," *IEEE Transactions on Power Electronics*, vol. 36, no. 2, pp. 2105–2118, 2021.

Hindawi
Journal of Sensors
Volume 2021, Article ID 1059517, 11 pages
https://doi.org/10.1155/2021/1059517

Research Article

Remote Sensing Big Data Analysis of the Lower Yellow River Ecological Environment Based on Internet of Things

Yuntong Liu,[1,2,3] **Kuan He**,[2,4] **and Fen Qin**[1,3]

[1]*The College of Geography and Environment, Henan University, Kaifeng Henan 475004, China*
[2]*Yellow River Conservancy Technical Institute, Kaifeng Henan 475004, China*
[3]*Henan Industrial Technology Academy of Spatio-Temporal Big Data, Zhengzhou Henan 450046, China*
[4]*School of Surveying and Land Information Engineering, Henan Polytechnic University, Jiaozuo Henan 454000, China*

Correspondence should be addressed to Yuntong Liu; liuyuntong@yrcti.edu.cn and Fen Qin; qinfen@henu.edu.cn

Received 1 November 2021; Revised 22 November 2021; Accepted 23 November 2021; Published 20 December 2021

Academic Editor: Gengxin Sun

This paper collects data on the ecological environment of the lower Yellow River through an IoT approach and provides an in-depth analysis of the ecological remote sensing big data. An impervious fusion of multisource remote sensing data cooperation and multimachine learning algorithm cooperation is proposed. The water surface extraction method has improved the extraction accuracy of the construction land and rural settlements in the Yellow River Delta. The data system, big data management platform, and application scenarios of the environmental data resource center are designed specifically, respectively. Based on the spherical mesh information structure to sort out environmental data, an environmental data system containing data characteristics such as information source, timeliness, and presentation is formed. According to the characteristics of various types of environmental data, the corresponding data access, storage, and analysis support system is designed to form the big data management platform. Strengthen the construction of ecological interception projects for farmland receding water. Speed up the construction of sewage treatment facilities. Carry out waste and sewage pipeline network investigation, speed up the construction of urban sewage collection pipeline network, and improve the waste and sewage collection rate and treatment rate. The management platform adopts the Hadoop framework, which is conducive to the storage of massive data and the utilization of unstructured data. Combined with the relevant national policy requirements and the current environmental protection work status, the application scenarios of environmental big data in environmental decision-making, supervision, and public services are sorted out to form a complete data resource center framework. Gray correlation analysis is used to identify the key influencing factors of different types of cities to elaborate the contents of the construction of water ecological civilization in different types of cities and to build a framework of ideas for the construction of urban water ecological civilization to improve the health of urban water ecological civilization. To realize the sustainable development of the lower reaches of the Yellow River, blind logging and reclamation should be avoided in the process of land development, and more efforts should be made to protect tamarisk scrub and reed scrub, which are vegetation communities with positive effects on the regional ecological environment. In urban planning, the proportion of green area and water area within the city should be reasonably increased, so that the city can develop towards a livable city that is more conducive to human-land harmony and sustainability.

1. Introduction

The rational use of resources and a good ecological environment are important conditions for sustainable development [1]. Although economic development and technological progress have brought unprecedented prosperity to human civilization, they have also brought incalculable impacts on various natural resources and the ecological environment. In the process of transforming nature, human beings have been intensifying the predatory exploitation of land to meet their growing needs, resulting in drastic changes in land surface form. Although these changes have met the needs of human production and life to a certain extent, the environmental effects caused by these changes have caused many

adverse effects on the long-term development of human beings. Wetlands are closely related to the development of human society, they are an important guarantee for the healthy and safe survival and development of human beings, provide an important supply of freshwater resources for human society, and are also home to many rare plants and animals [2]. AWEI classifies edge pixels more accurately, and the optimal threshold used to segment AWEI varies little with time and space. Therefore, the AWEI can be used as an important choice for water body extraction. Wetlands can improve water quality, reduce natural disasters such as floods and droughts, restore groundwater resources, and promote agriculture, forestry, animal husbandry, and fishery production. Wetlands also play an indispensable role in reducing the greenhouse effect on a global scale. While wetlands occupy only 6.4% of the world's total land area, the carbon content of wetlands is as high as 35% of the terrestrial biosphere, providing an important guarantee for the normal carbon cycle. Over the past century, coastal wetlands worldwide are facing increasing threats and severe losses in ecological integrity and service provision, with almost half of them having been lost because of human disturbance and climate change.

In the relatively immature period of remote sensing technology, wetland exploration was mainly carried out by traditional methods [3]. There are many disadvantages of traditional methods, such as being time-consuming, costly, and easy to damage wetland ecology, and all these shortcomings greatly hindered the improvement of the wetland database. The maturity of remote sensing technology has led to a breakthrough in wetland research. Because of the unique advantages of remote sensing technology, such as large detection range, dynamics, rapidity, and short repetition period, it is widely used in the interpretation of wetland features, landscape pattern analysis, and dynamic change monitoring of large areas. Satellite remote sensing technology, which can provide spatially continuous surface image data, has been used as an important tool for monitoring wetland dynamics, especially because of its ability to capture large-scale, up-to-date temporal wetland information repetitively, thus making it possible to obtain satellite data on a regional or even global scale. The Yellow River Delta is of interest to researchers because of its key role in wildlife conservation, energy production, and agriculture [4]. The Yellow River Delta wetlands are the largest and youngest coastal wetland ecosystem in China, providing habitat and migration stations for millions of wild birds and providing spawning and nursery grounds for numerous freshwater and marine organisms, making the Yellow River Delta wetlands an ecological barrier for inland areas [5]. The Yellow River Delta also provides enormous ecosystem service values, including nutrient cycling, carbon storage, and tourism and recreational values. China's second-largest oil field, the Shengli Oilfield, is also located in the Yellow River Delta wetland region, where energy production and related industrial activities have a significant impact on the surface and subsurface environment. Agricultural production also currently occupies a large portion of the newly formed delta land and utilizes a large amount of riverine and subsurface freshwater resources, and activities such as agricultural land reclamation and sea enclosures have also caused damage to wetland resources in the Yellow River Delta. As a result of human activities and natural evolution, the Yellow River Delta region is at increasing risk of degradation.

With the continuous improvement of the level of environmental information technology and the gradual expansion of the scale of environmental data collection, the State has continuously emphasized the requirement for environmental protection departments at all levels to build environmental data resource centers for the unified collection, storage, management, and utilization of various types of environmental data. However, at this stage, China has not yet formed a construction plan or guide for data resource centers; China's provinces and cities are currently in the mapping stage of environmental data resource center construction design and lack research on the construction of the overall framework of environmental data resource centers. There are some difficulties in selecting suitable attributes and methods for statistical analysis from multidimensional attributes. Therefore, a series of big data services have emerged for statistical analysis of big data. However, for spatiotemporal big data, it is necessary to focus on analyzing its spatiotemporal attributes, and for spatiotemporal big data with a similar structure, a common statistical template can be used for statistical analysis of spatiotemporal big data. This is associated with the characteristics of web services, that is, writing some statistical service interfaces; each interface implements a specific function, and users can call different interfaces to finally get the results of the desired statistical analysis. Therefore, we can use the idea of service-oriented to carry out the statistical work of spatiotemporal big data and refine the statistical process of spatiotemporal big data into different functions, each function corresponds to service, and these services are reusable. The user invokes different services in turn and finally can get a result of statistical analysis of data.

2. Current Status of Research

To better articulate the health of urban ecosystems and to conduct quantitative analysis, the indicator system approach is often used. There is a large amount of foreign literature on the study of urban ecosystem health, but fewer studies have been conducted on urban ecosystem health indicator systems [6]. In general, classifier-based methods for classifying remote sensing images can vary depending on the classification criteria. Supervised and unsupervised classification can be classified according to whether training samples are required for classification; parametric and nonparametric classification methods can be classified according to whether the assumption that the data obeys normal distribution is required; and image, subimage, and face-image object classification methods can be classified according to the smallest unit of classification [7], thereby forming an orderly and systematic hierarchical structure, making the selected indicators clearer and more specific, and better reflecting the health of the system. In wetland classification techniques and wetland conservation, the first use of the hybrid iterative

classification of remote sensing images for spectral aggregation analysis of wetland information, classification accuracy has been greatly improved compared with supervised and unsupervised classification. Using wetlands in central Kansas as the study area, multitemporal remote sensing data sources were used for the analysis, and the results showed that multitemporal remote sensing data can help in wetland change detection and can reflect the dynamic change of wetlands [8]. A multivariate adaptive regression curve development model was used to predict the risk of wetland habitat loss, and the study showed that the model has strong predictive power in the southern United States [9]. Policy analysts, land-use planners, and others can use the model to prioritize wetland conservation, assess wetland habitat connectivity, predict future land-use change trends, and evaluate effective conservation plans for wetlands [10].

With the arrival of the era of big data, the development direction of environmental information technology has started to change. A summary of the application of big data technology in environmental management is made [11]. The construction of an environmental monitoring data center proposed to realize the collection of environmental big data, the establishment of an environmental opinion monitoring and analysis platform to realize the mining of the massive value of the massive data from the Internet, and the establishment of an emergency warning application to assist environmental management. However, no detailed study of the specific implementation of these elements has been conducted [12]. In the era of big data, the organization and management of environmental data should be changed, the traditional environmental information coding content may no longer apply to the collection of environmental data in the era of big data, and environmental information should be more comprehensive and complete; at the same time, multisource heterogeneous environmental information is difficult to unfold with the traditional linear classification method and multidimensional tree classification, and the classification with a spherical mesh information structure can reflect the organization of the environmental information classification system [13]. It is proposed that in the era of big data, environmental information work should be changed. First is that the environmental quality and pollution source monitoring should change the traditional sampling monitoring, through the isolinear surface and other methods to achieve the monitoring of all environmental data; at the same time, the first-hand raw data instead of the traditional environmental analysis of the results of the data, to obtain more value, should be concurrent with the environmental protection in the cause and effect relationship and correlation and switch the role of data, so that the data itself is for decision-making [14].

Various studies have described the promotion of environmental informatization reform through big data technology. However, at this stage, the concept of big data is still vaguely defined in various studies, and the relationship between the development of environmental informatization and the application of environmental big data is not clear; at the same time, there is a lack of analysis of the current state of access to environmental data and whether the quality of data meets the relevant research on environmental big data, which makes it difficult to form the support of data-based research for the development of environmental protection work under the situation of big data. There has been some research base in regulation and environmental quality management. However, there has not been a clear study to sort out the current application needs of environmental big data in China in a unified manner. In addition, researchers lack a focus on how environmental data resource centers can provide support for environmental big data applications.

3. Remote Sensing Big Data Analysis of the Lower Yellow River Ecological Environment by the Internet of Things

3.1. Remote Sensing Big Data Design for the Internet of Things. In recent years, the concept of big data has been heating up, and all industries are trying to apply big data to change the traditional work management mode and innovate business content, and environmental management is no exception [15]. The flow capacity of the river channel has increased significantly; the increase in the height difference of the beach and channel makes the river channel tend to be narrow and deep, and the river channel develops towards a stable river pattern, which not only increases the longitudinal connectivity of the channel but also maintains the lateral connectivity of the beach and channel, so it needs to continue to maintain the water and sand regulation of the reservoir. This chapter first synthesizes the definitions of the concept of big data from various international research institutions and government departments to clarify the characteristics of big data and combines the practical application process of big data with the research objectives of this paper to clarify the definition of the concept of big data in this paper. Subsequently, this chapter sorts out the types and characteristics of environmental data and maps the concept of big data to the environmental field, clarifies the concept of environmental big data in this paper, and compares the differences and correlations between environmental big data applications and traditional environmental applications. Immediately after, based on the concept of environmental big data, this chapter defines the environmental data resource center and compares it with the traditional data resource center and establishes the content of the environmental data resource center design according to the definition. A large amount of data exists in the network environment and life, mainly including structured data in the SQL database, semistructured data in the network, and other unstructured data such as pictures and picture-based text; first, a large amount of structured data, unstructured data, and semistructured data are integrated and extracted through data collection techniques, subsequently, after preprocessing operations such as cleaning of the collected data. Then, after preprocessing operations such as cleaning of the collected data, a large amount of correlated data is stored; immediately afterward, the stored data is analyzed using machine learning, data mining, and other algorithms to achieve applications such as decision support and business

analysis; finally, the data results are expressed to users through visualization and human-machine interaction.

Water system connectivity refers to the longitudinal and transverse connectivity of the connecting channel and the structural connectivity of the water system. The mechanism of connecting channels is the principle of general river channel flushing and siltation evolution, the mechanism of lateral connecting channels is the theory of water and sand exchange in river channels, and the mechanism of connecting water system structures is the principle of diversion and dry and branch confluence in water system channels. The evolution of river channel flushing and siltation, beach and channel water and sand exchange, and river channel diversion and confluence is very classic and traditional research topics, and there are many mature research results, as shown in Figure 1.

In the process of acquiring data by satellite sensors, the influence of the sensors, the curvature of the Earth, atmospheric refraction, and the rotation of the Earth can cause distortion, deformation, and translation of the acquired images, so the geometric correction of the captured images is needed to restore the real coordinates and shape information of the features before subsequent applications are carried out [16]. Many factors cause geometric distortion in remote sensing images, and in general, geometric distortion errors can be divided into internal errors and external errors. Internal errors are caused by the structural factors of the satellite sensor itself, such as lens distortion, uneven scanning prism speed, and offset of image principal points. The size of internal errors may vary according to different sensor structures, and usually, the internal errors are not large. External errors are errors caused by factors other than the sensor (e.g., errors caused by outer azimuth elements characterizing the satellite position attitude, atmospheric refraction, terrain height and undulation, earth autotransfer, and earth curvature) under the normal operation of the satellite sensor. The purpose of geometric correction of remote sensing images is to eliminate the various image distortions caused by the above factors and to obtain orthophotos or approximate orthophotos that match the maps.

$$\begin{aligned} \mathrm{NDVI} &= \frac{p(\mathrm{NIR}) + p(\mathrm{Re}\ d)}{p(\mathrm{NIR}) - p(\mathrm{Re}\ d)}, \\ \mathrm{SAVI} &= \frac{p(\mathrm{NIR}) + p(\mathrm{Re}\ d)}{p(\mathrm{NIR}) - p(\mathrm{Re}\ d) - L} \times (1 - L), \\ \mathrm{MNDWI} &= \frac{p(\mathrm{NIR}) + p(\mathrm{MIR})}{p(\mathrm{NIR}) - p(\mathrm{MIR}) + L}. \end{aligned} \tag{1}$$

Changes in pollution source data will inevitably lead to changes in environmental quality data. Part of the data obtained through crossdepartment can characterize the intensity of daily human activities, that is, reflect the situation of natural and social parameters. The classifier is the final performer of the image classification task. There are many factors to be considered while selecting an image classification algorithm such as type of input data, the statistical distribution of categories, target accuracy, ease of use, speed of classification, scalability, and decipherabilit. Which classification method is appropriate for a specific study is a difficult question to answer. Parametric classifiers such as maximum likelihood usually achieve good classification results when dealing with input data with a single-peaked distribution.

However, since parametric classifiers always assume that the input data are normally distributed, they are not suitable for handling input data that are multitemporal and exhibit multipeaked distributions, and in addition, in many cases, the statistical distribution of land types in the study area is often unknown, and these limitations make it difficult for parametric classifiers to achieve satisfactory results when mapping surface cover over large and complex environments [17]. Nonparametric classifiers are in principle machine learning-based algorithms that do not require additional assumptions on the input data, and although some computational performance is sacrificed in the iterative process, nonparametric classifiers offer better flexibility, so when faced with complex scenarios such as unknown statistical distributions of data, multiple sources, multiple temporal phases of data being employed, and input data showing multipeaked distributions, the use of nonparametric classification algorithm for surface thematic information extraction is well suited.

This study was conducted to explore how soil enzyme activity responds to changes in land-use types and seasons and to elucidate the relationship between soil enzyme activity characteristics and soil carbon, nitrogen, phosphorus, and other elements in a typical hanging river section beach area and backwater depression of the lower Yellow River. The aim is to understand the soil properties and change characteristics along the hanging section of the lower Yellow River and provide theoretical support for sustainable land use and scientific management along the Yellow River. The influence of land use on soil properties along the Yellow River was explained from the perspective of soil enzyme activity to provide a basis for ecological environment management along the Yellow River. Through the comparison of the Yellow River beach area and the backwater depression, the basis for rational development of soil under the influence of the Hanging River was laid, which provided some support for further research on the Hanging River, as shown in Figure 2. Nonparametric classifiers are based on machine learning algorithms in principle. No additional assumptions are needed on the input data. Although certain computational performance will be sacrificed in the iterative process, nonparametric classifiers have better performance. The flexibility of using nonparametric classification algorithms to extract surface thematic information is very suitable.

The mudflats are mainly distributed in the coastal area, and some bare land and urban construction land with high water content in the inland area are found to affect the extraction accuracy of the mudflats. It is decided to separate the coastal area dominated by mudflats and use the maximum likelihood method to classify the distribution area of mudflats. The maximum likelihood method in supervised classification is widely used in the classification of remote

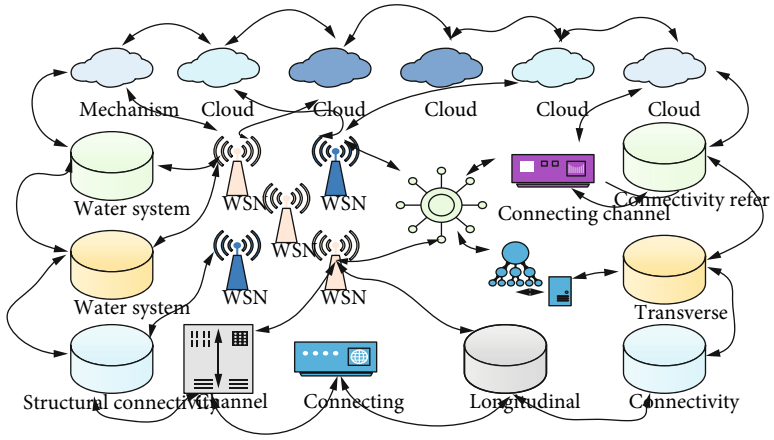

Figure 1: Remote sensing framework design for the Internet of Things.

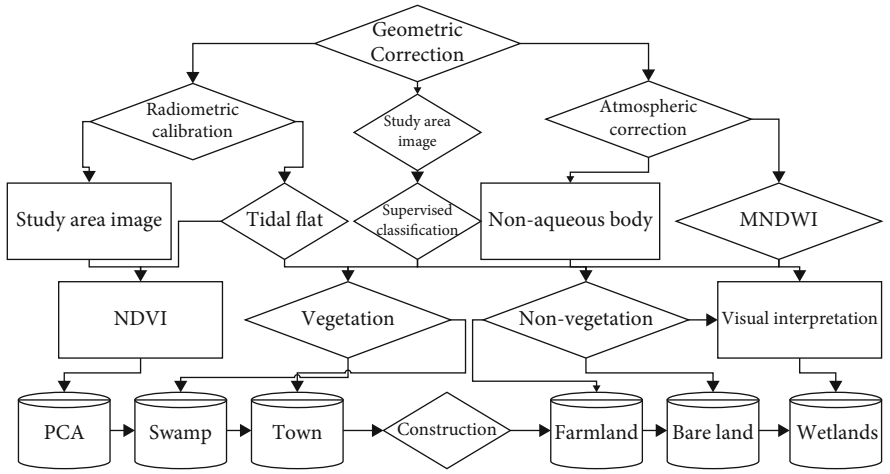

Figure 2: Hierarchical classification discriminant method.

sensing images, which firstly calculates the variance and mean value of each category in interest and then obtains a classification function.

$$\frac{\partial A}{\partial t} - \frac{\partial Q}{\partial x} - q_x = 0, \qquad Q_{\text{in}} = Q_{\text{out}} - \Delta Q. \tag{2}$$

In the first phase, data centers were only used in some organizations to demonstrate technology and train staff on technology to meet end-user needs; i.e., the function of the data center was to communicate information. Subsequently, with the development of database technology, the data center entered the second stage, where it began to guide and direct end-users to utilize and use data, and the function of the data center evolved into information presentation and interaction [18]. And in the third stage, with the development of artificial intelligence, machine learning, and other technologies, data centers have a more integrated nature of functions that can help all people to solve problems creatively.

Water flow continuity indicates that water resources can be allocated according to demand, but in the process of allocation, it is also necessary to meet the basic runoff of rivers and maintain a certain flow of water to shape the basic shape of river boundaries, maintain the transport and exchange of river sediment, meet the requirements of river water ecology and water environment, and ensure the normal function of rivers, otherwise, river connectivity will change. When river flow does not meet its natural evolutionary needs, it may trigger problems such as shrinking of river channels, river disconnection, and ecological degradation, which are all important features and extreme manifestations of the decline of water system connectivity.

3.2. Design of Big Data Analysis for the Lower Yellow River Ecosystem. At this stage, the public administration still pays little attention to environment-related data on the Internet, and Internet data can greatly enrich the scale amount of environmental data, expand the variety of environmental data, and update quickly, and the Internet contains a lot of environmental data values, so the acquisition and collection of Internet data are an important basis for improving the level of environmental big data. For example, the level of

concern of the population about environmental issues, the impact of environmental problems on the population, sudden environmental pollution in a certain area, and other environment-related information can be obtained from the Internet [19]. Environmental management departments should pay attention to the acquisition of environmental data on the Internet and effectively acquire all kinds of data on the Internet through technologies such as web crawlers to enrich the content of environmental big data, such as lens distortion, nonuniform scanning prism rotation speed, and deviation of the principal point of the image; the size of the internal error will vary with different sensor structures, and the internal error is usually not large. Under the perfect environmental big data scenario, environmental management departments should supervise all kinds of environment-related public opinion information on the Internet and the data released by third-party environmental protection agencies on the Internet from time to time and store the Internet data to effectively supplement the content of environmental data and improve the value of environmental big data.

In the context of perfect environmental big data, all kinds of environment-related data are intertwined and interrelated. Environmental quality monitoring data directly reflect the current environmental quality; data on environmental pollution sources characterize direct human activity changes on environmental quality, and changes in pollution source data will inevitably cause changes in environmental quality data. Some of the data obtained through crosssectoral can characterize the intensity of daily human activities, i.e., reflect the situation of natural social parameters, which indirectly affect the data changes of environmental quality through the form of environmental pollution. The data of environmental management operations, on the other hand, is the data situation of pollution control made by humans to improve environmental quality, which is the feedback of environmental quality data changes to pollution source data changes. Internet data then complements the above types of data content. And all the above types of data can be interconnected through the bond of time coordinate and space coordinate. Under the background of perfect environmental big data, through big data analysis, the relationship mining between data can be effectively completed, forming various kinds of highly valuable environmental big data applications to help environmental management, as shown in Figure 3.

At the same time, it also has an immeasurable impact on various natural resources and the ecological environment. The selected indicator system should be able to reflect the real situation of urban water ecosystems, establish the indicator system according to a certain purposefulness, diagnose the damage or degradation degree of urban water ecosystems caused by natural factors and human activities, serve the final assessment, issue an early warning, provide the basis for evaluation and countermeasure suggestions, and carry out optimal control. At the same time, the constructed indicator system should be consistent with the overall strategy of system health, thus serving as a guide for the future development behavior and direction of the city. The urban water ecosystem is a complex whole, and the elements

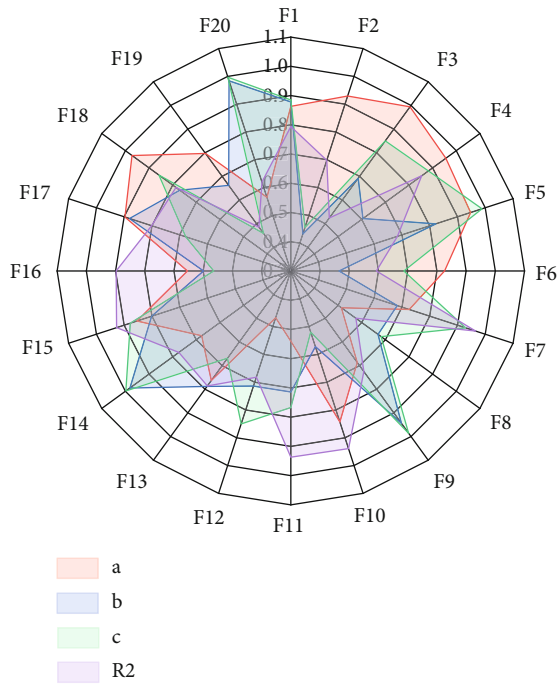

Figure 3: Crosscalibration factor.

within it are not independent but are interconnected and interacting with each other. Therefore, the indicator system should reflect its comprehensive characteristics more comprehensively and organically combine the evaluation objectives and the selected indicators to form a hierarchical whole. The relationship between evaluation indicators must be subordinated to the purpose and function of health evaluation but avoid overlap between indicators and maintain the relative independence between indicators. At the same time, it is also necessary to further decompose the indicator system into several levels according to the needs and complexity of urban water ecosystem health evaluation, from high level to low level one by one; each evaluation indicator expresses the subordination and interaction of evaluation indicators at different levels, thus constituting an orderly and systematic hierarchical structure, making the selected indicators more clear and specific, and better reflecting the health degree of the system.

In general, empirical methods used for specific emissivity estimation include classification-based methods and spectral index-based methods. The classification-based approach for estimating surface-specific emissivity is based on the idea of first obtaining accurate land-use/cover data based on remote sensing image classification algorithms and then assigning representative surface-specific emissivity values to each surface cover type; however, accurate land-use/cover data are difficult to obtain and the representative specific emissivity of different land-use/cover types may change with the change of surface state. The surface-specific emissivity values based on spectral indices are difficult to obtain. It is an important guarantee for human health, safe survival, and development; provides an important supply of fresh water resources for human society; and is also home to many rare

animals and plants. The estimation of surface-specific emissivity based on spectral indices relies on the statistical relationship between spectral indices and specific channel-specific emissivity, and NDVI is one of the commonly used spectral indices for surface-specific emissivity estimation. The data exchange platform is the core platform for interconnection and interoperability among interface systems, responsible for message transmission with different business systems and different networks, and provides a unified data transmission channel for information exchange among various application systems of environmental management, integration, and sharing of external data. Through the data exchange platform, data from various business systems of environmental management can be exchanged to various commissions and offices to realize data sharing services to other commissions and offices.

Environmental planning at the macrolevel is one of the important elements of environmental decision-making (Figure 4). According to the negative externality of environmental problems, the macroregulation of government management is a key factor in solving environmental problems, and all environmental protection work is carried out according to the macrolevel environmental planning of management. To achieve the goal of sustainable development, environmental planning should take the "social-economic-environmental" system as a comprehensive consideration and make decisions in time and space to achieve the purpose of coordinated development of the environment and social economy. In the process of environmental planning at the macrolevel, it is necessary to consider all factors, including the general urban planning, economic zoning, land planning, and national economic and social development planning, to make a comprehensive evaluation of the economic situation, social development situation, and environmental conditions and then make decisions and plans based on them [20].

From this, it can be seen that accurate judgment of the environmental development situation and analysis of the environment and economic and social relevance are important bases to support environmental macro-decision-making and planning. Due to human disturbance and climate change, almost half of the wetlands have disappeared. Traditional environmental planning is generally judged by human experience through expert consultation and social research, and there may be subjective errors in research and judgments or mistakes in decision-making; at the same time, the amount of data relied on by traditional decision-making is small, and objectively, there may be a lack of information that causes decision-making mistakes. With the development of environmental big data applications, management departments can rely on the massive environmental data resources through big data means that are used to study and judge the environmental and economic situation and make targeted planning decisions. The macroenvironmental decision-making planning supported by environmental big data can reduce the interference of human factors, accurately analyze the planning elements, and improve the accuracy of environmental decision-making planning.

4. Analysis of Results

4.1. Experimental Results of Remote Sensing Big Data for the Internet of Things. In particular, reservoirs and ponds that use Yellow River water as their water source are the main source of water for people's production and living, and these reservoirs and ponds are used as a source of drinking water for people on the one hand and for agricultural irrigation on the other hand, so the salinity of reservoirs and ponds is usually lower than that of farming water surfaces and salt fields, but since the groundwater in the Yellow River Delta is mostly brackish or slightly saline, for those small reservoirs or ponds that are not Yellow River water sources, the spectral characteristics of their water bodies are similar to those. However, for those small reservoirs or ponds with non-Yellow River water sources, the spectral characteristics of their water bodies are very similar to those of farming waters or salt fields (especially the underground brine before crystallization), which may be one of the factors causing the mixing of reservoirs and farming waters; most of the farming waters rely on the introduction of seawater for fish and shrimp farming, while the salt fields mainly use the extraction of underground brine as raw material and then crystallize and produce salt by evaporation through sunlight, and the concentration of the brine will change continuously during the crystallization process. Especially because of its ability to repeatedly capture large-scale and up-to-date wetland information, it is possible to obtain satellite data on a regional or even global scale. The higher the concentration of the brine, the greater the difference between its spectrum and that of aquaculture water. The higher the concentration of the brine, the greater the spectral difference between it and the farmed water surface. For the brine just extracted from the ground, the spectral difference between it and the farmed water surface is smaller due to the relatively low salt content, which in turn causes mixing between the brine and the farmed water surface.

Low albedo features on remotely sensed images (e.g., asphalt roads, shadows from mountains, buildings, and clouds) can cause some impact on the accuracy of water body classification. The presence of shaded areas can cause misclassification of water bodies and thus reduce the accuracy of surface water mapping because the spectral properties exhibited by the shaded areas have some similarity to the spectral properties of water bodies. In scenarios where nonwater low albedo features are present, two-band water body indices (e.g., MNDWI) do not accurately distinguish between water body pixels and shaded regions. Compared with MNDWI, the AWEI not only is better at suppressing shadows and other nonwater dark surfaces on the image but also classifies edge pixels more accurately, and the optimal threshold for segmenting AWEI has less variation in time and space, so the AWEI can be an important choice when extracting water bodies (Figure 5). Energy production and related industrial activities have had a huge impact on the surface and underground environment of the region.

Water environment-sensitive point predetermination refers to the water quality analysis and prediction big data model to reveal the relevant elements of the water

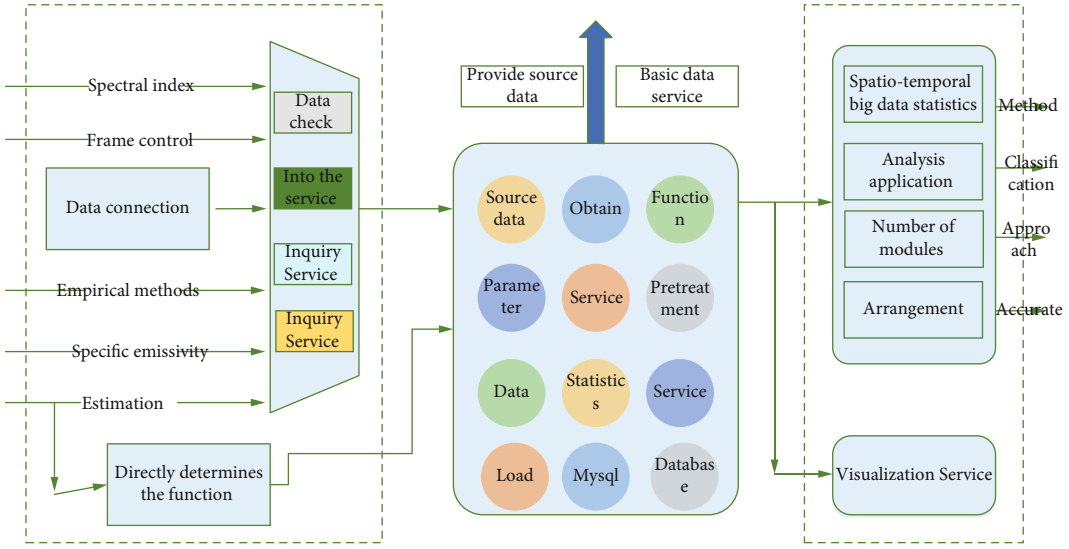

Figure 4: Flowchart for building a big data analytics application.

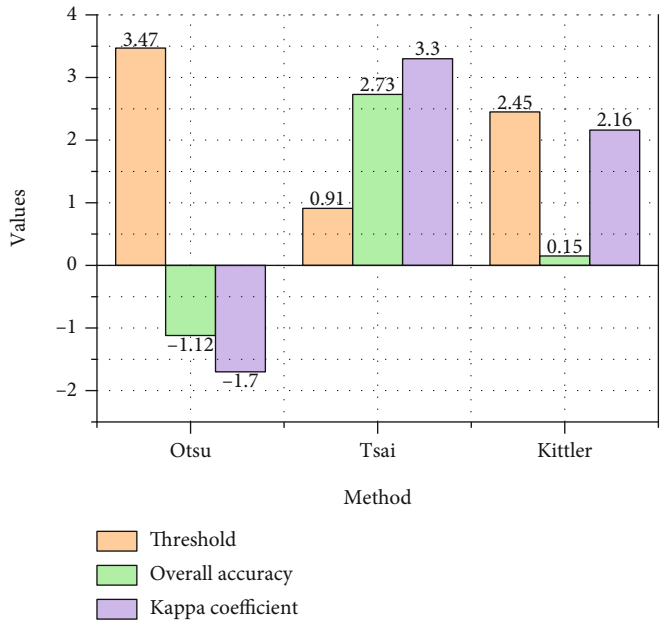

Figure 5: Accuracy of the thresholds calculated by the three threshold determination methods and the results of water segmentation.

environment and development trends, directly from the perspective of correlation between data to grasp the correlation between pollution sources and water quality, and then provide support for management decisions in areas such as prediction and early warning, which mainly includes water quality big data collection preprocessing, water quality big data offline learning, water quality big data online calculation, water big data visualization display, and other functions. Through the integration of meteorological forecasts and live data, pollution source data, air quality forecast data, socioeconomic and satellite remote sensing, other types of atmospheric environmental quality-related data, and the use of correlation analysis, cluster analysis, and other mathematical methods, data mining analysis, and the data of spatial and temporal analysis, component analysis, meteorological field clustering analysis, pollution, and economic factor correlation analysis, and other kinds of analysis, the interrelationship between the data can effectively provide sufficient support for the management of the atmospheric environment. It mainly includes atmospheric environment correlation analysis, atmospheric environment-sensitive point identification, and air quality early warning forecast, as shown in Figure 6.

Carrying out comprehensive improvement of the rural water environment, first, strengthen the treatment of rural domestic sewage and domestic waste. Promote the construction of rural domestic sewage treatment facilities, and promote the construction of small sewage treatment stations, artificial wetlands, oxidation ponds, and other domestic

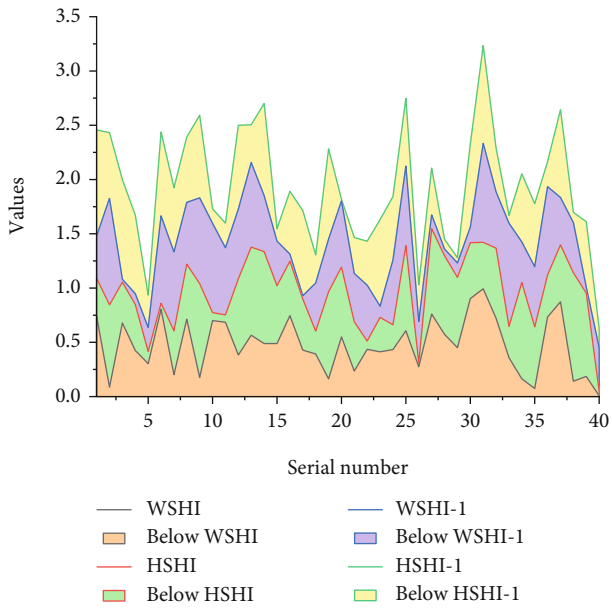

Figure 6: WSHI and HSHI thresholds.

sewage treatment facilities, laying sewage collection pipeline networks and unifying the treatment of domestic sewage in villages, because of the scattered nature of rural settlements and the high cost of building unified pipeline networks. Second, strengthen the prevention and control of pollution from concentrated livestock and poultry breeding in rural areas. Therefore, a series of big data services have emerged for the statistical analysis of big data. But for spatiotemporal big data, it is necessary to focus on analyzing its spatiotemporal attributes. For spatiotemporal big data with similar structures, a general statistical template can be used for statistical analysis of spatiotemporal big data. The city's livestock and poultry breeding will be verified, livestock and poultry breeding that cannot meet the standards will be treated by a deadline, and ecologically sensitive areas such as strictly controlled areas, drinking water source areas, and important reservoir catchment areas will be set as no-breeding areas. Livestock farms are encouraged to return manure and sewage to the land ecologically or use them to produce biogas, organic fertilizer, and other substances.

4.2. Results of Big Data Analysis of the Lower Yellow River Ecosystem. The integrated connectivity of the lower Yellow River channel is improved and maintained by carrying out reservoir water and sand transfer. River connectivity in the lower Yellow River has undergone a process from decreasing to increasing. Since the construction of Xiaolangdi Reservoir, the implementation of water and sand transfer has been strengthened, and the drainage of sand during floods has been enhanced, even shaping larger floods, and the frequency of flooding has increased; this has led to the obvious scouring of the river channel in the lower reaches, the siltation of the beach, and the obvious increase in the overflow capacity of the river channel; the difference in height of the beach channel has increased, making the river channel narrower and deeper, and the river channel has developed towards a stable river type, which has not only increased the longitudinal connectivity of the river channel but also maintained the lateral connectivity of the beach channel. Therefore, it is necessary to continue to maintain the water and sand transfer of Xiaolangdi Reservoir, to continue to maintain the balance of scouring or overall scouring and siltation of the lower Yellow River, not to return to the old way of siltation and uplift, and to maintain and promote the excellent state of longitudinal connectivity of the lower river, as shown in Figure 7.

In terms of the topography of the Yellow River Delta, urban development in the Yellow River Delta is less influenced by topography, thus providing a good spatial basis for urban expansion in all directions, which is one of the important factors that have enabled the rapid expansion of impervious surfaces in the Yellow River Delta in recent decades. Combining the actual application process of big data and the research goals of this article, the definition of big data in this article is clearly defined. Subsequently, this chapter sorts out the types and characteristics of environmental data, maps the concept of big data to the environmental field, clarifies the concept of environmental big data in this article, and compares the differences between environmental big data applications and traditional environmental applications. From the perspective of the soil characteristics of the Yellow River Delta, the spatial distribution of the Yellow River Delta soils determines the overall pattern of regional land use/cover and the direction of change of each type. Due to the high degree of salinization of tidal soils, these soils were mostly dominated by tamarisk scrub and unused land in the early period, and to meet the physical conditions required for population growth, humans increased the improvement of tidal soils, converting the former tamarisk scrub and unused land into arable land. The early land-use/cover types of saline soils were mostly unused land and mudflats, and since the salinity of saline soils is so high that it is difficult to improve them into arable land, most of these areas have been developed into highly economically productive land-use/cover types such as farmed water and salt flats.

The structure of land use/cover in the Yellow River Delta for each sampling year shows that arable land accounts for the largest share of all land-use/cover types, indicating that land use in the Yellow River Delta is mainly agricultural, and this type of use makes climate have a greater influence on land-use/cover change. In addition, global warming also has a driving effect on regional land-use/cover change, especially for those cities near the sea. This is because global warming causes sea-level rise, which in turn increases the erosive effect of seawater on coastal soils, resulting in increased salinization of soils, which in turn causes the more salt-tolerant vegetation on the seashore to no longer be able to adapt to this high salt growth environment, prompting the conversion of forested grasslands into mudflats and causing land-use/cover change, as shown in Figure 8.

Guided by the concept of water ecological civilization and the theoretical system of water ecological civilization construction, this paper analyzes the concept and connotation of urban water ecosystem health, as well as the

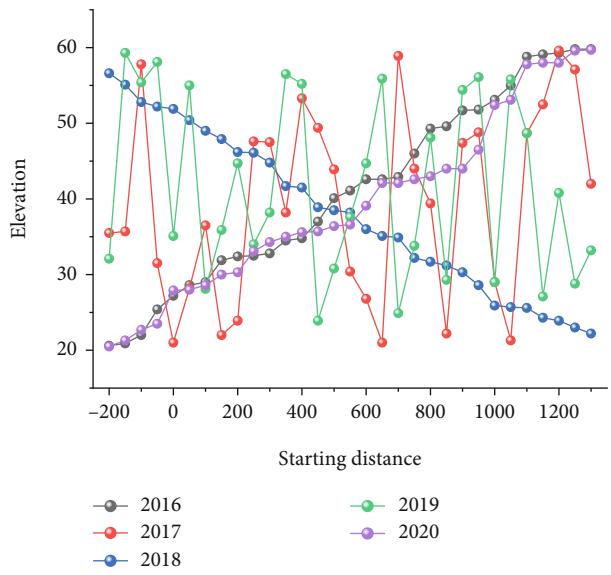

Figure 7: Hydrological station cross-sectional flushing and siltation variation.

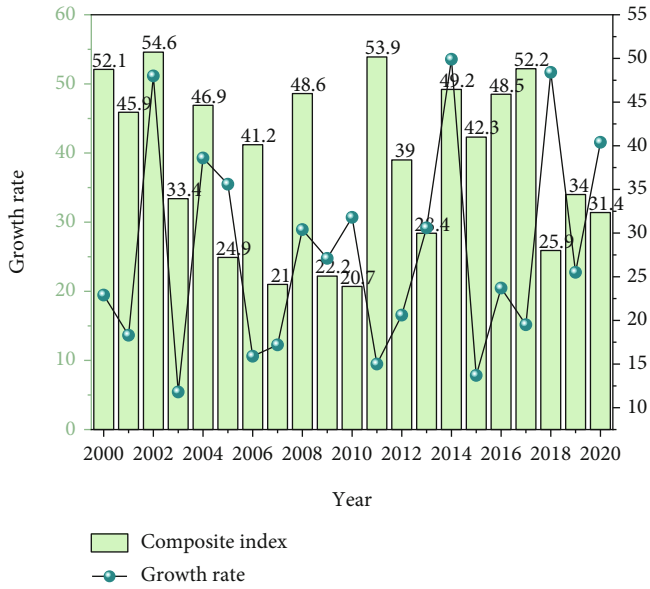

Figure 8: Evolution of the composite index and growth rate of the sustainable development system.

operating mechanism of urban water ecosystem health, and builds an evaluation model of urban water ecosystem health based on it. According to the evaluation results, a complete set of urban water ecological civilization construction idea frameworks is proposed. Strengthen industrial point source pollution treatment; carry out special rectification of chemical, pharmaceutical, and other heavy pollution enterprises; strengthen the transformation of sewage treatment facilities; promote the relocation of polluting enterprises and industrial upgrading and transformation; and investigate the key outfalls along with the more serious pollution of Naming River. Promote the treatment of surface source pollution, rational use of pesticides and fertilizers, and the implementation of clean agricultural production, and strengthen the construction of ecological interception projects for farmland retreat. There are semi-structured data and other unstructured data in the network; first, through data collection technology, a large amount of structured data, unstructured data, and semistructured data are integrated and extracted.

Carry out waste sewage network investigation, accelerate the construction of urban sewage collection network, improve the collection rate and treatment rate of waste sewage, and implement the upgrading of urban sewage treatment plants that do not meet the primary standard, reducing the number of pollutants entering the river from the process.

5. Conclusion

Based on the parallel random forest algorithm, the extraction method of typical vegetation types in the Yellow River Delta was constructed to improve the accuracy and efficiency of vegetation information extraction. In terms of extraction accuracy, the overall average accuracy of the extraction results of the Yellow River Delta time series was found to be 89.79% and the average kappa coefficient was 0.8838, which proved that the proposed method can achieve high accuracy in extracting typical vegetation types in the Yellow River Delta. In terms of computational efficiency, we found that the time spent on vegetation extraction with the proposed method is only 1/4~1/5 of that of the nonparallel random forest algorithm, and the average speedup ratio reaches 4.18, which proves that the proposed method can greatly improve the computational efficiency. Support vector machines, multiclass logistic regression, and multilayer perceptrons were used in the cooperation of multiple machine learning algorithms. The accuracy evaluation of the Yellow River Delta time series impervious surface extraction results shows that the overall average accuracy of the impervious surface extracted by the multistrategy synergistic method reaches 88.19% and the average kappa coefficient reaches 0.8647, which proves that the multistrategy synergistic method can obtain ideal results in extracting the impervious surface of the Yellow River Delta. The effectiveness of the method in extracting impermeable surfaces in the Yellow River Delta was verified. The transformation of wetland types was obvious, with many natural wetlands transformed into artificial wetlands or nonwetlands, and the main transformation types occurred between farming ponds, salt pans, and reservoir pits and mudflats, swampy wetlands, bare land, and agricultural land. Wetland transformation in the Yellow River Delta is influenced by both natural and anthropogenic factors, with human activities being the main influencing factor.

Data Availability

The data used to support the findings of this study are available from the corresponding author upon request.

Conflicts of Interest

The authors declare that there is no conflict of interest in this article.

Acknowledgments

This work was supported by the National Science and Technology Infrastructure Program Aid Financial Project (No. 2005DKA32300), the project of Science and Technology Project of Henan Province (152102110047), and the project of Major Science and Technology Project of Henan Province (121100111300).

References

[1] Q. Yue, F. Liu, C. Song, J. Liang, Y. Liu, and G. Cao, "Exploration and application of the value of big data based on data-driven techniques for the hydraulic internet of things," *International Journal of Embedded Systems*, vol. 12, no. 1, pp. 106–115, 2020.

[2] Y. Dong, B. Q. Hu, S. L. Zhang, Y. L. Huang, G. C. Nong, and H. Xin, "Research on North Gulf distributed big data submarine 3D terrain computing system based on remote sensing and multi-beam," *Soft Computing*, vol. 24, no. 8, pp. 5847–5857, 2020.

[3] C. Tomsett and J. Leyland, "Remote sensing of river corridors: a review of current trends and future directions," *River Research and Applications*, vol. 35, no. 7, pp. 779–803, 2019.

[4] P. Gao, H. Zhang, J. Yu et al., "Secure cloud-aided object recognition on hyperspectral remote sensing images," *IEEE Internet of Things Journal*, vol. 8, no. 5, pp. 3287–3299, 2021.

[5] H. Guo, J. Liu, Y. Qiu et al., "The Digital Belt and Road program in support of regional sustainability," *International Journal of Digital Earth*, vol. 11, no. 7, pp. 657–669, 2018.

[6] R. Yang and Y. Pan, "Rural vulnerability in China: evaluation theory and spatial patterns," *Journal of Geographical Sciences*, vol. 31, no. 10, pp. 1507–1528, 2021.

[7] A. Kamilaris, A. Anton, A. B. Blasi, and F. X. P. Boldú, "Assessing and mitigating the impact of livestock agriculture on the environment through geospatial and big data analysis," *International Journal of Sustainable Agricultural Management and Informatics*, vol. 4, no. 2, pp. 98–122, 2018.

[8] S. Yang, Y. Yang, and Q. Zhang, "Remote sensing tracking method for migration path of bar-headed goose under the impact of ecotourism," *Ekoloji*, vol. 28, no. 108, pp. 1203–1209, 2019.

[9] W. Hua, Z. Yuxin, W. Mengyu, N. Jiqiang, C. Xueye, and Z. Yang, "Spatial characteristics and driving forces of cultivated land changes by coupling spatial autocorrelation model and spatial-temporal big data," *KSII Transactions on Internet and Information Systems (TIIS)*, vol. 15, no. 2, pp. 767–785, 2021.

[10] A. Naboureh, J. Bian, G. Lei, and A. Li, "A review of land use/land cover change mapping in the China-Central Asia-West Asia economic corridor countries," *Big Earth Data*, vol. 5, no. 2, pp. 237–257, 2021.

[11] J. O. Payero, M. W. Marshall, A. M. Nafchi et al., "Development of an Internet of Things (IoT) system for measuring agricultural runoff quantity and quality," *Agricultural Sciences*, vol. 12, no. 5, pp. 584–601, 2021.

[12] Y. Leung, Y. Zhou, K. Y. Lam et al., "Integration of air pollution data collected by mobile sensors and ground-based stations to derive a spatiotemporal air pollution profile of a city," *International Journal of Geographical Information Science*, vol. 33, no. 11, pp. 2218–2240, 2019.

[13] Y. Wang and M. Li, "Urban impervious surface detection from remote sensing images: a review of the methods and challenges," *Ieee Geoscience and Remote Sensing Magazine*, vol. 7, no. 3, pp. 64–93, 2019.

[14] F. Mao, K. Khamis, J. Clark et al., "Moving beyond the technology: a socio-technical roadmap for low-cost water sensor network applications," *Environmental Science & Technology*, vol. 54, no. 15, pp. 9145–9158, 2020.

[15] G. Tran Thi Hoang, L. Dupont, and M. Camargo, "Application of decision-making methods in smart city projects: a systematic literature review," *Cities*, vol. 2, no. 3, pp. 433–452, 2019.

[16] J. Fell, J. Pead, and K. Winter, "Low-cost flow sensors: making smart water monitoring technology affordable," *IEEE Consumer Electronics Magazine*, vol. 8, no. 1, pp. 72–77, 2019.

[17] S. M. R. Alam and M. S. Hossain, "A rule-based classification method for mapping saltmarsh land-cover in south-eastern Bangladesh from Landsat-8 OLI," *Canadian Journal of Remote Sensing*, vol. 47, no. 3, pp. 356–380, 2021.

[18] B. Kong, H. Yu, R. Du, and Q. Wang, "Quantitative estimation of biomass of alpine grasslands using hyperspectral remote sensing," *Rangeland Ecology & Management*, vol. 72, no. 2, pp. 336–346, 2019.

[19] R. Jayaraman, B. S. Kumar, and S. K. Singh, "Remote sensing and GIS based site suitability analysis for tourism development in Vaishali block, Bihar," *Landscape & Environment*, vol. 15, no. 2, pp. 12–22, 2021.

[20] M. Deng, "Challenges and thoughts on risk management and control for the group construction of a super-long tunnel by TBM," *Engineering*, vol. 4, no. 1, pp. 112–122, 2018.

Hindawi
Journal of Sensors
Volume 2021, Article ID 9596606, 11 pages
https://doi.org/10.1155/2021/9596606

Research Article

Wireless Resource Management and Resilience Optimization of the M2M-Oriented Mobile Communication System

Li Liao [1,2] **and Chengjun Ji** [1]

[1] *School of Business Administration, Liaoning Technical University, Huludao, Liaoning 125105, China*
[2] *School of Economics and Management, Zhejiang University of Science and Technology, Hangzhou 310013, China*

Correspondence should be addressed to Li Liao; liaoli@zust.edu.cn

Received 1 November 2021; Revised 24 November 2021; Accepted 29 November 2021; Published 17 December 2021

Academic Editor: Gengxin Sun

Machine-to-machine (M2M) communication technology is an emerging technology that can connect smart wireless devices. The most obvious feature of M2M is that the communication between devices does not require human intervention. Therefore, ensuring the low-energy consumption of M2M devices is a necessary condition for prolonging the survival time of their devices. This paper first considers the coexistence of M2M and H2H scenarios. Aimed at the energy efficiency of M2M equipment and the channel capacity of H2H equipment, a multiobjective problem is constructed for joint spectrum and power resource management, and a weighted Chebyshev algorithm is proposed to solve this problem. Secondly, in view of the additional interference problems caused by the introduction of M2M communication, the intercell cooperative link selection algorithm is used to optimize its resilience. The effectiveness of the algorithm is proven by simulation results.

1. Introduction

The development of wireless communication technology and people's needs complement each other. Compared with the existing 4G (4th generation) technology, the upcoming 5G (5th generation) technology will provide higher transmission rate, lower transmission delay, and higher user satisfaction [1, 2]. Machine-to-machine communication (M2M) technology is not only the key component of Internet of things technology but also the basis of realizing information society. Therefore, this paper focuses on M2M technology [3, 4].

M2M uses sensor and other technologies to enable wireless communication equipment to have the ability of autonomous communication [5]. The biggest feature of this technology is that it does not need human intervention. Therefore, it can be applied to a variety of scenarios, such as intelligent transportation system, intelligent monitoring system, medical system, public security monitoring, and electronic meter reading [6]. These application scenarios are composed of a large number of mobile devices, and different devices have different quality of service, which will cause huge traffic consumption. According to literature [7], it is predicted that the total number of connections of M2M devices in 2022 will increase to 18 billion compared with the current total number of connections of M2M devices, accounting for 61% of the total accessible communication devices. Therefore, in the face of such a large number of M2M devices, people have paid more and more attention to their size, power, and cost. M2M technology and human-to-human communication (HTC) technology are different. The research focus of HTC technology is mainly to improve the user's transmission rate and reduce the delay, and the number of devices is far less than the number of M2M devices. When MTC devices and HTC devices coexist in the same cellular network and compete for spectrum resources together, the traditional communication quality between people will be affected by MTC. Therefore, in the future 5G ultradense M2M scenario and the network where MTC and HTC coexist, how to ensure the performance of MTC equipment without affecting the performance of HTC equipment is an important problem to be solved at this stage [8].

At the same time, in order to meet the QoS requirements of such large-scale M2M devices, it is necessary to effectively allocate the current wireless resources. Therefore, this paper proposes a new wireless resource management scheme. Secondly, for the additional interference caused by the introduction of M2M communication, it is necessary to provide corresponding wireless resource management and interference coordination strategies to optimize the system performance.

2. Related Knowledge

2.1. M2M. The network architecture of M2M specified by the technical committee of the European Telecommunications Standards Association is shown in Figure 1. M2M transfers data from one terminal to another, that is, the dialogue between machines. For example, access control cards for work, bar code scanning in supermarkets, and NFC mobile payment are more popular recently. Key M2M elements in the figure include the following: M2M device, M2M area network (device domain) providing connection between the M2M device and M2M gateway, personal local area network, M2M gateway using the M2M function to ensure interworking and interconnection between the M2M device and communication network, M2M communication network providing communication between the M2M gateway and M2M application, and M2M application program included in the application layer [9]. For M2M applications, their data passes through various applications and is processed and used by a specific business processing engine. M2M equipment forms an M2M regional network. Its applicable scenarios include not only small home networks but also larger scenarios, such as factory environment.

For the network architecture in Figure 1, the M2M device can be connected to the M2M server through WAN connection or M2M gateway. A gateway is an intelligent M2M device, which can easily collect and process data from M2M devices and manage their operations.

2.2. Research on M2M Wireless Resource Management. Different from the traditional communication system, in M2M communication, a large number of devices with multiple quality of service requirements access the network, which brings great challenges to resource allocation. At present, a large number of literatures have studied the radio resource management of M2M communication which is different from H2H communication, mainly including access control, spectrum allocation, and power control. This paper mainly focuses on spectrum allocation and power control [10].

At present, there are many possible architectures for M2M communication. Document [11] proposes three architectures, including direct communication between M2M devices and ENB, multihop transmission by gateway, and end-to-end transmission between M2M devices.

Because the uplink communication adopts single carrier frequency division multiple access (FDMA) multiple access mode, when M2M equipment communicates directly with ENB, the allocated frequency domain resource blocks are

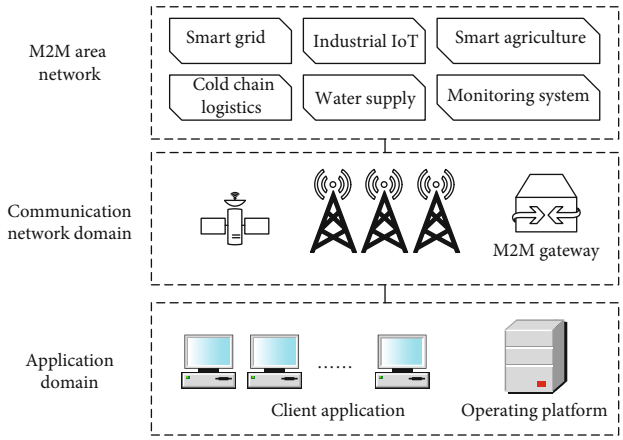

Figure 1: Network architecture of M2M.

required to be continuous, which increases the difficulty of resource allocation. C-FDMA single-carrier frequency division multiple access (single-carrier frequency division multiplexing) is the mainstream multiple access in the uplink of LTE. SC-FDMA is a single-carrier modulation mode. The basic processing methods can be divided into dft-s-gmc and dft-s-ofdm. In Reference [12], resource block allocation is transformed into resource block mode allocation, and the optimization problem is solved by combining the Lagrange dual method and ellipsoid method. According to the multiservice characteristics of M2M equipment, document [13] divides resource allocation into two steps. Firstly, the equipment is graded according to the equipment type and the allowable length of residual delay, and the equipment that can be scheduled is selected. Then, the appropriate resource block is selected according to the channel conditions of the equipment in different frequency bands. In Reference [14], user terminal equipment (UE) and M2M equipment are put into two queues, respectively, and the calculation formula of proportional fair scheduling algorithm is improved. This method not only considers the current channel conditions but also takes into account QoS and waiting delay. Based on this, they proposed a new scheduling algorithm. Both algorithms give M2M devices lower priority and ensure the performance of H2H communication when a large number of M2M devices join. However, in the case of heavy H2H load, these two methods can easily make it difficult for M2M equipment to communicate for a long time.

According to the mass characteristics of M2M devices, packet transmission of M2M devices is a good idea. Each section of information, together with the call control signal and verification information required for exchange, is arranged into a message packet according to the specified format. A packet is transmitted as a whole in the network, with high utilization of communication resources, which greatly improves the capacity and throughput of the channel. Document [15] proposes to group M2M devices and uses the traditional uplink spectrum resource allocation method for spectrum selection between groups and ordinary H2H devices. Device-to-device (D2D) communication is adopted in the group, and nonorthogonal spectrum is used with H2H equipment. In order to reduce the interference

of M2M equipment to H2H equipment, the whole problem is modeled as a bipartite graph, and the KM algorithm is used to allocate resources. Reference [16] uses a similar architecture, uses the KM algorithm to realize resource allocation in the case of M2M/H2H shared spectrum, and performs power control based on the interference level reflected by the proportional integral derivative (PID) controller. However, at present, most M2M devices do not support D2D communication, resulting in limited application scenarios. Document [17] proposes a nonorthogonal resource allocation method. M2M devices conduct random access in groups. Devices belonging to different groups can use the same group of resource blocks to improve spectral efficiency and adopt a continuous interference cancellation method to reduce interference. Literature [18] combines access control and resource allocation to reduce energy consumption and completes the determination of grouping, team leader selection, resource allocation, and packet size.

In addition, M2M equipment can also communicate with UE. Reference [19] proposed a distributed resource allocation method. Using the matching principle, the M2M device can negotiate with the UE device and give the UE certain compensation in exchange for the access of the subchannel. Document [20] proposes to use UE as the gateway of M2M equipment. In the first stage, the M2M device transmits the information to the corresponding UE. In the second stage, the UE transmits the information of the M2M device and its own information to the base station. By solving the optimization problem and setting the appropriate transmission power, the power consumption of M2M equipment is minimized on the premise of meeting the delay constraint, so as to improve the network lifetime of M2M equipment.

2.3. Optimize Interference and Signal Fading. Signal fading [21] and interference [22–24] are two important problems encountered in the design of the mobile communication system. Fading results in the reduction of coverage and reliability of point-to-point communication links. The existence of interference limits the reusability of wireless resources, thus limiting the improvement of spectral efficiency (BPS/Hz/area) per unit area [25]. In view of these two important problems, combined with the development process and trend of the mobile communication network, this section summarizes the research status of the M2M mobile communication scenario and the development trend of related mobile communication technologies.

As shown in Figure 2, in the mobile communication network based on intercell cooperation, it is assumed that the base stations are connected to each other through a backhaul network without delay and capacity limitation. Under this assumption, the base stations can share the global channel state information and all data information of their users. In this scenario, multibase station cooperation actually regards the whole multicell network as a large multiuser multiple input multiple output (MIMO) system [26, 27]. Therefore, the multibase station joint signal processing algorithm can eliminate interference, so as to greatly improve the system capacity [28–30].

3. Method

3.1. M2M Resource Allocation Algorithm. In the scenario of direct connection between MTC equipment and base station, MTC equipment and HTC equipment share the same frequency band resources, resulting in resource competition between the two system networks. At the same time, this paper maximizes the energy efficiency of MTC equipment and the rate of HTC equipment, so as to complete the reasonable allocation of bandwidth and power resources.

The system model diagram of this paper is shown in Figure 3. Suppose that there is only one base station (ENB) in this cell, and there are n MTC devices and M HTC devices in its coverage. These devices are randomly distributed in the cell, where the set of MTC devices is $\Omega = \{1, 2, \cdots, n\}$ and the set of HTC devices is $\Xi = \{1, 2, \cdots, m\}$. In this paper, it is assumed that all devices are directly connected to the base station for data transmission.

In this cell model, since the communication behavior of MTC equipment transmitting data mainly occurs in the uplink, the uplink is considered the main link. It is assumed that all access devices work in orthogonal frequency bands, so the interference between devices is ignored. The total shared bandwidth of all devices is set to $B_{\max}$, and this paper assumes that the base station can obtain the global channel side information (CSI) of all devices. In this paper, the gain between the MTC device n and the base station can be expressed as

$$d_n^{\alpha} g_n = h_n. \tag{1}$$

Similarly, the gain between the HTC device m and the base station is expressed as

$$d_m^{\alpha} g_m = h_m. \tag{2}$$

The signal propagating at multipath can reach the simultaneous interpretation of the field strength at the receiving point from different paths, and the delay time of each path is different. The superposition of the component waves in each direction produces a standing wave field strength, thus forming a fast fading signal, called Rayleigh fading, where HN represents that the variable has experienced slow fading and Rayleigh fading on the transmission link, DN represents the distance between MTC user n and the base station, and α is the path loss index.

In order to balance the performance of MTC devices and HTC devices, we will construct a multiobjective optimization problem. Compared with the single-objective optimization problem which can only obtain the unique solution, it is more suitable to solve the Pareto optimal solution in the coexistence scenario of MTC and HTC. Therefore, the weighted Chebyshev method is used in this paper.

The signal-to-noise ratio (SNR) of MTC equipment can be written as

$$p_n^{-1} \gamma_n = N_0^{-1} b_n^{-1} g_n. \tag{3}$$

Here, $p_n \geq 0$ and $b_n \geq 0$ represent the allocated

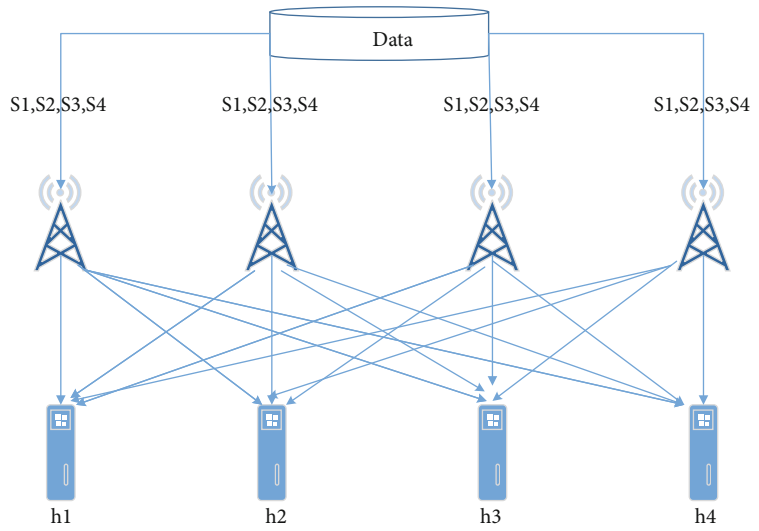

Figure 2: Cooperative multicell system model.

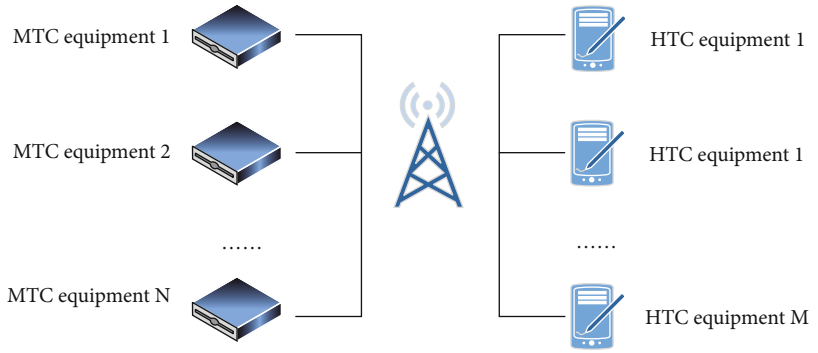

Figure 3: System model.

transmission power and bandwidth of MTC device n in the uplink, respectively, and n represents the power spectral density of additive white Gaussian noise (AWGN).

Therefore, the energy efficiency (EE) of a single MTC device can be expressed as

$$e_n = p_n^0 \log_2(\gamma_n + 1) b_n. \tag{4}$$

Here, r_n represents the transmission bit rate from MTC device n to the base station. In addition, $p_n^0 = p_n + p_e$, where p_e represents the fixed power consumption.

For HTC equipment, the uplink rate is also an important indicator in the future 5G communication. Therefore, the channel capacity requirements of HTC equipment are the focus of consideration. According to Shannon's theorem, the bit rate of HTC equipment m in the uplink can be written as follows:

$$r_m = b_m \log_2\left(N_0^{-1} b_n^{-1} g_n + 1\right). \tag{5}$$

$p_m = \{p_1, p_2, \cdots p\}$ and $b_m = \{b_1, b_2, \cdots, b\}$ are the optimized power and bandwidth variables of HTC devices, respectively. r_m represents the uplink bit rate of each HTC device, and b_m and p_m represent the bandwidth and power allocated to each HTC device, respectively. g_m represents the gain between HTC device m and base station.

Before introducing the weighted Chebyshev algorithm, this section first needs to deal with the weight factor accordingly. When a large number of MTC devices are connected to the cell network, more subcarriers are allocated to MTC devices, which will seriously affect the QoS of HTC devices. To solve this situation, this paper defines the ratio of the total number of subcarriers required by MTC devices to the bandwidth of the whole network The value is its demand factor (DF)p. Then, the weight function of energy efficiency of MTC equipment $\Phi_1(\rho)$ can be defined as follows:

$$\phi_1(\rho) = (1 - \exp sp)(1 - \exp s)^{-1}. \tag{6}$$

Here, s is a parameter greater than 1, which affects the curve slope of the weight function, and is set here as $\Phi_1(\rho) \in [0, 1]$, and the objective function increases with the increase in p. The gradient is a decreasing function, which shows that the sensitivity of the energy efficiency objective

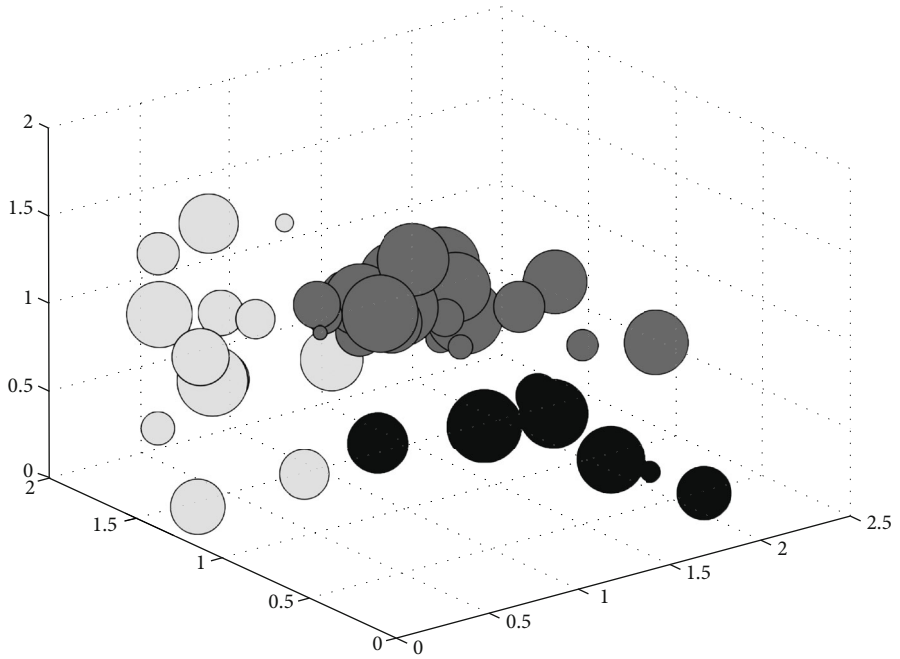

Figure 4: Cooperative multicell network layout and user distribution.

function of MTC equipment to a high DF factor is reduced. The energy consumption problem of MTC terminal can be solved by the communication unit deciding whether to enter the transmission state according to the relationship between the current channel signal-to-noise ratio and the preset threshold, which is obtained based on the maximum value of the energy efficiency function of MTC terminal. In addition, the weight function expression of HTC equipment can be calculated by $\Phi_2(\rho) = 1 - \Phi_1(\rho)$.

For the two optimization objectives, finding the minimum value is the core idea of the weighted Chebyshev algorithm.

$$\min_{\{p,b\}} \max_{n\in\Omega} \left\{ \phi_1 - f_1^u \phi_1 \sum r_n p_n^{-1}, \phi_1 - f_2^{-u} \phi_2 \sum r_m \right\}. \quad (7)$$

Here, Φ_1 and Φ_2 represent the positive weight factors of energy efficiency and system capacity functions, respectively. For the sake of fairness, the value of each single objective function is divided by its ideal point for normalization.

3.2. Optimization of Interference and Fading Signals. OFDMA combines OFDM and FDMA technology. After subcarriering the channel with OFDM, different subcarrier resources are allocated to different users to achieve multiple access. Consider a downlink OFDMA network jointly processed by multiple base stations, which contains k cooperative cells, and M users are evenly distributed in each cell, as shown in Figure 4. In each cell, the system bandwidth is divided into a series of continuous subcarrier sets orthogonal to each other, and each subcarrier set forms a subchannel. Because the subcarriers of OFDM overlap in the frequency domain, there is no guard frequency. Users access different subchannels in different time slots to achieve multiple access. Therefore, in the ideal synchronization case, there will be no multiuser interference in each cell. In this paper, a subchannel and a corresponding time slot are combined and defined as a basic resource allocation unit (AU). Assuming that each AU can only be occupied by a unique user, interference free multiuser access can be realized through the division of frequency and time resources.

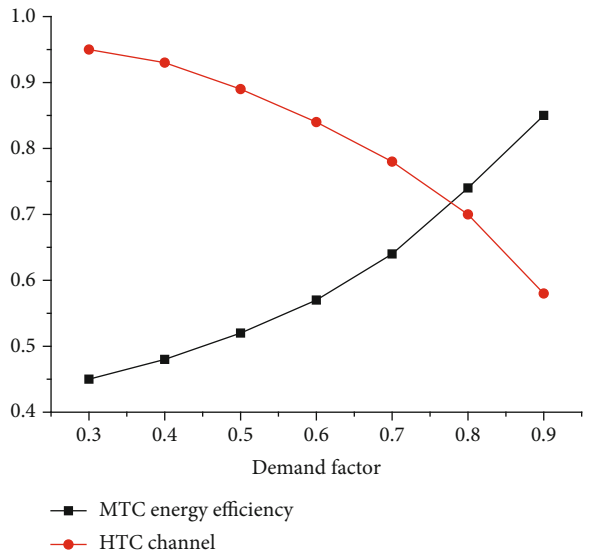

Figure 5: Relationship between multiobjective function and demand factor.

This paper considers two different physical frame structure models in the downlink OFDMA network, namely, ordinary physical frame and superframe. Each base station adopts different operations for radio resource management within and between cells under different frame structures.

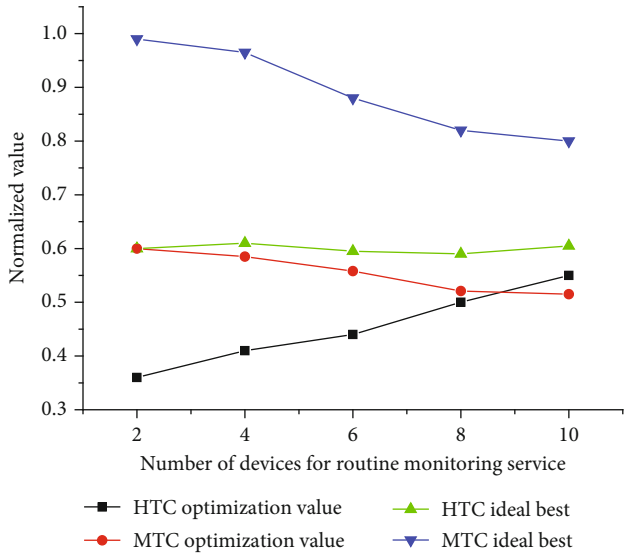

Figure 6: Relationship between multiobjective optimization value and the number of conventional monitoring service equipment.

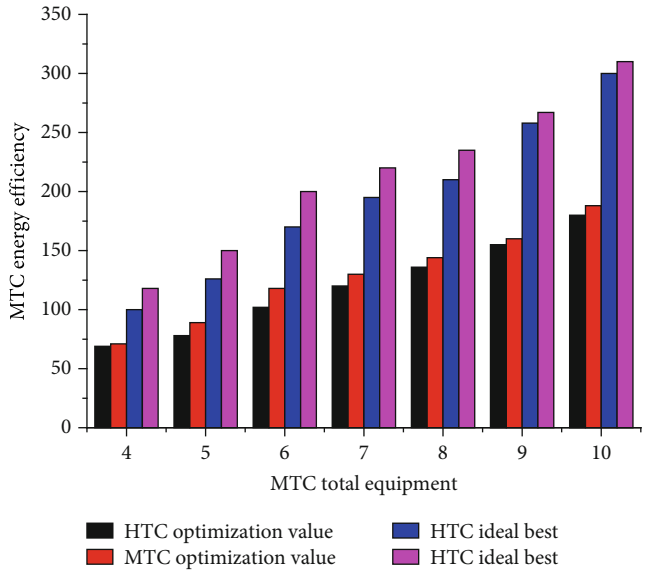

Figure 7: Relationship between multiobjective optimization value and total number of MTC equipment.

Suppose that when the working frequency band is divided into several continuous subchannels, the ordinary frame is composed of these subchannels and several continuous time slots. The super physical frame is composed of several time continuous ordinary frames.

On any AU_n, the signal-to-interference noise ratio received by user m from its serving base station K and other adjacent base stations can be expressed by the following formula.

$$\mathrm{SINR}_{k,m}^{n} = \frac{\left|h_{k,m}^{n}\right|^{2}}{N_0 p_i^{-n} \sum_{i=1}^{K} p_i^{n} \left|h_{i,m}^{n}\right|^{2}}, \tag{8}$$

where p represents the power of the transmitting base station K on the resource allocation unit (AU_n) and N_0 represents the power of the additive white Gaussian noise (AWGN). H_{nim} represents the complex channel response coefficient of the cofrequency interference channel on the AU_n from the base station master to the user m in cell K.

When the base station performs equal power allocation among AU in the physical frame, there are

$$p_t = N p_k^{n}, \tag{9}$$

where p represents the total transmission power of each base station and N represents the total number of radio resource allocation units (AU) contained in each physical frame.

Therefore, for the scheduling user m working on the AU_n in cell K, the downlink user rate can be expressed as follows:

$$r_{k,m}^{n} = \log_2\left(1 + \frac{\left|h_{k,m}^{n}\right|^{2}}{N_0 p_i^{-n} \sum_{i=1}^{K} p_i^{n} \left|h_{i,m}^{n}\right|^{2}}\right). \tag{10}$$

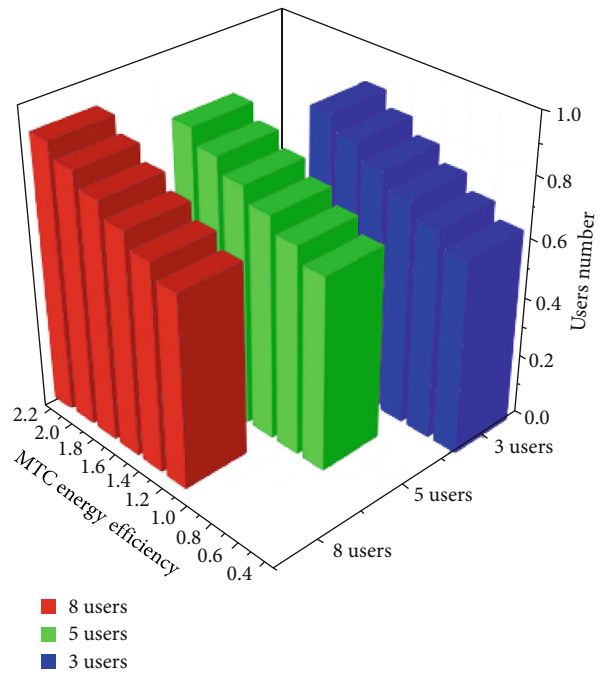

Figure 8: Pareto optimal solution.

Further, the total rate of scheduling user m in cell K can be expressed as

$$R_{k,m}^{n} = \sum_{n \in N} \log_2\left(1 + \mathrm{SINR}_{k,m}^{n}\right), \tag{11}$$

where NT, m represents the AU set composed of all resource allocation units occupied by user m in cell K.

By establishing intercell cooperative links to build a multicell joint signal processing system, interference can be eliminated and cooperation gain can be obtained. Therefore,

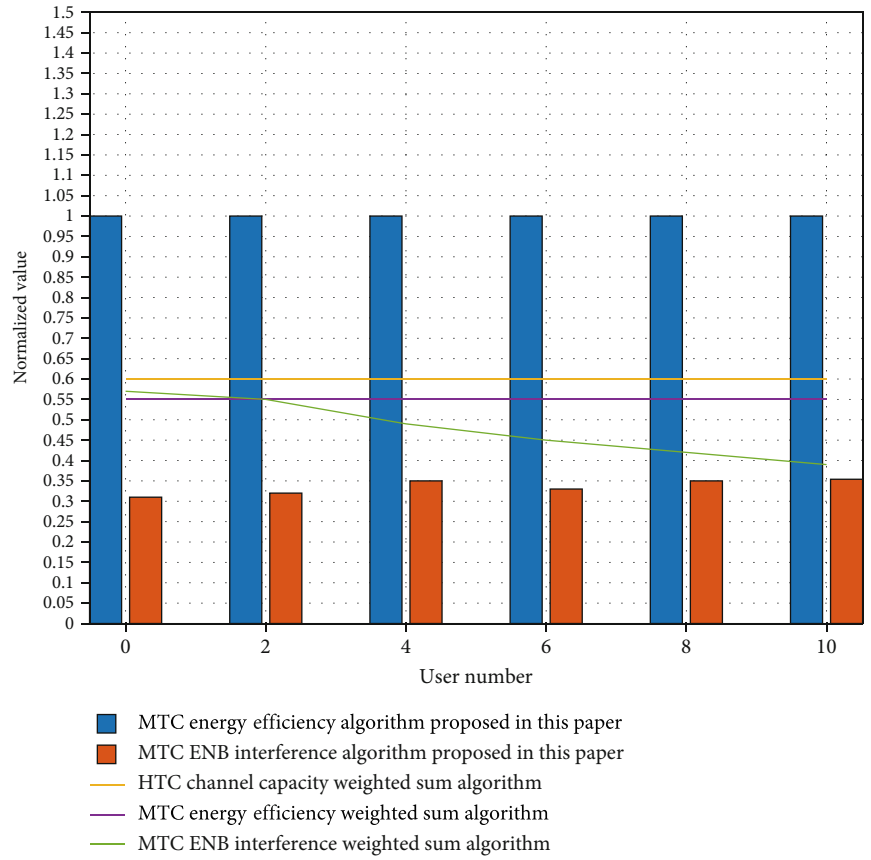

Figure 9: Relationship between normalized values of three objective functions and the number of users.

the network capacity gain of establishing cooperative links can be modeled as follows:

$$\text{benefit} = \frac{\widehat{r}_{k,m}^{n} - r_{k,m}^{n}}{\widehat{r}_{k,p}^{n}}, \tag{12}$$

$$\widehat{r}_{k,m}^{n} = \log_2\left(\frac{p_k^n \left|h_{k,m}^n\right|^2}{p_i^n \sum_{i=1}^{K} p_i^n \left|h_{i,m}^n\right|^2 + N_0}\right), \tag{13}$$

$$r_{k,m}^{n} = \log_2\left(\frac{p_k^n \left|h_{k,m}^n\right|^2}{\sum_{i=1}^{K} p_i^n \left|h_{i,m}^n\right|^2 + N_0}\right). \tag{14}$$

4. Results and Discussion

4.1. Performance Analysis in Orthogonal Resource Scenarios. The relationship between multiobjective function and demand factor p is simulated in Figure 5. In order not to lose generality, the energy efficiency of MTC and the channel capacity of HTC are normalized, respectively. The channel varies randomly, and the values vary from large to small, so the normalization of channel coefficients is for better data comparison. The number of three services of MTC equipment is $(n_{SM}, n_{EA}, n_{RM}) = (4,4,2)$. As shown in Figure 5, when the demand factor p changes from 0.3 to 0.9, the energy efficiency of the normalized MTC equipment continues to increase. This is because the higher the weight factor of MTC devices, the higher their priority to obtain band resources. On the contrary, the channel capacity of the normalized HTC device decreases with the increase in P. This is because fewer subcarrier resources are allocated to HTC devices. It is worth noting that even when p is very high, the normalized energy efficiency value will not increase sharply, which is conducive to protecting the QoS of HTC equipment from changing too fast.

The relationship between MTC energy efficiency and HTC energy efficiency and the number of equipment users served by RM is discussed in Figure 6. The increasing number of users means that the overall QoS requirements of the MTC system are improving. Therefore, it can be seen from the curve in the figure that as the proportion of service devices gradually increases, the bandwidth available for HTC devices gradually decreases. Therefore, the optimal value of HTC channel capacity calculated by the KM algorithm and its ideal point are in a downward trend. In addition, by observing the curve in the figure, we can know that the optimal value of MTC channel capacity and its ideal point are also in a downward trend. This is because MTC equipment improves its ability to obtain power resources to meet high QoS requirements, thus reducing the energy efficiency value of the system. As a comparison with the algorithm in this paper, the performance of the weighted sum (WS) algorithm is also reflected in this figure. Assuming that the weight ratio of the two objective functions of the weighted sum algorithm is also 1 : 1, it can be seen from the comparison curve in the figure that when the weighted

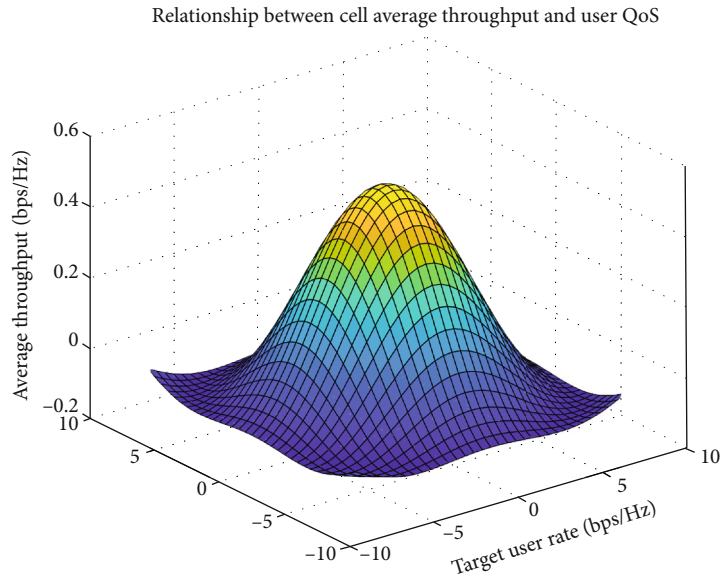

(a) Relationship between cell average throughput and user QoS

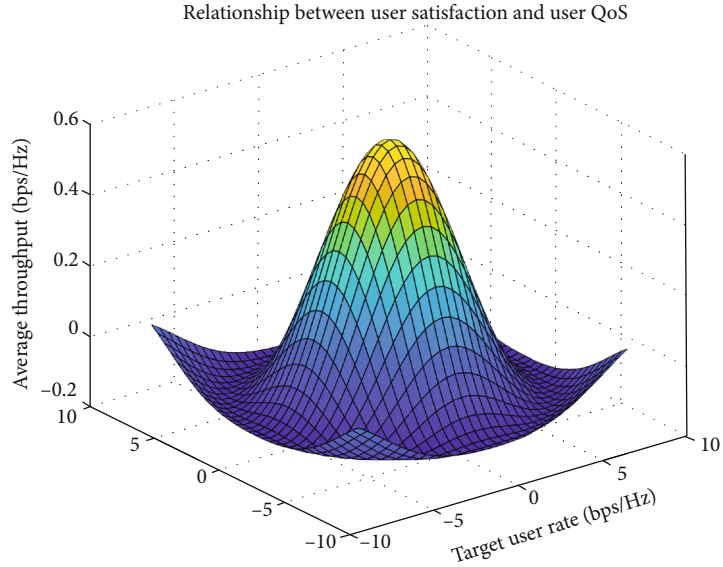

(b) Relationship between user satisfaction and user QoS

Figure 10: Performance analysis of multiple indicators.

sum algorithm is adopted, the MTC energy efficiency and HTC channel capacity curve decrease or increase significantly with the change of the number of devices. Using this algorithm, we can see that the fluctuation range of these two curves is not large. The weighted Chebyshev method is an iterative multivariable optimization method based on the Remez exchange algorithm, which can be used for polynomial interpolation. The corresponding interpolation polynomials can minimize the Runge phenomenon and provide the best uniform approximation of polynomials in continuous functions. It can be seen that the weighted Chebyshev algorithm adopted in this paper to solve the multiobjective optimization problem can better reflect the fairness of the compromise between the two objective functions than the weighted sum algorithm, which is more in line with the scene in the actual network.

The effectiveness of the proposed multiobjective optimization algorithm under different user equipment scenarios is proven in Figure 7. It can be seen from the figure that with the increasing number of users n, the curve of the ideal point and the optimization curve obtained by the KM algorithm are in an increasing trend. Therefore, in the scenario of different numbers of users, the multiobjective optimization algorithm proposed in this paper still has good applicability, which is more suitable for the actual needs of future wireless networks.

Figure 8 shows the trade-off between energy efficiency and channel capacity in the scenario of 8 users, 5 users, and 3 users. When the demand factor P changes from 0.65 to 0.9, the Pareto optimal solution of HTC equipment and MTC equipment changes. The Pareto optimal state is that there is no more room for Pareto improvement; that is,

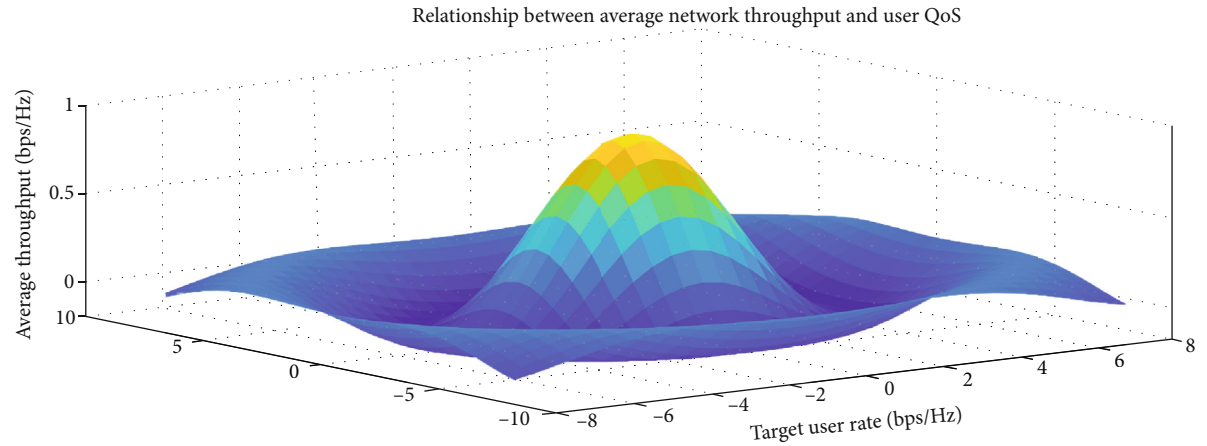

(a) Relationship between average network throughput and user QoS

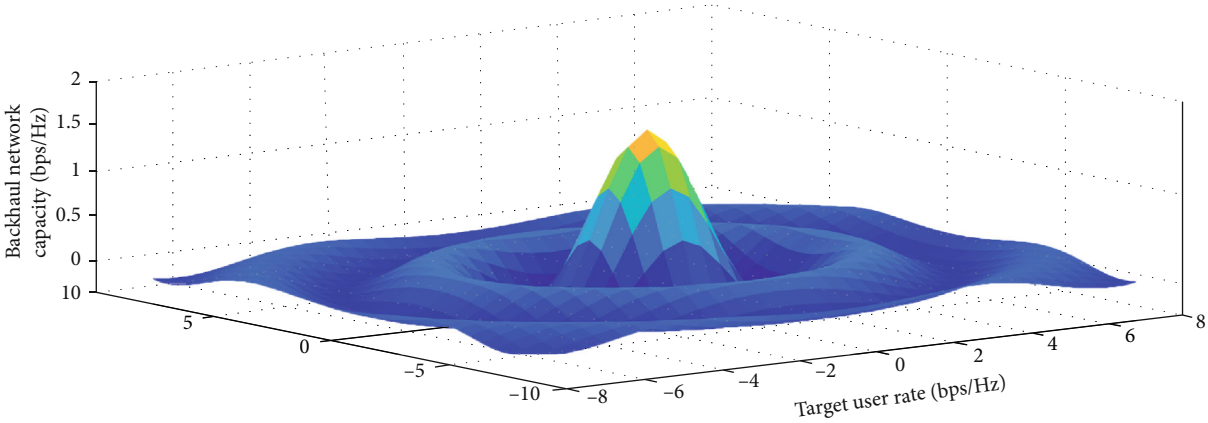

(b) Relationship between backhaul network capacity consumption and user QoS

Figure 11: Relationship between average network throughput performance and backhaul network capacity consumption and user requirements.

Pareto improvement is the path and method to achieve the Pareto optimal. The curve of the former shows a downward trend, and the curve of the latter shows an upward trend. This is because with the increase in P, MTC devices have higher priority in obtaining bandwidth and spectrum resources. Similarly, when p decreases, the curve in the graph will show the opposite trend. In short, in the actual scenario, according to the demand factor of MTC equipment, network managers can balance the system performance of MTC and HTC by adjusting the weight function.

4.2. Performance Analysis under the Interference Scenario. In performance analysis under the interference scenario in Figure 9, the performance of the weighted Chebyshev algorithm used in this paper is compared with that of the traditional weighted sum algorithm, the weight factor is set as $\Phi_1 = \Phi_2 = \Phi_3 = 0.33$, and the algorithm of three targets is normalized. As can be seen from the figure, when the weighted Chebyshev algorithm is adopted, the normalized value of MTC interference to ENB is reduced by 2%. In contrast, for different numbers of users, when using the weighted sum algorithm, the optimal channel capacity of HTC equipment is close to its ideal point value 1, which is much higher than that obtained by using the weighted Chebyshev algorithm. However, the optimization performance of MTC equipment is much lower than that of the weighted Chebyshev algorithm.

4.3. Optimized Performance Analysis. Figure 10(a) shows the relationship between the change of user QoS requirements and the change of network average throughput and compares the impact of the change of cell average number of users on throughput. It can be seen that with the increase in user QoS requirements, the average throughput of the cell also increases gradually. However, when the average number of users per cell increases, the average cell throughput decreases. Moreover, with the increase in user QoS requirements, this difference becomes more and more obvious. This is because there are too many users, resulting in fierce competition among users in the cell, and the available wireless resources are quickly allocated, making it difficult to maintain user demand.

Figure 10(b) shows the relationship between the change of user QoS requirements and user satisfaction in the same

case. It can be seen that when the user QoS is generally low, most users can meet their communication quality requirements regardless of the total number of users. However, with the increase in user QoS demand, the user dissatisfaction of cells with high user density increases sharply compared with cells with low user density. Figures 10(a) and 10(b) also show that relying solely on wireless resource management and user scheduling is difficult to meet the large number of users and high user communication requirements.

Figure 11(a) describes the relationship between the average cell throughput and the user QoS requirements. The results show that with the improvement of user QoS requirements, the performance of the three algorithms shows an upward trend. The performance of the proposed algorithm is between the other two, because the proposed algorithm is limited by the backhaul network capacity, and there is a trade-off between throughput performance and backhaul network consumption. The problem of limited backhaul link capacity is common in cellular communication systems, which is also the bottleneck to realize the potential performance gain of downlink comp.

The backhaul network is the return line of the line. Generally, the end users have a large download service and a small amount of uplink data. The throughput reflects the amount of data that can actually pass through the network and receive the backhaul network capacity limit. Figure 11(b) compares the backhaul network capacity consumption of the two algorithms in Figure 11(a). The global cooperation algorithm works better under the nonconvex setting, but it depends on the global learning rate. It can be seen that with the increase in user QoS requirements, the backhaul network communication pressure caused by the global cooperation algorithm increases approximately linearly, and the consumption is too large. Relatively speaking, the algorithm proposed in this paper maintains the performance improvement of the whole network brought by cooperation.

5. Conclusion

Firstly, this paper considers the coexistence of M2M and H2H and considers the allocation and management of band resources and power resources. A multiobjective problem is constructed for joint spectrum and power resource management, and the complex optimization problem is transformed into a single objective optimization problem that can be solved directly by the weighted Chebyshev algorithm. Secondly, in view of the additional interference caused by the introduction of M2M communication, an intercell cooperative link selection algorithm is proposed, which not only eliminates the interference and improves the rate but also effectively reduces the network capacity requirements of wireless resource management. From the performance simulation results, it can be seen that under the resource management of the proposed algorithm, MTC and HTC systems can coexist fairly. Moreover, the proposed scheme shows performance advantages in user fairness, average network throughput, and communication pressure relief for the backhaul network and maximizes performance gain by minimizing network redundancy overhead.

Data Availability

The data used to support the findings of this study are available from the corresponding author upon request.

Conflicts of Interest

The authors declare that they have no known competing financial interests or personal relationships that could have appeared to influence the work reported in this paper.

References

[1] H. Dujuan, "Mobile communication technology of sports events in 5G era," *Microprocessors and Microsystems*, vol. 80, article 103331, 2021.

[2] S. Buffa, M. Cozzini, M. D'Antoni, M. Baratieri, and R. Fedrizzi, "5th generation district heating and cooling systems: a review of existing cases in Europe," *Renewable and Sustainable Energy Reviews*, vol. 104, pp. 504–522, 2019.

[3] A. Esfahani, G. Mantas, R. Matischek et al., "A lightweight authentication mechanism for M2M communications in industrial IoT environment," *IEEE Internet of Things Journal*, vol. 6, no. 1, pp. 288–296, 2019.

[4] Y. Mehmood, N. Haider, M. Imran, A. Timm-Giel, and M. Guizani, "M2M communications in 5G: state-of-the-art architecture, recent advances, and research challenges," *IEEE Communications Magazine*, vol. 55, no. 9, pp. 194–201, 2017.

[5] G. Tuna, D. G. Kogias, V. C. Gungor, C. Gezer, E. Taşkın, and E. Ayday, "A survey on information security threats and solutions for machine to machine (M2M) communications," *Journal of Parallel and Distributed Computing*, vol. 109, pp. 142–154, 2017.

[6] X. Liu and N. Ansari, "Resource allocation in UAV-assisted M2M communications for disaster rescue," *IEEE Wireless Communications Letters*, vol. 8, no. 2, pp. 580–583, 2019.

[7] E. Lara, L. Aguilar, M. A. Sanchez, and J. A. García, "Lightweight authentication protocol for M2M communications of resource-constrained devices in industrial internet of things," *Sensors*, vol. 20, no. 2, p. 501, 2020.

[8] M. Kamel, W. Hamouda, and A. Youssef, "Uplink performance of NOMA-based combined HTC and MTC in ultra-dense networks," *IEEE Internet of Things Journal*, vol. 7, no. 8, pp. 7319–7333, 2020.

[9] V. Mancuso, P. Castagno, M. Sereno, and M. A. Marsan, "Modeling MTC and HTC radio access in a sliced 5G base station," *IEEE Transactions on Network and Service Management*, vol. 18, no. 2, pp. 2208–2225, 2021.

[10] D. Tokody and F. Flammini, "The intelligent railway system theory," *International Transportation*, vol. 69, no. 1, pp. 38–40, 2017.

[11] R. P. Centelles, F. Freitag, R. Meseguer, and L. Navarro, "Beyond the star of stars: an introduction to multihop and mesh for LoRa and LoRaWAN," *IEEE Pervasive Computing*, vol. 20, no. 2, pp. 63–72, 2021.

[12] A. Aijaz, M. Tshangini, M. R. Nakhai, X. Chu, and A.-H. Aghvami, "Energy-efficient uplink resource allocation in LTE networks with M2M/H2H co-existence under statistical QoS guarantees," *IEEE Transactions on Communications*, vol. 62, no. 7, pp. 2353–2365, 2014.

[13] H. Yang and S. An, "Robustness evaluation for multi-subnet composited complex network of urban public transport," *Alexandria Engineering Journal*, vol. 60, no. 2, pp. 2065–2074, 2021.

[14] M. A. Mehaseb, Y. Gadallah, A. Elhamy, and H. Elhennawy, "Classification of LTE uplink scheduling techniques: an M2M perspective," *IEEE Communications surveys & tutorials*, vol. 18, no. 2, pp. 1310–1335, 2016.

[15] K. Zheng, F. Hu, W. Wang, W. Xiang, and M. Dohler, "Radio resource allocation in LTE-advanced cellular networks with M2M communications," *IEEE Communications Magazine*, vol. 50, no. 7, pp. 184–192, 2012.

[16] S. Hamdoun, A. Rachedi, and Y. Ghamri-Doudane, "Graph-based radio resource sharing schemes for MTC in D2D-based 5G networks," *Mobile Networks & Applications*, vol. 25, no. 3, pp. 1095–1113, 2020.

[17] H. S. Jang, H. S. Park, and D. K. Sung, "A non-orthogonal resource allocation scheme in spatial group based random access for cellular M2M communications," *IEEE Transactions on Vehicular Technology*, vol. 66, no. 5, pp. 4496–4500, 2016.

[18] C. Yin, L. Shi, R. Sun, and J. Wang, "Improved collaborative filtering recommendation algorithm based on differential privacy protection," *The Journal of Supercomputing*, vol. 76, no. 7, pp. 5161–5174, 2020.

[19] D. Kim, D. Hyeon, J. Oh, W.-S. Han, and H. Yu, "Influence maximization based on reachability sketches in dynamic graphs," *Information Sciences*, vol. 394-395, pp. 217–231, 2017.

[20] Y.-H. Lin, J.-J. Huang, C.-I. Fan, and W.-T. Chen, "Local authentication and access control scheme in M2M communications with computation offloading," *IEEE Internet of Things Journal*, vol. 5, no. 4, pp. 3209–3219, 2018.

[21] G. R. MacCartney and T. S. Rappaport, "Millimeter-wave base station diversity for 5G coordinated multipoint (CoMP) applications," *IEEE Transactions on Wireless Communications*, vol. 18, no. 7, pp. 3395–3410, 2019.

[22] Y. J. Chun, S. L. Cotton, H. S. Dhillon, F. J. Lopez-Martinez, J. F. Paris, and S. K. Yoo, "A comprehensive analysis of 5G heterogeneous cellular systems operating over κ–μ shadowed fading channels," *IEEE Transactions on Wireless Communications*, vol. 16, no. 11, pp. 6995–7010, 2017.

[23] F. Wu, R. Tan, C. Zhang et al., "Mixed numerology interference recognition approach for 5G NR," *IEEE Wireless Communications Letters*, vol. 10, no. 10, pp. 2135–2139, 2021.

[24] K. S. Ali, H. Elsawy, A. Chaaban, and M.-S. Alouini, "Non-orthogonal multiple access for large-scale 5G networks: interference aware design," *IEEE Access*, vol. 5, pp. 21204–21216, 2017.

[25] F. Qamar, M. H. D. N. Hindia, K. Dimyati, K. A. Noordin, and I. S. Amiri, "Interference management issues for the future 5G network: a review," *Telecommunication Systems*, vol. 71, no. 4, pp. 627–643, 2019.

[26] M. Abdullah, S. H. Kiani, and A. Iqbal, "Eight element multiple-input multiple-output (MIMO) antenna for 5G mobile applications," *IEEE Access*, vol. 7, pp. 134488–134495, 2019.

[27] M. S. Sharawi, "Current misuses and future prospects for printed multiple-input, multiple-output antenna systems wireless corner," *IEEE Antennas and Propagation Magazine*, vol. 59, no. 2, pp. 162–170, 2017.

[28] E. Chen, M. Tao, and Y. F. Liu, "Joint base station clustering and beamforming for non-orthogonal multicast and unicast transmission with backhaul constraints," *IEEE Transactions on Wireless Communications*, vol. 17, no. 9, pp. 6265–6279, 2018.

[29] J. An, Y. Zhang, X. Gao, and K. Yang, "Energy-efficient base station association and beamforming for multi-cell multiuser systems," *IEEE Transactions on Wireless Communications*, vol. 19, no. 4, pp. 2841–2854, 2020.

[30] F. Liu, C. Masouros, A. Li, H. Sun, and L. Hanzo, "MU-MIMO communications with MIMO radar: from co-existence to joint transmission," *IEEE Transactions on Wireless Communications*, vol. 17, no. 4, pp. 2755–2770, 2018.

Hindawi
Journal of Sensors
Volume 2021, Article ID 9974170, 10 pages
https://doi.org/10.1155/2021/9974170

Research Article

Animation Art Design Online System Based on Mobile Edge Computing and User Perception

Jianzhi Liu

School of Shenyang Ligong University, Shenyang, Liaoning 110000, China

Correspondence should be addressed to Jianzhi Liu; fateloli@sylu.edu.cn

Received 25 October 2021; Accepted 1 December 2021; Published 14 December 2021

Academic Editor: Gengxin Sun

Based on mobile edge computing and user perception technology, this paper analyzes and discusses the respective advantages and disadvantages of the important optimization models and mobile models in the animation art design, as well as the wireless block data transmission mechanism and protocol. In order to solve the problem that user mobility cannot be sensed, a content-centric mobile edge animation art design mechanism based on user mobility perception is proposed. This mechanism comprehensively calculates the centrality of users' perception of nodes, the idle rate of animation design, and the staying time of users in a small area. The mobile edge network controller integrates the information of each edge user's perception node, calculates the importance of each edge user's perception node and prioritizes it, and selects the appropriate content animation to design the user perception node according to the ranking result. Finally, various simulation or platform test experiments were carried out for all the design schemes in this paper, and the experimental results were analyzed. The simulation experiment results show that compared with the traditional animation design mechanism, the animation art design system effectively reduces the average number of hops for users to obtain content by up to 15.9%, improves the hit rate of edge user perception node animation design by at least 13.7%, and reduces the traffic entering the core network by up to 32.1%. According to the comparison results, the various designs in this work can successfully use sensor data to preclassify migration tasks in the mobile edge network environment. Compared with the latest block data transmission protocol, it has a significant performance improvement, reducing the data distribution delay by 34.8%, thereby helping to improve the overall efficiency of mobile edge computing.

1. Introduction

Mobile edge computing has become a computing model that is expected to provide pervasive computing and storage services for mobile and big data applications. At the network edge, due to the deployment of small base stations, the mobile edge computing service network can be established [1]. These small base stations are usually able to directly connect to mobile users and provide them with fast feedback low-latency services. Therefore, mobile users can upload and migrate some computationally intensive or delay-sensitive tasks to the currently connected small base stations. Mobile edge computing networks use the hardware resources on small base stations to assist users in handling such tasks [2]. The decision to perform task migration in this new computing model faces many new challenges such as complex task requirements, high user mobility, diverse applications and services, and limited computing and storage resources of small base stations [3]. Therefore, how to collect and use the new features of the mobile edge network and improve the task allocation decision and data transmission efficiency involved in the task migration process are all topics and directions that are worthy of in-depth study [4–6].

With the rapid development of the entire mobile Internet and the development of a new generation of wireless networks, in order to solve the above problems, small base stations with certain computing and storage capabilities have been laid on the edge of the mobile network on a large scale [7]. Therefore, how to use these small base stations scattered on the edge of the network to provide users with lower latency and higher bandwidth services and to undertake

the task of reducing the burden on the core network has become particularly important [8]. Therefore, task migration under mobile edge computing can be used not only as a way to expand terminal resources but also as an effective method to increase network throughput and reduce task delay. In this context, the research on task migration decision-making, task migration allocation, and high-performance block data transmission mechanism has great practical significance [9]. Specifically, in terms of task migration decision-making and allocation, the unique data or device characteristics (such as sensor data) that can be provided by mobile smart terminals or mobile Internet of things terminals are used to combine the task's demand for computing resources and reduce task processing time. The goal of extending and reducing the energy consumption of equipment is designed to design a more optimized migration strategy, so as to achieve more detailed division and decision-making on whether the task is migrated or to which user-aware node is for processing [10].

On this basis, this paper mainly designs and verifies the following three aspects of work in mobile edge computing: a service model architecture that perceives the characteristics of mobile users and a migration task preclassification mechanism, a user-based mobile migration optimization algorithm, and a high-performance block data reliable transmission protocol. In order to solve the situation that the content animation design location and the marginal user perception node animation design space are insufficient, this paper proposes an animation design mechanism based on the age and popularity of the content information. This mechanism uses the three attributes of communication, computing, and animation design of the edge user perception node and uses the communication ability, computing ability, and animation design ability of the user perception node as an evaluation index to measure the importance of the user perception node. The node animation design content is required by users, and when the animation design space is insufficient, the information age and popularity of the animation design content in the animation design user perception node are used as reference indicators for content replacement. Simulation experiments show that compared with the animation design mechanism and probabilistic animation design mechanism, the algorithm in this paper improves the fault tolerance rate of edge user perception node animation design by 12.3% and 10.8%, respectively.

2. Related Work

The development of the mobile Internet has led to the vigorous rise of video applications, and video traffic occupies a dominant position in the explosive growth of data traffic on a global scale. With the growth of mobile data traffic, the traditional cloud computing-based mobile Internet architecture cannot meet the low-latency requirements of video applications, and the consumption of network bandwidth has increased sharply. Therefore, the center of the mobile communication network architecture has evolved from base stations to information and content. The mobile edge network (MEN) includes mobile fronthaul networks (between radio frequency units and distribution units), mobile midhaul networks (distribution units to centralized units), and mobile backhaul network (above the centralized unit) [11–13].

In terms of improving the recognition accuracy of user behavior characteristics, Cong et al. [14] started with sensor data such as different directions and positions of smart phones and provided experiments and analysis methods. In this work, two experiments of placing smart phones in different user carrying positions were carried out. The experiments included 10 users participating in the test and 6 daily user behavior characteristics. They built a feature vector based on the three-dimensional acceleration signal to calculate the average and standard deviation and built an instance-based classifier. By organizing the acceleration signals into the same coordinate system, the accuracy of its recognition has been significantly improved. Sha et al. [15] use acceleration sensors to distinguish seven behavioral features generated in the user's daily activities. It considered and clarified the placement of 6 kinds of mobile phones. Compared with the previous work, this work was able to construct more features because it collected more time-domain and frequency-domain features from the 7 users participating in the experiment. Finally, a support vector machine classifier is used to test the classification results. When the placement position is known, the overall F-score can reach 94.8%. Zhang et al. [16] tried to minimize the task execution delay with a one-dimensional search algorithm in a single-user scenario. The algorithm outputs whether a task determines the migration strategy according to the computing and processing capabilities of the user's mobile devices and small base stations, as well as the animation design queue status of the application tasks. In addition, the model proposed in this work also takes into account the characteristics of the wireless channel between the user equipment and the small base station. In the task migration calculation model proposed by the author, the task migration decision is completed by the task migration strategy module at the user equipment.

Wang et al. [17] proposed that the content of the animation design in the device is shared through D2D communication; that is, in each time period, each user should animate the design data at a constant rate, and then, each user transmits the D2D link at a constant rate as a convex optimization problem. In SBS animation design, the content animation is designed in the small base station (SBS). If the user's desired content animation is designed in SBS, the local SBS will directly distribute the content to the device. Generally, the information between SBSs in the same area is shared; that is, the data content or resource usage of the animation design in each SBS is known to neighboring SBSs. Miao et al. [18] proposed to perform animation design on SBS; that is, in each time period, it is ideal to design data at a constant rate and redefine the problem as a convex program. Then, the dual decomposition method is used to solve this convex problem, and a subgradient algorithm for finding the optimal dual variable is proposed. Finally, the optimal transmission power structure at MBS and the optimal animation design strategy at SBS are derived. Some scholars

use the relevance of user files and user social relationships to predict the popularity of content through collaborative filtering and predict the needs of certain users to provide active services by designing popular content in advance animation on base stations and devices. This approach can greatly reduce the peak demand for data traffic. Researchers make time-varying estimates of popularity based on user requests and the freshness of content and use the Poisson noise model to estimate the popularity distribution a priori [19–21].

3. Construction of an Online Design Model of Animation Art Based on Mobile Edge Computing

3.1. User Perception Level Distribution. The functions of the user-perceived data center mainly include mobile network control, management, and scheduling. The functions of the mobile core network mainly include control plane network functions such as mobility management (AMF), session management (SMF), and user data management (UDM). Gateway functions such as User Plane Function (UPF) are interconnected with the centralized unit of the mobile edge network or other macrobase stations to form a regional convergence network [22, 23]. The mobile edge network is composed of a mobile fronthaul network, a mobile midhaul network, and a mobile backhaul network. Figure 1 is the user-perceived hierarchical topology.

Each user perception node will operate according to the three states of the time slot—transmission time slot, reception time slot, and sleep time slot. Then, the work of data distribution and transmission will be completed in the form of page-by-page transmission; that is, a user perception node will only transmit the data of the next page after the current page data has been received by the subuser perception nodes in its structure.

$$\left(\frac{x-y}{a_1}\right)^2 - \left(\frac{x+y}{a_2}\right)^2 = 1. \tag{1}$$

The RAN network has evolved from a two-level structure consisting of a baseband processing unit and a remote radio frequency unit in a 4G network to a centralized unit (CU), a distributed unit (DU), and a radio unit (RU). The centralized unit and the distributed unit can be deployed separately or jointly. According to their different deployment methods, the RAN network is divided into different networks: the radio frequency unit and the distributed unit are between the fronthaul network and the distributed unit.

$$S = \frac{E(m=1)}{L} - \frac{N}{L} \times \left(1 - \frac{2}{L+d}\right)^{N-m}, \tag{2}$$

$$t' = [r \times \cos\theta, r \times \sin\theta, r \times \tan\theta_1 - t]. \tag{3}$$

Between the centralized units is the intermediate transmission network, and above the centralized unit is the backhaul network. The core network is split into two parts: a new core network unit and a mobile edge computing (MEC) unit. The mobile edge network is further divided into a mobile fronthaul network, a mobile midhaul network, and a mobile backhaul network.

$$f_{11} = \left(\frac{1}{n} \times \sum_{i=1}^{n} x_t^2, \frac{1}{n} \times \sum_{i=1}^{n} y_t^2\right). \tag{4}$$

Specifically, in terms of network resource management, with network virtualization technology as the technical support, the cloud control layer performs a unified and abstract description of physical and network resources to achieve resource pooling and unified scheduling. For different IoT applications, the cloud-based control layer builds dynamic edge networks on demand and implements collaborative management of edge network resources by deploying virtual gateways. First, it can support the data distribution transmission form of the multihop pipeline, and different page data can be transmitted at the same time in different hops, thus reducing the overall data distribution; the second is to establish a retransmission mechanism and ensure the reliability of the final data transmission.

$$g(m,t) = \frac{n * (h(m,t)/k(i,t))}{\sum_{i=1}^{n} h(i,t)/k(i,t)}. \tag{5}$$

A bitmap can be used in a request message to indicate the missing data packet, and for the entire file object, using a bitmap to represent it may occupy a large space in the limited message payload or even fail to represent it. However, it will be much smaller if a bitmap is used to represent a page of data, so it can also be appropriately placed in a request message. When all page data has been received, the reliability of block data transmission will be reduced. It is guaranteed.

3.2. Mobile Edge Computing Algorithm. The tasks of the mobile edge computing model can be processed in three ways, namely, letting the task be executed locally, through the edge small base station, or through the upper-level macrobase station to request the mobile edge computing service for task processing. By calculating the energy consumption and delay costs generated by different access methods, to achieve the lowest energy consumption cost as the optimization goal, it is combined with the minimum delay limit of user tasks.

In the algorithm at this stage, the criteria for judging the three categories are as follows: if the task is executed locally that can meet its minimum delay requirements and the energy consumption of the local execution does not exceed the energy consumption of the migration task, it will be retained for execution locally; if tasks that cannot meet the minimum latency requirements for local execution must be migrated to the mobile edge computing system for execution, tasks in other cases represent the third type and tasks in this type will eventually be in the first stage that determines whether to migrate tasks to the mobile edge computing user perception node according to the wireless

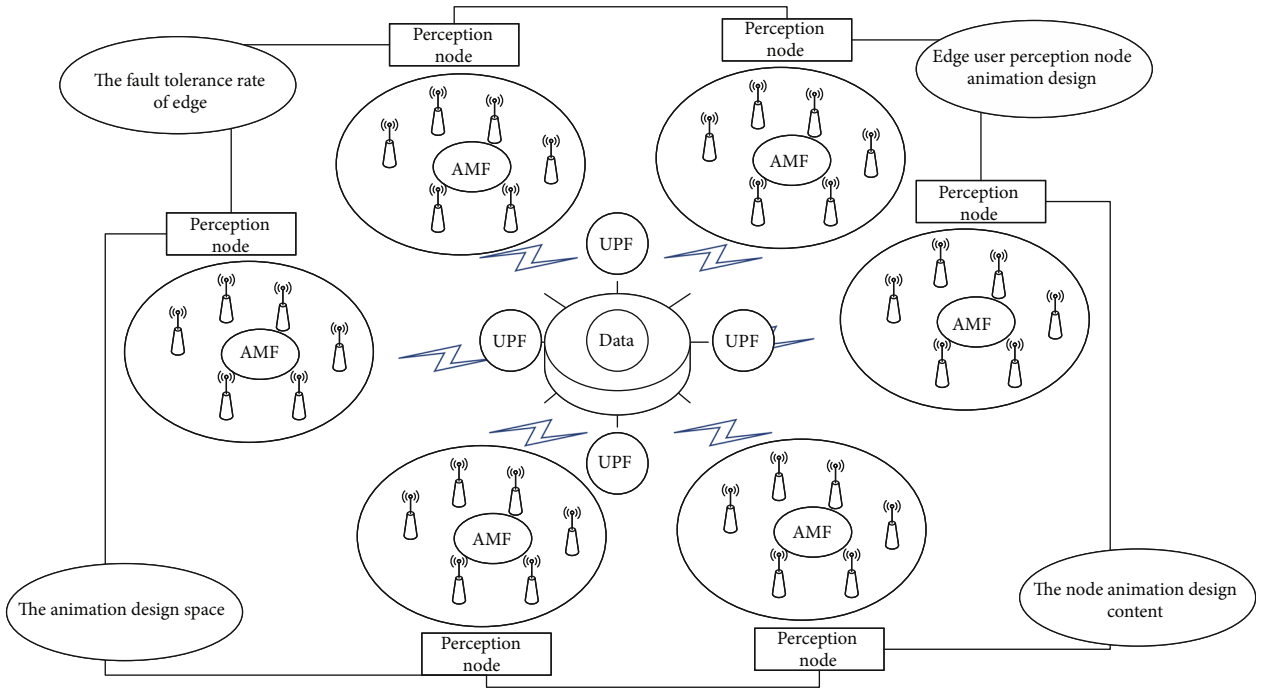

Figure 1: User-perceived hierarchical topology.

communication status. Figure 2 is a histogram of user perception nodes of mobile edge computing.

The core idea of the animation design mechanism based on the age and popularity of content information is as follows: first, according to the three inherent communication, computing, and animation design attributes of the edge user perception node, select the appropriate content required for the edge user perception node animation design. The process of determining the edge user perception node is by calculating the distance from the edge user perception node to the user perception node to characterize the communication capability of the user perception node; the number of collaborative edge user perception nodes sharing animation design content characterizes the computing ability of the user perception node. The free rate of the animation design space of the perception node represents the animation design ability of the edge user perception node. Finally, the total score of each edge user perception node is obtained and the animation design priority of the edge user perception node is sorted, and several are selected in order.

In the current network, video data traffic has replaced voice data traffic as the main traffic type. In many cases, D2D communication enables devices that are close to each other to share content or interact with each other, such as games and social networks. At the same time, D2D communication can improve network efficiency in many aspects: firstly, it saves a lot of signaling resources and reduces transmission delay; secondly, it saves a lot of elements compared to transmission through base stations; in addition, because the path loss is much smaller than that of base station-to-device communication loss, it can improve the spectral efficiency.

3.3. Composition of Animation Art Elements. In the animation art scene, mobile users migrate the computationally intensive and time-sensitive tasks on their devices to a mobile edge computing network composed of multiple small base stations with computing and storage capabilities. In this mobile edge computing system, we consider a small base station set N, where $N = \{1,2,3,\cdots,n\}$, and distribute the data in the network according to the similarly mentioned mesh topology distribution transmission. All of the small base stations can receive, execute, and transmit tasks that need to be relocated. In addition, we also assume that the software-defined network architecture is used in the mobile edge network; that is, all small base stations are controlled and monitored by the central controller. Among them, conditions C1 to C3 are guarantees of the delay conditions for using three different methods; conditions C4 to C6 are that the task can only choose one way to execute, and the purpose is to avoid task duplication and waste of computing and energy resources. It is to ensure that the channel allocation does not conflict; condition C8 restricts the total number of channels occupied not to exceed the number of channels that can be allocated.

The basic structure of MEC is given in the specification document. The MEC system is divided into three levels at a macrolevel, namely, the system layer, the host layer, and the network layer. Figure 3 is the distribution of the basic structure of animation art elements. The top layer is the system layer, which is the level management entity of the MEC system. It manages the MEC system globally and abstracts the system as an interface for users and third-party developers to use; the middle layer is the core host layer, which is hosted by the MEC. It consists of two parts and MEC host management, including the underlying hardware resource

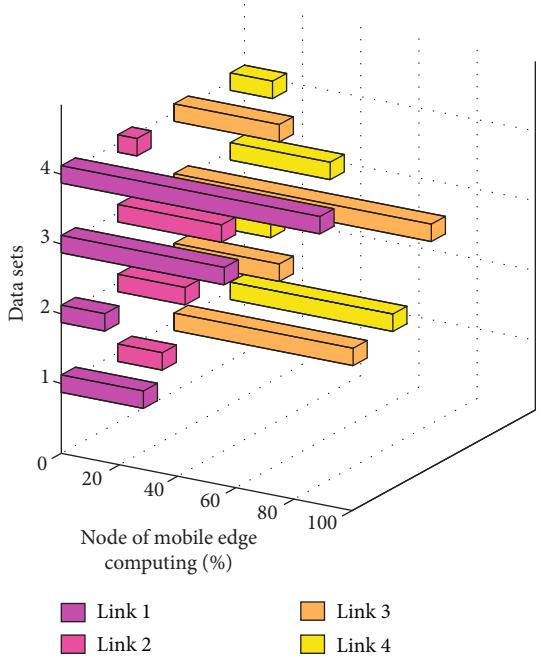

Figure 2: Histogram of user perception nodes of mobile edge computing.

layer and the virtualization layer, which provide guarantee for functions related to virtualized switching, storage, and computing.

Among them, unloadable tasks must be performed locally on the vehicle, such as user interaction, input and output, and peripheral interfaces. The unloadable part of the task can be executed by the animation processor, or it can be transmitted to the MEC server on the RSU side by establishing a connection with the roadside unit. The unloadable task generally does not need to interact with the local device. It is assumed that the tasks of each vehicle user cannot be divided into multiple subtasks in fine-grained granularity again; either all are handed over to the local execution or all are offloaded. The roadside unit detects the task status of the animation, minimizes the overall service delay according to the status of the animation and the task, plans the unloading strategy and arranges the order of task scheduling, and arranges the priority of the unloaded task.

3.4. Design Model Weight Iteration. In order to evaluate the control optimization decisions taken by the animation design system in each state, this section uses the resource usage cost under the time delay constraint to represent the cost function of the system. The main user's resource usage cost is mainly determined by the energy consumption and resource price generated by the system. In order to maximize the use of renewable elements, the cost of using renewable elements can be set to zero.

One advantage brought about by migrating the user's computationally intensive tasks to the mobile edge computing small base station is that it can reduce the execution delay. When the user's local device performs all computing tasks by itself (that is, no task migration is performed), the execution delay (Dl) represents the time it takes to perform tasks locally on the user device. In the case of migrating computationally intensive tasks to mobile edge computing small base stations for processing, the execution delay (Do) includes the following three parts: (1) transmission of migration data to mobile edge computing user perception node duration (Dot); (2) the calculation and processing time (Dop) of the migration task of the small base station in the mobile edge computing system; and (3) after the migration task is processed, the user equipment receives the processing transmitted back from the small base station to receive the result data (Dor).

Figure 4 is the level of the animation art design model. As the number of user-perceived tasks increases, the proportion of tasks processed on the local device also increases, because although offloading tasks can greatly reduce the delay, due to the single-channel characteristics, tasks need to be queued and the waiting time will also increase as the number of tasks increases, and local processing can be performed in parallel, so local computing has a significant advantage. We iterate 100 times to reach convergence, find the optimal unloading strategy, and achieve the minimum overall system time cost. And we compare the improved binary particle swarm algorithm and the original binary particle swarm algorithm, both can achieve convergence, and the convergence speed is faster, but the BPSO algorithm makes all the particles follow the position of the optimal particle and gradually tend to be the same. The phenomenon of prematurity has appeared, so that it has fallen into the local optimal situation and cannot jump out of finding the global optimal solution. The GA-BPSO algorithm strengthens the global search ability through crossover and mutation operations, so that the final result is obtained. Strategy performance is better than that of BPSO. Therefore, from the point of view of the convergence and convergence rate of the algorithm, although the convergence rate of the algorithm is not as fast as the BPSO algorithm, the discrete particle swarm optimization algorithm introduced with the genetic algorithm has a significant improvement in the optimization ability, and the system delay performance is improved about 9.2%.

4. Application and Analysis of the Animation Art Online Design Model Based on Mobile Edge Computing and User Perception

4.1. Mobile Edge Computing Data Preprocessing. The hardware environment of this experiment is Intel(R) Core(TM) i7-640m CPU @2.8 GHz and 8 G RAM, and the software environment is Ubuntu 16.04 LTS 64-bit MATLAB 2016a. Finally, it is compared with the animation design mechanism LCE and the probability cache mechanism Prob and compares and analyzes the three evaluation indicators of the content source user's perception node average number of requests, animation design hit rate, and average request delay.

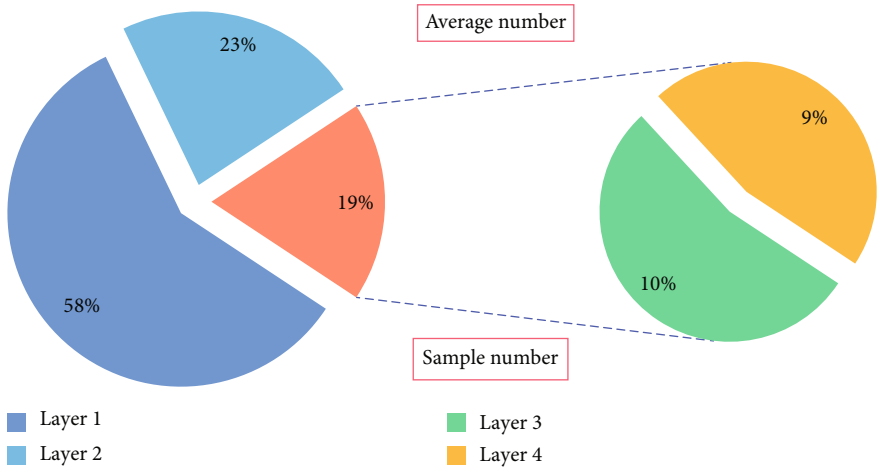

Figure 3: The distribution of the basic structure of animation art elements.

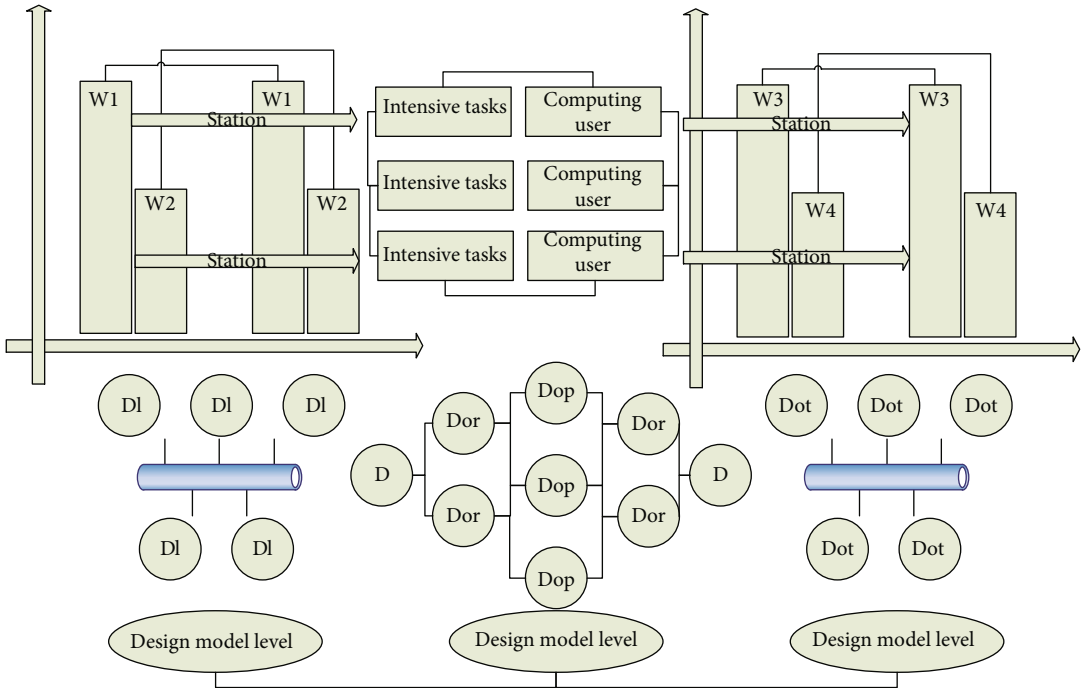

Figure 4: Animation art design model level.

The average number of requests accepted by the content source user perception node reflects the number of times the source user perception node has been visited. The lower the request load is, the higher the animation design hit rate of the edge user perception node will be; the traffic flowing to the core network will decrease, and the performance of the corresponding animation art design mechanism will be better. This paper uses the edge confidence based on the mean shift to describe the average probability that the detected edge information points are true edge points. The greater the degree of difference is, the higher the probability that the detected edge point is the true edge point. At the same time, we use the edge detection results to reconstruct the animation and calculate the reconstruction similarity index with the original image, to evaluate the integrity of the edge detection results and to make up for the defect of the edge confidence index; the reconstruction method adopts the linear interpolation reconstruction method.

Figure 5 is the similarity index curve of moving edge reconstruction. The experimental results show that as the number of auxiliary users increases, the total system cost based on Lyapunov's computing migration strategy shows a significant downward trend. This is because more auxiliary user SDs participate in D2D-ECN, and the joint optimization strategy of task offloading, power control, and computing resource allocation can be used to realize distributed task transmission and data processing and reduce the energy for each auxiliary user, thereby reducing system overhead. It can

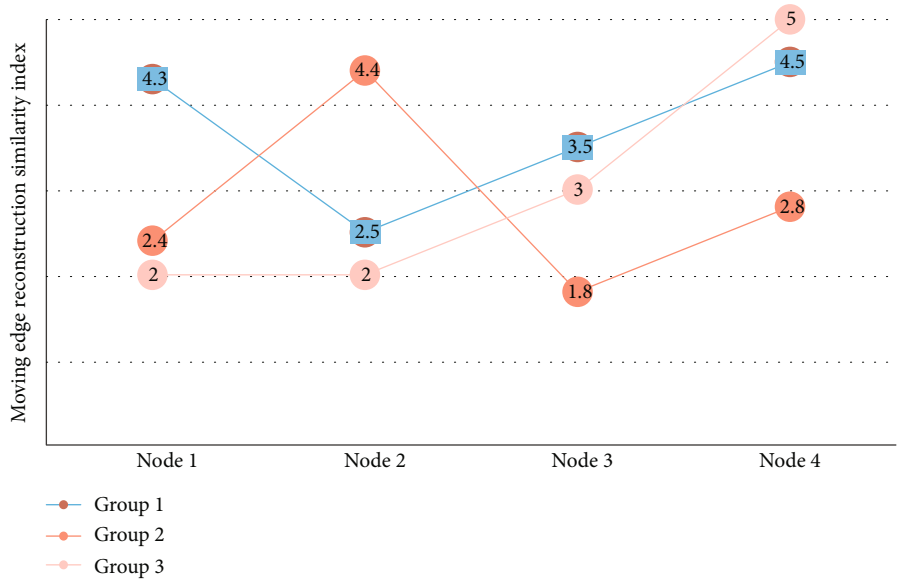

Figure 5: Moving edge reconstruction similarity index curve.

be seen that the average number of requests accepted by content source user perception nodes of the three animation design mechanisms gradually decreases with the increase in R. Among them, the AoIPC mechanism content source user perception node accepts the least number of requests and flows to the core network the least. This is because with the increase in R, most of the content requested by the user is directly animated at the edge user perception node, where the user can directly obtain the requested content, so the average number of requests received by the content source user perception node is large. Compared with the AoIPC mechanism, Prob is still insufficient in the diversity of animation design content at the user perception node, so it still causes a certain amount of content redundancy. In the end, the average number of requests received by the user perception node of the content source is relatively large. Compared with AoIPC and Prob, the LCE mechanism has the same animation design for all content resources at all user perception nodes. Even if the animation design capacity increases, there is still a lot of content redundancy. The content source user perception node obtains it, and the content source user perception node accepts the most requests on average.

4.2. Animation Art Online Design Simulation. In this section, MATLAB R2014b software is used to simulate and verify the task migration algorithm in a single cycle. In order to verify the performance of the two-way matching correlation algorithm, we used the random request correlation strategy as a benchmark to compare and analyze the animation utility and the edge server utility.

In addition, in the two-way matching process, the influence of animation and edge server as the association applicant or association decision-maker on the utility of their respective preferences was analyzed through simulation. On the other hand, in addition to adopting two-way matching to satisfy the respective preference utility of animation and edge servers, in the actual economic model, the resource supply and demand parties will also maximize the total income from the perspective of cooperation (social welfare) to design animation and edge servers. This problem can be described as a 0-1 linear programming problem that maximizes the weighted utility of animation and edge servers. With the help of the correlation analysis and screening unit, we can select all the sensor parameters that are positively related to the user's preferred applications and services and pass them to the learning unit for training. We use learning tools to classify, select which sensors are more critical to specific applications and services, and provide service references for small base stations in mobile edge computing networks accordingly.

Taking into account the richness and diversity of the edge details of the animation, the edge detection experiment is compared with the sample library composed of 20 images, and the average value and the mean square error are used to calculate the edge confidence and the results of the reconstruction similarity and combined with the t-test. When the P value of the significance test is greater than 0.05, it means that there is no significant difference between the effects of the two detection methods and vice versa and it indicates that the effects of the two detection methods are significantly different. Figure 6 shows the sensor parameters of mobile edge computing.

In order to achieve the optimal compromise between the long-term average task service delay and the long-term average energy consumption of the system, a joint optimization problem of task offloading, computing resource allocation, and energy scheduling is designed. From a time-domain perspective, network traffic shows periodic changes during weekdays and weekends. From a spatial point of view, network traffic presents single-peak and multipeak characteristics in different areas. Moreover, business traffic has strong randomness on the peaks and troughs. For a single IoT device, according to different business requirements, the generation of business data has stronger random

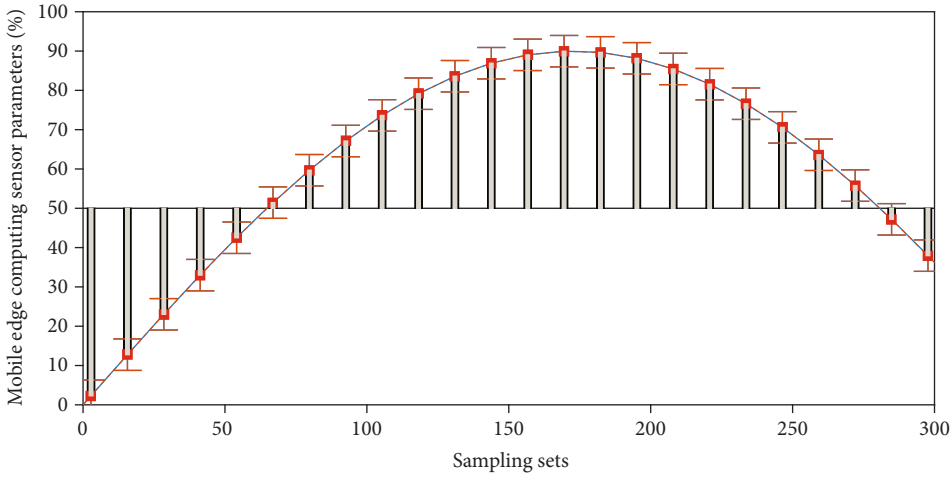

Figure 6: Mobile edge computing sensor parameters.

characteristics. It can be seen that the distribution of renewable elements presents the characteristics of periodic certainty, periodic uncertainty, and complete randomness. It can be seen from the temporal and spatial distribution characteristics of business data and renewable elements that in real network scenarios, it is difficult to use a deterministic distribution or closed expression to accurately reflect the characteristics of data and energy distribution under different temporal and spatial conditions. The simulation results prove that the algorithm proposed in this paper can effectively reduce the average response delay of system processing tasks by comparing it with other algorithms and ensure that the cost of application service providers for leasing base station resources is maintained at a relatively low level.

4.3. Example Application and Analysis. In this model framework, we choose to use the naive Bayes method as a concise learning tool. The edge confidence and reconstruction similarity are used to quantitatively evaluate the detected edge information points, the statistical samples are used to quantitatively evaluate the mean and standard deviation of the results, and the t detection method is used to count the edge confidence and reconstruction similarity of 20 images. Due to the differences in the detection effects of strong and weak edges in the method in this paper, the samples are divided into two categories: animations containing a large amount of strong edge information and animations containing a large amount of weak edge information.

For battery-powered equipment that may have computing interruptions, energy harvesting technology is used to ensure the continuity of data transmission and business processing. One aspect of this consideration is that Naive Bayes only needs a small amount of training data to estimate sensor parameters for classification. On the other hand, this section mainly proposes this innovative model framework rather than a specific learning algorithm. This learning tool was chosen because of the efficiency of its deployment in the framework. Therefore, the computing migration system needs to design a matching computing migration algorithm based on this randomness and uncertainty, so as to ensure the continuity of the computing migration process. Figure 7 shows the calculation uncertainty distribution based on the mobile edge.

The curve trends of the OCA-CLJP algorithm and the OCA-SSCR algorithm are very close, but the former will, under the condition of violating the long-term average cost constraint, seek a solution with better cost through continuous iteration. Therefore, in 0-20 time slots, the OCA-CLJP algorithm is constantly switching between finding a solution with better cost and a solution with better delay, which leads to greater volatility of the delay curve, but this also makes the cost converge faster. Among them, the HF algorithm does not have a mechanism for cooperation between base stations, so that a large number of tasks are routed to the remote cloud for processing, resulting in a higher average response delay of the system. However, the SFCC algorithm has a fixed overhead limit (set to 160) in the time slot. Compared with the OCA-OSCR and OCACLJP algorithms, the service chain can be animated and the processing tasks will be reduced, so its performance is better than that in this article.

It can be seen that the three performance indicators of the content animation design hit rate, the average number of requests accepted by the content source user perception node, and the average user access delay are the best when considering both the content information age and the content popularity, and only the content information is considered. The performance of the animation design system is second when the age does not consider the popularity of the content, but the performance of the animation design system is the worst when only considering the popularity of the content without considering the age of the content information.

Figure 8 shows the confidence of animation art design based on moving edges. It can be seen that the overall edge confidence of the method in this paper is slightly lower than that of the PCNN method. Combined with subjective qualitative observation, it can be found that the false detection of noise information by PCNN is the main reason for its high confidence, and the filter method has too many falsehoods.

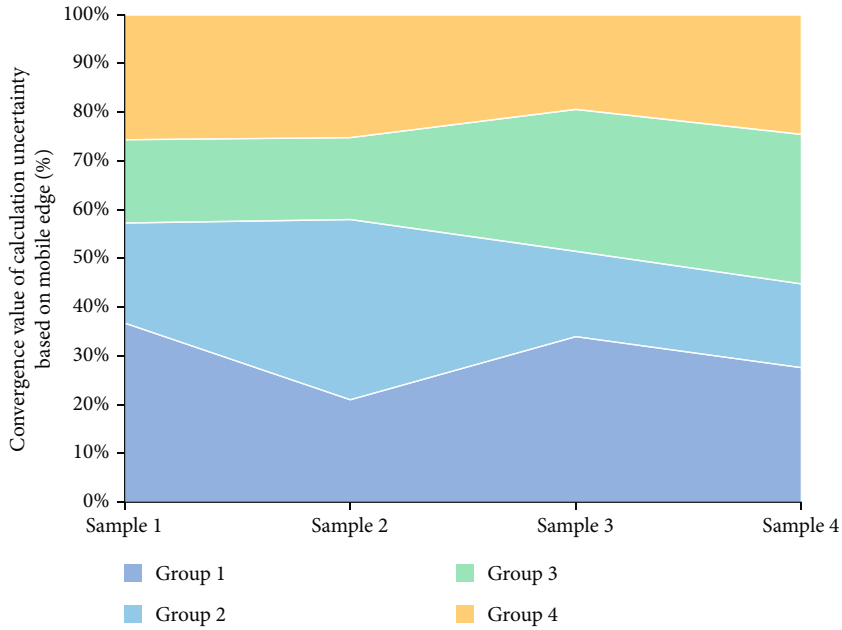

Figure 7: Distribution of calculation uncertainty based on mobile edge.

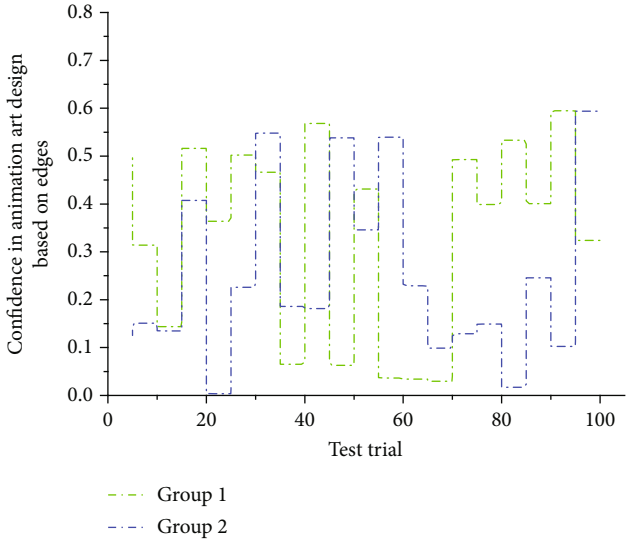

Figure 8: Confidence of animation art design based on moving edges.

Edges make their confidence low. Because of the effective suppression of noise information and false edges in this method, the confidence is more expressed as a judgment of true edges.

The reconstruction similarity of the method in this paper is basically greater than that of other methods, but it is worth noting that false edges will also lead to high reconstruction similarity. As mentioned above, the higher edge confidence in this paper indicates that the method in this paper has fewer false edges, and the reconstruction of animation is more based on true edges. It can be seen that the edges detected by the method in this paper are more complete and continuous. In summary, the method in this paper can effectively detect the edge information of animation, which has significant advantages in the accuracy and completeness of the edge compared with other methods. It can be concluded that the effect of using only a single indicator is worse than the effect of using two indicators at the same time, because each indicator of content measures different directions, and the information age of the content considers the popularity of the content at the current moment. The popularity of content considers the number of times the content has been requested in the past period of time, so this article considers the information age of the content and the popularity of the content as indicators to measure the content of the animation design to improve the performance of the animation design system.

5. Conclusion

In order to maximize the user's perception of the preferences of both parties, this paper designs an animation art design mechanism based on the mobile edge computing matching theory. Different from the 0–1 planning problem method of maximizing user perception preferences, the matching-based association algorithm is based on the participants' strict preference sequence, and after a limited number of mobile edge calculations, they achieve mutually satisfactory association results. First of all, according to the theory of open user-perceived hierarchical queuing network, this paper analyzes the average delay of processing tasks in the service chain and then quantifies the animation design and task routing decision-making of the service chain. Then, under the long-term average cost constraint set by the application service provider, this paper designs an online cost adaptive algorithm based on mobile edge computing technology, which converts the long-term minimization problem that requires future global task information into only single-

slot problem of current time-slot task information. On this basis, this article designs a joint optimization algorithm for animation access mode selection and task distribution for the high-speed animation environment, which is aimed at meeting the needs of diversified applications and taking into account the energy consumption of the system. Aimed at this complex mixed integer programming problem, this paper proposes a multiaccess coordinated computing migration strategy based on deep reinforcement learning. Both theory and simulation results prove that the computational migration algorithm proposed in this paper has good performance gain and convergence. The simulation results verify that the proposed collaborative computing migration algorithm can significantly reduce the average service delay of animation art design and reduce the energy consumption of the system.

Data Availability

The data used to support the findings of this study are available from the corresponding author upon request.

Conflicts of Interest

The author declares that he has no conflicts of interest.

Acknowledgments

This work was funded by the introduction of high-level talents research support program of Shenyang Ligong University (project name: Research on the relationship between visual symbols and design information transmission, project number 1010147001009).

References

[1] W. Rafique, L. Qi, I. Yaqoob, M. Imran, R. U. Rasool, and W. Dou, "Complementing IoT services through software defined networking and edge computing: a comprehensive survey," *IEEE Communications Surveys & Tutorials*, vol. 22, no. 3, pp. 1761–1804, 2020.

[2] N. Watkinson, F. Zaitsev, A. Shivam et al., "EdgeAvatar: an edge computing system for building virtual beings," *Electronics*, vol. 10, no. 3, p. 229, 2021.

[3] S. Friston, E. Griffith, D. Swapp et al., "Quality of service impact on edge physics simulations for VR," *IEEE Transactions on Visualization and Computer Graphics*, vol. 27, no. 5, pp. 2691–2701, 2021.

[4] T. Ouyang, Z. Zhou, and X. Chen, "Follow me at the edge: mobility-aware dynamic service placement for mobile edge computing," *IEEE Journal on Selected Areas in Communications*, vol. 36, no. 10, pp. 2333–2345, 2018.

[5] Z. Zhang, W. Zhang, and F. H. Tseng, "Satellite mobile edge computing: improving QoS of high-speed satellite-terrestrial networks using edge computing techniques," *IEEE Network*, vol. 33, no. 1, pp. 70–76, 2019.

[6] T. Ouyang, R. Li, X. Chen, Z. Zhou, and X. Tang, "Adaptive user-managed service placement for mobile edge computing: an online learning approach," *Computer Communications*, pp. 1468–1476, 2019.

[7] L. Tang and S. He, "Multi-user computation offloading in mobile edge computing: a behavioral perspective," *IEEE Network*, vol. 32, no. 1, pp. 48–53, 2018.

[8] L. Zhang, S. Wang, and R. N. Chang, *QCSS: a QoE-aware control plane for adaptive streaming service over mobile edge computing infrastructures*, Web Services, 2018.

[9] B. Gao, Z. Zhou, F. Liu, and F. Xu, "Winning at the starting line: joint network selection and service placement for mobile edge computing," *Computer Communications*, pp. 1459–1467, 2019.

[10] G. Mitsis, P. A. Apostolopoulos, E. E. Tsiropoulou, and S. Papavassiliou, "Intelligent dynamic data offloading in a competitive mobile edge computing market," *Future Internet*, vol. 11, no. 5, p. 118, 2019.

[11] R. Wang, Y. Cao, A. Noor, T. A. Alamoudi, and R. Nour, "Agent-enabled task offloading in UAV-aided mobile edge computing," *Computer Communications*, vol. 149, pp. 324–331, 2020.

[12] D. He, S. Chan, and M. Guizani, "Security in the Internet of things supported by mobile edge computing," *IEEE Communications Magazine*, vol. 56, no. 8, pp. 56–61, 2018.

[13] J. Zhang and K. B. Letaief, "Mobile edge intelligence and computing for the internet of vehicles," *Proceedings of the IEEE*, vol. 108, no. 2, pp. 246–261, 2019.

[14] P. Cong, J. Zhou, L. Li, K. Cao, T. Wei, and K. Li, "A survey of hierarchical energy optimization for mobile edge computing," *ACM Computing Surveys (CSUR)*, vol. 53, no. 2, pp. 1–44, 2020.

[15] K. Sha, T. A. Yang, W. Wei, and S. Davari, "A survey of edge computing-based designs for IoT security," *Digital Communications and Networks*, vol. 6, no. 2, pp. 195–202, 2020.

[16] Y. Zhang, B. di, P. Wang, J. Lin, and L. Song, "HetMEC: heterogeneous multi-layer mobile edge computing in the 6 G era," *IEEE Transactions on Vehicular Technology*, vol. 69, no. 4, pp. 4388–4400, 2020.

[17] Y. Wang, P. Lang, D. Tian et al., "A game-based computation offloading method in vehicular multiaccess edge computing networks," *IEEE Internet of Things Journal*, vol. 7, no. 6, pp. 4987–4996, 2020.

[18] Y. Miao, G. Wu, M. Li, A. Ghoneim, M. al-Rakhami, and M. S. Hossain, "Intelligent task prediction and computation offloading based on mobile-edge cloud computing," *Future Generation Computer Systems*, vol. 102, pp. 925–931, 2020.

[19] X. Zhang, H. Chen, Y. Zhao et al., "Improving cloud gaming experience through mobile edge computing," *IEEE Wireless Communications*, vol. 26, no. 4, pp. 178–183, 2019.

[20] R. Bruschi, F. Davoli, P. Lago, and J. F. Pajo, "A multi-clustering approach to scale distributed tenant networks for mobile edge computing," *IEEE Journal on Selected Areas in Communications*, vol. 37, no. 3, pp. 499–514, 2019.

[21] F. Zhang, G. Liu, B. Zhao, X. Fu, and R. Yahyapour, "Reducing the network overhead of user mobility–induced virtual machine migration in mobile edge computing," *Software: Practice and Experience*, vol. 49, no. 4, pp. 673–693, 2019.

[22] D. K. Baroroh, C. H. Chu, and L. Wang, "Systematic literature review on augmented reality in smart manufacturing: collaboration between human and computational intelligence," *Journal of Manufacturing Systems*, vol. 61, pp. 696–711, 2020.

[23] P. Wisessing, K. Zibrek, D. W. Cunningham, J. Dingliana, and R. McDonnell, "Enlighten me," *ACM Transactions on Graphics (TOG)*, vol. 39, no. 3, pp. 1–12, 2020.

Hindawi
Journal of Sensors
Volume 2021, Article ID 5981385, 11 pages
https://doi.org/10.1155/2021/5981385

Research Article

Cross-Modal Travel Route Recommendation Algorithm Based on Internet of Things Awareness

Yuran Zhang[1] **and Ziyan Tang**[2]

[1]*General Office of Chengdu Municipal CPC Committee, Chengdu, Sichuan 610041, China*
[2]*Interdisciplinary Center for Culture, Science and Technology, Sichuan University, Chengdu 610065, China*

Correspondence should be addressed to Ziyan Tang; 20130801@stu.nun.edu.cn

Received 25 September 2021; Accepted 16 November 2021; Published 13 December 2021

Academic Editor: Gengxin Sun

In recent years, the Internet of Things has developed rapidly in people's lives. This brand-new technology is flooding people's lives and widely used in many fields, such as medical field, science and technology field, and industry and agriculture field. As a modern technology, the Internet of Things has many characteristics of low power consumption and multifunction, and it also has the characteristics of data-aware computing. This is the characteristic of this new product. In people's daily life, the Internet of Things is also closely related to people's daily life. In the tourism industry, the Internet of Things can make the best use of everything and give full play to its various advantages as much as possible. The Internet of Things can perceive cross-modal tourism routes. So here, this paper summarizes various algorithms recommended by the Internet of Things for this tourist route and works out the experimental data methods of these algorithms for cross-modal tourism route recommendation. The proposed algorithm is verified by data simulation, compared with related algorithms. We analyze and summarize the simulation results. At present, there is no comparative analysis of the performance of ant colony algorithm, genetic algorithm, and its optimization algorithm in tourism route recommendation. On the basis of crawling the tourism data in the Internet, this paper applies ant colony algorithm, genetic algorithm, max–min optimization ant colony algorithm, and hybrid ant colony algorithm based on greedy solution to tourism route recommendation and evaluates and compares the algorithms from three aspects: average evaluation score, optimal evaluation score, and algorithm time. Experimental results show that the max–min optimization ant colony algorithm and the hybrid ant colony algorithm based on greedy solution can be effectively applied to automated tourist route recommendation.

1. Introduction

Internet of Things is interwoven by different modern technologies, including wireless communication technology and live data analysis technology, machine language learning technology, sensor technology, and built-in embedded system [1]. The sensors in the internal perception level of the Internet of Things sense all kinds of information about things around them regularly and transmit the information in the perception level to the upper application of the Internet of Things through data fusion and network transmission, thus realizing the Internet of Everything. Therefore, the related research on the key technologies of the Internet of Things based on perception provides a foundation for the development of the Internet of Things [2]. At present, all walks of life at home and abroad have increased the research and development of technologies related to the Internet of Things, which closely links the Internet of Things with life and production. The main application fields of Internet of Things include smart cities, smart homes, intelligent transportation, intelligent environment, and intelligent enterprises. In 2009, IBM Company put forward the innovative concept of "Smart Earth," that is, "Internet plus Internet of Things = Smart Earth" Internet

of Things detects and perceives object information through the perception layer, which is the Internet of Everything based on perception [3]. As a key technology in the sensing field of Internet of Things, a wireless sensor network is a special ad hoc network [4], which plays a very important role in the perception of Internet of Things. It does not need fixed network support and has the characteristics of fast development and strong survivability [5]. It can carry out remote monitoring and real-time monitoring and can replace people to work in harsh or special environments, such as polluted areas, where the environment cannot be destroyed, and temporary areas, where natural disasters occur. The main applications of wireless sensor networks are as follows: safe construction and monitoring of various large-scale projects; monitoring the environmental conditions of livestock and poultry, crop irrigation, soil air changes and large-scale surface detection, and water-saving irrigation control [6]; and marine physics research, pollution monitoring, data acquisition, resource exploration, underwater military target monitoring, positioning, tracking, and classification. Wireless sensor networks in a variety of applications have a common point, either through the location information of nodes in the sensor network to locate nodes or targets or using nodes to track moving objects [7]. With the in-depth application of wireless sensor networks in many fields, especially in the detection and monitoring of enemy bases in military surveillance and rapid location of injured persons in natural disasters, these applications for the need of target location information also make wireless sensor network node location and moving target tracking become the key issues to be solved urgently at this stage [8]. To sum up, the optimization of precision and energy consumption of target location and tracking technology has gradually become a research focus. Target tracking technology has become one of the key technologies of perception-based Internet of Things, which is widely used in military and civilian fields [9]. For the research of target tracking technology, the important factors to be considered are tracking accuracy and tracking energy consumption. At present, there are mature tracking algorithms, and their key research directions include prediction algorithm, tracking structure, and positioning algorithm [10]. At present, in this paper, the ant colony algorithm is used to study the data of cross-modal travel route algorithm under the Internet of Things, and its research direction is to track a single target under the perception of the Internet of Things [11]. The algorithm requires consistent maintenance time, and at the same time, the initial information of all node positions is known. It takes the staying time of the sensor network target as the weight value and adds appropriate calculation to this weight value so as to locate and track more reasonably [12]. The second is a tracking algorithm based on transmission tree, which uses genetic algorithm and optimization algorithm for tracking. The algorithm uses a dynamic tree structure to track dynamically, which is different from the centralized tracking algorithm. The transmission tree is composed of nodes near the target, and the number of nodes increases and decreases dynamically with the movement of the target [13], thus ensuring high-precision tracking, reducing the energy consumption of nodes, and prolonging the network life. In addition, a distributed dynamic cooperative tracking method is proposed, which uses a Gaussian mixture particle filter to estimate the target state [14]. The algorithm uses a Kalman filter to predict linear motion and an extended Kalman filter to predict nonlinear motion, which has high prediction accuracy and uses dynamic cluster structure to track in real time [15]. The algorithm has high tracking accuracy and strong applicability. The shortcoming of this algorithm is that it requires high computing power and storage capacity of sensor nodes [16]. In the diversified modern society, the practical application of multitarget tracking needs to make scholars at home and abroad step up the research and development of target tracking technology in the Internet of Things and thus has achieved many related research results. To sum up, the Internet of Things has great application prospects. The above algorithms are used in other fields for in-depth research, mainly for position tracking and location research. However, in a single algorithm, there is a large error in recommending tourist routes, which makes it impossible to achieve accurate positioning and tracking. The cross-modal model proposed in this paper applies the ant colony algorithm, genetic algorithm, max–min optimization ant colony algorithm, and hybrid ant colony algorithm based on greedy solution to tourist route recommendation and analyzes the average evaluation score and the optimal evaluation score of the selected routes, respectively. This is based on the application of the optimal model in the above research algorithm, which can greatly improve the execution efficiency of the algorithm.

In this paper, a variety of algorithms are studied to combine and optimize the route, and the best algorithm is selected. The path distance error value produced by different tourist attractions has the least influence and can fluctuate in a relatively stable interval value to calculate the optimal path solution, which can greatly reduce the efficiency of travel path selection and travel experience in people's daily life. In the second part of the article, the modeling basis of tourism route algorithm is explained. The third part explains the collection of wireless sensor network routing protocols and related algorithms applied to travel route planning model; the fourth part is the experimental comparison of algorithms combined with various mathematical models.

2. Overview of Travel Route Algorithm Modeling

When the traditional travel path engine provides users with search results, regardless of the background of people's travel, returning the same results for different trips does not return personalized results according to people's travel

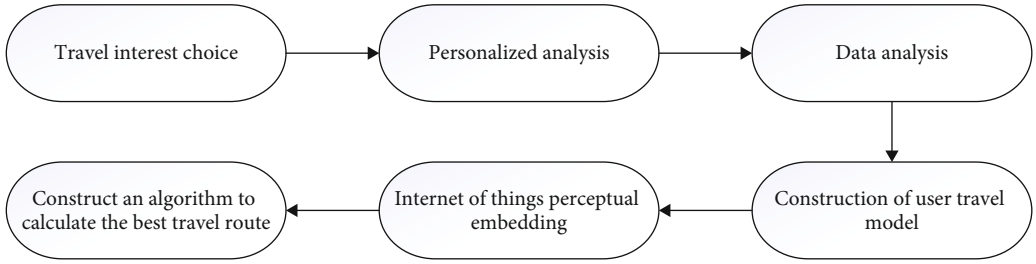

Figure 1: Construction diagram of user travel route modeling algorithm under physical network awareness.

route selection for specific travel modes, so it is necessary to model the route [17], mining people's travel route selection methods by analyzing the historical behavior of travel or the historical browsing content of travel routes. Traveling route modeling refers to the process of establishing the model of data analysis and representation of the same route from the selection of people's travel purpose and mode and the historical information of people's travel behavior, such as the selection mode of people's travel route and the time consumption of travel route. The main purpose is to show the results of selecting the best path for different scenic spots and destinations, so that people can travel quickly and efficiently, and avoid the waste of time caused by people's own path screening [18]. In terms of travel path data modeling, it can be seen from the literal meaning that the established model is based on the travel path, which is closely related to the path distance and time consumption, so it is sometimes called personalized modeling. The result of path selection is not to characterize the optimal path by a literal overview but to get people's optimal path solution by data mining or Internet of Things perception tracking and then express the data obtained from the optimal path solution in a certain data structure format, through the research data analysis of people's path selection for different paths to return targeted results for screening [19]. The second is the data calculation of the algorithm. Through data mining and cross-modal travel path algorithm analysis under the perception of Internet of Things, the collected time error data of various paths are modeled to obtain the calculation of travel path algorithm. This algorithm data calculation is a dynamic process, because the choice of scenic spots determines the length of the path, this data is not static, and the consumption content of different path time will also change [20]. Therefore, the travel path algorithm model also needs to change with the change of path time. As shown in Figure 1, only on the basis of establishing a high-quality travel path algorithm model can the data reliability, rigor, and scientificity obtained from the final optimal path solution be improved to a greater extent.

Choose the corresponding interest route for travel and plan the corresponding route. Enter the individual analysis, and recommend some interesting routes according to personal interest points. According to the above personalized data, the travel route of users is constructed. After in-depth analysis of the information such as people flow and road conditions perceived by the Internet of Things, the best travel route for users is finally constructed.

3. Routing Protocol for Energy Acquisition in Wireless Sensor Networks

A traditional Internet of Things routing algorithm has been quite mature, but for the energy acquisition of wireless sensor networks, routing algorithm research is not particularly in-depth [21]. At present, there have been some research results of routing algorithms with perceptual performance, and the existing research is mainly planar routing algorithm protocol. The invention relates to a routing protocol with a special energy collection mode, which can take the data energy collection work as a special consideration factor of an energy-saving routing protocol. The routing algorithm first proposes a hybrid routing metric which combines the residual energy and energy collection rate of nodes and then proposes a mechanism to update the information of neighbor nodes. According to this mechanism, the information of neighbor nodes is updated [22]. Nodes can choose the optimal data down-transform sampling location autonomously, considering the correlation between the hybrid routing metrics and the amount of node information in the adjacent location area. At present, an opportunistic routing protocol specially used for the best adaptation of Internet of Things awareness is obtained. Routing divides nodes into groups and determines the transmission priority of each node by considering the available energy of each node and the distance from the node to the sink node [23]. Simulation results show that adaptive opportunistic routing has better throughput, fairness, and scalability than other routes. Geographical routing is added to the routing of energy acquisition wireless sensor networks, and the routing is considered by geographical location, which makes the energy acquisition nodes get better performance [24]. Using the idea of geographic routing, we continue to optimize this route and get a geographic routing algorithm with repeatability detection; that is, we introduce a repeatability detection mechanism on the basis of geographic routing. Before forwarding data packets, we check whether the same data packets have been sent before, and if so, we discard the current data packets, thus improving network performance and network forwarding efficiency [25]. Different layouts and application scenarios of energy collection nodes are analyzed, different routing protocols are compared and analyzed, and the routing algorithm and node location indication suitable for the optimal path solution algorithm are found out. A cooperative path-aware algorithm for throughput optimization based on path algorithm model is

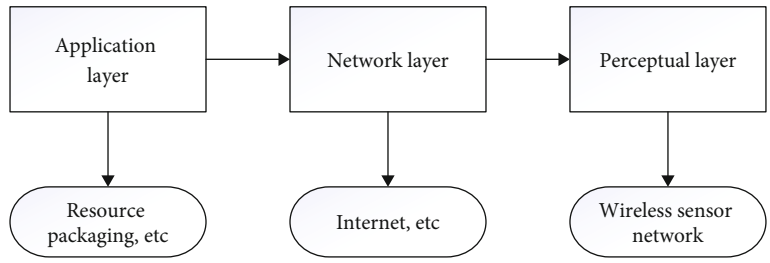

Figure 2: Construction diagram of Internet of Things awareness module.

proposed. These algorithms show effective improvement and performance improvement for power scheduling problems with different time delays. The existing routing algorithms for IoT awareness are mainly planar, while the traditional hierarchical routing algorithms for IoT applications are mainly aimed at isomorphic sensor networks; that is, the initial energy of each node is the same [26]. The nodes in the data acquisition wireless sensor network are heterogeneous; that is, the energy is different. If we use the classical clustering routing protocol in IoT awareness, the nodes with less energy will sleep or die because of excessive energy consumption, which will lead to network failure. Therefore, the traditional clustering routing algorithm in IoT awareness cannot be directly applied to the optimal path algorithm model. The structure diagram of each layer of the current Internet of Things is shown in Figure 2.

3.1. Solve the Mathematical Model of Tourism Route Planning. In order to compare the mathematical models based on the basic genetic algorithm of tourism route, in this paper, the central idea and architecture of hybrid ant colony algorithm are proposed. And the hybrid ant colony algorithm is used to recommend the best route for tourism. The main architecture of some mathematical algorithm models involved includes chromosome self-coding, fitness function selection, and data analysis operator architecture. The detailed mathematical evaluation methods and algorithms of these algorithm models are described as follows:

(1) Chromosome coding: people's common travel routes can be displayed by binary coding of machine language. For example, chromosome sequences in the number 10 dimension can be divided into (0, 1, 0, 1, 0, 0, 0, 0, 0, 1) to represent, and then 2, 4, and 10 are selected into the current best routes according to chromosome coding characteristics.

(2) Fitness function: in the general genetic algorithm, the key and most important thing is the construction mode of fitness function architecture model. At present, it is used to evaluate and select the target chromosome data source and can calculate the corresponding data genetic probability interval which affects the single target in the framework of selection operator, which is the key factor index reference of whether the popular genetic algorithm can achieve the optimal solution path. Therefore, the selection of appropriate fitness function can directly affect the convergence and occurrence speed of genetic algorithm and whether it is enough to find the optimal path solution function. The mathematical evaluation model of appropriate function constructed in this paper is as follows:

$$\begin{aligned} \mathrm{fit}(f(x), g(x)) &= (1-\partial)\left(\frac{A_{\max}}{1+A_{\min}+f_{(x)}}\right)^{y} + (g(x))^{\partial}, \\ \mathrm{pis} &= \frac{F_i}{\sum_{i-1}^{M} F_i} \quad (i = 1, 2, \cdots, M), \\ \sum_{k-1}^{m}\sum_{j-1}^{n-1} x_{ojk} - \sum_{k=1}^{m}\sum_{i=1}^{n-1} x_{iok} &= 0, \quad \forall k \in A, \end{aligned} \tag{1}$$

where fit $(f(x), g(x))$ is the fitness of tourism classic x; $f(x)$ is the objective optimization function of the scenic spot cost, which is composed of information such as scenic spot ticket price; $g(x)$ is the target optimization function of the scenic spot heat, which represents the total number of visitors to the scenic spot; $A_{\min}$ is the minimum cost and $A_{\max}$ is the maximum cost; and gamma is the scaling factor of cost and the scaling factor of heat. The function of Gamma is to prevent the value of cost or heat from fluctuating too much, in order to balance the influence of cost and heat on moderation.

(3) Select operator: using roulette, firstly, the sum of fitness corresponding to all populations is calculated; then, the relative fitness fit_i/sum of each individual is calculated as the probability of roulette, each probability value forms an area, and the sum of all probabilities is 1. Finally, a random value between 0 and 1 is generated, and the number of times each individual is selected and determined according to the occurrence of the random number in the above probability area. And adopt the elite rule, and forcibly copy the best individual of the previous generation directly into the next generation, so that the individual of the next generation will be superior to the previous generation. $U_{\max}$ and $U_{\min}$ are the maximum and minimum dependent variables, respectively.

$$
\begin{aligned}
p_i &= p_{i-1} + \frac{\text{fit}_i}{\text{sum}},\\
\text{sum} &= \sum_{i=1}^{n} \text{fit},\\
\delta &= \frac{U_{\max} - U_{\min}}{2^l - 1},\\
x &= U_{\min} + \left(\sum_{i=1}^{l} b_i \times 2^{i-1}\right) \times \frac{U_{\max} - U_{\min}}{2^l - 1}.
\end{aligned} \tag{2}
$$

(4) Genetic algorithm: a genetic algorithm is completely not used for other external comprehensive information in the process of systematic search and self-evolution. It only calculates the advantages and disadvantages of individual solutions through the evaluation of functions and uses this as the fundamental basis for the operation of subsequent genetic steps. Because of the construction of genetic algorithm and fitness function to compare permutation number and on this basis to calculate the size of the probability of the selection of data, so the fitness function of the selection of the value of the integer value should be selected. Therefore, in many cases, fitness function is especially necessary if the objective function is demapped to the traditional form of finding the maximum function value and the randomly selected function value is nonnegative:

$$
\begin{aligned}
f(x) &= x \cdot \sin\left(10 \cdot \pi \cdot x\right) + 2,\\
p_i &= \frac{f(x_i)}{\sum_{j=1}^{n} f(x_i)},\\
(b_0, \cdots, b_{20} b_{21})_2 &= \left(\sum_{i=0}^{21} b_i \cdot 2^i\right)_{10} = x^t.
\end{aligned} \tag{3}
$$

(5) Ant colony algorithm: literally speaking, it is equivalent to ants finding the shortest path, which is due to pheromones and environment. Assuming that there are two paths for ants to choose from the food point to return to the ant nest, the number of ants on the first two paths is equal. When an ant reaches the target point, it will immediately return according to the original path. The ants on the path with relatively short distance in the two paths consume a short time to go back and forth, and the frequency of repetition increases. The number of ants going back and forth in a certain period of time will increase, and the amount of information left in the path will also increase, which attracts other ants and leaves more information than before. On the other hand, the relatively long path will be the opposite, so more and more ants will leave information back and forth to reach the shortest path. In the data, T_t represents the path variable, n represents the dependent variable, t represents the distance independent variable, and P_u represents the number of ant independent variables, so the following ant colony algorithm formulas can be obtained:

$$
\begin{aligned}
T(t) &= (1-p) \cdot T_u(t-1) + \Delta T_u,\\
\Delta T_u &= \sum_{k=1}^{m} \Delta T_u^k + \lambda \Delta T_u^b,\\
p_u^k &= \frac{T_n^{\alpha} \partial_u^{\beta}}{\sum_j T_u^{\alpha} \partial_u^{\beta}},\\
T_u(n+1) &= p \times T_u(n) + \sum_{k=1}^{m} \Delta T_u^k.
\end{aligned} \tag{4}
$$

(6) Hybrid ant colony algorithm: the corresponding model formula is constructed by greedy solution combined with the ant colony algorithm. On the basis of ant colony algorithm, increase the number of matrix columns. The information amount structure is added. Therefore, the dependent variable will have more reference value intervals. Through the number in the interval, the error of the final calculation value will be smaller. Comparison based on the travel route recommendation algorithm can form a comparative data format, and the optimal solution can be obtained by studying the error interval of the data volume in combination with the perception of the Internet of Things. Therefore, the formula of the hybrid ant colony algorithm model is as follows:

$$
\begin{aligned}
m &= \sum_{k=2}^{n} b_i(t) (n \in k),\\
\Delta T_{ij}^k &= (1-p_1) \cdot T_{ij}(t) + p_1 \frac{1}{L_{\max}},\\
V_{i+1} &= \omega V_i + c_1 r_1 (P_a - X_i) + c_2 r_2 (G_1 - X_i),\\
\sum_{k=1}^{m} \sum_{j=1}^{n-1} x_{0jk} &\le m,\\
\sum_{k=1}^{m} \sum_{i=0}^{n-1} x_{ijk} &= 1, \quad \forall v_j \in C,\\
\sum_{i=1}^{n-1} q_i \sum_{j=0}^{n-1} x_{ijk} &\le G, \quad \forall k \in A.
\end{aligned} \tag{5}
$$

In the comprehensive algorithm, V_{i+1} is the optimal solution of data amount, P_1 is the distance variable, L is the distance return value, $c_1 r_1$ is the first product value of

the return value, $c_2 r_2$ is the second product value, and T is the termination variable. In order to select the best tourist route, an evaluation model is established to evaluate whether it is the best tourist route. The idea of modeling is that the selected tourist routes give priority to popular scenic spots, and the sum of scenic spot ticket price and hotel expenses is low. Therefore, an optimal score function of tourist routes is defined, which is used to evaluate the score values of tourist routes obtained by different algorithms, and a high score indicates that the route is excellent.

$$\begin{aligned} u_t &= \frac{E_1 \cdot R_t + E_2(k) \cdot R_k(t)}{N_c \cdot (E_x + E_1)}, \\ N_c &= 1 + \sum_{a \in c} N^a x^a, \\ X_C &= \partial X_c (u_c - u^a(x)), \\ u^a(x) &= \sum_{C_1} x_c \cdot u_c^a, \\ E_{eh} &= R_i(t) \cdot \Delta t, \\ R_i(t) &= a_i e^{(t-b_i)^2/2c_i{}^2}, \end{aligned} \tag{6}$$

where R_i is a variable frequency of wireless sensor in Internet of Things. Through the location and tracking of variable perception by frequency conversion, it can make the travel route more localizable. N_c is the network layer coefficient value of the Internet of Things. When the coefficient layer of the Internet of Things changes, the discreteness can become uncertain, and the calculation error becomes larger due to the influence of fluctuation. X_c is the wireless coefficient of independent variable, and the wireless coefficient increases with the increase of induction times. Finally, the cross-modal perception error value of u_t can be obtained through mathematical evaluation model calculation.

3.2. Selection and Analysis of Experimental Data of Travel Route. Scholars at home and abroad mainly focus on improving the ant colony algorithm; however, when the improved ant colony algorithm is efficient or can achieve their expected results, this often needs to be verified in examples. This chapter gives the comparison of the data before and after the algorithm is improved in the form of examples. When there are more data, the idealized data in the standard database is used. Some scholars use the given point coordinates when studying the route planning of vehicle routing and then use the given point coordinates to get the straight line distance between two points and use the obtained distance instead of the distance value in the actual road condition, which is obviously inconsistent with the actual road condition. What we can get from the current research data is that suppose a tourist enthusiast is going on a go on road trip and after traveling to 107 4A-level national key tourist attractions, these 107 tourist attractions are located in different provinces and places. In this way, the independent variable and dependent variable data of tourist route will be affected by the number of tours in different years and the number of days from departure to completion of a tour. The total expenditure of tourism, travel time, travel choice mode, travel time, and so on are constrained by external conditions, which can be summarized into discrete values to express this uncertain factor. Once again, the cost of travel can include many factors to constitute other expenses, such as the cost of expenses on the way, the toll of the road, and the accommodation expenses along the way. It is assumed that the mode of transportation for the whole journey is self-driving. If one or several factors are regarded as invariants, other factors can be determined, a mathematical model can be established, and the optimal route can be planned under the corresponding constraints. Because these 107 scenic spots belong to different provinces, therefore, we give priority to various scenic spots in the province as independent variables. Then, the shortest time ratio of each scenic spot in each different province is calculated. Then, the mathematical evaluation model under the perception of Internet of Things is established in turn to study. Then, the best travel path chart mode of different scenic spots in the same province is planned, and the big data perceived by the same Internet of Things finds out the distance between different scenic spots in the province. According to the planned road map, the time required from the unit scenic spot to the next unit scenic spot can be studied in turn. Moreover, the total travel time of scenic spots in each province and the total time required for a unit scenic spot to another unit scenic spot are the total travel time consumption data in each same province. Then, the provinces were taken as the unit, and the mathematical algorithm evaluation model is established in turn. Under the control of corresponding constraint indexes, the best road map between provinces is planned, and the time needed from one province to another is calculated. The total time loss of each trip is the total time needed from the target province to the unit province and the total time consumption data of playing in the province. As shown in Figure 3, based on the data selection and construction of people's travel routes, on the one hand, random sampling is adopted for the number and time of routes of each scenic spot, and on the other hand, random sampling is adopted for data selection to ensure the comparability and rigor of data. For sampling, it is necessary to ensure that batch calculation can be carried out in the research of path analysis and calculation of several algorithms, and wireless sensing embedded analysis data can be carried out for travel under the perception of Internet of Things. Combined with algorithms, uncertainty can be reduced and dimension interval can be controlled. Therefore, it is necessary to grasp the data selection of scenic spots. Recently, the tourism department published a report on China's tourism development. According to the data, there are 201 5A-level scenic spots in China. In the past two years, the growth rate decreased by 6.29% and 8.06%, respectively. The results show that the development of 5A-level scenic spots has entered a stable period, and the advantages of 5A-level scenic spots in tickets show a downward trend. By the second half of 2014, the peak season tickets of 5A scenic spots decreased by 22.15 percentage points and 1.94 percentage points, respectively, compared with 2018 and 2019, with an average ticket price of 103 yuan/ticket and an average off-

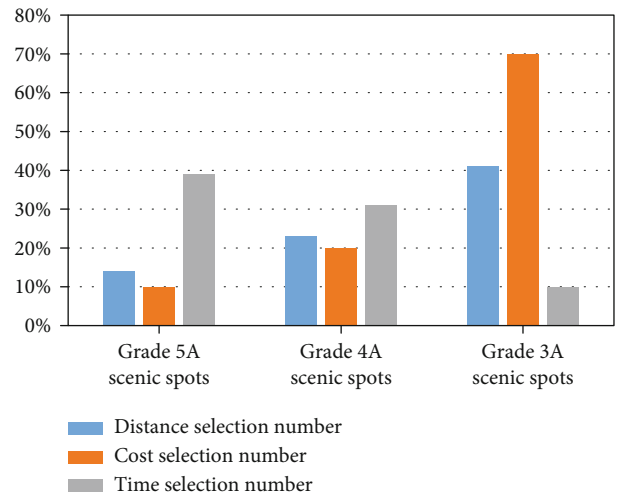

Figure 3: Histogram of selection of tourist route attraction data.

season ticket price of 93 yuan/ticket. Compared with that in 2019, the total price decreased by 19.88 percentage points as a whole, and for 2013, it decreased by 1.33 percentage points. In 2020, 186 5A scenic spots were searched for keywords, and the network attention of 5A scenic spots increased significantly compared with 13 years, with an increase of 21%. This research report counts the daily average of Baidu Index, and uses Baidu Index Search Platform to search the results, which reflects the network attention of 5A scenic spots in 2014.

Distance, cost, and time are important indicators for users to measure travel itinerary, so it is great research significance to choose these three indicators for comprehensive comparison. As can be seen from Figure 3, a scenic spot has an advantage in cost and low price, but the travel time is short and the user experience is not ideal. 4A scenic spot is the experience standard between 3A scenic spot and 5A scenic spot. According to the individual needs of customers, the corresponding concerns in these three indicators are selected, and the corresponding scenic spots are appropriately recommended, which has an efficient recommendation rate.

4. Experimental

For the recommendation experiment of tourism route recommendation algorithm based on Internet of Things awareness, in this paper, several randomly selected variable data such as route time, distance, and cost of scenic spots are applied to the algorithm model. Calculate the selected data to obtain the final data with the shortest path and the data with the least time consumption, modeling, and applying the algorithm; using the sensing technology of Internet of Things to track the path and time, this paper uses four algorithms to apply calculation to different scenic spot travel data, which are the ant colony algorithm, greedy algorithm, hybrid ant colony algorithm, and genetic algorithm. At present, these four algorithms have been partially studied, which are convenient for the construction and calculation of the algorithms. They are modern computing methods, which can effectively combine the Internet of Things sensing technology, and the tracking delay represents the time difference between the time when the location information is obtained by tracking and positioning and the specified time. The simulation start time of the three algorithms is the same, and the tracking delay is obtained by the average value of the difference between the determined time and the actual set time of the position information obtained by several tracking algorithms in the actual trajectory. The tracking simulation of networks with different numbers of nodes is carried out, and the trend of tracking delay with the number of nodes in the network is obtained. Sensor tracking and positioning is a simple and effective positioning method, which is suitable for a home environment. By judging the position, it can judge whether the user is located in the signal blind area and both sides of the wall and then give priority to the network access problem of users in this area. Tracking and positioning of indoor moving targets mainly include two steps: target position prediction and target positioning. Aiming at the characteristics of simple motion and low speed of moving targets and weak computing power of sensor nodes in smart homes, the dynamic cluster structure is used to track, the prediction algorithm adopts grey model based on wavelet denoising, and the trilateral positioning method based on RSSL is used to realize coordinate positioning.

4.1. Comparison of Experimental Data. The data comparison diagram of the four algorithms for the same path is shown in Figure 4. It can be seen that the ant colony algorithm can effectively infer the shortest path for scenic spots with short relative distance, and among the four algorithms, the ant colony algorithm is not particularly prominent in calculating the time of travel route. On the contrary, hybrid ant colony computing can greatly improve and analyze data on this basis. Under the tracking based on Internet of Things perception, the performance of the algorithm is evaluated by tracking accuracy, which is measured by the distance between the tracking position and the actual target moving position, and the average accuracy after 100 seconds of movement is taken. And compare the size of tracking structure. After 10 rounds of motion, the tracking accuracy map is obtained. Different curtain structure sizes affect tracking accuracy. The tracking distance radius is 1200, 1000, 800, and 600 meters, respectively, and the corresponding tracking accuracy is lower than 0.4 meters. The smaller the radius of dynamic cluster structure, the worse the tracking effect. When the cluster structure becomes smaller, it contains fewer tracking nodes, which leads to the reduction of tracking information and the decline of dynamic cluster tracking accuracy.

The accuracy of ant colony algorithm to path, the error rate of the calculated data of the average optimal path, and the theoretical optimal path under the change of discrete values are shown in Figure 5. It can be seen that the ant colony algorithm has values between 0.2 and 0.5, so some approximate discrete values between 0.2 and 0.5 can be obtained after synthesis, which are 0.2, 0.3, 0.4, and 0.5, respectively. The influence of the change of discrete value

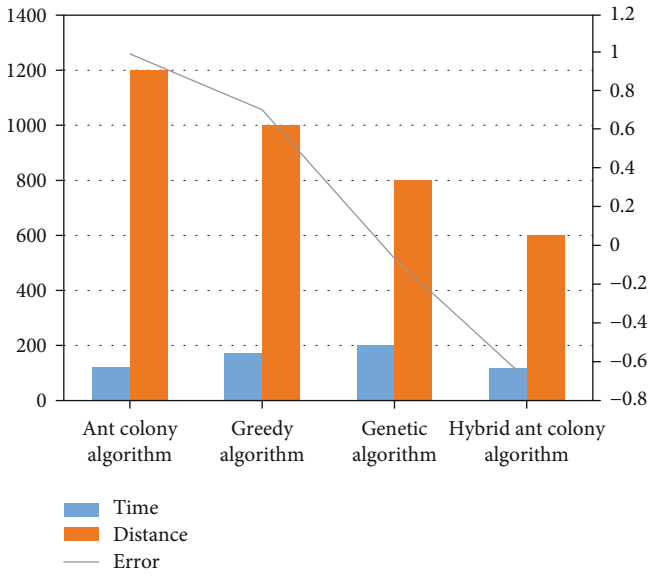

Figure 4: Comparison of time and distance data of four algorithms.

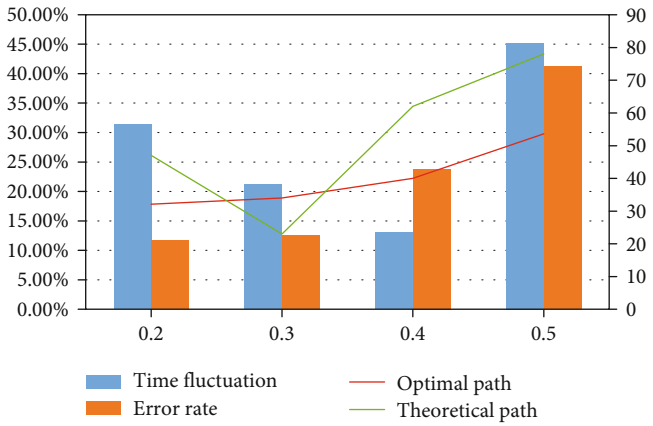

Figure 5: Influence of discrete numerical values on ant colony algorithm data comparison chart.

parameters on the operation results is expressed. When the discrete value is 0.2, the calculation error rate of ant colony algorithm is always maintained in a normal interval domain. Although the error value increases when the discrete value is 0.3, it still tends to a normal interval level. However, when the discrete value reaches 0.4, the error value gradually increases beyond the normal interval area, and when the discrete value reaches 0.5, the error value reaches its peak, which exceeds the normal interval a lot. It can be seen that for the ant colony algorithm, the influence of discrete values perceived by the Internet of Things on the calculation error rate of ant colony algorithm is not significant when the fluctuation is 0.2 and 0.3, but when it exceeds 0.3, the influence on the error rate of ant colony algorithm presents a positive increasing trend. Therefore, the comparison in the experiment should control the variable selection of discrete values.

When the constraint condition is invariant, the genetic algorithm uses multiple regression calculation and iterative calculation to calculate and analyze the path, so the error

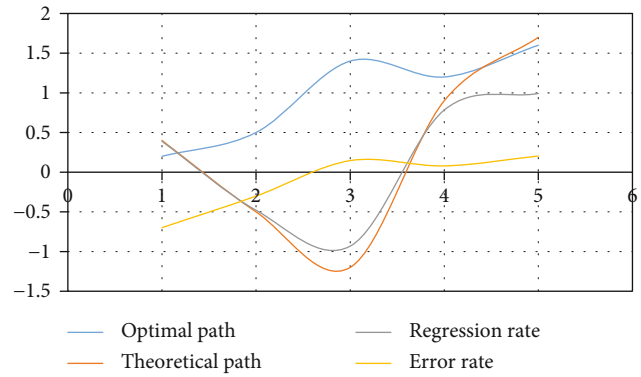

Figure 6: Comparison of error data in time selection by the genetic algorithm.

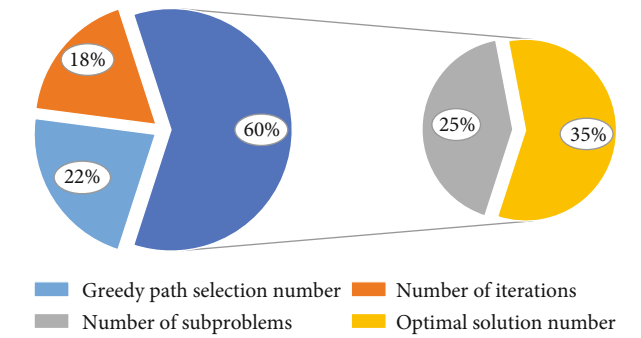

Figure 7: Data comparison graph between greedy path selection number and optimal solution of greedy algorithm.

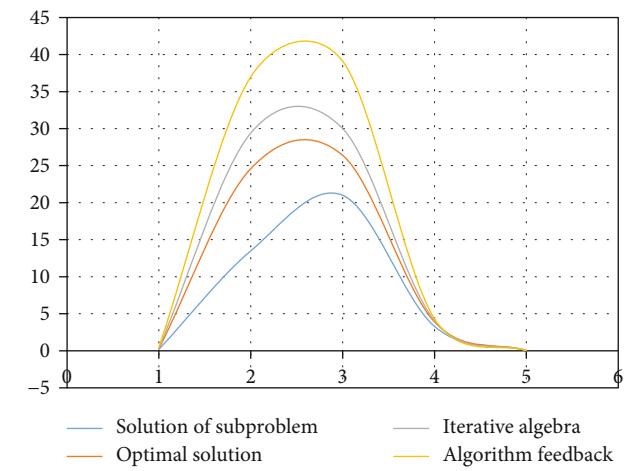

Figure 8: Data graph of the influence of greedy algorithm time scale on the optimal solution of subproblem.

value is not so obvious. But in terms of time calculation, the ability of genetic algorithm to analyze data produces a deviation value. Therefore, in the planning of travel routes, the selection of time parameters will have corresponding influence on the data of genetic algorithm. As far as the genetic algorithm is concerned, the selection of different time parameters can be seen from the data analysis diagram in Figure 6. When the time takes the normal interval number, the analysis and calculation of path by the genetic

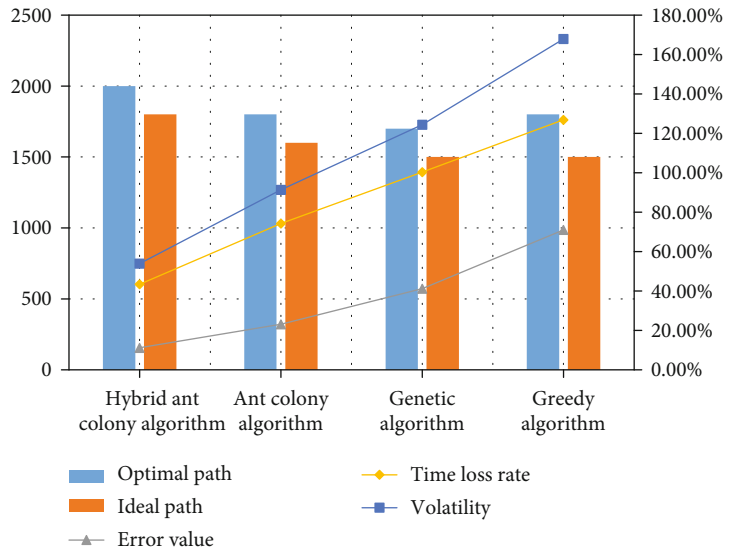

Figure 9: Comparison chart of experimental data of various algorithms.

algorithm are that there is no obvious fluctuation in a relatively normal area, and when the time is above 4 scales, the calculation data of the path gradually produces the deviation from the optimal path data, showing an increasing trend of proportional function. Therefore, when calculating the travel path by genetic algorithm, the time parameters should be selected in the positive range. When the unit time is selected to exceed 4.32, the deviation of the path reaches 41.2%, while the normal interval should fluctuate in the interval of 23%-30%. The results show that the optimal solution obtained by the genetic algorithm is within a certain error range with the known optimal solution; it can find the path sequence and path value which are very close to the known optimal solution provided by the database. The solution accuracy of ant colony algorithm in this paper is very close to the known optimal solution at present, which reflects the rationality of the genetic algorithm designed in this paper to solve the route from the side, and has reference significance.

In the greedy algorithm, the display form of data is more accurate, and the greedy algorithm is a kind of algorithm design theory that calculates the optimal data of some data more simply and quickly. Generally speaking, the biggest feature of greedy algorithm as travel path analysis is to calculate step by step. Usually, based on the current state as the theoretical basis, we seek an optimal test as the best selection of path data, but from this aspect, we abandon some data comparison of external conditions, which saves a lot of unnecessary time consumption and data calculation for seeking the optimal solution data. The greedy algorithm is different from other shortest path algorithms. It adopts a top-down calculation method. Through iterative model construction, the inherited greedy selection data is selected, so every time greedy data selection is carried out, and all complex problems will be reduced to a small sub-problem data to deal with, so as long as each step of greedy selection is carried out, the greedy data solution of a subproblem can be obtained. Although greedy data of subproblem can be obtained in every step, the unique solution of all problems cannot be guaranteed to be optimal data sometimes, so the greedy algorithm cannot take the way of data backtracking. As shown in Figure 7, it can be seen that the influence of greedy algorithm on the number of iterations and the number of subproblems fluctuates in the comparison data of the number of greedy path selections.

From the data obtained from the solution of the greedy algorithm to the optimal travel path, it can be seen that the influence of the fluctuation of discrete values on the greedy algorithm lies in the fact that the lower the discrete values, the greater the fluctuation. This is a reverse trend compared with the genetic algorithm. In terms of time consumption, a discrete value has little influence on the greedy algorithm, but in terms of error, when the discrete value is selected as 0.2, the volatility reaches its peak and exceeds the normal value interval, when the discrete value is selected as 0.3, the volatility gradually decreases, and when the discrete value is selected as 0.5, the error value is the smallest and the volatility is relatively stable. The calculated optimal path has the shortest solution distance and the least iteration times. The greedy algorithm based on Internet of Things perception calculates data pairs for travel paths, as shown in Figure 8.

In the greedy algorithm for the optimal solution of the subproblem, the subproblem solution, the optimal solution, iterative algebra, and algorithm feedback are analyzed. The optimal solution, iterative algebra, and algorithm feedback show the best performance at 2.5 times, while the subproblem solution shows better performance at 3 times. The whole algorithm shows the best performance from 2.5 to 3 times.

The hybrid ant colony algorithm is also called ant colony optimization algorithm. On the basis of ant colony algorithm, information source elements are used to construct information mutually. The optimization algorithm constructed by information particle swarm optimization can make use of the position information of single individual at present. The current iterative algorithm calculates the three information sources, namely, the limit value area of the single unit before calculation and the limit value area

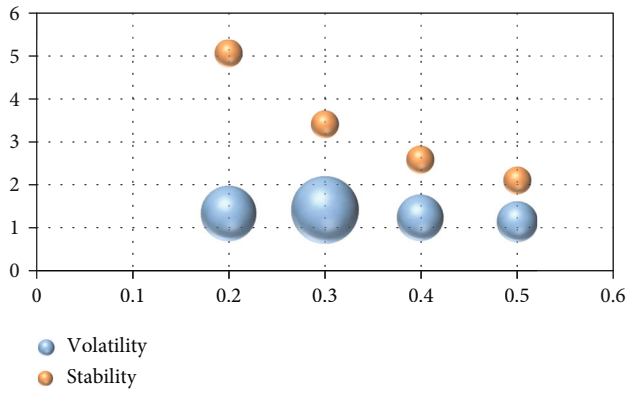

Figure 10: Comparison chart of volatility and stability data of hybrid ant colony algorithm.

constructed globally. Through the change of speed, the coverage and compilation of the position data of the single unit can be completed, and then the improvement measures can be produced for solving the optimal data of the path problem. According to the current experimental research, the above common ant colony algorithm is also particularly prone to resulting data and falling into the analysis of local optimal solution data. And the data solved by ant colony algorithm is not particularly fast. Therefore, the hybrid combination algorithm of common ant colony algorithm and data particle swarm optimization algorithm can be used, which is called the hybrid ant colony algorithm. It can complement the deficiencies in the path algorithm, thereby improving the data generation speed of the optimal solution of the algorithm and solving the problem of local optimum for a single problem path. It can be constructed according to the hybrid algorithm model of common ant colony algorithm and data particle swarm optimization algorithm. After the algorithm flow completes an overall calculation according to the normal ant colony algorithm, then, we let ants adjust and analyze their positions according to the individual optimal limit range in particle swarm optimization and the optimal problem data value of the whole path problem; then, this hybrid algorithm can be applied to the calculation of traveling salesman path problem at present. As shown in Figures 9 and 10, it can be seen that the hybrid ant colony algorithm has obviously improved the time of travel path analysis and the calculation of the optimal path. And the optimal path can be quickly obtained in a short time and reduce the time loss rate. When the discrete value is selected, it will not receive the fluctuation change, so that the data of the optimal solution of the path obtained by the algorithm will have an absolutely stable trend. In the theoretical path, the hybrid ant colony algorithm can also achieve the analysis of the target exponential rate and the overall calculation of the data, so that the distance of the travel path can be optimized.

5. Conclusion

Carrying the ant colony algorithm, genetic algorithm, greedy algorithm, and hybrid ant colony algorithm in the research of travel path data combined with Internet of Things sensing, by analyzing the theoretical path solution of these algorithms to the optimal path solution and time loss, according to the comparison of several data, such as the error of discrete value numerical selection analysis, the hybrid ant colony algorithm is an algorithm model recommended by cross-modal travel path comparison based on Internet of Things perception. Based on this algorithm model, the influence of path distance error value produced by different tourist attractions selection is minimized. The optimal path solution can be calculated by fluctuating in a relatively stable interval value. This can greatly reduce the efficiency of choosing travel routes and the travel experience in people's daily life. Under the perception of today's Internet of Things, although the other three algorithms have their own advantages and disadvantages, the path selection can be made in a short time, but the discrete values are 0.2. The error of the selection of 0.3, 0.4, and 0.5 is 18.7% beyond the normal value range. In the optimal path, the value produced by the fluctuation of iteration times of greedy algorithm is also in the fluctuation range of 42.3%~47.1%, and the time loss rate produced by the ant colony algorithm is repeated back and forth in the range of 13%~18.2%. But the hybrid ant colony algorithm solves this problem. In the selection of discrete values, the error value can also be kept fluctuating in the normal range of 10%~15%. And it can greatly reduce the peak data of about 17.32 in terms of time loss. In terms of regression value, the regression value of hybrid ant colony algorithm (3.971) is far lower than that of ant colony algorithm (0.23). When it is negative, the choice of optimal path also produces a negative interval domain of -1.172~1.42. Therefore, the construction and calculation of hybrid ant colony algorithm are recommended in the research of cross-modal travel path algorithm based on Internet of Things awareness. A future work focuses on multiroute optimization in the application of various algorithms and may consider the road conditions, traffic, and people flow of the routes for comprehensive application. According to the current application of tourism websites, this paper comprehensively evaluates the hot spots and whether to recommend the corresponding routes.

Data Availability

The experimental data used to support the findings of this study are available from the corresponding author upon request.

Conflicts of Interest

The authors declared that they have no conflicts of interest regarding this work.

References

[1] P. C. Garrido, G. M. Miraz, I. L. Ruiz, and M. Á. Gómez-Nieto, "A model for the development of NFC context-awareness applications on internet of things," in *2010 Second International Workshop on Near Field Communication*, pp. 9–14, Monaco, Monaco, 2010.

[2] L. Lim, P. Marie, D. Conan, S. Chabridon, T. Desprats, and A. Manzoor, "Enhancing context data distribution for the internet of things using qoc-awareness and attribute-based access control," *Annals of Telecommunications*, vol. 71, no. 3-4, pp. 121–132, 2016.

[3] M. Vazquez-Briseno, C. Navarro-Cota, J. I. Nieto-Hipolito, E. Jimenez-Garcia, and J. D. Sanchez-Lopez, "A proposal for using the internet of things concept to increase children's health awareness," in *CONIELECOMP 2012, 22nd International Conference on Electrical Communications and Computers*, pp. 168–172, Cholula, Puebla, Mexico, 2012.

[4] P. Pradeep, S. Krishnamoorthy, R. K. Pathinarupothi, and A. V. Vasilakos, "Leveraging context-awareness for Internet of Things ecosystem: representation, organization, and management of context," *Computer Communications*, vol. 177, pp. 33–50, 2021.

[5] Z. A. Almusaylim and N. Zaman, "A review on smart home present state and challenges: linked to context-awareness internet of things (IoT)," *Wireless Networks*, vol. 25, no. 6, pp. 3193–3204, 2019.

[6] J. Anesi, "Customer awareness, Internet of things influence IAQ products," *Air Conditioning Heating & Refrigeration*, vol. 254, no. 8, pp. 42–44, 2015.

[7] G. L. Shi and Y. X. Liu, "Research on key technologies for Internet of things," *Applied Mechanics & Materials*, vol. 190-191, pp. 308–312, 2012.

[8] M. A. Albreem, A. M. Sheikh, M. H. Alsharif, M. Jusoh, and M. N. Mohd Yasin, "Green Internet of things (GIoT): applications, practices, awareness, and challenges," *Access*, vol. 9, pp. 38833–38858, 2021.

[9] Y. Yuan and D. Wang, "Path selection model and algorithm for emergency logistics management," *Computers & Industrial Engineering*, vol. 56, no. 3, pp. 1081–1094, 2009.

[10] A. V. Donati, R. Montemanni, L. M. Gambardella, and A. E. Rizzoli, "Introduction to advanced system-on-chip test design and optimization, Erik Larson, Springer, Dordrecht (2005), 388 pp., Hardcover, plus XVIII, ISBN: 1-4020-3207-2," *Microelectronics Reliability*, vol. 48, no. 5, pp. 800-801, 2008.

[11] S. Behzadi, A. A. Alesheikh, and E. Poorazizi, "Developing a genetic algorithm to solve shortest path problem on a raster data Model," *Journal of Applied Sciences*, vol. 8, no. 18, pp. 3289–3293, 2008.

[12] Y. Zhang, J. H. Park, and K. T. Chong, "Model algorithm control for path tracking of wheeled mobile robots," *International Journal of Precision Engineering and Manufacturing*, vol. 11, no. 5, pp. 705–714, 2010.

[13] D. Q. Zhu, B. Sun, and L. Li, "Algorithm for AUV's 3-D path planning and safe obstacle avoidance based on biological inspired model," *Control & Decision*, vol. 30, no. 5, pp. 798–806, 2015.

[14] J. Dreo and P. Siarry, "Continuous interacting ant colony algorithm based on dense heterarchy," *Future Generation Computer Systems*, vol. 20, no. 5, pp. 841–856, 2004.

[15] G. L. Qin, "An improved ant colony algorithm based on adaptivelyadjusting pheromone," *Information and Control*, vol. 31, no. 3, 2002.

[16] L. Chen, J. Shen, L. Qin, and H. J. Chen, "An adaptive ant colony algorithm based on equilibrium of distribution," *Journal of Software*, vol. 14, no. 8, pp. 1379–1387, 2003.

[17] N. S. Safuan, M. Fathullah, Z. Shayfull, S. M. Nasir, and M. H. M. Hazwan, "Warpage improvement on wheel caster by optimizing the process parameters using genetic algorithm (GA)," *AIP Conference Proceedings*, vol. 1885, no. 1, pp. 1–5, 2017.

[18] T. A. Przylibski, "Radon and its daughter products behaviour in the air of an underground tourist route in the former arsenic and gold mine in Złoty Stok (Sudety Mountains, SW Poland)," *Journal of Environmental Radioactivity*, vol. 57, no. 2, pp. 87–103, 2001.

[19] T. Przylibski, "Changes in the concentration of radon-222 and its daughter products in the air of the underground tourist route in Walim (Lower Silesia)," *Antimicrobial Agents & Chemotherapy*, vol. 41, no. 3, pp. 196–205, 2000.

[20] D. E. Tchorz-Trzeciakiewicz and T. Parkitny, "Radon as a tracer of daily, seasonal and spatial air movements in the underground tourist route "Coal Mine" (SW Poland)," *Journal of Environmental Radioactivity*, vol. 149, pp. 90–98, 2015.

[21] Q. A. Huang, L. Dong, and L. F. Wang, "*LC* passive wireless sensors toward a wireless sensing platform: status, prospects, and challenges," *Journal of Microelectromechanical Systems*, vol. 25, no. 5, pp. 822–841, 2016.

[22] C. Mandel, B. Kubina, M. Schüßler, and R. Jakoby, "Metamaterial-inspired passive chipless radio-frequency identification and wireless sensing," *Annals of Telecommunications*, vol. 68, no. 7-8, pp. 385–399, 2013.

[23] S. M. Loo, M. Owen, J. Kiepert, A. Planting, C. Spicer, and S. W. Dean, "Modular, portable, reconfigurable, and wireless sensing system for the aircraft cabin," *Journal of ASTM International*, vol. 5, no. 4, p. 101638, 2008.

[24] Z. Zhang, S. Schwartz, L. Wagner, and W. Miller, "A greedy algorithm for aligning DNA sequences," *Journal of Computational Biology*, vol. 7, no. 1-2, pp. 203–214, 2000.

[25] P. Hadikhani, M. Eslaminejad, M. Yari, and E. Ashoor Mahani, "An energy-aware and load balanced distributed geographic routing algorithm for wireless sensor networks with dynamic hole," *Wireless Networks*, vol. 26, no. 1, pp. 507–519, 2020.

[26] S. Gu, G. Shi, W. Wu, and C. Lu, "A fast double greedy algorithm for non-monotone DR-submodular function maximization," *Discrete Mathematics Algorithms and Applications*, vol. 12, no. 1, 2020.

Hindawi
Journal of Sensors
Volume 2021, Article ID 6377024, 13 pages
https://doi.org/10.1155/2021/6377024

Research Article

EDF-Adaptive: A New Semipartitioned Scheduling Algorithm for Multiprocessor Real-Time

Shujuan Huang,[1] **Tiansen Li**,[1] **Zhihao Ma**,[1] **Feng Xiao**,[1] **and Wenjuan Zhang**[2]

[1]*School of Computer Science and Engineering, Xi'an Technological University, Xi'an 710021, China*
[2]*School of Sciences, Xi'an Technological University, Xi'an 710021, China*

Correspondence should be addressed to Shujuan Huang; huangshujuan@xatu.edu.cn

Received 18 October 2021; Revised 10 November 2021; Accepted 11 November 2021; Published 13 December 2021

Academic Editor: Gengxin Sun

Most of the multiprocessor real-time scheduling algorithms follow the partitioned approach, the global approach, or the semipartitioned approach which is a hybrid of the first two by allowing a small subset of tasks to migrate. EDF-fm (Earliest Deadline First-based Fixed and Migrating) and EDF-os (Earliest Deadline First-based Optimal Semipartitioned) are semipartitioned approaches and were proposed for soft real-time sporadic task systems. Despite their desirable property that migrations are boundary-limited such as they can only occur at job boundaries, EDF-fm and EDF-os are not always optimal and have higher tardiness and cost of overheads due to task migration. To address these issues, in this paper, we classify the systems into different types according to the utilization of their tasks and propose a new semipartitioned scheduling algorithm, earliest deadline first-adaptive, dubbed as EDF-adaptive. Our experiments show that EDF-adaptive can achieve better performance than EDF-fm and EDF-os, in terms of system utilization and tardiness overhead. It is also proved that EDF-adaptive is able to lessen the task migration overhead, by reducing the number of migrating jobs and the number of processors to which a task is migrated.

1. Introduction

The partitioned and global approaches are the classical scheduling algorithms for real-time multiprocessor systems. Because the former assigns tasks statically to processors and does not allow the tasks to migrate, it cannot achieve higher system utilization whereas the latter schedules tasks from a single run queue and the task hence can be migrated [1]. Although the global approach can attain higher system utilization but migrating tasks entails higher run-time overheads, especially in soft real-time (SRT) systems, many approaches have been proposed, based on these two algorithms [2–6] or the hybrid of the two [7–18]. Some approaches are aimed at reducing the switch context or preemption overheads and achieving higher system utilization [19–22].

Semipartitioned scheduling extends the partitioned scheduling by allowing a (usually small) subset of tasks to migrate, and these tasks cannot be feasibly assigned to two or more processors by a partitioned scheduling algorithm [23–26]. This type of approach is different from the global ones as the former use push migrations which are planned before execution whereas the latter use pull migrations which are reactive in nature and more difficult to account for and implement efficiently.

In this paper, we are particularly interested in two semipartitioned scheduling algorithms, EDF-fm [12] and EDF-os [13], because they are adaptive to SRT systems and allow a migrating task to migrate only between job boundaries, i.e., successive invocations. However, EDF-fm deals with per-task utilization restrictions according to the releasing sequence and cannot fully utilize the underlying hardware platform's available capacity that makes it nonoptimal. These restrictions preclude any task utilization from exceeding half the capacity of a processor. EDF-fm has two phases as follows:

(1) Offline assignment, where the tasks are assigned to the processors and meanwhile the tasks' attributions of fixed or migrating are given

(2) Online execution, where the extended earliest-deadline-first (EDF) scheduling is used to execute fixed tasks and migrating tasks on each processor. Note that a fixed task, i.e., a nonmigrating task, is the task assigned to only one processor and a migrating task is the task assigned to two or more processors in the phase of offline assignment

Like EDF-fm, EDF-os also has two phases, and in the online execution phase, the migrating tasks are statically prioritized over fixed ones. This ensures migrating tasks never miss deadlines. However, in the assignment phase, EDF-os is very different from EDF-fm. It assigns tasks as fixed ones as many as possible using a worst decreasing bin-packing heuristic. All remanent tasks are assigned in decreasing utilization order, by considering each processor and remanent tasks in turn. This approach allows migrating tasks to execute on any number of processors, instead of just two. However, the preemption overheads will be increased.

Though EDF-os increases the number of fixed tasks and reduces the number of migrating tasks, it may schedule a migrating task on three or more processors and thus the actual migrating times do not decrease. As a result, since the context switching overheads are also determined by the number of migrating jobs and the preemption times, EDF-os still has higher context switch overheads.

In this paper, we propose a novel EDF-based approach that overcomes the limitations of EDF-fm and EDF-os by reducing the number of jobs that miss deadline and making a balance between the cost of overheads and system utilization. The approach partitions tasks and schedules them adaptively, according to their utilization; thus, we dub it as EDF-adaptive. Given a real-time multiprocessor system with periodic tasks, EDF-adaptive first divides the tasks into two sets: one with high utilization denoted as S^H and the other with low utilization denoted as S^L. EDF-adaptive then chooses tasks from S^H and S^L whose utilization sum to an integer is less than the number of processors. We call these tasks complimentary. This selection process is repeated until the sum of all integers equals to the number of processors. During the execution, EDF-adaptive separates the processors into different scheduling queues according to the integers and puts these tasks into the corresponding queue. Our experiments have demonstrated that, compared with EDF-fm and EDF-os, EDF-adaptive is able to achieve lower job switching overheads, and the lowest degree of splitting and migrating, while in the meantime maintaining competitiveness in terms of system utilization and slack task minimum tardiness.

The remainder of this paper is organized as follows. Related works of semipartitioned algorithms are described in Section 2. The system model, definitions, and theorems about different utilization systems and EDF-adaptive algorithm in detail are introduced in Section 3. Experimental evaluations are undertaken to demonstrate the effectiveness of the proposed algorithm in Section 4. Finally, concluding remarks are drawn in Section 5.

2. Related Work

As mentioned in the previous section, there are two typical categories of scheduling algorithms for a real-time multiprocessor system, i.e., the global and the partitioned. Since our proposed approach in this paper concerns more on the latter, here, we focus on our review on semipartitioned schedulers, both for hard real-time (HRT) and soft real-time (SRT) systems. The difference between them is that the tasks in HRT are not allowed to miss their deadlines whereas those in SRT are allowed.

A variety of semipartitioned schedulers have been proposed for HRT that does not consider job boundary-limited. EDF-WM (Earliest Deadline First with Window constraint Migration) [14] assigns most tasks to processors, allowing some tasks to migrate between processors. But it is not only non-boundary-limited but also works by splitting tasks in a way guaranteeing no job misses a deadline while scheduling all jobs. When all processors share a single run queue, G-FL (Global Fair Lateness) [15] provides lateness bound for all tasks. For each job, G-FL uses a PP (Priority Point) that precedes its deadline. G-FL schedules each job based on the max-lateness bound which is minimized for any task system. C-FL (Clustered Fair Lateness) [16] defines the split factor of a task as the number of subjobs into which each of its jobs is split. By splitting job budgets to create subjobs with shorter periods and the worst-case execution times, such bounds can be reduced to near zero for implicit deadline sporadic task systems. Proposed for periodic task systems, EKG (Earliest Deadline First with task splitting and K processors in a Group) [17] is HRT-optimal when a configurable parameter is reduced in a way that increases preemption frequency.

Because non-boundary-limited schedulers above mentioned allow jobs to migrate in any time, it will be expensive in practice if jobs maintain a much-cached state. Some semipartitioned algorithms have been proposed to support SRT systems under bounded deadline tardiness. EDF-fm was first proposed, requiring utilization constraints that render it nonoptimal. To overcome the constraints, EDF-os was proposed by scheduling migrating tasks on three or more processors. Since none of the other migration algorithms mentioned above are job-boundary-limited, we will compare our proposed approach with EDF-fm and EDF-os.

3. Task Model and Scheduling Algorithm

3.1. Task Model. Assume a sporadic system consists of M processors and owns $N > M$ tasks $\tau = \{\tau_1, \tau_2, \cdots \tau_N\}$. These sporadic tasks are independent and to be scheduled upon a multiprocessor platform with $M \geq 2$ identical processors. In a sporadic task model, a sporadic task is a four-tuple $\tau_i(r_i, e_i, d_i, p_i)$ where e_i, d_i, and p_i are positive integer numbers and r_i is a nonnegative integer number and it

is characterized by a minimum interarrival time, also referred to as its period p_i, a worst-case execution cost e_i p_i, and a relative deadline d_i and a release time r_i. Every task τ_i may be invoked zero or more times with two consecutive invocations separated by at least p_i, time units. Each invocation of τ_i is referred to as a job of τ_i. The k^{th} job of τ_i, where $k \geq 1$, is denoted as $J_{i,k}$. The release time of the job $J_{i,k}$ is denoted as $r_{i,k}$. Each job of τ_i is executed for at most e_i, time units. The absolute deadline (or simply, deadline) of $J_{i,k}$, denoted as $d_{i,k}$, is the time at or before which $J_{i,k}$ should complete execution. Each task is sequential and at any time may be executed on at most one processor.

A periodic task system, in which every two consecutive jobs of every task τ_i are separated by p_i time units, is a special case of a sporadic task system. In this paper, we focus on the periodic task system and assume that $d_i = p_i$ holds for all τ_i and the first job of each task will be invoked or released at time zero. A task can then be represented using a two-tuple $\tau_i(e_i, d_i)$. The l^{th} processor is denoted as P_l, where $1 \leq l \leq M$. All tasks are synchronous and periodic and have the same initial release date. They are preemptive and independent. The overheads of other shared resources between tasks are not considered.

3.1.1. Utilization System and Tasks. To facilitate the description of our proposed EDF-adaptive, we categorize the real-time system aforementioned according to its task utilization.

Define $u_i = e_i/d_i$, where u_i is the utilization of task τ_i. Then, we have the utilization for all tasks $U(\tau) = \sum_{\tau_i \in \tau} u_i$.

We define the real-time system as follows:

(i) Single full utilization system, if $U(\tau) = 1$

(ii) All full utilization system, if $U(\tau) = M$

(iii) K full utilization system, if $U(\tau) = K$, where K is an integer. Under this scenario, the system may be either underloaded if $M > K > 1$ or fully utilized if $K = M$. For the latter, it may be an all full utilization system $K = M \geq 2$ or a single full system $K = M = 1$; overloaded utilization system, if $U(\tau) > M$

For the overloaded utilization system, we schedule the largest subset τ_{sub} so that the total utilization of the tasks' subset is very close to M. That is, $M - \sum_{i=1}^{k} u_i$ where $\varepsilon \in (0, 1)$ is a minimum float number and k is the number of the tasks in the subset τ_{sub}.

Each task is allocated a nonzero fraction, or share of one processor with the available utilization of 1.0. If there are k tasks being scheduled on the j^{th} processor, the remanent utilization of this processor is

$$U_j^{\tau} = 1 - \sum_{i=1}^{k} u_i, \tag{1}$$

where the fraction of the τ_i's utilization scheduled on this processor p_j, denoted as $u_{i,j}$, is U_j^{τ}. The total remanent utilization of this system is

$$U_{\text{rem}}^{\tau} = M - \sum_{j=1}^{M} U_j^{\tau}. \tag{2}$$

We define τ_i as a high utilization task if $u_i \geq 1/2$, and a low utilization task otherwise. Define S^H as a high utilization task set consisting of high utilization tasks, and S^L as a low utilization task set consisting of low utilization tasks. We represent S^H and S^L as follows:

$$S^H = \left\{ \tau_i \mid u_i \geq \frac{1}{2} \right\},$$
$$S^L = \left\{ \tau_i \mid u_i < \frac{1}{2} \right\}. \tag{3}$$

A high utilization system is defined as a system consisting of only S^H set.

3.1.2. Theorems for EDF-Adaptive Utilization. Here, we define several new theorems for the EDF-adaptive algorithm. First, we propose a concept of complementary tasks.

Definition 1. Given k periodic tasks $\tau_1, \tau_2, \cdots \tau_k$, $k > 1$, we regard k tasks are complementary if $\sum_{i=1}^{k} u_i = 1$. Then, we have the following lemma.

Lemma 2. *Complementary periodic tasks can be scheduled on uniprocessor, and their total utilization is 1.*

According to the DD scheduling algorithm [18], this lemma can be easily proved.

Given a time interval Δ, CPU utilization $U(\Delta) = \sum_{i=1}^{k} u_i$, where k is a set of periodic tasks executed in Δ, and u_i is the ratio of the execution time of τ_i task to Δ. Also, define the remanent utilization rate of a processor as $\beta(\Delta) = 1 - U(\Delta)$; then, the remaining time unit is

$$\text{spare}(\Delta) = \lfloor \beta(\Delta) \times \Delta \rfloor = \lfloor (1 - U(\Delta)) \times \Delta \rfloor. \tag{4}$$

Let T be the minimum common multiple of n tasks' period. Given $\sum_{i=1}^{n} u_i \leq 1$ if n tasks can be scheduled in $[0, T)$, then n tasks can be scheduled for the entire period of execution, according to [18]. This is because the corresponding scheduling method can be executed repeatedly in the future $[i * T, (i+1) * T]$, where $i \geq 1$.

Lemma 3. *Given n preemptive periodic tasks allocated to the j^{th} processor, the available time unit of the i^{th} periodic task $\tau_i = (e_i, d_i)$ in $[0, T]$ is spare $= T \times (1 - \sum_{k=1}^{n} u_k)$, where T is the minimum common multiple of the period of n tasks and τ_i. Define x as the available average time unit allocated to each activation of τ_i, and l as the number of τ_k' jobs allocated to this processor.*

We have

(1) A necessary and sufficient condition for τ_i to be assigned to the j^{th} processor as a fixed task without tardiness in $[0, T]$ is $x \geq e_i$ where $l = T/d_i$ and $x = \text{spare}/l$

(2) If τ_i is to be assigned to the j^{th} processor as a migrating task and $u_{i,j}$ is the fraction of the $\tau_i^{'}$ utilization is assigned to P_j, then $l = \lceil (T/d_i) \times (u_{i,j}/u_i) \rceil$ and $x = \text{spare}/l$. A sufficient condition for τ_i to be assigned to the j^{th} processor as a migrating task without tardiness in $[0, T]$ is $x \geq e_i$

Proof. For fixed tasks, firstly, we prove the necessary conditions under two scenarios.

One is for the first scheduled task, i.e., $n = 1$ and $\tau_1(e_1, d_1)$, where e_1 is the execution time and d_1 is the deadline or period. Obviously, this task is assigned to the processor as the fixed task. Given that the current spare time unit spare $= T = d_1$ time units and only τ_1 is allocated to this processor, we get

$$x = \frac{\text{spare}}{T/d_1} = d_1 \geq e_1. \tag{5}$$

The other is when $n = k - 1$, and the remanent time unit is spare $= T \times (1 - \sum_{i=1}^{k-1} u_i)$, we need to decide if the k^{th} task $\tau_k(e_k, d_k)$ will be allocated to this processor as a fixed task. T time unit including τ_k tasks' activation times is $l = T/d_k$. Because the time units that must be executed in each activation time are e_k and τ_k are scheduling on this processor with no tardiness, the remanent time unit spare must not be less than $l \times e_k$. Then, we get $x = \text{spare}/l \geq e_k$.

Secondly, we prove sufficient conditions. When $n = k - 1$, the remanent time unit is spare $= T \times (1 - \sum_{i=1}^{k-1} u_i)$. Because T is the minimum common multiple of the period of n tasks and τ_i, T is dividable to d_k. If the k^{th} task $\tau_k(e_k, d_k)$ is assigned to this processor as a fixed task, the activation times of τ_k, in $[0 ; T]$, is $l = T/d_k$ and the available average time unit allocated to each activation is $x = \text{spare}/l$. The time units that must be executed in each period are e_k. If $x \geq e_k$, there are enough time units for τ_k's every activation with no tardiness. □

For migrating tasks, when $n = k - 1$, the remanent time unit is spare $= T \times (1 - \sum_{i=1}^{k-1} u_i)$; we need to decide if the k^{th} task $\tau_k(e_k, d_k)$ will be allocated to this processor as a migrating task. Let $u_{k,j}$ be the fraction of τ_k's utilization. We can obtain the proportion of jobs allocated to this processor by $u_{k,j}/u_k$. The total activation time of τ_k in $[0, T]$ is T/d_k, but there are at most $\lceil (T/d_k) \times (u_{k,j}/u_k) \rceil$ jobs of τ_k allocated to this processor in $[0, T]$. Let l be the number of jobs, $l = \lceil (T/d_k) \times (u_{k,j}/u_k) \rceil$. If $x = \text{spare}/l \geq e_k$, there are enough time units for τ_k's jobs to be scheduled on this processor without any tardiness.

According to Lemma 3, given a task τ_i for a processor, we can decide whether it should be regarded as a fixed task or migrating task. If $n - 1$ tasks are assigned as fixed task and for the n^{th} task there always exists $x < e_i$ in $[0, T]$, τ_n is then removed. If the system becomes an underloaded utilization system after the removal, we call τ_n is a probable slack task.

Theorem 4. *A probable slack task $\tau_i(e_i, d_i)$ can be delayed, and its minimum tardiness is*

$$Tardiness_{\min} = e_i \times \left(\frac{1}{M - \sum_{i \neq j} u_j} - \frac{1}{u_j} \right). \tag{6}$$

Proof. If a probable slack task τ_i is removed, the system's remanent utilization is $M - \sum_{i \neq j} u_j > 0$. To schedule this system, the task has to be delayed in the whole process, and we assume the minimum period after delay is d_{new}, which is also the delay deadline for the soft real-time task. The tardiness can be derived as

$$\begin{aligned} \text{Tardiness}_{\min} &= d_{\text{new}} - d_i = e_i \times \left(\frac{1}{M - \sum_{i \neq j} u_j} \right) - d_i \\ &= e_i \times \left(\frac{1}{M - \sum_{i \neq j} u_j} - \frac{1}{u_i} \right). \end{aligned} \tag{7}$$

□

3.2. EDF-Adaptive Algorithm. Similar to EDF-fm and EDF-os, our EDF-adaptive also has two phases: offline task partitioning phase and task splitting execution phase.

3.2.1. Task Partitioning Algorithm. To partition tasks, we first arrange them in utilization ascending order. From S^H and S^L, we find all complementary task sets with their total utilization being $K (1 \leq K \leq M)$. Subsequently, we dispatch K sets into the K processors' scheduling queue. We assume that a center processor distributes new tasks to processors, and each processor sends a request and amends its own scheduling queue.

Though the DD scheduling algorithm can be used for the tasks in one processor with its scheduling queue, there exist two issues. One is that the complementary task sets may not be unique. For example, given six tasks with utilization as $\{0.1, 0.3, 0.4, 0.5, 0.7, 0.9\}$, we can divide them into two optional complementary tasks set: one is $\{0.1, 0.4, 0.5\}$, $\{0.7, 0.3\}$ and the other is $\{0.1, 0.9\}$, $\{0.7, 0.3\}$. EDF-adaptive always chooses the sets that include most tasks, unless the system species the priority of tasks. The other issue is to select the parameter ε so that all similar complementary tasks can be obtained. EDF-adaptive selects ε so that the total utilization is the nearest close to K.

Algorithm 1 presents the pseudocode to find complementary tasks set for K full utilization system. As shown in Algorithm 1, the overall approach is to find and add complementary tasks into Set_{comp} and then remove them from Q.

Input: i: the sequence number of the task with minimum utilization
j: the sequence number of the task with maximum utilization
U_{res}: the remanent utilization and initial value is K when the system is K full utilization system
Q: the set of all tasks in the system with their utilization in descending order
Output: Set_{comp}: the complementary task set.
1: if $Q \neq$ NULL and $U_{res} \neq 0$ and $j \neq i$ then
2: if $u_i + u_j == U_{res}$ then
3: $\text{Set}_{comp} \longleftarrow \tau_i, \tau_j$;
4: $U_{res} = 0$;
5: $Q \longleftarrow$ delete τ_i, τ_j;
6: return 1;
7: else
8: if $u_i + u_j < U_{res}$ then
9: $\text{Set}_{comp} \longleftarrow \tau_i, \tau_j$
10: $Q \longleftarrow$ delete τ_i, τ_j;
11: $U_{res} = U_{res} - u_i - u_j$
12: Find$(i + 1 ; j - 1, U_{res}, Q)$;
13: else:
14: if $u_i + u_j > U_{res}$ then
15: if $u_i == U_{res}$ then
16: $\text{Set}_{comp} \longleftarrow \tau_i$;
17: $U_{res} = 0$;
18: $Q \longleftarrow$ delete τ_i;
19: return 1;
20: else
21: if $u_j == U_{res}$ then
22: $\text{Set}_{comp} \longleftarrow \tau_j$;
23: $U_{res} = 0$;
24: $Q \longleftarrow$ delete τ_j;
25: return 1;
26: end if
27: end if
28: end if
29: end if
30: end if
31: $j = j - 1$
32: if $j \neq i$ then.
33: Find$(i, j - 1, U_{res}, Q)$
34: return 0;
35: end if
36: end if

Algorithm 1: Find complementary tasks.

When there are still tasks in Q or U_{res} is not 0 or $j = i$, Algorithm 1 recursively finds the complementary tasks set by adding u_i and u_j that is depending on the relationship between u_i, u_j, and U_{res}; there are several cases as follows:

If $u_i + u_j == U_{res}$, τ_i and τ_j belong to the complementary set.

If $u_i + u_j > U_{res}$, only one of them can be an element in the complementary set, depending on if $u_i == U_{res}$ or $u_j == U_{res}$.

If $u_i + u_j < U_{res}$, τ_i and τ_j may or may not be the elements in the complementary set.

If none of the conditions above is satisfied, the algorithm updates the sequence number $(j = j - 1)$ and continues to search.

3.2.2. Task Splitting and Execution Algorithm. To achieve higher system utilization, we split tasks assigned to K processors according to their utilization.

First, the tasks are arranged in descending order of utilization in the queue. The tasks with the highest utilization are assigned to the j^{th} processors and then removed from the queue. If $j \leq K$, calculate the remanent utilization of the j^{th} processor U_j. If $U_j > 0$, select the task which has the lowest utilization in the queue and calculate the split value by

$$f_{i,j} = \left(\frac{T}{d_i}\right) \times \left(\frac{u_{i,j}}{u_i}\right), \tag{8}$$

Input: Set_{comp}: a complementary utilization tasks set.
T: a global time counter.
Output: ProcessorSet$[N; K]$: the N tasks distribution results for the K processors the complementary task set.
1: if $\text{Set}_{\text{comp}} \neq$ NULL then
2: $\text{Set}_{\text{comp}} \longleftarrow \tau_i, \tau_j$
3: /*Sort all the tasks in Set_{comp} according to its period in descending order;*/
4: $i = 1$;
5: $j = 1$;
6: $U_i = 1$;
7: $U_i = u_i$;
8: while $j \leq K$ do:
9: if $U_i > U_j$ then.
10: $U_i = U_i - U_j$;
11: $u_{i,j} = U_j$;
12: $P_{\text{set}[j]} \longleftarrow \tau_i$;
13: $f_{i,j} \longleftarrow (T/p_i) \times (u_{i,j}/u_i)$;
14: ProcessorSet$[i, j] \longleftarrow f_{i,j}$;
15: $j = j + 1$;
16: else
17: $U_j = U_j - U_i$;
18: $u_{i,j} = U_i$;
19: $P_{\text{set}[j]} \longleftarrow \tau_i$;
20: $\text{Set}_{\text{comp}} \longleftarrow$ delete τ_i;
21: $f_{i,j} \longleftarrow (T/p_i) \times (u_{i,j}/u_i)$;
22: ProcessorSet$[i, j] \longleftarrow f_{i,j}$;
23: $i = i + 1$
24: if $U_j == 0$ then
25: $j = j + 1$;
26: end if
27: end if
28: end while
29: end if

Algorithm 2: Task splitting.

where $f_{i,j}$ is the number of jobs that τ_i will be scheduled on the j^{th} processor in $[0, T]$, according to Lemma 3. The task τ_i will be allocated to execute on the j^{th} processor in time $[0, T]$, i.e., the units of execution time units of τ_i on the j^{th} processor. τ_i will be divided and assigned to other processors if its remanent execution time unit is not zero. If $U_j \leq 0$, it means that the j^{th} processor has completed the assignment; if $j > K$, it indicates that the tasks of this group set have been allocated over, and it returns the corresponding processor with the allocated tasks. The pseudocode of the splitting approach is presented in Algorithm 2.

As shown in Algorithm 2, there are the following two scenarios:

If $U_i \geq U_j$, it means U_j cannot satisfy U_i. The τ_i's utilization share on processor P_j is $u_{i,j} = U_j$, and the remaining utilization of τ_i is $U_i = U_i - U_j$. The number of jobs that τ_i will be scheduled on the j^{th} processor in $[0, \text{T}]$ is $f_{i,j}$.

If $U_i < U_j$, it means that U_j can satisfy U_i. The share of task τ_i assigned on processor P_j is $u_{i,j} = U_j$. We calculate the number of jobs ($f_{i,j}$) that τ_i will be scheduled on the j^{th} processor in $[0, \text{T}]$ and record $f_{i,j}$ in the scheduling queue of processor P_j. Next, we update the remaining utilization of P_j, $U_j = U_j - U_i$, and remove the task τ_i from the complementary set before selecting the next task. If $U_j = 0$, it means that the remaining utilization of the j^{th} processor has been exhausted and the next processor must be selected.

In the execution phase, all released jobs of the fixed tasks are scheduled online without migration. Different from EDF-os and EDF-fm that the priority of migration tasks is higher than that of fixed tasks at any time, in EDF-adaptive's execution phase; the priority of migration tasks is only higher than that of fixed tasks with lower utilization. To compare the task splitting and scheduling of EDF-adaptive with EDF-fm and EDF-os, we use a task system $\tau = \{(9, 10), (7, 12), (3, 4), (2, 3), (3, 5), (1, 2)\}$ as an example, since $U(\tau) = 4$ is feasible on four processors. Because all task utilization but one exceed 0.5 and the other utilization is exactly 0.5, all the tasks belong to S^H. The comparing results are shown in Figures 1–6.

Figure 1 illustrates the offline assignment phase of EDF-fm functions, where tasks are assigned to the processors as either fixed task or migrating one. We can see that EDF-

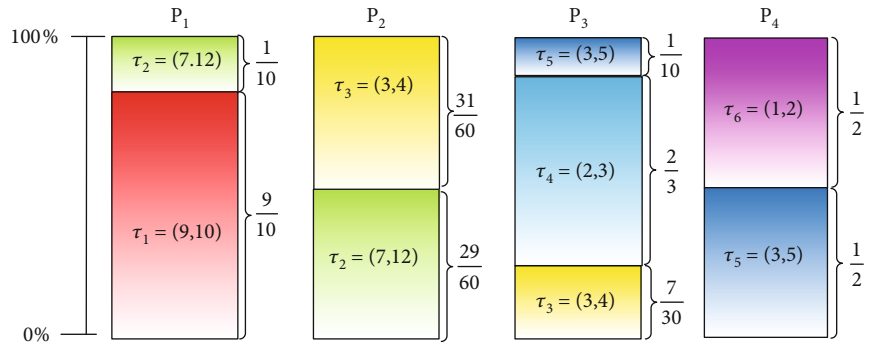

Figure 1: EDF-fm offline assigning tasks in 4 processors.

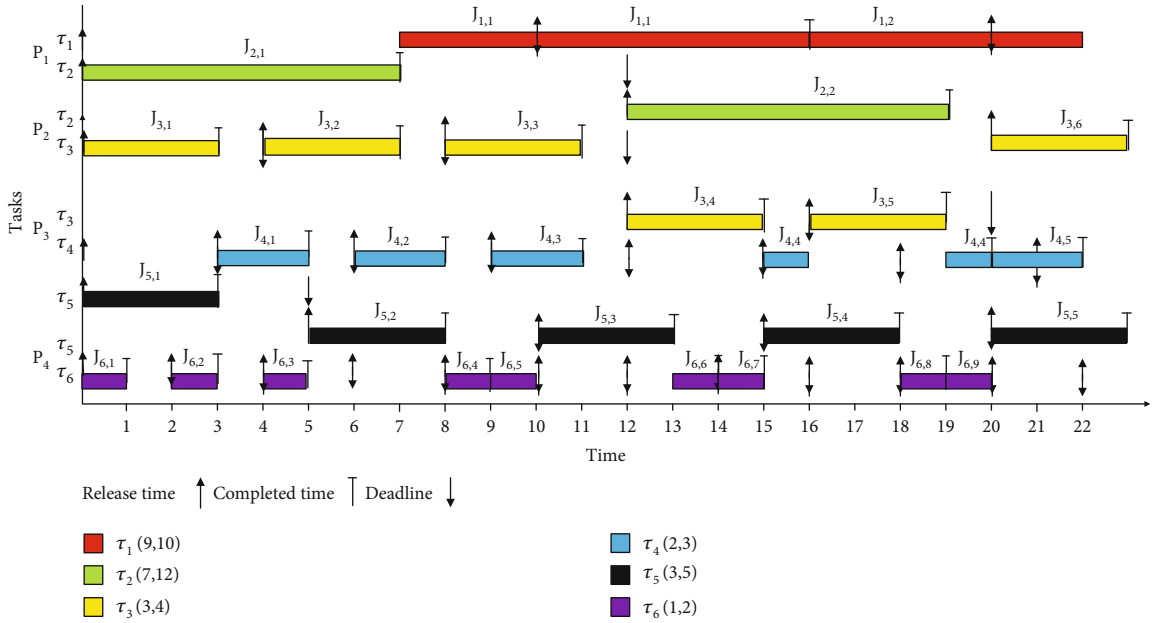

Figure 2: EDF-fm online scheduling results in 22 time units.

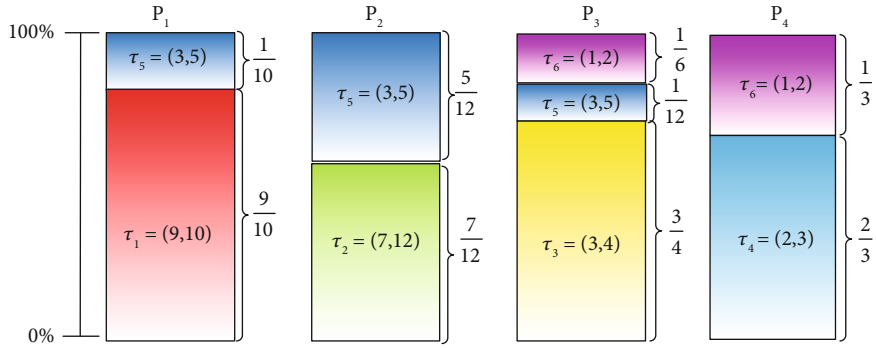

Figure 3: EDF-os offline assigning tasks in 4 processors.

fm has a simple assignment algorithm which dispatches tasks according to their order of coming. If the currently considered processor P_j has sufficient unallocated utilization, the currently considered task τ_i is assigned to it as a fixed task and $u_{i,j} = U_i$; otherwise, τ_i exhausts the remaining unallocated utilization of P_j and receives from P_{j+1} the rest of its allocation required. For example, τ_2 is assigned to P_1 and P_2, and its utilization has been divided into two parts: $u_{2,1} = 1/10$ and $u_{2,2} = u_2 - u_{2,1} = 29/60$; that means, τ_2 is a migrating task.

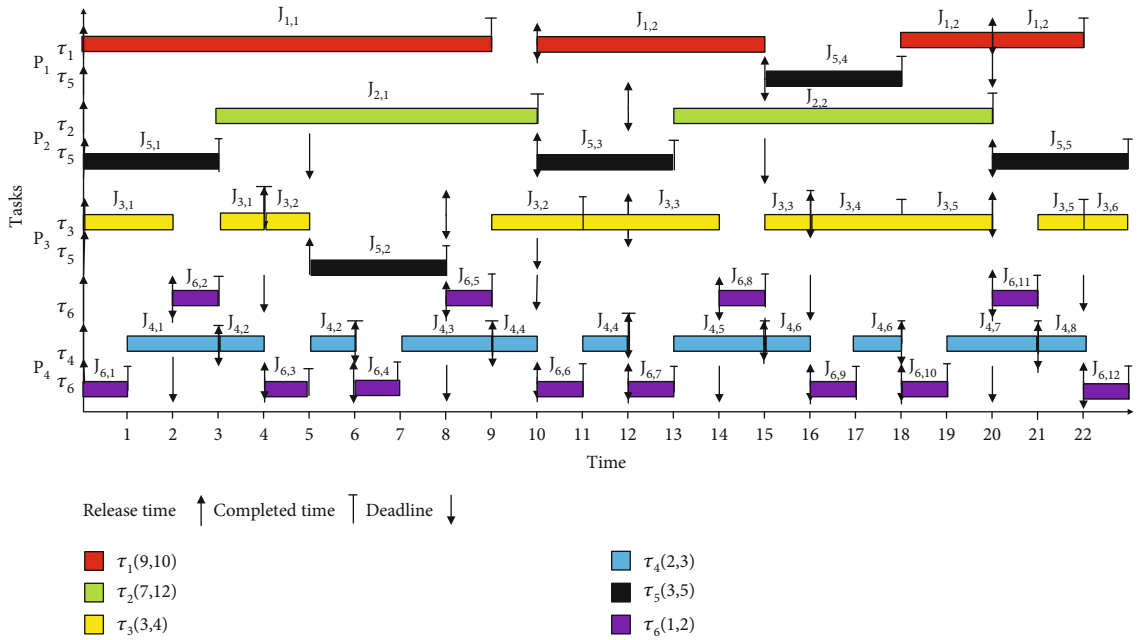

Figure 4: EDF-os online scheduling results in 22 time units.

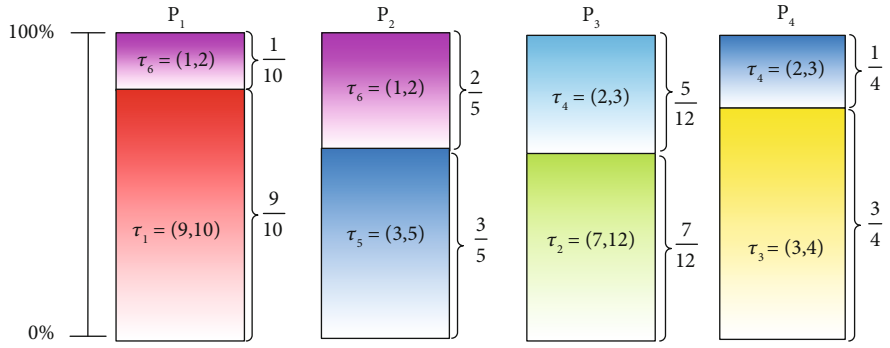

Figure 5: EDF-adaptive offline assigning tasks in 4 processors.

Figure 2 is EDF-fm's online execution phase that extends the earliest-deadline-first (EDF) scheduling to executed and migrating tasks. Specifically, each migrating task executes on two processors, and for each processor, at most two specific migrating tasks may execute upon it. Because the migrating tasks are prior to the fixed tasks for EDF-fm, the jobs of τ_1 cannot meet any jobs' deadline although it shares a 9/10 fraction of the processor P_1 of which the remanent utilization is given the migrating task τ_2. The jobs of τ_1 and τ_4 and τ_6 miss the deadline, and their total tardiness is 44 time units. The migrating tasks are τ_2, τ_3, and τ_5, and 9 time unit is unused. If the task's utilization restriction of EDF-fm is violated, migrating tasks may miss deadlines, which invalidates the tardiness analysis.

Figure 3 is the offline assignment phase of EDF-os. All the tasks' utilizations are assigned to the processors in decreasing order using a worst-t decreasing scheme rather than an arbitrary ordering. This phase tries to assign as many tasks as possible to be fixed; hence, the number of fixed tasks is as same as that of the processors at least. The remaining tasks are allocated nonzero shares from a succession of processors until the sum of its shares equals its utilization. Because the remaining tasks' utilization is considered in decreasing order, each processor must contain at least one fixed task with its utilization that is at least that of any migrating task. It is possible that such a task receives a nonzero share on only one processor, in which it is a fixed task; otherwise, it is migrating. This procedure ensures that there are at most two migrating tasks with nonzero shares on any processors. However, a migrating task under EDF-os can have nonzero shares on more than two processors. We can see there are τ_1, τ_2, τ_3, and τ_4 four tasks' utilization in decreasing order as fixed tasks and τ_5 has nonzero shares on three processors. P_3 contains one fixed task τ_3 and two migrating tasks τ_5 and τ_6.

Figure 4 is EDF-os's online execution phase. As in EDF-fm, migrating tasks are statically prioritized over fixed ones on any processor and each job executes on only one processor and fixed tasks are prioritized against each other using EDF. But if a processor has two migrating tasks τ_i and τ_{i+1}

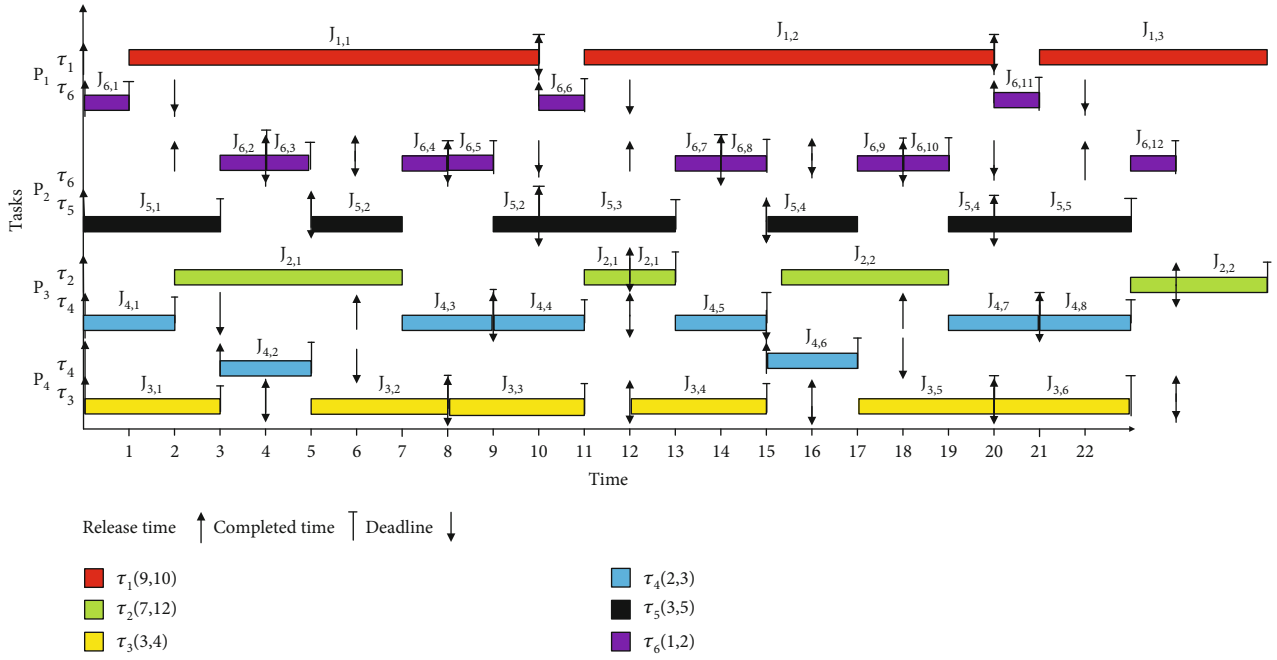

Figure 6: EDF-adaptive online scheduling results in 22 time units.

Table 1: Statistics for the example in 22 time units.

Algorithm	Tardiness (time units)	The number of migrating tasks	Unused (time units)	Context switch (time units)
EDF-fm	44	3	9	15
EDF-os	15	3	1	29
EDF-adaptive	3	2	1	23

assigned in this order, τ_i is statically prioritized over τ_{i+1}. This means a migrating task executes with the highest priority on any processor that is not its first processor. Note that the lowest-indexed processor to which a migrating task τ_i is assigned jobs is called $\tau_i^{'}$ first processor. For example, P_2 is τ_5's first processor and P_3 is τ_5's second processor, so τ_5 has the highest priority on P_3 and τ_6 has higher priority than τ_3.

EDF-os has better solutions for decreasing the number of jobs missing deadline, and it distributes the fixed tasks at first according to the processors, as shown in Figures 3 and 4. It can be seen that τ_2 and τ_3 in the EDF-fm have been scheduled as migrating tasks and assign them as the fixed tasks in the EDF-os, whereas the task τ_5 is split and assigned into three processors. The splitting will introduce more preemption overhead in the third processor. The jobs of τ_1 and τ_3 miss the deadline, and the total tardiness is 15 time units.

Figure 5 is the offline assignment phase of EDF-adaptive. Algorithm 1 divides these 4 (i.e., $K = 4$) full utilization systems into 2 full utilization subsystems that are $\{(9, 10), (3, 5), (1, 2)\}$ and $\{(9, 10), (3, 4), (2, 3)\}$. In each subsystem, the sum of tasks' utilization is 2. Meanwhile, the processors are divided into two parts $\{P_1, P_2\}$ and $\{P_3, P_4\}$ according to the subsystems, respectively. In each subsystems, as many tasks with the maximum period as possible are assigned as fixed tasks. We can see that the tasks with the minimum period such as τ_6 and τ_4 are the migrating tasks in the two subsystems, respectively.

Subsequently, according to Algorithm 2, we obtain the number of scheduling jobs for each task on processors. The scheduling results for this instance of EDF-adaptive are shown in Figure 6. We also consider the bounded tardiness restriction, i.e., the job is migrated at its boundary. Unlike EDF-os and EDF-fm, EDF-adaptive does not statically prioritized migrating tasks over fixed tasks. Instead, it always preempts the fixed tasks with the lowest utilization in its subsystems. It can be seen in Figure 6 that only the jobs of τ_2 miss the deadline and the total tardiness is 3 time units. The migrating tasks are τ_4 and τ_6, and only 1 time unit is unused. The context switch overhead is lower than that in EDF-os. With the statistic results depicted in Table 1, we can find that EDF-adaptive is prior to EDF-fm and EDF-os at the total tardiness but the context switch times are between the two. These figures also show us that EDF-os and EDF-adaptive need to increase the migrating times, preemptive times, and context switch times to meet more jobs' deadlines.

4. Evaluation

In this section, we evaluate the performance of EDF-adaptive by generating task sets for the SRT system and

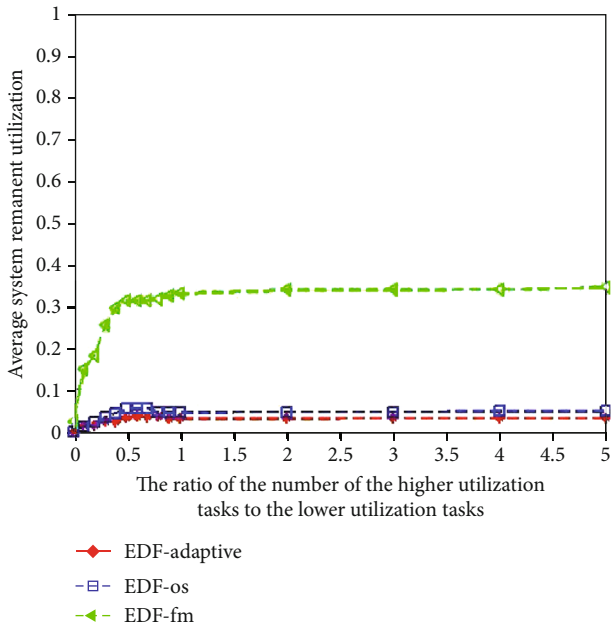

Figure 7: Average system remanent utilization.

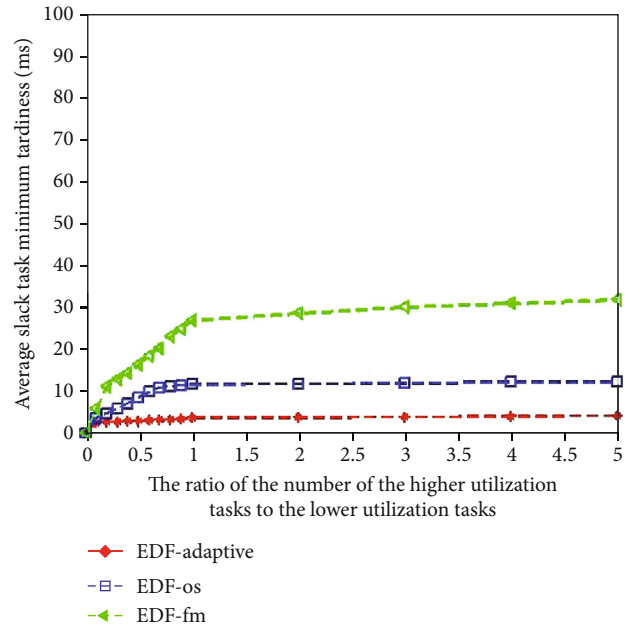

Figure 8: Average slack task minimum tardiness.

compare it with EDF-fm and EDF-os against five criteria as follows:

(1) Average remanent utilization, which is the ratio of the sum of the unused time units of the processors to the total time units

(2) Average slack task minimum tardiness, according to Theorem 4

(3) Average context switching overhead, which is the multiplication of the times of context switching jobs and the overhead of per job context switching

(4) Migrating degree, which is the ratio of the number of the migrating tasks to the total number of tasks

(5) Splitting degree, which is the ratio of the number of the tasks split and scheduled on more than three processors to the total number of tasks

4.1. Task Set Generation. We used an Intel (R) core (TM) 2 Quad Q8400 multiprocessors workstation with 4 processors shared on 4 MB L2 cache.

In the experiment, we randomly generated 100 task sets, and each task set has generated 20 soft real-time periodic tasks with different utilization and period parameters randomly. From each task set, three types of task sets, overloaded, underloaded, and all full utilization, are selected. We run each type of task set 10 times to calculate the average value. These tasks come with implicit deadlines and are either in S^H or in S^L because the utilization of half of them is less than 0.5, and the other half is greater than or equal to 0.5. The worst-case execution time (WCET) of each task is determined by the product of its period and utilization so that WCET of all tasks will be less than the deadline (which is equal to the period).

We set utilization caps in two sections, $[1, 4]$ and $(4, 5]$. This cap is a range when the sum of all task utilization is given. We calculate the system utilization and get the probable slack task according to Lemma 3. Then, we add or delete the probable slack task until an overloaded system, all full utilization system, or underloaded system is obtained. That is to say, when a set of 20 tasks is generated, the probable slack tasks will be added or subtracted so that the sum of the utilization of all tasks is less than 4 (underloaded system), equal to 4 (all full utilization system), or in the range of $(4, 5]$ (overloaded system), respectively.

4.2. Results and Discussions. To evaluate the performance of EDF-adaptive, EDF-fm, and EDF-os, we ran 100 times and obtained the average of each evaluation criterion. The results are shown in Figures 7–11. In each figure, the horizontal axis is the ratio of the number of tasks in S^H to the number of tasks in S^L, denoted as R. When the ratio increases, the system is moving from lower utilization to higher utilization.

Average remanent utilization. It can be seen from Figure 7 that for all algorithms, the remanent utilization increases with R, but it nearly stabilizes when R is greater than 1. Overall, EDF-adaptive and EDF-os get smaller remanent utilization than EDF-fm. This is because EDF-fm selects the tasks and executes them in releasing sequence while EDF-os sorts the utilization of the tasks with descending order first before execution, and EDF-adaptive chooses tasks to execute according to their utilization.

Average minimum tardiness. Figure 8 shows that EDF-adaptive and EDF-os have lower tardiness than EDF-fm because of their task selection, as it has been explained earlier. In fact, EDF-adaptive has the lowest tardiness because it can schedule the selective tasks that meet the full utilization system.

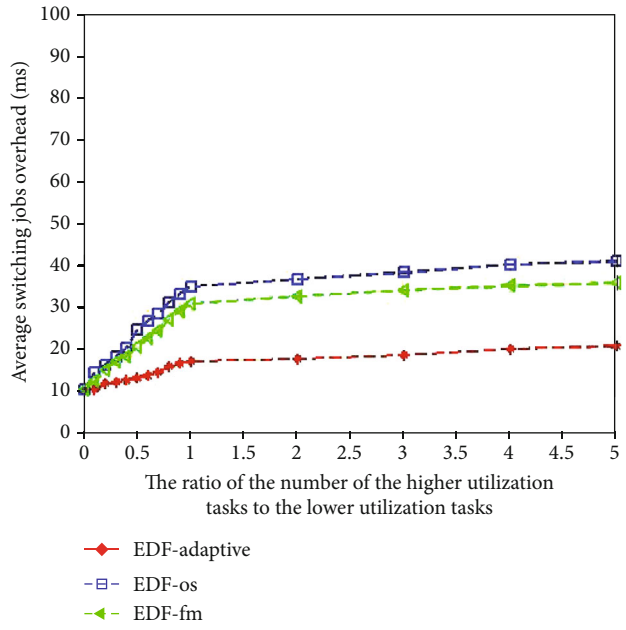

Figure 9: Average switching jobs overhead.

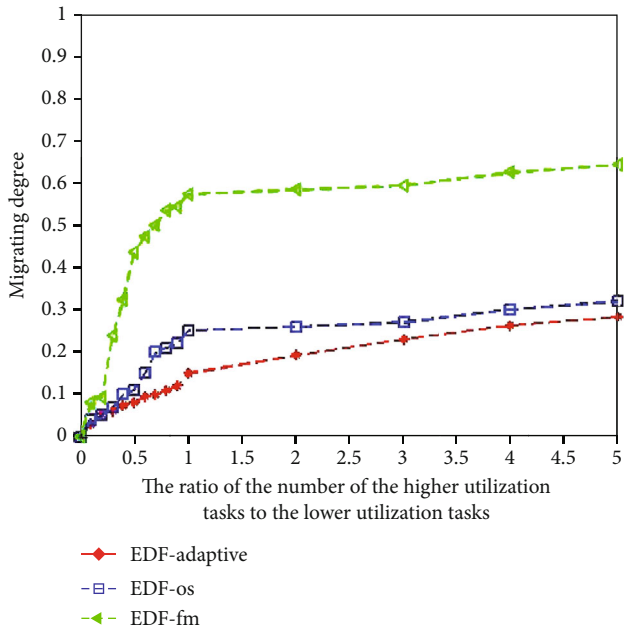

Figure 10: Migrating degree.

Average job switching overhead. Obviously, as shown in Figure 9, EDF-adaptive has lower overhead than EDF-os but has higher overhead than EDF-fm. Because EDF-adaptive and EDF-os are able to meet the jobs' deadlines, they have to increase the preemptive and migrating times which will give rise to context switch overhead. Although EDF-fm gets the lowest switch jobs overhead, many jobs miss their deadlines as shown in Figure 7. While EDF-os needs to meet the jobs' deadline and has no restrictions on task segmentation, some tasks may be partitioned into more than three processors that will introduce higher overhead than EDF-fm. EDF-adaptive partitions tasks to meet K full utilization rate in the

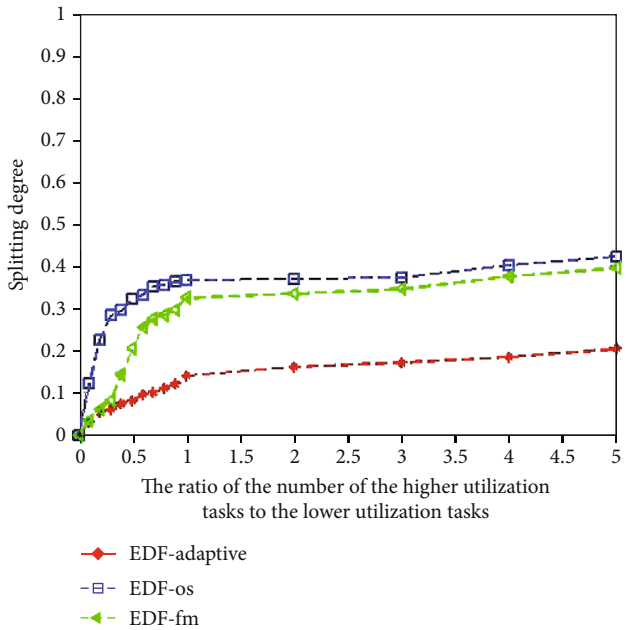

Figure 11: Splitting degree.

nondescending order integer value. As a result, it can reduce the switching cost of EDF-os. Obviously, EDF-adaptive can achieve almost as the same as EDF-os on system utilization and get the lowest tardiness in these algorithms and reduce the switch jobs overhead.

Migrating degree. Figure 10 shows that EDF-adaptive has a much smaller migration degree (thus lower migrating overhead) than EDF-fm and EDF-os, because there will be no migration between the different partition of processors when the maximal K full utilization is achieved.

Splitting degree. The higher the splitting degree, the more tasks have been scheduled on multiple processors. It can be seen in Figure 11 that EDF-adaptive has performed much better than EDF-fm and EDF-os, in terms of preventing tasks from being split into multiple processors. Figure 11 also shows that EDF-os has the highest splitting degree. This is because EDF-os allows tasks to be assigned to more than 3 processors. This increases the partitioning of tasks. Based on the discussion above, we can conclude that EDF-adaptive is able to schedule more tasks in overloaded systems than EDF-fm and EDF-os. Because EDF-adaptive can selectively schedule from the task queue, it keeps the system running at full capacity as much as possible. For example, in an overloaded system, EDF-fm only schedules tasks in releasing sequence and EDF-os schedules tasks in descending order of utilization and then schedules migration tasks first, followed by fixed tasks. EDF-adaptive is to select appropriate tasks to schedule from S^H and S^L. For example, EDF-os schedules tasks with a utilization of 0.3 in order, while EDF-adaptive can schedule two tasks with a utilization of, say, 0.1 and 0.2. And in terms of job switching, task migration, and splitting, EDF-adaptive complexity analysis. Despite better performance, EDF-adaptive suffers a higher time complexity than EDF-fm and EDF-os.

The time complexity of Algorithm 1 is $O(n^2)$ because the worst case for searching and selecting process is the total number of tasks n in S^H or S^L. And it uses a recursive approach for finding complementary tasks, mainly based on the number of S^H or S^L. Algorithm 2 schedules tasks onto the processors, and the time complexity is $O(m)$, where m is the number of processors. Hence, the time complexity of EDF-adaptive is $O(n^2 + m)$, while EDF-fm has the time complexity $O(nm)$ and EDF-os has the time complexity $O(n + nm)$. In our future work, we will investigate approaches to reduce the time complexity and simplify the process. One idea is to use hash functions to find the complementary tasks from S^H and S^L.

5. Conclusions

In this paper, we have proposed the EDF-adaptive algorithm for the soft real-time multiprocessor systems, which can be divided into three types of system: underloaded utilization system, full utilization system, and overloaded utilization system. The algorithm can allocate task sets onto the processors to achieve better performance than EDF-os and EDF-fm in terms of the degree of task's splitting and migrating. However, partition problems are generally Np hard and EDF-adaptive is not optimal because of its time complexity. In the future, we will try to apply EDF-adaptive for the heterogeneous systems and mixed-criticality systems, while investigating new approaches to reduce the time complexity.

Data Availability

The data used to support the findings of this study are available from the corresponding author upon request.

Conflicts of Interest

The authors declare that they have no conflicts of interest.

Acknowledgments

The authors would like to thank Professor Feng Tian for critically reviewing the manuscript. The research and publication of this article were funded by the National Natural Science Foundation of China (No. 62171361), Scientific and Technological Project in Shaanxi Province (No. 2021 JM-440), and Industrial Science and Technology Research Project of Shaanxi Province of China (No. 2020GY-066).

References

[1] A. Bastoni, B. B. Brandenburg, and J. H. Anderson, "An empirical com-parison of global, partitioned, and clustered multiprocessor EDF schedulers," in *Proc. 31st Int. Conf. IEEE Real-Time Systems Symposium*, pp. 14–24, San Diego, CA, USA, 2010.

[2] H. S. Chwa, J. Lee, K. Phan, A. Easwaran, and I. Shin, "Global EDF schedulability analysis for parallel tasks on multi-core platforms," *IEEE Transactions on Parallel and Distributed Systems*, vol. 28, no. 5, pp. 1331–1345, 2017.

[3] L. George and J. F. Hermant, "A norm approach for the partitioned EDF scheduling of sporadic task systems," in *Proc. 21st Euromicro Conf. Real-Time Systems*, pp. 161–169, Dublin, Ireland, 2009.

[4] R. Ayari, I. Hafnaoui, and G. Beltrame, "ImGA: an improved genetic algorithm for partitioned scheduling on heterogeneous multi-core systems," *Design Automation for Embedded Systems*, vol. 22, no. 1-2, pp. 183–197, 2018.

[5] J.-M. Chung, S.-W. Jo, and M. H. Ahn, "ARQ supportive EDF scheduling for wireless networks servicing real-time applications," *IEEE Communica-tions Letters*, vol. 17, no. 7, pp. 1329–1331, 2013.

[6] J. Li, Z. Luo, D. Ferry, K. Agrawal, and L. Christopher Gill Chenyang, "Global EDF scheduling for parallel real-time tasks," *Real-Time Syst*, vol. 51, no. 4, pp. 395–439, 2015.

[7] G. Kedar, A. Mendelson, and I. Cidon, "SPACE: semi-partitioned CachE for energy efficient hard real-time systems," *IEEE Transactions on Computers*, vol. 66, no. 4, pp. 717–730, 2017.

[8] E. M. Daoudiy and A. Kerfali, "Reducing the inter processor preemptions of the EDHS scheduling," in *Proc. 5th Int.Conf. Optimization and Applications*, pp. 1–6, Kenitra, Morocco, 2019.

[9] S. Moulik and Z. Das, "TASOR: a temperature-aware semi-partitioned real-time scheduler," in *Proc. IEEE Region 10 Conf. Technology, Knowledge, and Society*, pp. 1578–1583, Kochi, IN-DIA, 2019.

[10] V. Bonifaci, G. D'Angelo, and A. M. Spaccamela, "Algorithms for hierarchical and semi-partitioned parallel scheduling," in *Proc. 31st Int. Conf. IEEE Inter-national Parallel and Distributed Processing Symposium (IPDPS)*, pp. 738–747, Orlando, FL, 2017.

[11] A. Bastoni, B. B. Brandenburg, and J. H. Anderson, "Poster abstract: online semi- partitioned multiprocessor scheduling of soft real-time peri-odic tasks for QoS optimization," in *Proc. 22nd Int. Conf. IEEE Real-Time and Embedded Technology and Appli-cations Symposium*, pp. 1–1, Vienna, AUSTRALIA, 2016.

[12] J. Anderson, V. Bud, and U. Devi, "An EDF-based restricted-migration scheduling algorithm for multiprocessor soft real-time systems," *Real-Time Systems*, vol. 38, no. 2, pp. 85–131, 2008.

[13] J. H. Anderson, J. P. Erickson, U M.-S. C. Devi, and B. N. Casses, "Optimal semi-partitioned scheduling in soft real-time systems," *Journal of Signal Pro-cessing Systems*, vol. 84, no. 1, pp. 3–23, 2016.

[14] S. Kato, Y. Ishikawa, and R. R. Rajkumar, "CPU scheduling and memory management for interactive real-time applications," *Real-Time Systems*, vol. 47, no. 5, pp. 454–488, 2011.

[15] J. P. Erickson, J. H. Anderson, and B. C. Ward, "Fair lateness scheduling: reducing maximum lateness in G-EDF-like scheduling," *Real-Time Systems*, vol. 50, no. 1, pp. 5–47, 2014.

[16] J. P. Erickson and J. H. Anderson, "Reducing tardiness under global scheduling by splitting jobs," in *Proc. 25th Int. Conf. Real-Time Systems, ECE Grad Sch Engn*, pp. 14–24, Paris, FRANCE, 2013.

[17] E. M. Daoudi, A. Dargham, A. Kerfali, and M. Khatiri, "Reducing the inter-processors migrations of the EKG algorithm," *SCPE*, vol. 19, no. 3, pp. 293–300, 2018.

[18] C. L. Liu and J. W. Layland, "Scheduling algorithms for multiprogramming in a hard-real-time environment," *Journal of the*

Association for Computing Machinery, vol. 20, no. 1, pp. 46–61, 1973.

[19] Y. Liu, X. Zhang, H. Li, and D. Qian, "Allocating tasks in multi-core processor based parallel systems," in *Proc. 3rd Int. Conf. Network and Parallel Computing-Workshops*, pp. 748–753, Dalian, China, 2007.

[20] S. Senobary and M. Naghibzadeh, "First-fit semi-partitioned scheduling based on rate monotonic algorithm," in *Proc. 1st Int. Conf. Intelligent Computing, Communication and Devices, SOA Univ*, vol. 309, pp. 173–181, Bhubaneswar, INDIA, 2015.

[21] S. K. Dhall and C. L. Liu, "On a real-time scheduling problem," *Operations Research*, vol. 26, no. 1, pp. 127–140, 1978.

[22] W. A. N. G. Tao and L. I. U. Da-Xin, "The performance evaluation of rate monotonic tasks assignment algorithms on multiprocessor," *Computer Science of China*, vol. 34, no. 1, pp. 272–276, 2007.

[23] H. Xu and A. Burns, "A semi-partitioned model for mixed criticality systems," *Journal of Systems and Software*, vol. 150, pp. 51–63, 2019.

[24] A. Magdich, Y. Hadj Kacem, M. Kerboeuf, A. Mahfoudhi, and M. Abid, "A design pattern-based approach for automatic choice of semi-partitioned and global scheduling algorithms," *Information and Software Technology*, vol. 97, no. 5, pp. 83–98, 2018.

[25] H. A. Hassan, S. A. Salem, A. M. Mostafa, and E. M. Saad, "Deterministic harmonic segment-based semi-partitioning scheduling on multi-core real-time systems," *ACM Transactions on Embedded Computing Systems*, vol. 15, no. 4, pp. 1–29, 2016.

[26] S. Z. Sheikh and M. A. Pasha, "Energy-efficient multicore scheduling for hard real-time systems: a survey," *ACM Transactions on Embedded Computing Systems*, vol. 17, no. 6, pp. 1–26, 2019.

Hindawi
Journal of Sensors
Volume 2021, Article ID 2292580, 16 pages
https://doi.org/10.1155/2021/2292580

Research Article

Optimal Selection of the Cluster Head in Wireless Sensor Networks by Combining the Multiobjective Genetic Algorithm and the Gravitational Search Algorithm

Seyed Reza Nabavi,[1] **Vahid Ostovari Moghadam**,[2] **Mohammad Yahyaei Feriz Hendi**,[3] **and Amirhossein Ghasemi**[4]

[1]*Young Researchers and Elite Club, Arak Branch, Islamic Azad University, Arak, Iran*
[2]*Department of Industrial Engineering, Iran University of Science and Technology, Tehran, Iran*
[3]*Department of Computer Engineering, South Tehran Branch, Islamic Azad University, Tehran, Iran*
[4]*Department of Computer Engineering, Bozorgmehr University of Qaenat, Iran*

Correspondence should be addressed to Seyed Reza Nabavi; sr.nabavi95@iau-arak.ac.ir

Received 8 September 2021; Accepted 11 November 2021; Published 7 December 2021

Academic Editor: Gengxin Sun

With the development of various applications of wireless sensor networks, they have been widely used in different areas. These networks are established autonomously and easily in most environments without any infrastructure and collect information of environment phenomenon for proper performance and analysis of events and transmit them to the base stations. The wireless sensor networks are comprised of various sensor nodes that play the role of the sensor node and the relay node in relationship with each other. On the other hand, the lack of infrastructure in these networks constrains the sources such that the nodes are supplied by a battery of limited energy. Considering the establishment of the network in impassable areas, it is not possible to recharge or change the batteries. Thus, energy saving in these networks is an essential challenge. Considering that the energy consumption rate while sensing information and receiving information packets from another node is constant, the sensor nodes consume maximum energy while performing data transmission. Therefore, the routing methods try to reduce energy consumption based on organized approaches. One of the promising solutions for reducing energy consumption in wireless sensor networks is to cluster the nodes and select the cluster head based on the information transmission parameters such that the average energy consumption of the nodes is reduced and the network lifetime is increased. Thus, in this study, a novel optimization approach has been presented for clustering the wireless sensor networks using the multiobjective genetic algorithm and the gravitational search algorithm. The multiobjective genetic algorithm based on reducing the intracluster distances and reducing the energy consumption of the cluster nodes is used to select the cluster head, and the nearly optimal routing based on the gravitational search algorithm is used to transfer information between the cluster head nodes and the sink node. The implementation results show that considering the capabilities of the multiobjective genetic algorithm and the gravitational search algorithm, the proposed method has improved energy consumption, efficiency, data delivery rate, and information packet transmission rate compared to the previous methods.

1. Introduction

The wireless sensor networks (WSNs) are comprised of distributed microdevices with various measurement capabilities that monitor the environment and transmit information to the end users. The wireless sensor technology was introduced more than 20 years ago, and many projects have been conducted since then. Green calculations [1, 2] were presented in 2008 aiming to employ the limited resources and maximize the energy efficiency throughout the lifetime of a system. WSNs are usually comprised of a large number of sensor nodes equipped with limited energy resources, but

they should operate for a long time without charge or battery replacement. To increase the network lifetime and reduce energy consumption of the sensor nodes of the network, clustering techniques have been presented to achieve an efficient relationship among the sensor nodes [3, 4].

In the clustering techniques, the sensor nodes of a network are combined to constitute small separate clusters. Each cluster has a known leader called the cluster head (CH) and other nodes are known as the member nodes (MN). Selecting the CH is a fundamental challenge that is the topic of this study. The sensor nodes sense the environment information and transmit it to the corresponding CH. The CH nodes collect data from all sensor nodes of the cluster and transmit it to the base station after data aggregation and removing the duplicate data. Thus, the CH has to organize the network, collect data, and transmit data from the sensor nodes to the sink and the base station and it consumes more energy compared to other nodes [5–8].

Data collection based on clustering-based approaches has various advantages compared to the conventional schemes. First, collecting data received from various sensor nodes in a cluster decreases the amount of data transmitted to the base station, because the duplicate data is removed considering the CH analysis [9]. Second, the sensor nodes of each cluster can transmit data directly to the sink nodes. But since data transmission in long intervals requires more energy consumption, direct data transmission is avoided. Instead, transmitting data to the CHs in adjacency of the member sensor nodes consumes less energy; hence, the energy requirement in the whole network for data transmission is reduced [10]. Third, rotation of the CHs helps to ensure balanced energy consumption in the network, such that the hunger of particular nodes due to energy shortage is prevented. However, selecting a proper CH with optimal capabilities, while balanced energy consumption rate and network efficiency are met, is a well-known NP-hard problem in WSNs [11–13].

The NP-hard problems cannot be solved using linear or polynomial methods and require using artificial intelligence, swarm intelligence, or metaheuristic methods to find the nearly optimal solutions. In this regard, heuristic and metaheuristic methods have recently attracted attention in the context of sensor node clustering and CH selection in WSNs that aim at improving the contradicting objectives of the network simultaneously [14, 15].

Given that the main challenge in wireless sensor networks is energy constraint, so, the performance of most applications in the WSN depends on energy consumption [15]. Hence, the main goal of this paper is at saving energy consumption in wireless sensor nodes. Since the amount of energy required to sense data from the environment and receive packets from other sensor nodes in the WSN is constant, therefore, most of the energy consumption is related to sending packets. The farther the next hop is from the current node, the more energy it takes to send data. So, the closest next hop that has the most remaining energy and least distance to sink not only can save energy but also could improve the quality of service (QoS) parameters. On the other hand, since finding the optimal path in wireless sensor networks has been introduced as an NP-hard problem, the best option to find the optimal solution is to use metaheuristic algorithms. Metaheuristic algorithms can find local optimizations according to local search but may find weakness or deadlock in finding optimal global solutions. Therefore, the use of algorithms with global search properties or a combination of metaheuristic algorithms can achieve optimal global solutions.

Therefore, this study presents a novel optimization approach using the multiobjective genetic algorithm (MOGA) and the gravitational search algorithm (GSA) for clustering the WSNs. In this study, the multiobjective genetic algorithm based on reducing the intracluster distances and reducing the energy consumption of the MNs is used to select the CH and the nearly optimal routing based on the gravitational search algorithm is used to transfer information between the cluster head nodes and the sink node. Considering the capabilities of the multiobjective genetic algorithm and the gravitational search algorithm, the proposed method has improved energy consumption, efficiency, data delivery rate, and information packet transmission rate compared to the previous methods.

The main motivation of this paper is the combination of the multiobjective genetic algorithm and gravitational search algorithm in order to find the optimal local clusters and the optimal global path in the wireless sensor network. Hence, the main contribution of the article is summarized as follows:

(i) Use of multiobjective genetic algorithm to find the optimal thread nodes in each cluster locally

(ii) Reduce energy consumption and create a balance between service quality parameters by using the multiobjective fit function

(iii) Use the gravitational search algorithm to find the optimal global path

(iv) WSN simulation and evaluation of the proposed method based on important criteria in the wireless sensor network and comparison with previous methods

The rest of this paper is organized as follows. Section 2 reviews the literature. Section 3 describes the details of the proposed method. Section 4 presents implementation and evaluation of the proposed method. Finally, the paper is concluded in Section 5.

2. Literature Review

In this section, the routing protocols based on swarm intelligence for WSNs are studied. The protocols employed in WSNs, including the ant colony optimization (ACO) algorithm, particle swarm optimization (PSO), bacterial foraging optimization (BFO), and artificial bee colony (ABC) algorithms, are discussed.

The genetic algorithm-based energy efficiency clusters (GABEEC) is used to increase the network lifetime. The

Table 1: Comparison of the clustering methods based on swarm intelligence.

Protocol	Location	Clustering algorithm	Approach	Cluster head round	Routing the CH to the BS	Mobility	Node establishment	BS location
GABEEC	Unaware	Centralized	GA	All rounds	Direct	Stationary	Random	Outside the area
GCA	Unaware	Distributed	GA	All rounds	Direct	Stationary	Random	Center of the area
GAECH	Unaware	Centralized	GA	All rounds	Direct	Stationary	Random	Outside, corner, and center of the area
hACO	Unaware	Centralized	ACO	All rounds	Direct	Mobile	Random	Outside the area
ANTCLUST	Unaware	Centralized	ACO	All rounds	Direct	Stationary	Random	Outside the area
PSO	Unaware	Centralized	PSO	All rounds	Direct	Stationary	Random	Inside the area
PSO-SD	Unaware	Centralized	PSO	All rounds	Multihop	Stationary	Random	Inside the area
HAS-PSO	Unaware	Centralized	PSO	All rounds	Direct	Semistationary	Random	Inside the area
WSNCABC	Unaware	Centralized	ABC	All rounds	Direct	Stationary	Random	Center of the area
ABC-C	Unaware	Centralized	ABC	All rounds	Direct	Stationary	Random	Center of the area
Bee-Sensor-C	Unaware	Distributed	ABC	All rounds	Multi-hop	Mobile	Random	Outside the area
EABCA	Unaware	Centralized	ABC	All rounds	Multi-hop	Stationary	Random	Center of the area

GA evaluates all chromosomes by calculating the fitness function. The fitness function has three parameters, including the round in which the first node dies, the round in which the last node dies, and the cluster distance. This algorithm tries to reduce the network lifetime by reducing the distance of the nodes, but the communication at the CHs is reinforced due to transmitting information about the residual energy to the base station (BS). The genetic clustering algorithm (GCA) employs two parameters, including the total transmission distance in a cluster and the number of CHs to achieve a longer lifetime [16]. The genetic algorithm-based energy efficiency clustering hierarchy (GAECH) performs the GA twice and improves CH selection considering the residual energy and total transmission cost [17].

The ACO is one of the nature-inspired mechanisms that performs optimal routing. This protocol is dynamic and reliable and can provide data aggregation and collect the routing structure. Also, it prevents network congestion, reduces energy consumption, and supports multiroute data transmission to achieve reliable communications in WSNs. This protocol is aimed at preserving the maximum network lifetime during data transmission using an efficient method [18].

In the network routing, the ACO-based techniques achieve a better overhead due to real-time computations and less control. The ACO has various shortcomings, for example, its performance depends on the previous cycle. It seems that using the ACO-based routing protocol in dynamic networks is suitable for preventing the link failure (a number of artificial ants are generated at each round and search for the shortest route between the source and the destination). In the last decade, the ACO has been used to solve hybrid optimization problems like NP-complete problems. In addition, the performance of the proposed method in finding the shortest route is reinforced in terms of network lifetime and load balance in WSNs using various solutions like sensor node clustering [19].

In a study, the authors presented a CH selection algorithm using the ACO to construct balanced load clusters. This algorithm uses the residual energy of the node and the distance between the nodes to select the CH [20]. Another ACO-based clustering method organizes the energy efficient clustering protocol through local interactions among the sensor nodes. First, the CH nodes are selected among the nodes with high residual energy. Then, the clusters are constituted through random interaction of regular nodes. The interaction among sensor nodes is carried out via local message transmission. This algorithm puts pressure on the network by repeating the interaction of the sensor nodes and does not provide the sufficient energy clustering mechanism [21].

PSO is a subset of swarm intelligence based on a population-based random optimization approach. PSO applies the social behavior of the birds or fishes to the real-world problems. This approach preserves local solutions and global solutions and generates the best fitness of an objective [19]. Also, swarm intelligence is used in the WSN for clustering optimization. In a study, the authors presented a clustering algorithm using PSO. They considered two types of nodes: natural sensor nodes and high-energy nodes. The high-energy nodes operate as CHs while the normal sensor nodes operate as members of the cluster [22]. PSO is also used in the information broadcast protocol. The selection measure for the CH is the residual energy, intracluster distance, and node degree. A hybrid protocol that combines the harmony search algorithm (HSA) and PSO is also used for clustering optimization. This hybrid algorithm selects the CH using the fitness function that includes the residual energy of the nodes, node degree, and the distance between the nodes. The metaheuristic HAS-PSO algorithm is used to select a fixed number of CHs. It does not guarantee to cover the whole network for a specific number of CHs. The CHs in HAS-PSO employ direct communication to transmit data to the BS that reduces the energy efficiency [23].

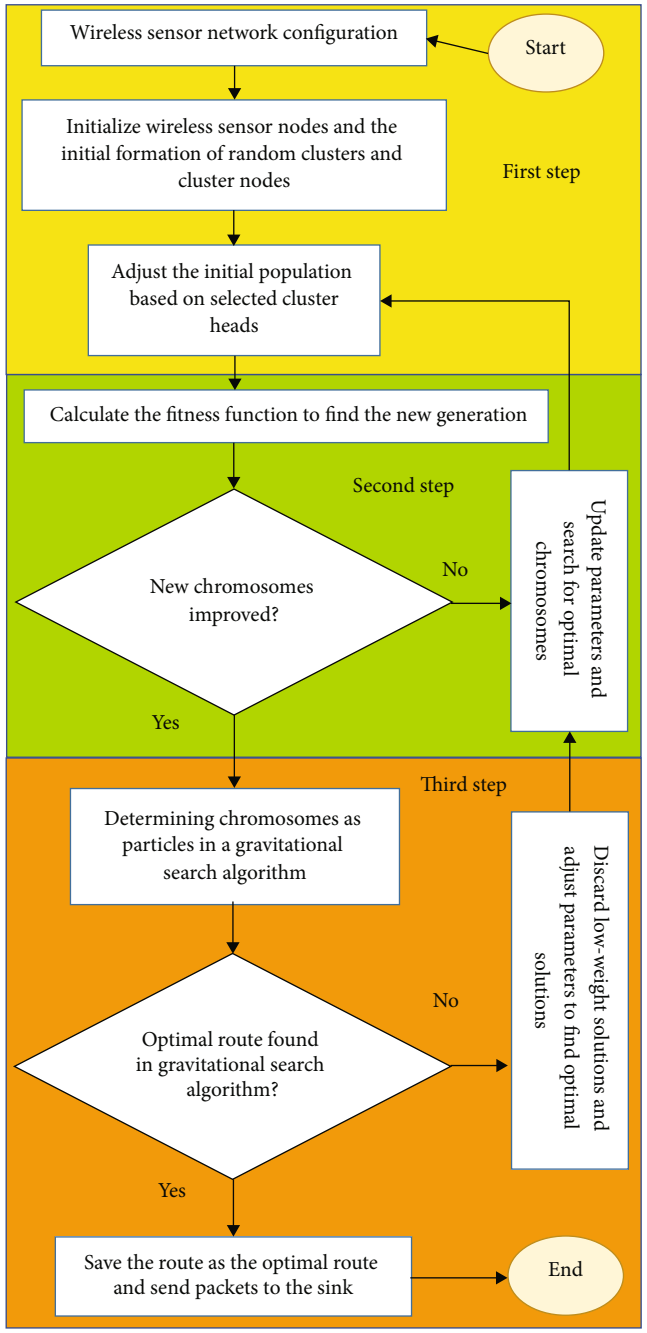

Figure 1: Flowchart of the proposed method.

The artificial bee colony (ABC) optimization also used constitute clusters in the WSN. WSN clustering using ABC (WSNCABC) employs the artificial bee colony to calculate the CH fitness using parameters like residual energy of the nodes and the distance between the BS and the nodes. However, this algorithm has a high cost for direct data transmission from the CH to the BS [24]. The clustering protocol based on ABC (ABC-C) has been presented in another study that improved the fitness function. The residual energy, distance of the node from the BS, and quality of the link are considered as the parameters of the fitness function. This algorithm selects the CH periodically [25]. The B-Sensor-C

G_1	G_2	G_3	G_4	G_5	G_6	G_7	G_8
5	14	25	39	42	65	9	86

Figure 2: Chromosomes of the proposed method.

algorithm has been developed for event-oriented SNs. When an event occurs, the protocol constitutes the clusters and selects the CH. The most important node that verifies this event should be the CH and others should follow it [26]. The energy-aware bee colony approach (EABCA) improves the network performance with the fitness function. Multihop communications between the CH and the BS are not required for data delivery [27].

Table 1 compares the clustering-based methods based on swarm intelligence regarding important parameters of WSN clustering.

3. The Proposed Method

As mentioned, in this study, a novel optimization approach is presented for WSN clustering using the multiobjective GA and the gravitational search algorithm. In this study, the multiobjective GA based on reducing the intracluster distance and energy consumption of the MNs is used to find the CHs and the nearly optimal routing based on the gravitational search algorithm is used to find the optimal route and transmit information between the CH nodes and the sink node. This study is presented to reduce the energy consumption of the sensor nodes, increase the network throughput, increase the data delivery rate, and reduce the information packet transmission delay. Figure 1 shows flowchart of the proposed method.

As shown in Figure 1, the proposed method has three main steps as follows:

(i) WSN configuration and random node clustering in the network

(ii) Determining the optimal CHs using GA

(iii) Determining the optimal route using the gravitational search algorithm

In the rest of this section, the aforementioned methods are described.

3.1. Initial Clustering. In the first section of the proposed method, the proposed WSN is simulated with 100 sensor nodes and one sink node. The initial parameters are considered based on the standard parameters of similar methods. Finally, the proposed method is compared with other available methods. After initial configuration of wireless sensor nodes in the network, a "Hello" message is transmitted by the sink node to all sensors to identify the nodes and determine the location of the existing nodes of the network. All sensors of the network transmit a routing reply (RREP) to the sink node after receiving the "Hello" message to obtain the exact location of each sensor node for initial clustering of the nodes. Since the energy required to transmit the RREP

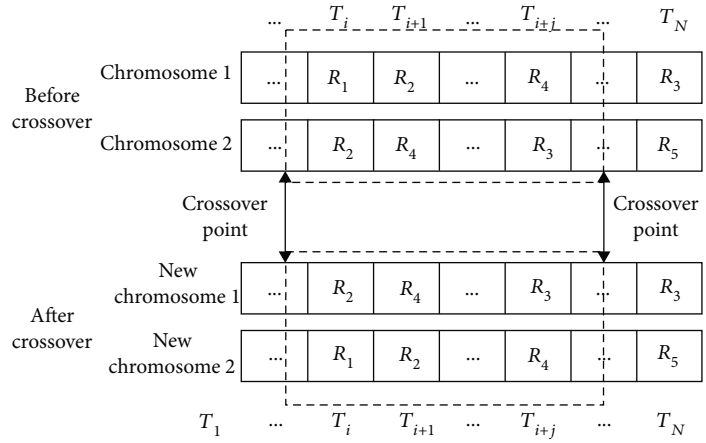

Figure 3: An example of crossover of two chromosomes.

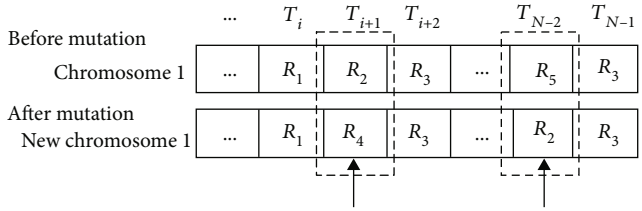

Figure 4: An example of population diversity of the chromosomes.

packets and data is different, different energy consumption constants are considered for each packet type. Thus, the energy consumption of the proposed method is examined accurately. In the next step, after receiving the RREP and identifying the initial location of the wireless sensor nodes, the proposed method clusters the nodes based on the random CHs. Since the initial energy of all nodes at the beginning steps is constant, random selection of the CHs does not interrupt the data transmission and early energy discharge of some sensor nodes does not occur. Then, the wireless sensor nodes are clustered based on their distance from the CH node. The distance of the sensor nodes from the CH node is measured based on the Euclidean distance, which is represented in equation (1) as follows.

$$\text{Euclidean} - \text{distance} = \left(\left(x_i - x_j \right)^2 + \left(y_i - y_j \right)^2 \right)^{1/2}. \quad (1)$$

in which (x_i, y_i) represents coordinate of the ith node. In this step, the CH nodes are given to the GA as the initial chromosomes so that the optimal location of the CH is found. In the proposed GA, an optimal node in the selected cluster might not be found as the CH. In this case, the cluster is wound up and upon finding an optimal CH around the cluster, clustering is carried out again.

3.2. Using GA to Determine the Optimal CHs. As mentioned, in the second step of the proposed method, the GA is used to find the new and optimal CHs instead of random CHs selected in the previous step. In the following, the chromosomes are configured and the fitness function of the GA for the proposed method is defined.

3.2.1. Chromosome Encoding. The proposed GA receives an initial set of CHs as input and initiates by generating an initial population of the chromosomes, where each chromosome represents a possible solution for the clustering problem. Therefore, a chromosome is a vector of genes and the numbers inside each chromosome represent the index of a CH node. In Figure 2, an example of the chromosomes of the proposed method is given.

As shown in Figure 2, the chromosomes of the proposed method include a vector of genes where each gene represents an index of a CH node. The numbers inserted in each gene represent the CH selected randomly in the initial step. At the beginning, each chromosome is considered as the probabilistic clustering in the WSN that changes by applying the fitness function and mutation and crossover operators. Finally, the chromosome with maximum fitness is selected as the nearly optimal cluster.

3.2.2. Fitness Function of the GA. The fitness function of each chromosome is determined considering the objective function that is a combination of residual energy of the CH, mean intracluster distance, and distance of the CH from the sink. For each possible clustering of the population, the fitness function is considered as the representative of the parameters of interest to balance the residual energy of the CH, mean intracluster distance, and distance of the CH from the sink. Since the scales of the distances between the nodes and energy of the sensor nodes is not the same, the values of the proposed method should be normalized to obtain a unit value as the fitness function; in the proposed method, MIN-MAX normalization, given in equation (2), is used [28].

$$NX = \frac{X(i) - \min(X)}{\max(X) - \min(X)}. \quad (2)$$

where NX is the normalized data, $X(i)$ is the main data, $\min(X)$ is the minimum possible value of the data, and $\max(X)$ is the maximum value of the data.

Table 2: Initial parameters of the proposed WSN.

Parameters	Value
Network dimension	100×100
Number of sensor nodes	100
Coordinate of the sink node	$(50, 50)$
Initial energy of the nodes	0.5 J
Initial energy of the sink node	50 J
Energy consumption of data transmission	5×10^8
Energy consumption of data reception	5×10^8
Energy consumption of routing packet transmission	1×10^{10}
Energy consumption of routing packet reception	13×10^{13}
Energy consumption of data aggregation	5×10^9
Initial probability of selecting the sensor node as the CH	0.01
Maximum number of rounds	3500
Data packet length	4000
Number of packet transmissions at each hop	10
Routing packet length	100
Radio range	5000

The fitness function used to evaluate the given chromosomes using the proposed objective function is calculated based on equation (3).

$$\text{Fitness} = \min\left(\sum_{i=1}^{M}\sum_{j=1}^{n} D_{i,j} + \sum_{i=1}^{M} DS_i - \sum_{i=1}^{M} E_{\text{res}_i}\right), \quad (3)$$

subject to

$$\sum_{i=1}^{M} E_{\text{res}_i} > E_{\min_i}, \quad (4)$$

$$\sum_{i=1}^{M} DS_i \le DS_{fa\text{res}r_j},$$

$$\sum_{i=1}^{M}\sum_{j=1}^{n} D_{i,j} \le \sum_{j=1}^{n} DS_j, \quad (5)$$

$$M_i \ge 0, DS_i \ge 0, D_{i,j} \ge 0,$$

Considering the fitness function given in equation (3), the proper chromosomes are selected from the initial population and other chromosomes are transmitted to the mutation and crossover operators to diversify the population and generate new superior chromosomes. Each chromosome of the new offspring population is checked to see if it is a possible solution for the problem or not (does it minimize the fitness function and satisfy the given constraints or not). The impossible chromosomes that violate the existing constraints are penalized considering their fitness value such that they have a lower probability to be selected for generation and conversion to new chromosomes. The most proper chromosome that represents the nearly optimal clustering solution is preserved at each iteration and sorted based on its optimality. This process continues until the termination condition is met.

3.2.3. The Crossover Operator. The crossover operator is an essential step of the GA to diversify the population and generate new chromosomes. To increase the search domain and public feasible solutions, the GA should apply the crossover operator between two chromosomes (parents) and generate new offspring as the new population. The crossover operator is performed as a random replacement of a number of genes of the first chromosome with the second chromosome. Thus, the parameter that is essential in the crossover operator is called the crossover probability or P-crossover, which is defined as follows for random crossover.

$$P - \text{crossover} = \text{round}(k * (G_{\max} - G_{\min})), \quad k \text{ is a rand in } [0, 1], \quad (6)$$

in which $G_{\max}$ is the maximum number of genes and $G_{\min}$ is the minimum number of genes of the chromosome. The parameter k is considered as a random number in the range of 0 and 1. The value of P-crossover is considered as a part of the chromosome that should be exchanged between the first chromosome and the second chromosome; the beginning and ending points are called the crosspoints. The beginning crosspoint might be selected from the beginning of the chromosome or any other part of the chromosome, and the ending crosspoints are added to the P-crossover. Figure 3 shows the crossover operator.

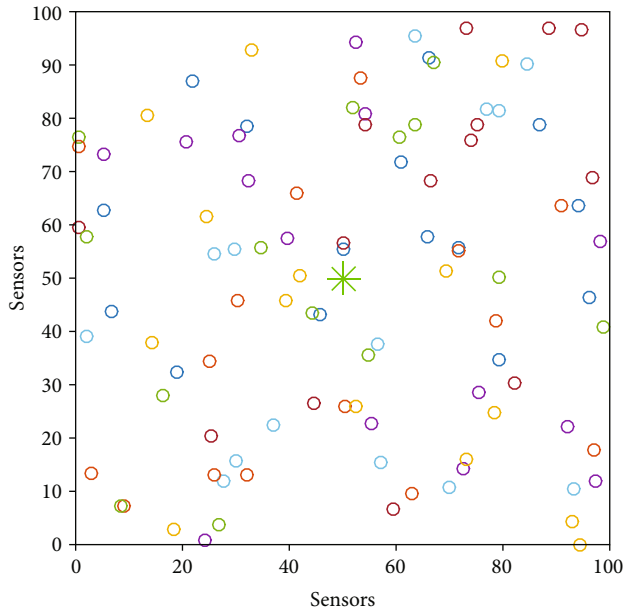

Figure 5: Initial configuration of the proposed WSN.

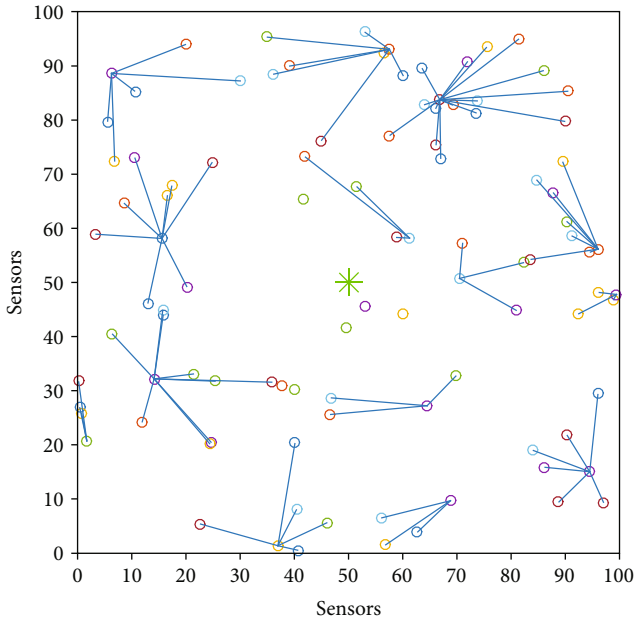

Figure 6: Initial clustering of the nodes in a WSN.

As shown in Figure 3, each gene, T_i, represents a CH node and R_i represents the cluster of each gene for any of the solutions.

3.2.4. Mutation Operator. The mutation operator, like the crossover operator, also plays a significant role in generating a new population and diversifying the chromosomes. This operator can increase the search domain and the possible solutions and generate new offspring as the new population. Thus, in this operator, the probability parameter is of great importance that is considered as a chromosome that should mutate. The P-mutate parameter or the mutation probability can be calculated.

Table 3: Information of the initial CHs.

CH no.	Node index
1	11
2	15
3	18
4	20
5	39
6	47
7	56
8	58
9	67
10	80
11	86
12	88
13	95
14	97

$$P - \text{mutate} = \text{round}(k * (G_{\max} - G_{\min})), \quad k \text{ is a rand in } [0, 1]. \tag{7}$$

The P-mutate parameter represents the mutation probability, and the parameter k can be considered as a value between zero and one; zero or one can be considered as the first or the last gene of the chromosome. The difference of the mutation and the crossover operators is that the crossover operator changes several genes of a chromosome with another chromosome but the mutation operator only changes the value of one gene to generate a new chromosome. Figure 4 shows the mutation operator.

As shown in Figure 4, there are two chromosomes with different genes that change at $(i+1)$ and $(N-2)$, independently. At $(i+1)$, the value of the gene changes from R_2 to R_4. Similarly, the value of the gene mutates from R_5 to R_2 at $(N-2)$. The gene mutation might yield excellent results. Sometimes the results might not be satisfactory. However, the gene mutation is essential to preserve population diversity.

3.2.5. Selection Operator. The selection operator, after the crossover and the mutation operators, selects the chromosomes with maximum fitness or the nearly optimal solution among the new population and the chromosomes generated as the next generation for the clustering problem to reduce energy consumption in the WSN. In this case, the CHs assigned to each cluster with maximum residual energy, minimum mean intracluster distance, and minimum distance to the CH are examined to balance the energy consumption of each cluster. Therefore, the efficiency of the clustering algorithm is optimized to balance the energy consumption of the WSN.

Table 4: Fitness value of the initial population.

CH no.	Node index	Fitness value
1	11	0.8884
2	15	0.8449
3	18	0.8094
4	20	0.8086
5	39	0.8653
6	47	0.8099
7	56	0.7486
8	58	0.6119
9	67	0.8012
10	80	0.5602
11	86	0.6077
12	88	0.4836
13	95	0.5802
14	97	0.0982

Table 5: Fitness values of the new population.

CH no.	CH index	Fitness value	CH index	Fitness value
1	11	0.8884	76	0.9485
2	15	0.8449	74	0.9678
3	18	0.8094	81	0.9438
4	20	0.8686	21	0.9721
5	39	0.8653	94	0.9631
6	47	0.8099	81	0.9844
7	56	0.7486	51	1
8	58	0.6119	28	0.9463
9	67	0.8012	55	0.9984
10	80	0.5602	51	1
11	86	0.6077	51	1
12	88	0.4836	51	1
13	95	0.5802	7	0.9742
14	97	0.9822	97	0.9822

3.3. Using the Gravitational Search Algorithm to Find the Optimal Route. As shown in Figure 1, in the third step of the proposed method, the gravitational search algorithm finds the best route based on the CHs selected by the proposed GA. In this step, considering the selected CHs, the information transmission routes from each cluster to the sink node are specified. Therefore, the CHs in each cluster are considered as particles of the gravitational search algorithm. Thus, at each information packet transmission step, the gravitational search algorithm measures the particles' weight and leaves the particles that do not have sufficient quality and other particles are selected as proper solutions.

The weight of the selected particles is determined based on the objectives. In other words, in the proposed method, at each information transmission step, the gravitational search algorithm checks if the route between the sensor nodes and the sink node that requires information transmission decreases the total energy consumption and the end-to-end delay and increases the data delivery rate and the network throughput or not. The routes that optimize these measures are selected as the optimal routes, and the routes that worsen even one of these measures are considered as the abandoned routes. Therefore, the fitness function of the proposed gravitational search algorithm is as given in equation (8).

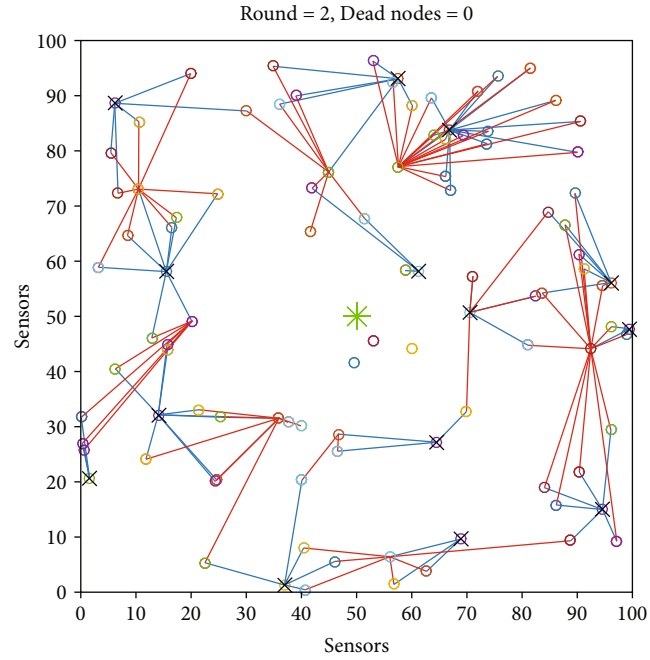

Figure 7: Replacement of the new CHs with previous CHs.

$$\text{CSfitness} = \min\left(\sum_{i=1}^{n}\sum_{j=1}^{n}\text{delay}_{i,j} + \sum_{i=1}^{n}E_{\text{cons}} - \sum_{i=1}^{n}\text{DDR}_i - \sum_{i=1}^{n}\text{throuput}_i\right), \tag{8}$$

subject to

$$\begin{aligned}
&\sum_{i=1}^{n}\sum_{j=1}^{n}\text{delay}_{i,j} \geq 0,\\
&\sum_{i=1}^{n}E_{\text{cons}} < E_{\text{init}},\\
&\sum_{i=1}^{n}\text{DDR}_i > 0,\\
&\sum_{i=1}^{n}\text{throuput}_i > 0,
\end{aligned} \tag{9}$$

where CSfitness is the fitness function value of the gravitational search algorithm, $\text{delay}_{i,j}$ is the end-to-end delay of nodes i and j, E_{cons} is the total energy consumption of the network, E_{init} is the initial energy of the network, DDR_i is

```
This solution of cluster heads as route must be abandoned
51 37 61 76 76 79 61 79 76 76 21 53
****************************************
This route is selected by probability 0.76915
========================================
76 21 59 79 51 37 10 29 41 25 69 87
****************************************
This solution of cluster heads as route must be abandoned
71 87 61 76 76 87 22 87 76 42 19 42
****************************************
This solution of cluster heads as route must be abandoned
22 87 42 87 76 76 76 76 76 71 87 51
****************************************
This route is selected by probability 0.8945
========================================
67 76 21 62 71 57 17 79 73 37 25 38
```

Algorithm 1: The output of the gravitational search algorithm for finding the high-quality routes.

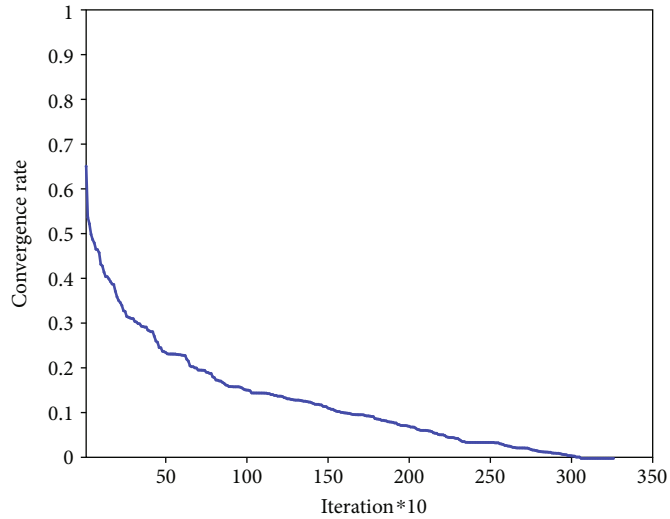

Figure 8: Convergence of the gravitational search algorithm to the optimal point.

the data delivery rate at each node, and throuput is the network throughput. According to the fitness function, each population that obtained the minimum fitness value can be selected as a practical solution for information transmission.

4. Implementation of the Proposed Method

To implement the proposed method, first, the WSN is configured based on the standard parameters. The proposed network is implemented in a 100×100 environment. To implement this scenario, MATLAB 2021a is used. Other parameters of the proposed network are given in Table 2. Figure 5 also shows the initial configuration of the proposed WSN.

As shown in Table 2 and Figure 5, the proposed WSN is simulated based on the initial parameters. This network is comprised of 100 sensor nodes that are distributed randomly in the network. The sink node is also at the center of the network that facilitates access to it.

In the first step, the sink node collects information about the location of the network sensors and selects multiple CHs accordingly. The CHs are selected randomly, and the sensor nodes also join the CHs based on their distance and constitute clusters. After formation of the first cluster and transmitting data to the CH, the information about the initial energy and the intracluster distances and distance of the CH from the source can be calculated. In Figure 6, the initial clustering of the WSN is shown. Table 3 represents the information of the initial CHs.

Information of Table 4 is given as the initial chromosome to the GA, and the second step of the proposed method is implemented. In the first step of the proposed GA, the initial population is evaluated considering the randomly selected CHs. To evaluate the input population of the proposed GA, the fitness function is applied to the initial

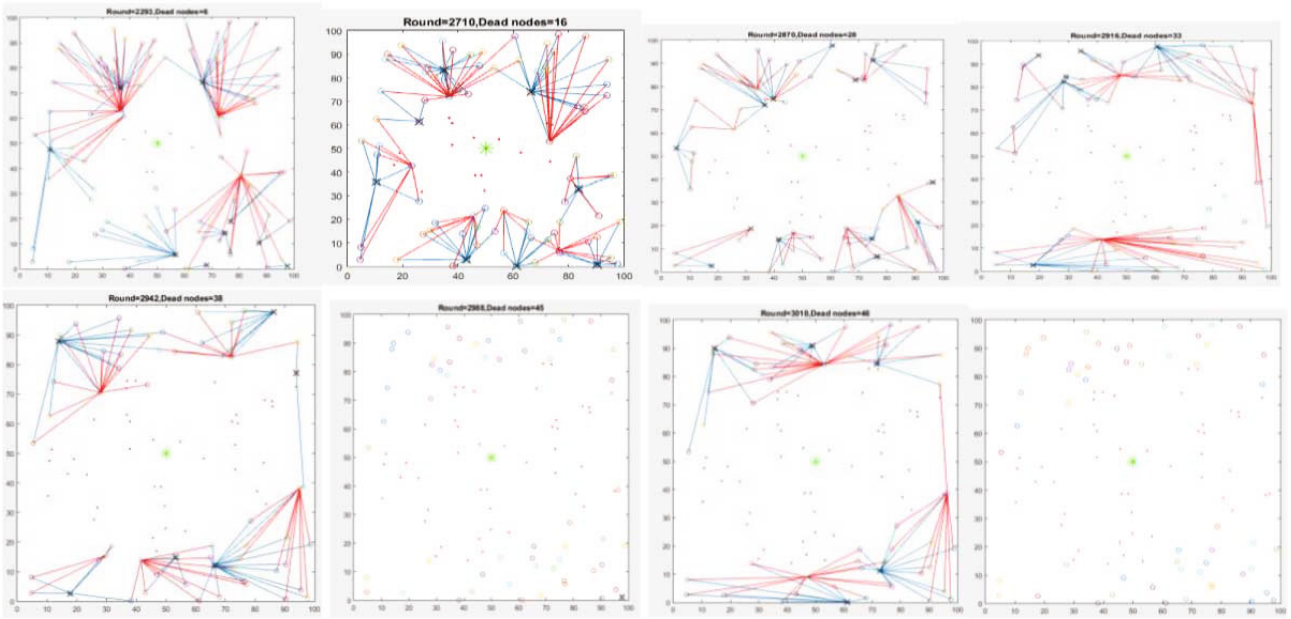

Figure 9: Death process of the sensor nodes by information transmission in the WSN.

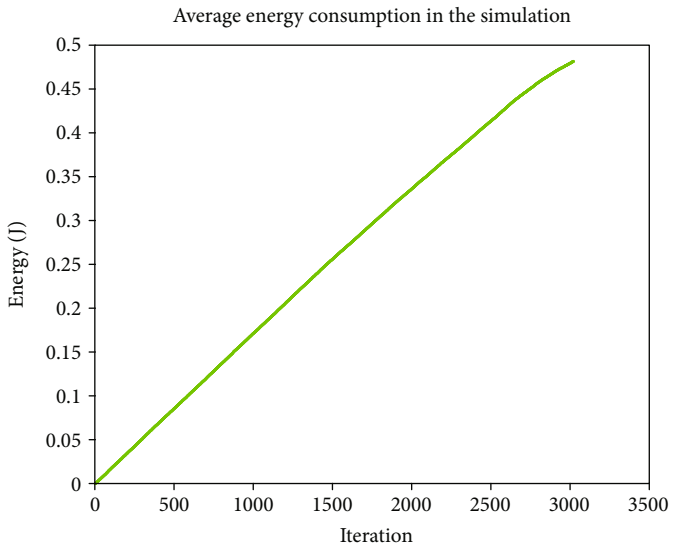

Figure 10: The average energy consumption in all nodes of the network.

population. Accordingly, the proposed GA evaluates the CHs in terms of the residual energy, mean intracluster distance, and distance from the sink node. Since no data is transmitted in the initial population, the initial energy of all CH nodes and MNs is the same. Thus, in the first step, the CHs are evaluated in terms of intracluster distance and distance from the sink node. In the following, since the optimal routes are found, information transmission, energy consumption, and residual energy affect the selection of the optimal CHs. To this end, Table 4 represents the fitness value of the initial population.

As shown in Table 4, the fitness value of each CH in the initial population is calculated. It is seen that some CHs have an excellent fitness but other are weak. Thus, in the next step, the new population is generated based on the crossover and mutation operators and the fitness value of the new population is examined. The new population of the proposed method is a combination of the CHs that have replaced the previous CHs, and their fitness is evaluated. Table 5 represents the expert population that have replaced the initial population considering their fitness.

As shown in Table 5, the fitness values of the new population are calculated. The clusters of three CHs with indexes of 86, 80, and 80 are broke down, and they are integrated in a cluster with CH 51. Also, it is seen that CH 97 is transferred from the previous population to the new expert population. Figure 7 shows the replacement of the new CHs with the previous CHs.

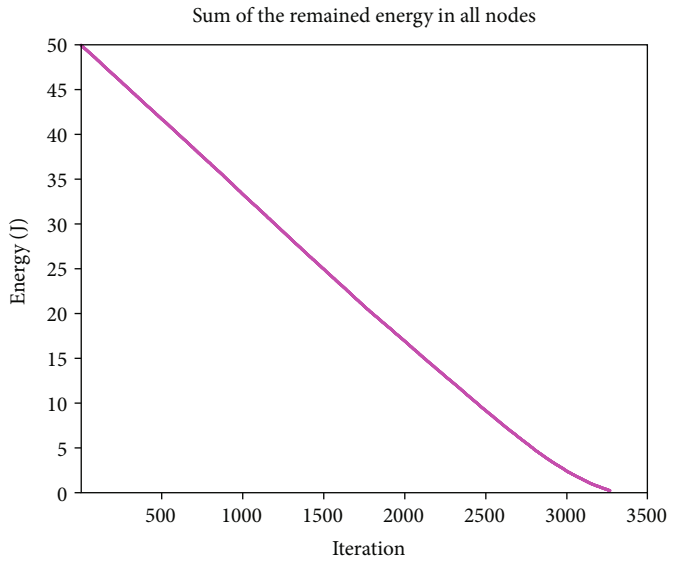

Figure 11: Total residual energy of the network nodes.

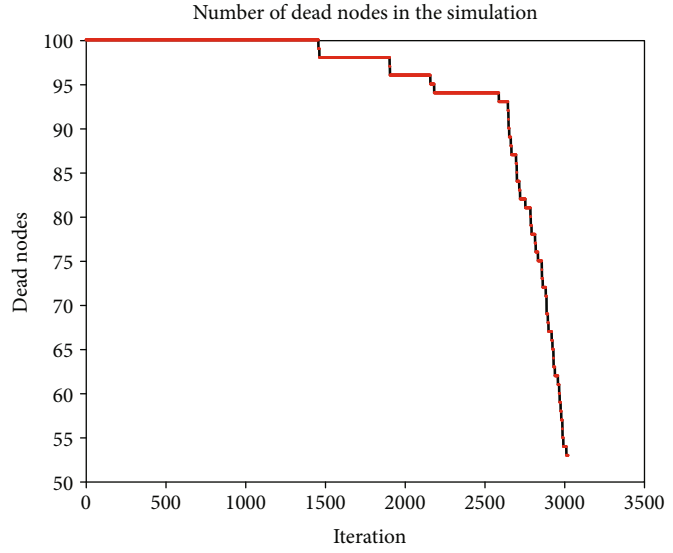

Figure 12: Death process of the sensor nodes of the network.

As shown in Figure 7, the previous CHs are represented with a black $\times$, the previous connections are represented in blue, and the connections with new CHs are represented in red. The new CHs are selected as the proposed solution for information transmission form sensor nodes, data aggregation, and data transmission to the sink node. Considering the distance of the CH nodes from the sink node, if a CH observes another CH along the direct route to the sink, the packet transmission is carried out in multihops between the CHs and the sink node.

Now, the proposed method enters the third step in which the gravitational search algorithm examines the quality of the route based on the CHs obtained using the GA. Considering the global search capability of the gravitational search algorithm, it can find the optimal route in the whole network. This step determines if the selected route is optimal for information packet transmission or there might be a more optimal route and the GA is trapped in local optimum. Algorithm 1 represents the output of the gravitational search algorithm for the routes proposed by the GA.

As shown in Table 5, the optimal routing of the proposed method is carried out using the gravitational search algorithm. The gravitational search algorithm examines the quality of the routes proposed by the GA based on the fitness function given in equation (11), and the routes that improve the network objectives are returned with their fitness value. Figure 8 shows convergence of the gravitational search algorithm to the optimal point.

As shown in Figure 8, since the employed fitness function is a minimization function, the gravitational search

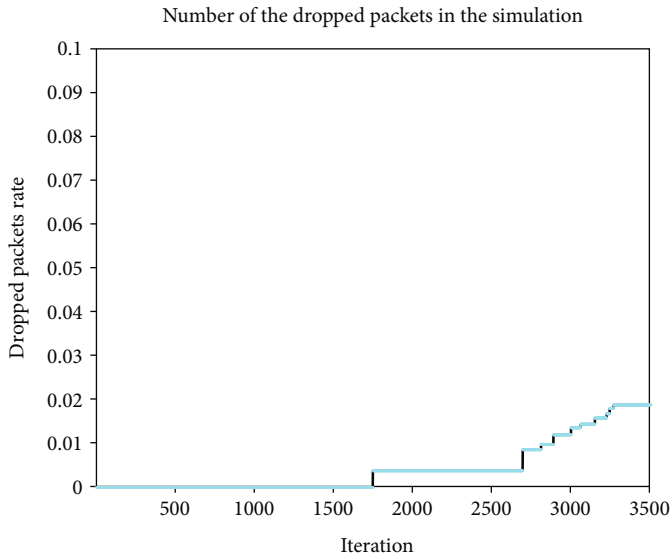

Figure 13: Lost packets in the proposed method.

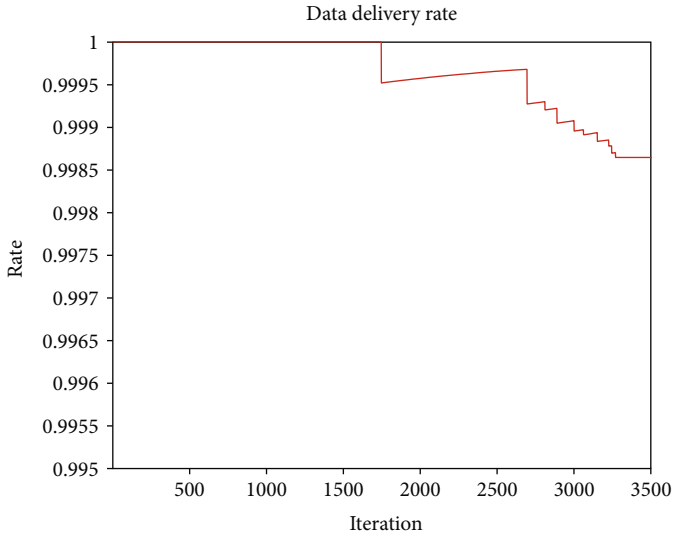

Figure 14: The data delivery rate of the proposed method.

algorithm reduces the objective function value at each step so that it converges to the optimal point. In the following, in Figure 9, the dead nodes of the WSN are represented.

As shown in Figure 9, the wireless sensor nodes run out of energy by information transmission and die. In Figure 9, small red dots show the dead nodes; as the information transmission steps increase, the number of dead nodes also increases until the network is interrupted. In the following, the proposed method is evaluated.

4.1. Evaluation of the Proposed Method. The proposed method is evaluated to examine its quality and improve the proposed method on the primary problem. Various measures have been presented in the literature to evaluate the WSNs, which are introduced considering the research objectives mentioned in the first section. In this section of the study, the proposed method is evaluated in terms of energy consumption, residual energy, message transmission delay, number of lost packets, data delivery rate, and network throughput. Thus, Figure 10 shows the average energy consumption of the network. Figure 11 also shows the total residual energy as the data transmission steps increase.

As shown in Figures 10 and 11, the slope of the energy consumption and residual energy curves is linear, indicating that energy consumption in the network nodes is symmetric. Thus, some nodes do not run out of energy earlier than other nodes and all nodes run out of energy almost the same. Thus, all nodes run out of energy gradually, indicating a long lifetime of the network. Figure 12 shows the death process of the sensor nodes of the network.

As shown in Figure 12, the first node in the proposed WSN has died after 1470 iterations. In WSN routing

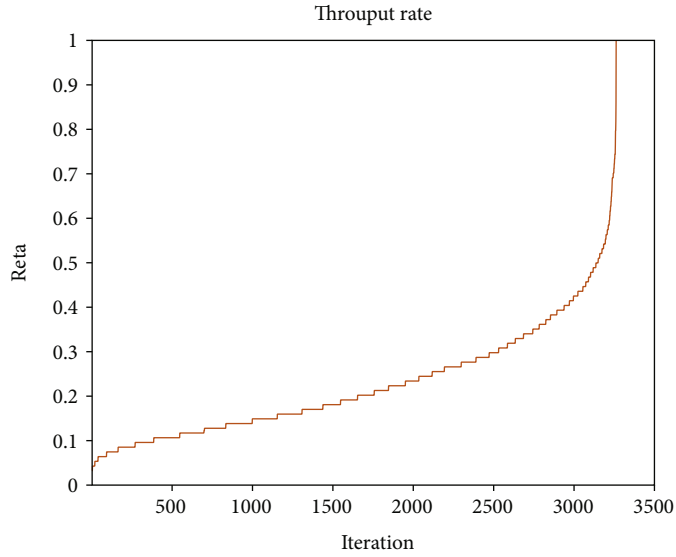

Figure 15: Network throughput.

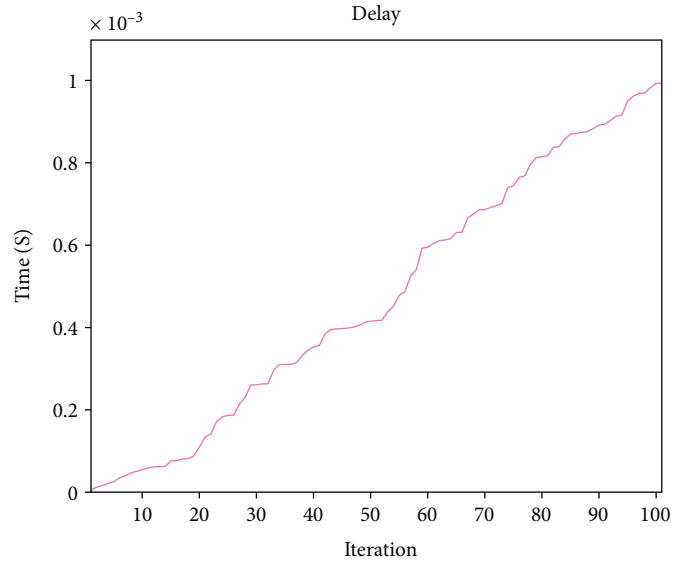

Figure 16: The cumulative end-to-end delay of the nodes.

methods, if a node dies, an alternative route might be found for information transmission but the information of that area cannot be aggregated. So, as long as a node's death does not interrupt the network, its death can be handled. In the proposed method, this has occurred in the 3020th round in which about half of the nodes have run out of energy and the network is interrupted.

Another measure used to evaluate the proposed method is the number of lost packets. The smaller is the number of lost packets in the information aggregation process, the quality of information collection and accuracy of the routing method are higher. Selecting nodes with congestion of transmitted packets that appear as the network bottleneck might be one of the main reasons of information packet loss. Figure 13 shows the lost nodes in the proposed method.

As shown in Figure 13, the number of lost packets in the proposed method is about 70 packets, yielding a maximum of 0.02 lost packets considering the 35000 total transmitted packets during routing. Therefore, it can be concluded that the proposed method is able to find the optimal route and deliver the information packets correctly. To this end, the date delivery rate, which is the ratio of received data to the transmitted data in the whole network can be examined. Figure 14 shows the data delivery rate of the proposed method.

As can be seen in Figure 14, the data delivery rate of the proposed method is high and reaches 99.8% for 3500 rounds of the network. As the method, this large value indicates the ability of the proposed method to find the optimal route and deliver and the information packets correctly. After this

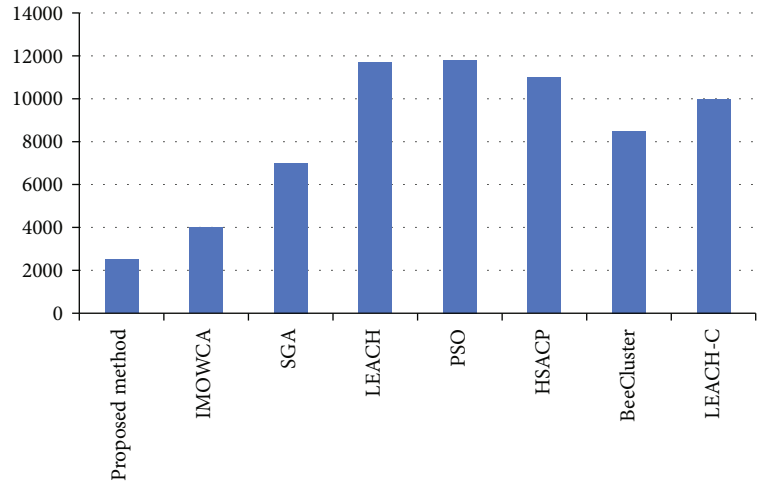

Figure 17: Comparison of the proposed method and the previous methods in terms of energy consumption.

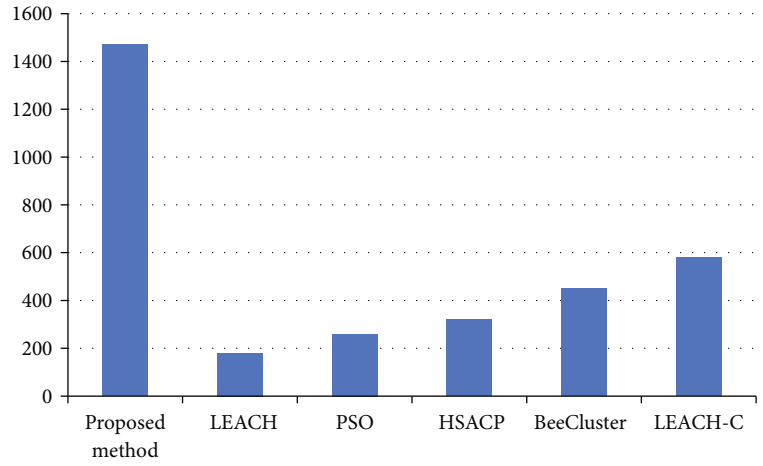

Figure 18: Comparison of the proposed method and the previous method in terms of lifetime.

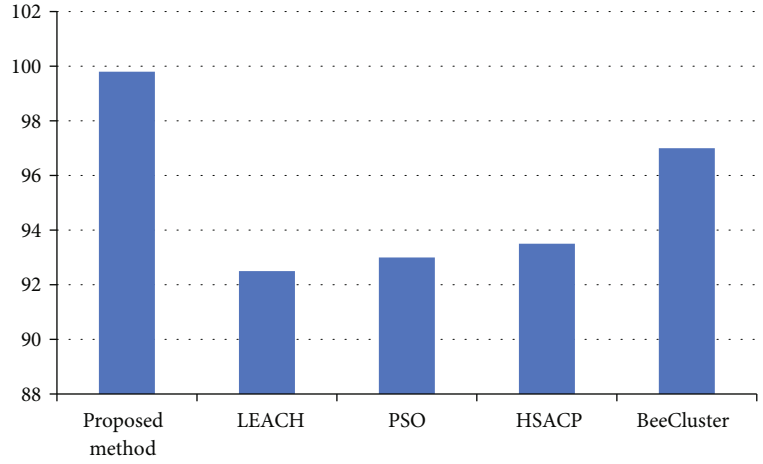

Figure 19: Comparison of the proposed method and previous methods in terms of data delivery rate.

measure, the network throughput can be examined. The throughput is the ratio of the transmitted packets per unit time to the bandwidth of the transmission medium. Since the bandwidth of WSNs is considered the same for all sensor nodes, the network throughput indicates the data delivery rate per unit time. Figure 15 shows the network throughput of the proposed method.

As shown in Figure 15, the network throughput has increased in an ascending order reaching 100% at the end.

The last measure that is evaluated is the end-to-end delay of the network nodes. Since the transmission time factor of a packet is fixed for the nodes, the main reason of the delay in end-to-end transmission is the distance between the nodes. Since in the proposed method, information is transmitted between the sensor nodes and the CH, the shorter distance between the CH and other nodes indicates accurate clustering and shorter mean intracluster distance, which is one of the objectives of the proposed GA. Figure 16 shows the cumulative effect of end-to-end delay of 100 nodes.

As shown in Figure 16, the proposed method has a 100 ms delay for 100 nodes and 3500 transmission rounds, demonstrating the high clustering accuracy of the proposed method.

4.2. Comparison of the Proposed Method with Previous Studies. Considering the importance of routing in WSNs for balancing the energy consumption of the nodes, the proposed method is compared with a previous method in terms of energy consumption and other evaluation measures. To this end, the proposed method is compared with [5, 11, 29] in terms of energy consumption and network lifetime. Figure 17 compares the proposed method with a previous method in terms of average energy consumption.

As shown in Figure 17, the proposed method has a lower average energy consumption for 100 nodes compared to the previous methods. Figure 18 also compares the proposed method and the previous methods in terms of lifetime and death of the first node.

As shown in Figure 19, the proposed method has a longer lifetime compared to the previous method and the first node in the proposed method dies later than other methods, indicating the balanced energy consumption of the proposed method. Figure 19 compares the proposed method and previous methods in terms of data delivery rate.

As shown in Figure 19, the proposed method has a higher data delivery rate compared to the previous methods, indicating the selection of the optimal route and avoidance of the bottlenecks and losing the minimum number of information packets.

5. Conclusion

The wireless sensor network is one of the most recent environments monitoring and controlling networks that collect information from the environment and aggregate data for network applications autonomously without any infrastructure. Thus, the popularity of these networks has resulted in various challenges, among which the unbalanced energy consumption can be mentioned. Considering the limited energy of the sensor nodes, unbalanced energy consumption might affect all performance measures of the network. Thus, in this study, a novel optimization approach using the multiobjective genetic algorithm and the gravitational search algorithm has been presented for WSN clustering. In this study, the multiobjective genetic algorithm based on reducing the intracluster distances and the energy consumption of the member nodes is used to select the cluster heads and the nearly optimal routing based on the gravitational search has been used to transmit information between the cluster heads and the sink node. The implementation results of the proposed method show that considering the capabilities of the multiobjective genetic algorithm and the gravitational search algorithm, the proposed method has improved the average energy consumption, data delivery rate, and network lifetime significantly compared to the previous methods.

Data Availability

The data used to support the findings of this study are included within the article.

Conflicts of Interest

The authors declare that they have no conflicts of interest.

References

[1] S. Murugesan, "Harnessing green IT: principles and practices," *IT Professional*, vol. 10, no. 1, pp. 24–33, 2008.

[2] S. R. Nabavi and M. Najafi, "An optimal routing protocol using multi-objective cultural algorithm for wireless sensor networks (ORPMCA)," *International Journal of Smart Electrical Engineering*, vol. 10, no. 2, pp. 79–86, 2021.

[3] L. Xu, R. Collier, and G. M. P. O'Hare, "A survey of clustering techniques in WSNs and consideration of the challenges of applying such to 5G IoT scenarios," *IEEE Internet of Things Journal*, vol. 4, no. 5, pp. 1229–1249, 2017.

[4] S. R. Nabavi and S. M. Mousavi, "A review of distributed dynamic key management schemes in wireless sensor networks," *Journal of Computers*, vol. 13, no. 1, pp. 77–89, 2018.

[5] H. Ouchitachen, A. Hair, and N. Idrissi, "Improved multiobjective weighted clustering algorithm in wireless sensor network," *Egyptian Informatics Journal*, vol. 18, no. 1, pp. 45–54, 2017.

[6] S. Misra and R. Kumar, "A literature survey on various clustering approaches in wireless sensor network," in *2nd International Conference on Communication, Control and Intelligent Systems, CCIS 2016*, pp. 18–22, Mathura, India, March 2017.

[7] T. T. Truong, K. N. Brown, and C. J. Sreenan, "Multi-objective hierarchical algorithms for restoring wireless sensor network connectivity in known environments," *Ad Hoc Networks*, vol. 33, pp. 190–208, 2015.

[8] S. R. Nabavi, N. Osati Eraghi, and J. Akbari Torkestani, "Temperature-aware routing in wireless body area network based on meta-heuristic clustering method," *Journal of Communication Engineering*, vol. 9, no. 2, 2020.

[9] S. Arjunan and S. Pothula, "A survey on unequal clustering protocols in wireless sensor networks," *Journal of King Saud*

University - Computer and Information Sciences, vol. 31, no. 3, pp. 304–317, 2019.

[10] A. Kumar Wadbude and R. Shyam Panda, "A survey on multi cluster head analysis scheme for wireless sensor network," *International Research Journal of Engineering and Technology*, vol. 6, no. 1, pp. 761–765, 2019.

[11] P. S. Mann and S. Singh, "Improved artificial bee colony metaheuristic for energy-efficient clustering in wireless sensor networks," *Artificial Intelligence Review*, vol. 51, no. 3, pp. 329–354, 2019.

[12] S. R. Nabavi, "An optimal routing protocol using multiobjective whale optimization algorithm for wireless sensor network," *International Journal of Smart Electrical Engineering*, vol. 10, no. 2, pp. 77–86, 2021.

[13] S. R. Nabavi, N. O. Eraghi, and J. A. Torkestani, "WSN routing protocol using a multiobjective greedy approach," *Wireless Communications and Mobile Computing*, vol. 2021, Article ID 6664669, 12 pages, 2021.

[14] F. Fanian and M. Kuchaki Rafsanjani, "Cluster-based routing protocols in wireless sensor networks: a survey based on methodology," *Journal of Network and Computer Applications*, vol. 142, pp. 111–142, 2019.

[15] S. R. Nabavi, N. Osati Eraghi, and J. Akbari Torkestani, "Wireless sensor networks routing using clustering based on multiobjective particle swarm optimization algorithm," *Journal of Intelligent Procedures in Electrical Technology*, vol. 12, no. 47, pp. 29–47, 2021.

[16] S. Mudundi and H. Ali, "A new robust genetic algorithm for dynamic cluster formation in wireless sensor networks," in *Proceedings of the 7th IASTED International Conferences on Wireless and Optical Communications, WOC*, pp. 360–367, Montreal, QC, Canada, 2007.

[17] B. Baranidharan and B. Santhi, "GAECH: genetic algorithm based energy efficient clustering hierarchy in wireless sensor networks," *Journal of Sensors*, vol. 2015, Article ID 715740, 8 pages, 2015.

[18] Y. Sun, W. Dong, and Y. Chen, "An improved routing algorithm based on ant colony optimization in wireless sensor networks," *IEEE Communications Letters*, vol. 21, no. 6, pp. 1317–1320, 2017.

[19] T. Gui, C. Ma, F. Wang, and D. E. Wilkins, "Survey on swarm intelligence based routing protocols for wireless sensor networks: an extensive study," in *Proceedings of the IEEE International Conference on Industrial Technology*, pp. 1944–1949, Taipei, Taiwan, May 2016.

[20] C. K. Ho and H. T. Ewe, "A hybrid ant colony optimization approach (hACO) for constructing load-balanced clusters," in *2005 IEEE Congress on Evolutionary Computation*, pp. 2010–2017, Edinburgh, UK, 2005.

[21] J. Kamimura, N. Wakamiya, and M. Murata, "A distributed clustering method for energy-efficient data gathering in sensor networks," *International Journal of Wireless and Mobile Computing*, vol. 1, no. 2, pp. 113–120, 2006.

[22] M. Azharuddin and P. K. Jana, "Particle swarm optimization for maximizing lifetime of wireless sensor networks," *Computers & Electrical Engineering*, vol. 51, pp. 26–42, 2016.

[23] B. Singh and D. K. Lobiyal, "A novel energy-aware cluster head selection based on particle swarm optimization for wireless sensor networks," *Human-centric Computing and Information Sciences*, vol. 2, no. 1, pp. 1–18, 2012.

[24] S. Okdem, D. Karaboga, and C. Ozturk, "An application of wireless sensor network routing based on artificial bee colony algorithm," in *2011 IEEE Congress of Evolutionary Computation, CEC 2011*, pp. 326–330, Orleans, LA, USA, 2011.

[25] D. Karaboga, S. Okdem, and C. Ozturk, "Cluster based wireless sensor network routing using artificial bee colony algorithm," *Wireless Networks*, vol. 18, no. 7, pp. 847–860, 2012.

[26] X. Cai, Y. Duan, Y. He, J. Yang, and C. Li, "Bee-Sensor-C: an energy-efficient and scalable multipath routing protocol for wireless sensor networks," *International Journal of Distributed Sensor Networks*, vol. 11, no. 3, 2015.

[27] D. Zaheeruddin, K. Lobiyal, and A. Pathak, "Energy-aware bee colony approach to extend lifespan of wireless sensor network," *Australian Journal of Multi-Disciplinary Engineering*, vol. 13, no. 1, pp. 29–46, 2017.

[28] S. Patro and K. K. Sahu, "Normalization: a preprocessing stage," 2015, https://arxiv.org/abs/1503.06462.

[29] Z. Ma, G. Li, and Q. Gong, "Improvement on LEACH-C protocol of wireless sensor network (LEACH-CC)," *International Journal of Future Generation Communication and Networking*, vol. 9, no. 2, pp. 183–192, 2016.

Hindawi
Journal of Sensors
Volume 2023, Article ID 9784172, 1 page
https://doi.org/10.1155/2023/9784172

Retraction

Retracted: Physiological Index Monitoring of Wearable Sports Training Based on a Wireless Sensor Network

Journal of Sensors

Received 3 October 2023; Accepted 3 October 2023; Published 4 October 2023

This article has been retracted by Hindawi following an investigation undertaken by the publisher [1]. This investigation has uncovered evidence of one or more of the following indicators of systematic manipulation of the publication process:

(1) Discrepancies in scope
(2) Discrepancies in the description of the research reported
(3) Discrepancies between the availability of data and the research described
(4) Inappropriate citations
(5) Incoherent, meaningless and/or irrelevant content included in the article
(6) Peer-review manipulation

The presence of these indicators undermines our confidence in the integrity of the article's content and we cannot, therefore, vouch for its reliability. Please note that this notice is intended solely to alert readers that the content of this article is unreliable. We have not investigated whether authors were aware of or involved in the systematic manipulation of the publication process.

In addition, our investigation has also shown that one or more of the following human-subject reporting requirements has not been met in this article: ethical approval by an Institutional Review Board (IRB) committee or equivalent, patient/participant consent to participate, and/or agreement to publish patient/participant details (where relevant).

Wiley and Hindawi regrets that the usual quality checks did not identify these issues before publication and have since put additional measures in place to safeguard research integrity.

We wish to credit our own Research Integrity and Research Publishing teams and anonymous and named external researchers and research integrity experts for contributing to this investigation.

The corresponding author, as the representative of all authors, has been given the opportunity to register their agreement or disagreement to this retraction. We have kept a record of any response received.

References

[1] Z. Lu, Z. Li, and L. Zhang, "Physiological Index Monitoring of Wearable Sports Training Based on a Wireless Sensor Network," *Journal of Sensors*, vol. 2021, Article ID 7552510, 10 pages, 2021.

Hindawi
Journal of Sensors
Volume 2021, Article ID 7552510, 10 pages
https://doi.org/10.1155/2021/7552510

Research Article

Physiological Index Monitoring of Wearable Sports Training Based on a Wireless Sensor Network

Zhihai Lu,[1] **Zhaoxiang Li**,[1] **and Lei Zhang**[2]

[1]*Capital University of Physical Education and Sports, Beijing 100191, China*
[2]*Beijing Dacheng School, Beijing 100141, China*

Correspondence should be addressed to Zhihai Lu; luzhihai@cupes.edu.cn

Received 25 October 2021; Revised 10 November 2021; Accepted 22 November 2021; Published 6 December 2021

Academic Editor: Gengxin Sun

According to the development needs of wireless sensor networks, this paper uses the combination of embedded system and wireless sensor network technology to design a network node platform. This platform is equipped with a sports training sensor module to measure the physiological indicators of the ward in real time. The network node sends the collected physiological parameters to a remote monitoring center in real time. First, according to the generation mechanism of the physiological index signal and the characteristics of the physiological index signal, the wireless sensor network analysis and processing method are used to denoise the physiological index signal, and the wireless sensor network package is used to extract the characteristics of the physiological index, indicating different types of respiration. The energy characteristics of the sound physiological index signals are different, which verifies the feasibility of the independent component analysis method for separating the physiological index and the physiological index signal of the heart sound. Secondly, the hardware system of physiological index signal acquisition is designed, and the selection principle of the hardware unit is introduced. At the same time, the system structure of the monitor is designed, and then, the wireless sensor network sensor node is researched, the hardware of the wearable monitor system is designed, and the hardware architecture and working mode based on the single-chip MSP430F149 are given. Finally, the wireless hardware platform includes the following main modules: sensor part, preprocessing circuit module, microprocessing module based on MSP430 low power consumption, wireless transceiver module based on RF chip CC2420, and power supply unit used to provide energy.

1. Introduction

The wireless sensor network (WSN) is composed of microsensor nodes deployed in the monitoring area. It is the result of a multidisciplinary development that combines sensor technology, wireless transmission technology, distributed information technology, and embedded technology. Processing technology can collect, process, and transmit object information to objects that need to be sensed [1–3]. The WSN has a wide range of applications, from environmental monitoring, industrial processing control to military applications; you can see the WSN [4]. The increasing demand for sports training and health care also requires continuous and real-time detection of human vital signs, integrating WSN technology into sports training, health care, diagnosis, and treatment and establishing a wireless sports training health monitoring system, which will become the future research and application hotspot [5]. At the same time, with the continuous development of science and technology in recent years, there has been a situation of multidisciplinary cross integration, and the detection of vital signs parameters based on wireless sensor network nodes has become a new auxiliary and support method in the clinical diagnosis and treatment process. At present, most of the main wireless sports training monitoring systems are aimed at the detection of conventional human physical parameters, and the related monitoring of the physiological index system, which is one of the four major systems of the human body, is not very common [6–8].

Regarding wearable devices, almost all current researches focus on the wearability of the device itself, while there is almost no research on data transmission, resource

sharing, and remote command between human bodies wearing wearable devices. Therefore, research on wearable wireless sensor networks has important value and significance [9–11]. The methods of physiological index signal analysis are generally divided into a time-domain analysis method, frequency-domain analysis method, and time-frequency joint analysis method. In digital physiological index signal processing, frequency domain analysis can be divided into periodogram and autocorrelation methods based on Fourier analysis and modern spectrum analysis methods based on non-Fourier analysis. Mao et al. [12] aimed at the current application status of wearable technology in the field of rehabilitation and discussed the possibility of wearable devices in the field in the future and the main problems. Masè and Micarelli [13], based on the concept of a wearable computer, proposed the concept of a wearable wireless network and built a wearable wireless network model using Bluetooth and Zigbee technology. Zhang et al. [14] proposed a wireless sensor network using a wearable computer as an intelligent interface, elaborated the architecture of the wireless sensor network, and proved the feasibility of the wireless sensor network. Khundaqji et al. [15] take the energy efficiency of human motion capture in wireless wearable devices as the main line, and in-depth research and exploration of energy efficiency improvement strategies are used in wearable computing in a low-power constrained environment. Kong and Wang [16] studied the sensor data fusion algorithm with the background of wireless wearable sensor network. The above literature mainly focuses on a brief overview of wearable wireless sensor networks. It does not analyze the network characteristics of wearable wireless sensor networks and the specific transmission process of the network, nor does it study the characteristics of network node mobility and real-time data transmission. Therefore, it is necessary for us to study the network optimization and routing algorithm of the wearable wireless sensor network based on the characteristics of the wearable wireless sensor network to improve the real-time and reliability of data transmission in the network [17–19]. Some scholars have pointed out the various problems and challenges faced by the WBAN network routing protocol through the research and analysis of various existing routing protocols in the WBAN network. In this environment, effective on-body communication routing has a significant impact on the performance of wearable wireless sensor networks [20–22]. For example, the researchers put forward a new opportunistic and mobile-aware routing protocol by studying the problems related to link quality and routing performance in high dynamic wireless body area networks [23–25].

Based on the multiresolution characteristics of the feature extraction method of wireless sensor networks, this paper conducts localized feature characterization of physiological indicator signals to obtain parameters that represent the characteristics of physiological indicator signals, which can be used to classify and recognize physiological indicator signals. Although modern processing technology has made some progress in analyzing physiological index signals, the diagnosis of physiological index system diseases still adopts auscultation. It is necessary to establish a complete physiological index collection, analysis, and recognition system and based on a wireless sensor network. This paper presents a research on the detection of wireless sensor network nodes that integrates collection, processing, and transmission of physiological indicators. At the same time, factors are selected according to the situation of this article to avoid the large prediction error caused by the incomplete consideration of input factors in the prediction model of this article. The key issue of this system is how to accurately collect, process, and short-distance wireless transmission of physiological index sounds. Physiological indicator signal pickup is to collect physiological indicator signals on the surface of the human body through the sensor; first, remove the interfering physiological indicator signals through the filter circuit; the processing module uses the microprocessor to analyze the physiological indicator signals on the basis of the collected physiological indicator sound physiological indicator signals. The collected and processed physiological indicator signals are transmitted to the next node or central station through short-distance wireless communication transmission technology, so as to provide diagnosis and treatment services for clinical sports training. Since the research in this paper is a wearable wireless sensor network applied to sports emergency scenarios, data transmission between human bodies should have a lower delay and a lower packet loss rate. The data aggregation in the physical communication network should be as energy-efficient as possible. Therefore, the research on the routing algorithm of On-Body network and B2B network in wearable wireless sensor network is very important.

2. Construction of a Wearable Sports Training Physiological Index Monitoring Model Based on a Wireless Sensor Network

2.1. Hierarchical Distribution of Wireless Sensor Networks. The wireless sensor network is composed of a large number of randomly distributed sensor nodes with real-time perception and self-organization capabilities, which can realize the purpose of overall monitoring of a certain area. In the On-Body network, the capabilities of sensor nodes are limited. It needs to use less power to transmit the collected data from the sensor nodes to the coordinator node in order to achieve the purpose of energy saving. However, because WSN and WBAN have different architectures and applications run under different conditions, the routing protocols in traditional wireless sensor networks cannot be directly applied to our On-Body network. Figure 1 is the hierarchical framework of the wireless sensor network.

It can separate hidden components from multidimensional statistical data. For linear transformation, the physiological indicator signal to be measured is a physiological indicator signal that is linearly mixed by multiple independent non-Gaussian physiological indicator signals. The independent physiological indicator signal can be regarded as the basis of linear space. The ICA technology calculates the source physiological index signal from the physiological index signal to be measured under an unknowable advance

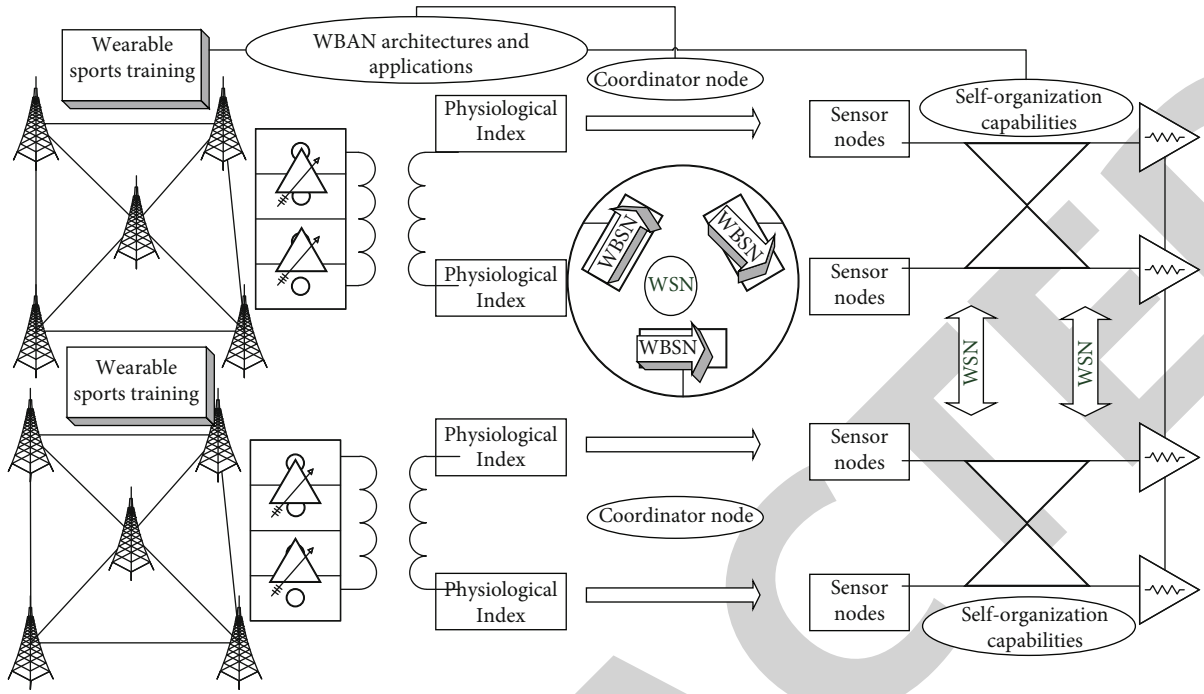

Figure 1: Hierarchical framework of wireless sensor network.

of the source physiological index signal and the linear transformation method.

$$L(x,y) = \sqrt{\sum [C_a(x,y) - C_b(x,y)]^2},$$
$$g(x,y) = \frac{|k(x,y)|^2}{t} \times \exp\left(-\|k\|^2 \times \frac{(x+y)}{2t}\right). \quad (1)$$

It remains unchanged for reversible linear transformations. Obviously, compared with the entropy that remains unchanged for the orthogonal transformation, the conditions for negative entropy are more relaxed. In ICA, this property makes it possible to take edge negative entropy and then find a linear transformation to maximize it.

$$R_A = \frac{X_A X_A{}^T}{\left|X_A X_A{}^T\right|},$$
$$R_B = \frac{X_B X_B{}^T}{\left|X_B X_B{}^T\right|}. \quad (2)$$

Because the Zigbee protocol uses a layered architecture similar to the OSI seven-layer model, each layer completes certain functions, and the layers and connected layers can call the functions of the layer each other. This layered structure is similar to the stack structure, so we also call it the protocol stack. Mutual information (MD) is a basic criterion used to measure the independence between random variables. Mutual information can be expressed in the form of K-L divergence. The mutual information between multiple random variables is defined as its joint probability density function between the products of each edge density function.

$$\begin{cases} F_1 = \dfrac{f_{11}}{\|f_{11}\|}, \dfrac{f_{12}}{\|f_{12}\|}, \\ F_2 = \dfrac{f^1}{\|f^1\|}, \dfrac{f^2}{\|f^2\|}, \\ F_{1,2} = \{F1, F2\}, \end{cases}$$

$$\exp \sum_{i=1}^{n} x(i) \times f(s,t) = \exp x(1) \times f(x) + \cdots + \exp x(n) \times f(x),$$
$$g\{w(i) \mid w(i-n+1), \cdots, w(i-1)\} = \frac{P[w(i-n+1), \cdots, w(i-1), w(i)]}{P[w(i-n+1), \cdots, w(i-1)]}. \quad (3)$$

Each layer provides services to its neighboring layers. These services are completed by two service entities: a data service entity and a management service entity. The former provides data transmission services, and the latter provides management and other services. These service entities all provide interfaces for their neighboring layers through service access points (SAP). The function functions defined by each layer can only be called by the functions of the layer or its connected layers, thus ensuring a clear hierarchical structure of the protocol.

2.2. Physiological Index Monitoring Module. The transmission of each sensor is scheduled in a synchronous manner, so that each sensor can efficiently transmit the collected data to the coordinator node. As we have introduced before, compared with other sensors, the coordinator node is

generally considered to be a more resource-rich device; it has less power constraints and is usually compatible with multiple standards and multiple communication modes. The coordinator node wirelessly interconnects the data sensed by the sensor node on the body to the coordinator node on other human body or external network infrastructure (GSM, GPRS, 3G, LTE, etc.) through off-body communication. In the case of unavailability or out of range, coordinator nodes can expand the end-to-end network connection in a multihop body-to-body manner by cooperating with each other, thereby forming self-organizing and dynamic wireless body-to-body networks. Among them, the main functions of the PHY physical layer include starting and closing wireless radio frequency transmission and reception, channel energy detection, link quality detection, channel selection, idle channel evaluation, and data packet transmission and reception through the radio frequency module; the main functions of the MAC layer include beacon management, time slot management, sending and receiving frame structure data, and providing appropriate security mechanisms; the network layer is mainly used for network connection, network information maintenance, data management, and network security.

According to the above summary and analysis of various sensor nodes, it can be seen that the transmission data rate of different sensor nodes is different, or even quite different. Figure 2 is a physiological indicator to monitor the transmission data rate. Therefore, in the subsequent simulation experiments, we need to consider the characteristics of different wearable sensor nodes and reasonably carry out location planning, speed setting, and initial energy setting. The classic theory of the central limit theorem in probability theory tells us that under certain conditions; the distribution of the sum of multiple independent distributions tends to be Gaussian. From the perspective of network topology, nodes can be divided into coordinator device nodes, router device nodes, and terminal device nodes. Among them, in addition to its own monitoring information, the coordinator node is also responsible for network formation, network related configuration, management of other network members, and link status information management. The terminal node only needs the functions of collecting data and sending and receiving data. Usually, the coordinator device node and the router device node are generally FFD nodes, and the terminal device nodes are RFD nodes.

2.3. Wearable Network Design. The wearable wireless sensor network is a self-organizing network based on the human body wearing the wearable device. Wearable wireless sensor networks can not only quickly network but can also accurately collect various physiological indicators of the human body and surrounding environment information in real time. At the same time, sports personnel can also collect information and data sensed by other sensor nodes on their bodies through the wearable node and conduct information interaction between each sports personnel and the command center in a single/multihop manner for accuracy. This not only saves lives and monitors the real-time health status of rescue team members and victims but also helps combat commanders make the best decisions in sports operations. Therefore, the wearable wireless sensor network plays an important role in the emergency sports system and has far-reaching significance for the development of the existing Public Safety Network (PSN). In order to reduce the interference of the electrode contact impedance on the detection result, the double-electrode impedance method is selected in the specific circuit for the detection of physiological index signal parameters. It borrows the chest monitoring electrode for measuring the PWM and adopts the PWM method integrated with the controller MSP430.

Figure 3 shows the topology of a wearable wireless sensor network. Conceptually, the physical layer should also include a physical layer management entity (PLME) to provide a management service interface that calls the physical layer management functions; at the same time, the PLME is also responsible for maintaining the physical layer PAN information base (PHY PIB). The physical layer provides physical layer data services through the physical layer data service access point (PD-SAP) and physical layer management services through the physical layer management entity service access point (PLME-SAP). The network coordinator first sets itself as a cluster header and sets the cluster identifier (CID) to 0 and, at the same time, selects an unused PAN network identifier for the cluster to form the first network in the network. Whether a device can become a cluster member is determined by the network coordinator. If the request is passed, the device will be added to the neighbor list of the network coordinator as a child device of the cluster. The newly added device will add the cluster head as the parent device to its neighbor list. According to the central limit theorem, if the random variable X is composed of the sum of many mutually independent random variables, as long as the ink has a finite mean and variance, no matter what distribution it is; the random variable X is closer to the Gaussian distribution than the ink. In other words, S is more non-Gaussian than X. Therefore, in the separation process, the non-Gaussian measurement of the separation results can be used to express the mutual independence between the separation results. When the non-Gaussian measurement reaches the maximum, it indicates that the separation of the independent components has been completed. BSS refers to recovering an independent source signal only from the mixed physiological index signal to be measured (usually the output of multiple physiological index signals). In the actual environment, since there is no prior knowledge about the mixed system, it is required to infer the mixed physiological indicator signal from the physiological indicator signal to be tested and realize blind source separation.

2.4. Model Data Collection Factors. In a clustered structure, all human bodies wearing wearable devices form multiple clusters according to corresponding conditions. The cluster head of each cluster can manage all members in the cluster and can act as a gateway between clusters to realize all clusters. Finally, in a distributed structure, each human body wearing a wearable device is responsible for its own On-Body network communication and communicates with the surrounding On-Body network in a self-organizing form.

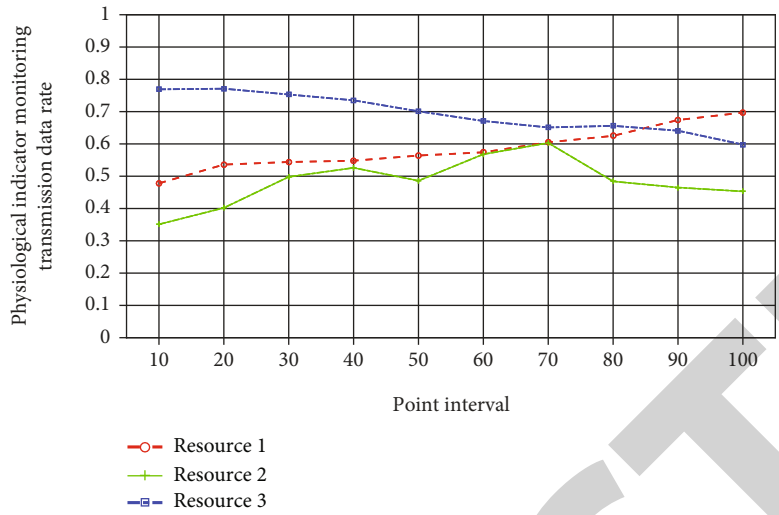

Figure 2: Physiological indicators monitor transmission data rate.

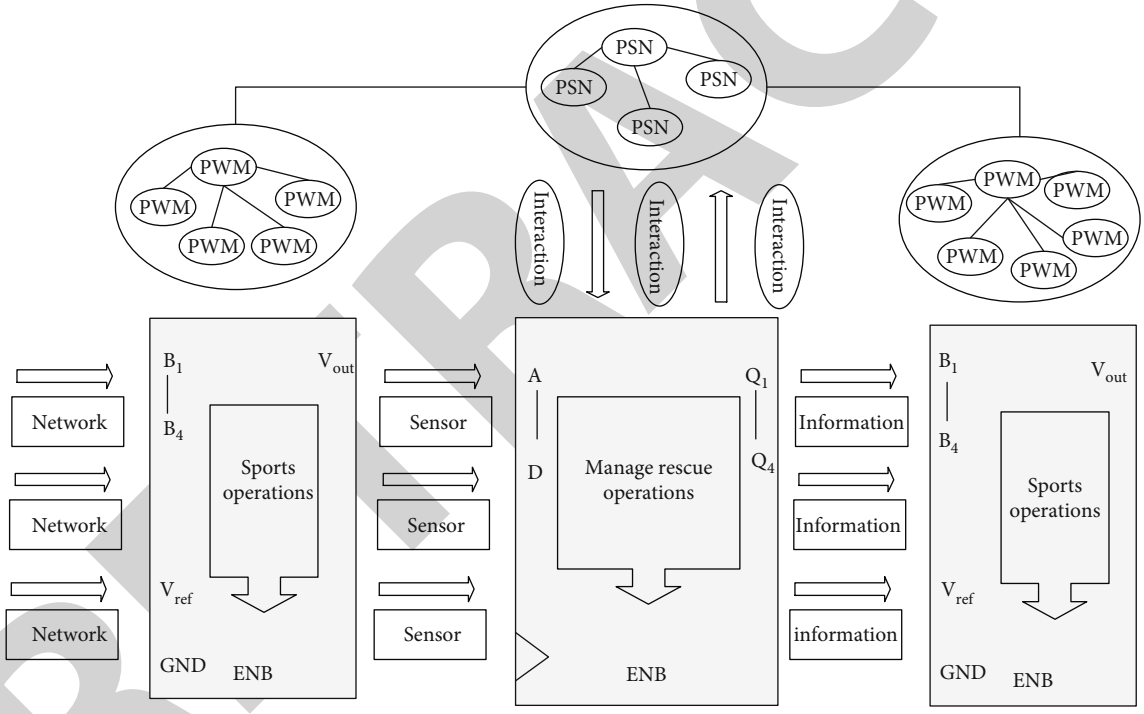

Figure 3: Wearable wireless sensor network topology.

The B2B network studied in this paper adopts a distributed network structure, and each mobile node forms a centerless, mobile, and self-organizing network. It cannot guarantee that the predicted result is completely accurate. The difference between the predicted load value and the actual load value is the error of the load forecast. The Zigbee node is composed of four parts: sensor module, information processing module, RF radio frequency module, and power module. The sensor module is used to monitor external information and pass it to the information processing module; the information processing module is responsible for coordinating the work of each part of the node, and it also needs to process and save the information obtained by the sensor module; the RF radio frequency module is responsible for sending and receiving of node data. Figure 4 is the distribution of physiological indicators of the wireless sensor network.

Reliable communication in sensor networks is very important. The communication requirements of different sports training sensors vary with the sampling rate, from 1 Hz to 1 kHz. One way to improve reliability is to perform signal processing of sensor physiological indicators. For example, feature extraction can be performed on an ECG sensor, and only information about a certain event (such as QRS features and the corresponding R peak time stamp) can be transmitted. For optimal system design, the balance

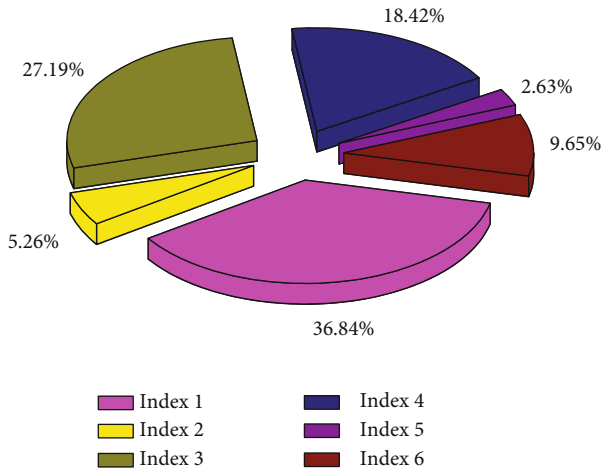

Figure 4: Physiological index distribution of wireless sensor network.

of communication and calculation is crucial. Based on the IEEE 802.15.4 protocol, the master node and each subnode together form a star network with simple structure, stability, and reliable operation. Once the network configuration is complete, the coordinator node manages the network and maintains channel sharing, time synchronization, data extraction and processing, and data fusion. Based on the synergy of information from multiple sports training sensors, sensor nodes display the user's health status and feed it back to the coordinator node through a wireless interface and then transmit it to the PC for further processing and storage of the collected data. If the user has an abnormal situation, an alarm will be sent on the sports training node and on the PC at the same time for the doctor to verify the user's status. The work flow of the information collection terminal mainly includes initialization, port configuration, communication module configuration, and main function loop functions. The initialization module includes data area initialization, parameter initialization, AD port configuration, and clock initialization. Port configuration includes network module configuration and Zigbee module configuration. The main functions include gas information collection, acceleration physiological index signal collection, pulse physiological index signal collection, body temperature physiological index signal collection, blood pressure physiological index signal collection, and Zigbee physiological index signal and network physiological index signal processing functions. The nodes work synchronously and at the same time transmit the received physiological indicator signals to the PC for processing and display.

3. Results and Analysis

3.1. Wireless Sensor Network Data Reception. This design uses the RC reset method to design the reset circuit, and the circuit adds a discharge loop. When the system power supply is stable, the circuit will cancel the reset physiological indicator signal. In order for the system to operate stably, after the system power supply is stable, the reset physiological indicator signal must be cancelled after a delay to prevent the power supply jitter from affecting the system reset. According to the Zigbee protocol standard, Zigbee equipment has a transmission output power of 0-3.6 dBm and a communication distance of 30-60 meters and can detect energy and link quality. According to these detection results, the transmission power can be automatically adjusted to minimize the energy consumption of the equipment under the condition of ensuring the quality of the communication link. Both the selectivity and sensitivity index of CC2420 exceed the requirements of the IEEE 802.15.4 standard. CC2420 hardware supports CSMA/CA, and it integrates functional modules such as digital RSSI module, power supply monitoring, and channel conversion that can be used to realize node ranging function, including hardware MAC and CRC automatic verification processing. In order to further suppress the common-mode interference with physiological indicator signals, in the design of the entire acquisition circuit, this topic has designed a shielding drive circuit and a right leg drive circuit. By studying the causes of errors and analyzing the error values to improve the forecasting model, it can effectively reduce errors and improve the accuracy of forecasting. It can be seen that error analysis is very important for load forecasting. Connecting the shielding wire to the amplifier output can not only separate the shielding layer from the ground but also drive the shielding the layer's potential to have the same potential as the lead core wire; eliminating the distribution between the shielding layer and the lead core wires improves the input impedance and common mode rejection ratio. After the networking is successful, the reliability of the Zigbee network will be tested. Generally, the received physiological index signal strength index (RSSI) is used to measure the communication quality of the network, and the packet error rate (PER) is used to measure the receiving ability of the test terminal.

Figure 5 shows the receiving capability of the physiological indicator monitoring terminal. The frequency of the useful part of the ECG physiological index signal is mainly concentrated at 0.05 Hz. In the range of 100 Hz, since the existence of 50 Hz power frequency physiological indicator signals will interfere with useful physiological indicator signals, according to different situations, high-pass filtering, low-pass filtering, and band-stop filtering are used to process the collected physiological indicator signals. The ECG physiological index signal extracted from the human body surface contains a large amplitude DC interference physiological index signal. In order to enable the operational amplifier to work in the amplification area, the operational amplifier gain of the designed pre-amplifier circuit should not be too large. If it is too large, the DC stability of the circuit will decrease. In this design, a metal film resistor of 8.25 K is selected in the operational amplifier, which can increase the gain of the first-stage amplifier circuit by about 7 times. It is not enough to rely solely on the high common mode rejection ratio of AD620. The interference physiological indicator signal amplitude still reaches the physiological level. In the wireless network system of multipoint networking, the wireless platform based on ANT module has the advantages of low power

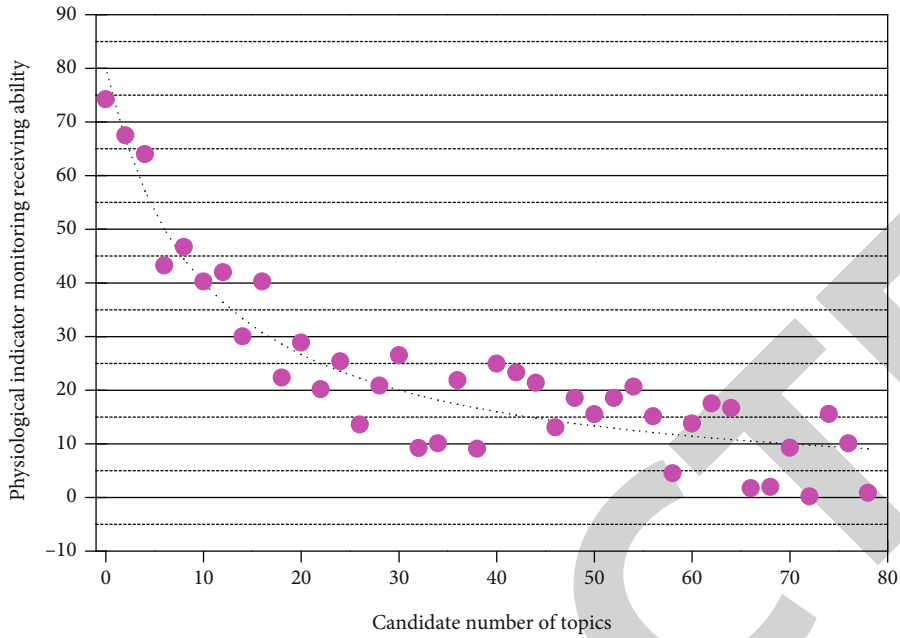

Figure 5: Receiving ability of physiological indicator monitoring terminal.

consumption, simple interface, convenient network protocol, etc.

3.2. Physiological Index Monitoring Model Simulation. The main part of a typical application circuit is to connect CC2420 to a microprocessor, with few external components such as crystal oscillator and load capacitors, input/output matching components, and power supply voltage decoupling capacitors. The single-chip microcomputer uses MSP430F149, which is a 16-bit low-power single-chip microcomputer with RISC architecture. It exchanges data with the personal computer through the serial port, receives the data of the sub-nodes in the cabin through the wireless module, and manages and coordinates the synchronization of the nodes in the cabin at the same time. When provided by the internal circuit, an external crystal oscillator and two load capacitors are required. The size of the capacitor depends on the crystal frequency and input capacitance and other parameters. For example, when a 16 MHz crystal oscillator is used, its capacitance value is about 22 pF. The RF input/output matching circuit is mainly used to match the input and output impedance of the chip so that its input and output impedance is 50 Ω, while providing DC bias for the power amplifier and low noise amplifier inside the chip. Figure 6 is the result of the radio frequency input/output matching ratio of the wireless sensor network.

There are two passive filter circuits in the design, both of which consist of three components to form a T-type, which is called a double-T network. When the frequency of the physiological index signal is relatively low, increasing the capacitor impedance will increase the output and reduce the feedback. As the frequency of physiological indicators increases, the impedance of the capacitor gradually decreases, resulting in a decrease in output and an increase in negative feedback. When the frequency of the physiological indicator signal reaches 50 Hz, the output value is the smallest. If the frequency of the physiological indicator signal continues to increase, the impedance of the capacitor will decrease successively, and the final output value will also become larger and larger. The collected data is transmitted to the coordinator node through the Zigbee wireless sensor network, and the coordinator transmits the data to the MCU of the information control terminal through the serial port for processing and display. The following figure shows the results after the measured temperature and pulse. The system test is divided into two parts: the first part is the test of the hardware part of the data acquisition module; the second part is the test of the background software system. In this system, the hardware part of the test is mainly based on the Zigbee development environment and the serial debugging assistant. Firstly, each submodule is tested separately, and then the output of the circuit and the communication connection between the modules are tested. Table 1 is the communication composition between wireless sensor circuit modules.

After sorting out and standardizing the original data, there are about 4500 pieces of original data. Since the data analysis in this article is based on system functions, the feature selection of training data is based on the selection of collection indicators in the front-end collection module of this system. The label of the data set is established based on the report results given by the doctor in the medical examination report. It can be seen from the model evaluation indicators that the model has a strong classification ability. The threshold can be adjusted by pressing the button. When the temperature or pulse exceeds the threshold, an alarm message will be sent to the preset guardian's mobile phone in the form of a short message. During the operation, the microprocessor can set the timer and interrupt program to make the two light sources alternately light up and to

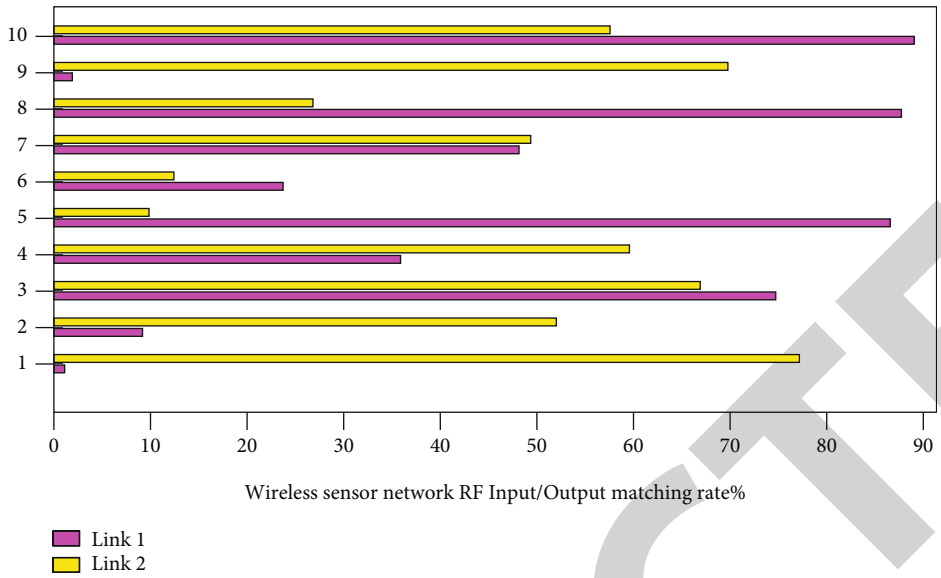

Figure 6: RF input/output matching rate results of wireless sensor network.

Table 1: Communication composition between wireless sensor circuit modules.

Module	Working frequency (GHz)	Distance (m)	Transmission rate (Mbps)
1	2.5	0-1000	250
2	3.0	20-800	500
3	4.0	200-1000	300
4	5.0	50-500	40

ensure a fixed frequency, to ensure that the sensor can run at high speed and stably.

3.3. Analysis of Experimental Results. In terms of node hardware design, the sensor module part is mainly designed for the collection temperature physiological parameters; for the wireless communication module part, this article uses direct sequence spread spectrum on the FPGA development platform Quartus II 10.1. In terms of node software design, this paper considers the feasibility of the scheme and the rational use of hardware resources, designs the overall workflow of the node, and adopts a divide-and-conquer method to design separate software for individual functions, including overall node scheduling, physiological and physiological indicator data acquisition, and wireless communication program. The simulation experiment is carried out on MATLAB as the platform. The experiment is divided into two groups of unconsidered factors and considered factors. When the outside world sends a physiological indicator signal to the chip, the boot area that stores the BOOTROM.

For the allocation of training set and test set, in this paper, 60% of the experimental data in the data set is used as the training sample, and 40% of the experimental data in the remaining data set is used as the test sample. Figure 7 shows the statistical distribution of the deviation of the wireless communication transmission. The model training experiment is implemented based on Python, and the support vector machine classifier SVC method is used to classify and train the data. The selection of the kernel function in the training method adopts the default Gaussian function, because it can obtain ideal results on most sample sets, and the support vector machine with Gaussian function as the kernel can usually show good performance. After the GPRS module is connected to the MSP430F149, the serial port will be initialized first, and then, the microcontroller will send the AT command to the GPRS module to make the module log in to the GSM network and establish a connection. After the configuration of the data transmission mode is completed, the data receiving function is used to the preset mobile phone in the form of short message. The temperature data obtained after DSl 8820 conversion is stored in the memory in the form of two-byte complement.

Since the data set contains continuous feature data with different value intervals, the data needs to be normalized. Normalization is to adjust the range of the data to the interval of $[0, 1]$ or $[-1, 1]$, eliminating the influence of different dimensions on the data. Figure 8 is a comparison of frequency measurement deviations of wireless sensors. The minimum-maximum normalization method is adopted for processing, and the value is mapped to the interval range of $[0, 1]$. Each group is divided into the BP neural network model, GABP neural network model, and PCA. The GABP neural network model was carried out by four groups. The acceleration movement amplitude in the vertical direction is greater than the lateral forward and backward movement, and the amplitude gradually increases from the head to the toe of the human body. In order to effectively reflect the motion state of the human body, this paper adopts the SMB38 three-dimensional acceleration sensor that measures the three-dimensional acceleration values of the front and rear, left and right sides, and upper and lower parts of the human body. For example, the uric acid value is generally three digits. The uric acid value is a single-digit value, which

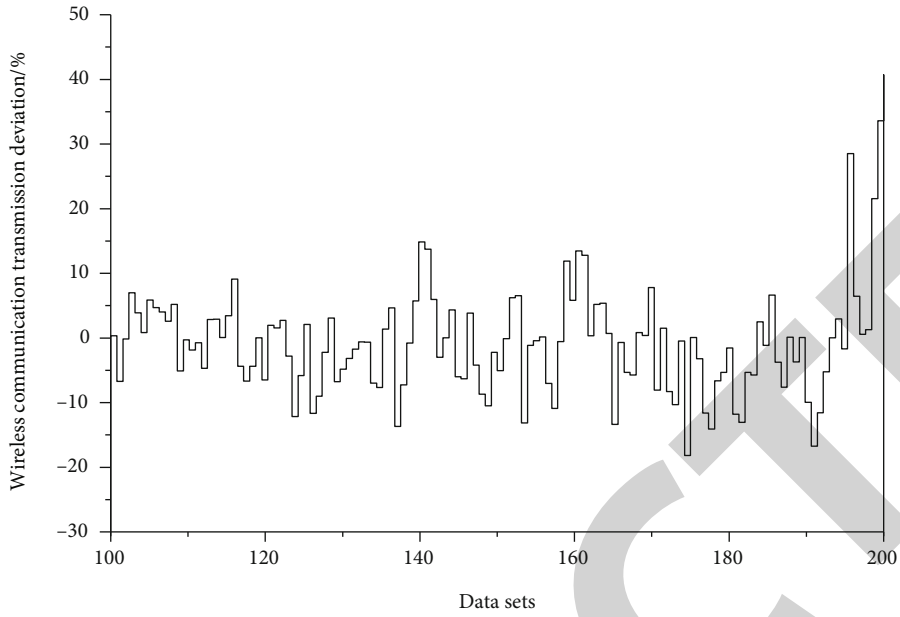

Figure 7: The statistical distribution of wireless communication transmission deviation.

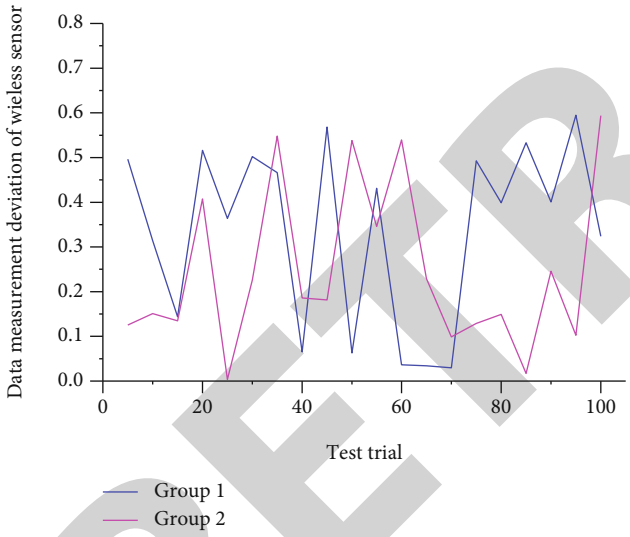

Figure 8: Comparison of frequency measurement deviation of wireless sensors.

is an abnormal value. The processing of outliers is to use the average value of the entire data set instead for correction. From the pulse test results, it can be seen that the pulse values of the three tested subjects are within the normal range, and there is not much difference between the test results of the medical pulse meter. It can be seen from the variance of the three sets of pulse test data that sometimes the result is not stable, but it can also be within the acceptable range. This is because the sensor element of the front-end pulse acquisition module is related to the circuit design. If there is a need for accurate measurement in the future, the pulse measurement module can be further improved and optimized.

4. Conclusion

According to the short-distance, low-complexity, low-power, low-cost, and high-stability requirements of wearable sports monitors, this paper chooses IEEE802.15.4 as the wireless communication protocol for a wireless sensor network. On this basis, the network structure, software, and hardware of the wearable sports monitor system are designed, and the technical difficulties and key points of implementing the monitoring device are analyzed and studied. The synchronization and coordination of the network carries out the collection and transmission of physiological indicator signals. The sensor module is responsible for the collection of physiological and physiological index signals and the conditioning of physiological index signals. In order to achieve a clear comparison effect, this paper uses the maximum relative error, the absolute value of the relative error, and the average relative error to do error analysis; we select the maximum relative error of the predicted load of 48 points. Each physiological and physiological index signal needs to be designed independently, based on different physiological physiology. For the reception and transmission of wireless data, this module mainly uses direct sequence spread spectrum technology for communication and uses FPGA development technology to complete the digital logic circuit of the direct sequence spread spectrum communication system to analyze and study the technical difficulties of wearable sensing detection and data collection of physiological and physiological indicator signals and design sensor nodes and coordinators by integrating these five detection circuits and radio frequency communication modules node. Through experimental verification, the physiological index signal denoising and feature extraction proposed in the paper have good effects and certain feasibility; the hardware system design scheme conforms to the principle of

Hindawi
Journal of Sensors
Volume 2021, Article ID 5204841, 17 pages
https://doi.org/10.1155/2021/5204841

Research Article

Research on Production Management and Optimization of Multisensor Intelligent Clothing in 5G Era

Xiang Chen,[1] **YouTang Gao**,[1] **and Bao Tian**[2]

[1]*Huang Huai University College of LEIZU Fashion Smart Manufacturing, Zhumadian City, 463000 Henan, China*
[2]*School of Intelligent Engineering, Zhengzhou University of Aeronautics, Zhengzhou Henan 450000, China*

Correspondence should be addressed to Xiang Chen; chen.xiang@huanghuai.edu.cn

Received 13 September 2021; Accepted 12 November 2021; Published 6 December 2021

Academic Editor: Gengxin Sun

The influence of 5G has penetrated into all aspects of people's lives. The field of garment production management is inevitably affected by 5G. The various advanced technologies it promotes can greatly promote the production and management of clothing. Learning and understanding these technologies can help you learn how to change in the changing garment factory to obtain more intelligent and efficient production methods without being excluded by age. The garment production line management system proposed in this paper is based on the garment production line, introduces Internet technology into the garment production process, and monitors all links of the garment production process through the Zigbee network. The system improves the automation degree of enterprises, greatly expands the application scope of wireless sensor networks, and improves the application level of data acquisition, monitoring, equipment maintenance, and diagnosis in China's industrial field. Wireless network node location technology is also an important supporting technology for managing wireless Zigbee networks. The visual display of a physical topology map can effectively help administrators manage and maintain wireless networks.

1. Introduction

5G is the fifth-generation wireless communication. The advantages of 5G include high speed, low delay, high throughput, and high security. It is impossible to simply understand the upgrade of traditional technology of the communication network. It should be regarded as a technological change with essential and subversive changes in various fields affecting people's production and life. Therefore, we have such a problem [1]. In the 5G era, how can the field of garment production management keep pace with the times and improve its own scientific and technological content? With the elimination of old technology, the field of garment production management is inevitably affected by 5G technology. This technology promotes production, and various advanced technologies are extremely convenient for garment factory production and garment management [2].

In the traditional garment production process, the site control is poor, and the bottleneck of the production line cannot be foreseen. In the process of production and processing, a large number of data such as material data, labor time, and output data need to be recorded manually. In addition, when product quality problems occur in the processing process, quality tracking cannot be carried out, and the classification of responsibilities is unclear. Finally, due to the lack of on-site systematic management, it is difficult to estimate the production progress of orders and the data that have been completed in the workshop. The production cost cannot be calculated correctly [3].

The automatic garment production monitoring system is equipped with RFID reader devices in each process and RF tag cards on each garment. When clothes pass through each process, employees can use the cards to observe the current line processing process and the completion of each process in real time and estimate the overall completion time, thus realizing the overall monitoring of the production line [4]. The monitoring process can also count the ratio of each employee and the labor effect in the cycle. These play an important and decisive role in stimulating the enthusiasm of employees. Combined with Internet of Things technology

and garment production management system, it can significantly improve efficiency and reduce costs [5].

A low-cost information collection system is used to manage the distribution of clothing production lines in order to ensure traceability of products throughout the supply chain, which is very important for any product. For the garment production line, the traditional way is to rely on the team leader's personal experience or intuition without relying on data. If the management team leader or workers are not on duty, it will directly affect the production efficiency and damage the production capacity. For such problems, the system uses information collection tools to continuously use the collected data in the supply chain and analyzes the data to display it [6]. In this way, even inexperienced leaders can use the data provided for management purposes. Research shows that team change can be achieved by assignment. With the development of science and technology, various new technologies are also applied in all walks of life, and nanotechnology is also applied to the clothing industry. The characteristics of nanomaterials determine that they can play a role in promoting and innovating the clothing industry. We summarized the nanodispersion theory by searching literature and then, combined with experiments, put forward the application of nanomaterials in safe and intelligent clothing design [7].

Military protective clothing is often threatened or destroyed by chemical components, coupled with a series of shortcomings such as its own bulkiness, so its practicality has been of wide concern. Researchers made graphene electronic fabric by laminating graphene, which is light, durable, and scalable. In addition, graphene intelligent protective clothing is provided by configuring a graphene triboelectric nanogenerator [8]. Through experiments, it is found that the clothing has high sensitivity to chemical warfare agents. Nowadays, with the rapid development of digitalization, many traditional industries have begun to change to digital industries, such as the clothing industry. Everyone is competing to launch the digital customization platform for clothing, but it is still in the exploratory stage, and the satisfaction is not very high in the actual use process. In fact, it is mainly caused by the low consumer participation and poor communication of the platform. To solve this problem, we first analyze the psychological needs of customers and then optimize and transform them in combination with the construction of the sales platform and design an intelligent interactive platform for personalized clothing customization [9]. Young people are exposed to more and more diversified things, and they also have a higher personalized pursuit of clothing. In order to meet the needs, we designed an intelligent clothing matching selection system, that is, a personalized clothing recommendation solution based on a self-organizing mapping SOM neural network. The system combines the collected personalized demand information with the objective elements of customers and then establishes a database to mine personal preferences. By using this system, we can provide customers with relevant reference for clothing [10]. Experiments show that the system has good accuracy and performance and has great development potential.

2. Detailed Design and Implementation of Each Module of the System

2.1. Grid Probabilistic Positioning Algorithm. The biggest feature of the DV-Hop localization algorithm is that it does not need any auxiliary hardware equipment, but the algorithm itself is not optimized and the localization accuracy of specific network applications is not high. Therefore, the system transforms the node location problem into the problem of identifying the correct location of network nodes in each grid [11].

For $\forall k \subseteq S\text{-}A$, we set the unknown node "k" in A and set the minimum number of hops $H^k = (h_1^k, h_2^k, \cdots h_{|A|}^k)$ for each anchor node of A. The unknown node "K" can be expressed as the probability distribution in the grid by the following formula.

$$F_k = \begin{pmatrix} f_{11}^k & \cdots & f_{1n}^k \\ \vdots & \ddots & \vdots \\ f_{n1}^k & \cdots & f_{nn}^k \end{pmatrix}, \quad \forall k \subseteq S - A. \tag{1}$$

The probability of unknown nodes in each grid satisfies the following equation.

$$f_{ij}^k = \begin{cases} \text{Probability that the sensor node ``}k\text{'' is located at the } (i,j)\text{position}, & (i,j) \notin A, \\ 0, & (i,j) \in A. \end{cases} \tag{2}$$

f_{ij}^k represents the probability that the sensor node "k" is located (i, j) in the grid. The calculation method of f_{ij}^k itself is expressed in equation (3). Of course, if the location (i, j) is the location of the anchor node, then the probability that the unknown node is in this grid is zero.

$$f_{ij}^k = \prod_{l=1}^{|A|} p_{ij}^{h_{ij}^k}. \tag{3}$$

$p_{ij}^{h_{ij}^k}$ in equation (3) represents the probability that the number of hops from the unknown node "k" to each anchor node is the number of hops represented by the vector H^k. The probability of the Poisson distribution is expressed as the following formula.

$$P_\tau \frac{\lambda^{\tau-1} e^{-\lambda}}{(\tau-1)!}. \tag{4}$$

In formula (4), $\tau = 1, 2, \cdots$ and λ are the hops and distances from the unknown node to the anchored node. Through this calculation, the probability that the unknown node "k" exists in each grid in the message topology can be obtained, in which case, only the location of the maximum probability or the estimated location of the location node "k" is determined.

2.2. Realization of RFID Data Acquisition. Users use RFID readers to collect data in the system. The identification stage includes the operation of finding the card, preventing collision, and operating the card. Authentication provides the password of the selected card through authentication, and the authentication authority of the card provides effective protection of the data in the card. You can start reading and writing the data in the card through authentication [12].

Figure 1 shows a flow of an RFID reader operation representing an implementation function of a corresponding function. Under normal circumstances, after receiving the card reading instruction, the card reader will first look for the card operation and then send a radio frequency signal to look for the response card. If a plurality of radio frequency tags exist within the identification range of the card reader, a plurality of cards respond to a card search signal sent by the card reader. At this time, the card reader adopts anticollision protocol. One of the many cards found to operate is selected. If a card is selected, we check whether we have access to the sectors that need to be read and written. The contents of the card are read and written only after passing the verification. After the final operation, the final operation card is needed. In this case, when the card cannot leave due to the test system, if the data in the card can be read again, the card reader needs to be reset.

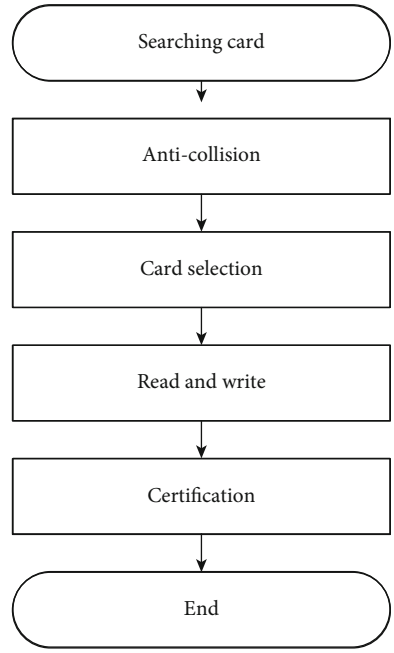

Figure 1: RFID reader operation flow.

Because the macroprocessor is single-column red, the idea of the main function design of the system is whether various tag bits polled continuously in the dead cycle are already located in it, and after initialization, they enter the dead cycle and become the state where their respective tags are polled. As you can see from the loop, if there is no identification location, the job of the system is to find the card. In the operation of the card, the buzzer prompts the user with a prompt sound of success or warning according to the operation result in Figure 2.

The system has two kinds of tag cards. One is the employee card assigned to the employee. The other is a card distributed by clothing. We call it the "packing card." When the card reader reads different types of cards, the screen will display different contents. The acquisition terminal reads data from the card, first judges the type of the card, and makes different responses to different types of the card.

The card operation trigger event is when the reader reads the legitimate tags belonging to the system, that is, the above two tags. In order to complete a friendly interaction with users, prompt information will be displayed on the LCD screen when operating the card. At the same time, if external instructions are needed in operation, keyboard operation will be involved. There is no mobile banking on the monitor. The word touch code of the word to be displayed is stored in an array in advance. It is just read directly when necessary. Keyboard operations are performed through external interruptions.

In order to count the accounting of employees, employees should first use their own employee cards before using the packaging cards. Therefore, when the card reader identifies the card, it must first determine whether the employee card is used in the current system. If there is an employee card recorded on the system, it will show the code of the current operator. Otherwise, the monitor will swipe the employee card first and then finish reading the card. If the unregistered card is detected, the LCD panel will also pay attention to the corresponding operation. Normally, if the confirmation card is an employee card, the current operator is prompted and the current employee number stored in the local cache is updated in Figure 3.

In order to improve CPU utilization, the macroprocessor uses the interrupt mechanism, because the macroprocessor operates in single-column red. Interruptions used during system implementation will interrupt timer interruptions and serial data reception. Timer interruption is mainly used for timing display. For example, the information of the current user will be automatically displayed after a certain period of time after swiping the card. Reception of serial data is interrupted. This is mainly used for receiving serial data. After receiving the serial data, the Serial Port Receive Interrupt Service Handling Subroutine is executed if the location of the tag is detected.

The crosstalk interrupt handler is responsible for receiving serial data. Crosstalk is received per byte, and the register flag bit RI is set to 1. The received data is set on the register SBUF. Therefore, our job is to set the received data into an arrangement. The process flow is shown in Figure 4.

If the register RI is set to 1, it indicates that new data has arrived at the serial port, where the data is received in byte form, and it is first determined whether the received byte is a frame header, and if it is the auxiliary flag bit Frame Start, it is determined whether the current byte is a data frame header or a frame trailer. Because the header and trailer use the same recognition, for Frame Start recognition, if 0 is the header, 1 represents the trailer. The flag position is set to 1 after the initial reception of the frame header, and if 0xC0 is encountered again after the

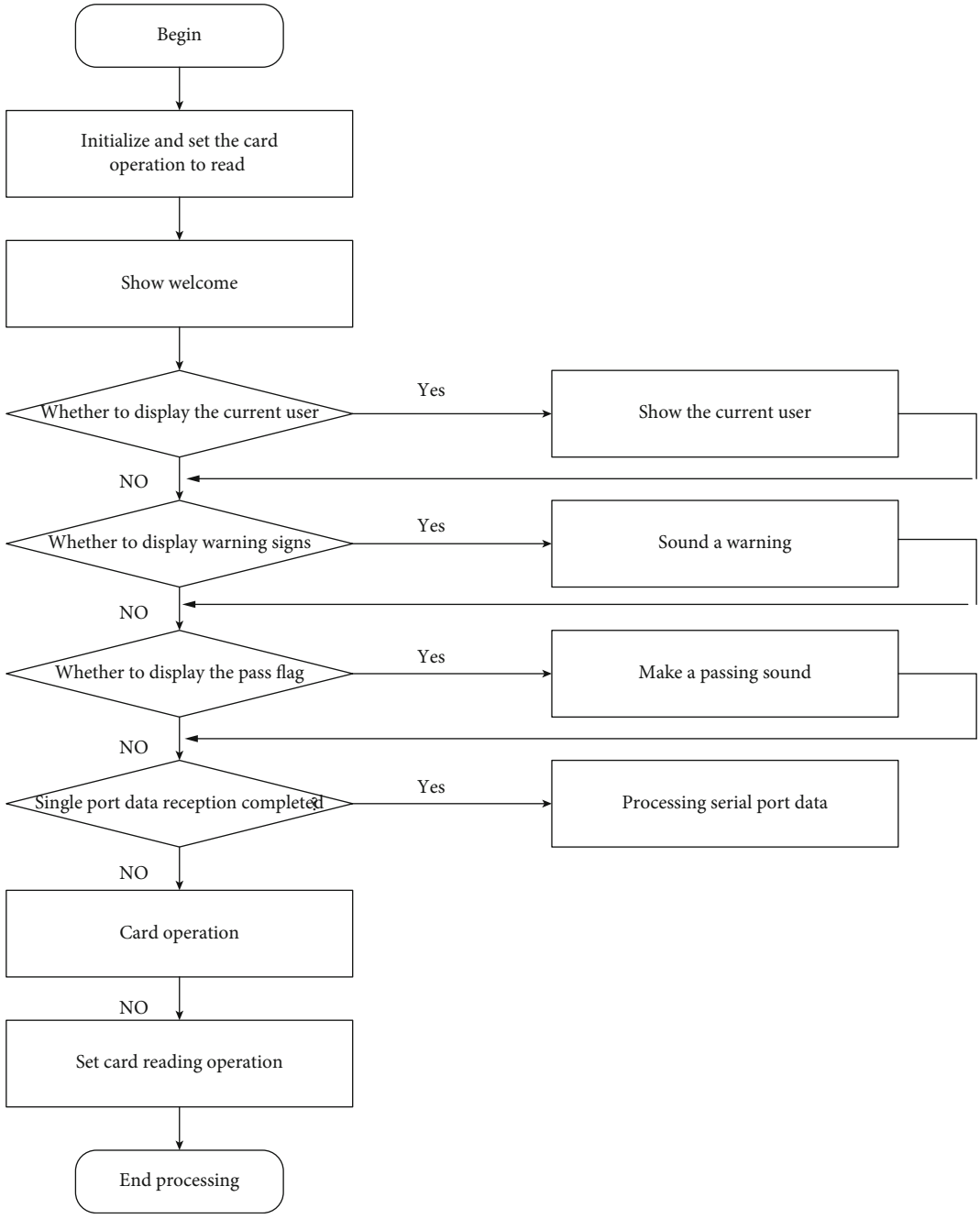

Figure 2: Main function execution flow chart.

reception of data, the current byte can be determined to be the last of the frame.

2.3. Design and Implementation of Reliable Communication in Zigbee. Zigbee is a wireless network protocol with low speed and short distance transmission. The bottom layer is the media access layer and physical layer which adopt the IEEE 802.15.4 standard specification. The main features are low speed, low power consumption, low cost, support for a large number of network nodes, support for a variety of network topologies, low complexity, fast, reliable, and safe. Zigbee is a new wireless communication technology, which is suitable for a series of electronic components and devices with short transmission range and low data transmission rate. It is a wireless network technology with short distance, low cost, and low power consumption, and it is also a technology suitable for star network topology. The Zigbee network transport software module sends data to the trusted module via crosstalk. The coordinator module is physically connected with the ARM9 gateway, and the main logic is implemented on the Linux platform, but the coordinator itself is only responsible for a data transceiver. There is not much processing logic [13]. Then this time, only the program of the Zigbee terminal is introduced.

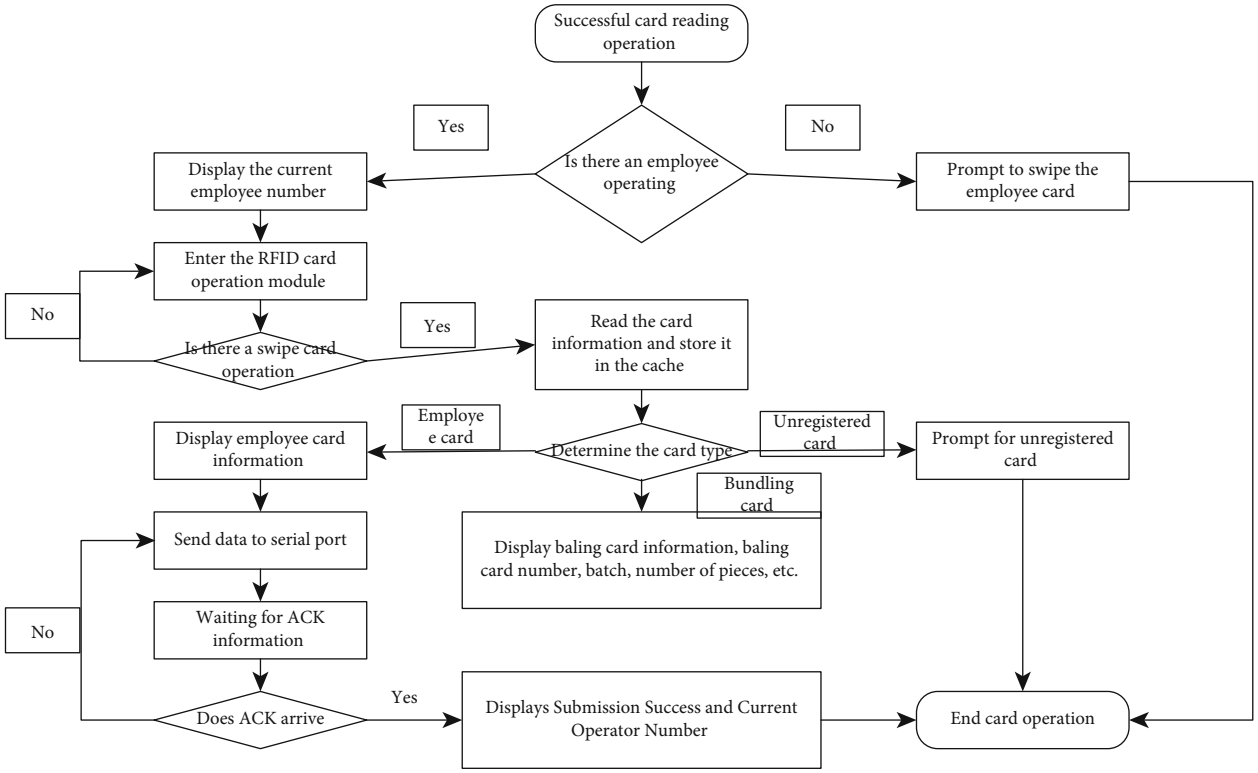

Figure 3: Main function execution flow chart.

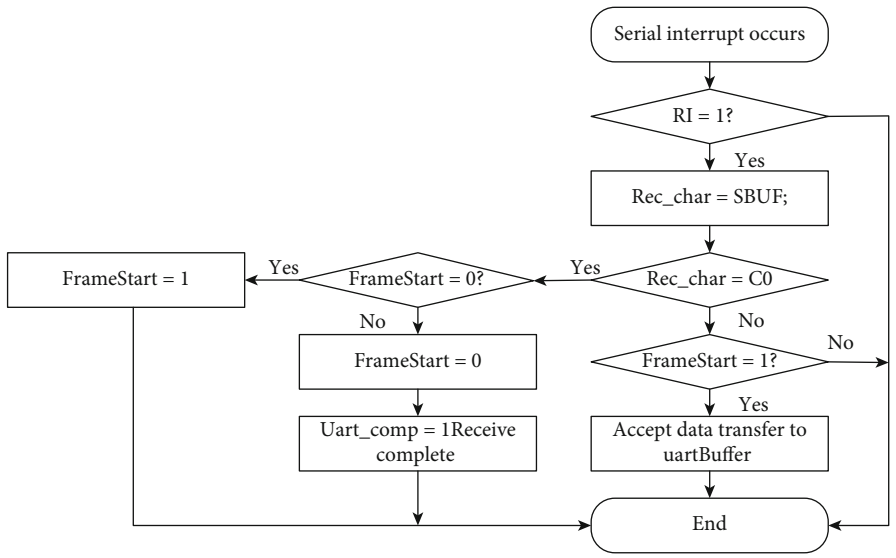

Figure 4: Flow chart of serial interrupt service program processing.

The whole Zigbee programming process is based on the model of event processing, which promotes the execution of the whole program through events. Figure 5 is a state switching diagram of the state machine. The coordinator node selects whether to receive data packets according to the report sequence number. The gateway node does not receive error messages. After the sequence number is reset, the state machine is in state 9 (trans_state_t_9), where tasks performed by the system send heartbeat packet messages to the gateway every 10 seconds. When the RFID terminal transmits a message to the Zigbee terminal, the Zigbee terminal determines the correctness of the message, modifies its format, generates a newspaper, inserts the newspaper into a waiting transmission matrix, and generates an event j (trans_state_convert_arc_t_j). When the event exists, the modified report is sent to the gateway together with the sequence number of the current state machine, and a timer is started to set the receiving waiting time of the ACK. If

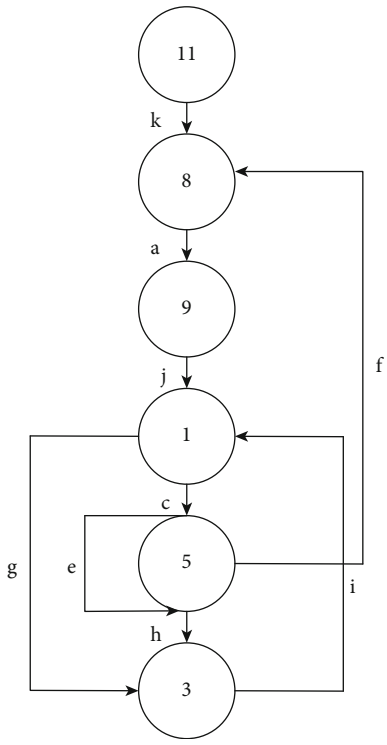

Figure 5: Implementation flow chart of Zigbee terminal based on state machine.

the Zigbee terminal does not receive an ACK within the specified time, we believe that an error occurred in the process of sending the newspaper. This report was not sent and needs to be sent again. After the newspaper is sent, according to whether the confirmation letter is received within the specified time, the system enters state 3 (trans_state_t_3) and state 5 (trans_state_t_5), respectively, indicating that the system enters the retransmission stage in state 5. If the retransmission times exceed the threshold set by the system, the event of resetting the serial number will occur, and the system enters state 8. In this case, the network failure or the serial number may be unsatisfactory in Tables 1 and 2.

According to the state machine, a normal state switching sequence, a state switching sequence when the transmission timeout is less than a threshold value, and a state sequence when the system fails or the sequence number is wrong are provided.

(1) *Transmission of messages under normal circumstances*. The usual sequence message transmission is k − >a−>b−>j−>g−>i−>g−>i−>⋯; that is, the program states are 11, 8, 9, 1, and 3, and it switches cyclically between state 1 and state 3. States 11, 8, and 9 are the state machine startup and initialization processes.

(2) *Temporary congestion on the network causes some messages to be lost*. In this case, some packets will be delayed or lost in the system network, and in this case, some packets may be transmitted repeatedly. At this point, the reported transport sequence is k − >a −>b−>j−>c−>e−>e−>. ⋯ −>e−>h−>i−>c−>g−>i ⋯

(3) *Network failure or message disorder*. In this case, the sequence of states corresponding to the above-mentioned switching graph is k > a − >b > j−>c−>e −>e−>⋯−>e−>f−>a−>b.

2.4. Implementation of Multiprotocol Conversion Gateway Module. The ARM9 gateway is the function of protocol conversion of the whole system. It is a service process that transforms the original data of the wireless sensor network collected by the Zigbee coordinator into TCP/IP data and transmits it to the background server. The overall workflow of the gateway is shown in Figure 6.

The three major functions of the gateway program are to obtain serial data, the boundary of the original data, and the repackaging of the data. Each function is shown in Table 3.

2.4.1. Obtain Serial Port Data. The gateway acquires raw data frames of undefined boundaries transmitted by the coordinator via crosstalk and stores them in the raw data queue, where each complete data frame is initiated by a delimiter 0xFE and the delimiter is a boundary that can be used to set the data frames. It is the thread uart_rcv_loop that gets the thread to receive the serial message. The thread execution flow chart is shown in Figure 7.

The data read from the serial is the original byte stream. The program checks the length of the data received from the sequence. If the data is complete, the data is saved to the queue. After the data is lost, the current operation is recorded in the error log. Each queue has a length. After reaching a certain length, the queue data is written as a buffer memory.

2.4.2. Data Delimitation and Encapsulation. The data boundary separates mixed data frames and discards incomplete data frames. The thread that completes this operation is package_analysis. The thread task extracts packets from the original data g_rawdata_queue, determines each packet, and reencapsulates each processed data frame into a packet in a new format, thus inserting it into the queue g_package_queue, waiting for the network thread to be sent for processing. The process diagram is shown in Figure 8.

The thread polls the original packet queue g_rawdata_queue, and if the queue is not empty, the data is fetched at the head of the queue. In the extracted queue array, the read state is set to be ready to receive the frame header, and the frame header identification 0xfe is searched at this time; after finding the frame header, the data reading state is set to prepare for receiving the frame length, and then, the frame length byte is read. The specific processing flow chart is shown in Figure 9.

The original packet queue g_rawdata_queue in the thread extracts data from the column header if the column is not empty. The data extracted at a time may include a plurality of raw packets each starting with 0xfx so that the data extracted from the queue is treated as a byte stream. In the extracted queue arrangement, the read state is first set to be ready to receive the frame header, and the frame header

Table 1: Definition and description of state in system.

Status	Abbreviation	Meaning
trans_state_t_1	1	The data transmission request is received
trans_state_t_3	3	ACK arrival
trans_state_t_5	5	The retransmitted data frame is in a timeout state
trans_state_t_8	8	The state in which the reset sequence number frame request is sent after receiving other states
trans_state_t_9	9	Reset the status of sequence frames after successful transmission
trans_state_t_11	11	Restart

Table 2: Definition and description of events in the system.

Events	Abbreviation	Meaning
trans_state_ convert_arc_t_c	c	The message was sent out of time for the first time
trans_state_ convert_arc_t_g	g	The message sent receives ACK within a given time
trans_state_ convert_arc_t_i	i	After this message is successfully sent, the next message will be sent
trans_state_ convert_arc_t_e	e	The message is sent out of time for the second time or more, but it is less than the maximum number of transmissions
trans_state_ convert_arc_t_f	f	The timeout times of message sending are greater than the maximum transmission times; request to send a reset sequence number frame
trans_state_ convert_arc_t_h	h	Receive ACK within a given time when the message is sent again after timeout
trans_state_ convert_arc_t_a	a	Sending a reset sequence frame to the coordinator
trans_state_ convert_arc_t_j	j	Start sending messages
trans_state_ convert_arc_t_k	K	State machine initialization, requiring a reset frame to be sent

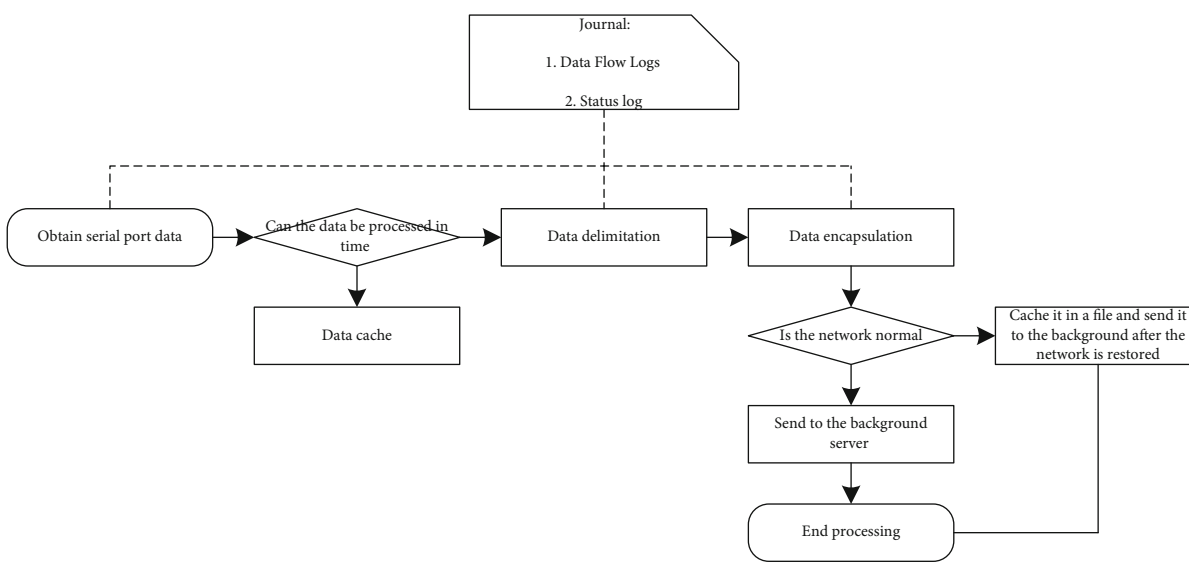

Figure 6: Business flow chart of gateway program.

identification 0xfe is sought at this time. After finding the frame header, the data reading state is set, the frame length is prepared to be received, and then, the frame length byte is read out. The frame content is read from the frame length byte. Finally, format conversion is carried out, and the conversion process is the process of data reencapsulation. The

Table 3: Function description of each thread in gateway programming.

Thread function name	Functional description
uart_rcv_loop	Processing data received from the coordinator
package_analyse	Delimitation and reencapsulation of original data packets
network_loop	Packet sending
pingtest_loop	Test the connection between the gateway and the server

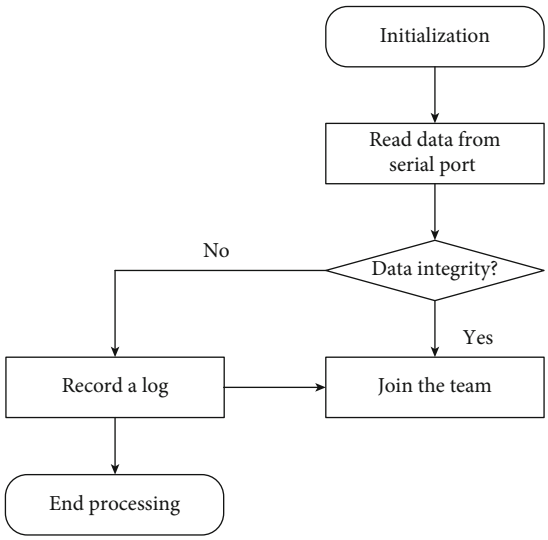

Figure 7: Flow chart of obtaining serial data thread execution.

processed new packet is inserted into the packet (g_package_queue). If the original queue is empty, the thread will go to sleep at intervals. The specific processing flow chart is shown in Figure 9.

2.4.3. Packet Sending. Packet sending sends the packet data to the background service program through the TCP/IP protocol. The thread of this process is the network_loop. A schematic diagram of the processing of this thread is shown in Figure 10 which is a flow chart of the design of a packet sending thread.

The network sending thread first creates a socket connection and sends a connection request to the server. If the request is successful, it reads the encapsulated packet queue and sends the data to the background server via the network. If this process fails, the socket is closed and the above process is reexecuted. When an error exception occurs during an operation, it is recorded in the error exception log.

2.4.4. Log Submodule. In order to improve the detection possibility of the system, the gateway module uses the log detection unit and now maintains the data flow log and the status log. By observing the data flow log, you can know the action details of the gateway. The status log is used to confirm whether the gateway is faulty in Figure 11.

2.5. File Cache Submodule. The gateway module uses two cache files in the storage of sequence data and the packaged data storage. In the gateway module, the upper limit of the queue size is set to 1024, and when the data volume exceeds 1024, it will be cached by external files. The logic of file caching is as follows:

(a) After processing the data in the queue (assuming there are N columns left blank at that time), you need to confirm the cache file and save N data at the end of the queue

(b) When new data enters the queue, the cache file is checked. If the cache file is not empty, the new data is saved directly to the cache file. If the cache file is empty, make sure the queue is full. If it is not filled, the new data is queued and filled, and the new data will be temporarily saved in the cache file

3. Design and Analysis of Probability Location Algorithm Based on DV-Hop Grid

This section will describe in detail the combined DV-Hop localization process and grid probabilistic localization algorithm execution process and, according to the specific application scenarios in this paper, improve the algorithm execution of the average hop distance and hop between nodes in the calculation method. Finally, the different factors that affect the bit accuracy of the method are analyzed.

3.1. Calculation of Average Jump Distance. In this part, the method of calculating the average hop distance between nodes by using the uniformity of nodes in the system is improved. In the current hypothesis, the number of nodes in a uniform network is the density of nodes (per square meter), the communication radius between nodes is$R$(m), and the total number of nodes in a circle has a radius$R$. The N nodes are arranged in the form of Figure 12, in which adjacent nodes of different layers represent equilateral triangles.

In the figure, there are about 19 nodes in a circle with radius R as the center, and the nodes are divided into two layers. The first layer (from inside to outside) contains 6 nodes, the second layer has 18 nodes, and generally, there are 6 m nodes in the m layer. The estimated total number of nodes n is suitable for the following equation.

$$n \leq \frac{m(6+6m)}{2}. \tag{5}$$

Equation (5) can transform the resulting equation (6) and solve the equation (6) to obtain equation (7). The value

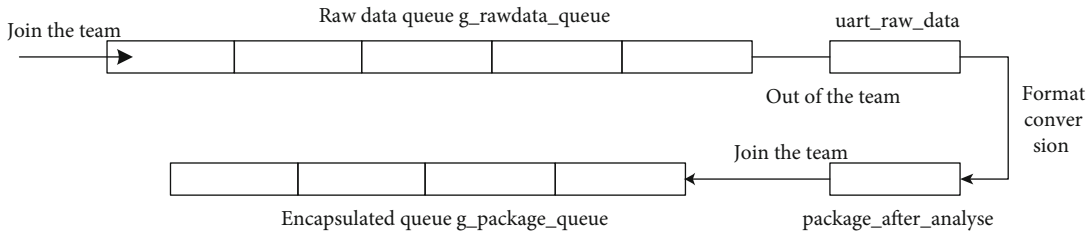

Figure 8: Schematic diagram of delimiting and encapsulating processing threads.

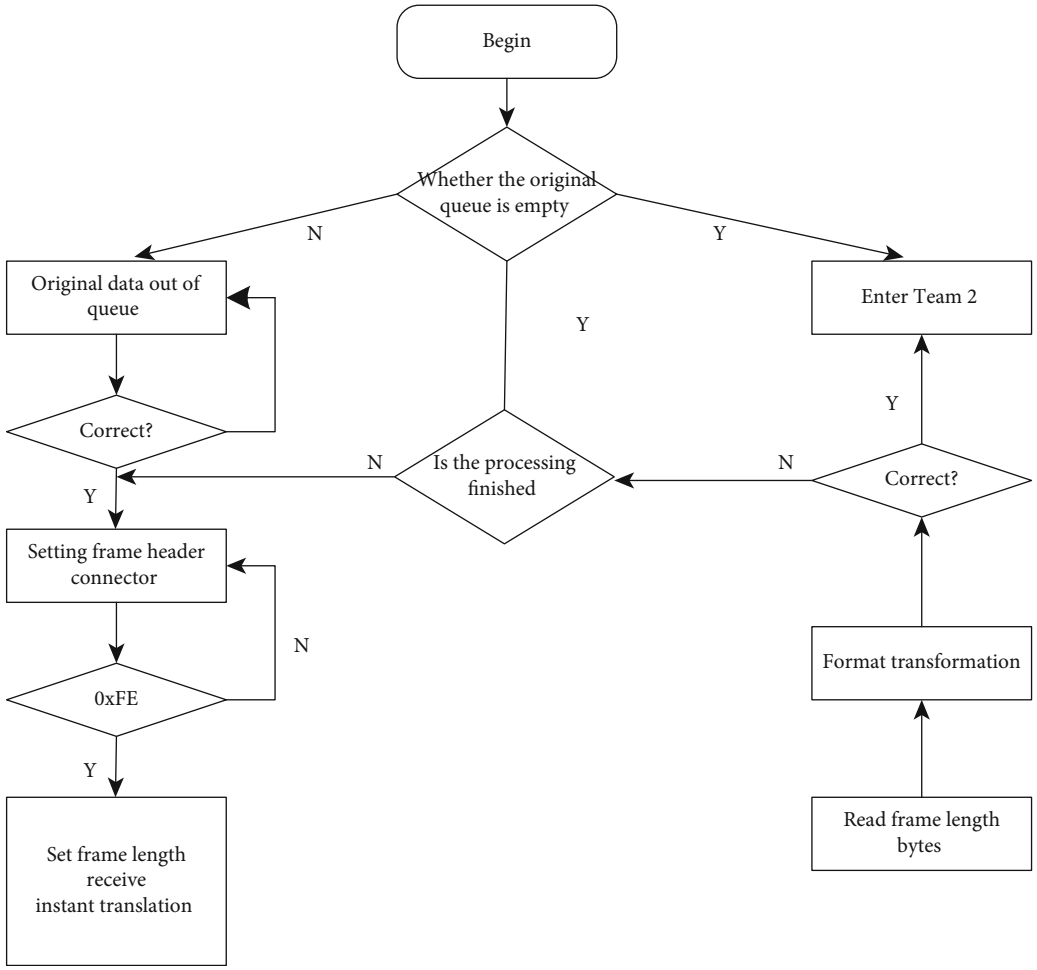

Figure 9: Flow chart of frame delimitation processing.

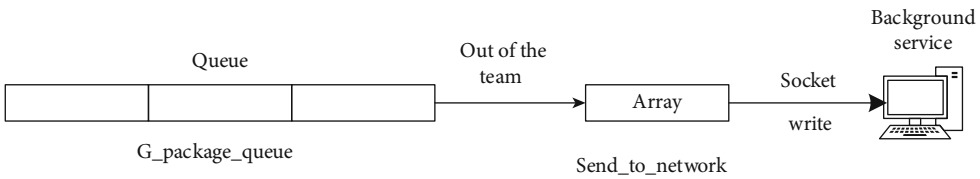

Figure 10: Schematic diagram of thread processing of network sending data packets.

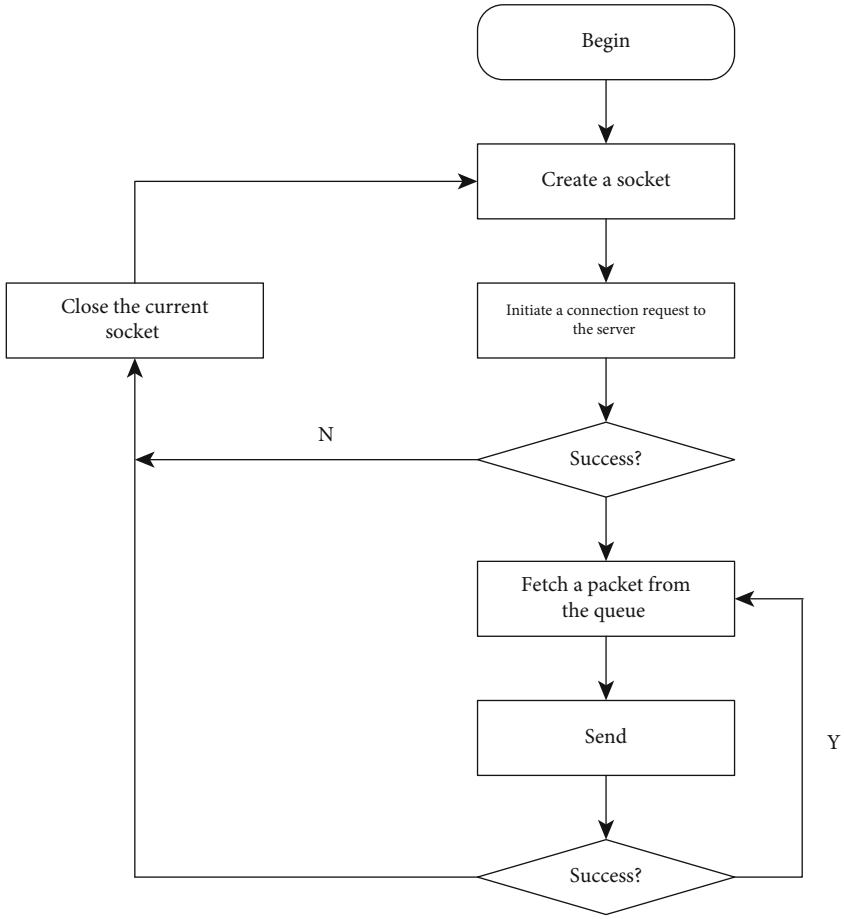

Figure 11: Network send thread design flow chart.

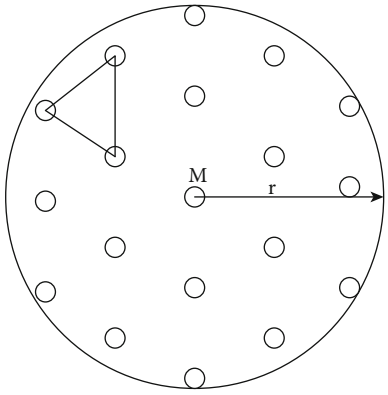

Figure 12: Node distribution diagram of single hop network.

of m is greater than 0, and the final value of m is shown in equation (7).

$$m^2 + m - \frac{n}{3} \geq 0, \tag{6}$$

$$m \geq \frac{-1 + \sqrt{1 + 4n/3}}{2} \text{or } m \leq \frac{-1 - \sqrt{1 + 4n/3}}{2}, \tag{7}$$

$$m \geq \frac{-1 + \sqrt{1 + 4n/3}}{2}. \tag{8}$$

Equation (10) can be obtained by appropriately scaling equation (8). Then, formula (9) is brought in, and the result of taking the minimum value of M to M is shown in formula (11).

$$n = \rho \pi r^2, \tag{9}$$

$$m \geq \sqrt{\frac{n}{3}} - \frac{1}{2}, \tag{10}$$

$$m \approx r\sqrt{\rho} - \frac{1}{2}. \tag{11}$$

From formula (11), it can be calculated that the circular area of n nodes is arranged in about m layers, so the distance between nodes is $H = R/M$. After expansion, it is shown in the following formula.

$$h = \frac{r}{m} \approx \frac{r}{r\sqrt{\rho} - 1/2} = \frac{2}{\sqrt{\rho} - 1/r}. \tag{12}$$

Because the value of h is greater than zero, we take $h = r$ when $\sqrt{\rho} - 1/r \leq 0$. Considering comprehensively, the

average jump distance h between nodes can be obtained as shown in the following equation.

$$h = \begin{cases} \dfrac{2}{\sqrt{\rho} - 1/r}, & \sqrt{\rho} - \dfrac{1}{r} > 0, \\ r, & \sqrt{\rho} - \dfrac{1}{r} \le 0. \end{cases} \tag{13}$$

Equation (13) is the average hop distance between nodes calculated in the ideal case of uniform arrangement of nodes.

3.2. Algorithm Design Flow. The process of mesh location determination algorithm based on the DV-Hop is similar to the DV-Hop location determination algorithm. The algorithm firstly calculates the minimum hops from each node in the network to the anchor node by broadcasting packets to the anchor node. In the location determination algorithm, each location node of course estimates that the barrier constructed by all nodes is the same [14]. The finishing execution flow of the algorithm is shown in Figure 13.

The calculation formula of parameter input is shown in the following equation.

$$\lambda = \frac{\text{Distance from grid point to anchor node}}{\text{Corrective factor}}. \tag{14}$$

λ in the above formula is the distance between grid point and anchor node in the unit of transmission hops, and the correction factor is calculated by equation (13). $p_{ij}^{h_1^k}$ is found, and $p_{ij}^{h_1^k}$ represents the probability that the unknown node k is located at the location (i, j) and reaches the anchor node through the h_1^k hop.

Formula (14) is the correction coefficient calculated theoretically, and the secondary factor needs to be further adjusted for the specific actual environment. In the next section, when the simulation experiment is carried out in the last paper, the small amplitude correction coefficient is given to obtain the best positioning effect of the system, and the ideal correction coefficient in the simulation environment is obtained under different network scales. Even in a real environment, this parameter must be adjusted to achieve the best positioning effect based on the specific network size and layout environment.

The experiment shows that the transmission hops of an unknown node and anchor node are integers, and the transmission hops have almost 0.5 error. In addition, considering that there is a certain error in obtaining the transmission hop count from the unknown node to the anchor node, the local average hop count is taken in this implementation, that is, the following equation.

$$S_i = \frac{\sum_{j \subseteq n(t)} h_j + h_i}{|n(i)| + 1} - 0.5. \tag{15}$$

$n(i)$ sends an adjacent node having a hop count of 1 from a surrounding node of the unknown node I to the node I itself. h_i and h_j are the hops of node i, node j, and anchor node, respectively. The formula calculates a local average for transmitting hops from the unknown node I to the anchor node. The hop count from the adjacent node to the anchor node is the reference information for calculating the hop count from the adjacent node to the anchor node. This calculation of hop count from unknown optimized node to anchor node is one of the improved parts based on the DV-Hop positioning algorithm. When the network scale becomes larger, the local average hop count is due to the significant differences between communication models of each part of the network, so it can further reflect the hop count from the location node to the anchor node. At this time, the hop count from the nodes around the node to the anchor node has certain reference significance for the hop count from the node itself to the anchor node.

3.3. Simulation Experiment and Result Analysis. According to the algorithm description provided in the previous section, the influence of grid size and the number of error nodes from two latitudes of the total network ratio on the algorithm error are observed. In this paper, we use formula (12) to calculate the error.

$$\text{error} = \sqrt{(x_{\text{dest}} - x_i)^2 + (y_{\text{dest}} - y_i)^2}, \tag{16}$$

where $(x_{\text{dest}}, y_{\text{dest}})$ is the location coordinates estimated by nodes located at positions (x_i, y_i).

Experiments show that the positioning accuracy of the DV-Hop-based probabilistic mesh location determination algorithm is directly related to the number of anchor nodes and the size of the network itself. Figure 14 is a diagram showing the change of positioning accuracy related to the number of anchor nodes when the network sizes are 30, 54, and 96, respectively.

It can be seen from the figure that with the increase of the number of anchoring nodes, the positioning accuracy index increases. When there are 20 anchored nodes, the accuracy of 96 nodes is only about 50%. This is because, as the network size increases, the proportion of anchored nodes decreases, affecting the correct speed.

In the experiment, the position configuration of anchor nodes is important, which directly affects the positioning accuracy. Figure 15 shows that when the anchor point is 5 and the total number of nodes is 20, the correct number of position nodes changes with the position of anchor nodes. In the figure, 50 tests indicate that the position of each locked node is randomly selected. It can be seen that the location of anchored nodes has a significant impact on the positioning accuracy of nodes.

From Figure 15, if the number of anchored nodes in the network significantly affects the error of the node positioning algorithm, and the proportion of the anchoring score increases to 30%, the error of the improved probabilistic grid positioning algorithm is as follows: it can be seen that it is about 7% of the communication distance. The location error of the DV-Hop algorithm and unimproved probabilistic grid algorithm is higher than this value.

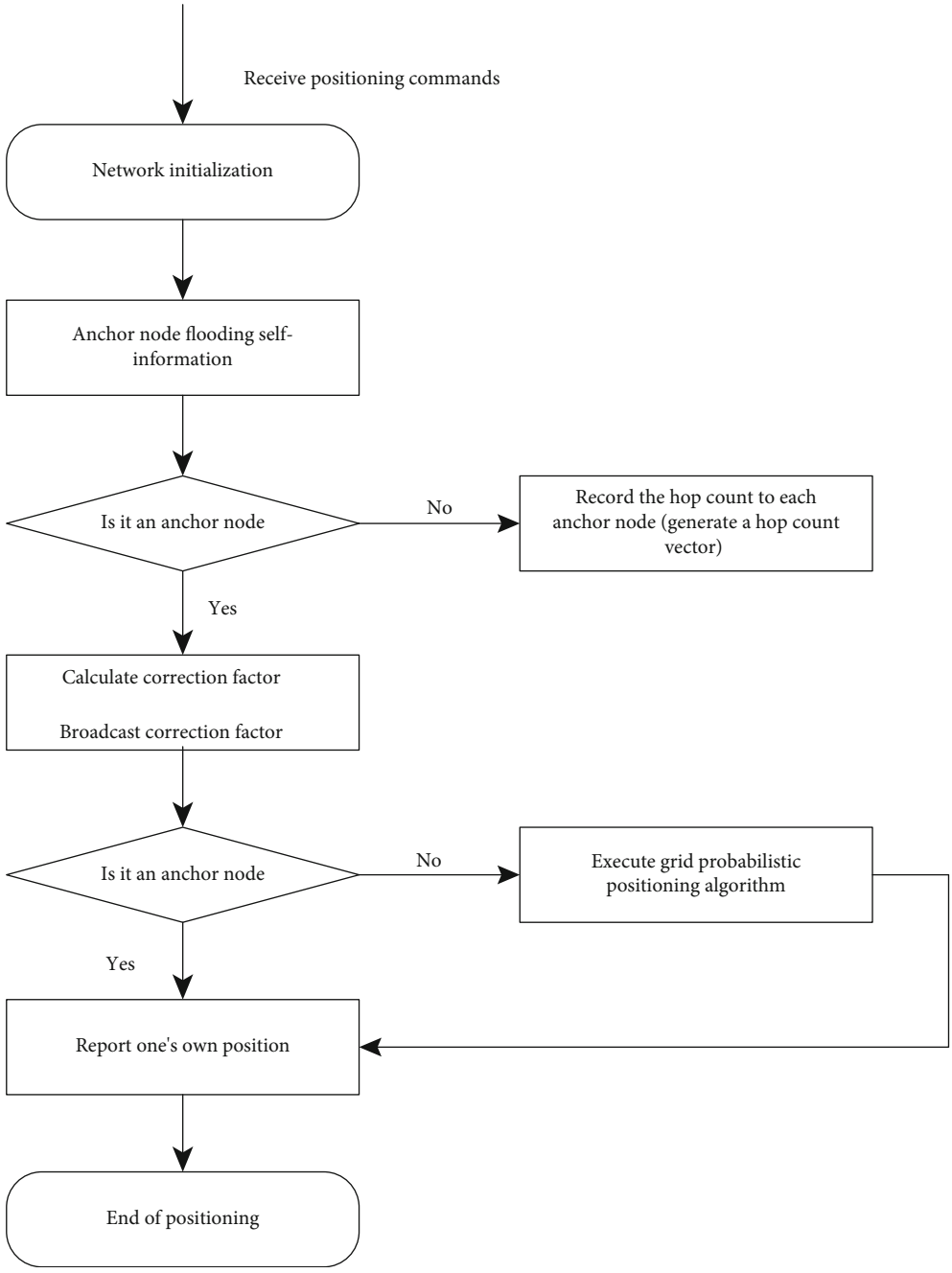

Figure 13: Flow chart of grid algorithm execution.

The selection of the correction coefficient has a significant influence on the positioning results. This paper introduces the change of the modification factor of the network scale through simulation experiment. According to the trend of the simulation curve, the correction coefficient can be dynamically adjusted according to the scale of the network in the practical application. If the ratio of anchor nodes in the network is assumed to be 10%, the curve of the optimal correction coefficient is shown here in Figure 16 according to the scale of the network expansion.

When the network size is more than 160 square meters, the configuration interval between nodes is 2 meters, and the change of correction coefficient begins to be stable.

4. Performance Test

4.1. Zigbee Network Performance Test. Figure 16 shows the operational topology of a single production line during system execution. The red node in the figure is the coordinator node, the blue node is the root node, and the yellow node is the terminal node. The whole network represents the tree structure.

During operation, the system tests the performance of the local Zigbee network of each line, and the Zigbee network is divided into a network establishment phase and a data transmission phase. It takes about 90% of the time in the process of network construction. Here, in the

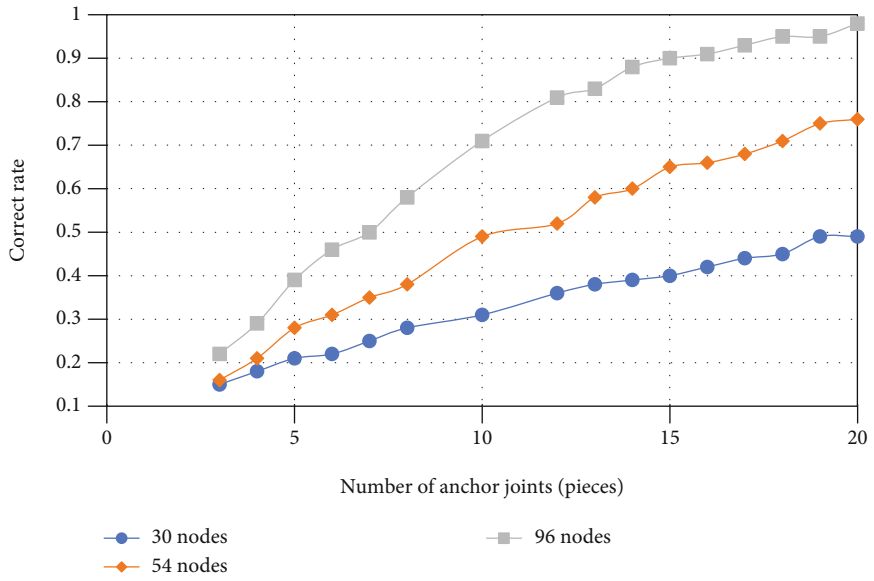

Figure 14: The change of the correct rate of positioning nodes with the number of anchor nodes.

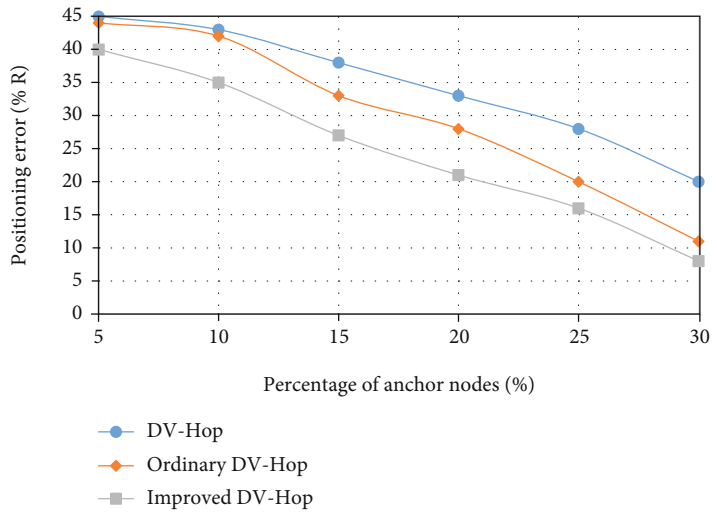

Figure 15: Influence of the proportion number of anchor nodes on positioning error.

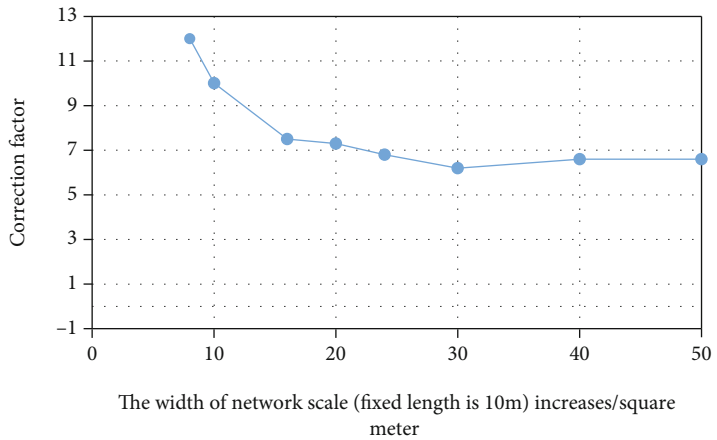

Figure 16: The curve of correction factor with the deployment scale of this network.

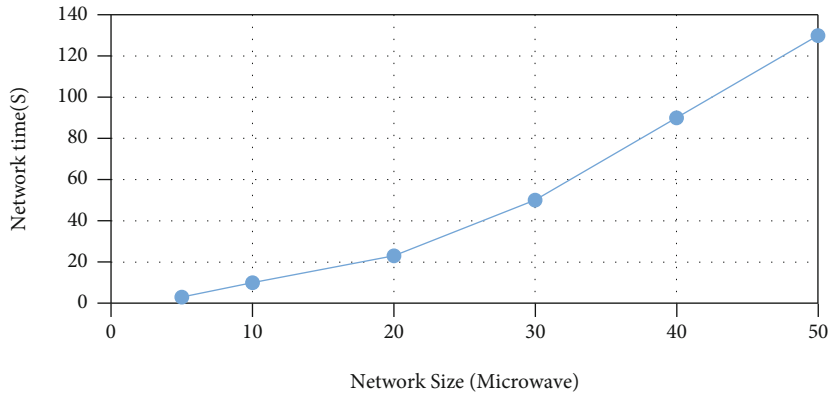

Figure 17: Relationship between the number of network nodes and the time required for networking.

Table 4: Gateway throughput test results.

Send rate (pieces/s)	Gateway output rate (pieces/s)
0.5	0.57
1	1.12
2	2.3
20	20.8
50	58
200	243

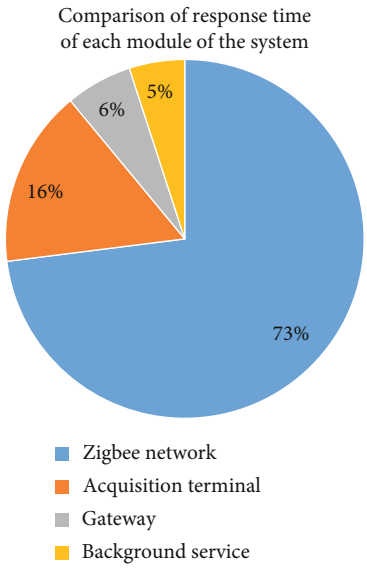

Figure 18: Response time ratio of each module of the system.

construction of the network, the time consumption of networks with different sizes is tested. The test results are shown in Figure 17.

As shown in the figure, with the increase of the network scale, the time required for network construction is getting longer and longer. If the network size is less than 80 nodes, the Zigbee network can be built within 10 seconds. If the network size is too large, the association space that coordination nodes must maintain will become larger, because it takes more time to maintain the terminal nodes in the network.

4.2. Gateway Performance Test. The throughput of the gateway is tested. It is the ability to transfer data without using cache files, that is, without losing data packets. The test results of this paper are shown in Table 4.

During the test, the input speed limit is 200 seconds. It can be seen from the table that the output speed increases linearly with the input speed, so the processing capacity of the gateway is in the crosstalk limit speed (38400 bps is used here), and the performance of the unsaturated gateway fully undertakes the transmission task of the Zigbee network. In addition, because the smaller the timer interval in the Zigbee protocol stack, the greater the error, and the greater the error for the two items at the back of the table.

4.3. Overall Response Time of Platform. The data is generated by the staff using the card from the collection terminal and then inserted into the database through the collection terminal, Zigbee network, gateway, and background server program. The whole process takes about 1.6 s. The system has made 28 measurements and obtained the average response time of each module. For example, the response time of each module is shown in Figure 18.

The Zigbee network module accounts for about 73% of the time. The coordinator needs to confirm the data sent by the terminal. This time, it is a two-way street. On the other hand, the processing power of the processors used by Zigbee coordinators and terminals is limited. When a terminal transmits a large amount of data, caching processing is needed to legally check the data. The background business processing module is equivalent to the time ratio of the gateway module. These processing tasks are similar, but the processing power of the background service is better than that of the gateway module.

4.4. Platform Performance Optimization Test

4.4.1. Data Acquisition Concurrent Stress Test. The employee's production data will eventually be inserted into the database through the wireless network. The concurrency of network transmission is not considered here. We simulated the production reports delivered to us during the

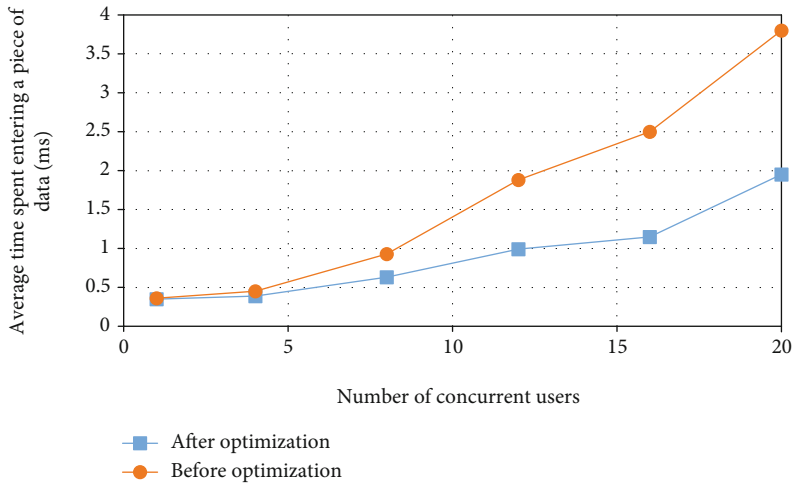

Figure 19: Data acquisition concurrent stress testing.

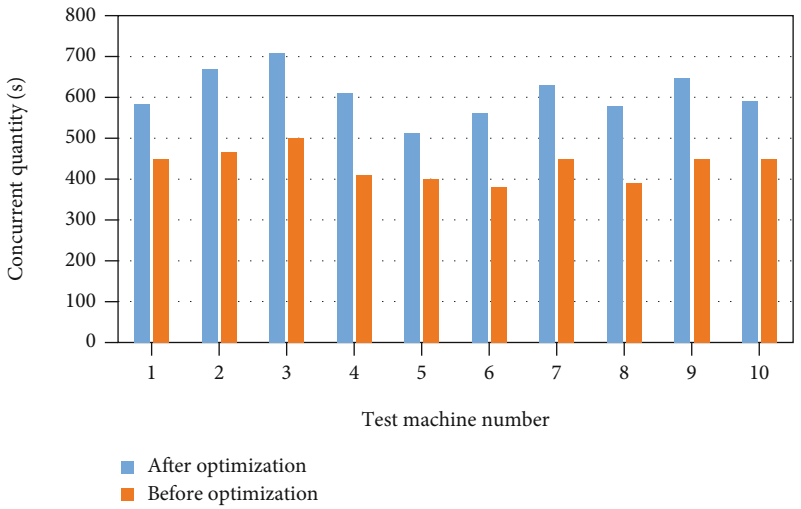

Figure 20: Concurrent stress test results of system client.

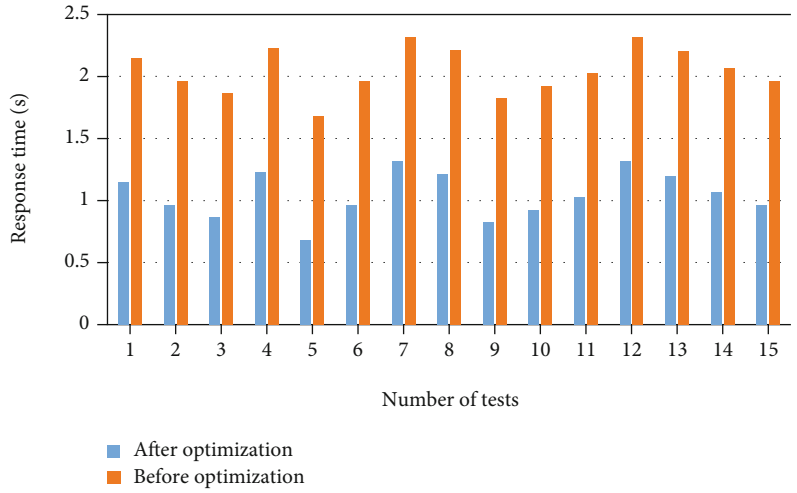

Figure 21: System page response time.

production process, increased the number of users linked to the database, and tested the average insertion time of data with different connection numbers. The following Figure 19 shows the results of data acquisition and simultaneous stress testing. When the number of simultaneous connections is 20, the average time for inserting one data after system optimization is 1.95 ms, which can meet the system requirements.

4.4.2. Concurrent Stress Test of System Client. In order to test the simultaneous user volume of the system, it is obviously impossible to install the system on hundreds of computers. In order to solve the above problems, first set the username and password of the database as regular passwords. We use the test database and can freely change the test account information. First, we modify the database with the program, so that the username and password of the test database are the same. At the same time, the program is changed, so that the system login program accepts the parameters of the command line, generates the simulated username and password for batch input, and executes the batch file to simulate the system registration and use of multiple users. In 10 computers, the simulated login and simultaneous stress test were carried out on the system client. Figure 20 shows the resulting test results. The test results show that the optimized system will be kept in the hands of more than 600 users at the same time, which can fully meet the scale requirements of client software installation and be used in large garment factories.

4.4.3. Performance Test of System Page Response Time. The paging response time of the system refers to the time from the time when the user sends out the paging request to the time when the corresponding data is obtained. The system page is the medium for the interaction between the system and the user. The paging response time of the system is the most intuitive evaluation standard for the user. The response time of the production status page was tested, and the test results shown in Figure 21 are obtained:

For the optimized system, the average response time of the production status page is 1.04 s. At the same time, the pages of different systems are tested in the same way, and the response time of each page is maintained at about 1 s. As for the paging response time of the system, there is an unwritten standard in the industry, with the principle of 2/5/10 seconds. The system with paging response time within 2 seconds is considered to bring excellent experience to users. It can bring a good user experience in 5 seconds and bad user experience in 10 seconds. The average user response time of this system is maintained at about 1 second, which can bring users a good experience.

5. Conclusion

This paper is aimed at the background of increasingly obvious advantages such as technological innovation and product manufacturing upgrade. The garment production line management system proposed in this paper is based on the garment production line, introduces Internet technology into the garment production process, and monitors every link of the garment production process through the Zigbee network. The system improves the automation degree of enterprises, greatly expands the application scope of wireless sensor networks, and promotes the application level of data acquisition, monitoring, equipment maintenance, and diagnosis in China's industrial fields. Through the Internet of Things technology, the clothing production process can be improved, production efficiency can be improved, and industrial upgrading can be realized.

Data Availability

The raw data supporting the conclusions of this article will be made available by the authors, without undue reservation.

Conflicts of Interest

The authors declared that they have no conflicts of interest regarding this work.

Acknowledgments

This work was supported in part by the Major Entrusted Project of the Zhumadian Industrial Innovation and Development Research Institute "Clothing Network Customization and Intelligent Manufacturing Training Platform Development and Application Promotion" Project No.: Huanghuai College [2020] No. 188-5.

References

[1] J. Vestin, A. Kassler, S. Laki, and G. Pongracz, "Toward in-network event detection and filtering for publish/subscribe communication using programmable data planes," *IEEE Transactions on Network and Service Management*, vol. 18, no. 1, pp. 415–428, 2021.

[2] Z. Guan, Y. Xu, H. Jiang, and G. Jiang, "International competitiveness of Chinese textile and clothing industry - a diamond model approach," *Journal of Chinese Economic and Foreign Trade Studies*, vol. 12, no. 1, pp. 2–19, 2019.

[3] X. Guan, X. Guo, L. Zhang, H. Zhao, and S. Xie, "Research on the development direction of marketing models of foreign trade enterprises in the new era," *E3S Web of Conferences*, vol. 251, article 01016, 2021.

[4] C. Gu, R. Zhou, L. Hu, and G. Gao, "A method of garment factory workers' performance monitoring using control chart based on RFID system," *The International Journal of Advanced Manufacturing Technology*, vol. 107, no. 3-4, pp. 1049–1059, 2020.

[5] X. Tang, "Research on smart logistics model based on Internet of Things technology," *IEEE Access*, vol. 8, pp. 151150–151159, 2020.

[6] O. Ayadi, N. Cheikhrouhou, and F. Masmoudi, "A decision support system assessing the trust level in supply chains based on information sharing dimensions," *Computers & Industrial Engineering*, vol. 66, no. 2, pp. 242–257, 2013.

[7] Y. Xin, D. Zhang, and G. Qiu, "Application of nanomaterials in safety intelligent clothing design," *Integrated Ferroelectrics*, vol. 216, no. 1, pp. 262–275, 2021.

[8] Y. Jin, D. Ka, S. Jang et al., "Fabrication of graphene based durable intelligent personal protective clothing for conventional and non-conventional chemical threats," *Nanomaterials*, vol. 11, no. 4, p. 940, 2021.

[9] Y. Wang and Z. Liu, "Personalized custom clothing for intelligent interaction design," in *Emerging Trends in Intelligent and Interactive Systems and Applications: Proceedings of the 5th International Conference on Intelligent, Interactive Systems and Applications (IISA2020)*, pp. 698–709, Shanghai, China, 2021.

[10] H. Liu and H. Ma, "Design of intelligent clothing selection system based on neural network," in *2019 IEEE 3rd Information Technology, Networking, Electronic and Automation Control Conference (ITNEC)*, pp. 1789–1792, Chengdu, China, 2019.

[11] X. Guo, Z. Chen, X. Hu, and X. Li, "Multi-source localization using time of arrival self-clustering method in wireless sensor networks," *IEEE Access*, vol. 7, pp. 82110–82121, 2019.

[12] Z. Xiao, W. Li, Y. Wu et al., "Preliminary study on regional technology architecture and planning of ubiquitous power internet of things part one overall architecture," *Procedia Computer Science*, vol. 175, pp. 752–757, 2020.

[13] W. Hamdy, N. Mostafa, and H. Layaway, "An intelligent warehouse management system using the internet of things," *International Journal of Engineering & Technology Sciences*, vol. 32, no. 1, pp. 59–65, 2020.

[14] N. Liu, J. S. Pan, J. Wang, and T. T. Nguyen, "An adaptation multi-group quasi-affine transformation evolutionary algorithm for global optimization and its application in node localization in wireless sensor networks," *Sensors*, vol. 19, no. 19, p. 4112, 2019.

Hindawi
Journal of Sensors
Volume 2021, Article ID 9398924, 9 pages
https://doi.org/10.1155/2021/9398924

Review Article

Application of Traction Power Supply for Metro Rail Transit Based on Electromagnetic Sensing Technology

Junxia Shang

Xi'an Railway Vocational and Technical Institute School of Electrical Engineering, Xi'an, Shaanxi 710026, China

Correspondence should be addressed to Junxia Shang; c309@wanfeng.edu.bi

Received 14 October 2021; Accepted 15 November 2021; Published 1 December 2021

Academic Editor: Gengxin Sun

With the gradual acceleration of modernization, metro projects have been opened for the development and construction of urban areas. How to ensure the smooth operation of subway project in public service has become the focus of urban public safety service research. In view of this content, this paper studies the subway field of urban rail transit operation and improves the public safety of urban rail transit operation. Firstly, the factors affecting the track traction power supply are analyzed, the anti-interference technology of ring array electromagnetic sensor is added, and the research scheme is formulated according to the track potential research standard to ensure the operation of the power supply system. Then, the electromagnetic sensor traction algorithm is used to detect the subway track power supply signal, and the working characteristics and advantages of single electromagnetic induction and double electromagnetic induction are analyzed. The experimental results show that compared with the traditional electromagnetic sensor power supply signal detection algorithm, the content of this paper can judge whether the power supply is normal according to electromagnetic induction, detect whether the subway traffic deviates from the track traction coordinates, and understand the size of the deviation from the track. It improves the efficiency of traction power supply detection, stabilizes the running track of subway traffic, and is conducive to the protection and development of urban public safety.

1. Introduction

With the rapid development of urbanization, the increase and expansion of scale are inevitable. The field of urban public security is facing many new problems and challenges [1]. How to control urban population management, improve social harmony governance scheme, innovate urban public security system, and enhance people's living standards are all problems that the country needs to face in the process of promoting urban construction [2, 3]. Among them, in the process of strengthening social governance, the field of urban public safety is a very important link [4]. Due to the combination of urban problems and security problems, the whole public link has become very complex, especially in the face of the rapid expansion of urban scale and the growth of population base [5]. At present, many provinces and cities in developed regions have made a lot of investment and energy investment in transportation hubs. With the intensive growth of population, the traffic environment is becoming more and more complex and bad. Expanding new modes of transportation is the main problem we cannot avoid. Subway track construction and development is a project content conforming to the social process. Most medium-sized cities have invested and studied subway construction projects [6].

Ensuring the stability and optimization of power supply system is an important support for subway construction and operation. In the metro power supply detection, most systems adopt relatively safe rigid catenary, which has the advantage of increasing the power supply safety in the traction process of metro rail transit. Therefore, it is vigorously applied and popularized in the field of metro power supply [7, 8]. However, in practice, the power supply link and operation technology of metro system are not very developed. A variety of environmental factors and facility factors lead to power supply contact failure, which affects the operation safety of metro rail transit and urban public safety [9]. Therefore, in addition to providing reliable contact equipment for the operation of metro system, we also need to

focus on the power supply detection mode, so as to finally improve the development of metro rail transit and urban public safety in China [10]. At present, most countries use sensor technology to support the research on the traction power supply system of metro rail transit. Common sensor technology includes multisensor technology, current sensor technology, and electromagnetic sensor technology [11, 12]. Through the understanding of the above technologies, we believe that electromagnetic sensor technology and equipment can better analyze the actual situation of rail transit power supply. The change of magnetic field is detected by electromagnetic sensor, and the interference factors and deviation of subway car body can also be detected and analyzed [13].

Based on the traction environment of metro rail transit in the field of urban public safety, this paper studies and analyzes the application of electromagnetic sensor technology in power supply detection mode. The innovative contributions include (1) the factors affecting track traction power supply are analyzed, and the anti-interference technology of ring array electromagnetic sensor is added. The error frequency in power detection is basically reduced. (2) The electromagnetic sensor traction algorithm is used to detect the subway track power supply signal, so as to improve the high sensitivity feedback efficiency and anti-interference performance under the power detection mode. (3) Further safe and effective application of electromagnetic technology to rail transit high-tech development.

This paper is mainly divided into three parts. The first part is about the development status of electromagnetic sensor technology in various countries. The second part is to use the subway track potential test to analyze whether the power supply system mode is normal and use the sensitive electromagnetic sensor to test the current noise to judge whether the power supply is normal and using electromagnetic sensor technology to improve the signal detection ability of upper position on electromagnetic track. Finally, the electromagnetic sensing measurement technology based on ring array improves the anti-interference performance of power supply system. The third part analyzes the detection results of electromagnetic sensor technology on traction power supply mode and the anti-interference performance of electromagnetic sensor to improve power supply environment.

2. Related Works

In recent years, China has made important breakthroughs in geological survey, oil resources, metal minerals, and other fields [14]. The technology of electromagnetic sensor equipment is gradually widely used, but the main production equipment of inductive electromagnetic sensors such as audio electromagnetic and transient electromagnetic are still in foreign countries [15, 16]. With the national attention, China has gradually caught up with the foreign standard level in the research and production of inductive electromagnetic sensors [17]. A series of high-tech research contents have been carried out for electromagnetic sensor technology. In the actual use environment, due to the interference of magnetic field, we will be subject to fluctuations and uncontrollable decline in accuracy when receiving the feedback effect of electromagnetic sensor [18]. This requires electromagnetic sensor technology to maintain high sensitivity and accuracy in the detection process. In the traction power supply detection mode of metro rail transit, we can use electromagnetic sensors to detect and analyze its current noise and know whether the power supply system operates normally. According to the current measurement requirements of power system, sensor magnetic array is the best way to combine electromagnetic sensor and magnetic core. It can solve the problems of space interference and environmental multifactor interference. Therefore, electromagnetic sensor technology can be widely used in various fault detection and anti-interference facilities and equipment [19, 20].

Sensor technology developed earlier. In the use of electromagnetic sensors, they are mainly aimed at the field of automation and military machinery [21]. Due to the rapid replacement of mechanical equipment, the working conditions of military aircraft and other engines are severe, which are prone to defects and wear. Researchers have improved the traditional sensor technology into electromagnetic sensor technology to detect the damage of complex structures of equipment. The wear detection is processed by the combination of electromagnetic sensor and digital locking detection [22].

Researchers collect and study the signal transmission and speed of the motor according to the electromagnetic sensor and spiral rotation signal equipment [23]. They can convert the speed signal into frequency pulse signal to realize current voltage conversion. The signal measurement and feedback based on the electromagnetic sensor is mainly used in the hull power supply control system, with the advantages of accuracy and real time.

The sensor research field is applied to the monitoring system, and the research technology also covers from infrared sensor to indoor transmission electromagnetic sensor [24]. The electromagnetic sensor can detect and analyze according to the circuit change and aging, which improves the safety guarantee of residents' life.

China's corresponding national call for scientific and technological innovation, explore energy security and strengthen technical deployment in the deep-sea field. The application of electromagnetic sensor technology in marine controllable power supply system provides a research and development basis for the exploratory process of deep sea [25]. Mainly according to the electromagnetic time-frequency acquisition principle, combined with the sensor, the acquisition performance is analyzed. Based on the above development status of electromagnetic sensor technology in various countries, this paper puts forward the research on the detection mode of traction power supply of metro rail transit. The electromagnetic sensor is used to analyze the current noise signal and test the subway track potential. Finally, the influence of interference factors of power supply system is improved. This research can improve the safety of metro rail transit and realize the control of urban public safety.

3. Research on Detection and Improvement of Traction Power Supply of Metro Rail Transit Based on Electromagnetic Sensor in the Field of Urban Public Safety

3.1. Research on Traction Power Supply Detection Mode of Metro Rail Transit Based on Electromagnetic Sensor. All electrical equipment in the power system must operate under the condition of not exceeding their allowable voltage, current, and frequency, not only in normal operation but also in accident. Therefore, the security of power system represents the ability of power system to maintain continuous power supply in case of accident in a short time, which belongs to the problem to be considered in the real-time operation of power system. Reliability refers to the probability index that the power system continuously supplies power to users for a long time, which belongs to the scope of power system planning and design. Stability refers to the state that the power system can continue to supply power to the load normally after being disturbed, that is, it has the ability to withstand disturbances. It is generally divided into power angle stability, frequency stability, and voltage stability.

The stability and reliability of power supply system are the basis for the normal operation of metro rail transit system. The analysis and detection of power supply environment are also an important link to monitor the normal operation of metro. In order to study the power supply detection mode, the electromagnetic sensor needs to have high sensitivity and real-time reliability. Firstly, the inductive electromagnetic sensor is used to test and analyze the current noise, mainly from the bottom noise and sensitivity performance, combined with the actual comparison to test whether the electromagnetic sensor can meet the requirements of metro track traction power supply detection task. In this paper, the electromagnetic sensor is designed by coil induction. The basic components include high conduction magnetic core, multi-induction coil group, calibration coil, and current bottom noise amplifier. At present, the current noise analysis of electromagnetic sensor is usually based on the sensor design principle and the numerical simulation of induction coil noise, so as to obtain the noise index and analyze whether the power supply link is normal. However, this method cannot represent the bottom noise of the whole sensor, the actual noise index is small, and cannot make accurate judgment. Therefore, this paper improves the original sensor to be a highly sensitive inductive electromagnetic sensor, and its bottom noise has a uniform power spectrum in sound domain and frequency domain. In order to study the influence of current white noise signal operation on noise, the mean variance is used for signal power detection, respectively. The signal and power spectrum are shown in Figure 1.

It can be seen from Figure 1 that the influence of signal value, energy, and power value is very high, so we need to carry out differential operation and summation. The calculation formula is as follows:

$$\begin{aligned} \mathrm{sub}_{(t)} &= f_{1(t)} - f_{2(t)}, \\ \mathrm{add}_{(t)} &= f_{1(t)} + f_{2(t)}. \end{aligned} \tag{1}$$

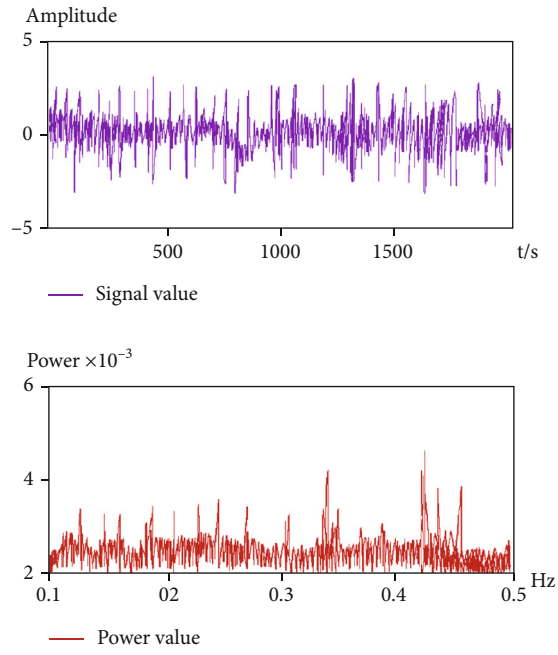

Figure 1: Signal and power spectrum.

$f_{1(t)}$ and $f_{2(t)}$ form the contrast variables of signal values, respectively. After difference operation and summation, the energy value also changes accordingly. In order to get the influence of interference analog signal on noise signal, we need to add sinusoidal signal for differential sum operation. The signal and power spectrum after adding sinusoidal signal are shown in Figure 2.

As can be seen from Figure 2, the same signal value can be offset by using the signal difference technology. The signal value after differential calculation is equal to the sum of the previous signal values. If the electromagnetic sensor with equal frequency characteristics is adopted, the interference of environmental factors can be solved by differential technology, so as to obtain the bottom noise of power supply current. In this paper, the synchronous test is carried out from the same track position, and the actual mapping data and prediction data of the electromagnetic sensor probe are obtained through data acquisition and processing, as shown in Figure 3.

As can be seen from Figure 3, the power efficiency of the electromagnetic sensor before differential calculation is between 0.0005 and 100 Hz, and the range is relatively stable. The actual measured data can basically agree with the predicted data. The difference signal also decreases obviously in this frequency band, which shows that this method can be applied to the bottom noise acquisition process of electromagnetic sensor. Before the electromagnetic sensor traction algorithm, it is necessary to analyze the current noise detection combined with the track potential. DC traction mechanism is the main mode of metro track power supply. The traction mechanism converts electric energy into power supply basis and supplies power through feeder grid. The current generally flows back to the power supply station through the rail to form a completed current loop. Due to

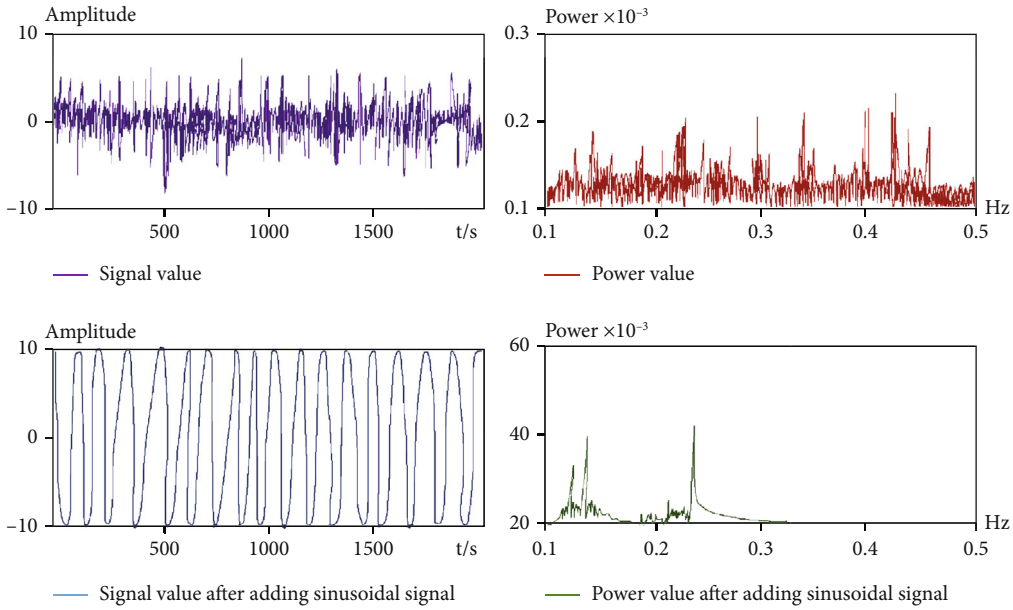

Figure 2: Signal and power spectrum after adding sinusoidal signal.

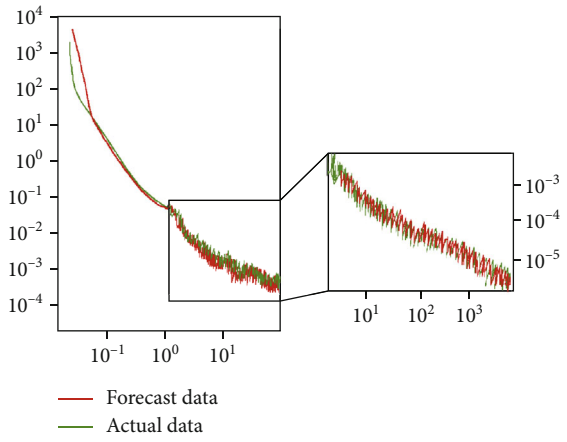

Figure 3: Comparison between actual mapping data and predicted data of electromagnetic sensor probe.

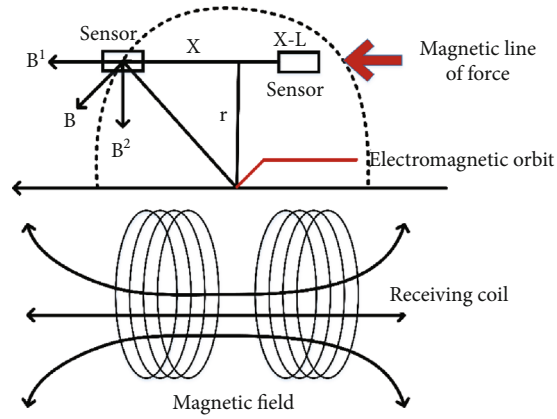

Figure 4: Internal setting of electromagnetic sensor.

the mixing of miscellaneous electricity, if there is a problem with the power supply mode, we cannot know according to the potential difference, so it will lead to instability such as potential frequency modulation. In urban public safety, if passengers cannot detect whether the power supply mode is normal when taking the subway, there will be step voltage and other personal hazards. The factors affecting the subway track potential include the maximum voltage during traffic operation and the leakage of stray current. The most frequent problem of power supply mode is in the return structure area. Based on the above situation, we need to use electromagnetic sensor magnetic field response to obtain the operation of power supply mode. First, learn about the setting of electromagnetic sensor, as shown in Figure 4.

As can be seen from Figure 4, since the electromagnetic track is close to the ground, the corresponding height is set to establish the coordinate axis. The sensor coil should be in a vertical parallel position. If the subway rail transit supplies power normally, the corresponding magnetic field will be generated and the induced electromotive force will be generated. We can obtain whether the traction power supply of metro rail transit is normal according to the reflection of magnetic field. The relationship between coil induction and coordinates is as follows:

$$E = C\frac{h}{x^2 + h^2}. \tag{2}$$

In the formula, C is the standard coefficient, that is, the induced electromotive force.

When the electromagnetic induction scheme is established, we can advance from single induction distribution to double inductance mode. Judge the position and operation of the subway car according to the change of the two inductances. The difference of electromotive force between

two inductors is

$$\Delta E = \frac{h}{x^2 + h^2} - \frac{h}{(x-L)^2 + h^2}. \quad (3)$$

The offset calculation formula of inductance electromotive force difference control is as follows:

$$e = \frac{\left(\left(h/\left(x^2 + h^2\right)\right) - \left(h/\left((x-L)^2 + h^2\right)\right)\right)}{\left(\left(h/\left(x^2 + h^2\right)\right) + \left(h/\left((x-L)^2 + h^2\right)\right)\right)}. \quad (4)$$

According to the above formula, we can get the induced electromotive force function diagram and its difference and sum value comparison diagram, as shown in Figure 5.

As can be seen from Figure 5, the difference can be realized that the center of the double inductor is located in the center and presents a monotonic function. This disadvantage is that the interval size is limited. If the vehicle track operation section changes sharply, it is likely to form error data. Therefore, the sum value calculation is carried out to solve it. The sum value image shows that this interval is almost a linear monotone interval, which can eliminate the signal processing error. According to the above research, we can use electromagnetic sensors for current detection and power supply potential judgment in the traction power supply detection of metro rail transit. It adds reliability guarantee for subway traffic safety in urban public safety.

3.2. Research on Improving Interference Detection of Traction Power Supply of Metro Rail Transit Based on Ring Array Electromagnetic Sensor. Facing the demand of traction power supply detection of metro rail transit, electromagnetic sensor array can solve the problem of spatial interference energy. With the reduction of research cost of sensors such as tunnel magnetoresistance (TMR), it is possible to form a variety of arrays. Compared with the traditional sensor equipment, the ring electromagnetic sensor array can have a centerless structure and there is no saturation problem. It greatly improves the performance of the whole power supply measurement process and can also be applied to power supply detection and protection equipment. The basic way of ring array detection is to use multiple TMR sensors to measure the change of magnetic field according to the ampere current path law. A closed current loop is added near the electromagnetic sensor to effectively resist interference and noise, so as to increase the accuracy of power supply detection.

According to the distance between the TMR sensor and the current carrier, the magnetic field range is sensed, so as to calculate whether the measured current is normal. Assuming that the conductor passes through the center of the ring array through a primary current and is vertical, the output signal of each single electromagnetic sensor is expressed as

$$V_{\text{tmr}} = K_s\left(H \cdot \hat{s}\right) = k_s \frac{I \times r}{2\pi r^2} \cdot \hat{s}. \quad (5)$$

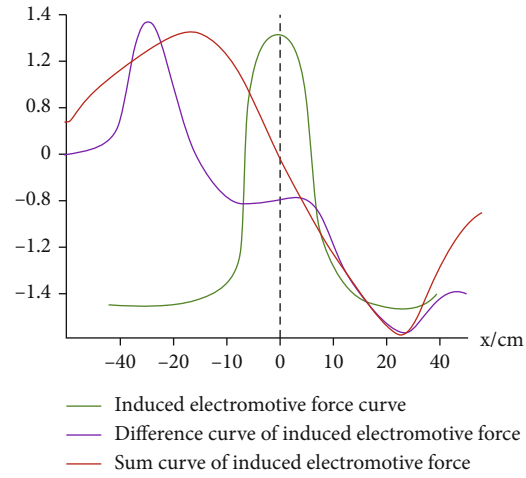

Figure 5: Induced electromotive force function diagram and its difference, sum value comparison diagram.

In the formula, K_s represents the sensitivity of the sensor after calibration, H is the magnetic field intensity variable generated by the carrier, and I is the measured current variable. The average output value of multiple sensors in the array is calculated as follows:

$$V_{\text{mean}} = \frac{1}{N}\sum_{n=1}^{N} V_{\text{tmr}}^{(n)}. \quad (6)$$

N in the formula is the total number of sensors. If the carrier does not pass through the center of the ring array, the output value will have different ranges. The measured current value can be calculated according to the sensitivity:

$$I_{\text{cal}} = \frac{2\pi r V_{\text{mean}}}{k_s}. \quad (7)$$

In the ring TMR array, the measurement error needs to be calculated, and the interference factor is the adjacent conductor magnetic field. Set the current variable and center distance in 3D coordinates. Define the angle between the variable and the x-axis, that is, the position of the first electromagnetic sensor. The corresponding variable expression is

$$a^{(n)} = \frac{2\pi n}{N} + a_0 (n = 0, 1, \cdots, N-1). \quad (8)$$

The distance relationship between the sensor and the measured current can be obtained from the basic principle of the ring array, that is,

$$V_{\text{mean}} = \frac{K_s}{2\pi}\left(\frac{I_0}{r_0} + \frac{I_1}{N}\right)\sum_{n=1}^{N} \frac{r_0 - d_{\text{cross}} \cos a^{(n)}}{r^2 + d_{\text{cross}}^2 - 2 r_0 d_{\text{cross}} \cos a^{(n)}}. \quad (9)$$

Then, calculate the measurement error caused by

interference:

$$\varepsilon_{\text{cross}} = \frac{I_{\text{cal,cross}} - I_0}{I_0} = \frac{I_1}{I_0}\Delta_{\text{cross}}, \tag{10}$$

$$\Delta_{\text{cross}} = \frac{r_0}{N} = \sum_{n=0}^{N-1} \frac{r_0 - d_{\text{cross}} \cos a^{(n)}}{r_0^2 + d_{\text{cross}}^2 - 2r_0 d_{\text{cross}} \cos a^{(n)}}. \tag{11}$$

$\varepsilon_{\text{cross}}$ is the measurement error. It can be known from formulae (10) and (11) that the error is the ratio of the interference current to the measured current. The spatial distance between two currents determines the ratio range. It can also be proved that after the initial array is determined, the error value can decrease with the increase of the number of TMRs, then

$$\lim_{N \longrightarrow +\infty} \Delta = 0 (r_0 < d_{\text{cross}}). \tag{12}$$

When the number of TMRs increases, the output of the ring array is closer and closer to the Abe loop principle. That is, the calculation along any path in the magnetic induction intensity is equal to the algebraic sum in the current path multiplied by the permeability. The relationship between the error value and the number of electromagnetic sensors and interference distance is shown in Figure 6.

As can be seen from Figure 6, in order to show the relative relationship between distance and current, it is assumed that there is interference. Most interference currents are the same, and the number of sensors changes from 1.5 to 6. It can be seen that the maximum measurement error occurs when the distance is between 16 and 20. With the increase of distance, the measurement error decreases exponentially and approaches 0. In the carrier measurement error, we also need to consider the eccentricity error of electromagnetic sensor in the influence of noninterference and geomagnetism. The influence of eccentricity error on annular TMR array is shown in Figure 7.

As can be seen from Figure 7, the intersection of the carrier and the annular array is no longer on the center of the circle, a variable d_{unc} is defined as the center offset variable, and the distance between the intersection and the electromagnetic sensor is calculated. The distance of each sensor is different due to the eccentricity of the carrier. Calculate the output current of the ring array, the distance from the carrier to the sensor, and the direction of the sensitive axis according to the Biot-Savart formula:

$$V_{\text{mean,unc}} = \frac{k_s I_{\text{cal}}}{2\pi r_0} = \frac{1}{N} \sum_{n-1}^{N} V^{(n)}. \tag{13}$$

Finally, the relative measured value of offset error is derived according to the above formula:

$$\varepsilon_{\text{unc}} = \frac{I_{\text{cal,unc}} - I_0}{I_0} = \Delta_{\text{unc}} - 1. \tag{14}$$

Through calculation, we can know that when multiple

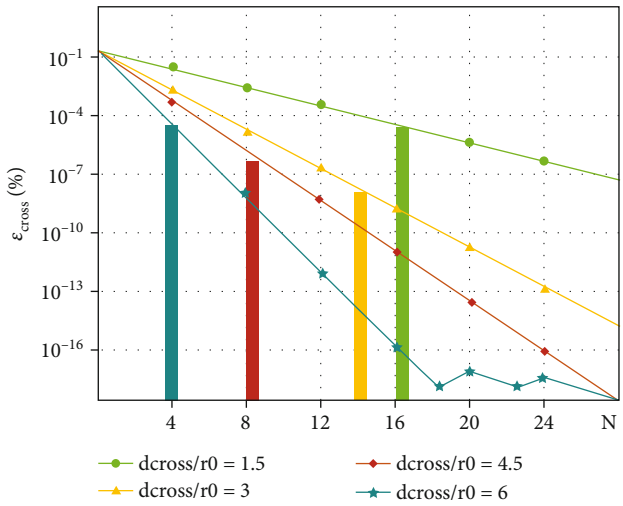

Figure 6: Relationship between error value and number of electromagnetic sensors and interference distance.

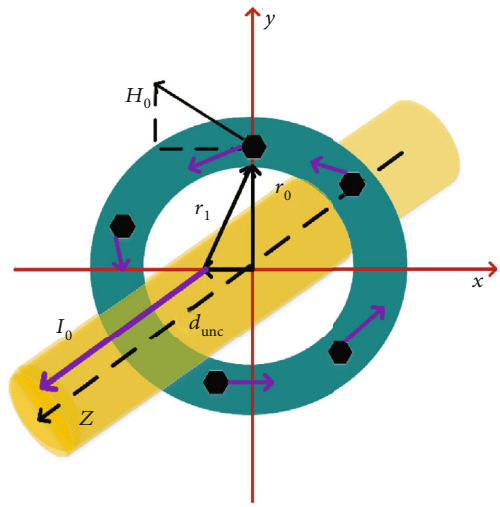

Figure 7: Influence of eccentricity error on annular TMR array.

TMR sensors are used, the maximum error caused by eccentricity is uncontrollable. This situation will lead to serious measurement failure. However, with the increase of the number of sensors, the error decreases exponentially. Therefore, in the detection process of traction power supply of metro rail transit, we can apply electromagnetic sensors to optimize the measurement error and anti-interference application. The annular array of electromagnetic sensors has excellent compensation ability for error offset, improves the accuracy of actual measurement, and gives the offset range.

4. Analysis of Research Results of Metro Rail Transit Traction Power Supply Detection and Improvement in the Field of Urban Public Safety Based on Electromagnetic Sensor

4.1. Analysis of Research Results of Traction Power Supply Detection Mode of Metro Rail Transit Based on

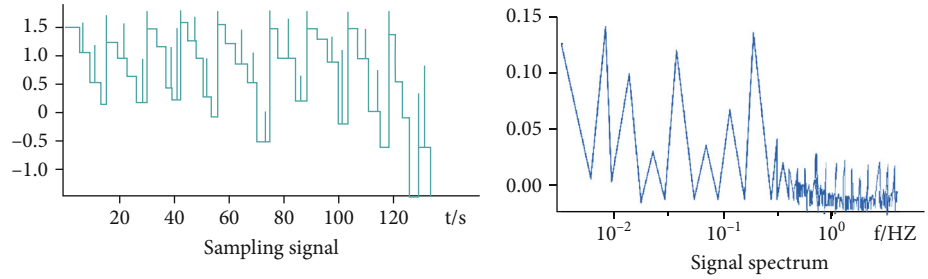

(a) Sampling signal (b) Signal spectrum

Figure 8: Sensitivity feedback curve after adding modulated square wave signal.

Electromagnetic Sensor. Firstly, the sensitivity of the induction effect of the electromagnetic sensor is tested. The ratio of the induced voltage to the magnetic field strength and frequency changes with the change of the magnetic field strength. In the high-frequency stage, the effective area of the magnetic core becomes smaller, which reduces the control of the electromagnetic sensor on the sensitivity of the power supply mode. Therefore, in this paper, the excitation coil is used to generate the corresponding magnetic field to realize the production of magnetic field strength within the limited power range. A modulated square wave signal is added to the excitation coil, and the frequency signal is collected at an interval of 0.1 seconds. The sensitivity feedback curve in the power supply system can be obtained by measuring the current output signal corresponding to the sensor, as shown in Figure 8.

As can be seen from Figure 8, when the magnetic field strength is weak and the frequency is low, the corresponding induced voltage is also low. The number of acquisition points generated in the interval seconds of the modulation frequency signal is larger and larger, and the feedback frequency is more and more dense. Experiments show that the electromagnetic sensor has high induction sensitivity in power supply detection mode. It can effectively detect the current direction and whether the output voltage is normal. We use the area with a length of 1.132 km from Hongshan station to Nanjing station for power supply detection. The actual test results are shown in Figure 9.

As can be seen from Figure 9, as the subway depth decreases, the section track resistance is also different. We represent the resistance change in different colors to obtain the current voltage and current. The closer the color to red, the higher the resistance. It can be seen that the power supply is in normal state and the resistance change is basically stable. The high sensitive feedback efficiency of electromagnetic sensor is also reflected in the actual detection, which provides a guarantee for urban public transport safety.

4.2. Analysis of Research Results on Improving the Detection Interference of Metro Rail Transit Traction Power Supply Based on Ring Array Electromagnetic Sensors. Based on the ring TMR array prototype, this paper adopts the full bridge structure design, including high-sensitivity sensing unit. In order to verify the performance of annular array electromagnetic sensor, we designed an error test system. When the carrier passes through the sensor array, connect the current power supply and DC power supply. The current mode is regulated by a selector switch. We take the collected high-precision resistance as the reference of the measured data. Control the eccentricity of the ring array and compare the actual value and theoretical value of the anti-interference error value, as shown in Figure 10.

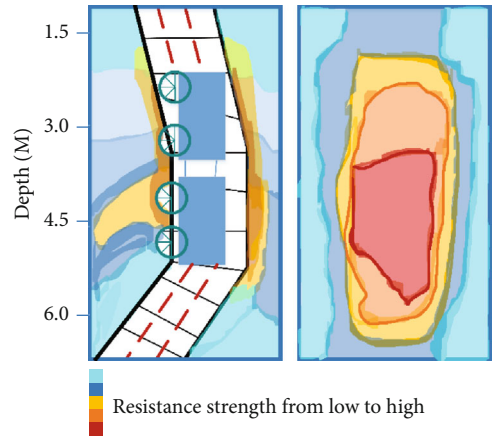

Figure 9: Diagram of metro car body current surround and power supply detection results.

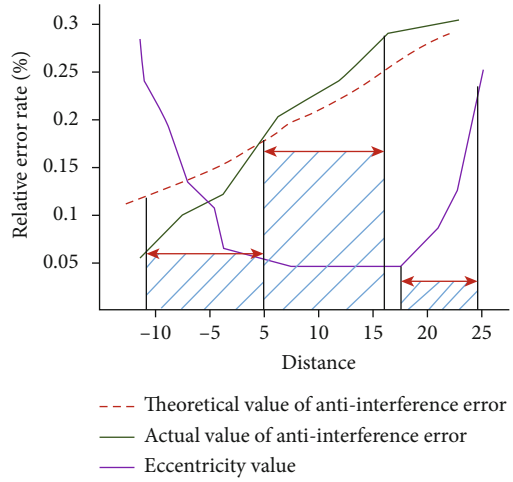

Figure 10: Comparison diagram of eccentricity value, anti-interference actual value, and theoretical value.

As can be seen from Figure 10, the current output is controlled at the same variable, and the distance change of the sensing conductor is adjusted for sampling. It can be seen that the actual test value of the experimental error value is almost the same as the theoretical value, which basically achieves the experimental purpose. It can effectively improve the interference in power supply detection in metro rail transit traction and increase the accuracy and sensitivity of power supply detection mode. In the field of urban public safety, metro rail transit has always been a content that cannot be ignored. If we can effectively improve subway traffic safety, we can further ensure urban public safety.

To sum up, this paper optimizes and improves the interference in the detection of metro traction power supply according to the ring array electromagnetic sensor technology. The error frequency in power detection is basically reduced, improving high sensitivity feedback efficiency and anti-interference performance in power detection mode. The above research results show that electromagnetic sensor technology can improve the safety of metro rail transit and ensure the timeliness and effectiveness of power supply detection. The study meets the needs of urban public safety and should be vigorously carried out and supported.

5. Conclusion

In the process of urbanization, with the growth of population base, the problem of public security is gradually revealed. Facing the complex social environment, how to safely and effectively apply high-tech development has always been an inevitable research content in people's life. Based on the traction environment of metro rail transit in the field of urban public safety, this paper studies and analyzes the application of electromagnetic sensor technology in power supply detection mode. Firstly, the functional gap between electromagnetic sensor and ordinary sensor is analyzed, and the appropriate research direction is found through the development status of various countries. Then, the electromagnetic sensor is mainly used to analyze the power supply mode of current noise detection and judge whether there is voltage fault through the change of potential difference. Analyze whether the power supply mode is normal according to the change of magnetic field and induced electromotive force, and effectively judge the vehicle body section where the fault occurs. Test the sensitivity of the electromagnetic sensor to prove whether it meets the power supply detection requirements. Finally, according to the ring array electromagnetic sensor technology, the interference in the traction power supply detection of metro rail transit is optimized and improved. Basically reduce the error frequency in power supply detection. Improve the high sensitivity feedback efficiency and anti-interference performance in power supply detection mode. The above research results show that electromagnetic sensor technology can improve the safety of metro rail transit and ensure the timeliness and effectiveness of power supply detection. The study meets the needs of urban public safety, so it should be vigorously developed and supported.

Although intelligent electromagnetic flow sensor has many advantages and is widely used in various fields of industrial production, it also has some shortcomings so that it is limited in use. Electromagnetic flow sensor cannot be used to measure gas, vapor, and liquid containing a large amount of gas. This has caused some obstacles in rail transit. Because the insulating lining material of the measuring pipe is limited by temperature, the industrial intelligent electromagnetic flow sensor cannot measure high-temperature and high-pressure fluid. In addition, it is also vulnerable to external electromagnetic interference. Therefore, in the future research, the research will continue to focus on the above problems.

Data Availability

The data used to support the findings of this study are included within the article.

Conflicts of Interest

The author declares that there are no conflicts of interest.

References

[1] Y. Guijuan and X. Huaizu, "Research on public safety management of urban rail transit from the perspective of situational prevention," *Urban fast rail transit*, vol. 34, no. 4, pp. 154–159, 2021.

[2] W. Rupeng, L. Yi, and H. Yaping, "Research on public safety emergency management from the perspective of smart city – taking a provincial capital city as an example," *Urban housing*, vol. 28, no. 7, pp. 238-239, 2021.

[3] Q. Sheng, J. Jiao, and T. Pang, "Understanding the impact of street patterns on pedestrian distribution: a case study in Tianjin, China," *Urban rail transit*, vol. 7, no. 3, pp. 209–225, 2021.

[4] H. Russell, "Sustainable Urban Governance Networks: Data-driven Planning Technologies and Smart City Software Systems [J]," *Geopolitics, History, and International Relations*, vol. 12, no. 2, pp. 9–15, 2020.

[5] C. Ye, "Research on the construction of urban public security system from the perspective of modernization," *Legal system and society*, vol. 14, pp. 96–98, 2021.

[6] X. Ming, L. Chuanjie, and W. Qi, "Research on key technologies of structured extraction of multi-source heterogeneous data for public security," *Digital communication world*, vol. 5, 2021.

[7] Z. Jingfeng, L. Qiong, L. Lei, M. Yunjie, and Y. Chao, "Research on evaluation system and method of urban public safety video surveillance system," *China security technology and application*, vol. 2, pp. 40–45, 2021.

[8] L. Weiyong, "Research on optimization of public safety and emergency management capacity of mountainous cities," *The Economist*, vol. 4, pp. 11–13, 2021.

[9] Z. Li, X. Jiang, P. Yin et al., "Towards self-powered technique in underwater robots via a high-efficiency electromagnetic transducer with circularly abrupt magnetic flux density change," *Applied Energy*, vol. 302, 2021.

[10] N. P. Aleshin, N. V. Krysko, A. G. Kusyy, S. V. Skrynnikov, and L. Y. Mogilner, "Investigating the detectability of surface volumetric defects in ultrasonic testing with the use of Rayleigh

waves generated by an electromagnetic-acoustic transducer," *Russian Journal of Nondestructive Testing*, vol. 57, no. 5, pp. 361–368, 2021.

[11] S. Peng, "Application of speed measurement device based on electromagnetic sensor in marine DC motor control system," *Marine power technology*, vol. 41, no. 5, pp. 10–12, 2021.

[12] L. Wang, Z. Tao, P. Zhenhua, L. Yi, M. Lianxun, and Z. Zidong, "Design and simulation of sensor based on transient field excitation," *Electronic measurement technology*, vol. 44, no. 5, pp. 171–175, 2021.

[13] J. Changcheng, "Inductance value processing scheme of intelligent vehicle based on electromagnetic sensor," *Automobile maintenance technician*, vol. 3, 2021.

[14] G. Song, D. Jin Xin, and L. Q. Xinwu, "Study on the influence of electrode roughness of electromagnetic flowmeter on measurement results," *Industrial instrument and automation device*, vol. 6, pp. 117–120, 2020.

[15] L. Hua, X. Yubao, W. Xin, W. Yao, W. Zhijun, and C. Changyong, "Design of camera and electromagnetic navigation intelligent vehicle and research on dual vehicle control," *Journal of Jiamusi University (Natural Science Edition)*, vol. 38, no. 4, pp. 90–94, 2020.

[16] B. Jian, C. Weisong, H. Libin, and H. Mengting, "Design and implementation of indoor patrol robot system based on electromagnetic navigation," *Electronic world*, vol. 7, pp. 110-111, 2020.

[17] Z. Bo, L. Bo, Z. Junbo, H. Xinyu, L. Meiyun, and S. Qingwen, "Research on grounding fault detection method of AC auxiliary power supply system of EMU," *Railway vehicles*, vol. 59, no. 3, pp. 40–45, 2021.

[18] L. Hu, C. Xiang, S. Li, and C. Jie, "Cause analysis and solution of false alarm in leakage current detection of train power supply system," *Electric locomotive and urban rail vehicle*, vol. 44, no. 3, pp. 60–63, 2021.

[19] S. Tianyu, "Short circuit current detection method for rail transit DC traction power supply system," *Machinery and electronics*, vol. 39, no. 3, 2021.

[20] W. Weifan, L. Yanlong, Y. Zhipeng, Z. Wenxuan, S. Liang, and H. Luping, "Study on inspection and evaluation method of power supply safety detection and monitoring system of high-speed railway," *Electrified railway*, vol. 31, no. S2, pp. 81–86, 2020.

[21] Z. Baoqi and L. Fangzhong, "Discussion on 1C detection and data analysis and application of power supply detection and monitoring system," *Electrified railway*, vol. 31, no. S2, 2020.

[22] F. Hui and L. Jinjian, "Analysis of common faults and detection technology of marine power supply cable," *Communication power technology*, vol. 37, no. 8, pp. 51–53, 2020.

[23] Q. Kaiqing, "Comparative analysis of domestic and foreign applications of railway traction power supply related technologies," *Electrified railway*, vol. 30, no. S1, pp. 1–4, 2019.

[24] Z. Keyong, "Analysis and research on the construction of power supply safety detection and monitoring system for high-speed railway," *Electrified railway*, vol. 30, no. 6, 2019.

[25] Q. Wang, S. Lin, T. Li, and Z. He, "Intelligent proactive maintenance system for high-speed railway traction power supply system," *IEEE Transactions on Industrial Informatics*, vol. 16, no. 11, pp. 6729–6739, 2020.

Hindawi
Journal of Sensors
Volume 2021, Article ID 3006397, 13 pages
https://doi.org/10.1155/2021/3006397

Research Article

Research on the Advantages of Digital Sensor Equipment in Language Audio-Visual and Oral Teaching

Wu Yufei,[1] **Wang Dandan**,[1] **and Zhu Yanwei**[2]

[1]*School of Foreign Studies, Tangshan Normal University, Tangshan 063000, China*
[2]*School of Mathematics and Computational Sciences, Tangshan Normal University, Tangshan 063000, China*

Correspondence should be addressed to Wu Yufei; 160409128@stu.cuz.edu.cn

Received 8 September 2021; Accepted 18 October 2021; Published 30 November 2021

Academic Editor: Gengxin Sun

Digital sensors use biotechnology and information processing technology to strengthen the processing of relevant visual and auditory information, which is helpful to ensure that the receiver can obtain more accurate information, so as to improve the learning effect and reduce the impact on the environment. This paper designs an experiment to explore the role of digital sensors in language audio-visual teaching, which provides a reference for the application of digital sensors in the future. The impulse response function in sensor technology is introduced. The speech time domain envelope and time-varying mouth area of the sensor device are calculated. The auditory attention transfer detection based on line of sight rotation estimation is carried out through the auditory attention decoding fusion technology and the sensor auditory attention conversion detection method. At the same time, the characteristic of sensor heog signal is analyzed. The results show that the algorithm proposed in this paper has good results.

1. Introduction

With the development of society, the research on image processing, pattern recognition, image and video compression, biometric recognition and information security, three-dimensional visual information processing, and intelligent human-computer interaction in the field of machine vision is gradually increasing. Visual auditory processing is widely used in the field of machine hearing. Machine auditory computing model and speech language information processing system are widely used. Many scholars have carried out artificial neural network and machine learning and carried out computational intelligence research in the field of intelligent information system. Research on neural computing model and physiological and psychological basis of vision and hearing mainly explores the perception mechanism of vision and hearing from the perspective of physiology and psychology, so as to provide basic theories and methods for visual and auditory information processing.

The most important thing in teaching is vision and hearing. Vision and hearing are important perceptual systems that people rely on in verbal communication. But in fact, because of many environmental factors, people in audio-visual and oral teaching cannot fully grasp the information. Digital sensor technology can strengthen information, so digital sensor began to appear in language audio-visual and oral teaching. Digital sensor equipment plays a better role in language audio-visual and oral teaching. Students using digital sensor equipment can learn better, so as to greatly improve the teaching effect.

Strengthening the processing of relevant visual and auditory information helps to ensure that the receiver obtains more accurate information, so as to improve the learning effect and reduce the impact on the environment. This paper creatively puts forward an experiment to explore the role of digital sensors in language audio-visual teaching, so as to provide reference for the application of digital sensors in the future. The impulse response function in sensor technology is introduced. The speech time domain envelope and time-varying nozzle area of the sensor device are calculated. Through auditory attention decoding fusion technology and sensor auditory attention conversion detection method,

auditory attention transfer detection based on line of sight rotation estimation is realized. At the same time, the characteristics of sensor heog signal are analyzed. The results show that the algorithm proposed in this paper has good results.

This paper is mainly divided into five parts. The first part is the background introduction. The second part is literature review, which mainly introduces the relevant research results of digital sensors. The third part is the introduction of related algorithms, mainly introducing the digital sensor and related technologies and algorithms. The fourth part is empirical analysis, which proves the advantages of digital sensor in language audio-visual and oral teaching through various studies. The fifth part is summary and analysis.

2. Related Work

In fact, sensor technology alone refers to information classification and processing technology here. The commonly used classifiers include decision tree (DT), support VEC tor machine (SVM), and neural network. Alhumayani et al. used the correlation coefficient, variance, frequency domain entropy, and mean value of acceleration sensor as behavior characteristics for the first time and combined with DT algorithm to realize the classification of 20 behaviors [1]. Yang realized the recognition of five gait based on FFT coefficient, quartile difference, and SVM algorithm [2]. Feng and Pan proposed using principal component analysis technology to reduce the dimension of mean, variance, and frequency domain features and using decision tree as classifier for classification [3]. In addition, Luo and Xiao use the compressed sensing method to efficiently process low dimensional sampling data for classification [4, 5]. In 2013, researchers from the University of Catalonia in Spain and the University of Genoa in Italy identified six behaviors such as walking, sitting, and standing by using the built-in sensors of mobile phones and disclosed the data set recorded in the experiment to volunteer researchers [6]. Because the traditional methods extract behavior features manually, there will be some empirical deviation in the description of behavior, and a lot of manual intervention is required, so the results are not very ideal. The development of big data technology and deep learning makes it possible to automatically learn the most distinctive behavior characteristics from massive raw data [7–9]. Jiang and Yin proposed a behavior recognition method using deep convolution neural network DCNN [10]. In this method, the data of gyroscope and acceleration sensor are converted into frequency domain signals through sliding window and Fourier transform processing, and the model is trained through supervised learning to obtain a feature extractor to identify human behavior. The experimental results show the superiority of this method on three public data sets (UCI, USC, and SHO) [11–13]. As an interpretable probability graph model, restricted Boltzmann machine is mainly divided into deep belief network (DBN) and deep Boltzmann machine (DBM) [14–17]. Among them, DBN belongs to a generation model, which can extract feature representation from unlabeled high-dimensional sensor data. For example, Fang and Hu and Bhattacharya and Lane used this method to extract irrelevant data in the data, realizing nonlinear dimensionality reduction of high-dimensional data [18, 19]. DBM learns features from sensor data by stacking undirected bipartite graphs. This method mainly uses sparse feature technology to reduce the sensitivity of data and combines cross-correlation feature extraction and sensor fusion methods [20–22]. Deep auto-encoder (DAE) includes two parts: encoder and decoder. First, it uses the encoder to find the correlation characteristics between sensor data, converts the high-dimensional data space to the low-dimensional space, and then uses the error back propagation algorithm to reconstruct the sensor sample data in the decoder [23]. Many research works use this method to reduce the feature dimension and use the method of approximate identity and compressed version to screen the feature vector, using DAE [24, 25]. It can be seen that there are many applications of digital sensors in information processing, but there are still few direct biological information enhancement at present. This paper also explores the enhancement of human information classification and collection by digital sensor technology.

3. Method

3.1. Introduction of Impulse Response Function in Sensor Technology. For the speech time domain envelope $s(t)$ sampled in discrete time $t(t = 1, \cdots, T)$ and the EEG signal $r(t, n)$ sampled in EEG channel $n(n = 1, \cdots, N)$, assuming that the auditory processing of mapping speech features to neural response is a linear time invariant system, the impulse response $w(\tau, n)$ of the forward system can be used to describe the system, as shown in the following formula:

$$r(t, n) = \sum w(\tau, n)s(t - \tau) + \varepsilon(\tau, n), \tag{1}$$

where $\varepsilon(\tau, n)$ represents the system residual. Impulse response $w(\tau, n)$ can be regarded as a set of temporal spatial filters, called TRFs. When solving TRFs, the inverse correlation method and ridge regression strategy can be used to solve the ill posed problem encountered in matrix inversion, see the following formula:

$$w = \left(S^T S + \lambda M\right)^{-1} S^T r. \tag{2}$$

The matrix $S \in R^{T \times \tau_{\text{win}}}$ is composed of the delay sequence of speech time domain envelope $s(t)$, and τ_{win} is the delay length; matrix $r \in R^{T \times N}$ is multichannel EEG data; matrix $M \in R^{T_{\text{win}} \times \tau_{\text{win}}}$ is regularization matrix; λ is a ridge parameter, which can be optimized by cross validation. The optimization index is the correlation coefficient (Pearson correlation coefficient) between the predicted $EEG\hat{r}(t, n)$ and the real $EEGr(t, n)$.

Similar to the forward system, if the system inversely mapped from EEG to speech time domain envelope is also a linear time invariant system and its impulse response is $g(\tau, n)$, the system can be described by formulas ((1))–((3)):…∗as the following formula

$$\hat{s}(t) = \sum\sum r(t + \tau, n)g(\tau, n). \tag{3}$$

$\hat{s}(t)$ represents the reconstructed speech time domain envelope, which can be regarded as linear regression of speech time domain envelope. Impulse response $g(\tau, n)$ is also a set of spatiotemporal filters, which integrates the neural response of specific delay τ and then sums the integrated signal between channels to obtain the reconstructed speech time domain envelope. The filter is also called a decoder. The solution of the decoder is similar to that of TRFs, as shown in the following formula:

$$g = \left(R^T R + \lambda M\right)^{-1} R^T s. \tag{4}$$

The matrix $R \in R^{T \times N - \tau_{\text{win}}}$ is composed of the delay sequence of multichannel EEG data $r(t, n)$, and τ_{win} is the delay length; matrix $s \in R^{T \times 1}$ is the time domain envelope of speech; matrix $M \in R^{N-\tau_{\text{win}} \times N-\tau_{\text{win}}}$ is the regularization matrix. The ridge parameter λ can be optimized by cross-validation. The optimization index is the correlation coefficient (Pearson correlation coefficient) between the reconstructed speech envelope $\hat{s}(t)$ and the actually noticed speech envelope $s_{att}(t)$, which is called reconstruction accuracy.

3.2. Speech Time Domain Envelope and Time-Varying Mouth Area Calculation of Sensor Equipment. For each clean speech signal, we first filter the speech signal by band through the bandpass filter bank (a total of 8 frequency bands). The center frequency of the bandpass filter bank is evenly distributed on the equivalent rectangular bandwidth (ERB) scale of 150–8000 Hz.

The relationship between ERB scale and frequency F_i (kHz) is shown in the following formula:

$$\text{ERB}_N \text{ number} = 21.4 \log_{10} 4.37 F_i + 1, \tag{5}$$

where F_i represents the passband center frequency of the $i\,(i = 1, \cdots, N)$ th filter. The output $x_i(t)$ of each filter is Hilbert transformed to obtain the analytical signal $H(x_i)$. Considering the nonlinear compression characteristics of the cochlea, we further model and compress the $H(x_i)$ (0.3 power) and conduct 8 Hz low-pass filtering to obtain the speech time domain envelope $e_i(t)$ of the corresponding frequency band, as shown in the following formula:

$$e_i = \text{LP}\left(|H(x_i)|^{0.3}\right), \tag{6}$$

where LP(•) represents low-pass filter operator. Finally, the speech time domain envelope $e\,(t)$ can be obtained by averaging the speech time domain envelope of all frequency bands, as shown in formula (7). For the convenience of writing, we will abbreviate it as speech envelope later.

$$e = \frac{\sum_N^{i=1} e_i}{N}. \tag{7}$$

The manually set features contain people's prior knowledge of the main features of the signal, but they cannot reflect all the features of the signal, such as the slope and small fluctuation of HEOG signal in the impulse process. Therefore, this paper further takes the heog signal waveform as the input and uses the DNN classifier in the sensor technology to automatically learn and extract the features related to the scanning angle in the signal. Considering that the time-domain characteristics of HEOG signal are most related to the scanning angle, and the cyclic neural network based on long short-term memory (LSTM) structure has good time series analysis ability, we use the classifier based on LSTM network. Because the signal waveform in this task is relatively simple, we use the cascade structure of single-layer LSTM (number of neurons: 64), single-layer fully connected network (FCN) (number of neurons: 12), and softmax classifier to map the HEOG waveform (sequence length is 160, corresponding to 5 s) to the scanning angle label.

In the training of LSTM, we use multiclassification cross-entropy as the loss function. Assuming that the one hot code of the sample category label is $y = [y_1, y_2, \cdots, y_c]$, and the prediction result of the LSTM classifier is $\hat{y} = [\hat{y}_1, \hat{y}_2, \cdots, \hat{y}_c]$, where C is the number of categories, the loss function is shown in the following formula:

$$\text{Loss}_{\text{CE}} = -\sum_c^{i=1} y_i \log\left(\hat{y}_i\right) = -\log\left(\hat{y}_c\right). \tag{8}$$

3.3. Fusion Technology of Auditory Attention Decoding and Auditory Attention Conversion Detection Method of Sensor. We can match the output of AAD method based on auditory selective attention neural mechanism (measured by EEG) with the auditory attention object of the listener, but the accuracy of linear decoding algorithm currently used is low and the detection delay of attention conversion is large (5–10 s).

Because the advantages and disadvantages of AAD and aad methods are complementary, the visual behavior-based aasd method (measured by heog and NEMG) has low alarm leakage rate and small detection delay (<2 seconds), but its output can only reflect the conversion of auditory attention and cannot correspond to the object of auditory attention. Therefore, this paper puts forward some "early warning and correction" strategies. Aad issues early warning to AAD. The output of the AAD method will be used to guide the implementation of the AAD method. When line of sight rotation is detected, the AAD algorithm will be executed once to detect the auditory attention object; otherwise, the final detection result will be maintained. This strategy can significantly reduce the amount of computation of the AAD algorithm. Aad directs aad to correct the test results. In order to alleviate the error propagation problem caused by aad errors, when the line of sight rotation is not detected for a continuous period of time, the AAD algorithm is executed once to compare and correct the new and old detection results.

Its formal expression is as follows.

That is, when no attention transition is detected in consecutive M frames, set the correction state $c(k)$ to 1. After calculating the warning and correction state of the k frame, the AAD operation state $p(k)$, that is, the final

detection result of the auditory attention object ID (k), can be calculated, as shown in the following formulas.

$$p(k) = a(k) + c(k), \tag{9}$$

$$\mathrm{ID}(k) = \begin{cases} \mathrm{ID}(k-1), & \text{if } p(k) = 0, \\ \boldsymbol{d}(k), & \text{if } p(k) = 1. \end{cases} \tag{10}$$

Note that the AASD algorithm is the operator $v(\bullet)$, and the AAD algorithm is the operator $d(\bullet)$. Boolean value $v(k)$ is the AASD state of frame k (1 indicates rotation is detected), Boolean value $a(k)$ is the early warning state of frame k (1 indicates early warning), Boolean value $c(k)$ is the correction state of frame k (1 indicates correction should be performed), and constant M is the correction window length; Then, it satisfies the following relationship formulas:

$$a(k) = \boldsymbol{v}(k-1), \tag{11}$$

$$c(k) = \neg\left(\sum_{M}^{i=1} v(k-i) + \sum_{M}^{i=1} a(k-i)\right). \tag{12}$$

In order to solve the problem of gradient saturation, ReLU activation function is selected in this paper. ReLU activation function was introduced into neural network by Nair and Hinton in 2010. It is essentially a piecewise function, which is defined as follows;

$$\mathrm{ReLU}(x) = \max\{0, x\} = \begin{cases} x & x \geq 0, \\ 0 & x < 0. \end{cases} \tag{13}$$

In this paper, L_2 regularization is used as the regularization method of convolutional neural network model. L_2 regularization is a very common model regularization method in traditional machine learning and deep neural network models. Two regularization techniques are also commonly used in depth model to regularize its convolution layer and classification layer. Finally, the overfitting phenomenon is avoided by constraining the model complexity of convolutional neural network. Assuming that the network layer parameter to be regularized is ω, the form of L_2 regularization term is as follows:

$$L_2 = \frac{1}{2}\lambda\|\omega\|_2^2. \tag{14}$$

Among them, λ reflects and controls the complexity of the regular term. The larger the value, the greater the model complexity, and vice versa. In the actual use of L_2 regular term, the regular term is usually added to the objective function set in advance, and the overall objective function is used to complete the error back propagation in the convolutional neural network model, so as to guide the training of convolutional neural network model by changing the regular term. L_2 regularization is commonly called "weight attenuation" in deep learning. In addition, L_2 regularization is also called ridge regression or regularization in machine learning.

Through the normalization of square difference, the distribution variance of input and output data can be consistent. The specific formula is as follows:

$$\mathrm{Var}(s) = \mathrm{Var}\left(\sum_{n}^{i} \omega_i x_i\right), \tag{15}$$

where s represents the output result of the layer network before nonlinear transformation, ω represents the layer parameters, and x represents the layer input data.

4. Results and Discussion

4.1. Auditory Attention Transition Detection Based on Line of Sight Rotation Estimation under Sensor Operation. This section will analyze the signal characteristics of heog, NEMG, and IMU sensors under the conditions of head fixation and head rotation, respectively, and explore the feasibility of applying these signal characteristics to AASD tasks by establishing the mapping relationship between these signal characteristics and the rotation angle of line of sight. Estimation of line of sight rotation is based on heog under fixed head. First, the experiment of line of sight rotation under the condition of fixed head is carried out in this section. Subjects induced sensor heog by paying attention to visual stimuli at different horizontal angle positions on the display. Through the feature analysis of heog signal, we will design a suitable classification algorithm to estimate the corresponding line of sight rotation angle. Four subjects with normal vision or corrected to normal vision (1 female, age range 22–25 years) participated in the experiment.

The experiment was conducted in the copper mesh shielded sound insulation room (IAC acoustics) of the speech and hearing research center of Peking University. In this experiment, the subject's head was fixed by the head support (wearing the sensor at the same time), and there was a 34.5-inch display (AOC) 0.4 m in front of the head. Visual stimulation is a red dot presented through the display, and the background of the display is black. The possible positions of red dots are located in the horizontal area on the display at the same height as the subject's eyes. There are five positions, which are 0° in front of the subject, 45° and 30° to the left in front of the subject, and 30° and 45° to the right in front of the subject. During the experiment, the red dot will only appear at a certain position at any time, and the subjects are required to always look at the red dot. We control the position change of the red dot to instruct the subjects to make horizontal scanning behavior, so as to induce heog. In one trial, the subjects were instructed to produce all 20 saccade behaviors once by setting the position change order of red dots. At the beginning of each trial, red dots will randomly appear in one position and continue to appear for 5 s and then jump to another position and continue to appear for 5 s. A total of 10 trials were conducted for each subject. The duration of each trial was 1 minute and 45 seconds. The presentation order of red dots in each trial

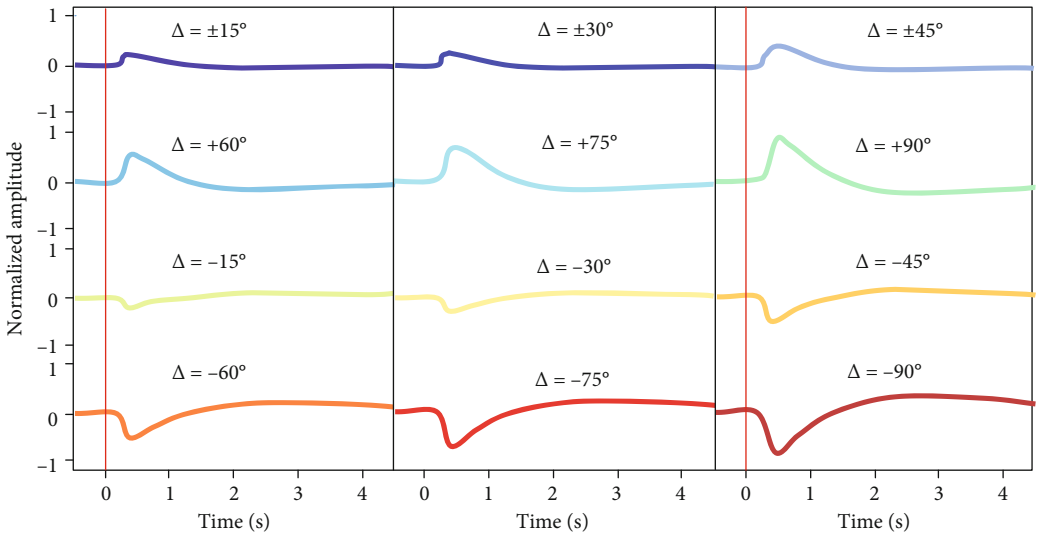

Figure 1: Normalized average sensor HEOG waveform (12 types of glance angles).

was randomly controlled. At the end of each trial, subjects will rest for a period of time to ensure sufficient attention. Before the formal experimental process, each subject should be trained to be familiar with the stimulation materials and experimental process. The whole experiment lasted about 0.5 hours for each subject.

4.2. Sensor Data Acquisition and Preprocessing. The recording and storage of sensor heog data are carried out through the NeuroScan synamps2 system. We used a pair of bipolar electrodes to record heog, which were placed outside the eyes. In addition, the midline of the forehead is used as the ground electrode, and the tip of the nose is used as the reference electrode. In order to ensure the data quality, the impedance between electrodes is kept below 5 k0hm. Heog is amplified (magnification: 20000), online bandpass filtered (frequency range: 0.15–100 Hz) and sampled (quantization accuracy: 16 bits, sampling rate: 250 Hz), and then stored for offline analysis. The generation and recording modes of trigger signal are similar to that in Section 3.2 of this paper. Each time the red dot changes its position, a trigger signal is generated to facilitate subsequent data preprocessing.

We use Matlab for digital preprocessing of heog signal, which is similar to previous work. For each test, we successively extract 20 heog signals according to 20 trigger signals with a window length of 5 s (0.5 s before the trigger signal to 4.5 s after the trigger signal), corresponding to each saccade behavior. Because the basic form of heog signal is slowly changing time-domain fluctuation, and its main components are located in the low-frequency band, the signal is further downsampled to 32 Hz, and 10 Hz low-pass filtering and baseline correction is performed. Finally, in order to ensure that the heog amplitude values of all subjects are comparable, we normalized all data of each subject within subject to ensure that the maximum amplitude is 1, and the minimum is -1 in all heog waveforms of each subject. Through the analysis of preexperiment, when the starting and ending positions of rotation are different but the scanning angle is the same (for example, the rotation amount of line of sight direction is +45° when turning from -45° to 0° and from 0° to 45°), the heog waveform shape is almost the same. Therefore, we classify the same rotation angle into one category, and finally, get the heog data corresponding to 12 types of scanning angles.

4.3. Characteristic Analysis of Sensor Heog Signal. The normalized average heog waveform corresponding to 12 types of scanning angles (Δ = ± 15°, ±30°, ±45°, ±60°, ±75°, and ±90°) is shown in Figure 1 (the error interval represents the standard deviation, and the red vertical line represents the time of trigger signal, which is the same later). It can be seen that in addition to the difference in amplitude, the heog waveform under each scanning angle is very similar. After the indication of saccade is given, the amplitude of heog begins to change significantly after about 0.2 S. At about 0.4 s, these results show that the extreme value of heog amplitude is an important feature of heog signal, which is consistent with previous findings. We further calculated the amplitude extreme value of each heog signal of each subject within the 2S segment at the beginning of the signal, and the average result is shown in Figure 2. It can be seen that the extreme value of heog waveform increases monotonically with the increase of rotation angle, indicating that it can be used as a manually set feature to estimate the change angle of line of sight orientation.

4.4. Estimation of Line of Sight Rotation Based on Heog Waveform and DNN in Sensor. The classification accuracy of the sensor built-in classifier based on heog amplitude feature is 81.8 ± 2.2%, which shows that the scanning angle can be better estimated by using heog amplitude feature under the condition of fixed head. The confusion matrix of classification results is shown in Figure 3(a). The elements i and j of the confusion matrix represent the proportion of class i samples classified to class j, which is the same later. It can be seen that confusion mainly occurs in the same

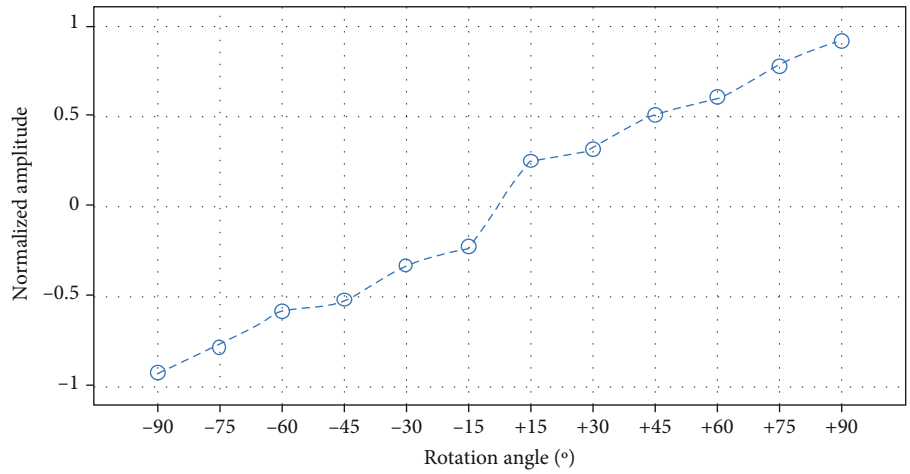

Figure 2: The normalized HEOG amplitude characteristics of the average sensor change with the saccade angle.

rotation direction and between adjacent rotation angles, especially between +60° and +45° and -60° and -45°, which is consistent with the trend in Figure 2. This shows that the spatial resolution of heog using amplitude features is still limited.

The classification accuracy based on heog waveform and LSTM classifier is 90.9 ± 2.0%, which is significantly higher than that of the sensor's own classifier. The confusion matrix of classification results is shown in Figure 3(b), and it can be seen that the degree of confusion is significantly reduced. This shows that compared with manually setting the feature (i.e., the amplitude extreme value of heog), the time-domain feature automatically learned after LSTM network enhancement reflects the information related to the scanning angle more finely and comprehensively and can be used as an enhanced version of the sensor.

4.5. Estimation of Line of Sight Direction Rotation of Sensor Based on HEOG and NEMG under Head Rotation. For example, although the algorithm using heog to estimate the scanning angle has achieved high accuracy under the condition of fixed head, the performance of the algorithm will be significantly reduced under the condition of head rotation. This is because under the condition of head rotation, the change of line of sight orientation no longer depends only on saccade, but also on head rotation, and the strategies of the two kinds of behavior are variable. In this experiment, subjects can perform natural saccade and head rotation when completing the task of line of sight rotation. We will use heog and NEMG to measure saccade and head rotation, respectively. By analyzing the characteristics of several sensor signals, a suitable classification algorithm is designed to estimate the corresponding line of sight rotation angle.

17 subjects with normal vision or corrected to normal vision (4 women, age range 21–28 years) participated in the experiment. All subjects ignored neurological diseases. The experimental process has been approved by the institutional review committee of Peking University, and the informed consent of each subject has been obtained. The experiment was conducted in the copper mesh shielded sound insulation room (IAC acoustics) of the speech and hearing research center of Peking University. The subjects (with sensors) had a 17-inch display (DELL) at 0.85 meters on the left and right in front of them. Visual stimulation is a red dot presented by the two monitors, and the background of the monitors is black. The possible positions of red dots are located in the horizontal area on the display at the same height as the subject's eyes. There are six positions in total, three of which are 45°, 30°, and 15° to the left in front of the subject, and the other three are 15°, 30°, and 45° to the right in front of the subject. During the experiment, red dots will only appear at a certain position of a display at any time. The subjects were asked to always turn their eyes towards the red dot. We instructed the subjects to turn their eyes by controlling the position change of the red dot. Before the change of position, the subjects were asked to minimize head movement and other body movements. When the transition occurred, the subjects were allowed to perform natural saccade and head rotation. In this experiment, in order to ensure that the subjects have obvious saccade and head movement behavior, the position of the red dot will only change between the two displays. We have set up a total of six line of sight orientation changes with different start and end positions: ±30°, ±60°, and ±90° (corresponding to -15° to +15°, +15° to -15°, -30° to +30°, +30° to -30°, -45° to +45°, and + 45° to -45°). In one trial, the red dot is continuously converted between two fixed positions for 40 times. The duration of continuous presentation at a certain position is still 5 s, and the duration of each trial is 3 minutes and 40 seconds. Therefore, two of the six line of sight rotation occurred in one trial, 20 times each. A total of 3 different trials were conducted for each subject to produce all six gaze orientations. At the end of each trial, subjects will rest for a period of time to ensure sufficient attention. Before the formal experimental process, each subject should be trained to be familiar with the stimulation materials and experimental process. The whole experiment lasted about 0.25 hours for each subject.

4.6. Characteristic Analysis of HEOG, NEMG, and IMU Signals in Sensor. In this section, the extreme value of heog waveform is still used as a manually set feature to estimate

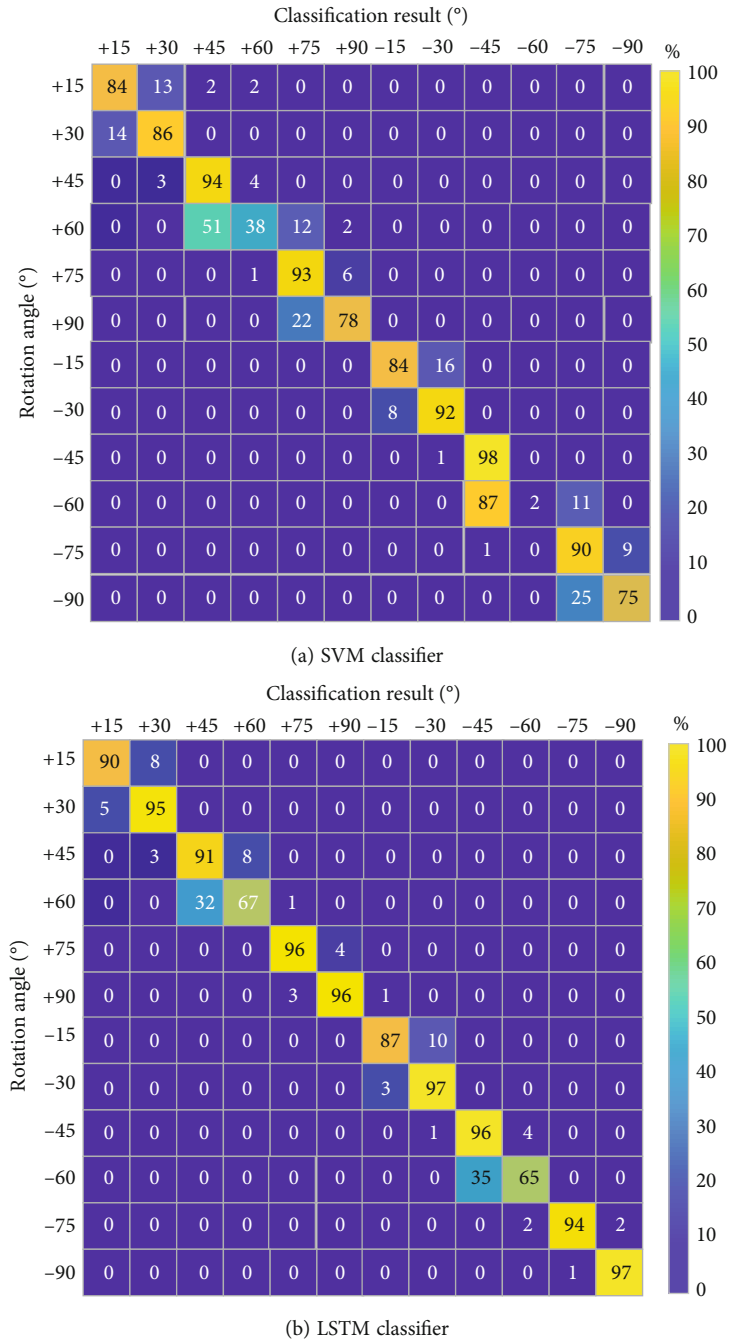

Figure 3: Confusion matrix of the classification results of the sensor's own classifier and the LSTM enhanced sensor classifier under the condition of fixed head (%).

the change angle of line of sight. When the line of sight rotates, different from the slow fluctuation of heog signal, NEMG signal will show obvious amplitude change in continuous and rapid neural discharge mode. It can be seen that the relationship between NEMG amplitude change trend and head rotation direction is expected, that is, within 1 s after head rotation, NEMG amplitude of contralateral SCM will increase and remain stable, while NEMG amplitude of ipsilateral SCM will decrease and remain stable. Therefore, the amplitude change of NEMG is its most significant signal feature. This characteristic will be described by calculating the short-term energy of NEMG signal. Figure 4 shows the normalized average heog waveform under head rotation. It can be seen that the heog waveform is similar to the heog waveform under the condition of fixed head.

We calculate the root mean square (RMS) of the signal to represent the signal energy and select the frame length of 0.1 s and the frame shift of 0.05 s. On this basis, the short-time energy of each NEMG is normalized, and the average short-time energy in the first 0.5 s is classified as 1. Figure 5 shows the change of normalized NEMG short-time energy with time under various line of sight rotation

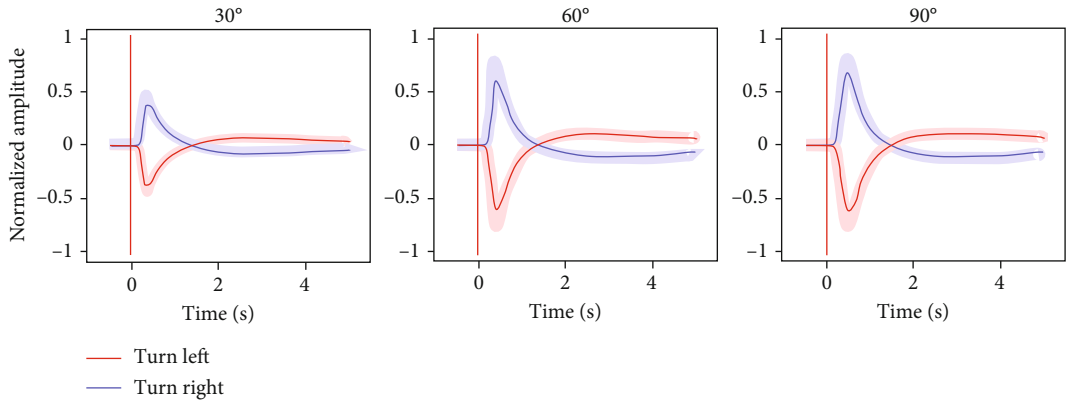

Figure 4: Normalized HEOG waveform of average sensor (6 types of sight rotation).

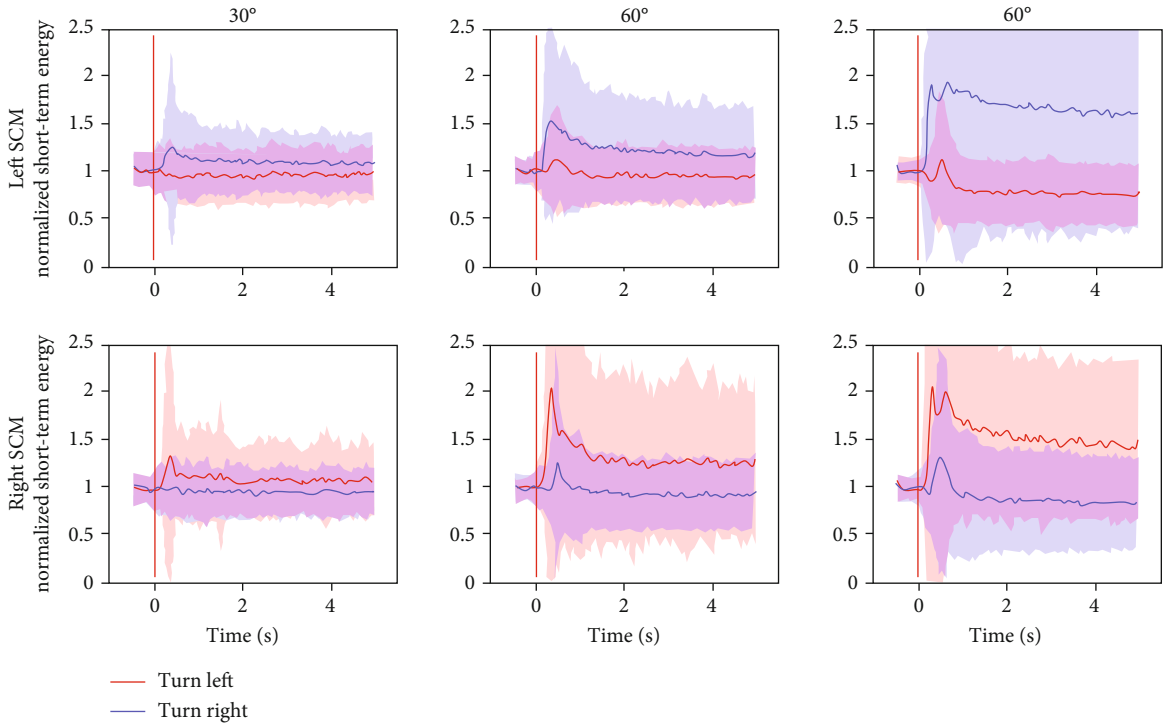

Figure 5: Normalized sensor NEMG short-term energy diagram (6 types of sight orientation changes).

angles. It can be seen that after the indication of line of sight rotation is issued, the NEMG short-time energy of the opposite SCM begins to change significantly after about 0.1 s, reaches the extreme value at about 0.4 s, and then remains at a high level, while the NEMG short-time energy of the ipsilateral SCM has little change. Similar to the trend of HEOG, the increment of NEMG short-time energy value increases with the increase of line of sight rotation angle. The results show that the extreme value of short-term energy can be used as a manually set feature to estimate the change angle of line of sight orientation.

We further analyze the differences between the results of different classifiers. It can be seen that under all input conditions, the accuracy of FCN classifier is not different from that of the sensor's own classifier, which may be because the network structure of FCN is relatively simple, and its automatically extracted signal features are similar to those set manually. Under all input conditions, the accuracy of LSTM classifier is the lowest, which may be because there is certain noise interference in the sensor signal under the condition of head rotation, and LSTM network is sensitive to the time information in the signal waveform, so its ability to extract features will be disturbed by noise. This also explains that the accuracy of univariate heog input (49.3%) is significantly lower than that in head fixation experiment (90.9%). Under the condition of univariate input, the performance of digital optimization classifier is similar to that of SVM and FCN classifier. Under the two bivariate input conditions, the performance of digital optimization classifier is the best, which is 72.6% (HEOG and NEMG) and 93.3%

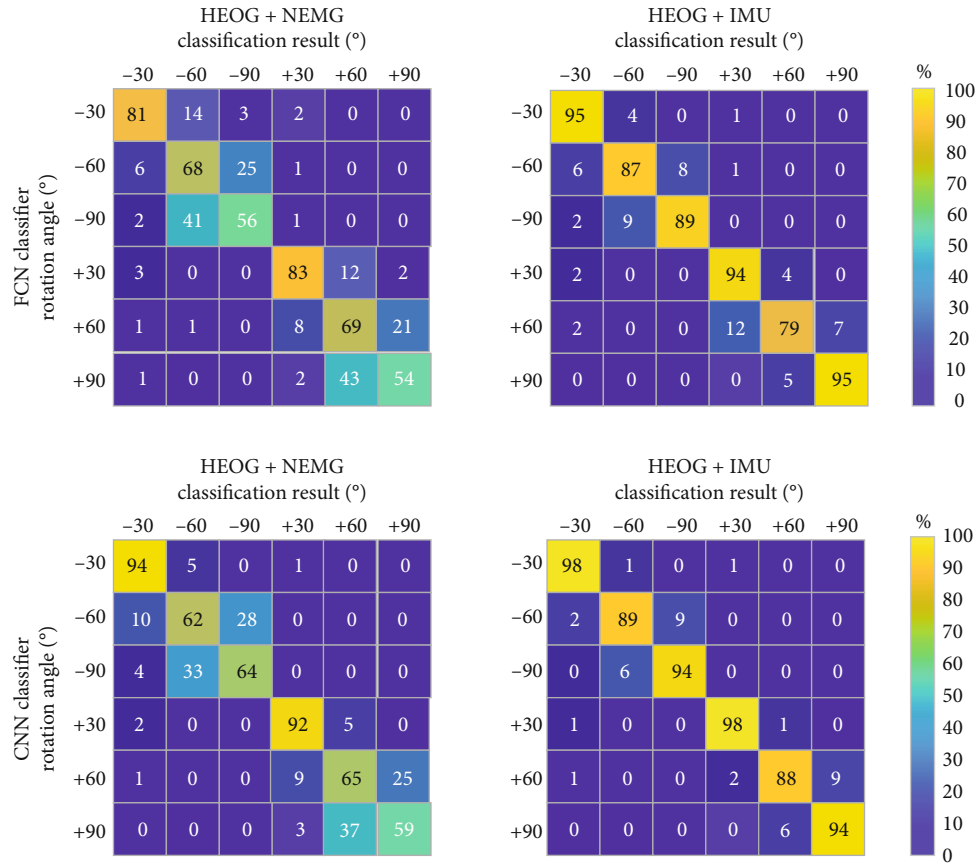

Figure 6: Confusion matrix of classification results of sensor with classifier and digital optimized classifier under head rotation condition (%).

(HEOG and IMU), respectively, indicating that digital optimization has better feature extraction ability than FCN and LSTM. This may be because the convolution kernel can observe the signal waveform in a certain time window at one time and has stronger ability to integrate the features between channels, so it reduces the possibility of noise interference to the digital optimization classifier. The confusion matrix of digital optimization classification results under two bivariate input conditions is shown in Figure 6, and the confusion mode is similar to the classifier provided by the sensor. The results also show that the algorithm can correctly judge the rotation direction under the condition of bivariate input. Compared with IMU, NEMG has poor resolution when measuring head rotation behavior.

In general, these results show that under the condition of audio-visual matching, the Los rotation estimation based on heog and NEMG can more accurately reflect the information related to auditory attention conversion, such as rotation time and rotation angle. Considering that the AASD task does not require accurate line of sight rotation angle information, we can reduce the line of sight rotation angle estimation to line of sight rotation detection, that is, the rotation label output by the classifier (class 7: 0°, ±30°, ±60°, and ±90°) is changed to rotation label (class 2: rotation, no rotation), so that while meeting the requirements of AASD task, the advantage of low detection delay (2 s) is also retained. Based on this change, this section will continue to explore the feasibility of AASD task based on line of sight rotation detection.

Based on the results in Figure 7, after remapping the output label of the classifier into rotation (±30°, ±60°, and ±90°) and nonrotation (corresponding to 0°), the experimental results of AASD task can be obtained, and the confusion matrix is shown in Figure 8. It can be seen that when two variables heog and NEMG are input, FCN is easier to misjudge the rotation condition as no rotation than digital optimization classifier (FCN: 6.3%, digital optimization: 3.1%) (see Figure 9). This missing alarm means that AASD algorithm fails to guide the calculation of AAD, which will affect the detection of auditory attention objects. On the contrary, false alarm has less impact, because AAD algorithm can correct it. In order to further quantify the performance of each algorithm in the AASD task under various input conditions, we calculate three indicators: $F1$ value, missed alarm rate and false alarm rate according to the confusion matrix. $F1$ value is the harmonic average of accuracy rate (the proportion of samples divided into positive examples) and recall rate (the proportion of samples divided into positive examples). The model can be comprehensively evaluated. The missed alarm rate is the proportion of the missed positive cases in all the positive cases. False alarm rate is the proportion of samples judged as positive cases, which are actually negative cases. It can be seen that the performance of the digitally optimized classifier is better, which has higher

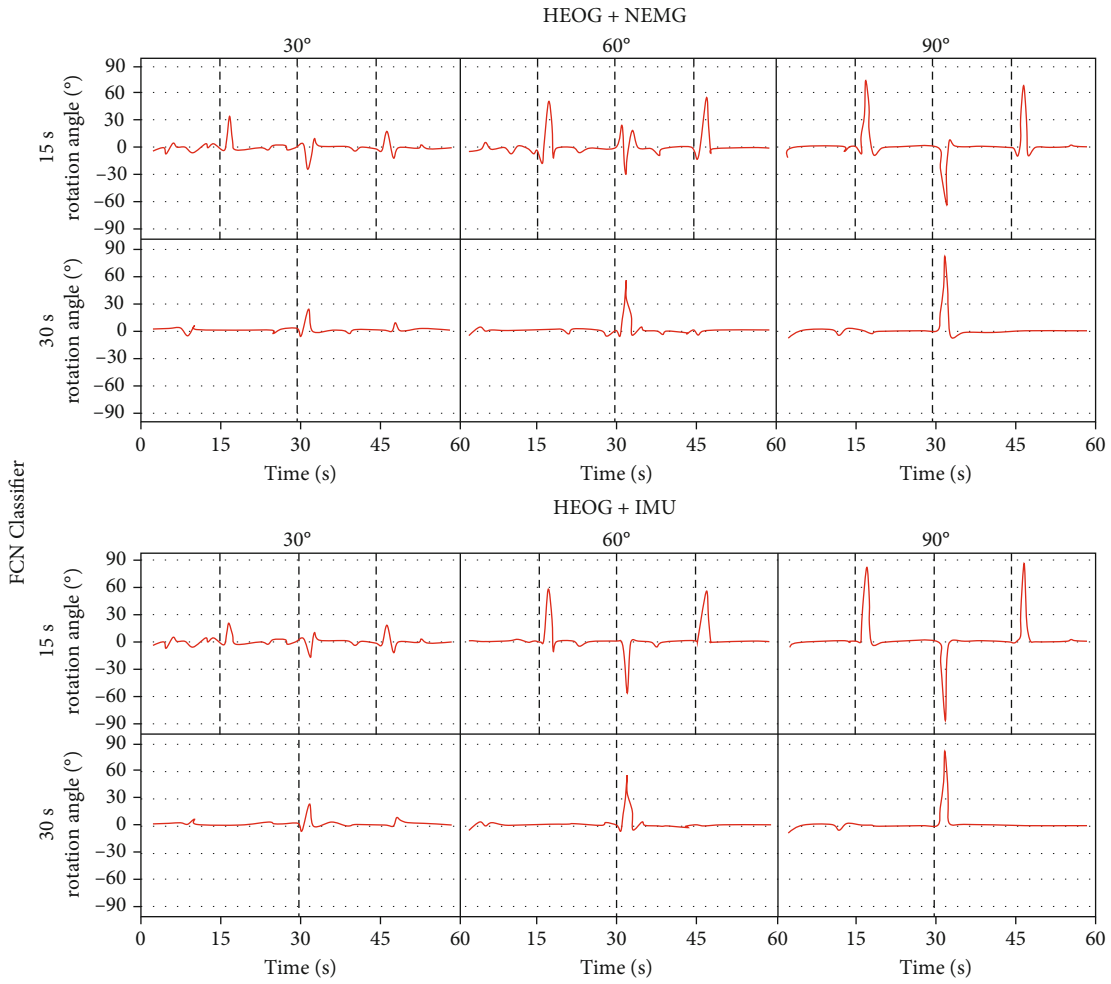

Figure 7: Result of continuous line-of-sight rotation angle estimation results during sensor trials.

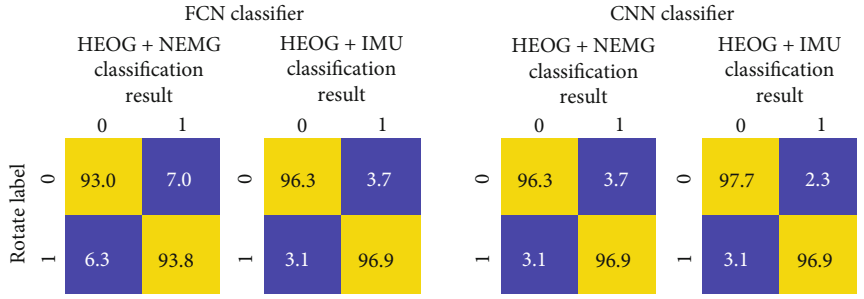

Figure 8: Confusion matrix of classification results of FCN and digital optimization classifiers (%).

$F1$ value, lower false alarm rate, and lower false alarm rate than the FCN classifier. This is similar to the comparison results of the two classifiers in the previous section, which proves that in this task, the digital optimization network has stronger feature extraction ability and is more robust to noise interference. In addition, although the results when using bivariate heog and NEMG are still worse than bivariate heog and IMU on the whole, the gap is not large, especially the missing alarm rate (both 3.1%) under the condition of using digital optimized classifier is almost no difference. The results show that the proposed AASD algorithm based on heog and NEMG is feasible.

One advantage of the fusion strategy is that it avoids the EMG artifact interference caused by saccade and head rotation. Figure 10 shows the signal waveforms of EEG, EOG, and NEMG recorded in a trial with an attention conversion interval of 15 s. In order to show the interference of EMG artifact on EEG, we selected some of the most representative EEG channels for display. They are either closer to the EMG artifact source in spatial position (for example, FPZ is close

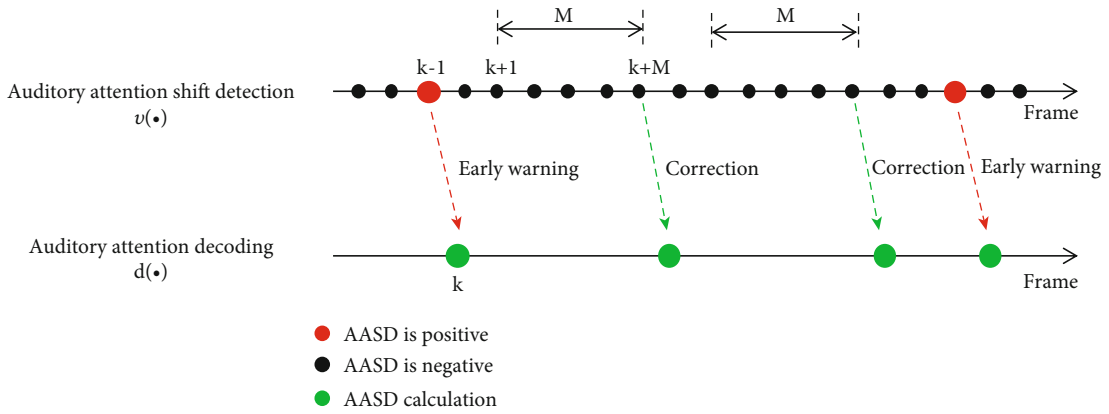

Figure 9: Schematic diagram of the fusion strategy of auditory attention decoding and conversion detection methods.

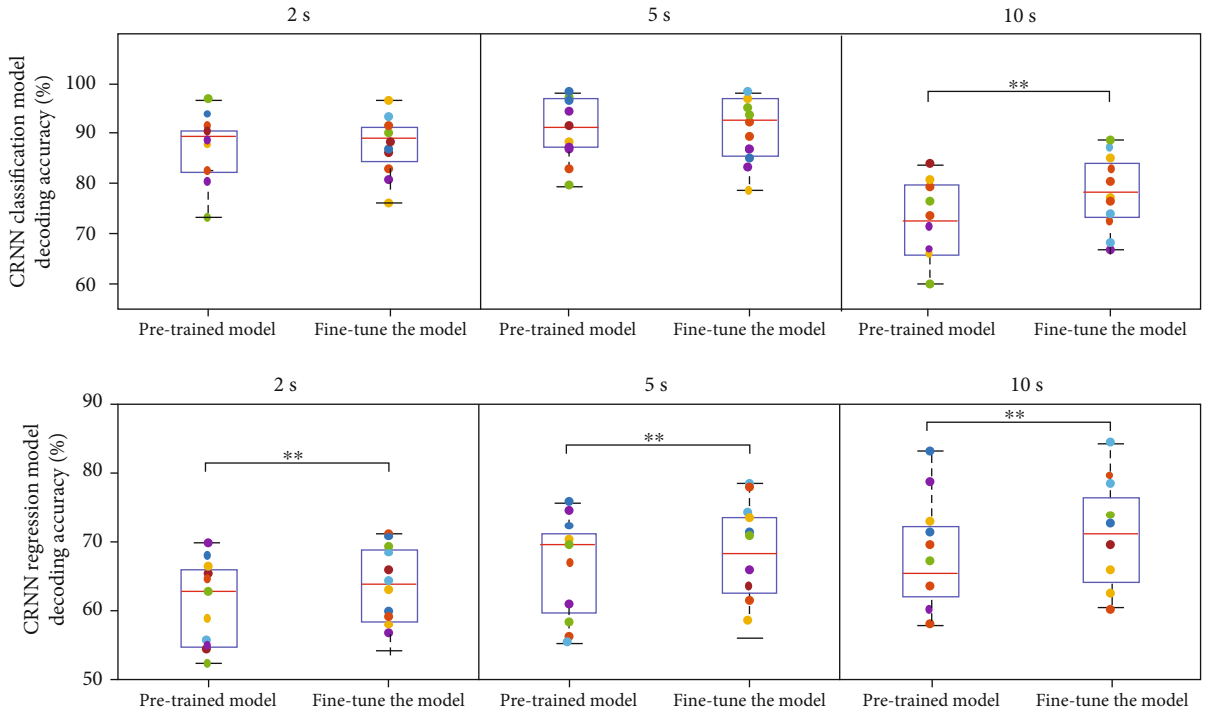

Figure 10: The decoding accuracy of CRNN classification and regression model before and after fine-tuning.

to the saccade and blink artifact source—eye muscle, T7, and T8 are close to the head rotation artifact source—SCM), or they contribute greatly to AAD (for example, FC5 and FC6 are located in the temporal lobe, and Oz is located in occipital lobe). In the channel FPZ close to the eye muscle, obvious interference from heog and VEOG can be seen; obvious interference from NEMG can be seen in channels T7, T8, and OZ close to SCM; FC5 and FC6 channels located in the temporal lobe may be disturbed by both heog and NEMG; the channel CZ located at the top of the skull is hardly disturbed by these artifacts due to its long distance. In general, almost all EEG electrodes are subject to artifact interference at the time of saccade and head rotation, so EMG artifact interference mainly comes from heog and NEMG induced by saccade and head rotation. In addition, the delay introduced by their volume conduction through the head is very small. This shows that the moment when EEG is disturbed by EMG artifact is the moment when AASD output is positive. Under the fusion strategy proposed in this paper, EEG segments interfered by EMG artifact will not participate in the calculation of AAD, so EMG artifact interference has no effect on the detection results of auditory attention objects.

The experimental results of model fine-tuning of CRNN regression and CRNN classification model under different decoding window lengths are shown in Figure 10, which shows the average decoding accuracy (box diagram) and individual decoding accuracy (scatter diagram) of the data of 12 subjects. It can be seen that under all decoding window length conditions, the average decoding accuracy of the fine-

tuning model is higher than that of the pre training model, but the improvement is significant only under the condition of 10 s ($t = -3.411$, $P = 0.006$). For the other two window length conditions, there may be two reasons why the gain caused by fine tuning is not significant. First, the accuracy of the pre training model itself is high and has ceiling effect; second, the classification model mainly relies on the spatial selective attention feature in EEG, which may have high consistency among subjects, so the pretraining model is also suitable for new subject data. On the contrary, the gain of fine tuning on CRNN regression model is significant under all window length conditions (2 s, $t = -3.688$, $P = 0.004$; 5 s, $t = -3.612$, $P = 0.004$; 10 s, $t = -3.597$, $P = 0.004$). This may be because the regression model relies on more complex spatiotemporal features in EEG related to the processing of audiovisual stimuli, which are less consistent among subjects. For example, different subjects may have different dependence on visual and auditory stimuli, which makes their EEG feature space different. It can be seen that compared with the subjects without sensors, the subjects with digital sensors have obvious advantages in language audiovisual teaching.

5. Conclusion

Digital sensor replacement equipment has obvious advantages in people's language audio-visual and oral teaching. Once in a noisy and complex environment, the effect of language audio-visual and oral teaching will decline. The help of digital sensors can help people improve their ability to accept information and reduce environmental obstacles. To some extent, sensor technology will also strengthen people's audio-visual response. In addition, daily face-to-face verbal communication is a scene of audio-visual matching. However, people's senses are often disturbed, which affects the learning in teaching. Under this condition, digital sensors can be selected to strengthen the processing of the obtained information, so as to get better learning and teaching results.

Data Availability

The experimental data used to support the findings of this study are available from the corresponding author upon request.

Conflicts of Interest

The author declared that they have no conflicts of interest regarding this work.

Acknowledgments

This study was funded by Research and Practice Project of English Teaching Reform in Higher Education of Hebei Province in 2020, Research on the Construction of Practical Curriculum System for Business English Major under the Background of Integration between Industry and Education (project no.: 2020YYJG059) and Project Supported by Scientific Research Fund of Tangshan Normal University, Research on the Construction Path of English Cloud Platform of Jidong Culture under the Background of New Infrastructure Construction (project no.: 2021B12).

References

[1] M. Alhumayani, M. Monir, and R. Ismail, "Machine and deep learning approaches for human activity recognition," *International Journal of Intelligent Computing and Information Sciences*, vol. 21, no. 3, pp. 44–52, 2021.

[2] Y. Xue, *Human Motion Pattern Recognition Based on a Single Acceleration Sensor*, South China University of Technology, Guangzhou, China, 2011.

[3] L. Feng and J. Pan, "Human motion recognition based on three-axis acceleration sensor," *Computer Research and Development*, vol. 53, no. 3, pp. 621–631, 2016.

[4] Y. Luo, S. M. Coppola, P. C. Dixon, S. Li, J. T. Dennerlein, and B. Hu, "A database of human gait performance on irregular and uneven surfaces collected by wearable sensors," *Scientific Data*, vol. 7, no. 1, pp. 1–9, 2020.

[5] L. Xiao, R. F. Li, and J. Luo, "Recognition of human activity based on compressed sensing in body sensor networks," *Journal of Electronics & Information Technology*, vol. 35, no. 1, pp. 119–125, 2013.

[6] D. Anguita, A. Ghio, L. Oneto, X. Parra, and J. L. Reyes-Ortiz, *A Public Domain Dataset for Human Activity Recognition Using Smartphones*, ESANN, Bruges, Belgium, 2013.

[7] A. Mcafee and E. Brynjolfsson, "Big data: the management revolution," *Harvard Business Review*, vol. 90, no. 10, p. 60, 2012.

[8] Y. LeCun, Y. Bengio, and G. Hinton, "Deep learning," *Nature*, vol. 521, no. 7553, pp. 436–444, 2015.

[9] J. Schmidhuber, "Deep learning in neural networks: an overview," *Neural Networks*, vol. 61, pp. 85–117, 2015.

[10] W. Jiang and Z. Yin, "Human activity recognition using wearable sensors by deep convolutional neural networks," in *Proceedings of the 23rd ACM International Conference on Multimedia*, pp. 1307–1310, Brisbane, Australia, 2015.

[11] M. Zhang and A. A. Sawchuk, *USC-HAD: A Daily Activity Dataset for Ubiquitous Activity Recognition Using Wearable Sensors*, ACM Conference on Ubiquitous Computing, 2012.

[12] M. Shoaib, S. Bosch, O. Incel, H. Scholten, and P. Havinga, "Fusion of smartphone motion sensors for physical activity recognition," *Sensors*, vol. 14, no. 6, pp. 10146–10176, 2014.

[13] D. Alberici, P. Contucci, and E. Mingione, *Deep Boltzmann Machines: Rigorous Results at Arbitrary Depth, Annales Henri Poincaré*, Springer International Publishing, 2021.

[14] L. A. Passos and J. P. Papa, "A metaheuristic-driven approach to fine-tune deep Boltzmann machines," *Applied Soft Computing*, vol. 97, article 105717, 2020.

[15] D. Alberici, A. Barra, P. Contucci, and E. Mingione, "Annealing and replica-symmetry in deep Boltzmann machines," *Journal of Statistical Physics*, vol. 180, no. 1-6, pp. 665–677, 2020.

[16] R. Salakhutdinov and H. Larochelle, "Efficient Learning of Deep Boltzmann Machines," in *Proceedings of the thirteenth international conference on artificial intelligence and statistics*, pp. 693–700, Sardinia, Italy, 2010.

[17] M. A. Alsheikh, D. Niyato, S. Lin, H. P. Tan, and Z. Han, "Mobile big data analytics using deep learning and apache spark," *IEEE Network*, vol. 30, no. 3, pp. 22–29, 2016.

[18] H. Fang and C. Hu, "Recognizing human activity in smart home using deep learning algorithm," in *Proceedings of the*

33rd Chinese Control Conference, pp. 4716–4720, Nanjing, China, 2014.

[19] S. Bhattacharya and N. D. Lane, "From smart to deep: robust activity recognition on smartwatches using deep learning," in *2016 IEEE International Conference on Pervasive Computing and Communication Workshops (PerCom Workshops)*, pp. 1–6, Sydney, Australia, 2016.

[20] V. Radu, N. D. Lane, S. Bhattacharya, C. Mascolo, M. K. Marina, and F. Kawsar, "Towards multimodal deep learning for activity recognition on mobile devices," in *ACM International Joint Conference on Pervasive and, Ubiquitous Computing: Adjunct*, pp. 185–188, Heidelberg, Germany, 2016.

[21] Y. Zhao and L. He, "Deep learning in the EEG diagnosis of Alzheimer's disease," in *Computer Vision - ACCV 2014 Workshops*, pp. 340–353, Springer, 2014.

[22] C. Y. Liou, W. C. Cheng, J. W. Liou, and D. R. Liou, "Autoencoder for words," *Neurocomputing*, vol. 139, no. 139, pp. 84–96, 2014.

[23] M. M. Al Rahhal, Y. Bazi, H. AlHichri, N. Alajlan, F. Melgani, and R. R. Yager, "Deep learning approach for active classification of electrocardiogram signals," *Information Sciences*, vol. 345, pp. 340–354, 2016.

[24] B. Jokanovic, M. Amin, and F. Ahmad, "Radar fall motion detection using deep learning," in *2016 IEEE Radar Conference (RadarConf)*, pp. 1–6, Philadelphia, PA, USA, 2016.

[25] M. Munoz-Organero and R. Ruiz-Blazquez, "Time-elastic generative model for acceleration time series in human activity recognition," *Sensors*, vol. 17, no. 2, p. 319, 2017.

Hindawi
Journal of Sensors
Volume 2021, Article ID 4819254, 10 pages
https://doi.org/10.1155/2021/4819254

Research Article

A Deep Learning Framework Based on Multisensor Fusion Information to Identify the Airplane Wake Vortex

Yi Ai, Yuanji Wang, Weijun Pan, and Dingjie Wu

Civil Aviation Flight University of China, China

Correspondence should be addressed to Yi Ai; aiyi@cafuc.edu.cn

Received 8 October 2021; Accepted 5 November 2021; Published 28 November 2021

Academic Editor: Gengxin Sun

Along with the rapid improvement of the aviation industry, flight density also increases with the increase of flight demand, which directly leads to the increasingly prominent influence of wake vortex on flight safety and aviation control. In this paper, we propose a new joint framework—a deep learning framework—based on multisensor fusion information to address the detection and identification of wake vortices in the near-Earth phase. By setting multiple Doppler lidar in near-Earth flight areas at different airports, a large number of accurate wind field data are captured for wake vortex detection. Meanwhile, the airport surveillance radar is used to locate the wake vortex. In the deep learning framework, an end-to-end CNN-LSTM model has been employed to identify the airplane wake vortex from the data detected by Doppler lidar and the airport surveillance radar. The variables including the wind field matrix, positioning matrix, and the variance sequence are used as inputs to the CNN channel and LSTM channel. The identification and location information of the wake vortex in the wind field image will be output by the framework. Experiments show that the joint framework based on a multisensor possesses stronger ability to capture local feature and sequence feature than the traditional CNN or LSTM model.

1. Introduction

Airplane wake is a special atmospheric turbulence phenomenon which occurs in the whole flight process. Jet flow and wingtip wake are the two main part of airplane wake. To be more specific, wingtip wake consists of two whirlpools with opposite rotation directions, which lasts for tens of seconds to several minutes. In space, airplane wake is a long cylindrical distribution medium target behind the airplane. Generally, it reaches a hundred times of wingspan at the rear of the airplane, with a length of several kilometers, which belongs to a very strong turbulence. In 2004, the Federal Aviation Administration (FAA) defined wake vortex or wingtip wake as "Round air mass caused by the movement of wings in the air during the process of generating lift" (see Figure 1). When the airplane flies through the clouds, the water vapor particles will be stirred by a strong air flow, which looks like a vortex [1–5].

Actually, every airplane creates wake but the strength of the different airplane type is determined by many factors, including the weight, speed, wingspan (or rotor design) of the airplane, and the atmospheric conditions during the process. Part of the reason for wake generation is the same as airplane lift [6–8]. Based on the propulsion of the airplane engine and the configuration characteristics of the wing surface, the pressure difference will be created when the air flows through the wing surface. For the reason that the air pressure of the lower wing surface is higher than that of the upper wing surface, the lift force is formed. At the same time, the high-pressure air from the lower surface of the wing will tumble around the tip of the wing and then get into the low-pressure air above the wing, forming two vortices at the rear. However, the structure of the vortex is small, the two wake vortices will induce each other to eventually form a horseshoe-shaped vortex.

As the aviation industry has grown, the quantity of airplanes has increased sharply, which means that the flight interval between airplanes has been reduced. So the impact of wake on the flight safety and air traffic control has become crucial. Another side effect of airplane wake is restricting airport throughput. That means that decreased utilization of airspace and runways will make it impossible to increase

Figure 1: Airplane wake vortex.

airport capacity and cause flight delays. In general, the adverse effects of the wake will damage the aerodynamic performance of the rear machine. In serious cases, flight accidents will be triggered, especially in the takeoff and landing, due to the decrease of flight speed and the poor aerodynamic performance [9, 10].

With the development of navigation technology and information technology, experts propose that the utilization of airspace can be improved by reducing the wake spacing of airplanes. However, the primary task of reducing wake separation is to detect and identify the wake of the airplane. The key to solve these problems is to detect and identify the dissipative characteristics of airplane wake by means of technology. In order to achieve this, the development of sensor technology and deep learning technology will provide us with a feasible scheme. The convolutional neural network (CNN) is considered to be one of the most widely used deep learning techniques such as target recognition and image processing, which can provide an idea of accurate eddy current identification based on a flow field image. With the addition of the CNN, the model can identify the flow field image and locate the wake accurately [11–16]. Concurrently, the long short-term memory (LSTM) network also has good performance in sequence feature extraction and data classification [17–19]. In addition, with the maturity of detection equipment technology, lidar has gradually become the most mature way to study airplane wake due to its high precision and high accuracy. At the same time, airport surveillance radar has been applied to airplane detection within the airport, which has also been proved to be effective in detecting and locating airplanes. The fusion of the two sensors can greatly improve the efficiency and accuracy of the wake location [20–31].

Therefore, this paper takes the detection and recognition of airplane wake in the near-Earth stage as the research content and detects the wind field in the flight channel of the airport with the help of Doppler lidar and a surveillance radar is used to obtain the real-time flight status of the airplane. Finally, deep learning technology is used to fuse information of different sensors and realize the accurate identification and prediction of the wake vortex. Effective identification of the wake vortex can improve flight safety and reduce the existing wake interval, so as to ensure flight safety. It is of great significance to the steady development of the civil aviation industry to reduce the second flight delay and relieve the capacity pressure of the airport.

2. Preliminary

As an important basis for studying the dissipation structure and characteristics of airplane wake, the field wind field measurement for wake can accumulate a large amount of measured data, which can be used to better mine the temporal and spatial characteristics of wake in different wind fields and through the auxiliary monitoring of the airport surveillance radar, so as to make the identification results more accurate, which is of great practical significance [5, 6, 31–36].

Coherent Doppler lidar is the product of the combination of traditional radar technology and modern laser technology, which possesses the characteristics of high range and angle resolution, accurate position information, strong antijamming ability, and all-weather operation. Due to unique four-dimensional scattering distribution, we need to fully consider the precise change of the tangential velocity of the wake in space and time and the working characteristics of the lidar. The detection content of coherent Doppler lidar includes the radial velocity information, signal-to-noise ratio information, Doppler spectrum, data and other information. In view of the above requirements, the continuous development of radar technology provides technical possibility for the field wind field measurement.

In order to obtain the 3D scanning of a complex wind field and the accurate data of airplane wake, wind3d 6000 coherent Doppler lidar was selected to collect the wind field data in airports through enough tests (see Figure 2 and Table 1).

Wind3d 6000 radars were placed in several airports to detect the wind field changes in the side direction perpendicular to the airplane wake vortices using the RHI scanning mode. By setting the change period of the pitch angle, we can get the wind field data image $H^k = (a_{ij})_{m\times n}$ in polar coordinates as shown in Figure 3, where a_{ij} is the radial

Figure 2: Wind3D 6000.

Table 1: Radar parameters.

Index item	Parameter
Laser wavelength	1.5 μm, invisible, and safe for the human eyes
Radial detection range	45 m~6000 m
Radial distance resolution	15 m/30 m/user setting
Data refresh rate	1 Hz~10 Hz, −37.5 m/s~37.5 m/s
Wind speed measurement accuracy	≤0.1 m/s
Scanning servo accuracy	Fixed point/DBS/VAD/PPI/RHI/ Cappi script programming

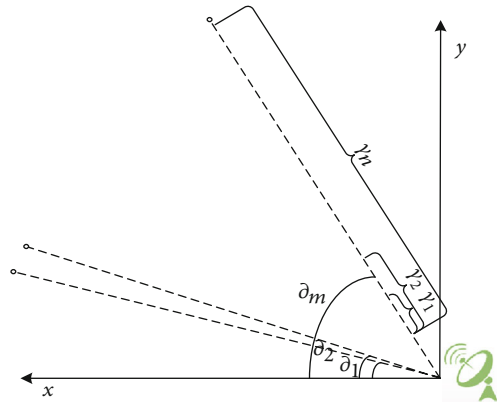

Figure 3: Detection principle in polar coordinates.

velocity of the wind field in different locations ($i = \partial_1, \partial_2, \cdots, \partial_m$ represents pitch angles and $j = \gamma_1, \gamma_2, \cdots, \gamma_n$ represents distances to range radar) [37–42].

Meanwhile, the airport surveillance radar can reliably monitor and track within 75–110 km of the airport and the flight altitude is less than 6000 m which can help coherent Doppler lidar to better obtain the flight state and airplane position (see Figure 4).

It is the fact that the data of the RHI wind field detected by the radar is easily interfered by the external atmospheric environment and the clutter of the equipment itself, in order to eliminate the interference of the signal echo in the transmission and detection process and to strengthen the tail vortex Doppler characteristics of the data. It is necessary to preprocess the data and eliminate the useless noise data and interference data [43–48]. At the same time, the surveillance radar data also needs corresponding spatiotemporal alignment and filtering.

3. Methodology

According to the characteristics of data generated by a multisensor, it is obvious that the data is fusion information composed of regional radial wind speed, wind field parameters, flight status, and airplane positioning. Supposing that it is necessary to identify the wake vortices in the wind field, the model needs to possess strong recognition ability for local features and sequence features.

In this paper, we employ a parallel DL framework—LSTM and CNN—to capture fusion information in wake vortex recognition. In this section, we first present a brief review of the traditional LSTM and CNN.

3.1. LSTM. Long short-term memory (LSTM) networks, a special RNN network, are designed to solve the problem of long dependence. The network was introduced by Hochreiter & Schmidhuber (1997) and has been improved and popularized by many people. Their work has been used to solve a variety of problems; until now, it has been widely used.

The core of LSTM is a cell state, which is represented by the horizontal line through the cell. Cells are in the same state as conveyor belts. It runs through the whole cell but has only a few branches, which can ensure that the information flows through the RNNs unchanged.

As a kind of deep learning model, long-term and short-term memory networks have a chain structure. Time stamps are used to connect cells, which can effectively enhance the memory ability of memory cells. Each memory cell is

Figure 4: Surveillance radar.

controlled by three parts: input gate, forgetting gate, and output gate. The input gate is mainly responsible for saving the input vector to the memory cell. In this process, some information will be deleted selectively by the forgotten door. After some processing, the new information will become the input information of the next memory cell and output the final result through the output gate after several iterations. The whole process schematic diagram of the LSTM model is shown in the figure below (see Figure 5).

3.2. CNN. As a convolutional neural network of the feedforward neural network, the connection mode of its neurons is inspired by the visual cortex of animals, with the least number of multilayer perceptron recognition variants. LeNet is an early convolutional neural network, which is Yann Lecun's successful work after many iterations. The convolution neural network can not only complete the work of the reading postal code and numbers but also accurately process images and recognize video data. Among them, the structure of the convolution neural network is mainly composed of four parts: the convolution layer, activation function, pooling layer, and fully connected layer.

3.2.1. Convolution Layer. The convolution layer is a kind of mathematical operation on the input variables. For example, convolution of variables will produce a third new variable. In the process of feature extraction, multiple filters are needed because the weights of different filters and data windows are different and fixed, so the content of each filter is different.

3.2.2. Activation Function. The activation function is to reflect the more complex mapping relationship in the model, that is, the acquired local features are mapped to the new feature map. At present, the common activation functions are sigmoid, $\tan h$, and ReLu. But the convolution layer usually uses ReLu as its activation function, because it can reduce the overfitting problem and make the calculation easier (see Figure 6).

3.2.3. Pool Layer. The pooling layer is a process of sample discretization, that is, to reintegrate the input sample data and reduce the dimension without reducing the sample characteristics. The most common pooling processes use

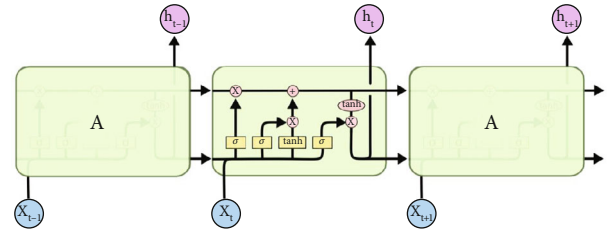

Figure 5: Structure of LSTM.

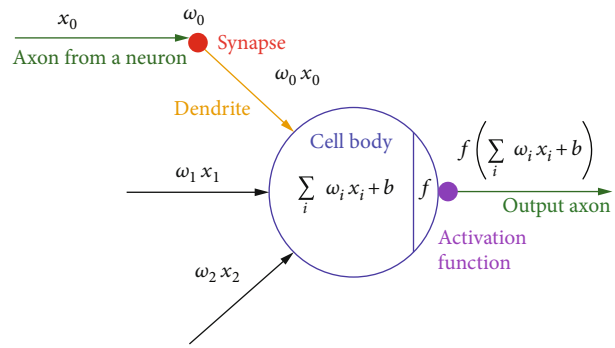

Figure 6: Activation function.

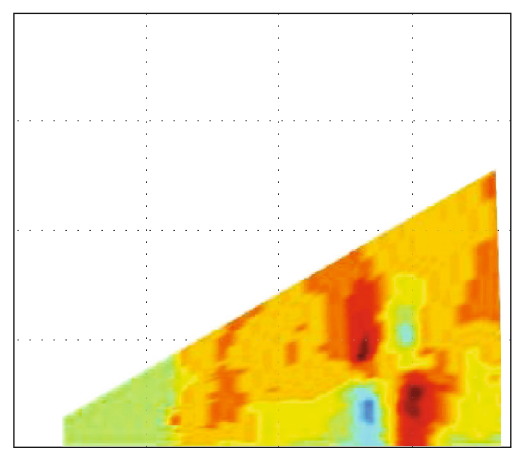

Figure 7: Wake vortex image in coherent Doppler lidar.

an abstract form to reduce the number of parameters and the difficulty of calculation.

3.2.4. Random Deactivation. As an artificial intelligence deep learning model, it has the advantages that the traditional model cannot compare; but because of too many parameter settings, it is easy to lead to model overfitting. When the problem of overfitting is solved by random deactivation (dropout layer), it is not necessary to add new constraints or train more models, only to change the eigenvalue of the hidden layer to 0 according to a certain proportion.

3.2.5. Full Connection Layer. As a multilayer perceptron, the all-connected layer refers to the connection between each

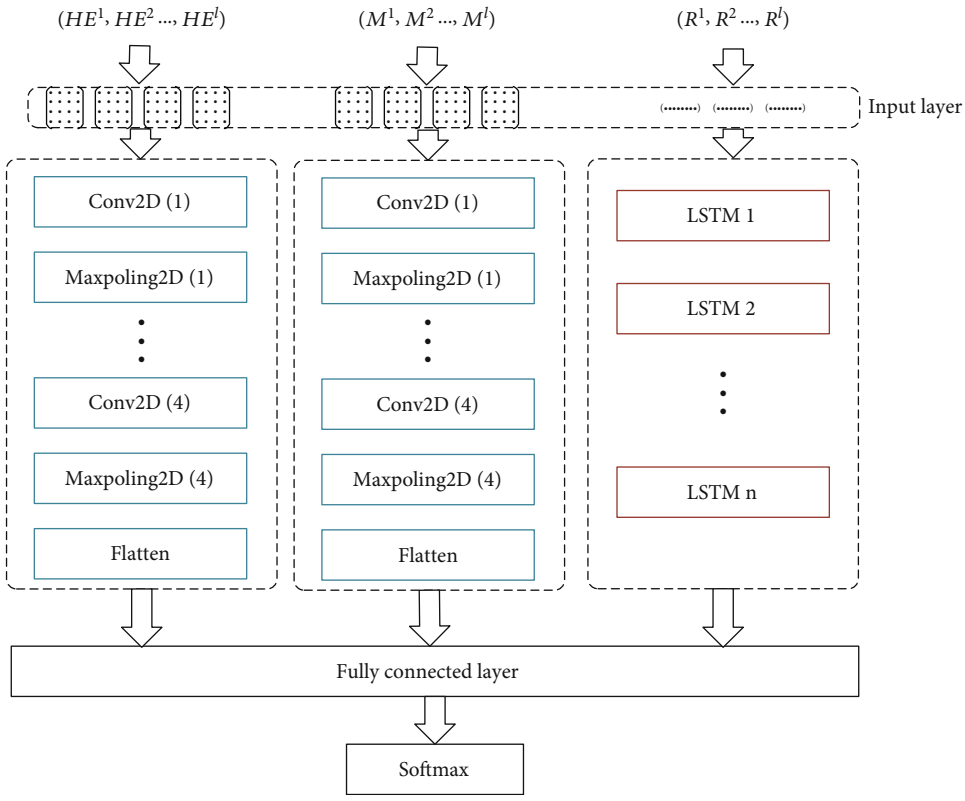

Figure 8: Framework of CNN-LSTM.

neuron in the former layer and each neuron in the latter layer. At the same time, the full connected layer calculates the hidden layer of the model through the linear function and obtains the final output results.

3.3. Combination of CNN and LSTM. Radar data usually appear in polar coordinates (see Figure 7). Therefore, the radar image must be accompanied by periodic characteristics and local characteristics. Focusing on the joint recognition of temporal and image features, the CNN and LSTM, respectively, show good performance in their respective fields. Local features will be better captured by CNN, and temporal features will be more suitable for LSTM. Hence, we will use a combined structure to recognize the wake vortex by a multisensor.

The spatial features in the radar image will be captured by the CNN in this paper. Firstly, due to the dimension requirement of the CNN for input variables, the wind field matrix produced by one radar scanning cycle will be expanded to the $n \times n$ matrix form which fills in the missing position with 0 ($H^k = (a_{ij})_{m\times n} \longrightarrow \mathrm{HE}^k = (a_{ij})_{n\times n}$). Supposing that we need to recognize the wake vortex in kth wind field images, the wake vortex will exhibit some special local characteristics which will trigger a series of wind field evolution. For these regular local features, the CNN will show a good learning ability.

In this paper, LSTM is applied to the learning of sequence features. For the wind field image, when the airplane wake is detected in the region, the wind field intensity around the wake vortex will show an obvious upward trend. In order to make the model better grasp this trend, this paper deals with the radar data according to the sequence characteristic. We can generate the variance sequence of the radial wind velocity of each radar record point at different pitch angles, and these sequences will contain wake vortex characteristics so that the LSTM model can grasp them.

$$R_j^k = \sum_i \left(a_{ij} - \mathrm{EX}_j\right)^2,$$
$$R^k = \left(R_1^k, R_1^k, \cdots, R_n^k\right), \tag{1}$$

where R^k is the variance sequence of the radial wind velocity and $j = \gamma_1, \gamma_2, \cdots, \gamma_n$ are data record points at different distances. EX_j represents the mean value of radial wind velocity of record point j at different pitch angles $i = \partial_1, \partial_2, \cdots, \partial_m$.

Furthermore, in order to better integrate airport surveillance radar information, we transform the spatial coordinate system of the airport surveillance radar into a 200×200 grid network, in which the grid accuracy is 20 m, where $M^k = (b_{ij})_{200\times 200}$ represents the airplane positioning matrix.

The applied combination of the CNN and LSTM is used to capture the spatial features HE^k, M^k and the sequence features $R^k = (R_1^k, R_1^k, \cdots R_n^k)$, where HE^k reflects the local change of regional wind field intensity, M^k can infer the accurate spatial position of airplane and wake, and R^k represents the difference characteristics of the wind field sequence. The

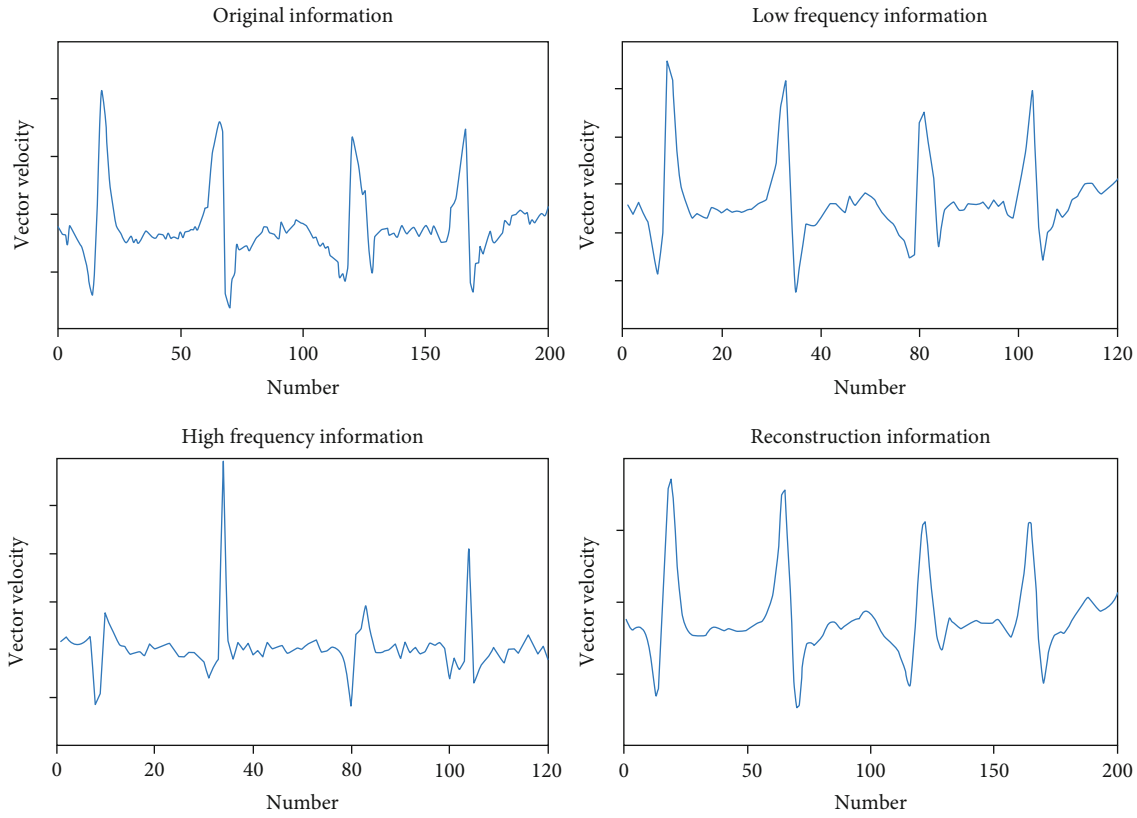

Figure 9: Data denoising results.

fusion of three spatial and sequential variables can greatly improve the detection accuracy of the airplane wake vortex.

Firstly, in order to realize the recognition of variable characteristics, the model will be divided into three channels for learning. Secondly, we add a full connection layer to achieve the fusion of local features and temporal features. Finally, a softmax layer is set to achieve information recognition and classification (see Figure 8).

4. Experiments and Results

4.1. Datasets. In this paper, the real-time wind field data has been generated by coherent Doppler lidars which have been located at Qingdao Liuting Airport (TAO) and Chengdu Shuangliu Airport (CTU) from Aug 16, 2018, to Oct 10, 2018. In addition, the airport surveillance radar data is also matched with the wind field data. In particular, various types of civil airplanes will take off and land at these airports, which will bring more promotion for the recognition accuracy and adaptability of the model.

Due to the low SNR of the echo signal, in order to reduce the interference of the high-frequency clutter in the sensor signal and retain the characteristics of the wake vortex contained in the low-frequency signal, this paper uses the discrete wavelet transform to process the signal. The discrete wavelet basis function is defined as follows:

$$\Psi_{b,c}(t) = \frac{1}{\sqrt{b}}\Psi\left(\frac{t-c}{b}\right). \quad (2)$$

Table 2: CNN parameters.

Layer (type)	Parameter
conv2d_1 (Conv2D)	(32, (3, 3), activation = "ReLu")
max_pooling2d_1	(2, 2)
onv2d_2 (Conv2D)	(64, (3, 3), activation = "ReLu")
max_pooling2d_2	(2, 2)
conv2d_3 (Conv2D)	(64, (3, 3), activation = "ReLu")
max_pooling2d_3	(2, 2)
conv2d_4 (Conv2D)	(64, (3, 3), activation = "ReLu")
dense_1 (dense)	64
dense_2 (dense)	1

Table 3: LSTM parameters.

Layer (type)	Parameter
dense_1 (dense)	64
dense_2 (dense)	32
Softmax	2

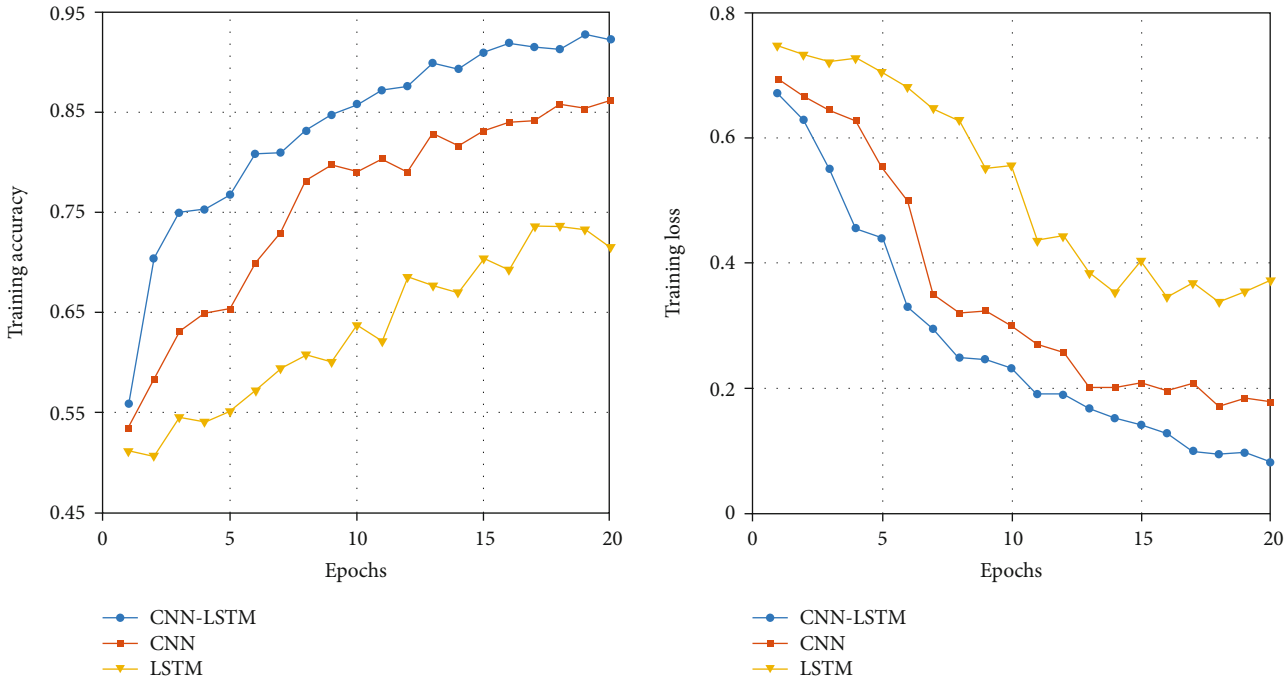

Figure 10: Training accuracy and loss.

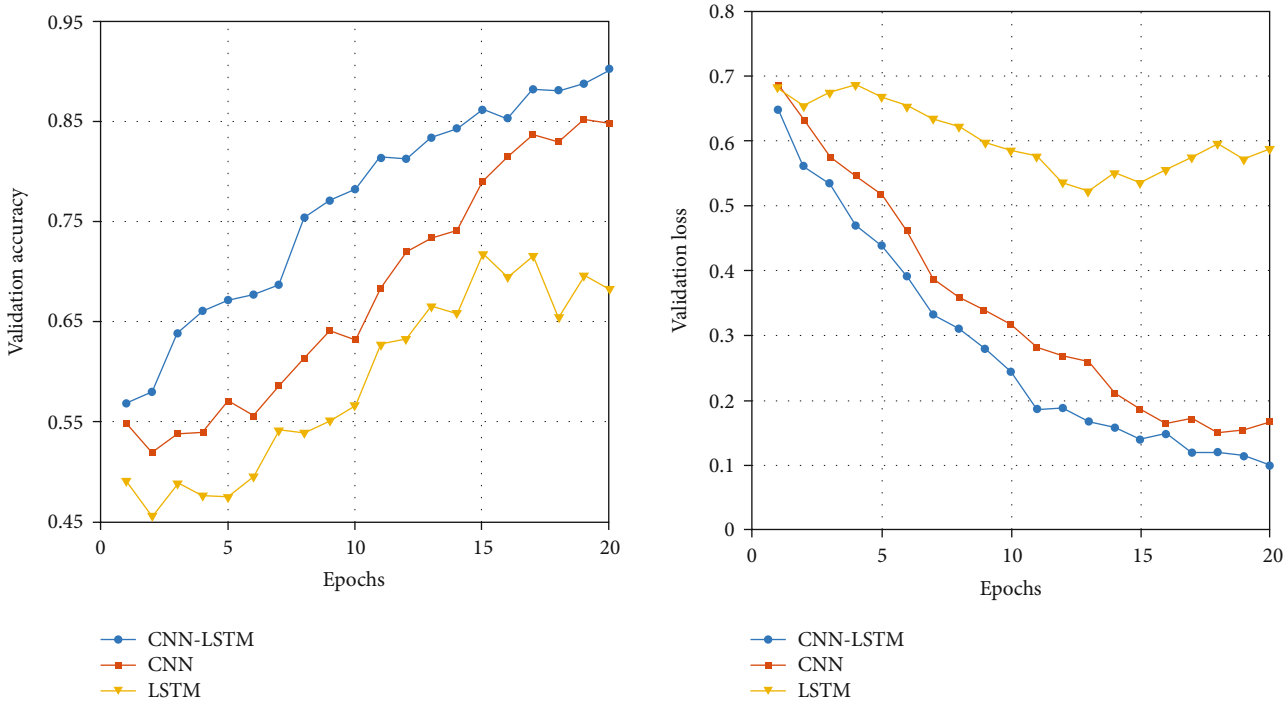

Figure 11: Validation accuracy and loss.

$\Psi_{a,b}(t)$ is wavelet basis, b is the scale factor, and c is the time translation factor.

In this paper, the high-frequency information and low-frequency information are separated with the wavelet denoising method:

It can be seen that after denoising, the signal-to-noise ratio of data has been significantly improved in Figure 9, which indicates that the data quality after denoising has been significantly improved.

For airport surveillance radar data, it includes the airplane flight number, registration number, wake level, longitude and latitude coordinates, and other parameters. However, track correlation and track filtering need to be carried out for all airplanes within the range based on the

Table 4: Predictive performance comparison.

Model	Training accuracy	Validation accuracy	Training loss	Validation loss
CNN-LSTM	0.922	0.901	0.083	0.099
CNN	0.862	0.847	0.179	0.167
LSTM	0.716	0.682	0.373	0.587

airplane registration numbers, so as to integrate them into relatively complete and smooth independent tracks.

In addition, the track coordinates and wind field coordinates of each aircraft are spatiotemporal aligned and standardized to ensure the real-time matching of the track and wind field.

4.2. Results. In this paper, the dataset will be partitioned into two parts: the first part is training data (40 days) and the second part is test data (16 days). The employed CNN-LSTM with full variables are trained on the training set and validated on the test set. Meanwhile, two CNN networks and a LSTM network with the same topology are adopted to train and test, respectively, where the wind field matrix HE^k, the airplane positioning matrix M^k, and the sequence features $R^k = (R_1^k, R_1^k, \cdots R_n^k)$ are used as the input variable of CNN and LSTM. The definitions of two models are shown in Tables 2 and 3 as follows:

Figures 10 and 11 show the learning performance of the CNN-LSTM, CNN, and LSTM on the training set, where the training accuracy and validation loss after each training epoch are recorded for all models. It can be observed that the training accuracy of CNN-LSTM increases faster than other models in the initial 5 epochs, and similarly, the training loss of CNN-LSTM also showed a faster decline rate. The training results indicate that CNN-LSTM has a higher convergence speed and learning performance than traditional model frameworks in wake recognition training. In addition, the training process of the LSTM network is relatively difficult due to the single information in variables.

In the following model validation process, the CNN-LSTM shows more excellent recognition ability than other models for the wake vortex in the wind field, which benefits from the fusion of sequence features and local features (see Figures 10 and 11). Moreover, the CNN also shows good image recognition ability, and on the contrary, the LSTM has some disadvantages for image features (see Table 4).

5. Conclusions

This paper presents a joint framework to detect and identify airplane wake vortices in the wind field based on a multisensor. The coherent Doppler radar has been proved to have excellent performance in the field of wind field detection. At the same time, airport surveillance radar data is innovatively introduced and fused with wind field data, where the integration of a track enables the model to capture the spatiotemporal variation characteristics of wake vortex easier. Besides that, the employed CNN-LSTM network can capture local features and sequence features simultaneously, which is especially desirable for image recognition with time series features. Therefore, aiming at the problem of wake recognition in the wind field, a fusion framework composed of CNN-LSTM and a multisensor has been regarded as an ideal solution. To validate the effectiveness of the proposed framework, the wind3d 6000 coherent Doppler radars have been installed to continuously monitor the wind field changes over the airport runway in several airports. After the discrete wavelet denoising, the fusion information from the multisensor is transformed into three input forms of the CNN-LSTM model—the wind field matrix and the variance sequence. Through the training and validation of the CNN-LSTM model, the recognition accuracy of this framework for the wake vortex in wind field reaches 90%, which is proved to have high practical value and research significance.

Furthermore, several future work can be considered in this study. Firstly, the model variables can be further integrated by introducing the time dimension. By combining the continuous wind field images into a continuous segment, the spatiotemporal information contained in variables will be significantly improved. It is worth noting that the deep learning framework also needs to be expanded on this basis, which will transform time variables and space variables into spatiotemporal variables. In addition, the influence factors of different meteorological conditions and wind conditions on the wake vortex can be introduced, which may greatly improve the recognition accuracy of the model.

This method provides a new idea for wake detection under multisensor and multisource data and innovatively realizes the real-time fusion and accurate prediction of the track and wake vortex.

Data Availability

The data used to support the findings of this study are available from the corresponding author upon request.

Conflicts of Interest

We declare that there is no conflict of interest.

Acknowledgments

This work was supported by joint funds of the National Science Foundation of China and the Civil Aviation Administration (grant number U1733203), Sichuan Science and Technology Project (grant number 2021JDRC0083), and funds of Civil Aviation Flight University of China (J2021-069 and J2020-075).

References

[1] S. Lang, J. Tittsworth, W. H. Bryant et al., *Progress on an ICAO Wake Turbulence Re-Categorization EffortAIAA Atmospheric and Space Environments Conference*, p. 7682, Toronto, Ontario, Canada, 2010.

[2] J. Babcock and R. Lind, "Aeroelastic Effects of Wing Stiffness on the Flight Dynamics of a MAV," in *AIAA Atmospheric Flight Mechanics Conference*, p. 4400, Minneapolis, Minnesota, 2012.

[3] T. Leweke and C. H. K. Williamson, "Experiments on long-wavelength instability and reconnection of a vortex pair," *Physics of Fluids*, vol. 23, no. 2, p. 024101, 2011.

[4] I. Hennemann and F. Holzäpfel, "Large-Eddy simulation of aircraft wake vortex deformation and topology," *Journal of Aerospace Engineering*, vol. 225, no. 12, pp. 1336–1350, 2011.

[5] R. E. Loucel and J. D. Crouch, "Flight-simulator study of airplane encounters with perturbed trailing vortices," *Journal of Airplane*, vol. 42, no. 4, pp. 924–931, 2005.

[6] D. Vechtel, "Flight simulator study on the influence of vortex curvature on wake encounter hazard using LES wind fields," *Aeronautical Journal*, vol. 116, no. 1177, pp. 287–302, 2012.

[7] D. Bieniek and R. Luckner, "Simulation of airplane encounters with perturbed vortices considering unsteady aerodynamic effects," *Journal of Airplane*, vol. 51, no. 3, pp. 705–718, 2014.

[8] G. Höhne, M. Fuhrmann, and R. Luckner, "Kritische Einflugbedingungen in eine Wirbelschleppe," *Aerospace Science and Technology*, vol. 8, no. 8, pp. 689–701, 2004.

[9] T. Sarpkaya, "New model for vortex decay in the atmosphere," *Journal of Airplane*, vol. 37, no. 1, pp. 53–61, 2000.

[10] T. Gerz, F. Holzäpfel, and D. Darracq, "Commercial aircraft wake vortices," *Progress in Aerospace Science*, vol. 38, no. 3, pp. 181–208, 2002.

[11] Y. LeCun, L. Bottou, Y. Bengio, and P. Haffner, "Gradient-based learning applied to document recognition," *Proceedings of the IEEE*, vol. 86, no. 11, pp. 2278–2324, 1998.

[12] A. Krizhevsky, I. Sutskever, and G. E. Hinton, "Imagenet classification with deep convolutional neural networks," *Advances in Neural Information Processing Systems*, vol. 25, no. 2, pp. 1097–1105, 2012.

[13] K. Simonyan and A. Zisserman, "Very deep convolutional networks for large-scale image recognition," 2014, http://arxiv.org/abs/1409.1556.

[14] C. Szegedy, W. Liu, Y. Q. Jia et al., "Going deeper with convolutions," in *Proceedings of the IEEE Conference on Computer Vision and Pattern Recognition*, pp. 1–9, New Orleans, LA, USA, 2015.

[15] K. He, X. Zhang, S. Ren, and J. Sun, "Deep residual learning for image recognition," in *Proceedings of the IEEE Conference on Computer Vision and Pattern Recognition*, pp. 770–778, New Orleans, LA, USA, 2016.

[16] J. Long, E. Shelhamer, and T. Darrell, "Fully convolutional networks for semantic segmentation," in *Proceedings of the IEEE Conference on Computer Vision and Pattern Recognition (CVPR)*, pp. 3431–3440, New Orleans, LA, USA, 2015.

[17] G. L. Tian, S. Zhou, G. X. Sun, and C. C. Chen, "A novel intelligent recommendation algorithm based on mass diffusion," *Discrete Dynamics in Nature and Society*, vol. 2020, Article ID 4568171, 9 pages, 2020.

[18] S. Bin and G. Sun, "Matrix factorization recommendation algorithm based on multiple social relationships," *Mathematical Problems in Engineering*, vol. 2021, Article ID 6610645, 8 pages, 2021.

[19] S. Hochreiter and J. Schmidhuber, "Long short-term memory," *Neural Computation*, vol. 9, no. 8, pp. 1735–1780, 1997.

[20] X. Ma, Z. Tao, Y. Wang, H. Yu, and Y. Wang, "Long short-term memory neural network for traffic speed prediction using remote microwave sensor data," *Transportation Research Part C: Emerging Technologies*, vol. 54, pp. 187–197, 2015.

[21] R. Zhao, R. Yan, J. Wang, and K. Mao, "Learning to monitor machine health with convolutional bi-directional LSTM networks," *Sensors*, vol. 17, no. 2, p. 273, 2017.

[22] S. Rahm, I. Smalikho, and F. Kopp, "Characterization of airplane wake vortices by airborne coherent Doppler lidar," *Journal of Airplane*, vol. 44, no. 3, pp. 799–805, 2007.

[23] S. Rahm and I. Smalikho, "Airplane wake vortex measurement with airborne coherent Doppler lidar," *Journal of Airplane*, vol. 45, no. 4, pp. 1148–1155, 2008.

[24] M. Keane, D. Buckton, M. Redfern et al., "Axial detection of aircraft wake vortices using Doppler lidar," *Journal of Airplane*, vol. 39, no. 5, pp. 850–861, 2002.

[25] F. Holzäpfel, "Probabilistic two-phase wake-vortex decay and transport model," *J. Airplane*, vol. 40, no. 2, pp. 323–331, 2003.

[26] D. C. Burnham and J. N. Hallock, "Decay characteristics of wake vortices from jet transport airplane," *J. Airplane*, vol. 50, no. 1, pp. 82–87, 2013.

[27] M. J. Pruis, D. P. Delisi, D. Jacob, and D. Y. Lai, "Summary of NASA wake and weather data collection. Memphis International Airport. 2013-2015," in *8th AIAA Atmospheric and Space Environments Conference*, p. 3274, Washington, DC, 2016.

[28] F. Holzäpfel, A. Stephan, T. Heel, and S. Körner, "Enhanced wake vortex decay in ground proximity triggered by plate lines," *Aircraft Engineering and Aerospace Technology*, vol. 88, no. 2, pp. 206–214, 2016.

[29] G. F. Switzer and F. H. Proctor, *Numerical Study of Wake Vortex Behavior in Turbulent Domains with Ambient Stratification*, AIAA, 2000.

[30] D. C. Lewellen and W. S. Lewellen, "The effects of Aircraft wake dynamics on contrail development," *Atmospheric Sciences*, vol. 58, no. 4, pp. 390–406, 2001.

[31] I. Hennemann and F. Holzäpfel, "Large-eddy simulation of airplane wake vortex deformation and topology," *Proceedings of the Institution of Mechanical Engineers, Part G*, vol. 225, no. 12, pp. 1336–1350, 2011.

[32] A. Stephan, F. Holzäpfel, and S. Zholtovski, "The effect of gusts on aircraft wake vortices," *Aircraft Engineering and Aerospace Technology*, vol. 89, no. 5, pp. 692–702, 2017.

[33] S. M. Mackey, F. Y. Wang, H. Wassaf, and M. Soares, "Comparison between arrival and departure wake vortex statistics near the ground," in *Proc. 1st CEAS European Air and Space Conf.,-Century Perspectives*, pp. 1049–1054, Berlin, Deutschland, 2007.

[34] D. Vechtel, "Simulation study of wake encounters with straight and deformed vortices," *Aeronautical Journal*, vol. 120, no. 1226, pp. 651–674, 2016.

[35] D. Bieniek, R. Luckner, I. De Visscher, and G. Winckelmans, "Simulation methods for aircraft encounters with deformed wake vortices," *Airplane*, vol. 53, no. 6, pp. 1581–1596, 2016.

[36] D. Bieniek and R. Luckner, "Simulation of Aircraft encounters with perturbed vortices considering unsteady aerodynamic effects," *Airplane*, vol. 51, no. 3, pp. 705–718, 2014.

[37] C. Schwarz and K.-U. Hahn, "Full-Flight Simulatorstudie zur Untersuchung von Wirbelschleppen- Gefahrdungsraumen," *Aerospace Science and Technology*, vol. 10, no. 2, pp. 136–143, 2006.

[38] R. Luckner, "Modeling and simulation of wake vortex encounters: state-of-the-art and challenges," in *AIAA Modeling and Simulation Technologies Conference*, p. 4633, Minneapolis, Minnesota, 2012.

[39] F. Holzäpfel, "Analysis of potential wake vortex encounters at a major European airport," *Aircraft Engineering and Aerospace Technology*, vol. 89, no. 5, pp. 634–643, 2017.

[40] R. Luckner, G. Höhne, and M. Fuhrmann, "Gefahrdungskriterien fur das Durchfliegen von Wirbelschleppen wahrend des Landeanfluges," *Aerospace Science and Technology*, vol. 8, no. 8, pp. 673–687, 2004.

[41] N. P. Schmitt, W. Rehm, T. Pistner, P. Zeller, H. Diehl, and P. Nave, "Der bordgetragene AWIATOR LIDAR Turbulenz-Sensor," *Aerospace Science and Technology*, vol. 11, no. 7-8, pp. 546–552, 2007.

[42] J. Ehlers, D. Fischenberg, and D. Niedermeier, "Wake impact alleviation control based on wake identification," *Airplane*, vol. 52, no. 6, pp. 2077–2089, 2015.

[43] J. Cheng, J. Tittsworth, W. Gallo, and A. Awwad, "The development of wake turbulence recategorization in the United States," in *8th AIAA Atmospheric and Space Environments Conference*, p. 3434, Washington, DC, 2016.

[44] J. N. Hallock, G. C. Greene, J. A. Tittsworth, P. D. Strande, and F. Y. Wang, "Use of simple models to determine wake vortex categories for new airplane," in *7th AIAA Atmospheric and Space Environments Conference*, p. 3172, Dallas, TX, 2015.

[45] D. A. Hinton, *Description of Selected Algorithms and Implementation Details of a Concept-Demonstration Airplane Vortex Spacing System (AVOSS)*, NASA TM-211027, 2001.

[46] F. Holzäpfel, K. Dengler, T. Gerz, and C. Schwarz, "Prediction of dynamic pairwise wake vortex separations for approach and landing," in *3rd AIAA Atmospheric Space Environments Conference*, pp. 15-16, Honolulu, Hawaii, 2011.

[47] I. Sölch, F. Holzäpfel, F. Abdelmoula, and D. Vechtel, "Performance of on-board wake vortex prediction systems employing various meteorological data sources," *Airplane*, vol. 53, no. 5, pp. 1505–1516, 2016.

[48] H. Frank, "Airplane wake-vortex evolution in ground proximity: analysis and parameterization," *AIA Journal*, vol. 45, no. 45, pp. 218–227, 2007.

Hindawi
Journal of Sensors
Volume 2021, Article ID 7193788, 9 pages
https://doi.org/10.1155/2021/7193788

Research Article

An IPv6 Passive-Aware Network Routing Algorithm Based on Utility Value Combined with Deep Neural Network

Zhiping Wan,[1] **Zhiming Xu**,[1] **Jiajun Zou**,[1] **Shaojiang Liu**,[1] **Weichuan Ni**,[2] **and Shitong Ye**[3]

[1]*School of Information Science, Guangzhou Xinhua University, Dongguan 523133, China*
[2]*Facility Management & Laboratory Division, Guangzhou Xinhua University, Dongguan 523133, China*
[3]*Department of Data Science, Guangzhou Huashang College, Guangzhou 511300, China*

Correspondence should be addressed to Shitong Ye; yst888_0@126.com

Received 23 October 2021; Accepted 12 November 2021; Published 28 November 2021

Academic Editor: Gengxin Sun

Passive sensing networks can maintain the operation of the network by capturing energy from the environment, thereby solving the energy limitation problem of network nodes. Therefore, passive sensing networks are widely used in data collection in complex environments. However, the complexity of the network deployment environment makes passive sensing nodes unable to obtain stable energy from the surroundings. Therefore, better routing strategies are needed to save network energy consumption. In response to this problem, this paper proposes an IPv6 passive-aware network routing algorithm for the Internet of Things. This method is based on the characteristics of passive sensing networks. By analyzing the successful transmission rate of the network node transmission link, transmission energy consumption, end-to-end transmission delay, and waiting delay of IPv6 packets, the utility evaluation function of the route is obtained. After the utility evaluation function is obtained, the network routing is selected through the utility evaluation function. Then, the utility value and the deep neural network method are combined to train the classification model. The classification model assigns the best routing strategy according to the characteristics of the current network, thereby improving the energy consumption and delay performance of the network.

1. Introduction

The Internet of Things is the expanding application and network extension of the communication network and Internet. It uses perception technology and intelligent devices to perceive and identify the physical world. It is interconnected by means of network transmission to complete the functions of numerical operation, signal processing, and information mining, so as to realize the information interaction and seamless connection between people, things and things, and between people and things, so as to achieve the purposes of real-time control, accurate management, and scientific decision-making of the physical world [1, 2]. The application range of the Internet of Things in the real world is very wide, including application fields such as smart home, vehicle network, underwater detection, human health monitoring, and industrial monitoring [3, 4]. The current research on the Internet of Things mainly revolves around the active perception network; that is, the nodes of the Internet of Things are equipped with power supplies by default, and there is no need to consider the energy problem of the Internet of Things nodes. However, the active perception network is no longer sufficient to meet people's actual application needs. Passive energy supply is an important link to truly solve the space and time constraints of the Internet of Things application and realize the large-scale application of the Internet of Things.

The passive sensing network refers to a network composed of passive sensing nodes. Its nodes are not equipped with themselves or are not mainly dependent on their own power supply equipment for power supply, but support their computing, sensing, communication, and networking by

obtaining energy from the environment [5, 6]. Since passive nodes can maintain the operation of the network by capturing the energy of the surrounding environment, they can adapt to many application scenarios with limited energy supply and are a very promising network form in the Internet of Things. However, the passive sensing network can capture the energy of the surrounding environment, but it does not mean that it can obtain energy supply stably for a long time. For example, for passive sensing nodes that rely on optical energy, they will also lack energy in the face of weak optical signals. Therefore, when selecting network routes, we still need to pay attention to the transmission energy loss of the network [7]. Moreover, passive sensing nodes are often deployed in complex environments to perform monitoring tasks, so the network transmission delay will be relatively high under the influence of environment and terrain. Therefore, the routing propagation delay of passive sensing networks is also a problem that needs to be paid attention to when studying routing protocols.

In the research of the passive network of the Internet of Things, Hadi et al. proposed a general QoS-aware scheduling program for passive optical networks. In this research, the author discussed the service differentiation dynamic bandwidth allocation scheme in time division and wavelength division multiplexing passive optical. In the network application, in order to further reduce the computational complexity, the optimized closed-form solution involved in each scheduling iteration is derived and the transmission delay is directly included in the scheduling, which effectively reduces the transmission delay [8]. Li-ting et al. proposed a passive network architecture of an optical data center with high throughput and low delay, using passive optical devices such as an arrayed waveguide grating router, coupler, and demultiplexer, and gave wavelength allocation and packet transmission methods for each scale of architecture, with lower delay and higher throughput [9]. Hong-Chao et al. propose an opportunistic routing protocol with energy consumption and delay balance in passive sensing networks. The protocol estimates the expected energy consumption of the node by analyzing the node communication process, so that the node selects the neighbor node with low energy consumption as the forwarding candidate. The protocol makes decisions by combining the duty cycle information of the next hop neighbor node of the candidate node, so that the transmitting node can select the candidate node that can forward data faster to reduce the delay, so as to achieve the balance of energy consumption and delay performance [10].

This paper mainly focuses on the routing transmission energy consumption and transmission delay of passive sensing nodes in the Internet of Things. In the second section, the successful transmission rate, transmission energy consumption, transmission delay, and waiting delay of IPv6 packets are analyzed, and the utility evaluation function of routing is obtained. In the third section, a model is trained by using the method of the deep neural network and the method of utility value, so that it can select the best routing strategy for the current network. The fourth section carries out simulation experiments on the research methods of this paper and analyzes the results.

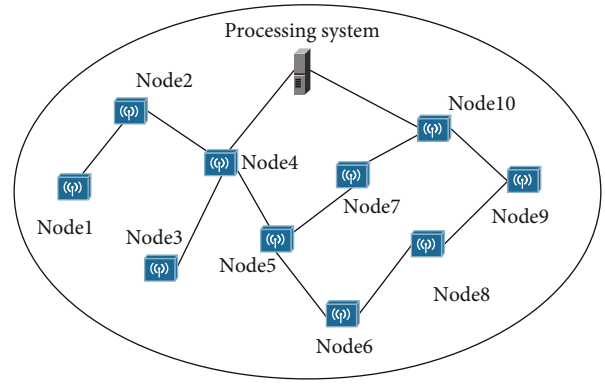

Figure 1: 10-node passive awareness network example.

2. Node Communication Link Analysis

In the passive sensing network of the Internet of Things, IoT devices located in the IPv6 network often need to send control/query commands to specific nodes in the passive sensing network, and these commands are encapsulated in IPv6 data packets. For example, the IoT center that performs monitoring tasks can send IPv6 packets to passive-aware network nodes deployed in complex environments through the IPv6 network to control the corresponding nodes to perform specific operations. This type of application requires that the transmission delay and transmission energy consumption be reduced as much as possible on the premise of reliable delivery of IPv6 packets. Figure 1 is a schematic diagram of a 10-node passive sensing network. The IoT node communicates with neighboring nodes within its communication radius to form a communication link, and there is a processing system in the network as the IoT center through the communication link sends control/query commands to IoT nodes.

2.1. Node Link Successful Transmission Rate. Using $(\text{node}_i, \text{node}_j)$ to represent the communication link between the i-th Internet of Things node node_i and the j-th Internet of Things node node_j in the network, the bit error rate of link $(\text{node}_i, \text{node}_j)$ is

$$\begin{aligned} \text{BRE}_{i,j} &= \frac{1}{2\pi}\int_a^{\infty} e^{-t^2/2}dt, \\ a &= \sqrt{\frac{2(P_t - P_{\text{loss}})B_N}{R}}, \end{aligned} \tag{1}$$

where $P_{\text{loss}} = P_l + 10\gamma \log_{10}(d_{i,j}) + P_t$.

P_l represents the power loss per unit distance, P_t represents the received power threshold of the device, and the received power threshold of all devices is the same by default. $d_{i,j}$ represents the distance between the i-th IoT node node_i and the j-th IoT node node_j, and γ represents the power attenuation coefficient.

In this network, assuming that IPv6 packets are sent using a dynamic allocation strategy, if $A_{i,j}$ is used to

represent the number of fragments used by node node_i in link $(\text{node}_i, \text{node}_j)$, the probability of success that node node_i successfully transmits a data packet to node_j by link $(\text{node}_i, \text{node}_j)$ for

$$p_{ij} = \left(1 - \text{BRE}_{i,j}\right)^{K_{v6}/A_{i,j}}, \tag{2}$$

where K_{v6} represents the length of the IPv6 packet.

2.2. Transmission Energy Consumption. For passive sensing networks, IoT nodes maintain the operation of the network by capturing energy from the environment. For example, nodes can perceive and capture energy from the surrounding environment such as sunlight, temperature, wind, and RF signals, so as to support the operation of IoT devices and solve the energy limitation problem of IoT. However, limited by the comprehensive impact of a complex environment, nodes cannot stably obtain energy from the surroundings for a long time. Therefore, reducing transmission loss and saving energy as much as possible is an important standard to evaluate node routing performance for passive sensing networks.

For the energy loss in the transmission link $(\text{node}_i, \text{node}_j)$, we use E_{ij} to represent the unit transmission loss of the link, which is expressed as

$$E_{ij} = \alpha^{-1} e_0 + \beta^{-1} e_1 D_i^2, \tag{3}$$

where α represents the transmission loss coefficient, e_0 represents the energy consumption of the node sending or receiving 1 bit on the circuit, e_1 represents the amplifier energy consumption for sending 1 bit of data under the communication radius D_i of the node i, and β represents the amplifier loss coefficient.

Then, a coded packet of length s is transmitted, and the sending energy consumption of node node_i is

$$E_{ij}{}^{t}(s) = sE_{ij}. \tag{4}$$

The receiving energy consumption of node node_j is

$$E_{ij}{}^{t}(s) = s\alpha^{-1} e_0. \tag{5}$$

Considering that the IPv6 packet adopts a dynamic allocation strategy, it needs to be decoded when $A_{i,j}$ coded packets are correctly received, so that node node_j can successfully receive a complete IPv6 packet. Therefore, here, we consider the transmission energy consumption in the case of successfully receiving an IPv6 packet. If the success probability ofnode_isuccessfully transmitting a data packet tonode_jthrough the$(\text{node}_i, \text{node}_j)$link is$p_{ij}$, the total transmission energy consumption of an IPv6 packet from node_i sending to node_j successfully receiving is

$${}^{*}E_{ij}{}^{t} = \frac{A_{i,j}\left(E_{ij} + \alpha^{-1} e_0\right)}{p_{ij}}. \tag{6}$$

2.3. End-to-End Transmission Delay. For passive sensing networks used in emergency scenarios such as disaster monitoring or battlefield environment monitoring systems, the requirements for link transmission delay are very high. Therefore, in order to construct a better node route, we also need to consider the transmission delay problem.

The transmission delay for node_i which transmits a data packet of length $l_{i,j}$ to node node_j is

$$\text{delay}_{ij} = t_p + \frac{l_{i,j}}{t_v}\left(1 + \varepsilon d_{i,j}\right), \tag{7}$$

where the subscript of $l_{i,j}$ means transfer from node_i to node_j, t_p represents the time required for a node to compete for channels and encode data before sending data packets, t_v represents the transmission rate of unit data, $l_{i,j}/t_v$ represents the transmission duration, and ε represents the loss factor per unit propagation distance.

We consider that$A_{i,j}$coded packets need to be correctly received before they can be decoded and reassembled into a complete IPv6 packet. According to the successful transmission probability p_{ij} of the data packet of the $(\text{node}_i, \text{nod e}_j)$ link, the delay from sending an IPv6 packet from node_i to node_j successfully receiving is

$${}^{*}\text{delay}_{ij} = \frac{t_p + \left(A_{i,j}/t_v\right)\left(1 + \varepsilon d_{i,j}\right)}{p_{ij}}. \tag{8}$$

2.4. Time Delay of Waiting IPv6 Packets. Because passive nodes may not be able to transmit IPv6 packets successfully due to insufficient energy, they need to wait until sufficient energy is captured from the surrounding environment to continue to complete the transmission of IPv6 packets. Therefore, for the transmission process of data packets, we also need to consider the waiting delay when the remaining energy of nodes is insufficient.

We assume that the remaining energy of node_i is E_i^p and that node_i needs to successfully send k IPv6 packets to node_j. If the remaining energy is insufficient, then the amount of energy that $node_i$ needs to capture is $E_{ij}^p(k)$:

$$E_{ij}^p(k) = k\frac{A_{i,j}E_{ij}}{p_{ij}} - E_i^p. \tag{9}$$

The electric energy that a node can obtain from the surrounding environment during the duration t is

$$E_c(t) = \delta\eta t, \tag{10}$$

where δ represents the charging efficiency coefficient of the node capacitor and η represents the average energy capture rate of the node.

According to formulas (9) and (10), when the remaining energy of node_i is E_i^p and k IPv6 packets need to be successfully sent to node_j, the required waiting delay t_{ij} is

$$t_{ij} = \frac{k\left(A_{i,j}E_{ij}/p_{ij}\right) - E_i^p}{\delta\eta}. \quad (11)$$

2.5. Routing Utility Evaluation Function. In order to enable the selected node routing strategy to comprehensively consider the performance of the link successful transmission rate, transmission energy consumption, transmission delay, and waiting delay of the passive sensing network of the Internet of Things, we adopt an optimal routing evaluation function to determine the utility value of node routing; a routing strategy with a higher utility value is more suitable for the current network. Taking the $(\text{node}_i, \text{node}_j)$ link as an example, we express the routing utility evaluation function as

$$Q_{ij} = \frac{w_1 p_{ij}}{w_2{}^* E_{ij} + w_3^* \text{delay}_{ij} + w_4 t_{ij}}. \quad (12)$$

w_1, w_2, w_3, and w_4 are the weighting factors of the link successful transmission rate, transmission energy consumption, transmission delay, and waiting delay, respectively, which can be specifically set according to the performance requirements of the network. ${}^*E_{ij}$ represents the total transmission energy consumption of the IPv6 packet from the sending of node_i to the successful reception of node_j, D represents the delay of the IPv6 packet from the sending of node_i to the successful reception of node_j, and the transmission delay calculated by t_{ij} includes the required when the remaining energy of the node is insufficient charging time.

Assuming that the route is $(\text{node}_1, \text{node}_2, \cdots, \text{node}_n)$, the best route evaluation function of the route is expressed as

$$\overline{Q_{1n}} = \frac{\sum_{i=1,j=i+1}^{n-1} Q_{ij}}{n-1}. \quad (13)$$

Through the best route evaluation function, we can determine the utility value $\overline{Q_{1n}}$ of the route $(\text{node}_1, \text{node}_2, \cdots, \text{node}_n)$. We can choose the node routing strategy according to the utility value. The route with the higher utility value is more likely to be selected as the best routing strategy.

However, currently, there are many routing strategies for the Internet of Things commonly used. To select the best routing strategy for the current network through the utility value method, the amount of calculation involved is very large. Therefore, in the following chapters, we use the deep neural network method, using specific network instances as input, 150 routing strategy IDs as labels, and the routing strategy ID with the largest utility value as the true label of the instance, to perform the deep neural network training. After the neural network model is trained, when a new network instance is inputted, the optimal routing strategy can be selected without performing utility value calculation.

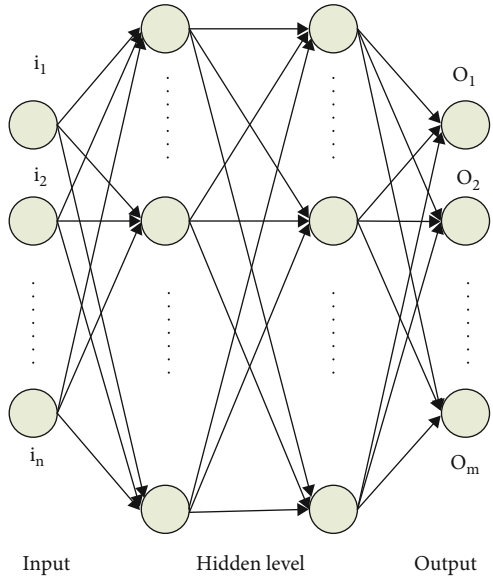

Figure 2: Deep neural network structure.

3. Routing Selection Based on Deep Neural Network

A deep neural network (DNN) is a neural network structure composed of a large number of neurons through an input layer, an output layer, and multiple hidden layers (usually at least two hidden layers). DNN has achieved great success in common tasks such as natural language processing, image processing, and other major machine learning problems [11, 12]. At present, the research field of the computer network also uses DNN technology to optimize the network. In the research of this paper, our node routing is selected by a deep neural network, and the neural network is trained by introducing a feedforward deep neural network and back propagation learning algorithm [13, 14]. In a feedforward network, information flows from the input node to the output node through the network without any feedback/loop connection. In the back propagation, the network model is optimized through the gradient optimization algorithm. The structure of the deep neural network is shown in Figure 2.

3.1. Neural Network Structure Used. In this algorithm, we construct the input layer node by taking the number of network nodes, node communication radius, network state, successful transmission probability of link, transmission energy consumption, end-to-end transmission delay of path, and waiting delay of the IPv6 packet as the characteristics of the instance. Taking the ID number of the optimal routing strategy corresponding to the example as the real output, the routing strategy is predicted by constructing the feedforward propagation from the input layer to the hidden layer and from the hidden layer to the output layer, and the parameters are learned by back propagation.

In order to make the constructed deep neural network play a role in routing selection, we used the characteristics

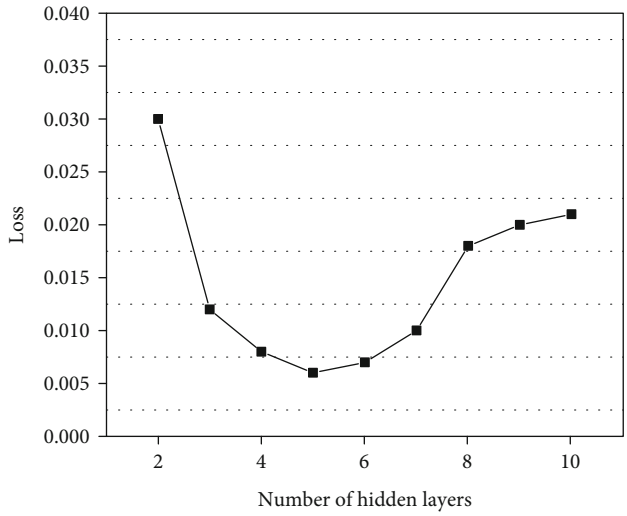

Figure 3: Model loss under different hidden layers.

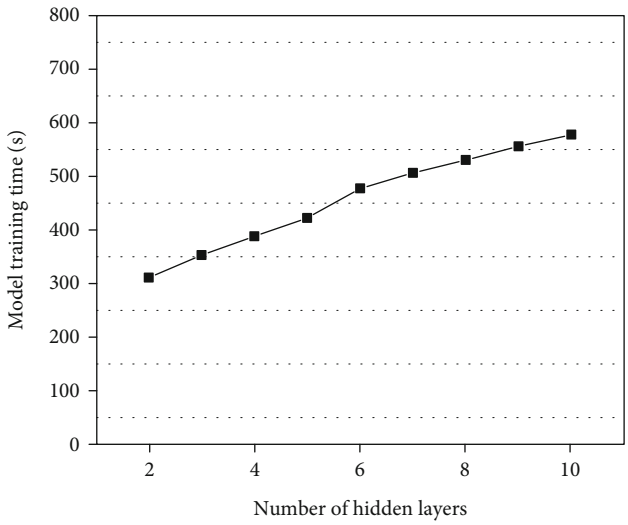

Figure 4: Model training time under different hidden layers.

of the data set, and the structure configuration of the constructed deep neural network model is as follows:

(1) *Network input layer*: the nodes of the input layer are determined according to the feature number of the data set. The input layer nodes are connected with the first layer hidden layer nodes, and the activation function of Relu is used. The form of the Relu function is as follows:

$$f(x) = \max(0,\infty). \tag{14}$$

x indicates that the Relu function gets inputted.

(2) *Network output layer*: the output layer uses the softmax function. The softmax function is often used in the multiclass structure of deep neural networks to normalize all output results. Each instance can only belong to one class (that is, a certain routing strategy):

$$S_i = \frac{e_i}{\sum_{i=1}^{m} e_i}, \tag{15}$$

where e_i represents the i-th output result; there are m outputs in total.

(3) *Network hidden layer*: we use 8 hidden layers. The number of nodes in the hidden layer can be adjusted according to the number of input characteristics of network instances. All hidden layers use Relu activation function.

(4) *Network loss function*: the loss function we use is "cross-entropy loss." Cross-entropy loss is very effective for estimating the loss of multiple classification methods. The form of the cross-entropy loss function used is as follows:

$$H(X) = -\sum_{i=1}^{n} p(x_i) \log(q(x_i)), \tag{16}$$

where x_i represents a specific instance and $p(x_i)$ represents the real label. In this article, when the label of the instance belongs to the real category, $p(x_i) = 1$. When the label of the instance does not belong to the true category, $p(x_i) = 0$. $q(x_i)$ represents the prediction result after the instance is processed by the model.

(5) *Network optimization method*: in this deep neural network model, we use Adam as the network optimizer. The learning rate is the default learning rate of the "Adam Optimizer," which is 0.001.

(6) *Number of network iterations*: the network model has been trained for multiple iterations in this article.

(7) *Index*: the performance evaluation index used is accuracy. The accuracy rate represents the proportion of the number of correctly classified instances to the total number of instances.

(8) *Verification data*: in order to verify the performance of the model, a verification split of 0.2 is used in this article; that is, we use 20% of the training data to verify the network model.

The flow of the entire algorithm is as follows:

(1) Select multiple routing strategies to build a routing set C

(2) For the data set composed of network instances, the label of each network instance is a routing policy in C, and the real label is the routing policy with the largest utility value of the network instance in C, wherein the utility value of the network instance is obtained according to the routing utility evaluation function of formula (12)

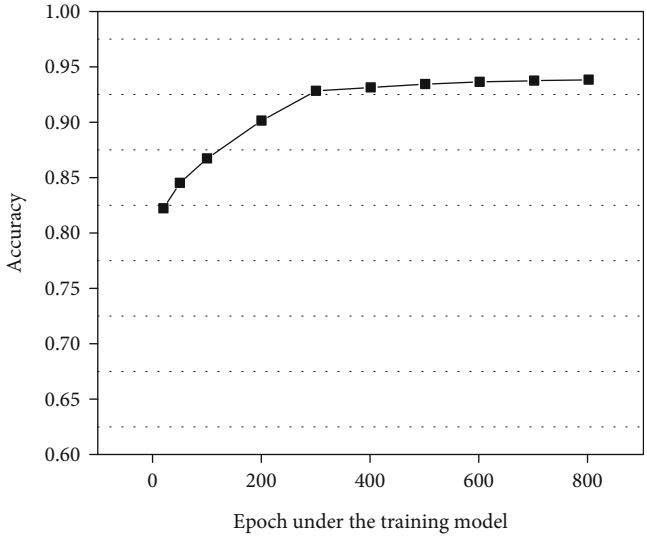

Figure 5: Model accuracy under different iterative training times.

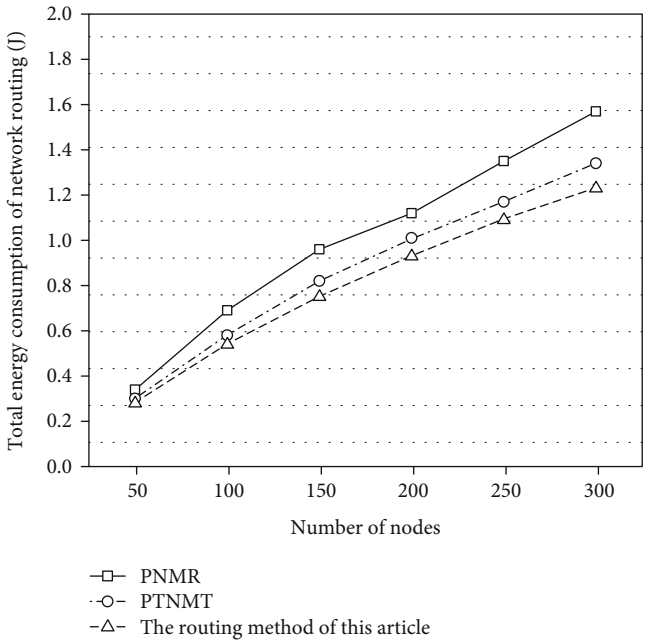

Figure 6: Total energy consumption of network routing under different numbers of nodes.

(3) After obtaining the real label of each network instance in the data set, the data set is divided into a training set, verification set, and test set, and is sent to the deep neural network model for training. The trained model can select the routing strategy with the maximum utility value for the network instance from the routing set C under the condition of a given network instance

3.2. Data Set Scheme. For the data set used for deep neural network model training, we use the OMNET++ simulator to obtain the simulated data set, which contains 50,000 instance samples. Each network instance sample contains

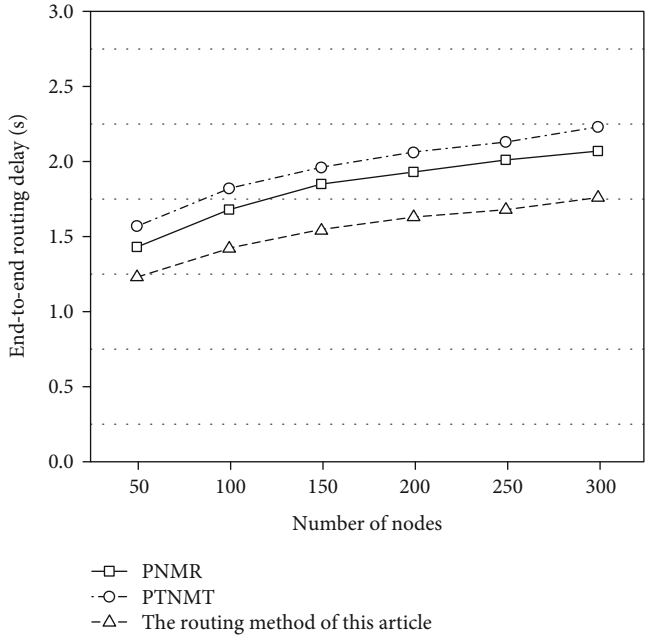

Figure 7: Total end-to-end routing delay under a different number of nodes.

several characteristics of the number of network nodes, node communication radius, network status, link's successful transmission probability, transmission energy consumption, end-to-end transmission delay of the path, and waiting delay of IPv6 packets. We equip the entire data set with 150 routing strategies as the classification result; that is, each network instance corresponds to an optimal routing strategy as the true label. The best routing strategy is determined according to the best routing evaluation mechanism proposed in this paper, which can make the routing strategy with the greatest utility value the best routing strategy. The 150 routing strategies include routing with minimum energy consumption, routing with minimum delay, general IoT node routing algorithms, and heuristic algorithms. The model obtains the best weights through training, so that when we enter a new network instance, we can base on the number of network nodes, node communication radius, network status, link's successful transmission probability, transmission energy consumption, and path. The end-to-end transmission delay and the waiting delay of IPv6 packets output an optimal routing strategy.

4. Experimental Simulation Results

Before getting the final usable deep neural network model, we first analyze the influence of different hidden layers on the model in the experimental test link, so as to determine an optimal number of hidden layers. We test the loss and training time of the model according to the number of hidden layers, and test the accuracy of our model under different iteration times. We show the results of the model on the test data set. The deep neural network model adopts the PyTorch framework and is implemented using Python language programming. The PC configuration used in the

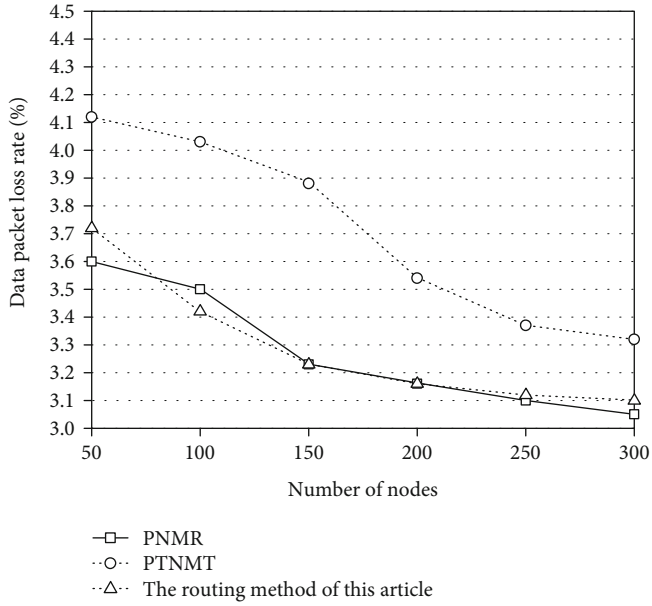

Figure 8: Average data packet loss rate.

experiment includes NVIDIA GeForce RTX 3080 Ti 12 GB GDDR6 video memory, Intel i9 processor, 32 G memory. Different hidden layers are all experimented on the same computer. The result obtained is shown in the following figure.

Figure 3 shows how the training loss of the model changes with the number of hidden layers. It can be seen from the figure that the training loss gradually increases after 5 hidden layers. In deep neural networks, the number of hidden layers is not as large as possible. Sometimes, using more hidden layers than required by the model will cause the model's classification ability to decrease. Therefore, for this article, using a 5-layer hidden layer deep neural network to achieve routing strategy selection will get better results.

It can be observed from Figure 4 that the training time of the model will increase as the number of hidden layers increases. Since we set the same number of neurons in each hidden layer, as the number of hidden layers increases, the number of neurons will also increase. In a deep neural network, each neuron has a weight, so more neurons will increase the amount of weight calculation, so the training time will increase as the number of hidden layers increases.

Figure 5 shows the accuracy of the model on the test set after training under different iterations of the training set. It can be seen from the figure that when the training set is iterated to 300 times, the accuracy of the model converges to a certain value, and then, the accuracy value will not change significantly.

Through the above experiments, we have determined that the deep neural network model of this article uses 5 hidden layers and only iterates 300 times during the training process to optimize the model parameters to obtain our final model results. In order to verify the effectiveness of the trained model in node routing, we use the trained model and other algorithms to compare the total energy consumption of routing transmission and the total end-to-end transmission delay. The comparison algorithms are the passive network multipath routing proposed in the literature [15] (here, we abbreviate it as PNMR for the convenience of expression) and the passive label network multihop routing protocol proposed in the literature [16] (here for the convenience of expression, we referred to it as PTNMT) for comparison. Among them, literature [15] conducts network multipath routing detection from link average delay and load balancing, and literature [16] considers the problems of asymmetry of communication links and transmission interference in passive sensing networks.

We first conducted a comparison experiment on routing energy consumption. With different numbers of nodes, we let the system randomly select the source node and the destination node, and then, we let the three comparison algorithms choose the node route by themselves, so that the source node can successfully transmit the IPv6 packet to the destination node. Figure 6 shows the total energy consumption of the PNMR method, PTNMT method, and the method in this paper under a different number of nodes in the network routing. It can be seen from the figure that as the number of network nodes increases, the total energy consumption of the network routing of the three algorithms continues to increase. When the number of network nodes is small, the total energy consumption of the routing of the three algorithms is relatively close. When the number of network nodes increases, the total energy consumption of routing in this paper will be less, because the deep neural network model of this paper will select the best routing strategy for the current network to reduce end-to-end transmission loss.

In another group of comparative experiments, we also let the system randomly select the source node and destination node under different number of nodes, then let the three comparison algorithms select the node route by themselves, and record the delay time when they successfully transmit

IPv6 packets from the source node to the destination node. As can be seen from the results in Figure 7, for Figure 7, the end-to-end routing delay of the network may increase with the increase of the number of nodes. This is because when the number of nodes increases, and the source node and destination node are randomly selected by the system, the number of routing hops from the source node to the destination node may need to be more and the delay will be greater. In Figure 7, we can see that the method in this paper has less end-to-end routing delay than the other two algorithms.

The following figure shows the comparison of the average data packet loss rate of the three algorithms. It can be seen from the results in Figure 8 that as the number of nodes increases, the distribution of the average data packet loss rate of the network will gradually decrease and tend to be flat. Since the source node and the destination node are randomly selected by the system, when the number of nodes is small, the probability of link interruption may increase, resulting in a higher network packet loss rate. From the comparison of the three algorithms, it can be seen that the data packet loss rate of the algorithm in this paper is close to that of the PNMR algorithm, and the packet loss rate of the PTNMT algorithm is smaller.

5. Conclusions

In the Internet of Things, a passive sensing network can capture energy from the surroundings through Internet of Things devices, so as to solve the problem of energy limitation when the Internet of Things is deployed in the field environment. However, the uncertainty of the field environment makes the Internet of Things devices unable to capture stable energy, and node routing still needs to reduce energy loss as much as possible. Therefore, this paper studies an IPv6 passive sensing routing strategy selection method for the Internet of Things, which is aimed at reducing the data transmission energy consumption and transmission delay of node routing, and at improving the operation efficiency of the network. Combined with the method of the deep neural network, this paper intelligently selects routing strategies for the current network through an artificial intelligence model. Simulation results show that the proposed method can reduce the transmission energy consumption and transmission delay of the network.

Data Availability

The data used to support the findings of this study are available from the corresponding author upon request.

Conflicts of Interest

The authors declare that they have no known competing financial interests or personal relationships that could have appeared to influence the work reported in this paper.

Acknowledgments

This research is supported by the Characteristic Innovation Projects of Ordinary Universities in Guangdong Province (2018KTSCX319) and Key Discipline Project Guangzhou Xinhua University (No. 2020XZD02).

References

[1] F. Piccialli, S. Cuomo, N. Bessis, and Y. Yoshimura, "Data science for the Internet of Things," *IEEE Internet of Things Journal*, vol. 7, no. 5, pp. 4342–4346, 2020.

[2] D. Cao, L. Li, C. Marina, L. Chen, Y. Xing, and W. Zhuang, "Special issue on Internet of Things for connected automated driving," *IEEE Internet of Things Journal*, vol. 7, no. 5, pp. 3678–3680, 2020.

[3] F. Li, K. Y. Lam, X. Li, Z. Sheng, J. Hua, and L. Wang, "Advances and emerging challenges in cognitive Internet-of-Things," *IEEE Transactions on Industrial Informatics*, vol. 16, no. 8, pp. 5489–5496, 2020.

[4] Z. Wan, Z. Xu, S. Liu, W. Ni, and S. Ye, "An Internet of Things roaming authentication protocol based on heterogeneous fusion mechanism," *IEEE Access*, vol. 8, pp. 17663–17672, 2020.

[5] Z. Zhou, "The connection engine of the Internet of Things: passive sensing network," *Computer Science and Application*, vol. 10, no. 11, pp. 2089–2094, 2020.

[6] S. Denis, B. Bellekens, A. Kaya, R. Berkvens, and M. Weyn, "Large-scale crowd analysis through the use of passive radio sensing networks," *Sensors (Basel, Switzerland)*, vol. 20, no. 9, pp. 2624–2632, 2020.

[7] H. Hwang, J. H. Lim, J. H. Yun, and B. Jeong, "Pattern-based decoding for Wi-Fi backscatter communication of passive sensors," *Sensors*, vol. 19, no. 5, pp. 1157–1176, 2019.

[8] M. Hadi, C. Bhar, and E. Agrell, "General QoS-aware scheduling procedure for passive optical networks," *Journal of Optical Communications and Networking*, vol. 12, no. 7, pp. 217–226, 2020.

[9] X. Li-ting, Z. Shao-biao, and J. Xu-han, "Research of two optical data center network frameworks with high throughput and low latency," *Study on Optical Communications*, vol. 222, no. 6, pp. 21–24, 2020.

[10] H.-C. Gao, X.-J. Chen, D. Xu, Y. Peng, Z.-Y. Tang, and D. Y. Fang, "Balance of energy and delay opportunistic routing protocol for passive sensing network," *Journal of Software*, vol. 30, no. 8, pp. 2528–2544, 2019.

[11] G. E. Dahl, Dong Yu, Li Deng, and A. Acero, "Context-dependent pre-trained deep neural networks for large-vocabulary speech recognition," *IEEE Transactions on Audio Speech & Language Processing*, vol. 20, no. 1, pp. 30–42, 2012.

[12] S. Liu, K. Hu, W. Ni, Z. Xu, F. Wang, and Z. Wan, "A cognitive relay network throughput optimization algorithm based on deep reinforcement learning," *Wireless Communications and Mobile Computing*, vol. 2019, Article ID 2731485, 8 pages, 2019.

[13] X. Zhang, Y. He, and S. Jian, "Channel pruning for accelerating very deep neural networks," in *IEEE International Conference on Computer Vision*, IEEE Computer Society, 2017.

[14] X. Huang, M. Kwiatkowska, S. Wang, and M. Wu, "Safety verification of deep neural networks," in *International Conference on Computer Aided Verification*, Springer, Cham, 2017.

[15] S. Pan, Y. Wang, M. Xiong, L. Gu, and G. Hu, "Detection of multipath routing with passive delay measurements," in *IEEE INFOCOM 2019-EEE Conference on Computer Communications Workshops (INFOCOM WKSHPS)*, Paris, France, 2019.

[16] C. Liu, Z. J. Haas, and Z. Tian, "On the design of multi-hop tag-to-tag routing protocol for large-scale networks of passive tags," *IEEE Open Journal of the Communications Society*, vol. 1, pp. 1035–1055, 2020.

Hindawi
Journal of Sensors
Volume 2021, Article ID 6441770, 9 pages
https://doi.org/10.1155/2021/6441770

Research Article

Application of Traditional Graphic Elements Based on Fiber Bragg Grating Tactile Sensor Technology

Jing Xu

Art College, Jimei University, Xiamen City, Fujian Province 361021, China

Correspondence should be addressed to Jing Xu; 2008110102@st.btbu.edu.cn

Received 23 September 2021; Accepted 18 October 2021; Published 17 November 2021

Academic Editor: Gengxin Sun

In today's era, sensing technology has been very developed in the fields of machinery, medicine, safety monitoring, and so on. In order to be applicable to more fields, new sensing technologies are also evolving. Tactile and sensory states are two important indicators of human induction to external things. Based on the contact force information between fiber Bragg grating tactile sensor and human body, this paper uses a new fiber Bragg grating tactile sensing system to study the artistic elements of ink painting in modern graphic design. Subsequently, the structure and specific performances of the sensor experimental data are analyzed. With its small volume, low cost, high sensitivity, and good compatibility with the observed body, the new fiber Bragg grating tactile sensor will not be affected by external electromagnetic interference, various noise signals, complex integration, and other problems. According to the data observed by ink painters in this paper, the new tactile sensing technology of fiber Bragg grating can well control the external interference factors. In general, the technology is of great social and practical value.

1. Introduction

Tactile sensing is not only an important function of fiber Bragg grating sensor but also an important correlation part between human and robot hand [1]. In order to obtain the specific strength, temperature, angle, and other information, tactile sensing is also required, so as to help the robot hand complete the difficult operation of ink painting. The so-called fiber Bragg grating sensor is equivalent to the "skin" of the robot hand [2]. Tactile sensors are widely used in all walks of life, such as in modern graphic design [3, 4]. In the past, there were many graphic designers in the modern graphic design industry, but there was a special lack of technical talents of traditional ink painting technology [5]. According to relevant water information, the design fees of graphic designers of ink painting are very high, which cannot be borne by the general public. In recent years, it has been learned from relevant news information that the relevant technology of robot hand replacing human work has been gradually widely used in all walks of life [6]. So far, in all kinds of large, medium, and small factories using assembly line operation, robots have completely replaced human manual production, and the completion efficiency is also very high [7, 8]. However, for the past sensor technology, the graphic design direction of ink painting studied in this paper is simply impossible to achieve. In recent years, with the progress of science and technology, there are more and more types of sensors. With the emergence of fiber Bragg grating sensors, robots have also appeared in the field of modern graphic design to replace human operations [9]. By wearing the sensor on the observation body, the designer receives the data of strength, temperature, and other aspects in the graphic design of ink painting and finally applies it to the machine [10, 11]. Instead of human operation, machines do not need to consider external abnormal factors, which improve the use efficiency.

Tactile sensors have evolved many different forms in recent years [12]. In the past, there were current type, voltage type, piezoresistive type, and so on. Ordinary tactile sensors have a lot of problems at the level of electromagnetic signal interference and signal interference [13]. Compared with the traditional tactile sensor, the tactile sensor based on optical fiber technology has better performance in precision measurement, performance stability, and sensitivity

[14]. In recent years, there are more and more researches in polymer optical fiber. Many researchers say that sensors based on optical fiber technology can indeed promote the development of science and technology. Then, based on the above development of tactile sensors, the fiber Bragg grating sensing technology is proposed [15]. This technology can accurately observe all kinds of tactile index information of ink painting graphic designers in design.

Based on the above, the sensor often has the problems of inaccurate test data, large volume, and high cost. This paper creatively uses a new fiber Bragg grating tactile sensing system to study the artistic elements of ink painting in modern graphic design. A fiber Bragg grating structure is added to the fiber Bragg grating tactile sensor. The new FBG (fiber Bragg grating) tactile sensor is applied to the design of traditional ink painting. The FBG new tactile sensing structure is very sensitive to small forces, and strain can be analyzed by various forces. The new fiber Bragg grating tactile sensor has the advantages of small volume, low cost, high sensitivity, and good compatibility with the measured object and will not be affected by external electromagnetic interference, various noise signals, complex integration, and other problems.

This paper is mainly divided into three parts. The first part briefly describes the development of tactile sensing technology and fiber Bragg grating sensor. In the second part, the fiber Bragg grating sensor technology is selected to study the tactile observation of ink painting designers. First, the sensor structure in tactile observation of ink painting graphic designers is optimized, and Bragg (FBG) structure is added. Finally, the overall performance of FBG tactile sensor is designed and studied. In the third part, based on the fiber Bragg grating sensing technology, the sensor structure is analyzed through the tactile information obtained by the observer. And the results of each performance are analyzed.

2. Related Work

Tactile observation of ink painting designers is a part of tactile sensor technology. First, the tactile sensor is used to observe the tactility of the ink painting designer. Finally, the observed tactile information is saved. However, in the process of observing the designer, the intervention of some external temperature cannot be avoided, such as poor contact, temperature, noise, and other influencing factors [16]. In order to achieve the correct and comprehensive tactile information, fiber Bragg grating sensing technology has been used in designers' tactile observation in recent years [17, 18]. The core content of fiber Bragg grating sensing technology is to observe the behavior information of the observer in all aspects. A new tactile sensing structure of FBG is added to the core technology of this paper. Compared with the normal fiber Bragg grating sensing technology, FBG new tactile sensor technology can better observe the detailed data information [19]. It is more suitable for the designer to check the tactile behavior in the process of designing ink painting. In the new FBG tactile sensor, the performance of the sensor is also improved and analyzed. Through the design and performance analysis of fiber Bragg grating sensor in sensitivity, resolution, repeatability, and hysteresis, the tactile observation of ink painting designers is finally realized.

Sensor technology is mainly used in the field of robot creation [20]. At the beginning of contact with the sensor, the fingers are made of composite materials. Finally, after various experimental tests, the machine fingers in the experiment can grasp objects accurately. The force of grasping objects is very close to the human force [21]. Up to now, the robot technology manufactured has always been a global leader [22]. It can be seen that the use of sensors has promoted the development of intelligent robots.

The application of sensors has a great impact in the field of medicine. As we all know, the success rate of retinal minimally invasive surgery is very high. It is incredible that the application of sensor technology is added to the probe used in the operation, which is also the key to greatly improve the success rate of surgery [23]. According to relevant data, the research team spent five years studying this technology. Nowadays, the development of medical technology is also very mature.

Sensors are widely used in the machinery industry [24]. The speed of development of the automotive industry is obvious to all. In the automobile manufacturing industry, Germany uses sensors to simulate manual manufacturing. Through the addition of a manipulator, the speed and performance of manufacturing various automobile parts are greatly improved, and a large part of expenses are saved.

The application of sensors has become more and more extensive in the past decade. Nowadays, sensing technology is applied in the research of promoting human sleep. The sensor itself cannot promote sleep quality. The sensor is placed under the mattress to detect a series of behaviors during human sleep [25]. After analyzing the information through sensors, we can infer the sleep stage of human beings. Finally, the data is changed into tracks, and the switch and volume of tracks are automatically adjusted, so as to improve the sleep quality. Based on the fiber Bragg grating sensing system under the sensor, this paper collects the tactile information of the target person. Then, the FBG structure is added to the fiber Bragg grating sensing system to improve the overall performance. Then, put the sample data into the FBG new tactile sensor for performance test, and finally, apply the FBG new tactile sensor to the graphic designer of ink painting.

3. Research on Tactile Observation Technology of Graphic Designers of Ink Painting Based on Sensor Technology

3.1. Research on Sensor Structure Design of Tactile Observation for Graphic Designers of Ink Painting Based on Sensor Technology. When the FBG sensor receives the influence of both force and temperature, it will change the wavelength of the reflection center. The sensor achieves the sensing effect by collecting the parameter information generated by the observer and the wavelength of the reflection center. The fiber Bragg grating sensing experimental

measurement system includes FBG sensor, PC, mediator, and other operating software. In this paper, the FBG sensor is combined with the fiber Bragg grating system. The demodulation software in the fiber Bragg grating system transmits the broadband light source to the FBG sensor. The FBG sensor modulates the light wave after receiving the light source information. Then, the modulated light wave is reflected into the fiber Bragg grating demodulation equipment through the sensor, the modulated light wave is decomposed, and finally, the decomposed light wave is transmitted to the PC. In short, the whole FBG new tactile sensor can feel the external parameter information on the ink painting designer. Finally, the information is transformed into wavelength change. The principle of the whole sensing system is shown in Figure 1.

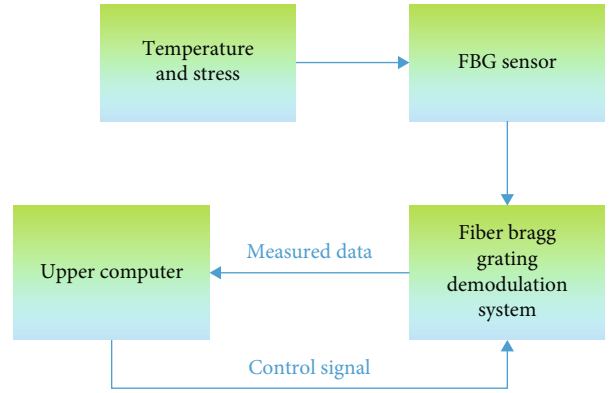

Figure 1: Schematic diagram of sensing system.

As can be seen from Figure 1 is the information transmission process of the whole system of the whole FBG sensor in sensing detection. After designing the overall structure of FBG sensor, the components are integrated into the new tactile sensor, and the preliminary design of the whole sensor has been completed. In the whole FBG sensor system, there is also a major structural basis called fiber Bragg grating system. The construction diagram of fiber Bragg grating system is shown in Figure 2.

As shown in Figure 2, the PC accurately controls and stores various indexes and motion parameters transmitted by the observer through the sensor. In this way, according to the experiment in this paper, the parameters generated by the ink painting designer when designing his works can be stored on the PC. It can be seen from the above that the external parameters are formed by the changes of force and temperature and are also the main factors that can affect the wavelength change in the grating reflection of fiber Bragg. Under the condition of temperature change, the thermal effect and expansion effect of temperature will affect the refractive index and fiber grating period. The relationship formula between the above temperatures is

$$\frac{\mathrm{d}\lambda_\beta}{\lambda_\beta} = \left(\frac{1}{\eta}\frac{d\eta}{dT} + \frac{1}{\wedge}\frac{d\wedge}{dT}\right)dT. \tag{1}$$

In this formula, it is assumed that the thermal coefficient is $\varepsilon = (1/\eta)(d\eta/dT)$ and the expansion coefficient is $\alpha = (1/\wedge)(d\wedge/dT)$. The influence formula of temperature on fiber Bragg grating can be deduced. See the following equation:

$$\frac{\mathrm{d}\lambda_\beta}{\lambda_\beta} = (\alpha + \varepsilon)dT. \tag{2}$$

The influence of force on Fiber Bragg grating is mainly based on the axial and transverse deformation caused by force on the basis of fiber Bragg grating. Because the optical fiber will undergo axial deformation when stretched by force, the transverse deformation can be directly ignored. Based on the above information, the reflection center wavelength formula and variable formula are

$$\lambda_\beta = 2\eta\wedge, \tag{3}$$

$$\frac{d\lambda_\beta}{\lambda_\beta} = (1 - P)\varepsilon_X. \tag{4}$$

P is the elasto-optic coefficient, and ε_X is the change of axial force. Combined with the above equation, the reflection center wavelength under the action of temperature and force is expressed as follows:

$$\frac{d\lambda_\beta}{\lambda_\beta} = (1 - P)\varepsilon_X + (\alpha + \varepsilon)dT. \tag{5}$$

With the addition of the technology of the above equation, the construction of the whole sensor can save more computation. The research direction of this paper is mainly based on a series of parameters produced by ink painting designers when painting. In selecting the types of sensors for observation, we should not only meet the conditions of small and portable but also meet the conditions of high performance and low cost. Compared with various devices, torque force sensing device is a good choice. The sensor is installed and detected by humans, as shown in Figure 3.

As shown in Figure 3, by installing the torque force sensing device on the brush, the parameter data can be observed when the ink painting designer holds the brush to draw. The sensitivity and resolution of the device are very high, which is very suitable for detecting more subtle tactile information. The probability distribution under the torque force sensing device is shown in Figure 4.

As can be seen from Figure 4, the torque force sensing device can recognize very small force, which also improves the tactile perception ability. When the torque force is added to the FBG tactile sensing system, deformation will occur, and the sensing element will feel the torque force. The

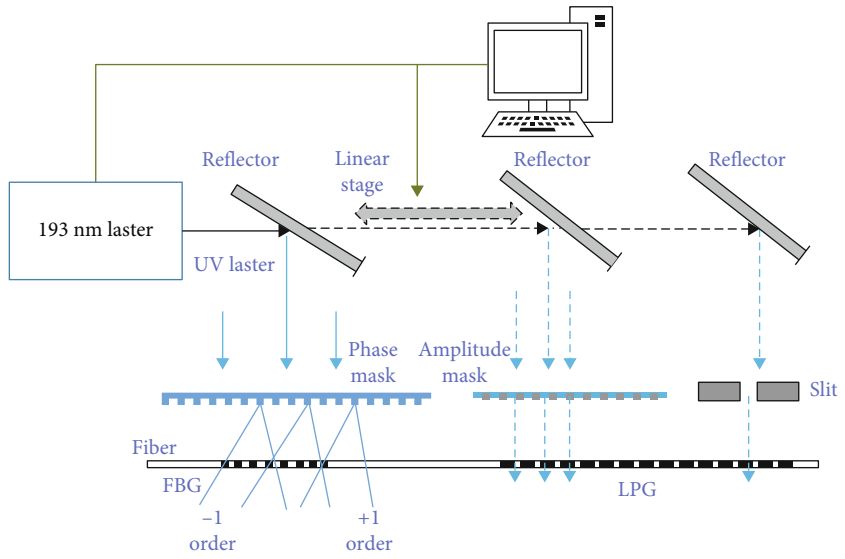

Figure 2: Construction diagram of fiber Bragg grating system.

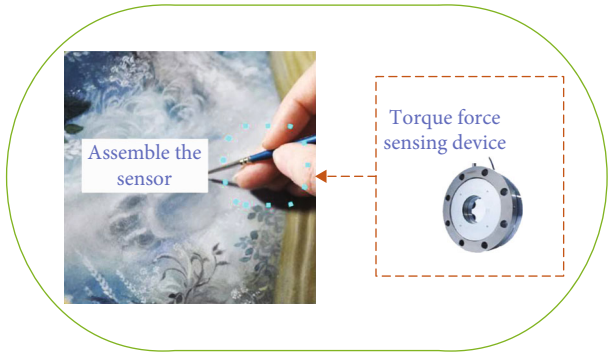

Figure 3: Application of torque force sensing device.

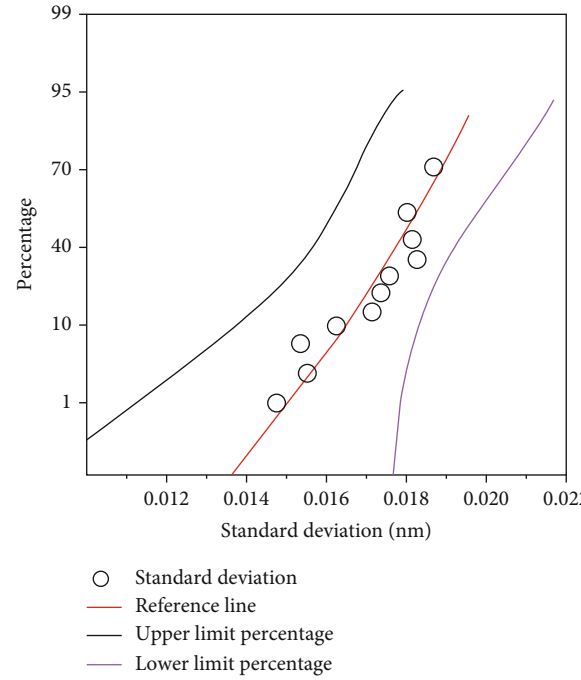

Figure 4: Probability diagram under torque force sensing device.

wavelength of the whole reflection center will also change, as shown in the following formula:

$$M = f\left(\Delta\lambda_\beta\right); F_z = f\left(\Delta\lambda_\beta\right), \tag{6}$$

$$\frac{\Delta\lambda_\beta}{\lambda_\beta} = K_T\Delta T + K_s\Delta\varepsilon. \tag{7}$$

Based on the above formula, the data generated under three different observation states are detected. The first torque detection expression is

$$\frac{\Delta\lambda_1}{\lambda_1} = K_T\Delta T + K_s\Delta\varepsilon 1. \tag{8}$$

The expression of the second reference optical fiber method is

$$\frac{\Delta\lambda_2}{\lambda_2} = K_T\Delta T. \tag{9}$$

The expression of the third reference axial force detection is

$$\frac{\Delta\lambda_3}{\lambda_3} = K_T\Delta T + K_{s2}\Delta\varepsilon 2. \tag{10}$$

In the above formula, the change value $\Delta\lambda$ of the reflection center offset, the initial center wavelength λ, and the sensitivity K between the torque force and the axial force

are all subjected to stress-strain. After adding different group forces, the expression of center wavelength minus initial wavelength is

$$\Delta\lambda_1 = \lambda_1{}' - \lambda_1 ; \Delta\lambda_2 = \lambda_2{}' - \lambda_2 ; \Delta\lambda_3 = \lambda_3{}' - \lambda_3. \quad (11)$$

It can be seen from the above formula that in the torque detection of FBG sensor, in addition to calculating the torque force, the influence of indoor temperature on the sensor is also very obvious. Due to the constant change of indoor temperature, the test value is not stable enough. Therefore, the interference caused by indoor temperature must be eliminated. When other conditions remain unchanged, the output signal will drift with the change of temperature. In order to reduce this phenomenon, a certain algorithm is adopted to correct the output result to eliminate the influence of temperature change on the output signal of components within a certain range. The reference method of indoor temperature compensation in this paper is the optical fiber method. The calculation formula of indoor temperature compensation effect is

$$\frac{\Delta\lambda_1}{\lambda_1} - \frac{\Delta\lambda_2}{\lambda_2} = \frac{\lambda_1{}' - \lambda_1}{\lambda_1} - \frac{\lambda_2{}' - \lambda_2}{\lambda_2} = \frac{\lambda_1{}' - \lambda_2{}'}{\lambda_1} = K_{\varepsilon 1}\Delta\varepsilon 1. \quad (12)$$

From the formula and algorithm of indoor temperature compensation effect, it can be seen that the principle of temperature compensation is the same as that of axial force detection. The elimination formula of axial force interference is

$$\frac{\Delta\lambda_3}{\lambda_3} - \frac{\Delta\lambda_2}{\lambda_2} = \frac{\lambda_3{}' - \lambda_3}{\lambda_3} - \frac{\lambda_2{}' - \lambda_2}{\lambda_2} = \frac{\lambda_3{}' - \lambda_2{}'}{\lambda_3} = K_{\varepsilon 3}\Delta\varepsilon 2. \quad (13)$$

The above two formulas adopt the optical fiber method. By deleting the interference to temperature in torque force and axial force, the sensitivity of the new FBG sensor system is greatly improved. To transmit the torque force to the new FBG sensor, it is also necessary to bond the sensing element with the elastic beam. The displacement formula of elastic beam when receiving small torque force is

$$\Delta y = \frac{9\pi R^{1/2}}{2Eht^{5/2}} \cdot \sqrt{R(b-t) - \frac{1}{4}(b-t)^2 M}. \quad (14)$$

The elastic beam will increase the displacement under the action of force, which can enable the new FBG sensor to detect smaller tactile information. Ink painting is a superb skill. By adding an elastic beam, it can analyze data more accurately and improve the ability to sense touch.

3.2. Research on Sensor Performance Detection Design in Tactile Observation of Ink Painting Graphic Designers Based on Sensor Technology. After the structure of FBG new tactile sensor is completed, it should be designed and analyzed according to the indicators of sensing performance. FBG new tactile sensor carries out 3D printing and tactile sensing experiment after tactile perception obtained by ink painting designers. In this design, the new tactile sensing structure needs to detect the strain of axial force and torque force when painting with a brush, so it needs the tactile performance index after applying force, respectively. The experimental data show that the new FBG tactile sensor has excellent performance. This paper mainly studies and analyzes the performance of sensitivity, repeatability, and hysteresis. The above performance is also an important index to detect the powerful performance of the new FBG tactile sensor. First, the experiment of strengthening the torque force is carried out, then the reflected wavelength data shall be recorded in the torque force interval of one millisecond per meter, and the wavelength value shall also be recorded. Use Origin software to fit the data collected by ink painting designers. Torque force, wavelength value, and change trend are shown in Figure 5.

As can be seen from Figure 5, the wavelength value in each torque force gradient is in a stable state. A total of ten test data points were recorded. After linear fitting of data points, it can be found that the linearity of the fitted curve has been greatly improved. Because the indoor temperature difference of the observer during the test is not obvious and there is no obvious difference in the fluctuation of the wavelength value of the above data, it has always been a relatively stable state. The applied linear equation and sensitivity equation are

$$Y_L = \pm\frac{\Delta L_{\mathrm{MAX}}}{Y_{\mathrm{FS}}} \times 100\%, \quad (15)$$

$$K = \frac{\Delta Y}{\Delta X} = \frac{dY}{dX}. \quad (16)$$

According to the fitting curve obtained after the experiment, the slope of the fitting curve is the embodiment of sensitivity. By adding the linear equation, the smaller the linearity of the fitting curve, it is proved that the fitting curve is more consistent with the actual curve. Finally, the sensitivity of the sensor can be proved by establishing the relationship between wavelength value, torque force, and axial force.

Repeatability is the degree of difference in the measurement curve repeated several times in the same and single stroke. In this paper, the tactile observation sample data on each gradient in the forward and reverse travel are compared. In order to more directly see the trend between the observed sample data and the standard deviation, a trend chart is made according to the standard deviation of tactile data, as shown in Figure 6.

As shown in Figure 6, the red and blue lines represent the change trend of positive and negative travel, respectively. The maximum difference is generated at the peak in the volume data. The equation for repeatability is

$$Y_R = \frac{(2 \sim 3)\sigma_{\mathrm{MAX}}}{Y_{\mathrm{FS}}} \times 100\%. \quad (17)$$

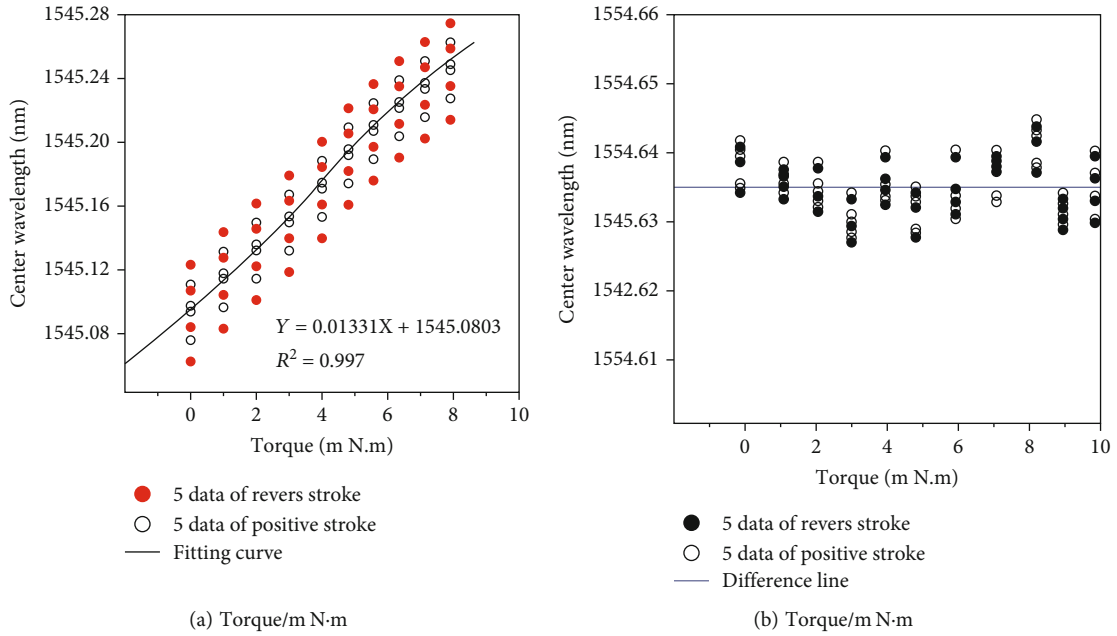

Figure 5: Torque force, wavelength value, and variation trend.

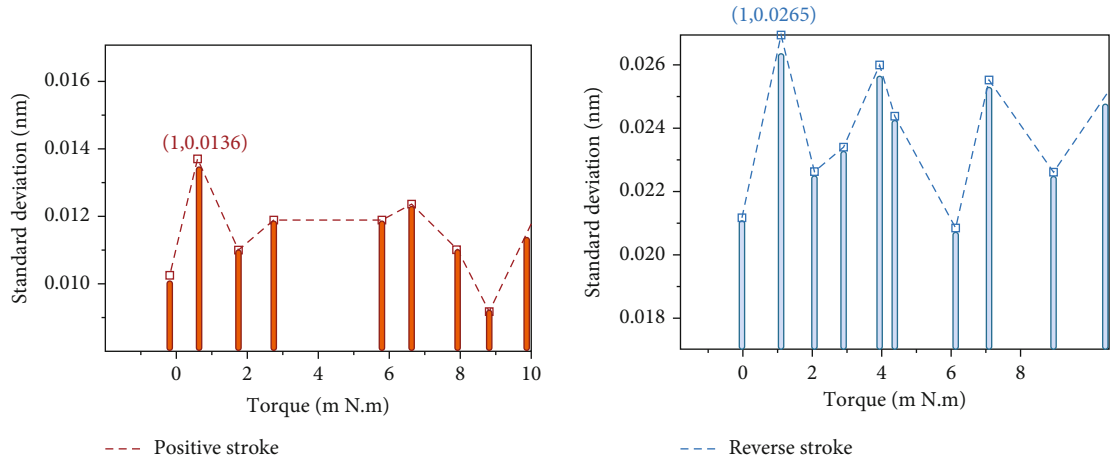

Figure 6: Trend comparison of standard deviation of tactile data.

According to the above formula, Bessel formula is used for calculation, as follows:

$$\sigma = \sqrt{\frac{\sum_{i=1}^{n}(y_i - \bar{y})^2}{n-1}}. \tag{18}$$

Through the repeated measurement of torque force and axial force under the same stroke, the repeatability detection of torque force and axial force performance of the sensor is finally achieved. In addition to the above two properties, there is another property called hysteresis. In the torque force sensing experiment, the performance is calculated by comparing the maximum deviation value formed by positive and negative with the full formed output value under the same torque force gradient. The experiment was also carried out using the sample data of the designer's touch. Finally, the overall change direction of the maximum deviation between the positive and negative calibration points is obtained, as shown in Figure 7.

As shown in Figure 7, the maximum deviation value between gradients appears at the maximum peak, which is obtained at 6 and 10, respectively. Bring the maximum deviation value into the following formula:

$$Y_H = \frac{\Delta H_{\mathrm{MAX}}}{Y_{\mathrm{FS}}} \times 100\%. \tag{19}$$

Finally, the hysteresis of the FBG tactile sensor in this paper can be obtained from the results. Through the comprehensive analysis of the above three performance experiments, it can be seen that the sensing performance of the new FBG tactile sensor is very good.

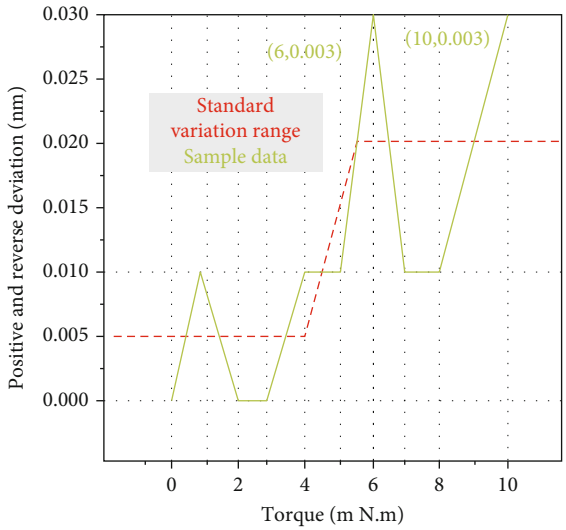

Figure 7: Variation trend of average calibration point deviation at each gradient.

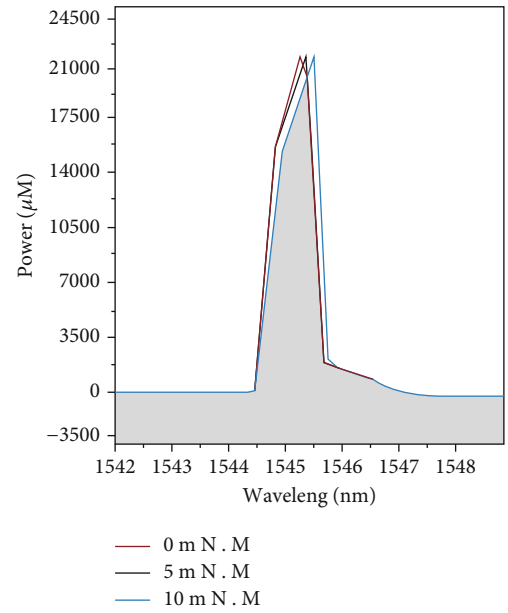

Figure 8: Reflection spectrum of torque force sensor.

4. Analysis of Research Results of Tactile Observation Technology for Graphic Designers of Ink Painting Based on Sensor Technology

4.1. Analysis of Sensor Structure Design in Tactile Observation of Ink Painting Graphic Designers Based on Sensor Technology. Based on the design of the sensing structure in the whole FBG fiber Bragg grating system, the reliability and speed of the FBG fiber Bragg grating demodulation analyzer for the collection of tactile information of ink painting designers can be seen. And the transmission of data to the PC is very considerable in the process of wavelength information demodulation. While the designer applies force to the brush, the fiber Bragg grating demodulator will quickly adjust the reflected center wavelength and refracted light intensity under different gradients. Finally, the torque force and axial force are stored under the tactile information data of the ink painting designer and then regenerated into the tactile reflection spectrum of the ink painting designer. The generated reflection spectrum can reflect the most intuitive result of FBG fiber Bragg grating system in observing the whole structure under the touch of ink painting designers. The torque force sensing reflection spectrum is shown in Figure 8.

It can be seen from Figure 8 that the reflection spectrum also has different change trends under different torque forces applied to the new FBG sensor. It is obvious that the displacement of the whole wavelength is also increasing with the increase of the applied force. Next, by applying axial force to the designer of FBG new sensor ink painting, the axial force reflection spectrum is generated, as shown in Figure 9.

As can be seen from Figure 9, after applying axial forces of different gradients to the new FBG sensor, with the increase of axial force, the wavelength displacement will also

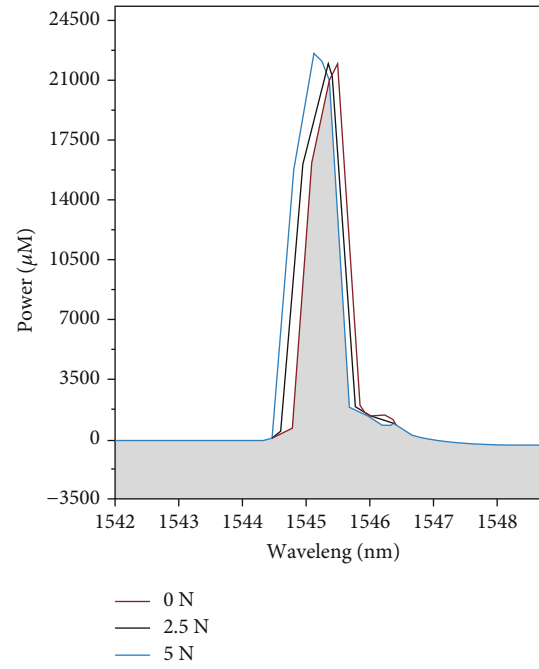

Figure 9: Reflection spectrum of axial force sensing.

increase. Through the above analysis, under the torque force and axial force applied by the ink painting designer to the FBG new sensor, the reflected wavelength value will increase synchronously with the increase of force. The experimental results also prove that the new FBG sensor achieves the purpose of force tactile sensing of the observation object by adding the new FBG structure.

4.2. Analysis of Sensor Performance Detection in Tactile Observation of Ink Painting Graphic Designers Based on Sensor Technology. Based on the multiangle performance

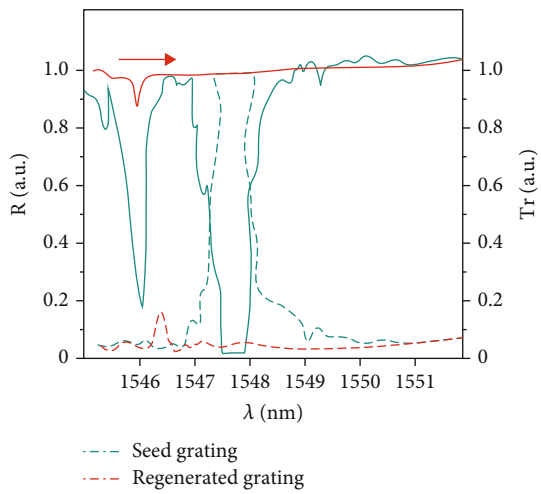

Figure 10: Initial reflection and projection spectrum and reflection and projection spectrum after data addition.

analysis of the new FBG sensor in the tactile experiment of ink painting designers, by using the optical fiber analysis method, the reflected wavelength is processed by difference, so as to achieve the experimental goal of temperature compensation. In order to further prove the influence of the optical fiber method on the data of temperature sensing performance, this paper makes an experimental study on temperature compensation. The purpose is to prove that the FBG new sensor system after passing the performance test can be better applied to the tactile collection of ink painting designers in different environments. The results show that temperature compensation can be made by recording simultaneous interpreting of two identical sensors in different environmental conditions. Different reflection spectra and projection spectra in the experiment are shown in Figure 10.

From Figure 10, we can see that the temperature compensation effect of two simultaneous interpreting sensors is similar under different environmental changes. Therefore, the experiment further proves the new FBG tactile sensor under the reference optical fiber method. The experimental results show that the new FBG tactile sensor can be applied to different external environments and can capture the tactile of ink painting designers normally. Therefore, the strain sensitivity of the whole tactile sensing system is greatly improved.

5. Conclusion

With the rapid development of science and technology, the FBG structure sensor is widely used in minimally invasive surgery, making fine parts, human tactile perception, and so on. The original ordinary tactile sensor cannot meet the capture and analysis of small movements at all. There are often some problems in the sensor, such as inaccurate test data, large volume, and high cost. After the sensors are used in various fields, the FBG structure can store and analyze small actions. Based on the above situation, the FBG structure is added to the fiber Bragg grating tactile sensor. The new FBG tactile sensor is applied to the design of traditional ink painting. The FBG new tactile sensing structure is very sensitive to small force and can analyze the strain through various forces. First, the new tactile sensing system is introduced, and the calculation algorithm related to torque force is added. The resulting difference data reflects the relationship with the FBG structure. The results show by adding the FBG structure. At the tactile data level, it contains more data of small forces. In the whole system structure level, the tactile perception of tactile sensor is greatly improved. Finally, the system structure is used to test the performance of the sample data of ink painting designers. In the research, the torque force and axial force are tested by the reference optical fiber method. The results show that the new FBG tactile sensor has very sensitive tactile sensing performance. In the tactile observation of ink painting designers, high-performance sensing devices can also better sense the occurrence of small forces and improve the comprehensiveness of data. However, the sensitivity of different axial forces of torque force is not discussed in this paper. Therefore, although the new fiber Bragg grating tactile sensor has very sensitive tactile sensing performance, the detailed parameters should be further discussed in the future research to obtain more mature applications.

Data Availability

The data used to support the findings of this study are included within the article.

Conflicts of Interest

We declare that there is no conflict of interest.

References

[1] A. Malandra, W. U. Rahman, N. Klimova et al., "Bordetella adenylate cyclase toxin elicits airway mucin secretion through activation of the cAMP response element binding protein," *International Journal of Molecular Sciences*, vol. 22, no. 16, p. 9064, 2021.

[2] K. T. Ehmsen, M. T. Knuesel, D. Martinez, M. Asahina, H. Aridomi, and K. R. Yamamoto, "Computational resources to define alleles and altered regulatory motifs at genomically edited candidate response elements," *Nucleic Acids Research*, vol. 49, no. 16, pp. 9117–9131, 2021.

[3] J. Hörberg, K. Moreau, M. J. Tamás, and A. Reymer, "Sequence-specific dynamics of DNA response elements and their flanking sites regulate the recognition by AP-1 transcription factors," *Nucleic Acids Research*, vol. 49, no. 16, pp. 9280–9293, 2021.

[4] D. V. Lopez, F. A. H. al-Jaberi, N. D. Damas et al., "Vitamin D inhibits IL-22 production through a repressive vitamin D response element in the il22 promoter," *Frontiers in Immunology*, vol. 12, 2021.

[5] D. Wang, C. T. Guo, X. B. Wan et al., "Identification of amino acid response element of SLC38A9 as an ATF4-binding site in porcine skeletal muscle cells," *Biochemical and Biophysical Research Communications*, vol. 569, pp. 167–173, 2021.

[6] S. Lee, J. Jin, J. Baek, J. Lee, and H. Chae, "Readout integrated circuit for small-sized and low-power gas sensor based on HEMT device," *Sensors*, vol. 21, no. 16, p. 5637, 2021.

[7] M. Stunnenberg, J. L. van Hamme, A. T. Das, B. Berkhout, and T. B. Geijtenbeek, "Variations in the abortive HIV-1 RNA hairpin do not impede viral sensing and innate immune responses," *Pathogens*, vol. 10, no. 7, p. 897, 2021.

[8] Y. T. Tang, Y. Li, Q. Li, K. Sun, H. N. Wang, and Z. R. Qin, "User input enrichment via sensing devices," *Computer Networks*, vol. 196, article 108262, 2021.

[9] C. Nnaji and I. Awolusi, "Critical success factors influencing wearable sensing device implementation in AEC industry," *Technology in Society*, vol. 66, article 101636, no. 66, 2021.

[10] Z. Ouyang, S. Cui, H. Yu et al., "Versatile sensing devices for self-driven designated therapy based on robust breathable composite films," *Nano Research*, vol. 31, no. 4, 2021.

[11] S. H. Kim, C. G. Wu, W. Y. Jia, Y. N. Xing, and R. S. Tibbetts, "Roles of constitutive and signal-dependent protein phosphatase 2A docking motifs in burst attenuation of the cyclic AMP response element-binding protein," *The Journal of Biological Chemistry*, vol. 297, no. 1, article 100908, 2021.

[12] S. P. Guo, H. C. Chang, L. S. Lu, D. Z. Liu, and T. J. Wang, "Activation of kelch-like ECH-associated protein 1/nuclear factor erythroid 2-related factor 2/antioxidant response element pathway by curcumin enhances the anti-oxidative capacity of corneal endothelial cells," *Biomedicine & Pharmacotherapy*, vol. 141, article 111834, 2021.

[13] S. M. Nayak, R. Anjum, J. Husain, H. Dattu, A. Afrooze, and G. Rahika, "PVA-ZNO nanocomposites thin films for sensing devices," *Ferroelectrics*, vol. 577, no. 1, pp. 221–228, 2021.

[14] S. Farokhimanesh, M. M. Forouzandeh, M. Ebrahimi, and Z. S. Hashemi, "Metastasis inhibition by cell type specific expression of BRMS1 gene under the regulation of miR200 family response elements," *Cell Journal*, vol. 23, no. 2, 2021.

[15] Y. Ying, Y. F. Zhang, Y. R. Tu et al., "Hypoxia response element-directed expression of aFGF in neural stem cells promotes the recovery of spinal cord injury and attenuates SCI-induced apoptosis," *Frontiers in Cell and Developmental Biology*, vol. 9, 2021.

[16] M. E. Wimmer, R. Cui, J. M. Blackwell, and T. Abel, "Cyclic AMP response element-binding protein is required in excitatory neurons in the forebrain to sustain wakefulness," *Sleep*, vol. 44, no. 6, 2021.

[17] G. Zhang, E. Anselmo, L. To, and S. Chattaraj, "692-P: preclinical study of a combined insulin infusion and glucose sensing device (duo)," *Diabetes*, vol. 70, Supplement 1, p. 692, 2021.

[18] S. Sahu, P. K. Jain, N. Mudgal, and G. Singh, "Glycosuria sensing based on nanometric plasmonic polaritons," *Materials Science and Engineering*, vol. 1136, no. 1, article 012064, 2021.

[19] G. Zonta, M. Astolfi, A. Gaiardo et al., "Medical parameters of a sensing device for colorectal cancer preventive screening through fecal odor analysis," *Electrochemical Society Meeting Abstracts*, vol. MA2021-01, no. 55, 2021.

[20] Q. Zhang, S. L. Koser, and S. S. Donkin, "Identification of promoter response elements that mediate propionate induction of bovine cytosolic phosphoenolpyruvate carboxykinase (PCK1) gene transcription," *Journal of Dairy Science*, vol. 104, no. 6, pp. 7252–7261, 2021.

[21] G. A. Giotopoulou, G. Ntaliarda, A. Marazioti et al., "cAMP response element-binding protein mediates immune-evasion of KRAS-mutant lung adenocarcinoma," *ERJ Open Research*, vol. 7, no. 84, 2021.

[22] S. Nyembe, T. Ntho, G. Ndlovu et al., "Indium phosphide nanowires: synthesis and integration into a gas sensing device," *Sensors and Actuators: B. Chemical*, vol. 333, article 129552, 2021.

[23] M. Liu, H. R. Li, L. Bai et al., "Real-time and visual sensing devices based on pH-control assembled lanthanide- barium nano-cluster," *Journal of Hazardous Materials*, vol. 413, article 125291, 2021.

[24] K. Kim, S. Park, C. Yeo et al., "A sensing device with the optical temperature sensors-based quad-RX module and a security module," *Sensors*, vol. 21, no. 5, 2021.

[25] C. C. Tu, S. Y. Wu, and Y. H. Tai, "36.1: invited paper: comparison in the performance of passive and active TFT pixel sensing circuits using PIN photodiode as the light sensing device," *SID Symposium Digest of Technical Papers*, vol. 52, no. S1, pp. 253–256, 2021.

Hindawi
Journal of Sensors
Volume 2021, Article ID 4903433, 14 pages
https://doi.org/10.1155/2021/4903433

Research Article

Effect Analysis of Language Education Based on Computer and Network Sensors

Wang Dandan[1], **Wu Yufei**[1] **and Zhu Yanwei**[2]

[1]*School of Foreign Studies, Tangshan Normal University, Tangshan 063000, China*
[2]*School of Mathematics and Computational Sciences, Tangshan Normal University, Tangshan 063000, China*

Correspondence should be addressed to Wang Dandan; 1212470926@st.usst.edu.cn

Received 8 September 2021; Accepted 20 October 2021; Published 17 November 2021

Academic Editor: Gengxin Sun

Language talent education is an essential education in education, but today's language talent education needs to be improved because of the influence of teaching methods and other factors. This paper puts forward an idea of sensor-assisted education. The sensor is connected to the computer to help improve the language ability and information acquisition ability of the educated by means of network sensing and try to intelligently classify the relevant languages in language education, so as to reduce the time for the educated to process information, so as to realize the matching between language and reception. At the same time, the research also found that the sensors based on computers and networks have the function of intelligently strengthening the language, and the meaning of expression is simpler and more accurate. By studying the improvement of the effect of language education based on computer and network sensors, this paper provides a reference for the application of network sensors in the future.

1. Introduction

A sensor is a new breakthrough in the modernization of educational means. With the continuous updating of various instruments and technologies, people try to expand their perception range with its advantages. Sensors, like human "five senses," are responsible for information collection. In physical experiments, they can perfectly integrate sound, light, force, heat, etc. These perceived physical quantities with electricity and amplify, transmit, and store them in measurement. Applying the advantages of sensor technology in physics experiment teaching presents digital experimental means. The successful examples of physics experiment teaching can show the visualization of physical phenomena and laws. The key to success in the experiment is to let the students "see the phenomenon." Although physics is science based on experiments, it is impossible to demonstrate all the experiments in middle school laboratories. At this time, the advanced technical means provided by digital sensing information systems play a very important role. For example, the effect of interaction is a common phenomenon in life. How to better understand the characteristics of interaction force from the law of physics is a teaching difficulty. Traditional experimental equipment can only measure the magnitude relationship of horizontal force with spring dynamometer, and the error of the result is relatively large. The advantage of digital sensors is shown at this time because it cannot provide students with valuable data for analysis. By introducing the sensor into the teaching of interaction force, students can clearly record the images of the two forces changing with time and the relationship between the two forces in the process of movement by pulling the force sensor on both sides in the experiment. With the organic combination of experimental technology and advanced experimental means, students not only see physical phenomena and summarize physical laws but also arouse their interest in physics, which is also the key factor of teaching.

The effect of language talent education pays more attention to the environment. Language teaching will also be related to learners' listening. A noisy environment will seriously affect the effect of language talent education. Not only is the language teaching of teachers easy to be affected but

also the information received by students is incomplete, which is not conducive to the communication between teachers and learners.

At present, intelligent sensor technology is applied in many aspects, and the characteristic of intelligent sensor technology is to retain information to the greatest extent. This feature makes the intelligent sensor be applied to the analysis of the effect of language talent education. Recently, the intelligent sensor has derived the function of strengthening information, which makes educators spend less energy on communication. With the combination of sensor and network, language talent education can also be applied to online teaching.

The first part is the introduction of the research background. The second part is the research on network sensors. The third part introduces the related algorithms based on computer and network sensors. The fourth part is experimental verification. The fifth part is the summary.

2. Related Work

The research of computer and network sensors has been very extensive, among which the most important is the transmission function of network sensors. S-mad introduces the idea of periodic sleep into wireless sensor network transmission for the first time. At the beginning of the protocol execution stage, nodes are divided into different virtual clusters and enter the sleep state according to different virtual clusters [1]. After the time synchronization phase, the node preempts the channel in the way of carrier listening, and the node that obtains the channel transmits data. However, because the node sleep time is determined by the virtual cluster, its sleep cycle is fixed. When the channel preemption is not successful, the node is still in the wake-up state, which increases the energy consumption of the network. Therefore, the T-MACt 22l protocol is improved. The node dynamically adjusts the length of wake-up time in the cycle according to the current network data volume, so as to reduce the idle listening time and avoid energy waste [2]. The above MAC protocols require nodes to perform synchronization. The synchronization mechanism generates not only unnecessary overhead but also periodic synchronization which will further increase the network delay. Therefore, the asynchronous low-power detection mechanism is proposed to solve the above problems. Its basic idea is that the node periodically wakes up and sends the detection frame, and the detection frame contains its own sleep plan. When a node receives the detection frame, it uses the obtained sleep plan to send data to the node, which will greatly reduce the waiting time of the sending node, so as to reduce energy consumption [3–5]. However, this method needs all nodes to send detection frames continuously, which increases the transmission cost of the whole network. At the same time, the detection frames sent by nodes will be received by multiple nodes. If these nodes wake up at the same time to send data, a large number of nodes wake up and seize the channel at the same time, resulting in low network channel utilization in the time domain. Therefore, the asynchronous low-power detection mechanism is only suitable for application scenarios with a small amount of low-power data. In order to overcome the above problems, B-MAC proposes a low-power listening mechanism for the first time. Its basic idea is that when a node preempts the channel, it first compares the currently measured minimum received signal strength of the sender with all received signal strengths through exponential weighted average by evaluating the current channel quality. When the signal strength of the sender is large, it indicates that the channel quality is good [6]. Secondly, when channel competition occurs in the network, in addition to using the initial back-off algorithm, the node will evaluate the congestion state according to the number of currently competing channel nodes and select a specific node for transmission to reduce the degree of network congestion. Finally, when the node data transmission is completed, the receiving node returns ACK to increase the reliability of the network. However, the preamble sequence of B-MAC is too long, which increases the transmission delay. X-mac proposes to fragment the preamble sequence, and each fragment contains the destination address information. When the destination address of the preamble sequence fragment received by the receiving node is not its own, it will immediately enter the sleep state. The node sends the fragment preamble sequence at a certain time interval. If the receiving node matches the destination address, it immediately returns an ACK to inform the sending node. The sending node stops sending the check-in sequence and sends the data to the receiving node. In this way, the receiving node does not have to wake up frequently to listen to whether a node sends data. At the same time, the node adjusts its duty cycle according to the load in the current network to further reduce energy consumption and network delay [7]. However, the cost of channel detection is further increased because the transmitting node needs to continuously send preamble sequence fragments. Especially in low load wireless sensor networks, the transmission cost ratio is too small to meet the needs of applications. Therefore, b0x-mac replaces the preamble sequence fragment with the data packet actually sent by the node. When the receiving node receives the data packet, it returns an ACK to the sending node, and other nodes directly ignore the data packet and turn to sleep. Thus, the cost of channel competition is further reduced, and the overall transmission cost ratio of the system is improved [8].

Although the above MAC layer protocol reduces the transmission energy consumption of the node to a certain extent, the duty cycle of the node is usually dynamically adjusted according to a fixed value or according to the traffic situation. The duty cycle adjustment method of the MAC layer protocol is based on the way that the node can transmit as much as possible, and there is no further description of adjusting the duty cycle. Therefore, these methods can not only guarantee the end-to-end transmission delay of nodes but also increase the duty cycle of nodes, resulting in a waste of energy. Researchers began to pay attention to the data transmission mechanism with guaranteed delay and optimal energy consumption. It was first proposed in wireless networks. Assuming that the arrival information of all scheduling packets is known and has the same transmission deadline, researchers minimize the transmission energy

under the condition of meeting the transmission delay and give off-line algorithm and on-line approximation algorithm. Without assuming the network packet rate and channel statistical characteristics, the average data transmission energy is minimized under the constraint of ensuring the average queue waiting delay [9, 10]. However, wireless sensor networks are different from traditional wireless networks. Therefore, EDF designs an anticollision delay guaranteed transmission protocol according to the prediction of wireless sensor network traffic. Rap proposes a prioritization method based on packet deadline and distance to sink node. The end-to-end transmission delay of data packets is controlled by adjusting the node transmission rate [11, 12]. Speedpi ensures end-to-end transmission delay by implementing a unified transmission rate in the whole network [13]. El Khediri et al. proposed a data stream transmission control mechanism to ensure the transmission delay of the network [14]. Some scholars have proposed a lazy transmission scheduling mechanism to minimize data transmission energy in single-hop wireless sensor networks [15]. At the same time, many articles have studied how to minimize the transmission energy consumption of the node with the worst link quality in the transmission path by reasonably allocating the single-hop data transmission time under the condition of limited total transmission time based on dynamically adjusting the constellation point scale in multihop wireless sensor networks [16]. In recent years, some work has used graph theory to ensure transmission delay. For example, for minimizing the transmission energy consumption in the process of data collection in wireless sensor networks, the algorithm of constructing a data collection tree is based on a greedy algorithm to dynamically allocate channels [17]. Some scholars have proposed the transmission scheduling problem to minimize the cost of data collection and used the connected dominating set to solve the above problem [18]. Some scholars put forward the transmission proportion requirements based on data packets and dynamically adjust the value of & (ruler) through the greedy algorithm to obtain that all data packets meet their own delay requirements [19]. The node periodic sleep mechanism is still not considered in the delay control problem of wireless sensor networks. Therefore, the delay control protocol combined with the node periodic sleep mechanism has been studied. In this paper, some scholars use the sleep cycle of scheduling nodes to control the end-to-end transmission delay in low-power wireless sensor networks for the first time. It divides the problem into two subproblems. One is how to adjust the sleep cycle of nodes; the other is how to place sink nodes and the number of sink nodes [20].

Edge proposes an energy-efficient end-to-end delay guaranteed transmission protocol. The protocol is divided into two parts. Firstly, the minimum energy cost path or minimum delay path from the node to sink node is found through energy cost formula EEC and end-to-end delay formula EED. Then, the number of wake-up time slices in the node cycle is dynamically adjusted to make the single-hop delay meet the requirements [21]. Therefore, dutycon proposes a method to dynamically adjust the sleep time C in the node cycle to ensure that the end-to-end delay expectation of the node meets a certain limit [22]. Some researchers began to introduce the routing protocol mentioned in wireless mesh networks into wireless sensor networks [23]. On the whole, the research of network sensors is relatively diverse, but the focus is on transmission. Few sensors take into account the application of language teaching [24]. This paper is to explore the effect of language talent education based on computer and network sensors [25].

3. Method

This paper puts forward the idea of sensor-assisted teaching. The sensor is connected to the computer to help the educated improve their language ability and information acquisition ability through network perception and try to intelligently classify relevant languages in language education, so as to reduce the time for the educated to process information, so as to realize the matching between language and reception. By studying the improvement of language teaching effect based on computer and network sensors, this paper introduces the sensor from three aspects: (1) intelligent recognition algorithm of network sensor language, (2) sensing related technology based on computer and network sensors, and (3) introduction to multilayer sensing structure of network sensors.

3.1. Introduction of Intelligent Recognition Algorithm for Network Sensor Language. The principle of language intelligent recognition of network sensors is variance normalization. The parameter initialization method can well solve the problem of variance normalization. In this paper, a sensor decoder is constructed using a PIC microcontroller and assembly language. When configuring parameter initialization, the parameter initialization method is used to make the parameter initialization distribution obey Gaussian distribution, and the network model can be trained after actual operation.

As shown in formula (1), $x_i \in R^k$ represents the ith vocabulary with K dimension in the input statement. Of course, K is set to 200 in this paper, which means that the dimension of vocabulary in this paper is 200. After the words in the input statement are converted into word vectors, they are input to the input layer through superposition as an input matrix. The i value of x_i can be defined according to the actual situation. In this paper, this value is set to 50, which means that the input statement is allowed to include up to 50 Chinese characters:

$$x_{(1:n)} = x_1 \wedge x_2 \wedge \cdots \wedge x_n. \tag{1}$$

As shown in equation (2), two parallel convolution calculations require a filter $y \in R^{jk}$. In this way, when applied to a window with j words, a new feature will be generated, which can be calculated by

$$a_i = f\left(y \cdot x_{i:i+j-1} + b\right). \tag{2}$$

In equation (2), $b \in R$ is the preset offset value and f is the nonlinear activation function. In the sigmoid type

function and ReLU function, this paper selects the ReLU function as the activation function. In this way, for the input statement, after being processed by the convolution kernel filter, each window will get a feature map, as shown in

$$c = [c_1, c_2, \cdots, c_{n-h+1}]. \tag{3}$$

It can be seen from equation (4) that $c \in R^{n-h+1}$; after that, this paper continues to maximize the pool of the obtained features, and $c' = \max(c)$ can be obtained as a new feature of the convolution kernel filter. The purpose of this is to facilitate the model to process input statements with different lengths. After the above steps, the input statement can be extracted into a group of features after convolution processing, and the extracted features become the basis for the final completion of intention recognition. In this process, the size of convolution kernels determines the window size. Generally speaking, small convolution kernels are selected, because compared with large convolution kernels, small convolution kernels can increase the complexity of the model and help to improve the accuracy of model training. Second, it can improve the network capacity and mine more hidden information of the input data. Third, it can reduce the number of convolution parameters. A cyclic neural network can be used in the sensor. The cyclic neural network uses the nonlinear function $f(\cdot)$ to convert the input statement sequence $x = \{x_1, x_2, \cdots, x_N\}$ into a hidden state output $h = \{h_1, h_2, \cdots, h_N\}$, where n is the sequence length of the input statement, and its network calculation unit is as shown in

$$h_t = f(x_t, h_{t-1}) = f(W_x x_t + W_h h_{t-1}). \tag{4}$$

The public Zi after heat treatment and the input query content instruction statement Qi are given, the public Zi is embedded in the matrix Zu, and the query content instruction statement Qi is embedded in the matrix Zq, so the public Zi and the statement Qi can be converted into a continuous hidden vector z_1^i and q_1^i. Finally, the coding is as follows:

$$h_{g,z}^i = \mathrm{LSTM}\left(w_{g,0}^i, z_1^i\right), \quad h_{g,0}^i = 0, \tag{5}$$

$$h_{g,q}^i = \mathrm{LSTM}\left(w_{g,2}^i, q_1^i\right), \quad h_g^i = h_{g,q}^i. \tag{6}$$

Formula (7) belongs to the further integration of formulas (5) and (6), and h_g^i is the output result obtained by the short-term and long-term memory network after processing the (z^i, q^i) sequence. On the basis that it can represent the user's query intention through the (z^i, q^i) sequence, the probability distribution of each alternative answer in the knowledge base to the intention can be obtained:

$$p^i = \mathrm{softmax}\left(Z_g \cdot h_g^i + b_g\right). \tag{7}$$

In equation (8), Z_g represents the linear transformation matrix and b_g represents the corresponding offset, which is mainly reflected in the matrix embedding of the input query statement which remains unchanged, but the invisible output h_g of the last layer is linearly transformed, and the results of the linear transformation are the initial input of the long-term and short-term neural network in this section:

$$q' = Z_g \cdot h_g + b_g. \tag{8}$$

In equation (8), Z_g is a linear transformation matrix and q' after linear change is more accurate than the original CC. In the training process of the long short neural network model, when using back propagation to calculate the gradient, h_g receives the gradient information from the global network for updating.

Equation (9) represents the calculation formula after the user input sentence is converted into a sentence vector. The sentence is represented by s, and W and V represent the words and word vectors that make up the sentence, respectively:

$$\vec{S} = \sum_{w \in S} V_w. \tag{9}$$

The similarity between the question sentences in the question answering database and the user input sentences can be calculated according to

$$\mathrm{sim}(S_1, S_2) = \frac{\vec{S_1} \cdot \vec{S_2}}{\left\|\vec{S_1}\right\| \cdot \left\|\vec{S_2}\right\|}. \tag{10}$$

3.2. Introduction of Sensing Related Technology Based on Computer and Network Sensors. Network sensing technology mainly involves the PMSM method, which is one of the common methods of network sensors. PMSM itself is a highly nonlinear structure, and the stator and rotor interact with each other, so the electromagnetic environment inside the motor is very complex. Since the magnetic circuit may have large current during operation, resulting in motor saturation, the sensing conduction equation of PMSM is

$$\begin{cases} u_a = R_s \cdot i_a + \dfrac{d}{dt}\psi_a, \\ u_b = R_s \cdot i_b + \dfrac{d}{dt}\psi_b, \\ u_c = R_s \cdot i_c + \dfrac{d}{dt}\psi_c, \end{cases} \tag{11}$$

where u_a, u_b, u_c is the phase voltage of three-phase winding, i_a, i_b, i_c is the current of three-phase winding, R_s is the equivalent resistance of three-phase winding, and ψ_a, ψ_b, ψ_c is the corresponding flux linkage of three-phase winding.

The stator flux linkage equation is

$$\begin{bmatrix}\psi_a\\ \psi_b\\ \psi_c\end{bmatrix}=\begin{bmatrix}L_{AA} & M_{AB} & M_{AC}\\ M_{AB} & L_{BB} & M_{BC}\\ M_{CA} & M_{CB} & L_{CC}\end{bmatrix}\begin{bmatrix}i_a\\ i_b\\ i_c\end{bmatrix}+\psi_f\begin{bmatrix}\cos\theta\\ \cos\left(\theta-\frac{2\pi}{3}\right)\\ \cos\left(\theta+\frac{2\pi}{3}\right)\end{bmatrix}, \tag{12}$$

where L_{AA}, L_{BB}, L_{CC} is the self-inductance of three-phase flux linkage, $M_{AB}=M_{BA}, M_{BC}=M_{CB}, M_{AC}=M_{CA}$ is mutual inductance between two-phase flux chains, ψ_f is the rotor flux linkage of the motor, and θ is the rotating electrical angle.

The electromagnetic torque equation is

$$T_c=-p_n\psi_f\left[i_a\sin\theta+i_b\sin\left(\theta-\frac{2}{3}\pi\right)+i_c\sin\left(\theta+\frac{2}{3}\pi\right)\right], \tag{13}$$

where p_n is the polar logarithm.

The motion equation of the network sensing factor is

$$J\frac{d\omega_m}{dt}=T_e-T_L-B\omega_m, \tag{14}$$

where ω_m is the speed of the network motor, J is the moment of inertia, B is the damping coefficient, and T_L is the load torque.

It can be seen that although the physical meaning of the mathematical model in the three-phase static coordinate system is easy to understand, it is not conducive to the application of the motor control algorithm due to the coupling of motor variables. Similarly, convert the ABC coordinate system to α-β. The process of the coordinate system is called inverse Clarke transformation, and the transformation formula is as follows:

$$[f_A \quad f_B \quad f_c]^T=T_{2S/3S}[f_a \quad f_\beta \quad f_0]^T. \tag{15}$$

3.3. Introduction of Multilayer Sensing Structure in Network Sensor. FCN is the most basic multilayer perceptron structure in sensor networks. First proposed a regression model based on FCN. The model uses FCN to reconstruct speech envelopes from EEG signals in the way of sample-wise prediction. Its network structure is shown in Figure 1. Considering that the system processing input speech into neural response is a causal system, and the input of stimulation reconstruction task is EEG signal and the output is speech time domain envelope, the reconstructed speech envelope at time 0 is only related to the neural response after time 0 + 1, but not to the neural response before time 0. Therefore, in order to predict the speech envelope value at time 0, FCN takes the EEG signal in a period of time after time 0 as the input. In the work of de Tailrez et al., the observation length of FCN is 27 sampling points, corresponding to 420 ms. After FCN expands all channels of EEG signals within 420 ms through one dimension (flatten) and activates two-

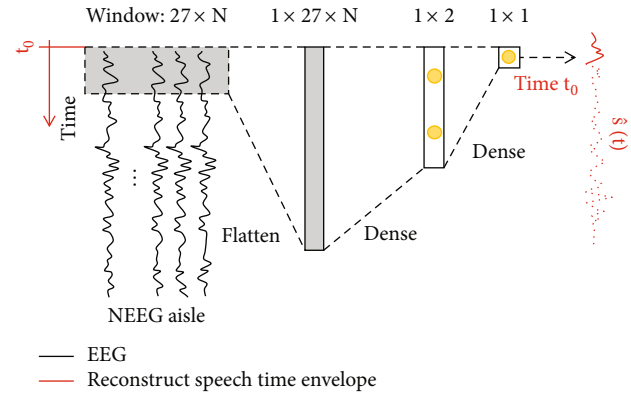

Figure 1: Flow chart of sensor's own sensing structure.

layer FCN (number of neurons: 2 and 1), the predicted value of the speech envelope at time 0 is obtained. When FCN slides continuously in the time dimension of EEG, the complete speech time domain envelope can be predicted (). Then, as in the second step of the linear decoding algorithm, the auditory attention object is determined by correlation analysis.

The authors conducted AAD experiments on data sets with only audio stimulation and spatial separation of sound sources (-45° and 45°). The results show that when the decoding window length is 10 s, compared with the linear decoding algorithm, the decoding algorithm based on the FCN regression model achieves higher accuracy (the accuracy is improved by about 20%). In addition, there are three findings in the experiment: (1) The accuracy of AAD using correlation coefficient loss function is higher than that using MSE loss function. This may be because the amplitude scale of the speech time domain envelope output by the network may not be fixed, the correlation value is independent of the signal amplitude, and the MSE value is related to the signal amplitude. Therefore, the loss function based on the correlation coefficient is better at capturing the consistency between the change trend of network output and the real speech envelope. (2) For the DNN decoder, the AAD accuracy when using broadband EEG is significantly higher than that when using narrowband EEG, while there is no significant difference in AAD accuracy when using two kinds of bandwidth EEG for the linear decoder. This result shows that compared with the linear decoder, the DNN decoder can use more information in the EEG signal and has stronger ability to describe the system. (3) After visualizing the weight of FCN, it is found that the neurons corresponding to the electrode channels of the temporal lobe (corresponding to the auditory cortex) have higher weight, which is similar to the temporal and spatial distribution patterns of the linear decoder. This result shows that the FCN regression model has certain interpretability. Ciccarelli et al. also used the above reconstruction model based on FCN regression. On the experimental data with only audio stimulation and single-channel presentation conditions, they also found that when the decoding window length is 10 s, the decoding accuracy of the FCN model (64%) is higher than that of the linear decoding algorithm (59%).

In addition to the above two studies, Nogueira and Dolhopiatenko proposed another decoding algorithm based on the FCN regression model. The difference from the previous model is that the causality between EEG and speech time domain envelope is realized by delaying EEG. FCN only observes the EEG signal at time $0 + \tau$ and then maps it to the predicted value of the speech envelope at time 0. Its network structure is shown in Figure 2. In the training, the author also uses the dropout strategy and the loss function based on the correlation coefficient. In addition, the operation of batch normalization (BN) is used to speed up the network convergence.

Compared with FCN, CNN is considered to have better spatial feature extraction ability. Nogueira and Dolhopiatenko proposed a decoding algorithm based on the CNN regression model, which uses the CNN structure to reconstruct the speech time domain envelope from EEG. Its network structure is shown in Figure 3. Similar to the FCN model proposed by the author, the causality between EEG and speech time domain envelope is realized by delaying EEG. In order to predict the speech envelope value at time 0, CNN takes the EEG signal in a period near time $0 + \tau$ as the input, which corresponds to the size of the convolution kernel in the time dimension. CNN used a size of $16 \times$ one -dimensional convolutions of N, corresponding to 250 ms. In the research using the linear decoding algorithm, it is found that the receptive field of this length can cover the most important delay range for speech envelope reconstruction; our results in this paper are also consistent with this conclusion. The EEG signal passes through single-layer one-dimensional CNN (number of convolution cores: 5, size: 16x). And two-layer FCN (number of neurons: 5 and 1) are activated to obtain the predicted value of the speech envelope at the time. With the convolution kernel sliding continuously in the time dimension of EEG, the model can predict the complete speech time domain envelope, so it can also be regarded as a point-by-point prediction algorithm. Then, as in the second step of the linear decoding algorithm, the object is noticed through correlation analysis. In the model training, the author also uses the dropout and batch normalization strategy, as well as the loss function based on the correlation coefficient. The experimental results on the same data set show that when the decoding window length is 10 s, the decoding algorithm based on the CNN regression model only achieves about 50% accuracy, which is equivalent to the opportunity level. This shows that the model does not learn the mapping relationship between EEG and speech time domain envelope, which may be due to the unreasonable implementation of the causal system.

4. Results and Discussion

4.1. Results and Discussion of the Decoding of Language by Sensors. In fact, there are 6 stimulation conditions (3 spatial separations × 2 auditory attention switching intervals). There is little difference between the decoders trained under the two auditory attention conversion intervals, so the AAD task uses the decoder jointly trained by all the data in the training set. At 90°, the masking release effect caused by spatial separation is the strongest, so its reconstruction accuracy is the highest. However, for 30° condition, although it has weaker masking release effect than 60°, the reconstruction accuracy is higher. This may be because the subjects have less language behavior, less EMG artifacts, and less interference with AAD at 30°, which offsets the disadvantage of low masking release effect to a certain extent. Although the single factor RM-ANOVA shows that the main effect of the conversion interval condition is not significant ($f1215 = 2.139$, $P = 0.897$, $2 = 0.009$), we can still observe that the reconstruction accuracy ($ATT = 0.0763$) under the conversion interval condition of 30 s is higher than that of 15 s ($ATT = 0.0729$), which is consistent with the trend that the AAD accuracy decreases with the decrease of the decoding window length, as shown in Figure 4.

Then, we use the above decoder to reconstruct the speech envelope frame by frame (5 s frame length, 1 s frame shift) for each trial and determine whether the AAD result of each frame is correct. Figure 5 shows the continuous decoding results after intertrial average under six stimulation conditions. The vertical axis in the figure represents the probability of being determined as speaker 1. The closer the curve is to 1, the greater the probability that the result of AAD is speaker 1. The closer the curve is to 0, the greater the probability that the result of AAD is speaker 2. It can be seen that the change trend of AAD results after average between trials over time is roughly consistent with the conversion setting of the attention object in the experiment (marked by vertical black dotted lines), but there are also two problems. Firstly, the accuracy of the algorithm is low; that is, the curve is close to the position with the longitudinal axis of 0.5; secondly, the algorithm has a delay of about 5–10 s; that is, the algorithm can stably judge that the attention object of the speaker has changed after about 5–10 s. These experimental results show that in the auditory selective attention task with language matching conditions and attention conversion, the EEG-based AAD method can be used for language attention object detection, but the accuracy is low and has obvious algorithm delay (about 5–10 s). This is mainly because the "linear system" assumption based on the linear decoding algorithm is too simplified, and the modeling ability of the mapping relationship between EEG signal and speech time domain envelope is limited. Nonlinear modeling can be used to solve this problem.

4.2. Application of Classifier in Sensor. As mentioned above, since the amount of data with a label of 0° in the experimental data is much higher than that of the other 6 types of labels, the classification accuracy index will be biased towards the results of this kind of data. Therefore, we show the results of FCN and CNN classifiers under various input conditions through the classification result confusion matrix, as shown in Figure 6. It can be seen that under all conditions, the classification accuracy of 0° is the highest and significantly higher than other rotation angles, because the data of each sensor is relatively stable under this condition. The confusion mainly occurs in the same rotation direction and between adjacent rotation angles, especially

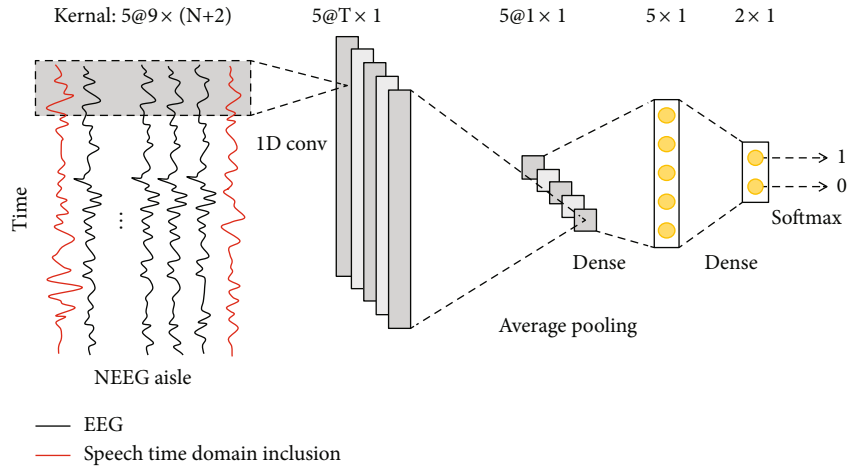

Figure 2: Flow chart of enhanced perception structure in network sensors.

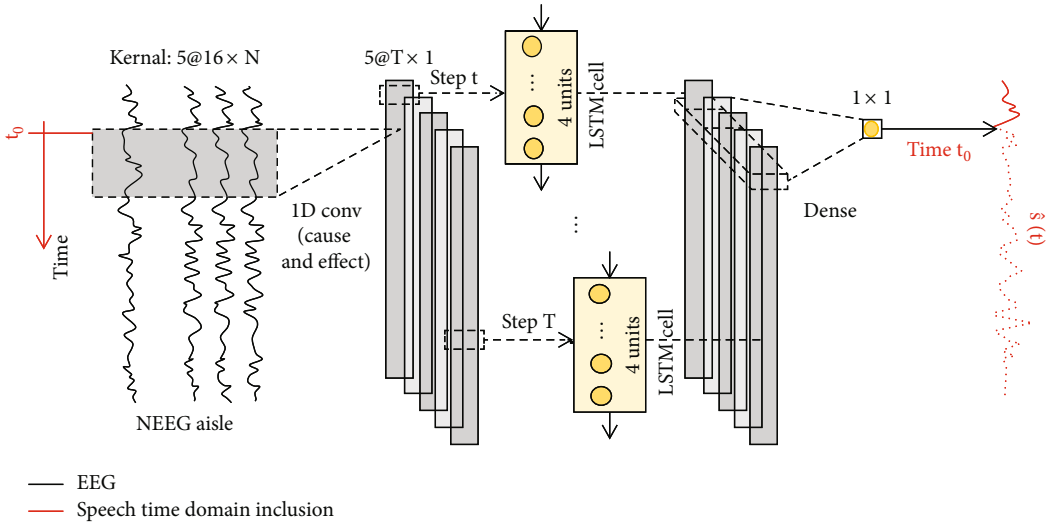

Figure 3: Flow chart of returning to the enhanced perception structure in network sensors.

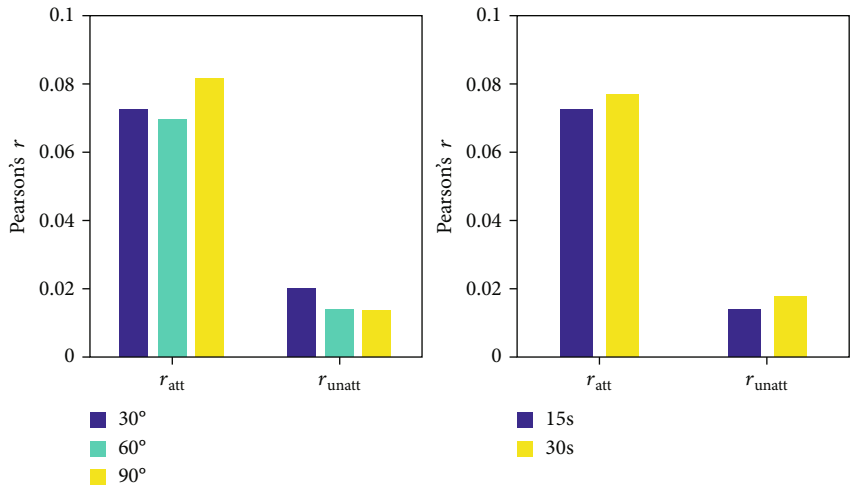

Figure 4: Comparison of reconstruction accuracy of network sensors under different language stimulation conditions.

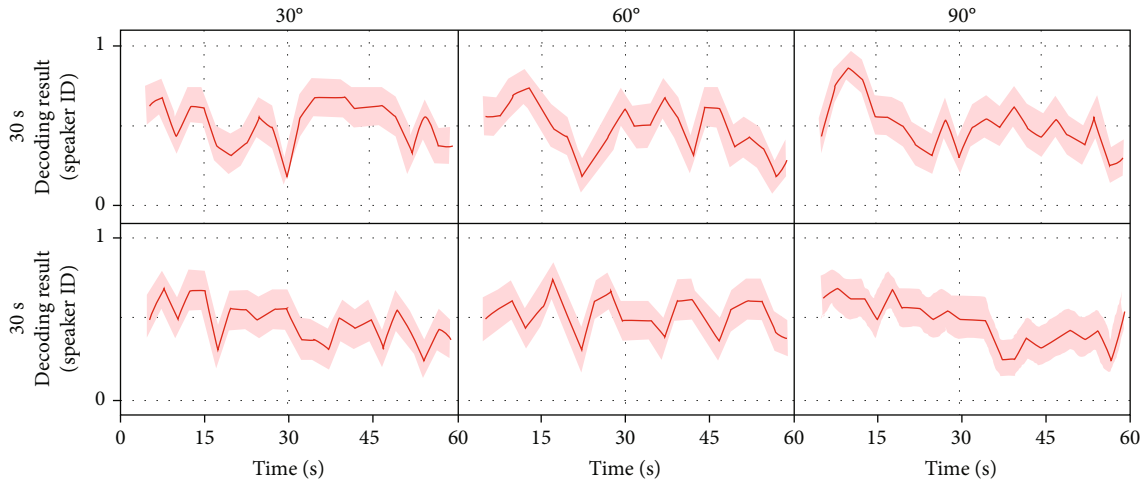

Figure 5: Continuous decoding results within a trial of the linear decoding algorithm in the network sensor.

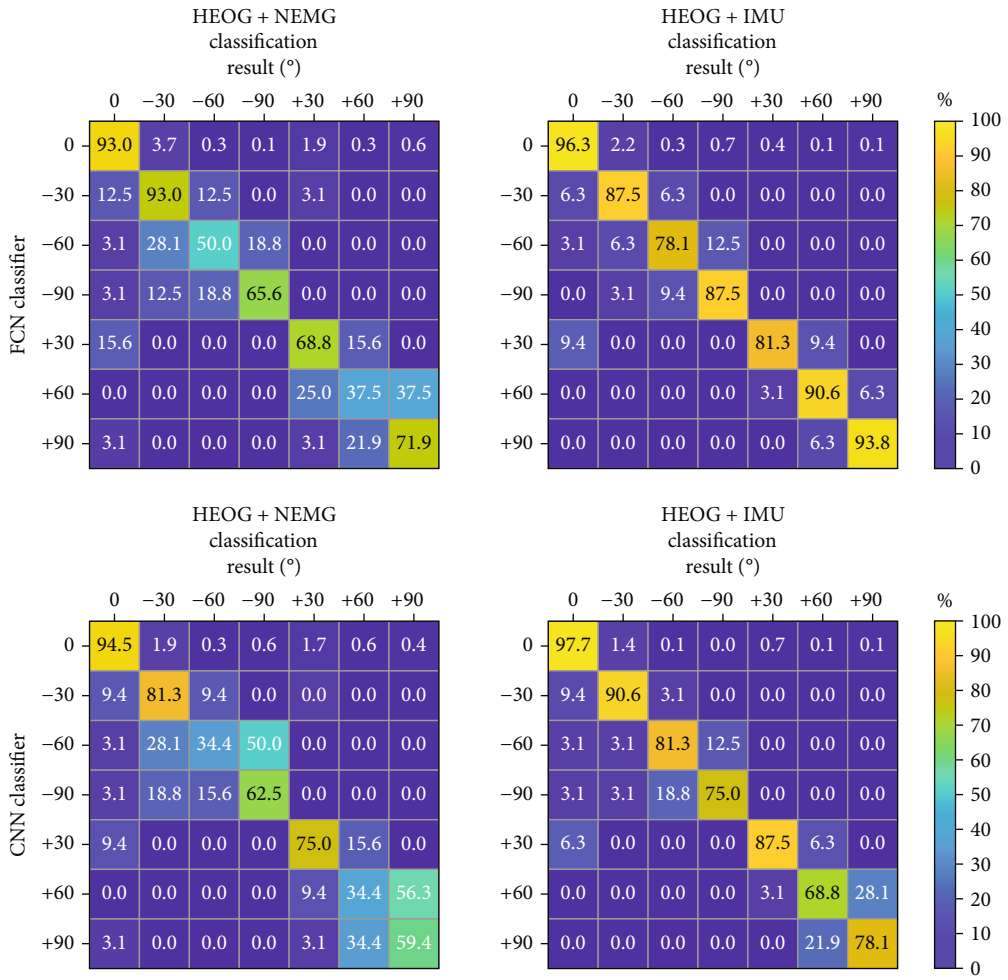

Figure 6: Confusion matrix of classification results of FCN and CNN classifiers in the sensor (%).

between +60° and +90° and -60° and -90°. For the two classifiers, the results of bivariate heog and NEMG are not as good as bivariate heog and IMU, which also shows that the effect of using NEMG to estimate head rotation is not as good as IMU.

We further calculated the continuous line of sight rotation estimation results for each trial in the test set. It should be noted that after the listener turns the line of sight, the sensor signal of several consecutive frames still fluctuates. Therefore, note that there is a certain oscillation in the

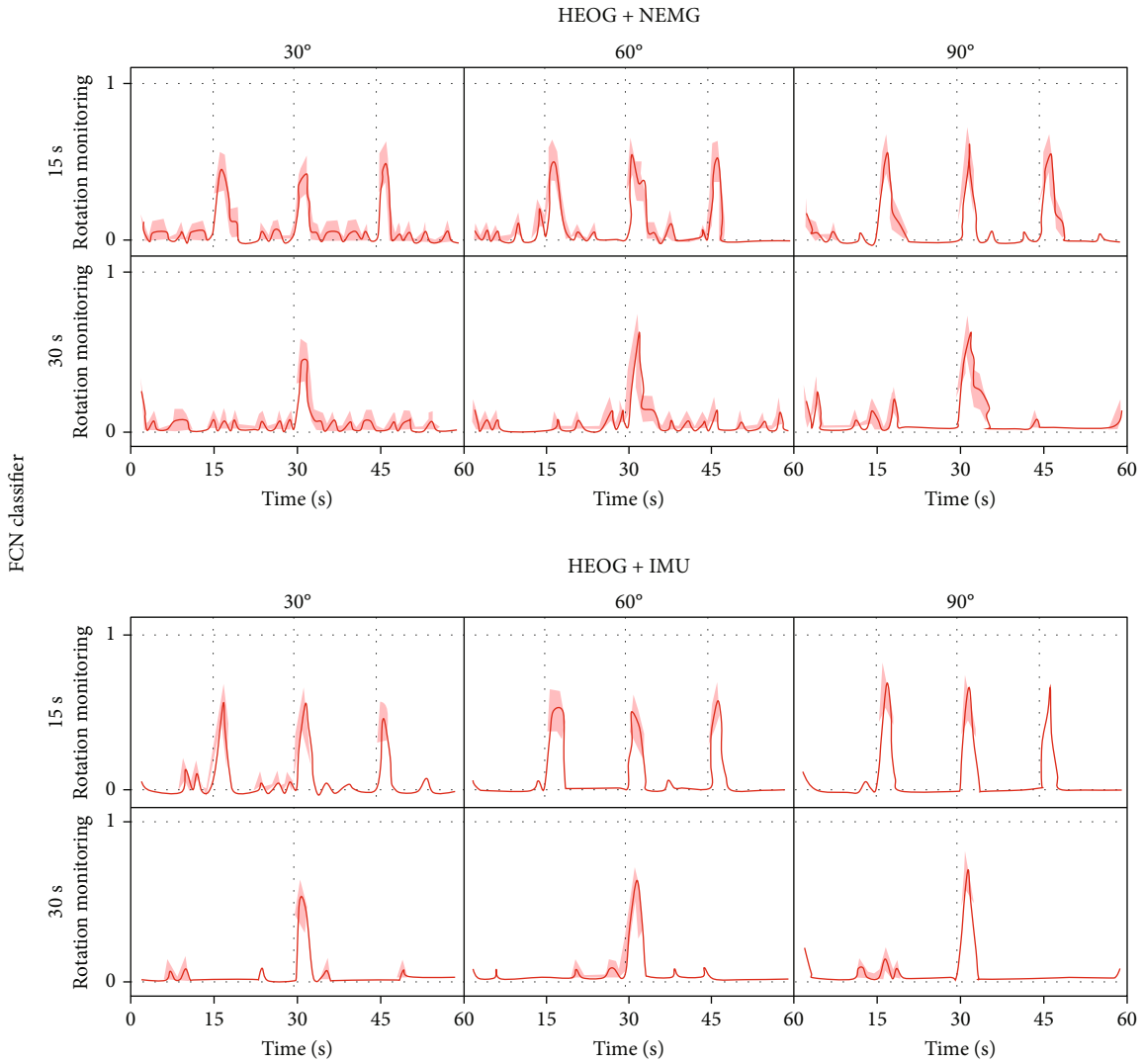

Figure 7: Estimation results of the rotation angle of the continuous line of sight within the trial.

estimation results of several consecutive frames after conversion. For example, as shown in Figure 6, after an impulse of a certain polarity occurs, the heog signal will gradually recover to the initial potential, and the latter process can also be regarded as a reverse impulse with a small amplitude. When we extract the signal waveform frame by frame, the forward and reverse impulse process will be divided into adjacent frames, so the algorithm may mistakenly classify the reverse impulse process as reverse line of sight rotation. Therefore, when calculating the estimation results of continuous line of sight orientation in the trial, when the estimation results of two consecutive frames are not 0°, we sharpen them. Set the smaller absolute value in the estimation result to 0°. Figure 7 shows the average continuous estimation results between trials under six stimulation conditions. Taking FCN classifier and bivariate heog and NEMG inputs as examples, it can be seen that the classifier can judge that the line of sight direction has rotated within 2 s after the attention conversion time (marked by vertical black dotted lines), and the estimated value output by the classifier increases with the increase of the spatial separation angle set in the experiment. In addition, it can also be observed that at the nonattention conversion time (i.e., the rotation angle should be 0°), the classifier may also output a rotation amount of non-0° (corresponding to the first row of the confusion matrix), which may be caused by the fluctuation in the sensor signal. The results using the CNN classifier show similar patterns. Under univariate (results not shown) and bivariate input conditions, the performance of the CNN classifier is slightly better than that of the FCN classifier, which is reflected in more accurate estimation of rotation angle, less misjudgment of nonrotation time, and smaller error interval. This is because the convolution kernel in the CNN structure can observe the signal waveform in a certain time window at one time and integrate the information in the window, which has stronger feature extraction ability and antinoise ability.

In general, these results show that under the condition of audiovisual matching, the Los rotation estimation based on heog and NEMG can more accurately reflect the information related to auditory attention conversion, such as rotation time and rotation angle. Considering that the AAD

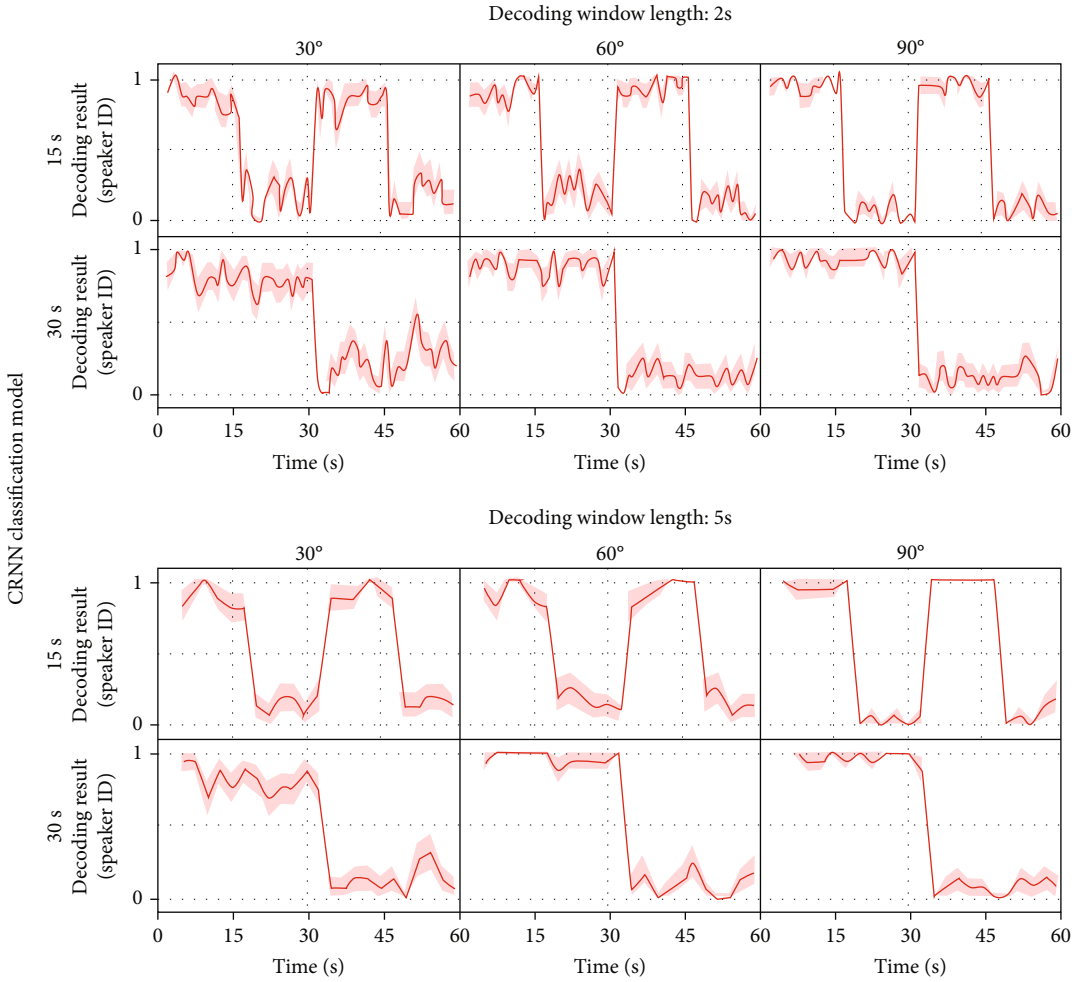

Figure 8: Continuous decoding results of the CRNN model in the sensor under different stimulus conditions.

task does not require accurate line of sight rotation angle information, we can reduce the line of sight rotation angle estimation to line of sight rotation detection; that is, the rotation label output by the classifier (Class 7: 0°, ±30°, ±60°, and ±90°) is changed to rotation label (Class 2: rotation, no rotation), so that while meeting the requirements of AAD task, the advantage of low detection delay (2 s) is also retained. Based on this change, this section will continue to explore the feasibility of the AAD task based on line of sight rotation detection.

Based on the results in Figure 7, after remapping the output label of the classifier into rotation (±30°, ±60°, and ±90°) and nonrotation (corresponding to 0°), the experimental results of the AAD task can be obtained, and the confusion matrix is shown in Figure 6. It can be seen that when the bivariate heog and NEMG are input, FCN is easier to misjudge the rotation condition as no rotation than the CNN classifier (FCN: 6.3%, CNN: 3.1%). This missing alarm means that the AAD algorithm fails to guide the calculation of AAD, which will affect the language object detection. On the contrary, a false alarm has less impact, because the AAD algorithm can correct it. In order to further quantify the performance of each algorithm in the AAD task under various input conditions, we calculate three indicators: F1 value, missed alarm rate, and false alarm rate according to the confusion matrix. F1 value is the harmonic average of accuracy rate (the proportion of samples divided into positive examples) and recall rate (the proportion of samples divided into positive examples). The model can be comprehensively evaluated. The missed alarm rate is the proportion of the missed positive cases in all the positive cases. The false alarm rate is the proportion of samples judged as positive cases, which are actually negative cases. It can be seen that the CNN classifier has better performance. It has a higher F1 value and lower false alarm rate than the FCN classifier. It is proved that in this task, the CNN network has stronger feature extraction ability and is more robust to noise interference. In addition, although the results when using bivariate heog and NEMG are still worse than bivariate heog and IMU on the whole, the gap is not large; especially when using the CNN classifier, the alarm leakage rate (both 3.1%) has almost no difference. The results show that the proposed AAD algorithm based on heog and NEMG is feasible.

The comparison and fusion of auditory attention decoding and auditory attention conversion detection methods combines the advantages and disadvantages of the AAD method based on the auditory selective attention neural mechanism (measured by EEG) and based on visual

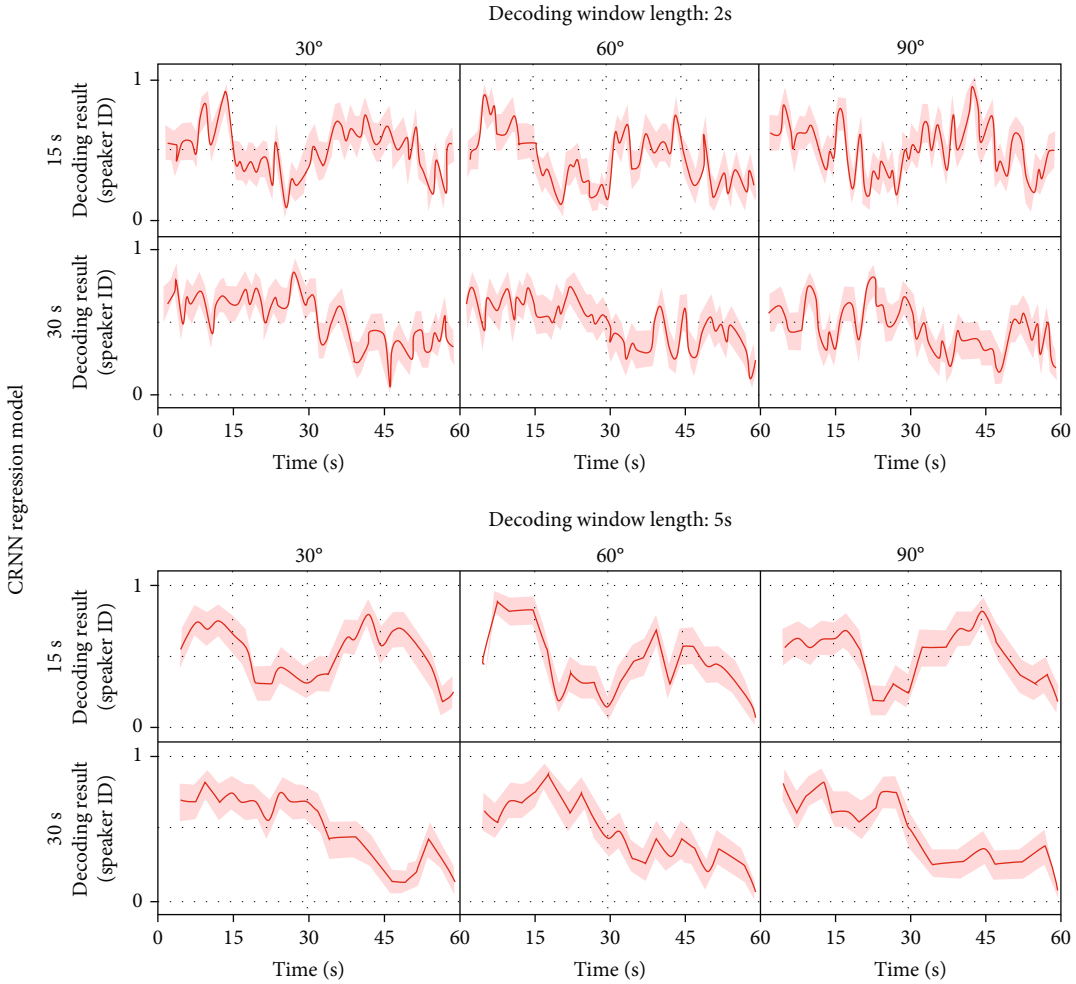

Figure 9: Continuous decoding results of the CRNN model in the enhanced sensor.

behavior (measured by heog and NEMG) and then puts forward the fusion strategy of the two kinds of methods. However, in the third chapter, due to the low accuracy of the linear decoding algorithm, the feasibility of this strategy is poor. Therefore, several AAD methods based on the DNN model are proposed to significantly improve the correct rate of understanding code, which makes the above fusion strategy possible. Therefore, in this section, we will recompare the performance of AAD methods and explore the feasibility of the fusion strategy proposed in this paper.

4.3. Research on Enhancement of Sensing Related Technology in Sensor Networks. Similar to Figure 6, we use the DNN decoder to perform AAD calculation frame by frame for each trial in the test set, where the frame length (i.e., decoding window length) is 2 s or 5 s and the frame shift is 50%. Considering that the classification and regression model based on the CRNN structure proposed in this paper is superior to other models in most cases, we will take these two models as examples for calculation. Figure 8 shows the continuous decoding results after intertrial average under six stimulation conditions. The vertical axis in the figure represents the probability of being determined as speaker 1. The closer the curve is to 1, the greater the probability that the result of AAD is speaker 1. The closer the curve is to 0, the greater the probability that the result of AAD is speaker 2. It can be seen that compared with the linear decoding algorithm, the decoding performance of the two CRNN models is significantly improved, and the change trend of AAD results after average between trials is more consistent with the conversion setting of the object of attention in the experiment (marked by vertical black dotted lines). In addition, the CRNN classification model has better performance than the CRNN regression model, which is reflected in higher accuracy and smaller error interval. The decoding performance under the condition of 90° spatial separation is better than the other two angle conditions.

For the CRNN classification model, when the decoding window length of 2 s or 5 s is used, the model can detect the auditory attention conversion in time under each stimulus condition, and the algorithm delay is the decoding window length. For the CRNN regression model, when the decoding window length of 2 s or 5 s is used, the model can also detect auditory attention conversion in time. However, due to its large error interval, the model needs longer time to achieve stable results. In conclusion, compared with the linear decoding algorithm, the AAD algorithm based on the CRNN model has higher accuracy and lower algorithm

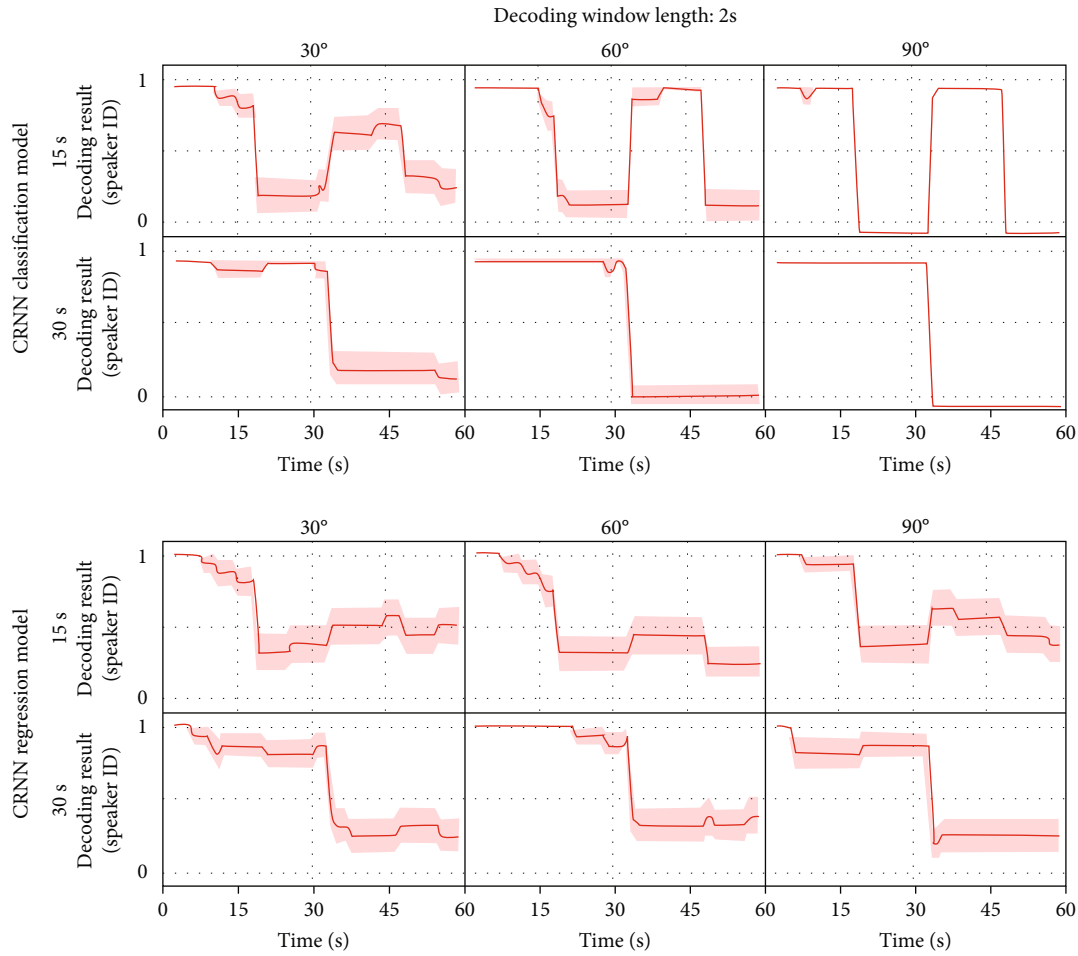

Figure 10: Continuous decoding results of the CRNN model in the sensor under the fusion strategy.

delay (about 2–5 s). Based on the above results, this paper summarizes the advantages and disadvantages of AAD, and the results are shown in Figure 9. Among them, the decoding window length is set to 2 s and the correction window length is set to 5 s. The AAD algorithm uses CNN classifier and bivariate heog and NEMG input. For the CRNN classification model, under the condition of 15 s attention conversion interval, the accuracy of auditory attention object detection after using the fusion strategy is reduced, and the accuracy of the initial part of the trial is higher than that of the second half, mainly because more attention conversion times will bring more cumulative errors (see Figure 10).

In addition, the decrease of this accuracy rate is greater than 60° and 90° under the condition of 30° spatial separation, because the accuracy of AAD itself is low under the condition of 30° and the algorithm cannot effectively correct the cumulative error. On the contrary, under the condition of 90° spatial separation, the AAD algorithm effectively corrects the cumulative error. For the CRNN regression model, under various stimulation conditions, the results after using the fusion strategy have been improved, and the model output can achieve stable results faster, reflecting the effectiveness of the fusion strategy. We can also observe that the result under the condition of 30 s attention conversion interval is significantly better than 15 s, which also indicates that the model has the problem of cumulative error. The error correction ability of the CRNN regression model is weaker than that of the classification model, which is mainly due to its low decoding accuracy. In addition, we statistically find that the fusion strategy significantly reduces the amount of computation of the AAD algorithm (about 70%), and the results show that the effect of language talent education based on computer and network sensors is better.

5. Conclusion

The key of network sensors is information request and enhancement. Because the sensor method is based on cortical phase-locked response, and the establishment of phase-locked response takes a certain time, there is a high delay (e.g., 5–10 s) in the detection of attention conversion using the sensor method. Under the condition of large interference of environmental factors, the sensor can play a better role in information capture. The experiment explores the strengthening effect of network sensors on language talent education. In addition, the accuracy of using the CNN classifier in the sensor is higher than that of other classifiers, indicating that the CNN model in the sensor has stronger ability to extract features from multichannel input signals. These results preliminarily verify the effectiveness of this method.

Simultaneously interpreting the influence of sensor signal types and classification algorithms on the transmission modes of different sensors, based on this, this paper proposes a fusion strategy of various sensor conduction modes, which initially verifies the feasibility of the strategy in language talent education. However, the research in this paper only preliminarily verifies the effectiveness of this method. Because there is no more in-depth data verification on the ability of the CNN model to extract features from multichannel input signals, it needs to be further discussed in future research.

Data Availability

The experimental data used to support the findings of this study are available from the corresponding author upon request.

Conflicts of Interest

The authors declared that they have no conflicts of interest regarding this work.

Acknowledgments

The study was funded by the following: (1) Research and Practice Project of English Teaching Reform in Higher Education of Hebei Province in 2020, Research on the Construction of Practical Curriculum System for Business English Major under the Background of Integration between Industry and Education (Project No.: 2020YYJG059), and (2) Project supported by Scientific Research Fund of Tangshan Normal University, Research on the Construction Path of English Cloud Platform of Jidong Culture under the Background of New Infrastructure Construction (Project No.: 2021B12).

References

[1] D. Kandris, C. Nakas, D. Vomvas, and G. Koulouras, "Applications of wireless sensor networks: an up-to-date survey," *Applied System Innovation*, vol. 3, no. 1, p. 14, 2020.

[2] A. Shahraki, A. Taherkordi, Ø. Haugen, and F. Eliassen, "Clustering objectives in wireless sensor networks: a survey and research direction analysis," *Computer Networks*, vol. 180, article 107376, 2020.

[3] M. Numan, F. Subhan, W. Z. Khan et al., "A systematic review on clone node detection in static wireless sensor networks," *IEEE Access*, vol. 8, pp. 65450–65461, 2020.

[4] D. K. Sah and T. Amgoth, "Renewable energy harvesting schemes in wireless sensor networks: a survey," *Information Fusion*, vol. 63, pp. 223–247, 2020.

[5] H. Patel, D. Singh Rajput, G. Thippa Reddy, C. Iwendi, A. Kashif Bashir, and O. Jo, "A review on classification of imbalanced data for wireless sensor networks," *International Journal of Distributed Sensor Networks*, vol. 16, no. 4, Article ID 155014772091640, 2020.

[6] S. Qu, L. Zhao, and Z. Xiong, "Cross-layer congestion control of wireless sensor networks based on fuzzy sliding mode control," *Neural Computing and Applications*, vol. 32, no. 17, pp. 13505–13520, 2020.

[7] X. Liu, P. Lin, T. Liu, T. Wang, A. Liu, and W. Xu, "Objective-variable tour planning for mobile data collection in partitioned sensor networks," *IEEE Transactions on Mobile Computing*, vol. 1, pp. 1–1, 2020.

[8] S. N. Mohanty, E. L. Lydia, M. Elhoseny, M. M. G. al Otaibi, and K. Shankar, "Deep learning with LSTM based distributed data mining model for energy efficient wireless sensor networks," *Physical Communication*, vol. 40, article 101097, 2020.

[9] X. Liu, M. S. Obaidat, C. Lin, T. Wang, and A. Liu, "Movement-based solutions to energy limitation in wireless sensor networks: state of the art and future trends," *IEEE Network*, vol. 35, no. 2, pp. 188–193, 2021.

[10] P. K. Singh, B. K. Bhargava, M. Paprzycki, N. C. Kaushal, and W.-C. Hong, *Handbook of Wireless Sensor Networks: Issues and Challenges in Current Scenario's*, Advances in Intelligent Systems and Computing, 2020.

[11] R. Priyadarshi, B. Gupta, and A. Anurag, "Deployment techniques in wireless sensor networks: a survey, classification, challenges, and future research issues," *The Journal of Supercomputing*, vol. 76, no. 9, pp. 7333–7373, 2020.

[12] B. D. Deebak and F. al-Turjman, "A hybrid secure routing and monitoring mechanism in IoT-based wireless sensor networks," *Ad Hoc Networks*, vol. 97, article 102022, 2020.

[13] X. Fu, P. Pace, G. Aloi, L. Yang, and G. Fortino, "Topology optimization against cascading failures on wireless sensor networks using a memetic algorithm," *Computer Networks*, vol. 177, article 107327, 2020.

[14] S. El Khediri, W. Fakhet, T. Moulahi, R. Khan, A. Thaljaoui, and A. Kachouri, "Improved node localization using K-means clustering for wireless sensor networks," *Computer Science Review*, vol. 37, article 100284, 2020.

[15] K. Khujamatov, K. Ahmad, E. Reypnazarov, and D. Khasanov, "Markov chain based modeling bandwith states of the wireless sensor networks of monitoring system," *International Journal of Advanced Science and Technology*, vol. 29, no. 4, pp. 4889–4903, 2020.

[16] S. R. Mugunthan, "Novel cluster rotating and routing strategy for software defined wireless sensor networks," *Journal of ISMAC*, vol. 2, no. 3, pp. 140–146, 2020.

[17] J. S. Raj, "Machine learning based resourceful clustering with load optimization for wireless sensor networks," *Journal of Ubiquitous Computing and Communication Technologies*, vol. 2, no. 1, pp. 29–38, 2020.

[18] R. Lin, H.-J. Kim, S. Achavananthadith et al., "Wireless battery-free body sensor networks using near-field-enabled clothing," *Nature Communications*, vol. 11, no. 1, p. 444, 2020.

[19] A. Ghosal, S. Halder, and S. K. Das, "Distributed on-demand clustering algorithm for lifetime optimization in wireless sensor networks," *Journal of Parallel and Distributed Computing*, vol. 141, pp. 129–142, 2020.

[20] H. Landaluce, L. Arjona, A. Perallos, F. Falcone, I. Angulo, and F. Muralter, "A review of IoT sensing applications and challenges using RFID and wireless sensor networks," *Sensors*, vol. 20, no. 9, p. 2495, 2020.

[21] A. Bulashenko, S. Piltyay, A. Polishchuk, and O. Bulashenko, "New traffic model of M2M technology in 5G wireless sensor networks," in *2020 IEEE 2nd International Conference on Advanced Trends in Information Theory (ATIT)*, pp. 125–131, Kyiv, Ukraine, 2020.

[22] R. Priyadarshi, B. Gupta, and A. Anurag, "Wireless sensor networks deployment: a result oriented analysis," *Wireless Personal Communications*, vol. 113, no. 2, pp. 843–866, 2020.

[23] J. A. Alzubi, "Bipolar fully recurrent deep structured neural learning based attack detection for securing industrial sensor networks," *Transactions on Emerging Telecommunications Technologies*, vol. 32, no. 7, article e4069, 2021.

[24] J. Singh, R. Kaur, and D. Singh, "A survey and taxonomy on energy management schemes in wireless sensor networks," *Journal of Systems Architecture*, vol. 111, article 101782, 2020.

[25] B. Bhushan and G. Sahoo, "Requirements, protocols, and security challenges in wireless sensor networks: an industrial perspective," in *Handbook of Computer Networks and Cyber Security*, B. Gupta, G. Perez, D. Agrawal, and D. Gupta, Eds., pp. 683–713, Springer, Cham, 2020.

Hindawi
Journal of Sensors
Volume 2021, Article ID 9357225, 12 pages
https://doi.org/10.1155/2021/9357225

Research Article

Study on Heart Rate and Energy Expenditure in College Sports Training Based on Multisensor Perception

Ge Liu and Baiqing Liu

Zhongnan University of Economics and Law, Hubei Wuhan 430074, China

Correspondence should be addressed to Ge Liu; z0004485@zuel.edu.cn

Received 31 August 2021; Accepted 13 October 2021; Published 13 November 2021

Academic Editor: Gengxin Sun

Heart rate is one of the important indices to calculate and evaluate the intensity and quality of motion. It can scientifically and objectively reflect the intensity level of momentum and exercise in the process of exercise. It is an important index of athletic strength and physical fitness of athletes in college sports training. This paper analyzes the basic metabolic model of the human body and energy supply and demand model and constructs a scientific energy consumption test model for special sports activity. An algorithm for heart rate detection and energy consumption based on acceleration data acquisition is proposed. Therefore, it is proposed to calculate motion acceleration using bone point data obtained from a portable telephone camera sensor for special sports activity and to calculate kinetic energy consumption through detection data. A model for evaluating the proposed algorithm is also established.

1. Introduction

In the past, heart rate measurement under exercise was carried out by using heart rate frequency band. This device needs to install conductive heart rate frequency band in the chest to collect ECG signals of users and analyze heart rate [1]. Now, in sports research in China, polar heartbeat band with high recognition is used [2]. Because the heart rate belt is inconvenient to wear and the price is high, the physical training in many colleges and universities is unbearable. With the popularity of people who value health and devices that can be installed, the number of people who want to record their exercise status and heart rate has increased. Many companies are developing corresponding products. These new products are almost all in the form of watches. These products exceed the limit of heartbeat band and greatly improve the comfort of users. Therefore, rapid development has been made in recent years. These devices generally use photoelectric volume pulse wave to measure heart rate, but the accuracy of heart rate measurement of these devices during exercise is not very good [3]. For example, like Huawei's HUAWEI Watch, when the arm is quiet, you can wait about 11 seconds to get the current heartbeat value. Static measurements are 2 BPM different from medical devices, but if the arm is shaken or swung in the test, the test will fail.

In addition, most of these watches have the function of motion state recognition, which can recognize various motion states such as running, walking, and rest [4]. The recognition of this motion state is mostly based on acceleration sensors. As an auxiliary function of heart rate meter, the recognition of action state is also the research content of this paper.

With the development of society, people's cognition of sports training has changed and new understanding. In colleges and universities, people have higher requirements for the effect of physical education teaching and training. After all, university is the last link and crucial link in personnel training. Having a healthy and ripped body requires creative thinking to strengthen students' physique in the process of exercise [5]. The rapid development of the Internet has brought many positive impacts on all aspects of people's lives. For example, we communicate more closely and frequently with foreign countries through the Internet, and we can shop and entertain

without leaving home. However, people's travel activities, exercise, and face-to-face communication are becoming less and less, which leads to obvious lack of physical fitness and deterioration of physical fitness of college students in China [6].

In order to change this situation, we analyzed the situation and put forward Tabata training method in physical education with high-intensity interval training as the focus, hoping to further improve the physical fitness and health level of college students. In the scheme of strengthening national physical fitness by sports put forward by our country, the overall level of aerobics in colleges and universities needs to be improved, so it is necessary to strengthen teaching, analyze the present situation, and prepare for improving the overall level. Combined with big data, the teaching methods of microcourses are applied to bodybuilding gymnastics in colleges and universities. Teachers can collect materials from the Internet, make videos, and then assign tasks to students, so as to achieve the purpose of learning and integrating knowledge. In addition, there are public online courses to realize the training of talents in the form of sharing, which shows that big data thinking provides a new perspective and ideas for the construction of aerobics online open courses [7]. Researchers collected and analyzed the physical exercise data of students from two Russian universities. Similarly, through the study of three courses, there are differences in physical preparation and functional status between students in nonphysical education colleges and physical education colleges, which show that the index value of functional status is related to training and its dynamic change is characterized by higher cost of adapting to physical functional status [8].

2. Motion State Recognition Algorithm Based on Acceleration Signal

2.1. Feature Extraction

2.1.1. Signal Preprocessing. Firstly, the acceleration signal is filtered. The original signal unit is converted to 9.8 N/kg (gravity acceleration g), and a 30-point smoothing filter is adopted.

The short acceleration signal does not contain enough signal to recognize the action. Long-time signals cause serious delay to real-time systems [9]. According to experience, the shorter sliding window does not contain enough information to identify different actions, and the sliding time window is long, which is not suitable for real-time systems. After repeated experiments, the data every 8 s is finally selected to form a feature matrix for motion state recognition [10]. The formula of the sum vector is as follows:

$$G = \sqrt{x^2 + y^2 + z^2}, \tag{1}$$

where x, y, and z are the components of acceleration in three directions, respectively.

Here, signal processing is to make use of systematic errors or noises produced by monitoring equipment in data acquisition. These signals need to be processed in normal data, which leads to large errors in later data processing. In this paper, filters are used for filtering, and some signals are adjusted to slide windows to reduce errors.

2.1.2. Time Domain Characteristics

(1) Standard Deviation. In motion state recognition, the time domain features are mainly mean, standard deviation, energy, sample entropy, peak degree, deviation, quartile difference, and correlation coefficient. Some literatures show that the deviation in the upper and lower directions can effectively distinguish the next layer. Kurtosis in front and back can effectively distinguish running. Coefficients in the left and right directions can distinguish between walking and going up.

The original signal is set as $x(1), x(2), x(3), \cdots, x(n)$ the mean value of $x(n)$ signals is, and the standard deviation is defined as

$$\delta = \sqrt{\frac{\sum_{i=1}^{n}(x_i - \bar{x})^2}{n}}, \quad i = 1, 2, \cdots, n. \tag{2}$$

In formula (2), n is the number of samples. The peak value in vertical direction is a time domain characteristic with good recognition effect.

(2) Sample Entropy. Sampling entropy is a method to detect the complexity of new time series. The larger the sampling entropy, the more complex the sequence and the worse the periodicity. The acceleration signal of human body motion has certain periodicity and unstable time series. Therefore, the sample entropy is suitable for being used as the eigenvalue in human operation state recognition. As shown in formula (3), the sample entropy calculation formula n is the length of the sequence, and m is the dimension.

Let the original signals be $X(1), X(2), X(3), \cdots, X(n)$, from which M numbers are continuously extracted to form a group of M-dimensional vectors. $y_m(i)$ represents a vector composed of m consecutive values starting from the i-th point.

$$y_m(i) = \{x(i), x(i+1), x(i+m-1)\}. \tag{3}$$

The distance between $y_m(i)$ and $y_m(j)$ is defined as $d[y_m(i), y_m(j))]$, and given the threshold r, the number of $i \le n - m$ is calculated for each value $d[y_m(i), y_m(j))] < r$. And the ratio of this number to the total distance is $n - m - 1$, which is defined as

$$B_i^m = \frac{\sum_{j=1}^{n=m}\{\mathrm{num}(\mathrm{d}[y_m(i) \boxtimes y_m(j))] < r)\}}{n - m - 1}. \tag{4}$$

Calculate its average for all i, add 1 to the dimension of m, and repeat the above steps to obtain

$$\mathrm{SampEn}(m, r) = \lim_{n \longrightarrow \infty}\left\{-\ln\left[\frac{B^{m+1}(r)}{B^m(r)}\right]\right\}. \tag{5}$$

Different values of m, r, and n will get different sample entropy values.

2.1.3. Frequency Domain Characteristics. For extracting feature vectors from human motion state recognition, many researches have been carried out using frequency domain features. The frequency domain features are FFT coefficients, DCT coefficients, spectral entropy, and energy spectral density. Comparing the performance of several frequency domain features, it is found that FFT coefficients have high resolution. Some scholars use PCA to reduce and reduce FFT coefficients and then have a significant impact on the accuracy of motion recognition. In the five exercises discussed in this section, FFT coefficients are applicable to the features identified as exercise states at the point that running, stepping, and walking cycles are good.

In this study, FFT coefficients are further analyzed, and it is suggested that the main frequency should be used as one of the eigenvalues. In this paper, the three-axis acceleration signals are converted by FFT, and the main frequency is extracted as the frequency domain feature. In this way, not only the high resolution of FFT is used but also the feature dimension is reduced and the computation is reduced.

2.2. Classifier Design

2.2.1. SVM Classifier. The basic idea of support vector machine is to transform the input space into high-dimensional space by linear transformation and obtain the best linear classification surface in the new space. To use the SVM Toolbox, you must select the kernel function to use. The following are the representations of several general kernel functions.

Linear kernel:

$$k(x, y) = x^T y + c. \tag{6}$$

Polynomial kernel:

$$k(x, y) = \left(ax^T y + c\right)^d. \tag{7}$$

Radial basis function:

$$k(x, y) = \exp\left(-\gamma \|x - y\|^2\right). \tag{8}$$

The radial basis function is a real function whose value depends only on the distance from the origin, that is, $\Phi(x) = \Phi(\|x\|)$, or it can also be the distance to any point c, which is called the center point, that is, $\Phi(x, c) = \Phi(\|x - c\|)$. Any function Φ satisfying the characteristic $\Phi(x) = \Phi(\|x\|)$ is called radial basis function, and the standard one generally uses Euclidean distance (also called Euclidean radial basis function), although other distance functions are also possible. In the neural network structure, it can be used as the main function of full connection layer and ReLU layer. Using various eigenvalues extracted in the previous section, Professor Lin Zhiren of Taiwan developed LibSVM for data training.

2.2.2. Decision Tree Classifier. Decision tree turns complex multicategory problems into several simple classification problems to solve. The key to tree creation is how to select features in each node to create a simple tree. Motion state recognition based on decision tree is generally divided into two steps. The learning of training set is used to generate decision tree. The generated decision tree is used to identify the motion state.

The flow of decision tree is simple, and the complexity of algorithm is low. The general decision tree algorithms are CART, ID3, C4.5, CHAID, and so on. Mr. Algorithm makes complex trees and cuts them according to the results of cross-validation and test group validation. It has a very powerful statistical analysis function. In addition, the rules contained in the results after data processing become easy to understand. Therefore, classification regression tree is a good method to establish statistical analysis model for characteristic data. According to the research, the prediction tree constructed by CART model is more accurate than the algebraic mathematical prediction benchmark constructed by general statistical methods in many cases. The more complex the data and the more variables, the more obvious the advantages of the algorithm. In CART (Classification and Regression Tree) algorithm, the Gini index structure is used to determine the tree, and the Gini index is defined as

$$\text{Gini}(D) = 1 - \sum_{i=1}^{m} p_i^2, \tag{9}$$

where m still denotes the number of classes C in the data set D, p_i denotes the probability that any record of D belongs to C, and p_i is defined as the ratio of the number of groups belonging to C_i in D to the total number of D. If all records belong to the same category, then $P_1 = 1$ and Gini $(D) = 0$, in which case the purity is the lowest. For each attribute that enumerates a nonempty proper subset of the attribute, the Gini coefficient after the attribute R is split which is taken

$$\text{Gini}_R(D) = \frac{|D_1|}{|D|}\text{Gini}(D_1) + \frac{|D_2|}{|D|}\text{Gini}(D_2). \tag{10}$$

D_1 is a nonempty proper subset of D, D_2 is the complete set of D_1, $D_1 + D_2 = D$, attribute R has multiple proper subsets, that is, Gini R (D) has multiple values, and the smallest value is selected as the Gini index of R.

$$\Delta\text{Gini}(R) = \text{Gini}(D) - \text{Gini}_R(D). \tag{11}$$

The maximum attribute of Gini (R) increment is used as the best splitting characteristic. In order to prevent the decision tree from fitting the sample, it needs to be pruned. CART adopts price. In the pruning method of complexity, price refers to the misclassification rate of samples. Complexity refers to the number of leaf nodes of a tree and defines the value complexity of a tree.

$$cc(t) = \alpha * \text{Leaf}_t + \frac{E}{N}. \tag{12}$$

In equation (12), N is the number of decision tree training samples, E is the number of decision tree error samples, and Leaf_t is the number of leaves and parameters of the tree.

α measures the relationship between price and complexity, indicating the relationship between the degree of complexity reduction of pruned trees and price. For t, cut down its subtree s and obtain a new tree new_t to replace the best leaf node in t. The training data can be divided into M by new_t than t, but the number of leaf points contained in new_t is less than t. Equate the price complexity after replacement.

$$cc(t) = cc(\text{new}_t) \Rightarrow \alpha * \text{Leaf}_t + \frac{E}{N} \Rightarrow \alpha = \frac{M}{N(\text{leaf}_s - 1)}. \tag{13}$$

In formula (13), M is the number of misdivided samples increased after replacing the S subtree of T with leaf nodes. leaf_s is the number of leaf nodes of the subtree s. The pruning step: the first step: calculate the α value of each nonleaf node of the complete decision tree $T_{\max}$; loop off the subtree with the smallest α value until the root node is left; a series of pruning trees $\{T_0, T_1, T_2, \cdots, T_m\}$ are obtained, where T_0 is the complete decision tree $T_{\max}$ and T_{i+1} is the result of pruning T_i. Step 2: using independent pruning set (nontraining set) to evaluate T_i in the first step to obtain the best pruning tree; standard error SE is shown in equation (14).

In formula (13), M is the number of error samples added after the leaf node replaces the T subtree. leaf_s is the number of leaf nodes of subtree s. Pruning steps are as follows.

Step 1. Calculate the complete decision tree. The value of each nonleaf node: cyclic cutting is minimal. α preserves the subtree of values before the root node. A series of pruning trees $\{T_0, T_1, T_2, \cdots, T_m\}$ are obtained, where T_0 is the complete decision tree $T_{\max}$ and T_{i+1} is the result of pruning T_i.

Step 2. Using independent pruning set (nontraining set) to evaluate T_i in the first step to obtain the best pruning tree, standard error SE defined as

$$\text{SE}\left(E^{'}\right) = \sqrt{\frac{E^{'} * \left(N^{'} - E\right)}{N^{'}}}. \tag{14}$$

In formula (14), N' is the number of pruning sets, and E_i is defined as the error fraction of tree T_i to pruning sets.

$$E^{'} = \min\left(E_i\right). \tag{15}$$

Optimal pruning tree: T best meets the following conditions and has the least number of nodes. The condition that needs to be met: $E \le E^{'} + \text{SE}(E')$.

3. Establishment of Energy Consumption Model of Sports Activities

The energy consumption of daily physical activity often cannot meet the total sports energy consumption demand of the balance of energy supply and demand of human body, so it is necessary to increase additional activity energy consumption [11]. At present, the common sports activities include running, skipping rope, swimming, and aerobic exercise. The common characteristics of these sports are planning, regularity, sports goals, etc. Therefore, this paper chooses four movements, namely, opening and closing jump, left and right small jump, skipping rope, and squat, which do not need additional fitness equipment and have lower requirements for sports environment. Compared with the commonly used acceleration sensor method, the skeleton point data collected by the mobile phone camera sensor can reflect the whole body motion trend, so the motion acceleration can be calculated by using the skeleton point data obtained by the mobile phone camera sensor in special sports activities.

Every movement completed by the human body depends on muscles and bones, and the work done by the body during exercise leads to energy consumption. A strand points out that there is a linear relationship between work, force product, and oxygen consumption for motion, and the force product is the integral of force and time, as shown in

$$W = \int_{t_2}^{t_1} F dt, \tag{16}$$

where F is the force acting on human muscles, according to Newton's second law:

$$W = \int_{t_2}^{t_1} mad t. \tag{17}$$

The differential of force product reflects the amount of activity per unit time, and the type and intensity of dipping and cutting are obtained by using the acceleration of movement. Under the changing trend of three dimensions of space, the energy consumption in a certain time is calculated by using the information of human motion intensity and time. Generally speaking, from the physical and mechanical point of view, researchers choose to fix the acceleration sensor at the hip joint because the hip joint is closer to the center of gravity of the human body. Compared with wearable devices, image recognition technology greatly reduces the invasion of motion and can simply and conveniently obtain the position of the human center of gravity and the change of acceleration value during human motion.

3.1. Data Acquisition of Bone Point and Center of Gravity. The bone point recognition algorithm adopts BlazePose algorithm in Blaze series algorithms released by Google. The algorithm is based on lightweight convolution neural network architecture, which not only pursues the implementation of mobile devices but also ensures high recognition accuracy. In the recognition process, the algorithm can provide up to 32 body key point information per frame, as shown in Figure 1. Running BlazePose algorithm on a mobile phone with Qualcomm Snapdragon 888 processor can provide 22 frames of bone point data per second [12], which is enough to meet the acquisition frequency requirements of acceleration data.

In the common calculation methods of center of gravity, the moment synthesis method needs to calculate the barycentric

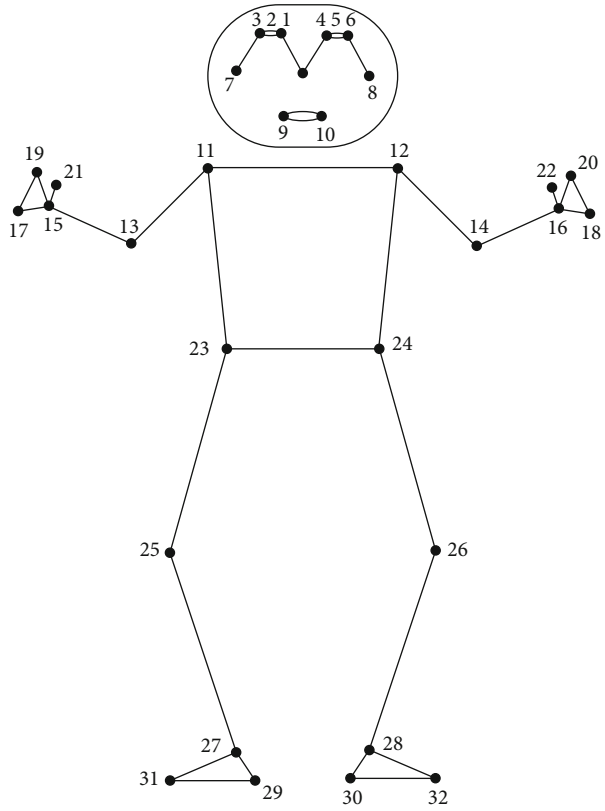

Figure 1: BlazePose algorithm bone point recognition diagram.

coordinates of the corresponding body parts by using the coordinates of bone points, while the multiplication coefficient method omits this step. On the basis of obtaining the coordinates of the center positions of each bone point of the body, it multiplies the corresponding bone point coefficient values and accumulates the results after multiplying each bone point to be the coordinates of the total barycentric of the human body. In this paper, the method proposed by Wei et al. is used to calculate the center of gravity of the human body in each frame image. The center of gravity is calculated according to the following equations:

$$X_c(t) = \sum_{i=1}^{15} k_i^* X_i(t), \tag{18}$$

$$Y_c(t) = \sum_{i=1}^{15} k_i^* Y_i(t). \tag{19}$$

In the formula, $X_c(t)$ and $Y_c(t)$ are the coordinates of bone point data obtained by BlazePose algorithm in X and Y axes, $X(t)$ and $Y_i(t)$ are the coordinates of a bone point I in X and Y axes when the number of frames is t, and k_i is the coefficient value corresponding to bone point I. The specific values are shown in Table 1.

Through the change trend of coordinate information of human skeleton points in each frame image, the displacement trend of human center of gravity in a period of movement is obtained by using the calculation method of center of gravity, as shown in Figure 2, which shows the displacement trend of the center of gravity of left and right small jumps in a period of time.

Table 1: Human skeleton points and corresponding coefficients.

Bone point	Mapping coefficient value (k)
Nose	0.0706
Shoulder	0.0356
Midpoint of shoulder connection	0.2391
Elbow	0.0580
Hand	0.0372
Hip	0.1297
Midpoint of the line between hips	0.1630
Knee	0.1630
Distance	0.0801

3.2. Filtering of Bone Point Data. In actual use, the information of human bone points obtained by BlazePose algorithm has high accuracy, but there is still bone point shaking. In order to avoid the large calculation error of acceleration information caused by bone point jitter, which will affect the accuracy of energy consumption fitting experiment of special sports activities and the accuracy of energy consumption detection in actual use, it is necessary to filter the bone point data obtained by camera sensor.

Considering the real-time and effectiveness of the filtering algorithm, the same filtering algorithm as the daily physical activity energy consumption detection is selected in the energy consumption detection of special sports activities, that is, the moving average filtering algorithm. Figure 3 shows the filtering effect of barycentric coordinates in the process of human movement.

3.3. Acceleration Calculation Method. The data of 15 bone points in each frame obtained by BlazePose algorithm can calculate the coordinates of the center of gravity of the human body in each frame by multiplication coefficient method. During a period of movement, the coordinates of the center of gravity of the human body constitute a discrete displacement variable function, and the velocity variable and acceleration variable are expressed by the change of displacement and time during the movement, while the solution of velocity and acceleration needs to build a continuous displacement differential equation. In this paper, the finite difference method is used to solve this problem. Its principle is to use discrete functions instead of continuous variable functions and to replace differential equations with difference equations, thus establishing finite difference equations. The acceleration problem solved in this paper is a second-order differential problem, so the second-order central difference method is selected as the method to construct the difference shown in Figure 4.

First-order difference:

$$\frac{\Delta f(x)}{\Delta x} = \frac{f(x + (h/2)) - f(x - (h/2))}{h}. \tag{20}$$

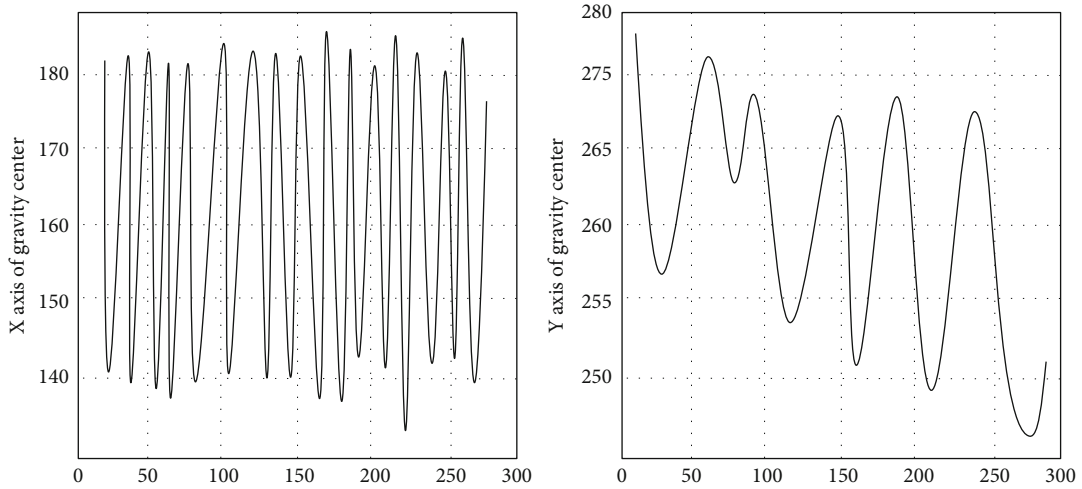

Figure 2: Relative displacement trend of left and right small jump center of gravity (a) X axis and (b) Y axis.

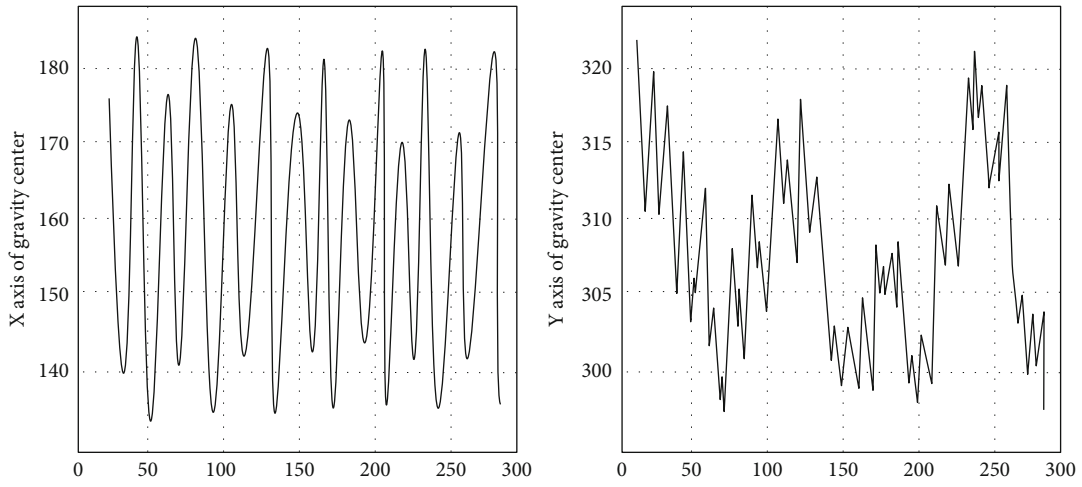

Figure 3: Filtering of (a) X axis and (b) Y axis of opening and closing jump center of gravity.

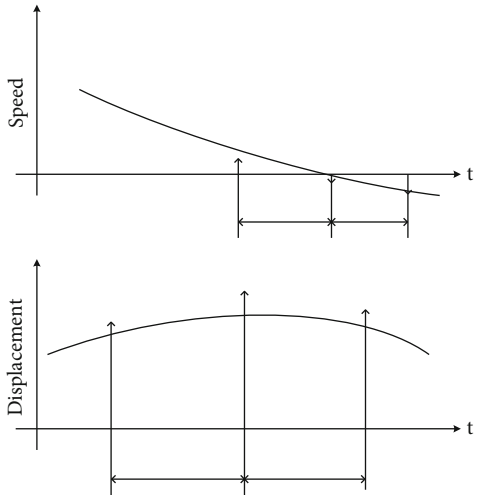

Figure 4: Schematic diagram of second-order central difference method.

Second-order difference:

$$\frac{\Delta^2 f(x)}{\Delta x^2} = \frac{f(x+h) - 2f(x) + f(x-h)}{h^2}. \tag{21}$$

At the beginning of the movement, time $t = t_0$:

$$m\ddot{v}_0 + c\dot{v}_0 + kv_0 = p_0. \tag{22}$$

The initial acceleration is

$$\ddot{v}_0 = \frac{1}{m}(p_0 - c\dot{v}_0 - kv_0). \tag{23}$$

The velocity at the midpoint of the step before and after $t = t_0$ is

$$\begin{aligned} \dot{v}_{-1/2} &= \frac{v_0 - v_{-1}}{h}, \\ \dot{v}_{1/2} &= \frac{v_1 - v_0}{h}, \end{aligned} \tag{24}$$

where H is an equal time step and the acceleration in the middle of time is calculated by velocity:

$$\ddot{v}_0 = \frac{\dot{v}_{1/2} - \dot{v}_{-1/2}}{h} = \frac{1}{h^2}(v_1 - v_0) - \frac{1}{h^2}(v_0 - v_{-1}). \quad (25)$$

Thus, it is concluded that

$$\ddot{v}_0 = \frac{1}{h^2}(v_1 - 2v_0). \quad (26)$$

Eventually,

$$v_1 = v_0 + h\dot{v}_0 + \frac{h^2}{2m}(p_0 - cv_0 - kv_0). \quad (27)$$

The coordinates of bone points obtained by BlazePose algorithm are relative coordinates. The relative height coefficient at present time can be obtained by the ratio of the relative distance between the real height information of the human body and the bone point data of the human body in each frame image, and the displacement value multiplied by the current relative height coefficient when calculating the acceleration information in the motion process is the real motion displacement data. The acceleration value of the human body during training is calculated by using the finite difference method described above.

3.4. Energy Consumption Calculation of Special Sports Activities. The nutrients ingested by the human body meet the fixed ratio relationship in oxidation reaction: the ratio of reactant consumption to product production and released energy is constant and has nothing to do with the reaction steps and conditions. Fixed ratio relationship is the basis of indirect calorimetry. By detecting the consumption of sugar, fat, protein, and other nutrients in the human body during a period of time, the total energy produced in the human body during this period can be obtained by using the heat price of each nutrient.

According to the law of fixed ratio, researchers put forward another index to evaluate the heat price of food, which is called the oxygen heat price of food, which refers to the energy released when a certain food consumes 1 L oxygen in the oxidation reaction in vivo. Oxygen and heat price of food is a key index of energy detection. The key parameters of oxidation reaction of basic nutrients for human energy supply are shown in Table 2.

Different nutrients consume different O and produce different CO_2 during oxidation reaction, and the energy produced is also different. The ratio of CO_2 production to O_2 consumption per unit time is called respiratory entropy, as shown in

$$\text{Respiratory entropy} = \frac{\text{Ml number of } CO_2 \text{produced}}{\text{Ml number of } O_2 \text{consumed}}. \quad (28)$$

The respiratory entropy of sugar is 1, and the oxygen thermal value provided by sugar is 21.1 kJ/L, that of fat is 0.71, that of oxygen thermal value is 19.6 kJ/L, that of protein is 0.80, and that of oxygen thermal value is 18.9 kJ/L. Under normal physiological conditions, most of the energy is produced by the reaction between sugar and fat, so in order to simplify the calculation method, the energy supply part of protein is ignored. According to the respiratory entropy, the reaction ratio of sugar and fat in this period of time was calculated, and the corresponding oxygen thermal valence was calculated.

4. Experiment

4.1. Motion State Recognition Experiment

4.1.1. Design of Exercise Experiment. According to the classification results of SCUT-NAA database, we propose an algorithm, which can effectively realize the recognition of motion state by using the acceleration sensor data of waist. However, the acceleration sensor of the heart rate meter is on the arm, and many literatures show that it is difficult to identify the motion state based on the acceleration sensor of the arm.

Firstly, this paper designs experiments and collects data. The subjects collected the sports data of 10 male college students in active service. First, they were required to stop for 1 minute, run for 3 minutes, rest for 1 minute, walk for 3 minutes, rest for 1 minute, stair for 2 minutes, rest for 1 minute, gymnastics for 2 minutes, and rest for 1 minute. All of them include five sports states: static, running, walking, jumping, and gymnastics.

4.1.2. Experimental Recognition Results and Analysis. The flowchart of multilevel motion recognition algorithm is designed by using decision tree classifier.

It can be seen from Tables 3 and 4 that the recognition rate of gymnastics is low. The main reason is that gymnastics has various sports states. When the human body does gymnastics, it is recognized as static, running, walking, etc., among which 21 are not recognized as static, which affects the overall recognition rate. There are two main reasons: (1) the gap between gymnastics and sports. (2) The feature values cannot better identify these five sports. These results show that the features extracted in the study cannot fully and effectively distinguish these sports states. The efficiency of the selected features needs to be further improved.

4.2. Energy Consumption Test

4.2.1. Experimental Design. Taking the energy consumption value detected by indirect calorimetry as the standard value and the front camera of mobile phone as the main tool, through the processing and calculation of the original image data, the energy consumption detection model is established on the basis of the recommended four sports and the validity of the equation is tested. The purpose is to establish a real-time, convenient, low-cost, and high-accuracy energy consumption detection method for special sports activities.

(1) Subjects. In this experiment, 45 subjects were selected. The body morphological indexes of the subjects are shown in Table 5. All the subjects were healthy and had no sports

Table 2: Parameters of oxidation reaction of nutrients.

Nutrients	Physiological heat value (kJ/g)	O_2 consumption (L/g)	CO_2 production (L/g)	Oxygen thermal valence (kJ/L)	Respiratory entropy
Sugar	17.2	0.83	0.83	21.1	1
Fat	39.8	2.03	1.43	19.6	0.71
Protein	18.0	0.95	0.76	18.9	0.80

Table 3: Recognition rate of motion experiment.

Kinds of sports	Recognition rate of action type
Static	79.41%
Running	88.64%
Escape	93.09%
Jump	79.26%
Do gymnastics	68.52%
Average	81.78%

Table 4: Confusion matrix of exercise experiment.

Status	Static	Running	Escape	Jump	Do gymnastics
Static	536	29	24	45	41
Running	23	359	0	11	12
Escape	15	0	377	1	12
Jump	27	5	3	214	21
Do gymnastics	53	2	17	13	185

injury. All the heads were called to return to the same equation with the superiority, and the other 15 subjects were used as the verification group. The linear regression equation of energy expenditure was constructed by using the training data of 30 people, and the training data of the remaining 15 people were used to verify the regression equation. There was no high-intensity activity before 24 hours and no dietary intake before 1 hour.

(2) Experimental Method. Before the beginning of the experiment, in order to avoid affecting the fitting results of energy consumption detection equation due to the sequence of actions, the sequence of actions that each experimenter needs to complete in the experimental group is disturbed. During the experiment, the experimenter followed the voice and action guidance video to complete four kinds of fitness actions, including opening and closing jump, left and right small jump, squat, and skipping rope. The completion time of each action is 1 minute, and the next action is started after 3 minutes of rest. During the rest of the experimenter, the staff recorded the detection data of each action for subsequent analysis.

The experimental scheme of the experimenters in the verification group is the same as that in the experimental group. In addition, in order to compare the accuracy of energy consumption detection model used in daily physical activities with that constructed in special sports activities experiments, the experimenters in the verification group need to fix a mobile phone device of the same model in the right pocket of trousers to record the motion acceleration information collected by the mobile phone acceleration sensor.

(3) Data Statistics. After completing the designed experimental program, the experimenter uses the exercise cardiopulmonary function instrument to record the data in the exercise process for calculation and gets the energy consumption value of each experimenter. This energy consumption value includes exercise energy consumption and basal metabolism. In order to build a physical activity energy consumption detection model, it is necessary to exclude basal metabolism energy consumption first, as shown in

$$\text{Exercise energy consumption after correction} = \text{Energy consumption of indirect calorimetry} - \text{Basal metabolism during exercise time}. \tag{29}$$

SPSS 20 software was used for statistical analysis, and the corrected energy consumption recorded by cardiopulmonary function instrument and the acceleration data calculated from image data were entered into the software in a one-to-one correspondence relationship. Pearson analysis was used to analyze the correlation between standard energy consumption and acceleration, sex of experimenter, BMI, and other indexes, and stepwise regression method was used to build an energy consumption detection model. The Bland-Altman (B-A diagram) analysis in MedCalc software

Table 5: Basic information of experimenters.

Indicators	Male ($n = 35$)	Female ($n = 10$)
Age (years)	25.2 ± 5.2	24.6 ± 3.8
Height (cm)	182.1 ± 5.2	161.2 ± 3.8
Body weight (kg)	80.5 ± 7.3	48.7 ± 5.6
BMI (kg/m^2)	24.3 ± 3.4	18.9 ± 2.8

is used to verify the consistency between the predicted value and the standard value, and the prediction accuracy of the energy consumption detection model is evaluated by calculating RMSE and MAPE coefficients of the predicted value and the standard value.

4.2.2. Establishment of Energy Consumption Model. In the energy consumption experiment of special sports activities, the acceleration values used include the activity information of all key body parts. Therefore, in the construction of energy consumption model of special sports activities, there is no need to build energy consumption detection models according to sports intensity, and the sports acceleration data and standard energy consumption data of the experimental group are only processed for different genders to build corresponding comprehensive energy consumption detection models.

Table 6 is a nested energy consumption model based on male VM value, in which Model 1 is a basic energy consumption model only considering VM value and R is 0.62. Compared with Model 1, Model 2 with BMI index has improved the prediction accuracy of the model to 0.65, so the comprehensive energy consumption detection model based on male VM value is shown in

$$\frac{\text{Energy consumption}}{5\text{s}} = 0.000525 \times \text{VM} + 0.0087 \times \text{BMI} = 0.261. \tag{30}$$

Table 7 is a nested energy consumption model based on women's VM value, in which Model 1 is a basic energy consumption model only considering VM value and R is 0.67. Compared with Model 1, Model 2 with BMI index has improved the prediction accuracy of the model, and R is increased to 0.70. Therefore, a comprehensive energy consumption detection model based on women's VM value is shown in

$$\frac{\text{Energy consumption}}{5\text{s}} = 0.000589 \times \text{VM} + 0.046 \times \text{BMI} - 0.581. \tag{31}$$

4.2.3. Band-Back Verification of Energy Consumption Model. The acceleration VM values and BMI values of 15 experimenters in the verification group were brought into the corresponding energy consumption detection model, the predicted values of the model were obtained, and the synchronous standard values were recorded. The Bland-Altman statistical method (B-A diagram) in MedCalc software is used to verify the consistency between the standard energy consumption value and the predicted energy consumption value, and the deviation confidence interval of the B-A diagram is 95%.

Table 6: Energy nesting model (based on male VM value).

	Model 1 Energy consumption	Model 2 Energy consumption
VM	0.000532 0.000	0.000525 0.000
BMI		0.0087 0.005
Constant	0.45 0.000	0.261 0.000
R^2	0.62 0.000	0.65 0.000

Table 7: Energy nesting model (based on female VM value).

	Model 1 Energy consumption	Model 2 Energy consumption
VM	0.000638 0.000	0.000589 0.000
BMI		0.046 0.000
Constant	0.345 0.000	-0.581 0.000
R^2	0.67 0.000	0.70 0.000

As shown in Figure 5, in the B-A graph of men in the verification group, 7 points fall outside 1.96 SD, accounting for 3.5% of the total data volume, and in the B-A graph of women in the verification group, 9 points fall outside 1.96 SD, accounting for 4.5% of the total data volume, all of which do not exceed the 5% standard. In addition, the average difference between standard and forecast is 0.00 and -0.02, respectively, which is close to the mean line 0. Therefore, it is considered that the two comprehensive energy consumption detection models constructed by experiments have strong prediction ability.

4.2.4. Comparison of Accuracy of Different Energy Consumption Models. VM values and BMI values collected by mobile phone acceleration sensors worn by 15 experimenters in the verification group were brought into the daily physical activity energy consumption detection model to obtain the energy consumption prediction value of the daily physical activity model, and at the same time, the energy consumption prediction values collected by the special sports activity energy consumption detection model were recorded. The RMSE and MAPE indexes of the predicted values and standard values of the two models are used to evaluate the prediction accuracy of the models, and the calculation methods are shown in formulas (32) and

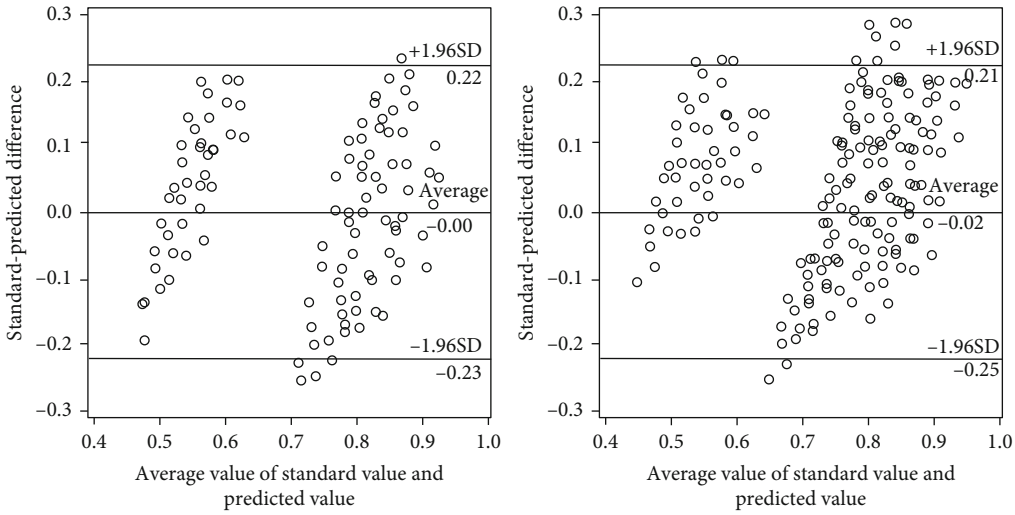

Figure 5: B-A diagram of (a) men and (b) women.

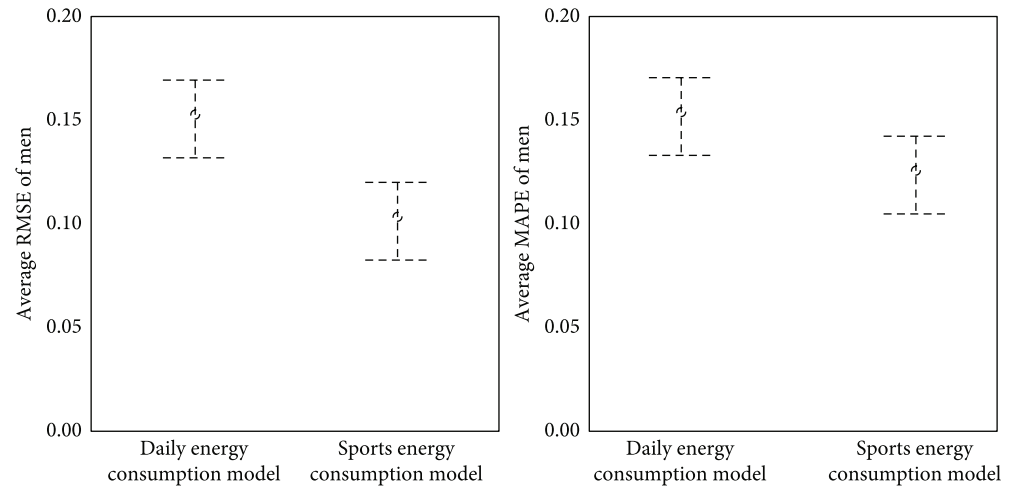

Figure 6: Comparison of indicators of male energy consumption detection models.

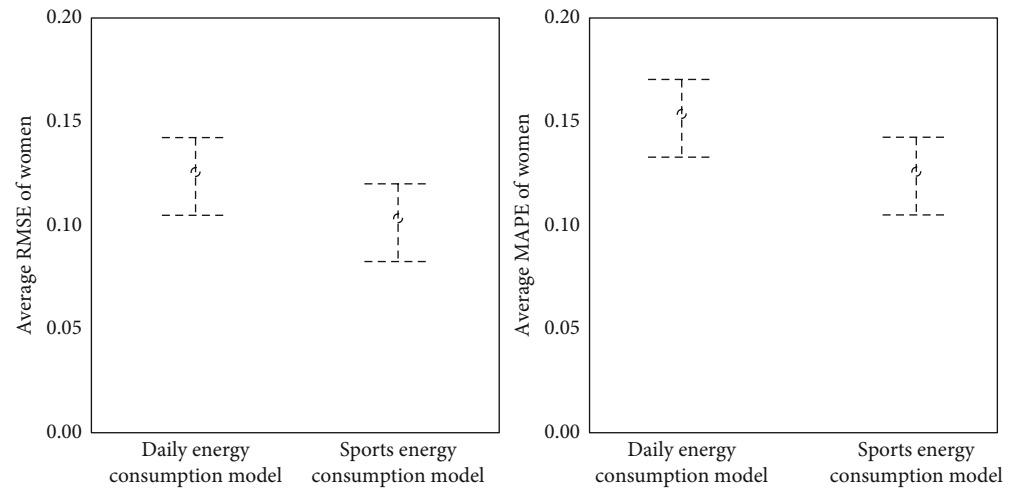

Figure 7: Comparison of indicators of women's energy consumption examination model.

(33). RMSE is the root mean square difference between standard and prediction, and the smaller RMSE, the higher the prediction accuracy of the model; MAPE is the average percentage difference between the standard and the forecast, and it is usually recognized that the MAPE value is less than 10%, which indicates that the accuracy of the model is high.

$$\text{RMSE} = \sqrt{\frac{\sum(\text{Predicted value} - \text{standard value})^2}{N}}, \quad (32)$$

$$\text{MAPE} = \sum \frac{|\text{Predicted value} - \text{standard value}|}{\text{Standard value}} \times \frac{100}{N}. \quad (33)$$

Figures 6 and 7 are the comparison charts of RMSE and MAPE indexes of two energy consumption detection models for men and women. It can be seen from the figure that RMSE and MAPE values of energy consumption detection model for special sports activities are lower than those of daily physical activity model. In the comparison of male energy consumption models, RMSE value of special sports energy consumption model is $0.12 + 0.03$, and the MAPE value is $6.45 \pm 0.72\%$. The RMSE value of daily physical activity energy consumption model is 0.15 ± 0.04, and the MAPE value is $7.93 \pm 0.726\%$. In the comparison of female energy consumption models, the RMSE value of special sports energy consumption model is 0.12 ± 0.04, and the MAPE value is $8.09 \pm 1.09\%$. The RMSE value and MAPE value of daily physical activity energy consumption model were 0.13 ± 0.04 and $9.63 \pm 1.01\%$, respectively. From the above RMSE value, we can see that the average value of men and women is less than 0.2, which indicates that the accuracy of energy consumption model is better. However, the average MAPE value of men and women is less than 0.1, which indicates that the accuracy of energy consumption model is high. From the analysis of the overall index value, it is concluded that the model constructed in this experiment has higher prediction accuracy.

4.3. Experimental Analysis. According to the comprehensive analysis of the data during the exercise, there is a significant correlation between sports energy consumption and morphological indexes such as gender, height, weight, and BMI. BMI is calculated from height and weight, while gender is used as classification index, and energy consumption between different genders is analyzed separately. Therefore, gender and BMI are considered as independent variables in the model construction. Under the same age and exercise type, men's activity energy consumption is higher than that of women, which is in line with the actual research conclusion: there are differences in fat situation and metabolic level between men and women, which leads to differences in energy consumption, so it is reasonable to include gender and BMI as independent variables in the construction of energy consumption detection model.

The comprehensive energy consumption detection model based on VM values of men and women is shown in

$$\text{Male}: \frac{\text{Energy consumption}}{5\text{s}} = 0.000525 \times \text{VM} + 0.0087 \times \text{BMI} + 0.261, \quad (34)$$

$$\text{Female}: \frac{\text{Energy consumption}}{5\text{s}} = 0.000589 \times \text{VM} + 0.046 \times \text{BMI} + 0.581. \quad (35)$$

After adopting stepwise regression method, the BMI index is brought into the energy consumption detection model, and the correlation between the predicted results and the standard values is increased from 0.62 to 0.65 and 0.67 to 0.70, respectively, which makes the interpretation of the model higher.

Figure 5 is the verification result of the energy consumption detection model of special sports activities. From the B-A diagram corresponding to male and female, it can be seen that the difference between the standard value and the predicted value of energy consumption of the experimenters in the verification group mostly falls within 1.96 SD, and the number of points falling outside the range is less than 5%. The reasons for this situation include the following:

(1) Considering that the data collected by mobile phone equipment and the data collected by exercise cardiopulmonary instrument are manually synchronized by the staff, there may be inconsistent data

(2) In the aspect of data processing, although the original skeleton point data is screened and processed, there may still be errors caused by skeleton point data shaking or disappearing

(3) The original data filtering algorithm is relatively simple, which may filter out some useful skeleton point information, resulting in some errors in the final energy consumption detection model verification results

This kind of error is within the acceptable range of experimental results, and the final energy consumption detection model is reliable. In order to verify the superiority of the energy consumption detection method and the constructed model of special sports activities, RMSE and MAPE indexes are used to verify the two energy consumption detection models of daily physical activity and special sports activities. The results are shown in Figures 6 and 7. The analysis results from the two energy consumption models in different genders are as follows. The prediction accuracy of the model constructed in this experiment is higher. The future work mainly studies the correlation and prediction of human body data perceived by human body multisensors, and the difference memory connection of different data can find the predictability of human body monitoring data as early as possible.

5. Conclusion

The basic metabolism model and energy supply and demand model of the human body were analyzed, and a scientific

energy consumption test model of special sports activities was constructed. An algorithm of heart rate detection and energy consumption based on acceleration data acquisition is proposed. Therefore, it is proposed to use the bone point data obtained by portable telephone camera sensor to calculate the motion acceleration and calculate the kinetic energy consumption through the detected data. A model for evaluating the proposed algorithm is also established, which can accurately collect human heart rate and energy consumption through sensor sensing information, thus providing health monitoring and further analyzing human health.

Data Availability

The experimental data used to support the findings of this study are available from the corresponding author upon request.

Conflicts of Interest

The authors declared that they have no conflicts of interest regarding this work.

References

[1] J. Geisheimer and E. Greneker, "A non-contact lie detector using radar vital signs monitor (RVSM) technology," *IEEE Aerospace & Electronics Systems Magazine*, vol. 16, no. 8, pp. 10–14, 2001.

[2] I. Waltering and G. Sl, "Identification of factors for a successful implementation of medication reviews in community pharmacies: using positive deviance in pharmaceutical care," *International Journal of Clinical Pharmacy*, pp. 1–11, 2021.

[3] A. Podolskij, "Reprint of: The system of planned, stage-by-stage formation of mental actions (PSFMA) as a creative design of psychological conditions for instruction," *Learning Culture and Social Interaction*, vol. 27, no. 4, p. 100474, 2020.

[4] V. Cantino, E. Giacosa, S. Alfiero, S. M. R. Shams, and A. Ferraris, "Introduction: smart tourism businesses (sustainability, measurability, awareness, recognition, & technology)," *Tourism Analysis*, vol. 24, no. 3, pp. 261–263, 2019.

[5] Y. Nie, K. Xiao, and J. He, "Exploring the cultivation path of public information literacy under the "information epidemic situation" (in Chinese)," *Shanxi Archives*, vol. 2, pp. 10–18, 2020.

[6] Y. Xiao, "Feasibility study of tabata training in the reform of physical education teaching in colleges and universities," *E3S Web of Conferences*, vol. 236, article 04022, 2021.

[7] J. Liu and D. Y. Huang, "Interpretation of the paths used in aerobics in colleges and universities under the background of big data," *Journal of Physics: Conference Series*, vol. 1574, no. 1, article 012118, 2020.

[8] A. A. Akhmatgatin, V. Y. Lebedinsky, G. K. Khomyakov et al., "The effectiveness of students' preparation in physical training at the universities of various departments," *Physical Education of Students*, vol. 24, no. 1, pp. 4–10, 2020.

[9] A. Rapp, "Design fictions for learning: a method for supporting students in reflecting on technology in human-computer interaction courses," *Computers & Education*, vol. 145, article 103725, 2020.

[10] J. Xiao, J. Qu, and Y. Li, "An electrooculogram-based interaction method and its music-on-demand application in a virtual reality environment," *IEEE Access*, vol. 7, pp. 22059–22070, 2019.

[11] C. Yang and H. Ming, "Detection of sports energy consumption based on IoTs and cloud computing," *Sustainable Energy Technologies and Assessments*, vol. 46, no. 3, p. 101224, 2021.

[12] M. Mason, "The elements of visitor experience in post-digital museum design," *Design Principles and Practices: An International Journal—Annual Review*, vol. 14, no. 1, pp. 1–14, 2020.

Hindawi
Journal of Sensors
Volume 2021, Article ID 7213595, 12 pages
https://doi.org/10.1155/2021/7213595

Research Article

An Indoor Positioning and Prewarning System Based on Wireless Sensor Network Routing Algorithm

Yanghua Gao, Weidong Lou, and Hailiang Lu

Information Center, China Tobacco Zhejiang Industrial Co., Ltd., Hangzhou 310008, China

Correspondence should be addressed to Yanghua Gao; yhgao@zju.edu.cn

Received 1 September 2021; Revised 27 September 2021; Accepted 12 October 2021; Published 5 November 2021

Academic Editor: Gengxin Sun

One of the most important means to position abnormal devices is to efficiently utilize the resources of wireless sensor network (WSN) and make proper analysis of the relevant data. Therefore, this paper constructs an indoor positioning and prewarning system that utilizes energy efficiently and achieves a long lifecycle. Firstly, the adjacent round iteration load balancing (ARILB) routing algorithm was proposed, which elects the cluster heads (CHs) by the adjacent round strategy. In this way, the random components were eliminated in CH election. Next, a short-distance multifrequency routing strategy was constructed between CHs to transmit the information to the sink, and a positioning algorithm was designed called ARILB-received signal strength (RSS). The ARILB-RSS positioning algorithm traverses the triangles formed by anchor nodes, forming multiple sets of ranging points; then, the optimal anchor node is recorded, and the path loss factor is iterated to reduce the positioning error. Simulation shows that the network survives 54.5% longer using ARILB than using the distributed energy-efficient clustering (DEEC) algorithm; the packet delivery rate using ARILB was about 139% higher than that of low energy adaptive clustering hierarchy (LEACH) algorithm and 35% higher than that of uneven clustering routing algorithm based on chain-cluster type (URCC) algorithm; ARILB-RSS reduced the ranging error by 14.31% and then the positioning error by 26.79%.

1. Introduction

Since its entry to the World Trade Organization (WTO) in 2001, China has maintained a rapid growth of economy for a long time, with its gross domestic product (GDP) growing at the rate of about 1,000% [1]. Meanwhile, there has been a significant increase in the fiscal revenue and economic capacity of the Chinese government and the hard power of the country. Against this backdrop, the Chinese people pursue long-term and better living standards [2]. Infrastructure, as an important carrier of living standards, has attracted more and more attention and policy support from the government [3]. In recent years, China has stepped up the construction of infrastructure, and completed numerous stations, stadiums, and shopping malls. Airports and residential communities are among these dense and complex buildings. The new airports are usually built together with transport facilities like high-speed rail and subway such as Hartsfield-Jackson Atlanta International Airport (Atlanta, USA), Heathrow Airport (London, UK), Frankfurt International Airport (Frankfurt, Germany), Narita International Airport (Narita, Japan), and Shanghai Pudong International Airport (Shanghai, China), making the building structure even more complicated. With the advancement of urbanization in China, newly built residential quarters in cities generally have a high floor area ratio.

While improving people's living standards, the above infrastructure adds difficulty to building maintenance and risk prewarning. The monitoring and positioning of personnel and equipment in buildings are essential to building maintenance and risk prewarning. For example, the building infrastructure in Europe is becoming older. Steel structures in industrial facilities and plant constructions are also affected by this ageing process. America needs to spend more than a quarter of a trillion dollars to bring its PreK-12 public school buildings up to working order, because these buildings lack building maintenance and risk prewarning. The health of building maintenance can be measured by

flow of people and the operation status of equipment. These metrics require continuous attention from the government and enterprises [4]. Nevertheless, it is extremely difficult to install, access, or manually maintain equipment in dense and complex buildings. This pushes up the operation and maintenance costs of buildings and reduces economic benefits. Meanwhile, the demand for effective monitoring and positioning of people in buildings has skyrocketed, owing to the rapid growth in the number of buildings [5]. Therefore, it is significant to realize reliable monitoring and positioning of indoor personnel and equipment.

The monitoring of people and equipment in buildings must be objective and consider various random factors. Objectivity is important because different equipment has different properties [6], which leads to the variation in sensor type and location. In order to ensure the improved type of the monitoring system, the development needs of the improved space and related instruments should be reserved when designing the system. The most significant random factor is people flow. The preset monitoring lines must account for the errors induced by the unpredictable people flow in the buildings. Hence, it is an inevitable trend in the development of indoor monitoring and positioning to improve the adaptability of the monitoring system.

Data is an inaccessible part of the various scientific and technological methods for digital indoor monitoring. As a key infrastructure for data acquisition, wireless sensor network (WSN) has been increasingly applied to various data collection tasks. WSN technology brings the data monitoring system multiple advantages, such as real-time uninterrupted monitoring, strong dynamic performance, and easy installation of facilities. WSN can effectively acquire data about the changes in equipment indices and personnel density in the monitoring range, eliminating the need for large-scale modifications to the original power supply lines. Although the WSN system is still in the test phase, there are some shortcomings, but it is still related to improvements and applied in actual operations. Therefore, our simulation only considers the data preprocessed by sensor chip. Then, it is a crucial issue to send these data to the data center.

WSNs can be an integral part of military command, control, communications, computing, intelligence, surveillance, reconnaissance, and targeting systems. The autonomous coordination capabilities of WSNs are utilized in the realization of a wide variety of environmental applications. For example, the developments in implanted biomedical devices and smart integrated sensors make the usage of sensor networks for biomedical applications possible. Smart sensor nodes and actuators can be buried in appliances such as vacuum cleaners, microwave ovens, refrigerators, and DVD players as well as water monitoring system. Routing algorithm [7–10], as an important means of data transmission in WSN, has received extensive attention from scholars. Recent years have witnessed a marked progress in routing clustering algorithms at home and abroad. Some of the latest routing algorithms are reviewed below:

Unequal cluster-based routing protocol (UCRP) is a routing algorithm to improve network throughput, packet delivery ratio, and energy of cognitive radio ad hoc networks. The UCRP realizes these goals by processing multilayer rings and normal nodes with different initial energies. Based on the optimal cluster radius, the UCRP was proved to outperform existing models through experiments [11]. Proactive source routing (PSR) protocol [12] is a lightweight routing algorithm that offers and provides new distance vector (DV) routing, link state (LS), and source routing method. Simulations have shown that PSR yields similar or better data transmission performance than other protocols.

The distributed probabilistic routing protocol (ProHet) abstracts a bidirectional route by finding a reverse path for every asymmetric link and using a probabilistic strategy to choose forwarding nodes, based on historical local information for WSN. ProHet realizes better efficiency, delivery rate, message cost, and coverage ratio than classic routing algorithms, such as prolong stable election routing (P-SEP) and unequal cluster-based routing protocol (UPRR) [13]. In 2013, Jin et al. proposed a practical passive cluster-based node-disjoint many-to-one multipath routing protocol, with the aim to enhance energy efficiency and maximize network lifecycle. This protocol searches for the optimal path through active clustering. The typical feature of the protocol is a node-disjoint many-to-one multipath routing discovery algorithm and the cost minimization on the multiple paths [14].

Centralized energy-efficient clustering routing protocol (CEECR) [15] provides a centralized cluster formation algorithm, detached nodes, and a mobile strategy. Compared to other routing protocols, CEECR reduces average energy dissipation and improves the packet delivery ratio. Aided efficient data gathering (AEDG) [16] is a novel approach to limit the number of associated nodes with the gateway nodes, with the aim to minimize network energy consumption and prevent gateway overloading. Through this approach, it is possible to obtain the suboptimal elliptical trajectory between nodes and ensure the duration, stability, and throughput of the network. Saleem et al. proposed a novel biological inspired self-organized secure autonomous routing protocol (BIOSARP) based on autonomous routing mechanism. The core of the protocol is to optimize the delay-reducing forwarding decision with the improved ant colony optimization (IACO). BIOSARP offers better results than many other protocols in WSN-based environmental monitoring [17].

To reduce the number of routes in conventional routing algorithms, Weng and Lai noted that the triangle routing algorithm saves much energy to transmit data between the transmitter and the receiver, by selecting sensors with a simple triangle rule. Therefore, they designed an enhanced relative identification and direction-based sensor routing (ERIDSR) algorithm, which effectively lowers the total energy in near-sensor nodes [18]. Ogundile et al. [19] put forward a clustered WSN that requires a sturdy energy-balanced (EB) and energy-efficient (EE) communication protocol. With the aid of the priority table, the protocol is formed by prioritizing the two shortest paths to the cluster head (CH) or sink, following some simple yet efficient rules. The purpose is to extend the lifecycle of WSN through balancing energy consumption.

The routing protocol of the WSN should prolong the lifecycle of the network and excel in data collection. The collected data should be analyzed by the server to judge whether the monitored area is abnormal. If the area is abnormal, it is necessary to locate the abnormality and make inspection and repair in a timely manner. So far, many scholars have explored WSN positioning algorithms. Depending on the necessity of node distance, the existing WSN positioning algorithms can be divided into two categories [20]: range-based algorithms and range-free algorithms. The typical range-based algorithms are time of arrival (TOA) algorithm [21], time difference of arrival (TODA) algorithm [22], angle of arrival (AOA) algorithm [23], and received signal strength indicator (RSSI) algorithm [24]. The range-free algorithms include approximate point-in-triangulation (PIT) test (APIT) [25], distance vector hop (DV-Hop) [26], and centroid algorithm [27]. Among them, the RSSI algorithm is low cost and easy to implement, because most wireless communication modules support RSSI ranging.

The above review shows that clustering and data transmission are the research focus of WSN communication. Therefore, this paper proposes the adjacent round iteration load balancing (ARILB) routing algorithm. Once the network is initialized, the number of CHs is optimized based on adjacent rounds to extend the network lifecycle. Then, the ARILB-received signal strength (RSS) algorithm was designed to enhance positioning accuracy. In the positioning phase, the ARILB-RSS algorithm determines the multilateral centroid more accurately. Finally, MATLAB simulations were conducted to demonstrate the performance of the proposed ARILB-RSS algorithm, compared with the ARILB algorithm.

2. Indoor Wireless Monitoring and Positioning System

2.1. Technical Roadmap. Figure 1 shows the technical roadmap of our indoor wireless monitoring and positioning system. There are two parts in the system: a routing algorithm and a positioning algorithm. The routing algorithm is the basis for running the positioning algorithm. The routing algorithm is the basis for running the positioning algorithm. First, the routing algorithm obtains various monitoring data based on WSN and sends the data to the server. Then, the server performs data analysis and discovers the anomalies. Finally, the location algorithm calculates the location of the anomalies.

(1) Routing algorithm

The routing algorithm collects data through sensors regularly arranged in the monitoring area and stores them in sensor memories. Then, the data are transmitted to the data center by the proposed ARILB algorithm, which is innovative in specificity analysis, CH election, and data transmission. Specifically, the sensor nodes are deployed evenly; adjacent rounds are introduced to the threshold equation to optimize the number of CHs; the optimal relay link is adopted to transmit the acquired data to the base station.

(2) Positioning algorithm (ARILB-RSS)

Firstly, the data obtained by ARILB algorithm are analyzed to find anomalies. Then, the abnormal equipment and people are located by ARILB-RSS in three phases: ranging, positioning, and correction. The ranging is realized with a classic ranging model. The positioning and correction are completed by ARILB-RSS, which is extended from the ARILB. The positioning is implemented in the following procedure: the triangles formed by anchor nodes are traversed to form multiple sets of range points. Then, the optimal anchor node is recorded by comparing the slope of each anchor node with that of the equilateral triangle. After that, the correction is made by periodically measuring the RSSI between anchor nodes near the unknown node. Then, the path loss factor of the next iteration is estimated based on multiple measured values, thereby minimizing the positioning error.

2.2. Specificity Analysis. With the expansion of application fields, WSN is facing more and more challenges. Unlike other monitoring systems, the indoor monitoring system does not need to focus on signal fluctuations in conventional deployment environments. For example, sensor nodes are sometimes arranged in liquid like water, which obstructs the signal transmission to a certain extent. Because of the uniform density of the liquid, the signal obstruction effect is uniform across the liquid. However, the signal might fluctuate due to crowd movement in buildings, as well as other random factors in indoor equipment and personnel monitoring. Therefore, wireless sensors need to be installed to suppress data fluctuations.

The indoor environment is different from the environment of classic routing algorithms. In indoor monitoring, the randomness brought by crowd movement is the key constraint on data transmission. There are many drawbacks of traditional data transmission methods in indoor monitoring. The WSN can transmit data in multihop mode or single-hop mode. In a single-hop transmission network, energy consumption is mainly affected by distance, the signal is dispersed, and the monitoring threshold is extremely low. As a result, single-hop transmission should be avoided in indoor monitoring.

In a multihop transmission network, the death of any CH has an immense impact, which can be mitigated by increasing the density and energy of CHs. However, increasing CH density will delay information transmission, while increasing CH energy will increase economic cost. Therefore, both single- and multihop transmission modes should be improved before being used for indoor monitoring and positioning.

3. Assumptions and Modeling

3.1. Assumptions. It is assumed that the monitoring area is a regular rectangle, all sensors are arranged randomly in this

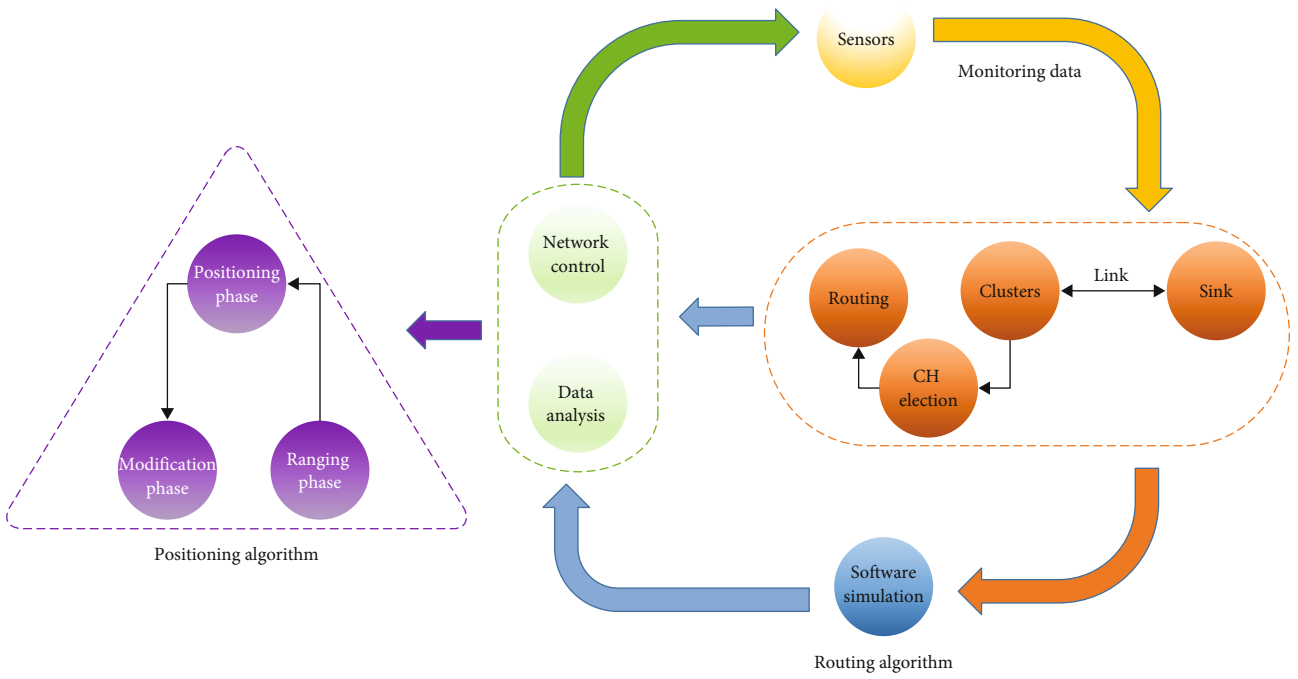

Figure 1: Technical roadmap.

area, and all sensors can cover the area effectively without sudden failure. The sensors installed by the ARILB algorithm have the following features:

(1) Every sensor installed in the network has a unique identification (ID) tag. Once a sensor fails, its ID will no longer be used

(2) The position of each sensor does not change after installation

(3) The sink has certain perception capabilities

(4) When the system is running (the main switch is not turned off), the energy of the sensors cannot be supplemented

(5) The sensors communicate via a symmetric two-way channel, which will never be blocked

Based on the above assumptions, N sensors are randomly arranged in an $L \times L$ rectangular area and transmit the acquired data back to the sink. Since the equipment and people flow are fixed, the sink (data center) should be installed in the geometric center to ensure the symmetry of data collection. Once the wireless monitoring system enters into operation, the network nodes will aggregate around CHs into clusters, and the data collected by the nodes in the same cluster will be sent collectively to the sink. Then, a clustering method should be adopted to mitigate the impact from the constantly changing network structure.

3.2. Energy Consumption Model. WSN mainly consumes energy in data sending and reception (Figure 2). By the transmission distance of nodes, the data sending energy can be described by two models. The energy consumed by a sensor to send each M-bit of data can be calculated by

$$\begin{aligned} ER(M) &= \mathrm{ME}_{\mathrm{elec}}, \\ ET(M,d) &= \mathrm{ME}_{\mathrm{elec}} + \mathrm{ME}_m d^{\tau}, \end{aligned} \tag{1}$$

where $\mathrm{ME}_{\mathrm{elec}}$ is the energy consumed to support equipment operation; $\mathrm{ME}_{\mathrm{fs}} d^2$ is the energy consumed by the radio frequency power amplifier, which accounts for a large portion of the energy consumption of the sensor node, within a communication distance (if the energy consumption surpasses $\mathrm{ME}_{\mathrm{fs}} d^2$, it will nosedive to $\mathrm{ME}_{\mathrm{amp}} d^4$); E_m is dependent on the transmission distance; $\tau = 2$ if $d < d_{\mathrm{th}}$ (d_{th} is the threshold of the transmission distance), and $\tau = 4$ if $d > d_{\mathrm{th}}$.

3.3. Protocol Matching by Classical Algorithm. Low energy adaptive clustering hierarchy (LEACH) algorithm [28] is the most classic routing algorithm, which effectively reduces energy consumption through clustering. However, its clustering rules have many defects in the matching of wireless routing protocols.

(1) CH election

LEACH generates CHs randomly by formula (2). In the initial state, each sensor node produces a number randomly in [0, 1] and uses this random number to influence CH election. Specifically, the random number is compared against the threshold $T(n)$. If the random number is smaller than

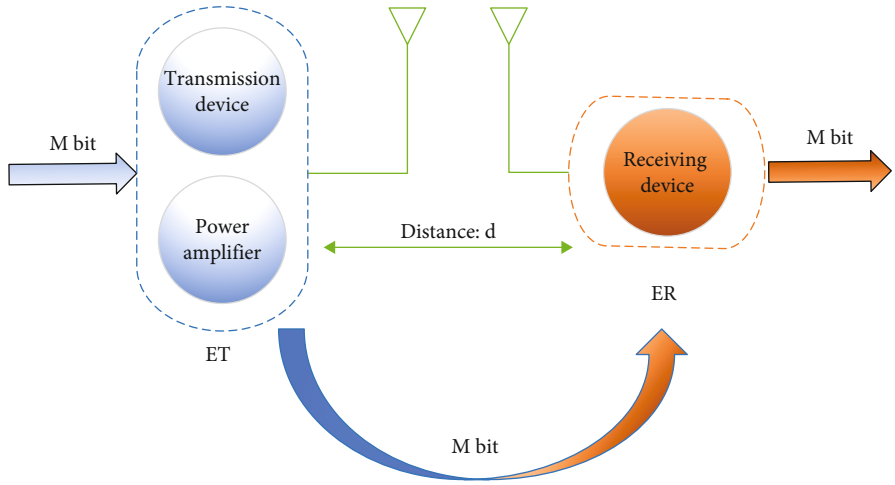

Figure 2: Energy consumption model.

$T(n)$, the node becomes the CH in this round.

$$T(n) = \frac{p}{1 - p(r \bmod (1/p))}, \tag{2}$$

where p is the percentage of the expected number of CHs among all nodes; r is the number of election rounds; and $r \bmod (1/p)$ is the number of nodes elected as CHs before this round. The nodes not elected as CH in this round are allocated to a set G.

Formula (2) ensures that every network node could be elected as CH and balances the energy consumption of all CHs. However, if this scheme is applied to a short-distance multifrequency scenario, the network nodes might cluster unevenly. To make matters worse, the heterogeneity of equipment properties determines that sensors differ greatly in adjustment. In other words, there is a huge difference in the data output in different areas. Therefore, formula (2) cannot be adopted for clustering alone.

(2) Data transmission

In LEACH, after a CH receives the requests from all non-CH nodes, it will create a scheduling table based on the number of sensors in its cluster and establish a scheduling sequence. Then, the CH sends the data directly to the sink. Nevertheless, in our monitoring scenario, some sensors might fail suddenly due to sudden changes in the monitoring area. Besides, the local data transmission is not smooth in the monitoring system. Therefore, it is necessary to enhance the degree of redundancy by improving the data transmission rules.

4. ARILB Routing Algorithm

In ARILB algorithm, CH election is usually implemented in the following stages. Before the algorithm starts, all sensors are fully charged, and the current state is by default the initial energy state of each sensor:

$$S(i) = \begin{pmatrix} R_P & \varphi \\ d_P & E_C \end{pmatrix}, \tag{3}$$

where i is the unique ID of the sensor, $R_P \in 0, 1$ is the ratio of the current round number to the total time, φ is an indicator of CH status (if $\varphi = 0$, the sensor is not a CH; if $\varphi = 1$, the sensor is a CH), E_C is the percentage of the remaining energy of the current node, and d_P is the relative distance between the node and the base station (%). Therefore, the initial state of sensor i can be denoted as $S(i)_{\mathrm{INIT}}$.

In WSN, the health of sensors can be largely measured by energy. Let $\ln(|S(i)|/|S(i)_{\mathrm{INIT}}|)$ be the health of a sensor at a certain moment, i.e., the energy factor. Obviously, the energy factor decreases continuously with the progression of data collection. The value of this factor falls in $-\infty, 1$. If $\ln(|S(i)|/|S(i)_{\mathrm{INIT}}|) = 1$, the sensor is in the healthiest state. If $\ln(|S(i)|/|S(i)_{\mathrm{INIT}}|)$ keeps dropping, the energy loss of the sensor is on the rise.

4.1. Structure of Monitoring Area. As suggested by signal characteristics [29] and Section 2.2, the monitoring area must be preprocessed to improve the monitoring effect. Considering the cost of sensors, the best preprocessing strategy is to optimize the spatial distribution rules. Therefore, this paper derives a suitable space model in the following process.

As mentioned before, the study area is an $L \times L$ square, with the sink at the geometric center. According to the equipment locations and mean speed of people flow [30], the interval of the sensors deployed in the network is smaller than the threshold mentioned in Section 2.2. The monitoring area could be divided into q square subareas with a side length shorter than d_{th}.The side length is related to various transmission paths and monitoring thresholds: $l_i = \{l_1, l_2, \cdots, l_q\}$. In addition, a circular area with a radius of d_{th} is planned near the sink and monitored directly by the base station (Figure 3). The purpose of this circular area is to

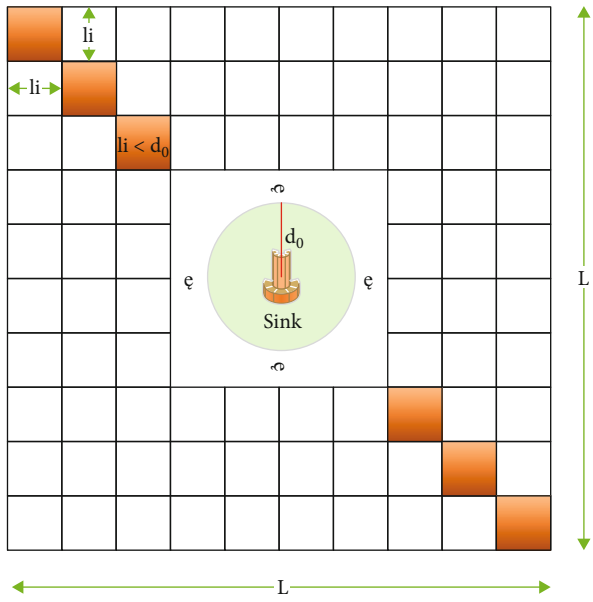

Figure 3: Schematic diagram of monitoring area.

prevent energy holes [31] and reduce path loss. Energy hole is a phenomenon in the traditional multihop mechanism: the nodes close to the sink are overloaded by data transmission tasks and thereby die prematurely. If the nodes close to the sink reduce or cancel the data transmission tasks, the energy consumed by them will be mostly utilized to transfer their own data. If $d < d_{\text{th}}$, the energy consumption will be greatly reduced.

4.2. CH Generation. CHs are constantly updated in the routing algorithm. In the beginning, the sink sends an initial signal to the entire monitoring area in a radiant manner. Then, each sensor starts to prepare for CH election. The proposed ARILB algorithm combines the classic routing algorithm with application scenarios into a CH generation scheme suitable for wireless monitoring of indoor equipment and personnel. The specific process is as follows:

Firstly, the sink broadcasts a "Hello" to the entire network. Upon receiving this information, each sensor waits to enter the working state. When all sensors are activated, the ARILB algorithm enters the CH generation phase. When a CH is elected, every network sensor will spontaneously generate a random number, rand, in the interval of (0, 1) and compare this number with a threshold function to finalize the CH election.

Specifically, the rand is contrasted with the new threshold function T_{new} for the following reasons: environmental factors (temperature, humidity, and wind speed) on the speed of crowd movement exert a combined effect on equipment monitoring, making it hard to balance the operation of the routing algorithm. In other words, the sensors are triggered at nonperiodic frequency.

ARILB has different requirements for CHs in different adjacent rounds. Therefore, this paper proposes a new threshold function T_{new} based on adjacent rounds. The function uses the energy factor defined above and introduces the iteration parameter $A_{\text{d}}(k)$:

$$T_{\text{new}} = T(n) \times (1 + A_{\text{d}}(k)), \tag{4}$$

where $A_{\text{d}}(k)$ can be calculated by

$$A_{\text{d}}(k) = \begin{cases} R_P \times \ln \dfrac{|S(i)|}{|S(i)_{\text{INIT}}|} & r = 2k + 1, \\ -R_P \times \ln \dfrac{|S(i)|}{|S(i)_{\text{INIT}}|} & r = 2k(k > 0), \end{cases} \tag{5}$$

where $R_P \in (0, 1]$ is the ratio of the current number of rounds to the total time. Formula (5) shows that clusters of different sizes can better match the frequency of a sensor triggered by random factors and make the CH election and cluster members more reasonable.

4.3. Routing Strategy. Energy consumption is the most pressing problem in the data transmission. As mentioned before, network data can be transmitted in single-hop mode or multihop mode. Under single-hop mode, each CH directly sends the collected data to the base station. Despite being simple to implement, single-hop mode has obvious shortcomings. Since the CH directly communicates with the sink, distance has a great impact on energy consumption. Different amounts of energy are consumed to transmit the same data over different distances. In the monitoring area, the sensors near the boundaries need to consume the greatest amount of energy. The excessive energy consumption of boundary sensors can be effectively prevented by the multihop mode. However, the multihop mode can hardly realize the continuity of data relay, which should not be interrupted. When multiple areas need to be monitored simultaneously, the multihop transmission links must meet higher requirements.

Through the above analysis, this section proposes a short-distance multifrequency routing scheme. It is assumed that, under multihop mode, each CH for data relay only forwards the information from the previous CH, without performing other relay tasks. Then, the problem of data transmission from boundary sensors to the sink can be converted into the selection of relay links.

To choose the right link, the CH $C_n (n < m)$ in the CH set $C = \{C_1, C_2 \cdots, C_m\}$ needs to find the next-level relay CHs $C_{n+1}, C_{n+2}, \cdots, C_m$. During data transmission, at least one relay CH needs to be found. Then, the total transmission distance of data in the link can be shown as

$$\begin{cases} \forall E_{C_i} \le \sum_{j=i+1}^{m} E_{C_j}, \\ \exists d_{\text{sum}} = \sum_{j=i}^{i+h} d^2 [C_j, C_{j+1}], \end{cases} \tag{6}$$

where E_{C_i} is the energy of CH; d_{sum} is the total transmission distance; $d^2[C_j, C_{j+1}]$ is the transmission distance of a relay interval; and h is the number of relays.

To transmit data, ARILB uses a partition-based multihop mode (Figure 4). Each CH can only transmit information once in a round. After receiving a piece of information, a CH will no longer receive any other information. At this time, the CH needs to forward the information to another CH that has not received the information in the subarea. If all CHs in the subarea have received the information, the CH will jump to another subarea, looking for a suitable CH. If the energy of the current CH is below the mean energy of the candidate CHs for next-level relay, the current CH will choose the closest CH as the next-level relay. This process will be repeated in turn, until the remaining energy of the current CH is greater than the mean energy of the remaining candidate CHs. In the latter case, the CH will directly send the data to the sink.

4.4. Positioning Algorithm. The distance-based positioning algorithms position nodes by the principle of space geometry, using the bases of distance and angle. Among them, the RSSI algorithm is simple, energy-efficient, and power-efficient, providing a suitable tool for the design of a low-power WSN. That is why this section presents the ARILB-RSS positioning algorithm. There are three stages of the RSSI-based positioning [32]: ranging, positioning, and correction.

4.4.1. Phase 1: Ranging. The distance between each anchor node and the unknown node is calculated based on the intensity of the transmitted signal to the unknown node. The most popular RSSI model can be expressed as

$$\mathrm{PL}(d) = A - 10n \lg\left(\frac{d}{d_t}\right) + X, \tag{7}$$

where d is the distance of the source; $d_t = 1$ m is the reference distance; n is the path loss factor; and A is the signal strength at $d_t = 1$ m. X represents the zero mean Gaussian variable. Then, a target can be positioned based on the location and signal strengths between two points. Formula (7) shows that the signal attenuates very quickly over a short distance. Therefore, the positioning error using RSSI signal attenuation is small in a short distance. This meets the short-range multifrequency requirements of the routing strategy in Section 4.3.

4.4.2. Phase 2: Positioning. The unknown node calculates the distance from an anchor node and locates its position. The greater the RSSI received by the unknown node, the smaller the signal attenuation, and the shorter the distance between the known node and the anchor node. Therefore, a high RSSI received by the unknown node means the environment and obstacles have a limited impact on positioning. It is possible to locate any object based on the positions of 3 sensor nodes, which are not in a straight line. Therefore, this paper proposes an improved positioning method (Figure 5).

In WSN, each anchor node sends RSSI signals to any unknown node. Then, the unknown node sorts the RSSI signals in a descending order by signal strength: PL + : PL − 1, PL − 2, ⋯, PL − N, with N being the number of received RSSI signals, i.e., the number of anchor nodes within the communication range. Since the corresponding anchor node position is known, the unknown node selects the three largest values: RSSI 1-3, namely, (x_1, y_1), (x_2, y_2), and (x_3, y_3). Then, the slope of the straight line connecting any two anchor nodes can be calculated by

$$\begin{aligned} f_{12} &= \frac{y_2 - y_1}{x_2 - x_1}, \\ f_{23} &= \frac{y_3 - y_2}{x_3 - x_2}. \end{aligned} \tag{8}$$

We can define the value of the error g, when the actual error is smaller than g; the ARILB-RSS considers that the three anchor nodes are close to an equilateral triangle and tends to locate unknown nodes as the optimal anchor node. Otherwise, the three anchor nodes that meet the conditions are selected, or the anchor nodes that meet the conditions are deemed as unqualified.

$$g = \frac{|f_{12} - f_E| + |f_{23} - f_E|}{2}. \tag{9}$$

4.4.3. Phase 3: Correction. To reduce the positioning error and improve positioning accuracy, the coordinates of the unknown node, which are estimated in the positioning phase, are optimized or corrected. Our algorithm is further improved to reduce the path loss factor n for ranging. Preset n is usually impractical and leads to a large deviation. Therefore, the actual n value should be approximated continuously in the actual environment. Our improved algorithm tries to iteratively update n in the following procedure: the RSSI between anchor nodes near the unknown node is measured periodically, and multiple measured values are used to derive the path loss factor of the next iteration, thereby minimizing the positioning error.

For the nodes in subarea l_i in the monitoring area, there are three possible scenarios near the subarea adjacent to l_i. In these three scenarios, there are 3, 5, and 8 square subareas, respectively (Figure 6).

Suppose there are multiple square subareas near the unknown node. Then, there should be at least y anchor nodes near this node: $y : y_1, y_2 \cdots \cdots$. The distance between anchor node y_p and the other $p - 1$ nodes can be expressed as $\{d_{y_1}, d_{y_2}, \cdots d_{y_{p-1}}\}$. Then, the following can be derived from formula (7):

$$\begin{cases} PL\left(d_{y_1}\right) = A - 10n_{p-1} \lg\left(\dfrac{d_{y_1}}{d_t}\right) + X, \\ \cdots\cdots \\ PL\left(d_{y_{p-1}}\right) = A - 10n_{p-1} \lg\left(\dfrac{d_{y_{p-1}}}{d_t}\right) + X. \end{cases} \tag{10}$$

Formula (9) can be simplified to obtain the n_p of the next iteration. The ranging error can be reduced through the constant updates of n.

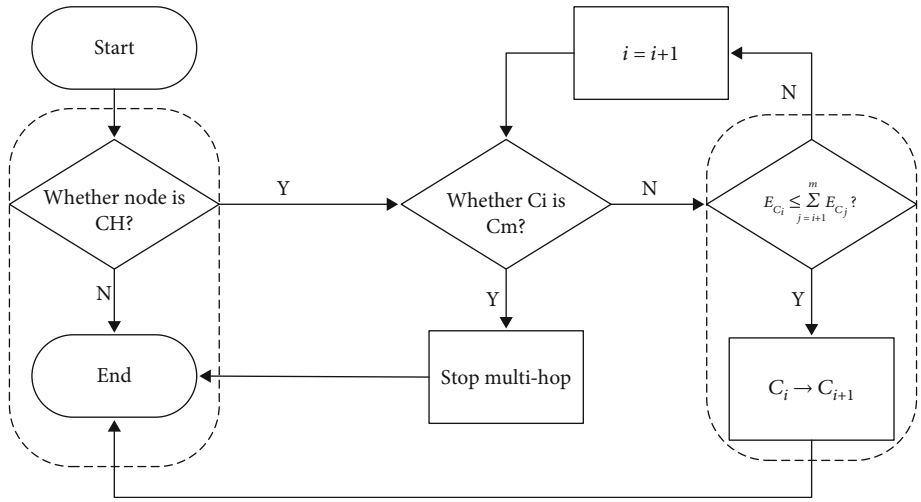

Figure 4: Routing process.

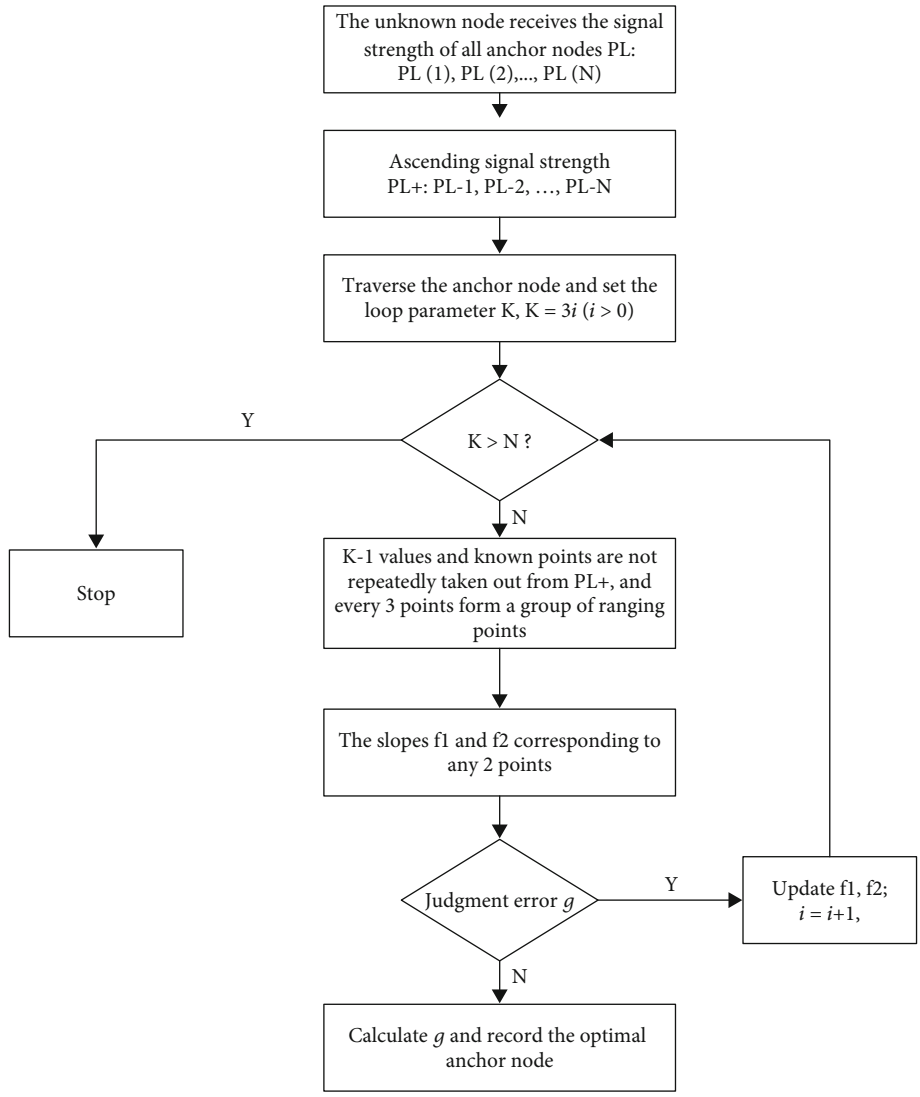

Figure 5: Positioning phase.

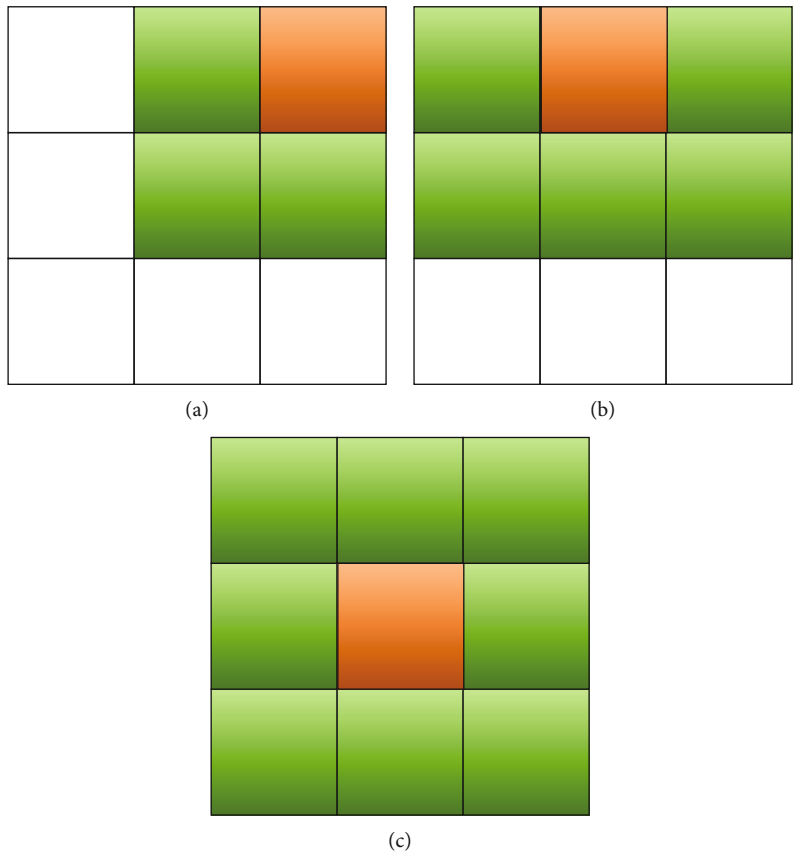

Figure 6: Scenarios of adjacent subareas.

5. Simulation and Result Analysis

5.1. Simulation Parameters. Our simulation was carried out on MATLAB. According to the proposed algorithm, 100 nodes were set up, with the sink at the geometric center (50 m, 50 m) of the monitoring area. Table 1 lists the simulation parameters.

5.2. Performance Analysis. This section compares the performance of our method, ARILB, with three other algorithms, namely, LEACH [33], distributed energy-efficient clustering (DEEC) [34], and uneven clustering routing algorithm based on chain-cluster type (URCC) [35], using metrics like stability time of the network, number of data packets received by the sink, and the total energy consumption of the network.

(1) Stability time

Figure 7 compares the stability time of the four algorithms, which is the top consideration in the design of wireless monitoring system. Only when the routing protocol survives long enough could the other performance indices be improved. In Figure 7, the stability time is demonstrated by the sensor failure rate in the same period. As shown in Figure 7, our algorithm boasts a rather long lifecycle. In the same period, our algorithm controlled the sensor failure rate below 20%, all the sensors in LEACH failed, and more than 54.5% of the sensors were damaged in DEEC and URCC. Therefore, our algorithm has an obvious advantage over LEACH, DEEC, and URCC in network lifecycle.

(2) Energy consumption

Energy is another key evaluation metric of WSN performance and an important consideration of protocol design. This paper quantifies the energy consumed by each protocol with the total energy consumption of the network in the same period. Figure 8 compares the energy consumption of the four algorithms. In the early stage (within 500 rounds), LEACH, DEEC, and URCC had similar slopes in their energy consumption curves. This means the three protocols have similar energy consumption rates in the early stage. In contrast, our algorithm had a smoother energy consumption curve in this stage, reflecting the good control of early energy cost. In addition, the network using our algorithm lasted longer than that using any other algorithm, under the premise of the same energy consumption. As the network operated, the network energy of LEACH, DEEC, and URCC was exhausted in 1,384; 1,844; and 2,200 rounds, respectively, while that of our algorithm was not exhausted before 2,500 rounds.

(3) Data packets

Apart from stability time and energy consumption, data transmission capacity is a nonnegligible performance index

Table 1: Simulation parameters.

Parameter	Value
Sink location	(50, 50)
Number of nodes	100
Short-distance transmission power amplifier	10 pJ/(bit·m^2)
Long-distance transmission power amplifier	0.013 pJ/(bit·m^2)
Data packets	4,000 bit
Initial energy	0.5 J
Area	100 × 100

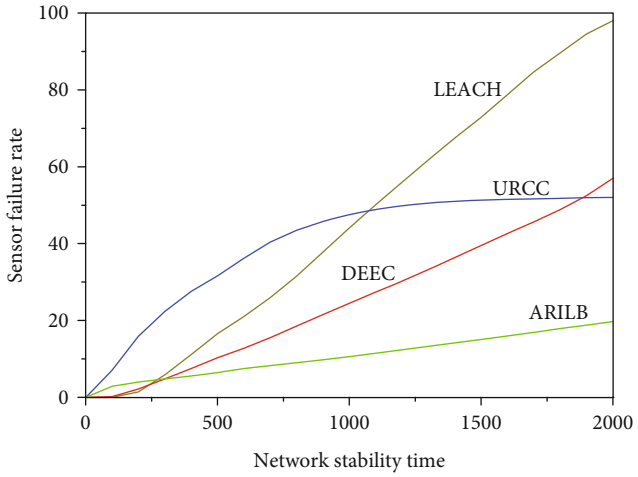

Figure 7: Stability time.

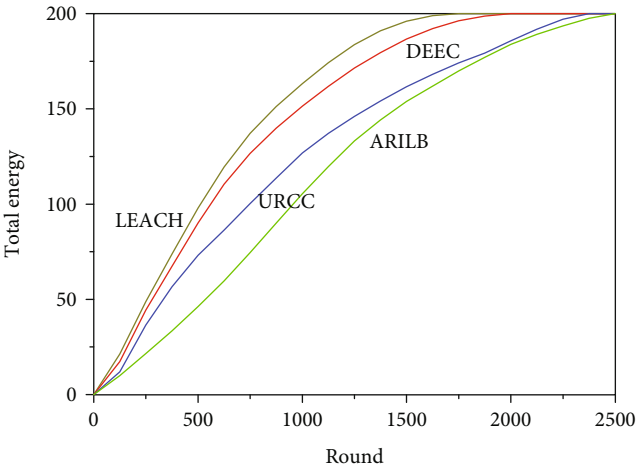

Figure 8: Energy consumption.

of routing protocols. In this paper, the data transmission capacity of the four algorithms is characterized by the number of data packets received by the base station in the same period (2,000 rounds). Figure 9 compares the data packets of the four algorithms. The base station under LEACH only received 41.71% of the data packets, which are received under our algorithm. The reason is that the single-hop mode

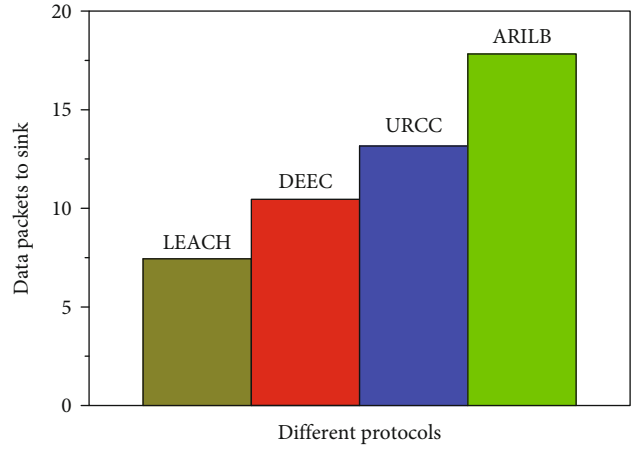

Figure 9: Data packets.

of sensors in LEACH may fail over time, resulting in a vacuum of data in some subareas. The data throughput of DEEC was less than 60% of that of our algorithm. This is because data transmission under DEEC is difficult, owing to link interruptions and the long time consumed to reestablish link distance. URCC achieved more data packets than LEACH and DEEC but never caught up with our algorithm. Throughout the simulation, our algorithm always realized more data packets than the other three protocols. The number of data packets of our algorithm was about 1.35-2.39 times that of the other protocols.

5.3. Comparison of Positioning Performance. Multiple wireless nodes were adopted for the simulation, one of which is an unknown node. The other nodes were placed in the same subarea as anchor nodes. Each anchor node sent an RSSI signal to the unknown node. Upon receiving the signal, the unknown node saves the information in the register and then transmits it through the gateway. Then, the host computer locates the unknown node by the positioning algorithm. The noise of each RSSI signal was designed by adding a random signal with a standard peak value of 1 at a certain probability, with a signal-to-noise ratio (SNR) of -5. The mean of 100 repeated simulations was taken as the final result. The simulation subareas are smaller than the subareas in the study area. Thus, the actual simulation range was set to 10-70 m.

Figure 10 compares the ranging errors of our algorithm and the traditional RSSI-based algorithm. When the subarea is small (e.g., 5 m), the two algorithms differed little in ranging error. With the growing distance, the error of the traditional algorithm increased rapidly since the subarea size of 40 m, while that of our algorithm rose slowly since the subarea size of 55 m. The results show that our algorithm can adapt effectively to multiple subarea sizes. As the distance increased, the error gap between the two gradually grew. The difference was 14.31% at the distance of 70 m.

Figure 11 compares the positioning errors of our algorithm with self-positioning algorithm (SPA) and ranging stratify unit (RSU) algorithms. When the noise and other factors were the same, the positioning errors of all three

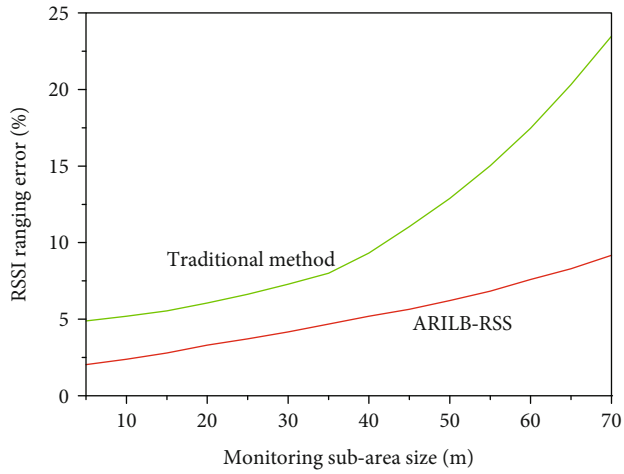

Figure 10: Ranging error.

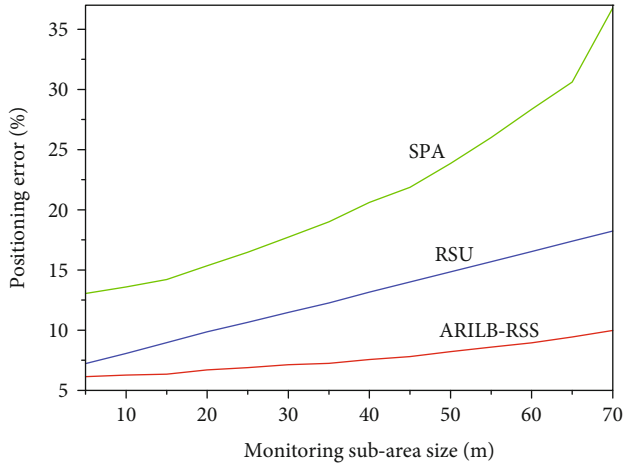

Figure 11: Positioning error.

algorithms increased with the subarea size. However, the error increment of our algorithm was the smallest. With the growing distance, the RSSI ranging error also increased. The positioning error of SPA rocketed up, because the algorithm cannot effectively eliminate the ranging error. Despite improving the positioning results, the RSU could not fully remove the influence of low-probability yet significant interferences during the processing of RSSI source data and the calculation of the mean of each data center. As a result, the positioning error of the RSU grew quickly with the increase of distance. In our algorithm, the path loss factor n is updated constantly with the growing number of anchor nodes. The updating factor slows down the growth of positioning error induced by the increase of subarea size. Within the distance of 40 m, the error gap between our algorithm and SPA and RSU was 7.45% and 5.61%, respectively. When the distance was 70 m, the difference was 18.54% and 26.79%, respectively. Therefore, our algorithm can get close to the true position, because the ARILB protocol can derive the accurate value of n, which reduces positioning error and improves positioning accuracy.

6. Conclusions

Considering the extensive application of WSN in indoor monitoring, this paper analyzes the rules of equipment installation and the features of human movement inside buildings and demonstrates the possibility and necessity of establishing an indoor data monitoring system. Then, the performance of the data monitoring network was simulated, and the protocol matching by a classic algorithm was discussed on computer software. On this basis, this paper proposes a novel adjacent round iterative load balancing routing protocol (ARILB). Simulation results show that the ARILB can achieve a good applicability and balance the network energy consumption. In addition, the protocol can balance the data throughput in each phase, delay the appearance of dead nodes, maximize the lifecycle of the network, and improve the overall energy efficiency. Furthermore, the ARILB was coupled with the division of monitoring area to propose the ARILB-RSS positioning algorithm. This new algorithm improves the positioning and correction performance, eliminates the ranging error, and controls the growth of positioning error. However, this research only discusses static WSN routing protocols for two-dimensional (2D) data. The future research will investigate the monitoring and positioning of mobile WSN nodes.

Data Availability

The data used to support the findings of this study are available from the corresponding author upon request.

Conflicts of Interest

The authors declare that they have no conflicts of interest.

References

[1] M. Amiti, M. Dai, R. C. Feenstra, and J. Romalis, "How did China's WTO entry affect U.S. prices?," *Journal of International Economics*, vol. 126, article 103339, 2020.

[2] X. Li, T. Li, H. Li, J. Qi, and L. Hu, "Research on the online consumption effect of China's urbanization under population aging background," *Sustainability*, vol. 11, no. 16, article 4349, 2019.

[3] J. Bai, J. Qu, T. N. Maraseni, J. Wu, L. Xu, and Y. Fan, "Spatial and temporal variations of embodied carbon emissions in China's infrastructure," *Sustainability*, vol. 11, no. 3, p. 749, 2019.

[4] W. Zhang, X. Wang, C. Shao, and X. Wu, "Optimal scheduling for urban micro integrated energy system considering decentralised high-rise buildings heating supply," *IET Generation, Transmission & Distribution*, vol. 13, no. 21, pp. 5005–5018, 2019.

[5] K. Chen, M. Guo, S. Liu et al., "Fiber-optic photoacoustic sensor for remote monitoring of gas micro-leakage," *Optics Express*, vol. 27, no. 4, pp. 4648–4659, 2019.

[6] L. J. Molofsky, J. A. Connor, C. J. Van De Ven et al., "A review of physical, chemical, and hydrogeologic characteristics of stray gas migration: implications for investigation and remediation," *Science of The Total Environment*, vol. 779, article 146234, 2021.

[7] M. Saleem, G. A. Di Caro, and M. Farooq, "Swarm intelligence based routing protocol for wireless sensor networks: survey and future directions," *Information Sciences*, vol. 181, no. 20, pp. 4597–4624, 2011.

[8] F. F. Wang and H. F. Hu, "An energy-efficient unequal clustering routing algorithm for wireless sensor network," *Revue d'IntelligenceArtificielle*, vol. 33, no. 3, pp. 249–254, 2019.

[9] F. F. Wang and H. F. Hu, "An improved energy-efficient cluster routing protocol for wireless sensor network," *Ingénierie des Systèmesd'Information*, vol. 24, no. 4, pp. 419–424, 2019.

[10] W. Wu, W. Liu, F. N. Zhang, and V. Dixit, "A new flexible parking reservation scheme for the morning commute under limited parking supplies," *Networks and Spatial Economics*, vol. 21, no. 3, pp. 513–545, 2021.

[11] J. F. Jiang, G. J. Han, L. Liu, X. Jiang, and J. F. Huang, "An unequal cluster-based routing protocol for wireless heterogeneous sensor networks," *Journal of Internet Technology*, vol. 16, no. 6, pp. 945–955, 2015.

[12] Z. Wang, Y. Chen, and C. Li, "PSR: a lightweight proactive source routing protocol for mobile ad hoc networks," *IEEE Transactions on Vehicular Technology*, vol. 63, no. 2, pp. 859–868, 2014.

[13] X. Chen, Z. Dai, W. Li et al., "ProHet: a probabilistic routing protocol with assured delivery rate in wireless heterogeneous sensor networks," *IEEE Transactions on Wireless Communications*, vol. 12, no. 4, pp. 1524–1531, 2013.

[14] R. C. Jin, T. Gao, J. Y. Song, J. Y. Zou, and L. D. Wang, "Passive cluster-based multipath routing protocol for wireless sensor networks," *Wireless Networks*, vol. 19, no. 8, pp. 1851–1866, 2013.

[15] J. Zhang and R. Yan, "Centralized energy-efficient clustering routing protocol for mobile nodes in wireless sensor networks," *IEEE Communications Letters*, vol. 23, no. 7, pp. 1215–1218, 2019.

[16] N. Javaid, N. Ilyas, A. Ahmad et al., "An efficient data-gathering routing protocol for underwater wireless sensor networks," *Sensors*, vol. 15, no. 11, pp. 29149–29181, 2015.

[17] K. Saleem, N. Fisal, and J. Al-Muhtadi, "Empirical studies of bio-inspired self-organized secure autonomous routing protocol," *IEEE Sensors Journal*, vol. 14, no. 7, pp. 2232–2239, 2014.

[18] C. E. Weng and T. W. Lai, "An energy-efficient routing algorithm based on relative identification and direction for wireless sensor networks," *Wireless Personal Communications*, vol. 69, no. 1, pp. 253–268, 2013.

[19] O. O. Ogundile, M. B. Balogun, O. E. Ijiga, and E. O. Falayi, "Energy-balanced and energy-efficient clustering routing protocol for wireless sensor networks," *IET Communications*, vol. 13, no. 10, pp. 1449–1457, 2019.

[20] J. Ren, S. Y. Huan, W. Son, and J. Han, "A novel indoor positioning algorithm for wireless sensor network based on received signal strength indicator filtering and improved Taylor series expansion," *Traitement du Signal*, vol. 36, no. 1, pp. 103–108, 2019.

[21] N. H. Nguyen and K. Doğançay, "Optimal geometry analysis for multistatic TOA localization," *IEEE Transactions on Signal Processing*, vol. 64, no. 16, pp. 4180–4193, 2016.

[22] M. R. Gholami, S. Gezici, and E. G. Strom, "TDOA based positioning in the presence of unknown clock skew," *IEEE Transactions on Communications*, vol. 61, no. 6, pp. 2522–2534, 2013.

[23] A. Arafa, S. Dalmiya, R. Klukas, and J. F. Holzman, "Angle-of-arrival reception for optical wireless location technology," *Optics Express*, vol. 23, no. 6, pp. 7755–7766, 2015.

[24] Y. G. Shi, T. Yang, S. Zhang, L. Liu, and Y. J. Cui, "A Wi-Fi positioning system for material transport in greenhouses," *Instrumentation MesureMétrologie*, vol. 19, no. 1, pp. 65–72, 2020.

[25] Z. G. Lin, L. Li, H. Q. Zhang, M. Li, and F. Q. Yao, "An APIT algorithm based on DV-HOP multi-hop," *Advanced Materials Research*, vol. 787, pp. 1038–1043, 2013.

[26] S. J. Xie, X. Wang, and H. Shang, "Security analysis on wireless sensor network in the data center for energy internet of things," *International Journal of Safety and Security Engineering*, vol. 10, no. 3, pp. 397–402, 2020.

[27] C. Leroux and C. Dainty, "Estimation of centroid positions with a matched-filter algorithm: relevance for aberrometry of the eye," *Optics Express*, vol. 18, no. 2, pp. 1197–1206, 2010.

[28] H. Zhou and K. M. Yu, "A novel wireless sensor network data aggregation algorithm based on self-organizing feature mapping neutral network," *Ingenierie des Systemesd'Information*, vol. 24, no. 1, pp. 119–123, 2019.

[29] L. Yu, Z. Yang, Q. He, R. J. Zeng, Y. Bai, and S. Zhou, "Novel gas diffusion cloth bioanodes for high-performance methane-powered microbial fuel cells," *Environmental Science & Technology*, vol. 53, no. 1, pp. 530–538, 2019.

[30] Z. Yuan, S. Zhang, F. Meng, H. Zhang, and K. Zuo, "Investigation of grain radius dependence of sensitivity for porous thin film semiconducting metal oxide gas sensor," *IEEE Sensors Journal*, vol. 20, no. 8, pp. 4275–4282, 2019.

[31] A. Lipare, D. R. Edla, and R. Dharavath, "Energy efficient routing structure to avoid energy hole problem in multi-layer network model," *Wireless Personal Communications*, vol. 112, no. 4, pp. 2575–2596, 2020.

[32] R. M. Sandoval, A. J. Garcia-Sanchez, and J. Garcia-Haro, "Improving RSSI-based path-loss models accuracy for critical infrastructures: a smart grid substation case-study," *IEEE Transactions on Industrial Informatics*, vol. 14, no. 5, pp. 2230–2240, 2017.

[33] F. Fanian, M. K. Rafsanjani, and V. K. Bardsiri, "A survey of advanced LEACH-based protocols," *International Journal of Energy Information and Communications*, vol. 7, no. 1, pp. 1–16, 2016.

[34] N. Jiang, H. You, and F. Jiang, "Distributed compressed sensing algorithm for cluster architectures of WSNs," *International Journal of Computers, Communications & Control (IJCCC)*, vol. 9, no. 4, pp. 430–438, 2014.

[35] O. Olayinka and A. Attahiru, "A survey on an energy-efficient and energy-balanced routing protocol for wireless sensor networks," *Sensors*, vol. 17, no. 5, article 1084, 2017.

Hindawi
Journal of Sensors
Volume 2023, Article ID 9864012, 1 page
https://doi.org/10.1155/2023/9864012

Retraction

Retracted: Sports Injury Risk Assessment Based on Blockchain and Internet of Things

Journal of Sensors

Received 10 October 2023; Accepted 10 October 2023; Published 11 October 2023

This article has been retracted by Hindawi following an investigation undertaken by the publisher [1]. This investigation has uncovered evidence of one or more of the following indicators of systematic manipulation of the publication process:

(1) Discrepancies in scope
(2) Discrepancies in the description of the research reported
(3) Discrepancies between the availability of data and the research described
(4) Inappropriate citations
(5) Incoherent, meaningless and/or irrelevant content included in the article
(6) Peer-review manipulation

The presence of these indicators undermines our confidence in the integrity of the article's content and we cannot, therefore, vouch for its reliability. Please note that this notice is intended solely to alert readers that the content of this article is unreliable. We have not investigated whether authors were aware of or involved in the systematic manipulation of the publication process.

In addition, our investigation has also shown that one or more of the following human-subject reporting requirements has not been met in this article: ethical approval by an Institutional Review Board (IRB) committee or equivalent, patient/participant consent to participate, and/or agreement to publish patient/participant details (where relevant).

Wiley and Hindawi regrets that the usual quality checks did not identify these issues before publication and have since put additional measures in place to safeguard research integrity.

We wish to credit our own Research Integrity and Research Publishing teams and anonymous and named external researchers and research integrity experts for contributing to this investigation.

The corresponding author, as the representative of all authors, has been given the opportunity to register their agreement or disagreement to this retraction. We have kept a record of any response received.

References

[1] J. Liu, "Sports Injury Risk Assessment Based on Blockchain and Internet of Things," *Journal of Sensors*, vol. 2021, Article ID 6820728, 13 pages, 2021.

Hindawi
Journal of Sensors
Volume 2021, Article ID 6820728, 13 pages
https://doi.org/10.1155/2021/6820728

Research Article

Sports Injury Risk Assessment Based on Blockchain and Internet of Things

Jihua Liu

Department of Physical Education, Beijing Union University, Beijing 100101, China

Correspondence should be addressed to Jihua Liu; jihua.liu@buu.edu.cn

Received 4 September 2021; Accepted 29 September 2021; Published 26 October 2021

Academic Editor: Gengxin Sun

With the increase of people's exercise in today's society, how to exercise scientifically and healthily has attracted much attention. Therefore, sports injury risk assessment and monitoring system has attracted more and more attention in real-time, flexibility, intelligence, and other aspects. To solve the above problems, this paper proposes a sports injury risk assessment based on blockchain and Internet of Things. By introducing computational power weight, a computational power balance D-H algorithm based on Internet of Things blockchain network architecture is proposed. It can provide a secure and trusted interactive environment for the Internet of Things. On the basis of blockchain and Internet of Things, a multisensor data fusion algorithm is proposed to be applied to the analysis and evaluation of sports injury. A variety of physiological parameters of human motion state are collected through multisensor, the collected physiological parameters are processed by data fusion, and finally, sports injury risk assessment is carried out. The built system takes the embedded esp8266wifi module as the hardware processing core and uses body temperature sensor, blood pressure sensor, EMG sensor, and pulse sensor to form wearable devices. By wearing wearable devices, four human physiological parameters such as body temperature, blood pressure, electromyography, and pulse can be collected. In the process of decision level fusion, different weights are set for the focal elements causing information conflict, and the optimized D-S evidence theory algorithm is used. Thus, according to the data detected by multisensor, the injury risk of user motion state is evaluated.

1. Introduction

Maintaining a healthy body requires not only a reasonable diet but also scientific exercise habits. A large number of studies have proved that regular aerobic exercise is beneficial to human health and can improve human exercise ability and physical fitness. In terms of health results and effectiveness of intervention programs, accurate quantification of physical exercise and physical health is very important [1]. If we can collect and analyze the health information and sports information of human body, we can give effective guidance and intervention to athletes in sports and health [2]. For ordinary athletes, real-time monitoring of their health and exercise status can help people adjust their exercise intensity or amount in time according to their daily exercise situation, so as to avoid physical discomfort caused by excessive or too little exercise and remind themselves to improve their exercise status in time and maintain a healthy body and healthy life. Research shows that sports enthusiasts and professional athletes in the process of sports, and sports risks are not only caused by a single reason but is also usually caused by the superposition of multiple factors. Traditional sports injury risk assessment methods focus on sports mode, and the risk calculation scope is limited. At the same time, there are some problems such as low efficiency and poor accuracy of evaluation, which are not suitable for large-scale evaluation [3]. According to the above problems, this paper proposes sports injury risk assessment based on blockchain and Internet of Things. Reanalysis of risk factors, introducing fuzzy D-S evidence theory algorithm [4], analyzing risk factors, adjusting calculation methods, and obtaining basic risk correlation data, thus, realizing the evaluation of sports risks. Through simulation experiments, three experiments are carried out: evaluation efficiency, evaluation accuracy, and evaluation ability. The experimental results show that the sports injury risk

assessment method designed in this paper is suitable for sports risk assessment of large, medium, and small scales and has high accuracy and high assessment efficiency.

Physical training in colleges and universities is an increasingly important part of college curriculum, and how to evaluate and determine the degree of sports risk should also be paid attention to. We propose a video summarization algorithm based on block sparse representation, combined with a certain heavy rainfall as the experimental background to study the factors affecting the risk of college sports, mainly establishing a fuzzy comprehensive evaluation model to determine the risk degree, weight, and prevention system. The purpose is to put forward reasonable suggestions, improve the safety awareness of teachers and students, strengthen the school safety management mechanism and improve various safety guarantees, and strengthen the management of school sports facilities [5]. As a professional athlete, injuries in daily training and competition are very common. Traditional three-dimensional knee joint moment (KJM) can provide early warning for athletes' knee injury risk. It mainly solves the portability problem by building a linear statistical extrapolation model, which relies too much on force plate and downstream biomechanical model. A pretrained CaffeNet convolution neural network (CNN) model has the strongest overall average correlation of 0.8895 with the source model, which is more accurate and belongs to a multidisciplinary research method, which can significantly promote the physical model and provide an effective application for athletes' training [6].

With the rapid development of Internet of Things technology, it is becoming more and more popular in our lives. It is applied to our traditional dragon boat training to solve our knowledge and understanding of the causes of injuries of athletes in this competition. The training intensity of dragon boat race is great, mainly based on strength and technology. The greater the training intensity, the higher the possibility of injury. We propose data fusion algorithm and clustering maintenance optimization algorithm to study the cause of injury and then use cluster maintenance optimization algorithm to improve the start-up time. Through analysis, the accuracy of the etiology detection system is almost perfect, which shows that it is consistent with the actual sports injury detection results [7]. Experiments show that the research on the causes of dragon boat sports injuries based on Internet of Things technology is effective, better detection of injury rules, so that athletes can effectively prevent injuries and a comprehensive understanding. Big data analysis of sports injury data realized by neural network is a new evaluation model of sports injury based on big data analysis and RBF neural network. In the constructed big data network, the evaluation of sports injury is realized by identifying hazard sources and various factors. After testing, the model is not restrained by various conditions, and its operation effect is good [8]. Badminton involves many injured parts, including legs, back, hands, and shoulders. We usually reduce injuries by increasing physical fitness plans and preventing training injuries [9]. Now we need to propose a more effective badminton evaluation system to make up for the lack of objective knowledge and method evaluation system.

2. Topology Model of Internet of Things Based on Blockchain Technology

Blockchain is a tamper-proof distributed network ledger technology that only contains real information. In addition, the peer-to-peer technology (P2P) of blockchain ensures that it does not need to rely on any central entity [10]. Therefore, blockchain technology can provide direct communication between IoT devices without centralized organization and can effectively solve the problems of computing node failure, transaction serial timeline error, privacy, trust, and reliability of new nodes in IoT [11]. In order to effectively apply blockchain technology to the Internet of Things network and realize the reliable identity authentication function of devices with certain computing power in the Internet of Things, this chapter proposes an Internet of Things network model based on blockchain technology under the Internet of Things network. At the same time, according to the characteristics of IoT equipment for sports injury risk assessment, the data structure of block body is improved, and a set of data interactive authentication method under this model is designed with cryptography algorithm. Ensure the stable transmission and safety of sports injury risk assessment data.

2.1. Design of New Block Structure. Blockchain is essentially different from traditional trading network and has many special characteristics. Their key features include encryption (asymmetric encryption), hashing, chaining blocks, and smart contracts. Blockchain transactions represent the interaction between two parties. For cryptocurrency, transactions represent the transmission of cryptocurrency between blockchain users. These transactions can also refer to message transmission or recording activities. Each block in the blockchain can contain one or more transactions, and the block structure is designed according to the things of the block.

Figure 1 illustrates the data structure of a general block body, which is a scattered, distributed, and common number composed of blocks. Typically, each block is connected to a timestamped transaction set. As you can see, this technique allows nodes to exchange data by creating transactions, each of which depends on another transaction, where the output of one transaction is referenced as an input in the other transaction, thereby creating a chain structure in it.

Blocks in blockchain are divided into block headers and block bodies. The block headers are like indexes in databases. The block header structure of Ethereum is too complex for the Internet of Things environment. In view of this situation, this paper cancels the data structures like GasLimit and Coinbase and simplifies the block headers data, as shown in Table 1, making the lightweight block headers more suitable for the Internet of Things environment.

Table 2 shows the main data structure of the new block body. According to the actual existence and uniqueness of Internet of Things devices, the device ID and company ID are used to locate the devices. The type field mainly stores the transaction type, which is used to locate and negotiate transactions between gateway nodes.

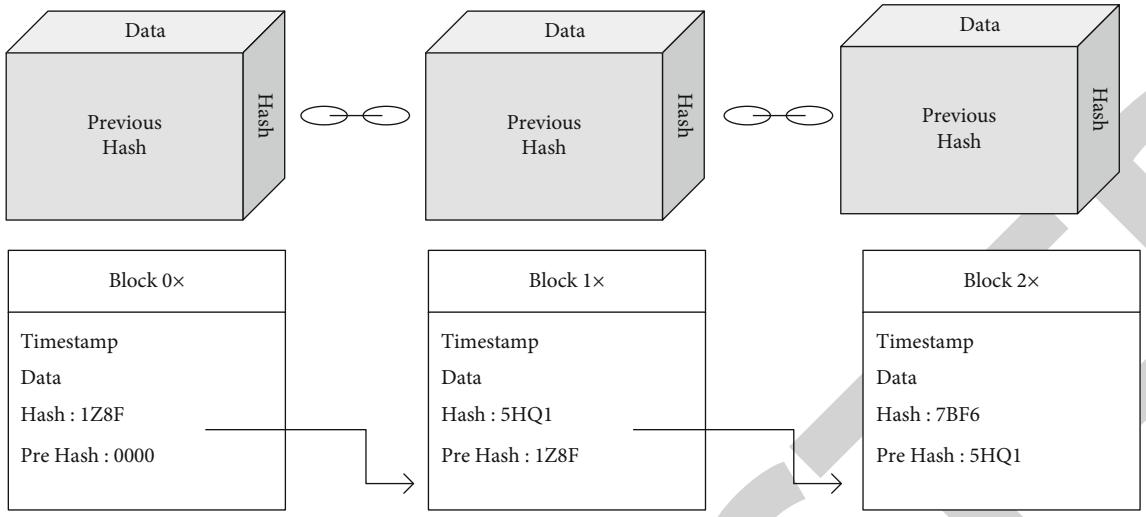

Figure 1: Logical structure of block body.

Table 1: Block structure of new area.

Attribute	Individual meaning
father_hash	Point to parent block (parentB1ock). Except for GenesisB1ock, each block has only one parent block.
Number	Serial number of the block. The number of a block is equal to its parent block number +1.
Merkel_root	The root of Merkel tree. Merkel tree is a kind of hash tree. Leaf node contains stored data or its hash value, middle node is the hash value of its two child nodes, and the top root node is composed of the hash value of its two child nodes.
Timestamp	The time when the block "should" be created. Determined by consensus algorithm, generally, it is either equal to parentB1ock. Time +10 s or equal to the current system time.

Table 2: Structure of new block body.

Attribute	Individual meaning
Type	0x00 stores type of things
Company	The number of the company is convenient for identity verification and ensures the global uniqueness of ID.
device_code	The number of the device is convenient for identity verification and ensures the global uniqueness of the ID.
dh_value	Field required for Diffie-Helman authentication, which is a struct, including a prime number and its source root.
ffs_value	The gateway node proves the set of global parameters through the zero recognition generated by its own random number R.
new_ffs_value	The updated set of zero recognition proof global parameters, which is empty when new devices are registered.
envelope_pk	Public key for envelope encryption.
Calculate	Node computing power weight is used to balance the computing power between nodes and improve efficiency.

2.2. D-H Algorithm of Computing Power Balance Based on Internet of Things-Blockchain Network Architecture. After completing the identity authentication of the blockchain gateway node, all the nodes in the network recognize the legitimacy of the node. One of the characteristics of the Internet of Things is that the computing power of devices is uneven, which will lead to a large time gap in the calculation of large numbers. In the process of establishing information interaction things such as instant messaging, it is inevitable that the party with strong computing power needs to wait for the party with weak computing power, which greatly wastes time and resources. In order to solve this inevitable problem in the Internet of Things environment, this section refers to Diffie-Hellman key exchange method [12] and proposes a key exchange method based on the Internet of Things-blockchain network architecture that can balance the computing power gap by introducing computing power weight.

Assuming that node A needs data interaction with node B, as shown in Figure 2, the node has calculated the intermediate shared value Y of random number S in advance and kept it confidential. The party with low computing power

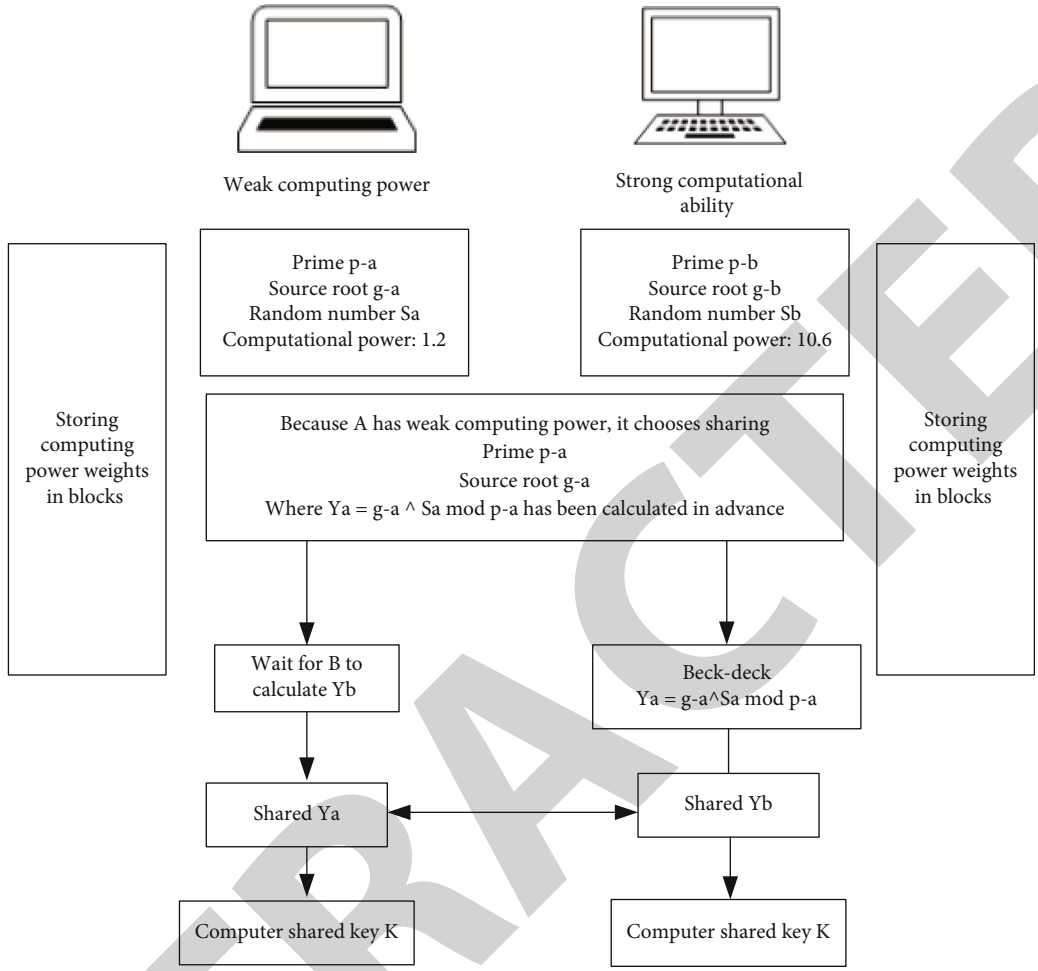

Figure 2: Balanced computing power key exchange process under blockchain-Internet of Things structure.

selects the calculated data as shared data. Suppose that node A needs time t_{ya} to calculate Ya, and node B needs time t_{ya} to calculate Ya, where $t_{ya} > t_{yb}$. The time for node A to calculate the shared key is t_{ka}, the time for node B to calculate the shared key is t_{kb}, and the communication network delay totals t_{network}. If the traditional D-H key sharing algorithm is adopted, the time for communicating and sharing keys between nodes is as follows:

$$T_{\text{total}} = t_{\text{network}} + \max\left(t_{ya}, t_{yb}\right) + \max\left(t_{ka}, t_{kb}\right). \quad (1)$$

If the sharing algorithm based on blockchain-Internet of Things computing power balance is adopted, the time for nodes to communicate and share keys is

$$T_{\text{total-new}} = t_{\text{network}} + \min\left(t_{ya}, t_{yb}\right) + \max\left(t_{ka}, t_{kb}\right). \quad (2)$$

The time savings of the whole process are

$$T_{\text{save}} = abs\left|\left(t_{ya} - t_{yb}\right)\right|. \quad (3)$$

In the Internet of Things environment, where the computing power of individual devices is quite different, this key exchange algorithm using cache and exchanging space for time saves considerable time.

Figure 3 shows the connection between a node A in the same node group and other devices by using ordinary D-H algorithm and computing force balance D-H algorithm, respectively. It is obvious that the new algorithm has shorter connection time.

3. Evaluation of Human Motion Data Based on Fuzzy D-S Evidence Theory Algorithm

The health monitoring system based on blockchain and Internet of Things proposed earlier brings convenience for users to detect their health status during exercise. The design of this system is mainly through the user's body temperature, blood pressure, EMG, and pulse four basic physiological parameters of human body data to judge the user's health status [13]. Through the optimized fuzzy set and D-S evidence theory, the discrimination algorithm proposed in this paper is introduced. In feature level fusion, fuzzy set theory algorithm is used. In the process of decision level fusion, a fuzzy D-S evidence theory discriminant algorithm is obtained by using the D-S evidence theory algorithm. This algorithm is applied in the sports injury risk assessment

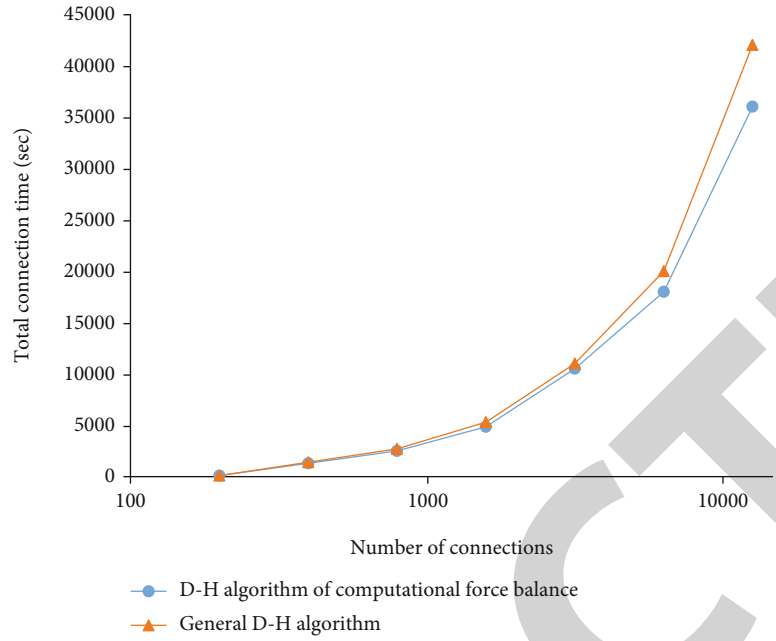

Figure 3: Comparison of the time required for devices to connect using different algorithms.

system and can be used to judge whether the user's sports behavior is healthy or not according to the data results detected by multiple sensors.

3.1. Intelligent Data Processing Algorithm. The information collected by each sensor and its observation information are combined according to certain optimization criteria, and these information are further processed. Considering the floating error of human health indicators and the difference of health representation weights of different health indicators, this study adopts the sports injury risk assessment algorithm based on fuzzy D-S evidence theory and realizes the evaluation of human health status to be detected based on the collected human health indicators data.

3.1.1. Fuzzy Sets. Fuzzy sets and fuzzy subsets are used to represent the whole thing with fuzzy definition characteristics.

Representation of fuzzy sets:

(1) Zadeh notation

$$A = \frac{A(u1)}{u1} + \frac{A(u2)}{u2} + \frac{A(u3)}{u3} + \cdots. \tag{4}$$

(2) When the number of elements in the fuzzy set is infinite, it is expressed by Zadeh method:

$$A = \int \frac{A(u)}{u}. \tag{5}$$

It is very important to test and analyze the accuracy, validity, and precision of information observation data in sensors, which is of great significance and helps to extract effective information observation data, ensure the reliability of data, and control the accuracy of final fusion results.

If the obtained absolute information amount of positioning is $Si\,(t)\,(i = l, 2, \cdots n)$ in positioning data, the absolute data information amount obtained at time t is used for positioning measurement, and the positioning value is placed on the number axis:

$$dis(t) = |si(t) - sj(t)|, \tag{6}$$

where $si(t)$ is the information data at time t, $d_i(t)$ is the distance between all the information data values, and $\bar{d}i(t)$ is the average distance.

$$di(t) = \sum_{j=1}^{n} disij(t), \tag{7}$$

$$\bar{d}i(t) = \sum_{i=1}^{n} di(t). \tag{8}$$

If dit satisfies the following conditions and regards all the data in the neighborhood of a set of valid information data as φ, then, this set is called the optimized fuzzy set.

$$di(t) < \bar{d}i(t) + M, \tag{9}$$

$$di(t) \geq \bar{d}i(t) - M. \tag{10}$$

The observation data set of n sensors of t-time fuzzy set is obtained by the definition of t-time optimal fuzzy set. For the optimized T-time fuzzy set of observation data, the smaller $Si\,(t)$ and $Sj\,(t)$ are, the more complex the fusion between T-time and observation data of two sensors is,

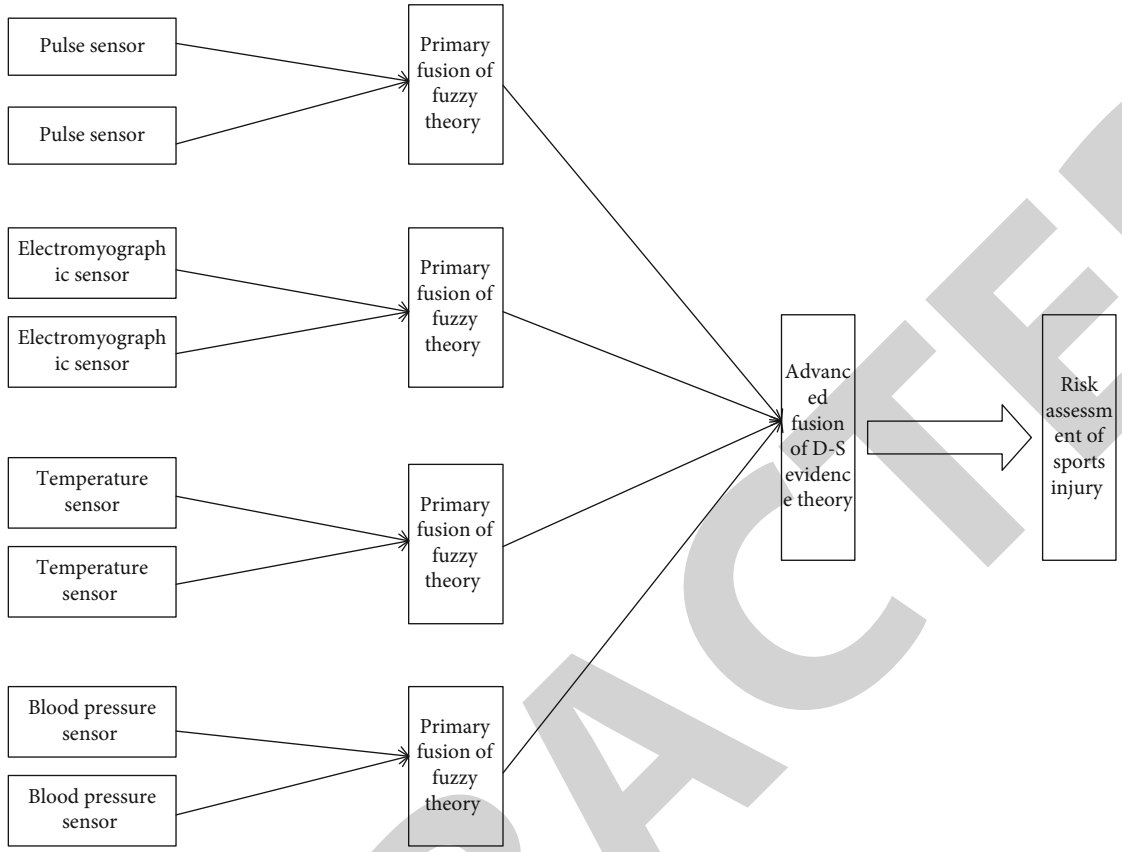

Figure 4: Flowchart of algorithm fusion.

and the higher the fusion complexity between data is. On the contrary, it shows that the lower the complexity of data fusion, the deviation of the fusion degree of observed data values between sensors. In order to facilitate the analysis and processing of the fusion complexity and values between the observed data of fuzzy sets, the concept that the fusion degree of fuzzy sets belongs to a function in mathematical theory is put forward. $Si(t)$ and $Sj(t)$ are mapped to each other to obtain a fusion degree membership function matrix $Cij(t)$, and the value range of $Cij(t)$ is [0, 1]. The membership function of the matrix $Cij(T)$ directly reflects the degree of fusion between the sensor and the observation data of the two sensors at T time. The expression defined by the fusion function is as follows:

$$Cij(t) = \exp\left\{-\frac{1}{2}|si(t) - sj(t)|\right\}. \tag{11}$$

It can be seen from the formula that the closer the $cij(t)$ value is to 1, the better the fusion of the two sensors and the higher the fusion degree of observation data. On the other hand, the $Cij(t)$ value is infinitely close to 0, and the fusion degree of the two sensors is worse. According to the definition of fusion degree, the data fusion degree matrix C is

$$C = \begin{bmatrix} 1 & C_{12}(t) & \cdots & C_{1m}(t) \\ C_{21}(t) & 1 & \cdots & C_{2m}(t) \\ \vdots & \vdots & \ddots & \ddots \\ C_{m1}(t) & C_{m2}(t) & \cdots & 1 \end{bmatrix}. \tag{12}$$

A larger sum of the elements of any row of matrix C indicates that $Si(T)$ is closer to the average. On the contrary, if the sum of the elements in this row is smaller, the greater the deviation of the observed data of sensor Si.

T is time, and the consistency fusion degree of sensor Si can be expressed as

$$\mu i(t) = \frac{\sum_{j=1}^{m} cij(t)}{m}. \tag{13}$$

However, the average consistency fusion degree cannot prove the stability of Si sensor. If the monitoring data transmission of sensor Si is very stable, the deviation between its fusion degree and sensors of other information sources will become very small. The deviation affects the distribution balance of fusion degree. Therefore, the definition of distribution balance is used.

Table 3: Mass values of body temperature, pulse, EMG, and blood pressure.

	S1	S2	S3	S4	S5	…
Electromyography	0.889	0.782	0.696	0.432	0.802	…
Pulse	0.754	0.723	0.512	0.231	0.772	…
Body temperature	0.709	0.689	0.594	0.302	0.632	…
Blood pressure	0.723	0.705	0.612	0.172	0.805	…

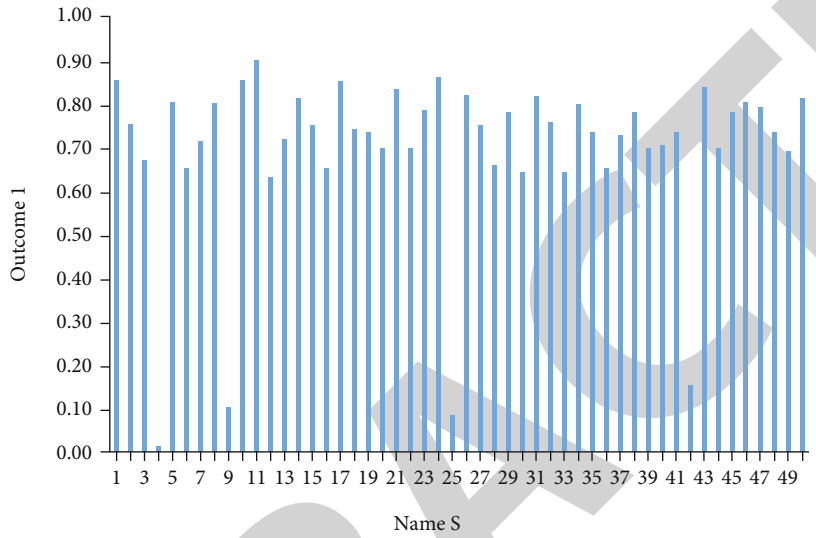

Figure 5: EMG and pulse fusion results 1.

The distribution balance of sensor Si at time t is

$$\tau i(t) = 1/\sum_{j=1}^{m}\left(ui(t) - cij(t)^2\right)/m. \tag{14}$$

In the actual process of sensor fusion, we should try to use sensors with consistent fusion degree and relatively balanced fusion degree distribution. The higher the uniformity and fusion coefficient of sensors, the more balanced the distribution of fusion degree and the greater the fusion degree weight of sensors. Therefore, the uniform fusion coefficient of a sensor can be multiplied by the distributed balance coefficient of the sensor as the fusion weight balance coefficient of the sensor.

The weight coefficient of sensor Si at time t is

$$\omega i(t) = ui(t) \times \tau i(t). \tag{15}$$

The above formula is normalized to obtain:

$$Wi(t) = \frac{\varpi(t)}{\sum_{i=1}^{m}\varpi i(t)}. \tag{16}$$

The fusion result is

$$\widehat{x} = \sum_{i=1}^{m} wi(t)si(t) = \sum_{i=1}^{m}\frac{\omega i(t)si(t)}{\sum_{i=1}^{m}\omega i(t)}. \tag{17}$$

Fuzzy sets are more valuable in multisensor data fusion. When used in multisensor information fusion, the first step is to observe the data monitored by each sensor, then use the concept of fuzzy set to complete the process of information synthesis according to relevant fusion rules, then use fuzzy set to complete multi-sensor information fusion or reasoning, and make the final information fusion decision.

3.1.2. D-S Evidence Theory. Evidence theory is a reasoning method using uncertainty. It can also be simply regarded as an improvement of subjective Bayesian estimation method. But it also has many advantages that Bayesian estimation reasoning method cannot match [14]. Bayesian estimation reasoning method usually needs to synthesize hypothetical prior probability and corresponding conditional probability, while the new generation D-S evidence analysis theory can calculate the probability of overcoming prior probability and corresponding condition according to its comprehensive basic reasoning rules. At present, it has been widely used in multisensor information fusion data processing system.

3.2. Data Fusion of Fuzzy Sets and D-S Evidence Theory. In order to minimize the decisive influence of low credibility evidence on conflict decision-making results, based on the research results of scholars at home and abroad, this paper proposes a new consistency algorithm of conflict evidence credibility synthesis. The algorithm basically combines the advantages of original reliability evidence consistency

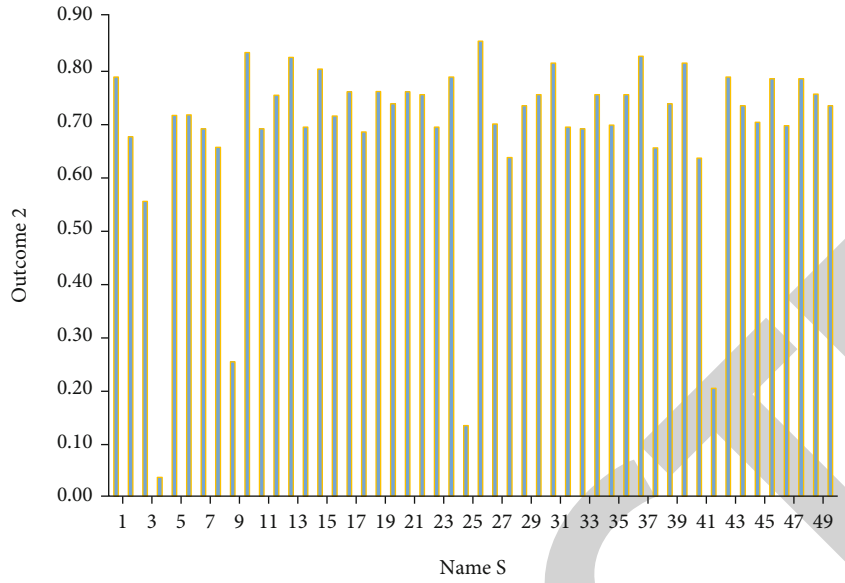

Figure 6: Results obtained by fusion of body temperature and blood pressure 2.

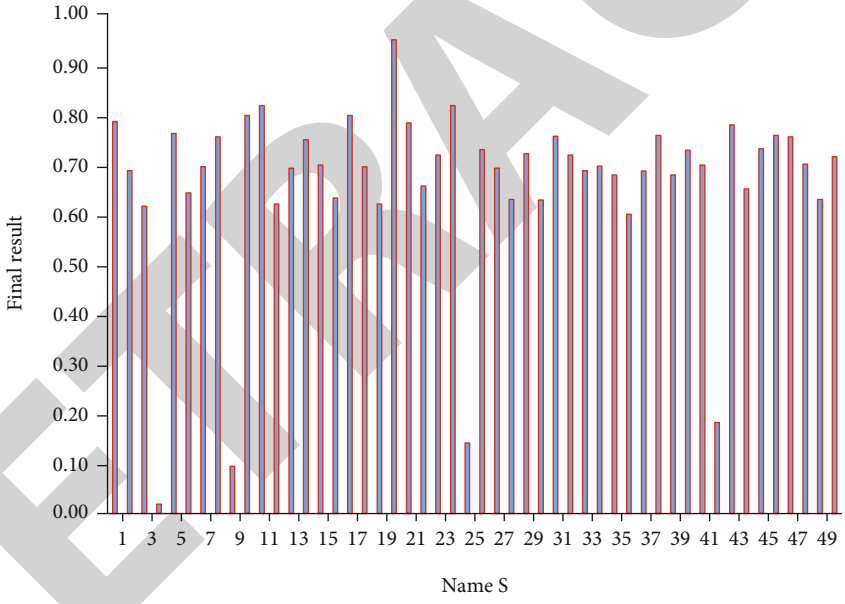

Figure 7: Final result.

modification and sensor combination rule consistency modification. In addition, the conflict evidence is not completely removed, and the conflict information and the consistency information between the conflict evidence are properly reserved. This new consistency algorithm not only improves the reliability of sensor evidence but also improves the accuracy of evidence fusion processing and reduces the risk that the weighted credibility evidence will affect the decision results.

Basic probability distribution function of combination:

$$m(A) = \begin{cases} 0 & A = \varnothing, \\ \dfrac{\sum_{AiBj=A} m_1(Ai) m_2(Bj)}{1 - \sum_{AiBj=\phi} m_1(Ai) m_2(Bj)} & A = \varnothing. \end{cases} \tag{18}$$

m_1 and m_2 represent their basic confidence distribution functions. Ai and Bi are the focus elements. The global reliability of each evidence in the fusion system can be calculated by equation (19). The evidence with the highest reliability after calculation is called the weight evidence of the fusion system, which can be expressed by u_k:

$$\mu_k(E_k) = \max_{1 \le i \le m} (\mu i(Ei)). \tag{19}$$

Taking the weighted evidence as a reference and the overall credibility of the evidence as the basis for measuring the weight coefficient of the evidence, the weight coefficients of other evidence can be expressed as follows:

$$\tau i = \frac{\mu i(Ei)}{\mu k(EK)} = \frac{\mu i(Ei)}{\max\limits_{1\le i\le m} \mu i(Ei)}. \tag{20}$$

Through normalization method, the basic confidence function $W\_i\,(t)$ can be obtained:

$$Wi(t) = \frac{\varpi i(t)}{\sum_{i=1}^{m} \varpi i(t)}. \tag{21}$$

The weight coefficient of each evidence is redistributed to obtain a new basic probability distribution function:

$$mi(A_k) = \begin{cases} \tau i \cdot mi(A_k), \\ 1 - \sum \tau i \cdot mi(B_k). \end{cases} \tag{22}$$

The improved combination rule is used to fuse the new basic probability distribution function, and the improved combination rule is shown in the following equation.

$$\begin{cases} m(\varphi) = 0 \\ m(A) = \sum\limits_{\substack{A_k \cap B_k = A \\ A_k \cdot B_k \subseteq \theta}} \tilde{m}i(A_k) \cdot mj(B_k) + \sum\limits_{\substack{A \cap B_k = A \\ B_k \subseteq \theta}} \lambda(A, B_k), \end{cases} \tag{23}$$

$$\lambda(A, B_k) = \frac{\tilde{m}i(A)^3}{\tilde{m}i(A)^2 + \tilde{m}j(B_k)^2} + \frac{\tilde{m}i(B_k)^3 \tilde{m}j(A)}{\tilde{m}i(B_k)^2 + \tilde{m}j(A)^2}. \tag{24}$$

From the consistency description of equation (21), it can be clearly seen that the new method fully excavates the information consistency between high-reliability evidences and the conflict consistency information between information and evidence and fully considers the security and reliability of relevant evidence information sources on the basis of assigning information weights to information conflict evidences.

4. Experiment

4.1. Application of 4.1 Fusion Algorithm in Sports Injury Risk Assessment System. Because the data transmitted based on the Internet of Things is human motion data transmitted at the same time, data-level fusion cannot be provided. According to the characteristics and functions of human physiology and data information, the two-level feature information data fusion technology is used to realize the information processing in the human sports injury risk assessment system and the judgment of human sports health results in Figure 4.

First, it is a feature level information analysis and fusion, which belongs to an intermediate level feature data fusion in the whole feature information processing process. Based on the analysis and fusion of feature data and the fusion of data processing information extraction, it is a fusion of global and local feature information. Second, information analysis and

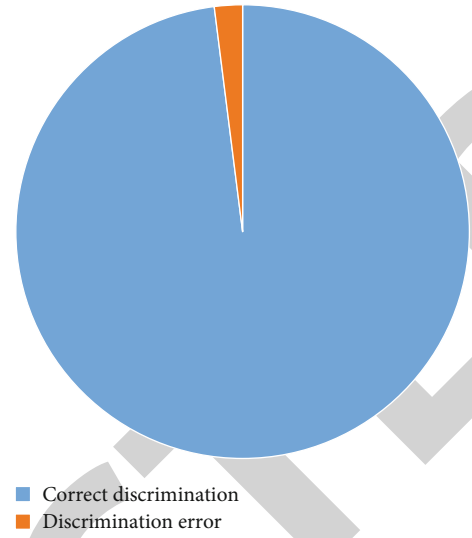

Figure 8: Correct rate of fuzzy D-S evidence theory algorithm.

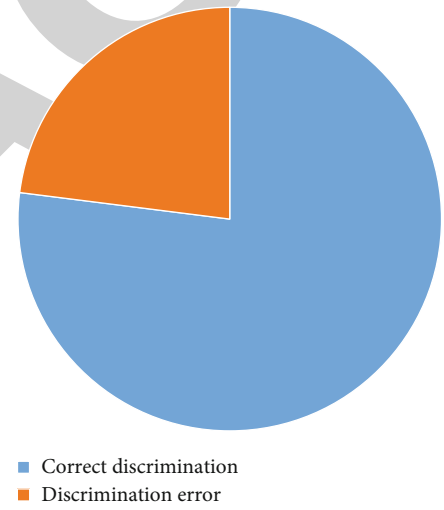

Figure 9: Correction rate of weighted average data fusion algorithm.

fusion at decision level are high-level technology of local feature information analysis and fusion [15]. It makes final decision analysis on the whole local feature information processing process formed by the fusion of local feature data and information of different feature types, that is, it makes the analysis and fusion of feature data and local information for each independent decision, so that the decision maker can obtain consistent whole feature information decision and judgment. The flow chart of algorithm fusion is shown in Figure 4.

The physiological data parameters of body temperature, pulse, EMG, and blood pressure were fused preliminarily. Then, the global credibility of each evidence is calculated, and the weight evidence of the fusion system is determined, defined as:

$$\mu_k(E_k) = \max_{1\le i\le m} (\mu i(Ei)). \tag{25}$$

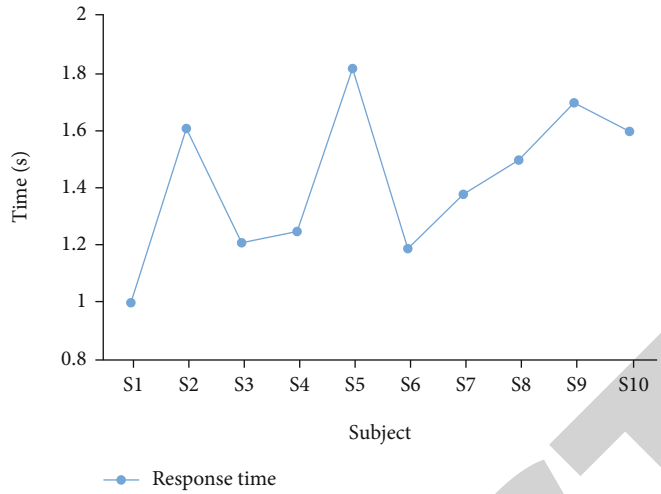

Figure 10: Response time of device in indoor environment.

Taking the weighted evidence as a reference and the overall credibility of the evidence as the basis for measuring the weight coefficient of the evidence, the weight coefficients of other evidence can be expressed as follows:

$$\tau i = \frac{\mu i(Ei)}{\mu k(Ek)} = \frac{\mu i(Ei)}{\max\limits_{1\le i\le m} \mu i(Ei)}. \tag{26}$$

Normalized to obtain the basic confidence function:

$$Wi(t) = \frac{\omega i(t)}{\sum_{i=1}^{m} \omega i(t)}. \tag{27}$$

From the above formula, it can be concluded that the primary fusion results of the three groups of sensors have the most normal pulse rate of 80, EMG of 210 mV, blood pressure of 86 mmHg, and body temperature of 36.7 degrees Celsius. Before the beginning of this experiment, the body temperature, pulse, EMG, and blood pressure of 50 subjects were tested with professional medical instruments. The subjects S4 and S9 showed hyperthermia, S25 showed high pulse rate, and S33 and S42 showed high blood pressure. Therefore, the physical movement state of subjects S4, S9, S25, S33, and S42 is "unhealthy."

In this experiment, we do not do any specific research on the basic probability distribution function, but get the assignment of the basic probability distribution function of the above sensors through the expert knowledge system, as shown in Table 3.

Fuse the body temperature and pulse of two sets of evidence related to human physiological parameters, and the fusion process is as follows.

First, the weight coefficients of the evidence are redistributed according to formula (28) to obtain a new distribution function.

$$\tilde{m}i(A_k) = \begin{cases} \tau i \cdot mi(A_k), \\ 1 - \sum \tau i \cdot mi(B_k). \end{cases} \tag{28}$$

Taking the value of τi as 1, we get a new mass function, as follows:

$$\tilde{m}i(A_k) = \begin{cases} mi(A_k), \\ 1 - \sum mi(B_k). \end{cases} \tag{29}$$

Then, S1-S50 is substituted into equation (29) to obtain a new expression for the basic probability distribution function, as follows:

$$\tilde{m}(X) \begin{cases} m(\delta 1) \cdots X = \delta 1, \\ m(\delta 2) \cdots X = \delta 2, \\ m(\delta 3) \cdots X = \delta 3, \\ m(\delta 4) \cdots X = \delta 4, \\ m(\delta 5) \cdots X = \delta 5, \\ 1 - m(\delta 1) - m(\delta 2) - m(\delta 3) - m(\delta 4) - m(\delta 5) \cdots X = \theta. \end{cases} \tag{30}$$

Using the basic probability distribution function calculated by Android platform of intelligent mobile terminal, EMG and pulse evidence are fused first. The result of ECG and pulse fusion is obtained, as shown in Figure 5.

Then, through the new principle of evidence combination, the blood pressure and body temperature are fused. The fusion of blood pressure and body temperature is obtained, as shown in Figure 6.

Finally, through the new evidence combination principle, the two groups of fusion results are fused. The final fusion result of the four items of data is obtained, as shown in Figure 7.

It can be seen from the final result diagram that the physical movement state detected by subjects S4, S9, S25, and S42 is "unhealthy," while other subjects are "healthy." Before the beginning of this experiment, the physical movement states of subjects S4, S9, S25, S33, and S42 were all "unhealthy" measured by professional medical instruments.

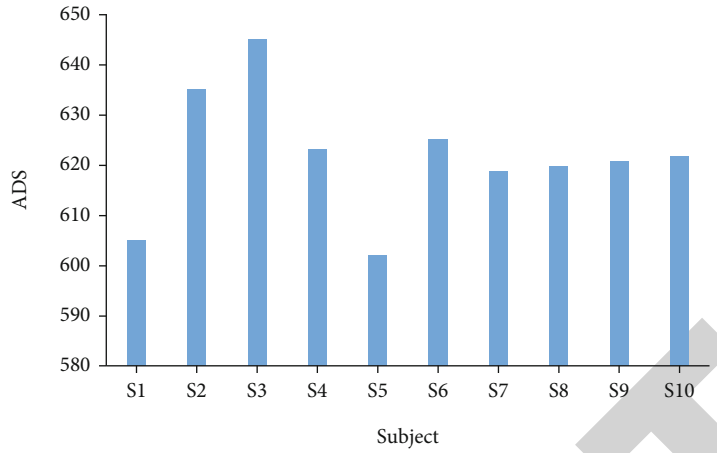

Figure 11: Change of AD value of EMG signal in indoor environment.

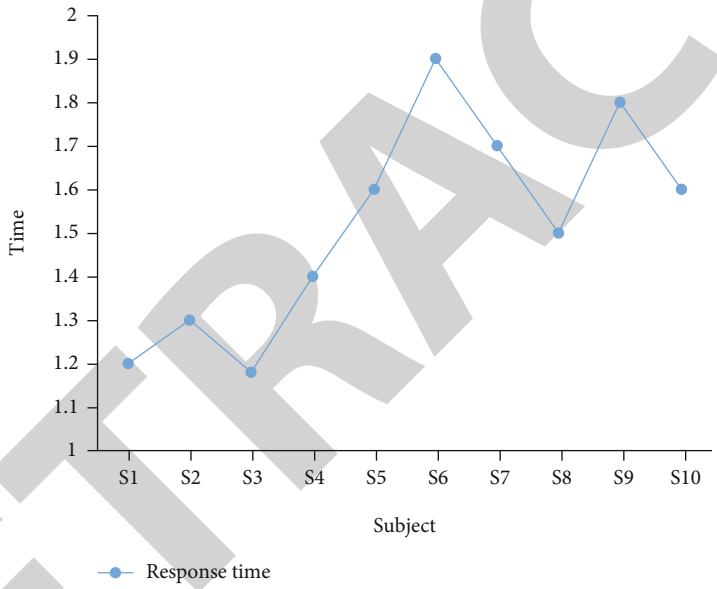

Figure 12: Response time of device in outdoor environment.

By comparison, it can be seen that the experimental results of S33 are inconsistent with those measured by professional medical devices. Therefore, this discriminant algorithm has a high accuracy in judging the status of human sports injuries, with a correct rate of 98% and an error of 2%. It conforms to the application standard in normal sports environment and has certain practical significance.

4.2. Comparison of Fuzzy D-S Evidence Theory Algorithm and Weighted Average Data Fusion Algorithm. In this section, the fuzzy D-S evidence theory algorithm and weighted average data fusion algorithm are compared, and the experimental results can be used to prove the effectiveness of the algorithm selected in this paper. First, the fuzzy D-S evidence theory algorithm is applied to 50 groups of experiments, and the experimental results are shown in Figure 7. The correct rate of human sports injury risk assessment is 98%, and the error is 2%. The accuracy of the experimental results of fuzzy D-S evidence theory algorithm is shown in Figure 8.

Using the same basic experimental data and applying weighted average data fusion algorithm, the sports injury risk detected by subjects S4, S9, S10, S12, S14, S16, S19, S20, S27, S33, S42, S45, S48, and S49 is assessed as "unhealthy," while other subjects are "healthy." Compared with the experimental results measured by professional medical devices, the correct rate is 77% and the error is 23%. The accuracy of experimental results of weighted average data fusion algorithm is shown in Figure 9.

From the comparison results of Figures 8 and 9, it can be seen that the correct rate of weighted average data fusion algorithm for human motion injury risk assessment is 77%. Although the correct rate is high, the correct rate of fuzzy D-S evidence theory algorithm for human motion injury risk assessment is 98%. In the application of human motion injury risk assessment, fuzzy D-S evidence theory algorithm

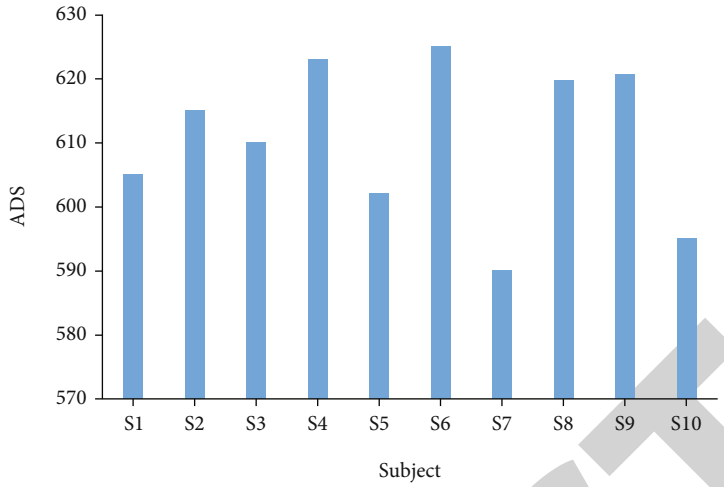

Figure 13: Change of AD value of EMG signal in outdoor environment.

has higher accuracy than weighted average data fusion algorithm and performs better and more stable in the overall performance. Therefore, fuzzy D-S evidence theory algorithm is more suitable for human sports injury risk assessment.

4.3. Human Muscle Fatigue Detection. If you exercise improperly or excessively, it may directly lead to severe muscle stiffness. Severe muscle stiffness is a natural physiological reaction of "self-defense signal," which indicates that your local muscles are completely tired. On the basis of realizing the risk assessment of human sports injury based on the system proposed in this paper, a muscle fatigue detection based on blockchain and Internet of Things is also designed in the experiment. This system judges the muscle fatigue state of users by detecting EMG signals on the surface of human skin. The following is the realization of human muscle fatigue detection and performance index evaluation.

Before the test, all the participants used the massager of the same specification to relax their muscles for 2 minutes. All the participants adopted standing posture, with their arms drooping naturally, holding 1.5 kg dumbbells of the same specification, repeating wrist flexion and extension for 10 times, and taking the average value of the final experimental data for 10 times. The test environment is indoor. Indoor environment: the temperature is 26 degrees, and the wind is weak, so it is regarded as calm in Figures 10 and 11.

Sometimes outdoor activities are also carried out. In order to facilitate the detection of anti-interference index and the evaluation of anti-interference performance of the adaptive system, a group of interference tests are also carried out in outdoor environment in Figures 12 and 13. Outdoor environment: temperature is 6 degrees, and wind level is 3.

Experiments show that environmental factors have little influence on the response time and accuracy of the system. With the help of the proposed system, the fatigue state of human muscles can be monitored in real time. The sports injury risk assessment is helpful to the healthy management of muscle fatigue and has high popularization and use value.

5. Conclusion

Blockchain and Internet of Things technology are developing rapidly and vigorously and have become a new development normal in the process of realizing information management of daily life for modern people. Internet data fusion applied to wireless sports health detection is also increasing day by day. To solve the above problems, a sports injury risk assessment based on blockchain and Internet of Things is proposed. In this chapter, through the application of fuzzy D-S evidence theory algorithm in human motion monitoring system, we can judge whether the user's motion state is healthy or not according to the results of multisensor detection data based on blockchain and Internet of Things. Experiments on 50 subjects show that the algorithm has high accuracy in judging human sports health status, which accords with the application standards in normal environment and has certain practical significance. It is compared with the risk assessment algorithm of human motion injury based on weighted average data fusion. Fuzzy D-S evidence theory algorithm is more accurate than weighted average data fusion algorithm, and it is better and more stable in the overall performance. Finally, the detection of human muscle fatigue is studied, and two groups of experiments are carried out under indoor and outdoor conditions. Experiments show that environmental factors have little influence on the response time and accuracy of the system, and it can monitor the state of human muscle fatigue in real time.

In this paper, D-S evidence theory algorithm is used to fuse the data of different sensors, and the benefits are ideal in this paper. However, the correlation between collected data has not been demonstrated, and the memory relationship of data sets has not been further analyzed. It is necessary to use other methods to analyze the correlation of data first and further analyze the independent data, so as to determine which are the main factors.

Data Availability

The experimental data used to support the findings of this study are available from the corresponding author upon request.

Hindawi
Journal of Sensors
Volume 2021, Article ID 4564143, 13 pages
https://doi.org/10.1155/2021/4564143

Research Article

Wireless Sensor Acquisition of Human Motion Parameters Based on Blockchain

Daibin Peng[1] **and Yonghong Liu**[2]

[1]*Professional Tennis College of Wuhan City Polytechnic, Wuhan, Hubei 430064, China*
[2]*College of Physical Education, Hubei University, Wuhan, Hubei 430064, China*

Correspondence should be addressed to Yonghong Liu; 20040752@hubu.edu.cn

Received 31 August 2021; Accepted 30 September 2021; Published 26 October 2021

Academic Editor: Gengxin Sun

With the rapid development of intelligent technology, people's lives have gradually entered the era of information and intelligence. Traditional vision-based and sensor-based human motion detection methods have shortcomings such as high illumination requirements, difficulty in preserving privacy, and poor portability. The wireless sensor detection method based on a wireless network can overcome the shortcomings of these methods, so it has become a hot research direction. Human motion parameters are very important data. If leaked, it may cause unimaginable harm to individuals. Blockchain technology is an emerging technology in the field of information technology. Its decentralized nature, distributed storage, and data is not easy. The modification provides a feasible solution for us to realize the data upload. Combining the advantages of wireless sensing and blockchain technology, this paper proposes a method of wireless sensing collection of human motion parameters based on blockchain, and designs a human motion recognition system. The experiment found that under the experiments given in this article, the traditional accuracy rate of sensor data collection is 71.82%, and the accuracy rate of the wireless sensing collection method of human motion parameters based on the blockchain in this article has reached 95.31%, which verifies the effectiveness and superiority of the system designed in this article.

1. Introduction

With the rapid development of artificial intelligence technology, people's lives have gradually entered the era of informationization and intelligence. The emergence of more and more intelligent devices is convenient for people's lives, and at the same time, people's actual needs have spawned the continuous development of various emerging technologies. Human motion detection technology has always attracted much attention. This technology mainly refers to the use of some special equipment and related detection algorithms to identify the motion state of the target person. The current motion state of the target user can be judged by the obtained motion state information, and corresponding services can be provided based on it, which can be widely used in smart homes, health care, entertainment games, and other related fields. From the technical means of human motion detection, human motion detection technology is mainly divided into three categories. The first is the use special sensor equipment to collect information; wearable devices containing specific sensors are worn on human bodies to collect human motion data to judge the human motion state. The advantages of this detection method include the simplicity of the equipment needed and the high precision achieved; however, the disadvantages are that the target person needs to wear auxiliary equipment actively, which will increase the burden on the target person to a certain extent, and it is difficult to complete the detection of motion state without cooperation. Second, with the development of computer vision, human motion detection based on vision has become a hot research direction. However, this method relies on (1) high-resolution video or images under line-of-sight, (2) high-precision cameras that are often costly, and (3) recognition performance that is greatly reduced in dark or poor line-of-sight conditions. In addition, it is easy to reveal users' personal privacy in some scenes because the

camera shoots directly. The third kind of motion state detection method based on radio frequency has become a new detection technology because of the following advantages: (1) it is not affected by illumination conditions, (2) it has strong expansibility, and (3) it can overcome non-line-of-sight and passive sensing. The detection method based on radio frequency uses specific receiving and transmitting equipment to obtain the signal change information of human motion state change, and then realizes motion state detection through preprocessing, feature extraction, training, and classification. In recent years, wireless sensor networks have been widely used in various fields. With the rapid development of wireless communication technology, sensor technology, and microcontrol technology, wireless sensor networks have been widely used to build a robust Internet of Things system. A sensor network is composed of a large number of sensor nodes, which are composed of an energy supply unit, a data acquisition unit, a data processing unit, and a data transmission unit [1]. In this paper, the advantages of wireless sensors, combined with the decentralization and distribution of blockchain technology, ensure the reliability of data uploading and enable designing a wireless sensor acquisition system of human motion parameters based on blockchain. Through experiments, its accuracy is much higher than that of the traditional human motion parameter acquisition system.

These results show that the wristband based on a pressure sensor can classify gestures very well and can also control mouse interaction. A new pressure signal processing framework has been developed, and it is a prototype system for real-time, robust gesture recognition [2]. It can make the gestures of the worn device intersect with the computer. Through the wristband experiment of a pressure sensor, it shows that people with or without experience can complete interactive tasks. In practice, the motion recognition system based on radio frequency is widely used, but it can be disturbed and lead to low accuracy. Therefore, we propose a new wireless sensor system, the Motion-Fi +, which can perform some motions simultaneously by multiple users because of its noninterfering characteristics and it does not depend on the template or contour of the scene. We built a backscatter wireless platform, and after 6 months of different scene designs, we added different people and directions to verify the system [3]. Experiments show that this method has high accuracy. With the development of research, a wireless inertial sensor system applied to human motion capture is a decoding strategy of human node displacement and attitude data based on the advantages of the previous two filtering methods. Evaluated on a built platform, wireless inertial sensor systems accurately measure human movement in the joints [4]. Nowadays, people live at a fast pace, and there are great pressures in work and study. They basically do not exercise at ordinary times, which has a great impact on their health. People gradually realize this and pay attention to their own health. Mild jogging and walking are the first choice for everyone to exercise. Wearing equipment plays an increasingly important role in the field of health, and its research is also of great significance [5]. Researchers put forward a wearable human body monitoring system based on wireless acceleration sensor technology, which can monitor the amount of running performed by a human body in time. Aiming at the confusing parts in the process of motion, this paper proposes a recognition method of human motion state based on single fractal and multifractal methods. Experiments show that this method is effective and feasible for recognition. In recent years, the wide application of artificial intelligence has also made a breakthrough in wireless network monitoring. It can identify abnormal events and has the global operation and maintenance capability of analysis. The video is captured and transmitted by camera, and then it is displayed in a browser by ActiveX control. Then, the linkage coordinate system of wireless network remote monitoring is established by the DH parameter method to realize intelligent control of a wireless network [6]. The above methods applied to human body monitoring and data collection are sensor-based data collection and are not applied to blockchain technology. There are some problems in the design accuracy and accuracy of the above methods, and the prediction effect is not ideal when analyzing the data after collection. Therefore, the method of collecting data from the human body with blockchain sensors can obtain more accurate data than traditional ones.

2. Characteristics of Blockchain Technology and Introduction of Related Technologies

Blockchain is a way to organize data skillfully, while blockchain technology is a technology that integrates many outstanding achievements of human intelligence, including database technology and network technology related to distributed books, network technology related to consensus algorithm, and asymmetric encryption technology and software technology related to intelligent contracts. Blockchain technology, which integrates these cutting-edge technologies, has challenged and confronted the mechanism based on central node credit since it was put forward. With the development of time, this characteristic of blockchain technology is becoming more and more obvious, which makes it no longer limited to digital cryptocurrency, but widely used in many fields of social and economic life, such as supply chain finance, data authentication, asset management, election voting, and fair security traceability introduced in this paper. Nowadays, blockchain technology has become an important technology that cannot be ignored among many high-end cutting-edge technologies.

2.1. Distributed Book of Accounts. Different from the traditional system network structure, the network architecture and data storage of a blockchain system choose distributed books with a decentralized architecture. The transmission of information in the network does not pass through the central node, and each member node retains complete data, which is embodied in the distribution of nodes in entity and the distribution of nonrelational databases on each node in logic. An account book is a storage form of data and a management unit of data. A nonrelational database is the logical carrier of data and an account book, and the physical carrier of data and the account book is a member node. Blockchain

is the underlying form of an account book, that is, the data form of a chain of blocks strung together. After the consensus process, consensus members will reach a consensus and write the same data into the blockchain system, so each member keeps a copy of the data. Because the data in each ledger cannot be deleted, the total amount of data will only increase, which is a great test for the ability of data storage; however, with the rapid development of technology, this problem will not be a problem. This is because the breeding nodes, slaughtering nodes, processing nodes, transportation nodes, and sales nodes in the livestock product supply chain are distributed in different places in the physical sense, in line with the distributed ledger technology in blockchain. In the ideal traceability model, the status of nodes where each link is located is expected to be equal, the information flow does not pass through the central node, and its network architecture naturally fits the characteristics of distributed books in blockchain technology; thus, it is reasonable and efficient for a livestock product traceability system to select the network architecture based on blockchain technology [7].

2.2. Cryptographic Algorithms. Cryptography is the core of a blockchain data layer, which escorts the whole data transmission and access of blockchain. Cryptographic algorithms will be used in three places in the blockchain platform of cold chain drug traceability, including the hash algorithm and the asymmetric encryption algorithm. This section will discuss the principle and selection of these two algorithms [8].

2.2.1. Hash Algorithm. The secure hash algorithm is an alias of the hash algorithm, which maps data of arbitrary length into hash strings of fixed length through certain rules. The more common ones are SHA-256, SHA-384, SHA-512, etc., which are widely used in various technologies requiring encryption including blockchain technology [9].

2.2.2. Asymmetric Encryption Algorithm. The asymmetric encryption algorithm comes from the secret key method in the cryptographic algorithm; the key consists of a public key and a private key. The key is generated at the same time, in which the public key is public as its name implies, while the private key is private and needs to be saved by itself. When encryption is needed, one of the same pairs of keys is used to complete the encryption operation, and only the other key can complete the decryption of the message. The asymmetric encryption algorithm plays an important role in blockchain, which is the cornerstone of the security of the whole blockchain system. The asymmetric encryption algorithm is mainly used in encrypted communication and for generating a digital signature in blockchain [10].

2.3. SM2 Digital Signature Algorithm. The SM2 algorithm is an improved national cryptographic algorithm based on ECC published in China in 2010, which includes the digital signature algorithm and the key exchange protocol and public key encryption algorithm. It has become the current public key algorithm standard GM/T 0003.2-2012 in China and entered the international standard ISO/IEC 14888-3.

2.3.1. Principle of the SM2 Digital Signature Algorithm. The elliptic curve equation $E(a, b)$ selected by the SM2 algorithm is as follows:

$$y^2 = x^3 + ax + b. \tag{1}$$

The Abelian group $(G, +)$ is defined on $Ep(a, b)$, where the unit element O of the group is defined as an infinity point. Let the elliptic curve be $y^2 = x^3 - x$. Take two points P and Q on the elliptic curve $(G, +)$ as straight lines intersecting the other point R' of the elliptic curve, and make parallel lines of the y axis intersecting R through R', and define $P + Q = R$. In this way, the sum of the additions made by two points on the Abelian group will also be on the elliptic curve, and it also satisfies the properties of the Abelian group. When the same points P are added, that is, when the two points P and Q coincide, the tangent of the point P is made. Repeat the above operation, and when k points P are added, it is recorded as k_P.

Ordinary elliptic curves are continuous and not suitable for encryption. In the national standard, the elliptic curves with 256 bits in the prime number field are used to transform the elliptic curves into discrete points. Let the prime number be p, the prime number field formed by the elliptic curves be F_p, and the elliptic equation be $E_{rp}(a, b)$:

$$y^2 = x^3 + ax + b \,(\text{mod } p), \tag{2}$$

where both a and b are elements in the prime field and satisfy $4a^3 + 27b^2 \neq 0 \pmod{P}$. SM2 can be encrypted by assuming that in the elliptic curve $P = d_G$, where P and G are two points on $E_p(a, b)$, N is the order of G, and D is an integer and its value is not higher than order N. Given D and G, it is easy to compute P in the front direction but difficult to compute D in the reverse, according to the definition of the Abelian group addition rule. Let the set $\{O, G, 2G, 3G, (n-1)G\}$ be a cyclic subgroup generated by G on $d \in [1, n-1]$. If d is selected as the private key and $P = d_G$ as the public key, the problem of finding d from P is the discrete logarithm problem on the elliptic curve group, which is the mathematical basis of the elliptic curve encryption algorithm [11].

2.3.2. SM2 Digital Signature Scheme. The digital signature scheme designed by the SM2 encryption principle is as follows: perform key generation with the input of SM2 elliptic curve parameter parms (elliptic curve equation E_p, large prime number p, base point G, and order n of base point), randomly generate private key $d \in [1, n-1]$ and keep it secretly, and use the public-private key relationship to generate the following public key:

$$P = [d]G. \tag{3}$$

In formula (3), P is the obtained SM2 public key, which is an important basis for SM2 to be used in encryption and signature. The SM2 signature process is as follows: input SM2 elliptic curve parameter parms, private key d and

message M to be signed, and calculate hash value Z_A at the same time:

$$Z_A = H_{256}(\mathrm{IDL}_A \| \mathrm{ID}_A \| a \| b \| x_G \| y_G \| x_A \| y_A). \quad (4)$$

In formula (4), ID_A is the user's distinguishable identification, IDL_A is the length of ID_A, a and b are the coefficients of the elliptic curve, x_G and y_G are the horizontal and vertical coordinates of base point G, respectively, and x_G and y_G are the horizontal and vertical coordinates of the public key, respectively.

The hash value Z_A is obtained, and then the hash digest e with the message M to be signed is calculated:

$$e = H_{256}(Z_A \| M). \quad (5)$$

Randomly generate $k \in [1, n-1]$ and calculate the elliptic curve point X_1 from it:

$$X_1 = (x_1, y_1) = [k]G. \quad (6)$$

Calculate the signature parameters r and s to output the signature (r, s):

$$r = (e + x_1) \mod n, \quad (7)$$

$$s = \left((1+d)^{-1}(k - rd)\right) \mod n. \quad (8)$$

The SM2 verification process is as follows: input parms, the public key P owned by the verifier, the message M to be verified, and the signature (r'', s') sent by the signer to obtain the hash digest e of the message M to be verified according to formula (8), and calculate the t value:

$$t = \left(r' + s'\right) \mod n. \quad (9)$$

Verify whether$t$is equal to equal, if it is equal to zero, the verification fails, otherwise calculate the elliptic curve point X_1'.

$$X_1' = (x_1, y_1) = \left[s'\right]G + \left[r'\right]P_A. \quad (10)$$

Verify whether $r' = (e' + x_1') \mod n$ is true, and if it is true, the verification is successful.

2.4. Consensus Algorithm. At present, the consensus algorithms commonly used in blockchain are Pow, Pos, DPos, and PBFT. Pow uses the workload proof mechanism to determine the node accounting rights and ensures the consistency of data through a large number of calculations. Pos adds the concept of currency age to the workload proof mechanism and uses currency age instead of computing power to reduce the difficulty of acquiring a block solution. DPOS uses digital cash holders to generate node sets with bookkeeping rights through elections and adopts rotation bookkeeping to generate blocks. PBFT is a distributed consensus algorithm based on state machine replication. Consensus is completed through three-stage communication between nodes. For the four consensus mechanisms in throughput, the performance of delay and scalability is compared. Details are as follows. The application of a consensus mechanism in blockchain is from PoW to PoS to DPOS to PBFT. In this process, computing power competition is gradually replaced by equity competition. The cost of obtaining node bookkeeping rights is gradually reduced. With the development of the blockchain application, the transaction speed gradually increases. At the same time, the consensus mechanism has gradually evolved from the initial decentralization to the current weak centralization. Each consensus mechanism has different advantages and disadvantages. PoW can realize decentralization to the greatest extent. It is safe, reliable, and has low consumption of network resources; however, it consumes too much computing resources. Computational attack can easily occur. Consensus time is longer. The emergence of PoS solves the problem of excessive waste of PoW computing power, but it makes the pressure of network traffic increase. The implementation is more complicated. DPOS has made appropriate compromises on centralization. The consumption of network resources is reduced. It has greatly shortened the consensus time. The throughput of the system is improved, but the security is reduced due to its weak centralization, which is prone to security loopholes. The PBFT algorithm solves the consistency problem of the distributed system with the Byzantine error nodes and improves the fault tolerance rate of the distributed system. However, due to the existence of a large number of point-to-point communications, it occupies a large amount of communication resources [12].

3. Wireless Sensor Network and Fingerprint Location Technology

When collecting human motion data, it is necessary to locate the human body accurately. This paper uses the characteristics of human heat source and chooses infrared sensors to identify the human body. In order to locate the human body more accurately, fingerprint positioning technology is selected to locate the human body. This section will briefly introduce these two technologies.

3.1. Wireless Sensor Networks. Typical wireless sensor networks are composed of a large number of low-cost and low-power sensor terminal nodes and gateway nodes, among which the structure of sensor terminal nodes is shown in Figure 1. As can be seen from Figure 1, the sensor terminal node not only has the function of data acquisition but also includes the functions of data processing and wireless data transmission. It ensures that each node can obtain the data of interest in the system in time, and accomplish specific supervision and control purposes by exchanging data or fusing the data of each sensor node. Usually, the sensor terminal nodes in the network are used as passive sensors. This type of sensor has the characteristics of low power consumption, low price, and convenient installation, which makes it meet the requirements of large-scale deployment and can be applied in large-scale sensor networks [13].

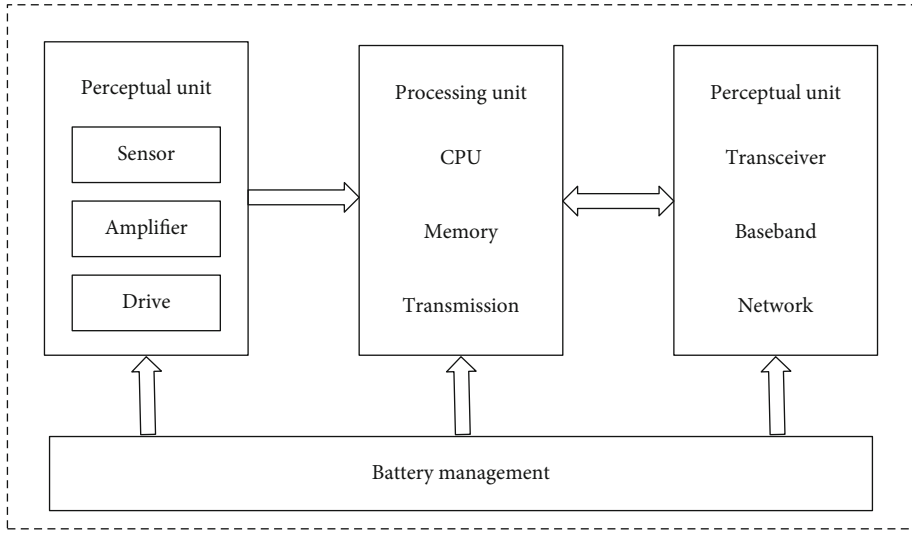

Figure 1: Wireless sensor network terminal node.

Because of the requirements of the deployment environment, sensor nodes often need to assemble batteries to supply power to the whole system, so that the whole network has the ability of data processing and transmission and node cooperation. The wireless sensor network structure is shown in Figure 2. In practical applications, wireless sensor networks not only need reliable communication channels but also need to prolong the life of network nodes as much as possible. Most of the energy consumption in WSNs comes from the wireless communication consumption in the network. However, considering the limited factors such as energy and economy, network nodes cannot be equipped with powerful communication and processing units, and sensor nodes are greatly limited in communication ability, computing ability, and data storage. These limitations will require further research on energy management, network topology optimization, node scheduling, distributed signal processing algorithms, and network communication protocols. The network topology and node scheduling guarantee the capacity of the network system and the real-time communication performance between nodes. The reliable communication protocol ensures that the data information can be transmitted in the network timely and accurately.

3.2. Fingerprint Location Technology

3.2.1. Principle of Fingerprint Location Technology. The location method based on position fingerprints firstly needs to collect infrared signals of a moving human body at each reference position in the off-line stage, then it needs to process these signals accordingly to build the PIR position fingerprint database, and then train these data through certain algorithms. Through training, a human body location model which can realize information matching is obtained. When positioning the position, firstly, the pyroelectric infrared signals generated when a human body walks on a certain path are collected online, then using the same data processing method as the off-line acquisition stage, the online acquisition signals are changed into position fingerprints. Finally, the trained model is matched with the fingerprints in the established PIR signal position fingerprint database, and the position positioning results are screened out.

3.2.2. Fingerprint Location Technology Algorithm

(1) Nearest Neighbor Algorithm (KNN). The NN algorithm is the most basic fingerprint-matching algorithm. It obtains the most similar reference point by calculating the Euclidean distance between the fingerprint data of the position to be measured and the fingerprint in the fingerprint database, and takes the reference point position as the approximate position of the target. The KNN algorithm is an improvement of the NN algorithm. Firstly, K similar reference points are selected as the initial measure of a position, and then the geometric centroid of K reference points is obtained as the final location result. Assume that there are N fingerprints in the off-line fingerprint database F_p, denoted $\{F_{p1}, F_{p2}, \cdots, F_{pN}\}$, and the reference point position corresponding to each fingerprint record is denoted $\{L_1, L_2, L_N\}$, where L_i is denoted (x_i, y_i). Assuming that the environment contains m PIR signal detection nodes, and the induced signal of each PIR node is denoted as a TSD vector, the fingerprint F_r is denoted $\{\mathrm{TSD}_{i1}, \mathrm{TSD}_{i2}, \mathrm{TSD}_{im}\}$, where TSD_{im} represents the signal time series of the mth PIR node detected at the i th reference position. In the online stage, the signal amplitude vectors $\{\mathrm{TSD1}, \mathrm{TSD2}, \cdots, \mathrm{TSD}_m\}$ generated when the human body moves are collected, and the similarity with the target reference point is calculated as follows [14]:

$$\mathrm{dist}_i = \left\{ \sum_{j=1}^{m} \left| \mathrm{TSD}_j - \mathrm{TSD}_{ij} \right|^2 \right\}^{1/2}. \tag{11}$$

In equation (11), dist_i represents the Euclidean distance between the target position and the ith reference point in the fingerprint database. K reference points with the smallest

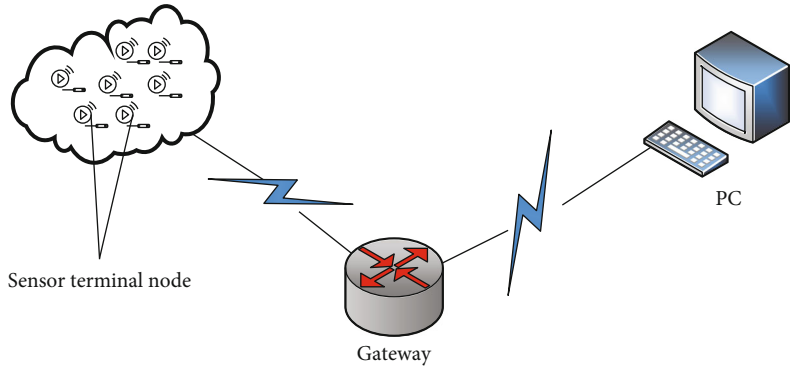

Figure 2: Structure diagram of a wireless sensor network.

distance are selected, and the position coordinates of the moving human body under K reference points are calculated as follows:

$$(x, y) = \frac{1}{k}\sum_{i=1}^{K}(x_i - y_i). \tag{12}$$

(2) Naive Bayesian Algorithm. The naive Bayesian algorithm is a learning algorithm based on statistical probability. In indoor location of PIR signals, conditional probability is used to establish the location fingerprint location model, and then the Bayesian law is used to calculate the position of the target. Suppose that there are N fingerprints in the off-line fingerprint database F_p, which are denoted as $\{F_{p1}, F_{p2}, F_{p3} \cdots F_{pN}\}$, and the reference point position corresponding to each fingerprint record is denoted as $\{L_1, L_2, L_3 \cdots L_N\}$, where L_i is denoted as (x_i, y_i). Assuming the existing fingerprint F_p, the posterior probability of the fingerprint appearing at each reference point is calculated by the naive Bayes algorithm, which is denoted as $P(L_i \mid F_p)$. The expansion formula is as follows [15]:

$$P(L_i \mid F_p) = \frac{P(F_p \mid L_i) * P(L_i)}{P(F_p)} = \frac{P(F_p \mid L_i) * P(L_i)}{\sum_{keL} P(F_p \mid L_K) * P(L_K)}. \tag{13}$$

In equation (13), $P(L_i)$ is a prior probability, which represents the probability that the real-time fingerprint appears at the reference point L_i; $P(F_p, L_i)$ is the conditional probability of the real-time target position at the reference fingerprint; $P(F_p, L_i)$ is the posterior probability obtained by the Bayesian algorithm. In the constructed system, it is assumed that the target can appear anywhere in the probe field of view. In the naive Bayesian algorithm, it is assumed that the output signals from different PIR nodes are independent of each other; that is, each fingerprint element is independent and irrelevant. On this basis, the conditional probability $P(F_p, L_i)$ can be decomposed into $P(\mathrm{DTS}_1 \mid L_i) \cdots P(\mathrm{DTS}_m \mid L_i)$. Assuming that the PIR signal detected at the reference point satisfies Gaussian distribution, the prior probability can be expressed as follows:

$$P\left(\mathrm{DST} \mid L_i = \frac{1}{\sqrt{2\pi} * \delta_i} \exp\left\{-\left(\frac{\mathrm{DTS} - \mu_i}{2\delta_i^2}\right)^2\right)\right\}. \tag{14}$$

In equation (14), μ_i and δ_i are the mean and standard deviation of signal strength at reference point L, respectively. The calculated posterior probability is taken as the weight coefficient, and the actual position coordinates of the moving target are estimated in combination with the position of the reference point.

$$(x, y) = \sum_{i=1}^{N} P(L_i \mid F_p) * (x_i, y_i). \tag{15}$$

(3) Neural Network Algorithm. The neural network algorithm is widely used in function approximation, classification, and other fields. In indoor positioning based on a PIR signal, the BP neural network model is mainly used. The BP network is mature in theory and performance, and it has a strong nonlinear mapping ability and a flexible network structure [16]. In the training process of the BP network, the input vector is firstly propagated backward to the output layer through the forward propagation process to obtain the result vector. If the deviation between the output value of the output layer and the expected output value exceeds the given threshold, the weight and bias parameters of the neural network are modified continuously through the error signal back propagation process until the value of the loss function meets certain requirements. The fingerprint location model of the PIR signal position under the BP network is shown in Figure 3.

The steps of BP algorithm in the PIR location process are as follows:

Step 1. The neural network model shown in Figure 3 is established, and the input dimension is the length n of the PIR signal sequence collected for a period of time; the output dimension m represents the category of time series; the number of hidden layers is $l = 1$; and each network parameter is initialized.

Step 2. According to the size of the fingerprint database, the sample data is divided into a certain proportion of training

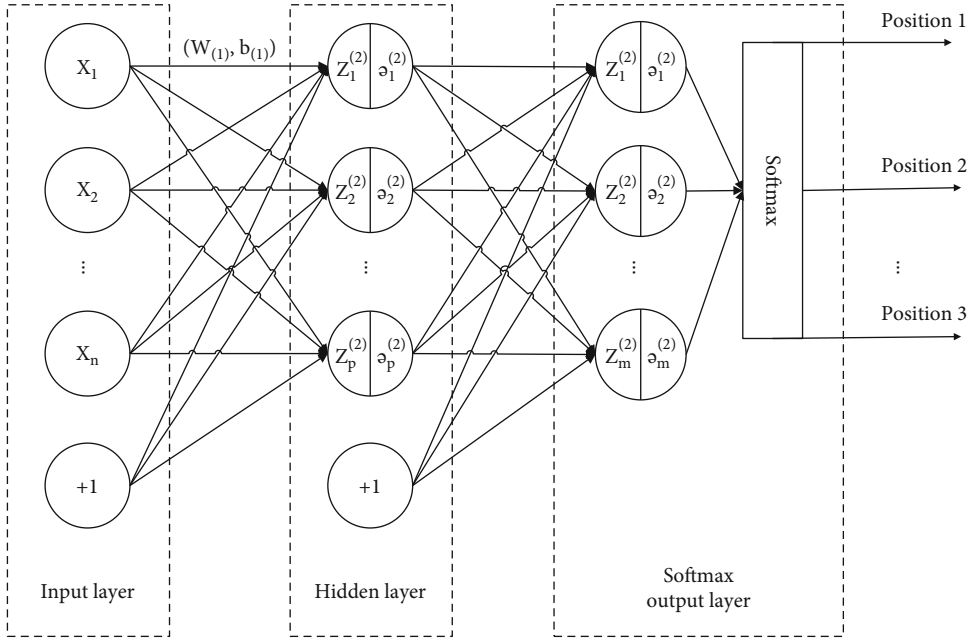

Figure 3: Fingerprint location model of the PIR signal position based on the BP neural network.

set and verification set, and the network model is trained by the training set.

Step 3. Calculate the sample output result through forward propagation, and calculate the error between the sample output result and the actual value. If the error does not meet the requirements or the iteration times are not reached, correct each network parameter through back propagation.

Step 4. Back propagation.

In view of the simple structure of the BP neural network and the strong generalization ability in signal sequence classification, the fingerprint location model of the PIR signal position based on the BP neural network will be adopted in the follow-up experiments of this paper.

4. Design and Implementation of Human Motion Recognition System

4.1. Design of Infrared Sensor Unit. A two-stage bandpass amplifier circuit is designed to filter, amplify, and resist the interference from the weak infrared signal detected by the pyroelectric probe. The circuit realizes the accurate acquisition of infrared signals of the human body, and its signal processing flow is shown in Figure 4.

The infrared sensing unit is composed of a Fresnel lens array, a pyroelectric probe, and a signal-conditioning circuit. When human bodies with different temperatures from the ambient background pass through the sensing area of the pyroelectric sensor, the sensor will output a weak AC signal of about 1 mV, and this AC signal is superimposed on a variable DC bias signal. Because of the interference of the environment and circuit noise, the weak signal will be annihilated in high-frequency noise, so a low-frequency bandpass filter circuit at $0.5 \sim 5$ Hz is designed. The signal-conditioning circuit can filter out the DC component of the sensor output signal, amplify the AC part, and filter out the environmental noise.

4.2. Design of Network Transmission Unit. The transmission network used in this design is a wireless network based on ZigBee technology. ZigBee technology is an area network protocol developed by ZigBee Alliance, which has excellent characteristics such as low power consumption and an ad hoc network; thus, it is widely used in wireless sensor networks. The ZigBee protocol stack is a specific implementation of the protocol, through which system developers can understand and use a certain part of the specific protocol. A complete ZigBee protocol stack includes a physical layer (PHY), a medium access control layer (MAC), a network layer (NWK), and an application layer (APL) from bottom to top. This is shown in Figure 5. Among them, the physical layer realizes the communication of the lowest level data, which will handle the receiving and sending of data from the physical end and is the basis of data communication between nodes. The medium access control layer completes the segmentation, recombination, and sequential transmission of the upper or lower layer data packets, thereby ensuring the reliability of data transmission, establishing network beacons, ensuring information synchronization, and establishing stable links between network nodes. The network layer function mainly realizes the establishment of an ad hoc network, configures the attributes and modes of nodes, and controls the transmission of data. The application layer develops the design of users' application requirements, and users can develop and design through the application layer to meet their own wireless sensor network needs.

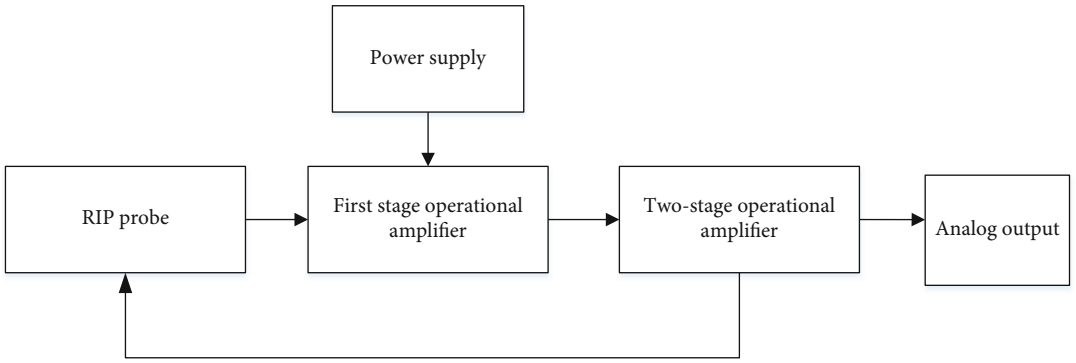

Figure 4: FIR signal processing flow.

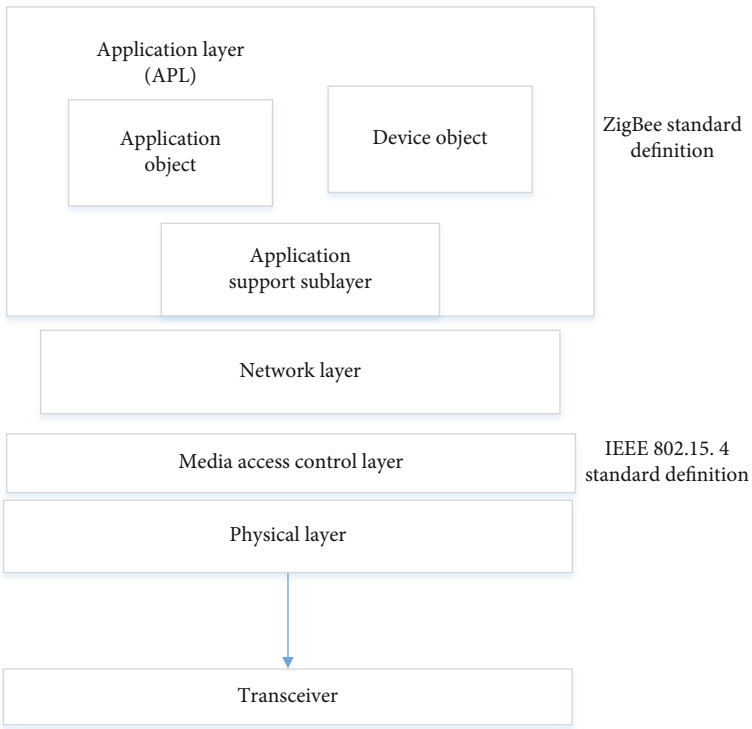

Figure 5: Structure diagram of a ZigBee protocol stack.

According to the different roles of nodes in wireless sensor networks, ZigBee nodes can be divided into the following three types:

(1) Coordinator (Coordinator): the coordinator is responsible for the creation and deployment of the entire network. As a data sink node in the network, it can communicate with any node in the network after the network is deployed

(2) Routing node (Router): as a signal relay node in the network, routing nodes are responsible for forwarding network data. The terminal node can communicate with the coordinator node through the routing node, and the network coverage can be expanded through the routing node

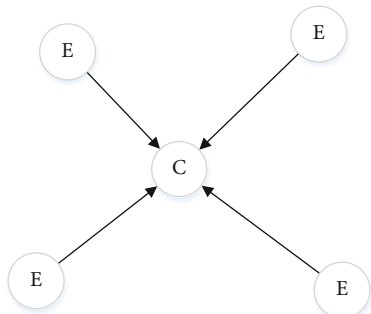

Figure 6: Star topology.

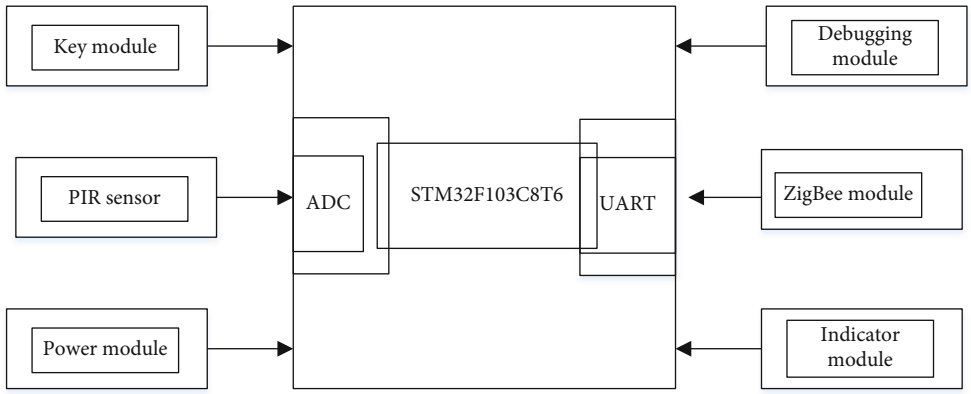

Figure 7: Design block diagram of an acquisition unit.

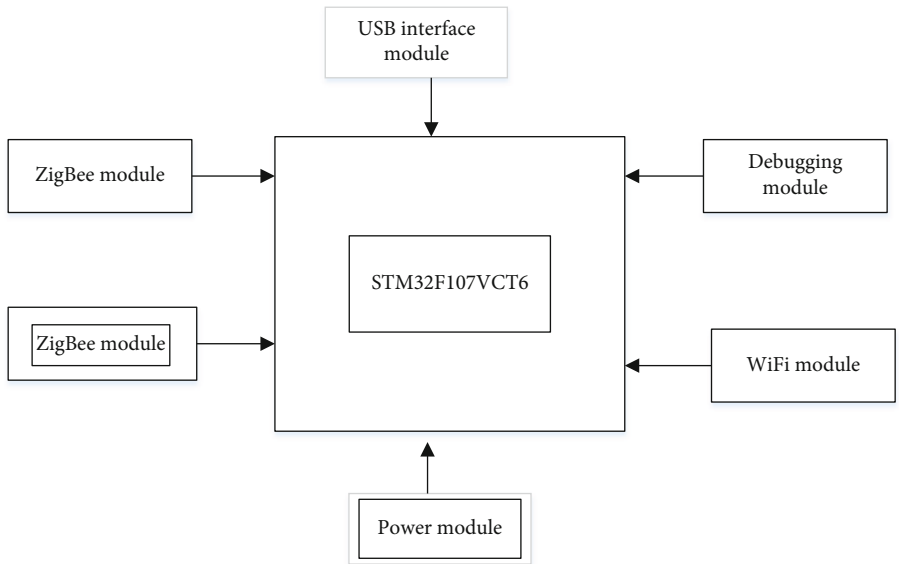

Figure 8: Gateway design block diagram.

(3) End node (EndDevice): as the bottom equipment in the network, terminal nodes have the functions of signal control, data processing, and transmission, and they are an essential part of the whole network

ZigBee network supports three kinds of topology: star, tree, and mesh. In this design, the star topology structure is adopted, and its topology structure is shown in Figure 6.

At present, the mainstream chips conforming to the ZigBee protocol specification in the market include the CC253x of Texas Instruments and the MC13224 of Freescale. In this design, the CC2530F256 chip of Texas Instruments is selected as the transmission unit in the network. The CC2530F256 chip is packaged in QFN40, the chip size is 6 mm ∗ 6 mm, and the working voltage is 2.0~3.6 V. It is an enhanced C8051 microprocessor with 2 USART serial ports and 21 fast I/O ports. In this design, the E18-MS1PA1-IPX model produced by Chengdu Yibaite Company is selected as the network transmission module of this paper, which integrates CC2530 and CC2592 (PA). A built-in ZigBee protocol stack, a 32.768 kHz clock crystal oscillator, a 256 kb flash, and an 8 kb RAM can realize the serial port transparent transmission function. This module is used in the signal acquisition terminal node and the network transmission unit in the coordinator gateway in this design system.

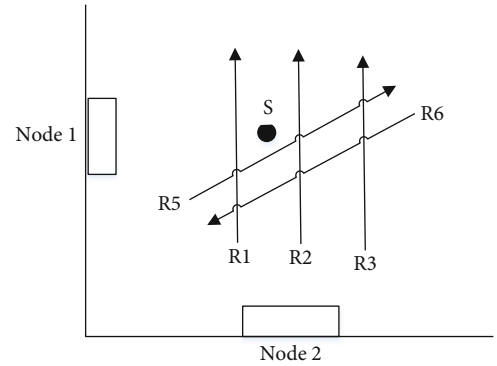

Figure 9: Some human movement paths in the experiment.

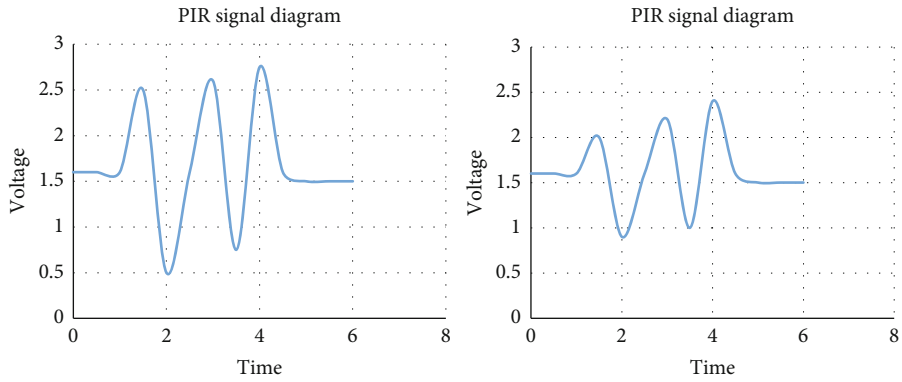

Figure 10: PIR signal diagram at different speeds.

4.3. Design of PIR Node Signal Acquisition Unit. The PIR node signal acquisition unit includes a power module and an MCU module, which can complete the data signal acquisition, filtering, packaging, transmission, and other functions. The design block diagram of the signal acquisition unit is shown in Figure 7.

4.3.1. MCU Module. The STM32F103C8T6 single-chip microcomputer used in this design has a 64 k flash and a 20 k SR AM, and the working voltage range is 2.0-3.6 V. It has two 12-bit A/D conversion modules, up to 16 conversion channels, conversion rates of up to 1 μs, a 7-channel DMA transfer controller, 26 fast I/O ports, an SWD debug interface, 7 timers, and 3 USART ports; these features are enough to meet the design requirements of this node and the expansion of future applications.

4.3.2. Power Module. Because the sensor node must be easy to deploy and install and its power consumption requirements are low, four 1.5 V dry batteries are selected for the external power supply, and the DC-DC voltage conversion module is selected for the internal power supply of the MCU and the peripheral sensor equipment. The AMS1117-33 V forward low-voltage regulator is selected as the voltage conversion module, which has 33 V stable output characteristics and supports overload and overheat protection.

4.4. Gateway Design. The gateway device includes a power module, an MCU module, a W-Fi module, a ZigBee module, and a USB serial port module. Through the gateway, the functions of the terminal nodes can be configured, and the network data can be received, unpacked, packaged, and sent. The design block diagram is shown in Figure 8.

4.4.1. MCU Module. The STM32F107VCT6 single-chip microcomputer in this design has a 256 K flash, a 64 K SRAM, a working voltage range of 2.0-3.6 V, a 12-channel DMA transfer controller, 5 USART ports, and an SWD debugging interface. These characteristics are enough to meet the design of this node and the expansion of future applications. The functions of the five serial ports in the gateway are as follows: one USB debugging interface, one W-Fi communication interface, and up to three ZigBee communication interfaces.

4.4.2. WiFi Module. The W-Fi module model selected is the Shanghai Hanfeng HF-LPB100, which has three working modes of STAIAP/STA + AP coexistence. The STA (station) mode is a site mode, which is equivalent to the terminal node in the network. The AP (access point) mode is the central node in the W1-Fi network. Other terminal nodes in the STA mode can communicate with each other through nodes in the AP mode. Usually, a wireless router is an AP node. In this design, the W-Fi module has the STA + AP mode, that is, the module supports an AP interface and an STA interface at the same time. Through the STA + AP coexistence mode, it is convenient for users to use mobile phones and other devices to monitor the terminal equipment in the network and realize the mode setting of the W-Fi module conveniently without changing its original network position. In the system, the mode configuration of the gateway and the acquisition of network data can be carried out through mobile phone equipment.

4.4.3. USB Adapter Module. The USB to serial port module adopts the CP2102 chip, which can realize data transmission with a PC through a USB cable.

4.4.4. Power Module. Externally, the gateway equipment adopts a general-purpose power adapter with 5 V-1 A and DC5 5 $*$ 2.1 mm interfaces; internally, the AMS1117-3.3 V LDO conversion module is adopted to supply power to the MCU, ZigBee, WiFi, etc.

5. Experiment

5.1. Experimental Environment and Data Processing. In the experiment, each sensor node is fixed at a height of 1.4 m. The MCU collects data at a sampling rate of 100 Hz and transmits it through the ZigBee sensor network in real time. The characteristics of sensor output signals in different motion states are analyzed through a MATLAB real-time interface. Part of the moving path in the experiment is shown in Figure 9, where Node 1 and Node 2 are two sensor nodes in the experimental environment. *S* is a static position point; R1, R2, and R3 are three paths parallel to Node 1; and

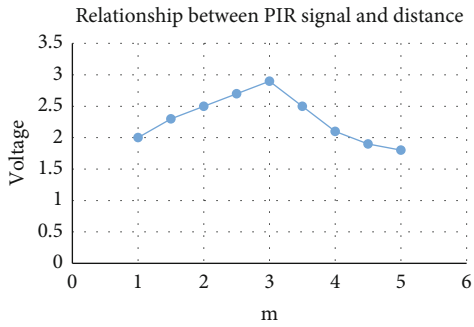

Figure 11: PIR signal and distance relationship.

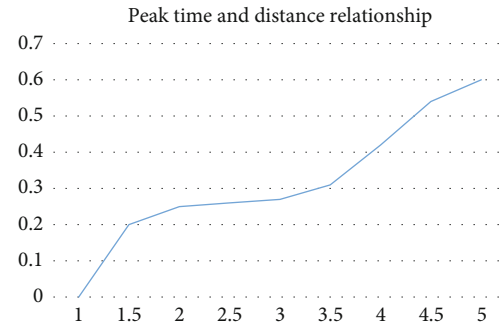

Figure 12: Relationship between peak time and distance.

their distances are D1 = 2 m, D2 = 3 m, and D3 = 4 m, respectively. R5 and R6 are the paths with 135 and -45 angles with Node 1, respectively.

Because different people move at different speeds, in order to eliminate the influence of speed on wireless sensor acquisition parameters, the same person walks along the R2 route at different speeds, and the results are shown in Figure 10.

According to the PIR1 output signal, when the human moving path is the same, different moving speeds will have an impact on the sensor output signal. In this experiment, when the speed is faster, the average amplitude of the sensor output signal is smaller; with the increase of the speed, the average peak time difference gradually decreases.

Because it is an infrared sensing unit, the distance between the equipment and the human body will also affect the collection of human motion parameters. Therefore, we let the experimenter walk parallel to different paths of Node 1 at the same speed and observe PIR signals. The results are shown in Figures 11 and 12.

According to the PIR1 output signal, when the human body moves at the same speed, different moving distances will have an impact on the sensor output signal. In this experiment, when the distance $D = 3$ m, the output signal amplitude of the sensor reaches the maximum value, and the average peak time difference increases with the increase of the distance. The relationship between the peak value and the peak time difference of the sensor output signal and the horizontal moving distance is shown in Figure 12.

From the above experiments, it can be seen that the infrared signal of a human body obtained by the system is a nonstationary random signal due to the tiny movements of the human body in the process of movement and the noise interference of the external environment. However, in this experiment, it is assumed that the human body walks along a fixed path, that is, the sensor will obtain the infrared waveform signal sampled for a period of time every time. By processing the infrared signal of this moving human body, the effective eigenvalue can be extracted, which can help this paper to make further judgment on the position of the human body.

Table 1: Classification and recognition results.

Dataset category	Node 1	Node 2	Node 1 and Node 2
Raw dataset	66.41%	64.06%	77.34%
Simplified feature data set	81.25%	82.81%	95.31%

In the experiment, this paper mainly considers the peak value of the signal waveform, the time when the peak value is located, and the number of the peak value. MATLAB firstly saves the collected data in frames and tags them. Then, the original infrared signal sequence is preprocessed, and the extracted effective eigenvalue vector is used as the input of the neural network. The valid eigenvalue data X is as follows:

$$x_i = \left[v_{p1}, \cdots, v_{pi}, \cdots, v_{pm}, t_{pp1}, \cdots, t_{ppj}, \cdots, t_{ppn}\right], \tag{16}$$

wherein I represents the index of the Ith peak element in the peak time series, and M is the number of peaks in the peak time series, including all peaks of the PIR1 output signal and the first two peaks of the PIR2 output signal; J represents the Jth peak element subscript in the peak time series, and $n$is the number of peaks in the peak time series, including all peak-to-peak pairs of the PIR1 output signal and the first peak-to-peak pair of the PIR2 output signal. V_{pi} represents the ith peak voltage in the peak time series in volts (V); t_{ppj} represents the Jth peak-to-peak time difference in the peak time series in seconds (s).

According to equation (16), for a group of real-time waveform signals collected by Node 1 in normal travel time at $D = 2$ m and $D = 3$ m, signal peak time series characteristics $x1$ and $x2$ can be extracted, respectively:

$$x1 : [2.48,0.61,2.29,1.11,1.89,1.37,2.48,0.98,1.87,2.24,1.01,0.24,0.20,0.19,0.23,0.30], \tag{17}$$

$$x2 : [2.44,0.52,2.74,0.80,2.60,0.77,2.74,0.69,2.05,1.85,1.50,0.30,0.25,0.24,0.25,0.33]. \tag{18}$$

Table 2: Accuracy rate of human motion recognition system.

Method	Parallel Node 1	Parallel Node 2	Slant line
Traditional human motion recognition system	72.31%	73.41%	71.82%
Wireless sensor human body recognition system based on blockchain	81.25%	82.81%	95.31%

According to equation (16), for a group of real-time waveform signals collected by Node 1, signal peak time series characteristics $x3$ and $x4$ can be extracted, respectively, when walking normally and fast at $D = 3$ m:

$$x3 : [2.44,0.52,2.74,0.80,2.60,0.77,2.74,0.69,2.05,1.85,1.50,0.30,0.25,0.24,0.25,0.33], \tag{19}$$

$$x4 : [2.45,0.56,2.45,0.94,2.31,0.93,2.51,0.87,1.98,1.76,1.68,0.26,0.20,0.21,0.20,0.10]. \tag{20}$$

From the characteristics of the waveform signal sequence, it can be seen that the distance between a moving human body and the sensor and the speed of the moving human body are related to the peak voltage, peak-peak time difference, and time series length of the sensor output signal.

5.2. Motion Recognition Analysis Process and Results. The task of this experiment is to verify the accuracy of the classification results of a PIR signal time series under the human infrared signal data set constructed in this paper. The experimental requirement is to collect infrared signals of a single human motion state. In this experiment, we mainly classify the position of a moving human body. At the horizontal distance $D_n = 1, 2, 3, 4$ m and the vertical distance $D_v = 1, 2, 3, 4$ m, the infrared signal of the human body is collected by normal walking and fast walking, respectively. In the experiment, a single person did 40 groups of experimental data at the above 8 paths with fast walking and slow walking; that is, a total of 640 groups of experimental data were generated.

In the design of the BP neural network, the number of hidden layers is 1. The conjugate gradient momentum algorithm (trainscg) is selected as the training algorithm, the tansig function is selected as the hidden layer transfer function, the softmax function is selected as the output layer transfer function, the learning rate is set to 0.1, and the mean square error is 1*e*-3. The number of hidden layer nodes is constantly revised, and a relatively stable neural network is obtained through multiple trainings.

The experimental results are analyzed as follows.

As shown in Table 1, the recognition results of the original data set and the peak time series feature (simplified feature) data set are analyzed, and the recognition results of a single node and a double node are analyzed, respectively. The original data dimension is 600, and the simplified feature dimension is 16. The experimental results show that Node 1 and Node 2 are similar in recognition rate, because each node has a higher recognition rate when moving horizontally with itself, but a lower recognition rate when moving perpendicularly with itself. When two nodes act at the same time, the recognition rate of the whole network is higher due to the data fusion between nodes. When the original data set is used, the time series obtained on the same path are quite different due to the difference of the intercepting position of the starting point of the time series, but the peak time series feature does not have these problems, and the accuracy rate of a moving human body position recognition is 95.31%.

In order to verify the superiority of this system, the accuracy of the wireless sensor human motion recognition system based on blockchain designed by us is compared with that of the traditional human motion recognition system. We mainly compared three kinds of motion routes: parallel to Node 1, parallel to Node 2, and diagonal line. The mean value of the five experimental results are shown in Table 2.

It can be seen from the experimental results that the system designed in this paper has high accuracy.

6. Conclusion

Traditional vision-based and sensor-based human motion detection methods have some disadvantages, such as high illumination requirements, difficulty in preserving privacy, and poor portability. To solve this problem, combining the advantages of wireless sensing and blockchain technology, a wireless sensor acquisition method of human motion parameters based on blockchain is proposed, and a human motion recognition system is designed. Experiments show that the accuracy of the wireless sensor acquisition method of human motion parameters based on blockchain in this paper reaches 95.31%, which verifies the effectiveness and superiority of the system designed in this paper.

Data Availability

The experimental data used to support the findings of this study are available from the corresponding author upon request.

Conflicts of Interest

The authors declared that they have no conflicts of interest regarding this work.

References

[1] J. Huang, Y. Hao, M. Zhao et al., "Biomass-based wearable and self-powered pressure sensor for human motion detection," *Composites Part An Applied Science and Manufacturing*, vol. 146, no. 5, p. 106412, 2021.

[2] Y. Zhang, B. Liu, and Z. Liu, "Recognizing hand gestures with pressure-sensor-based motion sensing," *IEEE Transactions on Biomedical Circuits and Systems*, vol. 13, no. 6, pp. 1425–1436, 2019.

[3] N. Xiao, P. Yang, Y. Yan, H. Zhou, and X.-Y. Li, "Motion-Fi+: recognizing and counting repetitive motions with wireless backscattering," *IEEE Transactions on Mobile Computing*, vol. 20, no. 5, pp. 1862–1876, 2021.

[4] H. Kim, S.-H. Shin, J.-K. Kim, Y.-J. Park, H.-S. Oh, and Y.-B. Park, "Cervical coupling motion characteristics in healthy people using a wireless inertial measurement unit," *Evidence-Based Complementray and Alternative Medicine*, vol. 2013, article 570428, 2013.

[5] J. Ren, F. Guan, M. Pang, and S. Li, "Monitoring of human body running training with wireless sensor based wearable devices," *Computer Communications*, vol. 157, pp. 343–350, 2020.

[6] J. Zhou, "Artificial intelligence driven wireless network remote monitoring based on Diffie-Hellman parameter method," *Computer Communications*, vol. 160, pp. 132–138, 2020.

[7] J. J. Sikorski, J. Haughton, and M. Kraft, "Blockchain technology in the chemical industry: machine-to-machine electricity market," *Applied Energy*, vol. 195, pp. 234–246, 2017.

[8] H. Bai, G. Zhou, Y. Hu et al., "Traceability technologies for farm animals and their products in China," *Food Control*, vol. 79, pp. 35–43, 2017.

[9] D. Ding, "From Ant Financial to Alibaba's Rural Taobao Strategy—how Fintech is transforming social inclusion," *Handbook of Blockchain, Digital Finance, and Inclusion*, vol. 1, pp. 19–35, 2018.

[10] K. W. Lye and J. M. Wing, "Game strategies in network security," *International Journal of Information Security*, vol. 4, no. 1-2, pp. 71–86, 2005.

[11] W. Gan, L. Chen, and Y. Liu, "Research on optical encryption system based on unequal modulus decomposition and polarized vortex optical holography," *Optics Communications*, vol. 482, p. 126609, 2021.

[12] M. Du, Q. Chen, and X. Ma, "MBFT: a new consensus algorithm for consortium blockchain," *IEEE Access*, vol. 8, pp. 87665–87675, 2020.

[13] P. Lorenz, "New path centrality based on operator calculus approach for wireless sensor network deployment," *IEEE Transactions on Emerging Topics in Computing*, vol. 7, no. 1, pp. 162–173, 2019.

[14] B. Jia, B. Huang, H. Gao, W. Li, and L. Hao, "Selecting critical WiFi APs for indoor localization based on a theoretical error analysis," *IEEE Access*, vol. 7, pp. 36312–36321, 2019.

[15] M. Hazas and A. Hopper, "Broadband ultrasonic location systems for improved indoor positioning," *IEEE Transactions on Mobile Computing*, vol. 5, no. 5, pp. 536–547, 2006.

[16] E. S. Tselishchev, A. G. Salin, I. S. Kudryashov, and S. V. Strakhov, "Application of new design automation in the development of the Pregolskaya TPP automated process control system," *Thermal Engineering*, vol. 66, no. 9, pp. 672–680, 2019.

Hindawi
Journal of Sensors
Volume 2021, Article ID 5775953, 12 pages
https://doi.org/10.1155/2021/5775953

Research Article

Tradeoff of Computation Bits and Computing Speed in an Edge Computing System for Sensor Networks

Jiaying Huang, Yawen Shi, and Fahui Wu

School of Information Engineering, Nanchang University, Nanchang 330031, China

Correspondence should be addressed to Fahui Wu; wufahui@ncu.edu.cn

Received 7 June 2021; Revised 4 August 2021; Accepted 12 August 2021; Published 15 September 2021

Academic Editor: Gengxin Sun

Unmanned aerial vehicle (UAV) enabled mobile-edge computing (MEC) has been recognized as a promising approach for providing enhanced coverage and computation capability to Internet of Things (IoT), especially in the scenario with limited or without infrastructure. In this paper, we consider the UAV assisted partial computation offloading mode MEC system, where ground sensor users are served by a moving UAV equipped with computing server. Computation bits (CB) and computation efficiency (CE) are two vital metrics describe the computation performance of system. To reveal the CB-CE tradeoff, an optimization problem is formulated to maximize the weighted sum of the above two metrics, by optimizing the UAV trajectory jointly with communication resource, as well as the computation resource. As the formulated problem is non-convex, it is difficult to be optimally solved in general. To tackle this issue, we decouple it into two sub-problems: UAV trajectory optimization and resource allocation optimization. We propose an iterative algorithm to solve the two sub-problems by Dinkelbach's method, Lagrange duality and successive convex approximation technique. Extensive simulation results demonstrate that our proposed resource allocation optimization scheme can achieve better computational performance than the other schemes. Moreover, the proposed alternative algorithm can converge with a few iterations.

1. Introduction

With the increasing popularity of computer terminals and the emergence of new applications (e.g. online games, face recognition, smart home, etc.), mobile data traffic continues to grow at a high speed, and users' demands for computing power and quality of experience (QoE) are also increasing [1]. However, the limited battery lifetime and low computing capacity make it difficult for mobile terminal to provide good QoE [2].

The computing offloading technology under the mobile cloud computing (MCC) architecture was first proposed to solve the above challenge, but the network bandwidth pressure and transmission delay problem make MCC unable to meet the application requirements well [2]. Therefore, mobile edge computing (MEC) has received widely attention as an advanced technology that can overcome these challenges [3]. The MEC serves are at the edge of the wireless sensor network, providing communication, computing, storage and other services to a large number of end users who are tightly deployed [2]. MEC enables rapid data analysis and processing, reduces the possibility of latency, and ensures high security [2]. However, terrestrial MEC systems have limitations in application scenario, such as infrastructures are destroyed due to natural disasters [4–6].

Unmanned aerial vehicles (UAV) can tackle this challenge due to the flexibility and controllability, they can be flexibly deployed in most scenarios, especially in the scenario with limited or without infrastructure. Moreover, the UAV-enabled MEC system has more reliable line-of sight (LoS) communication links thus improve the performance of computation tasks offloading and computation results downloading, significantly improved the computation performance eventually [7–9]. Furthermore, the trajectory of the UAV can be optimized to further improve the user computation performance [10–17].

For the above reasons, this paper considers an UAV-enabled MEC system. In order to achieve a good tradeoff

between computation bits and computation efficiency of all sensor users, a resource allocation scheme with jointly optimized computation performance and UAV's trajectory is proposed under partial computation offloading mode.

1.1. Related Work and Motivation. Resource allocation is one of the gordian technologies in mobile edge computing networks, MEC systems need to continuously optimize resource allocation algorithms to improve the computation performance. At present, there are a lot of researches on resource allocation in the conventional MEC networks [18–23]. Jian et al. [18] proposed a profit maximization problem based on the task-aware cloud radio access network with MEC system, which jointly optimizing offloading tactics, radio and computational resources allocation. In order to minimize the energy computation of the overall user, when multiple mobile users request for computation offloading to a public cloud server, Sardellitti et al. [19] defined the offloading problem specifically as the transmit precoding matrices of the multiple mobile users and the CPU cycles/second assigned by the cloud to each mobile user, thus proposing an optimization scheme for computing and radio resources. In order to provide high quality of experience, the issues about content caching strategies and computation offloading in wireless cellular network with MEC were considered, specifically, Wang et al. [20] designed the resource allocation scheme under the premise of considering the total network revenue, while the goal of Zhang et al. [21] is minimize the total delay computation during the computation process. Consider there is a delay of user's task completion, in order to avoid serious delay, Ding et al. [22] formulated a power and time allocation joint optimization scheme to decrease the energy consumption when performing computation offloading task in a NOMA-assisted MEC network. Du et al. [23] studied computation, communication and bandwidth allocation problem in a mixed fog/cloud system by considering computation resource allocation or offloading decision making while considering user fairness and tolerable delay.

In order to tackle the problem of achieving good communication and computation performance in complex environments, the resource allocation problems in UAV-enabled MEC networks have been studied [10, 11]. The authors of [10] first proposed a UAV-enabled MEC network and demonstrated that UAV can improve system's computing performance due to the LoS link and trajectory optimization, a testbed was developed for performance validation and results demonstrated that the UAV-enabled MEC reducing the processing time of recognition. In order to improve the computing performance, considering an UAV user is served by cellular ground base stations (GBSs) for computation offloading, Cao et al. [11] formulated an effective scheme that optimizes the computation offloading schedule and adjusts the trajectory to minimize the time for the UAV to complete the mission. Xiong et al. [12] studied a resource allocation scheme to minimize the sum of the maximum delay of multiple ground users in MEC system, a Block coordinate descent (BCD) based optimization algorithm was proposed to alternatively optimize the offloading decisions, bit allocations and the UAV trajectory in each iteration. Hu et al. [13] and Jeong et al. [14] proposed a resource allocation program to minimize the consumed overall energy of the system, the problem of jointly offloading and trajectory design in [13] with energy budget constraints was addressed by leveraging penalty dual decomposition-based algorithm, and the problem of jointly optimizing the bit allocation and path plan under energy consumption constraints was solved by leveraging successive convex approximation (SCA) strategies. Furthermore, Messous et al. [15] considered the tradeoff between execution time and energy consumption, a game theory model was adopted to minimize the cost function combination of energy overhead and delay. Zhou et al. [16] and Zhang et al. [17] designed resource allocation scheme by jointly optimizing the UAV's trajectory, the CPU frequencies, the offloading times and transmit powers of user to maximize the computation bits and computation efficiency, respectively.

Although a lot of literatures has been studied the resource optimization problems in the MEC networks, and UAV-enabled MEC system, none of the above works considered the tradeoff between computation bits and computation efficiency. Computation bits maximization aims to maximize the number of total computation bits by offloading and local computing. It can directly reflect the computation performance of UAV-enabled MEC system. However, the computation bits maximization overemphasizes the importance of computation bits, may lead to excessive energy usage. The computation efficiency maximization overemphasizes the importance of efficiency, the computation bits may too small to meet the computation requirement. In a word, consider only one metric maximization may fall into the trap of local (or partial) performance optimum. Thus, we study a tradeoff problem between computation bits and computation efficiency by jointly optimizing the UAV trajectory, the CPU frequencies, the offloading times and transmit powers of user in the UAV-based MEC system under the partial computation offloading mode. From the above discussion, this is the first study of considering the tradeoff between computation bits and computation efficiency in the UAV-enabled MEC system.

1.2. Contributions and Organization. An UAV-assisted MEC network is considered in the paper, where multiple ground sensor users receive energy and computation services from the UAV. In the system, each sensor user has an on-chip computing microprocessor that can perform simple computation tasks, and the UAV is equipped with a power computing processor that can execute computationally heavy tasks [11–15]. Even if the flight time is affected by battery capacity, which limits computing performance, it is promising due of the LoS links of UAV-to-ground communication channel [7]. The objective of this paper is to reveal and achieve a good tradeoff between the total computation bits and the computation efficiency of all users under partial computation offloading mode. Hence, our main contributions are summarized as follows:

(i) The resource optimization scheme is formulated in an UAV-enabled MEC system under partial

computation offloading mode. The tradeoff problem between computation bits and computation efficiency of users is formulated by jointly the CPU frequency, the offloading times, the transmit powers of users and the trajectory of UAV, subject to the time constraint, the maximum consumed energy constraint, the initial and final horizontal location constraints, and the speed constraint of the UAV.

(ii) We transform the challenging primal non-convex problem into a form that is easier to solve by decomposing it into two subproblems. Thus, a two-stage alternative optimization method is proposed to address the formulated original problem. With the UAV's trajectory fixed, the closed-form expressions for the optimal CPU frequencies, the offloading times and the transmit powers of users can be derived by the Lagrangian dual method. And the SCA method is used to optimize the trajectory of the UAV.

(iii) The simulation results demonstrate that the proposed resource allocation optimization scheme has better computational performance than the disjoint scheme. Moreover, it is seen that the convergence speed of the alternative algorithm is good, and it can converge after a few iterations.

The structure of the paper is as follows. The system model is introduced in Section 2. Section 3 formulates the resource allocation optimization problem under partial computation offloading and decomposed into two subproblems that are easy to solve. Section 4 presents the simulation results. Finally, Section 5 concludes this paper.

2. System Model

Consider a UAV-assisted MEC system as shown in Figure 1, where a UAV equipped with an MEC server to provide the computation capability for the ground sensors. The UAV is dispatched to fly from an appointed initial location to a final location. There are M sensor users fixed on the ground, denoted by $\mathcal{M} \triangleq \{1, 2, \cdots, M\}$. Each user offloads a portion of its computing tasks to the UAV and carries out the rest locally. Without loss of generality, a three-dimensional (3D) Euclidean coordinate is adopted, where the horizon coordinate of ground user m is denoted by $\mathbf{q}_m = [x_m, y_m]$,$m \in \mathcal{M}$. It is assumed that the ground users' locations can be detected by the UAV to facilitate the trajectory design [7–9]. Suppose that the UAV flies at altitude $H(H > 0)$ from the ground remains unchanged during a given flight period, H is the minimum height that can avoid obstacles on the ground and ensure normal communication.

2.1. System Model. The period time for the UAV flight is expressed by T. For convenience, the time duration T is divided into N time slots with equal length, which are expressed by a set $\mathcal{N} \triangleq \{1, 2, \cdots, N\}N$. And then, the horizontal plane coordinate of UAV over time slot n can be characterized by the discrete time locations $\mathbf{q}_u[n] = [x_u[n], y_u[n]], 0 \le n \le N$. Hence, the distance between the ground user $m \in \mathcal{M}$ and UAV in each time slot $n \in \mathcal{N}$ can be denoted by $d_m[n] = \sqrt{H^2 + \|\mathbf{q}_u[n] - \mathbf{q}_m\|^2}$, where $\|\cdot\|$denotes the Euclidean norm. The number of N should be large enough to ensure that the position of the UAV in each time slot (or the distance between the UAV and ground users) can be regarded as constant. Particularly, the UAV's initial and final horizontal positions are assumed to be determined before flight, which denoted as $\mathbf{q}_0$ and $\mathbf{q}_F$, respectively. Thus, we have the UAV's location and speed constraints:

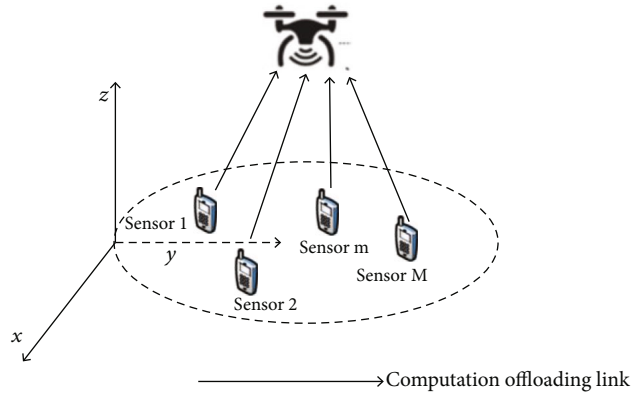

Figure 1: The system model.

$$\mathbf{q}_u[1] = \mathbf{q}_0 \tag{1a}$$

$$\mathbf{q}_u[N+1] = \mathbf{q}_F \tag{1b}$$

$$\|\mathbf{q}_u[n+1] - \mathbf{q}_U[n]\| \le \frac{\mathbf{1}}{N} V_{\max}, n \in \mathcal{N} \tag{1c}$$

where $V_{\max}$ is the maximum flying speed of the UAV. We consider block fading channel in this paper i.e., during each T, the channel remains static. Similar to [24–26], it is assumed that the wireless channel between the UAV and ground users is dominated by line of sight (LoS) link, hence the channels between the UAV and ground users are modelled by the free space path loss model. Thus, the channel power gain between the UAV and the mth user is denoted by $h_m[n]$, given as:

$$h_m[n] = \beta_0 d_m^{-2}[n] = \frac{\beta_0}{H^2 + \|\mathbf{q}_u[n] - \mathbf{q}_m\|^2}, m \in \mathcal{M}, n \in \mathcal{N} \tag{2}$$

where β_0 is the channel power gain at a reference distance $d_0 = 1$m.

2.2. Local Computation and Computation Offloading. In this paper, the partial computation offloading mode is adopted, the computing task of each user consists of local computing and computation offloading to the UAV. Each user can simultaneously perform the two tasks. Similar to the works in [27–29], let C denote the number of CPU cycles required to process one bit of date at each user and $f_m[n]$ denote the CPU frequencies of the mth user at the nth slot. Thus, the total computation bits and the total consumed energy of

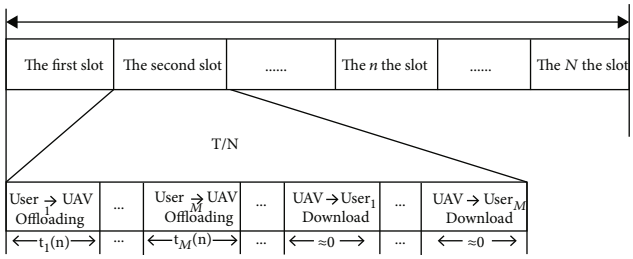

Figure 2: Computation offloading from user to the UAV.

the mth user when performing the local computing task during n slots are, respectively, denoted as:

$$R_{\text{local}} = \sum_{k=1}^{n} \frac{Tf_m[k]}{NC}, m \in \mathcal{M}, n \in \mathcal{N} \tag{3}$$

$$E_{\text{local}} = \frac{T}{N} \sum_{k=1}^{n} \gamma_c f_m^3[k], m \in \mathcal{M}, n \in \mathcal{N} \tag{4}$$

where γ_c denote the effective capacitance coefficient of the processor's chip at the mth user. Furthermore, each user's chip architecture determines γ_c. In the computation offloading part, as shown in Figure 2, a time-division multiple access (TDMA) protocol is applied. The computation process of mth user in each time slot can be divided into three stages: offloading, computation and downloading phase. In the offloading phase, M users execute their computation offloading task one after another during each slot. The UAV performs computing tasks and sends results to the user after all users have completed their computation offloading tasks at the nth slot. Similar to [16, 17], compare with the ground user, the UAV has a strong computation capability, thus, the computation time is much less than that of ground users. Moreover, the number of the bits related to the computation result is very small. Thus computation time and the downloading time of the UAV are neglected.

According to the works in [28], the total number of bits that the mth user offloads to the UAV at the nth slot is given by:

$$\frac{BTt_m[n]}{\nu_m N} \log_2\left(1 + \frac{h_m[n]P_m[n]}{\sigma_0^2}\right), m \in \mathcal{M}, n \in \mathcal{N} \tag{5}$$

where B represents communication bandwidth; $P_m[n]$ denotes the transmit power of the mth user at the nth slot; σ_0^2 is noise power of the mth user; $Tt_m[n]/N, 0 \le t_m[n] \le 1$ denotes the lasting time for the mth user offloads the computation tasks to the UAV at the nth time slot and ν_m denotes the redundant data in communication.

Moreover, the sum of the total offloading time of all users should not be greater than the duration of one time slot, thus:

$$\sum_{m=1}^{M} t_m[n] \le 1, m \in \mathcal{M}, n \in \mathcal{N} \tag{6}$$

We apply the energy available constraint to each ground user m so that the energy consumed for local computing and task offloading cannot exceed a threshold, denoted by Γ_m, $m \in M$. Thus, we have:

$$\frac{T}{N} \sum_{k=1}^{n} \left[\gamma_c f_m^3[k] + t_m[k]P_m[k]\right] \le \Gamma_m, m \in \mathcal{M}, n \in \mathcal{N} \tag{7}$$

Under the partial computation offloading mode, the total computation bits CB_m of the mth user is expressed as:

$$CB_m = \sum_{n=1}^{N} \left(\frac{Tf_m[n]}{NC} + \frac{BTt_m[n]}{\nu_m N} \cdot \log_2\left(1 + \frac{h_m[n]P_m[n]}{\sigma_0^2}\right)\right), m \in \mathcal{M}. \tag{8}$$

The total energy consumption of the mth user is given as:

$$E_m = \frac{T}{N} \sum_{n=1}^{N} \left[\gamma_c f_m^3[n] + t_m[k]p_m[n]\right], m \in \mathcal{M} \tag{9}$$

Therefore, the computation efficiency of the mth user can be expressed as:

$$CE_m = \frac{CB_m}{E_m} = \frac{\sum_{n=1}^{N}\left((Tf_m[n]/NC) + (BTt_m[n]/\nu_m N)\log_2\left(1 + \left(h_m[n]P_m[n]/\sigma_0^2\right)\right)\right)}{T/N\sum_{n=1}^{N}\left[\gamma_c f_m^3[n] + t_m[n]p_m[n]\right]}, m \in \mathcal{M} \tag{10}$$

3. Resource Optimization in UAV-Enabled MEC System

Our objective is to characterize the total computation bits CB and the computation efficiency CE tradeoff in the UAV-enabled MEC system under the partial computation offloading mode, by jointly optimizing CPU frequencies $f_m[n]$, offloading times $t_m[n]$, the UAV trajectory $\mathbf{q}_u[n]$ and the transmit power allocation $p_m[n]$, subject to the initial and final horizontal location constraints and the speed

constraint of the UAV in (1), the time constraint in (6), and the maximum consumed energy constraint in (7). Consequently, the resource and trajectory jointly optimization problem is formulated as:

$$\begin{aligned}\mathrm{P1}: &\max_{f_m[n],p_m[n],\mathbf{q}_u[n],t_m[n]} \left[\rho \sum_{m=1}^{M} CB_m + (1-\rho)\sum_{m=1}^{M} CE_m\right] \\ &\text{s.t.C1}: f_m[n] \geq 0, p_m[n] \geq 0, m \in \mathscr{M}, n \in \mathscr{N} \\ &(1), (6), \text{and } (7)\end{aligned} \tag{11}$$

where the constant ρ is a weight coefficient, and its value range is $[0, 1]$. In the special case, when $\rho = 1$, the above general problem becomes computation bits maximization problem, when $\rho = 0$, P1 is equivalent to the computation efficiency maximization problem.

It is easy to observe that P1 is non-convex problem since the presence of the non-linear couplings among the optimization variables, and the objective function is non-concave with respect to the trajectory of the UAV. An alternative two-stage algorithm is designed to address P1, the details are as follows.

3.1. Optimizing Transmit Power, Offloading Times and CPU Frequencies. For a given trajectory, P1 can be re-expressed as:

$$\begin{aligned}\mathrm{P2}: &\max_{f_m[n],P_m[n],t_m[n]} \left[\rho \sum_{m=1}^{M} CB_m + (1-\rho)\sum_{m=1}^{M} CE_m\right] \\ &\text{s.t.C1, (6), and(7).}\end{aligned} \tag{12}$$

Since the objective function is a fractional form, P_2 is still nonconvex. To obtain a tractable solution, a parameter problem based on the Dinkelbach's method is exploited to tackle the objective function [30]. Thus, P2 can be solved by iteratively solving P3, given by:

$$\begin{aligned}\mathrm{P3}: &\max_{f_m[n],P_m[n],t_m[n]} \left\{\rho \sum_{m=1}^{M} CB_m - (1-\rho)\eta\frac{T}{N}\left(\gamma_c f_m^3[n] + Z_m\right)\right. \\ &\left. + (1-\rho)\sum_{m=1}^{M}\left[\frac{Tf_m[n]}{NC} + \frac{BTt_m}{\nu_m N}\log_2\left(1 + \frac{h_m[n]Z_m}{t_m\sigma_0^2}\right)\right]\right\} \\ &\text{s.t.C1, and (6).}\end{aligned} \tag{13}$$

where $Z_m[n] = P_m[n]t_m[n]$, and η is a non-negative parameter. It is seen that P3 is a convex problem and can be solved by using Lagrange duality method [31]. The Lagrangian of P3 can be given by:

$$\begin{aligned}L(\Xi) = &\sum_{m=1}^{M}\sum_{n=1}^{N}\left[\frac{Tf_m[n]}{NC} + \frac{BTt_m[n]}{\nu_m N}\log_2\left(1 + \frac{h_m[n]Z_m[n]}{t_m[n]\sigma_0^2}\right)\right. \\ &\left. - (1-\rho)\eta\frac{T}{N}\left(\gamma_c f_m^3[n] + Z_m[n]\right)\right] \\ &- \sum_{m=1}^{M}\sum_{n=1}^{N}\left[\lambda_{m,n}\left(\frac{T}{N}\left(\gamma_c f_m^3[n] + Z_m[n]\right) - \Gamma\right)\right] \\ &+ \sum_{n=1}^{N}\mu_n\left\{1 - \sum_{m=1}^{M} t_m[n]\right\}\end{aligned} \tag{14}$$

In equation (14), $\lambda_{m,n}, m \in \mathscr{M}, n \in \mathscr{N}$ and $\mu_n > 0, n \in \mathscr{N}$ are the dual variables associated with the constraint in C1 and (6), respectively, and Ξ represents a collection of all optimization and dual variables. Let $\theta_{m,n} = \sum_{k=n}^{N}\lambda_{m,k}$ and $g_m(k) = \gamma_c f_m^3[k] + Z_m[k] - \Gamma_m$, then, the Lagrangian function can be rewritten as:

$$\begin{aligned}\mathscr{L}(\Xi) = &\sum_{m-1}^{M}\sum_{n=1}^{N}\left[\frac{Tf_m[n]}{NC} + \frac{BTt_m[n]}{\nu_m N}\log_2\left(1 + \frac{h_m[n]Z_m[n]}{t_m[n]\sigma_0^{1/n}}\right)\right. \\ &\left. - (1-\rho)\eta_N^T\left(\gamma_c f_m^3[n] + Z_m[n]\right)\right] \\ &- \sum_{m=1}^{M}\sum_{n=1}^{N}\left[\frac{T}{N}\theta_{m,n}g_m(k)\right] + \sum_{n=1}^{N}\mu_n\left\{1 - \sum_{m=1}^{M} t_m[n]\right\}\end{aligned} \tag{15}$$

Thus, the Lagrangian dual function expression of P_3 is written as:

$$\varphi(\lambda_m, n, \mu_n) = \max_{0 \leq f_m[n]} \mathscr{L}(\Xi) \tag{16}$$

According to equation (16), the optimal solutions of P3 can be obtained by solving its dual problem, given as:

$$\min_{\lambda,n,\mu_n} \varphi(\lambda_m, n, \mu_n) \tag{17}$$

Given dual variables, (17) can be decomposed into M parallel sub-problems, given as:

$$\begin{aligned}&\mathscr{L}_m(\lambda_{m,n},\mu_n, t_m[n], Z_m[n], f_m[n]) \\ &= \sum_{n=1}^{N}\left\{\frac{Tf_m[n]}{NC} + \frac{BTt_m[n]}{\nu_m N}\log_2\left(1 + \frac{h_m[n]Z_m[n]}{t_m[n]\sigma_0^2}\right)\right\} \\ &\quad - \sum_{n=1}^{N}\left\{(1-\rho)\eta\frac{T}{N}\left(\gamma_c f_m^3[n] + Z_m[n]\right)\right\} \\ &\quad - \sum_{n=1}^{N}\frac{T}{N}\theta_{m,n}g_m(n) + \sum_{n=1}^{N}\left\{\frac{\mu_n}{M} - \mu_n t_m[n]\right\}\end{aligned} \tag{18}$$

Therefore, let us take the derivative of (18) with respect to $f_m[n]$ and $Z_m[n]$, respectively, the optimal CPU frequency

$f_m^{\mathrm{opt}}[n]$ and transmit power of users $p_m^{\mathrm{opt}}[n]$ can be obtained, and their expressions are:

$$f_m^{\mathrm{opt}}[n] = \sqrt{\frac{1}{3C\gamma_c\left((1-\rho)\eta + \sum_{k=n}^{N}\lambda_{m,k}\right)}}$$

$$p_m^{\mathrm{opt}}[n] = \begin{cases} 0 & , t_m[n] = 0, \\ \left[\dfrac{B}{\nu_m \ln 2\left((1-\rho)\eta + \sum_{k=n}^{N}\lambda_{m,k}\right)} - \dfrac{\sigma_0^2}{h_m[n]}\right]^+ & , t_m[n] > 0, \end{cases} \tag{19}$$

where $[x]^+ = \max(x, 0)$ and $\max(x, 0)$ denotes the bigger value of x and 0.

And similar to the above, the optimal offloading time can also be obtained by deriving the following formula for a given trajectory $\mathbf{q}_u[n]$:

$$\log_2\left(1 + \frac{h_m[n]Z_m[n]}{t_m[n]\sigma_0^2}\right) - \frac{h_m[n]Z_m[n]}{\ln 2\left\{t_m[n]\sigma_0^2 + h_m[n]Z_m[n]\right\}} - \frac{\mu_n N \nu_n}{BT} = 0 \tag{20}$$

We can handle the (20) by applying the bisection method. Finally, the dual variables can be obtained by using subgradient method [30]. According to [30], the subgradient ensures convergence to the optimal values within a small margin of error.

3.2. Optimizing UAV Trajectory. For any given CPU frequencies, transmit power, offloading times of users, we can express the sub-problem about trajectory optimization as:

$$\begin{aligned} \mathrm{P4}: \max_{\mathbf{q}_u[n]} & \rho \sum_{m=1}^{M}\sum_{n=1}^{N}\left[\frac{BTt_m[n]}{\nu_m N}\log_2\left(1 + \frac{P_m[n]\beta_0}{\sigma_0^2\left(H^2 + \|\mathbf{q}_u[n] - \mathbf{q}_m\|^2\right)}\right)\right] \\ & + (1-\rho)\sum_{m=1}^{M}\sum_{n=1}^{N}\left[\frac{Bt_m[n]\log_2\left(1 + \left(P_m[n]\beta_0/\sigma_0^2\left(H^2 + \|q_u[n] - q_m\|^2\right)\right)\right)}{\nu_m\left(\gamma_c f_m^3[n] + t_m[n]p_m[n]\right)}\right] \\ \text{s.t.} & (1a), (1b), \text{and } (1c). \end{aligned} \tag{21}$$

Due to the objective function is non-concave with respect to $\mathbf{q}_u[n]$, and we can use SCA technology to handle the non-convex problem of P4. The obtained solution can be guaranteed to satisfy the Karush-Kuhn-Tucker (KKT) conditions of P4 [32]. Thus, the global underestimation can be obtained by using the first-order Taylor expansion method.

For any local trajectory $\mathbf{q}_u^j[n], n \in N$ at the jth iteration, we have:

$$\log_2\left(1 + \frac{\beta_0 P_m[n]}{\sigma_0^2\left(H^2 + \|\mathbf{q}_u[n] - \mathbf{q}_m\|^2\right)}\right) \geq y_m^j(\{\mathbf{q}_u[n]\}) \tag{22}$$

where:

$$\begin{aligned} & y_m^j(\{\mathbf{q}_u[n]\}) \\ & = \log_2\left(1 + \frac{P_m[n]\beta_0}{\sigma_0^2\left(H^2 + \left\|\mathbf{q}_u^j[n] - \mathbf{q}_m\right\|^2\right)}\right) \\ & \quad - \frac{P_m[n]\beta_0\log_2 e\left(\|\mathbf{q}_u[n]\|^2 - \left\|\mathbf{q}_u^j[n]\right\|^2\right)}{\left(\sigma_0^2 H^2 + P_m[n]\beta_0 + \sigma_0^2\left\|\mathbf{q}_u^j[n]\right\|^2\right)\left(\left\|\mathbf{q}_u^j[n]\right\|^2 + H^2\right)} \end{aligned} \tag{23}$$

where the equality holds when $\mathbf{q}_u[n] = \mathbf{q}_u^j[n]$.

By replacing the objective function of P4 with (22), the problem (21) is approximately transformed to:

$$\begin{aligned} \mathrm{P5}: \max_{\mathbf{q}_u[n]} & \rho \sum_{m=1}^{M}\sum_{n=1}^{N}\left[\frac{BTt_m[n]}{\nu_m N} y_m^j(\{q_u[n]\})\right] \\ & + (1-\rho)\sum_{m=1}^{M}\sum_{n=1}^{N}\left[\frac{Bt_m[n]y_m^j(\{q_u[n]\})}{\nu_m\left(\gamma_c f_m^3[n] + t_m[n]P_m[n]\right)}\right], \\ \text{s.t.} & (1a), (1b), \text{and } (1c). \end{aligned} \tag{24}$$

It is seen that P5 is convex and can be easily solved by using convex optimization tools such as CVX [32]. By solving P3 and P5, the two sub-problems alternate in an iterative manner. The specific process of the proposed algorithm is summarized in Table 1.

Here, we give the complexity analysis for the proposed Algorithm 1. It consists of solving resource allocation and optimizing UAV trajectory with CVX. Let L_1 and L_2 denote the number of iterations required for the Repeat 1 and Repeat 2 of Algorithm 1, respectively. The computation complexity of Repeat 2 is$\mathcal{O}(L_2N^3)$. For Repeat 1, the first aspect is calculate $f^{opt,i}[n]$ and $p^{opt,i}[n]$, the computation complexity is $\mathcal{O}(L_1 2MN)$; the computation complexity of bisection method for obtaining the $t^{Opt,i}$ is $\mathcal{O}[L_1 M \log_2(l_1/T)]$,where l_1 denotes the tolerance error for bisection method. The computation complexity of computing the dual variables is $\mathcal{O}(L_1/l_2^2)$, where l_2 denotes the tolerance error for

Table 1: Two-stage alternative optimization algorithm.

Algorithm 1. The alternative optimization algorithm for P1.

1: **Setting**

Γ, T, N, $V_{\max}$, $\mathbf{q}_0$,$\mathbf{q}_F$, and the tolerance errors ξ, ξ_1, inputting ρ;

2: **Initialization:**

The iterative index $i = 1$, $\lambda_{m,n}^i$, μ_n^i and $\mathbf{q}_u^i[n]$;

3: **Repeat 1**

Calculate $f^{\text{opt},i}[n]$ and $p^{\text{opt},i}[n]$ by solving problem P3 for given $\mathbf{q}_u^i[n]$;

Obtain $t^{\text{opt},i}$ using the bisection method to solve (20);

Update $\lambda_{m,n}^i$ and μ_n^i using the sub gradient algorithm;

Initialize the iterative number $j = 1$;

Repeat 2

Solve P5 by using CVX for the given $f^{\text{opt},i}[n]$, $p^{\text{opt},i}[n]$ and $t^{\text{opt},i}$;

Update $j = j + 1$, and $\mathbf{q}_u^i[n]$;

If $\sum_{n=1}^{N} \left\| \mathbf{q}_u^j[n] - \mathbf{q}_u^{j-1}[n] \right\| \le \xi$

$\mathbf{q}_u^i[n] = \mathbf{q}_u^j[n]$;

Break;

End

End repeat 2

Update the iterative index $i = i + 1$;

If $\left| \max_{n \in \mathcal{N}} \sum_i - \sum_{i-1} \right| \le \xi_1$ where $\sum_i = \rho CB_m + (1-\rho) CE_m$

Break;

End

End repeat 1

4: Obtain solutions

the subgradient method. Thus, the total complexity of Algorithm 1 is $\mathcal{O}[L_1(2MN + M \log_2(l_1/T) + 1/l_2^2 + L_2N^3)]$.

4. Simulation Results

In this section, the numerical results are presented to validate our proposed design. The parameter settings in the simulation process refers to the works in [16, 17]. In this paper, assuming that there are four ground users whose locations are set to $\mathbf{q}_1 = [3, 3]$, $\mathbf{q}_2 = [3, 8]$, $\mathbf{q}_3 = [8, 8]$, and $\mathbf{q}_4 = [8, 3]$, and the maximum consumed energy constraints are identical for multiple ground users, i.e., $\Gamma_m = \Gamma$, $m \in M$, the details of others parameters setting are shown in Table 2.

To illustrate the effectiveness of our proposed design, two benchmark schemes are considered. 1) The UAV flies from the initial position to final position follow a straight trajectory. 2) The UAV flies from the initial position to final position follow a semi-circle trajectory.

Figure 3 shows the available CB-CE region of the tradeoff for different schemes, in which the energy consumed threshold $\Gamma = 1$. This figure shows that available CB-CE region of proposed scheme is bigger than that of benchmark's, which indicate that through proper design the resource allocation and trajectory, the proposed UAV-MEC system design can achieve better computation performance and reduce the operation cost.

Table 2: Simulation parameters.

Parameters	Notation	Typical values
The height of the UAV	H	10 m
The time length of the UAV flying	T	2 sec
Communication bandwidth	B	40 MHz
The receiver noise power	δ^2	10^{-9} w
The number of time slots	N	50
The effective switched capacitance	N	10^{-28}
The channel power gain	β	-50 dB
The tolerance error	ξ, ξ_1	10^{-4}
The initial location of the UAV	$\mathbf{q}_0$	[0,0]
The final location of the UAV	$\mathbf{q}_F$	[10,0]
The maximum speed of the UAV	$V_{\max}$	10 m/s

We observe the values of the objective function about the tradeoff between computation efficient CE and computation bits CB for different weight parameter ρ and maximum consumed energy in Figure 4. For the proposed scheme, as ρ increases, the weight coefficient of the computation bits becomes larger, and the utility function gradually approaches the CB maximization problem. As ρ changes, we can obtain different tradeoff results between CB and CE. Besides, as shown in Figure 4, for a fixed weight parameter ρ, the objective function values increase with consumed energy Γ, and the rate of increase gradually slows down. When $\rho = 0$, since the value of the objective function is very small, the figure shows a straight line close to x axis. On the other hand, compared with CE, CB is more affected by the variation of tradeoff factor ρ and its range of change is larger, which indicates that on the premise of ensuring a large CB value, a relatively large CE value can be taken to optimize the resource allocation of the system. When $\rho \in [0.4, 0.8]$, both CB and CE values are relatively large, and the designed scheme achieves a good tradeoff effect.

Figure 5 depicts the UAV's flight trajectory in three different scenarios when $T = 2$ seconds. In the first scheme, the UAV flies in a straight line from the initial position to the end position and the flight speed remains unchanged; the second scheme, the trajectory of the UAV is a semi-circle with its diameter being $\|\mathbf{q}_F - \mathbf{q}_0\|$; the last one is the optimization scheme introduced in previous sections, where the weight parameter is set as $\rho = 0.5$and the maximum consumed energy of user is set as $\Gamma = 1.3$ joule. By comparing the three trajectories, it can be seen that when the weight of each user is not considered, the trajectory of the proposed scheme is more evenly approaching the location of four users and providing computation service to them. This means that when the UAV is closer to the users, the transmission distance is smaller and the channel power gain is larger, the ground user may tend to offloading more bits to the UAV, and UAV can provide more comupution services for the users.

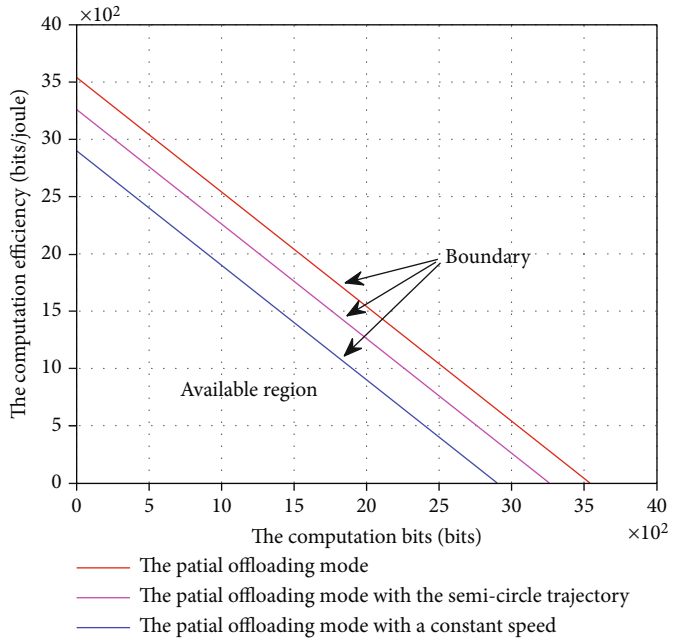

FIGURE 3: The available CB-CE region for different schemes when $\Gamma = 1$.

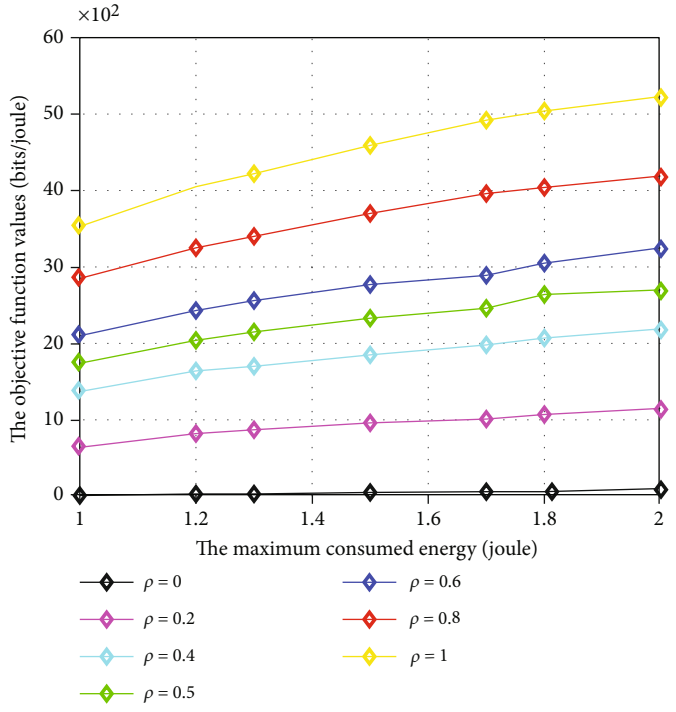

FIGURE 4: The relationship among the objective function values, the weight coefficient ρ, and the maximum consumed energy Γ.

Figure 6 shows the relationship between the values of objective function and the maximum consumed energy under three different trajectories when $\rho = 0.5$. It can be clearly seen that the value of the objective function increases with the maximum energy consumption under different schemes, and the objective function value of the designed optimization proposal is significantly higher than that of the UAV flying at a constant speed and flying in a semi-circular trajectory. This means that the designed resource allocation optimization algorithm by jointly optimizing the UAV trajectory is more effective to maximize the tradeoff between computation bits and computation efficiency.

Figure 7 shows the objective function values in three modes of local computation, global offloading, and partial computation offloading mode. The first mode is that the users only perform task of local computing, and the second mode is that the users only execute the process of offloading to the UAV. The two benchmark modes are jointly optimized in

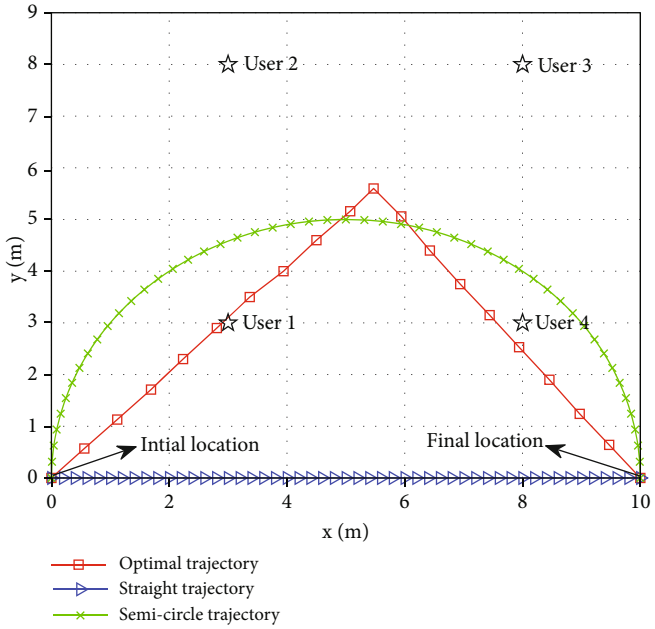

Figure 5: The trajectories of UAV under different schemes.

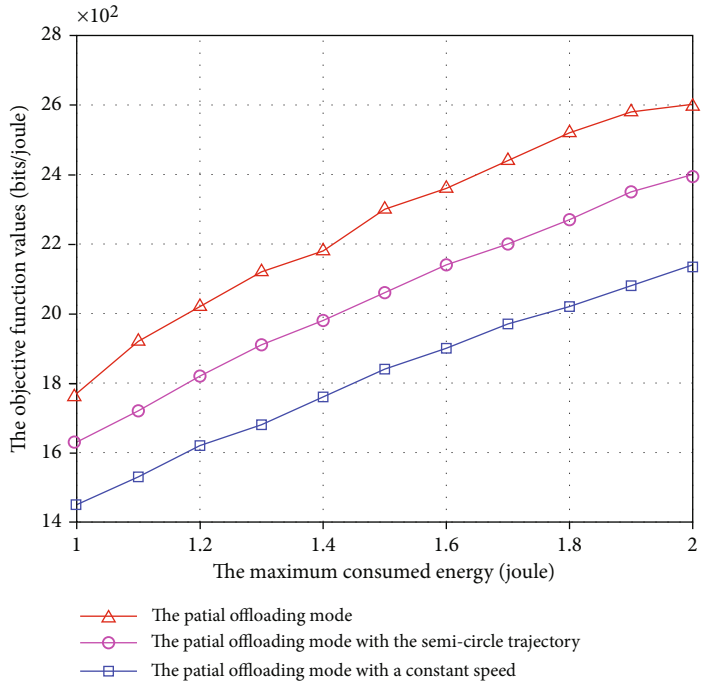

Figure 6: Values of the objective function versus the under three different trajectories when ?=0.5.

the trajectory of UAV and Algorithm 1 is used to obtain the curve of partial offloading mode presented in Figure 7. It is obvious that the value of the objective function of offloading mode (include global and partial) is directly proportional to the maximum energy consumed since energy can support users to perform computing tasks and offloading. Moreover, it can be seen that the performance obtained by partial offloading mode is better than that of global offloading modes. The reason is that although the UAV's computation ability is much stronger than ground users, the ground's energy and offloading time are both limited, thus the offloading bits are also limited, let the ground user's computation capability lain idle not a resource-efficiency way. Moreover, users can obtain higher quality channel state information (CSI) when performing tasks under partial offloading mode, so they can allocate resources dynamically and effectively. Furthermore, the performance of local computing mode is inferior to global offloading mode and not changes as the energy increases, this

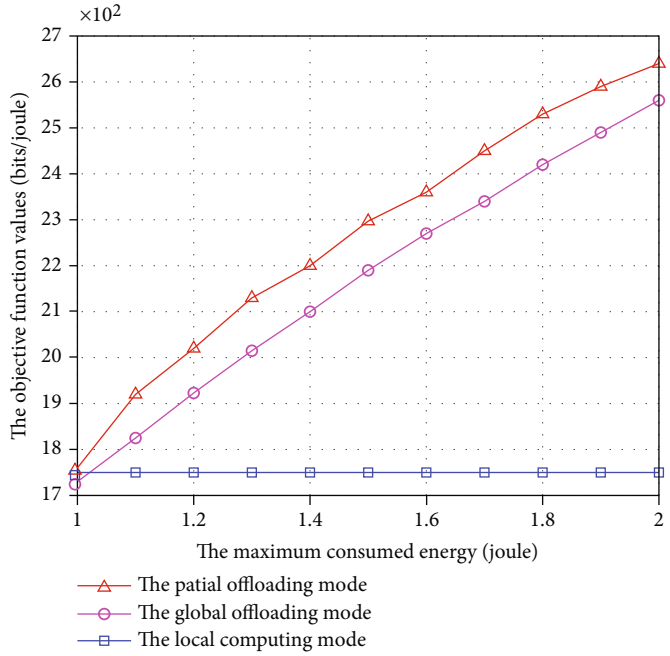

Figure 7: Values of the objective function versus the maximum consumed energy under three different schemes.

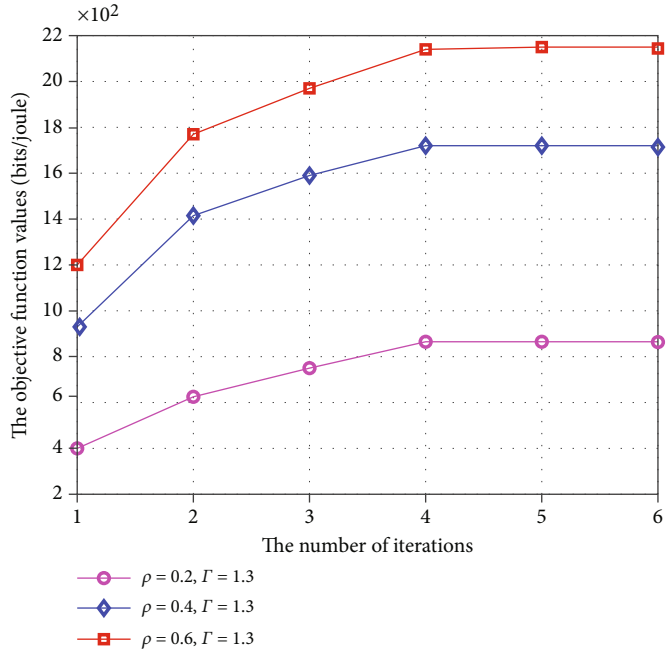

Figure 8: Values of the objective function versus the number of iterations with different values of ? and Γ.

because the ground users' computation ability is weak in general, within given time duration $T = 2$ sec, users energy consumption cannot exceed $\Gamma = 1$ due to limited computation ability.

Figure 8 is given to prove the proposed scheme can guarantee convergence. The figure shows the convergence performance when the maximum consumed energy of users is set as $\Gamma = 1.3$ joule and the weight coefficients take different values (ρ=0.2; ρ=0.4; ρ=0.6). It is seen that the algorithm can converge after a few iterations. Therefore, it can be concluded that the optimization algorithm adopted in this paper has fast convergence speed and low computational complexity.

5. Conclusion

In this paper, we studied the CB-CE tradeoff for the UAV enabled MEC system. The tradeoff optimization problem was formulated to maximize weighted sum of the CB and CE of all users. To tackle the nonconvex problem of jointly optimizing the computation performance and UAV's

trajectory, a two-stage alternative optimization method was exploited to address the primal non-convex problem by formulating it into two subproblems. A combination of the Lagrange duality, SCA method and CVX solver is employed to iteratively solve the subproblems. Simulation results demonstrated that the proposed resource allocation optimization scheme is superior to other benchmark schemes in terms of the computational performance. Moreover, the proposed alternative algorithm has a faster convergence speed, which converged within fewer iterations.

Data Availability

The data used to support the findings of this study are available from the corresponding author upon request.

Conflicts of Interest

The authors declare that they have no conflicts of interest.

Acknowledgments

This work is supported by National Natural Science Foundation of China (No. 62061027).

References

[1] F. Zhou, Y. Wu, R. Q. Hu, Y. Wang, and K. K. Wong, "Energy-efficient NOMA enabled heterogeneous cloud radio access networks," *IEEE Network*, vol. 32, no. 2, pp. 152–160, 2018.

[2] Q. Wu, Y. Zeng, and R. Zhang, "Joint trajectory and communication design for multi-UAV enabled wireless networks," *IEEE Transactions on Wireless Communications*, vol. 17, no. 3, pp. 2109–2121, 2018.

[3] L. Wei, R. Hu, Y. Qian, and G. Wu, "Key elements to enable millimeter wave communications for 5g wireless systems," *IEEE Wireless Communications*, vol. 21, no. 6, pp. 136–143, 2014.

[4] J. Zhang, L. Zhou, Q. Tang et al., "Stochastic computation offloading and trajectory scheduling for UAV-assisted mobile edge computing," *IEEE Internet of Things Journal*, vol. 6, no. 2, pp. 3688–3699, 2018.

[5] Y. Mao, J. Zhang, and K. B. Letaief, "Dynamic computation offloading for mobile-edge computing with energy harvesting devices," *IEEE Journal on Selected Areas in Communications*, vol. 34, no. 12, pp. 3590–3605, 2016.

[6] X. Hu, K. K. Wong, and K. Yang, "Wireless powered cooperation-assisted mobile edge computing," *IEEE Transactions on Wireless Communications*, vol. 17, no. 4, pp. 2375–2388, 2018.

[7] J. Xu, Y. Zeng, and R. Zhang, "UAV-enabled wireless power transfer: trajectory design and energy optimization," *IEEE Transactions on Wireless Communications*, vol. 17, no. 8, pp. 5092–5106, 2018.

[8] Y. Zeng, R. Zhang, and T. J. Lim, "Wireless communications with unmanned aerial vehicles: opportunities and challenges," *IEEE Communications Magazine*, vol. 54, no. 5, pp. 36–42, 2016.

[9] J. Xu, Y. Zeng, and R. Zhang, "UAV-enabled wireless power transfer: Trajectory design and energy region characterization," in *2017 IEEE Globecom Workshops (GC Wkshps)*, pp. 1–7, Singapore, December 2017.

[10] N. H. Motlagh, M. Bagaa, and T. Taleb, "UAV-based IoT platform: a crowd surveillance use case," *IEEE Communications Magazine*, vol. 55, no. 2, pp. 128–134, 2017.

[11] X. Cao, J. Xu, and R. Zhang, "Mobile edge computing for cellular-connected UAV: Computation offloading and trajectory optimization," in *2018 IEEE 19th International Workshop on Signal Processing Advances in Wireless Communications (SPAWC)*, pp. 1–5, Kalamata, Greece, June 2018.

[12] J. Xiong, H. Guo, and J. Liu, "Task offloading in *UAV*-aided edge computing: bit allocation and trajectory optimization," *IEEE Communications Letters*, vol. 23, no. 3, pp. 538–541, 2019.

[13] Q. Hu, Y. Cai, G. Yu, Z. Qin, M. Zhao, and G. Y. Li, "Joint offloading and trajectory design for *UAV*-enabled mobile edge computing systems," *IEEE Internet of Things Journal*, vol. 6, no. 2, pp. 1879–1892, 2018.

[14] S. Jeong, O. Simeone, and J. Kang, "Mobile edge computing via a UAV-mounted cloudlet: optimization of bit allocation and path planning," *IEEE Transactions on Vehicular Technology*, vol. 67, no. 3, pp. 2049–2063, 2017.

[15] M. A. Messous, H. Sedjelmaci, N. Houari, and S. M. Senouci, "Computation offloading game for an UAV network in mobile edge computing," in *2017 IEEE International Conference on Communications (ICC)*, pp. 1–6, Paris, France, May 2017.

[16] F. Zhou, Y. Wu, R. Q. Hu, and Y. Qian, "Computation rate maximization in UAV-enabled wireless-powered mobile-edge computing systems," *IEEE Journal on Selected Areas in Communications*, vol. 36, no. 9, pp. 1927–1941, 2018.

[17] X. Zhang, Y. Zhong, P. Liu, F. Zhou, and Y. Wang, "Resource allocation for a UAV-enabled mobile-edge computing system: computation efficiency maximization," *IEEE Access*, vol. 7, pp. 113345–113354, 2019.

[18] Z. Jian, W. Muqing, and Z. Min, "Joint computation offloading and resource allocation in c-ran with mec based on spectrum efficiency," *IEEE Access*, vol. 7, pp. 79056–79068, 2019.

[19] S. Sardellitti, G. Scutari, and S. Barbarossa, "Joint optimization of radio and computational resources for multicell mobile-edge computing," *IEEE Transactions on Signal and Information Processing over Networks*, vol. 1, no. 2, pp. 89–103, 2015.

[20] C. Wang, C. Liang, F. R. Yu, Q. Chen, and L. Tang, "Computation offloading and resource allocation in wireless cellular networks with mobile edge computing," *IEEE Transactions on Wireless Communications*, vol. 16, no. 8, pp. 4924–4938, 2017.

[21] J. Zhang, X. Hu, Z. Ning et al., "Joint resource allocation for latency-sensitive services over mobile edge computing networks with caching," *IEEE Internet of Things Journal*, vol. 6, no. 3, pp. 4283–4294, 2018.

[22] Z. Ding, J. Xu, O. A. Dobre, and H. V. Poor, "Joint power and time allocation for Noma–mec offloading," *IEEE Transactions on Vehicular Technology*, vol. 68, no. 6, pp. 6207–6211, 2019.

[23] J. Du, L. Zhao, J. Feng, and X. Chu, "Computation offloading and resource allocation in mixed fog/cloud computing systems with min-max fairness guarantee," *IEEE Transactions on Communications*, vol. 66, no. 4, pp. 1594–1608, 2017.

[24] A. M. Elsherbiny, A. M. Bayoumy, A. M. Elshabka, and M. M. Abdelrahman, "Unrestricted general solution of 6DoF inverse dynamics problem of a 3D guided glider," *Mathematical Modelling of Engineering Problems*, vol. 7, no. 3, pp. 465–475, 2020.

[25] S. Vrtagić, E. Softić, M. Ponjavić et al., "Video data extraction and processing for investigation of vehicles' impact on the asphalt deformation through the prism of computational algorithms," *Traitement Du Signal*, vol. 37, no. 6, pp. 899–906, 2020.

[26] Y. du, Y. Wang, X. Zhang, and Z. Nie, "Automatic separation management between multiple unmanned aircraft vehicles in uncertain dynamic airspace based on trajectory prediction," *Revue d'Intelligence Artificielle*, vol. 33, no. 3, pp. 171–180, 2019.

[27] R. Belmahdi, D. Mechta, and S. Harous, "A survey on various methods and algorithms of scheduling in fog computing," *Ingénierie des Systèmes d'Information*, vol. 26, no. 2, pp. 211–224, 2021.

[28] M. A. Messous, S. M. Senouci, H. Sedjelmaci, and S. Cherkaoui, "A game theory based efficient computation offloading in an UAV network," *IEEE Transactions on Vehicular Technology*, vol. 68, no. 5, pp. 4964–4974, 2019.

[29] S. Bi and Y. J. Zhang, "Computation rate maximization for wireless powered mobile-edge computing with binary computation offloading," *IEEE Transactions on Wireless Communications*, vol. 17, no. 6, pp. 4177–4190, 2018.

[30] W. Dinkelbach, "On nonlinear fractional programming," *Management Science*, vol. 13, no. 7, pp. 492–498, 1967.

[31] C. You, K. Huang, and H. Chae, "Energy efficient mobile cloud computing powered by wireless energy transfer," *IEEE Journal on Selected Areas in Communications*, vol. 34, no. 5, pp. 1757–1771, 2016.

[32] X. Zhang, Y. Wang, F. Zhou, N. al-Dhahir, and X. Deng, "Robust resource allocation for miso cognitive radio networks under two practical non-linear energy harvesting models," *IEEE Communications Letters*, vol. 22, no. 9, pp. 1874–1877, 2018.

Hindawi
Journal of Sensors
Volume 2021, Article ID 8776059, 13 pages
https://doi.org/10.1155/2021/8776059

Research Article

Gait Phase Recognition Using Fuzzy Logic Regulation with Multisensor Data Fusion

Gao Weidong[1] **and Zhao Zhenwei**[2]

[1]*School of Information and Communication Engineering, Beijing University of Posts and Telecommunications, Beijing 100876, China*
[2]*Information Center of the First Hospital of Jilin University, Changchun, Jilin 130021, China*

Correspondence should be addressed to Gao Weidong; gaoweidong@bupt.edu.cn

Received 23 July 2021; Revised 18 August 2021; Accepted 20 August 2021; Published 15 September 2021

Academic Editor: Gengxin Sun

The health challenges brought by aging population and chronic noncommunicable diseases are increasingly severe. Scientific physical exercise is of great significance to prevent the occurrence of chronic diseases and subhealth intervention and promote health. However, improper or excessive exercise can cause injury. Research shows that the sports injury rate of people who often exercise is as high as 85%. Aiming at the problem of low accuracy of single sensor gait analysis, a real-time gait detection algorithm based on piezoelectric film and motion sensor is proposed. On this basis, a gait phase recognition method based on fuzzy logic is proposed, which enhances the ability of gait space-time measurement. Experimental results show that the proposed gait modeling method based on ground reaction force (GRF) signal can effectively recognize and quantify various gait patterns. At the same time, the introduction of heterogeneous sensor data fusion technology can effectively make up for the accuracy defects of single sensor measurement and improve the estimation accuracy of gait space-time measurement.

1. Introduction

In 2019, the World Health Organization (WHO) proposed at the global health assembly that by 2030, the number of people actively participating in sports activities in the world will reach 100 million [1]. Scientific physical activity is one of the most important methods to manage chronic noncommunicable diseases and cope with the aging population. Regular physical exercise is helpful to slow down and prevent the occurrence of chronic diseases and is of great significance to the intervention of subhealth and the promotion of human health. However, improper exercise can lead to injury. Research shows that the sports injury rate of people who often exercise is as high as 85%. Sports activity monitoring provides individuals with health promotion awareness of personal habits. It is very important to accurately track the sports activities in people's daily life.

Walking is one of the most common sports activities in people's daily life. Whether the gait is healthy or not and the degree of health can reflect the health status of human body to a certain extent, therefore, gait evaluation is of great significance and has become a hot issue. The importance of gait analysis has been fully elaborated in many literature, and its application is also very wide, including pedestrian navigation, exercise fitness guidance, pathological gait evaluation, fall detection, exercise rehabilitation, age estimation and gender classification [2], balance functions evaluation [3], Parkinson diagnosis [4], and assessment of running asymmetry [5]. Gait analysis also has broad application prospects in emergency personnel search and rescue, blind path guidance, and other aspects [6]. In the past, gait analysis often relied on the experience of clinicians, and the qualitative evaluation of gait was easily affected by subjective factors. In recent years, large gait analysis systems such as infrared spot catcher, dynamometer, and electromyography have been used for quantitative analysis of human gait [7] in order to quantify the factors controlling lower limb function during walking. There are two gold standards that are often used to quantify gait: (1) 3D motion capture systems based on multicamera/infrared spot catcher [8],

such as Vicon system and Qualisys system, which capture the motion trajectory of human body markers, analyze and calculate the three-dimensional space coordinates of markers and obtain the motion parameters of human lower limbs. (2) Instrumented gait [9], such as treadmill system with pressure sensor and GAITRite pressure sensitive gait system, is used to measure and analyze biomechanical signals generated during walking. These systems are large-scale, high-cost, usually deployed in hospitals or professional gait analysis laboratories, and need professional personnel to operate. Long-time gait data recording is usually needed in clinical environment. Experienced clinicians need to interpret and evaluate gait performance in high-dimensional and massive data, which brings great complexity to gait analysis [10].

The rapid development of microelectromechanical system (MEMS) has promoted the application of wearable devices in personal health monitoring. Wearable health monitoring devices are usually composed of multiple physiological sensors and inertial sensors. These sensors are deployed on the human body to realize continuous and dynamic monitoring of the body status, and help people track their health status during exercise and fitness, or better monitor their personal health for medical rehabilitation [11]. The commonly used information in gait analysis include kinematics information and dynamics information. When designing wearable human activity measurement device, physiological sensors such as inertial measurement unit (IMU) and pressure sensor are usually used. IMU is usually deployed on human lower limbs to obtain human kinematic information, but the kinematic information of lower limbs is usually not equivalent to that of whole body. In order to obtain complete and accurate kinematic information, it is necessary to wear multiple IMUs in different parts, such as heel [12], waist [13], instep [14, 15], ankle [16–18], and thigh and leg [18]. In Reference [19], the influence of the position of inertial sensor on gait analysis is analyzed from the perspective of accuracy and repeatability. It is found that the performance of the algorithm depends on the position of inertial sensor, and the closer IMU is to the ground, the better performance can be obtained for gait event detection. In Reference [20], a foot switch is used to obtain the contact mode, but the binary signal generated by the foot switch cannot capture the subtle difference caused by the transfer of foot weight during walking. Most of the literature used the signals of four pressure sensors to analyze gait events, where the first sensor is located at the thumb, two sensors are located at the forefoot (the first and fifth metatarsals), and the other sensor is located at the heel [21, 22].

Although gait analysis algorithms have been widely studied, as far as we know, there is little research on real-time and accurate gait health evaluation using multisensor information fusion technology. Therefore, this paper designs and implements a gait evaluation system based on pressure sensor and inertial measurement unit. Through the collection and analysis of kinematic information and dynamics information, the gait behavior is explained accurately, which provides a richer application basis for future research.

The rest of this paper is organized as follows. In Section 2, the system model and signal composition are described. In Section 3, we propose the gait modeling method to realize gait phase recognition. We propose a gait health evaluation model in Section 4 using IMU-based gait detection, together with the analyses of accuracy and gait health score. Finally, the conclusions are drawn in Section 5.

2. Signal Acquisition with Heterogeneous Sensors

In view of the limitation that most of the existing researches use a single sensor for gait analysis, this paper designs a small gait detection device, which can monitor the motion state in real time and output the gait evaluation results. It not only cooperatively uses multiple pressure sensors but also uses a mixture of accelerometer and gyroscope for gait analysis. In addition to the dynamic data information, it also makes full use of the data collected by multiple sensors to jointly identify the motion state.

As shown in Figure 1, the developed wearable gait analysis system is composed of 8-way pressure sensor, ADC, IMU, MCU, and wireless communication module.

The signal acquisition subsystem consists of inertial measurement unit, pressure sensor, and ADC. In this paper, the sampling frequency of inertial measurement unit and pressure sensor is 50 Hz. A ZNX-01 resistance flexible film pressure sensor is used to collect the ground reaction force signal, and ADC has a 12-bit resolution. The results show that sole and heel are the main biomechanical regions during walking. Therefore, the distribution of 8-way pressure sensors is deployed as shown in Figure 2, where the pressure sensors GRF1-GRF3 are located at the heel, the pressure sensors GRF4-GRF7 are located at the phalanx, and the pressure sensor GRF8 is located at the thumb.

MPU6050 module is used to collect the kinematic data of human walking. The module is a 6-axis digital motion processor (DMP), which can not only greatly reduce the installation space but also connect with external magnetometer. In order to track fast and slow motion accurately, MPU6050 module integrates three-axis MEMS angular velocity sensor (gyroscope) and three-axis MEMS accelerometer. The sensing range of these inertial sensors can be programmed. The analog-to-digital converter of three-axis gyroscope and three-axis accelerometer in MPU6050 module is 16 bits, which can collect the digital output data of human kinematics.

The signal analysis subsystem includes gait phase recognition module and gait cycle segmentation module. The method of coordinate system rotation and attitude quaternion correction is used to improve the measurement accuracy. The wireless communication subsystem uses WiFi as the wireless data transmission mode to transfer the collected data.

3. Gait Modeling

3.1. Gait Parameters. Walking is a continuous and regular periodic movement. According to medical standards, gait

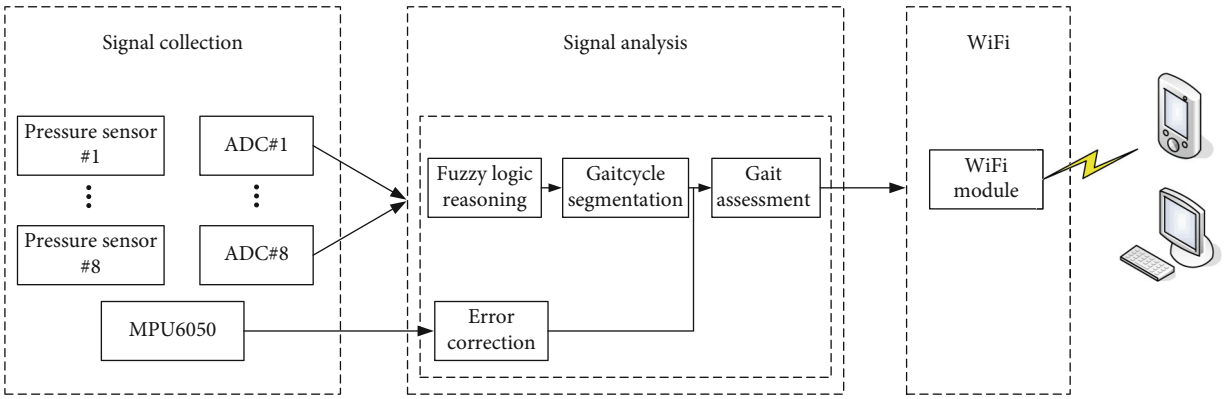

Figure 1: System architecture.

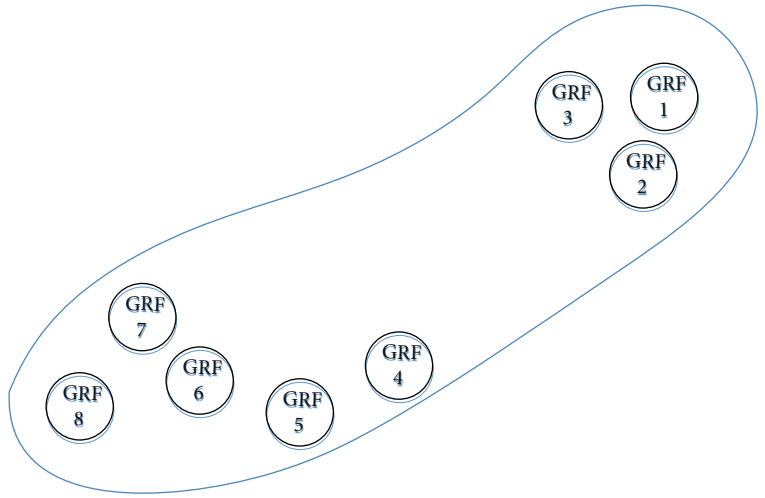

Figure 2: Pressure sensor distribution.

cycle is composed of stance stage and swing stage of a certain lower limb (such as right limb). The stance stage refers to the process when the feet touch the ground while walking, and the swing stage refers to the process when the feet leave the ground and move forward to land again. As shown in Figure 3, according to Perry gait model [23], each gait cycle is divided into eight phases, of which five phases belong to the stance stage, namely, initial contact (IC), loading response (LR), mid stance (MS), terminal stance (TS), and preswing (PS). The other three phases belong to swing stage, which are initial swing (IS), mid swing (MS), and terminal swing (TS).

The commonly used gait measurement methods are time measurement and space measurement. Time measurement parameters include gait cycle, cadence, velocity, percentage of stance stage, and percentage of swing stage. The parameter of space measurement is stride length. In the process of walking, normal gait shows reasonable stride length and cadence. Therefore, in gait health assessment, we should first study the parameter range of normal gait and then use it to detect abnormal gait. Gait parameters are defined as follows.

(1) Gait cycle: Gait cycle refers to the time interval between two consecutive events of the same lower limb, usually the time of two consecutive heel landing, also known as stride time

(2) Cadence: Cadence refers to the number of steps per unit time in the process of walking. The average cadence of healthy people is about 95~125 steps/min

(3) Velocity: Velocity represents the displacement along the walking direction per unit time. The average velocity of children aged 1-7 is 0.64 m/s-1.14 m/s, and that of normal adults is 1.2 m/s-1.5 m/s

(4) Stride length: It refers to the longitudinal linear displacement between two adjacent footholds of the same heel, which is equivalent to the sum of the lengths of a pair of left and right pedals. The stride length of normal adults is about 100-160 cm

For a particular lower limb, the duration of the stance stage and swing stage of different individuals may be completely different. We normalize them to gait cycles. The stance stage accounts for about 60% of the whole gait cycle, and the swing stage accounts for about 40% of the whole gait cycle. In the process of walking, the time percentage of the

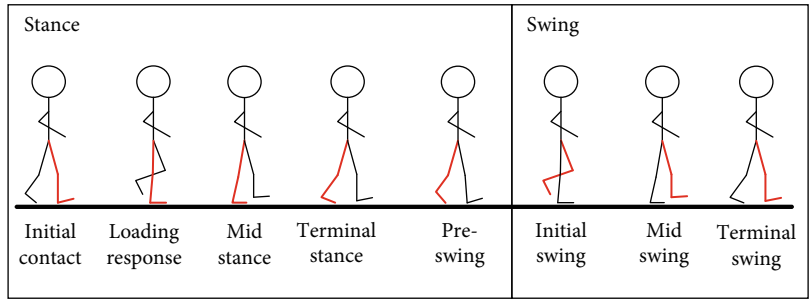

Figure 3: Structure of a complete gait cycle.

stance stage and swing stage of lower limbs is an indicator of gait symmetry.

3.2. Gait Phase Recognition. The quantification of gait time parameters requires accurate recognition of gait events. The dynamic information of gait phase analysis mainly refers to the ground reaction between the foot and the ground. The embedded pressure sensor can easily detect the ground reaction force generated in the process of movement and directly reflect the overall gait behavior of human body. A detailed description of each gait phase and its corresponding pressure sensor status is as follows.

(1) Initial contact phase: The lower limbs begin to contact the ground, and the GRF1~GRF3 pressure value of heel position is nonzero

(2) Loading response stage: The lateral part of the foot of the lower limb begins to contact the ground, and the body center of gravity is transferred from the heel to the whole foot. At this time, the pressure of GRF4~GRF5 is not zero

(3) Mid stance phase: The inner side of the lower limb begins to contact the ground, and the pressure value of GRF6~GRF7 is not zero. Due to individual gait differences, GRF8 may or may not have a nonzero pressure value

(4) Terminal stance phase: The gravity center of human body moves forward, and the heel of lower limb no longer contacts with the ground; that is, GRF1~GRF3 have zero pressure

(5) Preswing phase: It is the last phase of the stance stage, the thumb and toe of the lower limb contact the ground, and at this time, only GRF8 has nonzero pressure

(6) Swing phase: The measured lower limbs do not touch the ground, and no pressure signal is detected by GRF1~GRF8

Gait cycle is characterized by gait phases. Accurate detection of gait event/phase is of great significance for gait analysis. In the process of gait phase detection, the transition between adjacent gait phases is very subtle, and it is easy to misjudge each gait phase by using threshold method. In this paper, fuzzy logic algorithm is used to process the original GRF signal to realize the smooth and continuous recognition of gait phase. The gait phase recognition method based on fuzzy reasoning is as follows.

Firstly, the input variables are fuzzed. The sigmoid membership function is used to fuzzify the input GRF signal of each pressure sensor, as shown in Equation (1). According to the value of pressure signal, each pressure value is divided into L and S fuzzy values.

$$f(x; a, c) = \frac{1}{1 + e^{-a(x-c)}}, \tag{1}$$

where x is the range of input variables; we use the voltage collected by the piezoelectric sensor as the input; that is, $x \in [0, 3.3]$. The opening direction of the sigmoid function in Equation (1) is determined by the parameter a. The fuzzy value "L" is declared when a is positive and "S" is declared when a is negative. The value "L" means that the corresponding sensor is likely to contact the ground. The value "S" means that the possibility of the sensor contacting the ground is very small.

Then, the output variables are fuzzed. Each output variable is fuzzified by trapezoidal membership function and triangular membership function, and then, it is judged as one of the six fuzzy values of IC, LR, MS, TS, PS, and SW. The member functions are as follows.

$$f(y; a, b, c, d) = \max\left\{\min\left\{\frac{y-a}{b-a}, 1, \frac{d-y}{d-c}\right\}, 0\right\}, \tag{2}$$

$$f(y; a, b, c) = \max\left\{\min\left\{\frac{y-a}{b-a}, 1, \frac{c-y}{c-b}\right\}, 0\right\}, \tag{3}$$

where y is the output variable. The shape of membership function in Equation (2) is determined by parameters a, b, c, and d. Parameters a and d correspond to the left and right inflection points of the lower part of the trapezoid, and parameters b and c correspond to the left and right inflection points of the upper part of the trapezoid. In Equation (3), parameters a, b, and c determine the shape of triangle membership function. The maximum value of the function is 1 at point b and 0 at points a and c. Triangular membership function is a special form of trapezoidal membership function. In this algorithm, trapezoidal membership function is

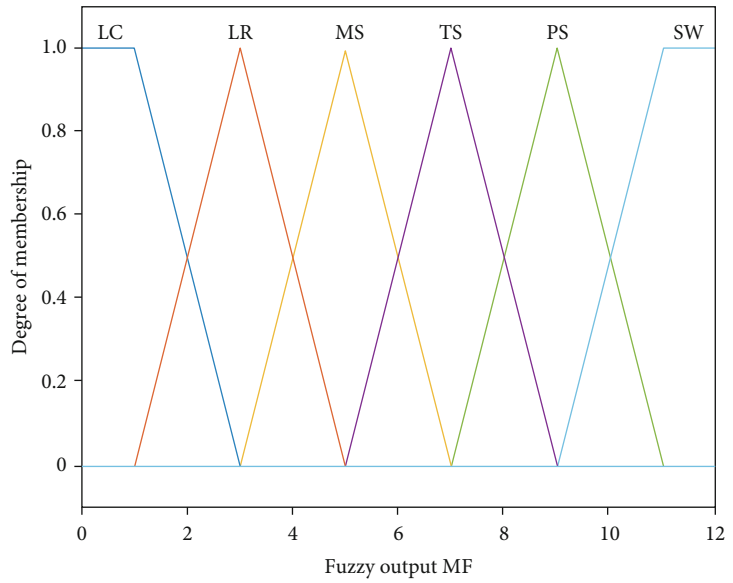

Figure 4: Output membership function.

Table 1: Fuzzy inference table.

Inference rules	GRFs								Gait phase
	GRF1	GRF2	GRF3	GRF4	GRF5	GRF6	GRF7	GRF8	
1	*L*	/	/	*S*	*S*	*S*	*S*	*S*	IC
2	/	*L*	/	*S*	*S*	*S*	*S*	*S*	IC
3	/	/	*L*	*S*	*S*	*S*	*S*	*S*	IC
4	*L*	*L*	*L*	*L*	/	*S*	*S*	*S*	LR
5	*L*	*L*	*L*	/	*L*	*S*	*S*	*S*	LR
6	*L*	*L*	*L*	*L*	*L*	*L*	/	/	MS
7	*L*	*L*	*L*	*L*	*L*	/	*L*	/	MS
8	*S*	/	/	*L*	*L*	*L*	*L*	/	TS
9	*S*	*S*	*S*	*S*	*S*	*S*	*S*	*L*	PS
10	*S*	*S*	*S*	*S*	*S*	*S*	*S*	*S*	SW

used for fuzzy sets IC and SW, and triangular membership function is used for other fuzzy sets, as shown in Figure 4.

Next, we will establish the fuzzy inference rules by using the change of pressure sensor signal and the landing position information that may appear in each gait phase as fuzzy rules. There are 8 output variables for 8-way pressure sensors, and each variable has two possible values, so there are totally $2^8 = 256$ fuzzy inference rules can be constructed. The formulation of fuzzy inference rules is the core content of fuzzy logic reasoning, and its performance depends on fuzzy inference rules to a great extent. We only use the rules with the greatest contribution to distinguish the possible phases and form the fuzzy inference rule table as shown in Table 1.

The form of fuzzy inference rule is "if... Then". For example, rule #10 can be described as "(GRF1 is *S*) and (GRF2 is *S*) and (GRF3 is *S*) and (GRF4 is *S*) and (GRF5 is *S*) and (GRF6 is *S*) and (GRF7 is *S*) and (GRF8 is *S*), then the gait phase is SW". The expression of fuzzy inference rules is complex, which is usually expressed by fuzzy inference rule matrix. For example, the rule vector corresponding to rule #10 is [2 2 2 2 2 2 2 2 6 1 1].

Finally, the fuzzy logic output is obtained. The average maximum membership method is used to solve the problem of multiple output maximum membership elements, and the corresponding fuzzy inference results are obtained through defuzzification operation as the following equation.

$$y_o = \frac{1}{N}\sum_{i=1}^{N} \max_{y \in Y}\left(\mu_y(y)\right), \tag{4}$$

where N is the total number of elements with the same maximum membership.

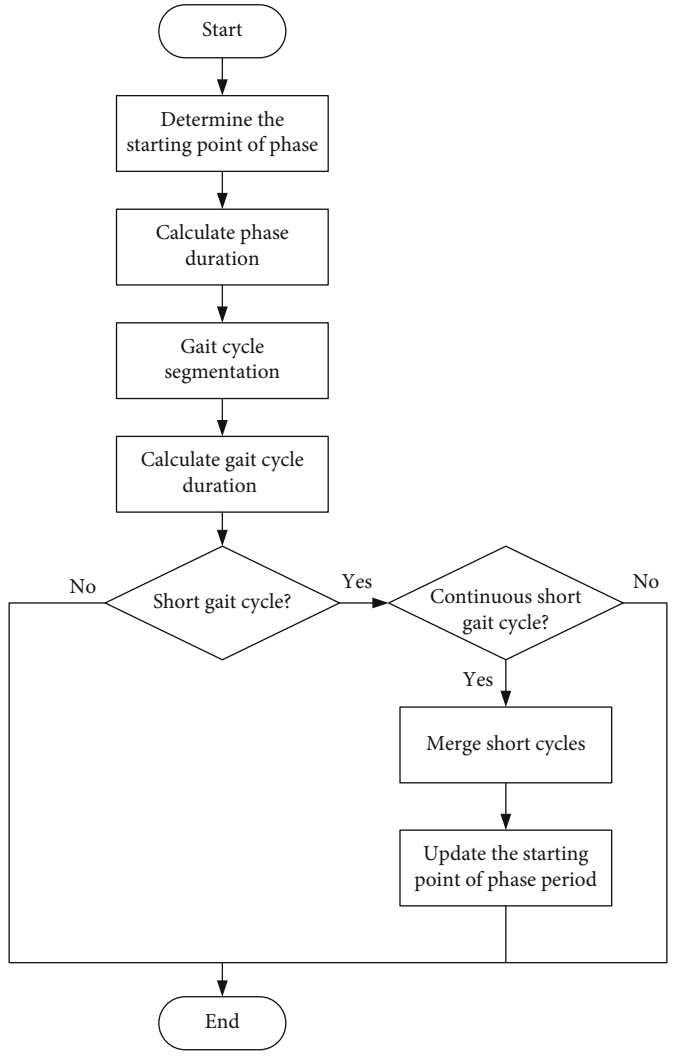

Figure 5: Flow chart of gait cycle segmentation.

3.3. Gait Cycle Segmentation. Accurate detection of key gait events is essential to the evaluation of gait. When we have detected continuous and smooth gait phases, we will segment them into gait cycles. Because of the difference of gait cycle composition among different people, the fixed threshold method cannot get accurate results. In this paper, a personalized gait cycle segmentation algorithm is proposed, which takes full account of the differences of individual gait cycle composition and uses fuzzy logic inference to get accurate gait cycle information.

The flow chart of the proposed gait cycle segmentation algorithm is shown in Figure 5. We have found that plantar pressure signal has obvious time-domain characteristics. Therefore, we analyze the gait phase signal $X = [x_1, x_2, \cdots, x_i, x_{i+1}, \cdots, x_n]$ after fuzzy processing in time-domain, which corresponds to a certain gait phase.

(1) Determine the starting point of gait phase

Accurate detection and marking of gait event transition from one gait phase to another is the premise of accurate gait cycle segmentation. In this paper, real-time gait phase output can be obtained according to the collected pressure signal. Gait phase transition can be declared when $x_{i+1} - x_i \neq 0$, and this position can be regarded as the starting point of the following gait phase. The starting point sequence of gait phase is recorded as the following equation.

$$\text{GaitPhaseSeq} = \left[y_1, y_2, \cdots, y_j, \cdots, y_{k-1}, y_k\right]. \quad (5)$$

(2) Obtain gait phase duration

In the starting point sequence of gait phase, the duration of current gait phase is equal to the time interval between adjacent elements, which can be calculated as follows:

$$\text{GaitPhaseDur} = \left[y_2 - y_1, \cdots, y_j - y_{j-1}, \cdots, y_k - y_{k-1}\right]. \quad (6)$$

Table 2: Measurement data of different subjects.

Index	Gender	Age	Height (cm)	Weight (kg)	BMI (kg/m^2)
1	Male	17	178	72	22.72
2	Male	20	175	65	21.22
3	Male	28	177	68	21.71
4	Male	45	172	70	23.66
5	Male	48	170	75	25.95

(3) Initial gait cycle segmentation

The initial gait cycle is segmented by using the sequence of gait phase starting points obtained in Step 1, and the composition and duration of each gait cycle are obtained as follows.

(a) The gait cycle begins at the stance phase. Therefore, the first detected gait phase that is different from the swing stage behind the swing stage is regarded as the beginning of the gait cycle. We can get the starting point sequence of $N + 1$ gait cycles

$$\text{GaitCycleIniSeq} = [z_1, z_2, \cdots, z_{N+1}]. \quad (7)$$

(b) Each gait cycle consists of a phase sequence between the starting points of two gait cycles, and the duration of each gait cycle is represented by GaitCycleDur_i. The number of gait cycles is N. The average duration of each gait cycle Mean_of_GaitCycleDur can be obtained from Equation (8)

$$\text{Mean\_of\_GaitCycleDur} = \frac{\sum_N \text{GaitCycleDur}_i}{N}. \quad (8)$$

(4) Due to the difference of individual gait structure, subjects may show different gait cycle patterns. At the same time, considering the possible abnormal mutation of pressure sensor signal, we combine the abnormal gait cycle with too small duration

(a) The gait cycles with duration less than Mean_of_GaitCycleDur $* 0.75$ are regarded as short cycles

(b) When two consecutive short cycles appear, the two consecutive short cycles are merged into one value

(c) The starting point sequence of gait cycle, the structure of gait cycle, and the duration of each gait cycle are updated to output the final result of gait cycle segmentation

3.4. Experimental Results and Analysis

3.4.1. Experiment Setup. Five subjects, aged 17-48 years old, with a height of 170 cm-178 cm, were selected. The detailed parameters of the subjects are shown in Table 2. During the experiment, all subjects walk in a straight line independently at a comfortable speed, and they can turn back and forth at will. There is no limit to the distance of straight line walking. Considering that the first step and the last step of each walk may not be a complete gait cycle, we remove these two incomplete gait cycles in the subsequent gait analysis.

3.4.2. Experimental Results and Performance Analysis. In Figure 6, the traditional gait cycle segmentation algorithm based on empirical formula is compared with the proposed algorithm. The proposed algorithm identifies the key gait event heel strike (HS) and key gait event toe off (TO) in the gait cycle and divides each gait cycle into two phases. In Figure 6, the red circle represents the key gait event HS, and the red pentagon represents the key gait event TO.

The gait modeling algorithm based on ground response signal is shown in Figure 7. As mentioned above, accurate detection of the starting point of gait cycle is the key to accurate recognition of gait cycle. In Figure 7, the red circle is the starting point of each gait cycle. The gait phase sequence of most gait cycles is the same as Perry gait model, i.e., IC > MS > PS > SW, but the duration of gait phase sequence of each gait cycle is different. Some gait cycles show different gait phase sequences from Perry gait model; for example, some of them may lack a certain gait phase, and some of them may have disorder gait phases. It can be seen from Figure 7 that the proposed gait modeling algorithm does not need to set the offset between each gait stage in advance. The algorithm can not only detect gait phase accurately and effectively but also recognize different types of gait cycle, which shows that the algorithm has strong adaptability to different groups of people, regardless of the age, gender, height, and weight of the subjects.

Figure 8 shows the frequency histogram of 446 gait cycles. The red dotted line indicates the threshold for identifying short periods. The duration of each gait cycle may be inconsistent. Regardless of the number of gait phases in each gait cycle, if the duration of a gait cycle is less than 0.75 times of the average duration, we regard it as a short cycle. It can be seen from Figure 8 that the threshold adopted can effectively identify the period with short duration and facilitate the subsequent integration of continuous short periods. It

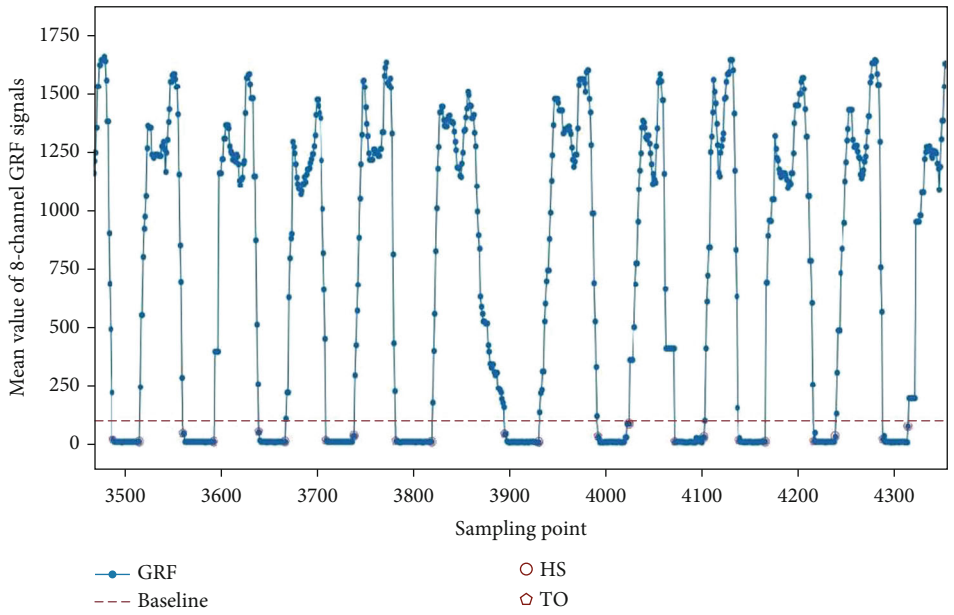

Figure 6: Gait cycle segmentation based on empirical formula.

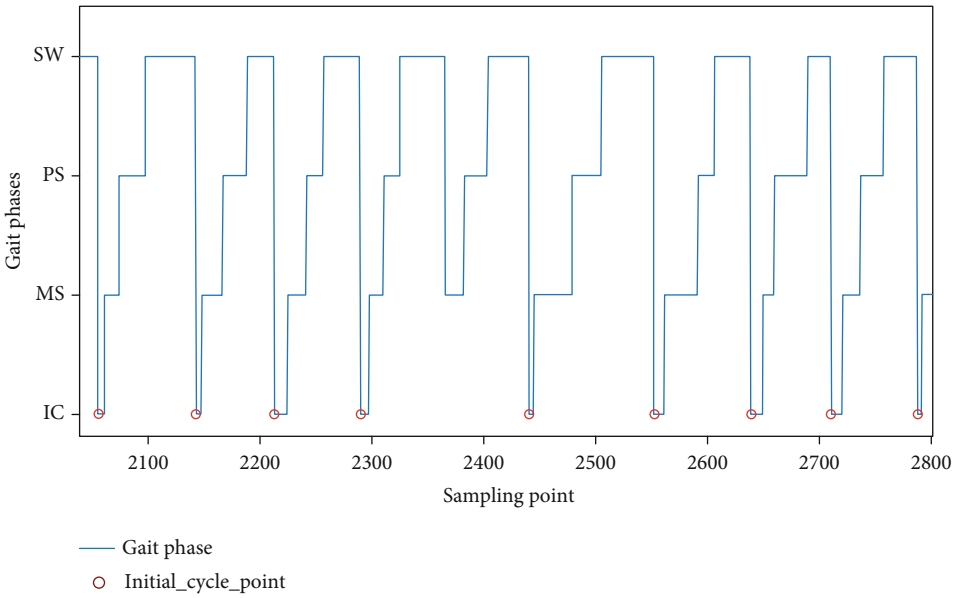

Figure 7: Gait cycle segmentation results.

is worth mentioning that the algorithm proposed in this paper has good robustness and has achieved good results in the subsequent gait modeling.

Figures 9 and 10 show examples of two consecutive short periods, wherein the purple solid line identifies the first short period and the red solid line identifies the second short period. In Figures 9 and 10, we can see that the duration of some phases in the gait cycle is too short, which will lead to the emergence of short cycles. Specifically, the first short period in Figure 9 lacks PS phase, the duration of SW phase is too short, and the second short period lacks IC phase and MS phase. Although the first short cycle in Figure 10 contains a complete gait phases, the duration of the IC phase, PS phase, and SW phase is too short. The appearance of a continuous short period is often accompanied by the abnormal mutation point of swing phase, which is due to the error caused by the high sensitivity of the pressure sensor in collecting the ground reaction force signal. If there are continuous short periods, no matter whether the number of phases in the gait period is complete or not, we will combine the continuous short periods to improve the accuracy of the gait period recognition.

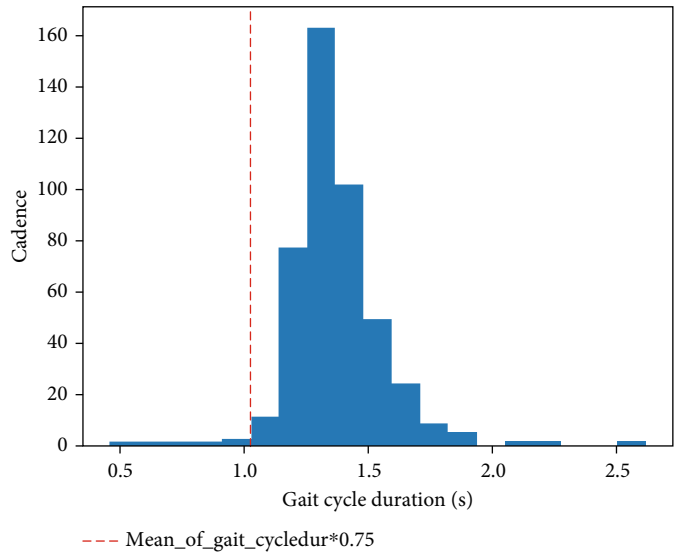

Figure 8: Frequency histogram of gait cycle duration.

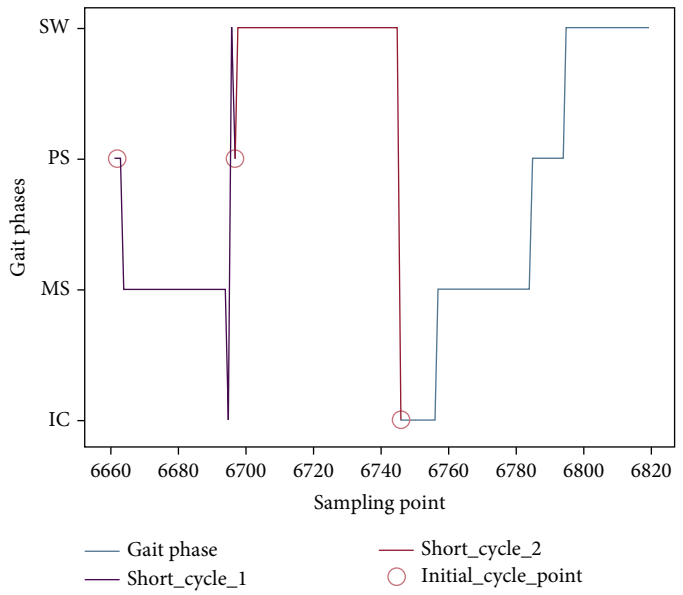

Figure 9: Example #1 of continuous short period.

4. Gait Health Assessment with Heterogeneous Data Fusion

4.1. IMU-Based Gait Detection. The acceleration data measured by the three-axis accelerometer is mapped into the corresponding reference coordinate system, and the velocity value can be obtained by one-time integration. The stride length can be obtained by integration of velocity; that is to say, the stride length can be obtained by quadratic integral of acceleration signal. In practical application, because of the noise and drift of the sensor, the stride obtained by directly integrating of velocity has a drift error. In the process of space measurement, resetting the integral window regularly can effectively alleviate the imprecision caused by error integral.

Most sports, such as walking and running, have identifiable repetition periods. In the process of activity, a gait cycle starts when the foot just touches the ground, and usually, the heel touches the ground first, which will cause a large peak acceleration and then vibration. In the stance stage, there is only a small duration of time when the foot fully contacts the ground. At this time, the foot and the ground are relatively static and the velocity is almost zero. These short periods are often referred to as the full standing phase and occur before the foot enters the swing phase. ZVU algorithm makes full use of the zero velocity information of the foot to

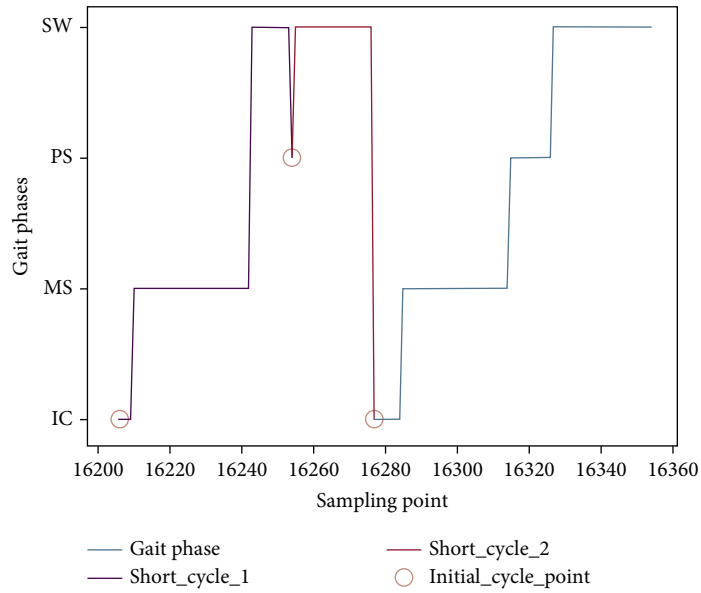

Figure 10: Example #2 of continuous short period.

correct the self-cumulative error by inputting the gait segmentation results; that is, when in the mid stance phase, the instantaneous speed is 0. ZVU algorithm is only suitable for the case of IMU on the foot, and its effectiveness depends on the detection of the zero velocity moment. The improved integration method is used to estimate the space measurement of gait. The flow chart of the algorithm is as follows.

(1) Step 1: Map the acceleration data measured by the three-axis accelerometer to the world coordinate system to obtain the acceleration value $a^W(t)$ in the world coordinate system

$$a^W(t) = \widehat{q}(t) \otimes a^b(t) \otimes q\wedge^*(t) = C_S^W(t) \cdot a^S(t). \quad (9)$$

(2) Step 2: Eliminate the influence of gravity acceleration to get the acceleration caused by motion

$$A(t) = a^e(t) - \vec{G}. \quad (10)$$

(3) Step 3: Integrate the acceleration caused by motion in the world coordinate system to obtain the instantaneous velocity in the process of motion

$$v(t) = \int_{T_1}^{T_2} A(t)dt, \quad (11)$$

where $[T_1, T_2]$ represents the sampling period.

(4) Step 4: After modeling the individual gait, when full stance is detected, ZVU algorithm is used to eliminate the instantaneous speed estimation error and the stride estimation error is also eliminated. Next, we describe the implementation of ZVU algorithm

Because of the intrinsic measurement error of the acceleration sensor, the acceleration data of each movement stage in the gait cycle consists of two parts:

$$a_m^e(t) = a_a^e(t) + \varepsilon, \quad t \in [0, T], \quad (12)$$

where $a_a^e(t)$ is the acceleration value caused by the real motion, ε is the drift error of the sensor, and T is the duration of each motion stage. Assuming that the drift error is constant in time $0 \sim T$, it can be regarded as a constant. Then, the speed of the foot before entering the full stance phase can be calculated by the following formula:

$$\begin{aligned} v_m^e(t) &= \int_0^t a_m^e(t)d\tau = \int_0^t (a_a^e(t) + \varepsilon)d\tau \\ &= \int_0^t a_a^e(t)d\tau + \int_0^t \varepsilon d\tau = v_a^e(t) + \varepsilon t. \end{aligned} \quad (13)$$

In Step 3, there is an error in the estimation of the instantaneous step speed. $v_a^e(t)$ is the instantaneous speed caused by actual motion, and εt is the speed error caused by drift error integral. When the foot enters the full stance stage of the following gait cycle, that is to say, when the foot contacts the ground completely once again, the instantaneous speed caused by the actual motion should be 0. The difference between the actual instantaneous speed and the nonzero $v_m^e(T)$ obtained by integration is used to

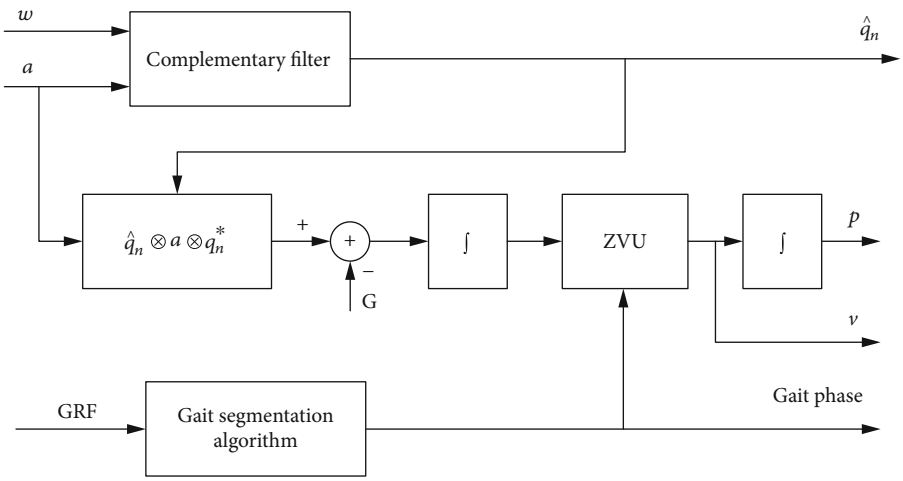

Figure 11: Flow chart of multisensor fusion gait health evaluation.

correct the acceleration drift error, and the drift error ε in a gait cycle can be estimated as follows:

$$\varepsilon = \frac{v_m^e(T)}{T}. \tag{14}$$

Then, the operation in Step 3 is used to integrate the corrected real acceleration value to obtain the instantaneous walking speed.

(5) Step 5: Integrating the corrected instantaneous step speed obtained in Step 4 once more to obtain the corresponding estimated position

$$p(t) = \int_{T_1}^{T_2} v(t)dt. \tag{15}$$

4.2. Gait Health Evaluation Model. The purpose of gait health evaluation is to establish a model that can identify the gait health status of different groups of people. On this basis, a quantitative evaluation model of gait health is constructed. Gait health evaluation is achieved by measuring the symmetry and homogeneity of gait. Gait disorder can affect the symmetry and homogeneity of gait. Symmetry indicates the similarity between the pressure signal and inertia signal measured by the left feet and right feet at each step, and homogeneity indicates the time repeatability of the same pressure mode and inertia mode between two adjacent steps of the same lower limb. In this paper, the monopedal gait analysis method is adopted, so the gait is evaluated by the homogeneity of gait, and the degree of abnormal gait is indicated by the range of departure from normal gait parameters. The flow of gait health evaluation algorithm is shown in Figure 11.

(1) Step 1: The GRF signal is used to model the individual gait. The gait phase sequence and duration of each gait cycle are recorded, and the parameters of gait cycle are obtained, including cadence, percentage of stance phase time, and percentage of swing phase time

(2) Step 2: Considering the homogeneity of gait, the individual gait is evaluated according to the phase sequence and the duration of each phase in the gait cycle. Compared with medical standard, IC, MS, PS, and SW account for 12%, 38%, 12%, and 38% of gait cycle, respectively. Taking the gait sequence IC > MS > PS > SW proposed by Perry model as the standard gait, the gait cycle that is different from Perry model and whose gait phase duration obviously deviates from the medical standard is regarded as abnormal gait cycle. Gait performance is expressed as ratio of normal gait cycles to total gait cycles, which can be expressed as follows

$$\text{Gait evaluation} = \frac{\text{Normal gait cycles}}{\text{Total gait cycles}}. \tag{16}$$

(3) Step 3: According to the measured acceleration and angular velocity, complementary filter is used to estimate the foot direction represented by quaternion, which is prepared for the spatial measurement and estimation in the follow-up gait evaluation

(4) Step 4: Estimate the stride length of each gait cycle and get the following average speed value

$$\text{Average velocity} = \frac{\sum \text{Stride length}}{\text{Walking time}}. \tag{17}$$

4.3. Experimental Results and Analysis

4.3.1. Experiment Setup. After the introduction of inertial measurement unit, in order to verify the adaptability of gait

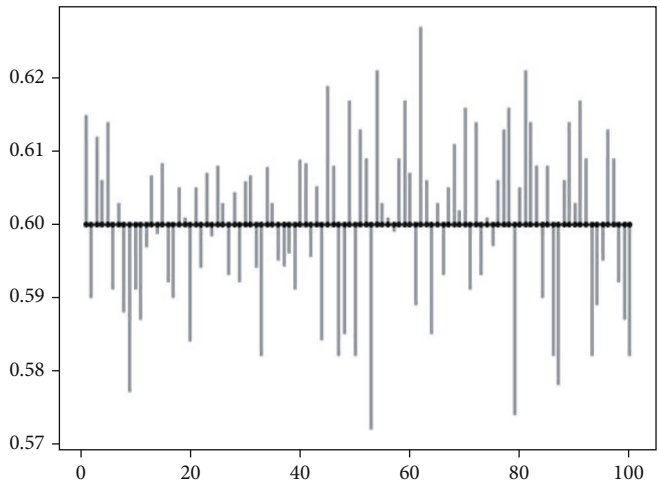

Figure 12: Single-step error analysis results.

Table 3: Gait assessment results.

Subjects	Actual step number	Gait cycle segmentation result	Accuracy (%)	Cadence (steps/min)	Average velocity (m/s)	Abnormal gait cycle number	Gait health score (points)
1	148	148	100	111	1.21	7	95
2	136	136	100	102	1.05	6	96
3	120	120	100	90	0.98	6	95
4	132	132	100	99	0.94	11	92
5	120	120	100	90	0.83	9	93

analysis algorithm based on heterogeneous sensor data fusion, two different cases are considered.

(1) Case 1: The subjects walk freely until they reach a fixed location, and the walking distance is fixed at 0.6 m

(2) Case 2: The subjects walk in a straight line at their comfortable speed, they may turn back and forth freely, and the straight line walking distance is not limited

4.3.2. Experimental Results and Performance Analysis. Figure 12 shows the deviation between the actual stride length and the single stride length measured by the proposed algorithm. The gait cycle starts from the starting of stance phase and ends at the beginning of the next gait cycle. The length of gray line segment in the graph indicates the degree of deviation, and it can be found that the deviation between them is less than 4.7%. Although there is no special research in the long-term experiment, the algorithm has no obvious error accumulation in the 5-minute walking process. This is due to the introduction of ZVU algorithm in the spatial metric estimation and accurate zero speed detection, which can effectively suppress the error accumulation.

Table 3 shows the gait evaluation results of each subject walking during 1 minute. We can see that the accuracy of the proposed algorithm is almost 100%, proving that it can be used for the subsequent time-space parameter analysis for gait. The accuracy of cadence is also relatively high, close to 100%. The average velocity and cadence of the experimental subjects are low, and the number of abnormal gait cycles is also at a low level. This is because most of the subjects choose a slower walking speed during the test. Gait health score is defined as the proportion of normal gait cycles to the total number of gait cycles multiplied by 100.

5. Conclusion

This paper presents a gait detection algorithm based on multisensor information fusion technology. The pressure sensor is used to collect the human body dynamics information, and the inertial measurement unit is used to collect the human body kinematics information to detect the temporal and spatial parameters of gait. Aiming at the problem that the traditional threshold-based gait phase recognition algorithm cannot distinguish the subtle changes between gait phases, a gait phase recognition algorithm based on fuzzy logic reasoning is adopted to realize the smooth and continuous recognition of gait phases. In order to overcome the attitude calculation error caused by inertial module measurement error and noise, quaternion correction and complementary filtering are used to correct the measurement accuracy and combined with zero speed update technology to suppress the accumulation of inertial module measurement error. The experimental data show that the gait evaluation algorithm based on heterogeneous sensor data fusion

can significantly improve the accuracy of gait spatiotemporal parameters and provide support for gait health evaluation. In the future, we will study more applications based on gait detection parameters, such as quantitative detection of energy consumption, fall prediction, and sports injury risk early warning.

Data Availability

The data used to support the findings of this study are available from the corresponding author upon request.

Conflicts of Interest

The authors declare that they have no conflicts of interest.

Acknowledgments

This work is supported by the National Key R&D Program of China under grant number (2020YFC203305).

References

[1] World Health Organization, *Global Action Plan on Physical Activity 2018-2030: More Active People for a Healthier World*, World Health Organization, 2019.

[2] S. I. Gillani, M. A. Azam, and M. Ehatisham-Ul-Haq, "Age estimation and gender classification based on human gait analysis," in *2020 International Conference on Emerging Trends in Smart Technologies (ICETST)*, pp. 1–6, Karachi, Pakistan, 2020, IEEE.

[3] B. J. Lee, N.-Y. Joo, S. H. Kim, C. R. Kim, D. Yang, and D. Park, "Evaluation of balance functions using temporo-spatial gait analysis parameters in patients with brain lesions," *Scientific Reports*, vol. 11, no. 1, p. 2745, 2021.

[4] B. E, B. D, V. K. Elumalai, and U. K, "Data-driven gait analysis for diagnosis and severity rating of Parkinson's disease," *Medical Engineering & Physics*, vol. 91, pp. 54–64, 2021.

[5] P. Tabor, D. Iwańska, O. Grabowska, M. Karczewska-Lindinger, A. Popieluch, and A. Mastalerz, "Evaluation of selected indices of gait asymmetry for the assessment of running asymmetry," *Gait & Posture*, vol. 86, pp. 1–6, 2021.

[6] H. Fourati, "Heterogeneous data fusion algorithm for pedestrian navigation via foot-mounted inertial measurement unit and complementary filter," *IEEE Transactions on Instrumentation and Measurement*, vol. 64, no. 1, pp. 221–229, 2014.

[7] D. T. H. Lai, R. K. Begg, and M. Palaniswami, "Computational intelligence in gait research: a perspective on current applications and future challenges," *IEEE Transactions on Information Technology in Biomedicine*, vol. 13, no. 5, pp. 687–702, 2009.

[8] C. Tunca, N. Pehlivan, N. Ak, B. Arnrich, G. Salur, and C. Ersoy, "Inertial sensor-based robust gait analysis in nonhospital settings for neurological disorders," *Sensors*, vol. 17, no. 4, p. 825, 2017.

[9] L. Zhou, C. Tunca, E. Fischer et al., "Validation of an IMU gait analysis algorithm for gait monitoring in daily life situations," in *2020 42nd Annual International Conference of the IEEE Engineering in Medicine & Biology Society (EMBC)*, pp. 4229–4232, Montreal, QC, Canada, 2020, IEEE.

[10] M. Karg, W. Seiberl, F. Kreuzpointner, J. P. Haas, and D. Kulic, "Clinical gait analysis: comparing explicit state duration HMMs using a reference-based index," *IEEE Transactions on Neural Systems and Rehabilitation Engineering*, vol. 23, no. 2, pp. 319–331, 2015.

[11] D. Dias and J. Paulo Silva Cunha, "Wearable health devices—vital sign monitoring, systems and technologies," *Sensors*, vol. 18, no. 8, p. 2414, 2018.

[12] Ö. Bebek, M. A. Suster, S. Rajgopal et al., "Personal navigation via high-resolution gait-corrected inertial measurement units," *IEEE Transactions on Instrumentation and Measurement*, vol. 59, no. 11, pp. 3018–3027, 2010.

[13] A. Alvarez-Alvarez, G. Trivino, and O. Cordon, "Human gait modeling using a genetic fuzzy finite state machine," *IEEE Transactions on Fuzzy Systems*, vol. 20, no. 2, pp. 205–223, 2011.

[14] I. Tien, S. D. Glaser, R. Bajcsy, D. S. Goodin, and M. J. Aminoff, "Results of using a wireless inertial measuring system to quantify gait motions in control subjects," *IEEE Transactions on Information Technology in Biomedicine*, vol. 14, no. 4, pp. 904–915, 2010.

[15] Z. Wang and R. Ji, "Estimate spatial-temporal parameters of human gait using inertial sensors," in *2015 IEEE International Conference on Cyber Technology in Automation, Control, and Intelligent Systems (CYBER)*, pp. 1883–1888, Shenyang, China, 2015, *IEEE*.

[16] Y. Chen, W. Hu, Y. Yang, J. Hou, and Z. Wang, "A method to calibrate installation orientation errors of inertial sensors for gait analysis," in *2014 IEEE International Conference on Information and Automation (ICIA)*, pp. 598–603, Hailar, China, 2014, IEEE.

[17] K. Hori, Y. Mao, Y. Ono et al., "Inertial measurement unit-based estimation of foot trajectory for clinical gait analysis," *Frontiers in Physiology*, vol. 10, p. 1530, 2020.

[18] S. R. Hundza, W. R. Hook, C. R. Harris et al., "Accurate and reliable gait cycle detection in Parkinson's disease," *IEEE Transactions on Neural Systems and Rehabilitation Engineering*, vol. 22, no. 1, pp. 127–137, 2014.

[19] G. Pacini Panebianco, M. C. Bisi, R. Stagni, and S. Fantozzi, "Analysis of the performance of 17 algorithms from a systematic review: influence of sensor position, analysed variable and computational approach in gait timing estimation from IMU measurements," *Gait & Posture*, vol. 66, pp. 76–82, 2018.

[20] V. Agostini, G. Balestra, and M. Knaflitz, "Segmentation and classification of gait cycles," *IEEE Transactions on Neural Systems and Rehabilitation Engineering*, vol. 22, no. 5, pp. 946–952, 2014.

[21] H. Ma and W. H. Liao, "Human gait modeling and analysis using a semi-Markov process with ground reaction forces," *IEEE Transactions on Neural Systems and Rehabilitation Engineering*, vol. 25, no. 6, pp. 597–607, 2016.

[22] I. González, J. Fontecha, R. Hervás, and J. Bravo, "An ambulatory system for gait monitoring based on wireless sensorized insoles," *Sensors*, vol. 15, no. 7, pp. 16589–16613, 2015.

[23] J. Perry and J. R. Davids, "Gait analysis: normal and pathological function," *Journal of Pediatric Orthopaedics*, vol. 12, no. 6, p. 815, 1992.

Hindawi
Journal of Sensors
Volume 2021, Article ID 1948103, 11 pages
https://doi.org/10.1155/2021/1948103

Research Article

Strange Attractors in Writing Competence Development from the Perspective of Complexity Theory Based on Sensor Data

Chao Zhang

College of Chinese Language and Literature, Qufu Normal University, Qufu, China

Correspondence should be addressed to Chao Zhang; xiangyuezc@hotmail.com

Received 22 July 2021; Accepted 19 August 2021; Published 3 September 2021

Academic Editor: Gengxin Sun

Writing competence is crucial for second language learners. Studying strange attractors in the development of writing competence is essential in understanding the laws of language development of foreign students. This study is aimed at investigating the state and laws of the development of Chinese as a second language (CSL) writing competence. Mathematical modeling and phase space construction methods in sensor research were used to investigate strange attractors in high-level Chinese learners studying in China in the development of CSL from the perspective of complexity theory based on the measurement framework of complexity, accuracy, and fluency. The results showed the following: (1) there are trends in the concentration and volatility of trigonometric function in different dimensions; (2) the group dynamic characteristics of writing development in CSL are simulated precisely by mathematical modeling; and (3) there are strange attractors with lexical density in CSL writing development. The development of CSL writing tends to maintain the state of strange attractors. The strange attractor reflects regularity in the dynamic, complex, and chaotic development of Chinese for international students, revealing the probabilistic prediction competence of different states in the development of CSL.

1. Introduction

Quantitative experimental research under the paradigm of reductionism has explored the statistical law of language development by controlling changes of factors, making this approach the mainstream method of second language writing research since the 1980s. However, research through the lens of complexity theory has found that the development of learners' written language is a nonliner adaptive system, in which interconnectedness and dynamic changes produce significant individual characteristics. Therefore, language development is difficult to precisely predict. Without constructing the unified research paradigm, researchers have aimed to explore the consilience of reductionism and complexity theory to probe the statistical characteristics of second language development hidden in the differentiated developments of second language writing [1–3]. The attractor in complexity theory is considered a crucial construct that combines the two paradigms. An attractor is the state or pattern that complex systems tend to develop and may be the key to revealing different patterns of learners' language development and revealing the statistical law of language development in chaotic, dynamic individual differences [4, 5]. This research is aimed at finding strange attractors in the development of Chinese as a second language (CSL) writing competence, with two novelties. (1) Few empirical studies have referred to attractors in second language development, which is still in the early stages of theoretical concept development [6–8]. The study of strange attractors in this research aids in further understanding this crucial construct in the complex system of language development; (2) there is a lack of effective methods to analyze attractors in the social sciences. The present study incorporates phase space construction and mathematical modeling methods used in sensor research to explore attractors. Previous studies have used a series of statistical methods, such as variance analysis, structural equation modeling, Monte Carlo simulation, and meta-analysis, which represent a challenge in exploring strange attractors. The application of interdisciplinary methods in the present research is the first instance of which academia has explored the strange attractors in the development of CSL writing competence,

providing a reference for future research. Accordingly, this research uses the interdisciplinary methods of mathematical modeling and phase space construction that have been widely used in the sensor research to detect strange attractors in the development of CSL among high-level international students studying in China.

2. Literature Review

In this section, two paradigms in second language research are introduced, after which the definitions of attractors and strange attractors, as well as relevant research and recent developments, are reviewed.

2.1. Theoretical Paradigms in Second Language Research. Reductionism and complexity theory are two paradigms in research into second language writing development. Reductionism has been the mainstream method of second language writing research for decades, on which the development of second language writing has long been recognized as a rule-based process in which the effect of experimental variables on development can be explored by controlling variables through experimental design and using statistical methods based on mean values to examine the law of the average value of language development in statistics. Complexity theory is a theoretical cluster on which case studies have been conducted to produce a blueprint of second language development characterized by dynamic and individualized paths [7, 9–12]. This field is challenging, and there is conflict between complexity theory and reductionism in perspectives and methods in that reductionism embraces the perspective of averaging individual differences in learners' language development.

The conflicting positions of the two paradigms hinder the unification of second language writing research in perspectives and methods. Therefore, researchers have called for the study of complex theory to concentrate on differences in language development and pay attention to statistical laws to explore language development patterns and the consilience between the two paradigms [2, 13–15]. However, there are a few studies from a complexity theory perspective that have focused on statistical pattern characteristics that emerge from individual differences. For example, Yu and Lowie [8] found improvements in general developmental trends of both complexity and accuracy, whereas there is a complex interplay between complexity and accuracy that has transformed from a competitive relationship to a supportive relationship on a group level. However, the rules of learners' language development process in the relevant research have been inducted by concentrating on observation and speculation methods, lacking a mathematical discussion of the group's CSL development patterns.

2.2. Attractors and Strange Attractors. Attractors in complex theories are a crucial construct in addressing research gaps. Attractors are the state or behavior patterns of preference to which the complex system has a tendency to develop [5]. Phase space is a technique for analyzing attractors and is a prescribed space that represents all possible states of the system, also known as state space. The state of the system is defined by different dimensions. As such, a one-dimensional phase space, for example, can be defined based on the writing scores of language learners, where each writing score of an international student corresponds to a unique point in the phase space. According to the characteristics of attractors in phase space, attractors can be divided into three types: fixed-point attractors, cyclic attractors, and strange attractors. The fixed-point attractor (Figure 1(a)) is a point in the phase space, which is a relatively constant state of the system in any dimension of the phase space. The cyclic attractor (Figure 1(b)) is multiple points in the phase space, representing the system in multiple states with periodic change. The strange attractor is the type of attractor and a feature of the complex system characterized with the most prominent chaos, also known as chaotic attractor. The butterfly-shaped area in Figure 1(c) is Lorenz's strange attractor [16]. The shape of the strange attractor is ambiguous, and its chaotic nature is reflected in the chaotic behavior of the system is disordered, but not random, and the trajectory has no obvious regularity [17]. Attractors are typical patterns emerging from system self-organization from the perspective of complexity theory, representing table and predictable aspects of development differences of the dynamic system, which are crucial ways in revealing different patterns of learner language development [4]. Studying strange attractors in the development of second language writing may reveal statistical rules contained in individual differences, which is a potential point of convergence to promote the unification of the two research paradigms.

Researchers have gained a limited understanding of attractors in the development of CSL in the field of applied linguistics. Complex theory originated in the field of natural sciences and has been widely applied in the field of sensor research, in which there exists proven methods for analyzing attractors in complex systems. The mathematical modeling method, for example, is an effective way of studying strange attractors by fitting development data captured by sensors. Through mathematical modeling, the state equation that characterizes the dynamic characteristics of the development of the CSL learners may be established, and the shape and boundary of the strange attractor in the phase space by simulating and drawing the state equation in the phase space can be analyzed. Therefore, using this interdisciplinary paradigm, this research takes international Chinese learners studying in China with high levels of language proficiency as the participants and examines strange attractors in the development of CSL writing, aiming to determine CSL development patterns hidden in individual differences based on complex theory.

3. Method

3.1. Research Questions. The present research focuses on patterns in the dynamic language development of high-level Chinese learners to examine potential strange attractors based on an analysis for characteristics of sensor data.

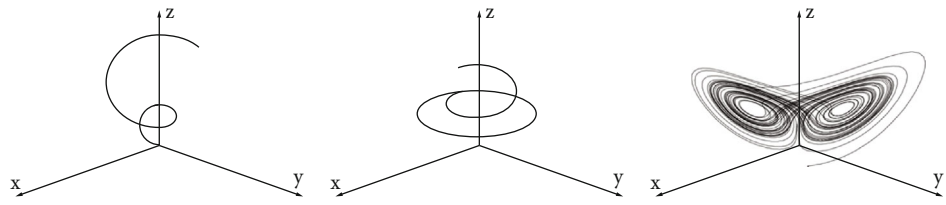

(a) Fixed-point attractor (b) Cyclic attractor (c) Strange attractor

Figure 1: Three types of attractors.

Therefore, the following three research questions are formulated.

(RQ1) What are the statistical dynamic characteristics of the development of CSL writing for international students in China?

(RQ2) Can the statistical dynamic characteristics of the development of CSL writing by international students in China be fitted by mathematical models?

(RQ3) Are there any strange attractors in the development of CSL writing for international students in China? If so, what are their characteristics in the phase space?

3.2. Participants. This research focuses on a group of high-level CSL learners' development of Chinese writing competence; 19 Chinese learners from four comprehensive universities in China were chosen as participants. Among these learners, 15 Thai international students studied in a first-class university in northern China, had passed the placement test, and were assigned to upper classes, all completing HSK Level 4. The other four international students were from two ordinary universities in the same province and had achieved HSK Level 5.

3.3. Writing Task. Sampling based on language teaching was used in this present research. In the research process, writing tasks were not assigned by the researchers; the writing texts produced by the learners within a limited time in class were collected. Participants were required to study teaching content ranging from six to eight units based on the writing curriculum. After each unit, there was a classroom writing task. The interval between the two tasks was approximately one month. The writing tasks were all based on selecting topics, involving learners' hometown, food, culture, personal career, daily life, school, critical thinking, etc. One-semester Chinese compositions written by international students were collected.

3.3.1. Writing Complexity. Complexity is a term that includes both lexical complexity and syntactic complexity. This research focuses on the lexical complexity of high-level Chinese learners. Lexical complexity, which is also called lexical richness, contains three dimensions, namely, lexical density, lexical sophistication, and lexical diversity. In the present research, lexical density was chosen to measure the learners' lexical complexity. Lexical density refers to the ratio of the number of content words in the text to all words in the text [18]. Chinese content words include nouns, verbs, adjectives, adverbs, distinguishing words, numerals, quantifiers, pronouns, interjections, and onomatopoeias. The formula for calculating the lexical density is as follows: lexical density = number of content words/number of words.

3.3.2. Writing Fluency. Writing fluency can be divided into process-based writing fluency and text-based writing fluency [19]. Process-based writing fluency is a time-related concept that mainly refers to the amount of text output per unit time, with a relatively single dimension. On the other hand, text-based writing fluency is related to text characteristics and is a multidimensional construct. Cluster analysis research shows that T unit length should be classified as complexity, and the number of words produced per minute is more appropriate for the concept of fluency, which represents the amount of text completed in a given time [20, 21]. Based on the characteristics of this research, the following process-based measure was used to calculate writing fluency: writing fluency = total number of symbols/total writing time.

When measuring total writing time used to calculate writing fluency, this research incorporated sensor technology. The sensor was able to accurately capture the writing time of the participants. When the pen tip touches the paper, the sensor under the paper will record the pressure-sensitive signal and start timing; when the pen tip leaves the paper, the sensor will stop timing. Through the sensor technology, the writing time of all participants was recorded.

3.3.3. Writing Accuracy. The accuracy of written CSL refers to the correct rate of words. Chinese composition is segmented into words, and the author and the writing teacher manually checked the words to measure accuracy. Word selection, collocation, and word meaning errors were all considered lexical errors. Lexical accuracy was measured by calculating the proportion of correctness in the composition text [22]. Since competence using letters and words belong to different constructs, they cannot be regarded as one dimension. As such, the present research did not consider letter errors when measuring lexical accuracy. The calculation method of accuracy is as follows: accuracy = number of errors/total number of symbols.

3.4. Phase Space. A tool for studying strange attractors is phase space in sensor research. After establishing the complexity, accuracy, and fluency index, Matlab was used to draw the three-dimensional phase space. A three-dimensional coordinate system was constructed, in which the accuracy was the x-axis, fluency the y-axis, and lexical density the z-axis ($0 < x < 1$, $y > 0$, $z > 0$). Any point in the

three-dimensional coordinate system corresponded to only one state for language learners' Chinese writing accuracy, fluency, and complexity. Accordingly, the three-dimensional coordinate system is the phase space of the CSL development. By constructing the phase space, the general scope of the development of complexity, accuracy, and fluency of international students' Chinese writing and the distribution characteristics of the development dynamics in each period in the phase space was observed. Based on this method, the strange attractors can be confirmed.

3.5. Data Analysis. The data analysis of this study was driven by the research questions. The first research question is aimed at examining the statistical characteristics of the development of Chinese writing text produced by learners. Therefore, the three indicators of complexity, accuracy, and fluency in the diachronic texts produced by studying abroad were calculated. The word segmentation software used the language technology platform developed by Harbin Institute of Technology [23], and the results of word segmentation and part-of-speech tagging were checked by the author of this study and a graduate student one by one to ensure that the word segmentation was correct. On the basis of this first stage, the number of content words, the number of errors, and the total number of characters were marked, and complexity, accuracy, and fluency were calculated one by one and recorded in a table in chronological order. An iterative graph of the development data of CSL writing competence was then constructed based on the task time as the abscissa and second language writing competence development indicator as the ordinate. The data of 21 participants were drawn into this coordinate system in turn. When fitting, coordinate time t is replaced by the real-time data by a function. For example, if the first learner is sampled seven times and the second learner is sampled eight times, the number eight on the coordinate axis is replaced by number one. If the number of samples is set to time t, complexity, accuracy, and fluency are a function of task time. In addition, task time was marked on the abscissa; and complexity, accuracy, and fluency data were marked on the ordinate, by which a scatter distribution graph was drawn to visualize the value range of international students' writing complexity, accuracy, and fluency in the given tasks. The iterative graph represented participants' individual characteristics and micro changes in language development, whereas the scattered point distribution graph highlighted participants' statistical characteristics.

The second research question is aimed at fitting the statistical characteristics of the development of Chinese writing by international students through mathematics. In the field of natural science, the premise of examining a strange attractor involves constructing an equation of state [24]. Although the development of CSL writing of international students does not follow a specific equation in the social sciences, it is still possible to use mathematical models to fit statistical development dynamics [25]. By analyzing the development trend of CSL writing competence using scatter distribution, a mathematical model was constructed to simulate the development trend. This study used Matlab to fit the group development dynamics of the complexity, accuracy, and fluency for the development of CSL writing in China, on which a fitted state equation for the development of CSL writing was constructed based on the data of these three indicators. The change of the state with the equation in the phase space indicated a tendency for the development of CSL writing. According to nonlinearity view on the complex system, Matlab was used to calculate the root mean square error (RMSE) of the fitted equation to evaluate the degree of model fitting.

The third research question is aimed at examining the strange attractor based on the fitted equation of state. Therefore, data were imported into Matlab to draw the curve of the fitting equation development in the phase space. By simulating a large amount of data, the corresponding position of the equation in the phase space was visualized. The higher the simulation time, the clearer the tendency area of the equation, and the clearer the outline of the strange attractor in the phase space [17]. Similar to the method of establishing development dynamics by simulating a large amount of data, this technique was applied to the research based on dynamic systems theory; the Monte Carlo simulation is based on this idea [26]. In the present research, 800 time simulations were performed to confirm the characteristics of the strange attractor in the phase space.

4. Results

4.1. The Dynamics of the Development of CSL Writing for International Students in China. The iterative graph of the development data of CSL writing competence (Figure 2) presents significant individual differences among learners. The maximum value of accuracy is close to 1, whereas the minimum value is close to 0.73. The maximum value of writing fluency is close to 0.4, and the minimum value is close to 0.05. The maximum value of lexical density is above 0.9, and the minimum is close to 0.6. In addition, no two segments of the same curve can be found in the graph, indicating that the development path of the Chinese language of international students is unique. The development of the second language writing is different, showing progress, retrogression, variability, and turbulence.

To visualize the development of CSL writing competence, a scatter plot of complexity, accuracy, and fluency data was drawn (Figure 3), in which accuracy and lexical density overlap and overall line changes are relatively stable. The lexical density (gray area), for example, presents fluctuates of maxima and minima over time, that is, from the first to the eighth writing index changes are approximated by a trigonometric function (a wavy line, closer to a sine function). In the change of lexical density, the index value reaches a lower maxima at the second time and reaches a higher maxima at the third time, dropping slightly and then rising. The overall range of changes is clear, in which the lowest value is approximately 0.6, and the highest value is 0.979.

The two-dimensional diagram provides a description of the individual characteristic and group development of learners' CSL writing competence, clarifying the direction

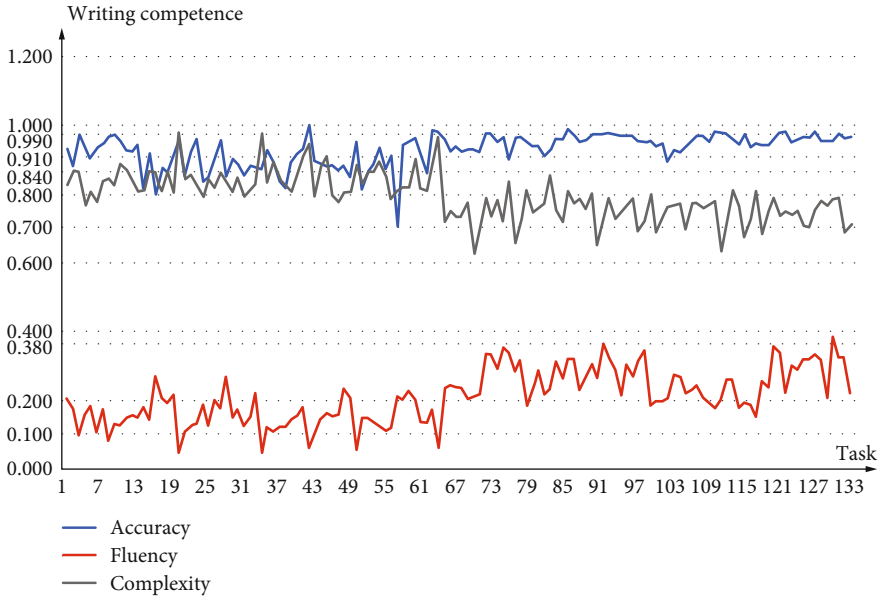

Figure 2: Iterative graph of the development data of CSL writing competence.

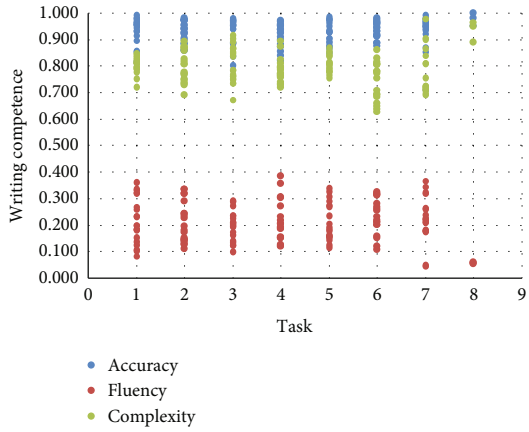

Figure 3: Scattered distribution map of the development data of CSL writing competence.

for examining strange attractors for the current research. There may be individual differences with fluctuations and variabilities in language competence development, showing stable characteristics in statistics and indicating that the statistical law exists. In addition, the fluctuation of the index shows the characteristics of trigonometric functions, and the development process is nonlinear, showing that it is reasonable for trigonometric function models (e.g., Fourier transform) to construct a mathematical model for the development tendencies of Chinese writing competence. Therefore, in the present study, sine and cosine functions were chosen to construct a mathematical model to fit learners' group development dynamics.

4.2. Mathematical Model of the Development of CSL Writing Competence. Mathematical modeling describes the dynamic trend of the development of international students' CSL writing competence. In the present study, function fitting was used with the task time as an independent variable, with complexity, accuracy, and fluency as dependent variables. After several adjustments, the fitting function of CSL writing competence was established (Table 1). After calculating accuracy (RMSE = 0.003), fluency (RMSE = 0.013), and complexity (RMSE = 0.034), the root mean square error of the fitting function was lower than 0.1, showing that the development of the three dimensions of complexity, accuracy, and fluency was effectively fitted for international students' CSL writing competence.

The graph of the fitting function in the abscissa [1, 5] interval is presented in Figure 4, which is fitted through discrete points; that is, there are only integer time of tasks on the abscissa, and the fitting data between two adjacent integer points only has mathematical meaning. The graph of the accuracy fitting function (Figure 4(a)) shows that the participants' CSL writing accuracy is approximately 0.95 in the first task, slightly increases in the second task, and continues to decline from the third to the fifth task. The graph of the fluency fitting function (Figure 4(b)) reflects the tendency of the participants' fluency in CSL writing from the first task to the third task and then continues to rise. The graph of the complexity fitting function (Figure 4(c)) shows an overall trend of the participants' CSL writing complexity falling and rising. The function graphs accurately present the statistical characteristics of the development of complexity, accuracy, and fluency in the scatter distribution map of the development data of CSL writing competence.

4.3. Strange Attractors in the Development of CSL Writing. The attractor is a tendency pattern for the development of complex systems and is mapped as a region in the phase space. Therefore, the phase space graph was constructed to examine a strange attractor with accuracy as the x-axis, fluency as the y-axis, and vocabulary density as the z-axis. The three-dimensional scatter graph of the state equation of

Table 1: Fitting function and evaluation of fitting degree of CSL writing development.

Dimension	RMSE	Function
Accuracy	0.003	$\text{Accuracy} = 0.917 + 0.075 \sin(3.272\,t)$
Fluency	0.013	$\text{Fluency} = 0.24 + 0.137 \cos(t)$
Complexity	0.034	$\text{Density} = 0.8 + 0.11 \sin(0.14\,t) \sin(0.052\,t + t^2)$

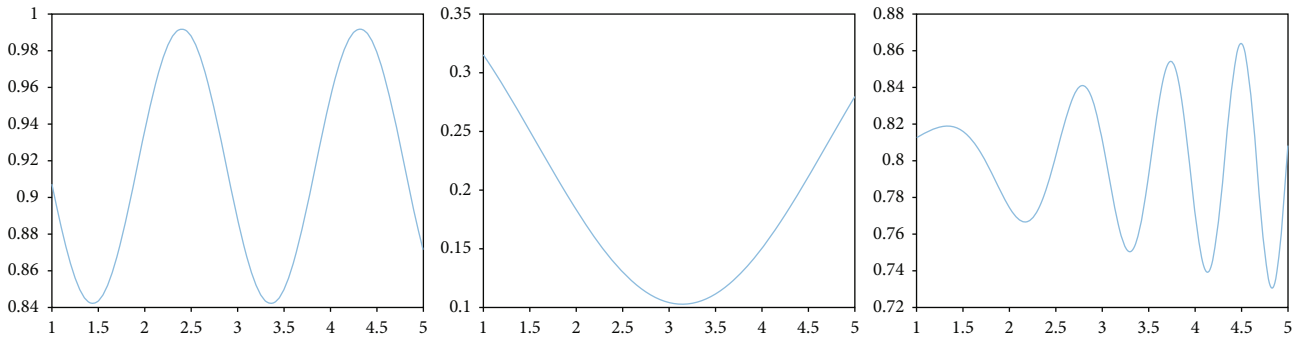

Figure 4: The fitting function graph of CSL writing accuracy, fluency, and complexity.

complexity, accuracy, and fluency development (Figure 5) shows that the scatter points are mainly blue and blue-green, indicating that the lexical density is distributed in interval [0.6, 0.9], demonstrating the possibility of the attractors and the tendency of the complex system of international students in CSL writing.

According to the analyses in Section 4.2, the fitted equation of state for strange attractor is as follows:

$$\begin{cases} x = 0.917 + 0.075 \sin(3.272\,t); \\ y = 0.24 + 0.137 \cos(t); \\ z = 0.8 + 0.11 \sin(0.14\,t) \sin(0.052\,t + t^2). \end{cases} \quad (1)$$

Based on the fitted equation of state, the function of the strange attractor simulated 800 times in the interval [1, 50] was drawn as three-dimensional graph (Figure 6), demonstrating that the data points are distributed in the interval of lexical density [0.70, 0.91], accuracy [0.84, 0.99], and fluency [0.10, 0.38] to form a rectangular area approximately, in which a large number of data points are distributed in the graph of fitted function, and a few data points outside the rectangular area will return to the area soon, indicating the tendency of development of CSL writing competence for international students. The behavior of the system in this phase space region is disorderly and unpredictable, though its boundary is relatively clear. Therefore, the rectangular area in the phase space is confirmed to be a strange attractor. Comparing Figures 2 and 3, the strange attractor is in the scatter of the development of CSL writing competence, and the fitting equation is consistent with development distribution.

By examining the language ability development data of 19 participants, the accuracy of their CSL writing development left strange attractors 10 times, accounting for 7.5% of total times. Furthermore, participants' fluency development left strange attractors eight times, accounting for 6.0% of total times, the complexity development left strange attractors 16 times, accounting for 12.0% of total times. The development of the second language writing of 17 participants escaped from the strange attractor, whereas the development of the second language writing of only two participants (Lin and Chen) escaped from the attractor for two consecutive tasks (the value of accuracy is 37 and 38, and the value of lexical density is 70, 71). The Chinese writing development data of two international students (Table 2) shows that Lin's writing accuracy was lower than the minimum (i.e., 0.84) of strange attractor twice in the third and fourth tasks, whereas Chen's writing complexity was lower than the minimum (i.e., 0.70) of strange attractor in the last two tasks. Once the second language writing development of other learners escaped from the rectangular area, they had to return to the strange attractor state in the next writing task. The above analysis shows that the development of Chinese writing by international students tends to develop towards and remain in strange attractors.

5. Discussion

A statistical analysis of the three indicator dimensions of the development of the CSL writing competence of international students was conducted to examine the statistical characteristics of the development of Chinese writing competence among international students and the strange attractors in the phase space. Through the development curve fitting and mathematical modeling, the strange attractor in the development of CSL writing competence was confirmed. These findings show difference, regularity, predictability, and complex are interconnected in language development. These features are discussed in the following section.

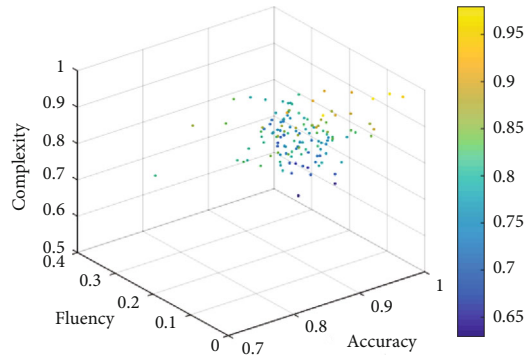

Figure 5: Scatter graph of the state equation of complexity, accuracy, and fluency development.

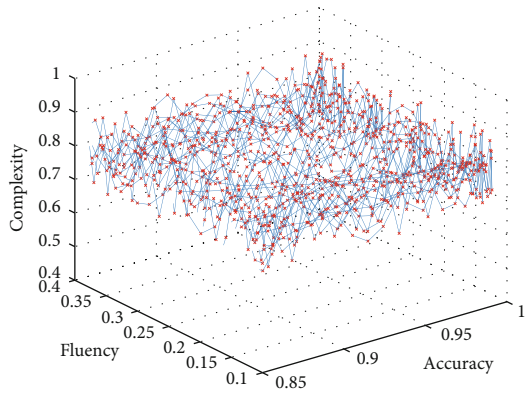

Figure 6: Strange attractor.

5.1. The Chaos of Strange Attractors in the Development of CSL. The results on the development dynamics of CSL writing competence show that there are a large number of individual differences in language development manifested in many aspects of development dynamics. There are no two participants with the same development dynamics, and the development curve of the learners' CSL writing competence shows increases, decreases, leaps, and temporary stagnation. The iterative graph of the complexity, accuracy, and fluency of the CSL writing competence shows that the development curve of international students in different dimensions is the identity of each participant. Therefore, learners' development dynamics in each dimension are unique, and the chaotic development trajectory of the strange attractor reflects this characteristic. Complexity theory provides a view that the environment as a complex system constantly changes, in which different learners have different system components in a period of time (for example, a month). Therefore, there are individual differences in the interconnectedness of the subsystems, and it is the dynamic interaction of the system elements that forms the dynamics of differentiated language development [27]. Interconnectedness, the prominent feature of the complex system, dominates the interactions of the subsystems of complexity, accuracy, and fluency in the development of CSL writing to form individual characteristics, in which learners' language development shows chaotic characteristics, making it almost impossible to precisely predict the development path of learners' language competence [13]. Due to the variability, interconnectedness, and sensitivity to the initial state of the system, the subsystems in a complex system are in constant change. As a consequence, learners will never follow the same path of second language writing development [11, 26].

5.2. Statistical Law of Strange Attractors in the Development of CSL Writing Competence. Strange attraction is a model of development of foreign students' Chinese in the dynamics of individual differences and chaos. The development of Chinese writing ability of foreign students in singular attractor changes dynamically throughout the process but tends to remain within a specific range with vocabulary density [0.70, 0.91], accuracy [0.84, 1], and fluency [0.10, 0.38] in a specific state area. The results of the lexical density dimension are consistent with previous research results on high-level CSL writing [28], indicating that the strange attractor found in this study may be a common state of the development of high-level Chinese in China. The dynamic development of learners' writing competence presents a tendency towards strange attractors, in which the development of Chinese writing for international students escapes for a short time but then returns (Figure 1). The graph of the equation of state (Figure 5) also displayed this feature of the strange attractors, indicating that the strange attractor is a state in which participants' Chinese writing competence tends to stay. In addition, the participants are CSL learners with high-level proficiency. Therefore, it may be considered that the strange attractor is a state achieved by the participant group through self-organization of the complex system of Chinese development after long-term acquisition; the strange attractor is also a state in which learners tend to develop. Strange attractors seem to "attract" the development of Chinese writing by international students in China from beginner to a high-level proficiency Chinese learners, which is the statistical law and certainty that emerges from the interaction and chaotic development of CSL writing competence.

The analysis of strange attractors in the development of Chinese writing competence by international students suggests that construction emergence may play a key role in this process. Construction is the pairing of form and semantics/-function with conventional characteristics [29]. Emergence is the showing of new states of the system that cannot be explained with existing parts and interactions [30]. Lexical density is the proportion of content words in a text, and using construction may help language learners to call on more language resources and organize more complex sentences, thus, significantly increasing their lexical density and generating more fluent language [31, 32]. Although the participants were Chinese learners with high-level proficiency, the analysis showed that some of the more advanced constructs (e.g., Chinese slot and frame construction) were in constant change, in which the degree of solidification of the construction representation was not high, and the constructs were still in the process of acquisition. The development system of CSL writing competence in the strange attractor is not stable; there are mismatches and

Table 2: Data on Chinese writing development of two international students in China.

	No.	Accuracy	Fluency	Complexity		No.	Accuracy	Fluency	Complexity
	1	0.930	0.123	0.837		1	0.957	0.235	0.719
	2	0.899	0.112	0.893		2	0.926	0.244	0.750
	3	0.835	0.123	0.846		3	0.941	0.239	0.736
Lin	4	0.819	0.122	0.828	Chen	4	0.923	0.235	0.736
	5	0.894	0.143	0.804		5	0.932	0.207	0.778
	6	0.919	0.158	0.861		6	0.930	0.213	0.629
	7	0.933	0.181	0.906		7	0.922	0.218	0.693

intensification in the process of construction emergence, which evolves on an individual level and shows as statistical characteristics. In addition, there is a feedback mechanism in the process of learners' interactions with the environment. Feedback refers to the impact of the current state on the subsequent state of the system, and the effect of the negative feedback is one of the most common attractor influence system mechanisms [33]. In this study, once the development path of CSL writing competence of international students in China leaves the strange attractor, there seems to be an invisible force that urges the development state to return to the singular attractor. This process derives from the system's negative feedback mechanism. The strange attractor of the learner's language complexity, accuracy, and fluency is the result of the long-term self-organization and stability of the system, in which the attractor is adapted to the cognitive resources that the learner is able to call. When the need of a certain dimension exceeds the learner's cognitive competence at a certain level (e.g., a learner tries to use an unfamiliar construction), the three dimensions of language performance compete for cognitive resources. A competitive growth forms in the internal dimensions, further decreasing available cognitive resources [34, 35]. The completive state is a negative experience for learners and cannot be maintained for an extended period, which triggers the negative feedback mechanism of the system and reduces the difference between the states of the complex system and the strange attractors, showing that the system tends to return to the strange attractor after leaving the strange attractor.

There are similarities in the development path of Chinese writing competence among learners with the same strange attractors, and the system shows order under these strange attractors. The self-organization of the system leads to the order of the complex system of CSL writing competence to reduce the degree of freedom of the system [36] and finally converge the development of the system to several possible patterns. Variability and self-organization are crucial characteristics of complex systems, in which variability leads to individual differences and unpredictability in the development of learners' CSL writing competence, whereas self-organization makes the development of learners' CSL writing more statistical to eventually form attractors. A stable system makes the macroscopic characteristics of nonlinear systems more prominent [33]. Strange attractors represent the tendency of learners' writing competence to develop in the form of accuracy, fluency, and complexity. The strange attractor, for example, corresponds to learners' tendency towards accuracy [0.84, 1], fluency [0.10, 0.38], and lexical density [0.70, 0.91] in the three-dimensional phase space region. The fitting function of the development state and the superimposed graph of writing competence development of all indicators show that the development of the group at a specific time presents a specific interval characteristic.

5.3. Probabilistic Predictability of Strange Attractors in the Development of CSL Writing Competence. The essence of science is predictability ([17] p.6). In the past, language research based on complexity theory has avoided mentioning the "predictability" of language, and the interconnectedness and openness of language development complex system make it almost impossible to precisely predict language development as a chaotic trajectory inside the strange attractor. Therefore, empirical research based on complex theory has used the "retrospective" approach in essence, concentrating on the reality of language development. The research source must be the dynamic trajectory of the system that has occurred [13]. The strange attractor indicates that, when the individual differences and laws of language development are considered, language development shows significant statistical laws that can be predicted to a certain extent. The characteristics of strange attractors in the development of CSL writing competence indicate that it may predict the dynamic range of language development in the next moment although it is difficult to precisely predict the development of the next moment and find clear rules from the dynamics, which is the consilience between individual differences and statistical rules, as well as reductionism and complexity in the development of a second language.

The development of learners' CSL writing competence tends to be in state with accuracy in [0.84, 1], fluency in [0.10, 0.38], and complexity in [0.70, 0.91], in which the accuracy of the second language writing of all participants in the state last for at least six months. The probability of the participant maintaining the strange attractor in the seventh month is higher than the probability of phase transition to other states. For individuals such as Chen, the probability that the lexical density of the next written text as [0.629, 0.778] is significantly higher than the probability of leaving this interval, in that the lexical density of her writing in the first six months is at the strange attractor. The language performance in the first six months is a condition, and the conditional probability of the state at time t may be expressed as $P(X_t \mid X_{t-1}, X_{t-2}, \cdots, X_1)$, showing that it is possible to

predict that the same attractor state will be maintained at a later time and predict the development interval for attractors. This prediction is reasonable based on the characteristics of the attractor based on previous sufficient observations. In other words, the language development state of the learner in the attractor at the next moment is not infinite, which conforms to the conditional probability distribution that the probability of being in a different state at the next moment is different, which may be predicted. The analysis shows that language development can be predicted to a certain extent, and this prediction conforms to the probability distribution. The extent to which language development can be predicted is determined by the state of the strange attractor, which depends on the conditional probability corresponding to the development of the learner in the dimension. The state of attractor, which is difficult to measure directly, is called the hidden state. The state of complexity, accuracy, and fluency, which can be measured directly, is the explicit state. The hidden state implies the complexity of the laws of language; it is difficult to find the laws from a bunch of individual data, and the hidden state must be found using statistical tools. However, the attractor, as a hidden state, provides the possibility of predicting the dynamic path of language development.

6. Conclusion

Based on an analysis of the characteristics of attractors, this study demonstrated the coexistence of individual differences and statistical laws in the development of CSL writing. Individual difference was manifested in the unique dynamic curve of language development, and statistical law was manifested learners' CSL writing development, which preferred certain intervals with fluctuations. In this study, the state equation for the development of CSL writing competence was constructed, and characteristics of participants' CSL writing competence development were simulated using mathematical modeling and phase space construction. The trajectory of the development of CSL writing in the phase space based on the equation of state suggests that there is a strange attractor in the development of CSL writing competence among international students in China, which are mapped in the phase space as accuracy in [0.84, 1], fluency in [0.10, 0.38], and complexity in [0.70, 0.91]. The strange attractor shows a more general, tendentious state in CSL dynamic development with significant individual differences, reflecting the statistical law of the development of the CSL and the probabilistic predictive characteristics of the state.

The theoretical significance of this research is to use the strange attractor as an approach to address key issues of complexity theory and reductionism, or to what extent is language development individual and to what extent do laws or patterns exist [2]. The emergence of complexity theory interrupts the authority of reductionism. However, there is a fundamental difference between the two paradigms on language development. The results indicate the consilience of complexity theory and reductionism in language research, and the research paradigm may be further expanded. In addition, this research has value for the teaching and research of second language writing. First, reductionist research can use diachronic experimental design to explore the dynamics and complexity of potential factors and confirm which types of learners are more in line with statistical law under reductionism. Research based on complexity theory may use a large sample, focusing on statistical law and patterning characteristics contained in the dynamics of individual differences. Second, as a hidden state, the strange attractor may become a classification label for learners to guide the implementation of differentiated teaching. This research used interdisciplinary paradigms such as mathematical modeling of dynamics in statistics, providing an effective method to detect strange attractors. Third, the strange attractor found was a law and phenomenon. The detection of attractors in learners' second language development helps language teachers to determine teaching strategies and analyze control parameters. Teachers could assist learners in maintaining a positive state and escaping from the negative aspects of CSL development. Fourth, using sensors to detect participants' writing time and sensor-based mathematical modeling methods to detect strange attractors in this study may provide references for language research.

The method of detecting the strange attractor in this study could be further improved. The study on attractors in the language development is still in its early stages, and the method of detecting attractors in language development is still in its exploratory stage. Therefore, this research used mathematical modeling, spatial mapping, and other sensor fields to establish strange attractors. These interdisciplinary methods still have limitations in the field of language research. The individual learner's development is complex and chaotic, making it impossible to accurately follow a certain mathematical equation. The fitted state equation is the mathematical simulation of the dynamic tendency of CSL learners' development. Although it may often be necessary to eliminate some details in language research to explore statistical laws, more accurate models need to be further explored to more precisely describe the actual state of language development.

7. Future Research

The limitations of this research may be addressed in future research. The method of probing strange attractors should be enhanced in said research. Because academic research into attractors in language development of learners is still in its early stages, the method of confirming attractors in language development is also still in its exploratory stage. In the future, more interdisciplinary methods may be incorporated to explore strange attractors in further detail (e.g., computer modeling based on deep learning). Furthermore, computer modeling can address limitations that are difficult to solve with mathematical modeling and more accurately depict the development of CSL writing competence among foreign students in China. In addition, a further study of a longer duration may be conducted to describe the attractor formation process and learners' language development dynamics more clearly, comprehensively describing the

distribution of attractors among language learners and the group law of attractors. Furthermore, future research may use a higher number of participants to more comprehensively reveal the distribution law and formation process of attractors.

Data Availability

The data used to support the findings of this study are included within the article.

Conflicts of Interest

The authors declare that they have no conflicts of interest.

Acknowledgments

The author is grateful for the comments of his Ph.D. advisor.

References

[1] L. M. Kallemeyn, J. N. Hall, and E. Gates, "Exploring the relevance of complexity theory for mixed methods research," *Journal of Mixed Methods Research*, vol. 14, no. 3, pp. 288–304, 2020.

[2] D. Larsen-Freeman, "Complexity theory," in *The Routledge Handbook of Second Language Acquisition*, S. M. Gass and A. Mackey, Eds., Routledge, London, New York, 2012.

[3] C. Zhang and R. Ma, "The effect of textual glosses on L2 vocabulary acquisition: a meta-analysis," *Language Teaching Research*, vol. 5, 2021.

[4] P. Hiver, "Attractor states," in *Motivational Dynamics in Language Learning*, Z. Dörnyei and P. D. MacIntyre, Eds., pp. 20–28, Multilingual Matters, UK, 2014.

[5] E. Thelen and L. B. Smith, *A Dynamic Systems Approach to the Development of Cognition and Action*, The MIT Press, Cambridge, MA, 1994.

[6] C. M. Amerstorfer, "The dynamism of strategic learning: complexity theory in strategic L2 development," *Studies in Second Language Learning and Teaching*, vol. 10, no. 1, pp. 21–44, 2020.

[7] G. G. Fogal, "Investigating variability in L2 development: extending a complexity theory perspective on L2 writing studies and authorial voice," *Applied Linguistics*, vol. 41, no. 4, pp. 575–600, 2020.

[8] H. Yu and W. Lowie, "Dynamic paths of complexity and accuracy in second language speech: a longitudinal case study of Chinese learners," *Applied Linguistics*, vol. 41, no. 6, pp. 855–877, 2020.

[9] K. Baba and R. Nitta, "Phase transitions in development of writing fluency from a complex dynamic systems perspective," *Language Learning*, vol. 64, no. 1, pp. 1–35, 2014.

[10] D. Larsen-Freeman, "On language learner agency: a complex dynamic systems theory perspective," *The modern language journal*, vol. 103, supplement 2016, pp. 61–79, 2019.

[11] D. Larsen-Freeman and L. Cameron, *Complex System and Applied Linguistics*, Oxford Univ. Press, New York, 2008.

[12] W. M. Lowie and M. H. Verspoor, "Individual differences and the ergodicity problem," *Language Learning*, vol. 69, Supplement 1, pp. 184–206, 2019.

[13] Z. Dörnyei, "Researching complex dynamic systems: 'retrodictive qualitative modelling' in the language classroom," *Language Teaching*, vol. 47, no. 1, pp. 80–91, 2014.

[14] T. Wrigley, "The problem of reductionism in educational theory: complexity, causality, values," *Power and Education*, vol. 11, no. 2, pp. 145–162, 2019.

[15] B. Yuan and Y. Lin, "Directionality and complexity of L1 transfer in L2 acquisition: evidence from L2 Chinese discourse," *International Review of Applied Linguistics in Language Teaching*, vol. 57, no. 4, pp. 377–416, 2019.

[16] E. N. Lorenz, "Deterministic nonperiodic flow," *Journal of the Atmospheric Sciences*, vol. 20, no. 2, pp. 130–141, 1963.

[17] J. C. Sprott, *Strange Attractors: Creating Patterns in chaos*, M & T Books, New York, 1993.

[18] J. Ure, "Lexical density: a computational technique and some findings," in *Talking about Text*, Birmingham: English Language Research, M. Coultard, Ed., pp. 27–48, University of Birmingham, 1971.

[19] M. M. A. Latif, "What do we mean by writing fluency and how can it be validly measured?," *Applied Linguistics*, vol. 34, no. 1, pp. 99–105, 2013.

[20] N. A. Chenoweth and J. R. Hayes, "Fluency in writing," *Written Communication*, vol. 18, no. 1, pp. 80–98, 2001.

[21] K. Wolfe-Quintero, S. Inagaki, and H.-Y. Kim, *Second Language Development in Writing: Measures of Fluency, Accuracy, & Complexity*, Second Language Teaching & Curriculum Center, Hawaii, 1998.

[22] J. Read, *Assessing Vocabulary*, Cambridge University Press, Cambridge, 2000.

[23] W. Che, Z. Li, and T. Liu, "LTP: a Chinese language technology platform," in *proceedings of the Coling 2010: demonstrations*, Beijing, China, 2010.

[24] R. A. Meyers, Ed., *Encyclopedia of Complexity and Systems Science. Springer Reference*, Springer, New York, London, 2009.

[25] S. C. Chapra, *Applied Numerical Methods with MATLAB for Engineers and Scientists*, McGraw-Hill Education, New York NY, Fourth edition edition, 2018.

[26] M. H. Verspoor, K. deBot, and W. Lowie, *A Dynamic Approach to Second Language Development: Methods and Techniques*, John Benjamins, Amsterdam, 2011.

[27] D. Larsen-Freeman, "Complexity theory: the lessons continue," in *Complexity Theory and Language Development: In Celebration of Diane Larsen-Freeman*, L. Ortega and Z. H. Han, Eds., pp. 11–50, John Benjamins, Amsterdam/Philadelphia, 2017.

[28] C. Huang and N. Xue, "Digital language resources and NLP tools," in *The Routledge Handbook of Chinese Applied Linguistics*, C.-R. Huang, J.-S. Zhuo, and B. Meisterernst, Eds., pp. 483–497, Routledge, London, 2019.

[29] N. C. Ellis, "Constructions, chunking, and connectionism: the emergence of second language structure," in *Blackwell handbooks in linguistics*, The handbook of second language acquisition, C. Doughty and M. H. Long, Eds., Blackwell, Malden, MA, Oxford, 2003.

[30] J. H. Holland, "Emergence: from chaos to order (3. Paperback print)," in *Helix books*, Perseus books, Cambridge, Mass, 1998.

[31] N. C. Ellis, "Language acquisition as rational contingency learning," *Applied Linguistics*, vol. 27, no. 1, pp. 1–24, 2006.

[32] A. E. Goldberg, *Constructions: A Construction Grammar Approach to Argument Structure Originally Presented as the*

Author's [PhD Thesis], University of California, Chicago, London, 1992.

[33] W. Banzhaf, "Self-organizing systems," in *Springer Reference. Encyclopedia of Complexity and Systems Science*, R. A. Meyers, Ed., pp. 8040–8050, Springer, New York, London, 2009.

[34] P. Skehan, *A Cognitive Approach to Language Learning*, Oxford University Press, Oxford, UK, 1998.

[35] P. Van Geert, "A dynamic system model of cognitive and language growth," *Psychological Review*, vol. 98, no. 1, pp. 3–53, 1991.

[36] T. DeWolf and T. Holvoet, Eds., *Emergence Versus Self-Organisation: Different Concepts but Promising when Combined*, vol. 1 of Engineering Self-Organising Systems: Methodologies and Applications, Springer, Berlin, 2005.

Hindawi
Journal of Sensors
Volume 2021, Article ID 4001584, 10 pages
https://doi.org/10.1155/2021/4001584

Research Article

Research on Underground Chemical Gas Monitoring and Target Location Based on an Improved Moth Flame Algorithm

Chunmei Tu[1] **and Guobin Chen**[1,2]

[1]*Chongqing Key Laboratory of Spatial Data Mining and Big Data Integration for Ecology and Environment, Chongqing Finance and Economics College, Chongqing 401320, China*
[2]*College of Computer Science and Technology, Chongqing University of Posts and Telecommunications, Chongqing 400065, China*

Correspondence should be addressed to Guobin Chen; d150201001@stu.cqupt.edu.cn

Received 30 June 2021; Revised 20 July 2021; Accepted 24 July 2021; Published 10 August 2021

Academic Editor: Gengxin Sun

The danger of downhole work is mainly due to the chemical toxic gases and flammable gases NO_2, CO, SO_2, H_2S, CH_4, CO_2, etc. When the concentration reaches a certain value, it will produce very great harm. With the continuous development of sensor technology and communication technology, it is necessary to monitor the relevant geographic features below the ground. Because of the complex environmental parameters of the coal mine roadway and the interference caused by various electrical equipment, the transmission of mine electromagnetic signals will be affected, resulting in low positioning accuracy. However, the underground chemical gas leakage leads to the life of underground workers which cannot be guaranteed, so it is necessary to effectively monitor the concentration of chemical gas components in underground mines. In this paper, a moth flame algorithm based on optimized inertia weights is proposed. By continuously improving the local inertia weights, the global optimum is determined by using the change of inertia weights in the iterative process of the algorithm. By testing the convergence and optimal value of several algorithms under common test functions, IMFO can obtain the global optimal solution. Finally, the concentrations of chemical gases NO_2, CO, SO_2, H_2S, CH_4, and CO_2 are monitored by setting specific areas to see if they reach the early warning values. Then, 16 coordinates in the region are used to predict the above method, and the IMFO algorithm can achieve the best prediction effect.

1. Introduction

Because the mining operation of coal resources is below the ground and has high harmfulness, there are still hundreds of people who pay their lives due to coal mining every year, and major accidents often occur. With the continuous development of sensor technology and communication technology, it has become a realistic need to monitor the relevant geographic feature information below the ground. Nowadays, with the development of wireless sensor network communication technology, smart mines also appear and Zigbee technology, radio frequency identification technology, WiFi network technology, and UWB technology are also gradually put into use in mine environment. Due to the complex environmental parameters of the coal mine roadway and the interference caused by various electrical equipment, the transmission of mine electromagnetic signals will be affected, resulting in low positioning accuracy [1]. Therefore, the wireless sensor network technology and algorithm used to realize accurate mine positioning are an important research direction of the mine positioning system at present. Whether the massive data generated under the above technical background can accurately measure the specific position has become a hot spot in the research of the positioning algorithm. Therefore, how to build a complete and reliable wireless sensor network combined with the actual positioning algorithm to complete the real-time positioning of underground personnel is an important issue in current research [2].

Considering the difference in testing accuracy and model mismatch between noise positioning algorithms [3], a nonlinear fading filtering algorithm with a single fading factor

is proposed to remove noise, and the sensitivity of the algorithm is improved by combining the least square algorithm. The results show that the positioning accuracy is better than Kalman filtering. The weights of different positioning algorithms are fused by fuzzy theory [4], and then, the positioning information is predicted by the weighted average method. The weights of three different positioning methods are applied to dynamically adjust the covariance of measurement noise. On the other hand, based on the theoretical model of wireless transmission signals, the weighted average value of the attenuation index of signal transmission paths is obtained periodically and optimized in combination with the genetic algorithm. This method is an intelligent swarm algorithm, a hot issue studied [5]. A large number of calculations by the genetic algorithm in underground environment lead to low search efficiency and poor stability in the later stage of evolution. In PSO [6], each particle in the best position is used to give inertia weights of different dimensions, different particles have different tasks, and the acceleration parameters of PSO are determined by different adaptive weights. Using the correlation sequencing function, the algorithm is tested, and the performance advantage of the proposed method is obvious in convergence speed. Considering that the underground environment is complex and affects the weighted centroid positioning [7], the genetic algorithm is used to optimize the weighting, and the improved method is superior to the traditional method in accuracy. In order to improve the positioning accuracy, a gradient enhanced regression tree positioning algorithm [8] is proposed, which fuses the positioning results of the KNN, random forest, SVM, and multilayer regression algorithm. It can see that the fused positioning can better improve the positioning accuracy of the algorithm. Aiming at the problem of low matching positioning accuracy such as MSD and MAD [9], the MPMD matching algorithm based on the feature vector product is used to improve positioning accuracy, and the results are better in error and pit noise. In view of the blind areas in the mining and monitoring of underground coal resources, document [10] proposes an improved DV-Hop positioning and monitoring system, which can accurately track personal operations, calculate the distance per jump of anchor nodes, and collect relevant operation safety data. To improve the positioning accuracy, ensure the safety of personnel and improve the production level underground in complex environment. In the wireless network environment, especially in the narrow underground space and complex working environment, there is a contradiction between its positioning error and wireless broadband. Literature [11] proposes a positioning algorithm based on PSO and Taylor-D. PSO provides optimized coordinate information, thus further reducing the positioning error and obtaining higher positioning accuracy. Literature [12] is aimed at the problems of unstable WLAN information and low positioning accuracy in narrow space; it is proposed to fuse GPS and WLAN data information, sample the integrated data, and realize particle weight by combining the Kalman filter and map. Thus, the advantages of GPS and WLAN positioning are realized, and the positioning accuracy is improved.

Inspired by moth navigation in nature, Mirjalili proposed a moth flame optimization algorithm (MFO) in 2015 [13], which is based on moth behavior and achieves a good balance between exploration and development through a special mechanism called lateral directional navigation to obtain global optimization performance. Because of the high efficiency of MFO in optimization, it has many applications in many fields and the effect is better [14]. Literature [15] constantly updates the flame position by adjusting the weight function, so as to achieve the goal of global optimization. Constantly accelerate the convergence efficiency, and calculate the adaptive value to infer the optimal position. Experiments show that the improved MFO algorithm can get the global optimization and the best performance in path optimization. Literature [16] proposes an improved IMFO based on exploration/development rate control in the field of machine learning for feature selection. Literature [17, 18] proposed a moth flame algorithm and solved the engineering optimization problem successfully. The improved MFO algorithm has achieved good results in specific applications. However, it must be admitted that, in solving complex peak function optimization problems, it is necessary to design a new improved MFO algorithm to improve the global optimization performance of MFO, aiming at the problem that MFO is easy to fall into local optimization and leads to low global search accuracy. In view of the difficulty in predicting the underground location, this paper puts forward an improved IMFO algorithm to improve the prediction accuracy of the underground geographical location. The algorithm can solve the problem of low position prediction accuracy and can improve the position prediction accuracy in different spaces. The above research is based on the position prediction in two-dimensional space or the existence of insufficient accuracy. At present, the accuracy of geographical position prediction is insufficient, and it is impossible to predict effectively in three-dimensional space. The second part introduces the MFO algorithm and explains the algorithm flow. In the third part, there are some problems in improving MFO, and the linear decreasing inertia weight adjustment strategy is used to improve MFO algorithm. In the fourth part, the performance of the improved IMFO algorithm is compared with those of other algorithms.

2. Moth Flame Optimization Algorithm

2.1. Population Initialization. In order to be able to simply describe the MFO algorithm, the moth as an individual is in the optimal position in the solution space. By continuously optimizing the position, we can achieve the goal of global optimization. The MFO model is described by

$$M = [\mathbf{m}_1, \mathbf{m}_2, \cdots, \mathbf{m}_n]^T,$$
$$\text{where } \mathbf{m}_i = [m_{i,1}, m_{i,2}, \cdots, m_{i,d}]^T, \tag{1}$$

where n is moths' number and d is the dimension of the optimization problem. The individual fitness value of moths

is stored in the OM matrix:

$$\mathrm{OM} = [\,\mathrm{OM}_1 \quad \mathrm{OM}_2 \quad \cdots \quad \mathrm{OM}_n]^{\mathrm{T}}. \tag{2}$$

The flame is the optimal position obtained in the local area. Formula (3) describes the optimal position relationship, and the adaptive value is described by OF.

$$\begin{aligned} F &= [\mathbf{f}_1, \mathbf{f}_2, \cdots, \mathbf{f}_n]^T, \\ \text{where } \mathbf{f}_i &= \left[f_{i,1}, f_{i,2}, \cdots, f_{i,d}\right]^T, \end{aligned} \tag{3}$$

$$\mathrm{OF} = [\,\mathrm{OF}_1 \quad \mathrm{OF}_2 \quad \cdots \quad \mathrm{OF}_n\,]^{\mathrm{T}}. \tag{4}$$

2.2. Location Update Mechanism. In the process of position optimization of the MFO algorithm, moonlight is used for positioning and navigation. However, moths are prone to fall into artificially set nonmoonlight navigation, which leads to the wrong position. In daily life, moths fly spirally under the light. This characteristic behavior puts forward the MFO algorithm, and moths constantly update their position relationship through moonlight navigation, so that they can search for the best position scheme.

(1) Flame catching behavior: moth M_j, which has phototactic characteristics in nature, will move towards the nearest light (flame) F_j. Choose the logarithmic spiral described in equation (5) as the moving track of moth catching flame:

$$S\left(M_i, F_j\right) = D_i \cdot e^{bt} \cdot \cos\left(2\pi t\right) + F_j, \tag{5}$$

where $S(M_i, F_j)$ is the updated moth position, b is a constant, t is a random number from -1 to 1, $t = -1$ is the closest to the flame, and $t = 1$ is the farthest from the flame. $D_i = |F_j - M_i|$ is the distance between moths M_j and flames F_j, that is, the step length.

(2) Abandoning flame: MFO constantly adjusts the adaptive value to reach an optimal position, and its flame is constantly decreasing as described by

$$\mathrm{no}_{\mathrm{flame}} = \mathrm{round}\left(N - t \times \frac{N-1}{T}\right). \tag{6}$$

In this, t represents the local maximum iteration number, T represents the global maximum iteration number, and N represents the maximum flame number. Local search is to continuously update the location information of subpopulations to get the optimal location solution. Formula (7) is as follows:

$$\begin{cases} D_i = \mathrm{rand}\,() * \left(x^F - x^M\right), & i = 1, 2, \cdots, m, \\ x^b = x^b + D_i, -D_{\min} \le D_i \le D_{\max}; & i = 1, 2, \cdots, m, \end{cases} \tag{7}$$

where $D_i \in (0, 1)$ and $D_{\min}$ and $D_{\max}$ denote the minimum and maximum moving steps. D_i is the offset of position update and constantly adjusts the current position, so as to achieve a certain position offset during position search, which is more conducive to achieving global optimization.

3. Improved Moth Flame Optimization Algorithm

The nonfree lunch optimization theorem shows that none of the optimization algorithm can solve all optimization problems, and the MFO algorithm also faces the above problems. MFO is prone to premature convergence and fall into local optimum when dealing with complex function problems, so it needs to be improved to improve its performance. Chaos refers to a nonrepetitive chaotic dynamic system with ergodicity. Kent chaos and logistic chaos are isomorphic, and it has been proven that they can search accurately with good distribution. Literature [14–16] compares the ergodicity of the two. The logistic probability distribution is uniform in the middle and high at both ends, resulting in uneven ergodicity of logistic mapping. However, Kent mapping is evenly distributed in each interval, and good randomness, ergodicity, and uniform distribution characteristics are beneficial for the MFO algorithm to mine around the local optimal solution to search for a better solution. In addition, weight parameters have an important influence on the global and local search of the MFO algorithm, and a single invariant fixed weight will restrict the function of weight adjustment. In order to further improve the convergence accuracy, besides considering the iterative stage of the algorithm, the fitness value of the moth in the iterative process should also be considered; that is, a linear decreasing inertia weight adjustment strategy determined by the iterative stage and the fitness value of the moth is proposed.

3.1. Linear Declining Inertia Weight Adjustment Strategy. With the continuous optimization of the current value of the MFO algorithm, the algorithm falls into the local optimum in the complex and high-dimensional optimization process and cannot jump out of the local search process. Experimental simulation shows that the global optimal effect can be achieved by adjusting the inertia weight. Therefore, this paper considers that the inertia weight will degrade the performance of the algorithm in the complex nonlinear optimization function. Combined with the adaptive degree value, a position updating method is proposed to change the inertia weight.

$$\begin{aligned} t_i &= \left(t_{\mathrm{start}} - t_{\mathrm{end}}\right)\frac{\mathrm{maxiter} - i}{\mathrm{maxiter}} + t_{\mathrm{end}}, \\ \Phi_{\mathrm{fit}} &= \frac{2}{1 + e^{-\mathrm{fit}_i/\mathrm{maxiter}}}, \\ w_i &= \Phi_{\mathrm{fit}} * t_i, \end{aligned} \tag{8}$$

where t_{start} is the initial value of the algorithm, t_{end} is the final value of the algorithm, $0 < t_{\mathrm{start}} < t_{\mathrm{end}} < 1$, maxiter is the

maximum number of iterations of the algorithm, i is the current number of iterations, t_i is the inertia weight, Φ_{fit} is the fitness value factor associated with fit, and w_i is the adaptive inertia weight.

In order to make better use of inertia weight adjustment to achieve local and global search ability, the object position update formula after inertia weight w_i is introduced into the algorithm which is updated to

$$D_i^k(t+1) = w_i * D_i^k(t) + v_i^k(t+1). \tag{9}$$

w_i plays a decisive role in the value range of D_i^k and decreases with the local optimal solution approaching the optimal solution. The learning experience optimization value of MFO is adopted to improve the optimization ability of MFO.

w_i represents the predicted trajectory of the MFO motion. When the local optimal solution appears, the inertia weight is relatively large, which leads to the local optimal value; when the global optimal solution appears, the inertia weight is characterized as relatively small, which is more conducive to the further search of the whole local optimal value. Further optimize the linear inertia weight:

$$\omega_i(t) = (\omega_{\max} - \omega_{\min}) \frac{\max \text{iter} * \sum_{i=1}^{m} \max it_i - \text{fit}_j * \sum_{j=1}^{it} \max \text{fit}_j}{\max \text{iter} * \sum_{i=1}^{m} \max it_i} + \omega_{\min}. \tag{10}$$

$\omega_i(t)$ represents the inertia weight of each i moth; $\omega_{\max}$ and $\omega_{\min}$ represent the maximum and minimum values of inertia weights. fit_j represents the number of iterations of the current subpopulation, and $\max it_i$ represents the maximum number of iterations of the subpopulation. The linear inertia weight decreases linearly with the increase in population iteration times. The linear decreasing strategy of inertia weight is simple and intuitive and has good optimization ability. However, the local search process of the population is a nonlinear and complex process, and the linear decrease in inertia weight cannot accurately reflect the search process. Therefore, this paper puts forward inertia weight:

$$\omega_i(t) = (\omega_{\max} - \omega_{\min}) \sqrt{\frac{\left(\text{fit}_j * \sum_{j=1}^{it} \max \text{fit}_j\right)}{it}}. \tag{11}$$

The above linear inertia weights are decreasing, and with the continuous iteration of the algorithm, the inertia weights will become smaller and smaller. When the inertia weight is initialized and when the inertia weight changes obviously, it shows that the local optimal situation is easy to appear. When the inertia weight algorithm does not change obviously in the later period, it shows that the algorithm is searching for the global optimal solution and it is easy to get the global optimal solution.

3.2. Moth Cross-Border Mirror Strategy. Formula (9) constantly optimizes the position, but the coordinates are easy to cross the boundary and will be limited to the boundary. In this way, the performance of the algorithm will be reduced a lot, and the global optimal value cannot be obtained, thus affecting the overall performance of the MFO algorithm. In view of the above problems, the boundary problem is adjusted by

$$m_{i,j} = \begin{cases} 2L_j - \text{rand}\,() \times m_{i,j}, & m_{i,j} \le L_j, \\ 2U_j - \text{rand}\,() \times m_{i,j}, & m_{i,j} > U_j, \end{cases} \tag{12}$$

where $m_{i,j}$ is the j-th dimension crossing position in the i-th moth; L_j and U_j are the value ranges of the j-th dimension. The multiple repetitive operation formula (12) can map $m_{i,j}$ to the range of the dimension, thus ensuring the diversity of the population and effectively improving the optimization performance of the MFO algorithm.

As the fitness value and iteration times show a nonlinear decreasing trend, Figure 1 shows the dynamic inertia weight change curve. The MFO algorithm iteration is the trend of change in Figure 1; when the algorithm is in the initial stage, the value is close to 1. It decreases rapidly with the change of iteration number and fitness value. When the iteration number is 35, the W value is about 0.293. The optimized position is shown in

$$S(M_i, F_j) = \omega_i \cdot D_i \cdot e^{bt} \cdot \cos(2\pi t) + (1 - \omega_i) \cdot F_j. \tag{13}$$

Dynamic inertia weights and iteration times and fitness value show a nonlinear relationship and artificial moth adaptive value to the better flame movement and effectively improve the search ability of the MFO algorithm.

3.3. IMFO Algorithm Steps. The IMFO is shown in Algorithm 1.

4. IMFO Algorithm Performance Test

This paper selects four commonly used functions for experimental comparison.

(1) Ackley function

$$f(x) = -20 * e^{\left(-0.2\sqrt{0.5\left(x_i^2 + x_j^2\right)}\right)} - e^{\left(0.5 * \cos(2\pi x_i) + \cos\left(2\pi x_j\right)\right)} + e + 20. \tag{14}$$

The optimal values are $\min(f(x*)) = 0$.

(2) Beale function

$$f(X) = \sum_{i=1}^{n} \left[x_i^2 - 10\cos(2\pi x_i) + 10\right], |x_i| \le 5.2. \tag{15}$$

The optimal values are $\min(f(x^*)) = 0$.

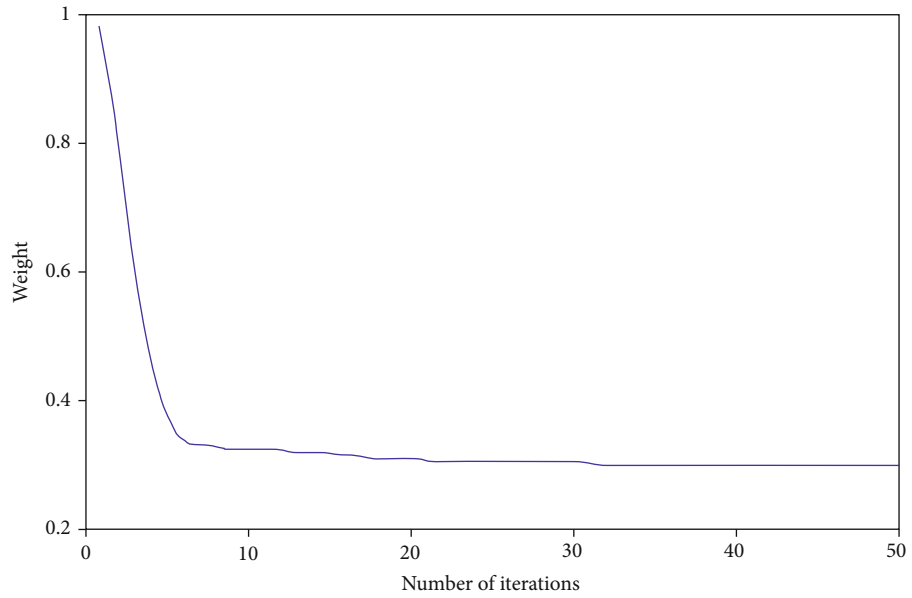

Figure 1: Dynamic inertia weight curve.

Parameter setting: population size (*sizepop*), dimension (*d*), maximum iteration number (*Maxiter*), current iteration number (*Iteration*), etc.
Initialize Moths and Flames
While (*Iteration* < =*Max_iterations*)
OM = FitnessFunction (*M*);
Update the number of MFO's algorithm flames according to equation (13);
If *Iteration*==1
F=*sort (m);*
OF=*sort (OM);*
Else
F=sort ($M_{t\text{-}1}$, M_t); //*t* is the current number of iterations
OF=sort ($OM_{t\text{-}1}$, OM_t);
End
For *i*=1: *sizepop*
For *j*=1: *d*
Calculate $D_i = |F_j - M_i|$;
Update D_i according to formula (7);
End
End
Update the new D_i according to formula (11);
Treat trans boundary moths according to formula (12);
Calculate $D_i = |F_j - M_i|$ and update the moth position according to Equation (13);
End
Terminate and output the global optimal solution moth.

Algorithm 1: IMFO implementation steps

(3) Rastrigin function

$$f(x) = -\left|\sin\left(x_i\right)\cos\left(x_j\right)\exp\left(\left|100 - \frac{\sqrt{x_i^2 + x_j^2}}{\pi}\right|\right)\right|. \quad (16)$$

The optimal values are $\min\left(f(x^*)\right) = 0$.

Table 1: Benchmark function.

Function	Function name	Value range	Optimal position	Optimal value
f_1	Ackley	$[-5, 5]^D$	$[0]^D$	0
f_2	Beale	$[-4.5, 4.5]^D$	$(3, 0.5)^D$	0
f_3	Rastrigin	$[-5.2, 5.2]^D$	$[0]^D$	0
f_4	Sphere	$[-100, 10]^D$	$[0]^D$	0

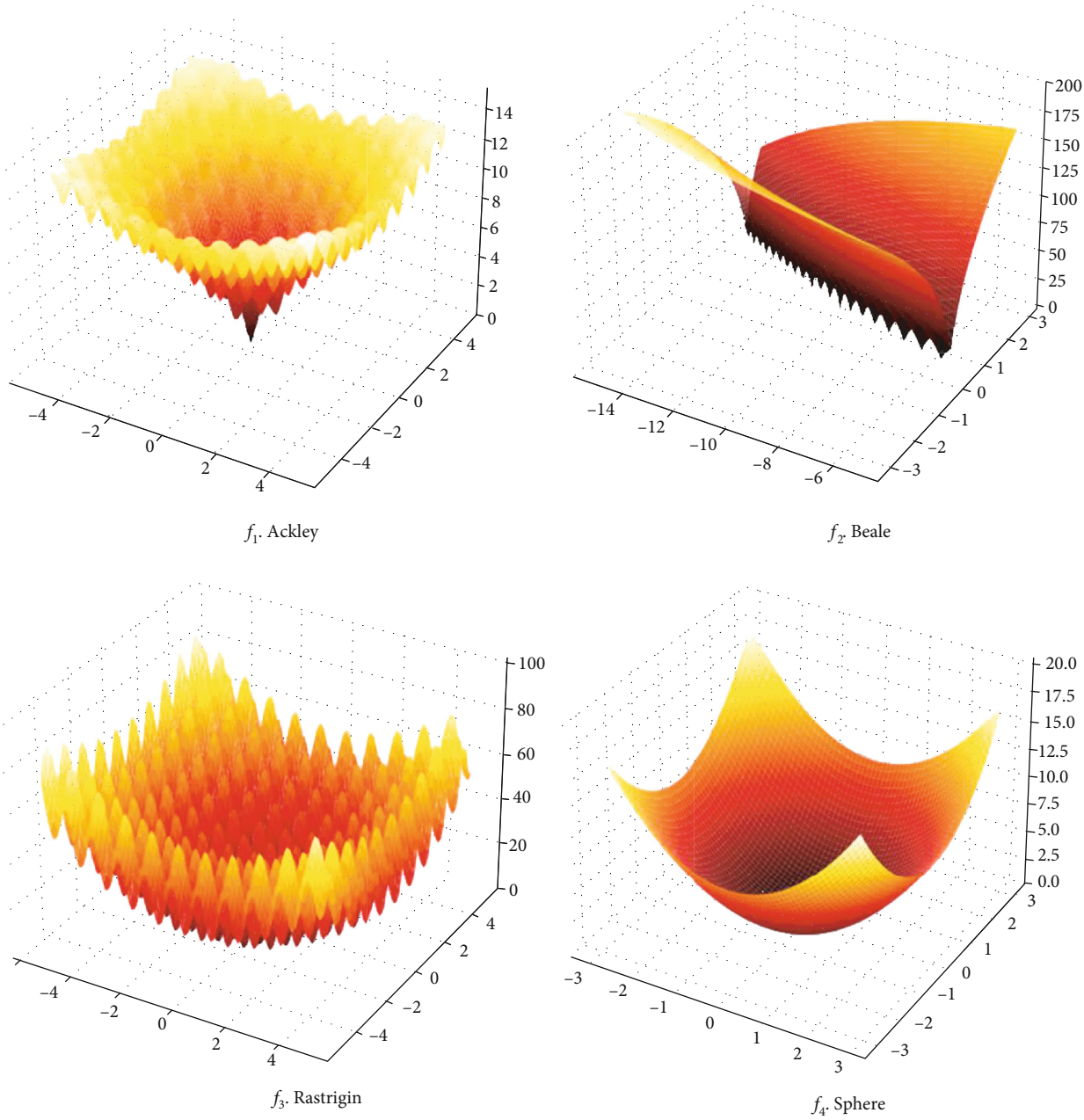

FIGURE 2: f_1-f_4 function schematic diagram.

(4) Sphere function

$$f(x) = \sum_{i=1}^{n} x_i^2. \tag{17}$$

The optimal values are $\min(f(x^*)) = 0$.

The Rastrigin function has many local optima, and global optimum is difficult; the Ackley function has less global optimum and more local optimum; the Griewank function has several local optimum solutions, and the global optimum solution is difficult to realize. The optimal range and global optimal value of the four functions are shown in Table 1. According to the above operation results, f_1-f_4 function is shown in Table 1.

The above $f1$-$f4$ function is tested, and its function image is shown in Figure 2.

f_1-f_4 test functions are representative, including unimodal functions and multimodal functions. The purpose of the test is to detect the advantages of the proposed algorithm in algorithm performance. From the sequencing effect of the f_1-f_4 function, the algorithm proposed in this paper has obvious advantages. The theoretical value is the global optimum value. Generally, there are one theoretical value and several

Table 2: Comparison of PSO, MFO, and IMFO results.

Function	Dimension	PSO		MFO		IMFO	
		Mean	MSD	Mean	MSD	Mean	MSD
f_1	10	2.435	6.325×10^{-1}	8.652×10^{-15}	4.551×10^{-14}	8.754×10^{-16}	0
	30	4.231	5.547×10^{-1}	3.578×10^{-2}	5.621×10^{-3}	8.654×10^{-16}	0
	50	7.914	1.314	1.135×10^{-1}	1.789	8.231×10^{-16}	0
f_2	10	4.937	1.634	2.451×10^{-1}	1.625×10^{-1}	0	0
	30	4.249×10^{-1}	3.467	1.235×10^{-2}	3.331×10^{-1}	0	0
	50	1.124×10^{-1}	5.657	3.142×10^{-2}	5.624×10^{-1}	0	0
f_3	10	7.984	3.741	2.451×10^{-1}	1.537×10^{-1}	0	0
	30	4.314×10^{-1}	6.754	2.145×10^{-2}	3.354×10^{-1}	0	0
	50	6.654×10^{-1}	5.625×10^{1}	2.578×10^{-2}	5.624×10^{-1}	0	0
f_4	10	3.147×10^{-9}	5.124×10^{-8}	6.514×10^{-31}	6.457×10^{-30}	7.985×10^{-192}	0
	30	1.987×10^{-2}	1.621×10^{-2}	3.245×10^{-3}	5.524×10^{-3}	2.547×10^{-107}	1.214×10^{-106}
	50	3.541×10^{-1}	7.951×10^{-2}	7.954×10^{-3}	7.714×10^{-3}	2.312×10^{-94}	1.112×10^{-93}

Table 3: Air quality index (gas concentration (ppm)) of downhole operation.

Status	NO_2	CO	SO_2	H_2S	CH_4	CO_2
Excellent	0-1	1-13	0-2.5	0-3	0-1000	1-2000
Good	1-2	13-23	2.5-4	3-5	1000-2000	2000-3000
Medium	2-3	23-30	2-6	5-13	2000-4000	3000-4000
Poor	3-4	30-49	6-8	13-20	4000-5000	4000-5000
Worst	>4	>49	>8	>20	>5000	>5000

local optimum values in multimodal functions. If the test result of the function reaches or approaches the theoretical value, it represents the global optimal value.

The design dimensions of the common functions are 10, 30, and 50, respectively. The test function is tested 100 times, and the average value is taken, and the optimal average value (mean) and standard deviation (SD) are taken. Table 2 lists the numerical results of PSO, MFO, and IMFO under four test functions.

From the test average and mean square error analysis of the four algorithms in Table 2, PSO and MFO algorithms have the same performance, and the IMFO algorithm is the best. For functions f_1-f_4, the performance of the IMFO algorithm is globally optimal. When the dimension is increased to 50, the IMFO optimization performance still has high accuracy, and the standard deviation is the smallest among the four algorithms. The optimal solution found by IMFO for the f_4 test function does not reach the theoretical optimal value and is still the smallest in value compared with other algorithms. For the multimodal function f_1, the IMFO algorithm is improved from 8.652×10^{-15}, 3.578×10^{-2}, and 1.135×10^{-1} optimized by MFO to 8.754×10^{-16}, 8.654×10^{-16}, and 8.231×10^{-16} in 10, 30, and 50 dimensions, respectively. The standard deviation is 0, and the IMFO algorithm has the best performance.

5. Experimental Simulation and Analysis

5.1. Monitoring of Chemical Gas Concentration. Due to the danger of CH_4, CO_2, CO, NO_2, H_2S, and SO_2 emitted from coal seam during mining, effective monitoring of these gas concentrations can improve the safety of downhole operation. The safety level of chemical gas is shown in Table 3.

Underground air quality monitoring can predict the danger, can effectively predict the future air quality, and can establish a set of safe methods.

The IMFO algorithm proposed in this paper is used to predict the air quality of underground operation and give early warning of possible dangers in time. The errors of using three algorithms to predict underground air quality are shown in Figures 3 and 4.

The IMFO algorithm in the prediction of chemical gas algorithm error is the best and can achieve the effect of prediction.

5.2. Location Prediction Algorithm. In order to verify and analyze the positioning accuracy and antinoise performance of this method, MATLAB simulation experiments are carried out and compared with PSO, MFO, and IMFO algorithms proposed in this paper. Because of the special underground environment, the accuracy of spatial ranging is affected, so the simulation environment is set to be in a cuboid three-dimensional area with a certain size.

Objective function is a standard to measure the advantages and disadvantages of IMFO. In each iteration of the algorithm, the position of moths needs to be updated according to the value of objective function. It is assumed that M beacon nodes are deployed in the location area, their coordinates are (x_i, y_i, z_i), $i = 1, 2, \cdots, m$; the coordinates of unknown nodes are (x, y, z); the distance measured by the RSSI method is d_i; and the average location error is the average value of the location error obtained by repeating the experiment 30 times. In order to reduce the ranging error,

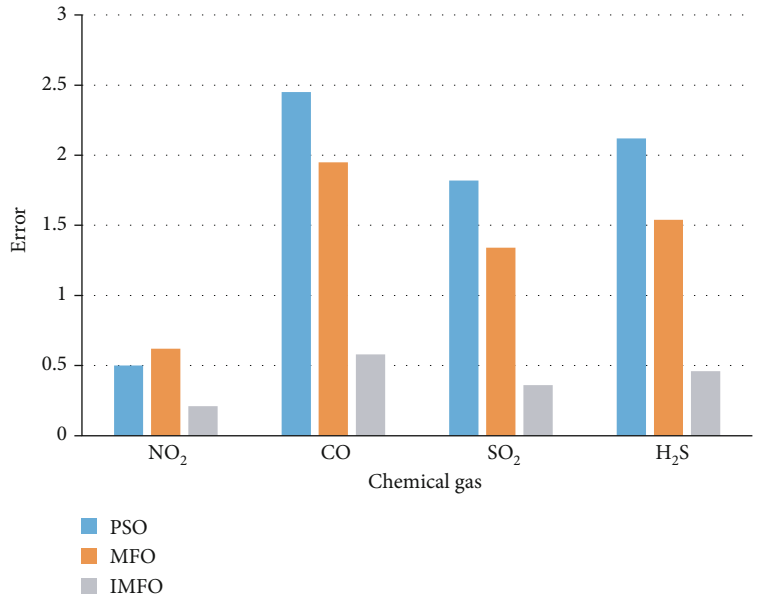

Figure 3: Comparison of prediction errors of chemical gases NO_2, CO, SO_2, and H_2S.

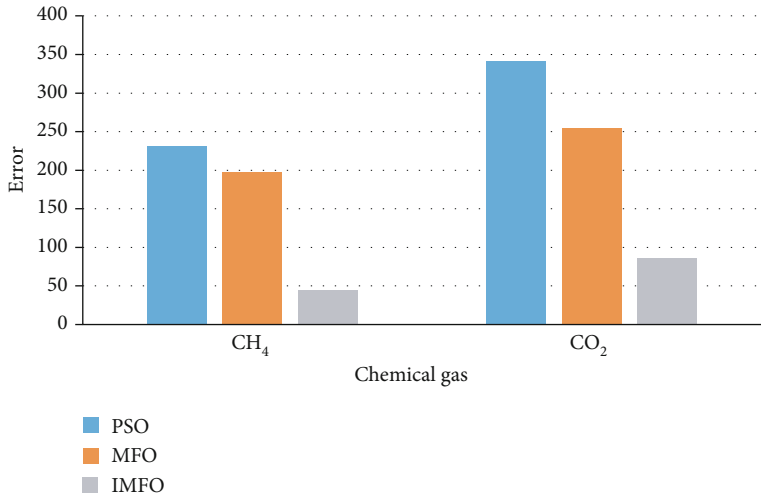

Figure 4: Comparison of prediction errors of chemical gases CH_4 and CO_2.

Table 4: Positioning simulation data.

Node ID	Actual coordinates	Node ID	Actual coordinates
1	(1, 2, 3)	9	(4, 1, 4)
2	(2, 2, 4)	10	(4, 2, 5)
3	(2, 3, 4)	11	(4, 4, 3)
4	(2, 5, 6)	12	(5, 2, 4)
5	(3, 1, 2)	13	(5, 3, 5)
6	(3, 2, 3)	14	(5, 4, 3)
7	(3, 4, 2)	15	(6, 3, 4)
8	(3, 5, 5)	16	(6, 4, 2)

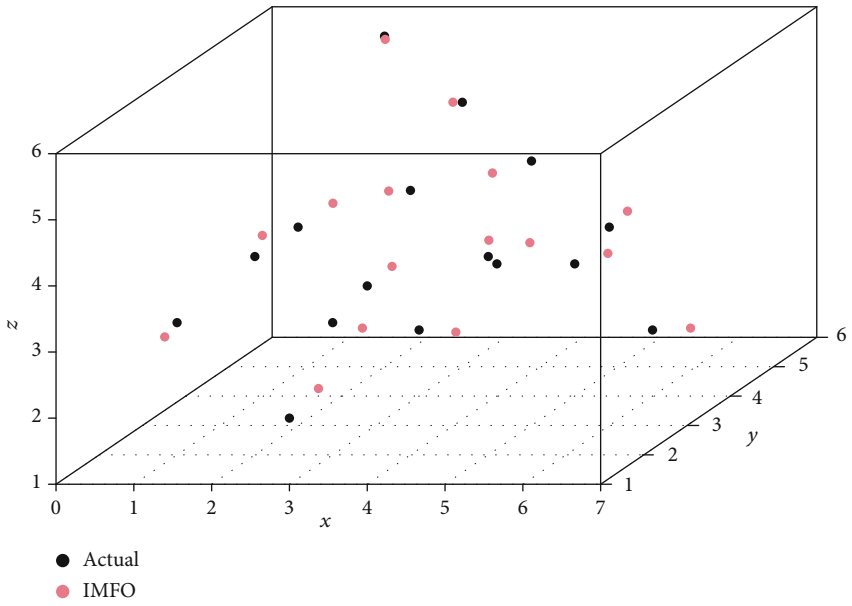

Figure 5: Spatial distribution of the IMFO algorithm and actual coordinates.

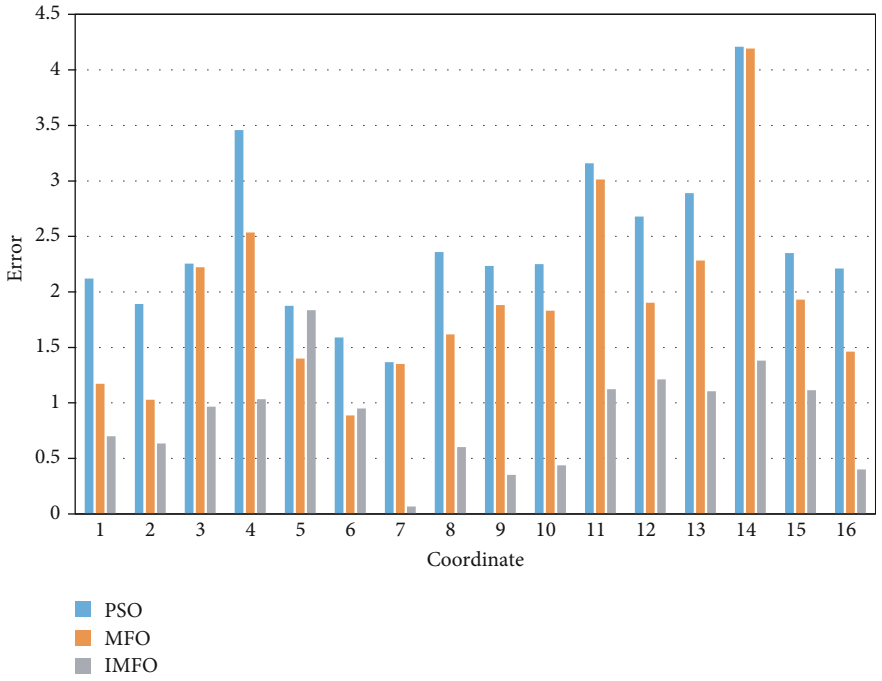

Figure 6: Comparison of errors under three algorithms.

the mean square error of the measured distance and the estimated distance of the unknown node and the beacon node is taken as the optimization objective function. The objective function is

$$f(x,y,z)=\sqrt{\frac{1}{m}\sum_{i=1}^{m}\left(\sqrt{(x-x_i)^2+(y-y_i)^2+(z-z_i)^2}-d_i\right)^2}. \tag{18}$$

The coordinate data in a specific area are shown in Table 4.

The IMFO algorithm is used to predict the actual coordinates, and the effect is shown in Figure 5.

The errors of PSO, MFO, and IMFO algorithms are compared below, and the errors are compared and analyzed by equation (18). The results are shown in Figure 6.

As can be seen from Figure 6, IMFO has the smallest error in different coordinates compared with other algorithms, and most values are less than 1.

6. Conclusion

The wireless sensor network technology and algorithm used to realize accurate mine positioning are an important research direction of the mine positioning system at present. Whether the massive data generated under the above technical background can accurately measure the specific position has become a hot spot in the research of the positioning algorithm. In this paper, the IMFO algorithm is proposed to compare the predicted coordinates with the actual coordinates in a specific area, and the prediction effect is good and the error is small. Further research in the future focuses on the problem of signal transmission, the diversity of prediction, and the application of algorithms in different scenarios. It can compare other intelligent algorithms and select the advantages of different algorithms to fuse to predict.

Data Availability

The raw data supporting the conclusions of this article will be made available by the authors, without undue reservation.

Conflicts of Interest

The authors declared that they have no conflicts of interest regarding this work.

Acknowledgments

This work was supported in part by the Science and Technology Research Program of Chongqing Municipal Education Commission (Grant nos. KJZD-K201902101 and KJQN-2019021002).

References

[1] J. J. Ramírez, "Radio frequency identification (RFID) technology for academic, logistics and passenger transport applications," *Ingeniería E Investigación*, vol. 32, no. 3, pp. 58–65, 2012.

[2] J. S. Lim, W. H. Jang, G. W. Yoon, and D. S. Han, "Radio map update automation for WiFi positioning systems," *IEEE Communications Letters*, vol. 17, no. 4, pp. 693–696, 2013.

[3] G. Li-Peng and J. Han-Wen, "A strong anti-interference capability location algorithm based on RSSI," in *2012 Second International Conference on Instrumentation, Measurement, Computer, Communication and Control*, pp. 290–295, Harbin, China, 2012.

[4] J. An, Y. Yu, J. Tang, and J. Zhan, "Fuzzy-based hybrid location algorithm for vehicle position in VANETs via fuzzy Kalman filtering approach," *Advances in Fuzzy Systems*, vol. 2019, Article ID 5142937, 11 pages, 2019.

[5] W.-B. Du, Y. Gao, C. Liu, Z. Zheng, and Z. Wang, "Adequate is better: particle swarm optimization with limited-information," *Applied Mathematics and Computation*, vol. 268, pp. 832–838, 2015.

[6] M. Taherkhani and R. Safabakhsh, "A novel stability-based adaptive inertia weight for particle swarm optimization," *Applied Soft Computing*, vol. 38, pp. 281–295, 2016.

[7] Y. L. Wang, Y. R. Huang, and L. G. Qu, *Improved Centroid Localization Algorithm in Application of Underground Personal Positioning*, M. Jixie, Ed., vol. 33, no. 8, 2012Coal Mine Machinery, 2012.

[8] F. Müller, D. Schug, P. Hallen, J. Grahe, and V. Schulz, "Novel DOI positioning algorithm for monolithic scintillator crystals in PET based on gradient tree boosting," *IEEE Transactions on Radiation and Plasma Medical Sciences*, vol. 3, no. 4, pp. 65–474, 2019.

[9] J. Wang, Y. Guo, L. Guo, B. Zhang, and B. Wu, "Performance test of MPMD matching algorithm for geomagnetic and RFID combined underground positioning," *IEEE Access*, vol. 7, pp. 129789–129801, 2019.

[10] K. Chen, C. Wang, L. Chen, X. Niu, Y. Zhang, and J. Wan, "Smart safety early warning system of coal mine production based on WSNs," *Safety Science*, vol. 124, p. 104609, 2020.

[11] B. Cao, S. Wang, S. Ge, W. Liu, S. Wang, and S. Yi, "Study on the improvement of ultra-wideband localization accuracy in narrow and long space," *Sensor Review*, vol. 40, no. 1, pp. 42–53, 2019.

[12] X. Liu, W. Jiang, Z. Li, H. Chen, and W. Zhao, "Comparison of convergence time and positioning accuracy among BDS, GPS and BDS/GPS precise point positioning with ambiguity resolution," *Advances in Space Research*, vol. 63, no. 11, pp. 3489–3504, 2019.

[13] S. Mirjalili, "Moth-flame optimization algorithm: a novel nature-inspired heuristic paradigm," *Knowledge-Based Systems*, vol. 89, pp. 228–249, 2015.

[14] N. S. Rebecca, H. S. Mohd, and M. Zuriani, "Optimal reactive power dispatch solution by loss minimization using moth-flame optimization technique," *Applied Soft Computing*, vol. 59, pp. 210–222, 2017.

[15] Y. Shen, "Research on fault reconfiguration of shipboard zonal distribution system based on improved moth-flame algorithm," *World Scientific Research Journal*, vol. 6, no. 3, pp. 118–125, 2020.

[16] E. Emary and H. M. Zawbaa, "Impact of chaos functions on modern swarm optimizers," *PLoS One*, vol. 11, no. 7, pp. 1–26, 2016.

[17] L. I. Zhiming, Z. H. O. U. Yongquan, and Z. Sen, "Lévy-flight moth-flame algorithm for function optimization and engineering design problems," *Mathematical Problems in Engineering*, vol. 2016, Article ID 1423930, 22 pages, 2016.

[18] C. Hou, Y. Wen, Y. He et al., "Public stereotypes of recycled water end uses with different human contact: evidence from event-related potential (ERP)," *Resources, Conservation and Recycling*, vol. 168, article 105464, 2021.